

isb2021.com



XXVIII Congress of the International Society of Biomechanics (ISB)

Program & Abstracts

Digital Congress 25-29, July 2021

Congress sponsor

QUALISYS
Motion Capture Systems

Major sponsors

VICON **XSENS**

Basic Sponsor

novel.de 

Qualisys Partners

 **DELSYS**
WEARABLE SENSORS
FOR MOVEMENT SCIENCES

 **AMTI**
FORCE AND MOTION

 **h/p/cosmos**

NORAXON

Arranged by

 International Society
of Biomechanics

 **GIH** THE SWEDISH
SCHOOL OF SPORT
AND HEALTH SCIENCES

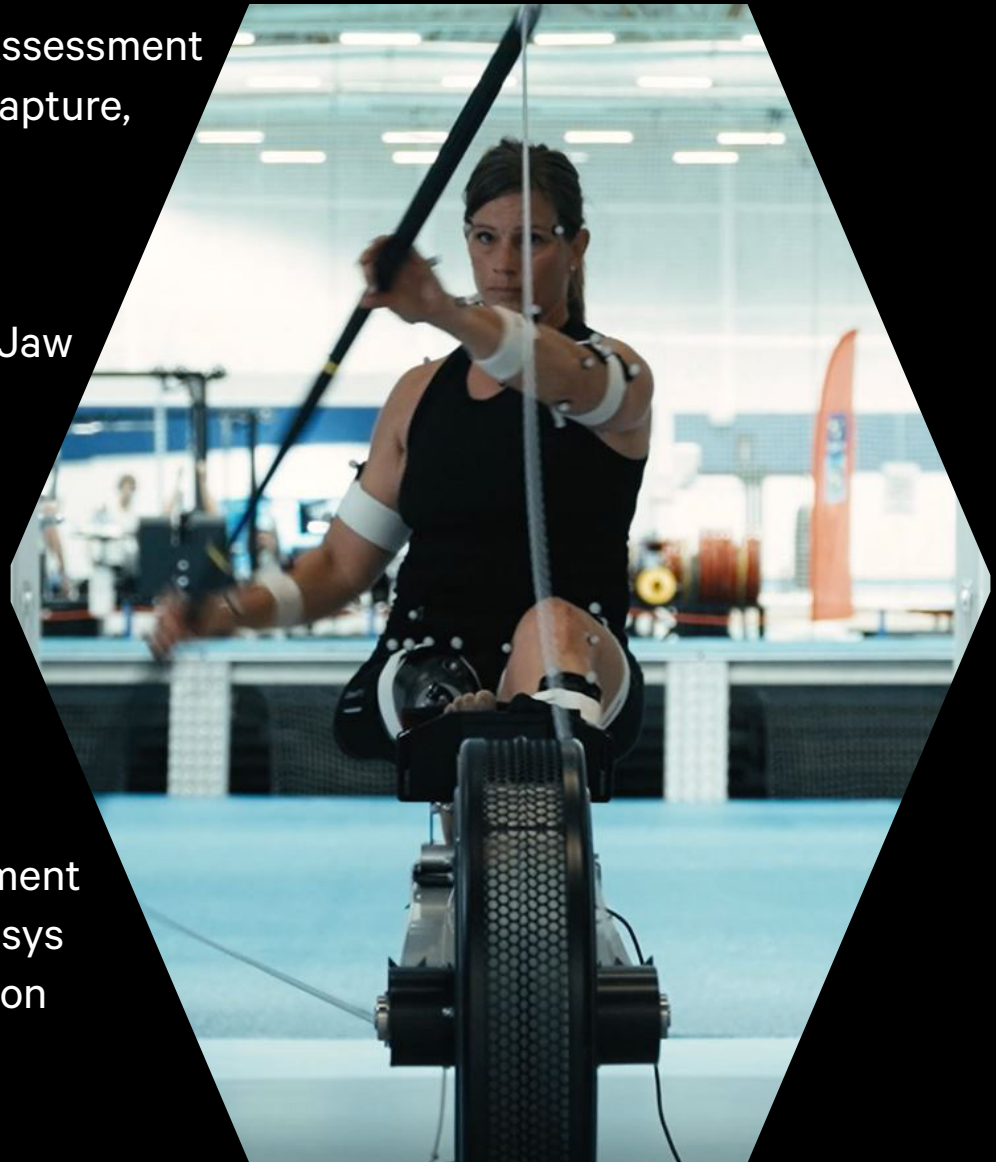


 **Karolinska
Institutet**

QUALISYS

QUALISYS is proud to support the biomechanics community by being main congress sponsor of ISB 2021. For more than 30 years, we have been supplying motion capture systems for researchers, athletes, coaches, and clinicians. Together with our partners, we run daily live workshops from Qualisys ISB Studio. Check the congress program for the schedule. We are looking forward to seeing you!

- Objective Functional Assessment with Qualisys motion capture, Delsys EMG and AMTI force plates
- Innovative Analysis of Jaw Movement with Delsys EMG and Qualisys Motion Capture
- Qualisys and Theia Markerless workflows: hands-on session
- Fully Integrated Movement Assessment with Qualisys Motion Capture, Noraxon EMG and h/p/cosmos instrumented treadmill



Helene Ripa, a World famous paralympic athlete, is practicing at Bosön, Sweden.



Contents

Welcome	4
Program overview	5
Detailed program–Monday	6
Detailed program–Tuesday	24
Detailed program–Wednesday	40
Detailed program–Thursday	61
Abstracts	81



Welcome

to the XXVIII Congress of the International Society of Biomechanics!

For the first time ever this meeting will be held fully digitally and we are sure we will set a benchmark for successful digital meetings. Despite the financial, travel and personal difficulties imposed by the Covid-19 pandemic, we are excited to announce that over 1000 people have registered and that companies continue to be attracted to support the ISB.

The congress will start with the traditional educational tutorials with the highly relevant and stimulating topics of wearable sensors, imaging and modelling, deep learning and optimal control in biomechanics: <https://isb2021.com/program/tutorials/>. We are also extremely proud to have attracted such an eminent list of Award and Keynote lecturers: <https://isb2021.com/speakers/>. In order to promote discussion and insight into some cutting edge and controversial issues in biomechanics we have a strong focus on five panel debates with world experts on the topics: the distribution problem in biomechanics and motor control; markerless vs marker motion capture; scientific peer review; biorobotics; computational approaches on studying locomotion disorders. Please visit here to find details concerning these debates and the internationally renowned biomechanists leading them: <https://isb2021.com/program/debates/> Special sessions have been organised by the ISB Hand and Wrist Biomechanics International and Motor Control Technical Groups and also one on Computer Simulation.

The congress will also include student social events, student mentoring possibilities and Advancing Women in Biomechanics sessions. Also, a new format is being explored for exposing the fantastic sponsors, whom, despite the difficulties experienced during the Covid-19 pandemic have remained loyal to ISB. The congress sponsor (Qualisys and partners) and the major sponsors (Vicon, Xsens) will have special sessions in which to present their companies to all delegates – we are sure this will be a new level of digital exposure for congress sponsors!

Every effort has been made to make the congress as attractive as possible in the digital format. We have staggered the days so that material is available to different time zones on different days, all oral and plenary presentations will be live so that a discussion is possible and all material will be recorded and available to registered delegates for 30 days after the congress.

Many generous scientific awards will be presented including two new ISB awards: the Jaqueline Perry Emerging Female Scientist Award and the World Athletics Award for Biomechanics.

We are confident that ISB2021 will be a truly exciting event with an exceptional level of scientific content! We are happy to welcome you to ISB2021, the most gender equal ISB congress ever.

Dr. Arndt
Professor in Biomechanics
Swedish School of Sport and
Health Sciences (GIH)

Dr. Gutierrez Farewik
Professor in Biomechanics
KTH Royal Institute of Technology

Dr. Felländer-Tsai
Professor and senior consultant
in Orthopaedics
Karolinska Institutet

	Sunday 25 July	Monday 26 July	Tuesday 27 July	Wednesday 28 July	Thursday 29 July
CET					
7 0	Welcome	Keynote lecture: Bronwen Ackermann Music Performance Biomechanics – using biomechanical principles to guide rehabilitation of injured musicians break		Short welcome	
15	A1	Oral A1		Oral F1	Oral F8
30	A2	Oral A2		Oral F2	Oral F7
45	A3	Oral A3		Oral F3	Oral F6
8 0	A4	Oral A4		Oral F4	Oral F5
15	A5	Oral A5		Conference sponsor: Qualisys	
30	A6	Oral A6		Panel debate: Special Oral: Developing Countries Grant Competition break	
45	A7	Oral A7		Computational approaches to studying locomotion disorders: NMSM Vs. AI break	
9 0	A8	Oral A8		Keynote lecture: Hazel Screen Tendon structure-function relationships in health and disease: Exploring the interfascicular matrix break	
15		Poster A		Advancing Women in Biomechanics meeting	
30			Student happy hour	ISB AGM	
45		Poster Quiz	Short welcome	Short welcome	
12 0	B1	Oral B1	Keynote lecture: Yves Vanlandewyck The Role of Biomechanics in Evidence-Based Paralympic Classification	Oral H1	Oral H8
15	B2	Oral B2		Oral H2	Oral H7
30	B3	Oral B3		Oral H3	Oral H6
45	B4	Oral B4		Oral H4	Oral H5
13 0	B5	Oral B5	Conference sponsor: Qualisys	Oral H5	Oral H4
15	B6	Oral B6	break	Oral H6	Oral H3
30	B7	Oral B7	Oral C1	Oral H7	Oral H2
45	B8	Oral B8	Oral C2	Oral H8	Oral H1
14 0		Lunch break	Oral C3	Poster C	
15		Panel debate: The Distribution Problem in Biomechanics and Motor Control	Oral C4	Poster quiz	
30		break	Oral C5	Lunch break	
45		Wartenweiler award lecture: Susan S. Margulies	Oral C6	Lunch break	
15 0		Social Mingle	Oral C7	Lunch break	
15			Oral C8	Lunch break	
30		Tutorial 3: Deep learning applications in biomechanics	Lunch break	Lunch break	
45			break	Lunch break	
16 0			Major sponsors	Keynote lecture: Lori Ploutz-Snyder How do biomechanical factors influence exercise prescription on the International Space Station?	
15			Panel debate: Peer review in science	Conference sponsor: Qualisys	
30			Panel debate: Biorobotics — How Biology will inform the next-gen machines	break	
45			break	Oral I1	
17 0		Tutorial 4: Optimal control in biomechanics	Oral D1	Oral G1	Oral I2
15			Oral D2	Oral G2	Oral I3
30			Oral D3	Oral G3	Oral I4
45			Oral D4	Oral G4	Oral I5
18 0			Oral D5	Oral G5	Oral I6
15			Oral D6	Oral G6	Oral I7
30			Oral D7	Oral G7	Oral I8
45			Oral D8	Oral G8	Oral I1
19 0			break	break	
15			break	break	
30			Muybridge award lecture: Scott L. Delp	ISB President's lecture: Toni Arndt	
45			Oral E1	break	
15			Oral E2	Awards presentations	
30			Oral E3	break	
45			Oral E4	Social Mingle	
20 0			Oral E5	Closing	
15			Oral E6	Social Mingle	
30			Oral E7	Social Mingle	
45			Oral E8	Social Mingle	
21 0			Advancing Women in Biomechanics meeting	Social Mingle	
15				Social Mingle	
30				Social Mingle	
45				Social Mingle	
22 0				Social Mingle	

Mon 26 Jul 2021

07:00 - 07:15

WELCOME

07:15 - 08:15

KEYNOTE LECTURE: MUSIC PERFORMANCE BIOMECHANICS - USING BIOMECHANICAL PRINCIPLES TO GUIDE REHABILITATION OF INJURED MUSICIANS (BRONWEN ACKERMANN)

Location: Online

BRONWEN ACKERMANN

Associate Professor Bronwen Ackermann is a specialist musicians' physiotherapist, musculoskeletal anatomist and medical science researcher focussing on musicians' health at the University of Sydney. Her research has focussed on interventions that can inform evidence-based approaches to optimising musical performance as well as preventing, assessing and managing performance-related injuries in musicians. Her research has utilised technologies including electromyography, 3D motion capture and fMRI imaging technology to better understand mechanisms underpinning healthy and pathological muscle usage patterns during musical performance. Additionally, she has worked extensively clinically with musicians using qualitative motion analysis, including video feedback and fine-motor coordination assessment, particularly for music-specific actions involving the upper limb, as well as orofacial and respiratory structures.



She was responsible for developing and leading the intensive Essentials of Performing Arts Medicine annual training course for the Performing Arts Medicine Association (PAMA) and American College of Sports Medicine (USA), authored an online e-health training program for musicians (www.soundperformers.com), led the first international occupational health and safety program for a national cohort of orchestral musicians (Sound Practice), and worked as the High Performance Consultant at the Australian National Academy of Music from 2012-2020. Internationally she collaborates extensively in research, teaches on a wide range of musicians' health topics, and has authored over 70 publications. Currently, she is a Humboldt Fellow in Germany, evaluating a clinical movement retraining program she designed to assess and treat task-specific movement dysfunctions, specifically embouchure (orofacial) dystonia and focal hand dystonia.

08:15 - 08:30

BREAK

Location: Online

08:30 - 09:30

OA1 - ARTIFICIAL INTELLIGENCE AND MACHINE LEARNING

Location: Online

Chair: Kim Duffy

Pres Time	Presentation title/Abstract title	Speakers/Authors
8:30	Generating 2D video frames from 3D motion capture data: a proof-of-concept study	Marion Mundt
8:42	Rib injury prediction using machine learning-based surrogate models	Shitij Malik
8:54	A machine learning approach for error detection in rowing	Oscar Sten
9:06	Validation of an AI assisted simple method to study muscle-tendon dynamics during running	Christoph Leitner
9:18	Optimal forefoot rocker parameter prediction using machine learning	Fredrik Olsson

08:30 - 09:30

OA2 - BIOMEDICAL ENGINEERING

Location: Online

Chair: Elizabeth Clarke

Pres Time	Presentation title/Abstract title	Speakers/Authors
8:30	Does a prosthetic toe joint affect mechanics or preference when persons with limb loss walk over uneven terrain?	Kirsty McDonald
8:42	Influence of excipients and lesions on drug-coated balloon therapy	Karthic Anbalakan
8:54	Change in mechanical properties of cortical bone under voltage application for formation of mineral components	Fuki Ota
9:06	Production of micro-structured hollow fiber membranes for membrane oxygenators - mimicking nature to increase mass transport	Markus Pekovits
9:18	Passive ankle exoskeletons influence muscle behaviour during unexpected perturbations	James Williamson

08:30 - 09:30

OA3 - CLINICAL BIOMECHANICS

Location: Online

Chair: Laura Diamond

Pres Time	Presentation title/Abstract title	Speakers/Authors
8:30	How does the prosthetic design affect muscle strength after knee arthroplasty surgery?	Iris Mittendorfer
8:42	Do bone defects of the greater trochanter affect the postoperative femoral fracture risk after total hip arthroplasty? A biomechanical study	Michael Saemann

8:54	Trunk kinematics during walking in adults receiving total knee arthroplasty: A systematic review	Tamaya Van Criekeing
9:06	Ambulatory knee mechanics after ACL repair with InternalBrace augmentation compared to healthy controls	Linda Bühl
9:18	Estimation and assessment of sagittal spinal curvature and thoracic muscle morphometry in different postures	Anoosha Pai S

08:30 - 09:30

OA4 - IMAGING

Location: Online

Chair: Geoffrey Handsfield

Pres Time	Presentation title/Abstract title	Speakers/Authors
8:30	Pose and shape registration of ankle bones using statistical shape and intensity model during walking	Jeongseok Oh
8:42	Preliminary Micro-CT imaging of the human tibial plateau under load	Kieran Bennett
8:54	Can synchrotron phase contrast micro-tomography uncover how in vivo loading affects the achilles tendon structure?	Maria Pierantoni
9:06	A principal component analysis of infant gastrocnemius growth in the first two years of life	Ricardo Florez
9:18	Quantitative comparison of fascicle length in lower limb muscles using 3D freehand ultrasound and diffusion tensor imaging	Zhongzheng Wang

08:30 - 09:30

OA5 - LOCOMOTION: GENERAL + CLINICAL GAIT

Location: Online

Chair: Rosemary Dubbeldam

Pres Time	Presentation title/Abstract title	Speakers/Authors
8:30	The feasibility and effectiveness of treadmill-based perturbations for assessing and improving walking stability in chronic obstructive pulmonary disease: a pilot study	Christopher McCrum
8:42	Simultaneous measurements of in vivo knee contact and tendon loading during walking	Colin Smith
8:54	Classification of spatiotemporal gait patterns in unilateral transfemoral amputees	Daisuke Ichimura
9:06	Series elasticity facilitates safe plantarflexor muscle-tendon shock absorption during perturbed human hopping	Taylor Dick
9:18	Musculoskeletal simulation of a gait for a person with unilateral transfemoral amputation: The cause of muscle atrophy	Isna Riski Safira

08:30 - 09:30

OA6 - LOWER EXTREMITIES

Location: Online

Chair: Logan Wade

Pres Time	Presentation title/Abstract title	Speakers/Authors
8:30	Comparative effects of conservative and arthroscopic management of femoroacetabular impingement syndrome on lower limb angles and moments	Tamara Grant
8:42	Accuracy estimation of a MIMU-based functional calibration for ankle kinematics assessment	Paolo Brasiliano
8:54	Effects of 12 different heel rocker designs, configured with different rocker radii, apex positions and apex angles, on plantar pressure	Athra Malki
9:06	The effect of a foot strengthening exercise intervention on restoring foot strength in people with diabetic peripheral neuropathy	Karen Mickle
9:18	The energetic function of the human foot and its muscles during rapid accelerations and decelerations	Ross Smith

08:30 - 09:30

OA7 - MUSCULOSKELETAL MODELLING

Location: Online

Chair: Sofia Brorsson

Pres Time	Presentation title/Abstract title	Speakers/Authors
8:30	Geometrical variations of the hind- and mid-foot and their associated functional consequences	Bryce A Killen
8:42	A mesh contact model for biomechanical simulations with automatic differentiation	Gil Serrancolí
8:54	A model of muscle mechanics elicits the important role of increased baseline tone in joint hyper-resistance in cerebral palsy	Jente Willaert
9:06	Wave propagation in muscles predicted by a Hill-type model with distributed mass	Jianqiao Guo
9:18	Accounting for vessel holes in finite element models of the femur affects strain prediction	Joeri Kok

08:30 - 09:30

OA8 - ORTHOPAEDICS

Location: Online

Chair: Gustavo Orozco

Pres Time	Presentation title/Abstract title	Speakers/Authors
8:30	Cumulative joint damage from repeated mild knee injuries over time	Carina Blaker

8:42	Muscle-tendon morphomechanical properties of non-surgically treated Achilles tendon 1-year post-rupture	Raad Khair
8:54	Analysis of post-operative osteoblastic activity patterns in unicondylar knee arthroplasties slated for revision	Félix Dandois
9:06	Dynamic knee loading in the ACL deficient knee	Georgios Giarmatzis
9:18	Influence of implant alignment on joint laxity following medially-stabilized total knee arthroplasty	Orcun Taylan

09:30 - 09:45

BREAK

Location: Online

09:45 - 10:15

OBJECTIVE FUNCTIONAL ASSESSMENT WITH QUALISYS, DELSYS AND AMTI

Location: Online

Qualisys invites you to experience the Swedish concept of "Fika": taking a break with friends or colleagues to relax, talk and share information. In this first session, our partners Delsys and AMTI will join us to demonstrate a fully integrated, digital workflow to generate a Functional Assessment report.

Our software, QTM, supports a range of force plates and EMG systems which enables force data and EMG capture along with the motion capture. During the session, we will present our integration with AMTI and Delsys and live demos.

The data will be presented in our online report that contains graphs, metrics, video, and a 3D visualization. The interactive report is easy to use, all data are synchronized, and the different sessions can be compared easily.

10:15 - 11:45

POSTER SESSION A

Location: Online

Pres Time	Presentation title/Abstract title	Speakers/Authors
	• Test test Running ISB 2021	Pärnilla Thompson
	• Analysis of biomechanical characteristics during the drop-landing phase with bionic shoes: A pilot study	Ukadike Chris Ugbohue
	• Can intraoperative intra-articular loads predict knee joint laxity? A Cadaveric Simulator Study	Darshan Shah
	• A proposal for the definition of anatomical reference systems for the bones of the foot and ankle complex	Michele Conconi
	• Muscle activity and fatigue in the context of musculoskeletal health complaints in high string musicians	Dirk Möller

- ACL injury prevention in high knee flexion conditions: a new musculoskeletal model Davide Pavan
- Design principles, mechanical testing and functional evaluation of a novel custom dynamic Ankle-Foot Orthosis for drop-foot patients Paolo Caravaggi
- Effects of Tai Chi exercise on postural stability among the elderly during stair descent under different levels of illumination Yaya Pang
- Quantification of arm swing during walking in healthy adults and patients with idiopathic Parkinson's disease Elke Warmerdam
- Meta-learning for personalized golf swing monitoring to overcome motion variability between users Myeongsub Kim
- Identifying the objective of human behavior using inverse reinforcement learning: A Case of human postural control SeongWoong Hong
- Classification of children with fragile X syndrome based on gait analysis: A supervised clustering approach Weronika Piatkowska
- FFH detection using SVM with SMOTE, normalization, and univariate feature selection Bummo Koo
- SEMG-based finger posture recognition considering the re-wearing of an armband sensor Jongman Kim
- Cerebral palsy gait classification based on 3D motion capture data using deep convolutional neural network Joongon Choi
- Upper Body Posture Monitoring Using Inertial Measurement Units and Recurrent Neural Network Hao-Yuan Tang
- A Biomechanical Testing Platform for the Stability and Mobility Assessment of Extracapsular Stabilization of Cranial Cruciate Ligament-Deficient Dogs Wei-Ru Hsu
- Acute effects of transcranial direct current stimulation on dynamic postural stability in healthy young adults Baofeng Wang
- Evaluation of Position and Variability of the Center of Pressure During Walking with Limited Knee Flexion Seobin Choi
- Visualising load distribution of the knee throughout kneeling tasks Simon Thwaites
- Effects of dual-task training on gait in stroke patients: a meta-analysis Xueyi Zhang
- Effects of transcranial direct current stimulation on dynamic postural control: A meta-analysis Changxiao Yu
- Evaluation of trunk muscles during horseback riding therapy on children with cerebral palsy Kenichi KANEKO
- Effects of different pressure lower-body compression garments on proprioception 思焱 王

- Comparison of foot kinematics of toe walking in the able-bodied to spastic equinus gait of cerebral palsy Beomki Yoo
- Systematic review of in vivo foot and ankle kinematics during gait measured using a dual fluoroscopic imaging system Dongqiang Ye
- Comfort assessments in a pneumatic cuff system Yejin Nam
- The differences between bonded and frictional contact settings in foot-sneaker finite element analysis Yi Yang
- Evaluation of muscle function by mechanomyography during dynamic contraction using microphone and accelerometer Yuki Haruta
- The functional role of collagen content in the human cartilage cell microenvironment Awuniji Linus
- Role of actin filament in dynamic changes of intranuclear strain induced by cyclic stretching Takumi Asakawa
- Dynamic responses of cells govern the boundary instability at the closing wound Jeong Hyuntae
- Hypoxic postconditioning on astrocyte activation in a 3D cortical stroke model Mong Lung Steve Poon
- Biophysical response of human bronchial epithelial cells to biocides Tae Yoon Kwon
- Arm Profile Score represents ability of activity using upper limb in individual with stroke. Dain Shim
- Lumbar and pelvis statistical shape model to characterize population shape variations Nikita Ghosh
- Evidence literature summary: Patellofemoral pain in adolescents and objective test routines for the movement analysis laboratory Beat Goepfert
- Kinematics Comparison of Two Posterior Stabilized Knee Implants During Daily Activities Chang Shu
- The effects of Joint Hypermobility Syndrome on the kinematics and kinetics of the vertical jump test Najla Alsiri
- Are biomechanics during gait associated with the structural onset and progression of lower limb osteoarthritis? A systematic review and meta-analysis Nicole D'Souza
- Influence of ankle joint angle on Achilles tendon stiffness Evan Crotty
- Assessment of role of iron in neural circuitry of motor intention on performance of Brain-Computer Interfaces Jagriti Natraj
- Imaging and image processing pipeline for enhanced connective tissue MRI Meeghage Randika Perera

- Detailed correlation between coronary artery disease and tissue speckle tracking Srisakul Chaichuum
- Differences in mechanical properties of hurdle bars Ryo Iwasaki
- Reliability of measuring ACL injury risk associated knee morphology in adolescent females Antonis Stylianou
- The effect of low back pain on plantar pressure during gait Clara Leyh
- Effects of different custom-made insoles on pressure-time integrals in cavus feet during running Mujia Ma
- Predictive simulation of walking with weak ankle plantar-flexor using an AI gait controller Young-Jun Koo
- ISB recommendations for skin-marker-based multi-segment foot kinematics Alberto Leardini
- Investigation of the function of walking shoes equipped with spring on the heel during gait Hayase Funakoshi
- The effect of functional biomechanics garment for walking Toshinori Miyashita
- Long-term Tai Chi practitioners performed better under dual-task condition during stair ascent Qipeng Song
- A longitudinal analysis of change of gait stability in older adults with dementia Sina Mehdizadeh
- Functional insoles improve plantar pressure distribution during race walking qipeng song
- Population study of kinematic gait parameters for biometric application Gunwoo Park
- A kinematic comparison of overground and treadmill walking using AI-based gait controllers Mingi Jung
- Developmental plasticity of locomotor economy in an avian bipedal model Talayah Johnson
- Plantar fascia stiffness is related to the foot arch deformability and performance in single-leg drop jump Hiroto Shiotani
- Adaptations of foot function when hopping on a damped surface Jonathon Birch
- Knee and ankle joint stiffness during running with different runaway surfaces Zihan Yang
- GaitSense: Estimation of knee joint angle for sit-to-stand (STS) movement activity in Osteoarthritis Gunjanbhai Patel
- Predictive tracking of the knee position for mobile x-ray imaging Seungwoo Yoon
- Identifying and comparing hip-knee coordination patterns in instep and punt kicking using functional data analysis Liwen Zhang

- Electromyography recordings of the tensor fascia lata muscle during dynamic tasks: A comparison of surface and fine-wire electrodes Manuela Besomi
- Removing artificial jumps from kinematic recordings with multiple cameras Charlotte Le Mouel
- Micro-biopsy fiber mechanics from the medial gastrocnemius of dancers Paige Rice
- Influence of intermittent blocking of visual information on corticomuscular coherence during walking Hitoshi Makabe
- Balance-dexterity task performance in and out of an episode of low back pain Jiaxi Tang
- The mechanical arrangement of the human semitendinosus muscle as assessed with shear wave elastography Adam Kositsky
- Surgical positioning of the hip joint center during total hip arthroplasty and its effects on muscle and hip joint reaction forces Jasvir Bahl
- Optimal Design of Elastic Ankle Exoskeleton Using Optimal Control of Musculoskeletal Model Karthick Ganesan
- Estimations of knee joint loading using generalized methods and muscle recruitment strategies Kieran Bennett
- Effect of sagittal alignment parameters on intervertebral compression forces in asymptomatic adolescent girls, during a pubertal growth spurt, using a thoracolumbar musculoskeletal model Mohammad Amin Shayestehpour
- Improving muscle geometry through via-point optimization Thomas Geijtenbeek
- The difference of bilateral tibial load in patients with unilateral anterior cruciate ligament reconstruction during jogging Ting Long
- The effect of functional knee alignment on the knee contact forces during execution of closed kinetic chain rehabilitation exercises Williane Bernardes
- Finite element solver based full-body musculoskeletal model for multiscale biomechanics Shihao Li
- Pre-operative planning of high tibial osteotomy using musculoskeletal and finite element models mousa kazemi
- Is hallux valgus responsible for metatarsus primus varus? Yuya Oishi
- Cartilage thickness is coupled to bone shape in healthy knees and varies with sex Marco Schneider
- How do Bone Measurements Change with Growth in a Paediatric Population? Laura Carman

- Increased Loading Rates During Gait Correlate with Morphology of Unaffected Hip in Juveniles with Treated Developmental Hip Dysplasia

WEI-CHUN LEE
- Whole-body sagittal plane angular momentum during running in unilateral transfemoral amputees

Genki Hisano
- Proprioceptive neuromuscular facilitation improves symptoms in older adults with knee osteoarthritis

Qipeng Song
- The effects of impaired foot plantar sensitivity on plantar pressure distribution during walking

Mengzi Sun
- Providing gravitational support using a direct-drive linear actuated assistive robot for shoulder rehabilitation

Soroosh Haji Hosseinejad
- Internal work could be used to estimate energy expenditure at various running intensities.

Bumjoon Kim
- Effects of training volume on lower limb kinematics in fast and slow running speed conditions in elite marathoners

Liqin Deng
- Shifts of tibiofemoral joint forces across the entire period of a half marathon

Tony Lin-Wei Chen
- Effects of running speeds and footwear on achilles tendon loading in elite marathoners with different training volumes

Xini Zhang
- Foot motion analysis using a stretch strain sensor during gait and running

Kodai Sakamoto
- Effects of training volume and running shoes on the patellofemoral joint loading in elite marathoners

Bin Shen
- Effects of the arch span of a carbon-plated midsole on running shoe energy transformation--a finite element study

Tony Lin-Wei Chen
- Influence of the functional foot supporter on the foot motion during locomotion

Shintarou Kudo
- FEM Driven plantar foot orthosis for diabetic foot prevention.

Alfredo Ciniglio
- Computational framework to perform parametric CFD studies from a patient-specific left atrium

Jorge Dueñas Pamplona
- Assigning trabecular bone material properties to total hip arthroplasty finite element models of the pelvis with peri-prosthetic osteolytic lesions

Thomas Grace
- Construction of subject-specific foot finite element model based on foot surface scan

Yinghu PENG
- Osteoporosis vertebral compression fracture finite element simulation and expendable bone implant system evaluation

Kit-leng Cheang

- Feasibility analysis of method for obtaining muscular data of forearm using musculoskeletal simulation TZU-LING CHEN
- An OpenSim-based musculoskeletal model controlled by neural oscillators that generates human gait patterns Makoto Yoshida
- Estimation of knee ligament forces during non-resisted and resisted pedaling using finite element analysis Yu-Ting Chen
- Simulating subject-specific spine mechanics: An integrated finite element and neuro-musculoskeletal modelling framework Laura Meszaros
- Biomechanical analysis of the stick handling in field hockey: kinematics and kinetics assessment Alfredo Ciniglio
- Intra-subject repeatability of joint angle measurement during skating on synthetic ice Aminreza Khandan
- Looking for the ideal sprint stride: how would sports results change if all strides were perfect Andrey Pomerantsev
- Grip socks reduce in-shoe sliding but not actual change of direction performance Charlotte Apps
- Reproducing the characteristics of muscle fatigue change through sEMG analysis based on joint mechanical work during upper limb repetitive rotation Jinsung Jung
- Feedback-based running retraining for impact reduction: The relationship between peak tibial acceleration and step frequency Pieter Van den Berghe
- The effect of cadences on lower extremity biomechanics during stair ascent and descent Qi Li
- Analysis flat service in tennis RAJINIKUMAR
PALANIYAPPAN
- Kinematics Analysis of a Malaysian Female Elite Tenpin Bowler A Case Study Victoria Chin Quan Weoi
- Analysis of pacing strategy adopted by long-distance cross-country skiers XIANSHUANG YUAN
- Biomechanics of fast bowling in men's cricket using wearable sensors Ammar Waheed
- Combinations of release parameters for accurate baseball pitching Ayane Kusafuka
- The applied analysis of kayaking ergometer with different drag resistance in kayak training: a pilot study Jiaxiang Yan
- Gait velocity influence dynamic gait stability in a dual-task paradigm Jingwen Wang
- The effect of different illumination levels and Tai Chi exercise on the postural stability of the elderly during stair ascent Qipeng Song

- Optimization of the whole-body motion to minimize the muscle-tendon length of biceps femoris long head during the late swing phase of high-speed running

Terumitsu Miyazaki
- Does the canoe-kayak ergometer with the electromechanical drag force have a good performance during training?

Weilan He
- The biomechanical characteristics and rules could improve injury risks during race walking

Song Qipeng
- Long-term Tai Chi Practitioners were less influenced by the dual-task paradigm during stair descending

Xiaoli Ma
- Backpack weight influence postural control among children with obesity during stair descent

Xinheng Che
- Sex differences in foot kinematics and kinetics during drop-jump using a novel multi-segment foot model

Yuka Sekiguchi
- Acute effect of transcranial direct current stimulation on rowing endurance performance: a double-blind, randomized, crossover plot study

Zhiqiang Liang
- Proprioceptive neuromuscular facilitation improves descending mechanics among knee osteoarthritis patients

Qipeng Song
- Development of squat-exercise support system using kinect sensor for persons with intellectual disabilities

Kazuyuki Mito
- Directional Dependence of Uniaxial Response Characteristics of the Porcine Thoracic Aorta

Manoj Myneni
- Ventricle of terrestrial Anura is stiffer than that of aquatic Anura due to differences in collagen density

Megumi Ito
- The importance of inertial measurement unit placement in assessing upper limb motion

Fredrik Öhberg
- Comparing surface and intramuscular electromyography patterns of the brachialis muscle during the dynamic elbow movement.

Shota Date
- System identification to characterise shoulder stiffness in a functional posture at various levels of muscle contraction

Yahya Z. Yahya
- Assessing Upper Extremity Function by Applying Sensor-Embedded Device

Charlie C. Ma
- Quantify hand tremor of Parkinson's disease based on Channel State Information

Hui-Hsin Chen
- Positioning effects of GPS Sensors during running

Clint Hansen
- Evaluating The Validity Of An Inertial Measurement Unit For Determining Knee And Trunk Kinematics During Athletic Landing And Cutting Movements

Lionel Chia

- Is the Standing Long Jump Specific-Shoe really Necessary for Chinese Students? Yang Song
- Development of snowboard force measurement system Yun Chen
- Locomotor changes in knee osteoarthritis patients during a 6-minute walk test Dominic Thewlis
- A study on the hip joint mechanism of the exoskeletal robot to improve the assistance performance Mingoo Jeong
- The 3D CoM kinematic estimation using a simple machine learning for portable gait monitoring Myunghyun Lee
- Design and verification of bio-mimetic knee joint mechanism for exoskeletal robots Taeyeon Kim
- Relationship between A2 Pulley Venting and resultant Flexor Tendon Superficialis Slack Tyler Shipley
- Archery gesture segmentation with wearables in both able-bodied and Paralympic athletes Lorenzo Rum

11:45 - 12:00

POSTER QUIZ

Location: Online

12:00 - 13:00

OB1 - CLINICAL BIOMECHANICS

Location: Online

Chair: Felipe Carpes

Pres Time	Presentation title/Abstract title	Speakers/Authors
12:00	In vivo mechanoresponse of articular cartilage before and after load modifying surgery in patients with medial compartment knee osteoarthritis	Annegret Mündermann
12:12	Tibio-femoral kinematics of natural versus replaced knees - A comparison using dynamic videofluoroscopy	Barbara Postolka
12:24	High tibial osteotomy effectively redistributes compressive knee loads during walking	Enrico De Pieri
12:36	Effect of additional training weight on tibiofemoral contact forces during a forward lunge	Ilse Jonkers
12:48	Assessment of variations in scapular morphology and bone quality in patients with B glenoids	Nazanin Daneshvarhashjin

12:00 - 13:00

OB2 - MUSCULOSKELETAL MODELLING

Location: Online

Chair: Taylor Dick

Pres Time	Presentation title/Abstract title	Speakers/Authors
12:00	Biomechanical analysis of industrial exoskeletons	Ulrich Glitsch
12:12	Impact of personalized geometry and motor control on musculoskeletal simulation results - How much detail is needed?	Hans Kainz
12:24	Predictive simulations of hemiparetic gait to explore the effects of muscle weakness on walking asymmetry and energetics	Tom Buurke
12:36	Altered triceps surae muscle dynamics and force demand at different stride frequencies	Wannes Swinnen
12:48	A multiscale constitutive description for load bearing soft biological tissue that incorporates the interfibrillar sliding of constituent collagen.	Christopher Miller

12:00 - 13:00

OB3 - SPECIAL: HAND & WRIST BIOMECHANICS I

Location: Online

Chair: Verónica Gracia Ibáñez, Co-Chair: Zong-Ming Li

Pres Time	Presentation title/Abstract title	Speakers/Authors
12:00	Scan-driven fully automated pipeline for a personalized, 3D printed low-cost prosthetic hand	Yair Herbst
12:12	Complementary functions of the joint morphology and ligaments in providing stability to first the carpometacarpal joint	Wan Mohd Radzi Rusli
12:24	Uniformity of performance during the collection of maximum voluntary contraction tasks for the muscles of the wrist	Mercedes Aramayo Gomes Rezende
12:36	The effect of wrist posture on grip and muscle force capacities: comparison of a prehensile and a non-prehensile task	Mathieu Caumes
12:48	Characteristics of palmar and dorsal flexion muscle strength in college baseball players	Kazuhiro IKEDA

12:00 - 13:00

OB4 - SPECIAL SESSION: MOTOR CONTROL IN IMPAIRED POPULATIONS

Location: Online

Chair: Paola Contessa, Co-Chair: James Richards

Pres Time	Presentation title/Abstract title	Speakers/Authors
12:00	Unrestricted age-related compensation in a daily life sit-to-walk task	Eline van der Kruk
12:12	Quantification of inter-limb coupling during bilateral stance in individuals with transtibial amputation	Peter Raffalt

12:24	Development of spontaneous motor activity with age in healthy infants and infants with infantile cerebral palsy	Catherine Disselhorst-Klug
12:36	Lumbar extensor muscle isometric torque steadiness and torque-HDsEMG coherence is altered in individuals with chronic low back pain	Michail Arvanitidis
12:48	Analysis of spectral attributes of surface electromyography during gait in children with Fragile X Syndrome	Weronika Piatkowska

12:00 - 13:00

OB5 - SPORT BIOMECHANICS

Location: Online

Chair: Ton van den Bogert

Pres Time	Presentation title/Abstract title	Speakers/Authors
12:00	Drop-landing asymmetries are related to knee symptoms 6-months following ACL reconstruction	Katherine Collins
12:12	Elbow load variability in youth elite baseball pitchers	Bart van Trigt
12:24	Whole-body angular momentum and external torque during the block phase of the sprint start	Paul Sandamas
12:36	Injury and surgery are associated with shoulder external rotation during exam and baseball pitching	Hannah Stokes
12:48	How running biomechanics influence the occurrence of iliotibial band syndrome	Qipeng Song

12:00 - 13:00

OB6 - SPINE & TRUNK

Location: Online

Chair: Veronique Feipel

Pres Time	Presentation title/Abstract title	Speakers/Authors
12:00	Cervical spine injuries observed in misdirected rugby tackles are not caused by a hyperflexion mechanism	Dario Cazzola
12:12	Spinal palpation error and its impact on marker-based spinal curvature estimation in adult spinal deformity	Pieter Severijns
12:24	Baricentricity of spinal alignment and posture in adolescent idiopathic scoliosis: Optical diagnosis	Saša Ćuković
12:36	Fear-avoidance beliefs are not related to stoop-squat-behavior during object lifting in healthy pain-free adults	Stefan Schmid
12:48	Subject-specific muscle forces in the lumbar spine are correlated to lumbar curvature	Jude Meakin

12:00 - 13:00

OB7 - SIMULATION TECHNIQUES AND APPLICATIONS

Location: Online

Chair: Maria Pierantoni

Pres Time	Presentation title/Abstract title	Speakers/Authors
12:00	FEBio and ABAQUS with fibril-reinforced biphasic models of knee articular cartilage produce similar mechanical responses during gait	Alexander Paz
12:12	The effect of soft tissue modeling on tibiofemoral stress distribution in models of high tibial osteotomy and its importance for making simulation-based clinical decisions	Elaheh Elyasi
12:24	An agent based model of the vibration-induced arterial growth: feeding the model parameters by cellular tests	Maha Reda
12:36	Numerical discretization of trabecular bone based on Voronoi tessellation	Yijun Zhou
12:48	Rapid X-ray-based 3-D finite element modeling of knee joint cartilage biomechanics	sana Jahangir

12:00 - 13:00

OB8 - POSTURE AND BALANCE

Location: Online

Chair: Andresa Germano

Pres Time	Presentation title/Abstract title	Speakers/Authors
12:00	Forefoot or ankle - which really affects balancing skills?	Rosemary Dubbeldam
12:12	How static and dynamic balance changes with age: the risk of sitting down	Lizeth Sloot
12:24	Concurrent assessment of posture and saccades -- connecting with cognitive function through immersive virtual reality	Yu Imaoka
12:36	Towards a new biomechanical model to explain upright postural control in unilateral transtibial prosthesis users	Cleveland Barnett T.
12:48	Sensitivity of biomechanical responses in path optimized follower loads considering the lumbosacral load sharing	Robin Remus

13:00 - 13:45

LUNCH BREAK

Location: Online

13:45 - 14:45

PANEL DEBATE: THE DISTRIBUTION PROBLEM IN BIOMECHANICS AND MOTOR CONTROL: HOW CAN WE MEASURE, PREDICT AND VALIDATE IN VIVO MUSCLE FORCES?

Location: Online

SPEAKERS:



Ton van den Bogert,
Cleveland State
University (USA)

– (experimental and
theoretical)



Friedl de Groote,
Katholieke Universiteit
Leuven (Belgium)

– (theoretical)



Walter Herzog,
University of Calgary
(Canada)

– (experimental)



Lanie Gutierrez-
Farewik, KTH
MoveAbility Lab
(Sweden)

MODERATOR:

13:45 - 14:45

PANEL DEBATE: MARKERLESS VS. MARKER-BASED MOTION CAPTURE

Location: Online

SPEAKERS:



Julia Stebbins,
PhD, Oxford Gait
Laboratory, Nuffield
Orthopaedic Centre
(United Kingdom)



Kevin Deluzio,
Professor, Queen's
University, Ontario
(Canada)



Michael Rainbow,
Assoc. Professor,
Skeletal Observation
Laboratory,
Queen's University,
Ontario (Canada)

MODERATOR:

14:45 - 15:00

BREAK

Location: Online

15:00 - 16:00

WARTENWEILER AWARD LECTURE: SUSAN S. MAGULIES

Location: Online

SUSAN S. MAGULIES

The Wartenweiler Memorial Lecture is given to honour Prof. Jürg Wartenweiler (1915-1976), first President of the ISB, who organized the First International Seminar on Biomechanics in Zürich, Switzerland (1967).

Wallace H. Coulter Chair, Biomedical Engineering

Georgia Institute of Technology and Emory School of Medicine

GRA Eminent Scholar in Injury Biomechanics



Dr. Margulies is the Chair of the Wallace H. Coulter Department of Biomedical Engineering at Georgia Tech and Emory University, and the Georgia Research Alliance Eminent Scholar in Injury Biomechanics. She received her BSE in Mechanical and Aerospace Engineering at Princeton and PhD in Bioengineering from the University of Pennsylvania, and was a post-doctoral fellow at Mayo. With over 30 years of experience in the areas of traumatic brain injury research and pulmonary biomechanics, Dr. Margulies has secured over \$35 million in federal, private, and industry funding to discover injury mechanisms on the macro and micro scales, and translate basic research findings to improve clinical outcomes. Dr. Margulies is a Fellow of the American Society of Mechanical Engineers, Biomedical Engineering Society, and American Institute for Medical and Biological Engineering, and a Member of the National Academy of Engineering and National Academy of Medicine.

The Wallace H. Coulter Department of Biomedical Engineering at Emory University and Georgia Institute of Technology is the only public-private inter-institutional BME department in the nation and is a national leader in translational biomedical engineering research and education. Faculty research focuses on cell manufacturing technologies, biomaterials, imaging and instrumentation, informatics and systems modeling, biomedical robotics, cardiovascular engineering, immunoengineering, neuroengineering, cancer technologies and innovative engineering education methods. Coulter BME is top ranked in the nation (#2) for PhD and undergraduate programs, and graduates the largest number of female and under-represented biomedical engineers annually.

16:00 - 22:00

SOCIAL MINGLE

Location: Online

Tue 27 Jul 2021

10:45-11:45

STUDENT HAPPY HOUR

Location: Online

11:45 - 12:00

SHORT WELCOME

Location: Online

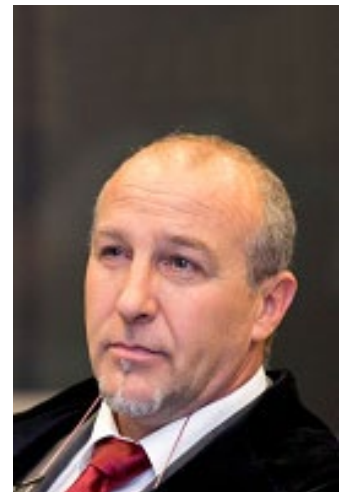
12:00 - 13:00

KEYNOTE LECTURE: THE ROLE OF BIOMECHANICS IN EVIDENCE-BASED PARALYMPIC CLASSIFICATION (YVES C. VANLANDEWIJCK)

Location: Online

YVES C. VANLANDEWIJCK

Yves C. Vanlandewijck is Professor in Rehabilitation Sciences at the Faculty of Kinesiology and Rehabilitation Sciences of the University of Leuven, Belgium, and guest-professor at the Swedish School of Sport and Health Sciences (GIH), Stockholm, Sweden. His research interests include exercise physiology, biomechanics and ergonomics, applied to individuals with locomotor impairment, in a rehabilitation to elite sports continuum. His main research applications focus on the development of evidence-based classification systems in Paralympic sports to ensure fairness in athletic competition categories. Since 2014, the research unit of Prof. Yves Vanlandewijck is recognized and funded by the International Paralympic Committee (IPC) as the Research & Development Centre for Classification in Athletes with Intellectual Impairment.



From 1997 to 2001, Prof. Yves Vanlandewijck was the vice-president of the International Federation of Adapted Physical Activity; he is the founding editor of the European Journal of Adapted Physical Activity and the editor of the IOC Series Books "The Paralympic Athlete" (2011) and "Training & Coaching the Paralympic Athlete" (2016). He was a member of the IOC Medical and Scientific Working Group and member of the Associations Board of the International Council of Sport Science and Physical Education. He is a member of the Sport Science Committee of the IPC since 1995 and Chairperson from 2003 to 2018. In 2017, Prof. Yves Vanlandewijck delivered the Joseph B. Wolffe Memorial Lecturer opening the ACSM Annual Meeting in Denver, Colorado, with a lecture entitled: "Crossroads and Conflicts – Olympics, Paralympics or Cyber Olympics". In 2019, he received the Paralympic Scientific Award for his lifetime contribution to Paralympic research and the Paralympic Movement.

13:00 - 13:30

INNOVATIVE ANALYSIS OF JAW MOVEMENT WITH QUALISYS AND DELSYS

Location: Online

In the second part of our daily "Swedish Fika" breaks, Delsys joins Qualisys to demonstrate the latest EMG and Motion Capture innovations, using Delsys Quattro sensors and Arqus A26 cameras to perform an analysis of jaw movement.

Our software, QTM support Delsys Quattro digital integration which enables EMG data capture along with the motion capture. During the session, we will present our integration together with the Delsys team and do a live demo.

13:30 - 13:45

BREAK

Location: Online

13:45 - 14:45

OC1 - LOWER EXTREMITIES

Location: Online

Chair: Janet Dufek

Pres Time	Presentation title/Abstract title	Speakers/Authors
13:45	Can electrical noise stimulation improve the perception of vibration stimuli in patients with diabetes mellitus?	Claudio Zippenfennig
13:57	Contraction intensity does not influence the elastic and contractile components of the muscle-tendon unit performance enhancement in stretch-shortening cycles	Denis Holzer
14:09	Comparing eight normalization methods for net joint moment data in the single-leg squat	Steven Hirsch
14:21	Is non-uniform achilles tendon displacement associated with calf muscle passive elastic modulus in young athletes?	Taija Finni
14:33	Modulating achilles tendon loading during gait with a resistive soft ankle exosuit	Dylan Schmitz

13:45 - 14:45

OC2 - MEDICAL DEVICES

Location: Online

Chair: Annegret Mündermann

Pres Time	Presentation title/Abstract title	Speakers/Authors
13:45	O2-enrichment device based on membrane separation for early phases of respiratory insufficiency	Christoph Janeczek
13:57	Fatigue resistance of nitinol stents subjected to walk-induced femoropopliteal artery motion	Ran He

14:09	Explicit and implicit FE-models capture the mechanical response of calcium phosphate-titanium cranial implants	Susanne Lewin
14:21	Experimental validation of the gross taper failure mechanism in total hip arthroplasty	Valerie Polster
14:33	Comparison of total ankle replacement designs using a dynamic computational model of the foot and ankle	Maria Ruiz

13:45 - 14:45

OC3 - METHODOLOGIES AND DATA ANALYSIS

Location: Online

Chair: Gillian Weir

Pres Time	Presentation title/Abstract title	Speakers/Authors
13:45	An open-source algorithm for automatic labelling of optical motion capture markers using deep learning	Allison Clouthier
13:57	The performance of open-source pose estimation algorithms during walking, running and jumping	Laurie Needham
14:09	Can leap motion controller replace conventional marker-based motion capture systems?	Amartya Ganguly
14:21	Under-shoe hydrodynamics correlate with film thickness predictions based on worn tread geometry	Sarah Hemler
14:33	Quantifying the hip-ankle synergy in short-term maximal cycling	Louise Burnie

13:45 - 14:45

OC4 - MUSCULOSKELETAL MODELLING

Location: Online

Chair: Claudia Mazzà

Pres Time	Presentation title/Abstract title	Speakers/Authors
13:45	Hill-type computational models of skeletal muscle-tendon actuators: a systematic review	Luca Modenese
13:57	Muscle-specific intramuscular passive properties are required to accurately scale passive muscle mechanics	Benjamin Binder-Markey
14:09	Motor-units matter: enriching continuum-mechanical skeletal muscle models with neuromuscular information	Harnoor Deep Singh Saini
14:21	A mechanistic model of muscle force and impedance	Matthew Millard
14:33	3D modeling of length and lever arm of sternocleidomastoid and scalenus muscles in respiratory movement	David Biteau

13:45 - 14:45

OC5- ARTIFICIAL INTELLIGENCE AND MACHINE LEARNING

Location: Online

Chair: Anne Koelewijn

Pres Time	Presentation title/Abstract title	Speakers/Authors
13:45	Automated and personalized pose registration from x-ray images using convolutional networks	Florian Vogl
13:57	Assessment of a novel deep learning-based marker-less motion capture system for clinical gait analysis	Laurent Gajny
14:09	Towards real-time estimation of joint moments during fast sidestepping	Sina David
14:21	Towards standardising a machine learning approach for automated and accurate event detection for human gait	Yong Kuk Kim
14:33	Muscle synergies enable accurate joint moment prediction using few EMGs	Yixing Liu

13:45 - 14:45

OC6 - SPORT BIOMECHANICS

Location: Online

Chair: Michael Asmussen

Pres Time	Presentation title/Abstract title	Speakers/Authors
13:45	The influence of bicycle lean on maximal power output during sprint cycling	Ross Wilkinson
13:57	Racing in the street -- Whole-body vibration during road cycling and the effect of different equipment choices to minimise it	Timothy Holsgrove
14:09	Sleep parameters and soccer kicking performance in youth players	Fabio Augusto Barbieri
14:21	Sagittal plane lower extremity joint demands of the golf swing in novice older adult golfers	Guanrong Cai
	Should major league baseball adjust the mound height?	Megan Stewart

13:45 - 14:45

OC7 - SPECIAL: HAND & WRIST BIOMECHANICS II

Location: Online

Chair: Kai-Nan An, Co-Chair: Angela Kedgley

MARC GARCIA-ELIAS

Dr. Garcia-Elias was born in Terrassa (Spain) the 6th of October of 1954.

He graduated in 1978 at the Universitat Autònoma Medical School, Barcelona, Spain. He obtained his certification as specialist in Orthopaedic Surgery in 1982, and his doctoral degree (PhD) by the University Autònoma of Barcelona, Spain in 1985. From 1986 to 1989, he worked as visiting scientist at the Orthopedic Biomechanics Laboratory of the Mayo Clinic. Since returning to his homeland, he has kept his interest in basic science of the upper limb. Since its foundation in 1994, Dr Garcia-Elias co-directs the Institut Kaplan for Hand Surgery in Barcelona, Spain. He is PhD coordinator of the Upper Limb Biomechanics laboratory of the Department of Anatomy of the Universitat Autònoma de Barcelona Medical School, in Bellaterra, Barcelona, Spain.



Since 2019, he is also President of the International Federation of Societies for Surgery of the Hand (see <https://www.ifssh.info/officers.php>). His areas of major interest are the anatomy and biomechanics of the wrist and the treatment of wrist and distal radioulnar instability. He has published 3 books, 74 chapters, and 168 peer reviewed (Pubmed indexed) articles, most of them on the anatomy and biomechanics of the wrist, or on surgery of the carpus and distal radioulnar joint instability.

Pres Time	Presentation title/Abstract title	Speakers/Authors
13:45	My current understanding of wrist dynamics	Marc Garcia-Elias
14:09	Fused with motion: A biomechanical comparison of dart throw motions after partial wrist fusions	Frederick Werner
14:21	In vivo validation of musculoskeletal model of the wrist featuring a consistent anatomical data set	Oluwalogbon Akinnola
14:33	Palmar musculature and its role as a dynamic compressor of the carpal tunnel	Ronit Wollstein

13:45 - 14:45

OC8 - CLINICAL BIOMECHANICS

Location: Online

Chair: Seong-won Han

Pres Time	Presentation title/Abstract title	Speakers/Authors
13:45	Biomarkers of knee joint healing following anterior cruciate ligament reconstruction: a systematic review	Lisa Ek Orloff
13:57	Biomechanical simulation of lung-tumor motion based on surface imaging	Maida Ranjbar
14:09	In-vitro bi compartmental approach to assess intra-capsular pressure in the hip joint during movements: Is the acetabular cavity also presents pressure fluctuations as the capsular chamber?	Marc-Olivier St-Pierre
14:21	Closing the kinetic chain: Weight-bearing versus non-weight bearing maximal force generation and its relation to patient reported outcomes in ACL injured males and females	Michael Del Bel
14:33	Towards the usage of embedded prosthesis sensors for real-life gait analysis of amputee subjects	Sabina Manz

14:45 - 15:30

LUNCH BREAK

Location: Online

MAJOR SPONSOR WORKSHOPS

15:30 - 16:00

GENERATING AUTOMATED REPORTS WITH XSENS, BRIDGING THE GAP BETWEEN DATA AND ANALYSIS

Location: Online

With MVN Reports you can easily generate automated reports for Health, Ergonomics and Sports. Powered by the new Xsens MotionCloud platform, MVN Reports instantly present complex movement data in an accessible, easy-to-read report. In this workshop we will show you how you can easily generate an automated Gait Analysis report with MVN Reports. In as little as a few minutes, a full standardized report with relevant data for that specific application is created. Also, the motion data is visualized as a 3D avatar. This report is automatically generated on the Xsens MotionCloud platform. The data is processed in the unique 'Xsens Sensor Fusion Engine, providing accurate and validated data. All that's required is an Xsens MVN motion capture setup and access to Xsens MotionCloud. During this workshop, we would like to give you an insight in the functionalities of MVN Reports and the reports roadmap. Also, we would like to give you an in-depth introduction to the Gait Analysis report specifically.

15:30 - 16:00

PANEL DISCUSSION ON HOW TECHNOLOGY IS USED IN RESEARCH AND WOMEN IN BIOMECHANICS.

Location: Online

Hear what 5 top biomechanists have to say about their own research, how they use technology to help answer those research questions, and Women in Biomechanics.

16:00 - 17:00

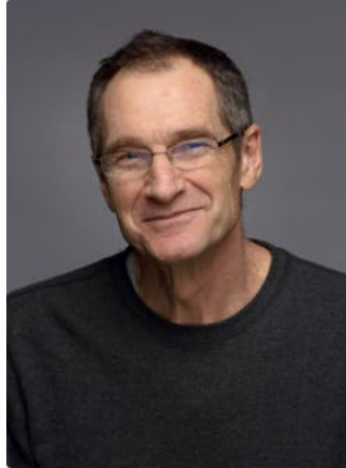
PANEL DEBATE: PEER REVIEW IN SCIENCE

Location: Online

SPEAKERS:



Benno Nigg
Founder and Chief
Science Officer



Walter Herzog,
University of
Calgary (Canada)

MODERATOR:



Katherine Boyer,
University of
Massachusetts
Amherst (USA)

16:00 - 17:00

PANEL DEBATE: BIOROBOTICS - HOW BIOLOGY WILL INFORM THE NEXT-GEN MACHINES

Location: Online

SPEAKERS:



Auke Ijspeert,
EPFL (Lausanne,
Switzerland)



Yulia Sandamirskaya,
University of Zurich and
ETH (Switzerland)

MODERATOR:



Francisco Valero-Cuevas,
University of Southern
California (USA)

17:00 - 17:15

BREAK

Location: Online

17:15 - 18:15

OD1 - WIRELESS SENSORS AND WEARABLE DEVICES

Location: Online

Chair: Lauren Benson

Pres Time	Presentation title/Abstract title	Speakers/Authors
17:15	Development of a channel identification algorithm for an autonomously usable 16-channel sEMG sensor system	Elisa Romero Avila
17:27	Surface EMG-based AAC technology for recognition of silent prosodic speech	Jennifer Vojtech
17:39	An open-source workflow for IMU-based kinematics over long durations	Johanna O'Day
17:51	From feasible to practical: Progress in the development & validation of wearables for accurately monitoring tibial bone forces in the real-world	Laura Judson
18:03	Measuring trunk motion during on-site wheelchair propulsion using inertial measurement units	Marit van Dijk

17:15 - 18:15

OD2 - INJURIES AND REHABILITATION

Location: Online

Chair: Hannah Rice

Pres Time	Presentation title/Abstract title	Speakers/Authors
17:15	Diffusion and advection of pro-inflammatory cytokines in injured articular cartilage under mechanical loading	Joonas Kosonen
17:27	Effects of functional resistance training on gait biomechanics following anterior cruciate ligament reconstruction	Alexa Johnson
17:39	A Prospective Study Linking Changes in Dynamic Center of Mass Motion With Lower-Limb Overuse Injuries Using a Single Trunk-Mounted Accelerometer	Gerard Aristizábal Pla
17:51	Consistency of athlete lower-limb work distribution across unilateral and bilateral tasks after ACL reconstruction	Holly Jones
18:03	A hierarchical clustering approach for examining potential risk factors for bone stress injury in runners	Jack Martin

17:15 - 18:15

OD3 - SPORTS AND EXERCISE FOR PERSONS WITH IMPAIRMENT

Location: Online

Chair: Mary Rodgers

Pres Time	Presentation title/Abstract title	Speakers/Authors
17:15	Effect of seat configuration on joint power distribution and performance in an elite Paralympic rower: a case study	Jørgen Danielsen
17:27	Validation of a new sport specific trunk test battery for paracanoe	Anna Bjerkefors
17:39	The impact of leg impairment on strength and race performance in elite para-cyclists	Johanna Liljedahl
17:51	Kinematic and kinetic performance variables during paddling among para-kayak athletes with unilateral above or below knee amputation	Johanna Rosén
18:03	Towards a standardized and individualized lab-based protocol for wheelchair-specific exercise capacity testing of wheelchair athletes: a scoping review	Rowie Janssen

17:15 - 18:15

OD4 - SPECIAL: HAND & WRIST BIOMECHANICS III

Location: Online

Chair: Frederick Werner, Co-Chair: Jennifer Nichols

Pres Time	Presentation title/Abstract title	Speakers/Authors
17:15	Biomechanical evaluation of a fracture fixation system for transverse fractures of the metacarpal neck	Rena Mathew
17:27	Reproducibility of Trapeziometacarpal Joint Angle Measurements Using Dynamic CT	Michael Kuczynski
17:39	Three-dimensional carpal tunnel reconstruction and analysis using multimodal co-registration of ultrasonography and computed tomography	Hui Zhang
17:51	Model of the Midcarpal Joint Accounting for Structural Difference	Ronit Wollstein
18:03	An implantable differential mechanism to restore individuated finger flexion following tendon transfer surgery	Suraj Chakravarthi Raja

17:15 - 18:15

OD5 - DAVID WINTER YOUNG INVESTIGATOR ORAL SESSION

Location: Online

Chair: Timothy Derrick

Pres Time	Presentation title/Abstract title	Speakers/Authors
17:15	Development and validation of FootNet, a new kinematic and deep learning-based algorithm to detect foot-strike and toe-off in treadmill running	Adrian Rivadulla

17:27	Semi-automatic quantification of muscles deformations during controlled exercises: application to the abdominal wall	Arthur Jourdan
17:39	Biceps femoris long head fascicle length increases after 3 weeks of eccentric exercise training are due to sarcomere lengthening rather than serial sarcomere addition	Melissa Boswell
17:51	Development of a high-density EMG-driven Hill-type muscle model	Arnault H D Caillet
18:03	Fibril-reinforced poroelastic properties of normal and osteoarthritic human femoral, tibial, and patellar cartilage	Mohammadhossein Ebrahimi

17:15 - 18:15

OD6 - SPECIAL: SIMULATION OF LOCOMOTION I

Location: Online

Chair: Friedl De Groot, Co-Chair: Tom Buurke

KAREN LIU

C. Karen Liu is an associate professor in the Computer Science Department at Stanford University. Prior to joining Stanford, Liu was a faculty member at the School of Interactive Computing at Georgia Tech. She received her Ph.D. degree in Computer Science from the University of Washington. Liu's research interests are in computer graphics and robotics, including physics-based animation, character animation, optimal control, reinforcement learning, and computational biomechanics. She developed computational approaches to modeling realistic and natural human movements, learning complex control policies for humanoids and assistive robots, and advancing fundamental numerical simulation and optimal control algorithms. The algorithms and software developed in her lab have fostered interdisciplinary collaboration with researchers in robotics, computer graphics, mechanical engineering, biomechanics, neuroscience, and biology. Liu received a National Science Foundation CAREER Award, an Alfred P. Sloan Fellowship, and was named Young Innovators Under 35 by Technology Review. In 2012, Liu received the ACM SIGGRAPH Significant New Researcher Award for her contribution in the field of computer graphics.



Pres Time	Presentation title/Abstract title	Speakers/Authors
17:15	Simulating Human Movements for Assistive Robotics	Karen Liu
17:39	Evaluating and combining cost function criteria to predict healthy gait	Kirsten Veerkamp
17:51	Simulations of walking with an ankle-foot exoskeleton to evaluate the predictive capability of neuromechanical models	Maarten Afschrift
18:03	Three-dimensional knee reduces metabolic cost and joint loading in simulated running	Ross Miller

17:15 - 18:15

OD7 - BIOMEDICAL ENGINEERING

Location: Online

Chair: Daniel Benoit

Pres Time	Presentation title/Abstract title	Speakers/Authors
17:15	Neck muscle network topology analysis in people with chronic neck pain	David Jimenez-Grande
17:27	Quantitative evaluation of hypomimia in Parkinson's disease: a face tracking approach	Elena Pegolo
17:39	A model for the biomechanical assessment of discoplasty in a laboratory setting	Salim Ghandour
17:51	Microfluidic integrated biosensor for the detection of osteoarthritis	Anupriya Singh
18:03	Micro- structured hollow fiber membranes - reducing the main transport resistance in membrane oxygenators	Paul Ecker

17:15 - 18:15

OD8 - ANIMAL AND COMPARATIVE

Location: Online

Chair: Judith Meakin

Pres Time	Presentation title/Abstract title	Speakers/Authors
17:15	Morphological determinants of glenohumeral mobility in primates	Erin CS Lee
17:27	Lateral stability and the frontal shape of land animals	Neelima Sharma
17:39	How some insects adhere to underwater surfaces	Pranav Sudersan
17:51	Relatively shorter muscle lengths increase the metabolic rate of cyclic force production	Owen Beck
18:03	Cadaveric demonstration of a novel stretchable sensor to wirelessly measure musculoskeletal soft tissue strains during passive limb motion	Qiang Zhang

18:15 - 18:30

BREAK

Location: Online

18:30 - 19:30

MUYBRIDGE AWARD LECTURE: SCOTT L. DELP

Location: Online

Chair: Friedl De Groot

SCOTT L. DELP

The Muybridge award is the most prestigious award of the Society. It is awarded for career achievements in biomechanics. The award is named after Eadward Muybridge (1830-1904), who was the first to use cinematography for the study of human and animal movement. Scott L. Delp, Ph.D., is the James H. Clark Professor of Bioengineering, Mechanical Engineering, and Orthopaedic Surgery at Stanford University. He is the Founding Chairman of the Department of Bioengineering at Stanford, Director of the RESTORE Center, a NIH national center focused on measuring real world rehabilitation outcomes, and Director of the Mobilize Center, a NIH National Center of Excellence focused on Big Data and Mobile Health. Scott is focused on developing technologies to advance movement science and human health.



Software tools developed in his lab, including OpenSim and Simtk.org, have become the basis of an international collaboration involving thousands of students and scientists who exchange simulations of human movement. Prior to joining the faculty at Stanford, Delp was on the faculty at Northwestern University and the Rehabilitation Institute of Chicago. He has published over 250 research articles in the field of biomechanics and has recently published a text from MIT Press entitled Biomechanics of Movement: The Science of Sports, Robotics, and Rehabilitation. Professor Delp has co-founded six health technology companies and is a member of the U.S. National Academy of Engineering.

19:30 - 20:30

OE1 - TISSUE

Location: Online

Chair: Anna Gustavsson

Pres Time	Presentation title/Abstract title	Speakers/Authors
19:30	Endoprosthesis size optimizes impaction force and circumferential stress in transtibial intramedullary prostheses	Carolyn Taylor
19:42	Mechanical fatigue in spinal joints: Viscoelastic responses to altered rate and frequency of compression loading	Jackie Zehr
19:54	Effects of cyclic loading on the mechanical properties and failure of human patellar tendon	Colin Firminger
20:06	Determining the Relationship Between Skull Diploë Morphometry and Mechanical Properties In Four-Point Bending	Kevin Adanty
20:18	A one-dimensional viscoelastic model of collagenous tissues with damage	Jeff Barrett

19:30 - 20:30

OE2 - ORTHOPAEDICS: BONE & CARTILAGE, SURGEON-GUIDED

Location: Online

Chair: Colin Smith

Pres Time	Presentation title/Abstract title	Speakers/Authors
19:30	Anterolateral versus medial plating for varus type pilon fractures	Ali Ammar
19:42	Quantification of 3-dimensional strength and pain in patients with shoulder osteoarthritis	Margaret Coats-Thomas
19:54	Mechanical fatigue of whole rabbit-tibiae under combined compression-torsional loading is better explained by strained volume than peak strain magnitude	Ifaz Haider
20:06	A biomechanical analysis of body mass index on frontal plane kinetics and kinematics between controls and total knee arthroplasty patients	Laura Linsley
20:18	The use of a wireless passive electronic strain sensor to measure hysteresis of sheep hindlimb tendons: A first step towards directly comparing in vitro and in vivo tendon properties	Fransiska M Bossuyt

19:30 - 20:30

OE3 - EDUCATION AND OUTREACH

Location: Online

Chair: Sarah Breen

Pres Time	Presentation title/Abstract title	Speakers/Authors
19:30	What womxn want: Using the international womxn in biomechanics organization to help womxn in biomechanics thrive	Anahid Ebrahimi
19:42	Using a physical sarcomere model to demonstrate titin's contributions to residual force enhancement	Heron B O Medeiros
19:54	Visual detection on simulated electromyography signals with varying signal-to-noise ratios: A training tool to enhance onset identification	Mario Lamontagne
20:06	Using hula hooping as a discussion point for STEM education and outreach	Polly Blaikie
20:18	Finite element modelling of the abdomen in developing a robotic patient for palpation examination training	Florence Leong

19:30 - 20:30

OE4 - LOCOMOTION: CLINICAL GAIT

Location: Online

Chair: Katherine Boyer

Pres Time	Presentation title/Abstract title	Speakers/Authors
19:30	Effect of low and high intensity strength training on muscle forces during walking in adults with knee osteoarthritis	Paul DeVita
19:42	Modular reorganization of gait in chronic but not in artificial knee joint constraint	Carlos Cruz
19:54	Lower back demands during load carriage with induced asymmetric gait	Jacob Banks
20:06	The use of the reference finite helical axis and high-speed biplanar videoradiography to characterize knee kinematics	Tomasz Bugajski
20:18	Gait asymmetries following ACL reconstruction differ based on sex and gait speed	Lindsay Slater

19:30 - 20:30

OE5 - RUNNING: BIOMECHANICS

Location: Online

Chair: Hermann Schameder

Pres Time	Presentation title/Abstract title	Speakers/Authors
19:30	Effects of foot core strengthening protocol on plantar arch biomechanics	Alessandra Matias
19:42	Subgroups of foot-ankle running movement patterns influence the responsiveness to a foot-core exercise program	Ricky Watari
19:54	Internal tibial forces and moments during graded running	Michael Baggaley
20:06	Tibial damage and osteogenic effects of high intensity interval and prolonged running	Stacey Meardon
20:18	Achilles Tendon and Patellofemoral Kinetics Following A Long Hilly Run in Traditional and Maximal Cushioning Shoes	James Becker

19:30 - 20:30

OE6 - SIMULATION TECHNIQUES AND APPLICATIONS

Location: Online

Chair: Dario Cazzola

Pres Time	Presentation title/Abstract title	Speakers/Authors
19:30	Hierarchical inverse kinematics via Bayesian inference	Andrew Pohl
19:42	The flow of tissue energy during whole muscle contraction in 3D	Stephanie Ross
19:54	Computational simulation of sideswipe collisions to predict head injury metrics	Shaun Jeffs
20:06	Inverse distance weighting to rapidly generate large simulation datasets	Kalyn Kearney
20:18	Kernel based modelling of intervertebral disc characteristics	Maria Hammer

19:30 - 20:30

OE7 - IMPACT BIOMECHANICS

Location: Online

Chair: Helen Bayne

Pres Time	Presentation title/Abstract title	Speakers/Authors
19:30	Loss of consciousness in national football league players is associated with high strain rate in the cerebellum and brainstem	Karl Zimmerman
19:42	Quantification of upper limb loading behind a ballistic shield using an adapted ATD arm	Julia de Lange
19:54	Evaluation of design and concept verification of a new figure skating blade with integrated damping system for reducing impact related overuse injuries	Ondrej Spiegl
20:06	Modelling of the pelvis and lumbar spine in high-rate axial loading	Corina Espelien
20:18	Statistical prediction of spinal injury using CIREN data	Sean Shimada

19:30 - 20:30

OE8 - LOWER EXTREMITIES

Location: Online

Chair: Victoria Chester

Pres Time	Presentation title/Abstract title	Speakers/Authors
19:30	Differences between loaded and unloaded bone kinematics of the foot and ankle complex	Michele Conconi
19:42	Patellofemoral contact forces after ACL reconstruction using statistical parametric mapping	Jack R. Williams

19:54	Out-of-plane motion reduces the knee extension moment arm	Mitchell Wheatley
20:06	Muscle-length dependence of residual force enhancement in the human patellar tendon during submaximal stretch-hold contractions	Patrick Bakenecker
20:18	The non-intuitive contributions of individual quadriceps muscles to patellar tracking	Seong-won Han

20:30 - 21:30

ADVANCING WOMEN IN BIOMECHANICS MEETING

Location: Online

Becoming an Ally

The goal of this one-hour workshop is to provide practice in recognizing and addressing bias through specific scenarios and discussion of positive responses. There will be break-out rooms where scenarios will be enacted. Participants in small groups will work together to recognize biases taking place and how best to respond. This session is open to all, and men are especially encouraged to participate. Scenarios will include hiring, reviews and promotions, meeting dynamics, mentorship and sponsorship, and everyday interactions. Our aim is to provide a safe environment for meaningful discussions. This workshop is organized by “Advancing Women in Biomechanics” (AWB).

Wed 28 Jul 2021

07:15 - 07:30

SHORT WELCOME

Location: Online

07:30 - 08:30

OF1 - ARTIFICIAL INTELLIGENCE AND MACHINE LEARNING

Location: Online

Chair: Julie Choisne

Pres Time	Presentation title/Abstract title	Speakers/Authors
7:30	Ground reaction force fusion for gait recognition	Kayne Duncanson
7:42	Data fusion of electromyography and motion data enhances locomotion intent recognition	Lin Meng
7:54	Predicting ground reaction force components from two-dimensional video using machine learning	Corey Morris
8:06	Estimation of knee flexion in knee arthroplasty patients using only shank mounted IMUs	Ted Yeung
8:18	Anomalous gait feature prediction using a neural network	Suil Jeon

07:30 - 08:30

OF2 - CLINICAL BIOMECHANICS

Location: Online

Chair: Corina Nüesch

Pres Time	Presentation title/Abstract title	Speakers/Authors
7:30	Femoral offset shortening after nailing of Hip fractures does not correlate with pelvic control during gait	Arj Sivakumar
7:42	Relationships between hip muscle strength and running biomechanics in femoroacetabular impingement syndrome	Benjamin Mentiplay
7:54	Personalised hip load modification using real-time biofeedback in hip osteoarthritis: a feasibility study	Laura Diamond
8:06	Effect of functional weightbearing versus non-weightbearing quadriceps strengthening exercise on contact force in varus-malaligned medial knee osteoarthritis: A secondary analysis of a clinical trial	Scott Starkey
8:18	A finite element analysis of foot with hammer toe deformity during walking	Mohammad Moayedi

07:30 - 08:30

OF3 - MUSCLE TISSUE AND ARCHITECTURE

Location: Online

Chair: Hazel Screen

Pres Time	Presentation title/Abstract title	Speakers/Authors
7:30	Statistical shape and fibre models to determine the effect of strength training on vastus lateralis shape and architecture	Bart Bolsterlee
7:42	Triceps surae muscle fascicle dynamics as a function of walking speed in young and older adults	Lauri Stenroth
7:54	Gender difference in architectural and mechanical properties of medial gastrocnemius-achilles tendon unit	Liqin Deng
8:06	Influence of muscle stiffness and architecture on gastrocnemii shape during isometric plantarflexion contractions	Nicole Yvette Kelp
8:18	Three-dimensional architecture of the medial gastrocnemius muscle in human infants in vivo	Brian Chow

07:30 - 08:30

OF4 - MUSCULOSKELETAL MODELLING

Location: Online

Chair: Glen Lichtwark

Pres Time	Presentation title/Abstract title	Speakers/Authors
7:30	Forward prediction of ankle joint moments using a generic feature set	Homayoon Zarshenas
7:42	Effect of meniscus material models on the mechanical responses of cartilage during walking: a finite element study	Tulashi Simkheada
7:54	A method to compare heterogeneous types of bone and cartilage meshes	Nynke Rooks
8:06	Free achilles tendon strain during common locomotor and rehabilitation tasks	Daniel Devaprakash
8:18	The deep hip stabilisers cannot stabilise	Evy Meinders

07:30 - 08:30

OF5- ORTHOPAEDICS

Location: Online

Chair: Carina Blaker

Pres Time	Presentation title/Abstract title	Speakers/Authors
7:30	Morphological variation in paediatric lower limb bones	Laura Carman

7:42	A semi-automated method for quantifying total hip arthroplasty related acetabular bone loss from CT scans: lesion volume measurement accuracy and overall method reliability	Thomas Grace
7:54	The effects of decellularisation and sterilisation processing on kangaroo tendon strength	Dylan Ashton
8:06	The free achilles tendon is shorter, stiffer, and thicker in trained runners compared to healthy controls	Claudio Pizzolato
8:18	Prediction of ACL tunnels: a comparison between model and surgeon	Marco Schneider

07:30 - 08:30

OF6 - REHABILITATION AND NEUROREHABILITATION

Location: Online

Chair: Polly McGuigan

Pres Time	Presentation title/Abstract title	Speakers/Authors
7:30	Does maintenance of whole-body balance take primacy over synchronization of footfalls to auditory beats during rhythm perturbed walking?	Deepak Ravi
7:42	The influence of a fatiguing wheelchair propulsion protocol on the neuromuscular activation of five shoulder muscles	Ursina Minder
7:54	Ankle kinematics during walking with a soft exoskeleton in people with dropfoot -- a case series	Eveline Graf
8:06	Influence of assistance timing on human gait biomechanics using a semi-passive ankle exoskeleton	Mahsa Momtahan
8:18	Real-time joint kinematics estimation in tele-rehabilitation	Marco Caruso

07:30 - 08:30

OF7 - MOTOR CONTROL II: MOTOR CONTROL IN SPORT

Location: Online

Chair: Walter Herzog, Co-Chair: James Richards

Pres Time	Presentation title/Abstract title	Speakers/Authors
7:30	Altered knee mechanics during weight acceptance in stair descent for athletes with anterior cruciate ligament reconstruction compared to asymptomatic athletes	Jonas Markström
7:42	Muscle shortening velocities and joint-specific powers at different external power and cadence requirements during cycling	Cristian Riveros-Matthey
7:54	Corticospinal excitability during the preparatory phase of preloaded concentric and eccentric contractions	Daniel Hahn
8:06	Variability of muscle synergies across skateboarding tricks with different levels of complexity	Lorenz Zweier
8:18	An exploration of the motor unit behaviour during squatting tasks performed at different speeds	Eva Orantes-Gonzalez

07:30 - 08:30

OF8 - RUNNING: BIOMECHANICS

Location: Online

Chair: Polly McGuigan; Antony Blazevich

Pres Time	Presentation title/Abstract title	Speakers/Authors
7:30	Changes in joint mechanics following repeated sprinting	Basilio Goncalves
7:42	The "spring-like" function of the subtalar joint in maintaining stability during running	Michael Asmussen
7:54	Increased segment coordination variability of the lower limb in runners accomplishing a half marathon	Tony Lin-Wei Chen
8:06	High-speed fluoroscopic imaging for investigation of 6 DOF knee kinematics during walking and running	Wenjin Wang
8:18	Mechanical energy transduction during running after unilateral transfemoral amputation	Hiroto Murata

08:30 - 09:00

QUALISYS AND THEIA MARKERLESS WORKFLOWS: HANDS-ON SESSION

Location: Online

In the third "Swedish Fika" break we will focus on how Qualisys markerless processing workflows integrate Theia software and review the state of validation studies.

09:00 - 10:00

PANEL DEBATE: COMPUTATIONAL APPROACHES TO STUDYING LOCOMOTION DISORDERS: NMSM VS. AI

Location: Online

SPEAKERS:

MODERATOR:



David Lloyd,
Griffith University
(Australia)



Eni Halilaj, Carnegie
Mellon University
(USA)



Ilse Jonkers,
University of
Leuven (Belgium)

09:00 - 10:00

SPECIAL ORAL: DEVELOPING COUNTRIES GRANT COMPETITION

Location: Online

Chair: Daniel Hahn

Pres Time	Presentation title/Abstract title	Speakers/Authors
	Investigating the performance of neck exoskeleton in prevention and reduction of neck pain problems	Ganesh M. Bapat
	Massage and adapted posture for correction of the spinal curvatures of 360 adolescent yam growers	Gerard Doussou
	Effects of exercise intervention on the biomechanics of occupational-related tasks among nurses with low back pain	Shazlin Shaharudin
	Electrical Impedance Tomography combined with Transcranial Doppler ultrasonography on monitoring stroke recovery: Biomechanical application at North Western Part of China	Li Le
	Foot-ankle physiotherapy as preventive strategy for biomechanical dysfunctions in people with diabetes	Isabel C.N. Sacco

10:00 - 10:15

BREAK

Location: Online

10:15 - 11:15

KEYNOTE LECTURE: TENDON STRUCTURE-FUNCTION RELATIONSHIPS IN HEALTH AND DISEASE: EXPLORING THE INTERFASCICULAR MATRIX (HAZEL SCREEN)

Location: Online

HAZEL SCREEN

Hazel Screen is Professor of Biomedical Engineering and Head of the School of Engineering and Materials Science at Queen Mary University of London. Her research centres on healthy and pathological tissue structure-function behaviour and its interplay with mechanobiology.

She has a particular long-standing interest in tendon and ligament, and leads a highly multidisciplinary group which spans human and animal in vivo and in vitro studies of tendon function and injury, taking a multiscale approach to exploring tendon mechanobiology from the nano- to micro-scale. She has established and is now further exploring a new paradigm associated with the aetiology of tendon injury.



Screen also leads the UK Organ-on-a-Chip Technologies Network and co-directs the Centre for Predictive in vitro Models at QMUL, within which she leads a research group specifically focused on developing novel in vitro models of musculoskeletal tissues which integrates her expertise in mechanobiology and structure-function into new models to explore health and disease.

11:15 - 12:15

ISB AGM

Location: Online

MAJOR SPONSOR WORKSHOPS

12:15 - 12:45

SNEAK PEEK: ACL PATIENT TRACKING PLATFORM GENERATES IMMEDIATE OBJECTIVE RESULTS

Location: Online

Objective measurements can now be visualized in automated reports as part of a new platform aimed at improving the rehabilitation phase of an ACL patient. Xsens MotionCloud generates a Knee Assessment Report which contains objective results of nine knee stability tests like 'single hop for distance' or a 'drop vertical jump'. Joint angles, distances, symmetries and automated LESS are visualized in the report.

The MotionCloud report is integrated into a patient tracking platform, where it is combined with the results of patient surveys (IKDC, Tegner, etc.) training specific programs and other measurement. This platform aids a physiotherapist to monitor a patient through the rehab phases, keeping the patient motivated. A dashboard displays the criteria that need to be met to elevate a patient to the next phase.

12:15 - 12:45

LIVE WORKSHOP: COMPARING TWO DIFFERENT SHOE TYPES WHILST HOPPING

Location: Online

LIVE from KIH Lab, we will be streaming a demo comparing two different shoe types whilst hopping. See how quick you can process the data and see the results.

12:45 - 13:30

LUNCH BREAK

Location: Online

13:30 - 14:30

OG1- LOCOMOTION: GENERAL

Location: Online

Chair: Isabel Sacco

Pres Time	Presentation title/Abstract title	Speakers/Authors
13:30	The effect of diabetic neuropathy progression on muscle fiber conduction velocity of proximal and distal leg muscles during isometric contractions at low level forces	Eneida Yuri Suda
13:42	Center of pressure control ensures mediolateral gait stability: Muscle driven foot placement and ankle moment control	Moira van Leeuwen
13:54	Tactical vest loading alters head-torso coordination in operational police officers during running	Matthew Ellison
14:06	Effects of unilateral swing leg resistance during walking on propulsion, braking and muscle activity	Sylvana Weiland
14:18	The effects of speed and footwear on 3D energy absorption during the braking phase of running: Distance matters	Steffen Willwacher

13:30 - 14:30

OG2- MUSCULOSKELETAL MODELLING

Location: Online

Chair: Tiago Jacques

Pres Time	Presentation title/Abstract title	Speakers/Authors
13:30	Sampling and modelling of motor unit-specific activation properties in the intact human in vivo	Antonio Gogeochea Hernandez
13:42	Estimating muscle and joint stiffness during plantar-dorsi flexion joint rotations via musculoskeletal modelling	Christopher P. Cop
13:54	Large-scale multi-channel electromyography and musculoskeletal modeling via wearable smart garments to support clinical decision-making	Donatella Simonetti
14:06	Voluntary control of a lower limb exoskeleton during walking using an EMG-driven biomechanical model	Guillaume Durandau
14:18	Predictive simulations of fixed-speed treadmill gait	Kayla Pariser

13:30 - 14:30

OG3 -CLINICAL BIOMECHANICS

Location: Online

Chair: Marco Vaz

Pres Time	Presentation title/Abstract title	Speakers/Authors
13:30	3D Body Landmark Detection for Markerless Motion Tracking	Alex Spencer
13:42	Neuromuscular activation patterns during challenged walking tasks in individuals with femoroacetabular impingement	Carson Halliwell
13:54	Eccentric training increases the cross-sectional area in different regions of the Achilles tendon after rupture	Emmanuel da Rocha
14:06	Is the side-stepping exercise effective on targeting gluteal muscles?	Heiliane de Brito Fontana
14:18	Biomechanical response of residual limb: combining shear-wave elastography and finite element analysis	Begum Zeybek

13:30 - 14:30

OG4 - SPECIAL SESSION: UPPER EXTREMITY MOTOR CONTROL

Location: Online

Chair: Michael Twardowski, Co-Chair: Mark Latash

MARK L. LATASH

Mark Latash is a Distinguished Professor of Kinesiology and Director of the Motor Control Laboratory at the Pennsylvania State University. His research interests are focused on the control and coordination of human voluntary movements, movement disorders in neurological disorders, and effects of rehabilitation. He is the author of "Control of Human Movement" (1993) "The Neurophysiological Basis of Movement" (1998, 2008), "Synergy" (2008), "Fundamentals of Motor Control" (2012), "Motor Control and Biomechanics: Defining Central Concepts" (with V.M. Zatsiorsky, 2016), and "Physics of Biological Action and Perception" (2019). In addition, he edited ten books and published over 400 papers in refereed journals. Mark Latash served as the Founding Editor of the journal "Motor Control" (1996-2007) and as President of the International Society of Motor Control (2001-2005). He has served as Director of the annual Motor Control Summer School series since 2004. He is a recipient of the Bernstein Prize in motor control.



Pres Time	Presentation title/Abstract title	Speakers/Authors
13:30	Synergic control of individual muscles and agonist-antagonist muscle pairs	Mark L. Latash
13:54	Size and structure of joint angle variability in young and old adults performing a fatiguing repetitive reaching task	Christopher Bailey
14:06	Individual finger movement control and association to brain activity in healthy participants	Helena Grip
14:18	Mirror-system-like excitability to kinaesthetic stimuli in the human motor cortex	Marc de Lussanet

13:30 - 14:30

OG5 - IMAGING

Location: Online

Chair: Arin Ellingson

Pres Time	Presentation title/Abstract title	Speakers/Authors
13:30	Quantitative assessment of a treatment addressing hypomimia in Parkinson's disease	Zimi Sawacha
13:42	Intra-assessor reliability of intrinsic foot muscles' size in older and younger adults using a portable ultrasound device	Lydia Willemse
13:54	Automated analysis of medial gastrocnemius muscle-tendon junction displacement in healthy young adults using deep neural networks	Rebecca Krupenevich
14:06	Development of an in-vivo tibiotalar kinematic protocol to investigate activities of daily living	David Williams
14:18	Fixation of tibial components in cementless total knee replacement measured with RSA and MRI	Jordan Broberg

13:30 - 14:30

OG6 - SPECIAL: HAND & WRIST BIOMECHANICS IV

Location: Online

Chair: Ronit Wollstein, Co-Chair: Benjamin Goislard de Monsabert

VERONIQUE FEIPEL

Veronique Feipel is a Professor of Functional Anatomy at the Université Libre de Bruxelles (ULB), Belgium. She is currently Dean of the Faculty of Motor Sciences and coordinator of the Research Master in Motor Sciences at ULB. She completed her PhD at ULB in 1997 and was a postdoctoral fellow in the LIS-3D – Sainte-Justine Hospital, Montreal, in 2000. Veronique has been a member of the ISB since 1999, has been a council member of ISB and has enjoyed the ISB meetings since attending her first ISB meeting in Calgary in 1999. She is Fellow of the ISB.

Veronique's research interests include spine, wrist and knee kinematics, clinical applications of musculoskeletal modelling and gait analysis. Over the past few years, her personal interest in sports led her to broaden her research efforts on the prevention of running related injuries and its link to running biomechanics.

Veronique leads a group of researchers in the Laboratory of Functional Anatomy aiming to facilitate clinical penetration of biomechanics research. She will continue supporting with energy research in the field of her first love, wrist biomechanics.



Pres Time	Presentation title/Abstract title	Speakers/Authors
13:30	Recent advances in wrist biomechanics	Veronique Feipel
13:54	A new radiographic index for early diagnosis of perilunate injuries	Fernando N Zambone Pinto

14:06	Force transmission via intertendinous linkages of the m flexor digitorum profundus	Guido Geusebroek
14:18	Monitoring development in children using hand function	Vasiliki Vardakastani

13:30 - 14:30

OG7 - PROSTHETICS AND ORTHOTICS

Location: Online

Chair: Carolin Curtze

Pres Time	Presentation title/Abstract title	Speakers/Authors
13:30	Knee implant wear predictions are altered by including fluoroscopy-measured kinematics in the boundary conditions	Michael J. Dreyer
13:42	Fuzzy-logic inference system for transfemoral socket rectification	Mike Karamousadakis
13:54	Plantar pressures in custom foot orthoses with and without heel plugs	Megan Balsdon
14:06	A case series of early swing perturbation recovery strategies in transfemoral prosthesis users	Shane King
14:18	Bi-linear Natural Ankle Quasi-Stiffness During Walking: Characterization and Implications for Orthosis Design	Luke Nigro

13:30 - 14:30

OG8 - SPECIAL: SIMULATION OF LOCOMOTION II

Location: Online

Chair: Friedl De Groote, Co-Chair: Marten Afschrift

PETER J. BISHOP

Originally from Australia, Peter has had a lifelong passion for palaeontology, geology and mathematics. He gained a BAppSc (Hons) in Geosciences from the Queensland University of Technology in 2012, completed his PhD in Evolutionary Biomechanics from Griffith University in 2017, and subsequently held post-doctoral research positions at Griffith University, the University of the Sunshine Coast and the Royal Veterinary College. Over this time he has studied many extinct animals including freshwater crustaceans, fish, stem tetrapods, lizards, early archosaurs and dinosaurs (avian and non-avian). Peter is particularly interested in integrating biomechanics with data from fossils and modern animals, using a rigorous, physics-based approach to examine the adaptive significance of evolutionary changes in the vertebrate skeleton. In his current role, his research focuses on the sprawling-to-erect postural transition that took place in synapsids on the line to mammals, where he is using biomechanical modelling and simulation to understand the anatomical and physical factors that influenced and constrained this transition. Since 2007, Peter has also been part of the Geosciences Program of the Queensland Museum, Brisbane, first as a student volunteer and more recently as an Honorary Research Fellow.



Pres Time	Presentation title/Abstract title	Speakers/Authors
13:30	Quo vadis, Tyrannosaurus? Predictive simulations of locomotor function and performance in modern and extinct animals	Peter J. Bishop
13:54	Trajectory optimization of a 3D musculoskeletal model with inertial sensors	Marlies Nitschke
14:06	Predictive simulation of human motion using SCONE	Thomas Geijtenbeek
14:18	Stochastic optimal control predicts features of sensorimotor control during walking	Tom Van Wouwe

14:45 - 15:45

KEYNOTE LECTURE: LEARNING HOW TO MOVE LIMBS WITH SOFT WEARABLE ROBOTS (CONOR J. WALSH)

Location: Online

CONOR J. WALSH

Conor Walsh is the Paul A. Maeder Professor of Engineering and Applied Sciences at the John A. Paulson Harvard School of Engineering and Applied Sciences. He is the founder of the Harvard Biodesign Lab, which brings together researchers from the engineering, industrial design, apparel, biomechanics, physical therapy and business communities to develop and translate new disruptive robotic technologies for augmenting and restoring human performance. Example application areas include, enhancing the mobility of healthy individuals, restoring the mobility of patients with gait deficits, assisting those with upper extremity weakness to perform activities of daily living and preventing injuries of workers performing physically strenuous tasks.



The soft exosuit technology is now commercially available in clinics for gait retraining through a collaboration with ReWalk Robotics and a lab spin-out, Verve, has launched a back assist product for workers performing physically strenuous tasks in industry. He is dedicated to training the next generation of biomedical engineering innovators and lab alumni have gone on to successful careers in academia, entrepreneurship, and high tech R&D positions in industry. Additionally, he co-founded the Soft Robotics Toolkit that serves as a platform the lab's extensive STEM outreach activities. He is the winner of multiple awards including the Presidential Early Career Award for Scientists and Engineers and the MIT Technology Review Innovator Under 35 Award.

15:45 - 17:15

POSTER SESSION B

Location: Online

Pres Time	Presentation title/Abstract title	Speakers/Authors
	• DIC-based stress-shielding analysis in compression of CoCrMo porous structures for orthopedic implants	Paolo Caravaggi
	• A gait pattern comparison between healthy adults and neurological patients at different walking speeds	Elke Warmerdam

- Effect of fatigue on hip, knee and ankle proprioception during a golf specific fatigue protocol Ukadike Chris Ugbolue
- A procedure for measuring the kinematics of the foot and ankle complex through Weight-Bearing CT Michele Conconi
- The project reflatperform - development of a reference laboratory for the evaluation of playing- and performance-related dysfunctions of performing artists to derive individual prevention and rehabilitation strategies Dirk Möller
- Step length asymmetry is associated with fear of falling activity avoidance in persons with unilateral transtibial amputation Noah Rosenblatt
- Multi-digit Force Coordination in Patients with Trigger Digit using Machine Learning and Deep Learning Kien Tran
- Inter-session repeatability of markerless motion capture gait kinematics Robert Kanko
- Novel computer vision and deep learning approaches for tracking 3-D spine motion during dynamic trunk flexion using an RGB-D camera Kristen Beange
- A supervised classification of children with fragile X syndrome and controls based on kinematic and sEMG parameters Weronika Piatkowska
- Ankle Joint Quasi-Stiffness of Quiet Unperturbed Standing in Chiari Malformation: A Fast Fourier Transform Approach Brittany Sommers
- Ground reaction forces during anteriorly-loaded overground walking Jiyun Ahn
- Automatic identification and segmentation of balance-related tasks using markerless motion capture Kieran J. Eveleigh
- Improved balance control following distance learning of yoga in novice practitioners Pranavi Depur
- Functional calibration to improve kinematic analysis in the clinics using inertial measurement units Clint Hansen
- A preliminary study comparing the effects of concurrent and terminal visual feedback on standing balance in older adults Jamie Ferris
- Changes in postural dynamics can be captured by a Wii Balance Board during standing tasks Takashi Sado
- Evaluation of postural sway for remote monitoring of vestibular rehabilitation Timothy Zehnbauer
- Characterizing the feasibility of progressive gait perturbation protocol for individuals poststroke Hala E. Osman
- Multifractal analysis of quiet standing in the young and old John H Challis

- Simple model of arch support: relevance to Charcot Neuroarthropathy Shaye Tiell
- Do relaxed sarcomeres return to their original length following repeated activations? Meng LI
- Classification of autism gait patterns in children using multisegment and single segment foot kinematic data Ashirbad Pradhan
- Firefighter turnout gear limits the ability to lift while maintaining a neutral spine posture Danielle Carnegie
- Does the time of day influence the clinical assessment of muscle strength in men and women? Karine Josibel Velasques Stoelben
- Gluteal activation cues reduce peak acetabular contact pressure during squatting in persons with femoroacetabular impingement syndrome: A finite element analysis study Jordan Cannon
- Lower extremity kinetics following an achilles speedbridge: A case study Kevin Valenzuela
- Is the dissipative energetic behavior of the human heel associated with thermal changes? Nikolaos Papachatzis
- The effects of using a rehabilitation technology on foot muscles strength in people with diabetic neuropathy: A preliminary data analysis Jane Suelen Silva Pires Ferreira
- Effect of maturation and limb dominance on knee flexion and extension torque in adolescent athletes Joanna Geck
- Upper and lower body inter-segmental coordination during unsupervised gait of older adults with dementia Lina Musa
- Biomechanical improvement and timing for total knee arthroplasty surgery Chang Shu
- Sex and anterior cruciate ligament injury effects on isometric and isokinetic force production in a paediatric population Christine Smith
- Knee joint kinetics during stationary cycling for unilateral total knee arthroplasty patients Erik Hummer
- Evaluating Muscle Recruitment During Lower Trapezius Early-Stage Exercises Performed Below 90° Shoulder Elevation Maria Herrera
- National biomechanics day: Past, present, and future Lisa MacFadden
- Development of a hands-on, wearables course as an alternative for physiology labs Patrick Mayerhofer
- Pilot study: Performance benefit of young athletes using a video-based feedback and instrumented starting blocks in athletics sprint start Beat Goepfert

- Active learning strategies using surface electromyography improve the undergraduate student's understanding of neuromuscular human movement control

Carlos De la Fuente
- Micromovements, low back pain, and computer task performance during prolonged sedentary postures

Liana M. Tennant
- Sex-specific neuromuscular adaptations to fatigue in a repetitive pointing task while sitting on a sit-stand stool

Chen Yang
- Sex-specific effects of anti-fatigue lenses on discomfort, kinematics and performance during a seated computer task

Samuel Lamanuzzi
- Relationship between the global movement of the hand and the forearm muscles during typing

Takanori Ito
- Combining wearable sensors and machine learning to monitor low back loading and injury risks in material handling

Emily Matijevich
- Correlation between wear region of shoes and contact region during early gait

Kurt Beschorner
- A scoping review on the applications of machine learning for primary work-related musculoskeletal disorder prevention

Victor Chan
- Drift-free algorithm for estimating muscle fascicle length from ultrasound images

Tim van der Zee
- Patient and implant performance between satisfied and dissatisfied total knee replacement patients

Jordan Broberg
- Investigation of the biofidelity of the MIL-Lx foot

Julia de Lange
- Occupant kinematic prediction model during rear-end collisions

Shimada Sean
- Most severely injured body regions in near side motor vehicle collisions involving head impact

Sean Shimada
- High risk glenohumeral joint forces during three pull-up techniques

Caryn Urbanczyk
- Classification of ACL reconstructed running dynamics using common gait features

Yannis Halkiadakis
- Use of Pressure-Measuring Insoles to Characterize Center of Pressure Length and Width under Simulated Reduced Gravity Conditions

Christian Ison
- In vitro mechanical effects of a specific neurodynamic mobilizations of the superficial fibular nerve: a preliminary study

Felix-Antoine Lavoie
- Drop height and sex differences in anterior cruciate ligament force during unilateral drop landings

Jake Melaro

- Effects of ACL reconstruction on in vivo quadriceps contractile behavior and association with knee joint biomechanics Amanda Munsch
- Optimization vs unscented filtering for measuring walking motion using IMUs Andy Bhateja
- Eight-week individualized gait modification intervention to reduce knee adduction moment: Preliminary analysis of a randomized controlled trial Bryndan Lindsey
- Home-based foot-ankle exercises program oriented by a booklet changed positively foot motion during gait in people with diabetic neuropathy Érica Silva
- Evaluation of a clinical walking test among unilateral lower-limb amputees Hananeh Younesian
- Foot progression angle modifications that maximally reduce the knee adduction moment do not decrease medial knee contact force Kirsten Seagers
- Are medial and lateral tibiofemoral compressive forces different in uphill compared to level walking for patients following total knee arthroplasty? Tanner Thorsen
- Dynamic gait stability during anteriorly loaded treadmill walking Caroline Simpkins
- Danger ahead: Fatigued obstacle negotiation in an unpredictable environment Joshua Vicente
- Modeling spatial asymmetry in visuomotor coordination Kolby Brink
- Effectiveness of a speed control based on auditive feedback during metabolic cost trials Leonardo Lagos
- Differences in ground reaction forces between children, adults, and elder people during walking Mauricio Delgado
- Impact of foot progression angle and/or lateral trunk lean gait modifications on lower limb joints external moments Thomas Legrand
- Spinal reflexes can produce a variety of bipedal gaits Frans van der Helm
- Walking aid selection for non-weight bearing ambulation: effects on stance limb plantar force, walking speed, perceived exertion, and device preference in adults 50 years of age and older David Kingston
- Data collection settings influence total body angular momentum: Effects of walking speed and participant sex Jackson Lordall
- Adaptations in mechanical limb power and metabolic energy cost after chronic growth-period limb loading Kavya Katugam
- Stepping kinematics indicate minimal disruptions to balance control when linking the arms and legs during walking Daisey Vega

- Lower-limb impact loading and bone stimulus in children during a week-long protocol Danilo Catelli
- Novel clamp protocol examines cause-effect relations between propulsive force, walking speed, and cost of transport Ricky Pimentel
- Contribution of the transverse arch to in vivo foot stiffness in humans Ali Yawar
- Movement decreases muscle and tendon stiffness compared to torque and angle matched isometric conditions Kristen Jakubowski
- Knee extensor moment increases with reduced moment arm in running and walking Mitchell Wheatley
- Simulation-based exploration of the anterior drawer test in juvenile patient populations Alexandria Mallinos
- Lower extremity biomechanical demands of a bend and pick-up task in healthy, older adults Jared Moore
- Validation of a non-invasive intra-abdominal pressure measurement tool in living and cadaveric specimen Natasha Jacobson
- Development of a Novel Tibiofemoral Dynamic Unloading Knee Brace with Air Bladder Insert and Wearable Control Box Run Ze Gao
- Biomechanical testing of proximal humerus fixation: a novel approach Patrick Williamson
- To filter, or not to filter force plate data for jump height determination? Brendan Pinto
- Timing of gait events affect time-continuous analysis outcomes Eric Honert
- Analysing the impact of sensor placement on the quality of sEMG signals on the human forearm Amartya Ganguly
- Stochastic Resonance and Heaviness Perception of an Occluded Object Alli Grunkemeyer
- Sex differences and fatiguing movement effects on task-specific stability Fariba Hasanbarani
- Movement preferences of the wrist and forearm combined during activities of daily living Steven Charles
- Information in EMG within and between pedal cycles Jaylene Pratt
- Ultrasound estimates of muscle quality: correcting for the confounding effect of subcutaneous fat Heiliane de Brito Fontana
- Probabilistic DTI tractography demonstrates better consistency with ultrasound estimates of muscle fascicle lengths in comparison to deterministic methods Divya Joshi

- Open vs closed articular architecture of the forearm for an analysis of muscle recruitment during throwing motions Claire Livet
- A quantitative test of soft tissue work analysis in human walking Koen Lemaire
- Can electrically induced contractions replicate walking in microgravity? Thomas Abitante
- Foot joint stiffness effects on maximum vertical jumps Daniel Davis
- Effects of maturation on estimated ACL loading in adolescent female soccer players Lauren Schroeder
- Dynamic foot model to study the syndesmotic variation during the rotation of the ankle Maria Ruiz
- Verification of a method to examine the effects of a knee brace on joint loading and muscle activity Ryan Baxter
- Effect of muscular fatigue on ACL loading in healthy and ACL-reconstructed females Shelby Peel
- Evaluating anthropometrically scaled models of lateral pinch to characterize the pediatric hand Tamara Ordonez Diaz
- Alignment of the normal ankle joint in neutral bilateral standing in six degrees of freedom Jordan Stolle
- How do dry needling and high-intensity focused ultrasound affect the mechanical properties of supraspinatus tendons? Sujata Khandare
- Spatial distribution of material properties influences gross and regional ACL load bearing function Jillian Beveridge
- Analyze the effect of the anterior oblique ligament injury and first dorsal interosseous function upon thumb CMC joint subluxation: a cadaver study Tai-Hua Yang
- Transfemoral prosthesis user stumble recovery responses for both limbs across swing phase Maura Eveld
- Motor unit action potential features for robust motion classification Michael Twardowski
- Exploring effects of prosthetic ankle and toe joint range of motion on activities of daily living Rachel Teater
- Bone contact differences of conical and cylindrical endoprostheses for transtibial percutaneous osseointegrated prostheses Carolyn Taylor
- Variable Stiffness Foot provides Users with Adjustment of Knee and Ankle Mechanics Kieran Nichols
- Effects of a physiotherapy exercise program for foot-ankle in people with diabetes on foot kinematics during gait Renan Monteiro

- Effects of short-term cycling intervention on knee biomechanics in cycling with augmented visual biofeedback for patients with total knee arthroplasty Songning Zhang
- Assessment of DCEF stimulation on the neuronal function using in vitro stroke model eumnin ko
- Predicting gait events from handle forces in an instrumented posterior walker Evan Dooley
- Protocol for improving familiarity with a lower-limb robotic exoskeleton in able-bodied, first-time Users Jan Lau
- Youth Running Biomechanics: The Influence of Footwear on Kinetics and Kinematics Andrew Traut
- The effect of fixation location and footwear type on peak impact accelerations from a consumer-grade IMU during running Christopher Napier
- Triceps surae muscle-tendon properties as determinants of the metabolic cost in trained long-distance runners Esthevan Machado dos Santos
- Mechanical symmetry in elite middle distance runners Geoffrey Burns
- In silico modeling of tibial fatigue life in physically active males and females during different exercise protocols Stacey Meardon
- Female runners demonstrate a greater decrease in knee flexion with age than males Heather Hamilton
- The effect of increasing step rate on foot progression angle during running Katie Farina
- Transverse thorax-pelvis movement patterns in runners with and without mild non-specific low back pain Maria Jesús Celedón
- Quantifying change of direction movements in youth soccer players using wearable technology Aki-Matti Alanen
- A systematic review: Long range correlations in running gait Taylor Wilson
- The between-day repeatability for peak tibial acceleration during track running Zoe Y.S. Chan
- Potential influence of stiffening elements on metatarsal-phalangeal joint flexion and running economy Scott Tucker
- A multiscale EMG-assisted muscle-force driven finite element analysis pipeline to investigate knee joint mechanics in functional movements: towards a rapid multiscale modeling toolbox Amir Esrafilian
- Development of a finite element model of the rat knee joint to estimate the articular cartilage biomechanics during gait Gustavo A. Orozco

- Approximation method to calculate the elasticity tensor for hyperelastic finite element models Manuel Lucas Sampaio de Oliveira
- A statistical shape model of the tibia-fibula complex: Effects of age on reconstruction accuracy from anatomical landmarks Olivia L Bruce
- Design and evaluation of a mixed reality spine surgical simulator benchtop configuration based on the workspace of haptic device and simulator users Sneha Patel
- Effect of transverse plane alignment on knee contact mechanics during running David Penaranda
- Learning from the measurable: Predicting changes in hill-type muscle parameters from lateral pinch Kalyn Kearney
- Objectively defining design parameters associated with self-selected lumbar support prominence Jessa Buchman-Pearle
- Trunk muscle co-activation in and out of an episode of low back pain during the balance-dexterity task Yue Ai
- Exploring the correlation between rotational and translational joint passive stiffness -- A porcine in-vitro investigation Jeff Barrett
- Reliability and accuracy of an on field methodology for ACL risk of injury screening Alfredo Ciniglio
- Multi-segment components of induced power generation during pitching in collegiate baseball players Arnel Aguinaldo
- Center of mass vertical velocity in short misses in the basketball shot Casey Wiens
- Correlation between the kinematic analysis and the field testing on the efficiency of the forehand throwing on ultimate frisbee Erika Salcedo Revelo
- Biomechanics of the landing for double salto backward stretched in the horizontal bar Franklin Camargo
- Characterizing tibial accelerations and exposure in collegiate basketball players during games and practices Jereme Outerleys
- Role of each leg in generating linear and angular impulse in baseball pitching Jun Liu
- Clinical tests can predict trunk control during unilateral landings Karine JV Stoelben
- Hip Range of Motion and Pitching Biomechanics in Adolescent Baseball Pitchers Cody Dziuk
- Sagittal plane kinematics of partnered and individual triple steps in swing dancing Meredith Wells
- Effects of dissociation on muscle activation and torque during stationary cycling Milena Santos

- Clinical estimation of movement behavior predictive of vertical ground reaction forces during athletic tasks Rachel K. Straub
- Neuromuscular profile of the lower limb in Colombian female soccer players in the training process Mauricio Daza
- Functional forearm fatigue response to changing stride length in baseball pitchers Ryan Crotin
- The Effects of Drive-Leg Knee Valgus Angle on Ground Reaction Forces During Baseball Pitching Anthony Fava
- Ground reaction force differences between two forms of squats Jason Wicke
- The influence of sports-related concussion on cognition and landing biomechanics in collegiate athletes Jason Avedesian
- Inertial measurement unit for determining elbow torque during baseball pitching Cody Dziuk
- Body composition and segmental sequencing in trained softball athletes Kenzie Friesen
- Should major league baseball adjust the mound distance? Megan Stewart
- Correlation of Glenohumeral Internal Rotation Deficit, Total Range of Motion, and Retroversion to Shoulder Kinetics in Collegiate Baseball Pitchers Marc Duemmler
- Are distal throwing arm kinematics predictive of maximum elbow valgus torque or ball velocity in youth baseball pitchers? Tessa Hulburt
- Limb symmetry during a cutting task in athletes with and without a history of sports-related concussion Warren Forbes
- Sprinting with prosthetic versus biological legs: an unfair advantage? Owen Beck
- Concurrent changes in median nerve deformation and displacement during gripping Aaron Kociolek
- In-vivo measurement of wrist angles during the dart-throwing motion using inertial measurement units Gabriella Fischer
- There is no repeated bout effect on the torque-frequency relationship of the elbow flexors Avery Hinks
- Effects of localized muscle fatigue on muscle activation during a multi-joint repetitive task Erika Renda
- Effect of thumb ip joint posture on cmc joint movement during thumb opposition Hiroshi Kurumadani
- Carpal bone arch changes in response to carpal bone rotation Jocelyn Hawk
- Inter- and intra-participant uniformity of muscle activation during wrist motion Oluwalogbon Akinola

- Capturing In-season Change of Direction Movement Pattern Variability in Youth Soccer Players with IMUs Aki-Matti Alanen
- Classification of high knee flexion postures using feature and time-series based distance approaches Annemarie F. Laudanski
- Validation of a wearable sensor OpenSense model for evaluating motor variability in gait Christopher Bailey
- Between-day and Between-condition Reliability for Accelerometer Measurements of Ground Contact Time Hannah Dimmick
- Using wearable technology to quantify adherence to a neuromuscular training warm-up in youth basketball and soccer players Lauren Benson
- Validation of In-Shoe Force Sensors for Measuring Ground Reaction Forces During Walking Kaleb Burch
- A Weighed K-Nearest Neighbors classifier as a tool for identification of activities of daily living in subjects with Parkinson's Disease ALBERTO ISAAC
PEREZNSANPABLO
- Implementation of inertial sensors for anaerobic resistance tests Andres Cervantes Villa
- Comparisons Between Researcher-Placed and Subject-Placed Wearable Sensors Matthew Ruder
- Examining the association of backward walking velocity with forward balance control in healthy adults Kirat Shukla
- Sex and height effects on unilateral landing on hip joint loading, ground reaction forces, and lower extremity kinematics Joshua Lardie
- Tasks used when determining return-to-activity in paediatric patients following an anterior cruciate ligament reconstruction: a systematic review Micheal Del Bel
- Design of a swelling suture anchor for improved fixation to osteoporotic bone Rena Mathew

17:15 - 17:30

POSTER QUIZ

Location: Online

17:30 - 19:00

SOCIAL MINGLE

Location: Online

17:30 - 18:30

STUDENT HAPPY HOUR

Location: Online

Thu 29 Jul 2021

10:30 - 11:30

ADVANCING WOMEN IN BIOMECHANICS MEETING

Location: Online

Becoming an Ally

The goal of this one-hour workshop is to provide practice in recognizing and addressing bias through specific scenarios and discussion of positive responses. There will be break-out rooms where scenarios will be enacted. Participants in small groups will work together to recognize biases taking place and how best to respond. This session is open to all, and men are especially encouraged to participate. Scenarios will include hiring, reviews and promotions, meeting dynamics, mentorship and sponsorship, and everyday interactions. Our aim is to provide a safe environment for meaningful discussions. This workshop is organized by "Advancing Women in Biomechanics" (AWB).

11:30 - 11:45

SHORT WELCOME

Location: Online

11:45 - 12:45

OH1 - CLINICAL BIOMECHANICS

Location: Online

Chair: Eva Andersson

Pres Time	Presentation title/Abstract title	Speakers/Authors
11:45	Biomechanical characterization of the primary fixation stability of different acetabular cups with respect to segmental acetabular bone defects	Christian Schulze
11:57	Superimposition of ground reaction force on tibial articular surface: a novel approach to support diagnosis and treatment of early knee osteoarthritis	Miriana Ruggeri
12:09	Supine versus weight-bearing computer tomography in surgically-treated patella instability: an investigation on ligament length change between two different loading conditions	Claudio Belvedere
12:21	Relationship between knee range of motion and gait function pre and post-total knee replacement	Marina De Vecchis
12:33	Recovery of weight-bearing symmetry after total hip arthroplasty depends on activity and pre-surgery values	Sónia A. Alves

11:45 - 12:45

OH2 - LOCOMOTION: GENERAL

Location: Online

Chair: Lizeth Sloot

Pres Time	Presentation title/Abstract title	Speakers/Authors
11:45	Which metabolic cost models most accurately predict energetics at different speeds of walking?	Abraham Israel Luis Pena
11:57	Model-based closed-loop control of locomotion via muscle reflexes and spinal synergies: A direct collocation-based system identification approach	Huawei Wang
12:09	Inclination of talocrural joint axis: In vitro studies and morphological considerations not confirmed in walking condition	Peter Wolf
12:21	Do different activation patterns between the lateral and medial gastrocnemius translate into different fascicle behavior during walking?	Raphaël Hamard
12:33	Bracing Results in Immediate Improvements in Gait Mechanics for Patients with Adult Spinal Deformity	Ruth Higgins

11:45 - 12:45

OH3 - MUSCULOSKELETAL MODELLING

Location: Online

Chair: Brian Umberger

Pres Time	Presentation title/Abstract title	Speakers/Authors
11:45	Bone alignments via weight-bearing CT scans and 3D reconstruction tools in the flat foot	Alberto Leardini
11:57	Computational modelling of proximal and distal epiphyseal and appositional growth of the femur in children	Andreas Lipphaus
12:09	Measuring knee joint laxity in four DOF in vivo using a robotics- and image-based technology	Hannah Katharina Fabro
12:21	Identification of optimal laxity tests to stretch individual parts of knee ligaments	Michael Skipper Andersen
12:33	Review of musculoskeletal modelling in a clinical setting: current use in rehabilitation design, surgical decision making and healthcare interventions	Samuel Smith

11:45 - 12:45

OH4 - ORTHOPAEDICS: BONE & CARTILAGE, TENDON & LIGAMENT

Location: Online

Chair: Jennifer Shin

Pres Time	Presentation title/Abstract title	Speakers/Authors
11:45	Mathematical modeling of degradation process of biodegradable metallic biomaterials in immersion and perfusion setups	Mojtaba Barzegari

11:57	Changes in ankle and foot joint kinematics after fixed-bearing total ankle replacement	Paul-André Deleu
12:09	In vivo length-change patterns of the medial collateral ligament throughout complete cycles of level walking	Seyyed Hamed Hosseini Nasab
12:21	Characterization of collagen structural response to in situ loading of the rat Achilles tendon	Isabella Silva Barreto
12:33	Functional performance associated with triceps surae muscle and tendon morphology in patients with achilles tendinopathy	Kayla Seymore

11:45 - 12:45

OH5 - MUSCULOSKELETAL MODELLING AND SIMULATION

Location: Online

Chair: Matthew Handford

Pres Time	Presentation title/Abstract title	Speakers/Authors
11:45	Sensitivity analysis of joint contact forces to individual muscles maximal isometric force using a Gaussian process emulator	Erica Montefiori
11:57	Musculoskeletal trunk model for simulation of scoliosis deformities	Hamed Shayestehpour
12:09	Hamstrings contraction regulates magnitude and timing of peak anterior cruciate ligament loading during drop vertical Jump in female athletes	Ryo Ueno
12:21	Application of a novel multiscale modeling toolbox to characterize knee joint mechanics during daily activities and rehabilitation exercises in knee osteoarthritis individuals	Amir Esrafilian
12:33	Applied biomechanics and computational modelling to prevent and manage upper extremity injuries in rowing	Caryn Urbanczyk

11:45 - 12:45

OH6 - ARTIFICIAL INTELLIGENCE AND MACHINE LEARNING

Location: Online

Chair: Emma Tole

Pres Time	Presentation title/Abstract title	Speakers/Authors
11:45	Lower-limb joint torque prediction using multi-step deep learning approach	Longbin Zhang
11:57	Prediction of finger movements via a reservoir-computing neural network driven by electromyographical data	Frederik Thies
12:09	Frontal-parietal delta microstate-based Brain computer interface improves Knee Gait Trajectory and Phase Prediction	Sanya Varghese
12:21	High density and bipolar sEMG based ankle joint torque prediction using machine learning	Asta Danauskiene
12:33	Prediction of the shape of human lumbar vertebrae from adjacent ones by singular values decomposition	Marco Sensale

11:45 - 12:45

OH7 - SPORTS BIOMECHANICS

Location: Online

Chair: Izzy Moore, Co-Chair: Molly McCarthyRyan

Pres Time	Presentation title/Abstract title	Speakers/Authors
11:45	Frontal plane knee control with regard to leg dominance in female adolescent competitive handball players during a drop vertical jump	Sabrina Erdrich
11:57	Anatomical predictors of sagittal hip kinematics during deep squat in adolescent males with and without CAM deformity	Dalia Al Otti
12:09	Development of a 3d musculoskeletal simulation model to estimate muscle and knee ligament forces during carved turns in alpine skiing	Dieter Heinrich
12:21	The validity of the GPS-based accelerometer to measure foot stance characteristics during running	Michael Lawson
12:33	Effects of 4-week transcranial direct current stimulation combined with foot core exercise on foot muscle strength and ankle kinesthesia	Songlin Xiao

11:45 - 12:45

OH8 - MOTOR CONTROL

Location: Online

Chair: Paola Contessa, Co-Chair: Jennifer Vojtech

Pres Time	Presentation title/Abstract title	Speakers/Authors
11:45	Pain-induced adjustments in motor Unit discharge depend on contraction speed	Eduardo Martinez-Valdes
11:57	Impact of personality on postural control - a pilot study	Justyna Kędziorek
12:09	Corticospinal excitability during and after stretch-shortening cycle contractions compared with pure shortening contractions	Lea-Fedia Rissmann
12:21	Uncontrolled manifold analysis of effects of different fatigue locations on coordination during a repetitive pointing task	Matthew Slopecki
12:33	Inter-individual variation in coordination and control of countermovement jumps	Stuart McErlain-Naylor

12:45 - 14:15

POSTER SESSION C

Location: Online

Pres Time	Presentation title/Abstract title	Speakers/Authors
	<ul style="list-style-type: none"> Increased postural threat alters control of dynamic stability in response to external perturbations that induce a step 	Noah Rosenblatt

- The relationship between 2D and 3D sacropelvic measurements Nikita Ghosh
- Musculoskeletal simulations of high knee flexion tasks: knee ligaments geometry definition Davide Pavan
- Musculoskeletal modelling: relevance of model anatomical consistency Michele Conconi
- Cadaveric knee simulator in orthopaedic training to quantify joint kinematics for active functional motions Darshan Shah
- Assessing the mechanical properties and stress distribution in dynamic Ankle Foot Orthoses: bench testing and FEA Paolo Caravaggi
- Kinematic Analysis of the Human Body using Machine Learning Technique Usman Saleem
- BrokenPose: why we need custom models for markerless motion analysis Neil Cronin
- Improved balance analysis accuracy using a functional base of support model Matthew Millard
- Differences in single leg postural control when assessed over time in professional rugby union players Molly McCarthy-Ryan
- Foot and ankle joint coupling in balance and gait Rosemary Dubbeldam
- Intra and intersession reliability of centre of pressure measures in older adults during bipedal static postural tests Diana Soares
- The effect of feet position on standing balance in pediatric patients with flatfeet alina khodorovvskaya
- Limits of stability in cognitively healthy individuals and mild cognitive impairment Andresa MC Germano
- The vertical balance control system in children with cerebral palsy is more synchronized compared to healthy children Galina Ikoeva
- Energy dissipation while landing from a jump Thibaut Toussaint
- Anticipatory Postural Adjustments During Gait Initiation in People with Mild Chronic Low Back Pain Lorenzo Rum
- Video game based kinematic assessment using a leap motion controller Dominik Buchmann
- A novel method to assess soft tissue overloading within the sole of the foot Chockalingam Nachiappan
- Friction coefficients of cancellous bone densified with autologous bone-particles in uncemented fixation Sebastian Manuel Zobel
- A finite element investigation of the tunability of non-pneumatic tyres for wheelchair use Otis Wyatt

- Development of a sensor assembly to measure vertical, horizontal and tilt motion of the glenoid edge during the ASTM F2028 test Leanne Haworth
- Robot-based method for analysis of knee prostheses in human cadaveric knees Adrian Gomez
- Increased muscle activity in acoustic startle response among children with recurrent pain in the head, neck and abdomen due to chronic stress Eva Andersson
- Unraveling human-rollator-interaction using a robot rollator simulator device Frieder C. Krafft
- Thumb range of motion in osteoarthritis and effect on hand function Jarque-Bou Néstor J.
- Hiking with total knee arthroplasty: In field kinematics in sloped walking in relationship to muscle strength Judith Bleuel
- Can knee valgus kinematics be predicted by clinical assessments during a unilateral landing task? Karine JV Stoelben
- Influence of mandibular reconstruction employing iliac crest flap and fibula flap on the long-term gait of patients Sybele E. Williams
- Evaluation strategies for assessing finger motion in rheumatoid arthritis to estimate impaired hand function Uday Phutane
- Musculoskeletal alterations in children with fragile X syndrome Zimi Sawacha
- Knee Joint Biomechanics Following Total Knee Arthroplasty with Posterior Stabilized Implants Chang Shu
- The effect of diabetic peripheral neuropathy on lower limb biomechanics: a systematic review and meta-analysis Erica Bartolo
- Reliability of a portable system for motion analysis in children and young adults with treated obstetrical brachial plexus palsy Helena Grip
- Quadriceps muscle and pain during daily activities for total knee arthroplasty patients Fangjian Chen
- Comparison between two mobile applications measuring shoulder elevation angle - A validity study Fredrik Öhberg
- Introducing a test setup to measure the tribological behaviour of shoe-factory interactions under biomechanically relevant conditions Lasse Jakobsen
- Functional assessment for passive and active back supporting exoskeletons Jasper Johns
- Fracture behavior of a composite of bone and calcium sulfate/hydroxyapatite Joeri Kok

- Microscale compressive behavior of hydrated lamellar bone at high strain rates Cinzia Peruzzi
- A high-fidelity finite element model of the cerebrovasculature for brain injury simulation Harry Duckworth
- The axial impact response and plantar load distribution of the hybrid III and MIL-Lx under altered ankle postures Julia de Lange
- Knee biomechanics of single leg hop landings after primary anterior cruciate ligament repair and InternalBrace™ augmentation Birte Luise Coppers
- New home exercise program for the Swiss Box Lacrosse National Team Beat Goepfert
- Experimental investigation of human head interaction with deformable elasto-plastic unsecured object placed in the vehicle during vehicular frontal crash Jaroslav Hruby
- Influence of a mixed reality training on gait in people with mental disabilities Alexis Laly
- Gait asymmetry results in symmetric relative efforts between affected and unaffected side musculature in children with hemiplegic cerebral palsy Juha-Pekka Kulmala
- The effect of lower limb loss on the stability and variability of kinematics and muscle activations during walking Natalie Egginton
- Hip contact forces in paediatric patients with increased femoral antetorsion Nathalie Alexander
- Comparison of the post-operative knee abduction-adduction angle measured during surgical navigation and treadmill gait: A preliminary study Xavier Gasparutto
- The change of foot clearance and cognitive performance between single and dual task conditions of healthy older adults and people with Parkinson's syndrome Elke Warmerdam
- The role of cutaneous afferents on mechanically induced stretch reflex excitability Kelly Robb
- Application of deep learning-based pose estimation methods for clinical gait outcome measures Logan Wade
- Kinematic and gait parameters classification of obesity by means of principal component analysis: a preliminary study Nicolas Houel
- Perturbed treadmill walking effect on cognitive vigilance Alex P. Moorhead
- The effect of gait speed on plantar pressure data measured with the GAITRite instrumented walkway Clara Leyh

- How does modulating load impact the limits of stability during walking? Inferences from simulated body-weight support and load carriage conditions Yong Kuk Kim
- Detecting gait from a shank-worn inertial measurement unit using harmonic frequencies Robbin Romijnders
- Moving from straight-line to curvilinear walking: effects on accuracy of marker-based gait event detections Tecla Bonci
- Validity and reliability of a mobile insole to measure vertical ground reaction force during walking Bernhard Dumphart
- Effect of aging and physical activity level on recovery within the stride during walking Léopoldine Kury
- Residual force depression is increased following greater in vivo muscle shortening work Brent Raiteri
- Relationship between metatarsophalangeal joint flexors and lower limb strength: a preliminary investigation Enrico Roma
- Comparison of leg muscle activity levels during different fitness tests in elderly individuals using surface electromyography Jonina Oddsson
- The utility and validity of high-intensity intermittent exercise protocols for biomechanical injury preventive screening in male jump-landing athletes Stefan Vermeulen
- Investigating osteoarthritis in the human hip using three-dimensional finite element models. James Osborne
- Relationship of contact time during cutting manoeuvres and lower extremity joint variability Johanna Robbin
- Sex influence on the neuromuscular fatigue examined by a force-velocity concentric test Robin Macchi
- Age-Related Lower Limb Muscle Co-Activation in Sit-to-Stand/Stand-to-Sit Performances Anna Brinkmann
- A new shoe sole technology that transfers the ground composition to the sole of the foot: a user experience evaluation Christoph Bauer
- An integrated cloud platform to perform in silico standard testing for orthopedic implants Vincenzo Carbone
- Can tibio-talo-calcaneal arthrodesis help to assess the effect of the soft tissue artefacts in hindfoot kinematics? Alexandre Naaim
- Reliability and repeatability of a methodology for real world gait and posture assessment in children Alfredo Ciniglio
- High density EMG based estimation of lower limb muscle characteristics using feature extraction Asta Danauskiene

- A modified vertex-wise Bhattacharya metric to compare statistical shape models of pediatric ankle bones Arnaud Boutillon
- Validation of kinematic models of the human whole body centre of mass Charlotte Le Mouel
- Reduction of number of tasks to obtain hand kinematic synergies Gracia-Ibáñez Verónica
- Falling Heads: biomechanical and neuromuscular responses to head-neck perturbations Isabell Wochner
- New approach on constitutive modeling of the pure titanium thermoplastic deformation Jakub Banczerowski
- Does multibody kinematic optimization increase reliability of knee joint angles and moments between thigh marker clusters in high knee flexion? Jessa Buchman-Pearle
- Periodic median filter for power line interference in force plate and bioelectric recordings Marc HE de Lussanet
- Studying the impact of internal and external forces minimization in a motion-based external forces and moments prediction method: application to fencing lunges Pauline Morin
- CNN-based markerless motion capture approach: a pilot study Silvia Zampato
- Evaluating methods of calculating jump height from force plate data Brendan Pinto
- A spot check to ensure comparability of stereophotogrammetric data in multicentric studies Kirsty Scott
- Influence of the balance of excitatory and inhibitory neurons on reservoir computing performance Myriam De Graaf
- Relationship between neck flexion in neurodynamic tests and lower limb muscle activity Dirk Möller
- Painful sinusoidal electrical stimulation decreases the firing rate of vastus medialis and lateralis motor units Alessio Gallina
- The efficacy of surface EMG decomposition to detect motor unit firing rates of the lower-limb muscles during high cadence cycling Brett Still
- The effect of load, speed and contraction phase on motor unit behaviour during a knee extension exercise EVA ORANTES-GONZALEZ
- The effects of passive hyperthermia on muscle-tendon unit mechanical properties Adèle Mornas
- 3D muscle morphology and intramuscular fat of lower legs in children with cerebral palsy ANTEA DESTRO
- Reliability of regional measurements of gastrocnemius muscle fibre lengths obtained from diffusion tensor imaging Jeroen Aeles

- Effect of muscle length on performance enhancement in a stretch-shortening cycle of the quadriceps femoris

Martin Groeber
- Quantifying mechanical loading and elastic strain energy of the human Achilles tendon during walking and running

Mohamadreza Kharazi
- Ultrasound investigation of muscle size and muscle properties in transfemoral amputees

Susann Wolfram
- In vivo submaximal force-angle relationship of the quadriceps based on net joint torque and shear-wave tensiometry

Tobias Weingarten
- Investigating the influence of personalized musculoskeletal models on the calculated muscles and joints forces

Ahmed Soliman
- Towards more effective training: A biomechanical comparison of three hamstrings exercises

Bas Van Hooren
- A forward-dynamics tracking simulation using a combined rigid body - FEM model to predict knee meniscus loading

Benedikt Sagl
- Estimated hamstring muscle function during sprinting is sensitive to modeling methods

Carlie Ede
- Musculoskeletal models for assessing surgical indications and outcomes in cerebral palsy

Claude Hayford
- A ligament-based enhancement via MRI in dynamic ankle modelling validated against corresponding experimental data

Claudio Belvedere
- Influence of optimization criteria on the prediction of knee-joint forces during walking and squatting

Heiko Wagner
- A note on the influence of tendon speed in musculoskeletal inverse dynamics

Joakim Holmberg
- A musculoskeletal parameter study of scapula characteristics affecting rotator cuff muscle forces

Johanna Menze
- Assistance level versus metabolic cost in a biarticular exoskeleton a simulation study

Karthick Ganesan
- Motion-based ground reaction forces and moments prediction method in a moving frame: a pilot study

Louise Demestre
- Automatic generation of personalized skeletal models of the lower limb using the STAPLE toolbox

Luca Modenese
- Evaluation of the impact of different scaling approaches in the model-based muscle forces estimation during locomotion in Parkinson's disease subjects

Marco Romanato
- Individual muscle contributions to knee bone-on-bone forces occurring during a maximal forward braking and backward acceleration in elite athletes

Rodrigo Bonacho Mateus

- Dynamic estimation of soft tissues stiffness of lower limb segments during squatting Sacha GUITTENY
- Impact of the quadratus lumborum muscle on the lumbar spine joint efforts via a parametrized model Simon Hinnekens
- Impact of femur length scaling errors on muscle and joint contact forces at all joints Willi Koller
- Predictive simulations of step initiation to study origins of age-related changes in weight shifting Wouter Muijres
- Which musculoskeletal model best predicts muscle excitations at different walking speeds? Abraham Israel Luis Pena
- Ex-vivo assessment of a novel technique for restoring native collateral ligament strains in total knee arthroplasty Orcun Taylan
- A numerical model to simulate crack propagation in articular cartilage under cyclic loading Gustavo A. Orozco
- Repeatability of cartilage oligomeric matrix protein kinetics in response to a walking stress test Simon Herger
- The effect of abduction angle and infraspinatus load on supraspinatus articular surface strain Patrick Williamson
- A predictive simulation study into the effect of below-knee prosthesis alignment on metabolic cost Anne Koelewijn
- Varying prosthetic knee and ankle combination affects gait biomechanics in unilateral transfemoral prosthesis users. Cleveland Barnett
- Impact of the acetabular component thickness on the implantation process and primary stability Miriam Ruhr
- Variability between surgeons in total hip arthroplasty Tobias Konow
- Are different foot models able to detect the same changes in kinematics due to foot orthoses? Graham J. Chapman
- Comparison of prosthetic liners for lower limb amputees using a 2D numerical model Vasja Plesec
- Ground reaction forces during walking of people with traumatic bilateral major lower limb amputations Brieuc Panhelleux
- A method to autonomously monitor the performance of rehabilitation exercises Asaad Sellmann
- Biophysical effects of steering on asynchronous and synchronous submaximal handcycle ergometry in able-bodied men Cassandra Kraaijenbrink
- Implications of a familiarization phase with a robot-assisted rehabilitation system on motor performance during simulated daily activities Sybele Williams
- F-A-I-T-H-kids method: A pilot evaluation of the clinical efficiency Beat Goepfert

- Impact of foot strike pattern on ankle plantar flexor muscle function during running at different speeds Bálint Kovács
- Local dynamic stability decreases above critical velocity in treadmill running Ben Hunter
- The relationship between running speed and footfall sounds during overground running Cristina Pirscoveanu
- Music-based biofeedback induced running-gait adaptations for lower impact running Rud Derie
- Running power estimation using body-worn inertial sensors: in-lab validation and sensor location comparison Salil Apte
- Runners don't bounce - power economy in springless legged locomotion Scott Tucker
- The physiological and biomechanical adaptations to acute-fatigue on running economy and pelvic-thorax coordination in sub-elite runners Craig Hicks
- Effect of the wear of city shoes on the variables characterizing the foot / ground interaction Elliot POLOME
- The effect of footwear on lower extremity joint functional indices in distance running Patrick Mai
- The effect of running shoes' milage on lower limb muscle activity Julia Habenicht
- Predictive neuromuscular simulation of the sit-to-walk movement Eline van der Kruk
- Estimating safe rehabilitation movements for rotator-cuff injuries from musculoskeletal modeling J. Micah Prendergast
- Kinematics and muscle activation patterns during a 30min walking test in patients with symptomatic lumbar spinal stenosis and healthy controls Corina Nüesch
- Altered timing in trunk rotation with the ToneFit reha compared to nordic walking in people with low back pain Eveline Graf
- 3D Characterisation of Isolated Disc Specimens Subject to Cyclic Loading Samantha Hayward
- Comparison of three approaches for calculating the CoM acceleration based on video analysis and plantar pressure data Alfredo Ciniglio
- Trunk center of mass position during a 90 degree cut in soccer players who go on to ACL injury and those who do not Celeste Dix
- Smartphone-based democratization of vertical jump height estimate Guido Mascia

- Relationships between strength, jump and kinematic variables during resisted sled sprinting

Katja Magdalena Osterwald
- Training to be an Olympic ski jumper in less than four years - a joint level perspective on the early development of simulated ski jump take-off performance in young athletes participating in a talent transfer program

Lauri Stenroth
- Validation of a monocular camera-based method to obtain 3D kinematics in strength training

Lisa Noteboom
- A deterministic model of the Bottom turn Technique

Micael Freitas De Sousa
- Lateral heel release reduces ACL strain in simulated backward twisting falls

Ryo Ueno
- Inertial measurement units to estimate drag forces and power output during standardised wheelchair tennis coast-down and sprint tests

Thomas Rietveld
- Biomechanical alterations as potential risk factors for ACL re-injury in soccer: a systematic review

Alberto Sanchez-Alvarado
- The simulation of kayak paddle blade based on individual stroke technique characteristics

Andrey Pomerantsev
- Toe flexor strength in elite female gymnasts compared to toe flexor strength-trained men

Jan-Peter Goldmann
- The applied analysis of kayaking ergometer with different drag resistance in kayak training: a pilot study

Jiaxiang Yan
- Joint moments have greater impact on vertical jump height than joint angular velocities

Marvin Zedler
- Kinematics of elite-board paddling in rescue sports

Stefan Kratzenstein
- Effects of Tai Chi exercise on postural stability among the elderly during stair descent under different levels of illumination

Yaya Pang
- Effect of exercise on muscle oxygen saturation during the posterior 11 hours

Jose Ignacio Priego-Quesada
- Mechanical work as a (key) determinant of metabolic cost in human locomotion: handcycling and handcycling-driven watercraft

Luca Ardigò
- Using in-fibre bragg grating sensors within the periodontal ligament space of an intact swine premolar: a cross-verification with a representative finite element model

Kathryn P Houg
- Multi-scale constitutive model of human trabecular bone

Krzysztof Jankowski
- Reliability and validity of a robotic manipulator to reproduce quasi-static physiological humerus motions

Florent Moissenet
- Foot health technology for the diabetic high-risk foot: A systematic Review

Claire Saliba Thorne

- Movement quality in subjects with osteoarthritis and after total joint arthroplasty assessed by a single accelerometer Jill Emmerzaal
- Lyapunov estimation from smartphone acceleration signals: Comparison between elderly and young adults Nahime Al Abiad
- The performance of a novel implantable strain sensor under replicated in vivo conditions Naomi Adam
- A novel method for equine gait event detection Eloise Briggs
- Improved accelerometer assessed physical activity patterns after an eight-week exercise intervention. Manne Godhe
- Validation of a LiDAR-based player tracking system during football-specific tasks Theodoros Bampouras
- Step count is related to habitual weight bearing asymmetry in the workplace: An occupational study in hotel employees Alison Agres
- An Automatic Inertial Measurement Unit Alignment Pipeline in Human Motion Measurement Qingyao Bian
- COVID-19 impact on physical activity: A covistress questionnaire evaluation Ukadike Chris Ugbolue
- Effect of total contact cast on lower limb kinematics and kinetics during walking gait Nachiappan Chockalingam
- Determining the optimal limb symmetry index threshold for classifying anterior cruciate ligament injury status in pediatric patients Micheal Del Bel
- A dynamic model of the ankle joint with artificial articular surfaces and its validation against corresponding experiments Maria Ruiz

14:15 - 14:30

POSTER QUIZ

Location: Online

14:30 - 15:15

LUNCH BREAK

Location: Online

15:15 - 16:15

KEYNOTE LECTURE: HOW DO BIOMECHANICAL FACTORS INFLUENCE EXERCISE PRESCRIPTION ON THE INTERNATIONAL SPACE STATION (LORI PLOUTZ-SNYDER)

Location: Online

LORI PLOUTZ-SNYDER

Lori Ploutz-Snyder earned her B.S. and M.S. degrees in zoology (1989) and Ph.D. in biomedical sciences (1994) from Ohio University. She conducted post-doctoral research at Michigan State in physiology and radiology especially developing muscle functional MRI techniques. In 1996, she joined the faculty of Syracuse University as an assistant professor in Exercise Science and rose to professor in 2008, while serving as the chair of the Department of Exercise Science from 2004-2008. She worked collaboratively at Syracuse and held joint appointments in Physical Medicine and Rehabilitation, Physiology and Neuroscience, and the Center for Policy Research. In 2008, she joined the NASA Johnson Space Center and University Space Research Association as NASA's Lead Scientist for exercise physiology and countermeasures. In this role, she was responsible for NASA's research portfolio for the preservation of cardiovascular, skeletal muscle and bone health during long duration spaceflight. In 2013, she was appointed as a musculoskeletal alterations team leader at the National Space Biomedical Research Institute at Baylor College of Medicine. In July 2016, she was appointed Professor of Movement Science and Dean of the School of Kinesiology at the University of Michigan.



Professor Ploutz-Snyder's research focuses on skeletal muscle physiology, the development and optimization of exercise programs for special populations and the integrative effects of exercise. This includes identifying targets for exercise intervention such as functionally relevant thresholds of muscle strength or aerobic fitness. She has worked with diverse populations ranging from athletes and NASA astronauts to frail elderly, stroke survivors, children with cerebral palsy and adults with Down Syndrome.

16:15 - 16:45

FULLY INTEGRATED MOVEMENT ASSESSMENT WITH QUALISYS, NORAXON AND H/P/COSMOS

Location: Online

h/p/cosmos and Noraxon join Qualisys to demonstrate how to create a fully integrated, digital workflow to analyse locomotion on an instrumented treadmill.

The session will be streamed live from German Sport University, Cologne

16:45 - 17:00

BREAK

Location: Online

17:00 - 18:00

OI1 - BALANCE AND POSTURE

Location: Online

Chair: Antonia Zaferoiu

Pres Time	Presentation title/Abstract title	Speakers/Authors
17:00	Triple inverted pendulum model links joint-specific contributions to postural sway in persons with lower limb loss	Courtney M. Butowicz
17:12	Control of the center of mass during standing on a uniaxial balance board; preliminary results	Maud van den Bogaart
17:24	Reactive gait stability in children with cerebral palsy and the effect of videogame-based balance training	Pieter Meyns
17:36	A progressive treadmill perturbation protocol for assessment of reactive balance responses in stroke survivors	Hala E. Osman
17:48	Anthropometric adiposity measures, not body mass index, relate to measures of trip-related fall risk in older adults	Noah Rosenblatt

17:00 - 18:00

OI2 - SPECIAL SESSION: MOTOR CONTROL IN GAIT

Location: Online

Chair: Walter Herzog

GELSY TORRES-OVIEDO

Gelsy Torres-Oviedo was a Ph.D. student of Prof. Lena Ting at The Georgia Institute of Technology and Emory University, where she developed analytical tools for understanding the neural control of balance and the functional consequences of changes in muscle activity. She was a post-doc in the laboratory of Prof. Amy J. Bastian at Johns Hopkins University and The Kennedy Krieger Institute, where she investigated factors that enhance motor learning and generalization of locomotor adaptation, which could improve the gait rehabilitation of patients beyond the clinical setting.



Pres Time	Presentation title/Abstract title	Speakers/Authors
17:00	Characterizing subject-specific adaptation of motor outputs and sensory inputs in locomotion	Torres-Oviedo Gelsy
17:24	Neuromechanical simulation with predicted ground reaction force in a reflex-based model	Binbin Su
17:36	Analysis of the activation modalities of the lower limb muscles in Parkinson's disease	Marco Romanato
17:48	Long-term savings of locomotor adaptation in human split-belt treadmill walking	Nikita Sharma

17:00 - 18:00

OI3 - SIMULATION TECHNIQUES AND APPLICATIONS

Location: Online

Chair: Stephanie Ross

Pres Time	Presentation title/Abstract title	Speakers/Authors
17:00	A framework for continuous integration in human body finite element model lineup	Jobin John
17:12	Crack patterns around an osteon simulated with the phase field method for fracture	Anna Gustafsson
17:24	A penalty contact implementation on a highly parallelisable cartesian mesh finite element solver	Frederik Trommer
17:36	Predicting the effects of knee extensor muscle weakening and strengthening on a post-stroke gait	Gilmar Fernandes dos Santos
17:48	Computational fluid dynamics in cerebral aneurysm	Alberto Brambila

17:00 - 18:00

OI4 - LOCOMOTION: GENERAL

Location: Online

Chair: Irene Davis

Pres Time	Presentation title/Abstract title	Speakers/Authors
17:00	Causal interactions between limbs walking with imposed leg constraints	Genevieve Williams
17:12	Initiation of arch recoil is asynchronous with the windlass mechanism in walking	Lauren Welte
17:24	Walking with increasing acceleration is achieved by tuning ankle torque onset timing and rate of torque development	Logan Wade
17:36	Lower Extremity Joint Moment Angular Impulse during Gait Transitions	Li Jin
17:48	A comparison of multisegment foot kinematics between younger and older adults during walking	Nayeli Marcial

17:00 - 18:00

OI5 - UPPER EXTREMITIES

Location: Online

Chair: Fredrik Öhberg

Pres Time	Presentation title/Abstract title	Speakers/Authors
17:00	Effect of operating setting on muscle activity of the upper body during tree harvester simulation	Jacqueline Toner
17:12	Posture (slouched versus erect sitting) affects upper limb maximal voluntary contraction levels: preliminary results	Aurélie Tomezzoli

17:24	Biomechanics during controlled forward descents on outstretched arms in response to Fall Arrest Strategy Training (FAST) in older men and women	Justin Pifko
17:36	Beyond euler/cardan analysis: true glenohumeral axial rotation during arm elevation and rotation	Klevis Aliaj
17:48	Effect of crutch fit on scapular motion and trapezius muscle activation	Gregor Kuntze

17:00 - 18:00

OI6 - MUSCLE TISSUE AND ARCHITECTURE

Location: Online

Chair: Ruoli Wang

Pres Time	Presentation title/Abstract title	Speakers/Authors
17:00	Regional variability of shear wave velocity is different between passive and active muscle	Allison Wang
17:12	Is there passive force-mediated enhancement of active force in skeletal muscles?	Eng Kuan Moo
17:24	3D soleus model predicts regional muscle displacements that are consistent with dynamic MRI measures	Katherine Knaus
17:36	Does increasing passive force at the start of activation increase the total isometric force of muscles?	Siwoo Jeong
17:48	Age-related changes to triceps surae muscle-subtendon interaction dynamics during walking	William Clark

17:00 - 18:00

OI7 - ARTIFICIAL INTELLIGENCE AND MACHINE LEARNING

Location: Online

Chair: Valentina Camomilla

Pres Time	Presentation title/Abstract title	Speakers/Authors
17:00	Prediction of Parkinsonian gait in older adults with dementia using joint trajectories and gait features from 2D video	Andrea Sabo
17:12	Comparison of data reduction techniques and their effect on neural network performance	Fabian Hoitz
17:24	Two-dimensional video-based analysis of human gait using pose estimation	Jan Stenum
17:36	Predicting ground reaction force waveforms from accelerometers during uphill and downhill running: A recurrent neural network solution	Ryan Alcantara
17:48	Classifying individuals with and without ankle sprain history using machine learning techniques	Monica Russell

17:00 - 18:00

OI8 - MUSCULOSKELETAL MODELLING

Location: Online

Chair: Ilse Jonkers

Pres Time	Presentation title/Abstract title	Speakers/Authors
17:00	Sharing the load: Strategies for modelling loads in OpenSim simulations of two-handed lifting	Mohammadhossein Akhavanfar
17:12	Simulating the effects of body weight loading on the arch of the foot using a dynamic model of the foot and ankle	Rostam Kojouri
17:24	The effects of extracellular matrix and sarcomere length changes in cerebral palsy on muscle stiffness	Ryan Konno
17:36	Personalized gait modifications improve pain and slow cartilage degeneration in individuals with medial knee osteoarthritis: a one-year randomized controlled trial	Scott Uhlrich
17:48	Measuring and modelling in vivo human gracilis passive force-length property	Lomas S Persad

18:00 - 18:15

BREAK

Location: Online

18:15 - 19:45

AWARDS PRESENTATIONS

Location: Online

19:45 - 20:00

BREAK

Location: Online

20:00 - 21:00

ISB PRESIDENT'S LECTURE: TONI ARNDT

Location: Online

TONI ARNDT

Toni Arndt performed his undergraduate studies in New Zealand and Australia in biology and Human Movement Sciences before receiving a scholarship for a PhD at the German Sport University, Köln. His PhD involved studies concerning asymmetrical loading of the Achilles tendon. This line of study continued at the Karolinska Institute in Sweden as a post-doc and he is still exploring new methods for investigating Achilles tendon function. At present Toni Arndt is a professor in biomechanics, specializing in lower extremity muscle-tendon function, athletic footwear and sports biomechanics, at The Swedish School of Sport and Health Sciences (GIH) in Stockholm. He was Dean of the Research and Doctoral Education Board at GIH for six years. He has published approximately 90 peer reviewed scientific articles and has supervised ten PhD students to completion. In 2020 Toni was awarded the Swedish senior prize for sport science research. He is President of the International Society of Biomechanics.



21:00 - 21:30

CLOSING CERMONY

Location: Online

21:30 - 22:30

SOCIAL MINGLE

Location: Online



Oral Abstracts

Rib Injury Prediction using Machine Learning-based Surrogate Models

Shitij Malik¹, Jobin D. John², Johan Iraeus², Mats Svensson²

¹Indian Institute of Technology Delhi, New Delhi, India

²Vehicle Safety Division (Injury Prevention), Dept. Mechanics and Maritime Sciences, Chalmers University, Gothenburg, Sweden

Email: jobin.john@chalmers.se

Summary

Although Finite Element (FE) Models of Human Body are extensively used in Vehicle Safety, they are computationally expensive for use in extensive investigations. In this paper, we explored the use of Machine Learning to build surrogate models as alternative fast models. Support Vector Regression and Decision-Tree based Ensemble Models were trained and validated for prediction of rib injury risk. Important variables influencing rib injury risk were evaluated from the surrogate models.

Introduction

Rib injury is a major risk of injury for vehicle occupants. FE human body models (HBM) are widely used for evaluation of rib fracture. These models are, however, computationally expensive and time consuming. Cheap and fast models will be useful for quick evaluations and to investigate scenarios where further investigations are required using the detailed HBM. Towards this end, the aim of this study was to develop surrogate models to predict risk of rib fracture in a vehicle occupant during car crash.

Methods

Rib injury risk data from FE simulations previously published, corresponding to a fracture of at least 3 ribs in a driver, was used as the training data for surrogate models [1], [2]. The training data had 25 variables (which included crash and vehicle features), which had been sampled using Latin Hypercube sampling to generate 1000 simulations. FE models of an average male along with a generic vehicle interior was used in these simulations. Details of the human body models and the simulation variables can be found in the cited studies.

In this study, the risk of rib injury was modeled using two methods: Support Vector Regression (SVR) with polynomial kernel and Decision-Tree based Ensemble Gradient Boosting Regression (GBR) with least squares loss function. The input variables were centered and scaled using Standard Scaler Transformation and the targets (risk values) were scaled using Quantile Transformation. Scikit-Learn was used to pre-process the data, train, and validate the surrogate models.

Results and Discussion

Five-fold cross-validation of the models yielded maximum scores of 0.87 for SVR and 0.93 for GBR. The cross-validation curves for both the methods plateaued at approximately 500 samples (Fig. 1). Decision tree ensembles are versatile enough to handle nonlinear relationships and interactions between variables, and hence may explain the better performance of GBR.

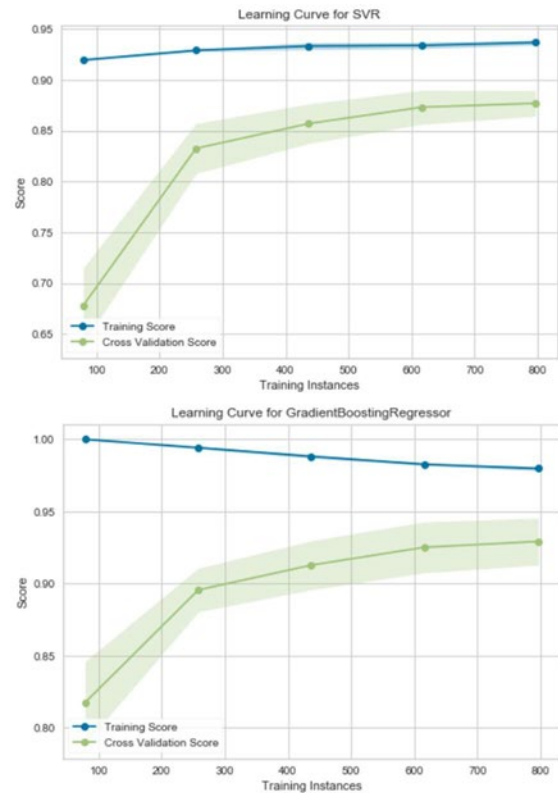


Figure 1: Learning curves for the two models.

The rib injury risks had a heavy right-skewed distribution, requiring transformation to obtain acceptable model accuracy. Quantile transformer, that converted the targets to an approximate uniform distribution, gave a better accuracy compared to other transformations like log.

The relative importance of the variables was evaluated on the GBR model. Change in velocity, airbag trigger time, and direction of impact influenced the risk of rib injury the most among the variables simulated in this study.

Conclusions

We developed surrogate models as fast and cheap alternative to finite element models for injury prediction. For a set of 25 variables, approximately 500 simulations were required to get an accuracy of 0.9. From the surrogate models, change in velocity and airbag trigger time during a crash were found to have the most influence on the risk of rib fracture for a driver.

References

- [1] Iraeus J. et al. (2015). *AAP*, **95**: 42-56.
- [2] Pipkorn B. (2019). *IRCOBI*. 175-192

Generating 2D video frames from 3D motion capture data: a proof-of-concept study

Marion Mundt¹, Henrike Oberlack², Jacqueline Alderson^{1,3}

¹Minderoo Tech & Policy Lab, The University of Western Australia, Perth, Australia

²Institute of General Mechanics, RWTH Aachen University, Aachen, Germany

³Auckland University of Technology, Sports Performance Research Institute New Zealand (SPRINZ), Auckland, New Zealand.

Email: marion.mundt@uwa.edu.au

Summary

Applying machine learning techniques to video data for improving our understanding of biomechanics in the field is increasingly popular. Historically, the bulk of biomechanical research relied on marker-based optical motion capture systems to determine joint kinematics and kinetics. This study proposes a method to synthesize two-dimensional (2D) video frames from three-dimensional (3D) motion data, to create datasets of scale that can leverage machine learning approaches for biomechanical analysis. The results of this proof-of-concept study indicates that the proposed synthesized data method provides a feasible alternative to experimental data capture.

Introduction

2D video data is becoming increasingly relevant for in-field biomechanical analysis. When coupled with pose-estimation (PE) algorithms, 2D video alone may be sufficient to determine joint kinematics and kinetics. Large datasets containing force plate, 2D video, 3D motion capture and/or inertial sensor data can be leveraged to improve the accuracy and validity of PE methods – especially for kinetic parameter estimations [1, 2]. Since such datasets are limited, this study presents a method to simulate 2D video frames and PE skeleton keypoints based on 3D motion capture data. In practice this method serves to facilitate the reuse of 3D motion capture databases by enlarging the available 2D video datasets for PE training, and also provides insight into the minimum number required, and optimal location of, 2D cameras.

Methods

This proof-of-concept study used previously collected and synchronized 2D video and 3D motion capture data.

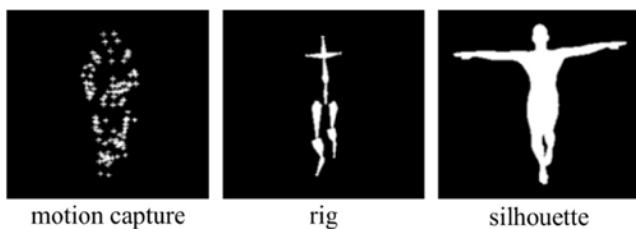


Figure 1: Workflow overview.

The motion capture data was used to create and drive a human silhouette in the open-source 3D computer graphics program blender (version 2.79). For this purpose, joint centers/locations of the bilateral ankle, knee, hip, shoulder and foot (endpoints), pelvis center, neck and head, were used to create a human skeleton rig. Using the MakeHuman plug-in for Blender, a

human silhouette was fitted to the rig and the marker data to model the participant's body shape (Figure 1). To validate the approach, the resulting model was screen captured in Blender software from the same camera view as the original 2D video. OpenPose [3] was used to determine keypoints in both the original video and the animated video. The Euclidean distance difference between the two associated keypoints over time was calculated to examine the accuracy of the method.

Results and Discussion

Mean Euclidean distance difference between the original and animation derived keypoints was smaller than 10 pixels (Figure 2). Only lower limb and trunk keypoints are shown as the 3D motion capture data used did not include arms. The method was validated for a single, perfectly orthogonal sagittal camera view, although different camera views can be constructed in blender to create 2D videos of the animated model. The position of the camera will most likely influence the keypoint PE results in a similar way for both, original videos, and animations.

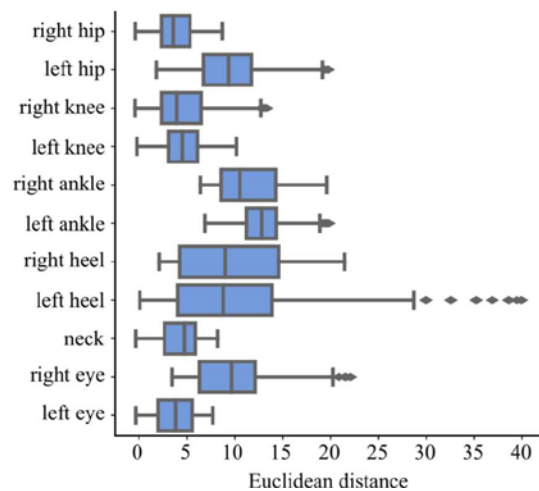


Figure 2: Euclidean distance between original video and animation.

Conclusions

The Python plug-in for Blender enables the automated creation of videos from multi-view camera angles, facilitating the reuse of 3D motion capture datasets for 2D video-based machine learning applications.

References

- [1] Johnson et al. (2019). *IEEE. Trans. Biomed. Eng.*, **66**(3): 689-694.
- [2] Mundt et al. (2019). *Med. Biol. Eng. Comput.*, **57**(8): 1833-1841.
- [3] Cao et al. (2021). *IEEE Trans. Pattern Anal Mach Intell.*, **43**(1):172-1

Validation of an AI assisted simple method to study muscle-tendon dynamics during running

Christoph Leitner^{1,2}, Stefan Kaltenböck¹, Christian Baumgartner², and Markus Tilp¹

¹Institute of Movement Science Sport and Health, University of Graz, Graz, Austria

²Institute of Health Care Engineering, Graz University of Technology, Graz, Austria

Email: christoph.leitner@uni-graz.at

Summary

Our study extends previous research by proposing a lightweight, AI based method to assess muscle and tendons unit (MTU) behaviour during fast locomotion. We demonstrate that our method does not significantly differ from the current gold-standard.

Introduction

Within the MTU, muscles and tendons have different properties, contribute differently to external loading and adapt dissimilar to training stimuli. Imbalances in muscle strength and tendon stiffness can lead to injuries or impede the interplay of muscles and tendons for efficient states of locomotion [1]. Investigations of muscle and tendon dynamics during locomotion involve several obtrusive sensors such as 3D motion capture, ultrasound (US), electromyography and force measurements [2]. This is complex, especially during fast movements like running due to high accelerations and skin perspiration. Therefore, simple methods overcoming these problems are desired. Kidzinski et al. [3] have demonstrated a quantitative movement analysis using single camera videos and deep neural networks. Our work aims to validate the estimation of MTU, muscle belly and Achilles tendon (AT) length changes using a lightweight laboratory setup consisting of an US probe and a single camera video during running.

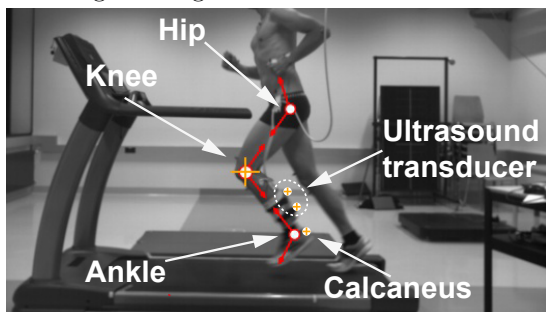


Figure 1: AI tracked landmarks. Red arrows in hip, knee and ankle indicate the joint angle. White markers with orange cross are used to estimate US probe and MTJ positions.

Methods

Data were collected from 14 participants. Videos were captured with one Miquis (Qualisys, Göteborg, Sweden) camera from the lateral view while running on a treadmill at various speeds between 6-18 km/h (Fig. 1). US recordings were collected on the medial gastrocnemius (MG) using the ArtUs EXT-1H with the LV8-5N60-A2 transducer (Teled, Vilnius, Lithuania) operated at 7.5MHz (image-rate: 80Hz). The US probe was tightly connected to the lower limb using a custom made cast. In 3 subjects we synchronously captured recordings using a Miquis 3D motion system. For the AI pose estimation we used an open-source deeplearning toolbox [4]. We re-trained provided networks to extract joint markers in our collected 2D video files. For the calculation of MTU lengths we used the estimation method by

Hawkins et al. [5]. The automated tracking of the muscle tendon junction (MTJ) in US images using deepMTJ [6] and markers on knee and calcaneus allowed the estimation of muscle and AT lengths. Subsequently, we compared MTU lengths calculated from joint angles of the 3D motion system with the 2D camera view. We used Bland Altman plots and two sample paired t-tests in 1dSPM [7] to estimate differences in the methods and time series of MTU length, respectively.

Results and Discussion

We observe that MTU lengths estimated with our proposed method (Fig. 2) do not significantly differ to the gold standard [$t(1,46)=4.13301$, $p < 0.05$] (Results for the AT and muscle belly use the same marker kinematics and are not shown). Thus, our work provides a lightweight and easily applicable setup for functional assessments of muscles and tendons during fast locomotion.

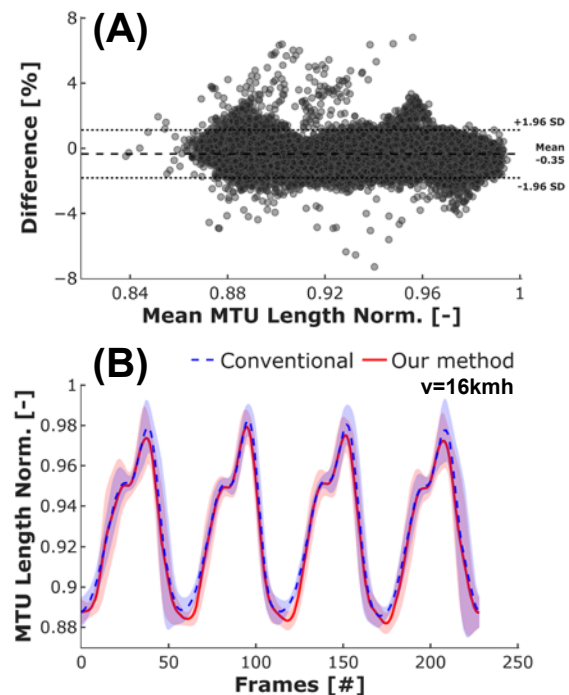


Figure 2: (A) The Bland Altman plot compares MTU length estimates using a conventional setup to our proposed AI based method (32.800 samples, 47 videos, 3 participants, running speeds 6-16 km/h). Our method underestimates MTU length by a mean of $-0.35 \pm 0.75\%$ to the current gold-standard. (B) Normalized MTU lengths over 4 gait cycles calculated with the regression equation by Hawkins et al. [5], captured in 10 recordings, of one representative participant, running at 16km/h.

References

- [1] Arampatzis, A. *et al. Front. Physiol.* **11** (2020).
- [2] Leitner, C. *et al. Sensors* **19**, 4316 (2019).
- [3] Kidzinski, L. *et al. Nat. Comm.* **11** (2020).
- [4] Mathis, A. *et al. Nat. Neuros.* **21**, 1281–1289 (2018).
- [5] Hawkins, D. *et al. J. Biomech.* **23**, 487–494 (1990).
- [6] Leitner, C. *et al.* 4770–4774 (IEEE, 2020).
- [7] Pataky, T. C. *J. Biomech.* **43**, 1976–1982 (2010).

Optimal Forefoot Rocker Parameter Prediction Using Machine Learning

Davit Soselia¹, Fredrik Olsson¹, Juha M. Hijmans³, Elena M. Gutierrez-Farewik^{1,2}

¹ KTH MoveAbility Lab, Dept. Engineering Mechanics, KTH Royal Institute of Technology, Stockholm, Sweden

²Dept. Women and Children's Health, Karolinska Institutet, Stockholm, Sweden

³ University of Groningen, Univ. Medical Center Groningen, Dept. Rehabilitation Medicine, Groningen, the Netherlands

Email: soselia@kth.se

Summary

Whether machine learning methods can successfully be employed for optimal shoe midsole rocker parameter selection for peak pressure minimization was evaluated. The study is motivated by the demonstrated benefits of peak pressure reduction in preventing the development of diabetic foot ulcers in diabetic patients. Random Forests and Convolutional Neural Networks were trained on data gathered from 9 healthy subjects.

Introduction

With the rise in diabetic cases, with estimated 422 million cases worldwide [1], related issues have garnered attention. One of such is diabetic foot ulcers, with a global prevalence of 6.3% [2]. If not successfully treated, these may result in amputation.

Previous research has shown that diabetic foot ulcers can be prevented by reducing plantar pressure. To achieve this, special shoes with varied midsole rocker profiles have been developed [3], with a goal to reduce maximum peak pressure to less than 200 kPa if possible, or if not, then by at least 30%. While such footwear shows promise, selecting and producing individualized shoes can be resource-intensive, and may rely on the intuition of orthopedic shoe technicians and trial-and-error. This study examines the possibility of using machine learning to predict individualized optimal rocker parameters that reduce peak plantar pressure.

Methods

Nine able-bodied subjects with shoe size of 42 were recruited. Each subject was tested with 24 forefoot rockers with varying parameters, including 3 rocker apex positions, 2 apex angles (both with respect to shoe's long axis), 2 rocker radii and either stiff or flexible sole (along forefoot rocker apex). This was achieved using a "sneaker" type shoe with replaceable forefoot mid- and outsole (Table 1). With first their usual sneakers then with each rocker shoe (in randomized order), each subjects were asked to walk on a treadmill at 3 different speeds (randomized) – normal, faster

Table 1. Midsole rocker parameters in the 24 tested shoes

Parameter	Values
Apex pos. (% sl)	55, 60, 65
Apex angle (°)	65, 85
Radius (mm)	177, 208
Sole stiffness	Flexible, stiff

and slower, defined as mean ± 1 SD of reported comfortable walking speeds adjusted for age and height [4], resulting in 75 trials per subject, with at least 12 strides in each trial. Plantar pressure was measured with instrumented insoles (pedar, Novel) at 100 Hz.

The data was then processed with derived features for the classification task. For each subject features extracted included average of peak pressure values over the steps recorded, 2D coordinates of the peak pressure value over all steps, mean and variance modelling pressure distribution from peak pressure point as measured for the control shoe. To prepare labels, for each rocker setting the average of peak pressures was compared to 200 kPa, and noted as 1 – positive sample if the value was less and 0 if the value was greater, resulting in a multi-label dataset.

Random Forests and Convolutional Neural Networks were used for classification. The dataset was split with a 7:2 ratio for training and testing.

Results and Discussion

The resulting accuracy was 0.76 for Random Forests, while CNN failed to converge with accuracy near to random guessing. The latter is likely caused due to insufficient number of samples. One possible way to amend the issue would be adding augmentation using gaussian noise to the training samples.

Another limitation is using only 2 data points for testing, which gives a limited idea of the generalizability of the model to the general population.

Conclusions

Random Forests show some promise in achieving the stated objective, while the data recorded is not enough to train Convolutional Neural Networks. Further study is required to choose the best method for the approach and better estimate the generalizability.

Acknowledgments

This project is funded by EIT Health (20250 IndiRock'nSole)

References

- [1] World Health Organization (2014).
- [2] Zhang et al. (2016) *Ann Medicine* 49 (2): 1-21
- [3] Reints et al. (2017) *Gait Posture* 58: 287-93.
- [4] Bohannon (1997) *Age and ageing*, 26 (1), 15-19.

A machine learning approach for error detection in rowing

Oscar Sten¹, Elena Bergamini², Federico Mari², Valentina Camomilla² and Andrea Mannini^{1,3}

¹Istituto di Biorobotica, Scuola Superiore Sant'Anna, Pisa, Italy

²Università degli Studi di Roma Foro Italico, Roma, Italy

³IRCCS Fondazione Don Carlo Gnocchi, Firenze, Italy

Email: o.sten@santannapisa.it

Summary

In this work, a system for automatic error detection in rowing technique is proposed, based on measurements from a single gyroscope. A machine learning method to classify correct vs incorrect strokes was cross-validated, based on motion capture data from nine subjects, obtaining a 79.5% accuracy.

Introduction

Sequential movement of the legs and trunk during rowing strokes is crucial during the drive phase, allowing greater acceleration of the boat and preventing raising the hull in the water. The legs should be in near complete extension before the initialization of trunk extension. A common error occurs if this does not happen which shows up as a double “hump” in the trunk velocity graph that otherwise has a unique peak for correct gestures. A similar trend can be observed in the generated force, causing a less efficient stroke [1]. In this work we hypothesized that this error could be detected using an inertial measurement unit (IMU) mounted on the athlete’s trunk (at C7 level). In particular, a machine learning based method to recognize incorrect gestures was proposed based on the analysis of angular velocity measurements.

Methods

Experimental data was collected involving nine male able-bodied participants, experienced rowers (17±3 years). The participants were asked to perform two trials of 15 rowing strokes on an ergometer (> 32 strokes/min). The participants wore: *a*) motion capture markers to track seat, trunk (C7 vertebra) and right hand wrists motion, and *b*) one IMU mounted on the trunk over the C7 vertebra, according to the experimental protocol already described in [2]. Data was automatically labelled in terms of correct/incorrect strokes using motion capture data according to the method proposed by Kleshnev et al. [1]. Labelling was obtained as follows: 1) single strokes were segmented by detecting peaks in the wrist position data, 2) trunk and seat position data were processed with a smoothing spline (smoothing parameter of 0.9999) and then differentiated to obtain a velocity estimation, and finally 3) the first peak of seat and trunk velocity from each individual stroke was detected. Strokes were labeled as correct if the first peak of the seat velocity preceded the peak of the trunk velocity, and as incorrect if the contrary took place [1]. After labelling the sequences, classification features were extracted from the segmented angular velocity data. In a correct stroke, during the initial part of the drive phase (marked as thick in fig 1), velocity should increase linearly and monotonically, therefore Pearson and Spearman correlation with time of this segment were proposed as

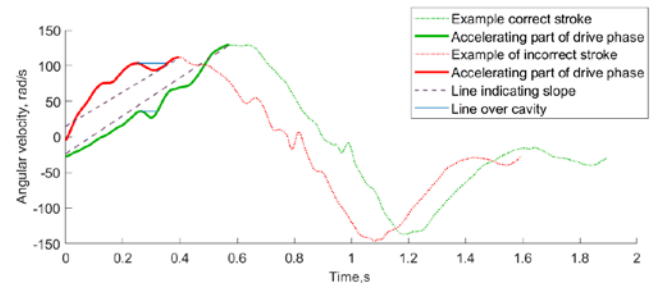


Figure 1: Two example strokes with features illustrated

discriminative features. In addition, the slope of the line between the start (median of the 10 first samples) and end (median of the 10 samples around the max) of this phase and the area of the main cavity in the graph (occurring if a non-monotonic behavior of the angular velocity was observed) were also proposed as features (fig. 1). Several machine learning models (Naïve Bayes, SVM, Random Forrest, and k-Nearest Neighbor) were compared, hyperparameters were selected through a grid search, and the models were cross validated by using Leave One Subject Out-Cross Validation (LOSO-CV). LOSO-CV was chosen since it allowed testing the inter-subject reliability of the method [3]. Processing was done using MatLab (vs2020a, The Mathworks, Natick, USA).

Results and Discussion

In total 273 strokes were identified, 141 were labeled as correct and 132 as incorrect. The k-NN classifier showed, through LOSO-CV, a best accuracy of 79.5% in recognizing incorrect and correct strokes (80.9% sensitivity, 78% specificity, F₁ score 0.8). The use of LOSO-CV was crucial due to the relatively small number of participants. In future works, we plan to collect a larger pool of participants to increase the robustness of this preliminary, but promising system. Since the proposed solution only requires one gyroscope, it could be easily embedded in a smartphone, opening scenarios for a fully portable solution for sport practitioners.

Acknowledgments

This study was funded by the Ministry of Defense under the WAVE project (Wearable Assistant for VEterans in sport).

References

- [1] Kleshnev V. (2011) *Rowing faster*; Human Kinetics 2: 105-121.
- [2] Lentola, A. et al., 15th 3D Analysis of Hum. Mov. Soc. Conf. (3DAHM), July 2018, Salford (UK).
- [3] Mannini, A. et al. (2013). *Med Sci Sport Exerc*, 45 11: 2193-20

Change in Mechanical Properties of Cortical Bone under Voltage Application for Formation of Mineral Components

Fuki Ota, Kazuhiro Fujisaki, Keita Osanai, Kazuhiko Sasagawa, Takeshi Moriwaki
 Graduate School of Science and Technology, Hirosaki University, Aomori, Japan
 Email: h20ms503@hirosaki-u.ac.jp

Summary

Mineral components relate to bone mechanical properties. We proposed a method to change the bone mineral configuration and mechanical properties by voltage application. In this study, hydroxyapatite formation of mineral components was confirmed in X-ray diffraction profiles. The change of bone elastic modulus in the voltage application process was obtained under bending test.

Introduction

Bone mainly consists of type-1 collagen and minerals such as hydroxyapatite, and the mechanical properties of bone tissue depend on the alignment and amount of the mineral components. Shah et. al. showed that bending strength of bone samples decreased in demineralization process using ethylenediaminetetraacetic acid (EDTA) [1]. We previously observed apatite formation on titanium surface and on bone surface located at the cathode side of voltage application with direct current (DC) in synthetic apatite solution [2]. In this study, we attempt to control the formation of mineral components on bone tissue and to change the mechanical properties of the tissue by voltage application.

Methods

Bone specimens cut out from the cortical region of a bovine femur were prepared to be 3×3 mm square area and more than 30 mm length for bending tests and wrapped by titanium wire used for electrode. Then, the specimens were immersed in phosphate buffered saline and respectively connected for both anode and cathode side of DC power supply. The specimens were applied constant voltage of 10 V for a day in 37°C. After that, they were observed by microscope and deposit on surface was analyzed with X-ray diffraction system. Finally, elastic modulus of the specimens was measured by 3-point bending test.

Results and discussion

Mineral deposit appeared on the bone surface located at cathode side of the voltage application and the deposit had unique X-ray diffraction peaks that were (002), (211), (213) and (004) of hydroxyapatite, as shown in Figure 1. Figure 2 shows the elastic modulus change (ΔE) of each bone specimen located at cathode and anode sides, respectively. Here, EDTA samples were used to confirm the effect in the case of progressive demineralization. As a result, elastic modulus of the bone located cathode side decreased similar to EDTA and of the bone located anode side increased. The deposit having hydroxyapatite crystal structure was formed under the voltage application although the components of hydroxyapatite were not fully contained in the phosphate buffered saline. It was confirmed that the hydroxyapatite components transferred from bone samples located at anode

side to cathode side, thereby mineral formation and elastic modulus change were realized in this process.

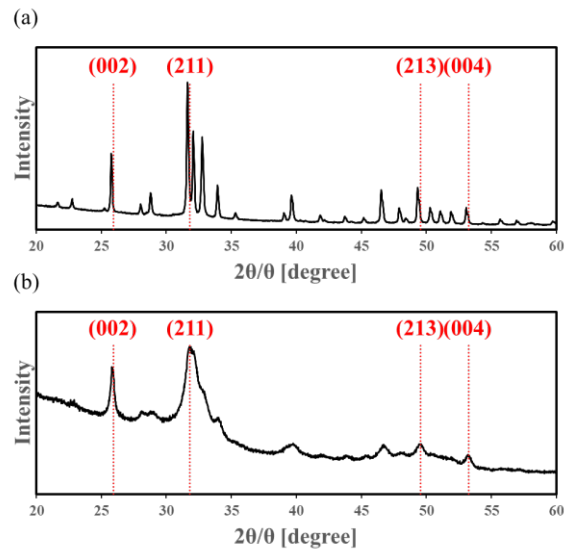


Figure 1: The X-ray diffraction pattern of (a)hydroxyapatite and (b)deposit.

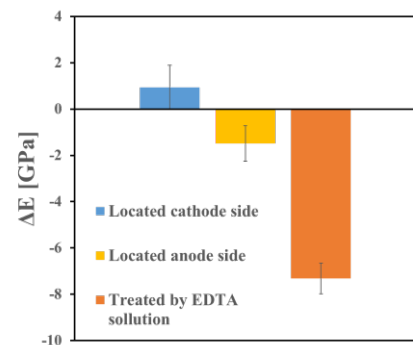


Figure 2: Comparison of elastic modulus change (ΔE).

Conclusions

Mineral formation on the bone surface and the changes of elastic modulus of specimens were induced by voltage application. This method is available for improving bone mechanical properties.

Acknowledgment

This study was funded in part by a Japan Society for Promotion of Science Grant-in-Aid for Scientific Research (C) # 20K04155.

References

- [1] Shah M. K. et. al. (1995). *Calcif Tissue Int*, **56**: 78-82.
- [2] Fujisaki K et. al. (2017). *Int. J. of Automation Technology*, **11**: 902-906.

Influence of Excipients and Lesions on Drug-Coated Balloon Therapy

Karthic Anbalakan¹, Toh Han Wei^{1,2}, Ang Hui Ying^{1,2}, Martin Lindsay Buist¹, Leo Hwa Liang¹

¹Department of Biomedical Engineering, National University of Singapore, Singapore

²National Heart Research Institute, Singapore

Email: E0011515@u.nus.edu

Summary

In this study, we evaluated the influence of different excipients on the efficacy of drug-coated balloon (DCB) therapy. We employed a previously established integrated model to quantify a variety of measures, associated with the treatment: tracking loss, vessel adhesion, drug release, uptake, and distribution. Moreover, we performed a parametric study to evaluate the potential influence different types of lesions would have on drug-coated balloon therapy. We found a strong correlation between the hydrophobicity of the excipient and its associated drug loss due to tracking and washout. In addition, we identified several key features of an atheroma that influences drug uptake and distribution.

Introduction

Cardiovascular interventional therapies have seen marked improvements to their design and performance in the last decade. However, there is still much to be desired when it comes to our understanding of how different excipients and lesions influence the treatment's efficacy.

Correspondingly, in our study, we used an integrated approach to quantify the key differences between urea, a common hydrophilic excipient, and butyryl-trihexyl citrate (BTHC), a common hydrophobic excipient. Additionally, we performed a parametric study to evaluate how different lesions influence the efficacy of treatment.

Methods

In this study, 60 percutaneous transluminal angioplasty balloon catheters were coated with sirolimus ($3\mu\text{g}/\text{mm}^2$) and either urea or BTHC as the excipient. The tracking loss and vessel adhesion, associated with each excipient, was determined by navigating the samples through an in-vitro model adapted from the ASTM standard F2394-07 [1].

Additionally, the drug release profile was determined by inflating the balloons in citrated porcine blood, at sink conditions, at various time points. The residual amount of sirolimus was evaluated using high-pressure liquid chromatography (HPLC).

Subsequently, to determine the drug uptake, retention and distribution, a non-linear multi-layered diffusion advection reaction model was solved computationally using the FEniCS library [2]. This integrated approach is discussed in greater detail in our recent study [3].

Results and Discussion

In this section, we summarize some of our key findings. Despite the significantly higher tracking loss (urea: 35.5% vs

BTHC: 8.13%) observed in the urea-based balloons, the drug uptake was almost two times greater than its hydrophobic counterpart: BTHC (Figure 1).

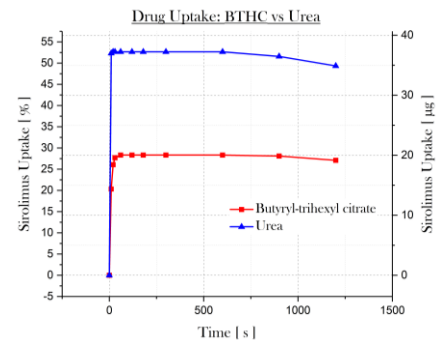


Figure 1: Sirolimus uptake over time observed with DCBs coated with different excipients: BTHC (red) against urea (blue)

Moreover, the distribution of drugs within the different layers of the tissue was found to vary most significantly between hard (Figure 2) and soft plaques.

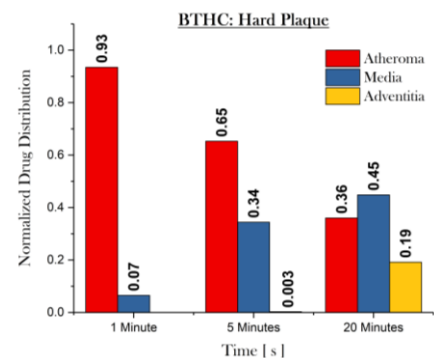


Figure 2: Normalized sirolimus distribution within different layers of the vessel at three distinct time points post-DCB therapy.

Conclusions

Ultimately, our results allude to a strong correlation between hydrophobicity of the excipients and tracking loss, which could potentially be a means of minimizing non-specific cytotoxic effects. Additionally, the porosity of the lesions and luminal calcification were found to be the chief contributors to drug distribution and uptake, respectively.

References

- [1] Seidlitz, A et al. (2013). *PLoS One*, **8**: e83992.
- [2] Alnæs, M et al. (2015) *The FEniCS project version 1.5*; Archive of Numerical Software **3**.
- [3] Anbalakan, K et al. (2020). *European Journal of Pharmaceutics and Biopharmaceutics*, **158**: 72-82.

PASSIVE ANKLE EXOSKELETONS INFLUENCE MUSCLE BEHAVIOUR DURING UNEXPECTED PERTURBATIONS

James L. Williamson^{1,2}, Nicole Y. Kelp¹, Glen A. Lichtwark², Taylor J. M. Dick¹

1.School of Biomedical Sciences, The University of Queensland, St Lucia, QLD, Australia

2.School of Human Movement & Nutrition Sciences, The University of Queensland, St Lucia, QLD, Australia

Email: james.williamson@uq.net.au

Summary

We present EMG and fascicle length data for the soleus (SOL) muscle during an unexpected drop task with and without passive ankle exoskeleton assistance. We find reduced SOL EMG and increased peak fascicle lengthening with exoskeleton assistance during unexpected perturbations. As passive exoskeleton devices move from the lab to the clinic – such important muscle level effects must be designed for.

Introduction

The behaviour with which lower limbs store and return energy during steady gait has inspired the design of passive wearable devices to assist walking [1], running [2] and hopping [3]. However, we still lack an understanding of how devices influence movement and neuromuscular function in real world environments (i.e. an unexpected drop, uneven terrain, or variable walking speeds). This has limited our ability to design and implement wearable assistive technologies in real-life scenarios. The aim of this study is to determine the influence of passive ankle exoskeletons on neuromuscular control and muscle fascicle dynamics during unexpected vertical perturbations.

Methods

Fifteen participants (9M,6F, 23±3Y) completed an unexpected ‘falling-in-a-hole’ experimental paradigm. A vertical perturbation was elicited via the rapid removal of a ground platform (15cm) at an unknown time during hopping. B-mode ultrasound (125Hz, ArtUS, Teleded, Lithuania) was used to determine SOL fascicle length during the hopping perturbations with exoskeleton assistance (91 Nm rad⁻¹) and without assistance.

Simultaneously, surface electromyography (sEMG) (2048Hz, Trigno EMG, Delsys Inc., USA) was used to measure muscle activity. sEMG signals were band-pass filtered (45-300Hz) and normalized to maximum jump trials. The RMS was calculated via a 20ms window over each ground contact (GC) and aerial (AER) hopping period for steady state hopping and the perturbation. Additionally, joint kinematics and kinetics were recorded using motion capture (100Hz, OptiTrack, USA) and bilateral force plates (2048Hz, Bertec, USA), respectively.

Results and Discussion

Exoskeletons Induce Altered Soleus Activation

Consistent with previous studies [3], we found that SOL muscle activity decreased by 4.8±5.2% during the GC phase of steady state hopping with passive ankle exoskeleton assistance (Figure 1). During the unexpected perturbation, we found a 5.4±14.31% and 2.4%±8.84% reduction in SOL muscle activity during AER and GC phases, respectively.

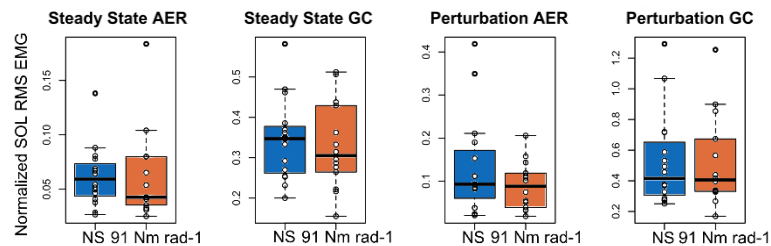


Figure 1: Normalized SOL RMS EMG for GC and AER phases in both steady state hopping and the perturbation hop. Blue denotes the no spring case; orange denotes exoskeleton assistance.

Exoskeletons Influence Soleus Fascicle Length Change

SOL fascicle length data from a subset of participants (N=4), showed that passive ankle exoskeletons use increased SOL fascicle lengths during both normal and perturbed hopping (Figure 2). Specifically, during steady state hopping, peak fascicle lengthening increased by ~8±3% with exoskeleton assistance compared to the no assistance case. During the perturbed hop, exoskeleton assistance increased peak SOL fascicle lengthening by ~9±5% more in comparison to the no assistance case.

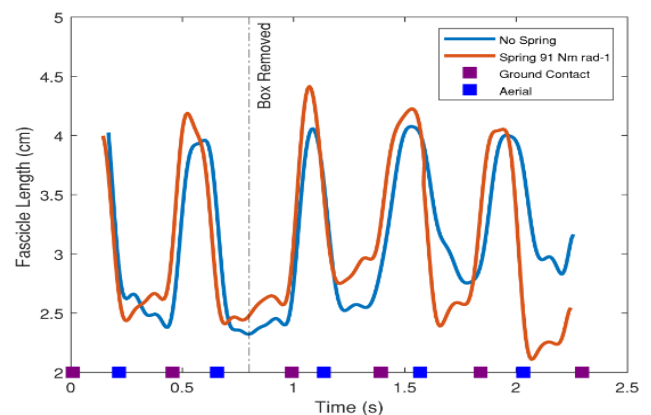


Figure 2: Fascicle length data (N=1) for hops before, during and after the perturbation. The blue line denotes the no spring case; the orange denotes exoskeleton assistance. Average ground contact and aerial phases of the hopping cycle are marked by coloured squares.

Conclusions

In summary we find reduced SOL EMG and increased peak fascicle lengthening with passive ankle exoskeleton assistance during unexpected vertical perturbations. However, further investigation is required to determine if these alterations impact capacity to respond to larger perturbations.

References

- [1] Collins S, et al. *Nature* **522**:212, 2015.
- [2] Nasiri, R, et al. *IEEE Syst Rehab Eng* **26**:2026, 2018.
- [3] Farris D, et al. *J Appl Physiol* **115**:579, 2013.

Does a prosthetic toe joint affect mechanics or preference when persons with limb loss walk over uneven terrain?

Kirsty A. McDonald¹, Rachel H. Teater², Karl E. Zelik²

¹School of Medical Sciences, University of New South Wales, Sydney, Australia

²School of Engineering, Vanderbilt University, Nashville, USA

Email: kirsty.mcdonald@unsw.edu.au

Summary

Lower limb prosthesis users have previously indicated a preference for a compliant prosthetic forefoot region during uneven terrain locomotion. This feature likely attenuates the destabilizing effect of the surface and thus, may also reduce the mechanical work requirements of the remaining biological lower limb joints. Here, we added a Flexible toe joint to a passive prosthesis and found that 5 of 9 participants preferred this Flexible toe to a Locked out joint (i.e., rigid foot keel). Positive prosthesis work (which predominantly occurs during Push-off) decreased with a Flexible joint, but so did prosthetic and intact limb positive hip work. Despite producing more positive prosthesis work, the Locked toe configuration was associated with greater positive hip work from both limbs, possibly required to enhance locomotor stability in the absence of compliance at the toe or forefoot.

Introduction

The challenges of walking over uneven terrain are exacerbated for people with lower limb loss [1]. Prosthetic device design modifications may improve user outcomes, e.g., prosthesis users (PUs) have been noted to prefer a more compliant forefoot region on uneven terrain [2], potentially because the compliance counteracts the destabilizing effects of the surface [3]. Thus, it is conceivable that mechanical work contributions of the remaining joints could decrease in response to the enhanced stability offered by a compliant forefoot on uneven terrain. Adding an articulating toe joint is a way to facilitate compliance of the keel in response to surface irregularities. Our group recently developed a prosthetic foot capable of switching between a Flexible (articulating) toe joint, and a Locked toe configuration [4]. We used this device to assess the effect of the two configurations on subjective preference and joint/prosthesis work when below-knee PUs walked over uneven terrain.

Methods

Active, below-knee PUs ($N=9$) participated. As detailed in McDonald et al. [4], participants completed a series of locomotor tasks using an experimental prosthesis configured with a Flexible and a Locked toe joint. During training and testing sessions, participants walked over a continuous series of 10 uneven terrain platforms. Each platform consisted of 24 plywood and foam blocks of varying heights relative to the ground (16, 46 and 58 mm).

Participant preference was recorded. For biomechanical analyses, participants were required to traverse the walkway at a velocity of 1 m s^{-1} . A minimum of five strides per limb of 3D motion capture data (Vicon) and synchronized ground reaction forces (AMTI) were collected. T-tests were applied

with an alpha level of 0.05 to compare gait mechanics for the Flexible vs. Locked toe joint.

Results and Discussion

Five participants preferred the Flexible configuration and four preferred the Locked configuration for walking over uneven terrain. Consistent with level walking, positive prosthesis work decreased for the Flexible toe configuration [4] (Fig. 1). However, positive hip work for both limbs also decreased. This is surprising because the positive prosthesis work occurs mostly during Push-off and therefore an increase in positive ipsilateral hip power in early stance is one method to overcome this reduction. Perhaps such a strategy did occur but was over-shadowed by inflated positive hip contributions in the Locked configuration that were required to offset the surface-level disturbances resulting from the non-compliant keel. Further research is required to explore or confirm.

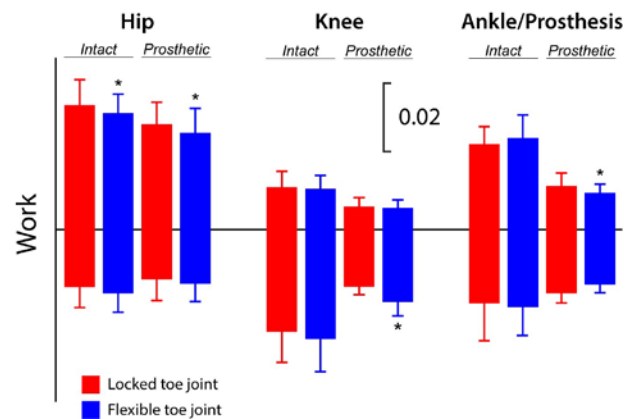


Figure 1: Intact and prosthetic side joint/prosthesis positive and negative work during a walking stride. ($N=8$ due to attrition).

Conclusions

A Flexible prosthetic toe joint may serve as a useful design feature or option for PUs on uneven terrain. Slightly over half the participants preferred the Flexible toe joint over a Locked toe, and the hip work of both limbs was reduced when walking with the Flexible toe joint.

Acknowledgments

This research is supported by NIDILRR (90IFRE0001).

References

- [1] Kim J et al. (2019). *PM&R*, **11**: 334-53
- [2] Raschke SU et al. (2015). *J Biomech*, **48**: 146-52
- [3] Childers WL et al. (2015). *ASB 2015*
- [4] McDonald KA et al. (2021). *Sci Rep*, **11**: 1924

Production of Micro-Structured Hollow Fiber Membranes for Membrane Oxygenators – Mimicking Nature to Increase Mass Transport

Markus Pekovits^{1,2}, Paul Ecker^{1,2}, Benjamin Lukitsch¹, Bahram Haddadi¹, Matthias Golda^{1,2}, Michael Harasek¹, Margit Gfoehler²

¹Institute of Chemical, Environmental and Bioscience Engineering, TU Wien, Vienna, Austria

² Institute of Engineering Design and Product Development, TU Wien, Vienna, Austria

Email: markus.pekovits@tuwien.ac.at

Summary

Microstructuring of hollow fiber membranes is a means to increase the gas exchange surface area of oxygenators, thereby increasing mass transport and making it more efficient. In this work, a method for fabricating micro-structured fibers is presented, process parameters are discussed, and feasibility in the size range of currently commercially available membranes is investigated.

Introduction

Modern extracorporeal membrane oxygenation (ECMO) devices use gas-permeable cylindrical polymeric hollow fiber membranes that act as a barrier between the blood and the gas phase. Although approximately 2 m² of these membranes are used to achieve the required gas transfer rates to best support the weakened human lung in its function, the efficiency of lung support devices is still subject to limiting factors [1]. The cylindrical hollow fiber membrane bundles cannot accurately replicate the small physical structures in the human lung, resulting in an increase in mass transfer resistance [1].

Micro-notches in fish gills not only increase the respiratory surface area but also lead to transverse flows, resulting in a decreased mass transfer resistance [2]. Initial CFD analyses of micro-structured membrane surfaces confirmed a significant increase in mass transfer rate with no evidence of increased risk of blood damage [3].

In this work the production of micro-structured hollow fiber membranes via the non-solvent induced phase separation (NIPS) technique is presented.

Methods

A membrane spinning system based on the NIPS fabrication process, designed by our institutes at TU Wien, was used to spin the hollow fiber membranes patterned on the outer surface in combination with a sinusoidally designed spinneret (Figure 1). The developed membrane spinning system allowed to vary the process parameters which are crucial for the NIPS manufacturing process. This ensured that the morphological and geometrical structure and consequently the gas separation properties of the membrane could be influenced. The polymer used was a 31 wt.% polyethersulfone (PES) + *N*-Methyl-2-pyrrolidone (NMP) mixture.

Scanning electron microscope (SEM) images provided a first impression about the geometrical properties of the hollow fiber membranes. In order to quantify the increase in separation performance of the patterned fiber, bundles of fibers are assembled into modules and compared with

modules prepared from cylindrical fibers with respect to their gas permeance properties.

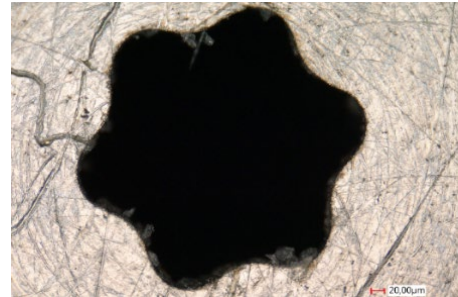


Figure 1: Sinusoidal outer shape of the spinneret ($OD = 400 \mu\text{m} + 50 \mu\text{m} * \sin(6\phi)$)

Results and Discussion

The SEM images of the first spun fibers (Figure 2) show a centrally and circumferentially closed hollow fiber without holes in the membrane wall, whose lumen as well as outer wall are circular in shape. The double finger pore structure typical for the NIPS manufacturing process is present.

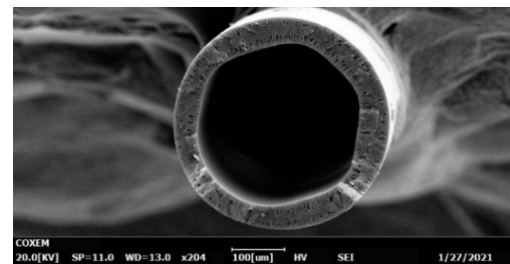


Figure 2: SEM picture of the preliminary spun PES hollow fiber membrane. OD and ID circularly shaped.

Conclusions

The production of polymeric hollow fiber membranes in ranges of a few hundred micrometers is possible with our NIPS based spinning plant. Geometry optimization and comparison of gas permeances require further spinning tests and parameter settings.

References

- [1] Evseev, A.K. et al. (2019), *Membranes and Membrane Technology*. **1**: 201–211
- [2] Maina, J. N. (2002), *Journal of Anatomy* **201** (4): 281-304
- [3] Haddadi et al. (2020) *Nordic Baltic Conference on Biomedical Engineering and Medical Physics, NBC2020 Online* from Reykjavik, Iceland 18.09.2020

Estimation and Assessment of Sagittal Spinal Curvature and Thoracic Muscle Morphometry in Different Postures

Anoosha Pai S¹, Honglin Zhang², Nima Ashjaee¹, Thomas R. Oxland²,
David R. Wilson², Stephen H.M. Brown³, John Street², Sidney Fels⁴

¹School of Biomedical Engineering, University of British Columbia, Vancouver, Canada. ²Department of Orthopaedics, University of British Columbia, Vancouver, Canada. ³Department of Human Health and Nutritional Sciences, University of Guelph, Guelph, Canada. ⁴Department of Electrical and Computer Engineering, University of British Columbia, Vancouver, Canada
Email: toxland@icord.org

Summary

Spine models are typically developed from supine imaging data, and hence do not fully replicate postures of subjects' clinical symptoms. A pipeline to estimate subject-specific sagittal spinal geometry in different postures (supine, flexion and sitting) from data (vertebral body center positions) in a reference posture (standing) was developed and validated. Dominant line-of-actions for two paraspinal muscles (erector spinae and transversospinalis) were computed in those postures. A correction factor (cosine between the MRI axial scan plane and fiber line-of-action) was computed and applied to the muscle parameters (CSA and moment-arm) computed from MR imaging. Overall, this work contributes to the growing literature of spine geometry and is a preliminary step in clinically relevant subject-specific modeling.

Introduction

Clinical imaging for spinal deformity typically consists of a standing x-ray of the whole spine and a supine MRI of only the pathological spinal levels. This does offer coherent data for the development of subject-specific, biomechanical spine models that reflect actual clinical symptoms. Additionally, muscle parameters measured from MRI are not perpendicular to the scan slices and must be corrected to be appropriately used in models. Objectives: 1) To develop and validate a method for estimating of subject-specific sagittal spinal geometry in different postures from vertebral body center (VBC) data in a reference posture (standing). 2) To correct for the cosine between the MRI axial scan plane and dominant fiber line-of-action for muscle parameters (CSA and moment-arms) in these postures.

Methods

Thoracic Spines of six healthy participants (age 26±6 y, BMI 24±3 kg/m²) were imaged (0.5T Open Upright MR scanner) in four postures (supine, standing, flexion, and sitting). VBCs from T1 to T10 were marked on sagittal MR images (Figure 1A). Muscle parameters, CSA, anterior-posterior (A-P) and medial-lateral (M-L) were computed for two muscles—erector spinae and transversospinalis on axial MR images (Figure. 1B). Sagittal spinal curvature was approximated using a circular spline parameterized with the segment angles (kyphosis or lordosis Cobb angle) and segment lengths (Figure 1C). The subject-spine geometry in any other posture was estimated by modification of these parameters and normalization with the reference posture. The estimated spine geometry was validated against the corresponding thoracic MRI data by rigid registration (Figure. 1D). The dominant muscle fiber line-of-action of erector spinae and

transversospinalis was computed for each posture. A correction factor based on published literature was then computed and applied to the muscle parameters [1].

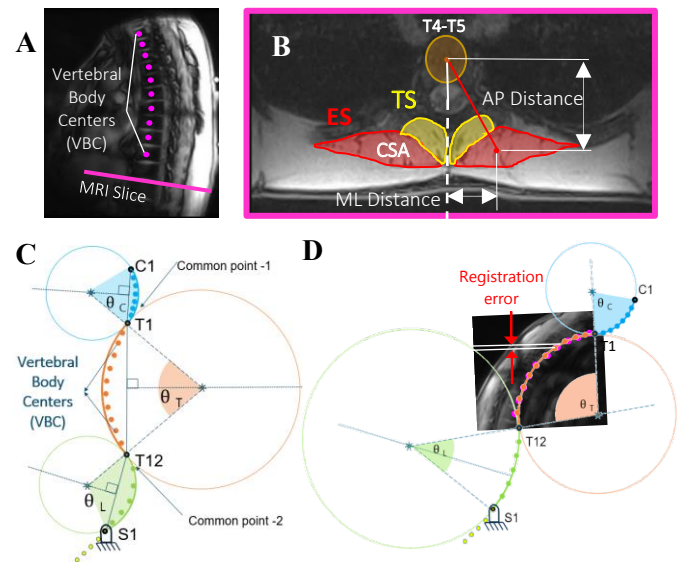


Figure 1: A) Sagittal MR image. B) CSA, A-P and M-L distances of erector spinae (ES) and transversospinalis (TS) on Axial MR image. C) Geometric construct of sagittal spinal curvature (standing). D) Estimated spine geometry (flexion) rigidly registered to ground truth data (MRI in flexion) showing registration error.

Results and Discussion

The maximum registration error between the estimated spine geometry and MRI data was small (average RMSE~1.2%). The correction factor reduced muscle parameters (~5% for erector spinae and ~25% for transversospinalis) when compared to raw, uncorrected MRI data. Compared to all existing methods for quantitative evaluation of sagittal spinal geometry [2], our method is simple, reliable, computationally inexpensive and easily digitizable for clinical images. Another novelty of this work is reporting trunk muscle properties for postures other than supine. Overall, our data contributes to the growing literature of trunk geometry evaluation and is preliminary step in clinically relevant subject-specific modelling.

Acknowledgments

We thank NSERC, CIHR and Medtronic Canada for funding.

References

- [1] L. Santaguida, et al. (1993) *Clin. Biomech.*, 8:171–178.
- [2] T. Vrtovec, et al. (2009) *Eur. Spine J.*, 18(5): 593–607.

How does the prosthetic design affect muscle strength after knee arthroplasty surgery?

Iris Mittendorfer¹, Igor Komnik², Steffen Willwacher³, Björn Michel¹, Judith Bleuel¹

¹Institute of Motion Analysis and Sports Medicine, Garmisch-Partenkirchen Medical Center, Garmisch-Partenkirchen, Germany

²Institute of Biomechanics and Orthopaedics, German Sport University Cologne, Köln, Germany

³Department of Mechanical and Process Engineering, Offenburg University of Applied Sciences, Offenburg, Germany
Email: iris.mittendorfer@klinikum-gap.de

Summary

Muscle strength condition after knee arthroplasty (KA) is crucial for returning to an active lifestyle. We showed that 5-14 months after surgery the hamstrings to quadriceps (HQ) ratio was significantly different between patients with total knee arthroplasty (TKA) and unicompartmental knee arthroplasty (UKA). When creating rehabilitation or training plans, therapists and patients should consider that muscle adaptations after KA differ between prosthetic designs.

Introduction

The number of KA, especially the UKA, increased significantly in the last 5 years in Germany [1], because of better function and higher patient satisfaction [2]. The muscular status of the knee surrounding muscles is one of the main factors for joint control after knee arthroplasty. It influences knee joint motion and loading. Different prosthetic designs aim to address the different anatomical and mechanical conditions of the arthritic joint. For instance, UKA only replaces one compartment of the knee and cruciate ligaments are preserved, while TKA replaces all articular surfaces at the knee [3]. The current data of recommendation after KA is mainly based on experts' expertise. Since return to sport with knee arthroplasty becomes increasingly important, we need a deeper understanding and scientific data of functional and biomechanical parameters of patients with UKA or TKA. The first specific aim of the study was therefore, to investigate if the muscle strength of the knee flexors and extensors 5-14 month after surgery is different in patients with UKA and TKA.

Methods

TKA and UKA patients conducted tests of concentric and eccentric isokinetic muscle strength (Isomed2000, D. & R. Ferstl GmbH, Hemau, Germany) of the knee flexors and extensors at two angular velocities (50°/sec, 120°/sec) 5-14 months after surgery. Additionally, participants reported their perceived pain (Visual analog scale) during the measurements and their functional impairments in the daily life using the WOMAC questionnaire.

Results and Discussion

Relative maximal muscle strength (maximal torque per body weight, MAX_{rel}) was similar in TKA (n=19) and UKA (n=12) for both muscle groups under all testing conditions.

However, HQ ratio in the operated limb was lower in UKA in concentric (TKA 86,81 ± 21,84; UKA 66,28 ± 16,13, p < 0,01) and eccentric (TKA 79,98 ± 22, 78; UKA 60,33 ± 21,47; p < 0,05) condition at 50°/sec, indicating a more pronounced quadriceps weakness in relation to the hamstrings muscles in TKA.

Eccentric quadriceps MAX_{rel} correlated with time post-op, showing higher torque values with more time after surgery. This was only quantifiable in TKA, but not in UKA. Similarly, multiple parameters of muscle strength (concentric hamstrings MAX_{rel} at 50 & 120°/sec, concentric quadriceps MAX_{rel} at 50°/sec, eccentric hamstrings MAX_{rel} at 50°/sec) correlated with the total WOMAC score or subscales only in TKA. Here, strength was lower with higher scores, representing worse pain, stiffness, and functional limitations (p < 0,05).

Conclusions

Although, patients with UKA and TKA have similar maximal strength (Nm/kg) in quadriceps and hamstrings muscles 5-14 months after KA, UKA patients show a more physiological muscular balance (closer to standard values) between agonist and antagonist. This may relate to a less invasive surgical approach, a better biomechanical performance of the prosthesis and a smaller preoperative damage in UKA. It indicates that factors like quadriceps weakness and proprioceptive impairment may be more present in TKA. This, in turn, can cause negative effects on gait patterns.

In an ongoing study, we are evaluating the effects of a specific training intervention on the deficits in muscle strength observed here in TKA and UKA patients. Furthermore, we are conducting kinematic analysis, to examine to what extent these muscular changes affect knee joint angles during different walking tasks in field.

Acknowledgments

The study was funded by the Dr. Auguste-Schaedel-Dantscher Stiftung für medizinische Forschung.

References

- [1] ERPD Jahresbericht 2019
- [2] Walker T et al. (2017). *Arthroscopie*, **30**: 302-311.
- [3] De Vroey H et al. (2019). *Gait and Posture*, **73**: 299-304.

Ambulatory knee mechanics after ACL repair with InternalBrace™ augmentation compared to healthy controls

Linda Bühl^{1,2}, Sebastian Müller¹, Corina Nüesch^{1,2,3,4}, Birte L. Coppers^{1,5}, Katherine A. Boyer^{6,7}, Erica Casto⁶, Geert Pagenstert⁸, Annegret Mündermann^{1,2,3,4}, Christian Egloff^{1,2,3}

¹Department of Orthopaedics and Traumatology, University Hospital Basel, Switzerland; ²Department of Biomedical Engineering, University of Basel, Switzerland; ³Department of Clinical Research, University of Basel, Switzerland; ⁴Department of Spine Surgery, University Hospital Basel, Switzerland; ⁵Institute of Sport and Sports Science, Karlsruhe Institute of Technology, Germany; ⁶Department of Kinesiology, University of Massachusetts Amherst, United States; ⁷Department of Orthopedics and Physical Rehabilitation, University of Massachusetts Medical School, United States; ⁸Praxis Clarahof Basel, Switzerland
email: linda.buehl@usb.ch

Summary

In recent years, repair of the anterior cruciate ligament (ACL) with InternalBrace™ has been increasingly used to treat patients after ACL rupture. We provide first evidence of only little side-to-side differences in knee biomechanics during walking in patients 2 years after surgery and brief differences at the beginning of stance in ground reaction force and in tibia translation but not in knee kinetics in the operated leg compared to age-matched knee healthy controls.

Introduction

While clinical outcome and patient satisfaction after repair of the anterior cruciate ligament with augmentation have been investigated and compared to patients after ACL reconstruction, information or comparative studies on knee function recovery in dynamic tasks are scarce [1,2]. We compared knee ambulatory biomechanics of patients 2 years after unilateral primary proximal ACL repair with InternalBrace™ (Arthrex, USA) with knee healthy subjects.

Methods

In 16 adult patients (6m/10f; 35.9±10.7 years; BMI 24.4±4.0 kg/m²; 25±2 months postoperatively) and 16 healthy control subjects (6m/10f; 36.0±11.1 years; BMI 22.6±3.9 kg/m²) bilateral 3D knee kinematics and kinetics during walking (stance phase) were measured with the Point Cluster Technique [3]. Differences in patients' operated leg compared with their healthy contralateral leg and with controls (non-dominant leg) were analyzed using statistical parametric mapping (t-tests, P<.05).

Results and Discussion

Patients had lower lateral ground reaction force (GRF) in the operated than the contralateral leg between 5-7% of stance phase (SP) (P=.037; max. difference: -1.0% body weight (BW)). Compared to controls, the patients' knees had significantly more valgus (P=.021, max. difference: 3.8°) between 11-32%SP and a more posterior tibia position at the beginning of stance (0-8%SP; P=.038; max. difference: 2.7mm; Figure 1). At heel strike, patients exhibited lower anterior (P=.049; difference: -1.4%BW) and vertical (P=.048; difference: -4.3%BW; Figure 1) GRF followed by shortly lower lateral (0-3%SP; P=.031, max. difference: -1.5%BW) and greater anterior (2-3%SP; P=.044, max. difference: 2.4%BW) GRF than controls.

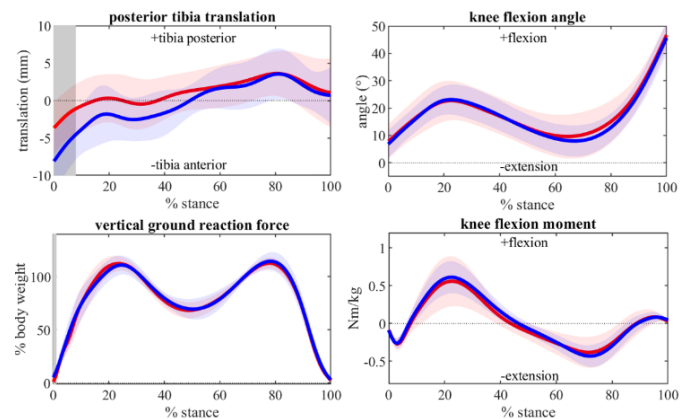


Figure 1: Mean values (solid line) and standard deviations (shaded color) of the operated leg in patients (red) and the non-dominant leg in controls (blue). The grey shaded area indicates significant differences.

Conclusions

Overall, interlimb comparison in patients' knee kinematics and kinetics demonstrated neither a systematic asymmetry nor a stiffer gait strategy and – in contrast to results after ACL reconstruction [4,5] – no offset in knee rotation. Differences in GRF and less anterior tibia position after heel strike compared to controls indicate a compensatory mechanism possibly to lower the load on the repaired ACL.

The patients' compensation strategy might be successful in achieving normal knee biomechanics during weight bearing. These promising results should be further explored by investigating the ankle and hip joints, (pre-) activation of relevant leg muscles, and the role of proprioception and muscle strength in more demanding activities and in comparison to patients after ACL reconstruction.

Acknowledgments

Funding: Department of Orthopedics and Traumatology, University Hospital Basel and Deutsche Arthrose-Hilfe e.V.

References

- [1] van der List P et al. (2019). *KSSTA*, **28**: 1946–1957
- [2] Nwachukwu BU et al (2019). *Arthroscopy*, **7**: 1-7
- [3] Boyer KA & Andriacchi TP (2016). *PloS one*, **11**: 1-12
- [4] Scanlan SF et al. (2010). *J Biomech*, **43**: 1817–1822
- [5] Stavro R et al. (2006). *Clin J Sport Med*, **16**: 111–116

Trunk kinematica during walking in adults receiving total knee arthroplasty: a systematic review

T. Van Criekinge¹, K. Claeys¹

¹ Department of Rehabilitation Sciences, KU Leuven Campus Bruges, Bruges, Belgium

Email: Tamaya.vancriekinge@kuleuven.be

Summary

Since trunk control seems to be an important contributor in the recovery process after total knee arthroplasty (TKA), increasing our understanding on trunk motion could aid in setting accurate rehabilitation goals and treatment strategies to enhance mobility outcomes. A literature review was performed, including 21 studies of which 11 examined trunk movements during walking. Pre-operative trunk kinematics were characterized by increased movement amplitudes in all three planes. Although amplitudes decreased post-TKA, they still differed from healthy controls. Recovery was time-, speed- and technique-dependent as mediolateral amplitude reductions proceeded anteroposterior improvements and better outcomes were observed when assessing at comfortable walking speed and when using minimal invasive techniques.

Introduction

Excessive trunk flexion has been related to a greater fall risk, while increased later trunk motion result in higher energy expenditures during walking in older adults.[1,2] Furthermore, it has been shown that enhanced trunk control improves mobility, balance and quality of life early after TKA. [3,4] As a result trunk control seems to be an important contributor to recovery after TKA. However, little is known about trunk motion in adults receiving TKA. By reviewing the available literature, we can increase our understanding on trunk deviations related to TKA, how they are altered due to surgery and which surgical technique is superior in the recovery process. This can aid in setting accurate rehabilitation goals and treatment strategies for improving mobility outcomes after TKA.

Methods

Five scientific databases were searched until October 2020 (Pubmed, WOS, Cochrane Central, Sportsdiscus, and Science Direct). Eligibility criteria consisted of outcomes assessing trunk motion in a population of adults undergoing TKA. Two reviewers independently screened studies and risk of bias was assessed by the Mixed Methods Appraisal Tool (MMAT).

Results and Discussion

Of the 341 studies retrieved from all databases, 21 studies were included (3 RCT and 18 cohorts). The cohort studies compared pre-post treatments (n=8 studies), case-control (n=11) and case-case (n=4). Mean MMAT score was 73%, which corresponds to an overall low score of risk of bias for the majority of studies.

In total 667 patients received TKA after OA and

were compared to 197 controls. The mean age of the participants in the TKA group was 70 years (range 58-76) and 69 years (range 55-76) in the control group. Time post-surgery varied from 68 days to 8 years. Eleven studies assessed trunk motion during walking or the relationship between trunk control and mobility. It was concluded that pre-operative trunk kinematics were characterized by increased three-dimensional movement amplitudes. After TKA, regardless of the technique, decreased movement amplitudes were observed but not all returned to normal, as compared to healthy adults. Minimal invasive TKA surgery lead to faster recovery by resulting in greater decreases in trunk movement amplitudes during walking within the first 3 months post-surgery, and afterwards these differences disappear when comparing to conventional methods. Recovery of trunk variability, on the other hand, seems to be both speed- and time-dependent in the frontal and transversal plane resulting in better outcomes when assessing at a normal comfortable walking speed (1.2 m/s) and leading to decreased variability with increasing time post-surgery, especially for TKA using computer-assisted navigation.

Conclusion

Excessive trunk motion amplitudes, as seen pre-operatively, decreased after TKA. Truncal recovery seemed to be time-, speed- and technique-dependent. Suggesting that post-surgery rehabilitation might influence sagittal kinematics more than the surgery itself, assessment should be executed at comfortable walking speed and minimal invasive techniques result in faster recovery. However, differences with healthy adults did remain after TKA which could indicate that current rehabilitation approaches are not yet optimal to return the walking pattern to normal standards. Incorporating a full biomechanical chain approach, including trunk exercises, could lead to better results after TKA as seen in other knee pathologies.[5] Future research should focus on the relationship between trunk control and post-surgery outcomes after knee arthroplasty.

Acknowledgments

The authors have no conflicts of interest to declare. This research received no specific grant or funding.

References

- [1] Grabiner MD, et al. (2008) J Electromyogr Kinesiol. 2008;18:197-204.
- [2] Nankaku M, et al. (2007) J Orthop Sci. 2007;12:550-4.
- [3] Sano Y, et al. (2018) PLoSONE13(10):e0204884.
- [4] Karaman A, et al. (2017) Physiother Theory Pract. 2017;33(4):289-295.
- [5] Hewett TE et al. (2011). Exerc Sport Sci Rev.39(4):161-166. doi:10.1097/JES.0b013e3182297439

Do bone defects of the greater trochanter affect the postoperative femoral fracture risk after total hip arthroplasty? A biomechanical study.

Michael Saemann¹, Martin Darowski¹, Rainer Bader¹, Manuela Sander², Daniel Kluess¹

¹Biomechanics and Implant Technology Research Laboratory, Department of Orthopaedics, Rostock University Medical Center, Rostock, Germany

²Institute of Structural Mechanics, University of Rostock, Germany
Email: michael.saemann@med.uni-rostock.de

Summary

Bone defects can lead to substantially impaired musculoskeletal biomechanics. A common reason for bone defects of the greater trochanter are intraoperative periprosthetic femoral fractures (PFF), which are a severe complication during total hip arthroplasty (THA) using uncemented hip stems. The intraoperative PFF of the greater trochanter (Vancouver classification A_G) is often treated with cerclage wire fixation or suturing and can result in a trochanteric bone defect. In our biomechanical study we analyzed, whether this bone defect affects the overall postoperative fracture risk of the femur equipped with an uncemented straight hip stem. We experimentally tested three cadaveric femurs without trochanteric defect and one fractured femur with a completely missing greater trochanter in a standing load case. Additionally, we conducted a corresponding Finite Element Analysis (FEA) of the three femurs with and without bone defect. Our preliminary results show that a defect of the greater trochanter did not significantly affect the postoperative fracture risk during standing or stumbling. Further research with a higher sample size is required.

Introduction

The intraoperative PFF of the greater trochanter (A_G) makes up for around 25 % of all intraoperative PFF during primary THA and is often treated only with cerclage wires or sutures and in around 16 % of the cases no treatment was given [1]. Therefore, A_G fractures resemble a common bone defect. Since intraoperative PFF are difficult to reproduce experimentally and an A_G fracture occurred during our cadaveric trials, we used this femur to analyze the influence on the postoperative fracture risk after total hip arthroplasty.

Methods

Experimental testing was conducted on three cadaveric human left unfractured femurs and one right fractured femur with trochanteric bone defect, each implanted with an uncemented straight hip stem. The femurs were distally embedded and axially loaded on the implant ball head to reproduce a standing or stumbling load scenario. The fracture load, load-displacement curves and stiffness at 1 mm axial displacement were compared. A FEA reproducing the experimental load scenario was conducted to compare the three left femurs without defect and with an artificially added A_G fracture as defect. The approaches described by Kluess et al. [2] and Miles et al. [3] were used as basis for model generation and physical modeling, respectively.

Results and Discussion

Experimentally and computationally, no significant differences between femurs with and without trochanteric defect could be shown. Nevertheless, the experimentally measured stiffness of the femur with defect was the lowest of the specimens, which, however, did not result in the lowest fracture load. Computationally, each femur showed a decrease in fracture load and stiffness with a trochanteric defect, although these were not significantly lower.

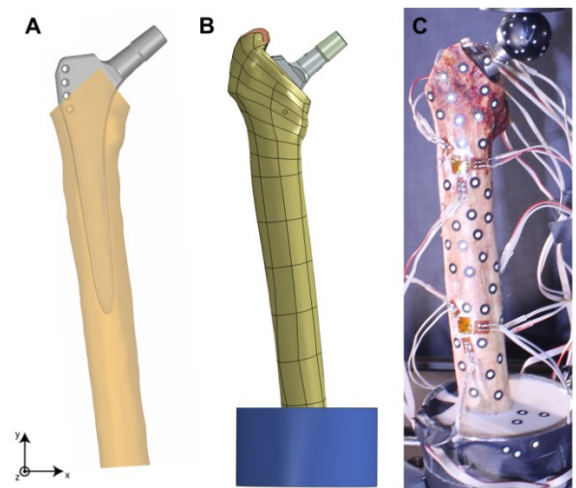


Figure 1: (A) Virtual positioning of the straight hip stem and added artificial A_G fracture as defect, (B) FE model of an unfractured femur, (C) experimental setup of the one femur with defect and added marker points for displacement measurement and strain gauges at representative locations.

Conclusions

From a biomechanical perspective it seems that a defect of the greater trochanter does not significantly affect the overall postoperative femoral fracture risk in a stumbling or standing load scenario, but further research with a higher sample size is necessary for confirmation.

Acknowledgments

This research was funded by the Deutsche Forschungsgemeinschaft (DFG, German Research Foundation) – KL 2327/5-1 and SA 960/8-1.

References

- [1] Abdel MP et al. (2016). *Bone Joint J*, **98-B**: 461-467.
- [2] Kluess D et al. (2009). *Comput Methods Programs Biomed*, **95**: 23-30.
- [3] Miles B et al. (2015). *Med Eng Phys*, **37**: 567-573.

Pose and Shape Registration of Ankle Complex using Statistical Shape and Intensity Model

Jeongseok Oh¹, Seungbum Koo¹

¹Department of Mechanical Engineering, Korea Advanced Institute of Science and Technology, Daejeon, Korea
Email: skoo@kaist.ac.kr

Summary

Accurate measurement of joint kinematics can help understand the pathomechanics of joint injuries. Recent development of bi-planar fluoroscopic imaging allows direct measurement of skeletal images but obtaining quantitative joint movements are laborious because of difficulties in the image processing and bone-to-image registration. We developed a method to find pose and shape of skeletons in the foot without patient's own bone geometry by using a statistical shape and intensity model (SSIM) and a digitally reconstructed radiograph specific to the SSIM. The accuracies in predicting three-dimensional pose were evaluated for the tibia, talus and calcaneus.

Introduction

Bi-planar fluoroscopic (BPF) image analysis is one of the methods to measure the position and posture of a joint accurately. It is utilized to study joint kinematics in vivo without human invasion. The accurate 2D-to-3D registration was able to find the 6 degree-of-freedom (DOF) parameter with error of less than 1mm and 1° for the long bones such as tibia or femur [1]. However, registration of the bones consisting ankle complex is still challenging compared to the long bones due to overlapping between neighboring bones and the bones appearing smaller on the images. It is also a common way to prepare a bone model before the 2D-to-3D registration, and to find the bone models, obtaining computed tomography (CT) should be preceded. The objective of this study was to develop a CT-less 6-DOF bone pose estimation method through the 2D-to-3D registration. A statistical model is used to find the shape without this process. A DRR is required to directly compare with BPF images without post-processing, such as feature extraction, and the SSIM is used.

Methods

The experiment was approved by the institutional review board and conducted by recruiting 18 healthy subjects with no abnormalities in walking. Bi-planar X-ray fluoroscopic images of the ankle were obtained. The positions of the two pairs of X-ray sources and image planes were obtained using a calibration phantom. Fluoroscopic images were taken at 60 fps and for about 2 seconds for each subject. The resolution of the images was 1024×1024. The ankle CT images were obtained and bone geometries were extracted to create a bone shape and intensity database to create a statistical model. The bone models were aligned, and the layers inside the volume were generated. The SPHARM-PDM [2] algorithm was used to find the corresponding points on the bone layers. The mean model and principal component (PC) were calculated using the principal component analysis. The

optimization proceeds by matching 6-DOF pose parameters and 10 PCs of shape parameters for each frame. The results of optimizations were compared with manually processed results.

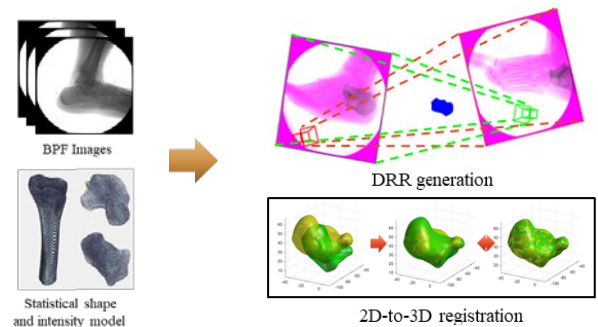


Figure 1: Registration process using SSIM and BPF images

Results and Discussion

The mean translation errors along the x-, y-, and z-axes were 1.35, 1.64, and 1.04 (mm), respectively. The mean rotational errors along the x-, y-, and z-axes were 3.31, 2.08, and 2.28 (°), respectively (Figure 1). The median Hausdorff distance of the registered model is 2.23 mm. The quality of registration is similar to the study using CT images to use the bone models [3], even the ground truth bone shape was estimated simultaneously.

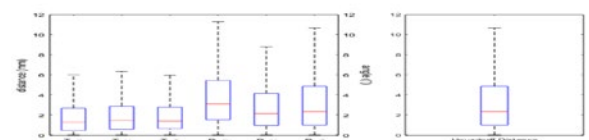


Figure 2: Translational and rotational registration error

Conclusions

The registration method using SSIM of bones that make up the ankle complex was developed, which shows an error of 1 -2 millimeters. We suggest that the procedures would be utilized for clinical applications and conducting studies comparing patients with foot disorders.

Acknowledgments

This work was supported by the Basic Science Research Program through the NRF (NRF-2020R1A2C2006057) of South Korea and the Samsung Research Funding Center of Samsung Electronics (SRFC-IT1902-01).

References

- [1] Yu, W. et al (2017). *Pattern recognit.*, 63:689-699.
- [2] Styner, M. et al (2006), *Insight*, 1071:242.
- [3] Pitcairn, S. et al (2020), *J Biomech*, 103:109

Preliminary Micro-CT Imaging of the Human Tibial Plateau Under Load

Kieran J. Bennett¹, Sophie Rapagna², Lauren Wearne², Saulo Martelli³, Gerald J Atkins¹, L Bogdan Solomon^{1,4}, Egon Perilli², Dominic Thewlis¹

¹Centre for Orthopaedics and Trauma Research, School of Medicine, The University of Adelaide, Adelaide, SA, Australia. ²The Medical Devices Research Institute, College of Science and Engineering, Flinders University, Adelaide, SA, Australia. ³Science and Engineering Faculty, School of Mechanical Medical & Process Engineering, Queensland University of Technology, Brisbane, QLD, Australia. ⁴Department of Orthopaedics and Trauma, Royal Adelaide Hospital, Adelaide, SA, Australia
Kieran.Bennett@adelaide.edu.au

Summary

In this preliminary study, we aim to use micro-CT analysis to determine the internal microstructural deformation of three tibial plateaus under physiological loading applied through their matching femur. Three cadaveric knees were scanned at 46 µm isotropic pixel size under a representative physiological load representing peak loading during stance, reconstructed, and co-registered, with the aim to determine the deformation of the articular surfaces while under load. From these images, the internal deformations can be elucidated using digital volume correlation and used to validate computational models.

Introduction

Micro-CT images of unloaded and loaded bones of entire articular surfaces, rather than excised biopsies, allows for investigation of the internal mechanics of bone and characterization of the responses of bone to external load [1, 2]. The aim of this study was to visualize bone the proximal tibia bone microstructure while under an inferior-superior load, using micro-CT imaging.

Methods

Cadaveric knee specimens (N=3) were obtained. All soft tissues except for the articular cartilage and meniscus were removed. The patella was also removed. The bones were potted and mounted within the loading stage wrapped in saline soaked paper. A custom-made loading stage developed earlier [3] was modified, to adjust the loading direction. The loading rig containing the specimen was positioned within a large-volume micro-CT scanner (Nikon XT H 225, Nikon Metrology, UK). Scans were performed in unloaded and then in loaded conditions, with the proximal tibia and the distal femur contained in the field of view (86 x 86 mm, width x height). Axial loads equivalent to three bodyweights were applied to each specimen, based on the donor's mass at time of death. Load was measured using a six degree-of-freedom load cell. Scans were acquired at 46µm isotropic pixel size at a 0.18° rotation step over 360°. The time to take a single scan was 66 minutes. Cross-section images were reconstructed using CTPro3D software (Nikon Metrology) and saved as grey level images. The loaded dataset was then co-registered DataViewer software (Bruker) to the unloaded and examined.

Results and Discussion

Three bodyweights of load was applied by displacing the femur vertically (1096-1563 N), with the angle of the femur altered to obtain a 60:40 medial:lateral loading ratio. Micro-

CT images (Figure 1) show the proximal tibial plateau in both preload and three bodyweight (3BW) loading conditions, with the joint space narrowing as the femur moves in the inferior direction. From this, the deformation of the articular surface will be evaluated.

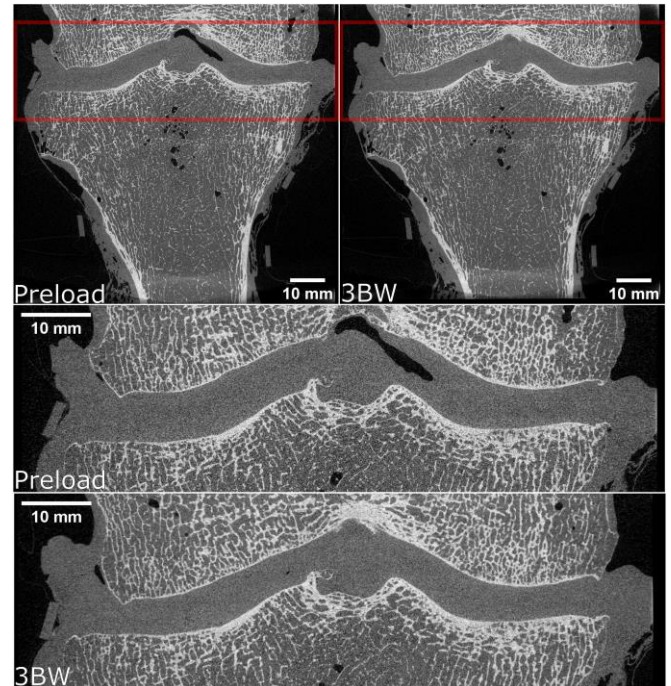


Figure 1: Micro-CT scan reconstructions (coronal) of one human tibial plateau under preload and 3BW load conditions. The highlighted regions (red) of the joint are below.

Conclusions

In this preliminary work, unloaded and loaded micro-CT scans of three human tibial plateaus were obtained. These data can be used to determine microstructural displacement due to joint loading within the tibial plateau. Future work will conduct digital volume correlation analysis to determine the internal deformations and strains. This will be used to inform computational models of bone mechanics.

Acknowledgements

This project was funded by the NHMRC (ID: 1126229) and the ARC (ID: LE180100136)

References

- [1] Grassi I. and Isaksson H. (2015). *J. Mech Behav Biomed Mater.* **50**: 43-54
- [2] Roberts B. et al. (2014) *J. Biomechanics.* **47**: 923-934
- [3] Martelli S. and Perilli E. (2015). *J. Mech Behav Biomed Mater.* **84**: 267-272

Can synchrotron phase contrast micro-tomography uncover how *in vivo* loading affects the Achilles tendon structure?

M. Pierantoni¹, I. Silva Barreto¹, M. Hammerman^{1,2}, E. Törnquist¹, V. Novak³, P. Eliasson², H. Isaksson¹

¹ Biomedical Engineering, Lund University, Sweden; ² Biomedical and Clinical Sciences, Linköping University, Sweden;

³ Paul Scherrer Institute, Switzerland;

Email: maria.pierantoni@bme.lth.se

Summary

Achilles tendons are mechanoresponsive and actively adapt to their mechanical environment. Yet little is known about tendon microstructural response to loading. Here we use synchrotron phase contrast micro-tomography (SR-PhC- μ CT) to visualize the microstructure and to determine the effect of *in vivo* mechanical (un)loading on rat Achilles tendons.

Introduction

Many studies consider the Achilles tendon as one homogenous tissue structure. Thus, less is known about tendons at the meso/microscale. Mechanical loading is believed to increase fiber orientation and packing density [1]. However, further investigation of the mechanobiological effects on the microstructure and mechanical properties is essential. Synchrotron X-ray tomography is a non-destructive method for 3D sub-micrometer visualization and quantitative analysis. In conventional X-ray tomography the contrast is given by the ability of the materials to absorb X-rays and imaging of soft biological materials is very challenging. Phase-contrast imaging was developed to image materials that weakly absorb X-rays, thus providing detailed visualization of soft tissues [2]. Our aim is to use SR-PhC- μ CT to investigate rat Achilles tendons to elucidate how different regimes of *in vivo* loading affect the microstructural properties.

Methods

Animal model: 14 Sprague-Dawley rats were divided into 2 groups: normal cage activity and unloading by Botox injections plus cast immobilization, following Hammerman et al. [3]. The tendons were harvested and kept frozen in saline solution until imaging. Imaging was carried out at the X02DA TOMCAT beamline at the Swiss Light Source, Paul Scherrer Institute, using the High Numerical Aperture Microscope (magnification: 4x, FOV: 4.2mm x 3.5mm and pixel size: 1.63 μ m).

To determine the effect of *in vivo* loading on the microstructure, the 3D orientation distribution of the fibers was determined and compared. A structure tensor analysis was conducted adapting a MATLAB script by Krause et al. [4]. The analysis permits to directly visualize fibers orientations by computing azimuth and elevation angles and to statistically describe how the orientations are distributed.

Results and Discussion

SR-PhC- μ CT imaging of fresh frozen Achilles tendons provides a comprehensive anatomical understanding of the complex internal fiber structure without invasive sample preparations (Fig. 1A). The 3D fiber orientation can be detected (Fig. 1B). The results indicate that angle

distributions depend on the *in vivo* loading regime and fibers are more organized along the main axis in the case of the loaded tendon and more crimped for the unloaded tendons (Fig. 1C and narrower Full Width at Half Maximum for both angles in Fig. 1D).

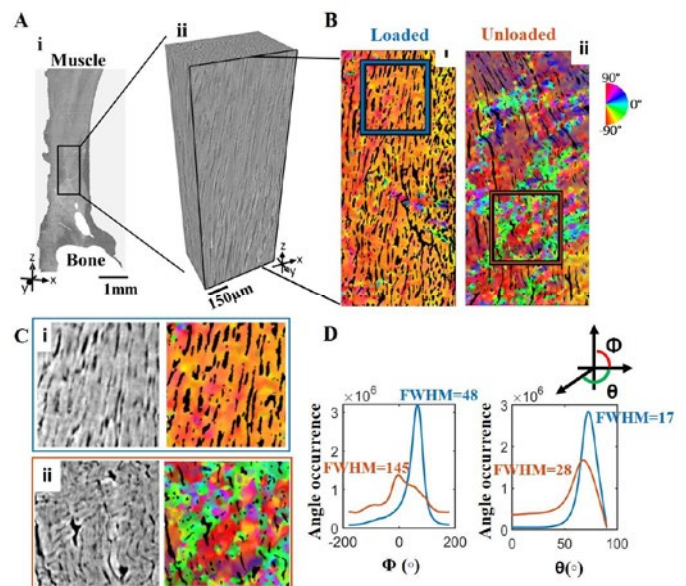


Figure 1: A) SR-PhC- μ CT of an Achilles tendon, i) the entire tendon, ii) magnification showing the collagen fibers. B) Colormap showing fiber orientations for *in vivo* loaded (i) and unloaded (ii) tendon orientations. C) Magnification of the areas indicated in B), showing straight fibers in the loaded tendon and crimped fibers in the unloaded tendon. D) Azimuth (Φ) and elevation (θ) angle distributions are narrower for the loaded tendon (blue curve) than the unloaded (red curve).

Conclusions

SR-PhC- μ CT imaging of Achilles tendons provides a comprehensive understanding of the 3D microstructure. The microstructure is affected by altered *in vivo* loading. Fibers are more crimped and less organized when mechanical stimulation is lacking.

Acknowledgements

We thank the Paul Scherrer Institut for the beamtime at the TOMCAT beamline X02DA of the SLS, and the Knut and Alice Wallenberg Foundation (2017.0221) and the Royal Physiographic Society of Lund, for funding.

References

- [1] Khayyeri H. et al. (2017). *Sci. Rep.*, **7**: 13067.
- [2] Iomoso A. et al. (1996) *Nat. Med.*, **2**: 473.
- [3] Hammerman M. et al. (2018). *PloS one*, **13**: e0201211.
- [4] Krause M. et al. (2010) *Nat. Med.*, **45**: 888–896.

A principal component analysis of infant gastrocnemius growth in the first two years of life

Ricardo Florez¹, Hyun Kyung Kim², Matthew Bell², Thor Besier¹, Sue Stott², Ali Mirjalili², Sian Williams², Justin Fernandez¹
¹Auckland Bioengineering Institute, The University of Auckland, Auckland, New Zealand
²Faculty of Medicine, The University of Auckland, Auckland, New Zealand
 Email: rflo977@aucklanduni.ac.nz

Summary

The medial and lateral gastrocnemius exhibit extraordinary growth in the first two years of life. Using 3D ultrasound we have tracked the growth of the infant gastrocnemius from 3 to 24 months of age. A principal component analysis has revealed that the medial gastrocnemius starts to increase in volume, relative to the lateral side, about the time when infants show autonomous walking skills. This is consistent with changes in spatiotemporal parameters, joint kinematics and kinetics which start to approach adult characteristics by age 2 years. When age related muscle volume increases were removed from the analysis, principal component analysis revealed that muscle belly width was the primary shape change, with the medial side showing increased muscle belly width relative to the lateral side. Understanding typical infant muscle growth has implications for better identification of muscle pathology, including in cerebral palsy.

Introduction

Infants experience rapid muscle changes during the first two years of life. During this time important biomechanical changes are observed. For instance, step width decreases, while step length and walking speed increases [1,2]. Kinematics and kinetics converge towards more adult like characteristics. Two of the most notable lower limb muscles for adequate gait function are the lateral gastrocnemius (LG) and medial gastrocnemius (MG) [3]. Little is known about form function relationships in infants less than 2 years of age. This is paramount because by 2 years of age mature features of gait and muscle function have already formed. In this study we evaluate infant muscle growth in the first 2 years. Understanding typical form function developments have important implications for clinical recommendations in pathologic gait.

Methods

Four OptiTrack cameras were integrated with a custom 3D ultrasound setup. Forty-four infants (3 to 24 months) were scanned using a single-sweep method for the MG and LG. Muscles were segmented from the femoral condyle to the distal musculotendinous junction [4] in the Stradwin/Stradview software suite. We used the musculoskeletal analysis software GIAS2 (Geometry Image-Analysis Statistics) to perform principal component analysis.

Results and Discussion

The gastrocnemius size increases across age and the LG and MG differentiate and become less symmetric (Figure A). Specifically, the LG appears more elongated and thinner while the MG shows a wider muscle belly with more volume. A secondary assessment (Figure B) involving a Procrustes analysis where muscle size is normalized revealed the primary shape change was in the muscle belly with the MG being wider than the LG as we get older. This is consistent with what we observe in children, and adolescents through to adulthood [5], where the MG is larger. Interestingly, we measured an increasing inversion ankle torque across the first year of walking and the MG muscle contributes to foot inversion [6].

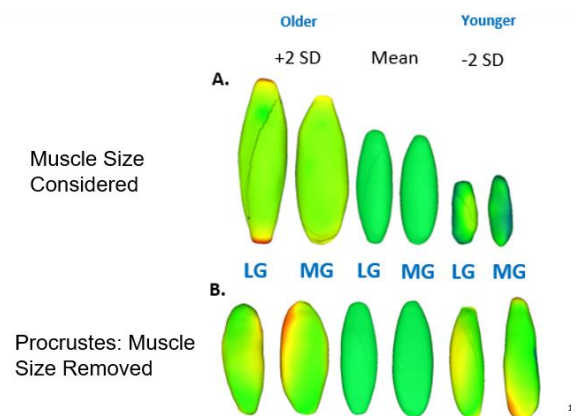


Figure: Muscle shape changes across age (A) and with muscle volume removed (B). Mean and ± 2 SD are shown with RED increase and BLUE decrease and GREEN the mean.

Conclusions

The medial gastrocnemius increases in size relative to the lateral gastrocnemius from the time independent walking occurs. This is in part explained by the developing inversion torque during the first year of walking.

References

- [1] Adolph et al., (2003). *Child Dev.*, 74(2), 475–497.
- [2] Snapp-Childs & Corbetta, (2009). *Infancy*, 14(1), 101–116.
- [3] Honeine et al., (2013). *PLoS ONE*, 8(1), 1–12.
- [4] Barber et al., (2019). *J. of Anat.*, 234(3), 384–391.
- [5] Luke (2018)., *Master Thesis*. The University of Auckland.
- [6] Vieira et al., (2013). *Hum Mov Sci.*, 32(4), 753–767.

Quantitative Comparison of Fascicle Length in Lower Limb Muscles using 3D Freehand Ultrasound and Diffusion Tensor

Imaging

Zhongzheng Wang¹, Ruoyu Huang¹, Francesco Cenni², Antea Destro¹, Sven Petersson³, Ruoli Wang¹

¹KTH MoveAbility Lab, Dept. Engineering Mechanics, KTH Royal Institute of Technology, Stockholm, Sweden

²Faculty of Sport and Health Sciences, University of Jyväskylä, Jyväskylä, Finland

³Department of Medical Radiation, Physics and Nuclear Medicine, Karolinska University Hospital, Stockholm, Sweden.

Email: zhowan@kth.se

Summary

Muscle morphological parameters, such as fascicle length (FL) can significantly influence the muscle function. In this study, FL in medial gastrocnemius (MG) of two healthy adults was quantified using 3D freehand ultrasound (3DfUS) and Diffusion Tensor Imaging (DTI), respectively. The preliminary data analysis showed that 3DfUS over-estimated the FL in MG compared to DTI-based measurement. Further investigation is necessary to yield a more precise comparison.

Introduction

2D ultrasound (US) and magnetic resonance imaging (MRI) are often used to quantify *in vivo* FL. However, 2D US only provides 2D images with limited field of view. DTI measures the diffusion of water molecules in the tissue and can be applied to reconstruct 3D muscle fascicles, serving as a reference standard of *in vivo* FL quantification. But DTI-based measurement has poor portability and limited accessibility. 3DfUS combines 2D US and a 3D motion capture system, which has been shown to have good accuracy in measuring muscle length and volume [1]. The purpose of this study was to compare the quantitative measurement of FL in lower limb muscles using 3DfUS and DTI, respectively.

Methods

Two healthy male subjects (age: 58.5 ± 3.5 yrs, weight: 77.0 ± 0.1 kg, height: 183.0 ± 5.7 cm) voluntarily participated in the study approved by the local ethics committee. B-mode US images of lower limbs were recorded using a 38-mm wide linear transducer (Mindray M9). A probe holder with four reflective markers is fixed rigidly to the transducer. A 10-camera optical motion capture system (Vicon Motion Systems) was used to simultaneously track the position and orientation of the transducer during the US image acquisition. The 3D reconstruction of 2D US images was performed based on a previously published pipeline [2]. Bilateral legs of the two subjects were previously scanned using a 3.0 Tesla MRI scanner (Siemens Trio). During both data acquisition sessions, subjects were lying in a supination position with identical joint alignment. T1-weighted MR and DT images were acquired. The FL was determined using DTI-based [3] and 3DfUS-based [2] method, respectively. Mean FL of the whole muscle volume was calculated. Furthermore, the

muscle was evenly divided into proximal, middle and distal parts to quantify variance in the FL in 3DfUS-based measurement (Figure 1).

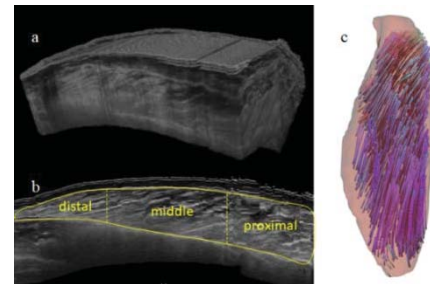


Figure 1: (a-b) 3DfUS based reconstruction of MG (c) 3D reconstruction of fascicles based on DTI measurement

Results and Discussion

Only FL in medial gastrocnemius (MG) were reported here. The FL was found the longest in the proximal part of the MG and shortest in the distal part (Table 1). Compared to the DTI-based method, the FL was longer using 3DfUS-based measurement. The observed differences may be due to the probe compression and manually defined plane for FL calculation in the 3DfUS-based measurement.

Conclusions

Based on this preliminary study, 3DfUS measurement overestimated FL in MG compared to the DTI measurement. Further investigation is needed to improve our measurement protocol in the 3DfUS in order to perform a precise comparison.

Acknowledgments

We would like to acknowledge financial support from Promobilia Foundation (19027) and Swedish Research Council (2018-04902).

References

- [1] Lee B et al. (2011) *J Anat*, **218**: 637-642
- [2] Francesco C et al. (2018) *Ultrasound Med Biol*, **12**: 2505-2518
- [3] Clara K et al. (2019) *Sci Rep*, **9**: 11836

Table 1: Fascicle length measured using 3DfUS- and DTI-based methods (mean \pm S.D.)

	Whole MG 3DfUS (mm)	Whole MG DTI (mm)	Proximal MG 3DfUS (mm)	Middle MG 3DfUS (mm)	Distal MG 3DfUS (mm)
Subject 1	55.99 \pm 8.23	40.21 \pm 23.71	61.76 \pm 5.96	58.15 \pm 5.14	48.07 \pm 6.50
Subject 2	42.63 \pm 8.37	29.56 \pm 13.57	44.21 \pm 7.43	43.84 \pm 8.59	39.84 \pm 8.63

The feasibility and effectiveness of treadmill-based perturbations for assessing and improving walking stability in chronic obstructive pulmonary disease: a pilot study

Christopher McCrum¹, Anouk W. Vaes², Jeannet M. Delbressine², Maud Koopman^{2,3}, Wai-Yan Liu^{1,2,4,5}, Paul Willems¹, Kenneth Meijer^{1#}, Martijn A. Spruit^{2,3#}

¹Department of Nutrition and Movement Sciences, NUTRIM School of Nutrition and Translational Research in Metabolism, Maastricht University Medical Centre+, Maastricht, The Netherlands. ²Research and Development, CIRO, Horn, The Netherlands.

³Department of Respiratory Medicine, NUTRIM School of Nutrition and Translational Research in Metabolism, Maastricht University Medical Centre+, Maastricht, The Netherlands. ⁴Department of Orthopaedic Surgery, Máxima Medical Center, Eindhoven, The Netherlands. ⁵Department of Orthopaedic Surgery, Catharina Hospital, Eindhoven, The Netherlands.

[#]Joint last authors

Email: chris.mccrum@maastrichtuniversity.nl

Summary

Chronic obstructive pulmonary disease (COPD) is linked with increased falls risk, but the mechanisms of this are not understood. Using treadmill-based perturbations during walking, we found that COPD does not appear to result in significant deficits in stability following sudden perturbations and patients do demonstrate some adaptability to repeated perturbations. The approach was also found to be feasible, meaning that perturbation-based balance training could be further explored in COPD.

Introduction

Falls risk is elevated in chronic obstructive pulmonary disease (COPD) but little is known about the contributing factors. We examined the feasibility of, and initial responses to, large walking perturbations in COPD, as well as the adaptation potential to repeated walking perturbations that might indicate potential for perturbation-based balance training in COPD.

Methods

12 participants with COPD undergoing inpatient pulmonary rehabilitation and 12 age-gender-matched healthy control participants walked on an instrumented treadmill at a stability-normalised walking speed [1] and experienced repeated treadmill-belt acceleration perturbations (first perturbation to the right leg, then up to eight times to the left leg as conducted in [2]). Three-dimensional motion capture was used to quantify the margin of stability [3] during perturbed walking. Feasibility, stability following the initial perturbations and adaptation to repeated perturbations were assessed.

Results and Discussion

Perturbations in this manner were feasible in COPD (no harness assists and 11 of 12 participants completed the minimum number of perturbations (5), with an average of 8). No significant deficit in reactive walking stability in COPD was found versus controls (Figure 1A). There were mixed results for the adaptability outcomes (no significant perturbation number effect but a significant interaction) which overall indicated some adaptability to repeated perturbations (Figure 1B), but not to the same extent as the healthy controls.

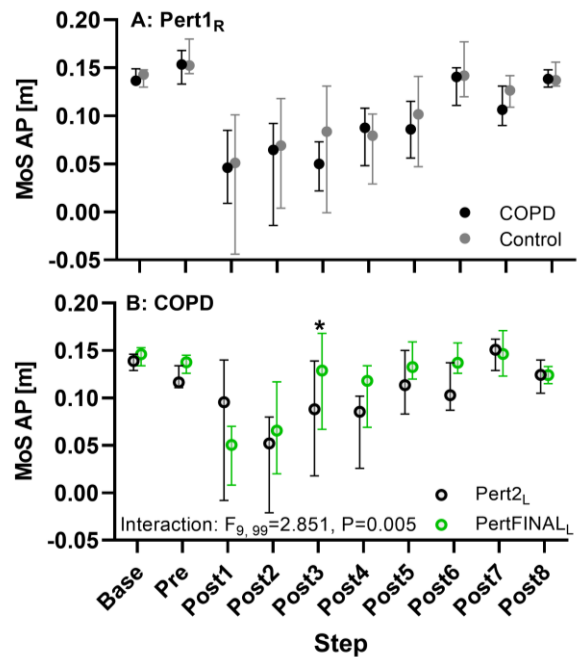


Figure 1: Medians and 95% confidence intervals of the AP MoS during unperturbed walking prior to each perturbation (Base), the final step prior to each perturbation (Pre) and the first eight recovery steps following the perturbations (Post1–8) for **A**, the first perturbation to the right leg in COPD and matched control participants, and **B**, during the first and final (for each individual) perturbation to the left leg within the COPD participants. *: Sidak's multiple comparisons test: $P=0.046$.

Conclusions

Treadmill-based perturbations during walking are feasible in COPD. COPD does not appear to result in significant deficits in stability following sudden perturbations and patients do demonstrate some adaptability to repeated perturbations. Perturbation-based balance training may be considered for fall prevention in research and practice in people with COPD.

References

- [1] McCrum C et al. (2019) *J. Biomech*, **87**: 48-53.
- [2] McCrum C et al. (2018) *Commun Biol*, **1**: 230.
- [3] Hof AL et al. (2005) *J. Biomech*, **38**: 1-8.

Classification of spatiotemporal gait patterns in unilateral transfemoral amputees

Daisuke Ichimura¹, Ryo Amma^{1,2}, Hiroto Murata^{1,2}, Genki Hisano^{1,3}, Hiroaki Hobara¹

¹National Institute of Advanced Industrial Science and Technology (AIST), Tokyo, Japan

²Tokyo University of Science, Chiba, Japan, ³Tokyo Institute of Technology, Tokyo, Japan

Email: d.ichimura@aist.go.jp

Summary

Understanding spatiotemporal gait strategies could help develop individualized transfemoral prostheses and provide better rehabilitation regimes. This study aimed to classify the spatiotemporal gait patterns across a range of walking speeds in unilateral transfemoral amputees (UTFAs). Hierarchical cluster analysis (HCA) was conducted on the step lengths and cadences at eight different speeds in 24 UTFAs. This HCA revealed three clusters based on a higher cadence, a longer step length, and a hybrid pattern. Current results suggest that there is more than one gait strategy in UTFAs.

Introduction

Walking is one of the most fundamental activities of daily life. In healthy subjects, spatiotemporal gait parameters, such as cadence and step length, have been shown to be automatically controlled by common mechanisms during steady gait [1]. In contrast, a previous study reported that below-knee prosthesis users have shown a greater variability of the parameters than healthy subjects across a range of walking speeds [2], indicating that prosthesis users are likely to have several different gait patterns. The aim of this study was to classify gait patterns using step length and cadence across a range of walking speeds in unilateral transfemoral amputees (UTFAs). We hypothesized that there would be two clusters of gait patterns based on a longer step length or a higher cadence.

Methods

Twenty-five UTFAs (18 M, 7 F; age 30.3 ± 9.0 years; mass 65.3 ± 14.3 kg; height 1.66 ± 0.75 m) participated in this study. Spatial and temporal footfall data were collected while each subject walked on a split-belt instrumented treadmill (FTMH-1244WA, Tec Gihan, Kyoto, Japan) at eight different speeds (2.0, 2.5, 3.0, 3.5, 4.0, 4.5, 5.0, and 5.5 km/h). The collected footfall data were processed to derive the cadence (step/s) and step length (m). The Mahalanobis distance criterion [3] was used to eliminate any outliers. Hierarchical cluster analysis (HCA) was then conducted to identify subgroups with homogeneous gait patterns, based on the relationships between cadence and step length in both the prosthetic limb and intact limb of each subject. Squared Euclidean distance was chosen as the metric for this analysis, and Ward's linkage method was adopted. After forming the clusters, a univariate analysis of variance (ANOVA) or a Kruskal–Wallis test was performed on cadence and step length. When a significant main effect was observed, post-hoc comparisons (*T*-test or Mann–Whitney U test) were performed on the variables between the clusters. Statistical significance was set to $p < 0.05$.

Results and Discussion

After an outlier was eliminated (Mahalanobis distance criterion > 4.0), a final sample of 24 participants was left for further analysis. HCA identified three clusters based on step lengths and cadences (Figure 1). Cluster 3 ($n = 9$) had a significantly longer step length than Cluster 2 in their intact limb over a wide range of walking speed and longer step length in their prosthetic limb at 2.5 and 3.5 km/h. Cluster 2 ($n = 7$) had a significantly higher cadence than Cluster 3 in their intact limb over a wide range of walking speeds, and in their prosthetic limb at 2.5 and 3.5 km/h. The step lengths and cadences in Cluster 1 ($n = 8$) exhibited nearly intermediate values between Cluster 2 and 3. These results indicate that the spatiotemporal gait parameters of UTFAs have different modes [4], suggesting the existence of different gait control mechanisms that adjust at least either their cadences or step lengths.

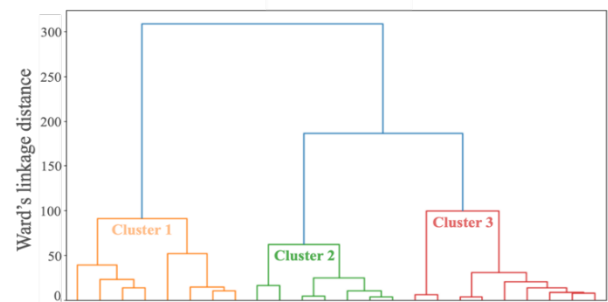


Figure 1: Dendrogram of hierarchical cluster analysis (HCA). Linkage distance is shown on the y-axis and UTFAs are shown on the x-axis. Three clusters were identified.

Conclusions

We showed that gait characteristics of UTFAs can be classified into three clusters based on their spatiotemporal parameters (cadence and step length) across a range of walking speeds, suggesting the existence of different gait control mechanisms in UTFAs. These results would help to develop individualized transfemoral prostheses, and to provide better rehabilitation regimes.

Acknowledgments

This study was partly supported by JSPS KAKENHI (Grant Number 19K11338).

References

- [1] Egerton et al., (2011). *Gait Posture*, **34**: 178-182.
- [2] Howard et al., (2013). *Gait Posture*, **38**: 883-887.
- [3] Kinsella and Moran, (2008). *Gait Posture*, **27**: 144-151.
- [4] Zijlstra et al., (1995). *Gait Posture*, **3**: 13-18.

Simultaneous Measurements of In Vivo Knee Contact and Tendon Loading during Walking

Colin R. Smith¹, Pascal Schütz¹, Barbara Postolka¹, Jörn Dymke³, Adam Trepczynski³, S.H. Hosseini Nasab¹, William R. Taylor¹, Darryl G. Thelen², Philipp Damm³, Jack Martin²

¹ Laboratory for Movement Biomechanics, Institute for Biomechanics, ETH Zürich, Switzerland

² Neuromuscular Biomechanics Lab, University of Wisconsin-Madison, USA

³ Julius Wolff Institute, Charité – Universitätsmedizin Berlin, Germany

Email: colin.smith@hest.ethz.ch

Summary

We collected simultaneous measurements of Achilles tendon, patellar tendon, and knee contact loading during walking in a patient with an instrumented total knee replacement. Tendon load was tracked using non-invasive shear wave tensiometers. This novel dataset will enable objective evaluations of predictions of internal tissue loading using either musculoskeletal modeling or machine learning approaches.

Introduction

The ability to characterize internal joint loads during walking from external measurements is hindered by muscle redundancy. Tensiometers are a novel wearable technology to assess *in vivo* loading by measuring shear wave propagation along superficial tendons [1]. Tensiometer data could potentially be used to resolve muscle redundancy when estimating internal tissue loads. This study aimed to collect coupled tensiometer and knee joint load data to assess the utility of tensiometer data to assess joint contact loads.

Methods

We performed simultaneous tensiometer, motion capture, ground reaction force, electromyography, and knee contact force measurements on a subject (K5R, Male, 93kg, 1.7m, 72 years) with an instrumented knee replacement [2] during overground level walking at the CAMS-Knee OpenSim 2020 Workshop (<https://cams-knee.orthoload.com/>). EMG was collected on the rectus femoris, tibialis anterior and medial and lateral hamstrings, quadriceps, and gastrocnemii. The inverse kinematics and dynamics tools in OpenSim were used

to calculate joint angles and moments. The measured and calculated metrics were analyzed against the gait cycle.

Results and Discussion

There was strong correspondence between the phasing of tendon wave speeds and knee contact forces. Specifically, the peak in the patellar tendon wave speed coincided with the first peak in the knee contact force, while the peak in Achilles tendon wave speed coincided with the second peak in knee contact force.

Conclusions

These unique measurements provide additional insight into the contributions of the patellar tendon and Achilles tendon loading patterns to *in vivo* knee contact forces during walking. These results suggest that with advanced analysis techniques, tensiometers show potential to be applied as a wearable technology to indirectly assess knee contact forces.

Acknowledgments

Swiss National Science Foundation Scientific Exchange Grant (IZSEZ0_191974), Wisconsin Alumni Research Foundation (WARF), OpenSim Pilot Project, OrthoLoad, OrthoLoadClub, DFG (TR 1657/1-1, Da 1786/5-1, SFB 1444).

References

- [1] Martin J et al. (2018). *Nat Comm*, 9: 1592.
- [2] Bergmann, G. et al. (2014). *PloS one*, 9(1), e86035.

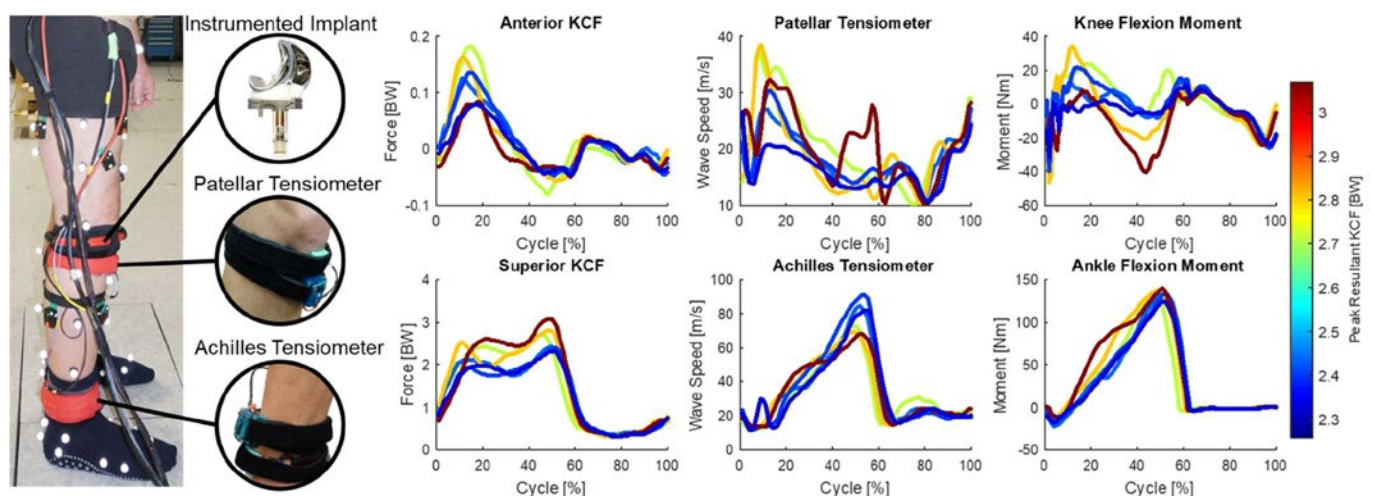


Figure 1: In vivo knee contact forces and Achilles and patellar tendon shear wave speeds were measured during six cycles of level walking.

Musculoskeletal Simulation of a Gait for a Person with Unilateral Transfemoral Amputation: The Cause of Muscle Atrophy

Isna Riski Safira, Motomu Nakashima

Department of Systems and Control Engineering, Tokyo Institute of Technology, Tokyo, Japan

Email: isna.r.aa@m.titech.ac.jp

Summary

Muscle atrophy information in transfemoral amputation is one essential factor to design better prosthesis and rehabilitation process. The previous study has explained the atrophy distribution, but the mechanism behind atrophy formation is yet to be known due to the difficulties in accessing deep muscles. The current study proposes the answer through musculoskeletal simulation using kinematic and kinetic gait dataset to calculate and compare the maximum muscle forces between amputated and intact limb. The result showed that the reduction in muscles' moment arms after surgery might cause lower muscle forces resulting in atrophy. On the contrary, muscles with higher force become hypertrophied. The largest difference in muscle force between amputated limb and intact limb was observed in the adductor longus muscle and indicated high contribution of this muscle to compensate for lack of force from the other muscles in amputated limb.

Introduction

Muscle atrophy in persons with transfemoral amputation (TFA) is one of the musculoskeletal comorbidities following surgery that occur in muscles at amputated limb (AL). However, a recent study shows that some muscles in AL become hypertrophied compared to the ones in intact limb (IL) [1], although the cause has yet to be confirmed. The cause can be elucidated by understanding the distribution of individual muscle forces, which has not been sufficiently studied before. For this purpose, a musculoskeletal simulation of a gait for a TFA was carried out in the present study.

Methods

Kinematic information and ground reaction force were obtained from open-source data of TFA [2] during gait. A subject with unilateral transfemoral amputation (male; age= 38 years, mass= 104.3 kg, height= 1.91m; gait speed= 1.4m/s) was modeled as shown in Figure 1. A musculoskeletal model was constructed using modified Gait 2392 of OpenSim [3], which has 12 body segments and 23 degrees-of-freedom. AL was modeled by removing muscles that have no origin or insertion point in the above knee. The distal ends of the transected muscles in AL were re-attached to the new insertion points near the medial ridges of linea aspera. The final model had 22 muscles on AL and 34 muscles on IL with the same muscle properties as a healthy person to simulate the condition before the atrophy.

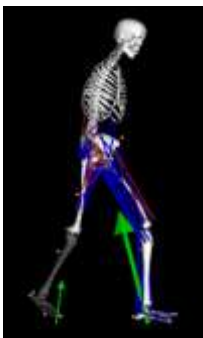


Figure 1: Musculoskeletal model of TFA

Results and Discussion

Table 1 shows the result of simulation with respect to the maximum muscle forces. Almost all muscles in AL have lower forces compared to IL due to the reduction in muscles' moment arms as the result of amputation. Muscles in AL with higher forces, including adductor longus (ADDL), were obtained due to having the same insertion point.

Table 1: Muscle force in AL compared to IL.

Muscle	AL Fmax (N)	Force Ratio	CSA Ratio (% in [1])
Iliopsoas	984.5	Higher	64.2
Gluteus maximus	254.5	Higher	63.6
Tensor fascialatae	0.0	Lower	46.1
Rectus femoris	203.3	Lower	56.5
Vastus medialis	0.09	Lower	54.5
Vastus intermedialis	0.0	Lower	75.1
Vastus lateralis	0.0	Lower	54.5
Sartorius	81.6	Lower	70.1
Biceps femoris	0.0	Lower	127.4
Semitendinosus	12.9	Lower	128.1
Pectineus	65.0	Higher	48.0
Gracilis	2.6	Lower	108.6
Adductor longus	246.0	Higher	143.8
Adductor brevis	53.1	Higher	75.0
Adductor magnus	18.3	Lower	85.9

The largest difference was observed in ADDL muscle force between AL (246 N) and IL (27 N). It indicates high contribution of this muscle to compensate for the lack of power in AL. ADDL in AL becomes more activated and generate higher cross-sectional area (CSA) with 143.8% ratio [1]. Our study suggests to take benefit of this muscle in prosthesis design and rehabilitation process.

Conclusions

The result showed that the reduction in muscles' moment arms might cause lower muscle forces resulting in atrophy. To compensate, AL muscles with the same musculature as before surgery will generate higher muscle forces. The largest difference in muscle force between AL and IL was observed in ADDL. It indicates the major contribution of ADDL to compensate the lack of force from the other muscles in AL.

References

- [1] Nakamura T et al. (2019). *JSP Journal*, **35**(3): 212-218
- [2] Hood S et al. (2020). *SciData*, **7**: 150
- [3] Delp et al. (2007). *IEEE Trans Biomed Eng*, **54**: 1940-50

Series elasticity facilitates safe plantarflexor muscle-tendon shock absorption during perturbed human hopping

Taylor J.M. Dick¹, Christofer J. Clemente^{1,2}, Laksh K. Punith³, Gregory S. Sawicki³

¹School of Biomedical Sciences, University of Queensland, St Lucia, QLD, Australia

²School of Science and Engineering, University of the Sunshine Coast, Sippy Downs, QLD, Australia

³George W. Woodruff School of Mechanical Engineering, School of Biological Sciences, Georgia Institute of Technology, USA

Email: t.dick@uq.edu.au

Summary

The ability for humans to stay upright in the face of unpredictable changes in their environment is remarkable, yet we understand little about this is achieved. Here, we determined how neuromuscular control and plantarflexor muscle-tendon dynamics are modulated to maintain stability during unexpected changes in ground height during hopping. We show that an unexpected drop in ground height introduces an automatic phase shift in the timing of plantarflexor muscle activity relative to ground contact and an increase in co-activation of the plantar and dorsi-flexor muscles. This leads to shorter fascicle lengths at ground contact and increased fascicle lengthening and forces during the perturbed step—enabling the plantarflexors to safely and effectively dissipate the energy injected by the drop.

Introduction

Animals display a remarkable ability to stay upright during movement in the face of uneven or unpredictable terrain. Yet much of our knowledge regarding locomotion has come from studies conducted under steady-state conditions on level surfaces. Our previous work has shown that humans use the most distal lower-limb joints to absorb energy and recover from perturbations [1]. However, the muscle-tendon dynamics and neural control strategies that accompany these responses are not yet understood. Previous unexpected drop landings in birds highlight that muscle-tendon unit (MTU) series elasticity acts as a buffer to rapidly absorb energy and protect muscle fascicles from potentially injurious strains [2]. Our aim is to provide fundamental insights into the mechanisms for stability during unexpected perturbations.

Methods

Participants performed steady-state hopping at their preferred frequency on a 20cm platform. We elicited an unexpected perturbation via rapid removal of the platform. Motion capture (Vicon, UK) was used to quantify the 3D positions of the lower limbs. MTU lengths were computed from a scaled musculoskeletal model and motion capture data. Ground reaction forces were measured during hopping using a static instrumented split belt treadmill (Bertec, USA). Surface electromyography (EMG) was used to record muscle activations in the medial (MG) and lateral gastrocnemius (LG), soleus (SOL), and tibialis anterior (TA) (Biometrics, UK). MG and SOL fascicle lengths were determined from B-mode ultrasound images (Telemed, Lithuania). Linear mixed effects models were used to examine variation in muscle activation and muscle-tendon dynamics between conditions.

Results and Discussion

The unexpected change in the height of the ground introduced an automatic phase shift that extended the aerial

phase of the perturbed hop. This altered the timing of muscle activation; MG and SOL activation shifted ~ 0.076 s earlier during the perturbation relative to ground contact and average muscle activation increased during the aerial and ground contact phases of perturbation compared to normal hopping ($P < 0.001$, Fig. 1). These alterations resulted in (1) more fascicle shortening prior to the perturbation, (2) shorter fascicles upon initial ground contact, and (3) increased fascicle lengthening during ground contact of the perturbed hop ($P < 0.001$). Similarly for the MTU, the perturbation leads to (1) increased MTU lengthening and shortening during the ground contact phase, and (2) shorter MTU lengths upon ground contact ($P < 0.001$) (Fig. 1A-D). These alterations in fascicle and MTU length changes together with increases in muscle force, led to increases in energy dissipation (negative power) during the perturbation. Finally, we find that the perturbation leads to co-activation of the plantarflexors and antagonist TA, which during normal hopping activate out of phase. This co-activation improves the capacity of the plantarflexors to rapidly absorb energy upon ground contact, and may also aid in avoiding potentially damaging strains.

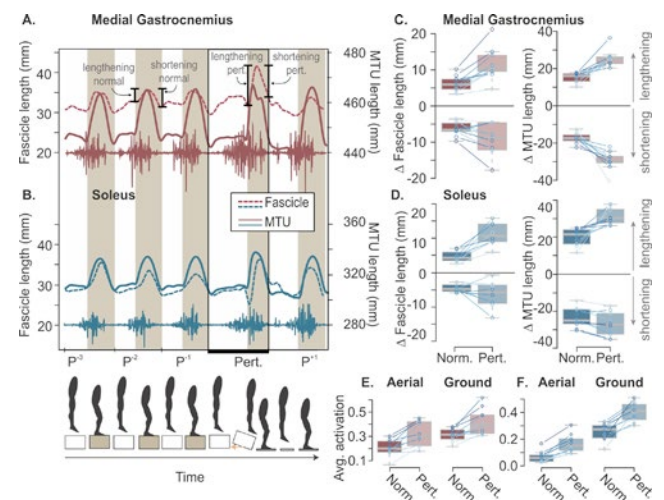


Figure 1: Muscle activation, MTU, and fascicle length during normal (Norm.) hopping (P^{-3} , P^{-2} , P^{-1}) and the perturbation (Pert.).

Conclusions

Our study provides novel insight into how humans alter their neural control to modulate *in vivo* muscle-tendon dynamics in response to unexpected perturbations. These data provide insight to guide design of lower-limb assistive devices that can perform within varied and unpredictable environments.

References

- [1] Dick, TJM et al. (2019). *Interface*, **16(159)**, 20190292.
- [2] Konow, N et al. (2012). *Proc B*, **279(1731)**, 1108-1113.

Effects of 12 different heel rocker designs, configured with different rocker radii, apex positions and apex angles, on plantar pressure

A. Malki¹, L. van Kouwenhove¹, G.J. Verkerke^{1,2}, R. Dekker¹, J.M. Hijmans¹

¹ University of Groningen, University Medical Center Groningen, Department of Rehabilitation Medicine, Groningen, The Netherlands

² University of Twente, Department of Biomechanical Engineering, Enschede, The Netherlands
Email: a.malki@umcg.nl

Summary

Rocker shoes are used to offload high-risk areas of the foot to prevent foot ulcers in diabetic patients with loss of protective sensation. Forefoot rocker shoes can reduce the peak plantar pressure of the hallux and MTH regions, however pressure in the heel region is often elevated by this type of footwear. Therefore, the effect of different heel rocker designs (12) on the heel plantar pressure (at 7 masks) is analyzed in this study. Results have shown a significant main effect of the rocker radius on the relative peak plantar pressure for the different heel masks. Patients with high risk areas in the proximal heel region benefit more from a rocker shoe with larger heel radii whereas smaller heel radii are beneficial for patients with high risk areas in the distal heel region.

Introduction

Rocker shoes are used to offload high-risk areas of the foot to prevent foot ulcers in diabetic patients with loss of protective sensation. These high-risk areas are the hallux, metatarsal heads (MTH) and heel region [1]. Forefoot rocker shoes can reduce the peak plantar pressure of the hallux and MTH regions, however pressure in the heel region is often elevated by this type of footwear, indicating great importance to focus on this region [2,3,4]. No studies have analyzed the effect of different heel rocker designs on the heel plantar pressure yet.

Methods

Shoes with 12 different heel rocker configurations were designed having different heel rocker radii, apex positions and apex angles (Figure 1). The relative peak plantar pressure (RPP) of each configuration at 7 heel locations (masks, Figure 1) was studied in 10 healthy participants.

Results and Discussion

There is a significant main effect of the rocker radius on the RPP for the different heel masks. Compared to a smaller radius (SR), a larger radius (LR) causes a significantly lower RPP in mask 1, 2 and 3 whereas the same radius causes a significant increase in RPP in mask 5 and 7. Moreover, a significant interaction effect between the rocker radius and the apex position for mask 1 and 3 was found. A LR, compared to a smaller, with a proximal apex position causes a significantly lower RPP in mask 1 and 3. The same result is seen in mask 1 with the mid-apex position.

The shape of the heel rocker affects heel pressure during the loading response of the first rocker. The radius of the

curvature influences how the pressure is redistributed. A steep curve (=SR) resulted in an increased RPP in the proximal heel region compared to a LR, probably due to a shortened rear curve rolling time. Lin et al. showed that the efficacy of rocker shoes is reduced when the curve rolling time is decreased, which could explain this finding [5].

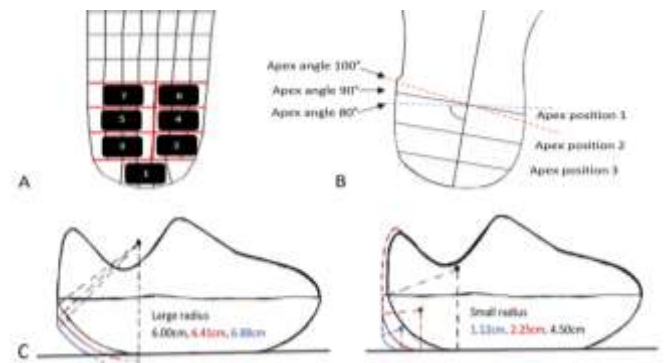


Figure 1: (A) The numbers represent the 7 masks (B) Red, black and blue lines respectively represent: apex angle of 100°, 90° and 80°. The distal, mid and proximal apex position are also shown in the same image. (C) Left image illustrates heel rockers with large radii (range: 6.00 - 6.88cm) and right image shows heel rockers with small radii (range: 1.12 - 4.50cm).

Conclusions

Patients with high risk areas in the proximal heel region benefit more from a rocker shoe with larger heel radii whereas smaller heel radii are beneficial for patients with high risk areas in the distal heel region.

Acknowledgments

The authors gratefully acknowledge EIT Health for funding the project.

References

- [1] Edmonds ME and Foster AV (2006). *BMJ (Clinical research ed.)*, **332**: 407–410.
- [2] Chapman JD et al. (2013). *Clinical Biomechanics*, **28**: 679–685.
- [3] Van Schie C et al. (2000). *Foot & Ankle International*, **21**: 833–844.
- [4] Reints R. (2020). *On the design and evaluation of adjustable footwear for the prevention of diabetic foot ulcers*; Rijksuniversiteit Groningen.
- [5] Lin S et al. (2017). *PLoS one*, **12**: e0169

Comparison of walking biomechanics following conservative or arthroscopic management for femoroacetabular impingement syndrome

Tamara M. Grant^{1,2}, Laura E. Diamond^{1,2}, Claudio Pizzolato^{1,2}, Trevor N. Savage^{1,2,3}, David G. Lloyd^{1,2}, David J. Hunter^{3,4}, Kim L. Bennell⁵, Michelle Hall⁵, David J. Saxby^{1,2}

¹Griffith Centre of Biomedical and Rehabilitation Engineering (GCORE), Griffith University, Gold Coast, Australia

²School of Allied Health Sciences, Griffith University, Gold Coast, Australia

³Kolling Institute of Medical Research, Institute of Bone and Joint Research, The University of Sydney, Sydney, Australia

⁴Department of Rheumatology, Royal North Shore Hospital, St Leonards, Sydney, Australia

⁵Centre for Health, Exercise & Sports Medicine, Department of Physiotherapy, The University of Melbourne, Melbourne, Australia

Email: tamara.grant@griffithuni.edu.au

Summary

Femoroacetabular impingement syndrome is commonly treated via arthroscopic surgery or conservative management. This randomised controlled trial compared the effects of these treatment approaches on external biomechanics during self-paced walking at baseline and 12-month follow-up. We observed no differences in trunk, pelvis, and lower-limb biomechanics between treatment groups, though both groups exhibited altered biomechanics at follow-up compared to baseline. The clinical implications of these relatively small changes require further investigation.

Introduction

Femoroacetabular impingement syndrome (FAIS) is a motion-related hip disorder, whereby an abnormally shaped femoral head/neck and/or acetabulum leads to mechanical impingement and hip pain [1]. FAIS may predispose an individual to hip osteoarthritis. Hip arthroscopy and physiotherapist-led conservative management are common treatments, though patient reported improvements in symptoms and function are modest. Although hip arthroscopy rates increased 460% from 2005 to 2013 [2], arthroscopic hip surgery does not restore normal walking patterns in those with FAIS [3]. The effects of conservative treatment on walking biomechanics in FAIS have not been explored, nor have treatment approaches been compared. We compared changes in trunk, pelvis, hip, knee, and ankle angles, and hip, knee, and ankle moments during self-paced walking following arthroscopy or conservative management of FAIS.

Methods

The Australian FASHIoN Trial recruited patients from waiting lists for arthroscopic treatment of FAIS (n=140), and a subset underwent biomechanical analysis (n=45). Patients were randomly assigned to arthroscopy (ARTH; n=21) or 12 weeks of conservative care (Personalised Hip Therapy, PHT; n=24) [4]. Three-dimensional body motion and ground reaction forces were measured prior to treatment (baseline) and at 12-months (follow-up) during four self-paced walking trials. Inverse kinematics and dynamics were performed in OpenSim [5]. Trunk, pelvis, and lower-limb angles (°), and lower-limb external moments (Nm/kg), were compared between baseline and follow-up and treatment groups using a two-way repeated measures analysis of variance via statistical parametric mapping ($p < 0.05$).

Results and Discussion

We observed no differences in treatment effects for any angles or moments during walking. Compared to baseline values, both ARTH and PHT patients walked with mean increased hip external rotation (mean difference (MD) 7.5° 95% confidence interval (CI) 3.2 to 11.8, $p < 0.001$) angles, reduced hip flexion (MD 0.12 Nm/kg 95%CI 0.02 to 0.23, $p = 0.03$), increased hip extension (MD 0.16 Nm/kg 95%CI 0.04 to 0.29, $p = 0.01$), hip external rotation (MD 0.02 Nm/kg 95%CI 0.004 to 0.04, $p = 0.04$), knee flexion (MD 0.09 Nm/kg 95%CI 0.04 to 0.14, $p = 0.01$), and plantarflexion (MD 0.07 Nm/kg 95%CI 0.04 to 0.11 $p = 0.02$) moments (Figure 1).

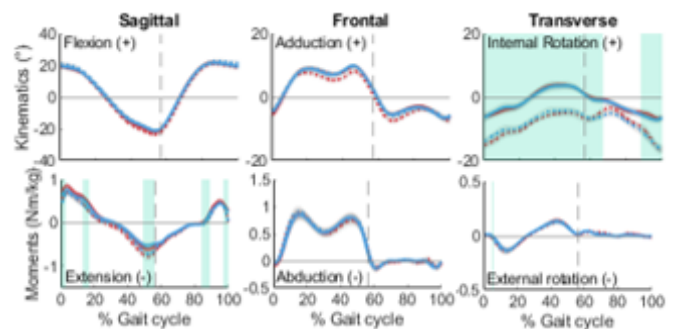


Figure 1. Ensemble average (± 1 standard deviation) hip angles (°) and moments (Nm/kg) for PHT (blue) and ARTH (red) at baseline (solid) and follow-up (dashed). Green shading indicates significant differences between baseline and follow-up for both treatment groups ($p < 0.05$). Grey dashed line - toe off (mean for all participants).

Conclusions

The effects of ARTH and PHT on walking biomechanics in patients with FAIS did not differ. Regardless of treatment, several lower-limb biomechanical parameters were altered at 12-month follow-up. The clinical and structural implications of these relatively small changes require further investigation over both the short- and long-term.

References

- [1] Griffin DR et al. (2016). *BJSM*, **50**: 1169-1176.
- [2] Maradit Kremers H et al. (2013). *J Arthroplasty*, **32**: 750-755.
- [3] Catelli DS et al. (2019). *Gait Posture*, **72**: 135-141.
- [4] Murphy NJ et al. (2017). *BMC M. D.*, **18**: 406.
- [5] Delp SL et al. (2007). *IEEE. Trans. Biomed. Eng.*, **54**: 1940-195.

The effect of a foot strengthening exercise intervention on restoring foot strength in people with diabetic peripheral neuropathy

Karen J. Mickle¹

¹School of Allied Health, Human Services and Sport, College of Science, Health and Engineering, La Trobe University, Melbourne, Australia

Summary

This study evaluates the effect of a specific foot strengthening exercise program on foot strength in people with diabetes and peripheral neuropathy. After 12 weeks, 20 participants returned to the laboratory for retesting (77%). We found a significant interaction between groups and time, whereby participants in the intervention group increased their toe strength compared to baseline. This study has provided good pilot data to show that a foot strengthening exercise program may be suitable for people with diabetic neuropathy.

Introduction

Diabetic polyneuropathy (DPN) is one of the most common complications associated with diabetes, present in 50-70% of older people with diabetes [1]. In later stage DPN, sensory and motor dysfunction occurs and muscle weakness develops, with muscle weakness progressing with the level of neuropathy [1]. Foot strength is particularly diminished in people with diabetes and peripheral neuropathy. Little is known as to whether strength can be altered through targeted exercise in people with diabetes and peripheral neuropathy. This study evaluates the effect of a specific foot strengthening exercise program on foot strength in people with diabetes and peripheral neuropathy.

Methods

A randomized control trial design was conducted to assess change in outcome measures following a 12-week foot strengthening exercise program. 26 participants presented with peripheral neuropathy and were eligible to be randomized to the foot strengthening exercise program (n = 15) or control groups (n = 11). Toe and ankle strength at baseline and after the intervention were measured [2]. A two-way repeated measures analysis of variance design, with one between factor (group: Toe-Training class and control) and one within factor (test session: pre and post), was then conducted to test whether the foot strengthening exercises affected foot strength over time.

Results and Discussion

20 participants returned to the laboratory for retesting (77%; control = 9, intervention = 11). Significant time x group interaction effects were found for both hallux and lesser toe

strength (Figure 1). For hallux strength, there was a decrease in the Control group ($M_{diff} = -0.99$ %BW), but there was a significant increase in hallux strength from pre- to post-intervention testing for the intervention group ($M_{diff} = 1.31$ %BW). Similarly, for lesser toe strength, there was a decrease in strength across time for the Control group ($M_{diff} = -0.87$ %BW), but there was a increase in lesser toe strength from pre- to post-intervention testing for the intervention group ($M_{diff} = 0.32$ %BW). There were no significant interactions for ankle strength (plantarflexion, dorsiflexion, inversion, eversion).

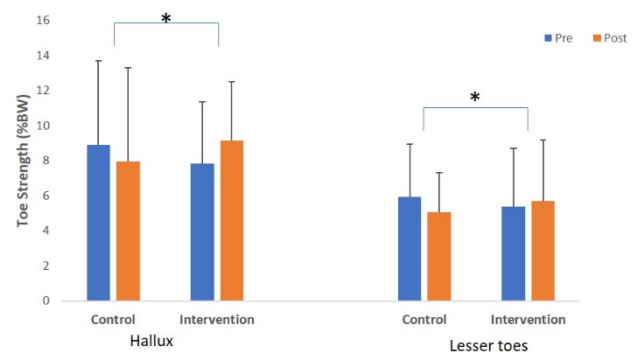


Figure 1: Change in toe strength for the control and intervention groups over the 12 week intervention period (* indicates significant group*time interaction $p \leq 0.05$)

Conclusions

This study has provided good pilot data to show that a foot strengthening exercise program may be suitable for people with diabetic neuropathy. The progressive, supervised 12-week exercise program class was able to increase both hallux and lesser toe flexor strength and minimize loss of foot and ankle strength associated with diabetic neuropathy.

References

- [1] Kirkman MS., et al. (2012). *Diabetes Care*, **35**: 2650-2664.
- [2] Mickle KJ., et al. (2016). *Clin Biomech*, **40**: 14-19.

Accuracy Estimation of a MIMU-based Functional Calibration for Ankle Kinematics Assessment

Paolo Brasiliano¹, Guido Mascia¹, Paolo Di Feo¹, Andrea Cereatti², Camomilla Valentina¹

¹Bioengineering and Neuromechanics of Movement, University of Rome Foro Italico, Rome, Italy

²Department of Electronics and Telecommunications, Polytechnic of Turin, Turin, Italy

Summary

Ankle kinematics was estimated from magneto-inertial measurement units (MIMU) data, devising an *ad hoc* functional calibration procedure. Intra/inter operator repeatability was tested to be in the range of 1 and 2 deg, respectively. The accuracy of the method, obtained as comparison with stereophotogrammetric data, showed high waveforms' shape similarity, even though with variable and ample posture angles disagreement, calling for further studies.

Introduction

In-field assessment of ankle joint kinematics is relevant in several different applicative settings. It can be obtained by positioning two MIMUs on shank and foot segments, estimating MIMU orientation in a common global coordinate system and then orienting them according to the anatomy of the relevant segment. To this aim, typically for the knee joint, functional calibration approaches are used that reconstruct selected anatomical axes starting from the direction of the average angular velocity vector measured during *ad-hoc* passive or active movements of a segment about two of its anatomical axes. However, this approach has not been applied to the ankle joint, possibly due to its complex functional anatomy and smaller range of motion. The aim of this study is to develop a MIMU-based functional calibration approach for the ankle joint which combines a functional and a reference pose imposition approach. The procedure inter and intra-operator repeatability and its accuracy, as a comparison to stereophotogrammetric gold standard measures, were also assessed during walking.

Methods

The functional calibration entails determining foot and tibia anatomical frames (AFs) using as key axes (Fig. 1): *i.* the plantar-dorsiflexion (PD) axis obtained through a passive functional movement (a_f); *ii.* the gravity direction when the subject is in orthostatic posture (shank vertical axis, a_v); *iii.* by aligning the foot to a wooden plate equipped with a MIMU (foot long axis, a_l). Determining a_v and a_l required the subject to be in orthostatic posture for a few seconds. The sequence to achieve foot and shank AFs is depicted in Figure 1.

Four healthy subjects (1F, 3M; age = 26.8 ± 3.2 years; mass = 69 ± 13 kg; height = 1.8 ± 0.1 m) were recruited. Candidates wore 2 MIMUs (Trident, Vicon, UK, @1200 samples/s), each attached to a plate equipped with retro-reflective markers captured by a 7-camera optoelectronic system (Vero/Bonita, Vicon, UK, @100 sample/s). A total of 3 operators performed 3 times the calibration procedure

performing 10 passive PDs, to estimate the PD functional axis (a_f) as the mean positive angular velocity vector. Three orthostatic posture measurements were performed. Each subject performed 3 linear gaits at chosen velocity. Ankle kinematics was computed according to ISB-recommendations [1]. Intra and inter-operator repeatability was quantified in terms of root mean squared distance between curves ($RMSD_{rep}$); $RMSD_{acc}$ and r correlation coefficient between MIMU- and optoelectronic-based kinematics were used to assess accuracy. Accuracy was computed for the posture angles and, after aligning the AFs to the same posture, for the task.

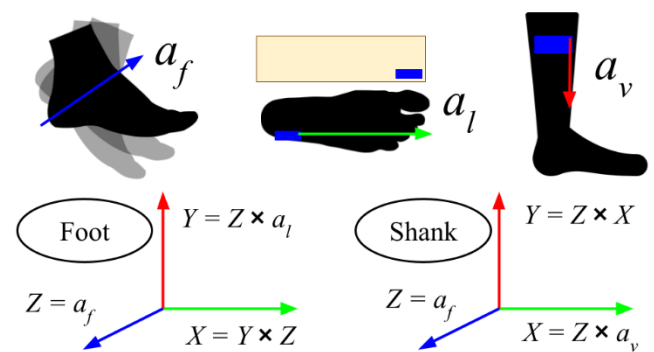


Figure 1: AFs definition for foot and shank.

Results and Discussion

Results relative to level walking PD angles revealed a good intra and inter-operators $RMSD_{rep}$ (0.8 ± 0.4 and 1.7 ± 1.0 deg, respectively). $RMSD_{acc}$ was of 8.5 ± 5.9 deg for upright posture and 4.3 ± 1.4 deg for walking, with r correlation coefficient of 0.94 ± 0.05 . Although $RMSD_{acc}$ values indicate the presence of an offset between the curves that may be related to different procedures to obtain a_v when using MIMUs or stereophotogrammetry, high r correlation coefficient suggests good waveforms' shape similarity.

Conclusions

The proposed functional methodology led to a repeatable estimation of lower limb kinematics. Inter/intra-operator repeatability were in line with those obtained with former anatomical calibration procedures [2] and denote it as promising approach for applied research. Discrepancies relative to the accuracy estimated here and elsewhere [2] may be attributed both to differences in calibration procedures and to different procedures to calculate the RMSD.

References

- [1] Wu G et al. (2002). *J Biomech*, **35**: 543-548.
- [2] Picerno P et al. (2008). *Gait Posture*, **28**: 588-595.

The energetic function of the human foot and its muscles during rapid accelerations and decelerations

Ross Smith¹, Glen Lichtwark¹, Luke Kelly¹

¹School of Human Movement and Nutrition Sciences, University of Queensland, Queensland, Australia

Summary

While growing literature has detailed the foot's energetic capacity during steady-state locomotion, its energetic capacity during accelerations and decelerations is unknown. Here we examined the foot and its intrinsic muscles' energetic contributions to non-steady state tasks with increasing work demands.

Introduction

When accelerating or decelerating, energetic demands at the centre of mass are met by generation (positive work) or dissipation (negative work) of energy of lower body joints like the hip, knee, and ankle. A recent study showed the foot and its intrinsic muscles also make energetic contributions to the centre of mass during stepping tasks [1]. However, the work magnitudes used in this study were small, and the force capacity of the small intrinsic foot muscles is likely limited. Therefore, we investigated the capacity for the foot to generate energy across a range of jumping heights, and dissipate energy over a range of landing heights. We hypothesized that the foot's net-work magnitudes would increase for both tasks (e.g. more negative foot work when landing from higher height) as work demands increased. We also compared normal task performance to a condition where recruitment of the intrinsic foot muscles was blocked, and further hypothesized that less net foot work would be performed at each height for each task in the blocked condition.

Methods

11 participants performed unilateral, submaximal jump trials onto three box heights and drop landings from three box heights (see Fig. 1). Then, a tibial nerve block was administered to participants' dominant leg to block recruitment of the intrinsic foot muscles. The task protocol was repeated. All tasks for both conditions were performed in a randomized manner. For all trials, motion capture (Oqus, Sweden) and force plate (AMTI, USA) data were collected at 250 and 2500 Hz, respectively. From motion data, inverse kinematics were calculated using a hip, knee, ankle, and foot chain. Kinematic data were combined with force data to calculate inverse dynamics (Visual 3D, USA). A unified-deformable foot model [2] was used to quantify the whole foot's (including soft tissue) energetic contributions from all structures distal to the calcaneus.

A 2 x 2 (Height x Condition) repeated-measures ANOVA was performed in order to assess the effects of the nerve block on task performance as work demands increased.

Results and Discussion

Negative foot work increased as landing height increased ($p=0.001$) but remained constant in relation to COM work ($p=0.288$). The nerve block resulted in a decrease in negative work performed by the foot during landing ($p=0.015$) and ~3% reduction relative to COM work ($p=0.02$). Positive foot work increased with increasing jump height ($p=0.004$)

without any changes in foot contributions to COM work ($p=0.102$). Also, the nerve block resulted in decreased positive foot work during jumping ($p=0.001$) and ~3% reduction in relation to COM work ($p=0.001$). The foot still played a large energetic role in both jumping (10% net positive COM work) and landing (12% net negative COM work) without the intrinsic foot muscles, which indicate the extrinsic foot muscles, which our nerve block did not affect, play a large role in the foot's energetic function. Also, our study highlights the importance of soft tissues like the plantar fat pads in energy dissipation when decelerating.

For jumping and landing in the blocked condition, relative ankle contributions to COM work decreased compared to normal conditions ($p=0.010$, $p=0.002$). This finding is consistent with previous literature employing a similar nerve block during running [3]. Previous authors have suggested the intrinsic foot muscles may act to control the centre of pressure, influencing to the ankle plantar flexors' external moment arm [4]. Through this mechanism, the reductions in ankle contributions observed in our data may stem from the intrinsic foot muscle block, but this remains speculative.

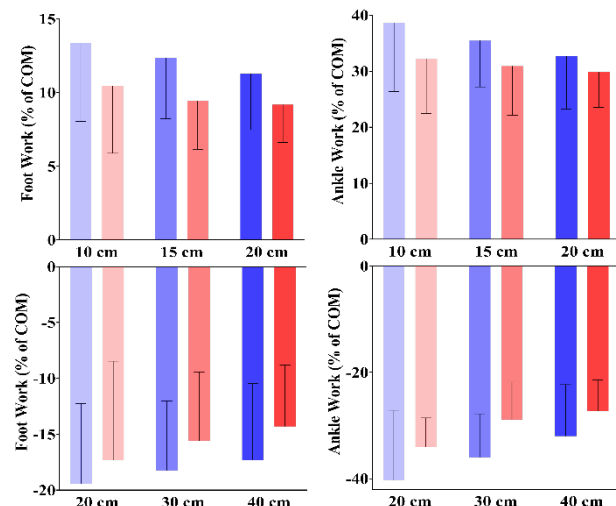


Figure 1. Group mean foot and ankle work values in relation to the COM work for jumps (top row) and landings (bottom row) at all heights. Blue bars are normal conditions, red bars are blocked.

Conclusions

While blocking recruitment of intrinsic foot muscles had small effects on net work contributions, their role in affecting proximal ankle work contributions may warrant further investigation.

Acknowledgements

This work was funded by an Australian Research Council Linkage Grant (LP160101316).

References

- [1] Riddick, R et al. (2018). *J. R. Soc. Interface*, **8**: 1-6.
- [2] Takahashi, K et al. (2012). *J. Biomech.*, **45**: 2662-67.
- [3] Farris, DJ et al. (2019). *P. Natl. A. Sci.*, **116**: 1645-50.
- [4] Kelly, et al. (2015). *J. R. Soc. Interface*, **12**: 20141076.

WAVE PROPAGATION IN MUSCLES PREDICTED BY A HILL-TYPE MODEL WITH DISTRIBUTED MASS

Jianqiao Guo¹, Yang Sun², Ligang Cui², Gexue Ren³, Qiang Tian¹

¹ MOE Key Laboratory of Dynamics and Control of Flight Vehicle, School of Aerospace Engineering, Beijing Institute of Technology, Beijing, China

² Department of Ultrasound, Peking University Third Hospital, Beijing, China

³ Department of Engineering Mechanics, Tsinghua University, Beijing, China

Email: iamguojq@163.com

Summary

Elastic wave propagation in skeletal muscles is essential in supersonic shear imaging and noninvasive therapies. This study examines the viability of using a Hill-type muscle model with distributed mass to simulate the shear wave propagation. A skeletal muscle with fixed ends is discretized by the proposed muscle element, and its wave propagation is initialized by the impact of a rigid ball. Numerical results of the shear wave velocity are validated by comparison with theoretical derivations, highlighting its use in the biodynamic analysis of musculoskeletal systems under large and impulsive loadings.

Introduction

Elastic wave propagation within human muscles is crucial for dealing with musculoskeletal disorders. For example, it is the basis of sonoelastography and extracorporeal shock wave therapy. Unfortunately, assessing *in vivo* wave propagation in muscles during active contractions remains challenging. Musculoskeletal models provide a systematic pathway to deal with the muscle contractile force, whereas conventional Hill-type muscle models do not account for the muscular mass. Günther et al. [1] have proposed contractile muscle models with inertial mass distribution. However, these models remain difficult to be utilized in large-scale models. Recently, we developed a novel muscle-tendon model based on a flexible multibody dynamics approach [2,3], which simultaneously takes the muscular mass and the Hill-type contractile element into account. The purpose of the current study was to investigate its potential for simulating elastic wave propagation based on a computational benchmark.

Methods

The skeletal muscle is discretized by the previously proposed flexible cable element [2,3]. Each end of this muscle is fixed to the ground by a spherical joint. The muscle geometry is idealized as a cylinder with a height of 1m, and other modeling parameters are taken from the rectus femoris within the OpenSim gait2392 model.

At the beginning of shock, a rigid ball of 0.1kg impacts the center node with a speed of 20m/s. After that, the muscle simultaneously produces the longitudinal wave and the shear horizontal (SH) wave at the middle node, and then these two waves spread to both ends. Numerical results of the SH wave velocity are compared with the analytical solution based on continuum mechanic theory.

Results and Discussion

As shown in Figure 1, the longitudinal wave travels back and forth until the muscle stress stabilizes. The more refined the mesh, the more longitudinal waves interact with each other at the same time. The first SH wave is reflected by the ground to form a higher stress peak. Simulation accuracy of the SH wave velocity is negatively correlated with muscle activation level a^{mus} because the contact duration cannot be ignored at low-level muscle contractions. Consequently, the root-mean-square error is decreased from 6.65% at minimal activation ($a^{\text{mus}} = 0.015$) to 3.96% at maximal activation.

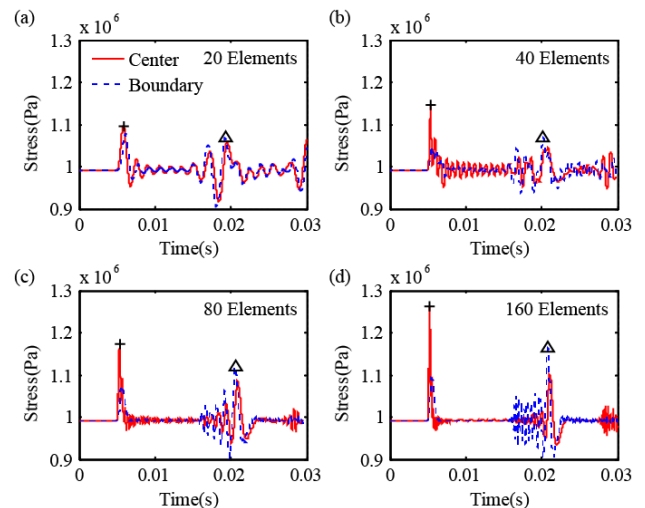


Figure 1: Muscle stress at maximal activation.

Conclusions

The present study demonstrates that the Hill-type flexible cable with distributed mass successfully captures the elastic wave propagation behavior, suggesting its potential use in large-scale musculoskeletal models under impulse loadings.

Acknowledgments

This work was supported in part by the China Postdoctoral Science Foundation under Grant 2020TQ0042.

References

- [1] Günther M et al. (2012). *Comput. Math. Method Med.*, **848**: 630.
- [2] Guo JQ et al. (2020). *Multibody Syst Dyn.*, **49**: 315–336.
- [3] Guo JQ et al. (2020). *Biomech. Model. Mechanobiol.*, **19**: 911–926.

Accounting for vessel holes in finite element models of the femur affects strain prediction

Joeri Kok¹, Karin Odin¹, Sofia Rokkones¹, Lorenzo Grassi¹, Hanna Isaksson^{1,2}

¹Biomedical Engineering, Lund University, Sweden; ²Orthopedics, Clinical Sciences, Lund University, Sweden
Email: Joeri.kok@bme.lth.se

Summary

Micro-CT (μ CT) images of cadaveric femora, previously used for mechanical testing [1], were used to create finite element models. The models include vessel holes in the cortex of the lateral neck. Strains were compared to the experimental data (fracture line and surface strains [1]). The detailed models reveal strain concentrations surrounding vessel holes that affect the femur's fracture behavior.

Introduction

Finite element (FE) models for prediction of the mechanical behavior of femora under sideways fall loading are becoming more and more accurate. Recently, bilateral digital image correlation (DIC) has been used to show strain concentrations surrounding vessel holes [1,2]. These strain concentrations could lead to fracture of the femur but are currently not captured by organ level FE models of the femur. The aim of this study was to more accurately predict surface strains and fracture locations in the femoral neck by including vessel holes in finite element models of the femur.

Methods

In a previous study, 12 female cadaveric femora (age 22-88) were mechanically loaded under simulated sideways fall until macroscopic fracture occurred [1]. Strains were measured in the medial and lateral femoral neck using DIC. μ CT images including hydroxyapatite calibration phantoms were taken before (isotropic voxel size of 52-60 μ m, 100 kVp, 0.2 mA) and after the mechanical testing experiment (isotropic voxel size of 60 μ m, 65 kVp, 0.13 mA). The images of the fractured bones were used to accurately determine the fracture line.

Linear elastic FE models of the proximal femur replicating the experiment were created (Figure 1A). The complete proximal femur was segmented from 8x downsampled μ CT images of the intact femur. The lateral neck was segmented from the full resolution μ CT images. From the segmentations a mesh was created with high detail in the lateral neck (element size \sim 0.25 mm) and lower detail in the rest of the femur (element size \sim 3 mm) (Figure 1B). The elements in the lateral neck were assigned a Young's modulus based on the mineral density obtained from the calibrated μ CT images. For the remaining elements, clinical calibrated CT images were used to assign Young's moduli. The applied load was set to 90% of the experimental peak force. Strains predicted by the high-resolution FE models were compared to the strains measured by DIC and the resulting fracture line.

Results and Discussion

Preliminary results from one subject show that the resulting fracture line goes through some of the larger vessel holes in the lateral neck (Figure 1C). From the high-resolution FE

model we can also see strain concentrations surrounding these vessel holes (Figure 1D). A comparison between the strains predicted by the FE model and the strains measured with DIC reveals similarities in strains surrounding a large vessel hole (Figure 2). Due to the higher spatial resolution of the FE model the high strains are limited to a smaller area and some smaller regions with high strains are revealed that are not captured by the DIC measurements.

Models of the remaining 11 femora are being created to confirm these preliminary findings.

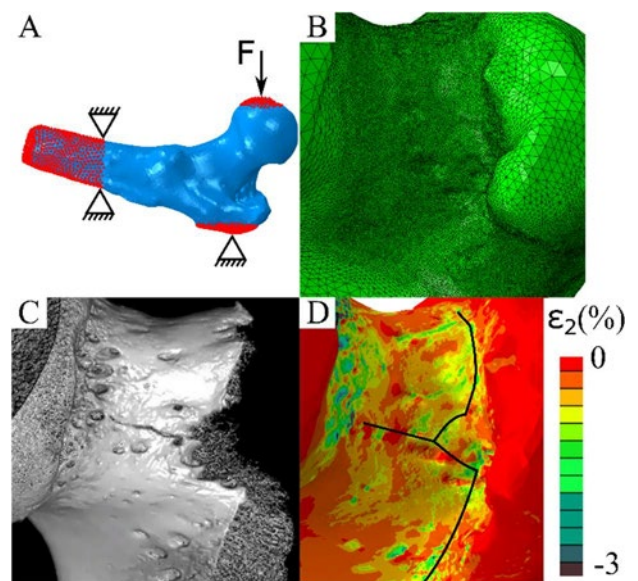


Figure 1: A) FE model with boundary conditions. B) Mesh in the lateral neck. C) μ CT of the fractured femur. D) Strain in the lateral neck with experimental fracture line indicated in black.

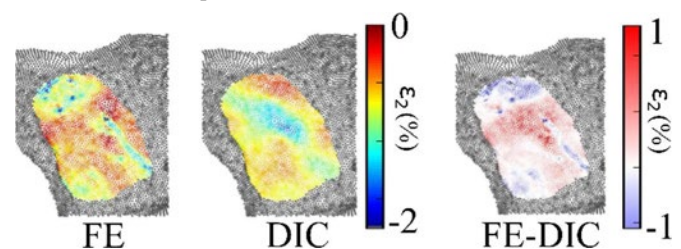


Figure 2: A comparison between strains predicted by the high-resolution FE model and strains measured with DIC.

Acknowledgments

Funding from the Swedish Research Council (2015-4795), the Birgit and Hellmuth Hertz' Foundation, and the Marie Skłodowska-Curie grant agreement No. 713645.

References

- [1] Grassi L. et al. (2020). *JBiomech.*, **106**:109826
- [2] Katz Y and Yosibash Z (2020). *JBiomech.*, **101**:109599

A model of muscle mechanics elicits the important role of increased baseline tone in joint hyper-resistance in cerebral palsy

Jente Willaert¹, Kaat Desloovere², Anja Van Campenhout³, Lena Ting⁴, Friedl De Groot¹

¹Department of Movement Sciences, KU Leuven, Belgium; ²Department of Rehabilitation Sciences, KU Leuven, Belgium;

³Department of Development and Regeneration, KU Leuven, Belgium; ⁴Neuromechanics Lab, Emory University & Georgia

Institute of Technology, USA

Email: jente.willaert@kuleuven.be

Summary

We propose a neuromechanical model based on a detailed model of muscle mechanics to identify neural and non-neural contributions to joint hyper-resistance as observed during the pendulum test in children with spastic cerebral palsy (CP).

Introduction

The pendulum test is a clinical test for measuring joint hyper-resistance. To perform this test, the examiner drops the lower leg of a seated and relaxed patient from the horizontal position [1]. The knee angle trajectory is recorded while the lower leg swings freely under the influence of gravity. With increasing levels of spasticity, as measured with the Modified Ashworth Scale (MAS), first swing excursion (FSE) decreases [1]. Yet there is large variability in FSE between children with the same MAS scores [1] (Fig. 1a), which might be caused by different neural contributions, i.e. hyperreflexia and muscle tone, and non-neural contributions, i.e. altered mechanical tissue properties, to joint hyper-resistance [2]. However, distinguishing these contributions based on clinical tests alone is challenging. Here, we propose a neuromechanical model to identify these different contributions. We previously demonstrated that modeling the interaction between short-range stiffness (SRS), a movement history-dependent increase in force upon stretch, and muscle tone was essential to capture the reduced FSE [3]. Yet our torque-driven model failed to explain fine details of experimental kinematics. We therefore modeled muscles by an extended Hill-type model that accounted for SRS. To test whether a muscle-driven model can explain the large variability in pendulum kinematics across typically developing (TD) children and children with spastic CP, we assessed (1) the quality of the fit between measured and simulated kinematics and (2) the differences in parameters between children with CP and TD children.

Methods

We modeled the lower leg as a pendulum actuated by two antagonistic Hill-type muscles extended with SRS. SRS acted in parallel with the contractile element during the first stretch only since SRS disappears with prior movement, and was proportional to muscle tone and muscle stretch up to a critical stretch [4]. We allowed the onset of passive force development to shift to smaller (< 0.1 , increased stiffness) or longer fiber lengths (> 0.1 , decreased stiffness). We estimated baseline tone of both muscles as well as this shift by optimizing the fit between simulated and measured knee angle trajectories for two to four trials from four children.

Results and Discussion

We could fit a wide range of pendulum test kinematics (Fig. 1a) by allowing only three parameters to vary (Fig. 1b). We found higher baseline muscle activations and passive forces in children with CP that had smaller FS excursions (Fig. 1b).

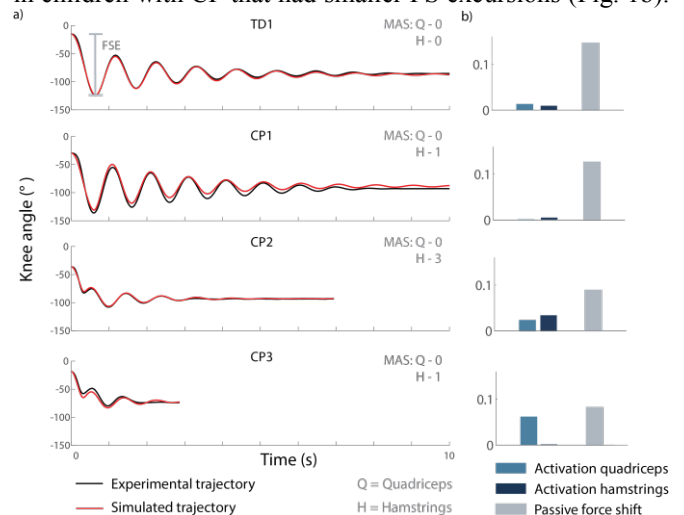


Figure 1: (a) Experimental and simulated pendulum kinematics. (b) Identified model parameters.

Through muscle mechanics, an increase in baseline tone was coupled to an increase in SRS force, muscle stiffness and damping, which captured changes in pendulum kinematics. Accurate models of muscle mechanics might therefore be important to identify contributions of abnormal muscle tone to joint hyper-resistance. We plan to extend our model with reflexes and to validate it by testing whether the identified model parameters capture the effect of pre-movement on pendulum test kinematics. We recently demonstrated that moving the leg prior to releasing it during the pendulum test, which reduced contributions from SRS, increased the FSE and that this increase was larger in children with CP [5].

Conclusions

A detailed model of muscle mechanics elicited the important role of increased muscle tone in joint hyper-resistance.

Acknowledgments

FWO-fellowship 1192320N to Jente Willaert.

References

- [1] Fowler E. et al. (2000). DMCN, 42:182-189. [2] Van der Noort J. et al. (2017). EU J, Neurol, 24(7):981, [3] De Groot F. et al. (2018), Plos One, 13(10). [4] De Groot F. et al. (2017), J. Biomech, 55:71-77. [5] Willaert J. et al. (2020). Front. Bioeng, Biotechnol, 8:920.

A mesh contact model for biomechanical simulations with automatic differentiation

Gil Serrancoli¹, Simone Perelli^{2,3}, Joan C. Monllau^{2,3}

¹Simulation and Movement Analysis Lab, Universitat Politècnica de Catalunya, Barcelona, Catalonia, Spain

²Institut Català de Traumatologia i Medicina de l'Esport (ICATME), Hospital Univ. Dexeus, UAB, Barcelona, Catalonia, Spain

³Department of Orthopaedic Surgery, Hospital del Mar. Universitat Autònoma de Barcelona, Barcelona, Catalonia, Spain

Email: gil.serrancoli@upc.edu

Summary

Estimation of contact forces is crucial for the assessment of a human joint. In this study, we present a contact model designed to work with automatic differentiation tools, recently shown to have sped up the computation of biomechanical simulations. The implemented contact model was applied in a knee pose estimation analysis, leading to both lower computational time and higher accuracy.

Introduction

Biomechanical simulations aimed at estimating or predicting joint contact forces need an efficient contact model to obtain feasible solutions in a short period of time. In musculoskeletal simulations, automatic differentiation (AD) tools have been shown to be computationally efficient [1]. Using AD, simulations with complex musculoskeletal models can be up to 20 times faster than using traditional finite differences (FD). These tools exploit the expression graph of the mathematical expressions to obtain derivatives efficiently. However, contact models based on mesh contacts are not suitable for AD tools, since many *if statements* are required during the computation of contact pairs. In this study, we formulated an elastic foundation contact model to be used with mesh contacts and AD tools. The model was applied to a knee-prosthesis pose estimation analysis.

Methods

The goal of the simulation is to obtain the poses of a tibial tray with respect to a femoral component. Experimental data of knee contact forces and moments and knee kinematics during a gait cycle were obtained from [2]. Before the optimization, the preprocess consisted of choosing the most appropriate mesh refinement and finding the potential pairs of faces to be in contact. The method to automatically calculate the penetration among faces of the mesh during the optimization iterations consists of the following steps: 1) Calculation of distances among potential contact faces (Figure 1); 2) Estimation of the potential penetration distances, similar to [3]; and 3) Identification of the maximum penetration based on a continuous function. After that, contact forces are estimated using the elastic foundation contact model from [4]. Finally, the resultant contact wrench is calculated at the center of the body.

An optimal control problem was formulated to pose the tibial tray as close to the experimental data as possible (cost function) so that the modelled contact forces and moments matched the experimental ones (constraints). The state variables were the six degrees of freedom of the tibial tray and their velocities. Accelerations of the tibial tray and residual

forces and moments were formulated as controls, and minimized in the cost function. The optimal control problem was formulated in CasADi and solved with AD and FD methods.

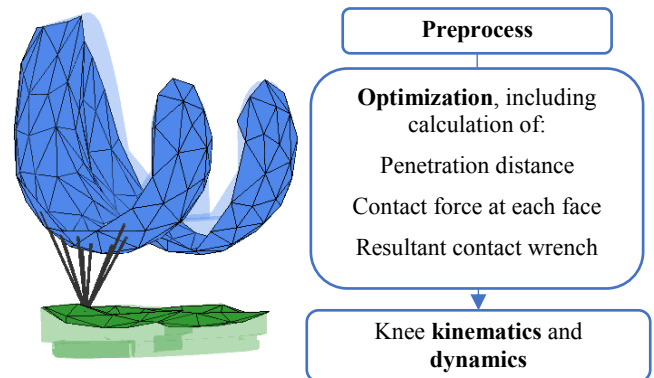


Figure 1. Meshes of the knee prosthesis with an example of potential contacting pairs (left). The process to compute the contact forces within the optimization (right).

Results and Discussion

The optimization found optimal solutions with both AD and FD methods. The results were faster and slightly more accurate using AD tools (Table 1).

Table 1. Results of the optimization for AD and FD.

	iterations	Time (s)	RMSE forces (N)	RMSE moments (Nm)
AD	794	330	14.1 ± 21.3	0.83 ± 0.21
FD	891	563	14.8 ± 18.5	1.15 ± 0.23

Conclusions

The results suggest that this model can be used in musculoskeletal simulations in combination with automatic differentiation tools. The model could be used to estimate joint contact parameters or to predict human movement.

Acknowledgments

G. Serrancoli acknowledges the support from the Serra Hünter Program, and the grant EIN2020-112411 from MICINN.

References

- [1] Falisse A et al. (2019). *PloS One* **14**: e0217730.
- [2] Fregly BJ et al. (2012). *J Orthop Res* **30**: 503-13.
- [3] Smith CR et al. (2018). *Comput Method Biomec* **6**: 491-498.
- [4] Bei Y and Fregly BJ. (2004). *Med Eng Phys* **26**: 777-789.

Geometrical variations of the hind- and mid-foot and their associated functional consequences

Bryce A. Killen¹, Sorin Siegler², Maria Rincon Ruiz², Jos Vander Sloten³, Ilse Jonkers¹

¹Department of Movement Science, ³Department of Mechanical Engineering, KU Leuven, Belgium

²Mechanical Engineering and Mechanics, Drexel University, United States of America

Email: bryce.killen@kuleuven.be

Summary

Using a database of 20 subjects, a statistical shape model (SSM) of the hind- and mid-foot was generated using open-source software. The SSM contained distal tibia-fibula, talus, calcaneus, tarsal, and metatarsal bones. SSM-based reconstructions of these bones, for the mean, and first principal component (PC) variations were subsequently used to generate a musculoskeletal model of the hind- and mid-foot. PC variations, variations in geometry and mechanical function of the models were then established.

Introduction

The ankle-foot is a highly complex structure containing > 20 bones. The complex structure is essential for the function of these joints during dynamic tasks such as walking providing an essential combination of flexibility, stability, and strength. Variations in the shape of any bone and subsequently joints, likely has an impact on the functionality of the ankle-foot. Previous research has applied statistical shape modelling (SSM) methods to assess variations in individual bones [1], and in isolated cases joint geometries [2]. Although providing valuable information, the potential functional impact of these structural variations is rarely considered. Such information could provide valuable information regarding functional interactions between the bones/joints of the hind- and mid-foot. Therefore, the aim of this study was to generate a SSM of the hind- and mid-foot to investigate (1) structural variability in a healthy cohort, and (2) the associated changes in function during simulated stance tasks.

Methods

Segmentations of the distal tibia-fibula, talus, calcaneus, tarsals, and metatarsals were performed from computed tomography (CT) scans of 20 healthy subjects. Due to irregular scan dimensions, tibia-fibula truncations were inconsistent between subjects. A previously validated SSM workflow [3] was used to (1) reconstruct full tibia-fibula bones for each subject, and (2) perform truncation to consistent anatomical regions. All segmentations were smoothed and re-meshed to the same number of vertices and faces (per bone) based on *a-priori* based on the lowest number of faces/vertices where reconstruction error was <1mm. Individual bones, for each subject, were then merged into a single mesh file. An established SSM workflow [4] was used to generate a SSM of the hind- and mid-foot in a three-step process. The first subject was used as a reference mesh, all remaining subject meshes were then morphed, using radial basis functions, to ensure node correspondence between subjects. Second, a rigid body transformation was performed to remove rotational and translational offsets. Finally, principal component (PC) analysis was used to extract the mean shape and statistical variations in geometry from the population. The mean shape model, and PCs were used to

generate bone models at the extremes of PC1 (i.e., ± 2 standard deviation). Mean model, and PC1+2, and PC1-2 bone models were implemented in a dynamic musculoskeletal model [4]. Each model was subjected to cyclic moments between +3.5Nm and -3.5Nm in inversion/eversion. Geometrical properties and load-displacement characteristics were then compared between models.

Results

Comparing morphological differences demonstrate the main differences to be size (PC1-2 < Mean (PC1) < PC1+2) as well as differences in foot type where PC1-2 corresponds to a flat foot, PC1 a normal arched foot and PC1+2 to a high arch foot.

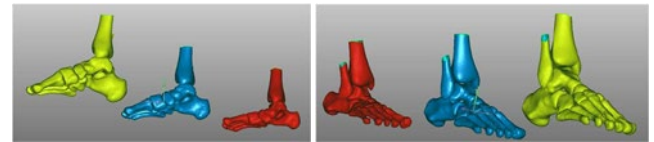


Figure 1: Comparison of bone model morphology of the three models: yellow (PC1+2), blue (Mean), and red (PC1-2).

Load-displacement characteristics in inversion/eversion obtained for each of the dynamic models (Figure 2) produced for mean, PC1+2 and PC1-2 were compared (Figure 3). The results clearly show a significant difference in the mechanical properties where PC1-2 (flatfoot) was the stiffest, followed by PC1 (normal arch), followed by PC1+2 (high arch).

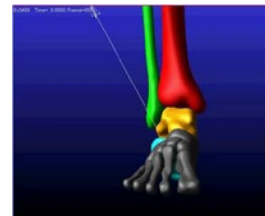


Figure 2: Dynamic model of the foot (shown PC1+2).

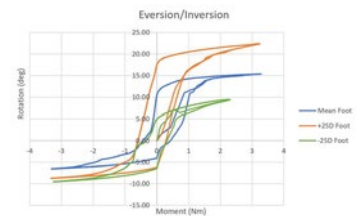


Figure 3: Comparison of the ad-displacement properties of the three models.

Discussion and Conclusions

Variation in the first PC of the SSM model of the foot are associated with variation both in size and foot type i.e., arch height (from flat arch to normal to high arch), these variations also produce significant changes in the mechanical characteristics. These differences may also manifest in other simulated tasks including gait like tasks.

References

- [1] Grant, T. et al. (2020). *PeerJ.*, **8**: e8397
- [2] Krähenbühl, N. et al (2020). *J. Orthop. Res.*, **12**: 2625-33
- [3] Zhang, J. et al (2014). *ISBMS.*, 182-192
- [4] Zhang, J. et al (2016). *Med Eng Phys.*, **38**: 450-7
- [5] Imhauser, C. et al. (2002). *F&A Int.*, **23**: 727-737

Muscle-tendon morphomechanical properties of non-surgically treated Achilles tendon 1-year post-rupture

Ra'ad Khair¹, Lauri Stenroth², Neil J. Cronin^{1,4}, Aleksi Reito³, Juha Paloneva³ and Taija Finni¹.

¹ Faculty of Sport and Health Sciences, University of Jyväskylä, Jyväskylä, Finland

² Department of Applied Physics, University of Eastern Finland, Kuopio, Finland

³ Central Finland Health Care District, Finland,

⁴ Department for Health, University of Bath, UK.

Email: raad.m.khair@jyu.fi

Summary

We investigated the mechanical and morphological properties of Achilles tendon rupture (ATR) in 24 patients as part of a prospective cohort study – NoARC. Ultrasonography and dynamometry were used to assess the muscle-tendon unit properties of non-surgically treated patients 1-year post rupture. Results showed that injured tendons were 13.5% longer and 93.2% thicker. MG-fascicles were 23.8% shorter and 21.7% more pennated in the injured limb. We found no difference in stiffness between the limbs. Inter-limb difference in MVC was moderately correlated with difference in stiffness ($r_s=0.45$, $p=0.026$) and MG-fascicles length ($r_s=0.55$, $p=0.005$). Poor self-evaluated functional outcome was associated with longer AT resting length ($r_s=0.64$, $p=0.004$). Even when stiffness of non-surgically treated tendons was similar to the un-injured, plantar flexion strength deficit was still present likely due to shorter muscle fascicle length.

Introduction

Achilles tendon (AT) rupture appears to impair stiffness and elongation of the AT [1,2]. These deficits may alter the overall function of AT in force transmission and affect the triceps surae muscles. Optimal tendon stiffness is essential for efficient economy and performance of locomotion [3]. Understanding how the mechanical properties of the muscle tendon unit change post-rupture is an important pre-cursor to understanding the recovery process.

Methods

Twenty-four participants (means: 43.2 y, 176.1 cm, 80.9 kg) were treated non-surgically in combination with early mobilization. The Ethics Committee of Central Finland Health Care District approved the study (2U/2018).

MG tendon resting length and AT thickness were measured using a 3.6-cm linear probe (UST-5411; 7.5 MHz, Aloka Alpha, Japan). MG fascicles length and pennation angle were assessed using a 6-cm linear probe (UST-5712; 7.5 MHz). Images were acquired with subjects in prone position with feet relaxed at the end of the table. Patients filled out Achilles tendon rupture score (ATRS) surveys (0-100= no-high impairments) during the 1-year follow up.

Force data were collected at 1 KHz via a transducer in the foot pedal of the ankle dynamometer. During maximal isometric contractions (MVC), displacement of MG muscle-tendon junction was imaged with 6-cm linear probe (UST-

5712; 7.5 MHz) in B mode while calcaneal movement was monitored using potentiometer. Tendon elongation and force were synchronised and fitted to a second order polynomial forced through zero. Tendon stiffness was defined as the slope of the fitted polynomial at 50% of the injured limb MVC. Bilateral differences were tested with t-test and associations with Pearson's correlation.

Results and Discussion

Injured tendons were longer with a mean difference of 2.5 cm (1.5-3.5 cm; $p<0.001$), and thicker 4.4 mm (3.5-5.1 mm; $p<0.001$). MG-fascicles were shorter in the injured limb with a mean difference of 1.1 cm (0.9 -1.4 cm; $p<0.001$) and more pennated 4.5° (2.6-6.4 $^\circ$; $p<0.001$). We did not find statistically significant difference in stiffness 1-year post rupture between injured 413.4 ± 186.6 N/m Vs un-injured 486.5 ± 210.2 N/m. The injured tendon showed lower AT elongation during MVC with a mean difference of 3.5 mm (1.9-5.1 mm, $p<0.001$). MVC difference between n limbs was correlated with difference in stiffness ($r_s=0.45$, $p=0.026$) and MG-fascicle length ($r_s=0.55$, $p=0.005$). ATRS was correlated with difference in AT resting length between limbs ($r_s=0.64$, $p=0.004$).

The persistence of plantar flexor torque deficits, even after stiffness of the tendon was similar to the un-injured, suggest that deficits in force production 1-year post-rupture may be largely due to the shorter length of MG fascicles.

Conclusions

Non-surgically treated tendons seem to heal at an elongated length, accompanied by MG remodeling at a shorter and more pennate fascicle. Tendon elongation seems to be the associated and likely factor leading to the observed objectively measured and self-reported functional disabilities.

Acknowledgments

Academy of Finland grant #323168, UNderstanding REStoration of Achilles Tendon function after rupture (UNRESAT).

References

- [1] Agres et al. (2015). Scand J Med Sci Sports. **25**:860–7.
- [2] Wang et al. (2013). Arch Phys Med Rehabil. **94**:1590–8.
- [3] Lichtwark, Wilson (2007). J Biomech. **40**:1768–75

Cumulative joint damage from repeated mild knee injuries over time

Carina L. Blaker^{1,2}, Ben Ventura^{1*}, Vanessa Lo Basso^{1*}, Cindy Shu², Christopher B Little², Elizabeth C Clarke¹

¹Murray Maxwell Biomechanics Laboratory and ²Raymond Purves Bone and Joint Research Laboratories, Institute of Bone and Joint Research, Kolling Institute, Faculty of Medicine and Health, University of Sydney, Northern Sydney Local Health District, Sydney, NSW, Australia

*Equal contribution

Email: carina.blaker@sydney.edu.au

Summary

The long-term effects of repeated mild joint injuries are an understudied area of research. This mouse model of double mild knee injury events separated by different lengths of time demonstrates cumulative joint pathology and early signs of osteoarthritic change. The greater change observed in injured joints with longer separation times between injuries may have implications for the timing of return to play.

Introduction

Mild knee injuries characterised by contusions and low-grade sprains are common occurrences in sports players [1]. Prior injuries are associated with a higher risk of recurrent injuries [2] but little is known about the cumulative effects of repeated mild injuries over time or the longer-term impacts on joint health and function. A mouse model was used to investigate the effect of single and repeated mild knee injuries on the risk of major injury (anterior cruciate ligament, ACL, rupture) and joint pathology associated with the onset of osteoarthritis.

Methods

Ten-week-old male C57BL/6J mice were randomly assigned to 1 of 4 mild knee injury groups: 1) naïve, no-injury (NI) control; 2) single injury (SI); 3) double injury separated by 2 weeks (DI-2w); 4) double injury separated by 4 weeks (DI-4w). Injury was induced by a single tibial compression load on the right hindlimb of anaesthetised mice. The injured knee was evaluated for changes in ACL biomechanics (tensile test: maximum load and stiffness; n=10/group at 14, 16 or 18 weeks of age) or osteochondral gene regulation in the patella and medial/lateral tibial epiphysis (RT-qPCR: *Acan*, *Coll1A1*, *Col2*, *Mmp-2,-3,-9*, *Timp-1,-3*; n=6/group at 14, 16, 18 or 26 weeks of age). A small subset of animals were assessed at 26 weeks for signs of structural histopathology (n=3/group). Data analysis was performed using mixed model regression for the biomechanical data and Kruskal-Wallis for gene expression.

Results and Discussion

ACL failure load and stiffness were not significantly different between groups, suggesting minimal direct damage to the ACL in this model. ACL stiffness at 18 weeks was significantly lower than earlier time points in all groups ($P \leq 0.008$) except DI-2w ($P \geq 0.759$). It is unclear if the absence of change in DI-2w is related to the timing of the second injury relative to the first injury.

Significant changes in gene expression occurred predominantly in the medial tibial epiphysis and the patella.

In the medial tibial epiphysis, the fold change of *Col2* increased significantly over time in both the SI and DI-2w groups ($P \leq 0.05$). In contrast, *Mmp-3*, *-9* and *Timp1* were significantly upregulated in DI-4w at 26 weeks compared with earlier time points ($P \leq 0.05$). In the patella, *Coll1A1*, *Mmp-2* and *Mmp-3* were significantly downregulated over time in both DI groups ($P \leq 0.05$). At 26 weeks of age, *Mmp-3*, *-9* and *Timp-1* were significantly higher in DI-4w compared with DI-2w ($P \leq 0.05$). These are genes which have been associated with the progression of osteoarthritis.

At 26 weeks all injury groups demonstrated signs of cartilage pathology compared with the smooth surface of NI joints (Figure 1). SI cartilage was roughened; DI-2w cartilage was fibrillated and the lamellar surface lost; DI-4w joints were marked by regions of partial thickness, non-calcified articular cartilage loss and more pronounced focal lesions. These findings suggest that repeated injuries, even when separated by 4 weeks, have cumulative effects on joint tissue integrity.

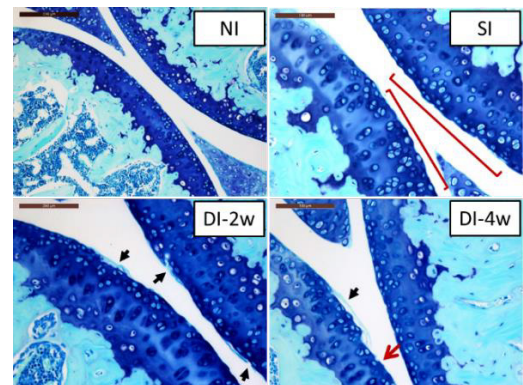


Figure 1: Sagittal toluidine-blue O sections of the knee. NI: smooth joint surface. SI: roughened joint surface (red bars). DI-2w: fibrillated articular cartilage (black arrows). DI-4w: fibrillated (black arrows) and loss of articular cartilage (red arrow).

Conclusions

In this model there was no increased risk of ligament injury following repeated mild knee injuries however, cumulative damage to other joint tissues was evident even when injuries were separated by longer recovery times (4 vs 2 weeks). Gene expression and structural pathology findings resemble indicators of early osteoarthritis which may have implications for treating patients with idiopathic or accelerated disease.

References

- [1] Powell JW et al. (1999). *J Athl Train*, **34**: 277-284.
- [2] Driban JB et al. (2015) *J Rheumatol*, **42**: 1463-1469

Analysis of post-operative osteoblastic activity patterns in unicondylar knee arthroplasties slated for revision

F. Dandois¹, L. Beckers¹, H. Vendenneucker¹, L. Scheys¹

¹Institute for Orthopaedic Research and Training, KU Leuven/University Hospitals Leuven, Belgium

Email: felix.dandois@kuleuven.be

Summary

Clinical evidence is often inconclusive to decide whether or not to revise unicondylar knee arthroplasty. Analysis of post-operative osteoblastic activity has potential to provide additional information to clinically corroborate this decision.

Introduction

Although revision rates of unicondylar knee arthroplasty (UKA) are higher compared to total knee arthroplasty, two-thirds of UKA revisions are performed without clinical evidence other than patient reported pain [1]. Furthermore, the main UKA failure modes leading to revision can be linked to osteoblastic activity which can be quantified with SPECT-CT imaging. Such imaging thus has clear potential to further our understanding of such failures towards reduced revision rates. Therefore, this study aimed to compare post-operative osteoblastic activity patterns in the tibia between successful UKA's and UKA's slated for revision surgery.

Methods

SPECT-CT scans were acquired in 23 patients (Age=61±8 years; BMI=29.23±4.71 kg/m²) with well-functioning medial UKA's at two years post-operatively. Additionally, SPECT-CT scans were also acquired in 10 patients slated for medial UKA revision surgery (Age=42±25 years; BMI=27.90±4.53 kg/m²). For these 10 patients, the interval time between initial UKA and scanning was on average 4.91 years (SD: 4.77, range: 0.96-13.96).

Using validated SCReg platform [2], spatial voxel-to-voxel correspondences were obtained between all SPECT-CT scans through a registration scheme. Osteoblastic activity was normalized according to activity in distal femur. Then, a statistical map was created by performing a Mann-Whitney U test on each voxel to compare successful UKA's and UKA's slated for revision. Finally, for each group, an aggregate map was created by averaging, for each voxel, normalized osteoblastic activity values over all specimens of the group.

Results and Discussion

Main areas with significantly different normalized osteoblastic activity (p<0.05) were located on (1) the lateral

tibial plateau, (2) the antero-medial cortex at implant level and (3) the lateral femoral epicondyle (Figure 1). For all these regions, increased activity was observed in the UKA's slated for revision (Table 1).

Significantly higher normalized activity on the antero-medial cortex of the tibia was expected as that region is known to be directly involved in two primary modes of UKA failures, i.e. tibial loosening and anterior tibial pain. Concerning the observed differences in the lateral femoral and tibial compartment, we hypothesize this to be related to lateral osteoarthritis progression as another common mode of UKA failure. Finally, the fact that this study cohort included different UKA designs should be noted as a limitation.

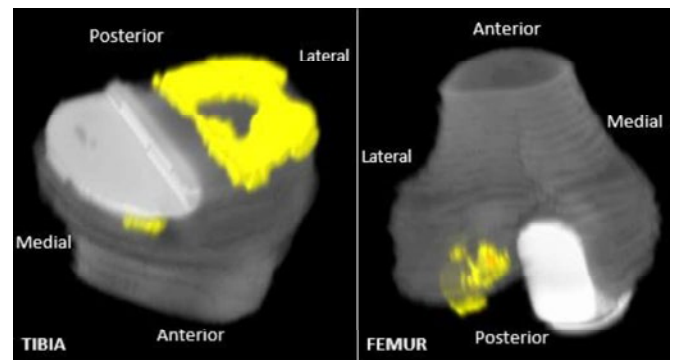


Figure 1: Location of voxels significantly different between successful UKA's and UKA's slated for revision in terms of post-operative normalized osteoblastic activity

Conclusions

Analysis of post-operative normalized osteoblastic activity using SPECT-CT imaging has diagnostic potential to confirm or infirm UKA revision surgery by elucidating failure mechanisms.

Acknowledgments

This study was partially funded by Zimmer-Biomet.

References

- [1] Kennedy JA et al. (2020). *KSSTA*, **28**: 3926-3934.
- [2] Dandois F et al. (2020). *BMC Musculoskelet Disord*, **21**

Table 1: Number of voxels significantly different (S.D.) and associated activity in aggregate maps.

	Number of voxels with S.D. in lateral tibial plateau	Normalized activity in lateral tibial plateau (mean±std)	Number of voxels with S.D. in antero-medial tibia	Normalized activity in antero-medial tibia (mean±std)	Number of voxels with S.D. in lateral femoral epicondyle	Normalized activity in lateral femoral epicondyle (mean±std)
Slated for revision	2448	2.46±0.40	452 (1293mm ³)	3.07±0.75	962 (2752mm ³)	2.30±0.25
Successful	(7044mm ³)	1.50±0.22		1.73±0.50		1.54±0.16

Influence of Implant Alignment on Joint Laxity following Medially-Stabilized Total Knee Arthroplasty

Orcun Taylan¹, Darshan Shah¹, Felix Dandois¹, Philippe van Overschelde², Lennart Scheys¹

¹Institute for Orthopaedic Research and Training, Department of Development and Regeneration, KU Leuven/University Hospitals Leuven, Belgium ²Kneeclinic.be, Sint-Martens-Latem, Belgium

Email: orcun.taylan@kuleuven.be

Summary

Patient satisfaction following total knee arthroplasty relies heavily on postoperative joint laxity, which is known to be influenced by intraoperative implant alignment. This cadaveric study aimed to quantify the influence of such implant alignment parameters on the postoperative knee laxity by performing abduction-adduction stress tests on cadaveric knees. A stepwise multivariate regression analysis indicated that while valgus laxity was influenced by all considered component alignment parameters, varus laxity was influenced only by component alignment in the frontal plane. The impact of individual alignment parameters on postoperative joint laxity revealed by this study could inform intraoperative decisions and related biomechanical outcomes.

Introduction

Postoperative patient satisfaction and biomechanical outcomes following total knee arthroplasty (TKA) are heavily dependent on intraoperative implant positioning [1]. Although novel techniques (e.g. kinematic alignment) and surgical tools (e.g. robotic-assisted surgery) specifically target improved component alignment [2], the influence of alignment parameters on biomechanical outcomes has not been studied to satisfactory depths. Therefore, this experimental study aimed at quantifying the biomechanical impact of several implant alignment parameters on postoperative joint laxity.

Methods

Computed tomography (CT) was performed on 14 fresh-frozen cadaveric legs (KU Leuven, Belgium, NH019 2018-11-01) in their native condition, and after performing medially-stabilised TKA (GMK Sphere, Medacta International, Castel San Pietro, Switzerland). Specimens were then mounted on a custom jig whereby the hip was rigidly fixed while the knee was subjected to abduction-adduction stress tests at fixed knee flexion angles (0°, 30°, 60°, 90°). Varus-valgus moments of 10 Nm were generated at the knee by applying controlled tensile loads at the ankle using a handheld digital dynamometer (Mark-10, Copiague, USA). A six-camera optical motion capture system (Vicon Motion Systems, Oxford, UK) was used to track the trajectories of retroreflective marker clusters attached rigidly to the femur and tibia, and compute corresponding tibiofemoral kinematics based on pre-defined anatomical landmarks [3].

3-Matic (Materialise, Leuven, Belgium) was used to measure specimen-specific implant alignment parameters from the available CT-data in terms of hip-knee-ankle angle (HKA), femoral valgus (FV) and tibial varus (TV) in the frontal plane, and tibial slope (TS) in the sagittal plane. Subsequently, a

stepwise multivariate regression model with backward elimination was performed with alignment parameters as independent variables (input) and joint angles as the dependent variables (output), to quantify the influence of component alignment on tibiofemoral kinematics during the varus-valgus stress tests. The Akaike information criterion (AIC) was used for statistical evaluation of parameter weighting.

Results and Discussion

Post-operative valgus joint laxity was influenced by all considered implant alignment parameters ($p < 0.001$), with TS having the largest impact based on AIC. In contrast, varus joint laxity was influenced only by FV and TV ($p = 0.002$), with the latter having a bigger impact.

Despite standardised intraoperative guidelines for implant sizing and alignment, often based on patient-specific instrumentation, surgeons also rely on experience-based intraoperative evaluation of the joint for subjective deviations from surgical plans. The impact of resulting individual alignment parameters on postoperative joint laxity revealed by this study could further inform such subjective intraoperative decisions, which would directly impact biomechanical outcomes following TKA.

	HKA	FV	TV	TS
Valgus laxity	0.93	-1.16	0.25	0.45
Varus laxity	-	-0.2	0.15	-

Table 1: Regression coefficients of various implant alignment parameters (inputs) for joint angles during varus-valgus laxity tests (outputs) calculated using stepwise multivariate regression analysis with backward elimination.

Conclusions

The positioning of implant components influences postoperative joint laxity following TKA, with certain alignment parameters more vital than others in terms of biomechanical impact. This should be especially considered for intraoperative alterations to patient-specific surgical plans.

Acknowledgments

This study was funded by Medacta International, Castel San Pietro, Switzerland.

References

- [1] Arnholdt J et al. (2020). *BMC Musculoskelet Disord*, **21**: 1-8.
- [2] Rivière, C et al. (2017) *OTSR*, **103**: 1047-1056.
- [3] Grood ES et al (1983). *J Biomech Eng*, **105**: 136-144.

Dynamic knee loading in the ACL deficient knee

Georgios Giarmatzis^{1,2}, Christos Kokkotis², Dimitrios Tsaopoulos², Konstantinos Moustakas^{2,1}

¹ Visual and Virtual Reality Group, Electrical and Computer Engineering Department, University of Patras, Greece

² Centre for Research and Technology-Hellas CERTH, IBO Institute, Greece

Email: giorgos.giarmatzis@gmail.com

Summary

The role of ACL on the pressure distribution at the knee cartilage during walking is still unclear. The current study showed that loss of ACL changes knee kinetics, resulting in higher pressure than normal at the medial side. Such findings shed light on post-traumatic knee loading conditions.

Introduction

Understanding how the anterior cruciate ligament (ACL) influences the pressure distribution of the knee during daily activities is crucial for addressing the problem of osteoarthritis onset and progression. Maximum pressure suffered by the knee cartilage during dynamic activities is thought to be the key determinant of local matrix failure [1]. This study aims to explore inherent dynamics and pressure distributions in the ACL deficient (ACLd) knee during walking and compare with the healthy side using knee-specific motion.

Methods

Patient cohort included nine participants who sustained an ACL rupture. Knee kinematics and kinetics were calculated during overground walking at self-selected speed for both healthy and ACLd knees, by means of motion capture and musculoskeletal modeling [2]. Medial knee contact pressures were calculated during stance phase for both sides. Muscle activations and knee kinematics were computed using the concurrent optimization of muscle activations and kinematics algorithm [2]. Mean maximum knee contact pressures (max KCP) were calculated and interpolated to 100 points across subjects and gait cycles for both healthy and ACLd knee. Wilcoxon signed rank tests were used to identify significant differences between the two knees across subjects for peak maximum KCP, medial vertical force and tibiofemoral contact area, along with anterior displacement, during the first and second half of the stance phase.

Results and Discussion

Average curves of medial max KCPs show a double peak profile for both healthy and ACLd knee (Figure 1). Higher variability seen in the ACLd knee compared to the healthy contralateral might indicate a rather highly variable post-

traumatic adaptive strategy for the inflicted side. Max KCPs in the ACLd knee were statistically higher (Table 1) than contralateral only during first peak of stance phase. This effect seems to be the result of higher medial vertical forces and smaller contact area estimated during the first half of the stance for the ACLd knee compared to the healthy side. The latter may be attributed in the excessive anterior translation of the tibia in respect to femur, leading to less available area for contact in the medial cartilage cup.

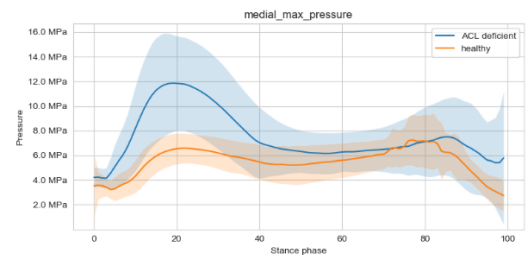


Figure 1: Knee medial max pressure in the healthy and ACL deficient knee along the stance phase of walking.

Conclusions

Loss of ACL can trigger gait alterations and lead to overloading of knee structures, possibly at the expense of local homeostasis. Larger max KCPs in the ACLd knee found in this study can be associated to high prevalence of knee osteoarthritis seen in this patient group. Current findings provide clinically relevant information regarding the effects of ACL deficiency on gait parameters.

Acknowledgments

This research has been co-financed by the European Regional Development Fund and Greek national funds (project code: T1EDK-04234).

References

- [1] K Montagne, Y Onuma, Y Ito, Y Aiki, K S Furukawa, and T Ushida *PLoS One* **12** 1 (2017).
- [2] C R Smith, K Won Choi, D Negrut, and D G Thelen *Comput. Methods Biomech. Biomed. Eng. Imaging Vis.* **6** 491 (2018).

Table 1: Maximum values during first (First Peak) and second (Second Peak) half of stance phase. Data are depicted as mean (SD) values. Asterisks denote statistically significant differences between healthy and ACLd knees for each peak

	First Peak		Second Peak	
	Healthy	ACLd	Healthy	ACLd
Vertical Force (xBW)	1.83 (0.54)	2.28 (0.42)*	2.51 (1.42)	1.82 (0.77)
Contact Area (cm ²)	3.55 (0.44)	3.19 (0.34)	4.03 (0.84)	3.49 (0.48)
Tibiofemoral Anterior translation (mm)	8.79 (1.61)	31.98 (8.49)*	9.59 (9.69)	22.21 (10.75)
Maximum pressure (MPa)	7.27 (2.01)	12.3 (3.91)*	8.13 (2.6)	8.91 (4.37)

In vivo mechanoreponse of articular cartilage before and after load modifying surgery in patients with medial compartment knee osteoarthritis

Annegret Mündermann^{1,2,3,4}, Corina Nüesch^{1,2,3,4}, Simon Herger^{1,3}, Anna-Maria Liphardt⁵, Christian Egloff^{1,3,4}

¹Department of Orthopaedics and Traumatology and ²Department of Spine Surgery, University Hospital Basel; ³Department of Biomedical Engineering and ⁴Department of Clinical Research, University of Basel, all Basel, Switzerland; ⁵Department of Internal Med. 3 – Rheumatology and Immunology, Friedrich-Alexander-University Erlangen-Nuremberg (FAU), Universitätsklinikum Erlangen, Erlangen, Germany; Email: annegret.muendermann@unibas.ch

Summary

In a walking stress test that may be suitable for assessing the acute mechanoreponse to interventions in patients with knee OA we observed that specific blood markers for articular cartilage (i.e. COMP, MMP-3, MMP-9 and resistin) consistently responded to an ambulatory load stimulus while other blood markers did not (i.e. MMP-1, C2C, CII, C2C/CPII, PRG-4, ADAMTS-4). The observed mechanoreponse was exaggerated after load modifying surgery for COMP but remained unaltered for all other markers.

Introduction

Ambulatory load plays an important role in the initiation and progression of knee osteoarthritis (OA) [1]. High tibial osteotomy (HTO) is a joint preserving surgery aimed at modifying the load distribution at the knee with the goal of slowing the rate of knee OA progression. The response of articular cartilage to ambulatory load can be measured as acute changes in blood biomarkers of articular cartilage [2]. The aim of this study was to determine if load-induced changes in blood markers of articular cartilage change after load modifying surgery in patients with medial compartment knee OA.

Methods

Seventeen patients with medial compartment knee OA (12 male; median [interquartile range], age: 44 [36–51] years; body mass: 85.0 [74.0–97.2] kg; height: 1.75 [1.63–1.80] m; body mass index: 29.4 [24.1–31.1] kg/m²) completed a walking stress test with blood sampling (30 minutes walking, 5.5 hours sitting) before and 8-months after HTO. Blood samples were taken after 30 minutes of rest immediately before (t₀) and 0h (t₁), 0.5h (t₂), 1.5h (t₃), 3.5h (t₄) and 5.5h (t₅) after the walking stress and analyzed using enzyme-linked immunosorbent assays for cartilage oligomeric matrix protein (COMP), matrix metalloproteinases (MMP)-1, -3, and -9, epitope resulting from cleavage of type II collagen by collagenases (C2C), type II procollagen (CPII), interleukin (IL)-6, proteoglycan (PRG)-4, A disintegrin and metalloproteinase with thrombospondin motifs (ADAMTS)-4 and resistin. We used a non-parametric test (Wilcoxon signed rank test) that does not rely on assumptions of absence of outliers and normality of the data (P<0.05).

Results and Discussion

COMP at t₀ and t₁ (Fig 1) and IL-6 levels at t₀, t₁ and t₃ were higher postoperatively than preoperatively. For all other

markers and time points, levels did not differ between baseline and 8-month follow-up. Compared to t₀ levels, COMP and MMP-3 levels were significantly different at t₁, t₃, t₄ and t₅, and MMP-9 and resistin levels were significantly lower at t₃ and t₅. Inconsistent mechanoreponses were observed for all other blood markers. The decreases in COMP from t₁ to t₂, t₃, and t₅ were significantly greater postoperatively than preoperatively (P=0.017; P=0.019; P=0.009, respectively; Fig 1). The load-induced changes in all other markers did not differ between the pre- and postoperative test.

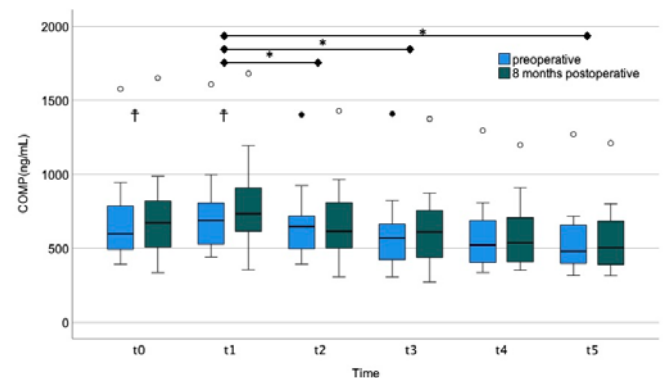


Fig 1: Box plots of COMP concentrations during the walking stress test. °outlier; †significant pre- to postoperative difference; *significant pre- to postoperative differences in decrease from t₁.

Conclusions

COMP was the only blood marker to respond to both the ambulatory load stimulus and to load modifying surgery further supporting the relevance of this marker in the context of knee OA and its treatment. Greater IL-6 levels 8 months postoperatively (when the osteotomy has completely healed) are surprising and should be closely monitored as they may counteract potential benefits of altering the load distribution at the knee regarding knee OA progression. In a next step, the relevance of the exaggerated delayed load-induced decrease in COMP levels but not MMP-3 after HTO regarding future progression of the disease and its relationship to the magnitude of ambulatory load must be determined.

Acknowledgments

Funding: Swiss National Science Foundation (SNSF #32003B_159871)

References

- [1] Andriacchi et al. (2004) *Ann Biomed Eng* **32**, 447-457.
- [2] Herger et al. (2020) *OA Cartilage* **28**, S320-S321.

Tibio-Femoral Kinematics of Natural *versus* Replaced Knees – A Comparison Using Dynamic Videofluoroscopy

Barbara Postolka¹, William R. Taylor¹, Renate List^{1,2}, Sandro F. Fucentese³, Peter P. Koch⁴, Pascal Schütz¹

¹Laboratory for Movement Biomechanics, Institute for Biomechanics, ETH Zürich, Zürich, Switzerland

²Human Performance Lab, Schulthess Clinic, Zürich, Switzerland, ³Balgrist University Hospital, Zürich, Switzerland

⁴Winterthur Cantonal Hospital, Winterthur, Switzerland

Email: barbara.postolka@hest.ethz.ch

Summary

In vivo knee joint kinematics of healthy subjects during level walking were compared to three different total knee arthroplasty geometries using dynamic videofluoroscopy. While individual tibio-femoral rotations and condylar translations could be guided by the implant geometry, variability among the healthy subjects indicates the necessity for different implant geometries, to address individual needs while aiming to restore physiological knee joint function.

Introduction

Despite the overall high success rates of total knee arthroplasty (TKA) surgery, 16-30% of all patients remain unsatisfied with the outcome, especially during dynamic functional activities [1]. To better identify the mechanisms leading to unsatisfactory results, and thus support correct implant selection in subjects with different limb alignments towards restoration of natural knee function, it is critical to understand the underlying kinematic deficits in TKA knees. Therefore, the aim of this study was to compare *in vivo* kinematics of healthy versus TKA subjects throughout complete cycles of level walking.

Methods

27 healthy subjects with different limb alignment (neutral: n=12, Hip-Knee-Ankle angle $0.5 \pm 1.6^\circ$; varus: n=10, HKA $5.7 \pm 1.8^\circ$; valgus: n=5, HKA $-5.6 \pm 1.5^\circ$) and 30 mechanically aligned ($-3^\circ \leq \text{HKA} \leq 3^\circ$) good outcome subjects with a TKA (GMK Sphere: n=10; GMK PS: n=10; GMK UC: n=10) [2] were assessed during 5-6 complete cycles of level walking using dynamic videofluoroscopy [3]. 2D/3D registration of the videofluoroscopic images was performed using 3D models of the bones (CT) or the implant components [4,5]. Tibio-femoral rotations, condylar A-P translations as well as the location of the centre of rotation (CoR) were determined.

Results and Discussion

While only the GMK UC showed a reduced range of flexion, all three implants exhibited smaller ranges of abduction/adduction as well as tibial rotation compared to the healthy subjects (Table 1). The additional constraints of the implant geometry, especially for the GMK Sphere and GMK UC, can therefore be assumed to restrict axial rotation. While the neutral, varus and GMK Sphere subjects,

exhibited less medial than lateral condylar A-P translation and an overall medial CoR, the valgus, GMK PS and GMK UC subjects demonstrated equal condylar translation and a more central CoR (Table 1, Figure 1). However, in all three alignment groups as well as in the GMK PS and GMK UC group, inter-subject variability was high, resulting in a contrary translational behaviour for certain subjects. Despite these differences, it seems that individual kinematic patterns can be guided by implant geometry but the necessity for different implant geometries to address individual functional needs is also evident.

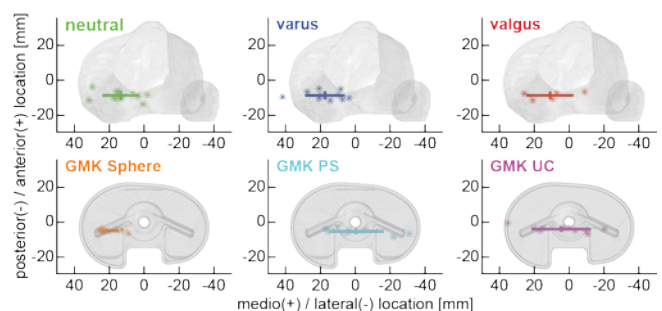


Figure 1: Location of the CoR over the complete gait cycle. Mean \pm STD over all subjects as well as individual subject means.

Conclusions

These results can provide a first basis to support clinical decision-making and help to further improve orthopaedic interventions aiming to restore physiological knee joint function. However, intra-operative component alignment remains controversially discussed and further evidence on component alignment and the desirable level of limb alignment correction is needed.

Acknowledgments

This study was partially funded by Medacta International and the Commission for Technology and Innovation.

References

- [1] Bourne RB et al. (2010). *COOR*, **468**:57-63
- [2] Schütz P et al. (2019). *J Orthop Res*, **37**:2337-2347
- [3] List R et al. (2017). *PLoS One*, **12**:e0185952
- [4] Postolka B et al. (2020). *Med Eng Phys*, **77**:107-113
- [5] Burckhardt K et al. (2005). *IEEE TMI*, **24**:676-688

Table 1: Range of motion for all three tibio-femoral rotations and range of A-P translation for the medial and lateral condyle point over complete cycles of level walking. Mean \pm SD for each group are presented.

		neutral	varus	valgus	GMK Sphere	GMK PS	GMK UC
tibio-femoral rotations [°]	flex/ex	66.1 \pm 3.9	63.3 \pm 4.0	63.5 \pm 6.4	62.7 \pm 4.9	63.5 \pm 4.7	57.2 \pm 4.8
	int/ext	15.5 \pm 2.6	13.8 \pm 1.6	13.3 \pm 0.8	11.9 \pm 4.2	10.5 \pm 1.9	8.1 \pm 2.5
condylar A-P translation [mm]	abd/add	7.0 \pm 1.9	5.7 \pm 1.6	7.6 \pm 2.3	2.8 \pm 0.8	2.9 \pm 0.8	2.3 \pm 0.6
	medial condyle	8.8 \pm 1.8	8.6 \pm 1.0	9.8 \pm 0.8	4.1 \pm 1.2	12.9 \pm 2.8	8.9 \pm 1.6
	lateral condyle	10.9 \pm 2.2	9.9 \pm 2.1	10.3 \pm 3.0	11.4 \pm 4.7	12.4 \pm 2.2	9.1 \pm 2.0

Effect of additional training weight on tibiofemoral contact forces during a forward lunge

Sam Van Rossom¹, Joséphine Evrard², Gitte Jacobs², Sabine Verschueren², Ilse Jonkers¹, **Jos Vanrenterghem²**

¹Human Movement Biomechanics Research Group, Dep of Movement Sciences, KU Leuven, Leuven, Belgium

²Musculoskeletal Rehabilitation Research Group, Dept. Rehabilitation Sciences, KU Leuven, Leuven, Belgium

Email: sam.vanrossom@kuleuven.be

Summary

This study investigated the effect of carrying handheld weights on knee joint loading, in terms of tibiofemoral contact forces during forward lunge as well as the effect of different positions to carry the weights. Resultant tibiofemoral contact forces increased as handheld load increased. No major effect of position was observed on total knee loading as well as the medial-lateral load distribution.

Introduction

After musculoskeletal injuries, it is crucial in rehabilitation to progressively reload the injured structures, avoiding to overload the damaged tissue yet providing sufficient stimuli to trigger mechanobiological adaptation processes underlying restoration of homeostasis. To date, exercises are selected primarily based on clinical experience rather than scientific evidence, assuming that when the level of difficulty is increased, higher loads are imposed on the structures [1]. Therefore, this study investigated the effect of adding additional handheld weights and different weight carrying positions during a forward lunge on knee joint loading, in terms of tibiofemoral contact forces.

Methods

10 healthy subjects performed a forward lunge while carrying handheld weights (0%, 10%, 20%, 30% of body weight) in 4 different positions (two hands either side of the body, two hands in front, one hand ipsilateral or contralateral side of the leading limb). Markers were attached to the body according to an extended plug-in-gait markerset and 3D motion capture data was recorded using a 10 camera vicon system (100Hz). Simultaneously, ground reaction forces were recorded under the leading limb (1000Hz). The data were processed using the Catelli model for deep knee flexion and a standard musculoskeletal modelling workflow in OpenSim 3.3 to estimate the peak resultant tibiofemoral contact forces of the leading limb during the weight-acceptance and push-off phase of the forward lunge [2,3]. The distribution of the vertical contact force over the medial and lateral compartment was calculated based on the method proposed by Winby et al., (2009) [4]. A two-way analysis of variance (ANOVA) was used to evaluate the effects of added weights and weight position on the peak knee contact forces as well as the joint kinematics and kinetics (external moments) and medial and lateral contact forces at instance of peak loading.

Results and Discussion

With increasing weight, external joint moments significantly increased. In addition, with increasing weight lumbar flexion increased significantly, whereas knee flexion angle was not

affected by adding weights. Resultant tibiofemoral contact forces significantly increased with increasing weight (Figure 1). During the different lunge variations, the medial compartment was loaded more compared to the lateral compartment.

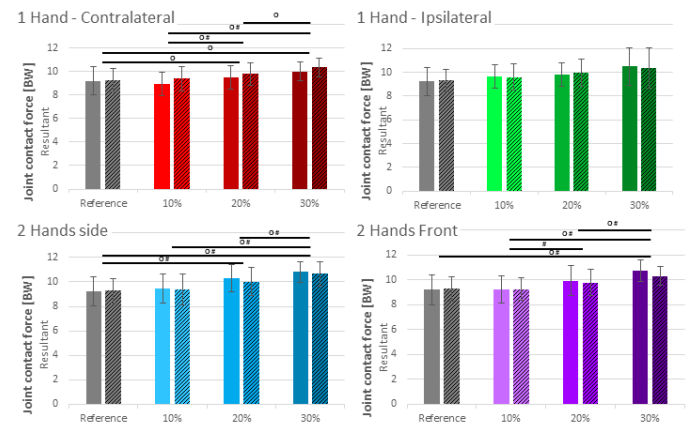


Figure 1: Effect of adding weights on peak knee contact forces during weight-acceptance (solid bars, # indicates significance) and push-off phase (hatched bars, O indicates significance).

Frontal plane knee moments were affected by weight position, where a significantly increased knee adduction moment was observed for the contralateral weight position and a significantly increased knee abduction moment for the ipsilateral weight position. However, no significant effect of weight-carrying position on resultant knee contact force was observed, nor did it affect the medial-lateral loading distribution, lateral contact forces were only increased when carrying the load at the ipsilateral side compared to the contralateral side in the 10%BW condition ($2.97 \pm 0.58 \text{ BW}$ vs $2.69 \pm 0.45 \text{ BW}$, respectively).

Conclusions

Resultant tibiofemoral contact forces increased as external load increased. No major effect of weights position was observed on total knee loading. However, carrying added weights had limited effect on load distribution (despite altered frontal plane joint moments) justifying further investigation in support of evidence-informed clinical care.

References

- [1] Riemann BL et al. (2012). *J. Athl Train*, **47**(4): 372-8.
- [2] Catelli DS et al. (2019). *Comp. Meth. Biomech. and Biomed. Eng.* **22**(1):21-24
- [3] Delp SL et al. (2007) *IEE Trans. Biomed. Eng.* **54**(11): 1940-50.
- [4] Winby CR et al. (2009) *J. Biomech*, **42**: 2294-2300

High tibial osteotomy effectively redistributes compressive knee loads during walking

Enrico De Pieri^{1,2}, Corina Nüesch^{2,3,4,5}, Elke Viehweger^{1,2,6}, Christian Egloff^{2,3,5}, Annegret Mündermann^{2,3,4,5}

¹Laboratory for Movement Analysis, University of Basel Children's Hospital, Basel, Switzerland; ²Department of Biomedical Engineering, University of Basel, Basel, Switzerland; ³Department of Orthopaedics and Traumatology, ⁴Department of Spine Surgery, University Hospital Basel, Basel Switzerland; ⁵Department of Clinical Research, University of Basel, Basel, Switzerland; ⁶Department of Neuro-Orthopaedics, University of Basel Children's Hospital, Basel, Switzerland; Email: enrico.depier@unibas.ch

Summary

This study analyzed ambulatory knee loads in patients who underwent high tibial osteotomy (HTO) by means of musculoskeletal modeling. HTO effectively unloads the medial knee compartment while increasing the compressive load on the lateral one.

Introduction

The development of degenerative joint diseases such as knee osteoarthritis (OA) is often determined by altered joint mechanics that lead to increased or abnormal intra-articular forces [1]. Individual variations in ambulatory knee mechanics can influence the rate of progression of cartilage degeneration [2]. High tibial osteotomy (HTO) is a well-accepted surgical procedure for patients with knee OA and varus alignment aimed at re-establishing a more even distribution of ambulatory load between the affected medial and the lateral knee compartment. We hypothesized that HTO would reduce the knee adduction moment and the medial compartment compressive force while increasing the compressive load in the lateral compartment in a cohort of patients with medial knee OA.

Methods

Twelve patients (mean ± 1 SD, age: 45 ± 9 years) diagnosed with isolated symptomatic medial compartment knee OA underwent opening wedge HTO. Kinematic and kinetic data were recorded using the Plug-In Gait model in 3D gait analysis sessions before (pre-) surgery as well as 9 ± 3 months postoperatively. The collected motion capture data was used as input for an inverse dynamics analysis (AnyBody Technology, Denmark) to evaluate external knee moments and knee contact forces. Personalized models were created from a generic lower-limb model [2], scaled according to marker data from a static trial. Knee varus/valgus alignment was estimated from the static trial and implemented as a fixed change in orientation of the knee joint axis. The distribution of the compressive knee force across the medial and lateral compartments was evaluated [4]. Differences between pre- and postoperative knee adduction moment, as well as total, medial, and lateral knee compressive forces were evaluated over the whole gait cycle through statistical parametric mapping (SPM), with one-tailed paired t-tests ($\alpha = 0.05$).

Results and Discussion

Modelled mean varus knee alignment in the cohort was $7.2 \pm 3.7^\circ$ preoperatively and reduced to $1.3 \pm 3.2^\circ$ after HTO. A statistically significant reduction in the postoperative external

knee adduction moment was observed during mid and terminal stance leading to a reduction in the medial compartment compressive force during mid stance and an increase in lateral compartment compressive force during most of the stance phase. The total compressive load through the knee did not present any statistically significant difference.

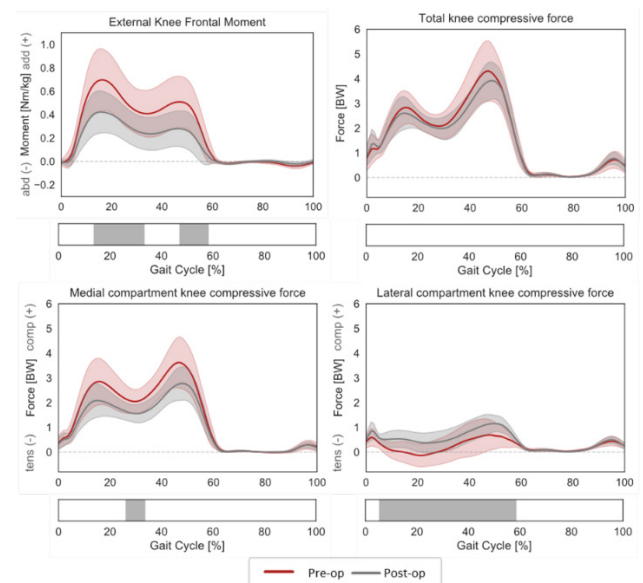


Figure 1: Predicted internal knee adduction moment, and total, medial, and lateral knee compressive forces in patients before (red) and after (grey) HTO. Significantly different phases of the gait cycle are indicated as grey bars below each force component.

Conclusions

HTO effectively unloads the medial knee compartment by redistributing part of the overall compressive force to the lateral compartment during gait. The timing of reductions in compressive force may not always coincide with the timing of reductions in knee adduction moments suggesting that the knee frontal moment may not adequately describe ambulatory load or changes induced by interventions at the compartment level.

Acknowledgments

Funding: Swiss National Science Foundation (SNSF #32003B_159871)

References

- [1] Felson DT (2013), *Osteoarthr Cartil*, **21(1)**, 10:15
- [2] Mündermann A et al (2004), *Arth Rheum*, **50(4)**, 1172-78
- [3] De Pieri E et al. (2018), *PLoS ONE*, **13(9)**.
- [4] Stoltze JS et al. (2018), *Int Biomech*, **5(1)**, 63-74.

Assessment of variations in scapular morphology and bone quality in patients with B glenoids

Nazanin Daneshvarhashjin¹, Filip Verhaegen, MD, PhD¹, Bernardo Innocenti, PhD², Lennart Scheys, PhD¹

¹Institute for Orthopaedic Research and Training, Department of Development and Regeneration, KU Leuven/University Hospitals Leuven, Belgium

²BEAMS Department (Bio Electro and Mechanical Systems), Université Libre de Bruxelles, Brussels, Belgium

Email: nazanin.daneshvarhashjin@kuleuven.be

Summary

A systematic description of variability in the scapular shape and bone mineral density (BMD) distributions in shoulder osteoarthritis (OA) can be valuable input for implant design and surgical intervention, especially in surgically challenging glenoids with asymmetric posterior erosion. Statistical shape (SSM) and intensity modeling (SIM) of these patients identified changes in the posterior and inferior shape of the glenoid cavity as main shape variations, whereas BMD variations were identified in all regions of the glenoid cavity, except for the posterior part of the bone consistently demonstrating the highest bone density.

Introduction

Shoulder osteoarthritis (OA) occurs in up to 20% of the population. In Bercik et al.'s classification, B glenoids comprise 32% of this population. It is characterized by asymmetric posterior wear of the glenoid and associated with regional bone density variations, which pose a known challenge for glenoid component fixation and survival in total shoulder arthroplasty surgery (TSA). Literature reports that at a minimum follow-up of 24 months after TSA surgery around 50% of the B glenoids demonstrated evidence of radiological glenoid component loosening [1]. Therefore, a systematic description of variations in BMD and morphology within this specific patient group can serve as valuable information for categorizing patients in terms of the risk of glenoid component loosening. The main objective of this study was therefore to develop a statistical shape and intensity model of the scapula for patients with B glenoids and describe their principal modes of variations.

Methods

The training dataset for the pathological SSM and SIM consisted of 31 CT images from subjects with B glenoids, as judged by an experienced shoulder surgeon. 3D surface full scapular models were constructed from the segmented images in Mimics (Materialise®, Belgium) after which an open-source non-rigid registration algorithm was used to obtain point-to-point correspondences between subjects and a generic surface template mesh [2]. For developing the SIM, volumetric registration was performed by elastically deforming the corresponding generic volumetric template mesh to each training subject driven by the known displacements between the surface nodes on the template and the corresponding surface nodes of each subject, using Abaqus software (Dassault Systemes Simulia Corp., Providence, RI, USA) [3]. Each scapular mesh was then transformed back into its original CT coordinates and Hounsfield units (HU) were assigned to each volumetric mesh' nodes. Corresponding BMD for each nodes was

defined using existing mathematical relationships between HU and BMD [3]. Finally, the SSM and SIM was established through principal component analysis after which the main modes of variations in both models were interpreted by perturbing the mean by ± 2 standard deviations.

Results and Discussion

The first five modes of the SSM and SIM represent 79.2% and 51.1% of their corresponding variability, respectively. Except mode 1 of the SSM, primarily describing a uniform scaling of the scapula, changes in the posterior and inferior shape of the glenoid cavity were observed in the subsequent four modes. Based on the SIM of this study, the posterior part of the glenoid was observed to have the highest average bone density in B glenoids. This contrasts with the glenoid bone of healthy subjects where the center of the glenoid typically has the best bone quality [3]; but is in agreement with previous studies investigating BMD in large sub-regions of asymmetric glenoids with OA [4]. Furthermore, the first principal mode of the SIM (15.6% of variability), described variations in glenoid BMD in the anterior-inferior region, while the second mode (13% of variability) primarily described differences in BMD affecting the other regions (Figure 1).

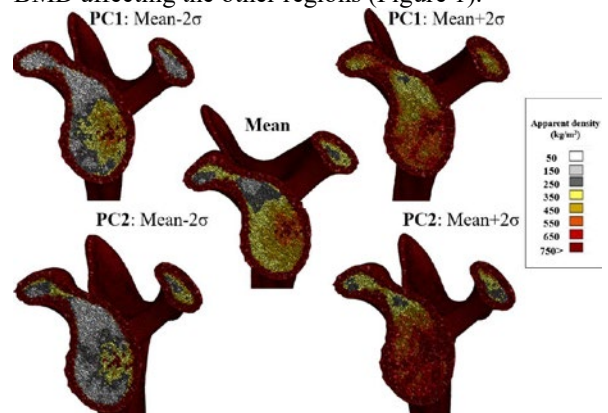


Figure 1: Variation in the bone mineral density of the B glenoids.

Conclusions

In B glenoids, higher bone density was found in posterior region of the glenoid. Nevertheless, important variations in the other regions should be taken into consideration before surgical intervention. These findings highlight the potential of SSM and SIM for assessing variations in shape and bone quality among pathological subjects.

References

- [1] Chin PC et al. (2015). *J shoulder Elb Surg*, **24**(12):1888–93.
- [2] White JD et al. (2019). *Sci Rep*, **9**(1):1–11.
- [3] Burton WS et al. (2019). *Comput Methods Biomech*, **22**(4):341–51.
- [4] Chen X et al (2017). *Clin Orthop Relat Res*, **475**:3090–3

Impact of personalized geometry and motor control on musculoskeletal simulation results – How much detail is needed?

Hans Kainz¹, Mariska Wesseling², Ilse Jonkers²

¹Neuromechanics Research Group, Centre for Sport Science and University Sports, University of Vienna, Vienna, Austria

²Human Movement Biomechanics Research Group, KU Leuven, Leuven, Belgium

Email: hans.kainz@univie.ac.at

Summary

We compared musculoskeletal simulation results from highly subject-specific models with less sophisticated models. The impact on gait deviation was evaluated based on root-mean-square-differences (RMSD) in simulation results between children with cerebral palsy (CP) and a typically developing (TD) child. The modelling choice had a minor impact on joint kinematics and kinetics. Muscle and joint contact forces were more sensitive to the modelling choice. The impact of including subject-specific musculoskeletal geometry was higher than the impact of including electromyography (EMG) data. Gait deviation was similar between modelling frameworks.

Introduction

Musculoskeletal simulations can improve clinical-decision making in children with CP [1]. Typically, linear scaling methods based on surface markers are used to personalize generic models to each participant's anthropometry [2]. Subject-specific musculoskeletal geometry and motor control is mostly neglected in the models and simulations due to the tedious process which is required to create highly personalized models. To assess the impact of these simplifications, we compared the simulations results from highly subject-specific models with linearly scaled generic models.

Methods

Magnetic resonance images (MRI) and gait data of one TD child and three children with CP were analyzed. For each participant a generic-linear scaled and MRI-based model were created based on a previously developed workflow [3]. Musculoskeletal simulations were performed using four modelling frameworks: 1) Generic-scaled model with static optimization, 2) Generic-scaled model with an EMG-informed approach [4], 3) MRI-based model with static optimization, and 4) MRI-based model with an EMG-informed approach. Joint kinematics, joint kinetics, muscle forces and joint contact forces were calculated with OpenSim [2] and compared between modelling frameworks. The impact on gait deviation was evaluated based on RMSD in simulation results between children with CP and a TD child.

Results and Discussion

RMSD in joint kinematics and kinetics between generic-scaled and MRI-based models were below 5° and 0.15 Nm/kg, respectively. RMSD over all muscles was below 0.2 body weight for every participant. Nevertheless, differences of ~200% in maximal individual muscles forces were observed in some participants (Figure 1). RMSD in joint contact forces between the different modelling frameworks were up to 2.2 body weight. Comparing the musculoskeletal simulation

results from the TD child with the results from the children with CP showed similar RMSD for all modelling frameworks (Figure 2).

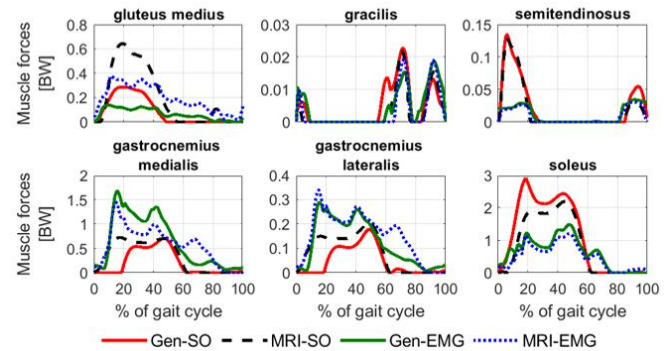


Figure 1: Example of muscle forces from one participant with CP calculated with the four different modelling frameworks.

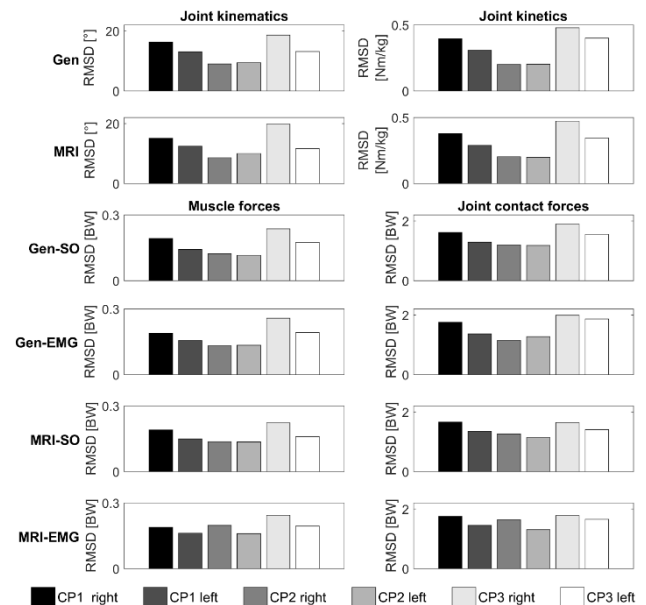


Figure 2: RMSD in simulation results between our participants with CP and the TD child. The overall trend was similar across modelling frameworks.

Conclusions

Overall group effects based on RMSD between CP and TD children are unlikely affected by the modelling choice, whereas caution is warranted if simulations are used to evaluate specific musculoskeletal parameters of an individual.

References

- [1] Rajagopal L et al. (2020). *PLoS One*, **15**: e0233706.
- [2] Delp SL. et al. (2007) *IEEE Trans Bio Eng*, **54**: 1940-50.
- [3] Schey L et al. (2008). *Gait Posture*, **28**: 358-65.
- [4] Wesseling M et al. (2020). *Gait Posture*, **82**: 54-60.

Altered triceps surae muscle dynamics and force demand at different stride frequencies.

Wannes Swinnen¹, Wouter Hoogkamer², Friedl De Groot¹, Benedicte Vanwanseele¹

¹Department of Movement Sciences, KU Leuven, Belgium

²Department of Kinesiology, University of Massachusetts Amherst, USA

Email: wannes.swinnen@kuleuven.com

Summary

While it is well recognized that the preferred stride frequency (PSF) in running closely corresponds with minimal energy consumption, the underlying mechanism is still unclear. Changes in ankle and knee joint mechanics when altering stride frequency are likely to affect triceps surae dynamics. Here, we investigated triceps surae muscle dynamics and force production in 10 runners while running at five different stride frequencies using ultrasound imaging (for Soleus, SOL and Gastrocnemius medialis, GM) and dynamic optimization. When deviating from PSF both SOL and GM muscles operated at shorter lengths during ground contact, implying a reduced force capacity, while average muscle force demand was increased. Differences were most pronounced at lower than preferred stride frequencies especially for SOL. Our results shed new light on the mechanisms that may be at least partly responsible for the increased energy consumption observed when deviating from PSF.

Introduction

Self-optimization, i.e. intrinsically adopting kinematics and kinetics associated with minimal energy consumption, is a well-known phenomenon in running with stride frequency often used as a textbook example. While the concept is well recognized, it is still unclear why a certain stride frequency corresponds with minimal energy consumption. Yet, previous research demonstrated that altering stride frequency affects lower limb kinetics and kinematics [1] presumably affecting muscle-tendon dynamics and thus possibly altering energy consumption. One important muscle-tendon unit is the triceps surae, spanning both the ankle and knee joint, and consuming 25% of the total metabolic energy rate [2]. Here, we investigated how the triceps surae muscle dynamics and force production are affected when changing stride frequency.

Methods

10 experienced runners ran on a force measuring treadmill at 12 km/h while adopting five different stride frequencies (PSF; PSF \pm 8%; PSF \pm 12%). During each trial, we measured lower limb kinematics and kinetics, metabolic energy expenditure and SOL (N = 9) and GM (N = 10) muscle fascicle behavior through dynamic ultrasound. Next, we used a dynamic optimization algorithm to individualize triceps surae muscle-tendon parameters of a musculoskeletal model (including 43 lower limb muscles), using the SOL and GM ultrasound images [3]. To estimate triceps surae muscle forces, we solved a new muscle redundancy problem, now including the individualized muscle-tendon parameters, by minimizing the muscle activation squared of all 43 lower limb muscles.

Results and Discussion

Runners consumed the least metabolic energy while running at PSF. During ground contact, we found significant shorter fascicle length and greater pennation angle when deviating from PSF for both muscles (**Figure 1**). In contrast, fascicle velocity was not different during mid-stance when muscle forces were highest. Average muscle force during ground contact was lower when running at PSF. Post-hoc analyses revealed significantly lower average force production at PSF compared to -15% for SOL and +15% for GM.

During running, the triceps surae muscles are operating on the ascending limb of the force-length relationship [4] and hence shorter lengths imply reduced force capacity. As our results also demonstrated increased triceps surae force demand when deviating from the PSF, muscle activation and subsequently muscle energy consumption is likely to be increased. Especially at frequencies lower than PSF, shorter operating lengths and increased force demand (only for SOL) are most prominent.

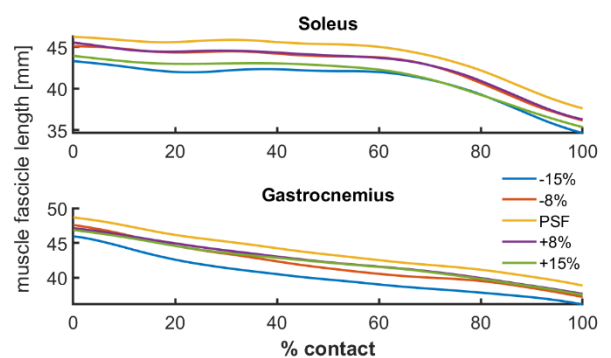


Figure 1: SOL and GM fascicles lengths throughout ground contact phase at different stride frequencies.

Conclusions

Our results indicate that increased energy consumption when deviating from PSF is at least partly the result of both reduced triceps surae force capacity and increased force demand.

Acknowledgments

WS obtained a PhD fellowship from the Research Foundation Flanders (11E3919N).

References

- [1] Heiderscheit B et al. (2011) *Med Sci Sports Exerc*, **43**: 296-302.
- [2] Swinnen W et al. (2019). *J Exp Biol*, **222**: jeb212449.
- [3] Delabastita T et al. (2020) *Ann Biomed Eng*, **25**: 722-733.
- [4] Bohm S et al (2019) *Proc R Soc B*, **286**: 20192560

Predictive simulations of hemiparetic gait to explore the effects of muscle weakness on walking asymmetry and energetics

Tom J.W. Buurke¹, Geert Verheyden², Friedl De Groot¹

¹Department of Movement Sciences, KU Leuven, Leuven, Belgium

²Department of Rehabilitation Sciences, KU Leuven, Leuven, Belgium

Email: tom.buurke@kuleuven.be

Summary

We used predictive simulations to explore the effect of unilateral muscle weakness on step length asymmetry and metabolic cost of transport. 90% unilateral plantar flexor, dorsiflexor, and knee flexor weakness, but not knee extensor or hip flexor/extensor weakness, led to step length asymmetry. Imposing step length symmetry increased the cost of transport for all simulations. These results suggest that walking with asymmetric step lengths after stroke may be more economical than imposing symmetric step lengths.

Introduction

Post-stroke hemiparetic walking is often characterized by step length asymmetry, which is associated with an increased metabolic cost of transport compared to able-bodied walkers. Research suggests that reducing step length asymmetry may reduce the cost of transport [1], but the different underlying impairments in muscle function, motor control, and sensory function and their interactions complicate investigation of the relationship between improving step length symmetry and cost of transport post-stroke [2]. With predictive simulations based on neuromusculoskeletal models [3], we can study the isolated effects of different impairments on walking symmetry and energetics. Here we study the isolated effects of muscle weakness of the hip, knee, and ankle flexor and extensor muscle groups on step length asymmetry and cost of transport. In addition, we impose step length symmetry on the simulations, to investigate the effect of reducing asymmetry on the cost of transport in hemiparetic walking.

Methods

We used an existing neuromusculoskeletal model with 31 degrees of freedom and 92 muscles. Gait mechanics and energetics were predicted by minimizing a multi-objective cost function containing muscle effort, metabolic cost, and joint accelerations while imposing gait speed (1.33 m s⁻¹) and periodicity as described in [3]. First, we performed a control simulation without weakness. Then, we simulated 90% unilaterally (left side) reduced maximal isometric force on six muscle groups (Fig. 1). Second, we added step length symmetry constraints to the simulations where a substantial asymmetry (>0.03) occurred in the initial simulation. Third, we imposed a step length asymmetry constraint on the control simulation, which matched the largest asymmetry from the weakness simulations. We compared step length asymmetry ($SL_{left} - SL_{right} / SL_{Left} + SL_{Right}$) and cost of transport (J kg⁻¹ m⁻¹) between simulations.

Results and Discussion

The results (Fig. 1) show a substantial step length asymmetry with a longer paretic step in the simulations of unilateral

plantar flexor (0.26) and knee flexor (0.03) weakness and shorter paretic step in dorsiflexor weakness (-0.06). Furthermore, we found an increase in the cost of transport in simulations of unilateral plantar flexor (7.2%), dorsiflexor (3.6%), and hip flexor weakness (6.4%). When we imposed step length symmetry upon the plantar flexor, dorsiflexor, and knee flexor weakness simulations, this led to a further increase in the cost of transport in all three simulations (resp. 5.9%, 2.1%, 1.1%). Finally, imposed step length asymmetry (0.28) in the control simulation led to a 6.4% increase in the cost of the transport.

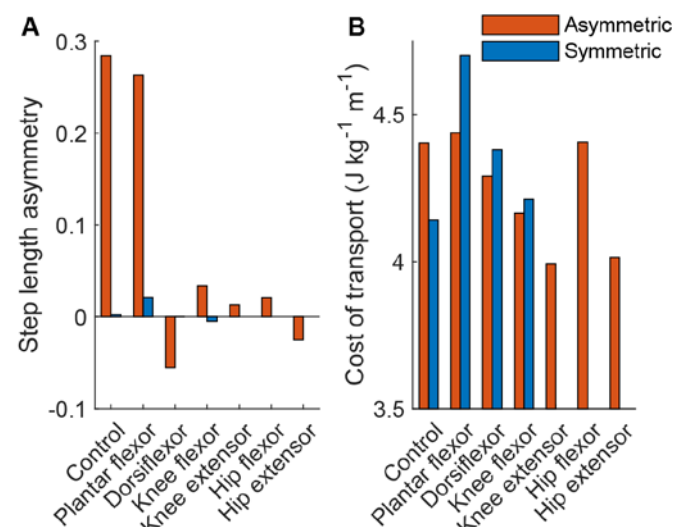


Figure 1: A) Step length asymmetry and B) cost of transport outcomes of predictive simulations of symmetric and asymmetric walking with weakness of different muscle groups.

Conclusions

Unilateral weakness of the more distal, but not proximal, muscle groups leads to step length asymmetry. Walking with asymmetric step lengths after hemiparesis may be more economical than walking with imposed symmetric step lengths. Further research is necessary to understand the effect of muscle weakness on walking stability and the interaction of muscle weakness with other impairments after stroke.

Acknowledgments

Tom Buurke was supported by KU Leuven Internal Funds.

References

- [1] Finley and Bastian (2017). *Neurorehabil Neural Repair*, **31(2)**: 168-177.
- [2] Sánchez and Finley (2018). *Neurorehabil Neural Repair*, **32(8)**: 701-713.
- [3] Falisse et al. (2019). *J Roy Soc Interface*, **16**: 20190402.

Biomechanical Analysis of Industrial Exoskeletons

Ulrich Glitsch, Jasper Q. Johns, Kai Heinrich

Institute for occupational safety and health (IFA), Sankt Augustin, Germany

Email: ulrich.glitsch@dguv.de

Summary

In an interventional study with 12 participants, the biomechanical effects of a passive trunk supporting exoskeleton during symmetric lifting tasks were investigated. Based on biomechanical motion analysis in combination with inverse dynamics modelling, the exoskeleton supportive function and the musculoskeletal loadings were determined. The presented approach aimed to provide comprehensive insights into the biomechanical effects of an industrial exoskeleton on the musculo-skeletal system, which could be applied in a similar manner to other exoskeleton types and working tasks.

Introduction

In recent years, more and more exoskeletons were introduced to the commercial market specifically for use in industrial workplaces. Although discrete benefits of exoskeletons were already described in numerous laboratory studies [1], the actual overall benefit in industrial practice is still largely unknown. Many studies provided only a very restricted set of parameters, which limits the biomechanical understanding of the exoskeleton's supporting function related to a designated working task.

The goal of the present study was to establish a fundamental biomechanical approach for analyzing the supporting effect of an industrial exoskeleton on the musculo-skeletal loading of the relevant body region.

Methods

Twelve healthy subjects (8 males, 4 females) volunteered in the interventional study, in which a passive commercially available trunk supporting exoskeleton consisting of a rigid segmented structure (mass = 3.3 kg) was used. Repeated symmetric lifting tasks (from below knee level to pelvis level) with weights of 10 and 20 kg were analyzed using a combined motion capture setup (12 cams Vicon, 2 Kistler force plates, bilateral lumbar and thoracic erector spinae EMGs). The support torque characteristic of the exoskeleton was experimentally determined using a digital force gauge and a digital inclinometer.

The lumbar moments and the compression forces (L4-L5) were determined by applying an inverse dynamics model [2, 3]. Repeated measures ANOVAs were conducted for each output variable of the lifting trials (SPSS V23).

Results and Discussion

During flexion, the supportive torque of the exoskeleton achieved a maximum of 45 Nm at about 84°. During

extension, the hysteresis effect reduced the supportive torque on average of about 50%.

Use of the exoskeleton significantly reduced the maximum lumbar joint moments by an average of 19% to 20% (10/20 kg). Averaged over the entire lifting phase, significant stress alleviation effects of 6% to 8% were observed. Similarly, the maximum lumbar compression forces were significantly reduced by an average of 17% to 18% (10 / 20 kg) (Figure 1). Averaged over the entire lifting phase, the forces were significantly reduced by an average of 5% to 7%.

The EMG of the back extensors revealed significant reductions of peak values by an average of 18% to 27%. In contrast, mean EMG-values did not change significantly.

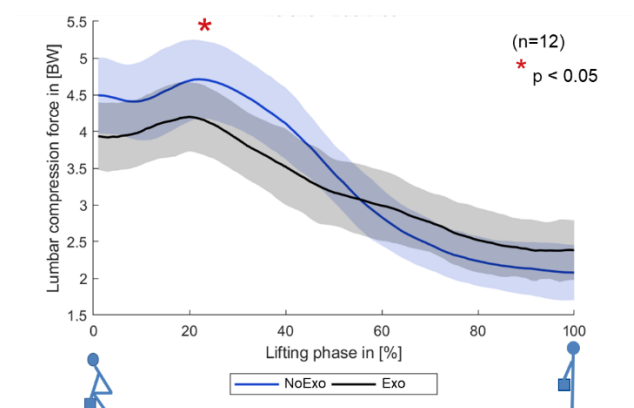


Figure 1: Mean and SD time histories of lumbar compression forces (\times bodyweight) during lifting of a 20 kg weight.

When using a (passive) exoskeleton, the effective reduction of the lumbar loads might be less than proposed by the manufacturer or even compared to other studies [1].

Conclusions

For the biomechanical assessment, a comprehensive approach is necessary to enlighten the functional interaction of an exoskeleton with the musculo-skeletal system and sufficient intermediate parameters have to be provided, making the assessment transparent. The presented approach may be a proposal for establishing a standardization in the biomechanical assessment of industrial exoskeletons.

References

- [1] De Looze M et al. (2016). *Ergonomics*, **59**, 671-681.
- [2] Jäger M and Luttmann A. (2007) *Int J Ind Ergon*, **37**, 823-824.
- [3] Glitsch U et al. (2020) *Z Arb Wiss*, **74**: 294-305.

A multiscale constitutive description for load bearing soft biological tissue that incorporates the interfibrillar sliding of constituent collagen.

C. Miller¹, T.C. Gasser^{1,2}

¹Solid Mechanics unit, Dept. Engineering Mechanics, KTH Royal Institute of Technology, Stockholm, Sweden

¹ Faculty of Health Sciences, University of Southern Denmark, Odense, Denmark

Email: chrismi@kth.se

Summary

A generalized multiscale constitutive framework is outlined that specifically accounts for several key features of the collagenous microstructure. Specifically, the continuous recruitment of undulated collagen fibrils and their time-dependent relative sliding are included. Macroscopic tissue properties are captured for numerous types of loading [1].

Introduction

Soft biological tissues are composed of numerous extracellular matrix (ECM) proteins. Their complex structural arrangement and interaction define their macroscopic material properties. Fibrous collagen is known to be the principal load bearing ECM constituent. Its hierarchical architecture and deformation mechanisms that act over multiple length scales, greatly determine observed physical phenomena. Furthermore, current evidence for various tissue types suggests that the interlinking of collagen fibrils by proteoglycans (PG's) promotes the relative sliding of fibrils and influences features such as stress relaxation, strain-rate sensitivity, and the transitioning point of the mechanical response [2,3].

Methods

A 1D model for a collagen fibril proteoglycan (CFPG) complex is employed, where overloaded fibrils are considered to reduce their loading through a time-dependent PG facilitated sliding. It is assumed that this sliding enables fibrils to reach a homeostatic target stress that can be inferred from physiological loading conditions. The sequential straightening of fibrils is described by a probability distribution, and the overall response of a collagen fiber is obtained through a novel integration strategy over all CFPG-complexes. The fiber model is subsequently numerically integrated over the unit sphere using spherical t-designs. This well established framework determines the macroscopic stress contribution of collagen at the Gauss point level and has been applied to the description of collagen fiber reinforced soft tissue previously [4]. Collagen fiber orientation varies greatly between different tissue types, a feature that greatly determines their overall mechanical response and function. This methodology readily accounts for this as it permits the inclusion of appropriate orientation density functions to characterise the tissue of interest. Furthermore, the contribution of non collagenous matrix material is described by a classical isotropic Neo-Hookean model.

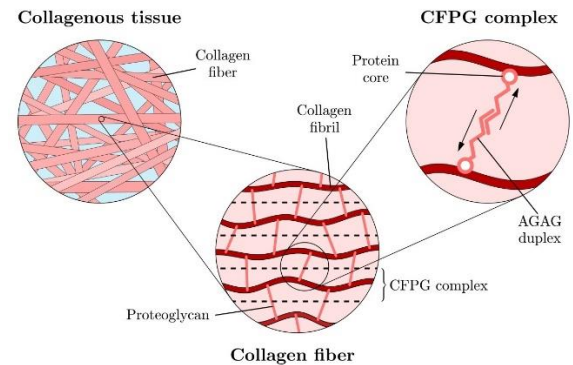


Figure 1: Hierarchical structural diagram of collagenous soft tissue microstructure. Collagen fibers are assembled by numerous CFPG-complexes, which consist of a collagen fibril and interconnecting PG's. PG's themselves are composed of a protein core and a GAG duplex that allows for a time dependent sliding deformation.

Results and Discussion

The outlined framework was applied to the uniaxial deformation of the human Calcaneal tendon. A transversely isotropic collagen fiber distribution was assumed as they are arranged predominantly along the axis of loading. The model was able to qualitatively capture nonlinear strain dependent stress relaxation in tendons, with increased strain leading to increased rates of relaxation. It was also able to characterize nonlinear creep phenomena, with significant applied stress leading to propagating creep failure. Finally, strain rate stiffening behavior was observed as increased strain rates inhibit the development of interfibrillar sliding, leading to a stiffer response.

Conclusions

The discussed constitutive model is informed by soft tissue histology and the microstructural deformation mechanisms that characterize the tissues overall mechanical response. Through accounting for interfibrillar sliding in particular, the model was able to successfully describe the non linear viscoelastic behavior of tendons, correlating well with experimental findings in the literature. The outlined framework is generally applicable to numerous soft tissue types and is well suited towards further expansion and the investigation of collagens role in both tissue failure and remodeling.

References

- [1] Miller et al (2021). *J Mech Phys Sol*, (under review)
- [2] Rigozzi et al. (2013). *J Biomech*; 46, 813-818
- [3] Mattson et al. (2017). *Biomech Model Mechanobio*; 16, 215-225
- [4] Martufi et al (2012). *J R SOC Interface*; 9(77), 3366-337t

Complementary Functions of the Joint Morphology and Ligaments in Providing Stability to First the Carpometacarpal Joint

Wan M.R. Rusli¹, Eushaa Mirza¹, Sarah Tolerton², Sarah Yong², Riem Johnson², Maxim D. Horwitz² and Angela E. Kedgley¹

¹Department of Bioengineering, Imperial College London

²Department of Hand Surgery, Chelsea and Westminster Hospital (London)

Email: w.rusli15@imperial.ac.uk

Summary

A morphology-function model was created to assess the influence of variability in bony anatomy of the first carpometacarpal (CMC) joint and the translation of the joint when there is disruption to the ligaments. Variation in first metacarpal torsion and articular tilt angles contributed the most to the variability in first CMC joint translation.

Introduction

The first CMC joint depends on its ligaments to provide stability. However, it is not clear how the morphology of the first metacarpal and trapezium works with the ligaments in maintaining joint stability. Hence, the objective was to use a morphology-function model to determine the interplay between the ligaments of the first CMC joint and its bony morphology in preventing joint subluxation.

Methods

Sixteen specimens (8 males; 52.4±11.7 years, 7 left hands) were used in this study. Semi-automatic segmentation was done to computed tomography images of the specimens using MIMICS (v.17, Materialise, Belgium) to obtain 3D models of the first metacarpal and trapezium. ***In-vitro experiment:*** The first and second metacarpals, trapezium and trapezoid were removed from each specimen, taking care not to violate the first CMC joint capsule. The distal end of the first metacarpal was fixed in a specimen holder. The trapezium, trapezoid and proximal end of the second metacarpal were similarly fixed. An Instron testing machine equipped with a customised jig was used to apply external loads to the specimen in its neutral orientation. Each specimen was tested during intact and ligament sectioned conditions. Four ligaments were sequentially sectioned – anterior oblique ligament (AOL), ulnar collateral ligament (UCL), intermetacarpal ligament (IML) and dorsal radial ligament (DRL). The position of the joint in its intact state was taken as the baseline. ***Anatomical features:*** The first metacarpal articular tilt and torsion angles and length and width of the first metacarpal facet on the trapezium were measured on the 3D model of each of the specimens (ver. 9, Materialise, Belgium). ***Principal component analysis (PCA):*** The anatomical features and the translation data of the first CMC joint were used to develop a morphology-function model. PCA was implemented to reduce the dimension of the morphology-function model and highlight the relationship between the ligaments and the anatomical features in the translations of the first CMC joint.

Results and Discussion

The first principal component indicated that, in all four directions, the first metacarpal torsion angle (-2.60° (-2SD) to

21.67° (+2SD)) contributed to the magnitude of translation. As this angle twisted more ulnarly (+2SD), the translations of the first CMC joint in the direction of loading increased after the transection of the IML and DRL (Figure 1). The second principal component indicated that variation in the first metacarpal articular tilt angle (-4.58° (-2SD) to 9.92° (+2SD)) also contributed to the magnitude of joint translation, for all four load directions. An increased first metacarpal torsion angle could enable a better match between the concavity of the trapezium articulating surface with the convexity of the first metacarpal articulating surface during opposition. This would maximise bony stability, preventing subluxation of the first CMC joint. An increase in the first metacarpal articular tilt angle could reduce bony stability in the volar region of the articulating surface of the joint. With this, disruptions in the ligaments may be more likely to cause first CMC joint subluxation. Hence, the joint may rely on its convex-concave articulating surface at the dorsal region to help prevent subluxation of the joint.

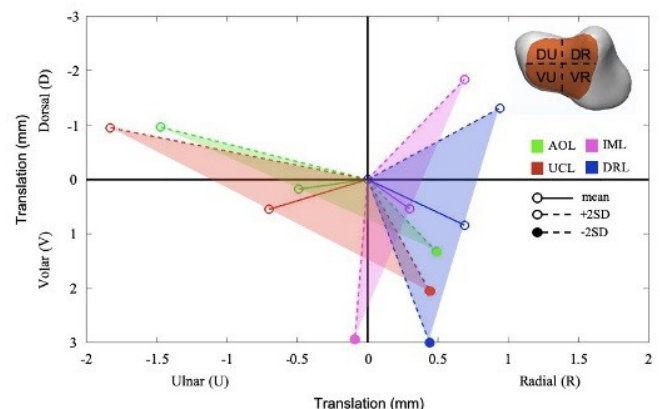


Figure 1: The translation (mean and ± 2 standard deviation) of the first CMC joint when displaced by load in the VD directions with variation in the first metacarpal torsion angle obtained in the first principal component. The colored region shows the region of subluxation of the joint that resulted from variations in the first metacarpal torsion angle with the presence of ligament disruption.

Conclusions

This study assessed the interactions between first CMC joint kinematics and its anatomical features. The morphology of the first metacarpal, particularly the torsion and articular tilt angles, was important in maintaining the stability of the first CMC joint.

Scan-Driven Fully Automated Pipeline for a Personalized, 3D Printed Low-Cost Prosthetic Hand

Yair Herbst¹, Shunit Polinsky¹, Anath Fischer¹, Yoav Medan², Ronit Schneor¹, Alon Wolf¹

¹Faculty of Mechanical Engineering, Technion, Israel

²Faculty of Electrical Engineering, Technion, Israel and Haifa3D organization, Israel

Email: yair.herbst@technion.ac.il

Summary

The loss of a hand can drastically reduce one's quality of life by decreasing the ability to perform activities of daily living. A prosthetic arm can help assist in such activities but cost of production and manual fitting processes limit the use and prescription of these devices. Moreover, prosthetic devices still have high rejection rates for various reasons, one of which is social acceptance. In this research we propose a novel, digital design process to create a personalized prosthetic hand. Our proposed fitting paradigm is entirely digital to minimize the design time and the high cost and dependency of trained professionals throughout the process, while potentially achieving a low-cost, tailor-made design that can be accessible from anywhere on the globe.

Introduction

Although there are many solutions in the field of upper limb prosthetics, financial resources play a crucial role in prescription of these devices, especially in children due to constant growth [1]. The cost of a prosthetic hand ranges from \$3,000 for a body powered prosthesis and up to \$100,000 for a neuro-prosthetic arm [2]. The very high price tag makes these devices inaccessible to large portions of the population. In many cases, the price is greatly affected by the time spent on manually fitting the device. Even when financial barriers are surpassed, rejection rates of prosthetic devices are considerably high and are usually related to the following causes: age of first fitting, lack of social acceptance, weight, vulnerability of the device and lack of sensory feedback [3]. Not using a prosthesis could lead to degeneration of joints and muscles, inflammations, and other complications.

Methods

The process, in general, is obtaining user data, then automatically generating a ready to print CAD model, a circuit

board and a bill of materials based on standard off-the-shelf parts and finally, assemble all parts together. The last step is the only manual one in the process but is shortened significantly by optimizing the previous steps. More specifically, we collect 2D images of the healthy hand for a parametrized model of the hand based on a functional *skeleton* and a *skin* to customize appearance thus increasing social acceptance and sense of ownership. In addition, we collect depth images of the residual limb for the hand's socket parametric design. The last type of user data collected is the user preferences which determines the user interface, such as simple body-powered or a motorized hand controlled by EMG, FMG or other interfaces, and haptic feedback. The entire process is illustrated in Figure 1.

Results and Discussion

Feedback from prospective users and from healthy subjects was collected in addition to inputs from professionals in the field. Based on the inputs received, the pipeline was improved and future research on each of the blocks will be conducted. In addition, validation tests for the hands performance and production were also conducted.

Conclusions

The proposed process and the outcome could potentially help overcome the above-mentioned difficulties and help push the prosthetic hands field into the digital design era. The entire research and final design are shared online for anyone in the world to use.

References

- [1] Krebs et al. (1991) Phys Ther. **71**: 920–934.
- [2] McGimpsey et al. (2008) Bioeng Inst Cent Neuroprosthetics Worcester Polytech Inst. 1–35.
- [3] Meurs et al. (2006) Prosthet Orthot Int. **30.2**:165–173.

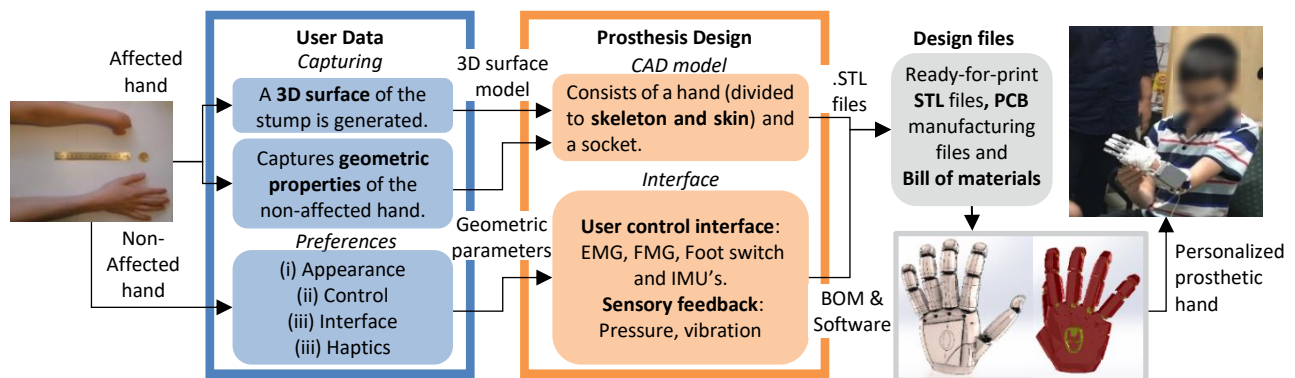


Figure 1: A block diagram of our proposed hand-fitting pipeline. Each of the blocks presents a component of the pipeline, which starts with user data and ends with a hand fitted to the user.

UNIFORMITY OF PERFORMANCE DURING THE COLLECTION OF MAXIMUM VOLUNTARY CONTRACTION TASKS FOR THE MUSCLES OF THE WRIST

Mercedes Aramayo Gomes Rezende¹, Oluwalogbon Akinnola¹, Angela E. Kedgley¹
¹Department of Bioengineering, Imperial College London, London, UK
a.kedgley@imperial.ac.uk

Summary

Maximum voluntary contraction (MVC) plays an important role in how we interpret electromyographical data. No protocol exists for finding MVC in forearm muscles though recommendations are available. This investigates the uniformity of MVC performance in recommended tasks and whether variance muscle activity is due to variance in force generated.

Introduction

Electromyography (EMG) is commonly used to record muscle activity. To enable inter- or intra-subject comparisons, measurements of maximum voluntary contraction (MVC) are used to normalize EMG data. There is no standardised protocol for obtaining MVCs of muscles of the upper limb. To create the most efficient protocol, it is important to understand the relationship between the forces and moments applied by participants during tasks designed to elicit MVCs. Therefore, the objective of this study was to quantify EMG signals and kinetics during a series of isometric tasks to provide a basis for an efficient and effective protocol to obtain MVCs in muscles of the forearm.

Methods

Fifteen right-handed participants (10 female, 5 male, 23.67 ± 4.5 years old) had nine surface EMG sensors (Delsys, Natick, MA) placed on their dominant forearm to capture muscle activity of the flexor carpi radialis (FCR), flexor digitorum superficialis (FDS), flexor carpi ulnaris (FCU), extensor digitorum communis (EDC), extensor carpi ulnaris (ECU), extensor carpi radialis (ECR), pronator teres (PT), biceps and triceps. Adapting the method from Ngo and Wells [1], participants performed tasks designed to elicit MVC of each muscle. These were: pull up, push down, radial pull, ulnar pull, pull, pronation, finger flexion, finger extension, grip, as well as two activities of daily living (ADL), which were turning a key in a lock and pouring a glass of water from a jar. The ADL tasks provided a baseline measure for expected muscle activations. A six degree of freedom load cell mounted to a handle measured the forces and moments applied.

Results and Discussion

The activity that elicited MVC for each muscle varied between participants (Fig. 1). For example, the MVC for PT occurred for most participants during the pronation-supination task, but it occurred during the pull up task and pull down tasks for two participants. Data from the load cell confirmed that the directions of the external forces exerted by the hand were the same for all participants (Fig. 2), indicating that the participants performed the activities correctly.

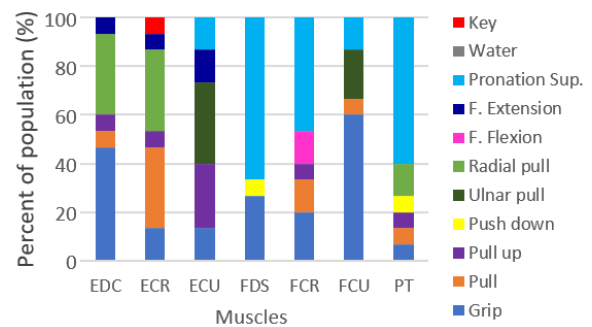


Figure 1: The percentage of people that generated maximum voluntary contraction for each muscle for all tasks.

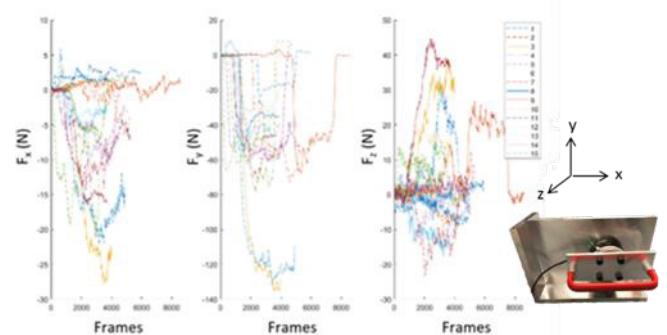


Figure 2: Load cell readings for all 15 participants for the push down task.

The forces and moments applied to the load suggest participants used different combinations of muscles to achieve the same external reaction force at the hand. Physiological differences may be the reason. This agrees with the findings of Maier et al., who investigated muscle synergies during precision grip and found that the interindividual variability was large enough to preclude the creation of a standard synergistic pattern [2]. They concluded that it was not the moments involved in the task but the central nervous system that chooses short-term, flexible synergies to achieve the task. This could result in participants using different muscles to achieve the same end task-oriented goal.

Conclusions

These findings indicate that, rather than prescribing a single activity to obtain the MVC of each muscle, a range of activities should be used to quantify the MVCs of wrist and hand extrinsic muscles to account for variations in activation strategies across the population.

References

- [1] Ngo, Wells, (2016) *J. Electromyogr. Kinesiol.* **26**, 66-72.
- [2] Maier, Hepp-Reymond, (1995). *Exp. Brain Res.* **103**, 108-122.

Characteristics of palmar and dorsal flexion muscle strength in college baseball players

Kazuhiro Ikeda¹, Yuki Hara², Ryuhei Michinobu³, Takeshi Ogawa³, Yuichi Yoshii⁴

¹ Department of Orthopedic Surgery, Kikkoman General Hospital, Chiba, Japan

² Department of Orthopedic Surgery, Faculty of Medicine, University of Tsukuba, Ibaraki, Japan

³ Department of Orthopedic Surgery, Mito Kyodo General Hospital, Ibaraki, Japan

⁴ Department of Orthopedic Surgery, Tokyo Medical University Ibaraki medical center, Ibaraki, Japan

Email: ikdkzhr1129.med@gmail.com

Summary (150/ 150 word)

The purpose of this study is to clarify the characteristics of wrist flexion and extension torques in college baseball players. Bilateral wrists of 50 college baseball players were evaluated. Throwing and non-throwing side, and hitting and non-hitting side were defined by the self-report. The players were divided into pitchers (P) and fielders (F) groups. In each group, the torques were compared between throwing and non-throwing side, hitting and non-hitting side. In addition, the wrist torques were compared between P and F groups for each of throwing side, non-throwing side, hitting side and non-hitting side. In group F, wrist extension torque was significantly larger on the throwing side compared to the non-throwing side. The wrist torques in F group were significantly larger than the P group in all conditions. This suggests that hitting requires more wrist flexion/extension torques than pitching. There were no significant effects in the throwing and hitting side.

Introduction

To prevent baseball pitching injury, it may be helpful to measure muscle strength related to the kinetic chain in the pitching motion. Although the wrist flexion is the end point of the kinetic chain, there is few knowledges of wrist flexion and extension torques in the baseball players. The purpose of this study is to clarify the characteristics of wrist flexion and extension torques in college baseball players. We hypothesized that the wrist flexion torque of the pitcher's is larger on the throwing side than on the non-throwing side, and is larger in the pitcher than in the fielder.

Methods

Bilateral wrists of 50 college baseball players (age: 18-21, all male, 24 pitchers and 26 fielders) were evaluated. We measured the maximum torques of wrist flexion and extension in the forearm neutral position using a self-designed wrist torque measuring machine (Three-One Design, Inc., Tsukuba, Japan) [1]. The throwing and non-throwing side, and the hitting and non-hitting side were defined by the self-report. The players were divided into pitchers (P) group and fielders (F) group. The results were divided into the throwing side or non-throwing side, and the hitting side or non-hitting side for group P and F. The wrist torques were compared between the P and F groups for each of throwing side, non-throwing side, hitting side and non-hitting side. In each group, the torques were compared between the throwing and non-throwing side, and between the hitting and the non-hitting side.

Results and Discussion

In the results of wrist flexion torques, there was no significant difference between throwing side and non-throwing side, and

hitting side and non-hitting side for both P and F groups. The measurements of F group were significantly larger than P group for all comparisons. (Fig.1).

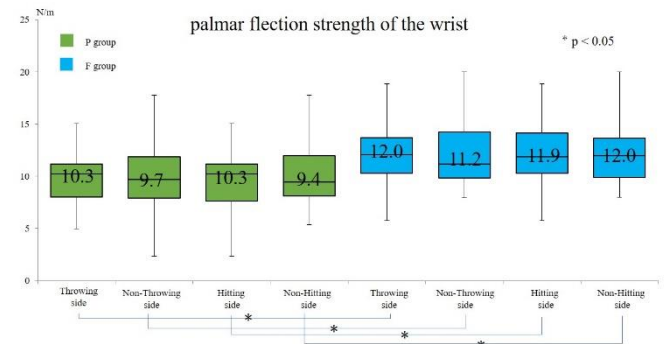


Figure 1: Results of wrist extension torques.

In the results of wrist extension torques, the throwing side torque was significantly larger than the non-throwing side in the F group. There were no significant differences in the other comparative items within the groups. The wrist extension torques in the F group were significantly larger than in the P group for all comparisons. (Fig.2).

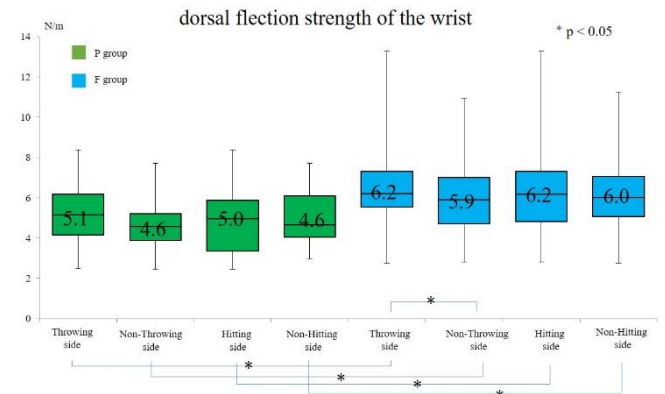


Figure 2: Results of wrist extension torques.

Conclusions

The wrist flexion and extension torque were larger in the fielders than in the pitchers in college baseball players. Fielder have more opportunities to hit, and this suggests that the wrist strength is more important in the hitting than in the pitching.

Acknowledgments: none

References

[1] Yuichi Yoshii et al. (2015). BioMed Eng Online,14:115

The effect of wrist posture on grip and muscle force capacities: comparison of a prehensile and a non-prehensile task.

Caumes. Mathieu¹, Vigouroux Laurent¹, Berton Éric¹, Goislard de Monsabert. Benjamin¹

¹Aix-Marseille Univ, CNRS, ISM, Marseille

Email: mathieu.caumes@univ-amu.fr

Summary

The wrist and finger are biomechanically coupled because of the hand extrinsic muscles, originating in the forearm. This coupling also influences the force-generating capabilities of the muscles crossing it. The goal of this study was to compare the effect of wrist posture on the grip and muscle force capabilities of 4 forearm muscles in a prehensile and a non-prehensile task. The non-prehensile task resulted in less co-contraction of extensors which modified the interaction between the force-length relationships of flexor and extensor muscles.

Introduction

The hand musculoskeletal system is composed of many joints and more than thirty muscles. The specific configuration of the hand musculature, including extrinsic muscles originating in the forearm, results in mechanical couplings between finger forces and the wrist joint equilibrium [1]. More precisely, it has been shown that the position of the wrist has a direct influence on the maximal grip force [2]. This influence seems to be explained by the interaction of the different force-length properties of forearm muscles [3]. However, this interaction could be modified in non-prehensile tasks, like finger pressing, as the wrist equilibrium constraints results in less antagonist activation [4]. The objective of this study was to compare the effect of wrist posture on grip and muscle force capacities for two different tasks: a finger pressing and a pinch grip task.

Methods

Nineteen volunteers (9 females, age: 21.7±2.5 years, hand length: 18.4±1.0cm) were instructed to exert a maximum force with their fingers in either a four-finger pressing or a thumb-index pinch grip configuration and in four different wrist postures. One posture was freely chosen by the participants, referred to as a “spontaneous” (S) position. The other three were imposed on the participants: a neutral (N) posture (0° of flexion and deviation), a maximal flexion (F) and a maximal extension (E). The force was recorded by a 6-axis force gauge (Nano25, ATI, Apex, NC). Simultaneously, the posture of the wrist and index finger was recorded using a 7-camera motion capture system (Qualysis, Göteborg, Sweden; 100Hz) tracking fourteen markers. Surface electromyographic (EMG) signals of six hand muscles were also simultaneously acquired (Trigno, Delsys, Natick, MA, 2000Hz).

For each trial, the maximal finger force was calculated as the mean on a window centered on the finger force peak. On this same window, joint angles were deduced from average marker positions and the activation from RMS of the EMG signal normalized by the maximal RMS. Muscle length and force of different forearm muscles were computed from joint angles

and activation using a biomechanical model [3, including a geometrical model of tendon excursion and muscle force-length-activation relationships [5].

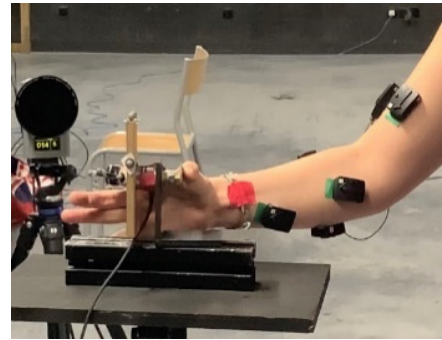


Figure 1: Photography of the experimental setup.

Results and Discussion

Wrist posture influenced differently the maximal force exerted in pinch grip and finger pressing. The highest maximal finger force in pinch grip was observed for the spontaneous wrist posture, as it has been observed for power grip [2,3]. This confirms participants spontaneously chose the wrist posture resulting in optimal flexor and extensors capabilities [3]. The maximal finger force during pressing task was less influenced by wrist posture. These different influences were explained by a change of muscle coordination, identified by EMG activity. The pressing task indeed reduced the level of co-contraction of finger and wrist extensors compared to the pinch grip task. As a result, the spontaneous posture is more variable. As the activation of extensors is low, the grip force is primarily influenced by force-length relationships of flexors which seems to produce a near-optimal force for a wide range of wrist posture. In this case, wrist posture might be more related to the participant's daily hand use, such as sports or professional activities.

Conclusions

This study showed that wrist posture influences differently the grip capabilities and the muscle mechanics in non-prehensile and prehensile tasks. These results could help surgeons in designing tendon transfers at the wrist or give insight to ergonomic engineers in optimizing hand-object interfaces.

References

- [1] Snijders, CJ et al. (1987). *Med Sci Sports Exerc*, **19**,5: 518-23.
- [2] O'Driscoll, SW et al. (1992). *The Journal of hand surgery*, **17**,1: 169-177.
- [3] Caumes, M et al. (2019). *Scientific reports*, **9**,1: 1-11.
- [4] Vigouroux L et al. (2011). *Neuroscience letters*, **504**,3: 290-294.
- [5] Goislard, B et al. (2020). *Med Biol Eng Comput.*, **58**,10: 2531-2549.

Development of Spontaneous Motor Activity with Age in Healthy Infants and Infants with Infantile Cerebral Palsy

C. Disselhorst-Klug¹,

¹ Department of Rehabilitation & Prevention Engineering, Institute of Applied Medical Engineering, RWTH Aachen University, Germany
Email: disselhorst-klug@hia.rwth-aachen.de

Summary

Abnormalities of age-appropriate motor development in infants may be a sign of a progressing motor impairment. This paper presents a method for objectively assessing the motor development of infants. It is demonstrated that and how the motor development of infants with ICP differs from that of healthy infants.

Introduction

Coordination between perception and action is required to interact with the environment successfully. This training is already undertaken by very young infants who perform spontaneous movements to learn how their body interacts with the environment. The strategies used by the infants for this purpose change with age. Therefore, investigations of motor development during the first month of life will give insight into the very early progresses made to control action. This information becomes even more important when it is reasonably expected that a newborn infant might develop a movement disorder due to infantile cerebral palsy (ICP).

In developmental neurology visual observation of spontaneous motor activity has turned out to be the most important diagnostic criterion. However, objective methods, which allow the evaluation of spontaneous movement development, are not available so far. This paper aims to introduce an objective methodology which allows the quantitative evaluation of the development of spontaneous motor activity in newborns.

Methods

The introduced methodology is based on the acquisition of spontaneous movements of the newborns by accelerometry. 4 lightweight accelerometers were attached to the infant's hands and feet (Figure 1). The unclothed babies lie prone and acceleration data are recorded over a 2-minute period.

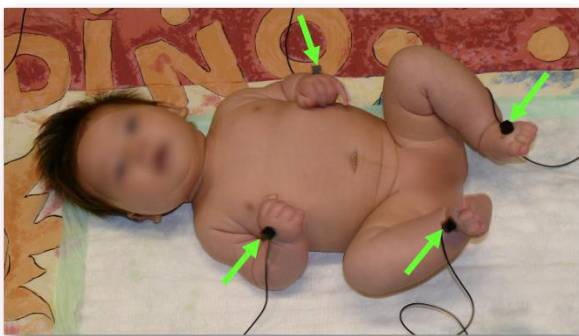


Figure 1: Acquisition of spontaneous movements of the hands and feet in newborns.

To evaluate the spontaneous movements, eight movement parameters, which have been shown to be sufficient to discriminate between normal and pathological movement patterns in infants [1], were extracted from the recorded accelerations.

The spontaneous movements of 24 infants, comprising 16 healthy full-term infants (mean gestational age 39.7 weeks, 11 female, 5 male) and eight pre-term infants (mean gestational age 28.6 weeks, 3 female, 5 male) with developing infantile cerebral palsy (ICP), were analyzed around the first, the third and the fifth months of life.

Results and Discussion

In the healthy group, three of eight parameter values showed significant changes between the first and the third month of life; values of two additional parameters changed significantly between the third and the fifth month of life. Figure 2 demonstrates with the example of the parameter "Cross-correlation coefficient of acceleration between left and right foot" how spontaneous movements in healthy infants change with motor development. In babies suffering from ICP, most differences to the healthy group can be found between the first and the third month of life (Figure 2), a trend which was reflected in this study in four of eight parameter values.

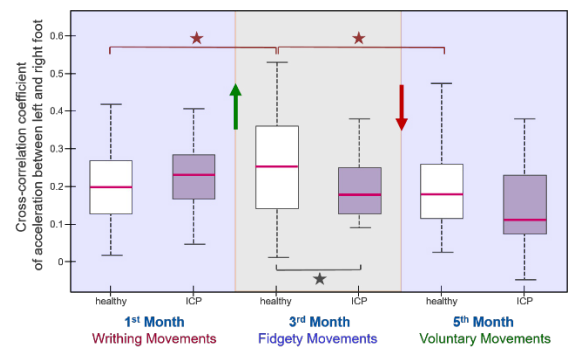


Figure 2: Parameter Cross-correlation coefficient of acceleration between left and right foot. Comparison between healthy subjects and patients with ICP. (* significant different $p < 0.05$)

Conclusions

It was possible to provide an objective description of motor development in healthy newborns. Furthermore, it was shown that pathologies influence development of motor activity significantly. Since the introduced methodology is objective and quantitative, it is suitable to monitor the development of spontaneous motor activity with age.

References

- [1] Heinze F et al. (2010). *Med Biol Eng Comput*, **48**: 765-772.

Quantification of inter-limb coupling during bilateral stance in individuals with transtibial amputation

Peter C. Raffalt^{1,2}, Jenny A. Kent^{2,3} and Nick Stergiou^{2,4}

¹ Department of Physical Performance, Norwegian School of Sport Sciences, Oslo, Norway

² Department of Biomechanics and Center for Research in Human Movement Variability, University of Nebraska at Omaha, Omaha, NE, USA

³ Department of Physical Medicine and Rehabilitation, Northwestern University, Chicago, IL, USA.

⁴ College of Public Health, University of Nebraska Medical Center, Omaha, NE, USA.

Email: peter.raffalt@nih.no

Summary

The inter-limb coupling of individuals with transtibial amputation (TTA) was investigated. The difference in inter-limb coupling between individuals with TTA and unimpaired individuals was direction-dependent and weaker in the anterior-posterior direction for the individuals with TTA.

Introduction

Balance control during upright standing requires the center of mass to be kept within the base of support whilst maintaining both the flexibility and stability to perform simultaneous actions and adjust to external perturbations. In individuals with permanent alterations to sensory input and to volitional control of movement due to unilateral foot or limb amputation, it is crucial to investigate the inter-limb coordination to fully understand how stable upright standing is controlled [1]. The aim of the present study was to determine how upright standing is controlled in individuals with unilateral TTA in terms of the inter-limb coupling of the center of pressure dynamics between the limb on the prosthetic side (COP_p) and the intact limb (COP_i).

Methods

Twenty-one individuals with TTA (male/female: 17/4; mean \pm SD age: 59.7 \pm 15.0 yrs; height: 1.79 \pm 0.07 m; mass: 100.3 \pm 15.6 kg) and 18 unimpaired individuals (male/female: 14/4; mean \pm SD age: 54.1 \pm 16.0 years; height: 1.73 \pm 0.10 m; mass: 85.2 \pm 18.4 kg) completed 90 seconds of upright standing with each foot on a separate force platform operating at 600Hz. The COP time series were filtered using a Daubechies wavelet, downsampled to 100Hz and the initial 15 seconds were removed. The inter-limb coupling was assessed from the COP_p and COP_i in terms of 1) the number of synchronization epochs between the signals (i.e. number of shifts between stable coordination states), 2) the total duration of the synchronization (i.e. stability of coordination), 3) the mean relative phase angle between the signals (i.e. coordination type) and 4) the deviation phase (i.e. coordination variability) [2]. A two-way mixed design ANOVA or Harrison-Kanjo test (for relative phase) with group and direction as independent factors was applied, Holm-Sidak post hoc test and level of significance at 5 %.

Results and Discussion

In the anterior-posterior direction, the TTA group had a significantly higher number of synchronization epochs, lower total synchronization duration, less in-phase relative phase angle and a greater deviation phase (Figure 1). No group

differences were observed in the mediolateral direction. The altered control of bilateral standing in individuals with TTA was characterized by more shifts between stable coordination states, less overall stability, a different coordination pattern and greater coordination variability compared to unimpaired individuals. This indicated a weaker inter-limb coupling in the AP direction for the individuals with TTA.

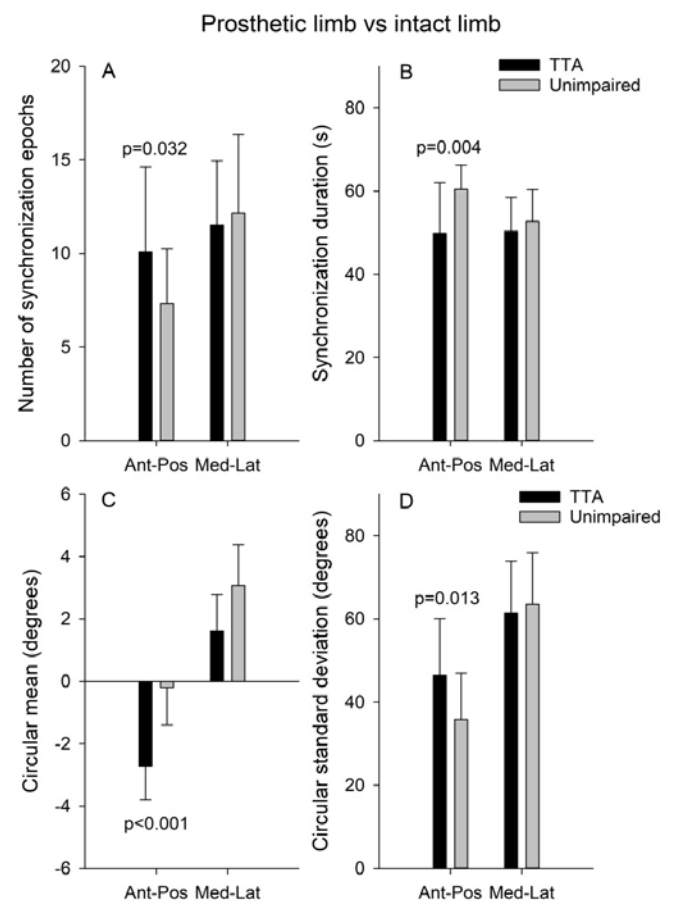


Figure 1: Inter-limb coupling characteristics for individuals with TTA and unimpaired individuals.

Conclusion

The difference in inter-limb coupling between individuals with TTA and unimpaired individuals was direction dependent and weaker in the AP direction for the individuals with TTA.

References

- [1] Hlavackova P. et al. (2011). *PLoS One*, **6**: e19661.
- [2] Wang and Newell (2012). *Neurosci Lett*, **507**: 47-51.

Unrestricted age-related compensation in a daily life sit-to-walk task

van der Kruk, Eline¹ & Bull, Anthony M. J.²

¹Biomechanical Engineering, Delft University of Technology, Delft, the Netherlands

²Department of Bioengineering, Imperial College London, London, UK

Email: e.vanderkruk@tudelft.nl

Summary

The prevention and treatment of age-related movement impairments, ideally, requires early diagnosis. As the human movement system has physiological and functional redundancy, movement limitations do not promptly arise at the onset of physical decline: humans will compensate. The aim of this study was to observe (early) compensation during the sit-to-walk task in relation to neuromuscular capacity and movement objectives in young and older adults. Participants' upper- and lower limb strength, nerve conduction, joint sense acuity, and balance were tested. Moreover, standardized questionnaires on fear of falling, pain, dizziness, lifestyle, and frailty were taken. Their kinematics and muscle activity during sit-to-walk tasks were recorded in an unrestricted experimental set-up. Key finding was that standing up from a chair by pushing off with the arms is not strictly a compensation strategy for a lack of muscular capacity.

Introduction

An important daily life activity is standing up from a seated position. This movement has been widely studied in biomechanics, however most studies have imposed standardizations on protocol, so the possibility of compensation is restricted [1]. For example, most studies on sit-to-stand did not permit participants to compensate using their arms. However, from the onset of age-related physical decline (mid-twenties) until the point that movement impairments arise, compensation is part of human movement strategies. Compensation can therefore be a clinically relevant early indicator of physical decline. Scientifically compensation is interesting as it tips the hand on how humans within the functional redundancy of the neuromuscular systems select a movement strategy. The aim of this experimental study was to capture unrestricted compensation in the sit-to-walk task and relate this to neuromuscular capacity and movement objectives (psychological considerations) in young and older adults.

Methods

This study (N=50) comprises 14 young women (YW) (age: 27.1±5 years), 13 young men (YM) (27.3±4.3), 12 relatively healthy older women (EW) (75±5.6), 11 relatively healthy older men (EM) (76.8±7.2). All participants gave their informed consent. Participants sat down on an instrumented chair with instrumented armrests with the seat at approximately knee height. Participants were asked to stand up and walk to a table 3m in front of them: 5x at self-selected speed, 5x at fast speed. Their kinematics (Vicon) and muscle activity (Delsys EMG) were recorded.

Additionally, to assess their neuromuscular capacity, we measured their maximum peak isokinetic joint moments for the knee, hip, ankle, and elbow on a dynamometer (Cybex), handgrip strength (Jamar), balance in a standing balance task, proprioceptive acuity with an ipsilateral matching task of knee flexion, joint range of motion of the hip and ankle (Cybex), and nerve conductivity and maximal muscle excitation with a nerve conduction test. To assess psychological considerations, a questionnaire reviewed their (former) profession, levels of activity, diet, general health, experienced injuries, level of frailty (Edmonton), fear of falling (FES-I short), hearing, level of Dizziness, hand dominance (Edinburgh), and pain (visual analogue scale).

For the purpose of this abstract we will focus on the results of the applied arm strategies.

Results and Discussion

Four arm strategies were observed: standing up without arms, swinging the arms, pushing off on the knees, and pushing off on the armrests. Note that all participants could stand up without arms. There was a distinct result: EM used an arm push off in 91% of all trials (N=55) at self-selected speed, and in *all* trials at fast speed, whereas YM, YW and EW only pushed off in less than half of all trials. The hypothesis was that EM had less lower limb joint strength than the other groups. However, their peak isokinetic strength corrected by bodyweight did not differ significantly from YW and was mostly higher than EW for all measures. Also, no differences were found between the means of the arm strategy groups with proprioceptive acuity, balance scores, hand grip strength, muscle excitation, or nerve conduction. Nor with the anthropometric data (BMI, length, weight), FES-score (fear of falling), or frailty score. The only significant difference was that the participants with an arm push-off had a significant lower hip flexion range of motion on the dominant side ($p<0.05$) and a lower ankle plantar-flexion range of motion on the non-dominant side ($p<0.01$).

Conclusions

Standing up from a chair by pushing off with the arms is not strictly a compensation strategy for a lack of muscular capacity in older men.

Acknowledgments

NWO-ENW Rubicon Grant 019.173EN.023, 2018

References

- [1] Van der Kruk & Bull (2019), Rising from a seated position, ISB 2019

Lumbar extensor muscle isometric torque steadiness and torque-HDsEMG coherence is altered in individuals with chronic low back pain

Michail Arvanitidis¹, David Jiménez-Grande¹, Nadège Haouidji-Javaux¹, Deborah Falla¹, Eduardo Martínez-Valdes¹

¹Centre of Precision Rehabilitation for Spinal Pain (CPR Spine), School of Sport, Exercise and Rehabilitation Sciences, College of Life and Environmental Sciences, University of Birmingham, Birmingham, UK

Email: marvanitidis@outlook.com

Summary

Lumbar extensor muscle isometric torque steadiness (TS) was evaluated in individuals with chronic low back pain (CLBP) and asymptomatic (AS) age- and gender-matched controls, during two submaximal torque-matching tasks at different torque levels. This study is the first to show that individuals with CLBP fail to increase common fluctuations in torque and electromyographic (EMG) activity when exerting higher forces. This finding shows that the CLBP group were still able to exert the requested amount of torque likely by utilising compensatory back-extension patterns.

Introduction

The ability of humans to exert steady torque during a submaximal voluntary contraction is defined as TS. Generation of smooth torque is essential for physical function, and the impairment of TS can influence the precision of voluntary movements. People with CLBP present with impairments in lumbar extensor muscle force accuracy compared to AS controls [1]. However, it is unclear whether people with CLBP also present with higher deficits in TS compared to AS controls. We investigated 1) whether individuals with CLBP present with reduced lumbar extensor muscle TS compared to AS controls, and 2) the neuromuscular mechanisms underlying reductions in TS by applying high-density surface EMG (HDsEMG)-torque coherence with principal component analysis (PCA).

Methods

15 individuals with CLBP and 15 AS controls were included. Submaximal isometric lumbar extensor TS was measured with an isokinetic dynamometer during two torque target-tracking tasks at 20% and 50% of their maximal voluntary contraction (MVC). HDsEMG signals were acquired from their lumbar erector spinae (ES) with a 64-electrode grid. Root mean square (RMS) was determined as an average for all electrode pairs (59 bipolar). TS was quantified as the coefficient of variation (CV) of torque. Coherence and cross-correlation analyses were conducted to quantify the degree of similarity between the filtered interference HDsEMG and torque signals for each submaximal contraction. PCA was used to reduce dimensionality of HDsEMG data, in order to improve HDsEMG-based torque estimation [2]. Coherence values were calculated for the δ (0-5Hz), α (5-15Hz) and β (15-30Hz) frequency bands and then they were transformed to z-scores to allow statistical comparisons.

Results and Discussion

Overall, TS was lower in individuals with CLBP ($p=0.029$; Figure 1A). Z-coherence in the δ band and cross-correlation

increased with the increase in torque for the AS controls but not in the CLBP group ($p=0.018$, $p=0.030$; Figure 1B, C). Coherence in the α and β bands did not differ between groups. Overall HDsEMG RMS amplitude, the center of ES muscle activity and co-activation levels did not differ between groups. As previously postulated, the neural drive to the muscles in the δ band mirrors the common drive to the muscle in the same bandwidth and is the main determinant for the control of torque [3]. Additionally, an increase in torque is commonly accompanied with an increase in δ band coherence, as seen in the AS group. Thus, the TS deficits observed in the CLBP group could be attributed to the lack of an increase in common synaptic input, with the increase in torque. This is also supported by the cross-correlation results, showing that in the CLBP group, the net increase in torque was not accompanied by an increase in the contribution of the ES muscle to the resultant torque fluctuations. Given that both groups exerted similar amount of torque during the task, the individuals with CLBP could be compensated by activating synergistic muscles. Interestingly, the RMS amplitude alone could not explain the differences in TS, but the proposed coherence analysis enabled us to explain the differences in TS, showing that HDsEMG can improve the estimation of the exerted torque, providing a more accurate assessment of lumbar ES activity than conventional RMS amplitude calculations.

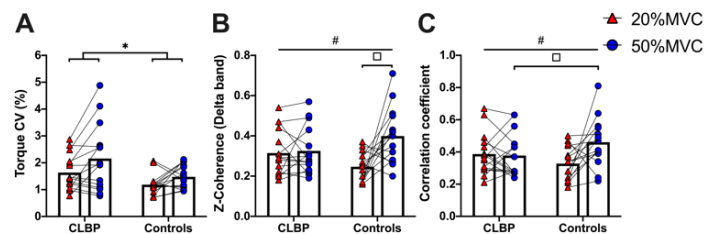


Figure 1: Torque CV (A), δ -band coherence (B) and cross-correlation (C) values (mean \pm SD) of the CLBP group and AS controls at 20% and 50%MVC respectively (*main effect of group, #interaction effect: group*torque, \square : post hoc tests).

Conclusions

This study uniquely demonstrates that individuals with CLBP have reduced TS and fail to increase the common fluctuations in torque and HDsEMG activity with increasing torque, likely due to the use of compensatory back extension patterns during this task.

References

- [1] Pranata A et al. (2017). *Clin Biomech*, **46**:46-51.
- [2] Staudenmann et al. (2006). *IEEE Trans Biomed Eng*, **53**(4):712-9.
- [3] Farina D et al. (2014). *J Physiol* **592**(16):3427-41.

ANALYSIS OF SPECTRAL ATTRIBUTES OF SURFACE ELECTROMYOGRAPHY DURING GAIT IN CHILDREN WITH FRAGILE X SYNDROME

W. PIATKOWSKA¹, M. ROMANATO¹, F. SPOLAOR¹, A. DESTRO¹, A. MURGIA², R. POLLI², Z. SAWACHA^{1,3}

¹ Department of Information Engineering, University of Padova, Italy

² DEPARTMENT OF WOMEN AND CHILDREN HEALTH, UNIVERSITY OF PADOVA, ITALY

³ Department of Medicine, DIMED, University of Padova, Italy

Email: weronikajoanna.piatkowska@studenti.unipd.it

Summary

Fragile X Syndrome (FXS) is a genetic condition, mainly characterized by intellectual disability, musculoskeletal alterations and behavioral problems. This project aims to investigate association between abnormal motor control and altered spectral attributes of electromyography signals in FXS. Results showed increased instantaneous mean frequency during gait in Rectus Femoris (RF) and Biceps Femoris (BF) in FXS children. Furthermore differences in the percentage of energy allocated in various frequency bands between analyzed populations were detected.

Introduction

FXS is the leading form of inherited intellectual disability and autism spectrum disorder, caused by a tri-nucleotide CGG repeat expansion in the promoter region of the FMR1 gene [1]. In these subjects, the most frequent musculoskeletal manifestations include severe flexible flat feet, excessive laxity of the joints, and possible scoliosis [1], that justifies a referral for gait analysis evaluation. The aim of the present study was to identify the relationship between observed musculoskeletal manifestation and altered motor control in FXS children. For this purpose surface electromyography (sEMG) was acquired within standard clinical ambulatory assessment conditions and its spectral attributes extracted.

Methods

After appropriate informed consent by the parents, 23 FXS children ((FXSC) mean (\pm SD) age and BMI respectively of 9,00 (\pm 3,92) years and 18,77 (3,07 \pm) Kg/m²) and 20 controls ((CS) mean (\pm SD) age of 9,68 (\pm 2,90) years and 21,52 (\pm 4,61) BMI of Kg/m²), were evaluated at the BiomovLab of the Department of Information Engineering, and at the Women and Children Health Department of the University of Padua. Kinematics and sEMG data were simultaneously acquired through four synchronized cameras (GoPro Hero3, 30fps) and an 8 channel sEMG system (FreeEmg, BTS, 1000Hz) that collected the activity of Tibialis Anterior (TA), Gastrocnemius Lateralis (GL), RF and BF. Each subject performed several gait trials and at least three trials per subject were processed. The following sEMG parameters were

extracted: instantaneous mean frequency (IMNF) and percentage distribution of signal energy in frequency bands.[2]

Results and Discussion

Results consistently showed the presence of an altered muscle activity (Fig. 1): FXS displayed increased IMNF values in RF and BF, decreased percentage of energy in the band between 10-60 Hz and increased percentage in the bands between 50-400 Hz.

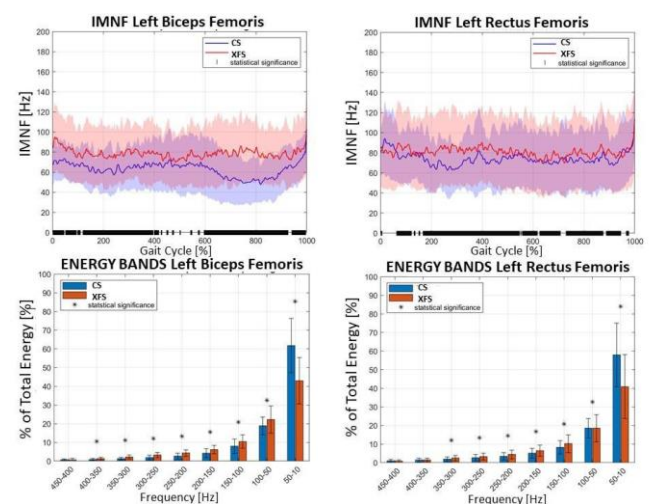


Figure 1: IMNF of left BF and RF (blue CS and orange FXSC; mean \pm SD) during gait cycle and percentage distribution of energy in the frequency bands of left BF and RF (blue CS and orange FXSC; mean \pm SD); (* - significant difference)

Conclusions

Results suggest that FXSC increases their muscle activity during the gait cycle and also the number of motor units in low frequencies. This information can help to determine the degree of improvement in FXSC walking ability.

References

- [1] Hagerman RJ et al. (2017). *Nat Rev Dis Primers*, 3, 17065
- [2] Pilkar, R et al. (2017). *Front Neurol* 8, 449

Injury and Surgery Are Associated with Shoulder External Rotation During Exam and Baseball Pitching

Hannah L. Stokes¹, Nigel Zheng¹, Koco Eaton²

¹Department of Mechanical Engineering and Engineering Science, University of North Carolina at Charlotte, NC, USA

²Tampa Bay Rays and University of South Florida, FL, USA

Email: nzheng@uncc.edu

Summary

The study included 109 college baseball pitchers and compared shoulder rotational properties, ball speed, and maximum external angle during baseball pitching with pitchers before and after injury and surgery and a healthy control group. One-way analysis of variance with Tukey post-hoc tests were performed using SPSS. The shoulder external rotation during exam and baseball pitching trended to being greater before surgery compared to those recovered from surgery, but there was not statistically significance.

Introduction

Baseball pitching is demanding on the shoulder and it is common for injuries to occur. The relationship of shoulder range of motion and injury has been studied [1]. A study showed that increasing ball speed also increased the risk for injury [2]. Improving performance and reducing injuries are a focus for both coaches and pitchers.

The purpose of this study is to investigate how elbow and shoulder injuries and surgeries are related to shoulder external rotation during exam and baseball pitching. This connection could allow for correction of baseball mechanics and reduce the number of injuries. We hypothesize that injuries and surgeries are not related to shoulder external rotation during exam and baseball pitching.

Methods

The study included 109 college baseball pitchers (height: 186±8 cm and weight: 85±9 kg). This study was approved by an institutional board and all pitchers gave informed consent. All pitchers were healthy during testing. The pitchers came into the lab for biomechanical testing and the self-reported injury questionnaire. The injury questionnaire reports if the pitcher has had a surgery or injury exclusively. Additionally, the pitchers were followed annually to complete the injury questionnaire. The shoulder rotational test measured the end-point angle (EPA), shoulder rotational flexibility (SRF), and resistant onset angle (ROA) using a custom-made wireless device [3] (Figure 1).

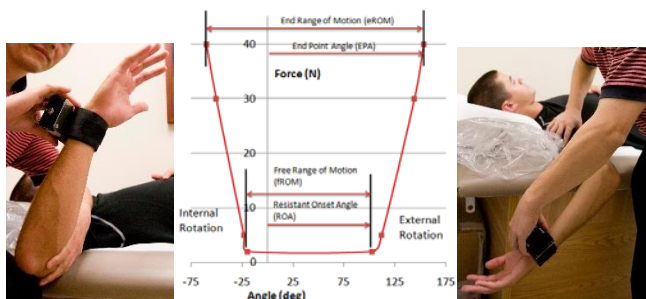


Figure 1: Shoulder rotational test performed during the exam.

Ten overhead fastball pitching motions were collected at 240 Hz using a motion capture system. Averages of top three strike pitches for ball speed and shoulder maximum external rotational (MER) angle were used for comparison. The surgery and injury groups had surgeries or injuries, respectively before or after testing. The healthy group had no reported surgeries or injuries before and after testing. One-way analysis of variance with Tukey post-hoc tests were performed using SPSS with an alpha set to 0.05.

Results and Discussion

Ball speed (mph), EPA (deg), SRF (deg/Nm), and MER (deg) were all greater in those before surgery (post-test) when compared to those after injury and surgery (pre-test) (Table 1). Eight subjects were excluded due to both pre-test and post-test surgeries or injuries.

Table 1: Results Mean±SD for the ball speed (mph), EPA (deg), SRF (deg/Nm), ROA (deg), and MER (deg).

	After Surgery	After Injury	Healthy	Before Injury	Before Surgery	P
N	19	16	41	12	13	-
Ball Speed	76±5	78±3	76±4	79±4	79±5	0.14
EPA	134±8	138±13	137±10	140±12	139±9	0.68
SRF	4.0±2.1	3.8±1.6	4.5±1.6	3.7±1.0	5.4±1.7	0.06
ROA	105±12	110±12	107±10	111±13	102±12	0.26
MER	169±11	173±12	173±10	179±13	178±12	0.12

Findings emphasize that shoulder rotational properties should be monitored in order to improve performance and reduce injury during baseball pitching. Future work should study shoulder rotational properties and injury mechanisms at the professional level for an extended duration of time.

Conclusions

The pitchers had trended to have greater ball speed, range of motion, flexibility and maximum external rotation during baseball pitching before surgery compared to after surgery; however, there was no significant difference.

Acknowledgments

This study is funded by a Clinical Research Grant from Major League Baseball.

References

- [1] Wilk K et al. (2015). *Am J Sports Med*, **43**: 2379-2385.
- [2] Bushnell B et al. (2010). *Am J Sports Med*, **38**: 728-732.
- [3] Zheng N. (2011). *Int J Sports Med*, **33**: 463-468.

Whole-body angular momentum and external torque during the block phase of the sprint start

Paul Sandamas¹, Elena M. Gutierrez-Farewik^{2,3} and Anton Arndt^{1,3},

¹BMC Laboratory, The Swedish School of Sport and Health Sciences, Stockholm, Sweden

²KTH MoveAbility Lab, Dept. Engineering Mechanics, KTH Royal Institute of Technology, Stockholm, Sweden

³CLINTEC Institution, Karolinska Institute, Stockholm, Sweden

Email: paul.sandamas@gih.se

Summary

Whole-body angular momentum (\mathbf{H}) and its time derivative, net external torque (\mathbf{T}), in the three spatial directions during the block phase of the sprint start were investigated. Nine competitive sprinters performed maximum effort block starts. A whole-body model was created and \mathbf{H} and \mathbf{T} computed from each athlete's trial with the greatest normalised average horizontal block power. The greatest peak block phase components of \mathbf{H} and \mathbf{T} were found in the sagittal plane whilst the smallest were found in the transverse plane. Sprinters generate two angular impulses in each plane. One during the double push (DP) phase followed by an opposite directed impulse during the single push (SP) phase. Regulation of angular impulses could explain segment motion outside the sagittal plane.

Introduction

From a force application perspective, the block phase in sprinting is a unique part of the race for several reasons. These include: initial simultaneous impulses from both feet, greatest contact time and greatest net external anterior impulse (i.e. greatest change in velocity) [1,2]. These present a challenge to the athlete in how to direct these large and varying external reaction forces in order to maximise external power whilst generating rapid upper and lower body segment rotations and rising from a crouched to an extended position at block exit. However, neither \mathbf{H} nor \mathbf{T} during the sprint start have been described in the scientific literature. Investigating the sprint start using the basic principles governing whole-body rotation is a basis for understanding why segment motions take place in the frontal and transverse planes. Therefore, the aim of this study was to investigate wholebody angular momentum and its time derivative, net external torque, during the block phase of the sprint start.

Methods

Nine competitive sprinters (8 male, 1 female) performed five maximum effort block starts. Block forces and three-dimensional kinematics were recorded throughout the block phase using a 12-camera (Oqus 4, Qualisys AB,) motion analysis system (250 Hz). A 15 segment full-body model was created using Visual3D, (C-Motion Inc.). The trial with the greatest normalised external block power was used to compute \mathbf{H} and \mathbf{T} with respect to the CoM. External torque was computed by taking the derivative of \mathbf{H} with respect to time. Each athlete started with their left foot on the front block. To allow comparison between athletes, \mathbf{H} and \mathbf{T} were normalised.

Results and Discussion

The largest peak magnitudes of \mathbf{H} and \mathbf{T} were found in the sagittal plane and the smallest were seen in the transverse plane (Figure 1a). Two angular impulses were generated in each plane, one during the DP phase followed by an opposite directed impulse during the SP phase (Figure 1b). The angular impulses in the transverse and frontal planes during the DP phase were virtually equal and opposite to their corresponding angular impulses during the SP phase.

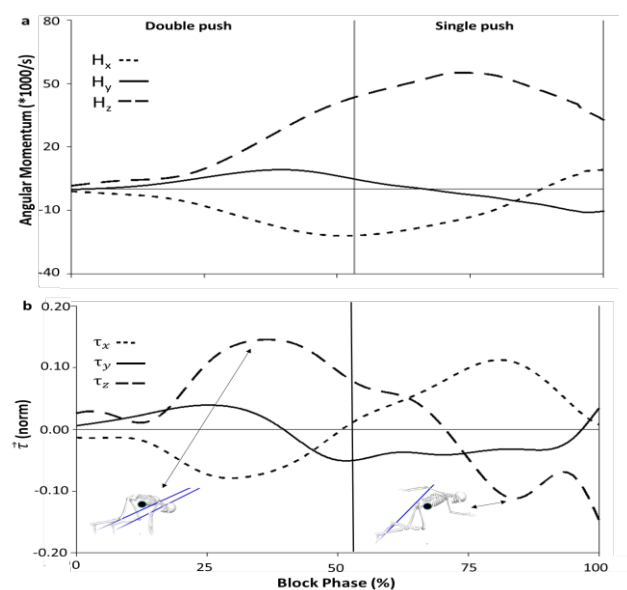


Figure 1: Ensemble average components of angular momentum (\mathbf{H}) (a) and external torque (\mathbf{T}) (b). Positive values indicate a counter clockwise rotation when viewed from the right side, front and above. The skeleton images give an illustration of the direction of the net external force vector(s) with respect to the CoM of the sprinter in the sagittal plane.

Conclusions

A possible reason for segment motion outside the sagittal plane is to help regulate the non-sagittal plane angular impulses to prevent unwanted whole-body rotation.

Acknowledgments

This work was supported by The Swedish Research Council for Sport Science [P2015-0029].

References

- [1] Otsuka et al. (2014). *J. App. Biomech*, **30**: 390-400.
- [2] Nagahara et al. (2017). *Int. J. Sp. Med.* **38**:534-540

HOW RUNNING BIOMECHANICS INFLUENCE THE OCCURRENCE OF ILIOTIBIAL BAND SYNDROME?

Qipeng Song¹, Peixin Shen², and Li Li³

¹College of Sports and Health, Shandong Sport University, Jinan, China

²Graduate School, Beijing Sport University, Beijing China

³Department of Health Sciences and Kinesiology, Georgia Southern University, Statesboro, 30460, USA

Corresponding author: Dr. Li Li, lili@georgiasouthern.edu

Summary

Iliotibial band syndrome (ITBS) is a leading knee overuse injury that is related to running biomechanics. A total of 192 male runners were recruited, and 179 of them finished the eight-week running program. Fifteen of them developed ITBS and comprised the ITBS group, and 15 matched healthy runners comprised the control group. One force platform and a motion capture system collected biomechanical data before and after the intervention. At week 9, the ITBS group exhibited greater anterior pelvic tilt angle and hip flexion angle than the control group. They showed increased trunk inclination angle, whereas the control group demonstrated lower hip flexion and adduction moments than those at week 0. Decreased hip flexion and adduction angles were gait adjustment strategies that could be used to avoid ITBS occurrence. Excessive trunk posture and pelvic activity during running are also ITBS risk factors.

Introduction

The popularity of running leads to an increased number of running-related injuries. ITBS is the second most common running injury, accounts for 1.6%–12% of all running-related injuries. The exact etiology of ITBS is unclear, but biomechanics is considered one of the factors [1]. Most of the previous studies on ITBS were retrospective ones. It was difficult to elaborate on the pathogenesis. Therefore, we designed a prospective study to explore the effects of running biomechanics of male runners on the occurrence of ITBS.

Methods

A total of 192 male runners were recruited, and 179 of them finished the eight-week running program. They run approximately 38 Km/week at approximately 3.7 m/s pace. Fifteen of them developed ITBS, comprised the ITBS group, and 15 matched healthy runners comprised the control group. Participants were asked to undergo two gait test trials, before and after the training. In each trial, all participants were asked to run on a 90 cm × 1500 cm platform at a velocity of 3.7 ± 0.2 m/s. A Kistler force plate with sampling at 1000 Hz was embedded at the center of the platform to collect ground reaction force data. An eight-camera motion capture system (Vicon, Oxford Metrics Ltd., UK) with sampling at 100 Hz was used to collect kinematic data synchronously (Figure 1). Group and training effects were examined by two-way ANOVA with mixed design. The significance level was set at 0.05.

Results and Discussion

At week 9, the ITBS group ($19.2 \pm 5.4^\circ$) exhibited greater ($p < 0.001$) anterior pelvic tilt angle than the control group ($11.8 \pm 6.3^\circ$), whereas the control group demonstrated lower hip flexion angle (week 0: $42.8 \pm 10.2^\circ$, week 9: $32.8 \pm 7.2^\circ$, $p = 0.006$), and hip adduction moment (week 0: 8.8 ± 2.6 Ng/kg, week 9: 6.4 ± 3.3 Ng/kg) than those at week 0.

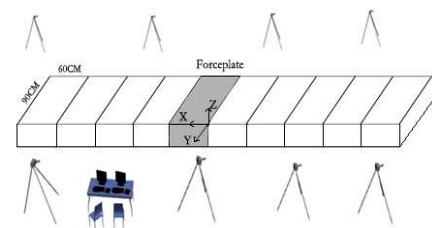


Figure 1: Laboratory settings

A greater anterior pelvic tilt angle in the ITBS group was observed than in the control group. This factor that may be linked to running injuries, such as ITBS. The increased anterior pelvic tilt may be due to weakness in the core muscles and the hip flexor musculature's tightness. Excessive pelvic activity during running is also an ITBS risk factor. The control group decreased the hip flexion after training to reduce strain and relieve tension in the Iliotibial band. It could be a gait adjustment strategy to avoid ITBS occurrence. The control group exhibited a significant reduction in hip adduction moment after training. This change may have been created to reduce the risk of developing ITBS because greater hip adduction is associated with tension and strain on the ITBS.

Conclusions

Decreasing hip flexion, adduction angle, and abductor moment may be a reasonable strategy to avoid ITBS. Risk of ITBS could be reduced by timely gait adjustment. Excessive trunk inclination and anterior pelvic tilt angles may be risk factors in the development of ITBS during running.

Acknowledgments

This work was funded by the Introduction and cultivation plan of young innovative talents of Shandong Provincial Department of Education (2019-183).

References

- [1] F.M., Cookingham et al. (2000). *Clin J Sport Med*, **10**:169-175.

Drop-Landing Asymmetries are Related to Knee Symptoms 6-Months Following ACL Reconstruction

Katherine Collins¹, Andrew Schorfhaar², Christopher Wilcox², Michael Shingles², Sheeba Joseph², Douglas Dietzel², Christopher Kuenze^{1,2}

¹Department of Kinesiology, Michigan State University, MI, USA

²Department of Orthopedics, Michigan State University, MI, USA

Email: colli784@msu.edu

Summary

Individuals with anterior cruciate ligament reconstruction (ACLR) demonstrate aberrant movement patterns associated with risk of re-injury. Individuals with ACLR also report persistent pain and symptoms. It is unclear how symptoms potentially influence lower extremity loading mechanics after ACLR. Therefore, the purpose of this study was to evaluate the relationship between symmetry of drop-vertical jump (DVJ LSI) kinetics and patient reported symptoms 6-months after ACLR. Symptoms (KOOS-symptoms) and vertical ground reaction force (vGRF) LSI was related in individuals with ACLR ($\Delta R^2 = 0.231$). A better understanding of how worse symptoms influence movement patterns post-ACLR is needed and may clarify an important link between symptom resolution and risk of re-injury.

Introduction

Individuals with ACLR exhibit aberrant knee joint biomechanics and loading patterns that increase risk of secondary ACL injury [1]. Almost 40% of individuals with ACLR report unacceptable symptoms for several years following surgery [2]. However, it is unclear how symptoms potentially influence lower extremity loading mechanics after ACLR. Therefore, the purpose of this study was to evaluate the relationship between DVJ LSIs and patient-reported knee symptoms (KOOS-symptoms) 6-months following ACLR.

Methods

Recreationally active individuals with primary unilateral ACLR participated in this study. All participants completed the Knee Osteoarthritis Outcomes Score symptoms (KOOS-symptoms) subscale at enrollment. Assessment of peak vGRF and knee extension moment (KEM) were conducted utilizing three-dimensional motion capture (120 Hz; Vicon Motion Systems, Ltd., Oxford, UK) and two integrated force platforms (1200 Hz; Advanced Medical Technology Inc., Watertown, USA). Participants were asked to drop off a 30-cm box and immediately jump upward to attain maximal height. The box was positioned at a distance $\frac{1}{2}$ participant height away from the force platform. Peak vGRF and KEM were extracted, normalized to body weight (BW), and LSIs were calculated using the following equation:

$$LSI \% = \frac{\text{involved limb value}}{\text{uninvolved limb value}} \times 100\%$$

Separate linear regression models were developed to evaluate the association between KOOS-symptoms, and peak DVJ vGRF and KEM LSIs. Age and time since surgery were entered as the first step in all regression models. Alpha was set a priori at 0.025 (0.05/2) to account for multiple comparisons.

Results and Discussion

Sixteen individuals (age: 18.4 \pm 3.0 years, 7 male/ 9 female, BMI: 27.2 \pm 6.4 kg/m², time since surgery: 6.3 \pm 0.5 months, graft type: 11 HAS/ 4 BTB/ 1 ALL, pre-injury Tegner activity score: 9 [5,10]) participated in this study. KOOS-symptoms (60.48 \pm 8.60) and vGRF LSI% (73.83 \pm 18.59) were associated (Table 1). KOOS-symptoms was not significantly associated with KEM LSI% (88.07 \pm 26.42).

Table 1. Regression Models

Model	Predictor Variables	R ²	ΔR^2	P-Value
Peak vGRF LSI %				
1	Age, TSS	0.289	0.289	0.010
2	KOOS-Symptoms	0.519	0.231	0.034
Peak KEM LSI %				
1	Covariates Age, TSS	0.149	0.149	0.351
2	KOOS-Symptoms	0.205	0.056	0.414

Table 1. Linear regression models to evaluate the relationship between KOOS-symptoms and DVJ peak vGRF and KEM LSI%. TSS= Time since surgery.

Conclusions

Patient symptoms are associated with ACLR limb underloading 6-months following ACLR. However, investigation of longitudinal changes in patient symptom burden and loading patterns in individuals with ACLR is needed in order to better understand the link between symptom resolution and risk of secondary injury.

References

- [1] Paterno M et al. (2010) *Am J Sports Med*, **10**: 1968-78
- [2] Wasserstein D et al. (2015) *Osteoarthr Cartil*, **10**:1674-84

Elbow load variability in youth elite baseball pitchers

Bart van Trigt^{1,1}, F.F. Bouman^{2,1}, A.J.R. Leenen^{3,2}, M.J.M. Hoozemans^{4,2}, F.C.T van der Helm^{5,1}, H.E.J. Veeger^{6,1}

¹Department of biomechanical Engineering, Delft University of Technology, Delft, The Netherlands

²Department of Human Movement Sciences, Faculty of Behavioural and Movement Sciences, Vrije Universiteit Amsterdam, Amsterdam Movement Sciences, Amsterdam, the Netherlands.

Email: b.vantrigt@tudelft.nl

Summary

Elbow injuries are a major problem in baseball pitching. The elbow internal varus torque is associated with elbow injuries in baseball pitching. It can be assumed that the within pitcher load variability is related to injuries, however, it is unknown what the pitcher within load variability is. Eleven youth elite Dutch baseball pitchers threw 25 fastballs. Peak internal varus torque was calculated and the variability was defined as the standard deviation of the 25 throws. The preliminary results show an indication of differences in within pitcher elbow varus torque variability between pitchers. Future research should investigate how this load variability is distributed over different elbow stabilizers.

Introduction

Baseball pitching exposes the upper extremity to high loads and is strongly associated with medial elbow injuries [1]. The most common medial elbow injury in baseball is the Ulnar Collateral Ligament (UCL) rupture. Inverse dynamics shows a peak external valgus torque around the elbow during pitching. This torque forces the forearm to move away from the upper arm. The UCL is one of the elbow structures that resist this torque and provide elbow stability but it is only possible to estimate the UCL load during pitching. Studies show that UCL injuries and UCL thickness are associated with internal varus torque [1,2]. Therefore, the internal varus torque can be used as proxy for UCL load.

It is hypothesized that an increased within pitcher load variability increases injury risk. It is, however, never investigated whether there is a difference in load variability between pitchers. Therefore, the aim of this study is to investigate whether there is a difference in within pitcher elbow internal varus torque variability between youth elite baseball pitchers.

Methods

Eleven youth elite baseball pitchers (age 15 to 23 year) threw twenty-five fastballs as fast and accurate as possible to the strike zone center at the regular distance of 18.4m. Body kinematics were measured in a motion laboratory with a VICON motion capture system sampled at 400 Hz. Ball speed was measured with a portable radar gun, positioned next to the strike zone. Peak internal varus torque was calculated by inverse dynamics for each throw with a custom-made model in Python. The standard deviation was used to quantify the within pitcher internal varus torque variability. Gaussian distribution was calculated to visualize within pitcher load variability.

Results and Discussion

Preliminary results of the within pitcher peak internal elbow varus torque are shown in figure 1. The results show a difference in the width of the normal distribution between pitchers. For example, participant 2 (orange line) shows a very low elbow internal varus torque variability compared to participant 6 (brown line). Indicating a difference in within pitcher load variability. The dashed horizontal lines in figure 1 show the mean internal varus torque of each pitcher. Some pitchers show higher internal varus torques compared to others, which is in line with the literature [1,2]. Future studies should investigate how this torque is distributed over different elbow stabilizers and thus investigate if there is a relation between internal varus torque variability and UCL load variability.

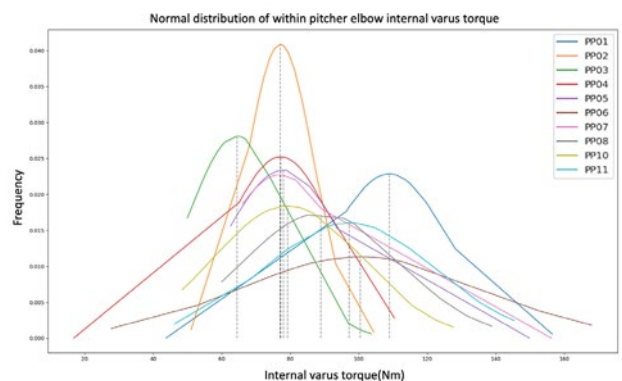


Figure 1: Normal distribution of the within pitcher elbow internal varus torque.

Conclusions

It can be concluded, based on the preliminary results, that there is a difference in peak elbow internal varus torque magnitude and variability between youth elite baseball pitchers. However, as this torque can also be resisted by muscle forces, understanding why some pitchers sustain an injury and others do not, cannot simply be explained with the magnitude of the internal varus torque.

Acknowledgments

This work was supported by the NWO Domain Applied and Engineering Sciences (AES). Project number [R/003635].

References

- [1] Anz et al. (2010). *Am J Sports Med*, **38**.
- [2] Hurd et al. (2011). *Am J Sports Med*, **39**

Spinal palpation error and its impact on marker-based spinal curvature estimation in adult spinal deformity

Pieter Severijns¹, Thomas Overbergh¹, Lieven Moke¹, Lennart Scheys¹

¹Institute for Orthopaedic Research and Training, KU Leuven/University Hospitals Leuven, Leuven, Belgium

Email: pieter.severijns@kuleuven.be

Summary

Palpation error (PE) is increased in deformed adult spines and relates to the severity of the deformity. Radiograph-based PE correction results in more accurate marker-based spinal alignment measurement, primarily in the coronal plane.

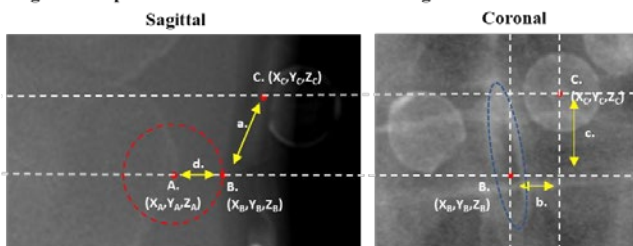
Introduction

Measurement of spinal alignment within adult spinal deformity (ASD) research is currently shifting from mainly two-dimensional, static radiography, towards three-dimensional (3D), dynamic assessment, through the use of marker-based motion analysis. However, information is lacking on the accuracy of spinal marker placement (i.e. palpation error), one of the main sources of variability in kinematic results, and its effect on spinal alignment estimation, in both healthy and deformed spines.

Methods

20 ASD and 10 control subjects underwent biplanar imaging with a spinal skin marker model attached. 3D spinous processes (SP) (T11, T12, L2, L3, L4) and corresponding 3D marker positions were extracted using custom software. The optimal marker position was obtained through a circle fitting method, defining the shortest distance from the respective spinous process to the skin surface. Palpation error was defined as the 3D Euclidean distance between the actual and optimal marker positions. Based hereon, also mediolateral (ML) and inferosuperior (IS) PE's were extracted. The 3D distance between the spinous process and the optimal marker position was used to quantify SP depth. PE was compared between ASD and controls and related to radiograph-based scoliosis and lordosis as well as body morphology (BMI and SP depth) through Spearman correlation (r_s). (Figure 1)

Figure 1. Palpation error calculation and circle fitting



A. Spinous process B. Optimal marker position C. Actual marker position

a. 3D palpation error = $\sqrt{[(X_B - X_C)^2 + (Y_B - Y_C)^2 + (Z_B - Z_C)^2]}$

b. Mediolateral error = $\text{Abs}(X_B - X_C)$

d. SP depth

c. Inferosuperior error = $\text{Abs}(Y_B - Y_C)$ = $\sqrt{[(X_A - X_B)^2 + (Y_A - Y_B)^2 + (Z_A - Z_B)^2]}$

To assess the effect of PE on marker-based spinal alignment measurement (lordosis and scoliosis), 10 ASD subjects were also measured in the motion lab. Lordosis and scoliosis were calculated by fitting a polynomial through both the uncorrected and palpation-error corrected marker positions [1]. The relation between these results and radiograph-based scoliosis and lordosis was investigated through Spearman correlation (r_s) and root mean square errors (rmse).

Results and Discussion

Table 1. Palpation error of ASD and control and impact on spinal curvature estimation using motion analysis

A. Palpation error quantification					
	ASD	Control	p-value		
3D PE _{mean} (mm)	15.5 (9.2)	14.0 (5.8)	0.502		
ML PE _{mean} (mm)	6.8 (9.1)	2.5 (1.9)	0.002		
IS PE _{mean} (mm)	8.1 (9.2)	12.4 (6.1)	0.091		
Incorrect level	37%	32%			
B. Correlation analysis: Mediolateral PE vs radiography/body morphology					
	ASD		Control		
	r_s	p-value	r_s	p-value	
Lordosis (°)	0.34	0.141	-0.08	0.829	
Scoliosis (°)	0.77	< 0.001	N.A.		
BMI (kg/m ²)	-0.08	0.734	0.78	0.008	
SP depth (mm)	0.33	0.158	0.66	0.038	
C. Spinal curvature estimation		Relation to Radiography			
1. Lordosis (°)		ASD	r_s	p	rmse
Radiography		44.4 (41.7)			
Uncorrected markers		15.0 (26.9)	0.77	0.009	28.7
PE-corrected markers		25.8 (27.8)	0.69	0.029	23.2
2. Scoliosis (°)					
Radiography		55.8 (38.2)			
Uncorrected markers		11.3 (12.5)	0.44	0.152	44.3
PE-corrected markers		18.1 (21.5)	0.84	< 0.001	32.7

Median (interquartile ranges) are reported. $\alpha=0.05$.

Although spinal level identification and inferosuperior palpation error were not different between deformed and healthy spines, significantly increased mediolateral palpation error was observed in ASD. Significant correlation ($r_s=0.77$) with radiographic scoliosis suggests a substantial contribution of the deformity itself, possibly due to the rotatory component of scoliosis, resulting in SP's directed towards the concave side of the curve. In contrast, PE in healthy spines was mainly related to body morphology. Correcting the marker positions towards their ideal position resulted in lordosis and scoliosis values, more similar to radiography (decreased rmse). For scoliosis, also a marked increase in correlation coefficient with radiography was observed.

Conclusions

Palpation error is increased in deformed adult spines and relates to the severity of the deformity. Radiograph-based PE correction results in more accurate marker-based spinal alignment measurement, primarily in the coronal plane.

Acknowledgements

This study was funded by a strategic basic research PhD grant of the Research Foundation – Flanders (FWO).

References

[1] Severijns P et al. (2019). *Spine J*, **20**: 934-946.

Fear-avoidance beliefs are not related to stoop-squat-behavior during object lifting in healthy pain-free adults

Stefan Schmid¹, Christian Bangerter¹, Magdalena Suter², Michael L. Meier²

¹Spinal Movement Biomechanics Group, Bern University of Applied Sciences, Bern, Switzerland

²Integrative Spinal Research ISR, Balgrist University Hospital, Zurich, Switzerland

Email: stefan.schmid@bfh.ch

Summary

To investigate whether “fear of round-back-lifting” is related to stoop-squat-behavior during object lifting, we developed a novel lifting style index, applied it to the motion capture data of 57 healthy pain-free adults and correlated it with scores from a self-report questionnaire for assessing fear-avoidance beliefs. The results showed no associations between “fear of round-back-lifting” and lifting style, indicating that fear-avoidance beliefs might not directly affect whole body motor control strategies.

Introduction

Although challenged by recent biomechanical evidence, many health care professionals still hold the opinion that lifting with a flexed spine (stoop lifting) is dangerous for the back and promote lifting with a neutral spine (squat lifting) as the safer way. In this regard, we previously showed that individuals with an elevated “fear of round-back-lifting” appear to reduce lumbar spine flexion during object lifting [1]. The question remains, however, whether this is related to lifting style in general (i.e. stoop or squat) or simply represents a localized motor control alteration.

In this study, we investigate the association between “fear of round-back-lifting” and lifting style in healthy individuals using a novel index for quantifying stoop-squat-behavior.

Methods

A cohort of 57 healthy pain-free adults (m/f: 30/27; age: 29.5±7.0 years) participated in this study. After completing the Photograph Series of Daily Activities-Short electronic Version (PHODA-SeV) [2], they were equipped with 58 retro-reflective markers [3] and asked to lift up and put down a 5kg-box with their preferred lifting style.

To quantify the lifting style, we developed a novel index, the Stoop-Squat-Index (StSq), which describes the relationship between trunk forward lean and lower extremity joint flexion based on the following formula:

$$StSq = 100\% - \left(\frac{(Vert_HJC_{Standing} - Vert_HJC_{Bending}) * 100\%}{Vert_C7_{Standing} - Vert_C7_{Bending}} \right)$$

whereby *Vert_HJC* and *Vert_C7* represent the vertical positions of the hip joint center and the C7 marker, respectively, during standing and bending. Hip joint centers were thereby established using the Plug-in Gait full-body model. An index of 100% indicates full stoop lifting and 0% full squat lifting behavior.

The association between “fear of round-back-lifting” (sub-score of PHODA-SeV between 0 and 100 (PHODA-Lift)) and StSq over a full lifting cycle was investigated using

linear regression models, which were implemented by means of one-dimensional Statistical Parametric Mapping [4].

Results and Discussion

Participants showed a large inter-subject variation of lifting styles (from almost full stoop to almost full squat lifting behavior), but no statistically significant associations between PHODA-Lift and StSq were found (Figure 1).

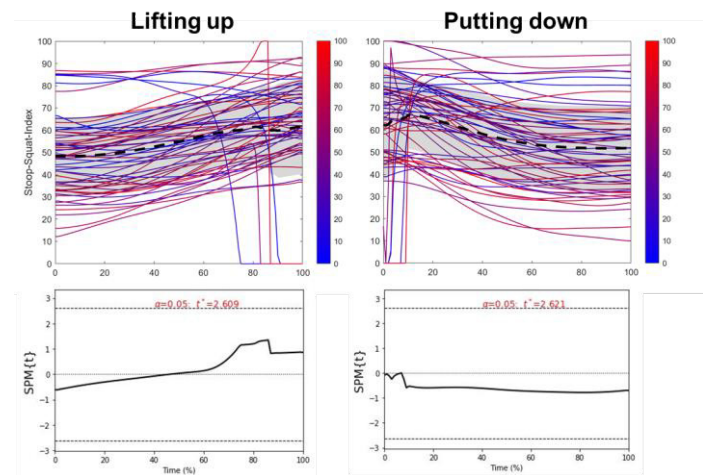


Figure 1: Stoop-Squat-Index for lifting up and putting down a 5kg-box and its relation to “fear of round-back-lifting” (PHODA-Lift).

Since this study only focused on lightweight objects, it remains unclear whether these results also apply for lifting heavier objects. Future studies might therefore use the newly introduced StSq to address this issue in more detail. If no motion capture information is accessible, the StSq might also be derived from conventional video recordings.

Conclusions

Fear-avoidance beliefs, particularly the “fear of round-back-lifting”, appears not to be related to the stoop-squat-behavior during object lifting, indicating that fear-avoidance beliefs might not directly affect whole body motor control strategies.

Acknowledgments

This work was supported by the Swiss National Science Foundation (SNSF, grant-no.: 185123).

References

- [1] Knechtle et al. (2020). *PAIN*, in press.
- [2] Leeuw et al. (2007). *J Pain*. 8(11):840-49.
- [3] Schmid et al. (2017). *Hum Mov Sci*, 54:73-81.
- [4] Pataky TC. (2012). *CMBBE*. 15(3):295-301.

Cervical spine injuries observed in misdirected rugby tackles are not caused by a hyperflexion mechanism

Pavlos Silvestros¹, Ezio Preatoni¹, Harinderjit S. Gill², **Dario Cazzola**¹
¹Department for Health, University of Bath, Bath, United Kingdom
²Department of Mechanical Engineering, University of Bath, United Kingdom
 Email: d.cazzola@bath.ac.uk

Summary

Rugby tackling carries with it a high proportion of all catastrophic cervical spine injuries in the game of rugby. In the literature, there is still an open debate on the injury mechanisms related to such injuries, with hyperflexion and buckling being under scrutiny. The aim of this study was to simulate the dynamic response of the cervical spine to loading conditions representative of misdirected rugby tackles injuries, and it was informed by experimental *in vivo* and *in vitro* data representing realistic rugby tackling conditions. Results showed that: i) neck flexion at the time of impact had the largest effect on neck internal loading; ii) the early generation of high compression, anterior shear and flexion loads provides additional evidence that hyperflexion is not the primary injury mechanism during rugby tackles.

Introduction

In the literature, quasi-static and dynamic *in vitro* cadaveric experiments have been conducted to investigate cervical spine injuries during head first impacts [1]. However, from an injury prevention perspective, such experiments are not often deemed conclusive as they are highly controlled by nature and may greatly differ from the real *in vivo* dynamics of rugby tackles. Computer simulations have since proven a valuable method in being able to recreate with high fidelity the internal and external loading conditions, and can be informed or driven by *in vivo* kinematics, kinetics, and electromyography data. We conducted an *in silico* investigation, informed and driven by a combination of *in vitro* and *in vivo* data, to examine the dynamic response of the cervical spine to loading conditions representative of misdirected rugby tackles.

Methods

One professional academy-level front-row rugby player (male, 22 years, 1.82 m, 113.7 kg) participated in this study. Experimental kinematics and neck muscles electromyography data was during staged rugby tackling trials, whilst external loading was collected during a set of head first impacts generated by accelerating a punch-bag against a dummy head. A subject-specific OpenSim musculoskeletal model [2] was firstly used in EMG-assisted inverse simulations to estimate neck muscles activation, and then in forward dynamics simulation (n=1638) where neck angles (n=117), loading conditions (n=7), and loading rate (n=2) were changed iteratively. The effects of initial neck angle and loading conditions were evaluated by analysing the maximal compressive loading, anteroposterior shear loading and flexion bending moment sustained during a 50 ms impact simulations.

Results and Discussion

From a tackling technique perspective, neck flexion at the time of impact had the largest effect on neck internal loading, and confirmed that compressive loading increases with neck flexion angle also in rugby tackling (Figure 1).

From an injury mechanism analysis perspective, the early generation of high compression, anterior shear and flexion loads provides additional evidence that hyperflexion is not the primary injury mechanism during rugby tackles.

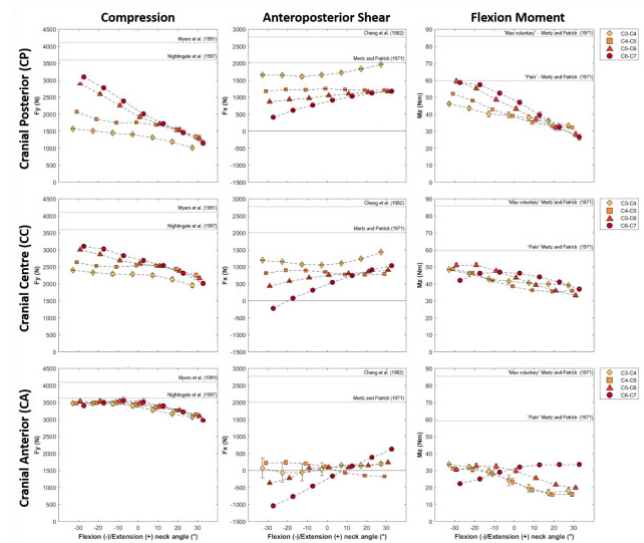


Figure 1: Mean and SD values for max compression and shear forces, and flexion moment of all initial neck angle conditions plotted against changes in neck flexion/extension angles for cranial loading conditions. Estimated injury thresholds from the literature for the entire cervical spine are also presented with horizontal lines.

Conclusions

During misdirected rugby tackles, loading patterns associated with buckling and anterior facet dislocations are generated much earlier than when physiological neck flexion ranges are exceeded. This indicates that the cervical spine injuries observed in misdirected rugby tackles are not caused by a hyperflexion mechanism.

Acknowledgments

The authors would like to thank the Rugby Football Union Injured Player Foundation for funding.

References

- [1] Nightingale et al. *J of Biomech* (1996); **29(3)**:307-318
- [2] Silvestros et al. *PLoS One* (2019); **15(5)**: e0216663

Baricentricity of Spinal Alignment and Posture in Adolescent Idiopathic Scoliosis: Optical Diagnosis

Saša M. Čuković¹, Vanja Luković², Christoph Heidt³, William R. Taylor¹

¹Laboratory for Movement Biomechanics, Institute for Biomechanics, ETH Zürich, Switzerland

²Faculty of Technical Sciences Čačak, University of Kragujevac, Serbia

³University Children Hospital - UKBB Basel, Switzerland

Email: sasa.cukovic@hest.ethz.ch

Summary

To avoid repetitive harmful effects of X-ray exposure in patients with Adolescent Idiopathic Scoliosis (AIS), new non-invasive approaches have been developed, with the aim to replace or reduce the need for X-ray imaging, especially in follow-up and monitoring stages. We recently developed ScolioSIM1.0, a software tool that produces 3D visualizations of the patient-specific deformity model and allows evaluation of AIS in a non-invasive manner. As it enables spatial visualization of the deformity, numerous geometrical parameters can be evaluated in all 3 body planes in 2D or 3D. One parameter of clinical importance is the barycenter (BC) of the spine, which describes the center point of the surface that envelops a projected Middle Spinal Alignment (MSA) in the plane normal to the local spinal axis DM-C7, located at L5's lower plate point.

Introduction

Traditional evaluation of AIS still relies on the 2D Cobb angle as a gold standard, which describes only one specific segment of the spinal curve in one plane, neglecting the 3D nature and spatial configuration of the deformity, especially axial projection of the MSA (Figure 1). In this study, we aim to determine transversal projections of the MSA and BC of the human spine using non-invasive optical techniques [1], as their shape and position can reveal important indicators of the deformity, as well as help clinicians to qualitatively describe a patient's posture [2].

Methods

We performed retrospective analysis of 26 3D optical samples of AIS patients' back surfaces using the ScolioSIM1.0 diagnostic tool (18 females and 8 males; 10.6 ± 1.37 and 11.5 ± 2.07 years old). For each patient, the BC location and surface area were calculated, and contour shapes were considered. Depending on the position of the BC from the local spinal axis (0,0), deformity may be left or right shifted. In addition, the BC was used to determine if the subjects' back posture deformities were flat (ventral) or sway (dorsal). As scoliosis is a 3D deformity, the BC was then placed in different quadrants in order to allow the pathology to be classified as an anterior shift, posterior shift, right or left shifted, or combined. Depending on the shape of projected contour, deformity could be qualified as isophasic (narrow contour) and anisophasic (rounded) (Figure 1).

Results and Discussion

Analysis of the collected datasets and parameters of BC points showed that the most dominant type of scoliosis in the

selected population of patients were right (84.6%) and posteriorly (57.7%) shifted. As datasets contained AIS patients only, all projected contours indicated mainly anisophasic deformities.

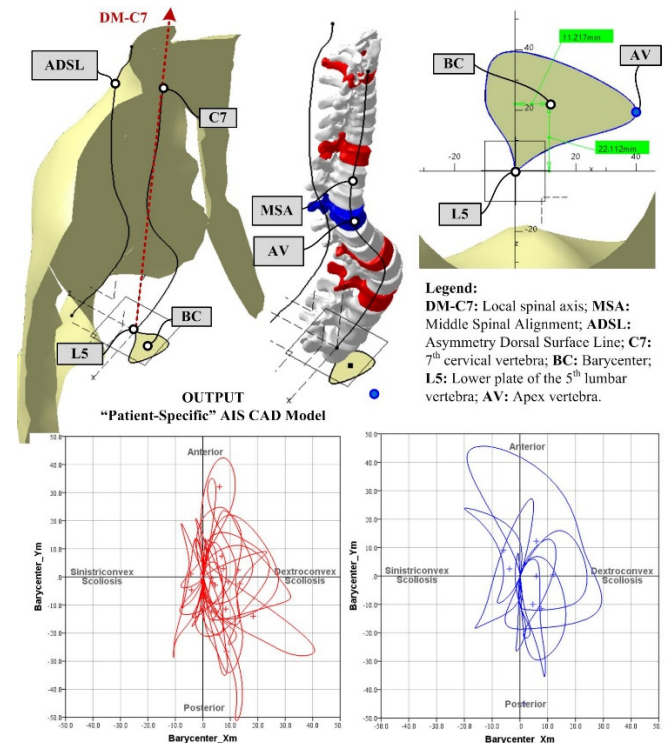


Figure 1: Barycenter points in pathological spines, presented for both female and male subjects

Conclusions

In many studies and current clinical practice, AIS is mainly diagnosed based on 2D frontal and sagittal plane parameters. Axial projection of the MSA is of crucial importance, and can now be accessed using optical techniques, hence providing access to the BC. Such approaches can clearly show balance of the patient and pave the way towards a new non-invasive 3D classification of scoliosis.

Acknowledgments

This project was partially funded by the EU Horizon 2020 research and innovation programme under the Marie Skłodowska-Curie grant agreement No 892729 and Serbian Ministry of Science under the project III-41007 (2012-2019).

References

- [1] Čuković S. (2015). *PhD Thesis*, Univ. of Kragujevac.
- [2] Negrini et al. (2016). *Scoliosis*, **20**:1-16.

Subject-specific muscle forces in the lumbar spine are correlated to lumbar curvature

Judith R. Meakin¹, Jonathan Fulford², Karen M Knapp²

¹Biomedical Physics, College of Engineering, Mathematics and Physical Sciences, University of Exeter, UK

²Medical Imaging, College of Medicine and Health, University of Exeter, UK

Email: j.r.meakin@exeter.ac.uk

Summary

Previous modelling has suggested that the muscle forces required to stabilize the lumbar spine are related to its shape. In this study, we performed subject-specific modelling on a sample of 41 healthy participants using a simple two-dimensional model. The predicted muscle forces correlated significantly with the lumbar lordosis suggesting that muscle force is subject-specific and related to spinal shape.

Introduction

The muscle forces required to maintain a stable lumbar spine have been shown to relate to lumbar spine shape [1]. Previous studies, however, have focused on single or idealized anatomy which may miss interactions between lumbar shape and other parameters such as muscle angulation. The aim of our study was therefore to investigate muscle forces in a sample of healthy individuals using subject-specific models.

Methods

Models were created using Matlab (R2020a, The MathWorks Inc.). The model geometry (Figure 1) was defined by the lumbar vertebrae and sacrum. Body forces (totaling 49 % of body weight) were distributed across the vertebrae according to [2]. Muscle forces were applied in directions defined by the vertebral body centroids and the sacrum.

The magnitude of the muscle forces and internal forces generated within the spine were determined using optimization for two cases (Figure 1b). In the 'optimum' case, the path of the internal forces was constrained to pass as close as possible to the vertebral body centroids. In the 'minimum' case the total muscle force was minimized without allowing the path of the internal forces to lie outside the vertebral bodies.

Subject-specific model data were derived from magnetic resonance images. The images were a subset of data from a study where participants had consented for their data to be used in subsequent research. The subset comprised 41 healthy female participants (26 to 46 years) with a body mass of 72 ± 13 kg (mean \pm sd). Lumbar lordosis was calculated as the angle between the superior endplates of L1 and S1.

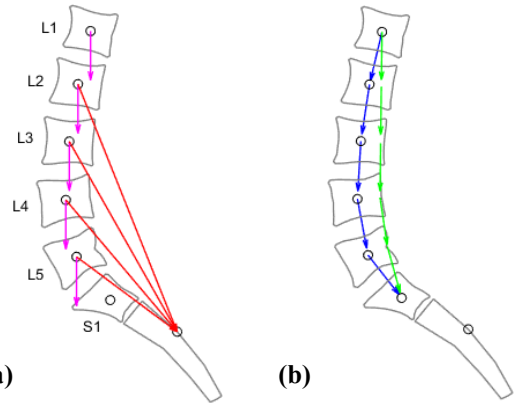


Figure 1: (a) Example model geometry with body forces (pink) and muscle forces (red) (b) Path of the resulting 'optimum' (blue) and 'minimum' (green) internal forces generated in the spine.

Results and Discussion

Predicted muscle forces (Table 1) increased from L2 to L5 in both the optimum and minimum case. Lumbar lordosis ranged from 37 to 72 degrees. The Spearman correlation between lordosis angle and muscle force was statistically significant for all optimum muscle forces and for minimum muscle forces at L4 and L5 (Table 1). The internal force magnitudes at L4L5 were consistent with measurements of intradiscal pressure from the literature [3], giving confidence in model validity.

Conclusions

The muscle forces required to maintain the upright lumbar spine in static equilibrium are subject-specific and are related to the curvature of the subject's lumbar spine.

Acknowledgments

We thank the volunteers for their image data.

References

- [1] Meakin and Aspden (2012) *J Mech Med Biol*, **12**: 1-10.
- [2] Duval-Beaupère and Robain (1987) *Int Orthop*, **11**: 261-269.
- [3] Sato et al. (1999) *Spine*, **24**, 2468-2474.

Table 1: Model results and statistics. Magnitude of muscle force at each vertebral level for the minimum and optimum cases is expressed as the median [interquartile range]. Correlation is expressed as the Spearman correlation coefficient (statistical significance).

		L2	L3	L4	L5
Optimum	Muscle force, N	7 [22]	59 [33]	160 [57]	927 [343]
	Correlation with lordosis	0.4 (0.01)	0.5 (<0.001)	0.5 (0.001)	0.4 (0.02)
Minimum	Muscle force, N	0 [0]	0 [0]	68 [46]	104 [69]
	Correlation with lordosis	-0.1 (0.5)	-0.1 (0.7)	0.6 (< 0.001)	0.5 (< 0.001)

FEBio and ABAQUS with Fibril-reinforced Biphasic Models of Knee Articular Cartilage Produce Similar Mechanical Responses During Gait

Alexander Paz^{1,2}, Gustavo A. Orozco¹, Petri Tanska¹, J.J. García², Rami K. Korhonen¹, Mika E. Mononen¹

¹Department of Applied Physics, University of Eastern Finland, Kuopio, Finland

²Escuela de Ingeniería Civil y Geomática, Universidad del Valle, Cali, Colombia

Email: alexander.paz@uef.fi

Summary

Finite element (FE) software ABAQUS and FEBio have been used to model time-dependent responses of fibril-reinforced poroelastic and biphasic tissues (FRPE), such as articular cartilage. However, knee joint models with depth-wise and split-line collagen fibril orientations have been simulated only in ABAQUS. Here, we propose a novel fibril-reinforced biphasic hyperelastic material formulation in FEBio, implemented in a knee joint model under a gait cycle loading. Results were compared with a previous validated FRPE model in ABAQUS. The mechanical outputs between the models corresponded well through the gait cycle. To conclude, we suggest using the easily accessible and free FEBio software to simulate the complex mechanical behavior of cartilage in the knee joint during gait.

Introduction

FRPE models of articular cartilage capture the mechanical interactions between tissue constituents (collagen fibrils, proteoglycans, interstitial fluid) and show how altered properties of the constituents in osteoarthritis affect tissue and joint mechanics [1]. These models have been implemented in FE software ABAQUS [2,3] and in the free open-source software FEBio [4,5]. However, FEBio models with the FRPE formulation of cartilage have not been generated for patient-specific knee joint geometries to simulate gait. Furthermore, the important split-lines patterns in a depth-dependent collagen network have not been incorporated in FEBio before, as has been done in ABAQUS. Thus, this study proposes a new material formulation of knee articular cartilage with a realistic orientation of collagen fibrils in FEBio. The results from the knee joint model during walking were then compared to those obtained from a corresponding model in ABAQUS.

Methods

Figure 1 shows the workflow of the study: (a) knee geometry generation, (b) optimization of the material parameters in FEBio, (c) boundary and loading conditions, and (d) result comparisons. The geometry was generated from MRI data of a healthy subject, obtained from the Osteoarthritis Initiative. In FEBio, articular cartilage corresponded to a fibril-reinforced biphasic hyperelastic material. The depth-wise collagen network consisted of primary and secondary fibrils that follow split-lines patterns. We simulated simple cubic models under tension and confined and unconfined compression tests to optimize the mechanical parameters in FEBio based on the FRPE model in ABAQUS. At the joint-level modeling, a simplified stance phase of gait was implemented in FEBio and ABAQUS models by applying time-dependent axial load and flexion angle boundary

conditions to the rigid-body femur reference point (Figure 1). Finally, mechanical responses of the knee joint cartilage were compared between software.

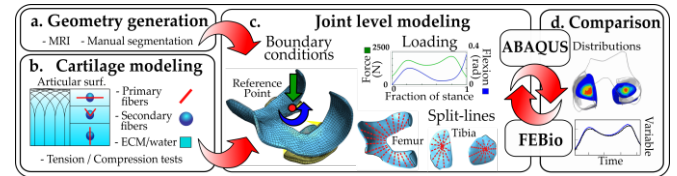


Figure 1: The workflow of the study.

Results and Discussion

Quantitative and qualitative results (Figure 2) show similar fluid pressures, stresses, reaction forces, and strains between FEBio and ABAQUS models. Small differences may arise from the different fibril formulations we used in the models. The results agreed with previous studies on the effect of depth-wise orientation of collagen fibrils of cartilage in FEBio, using simpler geometries [5], and ABAQUS [3], using knee joint geometries. As FEBio is easier accessible than ABAQUS and free for researchers, this work encourages its use in the modeling of knee joint mechanics.

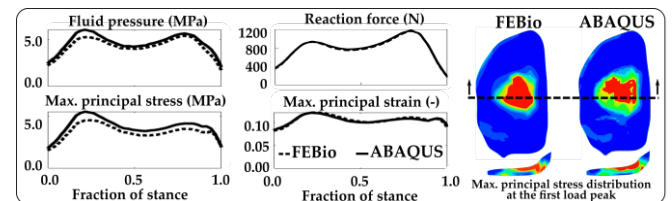


Figure 2: Mechanical responses in the medial tibial cartilage, modeled by fibril-reinforced biphasic and poroelastic material formulations, during simulated gait in FEBio and ABAQUS.

Conclusions

This study presents an approach to generate a 3D fibril-reinforced biphasic knee joint model in FEBio with realistic collagen fibril orientations of cartilage. Similar mechanical responses of cartilage during gait in FEBio and ABAQUS suggests that easily accessible FEBio can be used in future applications.

Acknowledgments

To the Academy of Finland (grants 324994, 328920).

References

- [1] Peters et al. (2018). *PeerJ*. **6**:1-48
- [2] Wilson et al. (2004). *J. Biomech*, **37**:357-366
- [3] Halonen et al. (2013). *J. Biomech*. **46**:1184-1192
- [4] Maas et al. (2012). *J. Biomech. Eng.* **134**:1-10
- [5] Meng et al. (2017). *J. Mech. Behav. Biomed*, **65**:439-453

Rapid X-ray-based 3-D Finite Element Modeling of Knee Joint Cartilage Biomechanics

Sana Jahangir¹, Ali Mohammadi¹, Jukka Hirvasniemi², Juha-Sampo Suomalainen³, Simo Saarakkala⁴,
Rami K. Korhonen¹, Mika E. Mononen¹, Petri Tanska¹

¹University of Eastern Finland, Kuopio, Finland; ²Erasmus University Medical Center, Rotterdam, The Netherlands; ³Kuopio University Hospital, Kuopio, Finland; ⁴University of Oulu, Oulu, Finland

Email: sana.jahangir@uef.fi

Summary

Recent developments in atlas-based finite element (FE) knee joint modeling have drastically reduced construction and computation time [1, 2]. However, that approach has been utilized only with magnetic resonance imaging (MRI) and computed tomography (CT) based imaging modalities. Radiographs of the knee joint are the most commonly used for knee osteoarthritis (OA) diagnosis. Hence, a capability to produce biomechanical knee joint models directly from radiographs would enable an efficient way to estimate knee cartilage failure and progression of knee OA. This study proposes an atlas-based FE modeling framework for an automatic model generation and simulation of knee joint cartilage mechanical responses using knee X-ray images. The developed framework was successfully verified against the simulation results obtained from MRI-based FE models.

Introduction

Current atlas-based FE models are based on images obtained through MRI [1] or CT [2]. However, these imaging modalities are typically available in specialized healthcare centers and are not standard knee OA diagnostics methods. However, radiography (planar X-ray imaging) is an economic diagnostic imaging modality at the primary healthcare level. Hence, 3-D knee joint model generation from radiographs would increase the scalability of the FE modeling – an important factor for clinical use. Thus, this study aims to develop a radiography-based 3-D knee joint model generation framework that would be a clinically feasible method to simulate knee OA progression.

Methods

Previously collected data from 28 patients (aged between 50 and 68 years) were used in the study [3]. In that study, each patient's knee MRI and X-ray images were acquired using clinical 3T MRI and X-ray devices, respectively. The X-ray images based FE modeling followed the previously developed atlas-based FE model generation method [1]. In order to generate FE models, the anatomical dimensions of the distal femur and tibiofemoral joint space widths were measured similarly from both imaging modalities (Figure 1A). To improve intra-observer reliability, the dimension measurements were repeated three times for each subject. Thereafter, the closest knee template to the patient's knee dimension measurements was selected from the knee atlas database (21 templates) and morphed to match the measured anatomical dimensions (Figure 1B). In total, 84 knee models for both modalities were constructed. Knee cartilages were modeled using fibril-reinforced poroviscoelastic material, and physiologically relevant time-dependent gait loading (stance phase) was applied to knee models in Abaqus (v2018) [1]. The model outputs (i.e., average values of maximum principal stress, strain and fluid pressure of tibial

cartilage obtained from the tibiofemoral contact area) of MRI and X-ray-based models were compared using a 1-D statistical parametric mapping.

Results and Discussion

In terms of the biomechanical responses, X-ray based approach offered similar outcomes compared with MRI based approach (Figure 1D). The maximum principal stress was different in the models in a narrow timeframe between the midstance and 2nd peak load as well as at the end of the stance (Figure 1D). The maximum principal strain was different at the loading response and at the same locations as the maximum principal stress. The fluid pressure was different only in a narrow timeframe along the midstance. These results suggest that to estimate knee cartilage mechanics and possible failure points, X-ray-based knee joint models can simulate similar results as MRI-based models.

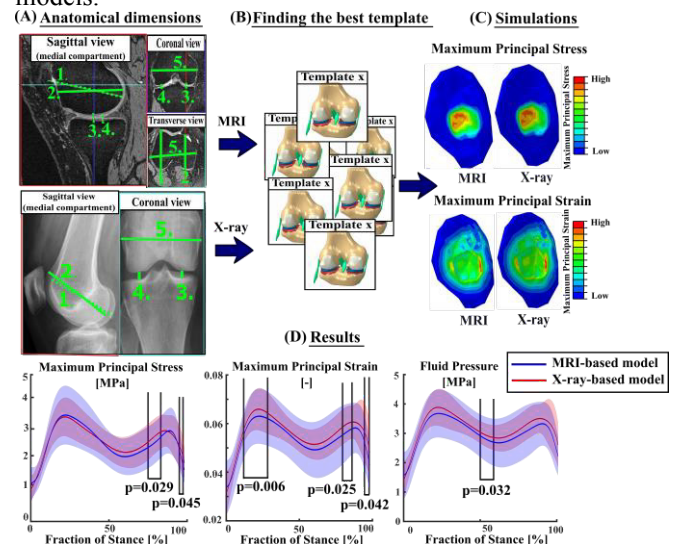


Figure 1: (A, B) Workflow of the atlas-based method for model generation, (C) the simulated maximum principal stress and strain distributions of a single subject in medial tibial cartilage in both X-ray and MRI-based models. (D) Mean and standard deviation (28 subjects, 84 models for both imaging modalities) of model outputs.

Conclusions

The presented modeling approach can offer a fast and cost-effective approach for simulation of biomechanical risks for the onset and progression of OA that could potentially be also used at the primary healthcare level.

References

- [1] Mononen et al., (2018). *Ann. Biomed. Eng.* **47**:813-825.
- [2] Mohammadi et al., (2020). *Ann. Biomed. Eng.* **48**:2965-2975.
- [3] Hirvasniemi et al., (2019). *Ann. Biomed. Eng.* **47**:1181-1190.

An agent based model of the vibration-induced arterial growth: feeding the model parameters by cellular tests.

M. Reda^{1,2}, C. Noel¹, N. Settembre³, J. Chambert², A. Lejeune², G. Rolin⁴ and E. Jacquet²

¹ Institut national de recherche et de sécurité (INRS), Vandœuvre-Lès-Nancy, France

² Univ. Bourgogne Franche-Comté, FEMTO-ST Institute, Department of Applied Mechanics, Besançon, France

³ Department of Vascular Surgery - Nancy University Hospital, France

⁴ Centre Hospitalier Universitaire de Besançon, Besançon, France

Email: christophe.noel@inrs.fr

Summary

Vibration-induced low Wall Shear Stress (WSS) flow inside digital arteries may cause arterial growth and remodeling. In this study, we propose an agent-based model of the WSS-modulated growth, supposedly induced by an intimal hyperplasia phenomenon. The modelled mechanisms depend on the Platelet-derived growth factor BB chain (PDGF-BB) secreted by endothelial cells (ECs) upon exposure to vibration. The PDGF-BB concentrations were obtained from flow experiments on cultured human umbilical vein ECs (HUVECs) exposed to a physiological level of WSS = 3 Pa and a vibration-induced level of WSS = 1 Pa. Results showed higher PDGF-BB level for WSS = 1 Pa. The arterial lumen narrowed around 50% when simulating a vibration exposure of 4 hours a day for 5 years (WSS = 1 Pa).

Introduction

A chronic exposure to Hand-Arm transmitted Vibration (HAV) can cause an arterial growth and remodeling inside digital arteries. In our study, we suppose that the growth is induced by a WSS-modulated intimal hyperplasia phenomenon (IH). Studies have shown that an acute exposure to HAV can decrease the WSS exerted by the blood on the arterial endothelium [1]. A low WSS can promote the EC-secretion of certain mitogens and chemoattractant acting on smooth muscle cells (SMCs), such as the PDGF-BB [2]. We suppose that this secreted PDGF-BB, will alter the dynamics of SMCs. On the long term, this can lead to the development of IH. In this present study, we propose an agent-based model that describes the SMCs dynamics inside the arterial wall during physiological state and for a low WSS resulting from vibration exposure. The secretion of PDGF-BB for different WSS values was investigated using in-vitro flow experiments on HUVECs. The results of the model will allow understanding the effects of the HAV on the onset of vascular pathologies.

Methods

The agent-based model, implemented in NetLogo[®], is based on biological laws derived from literature on ECs behaviors when exposed to low WSS. The initial geometry is a normal muscular artery including the endothelium (ECs) and the media layer (SMCs and Extracellular Matrix (ECMs)). The SMCs dynamics were modelled using probabilistic equations that describe biological mechanisms such as the proliferation/apoptosis, the migration and ECMs synthesis/degradation. Starting from an equilibrium state, the model was then disturbed by a WSS value resulting from a

vibration exposure. Our model took into account the acute cellular changes and simulated the chronic SMCs dynamics. Experimental data of the PDGF-BB concentrations secreted by HUVECs when exposed to a low WSS were used as input parameters for our model.

Results and Discussion

Results of the cellular tests on HUVECs showed that the ECs secreted almost 50% more PDGF-BB for WSS = 1 Pa (27.93 ± 5.14 pg/ml) than for WSS = 3 Pa (18.50 ± 7.97 pg/ml) ($p < 0.05$, $n = 7$). In addition, our model succeeded in simulating the physiological state, in the absence of vibration and the arterial growth resulting from vibration exposure (Figure 1).

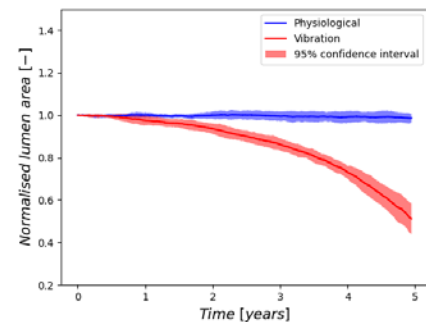


Figure 1. Change in lumen area for physiological and vibration exposure states (average of 5 simulations).

Figure 1 shows a 50% decrease in lumen area upon exposure to vibration, describing the arterial growth after 5 years of 4 hours exposure per day. We only took into account the change in ECs-secretion of PDGF-BB when exposed to a low WSS. However, other mitogens might be released from the SMCs as well and then modulate their dynamics. Our model offers the possibility to include more cellular mechanisms and to study other work conditions with different exposure times.

Conclusions

We presented an agent-based model of the vibration-induced intimal hyperplasia, enriched with experimental data. The model was able to describe the physiological state and predict the arterial growth resulting from vibration exposure.

References

- [1] Noel C. and Settembre N. (2017). *52nd Human Response to Vibration Conference & Workshop*, 202-209.
- [2] Hsieh H. J. et al. (1991). *Am. J. Physiol. Heart Cric. Physiol.*, **260**: 1-5.

The effect of soft tissue modeling on tibiofemoral stress distribution in models of high tibial osteotomy and its importance for making simulation-based clinical decisions

Elaheh Elyasi¹, Antoine Perrier¹, Yohan Payan¹

¹Univ. Grenoble Alpes, CNRS, TIMC-IMAG, 38000 Grenoble, France

Email: elyasi.elahesh@gmail.com

Summary

High tibial osteotomy (HTO) is a surgical procedure to treat unicompartmental osteoarthritis through correcting the lower limb alignment. Biomechanical models have been used for making simulation based decisions on the optimal alignment correction to achieve during HTO. However, in many models generated with this aim, the role of soft tissues has been neglected. Our objective was to investigate the impact that the connective tissues can have on simulation-based decisions.

Introduction

High tibial osteotomy (HTO) is a common surgical procedure used to relieve pain and improve joint function in patients with early-stage unicompartmental osteoarthritis. Its goal is to reduce the pressure of the damaged knee compartment by correcting the limb alignment. However, finding the required correction for each patient is challenging as indicated in the follow-up studies [1]. To overcome this challenge, biomechanical numerical simulations have been used, aiming to find the optimal correction that balances the contact force between knee compartments [2,3]. To our observation, these studies tend to oversimplify the problem by neglecting the impact of HTO on moments produced by the soft tissues. Our objective is to investigate the importance of realistically modelling the connective tissues impacted by HTO on the stress distribution in the cartilages. We propose to study the role of the superficial Medial Collateral Ligament (MCL) that is one of the most important soft tissue in this perspective.

Methods

MRI and CT images of a healthy subject were used to reconstruct the bone and soft tissue geometries through manual segmentation in Amira software. A model of the tibiofemoral joint at 25° flexion was generated in the Artisynth combined FE-multibody platform [4]. Virtual open-wedge HTO was performed on this model to simulate the HTO surgery with a 10° wedge opening. The model included the femoral and tibial cartilages and menisci all modeled with FE components and meshed with hexahedral dominant elements. Anterior and posterior cruciate ligaments, MCL with a deep and superficial layer, lateral collateral ligament, and the knee anterolateral ligament were modeled with bundles of nonlinear springs. An axial load along the mechanical axis of the limb was applied to the tibia at the center of the ankle while the femur was fully constrained and the knee flexion angle was fixed.

During HTO model generation, the superficial bundles of MCL were treated in three different ways: 1) Their length and tension were affected by wedge opening. 2) Their length and tension were not affected by wedge opening. 3) The superficial MCL was released after wedge opening.

Results and Discussion

Maximal principal stress distribution on tibial cartilages was observed in models with the three options for representing the superficial bundles of MCL, as presented in Figure 1. The results indicate that the approach we take towards modelling the MCL after HTO can significantly impact the stress distribution on the tibiofemoral compartments. Assuming that the insertion of superficial MCL is lower than the HTO cut and thus wedge opening results in increasing its length and tension, the maximum principal stress values (medial: -2.29, lateral: 1.40 MPa) show that the medial cartilage is noticeably under higher compression compared to the lateral cartilage. This means that the objective of HTO surgery is not achieved even after 10° wedge opening in this case. The stress in the medial cartilage is reduced to 48% of this value assuming that the superficial MCL is not impacted by surgery. Furthermore, releasing the superficial MCL reduces the medial stress to 34% of this value. This is while the lateral side experiences the highest stress values among the three models. As a result, it seems important to define the approach towards the MCL attachment/release when generating models of HTO as it can significantly impact the stress balance between compartments.

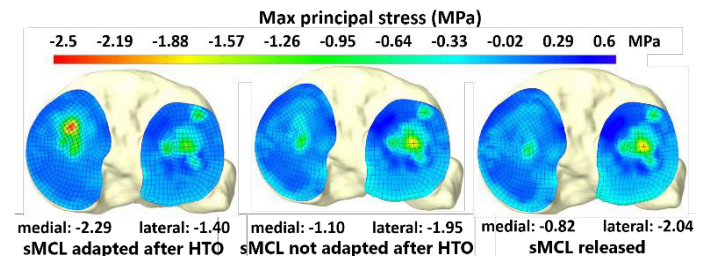


Figure 1: Maximum principal stress distribution on the tibial cartilages after 10° wedge opening.

Conclusions

Our results show that a clear approach towards the MCL in models of the HTO has to be defined to be able to propose relevant simulation-based decisions on the optimal lower limb alignment correction.

Acknowledgments

This work was funded by the Fondation pour la Recherche Médicale under the project FRM DIC20161236448.

References

- [1] Hernigou P et al. (1987). *J Bone Jt Surg*, **69(3)**: 332-354.
- [2] Martay JL et al. (2018). *J.Knee*, **25**:286-95.
- [3] Zheng K et al. (2017). *Med Eng Phys*, **42**:26-34.
- [4] Lloyd J.E. et al. (2012). *Soft T Biomech M CA Surg*, Springer.

Numerical discretization of trabecular bone based on Voronoi tessellation

Y. Zhou, P. Isaksson, C. Persson

Department of Materials Science and Engineering, Uppsala University, Sweden

Email: yijun.zhou@angstrom.uu.se

Summary

Discrete cellular three-dimensional structures were developed for numerical simulation of porous materials. The algorithms are based on Voronoi tessellation techniques and the morphometrical properties of the final structures are similar to trabecular human bone. Numerical and experimental evaluations of the mechanical behaviour of the structures reveal a reasonable agreement with human bone.

Introduction

The complexity of natural cellular structures, such as trabecular bone, imposes difficulties when discretizing them for numerical simulations. Although a good representation of the microstructure can be achieved with e.g. micro-CT imaging, it is limited to one specific specimen and does not permit for a rapid representation of structures from different sites and ages, which can display large variations in structural features. In recent years, several porous models have been proposed [e.g.1,2], however, they are often based on repeated unit cells, assembled to form a macroscopic homogenized structure, limiting stochastic features. In this study, a Voronoi tessellation technique was utilized to numerically discretize structures with mechanical and topological properties very close to those of human trabecular bone. The discretized geometries were numerically analyzed in finite element structural models and contrasted to compression tests on 3D-printed structures.

Methods

The basic steps in Voronoi tessellation to numerically generate a porous structure are well reported in the literature [e.g.3,4]. In contrast to previous studies, the discretized “core structure” was herein subdivided and scaled to achieve a smooth surface and the desired porosity. The discretized structures were compared to human and rabbit trabecular bone data to demonstrate the representability. Several numerical models were implemented in a commercial finite element software (ABAQUS). To validate the results, 3D-printed specimens were tested in quasi-static compression with a material testing machine.

Results and Discussion

One of the most important features of the derived algorithm is that it combines both open and closed cells. The different topologies are controlled by the relative porosity - a higher porosity results in higher connectivity between pores. Another important feature of the algorithm is that stochasticity is naturally included in the discretization process. Other important features, such as porosity, specific bone surface, trabecular thickness, or trabecular separation can easily be controlled in the algorithm to represent different types of bone [e.g.5]. Thus, several structural features of bone can be included in the algorithm, which demonstrates the universality

of the model. An example of discretized structures with roughly 60% porosity compared with a human trabecular bone is shown in Fig. 1.

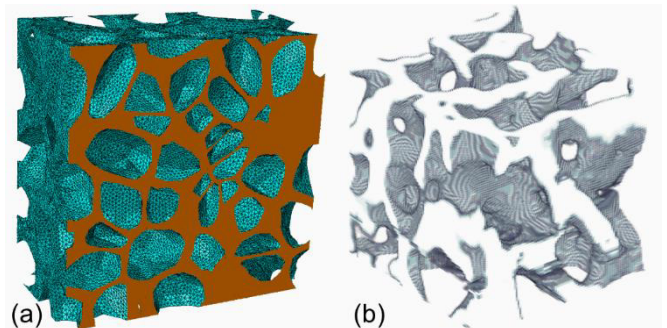


Figure 1: A part of finite element mesh with 200 randomly distributed pores (a), and a human trabecular bone (b).

When comparing the finite element models to the mechanical test results on 3D-printed structures, the stiffness was in general 25% higher in the finite element models. The main reasons could be differences in boundary conditions, test system compliance and defects resulting from the printing not being captured in the model.

Conclusions

An algorithm based on a Voronoi tessellation technique has been developed to numerically discretize trabecular bone tissue having different inherent properties such as relative porosity, orthotropy, connectivity, specific bone surface, etc. The mechanical testing shows reasonable agreements between numerical simulations and experimental results, suggesting that the discretized geometries may be utilized as test material for the development of new implants, e.g. in screw attachment tests.

Acknowledgements

This project has received funding from the European Union’s Horizon 2020 research and innovation program under the Marie Skłodowska-Curie grant agreement No 812765.

References

- [1] Wettergreen, M. A. et al. (2005). *Computer-Aided Design*, **37**: 1141-1149.
- [2] Ambu, R. et al. (2018). *Symmetry*, **10**: 361.
- [3] Kou, X. Y. et al. (2010). *Computer-Aided Design*, **42**: 930-941.
- [4] Fantini, M. et al. (2016). *Virtual and Physical Prototyping*, **11**: 77-90.
- [5] Bouxsein, M. L. et al. (2010). *Journal of Bone and Mineral Research*, **25**: 1468-1486

TOWARDS A NEW BIOMECHANICAL MODEL TO EXPLAIN UPRIGHT POSTURAL CONTROL IN UNILATERAL TRANSTIBIAL PROSTHESIS USERS

David F. Rusaw¹, Rasmus Alinder¹, Sigurd Edholm¹, Karin L.L. Hallstedt¹, Jessika Runesson¹, Cleveland T. Barnett²

¹Department of Rehabilitation, Jönköping University, Jönköping, Sweden

²School of Science & Technology, Nottingham Trent University, UK

Email: david.rusaw@ju.se

Summary

Investigations of balance and postural control in prosthesis users are often based on an implicit assumption that upright stance can be modelled as a single inverted pendulum. However, the validity of this assumption been shown to be questionable in this group. The current study suggests that a model incorporating the independent function of both the intact and prosthetic limbs better represents postural control in unilateral prosthesis users.

Introduction

Previous research has shown that the kinetic validity of the inverted pendulum model does not reflect the behaviour of the body during quiet standing for transtibial prosthesis users (TPU) [1].

The aim of the current study was to develop and to assess the efficacy of a biomechanical model representing the control of upright posture in unilateral TPUs, specifically by: (1) empirically establishing how closely the predicted outcomes of upright postural control from a theoretical model matched the measured outcomes from a group of unilateral TPUs and a group able-bodied individuals with mechanical constraints on the centre of pressure (CoP); and (2) assessing how closely matched the measured outcomes of upright postural control were between a group of unilateral TPUs and a group able-bodied individuals with mechanical constraints on the centre of pressure.

Methods

Two groups of participants were recruited (unilateral transtibial prosthesis users (TPU) (n=8) and controls (CON) (n=8). Participants stood quietly for 60 seconds on two parallel forceplates while full-body kinematics and kinetics data were collected. The CON group stood on a device which constrained the CoP to a fixed point. (CoP, centre-of-mass (CoM) and centre-of-mass acceleration (CoMacc) were extracted. Pearson

product-moment correlation coefficients (r) were calculated for the CoP-CoM (m) vs. (CoMacc) (m/s^2) for each foot and the resultant CoP in the ML- and AP-direction under three sensory conditions (eyes-open (EO), eyes-closed (EC), weightbearing feedback (FB)).

A three-way mixed ANOVA was used to compare mean coefficient for CoM-CoP distance under each foot/combined CoP and the CoM acceleration (CoM_{Acc}) in the mediolateral and anteroposterior directions.

Results and Discussion

There was no statistically significant three-way interaction between Group-Condition-Limb for the AP ($F(2.374, 30.858)=2.511, p=.089, \text{partial } \eta^2=.086, \epsilon=.593.$) or ML ($F(2.016, 26.212)=1.216, p=.313, \text{partial } \eta^2=.086$) direction.

There was one two-way interaction effect involving the group variable in the AP direction ($F(1.735, 30.858)=9.400, p=.002$) indicating increased positive correlation coefficients associated with the prosthetic/constrained limb factor vs. intact/unconstrained and total limb factors, particularly in the AB group.

Conclusions

For the intact and unconstrained limbs, coupling of CoM acceleration and CoP were stronger when contrasted against prosthetic and constrained limbs and suggest that both TPUs and constrained able-bodied individuals' postural control conforms well to that predicted by a unilaterally-constrained pin-controller model. These effects held independent of visual manipulation and weight-bearing asymmetry, suggesting that the proposed model has implications for the fundamental control of posture in transtibial prosthesis users.

References

- [1] Rusaw DF and Ramstrand S (2016). *Clinical Biomechanics*, **31**: 100-106.

Table 1: Mean (m) and 95% CIs of the Pearson product-moment correlation coefficient (r) for the CoP-CoM vs. CoMacc on each side (Intact, Constrained, Total), group (TPU-CON), condition (EO, EC, FB), in each direction (ML/AP).

Group		AP									ML									
		INTACT/UNCONSTRAINED			PROSTHESIS/CONSTRAINED			TOTAL			INTACT/UNCONSTRAINED			PROSTHESIS/CONSTRAINED			TOTAL			
		EC	EO	FB	EC	EO	FB	EC	EO	FB	EC	EO	FB	EC	EO	FB	EC	EO	FB	
TPU	m	-0.65	-0.47	-0.45	-0.02	0.05	0.07	-0.56	-0.36	-0.54	0.03	0.06	0.08	0.15	0.16	0.17	-0.73	-0.58	-0.63	
	95% CI	upper	-0.84	-0.79	-0.80	-0.26	-0.33	-0.27	-0.81	-0.69	-0.84	-0.09	-0.08	-0.11	0.04	-0.08	0.00	-0.93	-0.83	-0.87
		lower	-0.22	0.36	0.47	0.29	0.64	0.57	0.03	0.34	0.36	0.16	0.22	0.32	0.28	0.47	0.36	0.01	0.05	0.06
AB	m	-0.72	-0.60	-0.43	0.26	0.22	0.13	-0.82	-0.72	-0.71	0.07	0.06	0.11	0.13	0.10	0.20	-0.45	-0.31	-0.43	
	95% CI	upper	-0.88	-0.82	-0.62	0.18	0.11	0.04	-0.93	-0.91	-0.86	-0.03	0.02	0.00	0.04	0.04	0.12	-0.72	-0.62	-0.62
		lower	-0.33	-0.09	-0.16	0.35	0.36	0.24	-0.48	-0.14	-0.37	0.18	0.10	0.23	0.23	0.16	0.29	0.08	0.26	-0.15

Sensitivity of biomechanical responses in path optimized follower loads considering the lumbosacral load sharing

Robin Remus¹, Eike Uttich¹, Beate Bender¹

¹Chair of Product Development, Department of Mechanical Engineering, Ruhr-University Bochum, Germany

Email: remus@lpe.rub.de

Summary

In the optimization of a specific follower load (FL) path, usually only intervertebral rotations are minimized. In this study, we investigate the sensitivity of mechanical responses of a lumbosacral spine when including facet joint contact forces in the optimizations of FL paths. This consideration of load distributions results in substantial variations in FL paths and lumbosacral mechanical responses.

Introduction

Intervertebral disks and facet joints (FJ) of the lordotic lumbosacral spine (LSS) share compressive load in upright standing position [1]. Changes in their load sharing (LS) are associated with early degeneration and pain [2]. When modeling a LSS without muscles, a follower load (FL) is used to account for the axial compressive load from standing upright [3]. In the optimization of a specific FL path, however, usually only intervertebral rotations (IVR) are minimized [4]. FJ contact forces are excluded which omits possible effects of LS. We assume that this additional criterion has an impact on the FL path and mechanical responses of a LSS model. In this study, we investigate these effects and address the question of whether LS should be considered in future FL path optimizations.

Methods

We use a calibrated and validated passive hybrid model [5] of the ligamentous LSS built in ArtiSynth [6]. The LSS model consists of L1-S1 rigid vertebrae interconnected with fiber-reinforced finite element disks, ligaments, and idealized frictionless FJ with an initial gap width of 0.5 mm. Two sagittal symmetric tension-only cables implement the FL which is set to 600 N. The cables run through via-points attached to each vertebra. During optimization, via-point positions are automatically varied in a corridor (Figure 1B) starting at the approximate sideways centers of the vertebral bodies. In vivo estimations of FJ contact forces vary widely and may be influenced by the lumbar level or IVR [1]. Therefore, we compare the results of four different cases of objective functions used to optimize the FL path. They are minimized in MatLab® by PatternSearch with global search settings. Weighted objectives are the summarized absolute IVR and the targeted FJ forces as percentage of LS. The functions differ in the percentage of LS and in the lumbar levels for which the objectives are minimized: (1) minimize (min.) IVR; (2) min. IVR and 0% LS; (3) min. IVR (L1-L3) and 2% LS (L4-S1); (4) min. IVR (L1-L3) and 4% LS (L4-S1). For downstream LSS deflections, vertebra L1 is additionally loaded with ± 7.5 Nm in all principal directions.

Results and Discussion

Optimizations converge after 531-706 function evaluations. Calculated displacements (mean \pm SD) of the via points from the geometric centers in mm are -0.25 ± 1.80 , -0.22 ± 2.05 , -1.04 ± 1.03 , and -1.43 ± 2.54 . IVR with FL are 0.00° in (1) and $0.11 \pm 0.169^\circ$ in (2). IVR is maximal in (4) for L5 with 4.15° . Minimized IVR in (1) cause a FJ contact in L4/5 (5.2% LS). Lordosis and ROM of vertebra L1 (0.39° , 0.02° , 2.36° , and 3.44°) correlate with the mean FJ forces, which are lowest in (2) with 0.02 ± 0.03 N. Less the L1 ROM due to the FL, L1 ROM in flexion is maximal in (2) with 22.53° and min. in (4) with 20.37° . However, mean FJ force in extension is 105.31 ± 77.84 N in (1), highest in (2) with 112.2 ± 66.78 N and lowest in (4) with 102.9 ± 76.25 N. Coupled motion in axial rotation are altered by up to 4.5° .

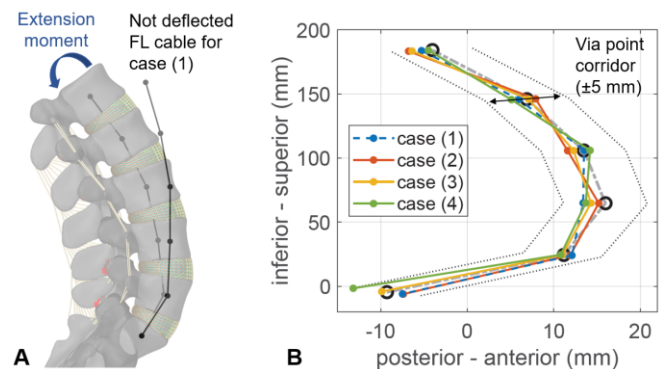


Figure 1: (A) LSS in extension for (1) plus the initial FL cable. (B) Vertebral body centers (O) and via point positions in sagittal plane.

Conclusions

Consideration of LS in FL optimization results in varying mechanical responses and FL paths. For better comparability of biomechanical data, even small LS ($<5\%$) due to FL should be discussed. Furthermore, influences of deviating anatomies, such as lordosis angle and facet joints, should be investigated in the future. Moreover, our study illustrates the sensitivity of LSS models to the defined boundary conditions, which will be particularly relevant in the context of a hybrid model extension with active skeletal muscles.

References

- [1] Bogduk N (2012). *Clinical and radiological anatomy of the lumbar spine*; Churchill Livingstone.
- [2] O'Leary et al. (2018). *Annu Rev Biomed Eng*, **20**:145-70
- [3] Patwardhan AG et al. (1999). *Spine*, **24**: 1003-9
- [4] Dreischarf M et al. (2010). *J Biomech*, **43**: 2625-28
- [5] Remus R et al. *PLoS One*, under Review.
- [6] Lloyd J et al. (2012). *Soft Tissue Biomechanical Modeling for Computer Assisted Surgery*; Springer.

How static and dynamic balance changes with age: the risk of sitting down

Lizeth H. Sloot¹, Matt Millard¹, Christian Werner², Katja D. Mombaur³

¹ORB Lab, Institute of Computer Engineering (ZITI), Heidelberg University, Heidelberg, Germany

²Center for Geriatric Medicine, AGAPLESION Bethanien Hospital, Heidelberg, Germany

³Dpt. Systems Design Engineering & Dpt. Mechanical Mechatronics Engineering, University of Waterloo, Waterloo, Canada
Email: lizeth.sloot@ziti.uni-heidelberg.de

Summary

Little is known about how older persons balance during stand-to-sit transitions even though this poses a higher risk for falls than walking. Compared to the young, we found older adults to be more statically balanced during both sit-down and stand-up. During sit-down, younger adults were unstable and fell into the chair. In contrast, older adults remained dynamically balanced but positioned more forward. This poses a risk for falling that could be addressed during fall training.

Introduction

The ability to get up from a chair is degraded in over 60% of long-term care residents, posing a risk of falling and affecting their independence [1]. To enable the assessment of balance during sit transitions, we recently presented an analysis of static versus dynamic balance, expressed relative to the person's base-of-support and using the foot-placement-estimator, thus taking into account the considerable linear and angular momenta during these movements [4]. Using this analysis, we found that older adults stay closer to being statically balanced than younger adults during stand-up.

Since nearly as many falls occur during stand-down [2,3], here we present the first analysis of the balance of younger and older adults during stand-to-sit.

Methods

Eight older adults (79±8 yrs; Short Physical Performance Battery 7-12 score) and 9 younger adults (28±5 yrs) stood up and sat down 5 consecutive times at comfortable speed with 2s rest in between. Full body motion capture and ground reaction force data were collected. Analyses focused on seat-on and seat-off, based on a >1N change in force measured under the stool (adjusted to knee-height), given the typically high velocities and instabilities at these moments.

Both static and dynamic balance were analyzed using the person's base-of-support (BOS), center-of-mass-ground-projection (COM_{GP}, IOR model Visual3D), center-of-pressure (COP), and the model-based foot-placement-estimator (FPE). The BOS was defined as the convex hull enclosing the area people could move the COP around in during flat foot standing [4]. A 2-factor mixed-model ANOVA (age vs. motion) was performed using SPSS.

Results and Discussion

Both age groups took more time to sit down compared to standing up ($p_{SIT} < 0.001$), but the older adults more so ($p_{INTER} = 0.02$; $\Delta Y = 0.47 \pm 0.39s$; $\Delta O = 1.61 \pm 1.25s$).

Being more conservatively statically balanced was defined as the COM_{GP} further within the BOS and closer to the COP, with lower COM speed. All 3 metrics indicated that older adults were more conservatively statically balanced compared to young, similarly during both tasks except for an even lower COM speed in older adults during sit-down (Figure 1A&B).

Being more conservatively dynamically balanced was defined as the FPE further within the BOS (larger dynamic balance margin); if the FPE is outside the BOS the person will need to take a step, or be caught by a chair, to prevent a fall. Both age groups were less dynamically balanced during sit-down compared to stand-up, with the younger adults becoming unstable (FPE far outside BOS; Figure 1C) and effectively falling onto the stool.

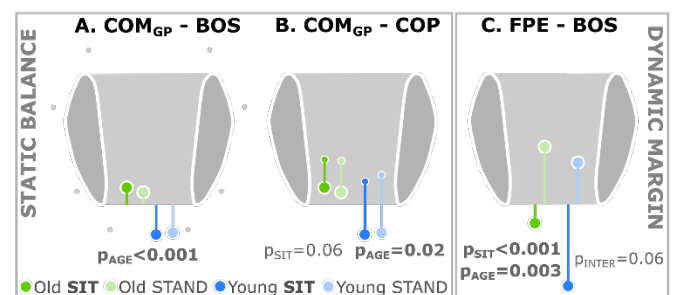


Figure 1: Static balance metrics and dynamic balance margin, with BOS hull and markers (A) in gray. Age effect, effect of sit vs. stand (P_{AGE}) and interaction effect (P_{INTER}) are given (p<0.05 significant).

Discussion

We showed that the balance dynamics between sit-down and stand-up motions are differently affected by age. While older adults sit down slower and more statically, younger adults fall into the chair. Paradoxically, the cautious approach of older adults might place them at a higher fall risk by leaning too far forward. Further research aims to relate balance in more frail older adults to typical falls seen in long-term care residents.

Acknowledgements

This study was part of the HeiAGE project, supported by the Carl-Zeiss Foundation (Germany).

References

- [1] Jeyasurya J et al. (2013). *J Rehab Res Dev*, **50**(6)
- [2] Rapp K et al (2012). *J Am Med Dir Assoc*, **13**(2)
- [3] Van Schooten KS (2018). *J Gerontol. A Biol*, **73**(6)
- [4] Sloot et al (2020). *Front Sports Act Living*, **2**

Forefoot or Ankle – Which really affects Balancing Skills?

Lena I. G. Fennen¹, Rosemary Dubbeldam¹, Heiko Wagner¹

¹Department of Movement Science, Sport Institute, Faculty of Sport and Psychology, University of Münster, Germany
Email: lena.fennen@uni-muenster.de

Summary

The idea of interpreting our foot as a simple connection to the ground during balancing is underrepresenting the foot's complexity and importance for posture [1,2,3]. Evolutional studies pinpointed the complexity of the foot and determined the medial longitudinal arch as a particularly unique part of human feet compared to the animal kingdom [1]. In this study, three-dimensional balance analysis with a multi-segment foot model showed that the segments midfoot and medial forefoot present extraordinary high movement activity during different balancing tasks. In contrast, rearfoot movements were much less. Hence, the role of mid- and forefoot in balancing should be reconsidered. Moreover, these findings suggest a re-evaluation of the so-called hip and ankle balance strategy. The insights may benefit rehabilitation.

Introduction

One of the common balance theories states that balancing is mostly managed by two joints: the hip and ankle [2]. Equivalently, in many biomechanical models, the human foot (26 bones, 20 muscles) is represented as one single segment [2,3]. But is this an accurate representation? Few approaches have been made to represent the foot's structures by multi-segment kinematic foot models [4]. Using such a model, assessing balance may reveal those foot segments, which influence balance abilities most. Such novel insights could be used to adjust rehabilitation approaches after, e.g., an ankle sprain. This study analyses the motion of the 6 foot segments from the Gent Foot Model (GFM) during balance tasks [4]. Additionally, so-called ankle joint motion was assessed using a 1-segment foot. The hypothesis is that not the rearfoot-tibia joint of GFM or the ankle joint present the highest amount of motion, but the midfoot and medial forefoot.

Methods

17 healthy subjects ($M_{age} = 24$ year, $SD \pm 5$) have been equipped with 21 infrared retro-reflective markers on the right foot [4]. Three balancing tasks were recorded using a 3-dimensional movement analysis system: two-limb stance, one-limb stance and one-limb stance with eyes closed. All tasks were performed for 60 seconds and repeated twice. The GFM's 6 segment angles, as well as the ankle joint angle (assuming the foot is one segment), were assessed in 3 dimensions. Cumulative ROM (cumROM) was calculated for each trial to derive the amount of movement over time (Figure 1). A linear mixed model was used to compare joint motion in all tasks for each joint and dimension.

Results and Discussion

The midfoot-medial forefoot joint is more active in

comparison to the rearfoot-tibia joint or the ankle joint, which difference further increases with increasing task difficulty (Figure 1). Task difficulty significantly predicted the joint's cumROM, $F(10, 491) = 3.7$, $p < 0.001$. When incorporating all 3 dimensions, significant changes remained, $F(20, 1324) = 5.94$, $p < 0.001$. The findings suggest that representing the foot by one rigid segment overestimates the role of the so-called ankle joint, and is not able to represent the role of the mid- and forefoot.

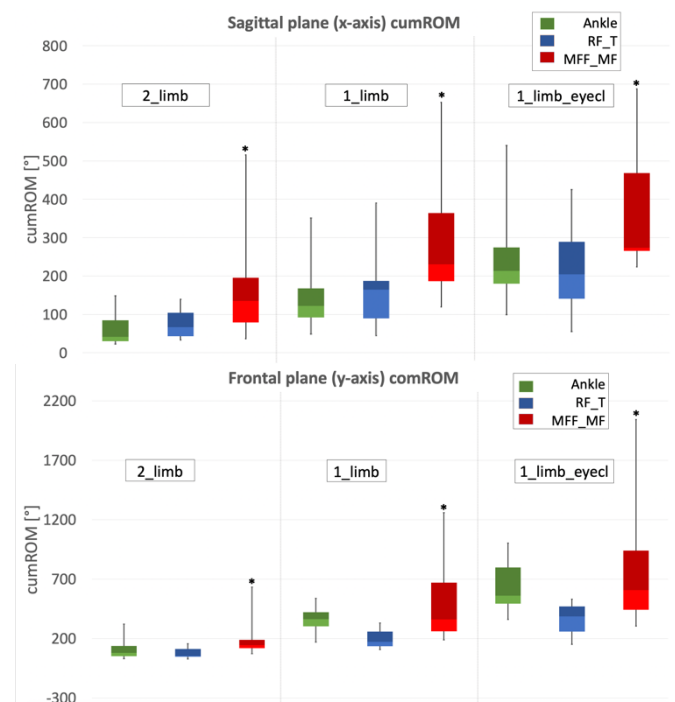


Figure 1: CumROM values with SD of two-limb (2_limb), one-limb (1_limb) and one-limb stance with eyes closed (1_limb_eyecld) of the ankle (Ankle), rearfoot-tibia (RF_T) and medial forefoot-midfoot (MFF_MF) joint on the sagittal and frontal plane.

Conclusions

New knowledge about the importance of the foot's segments motion while balancing provides an opportunity to redefine training interventions to increase balance abilities. Further, the assumption that the mid- and medial forefoot are of special importance can be confirmed. This can foster a different view on the foot and its influence on the body, which it is carrying.

References

- [1] Desilva J et al. (2019). *Am. J. Phys. Anthropol.*, **168**: 63-140.
- [2] Horak FB (2006). *Age Ageing*, **35**(2): 7-11.
- [3] Pollock AS et al. (2000). *Clin. Rehabil.*, **14**(4): 402-406.
- [4] Mits S et al. (2012). *J. Orthop. Res.*, **4**: 655-661.

Concurrent Assessment of Posture and Saccades with Visual Stimulation using Virtual Reality Technology; Construct Validity Testing in Healthy Older Adults

Y. Imaoka¹, A. Flury¹, E. D. de Bruin^{1,2}

¹ Motor Control & Learning Laboratory, Department of Health Sciences and Technology, ETH Zurich, Zurich, Switzerland
² Division of Physiotherapy, Department of Neurobiology, Care Sciences and Society, Karolinska Institute, Stockholm, Sweden
 Email: yu.imaoka@hest.ethz.ch

Summary

With the aim of early detection of dementia, a comprehensive assessment system with virtual reality (VR) technology was developed to measure posture and saccades simultaneously. Construct validity was evaluated with 14 healthy older adults (OA). We measured postural sway speed and saccade latency, provoking movements of posture and eyes with VR. Visual stimuli significantly affected on posture if saccade task was absent ($P=.01$, effect size (ES) = .66), and on saccade latency ($P>.002$, $ES<.78$).

Introduction

OA prone to mild cognitive impairment (MCI) can express dysfunction in posture and saccadic eye movement compared with healthy OA [1, 2]. Vestibular impairment is prevalent amongst people with MCI and is associated with poorer spatial cognitive skills [3]. Concurrent assessment of posture and saccades, provoking vestibular deficits, could broaden our understandings of mechanisms underlying MCI. Following prior studies, we integrated eye-trackers with our VR-based stabilometer and assess the validity of our construct in healthy OA [4]. We hypothesised that VR visual stimuli would more affect postural sway and cause longer saccade movement generation reaction times.

Methods

14 healthy OA (7 men / 7 women, mean age 71.9 ± 4.6 years) participated. We screened all participants using the Montreal Cognitive Assessment (MoCA). We measured postural sway and eye movement simultaneously with a newly developed VR-based stabilometer (GP-5000, ANIMA Corp. & VIVE Pro Eye VR headset, HTC Corp.), recording centre of pressure and gaze direction under 11 test conditions (eyes-open and -closed without VR; gaze, pro- and anti-saccade tests in 3 VR environments: black background (2D), non-oscillating stripes (NonOSC), oscillating stripes (OSC) in anterior-posterior (AP) direction). We started with non-VR tests and then randomised the other tests. Participants wore the VR headset while standing on the stabilometer with their feet at comfortable position. We measured both eye movements and posture for 60 seconds with 30 saccade trials per condition. We evaluated the effects of 1) visual stimuli by VR and 2) saccade types on postural sway speed and saccade latency by comparing the parameters between the test conditions.

Results and Discussion

The participants achieved MoCA scores of 27.5 ± 1.6 . We compared saccade latency between 2D and the other VR environments, and postural sway speed between 2D Gaze and

the other conditions. For mean saccade latency, we found significant differences between saccade types ($P<.001$, $ES=.88$), and between VR environments ($P>.002$, $ES<.78$). For posture, we observed significant difference only between 2D Gaze and OSC Gaze in AP direction ($P=.01$, $ES=.66$).

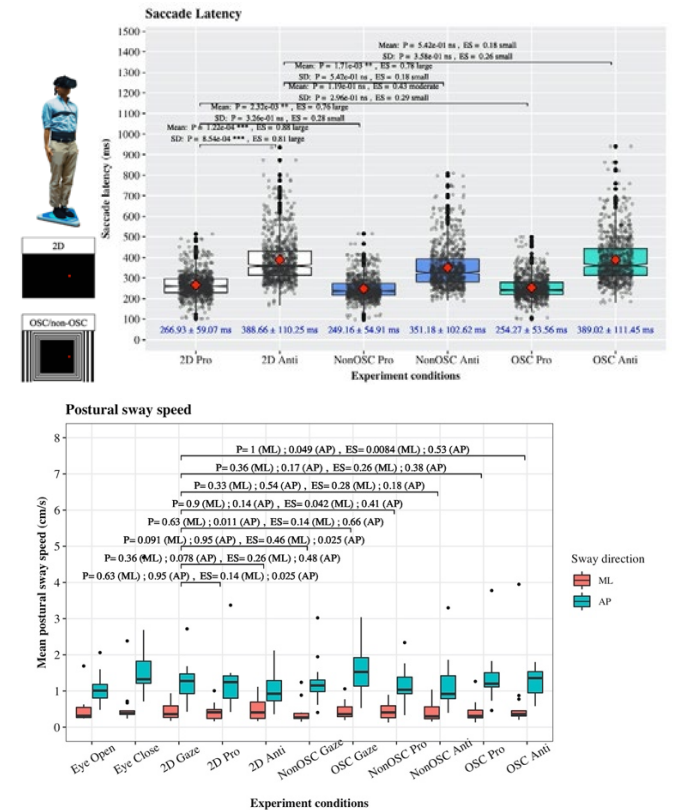


Figure 1: Distribution of saccade latency and postural sway speed

Conclusions

The results imply that OSC visual stimuli without saccade tasks induced more postural sway in healthy OA as hypothesised. OA had enough attentional resources to perform additional saccade tasks while lessening their postural sway in the OSC condition. Concurrent evaluation of posture and saccadic eye movements using VR might support assessing people with dementia more comprehensively and the results warrant further research where OA with and without MCI should be compared.

References

- [1] Bahureksa, et al. (2017). *Gerontology*, **63**:67-83.
- [2] Wilcockson, et al. (2019). *Aging-U.S.*, **11**: 5389-5398.
- [3] Agrawal, et al. (2020). *Aging Ment Health*, **24**:705-708.
- [4] Imaoka, et al. (2020). *Frontiers in Medicine*. 7:17.

Is non-uniform Achilles tendon displacement associated with calf muscle passive elastic modulus in young athletes?

Taija Finni¹, Ra'ad Khair¹, Iida Laatikainen¹, Pauline Eon^{1,2}, Antoine Nordez², Johanna Ihalainen¹

¹Faculty of Sport and Health Sciences, University of Jyväskylä, Finland.

² Université de Nantes, Mouvement – Interactions – Performance, MIP, EA4334, F-44000 Nantes, France

Email: taija.finni@jyu.fi, taija.m.juutinen@jyu.fi

Summary

We examined whether muscle-wise differences in passive elasticity, measured using shear wave elastography, are associated with non-uniformity in Achilles tendon displacement. In total 52 young athletes (18.3±3.2 years, 178±13.7 cm, 72±15.8 kg) were measured for soleus, medial and lateral gastrocnemius passive muscle elasticity during slow dorsiflexion. During submaximal isometric contraction, Achilles tendon internal displacement from the distal tendon was measured using B-mode ultrasonography and analysed by speckle tracking. Results showed that passive muscle elasticity was greatest in MG muscle and lowest in SOL without differences between sports or sex. Differences in absolute passive elasticity, measured as differential shear modulus between muscles did not correlate with tendon non-uniformity. Interestingly, female sex was the only significant predictor for greater non-uniformity in tendon displacement in this sample of young athletes.

Introduction

Athletes have 7.7 times greater chance of getting Achilles tendon (AT) rupture and 4.7 times greater chance for AT tendinopathy than controls [1]. AT injuries maybe long lasting and the factors leading to better recovery are still poorly understood. In healthy AT, non-uniform displacement is considered a healthy sign while in injury the non-uniformity is nearly nonexistent [2]. In search for functional factors influencing this phenomenon, we tested the hypothesis that non-uniform AT displacement is associated with non-uniformities in calf muscle passive elasticity in adolescent athletic population. We also examined if results were different between males and females or athletes in different sports.

Methods

Young athletes were recruited from local Sports Academy and training room -project. Total of 35 males (mean 18.5 yrs, 186 cm, 79 kg) and 17 females (17.8 yrs, 163 cm, 58 kg) from basketball (18), track and field (16) and gymnastics (18) visited laboratory for biomechanical assessments. Study had been approved by ethics committee and participants signed an informed consent.

Muscle elasticity was assessed using Supersonic shear wave elastography (SSI, France) when participants were sitting on an ankle dynamometer with knee fully extended. When relaxed, ankle joint was rotated from 40° plantarflexion to maximum of 20° dorsiflexion at 2°/s. These passive movements were repeated when imaging soleus (SOL), medial (MG) and lateral gastrocnemius (LG) muscle bellies in random order. Inter- and intrarater reliability was ICC>0.96 Shear modulus was extracted using ElastoGUI software.

AT proximo-distal displacements within a sagittal section of distal tendon were acquired with B-mode

ultrasonography (SSI, France) when participants were performing isometric ramp contractions up to 50 Nm target level. Displacements were assessed using 2D speckle tracking (Slane & Thelen 2015) in 6 locations across the tendon. Maximal nonuniformity was calculated as maximum-minimum displacement within the tendon cross-section. Correlations between maximal tendon non-uniformity and absolute differences in passive stiffness between muscles (MG-SOL, LG-SOL, MG-LG) were calculated. Results are presented from right leg. A linear stepwise regression to predict tendon non-uniformity was performed.

Results and Discussion

Passive muscle elasticity at maximal dorsiflexion was different between muscles (SOL 16.9±9.4 kPa, MG 89.2±25.2 kPa, LG 50.8±14.4 kPa, all p<0.001) but no differences were observed between sports or sex. Tendon displacement varied from 4.0. to 11.4 mm in the dorso-ventral plane, peak non-uniformity being non-significantly lower in males (7.0±2.9 mm) than females (9.3±5.0 mm) without differences between sports.

There were no bivariate correlations between non-uniformity in shear modulus of muscles and tendon displacement. While MG muscle had a much greater passive elastic modulus than SOL, the magnitude of elasticity difference did not correlate with the non-uniformity in AT displacement. It may be that active muscle dynamics plays the most important role in AT subtendon movement [3].

The regression model where differences in passive muscle elasticity and sex were included into the model revealed that females had more non-uniformity (standardized β 0.323, p=0.027). This novel finding needs further study in relation with the knowledge that males have more Achilles tendon ruptures [4].

Conclusion

Differential passive muscle properties were not associated with differential tendon displacement during isometric contraction. Female sex was the only significant predictor of AT non-uniformity in young athletes.

Acknowledgments

Academy of Finland (#323168/Finni) and Regional Council of Central Finland, European Union (A74999).

References

- [1] Kujala et al. (2005) *Clin J Sport Med* **15**(3):133-5.
- [2] Fröberg et al. (2017) *Knee Surg Sports Traumatol Arthrosc* **25**(6):1857-65.
- [3] Clark & Franz (2018) *PeerJ* **6**:e5182.
- [4] Ganestam et al. (2016) *Knee Surg Sports Traumatol Arthrosc* **24**(12):3730-7.

Modulating Achilles Tendon Loading during Gait with a Resistive Soft Ankle Exosuit

Dylan G. Schmitz^{1,2}, Krithika Swaminathan¹, Sungwoo Park¹, Fouzia Raza¹, Conor J. Walsh¹, Darryl G. Thelen²

¹Harvard Biodesign Lab, John A. Paulson School of Engineering and Applied Sciences, Harvard University, Cambridge MA, USA

²Neuromuscular Biomechanics Lab, Mechanical Engineering, University of Wisconsin-Madison, Madison WI, USA

Email: dgschmitz@wisc.edu and krithika@g.harvard.edu

Summary

This study combines shear-wave tensiometry with a soft exosuit to track Achilles tendon loading during exosuit-applied ankle resistance during gait. The results demonstrate the unique potential to actively modulate and track internal muscle-tendon loading during resistive training.

Introduction

Resistive training during gait rehabilitation in individuals with neuromotor disorders (e.g. cerebral palsy (CP), stroke) is often used to increase task intensity, which can improve retention of functional outcomes such as walking speed [1]. For post-stroke gait rehabilitation, one goal is to increase ankle push-off in the paretic limb, enhancing propulsion and walking speed. While clinics often use elastic bands to apply resistance and increase intensity, these methods do not directly target the paretic joint. Recent work showed that exoskeletons applying plantarflexor (PF) resistive torques increased PF muscle activity in patients with CP [2]. Still, it remains unknown how this translates into increased muscle-tendon (MT) loading, and how MT loading is modulated by the magnitude of applied resistance. The recent development of shear-wave tensiometry [3] enables noninvasive measures of tendon loading *in vivo* during dynamic movement, which has the potential to isolate the contributions of the triceps surae to net ankle torque. This is a distinction that cannot be made using traditional methods such as inverse dynamics, which only provide an estimate of the PF ankle torque. Here we demonstrate the feasibility of using shear-wave tensiometry to track modulations of Achilles tendon loading across a range of exosuit-applied resistances during gait.

Methods

One young healthy subject walked continuously for 9 minutes on an instrumented treadmill while wearing a unilateral soft exosuit on the left leg [4]. We collected data from optical motion capture, force plates, onboard exosuit sensors, and a tensiometer. The exosuit applied PF resistive force during the mid-late stance phase, such that the peak force increased monotonically each minute from 0N (slack) to 375N in 9 equidistant increments. The last 30 seconds of each condition was used for analysis. Net biological ankle torque was computed as the difference between exosuit-applied torque and net torque from inverse dynamics. Tendon loading is proportional to tendon shear wave speed squared, as measured by the tensiometer [3].

Results and Discussion

The peak exosuit resistance torque increased from 0 to 0.4 Nm/kg over the 9-minute walking trial. The corresponding

peak net biological ankle torque increased from 1.61 \pm 0.04 to 1.97 \pm 0.04 Nm/kg (+22%). Peak Achilles tendon wave speed increased from 50.1 to 58.9 m/s (+18%) over the trial, which we estimate to correspond to a 38.6% increase in tendon loading. A significant linear relation between tendon load and net biological ankle torque was observed, with the percent change in load exceeding the percent change in biological torque (ratio=1.49, $R^2 = 0.9529$, $p < 0.001$, Fig. 1). The strong correlation of tendon loading with resistance gives confidence that the tensiometer tracked modulations effectively. The deviation from a unity slope relationship suggests that estimations of net biological torque are insufficient to fully describe the modulation of individual muscle contributions.

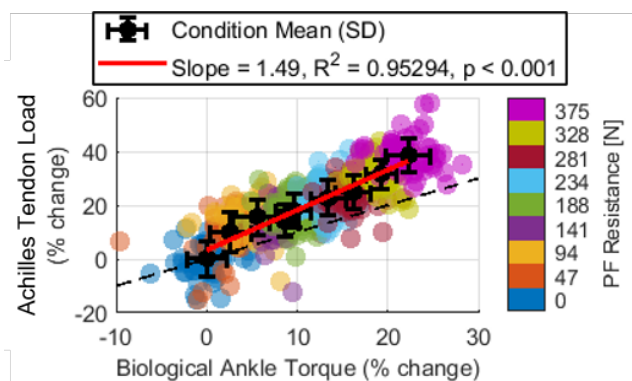


Figure 1: Relative change in peak biological ankle torque and peak Achilles tendon load with respect to slack walking ($F_{pk}=0$) across nine exosuit resistance magnitudes.

Conclusions

This study demonstrates that shear-wave tensiometry provides a unique methodology for directly assessing the effects of active exosuit resistance on MT loading during walking. The methodology obviates the need for a motion analysis laboratory, and hence is easily transferable to clinical environments. We believe that the coupled technologies could provide an objective approach to actively modulating MT loading during gait rehabilitation.

Acknowledgments

NSF DARE (2019621), NSF GRFP (2017250115) (DGE-1650114, DGE-1747503).

References

- [1] Ardestani et al. (2019). *Neurorehabil Neural Repair.*, **33**: 47-58.
- [2] Conner et al. (2020). *Ann. Biomed. Eng.*, **48**: 1309-1321.
- [3] Martin et al. (2018). *Nat. Commun.*, **9**: 1592.
- [4] Bae et al. (2018). *ICRA*. 2820-2827.

Contraction intensity does not influence the elastic and contractile components of the muscle-tendon unit performance enhancement in stretch-shortening cycles

Denis Holzer¹, Wolfgang Seiberl²

¹Biomechanics in Sports, Technical University of Munich, Munich, Bavaria, Germany

²Institute of Sport Science, Bundeswehr University Munich, Neubiberg, Bavaria, Germany

Email: denis.holzer@tum.de

Summary

This study investigates the interplay of the serial elastic and the contractile component of the muscle-tendon-unit (MTU) during pure shortening and stretch-shortening contractions among varying contraction velocity and range of motion. Thereby, we used nerve muscle stimulation, ultrasound, motion capture, and dynamometry. Our results suggest that a change in contraction intensity only affects the absolute concentric MTU work but does not lead to an increased SSC-effect.

Introduction

Stretch-shortening contractions (SSC) are the most common muscle action in sports or daily locomotion. During the concentric phase of a SSC, muscle force, work and power are increased by up to 50% when compared to pure concentric (CON) contractions [1]. This so-called SSC-Effect is discussed to be related to elastic energy preservation, reflex activity, activation dynamics or residual force enhancement (rFE) [2]. Thereby, the influence of contraction intensity on these performance-enhancing mechanisms is still rather poorly understood [3]. The aim of this study was to investigate how different contraction intensities influence the interplay of the serial elastic and the contractile component of the MTU during SSCs with varying range of motion (ROM) and contraction velocity.

Methods

Eleven participants performed submaximal plantar flexion contractions on a dynamometer using electrical nerve stimulation, including isometric, CON and SSC contractions at 30% and 60% of individual maximum voluntary torque (velocities: 40 & 120°/s; ROM: 15 & 25°). 3D motion capturing was used to track leg kinematics. In addition, two synchronized ultrasound probes were used to track changes in fascicle length of the gastrocnemius medialis and Achilles tendon, and to determine the dynamic Achilles tendon moment arm. The analysis focuses on the SSC-effect, defined as the ratio between the concentric phase of the SSC and CON contraction (Figure 1), using a repeated analysis of variance with the factors ROM, contraction speed and intensity.

Results and Discussion

The SSC-effect was confirmed as MTU work was significantly increased by 5-33% during SSC contractions ($p < 0.05$). The SSC-effect was unaffected by intensity as no change in MTU work ratio was found ($p = 0.096$). Contraction intensity changes had no effect on the relative behavior of the

series elastic and contractile component, as the ratio of Achilles tendon length change ($p = 0.242$), fascicle length change ($p = 0.549$), and fascicle and Achilles tendon shortening velocity ($p = 0.452$ and $p = 0.218$, respectively) was unaltered. Thus, intensity changes had no influence on fascicle work ratio ($p = 0.091$). Due to the measurement setup, reflex activity and activation dynamics should not have influenced the SSC-effect.

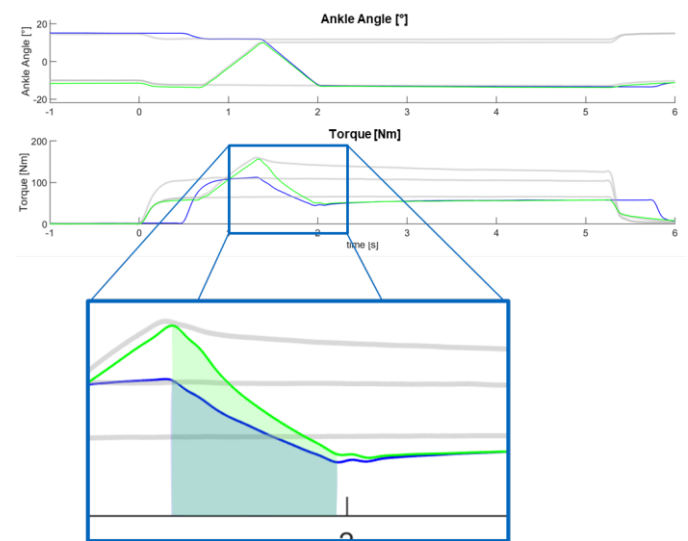


Figure 1: Exemplary ankle joint angle and torque of CON (blue), SSC (green), and isometric (grey) plantar flexions. During SSC contractions concentric work (green area under curve) was increased when compared to CON contractions (blue area under curve) throughout all contraction conditions (varying speed, ROM and intensity).

Conclusions

While the absolute values for all analyzed parameters were clearly affected by contraction intensity, these changes seemed to apply to SSC and CON contractions in a similar fashion so that the SSC-effect was unaffected. We did not find intensity-dependent changes in the contributions of the serial elastic and the contractile component of the MTU to the net SSC-effects. Further analysis focusses on rFE-related mechanisms that are not yet presented in this abstract.

References

- [1] Cavagna et al. (1968). *J. physiol.*, **24(1)**: 21-32.
- [2] Seiberl et al. (2015). *Physiol. Rep.*, **3(5)**.
- [3] Groeber et al. (2019). *J. Sports Sci. Med.*, **18(4)**, 604-614

Comparing Eight Normalization Methods for Net Joint Moment Data in the Single-Leg Squat

Steven M. Hirsch, Christopher J. Chapman, Tyson A.C. Beach
 Faculty of Kinesiology and Physical Education, University of Toronto, Toronto, Canada
 Email: steven.hirsch@mail.utoronto.ca

Summary

Recent ISB recommendations raise the question of whether the variance in kinetic data due to confounding anthropometric factors between groups (e.g., males vs. females) should be controlled by using statistical adjustments or (ratio) normalization techniques [1]. Although normalization facilitates between-group comparisons, certain techniques may misrepresent the relationship between kinetic and anthropometric data [2], fail to remove the correlation between them, or provide different interpretations to adjusted linear models. The purpose of this investigation was to assess eight normalization techniques using body mass, height, and limb length to normalize net joint moment (NJM) magnitudes. Normalizing NJMs by mass*height or mass*leg-length were the only methods that did not misrepresent the relationship between NJM and anthropometric data, removed the correlation between these data, and provided similar interpretations to adjusted linear models. Therefore, dividing NJM magnitudes by mass*height or mass*leg length is recommended to facilitate between-group comparisons.

Introduction

Anthropometric variables such as body mass, height, or limb length can influence the magnitude of NJMs. There is no consensus as to how, if at all, NJM data should be analyzed to account for differences in anthropometrics [1]. Commonly used ratio normalization techniques, where the NJM is divided by a "control" variable (e.g., body mass, height, or limb length), can potentially misrepresent the underlying relationship between NJM and anthropometric data if the regression line between these variables does not pass through the origin [2]. Further, it is unclear which methods successfully remove the correlation between the NJM and anthropometric variables while maintaining similar statistical interpretations to adjusted linear models (i.e., covariate analyses). Therefore, it is essential to consider how or if NJM data were normalized when interpreting research results, as it may affect the conclusions drawn. The purpose of this investigation was to compare the effects of eight different normalization techniques that involved dividing NJMs by various (combinations of) body mass, height, and limb length metrics during a single-leg squat (SLS) movement.

Methods

Sixteen males and 16 females performed five SLSs with their non-stance foot held back behind their body. A bottom-up inverse dynamical linked-segment modelling approach was used to quantify knee NJMs using standard methods. The data analyzed here were a subset of those reported elsewhere [3].

Net moments about the knee joint mediolateral axis were extracted when the knee was maximally flexed, and were then

divided by body mass, allometric mass ($\text{mass}^{0.67}$), height, limb length, mass*height, mass*limb length, allometric mass*height, and allometric mass*limb length.

Three methods were used to assess normalization techniques: 1) intercept analysis; 2) correlations between normalized NJM and anthropometric data; and 3) "mock" experimental analysis comparing normalized NJMs between males and females. The first method was used to assess the implicit assumption that the regression line between the NJM and anthropometric variables passed through the origin. If the regression line did not pass through the origin (i.e., the intercepts were significantly different from zero), then the ratio was deemed to misrepresent the relationship between these variables. The second method assessed the assumption that normalization removes the correlation between the NJM and anthropometric variables. The third method assessed the similarity of statistical interpretations when comparing NJMs between males and females using each normalization method relative to a statistically adjusted linear model.

Results and Discussion

The regression lines between NJMs and mass, mass*height, mass*limb length, allometric mass*height, and allometric mass*limb length passed through the origin (i.e., $p > 0.05$ for all intercepts). Correlations between NJMs and anthropometric data were only removed when normalizing by mass*height ($r = 0.04-0.19$), mass*limb length ($r = 0.06-0.11$), allometric mass*height ($r = 0.29-0.31$), and allometric mass*limb length ($r = 0.23-0.33$) (all $p > 0.05$). When comparing NJMs between males and females, only normalizing with mass*height and mass*leg length yielded similar statistical interpretations to an adjusted linear model.

Conclusions

Dividing NJMs by mass*height or mass*leg length is recommended to facilitate comparisons between groups. The traditional method of normalizing kinetic data based solely on body mass should be avoided for knee NJMs during a SLS.

Acknowledgments

The authors thank Steven Khuu for his assistance with data collection. Funding for this research was provided by the University of Toronto (Connaught New Researcher Award) and the Canadian Institute for Sport Ontario.

References

- [1] Derrick et al. (2019). *J Biomech.*, **99**
- [2] Curran-Everett (2013). *Adv in Physiol Ed*, **37**: 213-219
- [3] Hirsch et al. (2020). *J Strength Cond. Res.*, in press.

Can electrical noise stimulation improve the perception of vibration stimuli in patients with diabetes mellitus?

Claudio Zippenfennig¹, Tina J. Drechsel¹, Daniel Schmidt¹, Thomas L. Milani¹

¹Chemnitz University of Technology, Department of Human Locomotion, Chemnitz, Germany

Email: claudio.zippenfennig@hsw.tu-chemnitz.de

Summary

This study investigated the influence of an electrical noise stimulation (ENS) on plantar vibration perception thresholds (VPT) of 43 patients with diabetes mellitus (DM). ENS application was randomized during VPT measurements at 30 and 200 Hz. Although no significant differences were found, there were trends supporting a possible effect of ENS.

Introduction

Diabetic neuropathy is an incurable disease and mostly only symptomatic treatment with various drugs is available [1]. VPT are used to assess sensory deficits caused by DM; they are even used to assess neuropathy and ulcer risk [2]. A recent study showed that VPT can be enhanced by plantar mechanical noise stimulation (MNS) [2]. The phenomenon behind MNS is called stochastic resonance, which is the same for ENS [3,4]. To our knowledge, there are no studies investigating the effects of an ENS at the plantar foot on VPT in DM. Therefore, the present study investigated the effects of an ENS at the plantar foot on VPT in DM. Based on previous results, we hypothesized improved VPT due to ENS [2]. Furthermore, we hypothesized that ENS led to a reduction in the variability (CoV) of VPT.

Methods

43 DM subjects (27 ♂, 16 ♀; mean ± sd: 64.6 ± 9.3 yrs, 171.0 ± 9.8 cm, 88.9 ± 17.7 kg, 13.9 ± 10.6 yrs since diagnosis) participated in this study. VPT were measured at the first metatarsal head (MET I) at 30 and 200 Hz using a customized vibration exciter (type 4180, Brüel & Kjaer Vibro GmbH, Germany). ENS (white noise) was applied by an isolated bipolar constant current stimulator (Digitimer DS5, Digitimer Ltd, UK). Electrodes were placed at the plantar metatarsal heads and the dorsum of the toes/foot. Through a hole (∅ 10 mm) in the plantar electrode, the vibrating probe (∅ 7.8 mm) was positioned at MET I. VPT were measured three times with and without ENS (randomized). The stimulation intensity was 90% of the individual absolute current perception threshold.

Results and Discussion

Due to strict exclusion criteria, ENS was only performed on 38 DM subjects. Wilcoxon signed-rank tests showed no significant changes of VPT and CoV due to ENS (Table 1).

Table 1: Mean ± standard deviation of vibration perception thresholds (VPT) and coefficients of variation (CoV) for 30 and 200 Hz

	n = 38	stimulation off	stimulation on
VPT [μ m]	200 Hz	34.1 ± 22.1	34.7 ± 22.4
	30 Hz	89.5 ± 88.6	82.3 ± 78.5
CoV [%]	200 Hz	20.8 ± 17.2	17.0 ± 17.7
	30 Hz	22.7 ± 15.1	17.8 ± 12.9

VPT: $p_{200\text{Hz}} = 0.753$, $p_{30\text{Hz}} = 0.100$; CoV: $p_{200\text{Hz}} = 0.144$, $p_{30\text{Hz}} = 0.157$

Descriptively, DM with a diabetes duration ≤ 10 yrs showed an average improvement of ~ 6 -9% of their CoV. Although this was not significant, it shows a trend of variability reduction (Figure 1).

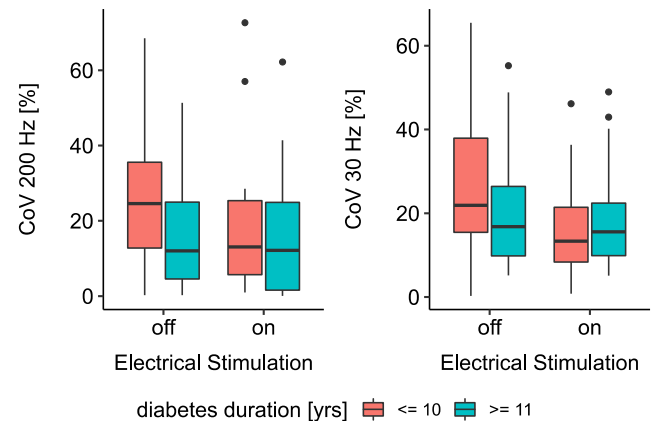


Figure 1: Coefficients of variation (CoV) for 30/200 Hz subdivided by diabetes duration (p range: 0.079 – 0.785).

Our results are in contrast to [2], but in line with the results of a previous study with healthy elderly subjects [3]. While MNS primarily acts on the receptors themselves, it is assumed that ENS modulates the nerve fiber [4]. This hypothesis is supported by improved VPT after ENS of the tibial nerve [5]. In contrast to MNS, skin properties play a major role in ENS, which are highly altered in DM. Since current seeks the path of least resistance, it is uncertain if the measured MET I area was also electrically stimulated, which could explain the lack of improvement in VPT.

Conclusions

Although our hypothesis was not confirmed, there seems to be a possible effect of ENS when considering diabetes duration and VPT variability. Hence, further studies are needed to provide evidence of the effect of ENS on VPT in DM patients.

Acknowledgments

Special thanks to all InSiDe project cooperation and network partners. This study is funded by the EU-EFRE.



References

- [1] Alsunousi S and Marrif HI (2014). *Front Neuroanat*, **8**:79.
- [2] Zwafernink JBJ et al. (2020). *J Diabetes Sci Technol*, **14**: 16-21.
- [3] Zippenfennig et al. (2018). *Clin Neurophysiol Pract*, **24**: 151-158.
- [4] Iliopoulos F et al. (2014). *J Neurophysiol*, **111**: 1238-1248.
- [5] Breen PP et al. (2016). *Med Eng Phys*, **38**: 822-825.

Experimental Validation of the Gross Taper Failure Mechanism in Total Hip Arthroplasty

V. Polster¹, S. Fischer¹, J. Steffens², M.M. Morlock¹, C. Kaddick²

¹Institute of Biomechanics, Hamburg University of Technology, Hamburg, Germany

²EndoLab Mechanical Engineering GmbH, Rosenheim, Germany

Email: valerie.polster@tuhh.de

Summary

Gross taper failure (GTF) is a rare but dramatic failure mode of the head-stem-taper connection of modular hip prostheses. The present study shows that the second stage of the GTF process - once initiated by bottoming-out - is associated with a linear increase in the wear of the stem taper and little further wear of the head taper caused by abrasive wear. The volume-time relationship is dependent on head length; with higher material loss for shorter heads.

Introduction

Gross taper failure (GTF) is a rare but dramatic failure mode of the head-stem-taper connection of modular hip prostheses, accompanied by massive material loss of the stem and head. GTF is suspected to be a two-stage process initiated by the corrosion-induced failure of the force locked taper, 'bottoming-out', leading to severe abrasive wear due to the subsequent rotation of the head on the stem taper.[1,2]

The objective of this study was to test the hypothesis of abrasive wear in the second stage in-vitro and to determine the time-material loss relationship.

Methods

Six cobalt-chromium alloy (CoCr) heads (36mm, 12/14 taper) with three different lengths ("S": -4mm, "M": 0mm, "L": +8mm) were assembled to stem taper replicas made from titanium-aluminium-niobium alloy (TiAl6Nb7). A small steel plug (S37) was used to simulate bottoming out. Dynamic gait loading according to ISO 14242-1 was applied for 2 million cycles using a hip simulator. Gravimetric wear was determined every 0.5 million cycles during serum exchange and volumetric wear was calculated with density of $\rho_{\text{CoCr}}=8,4\text{mg/mm}^3$ and $\rho_{\text{TiAl6Nb7}}=4,52\text{mg/mm}^3$.

Results and Discussion

Each stem taper surface developed a characteristic, head length-specific abrasive wear pattern (Figure1), comparable to those found in explants. At the time of serum exchange, the position of all heads was rotated to varying degrees from the initial position.

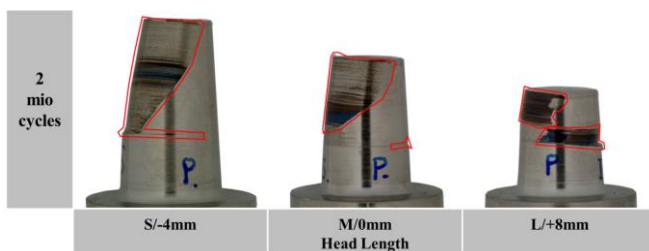


Figure 1: Taper wear after 2 million cycles. Red: Wear edges

Stem taper wear increased linearly with load cycles ($p<0.001$) and resulted in a mean volumetric material loss of $129\text{mm}^3/43\text{mm}^3/10\text{mm}^3$ per million cycles for head lengths S/M/L. The wear rate after 2 million cycles was significantly greater for the S head than for the M and L heads ($p=0.01$).

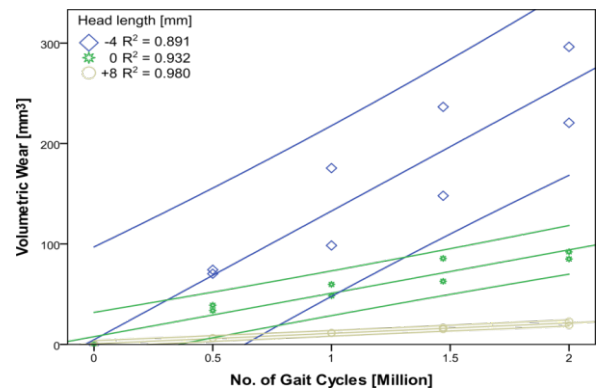


Figure 2: Volumetric wear of the stem tapers grouped by head length indicating a linear wear increase with time (Regression line with 95% confidence interval CI).

The head taper wear rates for the S/M/L head lengths were $2.5\text{mm}^3/2.6\text{mm}^3/4.1\text{mm}^3$ per million cycles. Only wear for the L head increased significantly with loading cycles ($p=0.016$). No difference was observed with respect to head lengths after 2 million cycles ($p=0.61$).

Conclusions

The present study shows that the second stage of the GTF process - once initiated by bottoming-out - is associated with a linear increase in the wear of the stem taper and little further wear of the head taper caused by abrasive wear. The volume-time relationship is dependent on head length; with higher material loss for shorter heads. Clinically, GTF is more common in association with longer heads [2]. This leads to the assumption that the total duration of the GTF process consists mainly of the first stage, where corrosion dominates, which is greater for longer heads [3,4] and thus leads to bottoming-out more quickly.

Acknowledgments

Materials were provided by Waldemar LINK GmbH and EndoLab provided the simulator time.

References

- [1] Bansal T et al. (2020). *IntOrth*, **44**: 609–21.
- [2] Morlock MM et al. (2018). *JoA*, **33**: 3581–90.
- [3] Falkenberg A et al. (2019). *J.Biomech*, **98**: 109424.
- [4] Pourzal R et al. (2018). *J.Arthroplasty*, **33**:2707-11.

Fatigue resistance of nitinol stents subjected to walk-induced femoropopliteal artery motion

Ran He¹, Liguao Zhao¹, Vadim V. Silberschmidt¹, Helen Willcock²

¹Wolfson School of Mechanical, Electrical and Manufacturing Engineering, Loughborough University, Loughborough, UK

²Department of Materials, Loughborough University, Loughborough, UK

Email: L.Zhao@lboro.ac.uk

Summary

Fatigue resistance of nitinol stents implanted in femoropopliteal arteries is a critical issue because of their harsh biomechanical environment. Limb flexions due to daily walk expose the femoropopliteal arteries and, subsequently, the implanted stents to large cyclic deformations, which may cause fatigue failure of the smart self-expandable stents. For the first time, this study utilised the up-to-date measurements of walk-induced motion of human femoropopliteal artery to investigate the fatigue behaviour of nitinol stent after implantation. The study was carried out by modelling the processes of angioplasty, stent crimping, self-expansion and deformation under repetitive bending, torsion and axial compression as well as their combination. The highest risk of fatigue failure of the nitinol stent occurs under a combined loading condition, with the bending contributing the most, followed by compression and torsion. The work is significant for understanding and improving the fatigue performance of nitinol stents through innovative design and procedural optimisation.

Introduction

Peripheral artery disease, narrowing of the peripheral arteries, is caused by the build-up of plaque on the inner wall of a blood vessel, which restricts the blood flow through the lower limbs. Peripheral artery disease is most found in the leg arteries, i.e., femoropopliteal arteries. Self-expandable nitinol stents were developed, which have excellent flexibility and can recover from deformation thanks to their unique superelastic behaviour. However, fracture of nitinol stents was frequently observed during follow-up examinations [1,2], which is directly associated with the repetitive external forces, i.e., fatigue loading, exerted on the stents during normal walk [3]. In this study, advanced finite-element simulations were carried out to investigate the fatigue resistance of nitinol stents subjected to walk-induced motion of an femoropopliteal artery.

Methods

In our numerical studies, a two-layer femoropopliteal artery, with an overall wall thickness of 1.15 mm, an inner diameter of 4 mm and a length of 50 mm, was modelled. The plaque was modelled as a symmetric layer inside the artery, with a length of 18 mm and a stenosis of 50% (i.e., an inner diameter of 2 mm). Finite-element model for the Zilver Flex® Vascular Self-Expanding Stent (Cook Medical, USA) was built using Abaqus CAE, with a length of 20 mm, an outer diameter of 5 mm and a strut thickness of 125 µm. A linear-elastic tube was

created in the numerical model to crimp and release the Zilver stent in the diseased artery. To simulate angioplasty, a three-folded non-compliant balloon model was also created, with a length of 21 mm and a nominal diameter of 4 mm.

Angioplasty was simulated before stenting, with a peak inflating pressure of 1.8 MPa applied to the inner surface of the balloon. The process of stent deployment in the diseased artery consisted of crimping and releasing steps. Following the stent deployment, its in-service fatigue behaviour was studied under a combined bending, torsion and axial compression fatigue caused by walking-induced artery motion.

Results and Discussion

In the constant-life's diagrams (Figure 1), the stent under combined loadings has the most elements in the dangerous zone above the fatigue strain limit line, indicating the highest risk of fatigue failure among all loading scenarios.

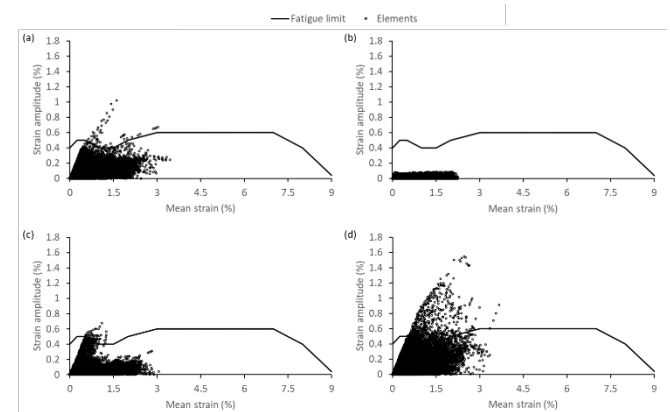


Figure 1: Constant-life diagrams for (a) bending, (b) torsion, (c) axial compression and (d) their combination.

Conclusions

The combined loadings imposed the highest risk to stent's fatigue failure, to which the main contribution was from bending, followed by axial compression and torsion.

Acknowledgments

We acknowledge the support from the EPSRC UK (EP/R001650/1).

References

- [1] Reis JMC dos et al. (2019). *J. Surg. Case Rep.*, **11**: 1-3.
- [2] Kim HT et al. (2020). *Cardiovasc. J. Afr.*, **31**: 1-3.
- [3] MacTaggart JN et al. (2014). *J. Biomech.*, **47**: 2249-2256.

Comparison of total ankle replacement designs using a dynamic computational model of the foot and ankle

Maria Ruiz¹, Rostam S. Kojouri¹, Sorin Siegler¹

¹Biomechanics Lab, Department of Mechanical Engineering, Drexel University, Philadelphia, PA

Email: mr3393@drexel.edu

Summary

Two different types of Total Ankle Replacement (TARs) are compared with a dynamic computational model of the foot. The foot is set to rotate in its three main directions in order to see the effect the implant designs have on the behavior of the ankle and subtalar joint. The saddle-shaped design approximates the anatomical surface of the bones, shows a better congruency and follows joint kinematics more realistically than the uniaxial design.

Introduction

TARs are used as a replacement of damaged cartilage and bone surfaces due to arthritis. These devices are getting more popular as their improved designs continue to accomplish better clinical results and good survival rates. While several Finite Element studies have been carried out to analyze critical stress concentrations due to wear [1], barely any project has managed to replicate *in vivo* motions of the ankle in a computational simulation. This study uses a validated numerical model [2] in order to compare the behavior of two TAR designs. One of the devices has a more constrained design, which mainly allows for uniaxial rotation (dorsiflexion/plantarflexion), such as the Infinity™ TAR. The other design instead, approximates the anatomical structure of the joint, thus making it more mobile, allowing the foot to rotate in all directions. A new implant (the Kinos™ TAR) is used as a representation of this second type of design. The study evaluates foot kinematics in the ankle complex, the talocrural joint and the subtalar joint.

Methods

The computational model used for this study includes the complete tibia and fibula bones, as well as the hindfoot and midfoot bones up to the metatarsals. These are considered 3D rigid bodies that were initially obtained from CT scans. The ligaments are modelled as tension-only springs with non-linear strain properties. The midfoot bones are also interconnected using specific springs with stiffness values in the 6 degrees of freedom. The articulating surfaces of the bones were offset for cartilage compensation, and the contact between them was considered frictionless. Regarding the implants, the talar dome and tibial tray were fixed to their respective bones, and the polymer component was attached to the tibial tray. The contact between the talar dome and the polymer is also assumed to have no friction. All the bones are completely free to move in any direction, only having the ligaments as constraints. In the simulations, the tibia was held fixed and rotational moments of 10Nm were applied to the calcaneus in dorsiflexion/plantarflexion, inversion/eversion and external/internal rotation. Also, a load of half-body weight was applied upwards as ground reaction force.

Results and Discussion

The results of these simulations show that the behavior of the two implants is very similar during dorsiflexion/plantarflexion, but larger differences can be seen during eversion/inversion and external/internal rotation (Figure 1). The Kinos implant is able to follow a very similar pattern to the natural joint, the Infinity design deviates more during those rotations.

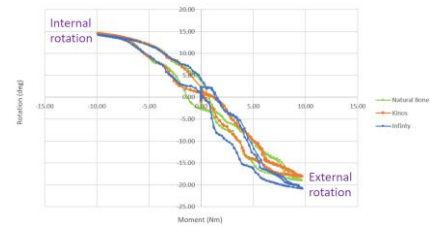


Figure 1: Rotation of the Ankle Joint Complex against the moment applied during External/Internal Rotation

Additionally, the distance between the interacting surfaces of the implants (the talar dome and the poly component) were studied using color maps. While the Kinos design showed good congruency, larger gaps between the surfaces were found in Infinity, as well as small areas of contact. This could lead in the future to stress concentration and wear.

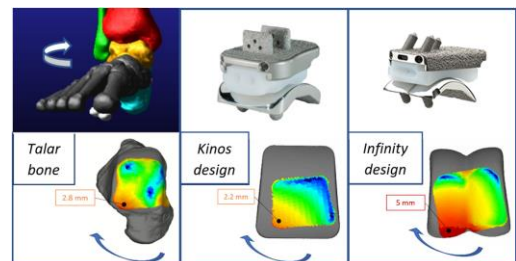


Figure 2: Distance mapping of the talus to the tibia, and the talar domes to the poly components, during External rotation

Conclusions

The dynamic computational foot/ankle model is a useful tool to compare the performance of different TAR designs. The saddle shaped implant, which approximates the anatomical joint surface, provides a better stress distribution, higher congruency and similar mechanics to that of the natural joint. This may suggest that such a replacement may provide less long-term wear and reduce failure rates.

References

- [1] Martinelli et al. (2017). *BMC Musculoskeletal Disorder*, **18(493)**: 1–9
- [2] Imhauser et al. (2008) *J Biomech.* **41(6)**: 1341-1349

Explicit and implicit FE-models capture the mechanical response of calcium phosphate-titanium cranial implants

Susanne Lewin¹, Ingmar Fleps², Dominique Neuhaus², Caroline Öhman-Mägi¹, Stephen J. Ferguson², Benedikt Helgason², Cecilia Persson¹

¹Dept. of Materials Science and Engineering, Uppsala University, Uppsala, Sweden

²Institute for Biomechanics, ETH Zurich, Zurich, Switzerland

Email: susanne.lewin@angstrom.uu.se

Summary

Cranial implants aim to provide cerebral protection after neurosurgery or skull trauma. With the increased use of patient-specific cranial implants, the mechanical response of each implant cannot be characterized experimentally in a practical way. However, computational models provide an excellent possibility to efficiently predict their mechanical response. This study developed finite element models of titanium-reinforced calcium phosphate (CaP-Ti) implants, the models predicted the mechanical response at both quasi-static and impact loading rates.

Introduction

Reconstruction of cranial defects with synthetic implants has a high clinical complication rate (~20%). Infection is the most frequent complication [1]. Most cranial implants have commonly been constructed from bioinert materials e.g. PMMA. The outcome could potentially be improved by using osteoconductive and bioactive materials. Promising clinical results have been reported for one such patient-specific calcium phosphate-titanium (CaP-Ti) implant, which consists of an additively manufactured titanium structure, covered by CaP tiles [2]. An important function of cranial implants is to provide cerebral protection. Recently, the mechanical behavior of generic CaP-Ti implants were experimentally investigated at quasi-static (QS) and impact loading rates [3]. However, computational models are required for investigating patient-specific designs. The primary aim of the present study was to develop a finite element modelling approach for CaP-Ti implants, and to validate it against experimental data of two implant designs at impact and quasi-static loading rates [4].

Methods

In the experiments, generically shaped implants were rigidly supported at the implant circumference and tested under QS (1 mm/min) or impact loading (5 kg, 1.52 m/s) [3]. Implant models were discretized (Ansa 17.1.0, Beta CAE Systems), and the boundary conditions were set to replicate the experiments. A rubber sheet (soft tissue surrogate) was used in the experiments, but only modelled in the impact model. The models were solved using implicit (QS) or explicit (impact) solvers (LS-Dyna R11.0.0, Livermore). For the CaP, a material model with tension-compression asymmetry was used. In the explicit model, damage was also implemented in the material model since CaP fractures had been observed experimentally. The material properties were determined by material testing or based on literature.

Results and Discussion

The FE models showed good agreement with experimental force-displacement data (Figure 1a-b). The failures indicated in the strain plots were observed at similar locations as in the experiments (Figure 1c). Initial peak loads were predicted with $\leq 11\%$ for implicit models, and $\leq 5\%$ difference for explicit models. The maximum displacement was predicted by the explicit models with $\leq 4\%$ difference.

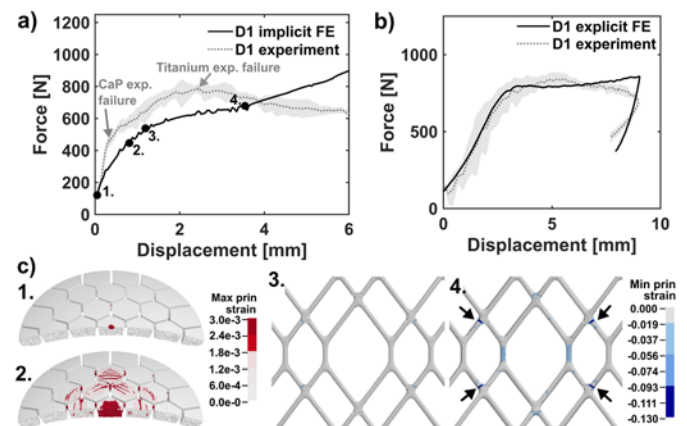


Figure 1: Force-displacement data for one implant design, QS (a) and impact (b). Implicit FE strain plots (c): CaP tiles (1, 2), red show failure. The titanium below the applied load (3, 4), blue show yield and failure. The strain plot locations are marked in a).

Conclusions

As demonstrated by this study on two implant designs, the mechanical response of CaP-Ti composite implants can be predicted by FE models at both quasi-static and impact loading rates. The models could be a valuable tool for the design and evaluation of patient-specific CaP-Ti cranial implants to optimize their performance and assure their safety. The framework developed for modelling the CaP-Ti implant used only literature based input and matched boundary conditions, hence it could be used in future studies for modelling CaP materials in other composite implants.

Acknowledgments

Funding from Eurostars-2 Joint EU, Horizon 2020 (E19741).

References

- [1] Van de Vijfeijken et al. (2018). *World Neurosurg.* **117**.
- [2] Kihlström et al. (2019). *World Neurosurg.* **122**.
- [3] Lewin et al. (2020). *J Mech Behav Biomed Mater.* **104**.
- [4] Lewin et al. (2020). *J Mech Behav Biomed Mater.* **112**.

O₂-Enrichment Device Based on Membrane Separation for Early Phases of Respiratory Insufficiency

Christoph Janeczek¹, Benjamin Lukitsch², Paul Ecker^{1,2}, Martin Elenkov¹, Bahram Haddadi², Christian Jordan²
Alexander Aloy³, Michael Harasek², Margit Gfoehler¹

¹ Institute of Engineering Design and Product Development, TU Wien, Vienna, Austria

² Institute of Chemical, Environmental and Bioscience Engineering, TU Wien, Vienna, Austria

³ Institute of Fluid Mechanics and Head Transfer, TU Wien, Vienna, Austria

Email: christoph.janeczek@tuwien.ac.at

Summary

High Flow Nasal Canula (HFNC) oxygen therapy can provide an effective treatment option in the early phase of respiratory insufficiency (e.g. for COVID-19 patients). Innovatively designed HFNC devices can be operated independently from medical O₂ supply infrastructure. In this study we present a simple, safe and cost effective HFNC system built with commonly available components utilizing membrane separation technology, which can support up to 10 patients in parallel depending on the clinically relevant flow rate.

Introduction

High Flow Nasal Cannula (HFNC) and Noninvasive Intermittent Positive Pressure Ventilation (NIPPV) via mask may have an advantage over controlled mechanical ventilation (CMV) [1]. Utilizing membrane separation technology in these noninvasive devices, O₂-enriched respiratory gas is directly produced via membrane separation from ambient air. An advantage permitting it for worldwide use due to the independence from medical O₂ supply infrastructure. For operation, only ambient air, an electrical power supply and water for humidification are required.

Methods

Based on a numerical model for the gas separation process, we designed an O₂-enrichment device for HFNC therapy. Key component of the device is an O₂-selective membrane module, in which pressurized and filtered ambient air (feed) is guided through the lumen of the hollow fiber membranes. O₂-enriched air is thereby separated as low pressure permeate and N₂-enriched gas is retained as high pressure retentate.

Pressure controllers ensure appropriate pressure levels and flow distribution in the flow paths of the system. We utilized an Arduino Mega 2560 with a TFT display as well as sensors for control and visualization of process parameters. Additionally, we developed a humidifier for the respiratory gas, comprising a pipe heating for the air flow combined with an evaporator.

Results and Discussion

The built prototype of the O₂-enrichment device measures 170 x 50 x 60 cm (height x width x depth). It provides respiratory gas with a O₂ concentration of 30 to 40 % for HFNC treatment of up to 10 patients in parallel depending on the clinically relevant flow rate. In order to generate a particle-free respiratory gas flow, the pressurized feed flow is first conditioned with a multistage filter unit. The permeate is then filtered in a second stage and subsequently heated and humidified. O₂ concentration is controlled via a pressure

control valve at the retentate exhaust. All described components are placed within an aluminum frame (Figure 1). Our prototype supports a working pressure of up to 10 barg on the feed side and a permeate flow of up to 200 L/min O₂-enriched respiratory gas for the patients.

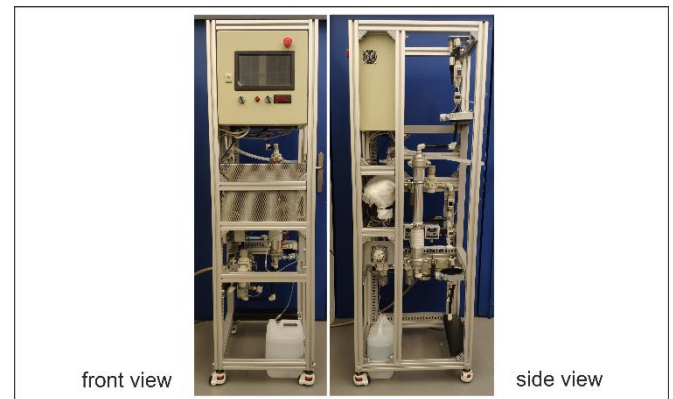


Figure 1: Lab prototype of the O₂-enrichment device

Figure 2 shows the dependency of O₂ concentration on the stage cut (permeate flow/feed flow) at a pressure of 7 barg in the feed stream.

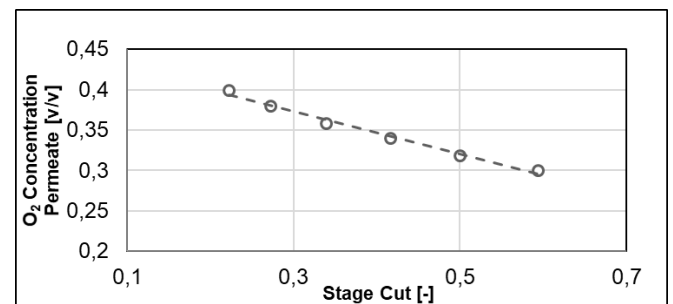


Figure 2: O₂ concentration in dependency on stage cut.

Conclusions

In this work we present a simple device for HFNC therapy of up to 10 patients suffering from respiratory failure (e.g. for COVID-19 patients) in parallel. The device is assembled using standard commercially available components and allows to provide HFNC therapy independently from medical O₂ infrastructure.

Acknowledgments

This study is self-funded by the institutes of the authors.

References

- [1] Dobler CC et al. (2020), *Mayo Clin Proc* 95, 12: 2594–2601

Quantifying the hip-ankle synergy in short-term maximal cycling

Louise Burnie^{1,2,3}, Paul Barratt⁴, Keith Davids², Paul Worsfold^{3,5}, Jon Wheat²

¹ Applied Sports, Technology, Exercise and Medicine Research Centre, Swansea University, Swansea, UK; ² Sport and Physical Activity Research Centre, Sheffield Hallam University, Sheffield, UK; ³ Biomechanics, English Institute of Sport, Manchester, UK; ⁴ Team INEOS, Manchester, UK; ⁵ Sports and Exercise Sciences, University of Chester, Chester, UK;

Email: l.a.burnie@swansea.ac.uk

Summary

A key mechanical feature of maximal cycling is hip and ankle joints working in synergy during the downstroke to enable the ankle to transfer power produced by the hip extensors to the crank. This study applied a modified vector coding technique to quantify the strength of the hip-ankle moment synergy in the downstroke during maximal cycling at varying pedaling rates: 60 and 135 rpm. There was a significantly stronger hip-ankle synergy for sprints at 60 rpm compared to 135 rpm, suggesting that as the task complexity increases (increase in pedaling rate) it is more difficult to coordinate the joint actions. Results suggest that this method could be used to assess riders' pedaling techniques and monitor effects of training or equipment interventions on coordination patterns.

Introduction

Musculoskeletal simulation studies have demonstrated during maximal cycling that the hip and ankle joints need to work in synergy through the downstroke, to enable the ankle to transfer power produced by the hip extensor muscles to the crank [1,2]. Consequently, the hip and ankle joints working in synergy during the downstroke is a key mechanical feature that represents functional maximal cycling coordination patterns. Therefore, developing a method to quantify the strength of this synergy in participant-based studies is important when investigating the stability of coordination behaviors in maximal cycling. The aim of this study was to apply a modified vector coding technique to quantify the strength of the hip-ankle moment synergy in the downstroke during short-term maximal cycling, and to compare the strength of the synergy to performance variations such as pedaling at differing rates of 60 and 135 rpm.

Methods

Twelve track sprint cyclists (4 males and 8 females, 24.1 ± 13.8 yrs, 68.2 ± 11.1 kg), performed 3 x 4 s seated sprints at 135 rpm, interspersed with 2 x 4 s seated sprints at a 60 rpm on an isokinetic ergometer. Joint moments were calculated via inverse dynamics, using measured pedal forces and limb kinematics, and interpolated to 100 points around the crank cycle. The hip-ankle moment synergy was quantified using a modified vector coding method [3]. First, the coupling angle was calculated from the hip-ankle moment-moment diagrams for each point on the crank cycle, with circular statistics used to calculate the mean coupling angles for each participant. The mean coupling angle was categorised into four coordination phases: in-phase, anti-phase, hip-phase and ankle-phase based on the system proposed by Chang and colleagues [3]. The frequency the mean coupling angle lay within each of these coordination patterns during the downstroke (0 to 180°) was calculated for each participant at each pedalling rate. Strength

of the hip-ankle synergy was quantified by the frequency of in-phase coordination pattern between the hip and ankle moments in the downstroke. Differences between coordination phase frequencies of the hip-ankle moments during the downstroke between sprints at 60 and 135 rpm were assessed using Wilcoxon matched-pairs tests.

Results and Discussion

In-phase coordination between the hip and ankle moments was significantly more frequent at 60 rpm compared to 135 rpm (Figure 1). Hip-phase coordination was significantly more frequent at 135 rpm compared to 60 rpm (Figure 1).

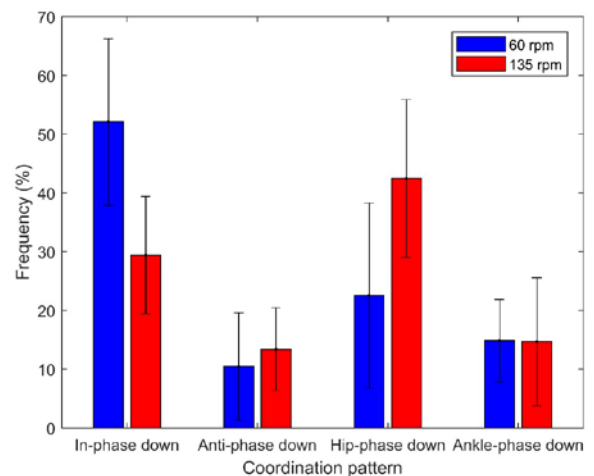


Figure 1: Hip-ankle moment coordination patterns during downstroke for sprints at 60 and 135 rpm. The P values for coordination patterns between sprints at 60 and 135 rpm: In-phase: $P = 0.001^*$, Anti-phase: $P = 0.119$, Hip-phase: $P = 0.005^*$, Ankle-phase: $P = 0.970$. *Indicates significant difference ($P < 0.01$)

There was a significantly stronger hip-ankle synergy for sprints at 60 rpm compared to 135 rpm, which might be due to the increased time available in the downstroke to coordinate the joint actions at 60 rpm. At 60 rpm, the ankle plantarflexion moment started to be produced just before TDC which was earlier than at 135 rpm, which meant it was increasing in conjunction with the hip extension moment, resulting in the stronger synergy at 60 rpm.

Conclusions

Results demonstrated that a modified vector coding technique can be used to quantify the strength of the hip-ankle moment synergy during the downstroke, and that the strength of the synergy is influenced by pedaling rate.

References

- [1] Fregly & Zajac (1996). *J Biomech.* **29(1)**: 81-90.
- [2] Raasch et al. (1997). *J Biomech.* **30(6)**: 595-602.
- [3] Chang et al. (2008). *J Biomech.* **41**: 3101-3105

An Open-Source Algorithm for Automatic Labelling of Optical Motion Capture Markers using Deep Learning

Allison L Clouthier¹, Gwyneth B Ross¹, Matthew P Mavor¹, Isabel Coll¹, Alistair Boyle¹, Ryan B Graham¹

¹School of Human Kinetics, Faculty of Health Sciences, University of Ottawa, Ottawa, ON, Canada

Email: allison.clouthier@uottawa.ca

Summary

We have developed and validated an open-source algorithm to automatically label optical motion capture markers. The algorithm uses deep learning and can be trained on existing data or simulated marker trajectories. We found that the algorithm had an accuracy of 99.6% when trained on existing data and 92.8% when trained on simulated trajectories. However, the later could be increased to 97.1% by applying transfer learning to existing data from a single participant. The algorithm and the provided user interface can help to reduce the time and effort required to label motion capture data, especially for those who have limited access to commercial software.

Introduction

Optical motion capture is a valuable tool for quantifying human movement. However, assigning labels to the 3D coordinate data in passive motion capture systems can be a tedious and time-consuming process. Previous methods have been proposed using machine learning to automate this process [1,2]; however, this typically requires a large dataset of ground truth data for training and some methods are negatively affected by extraneous or missing markers. Furthermore, few have made their algorithms publicly available. Therefore, our aim was to develop and share a deep learning-based algorithm that can be trained on existing or simulated marker trajectories to automatically label motion capture data.

Methods

In the proposed algorithm, a neural network based on long short-term memory units is used to predict label probabilities for unlabelled marker trajectories. Labels are assigned using the Hungarian algorithm, and corrections are made based on a pre-defined OpenSim marker set.

The algorithm was first trained on an existing dataset of 100 participants performing athletic movements and tested on a set of 42 participants performing the same movements. Simulated trajectories were then generated for a different marker set based on the motion of those 100 participants. The algorithm was trained on the simulated trajectories and tested on the data of nine participants that used this new marker and performed the athletic tasks and some other movements not included in the training set. The algorithm was updated using transfer learning on data from one participant and the accuracy was tested again. Labelling performance was compared to the commercial software Nexus (Vicon, Oxford, UK).

Results and Discussion

When trained on existing labelled data, the labelling accuracy was 99.6%. When trained on simulated trajectories, the

accuracy was 92.8%, but could be increased to 97.1% by updating the algorithm through transfer learning on labelled data from one participant. Performance was comparable to the commercial software, Vicon Nexus.

The labelling accuracy was better for movements contained in the training set of simulated marker trajectories (97.2%) than for those that were not (87.0%). However, the accuracy on unknown movements was increased to 95% following transfer learning. Additionally, markers were labelled successfully in the presence of missing and/or extraneous markers, although a large number of missing or extraneous markers did decrease the accuracy.

The Python code and data required to generate simulated trajectories for a custom marker set and to train the algorithm on existing or simulated trajectories is available at <https://github.com/aclouthier/auto-marker-label>. We have also created a graphical user interface to perform the labelling and make manual corrections as necessary (Figure 1).

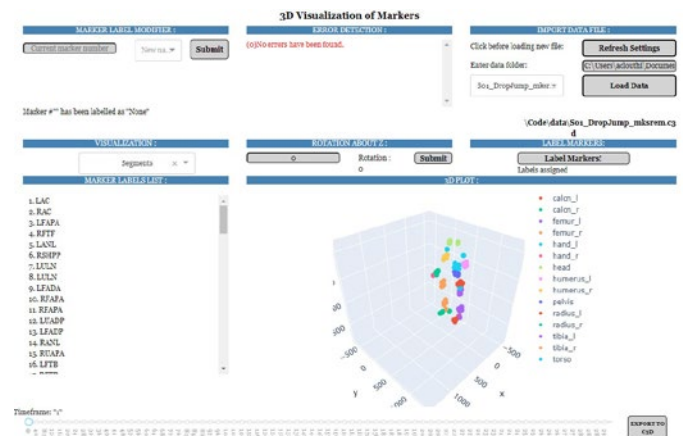


Figure 1: User interface that performs automatic labelling and allows user to make any necessary corrections.

Conclusions

The proposed marker labelling algorithm is able to accurately label motion capture markers without requiring any participant-specific model calibration and can be improved as data are collected, labelled, and used to update the algorithm. The algorithm and provided user interface have the potential to reduce the time and effort required to label motion capture data, especially for those with limited access to commercial software.

Acknowledgments

This work was funded in part by NSERC.

References

- [1] Ghorbani et al. (2019). *LNCS* **11542**: 167-178.
- [2] Han et al. (2018). *ACM Trans Graph* **37**(4).

The Performance of Open-Source Pose Estimation Algorithms During Walking, Running and Jumping

Laurie Needham¹, Murray Evans¹, Darren P. Cosker¹, Logan Wade¹, Polly M. McGuigan¹, James L. Bilzon¹, Steffi L. Colyer¹

¹Centre for the Analysis of Motion, Entertainment Research and Applications, University of Bath, Bath, UK
Email: ln424@bath.ac.uk

Summary

Several deep learning-based pose estimation methods (OpenPose, AlphaPose and DeepLabCut) were bench-marked against full-body marker-based motion capture. Joint centre locations between systems were evaluated during walking, running and jumping.

Introduction

Biomechanics research traditionally relies on vision-based motion capture tools, either using regular video data and manually annotating points of interest or using maker-based motion capture systems. Deep learning-based pose estimation methods are beginning to provide viable, non-invasive alternatives to traditional motion capture. However, markerless pose estimation methods were not developed specifically for biomechanics applications, thus there is a need to understand their performance in such settings against more established techniques, such as marker-based motion capture. The aim of this study was to evaluate the performance of several open-source pose estimation algorithms against maker-based motion capture during walking, running and jumping.

Methods

Fifteen participants performed walking, running and jumping activities wearing a full-body markerset (44 + clusters). Marker data were captured using a 15 camera Qualisys system (200 Hz) which was synchronised with 9 machine-vision cameras (200 Hz). Image data from each machine-vision camera were processed using OpenPose[1], AlphaPose[2] and DeepLabCut[3]. 2D image plane coordinates from each pose estimation method were back-projected into the 3D space, where the intersect of the back projected rays were taken to represent the 3D joint centre locations. Differences (mean \pm SD) in joint centre locations were determined by computing the 3D Euclidean distances between the marker-based (regressed from markers on the segment) and markerless joint centres. Additionally, 95% limits of agreement (LoA) values were computed for the differences in hip, knee and ankle joint centre positions.

Results and Discussion

For all three activities and methods, joint centre locations with the lowest mean differences and SD were observed at the ankle followed by the knee and hip, respectively (e.g., running in Table 1). A large portion of these differences were systematic in nature and likely represent systematic mis-

labeling of joint locations in the training data of the markerless pose estimation methods. Additionally, the large random errors that occurred were typically due to false positive detections of joint centres or erroneous switching of contralateral limbs by all pose estimation methods.

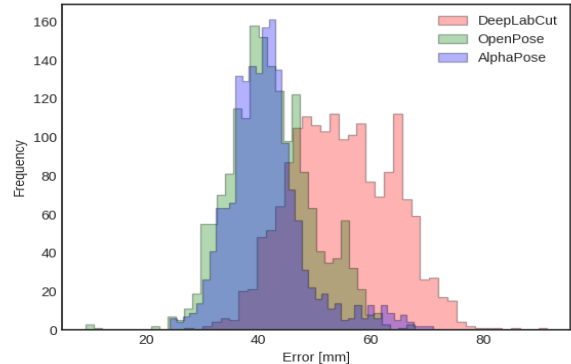


Figure 1: Hip joint location error distributions for each method during all activities.

The lowest mean differences were observed using AlphaPose, followed by OpenPose and then DeepLabCut (Table 1 & Figure 1). These results align with each method's performance on common computer vision benchmarks (COCO, MPII). Further processing of pose estimation results, e.g., outlier detection and inverse kinematics modelling, may be required before acceptable results can be obtained for biomechanics research applications.

Conclusions

OpenPose, AlphaPose and DeepLabCut were benchmarked against marker-based motion capture. Large systematic and random differences were observed for all methods but AlphaPose exhibited the lowest mean errors. Researchers should consider the accuracy and precision requirements of their research applications before implementing these markerless motion capture techniques.

Acknowledgments

This investigation was part-funded by CAMERA, the RCUK Centre for the Analysis of Motion, Entertainment Research and Applications, EP/M023281/1.

References

- [1] Cao, et al. (2019). *IEEE Trans.* 43(1), 172-186.
- [2] Fang, et al. (2017). In *ICCV* (pp. 2334-2343).
- [3] Mathis, et al. (2018). *Nat neurosci*, 21(9), 1281-1289.

Table 1: Mean 3D Euclidean differences for lower body joint centres during running.

	Mean Difference (Bias) (mm)			\pm SD			LoA (Bias + 1.96 SD)		
	OpenPose	AlphaPose	DeepLabCut	OpenPose	AlphaPose	DeepLabCut	OpenPose	AlphaPose	DeepLabCut
Hip	37.95	34.60	45.26	9.41	5.98	9.92	56.39	46.32	64.71
Knee	38.04	41.73	72.45	12.74	21.95	78.04	63.00	84.75	225.41
Ankle	18.50	29.99	89.69	11.09	20.29	154.02	40.25	69.76	391.57

Under-shoe hydrodynamics correlate with film thickness predictions based on worn tread geometry

S.L. Hemler¹, E.M. Pliner^{1,2}, M.S. Redfern¹, J.M. Haight³, K.E. Beschorner¹

¹Department of Bioengineering, University of Pittsburgh, Pittsburgh, PA, USA, ² Department of Aging & Geriatric Research, University of Florida, Gainesville, FL, USA, ³Department of Industrial Engineering, University of Pittsburgh, PA, USA

Email: slh148@pitt.edu

Summary

Greater shoe tread wear leads to increased slip risk. There is a need to standardize shoe replacement recommendations, but shoe wear is complex as the rate at which shoes wear varies across individual and shoe. This study found that the shoe's ability to disperse under-shoe fluids was positively associated with the shoe outsole wear geometry, independent of shoe type or individual. As such, shoe wear geometry may be a good indicator for shoe replacement across workplaces.

Introduction

Slips, trips, and falls are a major problem accounting for 28% of occupational injuries [1]. Footwear and particularly shoe outsole design are important factors for reducing slip risk [2]. Previous work has shown that the rate at which shoe tread becomes unsafe varies across individuals and shoe type [3]. This may prevent the distance walked in shoes from being an efficacious replacement recommendation. Therefore, replacement guidelines based on the condition of the shoe may be more advantageous.

Previous work by our group has applied lubrication theory to worn shoes to predict under-shoe hydrodynamics (film thickness) based on the worn region dimensions [4]. This approach provided valid predictions for the hydrodynamics for shoes worn via a controlled mechanical wear experiment [4]. The aim of this research is to extend that work to determine whether lubrication theory can predict changes in under-shoe hydrodynamics for *naturally* worn shoes.

Methods

Fifteen participants were each provided with two out of three types of slip-resistant shoes (shoes A and: B or C). A pedometer on the shoes tracked the distance walked. The under-shoe hydrodynamics (referred to as fluid force hereafter) were tested at baseline and after each month worn in the workplace. Fluid force was quantified from a robotic slip tester that applied a simulated slip under fluid-contaminated conditions (90% glycerol), while the load supported by the fluid was measured with fluid pressures sensors [5]. The shoe wear geometry was measured as the longest and widest regions of continuous wear. The under-shoe predicted film thickness (PFT) was calculated based on the wear geometry length and width, fluid viscosity, sliding speed, and vertical force [4].

Two repeated measures ANOVAs were used to assess predictors of fluid force. The primary predictor in model 1 was distance walked (current wear standard), and in model 2 was PFT (based on lubrication theory/wear geometry). Shoe type (A, B, C), and its interaction with distance walked/PFT were also independent variables. Distance walked was

square root-transformed and fluid force was natural log-transformed.

Results and Discussion

Participants walked 103-2053 km in the shoes across 1-11 months (199 total subject-months). Fluid force increased with the distance walked ($F_{1,276}=140.0$, $p<.001$) and PFT ($F_{1,205}=112.4$, $p<.001$). The shoe type was significant in both analyses ($F_{2,239}=29.2$, $p<.001$), ($F_{2,102}=29.2$, $p<.001$). An interaction was observed between shoe type and distance walked indicating the rate at which fluid force increased varied per shoe type ($F_{2,273}=7.5$, $p<.001$). This effect was not seen in the model with PFT ($F_{2,255}=2.0$, $p=0.141$).

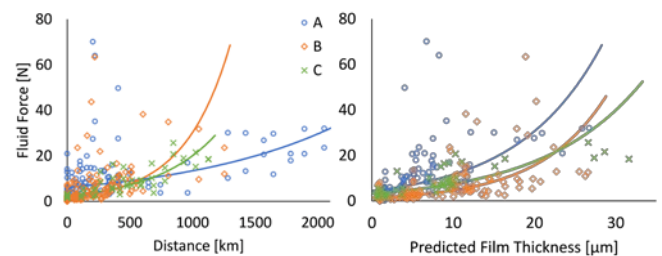


Figure 1: Fluid force vs. distance walked (left) and PFT (right) for the three shoe types with exponential trendlines.

Film thickness predictions based on the shoe outsole wear geometry consistently predicted increase in the fluid force across shoe types. The distance shoes are worn predicts fluid force though with greater variation across shoe type. Our results suggest lubrication theory, based on wear geometry, to be more versatile in predicting under-shoe hydrodynamics across multiple settings, shoes, and individuals than distance.

Conclusions

PFT based on outsole wear geometry was found to be a valid tool for assessing loss in fluid drainage capacity in naturally worn regions. Thus, this study shows that the previously developed models [4] are valid in the context of natural wear. This adds to the growing body of evidence for monitoring shoe wear based on the dimensions of the worn region rather than a time or distance walked measurement.

Acknowledgments

Funding was provided by the following grants: NIOSH R01 OH 010940, NSF GRFP 1747452, NIAMS R43AR064111.

References

- [1] US Dept. Labor, BLS. Occup Injuries & Illnesses, 2019.
- [2] Beschorner, et al. (2014). *J Biomech* 47(2), 458-463.
- [3] Hemler, et al. (2021). *Gait & Pos*, In Review.
- [4] Hemler, et al. (2020). *Trib Intl*, 106161.
- [5] Hemler, (2019). *App Ergo*, 80, 35-42.

Can Leap Motion Controller replace conventional marker-based motion capture systems ?

Amartya Ganguly¹, Gabriel Rashidi¹, Katja Mombaur²

¹Optimization, Robotics and Biomechanics, Institute of Computer Engineering, Heidelberg University

²Chair in Human-Centred Robotics & Machine Intelligence, University of Waterloo

Email: amartya.ganguly@ziti.uni-heidelberg.de

Summary

Over the last few years, the Leap Motion Controller (LMC) is progressively used in clinical environments to track hands, wrist and forearm positions as an alternative to the gold-standard motion capture systems. We compared performance of the LMC against gold-standard motion capture system to validate reliability of LMC. The two systems were time synchronised and performance validation was conducted for static as well as dynamic conditions i.e flexion and extension movements for all fingers. The study shows that currently, the LMC, is not yet suitable to replace gold-standard motion capture systems in clinical settings.

Introduction

The LMC device is a portable, marker-less motion capture system, and is often used as a low-cost alternative to standard marker-based motion capture systems, specially in clinical environments. The LMC is designed to track elbow, wrist, and finger joint positions. Few studies have attempted to validate the LMC against standard marker-based motion capture systems [1-3]. It is evident that the LMC is being used in a variety of applications, however, there is a lack of validation and replication studies with regards to clinical acceptance of this low-cost marker-less device. Specifically, there is a gap in evaluation of performance of LMC with respect to finger kinematics, as well as, lack of synchronised validation of LMC with a gold-standard motion capture system.

Methods

Ten right-handed subjects (6 male and 4 female) of mean age of 26.8 years were recruited for this study. The experimental protocol was completed successfully.

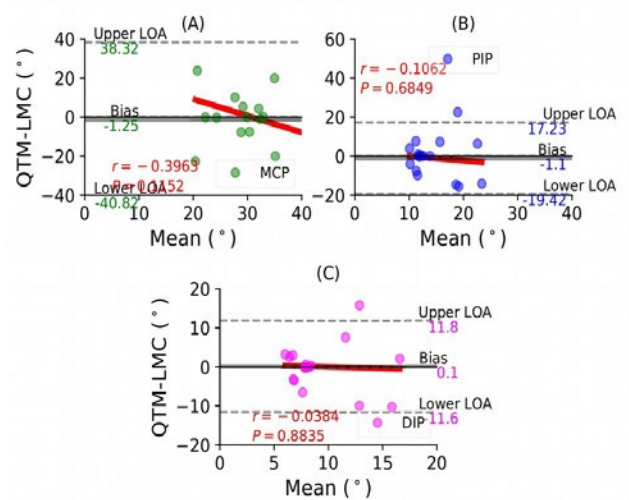
Ten Oqus 500 motion capture cameras (QTM; Qualisys, Goeteborg, Sweden) placed at appropriate locations, were used at a frame rate of 150Hz. The LMC generally is pre-calibrated, however, it was calibrated again with a calibration score of 95. Higher calibration score yields better stable measurements.

The two data acquisition systems were time synchronised as each system streams data with different sampling frequency. All participants performed a static trial and series of flexion/extension tasks. Instructions were prompted on the screen and all tasks were randomised. Two trials per subject were conducted. In each trial, the subjects performed flexion/extension movements three times. Overall, there were 10 successful static trials, and 120 dynamic trials.

Results and Discussion

The figure 1(A) shows a BA plot for MCP joint with a negative bias of 1.25° with $r = -0.3963$, $P = 0.1152$. Panel 1(B) shows a negative bias of 1.1° with $r = -0.1062$, $P = 0.6894$ of PIP joint. Lastly, Panel 1(C) shows a positive bias of 0.1° with $r = -0.0384$, $P = 0.8835$ of the DIP joint. During the index finger flexion movement, none of the joints demonstrated a positive correlation between the two measurement systems [4].

Figure 1: Bland-Altman plot for Index finger flexion, (A) MCP



joint, (B) PIP joint and (C) DIP joint

Conclusions

The LMC device has the potential to replace marker-based motion capture technology, however, it requires significant programming knowledge to extract data from the device for offline analysis. The variable sampling frequency is still a major problem with LMC when conducting such validation studies. At this juncture, we conclude that the LMC is acceptable in static conditions, however, for dynamic cases further validation studies are warranted.

Acknowledgments

We thank all the participants who volunteered for this study. We would also like to thank EIT Health 19340 for funding this study.

References

- [1] Guzsvinecz, T et al. (2019). *Sensors*, **19**: 1072.
- [2] Niechwiej-Szwedo, E et al. (2018). *PloS one*, **13**: e0193639.
- [3] Smeragliuolo, A. H. et al. (2016). *Journal of biomechanics*, **49**: 1742-1750.
- [4] Ganguly, A. et al. (2021). *Sensors*, **21**:1750.

A Mechanistic Model of Muscle Force and Impedance

Matthew Millard¹, David Franklin², and Walter Herzog³

¹Optimization, Robotics and Biomechanics Group, Heidelberg University, Heidelberg BW, Germany

²Neuromuscular Diagnostics Group, Technical University of Munich, Munich BY, Germany

³Human Performance Laboratory, University of Calgary, Calgary AB, Canada

Email: matthew.millard@ziti.uni-heidelberg.de

Summary

The intrinsic stiffness and damping of muscle are of great importance for force generation and stability. We present a muscle model with a force response dominated by a spring-damper in the short term but converges to a Hill model over time. The spring-like quality of the proposed model results in a gain and phase response that more closely follows biological muscle in the frequency domain than a Hill model.

Introduction

The intrinsic stiffness and damping of muscle vary linearly with activation [1] and are used by the central nervous system to stabilize the body's posture [2]. In this work, we present a muscle model that can reproduce the force-velocity [3] and force-length [4] properties by construction, and has stiffness and damping similar to biological muscle.

Methods

We model the musculotendon unit as a scaled half-sarcomere acting at a pennation angle of α to a rigid tendon (Fig. 1). The myosin filament attaches to the actin filament through a single lumped cross-bridge that attaches to the actin filament at a distance of ℓ^S from the Z-line. The intrinsic stiffness (K^X) and damping (β^X) of the lumped cross-bridge varies linearly with activation and the amount of overlap between the actin-myosin filaments. The attachment point ℓ^S , is driven at the acceleration-level primarily by the force imbalance between the spring damper and a Hill-type muscle model

$$dv^S/dt = [K^X \ell^X + \beta^X v^X - a f^L(\ell^S + L^M) f^V(v^S)]/T^S - \beta^S v^S \quad (1)$$

where 'v' stands for velocity, and T^S is a time constant. Given enough time, Eqn. 1 will drive ℓ^S to a length, velocity, and force consistent with the embedded Hill model. In the short term, the finite value of T^S ensures that the spring-damper system dominates the model's force response. We

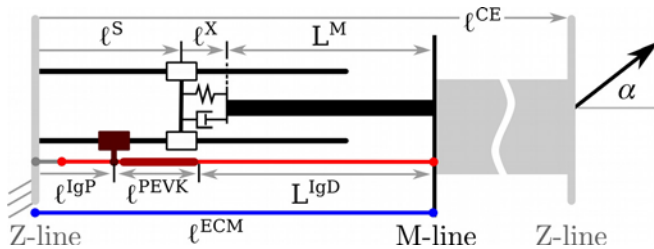


Figure 1: The proposed muscle model with a lumped cross-bridge

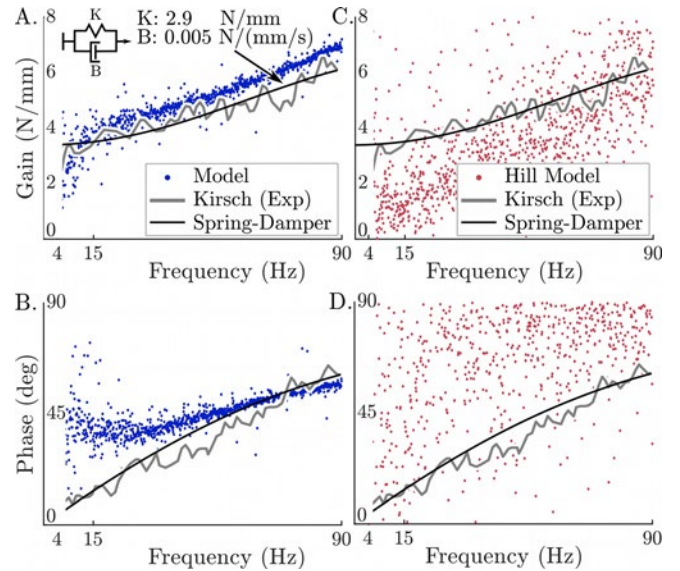


Figure 2: The frequency response of the models, Kirch et al.'s [1] processed data, and the spring-damper of best fit to the data.

simulate the experiments of Kirch et al. [1] and compare frequency domain responses of our proposed model and a Hill model [5] to Kirch et al.'s [1] results.

Results and Discussion

The gain and phase of both the proposed model and Kirch et al.'s analysis feline soleus [1] resemble the gain and phase curves of a spring-damper (Fig. 2A & 2B). In contrast, the gain and phase coefficients of the Hill model are scattered, due to the non-linearity of the model, and differ widely from Kirch et al.'s [1] observations (Fig. 2C & 2D).

Acknowledgments

Financial support from Deutsche Forschungs Gemeinschaft grant no. MI 2109/1-1, the Carl Zeiss Foundation, and NSERC of Canada is gratefully acknowledged.

References

- [1] Kirsch, Boskov, Rymer (1994). *IEEE T BIO-ENG.* **41**(8)
- [2] Burdet, Franklin, Milner (2013). *Human robotics: neuromechanics and motor control.* MIT press
- [3] Hill (1938). *P ROY SOC LOND B BIO.* **126**(843)
- [4] Gordon, Huxley, Julian (1966). *J PHYSIOL.* **184**(1)
- [5] Millard, Uchida, Seth, Delp (2013). *J BIOMECH ENG-T ASME.* **135**(2)

Hill-type computational models of skeletal muscle-tendon actuators: a systematic review

Arnault Caillet¹, Andrew T.M. Phillips¹, Dario Farina², Christopher P. Carty³, Luca Modenese¹

¹Dept Civil Engineering, Imperial College London, UK

²Dept Bioengineering, Imperial College London, UK

³School of Allied Health Sciences, Griffith University, Australia

Email: arnault.caillet17@imperial.ac.uk

Summary

Numerous articles and Hill-type muscle-tendon (MLT) models have been proposed in the past fifty years providing a rich but dense and thus hard-to-explore literature. This work presents the findings of a systematic review on skeletal MLT Hill-type phenomenological models. Current underdeveloped modelling aspects and other limiting factors for the field, such as inter-study inconsistency in terminology and notations, or scarcity of open-source models, are identified and discussed.

Introduction

Hill-type models [1,2] are computationally fast and fairly accurate models of muscle dynamics that are currently included in all biomechanical simulation platforms. As their popularity has increased in the last 50 years, they have become the subject of a dense literature that would gain from a contemporary assessment of the state-of-the-art, since the last milestone reviews date back 20-30 years [2,3]. This work offers such assessment by presenting the conclusions of a systematic review on phenomenological MLT Hill-type modelling aiming to identify current limitations and evaluate if updated recommendations would be beneficial to the field.

Methods

A systematic search of 20 key terms was performed on four online databases (PubMed, Web of Science, MedLine, EMBase). The eligible studies retained for review contained skeletal MLT Hill-type models including at least components for the neural controller, active and passive MLT properties and one methodological contribution (no duplicates). Each eligible model was first assessed for completeness against 23 possible phenomenological properties (Figure 1), for each of which inheritance diagrams representing the time-evolution of the published modelling approaches were created. The studies were finally scored on their methods for MLT model validation, calibration, reusability, and modelling strategy.

Results and Discussion

The systematic search yielded 478 studies including a Hill-type model among which 60 were eligible studies. Around 75% of the eligible models did not deviate from the traditional Hill-type modelling approach outlined in few classic studies [1-6]. Most used a linear activation-scaling of activation-independent Force-Length (FL) and Force-Velocity (FV) relationships [4], a first-order two-parameter differential equation for the activation dynamics [5], an instantaneous FL property with descending limb instability, exponential passive properties [4], and Hill's concentric and Mashima's eccentric instantaneous hyperbolic FV relationships [1,6]. Most models

did not account for accuracy-sensitive mechanisms such as time-history dependent properties (20% of the eligible models), motor unit recruitment dynamics (20%), or activation-dependency of the optimal fibre length (3%). We interpreted this as symptomatic of the limited reusability of the eligible models due to inter-study inconsistencies in the terminology and the notations, scarcity of open-source models (10%) and lack of good practices like validating simulations against experimental data (50%), providing objective quantitative or statistical analyses of the results (40%) or calibrating parameters using subject-specific data (50%).

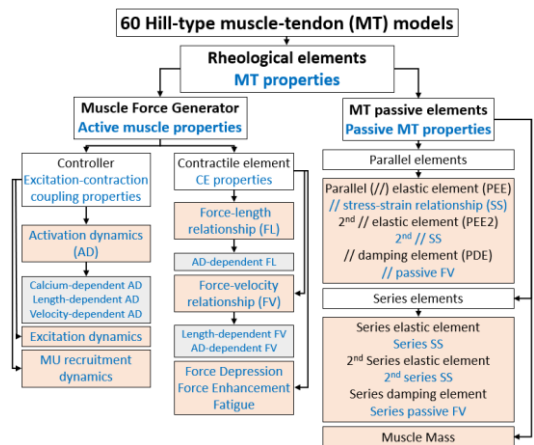


Figure 1: Rheological elements and their properties included in the 60 eligible Hill-type models. Black font: elements; blue font: properties; orange: main properties; grey: state-variable dependency

Conclusions

A review of 60 representative Hill-type muscle models unveiled that most models did not build upon previous advances, limiting further modelling innovations and the reassessment of older models. Recommendations aiming to standardize notation and terminology, clarify modelling assumptions and promoting model validation and sharing, could prove beneficial to the field.

Acknowledgments

Imperial College Skempton scholarship to A.C. and Imperial College Research Fellowship to LM.

References

- [1] Hill (1938). *Proc R Soc Lond B*, **126**:136-195
- [2] Zajac (1989). *Crit Rev Biomed Eng*, **17**:359-411
- [3] Winters (1990). *Multiple Muscle Systems*; Springer, NY
- [4] Hatze (1977). *Biol Cyb*, **25**:103-119
- [5] Winters et al. (1985). *IEEE Biomed Eng*, **10**:826-839
- [6] Mashima et al. (1972). *Jap J Physio*, **22**:103-120

Motor-units matter: enriching continuum-mechanical skeletal muscle models with neuromuscular information

Harnoor Saini¹, Thomas Klotz¹, Oliver Röhrle¹

¹Institute for Modelling and Simulation of Biomechanical Systems, University of Stuttgart, Stuttgart, Germany

Email: harnoor.saini@imsb.uni-stuttgart.de

Summary

Motor-unit (MU) physiology is fundamental to understanding skeletal muscle function and human movement. Continuum-mechanical, macroscopic muscle models often provide insights not practically obtainable via experimental techniques. Most of these models, however, neglect the spatial distribution of MUs and therefore may oversimplify muscle function. Here, we present a method to generate and incorporate physiological MU information within such models and demonstrate it via a prototype musculoskeletal model. We found that muscle deformation, pressure, and joint force were highly sensitive to MU distribution. This exploratory study highlights the importance of MU distribution in predicting muscle and joint function.

Introduction

Motor-units (MUs) are often restricted to sub-regions of a skeletal muscle, and their selective recruitment is partly responsible for the functional heterogeneity of muscles. That is, the same muscle may produce various “lines of action” depending on the subset of recruited MUs. To capture this phenomenon, we first present a method to incorporate micromechanically based MU activity and distribution within continuum-mechanical muscle models and second, to demonstrate the method via a prototype model of the masticatory system.

Methods

Constitutive modelling of skeletal muscles. The mechanical behaviour of the skeletal muscle is based on [1] and additively splits the active stress $\mathcal{S}_{ACT}(\alpha_M)$ from the passive response. The muscle activation parameter $\alpha_M \in [1,0]$ is decomposed according to $\alpha_M(t, \mathbf{X}) = \sum_i^{N_{MU}} \alpha_i(t) \kappa_i(\mathbf{X})$, where α_i and κ_i are, respectively, the temporal activity and spatial (fractional) distribution of MU i , and N_{MU} is the number of MUs.

Computing & integrating motor-unit information. Taking a scalar excitatory drive as an input to the MU pool, individual MU activities α_i are computed via a recruitment model coupled with cross-bridge and calcium dynamics models, e.g. [2]. MU distributions are computed by (i) reconstructing the microstructure in the muscle, (ii) assigning the (reconstructed) fibres to MUs via a novel algorithm (to control MU position, overlap, size, etc.) and (iii) homogenising the innervated microstructure within the FE mesh to obtain the fractional distribution $\kappa_i(\mathbf{X})$ of the MU.

Simulation trials. A masticatory system model, including the mandible and masseters, was used to simulate sub-maximal (34/50 MUs recruited) static bites. Only the MU distribution

was varied between trials, and the bite forces were used to quantify variations in motor-output. An additional simulation with spatially uniform MUs was carried out, representing the traditional modelling approach.

Results and Discussion

The distribution of the recruited MUs dictated active muscle stress (Figure 1). The range in peak bite forces for all MU distributions was 5N with a mean of 146N. Bite force angle (in the horizontal plane) exhibited a more drastic variation, with a range of 40° and a mean of -86° (-90° is oriented to the left). Such changes in the bite force can be explained by MU territory and masseter architecture. Since masseter fibre orientation and geometry are not uniform, changes in regional contraction influence the bite force. The traditional modelling approach yielded a steadier force, directed along the “average” fibre orientation of the masseters.

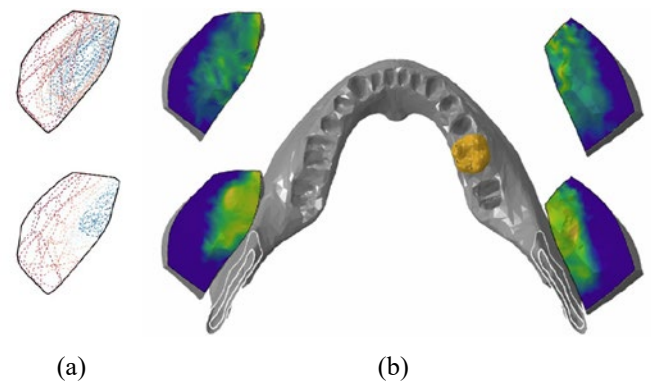


Figure 1: (a) MU territories in right masseter; MU 1 (dark blue) to 50 (dark red); recall only MUs 1-34 are active. (b) \mathcal{S}_{ACT} over the masseter cross-section at the same time instance; 0MPa (blue) to 1MPa (yellow)

Conclusions

Our method to enrich a continuum-mechanical model with MUs captured nuances in motor-output that were not possible with a traditional modelling approach.

Acknowledgments

This work was supported by the German Science Foundation (DFG GRK2198/I).

References

- [1] Röhrle et al. (2017). *Biomech. Model. Mechan.*, **16**(3): 743-762
- [2] Hiedlauf et al. (2017). *PLoS Comput. Biol.*, **13**(10): e1005773

Muscle-Specific Intramuscular Passive Properties are Required to Accurately Scale Passive Muscle Mechanics

Benjamin I Binder-Markey¹ and Richard L Lieber^{1,2,3}

¹Department of Physical Therapy and Rehabilitation Science, Drexel University, Philadelphia, PA, USA, ²Shirley Ryan AbilityLab & ³Department of Physical Medicine and Rehabilitation, Northwestern University, Chicago, IL, USA

Email: bb983@drexel.edu

Summary

Unlike whole muscle active length-tension properties, passive mechanical properties do not scale from the sarcomere to the whole muscle level. The source of this non-linear scaling is largely unknown. Thus, the purpose of this study was to directly measure muscle passive mechanical properties and then use modeling to identify potential sources contributing to non-linear scaling from fascicle to whole muscle. This study demonstrates that to accurately model muscle passive mechanical properties muscle-specific intramuscular model parameters must be included within models. Unfortunately, the actual structures that represent these mathematical terms are not currently clear.

Introduction

Generic whole muscle active length-tension properties with architecture parameters accurately scale from the sarcomere to the whole muscle level [1], but interestingly, in mammalian muscle, passive mechanical properties do not [1,2,3]. Recent work in rabbit muscle demonstrated that fiber, fiber bundle and fascicle mechanics did not simply scale to whole muscle mechanics [3]. We believe that this non-linear scaling is due to the poorly appreciated intramuscular connective tissues that increase with increasing scale. Thus, the purpose of this study was to measure whole muscle passive mechanical properties and use modeling to identify potential sources contributing to the non-linear scaling observed from fascicle to whole muscle.

Methods

Passive mechanical properties from three muscles of varying architecture and function were measured in 12-week C57Bl6 mice: rectus femoris (RF; n=6), semimembranosus (SM; n=6), and tibialis anterior (TA; n=5). Muscles were dissected, attached to a small 1N force transducer, and lengthened in static ~0.5mm increments. Muscle passive force was normalized to physiological cross-sectional area and muscle deformation converted to strain. These data were exponentially fit and curves were averaged to create a single exponential describing each muscle's passive stress-strain relationship (Fig. 1A).

To investigate potential sources contributing to the passive mechanics of muscle, we developed nine different Hill-type models of progressively increasing complexity. These models were created by sequentially including the fascicle passive property in the form of $\frac{a}{b}(e^{be} - 1)$, a parallel element elastic element (c_m) across the whole muscle, and an inter-fascicular shear factor (τ_m) resisting fascicle rotation, that were either generic or muscle specific (Table 1). For each model, parameters (a , b , c_m , and τ_m) were optimized in MATLAB to minimize the sum of the squared error (SSE) between the muscles' modeled stress-strain curve and the experimentally fit curve (Table 1).

Results and Discussion

Model 1 replicates most current muscle models that use a generic fascicle stress-strain curve scaled by architecture (Fig 1B). It provides a first approximation of each muscle's passive properties. However, it is clear that, to accurately replicate each muscle's mechanics, additional muscle-specific parameters are needed. Model 2 with muscle-specific fascicle properties had the lowest SSE and was able to replicate the previously fit curves (Fig 1C). However when incorporating other potentially physiologic relevant parameters we observe the best fits across muscles for models 3, 4, and 7 (Figs. 1D). Apart from model 2, the next best fit was model 4, using both muscle specific fascicle and parallel connective structure properties. To our surprise, the addition of shear did not improve the fit of any model.

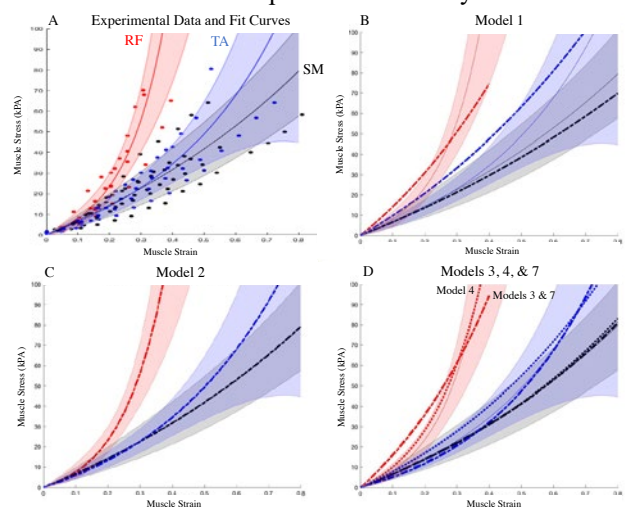


Figure 1: A) Stress-Strain data and fit curves average (solid lines) \pm SD (shaded region) for RF (red), SM (black), and TA (blue). Stress-strain fit curves with B) Model 1, C) Model 2, and D) Models 3, 4, and 7 in dashed lines, with experimentally fit curve in solid lines \pm SD in shaded regions.

Conclusion

These results demonstrate that, to accurately model muscle passive mechanical properties, muscle-specific intramuscular model parameters must be included. To a first approximation, architectural parameters helps, but in order to provide high resolution properties, additional terms are needed. Unfortunately, the precise structures that represent these mathematical terms are not currently clear and are the subject of ongoing investigations.

Acknowledgments: We acknowledge funding from the Brinson Fellowship and the Shirley Ryan AbilityLab.

Literature References

- [1] Winters *et al.* (2011). *J Biomech*, **44**: 109-115.
- [2] Meyer & Lieber (2018). *J Exp Bio*, **221**: 5.
- [3] Ward *et al.* (2020). *Front Physiol*, **11**: 211.

Table 1: Summary of Model Parameters and Total Sum of Squared Errors

	Model 1	Model 2	Model 3	Model 4	Model 5	Model 6	Model 7	Model 8	Model 9
Fascicle Properties	Generic	Specific	Generic	Specific	Generic	Generic	Generic	Generic	Specific
Parallel Elastic Element	-	-	Specific	Specific	-	-	Specific	Specific	Specific
Shear Factor	-	-	-	-	Generic	Specific	Generic	Specific	Specific
Total SSE	14738.69	0.04	5339.33	3145.45	14738.69	10514.17	5631.317	15511.35	28287.86

3D modeling of length and lever arm of sternocleidomastoid and scalenus muscles in respiratory movement

David Biteau¹, Véronique Feipel², Serge Van Sint Jan¹, Benoit Beyer²

¹ Laboratoire d'Anatomie, Biomécanique et Organogénèse, Université Libre de Bruxelles, Brussels, Belgium

² Laboratoire d'anatomie fonctionnelle, Université Libre de Bruxelles, Brussels, Belgium

Email: david.biteau@ulb.be

Summary

The aim of this study was to investigate length and lever arm (LA) variations of scalenus anterior (SAnt), medius (SMed) and sternocleidomastoid (SM) muscles in respiratory movement. We used a 3D modelling approach combining in vivo costovertebral joints kinematics from 12 asymptomatic adults and a generic model of the cervical spine (GMCS) scaled to in vivo data. Absolute and relative change in muscles length and LA relative to the helical axis of the first costovertebral joint was computed. Quantitative data and related 3D representation of the biomechanical features were obtained. Results showed that all muscles shortened during inspiration while LA increased.

Introduction

SAnt, SMed and SM muscles may be involved in various musculoskeletal and/or respiratory disorders. Biomechanical features such as moment generating capacity of these muscles were previously explored during cervical movements [1] but the effect of respiratory motion on length and LA is still to be determined. Therefore, the aim of the present study was to determine length and LA of the muscles of interest using 3D modelling approach.

Methods

Previously published kinematic data [2] computed from CTscan performed at three different lung volumes (TLC: total lung capacity, MIC: middle of inspiratory capacity and FRC: functional residual capacity) were used in the present study. 3D bone models and breathing kinematic data (ranges of motion, mean helical axis (HA) location and orientation) were combined to a GMCS. With LHPFusionBox software (<http://lhpfusionbox.org>), anatomical landmarks (AL) were positioned on each 3D bone model for registration and at the insertion sites of each muscle of interest for measurements on the first rib and on the sternum. The GMCS was then registered on the individual first thoracic vertebra of each subject using similarity transformation. (Figure 1 A). Finally, length muscle and LA according to the HA of the first costovertebral joint were computed (Figure 1 B) using direct method [3]. The relative variations were calculated as a percentage of the FRC reference position.

Results and Discussion

Globally, all muscles displayed an increasing length associated to a shortening of the LA from TLC to FRC. Absolute length variation was greater for SM (9.1 ± 4.1 mm) and smaller for SMed (7.1 ± 3 mm). The maximal relative length variation ranged between $5.3 \pm 2.5\%$ for SAnt and $-8.9 \pm 3.6\%$ for SM. Besides, LA ranged between 30.2 and 41.3mm at TLC and from 25.1 to 32.5mm at FRC for SAnt and SM respectively. LA displayed also the maximal change

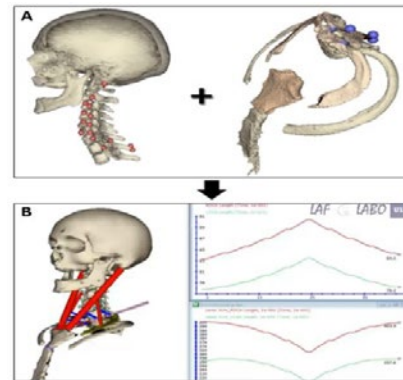


Figure 1: A: Left: GMCS with ALs on insertion sites and Th1; Right: Upper thorax model with ALs on Th1. B: 3D visualization of SAnt and SM with results of length and LA over the breathing cycle (right).

for SM (8.8 ± 4.9 mm) and minimal for SMed (5.1 ± 2.5 mm). The relative LA variations ranged between $22 \pm 18.3\%$ and $35 \pm 38.7\%$ for SAnt and SMed respectively. Note that the greatest variations of both length and LA occurred between MIC and FRC (i.e under 50% of the inspiratory capacity) and can be explained by the greater range of rib motion during this phase [2]. Considering the relative change in muscle length, this result combining a GMCS and in vivo rib kinematics are in line with previously published results [4]. Prior work [1] reported scalene muscles maximal LA close to 20mm for lateral bending of the cervical spine while the present study showed a minimum of 25.1mm for respiratory contribution. About the SM, the present minimal LA of 32.5mm represent approximately 50% of the value obtained for lateral bending of the cervical spine (55mm) and 200% of the value reported for axial rotation (15mm).

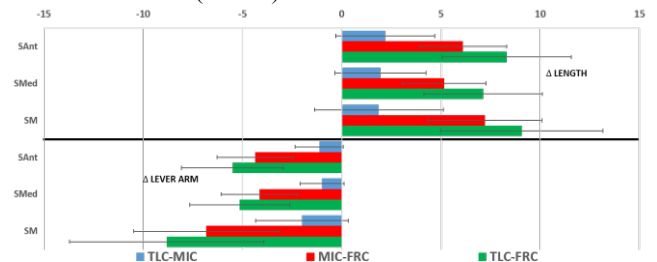


Figure 2: Mean difference in length/LA in millimeter of each muscle of interest between each respiratory position.

Conclusions

Length and LA changes of SAnt, SMed, and SM muscles during respiratory movement were quantified using a modelling approach. All muscles shortened during inspiration while LA increased. Further research will explore interaction of respiratory mechanics in clinical conditions.

References

- [1] Vasavada, A. N. et al. (1998). *Spine*, **23**(4) : 412–422.
- [2] Beyer, B. et al. (2016). *Resp. Phys. Neurobiol.* **232** :57-65
- [3] Hughes, R. et al. (1998). *J Biomech*, **31**(2): 157–160.
- [4] Legrand, A. et al. (2003). *J Appl Physiol*, **94**:1467-1472

Towards real-time estimation of joint moments during fast sidestepping

Sina David¹, Marion Mundt²

¹Department of Human Movement Sciences, Vrije Universiteit Amsterdam, Amsterdam, The Netherlands

²School of Human Science, The University of Western Australia, Perth, Australia

Email: s.david@vu.nl

Summary

This abstract presents the estimation results of lower limb joint moments using a long short-term memory neural network. The network was trained using linear accelerations and angular rates of the lower limb segments on predicting hip, knee and ankle joint moments during fast sidestepping. Data were obtained from 3D motion analysis. The average prediction accuracy is > 0.8 . The results are promising and indicate the possibility to apply neural networks for real-time feedback.

Introduction

A majority of collected biomechanical data from clinical and sports research is used to retrospectively analyze a participant's movement and the associated joint loading. Hence, direct feedback to the participant is limited due to the time arising from postprocessing and running musculoskeletal models. The application of neural networks and the development of inertial measurement units (IMUs) with direct output of linear acceleration and angular rate could provide the opportunity to estimate joint loading in real-time since no such data processing is needed. Long short-term memory (LSTM) neural networks are processing time series successively. This eliminates the need for time normalization, which is key for real-time applications. This study aimed to evaluate the ability of an LSTM neural network to predict joint moments from simulated IMU data in real-time.

Methods

Due to the limited availability of IMU data, linear acceleration and angular rate were simulated from a marker-based motion analysis study. Training a neural network based on these allows for the direct transition to measured IMU data when applicable [1]. The dataset consists of the 3D kinematics and kinetics of 67 healthy athletes (631 trials in total) during full effort 90° sidestepping [2]. To train the LSTM the linear acceleration and angular rate of the lower limbs was simulated and 3D joint moments from the touch-down of the execution to the take-off of the depart contact were extracted.

The dataset was split subject-wise into training (50 athletes), validation (8 athletes), and test set (9 athletes) for five-fold cross-validation. An LSTM neural network was trained on the time series. Different network architectures and hyperparameters were tested using a hyperband search [3].

The prediction accuracy of the network was evaluated on the test set only, assuring that these data were unknown to the network, and was measured using the root mean square error normalized to the range of the data (nRMSE) and the correlation coefficient. For this purpose, the time series were

split into execution and depart contact and normalized to the stance phase.

Results and Discussion

The hyperband search resulted in a single layer with 1024 LSTM cells to perform best. The initial learning rate was set to 0.0003, the activation function tanh, and dropout to 0.7.

The mean nRMSE of the execution step was 21.0% and 19.6% for the depart contact. The correlation coefficients were 0.8 and 0.9, respectively. Higher prediction accuracy was reached for the sagittal plane motion. The ankle joint rotation shows a low accuracy. The prediction accuracy for the depart contact is generally higher (Figure 1). These results are in accordance with previous studies [4,5]. The prediction accuracy in the main motion plane is generally higher due to the lower variance. Additionally, the minor motion planes do not necessarily show consistent behaviour in joint moment progression throughout all participants, which makes the prediction more difficult, especially based on a small dataset. As LSTM networks learn datasets successively, the first frames, which are part of the execution contact, are more difficult to predict than later ones, resulting in higher prediction accuracy of the depart contact.

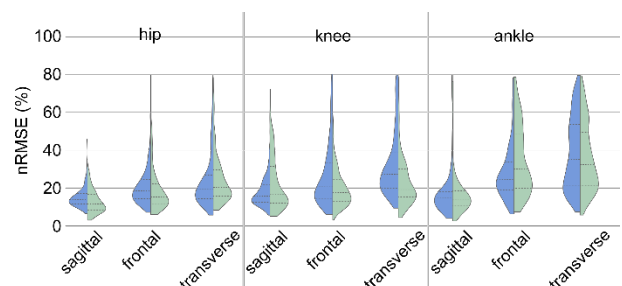


Figure 1: Violin plots of the nRMSE for all lower limb joints and motion planes for the execution (blue) and depart (green) contact.

Conclusions

Although further reduction of the prediction error needs to be achieved, the results are promising and show the general power of neural networks to develop motion analysis towards feedback applications.

References

- [1] Mundt M et al. (2020). *Front. Bioeng. Biotechnol.*, **8**: 1-16.
- [2] David S et al. (2018). *Hum Mov Sci*, **62**: 202-210.
- [3] Koeppe A et al. (2019). *Acta Mech*, **230**: 3279-3293.
- [4] Mundt M et al. (2019). *Med Biol Eng Comput*, **57**: 1833-1841.
- [5] Johnson WR et al. (2019). *IEEE Trans Biomed Eng*, **66**: 689-694.

Muscle synergies enable accurate joint moment prediction using few EMGs

Yixing Liu^{1,2}, Gunnar Ingi Fridriksson¹, and Elena M.Gutierrez-Farewik^{1,2,3}

¹KTH MoveAbility Lab, Department of Engineering Mechanics, KTH Royal Institute of Technology, Stockholm, Sweden.

²KTH BioMEX Center, KTH Royal Institute of Technology, Stockholm, Sweden.

³Karolinska Institutet, Department of Women's and Children's Health, Stockholm, Sweden.

Email: lyixing@kth.se

Summary

In this study, we predicted knee joint moments during walking from as few as 4 EMG sensors with a long short-term memory (LSTM) neural network by taking advantage of lower extremity muscle synergies. Results indicate that predicting joint moments from muscle synergies can reduce the number of EMG inputs required, with lower prediction error than predicting directly from EMG signals.

Introduction

Wearable sensors, i.e., electromyography (EMG) and inertial measurement units, can facilitate real-time detection of movement intention, estimation of appropriate torques in assistance-as-needed exoskeleton control, and even remote monitoring of patients' motor function, i.e., estimating joint torques and observing muscle activations during rehabilitation [1]. In these settings, it is important to minimize the required number of sensors in order to achieve practical applicability. To this end, the concept of muscle synergies has been useful in predicting unmeasured EMG signals within a measured subset [2] as well as in exoskeleton feedforward control [3]. The objective of this study was to identify and use muscle synergies to predict knee joint moment during walking in an LSTM network using a minimal number of EMG sensors.

Methods

Ten EMG signals (gluteus maximum, vastus medialis and lateralis, semitendinosus, biceps femoris, medial and lateral gastrocnemius, soleus, tibialis anterior, and rectus femoris) and knee joint moments during normal gait in six able-bodied subjects were collected through motion capture (Vicon cameras, AMTI force plates, Myon nano EMGs). Between 4 and 6 muscle synergies (n_{ms}) were identified from the 10 EMG signals using a non-negative matrix factorization (NNMF) algorithm. Two outputs were generated after NNMF – a weights matrix $W_{n_{emg} \times n_{ms}}$ and time-dependent synergy action signals $H_{n_{ms} \times n_{time}}$. The synergy action signals were then used as inputs to train an LSTM neural network prediction model. After training, the synergy action signals were then estimated with 4-7 EMG signals and the weights matrix using a non-negative least squares algorithm, and then used as inputs to evaluate the prediction performance. Four different testing conditions were conducted; predicting knee moments using the synergies-trained LSTM network from 1a) synergies estimated from all 10 EMG signals, 1b) synergies estimated from 4-7 EMG signals, as well as predicting knee moments using an LSTM network that was trained on the EMG signals directly, i.e., not trained with synergies, from 2a) all 10 EMG signals directly, and 2b) between 4-7 EMG signals. For

different EMG subsets, performance from both synergies-based and EMG-based predictions were compared with measured knee moments. Root-mean-square error (RMSE) of knee moment, as a percent of knee joint moment range, was used to assess the error between predicted and measured knee joint torques.

Results and Discussion

The model that takes advantage of muscle synergies predicted knee moments accurately (Figure 1) and with lower prediction error than the model that used EMG signals directly. In the synergies-trained LSTM model, when as few as 4

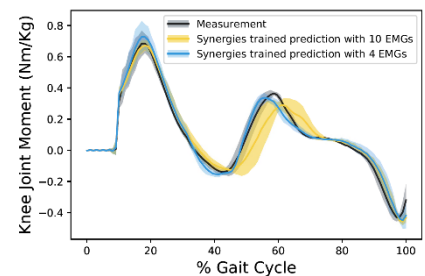


Figure 1. Measured and synergies trained predicted knee moments in 1 subject

EMG signals were used as inputs, knee moments were predicted with lower prediction error when predicting from 4 muscle synergies than that predicting from 5 and 6 muscle synergies (Table I), i.e., in an LSTM trained on 4 muscle synergies identified from 10 EMGs, knee moment could be accurately predicted using as few as 4 EMGs sensors.

Table I Average prediction RMSEs (% knee moment range)

	10 EMGs	7 EMGs	6 EMGs	5 EMGs	4 EMGs
4 synergies	5.85	4.35	4.42	4.48	4.48
5 synergies	5.67	5.07	5.17	5.71	7.48
6 synergies	4.70	4.54	4.73	5.85	7.85
No synergies	6.04	5.63	6.05	5.84	5.74

Conclusions

Taking advantage of muscle synergies can result in accurate joint moment prediction with fewer EMG sensors. By training an LSTM to predict joint moments from muscle synergies, rather than from EMG signals as independent observations, accurate prediction can be achieved with fewer EMG sensors. We believe this method can facilitate exoskeleton control and rehabilitation devices in daily uses by achieving accurate moment prediction with a minimum of wearable sensors.

Acknowledgments

This project was generously funded by the Promobilia Foundation (ref nr 18200).

References

- [1] Frechette et al., Current Neurol. Neurosci. Rep., 19:80
- [2] Gurchiek et al., IEEE.TNSRE, 2020, 28: 2478-2487
- [3] Alibeji et al., Front Bioeng Biotechnol, 2015, 3:203

Automated and personalized pose registration from x-ray images using convolutional networks

Florian Vogl¹, Pascal Schütz¹, Barbara Postolka¹, Renate List¹, William Taylor¹

¹Laboratory for Movement Biomechanics, Institute for Biomechanics, ETH Zürich, Switzerland

Email: fv@ethz.com

Summary

Measuring joint kinematics is a key requirement for a variety of biomechanical research and applications. While x-ray systems avoid the soft-tissue artefacts arising in optical systems, extracting an object's pose (translation and rotation) from the images is time-consuming, expensive, and operator-dependent. Based on 106'000 annotated images of knee implants collected using our moving fluoroscope during activities of daily living, we trained a deep-learning model to automatically estimate the poses for both implant components. By pretraining one stage of our architecture on renderings of the implant geometries, our approach offers predictions for unseen subjects personalized to their specific implants. In 90% of the test set, which included heavily occluded samples, our approach predicted both components' poses better than 2mm (in-plane translation), 25mm (out-of-plane translation), and between 1.5° and 3° (all Euler-angle rotations) without any additional user intervention.

Introduction

X-ray systems directly measure the skeletal structure and yield a series of x-ray images, from which the 3D kinematics are conventionally estimated by acquiring the 3D information and manually adjusting the object's pose until its projection matches the image. Even for high-contrast structures such as joint replacements, this process is time-intensive, expensive, and operator-dependent.

While automation methods for this task have been developed, their need for approximate poses means that extensive manual work is still required in practice [1,2]. Deep learning has recently achieved impressive results for pose estimation tasks, but requires large datasets including the annotated poses. With the aim to develop an accurate, automated, and personalized approach for 2D-3D registration, this study aims to take advantage of our unique dataset of 106'000 annotated images [3] to a) apply deep learning to pose estimation of knee replacements from x-ray images and b) personalize this process by considering the subject's particular implant geometries.

Methods

We split the 53 tibia/femur combinations in our dataset into a training- (90%) and test-set (10%). The network (Figure 1) consisted of a) a generic "shadow" network to extract the implant shadows from the image and b) a personalized "synthnet" network to estimate the poses from these shadows. Here, the intuition is that a human could extract the shadow solely by noting the components' absorption and recognizing the surrounding structures, while estimating the pose from this shadow requires the implant geometry. By pretraining a synthnet for each implant geometry on renderings in varying

poses, the synthnets learn what landmarks indicate what pose for a certain implant. Next, we trained the shadownet on our training-set by loading the correct synthnet with frozen weights for each sample, and performing backpropagation.

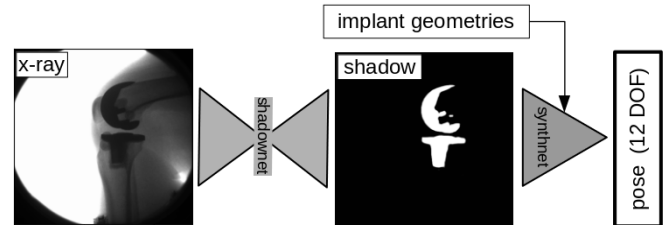


Figure 1: The network architecture. The synthnet is pretrained on renderings of the implant geometries in varying poses.

Results and Discussion

In-plane translations were predicted to within 2mm (about 3 pixels) in 90% of testsamples, while out-of-plane translations were only predicted to within 25mm because a change in this component only leads to a small change due to perspective (Figure 2). Because our approach struggled to extract the shadow from occluded images, we propose to iteratively feed the rendered shadows based on the estimated poses back into the shadownet to provide approximate information on the shadow it should be looking for.

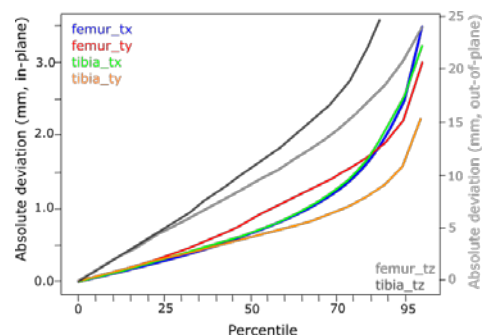


Figure 2: Testset-error between predicted and true translations

Conclusions

Our approach can either provide starting poses to other algorithms [1,2] or can be used directly to estimate poses from x-ray images in a personalized and automated manner, thus avoiding the laborious and expensive task of manually estimating the poses for each image.

References

- [1] Anderst W et al (2009), *Med. Eng. Phys.*, **31**:10–16
- [2] Flood PDL and Banks SA (2018), *IEEE Trans. Med. Imaging*, **37**:326–335
- [3] W. R. Taylor et al (2017), *J. Biomech.*, **65**:32-39

Assessment of a novel deep learning-based marker-less motion capture system for clinical gait analysis

Saman Vafadar¹, Laurent Gajny^{1,*}, Wafa Skalli¹

¹Institut de Biomécanique Humaine Georges Charpak, Arts et Métiers, Institute of Technology, Paris, France.

*Email: laurent.gajny@ensam.eu

Summary

A marker-less motion capture system designed based on four digital video cameras, novel deep learning techniques, and a dedicated dataset, is evaluated against a marker-based system in terms of spatiotemporal and kinematic gait parameters. The results indicate that the marker-less system is highly accurate for measuring spatiotemporal parameters; however, further improvement is required for some kinematic parameters if clinical applications are targeted.

Introduction

The effectiveness of clinical gait analysis is supported by the literature [1]. The gold standard systems are marker-based. However, their routine clinical use is limited to a few specialized centers mainly because of equipment and operating costs. Marker-less systems could be cost-effective alternatives. Deep learning techniques have demonstrated their potential on publicly available datasets for marker-less motion capture [2]. However, these techniques have not yet been adapted and assessed for 3D marker-less gait analysis. We aimed to design a marker-less system based on deep learning techniques and assess its performances in terms of gait outcomes.

Materials and Methods

The marker-less system was designed based on four calibrated and synchronized digital video cameras and a convolutional neural network (CNN) [2] that could estimate sixteen joints' 3D position. A novel dataset dedicated for gait study, was collected to train the CNN and test the marker-less system. Twenty-two asymptomatic, two adults with spinal disorder and seven children with bone disease, aged from 6-44 years performed ten walking trials, while being recorded by the marker-less and a reference marker-based system (VICON[®]). Biplanar radiographs (EOS[®]) were also acquired to improve the accuracy of anatomical frames determination according to the protocol published in [3].

The marker-less system was assessed on the test set (12 subjects including 4 pathological) in terms of gait parameters. A gait event detection algorithm [4], designed for marker-based systems, was adapted for the marker-less system. Then, spatiotemporal parameters were computed based on detected gait events. For kinematic parameters, since the marker-less system could only estimate one axis for each bony segment, to form an anatomical frame, the second axis was determined

using a priori knowledge – the gait data of sixty-six subjects, independent from the training and test sets, were used.

Results and Discussion

The difference between the gait parameters obtained by the marker-less and the reference systems is shown in Table 1. The biases of the spatiotemporal parameters were close to zero (<0.1 cm or sec), and the limits of agreement were smaller than the minimum detectable changes reported in [5] (e.g., step length: 1.56 < 6 cm). Thus, the designed system is accurate enough for measuring spatiotemporal parameters. Regarding kinematic ones, the limits of agreement of the joint-based (JB) knee extension-flexion angle, *i.e.*, the angle between the femoral and tibial segments was below 5°. However, knee and hip extension-flexion were higher than 5°. Indeed, the main limitation of the marker-less system was that it could only estimate the joint positions. Work is in progress to further develop the system to accurately determine anatomical frames, paving the way for using marker-less systems in clinical gait study.



Figure 1: Joint positions by the reference and marker-less systems.

Acknowledgments

This research was supported by ParisTech Foundation, BiomecAM Chair program, Covéa and Société Générale.

References

- [1] Benedetti et al. (2017). *Gait & Posture*, **58**:252-260
- [2] Isakov et al. (2019). *IEEE/CVF*, 7718-7727
- [3] Sauret et al., (2016). *Gait & Posture*, **50**:180-184
- [4] Zeni Jr et al., (2008). *Gait and Posture*, **27**:710-714
- [5] Meldrum et al., (2014). *Gait and Posture*, **39**:265-271

Table 1: The difference between the gait parameters obtained by the marker-less system and the reference system.

Parameter	Spatiotemporal parameters			Kinematic parameters (°)		
	Step length (cm)	Step width (cm)	Step time (sec)	JB knee ext.-flex.	Knee ext.-flex.	Hip ext.-flex.
Mean	-0.06	0.00	0.00	0.0	-3.4	2.6
Limit of agreement	1.56	0.72	0.01	4.8	7.2	15.6

Towards automated gait event detection using machine learning – what foot markers work best for what gait patterns?

Yong Kuk Kim¹, Rosa MS Visscher^{1,3}, Sailee Sansgiri², Marie Freslier³, Reinald Brunner¹, Florian Vogl¹, William R Taylor¹, Navrag B Singh¹

¹ *Laboratory for Movement Biomechanics, Institute for Biomechanics, ETH Zürich, Switzerland*

² *Department of Biomechanical Engineering, TU Delft, Netherlands*

³ *Orthopedic Department, Children's Hospital, University of Basel, Switzerland*

Summary

Conventionally, detecting gait events, such as initial contact (IC) and toe-off (TO), from kinematic data is performed through manual annotation or kinematic algorithms – both of which are operator-dependent and require substantial user-intervention. While Machine learning (ML) offers a data-driven alternative for detecting gait events in an automated manner, little is known about the performance for specific gait patterns, such as toe-walking. This study examined how well ML was able to detect gait events for different gait patterns by using a variety of foot-markers. Over 95% of the test-set, **our approach detected gait events to within 15ms (IC) and 23ms (TO)** when using the hallux and heel markers. While performance across all gait patterns did not improve when using other markers, **performance on individual gait patterns varied up to 8ms**. Thus, depending on the target population, different marker-sets are required to detect gait events in a repeatable and fully-automated manner.

Introduction

Clinical gait analysis is used to diagnose neuromotor deficits in pathologies such as Cerebral Palsy. This analysis requires the accurate detection of gait events, particularly IC and TO. In current clinical practice, experts have to manually detect these events based on kinetic (requiring force plates) or kinematic data, which is laborious, expensive, and operator-dependent. While ML techniques [1] have recently demonstrated promising results for detecting gait events using 3-D kinematic data, little is known about their performance in individual gait patterns (e.g. toe-walking). Furthermore, the effect of using different markers as inputs for the detection algorithms also remains unclear, which has significant practical relevancy as the number of kinematic markers and their locations can vary considerably.

Therefore, the goal of this study was to investigate a) how well ML is able to detect gait events in various gait patterns from foot-marker kinematics, and b) what combination of marker inputs optimises the performance for each gait pattern?

Methods

3-D kinematic and kinetic data were collected from **363 adolescent participants** (Age: 11.76 ± 3.16 years) who performed barefoot walking at a local hospital. The true events were found by setting a threshold of 20N for the vertical ground reaction force. This notably differs from similar works [1], in which the true events were identified by

manual annotation. To avoid overfitting, we assigned 80% of the data to the training-set, 10% to the validation-set used for hyperparameter tuning, and 10% to the test-set. Each gait event was categorised based on whether the heel, midfoot, or forefoot touched the ground first, yielding **5340 IC and 4937 TO events** with a ratio of about 4:2:1 between categories. The network consisted of a bidirectional long short-term memory (LSTM), a fully connected output layer, and a sigmoid activation function. The time-series of marker positions and velocities were cut to a length of 165 frames around the true event with a random offset and used as inputs to train the model with an ADAM optimiser (learning rate=0, momentum=0) and a binary-weighted cross-entropy loss.

Results and Discussion

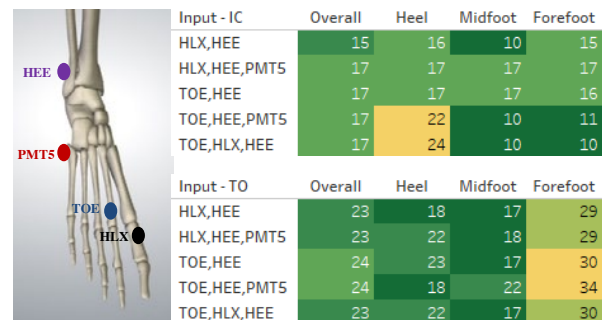


Figure 1: Marker placement on foot (left), Heat-map distribution of detection error in milliseconds (right)

Over 95% of the test-set, our approach detected gait events to within 15ms (IC) and 23ms (TO) when using only the hallux and heel markers (Fig. 1). These values are to be compared with an inter-rater variability of 25ms for manual annotations [1] and of 33ms for kinematic event detection [2]. While the use of other markers did not improve performance over all gait patterns, performance on individual patterns varied up to 8ms. Our results thus suggest that gait event detection could be improved by first identifying the gait pattern, and then choosing the optimal markers for this specific pattern and applying the appropriate detection algorithm. By training specialised algorithms for each gait pattern, the performance could be increased even further, thus ultimately providing optimal gait event detection in a repeatable and fully-automated manner.

References

1. Kidzinski, L et al (2019) *PLoS One* **14**(1): e0211466.
2. Bruening, D.A et al (2014) *Gait Posture* **39**(1): p.472-7.

Should Major League Baseball Adjust the Mound Height?

Megan S. Stewart^{1,2}, Alek Diffendaffer¹, Jon Slowik¹, Glenn Fleisig¹

¹The American Sports Medicine Institute, Birmingham AL, USA

²Concordia University of Chicago, River Forest, Illinois, USA

Email: megan.s.stewart19@gmail.com

Summary

With a decrease in runs scored, Major League Baseball (MLB) commissioned the American Sports Medicine Institute to conduct a biomechanical study looking at a potential change to height of the pitching mound.

Introduction

In 1903, the pitching mound was restricted to a maximum height of 15in. Following the 1968 season (“The Year of the Pitcher”), MLB lowered the mound to 10in in hopes of boosting run scoring^{1,2}. This seemed to work, as the number of runs scored bumped up in 1969 and remained relatively constant through the rest of the 20th century. However, from 2000-2014, there was a steady decrease leading to thoughts that the mound should be lowered again to boost scoring. Not only did scoring decrease during these years, but the number of pitching injuries and surgeries rose exponentially throughout professional and amateur baseball. Some baseball and medical experts suggested that lowering the mound may also reduce stress on the throwing arm and the number of injuries.

Methods

The research study was approved by the Institutional Review Board at St. Vincent’s Health System (Birmingham, AL, USA). Twenty collegiate pitchers were recruited from universities in the area of Raleigh, NC. All of the testing was performed at the USA Baseball Training Complex in Cary, NC where four custom dirt mounds with differing heights (6in, 8in, 10in, 12in) were built outdoors and covered by a tent.

Pitchers were instructed to throw 10 full effort pitches from each condition to a catcher. Three-dimensional pitching biomechanics were tracked with an 11-camera Motion Analysis System (Motion Analysis Corporation, Santa Rosa, CA) at 240 frames/second. Ball velocity was tracked with Rapsodo (Rapsodo Inc). All of the mounds were constructed with the same slope according to MLB specifications, starting at six inches in front of the pitching rubber the mound sloped downward at a rate of one inch per one foot over a distance of six feet. There were two 11-camera motion capture systems (Motion Analysis Corporation, Santa Rosa, CA) set up each surrounding a pair of mounds. For each of the mounds, homeplate was positioned 60.5 ft away and a ball tracking system was positioned 6 ft behind homeplate (Rapsodo Baseball System, Rapsodo Inc. Fishers, IN). The baseball tracking system utilized a high-speed video sampling at 240 frames per second and radar technology sampling at 50KHz to calculate ball movement

and spin. 40 pitches were collected, where the pitchers were instructed to throw five full-effort fastballs and five full-effort curveballs from each of the mounds in a randomized order. For all trials, three-dimensional motion data were collected at 240 Hz while the ball tracking system captured the ball speed, break, and spin. From the motion capture data, 31 kinematic and kinetic variables were calculated for each pitch as previously described.

For each of the eight testing conditions (four mound heights and two pitch types), the magnitudes of ball movement and biomechanical parameters were averaged by participant. Repeated measures analysis of variance (ANOVA) was utilized to determine significant differences in the mound heights for fastballs and curveballs separately. When a significant difference ($p < 0.05$) was found, a pairwise difference was analyzed with a Tukey post-hoc test ($p < 0.05$).

Results and Discussion

The pitchers were (mean \pm SD) 19.7 \pm 1.2 years old, 73 \pm 2 in tall, and had a weight of 205 \pm 19 lbs. There were no significant differences seen for ball velocity, movement, or spin when pitching from the four mound heights for both the curveball and fastball. The mean ball velocity for the fastball and curveball was 88.4 \pm 6.06 mph and 70.2 \pm 5.95 mph respectively. There were twelve biomechanical variables (seven kinematic variables and five kinetic variables) that were found to be significantly different when comparing the mound height for the fastball pitches. When comparing mound height and curveballs, there were eight kinematic variables shown to be significantly different.

Conclusions

The results from these two studies indicate that lowering the pitching mound may not increase run scoring, as there were no changes in fastball and curveball velocity, spin or movement. The differences seen in pitching kinematics with mound height variations were small and may lack practical significance. The shoulder and elbow kinetics of the fastball may be slightly lower with a lowered mound, which may reduce the risk of pitching injury.

Acknowledgments

We would like to acknowledge Major League Baseball.

References

1. McNeil WF. *The Evolution of Pitching in Major League Baseball*. McFarland & Company, Inc.; 2006.
2. MLB.com. MLB.com - Stats. Published 2017. Accessed November 1, 2017. <http://mlb.com/stats/sortable>

The influence of bicycle lean on maximal power output during sprint cycling

Ross D. Wilkinson and Rodger Kram

Locomotion Laboratory, The University of Colorado, Boulder, CO, USA

Email: ross.wilkinson@colorado.edu

Summary

We used a modified cycle ergometer to investigate if leaning (or not leaning) a bicycle side-to-side affects sprint power output. We found that leaning the ergometer *ad libitum* did not enhance maximal 1-s crank power compared to a locked condition. However, trying to minimize ergometer lean decreased maximal 1-s crank power by 5% compared to leaning *ad libitum*.

Introduction

Competitive cyclists typically sprint out of the saddle and alternately lean their bikes from side-to-side, away from the down-stroke pedal [1]. Yet, there is no direct evidence as to whether leaning the bicycle, or conversely, attempting to minimize lean, affects maximal power output during sprint cycling. Here, we investigated two questions related to maximal 1-s power output during non-seated, sprint cycling: 1) Does *ad libitum* lean affect maximal power output compared to a traditional stationary ergometer? and 2) Does trying to minimize lean affect maximal power output compared to *ad libitum* lean? To address these questions, we modified a cycle ergometer so that it could lean from side-to-side or be locked to prevent lean. This modified ergometer made it possible for riders to sprint under three different conditions: locked (no lean), *ad libitum* lean, and minimal lean. In the minimal lean condition, the ergometer could lean but we asked the subjects to try to minimize lean. Our first hypothesis (null) was that *ad libitum* lean would result in the same maximal 1-s crank power as the locked condition. Our second hypothesis was that trying to minimize lean would decrease maximal 1-s crank power compared to the *ad-lib* and locked conditions.

Methods

Nineteen healthy recreational cyclists (13M/6W, 28 ± 6 y, 1.75 ± 0.09 m, 69 ± 10 kg, mean \pm SD) pedaled a friction-loaded ergometer mounted atop a hinged chassis. The ergometer was equipped with a crank-based mechanical power meter (Quarq DZero, SRAM, Corp, Chicago, IL, USA) and a Monark 827E flywheel. In the *ad-lib* lean and minimal lean conditions, springs attached to the rear legs of the ergometer provided a restoring torque proportional to lean angle. In the locked condition, aluminum struts prevented lean. Subjects performed 9 maximal 5-s sprints from rest in a non-seated posture—3 locked, 3 *ad-lib* lean, and 3 minimal lean. We derived crank angle and ergometer lean angle from IMU acceleration data recorded at 500 Hz.

Results and discussion

Maximal 1-s crank power: In support of our first hypothesis, maximal 1-s crank power in the *ad-lib* condition (974 ± 33 W) was similar to the locked condition (982 ± 30 W), $p = 0.8$, $ES = 0.2$. In support of our second hypothesis, crank power was re-

duced by 47 W (5%) in the minimal lean condition (927 ± 32 W), compared to the *ad-lib* condition, $p < 0.001$, $ES = 1.3$.

Range of ergometer lean: The range of lean in the *ad-lib* condition (9.6 ± 2.3 deg.) was more than ten-times the locked condition (0.8 ± 0.3 deg.), $p < 0.001$, $ES = 1.7$, and more than twice the minimal lean condition (3.9 ± 1.0 deg.), $p < 0.001$, $ES = 1.3$.

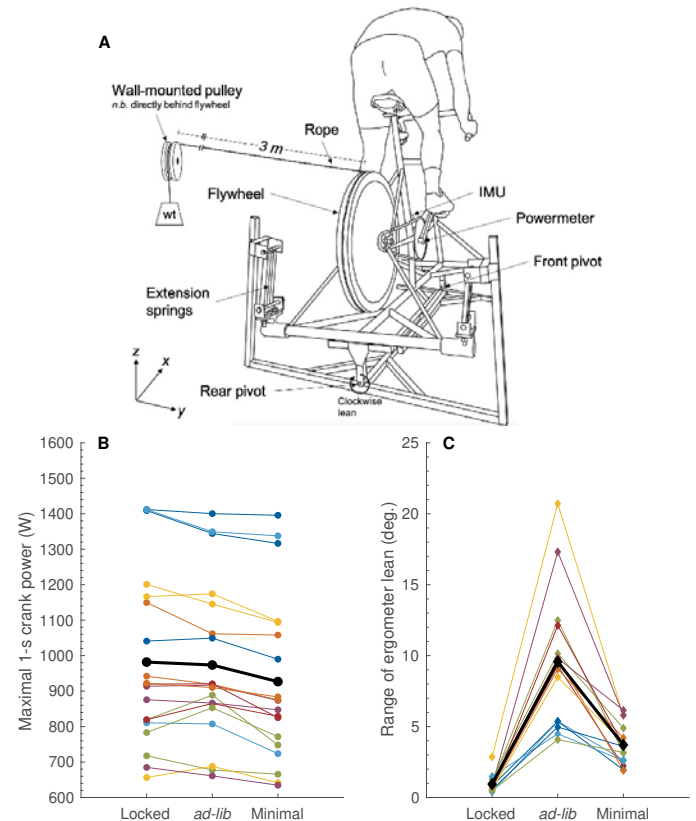


Figure 1: A. Diagram of modified cycle ergometer. B-C. Individual (color) and group mean (black) maximal 1-s crank power and range of ergometer lean, respectively.

Conclusion

Leaning the bicycle *ad libitum* did not enhance maximal 1-s crank power compared to a traditional stationary ergometer. Trying to minimize bicycle lean decreased maximal 1-s crank power by 5% compared to leaning *ad libitum*.

Acknowledgments

Supported by an ISB Student International Travel Grant to RDW.

References

- [1] Soden, P. and Adeyefa, B. (1978). *J Biom*, **12**:527–541.

Guanrong Cai¹, Jared Moore¹, Kiran Kanwar¹, Karen Lee¹, Roger Hawkes², and George Salem¹
¹Musculoskeletal Biomechanics Research Laboratory, University of Southern California, Los Angeles, CA.
²University College London, London, United Kingdom.
 Email: guanrong@usc.edu

Summary

Golf is a multimodal-activity that should be considered when designing training programs for older adults. This study quantified the lower extremity (LE) demands of the golf swing in healthy older adults (OAS) who acquired the skill through a 10-week golf training program. The average peak net extensor-(PEM) and support-moments (SM) of the lower extremity were calculated via 3D motion capture. PEM were found greater at the right hip and left knee compared to their contralateral counterparts, while no differences were found in the PEM of the ankles and SM. The LE demands of the golf swing were similar to common stepping activities in OAS. Understanding the demands associated with the physical tasks specific to golf will inform the design of safe and effective golf training programs in older adults.

Introduction

Proper exercise prescription is integral to quality of life in OAS [1]. Golf is a multimodal-activity that offers physical, psychosocial, cognitive, and health benefits [2, 3]. However, the physical demands associated with golfing activities have not been well characterized, and compared to other common exercises. The purpose of this study was to: 1) quantify the LE joint demands of the golf swing in OAS novel to golf after a 10-week golf training program, 2) examine the demand differences between limbs, and 3) to compare the demands to common stepping activities.

Methods

Fourteen of fifteen participants completed a 10-week golf training program with biomechanical, physical, and cognitive testing prior to and after the program. During post-testing, participants were instructed to hit 5 golf shots each with a pitching wedge, 7-iron, and driver while standing on 2 force plates. LE net joint moments were calculated via a marker-based, motion capturing system. PEM and SM of the hip, knee, and ankle during golf swings are reported. Independent-samples t tests were used to examine differences between left and right limbs ($p \leq 0.05$). To assess the relative magnitude of these moments, comparisons were made with common stepping activities using previously reported data, collected with similar methodology, from our laboratory [4]. Results are presented, in Nm normalized to body mass, as mean \pm standard deviation.

Results and Discussion

Participants completed 283/300 (94%) sessions with no program related adverse events. All were right-handed. The right hip PEM was greater than the left hip during the golf swing, regardless of the club ($p \leq 0.05$). At the knee, the left side had greater PEM than the right side for the 7 iron and driver ($p \leq 0.05$), but not the pitching wedge. No differences were found between limbs for ankle PEM. When comparing PEM in the sagittal plane, the golf swing moments appeared larger at the hips and similar at the

knees and ankles compared to common forward and lateral stepping exercise activities in older adults [4] (Figure 1.). In regards to SM, there were no differences between L and R limbs (Table 1.).

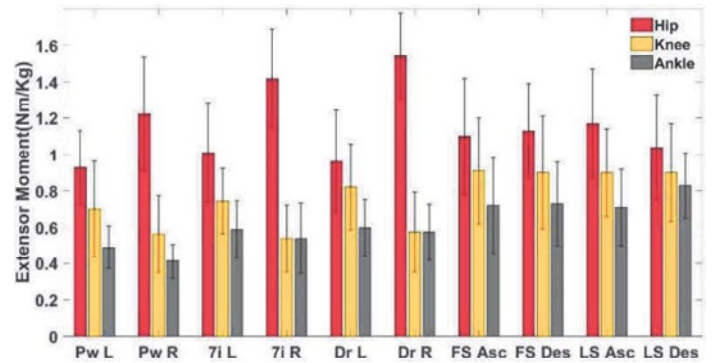


Figure 1. Average Peak Joint Moments in Golf Swings and Stepping Activities. FS: forward stepping; LS: lateral stepping; Asc: ascending phase; Des: descending phase.

Table 1. Golf Swing Support Moments in Three Types of Golf Clubs

	Pitching Wedge		7Iron		Driver	
	L	R	L	R	L	R
SM	1.55	1.34	1.68	1.58	1.64	1.62
(Nm/kg \pm SD)	± 0.33	± 0.29	± 0.38	± 0.48	± 0.43	± 0.41

Conclusions

Golf is a multimodal-activity that includes: swings, multi-terrain walking, and bending to mark or tee up the ball. These activities are likely responsible for the reported improvements in physical function (e.g., hip strength) associated with the golf-training program [3, 5]. Our findings suggest that golf swings generate sagittal plane PEM's that are similar or greater than those generated during stepping activities in OAS. Differences between left and right limb PEM's should be considered when prescribing golf as an exercise activity and suggest that other supplemental activities might be necessary to counteract these differences. Understanding the relative biomechanical demands associated with these activities will inform prescription of progressive, safe and effective golf training programs for OAS in the future.

Acknowledgments

Supported by R&A Grant GHA0012017.

References

[1] Garcia-Hermoso et al. (2020) *Sports Medicine*, **50**: 1095-1106
 [2] Tsuji et al. (2019) *J Sports Sci.* **38**: 422-429
 [3] Du Bois et al. *International Journal of Golf Science*, Accepted January, 2021.
 [4] Wang et al. (2003) *Clin Biomech.* **18(3)**: 214-221
 [5] Moore et al. SWACSM 2019

Racing in the street – Whole-body vibration during road cycling and the effect of different equipment choices to minimise it

Jon Ward¹, George L Ruell¹, Timothy P. Holsgrove¹

¹Department of Engineering, College of Engineering, Mathematics and Physical Sciences, University of Exeter, UK

Email: t.holsgrove@exeter.ac.uk

Summary

Whole-body vibration (WBV) exposure can lead to spinal injury and pain, and road cycling can expose participants to substantial WBV. Previous research has shown no difference between a standard seatpost compared to designs that aim to reduce vibration. This study provides further data in this area by focusing on the effect of saddle designs, tyre construction, and tyre pressure on WBV exposure. Our results again highlight the fact that daily WBV exposure limits are rapidly exceeded, and none of the equipment configurations we tested led to a substantial reduction in the WBV exposure. Alternative equipment, such as suspension, or larger volume tyres that can be used at lower pressures may be required to achieve meaningful reductions in WBV during road cycling.

Introduction

Exposure to whole-body vibration (WBV) substantially increases the risk of low back pain, spinal degeneration, and injury [1, 2]. Standard methods (ISO 2136-1) have been established to evaluate WBV [3], and there are daily WBV exposure action values (EAV) and exposure limit values (ELV) [4]. Cyclists who ride more than 160 km/week are 3.6 times more likely to have back pain compared to those that ride less than 160 km/week [5], and research evaluating seatpost designs during road cycling showed that daily WBV limits were rapidly exceeded with all seatposts [6]. This preliminary assessed the effect of saddle design, tyre construction, and tyre pressure on WBV.

Methods

Road cyclists completed a predetermined 6.42 km route [6]. The study was approved by the institutional ethics committee (eEMPS00007). One group (n=3) completed the route four times, each time with one of four saddles: Prologo Scratch 2 PAS Nack; San Marco Regal Evo; San Marco Regal; Brooks Cambium C13. Another group (n=3) completed the route six times: three times using Challenge Strada Race nylon vulcanized clincher tyres at pressures of 75, 85, and 95 psi; and three times using Challenge Strada Service Course cotton clincher tyres at pressures of 75, 85, and 95 psi. APDM Opal sensors were positioned at the seat cluster (SC), top of the seatpost (SP), and lumbar region (LB) in the saddle group, and at the rear hub (RH), saddle rails (SD) and lumbar region (LB) in the tyre group. The root-sum-of-squares vibration dose value (VDV_{RSS}) was calculated according to ISO 2136-1 [3]. Transmissibility (T) across the saddle was determined from the root mean squared acceleration (a_{rms}) at the SP and LB.

Results and Discussion

The vibration for all participants in all tests comprised both constant low-level vibration, and frequent shocks (Figure 1).

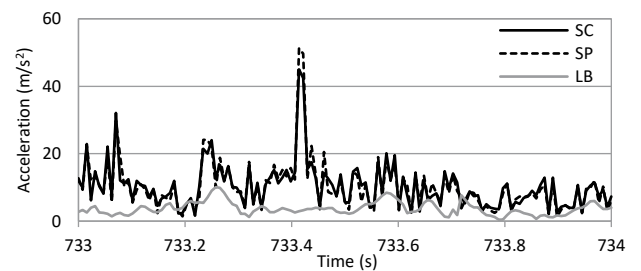


Figure 1: Typical data of the resultant acceleration magnitude.

The VDV_{RSS} measured at the RH, SC, SP, and SD exceeded the ELV in all tests, and the mean VDV_{RSS} at the LB position exceeded the EAV for all saddles, tyres, and tyre pressures, and the ELV in 40 % of cases (Figure 2). There was a large reduction in the acceleration between the SP and LB in all tests in the saddle group (T range 0.26-0.55), though it is likely that the clothing and soft tissue of the rider contribute to a large part of the observed reduction.

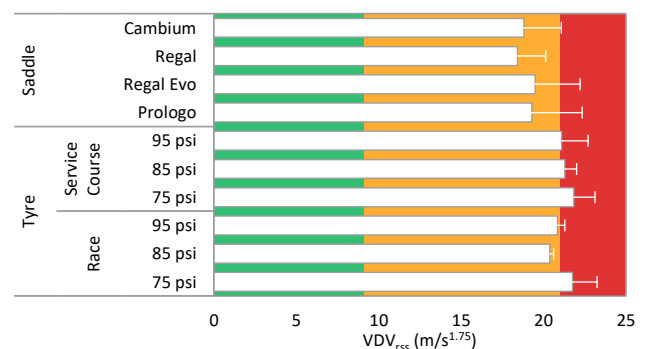


Figure 2: VDV_{RSS} at the LB position shown against daily WBV exposures: safe (green); EAV (amber); ELV (red).

Conclusions

Road cycling results in substantial WBV exposure. None of the test configurations reduced the WBV exposure to within occupational limits. Therefore, alternative equipment choices, are required to meaningfully reduce WBV.

References

- [1] Bovenzi M and Hulshof CT. (1999). *Int Arch Occup Environ Health*, 72(6):351-365.
- [2] Lan FY et al. (2016). *J Occup Health*, 58(1):118-127.
- [3] British Standards Institution. (2011). BS ISO 2631-1:1997.
- [4] EU Directive 2002/44/EC- (2002). *Official Journal of the European Communities*, L 117/13, 6.7.
- [5] Schultz SJ and Gordon SJ. (2010). *Int J Exerc Sci*, 3(3), pp. 79-85.
- [6] Edwards PI and Holsgrove TP. (2020). *J Sports Sci*, available online doi: 10.1080/02640414.2020.1829361.

Sleep parameters and soccer kicking performance in youth players

Fabio A. Barbieri¹, Michele Lastella², João Pedro da Silva¹, Tiago A. I. Cesário¹, Felipe B. Santinelli¹, Gabriel F. Moretto¹, Paulo R. P. Santiago³, Luiz H. Palucci Vieira¹

¹Human Movement Research Laboratory (MOVI-LAB), São Paulo State University (UNESP), Bauru, SP, Brazil

²Appleton Institute for Behavioural Science, Central Queensland University, Adelaide, Australia

³LaBioCoM Biomechanics and Motor Control Laboratory, USP University of São Paulo, Ribeirão Preto, SP, Brazil

Email: fabio.barbieri@unesp.br

Summary

The purpose of this study was to investigate the magnitude of relationships between sleep metrics and kicking performance in youth players. Twenty-eight under-17 players completed a kick testing protocol against a goalkeeper. We determined the approach run, foot and ball velocities, mean radial and bivariate variable error, and accuracy during kicking performance. Over 24h before field testing, players were monitored by wrist actigraphy. Self-reported sleep quality and chronotype scores were also collected. Multiple linear regressions indicated that the wake-up time and chronotype scores contributed to 40% of the mean radial error while self-reported sleep quality influenced respectively on 19% and 24% of the accuracy and bivariate variable error variances; taken together self-reported sleep quality and the time of final awakening explained 33% of the accuracy. In short, one-off self-reported or directly determined sleep measures using wrist actigraphy allowed for detecting inter-individual variations of kicking performance in youth-soccer players.

Introduction

Sleep is fundamental in the day-to-day recovery of physical capacity and motor skills [1]. A night with reduced sleep may disrupt central nervous system functioning, compromising visuospatial perception, decision-making and movements' execution [2]. In senior standards, variations in sleep duration, latency and efficiency produced no effects on match kicking accuracy [3]. However, results from senior players cannot be readily extrapolated to youth [4]. Therefore, the present study aimed to investigate the habitual sleep patterns experienced by youth soccer players and their influence on kicking performance features.

Methods

Thirty under-17 Brazilian soccer players were monitored using wrist actigraphy in the night immediately before kick testing. The following parameters were identified: sleep-wake phases, time in bed, wake-up time, time of lights out, total sleep duration, wake after sleep onset, latency of lights out and sleep starts, efficiency and number of awakenings [5]. Also, self-reported sleep quality, Karolinska Sleepiness Scale and individual's chronotype score were collected.

The soccer players performed seven kicks to each goal side and six requested to aim its centre. They kicked stationary balls positioned 18m away from the midpoint goal line, using the instep region of the dominant foot and aiming at the centre of 1x1m targets allocated in the goalpost. Two goalkeepers tried to block the shots. The kicks were recorded, and the

imagens were analyzed in DVIDEOW environment. We calculated the approach run, foot and ball velocities, mean radial (MRE) and bivariate variable error, and accuracy to analyzed kicking performance.

Partial correlations controlling for chronological age and body sizes were computed between sleep parameters and kicking performance indicators. Multiple linear regressions (stepwise method) were used to determine the relative contribution of sleep variables to the variance in kicking performance metrics.

Results and Discussion

The main findings (Figure 1) were: (1) both subjective and objective measures of sleep were associated with kicking performance ($r < 0.38, p < 0.05$); (2) higher perceived sleep quality was related to better kicking accuracy ($r^2 = 0.19, p < 0.02$) and lower placing variability ($r^2 = 0.24, p < 0.008$). In contrast, athletes with later wake-up time performed poorer kicks as illustrated by fewer kicks on-target ($r^2 = 0.15, p < 0.04$) and higher MRE ($r^2 = 0.40, p < 0.02$); (3) while either sleep quality and duration impacted on ball placement indices, kicking velocity properties were minimally influenced.

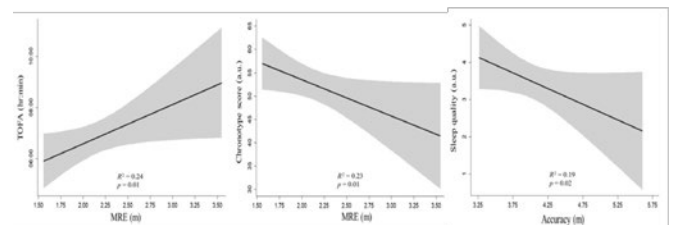


Figure 1: Associations between kicking performance with the sleep parameters. TOFA wake up time; MRE mean radial error.

Conclusions

Whilst sleep quality indicators had limited interference on kicking velocity components, good sleep quality and morning behavior may notably produce a better kicking accuracy.

Acknowledgments

FAPESP (2018/02965-7, 2018/21091-8, 2020/04282-4); CAPES; Brazilian Society of Biomechanics; Fogaíno Sports F.C at Bauru.

References

- [1] Fox JL et al (2020). *Sports Med*, **50**: 461-470.
- [2] Fullagar HH et al (2015). *Sports Med*, **45**: 161-186.
- [3] Begg MR (2015). *Thesis at Florida State University*.
- [4] Palucci Vieira LHP et al (2020). *Sports Med*, in press.
- [5] Lastella M (2015). *Eur J Sport Sci*, **15**: 94-100.

IN VIVO VALIDATION OF A MUSCULOSKELETAL MODEL OF THE WRIST FEATURING A CONSISTENT ANATOMICAL DATA SET

Oluwalogbon O. Akinnola¹, Vasiliki Vardakastani¹, ¹Angela E. Kedgley

¹Department of Bioengineering, Imperial College London, London, UK

Email: o.akinnola16@imperial.ac.uk

Summary

Activity of seven forearm muscles during wrist flexion-extension and radial-ulnar deviation was compared to muscle forces predicted from corresponding kinematics. The model predicted agonist muscle activity but perform poorly predicting antagonist activity. Co-contraction is needed for models to accurately predict forearm muscle activity.

Introduction

Musculoskeletal models of the wrist have been developed with averages of anatomical parameters, which has been shown to significantly affect model predictions [1]. The Imperial College London wrist model was developed from a consistent anatomical data set and previously validated in vitro [1]. However, in vitro validation risks omitting factors present in vivo. To improve the clinical applicability of the model, this study sought to validate the model outputs with electromyographical (EMG) data.

Methods

23 participants (1.71 ± 0.08 m, 68.26 ± 12.66 kg, 28.6 ± 4.60 years) took part in this study. Each performed 15 cycles of wrist FE and RUD with their dominant hand. Muscle activity of extensor digitorum communis (EDC), extensor carpi radialis (ECR), extensor carpi ulnaris (ECU), flexor digitorum superficialis (FDS), flexor carpi radialis (FCR), flexor carpi ulnaris (FCU), and pronator teres (PT) were recorded using surface EMG (Delsys, Natick, USA). Joint kinematics recorded using an eight-camera optical motion capture system (Qualisys, Gothenburg, Sweden) were used as inputs for the model. An inversion of the EMG-to-force method was used to generate model-predicted muscle activity [2]. These were qualitatively compared to the recorded EMG data using Statistical Parametric Mapping (SPM) t-testing, Magnitude-Phase-Comprehensive (MPC), and Pearson's Correlation Coefficients (PCC).

Results and Discussion

The qualitative comparison showed a good match between the model output and the recorded EMG. FCU and FCR were

observed to coactivate during flexion (Figure 1). ECU, ECRL and ECRB were observed to coactivate during extension, but muscles were only activated in the model when acting as agonists. The PCC between the predicted and recorded muscle activity was 0.04 on average. The average MPC values were 0.81 (M), 0.25 (P), and 0.83 (C). Only the ECRL predicted force was different ($p=0.01$) to in vivo estimates.

Both the qualitative comparison and the SPM statistical testing indicate that the model can accurately predict the muscle activation patterns of agonist muscles involved with wrist motion. However, the PCC values indicate that the model is not able to replicate the muscle activation pattern for all the muscles, specifically the antagonist muscles. This is further supported by the MPC values, which showed that the model underestimated muscle activity. The absence of co-contraction means that less activity is needed by the agonist muscles to generate the kinematics. As the model optimizes by minimizing muscle stress, if a muscle is not needed to generate the motion, it is effectively switched off. However, this is not the case in vivo, as antagonist muscles also act as stabilisers. Thus, there is a poor correlation as the model-predicted activity can be zero while the EMG shows activity. In conclusion, the model has been validated for the in vivo muscle activation patterns of agonist muscles during wrist motion. However, the inclusion of co-contraction in the model is needed to accurately capture the complete biomechanical picture.

Conclusions

In conclusion, the model has been validated for the in vivo muscle activation patterns of agonist muscles during wrist motion. However, the inclusion of co-contraction in the model is needed to accurately capture the complete biomechanical picture.

References

- [1] Goislard De Monsabert et al, (2018), *Ann. Biomed. Eng.*, **46**, 71–85.
- [2] Bogey et al, (2005) *IEEE Trans. Neural Syst. Rehabil. Eng.*, 13302–310.

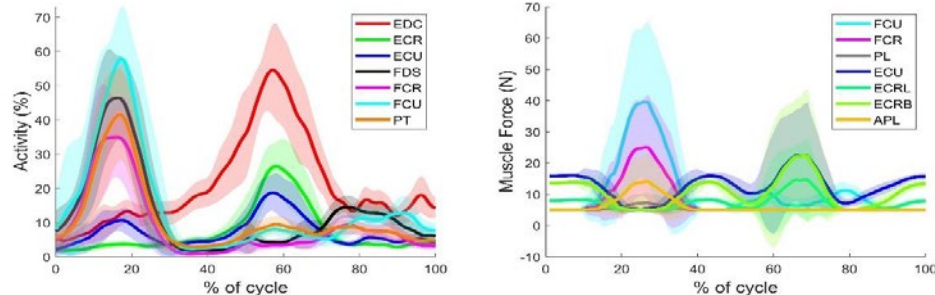


Figure 1: The muscle activity recorded by EMG (left) & simulated muscle force (right) for a participant performing flexion-extension of the wrist.

Palmar musculature and its role as a dynamic compressor of the carpal tunnel

Trevor Simcox, Lauren Seo, Kevin Dunham, Catherine Petchprapa, Ronit Wollstein

Departments of Radiology and Orthopedic Surgery, NYU Langone Health, New York, NY, USA

Email: ronitwollstein@gmail.com

Summary

It is possible that the musculature overlying and integrated with the transverse carpal ligament represent a dynamic force that exerts pressure over the median nerve contributing to the development of carpal tunnel syndrome (CTS). The aim of this study was to compare musculature overlying the carpal tunnel between subjects with and without the diagnosis of CTS. There was a very wide range of muscle mass measured. We found that there was a significant correlation between signs of CTS on MRI (median nerve cross-sectional area) and the amount of muscle overlying the carpal tunnel. Further study should refine the measurement method of these muscles to better understand their effect on CTS.

Introduction

The diagnosis of carpal tunnel syndrome (CTS) remains clinical. While much study has focused on the dimensions and size of the carpal tunnel, there has been little emphasis on possible dynamic factors of increased pressure in this anatomical space. During carpal tunnel release, variable amounts of muscle above the carpal tunnel are commonly observed. It is possible that this musculature may represent a dynamic force that exerts pressure over the median nerve contributing to the development of CTS. We believe these muscles, specifically those found immediately volar to the transverse carpal ligament and cross the carpal tunnel, have a dynamic role in the etiology of CTS especially in manual laborers who use their hands in a forceful and repetitive fashion. [1] This anatomic variant (muscles crossing the area of the carpal tunnel) may also be related to the "square" hand configuration contributing to increased incidence of CTS in these patients. The ability to recognize this "dynamic component" may improve our ability to understand and prevent the development of CTS. We hypothesized that patients with a clinical diagnosis of CTS have more muscle, as quantified by magnetic resonance cross-sectional imaging (MRI), overlying the carpal tunnel than normal controls.

Methods

Case control study of a database of wrist MRI. Cases were patient charts with a diagnosis of CTS. These were matched by age and gender to those without CTS (controls). Exclusion criteria included poor quality imaging, space-occupying mass in the carpal tunnel, concomitant neurological disorders, and previous carpal tunnel surgery. Axial cuts at the level of the hook of the hamate and scaphoid tubercle were used to measure the muscle mass overlying the carpal tunnel. Muscle mass was quantified using: thickness (mm) at 3 points (mid-capitate, capitate-hamate boarder, capitate-trapezoid border) and an average thickness (calculated by dividing the cross sectional area by the carpal tunnel width). Other MRI parameters from axial

cuts were measured: median nerve T2 signal, median nerve shape, and carpal tunnel cross sectional area.[2] Groups were compared with t-tests or Wilcoxon rank-sum tests and statistical significance was defined as $p < 0.05$. single-spaced,

Results and Discussion

A total of 21 cases and controls met the inclusion criteria for the study. There were no significant differences in age, gender, hand dominance, manual laborers, diabetes mellitus, hypothyroidism or nerve shape between case and controls. Average muscle depth in the carpal tunnel group was 2.61mm and control group 2.54mm ($p=0.83$). Muscle depth measurements for carpal tunnel and control groups were 2.36mm and 2.10mm ($p=0.46$) at the mid-capitate, 1.19mm and 0.67mm ($P=0.23$) at the capitate-hamate border, and 3.42mm and 4.30mm ($p=0.4$) and the capitate-trapezoid border respectively. The variability in measurements was significant in all areas measured. We did find a significant correlation between signs of CTS (median nerve cross-sectional area) on MRI and MRI measured muscle mass $p=0.008$.

Conclusions

We found no significant differences in muscle mass overlying the carpal tunnel using our method of evaluation between chart documented CTS and non-CTS wrist MRIs. We did find a correlation with MRI nerve cross sectional area.

It is possible that:

- 1) There truly is no difference.
- 2) Our method of evaluation is flawed:
 - The insertion (footprint) of the muscles may be more important in the mechanics of the carpal tunnel than the amount of muscle and this was not evaluated.
 - Anatomical variation was so great that our measurements were unable to identify true differences.
 - Advanced CTS can cause atrophy affecting the amount of muscle measured on MRI.
- 3) Future research should focus on a refining the measurement method of these muscles and their effect on CTS.

References

- [1] Bonfiglioli, R., et al., Course of symptoms and median nerve conduction values in workers performing repetitive jobs at risk for carpal tunnel syndrome. *Occupational Medicine*, 2006. **56**(2): p. 115-121.
- [2] Fowler, J.R., et al., *Comparison of ultrasound and electrodiagnostic testing for diagnosis of carpal tunnel syndrome: study using a validated clinical tool as thereference standard*. *J Bone Joint Surg Am*, 2014. **96**(17):p.1992-5

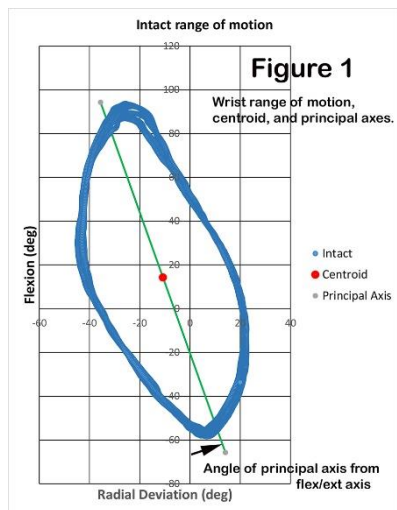
Fused with Motion: A Biomechanical Comparison of Dart Throw Motions after Partial Wrist Fusions

Frederick W. Werner, Dami O. Oluyede, Garrett Esper, Michael J. Schreck
 SUNY Upstate Medical University, Syracuse, NY, USA Email: wernerf@upstate.edu

Summary: Multiple partial wrist fusions exist for the management of wrist arthritis. The purpose of this study was to measure the motion allowed by different orientations of the dart throwing motion for 7 different partial wrist fusions and proximal row carpectomy.

Introduction: Partial wrist fusions may limit wrist motion differently during a dart throw style of wrist motion. The purpose of this study was to measure the retained motion for different orientations of the dart throwing motion for 7 different partial wrist fusions and proximal row carpectomy.

Methods: Eight fresh frozen cadaver wrists were tested with the wrist intact and for seven simulated fusions and proximal row carpectomy. In all cases, the wrists were passively moved through a minimum of 4 circumduction motions by 2 testers. Wrist motion was measured by a motion sensor,



attached to the dorsum of the 3rd metacarpal. The fusions were scaphocapitate (SC), scapholunate (SL), capitulate (CL), radiolunate (RL), radioscapolunate (RSL), scapho-trapeziotrapezoid (STT), 4 corner fusion (CF) and a proximal row carpectomy (PRC). For each circumduction motion, (figure 1) the area within the circumduction motion was computed, the principal axes of the motion were calculated as the angle it made with the flexion/extension axis, and the range of motion (arc) that a dart throw motion might have until it intersects the boundary of the circumduction motion was determined. The arc of motion was found for a pure flexion/extension motion, a pure radioulnar deviation motion and 11 motions oriented at increasing amounts from the flexion/extension axis. A one-way repeated measures ANOVA with a Bonferroni correction for multiple comparisons was used to compare the different simulated dart motions.

Results and Discussion: All fusions except for the SL fusion significantly reduced the area of motion ($p < 0.01$) compared to intact. The SC area was larger than the CL ($p = 0.04$). The SL area was larger than the CL and the RSL ($p < 0.03$). The SC and STT fusions principal axes were more closely aligned with the flexion/extension axis (ave 8 deg) than the intact axis

(19 deg). The SL had a larger angle (20 deg; more aligned toward the radioulnar deviation axis) than the STT (7 deg) or the PRC (8 deg; $p < 0.04$). The arc of motion (table 1) of the intact wrist oriented 20 deg from the flexion/extension axis was greater than any of the other 12 orientations ($p < 0.03$). At the 20 and 25 degree orientations, all fusions had a smaller arc of motion compared to intact ($p < 0.02$). The SC, CL and RSL fusions all had a smaller arc of motion than the intact at all 13 orientations ($p < 0.04$). The SL fusion was the only fusion which did not decrease the area of motion compared to the intact specimen. This finding makes intuitive sense biomechanically, and reinforces the importance of the SL ligament in linking the motion of the scaphoid and lunate bones under normal kinematic conditions of the carpus.

Table 1: Average Arc of Motion at Different Orientations of a Dart Thrower's Motion (angle from flexion/extension axis; mm)

Orientation	Fusion								
	Intact	SC	SL	CL	RL	RSL	STT	CF	PRC
Flex-ext	94	76	81	55	59	41	76	60	73
20 deg	116	73	102	59	83	54	67	65	70
25 deg	108	68	98	59	80	57	61	65	68
30 deg	99	62	92	58	75	57	55	65	63
35 deg	91	57	85	57	69	66	50	65	58
40 deg	83	53	78	55	65	53	46	63	55
45 deg	76	49	72	52	59	50	42	60	51
50 deg	70	46	66	50	55	47	39	57	48
55 deg	65	44	62	47	51	43	37	55	45
60 deg	61	41	58	45	48	40	34	52	43
65 deg	57	40	54	43	45	37	33	50	41
70 deg	54	38	51	42	43	34	32	48	40
Radio- ular	47	35	44	37	36	28	30	42	37

Conclusions: This study provides a comprehensive compilation of the range of motion in a functional plane "the dart throw motion" to be expected after various limited wrist fusions and proximal row carpectomy. These data provide the clinician with important information that can be used to educate the patient with regards to expectations after surgery.

Acknowledgments: Funded by the Department of Orthopedic Surgery, SUNY Upstate Medical University

My current understanding of wrist dynamics

Marc Garcia-Elias, Barcelona, Spain

The wrist is one of the most complex composite articulations of the human body, comprising 15 bones, 24 joint facets, and 24 ligaments. Furthermore, it incorporates a system of pulleys to control the moment arms of the tendons that cross the joint. The necessity of placing the hand in the best possible position that allows manipulating all sorts of objects with the minimal energy cost, on one side, and the need to ensure that the joint is capable to sustain considerable amount of forces without yielding explains why we are still struggling to understand how needs to be treated when is dysfunctional. In kinetic terms, a joint is meant to be stable when is able to sustain physiologic loads without yielding. To achieve this, when the wrist is loaded, capsular ligaments are the first to react. Some ligaments, however, may have difficulties resisting prolonged tensions, thus the need for muscles to protect the ligaments under the coordination by the sensorimotor system, a specialized group of neural elements that use the proprioceptive information to control stability. This session will cover what is the current understanding of the role of ligaments and muscles in the stabilization of the wrist.

Biomechanical Simulation of Lung-Tumor Motion Based on Surface Imaging

M. Ranjbar¹, P. Sabouri², S. Mossahebi³, A. Sawant³, P. Mohindra³, G. Lasio³, L.D. Topoleski¹

¹University of Maryland, Baltimore County, Baltimore, USA, ²Miami Cancer Institute, Miami, USA

³University of Maryland, School of Medicine, Baltimore, USA

Email: rmaida1@umbc.edu

Summary

Thoracic radiotherapy (RT) is restricted by breathing-related motion of the target and internal anatomy with limited options available for direct visualization of this motion during treatment. The current standard-of-care for motion mitigation expands the irradiated volume to encompass the entire range of tumor motion as assessed during the planning stages. We present a biomechanical model that predicts tumor motion during RT delivery sessions based on boundary conditions (BCs) derived by monitoring the patient's chest and abdomen surface. Our model can serve as a gold-standard for imaging-based models and can potentially lead to significant reductions in expansion margins, thereby better preserving healthy lung tissue.

Introduction

Surface images of the chest and abdomen are generally accessible during RT delivery and can be used to monitor patient motion. However, treatment of thoracic cancers require accounting for the motion of the internal anatomy. 4D computed tomography scan (4DCT) done as part of RT planning generates a sequence of volumetric images representing the range of internal anatomy motion over the "average" breathing cycle. To ensure RT delivery to the tumor, the irradiated volume is expanded into the internal target volume (ITV), which encompasses the range of motion observed in the 4D images. Irregularities in the breathing pattern can cause deviations from the average cycle. To account for breathing irregularities and setup uncertainties, the irradiated volume is further expanded into the planning target volume (PTV). These expansions expose healthy lung tissue to undesirable doses of radiation and pose a risk for radiation-induced toxicities. We present a finite element biomechanical model that uses chest and abdomen surface images acquired during RT treatment planning and delivery to predict motion of the internal anatomy including the tumor.

Methods

4DCT images, and VisionRT (VRT) surfaces of the chest and abdomen were collected from three lung cancer patients (Figure 1- top row). During RT treatments, two ~30s long datasets of VRT surfaces with concurrent fluoroscopic projections (FLs) were acquired pre- and post-RT delivery (Figure 1- bottom row). To generate BCs for the model, the end of exhale (EE) 4DCT image was mapped to the other images using deformable image registration. A mathematical basis for the observed deformation vector fields (DVs) was derived using principal component analysis. A previously validated surrogate motion model (SMM) that uses VRT surfaces as input was constructed to estimate EE lung surface DVFs. [1,2] The SMM applied concurrent VRT surfaces and FL projections to construct and update the internal-external correlation and predict lung surface DVFs. [3] An elastic, non-linear finite element model of the EE lung and tumor was generated in the ABAQUS finite element software. Lung and tumor material properties were optimized to minimize the error between model-estimated and 4DCT measured tumor centroid. The SMM-generated lung surface DVFs were used as boundary conditions and transient FE simulations were performed to compute tumor motion during the RT delivery session.

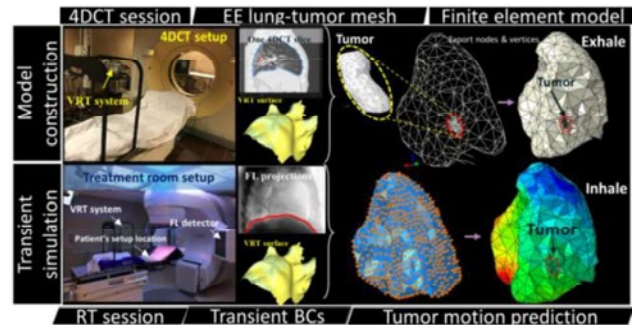


Figure 1 Biomechanical model construction. Top row: EE Lung and tumor contours were imported into ABAQUS and material properties were optimized. Bottom row: FL projections and VRT surfaces were concurrently acquired and used to construct the SMM that provides lung surface BCs based on input VRT surfaces. These BCs were supplied to the biomechanical model and lung-tumor motion was solved.

Results and Discussion

Our biomechanical model effectively estimated tumor position during 4D simulation (<3mm centroid error) and RT delivery sessions. For three out of six acquisitions, tumor motion was limited to within the PTV expansion. However, excursions outside of the ITV were observed during three acquisitions (Figure 2 a-b). For one patient (Figure 2 b), a shift in the base line was observed at the end of the fraction with the tumor spending more than 50% of its time outside of the PTV, suggesting the possibility for marginal failure. For another patient (Figure 2 c), the irradiated volume (PTV) overestimated tumor motion range.

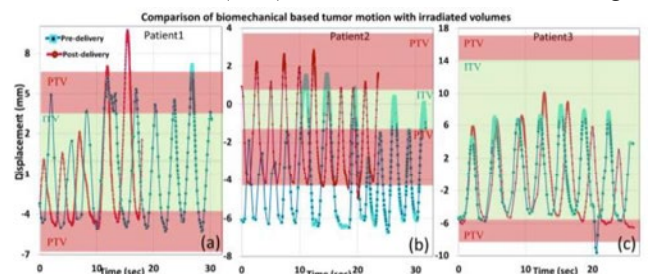


Figure 2: Tumor centroid motion estimated by the biomechanical model for patients 1-3 (a-c). Shaded green is the internal target volume (ITV) encompassing tumor motion (derived from 4D imaging protocol). Shaded red is the irradiated volume (PTV), generated by further expansion of the ITV.

Conclusions

Our biomechanical model used lung surface BCs estimated from chest and abdomen surface images to compute tumor motion during RT delivery sessions. Our findings show that the tumor can move outside the irradiated volume. Clinical implementation and application of our model can lead to improvements in RT delivery accuracy and target margin reductions.

References

- [1] M. Ranjbar et al. (2019) *Medical physics* **46.5**: 1995-2005.
- [2] M. Ranjbar et al. (2019) *Medical physics* **46.12**: 5407-5420.
- [3] M. Ranjbar et al. (2020) *Phys. Med. & Bio.* (in press)

Towards the usage of embedded prosthesis sensors for real-life gait analysis of amputee subjects

Sabina Manz^{1,2}, Dirk Seifert³, Thomas Schmalz¹, Thomas Maximilian Köhler¹, Michael Ernst¹, Strahinja Dosen², Jose Gonzalez-Vargas¹

¹Ottobock SE & Co. KGaA, Duderstadt, Germany

²Department of Health Science and Technology, Aalborg University, Aalborg, Denmark

³Ottobock Healthcare Products, Vienna, Austria

Email: sabina.manz@ottobock.de

Summary

This case study investigated the potential of the sensors embedded into a mechatronic prosthetic knee joint for clinical gait analysis. The results showed a strong correlation (~ 0.99) and small RMSE between the sagittal knee angle ($\sim 1.5\%$) and knee moment ($\sim 7\%$) recorded during over ground level walking using the gold standard (optoelectronic motion capture) and internal device sensor data.

Introduction

Clinical gait analysis is typically performed in a laboratory environment using optoelectronic motion capture systems and force plates [1]. Due to various limitations of the laboratory assessment (e.g., confined space, constrained pathway), the patient performance is often not representative of real-life gait [1].

To overcome these limitations, researchers have used inertial measurement units (IMUs) to replace optoelectronic motion capture systems and conduct accurate gait analyses in amputee patients outside of a laboratory environment (less than 1° knee angle error) [2]. However, the IMUs are external sensors that have to be placed on the subject and properly aligned to the limb segments. This requires an extra effort and can result in positioning errors that can translate into errors in the recorded movement [3].

Mechatronic lower limb prostheses are equipped with embedded sensors that collect information about orientation, acceleration, angular velocity, joint angles and loads [4]. The validity and potential usage of these sensor data for clinical gait analyses is, however, still unknown. Therefore, there is a need to investigate whether it is possible to accurately measure gait performance using the embedded device sensors, and to compare the performance of these sensors to that of the gold standard of laboratory assessments.

Methods

Kinematic and kinetic data were collected from one patient with transfemoral amputation (height: 169 cm, weight: 76 kg, knee joint: GeniumX3) using a gold standard (GS) motion capture system (Vicon, Oxford, UK) and force plates (Kistler, Winterthur, Switzerland). In addition, the device sensors (DS) were used to assess gait performance. The data recorded by the DS included hydraulic loading and knee joint angle. The data were collected during over ground level walking at comfortable walking speed while simultaneously using both systems (DS and GS).

The sagittal knee angle and moment were determined and the obtained profiles were compared between GS and DS using correlation coefficients, root mean square error (RMSE) and maximum error.

Results and Discussion

The results for a single walking trial are reported in Table 1 and the recorded knee angle profiles are shown in Fig. 1. We found strong correlations between both the knee angle and knee moment acquired by GS and DS ($\rho \sim 0.99$).

Further, the RMSE was below 1° for the knee angle and below 5 Nm for the knee moment (1.5% and 7.2% relative error, respectively). The maximum error was 3.27° and 7.41Nm, respectively. These results demonstrate that the embedded sensors can measure sagittal knee angles with a similar quality as the wearable inertial measurement units [2].

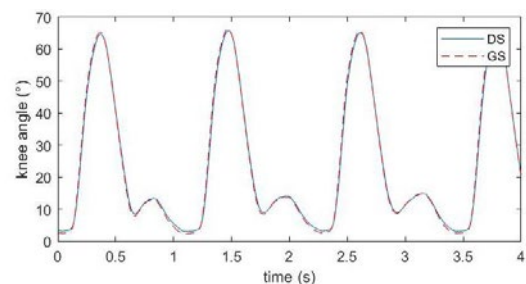


Figure 1: The knee angle recorded using device sensors (DS, continuous line) versus gold standard (GS, dashed line).

Table 1: Error and correlation between device sensors (DS) and gold standard (GS).

	RMSE	Max. Error	Correlation Coefficient (ρ)
Knee Angle ($^\circ$)	0.95	3.27	0.99
Knee Moment (Nm)	4.26	7.41	0.99

Conclusions

The preliminary results show the potential of embedded prosthesis sensors to assess knee angle and moments during amputee walking. A limitation is that this analysis only focuses on the affected limb. Additional experiments with other prosthesis sensors and more activities of daily living such as ramp and stair incline and decline, as well as a larger patient sample need to be conducted.

Acknowledgments

This work is supported by the Marie Skłodowska-Curie Actions (MSCA) Innovative Training Networks (ITN) H2020-MSCA-ITN-2019 - 860850 – SimBionics.

References

- [1] Cutti, A. et al. (2015) *G Ital Med Lav Ergon* **37**: 45-8.
- [2] Seel T. et al. (2014) *Sensors* **14**: 6891–909.
- [3] Bolink S. et al. (2016) *Med Eng Physics* **38**:225–31.
- [4] Bellmann M. et al. (2019) *Biomed Eng* **64**:407–20

In-vitro bi compartmental approach to assess intra-capsular pressure in the hip joint during movements: Is the acetabular cavity also presents pressure fluctuations as the capsular chamber?

St-Pierre Marc-Olivier^{1,2}, Lavoie Félix-Antoine^{1,2}, Hoffman Marion³, Begon Mickael³, Sobczak Stéphane^{1,2}

¹ Department of anatomy, Université du Québec à Trois-Rivieres, QC, Canada.

² Research Chair in Functional Anatomy, Université du Québec à Trois-Rivieres, QC, Canada.

³ Department of Kinesiology, Université de Montréal, QC, Canada.

Email : marc-olivier.st-pierre@uqtr.ca

Summary

The labrum separates the capsular chamber (CC) and the acetabular cavity (AC) of the hip joint. Hip extension and internal rotation bring high intra-capsular pressure within the CC. Therefore, high intra-capsular pressures in the CC are linked with pain. However, no assessment of pressures in the AC has been made and this information might have an impact in clinical assessment. The present study, using cadaveric specimens (n=6), reports variations of intra-capsular pressure in both, the CC and AC during five hip movements. Hip flexion and adduction showed the lowest pressure fluctuations in the CC. Hip extension showed a pressure increased in both compartments. Lastly, hip abduction and internal rotation showed an important depressurization in the AC.

Introduction

The labrum increases the contact surface of the acetabulum and helps to regulate the fluid exchanges between the AC and the CC [1]. Previous cadaveric studies have reported pressure fluctuations solely in the capsular chamber in different hip positions [2,3]. To date, no information is provided concerning the simultaneous pressure modifications into both, the AC and the CC of the hip joint during hip clinical assessment.

Methods

The specimens (n=6) were skeletonized from the lumbar spine (L5) to the distal femur and the hip capsular ligaments were carefully preserved. One cluster of reflective markers was placed on each of the following bones: coxal, femoral and tibial bones. CT-scan was performed for each lower limb to link osseous structures and the clusters. Hip kinematics were measured using six Optitrack cameras at 125 Hz. The coxal bones were stabilized in anatomical position on an experimental frame using two external fixators. Two intra-osseous tunnels were drilled to reach both CC and AC avoiding capsular tissue opening. The lateral tunnel was drilled over the greater trochanter with a latero-medial orientation to access the CC, medially to the trochanteric line. The medial tunnel was drilled through the iliac bone to access the AC with a supero-inferior orientation. To measure pressure fluctuations (125Hz), two fibre optic pressure sensors (FISO) were used and inserted in an injection chamber each, which were glued to the entrance of each tunnel. Before pressure measurement, 2.5 ml of mixture (Oil and latex) was injected into each compartment allowing the obstruction small arteries and avoiding leakages. Hip joints were tested in five different positions: 90° of flexion, maximal extension, abduction, adduction and internal rotation in 90° of flexion. Each movement was repeated five times and three trials were performed. Hip kinematics were synchronized with pressure fluctuations. Pressures were measured at the maximal ROM

of each movements described previously using Matlab (Version 2019b) (see Table 1).

Results and discussion

Pressure increased in the CC for all movements. Movements bringing high tension in the capsular ligament seemed to increase pressure in the capsular chamber (EXT, ABD, IR). Movements with lower hip capsular tension show little increase in pressure in the CC (F90, ADD) (p< 0.001). The pressure in the AC increased in two movements and decreased in the others. Flexion, abduction and internal rotation might have a more medio-lateral femoral head motion and create a depressurisation in the AC. The internal rotation showed the greatest difference between both compartments (60.06 mmHg).

Table 1. CC and AC mean intra-capsular pressures (SD). F90: 90° flexion, EXT: extension, ADD: adduction, ABD: abduction, IR: internal rotation. All values are in mmHg

	F90	EXT	ADD	ABD	IR
CC	5.93 (10.91)	18.57 (10.96)	3.40 (4.47)	14.71 (10.32)	17.31 (16.66)
AC	-8.58 (7.40)	15.44 (9.33)	7.51 (7.36)	-25.86 (33.85)	-42.75 (32.92)

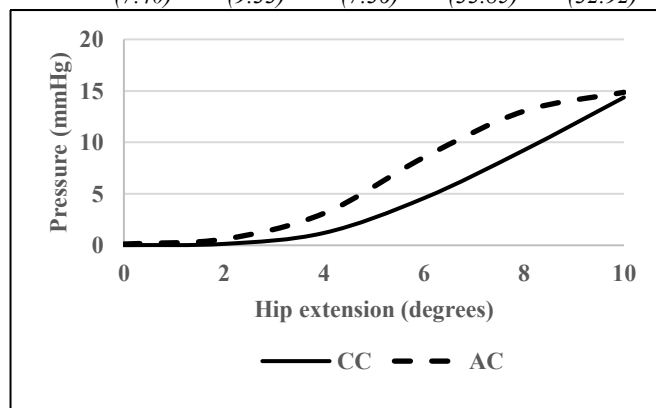


Figure 1. Capsular chamber (CC) and acetabular cavity (AC) pressure fluctuations in hip extension (0-10°).

Conclusion

This is the first study to provide simultaneous pressures measurements for the CC and AC without altering the capsular tissue. Hip kinematics and optic pressure transducers help to understand the link between hip movements, intra-capsular pressures and compartments. As increased pressure in the CC is linked with pain, these results might have a clinical impact.

References

- [1] Dwyer et al. (2014) *Am J Sports Med*, 4: 812-9
- [2] Tarasevicius et al. (2007) *J Arthroplasty*, 4: 596-600
- [3] Yen et al. (2009) *J Orthop Surg Res*, 4: 1-6

Closing the Kinetic Chain: Weight-bearing versus non-weight bearing maximal force generation and its relation to patient reported outcomes in ACL injured males and females

Michael J. Del Bel¹, Teresa E. Flaxman¹, Kenneth B. Smale¹, Tine Alkjaer², Erik B. Simonsen², Michael R. Krogsgaard³, Daniel L. Benoit¹

¹School of Rehabilitation Sciences, University of Ottawa, Ottawa, Canada

³Department of Neuroscience and Pharmacology, University of Copenhagen, Copenhagen, Denmark

⁴Section for Sports Traumatology M51, Bispebjerg-Frederiksberg Hospital, Copenhagen, Denmark

Email: michael.delbel@uottawa.ca

Summary

Clinicians often assess knee strength in patients with ACL injuries using open-kinetic chain (OKC) methods in the sagittal plane; yet, knee instability and pain are experienced while weight bearing in closed kinetic conditions (CKC) with multidirectional loading. Furthermore, the relationship or the effect of sex between subjective patient reported outcome measures (PROMs) and functional tasks is unclear. This study sought to determine whether differences exist in OKC vs. CKC force generation tasks, and if peak forces are associated to PROMs in ACL-injured males and females. We identified sex-dependent relationships for both subjective and CKC ground reaction forces (GRFs) measures, but no differences during the OKC task. Using a CKC task during patient assessment may provide additional insight into rehabilitation progression.

Introduction

Although PROMs are poorly related to postoperative outcomes, they have grown in popularity as they incorporate the patients' perceived function and can be easily administered [1]. It is nevertheless unclear what the relationship is between a patient's perceived and objective functional capacity [2]. Furthermore, despite the sex-bias in ACL injury risk [3], and the fact that over 70% of ACL injuries occur during non-contact CKC events, the influence of sex and ACL injury on knee joint strength during CKC multidirectional loading conditions has yet to be considered. As such, this study sought to i) evaluate differences in PROM scores and objective strength measures during OKC and CKC tasks, and ii) determine if relationships exist between subjective and objective measures of knee function among males and females with and without ACL injuries.

Methods

Thirty-eight adult patients with ACL injuries (17 females) and 34 (17 females) uninjured controls were recruited for this study and were matched for age and leg-dominance. Participants completed the Knee Injury and Osteoarthritis Outcome Score (KOOS), International Knee Documentation Committee (IKDC), Lysholm, and Tegner questionnaires. While maintaining 50% bodyweight per limb, they then performed a

standing isometric force-generating task [4] while producing maximal anterior, posterior, medial, and lateral GRFs respectively. Participants also completed maximum voluntary isometric knee extension and flexion on an isokinetic dynamometer. The GRFs and torque data were normalised to body mass (N/kg, Nm/kg) and Kruskal-Wallis and post-hoc Mann-Whitney U-tests were used to determine between group differences ($\alpha=0.05$). Spearman's rho correlation coefficients (rs) were calculated between subjective PROMs and objective outcome measures.

Results and Discussion

As expected, ACL-injured participants reported lower PROM scores. There were no differences in OKC torque, however, a main ACL injury effect for CKC torque, and subsequent post-hoc analysis identified lower posterior GRF production in ACL-injured females compared to their control counterparts (1.51 N/kg vs. 1.81 N/kg; $p=0.048$) but not among male participants ($p=0.413$). Maximum medial CKC GRFs were correlated to both the Lysholm ($r_s=-0.569$; $p=0.021$) and the Tegner ($r_s=-0.814$, $p<0.001$) scaling scores for ACL-injured females. No significant differences or correlations were found from the OKC task.

Conclusions

Our results indicate that (1) males and females with ACL injuries will display different relationships between subjective and objective assessments; (2) CKC measures detected functional deficits in females and (3) CKC evaluations are more closely related to perceived knee joint function in females. We conclude that clinicians should consider how sex affects perceived knee function with their patients and that CKC evaluations provide them additional insight into their functional capacity.

References

- [1] Bent et al. (2009) *Br J Sports Med* **43**;1006-12.
- [2] Alamangoush & Herrington (2014) *Int Sch Res Not.* **16**;613034.
- [3] Sutton & Bullock (2013) *Am Acad Orthop Surg* **21**;41-50.
- [4] Flaxman et al. (2012) *J Biomec* **45**;2570-6.

Biomarkers of Knee Joint Healing Following Anterior Cruciate Ligament Reconstruction: A Systematic Review

Lisa E. Ek Orloff¹, Michael J. Del Bel², Nicholas J. Romanchuk³, Sasha Carsen⁴, Pascal Imbeault¹, Daniel L. Benoit^{1, 2, 3}

¹School of Human Kinetics, ²School of Rehabilitation Sciences, ³CIBME Ottawa-Carleton Institute for Biomedical Engineering, ⁴Department of Surgery, University of Ottawa, Canada

Email: dbenoit@uottawa.ca

Summary

Rehabilitation and return to activity (RTA) guidelines following ACL reconstruction (ACLR) is typically guided by post-operative time, patient reported perceived function and functional capacity measures. The purpose of this systematic review was to determine biomarkers which may be used to accurately reflect knee joint healing in patients recovering from ACLR. Using the Preferred Reporting Items for Systematic Reviews and Meta-Analyses (PRISMA) guidelines, articles that included participants who had undergone ACLR and longitudinally measured biomarkers of knee joint healing were identified. Levels of interleukin-6 (IL-6; reflecting inflammation in the knee) and C-terminal crosslinking telopeptide of type II collagen (CTX-II; reflecting articular cartilage degradation in the knee) were identified as the most prevalent and accurate biomarkers at reflecting knee joint healing. Measuring the levels of these biomarkers during the recovery process in adolescents could lead to rehabilitation and RTA assessment informed by the healing status of the knee.

Introduction

ACL injuries are increasing in prevalence by 2.3% annually in adolescents [1] and lead to increased risk for early-onset knee osteoarthritis (OA) [2]. Current ACL rehabilitation guidelines do not directly reflect the physiological healing process of the knee joint. Instead, the sole focus is on a patients' perceived function and their ability to meet functional benchmarks in the lower extremities [3]. The physiological healing process could provide prognostic insight for clinicians and physiotherapists when rehabilitating ACL-injured patients. Thus, the purpose of this systematic review was to identify existing literature to determine i) the most prevalent and accurate biomarkers at reflecting knee joint healing in patients after ACLR, and ii) the quantity of these studies which include adolescents.

Methods

Following PRISMA guidelines, Medline, Embase, SCOPUS and Web of Science databases were searched up until September 2020. Studies were included if they (1) included

participants who had sustained a primary ACL injury and undergone a subsequent ACLR, and (2) measured at least one biomarker of knee joint healing at more than one time point. The NIH quality assessment tool (before-after (pre-post) study with no control group) was used to assess study quality. The following datum were extracted: participant age; biological sample(s); biomarker(s) analyzed.

Results and Discussion

Seven studies met inclusion criteria for this systematic review (Table 1). IL-6 and CTX-II were the most prevalent biomarkers (3/7 studies). These biomarkers reflected knee joint healing through consistent elevation and/or gradual decrease following ACLR. Six studies evaluated adult populations (age range; Table 1). One study (average age 19.6±4.5) evaluated the effect of age on biomarker levels of knee joint healing and showed a negative correlation between age and CTX-II concentrations ($r=-.769, p < 0.001$ [6]).

Conclusions

This systematic review identified (1) only 7 studies which evaluated healing using biomarkers following ACLR, (2) IL-6 and CTX-II were the most commonly used, and (3) there is a significant knowledge gap with respect to evaluating the healing process of the knee in adolescent patients following ACLR. Adolescents are unique from adults due to growth [4] and sex hormone variation [5]. Therefore, biomarker research in adults cannot simply be extrapolated to adolescents. In addition to existing biomechanical rehabilitation tasks (e.g. single-limb hops, limb-strength symmetry indices [3]), we propose that rehabilitation and RTA assessment following ACLR in adolescents could be informed by the healing status of the knee, improving outcomes and reducing their risk of early-onset knee OA.

References

- [1] Beck et al. (2017). *Pediatrics*, **3**: 139
- [2] Øiestad et al. (2010). *Am. J. Sports Med*, **11**: 2201-10
- [3] Wright et al. (2015). *Sports Health*, **3**: 239-243
- [4] Kronenberg et al. (2003). *Nature*, **423**: 332-336
- [5] Juul et al. (2001). *Hum. Reprod. Update*, **3**: 303-13
- [6] Chmielewski et al. (2012). *Osteoarthr Cartil*, **11**: 1294

Table 1: Biomarkers of knee joint healing after ACLR and participant age from included studies, specifying the most prevalent biomarkers.

Study	Anil, 2019	Beynnon, 2002	Chmielwesi, 2012	Larsson, 2017	Mendias, 2013	Sobue, 2017	Tourville, 2013
Age(mean±SD)	33.4±10.7	32.7±6.5	19.6±4.5	26±4.9	28±2.4	27.6±9.0	28.9±10.25
Biomarker type (biomarkers reoccurring in ≥3 studies)	Cytokines, cartilage metabolism (sIL-6)	Cartilage metabolism	Cartilage metabolism (uCTX-II)	Cytokines, cartilage/bone metabolism (sfIL-6, uCTX-II)	Muscle atrophy, cytokines, cartilage metabolism (sIL-6)	Cartilage metabolism	Cartilage metabolism (uCTX-II)

Abbrev: CTX-II, C-terminal crosslinking telopeptide of type II collagen; IL-6, Interleukin-6; s, serum; sf, synovial fluid; u, urine.

An open-source workflow for IMU-based kinematics over long durations

Johanna J. O'Day^{*1}, Mazen Al Borno^{*2}, Vanessa Ibarra, James J. Dunne¹, Ajay Seth³, Ayman Habib¹, Carmichael F. Ong¹, Jennifer L. Hicks¹, Scott D. Uhlich¹, Scott L. Delp¹

¹Department of Bioengineering, Stanford University, Stanford, CA, USA

²Department of Computer Science and Engineering, University of Colorado, Denver, CO, USA

³Department of Biomechanical Engineering, Delft University of Technology, Delft, Netherlands

*Authors contributed equally

Email: odayj@stanford.edu

Summary

We have developed an open-source workflow to estimate three-dimensional kinematics from inertial measurement unit (IMU) data over long durations (10min). We validated this workflow for common activities, finding minimal drift ($<1^\circ$) and 2-7° (median) RMS difference for all lower extremity joint angles except hip rotation (10-11° median RMS difference).

Introduction

The ability to track joint kinematics in natural environments over long durations using IMUs has the ability to extend biomechanics and rehabilitation research. An overwhelming number of studies have assessed accuracy over short durations (on the order of one minute) [1]. The majority do not report accuracies over multiple joints or for non-sagittal plane kinematics and lack open-source methods with which to replicate their results [1]. We developed an open-source workflow to estimate three-dimensional joint kinematics from IMUs and validated it for ten-minute trials of both walking and a varied sequence of lower-extremity tasks, including sitting, standing, stair-stepping, side-stepping, walking, and running.

Methods

We collected both IMU and optical motion capture data for 11 healthy subjects in a laboratory environment, which included significant amounts of electronic equipment and ferro-magnetic materials. Subjects wore eight IMUs (Xsens North America Inc., Culver City, CA) which were affixed to light, plexiglass frames along with a cluster of 4-5 markers, and placed on body segments (sternum, lower back (L5), thighs, shanks, feet). IMU data were streamed at 100 Hz. In addition, 15 reflective markers were placed on anatomical landmarks [2]. Marker positions were measured at 100 Hz using a six-camera motion capture system (Motion Analysis Co., Santa Rosa, CA). Experimental data was collected while each subject completed two trials: (i) ten minutes of walking and turning and (ii) ten minutes of a sequence of lower-extremity movements that included sitting, standing, stair-stepping, side-stepping, walking, and running. We used an open-source complementary filter by Madgwick and colleagues [3] to compute IMU orientations from the IMU sensor data. We used an open-source workflow (OpenSim 4.2 [4]) to compute inverse kinematics from either IMU orientations or optical marker positions, in both cases using a physiological skeletal model [5]. The placement of IMUs on the subject and corresponding skeletal model was determined using an initial pose calibration computed from optical motion capture data, as our main focus was assessing drift. We compared the joint angles computed with IMU orientations to

the joint angles computed from optical motion capture using descriptive statistics including root mean square (RMS) difference. All joint measures were pooled bilaterally.

Results and Discussion

Our workflow, which used a skeletal model for inverse kinematics and sensor fusion algorithms that incorporated magnetometer data, estimated lower extremity joint kinematics with minimal drift, $<1^\circ$ over ten minutes. We found RMS differences compared to optical motion capture of 2-7° for sagittal angles and 5-11° for non-sagittal angles over the ten-minute period of walking, which are within the reported variability and uncertainty of motion capture [6]. We saw the same results over the ten-minute sequence of varied lower extremity movements (not shown).

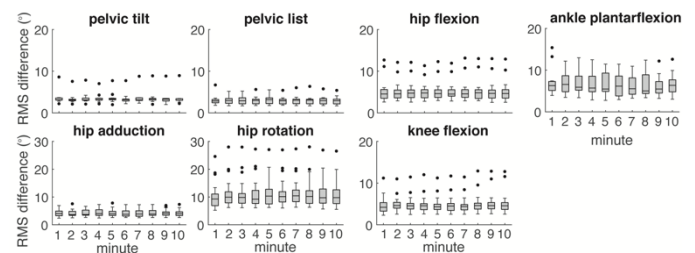


Figure 1: Root mean square (RMS) difference between IMU-based and optical-motion-capture-based lower extremity joint kinematics over a 10 minute-period of overground walking.

We discovered that we could monitor drift using the orientation errors from the inverse kinematics solution, which tracked drift when it was present. We also found we could reduce drift by reducing the relative weighting on distal IMUs (most affected by magnetic disturbances) when solving inverse kinematics.

Conclusions

We share our workflow along with the data, models and software (OpenSense, OpenSim 4.2 [5]) at simtk.org to allow researchers to reproduce and extend our work. This workflow enables accurate, long-duration measures, bringing the field one step closer to estimating IMU-based kinematics in natural environments.

References

- [1] Weygers et al. (2020). *Sensors*, **20**: 673.
- [2] Kadaba et al. (1990). *Journal of Ortho. Res.*, **8**: 383-92.
- [3] Madgwick et al. (2011). *IEEE Conf. Rehab Robotics*, 1-7.
- [4] Seth et al. (2018). *Plos Comp. Bio.*, **14**: e100622.
- [5] Rajagopal et al. (2016). *IEEE Bio. Eng.*, **63**: 2068-79.
- [6] Capozzo et al. (1996). *Clin. Biomech.*, **11**: 90-100.

SURFACE EMG-BASED AAC TECHNOLOGY FOR RECOGNITION OF SILENT PROSODIC SPEECH

Jennifer M. Vojtech¹, Michael D. Chan¹, Bhawna Shiwani¹, Serge H. Roy¹, James T. Heaton², Geoffrey S. Meltzner³, Paola Contessa¹, Gianluca De Luca¹, Rupal Patel^{3,4}, and Joshua C. Kline¹

¹Delsys, Inc and Altec Inc, Natick, MA

²Massachusetts General Hospital Department of Surgery, Boston, MA

³VocaliD, Inc. Belmont, MA

⁴Northeastern University, Boston, MA

Email: jkline@delsys.com

Summary

In this study, we evaluated the feasibility of using surface electromyographic (sEMG) recordings of articulatory muscle activity during silent speech for prosodic communication. Surface EMG signals were acquired from the face and neck as 4 speakers with and 4 without vocal impairments silently mouthed a speech corpus of prosodically varying phrases. Resulting signals were processed through a multi-stage architecture to recognize lexical content and categorize differences in phrase-level stress (realized via altered pitch, loudness, and/or duration). Cumulative word recognition and phrasal stress discrimination rates exceeded 90% accuracy across speakers with typical voices and speakers living with vocal impairments. These findings provide a solid foundation for using sEMG signals to recognize lexical and phrase-level prosodic content from silent, mouthed speech.

Introduction

Over 7.5 million people worldwide are unable to vocalize effectively [1]. Among these individuals are cancer survivors who underwent oropharyngeal/laryngeal surgery and must rely on augmentative and alternative communication (AAC) systems such as text-to-speech applications or artificial voice prostheses as substitutes for their natural voices. Yet most of these devices struggle to convey the expressive attributes of prosody, leading to lexical ambiguities and a lack of emotional content [2]. To address this need, we explored the use of sEMG to extract patterns for lexical and prosodic modulation from articulatory musculature during silent, mouthed speech.

Methods

Our existing algorithms for detecting words from silent speech [3,4] were expanded to recognize lexical content produced with specific prosodic contrasts. The algorithms—which recognize lexical content from articulatory sEMG signals via a hidden Markov model leveraging sEMG-derived Mel-frequency cepstral coefficients (MFCCs)—were augmented to detect prosodic patterns in silent speech by introducing two new processing stages: 1) speaker adaptive training via feature-space maximum likelihood linear regression for phoneme recognition in the presence of prosodic variations, and 2) a multilayer perceptron neural network to classify differences in phrasal stress (first word, last word, no stress) using sEMG features extracted from articulatory muscle patterns captured during silent speech. Our silent speech recognition models were then evaluated on sEMG signals recorded from the face and neck (**Figure 1**) as speakers with (N=4) and without (N=4) laryngectomy silently mouthed a speech corpus comprising 750 phrases

(650 phrases without stress and 100 phrases with first-word or last-word stress).

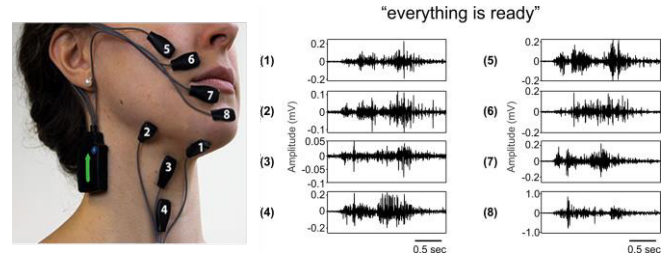


Figure 1. Trigno™ Quattro sensors are shown at 8 locations on the neck and face with examples of corresponding sEMG signals for the phrase “everything is ready.”

Results and Discussion

Mean word recognition rates ($96.3 \pm 3.1\%$) were comparable between speakers with (95.8%) and without (96.8%) laryngectomy (**Table 1**). Mean accuracy in predicting phrase-level stress ($91.2 \pm 4.5\%$) was also similar between speakers with (89.6%) and without (92.9%) laryngectomy (**Table 1**).

Table 1. Word recognition (WR) and phrasal stress discrimination (PSD) rates in speakers with (L) and without (C) laryngectomy.

ID	C1	C2	C3	C4	L1	L2	L3	L4
WR (%)	95.4	96.4	96.3	99.2	96.2	89.5	99.0	98.6
PSD (%)	99.0	86.7	90.0	95.7	86.8	88.0	90.0	93.4

Our results demonstrate a first-of-its-kind wearable system that accurately (>90%) recognizes lexical and prosodic content across speakers with typical voices and speakers living with vocal impairments.

Conclusions

This work highlights the feasibility of sEMG-based speech recognition to capture prosodic attributes of silent speech in combination with robust lexical content detection. This study is an impactful first step toward the development of a body-worn AAC system for use by individuals with vocal impairments to restore personalized and prosodic speech capabilities for communication.

Acknowledgments

This work was supported by the National Institutes of Health (R43 DC017097) and by the De Luca Foundation.

References

- [1] Statistics on Voice, Speech & Language, NIDCD, 2016.
- [2] Meltzner GS & Hillman RE (2005). *J Speech Lang Hear Res*, 48:766-79.
- [3] Meltzner GS et al. (2017). *IEEE/ACM Trans Audio Speech Lang Process*, 25:2386-98.
- [4] Meltzner GS et al. (2018). *J Neural Eng*, 15:046031.

Development of a channel identification algorithm for an autonomously usable 16-channel sEMG sensor system

Elisa Romero Avila¹, Catherine Disselhorst-Klug¹

¹Department of Rehabilitation and Prevention Engineering, Institute of Applied Medical Engineering – Helmholtz Institute, RWTH Aachen University, Aachen, Germany.

Email: romero@ame.rwth-aachen.de

Summary

sEMG technologies that enable the monitoring of muscle activation in clinical and out-patient settings are highly relevant for continuous, remote monitoring of patients. These technologies must be easy to use while providing high quality sEMG signals. The aim of this work is to develop an algorithm for the identification of relevant sEMG channels from an autonomously usable 16-channel sEMG sensor system (sEMG SS). The algorithm is based on a hierarchical approach, where channels are identified based on the highest RMS values. Testing of the algorithm was done during flexion and extension of the elbow and wrist to identify the flexor and extensor muscle group of the forearm and the brachioradialis muscle. Results showed the algorithm to be 92.5% effective in identifying these muscle groups. This algorithm in conjunction with the sEMG SS can particularly enhance and promote the autonomous use of rehabilitation devices and systems by patients with motor impairments.

Introduction

In rehabilitation, the use of wearable devices that record the muscle activation of patients with motor disorders during both therapy and the activities of daily living is extremely important for assessing the efficacy of therapy and patients' progress [1,2]. An autonomously usable sEMG SS has been recently introduced that has proven its effectiveness in obtaining high quality signals while being easy to use and size-adaptive [1]. This armband-shaped system consists of 16 sEMG channels distributed among 8 modules. So far, the device has been used to identify an sEMG channel in which the muscular activation of a specific muscle is recorded. The aim of this work is to develop an algorithm, which will enable the identification of 3 movement specific sEMG channels from the 16 of the sEMG SS.

Methods

Following a hierarchical approach, an algorithm was developed to identify 3 channels of interest in the sEMG SS, based on the highest RMS values in 80 ms windows [1]. The first relevant channel identified, corresponded to the muscle that could cause crosstalk in the sEMG signals of neighboring muscles. This channel is defined using an initial movement. Once this channel was identified along with adjacent channels in its module, they were removed from the algorithm to ensure a correct recognition of the other two predominantly active muscles, through a second movement.

To demonstrate the validity of the algorithm, two movements were performed: flexion and extension of the elbow and wrist. Thus, a group of forearm muscles (brachioradialis, flexor and extensor) were identified, where the risk of crosstalk was high.

During the measurements, the sEMG SS was autonomously positioned around the forearm, on the line connecting the axis through the wrist and the fossa cubit, at a location 1/3 from the fossa cubit. A series of 8 repetitions of elbow flexion (110°) and extension (0°) was then performed, followed by 8 repetitions of wrist flexion (40°) and extension (70°). These repetitions were performed with an external load of 1.5 kg while the subject was seated with the arms hanging at the side of the body. Then, the subject removed the sEMG SS. The procedure was repeated 40 times at a self-selected movement speed. As a result, 40 different positions of the device and 320 movement repetitions (8 repetitions x 40 positions) were achieved.

Results and Discussion

The algorithm misidentified the brachioradialis muscle in only two of the forty trials. Incorrect identification of either the flexor or extensor muscle groups occurred in only 1 trial. In addition, the algorithm mistook the flexor muscle group for the extensor muscle group in four of the forty trials. This represents 92.5% effectiveness for the algorithm.

Due to the muscle organization in the forearm, identification of these groups is particularly challenging. These results show that the design of the sEMG SS is effective in identifying the 3 selected muscles using 2 simple movements. The algorithm first identified, through the flexion and extension of the elbow, the sEMG channel corresponding to the brachioradialis muscle, as well as its adjacent channels. Thus, the risk of crosstalk was decreased when identifying the flexor and extensor muscle groups of the forearm. Additionally, the performance of an active wrist extension contributed to the differentiation between the two muscle groups.

Conclusions

The algorithm described has proven to be effective in identifying 3 movement specific sEMG channels from a multichannel sEMG SS through basic movements and without exact positioning around the limb. This bodes particularly well for the future usability of the sEMG SS, for monitoring and assessing patients with motor impairments.

References

- [1] Romero Avila, E. et al (2020). Introduction of a sEMG Sensor System for Autonomous Use by Inexperienced Users. *Sensors* **20**: 7348.
- [2] Disselhorst-Klug C and Williams S (2020) Surface Electromyography Meets Biomechanics: Correct Interpretation of sEMG-Signals in Neuro-Rehabilitation Needs Biomechanical Input. *Front. Neurol.* **11**:603550

From Feasible to Practical: Progress in the Development & Validation of Wearables for Accurately Monitoring Tibial Bone Forces in the Real-World

Laura J. Judson, Cameron A. Nurse, Anna E. Wolfe, Emily S. Matijevich, Lauren M. Grohowski, Peter Volgyesi, Karl E. Zelik
 School of Engineering, Vanderbilt University, Nashville, Tennessee, United States
 Email: laura.judson@vanderbilt.edu

Summary

The objective of this study is to characterize how accurately a multi-sensor wearable system can estimate tibial bone force during running. The system is comprised of one inertial measurement unit (IMU) on the foot/shoe, pressure-sensing insoles, and associated machine learning algorithms [1]. We previously showed the feasibility, accuracy, and benefits of this system using lab-based instrumentation and idealized (i.e., simulated) wearable sensor signals. Here, we seek to evaluate the use of real wearable sensors, and benchmark how bone force accuracy compares with estimates from idealized signals. Initial results are encouraging, with real wearable sensors demonstrating only slightly decreased accuracy ($r = 0.92$; correlation with lab-based estimates of tibial force) compared with idealized wearable sensors ($r = 0.95$). This combination of wearable sensors and algorithms continues to look promising as a practical solution for accurately monitoring tibial bone force in the real-world.

Introduction

Tibial bone stress injuries are amongst the most frequent injuries experienced by runners and are believed to result from the accumulation of microdamage due to repetitive tissue loading [1]. Developing a practical and accurate tool for monitoring tibial bone force outside of a laboratory setting could help us to understand, manage, and reduce overuse injury risks to the tibia. However, existing commercial tools are inadequate for monitoring tibial bone forces because ground reaction force (GRF) metrics (e.g., vertical average loading rate, impact peak) and IMU-based metrics (e.g., tibial shock) are not well correlated with tibial bone force during running and cannot be assumed to indicate loading on this bone or other tissues inside the body [2].

Tibial bone force can be estimated accurately using idealized wearable sensor signals [3], demonstrating the exciting potential of wearables to aid in understanding and mitigating overuse injury risks. However, these idealized signals were derived from lab-based data, and do not reflect the reduced measurement accuracy of real wearable sensors. Here we aimed to evaluate the accuracy of real wearable sensors for estimating tibial bone force when using sensor subsets and algorithms similar to those previously validated with idealized sensor signals [3]. This abstract provides preliminary results from four participants. At the conference, a dataset of approximately ten participants will be presented.

Methods

Four recreational runners (2 males, 2 females; age 21-26 years, stature 1.8 ± 0.05 m, mass 71 ± 11 kg) completed a series of running trials at different speeds (2.7, 3, 3.3 m/s),

slopes (0° , 3° , 6° , -3° , -6°), and stride patterns. Lab-based gold standard measures were collected using a force-instrumented treadmill (Bertec) and motion capture cameras (Vicon). Simultaneously, lower-body kinematics and in-shoe pressure data were collected using real wearable sensors: XSENS IMUs and Novel Pedar insoles. Peak tibial force each step was computed using (i) lab instrumentation (*target metric*), (ii) idealized wearable sensor signals distilled from lab-based kinematic and GRF signals (*idealized wearable estimate*), and (iii) real wearable sensor signals from portable pressure insoles and one IMU on the foot (*real wearable estimate*). Wearable estimates of tibial force were based on machine learning algorithms and training methods similar to [3]. Correlations between each wearable estimate and the target tibial force metric were then computed and compared.

Results and Discussion

Idealized and real wearable sensor estimates were strongly correlated with lab-based estimates of tibial bone force across running conditions (Table 1). The average correlation coefficient decreased from $r = 0.95$ with idealized wearable sensors to $r = 0.92$ with real wearable sensors.

Table 1: Correlation coefficients (r) between lab-based target tibial bone force and (i) idealized wearable estimates, and (ii) real wearable estimates, for first four participants.

Participant	Idealized Wearable	Real Wearable
1 (M)	0.99	0.93
2 (M)	0.98	0.95
3 (F)	0.97	0.93
4 (F)	0.91	0.77
Mean \pm SD	0.95 \pm 0.03	0.92 \pm 0.08

Conclusions

Preliminary results show promising potential for combining pressure insoles, a foot/shoe IMU, and machine learning to accurately monitor tibial forces during running, which could unleash various new opportunities to enhance scientific understanding, clinical care, and physical performance.

Acknowledgments

The authors gratefully acknowledge funding from Vanderbilt University and the National Institutes of Health.

References

- [1] Currey, JD. (2013). *Bones: Structures and Mechanics*; Princeton University Press.
- [2] Matijevich et al. (2019). *Plos One*, **14**: 1-19.
- [3] Matijevich et al. (2020). *Hum. Mov. Sci.*, **74**.

Measuring trunk motion during on-site wheelchair propulsion using inertial measurement units

Marit P. van Dijk¹, Monique A.M. Berger², Marco J.M. Hoozemans³, DirkJan H.E.J. Veeger¹

¹Department of BioMechanical Engineering, Delft University of Technology, Delft, The Netherlands

²Assistive technology for Mobility & Sports, The Hague University of Applied Sciences, The Hague, The Netherlands

³Department of Human Movement Sciences, Vrije Universiteit Amsterdam, Amsterdam, The Netherlands

Email: m.p.vandijk@tudelft.nl

Summary

Trunk posture and movement are reported to influence performance in wheelchair sports. However, an ambulatory system to measure on-site changes in trunk inclination is not yet available. Recently, a new inertial measurement unit (IMU)-based approach was proposed to improve the existing Madgwick filter using machine learning, such that body segment orientations can be determined more accurately in IMU challenging sports situations. This approach was applied to measure trunk motion during on-site wheelchair propulsion and the validity of these measures was determined. Twelve participants performed a series of wheelchair sport-specific tests with IMUs attached to their wheelchair and trunk, while simultaneously being measured with an optical motion analysis system to serve as gold standard. Results showed a mean absolute error of less than 5 degrees between IMU-based trunk inclination and a gold standard. With the application of an improved filter approach, IMUs can be validly used to assess instantaneous trunk inclination.

Introduction

The interaction between athlete and wheelchair is crucial in all wheelchair sports disciplines. More specifically, trunk posture and movement are reported to have an effect on performance in wheelchair sports. However, an ambulatory system to measure changes in trunk inclination in the field is not yet available. IMU-based systems seem to be suitable to measure changes in trunk inclination in daily wheelchair sport practice. To determine orientation from raw IMU signals, the data can be fused together using an Attitude Heading Reference system (AHRS). One commonly used and robust AHRS is the Madgwick filter, which was used in this study.

Although this filter has previously provided accurate orientation estimates, a problem with the use of IMUs to determine body segment orientation in sports, is that the filter assumes that the accelerometer only measures gravity and that the magnetometer only measures the magnetic north. As these assumptions do not hold for sports activities that are characterized by linear accelerations (e.g., every push in speed-skating or wheelchair propulsion) or by the presence of magnetic sources (e.g., because of a bike or a wheelchair), the estimated orientation shows errors that increase over time. For wheelchair sports, this is no different. An approach that improves the existing Madgwick filter, such that more

accurate body segment orientation estimates can be obtained during such sports activities has been proposed.

The aim of this study was to investigate whether this improved approach can be used to accurately measure IMU-based trunk inclination during wheelchair propulsion.

Methods

Twelve differently skilled participants performed a series of wheelchair sport-specific tests with IMUs attached to their wheelchair (frame) and trunk (sternum), while simultaneously being measured with an optical motion analysis system to serve as gold standard. Using these data, a machine learning model was trained and, accordingly, implemented to improve the existing Madgwick filter. To assess the validity of the 'improved' Madgwick filter approach, trunk inclination was calculated using the gold standard and using the IMU signals which were processed using this approach. In addition, the trunk inclination estimated using the proposed approach was compared with that of the 'regular' approach in which the Madgwick filter is applied.

Results and Discussion

Results show root-mean-square errors of less than 6 degrees and a mean absolute error of less than 5 degrees when IMU-based trunk inclination was compared with the gold standard. When performance of the regular Madgwick approach was compared with the performance of the improved Madgwick approach as proposed in the current study, a decrease of 2 degrees root-mean-square error was found.

Conclusions

In conclusion, the improved approach to apply the Madgwick filter provides accurate instantaneous trunk inclination estimates during wheelchair propulsion using IMU data. IMUs can thus be validly used to assess trunk inclination during wheelchair sports activities in the field.

Acknowledgments

This work was supported by ZonMw (Sport en Beweging 2018) under project number 546003002. This project, named 'WheelPower: wheelchair sports and data science push it to the limit' is a cooperative effort between TU Delft, UMCG, THUAS, VU Amsterdam and is in cooperation with several sports federations collected under the umbrella of NOC*NSF.

Consistency of athlete lower-limb work distribution across unilateral and bilateral tasks after ACL reconstruction

HSR. Jones¹, IS. Moore¹, E. King², V. Styles³, L. Laudani¹, K. Daniels^{2,4}

¹Cardiff School of Sport & Health Sciences, Cardiff Metropolitan University, Cardiff, UK

²Sports Surgery Clinic, Dublin, Ireland

³School of Sport and Health Sciences, Exeter University, Exeter, UK

⁴Department of Sport and Exercise Sciences, Manchester Metropolitan University, Manchester, UK

Email: st20057426@outlook.cardiffmet.ac.uk

Summary

Choosing which tests to include when designing a physical testing battery to monitor rehabilitation status following anterior cruciate ligament reconstruction (ACLR) is important for clinicians. The aim of the study was to examine the correspondence between movement strategies when the same task was performed bilaterally and unilaterally, and when two different unilateral tasks were performed. Participants performed a bilateral drop jump, a unilateral drop jump, and a 90° pre-planned cut. For each task, the proportion of work done at the ankle, knee and hip was calculated and compared between tasks. The joint contributing the highest amount of work done was also used to determine the dominant movement strategy for that task (e.g. ankle-, knee-, hip-dominant movement strategy). A significant, strong, positive relationship for proportion of work done was observed between the bilateral and unilateral drop jump, whereas a weak relationship was found for proportion of work done at each joint between the unilateral drop jump and the cut. The similarity between unilateral and bilateral drop jumps suggest that clinicians may only need to test one of the drop jumps and cut in future testing protocols.

Introduction

A dilemma for clinicians designing a physical testing battery for post-ACLR patients returning to sport is choosing which tests to include. Primarily, bilateral tasks have been used to monitor recovery, but ACL injury mechanisms are more commonly associated with unilateral landing and cutting tasks [1]. Consequently, these movements are becoming increasingly used in clinical testing batteries. The distribution of mechanical work between the ankle, knee and hip can be used to characterise athlete movement strategy for jumping, landing and cutting. Task redundancy can be identified by comparing movement strategies across both bilateral and unilateral tasks, facilitating the design of optimised physical testing batteries. The aim of the study was to examine movement strategies when the same task was performed bilaterally and unilaterally and when two different unilateral tasks were performed.

Methods

127 male, multidirectional field sport athletes aged 18 - 35 years who had undergone ACLR approximately 9 months prior to testing participated in the study (height: 1.81 ± 0.06 m; mass: 82.7 ± 9.3 kg). Participants visited the laboratory once, completing three movement tasks as part of a clinical testing battery: a bilateral drop jump, a unilateral drop jump and a 90° pre-planned cut. Non-invasive reflective markers were placed on the skin and shoes based on the Plug-in-Gait lower limb marker set. Only data collected from the reconstructed leg during the braking phase, defined as the time between initial contact and lowest vertical centre of

mass displacement, was used for analysis. The relative contribution of the ankle, knee and hip work to total lower extremity joint work in the sagittal plane was calculated. Spearman's correlation ($p \leq 0.05$) was used to determine the strength of the relationship between the proportions of work done at the ankle, knee and hip for the bilateral and unilateral drop jump and the unilateral drop jump and the cut.

Results and Discussion

A significant, strong, positive relationship was observed for proportions of work done at the ankle, knee and hip joints between the bilateral and unilateral drop jump, whereas a very weak relationship was found for proportion of work done at the ankle, knee and hip joints between the unilateral drop jump and the cut (Figure 1). Both drop jumps employed an ankle dominant strategy, whilst the cut utilised a knee dominant strategy, as indexed by the highest proportion of work observed at the ankle and knee, respectively.

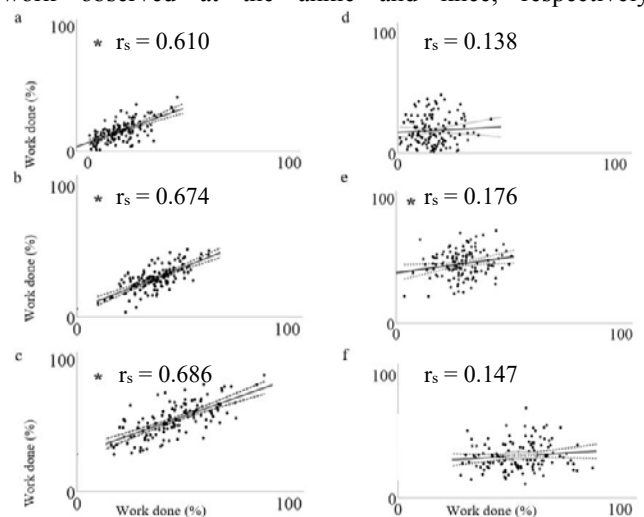


Figure 1. Correlation of proportion of work done between the unilateral and bilateral drop jump at the (a)hip, (b)knee, and (c)ankle, and between the cut and the unilateral drop jump at the (d)hip, (e)knee, and (f) ankle. * $p \leq 0.05$.

Conclusions

Movement strategies were similar (transferrable) between the same task performed bilaterally and unilaterally, but not across unilateral tasks. Thus, to assess movement strategies after ACLR, clinicians could consider omitting one of the drop jumps from assessment batteries but should include the 90° pre-planned cut.

Acknowledgments

The lead author, H Jones is funded by a Knowledge Economy Skills Scholarship (KESS 2).

References

[1] Alentorn-Geli E et al. (2009). *Knee Surg Sports Traumatol Arthrosc*, **17**: 705-729.

Effects of Functional Resistance Training on Gait Biomechanics Following Anterior Cruciate Ligament Reconstruction

Alexa K. Johnson¹, Scott R. Brown², Riann M. Palmieri-Smith^{1,3}, Chandramouli Krishnan^{1,4,5}

¹ School of Kinesiology, University of Michigan, Ann Arbor, MI, USA ² Department of Kinesiology, Aquinas College, Grand Rapids, MI, USA ³ Department of Orthopedic Surgery, University of Michigan, Ann Arbor, MI, USA ⁴ Physical Medicine and Rehabilitation, University of Michigan, Ann Arbor, MI, USA ⁵ Department of Biomedical Engineering, University of Michigan, Ann Arbor, MI, USA

Email: akjohns@umich.edu

Summary

The effect of 8-weeks of functional resistance training (FRT) on sagittal plane knee biomechanics was tested in individuals with recent anterior cruciate ligament (ACL) reconstruction. The changes in knee flexion moment symmetry were greater in individuals who underwent FRT with resistance bands than those who underwent FRT with a custom-designed brace or a target-match control condition.

Introduction

Persistent muscle weakness is pervasive after ACL reconstruction [1] and contributes to ongoing gait asymmetries [2] and the possible development of post-traumatic osteoarthritis [3]. FRT, or progressive low-load resistance training performed during walking, may be a safe and effective way early after ACL reconstruction to target gait deficiencies because it allows for task-specific muscle strengthening during gait. The purpose of this project, therefore, was to determine if FRT improves knee mechanics following ACL reconstruction.

Methods

Thirty individuals (9.5±2.9 weeks post-surgery) were assigned to one of three groups: 1) FRT with a custom brace designed to provide resistance primarily to the hamstring muscles, 2) FRT with custom resistance band device designed to provide resistance primarily to the quadriceps muscles, or 3) a target-match control group, where they received real-time kinematic feedback with no FRT during walking. All participants completed a 30-minute training session, 2-3 times a week for eight weeks [4]. Three-dimensional motion capture was used to assess knee biomechanics during overground walking at a self-selected speed before and after the first and last training session, respectively. Bilateral sagittal plane knee angles and internal knee moments were calculated. A change score for each variable was calculated as the time difference (post-training–pre-training) of the limb symmetry scores (ACL–uninjured). Statistical Parametric Mapping (SPM) was used to assess group differences in the swing and stance phase independently. Tukey's post-hoc tests were used to identify differences when group main effects were significant. Significance was set a priori at $p < 0.05$.

Results and Discussion

Ten individuals in the brace group (Age=18.7±6.2yrs; Mass=70.1±10.5kgs), eight individuals in the resistance band group (Age=23.1±4.3yrs; Mass=70.3±12.6kgs), and nine individuals in the control group (Age=20.4±5.6yrs; Mass=69.5±14.0kgs) completed this study. The changes in

flexion moment symmetry were different between groups from ~21 to 24% of the stance phase ($p=0.045$). The resistance band group had significantly greater improvements in stance phase flexion moment symmetry than the brace group ($p=0.043$) and the control group ($p=0.003$). No differences were found for stance or swing phase knee flexion angle, or swing phase knee flexion moments.

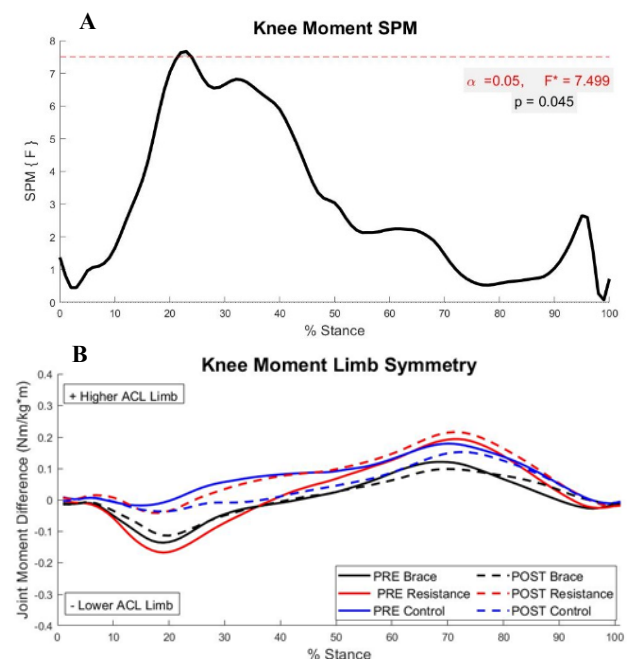


Figure 1: A: SPM Analysis in which the red dashed line indicates the critical threshold, when crossed data in that window is deemed significant. B: Limb symmetry values for before (Pre) and after (Post) intervention for the knee moment.

Conclusions

FRT targeting the quadriceps muscles may provide benefits to improve knee moment symmetry following ACL reconstruction. An improvement in gait symmetry after ACL reconstruction may help promote long-term knee joint health.

Acknowledgments

This research was supported by the NIH NICHD (R21-HD092614). The content is solely the responsibility of the authors and does not represent the views of the NIH.

References

- [1] Palmieri-Smith RM and Thomas AC. (2008). *Clin Sports Med*, **3**. 405-24.
- [2] Kaur M et al. (2016). *Sports Med*. **12**: 1869-95.
- [3] Lie MM, et al. (2019) *Br J Sports Med*, **53**: 1162-1167.
- [4] Brown SR, et al. (2020) *Sports Health*. Online First.

A Hierarchical Clustering Approach for Examining Potential Risk Factors for Bone Stress Injury in Runners

Jack A. Martin¹, Mikel R. Stiffler-Joachim¹, Christa M. Wille¹, Bryan C. Heiderscheit¹

¹Badger Athletic Performance, Dept. of Orthopedics & Rehabilitation, University of Wisconsin-Madison, USA

Email: jmartin8@wisc.edu

Summary

A hierarchical clustering approach was used to group runners based on kinematics and kinetics. Bone stress injury incidence was the highest in a group that tended towards a forefoot strike pattern with short stance phase and high peak forces.

Introduction

Machine learning techniques may be able to provide new insights into risk factors for running-related injury. Hierarchical clustering is an unsupervised learning approach that can group runners based on shared characteristics [1]. Injury incidence can then be studied in these groups to gain insight about potential risk factors for injury. The purpose of this study was to determine whether a hierarchical clustering approach can divide runners into meaningfully distinct groups based on kinematics and kinetics by examining: 1) whether any groups of runners have higher bone stress injury (BSI) incidence, and 2) whether groups of runners show differences in biomechanical metrics potentially relating to BSI risk.

Methods

Preseason running (4.47 m/s) gait mechanics data from 68 collegiate cross country runners (42F) were analyzed. At the time of testing, athletes were cleared for full participation, had no lower extremity injury in the prior 3 months, and had no history of lower extremity surgery. Standard inverse kinematics and dynamics approaches were applied to marker trajectories and ground reaction forces (GRF).

Joint kinematics (hip adduction and flexion, knee flexion, ankle dorsiflexion), kinetics (hip flexion, knee flexion, ankle dorsiflexion moments) and GRF (vertical, anteroposterior, mediolateral), were averaged across strides. Kinetics and GRF were normalized to body mass for each athlete. Data from each variable were normalized to the maximum and minimum value observed across all athletes, and data from all variables were collated into a single vector for each athlete.

Principal component (PC) analysis was used to reduce the dimensionality of the data. Hierarchical clustering was performed to divide athletes into groups exhibiting similar kinematics and kinetics based on their PC coefficients. A hierarchical cluster tree was created based on Euclidean distances between datapoints for each athlete using the Ward

algorithm, and distinct clusters of athletes were identified. Subsequent BSI incidence, confirmed by medical imaging, and biomechanical variables of interest were examined across these clusters.

Results and Discussion

Clustering identified 4 distinct groups of runners (Figure 1).

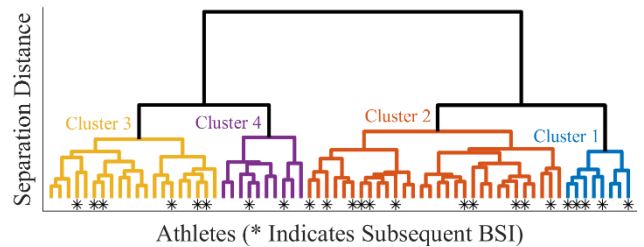


Figure 1: Hierarchical cluster tree based on running kinematics and kinetics. Endpoints along the x-axis represent individual athletes.

BSI incidence was highest in cluster 1 and decreased through cluster 4 (Table 1). Runners in cluster 1 tended towards shorter stance duration, greater peak vertical GRF and ankle plantarflexion moment, lesser peak knee flexion, and a forefoot strike pattern. Each of these showed a monotonic trend with BSI incidence. Of note, sex was disproportionately divided between clusters; however, similar trends held when only female athletes were included.

Conclusions

Hierarchical clustering can split runners into meaningfully distinct groups based on kinematics and kinetics. In this case, groups showed differences in BSI incidence and in several biomechanical variables potentially relating to BSI risk. This approach could yield insights into how and why injury risk may differ across different types of runners.

Acknowledgments

This work was supported by a grant from the Virginia Home Henry Fund for Women's Physical Education and Movement.

References

- [1] Jauhiainen S et al. (2020). *Scand J Med Sci Sports*, **30**: 732-740.

Table 1: Cluster splits, bone stress injury incidence, and several variables of interest showing differences between clusters.

Cluster	Females	Males	BSI Incidence	Stance Duration [ms]	Pk. Vertical GRF [N/kg]	Pk. Ankle PF Moment [Nm/kg]	Ankle DF Angle at Foot Strike [°]	Pk. Knee Flx. Angle [°]
1	3	5	5/8 (63%)	180 ± 10	29.5 ± 1.2	4.2 ± 0.3	-15.3 ± 6.0	39.9 ± 5.8
2	13	17	11/30 (37%)	191 ± 9	27.8 ± 2.0	3.9 ± 0.3	-5.5 ± 7.1	47.3 ± 4.0
3	17	3	6/20 (30%)	196 ± 8	25.7 ± 1.5	3.5 ± 0.3	1.3 ± 5.6	49.7 ± 3.6
4	9	1	2/10 (20%)	211 ± 13	24.2 ± 1.6	3.2 ± 0.2	5.5 ± 5.5	51.1 ± 3.2

Diffusion and advection of pro-inflammatory cytokines in injured articular cartilage under mechanical loading

Joonas P. Kosonen¹, Atte S.A. Eskelinen¹, Alan J. Grodzinsky², Rami K. Korhonen¹, Petri Tanska¹, Gustavo A. Orozco¹

¹Department of Applied Physics, University of Eastern Finland, Kuopio, Finland

²Departments of Biological Engineering, Electrical Engineering and Computer Science and Mechanical Engineering, Massachusetts Institute of Technology, Cambridge, MA, USA

Email: joonas.kosonen@uef.fi

Summary

In efforts to predict post-traumatic osteoarthritis (PTOA) progression, contemporary mechanobiological models implement cytokine diffusion-mediated inflammation. However, they lack an important biomechanical factor, the advection of cytokines along with the flow of interstitial fluid during physiological loading. Here, we refine the models predicting the PTOA progression by introducing combined diffusion and advection of cytokines in mechanically injured cartilage. Our theoretical model could be used for identifying lesions prone to accelerated inflammation-regulated cartilage degradation involved in PTOA.

Introduction

Traumatic knee injuries may cause chondral lesions and release of pro-inflammatory cytokines such as interleukin (IL)-1, which infiltrate the articular cartilage via the synovial fluid [1]. The latter occurs through diffusion and advection. Both solute transfer mechanisms have been previously studied in cartilage [2,3], but never in a mechanically injured fibril-reinforced porohyperelastic swelling (FRPHES) material. Here, we implement IL-1 diffusion and advection mechanisms within such material. We aim to estimate the combined effect of both mechanisms on the transport of pro-inflammatory cytokines into the cartilage tissue.

Methods

Our model is based on a previous experimental study including injurious and dynamic loading and culturing of bovine cartilage in exogenous IL-1 (1 ng/ml) [4]. This dynamical loading mimicking physiological loading was simulated in injured and intact cartilage models using a FRPHES material, incorporating depth-dependent structural and compositional properties [5]. The obtained time-dependent fluid velocity fields were imported into a previous diffusion-driven model [6] and interpolated to each simulation time point. Next, the cytokine diffusion–reaction equations were supplemented with an advection term where the scaling coefficient (Fig. 1, $\alpha < 1$) was inversely proportional to local glycosaminoglycan content and solute molecular weight [2,3]. For comparison, an injury model without advection was created.

Results and Discussion

Fluid velocities were higher near the lesion than in intact areas (Fig. 1AB). Advection increased IL-1 uptake locally compared to free diffusion (Fig. 1CEF) as suggested previously [2,3]. Our model predicted unevenly concentrated levels of IL-1 near the lesion and those were higher compared to the intact model predictions (Fig. 1CDF). These results

indicate that dynamic loading could locally increase concentrations of inflammatory mediators in injured tissue. If early cytokine infiltration is not mitigated pharmaceutically, elevated shear strains [5] might later degrade cartilage synergistically with inflammation [4].

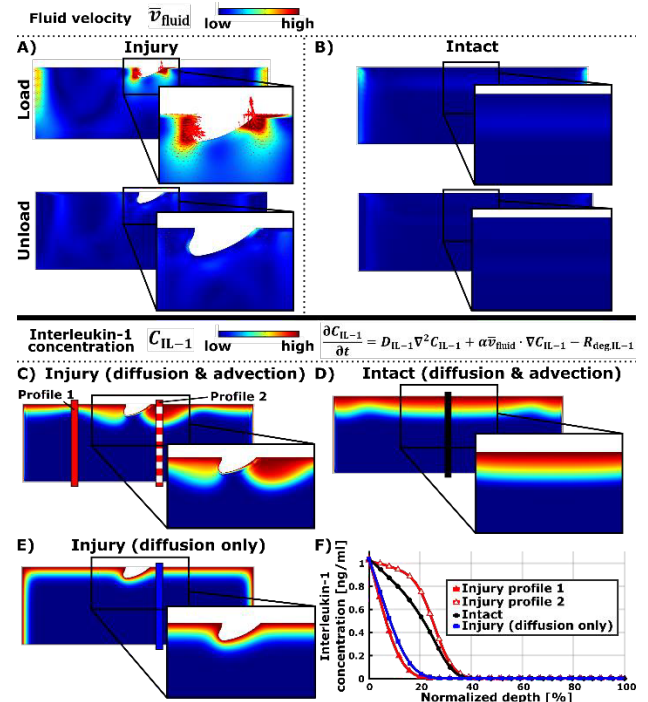


Figure 1: Fluid velocities during a single load/unload depth cycle in A) the injury and B) the intact model. Interleukin-1 infiltration due to diffusion and advection in C) the injury and D) the intact model. E) The cytokine concentrations in the injury model when advection was disabled. F) Depth-wise cytokine concentration profiles show a marked increase of cytokines near the side of the lesion, but not away from it, after simulated dynamic loading.

Conclusions

Uneven, rapid, and concentrated spread of pro-inflammatory cytokines near lesions could locally disturb the cartilage homeostasis. The adverse effects of advection-regulated cytokine infiltration should be blocked early *e.g.* with interleukin receptor antagonists to decelerate PTOA progression during prolonged dynamic loading.

References

- [1] Lieberthal et al. (2015) *Osteoarthr Cartil*, **23**: 1825-34.
- [2] Zhang et al. (2005) *Proc R Soc A*, **461**: 2021-42.
- [3] Zhang et al. (2007) *Arch Biochem Biophys*, **457**:47-56.
- [4] Eskelinen et al. (2021) *Trans Orthop Res Soc*, **67**:675.
- [5] Orozco et al. (2018) *Sci Rep*, **8**:15599.
- [6] Kar et al. (2016) *Arch Biochem Biophys*, **594**: 37-53.

A Prospective Study Linking Changes in Dynamic Center of Mass Motion With Lower-Limb Overuse Injuries Using a Single Trunk-Mounted Accelerometer

Gerard Aristizábal Pla^{1,2}, Enzo Hollville², Stijn Bogaerts³, Kurt H. Schütte², Sam Van Rossom², Benedicte Vanwanseele²

¹ University of Massachusetts Integrative Locomotion Lab, Department of Kinesiology, UMASS Amherst, Amherst, United States

² Human Movements Biomechanics Research Group, Department of Movement Sciences, KU Leuven, Leuven, Belgium

³ Department of Physical and Rehabilitation Medicine, University Hospitals Leuven, Leuven, Belgium

Email: garistizabal@umass.edu

Summary

The purpose of the current study was to investigate how accelerometry based-features changed in response to fatigue and their possible link with developing lower-leg overuse injuries (LLOIs). Our initial hypotheses were that: (i) fatigue would induce dynamic stability changes mainly occurring in the horizontal plane; and (ii) subjects who sustained an injury during a follow-up period of 6 months exhibited an increase in dynamic loading during a fatiguing protocol compared to subjects who did not sustain a LLOI. The findings of this study support our first hypothesis and partially the second one. With the accumulation of running fatigue, increased impact accelerations in the horizontal plane were detected for participants that would get injured during the 6 months follow-up that are different from the uninjured group.

Introduction

Fatigue protocols have been used to detect movement compensations [1] or changes in movement dynamics which can possibly be linked with a higher risk of overuse injury [2]. Wearable accelerometers can successfully identify movement deviations caused by running fatigue in indoor [3] and outdoor running conditions [4]. However, no prospective studies have ever attempted to link accelerometry-based measures of dynamic stability and dynamic loading to the development of running related injuries. We therefore investigated how these features changed in response to fatigue and their possible link with developing LLOIs.

Methods

One hundred and eighty-one participants aged 17-23 years completed the Cooper test. The following accelerometry based-measures of dynamic stability from all acceleration directions (Vertical, VT, Mediolateral, ML and Anteroposterior, AP) were extracted for consecutive ten percent of the Cooper test: the tri-axial ratio of acceleration root mean square normalized with the resultant vector RMS of all acceleration directions, step and stride regularity, and sample entropy. Dynamic loading measures, impact acceleration for all acceleration directions, and spatiotemporal measures, contact time and step frequency, were also extracted for consecutive ten percent of the Cooper test.

Participants then followed the same academic sports program at a common sport facility during 26 weeks per academic year and reported all LLOIs sustained during that period.

Results and Discussion

With the accumulation of running fatigue, increased impact accelerations in the horizontal plane were detected for

participants that would get injured during the 6 months follow-up that are different from the uninjured group (Figure 1).

The current study demonstrated that including a running fatiguing protocol has the potential to identify runners at risk for sustaining a lower-leg overuse injury. In addition, these findings build on limited available evidence linking an increased dynamic loading with the presence of LLOIs [5][6], as these changes in movement dynamics not only occur after but also prior onset of LLOI.

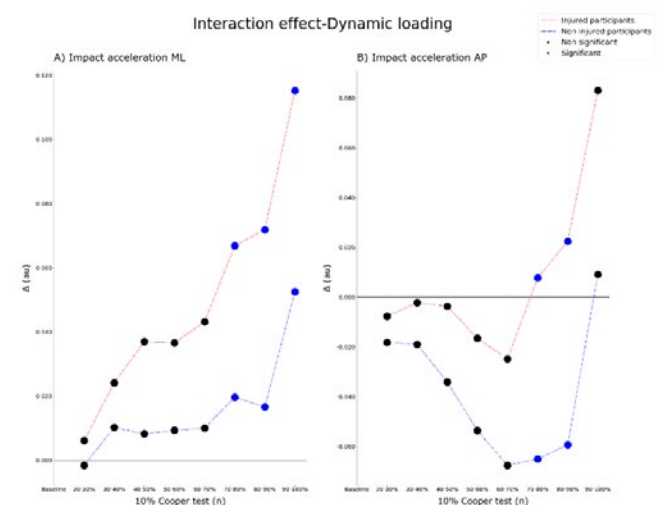


Figure 1: Significant interaction effects.

We also found that the fatigue accumulated with running had a significant effect in several dynamic stability, loading and spatiotemporal measures. Our findings are in line with previous investigations using similar trunk mounted accelerometer and accelerometer-based features [3] [4].

Conclusions

Our findings indicate that a single trunk-mounted accelerometer can detect changes in CoM motion that are exacerbated by running fatigue and linked to LLOIs.

References

- [1] R. Verrelst et al. (2014). *Am. J. Sports Med*, 42: 1219-1225.
- [2] Sanna G et al. (2008). *Clin Biomech*, 23: 946-954.
- [3] Schütte KH et al. (2015). *PLoS One*, 10: 1-12.
- [4] Schütte KH et al. (2018). *Gait Posture*, 59: 222-228.
- [5] Ribeiro AP et al. (2015). *PLoS One*, 10.
- [6] C.E. Milner et al. (2006). *Med. Sci. Sport Exerc*. 38: 323-328

Effect of seat configuration on joint power distribution and performance in an elite Paralympic rower: a case study

Jørgen Danielsen¹, Gertjan Ettema¹, Anna C. Severin¹

¹Center for Elite Sports Research, Department of Neuromedicine and Movement Science, Norwegian University of Science and Technology, Trondheim, Norway

Email: jorgen.danielsen@ntnu.no

Summary

We examined if altered seat configurations affected the contribution of power generated by the elbow, shoulder, and trunk in a world-class Paralympic PR1 rower during submaximal and maximal ergometer rowing. We found that configurations with a reclined back rest increased the total power generated during the maximal effort and increased the relative contribution from the trunk while decreasing relative shoulder contribution.

Introduction

Paralympic PR1 rowers have no leg function and minimal/no trunk function [1]. Because of the impairments, these rowers may benefit from individualized equipment for optimal technique and performance [2]. We recently reported that employing a seat configuration with a reclined backrest (Figure 1) increased performance and efficiency in a world-class PR1 Paralympic rower [3]. The adjusted seat resulted in higher peak force, longer stroke length, and lower stroke frequency compared to her usual configuration. These effects were mainly attributed to the increased trunk range of motion. In this study, we expanded on the previous analysis [3] and examined if the adjusted seats affected the distribution of power generation about the elbow, shoulder and trunk in the world-class female PR1 rower.

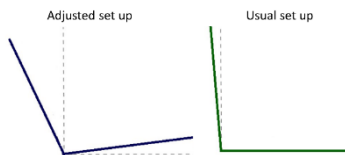


Figure 2 The tested set configurations (backrest/seat): Adjusted (A): 25°/5°, usual (B): 5°/0°.

Methods

The athlete performed one 4-min submaximal (ergometer power output (P_{erg}): 100 W) and one 4-min all-out (maximize average P_{erg}) bout of ergometer rowing (modified Concept2) in both configurations (Figure 1). Handle force (200 Hz) and kinematics (100 Hz) were collected, and inverse dynamics were used to compute elbow (P_{elb}), shoulder (P_{sho}), and trunk (P_{trunk}) power output and the relative contribution to P_{erg} . Work done during drive (W_{drive}) was calculated by time integration of instantaneous power.

Results and Discussion

Employing the adjusted configuration during submaximal rowing doubled $W_{erg\ drive}$ while stroke rate was halved compared to her usual set up (Table 1). Further, the increased trunk range of motion previously reported [3] coincided with an increase in P_{trunk} and a decrease in P_{sho} in the adjusted compared to the usual set up.

During maximal rowing, the athlete was able to increase P_{erg} by 43% in the adjusted setup compared to the usual setup. As in submaximal rowing, this was mainly due to an increase in P_{trunk} and $W_{trunk\ drive}$. Both during submaximal and maximal rowing, the more work performed during drive was mainly due to higher handle force (and moments) that were generated over a longer time as stroke length was longer (peak angular velocities during drive being quite similar between conditions, Fig. 2). Relative power contributions remained largely unaffected by intensity.

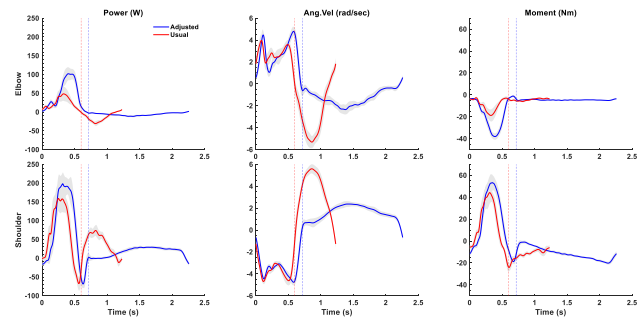


Figure 1. Power, angular velocity and moment about the shoulder and elbow during the submaximal bout of ergometer rowing in the two seat configurations. Vertical lines indicate end of drive phase.

Conclusions

The increased trunk range of motion permitted by the reclined backrest in the adjusted seat allowed for more work per stroke to be performed, with a considerable increase in trunk power generation, both during submaximal and maximal ergometer rowing in a world-class PR1 Paralympic rower.

References

- [1.] FISA Rule book. (2017). URL https://www.rowing.be/images/2017/kamprechtters/FIS_ArulebookEN2017finalweb_Neutral.pdf.
- [2.] Burkett B. (2010.) *BJSM*, **44**: 215-220
- [3.] Severin AC. et al. (2021.) *Front Sports Act Living*, **3**: 625656

Table 1. Effect of seat and backrest configurations on power generation and relative contribution to P_{erg} , W_{drive} , and stroke rate.

		P_{erg} (W)	P_{elb} (W)	P_{sho} (W)	P_{trunk} (W)	$W_{erg\ drive}$ (J)	$W_{elb\ drive}$ (J)	$W_{sho\ drive}$ (J)	$W_{trunk\ drive}$ (J)	Stroke rate (per min)
Submax	Adjusted	96	10 (10%)	35 (36%)	52 (54%)	219	32	53	128	26
	Usual	92	5 (6%)	51 (55%)	36 (39%)	113	14	39	60	49
Max	Adjusted	171	13 (8%)	61 (36%)	97 (57%)	198	23	40	133	52
	Usual	120	8 (6%)	71 (59%)	41 (34%)	119	15	45	54	61

Kinematic and kinetic performance variables during paddling among para-kayak athletes with unilateral above or below knee amputation

Johanna S. Rosén¹, Anton Arndt^{1,2}, Johnny Nilsson^{1,3}, Hans Rosdahl¹, Victoria L. Goosey-Tolfrey⁴, & Anna Bjerkefors^{1,5}

¹The Swedish School of Sport and Health Sciences (GIH), Stockholm, Sweden, ²Department of Clinical Sciences, Intervention and Technology (CLINTEC), Karolinska Institute, Stockholm, Sweden, ³Dalarna University, Falun, Sweden, ⁴Peter Harrison Centre for Disability Sport, School of Sport, Exercise and Health Sciences, Loughborough University, UK, ⁵Department of Neuroscience, Karolinska Institute, Stockholm, Sweden.

Email: johanna.rosen@gih.se

Summary

In para-kayak, athletes with unilateral above knee amputation (AK) and below knee amputation (BK) compete in the same class which is questionable since the legs are important for paddling performance. The purpose was therefore to examine differences in kinematic and kinetic performance variables between AK and BK para-kayak athletes and between the amputated (A) and non-amputated (NA) sides. No significant differences were observed between the groups in the majority of the examined variables suggesting that these group of athletes may be able to compete in the same class.

Introduction

Lower limbs may contribute to up to 21% of paddling force, 16% of kayak speed [1], and perhaps ultimately contributing to an increase in kayaking performance by 6% [2]. In para-kayak, athletes with unilateral AK and BK athletes compete in the same class. Since the leg movement during paddling is most likely a result of the flexion and extension of the knee joints, it is questionable whether athletes with these different impairment types should compete in the same class. The purposes of this study were therefore to examine the differences in kinematic and kinetic performance variables between AK and BK athletes and between the A and NA sides during kayak ergometer paddling.

Methods

11 AK and 6 BK international level competitive para-kayak athletes from 13 different countries participated in this study. The data collection was conducted by the athletes paddling on a kayak ergometer at an intensity level corresponding to the intensity of a 200 m race. Three-dimensional (3D) kinematic data from the body and paddle were recorded during the paddling using a 12-camera optoelectronic system. Force was measured using uniaxial piezoelectric force transducers attached at the paddle shaft, a force plate attached to the kayak seat and 3D piezoelectric force transducers attached to the footrest. Independent *t*-tests and two-way mixed model analysis of variance tests with one between-group factor *group* (AK, BK) and one within group factor *side* (A, NA) were performed. Significant interactions were followed up with Bonferroni post-hoc tests.

Results and Discussion

There were no significant differences between the groups in the main performance variables such as power output or paddle force which was quite unexpected. Differences

between the groups were only seen in the hip joint in flexion range of motion, flexion and extension velocity and flexion moment where the BK group demonstrated larger values. The NA side demonstrated greater values compared to the A side in posterior force at the seat (Figure 1) and in hip flexion moment. The posterior force at the seat during the drag phase of the A side was smaller compared to the NA side. For the AK athletes an anterior force could be seen for the A side, likely due to the majority of the athletes not wearing a prosthesis leading to an inability to push on the footrest during the drag phase of that side. This results in there only being a pull force on the footrest of the NA side resulting in the athletes gliding anteriorly on the seat, creating an anterior force.

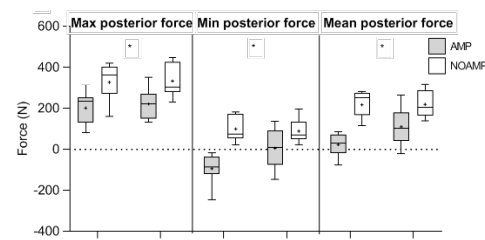


Figure 1: Maximal, minimal and mean posterior force at the seat.

Conclusions

The study examined differences in kinematic and kinetic performance variables between para-kayak athletes with unilateral AK and BK amputation as well as between the A and NA sides. There were only significant differences between the groups in the hip joint in flexion/extension ROM, flexion and extension velocity and flexion moment. Differences between the sides were seen in posterior force at the seat and in hip flexion moment. The limited number of variables in which differences between the groups were observed indicate that athletes with AK and BK amputation may be able to compete in the same class on similar terms.

Acknowledgments

We recognize financial contributions from the International Canoe Federation and The Swedish Research Council for Sport Science. Sincere gratitude is expressed to all the athletes who participated in this study.

References

- [1] Nilsson J & Rosdahl H (2016). *Int J Sports Physiol Perform*, **11**: 22-27.
- [2] Begon M et al. (2010). *Multibody syst dyn*, **23**: 387-400.

Towards a standardized and individualized lab-based protocol for wheelchair-specific exercise capacity testing of wheelchair athletes: a scoping review

Rowie J.F. Janssen¹, Sonja de Groot^{1,2,3}, Lucas H.V. van der Woude^{1,4,5}, Han Houdijk¹, Riemer J.K. Vegter^{1,5}

¹University of Groningen, University Medical Center Groningen, Center for Human Movement Sciences, Groningen, the Netherlands; ²Amsterdam Rehabilitation Research Center Reade, Amsterdam, the Netherlands; ³Department of Human Movement Sciences, Faculty of Behavioural and Movement Sciences, VU University, Amsterdam, the Netherlands. ⁴Center for Rehabilitation, University Medical Center Groningen, Groningen, the Netherlands, ⁵Peter Harrison Centre for Disability Sport, School of Sport Exercise & Health Sciences, Loughborough university, Loughborough, United Kingdom
Email: r.j.f.janssen@umcg.nl

Summary

Numerous equipment with various protocols to attain the wheelchair-specific anaerobic and aerobic exercise capacity of wheelchair athletes in a standardized lab environment have been used in previous research and practice. These are not necessarily wheelchair or athlete-specific and not very well standardised. This has implications for the comparison and generalizability of the results [1]. This review provides an overview of the assessment of lab-based wheelchair-specific exercise capacity by wheelchair athletes. Different characteristics of protocol designs are used interchangeably and from this review, conclusions cannot be drawn about the influence of the different aspects. Rather than to explore these differences we aim for more standardization and better reporting. Future studies should preferably use equipment that allow anaerobic sprint testing, that can accommodate an athletes own sports wheelchair and has the possibility of measuring power output. The anaerobic and aerobic protocol should be standardized, yet individualized towards their own capacity [2].

Introduction

This scoping review aims to provide an overview of the assessment of lab-based tests for the anaerobic and aerobic wheelchair-specific exercise capacity in wheelchair athletes. Accurate measurement of those entities provides a basis for individualized training programmes and if athletes are measured over time with the same methods their wheelchair-specific exercise capacity can be monitored. Our second aim is to generate a framework of protocols for standardized, yet individualized lab-based wheelchair-specific exercise capacity testing in wheelchair athletes.

Methods

A scoping literature search in Pubmed, Web of Science, Embase and CHINAL was conducted with the following search terms: (Wheelchair*) AND (Ergomet* OR Dynamomet* OR Simulator OR Treadmill) AND (Sport OR Athlet* OR Para-Athlet*) AND (Exercise test* OR Laboratory based test* OR Maximal incremental test* OR Multistage test* OR Aerobic test* OR Sprint test* OR Wingate OR Anaerobic test*).

Results and Discussion

The search resulted in 9 and 37 unique protocols for respectively wheelchair-specific anaerobic and aerobic exercise capacity testing. A variety of participants were included in the studies, numerous treadmills and ergometers were utilized and protocols vary widely. Also, several different outcomes to describe the wheelchair-specific exercise capacity were reported. Besides this, information regarding the participant characteristics or used methods was often missing.

Conclusions

Different characteristics of protocol designs are used interchangeably and from this review, we cannot draw conclusions about the influence of the different aspects. Rather than to explore these differences we aim for more standardized protocols and better reporting. Future studies should preferably use equipment that allow anaerobic sprint testing, that can accommodate an athletes own sports wheelchair and has the possibility of measuring power output. The anaerobic and aerobic protocol should be standardized, yet individualized. Protocols should be build towards the predicted outcome of the athlete which is based on an earlier performed test [2]. A checklist is provided together with this review, which shows the preferable equipment, protocol and all the relevant information and outcomes that should at least be reported by researchers and practitioners. With these guidelines we hope to work towards more individualization and standardization in future wheelchair-specific exercise testing and more international agreement.

Acknowledgements

This work was supported by ZonMw (Sport en Beweging 2018) under project number 546003002. This project, named ‘WheelPower: wheelchair sports and data science push it to the limit’ is a cooperative effort between UMCG, TU Delft, THUAS, VU Amsterdam and is in cooperation with several sports federations collected under the umbrella of NOC*NSF.

References

- [1] Kouwijzer I et al. (2019). *Eur J Appl Physiol*, **36**(4):4328.
- [2] Janssen TWJ et al. (1993). *Med Sci Sports Exerc*, **25**(7):863–70.

The impact of leg impairment on strength and race performance in elite para-cyclists

Johanna B. Liljedahl¹, Anna Bjerkefors^{1,2}, Carla F. Nooijen¹, Anton Arndt^{1,2}

¹The Swedish School of Sport and Health Sciences, Stockholm, Sweden

²Karolinska Institute, Stockholm, Sweden

Email: johanna.liljedahl@gih.se

Summary

Maximal isometric leg strength differs in three groups of para-cyclists with leg impairments while race speed does not, suggesting that the level of impairment in muscles important in cycling can be measured without predicting sport performance.

Introduction

In the C-class in para-cycling athletes compete on typical race bikes in time trials, mass starts and track cycling. To be eligible for the C-class, athletes must have impaired muscle strength or range of motion, limb deficiency, leg length difference, athetosis, ataxia or hypertonia. Activity limitations caused by impairments are expected to hinder cycling performance and therefore, the C-class covers five sport classes: C1 to C5 (C5 being least impaired).

Research describing the impact of different impairments on race performance is limited. The current classification system needs to be evaluated to assure evidence-based classification procedures, as highlighted by the International Paralympic Committee [1]. The aim of this study was to compare the impact of lower limb impairments on leg strength and cycling performance in the C-class.

Methods

Data from 58 para-cyclists was collected at four para-cycling events (World Cups and World Championships) in 2018-2019, sanctioned by the international cycling federation, UCI. The data collection protocol included isometric and dynamic strength testing and a sprint test.

In the isometric test, the athlete was seated in a custom-built strength setup with one foot on the floor and the tested leg reached horizontally out in front (knee flexion 50°) with the foot against a footrest equipped with force transducers. Maximal force (N) was exerted on the footrest in a leg push. The dynamic test was conducted on a cycling ergometer (Cyclus2, RBM Electronics, Germany) by pushing the pedal from the top (0° of the pedal revolution) to bottom position (180°), measuring peak power (W). A standardized 20-s all-out sprint test was performed to measure mean power output (MPO) (W). The three conducted tests were adjusted for body mass (kg). Time trial results (km/h) from the respective event where the athlete was tested were obtained [2].

Athletes were split into three groups based on impairments: impaired muscle strength (IM), transfemoral amputation (FA; one-legged cycling) and transtibial amputation (TA; two-legged cycling with prosthetics). One-way ANOVA with Tukey's HSD post-hoc test was conducted to compare effect of impairment on strength and performance variables.

Results and Discussion

The isometric test differed significantly ($F[2,55] = 12.47, p < .001$) between all groups. TA had significantly higher strength than IM ($p = .003$) and FA ($p < .001$), and IM had significantly higher strength than FA ($p = .037$). A significant difference was not evident in race speed ($F[2,53] = 1.74, p = .185$). The dynamic test ($F[2,55] = 9.20, p < .001$) and MPO ($F[2,54] = 6.79, p < .005$) were higher in TA than FA ($p = .002, p = .009$ for respective test) and in IM than FA ($p = .001, p = .001$ for respective test). The large variance in particularly the IM group is likely due to a large spread in impairment severity in IM athletes.

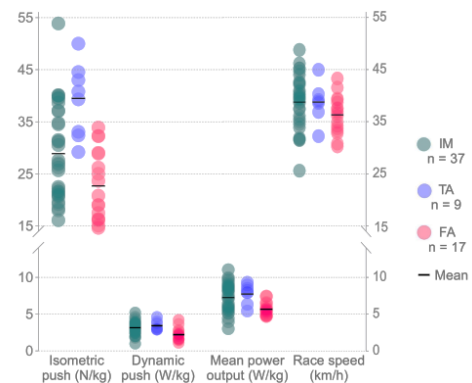


Figure 1: Effects of impairment on muscle strength tests (isometric and dynamic push) and performance (mean power and race speed).

Conclusions

To facilitate fair competition in para-cycling, classification methods need to assess activity limitation while not simultaneously impact the outcome of competition. The isometric strength results differ from race outcome results, indicating that the impact of impairment can be determined regardless of cycling performance. Further research is needed to explore confounding variables e.g. training, sex and experience and their role in test and race outcomes.

Acknowledgments

This project has been carried out with financial support from the Union Cycliste Internationale. The funding body was not involved in decisions concerning the design of this abstract, data analysis, interpretation of data or in reporting and publishing this project.

References

- [1] IPC (2015). *Athlete Classification Code*. Retrieved from www.paralympic.org
- [2] UCI (2019). *Official Book of Results*. Retrieved from www.uci.org

Validation of a new sport specific Trunk Test Battery for Paracanoe

Anna Bjerkefors^{1,2}, Johanna S. Rosén¹, Olga Tarassova¹, Martin Eriksson-Crommert³.

¹The Swedish School of Sport and Health Sciences (GIH), and, ²Department of Neuroscience, Karolinska Institute, Stockholm, Sweden, and ³University Health Care Research Center, Faculty of Medicine and Health, Örebro University, Örebro, Sweden.
Email: anna.bjerkefors@gih.se

Summary

The Trunk Test Battery (TTB) used in the Paracanoe medical classification is a valid test to measure trunk function in athletes with impaired muscle power, impaired passive range of movement and limb deficiency. A general form of the equation to predict power output from TTB, age and gender is Power output = 197.443 + (2.057*TTB) + (57.540*Gender) + (-3.118*Age).

Introduction

Para-kayak is one of two disciplines in the sport of Paracanoe and debuted in the Paralympic Games in 2016. In para-sport, athletes need to go through a classification process before they are able to compete. This process allocates athletes to different sport classes based on the impact of impairment on sport performance. In para-kayak, athletes with impaired trunk and/or leg function are allocated to and compete in one of three classes: KL1, KL2, or KL3 based on the results from the medical and technical classification. The medical classification involves tests of trunk and leg function. The Trunk Test Battery (TTB) consists of manual muscle tests (MMT) and functional assessment tests (FA). The outcome is scored on a 0 – 2-point ordinal scale.

The purpose of the study was to validate the TTB used in para-kayak classification. The research question was to examine the effect of age, gender, training intensity, TTB, MMT and FA on sport performance (power output), i.e. kayak ergometer paddling.

Methods

Fifty international or national level para-kayak athletes (16 females and 34 males) from 11 countries performed the TTB. A subgroup of 26 athletes (8 females and 18 males) completed a sport-specific performance test on a kayak ergometer. The TTB consisted of the MMT (six trunk muscle tasks performed in lying; flexion/extension, rotation left/right, lateral flexion left/right) and the FA (four tasks in unsupported sitting; static, dynamic and perturbation on stable and unstable surface). The kayak ergometer test was performed during high intensity paddling during 20 stroke cycles. Separate multiple linear regression analyses were carried out to investigate whether age, gender and training intensity and either a) TTB, b) MMT, c) FA, d) FA_{static}, e) FA_{dyn}, f) FA_{stable} or g) FA_{unstable} could significantly predict athletes' sport performance.

Results and Discussion

The mean power output during high intensity paddling on the kayak ergometer for males was 226.5 ± 108.6 W and for females 145.3 ± 57.9 W. The results of the regression analyses indicated that Model 3 in all analyses showed the highest R² (adjusted in %) in TTB, FA and FA_{dyn} (Table 1). In these analyses, the results showed that all independent predictors except training intensity significantly predicted sport performance outcome.

Table 1. Multiple linear regression analyses to evaluate if age, gender, training intensity and either a) TTB, b) MMT, and c) FA_{dyn}, predict changes in sport performance (power output) in paracanoe athletes (n=26).

	B	SE	P-value
a) TTB			
Gender	2.057	0.257	<0.001
Age	57.540	18.602	0.005
	-3.118	1.099	0.010
R2 adjusted in %			82.8
ANOVA F(3,22) = 41.189, p <0.001			
b) FA			
Gender	2.290	0.287	<0.001
Age	55.396	18.621	0.007
	-3.184	1.097	0.008
R2 adjusted in %			82.8
ANOVA F(3,22) = 41.048, p <0.001			
c) FA_{dyn}			
Gender	13.047	1.541	<0.001
Age	57.482	17.184	0.004
	-3.337	1.041	0.004
R2 adjusted in %			84.3
ANOVA F(3,22) = 45.577, p <0.001			

Notes: B=unstandardized beta coefficient, SE = standard error of the estimate, R²=explained variance adjusted in %. Training intensity was excluded in all three models.

Conclusions

To facilitate fair competition, the International Paralympic Committee requires all para-sports included in the Paralympic Games to develop and use classification systems based on evidence [1]. The new TTB was shown to be valid to measure sport specific trunk function and it was feasible to perform in Paracanoe classification. Further research on trunk function is needed where athletes with different impairment types are included and the impact of adaptive sport-specific equipment, strapping and positioning is evaluated.

Acknowledgments

We recognize financial contributions from the International Canoe Federation (ICF) and The Swedish Research Council for Sport Science (CIF). The authors would also like to express their sincere gratitude to all the athletes who participated in this study.

References

- [1] International Paralympic Committee classification Code, 2015 www.paralympic.org

Biomechanical Evaluation of a Fracture Fixation System for Transverse Fractures of the Metacarpal Neck

Rena Mathew¹, Nicholas Anastasi¹, Christopher Jones², Sorin Siegler¹

¹Department of Mechanical Engineering, Drexel University, Philadelphia, PA, 19103, USA

²Rothman Institute Orthopedics, Old Lancaster Road, Bryn Mawr, PA 19010

Email: rm3325@drexel.edu

Summary

Metacarpal fractures represent approximately 30% of all hand fractures that are evaluated in the emergency setting due to accidental falls or a direct blow to the fingers [1]. Intramedullary headless compression screw (HCS) fixation is a promising treatment method with the capacity to generate 60 N of compression [1]. Mechanical properties such as displacement with cyclic loading and stiffness were tested with this method to simulate a range of motion hand therapy exercises at 40 N. A test was also conducted to understand the peak load at which the metacarpal strength fails.

Introduction

Surgical techniques such as K-Wire and external fixation for metacarpal fractures lead to impediments such as infection, tendon injury and malunion [1]. Intermedullary HCS fixation is an alternative method to address high rates of complications post-surgery. The purpose of this study is to evaluate the mechanical properties such as stiffness and strength of HCS fixation of a metacarpal neck fracture.

Methods

A metacarpal neck fracture model was created in 13 fourth generation composite Sawbones by removing a volar-based bone wedge using a custom cutting jig to simulate a typical apex dorsal fracture, unstable in flexion (Figure 2). The bones were then fixed by 3.0 mm retrograde HCS fixation. A 3-D printed fixation jig was used to assure all hardware was identically placed. Models were potted at the base and mounted vertically in a material testing machine (Mark10:ESM1500), employing a cable tensioned over the metacarpal head to simulate forceful grip loading. Cyclic loading to 40N (simulating finger active range of motion exercises) and failure testing were performed. Load, displacement, and failure mode were recorded [2].

Results and Discussion

During cyclic loading to 40 N, the HCS models (n=4, 7.1±0.4 mm) exhibited significantly higher displacement with cyclic loading than a healthy metacarpal (5.4±1.2 mm). In addition, average displacement to failure of the HCS models (3.3±0.7 mm) were non—significantly lower and their corresponding loads to failure (137.4±30.17 N) were significantly higher than a healthy specimen (63.8±24.9 N) (Figure1a). Lastly, even though average final stiffness was higher than average initial stiffness, the average of the difference between them (5.1±3.8 N/m) was non-significantly higher than that of healthy specimen (4.7±1.3 N/m).

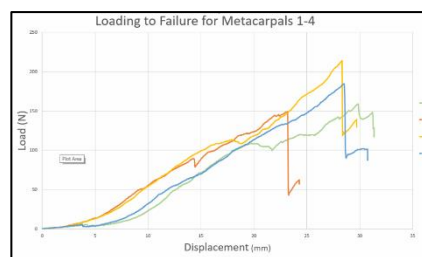


Figure 1: Plot of Total Force to mechanical failure

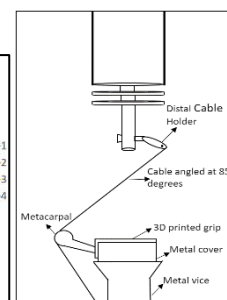


Figure 2: Experimental set-up

Conclusions

The HCS model provided comparable evidence of its mechanical properties which are similar to a simulated grip model (Table 1) [1]. The construct is also internally buried inside the bone and avoids the restrictive nature of pins that limit early motion exercises.

References

- [1] Hussain M, Ghaffar A, Choudry Q, et al. (2020) Management of Fifth Metacarpal Neck Fracture (Boxer's Fracture): A Literature Review. *Cureus* 12(7)
- [2] Jones, Christopher M et al. (2019) "Headless Screw Fixation of Metacarpal Neck Fractures: A Mechanical Comparative Analysis." *Hand (New York, N.Y.)* vol. 14,2

Table 1: Displacement with Cyclic Loading, Average Stiffness, Load to Failure, and Displacement at Failure of the HCS

ID	Displacement after cyclic loading (mm)	Stiffness(N/m)	Load to Failure (N)	Displacement to failure (mm)
1	5.84±2.5	7.4±0.1	159±30.2	8.6±0.2
2	2.44±3.4	6.7±2.3	149±13.8	9.4±3.4
3	2.64±7.5	7.9±0.7	214±22.4	9.7±2.5
4	4.84±3.1	6.5±4.4	184.5±10.5	8.2±3.1

Model of the Midcarpal Joint Accounting for Structural Difference

Ronit Wollstein¹, Martin Pendola¹

¹ NYU Grossman School of Medicine, Department of Orthopaedic Surgery, NY, USA

Email: ronitwollstein@gmail.com

Summary

There are multiple challenges to the study of in-vivo wrist mechanics. We present a preliminary model of the midcarpal joint based on computed tomography (CT) scans of normal wrists. By applying forces acquired in-vivo to the model we can study in-vivo biomechanics without invasive procedures. Our model predicted that the angle between the lunate and the capitate is significantly different between lunates type 1 and 2 in the midcarpal joint $p < 0.0001$. Significant differences in force transfer are predicted by the model, dependent on midcarpal joint type. Further study will delineate disparate measurements calculated from the model and may improve the model's ability to predict force transfer and kinematics.

Introduction

It is difficult to obtain in-vivo data to study structure of the wrist and its effect on wrist function[1,2]. We present a preliminary model of the midcarpal joint based on computed tomography (CT) scans of normal wrists. By applying forces acquired in-vivo to the model we can study in-vivo biomechanics without invasive procedures thus providing a platform for the study of wrist mechanics.

Previous models have not succeeded in accounting for variable patterns of bony shape and configuration likely due to the complexity of wrist structure.

Our purpose was to:

- 1) Generate an initial model of the midcarpal joint of the wrist based on normal wrist CT scans.
- 2) Generate separate models for the midcarpal joint based on 2 distinct wrist types (type 1 and type 2).

Methods

Thirty-five CT scans, (dicom files, anonymized, 2mm/slice resolution) were selected from a normal patient database and converted into 3-dimensional .stl files using OsiriX software (version 9, 2016, GNU LGPL), for classification. Solid Mechanics study in stationary conditions was used through the COMSOL library. Material properties for these models were generated from COMSOL materials library. The models were divided into 2 categories based on lunate type. Simulated loads were applied to the most distal articular

surface of the model. A load of 200N was applied in a distal to proximal direction, consistent with other studies. The predicted forces and movement were compared between the 2 wrist types.

Results and Discussion

Thirty-three percent of individuals displayed a Type 1 joint, and 67% of individuals in the sample presented with a Type 2 joint. The movements or displacement of the components in the midcarpal joint differed between wrist types 1 and 2. The angle between the lunate and the capitate was significantly different between lunates type 1 and 2 $p < 0.0001$. On force application, the surface stress and volume stress on the carpometacarpal (CMC) joints did not differ significantly between the 2 wrist types $p = 0.38$. However, the forces were predicted to travel more ulnarly in a type 1 wrist, and more radially-towards the scaphoid and scapholunate ligament- in type 2 wrists.

Conclusions

- The model can be used to predict movement after loading through the midcarpal joint.
- Significant differences in force transfer are predicted by the model, dependent on midcarpal joint type.
- Further study will delineate disparate measurements calculated from the model. And improve the model's ability to predict force transfer and kinematics

References

- [1] Sandow MJ, Fisher TJ, Howard CQ, Papas S. Unifying model of carpal mechanics based on computationally derived isometric constraints and rules-based motion - the stable central column theory. *J Hand Surg Eur Vol* 2014;**39**(4):3563.
- [2] Sandow MJ. 3D Dynamic Analysis of the Wrist. *Hand Surg* 2015; **20**(3):366-8.

Three-Dimensional Carpal Tunnel Reconstruction and Analysis Using Multimodal Co-Registration of Ultrasonography and Computed Tomography

Rakshit Shah, **Hui Zhang**, and Zong-Ming Li

Hand Research Laboratory, Departments of Orthopaedic Surgery & Biomedical Engineering

University of Arizona, Tucson, Arizona, United States

Email: lizongming@arizona.edu

Summary

A 3D carpal tunnel model was created by co-registering computed tomography scanning of carpal bones and robot-assisted ultrasound imaging of the transverse carpal ligament. The model allowed morphological analyses of bone and ligament arches at various tunnel locations and provided previously unknown information of carpal tunnel morphological properties. The developed multimodal imaging technique and the morphological analyses can be applied to examine pathomorphological changes of the wrist.

Introduction

The carpal tunnel is bounded by the transverse carpal ligament and carpal bones, which can be divided into the ligament and bone arches. The ideal imaging modality for morphology investigation of the carpal tunnel as an osseoligamentous structure is ultrasonography for ligament arch and computed tomography for bone arch. Therefore, the purposes of the study were to 1) establish methodology for reconstructing three-dimensional carpal tunnel by computed tomography scanning of carpal bones and ultrasound imaging of the ligament, and 2) investigate the morphology of the bone and ligament arches across carpal tunnel. We hypothesized that the ligament arch would occupy lesser carpal tunnel space as compared to the bone arch, and the bone and ligament arch spaces would be dependent on the location of the carpal tunnel.

Methods

Nine freshly frozen male cadaveric hand specimens were used. To reconstruct the ligament arch, multiple cross-sectional images of the ligament and the ligament-osseous attachments were collected using robot-assisted ultrasonography. Then the 2D image coordinates of anatomical features were spatially assembled to 3D point cloud of ligament arch using the positional information from the robot (Figure 1A). To reconstruct the bone arch, 3D surface of individual carpal bones was obtained by performing image segmentation on computed tomography scans. A 3D bone arch point cloud was reconstructed by filling the space between two adjacent bones with surrogate tissues of up to 3 mm thickness (Figure 1B).

The bone and ligament arches were co-registered into a common coordinate system to model a 3D carpal tunnel point cloud (Figure 1C) using the iterative closest points algorithm. The algorithm provided a rigid transformation matrix by performing a geometric match between the partial bone information from 3D ultrasonography and entire bone geometry from computed tomography scans.

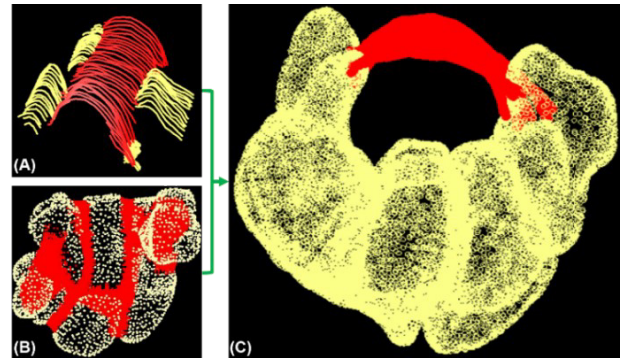


Figure 1: Sample reconstruction of ligament arch using ultrasonography (A), bone arch using computed tomography (B), and carpal tunnel using multimodal co-registration of both arches (C).

Results and Discussion

Total tunnel volume was $6820.8 \pm 1278.7 \text{ mm}^3$, agreed with a previous study [1]. The bone arch volume ($5719.6 \pm 1049.2 \text{ mm}^3$) was significantly greater than the ligament arch volume ($1101.2 \pm 230.5 \text{ mm}^3$, $p < 0.05$), consistent with previous findings [2]. The bone arch areas were significantly larger than the ligament areas at all tunnel levels (proximal, middle, distal, all $p < 0.05$). Additionally, both arches varied significantly with tunnel locations ($p < 0.05$). The ligament arch area progressively increased from distal to proximal locations, whereas the bone arch area was greatest at the middle location but tapered down towards the tunnel edges.

The robot-ultrasound incorporation allows for 3D ligament reconstruction from 2D ultrasound images, advancing the imaging of the carpal tunnel. The developed multimodal imaging technique and the calculated outcome parameters can be applied to examine the pathomorphological changes associated with the carpal tunnel.

Conclusions

A multimodal imaging technique was developed to reconstruct 3D carpal tunnel for advanced morphological analyses of bone and ligament arches, which advances our understanding of the carpal tunnel morphological properties.

Acknowledgments

NIH/NIAMS R01AR068278

References

- [1] Richman JA et al. (1987). *J Hand Surg Am*, **12(5)** 712-717
- [2] Shah R and Li ZM (2020). *J of Biomech Eng*, **142 (9)**

Reproducibility of Trapeziometacarpal Joint Angle Measurements Using Dynamic CT

Michael T. Kuczynski^{1,2,3}, Kendra Wang^{2,4}, Justin J. Tse^{2,3}, Sarah L. Manske^{1,2,3}

¹Biomedical Engineering Graduate Program, Schulich School of Engineering, University of Calgary, Canada

²McCaig Institute for Bone and Joint Health, Cumming School of Medicine, University of Calgary, Canada

³Department of Radiology, Cumming School of Medicine, University of Calgary, Canada

⁴Biomedical Engineering Undergraduate Program, University of Waterloo, Canada

Email: mkuczyns@ucalgary.ca

Summary

Dynamic computed tomography (CT) can be used to quantify joint motion. Joint angles are often calculated using manually placed anatomical landmarks (AL). This can be a highly subjective process and a better understanding of the associated errors resulting from manually placed AL on joint angles from dynamic CT scans is needed. Further, processing dynamic CT data can be prohibitively long. A semi-automated post-processing pipeline is proposed to improve processing times for joint angle quantification. Inter- and intra-rater analysis was performed on segment coordinate system (SCS) orientation and joint angles between three raters. Results show excellent reliability between raters for SCS orientation.

Introduction

Osteoarthritis (OA) is a degenerative joint disease that commonly affects the joints of the hand, including the trapeziometacarpal (TMC) joint [1]. OA is considered a complex and multifactorial disease in which biomechanics play a role [1]. While dynamic CT can provide real time visualization of bone and joint motion, structural joint changes caused by OA can impact the reproducibility of calculated joint angles from manually placed ALs. It is not clear how much variation in SCS orientation and resulting joint angles can be expected from this subjective task. A joint angle reproducibility study of the TMC joint using a joint coordinate system (JCS) is presented for dynamic CT data sets. Further, a semi-automated post-processing pipeline has been developed to quantify joint angles from dynamic CT scans of the TMC joint and improve upon the extensive processing times presented in literature [2].

Methods

Ten cadaveric hand specimens (5 female, age: 83.4±15.0 yrs) were scanned. Dynamic CT was acquired with 120kVp, 100mA, 4cm longitudinal coverage, 4vol/s gantry rotation, and 15s scan time. A custom passive motion device was used to move the thumb through radial abduction-adduction. Due to limitations in dynamic CT image quality and longitudinal coverage, high resolution peripheral quantitative CT (HR-pQCT) scans with 61µm isotropic voxels (XtremeCTII, Scanco Medical) were acquired to generate masks and for SCS definition (Figure 1). Static CT images were binarized using global thresholds, binary morphological operations, and connected component labelling. Dynamic CT images were binarized using intensity-based sequential registration of CT

bone masks. Joint angles were measured using a JCS representation [3]. SCS for each bone in the TMC joint were generated using ALs [4] selected by three raters. SCS orientation between raters was assessed by comparing angles between SCS axes and the principal axes of each segment. Inter- and intra-rater reliability was assessed using a two-way intraclass correlation coefficient (ICC) for SCS orientation and joint angle results between all three raters.

Results and Discussion

A semi-automated post-processing pipeline was developed that only required minor manual adjustments to the binary masks of each bone, due to narrow joint space and landmark placement. SCS orientation between raters showed excellent intra- and inter-rater reliability (Table 1). This study provides the groundwork for future studies that will assess the relationship between joint structure and function in osteoarthritic TMC joints using dynamic CT.

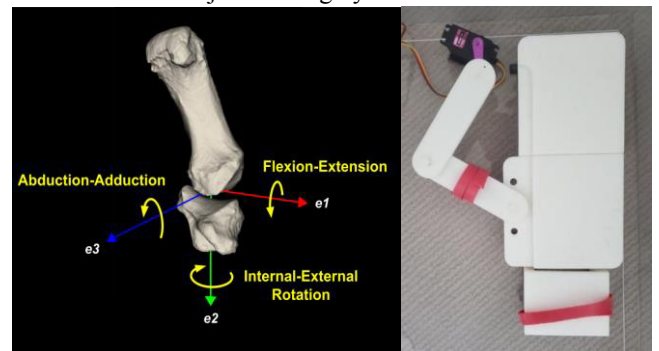


Figure 1: JCS defined on the TMC joint (left) and the passive motion device used during dynamic CT scanning (right).

Conclusions

Both inter- and intra-rater reliability was excellent when comparing orientation of both SCSs. This suggests that careful placement of AL on 3D bone models using detailed instructions and high-resolution bone models can provide reliable SCSs for the trapeziometacarpal joint.

References

- [1] Marshall M et al. (2018). *Nat Rev Rheumatol*, **14**:641-656.
- [2] Wang K et al. (2018). *J Hand Surg*, **43**:1088-1097.
- [3] Grood ES and Suntay WJ. (1983). *J Biomech*, **105**:136-144.
- [4] Chèze L et al. (2009). *Comp Methods Biomech Biomed Engin*, **12**:277-282.

Table 1: Inter- and intra-rater ICC values for segment coordinate system orientation, compared to principal axes of each segment.

	X_MC1	Y_MC1	Z_MC1	X_TRP	Y_TRP	Z_TRP
Inter-Rater ICC	0.988	0.994	0.908	0.978	0.989	0.976
Intra-Rater ICC	0.993	0.997	0.936	0.988	0.995	0.979

An Implantable Differential Mechanism to Restore Individuated Finger Flexion following Tendon Transfer Surgery

Suraj Chakravarthi Raja,¹ Won Suk You,⁴ Kian Jalaieeddini,² Justin C. Casebier,⁵ Nina R. Lightdale-Miric,⁶ Vincent R. Hentz,⁷ Francisco J. Valero-Cuevas,^{1,2,3} Ravi Balasubramanian,⁵

¹Ming Hsieh Department of Electrical and Computer Engineering, ²Division of Biokinesiology and Physical Therapy, and ³Department of Biomedical Engineering, University of Southern California, Los Angeles, CA, USA; ⁴UBTECH North America R&D Center, Pasadena, CA, USA; ⁵School of Industrial and Manufacturing Engineering, Oregon State University, Corvallis, OR, USA; ⁶Children's Hospital, Los Angeles, CA, USA; ⁷Stanford University, Stanford, CA, USA.
Email: surajcha@usc.edu

Summary

We developed a passive device implanted between the *flexor digitorum profundus* (FDP) tendons of insertion to construct a passive “differential mechanism” between the *extensor carpi radialis longus* (ECRL) muscle and the finger tendons (US Patents 9,925,035 and 10,595,984). This differential mechanism enables some finger(s) to continue to flex and make contact with the object even if other finger(s) are locked (checkreined) by already having made contact.

Introduction

High median-ulnar nerve injury paralyzes part of the FDP muscle and the entire *flexor digitorum superficialis* (FDS) muscle, resulting in limited grasp function by the patient. One of the current surgical solutions to restore flexion of the four fingers is a tendon transfer procedure that re-routes and directly sutures all four FDP tendons of insertion to the single tendon of insertion of the ECRL muscle, a wrist extensor innervated by the radial nerve.[e.g., 1] However, this procedure has a fundamental drawback: the surgery couples the previously independent movement of all four fingers because the excursion of the ECRL determines the excursion of all four FDP tendons of insertion. With this coupled finger flexion, all fingers cease to flex as soon as one finger makes contact with the object. This prevents all fingers from making contact when grasping irregularly shaped objects. Simple tasks such as holding an apple or using a knife with a contoured handle become challenging. This results in reduced function affecting quality of life.

Methods

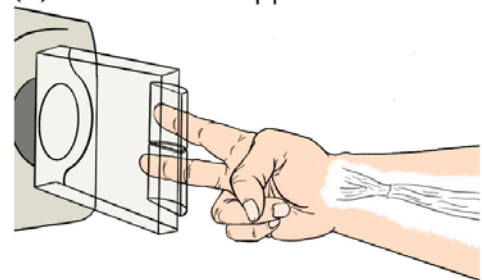
We tested the implant's ability to create differential flexion between the index and middle fingers during grasp when actuated by a single muscle in two human cadaver hands using a closed-loop computer-controlled actuation and measurement paradigm. In the cadaveric models, the implants enabled significantly more differential flexion between the index and middle fingers for a wide range of donor tendon tensions. The implants also redistributed fingertip forces between fingers.

Results and Discussion

When grasping uneven objects, the difference in contact forces between the index and middle fingers was reduced by 23% when compared with the current suture-based surgery. This means that force distribution is more even with the

implant in spite of the difference in flexion angle of the fingers. These results suggest that self-adaptive grasp is possible in tendon transfers that drive multiple distal flexor tendons with one donor muscle.

(A) Suture-based approach



(B) Implant-based approach

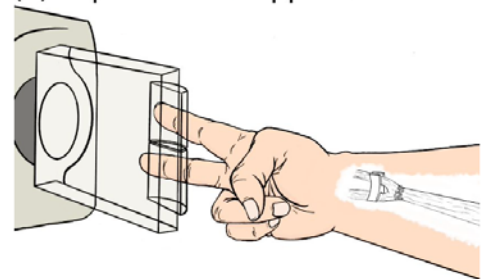


Figure 1: Experimental set up with cadaveric hands. For the traditional (A) and implant conditions (B), we measured the fingertip forces on the sensing paddle for a given tension in the donor tendon for different rotation angles of the sensing paddle.

Conclusions

The addition of an implant in the transfer of the ECRL to the FDP of the index and middle finger enhanced the cadaveric model's ability to flex each finger different amounts and apply variable pressure. Translating this biomechanical advantage to patients would likely enhance hand functional recovery after high median nerve palsy surgical reconstruction.

Acknowledgments

US Department of Defense grant *MR150091* to Balasubramanian and Valero-Cuevas; NIAMS *R01-AR050520* and *R01-AR052345* grants to Valero-Cuevas.

References

- [1] Seiler JG et al. (2013) *J. Am. Acad. Orthop. Surg.* 21(11):675–684.

Biceps femoris long head fascicle length increases after 3 weeks of eccentric exercise training are due to sarcomere lengthening rather than serial sarcomere addition

Melissa A. Boswell^{1*}, Patricio A. Pincheira^{2*}, Martino V. Franchi³, Scott L. Delp¹, Glen A. Lichtwark²

¹ Department of Bioengineering and Mechanical Engineering, Stanford University, Stanford, USA

² School of Human Movement and Nutrition Sciences, The University of Queensland, Brisbane, Australia

³ Department of Biomedical Sciences, University of Padova, Padova, Italy

*These authors contributed equally to this work

Email: boswellm@stanford.edu

Summary

Nordic hamstring exercise (NHE) is an eccentric exercise that elicits substantial changes in hamstring fascicle length, which potentially protects the muscle from subsequent injury. Yet, the macroscopic and microscopic changes that contribute to the mechanical load-induced hamstrings lengthening response remain poorly understood. In this study, we measured in vivo fascicle and sarcomere length changes in the biceps femoris long head (BFlh) in ten individuals after a three-week NHE training program. We found an increase in fascicle and sarcomere lengths in the distal but not the central portion of the BFlh. Our results suggest that fascicle lengthening is due to sarcomere lengthening rather than serial sarcomere addition at the outset of the adaptive process.

Introduction

Eccentric training helps enhance muscle strength, power, speed, and protection from subsequent exercise-induced muscle damage [1,2]. NHE is one such eccentric exercise that elicits changes in fascicle length; however, the mechanisms underlying these fascicle length changes and the role of muscle architectural adaptations in preventing injuries are still largely unknown. Therefore, this study aimed to measure multi-scale BFlh adaptations by in vivo measurement of fascicle and sarcomere lengths before and after NHE training.

Methods

Ten recreationally active participants (age: 27 ± 3 years, mass: 70 ± 14 kg, height: 174 ± 9 cm) completed three weeks (nine sessions) of NHE training. Participants performed NHE using a custom padded board with uniaxial load cells attached to ankle braces. We estimated eccentric knee flexion strength as the average of the load cells' highest measurements during three maximal NHE repetitions. We measured in vivo sarcomere and fascicle lengths in the central and distal regions of the BFlh using second harmonic generation microendoscopy [3] and freehand 3D ultrasonography, respectively. During imaging, participants laid prone with their hips and knees fully extended and their feet in a neutral position off the end of the bed.

Results and Discussion

Eccentric knee flexion strength increased after the training (15%, $P < 0.001$, $\eta_p^2 = 0.75$). Fascicle lengths significantly increased (21%, $P < 0.001$, $\eta_p^2 = 0.81$), as well as sarcomere

(17%, $P < 0.001$, $\eta_p^2 = 0.9$) lengths, in the distal but not the central portion of the BFlh.

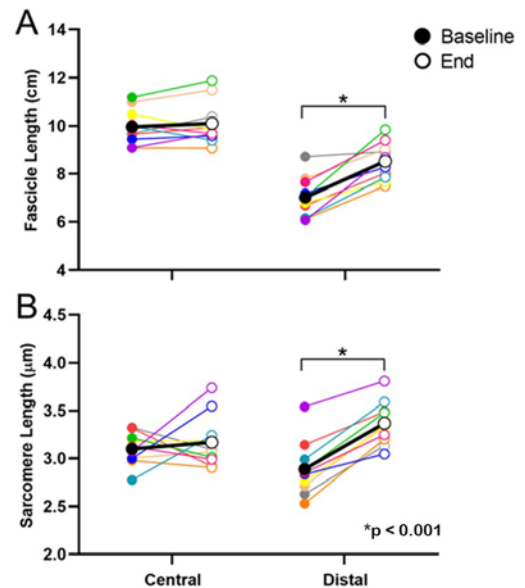


Figure 1: Fascicle lengths (A) and sarcomere lengths (B) in the central and distal portions of the BFlh at baseline (filled circles) and after NHE training (End, open circles). Each color is an individual participant, with the average across participant averages in black.

Conclusions

Fascicle length adaptations appear to be heterogeneous in the BFlh in response to three weeks of NHE training. An increase in sarcomere length, rather than the addition of sarcomeres in series, appeared to be underlying the initial BFlh adaptations we studied. The mechanism driving regional increases in fascicle and sarcomere length remains unknown, but we speculate it may be driven by regional changes in the passive tension of muscle or connective tissue adaptations.

Acknowledgments

This work was supported by a Company of Biologists Travelling Fellowship and the National Science Foundation Graduate Research Fellowships Grant No. DGE-1656518.

References

- [1] Douglas J et al. (2017). *Sports Med NZ*, **47**: 917-41.
- [2] Hyldahl RD et al. (2017) *Exerc Sport Sci Rev*; **45**:24–33.
- [3] Sanchez GN et al. (2015). *Neuron*, **88**:1109–20.

Development and validation of FootNet, a new kinematic and deep learning-based algorithm to detect foot-strike and toe-off in treadmill running

Adrian R. Rivadulla¹, Xi Chen², Gillian Weir³, Dario Cazzola¹, Grant Trewartha¹, Joseph Hamill³, Ezio Preatoni¹

¹Department for Health, University of Bath, Bath, UK

²Department of Computer Science, University of Bath, Bath, UK

³Department of Kinesiology, University of Massachusetts Amherst, Amherst, US

Email: arr43@bath.ac.uk

Summary

Foot-strike and toe-off detection is often critical in the assessment of running biomechanics. The onset and offset of the vertical ground reaction force is regarded as the “gold standard” method for step event detection, but several kinematics-based algorithms have been proposed to detect foot-strike and toe-off in the absence of force plates. However, the accuracy and generalisability of kinematics-based methods are often limited. Therefore, we developed FootNet, an algorithm using kinematic input and deep learning, to improve the detection of foot-strike and toe-off events during treadmill running in a variety of speed, foot-strike angle and incline conditions.

Introduction

The accurate detection of foot-strike and toe-off events based on kinematics has historically proved a challenging problem within locomotion biomechanics. Although several marker trajectory-based and segment/joint kinematics-based algorithms exist, these methods typically require markers to be affixed to highly deformable areas of the shoe which can be problematic. The accuracy of these methods can also be affected by running speed and a runner’s preferred foot-strike pattern (foot landing angle). Further, algorithm development and validation has typically been conducted in a single laboratory, potentially limiting their generalisability [1].

The purpose of this study was to develop and evaluate FootNet, a new kinematics and deep learning-based algorithm to detect foot-strike and toe-off in treadmill running.

Methods

Five treadmill-running datasets from three independent laboratories with different motion capture systems and instrumented treadmills were gathered from previous studies. These datasets included kinematics and kinetics of athletes of different abilities and foot-strike patterns running at multiple speeds and on different inclines. Marker trajectories were processed to calculate leg, foot and ankle kinematics. Running trials were divided in cycles and the non-contact and contact phases within each cycle were detected using the raw vertical ground reaction force (non-contact: vGRF < 50 N; contact: vGRF ≥ 50 N).

FootNet is based on a recurrent neural network with long, short-term memory (LSTM) units [2]. The network takes the distal tibia anteroposterior velocity, ankle dorsi/plantar flexion angle, and the anteroposterior and vertical velocity of the foot centre of mass as input features (entire time-series of a cycle) and predicts whether each time point belongs to the

contact or non-contact phases. Foot-strike and toe-off can then be simply identified by finding the first and last timepoints identified as contact. We used the five datasets for model development (70% participants from each set) and testing (30% participants of each set). The model underwent 5-fold cross-validation and the best set of weights was selected for final model testing.

Non-parametric Bland-Altman analyses (median bias and 2.5th and 97.5th percentile as 95% limits of agreement, 95LA) [3] and root mean squared error (RMSE) were used to assess the performance of FootNet against the onset and offset of the vertical ground reaction force method for the detection of foot-strike, toe-off and contact times. The linear association between detection errors and running speed, foot-strike angle and incline respectively were also investigated.

Results and Discussion

FootNet achieved close agreement with the force plate method (Figure 1), with a median bias of 0 ms for foot-strike (95LA = [-10, 7] ms, RMSE = 5 ms), toe-off (95LA = [-10, 10] ms, RMSE = 6 ms) and contact time (95LA = [-15, 15] ms, RMSE = 8 ms). These errors were two to four times smaller than those previously reported in the literature [1]. Linear associations between detection errors and running speed, foot strike angle and incline were small and practically negligible. Thus, FootNet seems robust to different running speeds, foot strike patterns and treadmill gradients, one of the main limitations highlighted in previous research.

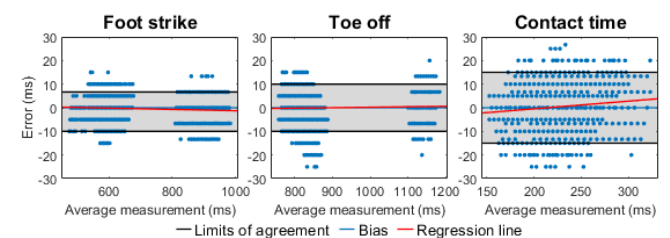


Figure 1: Bland-Altman plots.

Conclusions

FootNet improves the detection of foot-strike and toe-off events in treadmill running, and is robust to different speeds, foot-strike patterns and inclines. FootNet and its source code is publicly available for the biomechanics community.

References

- [1] King DL et al. (2019). *J Biomech*, **90**: 119-122.
- [2] Hochreiter S et al. (1997). *Neural Comput*, **9**: 1-38.
- [3] Bland Jet al. (1999). *Stat Methods Med Resl*, **8**: 135-160.

Fibril-reinforced poroelastic properties of normal and osteoarthritic human femoral, tibial, and patellar cartilage

Mohammadhossein Ebrahimi^{1,2}, Mikko A.J. Finnilä², Aleksandra Turkiewicz³, Martin Englund³, Simo Saarakkala², Rami K. Korhonen¹, Petri Tanska¹

¹ Department of Applied Physics, University of Eastern Finland, Kuopio, Finland;

² Research Unit of Medical Imaging, Physics and Technology, Faculty of Medicine, University of Oulu, Oulu, Finland;

³ Department of Clinical Sciences Lund, Orthopaedics, Clinical Epidemiology Unit, Lund University, Lund, Sweden

Email: mohammadhossein.ebrahimi@uef.fi

Summary

The fibril-reinforced poroelastic (FRPE) material properties of human femoral condyle cartilage and how these properties compare to other cartilage sites in knee are largely unknown. We combined multi-step stress-relaxation measurements with FRPE modeling to characterize these properties in the femoral condyle cartilage at different stages of osteoarthritis (OA) and compared them with other cartilage sites in knee. Our findings suggest that the strain-dependent fibril network modulus of femoral cartilage was smaller compared to that of tibial cartilage in normal and moderate OA, indicating less progressive fibril recruitment as a function of strain.

Introduction

Osteoarthritis affects the main constituents of articular cartilage (i.e., collagen network, PGs and interstitial fluid) [1,2]; thus, weakening the tissue function. FRPE modeling of cartilage tissue can quantify constituent-specific material properties and reveal their contributions to tissue mechanical response [1]. However, these properties are not known for human femoral cartilage. Thus, we aimed to quantify these properties and characterize how they compare to other cartilage sites in the knee joint at different stages of OA.

Methods

Osteochondral samples ($n = 35$) were extracted from medial and lateral femoral condyles of 14 total knee replacement patients and 10 donors without known clinical knee OA. A 3-step stress-relaxation protocol in indentation consisting of 5% strain and 15 minutes of relaxation at each step was applied. Sample-specific axisymmetric finite element models were created in Abaqus and cartilage tissue was modeled using the FRPE material model. The material parameters were obtained by minimizing the difference between the simulation results and experiments in the 2nd and 3rd stress relaxation steps (Matlab). Samples were histopathologically graded by OARSI score and grouped to *normal* (grade = 0-1, $n = 17$), *moderate OA* (grade = 2-3, $n = 15$) and *severe OA* (grade = 4, $n = 3$). An age-adjusted linear mixed model was used to compare the femoral cartilage material parameters **1**) between normal and moderate OA at medial and lateral condyle, **2**) with those of tibial [1] and patellar cartilages [2].

Results and Discussion

We did not observe essential differences between normal and moderate OA femoral condyle cartilage samples. However, in normal and moderate OA femoral cartilage, the strain-dependent fibril network modulus was smaller by 11.64 and

15.72 MPa compared to tibial cartilage (Figure 1), indicating that the superficial femoral cartilage has a more homogenous structure (homogenous structure leads to less progressive recruitment of fibers, represented in the model as a smaller strain-dependent fibril network modulus). In moderate OA, the initial fibril network and non-fibrillar matrix moduli of the femoral cartilage were greater than those of the tibial (0.77 and 0.18 MPa) and patellar cartilages (0.69 and 0.21 MPa); suggesting that the OA-related changes in PG and collagen matrices of femoral cartilage may occur later compared with other sites. In the severe OA, statistical tests could not be performed due to the small sample size ($n = 3$).

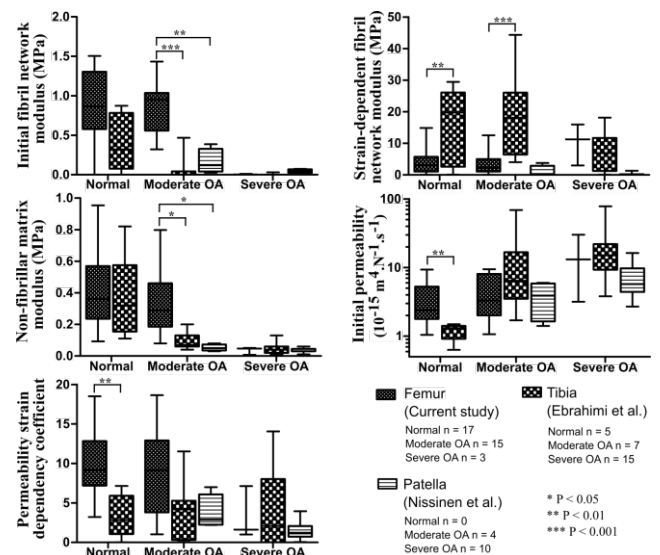


Figure 1: The fibril-reinforced poroelastic properties of human femoral cartilage compared to those of tibial and patellar cartilages.

Conclusions

The initial fibril network and non-fibrillar matrix moduli of femoral cartilage were greater compared to those of tibial and patellar cartilages, in the moderate OA, while the strain-dependent fibril network modulus of femoral cartilage was smaller compared to that of tibial cartilage in normal and moderate OA, suggesting less progressive fibril recruitment.

Acknowledgments

Emil Aaltonen Foundation, Academy of Finland, Finnish cultural Foundation, and The Swedish Research Council.

References

- [1] Ebrahimi M et al. (2019). *Ann Biomed Eng*, **47**:953-966.
- [2] Nissinen M et al. (2020). *ORS Annu Meet*, No.1500.

Development of a high-density EMG-driven Hill-type muscle model

Arnault Caillet¹, Andrew T.M. Phillips¹, Alessandro Del Vecchio³, Dario Farina², Luca Modenese¹

¹Dept Civil Engineering, Imperial College London, UK

²Dept Bioengineering, Imperial College London, UK

³Dept of Artificial Intelligence in Biomedical Engineering, University of Erlangen-Nürnberg (FAU), Germany

Email: arnault.caillet17@imperial.ac.uk

Summary

We developed a computational model of a muscle actuator composed of in-parallel Hill-type models of motor units (MUs) using as inputs the motor unit discharge times obtained from decomposed high-density surface EMG (HDEMG) signals. We then used the model to simulate isometric muscle contractions. This work extends the traditional Hill-type muscle models and enables further modelling possibilities such as HDEMG-based simulations and controllers.

Introduction

In computational muscle modelling, whole muscle dynamics are mostly described as a single functional MU modelled with a Hill-type model. This assumption requires lumping the MU neural contributions to a single control [1], that is dissociated from the physiological control of muscle forces, which limits the range of uses of these models. Recent advances in the acquisition and decomposition of HDEMG signals [2] open new possibilities for the definition and use of Hill-type models at the MU scale. In this work, we propose a multi-MU Hill-type muscle model driven by experimental motoneuron discharge times obtained from HDEMG recordings [2].

Methods

The time-histories of the discharge times $sp_i(t)$ of 32 identified MUs were obtained from blind source separation of HDEMG signals acquired during an isometric trapezoidal contraction up to 35% of the maximum force of the tibialis anterior (TA) muscle of a healthy subject (male, 27 years old, 189 cm, 77 kg) [2]. The whole muscle (Figure 1A) is modelled as 32 in-parallel Hill-type MU actuators. The excitation and activation dynamics of each MU are modelled using an updated Hatze's model [3] with parameters recalibrated using mammalian data. In this model, each neural discharge time $sp_i(t)$ fires a model of neural action potential which drives two cascading second-order differential equations of the dynamics of the muscle action potential (MAP) (excitation dynamics) and of the length-dependent calcium concentration transients in the sarcolemma (activation dynamics). The active state obtained from an adapted calcium-dependent 8-state model of cross-bridge attachment dynamics [4] scales a normalized isometric force-length relationship yielding the i^{th} MU normalized force. The following simplifying assumptions were made. The 32 identified MUs are representative of the population of recruited MUs at 35% maximum force and an exponential frequency distribution of the MU-specific maximum forces was considered. Accounting for the variation of optimal fibre lengths (l_0^M) with recruitment threshold, all MU dynamics are sub- l_0^M and passive parallel forces can be

neglected. The contribution of the short tendon of the TA is for now neglected. Finally, the 32 output MU forces are linearly summed to yield a whole muscle force profile $F^M(t)$.

Results and Discussion

The time profiles of the MAPs $u_i(t)$ and active state $a_i(t)$ of each i^{th} MU (Figure 1A) could be simulated from the HDEMG discharge times $sp_i(t)$, yielding a simulated whole muscle force $F^M(t)$ (red trace, Figure 1B) resembling experimental results (green trace, Figure 1B). Delays in force onset will be corrected by identifying or simulating the dynamics of supplementary representative MUs.

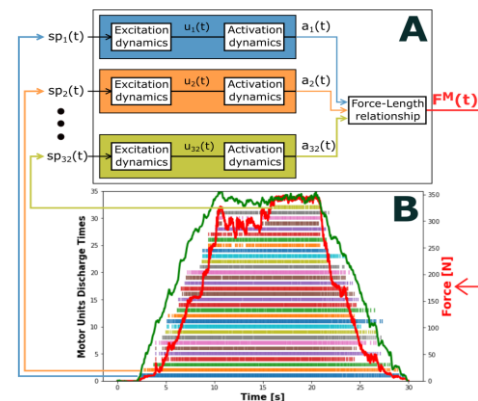


Figure 1: (A) Cascading dynamics of the 32-MU muscle model. (B) Discharge times of the 32 identified MUs. Experimental transducer force (green). Simulated whole muscle force (red).

Conclusions

This new muscle modelling approach enables the use of decomposed HDEMG signals with Hill-type muscle simulations. Defining a multi-MU muscle actuator with MU-specific properties clearly separates excitation and activation dynamics. Ongoing work will consolidate the current model by mapping the sample of identified MUs to an estimate of the entire population of active MUs, reducing the number of simplifications and using ad hoc experimental data for neural inputs and model calibration and validation.

Acknowledgments

Imperial College Skempton scholarship to A.C. and Imperial College Research Fellowship to L.M.

References

- [1] Sartori et al. (2017). *Sci Rep*, 7:13465
- [2] Del Vecchio et al. (2020). *J Elec Kin*, 53:1050-6411
- [3] Hatze (1977). *Biol Cyb*, 25:103-119
- [4] Zot et al. (2016). *Front Physiol*, 7:406

Semi-automatic quantification of muscles deformations during controlled exercises: application to the abdominal wall

Arthur Jourdan¹, Arnaud Le Troter², Pierre Daude², Stanislas Rapacchi², Catherine Masson¹, Thierry Bège^{1,3}, David Bendahan²

¹Aix-Marseille Univ, Univ Gustave Eiffel, IFSTTAR, LBA, F-13016 Marseille, France

²Aix Marseille Univ, CNRS, CRMBM, Marseille, France

³Department of General Surgery, Aix Marseille Univ, North Hospital, APHM, Marseille, France

Email: arthur.jourdan@univ-eiffel.fr

Summary

A genuine semi-automatic post-processing method has been designed for a fast and reliable quantification of abdominal wall muscles deformations during breathing and muscular contraction from real-time dynamic MR images.

Introduction

Kinetic imaging of the abdominal wall is largely underused in clinical practice. However, the quantification of abdominal muscles motion could bring valuable information in medical diagnosis of any situation involving abdominal muscle deficiency such as hernia, muscle dystrophy or obesity. It could also facilitate *in-vivo* patient-specific biomechanical characterization of muscle tissue.

A semi-automatic post-processing method dedicated to real-time dynamic MRI aiming at a fast and reliable quantification of abdominal wall muscles deformations during controlled exercises is reported.

Methods

Twenty healthy subjects (30.6 ± 8.7 y.o., 8 females) were scanned during a controlled breathing session, coughing and Valsalva maneuvering at the L3-L4 disc level using real-time dynamic MRI at 3T with a time resolution of 182ms.

In the corresponding image series, four regions of interest (ROIs) were segmented using a supervised 2D+ segmentation procedure [1]: right and left lateral muscles (RLM – LLM) and rectus abdominis muscles (RRA – LRA).

The evolution over time of the displacement magnitude of the muscles with respect to relaxed condition was computed from registration of the segmented masks [2].

Results and Discussion

As illustrated in Figure 1 for a typical subject, this evolution differs according to the type of exercise. During breathing and Valsalva maneuvering, maximum displacements (respectively 50mm and 25mm) are observed in the rectus abdominis muscles. The variation of RLM and LLM shape and thickness during Valsalva maneuver suggests greater muscle activation. During coughing the higher displacements (15mm) occurred in the deep zone of the lateral muscles, suggesting the activation of the transversus abdominis.

Our results support the specificity of muscle involvement during exercises and provide some quantitative metrics. The distribution of muscular displacements reported here supports the basic physiological knowledge regarding abdominal muscles activation [3] and is in agreement with previous studies reporting external measurements [4].

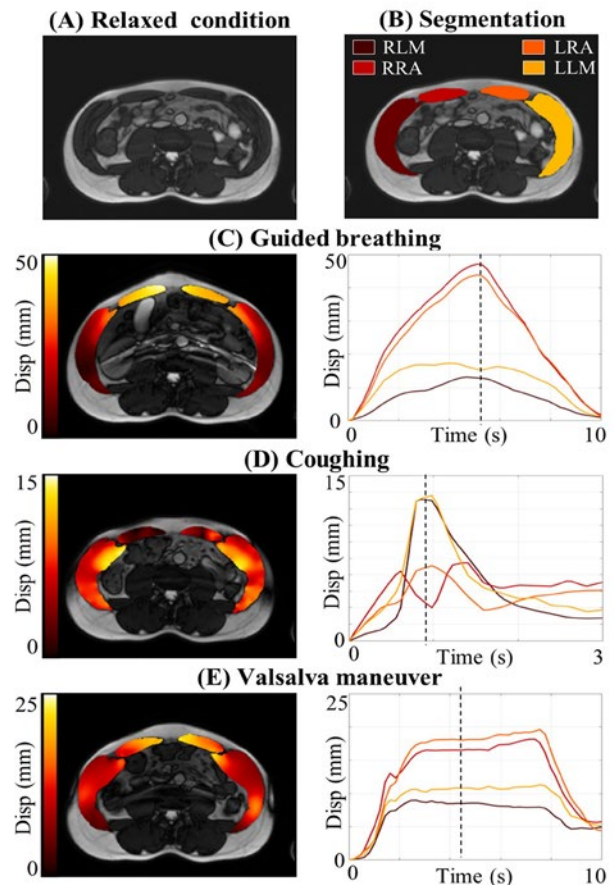


Figure 1: MR slice in relaxed condition (A); Segmentation ROIs (B); MR slice with 2D displacement field during: maximum inhalation (C), cough (D) and Valsalva maneuver (E); for each exercise the curves represent the evolution during time of the average displacement value in each ROI.

Conclusions

The present genuine post-processing method provides a quantitative analytical frame that could be used in further studies for the assessment of dysfunctions of the abdominal wall mobility and for a better understanding of abdominal wall biomechanics in physiological and pathological situations.

References

- [1] Ogier AC et al. (2020) *Magn Reson Med*, **83**:1825-1836
- [2] Jourdan A et al. (2021) *NMR Biomed*, **34**:e4470
- [3] Neumann P et al. (2002) *Int Urogynecol J*, **13**:125-132
- [4] Todros S et al. (2019) *Comput Methods Programs Biomed*, **175**:103-109

Evaluating and combining cost function criteria to predict healthy gait

K. Veerkamp^{1,2}, N.F.J. Waterval¹, T. Geijtenbeek³, C.P. Carty^{2,4}, D.G. Lloyd², J. Harlaar^{1,3,5}, M.M. van der Krogt¹

¹ Amsterdam UMC- Vrije Universiteit Amsterdam, Rehabilitation Medicine, Netherlands

² Griffith Centre for Biomedical & Rehabilitation Engineering (GCORE), Griffith University, Australia

³ Delft University of Technology, Dept. Biomechanical Engineering, Netherlands

⁴ Queensland Children's Hospital & Children's Motion Analysis Service, Australia

⁵ Erasmus Medical Center, Dept. Orthopedics, Netherlands

Email: k.veerkamp@amsterdamumc.nl

Summary

Accurate predictive simulations of human gait rely on optimization criteria to solve the system's redundancy. This study evaluated how well healthy gait could be predicted with a generic planar musculoskeletal model with 18 Hill-type muscles that were activated using a reflex-based, parameterized controller based on the weighted combination of different physiological-based cost function criteria (i.e., foot-ground impact, head stability, cost of transport, knee ligament use, and muscle activity). Criteria were first optimized individually, and then combined and weighted in a stepwise approach. The gait predicted with the combined, weighted cost function had better agreement with experimental data than when optimizing each criterion separately. Despite having a weak R^2 when minimized alone, cost of transport contributed most to the combined, weighted cost function.

Introduction

Predictive simulations of human gait rely on the optimization of criteria to handle system redundancy, yet these criteria are non-obvious. This study used different physiologically motivated criteria, and combined and weighted them in a stepwise manner to predict healthy gait and validate the predictions against experimental data.

Methods

A generic planar OpenSim [1] model with 18 Hill-type musculotendon actuators and nine degrees of freedom was controlled based on the model by Geyer and Herr [2]. Muscle excitations were generated using a combination of constant motor signals and reflexes based on muscle length and force, and active phases of gait. The parameterized controller was optimized using SCONE [3]. Each walk's simulation took 10 seconds and walking speed was free to vary. The initial pose and reflex gains were optimized for five cost function criteria: (1) cost of transport (CoT) using a muscle metabolic model [4], (2) muscle fatigue represented as activation squared, (3) head stability quantified by head acceleration per meter (HeadStab), (4) foot-ground impact quantified as the derivative of the ground reaction force per meter (FGImpact), and (5) extreme ranges of knee motion that minimized the use of knee ligaments (KneeInj). Coefficients of determination (R^2) quantified the agreements between simulated and experimental biomechanical variables, i.e., ground reaction forces (GRF); joint kinematics, moments and powers; and muscle activations. The average R^2 was calculated for each and across the variable categories.

The combined cost function was built in two stages. First, each criterion was optimized independently, except for KneeInj since it became zero when optimized alone. Second, the criteria were ranked by average R^2 and then added stepwise, in rank order, to create a combined cost function. At each step, criterion's cost-function weighting was systematically chosen to produce the best average R^2 , yielding the final combined, weighted cost function.

Results and Discussion

When optimizing for each criterion alone, the average R^2 was highest for FGImpact, followed by HeadStab, CoT, and MusAct (Figure 1). Average R^2 increased each step when combining the weighted criteria, yielding a combined cost function with an average $R^2=0.70$ (Figure 1 & 2). CoT had the highest normalized weighting in the combined cost function.

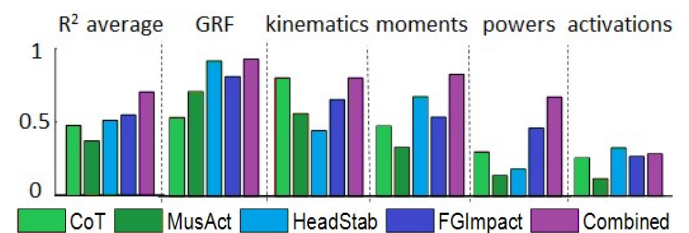


Figure 1: The agreement with experimental data (R^2) for each of the criteria separately and for the combined cost function.

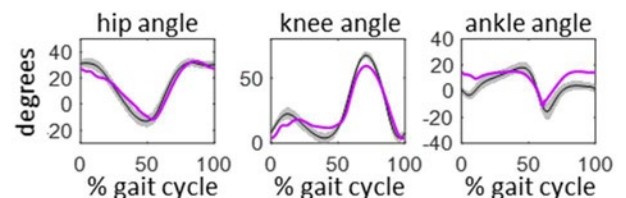


Figure 2: Kinematics predicted by the combined cost function (purple) compared to experimental data (black=mean; grey area=sd)

Conclusions

Tuning of the weightings in a cost function combining different criteria, in a stepwise approach, provided overall improved and acceptable agreement of the forward simulations of gait with experimental data. A next step is to validate the framework for pathological gait to be able to answer clinical what-if questions.

References

- [1] Delp S. L., et al., IEEE Trans Biomed Eng 54, 1940-1950, 2007
- [2] Geyer H. & Herr H., IEEE Trans Neural Syst Rehabil Eng 18, 263-273, 2010
- [3] Geijtenbeek T., JOSS 4, 1421, 2019
- [4] Uchida T. K., et al., PLoS One 11, 1-19, 2016

Simulations of walking with an ankle-foot exoskeleton to evaluate the predictive capability of neuromechanical models

Maarten Afschrift¹, Katherine Poggensee², Antoine Falisse³, Steve Collins², Friedl De Groot⁴

¹Robotics, Automation and Mechatronics, KU Leuven, Belgium, ²Biomechanics Lab, Stanford University, United States, ³Neuromuscular Biomechanics Lab, Stanford University, United States, ⁴Human Movement Biomechanics, KU Leuven, Belgium
Email: maarten.afschrift@kuleuven.be

Summary

We simulated walking with an ankle-foot exoskeleton to evaluate the predictive capability of a musculoskeletal model. Simulations were performed without prior knowledge of the experimental data. Predicted changes in muscle activity and metabolic rate were consistent with the direction, but not the shape or magnitude, of experimentally observed changes, while the simulation predicted some substantial changes in kinematics that were not observed experimentally.

Introduction

Forward simulations of human walking are currently being developed with the aim to predict the effect of interventions, such as a wearable robotic device, on human locomotion [1]. Even though these simulations capture important features of human walking [1], the predictive capability is unclear. In many studies, experimental data used for validation are also incorporated within the simulation (i.e. as a tracking term [2] or to tune high-level parameters), which limits the conclusions that can be drawn about predictive validity.

Here, we used physics-based simulations to predict the effect of an ankle-foot exoskeleton on human walking and evaluated model predictions against experimental observations that were shared after predictions were made.

Methods

We predicted walking with an ankle-foot exoskeleton using a framework for simulations of human movement [1]. A model (gait2392) was scaled to the subject [4]. The exoskeleton was modeled as rigidly connected to the foot and shank segments. Exoskeleton torque was a function of stride and was modeled as equal and opposite torques applied to the calcaneus and tibia. We predicted walking without the exoskeleton and with the exoskeleton in zero-torque mode and in active mode. Motions were predicted by minimizing a weighted multi-objective cost function consisting of (1) joint accelerations, (2) muscle activations, (3) metabolic energy [3], (4) passive forces and (5) actuators driving the arms while imposing average speed and periodicity of the movement [1].

We used integrated motion capture, electromyography and respirometry of one subject walking with and without bilateral ankle-foot exoskeletons, in zero-torque and assistance modes, to evaluate the simulations.

Results and Discussion

Simulation predictions of muscle activity were consistent with experimentally observed reductions in average activity, though not the timing of these reductions (figure 1). Soleus and gastrocnemius groups exhibited the largest changes.

The simulation predicted changes in kinematics that were not observed experimentally. The increase in ankle ROM in the active condition was overpredicted (figure 1). The simulation underpredicted step width by about 10 cm in all simulations.

The predicted decrease in cost of transport in the active mode was close to the experimental value, but the increase in cost of transport due to wearing the exoskeleton in zero-torque mode was underpredicted (figure 1).

Differences between the simulated and observed effects of wearing an exoskeleton on kinematics and cost of transport could only partly be explained by modelling the step width imposed by the split-belt experiment and adapting the baseline muscle activity in the simulation. In the next iteration, we will use a novel assistance profile to evaluate whether these adaptations improve the predictions.

Conclusions

Predictive simulations of human walking can anticipate some changes in muscle activity and energy consumption in response to ankle-foot exoskeleton assistance. Further development is needed for more accurate predictions, especially of metabolic energy and joint kinematics.

References

- [1] Falisse, A. et al. (2019). *J. R. Soc. Interface* **16**
- [2] Koelewijn, A. D. et al (2016). *Gait Posture* **49**: 219-255
- [3] Bhargava, L. J. et al. (2004) **37**: 81–88
- [4] Seth, A. et al (2011). *Procedia IUTAM* **2**:212-232

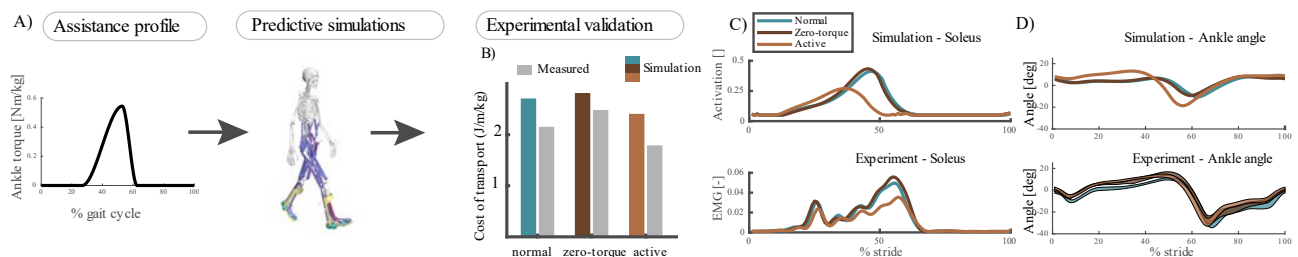


Figure 1: A) We simulated the effect of an ankle-foot exoskeleton and performed validation experiment afterwards. B) The effect of the exoskeleton on the cost of transport was underestimated in the prediction. C) Simulation predictions of soleus activity were consistent with observed reductions in average activity, though not the timing. D) The simulation predicted changes in ankle angle in the active mode were not observed experimentally.

Three-dimensional Knee Reduces Metabolic Cost and Joint Loading in Simulated Running

Ross H. Miller¹, Matthieu B. Trudeau²

¹Department of Kinesiology, University of Maryland, College Park, MD, USA

²Brooks Sports Inc., Seattle, WA, USA

Email: rosshm@umd.edu

Summary

Optimal control simulations of running with various cost functions were performed with knee models allowing one or three degrees of freedom. The results suggest non-sagittal knee motions can reduce metabolic cost and joint loading.

Introduction

“Overuse” running injuries at the tissue level can be viewed as biomechanical events that exhaust the fatigue-life of the injured tissue [1]. The Habitual Motion Path (HMP) theory suggests that knee injuries may be averted by running in footwear that affords movement along a trajectory in 3-D joint space that resembles its path in other activities of daily living [2]. HMP may also relate to running performance, e.g. perhaps economy is worsened by deviations from the HMP. HMP is conceptually similar to the “cartilage conditioning” theory which argues osteoarthritis results from joint loads that are “too unusual” compared to loads the joint typically sustains [3]. However, HMP remains untested as a causal factor to running injury or performance.

Computer simulations are useful for estimating internal loads that relate more directly to tissue damage than variables like ground reaction forces and joint motions. Most previous simulations of running have used knee models with one degree of freedom, making it difficult to test theories like HMP on the knee specifically. Our purpose was to compare running performance- and injury-related outcome variables from optimal control simulations between models allowing one vs. three degrees of freedom at the knee. As the study was exploratory, no hypotheses were posted, but we examined as outcome variables the metabolic cost and knee contact force.

Methods

Optimal control simulations of running were performed using a 3-D OpenSim model [4] (Fig. 1). Optimizations were performed in Moco software using direct collocation [5] to determine the muscle excitations and associated model states that minimized the cost function $J = J_{track} + w \cdot J_{effort}$, where J_{track} was the mean squared deviation from average human kinematic and ground reaction force data from instrumented gait analysis at an average speed of 3.2 m/s [6]. J_{effort} was defined with several different forms, the sum of muscle excitations raised to various integer powers, with or without muscle-specific weighting by muscle mass. The coefficient w had the same value for all simulations and was set so that the metabolic costs were realistic (~ 4 J/m/kg).

For the 3-D knee, torque-angle functions softly limiting frontal and transverse ranges of motion were defined using

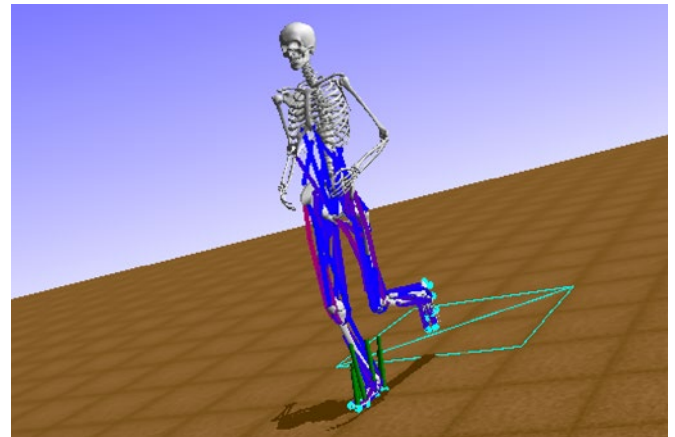


Figure 1: Modified Rajagopal model [4] in mid-stance from simulation of running at 3.2 m/s generated with Moco software [5].

cadaver data [7] and deviations of the frontal and transverse knee angles from zero were included in J_{track} .

Results and Discussion

Regardless of the cost function or knee degrees of freedom, the model tracked the experimental data with average errors less than 0.6 standard deviations away from the target means.

Regardless of the cost function, both metabolic cost (0.9-6.8% lower) and peak knee contact force (0.5-1.2 bodyweights lower) were reduced with a 3-D vs. 1-D knee, primarily due to less quadriceps force: peak force was up to 12% lower with the 3-D knee. Compared to joint angles from a simulation of squatting with minimum effort, the non-sagittal knee angles in running deviated from the squatting joint angles by up to 7° with the 1-D knee, compared to 3° with the 3-D knee.

Conclusions

A 3-D vs. 1-D knee reduced metabolic cost and knee contact forces even though the 1-D knee required no direct muscular effort to control non-sagittal motions. The theory that non-sagittal knee motions similar to habitual motions are beneficial for running performance and joint health warrants further attention. Suppressed or abnormal non-sagittal knee motions may cause unusual motions at other joints.

References

- [1] Edwards WB (2018). *ESSR*, **46**: 224-231.
- [2] Willwacher S et al. (2020). *Sci Reports*, **10**: 1363.
- [3] Seedhom BB (2006). *Rheumatology*, **45**: 146-149.
- [4] Rajagopal A et al. (2016). *IEEE TBME*, **63**: 2068-2079.
- [5] Dembia CL et al. (2020). *PLoS Comp Bio*, **16**: e1008493.
- [6] Miller RH et al. (2014). *MSSE*, **46**, 572-579.
- [7] Markolf KL et al. (1976). *JBJS*, **58-A**: 583-594.

Simulating Human Movements for Assistive Robotics

C. Karen Liu, Associate Professor of Computer Science, Stanford University

Unlike conventional robots, robots that physically assist humans need to embrace physical contacts and learn to utilize them for enabling human's activities of daily living. An immediate concern in developing such an autonomous and powered robotic device is the safety of human users during the early development phase when the control policies are still largely suboptimal. Learning from physically simulated humans and environments presents a promising alternative which enables robots to safely make and learn from mistakes without putting real people at risk. However, deploying such policies to interact with people in the real world adds additional complexity to the already challenging sim-to-real transfer problem. In this talk, I will present our current progress on solving the problem of sim-to-real transfer with humans in the environment, actively interacting with the robots through physical contacts. We tackle the problem from two fronts: developing more relevant human models to facilitate robot learning and developing human-aware robot perception and control policies. To contextualize our research effort, we develop a mobile manipulator to put clothes on people with physical impairments, enabling them to carry out day-to-day tasks and maintain independence.

Micro-structured Hollow Fiber Membranes – Reducing the Main Transport Resistance in Membrane Oxygenators

Paul Ecker^{1,2}, Markus Pekovits^{1,2}, Benjamin Lukitsch¹, Martin Elenkov², Christoph Janeczek^{1,2}, Bahram Haddadi¹, Margit Gfoehler², Michael Harasek¹

¹Institute of Chemical, Environmental and Bioscience Engineering, TU Wien, Vienna, Austria

²Institute of Engineering Design and Product Development, TU Wien, Vienna, Austria

Email: paul.ecker@tuwien.ac.at

Summary

Micro-structured hollow fiber membranes allow an increase of the available gas exchange surface area and offer a great potential for oxygenator optimization. In this study, experimental and numerical methods were used to investigate the flow within fiber packings with various fiber geometries. By calculating the local Sherwood number, we demonstrate that there is a tradeoff between increased surface area and flow stagnation zones and propose an optimized geometry.

Introduction

Enhancing mass transfer in membrane oxygenators is a key point in designing more efficient products. One way to achieve this is the use of micro-structured fiber geometries that offer an increased surface area [1]. Experimentally validated, numerical simulations offer the possibility to estimate mass transfer capabilities of different fiber geometries and arrangements [2].

Methods

Several fiber geometries with varying surface area, yet equal average diameter, were created and set in a staggered arrangement, mimicking the flow inside a membrane oxygenator. In order to quantify the mass transfer capability of each fiber geometry, the local Sherwood number ($Sh = k_c d/D$) was calculated on the membrane surface using computational fluid dynamics (CFD). Steady state simulations were carried out using the open source CFD code OpenFOAM®. Experimental validation of the numerical results was done by micro particle image velocimetry (μ PIV) measurements. For this purpose, an acrylic test channel resembling the investigated fiber structure was built and experiments with various Reynolds numbers were performed. Velocity profiles at the center plane of the channel were extracted and compared to the numerical results. Based on the obtained Sherwood numbers, the CO₂ removal performance was predicted using the specific area of the different geometries.

Results and Discussion

The calculated flow field for two different fiber geometries is given in Figure 1. In comparison to the circular geometry, Structure 1 has an increased specific area of about 80 %, however also a less uniform velocity distribution with areas of high velocity between the tips of the fiber and areas of low velocity inside the cavities. Areas of low velocity are of importance in membrane separation processes as they lead to concentration polarization, i.e., regions that obstruct mass transfer due to the lack of convective transport.

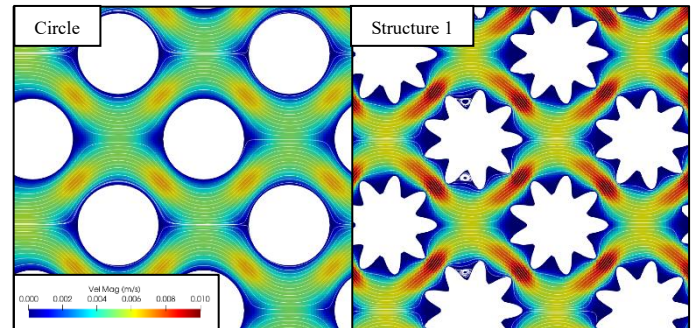


Figure 1: CFD result of the flow field for two different structures. Fluid flow is from left to right.

This is again reflected by the local Sherwood number along the circumference of the structures (Figure 2). Due to the low velocities, convective mass transfer is close to zero inside the cavities of Structure 1. Benefits of increased surface area are diminished by adverse flow structures if membrane module geometries are small.

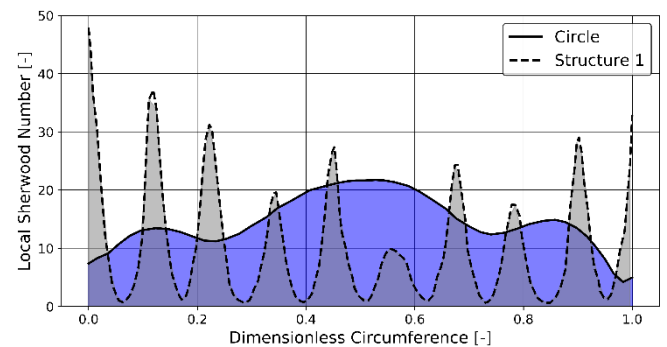


Figure 2: Local Sherwood number along the circumference of two structures.

Conclusions

Improving mass transfer by increasing membrane surface area is a feasible way to optimize oxygenators. Validated CFD simulations aid in the search for the best possible fiber geometry and arrangement.

Acknowledgments

This work is supported by the Austrian Research Promotion Agency (FFG). Project Nr. 23423220

References

- [1]. Liu, X. et al. (2011) *Chem. Fibers Int.*, **61**, 210–212.
- [2]. Santos, J.L.C. et al. (2007) *J. Membr. Sci.*, **305**, 103–117, doi:10.1016/j.memsci.2007.07.036.

Neck Muscle Network Topology Analysis in People with Chronic Neck Pain

David Jiménez-Grande¹, S. Farokh Atashzar², Eduardo Martínez-Valdes¹, Deborah Falla¹

¹Centre of Precision Rehabilitation for Spinal Pain (CPR Spine), School of Sport, Exercise and Rehabilitation Sciences, College of Life and Environmental Sciences, University of Birmingham, Birmingham, UK

²Electrical & Computer Engineering, as well as Mechanical & Aerospace Engineering, New York, United States

Email: dbj893@student.bham.ac.uk

Summary

This paper uniquely investigates how multi-muscle coordination in the neck is modified in people with chronic neck pain (CNP) through intermuscular coherence analysis.

Introduction

Neuromuscular impairments are frequent clinical features in patients with CNP; studies using electromyography (EMG) have revealed altered behavior of the neck muscles (e.g., increase co-activation, reduced specificity of activity, delayed onset) in patients with CNP compared to asymptomatic individuals [1]. We hypothesized that the connectivity between neck muscles will be modified in people with CNP. Verification of this hypothesis would provide further evidence of a common neuromuscular adaptation in people with CNP.

Methods

Twenty asymptomatic individuals and 20 people with CNP were recruited for this study. Participants were asked to walk barefoot at a self-selected speed along a curvilinear path (radius 1 meter) and along a rectilinear path (6 meters). EMG was recorded from the upper trapezius (UT), splenius capitis (SC), and sternocleidomastoid (SCM) muscles bilaterally.

Intermuscular coherence was used to map functional interactions between multiple muscles by the calculation of magnitude squared coherence (MSC). MSC generates a value of connectivity strength for each pair of filtered EMG signals at a specified frequency band, resulting in a weighted adjacency matrix per subject. This matrix is then thresholded in order to emphasize only significant connections and remove those that can obscure them. A proportional threshold was used to maintain the same connection density across participants. Once the average coherence matrix was obtained for each group, the connectivity between muscles can be represented graphically. Five frequency bands were considered in the calculation of the connectivity matrices to encompass the whole spectrum: δ (1–4 Hz), θ (4–8 Hz), α (8–12 Hz), β (12–25 Hz), and high β (25–30 Hz). To compare functional networks, we focused on strength and betweenness centrality (BC) features. BC identifies hot points of high information traffic and it is calculated as the proportion of shortest paths between all node pairs in the network that passes through a given index node. Strength is the sum of weights of links connected to the node that provides information about how strong the connections are between muscles [2].

Results and Discussion

The topology of complex networks was analyzed to compare functional interactions between neck muscles across different conditions and frequencies for both groups. The BC showed significance during curvilinear walking in the δ band between those with and without CNP ($p=0.021$). For rectilinear walking, BC was not significantly different between groups at the same frequency range ($p=0.068$). In contrast, the strength was not significant between groups. No significant differences were found in other frequency bands. Figure 1 shows neck muscle networks in the δ band for curvilinear and rectilinear walking where statistical differences were found. This band is the most relevant for the generation and control of force [3]. As can be seen in this figure, the muscle network in those with CNP presents thinner edges and a smaller number of connections, which suggests a weaker connectivity network between muscles during curvilinear walking [4].

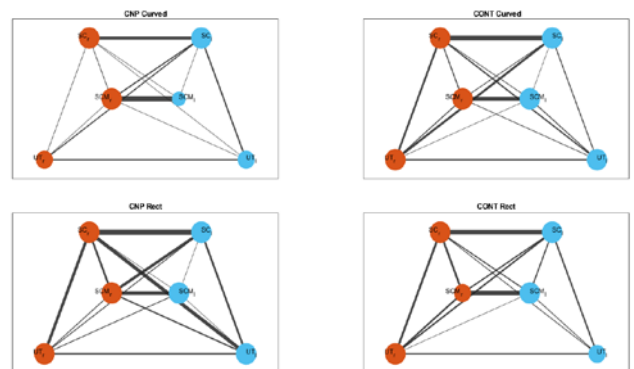


Figure 1: Functional networks of CNP and control groups during curvilinear and rectilinear task at δ band. Node's size represents the degree, which is the number of edges connected to other nodes (muscles). Connection strength is reflected by the width of the edge. Orange nodes represents left side muscles and blue nodes the right-side ones.

Conclusions

This study suggests different muscle synergies in people with CNP and the presence of task-specific muscle synergies that appear only when walking along a curved path.

References

- [1] D. Falla et al. (2009). *Clin Neurophysiol*, **5**: 744-53.
- [2] A. Fornito (2016). *Fundamentals of brain network analysis*; Academic Press.
- [3] Farina D et al. (2014). *J Physiol* **592(16)**:3427-41.
- [4] D.C. Hay et al. (2017). *Hum Mov Sci*, **54**: 101-109.

Quantitative evaluation of hypomimia in Parkinson's disease: a face tracking approach

E. Pegolo¹, L. Ricciardi^{2,3}, D. Volpe⁴, Z. Sawacha^{1,5}

¹ Department of Information Engineering, University of Padova, Padova, Italy

² St George's University of London, Molecular and Clinical Sciences Institute, London, United Kingdom

³ Medical Research Council Brain Network Dynamics Unit, Nuffield Dept. of Clinical Neurosciences, Oxford, UK

⁴ Fresco Parkinson Center, Villa Margherita, S. Stefano, Vicenza, Italy

⁵ Department of Medicine, University of Padova, Padova, Italy

Email: elena.pegolo@studenti.unipd.it

Summary

Parkinson's disease (PD) patients frequently experience an impaired facial expression with respect to healthy control (HC) subjects. In order to quantify the degree of hypomimia, we propose a preliminary assessment of facial expressivity using a face tracking methodology based on the Facial Action Coding System (FACS) [1]. A face mobility index is defined and compared between healthy and PD subjects in the six basic emotions.

Introduction

PD is a neurodegenerative disorder characterized by motor and non-motor symptoms. Among other features, hypomimia is considered one of the clinical hallmarks of this disorder [2]. However, quantitative measures of hypomimia are not currently available. FACS encodes changes in facial appearance by means of action units (AUs): AUs are associated with the contraction of specific facial muscles and completely describe the human basic emotions (anger, disgust, fear, happiness, sadness, surprise and neutral) [3]. Nowadays, FACS-based face tracking algorithms are mainly used for emotion recognition and classification, but they are not investigated in the medical research field. The aim of our study is to conduct a preliminary assessment to compare face mobility of HC and PD subjects exploiting a face tracking approach. Therefore, we propose a quantitative and easy-to-interpret index that can express the effects of the disease on the movement of face muscles involved in basic emotion expressions.

Methods

Data from 17 HC subjects (10 women and 7 men; mean(±SD) age: 66.53(±7.16) years) and 29 PD individuals (13 women and 16 men; mean(±SD) age: 68.48(±7.80) years) were analyzed. Frontal face videos of the subjects were recorded while they were instructed by a clinician to randomly perform the following facial expressions: anger, disgust, fear, happiness, sadness, and surprise. The neutral face expression was also acquired. Subjects were comfortably seated with a white background behind them at a distance of 1.36 m from a commercial camera placed at eye level. From the acquired videos, four frames were extracted per each expression. Based on the FACS encoding system, a set of 56 facial landmarks was defined and tracked in the 2D image space per each expression and frame, using a self-developed software (*TrackOnField, BBSof S.r.l.*) [4]. These coordinates were used to compute 35 Euclidean distances. Per each emotion, the ratio between the obtained distance and the one of the

neutral expression was derived (*ratio*). Values outside the interquartile range were excluded from the analysis. Moreover, a face mobility index (FMI) was defined and calculated per each subject as follows:

$$FMI_j = \frac{\sum_{i=1}^{n_dist} |1 - ratio_j| \cdot 100\%}{n_dist} \quad j = 1 \dots 6$$

Per each emotion ($j=1 \dots 6$) the FMI was determined as the summation of the percentage deviation from the neutral expression ($1-ratio$) of all the distances; the FMI was then normalized to the number of available distances (n_dist). The non-parametric Kruskal Wallis test ($p < 0.05$) was performed in order to compare the FMI in the two cohorts of subjects.

Results and Discussion

As expected, results showed a greater face mobility in HC subjects with respect to PD patients. Furthermore, statistically significant differences were highlighted in two expressions: anger and happiness (Figure 1).

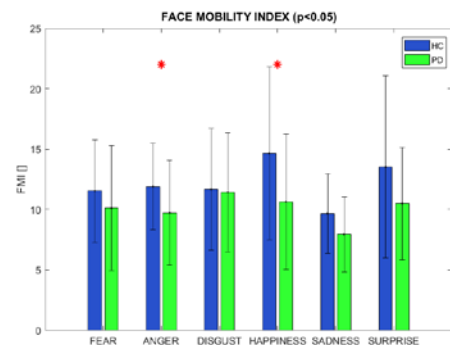


Figure 1: Comparison of FMI between HC and PD for the 6 emotions. The zero value corresponds to the neutral expression.

Conclusions

Besides some limitations (numerosity of the sample, subjectivity in the interpretation and expression of the emotion), promising results were achieved. The proposed face mobility index could be used as a quantitative measure for the degree of hypomimia in PD patients.

References

- [1] Ekman, P. (1978) *Facial Action Coding System: Investigator's Guide*; Consulting Psychologists Press.
- [2] Ricciardi L. (2017). *PLOS One*, **12(1)**:e0169110.
- [3] Wu P., et al. (2014). *Comput Math Methods Med*, **2014**.
- [4] Magalhaes FA et al. (2013). *J Sport Sci Med*; **12**:660.

Microfluidic Integrated Biosensor for detection of Osteoarthritis

Anupriya Singh^{1,2}, Walter Herzog³, Amir Sanati-Nezhad^{*1,2}

¹ BioMEMS and Bioinspired Microfluidic Laboratory, Department of Mechanical and Manufacturing Engineering, University of Calgary, Calgary, Canada

² Center for Bioengineering Research and Education, Schulich School of Engineering, University of Calgary, Calgary, AB, Canada

³ Human Performance Laboratory, Faculty of Kinesiology, University of Calgary, Calgary, AB, Canada

Email: amir.sanatinezhad@ucalgary.ca

Summary

A biosensor can detect as well as quantify the concentration of the biomarker in the body fluid, making it easy to monitor and or track the progression, making it effective to treat and change the course of treatment. Therefore, a microfluidic integrated electrochemical biosensor was fabricated to detect on-set and monitor the progression of the disease.

Introduction

Osteoarthritis (OA) is a common bone and joint disease and a leading cause of disability worldwide [1,2]. Biochemical markers of OA such as cartilage oligomeric matrix protein (COMP), C-terminal telopeptide, have been identified in bodily fluids, such as blood, and synovial fluid that are equally reliable be equally reliable for diagnostic and prognostic purposes as imaging technique [3]. The concentration of these markers classifies individuals as diseased or not, and its severity. Traditional ELISA-based analytical techniques detect biomarkers from the body fluids but cannot monitor the change in the biochemical signals. Conventional ELISAs-based analytical techniques can detect biomarkers from the body fluids but cannot monitor the change in the biochemical signals. Therefore, a more versatile detection system must be developed that can overcome the shortcoming of ELISAs and fulfill the clinical needs of OA. Sensors are compatible with different bodily fluids and detects up to picogram/mL analytes' concentrations. Microfluidics minimizes the use of synovial fluids and similar samples to a few microliters. Therefore, a microfluidic-integrated electrochemical biosensor must be developed for OA to detect and diagnose early-onset and monitor disease progression.

Methods

The microfluidic chip was fabricated using Polymethylmethacrylate (PMMA) sheet. The channels were designed in AutoCAD (student version), cut and engraved using LASER cutter. The active detection region was designed with the aim of working with 25 ul of sample.

The Biosensor was fabricated using a commercially available 3 electrode system with gold as active region Thiol-based self-assembled monolayer (SAM) surface modification was used to modify the surface of active region to facilitate immobilization of COMP specific antibody. Later, to block non-specific binding 0.01% bovine serum albumin was used as a blocking agent followed by 10 ng/ml COMP protein prepared in PBS that binds with the antibody. After incubating it for 30 min, the surface was cleaned with PBS and ready for

differential pulse voltammetry (DPV) measurements in the presence of redox probes.

Results and Discussion

Atomic force microscopy (AFM), and Scanning electron microscope (SEM), and Fourier transform infrared spectroscopy (FTIR) confirmed the successful surface modification of the biosensor. Electrochemical characterization using the DPV provides currents recorded for each step of the biosensor creation (Figure 1). The decreasing trend in the current peaks is indicates the active region's modification to a COMP-biosensor.

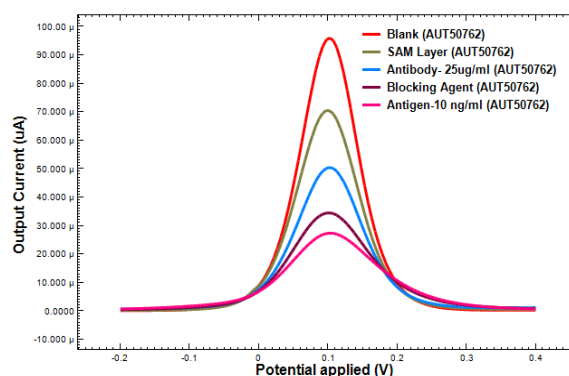


Figure 1: Characterization of the COMP biosensor by recording the DPV response in the presence of redox probes. Au bare (Red), Surface modification (green), COMP antibody (blue), and BSA blocking (brown), 10ng/ml COMP antigen.

The difference in the current peaks for the blocking step and 10 ng/mL COMP protein indicates the biosensor's ability to detect the quantify the target within the microfluidic chip.

Conclusions

The microfluidic biosensor fabricated is capable of selectively detecting the biomarker of OA by using just 25microlitre of sample. This can be used as a tool to monitor the progression of the disease by small sample volume.

References

- [1] Hip and Knee Replacements in Canada (2020) "Canadian Joint Replacement Registry Annual Report".
- [2] A Mobasheri, Y Henrotin, (2015) *Biomarkers of (osteo) arthritis*; Taylor & Francis.
- [3] WHO Department of Chronic Diseases and Health Promotion <http://www.who.int/chp/topics/rheumatic/en>.

A model for the biomechanical assessment of discoplasty in a laboratory setting

Salim Ghandour¹, Susanne Lewin¹, Konstantinos Pazarlis², Per Isaksson¹, Peter Försth², Cecilia Persson¹

¹Dept. of Materials Science and Engineering, Uppsala University, Sweden

²Dept. of Surgical Sciences, Uppsala University Hospital, Sweden

Email: salim.ghandour@angstrom.uu.se

Summary

Percutaneous cement discoplasty is a spinal surgical technique that has rarely been evaluated outside the clinical setting. This study aimed at developing an ovine model framework to allow testing and optimization of discoplasty in a controlled laboratory environment.

Introduction

Percutaneous cement discoplasty (PCD) is a minimally invasive surgical method developed for treating advanced degeneration in elderly patients whom, due to co-morbidities, cannot undergo major open surgery, in this case spinal fusion [1,2]. The procedure consists of the injection of poly(methyl methacrylate) (PMMA) into a disc via a Jamshidi needle entering either through the Kambin's triangle [1], or the vertebral endplate [2]. Insertion from the endplate avoids circumferential perforation of the disc.

To the best of the authors' knowledge, only one study has reported on the biomechanics of discoplasty [3]. In that study, the method of injury did not entail an overall annulus degeneration or an accurate representation of the vacuum phenomena. Therefore, the present study aims to develop a more clinically representative framework to explore PCD in a controlled laboratory setting. Papain-induced disc degeneration was used to this end. The obtained model could allow for optimization of the surgical procedure, materials used, and investigate the effect on the biomechanics of the spinal segments regardless of the needle's entry method.

Methods

Female sheep spines were cleaned, dissected and segmented to functional spinal units (FSU). They were submerged in phosphate buffer solution (PBS) and 1%vol penicillin-streptomycin for 24 h before testing. FSUs were scanned in a tabletop Skyscan 1172 CT and subsequently mechanically tested in dry conditions at a rate of 5mm/min on an MTS 858 Mini Bionix T/II.

A papain solution of 60 U/ml was prepared using a previously reported protocol [4]. Approximately 100 μ L was injected into the disc. The volume injected depended on the intradiscal pressure and size. The FSU was incubated at 60°C for 16 h. The FSUs were then rehydrated, scanned, and mechanically tested.

An orthopaedic surgeon (K.P) proceeded to perform the PCD procedure on the FSUs. A Jamshidi needle was guided using fluoroscopy into the intradiscal void. Vertebroplastic V-Steady™ PMMA bone cement (G21 srl, San Possidonio, Italy) was prepared and injected through the needle. The cement was left to harden for 24 h in PBS. The FSU was scanned and mechanically tested one final time.

Results and Discussion

Ten FSUs were used to optimize papain injection volume, as determined by comparison to the vacuum phenomena found in advanced degeneration in PCD candidate patients [5]. Figure 1 shows an L1-L2 FSU with a void created after degeneration with papain (left) and after treatment with cement (right). Three FSUs were successfully injected and scanned.

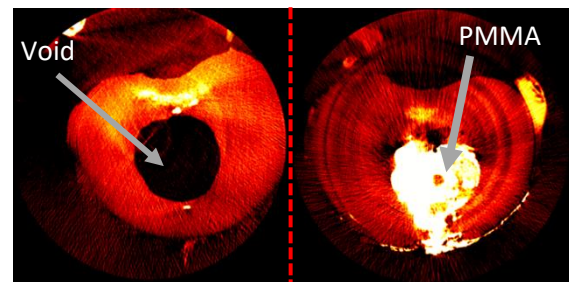


Figure 1: Shows CT images of a L1-L2 segment after degeneration with papain (left) and after treatment with cement (right).

The treated disc demonstrated increased mechanical stability, i.e. a significant increase in stiffness as opposed to the injured disc, confirming a positive biomechanical effect of the procedure in this aspect.

Future work includes increasing the sample size for statistical relevance, and further biomechanical investigation of treatment effects, e.g. after using different types of bone cements.

Conclusions

A methodology for the mechanical assessment of percutaneous cement discoplasty was developed. Early results show clinical relevance of the voids created in the intravertebral discs, and a biomechanically promising treatment demonstrated by an increased stiffness of the spinal segments.

Acknowledgments

This research has received funding from EIT Health (SOFTBONE, project nr 20519), supported by EIT, a body of the European Union and from the European Union's Horizon 2020 research and innovation programme under the Marie Skłodowska-Curie grant agreement No 812765.

References

- [1] Varga PP et al. (2015). *Orthopade*, **44**:1–8.
- [2] Yamada K et al. (2016). *Spine*, **41**:872–879.
- [3] Techens C et al. (2020). *Med Eng Phys*, **84**:51–59.
- [4] Schmocker A et al. (2016). *Biomaterials*, **88**:110–119.
- [5] Sola C et al. (2018). *Eur Spine J*, **1**:1–9.

How some insects adhere to underwater surfaces

Pranav Sudersan¹, Michael Kappl¹, Bat-El Pinchasik², Hans-Jürgen Butt¹, Thomas Endlein¹

¹Max Planck Institute for Polymer Research, Ackermannweg 10, 55128 Mainz, Germany

²School of Mechanical Engineering, Tel Aviv University, Tel Aviv-Yafo, Israel

Email: sudersanp@mpip-mainz.mpg.de

Summary

Some terrestrial beetles are able to walk underwater, presumably by trapping an air bubble around their feet. The bubble is thought to help in adhesion via surface tension forces, however its significance remained unclear. To investigate the exact role of the bubble, we performed *in-vivo* underwater adhesion measurements of a ladybug beetle's leg, as well as made theoretical estimates based on a simple model. Our experiments revealed that on a hydrophobic substrate, even without a bubble, the beetle exhibited similar adhesion underwater to that in air. On a hydrophilic substrate, underwater adhesion was significantly reduced, with or without a trapped bubble. Our results demonstrates that the wetting properties of the fluid secreted by the leg determines the insect's adhesion in both air and underwater conditions.

Introduction

Many small animals are able to adhere to smooth and slippery surfaces by using specialized adhesive pads on their feet, often consisting of a dense array of hair-like structures. The tip of each hair secretes an oily fluid, which promotes adhesion via surface tension, otherwise known as capillary forces. Typically, reversible and reliable underwater adhesion is complicated to achieve. However, a previous study [1] has revealed that terrestrial leaf beetles can attach quite well to surfaces underwater by trapping an air bubble around their pads. It has been hypothesized that a combination of capillary forces due the air bubble and hair contact within the de-wetted area results in its adhesion underwater. In this study, we aim to provide clarity on the source of insect adhesion underwater and the exact role played by the trapped bubble by a combination of experiments and theory.

Methods

Normal adhesion force measurements on a restrained leg of a live ladybug beetle (*Coccinella septempunctata*) were performed against smooth glass (hydrophilic) and fluorinated (PFOTS; hydrophobic) surfaces. Underwater measurements were also done in the absence of a trapped bubble by using degassed water.

The adhesive pad was then modeled as an array of cylindrical hairs with a certain amount of oil at the hair tips. Net adhesion was estimated as the sum of the capillary force contributions due to the oil bridges in contact with the substrate. Here, individual capillary forces due to the oil and the trapped bubble were calculated from Surface Evolver simulations. All model parameters were fixed corresponding to the ladybug beetle.

Results and Discussion

Experimental measurements (Figure 1) show that underwater adhesion on PFOTS surface is significantly larger than on glass. Here, the presence of a bubble does not appear to influence adhesion. But on glass, underwater adhesion is significantly lower than in air. The bubble's presence only slightly improves the adhesion underwater in this case.

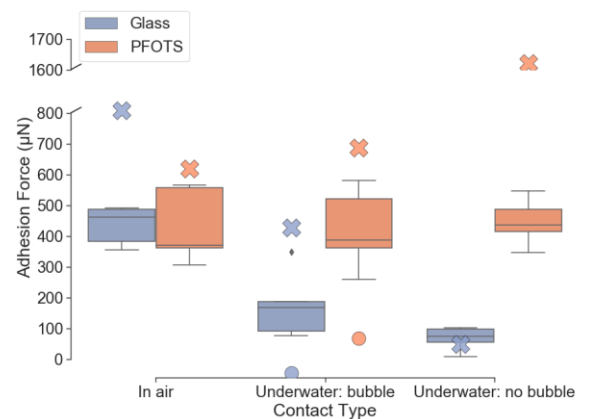


Figure 1: Single leg pull-off force of a ladybug beetle.

Theoretical predictions of the ladybug's adhesion from the model follow our experimental results ('x'). The model further shows that the bubble by itself has a negligible capillary contribution to the adhesion ('o'). The observed trend can be explained by the different oil interfacial tension and contact angles with each substrate in air and underwater, which determines the capillary adhesive force in each case. A similar reasoning also well predicts previously reported underwater measurements in geckos [2], which highlights the possibility of capillary contributions to gecko adhesion.

Conclusions

Animals can use its oily fluid secretions to adhere to surfaces even in underwater conditions. Due to the small contact angles of the oil to hydrophobic surfaces underwater, the animals achieve good adhesion even without a trapped bubble. Future studies should characterize the fluid secretion's interfacial properties with a substrate to better quantify the animal's adhesion, which may inspire reversible underwater adhesives.

References

- [1] Hosoda N and Gorb SN (2012). *Proc. R. Soc. B.*, **279**: 4236-4242
- [2] Stark AY, Badge I, et.al. (2013). *PNAS*, **110(16)**: 6340-63

Relatively Shorter Muscle Lengths Increase the Metabolic Rate of Cyclic Force Production

Owen N. Beck¹, Jordyn N. Schroeder¹, Lindsey H. Trejo¹, Jason R. Franz², & Gregory S. Sawicki¹

¹PoWeR Lab, School of Mechanical Engineering, Georgia Institute of Technology, Atlanta, GA, USA

²Applied Biomechanics Lab, Dept. Biomedical Engineering, University of North Carolina & North Carolina State University, Chapel Hill, NC, USA
Email: obeck3@gatech.edu

Summary

During locomotion, force-producing leg muscles are almost exclusively responsible for the entire body's metabolic rate. Animals can change the operating lengths of their leg muscles by altering body posture, kinetics, or the structural properties of their biological tissues via chronic exercise. Currently, it is uncertain whether muscle operating length has a measurable metabolic effect during cyclic locomotion-like contractions. Thus, we quantified the metabolic rate of human participants as they cyclically produce two distinct ankle moments at three separate ankle angles (90°, 105°, 120°) on a fixed-position dynamometer using their soleus. We found that increasing ankle angle decreased minimum soleus operating length by 17% ($p < 0.001$) and increased metabolic power by 208% ($p < 0.001$). Because we found an association between participant muscle fascicle operating length and metabolic power ($p < 0.001$), increasing the length of muscles that operate on the ascending-limb of their force-length relationship can likely reduce whole-body metabolic rate during locomotion.

Introduction

During locomotion, force-producing leg muscles are almost exclusively responsible for the whole-body's metabolic rate. One parameter that is not often considered to have a *measurable* effect on whole-body metabolism is relative muscle length. Perhaps, that is because muscle length is typically studied during isometric contractions [1], and it is difficult to isolate the metabolic effect of muscle length from other parameters during locomotor-like contractions (e.g., mechanical work). To help link locomotion biomechanics to metabolic rate, our goal was to determine the metabolic influence of cyclically producing force at different muscle fascicle lengths (Fig. 1). We hypothesized that cyclically producing the same average force at relatively shorter fascicle lengths would increase metabolic rate.

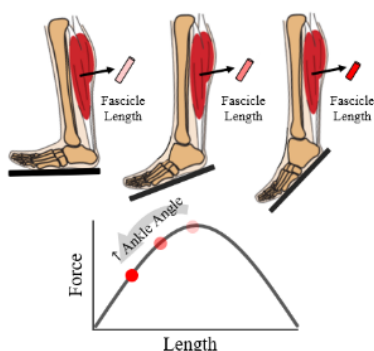


Figure 1. Three ankle angles (90°, 105°, and 120°) with the corresponding hypothetical soleus fascicle operating length and its region on a force-length curve.

Methods

Nine human participants cyclically produced ankle moments for five-minutes at two-distinct magnitudes and at three separate ankle angles (90°, 105°, 120°) on a fixed dynamometer using their soleus. During these trials, we collected rates of oxygen

uptake and carbon dioxide production, dynamometer torque data, motion capture data, soleus fascicle length via ultrasonography, and surface electromyography. We used linear mixed models and regressions to test the associations between independent and depend variables.

Results

Participants produced two distinct cycle average ankle moment levels: 4.85 Nm and 6.58 Nm ($p < 0.001$) (black & red symbols, respectively; Fig. 2). In each level, the duration of active force production ($p \geq 0.158$), force production cycle frequency ($p \geq 0.375$), and cycle average ankle moment ($p \geq 0.678$) were indistinguishable across ankle angles. Increasing participant ankle angle reduced their minimum soleus fascicle length by 17% ($p < 0.001$) and increased metabolic power by 208% ($p < 0.001$) (Fig. 2). Across moment levels, metabolic power was not driven by fascicle mechanical work ($p = 0.591$), fascicle force rate ($p \geq 0.235$), or active muscle volume ($p \geq 0.122$). Supporting our hypothesis, net metabolic power was correlated with participant average soleus fascicle operating length ($r = -0.72$ $p < 0.001$).

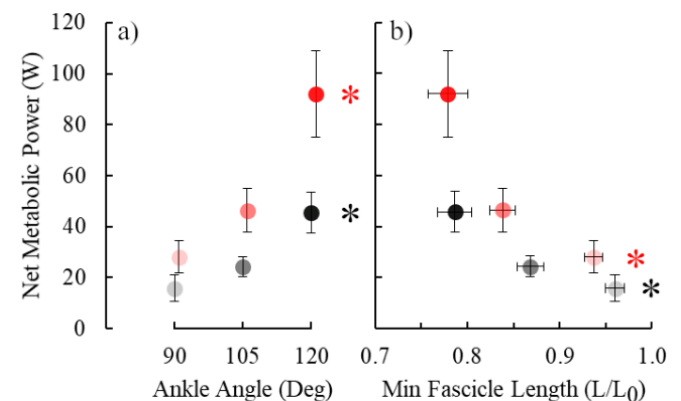


Figure 2: Average \pm SE net metabolic power versus a) ankle angle & b) minimum soleus fascicle length. Black and red symbols indicate lower and higher ankle moment levels, respectively. Asterisks (*) indicate statistical significance ($p < 0.05$).

Conclusions

Enabling active muscles to operate further up the ascending limb of the force-length curve may decrease metabolic rate during locomotion. These findings may help resolve why metabolic rate differs across and within animal species, in addition to informing biomechanical interventions aimed at augmenting locomotor performance.

References

[1] Hilber K et al. (2001) *J Physiol*, **531**: 771-780.

Cadaveric Demonstration of a Novel Stretchable Sensor to Wirelessly Measure Musculoskeletal Soft Tissue Strains during Passive Limb Motion

Qiang Zhang¹, Naomi Adam¹, Byron Llerena Zambrano², Katja Nuss³, Roland Küng⁴, William R. Taylor¹, Colin R. Smith¹

¹Laboratory for Movement Biomechanics, ETH Zürich, Zürich, Switzerland

²Laboratory of Biosensors and Bioelectronics, ETH Zürich, Zürich, Switzerland

³Musculoskeletal Research Unit, University of Zürich, Zürich, Switzerland

⁴Institute of Signal Proc. & Wireless Com., Zurich University of Applied Sciences, Winterthur, Switzerland

Email: bt@ethz.ch

Summary

To better understand musculoskeletal soft tissue (MST) strains in dynamic conditions *in vivo*, we have developed an implantable strain sensor capable of transmitting high-frequency data wirelessly across the skin. In this study, we surgically implanted one sensor on the quadriceps muscle of a sheep cadaver. Wireless measurements from the sensor indicated peak strains of 7.8% in the muscle during passive flexion of the stifle joint.

Introduction

Measurement of *in vivo* MST is critical for investigating muscle-tendon mechanics and informing data-driven treatment [1]. We developed a novel implantable strain sensor that innovates on existing designs through wireless data transmission and minimal impingement with neighboring tissues [2]. To prepare for *in vivo* applications, we performed a surgical implantation and demonstrated its efficacy in cadaveric sheep measurements.

Methods

A stretchable capacitive sensor was fabricated by embedding two nanowire layers within polydimethylsiloxane (PDMS). The capacitive sensor was connected to a coil antenna to form a passive inductor-capacitor-resistor resonator, and bonded to laser-cut PMMA suturing pads (Fig. 1, top). A custom pre-strain device facilitated suturing the sensor to muscle fascia and tendons. A readout system was developed to wirelessly excite the sensor and measure its resonance frequency (RF) across 1-2 cm of tissue with a rate up to 1024 Hz. Stretching the sensor resulted in a linear change in its RF over a 0-30% strain range, enabling wireless assessment of *in vivo* tissue strains. The sensor was calibrated using a custom stretching device. A 6 cm skin incision allowed the sensor to be implanted on the quadriceps muscle of a sheep cadaver (Fig. 1, bottom left), where the strain sensor was sutured onto the fascia of quadriceps muscle in a slack position. Subcutaneous pockets were formed to position the sensor coil, and the incision was closed. The lower limb was then manually manipulated through its full range of motion while the sensor RF was wirelessly measured across the skin.

Results and Discussion

The sensor design and surgical procedure enabled robust fixation to the MST. The wireless readout successfully

recorded the signal across the skin without disruption throughout the test. Post-experiment sensor calibration determined the sensor's sensitivity of 0.046MHz/mm. The peak strain in the quadriceps fascia during passive movement was 7.8%, which was measured at peak flexion of the stifle joint (Fig. 1, bottom right).

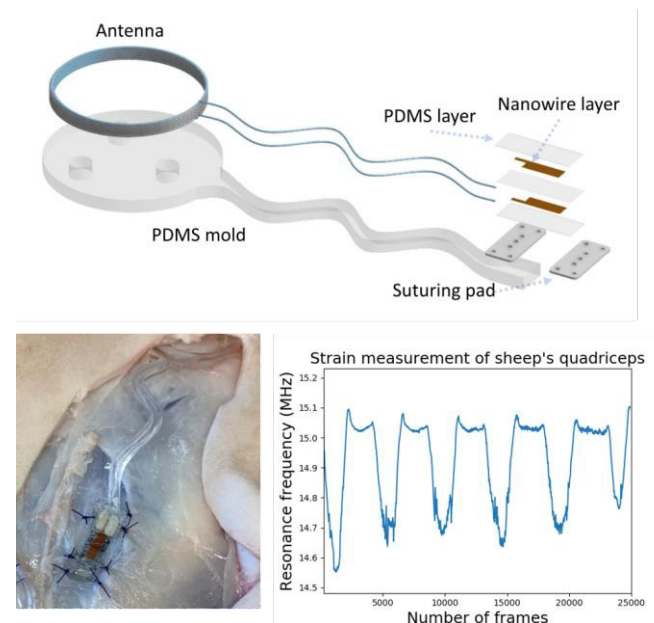


Figure 1: Top, Sensor structure; Bottom left, *In vitro* sensor implantation; Bottom right, Changes of sensor RF during test.

Conclusions

The successful surgical procedure and excellent sensor performance demonstrates that the stretchable sensor is ready for upcoming *in vivo* sheep measurements to investigate biocompatibility and muscle-tendon kinetic interactions during locomotion.

Acknowledgments

This study was funded by the Swiss National Science Foundation Project 182241.

References

- [1] Zhang Q et al. (2021). *Ann Biomed Eng*, **49**:7-28.
- [2] Stauffer F et al. (2018). *Adv Mater Technol*, **3**.

Morphological determinants of glenohumeral mobility in primates

Erin C.S. Lee¹, Nathan M. Young², Michael J. Rainbow¹

¹Mechanical and Materials Engineering, Queen's University, Kingston, Canada

²Orthopaedic Surgery, University of California, San Francisco, USA

Email: erin.lee@queensu.ca

Summary

Glenohumeral features are frequently used to infer functional demands in primates. The interactions among specific shape features and range-of-motion have been inferred but not quantified. Here, we use a congruence-based model to predict glenohumeral mobility across primate species and test its association with specific morphological features. Only glenoid orientation and glenoid surface area were correlated with mobility, indicating that the morphological pathways enabling mobility are more complex than previously assumed.

Introduction

Primate glenohumeral features are frequently used to infer functional demands in living and extinct taxa. For example, traits such as a relatively large humeral head, an oval-shaped glenoid, and a cranially-oriented scapula are found in suspensory apes and are thus assumed to enable enhanced range-of-motion (ROM) [1]. However, experimental ROM data opposes these assumptions [2], and the biomechanical pathways through which these features alter mobility remain largely untested. Computational models capturing the interaction between morphology and mobility can provide insight into glenohumeral mechanics and augment the current framework for mapping form-to-function.

Methods

Here, we use a 6dof model to estimate glenohumeral ROM, and test if specific morphological features are correlated with enhanced mobility. We acquired scapula and humerus meshes of sixteen subjects sampling living and extinct primate taxa (including lorines, suspensory monkeys, and apes) and used a novel congruence algorithm to simulate rotational positions spanning abduction, abduction plane angle, and long-axis rotation. The ROM was defined as positions where the humeral head and glenoid maintain congruence. We visualized these positions in Euler space and quantified *mobility* - a function of the size of the ROM (Figure 1) [3].

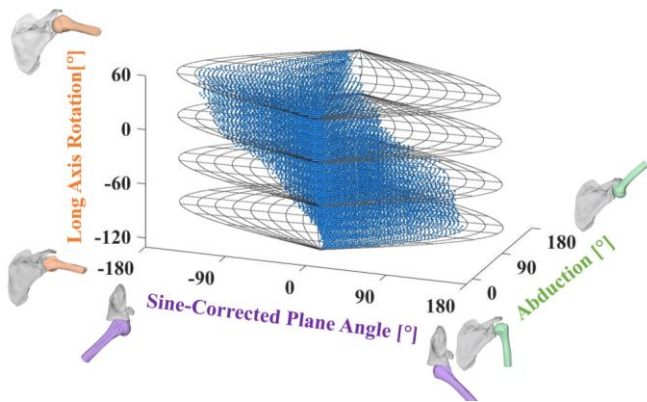


Figure 1: ROM positions of fossil hominin *Australopithecus sediba*. Plane angle is sine-corrected to account for distortion [3].

To determine morphological features important for mobility, we identified 22 and 20 landmarks on the scapula and proximal humerus, respectively. Following Procrustes superimposition, we regressed the landmark coordinates on mobility to visualize overall shape changes associated with enhanced ROM. Informed by the landmark visualization and long-held assumptions, we measured eight morphological parameters on scaled bone meshes and performed linear regression on mobility as a function of each parameter.

Results and Discussion

Predicted mobility was consistent with *a priori* expectations regarding locomotor repertoire, as mobility increased with suspensory behaviour. Contrary to previous assumptions, only two of the eight measured parameters – high cranial angle ($p=0.01$, $R^2=0.38$) and low glenoid surface area ($p<0.03$, $R^2=0.30$) – were associated with mobility (Figure 2). The landmark regression revealed potential factors for mobility requiring further investigation including acromion projection, humerus tubercle size, and glenoid curvature.

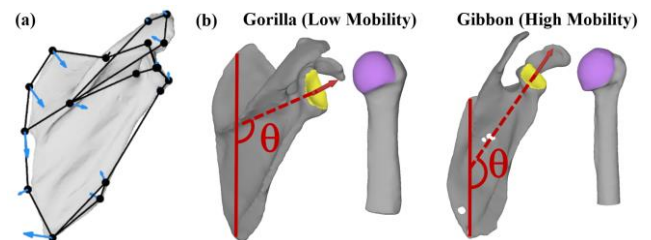


Figure 2: (a) Scapula landmarks and wireframe of mean shape, with blue arrows indicating landmark trajectories as mobility increases. (b) Comparison of least and most mobile subjects. The eight measured parameters were cranial angle (red) defined as the angle between the medial border and glenoid normal, glenoid surface area (yellow), humeral articular surface area (purple), critical shoulder angle, glenoid width, glenoid height, glenoid aspect ratio, humerus-to-glenoid surface area ratio, and humeral head radius.

Conclusions

Our congruence-based ROM predictions indicate that the morphological pathways enabling glenohumeral mobility are complex. Cranial angle and glenoid surface area are associated with mobility, but other features previously used to infer range-of-motion are not. Identifying shape features that best explain mobility in primates is necessary for reconstructing upper limb function in fossil taxa and may provide insight into why scapula shape is associated with shoulder injury in modern humans [4].

References

- [1] Arias-Martorell J. (2018). *Ecol. Evol.*, **9**: 703-722.
- [2] Chan LK. (2007). *Folia Primatol.*, **78**: 1-18.
- [3] Manafzadeh AR & Gatesy SM (2020). *J. Exp. Biol.*, **223**.
- [4] Lee ECS et al. (2020). *Clin Biomech.*, **78**: 105091.

Lateral stability and the frontal shape of land animals

Neelima Sharma^{1,*}, Madhusudhan Venkadesan^{1,§}

¹Department of Mechanical Engineering and Materials Science, Yale University, New Haven, CT, USA

Email: *neelima.sharma@yale.edu, §m.venkadesan@yale.edu

Summary

Among land animals, insects sprawl, small mammals crouch, and large mammals are upright, suggesting a scaling of frontal shape with size. We propose a scaling law for the frontal shape based on lateral stability considerations, governed by statistics of unevenness of natural terrain. Natural terrain is more uneven at the scale of small insects than larger animals. Therefore, to remain stable, we hypothesize that smaller land animals must have a landscape frontal profile, whereas larger animals can be portrait-shaped for stability. Using known terrain statistics across a range of sizes, we quantify frontal shape using the aspect ratio (a), the ratio of the base width to the center of mass height, and find that it scales with mass (m) such that $a \propto m^{-n}$, where $n=0.17$ for $a \ll 1$ and $n = 0.36$ for $a \gg 1$. Data from 369 species varying over 10^8 -fold in mass follow the predicted scaling and support the stability hypothesis.

Introduction

Control of balance during terrestrial locomotion is crucial to prevent falls, catch prey, and avoid predators. Lateral stability relies on the modulation of stance-width, so that wider is more stable [1]. A ubiquitous source of perturbations to lateral stability is the earth's uneven terrain. We hypothesize that animals have evolved their frontal shape to remain passively stable against the random height variations of natural terrain.

Methods

Natural terrain are well-approximated by a fractional Brownian process, namely a random process with fractional Gaussian increments [2]. The variance of the height difference z between two points that are horizontally separated by a distance l is given by $E[z^2] \propto l^{2H}$, where $0 < H < 1$ is the fractional exponent. Past measurements of natural terrain have characterized the unevenness using such a stochastic model and estimated values for H .

We consider an animal whose center of mass is at a height h above the ground, has width w for its base of support, and fore-aft length d . Its mass $m \propto dwh$, and the fore-aft length is known to scale according to $d \propto m^{1/3}$ [3]. These yield a relationship between mass and frontal plane dimensions. In order to remain barely stable, the critical angle of lateral tipping depends on the frontal aspect ratio $a = w/h$. When the tilt induced by the terrain z/l equals this critical angle, the animals is at the edge of becoming unstable (Figure 1a). We derive the scaling law for a critically stable animal and find $a \propto m^{-n}$, where $n=0.17$ for $a \ll 1$ and $n = 0.36$ for $a \gg 1$. In addition to a scaling for a typical animal, we derive a probability landscape for marginally stable animals as a function of their m and aspect ratio a (Figure 1b).

We collected data for the aspect ratio of the front profile and mass for 369 animals. Photographs of front profiles were analyzed to calculate the aspect ratio using Fiji (Version 1.0).

Results and Discussion

Data show systematic scaling of the aspect ratio with animal mass across over eight orders of magnitude such that small animals sprawl and larger animals are upright. The predicted scaling law and the probability densities agree with the trend in the data (Figure 1b).

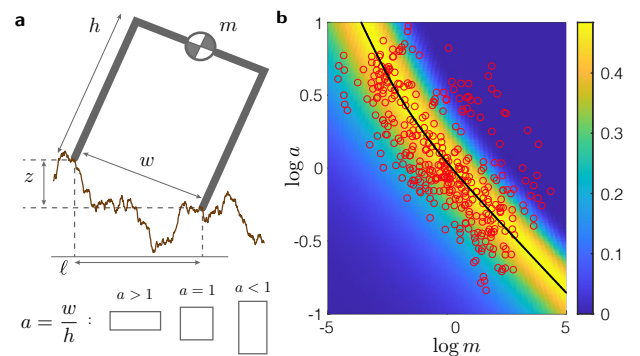


Figure 1: a. Terrain height perturbations inform the critical aspect ratio of the animal under the stability hypothesis. b. Data from 369 animals (red dots) follow the predicted scaling (black curve) and probability densities (heatmap) of aspect ratio and mass.

Conclusions

The frontal profile of diverse taxa, spanning a large range of body masses and habitats show systematic variation with mass in agreement with the scaling law derived using terrain unevenness statistics alone. The mean profile and the spread are consistent with the model. Underlying the model is assumption that marginal stability, and not maximal stability, is the driving factor. Although wider is generally more stable, being wide incurs other costs such as increased muscle stresses and metabolic energy for locomotion [4].

Acknowledgments

Larry Gall, Maishe Dickman, Peabody Museum (CT), Field Museum (IL), Joel Sartore, Prasenjeet Yadav for photographs.

References

- [1] Bauby CE and Kuo A. (2000). *Journal of Biomechanics*, **33(11)**: 1433-40.
- [2] Goodchild MF. (1982) *Modeling and Simulation*, **13(113)**: 3-1137.
- [3] Niklas KJ (1994). *Evolution*, **48(1)**: 44-54.
- [4] Biewener AA (1990). *Science*, **250(4984)**:1097-103.

Endoprosthesis size optimizes impaction force and circumferential stress in transtibial intramedullary prostheses

Carolyn E. Taylor^{2,3}, Heath B. Henninger^{2,3}, Kent N. Bachus^{1,2,3}

¹Department of Veterans Affairs, Salt Lake City, Utah, United States of America

²Department of Orthopaedics, University of Utah, Salt Lake City, Utah, United States of America

³Department of Biomedical Engineering, University of Utah, Salt Lake City, Utah, United States of America

Email: carolyn.taylor@utah.edu

Summary

Finite element analysis was used to estimate the force required for impaction and the circumferential stress around a conical endoprosthesis similar to those used for percutaneous osseointegration (OI) attachment of prosthetic limbs. This analysis revealed that there is an optimal size in each bone where force is maximized and stress minimized to improve initial fixation and decrease chances of fracture.

Introduction

Percutaneous osseointegration (OI) as a means of prosthetic limb attachment has experienced growing popularity with six systems in use worldwide. All of these devices were initially developed for transfemoral amputations, but many have been used in the tibia [1, 2] without translational research to indicate either similar, or better clinical results. While there has been some success, continued reports of aseptic loosening [3] indicate that tibia-specific endoprosthesis design may be needed for transtibial amputation patients.

This research examines the observations of cortical bone fracture during implantation of the endoprosthetic stem, occurring from excessive circumferential cortical stresses resulting from excessive impaction force.

Methods

Axial CT scans were collected with a calibration phantom (Mindways Software Inc., Austin, Texas) on three cadaver tibias (18, 34, and 46yr Caucasian males, 173, 188, and 183 cm tall, 86, 75 and 91 kg, respectively). 3D reconstructions were virtually amputated at 40% residual length and underwent a virtual surgical protocol to place an implant [4].

Bones were meshed with a coarse mesh proximally (1.2 mm edge length) tapering to a very fine mesh around the distal thin-walled region (0.2 mm). The endoprosthesis mesh had a uniform edge length of 0.7 mm. All meshes were constructed in 3-Matic (v13.0, Materialise, Plymouth, MI) and imported into FEBio Studio (v1.2, FEBio Software Suite, febio.org). Bones were assigned a neo-Hookean material, where density and Young's modulus values were derived from equations relating image intensity of the calibration phantom to bone in CT scans. A Poisson's ratio of 0.3 was assigned for the entire bone [5]. The endoprosthesis was assigned rigid body titanium material properties [5, 6].

The endoprosthesis was virtually implanted by positioning it into the bone according to a displacement ramp function. A sliding elastic contact interface was assigned between the bone and endoprosthesis [6]. A range of endoprosthesis sizes were simulated with the smallest barely in contact with the endosteal surface and largest just before penetration through the outer cortex. The impaction force and circumferential stress around the bone (first principal stress) were recorded. Results of each endoprosthesis size were normalized to the average diameter of the intact distal osteotomy.

Results and Discussion

The maximum impaction force of all bones modeled followed a bell curve with peak force occurring in the case where the endoprosthesis used was the same as the average diameter of the medullary canal at the distal osteotomy. Circumferential stress was lowest at or within one endoprosthesis size of this same endoprosthesis model (Figure 1). Larger endoprosthesis sizes caused an exponential increase in the circumferential stress.

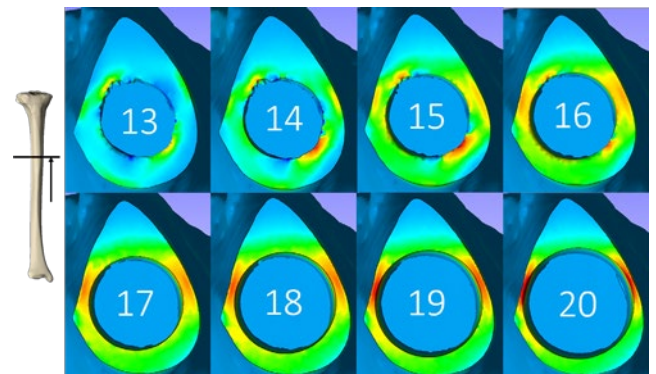


Figure 1: Circumferential stress distribution. Inset numbers indicate diameter (mm) of endoprosthesis used.

These data show that there is an optimal size endoprosthesis in each tibia where stress around the bone is minimized and force to impaction is maximized.

Conclusion

Size selection is determined by the operating surgeon when placing percutaneous OI implants. This research shows that the correct size selection determines initial fixation and fracture risk. Careful preoperative evaluation should be implemented to determine the implant size that minimizes stress while maximizing impaction force to encourage successful outcomes.

Acknowledgments

Research funding from the US Department of Veterans Affairs Rehabilitation Research and Development Service (#I01RX001246), the US Army Medical Research and Materiel Command (#W81XWH-15-C-0058).

References

- [1] Hoyt, BW, et al. (2020) *Expert Rev Med Devices*; **17**:17-25.
- [2] Thesleff, A, et al. (2018) *Ann Biomed Eng*; **46**:377-391.
- [3] Haque, R, et al. (2020) *BMJ Open*; **10**:e038346.
- [4] Drew, AJ, et al. (2020) *Clin Biomech (Bristol, Avon)*; **72**:108-114.
- [5] Robinson, DL, et al. (2020) *Clin Biomech (Bristol, Avon)*; **73**:201-212.
- [6] Tomaszewski, PK, et al. (2010) *Ann Biomed Eng*; **38**:2418-27.

Effects of cyclic loading on the mechanical properties and failure of human patellar tendon

Colin R. Firminger^{1,2}, W. Brent Edwards^{1,2}

¹Human Performance Laboratory, Faculty of Kinesiology, University of Calgary, Canada

²McCaig Institute for Bone and Joint Health, University of Calgary, Canada

Email: cfirring@ucalgary.ca

Summary

Nineteen human patellar tendons underwent cyclic loading until failure while anterior surface strain distributions were captured using digital image correlation (DIC). Creep rate and damage rate displayed high correlations ($r^2 \geq 0.86$) with the number of cycles to failure (N_f). Non-invasively tracking these measures – through ultrasound or other means – may provide meaningful predictions of patellar tendon failure *in vivo*.

Introduction

Patellar tendinopathy is a common overuse injury in basketball and volleyball athletes, owing to the repetitive loads their patellar tendons experience during jumping. Repetitive loading causes microdamage accumulation within the collagenous extracellular matrix, leading to a weakened tissue that is susceptible to injury [1]. This degeneration of stiffness and strength after submaximal repetitive loading resembles that of mechanical fatigue. Therefore, quantifying the fatigue behaviour of the patellar tendon may allow for the prediction of patellar tendon injury.

Methods

Nineteen whole patellar tendons, clamped at the patella and tibia bone, were cyclically loaded until failure. The cyclic loading protocol was segmented by four ramped loading tests to capture images for DIC analysis. Cyclic testing was performed in load control using a 2 Hz sinusoidal waveform. The minimum stress was set to 2 MPa and the maximum stress was randomly assigned to each tendon, ranging between 11% and 60% of the estimated ultimate tensile strength. Ramped loading tests were performed just prior to cyclic loading, and at timepoints corresponding to 10%, 20%, and 30% of maximum cyclic stiffness loss. Anterior surface strain distributions from the initial ramped test were used to calculate initial median strain. Creep rate (i.e., the rate of increase in peak cyclic strain) and damage rate (i.e., the rate of Young's modulus degradation) were calculated between 30-70% of N_f . N_f was correlated with the aforementioned variables, and anterior surface strains were visualized to examine the effect of cyclic loading on strain distributions.

Results and Discussion

Peak stress and initial median strain explained 65% and 60% of the variance in N_f , respectively. Creep rate had the strongest relationship with N_f ($r^2=96\%$, Figure 1), followed by damage rate ($r^2=86\%$). Anterior surface strain distributions illustrated strain concentrations within the tendon midsubstance that tended to grow in size and magnitude as the tendon fatigued (Figure 2).

Tendon failure at several length scales has been shown to be strain controlled [2]. Tendons with higher creep rates reached this limiting strain sooner and failed after fewer cycles, explaining the high correlation between this measure and N_f . Using DIC analysis, we observed the existence of localized strain concentrations that tended to increase in size and magnitude over the course of the cyclic loading protocol. This behaviour supports the hypothesis of load transfer between discontinuous fibrils via shear, which in turn begin to fail as peak strain increases with continued cyclic loading [3].

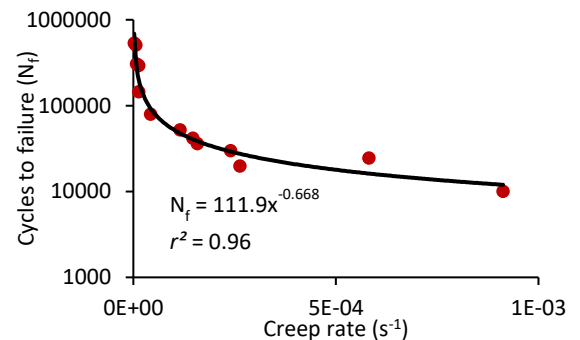


Figure 2: Creep rate versus cycles to failure.

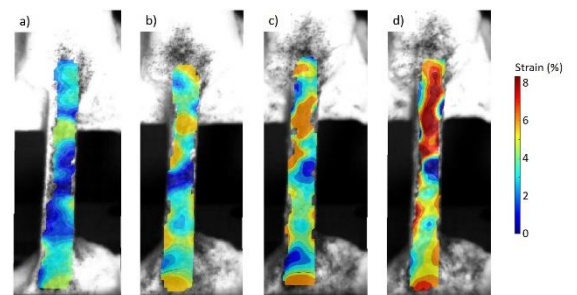


Figure 1: Axial surface strains of a representative sample at: a) 0%, b) 10%, c) 20%, and d) 30% of maximum stiffness loss.

Conclusions

Both creep rate and damage rate were highly predictive of patellar tendon fatigue failure. Thus, quantifying these rate-dependent measures with technologies such as ultrasound or shear wave elastography may be useful for the prediction and prevention of patellar tendon injury.

Acknowledgements

Research funding was provided in part by NSERC, Alberta Innovates, and the NBA/GE Healthcare.

References

- [1] Schechtman H et al. (2002). *J. Biomech.*, **35**: 347-353.
- [2] Zitnay JL et al. (2020). *Sci. Adv.*, **6**:1-10.
- [3] Szczesny SE et al. (2014). *Acta Biomater.*, **10**: 2582-2590

Mechanical Fatigue In Spinal Joints: Viscoelastic Responses To Altered Rate And Frequency of Compression Loading

Jackie D. Zehr, Jessa Buchman-Pearle, Jack P. Callaghan

Department of Kinesiology, University of Waterloo, Waterloo, Ontario, Canada

Email: jackie.zehr@uwaterloo.ca

Summary

This study examined a widespread experimental challenge associated with fatigue-failure analyses – the (potential) confounding effects of loading rate and frequency on the lifespan of spinal units. An *in vitro* paradigm was used to compare custom waveforms with equal compression rates and frequencies. Dose discrepancies were equalized between groups and revealed that the effect of loading rate on cyclic lifespan depends on loading frequency. Together, these findings have implications on the future examination of overuse injury pathways.

Introduction

Compression loads associated with habitual motor tasks can cause fatigue-failure in lumbar spine tissues [1]. Modulators of the demonstrated fatigue response in spinal joints [2] and isolated tissues [3] include load magnitude and frequency. Given that manipulation of these loading factors alters the applied loading rate, it is conceivable that the pattern of interaction may be influenced by viscoelastic tissue responses. As such, this study investigated the effects of loading rate and frequency on the fatigue response in isolated porcine functional spinal units (FSUs).

Methods

Thirty-two porcine FSUs (16 C3C4; 16 C5C6) were assigned to one of four experimental groups. Each group differed by average compression rate (4.2 kN/s \pm 0.25, 8.3 kN/s \pm 0.46) and frequency (0.5 Hz, 1 Hz). Custom haversine functions were developed (Figure 1).

Loading rates were controlled by normalizing the maximum compression to 20%, 40%, or 80% of the predicted ultimate tolerance and the minimum compression to 8% of the determined maximum. The discrepancies in compression dose – force-time integral – were normalized *post hoc* using dose correction factors computed from linear and nonlinear [4] risk-exposure relationships (Table 1).

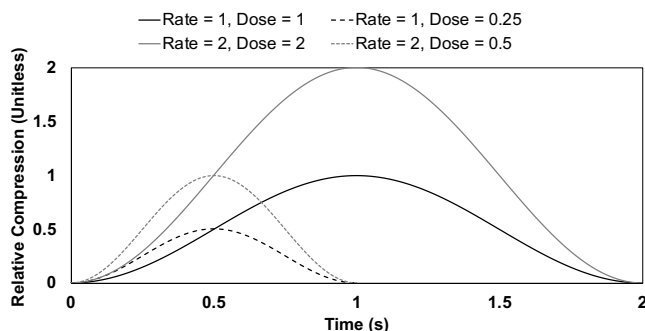


Figure 1. The relative compression signals.

Table 1. Dose correction factors for each condition.

	Linear		Nonlinear	
	4.2 kN/s	8.3 kN/s	4.2 kN/s	8.3 kN/s
0.5 Hz	1.00	2.00	1.0027	5.5
1 Hz	0.25	0.50	0.25	0.5013

Following a 0.3 kN preload and flexion-extension range-of-motion test, FSUs were positioned in the determined neutral posture. Cyclic testing was performed with a materials testing system until failure occurred or 10,800 cycles were tolerated. Force and displacement data were sampled at 100 Hz. Measurements of non-normalized and normalized (linear and nonlinear) cyclic lifespan were evaluated. A standard general linear model ($\alpha = 0.05$) was used to examine the effects of loading rate and frequency.

Results and Discussion

Significant main effects for loading rate and frequency were detected for the non-normalized cyclic lifespan ($p < 0.001$). FSUs tolerated 71% and 49% fewer cycles when loaded at 8.3 kN/s and 0.5 Hz, respectively.

A significant loading rate \times frequency interaction was observed following linear and nonlinear normalization ($p < 0.001$). The lifespan did not significantly differ (4%) between loading rates for a 1 Hz loading frequency ($p > 0.988$). At 0.5 Hz, the 8.3 kN/s loading rate reduced the lifespan by 97-99% ($p < 0.001$).

Conclusions

The effects of compression rate and frequency on fatigue-failure in isolated spinal joints were dependent on the normalization of differences in applied loading dose. Although the non-normalized lifespan findings align with the outcomes of previous fatigue studies [2,3], the emergent interaction between compression rate and frequency highlights the importance of dose-normalization for the examination of fatigue-failure at slower loading frequencies (i.e. 0.5 Hz).

Acknowledgments

The authors acknowledge funding from the Natural Sciences and Engineering Research Council of Canada.

References

- [1] Gallagher and Shall Jr. (2017). *Ergonomics*, **60**: 255-69.
- [2] Gooyers and Callaghan. (2015) *JBiomech*, **48**: 3701-08.
- [3] Wren et al. (2003). *Ann Biomech Eng*, **31**: 710-17.
- [4] Parkinson and Callaghan. (2005). *Theoret Issues Ergon Sci*, **8**: 171-8.

A one-dimensional viscoelastic model of collagenous tissues with damage

Jeff M. Barrett¹, Jack P. Callaghan¹

¹Department of Kinesiology, University of Waterloo, Waterloo, Canada

Email: jeffery.barrett@uwaterloo.ca

Summary

We present the addition of viscoelastic effects into an existing collagen distribution-based elastic model. The resulting model predicts a variety of established hyper-viscoelastic phenomena ubiquitous to biological tissues: hysteresis, stress-relaxation, creep, and, most notably, progressive failure.

Introduction

Macroscopic biomechanical models aiming to predict injury require biofidelic tissue models. The goal of this investigation was to present a biofidelic representation of biological tissues. We previously derived a partial differential equation (PDE) model which describes the rate of fibre-recruitment in a purely collagenous tissue [1], based on the Huxley muscle model:

$$\frac{\partial \rho}{\partial t} + v(t) \frac{\partial \rho}{\partial x} = -B(x, t) \rho(x, t) \quad (1)$$

Where $\rho(x, t)$ is the distribution of fibre strain (x) at the instant t ; $v(t)$ is the strain-rate; and $B(x, t)$ is the function describing the rate of failure of collagen fibres strained by x at an instant t .

Methods

We approximated $\rho(x, t)$ with a Gaussian distribution, and used the method of moments to reduce this PDE to a series of three ordinary differential equations (ODEs):

$$\begin{aligned} \dot{Q}_0 &= M_0 \\ \dot{Q}_1 &= M_1 + vQ_0 \\ \dot{Q}_2 &= M_2 + 2vQ_1 \end{aligned} \quad (2)$$

Where Q_0 , Q_1 and Q_2 are the estimated raw-moments of $\rho(x, t)$; M_0 , M_1 and M_2 are the approximations to the weighted product of $\rho(x, t)$ and $B(x, t)$, expressed as functions of Q_0 , Q_1 and Q_2 . Similar expressions have been derived for the DM approximation to the Huxley model [2]. A Voigt-element in series with this non-linear spring was used to represent the viscoelastic non-collagenous elements, which have been shown to play a critical role in viscoelasticity. Separate systems of differential algebraic equations (DAEs) were derived for strain-control and stress-control simulations.

Results and Discussion

The resulting model possessed several characteristics reminiscent of true biological tissues. These included stress-relaxation, hysteresis (Figure 1), failure, and, most notably, a three-phased creep curve. This curve begins with an initial deformation of the model, a prolonged quasi-static period, and an abrupt failure portion (Figure 2).

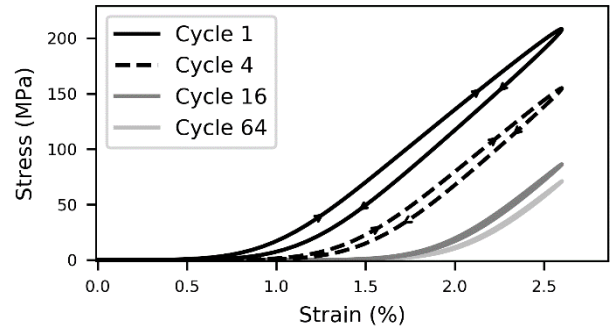


Figure 1: Cyclic loading demonstrating both the hysteresis (area between loading and unloading) and stress-relaxation predicted by the model.

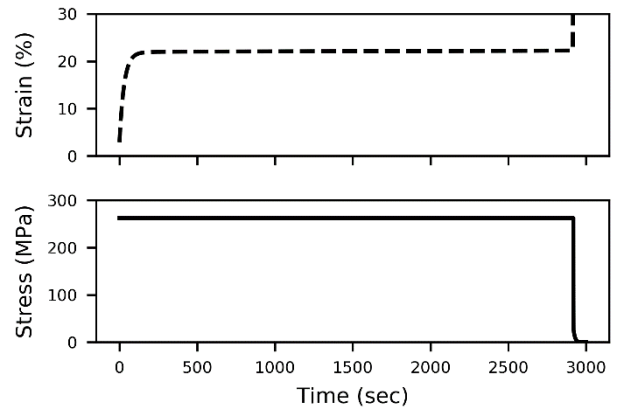


Figure 2: Model predictions during a prolonged creep protocol with strain (top) and stress (bottom).

Conclusions

The model agrees with several experimentally observed phenomena of biological tissues, including, most notably, fatigue. It may be used with macroscopic biomechanical models to aid in the understanding of these cumulative loading injuries and time dependent responses.

Acknowledgments

The authors acknowledge funding from the Natural Sciences and Engineering Research Council of Canada. JPC is the Tier 1 Canada Research Chair in Spine Biomechanics and Injury Prevention.

References

- [1] Barrett JM, Callaghan JP (2017). *JBiomech*, **61**: 11-17.
- [2] Ma S, Zahalak GI (1991) *JBiomech*, **24.1**: 21

Determining the Relationship Between Skull Diploë Morphometry and Mechanical Properties In Four-Point Bending

Kevin Adanty^{1,2}, Kapil B. Bhagavathula², Karyne N. Rabey³, Michael R. Doschak⁴, Dan L. Romanyk², James D. Hogan², Simon Ouellet⁵, Thomas A. Plaisted⁶, Sikhanda S. Satapathy⁶, Christopher R. Dennison^{1,2}

¹Biomedical Instrumentation Lab, University of Alberta, Edmonton, Canada

²Department of Mechanical Engineer, University of Alberta, Edmonton, Canada

³Medicine and Dentistry, University of Alberta, Edmonton, Canada

⁴Pharmacy and Pharmaceutical Sciences, University of Alberta, Edmonton, Canada

⁵Defense Research and Development Canada at Valcartier Research Centre, Valcartier, Canada

⁶US Army Combat Capabilities Development Command - Army Research Laboratory, Aberdeen, USA

Email: adanty@ualberta.ca

Summary

The mechanical properties of the human skull are influenced by its diploë morphometry. Trabecular thickness was positively correlated with bending modulus, whereas porosity and non-plate-like trabeculae were associated with a reduction of failure stress in bending. By identifying which morphometric properties are significantly associated with mechanical properties, surrogate designers and computational modelers can identify the morphometry to prioritize when designing a skull fracture model.

Introduction

Limited studies have examined the relationship between diploë morphometry and the mechanical response of cranial bone [1,2]. Adanty et al employed regression techniques to predict fracture strain from morphometry, however, the correlative relationship between morphometry and mechanical properties has not been examined [1]. Quantifying this relationship could increase our knowledge on the role of morphometry in mechanical response and provide morphometric data to design skull fracture models. The purpose of this work was to determine the correlation between diploë morphometry and mechanical properties of human skull specimens in quasi-static 4-pt bending. The null hypothesis was the correlation coefficient between morphometry and mechanical properties is equal to zero.

Methods

The methods were approved by the University of Alberta Research Ethics Board (ID: Pro00089218). All bodies were obtained through donation via the University of Alberta Anatomical Gift Program. From 10 embalmed cadavers (Male: 5, Female: 5), one parietal specimen was extracted from each skull (N=10). Each specimen was then scanned using micro-computed tomography (CT) (Bruker-Skyscan 1176) at a resolution of 18 μm to determine diploë morphometry: trabecular number (Tb.N), trabecular thickness (Tb.Th), porosity (%), and un-plate index (uPi). The specimens were then tested in quasi-static 4-pt bending using an Instron E3000 (Figure 1). The mechanical properties of interest were strain at failure measured using fiber Bragg gratings (FBGs), estimated failure stress, and an estimated effective bending modulus. Spearman's correlation tests were performed to determine the correlation coefficient (r_s) between morphometric and mechanical properties.

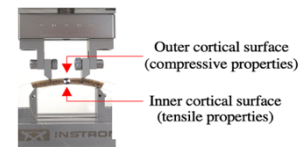


Figure 1: Specimen in 4-pt bending. Displacement rate: 2 mm/min

Results and Discussion

Table 1 presents significant r_s between morphometric and mechanical properties ($p < 0.05$). Porosity was negatively correlated with stress at failure. Non-plate-like trabeculae (uPi) was negatively correlated with stress and strain at failure. Tb.Th was strongly correlated (r_s close to 1) with compressive bending modulus. No significant correlations were found with Tb.N.

Table 1: Significant r_s between morphometric and mechanical properties ($p < 0.05$).

	Tb.Th	Porosity	uPi
Outer cortical failure stress	-	-0.78	-0.67
Inner cortical failure stress	-	-0.67	-0.70
Inner cortical failure strain	-	-	-0.68
Compressive modulus	0.89	-	-

Conclusions

Porosity, uPi, and Tb.Th had a significant association with the mechanical response of cranial bone during bending, thus rejecting the null hypothesis. These findings will support our next stage of work that will include the fabrication of a surrogate model of the skull for fracture simulation.

Acknowledgments

This research was sponsored by the Army Research Laboratory and was accomplished under Cooperative Agreement Number #: W911NF1920336. The views and conclusions contained in this document are those of the authors and should not be interpreted as representing the official policies, either express or implied, of the Army Research Laboratory or the U.S Government. The U.S Government is authorized to reproduce and distribute reprints for Government purposes notwithstanding any copyright notation herein.

References

- [1] Adanty K et al. (2020). *IRCOBI 2020*, 821-822.
- [2] McElhaney J et al. (1970). *J Biomech*, 3(5): 495-6.

Mechanical fatigue of whole rabbit-tibiae under combined compression-torsional loading is better explained by strained volume than peak strain magnitude

Ifaz T. Haider^{1,2}, Mattea Lee^{1,2,3}, Rebecca Page^{1,2}, Donovan Smith^{1,2}, W. Brent Edwards^{1,2}

¹Human Performance Laboratory, Faculty of Kinesiology and ²McCaig Institute for Bone and Joint Health, Cumming School of Medicine, University of Calgary, Calgary, Alberta, Canada

³School of Kinesiology, Western University, London, Ontario, Canada
Email: ifaz.haider@ucalgary.ca

Summary

We examined the mechanical fatigue behavior of whole rabbit tibiae under uniaxial compression and biaxial compression + torsion. In uniaxial loading, bones exhibited a logarithmic relationship between load and fatigue life ($r^2=0.68$). Similarly, fatigue life under biaxial loading decreased with greater superimposed torsion. Specimen-specific finite element (FE) modelling illustrated that spatial peak stress/strain poorly explained fatigue life variation under biaxial loads; variation was better explained by measures of stressed/strained volume. Strained volume based on pressure-modified von Mises strain explained 73% and 59% of the variation under uniaxial and biaxial loading, respectively. This highlights the importance of stress/strain distributions, not peak values, in the prediction of fatigue-life of whole-bone.

Introduction

Stress fractures are mechanical fatigue phenomena associated with progressive microdamage accumulation, material property degradation, and eventual structural failure with repetitive loading. Nonlinear relationships between load magnitude and fatigue life are well characterized in small material samples, but it is unclear if similar relationships can be extrapolated to more complex whole-bone structures. Material studies also identified that biaxial loading (compression + torsion), which occurs during running, may be particularly detrimental to fatigue life; again, this has not been demonstrated at the whole bone level. Finally, it is unclear how the complex distribution of stress/strain in whole bone structures relates to fatigue life. Thus, the purpose of this study was to quantify the fatigue life of whole-bones under uniaxial and biaxial loading, and to identify the relationship between fatigue life and FE predictions of stress/strain.

Methods

12 rabbit tibiae were cyclically loaded in uniaxial compression (peak load: 925-2450 N), until failure. Another 22 tibiae were loaded in biaxial compression + torsion. These bones were loaded to 50% compressive strength, and either 0% (n=10), 25% (n=6), or 50% (n=6) of torsional strength. Specimen-specific FE models were generated from computed tomography imaging prior to testing (220 mA, 120 kVP, 0.39 mm and 0.625 mm in-plane and between-plane resolution). Based on strain gauge testing, bone was modelled as a heterogeneous isotropic material, with modulus computed from CT intensity at each element. We examined principal, von Mises and pressure modified von Mises [1] equivalent

stress and strain, reporting the peak values and stressed/strained volume (volume above a threshold).

Results and Discussion

Under uniaxial compression, number of cycles to failure was well described by a logarithmic relationship ($r^2=0.68$; $p<0.001$). Similarly, fatigue-life in biaxial loading significantly decreased with the magnitude of superimposed torsion (Kruskal-Wallis test, $p=0.034$). From FE models, peak stress/strain demonstrated a poor correlation with fatigue life in biaxial loading conditions, explaining <38% of the variation; stressed/strained volume better explained variation in this loading mode (Fig 1). In particular, pressure modified von Mises explained 73% and 59% of variation under uniaxial and biaxial loading, respectively.

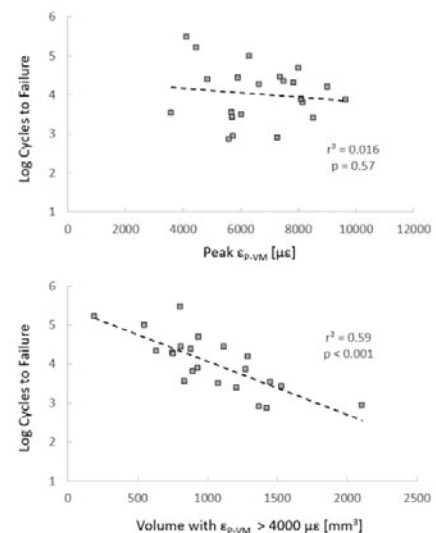


Fig 1 Log cycles to failure vs. pressure-modified von Mises Strain (ϵ_{p-VM}) under biaxial loading. Variation was better explained by strained volume (BOT; $r^2=0.59$) vs. peak strain (TOP; $r^2=0.016$)

Conclusion

Increased load was associated with nonlinear reductions in whole bone fatigue life under uniaxial and biaxial modes. Fatigue life variation was best explained by strained volume calculated from pressure modified von Mises strain. These results highlight the importance of stress/strain distributions, not peak values, in fatigue-life of whole bone. These findings have important implications for FE-based predictions of stress fracture risk.

References

[1] de Vree, J. et al. (1995). *Comput. Struct.* 7949, 581–588.

Quantification of 3-dimensional strength and pain in patients with shoulder osteoarthritis

Margaret S. Coats-Thomas^{1,2,5}, Emma M. Baillargeon^{1,2,4,5}, Daniel Ludvig^{1,5}, Guido Marra^{2,3}, Eric J. Perreault^{1,5}, Ameer L. Seitz^{2,4}

¹Biomedical Engineering, ²Feinberg School of Medicine, ³Orthopaedic Surgery, and ⁴Physical Therapy and Human Movement Sciences, Northwestern University, Chicago, IL, USA; ⁵Shirley Ryan AbilityLab, Chicago, IL, USA

Email: margaret.coats-thomas@northwestern.edu

Summary

Glenohumeral osteoarthritis (OA) can result in symmetric or asymmetric (eccentric OA) glenoid bone loss and causes pain and weakness. Unresolved strength imbalances are thought to contribute to inferior post-surgical outcomes in patients with eccentric OA, yet pre-operative strength has not been quantified. Further, current knowledge of strength in OA is confounded by pain. We sought to evaluate strength balance, accounting for pain, in patients with eccentric OA. As the shoulder functions in multiple degrees of freedom, we assessed 3-dimensional strength. Preliminary data suggest a pain-independent strength imbalance with relative weakness of extension and internal rotation in patients with eccentric OA compared to healthy adults. Our findings may provide insight to further enhance rehabilitation and surgical outcomes in patients with eccentric OA.

Introduction

Glenohumeral osteoarthritis (OA) results in shoulder weakness and pain. Post-surgical outcomes are inferior in patients with asymmetric glenoid wear (eccentric OA) [1], but it is not fully understood why. Imbalanced strength between agonist/antagonist rotator cuff muscles is theorized to play a role [2]; yet, strength balance has not been quantified in patients with eccentric OA. Further, pain likely impacts strength measures, but has not been accounted for previously [3]. We sought to determine if strength imbalances, when accounting for pain, exist in patients with eccentric OA, which may direct rehabilitation and improve surgical outcomes. The shoulder works in multiple degrees of freedom, so we measured strength in many directions to assess 3-dimensional (3D) strength.

Methods

Five patients with end-stage eccentric OA (2F; mean±SD: 58±17 yrs) and 26 healthy adults (14F; 59±13 yrs) participated. Participants performed maximal isometric contractions in 26 equally spaced directions spanning shoulder flex/extension, ab/adduction, and internal/external rotation. The affected (OA) or dominant (healthy) arm was casted, attached to a six degree-of-freedom load cell, and positioned in 90° abduction (healthy) or 50° scapular plane elevation (OA) to measure shoulder torque. Patients with OA rated pain (0-10) with each trial. Trials rated above the patient's average pain were plotted along the corresponding torque direction. Maximum torque in each direction was calculated. Strength magnitude was computed and normalized by bodyweight (Nm/kg). To quantify relative strength in opposing directions (strength balance), 3D torque data were averaged across all directions [4]. Mann-Whitney

U tests ($\alpha=0.05$) were used to test for differences in strength magnitude and strength balance between groups.

Results and Discussion

Preliminary results suggest strength magnitude is reduced in patients with OA compared to healthy adults (diff in mean rank, [95% CI]: -13.6, [-22.3,-4.9], $p=0.002$). We observed an unexpected shift in strength balance towards external rotation (-15.5, [-24.2,-6.8], $p=0.0005$, Fig. 1A) and flexion (+9.1, [+0.4,+17.8], $p=0.04$) in patients with OA compared to healthy adults. Among patients with OA, above-average pain was experienced in 13 unique directions. Only 3/13 directions were repeated in 2/5 patients.

The observed reduction in strength magnitude is expected with OA. Despite a consistent directional shift in strength balance, this was not observed in above-average pain (Fig. 1B). Our preliminary findings suggest patients with eccentric OA have pain-independent strength imbalances with relative weakness in extension and internal rotation.

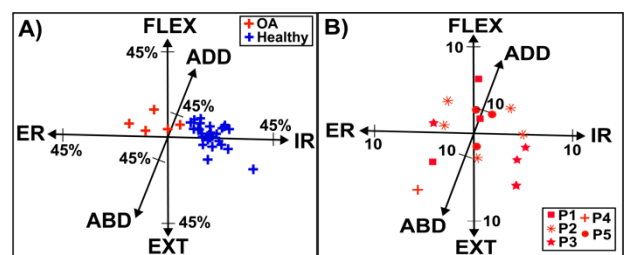


Fig. 1: **A)** 3D strength balance (% strength magnitude). **B)** Above-average pain in OA patients (P1-5). Flex/extension= FLEX/EXT. Ad/abduction= ADD/ABD. Internal/external Rotation= IR/ER.

Conclusions

Preliminary results suggest pain-independent strength imbalances with relative weakness of internal rotation and extension in patients with eccentric OA compared to healthy adults. These results highlight the utility of accounting for pain when measuring strength in this population. Our findings may guide rehabilitation to target strength deficits, potentially improving surgical outcomes. Future comparison to patients with symmetric glenoid bone loss is warranted.

Acknowledgments

NIH (F31-AR077426), Northwestern Orthopaedic Surgery

References

- [1] Walch G et al. (2012). *JSES*. **21**: 1526-33.
- [2] Donohue KW et al. (2018). *JBJS Am*. **100**: 381-7.
- [3] Sperling JW et al. (2008). *Int J Shoulder Surg*, **2**: 1-3.
- [4] Baillargeon EM et al. (2019). *J EMG Kinesiol*. **Online**

Anterolateral Versus Medial Plating for Varus Type Pilon Fractures

Marisa Kohut¹, Ali Ammar¹, Bashar Alolabi², Cheryl Quenneville^{1,3}

¹School of Biomedical Engineering, McMaster University, Hamilton ON, Canada

²Department of Surgery, McMaster University, Hamilton, ON, Canada

³Department of Mechanical Engineering, McMaster University, Hamilton ON, Canada

Email: ammara@mcmaster.ca

Summary

Pilon fractures occur mainly from high-energy impacts. Orthopaedic surgeons can repair these injuries using either anterolateral or medial fracture plates, but with little biomechanical basis for which provides superior stability. Paired cadaveric tibia-fibula specimens were ‘fractured’ and repaired with both types of plates (R/L randomized). Under axial loading, stiffness and strength were measured to determine which plating method provided the greatest stability. No benefits were found in choosing one plating technique over the other. These findings can be used to allow other factors such as soft tissues and surgeon preference to guide decision making.

Introduction

Pilon fractures are caused by high energy impacts, such as falls and automotive collisions, and typically result in a high level of comminution with articular surface involvement [1]. The most common treatment for pilon fractures is open reduction and internal fixation (ORIF) using medial or anterolateral plates. The current dogma is to put the plate across the opening side of the wedge, but there is no biomechanical data to support this. Patients after surgery report negative outcomes affecting their quality of life, regardless of the type of treatment [2]. The purpose of the present study was to evaluate different plating techniques on a varus fracture based on cadaveric specimen stiffness and strength.

Methods

A. Specimen Preparation: Six pairs of lower leg cadaveric specimens (tibia, fibula, and inter-osseous membrane) were used in this study. One specimen from each pair was randomly allocated to each plating type with the right and left assignment randomized. Specimens were potted proximally using dental cement in square metal tubing in an inverted position, vertically aligned using a bull’s eye level.

B. Fracture and Plating: Plates were pre-drilled and tapped into the specimen before the fractures were created. This allowed for planned positioning of the screws to ensure alignment post-repair. A typical Y-type intra-articular fracture was made on the articular surface using an oscillating saw. A varus wedge fracture was similarly created 4 cm from the medial gutter. A transverse fibular fracture was also created, aligned with the vertex of the wedge. Finally, plates were attached, lining the screws up to the pre-drilled holes.

C. Mechanical Testing: An artificial talus was made using bone cement (Simplex P, Stryker) to reduce unnatural stress

concentrations yet be able to transmit high loads to the tibial plafond. Cyclic loads were applied quasi-statically from 75-400N at a rate of 0.1 mm/s for 10 cycles using a material testing machine (Instron 5967, Canton MA, USA). The stiffness was calculated, then a ramp load was applied to failure, which was defined as a load drop greater than 100 N.

Results and Discussion

The medial plated specimens tended to be stiffer than the anterolateral plated specimens, but this was not significantly different (M: 601.7 ± 135.2 N/mm; AL: 472.6 ± 150.3 N/mm; $p=0.28$). The failure load for the medial plated specimens was not different from that of the anterolateral plated ones (M: 3096 ± 1826 N; AL: 2760 ± 1279 N; $p=0.73$) (Figure 1).

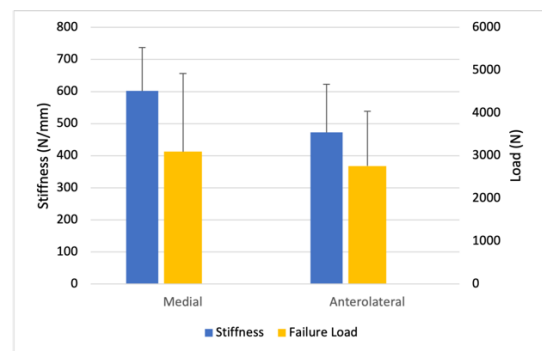


Figure 1: Repaired Stiffness and Load to Failure Results

Although there was no significant difference between the two plating methods (potentially attributable to the low number of specimens used), this study allowed for direct comparison by using paired specimens to assess both plating methods. As the biomechanical performance was similar, this allows other factors such as soft tissue access and surgeon preference to guide the decision making.

Conclusions

Based on stiffness and strength, both techniques appear to be valid for repairing varus pilon fractures.

Acknowledgments

Surgical materials (plates and screws) were provided by DePuy Synthes through an Investigator Initiated Study. Other funding is through NSERC Discovery program.

References

- [1] S.-jun Wei et al. (2014) *International Journal of Surgery*, **12**: 418-425.
- [2] M.B. Cutillas-Ybarra A et al. (2015). *Journal of Orthopaedics*, **46**: 2253–2257.

A Biomechanical Analysis of Body Mass Index on Frontal Plane Kinetics and Kinematics between Controls and Total Knee Arthroplasty Patients

Laura M. Linsley¹, Samantha Andrews², Cris Stickley¹ and Cass Nakasone²

¹University of Hawaii at Manoa, Honolulu, Hawaii

²Straub Medical Center, Honolulu, Hawaii

Email: lmflynn@hawaii.edu

Summary

Varus malalignment and increased knee adduction moment (KAM) in knee osteoarthritis (OA) and subsequent post-total knee arthroplasty (TKA) patients are associated with worsening symptoms and poor outcomes. These gait patterns were present in OA patients compared to controls in the current study, with the greatest KAM, KAM impulse and knee adduction angle in obese OA patients.

Introduction

While higher KAM and knee adduction angles have been linked to progression of OA and poor post-TKA outcomes [1], the deleterious effects may be even more pronounced in obese patients [2, 3]. Based on the lack of previous research comparing pre- and post-TKA patients to controls and with the increasing prevalence of both obesity and knee OA, the current study compared walking frontal plane gait in healthy controls and TKA patients pre- and 12-months post-surgery.

Methods

Pre- and 12-month post-TKA walking gait of 29 knee OA patients (40 knees) under 85 years old and able to walk without an aid was compared to 146 control participants (146 knees). Kinematics (240 Hz) of three walking gait trials were collected from 29 retroreflective markers and synchronized to kinetic data which was measured via a force plate. Repeated measures analyses of variance was performed to compare main effects over time, with Fisher's

least significant difference test to compare group means. Significance level was set at $p < 0.05$.

Results and Discussion

Pre-operatively, obese patients had significantly higher KAM, KAM impulse and knee adduction angle than healthy weight OA patients and all weight categories of controls. Post-TKA, no differences were noted between weight categories for TKA or control patients and only overweight TKA KAM and knee adduction angle were significantly lower than controls. The results indicate significant changes over time in KAM impulse and peak KAM for the overweight and obese TKA group. Significant changes over time were observed for peak knee adduction angle in the healthy, overweight, and obese TKA group.

Conclusions

Obese OA patients exhibit significantly greater deleterious gait patterns compared to less obese patients and controls. However, these differences were not noted following TKA.

References

- [1] Baliunas AJ et al. (2002). Increased knee joint loads during walking are present in subjects with knee osteoarthritis. *Osteoarthritis Cartilage*, **10**(7): 573-579.
- [2] Kortt M, Baldry J (2002). The association between musculoskeletal disorders and obesity. *Aust Health Rev*, **25**(6):239-246.
- [3] Kobayashi T, et al. (2000). Procollagen IIC-peptide ... *Ann Rheum Dis*, **59**(12):982-984.

Table 1 Group Mean Differences in Biomechanical Variables – Mean ± Standard Deviation

	Total Knee Arthroplasty			Controls		
	Healthy N=3 (4 knees)	Overweight N=9 (14 knees)	Obese N=17 (22 knees)	Healthy N=57 (57 knees)	Overweight N=55 (55 knees)	Obese N=34 (34 knees)
Pre-Operative						
KAM (Nm/kg)	0.31 ± 0.13	0.50 ± 0.27*	0.55 ± 0.18*†	0.47 ± 0.13	0.46 ± 0.12	0.44 ± 0.13
KAM Impulse (∫Nm/kg/s)	0.11 ± 0.07	0.18 ± 0.14	0.26 ± 0.12*^†	0.15 ± 0.05	0.16 ± 0.05	0.15 ± 0.05
Knee Adduction Angle (°)	3.00 ± 5.69	5.64 ± 8.32	8.32 ± 7.28*†	3.72 ± 3.18	3.56 ± 3.01	2.07 ± 3.80
12-Month Post-Operative						
KAM (Nm/kg)	0.37 ± 0.13	0.35 ± 0.10†	0.38 ± 0.08	0.47 ± 0.13	0.46 ± 0.12	0.44 ± 0.13
KAM Impulse (∫Nm/kg/s)	0.15 ± 0.06	0.12 ± 0.05	0.15 ± 0.05	0.15 ± 0.05	0.16 ± 0.05	0.15 ± 0.05
Knee Adduction Angle (°)	-0.74 ± 2.81†	0.93 ± 2.69†	1.66 ± 4.01	3.72 ± 3.18	3.56 ± 3.01	2.07 ± 3.80

N = number of patients; KAM = peak knee adduction moment; Nm Newton meter; kg = kilogram; s = second; ° = degrees

* = significantly different than Healthy; ^ = significantly different than Overweight; † = significantly different than Control

The use of a wireless passive electronic strain sensor to measure hysteresis of sheep hindlimb tendons:

A first step towards directly comparing *in vitro* and *in vivo* tendon properties

Bossuyt FM¹, Han S¹, Leonard T¹, Sawatsky A¹, Zhang Q², Smith C², Adam N², Taylor WR², Herzog W¹

¹Human Performance Lab, Faculty of Kinesiology, University of Calgary, Canada

²Laboratory for Movement Biomechanics, ETH Zürich, Zürich, Switzerland

Email: fransiska.bossuyt@ucalgary.ca

Summary

In order to better understand the dynamic mechanical properties of sheep hindlimb tendons, this study aimed to test the use of a wireless passive electronic strain sensor (PESS) on cadaveric tendons under tensile loading. Forced longitudinal sinusoidal oscillations were applied with 2% and 4% peak strains at 1 Hz. Tendon hysteresis decreased from the 1st to subsequent loading cycles.

Introduction

Hysteresis or energy dissipation in tendons during cyclic loading is considered to be an important factor in the efficiency of movements [1]. However, previously reported tendon hysteresis values are inconsistent and have never been obtained in conjunction with the corresponding directly measured *in vivo* muscle forces. Our wireless, passive electronic strain sensor (PESS, Figure 1A) [2] allows for the direct measurement of tendon strains during cyclic loading and offers an opportunity to gain new insights into tendon properties and muscle-tendon interactions *in vivo*. The goal of this pilot study is to answer the question: What is the hysteresis of a sheep hindlimb tendon *in vitro* when defined locally with the PESS, and how does this local hysteresis relate to global tendon hysteresis obtained from a servo-hydraulic tensile testing machine (MTS)?

Methods

A cadaveric sheep medial gastrocnemius tendon was clamped in the MTS, instrumented with a 1 kN load cell, and preloaded with 6.3 N (0.272MPa * 23.15mm² (cross-sectional area = mass / (density(1120 kg/m³) * length_{tendon})) (Figure 1B). Upon suturing the PESS onto the tendon, and a 20-min rest period in the preload position, the protocol started. The protocol consisted of a warm-up condition (101 cycles to 1% strain at 0.5 Hz), followed by two test conditions separated by 5 min of rest: 51 cycles to 2% at 1 Hz, and 51 cycles to 4% strain at 1 Hz. The tendon was kept hydrated by spraying a solution of 0.9% sodium chloride in water every two min. The output resonant frequency signal of the PESS was calibrated to the strain produced with sonomicrometry crystals aligned with the PESS. The tendon hysteresis was defined as the percent area between the force-displacement loading and unloading curves relative to the area under the force-displacement loading curve.

Results and Discussion

Table 1: Hysteresis (%) of sheep medial gastrocnemius tendon for the first 6 cycles of different loading conditions

2% strain	1st	2nd	3rd	4th	5th	6th	4% strain	1st	2nd	3rd	4th	5th	6th
Hysteresis _{MTS}	18.0	17.9	17.3	16.9	9.5	13.9	Hysteresis _{MTS}	24.0	14.0	16.5	15.4	17.8	17.6
Hysteresis _{PESS}	23.7	19.2	16.2	18.9	9.9	6.2	Hysteresis _{PESS}	20.2	18.1	37.1	10.4	19.8	38.6

This pilot test demonstrated a reduction in hysteresis from the 1st to subsequent loading cycles due to a reduction in the loading curve with minimal changes in the work under the unloading curve (Table 1, Figure 1). Overall, hysteresis values are slightly larger as compared to data from previous *in vitro* studies [1], and local hysteresis varied from the global hysteresis. Implications of these observations remain unclear and require further testing.

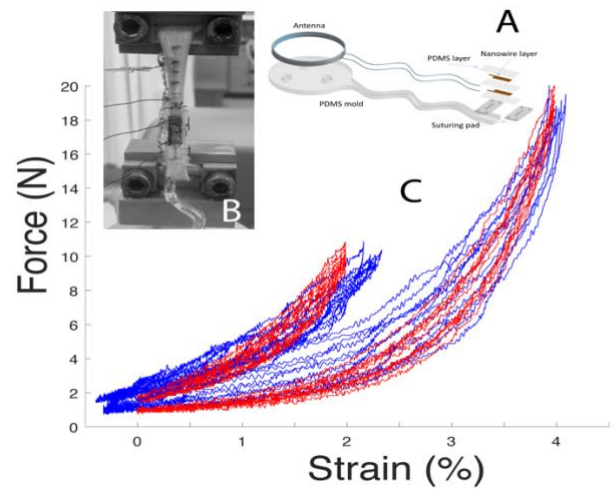


Figure 1: Hysteresis of sheep medial gastrocnemius tendon *in vitro* defined from a passive electronic strain sensor (blue) and a tensile test machine (red), for the 2% and the 4% strain conditions.

Conclusions

This study presented local and global hysteresis of a sheep medial gastrocnemius tendon *in vitro*. Following work will directly compare the *in vivo* tendon properties in freely walking/running sheep with the corresponding properties obtained *in vitro* and aims to measure the detailed interaction between tendon strain, fascicle strains and muscle forces *in vivo*.

Acknowledgments

Early postdoc mobility and project funding from the Swiss National Science Foundation (SNF 187793 and 182241). The Killam Foundation and the CRC programme (Tier 1, CIHR).

References

- [1] Finni T et al. (2012). *J Appl Physiol.* **114**: 515-517.
- [2] Stauffer F et al. (2018). *Adv Mater Technol.* **3**(6): 1-7.

Visual detection on simulated electromyography signals with varying signal-to-noise ratios: A training tool to enhance onset identification

Erik Kowalski¹, Danilo S. Catelli¹, Mario Lamontagne¹

¹Human Movement Biomechanics Laboratory, University of Ottawa, Ottawa, Canada

Email: mlamon@uottawa.ca

Summary

The aim of this study was to determine if a training tool that used simulated electromyography signals could be used to help improve visual onset detection. Eight participants completed two sessions, separated by a week, where they selected 120 muscle onsets on a custom-made graphical user interface. Signals were presented randomly and had signal-to-noise ratios of 5, 10, 20 or 40 dB. Participants received visual feedback at the end of each session. Visual onset detection improved during the second session for all signal-to-noise ratios. The concept of a training tool to help improve visual onset detection is warranted for further exploration.

Introduction

The detection of the onset of muscle activity is required to determine the temporal characteristics of muscle recruitment and its detection is accomplished by a variety of different methods including computerized methods or through visual detection (VD). Computerized detection methods were created to produce a reliable way to determine muscle onsets. However, when the signal-to-noise ratio (SNR) is low, researchers need to visually inspect these signals. VD is time-consuming, and its reliability has been questioned due to its poor reproducibility due to both human error and variability between researchers.

Having simulated electromyography (SIMEMG) would create a controlled repeatable environment where researchers could improve their VD ability. To assist and improve with VD, we have developed a training tool framework where researchers can practice detecting onsets on SIMEMG signals. The aim of this study was to determine if a training tool can improve visual onset detection.

Methods

Electromyography (EMG) signals were simulated using previously reported methods which controlled many signal features [1]. A white noise process was added to each SIMEMG signal which allowed for the configuration of a desired SNR. Eight signals, each with five bursts of muscle activity were simulated to create signals with SNRs of 5, 10, 20 & 40 dB. The training tool was created with a custom-made graphical user interface (GUI) which presented the SIMEMG signals in random order and allowed users to select where they believed the onset of each burst was for each signal.

Eight individuals with at least one year of EMG VD experience (7.1 ± 8.8 years) participated in the study and completed two VD sessions, separated by one week. Using the training tool, the participants completed three sets of 10 - SIMEMG signals, at four different SNRs, for a total of 120 onset selections. Feedback between their selected onset and the true onset was visually provided at the end of each session.

The absolute difference between the true from SIMEMG and selected onset was determined for each signal burst. A Wilcoxon signed-rank test was conducted to determine the effect of the VD training tool between the two sessions on the absolute difference between true and selected onset at the various SNRs ($p < .05$).

Results and Discussion

The second VD session elicited a significant median decrease in absolute difference with the selected onset from the true onset compared to the first VD session at all SNRs ($p < .001$) (Figure 1).

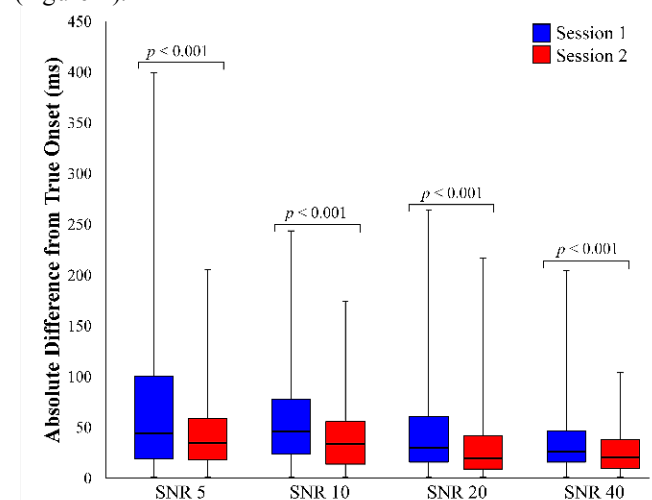


Figure 1: Absolute difference from true onset (ms) between the two VD sessions during SNRs of 5, 10, 20, and 40 dB.

The concept of a training method to improve VD muscle onset detection was shown with this small sampled study. The interquartile range was still large after the second session, so more training sessions are necessary to help further improve accuracy. Future improvements to the GUI are warranted to help improve learning outcomes, such as allowing users to select the SNR, providing immediate feedback instead of at the end of the session, as well as incorporating signal conditioning methods such as a Teager-Kaiser Energy Operator [2].

Conclusions

This study presented a training tool that used SIMEMG signals to help train participants for visual onset detection. Significant improvements were made between the two sessions. Several improvements could be made to the GUI to improve learning, however, the concept of a training tool to help improve visual onset detection is warranted for further exploration.

References

- [1] Rosa IG et al. (2008). *Comput Meth Prog Bio*, **89**:269-274
- [2] Solnik S et al (2010). *Eur J Appl Physiol*, **110**:

What womxn want: Using the International Womxn in Biomechanics organization to help womxn in biomechanics thrive

Anahid Ebrahimi¹, Sarah Kessler², Jana Montgomery³, Caitlin Banks⁴, Kirsty McDonald⁵, Kat Daniels⁶, Jayishni Maharaj⁷

¹University of Wisconsin-Madison, Madison, WI, USA; ²Harvard University, Cambridge, MA, USA; ³Providence Medical Technology, CA, USA; ⁴University of California-Davis, Davis, CA, USA; ⁵University of New South Wales, Sydney, NSW, AUS;

⁶Manchester Metropolitan University, Manchester, UK; ⁷Griffith University, Gold Coast, Queensland, AUS

Email: aebrahimi2@wisc.edu

Summary

The International Womxn in Biomechanics (IWB) organization was recently formed to increase representation of womxn in biomechanics. Here, we present the results of an anonymous survey highlighting the needs and challenges faced by womxn in our field, and the current and future role of IWB in addressing them.

Introduction

Women exit the professional pipeline at higher rates than men, in part due to challenges faced disproportionately by women (e.g. sexism and parental leave) and particularly during transitional periods, such as postdoctoral years [1]. Supportive environments and groups for women have shown women gain increased confidence, empowerment, and professional skills that enhance their career satisfaction and self-efficacy [2]. Thus, IWB was formed in June 2020 to increase the representation of women and non-binary individuals (collectively: womxn) in biomechanics. The purpose of this paper is to identify factors that contribute to the “leaky pipeline” in our field, and to discuss IWB’s ongoing and proposed efforts to support womxn in biomechanics.

Methods

In August 2020, we conducted an anonymous survey to characterize the experiences of womxn in biomechanics and identify the issues and challenges they encounter. The survey was sent to all members of the organization, which at that time contained approximately 200 womxn. Survey questions focused on the topics of: opportunities for training; research collaborations and grants; professional development; long-term goals; and mental health and wellbeing.

Results and Discussion

We received 128 responses from womxn at varying career stages (undergraduate students to faculty and industry professionals), with most recipients at the doctoral (54%) and postdoctoral (21%) stages. We identified common areas of concern for womxn biomechanists working in a male-dominated field. The most alarming of these included feeling a lack of respect, juggling personal and family commitments, overcoming discrimination, and dealing with sexism in the workplace. In addition, 48% of womxn believed stress and mental health challenges had a ‘high’ to ‘very high’ impact on their productivity. Finally, most (67%) respondents felt their current training was preparing them for their career goals; however, 47% of respondents were ‘somewhat’ or ‘not very’ satisfied with professional development offerings (Fig 1).

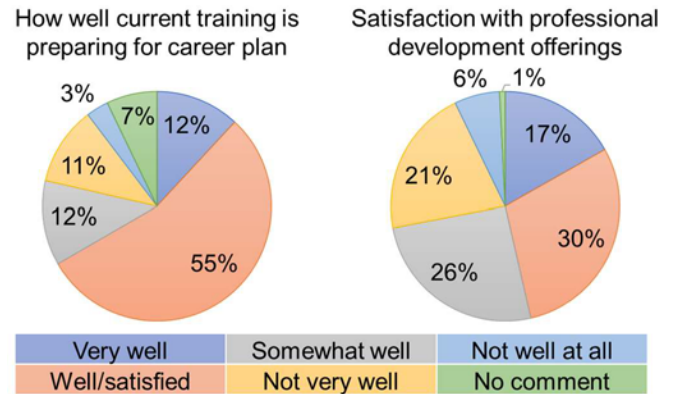


Figure 1: Survey responses related to career preparation (left) and satisfaction with professional development offerings (right).

IWB is providing a safe networking platform for our members (using Slack) to discuss career opportunities, professional development, feedback, advice, and professional support. Members use this platform to network, seek confidential support for personal and professional issues, celebrate each other’s successes, and learn from each other’s failures, among other things. We also host monthly meetings for our members, which, to date, have included topics such as applying for grants, fellowships, and awards (in collaboration with ASB, ISB, ISBS, and other biomechanics societies), discussing challenges faced by womxn in STEM, learning about racial and implicit bias in research spaces (in collaboration with the Black Biomechanists Association and Latinx in Biomechanics affinity groups). Many of these meetings are made freely available on our YouTube page for the biomechanics community [3].

As of January 2021, IWB includes over 500 womxn from over 20 countries. Our future efforts include (1) supporting our members’ personal and professional goals, (2) creating outreach opportunities to introduce young womxn to the field, and (3) empowering allies and advocates to create a more equitable workplace.

Conclusions

IWB was created to address the needs of womxn in biomechanics. Through continued support from the broader biomechanics community, we are committed to increasing representation of womxn in biomechanics.

References

- [1] Ysseldyk R, et al. (2019). *Front. Psychol.*, **10**: 1297.
- [2] Horner-Devine MC, et al. (2016). *Front. Ecol. Evol.*, **4**: 119.
- [3] IWB Youtube channel: <https://www.youtube.com/channel/UCjkQjsuNrwLpFmVUWVIndw>

Finite Element Modelling of the Abdomen in Developing a Robotic Patient for Palpation Examination Training

Florence Leong¹, Siamak F. Khosroshahi¹, He Liang¹, Thilina D. Lalitharatne¹, Simon de Lusignan²,
Thrishantha Nanayakkara¹, Mazdak Ghajari¹

¹Dyson School of Design Engineering, Imperial College London, London, United Kingdom
²Nuffield Department of Primary Care Health Sciences, University of Oxford, United Kingdom
Email: f.leong@imperial.ac.uk

Summary

Abdominal palpation is a very challenging procedure for medical trainees as there is rarely any immediate feedback about the findings or diagnoses of abdominal conditions. We are developing a robotic platform for trainees to sharpen their skills effectively with the aid of a Finite Element Model (FEM) of abdominal palpation that informs them of the stresses on the internal tissues based on the palpation forces.

Introduction

Physicians often perform palpation examination on patients to detect anomalies in the abdomen. This technique requires years of experience for accurate perception and diagnoses. Simulation-based learning platforms (e.g. manikins and virtual reality systems) are used for medical training in place of patients but they lack the flexibility to realistically simulate a patient's condition, and to provide required haptic and visual feedback desired for training [1]. Hence, we are developing a robotic patient (RoboPatient) that incorporates haptic [2] and visual feedback, i.e. facial expression [3] and that informed by FEM of palpation for training. We are constructing a high-fidelity FEM to simulate abdominal palpation to observe internal stresses (on the liver in this context) and to obtain information for the robot design. Our aim is to train a surrogate model based on FEM results using machine learning to provide real-time visual feedback (see Fig 1a) with respect to palpation forces and pain levels.

Methods

A high-fidelity FEM of the abdomen is constructed from 3D images generated by XCAT program, and is simplified to a lumped abdomen with ribs and liver. The simulations are set up in LS-Prepost (Fig 1b) using material properties in the GHBM model [4] for the flesh and ribs, and the Ogden parameters in [5] for the liver. A dummy finger is added to visualize the contact with the abdomen. Simulations are performed with indentation up to 20mm on the abdomen, and lateral motion across the liver emulating the palpation

motion we hypothesize physicians would feel the liver with. The resulting stresses on the liver are observed.

Results

From the simulation, we observed the largest principal stress on the liver of over 5kPa with a maximum resultant contact force of 10N at 20mm deformation on and across the abdomen. The displacement and stress on the liver tissue can be observed through the simulation with respect to the contact forces on the fingertip (Fig 1c), demonstrating that the finger perceives reaction forces from the liver and ribs translated from within the abdomen. The simulated stress can be mapped to real-time palpation forces measured using force sensors on RoboPatient system, and the corresponding abdominal pain levels for informed visual feedback.

Conclusions

The FEM simulations show that the internal stresses on the tissues inside the abdomen can be observed based on the palpation forces. This visual feedback allows physicians and trainees to condition their fingers behaviour to reduce pain onto patients while receiving immediate feedback on their finding. The model will also be simulated with different patient conditions for optimal RoboPatient platform design.

Acknowledgments

This work was supported by the Engineering and Physical Sciences Research Council (EPSRC) RoboPatient grant EP/T00603X/1. We also thank Dr Paul Segars from Duke University School of Medicine for the XCAT program.

References

- [1] Hollerbach J M et al. (1999). *IJRR*, **18(11)**: 1088–1100.
- [2] He L et al. (2018). *IEEE EMBC*, 2154–2157
- [3] Lalitharatne T D et al. (2021). *IEEE RAL*, 643-650.
- [4] Gayzik F S et al. (2011). *Ann. Biomed. Eng.*, **39**: 2568.
- [5] Sato F et al. (2013) *IRCOBI*, 736-750.

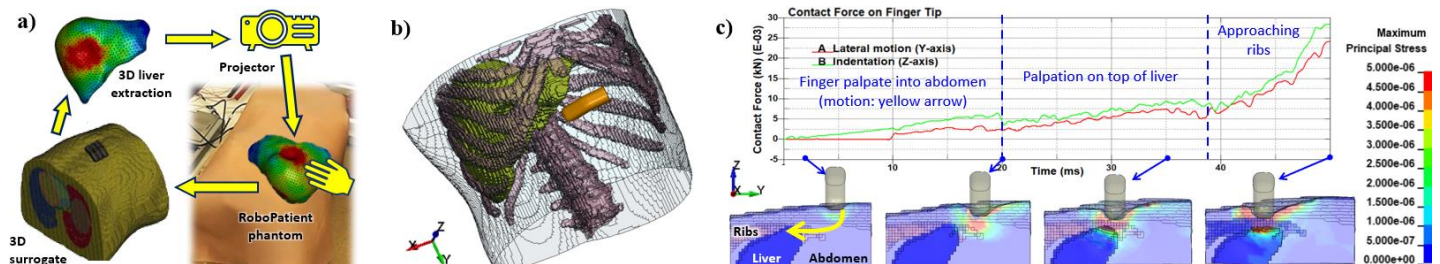


Figure 1: a) RoboPatient platform augmented with real-time deformation of abdomen or liver model during palpation training, b) Abdomen model in LS Prepost, and c) Visualisation of internal stress with respect to contact force on fingertip during palpation.

Using hula hooping as a discussion point for STEM education and outreach

I. Bold¹, C. Holt¹, P. Blaikie¹, D. Syrop¹

¹Cardiff University School of Engineering, Cardiff, Wales

Email: blaikiep@cardiff.ac.uk

Summary

The aim of this project was to develop a public engagement Science Technology Engineering and Mathematics (STEM) activity using Hula Hooping to introduce subjects including Biomechanics and Medical Engineering. The activity is intended to demonstrate a wider range of STEM careers available to young people, their parents, and teachers. It also provides an opportunity to include broader science and maths concepts and skills, and how learning about them can help people and improve lives.

Introduction

The UK is facing a skills gap in STEM which is effecting how industry operates and their ability to recruit and train their workforce.

ASPIRES [1], a large scale survey of children from age 10 to 14, showed that while 70% would class science as one of their favourite subjects and 90% would like a job that helps others, less than 20% would actually think about pursuing a career in science. The report showed that this was due to several reasons including, how much interaction young people have with science at home, the idea that science is for 'clever people' and whether there was a STEM club at school. The aim of this project was to develop a public engagement Science Technology Engineering and Mathematics (STEM) activity using Hula Hooping to introduce subjects including Biomechanics and Medical Engineering.

Methods

Three dimensional motion analysis was performed on one professional hula hoop instructor using 10 Oqus 700+ Cameras (Qualisys, Sweden). EMG (Delsys Inc.) and force data (Berotec, USA) was also collected in the session. This data was processed using QTM 2020.3 (Qualisys, Sweden) and MATLAB 2020a (MathWorks Inc.). The participant wore a CAST marker set, with additional markers included on the upper body, and lower limb EMG sensors applied following the SENIAM guidelines. Two hula hoops were used one with 8 markers and one with 6 to allow identification during post-processing (see Figure 1).

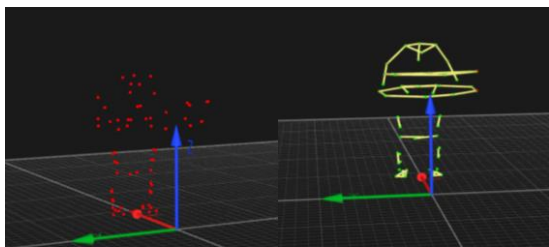


Figure 1: An example of the hula hooper with two hoops before and after processing.

The motion analysis data was used for several purposes. Firstly to demonstrate the stages of data processing (see Figure 1), and the creation of wire model videos to show how the hula hooper is moving. Secondly using marker trajectory, force and EMG data to create sounds associated with the different waveforms. Thirdly, to demonstrate muscle activation associated with human movement.

A literature review undertaken to assess the availability of information on hula hoop biomechanics found a small number of studies, including a trial to develop a robot that can hula hoop [2]. The design that was developed for the robot which shows the abdominal muscles was developed into a craft activity (see Figure 2).

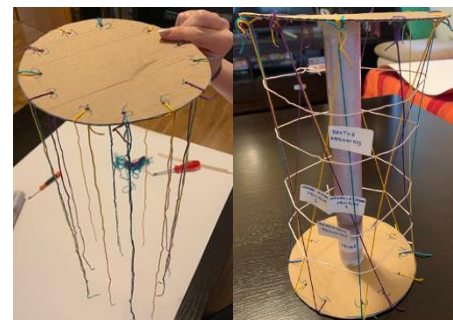


Figure 2: An example of the steps and final abdominal muscle model craft activity

Results and Discussion

The main output of the project to date is the creation of a craft activity (Figure 2) and an interactive webinar for Cardiff Science Festival due to launch on 19th Feb 2021. Feedback recorded from this pilot public engagement event will be then used to inform activities for National Biomechanics Day 2021 which is likely to be a virtual event.

Further work is required, with the aspiration to recruit more hula hoopers, to develop this as a resource pack for schools or youth groups.

Conclusions

Hula hooping is an activity that can be used as a starting point from which to talk about physics, engineering, and biomechanics. This work aims to demonstrate the breadth of careers in STEM, how maths and science concepts that young people are learning at school can be applied to interesting questions, and to highlight the range of different careers and opportunities available in the field of medical engineering.

References

- [1] Archer Ker, L. et al. (2013) *ASPIRES Report: Young people's science and career aspirations, age 10–14*
- [2] Kekehashi, Y. et al. (2011) *11th IEEE-RAS International Conference on Humanoid Robots*, pp. 423–428.

Using a physical sarcomere model to demonstrate titin's contributions to residual force enhancement

Heron B. O. Medeiros¹, Heiliane B. Fontana^{1,2}, Walter Herzog³

¹Biomechanics Laboratory, Federal University of Santa Catarina, Florianópolis, Brazil

²Morphological Sciences Department, Biological Sciences Center, Federal University of Santa Catarina, Florianópolis, Brazil

³Human Performance Laboratory, Faculty of Kinesiology, University of Calgary, Calgary, Canada

Email: heronbomed@gmail.com

Summary

We built a physical sarcomere model aimed at helping students and trainees in understanding the role of titin in the production of active force in skeletal muscle. Using a simple sarcomere prototype we are able to demonstrate actin-myosin cross-bridges interactions and illustrate the different ways of force production by titin in the active and passive muscle. Specifically, the model illustrates the role of titin in residual force enhancement through calcium binding to titin and titin binding to actin. The model is simple, and demonstration to students resulted in positive feedback about the clarity and improved understanding of a complex molecular mechanism.

Introduction

Titin is a structural protein in striated muscle sarcomeres. Recently, titin has been associated with active force regulation in muscles, specifically during eccentric (lengthening) contractions, resulting in increased force and reduced metabolic cost for eccentric compared to isometric or concentric contractions [1]. However, the molecular mechanisms causing titin's force regulation remain unknown, although it is generally accepted that it has to do with an activation or a force-dependent change in **titin's stiffness** [1].

In order to illustrate the complex manner in which titin is thought to contribute to active force regulation, we built a physical sarcomere prototype that allows for illustration of titin's proposed function specifically as it relates to the residual force enhancement (RFE) property of skeletal muscle [2]. Thus, the aim of this educational outreach research was to build a physical model of a sarcomere that illustrates the proposed action of titin in RFE.

Methods

The physical sarcomere prototype contains a Z-band structure (2 cm x 15 cm x 2 cm), actin filaments (15 cm x 2 cm x 2 cm), myosin filament (20 cm x 2 cm x 2 cm), cross-bridges interactions represented by small, stiff springs, and titin, represented by long, soft springs. We used a sole paper of 3 mm to build the sarcomere structure (Figure 1) to arrive at a mostly 2D model with some 3D representation.

The small, stiff springs representing cross-bridge connections between actin and myosin can be attached to three hooks on actin spaced by 2.5 cm and three corresponding hooks per half-myosin, also spaced by 2.5 cm (attached only two cross-bridges in the figure). To allow for rotational and planar stability of the sarcomere model, opposing actin filaments were connected using 30 cm x 1.2 cm x 1.2 cm insert piece (in black).

Results and Discussion

The primary mechanisms of titin's contribution to the RFE property are related to *changes in titin's inherent stiffness* through binding of calcium to selected immunoglobulin and glutamate regions and by *binding of titin to actin*, thereby

reducing its free spring length, upon muscle activation [1]. The increased titin stiffness with calcium binding is represented by clips in the model that prevent small segments of the titin spring from elongating (Figure 1C). The increased titin stiffness caused by titin binding to actin is represented by hooking the proximal segment of titin to actin (Figure 1D).

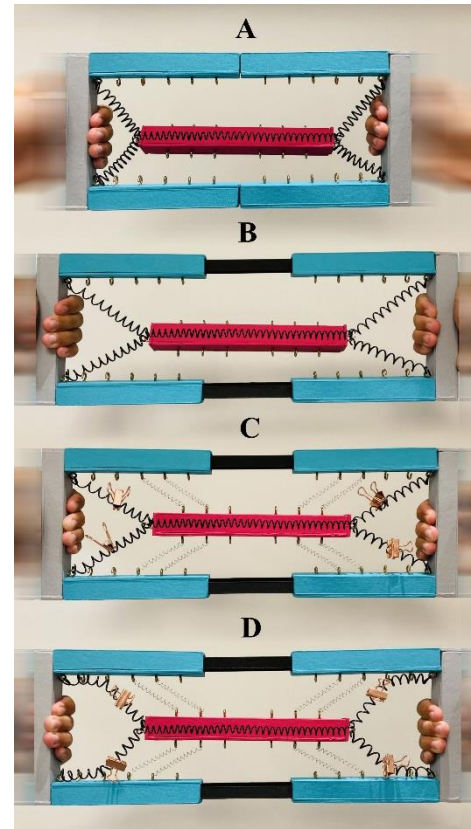


Figure 1: Three-filament sarcomere model bordered by the Z-bands (gray), myosin filament (pink), actin filaments (blue), titin (black spring), and cross-bridges (small gray springs). (A) passive sarcomere, short length; (B) passive sarcomere, long length (titin elongates unrestricted); (C) active stretch with cross-bridges attached and calcium bound to titin; (D) active stretch with cross-bridges bound, calcium bound to titin, and titin bound to actin.

Conclusions

The prototype sarcomere model with a titin whose stiffness can be changed through calcium-titin binding and titin-actin binding allows for a visual, macro-structural representation of titin's force regulation mechanisms in muscle – a complicated process. Class demonstrations have proved successful and resulted in positive feedback.

Acknowledgments

Funded by CNPq of Brazil, and NSERC of Canada.

References

- [1] Herzog W. (2018). *Biophys Rev*, **10**: 1187-1199.
- [2] Edman et al. (1982). *J Gen Physiol*, **80**: 769-84.

Modular reorganization of gait in chronic but not in artificial knee joint constraint

Carlos Cruz-Montecinos^{1,2,3}, Sofia Pérez-Alenda¹, Mauricio Cerda^{4,5}, Huub Maas².

¹. Department of Physiotherapy, University of Valencia, Valencia, Spain.

². Department of Human Movement Sciences, Vrije Universiteit Amsterdam, Amsterdam, Netherlands.

³. Laboratory of Clinical Biomechanics, Department of Physical Therapy, University of Chile, Santiago, Chile.

⁴. SCIAN-Lab, Programme of Anatomy and Developmental Biology, ICBM, University of Chile, Santiago, Chile.

⁵. Biomedical Neuroscience Institute, Santiago, Chile.

Email: carloscruz@uchile.cl

Summary

Muscle synergies can be characterized by electromyographic (EMG) activities of muscles represented by combinations of time-dependent coefficients (motor primitives) and time-independent weights (motor modules). The motor modules and motor primitive represent together the modular organization. It is currently unknown if modular reorganization (i.e., merging of muscle synergies) does occur if not the central nervous system, but the musculoskeletal system is affected. The aim of this study was to assess short-term (immediate to a few minutes following application) and long-term (years) effects of a constraint of the knee ROM on the modular organization of gait. For this purpose, we used the Non-negative matrix factorization (NNMF) to extract muscle synergies from EMG data of eleven leg muscles in healthy subjects with an artificial knee joint constraint and people with a similar but chronic knee joint constraint. This study showed that in the short-term a knee constraint does not affect the modular organization of gait, but that constraining the knee long-term results in modular reorganization.

Introduction

It is currently unknown if modular reorganization (i.e., merging of muscle synergies) does occur if not the central nervous system, but the musculoskeletal system is affected. We hypothesize that the modular organization of gait will not be affected in the short-term, but substantially changed in the long-term. For this purpose, we assessed (i) the acute effects of an artificial knee joint constraint on the modular organization in healthy subjects; (ii) the differences in modular organization between healthy subjects with an artificial knee joint constraint and people with a similar but chronic knee joint constraint.

Methods

Eleven healthy subjects and eight people with a chronic knee joint constraint due by haemophilic arthropathy walked overground at 1 m/s. The healthy subjects also walked with an articulated knee brace limiting knee movement to 20°. NNMF was used to extract muscle synergies from EMG data of eleven leg muscles [1]. Ten cycles corresponding to the middle 10 meters of the 30-meter corridor were used for data analysis (20 cycles in total). The total variance accounted (tVAF) for one to four synergies and modular organization were assessed. Two independent assessments were made: (a) comparison between control group no constraint (control) and

artificial knee joint constraint (artificial) (b) and between artificial joint constraint and people with chronic knee constraint (chronic constraint).

Results and Discussion

The distributions of number of synergies were not significantly different between groups. The tVAF and modular organization of gait were not significantly affected by the artificial knee constraint. A higher tVAF for one and two synergies, as well as merging of synergies (i.e., acceptance and propulsion, and acceptance and deceleration) were observed in the chronic knee constrain group (Fig 1). The finding that modular reorganization occurred only after long-term exposure to a joint constraint may be explained by secondary changes in the musculoskeletal and the central nervous systems. Up to now, such merging of synergies has been reported only in people with neurological diseases (i.e., chronic stroke, cerebral palsy) [2,3].

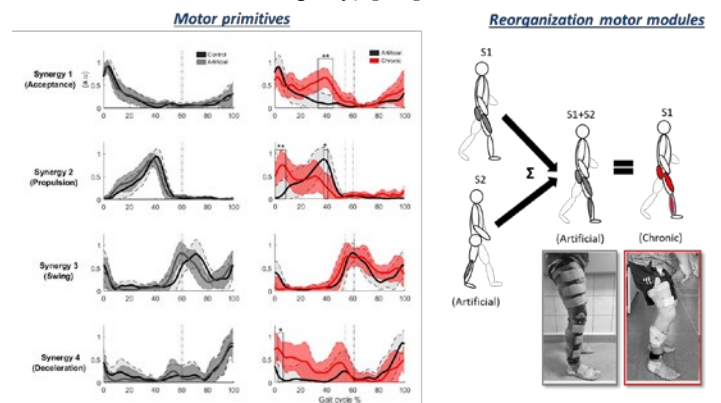


Figure 1. Motor primitives and reorganization of motor modules. * <0.05 . ** <0.001 . S1, acceptance synergy. S2, propulsion synergy.

Conclusions

We conclude that merging of muscle synergies may also occur when changes in the mechanics of the musculoskeletal system is the primary cause of the motor impairment. The present results offer a new perspective on the adaptations of the central nervous system to joint restriction.

Acknowledgments

National Agency for Research and Development (ANID) projects ICN09_015, PIA ACT192015, and EQM140119.

References:

- [1] Tresch MC. et al. J Neurophysiol 95: 2199–2212, 2006.
- [2] Van Crielinge T et al. Disabil Rehabil 0: 1–10, 2019.
- [3] Allen JL. Clin Biomech (Bristol, Avon) 28: 697–704, 20.

Effect of Low and High Intensity Strength Training on Muscle Forces During Walking In Adults With Knee Osteoarthritis

Paul DeVita¹, Daniel Beavers², David J. Hunter³, Kim L. Bennell⁴, Richard F. Loeser⁵, Shannon Mihalko⁶, Stephen P. Messier⁶

¹Dept of Kinesiology, East Carolina University, Greenville, U.S., ²Department of Biostatistical Sciences, Wake Forest School of Medicine, Winston-Salem, U.S., ³Rheumatology Department, University of Sydney, Sydney, Australia, ⁴Department of Physiotherapy, University of Melbourne, Melbourne, Australia, ⁵Division of Rheumatology, University of North Carolina School of Medicine, Chapel Hill, U.S. ⁶Department of Health & Exercise Science, Wake Forest University, Winston Salem, U.S.

Email: DeVitaP@ECU.edu

Summary

An 18 month, randomized clinical trial (RCT) with 377 adults with knee pain and radiographic knee osteoarthritis (OA) were enrolled into either low- (N=126) or high- (N=127) intensity strength training (ST) or attention control (N=124) groups. Muscle strength, knee pain, and gait biomechanics during walking were analyzed at 0, 6, and 18-months. Low- and high-intensity ST groups had greater quadriceps and hamstrings strength vs control at 18-months, but pain and maximum quadriceps and hamstrings forces during walking were not statistically significantly different between groups.

Introduction

Since quadriceps muscle weakness is prevalent with knee OA, standard of care often includes ST to strengthen this and other muscles [1]. Additionally, ST also reduces pain and disability in this population [1]. The actual mechanisms for these beneficial outcomes remain unknown but are thought to be due to improved muscle function in gait after strengthening [2]. Recent preliminary evidence suggests however that strengthening does not alter lower extremity muscle forces during locomotion [3]. The purpose of this study was to compare the effects of low and high intensity ST and attention control on muscle strength, knee pain, and muscle forces during level walking in adults with knee OA.

Methods

An 18 month RCT on 377 adults (40% women, BMI: 31kg/m², Age: 65 yrs) with knee pain and radiographic knee OA and enrolled into low- (N=126) or high- (N=127) intensity ST or an attention control (N=124) group was completed. with tests at baseline, 6 and 18 months. Muscle strength was assessed with isokinetic dynamometry, knee pain with WOMAC questionnaire, and gait data with 3D motion capture and force plate. A musculoskeletal model [4] predicted quadriceps and hamstrings forces during level walking at self-selected speeds. Data were analyzed with a mixed-effects model including time (0, 6 and 18 months), treatment group, time by treatment interaction while adjusting for sex, baseline BMI and baseline outcome values.

Results & Discussion

Quadriceps strength increased 10, 18 and 25% in control, low and high intensity groups over 18 months and was significantly greater in high vs control group at 18 months, $p < 0.002$. Hamstrings strength followed a similar pattern, increasing 6, 13, and 17% in the three groups over 18 months

and was statistically significantly greater in both ST groups compared to control at 18 months, $p < 0.001$. ST groups did not differ in hamstrings strength at 18 months. Knee pain was not significantly different between groups at 18 months, $p < 0.22$ and improved on average 33% over 18 months in all groups.

The primary results for this abstract were maximum quadriceps and hamstrings muscle forces during level walking. Despite increased strength in both muscles in ST groups relative to attention control at 18 months, neither low or high intensity ST altered maximum muscle forces during walking relative to attention control, $p < 0.99$ & 0.44, figure 1.

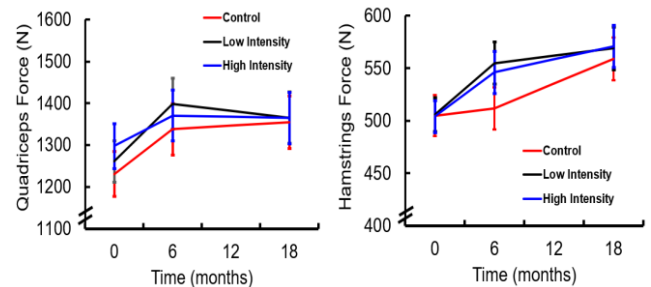


Figure 1. Maximum quadriceps and hamstrings forces during stance phase of walking.

Present results confirm previous data [3] showing that despite increased muscle strength, muscle function during locomotion was not altered after ST. These data also agree with our report that knee joint compressive force was not significantly different among these groups at 18 months [5].

Conclusions

Both low- and high- intensity ST increased muscle strength relative to attention control after 18 months but did not alter muscle function through maximum muscle forces during level walking relative to attention control in adults with knee OA. The mechanism of reduced pain and disability after ST remains elusive.

Acknowledgements

National Institute of Arthritis, Musculoskeletal and Skin Diseases: 1R01AR059105-01 & National Institute of Aging, P30 AG21332: Strength Training for Arthritis Trial (START)

References

- [1] Ettinger et al. (1997). *JAMA*, 277:25-31.
- [2] Bennell et al. (2018). *Osteo & Cart*, 26:495-500.
- [3] DeVita et al. (2018). *Clin Biomech*, 59:199-206.
- [4] DeVita et al. (2001). *J Appl Biomech*, 17:297-311.
- [5] Messier et al (*In Press*), *JAMA*.

Gait asymmetries following ACL reconstruction differ based on sex and gait speed

Lindsay Slater¹, Joe Hart²

¹Department of Physical Therapy, University of Illinois at Chicago, Chicago, Illinois

²Exercise and Sport Injury Laboratory, Department of Kinesiology, University of Virginia, Charlottesville, Virginia

Email: slaterlv@uic.edu

Summary

Sex differences have been previously reported in gait symmetry following anterior cruciate ligament reconstruction (ACLR) in knee and hip kinematics. The purpose of this study was to investigate sex differences in limb asymmetry in knee, hip, and trunk kinematics in walking and running gait. Females demonstrated more knee extension, knee valgus, hip abduction, and lateral trunk flexion towards the contralateral side on the ACLR limb compared to the contralateral side during walking. In contrast, females demonstrated more knee external rotation, hip external rotation, trunk extension, and trunk rotation towards the contralateral side on the ACLR limb compared to the contralateral limb during running. Sex differences exist in knee, hip, and trunk triplanar kinematics in both walking and running gait up to two years following ACLR. Gait asymmetries are not uniform based on sex and gait speed in individuals with unilateral ACLR.

Introduction

Gait symmetry is often measured following ACLR as an indicator of restoration of normal gait patterns and readiness to return to activity. There is some evidence to suggest sex differences are present in knee gait asymmetries following ACLR [1,2], however there is little information regarding triplanar proximal gait asymmetries following ACLR. Further, gait speed varies between studies. Therefore, the purpose of this study was to identify limb differences based on sex in knee, hip, and trunk kinematics during walking and running gait in individuals with unilateral ACLR.

Methods

Twenty-two females and 11 males with primary, unilateral, uncomplicated ACLR (19.9±2.2 years, 170.4±8.4 cm, 68.3±10.9 kg, 22.7±23.3 months postop) walked (1.34m/s) and ran (3.33m/s) on a split-belt instrumented treadmill with eight clusters of reflective markers attached to the thorax, sacrum, bilaterally over the lateral mid thigh, midcalf, and forefoot. Twelve nonconsecutive strides were analyzed for each speed and limb. Kinematic data were reduced to 101 points to represent 0-100% of the gait cycle, with 40% representing toe off during running and 60% representing toe off during walking. Heel strike was defined as the point when vertical ground reaction forces exceeded 20N. Kinematics were presented as limb differences by subtracting the contralateral healthy limb from the ACLR limb. Mean limb differences and 90% confidence intervals were calculated for each 1% of the gait cycle. Mean differences (degrees) and associated pooled standard deviations were calculated for periods of the gait cycle when confidence intervals did not overlap for three or more consecutive points.

Results and Discussion

Females demonstrated more knee extension (2.06°), knee valgus (2.86°), hip abduction (1.44°), lateral trunk flexion towards the contralateral side (2.03°), and trunk rotation towards the contralateral side (1.65°) on the ACLR limb compared to males during walking gait. During running gait, females demonstrate more knee external rotation (4.32°, Figure 1), hip external rotation (1.77°), trunk extension (1.68°), and trunk rotation towards the contralateral side (3.09°). Sex differences in gait asymmetries exist in both walking and running gait following ACLR, however asymmetries in walking gait tended to be more evident in sagittal and frontal planes while running asymmetries tended to be larger in transverse plane motion. These sex differences suggest that asymmetrical gait observed during walking and running gait are not interchangeable and gait profiles depend on both sex and gait speed even two years following ACLR.

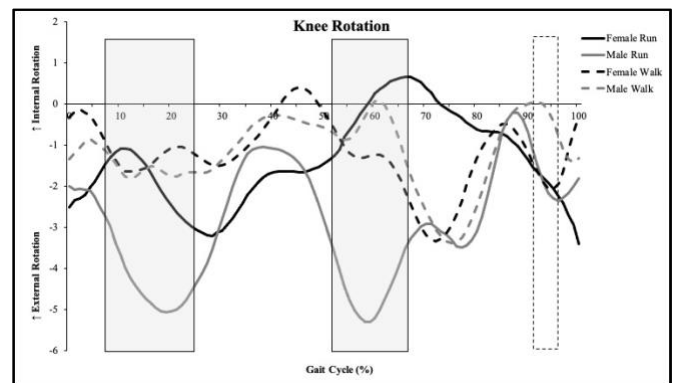


Figure 1: Sex differences in limb symmetry following ACLR during walking (dashed line) and running gait (solid line). Negative values indicate the ACLR was more externally rotated compared to the contralateral limb and boxed areas are where 90% confidence intervals did not overlap for at least three consecutive points during walk (open box) and run (grey box) gait.

Conclusions

There are significant sex differences in limb symmetry during gait in those with unilateral ACLR. Sex differences are largely present in knee mechanics, however larger differences are present in transverse plane and more proximal joints during running. These results suggest that walking and running are not interchangeable when evaluating gait asymmetries following ACLR.

References

- [1] Asaeda M et al. (2017). *Knee*, **24**: 280-288.
- [2] Di Stasi SL et al. (2015). *J Orthop Sports Phys Ther*, **45**: 207-21.

Lower Back Demands During Load Carriage with Induced Asymmetric Gait

Jacob J. Banks^{1,2} and Graham E. Caldwell²

¹Center for Advanced Orthopedic Studies, Beth Israel Deaconess Medical Center & Harvard Medical School, Boston MA, USA

²Department of Kinesiology, University of Massachusetts, Amherst MA, USA

Email: jbanks3@bidmc.harvard.edu

Summary

Are L5/S1 vertebral joint forces (VJF) during load carriage with an artificially induced gait asymmetry different than during normal ‘symmetric’ gait? To test this, participants carried dumbbells in one or two hands while walking on a treadmill with and without a walking boot on their right lower leg. VJFs were estimated with a musculoskeletal model incorporating participant-specific muscle recruitment strategies. Results indicated that several key metrics of VJF demand were generally larger during load carriage in asymmetric compared to symmetric gait.

Introduction

Asymmetric gait is related to a high incidence of lower back pain (LBP)[1]. Though force and repetition are often synonymous with LBP risk[2], biomechanical studies on those with asymmetric gait have been inconclusive[3]. However, most studies have focused on amputees during unloaded gait and applied a generic muscle recruitment algorithm to estimate muscle forces[2-5]. Such studies are limited by between group heterogeneity, the assumption that unloaded gait is the primary LBP catalyst, and the inherent limitations of static optimization[2-4]. Therefore, the purpose of this research was to examine VJF demands in able-bodied participants during load carriage with and without an artificially induced lower limb asymmetry, using a computer model with participant-specific muscle recruitment strategies.

Methods

Twelve healthy participants consented to have their biomechanics recorded while carrying loads on a treadmill with and without a ~1kg ankle restricting walking boot worn on the right ankle (Figure 1). Dumbbells of 7.5% and 15% of bodyweight were carried uni- and bilaterally with the treadmill set to 90% of preferred symmetric unloaded walking speed. Based on previous work showing location differences[3], unilateral asymmetric carries were conducted with the dumbbell in the left hand.

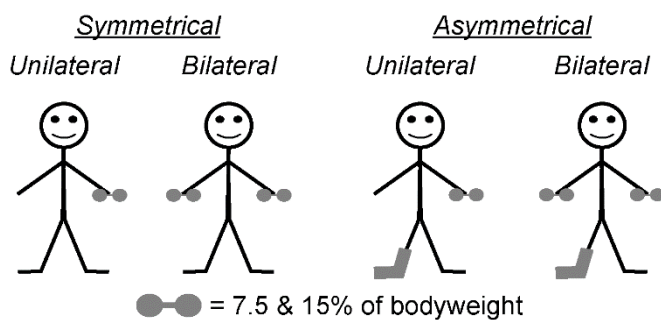


Figure 1: Cartoon of experimental carrying conditions.

A full-body OpenSim[5] model estimated bodyweight normalized peak and average L5/S1 VJF compression and resultant shear averaged from three consecutive strides. The model incorporated a custom EMG optimization[4] API to resolve the indeterminate muscle forces and had been evaluated for gait applications[3]. Three-way ANOVAs compared ($\alpha < .05$) VJF metrics for main effects of gait (a)symmetry, carrying location, and dumbbell load.

Results and Discussion

VJF peak and average resultant shear and compression forces increased with dumbbell load (p -values all $< .01$). Carrying location impacted VJF, with one hand carries resulting in mostly larger metrics (p -values $< .02$, except for peak compression force $p = .10$). Overall, gait asymmetry tended to increase VJF metrics (Table 1; p -values .03 to .42), but only average compression force was significantly different.

Table 1: L5/S1 VJF (% bodyweight) gait (a)symmetry effects.

		Symmetric	Asymmetric	p
Resultant	Peak	52.2 (12.6)	53.8 (13.8)	.42
	Average	34.7 (6.8)	36.0 (8.4)	.10
Compression	Peak	348.1 (67.0)	358.8 (62.7)	.10
	Average	261.2 (39.5)	271.2 (45.7)	.03

Previous work has demonstrated similar load carriage and location effects with symmetric gait[6]. Load carriage with a lower limb asymmetry could impact VJFs during weight transfer from the less comfortable lower limb, with acceleration differences and inertia of the carried load increasing kinetic demands. Although not all VJF metrics were different and are below joint acute failure tolerances, repeated steps in conjunction with non-neutral postures and small VJF increases could be a potential catalyst for LBP[2].

Conclusion

Load carriage with gait asymmetry induced by a walking boot led to increases in some VJF metrics. Therefore, in addition to encouraging lower load and bilateral carries, clinicians and ergonomists aiming to reduce lower back demands should also consider gait asymmetry in their recommendations.

Acknowledgments

UMass Amherst Dissertation Grant & P. Clarkson Scholarship

References

- [1] Dananberg HJ (1993) *JAPMA*, **83**: 615-624.
- [2] Marras WS (2008) *The Working Back*; J. Wiley & Sons Inc.
- [3] Banks JJ (2021) *University of Massachusetts Amherst Dissertation*.
- [4] Cholewicki et al. (1995) *JBmch*, **28**: 321-331.
- [5] Delp et al. (2007) *IEEE Trans. BE*, **54**: 1940-1950.
- [6] Badawy et al. (2018) *Ergo*, **61**: 1345-1354.

The Use of the Reference Finite Helical Axis and High-Speed Biplanar Videoradiography to Characterize Knee Kinematics

Tomasz Bugajski¹, Jessica Kupper², Gregor Kuntze³, Janet Ronsky²

¹Biomedical Engineering Graduate Program, University of Calgary, Calgary, Canada

²Department of Mechanical and Manufacturing Engineering, University of Calgary, Calgary, Canada

³Faculty of Kinesiology, University of Calgary, Calgary, Canada

Email: tbugajsk@ucalgary.ca

Summary

The reference finite helical axis (rFHA, the FHA relative to a reference frame) provides different kinematic measures than Cardan angles and has distinguished healthy and osteoarthritis (OA) prone knees. The rFHA has not been used to assess walking, a daily task that may influence OA progression. To understand its ability to distinguish kinematics during walking, it is first important to understand the variability of healthy walking rFHA measures. This study used the rFHA, in conjunction with high-speed biplanar videoradiography (HSBV), to determine the variability of specific rFHA outcomes during walking. The variability of the rFHA outcomes were similar in magnitude to Cardan angles, showing promise as a supplemental source of information to kinematic analyses.

Introduction

The rFHA (FHA relative to a reference frame) has shown to be a useful kinematic measure in optical camera systems, providing different information to Cardan angles. It has distinguished kinematics of healthy and OA prone knees during leg swings and single leg squats [1]. Walking, a daily activity that may influence OA progression [2], has not been assessed with the rFHA. To understand the rFHA's ability to distinguish kinematics during a walking task, variability of healthy rFHA measures must first be known. Therefore, the purpose of this study was to determine what variability of measures the rFHA provides (using HSBV to record direct bone movement) within a healthy sample during walking, and how it compares to the variability of the Cardan angles.

Methods

Five healthy males (25.8 ± 1.9 years) were recruited for this ethics approved study (REB15-0554). Magnetic Resonance images (GE 3T Discovery 750, Steady State Free Precision) of the right limb were captured and segmented (AMIRA, Germany), providing bone models of the femur and tibia. HSBV images were recorded (120 Hz) while walking (1.2 ms^{-1}) on a treadmill. Bone movements were quantified using 2D-3D registration (Joint Track Biplane, USA). The rFHAs of the knee were calculated from heel strike to mid-stance (0-25% of the gait cycle) relative to a reference position (60° knee

flexion in swing phase). The rFHA was computed using a custom MATLAB program (MathWorks, USA) and included four outcomes: **location** - mean anteroposterior (AP) and proximodistal (PD) intersection of the rFHA and femoral sagittal plane, **translation** - summed translation along the rFHA throughout the movement, **orientation** - mean angle between the rFHA and femoral transverse plane, and **dispersion** - mean angular deviation of each rFHA from the average rFHA [3]. Variabilities (i.e. standard deviations [SD]) across participants for the rFHA outcomes and maximum Cardan angles were compared.

Results and Discussion

The rFHA location showed large variability (AP location: 40.68 mm, PD location: 31.36 mm, Table 1). Conversely, the translation, orientation, and dispersion had small variability (SDs of 1.92 mm, 2.31 deg, and 0.32 deg, respectively, Table 1). Abnormal knees, such as injured or arthritic, may reveal different variabilities in these kinematic outcomes [3]. The Cardan angles showed slightly greater magnitudes of variability compared to the rFHA outcomes, with SDs ranging from 4.83 deg - 5.62 deg. The rFHA may provide useful measures of knee kinematics and support traditional methods such as Cardan angles.

Conclusions

The rFHA and Cardan angles provided similar magnitudes of variability during walking in a healthy group. This may provide the framework of future comparisons to other knee conditions, such as aged or injured knees. The application of the rFHA to these conditions may supplement Cardan angles for distinguishing biomechanical markers of the knee (e.g. joint stability).

Acknowledgments

NSERC, CIHR, AITF, and T. Chen Fong Doctoral, I.W. Killam Doctoral, and Dean's Doctoral Scholarships.

References

- [1] Bishop EL et al. (2014). *Osteoarthr. Cartil.*, **22**: S120.
- [2] Andriacchi TP et al. (2009). *J. Bone Jt. Surg.*, **91**: 95-101.
- [3] Kiss RM. (2011). *J. Electromyogr. Kines.*, **21**: 695 – 703.

Table 1: Means (SD) of the rFHA outcomes across all participants.

	rFHA Outcome Measure					Cardan Angles		
	AP location (mm)	PD location (mm)	Translation (mm)	Orientation (deg)	Dispersion (deg)	Flexion (deg)	Adduction (deg)	Internal Rotation (deg)
Mean (SD)	-2.05 (40.68)	-4.36 (31.36)	-5.42 (1.92)	8.55 (2.31)	2.78 (0.32)	38.11 (5.62)	3.00 (5.52)	1.87 (4.83)

Tibial Damage and Osteogenic Effects of High Intensity Interval and Prolonged Running

S. Meardon¹, A. Vahdati², C. Campbell¹, D. Sampson¹, J. Willson¹

¹Human Movement Analysis Laboratories, East Carolina University, Greenville, NC, United States

²Multi-disciplinary Mechanics and Modeling Laboratory, East Carolina University, Greenville, NC, United States

Email: meardons@ecu.edu

Summary

Tibial stress during prolonged running was compared to a HIIT protocol of high-speed running with walking recovery bouts. HIIT was more osteogenic with lower cumulative peak stress and damage formation. These results suggest HIIT may be a safe alternative to prolonged running for bone health.

Introduction

Bone stress injury results from microdamage accumulation associated with repetitive high-impact load cycles in activities like long distance running. Inserting bouts of rest into high impact activity, like those inherent to high intensity interval training (HIIT), may retain the high impact stimulus needed for bone formation while reducing damage accumulation. Evidence related to biomechanical effects of HIIT running protocols is limited. The purpose of this study was to compare cumulative peak stress, osteogenic potential and damage formation rates during a HIIT run protocol to a prolonged run.

Methods

On day 1, 20 runners (10M, 10F; 25.3±2.6 years; 22.6±2.9 kg/m²) completed 5 repetitions of a HIIT protocol consisting of 2-minute run periods at a 95% estimated VO₂ max speed and 3-minute walk periods at preferred speed. On day 2 (>48 hours later), runners completed a 25-minute prolonged run at their self-selected 5k training pace. 3-dimension motion capture and ground reaction force (GRF) data from 5 stance phases were collected in the last minute of each HIIT run and walk period and every 3 minutes during the prolonged run. Kinematics and kinetics were input to an anthropometric-scaled musculoskeletal model to determine internal forces at the distal 1/3 tibia, a common site of injury. Tibial forces and moments were applied to scaled, sex-specific cross-sectional

distal tibia models to estimate compressive and tensile tibial stress using a combination of prismatic beam theory and finite element analysis [1,2]. Peak stress and the number of strides per period were input to cumulative stress, osteogenic index [3] and damage formation rate equations [4]. Session effects were examined with paired t-tests ($\alpha=0.05$) and effect sizes (d_z).

Results and Discussion

Peak compression and tension were greatest in the HIIT run condition (-148±27; 115±23 MPa), followed by preferred run (-136±24; 104±29 MPa) and walk (-61±8; 43±6 MPa). Fig. 1 a and b illustrates that HIIT resulted in lower cumulative peak tibial stress ($p<0.01$, $d_z=3.28-3.52$) and damage formation rates ($p<0.01$, $d_z=0.61-0.88$) than a time-matched, 25-min run. The beneficial effects of HIIT were likely due to fewer high-impact load cycles relative to prolonged running (873±60 vs. 2299±150). To the extent that walking is osteogenic in this population, HIIT was also more osteogenic (Fig. 1b) than prolonged running ($p<0.01$, $d_z=4.66-4.68$).

Conclusions

While not without risks, incorporating periods of walking into HIIT running bouts appeared to offset the cumulative damage effects of prolonged running while maintaining, and possibly, increasing osteogenic potential.

Acknowledgments

NSF 1359183, L.Goel, J. Liu, T. Derrick

References

- [1] Derrick TD et al. (2016). *J Biomech*, **49**: 429-435.
- [2] Kourtis LC et al. (2009). *J Mech Mater*, **4**: 659-674.
- [3] Turner CH et al. (2003). *Exerc Sport Sci Rev*, **31**: 45-50.
- [4] Hazelwood et al. (2001). *J Biomech*, **34**: 299-30.

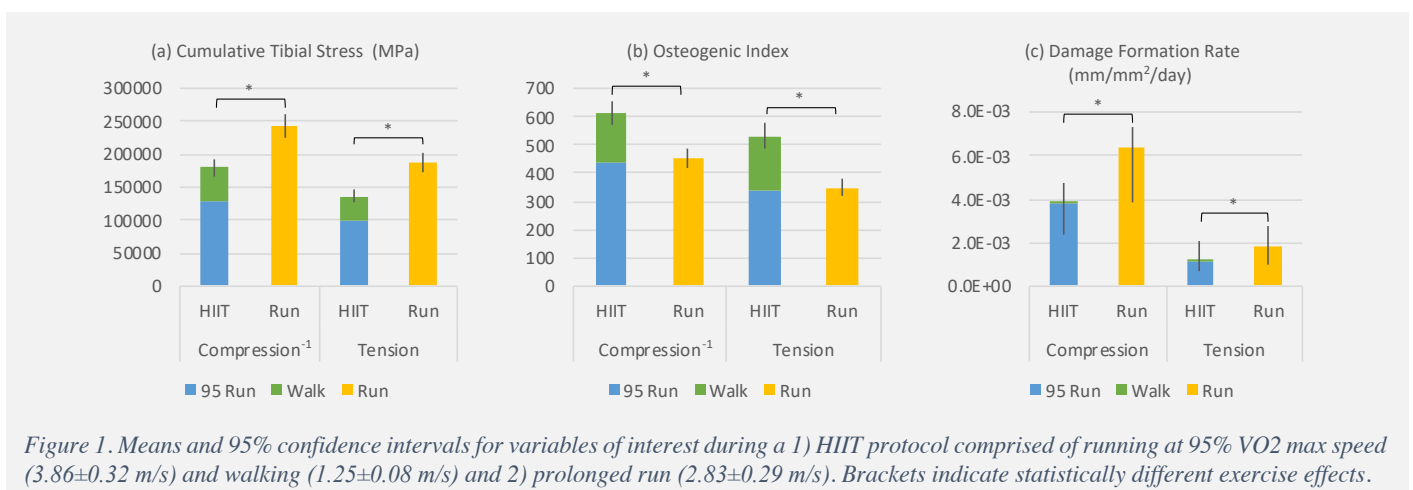


Figure 1. Means and 95% confidence intervals for variables of interest during a 1) HIIT protocol comprised of running at 95% VO₂ max speed (3.86±0.32 m/s) and walking (1.25±0.08 m/s) and 2) prolonged run (2.83±0.29 m/s). Brackets indicate statistically different exercise effects.

Subgroups of foot-ankle running movement patterns influence the responsiveness to a foot-core exercise program

Ricky Watari¹, Eneida Y. Suda¹, João P. S. Santos¹, Alessandra B. Matias¹, Ulisses T. Taddei¹, Isabel C. N. Sacco¹

¹Dept. Physical Therapy, Speech and Occupational Therapy, Faculty of Medicine, Universidade de São Paulo, Sao Paulo, Brazil
Email: rickywatari@usp.br

Summary

The purpose of this study is to identify subgroups of foot-ankle (FA) kinematic patterns among recreational runners and investigate whether differences in baseline movement patterns can influence the mechanical responses to a foot-core exercise intervention program. This is a secondary analysis from a randomized controlled trial investigating the effects of a foot-core exercise program. The kinematic time-series during treadmill running, based on a multi-segment foot model, underwent principal component analysis, and the reduced data was used in a hierarchical cluster analysis. Two clusters of FA running patterns were identified, with cluster 1 (n=36) presenting forefoot abduction, while cluster 2 (n=49) displayed a rearfoot adduction and midfoot abduction throughout the stance phase of running. Runners from cluster 1 (n=16) who underwent foot-core exercises presented changes in foot kinematics that approximated them to the patterns displayed in cluster 2 (n=13). The findings of this study indicate that individual FA patterns can influence the response to exercise interventions.

Introduction

Foot-core exercise intervention has been shown to reduce running-related injury (RRI) incidence in recreational runners [1]. However, the response to an exercise-based therapeutic approach can present individual differences that could be related to baseline biomechanical patterns. Thus, the aim of this study is to identify homogenous subgroups of foot-ankle (FA) kinematic patterns among recreational runners and further investigate whether differences in FA movement patterns can influence the mechanical responses to a foot-core exercise program.

Methods

This is a secondary analysis of data from a single-blind parallel controlled trial (clinicaltrials.gov - NCT02306148), in which the effects of a foot-core exercise program on the incidence of RRIs were investigated [2]. 3D kinematic data was acquired from 85 recreational runners, using the Rizzoli Foot Model [3], during barefoot treadmill running. Joint angle time-series from the angles between shank and calcaneus (Sha-Cal), calcaneus and midfoot (Cal-Mid), and midfoot and metatarsal bones (Mid-Met) were calculated; kinematic features were extracted using principal component analysis; and the resulting principal components (PCs) served as input to a hierarchical cluster analysis. Optimal cluster division was determined based on the Silhouette index. PCs that presented significant differences between the formed clusters were used to analyze the mechanical differences between them. Data from runners that underwent the foot-core intervention (n = 29) were compared between baseline and week-8 (post-

intervention) assessments, also based on the PCs that presented significant differences.

Results and Discussion

The optimal cluster division presented a two-cluster solution. Cluster 1 (n=36) and cluster 2 (n=49) had significant differences at baseline in PC1 (p<0.001) and PC3 scores (p=0.037). Cluster 1 maintained the rearfoot and midfoot closer to neutral position and a forefoot abduction during the stance phase of running, whereas cluster 2 presented greater rearfoot adduction and midfoot abduction, while keeping the forefoot closer to neutral position (Figure 1).

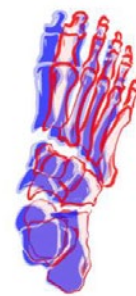


Figure 1: Between-cluster differences of foot and ankle movement patterns. Cluster 1 is represented in red and cluster 2 in blue.

There was a significant cluster X intervention interaction only for PC1 scores (p=0.01), wherein only cluster 1 presented a significant change after the foot-core exercise protocol. Runners from cluster 1 presented an increase in rearfoot adduction and a decrease in forefoot abduction, making their movement pattern more similar to the runners in cluster 2.

Conclusions

We identified two clusters of FA movement patterns among recreational runners, with one subgroup presenting a more pronounced forefoot abduction, while the other displayed greater rearfoot adduction and midfoot abduction. There was a different response to a foot-core exercise-based intervention between clusters, indicating that individual foot biomechanical patterns can influence the response to exercise interventions.

Acknowledgments

FAPESP: 2015/14810-0; 2017/15449-4; 2019/19291-1; 2016/17077-4. CNPq: 304124/2018-4.

References

- [1] Taddei UT et al. (2020). *Am J Sports Med*, **48**: 3610-9.
- [2] Matias AB et al. (2016). *BMC Musculoskel Dis*, **17**: 160.
- [3] Leardini A et al. (2007). *Gait Posture*, **25**: 453-462.

Effects of Foot Core Strengthening Protocol on Plantar Arch Biomechanics

Alessandra Matias¹, Marcus Fraga Vieira², Ricky Watari¹, Eneida Yuri Suda¹, Ulisses Taddei¹, Isabel Sacco¹

¹Faculdade de Medicina FMUSP, Universidade de Sao Paulo, Sao Paulo, SP, Brazil

²Bioengineering and Biomechanics Laboratory, Federal University of Goiás, Goiânia, Brazil

Email: alessandra.matias@usp.br

Summary

The aim of this study was to investigate the influence of a foot-core strengthening protocol on medial longitudinal arch (MLA) biomechanics in recreational runners. Multi-segment foot kinematics was recorded from 87 runners randomly allocated in control or intervention group. Significant interaction effect was found for metatarsus-calcaneus angle on frontal plane, and intervention group exhibit less inverted metatarsus, suggesting that the strengthening protocol has a positive effect on foot control.

Introduction

The intrinsic foot muscles contribute to regulation of foot stiffness during running [1], allowing the MLA storage and return elastic energy and contributing to metabolic energy savings. The inefficient active support of the foot caused by dysfunction or weakness of those muscles is related to injuries in runners [2]. Thus, the aim of this study was to investigate the influence of a foot-core strengthening protocol on MLA biomechanics in recreational runners.

Methods

A total of 87 injury-free runners (42M, 45F; 40.3±6.9 yrs) with at least 1 year of running experience, running in traditional running shoes, minimum weekly training volume of 20 km, were enrolled to a larger single-blind parallel controlled trial (clinicaltrials.gov - NCT02306148). Runners were randomly allocated in a control group (CG, n=46) or an intervention group (IG, n=41). Kinematic data were collected while running on an instrumented treadmill at self-selected speed (2.7±0.24 m/s). Runners were evaluated at baseline (T0), and after 8 weeks of foot-core training (T8). Participants in the IG went through an 8-week foot-core training exercising 3-times/week while the CG followed a placebo stretching protocol. In order to provide detailed insights into the contribution of individual foot segments to the running biomechanics, MLA and metatarsus with respect to the calcaneus (Cal-Met) angles were calculated in the sagittal, frontal and transverse planes [3]. Joint angles time series were compared using statistical parametric mapping with two factors, 1 repeated (SPM{F}, posthoc SPM{t}) [4].

Results and Discussion

Following SPM, significant interaction effect was observed in Cal-Met angle on frontal plane between 12.5% and 80% stance phase (p=0.008). The IG showed a larger metatarsus inversion at T8 compared to the CG, suggesting that the IG

was able to increase the foot deformation during stance phase after foot-core training (Figure 1). The range of motion of Cal-Met angle increased, suggesting that the foot improved its stiffness capability on IG. A larger metatarsus inversion may represent a better contribution of the foot structures in transferring and dampening forces during running. The Cal-Met angle on sagittal and transverse planes did not present significant differences. As expected, the MLA, in agreement with the Cal-Met sagittal result, did not show interaction effect. Both groups, IG and CG, showed a large dispersion in the behavior of the participants at T8.

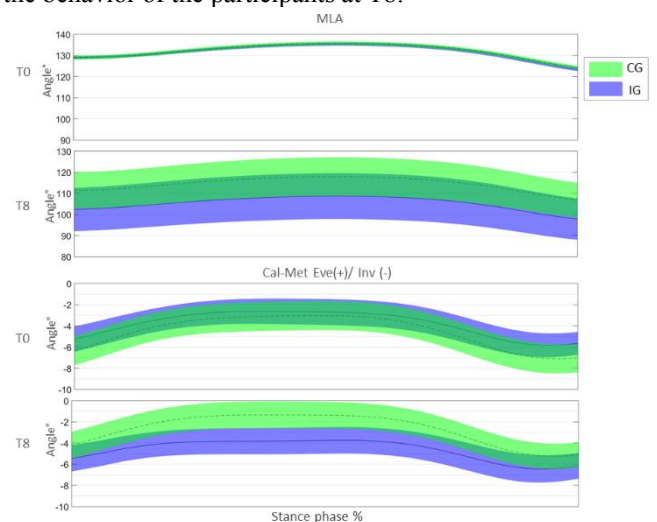


Figure 1: MLA (top plot) and Cal-Met angle (Inv/Eve) in frontal plane (bottom plot) waveforms at T0 and T8 for control (green) and intervention (light purple) groups.

Conclusions

There was a positive effect of the foot-core training on the foot dynamics during running. Foot-core exercises can help the foot structure regarding control of its segments and maintaining stiffness during running.

Acknowledgments

Supported by FAPESP: 2016/17077-4; 2015/14810-0; 2017/15449-4; 2019/19291-1; CNPq: 304124/2018-4.

References

- [1] Kelly LA et al. (2014). *J. R. Soc. Interface* **11**:1-9
- [2] Williams III et al. (2001). *Clin Biomech*, **16**:341-347.
- [3] Leardini A et al. (2007). *Gait Posture*, **25**: 453-462.
- [4] Pataky et al. (2013) *J Biomech*; **46**: 2394-2401.

Internal Tibial Forces and Moments During Graded Running

Michael Baggaley¹, Timothy R. Derrick² W. Brent Edwards¹
¹Faculty of Kinesiology, University of Calgary, Calgary, Canada
²Department of Kinesiology, Iowa State University, Ames, USA
 Email: michael.baggaley1@ucalgary.ca

Summary

The forces and moments acting on the tibia during running play an essential role in the development of tibial stress fractures. The present study observed that downhill running resulted in lower tibial forces and moments compared to level and uphill running. Small reductions in tibial axial and medio-lateral force were observed between steep uphill and level running, yet this did not translate to differences in bending moments. Considering that bending moments are responsible for most of the normal stress placed on bone, these results suggest that downhill running may be associated with a lower risk of tibial stress fracture than either level or uphill running.

Introduction

Internal bone loads play an important role in stress fracture development. Stress fractures frequently occur at the tibia, and while several studies have examined internal tibial loads in level running, little is known about tibial loads in up- and downhill running. Graded running is associated with large alterations in gait mechanics [1], which are likely to influence the magnitude and orientation of forces and moments acting on and within the tibia. While recent studies have quantified the axial force acting on the tibia to infer bone load and injury risk [2,3], the bending and torsional moments acting on the tibia are responsible for the majority of the stress experienced by the tibia in running [3] and may be more indicative of injury risk. The purpose of this study was to examine the influence of running grade on internal tibial forces and moments.

Methods

17 (9M/8F, 25.7±6.9 yrs, 22.3±2.1 kg/m²) participants ran on an instrumented treadmill while motion-capture and force platform data were collected. Participants ran at 0°, ±5°, and ±10° in a random order at a speed of 3.33 m/s. Ankle joint contact force was estimated using inverse dynamics-based static optimization [4] with muscle moment arms, orientations, and force bounds obtained from a scaled musculoskeletal model [5]. Internal tibial forces and moments were quantified at a cross section located at the distal 1/3rd of the tibia, by ensuring static equilibrium with all applied forces and moments. Linear mixed models were used to evaluate the effect of grade on peak forces and moments. Post-hoc testing was performed using Bonferroni adjusted pair-wise comparisons (adjusted $\alpha=0.005$).

Results and Discussion

Internal tibial moments were lower in downhill running than level running and both uphill running conditions ($p<0.001$), while internal forces were lower in downhill running than

level and shallow (+5°) uphill running ($p<0.001$). Only axial and medio-lateral forces were lower in steep uphill running than level running ($p\leq0.005$). Differences between conditions were driven by changes to the magnitude and orientation of forces acting on the tibia. Specifically, the resultant ankle joint contact force was lower during ±10° and -5°, compared to 0°. However, the lower contact force in +10° did not result in lower bending moments due to changes in the orientation of the contact force vector. During +10°, the contact force was oriented more in the anterior-posterior, which acted to reduce the axial force, while maintaining a similar anterior-posterior tibial force ($p<0.001$) and sagittal plane moment ($p<0.001$) (Figure 1). During downhill running, the changes in forces and moments were mainly the result of the large reduction in contact force magnitude, as orientation of the contact force was only different during -10°. However, this explains the large reduction in bending moments (Figure 1) observed in -10°, as the change in orientation would result in more force acting in the axial direction, thereby producing a lower moment. Overall, graded running altered the forces and moments acting on the tibia. Downhill running may be associated with a lower risk of tibial stress fracture than either level or uphill running.

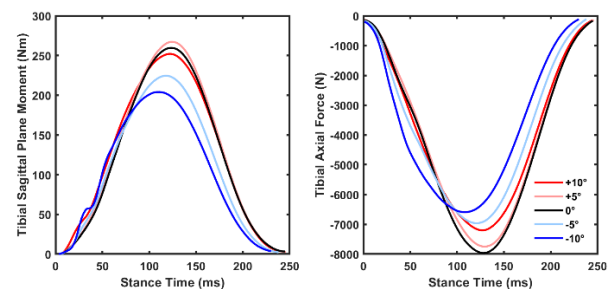


Figure 1: Tibial sagittal plane bending moment (left) and axial force (right) during running.

Conclusions

Changes to gait mechanics during graded running alter the forces and moments acting on the tibia. However, only downhill running resulted in both lower tibial forces and moments compared to level and uphill running, suggesting that it may be associated with a lower risk of tibial stress fracture development.

References

- [1] Vernillo G et al. (2017). *Sports Med*, **47**:615-29.
- [2] Matijevich E et al. (2019). *PLoS ONE*, **14**:e0210000.
- [3] Hunter J et al. (2019). *Med Sci Sports Exerc*, **51**:1178-85
- [4] Derrick T et al. (2016). *J Biomech*, **49**:429-35.
- [5] Edwards WB et al. (2008). *Clin. Biomech*. **23**:1269-78.
- [6] Arnold E et al. (2010). *Ann. Biomed. Eng.* **38**: 269–79.

Achilles Tendon and Patellofemoral Kinetics Following A Long Hilly Run in Traditional and Maximal Cushioning Shoes

James Becker, Christopher Casillas

¹Neuromuscular Biomechanics Laboratory, Montana State University, Bozeman, MT, USA

Email: james.becker4@montana.edu

Summary

This study evaluated Achilles tendon (AT) and patellofemoral (PF) kinetics before and after a long hilly run in traditional (TRAD) and maximal cushioning (MAX) shoes. AT impulses increased following the run in both shoes while knee extensor moments and PF contact forces were greater in the MAX shoes, both before and following the run. These results add to a growing body of literature suggesting running in MAX shoes may load the PF joint more than traditional shoes.

Introduction

Several studies have evaluated loading at common injury sites such as the AT or PF joint while running in MAX shoes [1,2]. However, these studies used level ground running over short durations. Both running over graded terrain [3] and long durations [4] has been shown to influence loading at common injury sites. Therefore, the purpose of this study was to compare AT and PF kinetics before and after a long hilly run (LHR) in TRAD and MAX shoes. We hypothesized that MAX shoes would have lower AT and greater PF loading before the run and this difference would increase following the run.

Methods

Seventeen highly trained trail runners (13 male/ 4 female, age: 26.4 ± 8.2 years, weekly volume: 65.4 ± 22.2 km) were randomly assigned to run in either TRAD (n=8) or MAX (n=9) shoes. After a 10-minute warmup, participants completed a 16 km LHR on an instrumented treadmill. The grade varied to match the elevation profile of a popular local trail run, with a total gain and loss of 337.8 m and 918.8 m, respectively.

Whole body kinematics (250 Hz) and ground reaction forces (1000 Hz) were collected during 2-minutes of level running before and immediately following the completion of the course. Kinetics of the AT and PF joint were calculated using

a musculoskeletal model [5]. Differences in AT and PF kinetics were evaluated using a 2x2 mixed ANCOVA, with time to complete the run used as a covariate.

Results and Discussion

There were no significant shoe x time interactions for any variable. AT impulse was greater following the LHR (p=.028, Table 1). Both peak knee extensor moments (p=.032) and PF contact forces (p=.042) were greater in the MAX shoes (Table 1).

The increased knee extensor moments in MAX shoes adds to the growing body of literature showing that running in MAX shoes loads the PF joint more than TRAD shoes. Additionally, compared to TRAD shoes, highly cushioned MAX shoes are not protective against potentially detrimental changes in mechanics which occur with fatigue following long graded running.

Conclusions

Changes in running mechanics following a LHR are similar between TRAD and MAX shoes, however MAX shoes result in greater PF joint loading when running both fresh and fatigued.

Acknowledgments

Footwear for this study was provided by New Balance, Inc. through the 2017 New Balance Footwear Research Award.

References

- [1] Sinclair, J et al. (2016). *J Applied Biomech*, **32**: 359-364.
- [2] Sinclair, J et al. (2015) *Comp Ex Phys*, **11**: 239-244.
- [3] Neves, K et al. (2014) *J Sports Sci Med*, **13**: 823-828.
- [4] Fletcher, J et al. (2018) *Plos One*, **13**: 1-17.
- [5] Willy, R et al. (2016) *J Ortho Sports Phys Ther*, **46**: 664-671.

Table 1: Mean and standard deviations for Achilles tendon (AT) and patellofemoral (PF) metrics. Bold values are significantly different between pre and post while italicized values are significantly different between shoes.

AT Variables	TRAD pre	TRAD post	MAX pre	MAX post	PF Variables	TRAD pre	TRAD post	MAX pre	MAX post
DF (°)	17.5 ± 5.6	17.1 ± 5.6	18.6 ± 3.5	19.2 ± 3.2	KF (°)	35.7 ± 4.9	37.1 ± 3.8	37.5 ± 2.1	39.3 ± 3.2
PFM (Nm/kg)	1.6 ± 0.5	1.6 ± 0.4	1.6 ± 0.3	1.6 ± 0.2	<i>KEM (Nm/kg)</i>	<i>0.9 ± 0.2</i>	<i>1.0 ± 0.2</i>	<i>1.1 ± 0.1</i>	<i>1.2 ± 0.2</i>
ATF (BW)	6.1 ± 1.7	6.0 ± 1.3	6.2 ± 1.1	6.0 ± 0.9	<i>PF CF (BW)</i>	<i>3.8 ± 1.3</i>	<i>4.1 ± 0.8</i>	<i>4.6 ± 0.6</i>	<i>4.9 ± 1.0</i>
ATLR (BW/s)	77.9 ± 26.1	71.3 ± 22.4	79.1 ± 15.0	73.5 ± 12.8	PFJS (MPa)	5.8 ± 1.5	6.1 ± 1.1	6.1 ± 1.1	6.3 ± 1.1
Imp. (BW*s)	0.7 ± 0.2	0.8 ± 0.2	0.7 ± 0.1	0.9 ± 0.2	PFJSLR (MPa/s)	107.2 ± 26.5	114.5 ± 17.2	107.7 ± 16.0	110.1 ± 18.9
					Imp. (MPa*s)	0.6 ± 0.2	0.6 ± 0.1	0.6 ± 0.1	0.7 ± 0.1

Note: All values except impulses are peak during stance. DF: dorsiflexion, PFM: plantar flexor moment, ATF: Achilles tendon force, ATLR: Achilles tendon loading rate, Imp: impulse per step, KF: knee flexion, KEM: knee extensor moment, PFCF: patellofemoral contact force, PFJS: patellofemoral joint stress, PFJSLR: patellofemoral stress loading rate.

Hierarchical Inverse Kinematics via Bayesian Inference

Andrew J. Pohl¹, Reed Ferber¹, Matthew R. Schofield²

¹ Faculty of Kinesiology, University of Calgary, AB, Canada

² Department of Mathematics and Statistics, University of Otago, New Zealand

Email: andrew.pohl@ucalgary.ca

Summary

Bayesian inference is applied to a novel hierarchical model to solve an inverse kinematics problem for a set of stance phases collected from a healthy runner. Uncertainty in the resulting joint angle estimates is 2° less than when a hierarchical model is not used. Estimated stride to stride variability suggests that movement variability is reduced in the vertical direction but highest for the angle of the shank.

Introduction

Recently Bayesian inference has been suggested as an effective approach to solving inverse kinematics problems related to determining gait pose parameters from noisy marker position data [1-2]. A valuable contribution of Bayesian inference, not yet explored with regards to inverse kinematics problems, is the ability to effectively model the hierarchical manner in which data is collected, including parameters to describe stride-to-stride, often ignored in a standard biomechanical analysis. Therefore, we aim to develop a hierarchical model which describes the stride to stride variability in kinematics along with underlying measurement noise and fit this model via Bayesian inference. Secondly, we wish to explore differences in stride to stride variability across the stance phase of gait hypothesising that variability will be lowest for movement in the vertical direction and will decrease for distal segments.

Methods

3D marker trajectories were extracted from a pre-existing database of gait kinematics [3] for one healthy female runner running on a treadmill. Marker trajectories were projected into the sagittal plane where 20 stance phases were identified and time normalized to 101 points [4]. To determine the typical kinematics and the associated stride-to-stride variability the lower limb was modelled as an $i = 3$ link kinematic chain and the observed positions of $j = 1, \dots, 4$ markers for $k = 1, \dots, 20$ strides (\mathbf{y}_{ijk}) were modelled via a multivariate Gaussian distribution where the expected position of markers results from rigid body transformation α_{ijk} acting on the known positions of markers within their local coordinate system \mathbf{x}_{ij} with variation determined by measurement noise σ :

$$\mathbf{y}_{ijk} | \mathbf{x}_{ij}, \mathbf{q}_k, \sigma \sim \text{Multivariate-Normal}(\alpha_{ijk}, \sigma^2 I_2) \quad (1)$$

$$\alpha_{ijk} = \mathcal{J}_{ik}(q) + \Gamma(\theta_{ik})\mathbf{x}_{ij},$$

where $\mathcal{J}_{ik}(q)$ defines the position of each joint:

$$\mathcal{J}_{ik}(q) = \begin{cases} \mathbf{r} & i = 1 \\ \mathcal{J}_{i-1,k}(q) + \Gamma(\theta_{i-1,k})[L_{i-1}, 0]^T & i > 1 \end{cases} \quad (2)$$

and $\Gamma(\theta_{ik})$ defines a planar rotation matrix given angle θ_{ik} with L_i the known length of link i . In the second stage, pose parameters θ_{ik} and \mathbf{r}_{ik} are modelled as having arisen from a Gaussian distribution with mean ω_i and μ and stride to stride variance and κ_i, ε :

$$\begin{aligned} \theta_{ik} &\sim \text{Normal}(\omega_i, \kappa_i) \\ \mathbf{r}_{ik} &\sim \text{Multivariate-Normal}(\mu, \varepsilon I_2), \end{aligned} \quad (3)$$

For unknown parameters weakly informative prior distributions were used and 10000 samples from the respective posterior distribution were obtained using Markov Chain Monte Carlo methods [5].

Results and Discussion

This model resulted in more accurate measures of average kinematics with less uncertainty than when a single stride was modelled in isolation. For example, uncertainty of knee and ankle angles was reduced by 2° likely in response to increased information being available for parameter estimation. Stride to stride variance highlighted in Figure 1 demonstrates partial support of our hypothesis with significantly greater variation in the horizontal direction (ε_x) than the vertical direction. In addition the variability in foot angle was less than that of the shank and thigh, however, the variability of the shank segment is greater than that of the thigh segment.

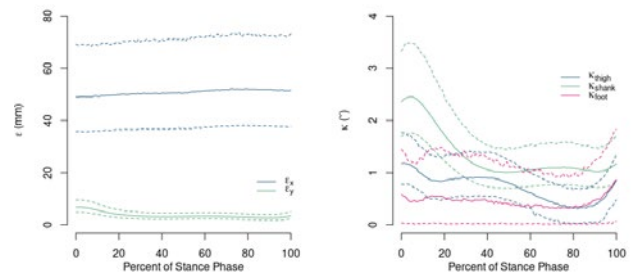


Figure 1: Stride to stride variance across the stance phase for hip joint center (left) and segment angle (right)

We suggest that observed reductions in variability are likely in response to constraints imposed by the length of the lower limb. However, further analysis of such variation may provide insights as to the control of the lower limb during gait.

Conclusion

A hierarchical model, fit using Bayesian inference, was successful in reducing uncertainty with respect to key kinematic quantities and partitioning stride to stride variance. Such an approach may lead to future insights into the motor control of the lower limb and also present researchers with improved statistical methods in which to analyse the effects of gait interventions.

Acknowledgements

NSERC CREATE Wearable Technology Research and Collaboration Training Program; Alberta Graduate Excellence Scholarship; Alberta Innovates Graduate Student Scholarship.

References

- [1] Pataky et al. (2019). *J. Biomech.*, **82**, 324-329
- [2] Serrien et al. (2020). *J. Biomech.*, **109**, 109902
- [3] Ferber et al. (2016). *J. Biomech.*, **49**, 16, 3759-3761
- [4] Osis et al. (2016). *Gait Posture*, **46**, 86-90
- [5] Plummer, M. (2017). JAGS v.4.3.0.

Computational Simulation of Sideswipe Collisions to Predict Head Injury Metrics

Shaun B. Jeffs¹, Dominic R. Demma¹, Karla J. Petroskey¹, Megan L. Bland¹, Steven A. Rundell¹

¹Explico Engineering Co., Novi, Michigan, USA

Email: sjeffs@explico.com

Summary

Subjective allegations of mild traumatic brain injury (mTBI) are common following low-energy motor vehicle collisions. In particular, sideswipe collisions between passenger vehicles and heavy trucks often result in substantial vehicle damage and significant claims of injury. Full-scale crash testing of these collisions on a case-by-case basis is not financially feasible. Therefore, we present a validated computational method to predict biomechanical responses of an occupant's head during a sideswipe collision. Vehicle accelerations from published instrumented sideswipe tests were applied to a digital model of the test vehicle in MADYMO. A virtual anthropometric test device (ATD) predicted head injury metrics, which compared favorably with those recorded in the physical tests. The head accelerations were of the same magnitude as those experienced during benign activities of daily living (ADLs). This simulation technique can provide a valuable resource in assessing occupant injury risk during sideswipe collisions.

Introduction

The considerable physical damage that may be sustained by passenger vehicles during sideswipe collisions with heavy trucks is often disproportionate to the loading experienced by the occupant. Due to characteristically long impact durations during sideswipes, vehicle accelerations are typically lower than in other collision modes. Nonetheless, substantial injuries are often claimed by sideswipe occupants.

Few studies have sought to quantify occupant loading through full-scale sideswipe collision tests. Fittanto et al. conducted four low-speed sideswipe collisions between a tractor-semitrailer and a sedan with an instrumented ATD driver [1]. The ATD responses at various body regions, including the head, were evaluated by Rodowicz et al. [2].

As medical diagnoses of mTBI, i.e. concussion, are generally based on subjective complaints, biomechanical analyses are useful in providing a quantitative means for determining the likelihood of sustaining mTBI. The objective of this study was to establish a validated simulation technique that accurately computes occupant head injury metrics in a sideswipe collision given known vehicle dynamics.

Methods

A simplified model of the occupant compartment of a 1990s-era Ford Taurus was built in MADYMO based on images from a published crash test (NHTSA #5981). A digital 50th percentile male Hybrid III (HIII) was positioned to match the tested ATD (Fig. 1A). This configuration was consistent with the setup used in Fittanto et al. Baseline seat properties were based on literature values [3].

Vehicle acceleration data from sideswipe Test 1A of the Fittanto et al. study were digitized and applied to the model. Linear head acceleration (LHA) and head injury criterion (HIC) 15 were evaluated. Seat properties were then modulated slightly (within real-world ranges) in order to optimize the head accelerations between the physical test and simulation. Once acceptable agreement was found, vehicle dynamics from the remaining three Fittanto et al. tests (1B, 2A, and 2B) were simulated using the same model properties for further validation.

Results and Discussion

The MADYMO ATD LHA data from Test 1A matched the physical test data with a high degree of fidelity (Fig. 1B). Although the physical test data showed greater noise than the MADYMO data, the peak resultant LHA differed by less than 0.1 g, while HIC varied by only 0.4 (Table 1). Further, the MADYMO ATD's head contacted the head restraint in a similar fashion as described by Rodowicz et al. [2].

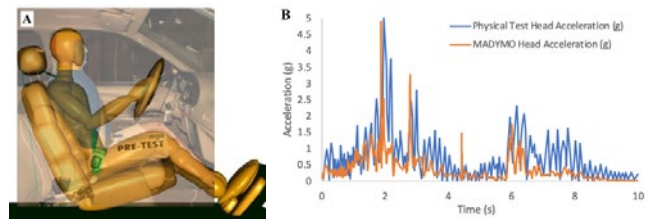


Figure 1: (A) MADYMO setup. (B) Resultant head accelerations.

Table 1: Peak LHA and HIC for physical tests and simulations.

Test No.	Physical Tests				MADYMO Simulation			
	1A	1B	2A	2B	1A	1B	2A	2B
LHA (g)	5.0	2.6	2.2	1.6	5.0	1.7	1.2	1.2
HIC-15	0.7	0.1	0.1	0.0	0.3	0.0	0.0	0.0

For Tests 1B, 2A, and 2B, LHA and HIC differed by a maximum of 1.0 g and 0.1, respectively, between simulation and physical test data. The LHA values across all tests were within a range associated with benign ADLs (e.g. sitting in a chair, hopping) and far below mTBI thresholds [4].

Conclusions

The present MADYMO simulation predicted occupant head injury metrics during staged sideswipe collisions within a reasonable degree of accuracy. Thus, this technique may be applied to forensic investigations of low-speed sideswipe collisions to assess mTBI risk.

References

- [1] Fittanto et al (2011) *J Pass Cars-Mech Sys*, 4: 304-31.
- [2] Rodowicz et al (2011) *SAE Tech Paper*, 2011-01-1125.
- [3] Cruise et al (2020) *SAE Tech Paper*, 2020-01-0524.
- [4] Funk et al (2010) *ABME*, 39: 766-76.

Kernel Based Modelling of Intervertebral Disc Characteristics

Maria Hammer^{1,2}, Tizian Wenzel^{2,3}, Gabriele Santin⁴, J.Paige Little⁵, Bernard Haasdonk^{2,3}, Syn Schmitt^{1,2}

¹Institute for Modelling and Simulation of Biomechanical Systems, University of Stuttgart, Germany

²Stuttgart Center for Simulation Science (SC SimTech), University of Stuttgart, Germany

³Institute for Applied Analysis and Numerical Simulation, University of Stuttgart, Germany

⁴Center for Information and Communication Technology, Fondazione Bruno Kessler, Italy

⁵Biomechanics and Spine Research Group, Queensland University of Technology, Brisbane, Australia

Corresponding author email: maria.hammer@imsb.uni-stuttgart.de

Summary

The aim of this study was to develop surrogate models of the non-linear elastic behaviour of six lumbar intervertebral discs for implementation in a multi-body spine model. Based on greedy kernel approximations in combination with force-displacement datasets from detailed finite element disc models, the surrogates were capable of predicting level-specific disc forces exerted onto the adjacent vertebra endplates in the full physiological range of motion and for coupling of all six degrees of freedom of an intervertebral joint.

Introduction

Computer modelling and simulation is a key technique for research in spine biomechanics, where soft tissue elements like ligaments, muscles, and intervertebral discs (IVDs) play a major role. IVDs as a sub-model in multi-body (MB) spine models are typically implemented as a force-torque element acting on the adjacent vertebrae while being dependent on the vertebrae's relative translational and rotational displacements. Disregarding the non-linear characteristics of this soft cartilaginous tissue, the elastic responses are commonly estimated by (bi-)linear spring-damping elements [1]. Even though these so-called 'bushing elements' do not allow for coupling of different degrees of freedom (DOFs), they are the currently most sophisticated approach for modelling elastic IVD responses in MB simulation frameworks in terms of considering basic physical principles. By deriving vectorial forces and torques from a single scalar force potential [2], they conserve mechanical energy in spine simulations. Alternative surrogate models of IVDs include coupling of several DOFs and the non-linear behaviour by fitting force-displacement data for single force or torque components separately, e.g. with polynomials [3] or kernel approximations [4]. Due to the lack of a common force potential and, by that, a loss of physical information, such models violate energy balance.

We, here, combine the physical approach with machine learning techniques based on recently developed greedy kernel methods [5] to mathematically describe the mapping of displacements in all six DOFs of an intervertebral joint to the six elastic response forces and torques exerted by an IVD. To account for energy conservation, we generate kernel models for the force potential of individual IVDs rather than for single force and torque components.

Methods

Following the procedure presented in [6], a biomechanical finite element (FE) model of a healthy spine was built using anatomical landmarks selected from CT scans of the Visible Human Project (National Library of Medicine, Bethesda, USA, 1994). FE models of the six lumbar IVDs (from sacrum to the lowest thoracic vertebra) were separated from this thoracolumbar spine model. Afterwards, FE simulations of every single IVD were performed in ABAQUS 6.14, representing different load cases: translational and rotational

displacements of the upper IVD endplate along single axes, along two DOFs simultaneously and full 6-dimensional movements. This resulted in datasets of response forces and torques onto the adjacent vertebra endplates and their corresponding displacements. Greedy kernel methods, as described in [5], were applied to create one surrogate model of the force potential for every IVD. Finally, the six level-specific models were included in a MB generic spine model [7]. During simulated spinal movements about different rotation axes, the elastic IVD forces and torques are constantly derived from their corresponding force potential surrogates.

Results and Discussion

The kernel model generates forces, which are in good agreement with the FE simulation results not only for training data but even for unseen data and coupled DOF motions. At the same time, it is a fast and efficient method to map the non-linear force-displacement characteristics of an IVD. The six-dimensional kernel basis enables to include kinetic coupling of DOFs while the development of surrogate models for the force potential ensures physical validity. Since the underlying FE model only captures elastic behaviour of IVDs, all dissipative processes are neglected in the presented models. Further-more, the assumption of generic IVD material parameters might not hold for different subjects. Instead, the kernel approximation algorithms could be applied to in vivo data of elastic IVD responses or other soft tissue elements in the human body.

Conclusions

With the established algorithm, we are capable of predicting the non-linear characteristics of subject- and level-specific IVDs in a multi-body spine simulation. Using this approach, it is also possible to generate IVD surrogates for pathological geometric deformations, such as scoliotic spines.

Acknowledgments

Funded by Deutsche Forschungsgemeinschaft (DFG, German Research Foundation) under Germany's Excellence Strategy - EXC 2075 - 390740016.

References

- [1] Christophy et al. (2013). *Multibody Syst Dyn*, **30**: 413-432.
- [2] Senan et al. (2009). *Int J Eng Sci*, **47**:595-609.
- [3] Karajan et al. (2013). *Biomech Model Mechanobiol*, **12**: 453-466.
- [4] Wirtz et al. (2015). *IJNME*, **101**:1-28.
- [5] Wenzel et al. (2021), *J Approx Theory*, **262**:105508.
- [6] Little et al. (2009). *Spine*, **34**:E76-E82.
- [7] Mörl et al. (2020). *Biomech Model Mechanobiol*, **19**: 2015-2047.

Inverse Distance Weighting to Rapidly Generate Large Simulation Datasets

Kalyn M. Kearney¹, Joel B. Harley², Jennifer A. Nichols¹

¹J. Crayton Pruitt Family Department of Biomedical Engineering, University of Florida, Gainesville, United States

²Department of Electrical and Computer Engineering, University of Florida, Gainesville, United States

Email: kalynkearney@ufl.edu, joel.harley@ufl.edu, jnichols@bme.ufl.edu

Summary

Advances in machine learning have increased demand for large, biomechanical datasets. Musculoskeletal simulation techniques, such as computed muscle control (CMC), have the potential to quell this demand at little expense. Yet, calculating one second of muscle activations using CMC can take minutes. We tested the accuracy of using inverse distance weighting (IDW) to approximate muscle activations across models scaled by mass and height. Our results suggest that IDW can accurately predict muscle activations with little cost.

Introduction

Given sufficient data, machine learning approaches can elucidate complex biomechanical relations. Physics-based simulations provide one approach for generating these large datasets. However, some simulation approaches have a high computational cost, thereby hindering the number and type of observations achievable in a reasonable time. For example, CMC, which computes muscle activations from target kinematics and forces [1], can take minutes to simulate seconds of movement. Across thousands of simulations, this can result in weeks of calculations. In contrast, interpolation methods, such as IDW, are computationally fast. The objective of this work was to investigate the utility of IDW for interpolating muscle activations from sparse CMC datasets.

Methods

We generated three CMC datasets with different levels of sparsity. Briefly, using OpenSim v. 4.1, we scaled a generic thumb model [2] across uniformly-spaced combinations of 30 masses and 10 heights chosen to represent 5th-95th percentile adults [3]. For each model, muscle activations to achieve a 40 N lateral pinch force were calculated using CMC. 117 CMC simulations ran to completion, providing muscle activations for a population roughly 63-103 kg and 1.72-1.88 m tall. This dataset was divided into three uniformly-spaced grids: 17 masses by 7 heights (high density), 9 masses by 4 heights (medium density), and 5 masses by 3 heights (low density).

To evaluate IDW's ability to approximate muscle activations, we selected 108 random mass-height pairs that did not correspond to the 117 computed grid vertices. We scaled the thumb model to each mass-height pair and identified the 3 closest grid vertices on a normalized scale. We used IDW with an inverse power weighting function [4] and power parameter of 1 to interpolate the 108 sets of activations. This approach preferentially weighted activations from closer grid vertices. We repeated this procedure for all three grid densities.

To compare against the interpolated muscle activations, we simulated lateral pinch using CMC for each randomly selected

mass-height pair. We quantified the root mean square error (RMSE) between the interpolated activations and the CMC activations. We report the mean RMSE for each simulation (averaging across all muscles) as well as the mean RMSE for each muscle (averaging across simulations).

Results and Discussion

IDW approximated muscle activations in lateral pinch with minimal error and substantially less computational cost than CMC alone. Fig. 1 illustrates the low density and high density RMSE results. The RMSE associated with interpolated muscle activations never exceeded 4%. Increasing the grid density slightly decreased RMSE, which averaged 0.33%, 0.40%, and 0.45% for high, medium, and low density grids, respectively. At the grid boundaries, the high density grid had higher RMSEs. As CMC simulations outside the grid failed to run to completion, CMC solutions at the boundary may have been less stable. The *flexor pollicis longus* and *extensor carpi ulnaris* had the highest mean RMSE, peaking at 3.2% and 3.7%, respectively, on the low-density grid. No other muscles exceeded a mean RMSE of 1.5%. Furthermore, computation time for CMC simulations averaged 4.22 core-minutes, while IDW averaged 0.95 core-seconds per mass-height pair.

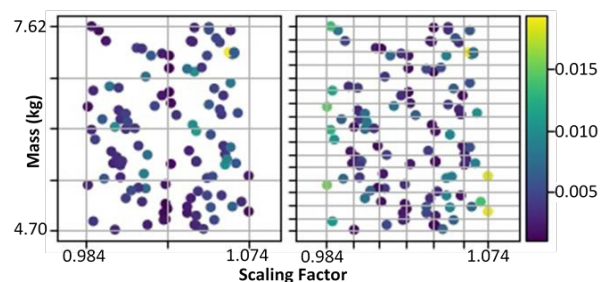


Figure 1. Mean RMSE of interpolated muscle activations across each randomly selected mass-height pair (colored). Muscle activations from CMC were calculated at the grid vertices (gray).

Conclusions

The present work proposed and tested a method for efficient and accurate estimation of muscle activations using a grid of CMC simulations and IDW. This work indicates IDW is a powerful approach for rapidly estimating muscle activations from sparse CMC datasets. Rapid generation of data will facilitate machine learning analyses of human movement.

References

- [1] Thelen et al. (2003). *J Biomech*, **36**: 321-328.
- [2] Nichols et al. 2017. *J Biomech*. **58**:97-104.
- [3] Fryar et al. (2016). *Vital Health Stat*, **39**: 1-46.
- [4] Shephard, D (1968). *Proc. of ACM Nat. Conf.*, 517-524.

The flow of tissue energy during whole muscle contraction in 3D

Stephanie A. Ross^{1,*}, Sebastián Domínguez², Nilima Nigam³, James M. Wakeling^{1,3}

¹Neuromuscular Mechanics Laboratory, Dept. Biomedical Physiology and Kinesiology, Simon Fraser University, Burnaby, Canada

²Dept. Mathematics and Statistics, University of Saskatchewan, Saskatoon, Canada

³Dept. Mathematics, Simon Fraser University, Burnaby, Canada

*Email: saross@sfu.ca

Summary

In this study we examined how energy is distributed through whole muscle tissue during cyclic contractions, and how this impacts the external mechanical work done, using a three-dimensional (3D) continuum model of muscle. We found that muscles with higher initial pennation angles stored more energy in the aponeurosis and base material during contraction, and this was associated with higher muscle mechanical work per cycle. These results highlight that the structural and material properties of whole muscle tissue affect the mechanical performance of a muscle.

Introduction

Skeletal muscles are the motors that drive human and animal locomotion. While muscles have historically been assumed to behave as massless one-dimensional actuators, whole muscles deform and change shape in all three dimensions during contraction [1]. Energy is stored in the tissue as it deforms which alters the amount of energy that is available to do external mechanical work during contraction. Here we examine the distribution of energy through whole muscle in three dimensions during contraction, and how this alters the overall performance of the muscle in the longitudinal direction.

Methods

To simulate the behaviour of whole muscle, we used a 3D continuum model (Figure 1) that is fully dynamic and accounts for the effects of tissue mass, velocities, and accelerations [1,2]. The model is composed of one-dimensional fibers embedded in an isotropic base (or background) material, resulting in an overall anisotropic tissue behaviour. We chose the size of the geometry to approximate the dimensions of a human medial gastrocnemius muscle.



Figure 1: Image of 3D continuum model of muscle during an active cyclic contraction. The color gradient shows the deformation of the tissue, with red and blue representing greater and lesser deformation, respectively.

We examined the deformations and flow of energy through the muscle tissue during cyclic contractions (Figure 2) with different initial fibre pennation angles (11.5 to 22.7 deg), cycle strain amplitudes (2.5 to 7.5%), and maximum excitations (40 and 100%). We additionally explored how

these tissue deformations and energies were associated with changes in mechanical work per cycle.

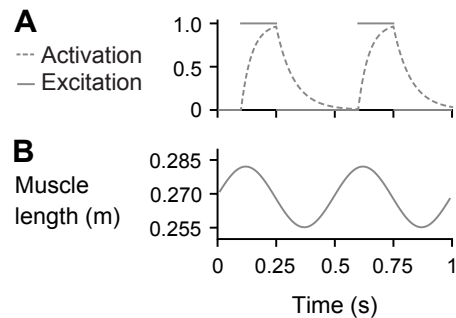


Figure 2: Sample traces of prescribed excitation (solid) and activation (dashed) (A) and muscle length (B) over time.

Results and Discussion

For simulations with maximal excitation and a cycle strain amplitude of 5% of the muscle resting length, the energy of the active contractile elements increased as the activation increased, and this was greater for more pennate muscles (with higher initial pennation angles). The base material, which represented the extra- and intra-cellular material besides the contractile elements, and the aponeurosis both had greater peak energy storage during the contraction cycles for muscles with higher initial pennation angles. In terms of the mechanical work, we found that muscles with higher initial pennation angles did greater mechanical work per contraction cycle, possibly due to the greater energy storage in the aponeurosis and base material.

Conclusions

This study shows how the 3D shape of muscle, and the storage of energy in the tissue during contraction, has important implications for its mechanical behaviour.

Acknowledgements

This work was supported by NSERC Discovery Grants to JMW and NN and an Alexander Graham Bell Canada Graduate Scholarship-Doctoral to SAR. We are also grateful for funding to SD from the Pacific Institute for the Mathematical Sciences, Canada.

References

- [1] Zurbier CJ and Huijing PA (1993). *J. Morphol.*, **218**: 167-180.
- [2] Wakeling JM et al. (2020). *Front. Physiol.*, **11**: 813.
- [3] Ross SA et al. (2018). *Integr. Comp. Biol.*, **58**: 232-250.

Statistical Prediction of Spinal Injury Using CIREN Data

Sean Pham¹, Sean D. Shimada¹
¹Biomechanical Consultants, Davis, CA
 Email: sean@motionsandforces.com

Summary

To compensate for the lack of available research defining the lateral shear thresholds for spinal injury, crash injury data from 2017 to 2019 was surveyed to develop statistics to gauge the likelihood of spinal injury due to side impact.

Introduction

This investigation was motivated by the lack of research defining lateral shear thresholds for spinal injury. The goal of this study was to develop probabilistic measures to predict spinal injury occurrence based on crash data from the current Crash Injury Research Engineering Network (CIREN) compiled for years 2017 to 2019. Though there have been studies that use crash data from national databases to separately study side impact [1] and spinal injury [2], the literature correlating side impact dynamics to spinal pathology is sparse.

Methods

110 incidents, involving a total of 1216 injuries, were surveyed in the current CIREN database. Non-horizontal impacts and incidents with no reported delta-v were excluded. The remaining incidents were indexed for spinal injuries and extracted with accompanying data on impact delta-v, clock direction, spinal section, and injury type. Statistics were calculated based on these parameters to develop Bayesian probabilities for the determination of spinal injury in side impacts.

Results and Discussion

After downselecting based on the aforementioned criteria, 33 incidents were found that resulted in a total of 78 spinal injuries. Lumbar fractures, including fractures of the vertebral body, spinous, and transverse processes, were the highest likelihood injury with a 51.3% incidence across all impact conditions (Figure 1). Fractures amongst all spinal sections were the prevalent injury mechanism.

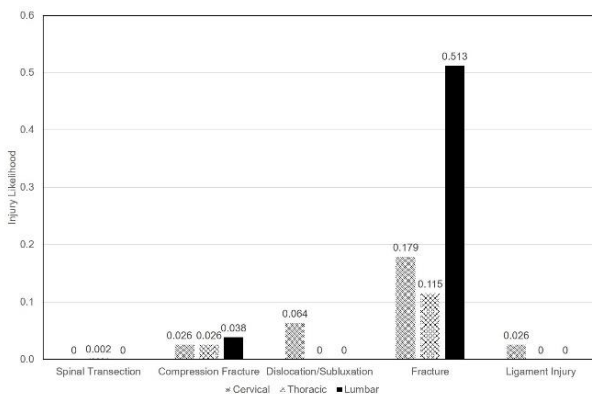


Figure 1: Summary of spinal injuries and their likelihood for each section of the vertebral column for all crash types.

To classify side impact injuries, clock directions of 2-4 o'clock (right) and 8-10 o'clock (left) were considered. 24 spinal injuries from 8 side impacts were identified. Injuries were further classified into four delta-v bins (0-25 km/h, 25-50 km/h, 50-75 km/h, 75-100 km/h). Using Bayes' Theorem, the probability of an injury in a specified spinal section for a side impact at a given delta-v was approximated (Table 1).

Table 1: Summary of Injury Probabilities for Given Delta-V Classes.

	0-25 km/h	25-50 km/h	50-75 km/h	75-100 km/h
Cervical	6.95%	8.67%	17.1%	2.50%
Thoracic	6.10%	4.15%	8.49%	0.00%
Lumbar	4.67%	43.5%	3.68%	4.67%

Conclusions

The crash data compiled in the CIREN database provides a good basis for developing statistical tools for accident reconstruction. However, the current CIREN repository lacks sufficient data to adequately gauge the likelihood of a lateral shear spinal injury; the sample size for side impact crashes is small, and the reported injuries do not cover a broad spectrum of injury mechanisms, locations, or severities. Because of the lack of data for high delta-v impacts, the injury probabilities appear artificially low. Addition of data in the 50+ km/h regime will provide more robust probabilistic characterization of spinal injury. Future work will focus on incorporating data from the older CIREN database to build more reliable metrics to capture the dynamics of lateral shear spinal injury. A more diverse array of spinal injuries would allow for further discrimination based on vertebral location and injury severity, amongst other parameters, to improve the precision of spinal injury prediction.

References

- [1] David C. Viano & Chantal S. Parenteau (2010) Severe Injury to Near- and Far-Seated Occupants in Side Impacts by Crash Severity and Belt Use, *Traffic Injury Prevention*, **11:1**, 69-78.
- [2] Darrin Richards et al. (2006) Incidence of Thoracic and Lumbar Spine Injuries for Restrained Occupants in Frontal Collisions, *Association for the Advancement of Automotive Medicine*, 50th Annual Proceedings, 125-139.

Evaluation of design and concept verification of a new figure skating blade with integrated damping system for reducing impact related overuse injuries

Ondrej Spiegl¹, Lina E. Lundgren², Olga Tarassova¹, Daniel Neuman³ & Anton Arndt^{1,4}

¹The Swedish School of Sport and Health Sciences (GIH), Stockholm, Sweden

²Rydberg Laboratory of Applied Sciences, Halmstad University, Halmstad, Sweden

³Department of Physics, Royal Institute of Technology (KTH), Stockholm, Sweden

⁴Karolinska Institute, Stockholm, Sweden

Email: spiegl.ondrej@gmail.com

Summary

In this study, a new figure skating (FS) blade with an integrated damping system (FSB-IDS) was developed, assisted by a needs analysis, computer-aided design and finite element analysis. The FSB-IDS enables a blade runner to slide upwards inside a frame against elastic damping elements that deflect under the impact load, reducing landing accelerations. Furthermore, the blade runner interacts with the direction and the location of the force vector during the individual phases of the landing impact. Prototype damping elements of stiffnesses relevant for high landing impacts (about 3000 N), with minimal effect on propulsive forces at take-offs (about 1000 N), were tested using a universal test system. A landing impact from a 60 cm high box onto artificial ice using the FSB-IDS prototype verified the intended functionality. In addition, the FSB-IDS can be considered as a lightweight blade.

Introduction

Today's FS blades have more or less the same characteristics as those from more than a century ago. Apart from incorporating new materials in the construction of the blade, the innovation and emphasis on injury prevention have been inconsistent with the increase in the jump demands of today's competitive FS and the associated rising frequency of chronic overuse injuries. The chronic overuse injuries in singles and pair skaters are attributed to the high loads absorbed during repeated take-offs and landing impacts [1, 2]. Furthermore, the FS equipment contributes to the high impact forces and injury risk, due to its stiff characteristics [3, 4].

Methods

Based on the requirement specifications, computer models (Fusion 360, Autodesk Inc.) of different FSB-IDS designs ($n=3$) were developed, all consisting of a frame, a blade runner and damping elements. The permissible movement of the blade runner is in vertical direction (V), and diagonally upwards forward and rearward along the (F) and (R) axis (Figure 1).

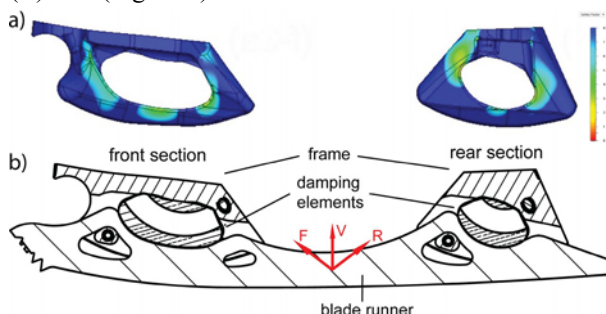


Figure 1: a) FEA, Safety factor of FSB-IDS frame under 1000 N perpendicular load to the frame; b) Cross-sectional view of the FSB-IDS, the red arrows indicate the direction of the permissible movement of the blade runner inside the frame (V), (F) and (R).

Finite element analysis (FEA: nonlinear static stress simulation, Fusion 360) was used to initially assess the performance of different shapes and materials, placement of damping elements, including stress distribution. Prototypes of the selected damping elements (thermoplastic polyurethane (TPU) 90 A shore hardness) were evaluated in regards to force-displacement in an electromechanical universal test system (MTS Criterion C42.503). Finally, the prototype of the FSB-IDS was tested during simulated landing impact (replicating a waltz jump from a 60 cm high box) to verify the functionality.

Results and Discussion

The FSB-IDS concept uses two thick elastic damping elements of TPU material that compress during the impact and thereby reduces the acceleration of the impact [5, 6]. A simulated landing impact using the FSB-IDS prototype showed that the blade runner slides inside the frame and interacts with the direction and the location of the force vector during the individual phases of the landing impact as the damping elements deflect under the load (Figure 2).

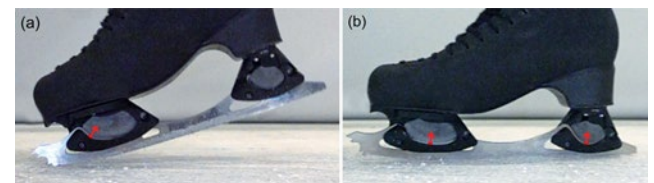


Figure 2: a) Initial contact of the FSB-IDS with the ice surface; b) Full contact of the FSB-IDS with the ice surface.

Theoretical displacement of the blade runner supported by two damping elements ranged from 1.1 ± 0.4 mm under a load of 1000 N to 4.8 ± 2.4 mm under a load of 3000 N.

Conclusions

The current FSB-IDS has a simple, compact design in which the combined effect of low weight and damping is adequate to the demands of high-performance FS today.

Acknowledgments

This work was supported by the Swedish Research Council for Sport Science under Grant P2019-0078. A patent (pending) application was submitted on the FSB-IDS.

References

- [1] Han JS et al. (2018). *Sports Health*, **10**(6): 532-537.
- [2] Porter EB et al. (2007). *WMJ*, **106**(6): 330-334.
- [3] Bruening DA and Richards JG (2006). *J Appl Biomech*, **22**(4): 285-295.
- [4] Spiegl O et al. (2019). *Footwear Sci*, **11**(2): 121-129.
- [5] Gawlak D et al. (2017). *Acta Bioeng Biomech*, **19**(1): 89-95.
- [6] Li K and Darby AP (2006). *J Vib Control*, **12**(5): 445-464.

Loss of consciousness in National Football League players is associated with high strain in the thalamus and brainstem.

Karl A. Zimmerman^{1,2}, Janie Cournoyer³, Clara Karton³, Blaine Hoshizaki³, Mazdak Ghajari², David J. Sharp¹

¹ Computational, Cognitive and Clinical Neuroimaging Laboratory, Department of Brain Sciences, Hammersmith Hospital, Imperial College London, London, UK

² HEAD Lab, Dyson School of Design Engineering, Imperial College London, UK

³ Neurotrauma Impact Science Laboratory, University of Ottawa, Canada

Email: kaz11@ic.ac.uk

Summary

Zimmerman et al., show using video and computational modelling analysis of head impacts leading to a mild TBI in the National Football League, patterns of brain deformation (strain) differ based on whether players lost consciousness or not. In particular, strain was higher in the thalamus and brain stem in players who lost consciousness compared to those who did not.

Introduction

Sports traumatic brain injury (TBI) can produce transient neurological signs such as loss of consciousness (LOC) and dystonic posturing. However, it is unknown why impacts produce a range of neurological effects. Video surveillance allows the biomechanics of impacts to be calculated from impact reconstructions. The biomechanics can then be used to estimate the patterns of strain produced in different brain regions. Here we use a 3D model of brain injury biomechanics to investigate the strains produced by National Football League impacts that produce mild TBI leading either to LOC, dystonic posturing, or producing no neurological signs. We test the hypotheses that LOC is associated with high strain within the brainstem and thalamus, whereas dystonic posturing is associated with high strain in the motor cortex.

Methods

82 videos of mild TBIs in the NFL were classified as showing either LOC (20), posturing (21) or no neurological signs (No Signs - 41). Videos were analysed and impacts simulated using previously published methodology [1]. In brief, video analysis was used to estimate impact velocity and location/orientation. Laboratory reconstructions using Hybrid III headforms with mounted accelerometers were used to capture head impact kinematics (Fig 1A). A 3D finite element model was used to calculate brain deformations from each head impact (Fig 1B). The estimated magnitude and location of mechanical strain in specific brain regions were then statistically compared across the groups.

Results and Discussion

Impacts leading to LOC had significantly higher impact kinematics and whole brain measures of brain deformation compared to No Signs impacts. A voxelwise analysis of brain deformation corrected for the magnitude of strain showed regions of disproportionately higher strain in the thalamus, brain stem and cerebellum in impacts leading to LOC compared to No Signs (Fig 1C). Impacts leading to posturing also showed regions of higher strain, however these areas

were constrained to the cortical regions including the motor cortex.

A. Impact reconstruction



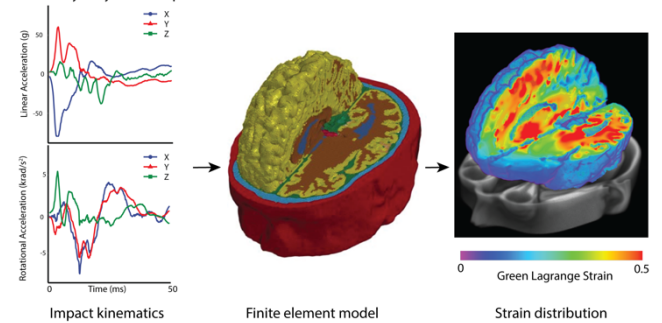
Impacts analysed on video for visible signs post injury, impact velocity, location and orientation



Videos used to guide laboratory reconstructions with mounted accelerometers

B. Computational modelling of traumatic brain injury

Case study: Player who experienced loss of consciousness: kinematics and brain deformation



C. Voxelwise analysis across the groups

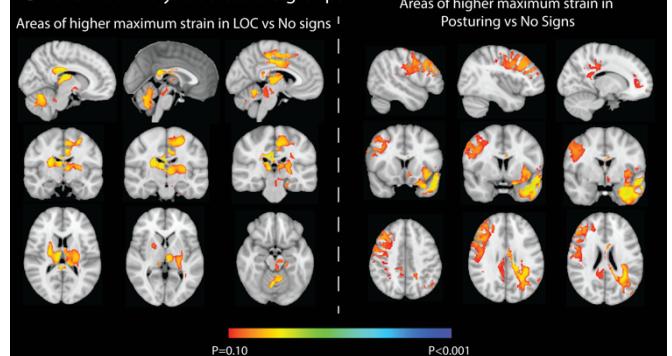


Figure 1: A. Impact reconstruction and physical simulation B. Finite element modelling of brain injury biomechanics. C. Maximum strain comparison across groups.

Conclusions

We show that strains are particularly high in the thalamus and brain stem in those players who lose consciousness. In contrast, impacts leading to posturing appear to disproportionately affect cortical regions, including the motor cortex. These results provide evidence that loss of consciousness is produced by head impacts that produce high strain in the brainstem and thalamus.

References

[1] Zimmerman K.A, et al., (2021). *Journal of Biomechanics*

Modelling of the Pelvis and Lumbar Spine in High-Rate Axial Loading

Corina Espelien¹, Katarzyna Rawska¹, Rob Salzar¹

¹Center for Applied Biomechanics, University of Virginia, Charlottesville, USA
Email: cme2kd@virginia.edu

Summary

This study creates a framework to efficiently evaluate the injury risk in an underbody blast (UBB) impact with computational human body models (HBM). Input curves examined in this study varied in terms of peak acceleration and loading rate, as well as HBM posture and axial loading angle. Relative trends of peak forces and accelerations, in addition to the probability of injury, are discussed.

Introduction

UBB are extremely high rate and high magnitude loading events that can occur in the combat theater, where personnel are subjected to axial loadings due to the detonation of an explosive beneath a military vehicle. While the vehicle can shield occupants from projectiles and blast shock waves, there is a massive amount of energy imparted from the floor and seats of the vehicle directly to the occupants.

Post-mortem human subject (PMHS) testing has helped identify the pelvis and vertebrae injuries from a UBB motivated loading and develop injury risk curves [1]. For any given loading scenario, the injury risk curves use an input variable, such as resulting pelvic acceleration, to determine the probability of injury. Using computational HBM, resultant accelerations, forces, and moments can be approximated for a given load curve. Comparing these resultant metrics to the injury risk curves from PMHS testing provides a low-cost and efficient screening method to determine the types of inputs that may be injurious or not injurious.

Methods

Simulations in MADYMO, a multibody solver, used with a passive musculature, 50th percentile male model were performed to obtain the resultant accelerations and forces of the pelvis and lumbar spine. The peak values for these metrics were compared to the appropriate injury criteria. A finite element model (FEM) of the isolated pelvis and lumbar spine of the 50th percentile male model was run in LS-Dyna to assess the strain distribution in the cortical and trabecular bone and the corresponding locations likely to fracture.

The test space and corresponding injury risks were bracketed by two baseline triangular acceleration curves of approximately equal energies, defined by peak accelerations and time-to-peaks. The first baseline impact curve, based on a pilot ejection seat, typically does not result in injury (given the appropriate alignment), with a peak of 17g in 107 ms. The second baseline impact curve, based on average UBB acceleration curves, is considered injurious with a peak of 730g in 2.5 ms. The tilt of the pelvis and the tilt of the entire seat pan relative to the global coordinate system were considered, as they have potential analogs to injury concerns and mitigation strategies.

Results and Discussion

The MADYMO model output pelvic accelerations for the ejection seat (low-rate) and UBB (high-rate) curve corresponded to injury probability of 0% and 100%, respectively. Compared to a nominal position of the pelvis, an anterior positional tilt resulted increase of L5/sacrum peak axial force by 16%. Reclining the entire seat decreased the peak forces at L5/sacrum and T12/L1 by 24% and 59%, respectively. The FEM strain maps of the cortical bone illustrate the differences resulting from the low-rate and high-rate inputs (Figure 1).

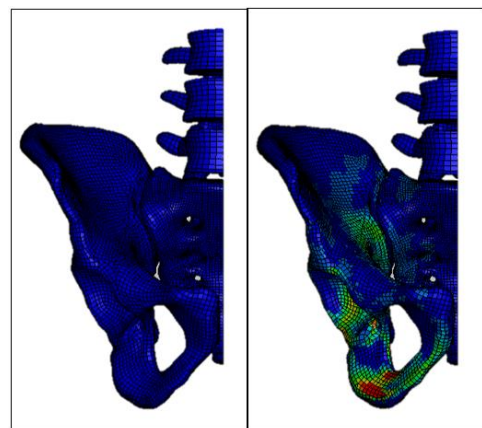


Figure 1: Strain of cortical bone at 5 ms for low-rate (left) and high-rate (right) load input curves. Scale from 0% to 0.3% strain.

Conclusions

The MADYMO model can quickly output metrics which can be used to assess the probability of injury risk to the pelvis or lumbar vertebrae, while the FEM provides more detailed information about locality of strains. This framework provides a method to assess potential injuries for a given high-rate axial load curve, which can be modified based on UBB mitigation strategies.

Acknowledgments

The authors are grateful to the University of Virginia School of Engineering and Applied Sciences and Luna Innovation, Inc., for supporting the work leading to the development of this work.

References

- [1] Bailey AM et al. (2015). *Annals of Biomedical Engineering*, **43**: 1907-1917.

Quantification of Upper Limb Loading Behind a Ballistic Shield Using an Adapted Anthropomorphic Test Device Arm

Noah Steinmann¹, Julia de Lange², Jean-Sébastien Binette³, Cheryl E. Quenneville^{1,2}

¹Mechanical Engineering Department, McMaster University, Hamilton, Canada

²School of Biomedical Engineering, McMaster University, Hamilton, Canada

³Defence Research and Development Canada, Valcartier Research Centre, Quebec City, Canada

Email: quennev@mcmaster.ca

Summary

The back-face deformation caused by small arm projectiles impacting ballistic shields used by military and police members can contact the arm, potentially causing an upper extremity injury. This study modified an Anthropomorphic Test Device (ATD) to be used for the characterization of behind ballistic shield blunt impact loading profiles. It was then used to comparatively assess the protective capabilities of two shields with the same ballistic protection rating. The shields exhibited different deflections and loading profiles, indicating a need for a back-face injury metric.

Introduction

Behind Armor Blunt Trauma (BABT) is a non-penetrating injury that results from contact from back-face armor deformation to the body. Standards have been developed to specify allowable back-face deformation on worn body armor, but these do not directly relate to ballistic shields. When a ballistic shield is struck by a projectile, even if there is no perforation, the back-face deformation may result in fractures of the upper limb. A tool for measuring loading behind shields to assess injury risk and develop appropriate standards to evaluate shield protective capabilities is needed. The purpose of this work was first to modify an ATD to quantify impact responses behind ballistic shields and second, to assess two types of composite ballistic shields (flat and curved), both with the same ballistic protection rating in NIJ 0108.01 [1].

Methods

Four vulnerable locations were identified: elbow, forearm, wrist and hand. A World SID 50th percentile upper extremity (Humanetics Innovative Solutions) formed the basis of the new device, including integrated six-axis (forearm) and two-axis (elbow) load cells. Uniaxial piezoelectric washer-style force sensors (PCB Piezotronics, Model 201B05, 22.24 kN capacity) were added at the wrist and elbow to measure the applied force. A new hand employed to facilitate gripping of the handle and was similarly instrumented (PCB sensors).

Ballistic testing was conducted at Defence Research and Development Canada (RDDC) - Valcartier Research Centre (VRC), where the ATD, positioned behind the composite shields, was subjected to ballistic impacts (projectile mass 9.6 g, velocity 847.7 ± 9.8 m/s, mean \pm SD). Impacts were delivered to the elbow and hand, at two stand-off distances (defined as the distance between the back of the shield and the surface of the ATD's sensor). For each impact, the peak forces, moments, and impact duration were recorded, and a high-speed camera (Photron, Fastcam SA-X2, 20,000 fps) was used

to characterize and compare the responses of the shields. The apex of the deformation profile was tracked to determine the total shield displacement and velocity.

Results and Discussion

For the flat shield, the maximum deflection was 1.77 ± 0.3 cm, whereas the curved shield was 3.84 ± 0.3 cm. Furthermore, the flat shield had a 32% lower ($p=0.022$) peak back-face velocity compared to the curved shield. The four elbow impacts at each of the two stand-offs (10 mm and 20 mm) for the flat shield showed impact force increased by 40% (although not significantly, $p=0.18$) when decreasing the stand-off distance. The five hand impacts at each of the two stand-offs (30 mm and 40 mm) for the curved shield, showed the peak force increased significantly by 44% ($p=0.0022$) when decreasing the stand-off.

Each of the ballistic shields were designated Level III under NIJ 0108.01 [1]; however, they performed very differently under the same testing conditions as their resulting back-face response differed greatly. There is no BABT criterion or specification under this standard, only perforation performance. The curved shield required a greater stand-off to keep loading on the arm consistent, as compared to the flat shield. Increasing stand-off distance is a potential method for manufacturers to reduce loading to the upper limb, to a certain point. A standard is needed (along with injury criteria for these regions of the upper limb) to evaluate shields so that consideration is given to both the risk due to projectile penetration, and the back-face deformation.

Conclusions

This represents the first highly instrumented ATD upper limb capable of evaluating high energy, short duration impacts typical of BABT. This newly developed ATD quantified the back face loading experienced by the upper limb for two different shields with the same ballistic protection rating. Although rated the same, they had very different deflections which affected their loading at altered stand-off distances, and thus may have different protective capabilities for BABT of comparable impacts.

Acknowledgments

The authors acknowledge the contributions of Daniel Bourget, Benoit Gauthier and Steven Kelley (DRDC-VRC). This work was also funded by DRDC.

References

- [1] National Institute of Justice (1985). *NIJ Standard 0108.01*

Patellofemoral Contact Forces after ACL Reconstruction using Statistical Parametric Mapping

Jack R. Williams¹, Kelsey Neal¹, Abdulmajeed Alfayyadh¹, Ashutosh Khandha¹,
Kurt Manal¹, Lynn Snyder-Mackler¹, Thomas S. Buchanan¹

¹University of Delaware, Newark, Delaware, U.S.A

Email: jackrw@udel.edu

Summary

Patellofemoral osteoarthritis (OA) after ACL reconstruction (ACLR) is prevalent. Limited evidence suggests patellofemoral underloading in the involved limb (vs. uninvolved) occurs early after surgery; however, it is unknown if this underloading persists with time. 10 participants underwent motion analysis during overground walking at 6 and 24 months after unilateral ACLR. Muscle forces from a validated EMG-driven musculoskeletal model, in combination with kinematic and anthropometric information, were used to calculate patellofemoral contact forces. Statistical parametric mapping was used to conduct a 2x2 repeated measures ANOVA (Limb x Time) to evaluate patellofemoral contact forces. A significant interaction effect was observed early in stance. Patellofemoral underloading was present at 6 months but did not persist with time. It remains to be seen if this loading pattern is related to eventual OA development.

Introduction

Patellofemoral osteoarthritis development after ACLR is common; however, the pathogenesis of the disease remains unknown [1]. Underloading of the involved limb has been associated with tibiofemoral OA development after ACLR [2]. Limited evidence suggests a similar underloading mechanism may be occurring within the patellofemoral compartment [3]. However, it is unknown if this underloading persists with time. Thus, the purpose of this study was to examine how patellofemoral contact forces change from 6 to 24 months after ACLR. We hypothesized that there would be involved limb underloading (vs. uninvolved) at 6 months but not at 24 months.

Methods

10 participants (5 female, mean age: 21 ± 5 yrs) underwent motion analysis during walking at 6 and 24 months after unilateral ACLR with a bone-patellar tendon-bone graft. Kinematic, kinetic, and electromyography (EMG) data were collected bilaterally and used as inputs into a validated, EMG-driven musculoskeletal model to determine subject-specific muscle forces [2]. These muscle forces, in conjunction with kinematic data and anthropometric information, were used to calculate patellofemoral contact force [4]. Statistical parametric mapping (SPM) was used to perform a 2x2 (Limb x Time) repeated measures ANOVA throughout stance ($\alpha = 0.05$) in order to gain insight into patellofemoral forces throughout the entirety of the movement pattern.

Results and Discussion

Our hypotheses were supported. Underloading of the involved limb's patellofemoral compartment (vs. uninvolved) occurred

6 months after ACLR during the early portion of stance; at 24 months the involved and uninvolved limb displayed similar patellofemoral contact forces (Figure 1A). No main effects of limb or time were observed. However, a limb by time interaction was seen during early stance (Figure 1B). Restoration of patellofemoral contact force symmetry with time is likely driven by restoration of quadriceps strength after surgery; however, this remains to be investigated. Future work should also determine if these changes in patellofemoral contact forces are associated with eventual OA development.

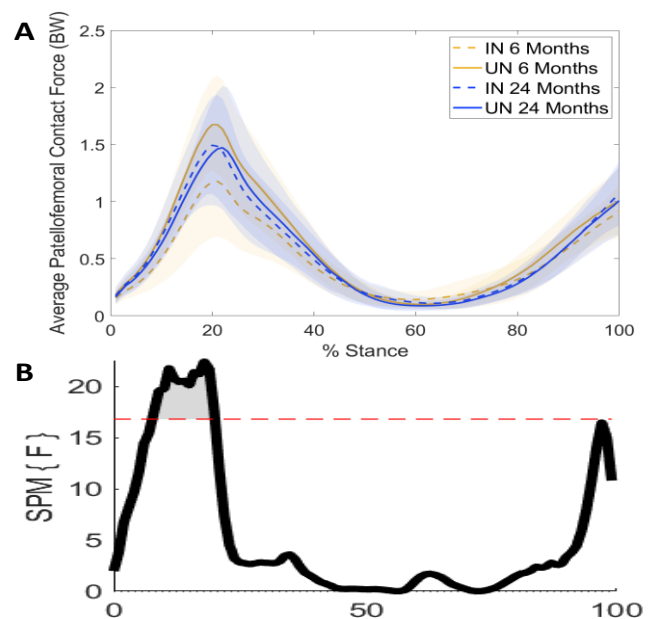


Figure 1: A. Involved limb (dashed) and uninvolved limb (solid) patellofemoral contact force at 6 (yellow) and 24 months (blue) after ACLR. Shaded boundaries represent ± 1 SD. B. 2x2 repeated measures ANOVA F statistic throughout stance for the interaction term; dashed red line indicates significance threshold ($\alpha = 0.05$), shaded area represents significance.

Conclusions

Involved limb patellofemoral underloading (vs. uninvolved) is present 6 months after ACLR but absent at 24 months. The implications of these loading changes in the context of patellofemoral OA development remains to be explored.

Acknowledgments

NIH R01-HD087459

References

- [1] Culvenor AG et al. (2013). *AJSM*, **47**: 66-70.
- [2] Wellsandt E et al. (2016). *AJSM*, **44**: 143-151.
- [3] Sritharan P et al. (2020). *AJSM*, **48**: 1711-1719.
- [4] Yamaguchi G & Zajac FE. (1989). *J. Biomech.*, **22**: 1-10.

Differences between loaded and unloaded bone kinematics of the foot and ankle complex

Michele Conconi^{1*}, Alessandro Pompili¹, Nicola Sancisi¹, Alberto Leardini², Stefano Durante², Claudio Belvedere²

¹Department of Industrial Engineering - DIN, University of Bologna, Italy

²Movement Analysis Laboratory, IRCCS Istituto Ortopedico Rizzoli, Bologna, Italy

Email: michele.conconi@unibo.it

Summary

We investigated the motion of the foot and ankle bones from a series of static Weight Bearing CT (WBCT) scans, evaluating load related variation through principal component analysis (PCA). For the two investigated feet, unloaded motion can be explained with three synergies. When load is considered, a fourth synergy is needed. In both cases, all the bones participated to the overall foot motion. Synergies matched very well among the feet.

Introduction

The human foot and ankle complex is a multi-joint mechanism that plays a fundamental role in limb-to-ground interaction. As reported in the literature, its behavior is load-dependent [1-3]. However, a description of the loaded 3D foot kinematics including all bones is still missing, mainly due to the complexity in accurately tracking the motion of all the bones at once. The aim of this work is to fill this gap, by reconstructing the foot bone motion from a series of static scans performed both with and without load. To provide a compact representation of the motion of the foot and ankle complex, data are analyzed through PCA to identify significant synergies among the bone kinematics.

Methods

We analyzed two feet from cadaver dissection, free from anatomical defects. First, the legs were casted with extended knee (fig. 1.a), leaving the foot and ankle free to move. The feet were then scanned via Cone Beam CT (fig. 1.c) in 15 positions, varying ankle dorsiflexion among $[-30^\circ -10^\circ 0^\circ 10^\circ 20^\circ]$ and foot supination among $[-10^\circ 0^\circ 10^\circ]$ through a set of wedges (fig. 1.b), while keeping the leg vertical and suspended by cables, to make it unloaded. The same scans were repeated by applying a vertical load equal to the subjects' half weight (35 kg). Two additional scans were taken by rotating the tibia internally and externally to its max, with the foot in neutral position. CBCT scans were segmented through a semi-automatic procedure (DICE > 95%). Anatomical reference systems were defined for the neutral foot and registered automatically to those from the other scans (accuracy $<0.5^\circ$ and 0.1 mm). Bone position and orientation were expressed through a cardanic sequence defined for this study (z-y-x). PCA was carried out on two different databases: one with only unloaded poses (15) and the other with all the poses (32).

Results and Discussion

When foot is unloaded, 3 synergies explained more than 97 % of the variance in bone motion. To explain the same variance with load, a fourth synergy is needed. All the bones participate

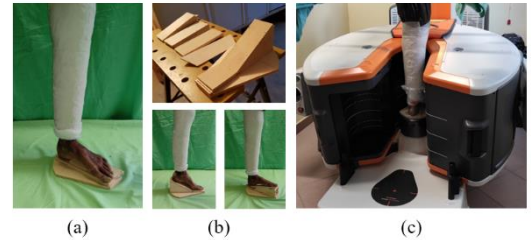


Figure 1: casted leg (a); wedges to set the foot pose (b); the leg in the CBCT (c)

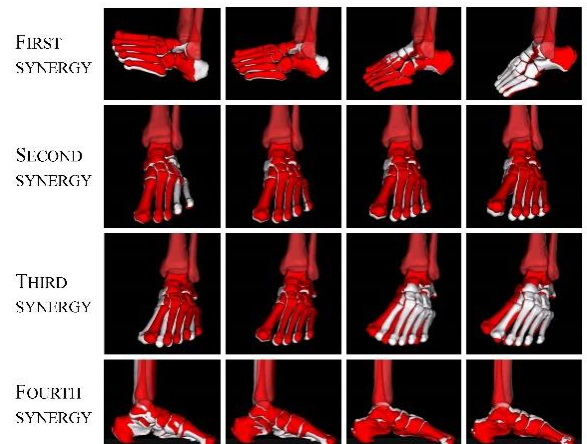


Figure 2: The first four foot without load (grey) and with load (red).

to the overall motion of the foot-ankle complex. The first synergy mainly maps ankle flexion, the second the overall foot pronation, the third abduction at the Chopart joint. These synergies are similar between unloaded and loaded dataset, although the ROM is typically wider for the second. The fourth synergy represents deformation of the foot arches, thus explaining why it is observable only under load (fig. 2). The motion of the two feet is mapped by the same four synergies, however with different variance, confirming that the joint mobility may change among individuals.

Conclusions

This work reveals the complexity of relative motion among the bones of the foot and ankle complex and the need for weight-bearing CT based investigations, also in patients. While the tibiotalar and subtalar joints provide the main foot mobility about two almost decoupled directions, the other joints behave synergically to support loads and are thus essential to the functionality of the foot.

References

- [1] Hirschmann et al. (2013). *Eur Radiol*, **24**: 553-558.
- [2] Fassbind et al. (2011) *J. of Biom. Eng.*, **133**: 104502-1.
- [3] Phan et al. (2017). *J. Biomech* **95**: 109287.

The Non-Intuitive Contributions of Individual Quadriceps Muscles to Patellar Tracking

Seong-won Han^{1*}, Andrew Sawatsky¹, Walter Herzog¹

¹Human Performance Laboratory, Faculty of Kinesiology, University of Calgary, Calgary, AB, Canada

*Email: seongwon.han@ucalgary.ca

Summary (150 words)

The purpose of this study was to quantify the contribution of the individual quadriceps muscles to patellar tracking. The individual and/or combined quadriceps muscles were activated in rabbits (n=6) during knee flexion/extension. Three-dimensional patellar tracking was measured for the vastus lateralis (VL), vastus medialis (VM) and rectus femoris (RF) when activated alone, and when activated simultaneously. Our results showed that when all quadriceps muscles were activated simultaneously, the patella was shifted, rotated and tilted more medially, compared to when VL or RF were activated alone ($p < 0.05$). Interestingly, VM activation alone produced a similar tracking pattern to that observed when all quadriceps muscles were activated simultaneously, even though the knee extensor torque of VM was much smaller than the torque produced when all quadriceps muscles were activated simultaneously. We conclude that VM affects patellar tracking in a distinctly different way than VL and RF.

Introduction

Patellar tracking, the movement of the patella relative to the long axis of the femur during knee movements [1], has been found to depend significantly on the force applied to the joint exerted by knee extensors [2]. For example, the patella was found to shift and rotate more medially, as knee extensor torques increased by increasing the level of quadriceps muscle activation [2]. However, it is uncertain how the individual quadriceps muscles contribute to patellar tracking when they are activated individually in isolation.

Recently, we developed a novel technique whereby the individual quadriceps muscles of the rabbit can be stimulated in isolation or in synchrony in any manner desired [3].

The purpose of this study was to quantify the contribution of the individual quadriceps muscles to patellar tracking. Based on previous findings [2], we hypothesized that patellar tracking during knee extension for individual muscles is similar to conditions when all quadriceps muscles are activated simultaneously (this condition is hereafter referred to as "ALL").

Methods

All experiments were performed on skeletally mature New Zealand white rabbits (n=6). VL, VM, and RF were individually activated through home-built cuff-type electrodes that were implanted surgically [3]. Rabbit knees were held in place by bone pins, and a motor bar was used to move the knee joint from 30° to 90° (0° = full extension), and to measure the resultant knee extensor torque. Two high speed cameras were used for patellar tracking in three dimensions during knee flexion and extension while activating individual quadriceps muscles in isolation and simultaneously.

Results and Discussion

The knee extensor torques for individual muscle activation were always smaller than those obtained for the ALL condition (Fig 1a; $p < 0.05$).

As a representative result, the medial-lateral shifts of the patella are shown (Fig 1b). The patella always shifted medially upon muscle activation. Tracking in the medial-lateral direction differed between ALL and VL, and between ALL and RF ($p < 0.05$), while it was similar for ALL and VM (Fig 1b).

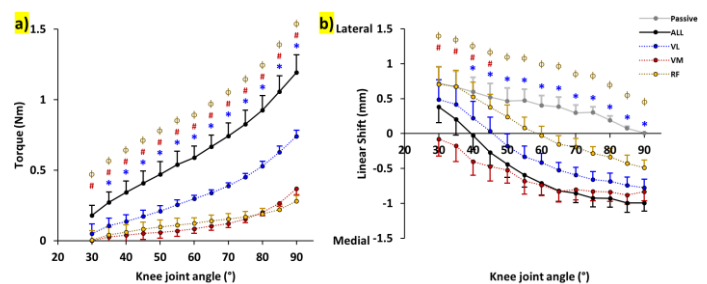


Fig 1. Mean (± 1 SE) of knee extensor torque (a) and medial-lateral linear shift of the patella (b) during knee extension (from 90° to 30°). Black circles with solid black lines represent the ALL condition; the blue, red, and yellow circles represent the VL, VM, and RF conditions, respectively. In figure (b), the grey circles with the grey line is the passive patellar tracking (no muscle activation). Statistical difference: *, differences between ALL and VL; #, differences between ALL and VM; ϕ , differences between ALL and RF.

If our hypothesis was correct, the medial-lateral shift for VM and RF should be similar, due to the similar force of these two muscles. However, patellar tracking differed between VM and RF. Furthermore, VM activation caused medial patellar shifts similar to the ALL condition, despite much smaller forces. These results suggest that VM plays a unique role in patellar tracking that cannot be achieved by any of the other muscles.

Conclusions

We conclude that VM contributes in a unique way to patellar tracking, while VL and RF contribute as would be expected based on their force contributions to knee extension.

Acknowledgments

The Canadian Institutes for Health Research; Canada Research Chair Program; The Killam Foundation; Eyes High International Doctoral Studentship (UofC); CONNECT! NSERC CREATE Program.

References

- [1] Katchburian, M. V. et al. (2003). *Clin Orthop Relat Res*, 412:241-259
- [2] Han, S.W. et al. (2021). *J Biomech*, (submitted)
- [3] Han, S.W. et al. (2019). *J Exp Biol*, 222 (Pt 6)

Out-of-plane motion reduces the knee extension moment arm

Mitchell G.A. Wheatley¹, Darryl G. Thelen², Daniel P. Borschneck³, Kevin J. Deluzio¹, Michael J. Rainbow¹

¹Department of Mechanical and Materials Engineering, Queen's University, Kingston, Canada

²Department of Mechanical Engineering, University of Wisconsin-Madison, Madison, USA

³Department of Surgery, Kingston General Hospital, Kingston, Canada

Email: mitchell.wheatley@queensu.ca

Summary

The knee extension moment arm is often modelled using equations derived from cadaveric studies or using measurements limited to the sagittal plane. The objective of this study was to determine if out-of-plane motion affects moment arm length. Using a musculoskeletal model that optimizes three-dimensional patella kinematics, out of plane knee motions, and soft tissue forces, we determined the knee extension moment arm for walking and running across individuals. We found that out-of-plane motion explained a large range of inter-subject variation in the moment arms. This demonstrates the importance of fully describing patella and knee motion when determining the knee extension moment arm.

Introduction

The patella increases the knee extension moment arm and allows for moment arm variation throughout gait as the patella and tibia articulate with the femur. The knee extension moment arm is measured between the tibiofemoral axis of rotation and patellar ligament [1]. Many models constrain the knee flexion axis and limit moment arm measurements to the sagittal plane. Therefore, these models do not account for all translational and rotational degrees-of-freedom at the knee. Cadaver studies have accounted for out-of-plane knee motions; however, they may not capture accurate *in vivo* behavior from activated muscles [2].

In this study we use a data driven musculoskeletal model with an optimizer that solves for three-dimensional patella mechanics, out of plane tibiofemoral kinematics, muscle and ligament forces, and cartilage contact in a 12 degrees-of-freedom knee [3]. The objective of this study was to determine if out-of-plane motion would affect moment arm length for a given degree of knee flexion.

Methods

We simulated of walking and running trials from ten subjects with a lower-limb MSK model with a twelve degrees-of-freedom knee [3]. The simulations were driven by marker-based optical motion capture and ground reaction force data. We scaled mean bone geometry from a previously collected dataset of fourteen asymptomatic knee MRIs [4] and incorporated the scaled geometry across all trials to focus on kinematic effects instead of morphology. The model specified tibiofemoral flexion from motion capture data and allowed other degrees of freedom at the tibiofemoral and patellofemoral joints to evolve based on optimization of contact, muscle, and ligament forces. We reduced inherent noise of the rotation axis by sectioning gait based on direction of knee motion. Poses of the tibia with respect to the femur at the beginning and end of each section were used to calculate the rotation axes.

We calculated the knee extension moment arm for each trial using a geometric method [1]. To compare the large variation in moment arms found among subjects, we selected 20° of knee flexion—common across all trials within stance—and determined the moment arm and direction cosines of the rotational axis for each trial. F-tests determined if the correlation between moment arm length and the direction cosines were non-zero with an alpha of 0.05. Paired t-tests compared simulated moments arms and moment arms calculated if the rotation axis was purely medial-lateral.

Results and Discussion

Moment arms at 20° knee flexion varied by 42.3% and decreased as rotation axes became less aligned with the flexion-extension axis. Moment arms were larger if the rotation axis was more aligned with the medial-lateral axis of the knee ($R^2=0.67$, $p<0.001$). Moment arms decreased with anterior-posterior ($R^2=0.71$, $p<0.001$) and superior-inferior ($R^2=0.58$, $p=0.001$) rotational axis orientation. Moment arms were larger when isolating the rotation axis to the medial-lateral direction ($p<0.002$).

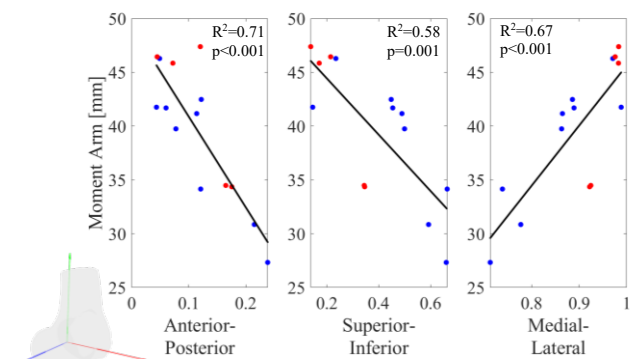


Figure 1: Moment arms for walking (blue) and running (red) trials versus the directional cosines aligned with femur axes.

Conclusions

Differences in out-of-plane knee motion across subjects explained the large range of inter-subject variation observed in the knee extension moment arm during both walking and running. These findings highlight the importance of using three-dimensional models that fully describe all translation and rotational degrees-of-freedom at the knee to properly describe the knee extension moment arm.

References

- [1] Krevolin JL et al. (2004). *J Biomech*, **37**(5): 785-8.
- [2] Tsaopoulos, DE et al. (2006). *Clin Biomech*, **21**(7): 657-67
- [3] Lenhart, RL et al. (2015). *Ann. Biomed. Eng.*
- [4] Clouthier, AL et al. (2019). *Med Eng Phys*, **66**: 47-55.

Muscle-length dependence of residual force enhancement in the human patellar tendon during submaximal stretch-hold contractions

Patrick Bakenecker¹, Tobias Weingarten¹, Brent J. Raiteri¹ and Daniel Hahn^{1,2}

¹Human Movement Science, Faculty of Sport Science, Ruhr University Bochum, Bochum, Germany

²School of Human Movement and Nutrition Sciences, University of Queensland, Brisbane, Australia

Email: patrick.bakenecker@rub.de

Summary

Little is known about the influence of muscle length on residual force enhancement (rFE) following *in vivo* lengthening contractions. This is because only a limited range of muscle lengths has been tested and because rFE *in vivo* needs to be estimated from net joint torque measurements. We therefore estimated rFE within the patellar tendon using a new non-invasive technique known as shear-wave tensiometry [1]. Preliminary data shows that rFE can be detected within the patellar tendon and that rFE is affected by the length of the muscle.

Introduction

rFE refers to a long-lasting force enhancement following active muscle lengthening compared with a fixed-end reference contraction at the same final muscle length and activation level [2]. *In vivo* rFE has been repeatedly observed in humans indirectly from net joint torque measurements [2]. However, the influence of muscle length on *in vivo* rFE remains unclear [3]. This is because the range of tested *in vivo* muscle lengths is limited and whether rFE occurs at very long muscle lengths is unknown. Further, net joint torque measurements to infer rFE can be problematic because torque is influenced by gravitational forces and forces generated by agonist and antagonist muscles. One potential solution for more directly quantifying *in vivo* rFE involves using a new non-invasive technique known as shear-wave tensiometry [1]. This technique estimates tendon load based on tendon wavespeed measurements. We therefore used this technique and compared it with net joint torque measurements to examine rFE at short, long and very-long muscle lengths.

Methods

Preliminary data was recorded from one healthy participant who had their right shank fixed to the lever arm of an isokinetic dynamometer while they sat with 90° hip flexion (IsoMed2000, D&R Ferstl GmbH, GER). Net knee joint torque and crank arm angle were measured at 2 kHz and muscle activities of the vastus lateralis (VL), vastus medialis (VM), and rectus femoris (RF) were obtained at 2 kHz using surface EMG (sEMG; NeuroLog System NL905, Digitimer Ltd, UK). The participant performed a maximum voluntary contraction at 70° knee flexion and then fixed-end ramp contractions from rest to 50% of maximum combined knee extensor muscle activity (i.e., by matching their real-time sEMG level to a predefined trace displayed on a screen) at knee flexion angles ranging from 30° to 110° (10° increments). From the resulting wavespeed-angle

relationship ($W_s-\theta-r$), we selected one target knee joint angle on the ascending limb (short muscle length) and two target knee joint angles on the descending limb (long and very-long muscle lengths) of the $W_s-\theta-r$. Then, 50% of maximum sEMG-controlled fixed-end contractions at the three target knee joint angles were performed. 50% of maximum sEMG-controlled stretch-hold contractions were also performed over a 15° ($60^\circ\cdot s^{-1}$) stretch amplitude and ended at each target joint angle with an isometric-hold phase of 4-s. During both contraction types, patellar tendon wavespeeds were determined using a piezo-actuated tapper that delivered micron-scale impulses through the skin to the superficial patellar tendon, which induced a transient wave (i.e., transverse tendon motion). The transient wave was detected by two adjacent miniature accelerometers sampling at 100 kHz [1]. All data were synchronized using a 16-bit A/D card within a Power1401 data acquisition interface (Spike2, CED, UK). Calculated wavespeed was smoothed using a moving average over 200-ms. rFE was calculated based on torque and patellar tendon wavespeed data as the percent difference in mean knee extension torque/patellar tendon wavespeed from 2-2.5-s after stretch relative to the time-matched torque/wavespeed during fixed-end contractions.

Results and Discussion

Based on torque measurements, preliminary results show no rFE at a short muscle length (1%) and similar rFE at long (9.5%) and very-long (8.1%) muscle lengths. Based on wavespeed data, rFE was not observed at a short (-9.4 %) muscle length and rFE was observed at long (5.9%) and very-long (8.2%) muscle lengths. Differences in rFE between net joint torque and wavespeed measurements might be due to axis misalignment of the knee joint relative to the dynamometer axis or might arise from force contributions from antagonist muscles.

Conclusions

These preliminary results indicate that rFE can be observed within the patellar tendon using shear-wave tensiometry. Similar to *in vitro* experiments, there might be an increase in rFE from long to very long muscle lengths when *in vivo* rFE is assessed more directly via shear-wave tensiometry.

References

- [1] Martin J.A. et al. (2018). *Nat. Commun.*, **9**: 1-9.
- [2] Seiberl W et al. (2013). *J. Biomech.*, **46**: 1996-2001.
- [3] Bakenecker P et al. (2020). *Eur. J. Appl. Physiol.*, **120**: 2597-2610.

Data fusion of electromyography and motion data enhances locomotion intent recognition

Lin Meng¹, Jun Pang¹, Ziyao Wang², Dong Ming^{1,3}

¹ Academy of Medical Engineering and Translational Medicine, Tianjin University, Tianjin, China

² International Engineering Institute, Tianjin University, Tianjin, China

³ School of Precision Instrument & Opto-Electronics Engineering, Tianjin University, Tianjin, China

Email: linmeng@tju.edu.cn

Summary

Locomotion recognition is of significance for adapting different control modes of assistive robots. In this study, we proposed a novel recognition method that incorporates electromyography (EMG) and 3-axis acceleration of body segments. Ten healthy young participants were enrolled in the experiment where they performed seven locomotion tasks including standing, sitting, walking, stair ascent, stair descent, ramp ascent and ramp descent. Four classifiers were used and their performance was compared. The results show that all four classifiers could recognize all locomotion tasks with high accuracy (>95%) and more importantly the method can predict movement intention (~229.91ms). The method is expected to significantly improve the effectiveness of a lower-limb assistive device.

Introduction

Locomotion recognition is crucial for adaptive control of lower-limb assistive system, and detection of user's motion intention enables the wearable robot to deliver a smooth and seamless assistance. As electromyographic (EMG) measures muscle activation resulting in joint movements, intention of locomotion can be decoded based on EMG signals. However, due to its low signal-to-noise ratio and high variance between individuals [1], EMG-based recognition model usually has relative lower accuracy [2]. On the other hand, motion data has been widely used in locomotion modes identification with high recognition accuracy [3]. Therefore, we proposed a locomotion recognition method by combing EMG and motion signals in order to predict locomotion intention.

Methods

10 healthy young participants (5 males and 5 females, 23.00±0.82 years old, 60.71±11.25 kg) were recruited in the experiment. Each participant wore 7 inertial sensors on the pelvis, thigh shank and foot while 16 muscles were selected, namely rectus femoris, vastus lateralis, biceps femoris, semitendinosus, tibialis anterior, lateral gastrocnemius, and medial gastrocnemius of both legs. They were required to perform 7 locomotion tasks, such as sit, stand, walk, stair ascent, stair descent, ramp ascent and ramp descent. During tasks, EMGs and tri-axis acceleration data were recorded by motion analysis system (Ultium EMG and myoMOTION, Noraxon U.S.A.,Inc.) with a sample rate of 2000Hz.

The root mean square (RMS) amplitudes of EMG and acceleration were normalised within gait cycles. Sliding window analysis was used for feature extraction. The window length was set to 150 ms with a sliding step of 50

ms. Four classification methods were used for locomotion recognition, including Support vectors machine (SVM), K-Nearest Neighbor (KNN), linear discriminant analysis (LDA), and artificial neural networks (ANN). After models were trained offline, we tested and analysed real-time model performance on new data.

Results and Discussion

The offline recognition performance of 7 locomotion tasks was shown in Table 1. The results demonstrated that all classifiers achieved high recognition accuracy (>96%), specificity (>95%) and sensitivity (>99%) and responded to locomotion transitions earlier of actual movements.

Table 1: Performance comparison of classifiers.

	SVM	KNN	ANN	LDA
Accuracy (%)	97.80±1.48	96.75±1.19	97.00±1.67	96.45±1.13
Sensitivity (%)	97.86±1.45	96.75±1.19	97.00±1.67	95.45±0.13
Specificity (%)	99.64±0.24	99.46±0.20	99.50±0.28	99.24±0.02
Response Time (ms)	-229.91± 289.80	-185.64± 349.08	-194.31± 287.98	-178.08± 213.70

Conclusions

The proposed method achieved high accuracy of locomotion recognition and could predict locomotion tasks with combining EMG with acceleration data.

Acknowledgments

This work was supported by the National Natural Science Foundation of China (82001921) and the National Key R&D Program of China (2020YFC2004300, 2020YFC2004302).

References

- [1] J. Ning et al. (2012). *IEEE Signal Process Mag*, **29**: 152-150.
- [2] T. Afzal et al. (2017). *IEEE Trans. Neural Syst. Rehabilitation Eng.*, **25**: 608-617.
- [3] S. Kyeong et al. (2019). *Front. Inf. Technol. Electron. Eng.*, **20**:342-352.

Ground reaction force fusion for gait recognition

Kayne A. Duncanson¹, William S. P. Robertson², Ehsan Abbasnejad³, David Booth⁴, Simon Thwaites¹, Dominic Thewlis¹
¹Adelaide Medical School, University of Adelaide, SA, 5000, AUS; ²School of Mechanical Engineering, University of Adelaide, SA, 5000, AUS; ³Australian Institute for Machine Learning, University of Adelaide, SA, 5000, AUS; ⁴Defence Science and Technology Group, Australian Government Department of Defence, Edinburgh, SA, 5111, AUS
 Email: kayne.duncanson@adelaide.edu.au

Summary

Gait has been posited as a biometric for person re-identification (*re-ID*) in authentication and surveillance scenarios. A novel data fusion Siamese deep neural network (*GRFNet*) was developed and evaluated to determine the most discriminant kinetic components during self-selected speed walking in consistent footwear. Across ten runs of network evaluation, an average re-ID accuracy of $92.33 \pm 1.53\%$ was obtained on 118 healthy participants. Findings from this study confirm the baseline utility of deep neural networks for force platform based gait recognition. The present system is appropriate for authentication tasks that require user cooperation.

Introduction

Gait is expressed differently between individuals in accordance to their unique structure, physiology and behaviour [1]. State-of-the-art gait recognition systems employ deep neural networks (*DNNs*) to extract features on body appearance or motion from key frames of video data [2]. These systems depend on unreliable appearance features that encode at least some irrelevant, and perhaps confounding, information. Force platforms may be suitable for gait recognition because they record high-resolution kinetic data without influence from lighting conditions. The aim of this study was to develop and evaluate a gait recognition system that incorporates the most discriminant components of walking gait kinetics.

Methods

The dataset contained 1168 trials of self-selected speed walking from 118 healthy participants with consistent (personal) footwear (57% M, age 27 ± 7 years, mass 71 ± 17 kg, height 1.72 ± 0.10 m). Two sessions were attended within a two week period (3-14 days). Each sample contained *GRFs* (F_x , F_y , and F_z), *GRMs* (M_x , M_y , and M_z), and *COP* coordinates (C_x and C_y) from two OPT400600-HP force platforms (AMTI, USA) at 2000 Hz. Signals were filtered using a fourth-order Butterworth low-pass filter (cut-off=30Hz) then interpolated to 400 frames. Samples were separated by stance side to prevent sequence bias and represent the asymmetry of walking gait. Finally, signals within each component were standardised ($\bar{x}=0$, $\sigma^2=1$). Neural architecture search and hyper-parameter tuning were conducted manually through bias-variance analysis. The network consisted of four convolutional blocks followed by one long-short term memory layer and one fully-connected layer. Left and right stance inputs were passed through the network in parallel and feature vectors were fused via element-wise summation. The

network was trained, validated and tested ten times for each condition using online batch hard triplet loss (margin=0.3) and AMSGrad optimiser. *Re-ID* accuracy was the primary performance metric.

Results and Discussion

GRFNet was $92.33 \pm 1.53\%$ accurate on test sets using F_y and F_z concatenated along the channel dimension. Training accuracy reached 100% and validation accuracy reached above 90% in all runs (Figure 1). Input-level fusion of sagittal plane GRFs and output-level fusion of stance side features appears to be an effective strategy for force platform based gait recognition.

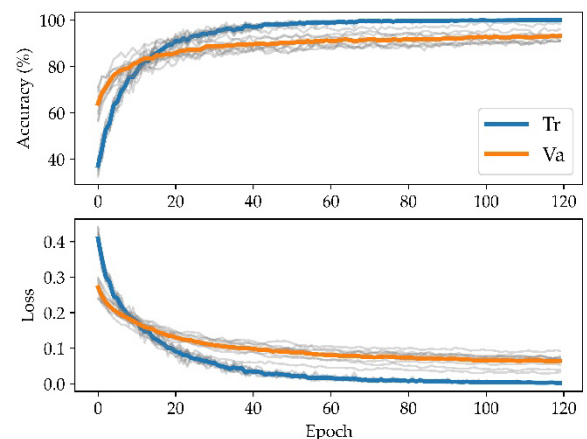


Figure 1: Mean accuracy and loss of the dual component *GRFNet* during training (blue) and validation (orange) overlaid with individual runs (grey).

Conclusions

This study provides evidence that *DNNs* can reliably extract useful features from multi-dimensional representations of force platform data. In future, force platform based gait recognition systems should be tested in unconstrained walking conditions to validate their utility for unobtrusive and discreet *re-ID*.

Acknowledgments

Defence Science & Technology Group and the NHMRC (ID: 1126229) funded this work.

References

- [1] Vaughan CL et al. (1992). *Dynamics of human gait*; Human Kinetics.
- [2] Sundararajan K, & Woodard DL (2018) *ACM Comput. Surv.*, **51**: 1-34.

Anomalous gait feature prediction using a neural network

Suil Jeon¹, Gunwoo Park¹, Kyoung Min Lee², Seungbum Koo¹

¹Department of Mechanical Engineering, KAIST, Daejeon, South Korea

²Department of Orthopedics, Seoul National University Bundang Hospital, Kyungki-do, South Korea

Email: skoo@kaist.ac.kr

Summary

Gait is one of the complex motor skills associated with neurological and musculoskeletal conditions. Understanding the association between musculoskeletal disease and gait kinematics is essential for the treatment of the disease. However, it requires training and expertise to read and understand gait kinematics graphs for clinical application. Here, we proposed a classification network architecture that predicts anomalous gait features from three-dimensional gait kinematics data. The first part of the network is an encoder that extracts a latent gait vector from high-dimensional gait kinematics data. The second part is a classifier for predicting anomalous gait features from the latent gait vector. The proposed method showed a classification accuracy of 83% on average for five different anomalous gait features.

Introduction

The gait analysis has been used to assess musculoskeletal diseases [1]. However, clinical assessment of gait kinematics requires physicians trained for gait analysis. The gait deviation index can compare the differences in the patient's gait kinematics from those of the normal population using three-dimensional motion capture data. Still, it provides only a single value for the deviation [2]. Recently, there have been fast advancements in machine learning methods for classifying features using a neural network with high accuracy. The objective of the study was to develop a network model that could classify five anomalous gait features from 3D gait kinematics data.

Methods

Four hundred eighty-eight subjects (248 males, 240 females, and average age: 37.1±16.8 years) participated in the experiment. Three-dimensional gait kinematics were captured at the subjects' self-selected walking speed using ten motion capture cameras. A physician trained for gait analysis labeled five anomalous gait features – out toe, hindfoot valgus, planovalgus, genu varum, and turtle neck – from using the gait kinematics data. The proposed neural network model and framework to perform anomalous gait feature classification are shown in Figure 1. A 4848-dimensional gait vector was created from a cycle of 3D gait kinematics. Four gait vectors were prepared for each subject. A variational autoencoder was trained to reduce the dimension of the gait vector to 256 dimensions to obtain a latent gait vector. A two-layer neural network was trained to classify the five gait features using

binomial logistic regression. The trained classification network calculated a gait feature vector with five components. The gait feature vector was rounded at 0.5 to classify the five anomalous gait features. The proposed method was compared with the reconstruction-based model in a previous study [3].

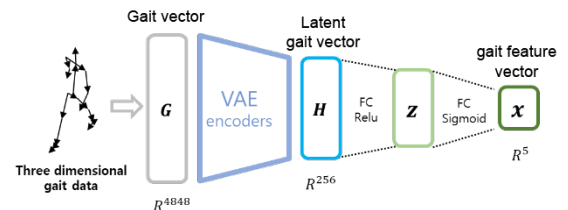


Figure 1: Anomalous gait feature classification network

Results and Discussion

The classification performances of the proposed method and the method in a previous study were summarized as sensitivity, specificity, and balanced accuracy as shown in Table 1. The results show that the anomalous gait features could be predicted and classified through 3D gait kinematics, and that our proposed model has a high performance that is superior to the previous method. The five types of anomalous gait features had a slight kinematics difference that can only be detected by trained physicians.

Conclusions

The five anomalous gait features could be detected from 3D gait kinematics data using a neural network with a balanced accuracy of 83% on average. Our method could provide assessments on five different clinical gait features. The features could increase if a larger cohort data is provided. It showed the possibility of using the proposed method as a clinical tool to screen subjects with potential gait-related disease.

Acknowledgments

This work was supported by the Basic Science Research Program through the NRF (NRF-2020R1A2C2006057) of South Korea and the Samsung Research Funding Center of Samsung Electronics under Project Number SRFC-IT1902-01.

References

- [1] Winter DA. (1989) *J Motor Behav*, 21(4):337-355.
- [2] Schwartz MH, Rozumalski A. (2008) *Gait Posture*, 28(3):351-357.
- [3] Nguyen, et al. (2018) *2018 IEEE Seventh ICCE*, 311-315.

Table 1: Classification accuracies for five anomalous gait features

Gait features	Out toe	Hindfoot valgus	Planovalgus	Genu varum	Turtle neck
Nguyen et al. [3]	55.2 %	51.5 %	55.2 %	44.0 %	54.7 %
Proposed method	82.8 %	85.9 %	80.2 %	73.2 %	92.9 %

Estimation of Knee Flexion in Knee Arthroplasty Patients using only Shank Mounted IMUs

Ted Yeung¹, Astrid Cantamessa², Bruno Batinica³, Scott Bolam³, Andreas W. Kempa-Liehr³, Paul Monk¹, Thor Besier^{3,1}

¹Auckland Bioengineering Institute, Auckland, New Zealand

²University of Liège, Belgium

³School of Medicine, University of Auckland, Auckland, New Zealand

⁴Department of Engineering Science, University of Auckland, Auckland, New Zealand

Email: tyeu008@aucklanduni.ac.nz

Summary

Obtaining accurate knee kinematics from inertial measurement units (IMUs) typically requires sensors on the thigh and shank and data fusion algorithms to obtain accurate orientation data. Here we present a machine learning model to predict knee flexion angles directly from raw acceleration and angular velocity data from two ankle-mounted IMUs. The model was compared to optical motion capture data on four patients who had undergone total knee arthroplasty. Our machine learning model showed an average root mean square error of 4.5 degrees. This approach is suitable for tracking knee flexion angles of patients outside of the gait laboratory.

Introduction

Restoring normal knee kinematics is a primary outcome following total knee arthroplasty. Accurate estimation of knee flexion during gait typically requires optical motion capture (OMC), which restrict data collection to laboratory settings. Ideally, wearable sensors, such as inertial measurement units (IMUs) would provide these data to monitor patients in their home environment.

IMUs have been used as input to Kalman filters [1], to provide orientation information, which can then be used to estimate body segment kinematics. However, these require IMUs on multiple body segments with complicated calibration procedures. We present a machine learning approach to estimate bi-lateral knee flexion angles using shank mounted IMUs. The approach requires gait data to be collected for model training, but following training, can be used to obtain reliable and accurate kinematics in the field.

Methods

A modelling pipeline was developed using the Python package tsfresh [2] to semi-automate feature selection and extraction from IMU data [3]. We used a random forest regressor to generate person-specific models to estimate knee flexion angle from features extracted from IMUs mounted on the distal tibia of both limbs. Synchronised OMC and IMU data (VICON-IMeasureU) were collected from four knee arthroplasty patients walking at a self-selected speed over ground. A scaled OpenSim model [4] was used to obtain sagittal plane knee kinematics, which were used to train the surrogate model.

The model training involved the following steps: 1) parsing the IMU data for each of the recorded joint angles, 2) feature extraction using tsfresh, 3) feature selection based on their importance (we selected the top 100 features); and 4) fitting regression model to generate the final surrogate model.

We performed a temporal cross validation by training the models on 70% of the individual's data and comparing model predicted knee flexion of the last 30% to OMC-derived knee flexion. Root mean square error (RMSE) and coefficient of determination (R^2) was used to compare the surrogate model to the OMC 'ground truth'.

Results

The surrogate model predicted knee flexion angles to within 4.5 degrees with an average R^2 of 0.93 (Table 1). An example of knee flexion angle prediction is presented in Figure 1.

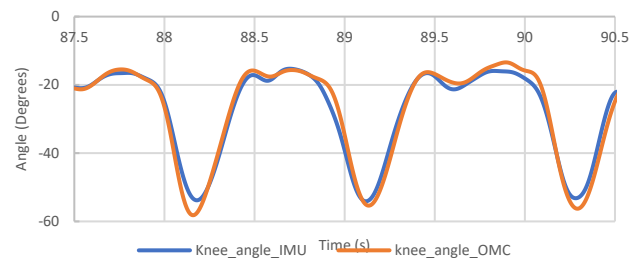


Figure 1: Predicted knee flexion from IMUs compared to optical motion capture (Patient 3).

Table 1: Overground walking surrogate model's RMSE (R^2)

Patient #	1	2	3	4	Average
RMSE °	5.35°	4.61°	3.54°	4.56°	4.52°
R^2	0.92	0.95	0.95	0.91	0.93

Conclusions

We developed a surrogate model capable of predicting knee flexion angles using only shank mounted IMUs in a small cohort of knee joint replacement patients. Our model showed close agreement to OMC-derived knee flexion, which indicates that this approach could be suitable for collecting kinematics in the field. Additional patient data is being collected for validating this approach.

Acknowledgments

We would like to acknowledge VICON-IMeasureU for their funding and technical support for this project. We also thank Sivani Patel for technical support during data collection.

References

- [1] E.-H. Shin et al. (2004). *PLANS*. pp. 273–279.
- [2] M. Christ et al. (2018). *Neurocomputing*: **307**, pp. 72–77
- [3] A. W. Kempa-Liehr et al. (2019). *CCIS*: **1180**, pp. 223–231
- [4] S. L. Delp et al. (2007). *IEEE Trans. Biomed. Eng.* **54**, no. 11, pp. 1940–1950.

Predicting ground reaction force components from two-dimensional video using machine learning

Corey Morris¹, Marion Mundt¹, Molly Goldacre¹, Jason Weber¹, Ajmal Mian², Jacqueline Alderson^{1,3}

¹Minderoo Tech & Policy Lab, The University of Western Australia, Perth, Australia

²School of Computer Science, The University of Western Australia, Perth, Australia

³Auckland University of Technology, Sports Performance Research Institute New Zealand (SPRINZ), Auckland, New Zealand.

Email: corey.morris@research.uwa.edu.au

Summary

On-field athlete mechanical ‘workload’ monitoring is of high interest in sport to inform decisions about performance and injury risk management. However, the direct recording of mechanical workload is predominantly locked to laboratory environments, with field-based efforts inhibitive or unsafe for athletes, or otherwise restricted or regulated. This study aims to use an artificial neural network (ANN) to estimate three-dimensional (3D) ground reaction force components using two-dimensional (2D) video and human pose estimation. Results demonstrated the feasibility of machine learning techniques to remotely estimate ground reaction forces (GRFs) during walking and running for female Australian Rules Football (ARF) players.

Introduction

The ability to quantify athlete mechanical workload is an integral part of a biomechanist’s role. These workloads can serve as an indicator of athlete performance and injury risk, and can help inform rehabilitation. Current approaches to monitor workload in sport settings have shown the feasibility of neural networks to predict kinetics using wearable inertial motion units (IMUs) and motion capture data [1, 2], although an ecologically valid method to estimate GRF remotely is still required. This study aims to remotely predict 3D GRF components using ANNs from 2D video inputs.

Methods

Fifteen semi-professional and professional female ARF players (23±3.74 years, 62.77±5.41 kg) performed 10 walking and 21 running trials. Running trials were completed between 4.5 - 5.5 ms⁻¹. 12 months following data collection a further four volunteers, ([2♀; 2♂] 25.75±4.69 years, 73.5±7.05 kg) completed three walking, and three running trials to test the trained ANN robustness. All participants provided informed consent with the study approved by the UWA Human Ethics Committee (RA/4/1/2593).

Three video data views were captured (Sony HDR-CX700, 25 Hz); anterior sagittal, sagittal and posterior sagittal. Force plate data was collected at 2000 Hz (Advanced Mechanical Technology Inc., Watertown, MA, USA). Estimated joint centers, or ‘keypoints’, were determined using OpenPose [3] and were used as input data to the ANN. The full video dataset comprised 1130 walking and 1219 running trials. Network architecture is displayed in Table 1.

Table 1: Neural network hyperparameter search conditions.

Network Architecture	Hyperparameter Search	Walking Architecture	Running Architecture
Dropout	0.1 - 0.7	0.3	0.3
Layer size	8 - 650	500-400-900	500-350-900
Learning rate	3E-02 & 1E-02 - 3E-05 & 1E-05	3E-03	3E-03
No. epochs	1, 11, 21, 31	31	31

ARF player data was used for training and internal validation, performing 3-fold cross validation without data leakage. The additional volunteer data was used to externally validate the ANN, consisting of 34 walking and 20 running trials.

Results and Discussion

Figure 1 shows that high mean correlation coefficients were achieved for all GRF component estimates for walking ($r_{\text{med-lat}} = 0.843$, $r_{\text{ant-post}} = 0.988$, $r_{\text{vert}} = 0.957$), however only two components for running ($r_{\text{med-lat}} = 0.501$, $r_{\text{ant-post}} = 0.981$, $r_{\text{vert}} = 0.978$). The same trend was observed for external validation, walking ($r_{\text{med-lat}} = 0.864$, $r_{\text{ant-post}} = 0.989$, $r_{\text{vert}} = 0.969$) and running ($r_{\text{med-lat}} = 0.678$, $r_{\text{ant-post}} = 0.892$, $r_{\text{vert}} = 0.962$). The lowest prediction accuracy was in the medio-lateral direction. Vertical and anterior-posterior predictions showed similar accuracy to other machine learning approaches utilising wearable sensors [1, 2].

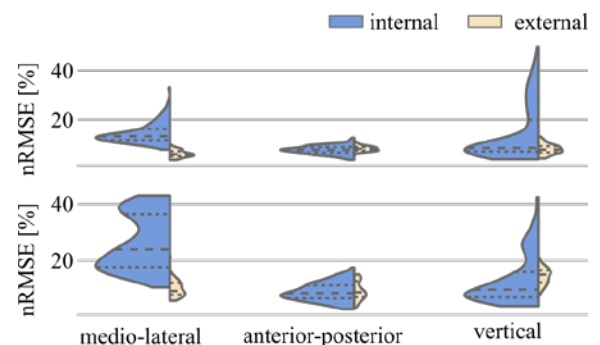


Figure 1: Violin plot of the distribution of normalised RMSE for internal and external validation datasets. Walk (top), run (bottom). X axis = force components X, Y, Z.

Conclusions

This novel machine learning method to predict 3D GRF components outlines a feasible approach to the remote estimation of mechanical workloads from 2D video.

Acknowledgements

This study was supported by Fremantle Football Club.

References

- [1] Johnson, WR. et al. (2020). *IEEE Trans Biomed Eng*, **68**(1):289-297.
- [2] Mundt, M. et al. (2020). *Med Eng Phys*, **86**:29-34.
- [3] Cao, Z. et al. (2019). *IEEE Trans Pattern Anal Mach Intell*, **43**(1):172-186.

Relationships between hip muscle strength and running biomechanics in femoroacetabular impingement syndrome

Benjamin Mentiplay¹, Joanne Kemp¹, Kay Crossley¹, Mark Scholes¹, Sally Coburn¹, Danilo de Oliveira Silva¹, Richard Johnston¹, & Matthew King¹

¹La Trobe Sport and Exercise Medicine Research Centre, La Trobe University, Melbourne, Australia

Email: b.mentiplay@latrobe.edu.au

Summary

Femoroacetabular impingement syndrome can result in impaired movement patterns and muscle strength. This study aimed to explore the relationships between hip muscle strength and running biomechanics in adults with femoroacetabular impingement syndrome.

Introduction

Femoroacetabular impingement (FAI) syndrome is a motion-related condition associated with an increased risk of developing hip osteoarthritis [1]. Biomechanical impairments (i.e., kinematics and kinetics) have been shown in FAI syndrome compared to controls during walking and squatting [2]; however, hip biomechanics during higher impact tasks (e.g., running) have yet to be examined.

As well as altered movement patterns, people with FAI syndrome have demonstrated lower hip strength compared to controls [3]. Importantly, hip strength has been shown to relate to self-reported symptoms [3]; thus, hip strengthening is often recommended as a non-surgical treatment strategy. The relationship between hip strength and running biomechanics has been examined in numerous healthy and clinical cohorts, but not in FAI syndrome. If a relationship exists, this will provide further impetus to the prioritization of hip strengthening as a treatment strategy in FAI syndrome.

The aim of this study was to explore the relationship between hip strength and hip biomechanics during running in FAI syndrome, and whether relationships were dependent on sex.

Methods

This study involves a subset of participants enrolled in a large RCT investigating physiotherapist-led treatment for FAI syndrome. Data were collected at the baseline (pre-randomization) assessment. Inclusion criteria were adults aged 18-50 years, hip-related pain ($\geq 3/10$ on a numerical pain scale for ≥ 6 weeks), cam morphology ($\geq 60^\circ$ alpha angle), and a positive flexion-adduction-internal rotation test. Exclusion criteria were recent physiotherapy treatment or intra-articular hip injections, previous or planned surgery, radiographic hip osteoarthritis, or other musculoskeletal conditions. All participants provided written informed consent and ethical approval was obtained from the institutional ethics committee.

Overground running biomechanics data were collected with a 10-camera motion capture system (Vicon, UK) and an embedded force plate (AMTI, USA). Participants underwent overground running trials at a target running velocity of 3 to 3.5m/s. Marker trajectories and ground reaction force data were filtered using a fourth-order low-pass Butterworth filter with zero-lag and a cut-off frequency of 10Hz as per previous

research [4]. A previously used biomechanical model [4] was used to calculate joint angles and ‘external’ joint moments over the stance phase of the gait cycle. Discrete variables of interest included peak hip joint angles, and peak and impulse of the hip joint moments.

Following biomechanical assessment, a hand-held dynamometer (JTECH Medical, USA) was used to assess the isometric strength of the hip abductors and adductors (supine), extensors, internal rotators, and external rotators (prone), and flexors (seated). A single assessor performed all strength testing. Three maximal efforts for each muscle group were recorded, with the peak of the three trials used in the analyses.

Relationships between hip strength and hip running biomechanics were explored using linear regression models. Biomechanical variables ($^\circ$, Nm) acted as the dependent variable, with muscle strength (N), body mass (kg), velocity (m/s), and sex (men/women) entered into the model as independent variables. A sex*strength interaction term was examined; if significant, data were dichotomized by sex and examined in separate models, and if non-significant, the interaction term was omitted.

Results and Discussion

Forty-two participants with FAI syndrome were analyzed (22 men and 20 women; 36 ± 9 years of age; 73 ± 15 kg; 1.7 ± 0.1 m; $73 \pm 8^\circ$ alpha angle). During the stance phase of running, a significant negative relationship was observed for hip frontal range of motion and peak hip external rotation strength, independent of sex ($P=0.03$). Furthermore, an interaction effect was observed for the relationship between peak hip external rotation strength and peak and impulse of the hip extension moment ($P=0.04$ and 0.02 , respectively), with stronger external rotators related to increased ‘external’ hip extensor moments in women but not men.

Conclusions

This study is the first to explore the relationships between hip strength and running biomechanics in FAI syndrome. We found relationships to be minimal, with external rotation the only strength measure to demonstrate significant relationships to hip biomechanics during running. Due to the cross-sectional nature of this study, causation is unable to be determined. Future FAI syndrome research should explore changes in hip strength and biomechanics after intervention.

References

- [1] Van Klij P et al. (2018). *JOSPT*, **48**: 230-238.
- [2] King MG et al. (2018). *BJSM*, **52**: 566-580.
- [3] Kierkegaard S et al. (2017). *JSAMS*, **20**: 1062-1067.
- [4] King MG et al. (2020). *MSSE*, **52**: 1776-1784.

Personalised hip load modification using real-time biofeedback in hip osteoarthritis: a feasibility study

Laura Diamond^{1,2}, Daniel Devaprakash^{1,2}, Bradley Cornish¹, Melanie Plinsinga¹, Andrea Hams^{1,2}, Michelle Hall³, Rana Hinman³, David Saxby^{1,2}

¹School of Allied Health Sciences, Griffith University, QLD, Australia

²Griffith Centre of Biomedical and Rehabilitation Engineering (GCORE), Griffith University, QLD, Australia

³Centre for Health, Exercise and Sports Medicine, The University of Melbourne, VIC, Australia

Email: l.diamond@griffith.edu.au

Summary

Mechanical loading plays a fundamental role in osteoarthritis (OA) worsening and is potentially modifiable through movement retraining. This feasibility study evaluated whether hip load could be modified by changing external biomechanical parameters with assistance from real-time biofeedback during walking in people with hip OA. Most participants with hip OA could immediately alter their hip loading through personalised movement retraining and reported a clinically meaningful improvement in pain after a 6-week intervention.

Introduction

Non-surgical and non-drug treatments are recommended globally for management of hip OA, despite many patients reporting only small-to-modest improvements in symptoms [1]. These poor outcomes exist because targets for treatment are not well defined, not personalised, and largely extrapolated, inappropriately, from studies of people with knee OA. Mechanical loading plays a fundamental role in OA worsening [2] and is potentially modifiable through movement retraining. Lower hip loads are characteristic of individuals with mild-to-moderate hip OA [3], who are early in the disease course and therefore prime candidates for targeted disease modifying interventions. This study aimed to determine: 1) whether hip load could be increased by changing external biomechanical parameters with assistance from real-time biofeedback during walking; (2) which biomechanical parameter(s) are most effective for increasing hip load; and (3) any associated change in pain following 6-weeks of walking using a personalised load modification strategy.

Methods

Seven participants (age=57.6±4.9 yrs, BMI=30.8±5.8 kg.m⁻², 57% male) walked on an instrumented split-belt treadmill (Bertec Corporation, USA) while three-dimensional whole-body motion (Vicon, UK), ground reaction forces, and surface electromyography (Cometa, ITA) of 14 lower limb muscles were synchronously recorded. Participants walked for 5-minutes at a self-selected pace, then under each of the following conditions: (i) neutral trunk lean; (ii) neutral pelvis; and (iii) increased step length. For each condition, the biomechanical parameter of interest and a corresponding target value was displayed in front of the treadmill in real-time. The personalised target was calculated from the normal walk condition and was set to increase hip load by ~5%. Participants were asked to rate their pain and confidence on 11-point numerical rating scales (NRS, 0=none, 10=extreme) following each condition. A decision tree, based on

competence, confidence, and pain, was used to assign a personalised load modification strategy to each participant for integration into their walking routine over 6-weeks. A calibrated EMG-assisted model [3] was used to estimate hip contact forces (i.e. load, N) across five gait cycles per walking condition. Peak hip load was compared between walking conditions using a repeated measures analysis of variance ($p < 0.05$).

Results and Discussion

Five of seven (71%) participants increased peak hip load >5% when walking using their personalised load modification strategy (Figure 1). Walking under all conditions increased peak hip load compared to normal walking, albeit not a statistically significant amount ($p > 0.05$). All but one participant reported a clinically important difference in pain (>1.8 NRS units) following the 6-week intervention.

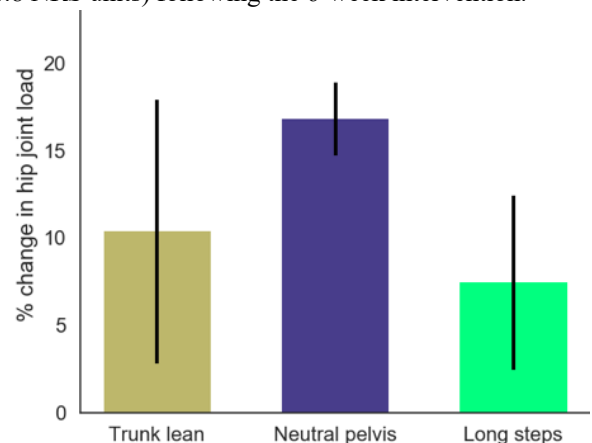


Figure 1: Percent change (± 1 standard deviation) in hip load relative to normal walking when participants with hip OA walked under three load modifying conditions (neutral trunk lean $n=3$; neutral pelvis $n=2$; increased step length $n=2$) with assistance from real-time visual biofeedback.

Conclusions

Most participants with hip OA could immediately increase their hip loading through personalised movement retraining and reported a clinically meaningful improvement in pain after 6-weeks. However, the hip's load response to each biomechanical condition was not universal, emphasising the need for an intervention customised to the individual.

References

- [1] Fernandes L et al. (2013). *Ann Rheum Dis*, **72**:1125-1135.
- [2] Felson DT (2013). *Osteoarthritis Cartilage*, **21**:10-15.
- [3] Diamond LE et al. (2020). *Osteoarthritis Cartilage*, **28**:921-931.

Femoral Offset Shortening After Nailing of Hip Fractures Does Not Correlate with Pelvic Control During Gait

Arjun Sivakumar¹, Mark Rickman^{1,2}, Dominic Thewlis¹

¹Centre for Orthopaedic & Trauma Research, The University of Adelaide, Adelaide, SA, Australia

²Department of Orthopaedics & Trauma, Royal Adelaide Hospital, Adelaide, SA, Australia

Email: arjun.sivakumar@adelaide.edu.au

Summary

Femoral nailing of elderly trochanteric fractures often result in shortening of the femoral neck, negatively impacting patient function and spatiotemporal parameters of gait. This study aimed to determine if femoral offset shortening is associated with pelvic control during gait. Results from this interim analysis showed a trend towards a significant correlation between the amount of femoral offset shortening and contralateral pelvic drop.

Introduction

Intertrochanteric (IT) fractures are commonly treated with proximal femoral nails (PFN) that promote compression at the fracture site during loading. While desirable for fracture stability and healing, shortening of the femoral neck is commonly reported postoperatively [1], negatively impacting physical functioning scores [2] and spatiotemporal parameters of gait [3]. Theoretically due to shortening of the hip abductor moment arm, there exists no published literature on gait kinematics in geriatric trochanteric fracture patients to date, leaving this recovering cohort poorly understood. In particular, the relationship of femoral offset shortening on pelvic control during gait remains unclear. This study aims to determine if femoral offset shortening is associated with pelvic control during stance phase of gait after femoral nailing of intertrochanteric fractures.

Methods

Thirty elderly patients (n=30) sustaining IT fractures were prospectively enrolled and treated with a PFN. Patients were followed up at six months post-operatively where radiographs of the affected hip and three-dimensional gait analysis data were collected. An OpenSim lower limb model (gait2392) was scaled using an atlas based statistical shape modelling method (MAPClient) [4] by fitting principal components of an articulated shape model to landmarks collected from the motion capture static trials. Segment angles were calculated for each patient according to ISB recommendations [5]. The amount of contralateral pelvic drop/rise at midstance (30% of the gait cycle) was calculated by subtracting the degree of pelvic obliquity at midstance from that at footstrike of the operated limb. Femoral offset (FO) was measured at baseline using post-operative image intensifier radiographs and at six months using flat panel radiographs. The change in FO was then calculated between the immediate post-operative and six-month time points. A Pearson correlation was used to assess the relationship between the FO shortening and contralateral pelvic drop (Trendelenburg sign) during the stance phase of gait.

Results and Discussion

The results presented are an interim analysis of thirteen patients. The measured change in FO at six months post-operative and pelvic obliquity across a gait cycle is shown for each patient in (Figure 1). For measured increases in FO and changes < 2 mm, FO shortening was assumed to be 0 mm, due to limitations in accurately measuring FO from plain film radiographs. Up to 8 mm of FO shortening was measured at six months postoperative. Degree of contralateral pelvic drop from footstrike to midstance ranged between -2 to 2 degrees. There was a minor trend between FO shortening and contralateral pelvic drop during the stance phase of gait, $r = 0.420$, $n = 13$, $p = 0.153$.

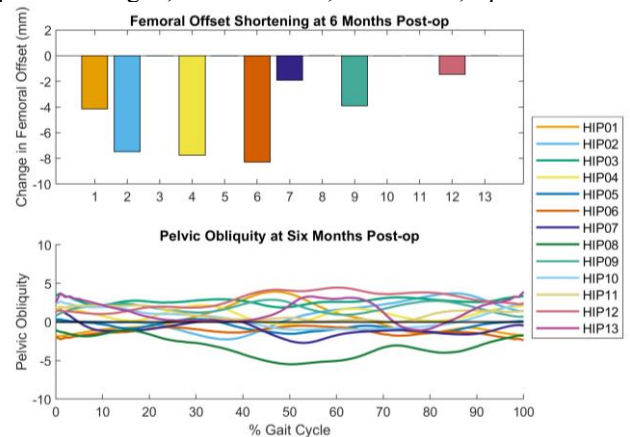


Figure 1: Changes in femoral offset per patient at 6 months postoperative and pelvic obliquity over the gait cycle.

Conclusions

The magnitude of FO shortening varied between individuals and presented a trend towards a significant correlation with contralateral pelvic drop during the stance phase of gait. Analysis of the updated dataset is required to better discern whether this is statistically significant. Patients exhibited rigid angular pelvic motions, likely resulting from age related changes to pelvic, trunk and lower limb motions, reported by previous authors. [6]

References

- [1] Gilat R et al. (2017). *J Orthop Trauma*, **31**: 311-315.
- [2] Zlowodzki M et al (2008). *J Bone Joint Surg Br*, **90**: 1487-94.
- [3] Gausden E et al (2018). *J Orthop Trauma*, **32**: 554-558.
- [4] Zhang et al (2014), *ISBMS*. **8789**: 182-192, 2014.
- [5] Wu G et al (2002). *J Biomech*, **35**: 543-548.
- [6] Gimmon Y et al (2015), *J Electromyogr Kinesiol*, **25**: 791-799

A FINITE ELEMENT ANALYSIS OF FOOT WITH HAMMER TOE DEFORMITY DURING WALKING.

M. Moayedi¹, M. Salehi¹, A. R. Arshi², M. Akrami³, R. Naemi⁴

¹Department of Mechanical Engineering, Amirkabir University of Technology, Tehran, Iran

²Biomechanics and Sports Engineering Groups, Biomedical Engineering Department, Amirkabir University of Technology, Tehran, Iran

³Department of Engineering, College of Engineering, Mathematics, and Physical Sciences, University of Exeter, Exeter EX4 4QF, U.K.

⁴Centre for Biomechanics and Rehabilitation Technologies, Staffordshire University, Stoke-on-Trent, UK
Email: R.Naemi@staffs.ac.uk

Summary

A three-dimensional finite element model of a diabetic neuropathic foot with hammer toe deformity was constructed. The geometry of the FE model was formed based on segmentation and reconstruction of MRI images. A multi-body musculoskeletal simulation based on 3D gait analysis was carried out for predicting six muscle forces. Validation of the derived muscle forces were performed using EMG. FE simulations were run at five stages of stance phase of gait. The derived muscle forces and measured GRFs during gait were added to the model as boundary conditions. The validation of FE results indicated a good agreement between simulated plantar pressures (PP) against the measured values from pressure plate. The analyses showed that the presence of hammer toe causes stress concentration on metatarsals. However, the stress concentration seems to shift from the 5th metatarsal to the 3rd metatarsal as the gait progresses from early stance to toe-off.

Introduction

Finite Element analysis can overcome the restriction of experimental methods, by providing a mean to measure internal stresses [1,2].

The aim of this study was to investigate the effects of hammer toe on the internal stress distribution on the bone during walking.

Methods

A participant (male; age: 53 years; BMI: 34 kg/m²) with diabetic neuropathic diabetic foot with non-deformed right foot and hammer toes deformity in the left foot, participated in this study. Following informed consent, MRI scan and 3D gait analysis were carried out. To predict the muscle forces, 'gait 2392' model in OpenSim software was used [3]. A 3D model consisted of a soft tissue and 30 bony structures were reconstructed based on MRI images using mimics software (Materialise, Leuven, Belgium). The obtained model was then imported to ABAQUS software (SIMULIA, Providence, USA) where the plantar fascia and ligaments were modelled as 2174 truss elements, while 74 layers of cartilage was added to the model. The material properties were assigned based on previous study [1]. The 3D foot orientation angles were obtained from the gait analysis of the participant. As boundary conditions, the GRFs were applied at the COP while the muscle forces (including: lateral gastrocnemius, medial

gastrocnemius, tibialis posterior, tibialis anterior, soleus, peroneus longus) were applied at the corresponding insertions points at five stages of stance phase of gait (5%, 25%, 50%, 75% and 90%)

Results and Discussion

The FE model showed to be able to predict peak plantar pressure with less than 11% errors. FE results showed internal stresses distribution in bony structures (Figure 1). As shown in this figure, maximum Von-misses (internal) stress occurred at 3rd metatarsal during of late stance phase of gait.

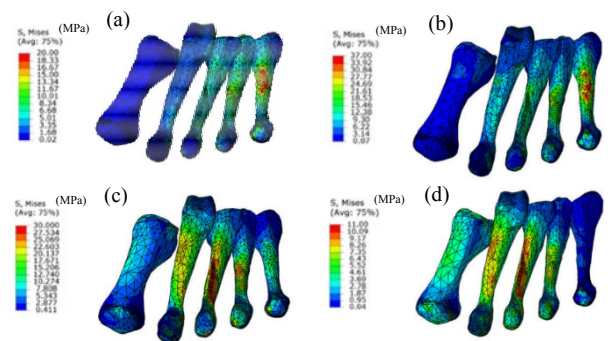


Figure 1: Finite element internal stresses in metatarsals at four walking events. Early stance (a), mid-stance (b), late stance (c) and toe off (d).

Conclusions

In a foot with hammer toe deformity stress concentration appears to be on the 5th metatarsal during the early and mid-stance stages of gait. The stress concentration shifts to 3rd metatarsal during the late stance and toe-off. The findings can have practical implications in clinical management of hammer toe deformity.

References

- [1] Akrami, M., Qian, Z., Zou, Z., Howard, D., Nester, C.J. and Ren, L. (2018). *Biomechanics and modeling in mechanobiology*, **17**: 559-576,
- [2] Scarton, A., Guiotto, A., Malaquias, T., Spolaor, F., Sinigaglia, G., Cobelli, C., Jonkers, I. and Sawacha, Z. (2018). *Gait & Posture*, **60**: 279-285.
- [3] Delp, S.L., Anderson, F.C., Arnold, A.S., Loan, P., Habib, A., John, C.T., Guendelman, E. and Thelen, D.G. (2007). *IEEE transactions on biomedical engineering*, **54**: 1940-1950.

Statistical shape and fibre models to determine the effect of strength training on vastus lateralis shape and architecture

Bart Bolsterlee^{1,2}, Junya Eguchi^{1,2}, Jeanette Thom^{1,2}, Rob Herbert^{1,2}

¹Neuroscience Research Australia (NeuRA), Randwick, New South Wales, Australia

²University of New South Wales, Randwick, New South Wales, Australia

Email: b.bolsterlee@neura.edu.au

Summary

We used statistical shape modeling, and developed a novel method called statistical fibre modeling, to determine the effects of strength training on the three-dimensional (3D) shape and fibre architecture of the vastus lateralis muscle. Mean muscle shape and architecture, and their main modes of variations, were determined from magnetic resonance and diffusion tensor imaging scans obtained before and after eight weeks of strength training. Shape modes that were closely associated with changes in volume were significantly affected by training. The two major modes of variation in fibre orientations were significantly affected by training, suggesting complex three-dimensional fibre reorientations when muscles hypertrophy.

Introduction

The effect of strength training on muscle architecture is typically measured as the change in volume, cross-sectional area, thickness, mean fascicle length and/or pennation angle of a muscle [1]. However, these measures do not capture the potentially complex changes in 3D shape and architecture when muscles hypertrophy.

Here, we apply *statistical shape models* (SSM) – an analysis technique to describe and analyze complex geometrical properties of shapes [2] – to determine the effects of knee extensor strength training on vastus lateralis shape. We also introduce statistical fibre models – a method to describe and analyze changes in 3D fibre orientations – and use these models to determine how fibres of the vastus lateralis reorient following strength training.

Methods

We created surface models of the left vastus lateralis from segmentations of the muscle on mDixon MRI scans of the upper legs of 11 healthy participants (9 females, age 21±2 years; height 163±7 cm), before and after eight weeks of progressive knee extensor strength training. Distance maps of all surface models were transformed with a b-spline transformation to a reference model. Using statistical shape modeling techniques (principal component analysis), all shapes were expressed as weighted deviations, from the mean shape, of a series of principal shape modes.

Similar to statistical shape modeling methods, but now using fibre orientation vectors instead of surface node locations, we created *statistical fibre models*. Muscle fibre orientation vectors, derived from diffusion tensor imaging data, were sampled at corresponding locations in muscles at a resolution of 3×3×3 mm. The mean fibre orientation (per location) and

the major modes of variation were then determined. Fibre orientations in each muscle were expressed as weighted deviations, from the mean fibre orientations, of a series of principal fibre orientation modes.

Shape weights and fibre weights of muscles before and after training were compared using paired sample t-tests, using Bonferroni correction to adjust the significance level for comparing multiple modes.

Results and Discussion

Muscles increased in volume by 14±9% (mean±SD, across participants, $p < 0.01$). Training significantly altered shape weights of modes that were strongly correlated with muscle volume. Visualisation of the patterns of hypertrophy revealed some degree of regional variations in shape change (Fig. 1). Fibre weights associated with the two major modes of variation in fibre orientations changed significantly with training. These modes were associated with complex patterns of fibre reorientations.

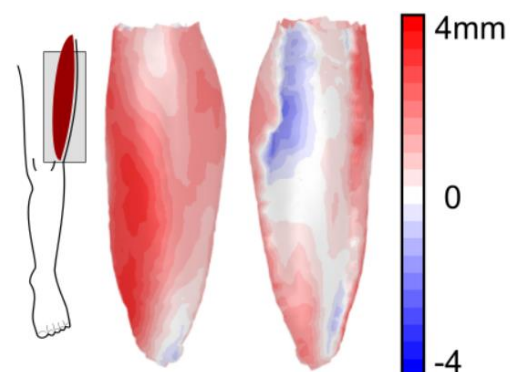


Figure 1: Lateral (left) and medial view of the vastus lateralis muscle, colored to visualise the effect of strength training on muscle shape. Red/blue shades indicate the distance between the (mean) muscle surface after and before training (red=local expansion, blue=local contraction).

Conclusions

We demonstrated the use of statistical shape and fibre models for comprehensive investigations of shape and architectural changes in human muscles. We propose the further use of these techniques for future investigations into architectural adaptations of muscles, and to inform anatomically realistic continuum models of skeletal muscle.

References

- [1] Marzilger R et al. (2019) *Front Physiol*, **10**:957
- [2] Heimann R et al. (2009) *Med Image Anal* **13**(4):543-6

Triceps surae muscle fascicle dynamics as a function of walking speed in young and older adults

Lauri Stenroth¹, Williane Bernardes¹, Santtu Mikkonen¹, Taija Finni², Neil J Cronin²

¹Department of Applied Physics, University of Eastern Finland, Finland

²Faculty of Sport and Health Sciences, University of Jyväskylä, Finland

Email: lauri.stenroth@uef.fi

Summary

A decline in plantarflexor muscle function is considered a key contributing factor to age-related gait impairments. The loss of plantarflexor muscle function may be partially due to compromised muscle-tendon interaction resulting in unfavorable alterations in muscle fascicle dynamics. Here, we investigated *in vivo* muscle fascicle dynamics of the soleus and medial gastrocnemius at a wide range of walking speeds in young and older adults. We were able to detect age-related differences in soleus muscle fascicle velocity with potential implications for walking performance in older adults.

Introduction

A decline in plantarflexor muscle function is considered a key contributing factor to age-related gait impairments such as reduced maximal and preferred walking speeds and increased energy cost of walking. Previous studies suggest that alterations in muscle-tendon interaction and muscle fascicle dynamics may partially explain the decline in plantarflexor muscle function [1,2]. However, the current knowledge is based on observations from a narrow range of walking speeds and the contribution of gastrocnemius and soleus muscles to the decline in ankle function is not clear. This study aimed to examine age-related differences in medial gastrocnemius (MG) and soleus muscle fascicle dynamics at a wide range of walking speeds.

Methods

Thirteen young (24.4 ± 3.7 y) and 13 older (73.5 ± 3.7 y) males walked on a treadmill at seven speeds ranging from -45% to +45% of the preferred walking speed in random order for four minutes per speed. During the last minute at each speed, ground contact timing (footswitch), ankle and knee kinematics (electrogoniometers), and B-mode ultrasound images (80 Hz) of the medial gastrocnemius (MG) and soleus muscles were collected. Ten strides were identified, and muscle fascicle lengths were tracked [3]. Fascicle lengths and velocities were extracted from the time instant of peak tendinous tissue lengths, approximating the time instant of peak muscle force, and normalized to the resting fascicle lengths measured in passive condition with the knee extended and neutral ankle. Linear mixed-effects models were used to investigate the effects of age and walking speed on fascicle dynamics.

Results and Discussion

MG fascicle length at the instant of estimated peak force generation was unaffected by age ($p=0.446$) and invariant to changes in walking speed ($p=0.128$). Soleus fascicle length was not affected by age ($p=0.142$) but showed a linearly de-

creasing trend with an increase in walking speed ($p<0.001$). Both MG and soleus showed a curvilinear increase in the fascicle shortening velocity with an increase in walking speed ($p<0.05$, Figure 1) with no difference between age groups in MG ($p=0.422$) In soleus, fascicle velocity differed between groups ($p<0.001$). The lengthening behavior of the fascicles at the instant of estimated peak force generation observed in older adults was absent in young adults.

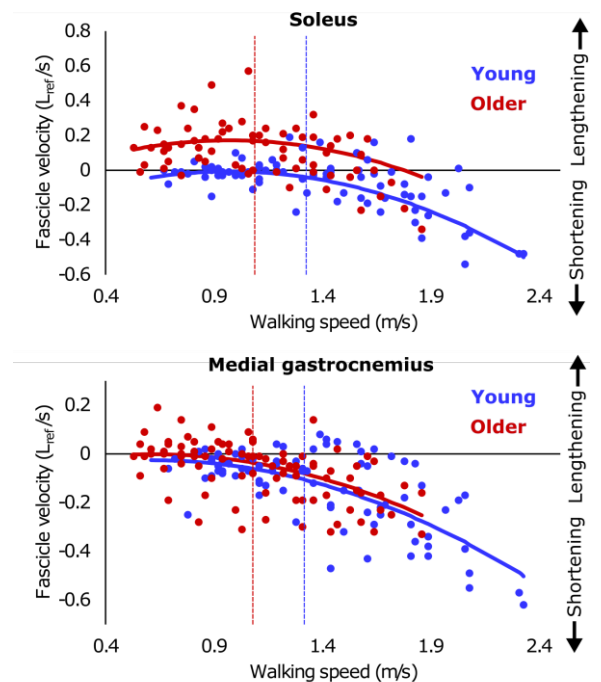


Figure 1: Soleus and medial gastrocnemius muscle fascicle velocities at the instant of estimated peak force generation during walking at different speeds. The curves represent the values predicted by the linear mixed-effects models. The vertical dotted lines represent the preferred walking speeds for both age groups.

Conclusions

Using data from a wide range of walking speeds we were able to identify the effects of age and walking speed on triceps surae muscle fascicle dynamics. The observed lengthening behavior of soleus at the instant of peak force generation in older adults may negatively affect elastic energy storage and return and have a role in age-related walking impairments.

References

- [1] Stenroth L et al. (2017). *Med Sci Sports Exerc*, **49**: 158-166.
- [2] Conway K and Franz J (2020). *Gait Posture*, **77**:88-94.
- [3] Cronin NJ et al. (2011). *J Appl Physiol*, **111**: 1491-1496.

Three-dimensional architecture of the medial gastrocnemius muscle in human infants *in vivo*

Brian V. Y. Chow^{1,2}, Bart Bolsterlee^{1,3}, Robert D. Herbert^{1,2}, on behalf of the MUGgLE Study research team
¹Neuroscience Research Australia (NeuRA), Randwick, NSW, Australia
²School of Medical Sciences, University of New South Wales, Randwick, NSW, Australia
³Graduate School of Biomedical Engineering, University of New South Wales, Randwick, NSW, Australia
 Email: b.chow@neura.edu.au

Summary

There is a paucity of data on muscle architecture in human infants. This study used magnetic resonance and diffusion tensor imaging (MR-DTI) methods to describe, for the first time, the three-dimensional (3D) architecture of the medial gastrocnemius (MG) muscle in human infants *in vivo*. Mean muscle volume, physiological cross-sectional area (PCSA), and fascicle length were 68, 19 and 3 times smaller, respectively, in infants than in adults.

Introduction

Several studies have measured muscle architecture in children to investigate childhood muscle growth. To our knowledge, only one study (on cadaveric muscle from a 6-month old [1]) has quantified skeletal muscle architecture in human infants, so little is known about the “starting point” of postnatal muscle development. In this study we used anatomically constrained DTI tractography to measure the 3D architecture of MG muscles from two infants *in vivo*.

Methods

Two healthy infants (S1 & S2), both aged 3 months, were firmly swaddled and, while sleeping, placed supine in a 3-T MRI scanner. T1-weighted MRI and DTI scans were obtained from both lower legs of participants but only one leg was used for analysis (S1: left; S2: right). The MRI protocol has been described elsewhere [3]. A 3D surface model of the MG, from which muscle volume was calculated, was created from manual segmentations of the T1 scan (Fig. 1A). Anatomically constrained tractography [3] was used to reconstruct and quantify the 3D architecture of the MG (Fig. 1B). The average fascicle length and pennation angle were calculated for each muscle. PCSA was calculated by dividing muscle volume by mean fascicle length. Shank length was measured as the distance from the lateral femoral condyle to the lateral malleolus.

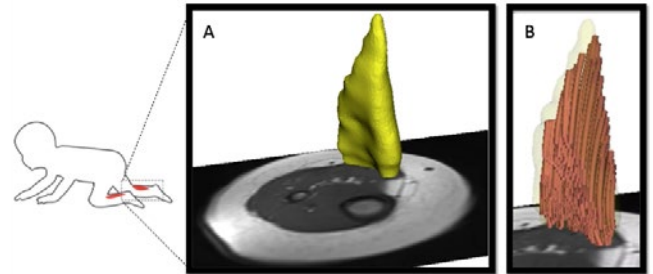


Figure 1: (A) 3D surface reconstruction and (B) fascicle reconstruction of the MG muscle.

Results and Discussion

Data from the current study and two previous studies [1-2] are given in Table 1. The mean MG muscle volume measured here was >3 times greater than MG muscle volume measured on the cadaver of one 6-month old infant. Mean muscle volume, PCSA, and fascicle length were 68, 19 and 3 times smaller, respectively, than in adults. Normalized to bodyweight, the infant MG volume was 7 times smaller than in adults. Normalized to shank length, the infant MG fascicle length was similar to (9% longer than) in adults.

Conclusions

We demonstrated feasibility of using MR-DTI for measuring infant muscle architecture. To a rough approximation, fascicle length, PCSA and volume scaled with the first, second and third powers of tibia length, respectively. The generality of this scaling needs to be further tested with more data.

Acknowledgments

The study was supported by NHMRC grants APP1156394 and APP1117192. BC is supported by a UNSW Scientia scholarship. None of the authors have a conflict of interest.

References

- [1] Bradshaw LR et al. (2020). *Eur. J. Anat.*, **24**: 491-499.
- [2] Bolsterlee B et al. (2017). *J Appl Physiol*, **122**: 727.
- [3] Bolsterlee B et al. (2019). *J Biomech*, **86**: 71-78.

Table 1: Anthropometry, muscle volume and MG muscle architecture from this study (A) and previous studies on an infant [1] and adults [2].

Study	Age, year	Gender (Male: Female)	Height, cm	Body mass, kg	Shank length, cm	Muscle volume, cm ³	Fascicle length, mm	PCSA, cm ²	Pennation angle, °
A	0.3 ± 0.0	1:1	60.8 ± 2.5	6.6 ± 1.8	10.6 ± 0.0	2.9 ± 0.7	15.5 ± 0.9	1.9 ± 0.6	26.3 ± 4.2
[1]	0.5	0:1	-	-	-	0.8	19.8 ± 3.2	0.4	14.7 ± 3.5
[2]	29.3 ± 5.2	4:4	168.5 ± 8.3	63.6 ± 5.8	39.5 ± 2.8	193.4 ± 39.4	52.8 ± 6.4	36.8 ± 6.9	22.2 ± 2.6

Gender Difference in Architectural and Mechanical Properties of Medial Gastrocnemius-Achilles Tendon Unit

Liqin Deng, Xini Zhang, Faning Zhang, Weijie Fu
 School of Kinesiology, Shanghai University of Sport, Shanghai, China
 E-mail: fuweijie@sus.edu.cn

Summary

In this study, the gender difference in architectural and mechanical properties of medial gastrocnemius-Achilles tendon unit (MTU) was explored. The results showed the pennation angle (PA_{MG}), thickness (TK_{MG}), stiffness (k_{MG}) of the medial gastrocnemius (MG), and Achilles tendon (AT) length (L_{AT}) and cross-sectional area (CSA_{AT}) was greater or longer in males. Besides, females had greater MG logarithmic decrement (D_{MG}). The results indicated males potentially had greater MG force-producing capacities, mechanical efficiency, and AT load-bearing capacities, while less compliance of MG.

Introduction

As the largest muscle-tendon unit, the architectural and mechanical properties of the MTU could affect sport performance and the incidence of MG & AT injury. One of the major influence factors for the architectural and mechanical properties of the MTU is gender. It was reported males tended to have greater absolute strength and better performance in speed and strength-oriented sports compared to females [1]. Nevertheless, the majority of AT and MG sports injuries occur in males [2]. Thus, the purpose of this study was to explore the gender difference in the architectural and mechanical properties of the MTU.

Methods

18 healthy male (age: 25.1 ± 1.6 yrs) and 18 healthy female (age: 24.4 ± 2.1 yrs) collegiate students with no training experience were recruited.

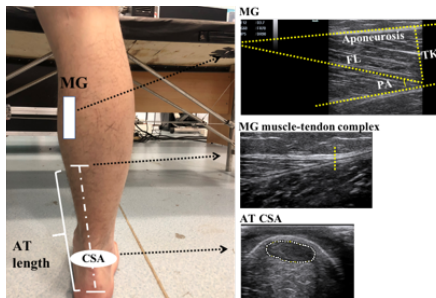


Figure 1: Diagram and ultrasound images of medial gastrocnemius (MG) and Achilles tendon (AT).

The MG fascicle length (FL_{MG}), PA_{MG} , TK_{MG} , L_{AT} , and CSA_{AT} were acquired by ultrasonography. The ultrasound imaging was analyzed via the Image J software (Figure 1). Stiffness and logarithmic decrement of MG (k_{MG} and D_{MG})

and AT (k_{AT} and D_{AT}) was measured by MyotonPRO at MG belly and 3cm above AT insertion point, where D_{MG} and D_{AT} represents the dissipation of the mechanical energy.

Independent *t*-tests were used to quantify the gender effect on the architectural and mechanical properties of the MTU.

Results and Discussion

For architectural properties, the PA_{MG} , TK_{MG} , L_{AT} , and CSA_{AT} were significantly greater or longer in males than females ($p < 0.05$). These results indicated the MG force-producing capacities, mechanical efficiency, and AT load-resisting capacities, and performance were greater in males (Figure 2).

For mechanical properties, females had significant smaller k_{MG} and greater D_{MG} than males ($p < 0.05$). The former may explain the lower AT injuries rate of females [3]. However, no gender differences were observed in k_{AT} and D_{AT} (Table 1).

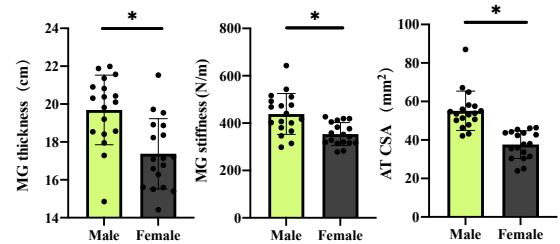


Figure 2: Gender difference in medial gastrocnemius (MG) thickness, stiffness, and Achilles tendon cross-sectional area (AT CSA) (*: $p < 0.05$).

Conclusions

Compared to females, males had greater or longer k_{MG} , PA_{MG} , TK_{MG} , L_{AT} , and CSA_{AT} and had smaller E_{MG} . These findings indicated males had larger MG and potentially had greater MG force-producing capacities, mechanical efficiency, and load-resisting capacities of AT. However, the higher k_{MG} might be a reason for the higher injury risk of AT in males.

Acknowledgments

This study was supported by NNSFC (11772201, 11932013).

References

- [1] Chow S et al. (2000). *Eur J Appl Physiol*, **82**, 236-44.
- [2] Fields B et al. (2016). *Curr sport med rep*, **15**, 320-24.
- [3] Zhou, J et al. (2019). *J Sports Sci Med*, **18**, 454-61.

Table 1: Gender difference in medial gastrocnemius fascicle length (FL_{MG}), pennation angle (PA_{MG}), thickness (TK_{MG}), elasticity (D_{MG}), stiffness (k_{MG}), Achilles tendon length (L_{AT}), cross-sectional area (CSA_{AT}), elasticity (D_{AT}), and stiffness (k_{AT}).

	FL_{MG} (cm)	PA_{MG} (°)	TK_{MG} (cm)	D_{MG}	k_{MG} (N/m)	L_{AT} (cm)	CSA_{AT} (mm ²)	D_{AT}	k_{AT} (N/m)
Female	5.7 ± 0.6	$18.2 \pm 2.2^*$	$1.7 \pm 0.2^*$	$1.0 \pm 0.2^*$	$337.4 \pm 89.8^*$	$18.7 \pm 1.9^*$	$37.6 \pm 7.2^*$	0.6 ± 0.3	1205.4 ± 187.3
Male	5.9 ± 0.4	21.2 ± 2.4	2.0 ± 0.2	0.9 ± 0.1	438.6 ± 86.4	20.9 ± 2.6	55.2 ± 10.2	0.8 ± 0.3	1228.6 ± 162.8

Note: * indicates a significant difference between females and males with $p < 0.05$.

Influence of muscle stiffness and architecture on gastrocnemii shape during isometric plantarflexion contractions

Nicole Yvette Kelp¹, Sabrina Pinel¹, Kylie Tucker¹, Francois Hug^{1,2}, Taylor Dick¹

¹ School of Biomedical Sciences, University of Queensland, St Lucia, Queensland, Australia

² Movement, Interactions, Performance Laboratory (EA 4334), Nantes Université, Nantes, France

Email: n.kelp@uq.net.a

Summary

Shape changes allow skeletal muscle to extend its functional range, yet we still lack an understanding of how internal constraints play a role in this process. Using aging as a model, the aim of this study was to determine the effects of muscle shear modulus (an index of stiffness) and muscle architecture (volume and pennation angle) on muscle shape changes and fibre rotation during isometric plantarflexion contractions. We found internal muscle properties such as, muscle volume, resting pennation angle, and muscle shear modulus to not be affected by age, however all muscle properties had a significant effect on changes in pennation angle at 100% contraction level in the medial gastrocnemius.

Introduction

A muscle's ability to produce force across a wide range of mechanical demands is due, in part, to changes in pennation angle and muscle shape. Muscle fibre rotation and muscle bulging allows belly shortening to be uncoupled from fibre shortening during a contraction, optimizing the fibre's ability to produce force and power [1]. Our recent work has shown synergistic muscles have different shape change patterns at similar contraction levels [2]. However, the degree to which muscle changes shape may be due to internal constraints such as connective tissue properties and resting muscle architecture and remains untested in humans [3]. Aging is often associated with greater muscle stiffness, lower resting pennation angle, and lower muscle volume [4]. The aim of this study was to determine the effects of passive muscle shear modulus (an index of stiffness) and resting muscle architecture, such as volume and pennation angle, on muscle shape change and fibre rotation during isometric contractions *in vivo* in humans.

Methods

10 younger (23.6 ± 3.6 yrs) and 10 older (70.3 ± 2.9 yrs) adults participated in this study. Each participant underwent a T1-weighted MRI scan (3T Magnetom Prisma, Siemens, Germany) of the dominant lower limb. MRI images were segmented to determine volume of the medial (MG) and lateral gastrocnemius (LG). Passive muscle shear modulus was measured from 20° plantarflexion to 15° dorsiflexion using shear wave elastography (Aixplorer, Supersonic Imagine, Aix-en-Provence, France). Participants performed isometric plantarflexion contractions at 10%, 30%, 50% and 100% of maximum voluntary contraction. A dual probe B-mode ultrasound (Telemed, Lithuania) configuration was used to image MG and LG during each contraction. Linear mixed effects models were used to determine the effect of Muscle Volume, Resting Pennation Angle and Shear Modulus at slack +5°, on changes in pennation angle and muscle thickness. Differences were considered significant at $p < 0.05$.

Results and Discussion

Age did not have a significant effect on muscle volume, resting pennation angle, or shear modulus (All: $p > 0.05$). Muscle had a significant effect on all three muscle properties, with the MG displaying greater muscle volume ($p < 0.001$), greater resting pennation angle ($p < 0.001$), and greater shear modulus ($p < 0.001$), compared to the LG. We found an effect of Muscle Volume, Resting Pennation Angle and Shear Modulus on the change in pennation angle only at higher contraction levels of 50% and 100% MVC. In both muscles, there was a positive relationship between muscle architecture (volume and resting pennation angle) and change in pennation angle at 100% MVC. A negative relationship between shear modulus and change in pennation angle was found only in the MG at 100% MVC (Figure 1). There was no relationship between Muscle Volume, Resting Pennation Angle, and Shear Modulus on the change in muscle thickness.

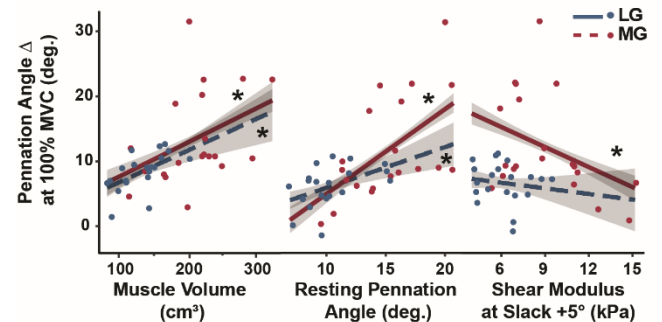


Figure 1: Relationships between internal muscle properties and change in pennation angle at 100% MVC. * $p < 0.05$

Conclusions

Internal muscle properties influence muscle fibre rotation at high contraction levels such that muscles with greater volumes and higher resting pennation angle display more fibre rotation while muscles with greater shear modulus display less fibre rotation. It is likely that differences in internal muscle properties are related to the differing shape change and fibre rotation behaviors in synergistic muscles at similar contraction levels.

Acknowledgments

We would like to acknowledge the UQ Centre for Advanced Imaging for help in MRI imaging and Romain Feigean and India Lindemann for help collecting and processing data.

References

- [1] Azizi et al. (2008). *PNAS*, **105**:1745-1750
- [2] Kelp et al. (2021) *In Review*
- [3] Eng et al. (2018) *Integr. Comp. Biol.*, **58**:207-218
- [4] Holt et al. (2016). *J Exp Biol.*, **219**: 998-1003

Forward Prediction of Ankle Joint Moments Using a Generic Feature Set

Homayoon Zarshenas¹, Thor F. Besier¹, Bryan P. Ruddy¹, Alexander Woodall¹, Andreas W. Kempa-Liehr²

¹ Auckland Bioengineering Institute, University of Auckland, New Zealand

² Department of Engineering Science, University of Auckland, New Zealand

Email: hzar638@aucklanduni.ac.nz

Summary

Musculoskeletal models can estimate joint moments from electromyography (EMG), but these are subject-specific, with a time-consuming training process, and are not capable of forward prediction. In this study, we developed a generic model to use a unique set of features to train a regression model to predict ankle moments across ten participants and compared this to a subject-specific feature set.

Introduction

Musculoskeletal modeling can be used to estimate joint moments from EMG. However, because of the nonlinear relationship between muscle activation and joint torque, model calibration is computationally expensive and unsuitable for real-time applications. Machine learning (ML) models show promise as an alternative method to predict joint moments [1]. However, these models are subject-specific, and training each individual's model is tedious and time-consuming. The objective of this study is to introduce a generic model to have a smooth and continuous prediction of ankle moments, 30 msec forward in time, during walking at a constant speed, which applies to multiple individuals. This model can be used to control assistive robots.

Methods

Ten healthy participants were asked to walk at the constant speed of 1 m/s for 30 seconds on a force-instrumented treadmill. Motion capture cameras were used to reconstruct lower limb kinematics. Muscle activities from vastus lateralis, medial, gastrocnemius, tibialis anterior, soleus, and medial hamstring were recorded. Motion capture data and ground reaction forces were low-pass filtered at 10Hz and used as input for OpenSim to calculate the right ankle's kinematics and moments [2]. The input time series for the ML model included 1-sec length and 0.01-sec sliding length of; right ankle angle, angular velocity, and muscle activity (full-wave rectified and low-pass filtered at 6Hz).

The proposed pipeline for using EMG signals and kinematic features as input to predict ankle moments comprises three main steps; a) feature extraction, b) feature selection, and c) regression model development. The Python-based package TSFRESH (Time Series FeatuRe Extraction on basis of Scalable Hypothesis tests) was used for feature extraction [3]. The features were sorted based on their importance score in the feature selection phase. The top 50 features were selected to represent each window of input signals. To generate a generic feature set, cross-validation was used by leaving one subject out and using the rest to select the features (generic feature set), then the regression model was trained and tested for the unseen individual. A random forest regression model correlated selected features to the desired output, which was

given as calculated joint moments from the inverse dynamics. The model performance was assessed under three scenarios: 1) train the regression model based on the selected feature set for the same individual (personalized feature set), 2) generic feature set, and 3) using the tuned feature set of one participant and train and test the regression model for another individual (mismatched feature set). The regression model accuracy was reported using a coefficient of determination (R^2), and root mean square error (RMSE).

Results and Discussion

Using the generic set of features to develop the regression model increased the accuracy of moments prediction compare to the mismatched feature set. Also, the generic model results were close to the personalized model (Table 1).

Table 1: The regression model accuracy comparison (mean \pm SD).

	R^2 (%)	RMSE (mN.m)
Mismatched feature set	92.0 \pm 3.10	1.32 \pm 1.6
Generic feature set	98.4 \pm 0.97	0.897 \pm 0.89
Personalized feature set	98.9 \pm 0.77	0.654 \pm 0.62

Error reduction and smoother tracking of the moments' profile result of using the generic feature set compared to the mismatched feature set (Fig. 1). The highest similarity to calculated moments via inverse dynamics is a critical characteristic for EMG-based models to provide effortless interaction between human and assistive robots.

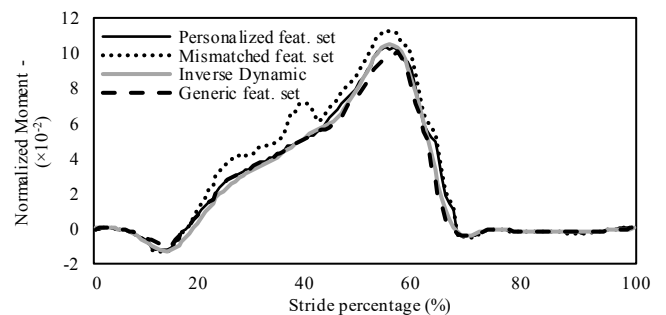


Figure 1: Ankle moments prediction of personalized, genetic, and mismatched feature set. Target moments from inverse dynamics.

Conclusions

In this study, we presented a model based on a generic set of features that is capable of accurately predicting ankle joint moments up to 30 msec into the future. This model does not require calibration to new participants, and its performance was comparable to personalized models.

References

- [1] Zarshenas H. et al. (2020). *IEEE EMBC*: 4854-4857.
- [2] Delp, S. L., et al. (2007). *IEEE TBME*, **54.11**:1940-1950.
- [3] Christ, M., et al. (2018). *Neurocomputing*, **307**: 72-77.

A Method to Compare Heterogeneous Types of Bone and Cartilage Meshes.

N. Rooks¹, M. Schneider¹, A. Erdemir^{2,3}, J. Halloran⁴, P. Laz^{5,6}, K. Shelburne^{5,6}, D. Hume^{5,6}, C. Imhauser⁷, W. Zaylor^{8,9}, S. Elmasry⁷, A. Schwartz^{2,3}, S. Chokhandre^{2,3}, N. Abdollahi Nohouji^{2,3,8,9}, T. Besier^{1,10}

¹Auckland Bioengineering Institute, University of Auckland, Auckland, New Zealand

²Department of Biomedical Engineering, Lerner Research Institute, Cleveland Clinic, Cleveland, USA

³Computational Biomodeling (CoBi) Core, Lerner Research Institute, Cleveland Clinic, Cleveland, USA

⁴Applied Sciences Laboratory, Institute for Shock Physics, Washington State University, Spokane, USA

⁵Department of Mechanical and Materials Engineering, University of Denver, Denver, USA

⁶Center for Orthopaedic Biomechanics, University of Denver, Denver, USA

⁷Department of Biomechanics, Hospital for Special Surgery, New York, USA

⁸Department of Mechanical Engineering, Cleveland State University, Cleveland, USA

⁹Center for Human Machine Systems, Cleveland State University, Cleveland, USA

¹⁰Department of Engineering Science, Faculty of Engineering, University of Auckland, Auckland, New Zealand

Email: nroo469@aucklanduni.ac.nz

Summary

Comparing bone and cartilage meshes of different types is a significant challenge. We established a method to register and compare bone and cartilage meshes agnostic to mesh type and nodal density, by looking at bone mesh-to-mesh distance, subchondral bone area and cartilage thickness.

Introduction

Accurately capturing the bone and cartilage morphology and generating a mesh remains a critical step in the workflow of computational knee modeling. Currently there is no standardized method to compare meshes of different element types and nodal densities (and therefore underlying geometries). For example, different mesh-to-mesh distances are found when comparing mesh A to B or mesh B to A. This makes comparisons across research teams a significant challenge. To overcome this problem, a method to quantify differences in knee joint bone and cartilages meshes, independent of bone and cartilage mesh topology was established.

Methods

To calculate bone mesh-to-mesh distances, the meshes were registered and resampled after which a dense point cloud was Radial Basis Function (RBF) fitted [1] to the femur (200,000 points), tibia (100,000 points) and patella (100,000 points) meshes. Cloud-to-cloud distances were obtained using CloudCompare (CloudCompare, version 2.10-alpha).

For cartilage mesh comparisons, a common frame of reference was created by RBF fitting parametric templates to resampled bone meshes. The subchondral bone boundaries and cartilage thicknesses were then calculated and visualized in a common frame of reference.

Cartilage thickness was calculated for each subchondral point in the fitted common frame of reference. Cartilage thickness was calculated as the distance along the normal of the subchondral bone point from the bone to the articular cartilage layer. The subchondral bone boundaries were obtained by selecting the bone points closest to the articular cartilage points.

The methods were applied to bone and cartilage meshes generated by five knee modelling teams [2].

Results and Discussion

Bone mesh-to-mesh distances between all teams' meshes were obtained. The average (\pm SD) absolute distance difference between the two calculations (mesh A to B vs. mesh B to A) was 0.0041 ± 0.0031 mm for the femur, 0.0178 ± 0.0254 mm for the tibia, and 0.0091 ± 0.0085 mm for the patella.

Cartilage thicknesses and subchondral bone areas were obtained for all teams (Figure 1).

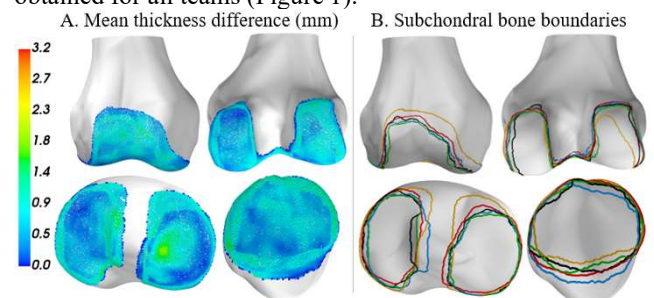


Figure 1: Mean absolute thickness difference ($n=5$) (A) and subchondral bone area (B), where each color presents one team.

Conclusions

A new method was established to quantify differences in knee joint bone and cartilage meshes independent of mesh type and nodal density. This method can easily be implemented in any study comparing bone and cartilage meshes with different characteristics. Other potential applications exist in unifying the description of anatomical coordinate systems and in mesh generation independent of segmentation method or software.

Acknowledgments

This work was funded by the US National Institutes of Health (NIH, NOA_1R01EB024573-01).

References

- [1] Zhang J. et al. (2018). *Comput Methods Biomech Biomed Eng*, **21**(7): 498-502.
- [2] Erdemir A. et al. (2019) *J. Biomech. Eng.*, **141**(7).

The deep hip stabilisers cannot stabilise

Evvy Meinders^{1,2}, Basilio AM Goncalves^{1,2}, David G Lloyd^{1,2}, David J Saxby^{1,2}, Claudio Pizzolato^{1,2}, Laura E Diamond^{1,2}

¹School of Allied Health Sciences, Griffith University, Gold Coast, Australia,

²Griffith Centre of Biomedical and Rehabilitation Engineering, Griffith University, Gold Coast, Australia

Email: evvy.meinders@griffithuni.edu.au

Summary

This study aimed to understand the contribution of deep hip muscles to hip stability during walking. We defined hip stability as hip stiffness in the sagittal plane, calculated via electromyography (EMG)-assisted neuromusculoskeletal modelling. Hip stiffness was compared between three model configurations: (i) deep hip muscles informed by EMG measurements, (ii) no deep hip muscles, and (iii) deep hip muscles imposed by maximal activation. Hip stiffness was 1-5% less over the gait cycle when the model had no deep hip muscles compared to normally activated deep hip muscles, whereas maximally activated deep hip muscles had no significant effect on hip stiffness. Findings suggest the deep hip muscles have a minimal role in modulating hip stiffness and contest their widely proposed role as hip stabilisers.

Introduction

The deep hip muscles have long been considered hip stabilisers based on their morphology and lines of action [1]. Irrespective of the nebulous definition of “stability” used in clinical literature, it remains unclear whether the deep hip muscles can generate enough force to stabilise the hip. We defined hip stability as hip stiffness in the sagittal plane, a mechanical quantity that measures the joint angle displacement following force perturbation. This study aimed to understand the contribution of deep hip muscles to hip stability during walking.

Methods

Three-dimensional marker trajectories and ground reaction forces, together with EMG from 12 superficial and 4 deep muscles of the lower limb, were recorded during self-paced walking in nine healthy participants (age: 24±4 yrs). Inverse kinematics, inverse dynamics, and muscle analysis were performed in OpenSim [2] using a linearly scaled modified generic model [3], including all 22 hip spanning muscles. Muscle-tendon parameters were calibrated to the individual using CEINMS [4]. EMG-assisted neuromusculoskeletal modelling was used to calculate muscle-tendon unit stiffness [5] for the hip spanning muscles in the model, followed by hip stiffness in the sagittal plane over the gait cycle.

Hip stiffness was calculated for each participant using three model configurations: (i) deep hip muscles included in the model and informed by

EMG measurements, (ii) no deep hip muscles in the model, and (iii) deep hip muscles included in the model imposed by maximal activation. Hip stiffness was compared between configurations over the gait cycle using within-participant analysis of variance with statistical parametric mapping (SPM) methods [6] ($p < 0.05$). A Bonferroni post-hoc analysis was performed if statistical differences were found.

Results and Discussion

The model with no deep hip muscles (ii) had 1-5% lower hip stiffness than the model that was informed by EMG measurements (i). Few significant differences were found for the other comparisons.

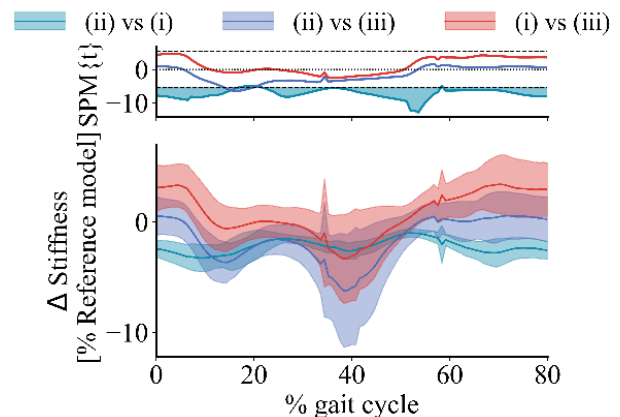


Figure 1: Statistical parametric mapping post-hoc results for within-participant comparison (top). Mean difference in hip stiffness between configurations (± 1 standard deviation) in sagittal plane (bottom).

Conclusion

The deep hip muscles have limited potential to modulate hip stiffness, with no increase in hip stiffness when the deep hip muscles are maximally activated. The merit of targeting these muscles in the management of hip conditions associated with hip instability is unclear.

References

- [1] Retchford TH et al. (2013). *J Musculoskeletal Neuronal Interact*, **13**: 1-12.
- [2] Delp S et al. (2007). *IEEE Trans Biomed Eng*, **54**: 1940-50.
- [3] Rajagopal A et al. (2016). *IEEE Trans Biomed Eng*, **63**: 2068-79.
- [4] Pizzolato et al. (2015). *J Biomech*, **48**: 3929-36.
- [5] Sartori et al. (2015). *J Neurophysiol*, **114**: 2509-27.
- [6] Pataky T (2010). *J Biomech*, **43**: 1976-1982.

Effect of meniscus material models on the mechanical responses of cartilage during walking: a finite element study

Tulashi Simkheada¹, Gustavo A. Orozco¹, Rami K. Korhonen¹, Petri Tanska¹, Mika Mononen¹

¹Department of Applied Physics, University of Eastern Finland, Kuopio, Finland

Email: tulasi@uef.fi

Summary

Biomechanical behavior of meniscus can be modeled using different constitutive material models. An isotropic elastic (IE) model offers the simplest approximation, while a fibril reinforced poroelastic (FRPE) model is capable to separate contributions of fluid, and fibrillar and nonfibrillar parts. However, the FRPE material is complex to implement and computationally demanding in 3D geometries. Here, we aimed to quantify the most suitable and efficient constitutive model of meniscus for simulation of cartilage responses in the knee joint during walking. We demonstrated that simpler models can reproduce identical cartilage responses compared with the knee model with the FRPE meniscus. However, the material anisotropy should be considered, if internal responses are of interest.

Introduction

Meniscus is a poroelastic connective tissue in the knee joint, which distributes joint loads efficiently on cartilage surfaces [1]. The FRPE material model has been used in many studies to characterize anisotropy in meniscus and other soft tissues [2]. However, implementation of such a model in 3D geometries and model simulation are time-consuming processes. The application of a simpler material model for meniscus would accelerate the generation and simulation of biomechanical knee joint models. Hence, we aimed to evaluate how complex material model is required for meniscus so that the cartilage mechanical responses in the knee joint are the same when meniscus is modeled using the FRPE material. We hypothesize that the mechanical function of the FRPE meniscus in the knee can be captured using a simpler material model.

Methods

A finite element (FE) knee joint model geometry and material properties for the FRPE cartilage and meniscus were obtained from a previous study [2]. In addition to the FRPE meniscus, the following formulations were considered: isotropic elastic (IE), orthotropic elastic (OTE), and orthotropic poroelastic (OTPE). First, the IE, OTE, OTPE material parameters were obtained by fitting the force, stress, and strain responses to those obtained from the FRPE meniscus under 10% deformation (compression and shear) in a simple cubic geometry (Table 1). Then, the fitted material properties of different meniscus models were implemented in the knee joint level models under gait loading (stance phase) [2]. Finally, reaction forces through tibial cartilage and meniscus, and tissue stresses and strains, were compared to the knee model with the FRPE meniscus.

Results and Discussion

The simulated reaction forces through the tibial cartilages were identical for all meniscus models (Figure 1a, c). This suggests that a properly calibrated and simple meniscus material model can reproduce the same knee joint contact

forces compared to knee model with more complex meniscus. Likewise, the simulated reaction forces through the IE, OTE, OTPE, and FRPE menisci were similar (Figure 1b, d). However, we observed that only OTE and OTPE meniscus models were able to replicate the internal material responses (stresses and strains) of the FRPE meniscus (data not shown), indicating that meniscus anisotropy must be considered to adequately simulate internal tissue responses of the FRPE material.

Table 1: Material parameters for the meniscus material models.

Models	Material parameters	Meniscus	Parameter description
Fibril-reinforced poroelastic	E_f (MPa)	184	Fibril network modulus
	E_m (MPa)	0.08	Non-fibrillar matrix modulus
	ν_m (-)	0.3	Poisson's ratio of the non-fibrillar matrix
	M (-)	12.1	Strain dependent permeability coefficient
	k_0 ($\times 10^{-15} \text{m}^4 \text{N}^{-1} \text{s}^{-1}$)	0.08	Initial permeability
Orthotropic poroelastic	E_x (MPa)	6	Young's modulus (radial)
	E_y (MPa)	0.08	Young's modulus (axial)
	E_z (MPa)	184	Young's modulus (circumferential)
	ν_{xy} (-)	0.4	Poisson's ratio
	ν_{yz} (-)	0.02	
	ν_{zx} (-)	0.0001	
	G_{xy} (MPa)	0.62	Shear modulus
	G_{xz} (MPa)	1.99	
	G_{yz} (MPa)	1.99	
	k ($\times 10^{-15} \text{m}^4 \text{N}^{-1} \text{s}^{-1}$)	0.08	Permeability
Orthotropic elastic	E_x (MPa)	6.2	Young's modulus (radial)
	E_y (MPa)	6.2	Young's modulus (axial)
	E_z (MPa)	184	Young's modulus (circumferential)
	ν_{xy} (-)	0.91	Poisson's ratio
	ν_{yz} (-)	0.02	
	ν_{zx} (-)	0.03	
	G_{xy} (MPa)	1.41	Shear modulus
	G_{xz} (MPa)	2.6	
	G_{yz} (MPa)	2.6	
	Isotropic elastic	E (MPa)	40
ν (-)		0.49	Poisson's ratio

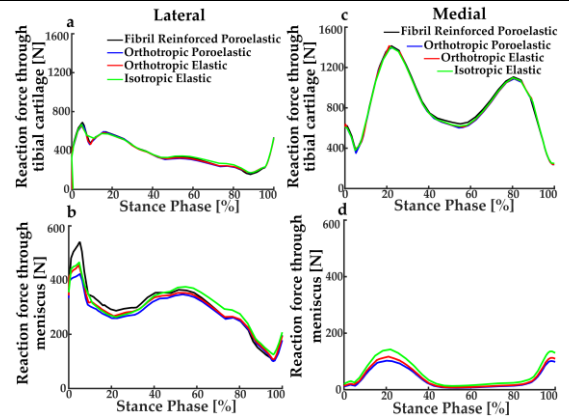


Figure 1: Reaction forces through tibial cartilage and meniscus in (a,c) lateral and (b,d) medial compartment.

Conclusions

The OTE and OTPE menisci are feasible to be used in knee joint models as they are capable of producing similar joint contact forces and internal tissue responses of meniscus as simulated with the FRPE meniscus.

References

- [1] Makris et al. (2011). *Biomaterials*. **30**: 7411-7431.
- [2] Halonen et al. (2016). *J. Biomech*. **49**: 2566-2576.

Free Achilles tendon strain during common locomotor and rehabilitation tasks

Daniel Devaprakash^{1,2}, David F. Graham^{1,3}, Rod S. Barrett^{1,2}, David G. Lloyd^{1,2}, Steven J. Obst^{1,4}, Ben Kennedy¹, Kahlee L. Adams⁵, Adam Hunter⁵, Nicole Vlahovich⁵, David L. Pease⁵, Claudio Pizzolato^{1,2}

¹School of Allied Health Sciences, Griffith University, QLD, Australia

²Griffith Centre of Biomedical and Rehabilitation Engineering (GCORE), Griffith University, QLD, Australia

³Department of Health and Human Development, Montana State University, Bozeman, MT, United States

⁴School of Health, Medical, and Applied Sciences, Central Queensland University, Bundaberg, Australia

⁵Movement Science, Australian Institute of Sport, Canberra, Australia

Email: d.devaprakash@griffith.edu.au

Summary

We used a personalized electromyogram-informed neuromusculoskeletal model to assess Achilles tendon strain during dynamic motor tasks. Our model estimates of Achilles tendon force agreed with direct measures reported in the literature. Peak free Achilles tendon strain was highest during running at 5 m/sec, and the average free Achilles tendon was highest during maximal hop landing.

Introduction

In vivo studies have shown that Achilles tendon (AT) geometry and mechanical properties adapt based on the magnitude and duration of tissue strain [1]. 2D ultrasound has been commonly used to measure AT-aponeurosis strain during dynamic tasks, but this method is susceptible to motion artefacts and cannot be used to estimate free AT strain. The primary aim of this study was to estimate free AT strain during locomotor and rehabilitation tasks using neuromusculoskeletal models informed by 3D medical imaging data and surface electromyography (EMG). Our model was validated using direct measurements of AT force reported in literature.

Methods

Sixteen trained runners (run > 80 km/wk) (10 male, 6 female, age: 25.2±5 yrs, BMI: 20.9±1.8 kg.m⁻²) with no prior history of AT injury completed a range of locomotor and rehabilitation tasks: single leg heel drops and rise, single leg heel drops and rise with added mass (20% BW), walking at 1.3 m/s, running (3 m/s, 5 m/s), counter movement jump, squat hop landing, and maximal hop landing. Motion capture, ground reaction force, and surface electromyography data were synchronously recorded during all tasks. Calibrated EMG-informed neuromusculoskeletal model [2] with tuned muscle-tendon parameters was used to estimate triceps surae muscle forces and tendon strain across all tasks. Personalised models were generated by: 1) linear scaling of the OpenSim model [3], 2) recalculating muscle maximal isometric forces based on linear regression, 3) adjusting triceps surae insertion point to match model moment arm data with experimental data, 4) optimising optimal fibre length and tendon slack length using morphological scaling methods, and 5) modifying normalised force-strain curves of tendons of triceps surae muscles based on experimental data [4]. Differences in average and peak free AT strain across all tasks were assessed using ANOVA (Greenhouse-Geisser corrected), and planned contrast tests. Model estimates of free AT force were compared with direct measures of AT force

reported in the literature as part of the model validation process.

Results and Discussion

Average strain during walking was significantly lower than the other tasks (Figure 1). Average and peak free AT strains were significantly higher in added mass (20% BW) condition during heel rise and heel drop (Figure 1). Average free AT strain during running at 5 m/sec was significantly higher when compared to running at 3 m/sec (Figure 1).

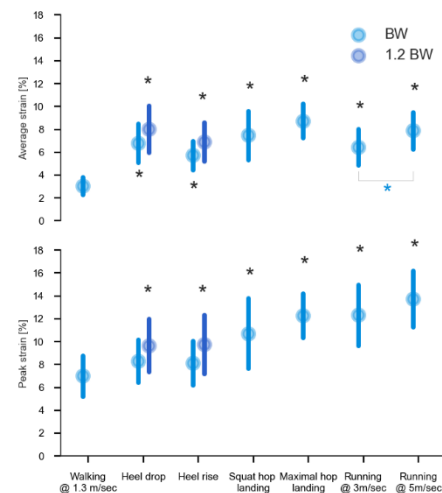


Figure 1: Average and peak strain during locomotor and rehabilitation tasks. Data are mean and standard deviation. * indicates significant difference between walking and the given task

Our measures of free AT force were close to direct measures of AT force during walking (R^2 : 0.94), counter movement jump (R^2 : 0.86), and running (R^2 : 0.92 – 0.94).

Conclusions

Average and peak free AT strain were not different between heel drop and heel rise tasks. During locomotor tasks, average and peak free AT strain increased as the average speed of the task increased. Neuromusculoskeletal models can be used to better inform AT rehabilitation programs.

References

- [1] Arampatzis A et al. *J Biomech*, **43** 3073-3079.
- [2] Pizzolato C et al. (2020) *Front. Bioeng. Biotechnol*, **8**, 878.
- [3] Delp et al. (2007) *IEEE Trans. Biomed Engg*, **11** 1940-1950.
- [4] Devaprakash D et al. (2020) *Front. Physiol*, **11**

Morphological Variation in Paediatric Lower Limb Bones

Laura Carman¹, Thor Besier¹, Julie Choisne¹

¹Auckland Bioengineering Institute, The University of Auckland, Auckland, New Zealand

Email: icar475@aucklanduni.ac.nz

Summary

Here we present a statistical shape model (SSM) from a population of 333 children (aged 4-18 years) to characterise the morphological variation and prediction of new skeletal geometry. Shape and size variation were captured using principal component analysis (PCA) and Procrustes analysis. This model captures morphological variations in growth and can predict bone geometry with errors of 3.6 ± 1.3 mm using demographic information and five linear bone dimensions.

Introduction

The skeletal anatomy of children differs significantly from adults, yet we often scale down musculoskeletal models that have been developed from adult datasets. Subject-specific models can be built using medical imaging [1], but this is costly and time-consuming. Ideally, we would scale musculoskeletal models using a population of paediatric bones that capture morphological variation of the growing skeleton. The aims of this study were to: 1) characterise bone shape variation in a typically developed paediatric population and 2) evaluate bone shape prediction error using a SSM.

Methods

Post-mortem CT scans of 333 children (137 F, Age: 12 ± 5 Y, H: 148 ± 24 cm, M: 49 ± 22 kg) were obtained from the Victorian Institute of Forensic Medicine (VIFM, Melbourne, Australia). The pelvis (P), sacrum, femurs (F), tibiae, and fibulae were segmented using Mimics (Materialise, Leuven, BE) and a convolutional neural network. Bones were aligned according to the ISB coordinate system [2]. Right bones for the femur, tibia, and fibula were mirrored to the left side and the tibia and fibula (TF) were considered as a single bone. Each bone was non-rigidly registered and fitted to a template mesh, using radial basis functions to achieve nodal correspondence, and then rigidly aligned. The shape model was characterized using PCA [3]. A Procrustes analysis was performed to characterize the shape variation within the dataset by performing PCA on bones scaled to the size of the mean bone. The accuracy of the shape model was assessed using fitting error, compactness, specificity, and generality. The predictive power of the shape model was assessed with a leave one out (LOO) analysis using demographic (age, height, mass, sex) and bone measurements (thigh and shank length, hip, knee, and ankle width).

Results and Discussion

The first PC of the general shape model captured most of the variation in the dataset (F: 98%, TF: 97%, P: 91%). This was reduced using the Procrustes analysis (first 9 PC's F: 66%, TF: 74%, P: 74%), where the first PC shows the changes in bone shape within the dataset (Figure 1). The results from the LOO analysis gave average RMSE of 5.6mm (F: 6.1 ± 3.3 mm, TF: 5.5 ± 2.8 , P: 5.1 ± 2.1 mm) using demographic

measurements, which was reduced to 4.32mm (F: 4.5 ± 2.1 mm, TF: 4 ± 1.8 mm, P: 4.4 ± 1.6 mm) when linear bone measurements were included. Results from the femur show that first scaling the bones by length reduces this error to 3.6 ± 1.3 mm.

Conclusions

This unique dataset characterises morphological variation in paediatric bone and allows for prediction of new bone shapes with low errors for use in clinical settings and musculoskeletal modelling. Future work will assess the best method of bone prediction for the remaining bones (tibfib, pelvis, and sacrum) by calculating errors in LOO analyses.

Acknowledgments

Data from the VIFM made this research possible. This research is funded by the University of Auckland doctoral scholarship and the Health Research Council of NZ emerging researcher first Grant.

References

- [1] Scheys L et al. (2011). *Gait Posture*, **33**: 158-164
- [2] Wu G et al. (2002). *J. Biomech.*, **35**: 543-548
- [3] Zhang J et al. (2016). *Med. Eng. Phys.*, **38**: 450-457

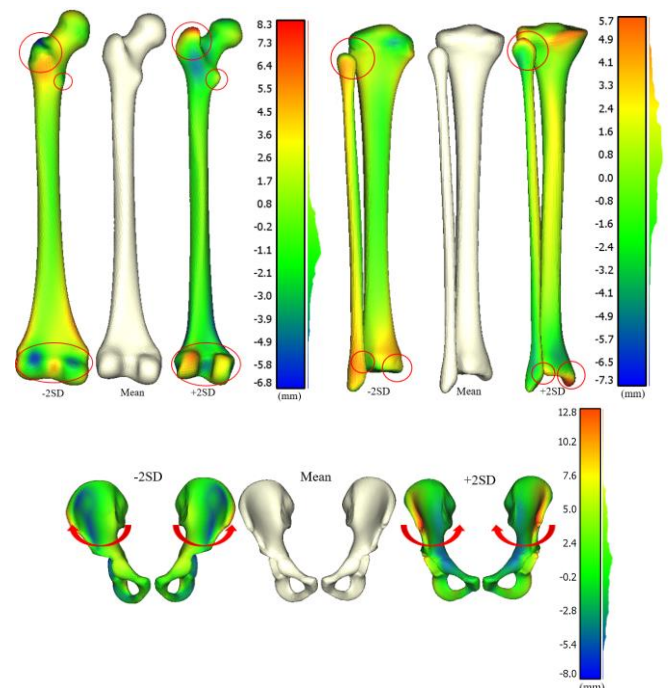


Figure 1: First principal component of the Procrustes analysis. Top left: femur, top right: tibia/fibula, and bottom: pelvis. Represented as the mean shape in cream and -2SD/+2SD to the left and right. Point distances from the mean shape are represented as displayed on the corresponding colour bars.

A Semi-automated Method for Quantifying Total Hip Arthroplasty Related Acetabular Bone Loss from CT scans: Lesion Volume Measurement Accuracy and Overall Method Reliability

Thomas M. Grace¹, Dermot O'Rourke², Thomas Robertson^{1,3}, Egon Perilli², Stuart Callary^{1,3}, Mark Taylor², Gerald J. Atkins¹, Lucian B. Solomon^{1,3} and Dominic Thewlis¹

¹Centre for Orthopaedic & Trauma Research, University of Adelaide, Adelaide, SA, Australia

²Medical Device Research Institute, College of Science and Engineering, Flinders University, Adelaide, SA, Australia

³Department of Orthopaedics and Trauma, Royal Adelaide Hospital, Adelaide, SA, Australia

Email: thomas.grace@adelaide.edu.a

Summary: Periprosthetic osteolysis remains a serious complication of joint replacement surgery and can lead to revision surgery. Accurate assessment of bone loss after total hip arthroplasty (THA) has the potential to assist with surgical planning and decision making. However, it is difficult due to the complex morphology of the hip joint and the presence of a metallic implants decreasing CT image clarity. This study describes a semi-automated method to extract this from pelvic computed tomography (CT) scans. Ex vivo accuracy and reliability tests of lesion volume measurement were performed. Accuracy and reliability were found to be sufficient (all mean absolute relative error (MARE) below 10% and all coefficient of variation (CoV) below 10% for accuracy and reliability respectively). This new method is accurate and reliable and may be of use when studying acetabular periprosthetic bone loss.

Introduction: Implant loosening and periprosthetic fracture are two of the most common causes of THA failure and are associated with acetabular bone loss [1]. High sensitivity and specificity when identifying and monitoring such defects from CT scans are of diagnostic and surgical importance [2]. It is also necessary to measure bone loss within specific three-dimensional (3D) acetabular regions of interest (ROI) [3]. However, there is no established method to achieve this. The primary aim of this study was to develop a semi-automated method for measuring lesion volume and the BMD distribution in the acetabulum. Our secondary aim was to test the accuracy of lesion volume measurements and to test the reliability of the method.

Methods: CT scans (0.8 mm pixel size, 1 mm slice thickness) were taken of cadavers with varying numbers of implants *in situ* (as metal implants reduce CT clarity) for the accuracy and reliability tests (four cadavers with one and then two implants and one cadaver with the native anatomy, one implant and two implants respectively). For each cadaver, a physical lesion was created prior to insertion of the first implant. For the accuracy tests, large-volume micro-CT scans were employed as a reference.

Points around the acetabular rim and the Anterior Superior Iliac Crest and the Pubic Tubercle anterior landmarks were located manually on the 3D reconstruction of the CT and exported as coordinates (nms Builder). The 3D model and landmarks were inputted into custom written code (MATLAB), which applied an acetabular sphere fit via the Pratt method using the acetabular rim coordinates and a local patient-specific coordinate system based on the center of the sphere and the anterior landmark coordinates. The sphere radius was increased by 40%, then the sphere was split into

thirds and the containing areas exported. Regions were overlaid over the original CT image and segmented to determine lesion volume in mm³ and BMD in Hounsfield units (HU), (Fig. 1).

To test accuracy, lesion volume was measured five times per CT scan (two per cadaver, ten in total) and the MARE between the CT measurements and reference values was calculated. The intra- and inter- operator reliability (three repeats and two repeats respectively) was tested for lesion volume, HU and ROI volume and reported as the CoV.

Results and Discussion: For the accuracy tests, all MARE values were less than 10% for lesion volume measurement. For the intra- and inter-operator reliability tests, all CoV values were less than 10%.

Accuracy and reliability of quantifying lesion volume decreased with increasing number of implants by 0.6% - 3.6% MARE and 1.6% - 2.6% CoV respectively, as did the reliability of BMD measurements in the region most disrupted by metal artefacts (2% - 2.9% decrease in CoV).

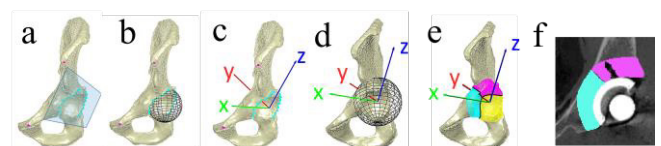


Figure 1: Splitting the acetabulum into three ROI to measure bone loss: a. Acetabular plane b. Acetabular sphere c. Acetabular coordinate system d. Increasing sphere radius by 40% e-f. Acetabulum split into ROI and overlaid over CT with lesion.

Conclusions: This study presents a new accurate and reliable semi-automated method to quantify BMD (HU) and lesion volume within 3D anatomical ROI of the human acetabulum from CT scans, which may assist towards developing of a standardized approach.

Acknowledgments: This study was supported by National Health and Medical Research Council (ID: 1126229), a research grant from Zimmer Biomet Pty Ltd (Warsaw, IN), the Royal Adelaide Hospital Research Fund and the Australian Research Council (LE180100136)

References

- [1] Fernández-Fernández R (2020). *Revision Total Joint Arthroplasty*; Springer.
- [2] Ries MD et al. (2012). *J. Bone Jt. Surg.* **94**: 2097-2105
- [3] Horas K et al. (2017). *Der Orthopäde.* **46**:168-178

Prediction of ACL tunnels: a comparison between model and surgeon.

Marco T. Schneider¹, Paul Monk¹, Alan Wang^{1,2}

¹Auckland Bioengineering Institute, The University of Auckland, Auckland, New Zealand

²Faculty of Medical and Health Sciences, The University of Auckland, Auckland, New Zealand

Email: marco.schneider@auckland.ac.nz

Summary

The outcome of ACL reconstruction is strongly related to the placement of the femoral and tibial tunnels. Patient specific anatomy affects tunnel positioning and is a challenge for low-volume surgeons. We developed a computational model that characterised the ACL attachment site in a population of 51 knees and evaluated the model with a leave-one-out (LOO) analysis. We compared the accuracy and variance of the predictions with those of an experienced orthopaedic surgeon.

Introduction

Anterior cruciate ligament (ACL) ruptures are one of the most common sport injuries in the world, with ~ 350,000 reconstructions performed annually in the US alone and 1 million performed globally [1]. Orthopaedic dogma maintains that the outcome of anterior cruciate ligament (ACL) reconstruction is dependent on accurate surgical placement of the graft. However, the procedure is technically challenging and approximately 40% of ACL grafts are misplaced as a result [2]. Patient-specific anatomy is believed to affect tunnel positioning, and improper graft tunnel placement can lead to costly premature degeneration of knee structures, eventually leading to total knee joint replacement.

This study has three aims: 1) quantify ACL attachment sites in a cohort of knees (n=51) with in-tact ACL; 2) develop a computational model to characterise the natural variation of the ACL attachment site across the cohort; 3) compare the model predictions to those of an experienced surgeon.

Methods

MR images of 51 healthy adult knees (28.4 ± 4.1 years) were obtained from a previous study [3]. The bones, including the femur and tibia, and the ACL were manually segmented to generate triangulated models. The footprints of the ACL on the femur and tibia were obtained by finding the surface of the bone that overlapped with the ACL. The centroid of each footprint was then quantified. A published method [4] was adapted to characterise the natural variation of the ACL centroids. A machine learning model was developed to predict ACL centroids. The predictive performance of the model was evaluated in a LOO analysis. An experienced surgeon

performed virtual ACL reconstructions and the distance to the ACL centroids were calculated. The accuracy was compared between model and surgeon.

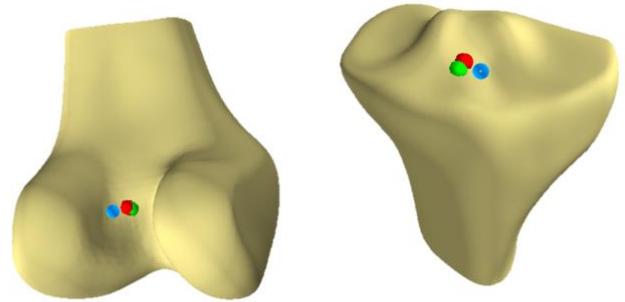


Figure 1. Model prediction (green) and surgeon's prediction (blue) compared with anatomical site (red) in one subject.

Results and Discussion

ACL attachments were quantified in our cohort of knees (n=51) and a computational model that characterised the natural variation of ACL attachment sites was developed.

Mean LOO prediction accuracy for femoral attachments was 1.89 ± 1.41 mm and 2.21 ± 1.32 mm for tibial attachments. The experienced surgeon had an accuracy of 6.69 ± 1.38 mm for the femoral attachments and 4.96 ± 2.74 mm for the tibial attachments (Table 1).

Conclusions

ACL attachment sites are dependent on bone morphology. Our computational model was more accurate and consistent at predicting the ACL tunnels than an experienced orthopaedic surgeon.

References

- [1] Mather RC et al. (2013). *J Bone Joint Surg Am*, **95**(19):1751-1759.
- [2] Trojani C et al. (2011). *Knee Surg. Sports Traumatol. Arthrosc.* **19**(2), 196-201.
- [3] Draper C et al. (2006). *Osteoarthr. Cartil.*, **14**:931-937.
- [4] Schneider et al. (2018). *Osteoarthr. Cartil.*, **26**:1338-1344.

Table 1 – Errors (in mm) in ACL attachment prediction from bone.

Predictor	Femoral tunnels					Tibial tunnels				
	Mean Error	Std.	Max Error	Min Error	RMS	Mean Error	Std.	Max Error	Min Error	RMS
LOO model	1.89	1.41	8.56	0.23	2.35	2.21	1.32	6.05	0.48467	2.57
Surgeon	6.69	1.38	8.72	4.31	6.83	4.96	2.74	9.83	1.38	5.67

The free Achilles tendon is shorter, stiffer, and thicker in trained runners compared to healthy controls

Daniel Devaprakash^{1,2}, Steven J. Obst^{1,3}, David G. Lloyd^{1,2}, Rod S. Barrett^{1,2}, Ben Kennedy¹, Kahlee L. Adams⁴, Tyler J. Collings^{1,2}, Giorgio Davico^{1,2}, Adam Hunter⁴, Nicole Vlahovich⁴, David L. Pease⁴, Claudio Pizzolato^{1,2}

¹School of Allied Health Sciences, Griffith University, QLD, Australia

²Griffith Centre of Biomedical and Rehabilitation Engineering (GCORE), Griffith University, QLD, Australia

³School of Health, Medical, and Applied Sciences, Central Queensland University, Bundaberg, Australia

⁴Movement Science, Australian Institute of Sport, Canberra, Australia

Email: d.devaprakash@griffith.edu.au

Summary

Achilles tendon structure and function are intimately coupled. We show that free Achilles tendons in trained runners were stiffer when compared to healthy controls. This was due to shorter length and larger cross-sectional area, but not increased Young's modulus, the latter having no relationship with T2* relaxation time from MRI's. Achilles tendon T2* relaxation time was significantly longer in trained runners compared to healthy controls.

Introduction

The relationship between tissue structure (i.e., geometry and mechanical properties) and function is complex, dynamic, and affected by aging, disease, and, possibly, physical activity levels. For instance, free Achilles tendon (AT) average cross-sectional area (CSA) is larger, and the Young's modulus is lower, in tendinopathic tendons when compared to healthy controls [1]. But how does AT structure vary between low and high physical activity levels? This study compared free AT geometry, mechanical properties, and T2* relaxation time between trained runners and healthy controls, and determined the relationship between T2* relaxation times and Young's moduli.

Methods

Sixteen trained runners (run > 80 km/week) (10 male, 6 female, age: 25.2±5 yrs, BMI: 20.9±1.8 kg.m⁻²) and healthy controls (11 male, 5 female, age: 30.3±4.9 yrs, BMI: 23.8±4.5 kg.m⁻²) with no prior AT injuries participated in this study. Participants refrained from strenuous physical activity prior testing. Following AT preconditioning, participants underwent magnetic resonance imaging (MRI) of their free AT using a Philips Ingenia 3.0T (T1W 3D FFE, TR/TE 8.0/4.1 ms; slice thickness 0.6 mm, slice gap 0.3 mm) [2,3]. Ultrashort echo time (UTE) T2* sequence data was acquired using a 16-channel knee coil to estimate T2* relaxation time of the free AT [3]. The free AT was then imaged using an established 3DUS method (transducer: Canon PLT-805, motion capture: Vicon). All 3DUS data were acquired with the participant lying prone and ankle locked in a neutral position during rest and three isometric loading levels (25%, 50%, and 70% maximum voluntary contraction) [3]. Ankle torque data were synchronously recorded using isometric dynamometer (Humac Norm, FUTEK).

Free AT volume, CSA, length, and moment arm were obtained from MRI data. Mechanical stiffness and Young's modulus were obtained from 3DUS and dynamometer data. ANOVA was used to compare differences in free AT

geometry (discrete measures) and mechanical properties between trained runners and controls. Kruskal-Wallis test was used to compare T2* relaxation time between the two groups. Relationship between T2* relaxation time and Young's modulus were determined using Pearson product moment correlation.

Results and Discussion

Average CSA of the free AT was significantly larger in trained runners when compared to healthy controls (p=0.009) (Figure 1). Length of the free AT was significantly shorter in trained runners when compared to healthy controls (p=0.01) (Figure 1). Trained runners had a stiffer free Achilles tendon when compared to healthy controls (p=0.003) (Figure 1). Free AT T2* relaxation time was significantly longer in trained runners compared to healthy controls. There was no significant relationship (p>0.15) between T2* relaxation time and Young's modulus indicating that T2* relaxation time cannot be used as a valid proxy for tissue material properties.

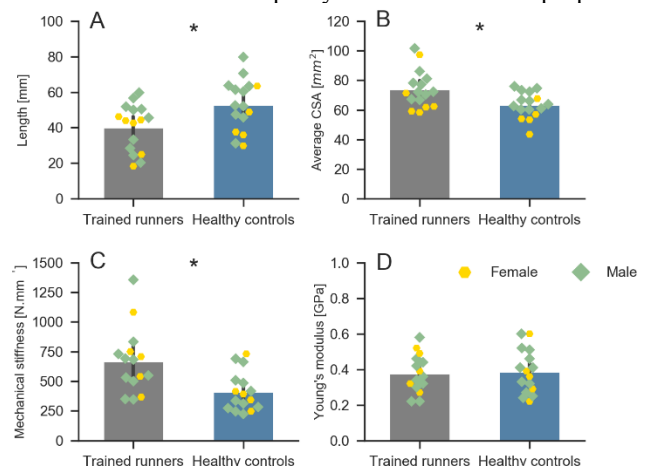


Figure 1: Length, average CSA, mechanical stiffness, and Young's modulus of trained runners and healthy controls.

Conclusions

Trained runners have a shorter, thicker, and stiffer free AT when compared to healthy controls. T2* relaxation time is not a valid proxy to assess AT material properties.

References

- [1] Arya & Kulig (2010) *J App Phys*, **108**, 670-675.
- [2] Devaprakash D et al. (2019) *Ultrasound Med Biol*, **31**, 126-135.
- [3] Devaprakash D et al. (2020) *Front. Physiol*, **11**.

The effects of decellularisation and sterilisation processing on kangaroo tendon strength

Dylan M. Ashton^{1,2}, Carina L. Blaker^{1,2}, Nicholas J. Hartnell³, Christopher B. Little^{1,4}, Elizabeth C. Clarke^{1,2}

¹Faculty of Medicine and Health, University of Sydney, Sydney, Australia

²Murray Maxwell Biomechanics Laboratory, Institute of Bone and Joint Research, Kolling Institute, Sydney, Australia

³Bone Ligament Tendon Pty Ltd (BLT),

⁴Raymond Purves Bone and Joint Research Laboratories, Institute of Bone and Joint Research, Kolling Institute, Sydney, Australia
Email: dylan.ashton@sydney.edu.au

Summary

Escalating incidences of primary and secondary ACL injuries has created substantial demand for a superior graft option for human ACL reconstruction. Kangaroo tendon, processed into an acellular tissue, has potential as a new xenograft tissue source for ACL reconstruction. The present study screened four proprietary decellularisation protocols and two doses of gamma sterilisation, assessing their effect on kangaroo tendon strength. All combinations of decellularisation and sterilisation protocols provided xenografts with higher strength compared to published values for native human ACL.

Introduction

Rupture of the anterior cruciate ligament (ACL) is one of the most common musculoskeletal injuries in humans. Surgical reconstruction requires the use of either tendon autograft (harvested from the patient), allograft (sourced from a deceased tissue donor), or synthetic construct; each with inherent limitations. These challenges are further exacerbated by increasing incidences of both primary and secondary (re-injury) ACL injury, especially in younger patients. Kangaroo tendon, processed into an acellular tissue, has potential as a new xenograft source for ACL reconstruction. A major challenge faced by loadbearing xenografts is retaining sufficient mechanical strength following necessary decellularisation and sterilisation processing. The present study screened four candidate decellularisation protocols and two doses of gamma irradiation, assessing their effect on kangaroo tendon strength.

Methods

Kangaroo tendons were processed using one of four proprietary decellularisation protocols (A-D), followed by gamma irradiation with either low (15kGy) or standard (25kGy) dose (n=8/group). Unprocessed (“*ex vivo*”), and non-irradiated (decellularised only) controls were also prepared. Biomechanical evaluation was performed by tensile loading to failure at 5% strain/s, with ultimate tensile strength normalised (%) to *ex vivo* controls. Results were analysed using mixed model regression, followed by pairwise comparisons between groups, adjusting for multiple comparisons using the Benjamini Hochberg procedure with false discovery rate of 0.05.

Results and Discussion

All four decellularisation protocols significantly reduced non-irradiated tendon strength compared to *ex vivo* controls (p<0.007). Decellularisation protocol A retained the highest

tendon strength (89.0% of *ex vivo*) compared to protocol B (64.7%, p<0.001), protocol C (76.2%, p<0.001) and protocol D (64.1%, p<0.001) in nonirradiated groups (Figure 1). Gamma irradiation further reduced tendon strength when compared to nonirradiated controls (p<0.001 both doses), however there was no main effect of irradiation dose (p=0.351 between doses).

Pairwise comparisons between, and within, decellularisation groups showed no consistent effect of decellularisation or sterilization protocol on the reduction in tendon strength (Figure 1). Significant differences observed between non-irradiated decellularisation groups were not maintained after sterilisation; with the singular exception of protocol C (62.5%) retaining significantly higher strength than protocol B (53.3%) in the low irradiation dose group only (p<0.001).

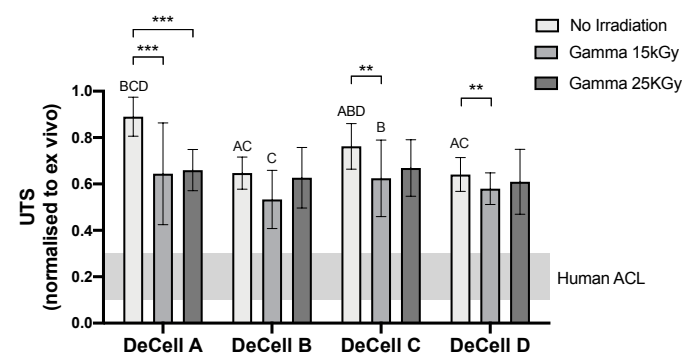


Figure 1. Effects of Decellularisation and Sterilisation Protocols on Kangaroo Xenograft Strength.

Despite processing-induced reductions, all combinations of decellularisation and sterilization protocols retained a higher strength when compared to published values for native human ACL [1,2].

Conclusions

All four decellularisation protocols and both irradiation doses provide grafts with sufficient mechanical strength and remain as viable candidate methods for future development of this novel ACL xenograft. Sufficient mechanical strength only represents one facet of a successful graft, and ongoing biocompatibility studies may highlight more imperative differences between processing protocols to direct future xenograft development.

References

- [1] Noyes FR, et al., *J Bone Jt Surg Am* **58**: 1074-1082, 1976.
- [2] Butler DL, et al., *J Biomech* **19**: 425-426, 1986

Ankle kinematics during walking with a soft exoskeleton in people with dropfoot – a case series

Eveline S. Graf, Markus Wirz, Carole Pauli, Christoph M. Bauer

Institute of Physiotherapy, School of Health Professions, Zurich University of Applied Sciences, Winterthur, Switzerland

Email: eveline.graf@zhaw.ch

Summary

The effect of XoSoft, a soft exoskeleton providing support during dorsiflexion at the ankle, was analyzed in people with drop foot. This study identifies areas of future research in order to achieve the goal of a support system at the ankle that results in high adherence.

Introduction

Dropfoot, caused by neurological conditions, is characterized by weakness of the dorsiflexor muscles at the ankle. It results in altered walking mechanics and increased risk of falling due to reduced foot-ground clearance [1]. While there are orthotic solutions available, limited comfort and wearability as well as their limited mobility result in a low adherence of patients. Consequently, a novel comfortable and dynamic solution has great potential, but its functionality must be demonstrated. The aim of this study was to assess the influence of a prototype soft exoskeleton on ankle kinematics in individuals with dropfoot during walking.

Methods

Three participants with dropfoot (2 female, 2 incomplete spinal cord injury/1 stroke, 2 with unilateral impairment) walked without support (none) and with the XoSoft prototype. A minimum of four trials were recorded and averaged. Ankle kinematics was recorded with a camera system (240 Hz, Vicon Vantage, Vicon Motion Systems Ltd.) and a cluster marker approach [2]. In agreement with the case study characteristics, data were analyzed descriptively.

The XoSoft prototype consisted of a soft, pneumatic clutch in series with an elastic band [3]. The two ends were anchored at the shoe and the shin. The clutch was active from 50 to 0 % of gait cycle. The elongation of the distance of the anchor points during push-off (clutch activated) was thought to result in elongation of the elastic band which released its energy during the swing phase, keeping the foot in a dorsiflexed position.

Results and Discussion

For all three participants, XoSoft was able to increase dorsiflexion during the swing phase; the effect was, however, small with less than 10° difference between conditions (Figure 1). Participant 2 reaches a plateau with XoSoft between 60-80% of gait cycle. It is assumed that the participant may not be able to push-off actively and, therefore, cannot elongate the dorsiflexion clutch enough. When the foot is lifted off the ground, the elastic band can maintain the foot at this position but not actively pull it up. The inertia of the foot during the swing phase may cause the

decrease in dorsiflexion in later swing. Consequently, the participant would benefit from a stiffer dorsiflexion elastic band in combination with active support of the plantarflexion during the push-off movement.

All participants (except participant 1) had a plantarflexion movement at the beginning of the gait cycle that was enabled or increased with XoSoft. Having an initial plantarflexion movement represents a more physiological pattern with heel-strike, followed by flattening of the foot. Participant 1 had a reduced active and passive range of motion in dorsiflexion. It is concluded that the elastic band was not stiff enough to maintain the ankle in dorsiflexion while landing.

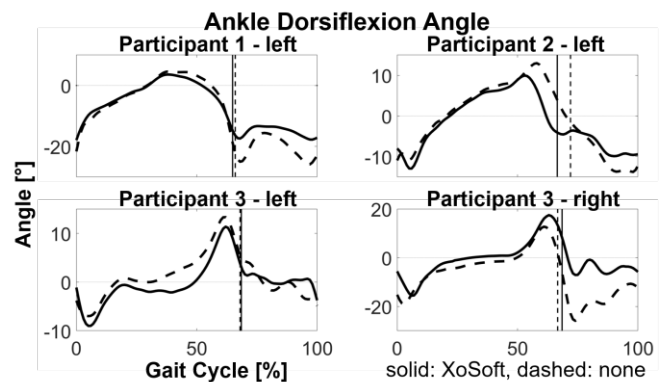


Figure 1: Ankle dorsiflexion angle [in degrees] during walking with XoSoft (solid line) and no support (dashed line) for each participant (participant 3 had bilateral actuation). Please note the difference in scale of the y-axis between figures.

Conclusions

Overall, these results indicate that XoSoft can alter gait pattern of the ankle and allow a more natural gait despite an inability of the participants to perform this movement actively. Additional research looking into actuation of the plantarflexion during push-off in combination with a fine tuning of the elastic band is necessary.

Acknowledgments

The authors would like to acknowledge the entire XoSoft consortium for their contribution during the project. This work has received funding from the European Union's Horizon 2020 research and innovation programme under grant agreement No. 688175 (XoSoft).

References

- [1] Graham J (2010). *Br J Neurosci Nurs*, **6**: 168-172.
- [2] List R et al. (2013). *J Strength Cond Res*, **27**: 1529-38.
- [3] Ortiz J et al. (2019). *Wearable Robotics: Challenges and Trends*, Springer, Cham.

Influence of assistance timing on human gait biomechanics using a semi-passive ankle exoskeleton

Mahsa Momtahan¹, Thor Besier^{1,2}, Homayoon Zarshenas¹, Bryan Ruddy^{1,2}

¹ Auckland Bioengineering Institute, The University of Auckland, Auckland, New Zealand

² Department of Engineering Science, University of Auckland, Auckland, New Zealand

Email: mmom109@aucklanduni.ac.nz

Summary

In this paper, we used a semi-passive clutched spring ankle-foot exoskeleton (Figure 1) that enables us to study different assistance onset timings on healthy individuals' gait biomechanics. The results obtained from this study suggest that controlling timing of assistance in clutched elastic ankle exoskeletons can influence the assistive performance and further improve gait efficiency.

Introduction

Previous studies have shown that incorporating clutches and elastic elements in parallel with the ankle muscles can offload substantial muscle force and therefore reduce the metabolic cost of walking [1]. However, optimal assistance timing with clutched elastic exoskeletons remains unclear. The purpose of this study was to evaluate the effect of different assistance onset timings on human gait mechanics and energetics by regulating the activation of a controllable clutch in an elastic ankle exoskeleton. This mechanism uses the principle of controlled energy storage and release and has been designed to optimize the functionality of a passive elastic exoskeleton.

Methods

A healthy adult (male; mass = 83.7 kg; height = 1.81 m) participated in the study and completed a series of walking trials at 1.5 m s⁻¹ on a force-instrumented treadmill. The participant read and signed a written consent prior to participation. The participant walked for 28 min (4 blocks of 7 minutes) with the device unpowered ($k_{Exo}=0$) and then with the moderate exoskeleton stiffness ($k_{Exo}=105$ N m rad⁻¹) with the clutch engaging at three angle points during early stance (P0: heel-strike, P1: foot-flat, and P2: single-support) and disengaged at the same angle during the late stance. In all trials, lower limb joint kinematics, muscle activation, and whole-body metabolic rate were measured.

Results and Discussion

We found that using a controllable clutched elastic ankle exoskeleton can improve walking economy by an average of 11.7% as compared to the unassisted walking ($k_{Exo}=0$) at 1.5 m s⁻¹ (Table 1). This suggests that the assistance provided by our semi-passive ankle exoskeleton can compensate for the

distally added mass of the device and reduce plantarflexion muscle activity (Table 1).

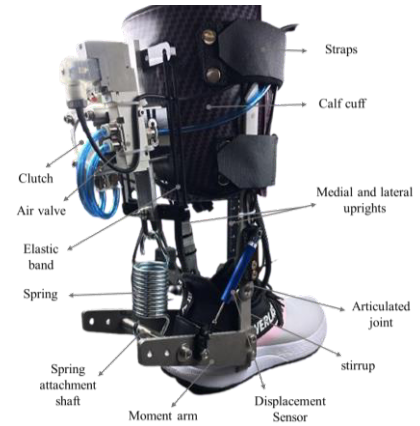


Figure 1: Semi-passive clutched spring ankle exoskeleton.

Additionally, we found that among the tested onset times, the heel-strike timing (P0) led to higher reduction (13.5%) in the metabolic rate. Further reduction in the metabolic cost and soleus muscle activation might be achieved by adjusting the spring stiffness and mass of the exoskeleton. However, since stiffness, timing and walking speed mutually influence the effect of powered walking with ankle exoskeletons, metabolically “optimal” assistance timing needs to be adjusted on a subject-by-subject basis for different walking speeds [2]. This emphasizes the importance of using a controllable clutch along with a passive elastic ankle exoskeleton to optimize assistance during human gait.

Conclusions

This study presents a first attempt to illustrate that controlling the timing of assistance in passive elastic ankle exoskeletons can influence the assistive performance of a compliant ankle exoskeleton on human gait biomechanics.

References

- [1] Collins, S. H., Wiggin, M. B., & Sawicki, G. S. (2015). *Nature*, 522(7555), 212-215.
- [2] Galle, S., Malcolm, P., Collins, S. H., & De Clercq, D. (2017). *Journal of neuroengineering and rehabilitation*, 14(1), 1-16.

Table 1: Change in net metabolic rate and soleus activation with the moderate exoskeleton stiffness at 1.5 ms⁻¹ for three assistance timings.

	P0: heel-strike	P1: foot-flat	P2: single-support
Reduction in net metabolic rate (% unpowered)	13.5	9.6	12.2
Reduction in peak soleus activation (% unpowered)	29.3	12.0	20.1

Does maintenance of whole-body balance take primacy over synchronization of footfalls to auditory beats during rhythm perturbed walking?

Deepak K Ravi, William R Taylor, Navrag B Singh

Laboratory for Movement Biomechanics, Institute for Biomechanics, ETH Zürich, Switzerland

Email: deepak.ravi@hest.ethz.ch

Summary

Towards understanding resilience in walking behavior, this study aimed to investigate the relationships between footfall rhythmicity, auditory perturbations, and dynamic stability. To achieve this, novel techniques for the quantification of resilience were applied after young adults were subjected to a beat delayed perturbation in a metronome sequence.

Introduction

Impaired regulation of rhythmic walking patterns results in either random or stereotypical behavior that limits one's ability to adapt to perturbations, as observed in individuals with an increased risk of falling. To investigate and identify subtle impairments in rhythmicity, one proposed approach has been to exploit the sensorimotor synchronization paradigm, which evaluates a subject's ability to match the rhythmic oscillations of a limb with an external (often auditory) stimulus, including infrequent temporal perturbations (where beats are presented earlier or later than expected). In synchronizing to rhythm-perturbed metronome beats, the maintenance of stable whole-body (center of mass, CoM) movement patterns can directly influence the timing of footfall correction response to the perturbation [1]. Importantly, the inverse effect of footfall perturbations on the dynamic stability of walking remains unaddressed, hence overlooking the critical aspect inherent in this paradigm for understanding an individual's resilience to falling.

Methods

Twenty healthy young adults (13 males and 7 females; with mean age: 24.90 (standard deviation: 2.29) years; height: 1.76 (0.07) m; mass: 72.66 (6.33) kg) participated in this study. Participants performed three walking trials: baseline walking 1 (BW1), paced walking (PW) and baseline walking 2 (BW2), each 6 minutes in duration, at self-selected walking speed. The inter beat intervals (IBIs) of an auditory metronome (0.1s of the note A, sine wave with frequency 440Hz) were matched to the mean step time evaluated from BW1. The created track was adjusted by embedding 5 perturbation intervals, increased by 20x the standard deviation of the step time, introduced around 3 minutes of the track (Figure 1A). Participants completed PW listening to the metronome track at their previously selected walking speed. They were explicitly instructed to step in time to the metronome beats while maintaining a natural walking pattern. The vertical displacement time series of the sacrum marker (used as a simple approximation of the body CoM) was used to assess the recovery of whole-body balance to steady-state patterns after a perturbation (Figure 1B and 1C, [2]). Recovery of footfall synchrony to pre-perturbation limits was evaluated

using the approach presented by Bank, Roerdink [3] and compared to the former.

Results and Discussion

Of the 20 participants recruited for the study, 5 did not show qualitative evidence of effects of perturbation to sacrum kinematics. For the remaining 15 participants, average time between start of the perturbed cues and recovery of CoM kinematics was 11.45 (8.80) sec and similarly to recovery of footfall synchrony was 9.34 (2.39) sec. Here, 8 participants recovered the CoM kinematics ahead of the recovery of footfall synchrony (effect size = -0.31, Figure 1D).

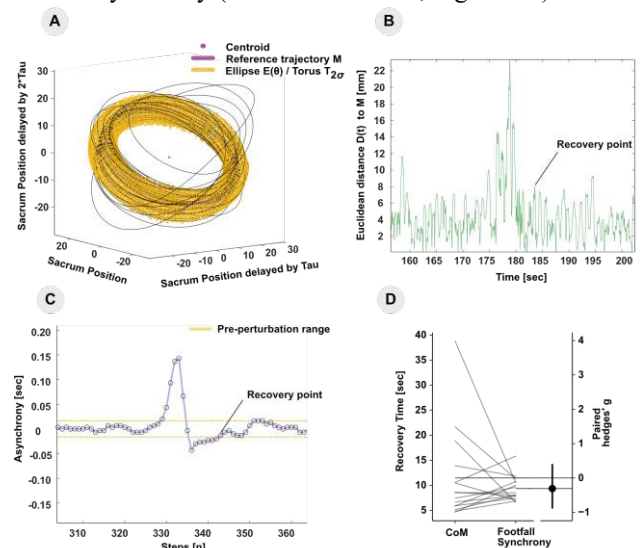


Figure 1: A. Resilience Quantification; B. Recovery of CoM to steady-state patterns; C. Recovery of footfall synchrony; D. Comparison of recovery times

Conclusions

The ability to reliably measure recovery of movement behavior thus clearly provided an improved understanding of the relationships between task level synchronization outcomes (i.e. number of walking steps to return to footfall synchrony) and dynamic stability of walking (i.e. number of walking steps to return to steady state COM kinematics). Future research could attempt to delineate such relationships in balance impaired older adults subjected to rhythmic auditory stimulation.

References

1. Wright R.L. et al. (2014). *Front. Hum. Neurosci.*, 8.
2. Ravi D.K. et al. (2021). *J. Exp. Biol*, Accepted.
3. Bank P.J. et al. (2011) *Exp. Brain. Res.*, 209: 159-69.

Real-time joint kinematics estimation in tele-rehabilitation

Marco Caruso^{1,3}, Andrea Zedda², Elisa Gusai², Stefano Bertuletti³, Salvatore Spanu², Andrea Pibiri⁴, Marco Monticone⁴, Danilo Pani², Andrea Cereatti^{1,3}

¹ Polito^{BIO}Med Lab and Department of Electronics and Telecommunications, Politecnico di Torino, Torino, Italy

²Electrical and Electronic Engineering Department (DIEE), University of Cagliari, Cagliari, Italy

³Biomedical Sciences Department, University of Sassari, Sassari, Italy.

⁴Department of Medical Sciences and Public Health, University of Cagliari, Cagliari, Italy.

Email: marco.caruso@polito.it

Summary

Telerehabilitation can promote innovation in the definition of optimal rehabilitation pathway by treating chronic patients at home. In this perspective, DoMoMEA project aimed at developing a tele-rehabilitation system based on multiple inertial sensors specifically designed for neuro-muscular rehabilitation for stroke patients. In this specific study, the algorithms for real-time joint kinematics estimates and evaluation are presented. For each task, and each joint, a quantitative assessment of the movement quality is obtained and relevant feedbacks are provided to the patients for guide and correction.

Introduction

Rehabilitation is fundamental for stroke survivors to relearn motor skills and to compensate for residual abilities. In this context, home-based telerehabilitation adopting low-cost wearable technology can be used to provide rehabilitation services, overcoming geographical barriers, and allowing to implement personalized rehabilitation pathways. The aim of this work is to present, within the framework of the research project DoMoMEA, the methods developed for real-time multi-joint kinematic estimation based on the use of seven miniaturized inertial sensors (IMUs).

Methods

The protocol consists of 14 planar exercises involving the main joints of upper and lower limbs aimed at recovering joint angular excursions, stability, and muscle strength. Each body segment of interest is equipped with a IMU aligned along the longitudinal axis thereby avoiding the need for functional movements [1], thus minimizing the patient's effort. The accelerometer and gyroscope data are fused to estimate the IMU orientation by using the filter described in [2], [3]. The orientation is estimated without the magnetometer to prevent any corruptions due to ferromagnetic disturbances (very likely in a domestic environment). The orientation computed by each IMU is then transmitted to an Android device at 50 Hz. At the beginning, the patient is asked to maintain the neutral standing posture for 10 s to allow the skeleton calibration by exploiting gravity direction. This ensures the kinematics to be less dependent on IMU positioning. The resulting joint kinematics is then decomposed into the triplet of Euler angles according to the ISB conventions, one of which represents the joint angle of interest. The amplitude of the secondary rotations is used to quantify undesired compensatory movements. A visual real-time feedback is provided to the

patient to support the correct execution of the rehabilitation protocol (e.g., during elbow flexion-extension the forearm pronation-supination is monitored). The joint kinematics is used to animate the exergaming and to quantitatively evaluate the execution performance by counting the repetitions and computing the range of motion and the repetition time in both ascending and descending parts (identified through the derivative of the joint angle).

Results and Discussion

Figure 1 shows, as example, the elbow angle and the feedback. Table 1 shows the range of motion (ROM) and the repetition time averaged over 10 repetitions during a shoulder ab-adduction exercise executed at three different amplitudes.

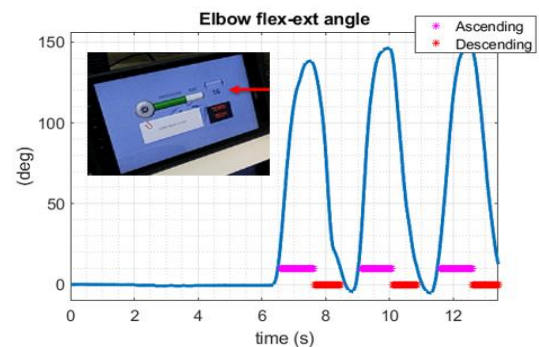


Figure 1: elbow flexion-extension angle from which it is possible to compute the ascending/descending parts.

Table 1: ROM and execution time for a shoulder ab-adduction exercise repeated at three increasing amplitudes (columns).

ROM (deg)	52.7 ± 2.8	70.7 ± 3.4	100.6 ± 4.5
Time (s)	1.25 ± 0.06	1.41 ± 0.06	1.77 ± 0.09

Conclusions

The use of a scalable IMU network represents a promising solution for real-time motion capture and assessment in tele-rehabilitation applications.

Acknowledgments

The DoMoMEA Project is funded by Sardegna Ricerche with POR FESR 2014/2020 funds, Priority Axis I "Scientific Research, Technological Development and Innovation".

References

- [1] Cereatti et al. (2015). *IEEE ISISS*: 1-4.
- [2] Madgwick et al. (2011) *ICORR*.
- [3] Caruso et al. (2020). *IEEE Sensors*, **21**: 3408 - 3419

The influence of a fatiguing wheelchair propulsion protocol on the neuromuscular activation of five shoulder muscles

Minder U¹, Arnet U², Müller E¹, Boninger M⁴, Bossuyt FM^{2,3}

¹Department of Sport and Exercise Science, University of Salzburg, Austria

²Shoulder Health and Mobility Group, Swiss Paraplegic Research Nottwil, Switzerland

³Human Performance Lab, Faculty of Kinesiology, University of Calgary, Canada

⁴University of Pittsburgh, Pittsburgh, USA

Email: ursina.minder@hotmail.com

Summary

In order to better understand the influence of fatigue measured on a muscular level on the development of shoulder pain in paraplegic wheelchair users, this study investigated changes in the root mean square (RMS) of the electromyography (EMG) signal of five shoulder muscles during a wheelchair propulsion fatigue protocol. Fatigue was demonstrated in the pectoralis major pars sternalis and upper trapezius with a significant increase in the RMS after the demanding sections of the protocol and a decrease after the recovery times.

Introduction

Shoulder pain is common in persons with spinal cord injury (SCI) [1] and has been associated with wheelchair use. Previous studies investigated fatiguing propulsion with an overground protocol and identified compensation strategies that could impact the development of shoulder injury and pain [2]. In addition, neuromuscular fatigue was identified as a possible cause for shoulder injury in overhead athletes [3]. To further investigate fatigue's contribution to shoulder pain in wheelchair users with SCI, the aim of this study was to determine changes in neuromuscular activation during the fatiguing task itself and thereby validate the previously used figure 8 fatigue protocol [4].

Methods

Wheelchair users with paraplegia (n = 43, age = 50.2±10.1 years, body weight = 72.1±13.3 kg, time since injury = 27.1±11.6 years) completed a fatigue protocol introduced by Collinger et al. [4]. The fatigue protocol consists of 3 repetitions of 4 minutes maximum voluntary propulsion along an 8-shaped course with 90 seconds of rest between the repetitions. Every lap includes a right and left turn and two full stops at the crossing point. The surface EMG signal (Telemyo 2400T DTS, 305 Noraxon, Inc. USA) of the biceps brachii, pectoralis major pars sternalis, deltoideus pars acromialis, lower and upper trapezius of the non-dominant shoulder was recorded, offset corrected, rectified, filtered with a high pass (20Hz) and low pass (3Hz) 3rd order Butterworth filter. The generated linear envelope was used to calculate the RMS. RMS means were normalised to the starting RMS value. A one-way repeated measure ANOVA was used to analyse changes in the dependent variable RMS over time ($\alpha=0.05$).

Results and Discussion

The results demonstrated a significant increase in %RMS of the pectoralis major and the upper trapezius throughout the fatigue protocol (resp. $p < .01$, partial $\eta^2 = .18$; $p < .001$, partial $\eta^2 = .19$) (Figure 1).

The RMS of these two muscles showed the expected increases at the end of the demanding parts of the protocol (240s, 570s and 900s) demonstrating a shift in the power of the EMG signal indicating fatigue. Exercise programs targeting the trapezius and pectoralis major may have a role in preventing fatigue related injury [5, 6].

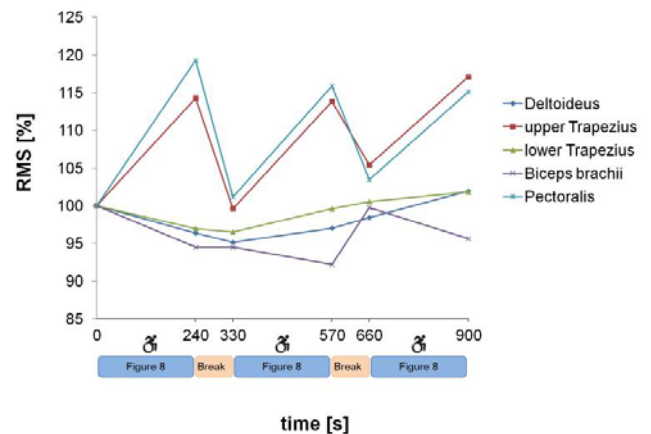


Figure 1: Mean of root mean square (RMS) in percentage of the start RMS of the EMG signal of all five muscles measured during the figure 8 fatigue protocol.

Conclusions

The detected changes in RMS of the upper trapezius and pectoralis major support the protocol introduced by Collinger et al. [4] as an adequate choice to evaluate the effect of wheelchair propulsion induced fatigue in wheelchair users with paraplegia. Furthermore, these findings support strategies to prevent shoulder pain and injury in wheelchair users with paraplegia including strengthening of these muscles.

Acknowledgments

This study was financed in the framework of the Swiss Spinal Cord Injury Cohort Study supported by the Swiss Paraplegic Foundation.

References

- [1] Bossuyt FM et al. (2018). *Disability and rehabilitation*, **40**(7): 798-805.
- [2] Bossuyt FM et al. (2020). *American Journal of Physical Medicine & Rehabilitation*. **99**(2): 91-98.
- [3] Joshi M et al. (2011). *National Athletic Trainers' Association*. **46**(4):349-57
- [4] Collinger JL et al. (2010). *PM&R*. **2**(10): 920-925.
- [5] van Straaten MG et al. (2014). *Archives of physical medicine and rehabilitation*. **95**(10): 1810-1817.
- [6] Mulroy SJ et al. (2015) *Physical therapy*. **95**(7): 1027-1038

An exploration of the motor unit behaviour during squatting tasks performed at different speeds

E. Orantes-Gonzalez¹, J. Heredia-Jimenez^{2,1}, J. Richards³, G. Chapman³, S. Lindley⁴

¹Human Behavior and Motion Analysis Lab (Hubema Lab). University of Granada. Ceuta, Spain.

²Dpt. Physical Education and Sport. Faculty of Education, Economy and Technology. University of Granada. Ceuta, Spain.

³Allied Health Research unit, University of Central Lancashire, UK

⁴Delsys Europe, Manchester, UK

Email: maevor@ugr.es

Summary

Squatting is a closed chain kinetic exercise frequently performed in activities of daily living and sporting tasks. The decomposition of EMG signals can give specific information on motor unit behaviour during muscle contractions. In this study we analysed the motor unit firing rates from vastus medialis and vastus lateralis using dEMG sensors during a double limb squat at 15 and 25 repetitions per minute (RPM). Twenty-two healthy adults were tested. The faster speed produced an increase in the firing rate during the eccentric phase. These results indicate the importance of movement speed and contraction phase on motor unit recruitment.

Introduction

Squats are often recommended for strength training [1] or rehabilitation exercises [2], however the influence of the speed that the task is performed at on muscle recruitment is still unknown. The use of surface EMG decomposition (dEMG) to describe motor unit behaviour within muscles has previously been restricted to isometric tasks [3], however this has been recently reported during cyclic dynamic contractions [4]. The aim of this study was to explore the motor unit firing rates in the vastus lateralis (VL) and medialis (VM) in the concentric and eccentric phases during a double limb squat at 15 and 25 RPM to gain more insights into the motor control demands.

Methods

Twenty-two healthy adults (10 females and 12 males) volunteered and participated in this study. The average (standard deviation) age was 31.2 (6) years, height 1.78 (0.10) m and weight 78.4 (14.6) kg. Surface EMG signals were recorded at a frequency of 2222 Hz using two four-channel dEMG Trigno Galileo wireless sensors (Delsys Inc., Boston, USA). The dEMG sensors were attached to the skin using hypoallergenic double-sided tape over the VM and VL of the dominant leg of each participant. An additional two IMUs sensors (Trigno Avanti, Delsys Inc., Boston, USA) were attached to the skin on the thigh to record angular velocity sampling at 148Hz.

From an upright standing position, participants completed double leg squats flexing their knees to 90° at two different speed conditions, 15 and 25 RPM, for 45 seconds per trial. NeuroMap software v.1.1.0 (Delsys Inc., Boston, USA) was

used to decompose the EMG signals from VM and VL into their constituent motor units. Motor units over an 80% accuracy threshold were then combined with the segment angular velocity data and imported into Visual 3D. The mean, maximum, and tertiles (upper, middle and lower) of the firing rates were then calculated for the different speeds during the eccentric and concentric phases. A 2-factor repeated measures ANOVA was used to examine differences in the two squat speeds and contraction phases. Any interactions between speed and phase were further explored using post hoc paired t-tests. The statistical significance level was set to $p < 0.05$.

Results and Discussion

The repeated measures ANOVA showed significantly higher firing rates during the concentric phase, with VM having higher firing rates than VL (Figure 1). However, significant interactions were seen between speed and phase (see Figure 1). Post hoc tests revealed significant differences between speeds in VM for the maximum firing rate ($p=0.01$), upper and mid tertials all in the eccentric phase only. For VL significant differences were seen between speeds in the maximum ($p=0.02$) and lower tertial ($p=0.04$) firing rates, and a trend towards significance was seen in the mid tertial ($p=0.05$) firing rates, again these differences were only seen in the eccentric phase, Table 1.

Conclusions

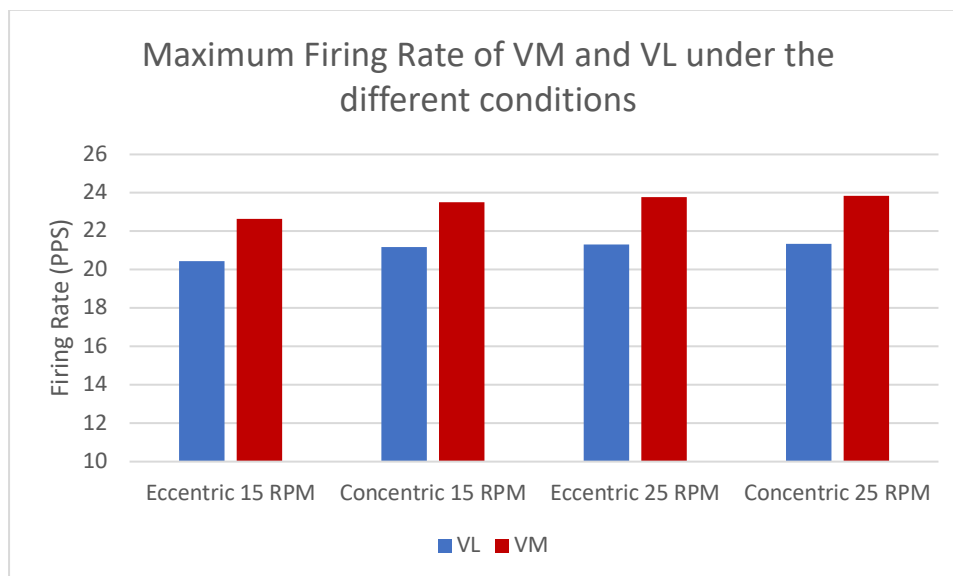
This study showed that faster speeds produce an increase in the motor unit firing rates in the VM and VL during the eccentric phase only. This highlights the previously unreported effects of movement speed and phase during squatting in healthy adults, and provides insights into the differences in motor unit behaviour when performing closed chain kinetic exercises.

References

- [1] Wu et al. (2019). *J Sports Med Phys Fitness*, **37**: 240-45.
- [2] Stephen. (2020). *Designing a rehabilitation*; Springer.
- [3] Nawab (2010). *Clin Neuroph*, **121**: 1602:15
- [4] De Luca et al. (2015). *J Neurophysiol*, **113**:6, 1941-1951

Table 1: Mean (SD) for motor unit behaviour for Vastus Lateralis (VL) and Medialis (VM). *: differences between speeds (15 RPM and 25 RPM); ^: differences between contraction phases (eccentric and concentric).

Variables	Squat 15 RPM		Squat 25 RPM		
	Eccentric	Concentric	Eccentric	Concentric	
VL	Upper Tertial (pps)	18.29 (3.6)	19.33 (3.9)^	19.01 (3.2)	19.17 (3.6)
	Middle Tertial (pps)	14.07 (3.4)	15.36 (3.7)^	14.96 (2.6)	15.31 (2.8)
	Lower Tertial (pps)	7.99 (2.1)	9.27 (2.5)^	8.69 (1.9)*	9.17 (1.9)^
VM	Upper Tertial (pps)	20.40 (4)	21.52 (4.2)^	21.46 (3.6)*	21.56 (3.7)
	Middle Tertial (pps)	15.40 (3.6)	16.95 (3.3)^	16.59 (3.1)*	16.75 (3.2)
	Lower Tertial (pps)	8.51 (3)	9.99 (2.6)^	8.97 (2.3)	9.21 (1.8)
	Angular velocity (°/s)	64 (20.2)	66.3 (17)	96.1 (20.5)	100.2 (18.1)



Altered knee mechanics during weight acceptance in stair descent for athletes with anterior cruciate ligament reconstruction compared to asymptomatic athletes

Jonas L. Markström^{1,3}, Dario G. Liebermann², Lina Schelin³, Charlotte K. Häger¹

¹Department of Community Medicine and Rehabilitation, Section of Physiotherapy, Umeå University, Sweden.

²Department of Physical Therapy, Stanley Steyer School of Health Professions, Tel Aviv University, Israel.

³Umeå School of Business, Economics and Statistics, Section of Statistics, Umeå University, Sweden.

Email: jonas.markstrom@umu.se

Summary

We evaluated trunk and lower limb kinematics and kinetics in athletes treated with unilateral anterior cruciate ligament reconstruction (ACLR). These individuals were divided into three groups according to time post-ACLR, and compared to asymptomatic athletes and between legs within groups (asymmetry) during weight acceptance in stair descent. We found adaptations independent of time post-ACLR, with greater knee flexion angle and moment for both the injured and non-injured legs. This could presumably be attributed to a change of strategy needed to maintain knee control, since asymmetries were observed only at an early time post-ACLR.

Introduction

Injury of the ACL is a common and serious knee injury with both short-term and long-term physical and psychological consequences, irrespective of treatment with ACLR or only physiotherapy. The loss of mechanically sensitive receptors originally found in the ruptured ACL is believed to result in poorer knee proprioception, and a functional reorganisation of the cortex for movement compensation [1-2]. This in turn might lead to chronically adapted compensational movement strategies to increase knee control.

The current aim was to evaluate trunk and lower limb kinematics and kinetics for athletes with unilateral ACLR, in relation to time post-ACLR, compared to asymptomatic athletes and between legs within groups during the weight acceptance phase of stair descent.

Methods

Forty-nine athletes with ACLR (24.4±4.7 years) were classified into three groups according to time post-ACLR (EARLY <6 months, n=17; MID 6-18 months, n=16; LATE ≥18 months, n=16) and compared to 18 asymptomatic athletes (ATH). Data from an eight-camera motion capture system (Qualisys, 240Hz) and a force plate (Kistler, 1200Hz) installed on the first step were used to calculate sagittal plane trunk, hip, knee and ankle kinematics (angle curves) and kinetics (body-mass normalised curves of moments, powers, and vertical ground reaction force [vGRF]). Five stair descent trials per leg were collected to calculate individual mean curves used for analysis. The injured leg was compared to the non-dominant leg of ATH, and the non-injured leg was compared to the dominant leg. The weight acceptance phase was defined from initial contact on the first step of the leading leg, to toe-off of the lagging leg, and time-normalised to 101 data points. Inferential methods for curve (time-series) data were used. In detail, a linear model was used to compare each ACLR-group to ATH, while paired t-tests were used for within-group analyses. Statistical significance was evaluated with adjusted p-values, set *a priori* at 0.05. The statistical analyses were performed using R (v.3.6.1).

Results and Discussion

Between-group comparisons: For the injured leg, EARLY showed different kinematics and/or kinetics compared to ATH at the trunk, hip, knee, and ankle, while MID and LATE displayed differences primarily at the knee. Similar findings between groups were also observed for the non-injured leg. Notably, all ACL groups had greater knee flexion angles and external moments (0-100% and ~final 60-80% of weight acceptance, respectively) than ATH for both legs (Figure 1).

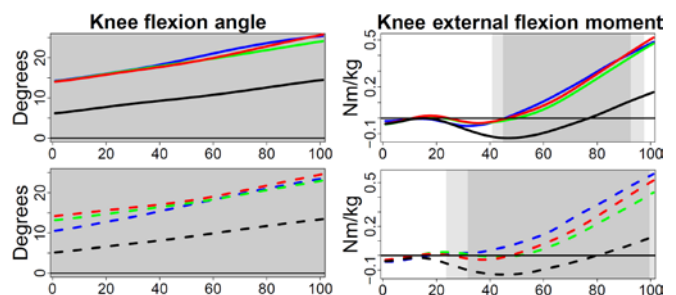


Figure 1: Group mean curves of knee angles and external moments for the injured (solid lines) and non-injured legs (dashed lines). Light and dark grey areas indicate p-values <0.05 and <0.01, respectively. Blue = EARLY, Green = MID, Red = LATE, Black = ATH.

Between-leg comparisons within groups: Asymmetry was found for EARLY, where the injured leg had greater external hip flexion moment, the ankle had greater dorsiflexion angle while the external dorsiflexion moment and negative power (absorption) were lower, accompanied by lower vGRF. For the other groups only MID displayed significant asymmetry restricted to lower negative ankle power for the injured leg.

Our results with greater knee flexion angle and moment (independent of time post-ACLR) might be an expression of a strategy to maintain knee control. This may be explained by a poorer generation of appropriate motor responses [3], resulting in a sensation of knee instability in the sagittal plane when loading a relatively extended knee at weight acceptance. The differences observed between groups, despite the lack of asymmetry, highlight the importance of including a control group when analysing movement patterns.

Conclusions

Individuals with unilateral ACLR independent of time post-ACLR (<6 months, 6-18 months, ≥18 months) show compensatory movement strategies to load the knee for both the injured and non-injured legs with greater flexion angle and moment, which may presumably be a strategy to maintain knee control, during weight acceptance in stair descent.

References

- [1] Kapreli E et al. (2009). Am J Sports Med. **37**: 2419-2426.
- [2] Grooms DR et al. (2017). JOSPT. **47**: 180-189.
- [3] Needle et al. (2017). Sports Med. **47**: 1271-1288

Variability of muscle synergies across skateboarding tricks with different levels of complexity

Lorenz Zweier¹, Florentina De Comtes¹, Lorenzo Pitto², **Hans Kainz¹**

¹Neuromechanics Research Group, Centre for Sport Science and University Sports, University of Vienna, Vienna, Austria

²Human Movement Biomechanics Research Group, KU Leuven, Leuven, Belgium

Email: hans.kainz@univie.ac.at

Summary

Muscle synergies are used to increase our insights in the motor control of the central nervous system. We compared synergies across skateboard tricks with different levels of complexity. The number of synergies were similar between the different tricks. The synergies from the least complex trick, however, were not capable to reconstruct the electromyography data of the more complex tricks in a sufficient way. Based on the findings of our study, it seems that different motor modules are required for different tricks, which might explain why it takes several years of practice before skateboarders are able to perform complex tricks.

Introduction

Muscle synergy can be used to model how the central nervous system solves the redundancy problem of the musculoskeletal system [1]. It is assumed that each synergy controls several muscles with a single activation command. Previous studies found shared synergies (muscle weightings) across different movements, e.g. walking and cycling [2], overground and beam walking [3] or pedaling with different constraints [4]. So far, no studies, evaluated if more complex movements also share the same synergies.

From a motor control perspective skateboarding is a very complex sport, which has barely been studied. It usually takes beginners weeks to months to be able to do a simple jump, the so called ‘ollie’, with the skateboard. More experienced skateboarders are able to do very complex tricks such as kickflips and 360-flips (Figure 1A).

Our aims were to (i) investigate if the number of synergies differ between skateboard tricks and (ii) evaluate if muscle synergies from a simple skateboard trick, i.e. ollie, can be used to reconstruct the muscle activation pattern from more complex tricks, i.e. kickflip and 360-flip. Considering that it usually takes many months and several years before skateboarders can do a kickflip and 360-flip, respectively, we hypothesized that (i) the number of synergies increases with the complexity of the trick and (ii) synergies from a simple ollie are insufficient to reconstruct muscle activation patterns from more complex tricks.

Methods

Three-dimensional motion capture data (Plug-in-Gait marker set, 12-camera Vicon system, Oxford, UK) and electromyography (EMG) data (Menios, Ratingen, Germany) of 16 lower limb muscles (eight on each leg) were collected from 8 healthy participants with several years of skateboarding experience. EMG data of six successful trials per trick (ollie, kickflip and 360-flip) were filtered, demeaned, time- and amplitude-normalized, and used to calculate muscle synergies using non-negative-matrix-factorization. We

calculated the total variance accounted for (tVAF) for all synergies and tricks. We chose a threshold of 90% for the tVAF to quantify the necessary synergies for each trick. To address our second hypothesis, we used an optimization in which we kept the synergy weightings from the ollie fixed and allowed the activation profile to change to optimize the fit with the EMG data of the kickflip and 360-flip [5]. Afterwards, we calculated the tVAF based on the optimized activation profile and ollie synergies and compared the results with the tVAF based on the synergies and activation profile of each trick.

Results and Discussion

In all except of one participant five or six synergies were enough to get a tVAF above 90% for all tricks. Surprisingly, the number of synergies was not significant different between tricks (Figure 1B). Synergies from the simplest trick, i.e. ollie, were not capable to reconstruct the majority of EMG signals (Figure 1C).

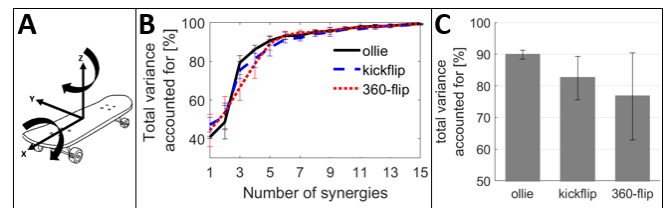


Figure 1: A: Skateboard with rotation axes. Ollie=jump without any rotation; kickflip=jump with a 360° rotation around the x-axis; 360-flip= jump with a 360° rotation around the x- and z-axis. B: tVAF (mean+/-SD over all participants) for all tricks. C: tVAF (mean+/-SD) obtained with synergy weightings from the ollie.

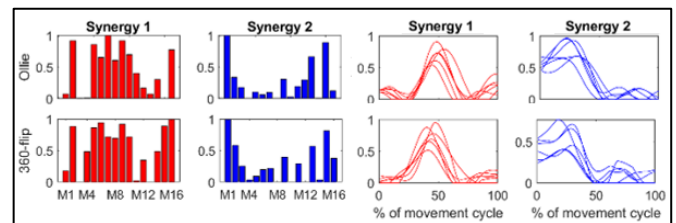


Figure 2: Example for muscle synergies (only two synergies are shown) and activation pattern for two tricks from one participant.

Conclusions

Different tricks require different motor modules, which might explain why it is so difficult and time-consuming to learn new complex movements.

References

- [1] Ting et al. (2005). *J Neurophysiol*, **93**: 609-13.
- [2] Barroso et al. (2014) *J Neurophysiol*, **112**: 1984-98.
- [3] Sawers et al. (2015) *J Neurophysiol*, **114**: 3359-73.
- [4] Hug et al. (2011) *J Neurophysiol*, **106**: 91-103.
- [5] Pitto et al. (2020) *PLoS ONE*, **15** (2): e0228851.

Corticospinal excitability during the preparatory phase of preloaded concentric and eccentric contractions

Daniel Hahn^{1,2}, Rica Gerdesmeyer¹, Brent J. Raiteri¹

¹Human Movement Science, Faculty of Sport Science, Ruhr University Bochum, Bochum, Germany

²School of Human Movement and Nutrition Sciences, University of Queensland, Brisbane, Australia

Email: daniel.hahn@rub.de

Summary

The control of eccentric contractions has been linked with neural inhibition that might already be evident prior to movement onset. Therefore, this study investigated whether corticospinal excitability as measured by motor evoked potentials differs during the preparatory phase of preloaded concentric and eccentric contractions. Our results indicate that corticospinal excitability 150-ms before movement onset is not significantly different between contraction types.

Introduction

When an active muscle is stretched during an eccentric contraction, its force capacity is enhanced (i.e., force enhancement, FE) compared with a fixed-end reference contraction at the same muscle length and activation level. As FE is commonly observed in isolated muscle preparations, but not during human voluntary eccentric contractions, absent FE *in vivo* has been suggested to arise from neural inhibition [1]. Evidence suggests that neural inhibition can exist even prior to movement onset [2], which indicates that neural inhibition might be based on movement planning rather than sensory feedback during the contraction. As the evidence for neural inhibition prior to movement onset is based on EMG and EEG activity only, the aim of this study was to investigate corticospinal excitability via transcranial magnetic stimulation (TMS) of the motor cortex. Based on the neural inhibition reported in the literature, we predicted that corticospinal excitability would be reduced in the preparatory phase of voluntary eccentric contractions.

Methods

Ten healthy participants (4 females) performed fixed-end, concentric and eccentric knee extension contractions with their right leg, while torque and EMG of the vastus lateralis (VL), vastus medialis (VM) and rectus femoris (RF) muscles were recorded. All contractions started at 60° knee flexion and were performed up until 50% of maximum voluntary torque with a 2-s ramp and 3-s hold phase. At the end of the hold phase, the crank arm of a dynamometer either remained at 60° knee flexion (fixed-end contraction) or was triggered to rotate the knee at an angular velocity of 60°·s⁻¹ either into further extension (concentric contraction) or further flexion (eccentric contraction). During the rotations, participants were asked to maintain the same level of effort as during the preceding hold phase. 150-ms prior to movement onset, participants received an electrical femoral nerve stimulation (ENS) or a TMS of their left motor cortex. The time of movement onset was marked with a cursor on a screen in front of the participants. Overall, participants performed 13 contractions of each type, with three of them involving ENS

and ten of them involving TMS. Contraction types were performed in a randomized order.

Net knee joint torque and crank arm angle were measured by an isokinetic dynamometer (IsoMed2000, D&R Ferstl GmbH, GER) and sampled at 1000 Hz. Muscle activity and neural responses to ENS and TMS were recorded from VL, VM and RF using bipolar surface EMG (AnEMG12, OT Bioelettronica, IT) and sampled at 5 kHz. ENS over the femoral nerve was delivered by 1-ms single pulses with a supramaximal stimulation intensity (DS7AH, Digitimer, UK) to evoke maximal M-waves (M_{max}). TMS (MagPro Compact, MagVenture, DK) over the left motor cortex was done using a double-cone coil (D-B80, MagVenture, DK) delivering 280- μ s single pulses with a stimulation intensity that resulted in motor evoked potentials (MEPs) of 30-50% M_{max} .

The sizes of M-waves and MEPs were determined as peak-to-peak amplitudes and responses were averaged. MEPs were normalized to M_{max} of the same contraction type. The duration of the silent period (SP) after MEPs was determined as the time from stimulation onset to the instance of time when the EMG signal reappeared. All data were checked for normality using Shapiro-Wilk tests. One-way repeated measures ANOVAs were used to compare dependent variables between different contraction types. The alpha level was set to 5%.

Results and Discussion

Torque ($p = 0.374$) and background EMG ($p > 0.305$) did not differ between contractions types during the hold phase 1-s prior to the onset of stimulation. Average normalized MEPs ranged between 36% and 49% M_{max} and MEP amplitudes were not significantly different prior to eccentric contractions compared with fixed-end and concentric contractions ($p > 0.67$). The mean durations of SPs ranged between 112-ms and 121-ms and SP durations were not significantly different between contractions types ($p > 0.397$).

Conclusions

Our results suggest that corticospinal excitability is not specifically modulated 150-ms prior to the execution of eccentric contractions in comparison with fixed-end and concentric contractions. This is in line with earlier research that found no signs of neural inhibition during voluntary eccentric contractions [3].

References

- [1] Duchateau J and Enoka RM (2016). *J. Exp. Biol.*, **219**: 197–204.
- [2] Grabiner MD and Owings TM (2002). *Exp. Brain Res.* **145**:505–511
- [3] Hahn D (2018). *J. Sport Health Sci.*, **7**: 275-281.

Muscle shortening velocities and joint-specific powers at different external power and cadence requirements during cycling

¹Cristian Riveros-Matthey, ¹ Timothy J. Carroll, ¹ Glen A. Lichtwark, ¹ Mark J. Connick

¹ The University of Queensland, School of Human Movement & Nutrition Sciences, Centre for Sensorimotor Performance, Brisbane, Australia

Email: c.riverosmatthey@uq.net.au

Summary

This study aimed to quantify the effect of cadence and external power requirements on vastus lateralis (VL) fascicle shortening velocities and joint-specific powers during cycling. VL fascicle shortening velocities and joint-specific powers were measured between 60 and 120rpm along with the self-selected cadence (SSC) at 10%, 30% and 50% of peak maximal power (Pmax). The VL shortening velocity showed a tendency to increase as cadence increase. Contrarily, joint-specific powers may be affected by the external requirement increase.

Introduction

Humans tend to locomote in ways that minimize energy consumption (1). For example, people tend to select a step frequency near that which minimizes the metabolic energy cost during submaximal walking (2). However, people do not show the same behavior in cycling tasks, where riders tend to use higher cadences than the metabolically optimal one (3). Apparently, other criteria besides energetic economy are at play in the SSC during cycling. Alternative factors that influence cadence selection might be related to mechanical advantage (4-5). Based on intrinsic contractile properties of the VL muscle, empirical measurements have demonstrated that cadences close to the SSC provide an optimal shortening velocity condition for producing knee extensor muscle power during submaximal cycling (5). However, it is still questionable whether maximization of power generation capacity remains a priority in external power requirement near to the maximal conditions. This study, therefore, aimed to quantify the effect of cadence and external power requirements on VL fascicle shortening velocities and joint-specific powers during cycling.

Methods

Ten level 3-4 cyclists were recruited for this study. Each rider used a bike ergometer (Excalibur Sport, Lode BV, Groningen, The Netherlands) adjusted according to individual anthropometric characteristics. The experimental design was conducted in two days-assessments. The first day comprised a force-velocity test, which aims to obtain the Pmax that the participant can exert during pedalling. Secondly, the self-selected cadence test will be applied aiming to establish the preferences in cadence of each participant. During the second-day assessment, cyclists pedaled at eight different cadences (ranging from 60 to 120rpm plus the SSC) at 10%, 20% and 50% of the Pmax. During the experimental protocol, the VL muscle shortening velocities were measured using double ultrasound transducers in series (LV7.5/60/96Z, TELEMED, Vilnius, Lithuania). An inverse dynamic (OpenSim) approach was run from kinematic and kinetic data to calculate joint-specific powers. Two-way ANOVA was used to test the main effects of cadences and external power requirements on muscle shortening velocities, and joint powers with an alpha of $p =$

0.05. The local ethics committee approved this study (2020000111). Also, a written informed consent was obtained from the participants.

Results and discussion

Preliminary results of two participants, indicate that VL muscle fascicle shortening velocities increase as cadence increases per intensity condition, reaching an approximate peak value between 20 and 30cm/s in both participants (see Fig. 1). Knee and hip extension powers show a tendency to increase as the external power requirements increase (Table 1).

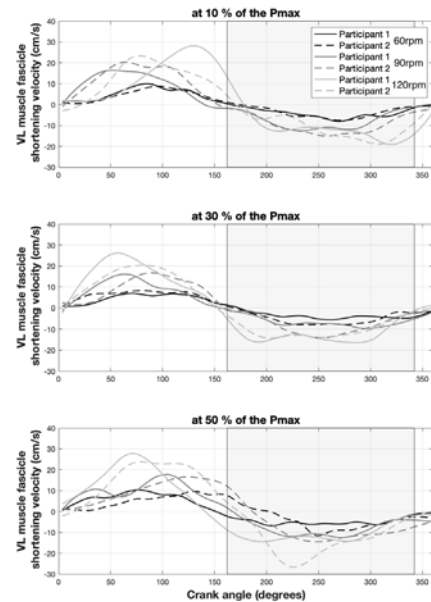


Figure 1: VL fascicle shortening velocity waveforms at 60rpm, 90rpm and 120rpm across 10%, 30% and 50% of the Pmax. The shaded area represents the knee flexion phase that was not included in the analysis. The crank angle is 0 at top-dead-center. The 70, 80, 100, 110rpm and SSC cadences are omitted for each intensity conditions for clarity.

Table 1: Mean of joint extension powers of hip and knee at 60, 90 and 120rpm at different external power requirements.

Cadence (rpm)	10% of the Pmax		30% of the Pmax		50% of the Pmax	
	Hip ext. power (W)	Knee ext. power (W)	Hip ext. power (W)	Knee ext. power (W)	Hip ext. power (W)	Knee ext. power (W)
60	9.9	32.3	12.48	69.5	49.34	91.8
90	5.6	30.7	15.23	68.8	32.96	107.7
120	16.3	29.0	28.66	68.2	45.28	99.5

Conclusions

Although the analysis is restricted to two participants, preliminary results showed that VL shortening velocity responses may be affected by cadence. Conversely, joint-specific powers would be affected by the increase of external powers requirements. The data analysis continues and the complete data set will be prepared for presentation.

References

- Alexander McN. R. (1989). *Physiol Rev.* **4**:1199–227.
- Donelan JM. (2001). *Proc Soc B Biol Sci.* **1480**:1985–92.
- Brisswalter J. (2000). *Int J Sports Med.* **1**:60–4.
- Marsh AP. (2000). *J Biomech.* **2**:173–80.
- Brennan SF. (2019). *Med Sci Sports Exerc.* **51**:941–950.

High-Speed Fluoroscopic Imaging for Investigation of 6 DOF Knee Kinematics during walking and running

Wenjin Wang¹, Tsung-Yuan Tsai², Jixin Li¹, Yaqi Zhao¹, Junjie Li¹, Fei Tian¹, Yu Liu¹, Shaobai Wang^{1,*}

¹School of Kinesiology, Shanghai University of Sport, Shanghai, China

²School of Biomedical Engineering, Shanghai Jiao Tong University, Shanghai, China

Email: wangs@innomotion.biz

Summary

Objective: To analyze six-degrees-of-freedom (6-DOF) knee kinematics before, at, and after heel strike during walking and running using high-speed fluoroscopy and magnetic resonance imaging (MRI) technique. **Methods:** Knee models were constructed from MRI scans of 10 healthy male participants. Participants walked and ran on a treadmill while fluoroscopic images were acquired. **Results:** During walking, knee extension and internal femoral rotation were higher at heel strike than before and after heel strike. At heel strike, the proximal-distal distance decreased by 0.32 mm as the knee loaded. During running, the knee flexion was higher before and after heel strike than at heel strike, and knee flexion before heel strike was higher than after heel strike, whereas the proximal-distal distance decreased by 0.22 mm as the knee loaded at heel strike. **Conclusion:** Revealed differences in 6-DOF knee kinematics during gait, providing insight into knee function and normal reference data for sports injury research.

Introduction

Walking and running are popular fitness activities with many associated health benefits [1]. However, running-related injuries, especially involving the knees, are prevalent [2]. The aim of this study was to evaluate in-vivo knee kinematic data with 6-DOF during treadmill walking and running using a combined high-speed fluoroscopic and MRI technique to reveal the differential effects of these gaits on the knee joint kinematics.

Methods

Three-dimensional (3D) knee models were constructed from MRI scans of 10 healthy adult male participants. Participants walked and ran on a treadmill while fluoroscopic images were acquired at 200 Hz; 3D knee bone models were then related to the fluoroscopic images to capture the 3D motion of the joint. Instantaneous knee kinematic characteristics were calculated at three time points: 0.05 s before heel strike, at 0.00 s relative to impact (heel strike), and 0.05 s after heel strike.

Results and Discussion

During walking, knee extension and internal femoral rotation were higher at heel strike than before and after heel strike. At heel strike, the proximal-distal distance decreased by 0.32 mm as the knee loaded. During running, the knee flexion was higher before and after heel strike than at heel strike, and knee flexion before heel strike was higher than after heel strike, whereas the proximal-distal distance decreased by 0.22 mm as the knee loaded at heel strike. Compared with walking, the knee before heel strike during running was 11.97° more flexed,

3.42° more externally rotated, and 1.00 mm more distracted. Similar differences between running and walking were observed at heel strike (9.95°, 7.85°, and 0.95 mm, respectively) and after heel strike (6.45°, 2.24°, and 0.85 mm, respectively). Posterior femoral translation at heel strike was also increased during running relative to walking.

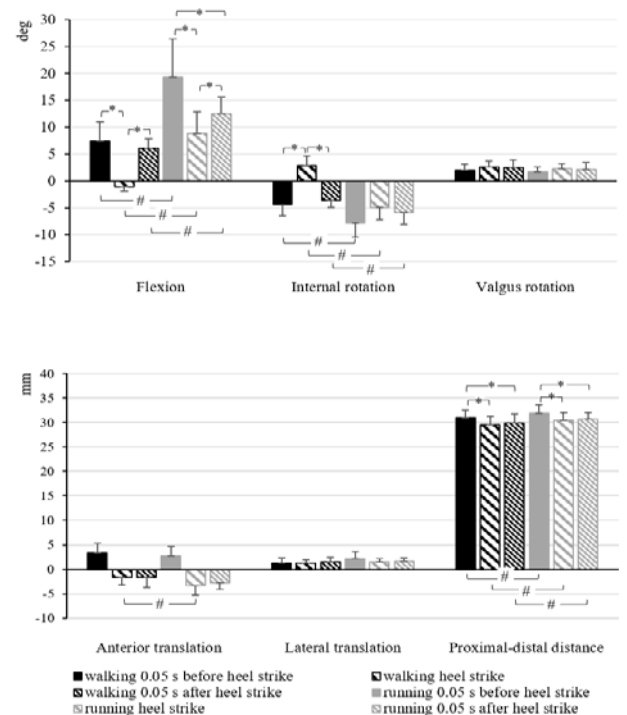


Figure 1: Kinematics changes of the knee seen 0.05 s before heel strike, at heel strike, and 0.05 s after heel strike during walking and running; * $p < 0.05$ among time points; # $p < 0.05$ walking vs. running.

Conclusions

Combined fluoroscopy-MRI derived 3D-image analysis revealed differences in 6-DOF knee kinematics between walking and running in healthy participants, providing insight into knee function and normal reference data for sports injury research.

Acknowledgments

study was supported by Natural Science Foundation of China (No. 81702211) and the National Key R&D Program of China (No. 2018YFF0300504).

References

- [1] Van Gent RN et al. (2007). *Br J Sports Med*, **41**:469-80.
- [2] Fredericson M et al. (2007). *Sports Med*, **37**:437-9.

Increased segment coordination variability of the lower limb in runners accomplishing a half marathon

Tony Lin-Wei Chen^{1,2}, Duo Wai-Chi Wong^{1,3}, Wing-Kai Lam^{2,4}, Ming Zhang^{1,3}

¹Department of Biomedical Engineering, Faculty of Engineering, Hong Kong Polytechnic University, Hong Kong SAR, China

²Li Ning Sports Science Research Center, Li Ning (China) Sports Goods Co. Ltd, Beijing, China

³Hong Kong Polytechnic University Shenzhen Research Institute, Shenzhen, China

⁴Department of Kinesiology, Shenyang Sports Institute, Shenyang, China

Email: gilbertlam@li-ning.com.cn and ming.zhang@polyu.edu.hk

Summary

Segment coordination variability (CV) indicates the degrees of fluctuations in a movement pattern and relates to injury incidence. We observed the changes in lower limb segment CVs and vertical loading rates in fifteen runners accomplishing a half marathon. Synchronized kinematic/kinetic data were collected every 2 km (from 2 km to 20 km) and processed with musculoskeletal modeling to report the outcomes. We found no alterations in loading rates across the running mileages. At early stance, the CV of pelvis frontal vs. thigh frontal was higher at 20 km than at 8 km ($p = 0.022$). The CV of shank transverse vs. rearfoot frontal increased from 2 km to 18 km and 20 km, respectively ($p < 0.001$). The unchanged loading rates could be attributed to stable CVs on the sagittal plane. The increased CVs on the frontal/transverse plane may be an early sign of fatigue and possible injury risks.

Introduction

Two adjacent body segments coordinate to produce specific movements that fulfill a locomotion task. Segment CVs measure the degrees of fluctuations in a coordination pattern. Maintaining a consistent coordination pattern, or namely a stable CV, is considered one of the knacks to avoid injuries during a prolonged run [1]. Increased CVs could be seen in fatigued runners with decreased neuromuscular control of the body and contribute to pathologies [2], despite the lack of supporting evidence.

In the study, we assessed the runners' lower limb segment CVs and vertical loading rates at different distance checkpoints of a half marathon. We hypothesized that both variables would increase as running mileage accumulated.

Methods

Fifteen experienced runners were recruited to finish a half marathon on an instrumented treadmill. The kinematic and kinetic data were collected every 2 km (from 2 km to 20 km) and processed by a musculoskeletal model. Segment CVs were computed from the angle-angle plots of selected pelvis-thigh, thigh-shank, and shank-rearfoot couplings using a modified vector coding technique. Segment CVs and vertical loading rates were averaged across ten running steps using circular and linear statistics respectively.

Results and Discussion

MANOVA reported no changes in vertical loading rates across the distance checkpoints ($p = 0.881$). CVs of the pelvis frontal vs. femur frontal during the early stance (Figure 1) were significantly increased at 20 km compared to that at 8 km ($g = 0.59$, $p = 0.022$). CVs of shank transverse vs. rearfoot frontal during early stance were higher at 18 km than at 2 km ($g = 0.05$, $p < 0.001$) and higher at 20 km than at 2 km, 4 km, and 8 km, respectively ($g = 0.36-0.66$, $p < 0.036$). The results showed that segment CVs increased on the frontal/transverse planes but not on the sagittal plane. CVs on the frontal/transverse planes were driven by small muscles and therefore possessed lower stability under fatigue [3]. Conversely, large muscle groups regulate coordination on the sagittal plane and are more robust in attenuating landing impacts during a prolonged run.

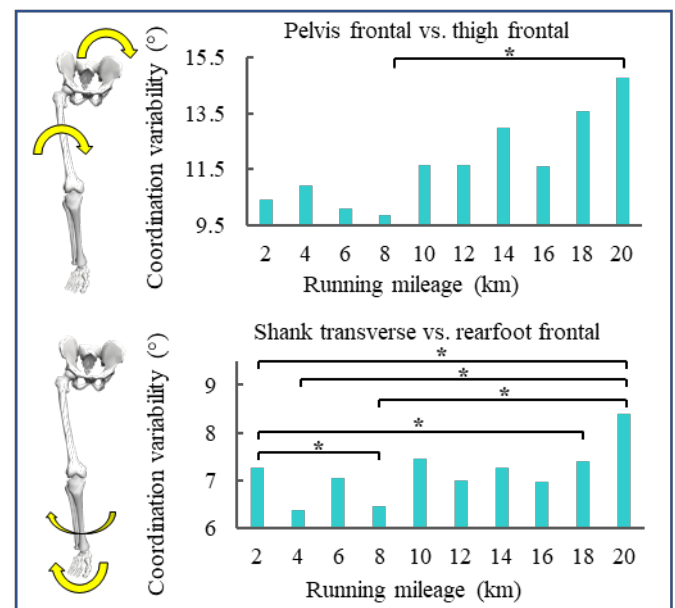


Figure 1: CVs of selected segment couplings over the course of a half marathon. * significant difference in pairwise comparisons.

Conclusions

The runners' coordination patterns were more variable on the frontal/transverse plane as the half marathon progressed, which may be related to fatigue onset and injury risks.

References

- [1] Nigg BM. (2001). *Clin J Sport Med*, **11**: 2-9.
- [2] Baida SR. (2018). *Scand J Med Sci Sports*, **28**: 1320-38.
- [3] Vishram S. (2014). *Textbook of Anatomy: Abdomen and Lower Limb*; Elsevier.

Mechanical energy transduction during running after unilateral transfemoral amputation

Hiroto Murata^{1,3}, Genki Hisano^{2,3}, Ryo Amma^{1,3}, Daisuke Ichimura³, Hiroshi Takemura¹, Hiroaki Hobara³

¹Tokyo University of Science, Chiba, Japan, ²Tokyo Institute of Technology, Tokyo, Japan

³National Institute of Advanced Industrial Science and Technology (AIST), Tokyo, Japan

Email: hiroto.murata12@gmail.com

Summary

The recovery of mechanical energy during running is important for evaluations of bouncing steps performed by spring-like leg behaviors, but little is known about energy transduction in unilateral transfemoral amputees (UTFAs) with running-specific prostheses (RSPs). Since, energy transduction can be expressed as the recovery R (%), we investigated the R at different running speeds in UTFAs. On an instrumented split-belt treadmill, 14 UTFAs ran at incremental speeds (30%, 40%, 50%, 60%, and 70% of the average speed of their 100-m personal records). At all running speeds, the R of the unaffected limb was significantly greater than that of the affected limb. These results suggest that UTFAs with RSPs perform bouncing steps using limb-specific elastic behavior.

Introduction

Running-specific prostheses (RSPs) have enabled unilateral transfemoral amputees (UTFAs) to run by partly providing a spring-like leg function in their affected limbs. When non-amputees run at a constant speed on level ground, the gravitational-potential and kinetic energy curves of the body center of mass (COM) are in phase for each step because of the elastic behavior of their lower limbs [1]. The energy transduction can be expressed as the recovery R (%); $R = 0\%$ indicates that the curves are perfectly in phase. Although the R is important for evaluating bouncing steps performed by spring-like leg behaviors, little is known about the energy transduction in UTFAs during running. This study aimed to investigate the R at different running speeds in UTFAs with RSPs.

Methods

14 UTFAs with RSPs participated in this study (age: 29 ± 10 years, height: 1.63 ± 0.08 m, mass: 59.8 ± 9.3 kg, 100-m personal records: 17.70 ± 2.83 s, mean \pm SD). Each participant ran on an instrumented split-belt treadmill (FTMH-1244WA, Tec Gihan, Kyoto, Japan) at incremental speeds of 30%, 40%, 50%, 60%, and 70% of the average speed of their 100-m personal records. The anteroposterior and vertical ground reaction forces were used to calculate the mechanical energy of the COM (E_{ap} and E_v), respectively. The total mechanical energy of the COM (E_{tot}) was the sum of E_{ap} and E_v . The negative (W_{ap}^- , W_v^- , and W_{ext}^-) and positive work (W_{ap}^+ , W_v^+ , and W_{ext}^+) per step were computed as the negative and positive increments of the E_{ap} , E_v , and E_{tot} curves, respectively [1]. Consequently, the recovery R (%) was computed as follows [2]:

$$R = 100 \frac{W_{ap}^+ + |W_{ap}^-| + W_v^+ + |W_v^-| - (W_{ext}^+ + |W_{ext}^-|)}{W_{ap}^+ + |W_{ap}^-| + W_v^+ + |W_v^-|} \quad (1)$$

We analyzed 10 consecutive steps and averaged 5 steps for the affected and unaffected limbs to determine R at all speeds.

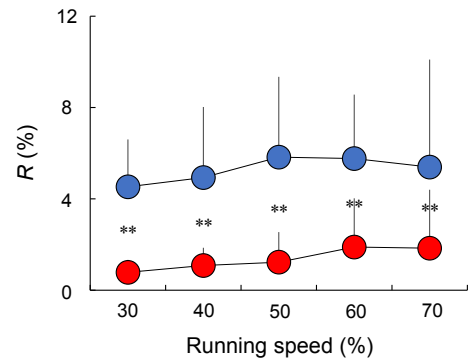


Figure 1: The recovery R of unaffected (blue) and affected (red) limbs across five running speeds. Error bars represent 1 standard deviation. The asterisks (**) indicate there are statistically significant differences ($P < 0.01$) between both limbs at each speed. Statistical significance was set to $P < 0.05$.

Results and Discussion

As shown in Figure 1, no significant main effect of speed was observed ($P = 0.70$) on the recovery R . However, there was a significant main effect of limb ($P < 0.01$), where the R of the unaffected limb was significantly greater than that of the affected limb for all running speeds ($P < 0.01$). In non-amputees, R is known to be less than 5% across a range of speeds because of the elastic behavior of the musculoskeletal system in the lower limbs during running [1]. The unaffected limb in UTFAs wearing RSPs would work similarly to non-amputee limbs because both types of limbs have the same biological structures. In contrast, the R in the affected limb was significantly smaller than that in the unaffected limb at all speeds. These results suggest that affected limbs would behave as a springy leg compared to unaffected limbs using the energy storing and restoring capabilities of RSPs [3].

Conclusions

As the recovery R shows the energy transduction for each step during running, the difference of the R in both limbs indicates that UTFAs wearing RSPs performed bouncing steps using limb-specific elastic behavior across different running speeds.

Acknowledgments

This study was partly supported by JSPS KAKENHI (Grant Number 19K11338). The authors thank Mr. Hiroyuki Sakata, Tokyo University of Science, for the initial data analysis.

References

- [1] Cavagna GA et al. (1976). *J. Physiol.*, **262**: 639-657.
- [2] Mesquita RM et al. (2020). *Eur. J. Appl. Physiol.*, **120**: 1575-1589.
- [3] Nolan L. (2008). *Foot Ankle Surg.*, **14**: 125-129.

The “spring-like” function of the subtalar joint in maintaining stability during running

Michael J. Asmussen¹, Glen Lichtwark², Jayishni Maharaj³

¹Mount Royal University, Calgary, Alberta, Canada, ²University of Queensland, Brisbane, Queensland, Australia. ³Griffith University, Gold Coast, Queensland, Australia. Email: masmussen@mtroyal.ca

Summary: We studied the mechanical and energetic function of the subtalar joint during running and how it responds to custom-made footwear that perturbs frontal plane kinematics. We found that in all footwear conditions the tissues at the subtalar joint absorbed energy in early stance and released this energy in late stance in a “spring-like” manner. We believe that this behaviour is largely attributed to the tibialis posterior (TP) tendon and may be important for maintaining mediolateral (ML) stability during gait.

Introduction: Muscles contribute to joint stabilization and are important for maintaining ML stability during locomotion. The subtalar joint allows for rotation in the frontal plane and given its proximity to the ground, excessive rotation at this joint would create instabilities during locomotion. The TP muscle has the largest moment generating capacity to control rotation of the subtalar joint [1, 2]. In fact, during walking, it has been shown that the TP stores and releases energy about the subtalar joint through stance in a “spring-like” manner by utilizing its tendon [3]. During running, when large forces are produced at high rates, it is unknown if the subtalar joint can maintain this “spring-like” function or whether it may absorb more energy than it returns, which could ultimately make a person unstable in the frontal plane (i.e., ML stability). The purpose of this study was to determine the mechanical and energetic function of the subtalar joint during running while wearing footwear that would induce kinematic perturbations in the frontal plane.

Methods: Ten participants ran on an instrumented treadmill in three footwear conditions (**Figure 1**) that were designed and 3D printed to perturb stability of the subtalar joint: **1.** supination perturbation (blue), **2.** no ML perturbation (purple), **3.** pronation perturbation (green). Motion capture (Qualisys: 29 reflective markers) were used to capture kinematics of each participant’s right leg. Intramuscular EMG was inserted into the TP muscle to determine relative muscle activation. A validated multi-segment musculoskeletal foot model was used to model joint moments and powers using inverse kinematics and dynamics, with *OpenSim*.

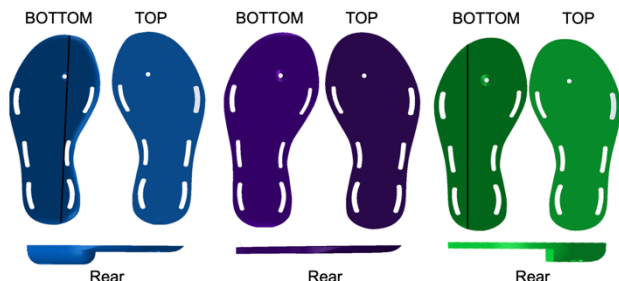


Figure 1: Shows supination 1 (blue), no ML (purple), and pronation (green) perturbation conditions. Top, bottom, and rear views of the footwear conditions are displayed. The foot is placed on the “Top”.

Results and Discussion: In the no ML perturbation condition, soft tissue structures at the subtalar joint absorbed mechanical

energy during early stance, as TP muscle activation increased. In late stance, positive power was generated about the subtalar joint, which was coupled to decreasing TP activation. Energy absorption and power generation decreased in the supination perturbation condition (condition 1, blue) and increased in the pronation perturbation condition (condition 3, green) relative to the no ML condition (see **Figure 2**). Peak subtalar joint moments, summed negative and summed positive power, and TP EMG were different across the conditions ($p < 0.05$).

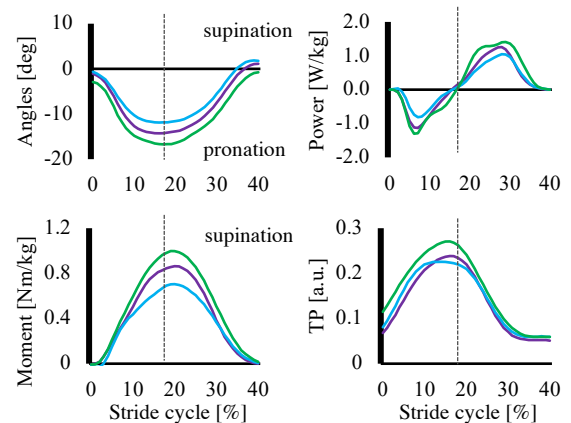


Figure 2: Shows the mean (n=10) time-series data of subtalar joint angles, moments and powers and TP EMG across Footwear conditions 1 (blue), 2 (purple), 3 (green). The dashed line marks the periods of negative (left) and positive power (right).

The negative followed by positive power phases suggest that the subtalar joint functioned in a “spring-like” manner during running. We speculate that the TP muscle and tendon contribute to the “spring-like” function of the subtalar joint, storing energy with increasing muscle activation during subtalar pronation, and releasing this energy during subtalar supination when the muscle deactivated. This resembles the function during walking [2], although energy return seems to immediately follow absorption in running. Given that the subtalar joint continued to absorb and return more energy in the pronation perturbation condition compared to absorbing more energy than it returns suggests that this “spring-like” function of the subtalar joint is important for maintaining ML stability during gait. We speculate that the TP muscle and tendon is the main source of this function, but further investigation will confirm these speculations.

Conclusions: The subtalar joint functions in a “spring-like” manner during running even in response to footwear conditions that perturbs an individual’s ML stability. We suspect that this function is driven by TP muscle and tendon.

Acknowledgments: Mount Royal University FST funds

References

- [1] Klein et al., (1996). *J. Biomch.*, **29**:21-30
- [2] Ward et al., (2009). *Clin. Ortho. Relat. Res.* **467**: 1074-82
- [3] Maharaj et al., (2016). *J. Biomch.*, **49**:3238-43

Changes in joint mechanics following repeated sprinting

Basilio A.M. Goncalves^{1,2}, Evy Meinders^{1,2}, David J. Saxby^{1,2}, Matthew N. Bourne^{1,2,3}, Rod S. Barrett^{1,2}, Laura E. Diamond^{1,2}

¹School of Allied Health Sciences, Griffith University, Gold Coast, Australia

²Griffith Centre for Biomedical and Rehabilitation Engineering (GCORE), Griffith University, Gold Coast, Australia

³La Trobe Sport and Exercise Medicine Research Centre, La Trobe University, Melbourne, Australia

Email: b.goncalves@griffith.edu.au

Summary

Repeated sprinting is a common activity in team and court sports that has been linked to team performance. Here we demonstrate, for the first time, the changes in the work done by the hip, knee, and ankle joint moments during a 10-metre sprint, following a repeated-sprint protocol. In summary, the main reductions in joint work were observed at the hip and knee during the swing phase while no changes were observed during the stance phase for any of the three joints..

Introduction

To succeed in their respective sports, athletes often depend on repeated sprint ability. A better understanding of lower limb mechanical adaptations to repeated sprinting can inform strategies to improve performance and reduce injury in running-based sports. Point mass mechanics have received much attention in the past [1] but do not resolve the mechanical work done by muscles. Joint work can be used as a surrogate for mechanical energy transferred by muscles [2]. The aim of this study was to quantify changes in work done by lower limb joint moments during maximal running accelerations following a sports-specific repeated running protocol.

Methods

Recreational athletes (n=18, 9 female, age=25±8 years) performed a repeated running protocol consisting of 12 maximal 30-metre sprints on a self-paced treadmill with 60 seconds of physical testing and active rest between sprints. Three-dimensional kinematics (200 Hz) and ground reaction forces (2000 Hz) were recorded during a maximal 10-metre overground sprint before and immediately after the repeated running protocol. Data collected during overground sprints were used to calculate normalised sagittal plane joint power

(J/kg) for the hip, knee, and ankle. Individual power bursts were identified for each joint based on direction of net joint moment (i.e., flexion or extension), direction of angular velocity (i.e., flexing or extending), and sign of power (i.e., + or -) [3]. Work done by net hip, knee, and ankle moments (J/kg) was calculated using a trapezoidal numerical integration of power-time curves for each power burst (Figure 1). Work done by net joint moments before and after the repeated running protocol was compared using univariate analyses of variance ($p < 0.05$). Pearson product-moment correlation coefficient (r) was used to assess the correlation between maximum running speed and joint work.

Results and Discussion

Maximal running speed decreased 19% after the repeated running protocol and was accompanied by significant reductions in work done by hip (H3= -29%, H4= -45%, $p = 0.002$) and knee (K3= -31%; K4= -24%, $p = 0.005$) moments during swing (Figure 1). No changes in work done by the ankle were observed (A1= -1%; A2= -8%, $p > 0.05$). Reductions in work done by hip and knee moments during swing were significantly correlated with reductions in maximum running speed ($r = 0.61-0.89$).

Conclusions

Our results suggest strategies to maintain sprint performance should focus on maintaining positive work done by hip extensors and negative work done by knee flexors during the swing phase of running.

References

- [1] Edouard et al. (2018) *Front. Physiol.* **9**: 1706.
- [2] Farris & Sawicki (2012) *J. R. Soc. Interface.* **9**: 110-118.
- [3] Winter (1983) *Clin. Orthop. Relat. Res.* **May**: 147-154.

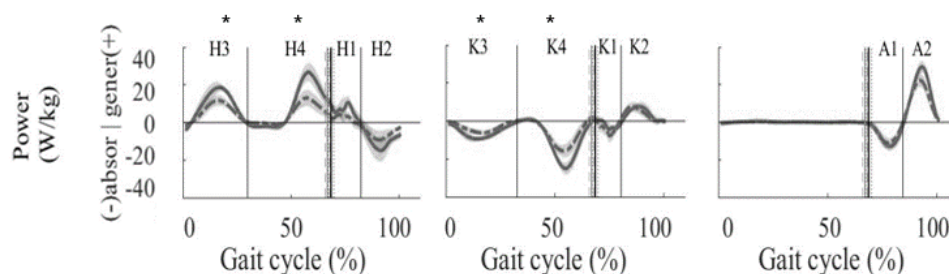


Figure 1. Ensemble averages \pm 95% confidence intervals of hip (left), knee (middle), and ankle (right) joint powers before (solid) and after (dashed) the repeated running protocol. * indicates significant differences ($p < 0.05$) in the work (area under the curve) from before to after the running protocol. Gait cycle represented as toe-off to toe-off with the vertical dashed line representing foot contact.

The effects of speed and footwear on 3D energy absorption during the braking phase of running: Distance matters

Steffen Willwacher^{1,2}, Johanna Robbin^{1,2}, Patrick Mai²

¹Department of Mechanical and Process Engineering, Offenburg University of Applied Sciences, Offenburg, Germany

²Institute of Biomechanics and Orthopaedics, German Sport University Cologne, Cologne, Germany

Email: steffen.willwacher@hs-offenburg.de

Summary

We analyzed the distribution of negative work performed during the first half stance among the major lower extremity joints and within all three motion planes. Further, we investigated the effects of running speed and footwear use on these distributions. Since step frequencies differed between speeds and footwear conditions, we found different directions and effect size of changes when performing the analysis over a single stance phase compared to performing the analysis over a fixed running distance (1000 m). Depending on the purpose of the analysis, studies on running mechanics should consider the effects of spatiotemporal parameters when determining work or load magnitudes.

Introduction

During ground contact, runners' legs typically show a spring-like behavior, overall performing negative work in the first and positive work in the second half of stance. Researchers frequently analyze joint work patterns in human locomotion by lumping together the contributions from different planes of movement, limiting the ability to locate sources of energy absorption/generation in greater anatomical detail. Further, when analyzing running interventions, work analyses are often performed for individual gait cycles or stance phases, ignoring that these phases' duration might change with the intervention. Therefore, a runner might perform a different number of gait cycles and different work quantities when considering the entire running distance.

Therefore, the purpose of this study was to analyze changes in 3D negative work patterns within the initial half of the stance phase in running when changing running speed and when using cushioned footwear compared to barefoot running.

Methods

We recruited three female and ten male participants (age: 25.5 ± 2.76 years; height: 1.82 ± 0.08 m; body mass: 73.3 ± 9.71 kg; leg length: 0.93 ± 0.05 m) and captured the 3D running kinematics and kinetics of their right lower extremity joints on a force-instrumented treadmill using previously described methods [1]. The participants ran in a barefoot and neutral cushioned running shoe condition at five different leg-length (l) normalized speeds (0.7, 1.375, 2.05, 2.725, and 3.4 Froude Number; $N_F \tau = v^2/g$) in randomized order. Joint power was calculated as the product of the resultant internal joint moment and joint angular velocity. We determined negative work during the first half of stance by integrating joint power over time. We quantified the number of steps needed to run 1000 m and calculated the cumulated negative work for each joint in each plane of motion for each running speed. We then performed a two-factor (speed, footwear) repeated measures

ANOVA to identify their effects on joint work-related parameters ($\alpha=0.05$).

Results and Discussion

Analyzing the effects of speed on negative work patterns over just the first half of the stance phase resulted in a different direction of change compared to analyzing them per running distance (Fig. 1). Most negative work was performed by ankle plantarflexion, knee extension, and hip abduction moments. We found several speed*footwear interaction effects, highlighting the differential response to speed changes in initial stance energy absorption patterns between barefoot and shod running.

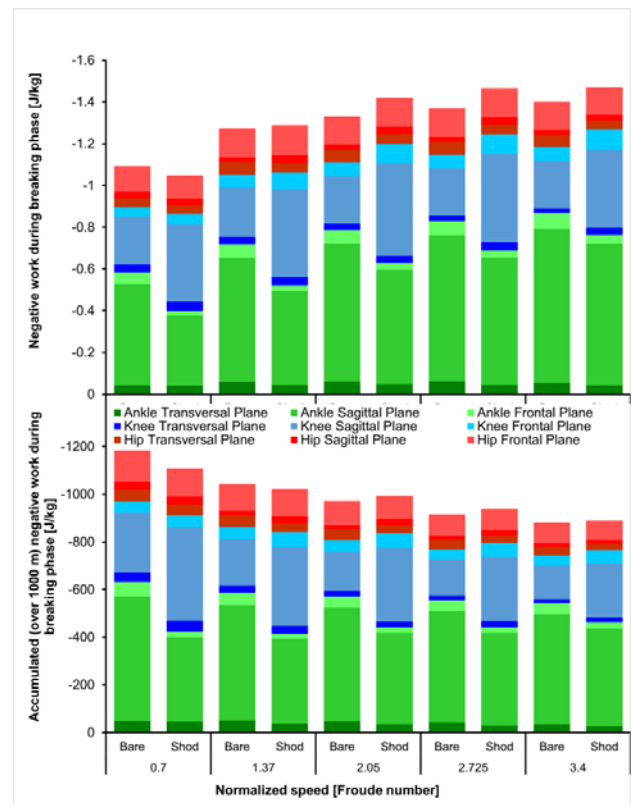


Figure 1: 3D-negative work patterns during the braking phase of stance per stance phase (top) and per 1000 m distance (bottom).

Conclusions

Intervention studies analyzing work-related parameters should consider potential changes in step frequency due to the intervention.

References

- [1] Sanno et al. (2018). *Med. Sci. Sports. Exerc.*, **50(12)**:2507-17.

The effect of diabetic neuropathy progression on muscle fiber conduction velocity of proximal and distal leg muscles during isometric contractions at low level forces

Eneida Yuri Suda¹, João Pedro Silva Santos¹, Taian Martins Vieira², Isabel CN Sacco¹

¹ Physical Therapy, Speech and Occupational Therapy Dept, School of Medicine, University of São Paulo, Brazil

² Laboratorio di Ingegneria del Sistema Neuromuscolare (LISiN), Politecnico di Torino, Torino, Italia.

Email: yurisuda@usp.br

Summary

This study investigated whether muscle fiber conduction velocity (MFCV) of lower limb muscles is sensitive to different degrees of diabetic polyneuropathy (DPN). Ten control subjects and 36 diabetic patients with different neuropathy degrees were evaluated. Multichannel Surface EMG (64 electrodes matrix: 16 x 4) was acquired during 10%, 20% and 30% of maximum isometric voluntary contractions (MIVC) of tibialis anterior (TA) and vastus lateralis (VL) muscles. MFCV was determined using a modified, beamforming algorithm, that estimate the delay of motor unit action potentials across the 2-D grid. Correlation analysis between MFCV and neuropathy degree, and ANOVAs analysis followed by Bonferroni post-hoc test comparing control, non- DPN and DPN groups were performed ($P < 0.05$). MFCV decreased progressively with neuropathy progression. The TA muscle showed a more consistent pattern of changes across all the studied force levels. These results suggest that DPN causes changes in the muscle fiber contractile properties with disease progression.

Introduction

DPN is one of the most prevalent complications of diabetes mellitus, affecting both sensory and motor nerve fibers and leading to pronounced motor dysfunction. Neuromuscular impairment is related not only to nerve integrity but to factors like the state of motor end plates and skeletal muscle fibers as well. The DPN is a progressive phenomenon and related alterations could be different for earlier and more advanced stages of the disease. The MFCV is a parameter that represents the mechanisms underlying the muscle functional status and can be a sensitive tool to detect signs of motor axonal dysfunction with DPN progression. Therefore, the aim of this study is to investigate whether MFCV is sensitive to different degrees of DPN, during isometric contractions at low level forces for one proximal and one distal lower limb muscle.

Methods

Ten control subjects (49.4±9.6yrs) and 36 diabetic patients (58.6±4.8yrs, 14.8±13.1yrs of diabetes diagnosis, 196.9±79.1 mg/dL blood glucose) were evaluated. Participants were assessed for (i) vibratory perception, (ii) tactile sensitivity (10g monofilament) and (iii) presence of typical neuropathy symptoms. These three groups of variables were used as linguistic inputs in a fuzzy system to determine the DPN degree (score 0-10). Diabetic subjects with the score > 2.5 were considered neuropathic. Multichannel Surface EMG (64 electrodes matrix: 16 x 4, OT Bioelettronica, Torino, Italy) was acquired during 10%, 20% and 30% MVC of TA and VL

muscles. MFCV was determined using a modified, beamforming algorithm, that estimate the delay of motor unit action potentials across the 2-D grid, as moving high-potential regions across the skin's surface [1]. Correlation analysis were performed in order to analyze the association between MFCV and DPN degree. Control, non-DPN and DPN groups were compared using ANOVAs, followed by Bonferroni post-hoc tests ($P < 0.05$).

Results and Discussion

MFCV decreased significantly for TA muscle in all studied force levels and for VL muscle at 20% MVC with DPN progression (Table 1). DPN subjects showed lower MFCV values for TA at 30% MVC and VL at 10% MVIC regardless the DPN degree (Table 2).

Table 1: Correlation analysis results.

Muscle	Force level	Person's correlation analysis	
		r	P
TA MFVC	10 % MVC	-0.362	0.016*
	20 % MVC	-0.306	0.041*
	30 % MVC	-0.338	0.023*
VL MFVC	10 % MVC	-0.209	0.155
	20 % MVC	-0.340	0.018*
	30 % MVC	-0.269	0.068

Table 2: MFCV values (m/s) for tibialis anterior and vastus lateralis muscles for the studied groups and ANOVA results.

Muscle	Force level	Control (n=10)	Non-DPN (n=12)	DPN (n=24)	P
TA	10 %	5.1±0.4	4.9±0.6	4.7±0.6	0.18
	20 %	5.1±0.3	4.9±0.5	4.8±0.5	0.20
	30 %	5.1±0.5 ^a	4.9±0.5	4.7±0.4 ^a	0.04*
VL	10 %	5.9±0.3 ^b	5.4±0.6	5.1±0.8 ^b	0.01*
	20 %	5.5±0.6	5.2±0.5	4.9±0.7	0.08
	30 %	5.3±0.5	4.9±0.6	4.8±0.7	0.08

*Statistically differences. ^{a, b} Differences between groups.

Conclusions

MFCV decreases progressively with DPN progression in TA and VL muscles. MFCV presented lower values in later stages of DPN, presumably related to changes in muscle fiber contractile properties. The greater proportion of type I fibers lost in the course of the disease in TA may explain the differences observed in a more consistent way for TA muscle.

Acknowledgments

FAPESP (processes 2013/05580-5, 2017/15449-4, 2019/15744-1).

References

[1] Grönlund C et al. (2005). *Med Biol Eng Comput*, 43: 63-70

Center of pressure control ensures mediolateral gait stability: Muscle driven foot placement and ankle moment control

A.M. van Leeuwen^{1,2}, L.A. Hoogstad¹, J.H. van Dieën^{1,2}, A. Daffertshofer^{1,2}, S.M. Bruijn^{1,2,3}

¹Department of Human Movement Sciences, Faculty of Behavioural and Movement Sciences, Vrije Universiteit Amsterdam, Amsterdam Movement Sciences, Amsterdam, The Netherlands

²Institute of Brain and Behavior Amsterdam

³ Biomechanics Laboratory, Fujian Medical University, Quanzhou, Fujian, PR China

Email: a.m.van.leeuwen@vu.nl

Summary

During steady-state walking, active control is exerted to maintain mediolateral gait stability. To this end, the center of pressure (CoP) location relative to the center of mass (CoM) can be modulated to control CoM acceleration. During steady-state treadmill walking, muscle driven foot placement control largely determines the CoP location relative to the CoM. As a compensation for errors in foot placement, muscle driven mediolateral ankle moments caused corrections of CoP location by shifting it underneath the stance foot. We tested whether constraining ankle moments would acutely cause tighter foot placement control, but instead participants walked with wider steps and increased their stride frequency. Training with constrained ankle moments did enhance foot placement control, which may be a more energetically efficient strategy for stability control.

Introduction

Understanding the mechanisms underlying mediolateral gait stability can help in designing training interventions for those with impaired stability control. Earlier studies have shown active stability control in response to perturbations and during steady-state walking. We focused on step-by-step muscle driven foot placement control during steady-state walking, replicating [2, 3] and providing support for active control of foot placement. Here we hypothesized that active ankle moment control would compensate for foot placement errors. Concurrently, we expected tighter foot placement control when walking with ankle moment constraints.

Methods

Healthy adults walked on a treadmill at normal walking speed. Participants walked normally, or while wearing a shoe with a narrow ridge attached to the sole. This flexible ridge constrained mediolateral CoP shifts, yet retained push-off. A constant stride frequency was dictated by a metronome. We used linear regression models to analyse the measured full body kinematics and EMG data. Foot placement control was defined as the relationship between foot placement and CoM kinematic state in preceding swing. The R^2 of this model quantified how tight foot placement was controlled. Ankle moment control was defined as the relationship between errors in foot placement and the subsequent CoP shift. We correlated gluteus medius and adductor longus activity with foot placement to test for active control. We correlated peroneus longus, tibialis anterior and soleus activity with the CoP shift due to ankle moment control.

Results and Discussion

Bayesian statistics revealed evidence for active foot placement control ($BF_{10} > 100$) and active ankle moment control partially accounting for errors in foot placement ($BF_{10} > 100$). Yet, constraining ankle moment control did not lead to tighter foot placement control (Figure 1A). Instead, participants increased their step width and stride frequency.

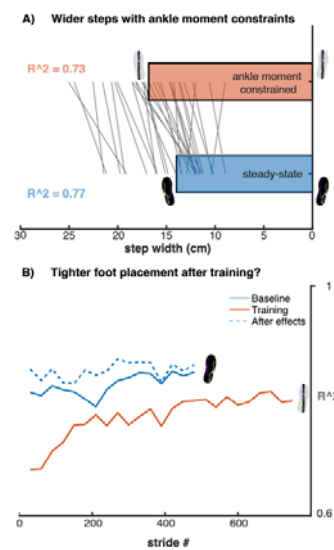


Figure 1: Effects of ankle moment constraints. **A:** Wider steps ($BF_{10} > 100$) and decreased mean R^2 (less tight foot placement control). **B:** Tighter foot placement control after longer exposure and as an after effect (no statistics).

Thus, ankle moment constraints perturbed foot placement, and participants resorted to general compensatory strategies [1, 4]. This emphasizes the interdependence of stability control mechanisms and suggests that ankle moment constraints can be used for training, similar to e.g. [5], to enhance foot placement control. Longer exposure to ankle moment constraints indeed showed a potential training effect (Figure 1B). Tighter foot placement control may allow for narrower steps, associated with lower metabolic cost [6].

Conclusions

Foot placement and ankle moment control are interdependent in coordinating the center of pressure with the center of mass. Constraining ankle moment control holds potential as a training tool to enhance foot placement control.

References

- [1] van Leeuwen AM et al. (2020). *Plos one*, **15**.
- [2] Rankin BL et al. (2014). *Journal of neurophysiology*, **112**, 374-383.
- [3] Wang Y and Srinivasan M (2014). *Biology letters*, **10**.
- [4] Wu M et al (2015). *Plos one*, **10**.
- [5] Reimold NK et al. (2020). *Scientific reports*, **10**: 1-15.
- [6] Donelan JM et al. (2004). *Journal of biomechanics*, **37**: 827-835.

Effects of unilateral swing leg resistance during walking on propulsion, braking and muscle activity

Sylvana Weiland^{1,2}, Han Houdijk¹, Heleen A. Reinders-Messelink^{2,3}, Luc H.V. van der Woude¹, Paul P. Hartman², Rob den Otter¹

¹ University of Groningen, University Medical Center Groningen, Department of Human Movement Sciences, Groningen, The Netherlands.

² Rehabilitation Center "Revalidatie Friesland", Beetsterzwaag, The Netherlands.

³ University of Groningen, University Medical Center Groningen, Center for Rehabilitation, Groningen, The Netherlands.

Email: s.m.weiland@umcg.nl

Summary

Unilateral swing leg resistance (SwR) may be used in rehabilitation post stroke. When walking with SwR, more power is required to progress the trunk and the loaded leg through swing. Arguably, this will stimulate propulsion. This study assessed the bilateral effects of SwR on propulsion, braking and muscle activity. The results show that propulsion increased in duration and magnitude while braking decreased in duration and magnitude, in both legs with SwR. In addition, activity of muscles related to propulsion was altered bilaterally. Activity of Rectus Femoris in the loaded leg increased during swing when SwR was applied. Simultaneously, activity of Biceps Femoris in the unloaded leg increased. The Medial Gastrocnemius increased in activity during stance in the loaded leg while a small decrease could be observed in the unloaded leg. The stimulation of propulsion and muscles related to propulsion can be promising for the training of walking ability post stroke.

Introduction

The ability to generate propulsive force on the affected side is often severely affected after stroke [1]. Propulsion can be defined as the impulse of the positive anterior component of the ground reaction force (GRF) [2] and is essential for forward progression. A decreased propulsive capacity is associated with a diminished walking ability [1]. Therefore, improving propulsion should be an important focus in rehabilitation post stroke. When walking with SwR, more power is required to actively progress the body and the loaded leg through swing. Arguably, the increased demand for propulsion may stimulate propulsive behavior after stroke. Before resistance forces can be applied in rehabilitation settings, the precise effects on propulsion, braking and muscle activity related to propulsion need to be assessed.

Methods

To assess the effects of SwR on propulsion, braking and muscle activity independent of gait pathology, 14 able-bodied participants walked on a treadmill with and without unilateral SwR at 0.56m/s. SwR was applied by attaching a weight of 1.25kg to a rope that was carried by pulley wheels and horizontally attached to the subject's right ankle. The effect of SwR was assessed on (1) propulsive force in terms of peak, impulse and duration, (2) braking force in terms of peak, impulse and duration and (3) muscle activity of Biceps Femoris (BF), Rectus Femoris (RF) and Medial Gastrocnemius (MG).

Results and Discussion

SwR alters the demand for propulsion, braking and muscle activity bilaterally. When SwR was applied:

- (1) Propulsive impulse, peak force and the relative duration of the propulsive phase increased in both legs (Figure 1).
- (2) Braking impulse, peak force and the relative duration of the braking phase decreased in both legs (Figure 1).
- (3) RF activity in the loaded leg increased during swing to progress the leg. Since the demand for deceleration of the swing leg decreased, BF activity in the loaded leg decreased during late swing. In contrast, BF activity in the unloaded leg increased during its single stance phase to generate propulsion. To maintain stability and to progress the loaded leg through swing, MG activity increased during stance in the loaded leg. A small decrease of MG activity during stance was found in the unloaded leg.

Stimulation of propulsion and muscle activity can be relevant for training settings as these gait features are often considered to be a limiting factor for functional gait ability [3].

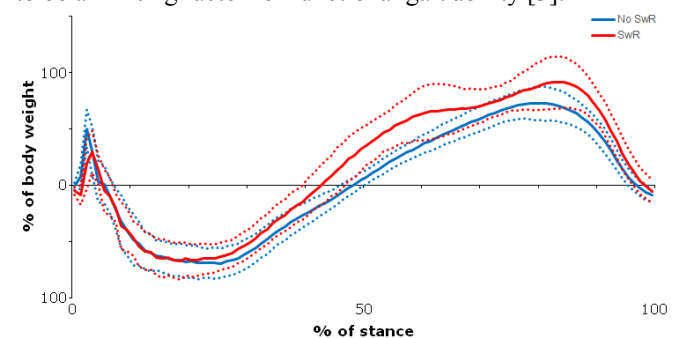


Figure 1: Group-averaged profiles (solid lines) and standard deviations (dashed lines) of the anterior-posterior ground reaction force in the loaded leg during walking with (blue line) and without (red line) unilateral swing leg resistance (SwR).

Conclusions

Unilateral SwR increases propulsion and muscle activity bilaterally in able-bodied participants. The provision of unilateral SwR may stimulate propulsive capacity after stroke.

References

- [1] Awad et al. (2014). *Arch Phys Med Rehabil.* **95**: 840-848.
- [2] Hsiao et al. (2016). *J. Biomech.* **49**: 388-395.
- [3] Perry J and Burnfield JM. (1992) *Gait analysis: normal and pathological function*; SLACK Incorporated.

Tactical Vest Loading Alters Head-Torso Coordination in Operational Police Officers During Running

M.A. Ellison¹, F. Mulloy¹, A.J. Gorman¹, O. Brown¹, D.R. Mullineaux¹

¹School of Sport and Exercise Science, University of Lincoln, Lincoln, United Kingdom

Email: mellison@lincoln.ac.uk

Summary

Loaded carriage has been associated with injury, with police populations showing a high prevalence of neck and shoulder pain. Kinematic data was collected during running with typical police tactical vest loads. Peak torso lean, head-torso displacement and the coupling angle between head and torso were assessed. Findings indicate that there is a delayed torso motion when loaded with no corresponding changes in head motion to accommodate. This suggests a possible mechanism for the prevalence of shoulder and neck pain amongst police officers.

Introduction

The modern police force is required to carry operational equipment, but to date there has been little consideration of an officers' capacity to effectively carry this load. Loaded carriage is associated with an increased risk of injury [1] and police populations display high injury rates when compared to other occupations, specifically with neck and shoulder injuries shown to be problematic [2]. Loaded carriage effects on lower limb joint kinematics [3] and ground reaction and joint forces [1] have been assessed in military populations, however there is little understanding of the mechanisms that may cause injury to the neck and shoulders, with only limited research investigating the effects of typical police load carriage systems. Vector coding is a method by which the coordination of interacting segments can be investigated [4] and may provide more information than a comparison of discrete variables or individual segments alone. This study aimed to assess the effects of police equipment carriage on head-torso co-ordination, during running, using three different loading distributions.

Methods

Following ethical approval, 29 police officers from a UK police force participated in this study (14 females; age 42±8 years; mass 85.9±15.2 kg; height 1.74±0.08 m). Participants wore a commercially available tactical vest used globally by international police forces (P9MPS, Arktis Endurance Textiles, Exeter, UK). Customised sandbags were used to replicate equipment masses of items typically carried (total 2.54 kg). These were positioned in Low, High and Distributed configurations on the torso. Participants ran at a self-selected pace with each load and an unloaded control condition, on a treadmill for 60s. 15 Raptor cameras and Cortex software (Motion Analysis, CA) recorded kinematic data at 150 Hz for the final 30s. Peak forward torso lean, and peak head-torso displacement were calculated across the stance phase, along with the head-torso coupling angles using vector coding [4] and the torso and head angle time-series. Configurations were compared using one-way repeated

measures ANOVA (SPSS v25, IBM, NY) (discrete variables) and statistical parametric mapping (SPM) in MATLAB R2020a (Mathworks, MA) (time-series variables).

Results and Discussion

Analysis indicated no differences in peak torso lean ($F = 1.603$, $p = 0.196$) or peak head-torso displacement ($F = 0.190$, $p = 0.903$). All loading conditions altered the head-torso coupling angle compared to the control (Figure 1). SPM indicated torso orientation was significantly different between control and all loaded conditions at 37 to 53% stance ($p < 0.001$), but no differences existed between loaded conditions ($p > 0.05$). No differences were found in head angle orientations between conditions ($p > 0.05$), but the torso reached peak forward lean later in stance when loaded compared to the control conditions. The head and torso move out of phase during this time, with the head effectively tilting back as the torso tilts forwards. The smaller postural neck muscles are likely stretched more in the loaded conditions, and eccentrically loaded during weight acceptance presenting a possible mechanism for neck pain in these populations.

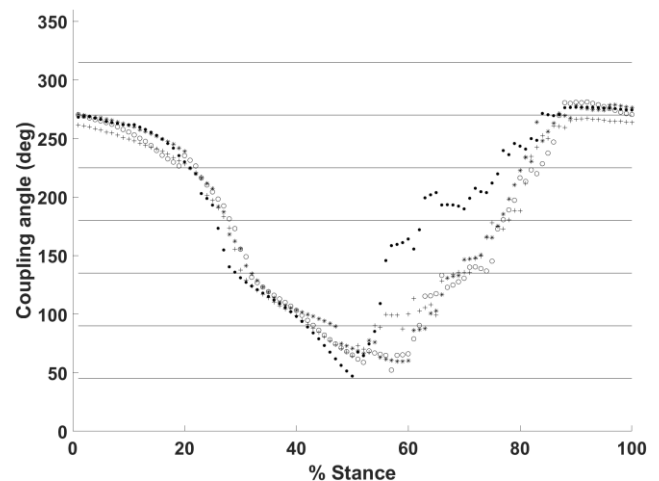


Figure 1: Coupling angle of head tilt and torso lean for control (.) and Low (*), High (o), Distributed (+).

Conclusions

Typical police load carriage alters head-torso coordination during running. Specifically, torso orientation is altered during weight acceptance, while the head does not move, which may contribute to the incidence of neck and shoulder pain in police officers.

References

- [1] Birrell, S.A., *et al.*, (2007). *Gait Posture*, **26**:611-614
- [2] Lentz, L., *et al.*, (2020). *J Occ Med Env Health*, **33**:59-66
- [3] Birrell, S.A., *et al.*, (2009). *Ergonomics*, **52**:1298-1304
- [4] Needham, R.A., *et al.*, (2015). *J Biomech*, **48**:3506-11

Predictive Simulations of Fixed-Speed Treadmill Gait

Kayla M. Pariser, Jill S. Higginson

Department of Mechanical Engineering, University of Delaware, Newark, DE USA

Email: pariserk@udel.edu

Summary

Fixed-speed treadmill gait training is a common gait rehabilitation method, but it can be challenging to experimentally determine the optimal training speed for an individual. This study develops and validates the first predictive simulation framework to estimate user response to various treadmill belt speeds. Overall, the framework captured many experimental kinematic, kinetic, and spatiotemporal trends of gait with increasing speed. This is the first step to establishing a workflow to effectively and efficiently design treadmill-based rehabilitation protocols to target specific therapeutic goals.

Introduction

Treadmill gait training is a commonly used rehabilitation strategy to improve walking function for individuals with diseases or injuries impacting the neuromusculoskeletal system [1]. Musculoskeletal models and simulations generated from experimental treadmill gait data have shown that training at faster speeds can be used to promote increased soleus positive work, resulting in increased propulsion and gait speed [2]. However, simulations generated from experimental data cannot answer what-if questions about the ideal training speed for an individual or to estimate user response to a novel speed.

An emerging approach to addressing these questions is predictive simulations that estimate movement via trajectory optimization of high-level task goals without relying on experimental data [3]. The objective of this study is to develop and validate a predictive simulation framework for fixed-speed treadmill gait at three treadmill speeds.

Methods

A 2D lower limb gait model with 10 degrees of freedom, 18 musculotendon actuators, two contact spheres on each foot, and a mass of 63 kg was modified to include a treadmill body with prescribed linear motion. The ground contact was defined between the contact spheres and the top plane of the treadmill. The slope of the linear function defining the treadmill motion was set to -0.7, -1.3, and -1.8, to represent the speed and posterior movement of the treadmill belt at slow, medium, and fast speeds.

To predict the model's motion at the three belt speeds, a two-step framework was established: (1) motion tracking and (2) motion prediction, using direct collocation optimal control in OpenSim Moco [4]. The tracking simulation minimized the control effort and the error between reference and simulated states and ground reaction force data. The tracked motion was set as the initial guess to the predictive problem. The predictive problem calculated the motion that minimized the sum of muscle activations cubed while enforcing the boundary constraints of bilateral periodicity and zero average speed of the center of mass relative to the ground.

Results and Discussion

The treadmill simulation framework successfully predicted many trends, values, and trajectory curves observed in experimental data [5]. Peak hip extension and ankle plantarflexion increased with increasing speeds. The peak anterior and vertical ground reaction forces also increased with increasing belt speed (Figure 1). In addition, predicted spatiotemporal parameters, cadence and step length, increased with increasing belt speed, matching well-established experimental trends [6].

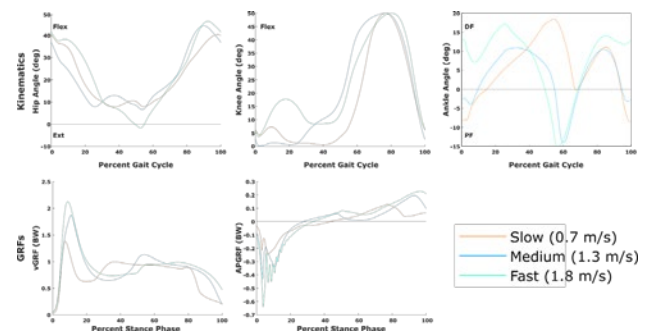


Figure 1: Predicted kinematics and GRFs at 3 treadmill speeds.

Our predictions did not capture increasing swing phase knee flexion with increasing speeds [5]. This is most likely due to bounding the knee flexion at 50° for all three simulations thereby not enabling the flexion angle to increase at faster speeds. Also, predicted hip extension angle values are small and likely due to the small hip extension angles in the reference coordinates applied to the tracking simulation.

Conclusions

The simulation framework correctly predicted several kinematic, kinetic, and spatiotemporal trends with increasing treadmill belt speed. Future work should seek to predict increasing knee flexion with increasing speed and improve the match of hip extension angle values with experimental data using subject-specific scaling and reference data. In addition, we will explore whether this framework will predict gait adaptations on a fixed-speed treadmill when modeling impairments such as unilateral muscle weakness.

Acknowledgments

Funding: NSFGRFP, NIH U54-GM104941, and University of Delaware Helwig Mechanical Engineering Fellowship.

References

- [1] Yamada S et al. (2015). *J Phys Ther Sci*, **27**: 1247-1250.
- [2] Neptune R et al. (2008). *Gait Posture*, **28**: 135-143.
- [3] Falisse A et al. (2019). *J R Soc Interface*, **30**: Epub.
- [4] Dembia C et al. (2020). *PLoS Comput Biol*, **16** (12).
- [5] Schwartz M et al. (2008). *J Biomech*, **41**: 1639-1650.
- [6] Fukuchi C et al. (2019). *Syst Rev*, **8** (153).

Voluntary control of a lower limb exoskeleton during walking using an EMG-driven biomechanical model

Guillaume Durandau¹, Herman van der Kooij^{2,1}, Massimo Sartori¹

¹Department of Biomechanical Engineering, Technical Medicine, University of Twente, The Netherlands

²Department of BioMechanical Engineering, Delft University of Technology, Delft, The Netherlands

Email: g.v.durandau@utwente.nl

Summary

Assisting walking via an exoskeleton is still challenging. Even more challenging is the task to give complete voluntary control of the exoskeleton over to the user, giving him the freedom to move as desired. Here, we present a controller based on biomechanical modelling of the human body controlled by the user's EMG signals. We tested the developed controller on four healthy subjects and on one uninterrupted recording containing a mix of two different walking speeds and three different elevations as well as the change between them. Results showed that for all conditions and between the transition of those conditions, reduction of EMG and joint torque levels were observed. These results open new avenues for biomechanical based control informed by bio-electrical signals for wearables robotics.

Introduction

Current commercial exoskeleton controllers are position-based and state of the art research controllers are based on predefined torques patterns. Those have shown remarkable results in controlled sessions aimed at rehabilitation but are still limited for assisting in everyday life in unknown and rough terrain. To circumvent current limitations, internal biomechanics variables and user's intention knowledge is desired. For this purpose, we developed a real-time neuromusculoskeletal framework that can inform in real-time on the user muscle forces and joint torques [1]. Later, this framework was used to control an ankle-knee exoskeleton during sited exercises with strokes and spinal cord injury patients [2].

Methods

The developed method is based on real-time Hill-type muscle modeling driven by recorded EMG and joint position. To obtain subject-specific results the model is first calibrated using experimental data. More information about the developed real-time framework can be found in [1]. The framework was adapted to work with the ankle modules of the WR2 exoskeleton presented in [3]. Experiments were done on four subjects (30±4 years, 177±6 cm, 71±6 Kg) and consisted on one long walking recording on a treadmill comprising a mix of two different speeds (1.8 km/h and 2.8 km/h) and three elevations (-5%, 0%, and 12%). This was repeated two times for each tested conditions, I) minimal impedance where the exoskeleton try to be as transparent as possible to the user and II) assistance where a percentage of the computed joint torques by the framework is given back to the user as assistance.

Results and Discussion

Results showed that EMG levels for each tested walking conditions were reduced when assistance was provided compared with minimal impedance (Figure 1). Reductions were also observed in the transition between walking conditions. At the muscle level, the Soleus muscle showed the biggest reductions contrary to the tibialis anterior that showed slight increases. The developed framework showed the possibility to reduce EMG levels for all tested conditions as well as in the transition between them. Importantly, these reductions were achieved without having to change any parameters in the exoskeleton controller or in the biomechanical model use. This is possible because the user's intention is known through the EMG signal, which allows for voluntary control of the exoskeleton by the user. Future works will make use of the rich level of internal information given by the biomechanical model such as muscle forces, joint stiffness, and joint loading to design wearables controller that offers personalized assistance to reduce effects of affliction.

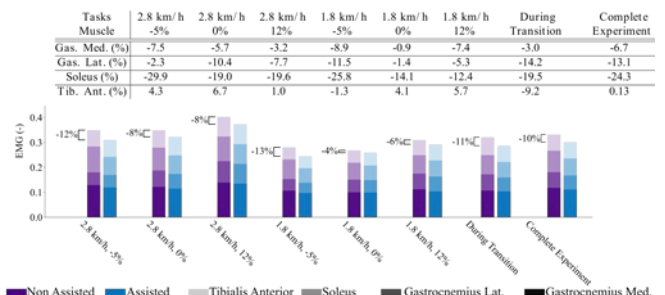


Figure 1: EMG results for all tested conditions. The table shows results at the muscle levels.

Conclusions

Real-time biomechanics combined with wearables robotics open new opportunities to develop controllers that can offer biomechanical benefits (EMG reduction) on a broad range of walking conditions. This method also offers the unique opportunity to observe changes in the neuromusculoskeletal system user as they happen.

References

- [1] Durandau et al, 2017, *IEEE-TBME*, **65**, 556-564
- [2] Durandau et al, 2019, *JNRE*, **16**, 1-18
- [3] Meijneke et al, 2021, *IEEE-TNSRE*

Large-scale multi-channel electromyography and musculoskeletal modeling via wearable smart garments to support clinical decision-making

D. Simonetti¹, B. F. J. M. Koopman¹, M. Sartori¹

¹Department of Biomechanical Engineering, University of Twente, Enschede, The Netherlands

Email: d.simonetti@utwente.nl

Summary

Clinical decision-making requires above all rapidity. Currently, motor deficit evaluation is based on a simplistic and subjective assessment, i.e. a simple 10m walk. It fulfills the main requirement, but it is not accurate, and it is just based on the evaluator's knowledge and experience. Greater accuracy is achieved in biomechanical laboratories where advanced technology together with neuro-musculoskeletal modeling allows to quantify the subject impairment. However, this is made at the expense of rapidity. The lengthy set-up and time-consuming post-processing do not allow the translation of this technology in the clinical environment. Our work aims to blend the two worlds, clinical rapidity and biomechanical accuracy, through an advanced technology quick to set up like a sock. The integration of advanced signal processing and real-time musculoskeletal modeling integrated into a smart wearable garment could become a promising asset helping clinicians to better and quickly characterize stroke patients.

Introduction

The key aspect in clinical environments is rapidity. A large number of people with motor deficit forces clinicians to rely on a simplistic but rapid tool to assess the motor function. It is common to use functional ambulatory categories (FAC)[1], i.e. 10m walk. The evaluation is rather subjective based on the knowledge and experience of clinicians. On the other hand, in biomechanical laboratories, the availability of advanced technology combined with musculoskeletal modeling techniques can give more accurate insights into the actual patients' state. However, the accuracy is achieved at the expense of rapidity so that the lengthy setup, data acquisition, and the time-consuming post-processing prohibit the translation of this advanced technology in the clinics. Our work is aimed to balance clinical rapidity and biomechanical accuracy. We propose to use advanced signal processing techniques and real-time neuro-musculoskeletal modeling integrated into a smart wearable garment. The garment is a simple lower leg sock instrumented with a large-scale multi-electromyography (EMG, 64 channels) grid and inertial sensors (IMUs) allowing to get over the lengthy setup and to prevent human error in the manual electrodes' placement. The smart clothing together with advanced signal processing techniques provides muscle activation and muscle-tendon unit (MTU) kinematics necessary to finally model the subject-specific musculoskeletal properties. In the following paragraphs, we show the results on (1) the automatic extraction of 5 muscle activations and (2) the torque estimation at ankle joint during different locomotion speeds using EMG-driven musculoskeletal modeling.

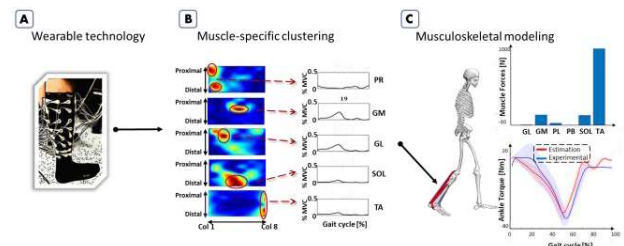


Figure 1: Schematics of the proposed technology: (A) fully wearable soft sensorized garment, (B) signal processing techniques to extract MTU activations (C) framework for patient-specific musculoskeletal modeling.

Methods

Seven healthy subjects were equipped with 33 reflective markers and a lower leg flexible garment instrumented with 64 equally distributed EMG monopolar electrodes. The 64-electrode space is reduced in 5 muscle-specific clusters applying iterative non-negative matrix factorization (NNMF) [2] during slow locomotion at 1km/h. Afterward, 5 average muscle activations were extracted during locomotion at different speeds 1, 3, and 5 km/h, and used as input to EMG-driven musculoskeletal model to estimate ankle torque.

Results

The NNMF-approach seems to be able to locate the muscle location and to extract averaged activations during each locomotion speed that resembled with good accuracy the activation recorded with bipolar EMG. Afterward, the musculoskeletal model driven by the automatically extracted muscle-specific activation reproduced experimental ankle torques during gait at different speeds.

Discussion and Conclusions

The combination of a soft sensorized garment and the automatic procedure for the extraction of muscle activations added to the framework for neuromuscular modeling has a good potential to become a resource for fast and more accurate clinical decision-making.

Acknowledgment

This work was funded by EFRO Op Oost GUTs (20913301). The garment is developed in collaboration with TMSi.

References

- [1] Mehrholz J et al. (2007), *Arch. Phys. Med. Rehabil.*, **88**: 1314–1319.
- [2] Kim J. and Park H., (2008), *IEEE Data Mining*

Estimating muscle and joint stiffness during plantar-dorsi flexion joint rotations via musculoskeletal modelling

Christopher P. Cop¹, Alfred C. Schouten^{2,1}, Bart F. J. M. Koopman¹, Massimo Sartori¹

¹Department of Biomechanical Engineering, University of Twente, Enschede, The Netherlands

²Department of Biomechanical Engineering, Delft University of Technology, Delft, The Netherlands

Email: c.p.cop@utwente.nl

Summary

Modelling muscle stiffness-generating capacity under different types of dynamic contractions and history-dependencies is an open challenge. We present an experimental dataset that captures history-dependent phenomena *in vivo* as well as an initial resulting *in silico* model that also takes muscle architecture-contribution to stiffness generation into account. We compare the proposed model against joint stiffness reference values obtained via system identification during dynamic plantar-dorsi flexion joint rotations and show preliminary results.

Introduction

Quantifying human joint stiffness *in vivo* during movement remains a challenge. Here we propose a data-driven musculoskeletal model-based approach to estimate multi-muscle stiffness as well as resulting joint stiffness. Importantly, the proposed model-based approach does not require joint perturbations, in contrast to well established system identification methods. Musculoskeletal models often use a standard Hill-type muscle model that does not capture history-dependent properties, *e.g.* stretch-induced force enhancement (FE) and shortening-induced force depression (FD). Moreover, muscle architecture features, specifically pennation angles, are often neglected when estimating equivalent muscle-tendon stiffness. Our goals are: 1) to experimentally capture history-dependent muscle contraction mechanisms to further implement them in the model; 2) to include pennation angles into the current muscle-tendon unit stiffness model; and 3) validate the joint stiffness profiles predicted by our extended muscle model against an ensemble-based system identification method during ankle rotations.

Methods

A young healthy voluntary participant was instructed to keep the tibialis anterior muscle's (TA) activation level between 15% and 20% of maximum voluntary contraction while the resulting ankle torque was recorded by a dynamometer. The subject performed a) isometric contractions, b) an active stretch followed by an isometric contraction, and c) an active shortening followed by an isometric contraction.

Additionally, the subject was instructed to follow a sinusoidal plantar-dorsi flexion angle target (amplitude: 0.15 rad, frequency: 0.6 Hz). Electromyography (EMG) and kinematic data were used to estimate joint stiffness using an extended EMG-driven musculoskeletal model that considers the muscle fiber's pennation angle in the equivalent muscle stiffness computation: $K_{eq}^m = dF^m/dl^m \cos^2\alpha + F^m/l^m \sin^2\alpha$, where F^m and l^m are the force and length, respectively, of the

muscle fiber, and α represents the muscle fiber's pennation angle [1]. Joint stiffness predictions were compared to an ensemble-based system identification method [2].

Results

Preliminary results (Figure 1) show that we were able to elicit FE (19% torque increase compared to the reference) and FD (14% torque decrease compared to the reference) on the TA. The aforementioned values were computed by averaging the relative torque change in a one-second window one second after the joint angle transition was completed. Our extended model's joint stiffness prediction was comparable to the system identification reference profile ($R^2 = 0.69$ and root mean squared error, RMSE, = 3.33 Nm/rad).

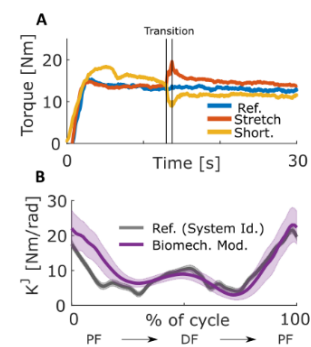


Figure 1: A) Measured ankle isometric DF torque in three conditions: reference (blue), and after muscle lengthening (red) and shortening (yellow). The vertical lines indicate the transition from the initial to the reference joint angle. B) Ankle joint stiffness during a plantar-dorsi flexion task estimated by the reference system identification method (grey) and predicted by our proposed model-based approach (purple).

Discussion and Conclusions

We captured history dependent muscle properties *in vivo* and we extended our joint stiffness formulation to consider the muscle's pennation angle. The inclusion of physiological features in musculoskeletal models may be beneficial for joint stiffness estimation. Next steps include the implementation of FE and FD models, as well as a short-range stiffness module, in the Hill-type muscle model to improve its capabilities of force and stiffness estimation during complex tasks involving eccentric, concentric and isometric contractions.

Acknowledgments

ERC Starting Grant INTERACT (803035) funded this work.

References

- [1] Cop CP et al. (2020). *ICNR*: in Press.
- [2] Moya-Esteban A et al. (2019). *IEEE EMBC*: 2119-2122.

Sampling and modelling of motor unit-specific activation properties in the intact human in vivo

Antonio Gogeochea¹, Utku S. Yavuz², and Massimo Sartori¹

¹Department of Biomechanical Engineering, University of Twente, Enschede, The Netherlands

²Biomedical Signals and Systems Group, University of Twente, Enschede, The Netherlands

Email: antonio.gohz@gmail.com

Summary

Human motor function is highly variable across motor tasks, pathology, and training, within the same person and between individuals. This is a major problem for devising neurorehabilitation strategies to restore natural movement. Although current signal-driven neuromusculoskeletal models can predict accurate joint moments, there is room for improvement in reproducing neuro-mechanical processes across different conditions. For this, we propose an motoneuron-based approach to extract relevant alpha-motor unit (a-MU) properties, and to employ their statistical distributions for generating a-MU-specific muscle activation dynamics. We expect that this will enable better torque predictions across multiple conditions, as well as a better understanding of how alpha motor neurons interact with muscles, and how they modulate in response to neurorehabilitation devices (e.g. spinal electrical stimulators).

Introduction

The development of closed-loop neuro-modulative techniques is currently hampered by the inability of interfacing with neural targets responsible for motor function. State of the art electromyography (EMG)-driven models [1] aim to provide a deeper insight into force-generation processes of movement, however, they do not offer detailed information on individual a-MU behavior. The ability of decomposing several MUs from high density-EMG opens up new avenues to extend current generalized neuromusculoskeletal models into MU-specific formulations. This work presents a technique for sampling a-MU distributions, and creating more detailed models that account for MU-specific twitch properties.

Methods

Four healthy men performed a series of isometric plantar-dorsi flexion tasks as described in [2]. We recorded high density-EMGs from the lower leg muscles, and decomposed them into constituent MU spike trains using a convolutive blind source separation technique [3]. The non-physiological spike trains were eliminated using quantitative accuracy indices [4]. We then calculated the mean discharge rate (normalized to 40 Hz) and recruitment threshold of each MU across all trials for each subject. We obtained a linear combination from these features through principal component analysis, and projected the data onto the first eigenvector (Figure 1). Moreover, we designed a piecewise parametric function that models a critically damped system where shape parameters (amplitude, time-to-peak and half-relaxation time) can be fine-tuned based on the MU distribution (Figure 2).

Results and Discussion

The probability density functions of the first eigenvector showed an overlapping mixture of two gaussians (Figure 1).

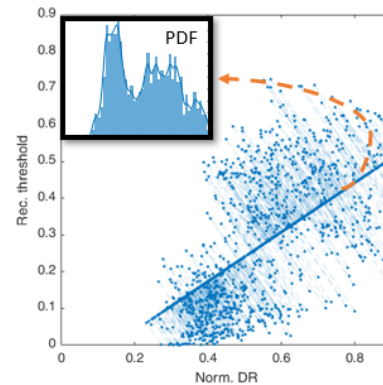


Figure 1: Scatter plot of norm. discharge rate and rec. threshold.

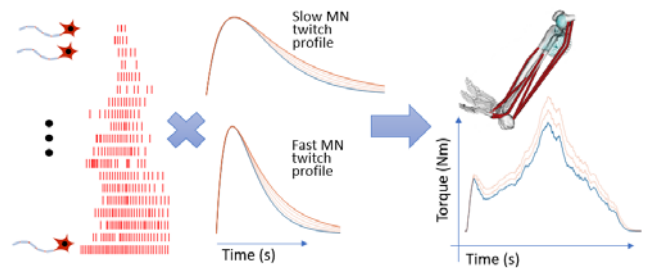


Figure 2: The convolution between decode spike trains and their specific twitch response will allow a better torque estimation.

These may correspond to slow and fast MU populations. The slow MU population had the ranges (95% confidence interval): 0.091-0.104 for rec. threshold, and 0.41-0.43 for norm. discharge rate; whereas the ranges for the fast MUs were: 0.38-0.45 for rec. threshold, and 0.61-0.71 for norm. discharge rate. Future work aims at coupling this sampling technique with our proposed twitch model to generate a MU-specific formulation of activation dynamics.

Conclusions

We proposed a technique to sample MU distributions and to model specific twitch responses based on their properties. This enables MU-specific activation dynamics which, in turn, may provide better torque predictions in comparison to current EMG-driven models. In a rehabilitation scenario, this would enable developing personalized neurorehabilitation strategies tailored to specific neural targets.

Acknowledgments

This work was supported by the European Research Council Starting Grant INTERACT (grant no. 803035).

References

- [1] Pizzolato C et al. (2015). *J. Biomech*, 48(14): 3929–3936.
- [2] Sartori M et al. (2017) *Sci. Rep.*, 7:13465.
- [3] Holobar A et al. (2007). *IEEE Trans.Sig. Process.*, 55(9): 4487-4496.
- [4] Gogeochea A et al. (2020) *Front. Neurol.*, 11:493

Is the side-stepping exercise effective on targeting gluteal muscles?

Heron B. O. Medeiros¹, Géssica A. Silvano¹, Erik M. Roesler¹, Marcio O. Nunes², Walter Herzog³, Heiliane B. Fontana^{1,4}

¹Biomechanics Laboratory, Federal University of Santa Catarina, Florianópolis, Brazil

²Physical Education Department, University Center of Brusque, Brusque, Brazil

³Human Performance Laboratory, Faculty of Kinesiology, University of Calgary, Calgary, Canada

⁴Morphological Sciences Department, Biological Sciences Center, Federal University of Santa Catarina, Florianópolis, Brazil

Email: heronbomed@gmail.com

Summary

In this study, we tested the commonly made assumption that the side-stepping exercise with an elastic band around the forefeet creates a torque of adduction and medial rotation of the femur around the pelvis resulting in the activation of gluteal muscles in opposition to the external moments created.

Introduction

Strengthening hip abductor and lateral rotator muscles has been a common goal in lower limb rehabilitation and injury prevention exercise programs, with great emphasis given on maximizing gluteal muscle activation during movement-based exercises [1].

The side-stepping exercise is typically performed in a squatted posture with the individual moving laterally with a looped resistance band around the forefeet. Both, the use of a squatted posture and the forefeet band position were shown to be optimal for enhancing gluteal activity [2,3], which has contributed to the popularity of side-stepping with the band around the forefeet.

It is assumed that **the band** around the forefeet **produces** a hip adduction and medial rotation torque, which is counteracted by gluteal muscles. However, this assumption seems to ignore the mechanics of the exercise [4] and the changes in gluteal muscle action that occurs with hip flexion in the squatted position [5].

Here, we investigated simultaneously the electromyography (EMG) of gluteal muscles (and tensor fascia lata (TFL)) and hip moments in the sagittal, transverse, and frontal plane during side-stepping and tested the hypotheses that: i) hip muscle torques during side-stepping are of extension, medial (not lateral) rotation and abduction, and ii) the increase in gluteal activation in the squatted posture compared to the upright posture in this exercise is not related to an increase in hip lateral rotator or abductor torque but to an increase in hip extensor torque.

Methods

Thirty-six adults performed side-stepping with an elastic band around the forefeet in an upright and a squatted posture while 3D kinetic/kinematic and EMG data were collected. An inverse dynamics approach was used to estimate hip joint torques. EMGs of the gluteus medius (GMED), TFL, and superior and inferior fibers of gluteus maximus (GMAXS and GMAXI) were analyzed.

Results and Discussion

Average EMG of GMAXS and GMAXI was greater in the squatted posture than the upright posture (Figure 1, $p \leq 0.001$), while no differences were observed for the GMED and TFL ($p > 0.133$).

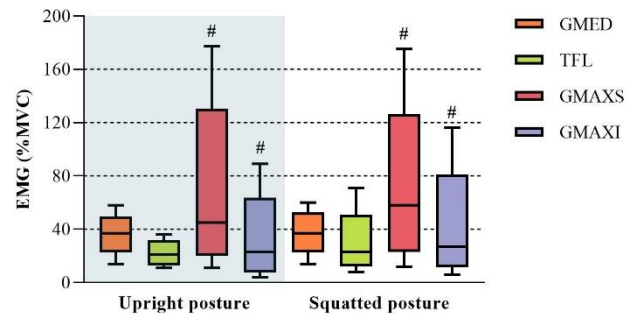


Figure 1: Hip muscle activity (median \pm QI) during side-stepping (#: significant differences between postures with Wilcoxon).

Regardless of posture, a hip muscle torque of extension, medial rotation and abduction was necessary during all phases of side-stepping, challenging the assumption that GMAX activity during side-stepping results from the need to **laterally** rotate the hip during this exercise. Side-stepping in a squatted posture resulted in an increase in hip extensor and **medial** rotator torque but not hip abductor torque (Figure 2).

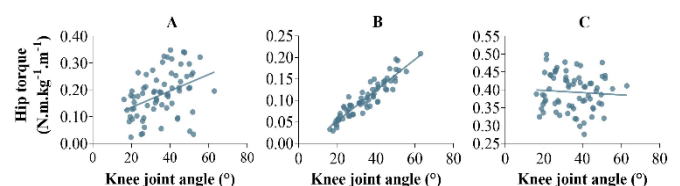


Figure 2: Association between knee joint angle and hip extensor (A), medial rotator (B), and abductor torques (C).

While the role of gluteal muscles in the transverse plane may change with hip flexion [5], transverse hip muscle torque of medial rotation is required in both postures (Figure 2B) and for all phases of the exercise (data not shown).

Conclusions

The assumption that the side-stepping with the band around the forefeet targets gluteal muscle action towards hip lateral rotation and abduction is not correct. Hip muscle torques required are of abduction, extension and **medial** rotation.

The increase in gluteal muscle activity observed in the squatted posture compared to an upright posture might be related to the increase in hip extensor torque and hip medial rotator torque as GMAXS fibers change their moment arm to medial rotation as the hip is flexed.

References

- [1] Chia L et al. (2020). *J Orthop Sports Phys Ther*, **50**: 476-489.
- [2] Cambridge EDJ et al. (2012). *Clin Biomech*, **27**: 719-724.
- [3] Lewis CL et al. (2018). *J Athl Train*, **53**: 1071-1081.
- [4] de Brito Fontana H et al. (2020). *J Funct Morphol Kinesiol*, **5**: 74.
- [5] Delp SL et al. (1999). *J Biomech*, **32**: 493-501.

Biomechanical response of residual limb: combining shear-wave elastography and finite element analysis

Begum Zeybek¹, Susann Wolfram¹, Alvaro Dueñas Ruiz², Victor M. Encinas-Tobajas³

¹School of Health and Life Sciences, Teesside University, Middlesbrough, UK

²Institute of Biomedicine of Seville, Virgen del Rocío University Hospital, Sevilla, Spain

³Radiology Department, Virgen del Rocío University Hospital, Sevilla, Spain

Email: b.zeybek@tees.ac.uk

Summary

This study aimed to combine shear wave (SW) elastography for the quantitative assessment of muscle tissue stiffness variations after transfemoral (TF) amputation and used simplified finite element (FE) simulations to map numerical material inputs for different muscles to replicate the biomechanical response of the residual limb at the residual limb-prosthetic socket interface under loading.

Introduction

The residual limb shape changes in time with muscle atrophy and stiffening of loaded tissue regions; this constantly evolving interface is an important parameter to consider for personalized and comfortable socket development. FE modeling has been used to support prosthetic socket design for many years because of its potential to offer insights into soft tissue load distributions. It has been shown that variation of the muscle stiffness in numerical models caused substantial differences in the predicted strains between liner and skin interface [1]. Here we aimed to determine the differences of elastic modulus in different muscle regions of TF amputee using SW elastography and the effect of muscle material parameter inputs on predicted numerical strains for the residual limb which is ultimately related with socket comfort.

Methods

SW elastography measurements were performed on muscles of the residual and sound limb in five (2 males and 3 females) TF amputees with mean age of 38.4 ± 5 years. TF amputees' rectus femoris (RF), vastus lateralis (VL), vastus medialis (VM), biceps femoris (BF), semitendinosus (ST), semimembranosus (SM), adductor magnus (AM) muscles were measured. Shear wave propagation speeds were captured using ultrasound scanner for shear wave elastography. from the participants' amputated (Figure 1.a) and sound limb. For each muscle, shear modulus was measured three times. All participants were recruited at Hospital Universitario Virgen del Rocío and ethics committee approval was obtained. FE models were developed with ABAQUS software. The shear modulus data was converted to linear elastic modulus (Figure 1.c) and simplified model geometry was developed (Figure 1.b). The contact interface between the skin and liner was modeled as a tied interface to demonstrate if slip not occurred. A rigid interface between bone and muscle was also defined to prevent separation. The load conditions were obtained from

literature and 25mm displacement [2] and 5 kPa distributed pressure [3] was applied to liner surface.

Results and Discussion

Different elastic moduli values were found in TF amputees' residual limb muscles at relaxed state. The AM had a significantly ($p < 0.05$) higher elastic modulus compared to the other muscles. The FE simulations with corresponding muscle material models resulted in varying biomechanical responses to same levels of load conditions at the residual limb-liner interface. As expected less stiff muscle regions experienced higher levels of compressive strain. Young's moduli of the residual limb tissues were significantly ($p < 0.05$) smaller than those of their sound sides for BF muscle (Figure 1.c).

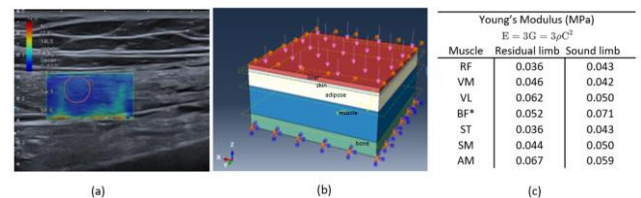


Figure 1: (a) Longitudinal sonogram of RF, color-coded box represent elasticity (stiffer areas were coded in red and softer areas in blue), (b) Simplified geometry of FE model, (c) Measurements of elastic modulus for residual limb and sound limb where C is the SW propagation speed and ρ is the tissue's density. *Significant difference between residual limb and sound limb ($p < 0.05$)

Conclusions

Different muscle groups of TF amputee's residual limb had varying elastic modulus stiffness which influences the numerical model outcomes of the simplified FE models. This is an important aspect to take into consideration while modelling bulk soft tissue representations for the entire stump.

Acknowledgments

This project has received funding from the European Union's Horizon 2020 research and innovation program under grant agreement No 825429.

References

- [1] Steer J.W. et al. (2020) *Prosthet. Orthot. Int.* 1-9
- [2] Kahle J. T. et al. (2013) *J. Rehabil. Res. Dev.*, **50**, 1241–1252
- [3] Lenz A. L. at al. (2018) *J. Biomech.*, **74**, 213–219

Eccentric training increases the cross-sectional area in different regions of the Achilles tendon after rupture
Emmanuel S da Rocha, Francesca C Sonda, Klauber D Pompeo, Mariane B Scheeren, Jeam M Geremia, Marco A Vaz
 Biomechanics and Kinesiology Research Group, Federal University of Rio Grande do Sul, Porto Alegre, RS, Brazil
 Email: emmarocha@gmail.com

Summary

Here we verified the effects of 12 weeks of eccentric training on the Achilles tendon (AT) cross-sectional area (CSA) from patients with AT rupture (mean=4.6 years post-surgical repair). We compared the effects of two different training programs (isokinetic and conventional) on the CSA of 10 different regions of the AT. AT rupture leads to morphological adaptations (higher CSA) in the injured tendon after years from the surgery that is different among regions of the tendon. We showed that the tendon adapts after 8 weeks, and that eccentric training hypertrophied the tendon (18% increase in CSA).

Introduction

Achilles tendon (AT) rupture is associated with an increase in tendon cross-sectional area (CSA) because the healing process generates a tendon callus that affects the plantar flexor function, with deficits persistent several years post-surgery [1]. AT morphology is an important measure to investigate tendon plasticity in response to training [2] and rehabilitation post-rupture [3]. Mechanical load from exercise stimulates biochemical signals eliciting tissue adaptation. Changes in the extracellular matrix [4], as well as fibre re-alignment, change the AT's CSA [2]. Eccentric contractions are the muscle actions with the highest force production capacity, and, therefore, elicit the highest tendon loading). However, the effects of different types of eccentric training [conventional (CONV) and isokinetic (ISOK)] on AT CSA remain unclear. The purpose of this study was to verify the effects of 12 weeks of these two eccentric training modalities in 10 different regions of the tendon of patients that underwent AT surgical repair.

Methods

This is a randomized evaluator-blind controlled clinical trial (NCT03861572) that was approved by the university's ethical committee (#96310118.4.0000.5347). AT CSA was obtained from 10 consecutive ultrasound images (1 cm apart) obtained from the calcaneus insertion to the myotendinous junction. An experienced evaluator used B-mode ultrasonography before training (Pre-training), and after 4, 8 and 12 weeks of training. We randomized participants using a computer program to generate random numbers in permuted blocks thereby assigning them into two groups: the ISOK training [n: 14 (13 men), age: 38.4 ± 6.8 years old, body mass: 87.5 ± 14.8 kg, postoperative follow-up: 5.1 ± 5.2 years]; and the CONV training [n: 14 (13 men), age: 37.7 ± 4.3 years old, body mass: 87 ± 10 kg, postoperative follow-up: 4.1 ± 3.5 years]. Volunteers trained twice a week. Two to four series of 8 to 12 repetitions were performed. The load

was increased from 60% to 80% of maximal effort in the three mesocycles (1st-2nd week: 2x8, 60%; 3rd-4th week: 3x8, 60%; 5th week: 3x8, 70%; 6th-8th week: 3x10, 70%; 9th-10th week: 3x12, 80%; 11th-12th week: 4x10, 80%). Both legs were trained.

Results and Discussion

Eccentric training increased (18%) the injured leg's tendon CSA in region 5 (Figure 1) in the CONV group after 8 weeks (p=0.048; 95% CI -0.50, -0.001; d=0.67). The injured tendon in the CONV group had higher CSA at post-12. ISOK showed higher (21-35%) CSA at the uninjured leg than CONV at the end of the training period.

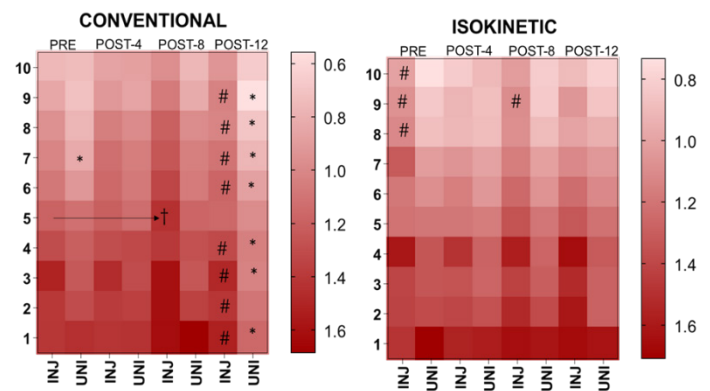


Figure 1. Cross-sectional area. Heat map where higher area values are depicted with darker or stronger colour. † means training effect; * means differences between groups; # differences between legs.

Conclusions

CONV eccentric training increased the injured AT CSA by 18%, while the ISOK training increased the uninjured AT CSA by 21-35% at the end of the training program.

Acknowledgments

This study was financed in part by the Coordenação de Aperfeiçoamento de Pessoal de Nível Superior - Brasil (CAPES) - Finance Code 001.

References

[1] Zellers, JA et al. (2019). *Knee Surg Sports Traumatol Arthrosc*, **28**(1):245-252.
 [2] Geremia, JM et al. (2018). *Eur J Appl Physiol*, **118**(8):1725-1736.
 [3] Geremia, JM et al. (2015). *Clin Biomech*, **30**(5):485-492.
 [4] Nourissat, G et al (2015). *Nat Rev Rheumatol*, **11**(4):223-233.

3D Body Landmark Detection for Markerless Motion Tracking

Alex Spencer¹, Serge H. Roy¹, Paola Contessa¹, Gianluca De Luca¹, Joshua C. Kline¹, and Bhawna Shiwani¹
¹Delsys Inc. and Altec Inc., Natick, USA
 Email: bshiwani@delsys.com

Summary

Rapid advances in depth-sensing and computer vision technologies have provided unique opportunities for the translation of traditional marker-based kinematic tracking into markerless assessments for clinical practice. We evaluated the feasibility of providing clinical outcome measures from depth-based features of the human body detected using a single video and depth (RGB-D) camera. Our 3D Body Landmark Detection algorithm leverages point-cloud processing techniques to localize and track body landmarks. We evaluated this approach by tracking body movement during commonly assessed motor tasks in a neurological exam (finger tapping, toe tapping, heel tapping, and gait) and calculating the resulting landmark position-based outcomes. The mean accuracy of the 3D Body Landmark Detection algorithm with respect to a marker-based motion capture system was 93.1% across tasks, which was 30% higher than a traditional pose estimation algorithm. These findings provide a foundation for using 3D landmark-based localization and tracking techniques for the assessment of clinical outcomes.

Introduction

Motor assessments are an essential part of most clinical examinations. While traditional multi-camera optical motion capture solutions have proven effective in delivering kinematic accuracy during such assessments, they are confined to a research lab and require significant setup. Other single camera efforts to localize features of the body primarily utilize pose estimation algorithms, which have known limitations in computing clinically relevant outcomes (e.g., distance between body segments or locations in space), especially during motor assessments tasks [1, 2]. To overcome these limitations, we designed a 3D Body Landmark Detection algorithm that bypasses the need for pose estimation to obtain clinical outcomes by automatically localizing and tracking body landmarks directly from a single RGB-D camera during standardized motor assessment tasks.

Methods

Six healthy participants (3 F, 3 M; 21-30 y.o.) performed the following motor-activities: finger tapping, toe tapping, heel tapping, and gait. All tasks were completed at three different self-selected speeds (>500 cycles per movement). Movements were concurrently recorded with an 8-camera optical motion capture system (Vicon, Oxford, UK) and a single RGB-D camera (Microsoft Kinect Azure). The point-cloud data was processed through a multi-stage algorithm architecture (Figure 1) including: 1) Background Removal using depth-based spatial filters; 2) Landmark Extraction via geodesic path tracking and body segment identification; and 3) Movement Tracking by extrema detection and neighborhood cluster

tracking. Task-relevant clinical outcomes were computed as the peak-to-peak amplitude between relevant landmarks for each activity – index finger and thumb (finger tap); toe/ foot and floor (toe tap and heel tap); and alternate feet (step length and step width during gait). We compared the proposed 3D Body Landmark Detection algorithm with Kinect body tracking software to gauge its outcome accuracy with respect to an established joint estimation-based solution [3].

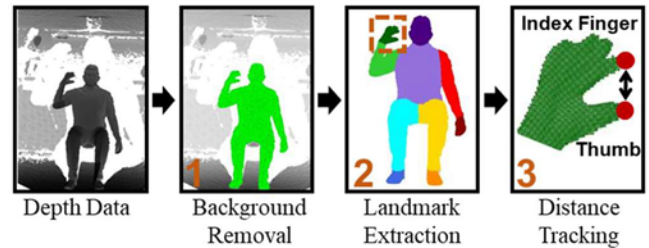


Figure 1: 3D Body Landmark Detection approach for distance tracking, illustrated for a finger tapping task

Results and Discussion

The 3D Body Landmark Detection algorithm achieved greater than 90% accuracy (Table 1) across the range of fine-motor and whole-body assessments with respect to gold-standard motion capture recordings. Mean accuracy margins were 30% higher than traditional Kinect pose estimation algorithms.

Table 1: Accuracies for the 3D Body Landmark Detection and Kinect pose estimation

Motor Activity	3D Landmark Detection		Kinect Pose Est.	
	Absolute Error (cm)	Relative Accuracy (%)	Absolute Error (cm)	Relative Accuracy (%)
Finger Tap	0.6 ± 0.5	93.1 ± 6.3	6.0 ± 1.4	39.5 ± 15.4
Toe Tap	0.4 ± 0.3	94.3 ± 4.2	3.8 ± 1.6	40.6 ± 14.5
Heel Tap	1.5 ± 1.2	93.1 ± 4.6	6.7 ± 3.0	66.2 ± 15.5
Step Length	3.6 ± 2.9	93.2 ± 5.9	8.5 ± 3.8	84.8 ± 6.4
Step Width	1.7 ± 1.4	91.9 ± 6.1	4.3 ± 3.1	80.9 ± 12.8

Conclusions

The 3D Body Landmark Detection algorithm provides a useful alternative to traditional pose estimation methods by directly localizing relevant body landmarks using a single-camera system. This study demonstrates the proof-of-concept feasibility of using markerless movement tracking systems to supplement clinical assessments with quantitative metrics that facilitate objective and evidence-based practice.

References

- [1] Galna B. et al. (2013). *Gait & Posture* **39** (4): 1062-1068.
- [2] Albert J. et al. (2020). *Sensors* **20** (18): 5104
- [3] Microsoft Azure Kinect DK. Available online: <https://azure.microsoft.com/en-us/services/kinect-dk/>

NEUROMUSCULAR ACTIVATION PATTERNS DURING CHALLENGED WALKING TASKS IN INDIVIDUALS WITH FEMOROACETABULAR IMPINGEMENT

Carson Halliwell^{1,2}, Derek Rutherford^{1,3}, Janice Moreside⁴, Ivan Wong⁵, Rebecca Moyer^{1,2}

¹School of Physiotherapy, Faculty of Health, Dalhousie University, Halifax, B3H 4R2, Canada

²Laboratory for Clinical Biomechanics and Rehabilitation Research, Dalhousie University, Halifax, B3H 4R2, Canada

³School of Biomedical Engineering, Faculty of Engineering, Dalhousie University, Halifax, B3H 4R2, Canada.

⁴School of Health and Human Performance, Faculty of Health, Dalhousie University, Halifax, B3H 4R2, Canada

⁵Department of Surgery, Division of Orthopedics, Nova Scotia Health Authority, Halifax, B3H 2E2, Canada

Email: carson.halliwell@dal.ca

Summary

Femoroacetabular impingement (FAI) is a motion related clinical disorder of the hip represented by symptomatic contact of the hip joint surfaces. Hip mechanics in this population during level walking are inconsistent and question whether more challenged walking is necessary to evaluate the role of mechanics in this disease. The current study examines lower limb neuromuscular activity to better understand hip joint mechanics in individuals with FAI compared to asymptomatic individuals. Effect sizes suggest that individuals with FAI may walk with reduced activation of the knee and hip extensors as well as hip abductors.

Introduction

FAI is a proliferative musculoskeletal diagnosis in young adults. Although level walking is considered the gold standard for quantifying lower limb muscle activation, reported neuromuscular changes in this population are limited and inconsistent, thus highlighting the need for more challenged walking tasks to better understand hip joint mechanics in individuals with FAI. The purpose of the current study was to investigate neuromuscular activation during challenged walking in individuals with FAI compared to age matched controls.

Methods

Seven individuals with a clinical diagnosis of FAI (3M/4F) and seven asymptomatic individuals (2M/5F) were recruited to participate. Participants were prepared for surface electromyography (EMG) using a standardized protocol. Surface electrodes were placed bilaterally in a bipolar configuration over the vastus medialis (VM) and lateralis (VL), rectus femoris (RF), medial (MH) and lateral (LH) hamstrings, as well as gluteus maximus (GMax) and medius (GMed). The treadmill walking protocol consisted of level walking and four randomized walking conditions including: 5° and 10° inclines, and 5° and 10° declines. Participants walked for three minutes in each condition, and during the third minute a 20-second data collection was recorded. Maximum voluntary isometric contractions (MVIC) were collected for the knee and hip flexors and extensors, and hip abductors. Surface EMG profiles were amplitude normalized using the maximum amplitude calculated for all corresponding MVIC trials (%MVIC). For asymptomatic participants, the study limb was randomly selected for analysis. Peak activations (%MVIC) during stance and their

mean between group differences were calculated for each condition. Cohen's *d* was calculated using the mean difference between groups for each walking condition divided by the pooled standard deviation and interpreted using cut points including 0.2 (small), 0.5 (moderate), and 0.8 (large).

Results and Discussion

Moderate to large between group effect sizes for VM ($d=0.61-1.39$) and VL ($d=0.67-0.88$), and small to moderate effect sizes for RF ($d=0.22-0.52$), were observed for all walking conditions. Individuals with FAI consistently walked with lower quadriceps (VM and VL) activation during all conditions (15%-37%MVIC). Between group differences increased two-fold during inclined and declined walking with larger activation increases for asymptomatic individuals. Minimal between group differences were observed for RF (4%-7%MVIC) during all conditions. Small to moderate between group effect sizes were observed for MH ($d=0.0-0.39$) and LH ($d=0.10-0.57$). Although the between group differences for hamstring activation were small (<9%MVIC) for all walking conditions, individuals with FAI consistently walked with higher activation. Their increases in MH and LH activation were larger (12-19%MVIC) during inclined walking conditions compared to asymptomatic individuals (9%MVIC), but both groups had similar decreases in activation (5-7%MVIC) during declined walking. Small to large between group effect sizes were observed for GMax ($d=0.26-0.73$) and GMed ($d=0.60-0.87$) for all walking conditions. Individuals with FAI consistently walked with lower GMax (8%-25%MVIC) and GMed (13%-20%MVIC) activation during all conditions, with larger between group differences observed during inclined walking.

Conclusions

The present results suggest that neuromuscular activation patterns differ between individuals with FAI and asymptomatic individuals, and between group differences increased during challenged walking. Individuals with FAI may walk with learned strategies to minimize hip joint movement that mirrors hip impingement. Future research to understand these patterns and their relationship with hip joint loading is warranted.

Acknowledgments

Funding for this work was provided by Research Nova Scotia, and Scotia Scholar Award.

Size and structure of joint angle variability in young and old adults performing a fatiguing repetitive reaching task

Christopher A. Bailey^{1,2}, Fariba Hasanbarani^{1,2}, Matthew Slopecki^{1,2}, Chen Yang^{1,2}, Julie N. Côté^{1,2}

¹Department of Kinesiology and Physical Education, McGill University, Montreal, Canada

²Center for Interdisciplinary Research in Rehabilitation of Greater Montreal, Jewish Rehabilitation Hospital, Laval, Canada
Email: cbailey2@uottawa.ca

Summary

Fatigue is a risk factor for musculoskeletal disorders and older adults have been shown to experience more fatigue in everyday life. Motor variability has been shown to mitigate fatigue in repetitive tasks, but the influence of old age is unclear. Young and old adults completed a fatiguing repetitive reaching task while seated. Trunk and upper limb joint angles were computed for the forward reaches of the first (no fatigue: NF) and final (fatigue terminal: FT) minutes. Variability size was quantified by the reach-to-reach standard deviation (SD) of joint angles and variability structure was quantified by uncontrolled manifold outcomes. Old adults had smaller SD in shoulder and wrist angles and less variance parallel to the manifold, but old age did not affect synergy index at NF or FT. Findings suggest that old adults preserved the synergy that stabilized the forward reach motion despite using less motor flexibility.

Introduction

Fatigue has been identified as a risk factor for musculoskeletal disorders. Fatigue from repetitive movements may be mitigated by motor variability and some studies have shown that older adults have more variable motor patterns in repetitive tasks such as gait [1]. However, how older adults use motor variability to mitigate fatigue in the upper limb is unclear. With fatigue from occupational assembly, old and young adults had different changes in the SD of elbow posture [2], a measurement of the size of variability. Without fatigue, old adults have been reported to have higher [3] or no difference [4] in the synergy amongst the joint elements, a structural component of variability. Investigating the size and structure of motor variability together could provide new insights on control of repetitive reaching. Thus, our purpose was to determine the effects of age and fatigue on the *size* and *structure* of joint angle variability during forward reaching.

Methods

Healthy young (N = 18, 9 females, 24.4 ± 2.9 years) and old (N = 16, 11 females, 73.5 ± 7.3 years) adults performed a seated repetitive reaching task with the dominant arm between targets placed at 30% and 100% of functional reach, at a frequency of 1 Hz [5]. Perceived exertion (Borg CR-10 scale) was recorded each minute and, after a rating ≥ 8, the participant performed the task for one final minute. Optoelectronic marker data were used to model joint angles across 11 degrees of freedom of the trunk and upper limb for the last 30 seconds of the first and final minutes, defined as the NF and FT conditions. Angles were partitioned into 15 time-normalized (0-100%) forward reaches.

Size of motor variability was measured by the reach-to-reach standard deviation (SD) of individual joint angles. Structure of motor variability was quantified by the uncontrolled manifold that predicted endpoint position from the 11 joint angles.

Measurements were variance not affecting performance (V_{UCM} , i.e. “good” variability) and variance affecting performance (V_{ORT} , i.e. “bad” variability), as well as the synergy index (ΔV_z). Means were calculated for the early (0-10%), middle (40-60%), and late (90-100%) phases of the reach for each condition, then compared in Age*Condition*Phase general estimating equations that covaried for sex and body mass index.

Main Results

Size of reach-to-reach variability: Generally, SD of trunk, shoulder, and wrist angles increased from NF to FT. SD of shoulder abduction/adduction, shoulder flexion/extension, wrist pronation/supination, and wrist flexion/extension in the early phase were larger in young than in old adults.

Structure of reach-to-reach variability: No age effects were seen in ΔV_z (young: 0.27-0.54; old: 0.45-0.65). V_{UCM} increased from NF to FT at the late phase in both age groups, and V_{UCM} was larger in young than in old adults at the early phase (interaction effect: $p < 0.001$; Figure 1).

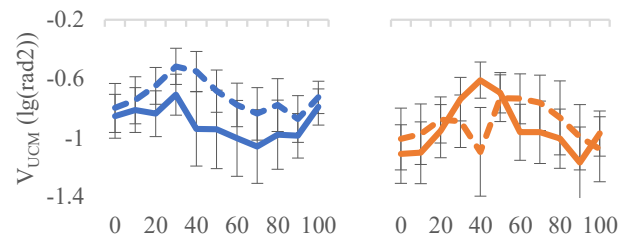


Figure 1. Mean forward reach V_{UCM} of young (left) and old (right) adults at no fatigue (solid line) and fatigue time (dashed line).

Conclusions

In seated repetitive forward reaching, fatigue similarly affected the size and structure of variability of young and old adults. While old adults had less motor flexibility in the early phase of reaching than young adults, due to greater variability in shoulder and wrist angle, old adults still produced a similar motor synergy that stabilized endpoint motion.

Acknowledgments

This project was supported by funding from the Natural Sciences and Engineering Research Council of Canada.

References

- [1] Bailey et al (2020). *J Biomech*, **99**: 109574.
- [2] Greve et al (2017). *Eur J Appl Physiol*, **117**:955-67.
- [3] Qin et al (2014). *J Electromyogr Kinesiol*, **24**:404-11.
- [4] Xu X et al (2013). *Exp Brain Res*, **231**:249-56.
- [5] Bailey et al (2020). *J Aging Phys Act*, **28**:556-66.

Mirror-system-like excitability to kinaesthetic stimuli in the human motor cortex

Marc H. E. de Lussanet^{1,2}, Volker Zschorlich³, Frank Behrendt⁴

¹Movement Science, University of Münster, Münster, Germany

²OCC Center for Cognitive and Behavioral Neuroscience, University of Münster, Münster, Germany

³Department of Movement Science, University of Rostock, Ulmenstraße 69, 18057 Rostock, Germany

⁴Reha Rheinfelden, Research Department, Salinenstraße 98, CH-4310 Rheinfelden, Switzerland

Email: lussanet@uni-muenster.de

Summary

The mirror neuron system integrates sensory stimuli into our own motor control. Initially, mirror behavior is known in human and monkey motor neurons when seeing or hearing another individual's actions. An open question is how this mirror behavior relates to one's own kinaesthetic input. Here we present data showing that motor evoked potentials (MEP) by transcranial magnetic stimulation (TMS) are the same for passive viewing of other's wrist movement and passive movements of one's own wrist. The kinaesthetic influence on the motor threshold was even slightly stronger than the visual stimulation, whereas combined visual and kinaesthetic stimulation further increased the MEPs. We thus provide, for the first time, evidence for the integration of passive kinaesthetic- and visual-sensory stimuli.

Introduction

Cells of the mirror neuron system have originally been described as motor neurons from the premotor cortex that also respond if motor action is seen while the individual is passive [1], but such mirror activity has later been found for the entire frontal cortex [2]. In humans, mirror neuron activity is typically studied using Motor Evoked Potentials (MEPs) [3]. MEPs can be evoked by placing an electromagnetic coil over the skull which directs a brief, focal electromagnetic pulse into the cortex, known as Transcranial Magnetic Stimulation (TMS). When placed over the motor cortex, such a magnetic pulse may evoke brief, local, involuntary muscle contractions. When a wrist movement is seen by a passive subject, even subthreshold TMS pulses over the hand region of the contralateral motor cortex can evoke an MEP [2].

Since mirror neurons are motor neurons [1], we hypothesized that kinaesthetic sensory information should also affect the mirror neurons. However, it is not known if this is so. Moreover, it is not known if kinaesthetic sensory information from passive movements can activate the motor system in the way that visually perceived motor actions do.

The goal of the present experiment was to find out how the seeing of passive wrist movement and the kinaesthetic sensory information from the passively moved wrist relate, by implementing an MEP paradigm [4].

Methods

Twenty healthy participants with a mean age of 28.3 years (± 8.3) with no history of neurological disease or upper limb impairment were included.

60 stimulations were applied for the three conditions in random order: KIN: the kinaesthetic stimulus was applied by a passive, motor controlled, wrist extension movement, VIS: visual presentation of an animated wrist extension movement, and VIS&KIN: the synchronously applied

visual and kinaesthetic stimuli. For the control condition (CC) 20 Stimulations were applied. Subjects could not see their arm, were requested to keep their wrist relaxed all the time.

For TMS a magnetic stimulator R30 MagPro with MagOption (MagVenture, Skovlunde Denmark) and a parabolic coil type MMC-140 were used. For recording of the EMG, two electrodes (surface area of 3 mm^2) were placed with a distance of 1 cm longitudinally over the belly of the *extensor carpi radialis* muscle.

Results and Discussion

All differences were statistically significant (Fig. 1). Both VIS and KIN stimulation resulted in stronger MEPs than the control condition. The combined condition VIS&KIN showed an even stronger MEP, but less than the sum of VIS and KIN.

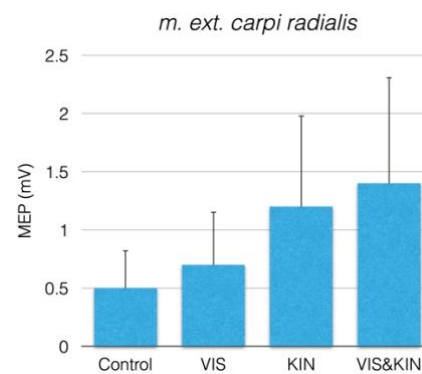


Figure 1: Evoked potentials in the wrist extensor muscle.

The kinaesthetic information from passive wrist extension lowers the motor threshold for wrist extension. This result shows, that on a cortical level, the motor system does not oppose passive movement, but rather releases it.

This result is fully consistent with the known mirror neuron mechanism. The low level of summation indicates, that at least some of the VIS and KIN sensorimotor integration depends on a shared pool of motor neurons.

Conclusions

Our results support the implicit assumption of the mirror neuron theory, that the motor system processes afferent kinaesthetic information and sensory information about others' actions in a coherent manner [4].

References

1. Rizzolatti G, et al. (1996). *Cogn Brain Res.* **3**: 131–141.
2. Fadiga L et al. (2005). (1995). *J Neurophysiol* **73**: 2608–2611.
3. Rizzolatti G and Craighero L (2004). *Annu Rev Neurosci* **27**: 169–197.
4. Zschorlich VR, Behrendt F, de Lussanet MHE (2021). *Brain Sci*, also available on *bioRxiv*

Individual finger movement control and association to brain activity in healthy participants

Helena Grip¹, Anna-Maria Johansson², Carl-Johan Boraxbekk^{3,4,5}, Jonas Selling⁶, Louise Rönnqvist², Charlotte K Häger⁶

¹Department of Radiation Sciences, Umeå University, Umeå, Sweden; ²Department of Psychology, Umeå University, Umeå, Sweden; ³Danish Research Centre for Magnetic Resonance (DRCMR); ⁴Centre for Functional and Diagnostic Imaging and Research, Copenhagen University Hospital Hvidovre, Copenhagen, Denmark; ⁵Umeå Center for Functional Brain Imaging (UFBI), Umeå University, Umeå, Sweden; ⁶Department of Community Medicine and rehabilitation; Physiotherapy, Umeå University, Umeå, Sweden. Email: Helena.grip@umu.se

Summary

Our study addresses the control of individual finger movements in humans and the associated brain response. We investigated this by simultaneous recordings of finger kinematics and functional Magnetic Resonance Imaging (fMRI) in 26 asymptomatic individuals. Preliminary results show that finger independence differed between fingers, and that there were associated, overlapping finger movement representations primarily found in the contralateral sensorimotor areas of the brain.

Introduction

Digits are represented as a fine-grain somatotopy in the primary somatosensory cortex [1] but it is not known to which extent finger movement control can be broken down to the digit specific level. The current study aims to examine the underlying neural correlates of individual finger movements. Specifically, we want to associate kinematic indices of finger movement independence [2], with brain activity estimated with fMRI in healthy individuals.

Methods

Twenty-six right-handed participants (Mean age 62 years) performed cyclic flexion-extension movements of one finger at a time while keeping the other fingers still (Figure 1), lying in a 3T MR scanner. The blood-oxygen-level-dependent imaging technique (fMRI) quantified brain response while four 3D optical special non-magnetic cameras (Qualisys AB, Gothenburg) simultaneously recorded the positions of ten reflective markers affixed to each finger. Test instructions were presented on a screen via a tilted mirror.

Movements of the dominant hand's fingers were analyzed. Motion capture data were exported to Visual3D software and filtered with a 6 Hz low-pass filter. Automated scripts identified the start and stop of each flexion-extension. An Individuation Index (II) computed each finger's movement independence by the ratio of the finger's normalized movement in relation to the others; "1" represented excellent finger independence and "0" represented no independence [2]. Brain response associated to each finger's movement was analyzed, both in comparison to rest and in comparison to the thumb movement using statistical parametric mapping (SPM12, Wellcome Trust Centre for Neuroimaging).

Results and Discussion

The thumb had the highest II (0.98 ± 0.01) followed by the index finger (0.95 ± 0.02), the little finger (0.91 ± 0.05), the ring finger (0.91 ± 0.04) and the middle finger (0.90 ± 0.03), in line with previous studies [2]. Preliminary results reveal differences in the associated brain activation (Figure 3), with overlapping regions primarily found in the contralateral sensorimotor areas (Fig 3).

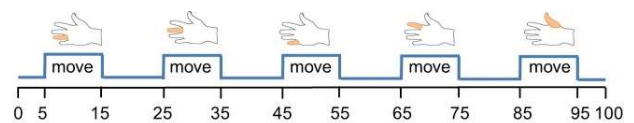


Figure 1: A block design was used where the finger either moved or were held still during a period of 10 seconds.

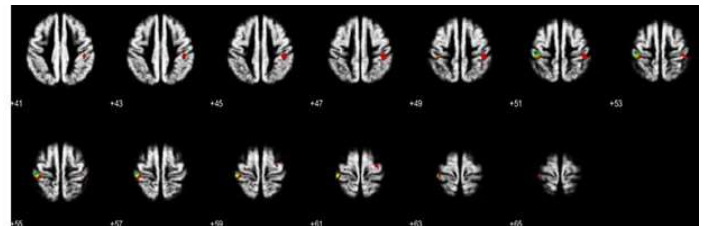


Figure 3: Statistical brain maps (familywise corrected, $p=0.05$, voxel threshold 15) describing overlapping regions for the fingers when contrasted against the thumb (Index finger: blue, long finger: green, Ring finger: yellow, Little finger: red)

Conclusions

The movement independence was lower in all fingers compared to the thumb, and the ranking seems to also be corresponding to activation of different but yet overlapping somatosensory areas of the brain. Further analysis is in progress.

Acknowledgement

This study was funded by Stiftelsen Promobilia, Norrbacka-Eugeniastiftelsen, Foundation of Stroke research I Norrland, Stroke-Riksförbundet and Konung Gustaf V:s and Drottning Victorias frimurarstiftelse.

References

- [1] Kolasinski J. et al (2016) *J NeuroSci*, **36**: 1113-1127.
- [2] Häger-Ross C and Schieber MH (2000). *J NeuroSci*, **20**: 8542-8550.

Synergic control of individual muscles and agonist-antagonist muscle pairs

Mark L. Latash

(Pennsylvania State University, University Park, PA 16802)

According to the original concept of synergy introduced by Nikolai Bernstein, numerous muscles, which take part in natural movements, are united into stable groups, and the group involvement co-varies to ensure dynamical stability of salient performance variables. Recently, we have extended this concept to within-a-muscle recruitment patterns of motor units (MUs). During accurate cyclical force production, MUs in extrinsic hand muscles (flexor digitorum superficialis, FDS, and extensor digitorum communis, EDC) form stable groups – MU-modes. Within-a-muscle analysis of MU-mode variance across force cycles has shown much larger variance within the space that leads to no force change (uncontrolled manifold, UCM) compared to the orthogonal to the UCM space (ORT). These signatures of force-stabilizing synergies were present in spaces of the MU-modes defined for FDS and for EDC separately. Analysis of MUs combined over FDS and EDC has revealed two MU-modes corresponding to the reciprocal and coactivation commands as introduced within the theory of control with spatial referent coordinates – a major support for the theory. The existence of MU-based synergies suggests an important role of segmental reflex mechanisms in synergic control of movements.

Automated Analysis of Medial Gastrocnemius Muscle-Tendon Junction Displacements in Healthy Young Adults Using Deep Neural Networks

Rebecca L. Krupenevich, Callum J. Funk, Jason R. Franz

¹Joint Department of Biomedical Engineering, UNC Chapel Hill and NC State University, Chapel Hill, NC
Email: rkrup@email.unc.edu

Summary

We show that deep neural networks (DNNs) created with open-source software are capable of accurately tracking muscle-tendon junction (MTJ) positions in cine B-mode ultrasound images in tasks spanning controlled loading during isolated contractions to physiological loading during treadmill walking.

Introduction

Direct measurement of MTJ position is important for understanding dynamic tendon behavior and muscle-tendon interaction in healthy and pathological populations [1]. Obtaining MTJ position during functional activities is often accomplished by manually labeling the MTJ in cine B-mode ultrasound images, a laborious and time-consuming process. Advancements in deep learning have facilitated the availability of open-source software for automated video tracking [2]. However, these tools were originally intended for animal pose estimation and have not been widely applied to ultrasound images. The purpose of this paper was to evaluate the efficacy of DNNs to track medial gastrocnemius MTJ position in cine B-mode ultrasound images from isolated contractions and treadmill walking.

Methods

Cine B-mode ultrasound images of the medial gastrocnemius MTJ were collected from 15 subjects (6M/9F, 23 yr, 71.9 kg, 1.8 m) during treadmill walking at 1.25 m/s and during maximal voluntary isometric plantarflexor contractions (MVCs). Subjects were randomly shuffled into five combinations of 12 training and 3 test subjects - each combination was trained using 480 manually labeled images collected during walking (40 per training subject) - which we used to predict MTJ position in images from test subjects during walking (novel subject) and MVCs (novel condition).

Results and Discussion

Overall root mean square error (RMSE) was 2.72 mm and 6.24 mm between manually labeled and predicted MTJ position in novel-subject and novel-condition evaluations, respectively – comparable to previous DNNs trained with larger training sets [3]. A modified median filter reduced overall RMSE to 2.37 mm and 5.05 mm in the novel-subject and novel-condition evaluations, respectively.

Conclusions

Our results support the use of open-source software for creating DNNs to reliably track MTJ positions in B-mode ultrasound images. We believe this approach to MTJ

position tracking is an accessible and time-saving solution, with broad applications for many fields, such as rehabilitation or clinical diagnostics.

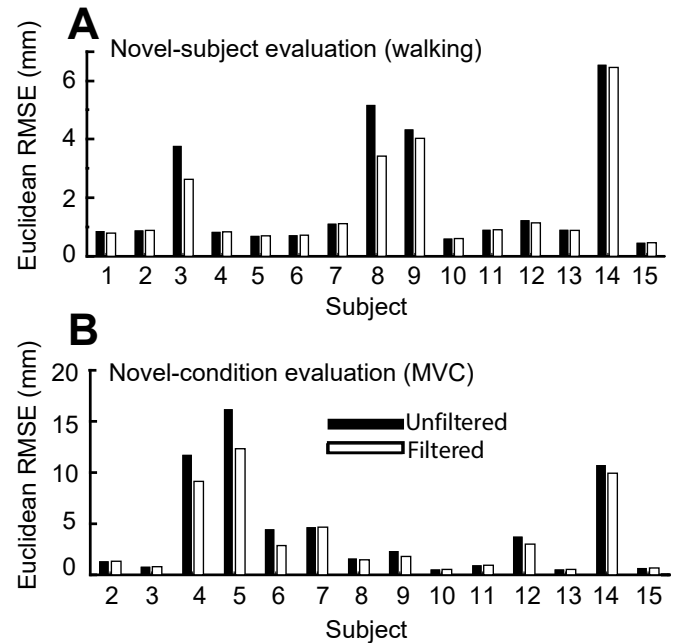


Figure 1: Unfiltered (black) and filtered (white) root mean square error (RMSE) for A) each individual subject in the novel-subject evaluation (walking), and B) each individual subject in the novel-condition evaluation (MVC).

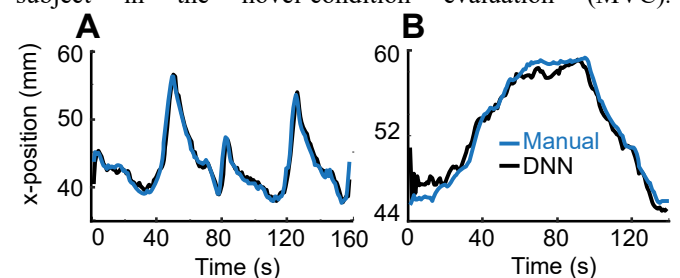


Figure 2: Manually labeled (blue) and predicted (black) MTJ positions for one representative subject during A) walking, and B) MVC.

Acknowledgments

This work was supported by grants from the NIH: R01AG058615 to JRF and F32AG067675 to RLK.

References

- [1] Cronin and Lichtwark (2013). *Gait Posture*, 37:305-12.
- [2] Mathis A et al. (2018) *Nat Neurosci*, 21(9): 1281-86.
- [3] Leitner et al. (2020) *Bioarxiv*:2005020

Intra-assessor reliability of intrinsic foot muscles' size in older and younger adults using a portable ultrasound device

Lydia Willemse^{1,2,3}, Eveline Wouters^{1,3}, Martijn Pisters^{1,4,5}, Benedicte Vanwanseele^{1,2}

¹Department of Health Innovations and Technology, Fontys University of Applied Sciences, Eindhoven, The Netherlands

² Department of Movement Sciences, KU Leuven, Leuven, Belgium

³Tranzo, School of Social and Behavioral Sciences, Tilburg University, Tilburg, The Netherlands

⁴Department of Rehabilitation, Physiotherapy Science & Sport, University Medical Center Utrecht, Utrecht, The Netherlands.

⁵Center for Physical Therapy Research and Innovation in Primary Care, Julius Health Care Centers, Utrecht, The Netherlands

Email: Lydia.willemse@fontys.nl

Summary

To determine the intra-assessor reliability of ultrasound measurements of intrinsic foot muscles' size in older and younger adults, we used a portable tablet-based device. Measurement errors relative to the mean muscle size did not exceed 6.3% in older adults. The intrinsic foot muscles' size measurements are sufficiently reliable to be used in the assessment of force generating capacity of these muscles in older adults.

Introduction

Intrinsic foot muscles have an essential role in foot function during walking. The size of the foot's intrinsic muscles serves as a measure of the strength and has been associated with balance [1] and gait biomechanics [2] in healthy younger adults. In order to study foot function in older adults, the reliability of ultrasound measurements of intrinsic foot muscles' size in this specific population needs to be investigated. The purpose of the study was to determine the intra-assessor reliability of ultrasound measurements of intrinsic foot muscles' size in older and younger adults.

Methods

A single assessor test-retest study was performed in 10 older (5 male, 5 female, 74.5 ± 5.6 years) and 10 younger adults (4 male, 6 female, 21.9 ± 1.8 years) not presented with conditions that compromise gait. Ultrasound images of abductor hallucis (AbH), flexor digitorum brevis (FDB), quadratus plantae (QP), flexor hallucis brevis (FHB) and abductor digiti minimi (AbDM) were captured on two separate occasions (1-7 days apart) using a portable tablet-based Philips Lumify ultrasound device.

The scan protocol [3] was carried out by a single operator. Three longitudinal and transverse (only for AbH and FDB) images per muscle and for each occasion were post-processed using Image J software to obtain the mean thickness and cross-sectional area (CSA). The intraclass correlation coefficient (ICC; 3,3; absolute agreement) and standard error of measurement (SEM) were calculated.

Results and Discussion

For all, but the FDB thickness, the SEM was smaller for younger adults (Table 1). This may be explained by the increased intramuscular adipose and connective tissue with advancing age that is detrimental for image quality. Even

though this difference, the SEM relative to the mean did not exceed 6.3% for older adults. This SEM is smaller compared to other foot muscle strength measures, such as those obtained with dynamometry [4], and also smaller than the effect that is expected from a strengthening exercise intervention [4].

The SEM of the CSA is slightly smaller than the SEM of the thickness of the same muscles in the older adults. Considering that the CSA is a more representative measure of the force generating capacity of a muscle, we recommend to use the CSA to measure the size of AbH and FDB in this population.

Table 1: Measurement properties of muscles' size measures.

Muscle	Size measure	Older		Younger	
		ICC	SEM (%)	ICC	SEM (%)
AbH	CSA	0.97	9.86 (4.8)	0.98	8.04 (4.2)
	thickness	0.95	0.56 (5.4)	0.99	0.18 (1.6)
FDB	CSA	0.98	11.0 (4.4)	0.98	7.57 (3.6)
	thickness	0.96	0.52 (5.0)	0.87	0.81 (7.6)
QP	thickness	0.94	0.34 (3.8)	0.94	0.26 (2.6)
FHB	thickness	0.79	0.84 (6.3)	0.93	0.57 (4.0)
AbDM	thickness	0.89	0.49 (5.3)	0.96	0.41 (3.7)

AbH: abductor hallucis, FDB: flexor digitorum brevis, QP: quadratus plantae, FHB: flexor hallucis brevis, AbDM: abductor digiti minimi, CSA: cross-sectional area, ICC: intraclass correlation coefficient, SEM: standard error of measurement.

Conclusions

Based on our findings, we conclude that the size of intrinsic foot muscles can be reliably assessed in older adults by the same assessor using a portable ultrasound system and hence can be used to investigate foot function in this population.

Acknowledgments

This work was supported by the doctoral grant for teachers from the Dutch Research Council (NWO) and is registered under the NWO project number 023.013.063.

References

- [1] Zhang X et al. (2017). *Gait & Posture*, **57**:52-6.
- [2] Zhang X et al. (2017). *Gait & Posture*, **54**:290-4.
- [3] Mickle KJ et al. (2013). *J Foot Ankle Res*, **6**:12.
- [4] Ridge ST et al. (2019). *Med Sci Sports Exerc*, **51**:104-113.

Quantitative assessment of a treatment addressing hypomimia in Parkinson's disease

E. Pegolo¹, L. Ricciardi^{2,3}, D. Volpe⁴, Z. Sawacha^{1,5}

¹ Department of Information Engineering, University of Padova, Padua, Italy

² St George's University of London, Molecular and Clinical Sciences Institute, London, United Kingdom

³ Medical Research Council Brain Network Dynamics Unit, Nuffield Dept. of Clinical Neurosciences, Oxford, UK

⁴ Fresco Parkinson Center, Villa Margherita, S. Stefano, Vicenza, Italy

⁵ Department of Medicine, University of Padova, Padua, Italy

Email: elena.pegolo@studenti.unipd.it

Summary

Hypomimia is one of the clinical hallmarks of Parkinson's disease (PD). Patients experiencing this symptom have a limited facial expression that could lead to a reduction of their social well-being. We conducted a preliminary study on ten PD patients who underwent a specific rehabilitation treatment and quantified its effects exploiting a face tracking algorithm.

Introduction

PD is a progressive disease that mainly affects the movement. The most frequent symptoms are tremor, rigidity, and bradykinesia, that have been widely investigated in the upper and lower limbs. However, they can also affect facial muscles causing hypomimia: a reduced facial expression both in spontaneous and voluntary facial movements. Hypomimia can lead to a significant reduction of the patient's quality of life who may experience social interaction difficulties. Limited data are available on validated treatments and on the evaluation of their possible effects [1]. The aim of our study is to quantitatively assess the effects of a hypomimia treatment in PD patients comparing the pre- and post-treatment conditions. We exploited a face tracking algorithm based on the Facial Action Coding System (FACS) [2,3].

Methods

Ten PD patients (mean(±SD) age: 68.4(±8.46) years) were analyzed. Patients underwent a hypomimia rehabilitation treatment consisting of 9 sessions of 60 minutes each, in a time window of two months. Data acquisition took place before (T₀) and after the treatment (T₁). MDS-UPDRS values were collected (Table 1). Moreover, frontal face videos of the subjects were recorded while they were instructed by an operator to perform the face expressions described in [3]. A GoPro Hero 3 camera (1920x1080 pixels, 30 fps) placed at eye level, at 1.36 m from the patient seated with a white background behind was used. Videos were segmented into 4 frames per each emotion; using an ad-hoc set of 56 features tracked in the 2D-image space (*TrackOnField*, self-developed software, *BBSof S.r.l.*) [4], 35 distances were calculated

(Fig1). Each distance was normalized on the corresponding one in the neutral expression. The two conditions were compared through Wilcoxon signed-rank test (p<0.05).

Results and Discussion

Along with the improvements in the MDS-UPDRS scale values (Table 1), results showed an enhancement in facial mobility at T₁ (Figure 1).

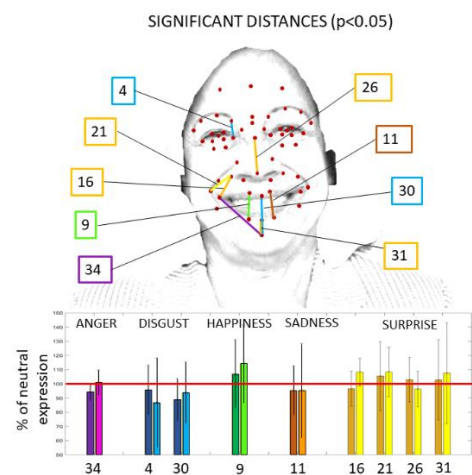


Figure 1: Statistically significant distances per emotion. Darker colors refer to T₀. The red line represents the neutral expression.

Conclusions

Preliminary results on the quantification of the treatment outcomes are encouraging. This method can be used in future investigations increasing the dataset and studying different rehabilitation treatments.

References

- [1] Ricciardi L. (2017). *PLOS One*, **12(1)**:e0169110.
- [2] Ekman, P. (1978) *Facial Action Coding System: Investigator's Guide*; Consulting Psychologists Press.
- [3] Wu P., et al. (2014). *Comput Math Methods Med*, **2014**.
- [4] Magalhaes FA et al. (2013). *J Sport Sci Med*; **12**:660.

Table 1: MDS-UPDRS values in the pre- (T₀) and post-treatment (T₁) conditions

(Part). Item	(III) .2	(III) .1	(II) .1	(I) .3	(I) .5	Total UPDRS score	
Description	Facial expression	Speech	Speech	Depressed mood	Apathy		
T₀	mean ± SD	1.90 ± 0.32	2.10 ± 0.88	2.10 ± 0.99	2.30 ± 1.16	1.90 ± 1.66	116.3 ± 27.93
T₁	mean ± SD	1.40 ± 0.52	1.80 ± 1.03	1.60 ± 1.26	1.22 ± 0.83	1.11 ± 1.05	87 ± 33.11

Development of an In-Vivo Tibiotalar Kinematic Protocol to Investigate Activities of Daily Living

D. Williams¹, L. Esquivel¹, G. Chapman², C. Brockett³

¹Musculoskeletal Biomechanics Research Facility, School of Engineering, Cardiff University, Cardiff, UK

²Allied Health Research Unit, School of Sport and Health Sciences, University of Central Lancashire, UK

³Institute of Medical and Biological Engineering, School of Mechanical Engineering, University of Leeds, Leeds, UK

Email: williamsd37@cardiff.ac.uk

Summary

It is an important and technical challenge to measure the in-vivo kinematics to evaluate the biomechanical and functional effects of ankle injury. To fully understand these difference healthy comparator data is needed. This pilot study develops imaging protocols to measure the direct bone movements of the tibia and talus using biplane video X-ray and MRI. The pilot results demonstrated the differences between the activities and provided suggestions on stratification of future healthy cohorts.

Introduction

To be able to evaluate the biomechanical and functional effects of ankle injury and disease, and the interventions used to treat them, it is first necessary to characterize ankle kinematics in a healthy population. Due to the anatomical complexity of the ankle, it is difficult to accurately measure the Tibiotalar and Subtalar joint angles using traditional marker-based motion capture techniques. Biplane Video X-ray (BVX) is an imaging technique that allows direct measurement of individual bones using high-speed, dynamic X-rays. It has been suggested in a recent review that there is a lack of research on healthy ankle joint kinematics and different activities need to be investigated [1]. This pilot study is focused on developing an in-vivo protocol for the ankle joint looking initially at the tibiotalar joint for two different activities of daily living.

Methods

A custom-built raised walkway was manufactured to position the foot and ankle inside the field of view of the BVX system.

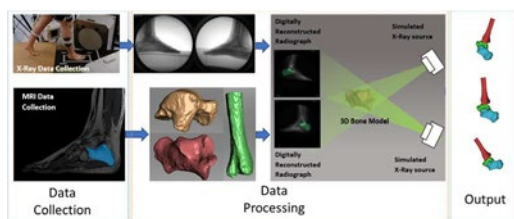


Figure 1: Data collection and processing pipeline

Two healthy volunteers performed five gait and step-down trials while capturing Biplane Video X-Ray (125Hz, 1.25ms pulse width, 80kVp and 160 mA). Participants underwent MR imaging (Magnetom 3T Prisma, Siemens) which were manually segmented into 3D bone models (Simpleware Scan IP, Synopsis). Anatomical coordinate systems were applied to the 3D bone models using the centroid and inertial axes of each bone. Bone position and orientation for the Talus and Tibia were calculated by manual matching of 3D Bone models

to X-Rays (DSX Suite, C-Motion, Inc.) (Fig 1). Kinematics were calculated using MATLAB (MathWorks, Inc. USA).

Results and Discussion

For this pilot study it was found that for the two activities of daily living there was a larger range of motion (ROM) for the sagittal plane rotations (Fig. 2) for step down (26.1°) compared with gait (16.2°) at the tibiotalar joint. For frontal and transverse plane rotations the ROM were found to be larger for gait (frontal: 13.9°, transverse: 9.5°) when compared with step down (frontal: 11.0°, transverse: 6.5°). When comparing the two volunteers it was found that they performed varying movement strategies for the different activities. For gait it was found that HV002 had reduced plantarflexion during heel strike and ROM during stance compared with HV001 (Fig. 2). For step down, HV001 used a forefoot strike during step down whereas HV002 used a midfoot strike strategy to step down. This is shown in Fig. 2 by the reduced plantar flexion at initial contact of step down. These results suggest that for future data collection it may be necessary to stratify by movement strategy for different activities of daily living to fully understand the variation within healthy ankle functioning.

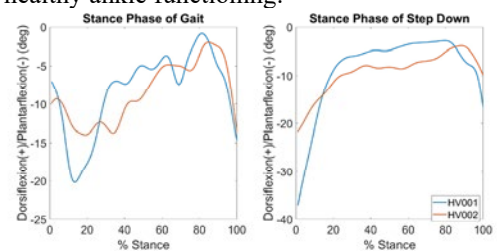


Figure 2: Sagittal plane Tibiotalar joint angles during gait and step down

Conclusions

The developed protocol successfully calculated the in-vivo kinematics of the tibiotalar joint for different dynamic activities of daily living. These pilot results show the varying kinematics between two different activities of daily living and highlight the need for a larger cohort study. Future work would look to expand the analysis to the other joints in the ankle complex and investigate further activities of daily living.

Acknowledgments

Funding received from the OATech Network+ Biomechanics and Mechanobiology Pump-priming Project.

References

- [1] Canton et al. 2020. *Current Reviews in Musculoskeletal Medicine*, **13**: 77-85.

Fixation of tibial components in cementless total knee replacement measured with RSA and MRI

Jordan S. Broberg¹⁻³, M.F. Koff⁴, J.L. Howard⁵, B.A. Lanting⁵, H.G. Potter⁴, and M.G. Teeter^{1-3,5}

¹Department of Medical Biophysics, Schulich School of Medicine & Dentistry, Western University, London, Canada

²Robarts Research Institute, London Canada; ³Lawson Health Research Institute, London, Canada

⁴Department of Radiology and Imaging, Hospital for Special Surgery, New York, USA

⁵Department of Surgery, Schulich School of Medicine & Dentistry, Western University, London, Canada

Email: jbroberg@uwo.ca

Summary

This study aims to investigate cementless total knee replacement (TKR) implant fixation using radiostereometric analysis (RSA), and to study the corresponding bone-implant interfaces for bone ingrowth using modified magnetic resonance imaging (MRI). Early results show a potential relationship between the amount of migration and the type of bone-implant interface.

Introduction

Modern cementless TKR implants have porous metal surfaces that allow for bone ingrowth to create a biological fixation mechanism. The gold standard for investigating implant fixation is RSA, which has previously been used to study cementless TKR [1]. Modified MRI techniques have been developed to analyze the bone-implant interface and classify an implant as loose if there is poor bone integration. However, there is yet to be a study that uses both modalities to determine if there is a relationship between implant fixation and the type of bone-implant interface. Therefore, the objective of this study is to investigate cementless TKR implant fixation using RSA, and to study the corresponding bone-implant interfaces for bone ingrowth using modified MRI.

Methods

Thirty patients will be recruited and implanted with cementless titanium tibial components and cobalt-chromium femoral components. Supine RSA and MRI exams will be performed at a baseline of one day after TKR surgery and again at 2-weeks, 6-weeks, 3-months, and 6-months postoperatively. Additional standing weight-bearing RSA exams will be done at all non-baseline timepoints. Supine RSA is used to measure implant migration at different fictive points (Figure 1) on the tibial component relative to bone over time. Standing RSA exams are compared to their supine counterparts to determine inducible displacement, a measure of how much an implant shifts in weight-bearing conditions.

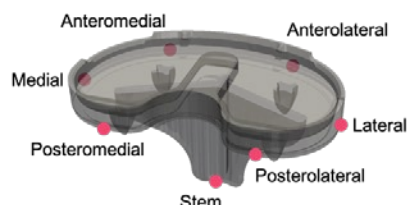


Figure 1: Location of fictive points on the tibial component.

MRI is performed using a 3T clinical scanner and the MAVRIC metal artifact suppression sequence, from which the bone-implant interface is classified as: normal, fibrous, fluid, or osteolytic and the percent contact of bone with the porous metal implant surface is assessed. Implants are then scored as either loose or not loose.

Results and Discussion

Two patients have been recruited at time of submission and data has been collected up to 3-months. Figure 2 displays the fictive point migration of the tibial component for both patients. For Patient S01, the maximum inducible displacement was 0.61 mm at 2-weeks (posteromedial), 0.67 mm at 6-weeks (medial), and 1.06 mm at 3-months (lateral). For Patient S02, the maximum inducible displacement was 0.50 mm at 2-weeks (stem), 1.75 mm at 6-weeks (posteromedial), and 0.93 mm at 3-months (posteromedial). MR images at all timepoints revealed >66% contact of bone with the porous implant surfaces. Patient S01 had normal bone-implant interfaces in all regions of the tibial component. Patient S02 had fibrous tissue in the anteromedial and anterolateral regions at Day 1 and 2-weeks, but these regions scored normal at 6-weeks and 3-months. All other bone-implant interfaces were normal. Both patients' implants were scored as not loose.

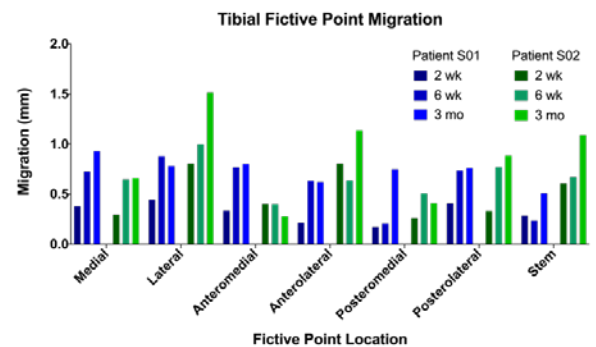


Figure 2: Migration of each fictive point on the tibial component for Patient S01 and S02 at 2-weeks (2 wk), 6-weeks (6 wk), and 3-months (3 mo).

Conclusions

Early results show a potential relationship between the amount of migration and the type of bone-implant interface, as a high amount of migration was seen at fictive points in regions where a fibrous membrane interface was located.

References

[1] Hasan S. et al. (2020). *Bone Joint J*, **102-B**:1016–1024.

Force transmission via intertendinous linkages of the m. flexor digitorum profundus

G. Geusebroek¹, G.C. Baan¹, H.E.J. Veeger^{1,2}, H. Maas¹

¹Dept. of Human Movement Sciences, Vrije Universiteit, Amsterdam

²Dept. of Biomechanical Engineering, TU Delft

Email: g.m.geusebroek@vu.nl

Summary

Force transmission via intertendinous linkages of the extrinsic finger flexors has been proposed as one of the factors causing limited independent finger movement. We assessed force transmission via linkages between the tendons of the flexor digitorum profundus (FDP) in fresh frozen cadaver hands by exerting force on the tendon of one finger and measuring the flexion force exerted by the other fingers. Our results show that intertendinous linkages of the FDP transmit force to neighboring fingers and that the extent of such force transmission increases upon flexion of the target finger (TF).

Introduction

The independent movement of fingers is limited [1]. Unintended movement or force production of fingers is termed enslavement [2]. Besides neural factors, mechanical coupling between finger flexor tendons via intertendinous tissue may cause enslavement [3], but this has not been investigated. We assessed the effects of finger position on force transmission between FDP tendons via mechanical linkages.

Methods

In six fresh-frozen cadavers, lower arms were amputated, the volar skin was removed until the carpal tunnel, and the myotendinous junctions of the FDP were severed. The arm was secured to a frame with the fingers pointing upward and the wrist fixed at $\sim 20^\circ$ dorsiflexion. The dorsal aspect of each proximal phalangeal bone of the fingers was connected to force transducers to measure flexion force. Each non-targeted finger (NTF) tendon was loaded with a weight of 3N. Then the TF tendon was loaded with 10N. Flexion force of each finger was measured before and after loading the TF tendon and the difference was calculated (Δ Force). Each of the four fingers was tested with the TF extended and flexed in $\sim 90^\circ$. Δ Force exerted at each NTF was expressed as a percentage of the total flexion force exerted at all fingers.

Results and Discussion

For all fingers, applying a load on the TF tendon resulted in changes of force exerted at the adjacent NTFs (Table 1). Δ Force was higher for fingers adjacent to the TF than for fingers not adjacent to the TF. Δ Force of adjacent NTFs increased upon TF flexion, ranging from 18 to 58%, except for the index finger when the middle finger was targeted (Figure 1).

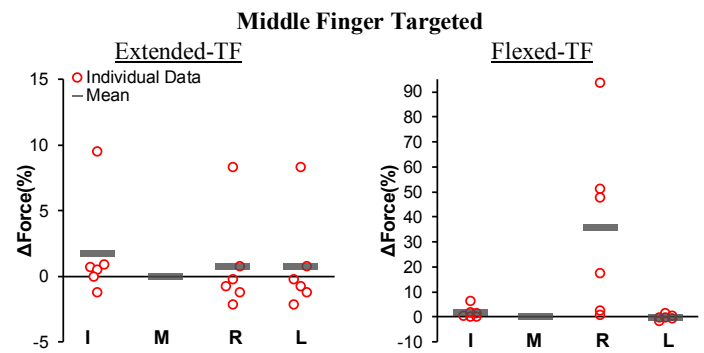


Figure 1: Δ Force(%) exerted by the NTF of each hand when the middle finger(M) was the TF; tested in extended and flexed position.

Results indicate that the linkages between the FDP tendons do transmit force when pulled on only one of the tendons and that force transmission increases upon TF flexion. Thus, intertendinous linkages of the FDP do contribute to finger enslavement, especially when one finger is moved relative to the other fingers. Intertendinous force transmission should be taken into account in the design of musculoskeletal models of the hand.

Acknowledgements

Funded by the European Commission through MOVE-AGE, an Erasmus Mundus Joint Doctorate program (2011–0015).

References

- [1] Van den Noort et al. (2016) *PLoS One* **10**: 1–18
- [2] Van Duinen et al. (2011) *J. Physiol.* **589**, 23: 5583–5593
- [3] Mirakhorlo et al. (2017) *PLoS One* **12**: 1–9

Table 1: Mean \pm SD per NTF for each TF. Significant ($p < 0.05$) *main effects of position and interaction effects assessed with a mixed ANOVA.

Δ Force(%)		Targeted Finger							
		Index-finger		Middle-finger*		Ring-finger		Little-finger*	
		Extended	Flexed	Extended	Flexed	Extended	Flexed	Extended	Flexed
NTF	Index	-	-	1.7 \pm 3.9	1.8 \pm 2.3	1.1 \pm 0.7	1.2 \pm 1.6	0.3 \pm 1	0.5 \pm 0.6
	Middle	3.1 \pm 9.1	18.3 \pm 34.8	-	-	5.3 \pm 8.4	17.9 \pm 26.5	1.9 \pm 3.1	0.8 \pm 1.8 *
	Ring	0.7 \pm 1.4	2.4 \pm 3.7	0.8 \pm 3.8	35.6 \pm 35.8	-	-	13.7 \pm 20.7	57.9 \pm 33.5
	Little	0.6 \pm 1.4	0.3 \pm 0.7	0.2 \pm 0.9	-0.1 \pm 1	1.9 \pm 3.1	22.8 \pm 30.8	-	-

Monitoring Development in Children using Hand function

Vasiliki Vardakastani¹, Oluwalogbon O. Akinola¹, Angela E. Kedgley¹
¹Department of Bioengineering, Imperial College London, London, UK
 Email: v.vardakastani13@imperial.ac.uk, akedgley@imperial.ac.uk

Summary

This study aims to investigate the effectiveness of different metrics of hand function as a valid and reliable measure of children development. Four tests were used to acquire strength and dexterity measurements of a group of 184 children [range between 5-18 years old]. Our findings show that grip strength and the box and block dexterity tests are appropriate to assess children development.

Introduction

There are a number of clinical tools and assessment tests used to evaluate development in children. Object manipulation is one of the standard metrics for evaluating mental development. Hand function also can be assessed objectively by measuring strength and dexterity. However, there is currently little evidence of the effectiveness of these tests in monitoring developmental changes in children. The aim of this study is to investigate whether specific metrics of hand function can be better correlated with child development and to show whether age can be expressed as a function of such measurements.

Methods

A group of 184 children (100 female, range between [5-18] years old) were recruited for this study. Demographic information about their age, height, weight and hand dominance was collected. Four tests were used to assess the manual strength and dexterity of the participants: the box and block (BBT) and the functional dexterity (FDT) tests and the maximum grip and lateral pinch strength tests. Each participant was randomly assigned to one dexterity and one strength test and they were asked to perform all tests with their dominant hand. For the BBT, the participant was asked to transfer as many blocks as they could in 60 seconds. For the FDT, the participant was asked to turn over all 16 pegs on the board as quickly as possible. Grip and lateral pinch strength were measured using a Jamar dynamometer G200 and a pinch meter P200 (Biometrics Ltd, Newport, UK), respectively. A multiple regression analysis was performed between the test results and the demographic parameters. To avoid overfitting, the models presented below were generated using only parameters with significant effect on the regression.

Results and Discussion

From the four tests investigated in this cohort, only the results of grip and BBT showed large association (Pearson Correlation Coefficient > 0.5) with development parameters age (0.874 for grip, 0.719 for BBT), height (0.858 for grip,

0.612 for BBT) and weight (0.856 for grip). Grip strength showed significant correlations with both dexterity tests ($p = 0.001$ for BBT and $p = 0.002$ for FDT). A linear regression was able to express 63.2% of the variance of the age with respect to grip strength ($R^2=0.632$). However, a second linear regression where both grip and BBT results were used (Figure 1) expressed 78.6% of the age variance within our group ($R^2=0.786$). Both factors had a significant contribution to the regression with a final equation:

$$\text{Age} = 0.175 \cdot \text{Grip strength} + 0.136 \cdot (\text{Box and Block test}) - 0.594$$

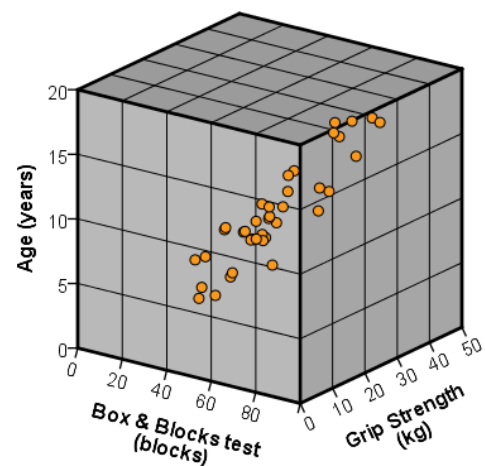


Figure 1: Linear regression between age and grip strength and box and blocks test results.

Our results show that the grip strength and BBT dexterity tests are appropriate for monitoring development. While grip strength alone was able to express a large proportion of the variance within the group, the regression including both grip and BBT presents a more spherical expression of the functional changes during a child's development. Both tests are non-invasive and standardized and they have been previously used to assess hand function in children with myopathy and cerebral palsy [1,2].

Conclusions

The application of these findings can be extended further to healthy cohorts as a sufficient and non-invasive metric to evaluate development in children.

References

- [1] Van den Beld et al. (2011), *Eur J Paediatr Neurol*, **15**(6): 512-518.
- [2] Araneda et al. (2019), *Dev Med Child Neurol*, **61**(10): 1182-1188

A new radiographic index for early diagnosis of perilunate injuries

Pinto FNZ¹, Fernandes CH¹, Meirelles LM¹, Ejnisman B¹, Cohen M¹, Faloppa F¹

¹Department of Orthopedic Surgery, Universidade Federal de São Paulo, São Paulo, Brazil

Email: drfernandozambone@gmail.com

Summary

The objective of this study was to develop radiographic indexes that help the diagnostic confirmation of perilunate injuries. A descriptive, cross-sectional, retrospective study was carried out with the objective of finding radiographic indexes that facilitate the diagnosis of perilunate injuries. Eighty lateral wrist radiographs were evaluated, divided into 20 radiographs without changes and 20 radiographs with the following diagnosis: scapholunate ligament injury, transscaphoid fracture dislocation, lunate dislocation. Bone points were selected that originated lines to evaluate the anatomical relationship between the carpal bones.

So the radiolunate index was calculated and a statistical analysis were made.

Introduction

Perilunate injuries can present very subtle changes in the initial imaging exams, which go unnoticed in emergency care [1,2,3]. Despite its severity, 25% of patients do not have their diagnosis identified in the initial assessment [4]

Methods

This index was created to assess the position of the lunate bone in relation to distal surface of the radius. For this purpose lateral radiographs of the wrist were evaluated. Despite the possibility of difficult identification of the carpal bones, we chose intracarpal landmarks. The D line connects the dorsal edge of the distal surface of the radius to the dorsal edge of the distal surface of lunate. The P line connects the volar edge of the distal surface of the radius to the volar edge of the distal surface of the lunate. By measuring the length of lines D and P, we created the radiolunate index, that was calculated from the P/D ratio (figure1).



Figure 1: Production of the lines P and D, which measurements allows the calculation of the radiolunate index (RLI).

The Kruskal-Wallis test, Mann-Whitney test and graphical analysis using box-plot was used in the statistical analysis. The result of each comparison presents a p, being defined as a significance value of 0.05 (5%).

Results and Discussion

The radio-lunate index (RLI) on the radiographs of the wrists without changes ranged from $1,136 \pm 0,172$. In the radiographs with diagnosis of scapholunate ligament injury, the index ranged from $1,907 \pm 0,428$, in the radiographs with diagnosis of transscapho-lunate fracture dislocation, it varied from $0,743 \pm 0,099$ and in the radiographs with diagnosis of lunate dislocation it ranged from $0,47 \pm 0,086$. The p-value for RLI was less than 0.001.

	Group	Interval
IRS	Without changes	$1,136 \pm 0,172$
	Scapholunate ligament injury	$1,907 \pm 0,428$
	Transscaphoid fracture dislocation	$0,743 \pm 0,099$
	Lunate dislocation	$0,47 \pm 0,086$

Table 1: Radiolunate index range for different diagnoses

When comparing the ratio of the RLI of the radiographs of the wrist without changes with the ratio of the RLI of the radiographs with perilunate injuries, there was a statistically significant difference between the groups.

So the proposed method demonstrated an easy and quick way to facilitate the radiographic analysis of perilunate injuries, which can provide a faster diagnosis and may reduce misdiagnosis in these injuries.

In the next studies we intend to evaluate intraobserver and interobserver variability, in order to determine the accuracy of this method.

Conclusions

The application of the IRS demonstrated that there is a change in the position of the lunate in relation to the articular surface of the radius in perilunate injuries. Thus, it can be applied clinically to aid in the diagnosis of perilunate injuries.

References

- [1] Garcia-Elias M et al. (1989) *J Hand Surg Am.*, **14**:1017-1021
- [2] Gyftopoulos S et al. (2014). *Am J Roentgenol.* **203**:477-479
- [3] Çolak I et al. (2018). *Acta Orthop Traumatol Turc.* **52**:32-36.
- [4] Herzberg G et al. (1993). *J Hand Surg Am.*, **18**(:768-779.

Recent advances in wrist biomechanics

Veronique Feipel, Université Libre de Bruxelles, Brussels, Belgium

With the advances of technology and methodologies used in Biomechanics, our understanding of wrist biomechanics has progressed over the past decades and has led to improved patient care.

The techniques used today to measure global and segmental wrist kinematics *in vivo* will be discussed and obtained results will be reviewed in a practical (clinical) context. State of the art knowledge on load transfer across the wrist joints suggests the high relevance of musculoskeletal modelling. In this context, the biomechanics of wrist muscles and ligaments will be presented. The role of these structures on wrist stability will be highlighted and linked to current concepts on neural control and cognitive factors.

Even if the main accent of the lecture will concern recent advances in *in vivo* wrist biomechanics, we will remember that our current understanding of this topic was shaped by the work of pioneers many decades ago. We will also summarize the contribution of *in vitro* and *in silico* studies to the fundamental and applied knowledge of wrist biomechanics.

Knee Implant Wear Predictions are Altered by Including Fluoroscopy-Measured Kinematics in the Boundary Conditions

Michael J. Dreyer^{1,2}, Colin R. Smith¹, Seyyed Hamed Hosseini Nasab¹, William R. Taylor¹, Rowena Crockett², Bernhard Weisse²

¹Laboratory for Movement Biomechanics, Institute for Biomechanics, ETH Zürich, Zürich, Switzerland

²Laboratory for Mechanical Systems Engineering, Empa, Dübendorf, Switzerland

Email: michael.dreyer@hest.ethz.ch

Summary

The CAMS Knee datasets provide novel in vivo measurements of knee implant forces and kinematics during walking. We simulated the wear on knee implants using these datasets and the ISO standard wear testing boundary conditions (BCs). The choice of force or displacement BCs impacted wear location and magnitude. Wear produced by the ISO standard force BCs was similar to that produced by applying in vivo forces, but the application of in vivo kinematics yielded more posterior wear.

Introduction

Wear of the polyethylene (PE) inlay limits the longevity of knee implants. Currently, implant wear is evaluated using the ISO 14243 force- and displacement-controlled BCs derived from analytical musculoskeletal models. The novel CAMS-knee datasets provide synchronized knee contact forces measured using instrumented implants and implant kinematics measured using a moving fluoroscope for six subjects [1]. We investigated if applying these in vivo implant kinetics and kinematics to simulated wear tests leads to altered predictions of inlay wear compared to the ISO standard.

Methods

We developed finite-element models of the Innex FIXUC implant (Zimmer Biomet, CAMS-knee datasets) and simulated ISO standard knee implant wear tests with force control (FC) and displacement control (DC) in Abaqus. Both prescribe the knee flexion angle and axial force. The DC model further prescribes anterior-posterior (AP) displacement and internal-external (IE) rotation. The FC model prescribes an AP force and an IE torque instead and has nonlinear AP and IE spring restraints added. We derived representative knee loads and kinematics from the CAMS walking dataset using the Orthoload HIGH100 averaging method [2] and applied the corresponding components to the DC and FC ISO models.

The tibial inlay was assigned an elastic-plastic PE model, while the femoral component was modelled as rigid. The mesh size of the inlay (quadratic tetrahedral elements) and femoral component (rigid shell elements) was chosen based on a mesh convergence study. A coefficient of friction of 0.04 [3] was used for the tibiofemoral penalty contact formulation.

PE wear and creep were predicted for 3 million cycles using a cross-shear and contact-pressure dependent wear model [4] and compressive creep model [5] using custom Python scripts. The inlay geometry was updated intermediately to reflect the geometry change caused by wear and creep.

Predicted wear volume, rate, and location produced by the FC and DC CAMS models was compared to that of the standard

FC ISO model. The standard DC ISO model was excluded due to unrealistic contact conditions.

Results and Discussion

The FC ISO model showed the highest wear rate followed by the FC CAMS model and the DC CAMS model (Table 1). The FC models showed larger average contact area and more relative sliding than the DC CAMS model, which showed much higher maximum cycle-averaged contact pressure. This suggests a weak dependence of wear volume on contact pressure and a stronger dependence on contact slip and area.

Table 1: Predicted wear rate, cycle-averaged contact area, max. total sliding distance and max. cycle-averaged contact pressure.

	wear rate [mm ³ /Mc]	avg. area [mm ²]	max. sliding dist. [mm]	max. avg. press. [MPa]
CAMS FC	11.6	671	51.2	5.2
CAMS DC	10.0	363	33.1	12.6
ISO FC	13.7	442	46.2	3.2

A small average cross-shear-ratio (≤ 0.01) across all models indicated unidirectional sliding. For all models, the medial side showed 2–4 times more wear, even though the medial contact force was only 1.5 times higher. For the DC CAMS model the medial and lateral wear scar centroids were located ~10mm more posterior than for the FC models (Figure 1).

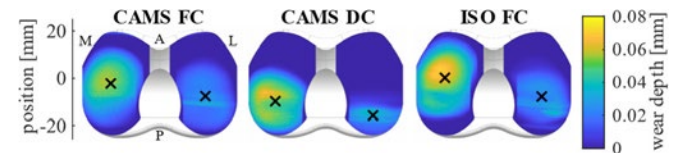


Figure 1: Wear scar depth and centroid after 3 Mc.

Conclusions

Wear predicted by the FC ISO loads provides a good approximation of that produced by in vivo loads for this highly constrained implant. However, neither set of FC BCs resulted in wear locations that corresponded with those predicted from measured in vivo kinematics, thus indicating the value of fluoroscopy to improve future wear testing standards.

Acknowledgments

We thank Zimmer Biomet, Dr. P. Damm and Dr. A. Trepczynski for their contributions to this research.

References

- [1] Taylor, WR et al. (2017) *J. Biomech.*, **65**: 32–39.
- [2] Bergmann, G et al. (2014) *PLoS ONE*, **9**: e86035.
- [3] Godest, AC et al. (2002) *J. Biomech.*, **35**: 267–275.
- [4] Saikko, V. (2006) *Proc. Inst. Mech. Eng. H*, **220**: 723–731.
- [5] Lee, K-Y (1998) *J. Biomed. Mater. Res.*, **39**: 261–265.

Plantar pressures in custom foot orthoses with and without heel plugs

Megan E.R. Balsdon¹, Colin E. Dombroski^{1,2}

¹SoleScience Inc., Fowler Kennedy Sports Medicine Clinic, London, Ontario, Canada

²School of Physical Therapy, Faculty of Health Sciences, Western University, London, Ontario, Canada

Email: megan@solescience.ca

Summary

The goal of foot orthoses (FOs) for treating plantar fasciitis (PF) is to decrease pain and increase function by reducing pressures on the heel at the insertion of the plantar fascia. This study compared two types of custom foot orthoses (CFOs) that are typically made to treat PF – one with a heel plug, and one without. Plantar pressure measurements objectively compared average pressure, peak pressure, and pressure contact area at the hindfoot, midfoot and forefoot in fourteen healthy participants during treadmill walking. The heel plug CFO showed a statistically significant reduction in all three metrics at the hindfoot while a significant increase was seen at the midfoot for average and peak pressures ($p < .05$), compared to the CFO without the heel plug. These findings are significant as offloading the hindfoot is critical for people with PF to decrease pain while walking, lessening compensation.

Introduction

Studies have shown that custom-made foot orthoses (CFOs) were better at improving morning pain in people with plantar fasciitis compared to both prefabricated foot orthoses (FOs) and sham devices[1]. Foot specialists aim to reduce the pressure at the heel with FOs by increasing support in other areas of the foot. FOs have shown to decrease pressures in the heel compared to a flat insole[2] and shoe alone[3]. A finite element study identified the effect of plugs on peak pressure and pressure distribution under the calcaneus, while validating the simulation with in-shoe pressure measurements using a single subject[4]. This study quantified plantar pressures in two CFOs, one with a heel plug, and one without.

Methods

Fourteen healthy participants (8 male) who were free of lower extremity injuries participated in the study after providing informed consent (35.4 years; 174.9cm; 76.3kg). The regular (REG) orthosis was made with a 3mm RCH 500 Shell, 45 durometer posting material, 3mm Multiform top cover, 1.5 puff bottom cover, and blue poron with 3mm heel lifts, while the full length heel plug (HP) orthotic was made with the same materials but with a heel hole cut out and a blue poron heel plug added. Plantar pressure measurements (F-scan, Tekscan) were recorded in both FOs, the order randomized among

participants, while walking on a treadmill (4.2±0.6 km/h). Three regions of the foot – the hindfoot, midfoot and forefoot were measured with three metrics: average pressure (kPa), peak pressure (kPa) and pressure contact area (kPa/cm²). A paired samples t-test determined differences between the two conditions ($p < .05$).

Results and Discussion

The results across all participants showed that the HP CFO significantly reduced the average pressure, peak pressure, and pressure contact area across all participants ($p < .05$). The HP device also saw a significant increase in average and peak midfoot pressures ($p < .05$) (Table 1). These findings were expected since the goal was to reduce pressure at the heel by increasing pressures in the midfoot to aid in offloading. These findings are consistent with a study that simulated insoles with heel plugs where reductions in peak pressures were greater as the heel plugs increased in width of the calcaneus (95%)[4]. Direct *in vivo* comparisons cannot be made; however, one study showed a CFO device was the only device (among EVA and flat sham FOs) to show both lower peak pressures at the medial heel and higher peak pressures at the midfoot, compared to the control condition, demonstrating the efficacy of CFOs in redistributing pressures in the foot[5].

Conclusions

This study investigated the objective effects of two CFOs on plantar pressures in healthy participants. CFOs with heel plugs were more effective at offloading pressures at the hindfoot, while increasing pressures at the midfoot. Future research should investigate this same effect on patients with plantar fasciitis and include subjective efficacy measures such as the foot function index and comfort rating.

References

- [1] Wrobel JS et al. (2015). *J Am Podiatr Med Assoc*, **105**(4): 281-294.
- [2] Khodaei BC et al. (2017). *Foot*, **33**: 76-80
- [3] Ki SW et al. (2008). *Prosthet Orthot Int*, **32**(3):356-362.
- [4] Gu YD et al. (2011). *Comp Meth Biomech Biomed Engin*, **14**(8):747-753.
- [5] McCormick CJ et al. (2013). *J Foot Ankle Res*, **6**(1):19.

Table 1: Mean, SDs and p-values of the differences in plantar pressure metrics in the hindfoot, midfoot and forefoot (n=14).

Region	Average Pressure (kPa)			Peak Pressure (kPa)			Pressure Contact Area (kPa/cm ²)		
	Mean	SD	p-value	Mean	SD	p-value	Mean	SD	p-value
Hindfoot	-13.1	13.2	0.003*	-36.7	26.9	<0.001*	-0.98	0.89	0.001*
Midfoot	7.9	12.2	0.03*	12.8	20.0	0.03*	0.10	0.34	0.28
Forefoot	3.1	16.6	0.50	2.0	33.9	0.83	0.14	1.03	0.61

*significant at the level of $p < 0.05$

A case series of early swing perturbation recovery strategies in transfemoral prosthesis users

Shane T. King, Maura E. Eveld, Karl E. Zelik, and Michael Goldfarb
 Department of Mechanical Engineering, Vanderbilt University, Nashville, TN, USA
 Email: shane.t.king@vanderbilt.edu

Summary

In contrast with healthy individuals who typically employ an elevating strategy (immediately lifting the swing leg over the obstacle) [1], transfemoral prosthesis users utilize a variety of recovery strategies when reacting to early swing, prosthetic-side obstacle perturbations. Here we examine how these recovery strategies relate to a user's prosthetic knee type (e.g., hydraulic vs. mechanical) to inform the design of future prosthetic devices that further improve stumble recovery and reduce fall risk.

Introduction

Healthy individuals use an elevating strategy to recover from early swing perturbations and maintain their balance [1]. While the elevating strategy is a common reflexive response in this population, it is not for transfemoral prosthesis users, who are 200 times more likely to fall than their age-matched, healthy equivalents [2,3]. Early swing phase perturbations are a fall-risk for this group because most commercial prostheses provide no way to easily control the leg's trajectory after the perturbation. Limitations in prosthetic knee functionality force users to adopt a variety of stumble recovery strategies with varying degrees of effectiveness. While multiple strategies may be effective in preventing a fall, certain strategies may be superior in terms of reducing recovery effort, such as the number of recovery strides required to return to steady state.

This work investigates a case series demonstrating the varying recovery strategies of transfemoral prosthesis users in response to early swing, prosthetic-side perturbations while wearing their prescribed prosthesis to determine how effective each strategy is and which features of each strategy provide the most potential benefit, to better inform future prosthetic designs.

Methods

Six participants were introduced to a series of swing phase obstacle perturbations, including 1-2 early swing, prosthetic-side perturbations, while walking on a treadmill at 0.8 m/s. The perturbation system is detailed in [1]. Motion capture and force plate data were collected and falls were monitored through a load-instrumented harness (>50% bodyweight = "likely fall"). Participants included: four Ottobock C-Leg users, one Ottobock 3R80 user, one Blatchford KX06 user.

Results and Discussion

Nine early swing phase, prosthetic-side perturbations were recorded across the six participants. Five perturbations resulted in falls (56%) with four out of six participants falling at least once (67%). The majority of participants utilized a lowering strategy in which the user terminated their swing phase after the perturbation and took a quick contralateral step to recover [1]. Healthy individuals often use this strategy in response to perturbations much later in swing when the stride is nearly complete, as it is typically difficult to transfer one's weight back to the swing limb early in the swing phase due to the body's momentum [1]. This lowering strategy was the

only strategy used by C-Leg users, likely due to the higher swing impedance of the knee joint compared to other prostheses, preventing enough swing flexion to clear the obstacle. However, mechanical knee users (3R80 and KX06) attempted an elevating strategy, similar to what healthy individuals use in early swing phase. These mechanical knee users were able to effectively emulate an elevating strategy, which was enabled in part by the low swing impedance of their knees which resulted in exaggerated knee flexion in response to the perturbation, which then provided enough clearance to pass over the obstacle prior to subsequent knee extension. The elevating strategy resulted in one successful recovery out of the two attempts (50%) by the mechanical knee users, while the lowering strategy was successful three out of seven attempts (43%) with three out of the five participants successfully recovering using this strategy (60%). Further analysis will be presented to gain insight into which aspects of these strategies are most effective, and how they might be improved in future powered prosthesis interventions.

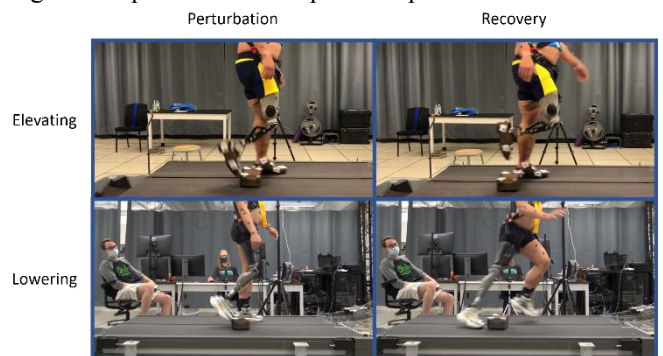


Figure 1. Two examples depicting the elevating (top, KX06) and lowering (bottom, C-Leg) recovery strategies, showing the moment of perturbation (left) and the recovery (right).

Conclusions

Unlike healthy individuals, C-Leg users exhibited a lowering strategy in response to early swing perturbations, relying on their prosthetic knee's stance resistance to flexion to support them when lowering, while mechanical knee users employed an elevating strategy due to the low swing impedance and quick swing extension of those devices. C-Leg users required more time to return to steady state gait relative to the mechanical knee user who successfully employed an elevating strategy. The authors hypothesize that the desirable characteristics from each type of prosthesis could be combined into a single robotic prosthesis in the future to improve the ability of users to recover from various perturbations.

Acknowledgments

Funding from NIH R01HD088959.

References

- [1] King & Eveld et al. (2019). *J NeuroEng Rehab*, **16**: 69.
- [2] Kahle JT et al. (2008). *J Rehabil Res Dev*, **45**: 1-14.
- [3] Talbot LA et al. (2005). *BMC Public Health*, **5**: 86.

Bi-linear Natural Ankle Quasi-Stiffness During Walking: Characterization & Implications for Orthosis Design

Luke Nigro¹, Elisa S. Arch, PhD²

¹Dept. of Mechanical Engineering, University of Delaware, Newark, DE, USA

²Dept. of Kinesiology & Applied Physiology, University of Delaware, Newark, DE, USA

Email: lnigro@udel.edu

Summary

This research expands on an existing definition of natural ankle-quasi stiffness (NAS) as *bi-linear* – using two distinct portions of the loading phase of stance instead of one single region – to understand how ankle joint mechanics change during stance. A bi-linear ankle-foot orthosis (BL-AFO) prototype was constructed and tested as proof-of-concept for future AFO designs that can implement bi-linear stiffness.

Introduction

Natural ankle quasi-stiffness (NAS), defined as a linear regression of the sagittal ankle moment vs. ankle angle during the loading (second rocker) phase of stance, can be used as a design parameter to customize passive-dynamic AFO (PD-AFO) bending stiffness. This spring-like stiffness can substitute for lost plantar flexor (PF) function for individuals with PF weakness [1]. Historically, a single NAS value has been defined over the entire loading phase of stance [2]. NAS increases during the loading phase of stance in healthy gait [3] often with two regions of nearly linear stiffness – a lower stiffness early in loading and higher stiffness later in loading (Fig. 1). Tuning a single PD-AFO bending stiffness to the entire loading phase of stance may result in a device stiffness that is too stiff to initiate bending, or not stiff enough to provide appropriate support in late loading. This research focuses on characterizing *bi-linear* NAS – or dividing the loading phase into two distinct regions of stance, each with its own stiffness [4]. A PD-AFO prototype with bi-linear bending stiffness (BL-AFO) was then built as proof-of-concept that such a device could be designed around this concept of bi-linear NAS.

Sagittal ankle angle vs. sagittal ankle angle (NAS curve)

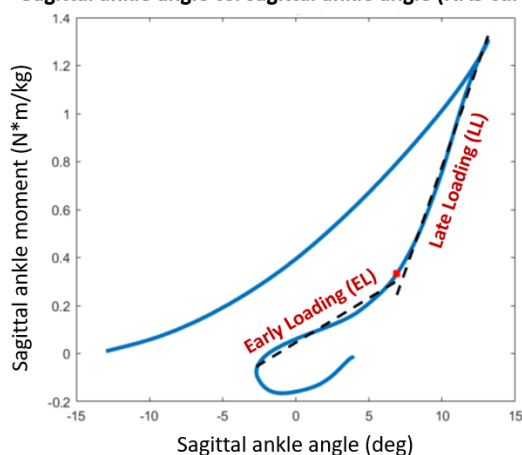


Figure 1: NAS curve of typical stance phase with the loading phase divided into EL and LL phases.

Methods

10 individuals walked at three speeds (0.6, 0.8, and 1.0 statures/s) over level ground. Sagittal ankle angles and moments were calculated from 3D kinematics and ground reaction forces (GRFs). Early loading (EL) and late loading (LL) phases were separated at the instant at which the vertical GRF reached a local minimum in the typical M-shaped profile at ~50% stance [4]. Ankle angles at the transition were calculated as the difference between the angle at that instant and the angle at which loading phase began. NAS was calculated for EL and LL regions separately for each trial and each speed. One-way ANOVA tests were used to determine significant differences in speed conditions. A BL-AFO was constructed from a single-stiffness PD-AFO with steel strips attached to a rear strut. As the BL-AFO flexes, only the rear strut bends initially. An adjustable grabber engages the steel strips once a certain angle is reached, thus adding their stiffness to the rear strut.

Results and Discussion

Average EL-NAS was 0.056 N*m/deg/kg and did not change significantly with walking speed. Average LL-NAS was 0.113, 0.162, and 0.210 N*m/deg/kg at 0.6, 0.8, and 1.0 statures/s, respectively, which is significantly greater than LL-NAS at every speed ($p < 0.001$). The average transition angles for each speed were 8.7, 9.1, and 8.1 degrees for 0.6, 0.8, and 1.0 stat/s, respectively. Transition angles were significantly different from 0.8 to 1.0 stat/s only ($p < 0.001$). The BL-AFO was able to achieve distinct bi-linear stiffness properties with an EL stiffness of 2.2 N*m/kg and LL stiffness of 4.2 N*m/kg and an adjustable transition angle (7-11 deg).

Conclusions

This research presents a thorough investigation of bi-linear NAS and its changes with walking speed. It also presents a BL-AFO prototype as a proof-of-concept that bi-linear stiffness can be used as design criteria for AFOs in the future.

Acknowledgments

Luke Nigro acknowledges the National Science Foundation's Graduate Research Fellowship no. 1940700 for funding, and Ralph Nigro, MS, for assistance with device construction. None of the authors have conflicts of interest to disclose.

References

- [1] Arch & Reisman (2016), *J.Prosthet.Orthot.*, 28(2):60-67.
- [2] Davis & DeLuca (1995), *Gait & Posture*, 4:224-231.
- [3] Nigro et al. (2021), *Gait & Posture*, 84:58-65.
- [4] Shamaei et al. (2013), *PLOS One*, 8(3).

Fuzzy-logic Inference System for Transfemoral Socket Rectification

Mike Karamousadakis¹, Antonis Porichis¹, Panagiotis Vartholomeos¹

¹TWI-Hellas, Athens, Greece

Email: panagiotis.vartholomeos@twi.gr

Summary

A Decision Support System (DSS) is developed that outputs suggestions for rectification action to the prosthetist, aiming to improve the fitness of transfemoral prosthetic socket design. For this purpose, the DSS employs a fuzzy-logic inference engine (IE). A set of rules are used by the IE, which models the thought process followed by the prosthetist for deciding rectification actions. The novel feature of the proposed DSS is that the rules of the IE take into account measured pressures on the stump, provided by sensors embedded in the socket's walls. The rectification actions (proposed by the IE) are then processed by an algorithm which receives, manipulates and modifies a 3D digital socket model as a triangle mesh formatted inside an STL file. The updated STL file offers to the prosthetist a visual representation of the suggested rectifications in 3D.

Introduction

Many patients experience serious discomfort wearing a conventional prosthetic limb because of pain, instability during walking, and skin irritation [1]. These are due to poor socket fitness, which results in pistoning, friction and instability of the socket with respect to the stump. The current practice for improving the socket design is based on empirical rules and visual inspection and involves skilled manual crafting. Usually, the patient is required to visit a clinic multiple times over one or more weeks for a complete socket rectification (i.e. socket design corrections). Hence, there is a need for improved design tools that exploit digital technology to expedite and improve the rectification procedure. To this end, computer aided methods for socket re-design are presented in [1-2]. These approaches redesign the socket based on biomechanical models and patient's characteristics. In this work, we present a computer aided method which takes into account socket-stump interaction pressures, based on measurements made by embedded sensors, and suggests rectification actions of the socket, so that the pressures are adjusted in a way to improve the socket fitness and comfort.

Methods

The first step is the input data generation. For this purpose, the patient dons the socket and stands upright. Pressure measurements, taken by the embedded sensors, are sent as crisp inputs to the DSS. Next, the crisp inputs are fuzzified into membership functions that represent the degree of certainty that a pressure over each anatomical region of the socket is high. A set of fuzzy rules that encode the thought process followed by a prosthetist are expressed using propositional logic whose premisses are the membership functions values. The IE processes the rules and produces a set of implied fuzzy sets, which are aggregated into one set representing the proposed rectification conclusions. Defuzzification generates the most certain rectification output (crisp value), meaning that this output has the highest

certainty to be the action of the prosthetist. The rectification actions are visualized by modifying the 3D mesh of the socket STL file. The proposed IE workflow is depicted in Figure 1.

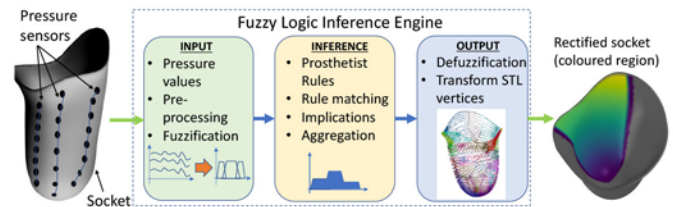


Figure 1: Fuzzy logic-based expert system for socket rectification.

Results and Discussion

Consider the following typical case. The rule states that:

$$P \wedge (\neg Q) \Rightarrow R \text{ and } P \wedge Q \Rightarrow S$$

Where P is "high pressure at distal-end", Q is "high pressure at scarpas's triangle", R is "reduce volume of anterior area" and S is "socket is too short and has to be replaced". Measured pressures indicate high degree of certainty for linguistic statement P and low for Q . The IE workflow is executed and outputs the rectification depicted in Figure 2.

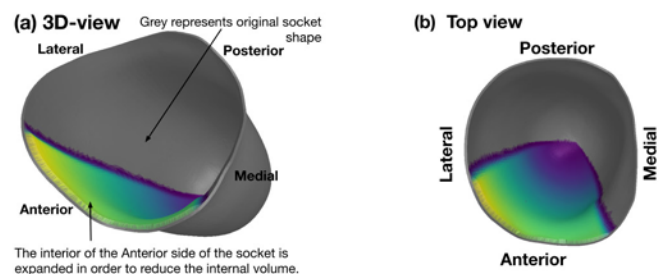


Figure 2: (a) 3D view, and (b) top view of the rectified socket.

The light-green is max expansion; the purple is min expansion. From the proximal to the distal anterior, expansion reduces smoothly. This rectification offers a tighter socket at proximal regions that prevents the stump sliding towards the distal-end. Therefore, no high pressures are exerted on the stump distal-end and the user does not experience discomfort.

Conclusions

A DSS has been developed that outputs rectification suggestions to the prosthetist aiming to improve the fitness of the prosthetic socket design and increase patient's comfort.

Acknowledgements

This work was supported by the EU Horizon2020 research and innovation project SocketSense, No 825429.

References

- [1] Richard Torres-Moreno et al. (1992). *Journal of Rehabilitation Research*, 29(3): 35-44.
- [2] Ellankavi Ramasamy et al. (2018) *Frontiers in Bioengineering and Biotechnology*, 6(126).

Predictive Simulation of Human Motion using SCONE

T. Geijtenbeek¹, F.C.T. van der Helm¹

¹Biomechatronics and Human-Machine Control, Delft University of Technology, Delft, The Netherlands
Email: t.geijtenbeek@tudelft.nl

Summary

Predictive simulation is a powerful tool for research on human motion, with enormous potential for the development of assistive devices and clinical treatment. Despite its promise, adoption in the biomechanics community has been limited – largely due to its complexity and multidisciplinary nature. SCONE is open source that aims to remove these barriers and make predictive simulations accessible to a wide audience of researchers, clinicians and developers.

Introduction

Despite a wealth of knowledge of the individual components comprising biological motion, the fundamental question of how the neural, muscular and skeletal systems operate together to produce efficient and purposeful motion remains largely unanswered. Predictive simulations from first principles provide an exciting avenue for exploring human motion on a systems level, allowing a level of control and inspection that is unimaginable in real-world experimentation.

In predictive simulations, motion is generated based on controller output, which is optimized to perform a given task according to high-level objectives, such as energy efficiency and pain avoidance. They permit fundamental *what-if?* questions, allowing researchers to investigate the effects of individual model parameters on the motion as a whole, and enable many real-world applications, such predicting treatment outcome and optimizing assistive devices *in silico*.

Unfortunately, the number of studies that successfully employ predictive simulations is limited. One important contributing factor is complexity: predictive simulations require expertise in musculoskeletal simulation, neuromuscular control and optimization – plus the software development skills to tie these components together. Software from successful projects is often either unavailable or lacks proper structure and documentation, limiting collaborations between researchers.

SCONE [1] is a free, open-source software initiative designed to help overcome these obstacles, and has been applied to answer various neuromuscular research questions.

Methods

Neuromuscular control. SCONE implements several building blocks for neuromuscular control, including spinal feedback from proprioceptive sensors, neural delays, finite state machines for gait [2], feedforward control, neural network control, and controllers based on *Lua* scripting. Together, these can be combined to develop a wide range of neuromuscular control strategies for a variety of tasks.

Musculoskeletal simulation. SCONE uses external simulation software to evaluate controllers, through a software API. Currently supported are the free and open-source *OpenSim*

(<https://opensim.stanford.edu>), as well as the commercially available *Hyfydy* (<https://hyfydy.com>), which allows for a 50-100x speed-up in simulation time over OpenSim.

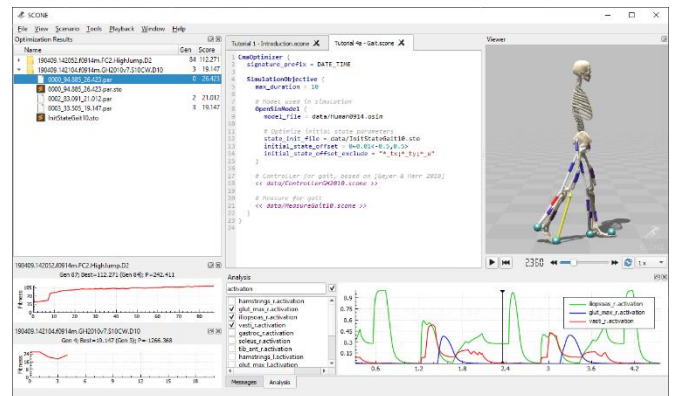


Figure 1: The SCONE User Interface

Optimization. Both model and control parameters can be optimized for user-defined objectives, which are made up from individual components including gait velocity, energy consumption, muscle activation, *etc*. Parameters are optimized through shooting-based methods (the Covariance Matrix Adaptation Evolutionary Strategy by default).

User interface and documentation. The SCONE user interface allows users to perform optimizations and analyze the results without software development skills. Tutorials, examples and documentation are available on-line (see link below).

Results and Discussion

SCONE has been successfully applied in a number of scenarios, including investigation of plantarflexor weakness [3], the development of assistive robotic devices, optimization of the stiffness for ankle-foot-orthoses, and prediction of treatment outcome. SCONE has also been part of a teaching program for biomechanics MSc students.

Conclusions

SCONE provides access to predictive simulations for a wide audience of researchers, clinicians and developers, and we believe further adoption will greatly benefit the biomechanics community. SCONE is freely available under the GNU Public License. See <https://scone.software> for more details.

References

- [1] Geijtenbeek, T. (2019). *Journal of Open Source Soft*, **4**(38)
- [2] Geyer, H., & Herr, H. (2010). *IEEE Trans. Neural Systems and Rehabilitation Engineering*, **18**(3), 263–273.
- [3] Ong, C. F., et al. (2019). *PLoS Comp. Biology*, **15**(10).

Trajectory Optimization of a 3D Musculoskeletal Model with Inertial Sensors

Marlies Nitschke¹, Eva Dorschky¹, Bjoern M. Eskofier¹, Anne D. Koelewijn¹, Antonie J. van den Bogert²

¹Machine Learning and Data Analytics Lab, Friedrich-Alexander-Universität Erlangen-Nürnberg (FAU), Germany

²Department of Mechanical Engineering, Cleveland State University, Cleveland, OH, USA

Email: marlies.nitschke@fau.de

Summary

We propose trajectory optimization for estimation of three-dimensional (3D) kinematics and kinetics of running from inertial data which resulted in high correlations for the sagittal plane and moderate for the frontal and transverse plane.

Introduction

Inertial measurement units (IMUs) consist of accelerometers and gyroscopes and are light weighted and cheap wearable sensors which have the potential to replace lab-based optical motion capturing (OMC). For walking, conventional inverse dynamic methods were used after estimating kinematics and ground reaction forces and moments from inertial data [1]. In contrast to that, we first presented trajectory optimization to directly track noisy inertial data with a planar musculoskeletal model for walking and running [2]. Trajectory optimization ensures a dynamically consistent simulation. However, the planar lower-body model used in [2] is not capable of capturing for example lateral stability required to evaluate running shoes. Here, the trajectory optimization driven by IMU data is extended towards the estimation of 3D kinematics and kinetics of running.

Methods

A 3D musculoskeletal model with 33 degrees of freedom and 92 Hill-based muscle tendon units [3] was used to track inertial data of seven IMUs at the lower body in a trajectory optimization. Sensor signals were simulated by placing virtual sensors on the model. Gyroscope signals were obtained from the skew-symmetric matrix $[\omega]_{\times} = \mathbf{R}^T \dot{\mathbf{R}}$, where \mathbf{R} describes the global orientation of the segment and $\dot{\mathbf{R}}$ its time derivative. Accelerations \mathbf{a} were computed as follows:

$$\mathbf{a} = \mathbf{R}^T (\ddot{\mathbf{r}}_{Seg} + \dot{\mathbf{R}} \mathbf{p}_{Sen} - \mathbf{g}),$$

where $\ddot{\mathbf{r}}_{Seg}$ denotes the global acceleration of the segment, \mathbf{p}_{Sen} denotes the sensor position in the segment coordinate system, and \mathbf{g} denotes the global gravity vector.

The state $\mathbf{x}(t)$ and control $\mathbf{u}(t)$ trajectories of a gait cycle were simulated by minimizing a combination of tracking error, cubic neural excitation, torque controls actuating the arms, and a small regularization term. The tracking error of the 42 sensor axes was expressed as squared difference between the virtual signal and the mean measured signal normalized to the measured variance. The trajectory optimization was constrained to be periodic and by the model dynamics which were formulated implicitly as $\mathbf{f}(\mathbf{x}, \dot{\mathbf{x}}, \mathbf{u}) = \mathbf{0}$ [3]. The simulation was solved by 100-node direct collocation using Backward Euler and IPOPT.

The approach was evaluated using running at three different speeds of nine subjects with OMC as reference [2]. Coefficients of multiple correlation (CMCs) [4] were

computed between IMC and OMC for joint angles and joint moments of the hip, knee, ankle, subtalar and mtp joint and for ground reaction forces. Finally, CMCs were averaged over running speeds and subjects using Fisher's z-transform.

Results and Discussion

The simulation tracked the measured IMU data well and rejected soft tissue artifacts. Sagittal plane kinematics and kinetics showed excellent (CMC: 0.93-0.98) and strong (CMC: 0.81-0.92) correlations, respectively (see Figure 1). However, correlations were weak for joint angles and moments of the subtalar and mtp joint.

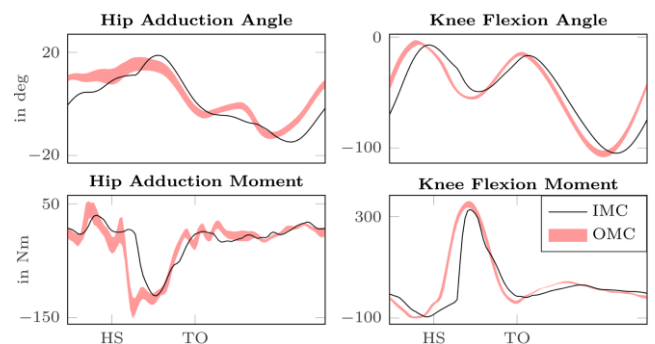


Figure 1: Comparison of inertial motion capturing (IMC) and optical motion capturing (OMC) for running of one subject.

Similar correlations have been reported for sagittal plane kinematics and kinetics [1,2] whereas frontal and transverse plane variables appear to be harder to estimate [1]. Variables of the subtalar and mtp joint are sensitive to the ground contact model which could be further improved. Trajectory optimization results in consistency between kinematics and kinetics in contrast to inverse dynamics [1] or machine learning. Simulation quality for motions with directional changes, like curved running, will be further evaluated.

Conclusions

We have shown that the full state and muscular control of a 3D musculoskeletal model can be estimated by tracking inertial data with trajectory optimization. The results agreed well with optical motion capturing for the sagittal plane and moderately for the frontal and transverse plane.

Acknowledgments

We acknowledge the support of adidas AG and the German Research Foundation.

References

- [1] Karatsidis A et al. (2019). *Med Eng Phys*, **65**: 68-77.
- [2] Dorschky E et al. (2019). *J Biomech*, **95**: 109278.
- [3] Nitschke M et al. (2020). *Sci Rep*, **10**: 17655.
- [4] Ferrari A et al. (2010). *Gait Posture*, **31**(4):540-2.

Stochastic optimal control predicts features of sensorimotor control during walking

Tom Van Wouwe¹, Lena H. Ting², Friedl De Groot¹

¹Department of Movement Sciences, KU Leuven, Belgium

²W.H. Coulter Dept. Biomedical Engineering, Emory University and Georgia Institute of Technology, Atlanta, GA, USA

Email: tom_van_wouwe@hotmail.com

Summary

It is unclear whether stochastic optimal control theory explains motor control of walking. Here, we applied a novel optimal control framework to simulate gait based on a five degree-of-freedom (dof) torque-driven model controlled by both feedforward and time-varying full-state feedback in the presence of sensorimotor noise. We solved for control policies that resulted in stable gait patterns while minimizing expected effort at two gait speeds. Our model predicted experimentally observed motor control features that were not prescribed, such as downregulation of feedback gains with speed and COM feedback to control the ankle torque during perturbed walking.

Introduction

Deterministic optimal control simulations capture main features of gait mechanics and energetics, but provide limited insight into the underlying control. In contrast, stochastic optimal control simulations that take into account physiological noise, have described underlying control mechanisms for movements that could be simulated with simple, linearized models (e.g. reaching and standing balance) [1]. Here, we leveraged recent computational advances that improved efficiency of deterministic simulations of movement [2]. This allowed us to simulate more complex, non-linear models in the presence of sensorimotor noise. Applying this framework to gait, we demonstrated that stochastic optimal control predicts experimentally observed motor control features.

Methods

We simulated a five dof torque-driven walker model with contact mechanics approximated as impulsive collisions [3]. Joint torques were determined by a combination of feedforward and time-varying linear feedback of the observed states. Dynamics were stochastic in the sense that sensory noise ($\sigma_{pos}^2 = 0.25 [(\text{°})^2 \cdot \text{s}]$; $\sigma_{vel}^2 = 2.25 [(\text{°}/\text{s})^2 \cdot \text{s}]$) was added to the feedback signal and motor noise ($\sigma^2 = 0.2 [\text{Nm}^2 \cdot \text{s}]$) was added to the torques.

We approximated the stochastic state trajectory by the state mean trajectory and state covariance trajectory. We described the propagation of the state covariance by the Lyapunov equation [4]. The resulting deterministic optimal control problem was solved using direct collocation.

We solved for feedforward torques and feedback gains by minimizing expected effort, (time-integral of the expected control torques squared), while imposing an average speed of 0.625m/s and 1m/s. To achieve a stable limit cycle, we imposed periodicity of the state mean and the state covariance trajectory.

We evaluated whether our simulations predicted (1) modulation of local reflexes throughout stance and with gait speed in agreement with observed modulation of the H-reflex, and (2) experimentally observed correlations between

corrective ankle torques and COM kinematics in perturbed walking. We therefore simulated treadmill walking with random belt accelerations and decelerations [6] and analyzed how much of the corrective ankle torque (ΔT_{corr}), was explained by COM feedback: $\Delta T_{corr}(t) = K_p(t) \cdot \Delta COM_x(t) + K_v(t) \cdot \Delta \dot{COM}_x(t)$. We compared the gains identified from stochastic optimal control simulations to those identified from experiments [7].

Results and Discussion

Similar to the soleus H-reflex, simulated local ankle feedback gains are downregulated at increased walking speed (Fig. 1 – B). Deviations in COM kinematics from the nominal trajectory due to perturbations were correlated (high R^2 values) with ankle torque as observed in walking experiments (Fig. 1 – C). Both COM feedback gains identified from experiments and simulated COM feedback gains are downregulated at increased walking speed (Fig. 1 – C). Differences in simulated and experimental modulation of feedback gains might be due to the absence of double support and feet in our model.

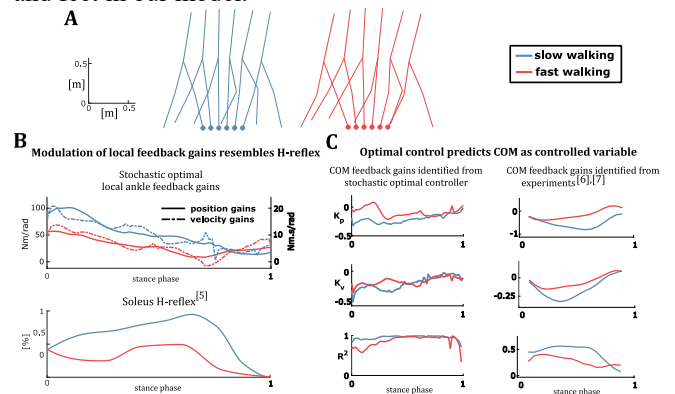


Figure 1: A: Gait pattern at slow and fast walking speeds. B: Optimal local ankle feedback gains; soleus H-reflex. C: Identification of COM feedback gains from perturbed walking in simulation and experiments. K_p COM position feedback, K_v COM velocity feedback, R^2 goodness-of-fit of COM feedback model.

Conclusions

Stochastic optimal control predicts experimentally observed motor control features that were not prescribed. This suggests that control of walking might be governed by the single overarching goal of minimizing effort in the presence of sensorimotor noise.

References

- [1] Falisse et al. (2019), *J. R. Soc. Interface*, **16**(157)
- [2] Todorov et al. (2002), *Nat. Neurosci.*, **5**(157)
- [3] Kelly et al. (2017), *SIAM Review* **59**(4)
- [4] Houska et al. (2010), *Proc. Control Appl.* 2172 – 2177
- [5] Capaday et al. (1986), *J. Physiol.*, **392**, 513-522
- [6] Moore et al. (2015), *PeerJ*, 3
- [7] Afschrift et al. (2020), *Biorxiv*

Quo vadis, *Tyrannosaurus*? Predictive simulations of locomotor function and performance in modern and extinct animals

P.J. Bishop^{1,2,3}.

¹Museum of Comparative Zoology and Department of Organismic and Evolutionary Biology, Harvard University, Cambridge, Massachusetts, USA

²Structure and Motion Laboratory, Royal Veterinary College, Hatfield, Hertfordshire, UK

³Geosciences Program, Queensland Museum, Brisbane, Australia

The study of locomotor function in non-human species – both living and extinct – can improve our understanding of the complex interplay between anatomy, mechanics, function and performance in a range of behaviours. Yet, animals are frequently difficult to study experimentally; combined with other logistical constraints or data scarcity, this can limit the breadth or depth of insight able to be gained in a given system. Computational musculoskeletal modelling provides a means of addressing this problem, shedding insight on aspects that are otherwise difficult or impossible to study. In particular, predictive simulations using these models hold incredible potential, because they are freed from the constraints of available empirical datasets, such as those involved with collecting experimental data, or the limited anatomical variation observed across living species. By facilitating investigation of “what if” questions, predictive simulations allow us to explicitly and mechanistically relate observed anatomy to whole-animal function, behaviour and performance. This talk will summarize recent predictive simulation efforts of walking, running and jumping in modern animals (e.g., birds), using this as a vehicle to demonstrate the promises and challenges of predictive simulations for understanding animal function. A wide variety of questions are able to be explored, and key areas requiring future research (e.g., tendon properties) will be outlined. The talk will culminate with discussion of application to extinct species, using high-speed running in theropod (carnivorous) dinosaurs as an example. Theropods stood and moved with a pronograde trunk and possessed a long, heavy tail, and so this provides a powerful demonstration of where predictive simulations can unravel the function of anatomies that have no modern equivalent, further broadening our perspective on the interplay between biology and physics.

Supine versus weight-bearing computer tomography in surgically-treated patella instability: an investigation on ligament length change between two different loading conditions

Belvedere C.¹, Weyer H.¹, Marcheggiani Muccioli G.M.², Lullini G.¹, Durante S.³, Zaffagnini S.², Leardini A.¹
¹Movement Analysis Laboratory, ²II Clinical Department & ³NTRAS, IRCCS Istituto Ortopedico Rizzoli, Bologna, Italy
 Email: belvedere@ior.it

Summary

Many knee-related image-based evaluations are performed in supine but a more realistic joint loading should be in weight-bearing. In this study on patients treated for patellar instability, differences in the knee ligament lengths were observed between these two different joint loading conditions, these revealing interesting biomechanical aspects.

Introduction

Abnormal Patello-Femoral (PF) joint motion may result from unnatural load transfer between the knee articulating bones, this altering the stabilizing/guiding role of a number of soft tissues. This may result from several causes, acting even in combination, like congenital deformities, e.g. bone dysplasia, altered nearby joints function, and lifestyle, including sport activity [1]. More specifically, patellar instability (PI) is a common knee disorder in the young and active population. PI is associated with Medial PF Ligament (MPFL) injury, and is treated surgically via ligament reconstruction [1,2]. PI is diagnosed via medical imaging, but controversies exist on how image-based inspections must be carried out to depict the real bone-ligament interaction [2]. Accordingly, reliable and more PI revealing evaluations are needed both for diagnosis and in surgically treated patients. In conventional, i.e. Supine, Computed-Tomography (SCT), PI is evaluated routinely with the patients lying on CT scanner bed, i.e. in non-weight-bearing. Recently, Weight-Bearing-CT (WBCT) has been introduced in the clinical practice, and allows patient imaging in upright-standing position. The aim of this study is to assess via CT the fibre length changes between supine and weight-bearing conditions of those knee ligaments associated to PI.

Methods

16 patients (BMI<25; 18-35 years) affected by PI were treated with MPFL reconstruction. At 5-year follow-up, all patients were scanned via SCT and WBCT, the latter based on cone-beam technology (Fig. 1). A 3D image-based methodology was adopted to reconstruct the bone CAD models for the femur, tibial and patella, and to identify the attachment footprints of the Patellar Tendon (PT), natural Lateral PF Ligament (LPFL) and reconstructed MPFL. The latter was modelled with 3 bars connecting the PF insertion grafts. LPFL and PT were modelled with 3 and 5 bars, respectively, joining the natural bone-ligament attachments. Relevant fibre lengths were calculated in the two loading conditions as the distance between the bar extremities. Tibio-femoral and PF joint alignments in both conditions was also

assessed using original proposals [3]. Pearson correlation and paired t-test analysis were used to extract significance differences. This study was IRB-approved.

Results and Discussion

Considerable differences in fibre lengths between the two loading conditions were observed, these being up to about 9, 6 and 14 mm for MPFL, LPFL and PT, respectively. For MPFL and LPFL, these length changes were found not consistent over the patients; conversely, a significant negative correlation ($R=-0.51$; $p=0.03$) between the length change of the two ligaments was observed, this confirming the opposition in lengthening for these two structures. Only the LPFL and PT fibres were significantly longer in weight-bearing ($p<0.001$). The length changes of MPFL and LPFL were found significantly correlated, directly and inversely respectively, with the PF tilt angle change between the two loading conditions.



Figure 1: WBCT scan. The patient is in monopodal upright posture. The moving bore is centered at the knee level.

Conclusions

The reported differences between SCT- and WBCT-based assessments support joint loading as a key factor in the assessment of ligament tensioning and PI. Furthermore, these confirm the knee as a complex mechanism coupling translations and rotations when moving between different loading configurations. In this context, within medical imaging, WBCT offers the possibility to extract more realistic information depicting the knee during its natural function, i.e. load transmission, this potentially leading to more reliable clinical and biomechanical evaluations.

References

- [1] Marzo J et al. (2016). *Orthop J Sports Med*, **4**: 2325967116673560.
- [2] Desio SM et al. (1998). *Am J Sports Med*, **26(1)**: 59-65.
- [3] Belvedere C et al. (2007). *KSSTA*, **15(8)**: 985-93.

Recovery of weight-bearing symmetry after total hip arthroplasty depends on activity and pre-surgery values

Sónia A. Alves¹, Marco Preuß², Hagen Hommel², Georg N. Duda¹, Alison N. Agres¹

¹Julius Wolff Institute, Charité – Universitätsmedizin Berlin, Berlin, Germany

²Klinik für Orthopädie und Traumatologie, Krankenhaus Märkisch-Oderland GmbH, Wriezen, Germany

Email: sonia.alves@charite.de

Summary

It remains unclear if the short-term recovery of weight-bearing symmetry (WBS) after total hip arthroplasty (THA) improves upon pre-THA function with time similarly across different activities of daily living. Here, only two activities showed lasting improvements in post-THA WBS compared to pre-THA, suggesting that WBS recovery is sensitive to the activity investigated. Additionally, pre-THA WBS appears to have a critical role when assessing post-THA functional recovery, which may assist to optimize rehabilitation by clarifying the origin of post-THA deficits in WBS.

Introduction

Deficits in WBS often persist after THA, with reduced ipsilateral limb loading observed in various activities [1]. Over time, this may overload the contralateral joint and contribute to the development of contralateral osteoarthritis [2]. It remains unclear if THA patients improve upon pre-THA deficits in WBS with time similarly across different activities of daily living. This study investigated WBS both pre- and post-THA across different activities of daily living, in order to identify if deficits in pre-THA WBS are similarly improved upon.

Methods

Twenty-two patients (13 female, 66.5±7.0 years, 32.1±5.9 kg/m²) were recruited pre-THA. Instrumented insoles (novel GmbH) measured plantar normal force at 1 week pre-THA (V1), at 1, 3 to 6, and 6 to 12 weeks post-THA (V2, V3 and V4, respectively). Standing comfortably (SC), standing 50-50 (S50, patients directed to load limbs evenly without feedback), walking (W) and sit-to-stand-to-sit (chair test, CT) activities were performed. The weighted Universal Symmetry Index (wUSI) [3] computed WBS, where wUSI=0 indicates perfect WBS and wUSI<0 indicates higher contralateral loads. Depending on data normality, either one-way ANOVA or Kruskal-Wallis tests examined the effect of time point on wUSI for each activity (significance $p<0.05$).

Results and Discussion

A significant effect of time point ($p<0.05$) on wUSI values was identified for SC, W and CT. S50 did not yield wUSI differences across visits ($p=0.08$). Post hoc tests revealed further significant differences (Figure 1), which were not consistent across activities. This indicates that WBS recovery differs across activities, in agreement with previous findings [1]. Between V1 and V2, differences were only identified for W and CT ($p<0.01$). Between V1 and V3, no wUSI significant differences were found for W and CT ($p>0.1$), revealing that patients reached pre-THA wUSI levels, whilst SC wUSI values improved significantly ($p=0.013$). Between V1 and V4,

differences were only observed for SC and CT ($p<0.01$), indicating an improvement of WBS from pre-THA deficits. Pre-THA (V1), W was the most symmetrical activity, yet patients still applied more weight to the contralateral limb. This was not significantly improved upon at V3 and V4, which supports previous suggestions that gait adaptations learned pre-THA may be carried over throughout post-THA recovery [4]. When considering only post-THA periods, wUSI differences (V2-V3 and V2-V4) were observed for SC, W and CT (all $p<0.05$) with no differences observed between V3 and V4. This suggests that the majority of the WBS recovery occurs between V2 and V3 for the three activities, with reduced recovery between V3 and V4.

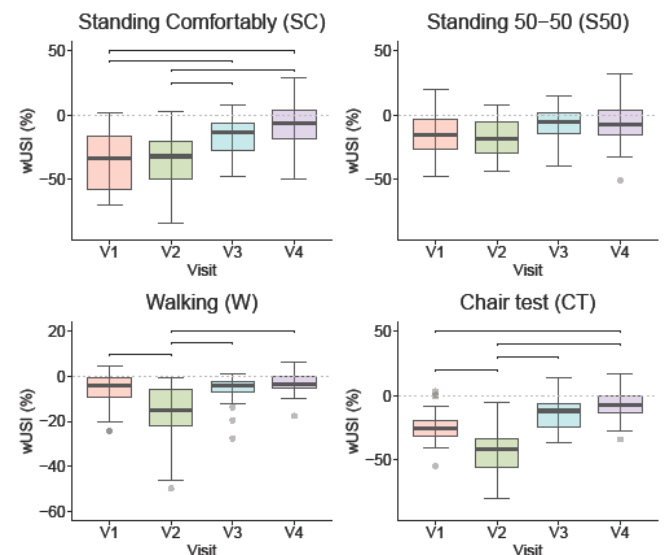


Figure 1: Boxplot depicting wUSI (%) values at all visits (V1, V2, V3 and V4) for the standing comfortably, standing 50-50, walking and chair test activities. Brackets indicate post hoc test results.

Conclusions

The recovery of WBS depends on the activity performed and on the inclusion of pre-THA values. Only two of the four investigated activities (SC and CT) exhibited functional improvements in WBS compared to pre-THA levels. This work highlights the critical role of pre-THA WBS in assessing functional recovery, as they can further optimize rehabilitation by clarifying the origin of post-THA deficits in WBS.

References

- [1] Miura et al. (2017) *Physio Theory Pract* **34**: 529-533.
- [2] Shakoor et al. (2003) *Arthritis Rheum*, **48**: 1556-61.
- [3] Alves et al. (2020) *Front. Bioeng. Biotechnol*, **8**: 57951.
- [4] Talis et al. (2008) *Clin Biomech* **23**: 424-43.

Superimposition of ground reaction force on tibial articular surface: a novel approach to support diagnosis and treatment of early knee osteoarthritis

Belvedere C.¹, Gill R.⁴, Ruggeri M.¹, Ortolani M.¹, Durante S.², Grassi A.³, Zaffagnini S.³, Leardini A.¹
¹Movement Analysis Laboratory, ²NTRAS & ³II Clinical Department, IRCCS Istituto Ortopedico Rizzoli, Bologna, Italy
⁴Department of Mechanical Engineering, University of Bath, UK
 Email: belvedere@ior.it

Summary

External forces, as assessed in gait analyses, suitably characterized with respect to the knee anatomy may be of help in revealing instant and location of forces peaks. In this study an original methodology merging patient-specific knee anatomy, from medical imaging, and ground reaction forces is reported potentially useful for diagnosis and surgery.

Introduction

Medial Knee Osteoarthritis (MKO) is generally associated with abnormal varus joint alignment [1]. During locomotion, this results in altered lower limb locomotion and loading, especially at the knee level. To delay or prevent end-stage disease, misalignment correction via high tibial osteotomy (HTO) may be considered at an early disease stage to restore normal alignment restoration and provide medial compartment decompression [1,2]. For the latter, efficacy information may be provided by the analysis of the ground reaction forces (GRF), whose orientation would reflect knee misalignment if depicted upon real patient-specific knee anatomy.

Unfortunately, although multi-instrumental evaluations are reported, this rarely involves combination of medical imaging and gait analysis (GA), including GRF data, in a fully personalized way. The aim of this study was to create an original methodology merging CT imaging with GA and GRF data in order to depict a realistic patient-specific representation of the knee status during motion.

Methods

25 patients (BMI<25; 40-65 years) affected with MKO and with a <20° varus deformity were selected for HTO. So far, 16 patients received pre-operative clinical scoring, and radiological, and instrumental evaluations. In detail, standard GA [3] was performed during walking, squatting and stair climbing/descending. An 8-camera motion systems (Vicon, Oxford, UK), combined with wireless electromyography, and force platforms (Kistler, Einterthur, CH) for GRF tracking, was used together with updated standard procedures. The latter implied data collection of 4 additional skin-based non-collinear markers, positioned around palpated tibial plateau bony rim. By still wearing the GA markers, patients received medical imaging examinations, i.e. full lower-limb X-ray and CT in weight-bearing condition (Carestream, Rochester, NY-USA). In data processing, relevant DICOM files were segmented to extract STL models for the tibia and the 4 additional reference markers; an anatomy based reference frame was defined on

the tibia, centered on the tibial plateau spine. The trajectories of the 4 additional markers as derived from GA during motion were then registered on the corresponding from CT reconstruction. Resulting registration matrices were used to superimpose GRF data on the reconstructed tibia model. Marker cluster deformation with respect to the target was assessed; intersections of GRF vectors with the tibial plateau were calculated/depicted throughout motions.

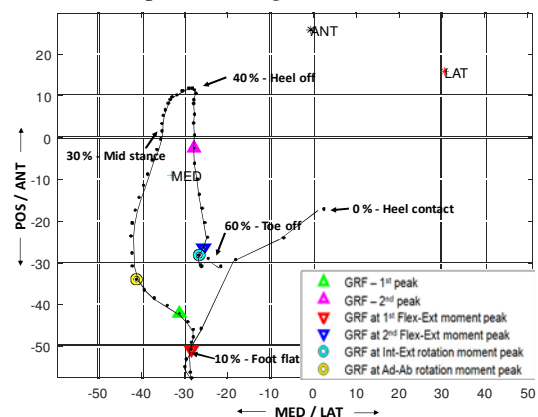


Figure 1: GFR pattern and peaks reported on patient-specific tibial plateau from a representative patient during walking phases

Results and Discussion

Clinical scoring confirmed the expected impaired knee status. Abnormal varism, up to 18° was confirmed via X-ray inspections. Cluster deformation resulted in <1.5 mm error. The morphological characterization of GRF (Fig. 1) was successfully achieved on patient-specific tibial plateau morphology, barring an acceptable level of error. Generally, GFR patters and peaks, including those related to anatomical joint moments, are concentrated on the medial compartment, as expected in varus knees.

Conclusions

This novel approach allows a linkage between motion data, including GFR, and knee misalignment exactly at the knee level. Relevant pre-/post-operative routine application, as in HTO, may offer a quantification of the effect of the executed joint realignment and as well assisting surgery planning.

Acknowledgments: TOKA, 3DMP Ltd, Bath, UK.

References

- [1] Zaffagnini S et al. (2013). *KSSTA*, **21**:934-941.
- [2] MacLeod AR et al. (2019). *Bone Joint Res*, **7**: 639–649.
- [3] Leardini A et al. (2007). *Gait Posture*, **26**:560-71.

Relationship between knee range of motion and gait function pre and post-total knee replacement

Marina De Vecchis¹, David E. Williams¹, Jake B. Bowd¹, Christopher Wilson^{1,2}, Gemma M. Whatling¹, Cathy A. Holt¹

¹Biomechanics & Bioengineering Centre Versus Arthritis, Cardiff University, UK

²Cardiff and Vale University Health Board, Cardiff, UK

Email: devechism@cardiff.ac.uk

Summary

Total knee replacement (TKR) surgery aims at improving pain, knee range of motion (ROM) and lower limb function in people with end-stage knee osteoarthritis (OA). In this study, knee ROM did not improve one-year post-TKR. Gait function improved post-TKR but less than 23% of patients displayed a gait pattern similar to non-pathological participants. There was a moderate relationship between knee ROM and gait function both pre and post-TKR suggesting that there may be other factors affecting the lower limb function.

Introduction

Knee OA is a degenerative disease that causes pain and functional limitations. TKR surgery aims at reducing symptoms and improving lower limb function in people affected by knee OA [1]. Knee ROM is frequently used as an objective outcome measure for TKR. However, it is not clear whether an increased knee ROM post-TKR is sufficient to ensure an improved gait. This study aims to investigate whether knee ROM and gait improve after TKR and if knee ROM correlates with an objective classification of gait function (Cardiff Classifier (CC)) [2] in patients pre and one-year post-TKR.

Methods

In this longitudinal study, 3D gait analysis (Qualisys system, Bertec force plates) was performed on 41 participants walking at self-selected speed (20 non-pathological (NP), 21 with knee OA – 22 knees – pre and post-TKR). The patients' knee active-assisted ROM (AAROM) was measured. Patients' data were recorded pre and one-year post-TKR. Principal Component (PC) analysis was performed on pelvis, hip, knee and ankle biomechanics waveforms of the affected side and of a randomly selected side in NP (frontal, sagittal and transverse planes). The first 3 PCs of each variable were used to train the CC, a classification system based on the Dempster-Shafer theory. The CC outputted three values for each participant: belief in NP (BNP), belief in OA (BOA) and belief in uncertainty (BU), each ranging from 0 to 1 and whose sum is 1. A predominant BOA value indicated the presence of a pathological gait. The 18 PCs that ranked the highest in classifying each participant as NP or with knee OA were retained and used to quantify the biomechanical changes pre and post-TKR. The significance of the changes in AAROM and BOA pre to post-TKR was explored with the Wilcoxon matched-pair test ($p \leq 0.05$). The correlations between patients' BOA and AAROM values pre and post-TKR were tested with Spearman's correlation coefficient ($p \leq 0.05$).

Results and Discussion

The CC identified NP and OA patients pre-TKR with 97.6% accuracy (Figure 1). Interestingly, the CC highlighted that the highest-ranking features classifying the gait as pathological or NP, are related to the joints that are distal or proximal to the knee. In fact, the PCs that had the highest accuracy ($>79\%$) in classifying each participant as NP or OA were ground reaction force, hip and ankle moments, pelvis, hip and ankle angles; the PCs representing knee sagittal angles and moments only ranked 11th, 14th and 15th in terms of classification accuracy. Knee AAROM did not improve significantly post-TKR (median difference=2.65°, $p=0.149$), with 45.5% of patients ($n=10$) experiencing a decrease in AAROM. The BOA value improved significantly post-TKR (median difference=0.15, $p<0.001$) but it was still predominant over the BNP and BU values in 77.3% of patients ($n=17$). There was a moderate, negative correlation between BOA and knee AAROM both pre-TKR ($r_s = -0.596$, $p=0.003$) and one-year post-TKR ($r_s = -0.448$, $p=0.037$). This means that pre and post-TKR, a more restricted knee AAROM was associated with a more compromised gait pattern. This relationship was weaker one-year post-TKR.

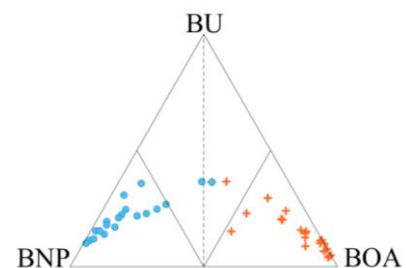


Figure 1: Cardiff classifier simplex plot: classification of NP (blue dots) and OA patients pre-TKR (orange crosses); the black, dashed line indicates the boundary between BNP and BOA.

Conclusions

One-year post-TKR, knee AAROM did not improve, the gait pattern improved but it was still classed as pathological for most patients. The moderate relationship between knee AAROM and gait classification both pre and post-TKR may suggest that knee AAROM on the affected side is not the sole variable influencing the gait pattern in people with knee OA and especially after TKR. The findings from the CC suggest that pelvis, hip and ankle joints should also be considered when assessing gait function in patients with end-stage knee OA and when examining the outcome post-TKR.

References

- [1] Zhang et al (2008). *Osteoarthritis and cartilage*, **16**:137-162.
- [2] Biggs et al (2019). *Gait & posture*, **70**: 65-70.

Biomechanical characterization of the primary fixation stability of different acetabular cups with respect to segmental acetabular bone defects

Christian Schulze¹, Maeruan Kebbach¹, Rainer Bader¹

¹ Biomechanics and Implant technology Research Laboratory, Department of Orthopaedics, Rostock University Medical Center, Rostock Germany

Email: christian_schulze@med.uni-rostock.de

Summary

In the present study we compared the primary stability of a commonly used primary and revision acetabular cups by push-in and lever-out tests in a biomechanical cup block model considering segmental acetabular bone defects. Thereby the revision cup showed higher push-in forces and lever-out moments in all defect types.

Introduction

Fixation stability of cementless acetabular cups is influenced by the implant design and the quality of the acetabular bone stock. Particularly, fixation can be compromised by joint dysplasia and acetabular bone defects. Therefore, our experimental study aimed to characterize the primary fixation stability of a primary acetabular cup in comparison to a revision cup design with respect to different stages of segmental acetabular bone defect.

Methods

For the characterization of the fixation stability of uncemented primary acetabular and revision cup designs (Allofit[®] 54/JJ vs. Trabecular Metal[™] Acetabular Revision System, Zimmer GmbH, Wintherthur, Switzerland) a standardized supero-lateral acetabular defect model [1] was used. The extent of the segmental defect (α/β) is defined in anterior-posterior direction by the angle α and in lateral-medial direction by the angle β with regard to the center of rotation of the reamed acetabulum. Three stages of acetabular defects (α/β) were considered, intact cavity (0/0) (A), a 90/45 defect (B) and a 120/45 defect (C). For each type of uncemented cup, $n = 5$ cavities per defect type were created in blocks made of 20 pcf Polyurethane foam (Sawbones[®], Malmö, Sweden) using CNC milling. Both acetabular cup types ($n = 2$ cups for each type) had a nominal outer diameter of 56 mm and were displacement controlled pushed ($v = 20$ mm/min) into the cavities with a diameter of 54 mm by means of a universal testing machine (Zwick/Roell Z050, Zwick GmbH & Co. KG, Ulm, Germany) until the recommended final implant position was reached. Subsequently, the acetabular cups were displacement controlled ($v = 20$ mm/min) levered out of the cavities in the opposite direction to the defect. The push-in force and the lever-out moment were continuously recorded during the experimental testing.

Results and Discussion

For the primary cup, push-in forces were determined in a range from 8.46 ± 0.36 kN (intact) to 4.33 ± 0.23 kN (120/45) and for the revision cup from 13.77 ± 1.92 kN (intact) to 10.34 ± 0.61 kN (120/45). The

primary cup showed lever-out moments in a range from 14.89 ± 0.77 Nm (intact) to 6.50 ± 0.26 Nm (120/45), while the revision cup showed lever-out moments in a range from 29.55 ± 1.81 Nm (intact) to 13.53 ± 0.88 Nm (120/45) (Figure 1). The 90/45 defect reduced in comparison to the intact cavity the lever-out moment of the primary cup by about 38% and of the revision cup by about 46%, whereas the 120/45 defect reduced lever-out moment of the primary cup by about 56% and the revision cup by about 54%.

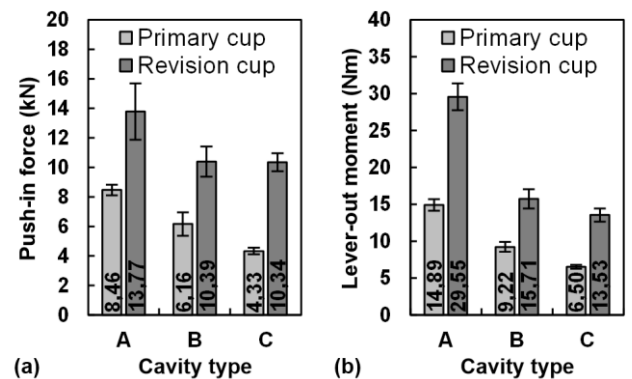


Figure 1: Experimentally determined test parameters (a) push-in force and (b) lever-out moment for the primary and revision acetabular cup with respect to different defect cavities. The bars represent the mean values and the error bars represent the standard deviation of each test group ($n = 5$).

In the case of the 90/45 defect, the lack of superior bone support leads to a significant decrease in moment in both cup types. In contrast to the primary cup, an increase in the anterior-posterior defect extend (angle α) from 90° to 120° only slightly reduces the lever-out moment for the revision cup. The push-in forces show a similar behavior; however, the high push-in forces of the revision cup should be noticed. The higher fixation stability of the revision cup is due to higher press fit within the bone cavity at the level of the cup equator. It should be noted that the defect model and the artificial bone material used do not reproduce all the anatomical and material properties of the native acetabular bone cavity.

Conclusions

Compared to the primary cup, the revision cup investigated showed higher push-in forces and lever-out moments, which are associated with a higher equatorial press fit.

References

[1] Schulze C et al. (2020). *J Arthroplasty*, **35**: 1720-1728.

Inclination of talocrural joint axis: In vitro studies and morphological considerations not confirmed in walking condition

P. Wolf¹, R. Moor¹, E. Graf²

¹Sensory-Motor Systems Lab, Department of Health Sciences and Technology, ETH Zurich, Zurich, Switzerland

²Institute of Physiotherapy, ZHAW School of Health Professions, Winterthur, Switzerland

Email: pwolf@ethz.ch

Summary

Knowledge about the orientation of the talocrural joint axis is limited to studies on tarsal morphology and quasistatic studies. Here, we determined the talocrural joint axis during walking. In contrast to literature, the mean axis was inclined upwards laterally during dorsiflexion while being inclined rather upwards medially in plantarflexion.

Introduction

Already 70 years ago, the two different arcs and radii of the medial profile of the talus were used to highlight that the talocrural joint has no fixed axis of rotation. It was postulated that in talocrural dorsiflexion the axis of rotation is inclined upwards medially whereas in talocrural plantarflexion the axis of rotation is inclined upwards laterally [1]. Subsequent studies confirmed this postulation *in vitro*, e.g. [2], as well as (at least partly) *in vivo* [3]. As related studies were either based on morphological data only or on data gained quasi-statically, the aim of this study was to determine the orientation of the finite helical axis (FHA) of the talocrural joint during the stance phase of walking.

Methods

Using intracortical pins, kinematics of the talus and tibia were recorded during self-paced walking of five participants [4]. The FHA was determined [5] for a moving window of 10% stance phase and reported when the rotation was more than 2° to reduce the influence of noise. The mean helical axis was calculated for 15-30% stance phase, i.e. a phase known for talocrural dorsiflexion, and for 80-95% stance phase, i.e. a phase known for talocrural plantarflexion. Computer tomography of the bones was done while the pins were inserted to facilitate the visualization of the FHA.

Results and Discussion

As expected, we could confirm that the talocrural joint acts not like a hinge joint with one single fixed axis of rotation (Figure 1). In contrast to existing literature, however, we observed that during a phase of talocrural dorsiflexion the axis of rotation was inclined upwards laterally and that in talocrural plantarflexion the axis turned more medially upwards (Figure 2).

Conclusions

Although recent designs of ankle joint prostheses have considered different inclinations for dorsi-/plantarflexion axes, their necessity could be justified differently than previously thought as in waking, we observed axes inclinations opposite to the expected ones.

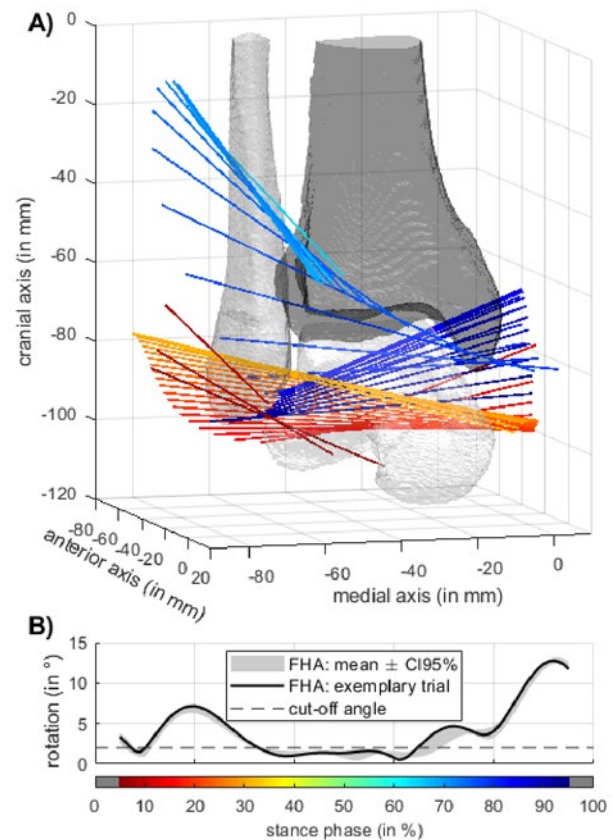


Fig. 1 (A) Exemplary trial: Bones displayed in reference (standing) position. (B) Rotation along the FHA of exemplary trial (black) and of all trials of participant p4 (grey).

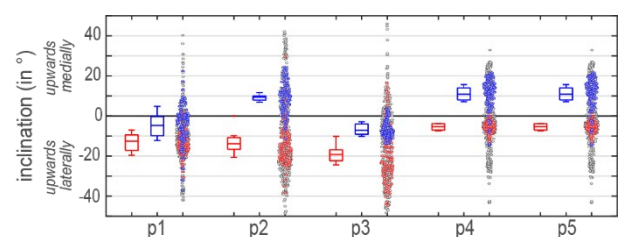


Fig. 2 Inclination of helical axes: Red (blue) boxplots represent mean helical axes of all trials of participant p1 to p5 in early (late) stance phase. Grey dots of swarm plot represent inclination of all FHA, red (blue) those of early (late) stance phase.

References

- [1] Barnett CH and Napier JR (1952) *J Anat*, **86**: 1-9.
- [2] Van Langelaan EJ (1983) *Acta Orthop Scand*, **54**: 1-269.
- [3] Lundberg A et al. (1989) *J Bone Joint Surg*, **71**: 94-99.
- [4] Maiwald C et al. (2017) *Gait & Posture*, **52**, 129-134.
- [5] Woltring HJ et al. (1985). *J Biomech*, **18**: 379-389.

Which metabolic cost models most accurately predict energetics at different speeds of walking?

Israel Luis¹, Maarten Afschrift², Friedl De Groot², Elena M. Gutierrez-Farewik¹

¹KTH MoveAbility Lab, Dept. Engineering Mechanics, KTH Royal Institute of Technology, Stockholm, Sweden

²Department of Movement Sciences, KU Leuven, Leuven, Belgium

Email: ailp@kth.se

Summary

Energy expenditure during walking at 7 different speeds was predicted based on motion capture, musculoskeletal simulation, and 6 different metabolic cost models, and compared to measured energy expenditure and gross cost of transportation. All metabolic cost models predicted a U-shaped relation between walking speed and cost of transport but the models from Uchida 2016 and Lichtwark and Wilson 2005 agreed better with the measured metabolic cost than the other models.

Introduction

Energy expenditure (EE) provides a quantitative measurement to assess metabolic demand of locomotion; accurate prediction may support rehabilitation treatments or design of assistive devices. The metabolic cost models (MCMs) formulated by Bhargava 2004 (BH04), Lichtwark and Wilson 2005 (LW05), Houdijk 2006 (HO06), Umberger 2003 (UM03), Umberger 2010 (UM10), and Uchida 2016 (UC16) consist of a set of equations that relate muscle excitations, states and state derivatives to metabolic energetics from different animal species, and have served to explain muscle energetics [1,2]. There are, however, significant differences between them: BH04, HO06, and UM03 allow negative mechanical work to decrease EE. UM03, UM10 and UC16 were derived from similar experimental data sets. Whether these relationships are able to predict salient characteristics of walking energetics such as the U-shaped cost of transport (COT) curve and optimal speed (OS) has not been examined. The objectives of this study were to evaluate six MCMs and determine which provides the best prediction of EE and COT across different speeds of walking.

Methods

Ten able-bodied adults were asked to walk at 55%, 70%, 85%, 100%, 115%, 130% and 145% of their preferred walking speed in two conditions: treadmill (TRE) and overground (OVG). In TRE trials, gross EE was recorded as O₂/CO₂ consumption (Cortex Metamax 3B) during 6-minute trials at each speed (randomized). Net EE measured was then computed as gross EE minus EE during resting/sitting. Each subject's average cadence at each speed was recorded.

In OVG trials, gait kinematics (Vicon V16), ground reaction forces (AMTI Optima) and EMG (Myon nano) were recorded. Participants were asked to walk at approximately the same 7 speeds by matching their cadences from TRE trials. Data from all OVG trials was processed (inverse kinematics and inverse dynamics) using OpenSim 4.1 based on the musculoskeletal model proposed by Lai Arnold 2017 [3] scaled to the subject's dimensions. A muscle-redundancy solver based on direct collocation [4] was used to estimate the muscle states. EE and

COT (energy required to move 1 kg per meter) were computed from the 6 MCMs (BH03, LW05, HO06, UM03, UM10 and UC16) at each speed and compared to the measured net EE. Net EE in the different speeds was linearly fit and COT was fit to second order equations.

Results and Discussion

All MCMs captured main trends, i.e., predicted EE increases and predicted COT follows a U-shape with respect to walking speed (Fig. 1). Among different subjects, LW05 and UM10 usually overestimated net EE, while BH04 underestimated it. Overall, EE estimated from UC16 and LW05 agreed best with experimental data, and HO06 agreed least.

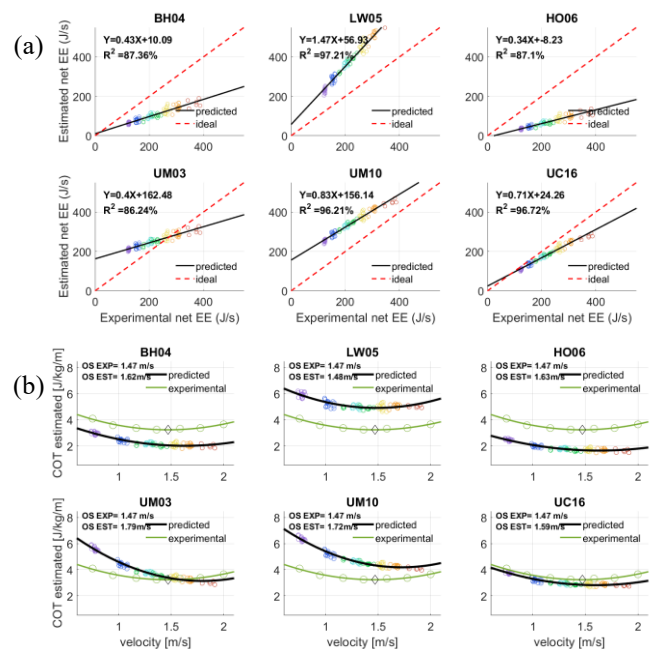


Figure 1: a) experimental and predicted net EE and (b) COT and OS for one representative subject walking at 7 speeds ranging from very slow (purple) to very fast (red).

Conclusions

While none of the MCMs entirely predicted EE that matched with experimentally measured EE, UC16 and LW05 agreed better than the other 4 models. All MCMs predicted U-shape relation, wherein the models of UC16 and LW05 tend to provide the best estimates.

References

- [1] Koelewijn et al. (2019). PLOS ONE, pp 1-19.
- [2] Miller (2014). J. Biomech, vol 47, no. 6, pp 1373-1381
- [3] Lai et al. (2017). Ann Biomed Eng. 45 pp 2762-2774
- [4] De Groot et al. (2016). Ann. Biomed. Eng., vol. 44, no. 10, pp. 2922–2936

Do different activation patterns between the lateral and medial gastrocnemius translate into different fascicle behavior during walking?

Raphaël Hamard¹, Jeroen Aeles¹, Nicole Y. Kelp², Romain Feigeau^{1,2}, François Hug^{1,2}, Taylor J. M. Dick²

¹Nantes University, Laboratory "Movement, Interaction, Performance" (EA 4334), Nantes, France

²The University of Queensland, School of Biomedical Sciences, Brisbane, Queensland, Australia

Email: raphael.hamard@univ-nantes.fr

SUMMARY

The aim of this study was to determine whether the higher activation in the medial gastrocnemius (MG) compared to the lateral gastrocnemius (LG) during walking translates into different mechanical behavior of the fascicles. To address this aim, we used an experimental approach, which combined electromyography (EMG) and ultrasound imaging. Our results show that the higher activation of MG compared to LG translates into less MG fascicle lengthening and a greater change in MG pennation angle during the fascicle shortening period. No difference in the amount of fascicle shortening or peak shortening velocity were found.

INTRODUCTION

The triceps surae contributes more than half of the total propulsive power during the push-off phase of walking [1]. Although functional differences between the soleus and the gastrocnemii are well documented, MG and LG muscles are often considered to share the same functions and thus to behave similarly. Evidence suggests that during walking, muscle activity is greater in the MG than the LG [2]. However, it is unknown whether these differences in activation translate to differences in the mechanical behavior of the fascicles. The aim of this study was to determine whether the differences in activation between the MG and the LG during walking translate into different mechanical behavior.

METHODS

Fifteen healthy participants walked on a treadmill at their preferred walking speed under two conditions: (1) level walking and (2) incline walking (10% grade). Participants performed both conditions twice, to first record MG and LG muscle activations using surface EMG (Trigno Delsys Inc., USA; 10 mm interelectrode distance) and second to measure MG and LG fascicle behaviors using B-mode ultrasound imaging (120 Hz, 5-8 MHz, 60mm field-of-view, LV8-5L60N-2, ArtUS, Teleded, Lithuania).

Raw EMG signals of fifteen strides were filtered, rectified and normalized to the maximal activation level previously determined during maximal voluntary contractions. We used a semi-automated tracking algorithm to determine fascicle length and pennation angle during five strides of walking.

To assess the muscle effect, the condition effect and the muscle x condition interaction, we conducted a two-way repeated measures ANOVA on the EMG and ultrasound parameters. Then, we used correlations to determine the relationship between activation and mechanical behavior.

RESULTS AND DISCUSSION

Peak EMG amplitude was higher in MG than LG ($p=0.01$), regardless the condition, with no interaction effect ($p=0.67$).

During early stance, the LG fascicle lengthened 26% more ($p=0.02$) and rotated 1 degree more ($p<0.01$), compared to the MG. However, we found no differences in the amount of fascicle shortening following this lengthening ($p=0.21$) (Figure 1) or in peak shortening velocity during this shortening ($p=0.85$) between the MG and LG. During the fascicle shortening period, the MG underwent greater increases in pennation angle compared to the LG ($p=0.04$). We did not find any significant interaction effects (All: $p>0.29$).

Finally, we did not find any significant correlation between EMG parameters and ultrasound parameters.

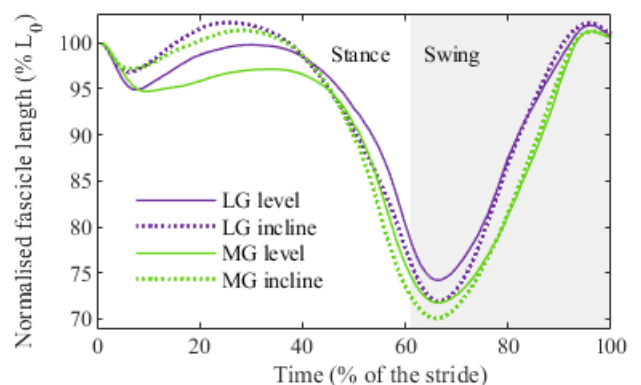


Figure 1 : MG and LG fascicle length change patterns during level (solid) and incline (dashed) walking.

CONCLUSIONS

In this study, we found that during walking the MG is activated more than the LG, consistent with previous studies. The higher MG activation was associated with a less fascicle lengthening and greater increases in the change in pennation angle, compared to the LG. However, the greater MG activation did not lead to more fascicle shortening or changes in peak shortening velocity, suggesting the motor coordination control and fascicle dynamics are uncoupled.

Acknowledgments

Support: University of Queensland (ECR Grant to T. Dick), *Institut Universitaire de France* (IUF), *Société de Biomécanique*, ANR-19-CE17-002-01.

References

- [1] Neptune et al. (2001). *J. Biomech*, **34(11)**: 1387-1398.
- [2] Ahn et al. (2011). *Biol. lett.*, **7(4)**: 539-542.

Model-based Closed-loop Control of Locomotion via Muscle Reflexes and Spinal Synergies: A Direct Collocation-based System Identification Approach.

Huawei Wang, Massimo Sartori

Neuromechanical Modeling and Engineering Lab, Technical Medical Centre, University of Twente, Enschede, The Netherlands
Email: h.wang-2@utwente.nl

Summary

Computational models of motor control (i.e., spinal synergies, and muscle reflexes) in human locomotion are often based on empirical knowledge and hence are not subject-specific. This study showed that detailed reflex structures for leg muscles can be directly identified from human walking data *in vivo*, which has the potential to explain specific individuals' movement neuromechanics. The identification framework can also be extended to a variety of movements, such as sit-to-stand and jumping.

Introduction

Muscle reflexes and spinal synergies have been studied via both avatar-based simulations and *in vivo* experiments [1,2], showing that they can explain complex locomotion tasks. In addition, they can also be used to close the control loop between real-time neuromechanical model-based (NM) controllers and wearable robots (i.e., robotic exoskeleton and bionic limbs), to relax or even eliminate the needs of electromyography sensors [3]. In this study, we answer the question about whether can personalized reflex models be directly identified from walking data.

Methods

Kinetic and muscle activation data of 5 healthy adults at 4 walking speeds (0.9, 1.8, 2.7, 3.6km/h) were collected. Models of muscle reflexes are identified from this dataset, through an indirect identification approach (Figure 1). These identification problems were solved through trajectory optimization with the direct collocation method [4].

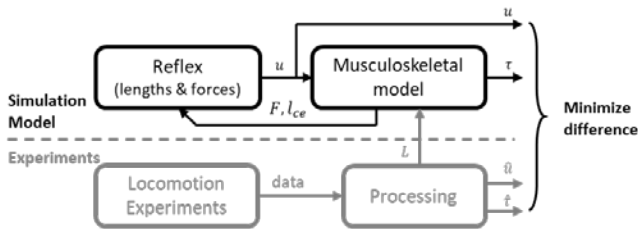


Figure 1: Structure of the reflex-synergy controller identification. Where, u represents muscle excitations; τ represents joint torques; F represents muscle forces; L represents muscle lengths; l_{ce} represents lengths of muscle contractile element.

In the identification, reflex model was defined as a fully connected network with all possible muscle force and length linear feedback loops. To find the minimal reflex structure, besides the data tracking terms, another term was added to the objective function: $O_{min-loops} = \sum_{j=1}^{M_f} |\bar{k}_f|^{\frac{1}{2}} + \sum_{j=1}^{M_l} |\bar{k}_l|^{\frac{1}{2}}$, where \bar{k}_f and \bar{k}_l are the normalized reflex gains. By minimizing the objective function, one strong reflex loop was preferred, instead of two weak reflex loops, in explaining muscle excitations. The optimization problem was defined as:

$$\text{optimize: } [\bar{k}_f, \bar{k}_l, u(t), l_{ce}(t)]$$

$$\text{minimize: } \int_{t=0}^T [(u(t) - \hat{u}(t))^2 + (\tau(t) - \hat{\tau}(t))^2] \cdot dt + O_{min-loops}$$

$$\text{subject to: } f_r(l_{ce}(t), F(t), \bar{k}_f, \bar{k}_l) - u(t) = 0$$

$$f_m(L(t), u(t), l_{ce}(t), \dot{l}_{ce}(t)) - F(t) = 0$$

$$F(t) \cdot r - \tau(t) = 0$$

$$0.01 \leq u(t) \leq 1$$

$$K_{lb} \leq \bar{k}_{f,l} \leq K_{ub}$$

Results and Discussion

Preliminary results (Figure 2) showed that similar but more detailed reflex structures can be identified from the walking data, comparing to the commonly used reflex model [1].

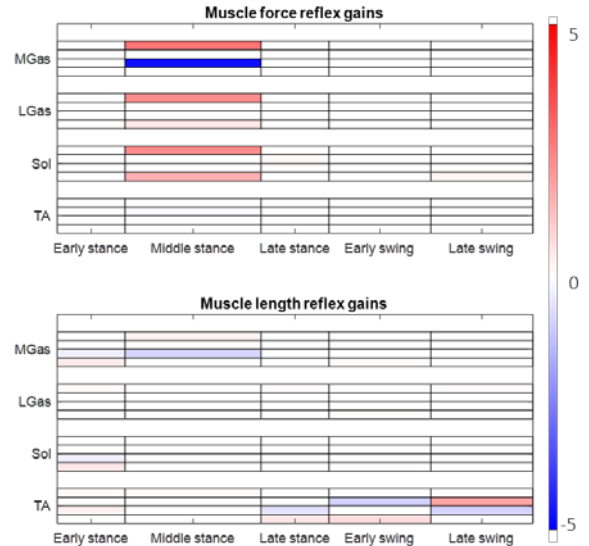


Figure 2: Identified reflex gains. An averaged gait cycle was divided into five phases. One constant reflex gain was defined in each phase and each reflex loop. Each muscle has four reflex feedbacks (four sub-rows) from four muscles. Colors in each block indicate the significance of this reflex loop in explaining the muscle excitation.

Conclusions

Our study showed that subject-specific muscle reflex models can be directly identified from locomotion data.

References

- [1] Song, SE and Hartmut GE (2015). *The Journal of physiology*, **593.16**: 3493-3511.
- [2] Sartori MA, et al. (2013). *Frontiers in computational neuroscience*, **7**: 79.
- [3] Durandau GU et al. (2019). *Journal of neuroengineering and rehabilitation*, **16.1**: 91.
- [4] Von Stryk OS. (1993) *Optimal Control*; Springer.

Bracing Results in Immediate Improvements in Gait Mechanics for Patients with Adult Spinal Deformity

Ruth Higgins¹, Ram Haddas², Isador Lieberman², Joshua M. Tome³, Runit Singh Kakar¹

¹School of Rehabilitation Sciences, Old Dominion University, Norfolk, VA, USA

²Texas Back Institute, Plano, TX, USA; ³Ithaca College, Ithaca, NY, USA

Email: rhigg002@odu.edu

Summary

Effects of bracing on trunk and pelvis range of motion (ROM) for patients with adult spinal deformity (ASD) were compared for immediate- and short-term benefits. When wearing brace, normal trunk ROM was maintained, and pelvic kinematics during gait were improved. Bracing could help improve gait mechanics in addition to pain reductions.

Introduction

ASD is characterized as a spectrum of abnormalities that affect the thoracolumbar or lumbar spine throughout the ageing process. Literature supports significant reductions in worst pain, back pain, and leg pain with bracing in adult female idiopathic scoliosis patients [1]. Due to the rigidity of adult spines, bracing in patients with ASD is not meant to correct spinal curvature, but rather aims to relieve the pain and other symptoms by temporarily placing their spine/trunk into the best physiological alignment possible [2]. Paucity of investigations on effects of bracing on trunk or pelvis ROM during gait is known [2]. Therefore, the purpose of this study was to investigate the impact of bracing on trunk and pelvis ROM during gait for individuals with ASD.

Methods

Thirty patients (26 females, age: 72.7±4.5, Height: 1.58±0.09m, Weight: 67.7±16.1kg) with clinically diagnosed thoracolumbar and/or lumbo-sacro-pelvic deformity (SRS/Schwab classification; Cobb angle >25°) were recruited. Three-dimensional (3D) trunk and pelvis kinematics were recorded as each patient performed 5 acceptable trials of 10-meter walk test at self-selected speed (Vicon®-100Hz) at initial evaluation (pre), 45min post fitting (post45m) with Peak™ scoliosis brace and after 8 weeks (average 4.5 hour/day) of bracing (post8w). A one-way RM-ANOVA was performed to determine kinematic differences between the 3 time points. Post-hoc analyses were also performed using the Bonferroni correction (p<.05).

Results and Discussion

Statistically significant changes in trunk ROM were found in all three planes of motion (p<0.01), and in the frontal and transverse planes (p<0.019) for pelvis ROM. Post-hoc analyses showed significant reductions between Pre- and Post45m measurements in trunk ROM in all three planes (p<0.01), and the frontal and transverse (p<0.05) planes for pelvis ROM (Figure 1). No other significant changes were observed. Difference in Post45m and Post8w could be due to testing performed without the brace for Post8w session.

For the trunk sagittal and frontal planes, both the Pre- and Post45m motion stayed within the normal ranges compared to

the literature [3]. However, for Post45m, transverse plane ROM was lower than the expected mean ranges. These results indicate the brace does not restrict trunk movement in a way that would cause gait or balance impairments related to trunk and head stiffness as seen with other bracing methods [4].

Pre-bracing, all three planes of pelvis motion were outside of the normal ranges reported in the literature [5]. Immediately after bracing, frontal and transverse plane ranges reduced to within the normal limits but not for the sagittal plane. Restoring pelvic motion to a normal range could lead to a smoother and energetically more efficient gait [5]. Minimal changes were observed with 8 weeks of bracing, suggesting a need for continued use during activities of daily living or increased hours/day compliance for sustained effects.

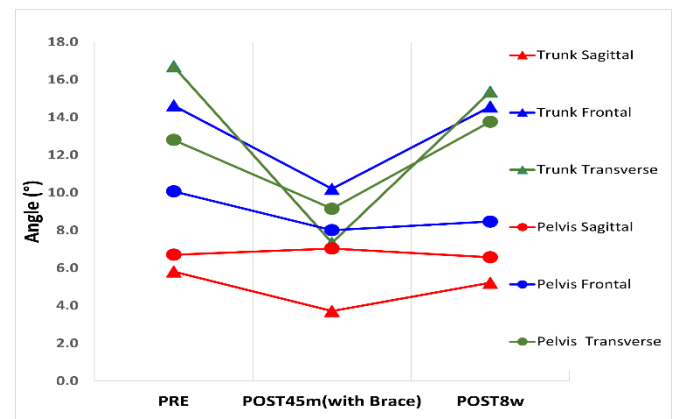


Figure 1: Pre-, Post45m, and Post8w kinematics

Conclusions

Bracing for individuals with ASD resulted in a healthy reduction in pelvis ROM and although trunk ROM was reduced, it remained in normal range in the sagittal and frontal planes. With immediate use, these kinematic changes could lead to improved gait biomechanics in patients with ASD in addition to the previously shown reductions in pain [1].

Acknowledgments

The study was supported by a research grant from Aspen Medical Products.

References

- [1] Zaina F et al. (2018) *Prosthet Orthot Int.*, **4**: 410-414.
- [2] McAviney J et al. (2020) *BMC Musculoskelet Disord*, **21**: 87
- [3] Chung C et al. (2010) *J NeuroEng Rehabil*, **7**: 9
- [4] Morrison S et al. (2015) *J. Neurophysiol.*, **114**: 1773-1783
- [5] Lewis CL et al. (2017) *Anat Rec*, **300(4)**: 633-6

Review of musculoskeletal modelling in a clinical setting: current use in rehabilitation design, surgical decision making and healthcare interventions

Samuel H L Smith^{1,2}, Russel J Coppack^{1,3}, Antonie J van den Bogert⁴, Alexander N Bennett^{1,5}, Anthony M J Bull²

¹Academic Department of Military Rehabilitation, Defence Medical Rehabilitation Centre (DMRC), Stanford Hall, UK;

²Department of Bioengineering, Imperial College London, UK; ³Centre for Sport, Exercise & Osteoarthritis Research Versus Arthritis, Department for Health, University of Bath, UK; ⁴Department of Mechanical Engineering, Cleveland State University, Cleveland, OH, USA; ⁵National Heart & Lung Institute, Faculty of Medicine, Imperial College London, UK

Email: samuelhsmith@gmail.com

Summary

Despite the ability to assess joint loading and muscle force, musculoskeletal models (MSM) are still not widely used clinically. A review of the recent literature revealed that over the last 10 years, only 39 published works featured the use of these models in the design of training programs, surgical decision making, and informing general healthcare practice. Collaborations should be encouraged between model developers and clinical teams to create accessible software, usable with minimal input and programming skills.

Introduction

MSM are simulation tools through which biomechanical analysis of human movement can be performed non-invasively, the outputs of which include muscle and joint contact forces (JCF). This enhanced analysis requires complex optimization [1], which can be time-consuming and requires additional expertise beyond that of routine clinical training. The utility of such models in a healthcare environment is largely unknown. Therefore, a narrative review was performed to classify the most recent uses of MSM in clinical practice.

Methods

A search of the literature was performed using the online databases Scopus and PubMed. Titles, keywords and abstracts were searched using terms which included *Musculoskeletal model**, *biomechanical model**, *inverse dynamic**, *joint contact force**, *joint reaction force**, and *muscle*. Papers were collated up to 24th August 2020.

Only peer reviewed articles, published in 2010 onwards, were considered. Exclusions included: robotics, finite-element analysis, animals, cadavers, unrelated to clinical outcomes, validation/model development, not using MSM, or not featuring a patient population or clinical intervention. Work containing only healthy controls was included if assessing a clinical intervention for patients. Articles were classified by use, iterating groups to find the minimum number that would contain all included studies. The authorship of each article was also noted as a surrogate measure of clinical utility.

Results and Discussion

4662 abstracts were found and 39 full papers were deemed appropriate for review. Of these papers, 38 were co-authored by clinical and engineering/modelling authors, with 1 paper

authored solely by the latter. Five distinct categories were created: Assessment of non-surgical treatment (3/39); Assessment of orthotic devices (10/39); Surgical decision making (3/39); Assessment of surgical interventions (10/39) and the assessment and/or design of exercises and rehabilitation programmes (13/39). Reviewed work included the assessment of knee braces in the treatment of osteoarthritis [2], optimizing rehabilitation programmes using JCF [3], and deciding on the necessity of hamstring lengthening surgery in adolescents with cerebral palsy [4].

Only 7 of the reviewed papers analysed movements other than gait. Expanding the list of tasks analysed in treatment decision making is vitally important in improving outcomes. Higher functioning patients, such as elite athletes and those in the military, will desire a return to activity beyond ambulation. Validation studies should routinely address a greater number of tasks to ensure the needs of a population are met.

Reviewed articles regularly commented that individualised care could be optimised through the use of MSM. However, there is still a lack of published work showing the use of MSM as tools for patient care despite the ability to assess long- and short-term joint loading, and muscle overuse, during clinical decision making. The large number of papers focused on the development/validation of MSM, and associated authorships of the reviewed papers, highlight the absence of mature software available for clinical use.

Conclusions

There is an absence of evidence, and therefore numerous challenges to overcome, for the use of MSM in regular clinical practice. The reviewed work mainly contained efforts to assess existing treatment methods, as opposed to employing MSM as a tool itself. The authors call for further model developer collaborations and increased awareness of these modelling techniques in clinical fields, combining the numerous available platforms to produce MSM which can be used in the healthcare decision-making process.

References

- [1] Crowninshield & Brand (1981). *J Biomech*, **14**: 793-801.
- [2] Brandon et al. (2019) *Knee*, **26**: 564-577.
- [3] Van Rossom et al. (2018). *J Orthop Sports Phys*, **48**: 162-173.
- [4] Laracca et al. (2014). *Gait Posture*, **39**: 847-851

Computational modelling of proximal and distal epiphyseal and appositional growth of the femur in children

Andreas Lipphaus¹, Andreas Wegener-Panzer², Ralf-Bodo Tröbs³, Ulrich Witzel¹

¹Biomechanics Research Group, Chair of Product Development, Ruhr-University Bochum, Bochum, Germany

²Department of Radiology, Children's Hospital Datteln, University Witten/Herdecke, Datteln, Germany

³Department of Pediatric Surgery, Helios Hospital St. Johannes, Duisburg, Germany

Email: andreas.lipphaus@rub.de

Summary

Mechanical loading of the growth plate modulates bone shape. Combined modelling of epiphyseal and appositional growth can predict bone development.

Introduction

Longitudinal growth of the femur occurs at the epiphyseal plates where the distal plate contributes to 70% of femoral growth. Epiphyseal growth is influenced by biological and mechanical factors. The predominant mechanobiological theory states that mechanical stimulated growth accounts for 50% of the total growth and is determined by deviatoric shear and hydrostatic stress [1]. Appositional growth takes place at the bone surfaces and increases the bone diameter. It has been assumed that the benefit of mechanical modulation of pediatric bone growth is to correct deformities [2], leading to bending-minimized lightweight design. Several computational models of bone growth have been established. However, most models only include a single growth plate, neglect different plate specific growth rates or do not include appositional growth. Our aim is to provide a comprehensive mechanobiological model of femoral growth.

Methods

A finite element model from literature of a femur based on MRI scans of a healthy 8-year-old child (20.4 kg, 1.24 m) is used [3]. The growth plate in the femoral neck and the distal growth plate are modeled as two layers each 0.6 mm thick representing the proliferative and the hypertrophic zone. Hypertrophic growth is modeled as unidirectional expansion in the direction of the highest absolute principal stress and proliferation by isotropic expansion. Biological baseline growth is 0.9 month⁻¹ for the proximal and 2.1 month⁻¹ for the distal growth plate. Mechanically stimulated growth is described by the weighted sum of the deviatoric shear stress σ_S and hydrostatic stress σ_H . Appositional growth is simulated by displacement of the external nodes normal to the bone surface. Periosteal apposition rate is fixed at 2 $\mu\text{m}/\text{day}$ for areas with compressive 3rd principal stresses of more than 20 MPa. Young's modulus is 12000 MPa for cortical and 500 MPa for spongy bone and 6 MPa for the growth plate. All calculations are performed in ANSYS Mechanical 19.2 (ANSYS Inc, Canonsburg). One iteration represents growth during one month and six iterations are performed.

Results and Discussion

After six simulated months, an increase of femoral length by 16.8 mm is predicted. The femoral shaft diameter enlarges

by 0.36 mm. Appositional growth is highest on the concave side of the bone leading to a reduced curvature and hence a more homogenous stress distribution in the femoral shaft. However, structural adaptations are relatively slow and cannot fully compensate bending stresses after six simulated months. Muscle forces seem to play a predominantly role in skeletal lightweight design. Limitations of this study include the non-consideration of changes in muscle lines of actions, muscles forces, or the bone density during growth as well as resorption of bone.

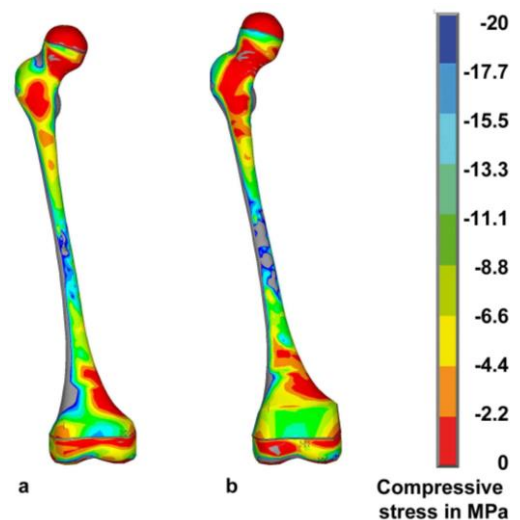


Figure 1: Frontal view of bone shape and 3rd principal stresses a) before and b) after 6 months of simulated growth

Conclusions

Combination of epiphyseal and appositional growth is necessary to model bone development. The contribution of both mechanisms to reduce bending stress in terms of lightweight design needs further investigation.

Acknowledgments

This research was supported by the Deutsche Forschungsgemeinschaft (DFG, German Research Foundation) – 445465815. The finite element model of the pediatric femur was provided by Bryce Killen, Hans Kainz, and Ilse Jonkers on SimTK under MIT licence.

References

- [1] Stevens SS et al. (1999). *J Orthop Res*, **17**: 646-653.
- [2] Pauwels F. (1980). *Biomechanics of the Locomotor Apparatus*; Springer.
- [3] Kainz et al. (2020). *PLOS ONE*, **15**: e023596

Bone alignments via weight-bearing CT scans and 3D reconstruction tools in the flat foot

Belvedere C., Pavani C., Scicolone S., Ortolani M., Berti L., Girolami M., Bevoni R., Durante S., Leardini A.
 IRCCS Istituto Ortopedico Rizzoli, Bologna, Italy
 Email: claudio.belvedere@ior.it

Summary

Acquired adult flatfoot is a frequent deformity which implies multiple, complex and combined 3D modifications of the foot skeletal architecture. Exact assessment of bone alignments now can be provided by CT in weight-bearing. These scans were taken from 21 patients before surgical correction. 3D bone models were obtained by two segmentation tools with different levels of automatization: MIS (Materialise) and Bonelogic® Ortho Foot and Ankle (Disior). Principal Component Analysis defined anatomical reference frames for each bone model. Absolute and relative angles were calculated, in anatomical plane projections and in 3D. Between the two tools, statistically significant linear correlations were found for all measurements, and no statistical difference was found for most of these.

Introduction

Acquired adult flatfoot is a frequent deformity which implies multiple, complex and combined 3D modifications of the foot skeletal architecture. A thorough assessment of the degree of severity, of the effect of orthotics, and of the post-operative outcome can take advantage by modern Cone-Beam CT technology [1, 2]. This finally gives access to foot bones in 3D and in weight-bearing (WBCT). This study reports on original measurement techniques to quantify overall foot bone deformities, here exploited to severe flatfoot patients. A comparison of two segmentation tools is also provided.

Methods

Twenty-one patients were scanned while standing on the foot to be operated, via WBCT (OnSight 3D Extremity System, Carestream®, US). The CT scans were sliced at 0.26 mm, and 3D models of each of the bones were reconstructed from these DICOM files. A more manual segmentation was performed with a state-of-the-art tool (MIS, Materialise, Belgium); a more automatic segmentation was also performed by Bonelogic® Ortho Foot and Ankle (DISior, Finland). From both 3D reconstructions, Principal Component Analysis was used to define anatomical reference frames for each bone model. Traditional angular and linear measures were taken from these frames, mostly based on the longitudinal axis. This was obtained as absolute orientation for single bones and as relative orientation from two bones, in the three anatomical plane projections as well as in 3D [3].

Results and Discussion

Both reconstructions revealed a considerable valgus of the calcaneus, plantarflexion and internal rotation of the talus, and typical Meary's angles in the sagittal and transverse planes. 3D angles were found different from and more consistent than

corresponding planar projections. The difference between manual and automatic segmentation tools was within 3 degrees for most of these angles, in front of about 15 person-hour difference for the two tools. Many correlations were found between measurements of deformity from the rear- and the fore-foot. Correlations were found with the Foot Posture Index: for Meary, FAO [4] and talus distance from the floor.

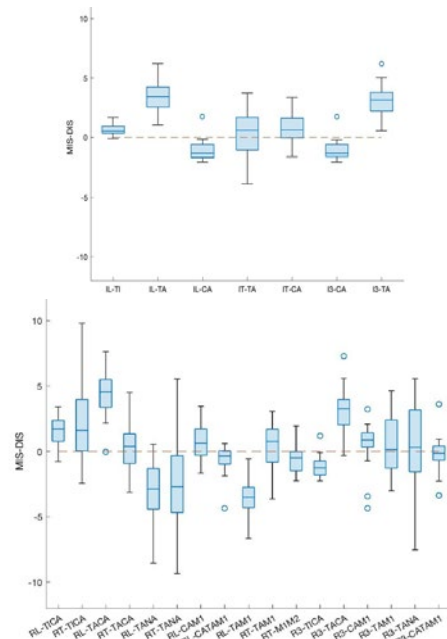


Figure 1: Boxplots with outliers of the difference between the major angular measurements from MIS and DIS bone models, in 2D (RLateral, RTransverse) and in 3D (R3); the rest of the acronym reports the bone (single - above) or the two bones involved (e.g. Tlbia and CAlcaneus - below).

Conclusions

WBCT finally provides accurate 3D assessments of complex foot and ankle deformities, to be exploited in a number of clinical evaluations [5]. Modern software tools allow for accurate and fast reconstructions of bones, which now give access to a huge spectrum of traditional and novel angular measurements. 3D measurements also limit the projection artifacts associated to malposition and deformity of the foot as in traditional radiographs [3]. Analysis of the corresponding post-operative alignments of this population is in progress.

References

- [1] Barg A et al. (2018). *Foot & Ankle Int*, **39**(3): 376-386
- [2] Richter M et al. (2020). *Foot Ankle Surg*, **26**(5):518-522
- [3] Carrara C et al. (2021). *Foot Ankle Surg*, **27**: 168-174
- [4] Lintz F et al. (2017). *Foot Ankle Int*, **38**(6):684-689
- [5] Leardini A et al. (2019). *Sem Musc Rad*, **23**(6):643-656

Identification of Optimal Laxity Tests To Stretch Individual Parts of Knee Ligaments

Michael S. Andersen¹, Dennis Pedersen²

¹Biomechanics Research Group, Department of Materials and Production, Aalborg University, Aalborg, Denmark

² Regional Development, Central Denmark Region, Denmark

Email: msa@mp.aau.dk

Summary

We developed a novel approach to identify optimal knee laxity tests to stretch knee ligaments relatively more than other ligaments and applied it to identify optimal tests on a biomechanical model. For some ligaments, the optimal load cases resemble those applied clinically while for others, the optimal tests are much different. Our results have implications for the development of new laxity tests to diagnose ligament injuries or identify ligament properties from laxity tests.

Introduction

Knee instability can arise for several reasons and can lead to pain, joint degradation and an overall reduced quality-of-life [1]. To advance our understanding of knee instability, it is important to gain insight into the mechanical properties of the knee ligaments *in vivo*, which cannot be measured directly.

Recently, we developed a novel 3D laxity measurement technology [2] that enables applying any load case to the knee. This provides an opportunity to re-think how laxity tests are performed and tailor the applied loads to stretch some ligaments relatively more than others and thereby having the best data to estimate the ligament properties from. The purpose of this study was to identify such optimal laxity tests.

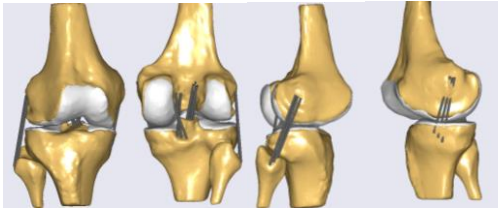


Fig. 1 Illustration of the applied knee model.

Methods

A subject-specific knee model based on a MRI scan of a female subject (27 year-old, 1.72 m, 61 kg) was developed in the AnyBody Modeling System (AnyBody Technology, Denmark) using the Force-dependent Kinematics (FDK) approach [3](Fig. 1). The contact between the tibial and femoral cartilage and the four major ligaments were included.

As inputs to the model, we provided the knee flexion angle as well as an applied force and an applied moment to tibia. The force was applied to the tibial tuberosity and the moment as a pure moment in a tibial ISB anatomical coordinate system.

We introduced five FDK degrees-of-freedom that were allowed to equilibrate according to the applied loads, ligament and contact forces. A reaction moment around the knee flexion axis was included to simulate a fixated knee flexion as typically done during laxity tests. To identify what we will denote the optimal load cases to stretch each element of the ligaments, we solved the following optimization problem:

$$\max_{\mathbf{x}^1, \mathbf{x}^2} (F_i^2 - F_i^1)^2 - \frac{1}{N-1} \sum_{j=1, j \neq i}^N (F_j^2 - F_j^1)^2 \quad (1)$$

where \mathbf{x}^1 and \mathbf{x}^2 denote two load cases (i.e. each containing the knee flexion angle and applied force and moment on tibia). F_k^1 and F_k^2 denote the force in the k th ligament bundle under load cases \mathbf{x}^1 and \mathbf{x}^2 , respectively. The first term in the equation specifies the squared difference in the ligament bundle of interest (i th) from which the second term subtracts the average force in all other ligament bundles. N denotes the number of ligament bundles in the model.

Results and Discussion

Load cases for all ligaments were found but for the sake of brevity, we present the results for the antero- and posterior-medial bundles of the Anterior Cruciate Ligament (ACL) only (Table 1). For the anteromedial ACL bundle, the optimal knee angles were found to be 6.0° and 22.4° and with a clear anterior and posterior force difference between the two loads. The posteromedial bundle of ACL, however, required one load at 7.3° of knee flexion, primarily directed anteriorly and the other at 93.2° directed posterolaterally.

Conclusions

In this study, we presented a method to identify optimal loads to stretch individual ligament bundles. This approach, and the obtained results, can be applied to develop future measurement protocols, ultimately leading to a better estimation of knee ligament properties *in vivo*.

References

- [1] Nevill MC, et al., *Arthritis Care Res*, **68**:1089-1097, 2016.
- [2] Pedersen et al., *J Biomech*, **82**:62-69, 2019.
- [3] Andersen et al., *J Biomech Eng*, 139: 091001, 2017.

Table 1: Optimal loads for selected ACL bundles. Standard abbreviations for anterior-posterior (ap) etc. are used.

Ligament	Knee flexion [°]	F _{AP} [N]	F _{SI} [N]	F _{ML} [N]	M _{vv} [Nm]	M _{IE} [Nm]	M _{FE} [Nm]
ACL anteromedial	6.0	-120.0	-44.3	-28.0	-8.4	5.3	-0.6
	22.4	95.8	65.0	-92.6	-5.4	6.1	-0.2
ACL posteromedial	7.4	137.9	16.8	-19.5	-1.1	7.4	-4.9
	93.2	-74.3	-29.6	-114.4	-0.3	4.2	2.2

Measuring knee joint laxity in four DOF *in vivo* using a robotics- and image-based technology

Hannah K. Fabro¹, Jana Kümmerlin¹, Peter H. Pedersen², Kenneth K. Jensen³, Dennis Pedersen⁴, Michael S. Andersen⁵

¹Department of Mechanical Engineering, Ostbayerische Technische Hochschule, Galgenbergstr.30, 93053 Regensburg, Germany

²Department of Orthopedic Surgery, Aalborg University Hospital, Hobrovej 18-22, 9000 Aalborg, Denmark

³Department of Radiology, Aalborg University Hospital, Hobrovej 18-22, 9000 Aalborg, Denmark

⁴Regional Development, Central Denmark Region, Skottenborg 26, 8800 Viborg, Denmark

⁵Department of Materials and Production, Aalborg University, Fibigerstræde 16, 9220 Aalborg, Denmark

Email: msa@mp.aau.dk

Summary

This paper presents the development of an *in vivo* 3D knee laxity measurement method, combining robotics- and image-based technologies, to measure tibiofemoral poses under static 3D loads. With the robotic device, single and combined loads can be applied and it allows measurements of primary and secondary knee laxity, providing information about knee ligament integrity. The method also serves as a basis for improved patient-specific computational modeling, diagnoses and treatment.

Introduction

Instability in the knee joint, which is often attributable to instable knee ligaments, can lead to meniscal tear and osteoarthritis [1]. Therefore, knee ligament properties and knee stability are increasingly important areas in orthopedic treatment, surgery planning as well as prosthesis design [2].

Because of drawbacks such as soft tissue artifacts and constrained range-of-motion in the knee joint within current knee laxity investigations, Pedersen et al. [3] developed a methodology to measure knee ligament laxity in four degrees of freedom (DOF) *in vitro*, thereby overcoming aforementioned complications. As this technology has only been applied *in vitro*, this study provides a proof-of-concept of 3D knee laxity measurements of healthy subjects *in vivo*.

Methods

The device (see Figure 1) was designed to fit into the EOS bi-planar imaging system (EOS imaging, France). To demonstrate the method, it was applied to four healthy male subjects. Seven different loads were applied during the experiment: No load, Internal/External (IE) rotation (6Nm), Anterior/Posterior (AP) translation (100N), Medial/Lateral translation loads (ML) (10Nm).

During peak stationary application of the load, x-rays were simultaneously taken from the frontal and lateral side. Magnetic Resonance Imaging (MRI) scans were obtained from whole lower limbs. After completion of data acquisitions, the following steps were accomplished: 1) segmentation of the 3D bone geometries from the MRI scans, 2) registration of the 3D bone geometries to the EOS bi-planar x-rays for each load case using an iterative closest point algorithm developed in MATLAB 2017b (Mathworks, USA) and 3) computation of the tibiofemoral poses in accordance with the ISB recommendations using the AnyBody Modeling System 7.3.0 (AnyBody Technology, Denmark).

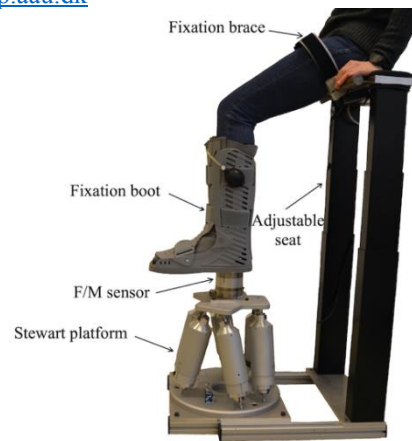


Figure 1: Experimental setup showing all important components.

Results and Discussion

Primary laxity, which refers to the knee laxity in the direction of the load application, was obtained. AP loading resulted in a tibial translation of 1.8 ± 1.2 mm and 1.4 ± 2.2 mm, respectively. IE rotational loading resulted in a tibial rotation of $11.3 \pm 7.7^\circ$ and $6.0 \pm 4.6^\circ$, respectively. ML loading resulted in a tibial translation of -1.5 ± 1.3 mm and 1.3 ± 1.0 mm, respectively.

Secondary laxity measurements, which refer to the knee laxity in all other directions, revealed an association between AP translations and IE rotations during AP loading.

Due to the fact that only healthy subjects were included in the study, the calculated mean of AP translations in part did not exceed the reported measurement uncertainty. This was expected, as intact ligaments do not allow for bigger than reported poses under a medically justifiable load application.

Conclusions

A methodology that combines robotics- and image-based technology to assess knee laxity in four DOF *in vivo* was presented. The advantages of this new approach include accurate measurements of primary and secondary laxity, the ability of making unconstrained measurements as well as the ability of applying multiplanar load cases.

References

- [1] Pugh L et al (2009). *Am. J. Sports Med.*, **37**: 199-210
- [2] Beldame J et al (2011) *Orthopaedics & Traumatology: Surgery & Research*, **97**: 34-43.
- [3] Pedersen et al (2019) *J. Biomech.* **82**:62-69.

Characterization of collagen structural response to *in situ* loading of the rat Achilles tendon

I. Silva Barreto¹, M. Pierantoni¹, M. Hammerman¹, E. Törnquist¹, S. Le Cann^{1,3}, A. Diaz⁴, J. Engqvist¹, M. Liebi^{5,6}, P. Eliasson², H. Isaksson¹

¹Lund University, Sweden; ²Linköping University, Sweden; ³CNRS, Paris, France; ⁴Paul Scherrer Institut, Switzerland; ⁵Chalmers University, Sweden; ⁶EMPA, Switzerland

Email: isabella.silva_barreto@bme.lth.se

Summary

The collagen response in rat Achilles tendons to *in situ* tensile loading was studied using small-angle X-ray scattering (SAXS), to evaluate the relationship between the elastic and viscoelastic behavior of the tissue and collagen fibrils. The fibril strains were substantially lower than the applied tissue strains. Fibril strains increased linearly before yielding and breaking prior to tissue failure.

Introduction

The mechanical properties of tendons are depending on a complex hierarchical design, where collagen is arranged into fibrils in a periodic, quarter staggered pattern at an intermolecular distance referred to as d-spacing. This study aimed to characterize the Achilles tendon's mechanical response to *in situ* loading at the nanoscale and how it relates to the resulting macroscopic tissue mechanical behavior.

Methods

Achilles tendons (n=16) were harvested from Sprague Dawley rats (10-14 weeks) and stored frozen in NaCl until measurements at the SAXS beamline (cSAXS, Swiss Light Source, PSI) (energy 12.4keV, beam size 150 μ m). The tendons were loaded using a custom-made uniaxial tensile device (Fig 1) [1] while SAXS patterns ($q=0.05$ - 1.45nm^{-1}) were acquired simultaneously from the center of the tendon. A radiation damage test was conducted prior to testing which ensured that all analysis was conducted below 28kGy. The tendons were loaded (5mm/min) in ramp to failure (N=5), cyclic loading (N=5) or stress relaxation (N=6). From collagen peaks identified from the azimuthally integrated scattering intensity over the angular sector θ (Fig 1.A), local fibril strain and collagen structural parameters were extracted [2,3]. All analysis was performed using MATLAB.

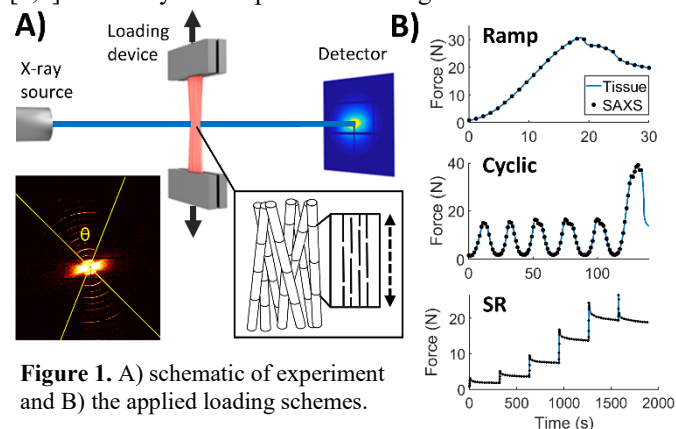


Figure 1. A) schematic of experiment and B) the applied loading schemes.

Results and Discussion

For all loading schemes, the fibril strain, strain heterogeneity and overlap followed the macroscopic load. During ramp to

failure, the fibril strain increased linearly with tissue strain in the elastic region (Fig 2.A). The fibrils in the beam path yielded and broke (fibril strains $1.3\pm 0.3\%$) prior to global tissue failure, which could be the result of an accumulation of nanoscale ruptures throughout the specimens. With increasing load, the fibril d-spacing increased and the overlap region decreased, which indicates fibril stretching and sliding simultaneously. During cyclic loading, the tissue hysteresis decreased with number of cycles (Fig 2.B, i). Interestingly, while the d-spacing at maximum load remained constant for all cycles ($0.9\pm 0.5\%$), it decreased sequentially at the end of each cycle (Fig 2.B, ii). This suggests that the initial decline in tissue hysteresis is accompanied by an increase in fibril recovery and stretchability. During stress relaxation, most of the collagen parameters experienced transient relaxation simultaneously as the tissue (Fig 2.C).

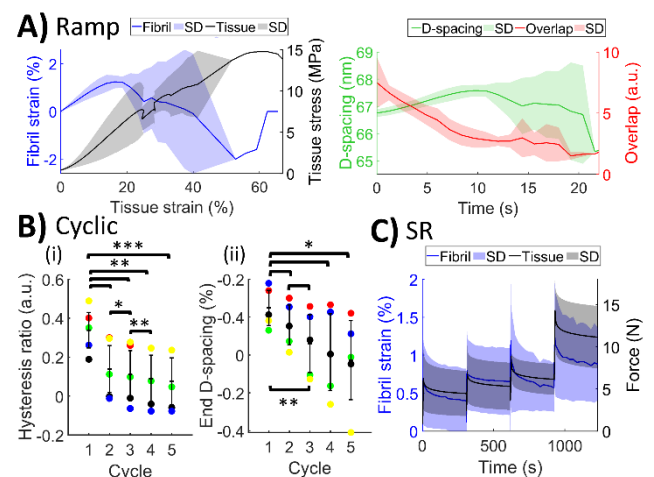


Figure 2. Changes in fibril parameters during A) ramp to failure, B) cyclic loading and C) stress relaxation.

Conclusions

Different loading scenarios enabled linking of the nano and macroscale in the Achilles tendon in terms of mechanics, such as accumulation of local fibril ruptures before global failure and adaptation of the nanostructure to the applied load.

Acknowledgments

This project was funded by the European Union's Horizon 2020, No 731019 (EUSMI) through beamtime at cSAXS beamline, PSI, and by the Knut and Alice Wallenberg Foundation.

References

- [1] J. Engqvist et al. (2014). *Exp Mech*, **54**;1373-1383.
- [2] H. Khayyeri et al. (2017). *Sci Rep*, **7**;13067.
- [3] G. Fessel et al. (2014). *PLOS one*, **9**;e110948.

Functional Performance Associated with Triceps Surae Muscle and Tendon Morphology in Patients with Achilles Tendinopathy

Kayla D. Seymore^{1,2}, Haraldur B. Sigurðsson¹, Karin Grävare Silbernagel¹

¹Dept. of Physical Therapy, University of Delaware, Newark, DE, USA

²Biomechanics and Movement Science Program, University of Delaware, Newark, DE, USA

Email: seymorek@udel.edu

Summary

This study determined the association between functional performance and triceps surae muscle and tendon morphology in patients with Achilles tendinopathy. Eighty-nine participants with confirmed Achilles tendinopathy had triceps surae muscle size and Achilles tendon viscoelasticity quantified with ultrasound imaging and continuous shear wave elastography (cSWE) prior to functional performance testing. Heel rise and hopping performance was associated with triceps surae muscle size and tendon shear modulus in patients with Achilles tendinopathy, when controlling for sex, limb, age, weight, and physical activity level.

Introduction

Achilles tendinopathy is an overuse injury, often accompanied by alterations in tendon morphology, triceps surae muscle weakness, and impaired functional performance [1,2]. Though these tissues have complimentary roles in ankle and knee joint mechanics, the contribution of triceps surae muscle and tendon morphology to lower limb function has not been established in the Achilles tendinopathy population. Thus, the purpose of this investigation was to determine the association between functional performance and the triceps surae muscle size and tendon material properties of patients with Achilles tendinopathy.

Methods

Eighty-nine (44 F, 47.6 ± 11.7 yrs) participants with clinically confirmed mid-portion Achilles tendinopathy were included in the study. Triceps surae size was obtained with B-mode ultrasound and characterized by cross-sectional area (CSA) of the medial (MG) and lateral (LG) gastrocnemius muscle, as well as thickness of the soleus (SOL) muscle, according to previously published protocol [3]. Achilles tendon material properties of shear modulus and viscosity were obtained in accordance with previously published cSWE protocol [4].

Functional performance was then quantified with a test battery. Total work and repetitions for a single-leg maximum endurance heel-rise test were measured using a linear encoder affixed to the heel. Hop frequency was calculated using a light

field comprised of infrared beams, which triggered a timer when the field was disrupted. The middle 20 hops during a 25-repetition continuous single-leg hopping test were analyzed.

Dependent variables of triceps surae muscle size and tendon material properties and independent variables of heel rise and hopping tests were analyzed with a two-way multivariate analysis of covariance to determine the association between functional performance and triceps surae muscle and tendon morphology, when controlling for sex, limb, age, weight, and physical activity level, measured via Physical Activity Scale questionnaire. Alpha was $p < 0.05$.

Results and Discussion

Heel rise work ($p=0.004$) and heel rise repetitions ($p=0.031$), but not hop frequency ($p=0.081$), were associated with triceps surae muscle and tendon morphology. Heel rise and hopping performance correlated to MG ($p<0.001$, $r^2=0.539$), LG ($p<0.001$, $r^2=0.490$), and SOL ($p<0.001$, $r^2=0.168$) muscle size and tendon shear modulus ($p=0.001$, $r^2=0.145$), after controlling for sex, limb, age, weight, and physical activity level. However, large differences in performance were required for appreciable change to morphology (Table 1). There were significant effects of sex, age, weight, and physical activity level ($p<0.01$), with no effect of limb nor interaction of sex and limb on muscle and tendon morphology.

Conclusions

Functional performance correlates to the triceps surae muscle size and Achilles tendon shear modulus of patients with Achilles tendinopathy. Future studies are needed to investigate the impact of changes in calf tissue morphology on functional performance.

References

- [1] Silbernagel KG et al. (2020). *J Athl Train*, **55**: 438-447.
- [2] O'Neill S et al. (2019). *Phys Ther Sport*, **37**: 69-76.
- [3] Zellers JA et al. (2019). *J Orthop Res*, **37**: 933-941.
- [4] Cortes DH et al. (2015). *Ultrasound Med Biol*, **41**: 1518-1529.

Table 1: Regression coefficient estimates (β), 95% confidence intervals (CI), and p-values for the fit model.

	Heel Rise Work			Heel Rise Repetitions			Hop Frequency		
	β	95% CI	p-value	β	95% CI	p-value	β	95% CI	p-value
Shear Modulus	0.005	(-0.002, 0.012)	0.184	-0.233	(-0.770, 0.304)	0.392	11.266	(2.364, 20.169)	0.014
MG CSA	0.001	(0.000, 0.002)	0.007	-0.105	(-0.173, -0.037)	0.003	-0.560	(-1.686, 0.567)	0.327
LG CSA	0.001	(0.000, 0.001)	0.029	-0.040	(-0.083, 0.002)	0.063	0.004	(-0.701, 0.709)	0.991
SOL Thickness	0.000	(0.000, 0.000)	0.077	-0.002	(-0.009, 0.006)	0.637	-0.002	(-0.124, 0.119)	0.971

Mathematical modeling of degradation process of biodegradable metallic biomaterials in immersion and perfusion setups

Mojtaba Barzegari¹, Di Mei², Sviatlana V. Lamaka², Liesbet Geris^{1,3}

¹ Biomechanics Section, Department of Mechanical Engineering, KU Leuven, Leuven, Belgium

² Institute of Surface Science, Helmholtz-Zentrum Geesthacht, Geesthacht, Germany

³ Biomechanics Research Unit, GIGA in Silico Medicine, University of Liège, Liège, Belgium

Email: mojtaba.barzegari@kuleuven.be

Summary

Despite the advantages of using biodegradable metals in implant design, their uncontrolled degradation and release remain a challenge in practical applications. A validated computational model of the degradation process can facilitate the tuning of implant biodegradation by changing design properties. In this study, a physicochemical model was developed by deriving a mathematical description of the chemistry of magnesium biodegradation and implementing it in a 3D computational model. The model was validated by comparing the predicted and experimentally obtained hydrogen evolution and change of pH during the corrosion tests in both immersion and perfusion setups, showing a good agreement between the results.

Introduction

Due to their bio-friendly properties and non-toxic contribution to body metabolism, biodegradable metallic biomaterials, including magnesium (Mg), iron (Fe), and zinc (Zn), are regaining attention in recent years for fixation applications [1]. Despite these advantages, their fast degradation rate and uncontrolled release have always been a challenge. These issues are usually investigated by conducting *in vitro* and *in vivo* tests of biodegradable metallic scaffolds and implants, which requires conducting multiple experiments for different scenarios. In this research, we have developed a mathematical model to predict the degradation behavior of biodegradable metallic materials *in silico*, which makes it possible to study their corrosion in a simulated environment.

Methods

In this study, a mathematical model of the biodegradation process of commercially-pure Mg was developed by deriving a set of partial differential equations (PDE), formulating the mass transfer and fluid flow phenomena as well as tracking the location of the moving corrosion surface during degradation. The equations were derived from the chemistry of biodegradation of Mg in saline (NaCl) and buffered (SBF) solutions, which includes the oxidation of the metallic part, reduction of water, changes in pH, formation of a protective film on the surface, the effect of different ions in the medium, and the effect of a perfusion setup. Tracking the movement of the surface was done by constructing a PDE based on the level set method, which captures the movement of the medium-scaffold interface by defining an implicit surface. The derived equations were coupled and solved using finite element methods. The degradation data to validate the models was collected from corrosion tests performed by using circulating media for simple scaffolds made of Mg. The model parameters were calibrated using a Bayesian optimization

approach, and the obtained parameters were used to simulate the pH changes in NaCl and SBF solutions.

Results and Discussion

In order to obtain the degradation rate over time, instead of direct mass loss measurement, we measured the volume of formed hydrogen gas in Mg corrosion, which can be converted to mass loss by considering the stoichiometry of the reactions. Figure 1 shows the model output for the predicted produced hydrogen and the pH changes in immersion tests. The graph of the evolved hydrogen is used as input during the parameter calibration process, but the pH results are produced by the simulations using the optimized parameters to demonstrate the validation of the developed mathematical and computational models. The predicted pH result shows a difference of 5.35% for the simulation in NaCl and 1.03% for SBF simulation. Although the pH simulations are insufficient in terms of experimental input to call the model fully validated, the obtained validation results show that the developed mathematical and computational models give a correct *in silico* representation of the studied process.

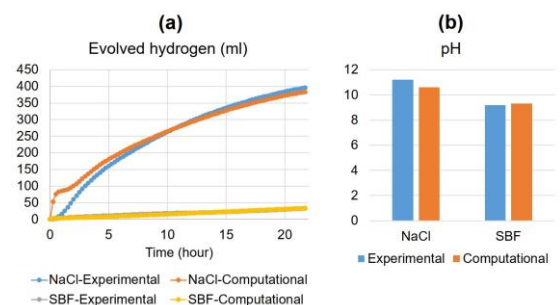


Figure 1: Comparing the quantitative output of the model for the rate of degradation (a) and the pH changes (b) in NaCl and SBF solutions with experimentally measured values.

Conclusions

Once fully validated, the models will serve as an important tool to find the biodegradable metal properties and predict their biodegradation behavior for improving the current workflows of designing biomedical implants and scaffolds.

Acknowledgments

This research is financially supported by the Prosperos project, funded by the Interreg VA Flanders - The Netherlands program, CCI grant no. 2014TC16RFCB046 and by the Fund for Scientific Research Flanders (FWO), grant G085018N.

References

[1] Zheng Y. et al. (2014). *Mat Sci Eng R*, **77**: 1-34.

Changes in ankle and foot joint kinematics after fixed-bearing total ankle replacement

P.-A. Deleu^{1,2}, B. Devos Bevernage¹, L. Chèze², R. Dumas², A. Naaïm², J.L. Besse², T. Leemrijse¹.

¹Foot & Ankle Institute, Brussels, Belgium

²Univ Lyon, Univ Gustave Eiffel, LBMC UMR_T9406, Lyon, France

Email: pa.deleu@footandankleinstitute.be

Summary

Total ankle replacement (TAR) is considered to be an optimal treatment strategy to relieve pain during walking in patients suffering from end-stage ankle osteoarthritis. The aim of this study was to investigate the post-operative effect of TAR on the foot joint angles. We included 28 patients suffering from post-traumatic end-stage ankle osteoarthritis scheduled for primary TAR. A multi-segment foot model was used to measure the kinematics of Ankle, Chopart, Lisfranc and MTP1 joints during gait. Post-operatively, patients demonstrated a significant increase in plantarflexion ankle joint angle and in dorsiflexion Chopart joint angle during loading response. No differences in joint angles were observed during midstance. During propulsion, an increase in the MTP1 dorsiflexion was observed. Clinical significance of this study dictates that patients after TAR preserve their residual pre-operative ankle dorsiflexion and the neighbouring foot joints seem also to be affected.

Introduction

Recently, multi-segment foot models showed that one-segment foot model could lead to clinical misinterpretations of the benefits of TAR on estimates of range of motion [1]. Furthermore, one-segment foot model neglects our clinical understanding of how TAR benefits the function of neighbouring foot joints. Nevertheless, gait analysis studies continue to implement a one-segment foot modeling approach to assess the effect of TAR [2]. Therefore, the purpose of this study was to assess changes in the intrinsic foot angles after TAR providing in-depth insight into the joints distal to the affected joint.

Methods

This study investigated 28 patients suffering from post-traumatic end-stage ankle osteoarthritis scheduled for primary TAR between May 2017 and January 2020. The subjects were asked to walk at self-selected speed barefoot over a 10 m walkway. Inter-segment foot kinematics were obtained using a motion-capture system of 10 Miquis cameras (Qualysis, Sweden) at a 200Hz frequency. An adapted Rizzoli foot model proposed by Deschamps et al. [3] was used. All 1D data were time-normalized to 100% of the stance phase. A paired Hotelling's T^2 (SPM{T2}) was performed to assess the time varying 3-component angles of the Ankle, Chopart, Lisfranc and MTP1 joints.

Results and Discussion

A waveform comparison of foot joint angles is displayed in Figure 1. Differences in waveform patterns were limited to dorsi-/plantarflexion inter-segment joint angles. At loading

response, the ankle plantarflexion joint angle as well as the Chopart joint dorsiflexion increased slightly. These differences may be explained by the fact that patients were not afraid to land properly on their affected ankle joint after surgery during walking. No differences in joint angles were observed during midstance. This finding confirms that TAR preserves the residual pre-operative dorsiflexion range of motion after surgery. During propulsion, an increase in the MTP1 dorsiflexion was observed. The results of this analysis suggest that the kinematic behavior of the foot joints distal to the affected ankle joint seem to improve post-operatively. The reason for this is not clear to determine conclusively to what extent the changes in joint foot angles are attributable to pain relief and to what extent they are related to improvement in a more "functional" foot. The main limitation of this study is the use of skin markers to estimate segment foot kinematics. Soft-tissue artefact reported as angular errors in the dorsi-/plantar-flexion, ev-/inversion and add-/abduction axes respectively has been estimated to be as much as 2.45°, 3.57° and 4.28° [4]. Through, this artifact is supposed to affect similarly pre- and post-operative kinematics, allowing for comparative analysis.

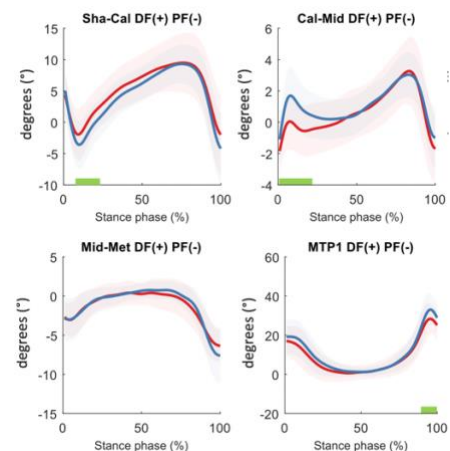


Figure 1: Pre- and Post-operative kinematic of the Ankle, Chopart, Lisfranc and MTP1 joints (Red line : pre-op; Blue line : post-op; significant differences highlighted with a green box)

Conclusions

The outcome of this study showed that changes in foot joint angles after TAR are not restricted to the affected ankle joint, but seem also to affect the neighbouring foot joints.

References

- [1] Deleu PA et al. (2021). *Gait & Posture*, **84**: 308-314.
- [2] Deleu PA et al. (2020). *Clin Biomech*, **73**: 213-225.
- [3] Deschamps KD et al. (2017) *Gait Posture*, **52**: 40-44.
- [4] Kessler SE et al. (2019) *Front Bioeng Biotech*, **7**: 199.

Musculoskeletal trunk model for simulation of scoliosis deformities

Hamed Shayestehpour^{1,*}, Mohammad Amin Shayestehpour³, Christian Wong², and John Rasmussen¹

¹Department of Materials and Production, Aalborg University, Aalborg East, Denmark

²Department of Orthopedics, University Hospital of Hvidovre, Hvidovre, Denmark

³Department of Mechanical Engineering, Sharif University of Technology, Tehran, Iran

Email: hs@mp.aau.dk

Summary

This work presents an improved spine model with an articulated ribcage capable of simulating scoliosis deformities. In this model, joint constraints were defined based on experimental data. A set of clinically accepted parameters that can be measured from bi-planar radiographs, controls the spine curve and ribcage configuration of the model. The normalized compression and lateral shear forces of the intervertebral joints along the spine were reported for a normal and a scoliotic spine. Future use of the model will include investigation of the pathomechanism behind adolescent idiopathic scoliosis, simulation of brace effects, and optimization of brace treatments.

Introduction

The pathomechanism underlying Adolescent Idiopathic Scoliosis (AIS) has remained unclear [1], and a better biomechanical understanding of the phenomenon might contribute to uncovering the phenomenon. The linked system of spinal vertebrae, ribs, and sternum is highly constrained with multiple closed loops, and an anatomically valid constraint definition is essential for reliable force transmission through the model. This work presents an improved and kinematically determinate musculoskeletal spine model with an articulated ribcage, capable of simulating various spine deformities.

Methods

A previously presented spine model [2] forms the basis of the new model. The model was developed in the AnyBody Modeling System, and different types of kinematic joints were implemented [3], based on reported clinical data of intact ribs, leading to a kinematically determinate model, which can simulate healthy spines and ribcage kinematics as well as scoliotic deformations without violations of anatomical constraints.

The posture is defined by a set of fifteen clinically accepted measures (such as Cobb angle) and anatomical degrees-of-freedom (DOF) from the patient's bi-planar radiographs. Muscle and joint reaction forces are simulated by an inverse dynamics analysis.

Results and Discussion

The patient's spine curve and rib rotations were constructed from radiographs (Figure 1). The normalized compression (NC) and normalized lateral shear forces (NLS) of the intervertebral joints along the lumbar and thoracic spine were presented for normal and scoliotic spines, and polynomial curves were fitted to them.

The lumbar and thoracic apical vertebrae of the scoliosis patient were L3 and T8, respectively. The NLS of the normal spine is zero. However, scoliosis seems to increase the NLS corresponding to the curve shape, indicating that the turning points of the spine curve (L1 and T6) occurred where the NLS polynomial curve hits zero. Besides, the progression of scoliosis appears to increase the NC, especially in the lumbar region.

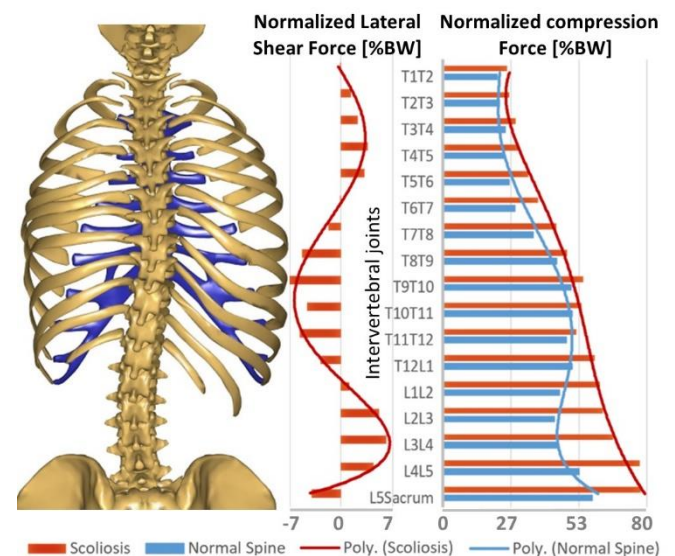


Figure 1: Posterior view of the scoliosis model. Normalized lateral shear and compression forces of the intervertebral joints for the normal and scoliotic spine, and their fitted polynomial curves. All forces are normalized to body weight [BW].

Conclusions

This work presents an improved spine-ribcage model for simulation of scoliosis deformities, suitable for investigating the pathogenesis of AIS by analyzing force trends. In a future perspective, the model can simulate the effect of supportive forces from braces, which can contribute to an optimization of brace interventions.

Acknowledgments

The project has received funding from the European Union's Horizon 2020 research and innovation programme under the Marie Skłodowska-Curie grant agreement NO. [764644].

References

- [1] C. Wong (2015). *Scoliosis*, 10: 1–5.
- [2] D. Ignasiak et al. (2016). *J. Biomech*, 49: 959–966.
- [3] H. Shayestehpour et al. (2021), *Multibody Syst Dyn*, Accepted.

Applied Biomechanics and Computational Modelling to Prevent and Manage Upper Extremity Injuries in Rowing

Caryn A. Urbanczyk^{1,2}, Alison H. McGregor², Anthony M.J. Bull¹

¹Musculoskeletal Mechanics Lab, Dept. Bioengineering, Imperial College London, London, UK

²Biodynamics Lab, Dept. Surgery & Cancer, Imperial College London, London, UK

Email: c.urbanczyk17@imperial.ac.uk

Summary

Investigating shoulder loading during rowing is a major step toward understanding mechanisms of injury, tailoring training programs, and improving performance coordination across all rowing athletes. Optical motion capture and musculoskeletal modelling were used to assess 3D shoulder biomechanics during rowing. Differences between athlete cohorts in glenohumeral joint forces, shoulder stability and muscle recruitment have implications for performance and pathology.

Introduction

Coaches and trainers rely on years of experience to visually assess athlete movement and posture relative to aesthetic characteristics representing an ideal style, [1] ultimately used as a surrogate to indicate high performance. When movements deviate from the circumscribed style, rower technique is manipulated through visual and audio cues to improve performance characteristics of force and timing.

Expert testimony, observational data and visual analysis are powerful and beneficial but lack rigor needed to sufficiently quantify the rowing stroke. Quantitative methods like computational modelling can identify biomechanical parameters crucial to rowing performance and athlete health.

Methods

A 10-camera optical motion capture system (Vicon, UK) was used to track kinematics ($f_c=100\text{Hz}$) of 39 athletes (22 female/17 male) regularly rowing at the time of study participation. 24 reflective markers tracked the torso, scapula, arm, and hand while athletes performed four, 3-minute rowing trials at increasing rate (18/24/28/32 strokes per minute, spm) on an instrumented ergometer (Concept 2, USA), with load cells at the handle and seat, strain gauges under the footplates, and a rotary encoder on the flywheel.

Motion data and external forces, normalized to percent stroke completion, where 0% is the *catch*, provided inputs to the UK National Shoulder Model [2], Glenohumeral joint reaction forces and surrounding shoulder muscles forces at the *catch*, max handle force (*MHF*), and *finish* were analyzed by repeated measures ANOVA ($\alpha<0.05$).

Results and Discussion

Males generate force through prime shoulder movers, latissimus dorsi ($p=0.048$) and serratus anterior ($p=0.005$), focusing on large back muscles for humeral extension and internal rotation. However, women show a wider distribution of cumulative muscle force (Figure 1), including higher max force in trapezius ($p=0.003$). Females also emphasize biceps brachii and brachialis muscle recruitment for shoulder extension and abduction.

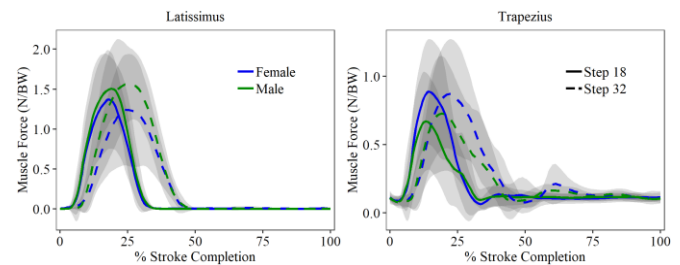


Figure 1: Male v. female BW normalized muscle force (mean \pm sd).

Age related decline in skeletal muscle mass, aerobic fitness [3] manifest in biomechanical changes in ergometer rowing. Compared to younger rowers in university, club, and elite cohorts, masters rowers ($>27\text{yrs}$) show less GH compression, S/I shear ($p=0.013$), and a distinct shoulder stability pattern (SSR) near the *finish* position (Figure 2).

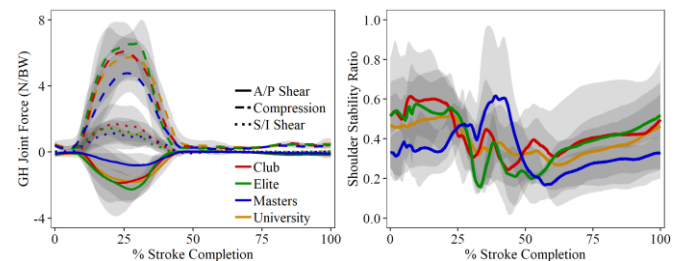


Figure 2: GH joint forces (mean \pm sd) at 32spm (*left*) & SSR at 18spm (*right*) per age/competition level.

Conclusions

Training programs should include greater focus on shoulder muscular endurance to minimize effects of fatigue, and females may benefit specifically from upper extremity strength and conditioning programs. GH instability is affected by stroke rate and position within the stroke. Chronic shoulder pain in rowers results from compromised shoulder positioning [4], instability under high load and acceleration, and likely worsens with age. Computational modelling can sensitively delineate the effects of rowing dynamics, making it valuable to athletes, coaches, and trainers for technique optimization, training impact, and strength and conditioning balance. In this case, specifically to ensure proper scapular and glenohumeral mechanics.

Acknowledgments

Imperial College President's PhD Scholarship for funding.

References

- [1] Smith R & Spinks W (1995) J Sport Sci., 13: 377-85
- [2] Prinold J et al. (2011) J. Biomech., 44(10): 2004-7
- [3] Arumugam S et al. (2020) Ind. J. Ortho., 54:246-55
- [4] Thornton J (2017) Sports Med., 47(4): 641-61

Sensitivity analysis of joint contact forces to individual muscles maximal isometric force using a Gaussian process emulator

Erica Montefiori¹, Ivan Benemerito¹, Alberto Marzo¹, Claudia Mazzà¹

¹Department of Mechanical Engineering & INSIGNEO Institute for *In Silico* Medicine, The University of Sheffield, UK

Email: e.montefiori@sheffield.ac.uk

Summary

Identifying model parameters that mostly influence the outputs of musculoskeletal models (MSKMs) would allow to simplify model personalisation. In this study, a Gaussian process emulator (GPE) enabled a sensitivity analysis to identify seven muscles in the lower limb whose muscle maximal isometric force (F_{max}) mainly influences the estimate of joint contact forces (JCFs). This suggests that their personalisation should be prioritised among others.

Introduction

MSKMs, widely adopted to estimate JCFs, require numerous input parameters, ideally to be personalised to increase their accuracy. An example is muscle F_{max} , computed from personalised muscle volumes, characterised by high between- and within-subject variability [1]. Sensitivity studies analysing the effect of F_{max} on model output reached contrasting conclusions depending on the range of values assigned to each muscle's F_{max} and on the adopted MSKMs [2] highlight the need to further investigate the model- and subject-specificity of MSKM outputs. Moreover, previous analyses were limited to one muscle at the time over few thousands of simulations, due to model complexity and computational time. GPEs are statistical tools using minimal training data to investigate models' input-output relationship, enabling low-cost sensitivity analyses [3]. This study investigated the suitability of GPEs to test the sensitivity of JCFs to lower-limb muscle F_{max} and identify those muscles whose F_{max} mostly affects the estimate of JCFs.

Methods

Gait analysis and magnetic resonance imaging (MRI) were collected from one woman (70.5y, 61.4kg, 1.64m). MRI was used to build a MSKM of the lower limb following established methods [4]. F_{max} was personalised for twenty-nine muscles according to $F_{max} = \sigma * V_M / (l_{opt})$, where V_M is the volume of the MRI-segmented muscle, σ is the specific tension, l_{opt} is the optimal fibre length estimated from the MSKM [1,4].

Normal distributions of F_{max} were calculated from mean and standard deviation of twenty-nine muscle volumes measured across a cohort of eleven older women [1]. Random sampling of F_{max} distributions allowed to determine two hundred combinations of lower-limb muscle F_{max} input to the original MSKM, i.e. generating two hundred variations. MSK simulations were run in OpenSim (<https://simtk.org/>) for one walking trial to estimate resultant JCFs.

F_{max} and associated JCFs (hip, knee and ankle) were used to train ($n = 50$) and validate ($n = 150$) the emulator, whose quality was quantified as the root mean square percentage error between predicted (from GPE) and simulated (from OpenSim) JCFs. 150000 F_{max} -JCF couples generated by the GPE were used to investigate the effect of each F_{max} on the JCFs, as quantified by the Sobol's index (S_i) [3].

Results and Discussion

GPE predictions showed $1.08 \pm 0.54\%$, $2.06 \pm 1.1\%$ and $1.47 \pm 1.22\%$ error for the hip, knee, and ankle validation data, respectively. The sensitivity analysis showed that the hip JCF was mainly influenced by Gluteus medius, Rectus femoris, and Tensor Fasciae Latae (Tfl) (max S_i : 0.31, 0.75, and 0.65, respectively), especially at the two force peaks (Figure 1). Knee JCFs were influenced by Rectus femoris, Soleus, and Tfl (maximum S_i : 0.90, 0.76, and 0.55, respectively), and ankle JCFs by Semimembranosus, Soleus, and Tibialis anterior and posterior (maximum S_i : 0.30, 0.68, 0.90, 0.55, respectively). Indeed, these muscles are known to contribute maximally to the JCFs of the respective joint [2] and our results confirm that their personalisation should be prioritised.

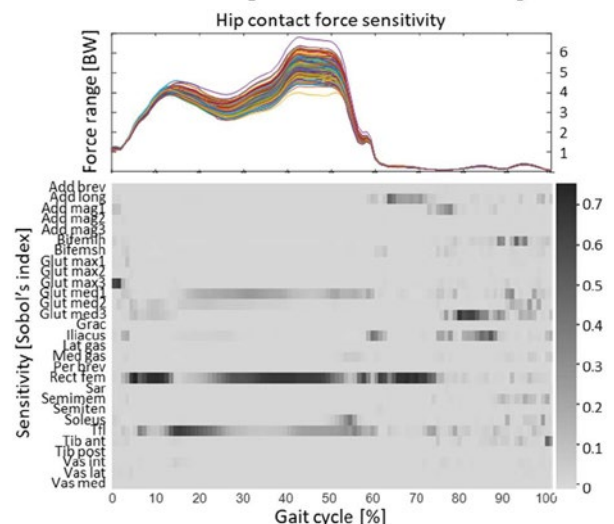


Figure 1: Two hundred hip JCF curves resulting from changes in F_{max} (top) and sensitivity to muscles' F_{max} over time (bottom).

Including measurable input and more subjects in a comprehensive analysis, using computationally efficient tools such as GPE, will enable to unveil dependence between each parameter and model output.

Conclusions

Personalisation of MSKMs can be informed by GPE to discriminate between the parameters that need personalisation and those that can be scaled from literature values.

Acknowledgments

This study was supported by the UK EPSRC (EP/K03877X/1, EP/S032940/1) and EU H2020 (CompBioMed2, No.823712).

References

- [1] Montefiori E et al. (2020) *PloS One* **15.12**:e0242973
- [2] Valente G et al. (2014) *PloS One* **9.11**:e112625
- [3] Melis A et al. (2017) *IJNMBE* **33.12**:e2882
- [4] Modenese L et al. (2018). *JBiomech* **73**:108-118

Application of a Novel Multiscale Modeling Toolbox to Characterize Knee Joint Mechanics During Daily Activities and Rehabilitation Exercises in Knee Osteoarthritis Individuals

Amir Esrafilian¹, Lauri Stenroth¹, Mika E. Mononen¹, Paavo Vartiainen¹, Petri Tanska¹, Pasi A. Karjalainen¹, Juha-Sampo Suomalainen², Jari Arokoski³, David G. Lloyd⁴, Rami K. Korhonen¹

¹Department of Applied Physics, University of Eastern Finland, Kuopio, Finland

²Department of Clinical Radiology, Kuopio University Hospital, Kuopio, Finland

³Department of Physical and Rehabilitation Medicine, Helsinki University Hospital and University of Helsinki, Helsinki, Finland

⁴Griffith Centre of Biomedical and Rehabilitation Engineering (GCORE) | Menzies Health Institute Queensland | School of Allied Health Sciences, Griffith University, Gold Coast, Queensland, Australia

Email: amir.esrafilian@uef.fi

Summary

Herein, a novel atlas-based multiscale musculoskeletal (MS) finite element (FE) modeling pipeline was used to investigate mechanics of knee cartilage and menisci during different daily activities and rehabilitation exercises of individuals with knee osteoarthritis (KOA). The pipeline comprised of an electromyography (EMG) assisted MS model linked to an FE model with fibril-reinforced poroviscoelastic (FRPVE) cartilages and menisci. In general, smaller tissue mechanical responses were observed during walking (compared to other daily activities), and during the non-weight-bearing exercise (compared to other rehabilitation exercises).

Introduction

Knee joint contact force (JCF) and tissue mechanics (such as stress and strain) are known as important quantities in the onset and progression of MS disorders and the success rate of rehabilitation protocols. Yet, no studies have investigated all these quantities during different activities in KOA individuals. Hence, we utilized a novel pipeline, developed as a rapid MS-FE analysis toolbox, to investigate joint- and tissue-level cartilage mechanics during different daily activities and rehabilitation exercises of individuals with KOA.

Methods

Data Collection: Fifteen participants with KOA performed six different daily tasks and seven rehabilitation exercises [1] while marker trajectories, ground reaction forces, and EMGs (from 8 muscles of the leg of interest) were recorded. Magnetic resonance images were acquired to create FE models.

Analyses: The pipeline consisted of an EMG-assisted muscle-force driven FE model with FRPVE cartilages and menisci [2]. EMG-assisted MS analyses were done within CEINMS toolbox [3]. An atlas-based FE modeling toolbox [4] was utilized to rapidly create the FE model geometries (i.e., 15 FE models), which consisted of subject-specific femoral, tibial, and patellar cartilages, menisci, and knee ligaments. The maximum JCFs, stresses, collagen fiber strains, and fluid pressures within different regions of knee cartilages and menisci were compared between activities using repeated measures ANOVA. Also, similar analyses were done with a static-optimization (SO) driven MS-FE pipeline [5] to investigate how the exclusion of subject-specific muscle activations alters tissue mechanics.

Results and Discussion

The EMG-assisted pipeline estimated either comparable or greater magnitudes in tissue mechanics compared to the SO

pipeline, due to higher muscle activations/co-contractions. In general, mechanical stresses of smaller magnitudes were observed during walking compared to other activities ($p < 0.05$, Figure 1A-B), and during knee extension exercise compared to other dynamic exercises ($p < 0.001$, Figure 1C).

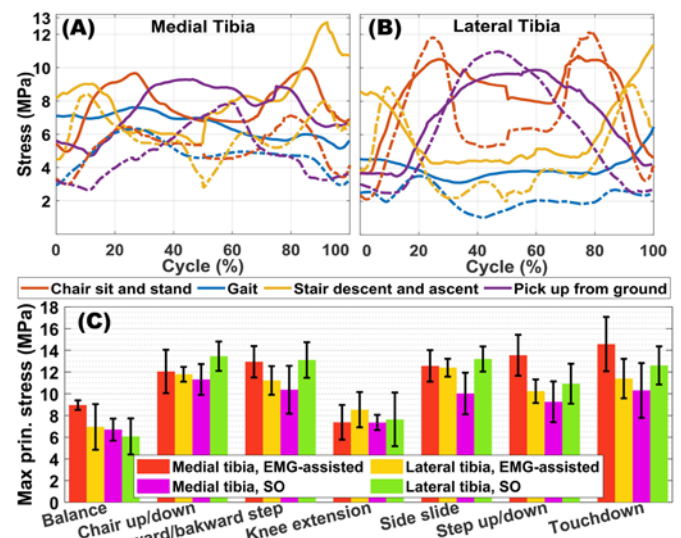


Figure 1: Maximum principal stresses: (A, B) timeseries during daily activities (solid-lines = EMG-assisted, dashed-lines = SO), and (C) maximum of entire rehabilitation exercises that is averaged over all study participants (error bars = 95% confidence interval). Statistics are not included to improve readability.

Conclusions

This study's results provide insights into the more efficient design of subject-specific rehabilitation protocols and daily activity modifications concerning the onset and progression of KOA or post-surgery rehabilitation. Assisting the pipeline with EMGs significantly altered estimated knee mechanics, which may emphasize the importance of considering the subject's muscle activation patterns when subject-specific mechanically-induced cartilage remodeling is of interest.

Acknowledgments

Marie Skłodowska-Curie 713645; Academy of Finland 324529, 324994, 328920; ERDF A73200 and A73241

References

- [1] Bennell K et al. (2014), *Arthritis & Rheu.*, **66**:950-959
- [2] Esrafilian et al. (2020), *IEEE Trans. Reh. Eng., In press*
- [3] Pizzolato C et al. (2015), *J Biomech*, **48**:3929-3936
- [4] Mononen M et al. (2018), *Ann. Biomed. Eng.*, **47**:1-13
- [5] Catelli D et al. (2019), *Com. Meth. Bio. Eng.*, **22**:21-24

Hamstrings Contraction Regulates Magnitude and Timing of Peak Anterior Cruciate Ligament Loading during Drop Vertical Jump in Female Athletes

Ryo Ueno^{1,2}, Alessandro Navacchia³, Nathan D. Schilaty², Gregory D. Myer⁴, Timothy E. Hewett⁵, Nathaniel A. Bates²

¹ Department of Sport Science, University of Innsbruck, Innsbruck, Austria

² Department of Orthopedic Surgery, Mayo Clinic, Rochester, Minnesota, USA

³ Smith & Nephew, San Clemente, California, USA

⁴ The SPORT Center, Division of Sports Medicine, Cincinnati Children's Hospital Medical Center, Cincinnati, Ohio, USA

⁵ Hewett Global Consulting, Rochester Minnesota, USA

Email: ryo.ueno@uibk.ac.at

Summary

Anterior cruciate ligament (ACL) loads during drop vertical jump (DVJ) were estimated via a musculoskeletal finite element (MSFE) model. Simulation conditions with or without inputs of ground reaction force (GRF) and muscle forces showed hamstrings activation significantly decreased and regulated magnitude and timing of ACL loading.

Introduction

ACL injury reduction training focused on lower body strengthening and landing stabilization [1]. *In vitro* studies showed that quadriceps forces increase ACL strain, as opposed to hamstring forces that decrease strain. However, the magnitudes of the effects of quadriceps and hamstrings forces on ACL loading and their timing during *in vivo* landings has remained unclear. The purpose of this study was to investigate the effects of knee muscle forces on ACL loading and their timing during landing.

Methods

Thirteen young female athletes performed three DVJ trials and their motion was recorded with three-dimensional motion capture. Electromyography-informed optimization was performed to estimate lower-limb muscle forces with an OpenSim musculoskeletal model [2]. To estimate ACL loading during landings, a whole body MSFE model was developed with a previously validated FE knee model [2]. The joint motion and muscle forces obtained from the OpenSim simulations were applied to the MSFE model. In the FE simulations, pelvis, knee, and ankle joint centers were kinematically driven while the muscle forces and GRF were applied. Hip rotations and knee rotational and translational degrees of freedom (DOF) remained free. This strategy was used to simulate knee biomechanics, in which hip rotation and knee abduction/adduction and knee translational DOF adjust their position as a function of forces at the knee.

The FE simulation was conducted with five different conditions in order to investigate the individual effects of GRF and muscle forces on ACL loading:

1. Kinematics (No application of GRF or muscle force)
2. GRF (kinematics + GRF)
3. Quadriceps (kinematics + GRF + quadriceps)
4. Hamstrings (kinematics + GRF + hamstrings)
5. Normal (kinematics + GRF + all muscles)

The Friedman test with a *post-hoc* Nemenyi multiple comparison test was used to examine the differences in ACL loading and peak time between the 5 conditions.

Results and Discussion

Simulation of landing kinematics without GRF or muscle forces yielded an estimated median ACL strain and force to be 5.1% and 282.6 N, respectively (Fig. 1). Addition of GRF to kinematic simulations increased ACL strain and force to 6.8 % and 418.4 N ($P < 0.05$). Addition of quadriceps force to kinematics + GRF simulations insignificantly increased ACL strain and force to 7.2 % and 478.5 N. Addition of hamstrings force to kinematics + GRF simulations decreased ACL strain and force to 2.6 % and 171.4 N ($P < 0.001$). Addition of all muscles to kinematics + GRF simulations decreased ACL strain and force to 3.3 % and 195.1 N ($P < 0.001$). ACL loading in the simulation with hamstrings force decreased from initial contact (time of peak: 1–18 ms) while the simulations without hamstrings force showed peak values at 47–98 ms ($P = 0.024-0.001$; Fig. 1-c,f). These findings provide strong evidence that hamstring muscle activation contributes to protection of the ACL during landing tasks.

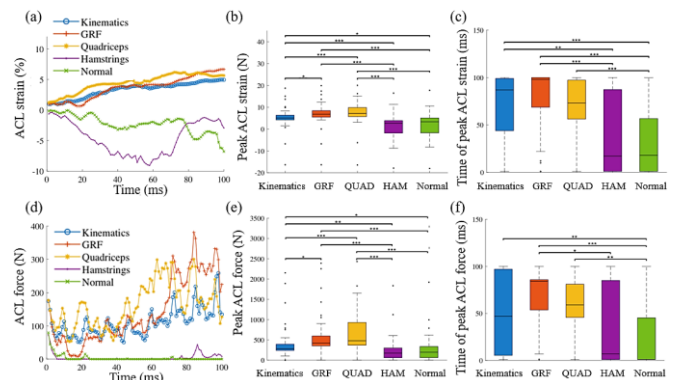


Figure 1: (a,d) Median waveforms and (b-c,d-e) comparisons of magnitude and timing of peak ACL strain and force with 5 different conditions (***) $P < 0.001$; **) $P < 0.01$; *) $P < 0.05$.

Conclusions

Hamstrings muscle activation had both a protective and greater relative effect to GRF and quadriceps activation on ACL loading and significantly decreased and regulated magnitude and timing of ACL loading during landing *in vivo*.

Acknowledgments

NIH grants: R01AR049735, R01AR056259, R01AR055563, K12HD065987, and L30AR070273.

References

- [1] Petushek et al., (2019). *Am J Sports Med*, **47**:1744-1753.
- [2] Ueno R et al., (2021), *Orthop J Sports Med*, in Press.

Prediction of the shape of human lumbar vertebrae from adjacent ones by Singular Values Decomposition

Marco Sensale^{1,2}, Tanguy Vendeuvre³, Arnaud Germaneau⁴, Christelle Grivot¹, Enrico Dall'Ara², Michel Rochette¹

¹ANSYS France, Lyon, France

²Department of Oncology and Metabolism, Insigneo Institute, University of Sheffield, Sheffield, UK

³Spine & Neuromodulation Functional Unit, University Hospital of Poitiers, Poitiers, France

⁴Prime Institute, Centre National de la Recherche Scientifique, ENSMA, University of Poitiers, Poitiers, France

Email: marco.sensale@ansys.com

Summary

Reduction is a primary objective of most treatments for vertebral fractures. However, the pre-fracture height and 3D shape of the vertebral body are unknown. Therefore, it is unclear how much height to restore in order to reestablish the pre-fracture biomechanics of the spine. In this study we propose a method based on Singular Values Decomposition (SVD) to predict the shape of a lumbar vertebral body from adjacent ones. A dataset of 20 patients was processed in a leave-one-out experiment. The L1 shape of the left-out vector was reconstructed with good accuracy. This method, once validated on a large cohort of patients, could be used to estimate the pre-fracture shape of a vertebra during the planning of the treatment strategy.

Introduction

Vertebral fractures are a widespread disease which is often related to age and low bone mineral density [1]. The main goals in treating vertebral fractures are the reduction of the fracture and the stabilization of the structure to allow bone healing [2], but the shape of the vertebral body before the fracture is unknown. The goal of this study was to develop and evaluate a method based on SVD to predict the shape of the vertebral body of L1 from the shapes of T12 and L2.

Methods

The geometries of T12, L1 and L2 of 20 patients were extracted from the VerSe'20 database [3]. The STL file of each vertebra was cut to remove the posterior elements. The resulting surfaces of the vertebral bodies were aligned based on 14 anatomical landmarks identified on the two endplates. Each surface was morphed to a template mesh in Scalismo [4]. For each patient, a vector \mathbf{h} with the nodes coordinates of the morphed T12, L1 and L2 surface meshes was built. Each time, one vector was left out, and the dataset of 19 remaining vectors was compressed with SVD keeping the first 15 modes. The left-out vector can be expressed as a linear combination of the 15 modes as: $\mathbf{h}_{proj} = \mathbf{A} * \boldsymbol{\alpha}$, where \mathbf{A} is a matrix composed of the 15 modes and $\boldsymbol{\alpha}$ is a vector of 15 parameters. The L1 vertebral body was reconstructed from \mathbf{h}_{proj} and compared with the reference shape (morphed) to evaluate the compression. Then, a vector \mathbf{h}_{T12-L2} was obtained by considering only the coordinates of T12 and L2 from the left-out vector. The following linear system of equations was considered: $\mathbf{A}_{T12-L2} * \boldsymbol{\alpha} = \mathbf{h}_{T12-L2}$, where \mathbf{A}_{T12-L2} is the part of the \mathbf{A} matrix that includes only the coordinates corresponding to T12 and L2 from the 15 modes. A linear-least-squares (LLS) solution $\boldsymbol{\alpha}'$ of the system was

calculated. These coefficients $\boldsymbol{\alpha}'$ were used to reconstruct the vector of coordinates of L1 (\mathbf{h}_{L1}) as: $\mathbf{h}_{L1} = \mathbf{A}_{L1} * \boldsymbol{\alpha}'$, where \mathbf{A}_{L1} includes only the nodes coordinates corresponding to L1 from the 15 modes. The mean and max relative distances between the predicted and the morphed shapes of L1 were calculated for each left-out vector.

Results and Discussion

The mean and max projection distances between the morphed and original vertebral bodies, averaged over the 60 vertebrae, were 0.31 ± 0.03 mm and 2.51 ± 0.44 mm. The mean and max projection distances between the L1 vertebral body projected in the basis of modes and the reference morphed shape were 0.93 ± 0.19 mm and 4.08 ± 0.71 mm. The mean and max projection distances between the shape of L1 predicted from the shapes of T12 and L2 and the reference morphed shape were 0.95 ± 0.22 mm and 4.23 ± 0.83 mm, on average over the 20 bases built during the leave-one-out (Figure 1). The results suggest that this method can predict the shape of the vertebral body of L1 from the shapes of the two adjacent vertebrae with a reasonable accuracy. The distances obtained by LLS optimization were similar to the distances obtained by projecting the left-out vector in the basis of modes.

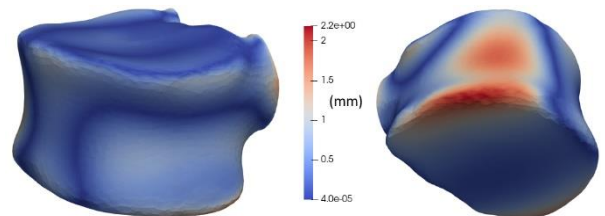


Figure 1: Distance map between predicted and morphed shapes (Patient #10).

Conclusions

The shape of a L1 vertebral body could be predicted by the adjacent ones. This method will be tested on a large database of patients.

Acknowledgments

This project was funded by the EU H2020 Marie Skłodowska-Curie grant agreement Spinner No. 766012.

References

- [1] Cosman et al. (2017). *Osteoporos Int*, **28**(6): 1857-1866.
- [2] Aebi et al. (2007), *AOSpine Manual*; Thieme.
- [3] Löffler et al. (2020), *Radiol Artif Intell*, **2.4**: e190138.
- [4] Clogenson et al, (2015), *Int J CARS*, **10.7**: 1097-1107.

High Density and Bipolar sEMG Based Ankle Joint Torque Prediction Using Machine Learning

Asta Danauskiene¹, Federica Aresu¹, Balázs Szabó¹, Ruoli Wang¹

¹KTH MoveAbility Lab, Dept. Engineering Mechanics, KTH Royal Institute of Technology, Stockholm, Sweden
Email: astad@kth.se

Summary

The relationship between electromyography (EMG), muscle force and associated joint torque provides valuable information for development of rehabilitation robotics. In this study, high density surface EMG (HD-sEMG) data was collected simultaneously with ankle joint torque during sub-maximal and maximal voluntary contractions (MVCs) of plantar- and dorsi-flexors at different ankle angles. Machine learning (ML) approaches were implemented and evaluated to best predict measured joint torque profiles given extracted features from bipolar-sEMG and HD-sEMG recordings in two study cases. In both study cases, the usage of HD-sEMG data leads to a higher prediction accuracy.

Introduction

Torque prediction driven by sEMG data has a great potential for use in rehabilitation [1]. This study aims to improve the accuracy of sEMG data driven joint torque prediction by employing HD-sEMG data and evaluate the prediction accuracy under different test protocols using Multi-Layer Perceptron (MLP) and Long short-term memory (LSTM).

Methods

Five healthy adults (3F/2M, age: 28.6 ± 5.4 yrs) voluntarily participated in the study approved by the local ethics committee. The experiments were designed as isometric contractions of plantarflexors and dorsiflexors at 4 angles (15° and 7.5° plantarflexion, neutral position, and 10° dorsiflexion) in a random order. Muscle contraction was performed at each angle with 70%, 50% and 30% of MVC by instructing subjects to follow a real-time trapezoidal force profile on the display with $\pm 10\%$ error allowed. HD-sEMG signals of medial and lateral gastrocnemius, soleus, peroneus longus and tibialis anterior were collected using a multichannel bioelectrical signal amplifier (Quattrocento, OT Bioelettronica) simultaneously with torque data recorded using a load cell. The HD-sEMG data was filtered with a bandpass filter at 10 - 500Hz and two consecutive channels from each grid were chosen to represent bipolar sEMG signals. Features such as Maximum Absolute Value, the Waveform Length and the Root Mean Squared were used as input to predict torque using MLP and LSTM algorithms. Each algorithm is used for torque prediction in intra-session (prediction of torque profile on same conditions) and intra-subject (prediction of torque profile on a different footplate

angle) study cases and the performances were evaluated using RMSE and R^2 scores.

Results and Discussion

Preliminary results based on one subject are presented here. In both study cases, it was shown that the usage of HD-sEMG data, instead of bipolar sEMG data leads to a superior prediction accuracy (Table 1, Figure 1) due to the additional spatial distribution information given by HD-sEMG. Overall, MLP and LSTM performed similarly when applied on the same data set (Table 1).

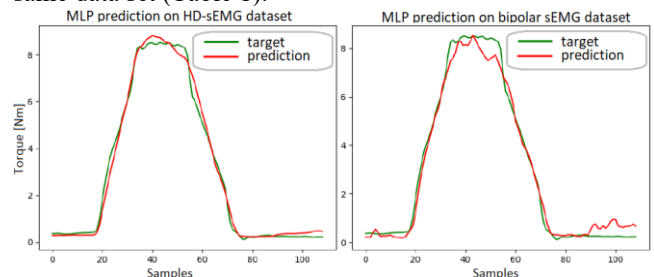


Figure 1: A sample torque prediction in 70% MVC of dorsiflexors at 7.5° plantarflexion in an intra-session case using MLP

Conclusions

This study investigated the ankle torque prediction using HD-sEMG and bipolar sEMG recordings during sub-maximal isometric contraction. The preliminary results showed that using HD-sEMG data as an input can give a more accurate torque prediction, as compared to bipolar sEMG input. Detailed analysis of the input data type and ML algorithms can provide useful information in design sEMG-informed rehabilitation devices. Further investigation with more subjects and other ML algorithms are needed to determine whether HD-sEMG is preferable in joint torque prediction.

Acknowledgments

We would like to acknowledge financial support from Promobilia Foundation (19027) and Swedish Research Council (2018-04902).

References

- [1] Peng, L. et al. (2016) *6th IEEE International Conference on Biomedical Robotics and Biomechanics (BioRob)*, pp. 810-814

Table 1: Performance results of LSTM and MLP algorithms on intra-session and intra-subject study cases.

	Intra-session HD-sEMG		Intra-subject HD-sEMG		Intra-session bipolar sEMG		Intra-subject bipolar sEMG	
	MLP	LSTM	MLP	LSTM	MLP	LSTM	MLP	LSTM
R^2	0.992	0.992	0.989	0.987	0.987	0.988	0.968	0.966
RMSE	0.062	0.018	0.070	0.041	0.194	0.029	0.015	0.099

Lower-limb Joint Torque Prediction using Multi-Step Deep Learning Approach

Longbin Zhang^{1,2}, Davit Soselia¹, Ruoli Wang^{1,2}, and Elena M. Gutierrez Farewik^{1,2,3}

¹KTH MoveAbility Lab, Dept. Engineering Mechanics, KTH Royal Institute of Technology, Stockholm, Sweden

²KTH BioMEX Center, KTH Royal Institute of Technology, Stockholm, Sweden

³Department of Women's and Children's Health, Karolinska Institutet, Stockholm, Sweden

Email: longbin@kth.se

Summary

In this study, sagittal plane ankle and knee torques, and both sagittal and frontal plane hip torques during several different motions were predicted using two alternative deep learning approaches; a direct Long short-term memory (LSTM) [1] approach and a multi-step approach based on movement clusters. The agreement between predicted and measured joint torque using these two methods were analysed and compared.

Introduction

In exoskeleton control and rehabilitation robotics, deep learning algorithms have been widely studied to predict limb joint torque, as they do not require explicit descriptions of the complex relationships between body kinematics and muscle states. There are, however, few studies that describe torque prediction in multiple lower-limb joints and degrees of freedom, nor evaluate the generalizability of deep learning models across subjects and daily activities. The objective of this study is to compare two deep learning approaches that predict lower-limb joint torques. Our hypothesis was that a multi-step approach based on clustering movement types would have a better performance than a direct approach.

Methods

Twelve able-bodied subjects performed ten types of daily activities, including fast walking, normal walking, slow walking, jump down from a stair, jump up to a stair, jump up, land, squat, sit to stand and stand to sit. Surface EMG electrodes (Myon nano) were placed on 13 muscles, including soleus, peroneus longus, tibialis anterior, gastrocnemius medialis, gastrocnemius lateralis, rectus femoris, vastus medialis, vastus lateralis, biceps femoris, semitendinosus, gluteus maximus, gluteus medius, and tensor fasciae latae of one leg. Marker trajectories were recorded (Vicon V16 cameras, AMTI Optima force plates), and kinematics and kinetics were computed based on the CGM2.3 model [2].

Hip flex/extension, hip abd/adduction, knee flex/extension and ankle dorsi/plantarflexion torques were predicted using two deep learning approaches, with EMG signals and joint angles as inputs. In the first direct approach, torque values were predicted using a single LSTM model. In the multi-step approach, t-distributed stochastic neighbour embedding was first used to reduce dimensionality and define clusters of movements with similar features, and then separate LSTM regression models were trained for each cluster. During the inference, the first 0.01 second is used to identify which cluster the movement belongs to, and the corresponding LSTM network is used for regression. Predicted torques from both deep learning methods were compared to measured

torques from motion analysis. Agreement between measured and predicted joint torque using the two approaches were compared with paired t-tests.

Results and Discussion

Both approaches predicted lower limb joint torques accurately and with relatively low error (Figure 1). Root mean square error (RMSE) of predicted torque was slightly lower in the cluster model than in the direct model, but there was no significant difference between the two approaches.

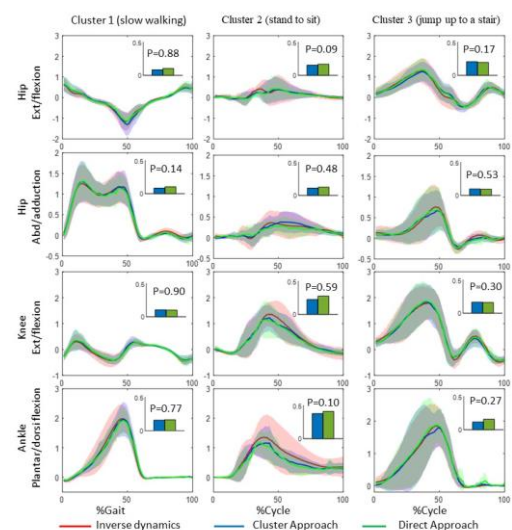


Figure 1: Lower limb torques (Nm/kg) in seven subjects during slow walking, stand to sit and jump up to stair, computed from inverse dynamics and predicted by the cluster and the direct approach. Both models' prediction RMSEs are illustrated in the small column plots.

Conclusions

Both approaches predicted lower limb joint torques during various activities accurately and with relatively low error. Our findings indicate no apparent benefit of the cluster method based. Further investigation to study whether one of approaches performs better in more activities and more subjects, is currently underway.

Acknowledgments

We would like to acknowledge financial support from Promobilia Foundation (ref nr 18200 and 18014) and Swedish Research Council (2018-00750 and 2018-04902).

References

- [1] Hochreiter S. et al. (1997). *Neural Computation*, **9**: 1735-1780.
- [2] Leboeuf F. et al. (2019). *Gait & Posture*, **69**: 235-241.

Prediction of finger movements via a reservoir-computing neural network driven by electromyographical data.

Frederik Thies¹, Luis Mochizuki², Myriam L. De Graaf^{1,3}, Heiko Wagner^{1,3}

¹Movement Science, University of Münster, Horstmarer Landweg 62b, 48149 Münster, Germany

²School of Arts, Sciences and Humanities, University of São Paulo, Brazil

³Otto Creutzfeldt Center for Cognitive and Behavioral Neuroscience, University of Münster, Germany

Email: f_thie20@uni-muenster.de

Summary

Intuitive control of myoelectric hand prostheses is still far from being precise, fast and robust. Machine learning is a promising field to decode user's intention in real-time and drive a prosthesis accordingly. We inspected if a reservoir-computing neural network (RC-NN) can predict the finger kinematics from electromyographical (EMG) data. RC-NN were able to predict kinematic data with an average R^2 of 0.82 ± 0.01 .

Introduction

A limb loss is an incisive event and has major impact on daily life and quality of life. Muscle-driven prostheses rely on remnant muscle activity and may reduce the patients' burden. An approach to intuitively control such prostheses is to use machine learning to decode user intention from muscle activation in real-time. The aim of this study is to investigate the use of a RC-NN to predict the corresponding hand movement with given EMG signals after training with the fullFORCE method [2]. We do it by training the RC-NN on EMG and kinematic data provided by the first iteration of the Ninapro dataset [1] and test with EMG and kinematic data not used during training. Accordance was defined as the absolute error and coefficient of determination between measured and predicted data.

Methods

Our analyzes are based on the Ninapro dataset's [1] first iteration. Network training was done by splitting data into a training set with 5 repetitions, and a testing set with 4 repetitions of each movement. EMG data and corresponding kinematic data of the training set was fed into a RC-NN of 3000 neurons) using the fullFORCE method [2]. For network training, the learning took place online by feeding training data sets in sequence rather than parallel. Each training sequence consisted of 20 repetitions, and reservoir weights were updated. After each sequence, current network error was calculated separately for each finger. Furthermore, a coefficient of determination index was calculated between measured and calculated output [4].

Results and Discussion

After learning, the RC-NN could describe the measured finger angles based on the time-depending EMG input (Fig. 1 left). For the training sets, the coefficient of determination showed values of $R^2 = 0.97 \pm 0.06$ and absolute errors 0.13 ± 0.02 . Depending on the repetition, coefficient of determination

showed values around $R^2 = 0.82 \pm 0.01$ and mean absolute error of 13.72 ± 3.81 .

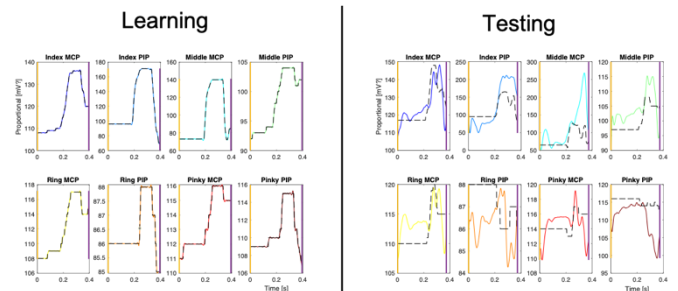


Figure 1: Predicted values (colored lines) and the measured values (dashed line) for each of the eight finger angles used. Left: Measured and Estimated Data after training. Right: Measured and Estimated Data after testing.

Testing on untrained data lead to a decrease in R^2 and an increase in prediction absolute error (Fig. 1, right). Due to motor variability during measurement, subjects perform same movements slightly different. This results in differences between each repetition, which reflects on network performance. Furthermore, the measurement was continuous, so splitting the data in training and testing sets led to a loss information regarding starting values for each repetition and previous recorded repetitions. To better mimic daily use of a prostheses, no feature extraction or dimensionality reduction was performed, which showed improvement of accuracy in other studies [4, 5].

Conclusions

It is possible to predict the corresponding hand movement with a given EMG signal after training a RC neural network with the fullFORCE method. To further increase prediction accuracy of the network, additional improvement e.g through data processing and different network parameters must be tested.

References

- [1] Atzori et al. (2015) *IEEE Trans. Neural Syst. Rehabilitation Eng.* **23**: 73-83
- [2] DePasquale et al. (2018) *PLoS One* **32**: 880-898
- [3] Krasoulis et al. (2015) *IEEE EMBS NER* 631-634
- [4] Ahmad et al. (2018) *IEEE IMCEC* 455-461.
- [5] Hargrove et al (2009). *IEEE Trans. Biomed. Eng.* **56**: 1407-1414.

Frontal-parietal delta microstate-based Brain computer interface improves Knee Gait Trajectory and Phase Prediction

Sanya Varghese^{1,2}, Vijayakumar Chinnadurai²

¹Pune Institute of Computer Technology, Pune, Maharashtra, India

²NMR Division, Institute of Nuclear Medicine and Allied Sciences, DRDO, Delhi, India

Email: varghese.sanya@gmail.com

Summary

Brain-Computer Interfaces (BCI) [1] has recently shown potential in predicting gait kinematics by assessing motor intentions. However, neural signals based on Electroencephalogram (EEG) are nonlinear and nonstationary which makes their synchronization with knee positional information for gait trajectory and phase prediction difficult. This study presents a novel frontal-parietal delta microstate BCI for improvising performance of traditional position based Long Short Time Memory (LSTM) in Knee Gait Trajectory and Phase Prediction.

Introduction

Knee gait trajectory and phase prediction [2] play vital role in the development of lower extremity exoskeletons. Frontal-posterior cortical networks [3] are known to be involved in gait motor intention decision making. However, decoding motor intentions from these cortical regions is a challenging task due to the non-stationary nature of EEG signals. This makes the synchronization of neural intention decoders with positional information difficult. Hence, present study estimates a stable microstate-based frontal-parietal delta information and evaluates its ability in improving performance of traditional position-based LSTM model.

Methods

20 healthy volunteers walked for ten rounds of 100 meters distance and their gait information were acquired using wireless 8 Channel EEG and Noraxon IMU system with sampling rates of 500 and 60 Hz respectively. The acquired data was initially subjected to the development of traditional IMU - LSTM based knee gait trajectory and phase prediction system. Subsequently stable microstate-based frontal-parietal delta information is estimated and synchronized with traditional IMU-LSTM gait prediction system. At first, the acquired knee gait has been classified into 4 gait phases [Initial-Contact (IC), Mid-Swing (MS), Pre-Swing (PS), Terminal-Swing (TS)]. Non-Walking Gait (NWG) were also marked from extracted knee gait cycles. Encoder-decoder based LSTM architecture was employed for both traditional and BCI enabled gait prediction system. At first, both knees angle data were processed through a sliding window to form 12 features (2 knee angles, 2 synchronization of peaks of both knees and 4 distinct crests and trough of each knee). This information was subjected to LSTM model with an input window of 120 frames (2 sec), an output window to predict the next 60 frames (1 sec). The hidden state and the cell state generated from the last timestep(context) is fed into the decoder LSTM. The decoder outputs hidden state for every timestep, the vectors are connected to a dense layer and reshaped into the next 60 frames vector. The network weights and biases were updated at the end of each batch using an adaptive moment estimation (Adam) optimization algorithm with mean square error (MSE). The training was carried out till MSE reached less than 0.05. 50%of the dataset was used for the

training and rest each 25% of the data was utilized as validation and testing set. Subsequently, to improve the gait trajectory and phase prediction, a deep neural BCI system based on stable frontal-parietal motor intention neural mechanism was developed. For this purpose, the acquired, preprocessed, and filtered (1 to 4Hz: Delta) EEG data of F3, F4, Fz, C3, C4, CP3, CP5, and Pz were subjected to k-means based microstate analysis [4]. The resultant microstates were back fitted to every individual's EEG data and subsequently appended to the input feature data used to train the LSTM gait prediction system. Training and testing of BCI enabled prediction system is similar to IMU-LSTM.

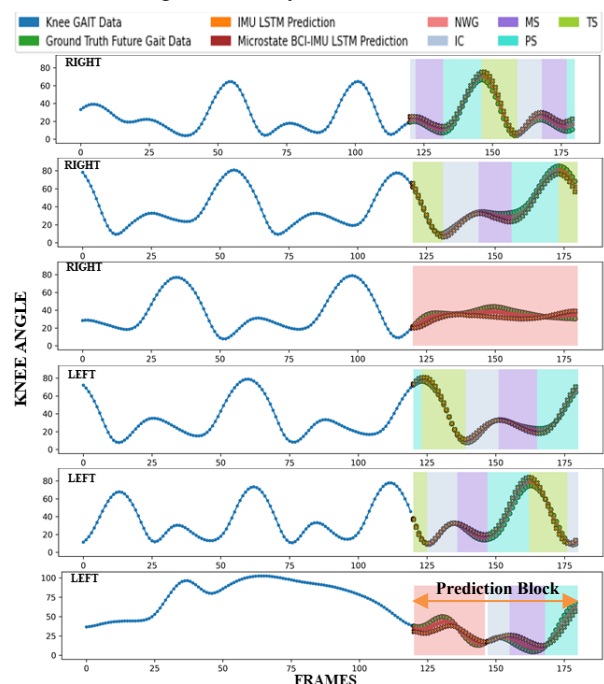


Figure 1: Overall performance of methodologies employed.

Results and Discussion

The accuracy of IMU-LSTM system in predicting gait phase's trajectories are as follows. Right knee: - IC :91.4%, MS: 91.5%, NWG: 90.0%, PS: 91.2%, TS: 92.2% and Left knee: - IC :90.8%, MS: 91.8%, NWG: 90.0%, PS: 91%, TS: 92%. On the other hand, frontal-parietal delta microstate-based BCI enabled LSTM's accuracy for right knee are as follows. IC :91.9%, MS: 92.3%, NWG: 93.1%, PS: 92.2%, TS: 93.6% and Left knee: - IC :92.5%, MS: 93.2%, NWG: 93.1%, PS: 93%, TS: 93.1%.

Conclusions

The frontal-parietal delta microstate-based BCI enabled LSTM system performs better than traditional IMU-LSTM based knee gait trajectory and phase prediction system.

References

- [1] Nakagome et al. (2020). *Sci re*, **10**: 1-17.
- [2] Su et al. (2020). *Sensors*, **20**: 1-8
- [3] Praamstra et al. (2005). *J Neurophysiol*, **94**: 764-774
- [4] Kaur et al. (2020). *Sci rep*, **10**: 1-25

Development of a 3d musculoskeletal simulation model to estimate muscle and knee ligament forces during carved turns in alpine skiing

D. Heinrich¹, A.J. van den Bogert², W.Nachbauer¹

¹Department of Sport Science, University of Innsbruck, Innsbruck, Austria

²Department of Mechanical Engineering, Cleveland State University, Cleveland, OH, USA

Email: dieter.heinrich@uibk.ac.at

Summary

A novel three-dimensional musculoskeletal model of an alpine skier with two skis (53 degrees of freedom, 94 three-element Hill-type muscles) was developed. The model was successfully applied to track experimental data of a turning maneuver and to investigate muscle and knee ligament forces.

Introduction

During turning maneuvers in alpine skiing, competitive skiers face a high risk of sustaining a serious knee injury. Musculoskeletal simulation models can estimate individual muscle forces, provide insight into tissue loading and neural control and can thus contribute to a better understanding of injury mechanisms during dynamic movements.

The purpose of the present study was to develop a three-dimensional musculoskeletal model of an alpine skier. The model was applied to determine muscle and knee ligament forces during a turning maneuver in alpine skiing.

Methods

We developed a three-dimensional musculoskeletal model of an alpine skier and two skis with 53 degrees of freedom (19 for the skier and 17 for each ski) and 94 three-element Hill-type muscles (43 per leg and 8 actuating the lumbar joint). The model of the skier was based on the full-body OpenSim model of Catelli et al. (2019), where we added additional muscles for the lumbar and hip joints.

Each ski was discretized into 18 rigid segments (7 rear segments, 1 center segment and 10 front segments) and connected by revolute joints with spring damper elements to incorporate mechanical properties of the skis (bending stiffness and damping). We modeled the ski-snow contact using three types of forces acting on each segment of the ski (Mössner et al., 2014). We applied a frictional force, a penetration force acting normal to the snow surface, and a shear force parallel to the snow surface, which provided resistance against lateral shearing.

To simulate a turning maneuver, we formulated an optimal control problem (OCP), where measured experimental data of an alpine skier was tracked. Muscle redundancy was resolved by minimizing the sum of squared muscle activations. The OCP was solved using direct collocation and the nonlinear optimization solver IPOPT. To increase computational speed, we provided analytical derivatives of the objective function and constraints (van den Bogert et al. 2011). Knee ligament forces were estimated in a postprocessing step using the 3D knee model of Weinhandl et al. (2014).

Results and Discussion

Tracking the measured kinematics of the turning maneuver (right turn) by the musculoskeletal skier model converged in about 40 min of computational time on a single core of a workstation (Thinkstation 330, 3.5 GHz E-2146 CPU). The speed of the skier was about 14 m/s and the duration of the turning maneuver was 1.5 s. Root mean squared differences between the measured joint angles and the joint angles obtained by the musculoskeletal skier model ranged from 0.75 to 2.77 deg. The primary activated muscle groups were the lateral and dorsal trunk muscles, the vasti, hamstrings and glutei of the inner leg as well as the glutei, vasti, soleus and hamstrings of the outer leg. Anterior cruciate ligament (ACL) forces peaked when the skier passed the gate at the fall line and amounted to 87 N on the outer left leg. The main contribution to the loading of the ACL was due to an external abduction moment acting on the knee joint. Sagittal plane contributions were low due to consistently high knee flexion (> 58 deg) and substantial coactivation of the hamstrings.

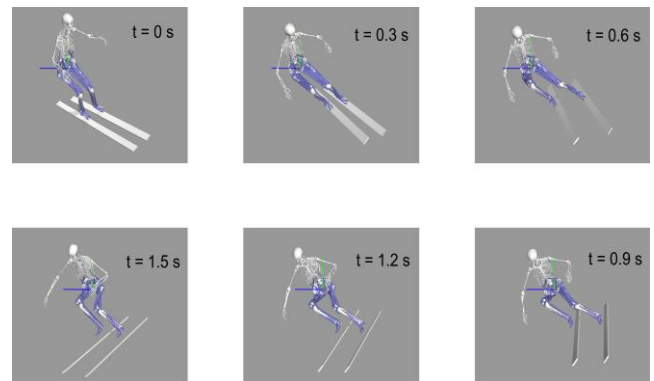


Figure 1: Musculoskeletal skier model visualized in OpenSim

Conclusions

A novel three-dimensional musculoskeletal model of an alpine skier was developed and applied to investigate muscle and knee ligament forces during a turning maneuver. In future research the model will be applied to study the effect to equipment, injury prone situations and predictive simulations.

References

- [1] Catelli DS et al. (2019). *Comp Methods Biomech Biomed Engin*, **22**: 21-24.
- [2] Mössner M et al. (2014). *Scand J Sci Sport*, **24**: 577-585.
- [3] Weinhandl et al. (2014). *Clin Biomech*, **29**: 752-759.
- [4] van den Bogert et al. (2011). *Procedia IUTAM*, **2**: 297-316.

Anatomical Predictors of sagittal hip kinematics during deep squat in adolescent males with and without CAM deformity

Dalia Al Otti¹, Stijn Ghijselings¹, Filip Staes², Lennart Scheys¹

¹Institute for Orthopaedic Research and Training, Department of Development and Regeneration, KU Leuven/University Hospitals Leuven, Leuven, Belgium; ²Research Group for Musculoskeletal Rehabilitation, Department of Rehabilitation Sciences, KU Leuven, Belgium;.

Corresponding author: Dalia.alotti@kuleuven.be

Summary

The aim of this ongoing study is to investigate the spinopelvic parameters and movement patterns of highly active adolescent males with and without CAM deformity during 2 deep squat tasks. Preliminary results show that subjects with CAM exhibit altered sagittal pelvic and hip kinematics in a manner similar to adults with symptomatic FAI.

Introduction

CAM-type Femoroacetabular Impingement (FAI) is a motion related disorder of the coxo-femoral joint characterized with groin pain. The aetiology of CAM-FAI is still unclear, specifically in relation to possible biomechanical factors influencing CAM-formation during final skeletal maturation.

Previous studies have demonstrated significant difference in certain spinopelvic parameters as well as the execution of movements like stair climbing and squats between FAI adult subjects and healthy controls [1]. However, there has been no similar investigations on adolescent males subjects. Nevertheless, research identifies this specific age population as most prone to developing cam deformity and subsequently FAI in adulthood [2]. Therefore, a multidimensional biomechanical exploration of movement execution and its association with radiological spinopelvic parameters as aimed for in this study is imperative.

Methods

Recruitment is currently ongoing for this study in collaboration with a local elite soccer school. Players are included if they train for a minimum of 12 hrs/week and subsequent physical screening ruled out current pain or injury.

All subjects undergo a hip radiographic examination that consists of a modified Dunn view scan and a low-dose bi-planar x-ray scan) during deep squatting. Therefrom following parameters are extracted: alpha angle ($>55^\circ$ = CAM present), pelvic incidence, pelvic tilt, and sacral slope.

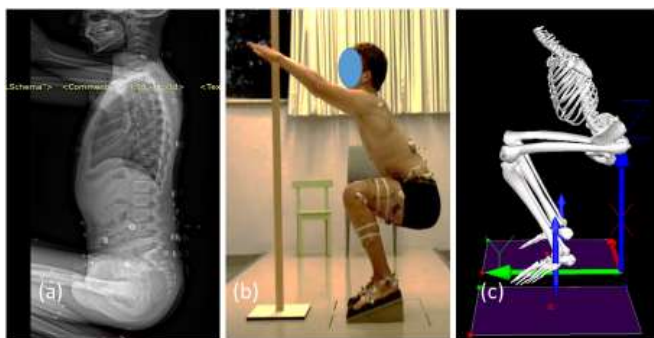


Fig. 1: Image (a) shows an EOS® scan in deep squat, image (b) shows the squat standardization method used, and image (c) shows the constructed kinematics skeletal model.

This is followed by a 3D kinematic analysis captured with 12–infrared camera system (Vicon, UK). Each participant is asked to perform, in triplicate, (1) a free deep squat at their own pace followed with (2) a standardized deep squat in which the ankle’s plantar flexion and excessive trunk flexion where controlled for. Resulting data is exported to Visual3D software (C-motion, USA) for skeletal model computation and subsequent analysis of hip flexion and pelvic anteversion.

Results and Discussions

Statistical significance was set to ($p < 0.05$) for all tests. The currently available cohort consists of 11 subjects (age= 15 ± 2 years). Peak hip flexion and pelvic anteversion during standardized squat were found to be significantly different between the CAM and no CAM Groups. A Pearson’s correlation test furthermore revealed a negative relationship between pelvic incidence and hip flexion during both free ($r = -.66$) and standardized squats ($r = -.62$). Additionally, alpha angle was positively correlated with both the peak hip flexion during the descend phase of the standardized squat ($r = .68$) and anteversion values at the peak depth of the standardized squat ($r = .75$).

Table. 1: The results of the 4 primary outcome parameters and their respective independent t-test p-values for the 2 study groups.

Group	n	Alpha Angle	Pelvic Incidence	Peak Hip Flexion (standard squat)	Peak Pelvic Anteversion (Standard squat)
CAM	5	64.5±5.3	47.3±3.8	109 ±8.2	30 ±6.5
No CAM	6	47.6±3.4	53±8.7	95 ± 7.7	18 ± 7.9
Significance	-	.000*	.193	.032*	.043*

* Significance less than 0.05

Conclusions

Our preliminary results show that adolescent males with asymptomatic CAM exhibit significantly higher sagittal ROM of the hip and the pelvic compared to controls during a standardized deep squat. The high correlation between alpha angle and anteversion at peak depth of the standardized squat points to inability of subjects with larger CAMs to retrovert their pelvic adequately at high hip flexion. Interestingly, this altered pattern of movement has been previously reported in symptomatic adults with FAI as a mechanism of excessive anterior femoral head coverage that can lead to impingement [3].

References

- [1] King, Matthew G. et al. (2017) *Br. J. Sports Med.*, **52**:566–580
- [2] I. Tak et al., (2015 *Br. J. Sports Med.*, **49**: 630–634
- [3] M. Lamontagne et al., (2009) *Clin. Orthop. Relat. Res.*, **467**: 645

Frontal plane knee control with regard to leg dominance in female adolescent competitive handball players during a Drop Vertical Jump

Sabrina Erdrich

SNL_H – Sports Neuromechanics Lab Heidelberg, Heidelberg, Germany

Email: erdrich@snlh.de

Summary

Dynamic knee valgus is considered a risk factor for anterior cruciate ligament (ACL) injuries in team handball. The study demonstrates the magnitude of this biomechanical risk factor in healthy female adolescent handball players with respect to leg dominance, highlighting the potential higher injury risk for the non-dominant side. The results may help to optimize preventive training strategies.

Introduction

Females have a distinct higher risk to injure their ACL than males in the same sports [1]. It has also been shown that in ski and soccer sports females are more likely to injure their non-dominant side compared to their male counterparts, who seem to more frequently injure their dominant side (defined as the kicking leg) [2,3]. There is no such evidence in team handball sports. Faulty biomechanics might give a hint for one side being at higher risk than the other. The purpose of this study was to define the extent of 2D dynamic knee valgus with respect to leg dominance, during the stretch-shortening-cycle (SSC) from a two-legged Drop Vertical Jump (DVJ) at the start of the season in female handball players.

Methods

10 competitive female handball players ($16,5 \pm 0,8$ yrs; $171,9 \pm 5,7$ cm; $65,5 \pm 8,4$ kg; $10,3 \pm 2,6$ yrs experience; $94,0 \pm 8,1$ KOOS sports/recreational Score; Baden League Level) took part in this preseason cross-sectional study. Subjects performed a DVJ from a 37 cm box (feet 35 cm apart [1]), placed under a basket to create an overhead goal, which has been shown to increase performance. Two rectangles (60 x 40 cm) were marked with a colored tape in front of the box (the midpoint being 60 cm away from the leading edge of the box) in order to simulate two force plates. To define knee alignment 8 colored 1 x 1 cm tape stripes were placed bilaterally at predefined anatomical landmarks: Anterior superior iliac spine (ASIS), mid patella, ankle joint center and proximal thigh 30 cm above the knee marker in line with the ASIS and patella marker [4]. Subjects performed 3-5 practice trials, before 2 trials were recorded. Tests were conducted barefoot to avoid variability of the performance due to different shoe materials and to be able to observe foot landing strategies for subsequent analysis. A trial was successful when the SSC and the landing were in the marked area and the subject landed stable on both feet. A digital camera (Fujifilm, model X-T10, 60 Hz) placed in the frontal plane (4,50 m ahead of the box, at 1,30 m height) captured the movement. Recorded videos were processed using Kinovea Software (Version 0.8.15, Kinovea Open

Source Project). Peak knee valgus was defined as knee valgus at the deepest point of the eccentric phase by assessing the player's navel height during the movement. For further analysis the worse valgus angle of the two trials was used. The dominant leg was defined as the jumping leg. Due to normally distributed data side-to-side differences were compared using paired t-tests ($\alpha = .05$).

Results and Discussion

All players demonstrated dynamic knee valgus during the SSC of the DVJ (Fig. 1).

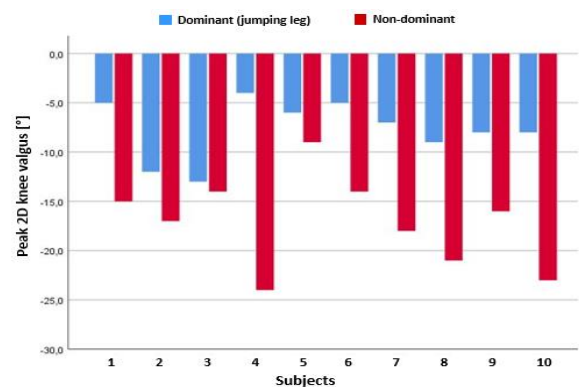


Figure 1: Peak 2D knee valgus angles during the SSC from a Drop Vertical Jump with arm swing (dominant vs. non-dominant side).

Throughout the group frontal plane knee control was more deficient on the non-dominant side ($-17.1 \pm 4.6^\circ$) compared to the dominant side ($-7.7 \pm 3.0^\circ$) ($p < .001$). The consistency of the side-to-side valgus pattern supports the approach to define the dominant leg as the jumping leg in team handball, as it shows better neuromuscular control for the selected parameter.

Conclusions

The magnitude of faulty frontal plane knee control in healthy adolescent competitive female handball players at the start of the season underlines the need for targeted ACL injury prevention training for this population. Due to the results the non-dominant side seems to be at distinct higher injury risk; this should be considered in preventive training concepts. Further research with bigger sample sizes is needed to substantiate these findings.

References

- [1] Hewett et al. (2005). *Am J Sports Med*, **33**: 492-501.
- [2] Ruedl et al. (2012). *Am J Sports Med*, **40** (6): 1269-1273
- [3] Brophy et al. (2010). *Br J Sports Med*, **44**: 694-697
- [4] Wouters et al. (2012). *IJSPT*, **7** (6): 637-646

Effects of 4-week Transcranial Direct Current Stimulation Combined with Foot Core Exercise on Foot Muscle Strength and Ankle Kinesthesia

Songlin Xiao, Xini Zhang, Baofeng Wang, Changxiao Yu, Weijie Fu*

Key Laboratory of Exercise and Health Sciences of Ministry of Education, Shanghai University of Sport, Shanghai, China

*corresponding author: fuweijie@sus.edu.cn

Summary

This study aims to investigate the effects of transcranial direct current stimulation (tDCS) combined with foot core exercise on foot muscle strength and ankle kinesthesia. Thirty participants randomly assigned to either anodal tDCS (a-tDCS) or sham tDCS (s-tDCS) combined with foot core exercise group, received twelve sessional tDCS combined with foot core exercise over four weeks. The results showed that compared to the pre-intervention and s-tDCS, a-tDCS combined with foot core exercise can significantly decrease the passive kinesthesia threshold of ankle eversion and increase toe flexor strength ($p < 0.05$), which suggested that a-tDCS combined with foot core exercise can effectively improve the physical performances of the foot and ankle.

Introduction

Currently, the tDCS is a safe noninvasive approach for modulating the excitability of brain regions. Our preliminary study showed that single-session a-tDCS may potentially improve the physical performances of the foot and ankle [1]. However, to date, there has been little research on exploring the long-term effect of tDCS alone, particularly combined with physical training. Therefore, this study aims to determine the effects of 4-week tDCS combined with foot core exercise on foot muscle strength and ankle kinesthesia.

Methods

In this double-blinded sham-controlled study, thirty healthy participants were randomly evenly assigned to two groups (i.e., a-tDCS or s-tDCS combined with foot core exercise). Each group received a 4-week intervention protocol over twelve sessions, which applied tDCS during performing foot core exercise. A-tDCS was applied over sensorimotor regions with an electric current intensity of 2 mA for 20 min using 4 × 1 ring electrodes, while s-tDCS followed the same protocols except that active stimulation remained on for only 30 s before the beginning and end of stimulation. Foot core exercise included short foot exercise, towel curling training, toe spread training, and balance board training. Two-way repeated-measures analysis of variance was used to examine the effects of tDCS combined with foot core exercise on metatarsophalangeal joint (MPJ) flexor strength, toe flexor strength, and the passive kinesthesia threshold of ankle joint.

Results and Discussion

A significant intervention by time interaction effect for the passive kinesthesia threshold of ankle eversion and toe flexor strength was observed ($p < 0.05$). Post-hoc analysis showed that compared to pre-intervention and s-tDCS, a-tDCS combined with foot core exercise can significantly increase

the toe flexor strength and decrease the passive kinesthesia threshold of ankle eversion (Figure 1).

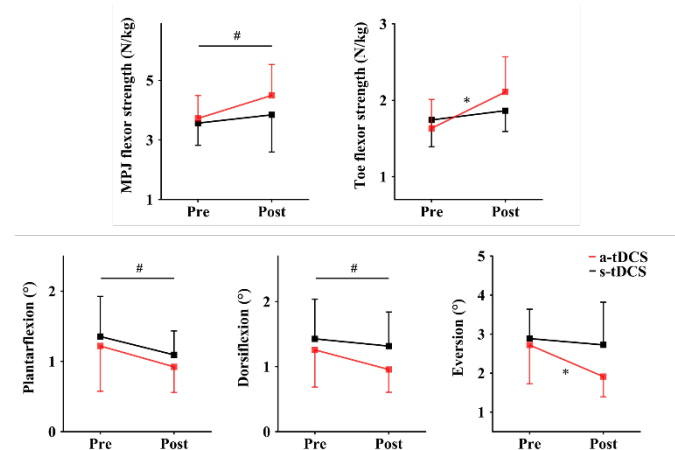


Figure 1: Comparisons of foot muscle strength and the passive kinesthesia thresholds of ankle joint before and after intervention between a-tDCS and s-tDCS groups. MPJ, metatarsophalangeal joint; # indicates significant differences between pre- and post-intervention regardless of groups; * indicates significant differences between pre- and post-intervention in a-tDCS group; $p < 0.05$.

A significant time effect was observed for MPJ flexor strength, toe flexor strength, the passive kinesthesia thresholds of ankle plantarflexion, dorsiflexion, and eversion (Figure 1).

Four-week foot core exercise combined with a-tDCS or s-tDCS can enhance foot muscle strength and ankle sensory function. Moreover, a-tDCS combined with foot core exercise can induce a more positive improvement in toe flexor strength and ankle eversion kinesthesia than s-tDCS. Similarly, a previous study found that multi-session a-tDCS can activate the cortical sensorimotor regions and promote the effects of physical training on the physical performances of the foot and ankle [2].

Conclusions

The findings of this study suggested that tDCS, especially a-tDCS, combined with foot core exercise can sufficiently improve toe flexor strength and passive ankle kinesthesia.

Acknowledgments

This study was supported by NNSFC (11772201, 11932013), NKRDPC (2019YFF0302100), DPSCEC (19SG47).

References

- [1] Xiao SL et al. (2020). *Brain. Sci.*, **10**: 246.
- [2] Bruce AS et al. (2020). *Med. Sci. Sports Exer.*, **52**: 335-344.

THE VALIDITY OF THE GPS-BASED ACCELEROMETER TO MEASURE FOOT STANCE CHARACTERISTICS DURING RUNNING.

Michael Lawson^{1,2}, Robert A. Needham¹, Nachiappan Chockalingham¹, Roozbeh Naemi¹

¹Centre for Biomechanics and Rehabilitation Technologies, Staffordshire University, Stoke-on-Trent, United Kingdom

²AIK Fotboll, Solna, Sweden

Email: mike.lawson@aikfotboll.se

Introduction

GPS technology is commonly employed within team sports to quantify work rate through derivatives of speed and distance. These sensors also contain high frequency accelerometers which provides an opportunity to gain further information into an athlete's locomotion. Accelerometers have been previously validated against a motion capture system to capture foot stance time characteristics during running mounted at the center of mass [1] and sternum [2]. The GPS sensors are mounted on the posterior aspect of upper trunk within a specially designed vest. The purpose of this study was to investigate whether the GPS-based accelerometer can accurately determine foot stance time characteristics during running at different running speeds.

Methods

Thirteen experienced male runners (age: 27 ± 3.7 years) ran on a treadmill with 1-degree inclination for 40 seconds at 9 different speeds ranging from 10-18km/h. Participants wore an GPS sensor (STATSports Apex, Northern Ireland) containing a high frequency tri-axial accelerometer housed in an appropriately sized GPS vest and were provided with standardized running shoes (Puma Anzarun). An eighteen-camera motion capture system (VICON, Oxford, UK) recorded marker coordinate data at 100 Hz, which was filtered (4th order Butterworth, 10 Hz cutoff frequency) and analyzed in Visual3D (C-Motion Inc, MD, USA). Initial foot contact (IFC), midstance (MS) and terminal foot contact (TFC) were determined with a kinematic method [1,3]. Foot stance time characteristics from the accelerometer data (recorded at 100 Hz) were processed and analyzed in Visual3D. A zero cross over method of the Y-axis was used to determine IFC (negative to positive) and TFC (positive to negative). MS was determined as the second acceleration peak following IFC. Time between IFC and TFC was determined as stance time. Stance time and time between IFC, MS and TFC were compared between the motion capture system and accelerometer across each running speed. Mean biases, 95% limits of agreement and Hedges g effect sizes were used to quantify the level of agreement between the two systems.

Results and Discussion

The accelerometer underestimated stance time for running speeds 10km/h (-0.03s) to 15km/h (-0.01s) and overestimated between speeds 16km/h (0.01s) to 18km/h (0.02s) (Figure 1a). The time between MS and TFC caused the stance time underestimation in the lower speeds, however, the time between IFC and MS also contributed to the overestimation in the higher speeds (figure 1b). A small effect size was noted at

15km/h (-0.26). Reasonable agreement was observed in 12km/h, 14km/h and 15km/h. The decrease in bias as speed increased in the lower speeds is similar to previous studies that investigated foot stance time with sternum mounted accelerometers [2]. This may be due to the greater center of mass vertical oscillations typically observed at lower running speeds [2] which increases noise within the accelerometer.

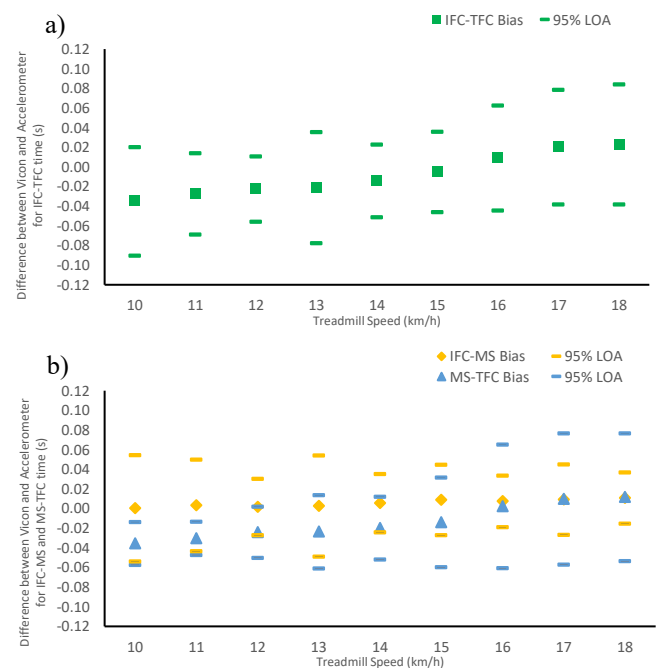


Figure 1: Bland-Altman plots of the difference between the Vicon and Accelerometer in timings between a) Stance time, b) IFC and TFC, MS and TFC. LOA= limits of agreement.

Conclusions

The present study showed that the ability of the GPS-based accelerometer to measure foot stance characteristics is speed dependent. The highest agreement between the two systems with low bias was observed at 15km/h. At 12km/h and 14km/h there was an underestimation of stance time, however, these speeds showed reasonable limits of agreement. Therefore, this study has shown valid estimations of stance time characteristics with the GPS based accelerometer at speeds of 12km/h, 14km/h and 15km/h.

References

- [1] Lee JB et al., (2010) *J Sci Med Sport.*, **13**(2):270-3.
- [2] Backes A et al., (2020) *Scand J Med Sci Sports.*, **30**(12):2399-2407.
- [3] Lussiana T et al., (2017) *Eur J Sport Sci.*, **17**(7):847-857.

Uncontrolled manifold analysis of effects of different fatigue locations on coordination during a repetitive pointing task

Matthew Slopecki^{1,2}, Fariba Hasanbarani^{1,2}, Chen Yang^{1,2}, Christopher A. Bailey^{1,2}, Julie N. Côté^{1,2}

¹BOS Laboratory, Department of Kinesiology and Physical Education, McGill University, Montreal, Canada

²Occupational Biomechanics and Ergonomics Laboratory, Michael Feil and Ted Oberfeld / CRIR Research Centre, Jewish Rehabilitation Hospital, Laval, Quebec, Canada

Email: matthew.slopecki@mail.mcgill.ca

Summary

Muscle fatigue is thought to contribute to incidence rates of musculoskeletal disorders (MSD). When one muscle is fatigued, in order to accomplish a whole-body repetitive task, a person can develop compensation strategies, such as increasing motor variability (MV); however, the effects of localized muscle fatigue has only been assessed on single-joint or inter-segment variability. In the present study, we employed the uncontrolled manifold (UCM) framework to compare how fatiguing different muscles affects whole-body coordination. Shoulder fatigue caused significant increases in variance components, and a significant decrease in synergy index. This suggests that fatigue of the shoulder joint forced a greater reorganization of the motor control system, compared to other fatigue locations and no fatigue.

Introduction

Repetitive, upper limb, fatiguing movement is a common component of workplace tasks, associated with the development of MSD. Compensation strategies exist in motor patterns after muscular fatigue [1]. Variability and multi-joint adaptations compensate against muscular fatigue, however current research has only investigated how localized muscle fatigue affects single-joint or inter-segment variability [1]. The objective of this project was to simultaneously link changes in individual joint variability to task performance to investigate the effect of different fatigue locations on motor variability, using the uncontrolled manifold framework.

Methods

Twelve (5m/7f) participants completed a repetitive pointing task (RPT), consisting in repetitively moving the dominant index finger between two targets (30% and 100% of maximal reach) placed at shoulder height, at rest and after maximal fatiguing protocols of the shoulder (SF), elbow (EF) and trunk (TF), as described by Yang et al. [1]. Kinematics of the trunk and upper limb were collected using a 7-camera motion capture system collecting at 120hz. A kinematic model was created following ISB recommendations [2]. A UCM framework [3] was applied to the kinematic model, linking elemental variables (degrees of freedom at a joint) to endpoint fingertip position.

Reaches were separated into Early (0 - 30%), Middle (40 - 60%) and Late (70 - 100%) phase. A mixed ANOVA determined effects (Phase, Fatigue location) on variance components (V_{UCM} and V_{ORT}). A one-way ANOVA determined effects (Phase, Fatigue Location) on Synergy Index (ΔV_Z) data. Post-hoc pairwise comparisons of Bonferroni were used.

Results and Discussion

Significant main effects of Fatigue Location: $F(3, 516) = 5.41$, $p < 0.01$, $partial\ n^2 = 0.03$; and Phase: $F(2, 516) = 8.23$, $p < 0.01$, $partial\ n^2 = 0.03$, were observed on the variance data. No interaction effects were found. Specifically, SF caused significant increases in variance components. Results of the effects of fatigue on ΔV_Z revealed significant main effects of Fatigue Location: $F(3, 516) = 5.30$, $p < 0.01$, $partial\ n^2 = 0.03$; and Phase: $F(2, 516) = 8.13$, $p < 0.01$, $partial\ n^2 = 0.03$. No interaction effects were observed. Decreased ΔV_Z in late phase of movement was observed after SF.

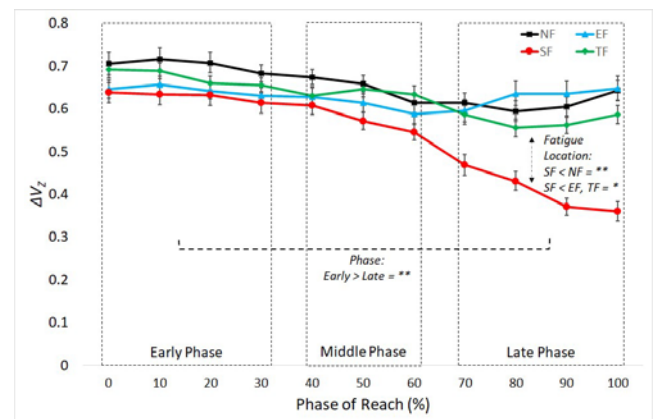


Figure 1: Changes in ΔV_Z during phases of reach. * indicates a significant pairwise comparison with significance set at $P < 0.05$. ** indicates a significant pairwise comparison with significance set at $P < 0.01$.

Conclusions

SF, compared to other conditions, caused significant increases in V_{UCM} and V_{ORT} . A decreased ΔV_Z in the late phase of the movement was observed, which is particularly noticeable in SF (Figure 1). This shows that fatigue of the shoulder joint, compared to other fatigue locations, forced a greater degree of reorganization in the motor control system to maintain performance of the RPT, surrogated as the accurate endpoint position of the fingertip

References

- [1] Yang et al. (2019). *PLOS ONE*, **14(12)**: 1-14.
- [2] Wu et al. (2005). *J Biomech*, **38(5)**: 981-992.
- [3] Hasanbarani, F. and Latash, M. L. (2020). *Motor Control*, **24(2)**: 238-252.

Impact of personality on postural control – a pilot study*

J. Kędziołek¹, M. Błażkiewicz¹

¹Józef Piłsudski University of Physical Education in Warsaw, Poland

Email: justyna.kedziorek@awf.edu.pl

Summary

Postural control is a term used to describe the way in which the central nervous system (CNS) regulates sensory information from other systems in order to produce adequate motor output to maintain a controlled, upright posture. Emotions and therefore personality type (especially fear, anxiety) can affect the strategy of body control. The aim of this study was to evaluate the impact of personality on postural control. Thirty three healthy individuals participated in this study. The Big Five Model was used in order to examine personality traits. Each participant performed in total 6 different standing tasks with eyes open and closed. Increased entropy values mean high irregularity and high complexity of the postural control system. A positive correlation was found between high values of Sample Entropy during one leg standing and Emotional Stability while negative correlation appeared between Agreeableness and Intellect.

Introduction

Postural control includes complex work of somatosensory, vestibular and visual systems. Such complexity allows the body to perform dynamic and complex tasks. Little is known about the impact of personality on postural control. Studies have shown that poor balance management is associated with panic disorder, agoraphobia and ADHD. People with these disorders have increased levels of anxiety which occurred in high level of neuroticism according to the Big Five Model of personality. This phenomenon is observed in children who have poor balance and motor skills exhibit elevated anxiety and insular behavior [1]. The aim of this study was to examine the relationships between the postural control and the Big Five personality Model.

Methods

Thirty three healthy individuals (21.94±1.64 yrs; 67.45±10.89 kg; 173.85±6.56 cm) participated in this study. Personality traits were assessed using IPIP-BFM-50 questionnaire based on the Big Five Model of personality. Participants underwent six balance measurements (each - 30sec) in the following order: both leg standing with eyes open (2eo), eyes closed (2ec), one leg standing with eyes open (1eo), eyes closed (1ec) and tandem standing with eyes open (teo) and eyes closed (tec). Center of pressure (CoP) trajectories in the anterior-posterior (AP) and medio-lateral (ML) directions were measured using the AMTI AccuSway at a sampling rate of 100 Hz. The study used Sample Entropy (SampEn) to assess CoP dynamics. The SampEn was calculated according to [2] using MatLab software. All statistical analysis was performed using Statistica software.

The Wilcoxon test was used in order to find differences between balance tasks. Pearson's correlation was used in order to find association between personality and nonlinear measure.

Results and Discussion

A significant, positive correlation was found between SampEn (1_ec) in ML direction and Emotional Stability ($r = 0.345^*$). Moreover, a significant, negative correlation was noted between SampEn (1_ec)_ML and Agreeableness ($r = -0.383^*$) and Intellect ($r = -0.455^*$). Significant difference was found for SampEn in AP direction between 2_eo and 1_eo ($p = 0.0001$) (Fig. 1).

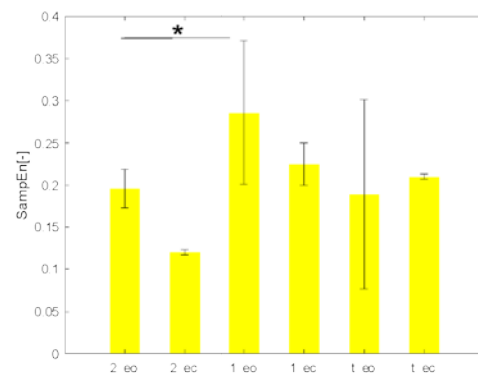


Figure 1: Mean and standard deviation of Sample Entropy values in AP direction for all trials, where: * - significant differences.

Conclusions

The highest values of SampEn in AP direction during 1_eo and 1_ec tasks indicated a high irregularity of CoP signal. These conditions required a lot of attention and concentration, due to the small surface of support and lack of visual control. The lowest values of SampEn in AP during the 2_ec task highlighted the ease and comfort of task execution. When the SampEn in that task increased, the extroversion in these subjects decreased. It is important to conduct study on a larger sample size to understand how some types of personalities may react to different postural tasks and connect emotions, temper with future problems like risk of falls and elevated anxiety in the elderly.

References

- [1] Kogan E et al. (2008). *The Journal of Psychology*, **142(6)**: 601-613.
- [2] Goldberger AL et al. (2000). *Circulation*, **13**: E215-220.

*- The project was carried out as part of the Science School no. 3, AWF Warsaw

Corticospinal excitability during and after stretch-shortening cycle contractions compared with pure shortening contractions

Lea-Fedia Rissmann¹, Antonia Zehentbauer¹, Brent J. Raiteri¹, Daniel Hahn^{1,2}

¹Human Movement Science, Faculty of Sport Science, Ruhr University Bochum, Bochum, Germany

²School of Human Movement and Nutrition Sciences, University of Queensland, Brisbane, Australia

Email: Lea-Fedia.Rissmann@rub.de

Summary

The aim of this study was to investigate cortical and spinal excitability during and after stretch-shortening cycles (SSCs). For this purpose, net ankle joint torque, motor-evoked potentials (MEPs), cervicomedullary motor-evoked potentials (CMEPs) and M-waves of the triceps surae muscles were obtained during and after SSCs. Preliminary data indicates enhanced torque output during and after the shortening phase of SSCs compared with pure shortening contractions (SHO), while cortical excitability was increased during and after SSCs and spinal excitability was increased during SSCs only.

Introduction

Force, work, and power output during the shortening phase of SSCs is enhanced compared with SHO, which is called the SSC effect [4]. The SSC effect has partly been explained by residual force enhancement (rFE), which is triggered by active stretch contractions (STR) [3]. Further, STR were shown to induce long-lasting modulations in cortical and spinal excitability during an isometric-hold phase after STR [1, 2]. However, little is known about cortical and spinal excitability changes during and after the shortening phase of SSCs, which is what this study sought to assess. In line with enhanced torque output during and after SSCs compared with SHO, we expected increased cortical and similar spinal excitability during the shortening phase and similar cortical and increased spinal excitability after the shortening phase of SSCs.

Methods

One participant laid prone on the bench of an isokinetic dynamometer (IsoMed2000, Ferstl GmbH, GER) with their right foot strapped onto a footplate attachment. Net ankle joint torque and crank arm angle were recorded at 1000 Hz. Voluntary fixed-end reference contractions (REF) were performed at +10° plantar flexion (PF) and -15° dorsiflexion (DF); voluntary STR, SHO and SSCs were all followed by isometric-hold phases at DF or PF, respectively. Stretch velocity was 40°·s⁻¹ and shortening velocity was 120°·s⁻¹. All contractions were performed at a joint-specific 40% of maximum soleus (SOL) muscle activity level. SOL, gastrocnemii and tibialis anterior muscle activities were recorded at 5000 Hz using surface EMG. All data were synchronized using a 16-bit A/D card within a Power1401 data acquisition interface with Spike2 software (CED, Cambridge, UK). Different stimulation types were superimposed on the voluntary contractions during REF_{PF}, SHO and SSCs. Stimulations were delivered during and 3-s after the shortening phase of SHO and SSCs and at time-matched instants during REF_{PF}. M-waves (M_{max}) were evoked by 1-ms single-pulse electrical tibial nerve stimulations (DS7AH, Digitimer, UK). CMEPs were obtained

after a single pulse (100-μs) stimulation of the spinal cord at the cervicomedullary junction (D185, Digitimer, UK). MEPs were evoked by a single-pulse (280-μs) magnetic stimulation of the motor cortex by positioning a double-cone coil (D-B80, MagPro Compact, MagVenture, DK) over the left vertex [1]. MEPs & CMEPs were matched to 10-30% of M_{max} and normalized to M_{max} obtained during the same contraction condition [2]. The SSC effect was calculated as the mean torque difference over a 150-ms window prior to stimulation during the shortening phase of SSCs relative to SHO. rFE and residual force depression (rFD) were calculated as mean torque differences between STR, SHO or SSCs relative to REF_{DF} or REF_{PF} at time-matched instants, respectively [1].

Results and Discussion

Preliminary results indicate a SSC effect, as well as rFE after STR and rFD after SHO and SSCs. rFD was lower in SSCs compared with SHO. MEP/M_{max} and CMEP/M_{max} ratios were higher during SSCs than during SHO. These findings indicate increased cortical and spinal excitability during SSCs compared with SHO during the shortening phase. MEP/M_{max} ratios were increased in SHO and even higher in SSCs compared with REF_{PF}. CMEP/M_{max} ratios were similar in REF_{PF} and SSCs, but reduced in SHO. Larger MEP/M_{max} ratios after SSCs than after SHO and than during REF_{PF} indicate increased cortical excitability. Similar CMEP/M_{max} ratios during REF_{PF} and after SSCs indicate no change in spinal excitability after the shortening phase of SSCs.

Conclusions

Our preliminary results suggest that stretch-induced rFE was not completely abolished during the shortening phase of SSCs as indicated by the reduced rFD after SSCs relative to after SHO. Furthermore, the SSC effect and reduced rFD were accompanied by increased cortical and spinal excitability during the shortening phase and increased cortical excitability after the shortening phase of SSCs, respectively. Increased cortical and spinal excitability might be evoked by the preceding stretch phase during SSCs and could potentially explain enhanced muscle performance during and after SSCs.

Acknowledgments

This work was supported by the German Research Foundation (DFG, grant #354863464).

References

- [1] Hahn D et al. (2012). *PLOS One*, **7**: e49907.
- [2] Sykes CT et al. (2018). *PeerJ*, **6**: e5421.
- [3] Seiberl W et al. (2015). *Physiol. Rep.*, **3**: e12401.
- [4] Fukutani A et al. (2015). *SpingerPlus*, **4**(1): 82.

Inter-individual Variation in Coordination and Control of Countermovement Jumps

Stuart A. McErlain-Naylor¹, Robert A. Needham²

¹School of Health and Sports Sciences, University of Suffolk, Ipswich, UK

²Centre for Biomechanics and Rehabilitation Technologies, Staffordshire University, Stoke-on-Trent, UK

Email: s.mcerlain-naylor@uos.ac.uk

Summary

A modified vector coding technique was used to quantify coordination and control during countermovement jumps by 16 males. Previously reported group-level coordination patterns were confirmed, although substantial inter-individual variation existed. Patterns of thigh-shank coordination and control were observed corresponding to a ‘deep’ or ‘shallow’ countermovement strategy, each used successfully within the cohort.

Introduction

Coordination patterns during countermovement jumps (CMJ) have previously been described at the group level [1]. Thigh-shank segment coupling showed a general anti-phase and thigh dominated coordination pattern during both the eccentric and concentric phases, except at the transition where an in-phase and shank dominated coordination pattern was observed. However, inter-individual variation in these coordination and control strategies is yet to be explored.

Methods

Sixteen males each performed three maximal CMJs, with segmental kinematics recoded via 3D motion capture. For each participant’s highest jump, a modified vector coding technique [2] was used to quantify inter-segmental coordination (Figure 1). Readers are directed elsewhere for further information on vector coding, coordination pattern classification, and associated data visualisations [2].

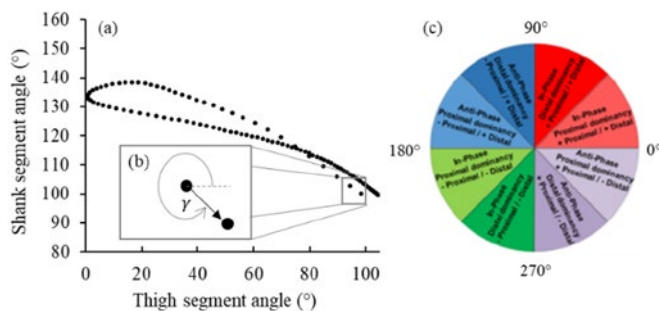


Figure 1: (a) angle–angle plot representing thigh and shank segment angles during a CMJ; (b) expanded view of one coupling angle that is assigned to a coordination pattern classification (c) [2].

Results and Discussion

At the group level, previous results [1] were confirmed (Figure 2a): an anti-phase and thigh dominated thigh-shank coordination pattern during both the eccentric and concentric phases, except at the transition where an in-phase coordination pattern was again observed. Inter-individual variation was greatest at movement initiation and transition between

concentric and eccentric phases. Coupling angle mapping and profiling techniques highlighted patterns of thigh-shank coordination and control corresponding to a ‘deep’ (greater inter-data point range of motion, early anti-phase coordination) or ‘shallow’ (lesser range of motion, early in-phase coordination) countermovement strategy (Figure 2b). Both strategies were used successfully within the cohort (*e.g.*, by P1 and P2, respectively). Analysis of alternative segment couples will also be presented and discussed.

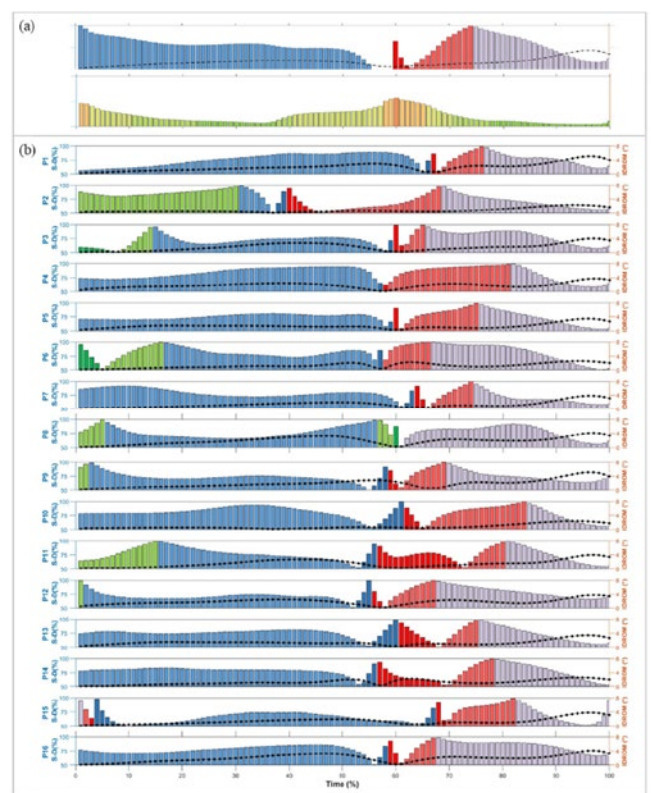


Figure 2: Coupling angle mapping (coordination pattern classification: colour-scale, Figure 1c), segmental dominance (bar height, 50-100%) and dominant segment inter-data point range of motion (IDP-ROM: dotted line, 0-8°) profiling of thigh-shank coordination in the sagittal plane: (a) group means (top) and inter-individual coordination variability (bottom); (b) individual participants ordered from highest to lowest jump height.

Conclusions

Group-level analysis of CMJ coordination and control masks important inter-individual variation in movement strategies.

References

- [1] Raffalt PC et al. (2016). *Hum Mov Sci*, **46**: 63-77.
- [2] Needham RA et al. (2020). *The Foot*, **44**: 101678.

Pain-induced Adjustments in Motor Unit Discharge Depend on Contraction Speed

Eduardo Martinez-Valdes¹, Francesco Negro², Michail Arvanitidis¹, Dario Farina³, Deborah Falla¹

¹Centre of Precision Rehabilitation for Spinal Pain (CPR Spine), School of Sport, Exercise and Rehabilitation Sciences, College of Life and Environmental Sciences, University of Birmingham, Birmingham, UK

²Department of Clinical and Experimental Sciences, Università degli Studi di Brescia, Brescia, Italy

³Department of Bioengineering, Imperial College London, London, UK

Email: e.a.martinezvaldes@bham.ac.uk

Summary

Variations in the proportion of low-and high-threshold motor units recruited during contractions at diverse speeds can induce different effects in the firing behavior of motor units in response to pain. Here we show that that pain reduces motor unit discharge rate and prolongs the neuromechanical delay (NMD) at slow contraction speeds only. This new evidence supports the presence of differential nociceptive inhibitory inputs across the MU pool, which allow exerting fast submaximal contractions in response to pain.

Introduction

At high forces, the discharge rates of low-and high-threshold motor units are influenced in a different way by muscle pain [1]. These differential effects may be particularly important for performing contractions at different speeds since the proportion of low and high-threshold motor units recruited varies with contraction velocity [2]. Therefore, we investigated whether motor unit discharge and recruitment strategies are differentially affected by pain depending on their recruitment threshold, across a range of contraction speeds.

Methods

Fifteen participants (26 (3) years, 9 men) performed ankle-dorsiflexion sinusoidal-isometric contractions at two frequencies (0.25Hz and 1Hz) and two modulation amplitudes [5% and 10% of the maximum voluntary contraction (MVC)] with a mean target torque of 20%MVC (Figure 1). High-density surface electromyography recordings from the tibialis anterior muscle were decomposed with convolutive blind-source separation and the same motor units were tracked across painful (intramuscular hypertonic saline injection) and non-painful (baseline, isotonic saline, post-pain) conditions. Mean discharge rate, recruitment threshold and the delay between the cumulative spike train and the resultant torque output (NMD, [3]) were assessed.

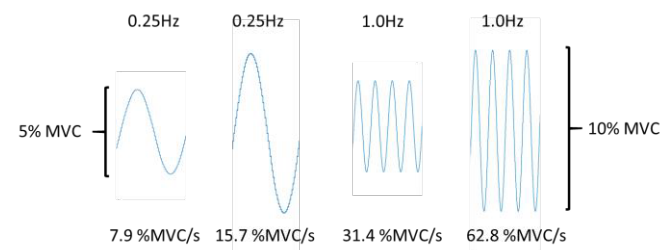


Figure 1: Sinusoidal torque targets representing different contraction speeds.

Results and Discussion

Mean discharge rate decreased significantly during pain at slow contraction speeds only (0.25 Hz, $p=0.04$). Moreover, NMD only increased during pain at slow contraction speeds (0.25 Hz, $p=0.03$). Recruitment threshold increased significantly with contraction speed ($p=0.01$) but was not affected by pain. Results from a representative participant can be seen in Figure 2.

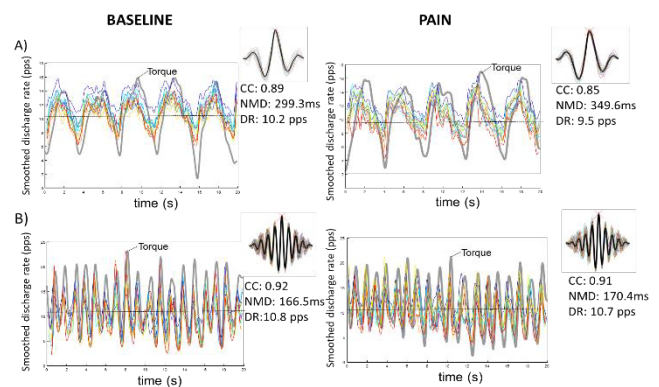


Figure 2: Representative results from one participant. Sinusoidal contractions were performed at 20% MVC with 10% amplitude modulation at a frequency of 0.25Hz (A) and 1Hz (B) during baseline (left) and painful (right) conditions. Smoothed discharge rates (DR, low pass filtered at 2Hz), torque profiles and results from the cross correlation (CC) between the cumulative spike train and torque can be seen for each of the contractions. An increase in neuromechanical delay (NMD) and decrease in discharge rate can be seen for the painful condition at low contraction speeds only (A). At high speed contractions (B), both the NMD and DR were similar between baseline and the painful condition.

Conclusions

The firing behaviour of motor units in response to muscle pain is dependent on contraction speed. The preserved firing frequency and NMD at faster contraction speeds suggests that higher threshold motor units compensate for the decline in firing frequency of low threshold motor units when a low force is exerted (20% MVC). Such a mechanism allows for the execution of fast submaximal tasks to be maintained despite the presence of pain, but could increase fatigability and persistence of symptoms in the long term.

References

- [1] Martinez-Valdes et al. *J Physiol* 598: 2093-2108, 2020
- [2] Desmedt JE, and Godaux E. *J Physiol* 264: 673-693, 1977.
- [3] Del Vecchio et al. *J Appl Physiol* (1985) 125: 1404-1410, 2018

Anthropometric adiposity measures, not body mass index, relate to measures of trip-related fall risk in older adults

Noah J. Rosenblatt¹, Michael L. Madigan²

¹Center for Lower Extremity Ambulatory Research, Rosalind Franklin University of Medicine and Science, North Chicago, USA

²Department of Industrial and Systems Engineering, Virginia Tech, Blacksburg, USA

Email: noah.rosenblatt@rosalindfranklin.edu

Summary

We investigated the effects of anthropometric adiposity measures (AAM) on trip-related gait kinematics and kinematics following a lab-induced trip in community-dwelling older adults. We recruited N=55 adults ≥ 65 years of age, with obese and normal-weight body mass index (BMI) and collected trip-risk measures based on motion of the toe during gait, trip-recovery measures reflecting trunk and step control after a lab-induced trip, and AAM. Trip-risk measures were significantly associated with waist-to-hip circumference ratio (WHR) and thigh circumference, but not BMI. Participants with obese WHR had significantly more variable minimum toe clearance (MTC) than non-obese. Trip-recovery measures were significantly associated with hip circumference, thigh circumference, fat mass index (FMI), and total fat, but not BMI. Participants with obese FMI had impaired trunk control relative to non-obese following a trip. Central obesity and overall adiposity may more closely relate to trip-induced falls risk than BMI.

Introduction

Obesity increases fall risk in older adults and trip-related falls are the lead fall-cause in older adults. Thus obesity-related increased fall-risk could reflect more frequent tripping and/or impaired recovery responses after tripping. Indeed, older adults with obese BMI have lower MTC (Garman et al 2015) and impaired kinematics of trip-recovery compared to those with normal-weight BMI (Rosenblatt et al 2012). However, dichotomizing obesity based on BMI may poorly indicate excessive fat. When assessing obesity-related health conditions it is recommend to combine BMI with other obesity measures, a concept that may extend to falls. We investigated the effects of AAM on trip-related fall risk. We hypothesized that measures of trip-risk and trip-recovery would: 1) associate with AAM other than BMI; 2) be less favourable in obese vs. non-obese older adults, characterized by AAM other than BMI.

Methods

28 community-dwelling older adults with normal-weight BMI and 27 with obese BMI participated. We calculated the following AAM using a tape measure, scale, and DEXA scan: waist, hip and thigh circumference; BMI; WHR; index of central obesity (waist circumference/height); percent leg, trunk, and total fat; and FMI (fat mass/height²). Participants donned a safety harness then walked along an 8 m walkway 10-20 times. During the last pass, an obstacle unexpectedly rose from the walkway to obstruct the swinging limb and induce a trip. From motion capture markers we derived three measures of trip-risk: median and interquartile range (IQR) of MTC and the probability of tripping as per Byju et al

(2016), and four trip-recovery measures: trunk flexion angle and angular velocity (θ and ω , respectively); anterioposterior distance between the toe marker on the stepping limb and the center of mass (COM_{dist}), and recovery step time. For HI , we separately ran principal component (PC) analysis on the set of trip-risk then trip-recovery measures. For each included PC, we calculated PC scores and correlated them with AAM. To address $H2$, we grouped participants according to the AAM that most strongly correlated with a given PC score and had an established obesity cut off, then ran between-group comparison for measures that loaded on the PC.

Results and Discussion

We induced a trip in 47 participants, and 80% used a lowering strategy. A single PC explained 83% of the variance in trip-risk measures, all of which strongly loaded on the PC. WHR ($r=0.29$) and thigh circumference ($r=0.31$) were significantly associated with PC scores, while BMI was not. When grouping participants based on WHR, obese participants exhibited a significantly higher MTC-IQR than non-obese (Cohen's $d=0.64$). Two PCs explained 80% of the variance in trip-recovery measures, with θ , ω and COM_{dist} strongly loading on the first PC (PC1). Hip circumference ($\rho=0.40$), thigh circumference ($r=0.43$), FMI ($\rho=0.34$), and total fat ($r=0.33$) were significantly associated with PC1 scores, while BMI was not. When grouping participants based on FMI, obese participants exhibited less favorable ω ($d=0.84$; Figure 1) than non-obese. Only step time loaded on PC2, but PC2 scores were not associated with any AAM. While biomechanics studies traditionally use BMI when assessing the effects of obesity on fall risk, alternative should be considered. Indeed, a 2020 study by Meng et al found android to gynoid fat ratio provided better insight into postural control than BMI. Similarly, fall-risk is elevated in adults ≥ 50 years of age with central obesity but not with obese BMI (Cho et al 2018).

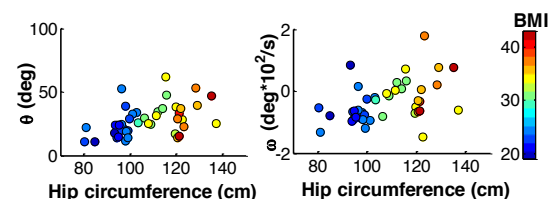


Figure 1: Scatters of trunk control measures and hip circumference.

Conclusions

Central obesity (WHR above established thresholds) and greater adiposity (high FMI) affect trip-related fall risk in older adults, perhaps more strongly than increased BMI.

Acknowledgements

This work was supported by award 1R03AR066326-01A1.

Control of the center of mass during standing on a uniaxial balance board; preliminary results

Maud van den Bogaart^{1,2}, Sjoerd M. Bruijn¹, Jaap H. van Dieën¹, Pieter Meys²

¹ Department of Human Movement Sciences, Vrije Universiteit, the Netherlands

² Rehabilitation Research (REVAL), Faculty of Rehabilitation Sciences, Hasselt University, Belgium

Email:maud.vandenbogaart@uhasselt.be

Summary

Balance during feet-in-place standing can be maintained by the ankle mechanism and the counter-rotation mechanism. A balance board limits the effectiveness of the ankle mechanism. However, preliminary results of this study on four young adults revealed that the contribution of the counter-rotation mechanism to the CoM acceleration was limited compared to the contribution of the ankle mechanism. The participants kept their head relatively stable compared to the balance board rotations, which could be preferable to keep the field view constant. It could be that trunk rotations are used to regulate the orientation of the head in space, rather than to control CoM accelerations.

Introduction

Balance control, defined as controlling the Center of Mass (CoM) within the base of support (BoS) during standing, can be achieved by applying ankle moments to shift the center of pressure (CoP) within the BoS ('ankle mechanism') [1], or by changing the angular momentum of segments around the CoM, e.g. arm and trunk movement ('counter-rotation mechanism') [1]. This study aims to reveal the influence of standing on a balance board, which reduces the effectiveness of the ankle mechanism, on the relative contribution of both mechanisms to balance control.

Methods

Children (6-9y), young adults (18-24y) and non-falling older adults (65-80y) performed trials of 16 seconds of standing on uniaxial balance boards varying in height (15,17 and 19 cm), creating an unstable support in the sagittal (AP) or in the frontal plane (ML). A greater height will create a larger

mechanical perturbation by reducing the effectiveness of the ankle mechanism [2]. This abstract contains preliminary results of four young adults (2 males, 2 females, mean age; 21.1 years old) standing on the highest ML balance board. Full body kinematics (16 segments, 48 markers, using SIMI 3D-motion analysis system (GmbH)) and kinetics (using the imbedded AMTI force plate) were recorded. The contributions of the ankle mechanism and counter-rotation mechanism to the CoM acceleration, as described by Hof (2007) [1] were calculated for the ML direction.

Results and Discussion

The contribution of the counter-rotation mechanism to CoM acceleration was limited (Figure 1A and Table 1A). Participants did not aim to keep the balance board horizontal. The amplitude of the rotations angles was greater for the balance board than the head (Figure 1B and Table 1B). This suggests that people attempt to stabilize the head in space. Keeping the head aligned may conflict with using the counter-rotation mechanism in regulating the CoM acceleration. In future work we will assess age differences in the use of the balance control mechanisms.

Conclusions

The ankle mechanism contributed the most to CoM acceleration. Participants tended to limit head rotation. It could be that trunk rotations regulate the orientation of the head in space, rather than CoM acceleration.

References

- [1] Hof (2007). J Biomech.;40(2):451-7.
 [2] Horak FB et al. (2001). J Neurophysiol.;86(2):575-85.

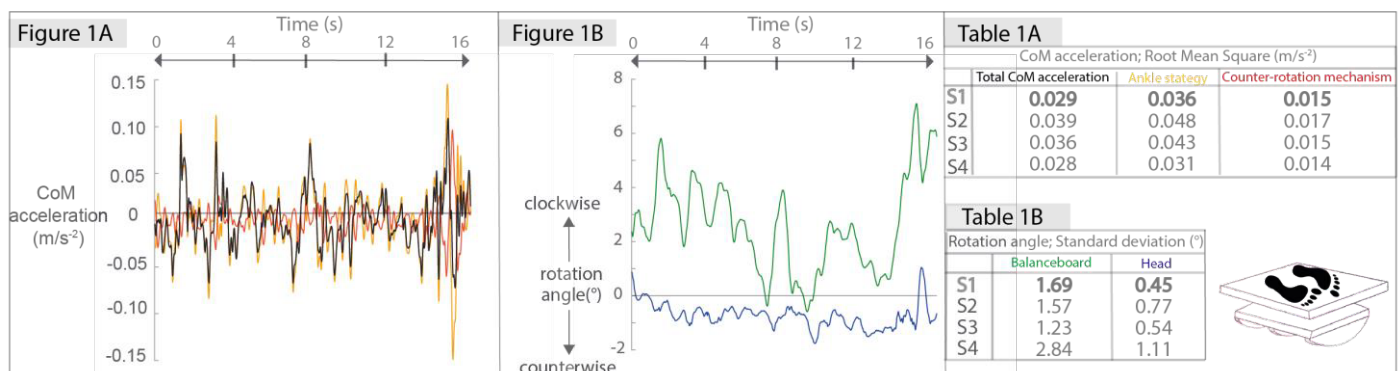


Figure 1A) Time series of the CoM accelerations for subject 1 (S1). **Figure 1B)** Time series of the head and board rotation angles for S1. **Table 1A)** Root Mean Square of the CoM accelerations per subject. **Table 1B)** Standard deviation of the rotation angles for all subjects.

Reactive gait stability in children with cerebral palsy and the effect of videogame-based balance training

Pieter Meyns¹, Chloé Bras², Jaap Harlaar³, Marjolein van der Krogt², Laura van de Pol⁴, Annemieke Buizer²

¹REVAL (rehabilitation research), faculty of Rehabilitation Sciences, Hasselt University, Hasselt, Belgium

²AmsterdamUMC, Dept. Rehabilitation Medicine, AmsterdamMovementSciences, Vrije Universiteit, Amsterdam, the Netherlands

³Dept. Biomechanical Engineering, TUDelft, Delft, the Netherlands

⁴Child Neurology, Amsterdam UMC location VUmc, Amsterdam, the Netherlands

Email: pieter.meyns@uhasselt.be

Summary

Children with bilateral spastic cerebral palsy (CPc) experience poor postural control including affected reactive standing balance control and steady-state gait stability. We examined to what extent reactive gait stability is affected in CPc compared to typically developing children (TDc) and whether 6-weeks home-based videogame-based balance training (VGBT) can improve reactive gait stability in CPc. Reactive gait stability was assessed using medio-lateral and backward margins of stability during a perturbed step during treadmill walking and the recovery step after perturbation in 17 CPc and 9 TDc. We found that reactive gait stability was affected in CPc compared to TDc in medio-lateral and antero-posterior direction. However, no improvements were found in reactive gait stability after VGBT in CPc.

Introduction

CPc experience poor postural control due to sensorimotor disorders resulting from non-progressive brain lesions [1]. They show affected reactive standing balance control [2] and steady-state gait stability [3]. However, it is unclear to what extent reactive gait stability is affected in CPc compared to TDc. Previous work suggested a transfer from standing VGBT to steady-state gait stability in CPc [4]. Therefore, we investigated to what extent reactive gait stability is affected in CPc compared to TDc, and whether VGBT can improve reactive gait stability in CPc.

Methods

In our registered trial (NTR6034), 17 CPc and 9 TDc were included. Inclusion-criteria of CPc were: bilateral spastic CP, GMFCS-level II (i.e. walking without assistive devices, with difficulty on uneven surfaces), no surgical interventions <12 months nor Botulinum Toxin A-injections <6 months. CPc performed 6 weeks home-based VGBT using the X-box One (Microsoft). Kinect games focusing on balance (tennis, football, bowling) were used 5x/week, 30min/session. Pre-VGBT (CPc & TDc) and post-VGBT (CPc), participants performed split-belt treadmill walking at preferred speeds including slip perturbations. At right foot contact, the right belt speed accelerated and then decelerated back to normal speed to induce a slip-like perturbation. Ten perturbations were unpredictably elicited. A perturbation was followed by approximately 10 unperturbed strides. Total body (Plug-In-Gait) kinematics were collected using a 10-camera Vicon motion-capture system at 120 Hz. Medio-lateral and backward margins of stability (ML-MoS, BW-MoS) were calculated as the position of the extrapolated center of mass (XCoM) relative to the lateral malleolus and heel of the

leading foot, respectively[5]. XCoM was defined as CoM, plus its velocity times a factor: $\sqrt{(\text{CoM height}/\text{acceleration of gravity})}$. Negative ML-MoS results in deviation from straight walking, and negative BW-MoS in interruption of forward progression. MoS was calculated for the perturbed step and the next step. Additionally, MoS variability (sdMoS) was determined. Mann-Whitney tests were performed to assess baseline differences between CPc and TDc. Wilcoxon signed-rank tests were performed to assess the effect of intervention in CPc.

Results and Discussion

Reactive gait stability was less in CPc compared to TDc in medio-lateral and antero-posterior direction. The perturbed step and step afterward showed higher ML-MoS (Figure 1) and lower BW-MoS than TDc. This suggests a protective strategy of increasing ML gait stability with reduced forward progression when perturbed. Variability of reactive gait stability appeared similar between the groups. Contrary to preliminary findings in steady-state gait stability [4], no improvements were found in reactive gait stability after VGBT, except for a counter-intuitive increase in variability of BW-MoS of the perturbed step. It should be investigated whether task-specific reactive gait training can improve reactive gait stability in CPc.

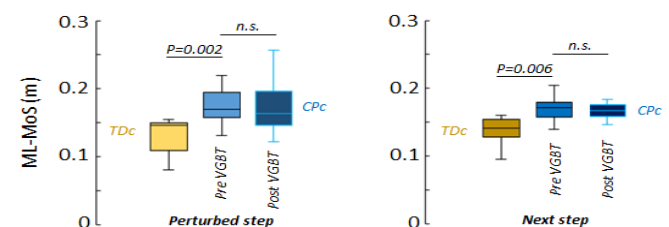


Figure 1: ML-MoS in CPc (blue) and TDc (orange).

Conclusions

Reactive gait stability is affected in CPc. VGBT while standing does not improve reactive gait stability in CPc.

Acknowledgments

This research was supported by FWO [1503915N], Phelps Foundation [2016025], and EU (MSCA fellow) [660458].

References

- [1] Bax et al. (2005) *Dev Med Child Neurol*, **47**:571-6.
- [2] Cherng et al. (1999) *Am J Phys Med Rehabil*, **78**:336-43.
- [3] Bruijn et al. (2013) *Res Dev Disabil*, **34**:1689-99.
- [4] Meyns et al. (2018) *Gait Posture*, **65**:105-6.
- [5] Hak et al. (2013) *PLoS One*, **8**:e82842.

Triple Inverted Pendulum Model Links Joint-Specific Contributions to Postural Sway in Persons with Lower Limb Loss

Courtney M. Butowicz^{1,3}, Adam Yoder^{1,4}, Shawn Farrokhi^{1,4}, Brittney Mazzone^{1,4}, Brad D. Hendershot^{1,3}

¹DoD-VA Extremity Trauma and Amputation Center of Excellence, USA

²Department of Rehabilitation, Walter Reed National Military Medical Center, Bethesda, MD, USA

³Department of Rehabilitation Medicine, Uniformed Services University of the Health Sciences, Bethesda, MD, USA

⁴Department of Physical & Occupational Therapy, Naval Medical Center, San Diego, CA, USA

Email: courtney.m.butowicz.civ@mail.mil

Summary

Among persons with lower limb loss, wearable sensors determined that intact limb hip, knee, and ankle joint motions contribute to increased postural sway, supporting the use of a triple inverted pendulum model.

Introduction

Persons with lower limb loss often rely on the intact limb, exhibit impaired balance and a high incidence of fall-related injury [1]. Postural sway (i.e., balance) is typically explained by double or single inverted pendulum models of the hip and/or ankle, neglecting contributions of the knee joint. However, recent work suggests knee joint motion influence and work in concert with the hip and ankle to stabilize the center of mass (COM) kinematics [2]. Yet, the extent to which ankle, knee, and hip motion contributes to postural sway in persons with limb loss is unknown. This study used a triple inverted pendulum model to determine the contributions of lower limb joint motion to standing postural sway using wearable sensors. We expected combinations of hip, knee, and ankle motions would predict sway parameters.

Methods

Forty-two participants with unilateral lower limb loss (30 transtibial, 12 transfemoral; 25m/17f, 35±8yrs, BMI: 27.3±5.2kg/m²) stood quietly for 30s on a firm surface, with eyes open and eyes closed, while wearing 4 accelerometers on the sacrum, thigh, shank, and foot of the intact limb (128Hz, Opal Gen2, APDM Inc, Portland, OR). Triaxial accelerations were transformed to inertial anterior-posterior components, from which 3 sway parameters were computed [3]: ellipse area (EA), root-mean-square (RMS), and jerk. A state space model with a causal Kalman filter calculated hip, knee, and ankle joint flexion-extension angles and ranges of motion (ROM; max-min joint excursion). Multiple linear regression predicted postural sway parameters from the intact lower limb joint ROMs, with BMI and amputation level as covariates ($p < 0.05$).

Results and Discussion

With eyes open, hip ROM predicted sway EA, whereas hip

and knee ROM predicted sway RMS, and hip (2.8±1.9°), knee (2.1±1.5°), and ankle (1.5±0.9°) ROM predicted sway jerk (Table 1; EA: .04±.03 m², RMS: .08±.04, jerk: 1.8±1.5 m/s³). With eyes closed, hip ROM (3.6±2.1°) persisted as the predictor of sway EA (.06±.06 m²); no other lower limb joint motions (knee: 3.2±2.5°, ankle: 2.1±1.4°) influenced other sway parameters in this condition. As hip motion increased, sway parameters also increased, regardless of visual condition. Consistent with our hypothesis, and the suggested use of a triple inverted pendulum model, knee and ankle joints have negative and positive relationships to sway parameters, respectively. Thus, increasing intact-side hip flexion, knee extension, and ankle plantarflexion ROM increased COM postural sway during quiet standing with limb loss. Given the increased dependence on vision for postural control among persons with lower limb loss [4], the lack of relationship between sagittal lower limb joint motion and postural sway with eyes closed is surprising, but may be explained by motions and coordination strategies in other planes, segments, and prosthetic limb control.

Conclusions

Motions from all intact lower limb joints contribute to postural sway in persons with lower limb loss during quiet standing, with eyes open, supporting the use of a triple inverted pendulum model of balance. Improving coordination of the biarticular muscles of the intact hip and knee may have important implications for balance control.

Acknowledgements

This work was supported by the DoD-VA EACE. The views expressed herein are those of the authors and do not reflect the official policy of the U.S. Department of the Army/Navy/Air Force, Department of Defense, nor the U.S. Government.

References

- [1] Miller, W. (2002) *Phys Therapy*. **82**:856-65.
- [2] Yamamoto A. (2015) *Gait & Posture*. **41**:291-94.
- [3] Mancini M. (2012) *J Neuroeng Rehabil*. **9**:1-8.
- [4] Ku (2014). *Gait & Posture*, **39**: 672-82.

Table 1: Regression model results for sway parameters and model predictors in eyes open condition. *Indicate model $p < 0.0001$.

Sway	Joint ROM	R ²	β	P-value	Sway	Joint ROM	R ²	β	P-value	Sway	Joint ROM	R ²	β	P-value
Ellipse Area	Hip	0.48*	0.81	<0.0001	RMS	Hip	0.62*	0.91	<0.0001	Jerk	Hip	0.61*	0.79	<0.0001
	Knee		-0.33	0.05		Knee		-0.51	0.001		Knee		-0.53	<0.0001
	Ankle		0.05	0.72		Ankle		0.17	0.18		Ankle		0.43	0.001

A progressive treadmill perturbation protocol for assessment of reactive balance responses in stroke survivors

Hala E. Osman¹, Antonie J. van den Bogert², Ann Reinthal³, and Debbie Espy³

¹ Cleveland State University, Department of Biomedical Engineering, Cleveland, OH, USA

² Cleveland State University, Department of Mechanical Engineering, Cleveland, OH, USA

³ Cleveland State University, College of Sciences and Health Professions, Cleveland, OH, USA

Email: h.osman@vikes.csuohio.edu

Summary

Gait was unexpectedly perturbed by rapid acceleration-deceleration once per trial at mid-stance of the unaffected leg during a randomly selected gait cycle. The initial perturbation was determined as the percentage of participant's maximum walking speed and increased or decreased in each trial, based on success or failure of recovery. Participants had fewer falls and more recoveries and had a higher recoverable perturbation. The protocol was found to be feasible in stroke survivors with moderate gait deficits.

Introduction

Stroke survivors show a high risk of falls with unexpected external perturbations during walking [1]. Fear of falling is one of the problems that stroke survivors encounter daily. Regaining balance after stroke is thus imperative. Assessment of gait may be key to use as a fall risk prediction tool [2]. Despite the number of studies that focus on gait stability, ways to quantify dynamic stability of human gait are still not fully clear [3]. Thus, the purpose of this work is to develop treadmill-based midstance gait-perturbation for a poststroke population.

Methods

Twelve participants were randomly assigned to one of the three intervention groups: clinical physical therapy, reactive standing slip, and active video gaming. Reactive balance was tested by a progressive perturbation protocol on the R-Mill treadmill before and after the 10 weekly intervention sessions.

The protocol consisted of a maximum of fifteen 90-second walking trials, each trial with three 30-second periods: pre-perturbation, perturbation, and recovery. The perturbation was induced by increasing the treadmill belt speed to a specified perturbation magnitude for 0.25 seconds, then returning it to its previous speed. All speed changes were done at a constant acceleration of 15 m/s².

These belt speed perturbations, which induce a forward fall, were applied once per trial at mid-stance of the unaffected leg, during a randomly preselected gait cycle within the perturbation period.

Average stance time was determined from vertical force data from gait cycles prior to the perturbation and used to calculate the half stance time (mid-stance) after the randomly selected heel-strike event; this mid-stance was the point at which the perturbation was induced. A stepwise progression based on

trial outcome was followed to modulate the perturbation magnitude for subsequent trials.

Results and Discussion

We were able to implement an individualized, treadmill-based, midstance gait-perturbation protocol for reactive balance assessment. Participants demonstrated improvements from pre-intervention to post-intervention in trial outcomes (fall vs. recover), and maximum recoverable perturbation (MRP) in Figure 1. Compared to the pre-session, there were fewer falls at post-testing and more recoveries and had a higher MRP.

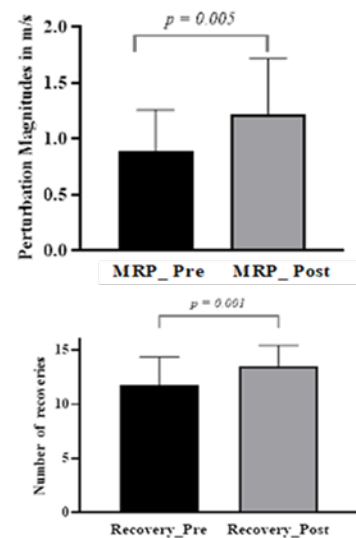


Figure 1: Comparing pre to post tests for maximum recoverable perturbation magnitudes and recoveries.

Conclusions

The capability to induce a perturbation at mid-stance, during a randomly selected gait cycle, within a given perturbation period, in a research laboratory setting has potential in assessing balance control among stroke survivors and in providing a more consistent test across- subjects and within-subjects.

References

- [1] M. Punt et al. (2017). *J. Biomech.*
- [2] A. Mansfield et al. (2015). *Physiother.*, **101**:373–380.
- [3] S. M. Bruijn, et al. (2013). *J R Soc Interface*, **10**:83

Long-term savings of locomotor adaptation in human split-belt treadmill walking

Nikita Sharma^{1*}, Tom JW Buurke^{1,2}, Lucas HV van der Woude^{1,3}, Rob den Otter¹, Claudine JC Lamoth¹.

¹University of Groningen, University Medical Center Groningen, Department of Human Movement Sciences, Groningen, The Netherlands

²Department of Movement Sciences, KU Leuven, Leuven, Belgium

³University of Groningen, University Medical Center Groningen, Center for Rehabilitation, Groningen, The Netherlands
Email: 07.nikitasharma@gmail.com

Summary

Locomotor adaptation and savings are hypothesized to underlie locomotor learning and are often studied through split-belt walking. We studied locomotor savings of split-belt adaptation after three weeks in healthy human adults. Fourteen participants adapted to split-belt walking for ten minutes upon first exposure and completed the same protocol again after three weeks, without any training in between. Measures of spatiotemporal asymmetry were used to assess adaptation. We applied Singular Spectrum Analysis, a non-parametric approach, to quantify adaptation and washout trends. Participants exhibited savings after three weeks in both adaptation and washout phase. Collectively, our results demonstrated locomotor savings of split-belt adaptation within ten minutes of total adaptation time and were more prominent in the spatial domain than the temporal domain.

Introduction

Locomotor adaptation is the ability to continually adjust one's locomotion pattern which aids in humans to move through their surroundings. Short term locomotor adaptation and savings have been studied experimentally using a split-belt treadmill [1]. We assessed the long-term savings of split-belt adaptation by re-exposure to split-belt adaptation after three weeks in able-bodied participants. Furthermore, step length's spatial and temporal characteristics have been studied and spatial information was reported to exhibit savings [1], therefore, we expected greater savings to be present in spatial (Step Length) rather than temporal (Double Support and Swing Time) gait asymmetry parameters.

Methods

Fourteen healthy young adults completed the same split-belt treadmill protocol during first exposure and then second exposure after three-weeks. During the Split-belt protocol participants walked five minutes fast tied-belt baseline (1.5 m s^{-1}), five minutes slow tied-belt baseline (0.5 m s^{-1}), ten minutes split-belt adaptation ($1.5: 0.5 \text{ m s}^{-1}$), and five minutes slow tied-belt washout (0.5 m s^{-1}) [2]. Step Length Asymmetry (SLA) and Double Support Asymmetry (DSA) were calculated from the force plates embedded in the treadmill. Singular Spectrum Analysis (SSA) was used to extract trend parameters like adaptation volume (i.e., total amount of adaptation during adaptation phase) and shape (i.e., percentage of total adaptation volume) of SLA and DSA to quantify adaptation and magnitude of savings [3]. Statistical non parametric test (paired Wilcoxon-signed rank test) was used to compare first and second exposure.

Results and Discussion

One-sample Wilcoxon signed rank test indicated adaptation in SLA volume ($M = 0.413$, $SD = 0.133$, $V = 105$, $p < 0.001$), SLA shape ($M = 0.638$, $SD = 0.180$, $V = 105$, $p < 0.001$), DSA volume ($M = -0.095$, $SD = 0.127$, $V = 14$, $p = 0.013$). Paired Wilcoxon signed rank test showed long term savings in SLA volume ($V = 105$, $p < 0.001$) and DSA volume ($M1 = -0.095$, $SD1 = 0.127$, $M2 = -0.042$, $SD2 = 0.065$, $V = 30$, $p = 0.172$) in adaptation phase.

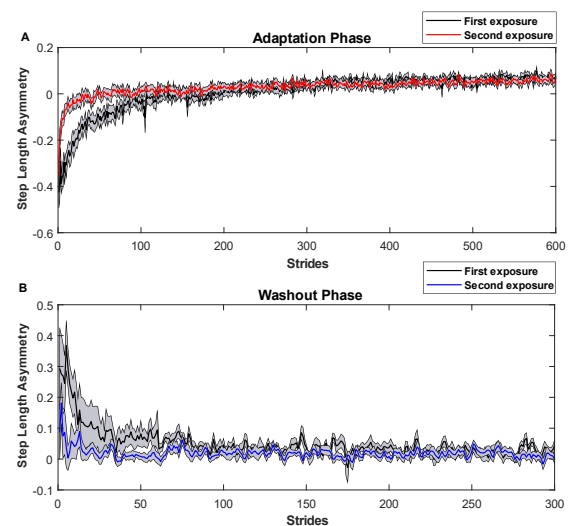


Figure 1: Group-averaged results (N=14) of Split-belt adaptation. Group averaged SLA - A (adaptation phase), B (washout phase).

Conclusions

We found locomotor savings within 10 minutes of split-belt adaptation after three-weeks of washout period in healthy adults. Also, savings of locomotor adaptation were more prominent in spatial gait parameters than temporal gait parameters.

Acknowledgments

Tom Buurke was supported by KU Leuven Internal Funds.

References

- [1] Malone, L. A. et al. (2011). *J. Neurosci.*, **31(42)**, 15136–15143.
- [2] Buurke, T. J. W. et al. (2019). *IEEE Trans. Neural Syst. Rehabil. Eng.*, **27(9)**, 1753–1759
- [3] Sanei, S., & Hassani, H. (2015) *Singular spectrum analysis of biomedical signals*; Boca Raton: CRC Press.

Neuromechanical simulation with predicted ground reaction force in a reflex-based model

Binbin Su^{1,2}, Elena M. Gutierrez Farewik^{1,2,3}

¹KTH MoveAbility Lab, Dept. of Engineering Mechanics, Royal Institute of Technology, Stockholm, Sweden

²KTH BioMEX Center, Royal Institute of Technology, Stockholm, Sweden

³Dept. of Women's and Children's Health, Karolinska Institute, Stockholm, Sweden

Email: binbins@kth.se

Summary

We introduced a reflex-based model to perform forward dynamics with ground contact information in a range of walking speeds without known motion beforehand. The model successfully predicted normal walking at different speeds. The model can also generate stable gait kinematics and predict ground reaction force (GRF). It has potential applicability in predicting GRFs in patient populations for eventual use in assistive device control aimed at achieving a more normal walking pattern.

Introduction

A neuromechanical simulation consists of a control model that represent the central nervous system and a musculoskeletal model that represents the body. Movements such as walking can be forward-simulated in control and musculoskeletal models based on physical laws. A reflex-based controller [1] can generate muscle activations during gait. The two lower limbs have separate stance and swing reflexes, which are selected based on ground contact sensing. The reflex outputs depend on the dynamic interplay between legged mechanics and the ground. As resulting GRFs are unknown, a recurrent dynamic network was introduced to approximate the GRFs.

Methods

In an OpenSim [2] musculoskeletal model, we used an optimization control framework (CMA-ES) [3] to implement the reflex-based controller [1]. The 3D musculoskeletal model consists of seven segments connected with eight rotational joints and is actuated by 22 muscles. Each foot segment has three contact spheres that can dynamically interact with the ground. We first developed a reward function that the optimization aimed to maximize during a specified time interval. The reward was designed so that the total reward was high when the musculoskeletal model walked at desired velocities with minimum effort.

After the optimization, we trained a recurrent dynamic network to map the joint kinematics to the GRF. Then we predicted the GRFs with new joint kinematics using the trained network. The predicted GRF was then fed back to the input of the controller to drive the forward simulation.

Results and Discussion

Realistic joint kinematics were produced over a range of desired walking velocities between 1.1m/s and 1.8m/s. All simulations produced a stable gait pattern at all walking speeds with the reflex-based controller using predicted GRFs. Peak extensions in the hip and the ankle increased

with increasing walking speed. Knee kinematics were more realistic with higher walking speeds than with lower.

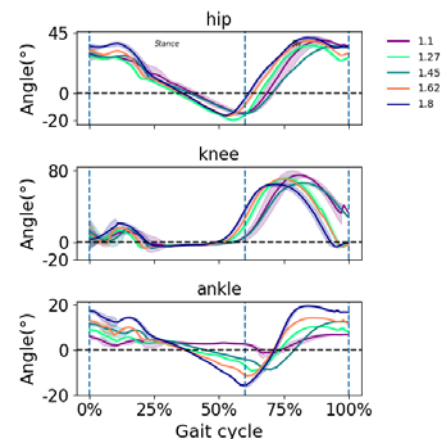


Figure 1: Kinematics of simulated walking over a range of speeds.

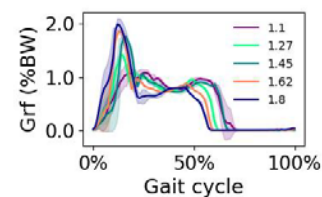


Figure 2: Predicted GRF over a range of speeds.

Conclusions

The neuromechanical model and optimization framework presented based on a reflex-based controller simulated reasonable walking kinematics over a range of desired speeds without any experimental data. It can also predict GRFs associated with the simulated joint kinematics to control the model. It has potential applicability in predicting GRFs in patient populations whose kinematics can be reasonably well predicted with the reflex-based model, which can be useful in designing control algorithms in assistive devices that aim to achieve more normal walking patterns.

Acknowledgments

This project was generously funded by the Promobilia Foundation (ref nr 18200) and by the Swedish Research Council (Grant no 2018-00750).

References

- [1] Song & Geyer (2015). *J Physiol*, **593**: 3493–3511.
- [2] Delp et al. (2007). *IEEE Tran Bio Eng*, **11**: 1940-1950.
- [3] Hansen (2006). *J EDAs*, 75-102

Analysis of the activation modalities of the lower limb muscles in Parkinson's disease

Marco Romanato¹, Weronika Piatkowska¹, Fabiola Spolaor¹, Daniele Volpe², Zimi Sawacha^{1,3}

¹Department of Information Engineering, University of Padova, Padova, Italy

²Fresco Parkinson Center, Villa Margherita, S. Stefano, Vicenza, Italy

³Department of Medicine, University of Padua, Padua, Italy

Email: romanato@dei.unipd.it

Summary

The aim of this work was to analyze how PD affects the motor plan. We hypothesized that the EMG sequence can be considered as a motor program. To be able to address and quantify the motor control abnormalities will allow us to identify how the PD disrupts normal control processes.

Introduction

Parkinson's disease (PD) is the second most prevalent neurodegenerative disorder affecting people worldwide. Gait disorder is one of the cardinal features of PD and might be affected by a modified pattern of motor unit activation and rigidity [1]. State of the art showed that basal ganglia dysfunction affects not only the automatic maintenance of the movement [2] but also each component of the motor plan in terms of timing. For a voluntary movement of a given amplitude and speed, a motor program is meant to specify the muscles to be used and their relative spatio-temporal parameters of activation [3].

Methods

The data of eighteen PD subjects (age 65.6 ± 10.5 years, BMI 26.5 ± 3.5 kg/m²) and ten controls subjects ((CS) age 62 ± 6.5 years, BMI 26.4 ± 3.7 kg/m²), have been acquired at the Human Movement Bioengineering Laboratory (10m walkway) of the Department of Information Engineering at the University of Padova (Italy). Data from an 8-channels EMG system (1000Hz, BTS, Italy) were collected to record the electrical activity of four lower limb muscles bilaterally: Tibialis Anterior, Gastrocnemius Lateralis (GL), Rectus Femoris and Biceps Femoris. The EMG signals were band pass filtered with a double 5th order Butterworth filter and full wave rectified. The cut-off frequencies varied between 15 and 20 Hz for high pass filter, and between 450 and 495 Hz for low pass filter. A double-threshold statistical detector [4] was applied for activation detection. Peak of the envelope (PoE) and its position (PPoE) per each accepted burst were extracted together with burst duration. Subjects were then grouped per activation modality types.

Results and Discussion

The most representative activation modalities, i.e., 1, 2 and 3 bursts, were reported in Table 1. In Figure 1 is reported the distribution of the activations over the gait cycle for each group of participants and each muscle for the two-activations modality. Red bars represent the PPoE for each burst. Greatest in between group differences were appreciated in the GL.

Table 1: Frequency of activation modalities in percentage of the total amount of trials for each group.

	TA		BF		RF		GL	
	CS	PD	CS	PD	CS	PD	CS	PD
1	10.3	7.2	23.2	21.3	25.5	43.9	43.1	59.8
2	63.8	61.9	44.6	51.1	45.5	41.8	48.3	37.1
3	17.2	21.6	26.8	19.1	23.6	9.9	5.1	2.1

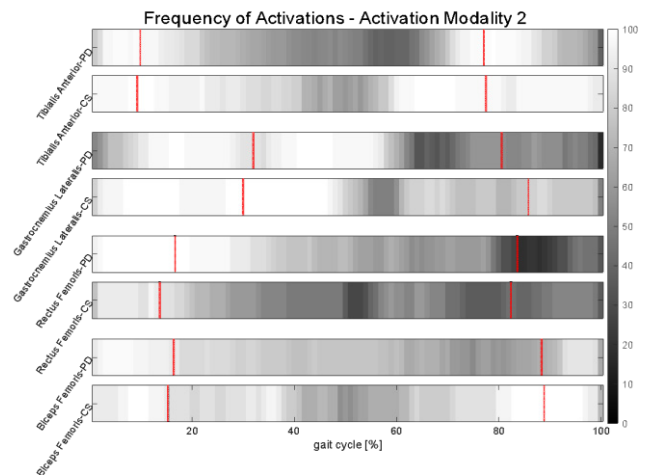


Figure 1: Activation frequency. Red vertical bars indicate PPoE for the second modality.

Conclusions

We propose a representation to characterize PD's motor control for lower limb muscles. PD subjects displayed a different motor plan during walking. The objective assessment of a different motor control strategy could be useful for planning interventions aiming at improving the walking pattern of PD's subjects.

Acknowledgments

Marco Romanato's PhD course grant is supported by Fondazione Fresco Parkinson Institute Italia Onlus.

References

- [1] Volpe D et al Gait & Posture.2020: 80:185–191.
- [2] Horak FB et al. J Neurol Sci. 1992;111(1):46-58.
- [3] Crenna P, Frigo C. J Physiol. 1991; 437: 635–653.
- [4] Bonato P et al. IEEE Trans Biomed Eng. 1998 Mar;45(3):287-99

Predicting the effects of knee extensor muscle weakening and strengthening on a post-stroke gait

Gilmar F. Santos¹, Eike Jakubowitz¹, Nicolas Pronost², Thomas Bonis², Christof Hurschler¹

¹Laboratory for Biomechanics and Biomaterials, Department of Orthopedics, Hannover Medical School, Hanover, Germany

²Université de Lyon, Université Claude Bernard Lyon 1, CNRS LIRIS, Lyon, France

Email: FernandesdosSantos.Gilmar@mh-hannover.de

Summary

Stroke may cause different gait abnormalities, such as knee hyperextension and stiff-knee gait. This study used predictive simulation to investigate how the weakening and strengthening of the knee extensor muscles affect the gait pattern of a post-stroke patient. The prediction result showed impairments similar to those observed in the gait obtained by the inverse dynamics. While the predictive simulation of muscle weakening corrected the stiff-knee gait, the gait prediction of muscle strengthening decreased the knee hyperextension exhibited in the gait pattern of the patient.

Introduction

Individuals who suffered stroke may present impaired gait. Knee hyperextension and stiff-knee gait (SKG) are deviations commonly exhibited by this population, but these gait patterns could have different causes [1]. Understanding how to improve these impairments may support the rehabilitation. Predictive simulation was used in order to investigate the cause-effect relationship between changes in the musculoskeletal system and the observed gait abnormalities in a typical post-stroke patient. In a simplified approach, the purpose of this study was to predict the effects of the weakening and strengthening of the knee extensor muscles on pathological gait, and to investigate whether the specific changes could improve the gait pattern of the patient.

Methods

The gait analysis was performed for a female patient (age: 46 years; height: 1.60 m; mass: 63.8 kg) walking overground at a self-selected gait speed (0.55 ± 0.04 m/s). Inverse dynamics (ID) results were obtained using a scaled lower body model (gait2392) and the tools available in OpenSim (v. 3.3). The 3D musculoskeletal model used for predictive simulations (PS) was based on the one used in ID. The PS was formulated as an optimal control problem [2]. The observed speed in the gait analysis was imposed. Personalized muscle-tendon parameters (optimal fiber length, maximal isometric force and tendon slack length) were used for PS. An optimal control problem was solved using the ID joint moments to estimate the personalized muscle-tendon parameters [2]. With this parameter set, it was possible to predict a pathological gait without directly relying on the kinematics and kinetics of the collected gait data. In order to investigate the effect of muscle weakening (PS-weak), maximal isometric force of the knee extensor muscles in PS was decreased by 50%. Similarly, muscle strengthening (PS-strong) was predicted by increasing maximal isometric force by 50%.

Results and Discussion

The knee hyperextension and SKG observed in the ID were predicted, but PS resulted in less knee extension during the stance phase than the ID (Fig. 1A). PS-weak increased knee hyperextension and corrected the SKG, while the opposite was observed for PS-strong (Fig. 1A). These results indicate that weak knee extensor muscles is related to knee hyperextension in this patient, as also reported by Mulroy et al. [3]. The decreased peak of knee flexion in the swing phase was accompanied by low knee flexion velocity (Fig. 1B), which has been identified as a cause of SKG [4]. The change of dominance from knee flexion to extension moment in early stance phase in PS-strong (Fig. 1C) allowed knee flexion, which corrected knee hyperextension.

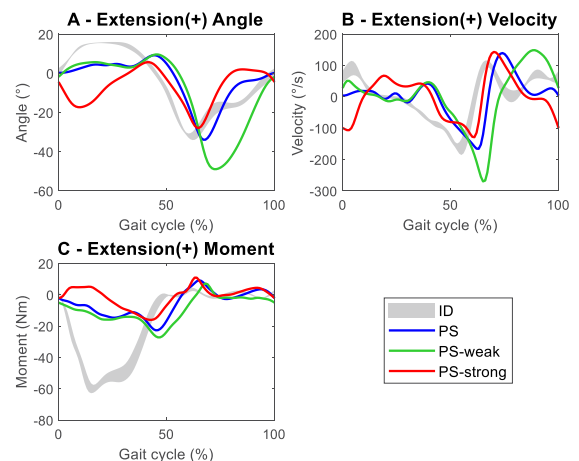


Figure 1: Knee extension (A) angle, (B) velocity and (C) moment for inverse dynamics, predictive simulation, knee extensor muscle weakening and knee extensor muscle strengthening results.

Conclusions

The alteration of the knee extensor muscle strength predicted improvements in the post-stroke gait and identified possible causes of the knee hyperextension and SKG. Future studies may investigate other gait abnormalities and should include more patients in the analysis.

Acknowledgments

This study is part of the OMEGA project funded by DFG (316739714) and ANR (16-CE92-0042).

References

- [1] Balaban B and Tok F (2014). *PM&R*, **6**: 635-642.
- [2] Falisse A et al. (2020). *Front Hum Neurosci*, **14**: 40.
- [3] Mulroy S et al. (2003). *Gait Posture*, **18**: 114-125.
- [4] Goldberg SR et al. (2003). *J Biomech*, **36**: 1111-1116.

Crack patterns around an osteon simulated with the phase field method for fracture

Anna Gustafsson¹, Hanna Isaksson¹

¹Department of Biomedical Engineering, Lund University, Lund, Sweden

Email: anna.gustafsson@bme.lth.se

Summary

The microstructure is key for good fracture resistance in cortical bone. In this study we evaluate the potential of using the phase field method to simulate crack growth around an osteon and compare the results to our previous extended finite element models. We show that the phase field models can capture realistic crack patterns in cortical bone, such as crack deflections along cement lines. In future studies, the phase field method will be a valuable tool for elucidating the underlying reasons for bone fragility in osteoporotic patients.

Introduction

Cortical bone tissue is a composite material (Fig. 1A) with good fracture resistance in healthy conditions. Potent toughening mechanisms arise when cracks interact with the microstructure. Although local fracture properties cannot be quantified experimentally, indentation tests suggest that osteons have slightly higher fracture toughness than the surrounding matrix [1].

We have shown using the extended finite element method (XFEM) how weak cement line interfaces can deflect cracks that approach an osteon [2]. However, the osteon fracture properties did not influence the crack patterns in our XFEM models [2]. The phase field method is a new promising method for modelling fracture [3], not yet applied in biomechanics. The aim of this study is therefore two-fold: 1) to evaluate the potential of using the phase field method to simulate crack growth in cortical bone at the microscale and 2) to analyze if the fracture energy of the osteon affects the crack pattern.

Methods

We adopted a phase field model for fracture previously applied on wood [4]. The same osteon geometry as in [2] was used with material parameters given in table 1. The fracture energy G_{cl} in the cement line was compensated following [4] to account for energy dissipation in the surrounding materials from the regularized phase field crack. The model was loaded quasi-statically in tension (Fig. 1A) and crack patterns were evaluated for interface fracture energies 4-5 times lower than the matrix. The fracture toughness of the osteon was assumed to be equal to or 20% higher than the matrix.

Table 1: Material parameters [2].

	Matrix (mat)	Osteon (ost)	Cement line (cl)
E (GPa)	15	12	18
ν	0.3	0.3	0.3
G (N/mm)	0.4	0.4 (0.48)	0.1-0.08

Results and Discussion

The phase field models predicted similar crack patterns as seen in our XFEM models [2], where weak interfaces deflected cracks and hindered them from growing through the osteons. Crack deflections occurred for interfaces approximately 5 times weaker than the matrix.

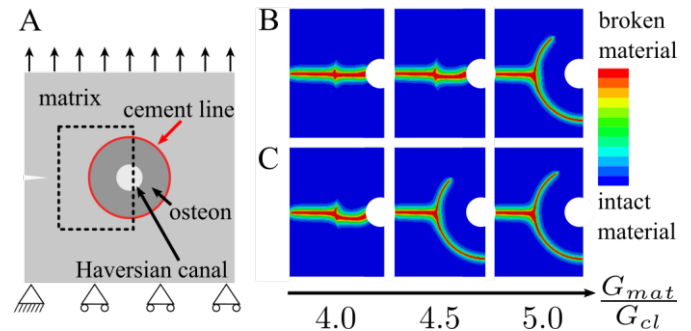


Figure 1: A) Finite element model. Crack patterns inside the dotted region are shown for B) $G_{ost}=0.4$ N/mm, and C) $G_{ost}=0.48$ N/mm, for different cement line fracture energies.

Increased fracture energy in the osteon further promoted crack deflection in the cement line (Fig. 1B and C). This is reasonable, as it indicates that osteons also, in combination with cement lines, play a role in protecting the Haversian canals from damage. This effect was not captured by the XFEM models [2].

Conclusions

To capture the competition between crack deflection and crack penetration at the osteon boundary is key for understanding the relationship between microstructure and tissue fracture toughness in cortical bone. This preliminary study shows that the phase field method is a suitable candidate for analyzing such relationship. Future studies should focus on simulating damage in more realistic bone geometries to elucidate the underlying reasons for bone fragility in osteoporotic patients.

Acknowledgments

Swedish Research Council (2015-04795).

References

- [1] Mullins et al. (2009). *Ann Biomed Eng*, **37**: 2574-2582
- [2] Gustafsson et al. (2019). *BMMB*, **18**: 1247-1261
- [3] Miehe et al. (2010). *IJNMBH*, **83**: 1273-1311
- [4] Carlsson, Isaksson (2020) *Eng Fract Mech*, **232**:107030

A Framework for Continuous Integration in Human Body Finite Element Model Lineup

Jobin D. John¹, Johan Iraeus¹, Mats Y. Svensson¹

¹Injury Prevention Group, Vehicle Safety Division, Mechanics and Maritime Sciences, Chalmers University of Technology, Gothenburg, Sweden
Email: jobin.john@chalmers.se

Summary

Human body models (HBMs) are becoming an indispensable tool to assess safety for current and future transportation systems. In this study, a framework for the design of open-source VIVA+ HBM lineup is presented. A workflow was developed where a single model serves as the baseline model, while all the other models in the lineup (other anthropometric design points and postures) are closely linked derivatives. Such an approach facilitates continuous integration for efficient model development, where the model development is focused on the baseline HBM while all the other models concurrently receive updates.

Introduction

Recent trends in automobile injuries indicate that safety should be evaluated for a wider population [1,2]. Finite element (FE) HBMs are well suited for performing virtual safety evaluations at multiple anthropometric design points and for various road users. Traditionally, however, developing and maintaining a lineup of HBMs require considerable modeling effort.

Methods

The goal for the VIVA+ HBM framework was to have one model as the baseline model and rest of the models in the lineup defined as closely linked derivatives. Such a workflow was implemented by having a common FE mesh for all the models in the lineup and by using mesh morphing to obtain the new geometry for specific anthropometries or postures [3]. In addition, material properties not affected by mesh morphing, were parametrized for easy adjustment.

As the first step, the FE mesh for an average female was developed on a statistical average geometry to serve as the baseline. This mesh was defined using hexahedral elements with seamless mesh flow about the joints, so that the mesh can accommodate large changes in joint angles to represent different postures. Models of different anthropometry and postures were then derived from the baseline model using mesh morphing.

Results and Discussion

Figure 1 shows the outcome of generating standing female and seated average male HBMs from the baseline VIVA+ seated female HBM. The only differences between the models are the node coordinates of the mesh. With this approach, the models benefit from having consistent definitions between them and enables more reliable comparisons of the outcomes between the models.

This workflow enables continuous integration for the models at two levels. First, it allows all the model development to be focused on the baseline model. All the changes are continuously relayed to all the derivative models in the VIVA+ lineup. This establishes a strong link between all the models and helps to keep all the models consistent with minimal effort.

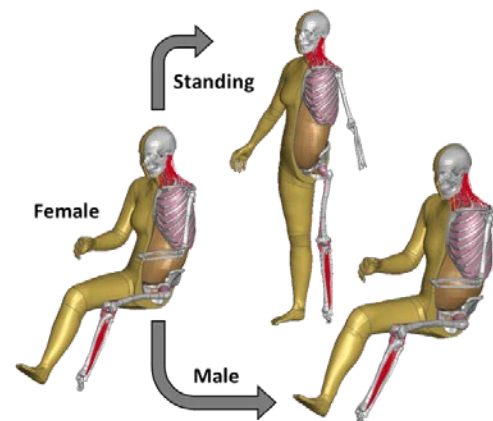


Figure 1: Derivative standing and male models from the baseline average female VIVA+ model.

Second, as the best practice in the development of digital products today, this workflow for HBMs enables frequent releases with smaller updates rather than a bigger release with many updates. With this framework, new features or model improvements can be released regularly, with the updates available on all the models in the VIVA+ lineup. We also see this as an important aspect of open-source sustainability, where a VIVA+ contributor needs to make an update only on the baseline model and the changes are reflected on all the derivative models.

Conclusions

In this work, we demonstrated a workflow for establishing continuous integration for a lineup of HBMs, which is critical for sustainability of open-source and collaborative model development.

Acknowledgments

This work was done in VIRTUAL project (<https://projectvirtual.eu/>), EU Horizon 2020, No. 768960.

References

- [1] Forman J et al. (2019) *Traffic Injury Prev*; **20**: 607-612.
- [2] Linder A and Svensson MY. (2019) *Interdisc Sci Rev*; **44**: 140-153.
- [3] Zhang K et al. (2017) *J Biomech*; **60**: 253-260.

A Penalty Contact Implementation on a Highly Parallelisable Cartesian Mesh Finite Element Solver

Frederik Trommer², Pinaki Bhattacharya¹

¹Insigneo Institute for in silico Medicine, University of Sheffield, United Kingdom

²Department of Mechanical Engineering, University of Sheffield, United Kingdom

Email: fntrommer1@sheffield.ac.uk

Summary

Elastic-elastic penalty contact was implemented in the highly parallelizable voxel based micro finite element solver ParOSol. Displacements for a simple contact problem were predicted and were found comparable to a commercial solver. This serves as an intermediate step towards implementing in ParOSol a novel contact formulation which has been shown to reduce errors associated with the jagged voxel surface.

Introduction

Micro finite element analysis (uFE) is a validated tool for non-invasively quantifying bone mechanics using high resolution computed tomography (CT) images. MicroFE solvers for Cartesian mesh (or voxel) models, such as ParOSol [1], can efficiently solve problems with billions of degrees of freedom. As yet, such solvers do not accurately compute contact induced stresses due to the artificially jagged Cartesian mesh surface. The novel simulated smoothed surface, sliding contact (SS-SC) formulation [2] addressed this by simulating a smooth surface within a penalty contact approach, resulting in a reduction of errors associated with contact from 42% to 2%. The usability of the SS-SC formulation is limited by the fact that it is currently implemented in an in-house FE solver. As an intermediate step towards implementing the SS-SC formulation in the highly parallelized octree-based multigrid ParOSol solver, the present study implements the standard penalty contact formulation in ParOSol.

Methods

The disjoint deformable bodies involved in contact are initially aligned along the same Cartesian grid. Initial rigid-body transformations orient these bodies such that contact is incipient. An incremental solution strategy is implemented to capture intermediate contact states leading to the final state of deformation and/or load. Within each increment, contact iterations are performed to solve the nonlinear contact boundary conditions. Specifically, in each iteration, the global stiffness matrix and the global load vector are updated by contributions from the tangent contact stiffness and the contact reaction forces. These contributions are computed based on [3]. The implementation was used to analyse the problem of two linear elastic, homogeneous and isotropic bodies (A and B) with hard, frictionless contact interaction (Figure 1). The nine nodes on the bottom plane of body B (comprising four voxels) are fixed in all dimensions; the 4 nodes on the top of body A, comprising a single voxel, are restricted in x and y directions; body A is displaced in -z direction onto body B such that they penetrate by 10% of the

voxel size. Two equally weighted master–slave pairs were defined with the opposing surfaces of A and B as master and slave respectively and vice versa. Model prediction is verified against an identical formulation in the commercial FEA solver Abaqus v6.14.

Results and Discussion

Figure 1 compares the predictions from ParOSol and Abaqus for the displacement of the bodies.

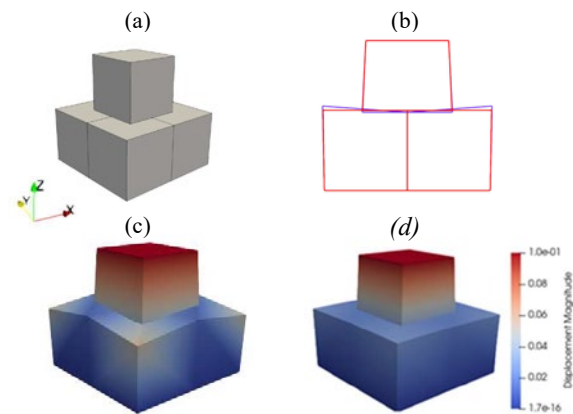


Figure 1: a) Model geometry in reference configuration. b) Outlines of the solutions at a central cross section, blue: Abaqus, red: ParOSol. Magnitude of contact induced displacements predicted by c) Abaqus and d) ParOSol.

Conclusions

The implemented penalty contact formulation converged, and predicted deformations comparable to a commercial solver. The solution obtained by Abaqus shows more overclosure and a larger bulge in body B, probably owing to numerical artifacts due to the small size and the constrained nature of the problem. Future implementations will engage the multigrid cycles in the solution process and include a simulated smooth surface definition, thus improving the prediction of surface interactions and integrating the SS-SC formulation more completely into ParOSol.

Acknowledgments

This work was supported by partially supported by the EPSRC UK grant MultiSim2 (No. EP/S023940/1).

References

- [1] Flaig (2012) PhD Thesis ETH Zürich.
- [2] Bhattacharya et al. (2018) *Int J Numer Meth Eng*, **115**(4):411–26.
- [3] Parisch (1989) *Int J Numer Meth Eng*, **28**:1803–12.

Computational fluid dynamics in cerebral aneurysm.

A. Brambila Solórzano¹, C. Escobar del Pozo²

¹Termofluids Department, Faculty of Engineering, UNAM, México City, México

²Faculty of Mechanical and Electrical Engineering, Universidad de Colima, Colima, México

Email: alberto.brambila@colima.tecnm.mx

Summary

A methodology for the study of fluid dynamics in intracranial aneurysms was developed to try to understand the pathophysiology of the disease. Besides, this methodology can help doctors in making clinical decisions on which aneurysms to operate, since the risk of rupture and postoperative complications are comparable.

Introduction

The incidence of intracranial aneurysms is extremely high: 2-5% of the adult population are affected. Fortunately, the majority remain asymptomatic and, the risk of rupture is very low: 0.1-1% [1]. The rupture of an aneurysm and its consequent subarachnoid hemorrhage has a mortality rate of 45% with significant neurological residues in half of the survivors [2]. Aneurysm detection has increased due to advances in imaging, the decision of which aneurysms to treat should not be taken lightly because the risk of rupture and the risk of the clinical procedure are comparable. Hemodynamics is one of the most accepted factors in the development of intracranial aneurysms. The aim of this work is developing a methodology to analyze fluid dynamics, pressure, and shear stress in intracranial aneurysm in order to help the doctors to choose the best treatment.

Methods

It is necessary to know the exact geometry of each patient's aneurysm to perform the fluid dynamics study. This is done by obtaining digital subtraction angiography (DSA) and reconstruct the geometry of the artery and aneurysm with the software 3D Slicer. Geometry preprocessing and simulation is done with open-source software.

OpenFOAM software is used to solve the fluid dynamics simulation. This software uses the finite volume method (FVM) to solve the discretized equations and store the value of the variables in the computational nodes.

Blood is modeled as Newtonian fluid with viscosity $\mu = 0.0035 \text{ Pa}\cdot\text{s}$ and constant density $\rho = 1050 \text{ kg/m}^3$. The boundary conditions are as follows: a pulsatile flow with a mean Reynolds of 400 was imposed at the inlet, a pressure of 0 pascals was imposed at the outlet, and a no-slip boundary condition was used on the wall, that was considered rigid.

Results and Discussion

Complex flow patterns were observed within the aneurysm, especially in the dome of the aneurysm where recirculation zones are formed. The fluid remains stagnant for a certain

time, increasing the residence time of the particles on the endothelium. Besides, these recirculation zones cause low values of shear stress throughout the cardiac cycle, which favors destructive cell remodeling, since a shear stress greater than 0.5 pa is needed to maintain the integrity of the artery wall [3].

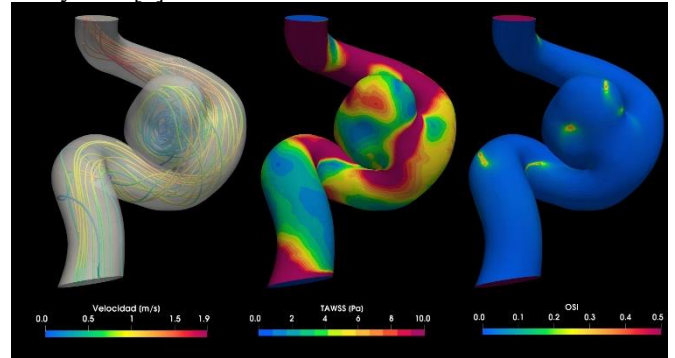


Figure 1: Hemodynamics in intracranial aneurysm in middle cerebral artery.

Also, results were obtained from some indices proposed by other authors to quantify the development of aneurysms, such as the shear stress gradient (WSSG), the oscillatory shear index (OSI), time-average shear stress (TAWSS), number of oscillatory gradient (GON), as well as relative residence time (RRT). These parameters show potential areas that can be affected that lead to a destructive remodeling of the arterial wall.

Conclusions

Areas with low values of shear stress and high oscillatory shear index have been linked to risk areas where the aneurysm could grow or even rupture. The methodology used allows access to these values of shear stress and the different indices used in the literature through open-source software. Computational fluid dynamics can be used as a support tool for clinical decision making in intracranial aneurysms.

Acknowledgments

This research used resources of the Oak Ridge Leadership Computing Facility, which is a DOE Office of Science User Facility supported under Contract DE-AC05-00OR22725.

References

- [1] Juvela, S. (2004). *Strokes*, **35**: 372-374.
- [2] Villablanca, J. P., et al. (2013). *Radiology*, **269**: 258-265.
- [3] Malek, A. M., et al. (1999). *Jama*, **282**: 2035-2042.

Causal interactions between limbs walking with imposed leg constraints

Genevieve K.R. Williams¹, Domenico Vicinanza¹, Attias, Michael³, Stéphane Armand³,

¹Faculty of Sport and Health Sciences, University of Exeter, Exeter, UK; ²Faculty of Science and Engineering, Anglia Ruskin University, Cambridge, UK; ³Laboratory of Kinesiology Willy Taillard, Geneva University Hospitals and University of Geneva, Geneva, Switzerland; email: g.k.r.williams@exeter.ac.uk

Summary

To provide new insights into motor control underpinning human walking we quantify the causal interaction of the leg motions during walking with bi and unilateral constraints induced by a passive exoskeleton emulating gastrocnemius contractures. Normal walking was characterised by a high mutual drive of each leg to the other. The effect of bilateral emulated contractures on one leg was a reduced drive of each leg to the other. With unilateral emulated contracture, the mechanically constrained leg strongly drives the free leg. Redundancy is used to support causal interactions where optimal walking may be driven by the most constrained leg.

Introduction

Walking is a fundamental human action that underpins daily activities throughout the lifespan. In satisfying walking, the human biomechanical system is redundant and adaptable when faced with neurological or musculoskeletal impairments.

Examining causal interactions based on nonlinear dynamics approach provides a framework to determine the extent to which one part of the biomechanical system drives another. Appreciating the nature and strength of drive of one limb to another in gait, in particular when that gait is impaired, unveils novel information on the motor control solution.

Contractures of the lower limbs are a common impairment resulting from conditions such as spinal cord injury, brain injury, or muscular dystrophy. Associated gait adaptations have been demonstrated in Armand and Attias (2019; pegs.unige.ch), with the aim to provide important understanding of the mechanisms underpinning characteristics of pathological gait, as well as the biomechanical solution to walking in their presence. The aim of this paper was to explore the causal drive of the legs during walking when contractures were emulated by a passive exoskeleton to the gastrocnemius.

Methods

Data acquired during the protocol reported in Attias et al. studies [1] were used for this study. Nine healthy participants (age: 27 ± 5.7 years; height: 1.70 ± 0.09 m; weight 66.3 ± 7.8 kg) wore a passive exoskeleton to replicate the contractures of the gastrocnemius with 34 reflective markers according to the conventional gait model. Participants walked along a 10-meter walkway at a self-selected speed. Marker trajectories were recorded and computed with a 12-camera motion analysis system (Vicon Peak Mx3, Oxford, UK, 100 Hz). The three experimental conditions were normal walking,

contractures both legs (bilateral exoskeleton), contracture on the left leg only (unilateral exoskeleton). Causality based on CCM was calculated to assess the driving strength of each leg to the other using the multispatialCCM library in R-Studio [2].

Results and Discussion

During normal walking there was the strongest mutual drive of each leg to the other, suggesting that the leg-leg system is able to influence itself bilaterally and a strong coupling exists. With bilateral exoskeleton the drive of each leg to the other reduces (significantly compared to normal walking, $p = 0.003$ left to right, and $p = 0.000$ right to left), indicating a mutual decrease in the legs ability to drive each other. In the unilateral exoskeleton condition, the left leg strongly drives the right, but the drive of the right leg to the left leg is reduced compared to normal walking ($p = 0.000$ right to left).

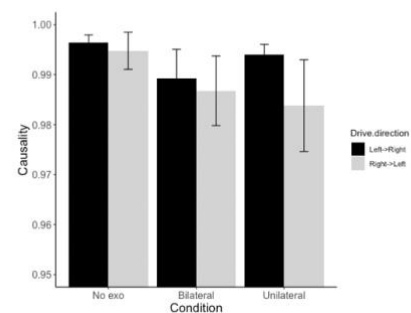


Figure 1: Causal drive of the left to the right leg (black) and right to left leg (grey) across the three experimental conditions.

This nontrivial finding suggests the system uses redundancy in free parts of the system to be driven by the constrained limb, exploiting a degenerate technique that can be used to compensate for the constrained leg. The motor control solution is then defined by the optimal solution in light of the constraints imposed, and adaptability and exploiting redundancy is key to supporting functionality.

Conclusions

Optimal walking gait may be driven by the most constrained leg, and while less resembling ‘healthy’ walking kinematics, may provide a more optimal motor control solution.

Acknowledgments: Supported by Geneva-Exeter funding, and the Swiss National Science Foundation 325230_146801.

References

- [1] Armand A & Attias M. (2019). *Contracture and gait deviations*. Springer.
- [2] Clark AT et al. (2015). *Ecology*, **96**(5): 1174-1181.

Walking with increasing acceleration is achieved by tuning ankle torque onset timing and rate of torque development

Logan Wade^{1,2}, Jonathon Birch^{2,3}, Dominic James Farris³

¹Department for Health, University of Bath, Bath, United Kingdom

²School of Human Movement and Nutrition Sciences, University of Queensland, Brisbane, Australia

³Sport and Health Sciences, University of Exeter, Exeter, United Kingdom

Email: lw2175@bath.ac.uk

Summary

Three-dimensional kinematics and kinetics were collected from fifteen participants who performed over-ground walking at a constant speed, as well as a low, moderate and maximal walking acceleration. During accelerative walking, ankle coordination was substantially altered by timing of torque onset and peak, rate of torque development and peak torque magnitude. These results have implications for clinical rehabilitation, as well as robotic and powered assistive devices, where adaptations in ankle coordination may facilitate functional accelerative gait.

Introduction

Changes in joint coordination (joint movement patterns and torque development) are generally examined at a constant speed, despite accelerative gait comprising a large portion of locomotion. Previous research has demonstrated that during accelerative walking, increased net work about the ankle was due to muscles contracting to store energy in the tendon, compared to constant speed walking where energy was stored from external sources [1]. Therefore, acceleration likely requires more than simply increasing torque about the ankle, as timing of torque production will also play an important role.

However, previous work has only examined a single acceleration magnitude and temporal characteristics of torque development were not explored. Therefore, it is unknown how ankle coordination is altered as acceleration increases. We hypothesised that an increase in net work about the ankle, intended to increase walking acceleration, would not be due to solely increasing torque magnitude, and instead would also be a product of temporal adjustments to the ankle torque profile.

Methods

Fifteen participants (27 ± 4 years, 175 ± 9 cm, 70 ± 11 kg) performed over-ground walking at a constant speed, as well as a low, moderate and maximal walking acceleration. Participants walked over an in-ground force plate for eight successful trials; defined as approaching the plate at a constant speed, striking the plate with the entire right foot and then performing constant or accelerative gait for three steps. Three-dimensional kinematic (200 Hz) and kinetic data (1000 Hz) were recorded in ODIN (Codamotion) and processed in Visual3D (C-Motion) to calculate ankle joint angle, moment and work. Statistical analysis was performed using linear mixed modelling, where the outcome variable was analysed with acceleration magnitude as a fixed effect and participant as a random effect.

Results and Discussion

Net work about the ankle increased 0.384 J/kg as acceleration increased from 0–100% ($P < 0.001$) due to an increased

maximal moment (Fig. 1B, $P < 0.001$), combined with an increased time between heel strike and start of plantar flexion moment (Fig 1B, $P < 0.001$), and a decreased time between the start and peak plantar flexion moment (Fig. 1B, $P < 0.001$). Thus, onset of plantar flexion moment was delayed as acceleration increased, which when combined with a shorter time to produce maximal torque, resulted in a 5.55 Nm/s increase in rate of torque development from constant speed to maximal accelerative walking ($P < 0.001$).

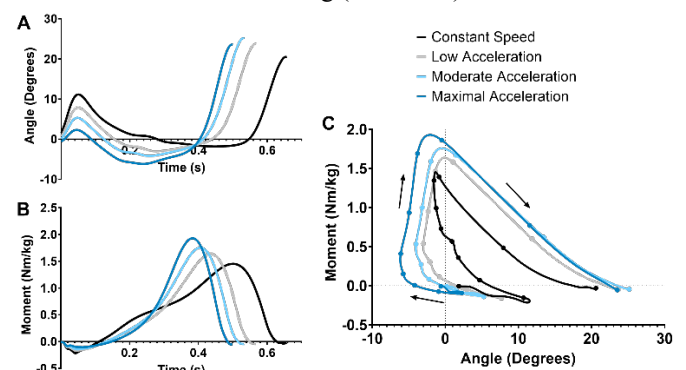


Figure 1: Mean ankle joint angle (A) and moment (B) for each walking condition (plantar flexion = positive). Dots on moment-angle curve (C) represent 10% portions of stance. Heel-strike to toe-off occurs in a clockwise direction as indicated by arrows.

During acceleration, there appears to be a period where dorsiflexion occurs without any change in torque (Fig. 1C), followed by a rapid increase in ankle torque without any change in ankle angle. These results demonstrate that ankle coordination is significantly altered as walking acceleration increases, which may have a range of implications in the treatment of neuromuscular disorders and the development of powered exoskeletal and prosthetic devices. Currently powered assistive devices are commonly controlled by altering peak torque based on a set time delay after heel strike [2]. These results support previous work that has highlighted the importance of adapting timing of torque onset and peak, magnitude of peak torque and rate of torque development in the design and application of assistive devices [3].

Conclusions

Timing, magnitude and rate of torque development during acceleration is altered compared to constant speed walking, which has implications for clinical, robotic and rehabilitation applications.

References

- [1] Farris & Raiteri. (2017). *R. Soc. Open Sci.*, **4**: 160901.
- [2] Young & Ferris. (2017). *IEEE Trans. Neural Syst. Rehabilitation Eng.*, **25**: 171-182
- [3] Zhang et al. (2017). *Science*, **356**: 1280–1284.

Initiation of arch recoil is asynchronous with the windlass mechanism in walking

Welte L.¹, Arndt A.², Kelly LA.³, Holowka NB.⁴, Rainbow MJ.¹

¹ Queen's University, Kingston, Canada

² Swedish School of Sports and Health Sciences, Stockholm, Sweden

³ The University of Queensland, Brisbane, Australia

⁴ University at Buffalo, Buffalo, USA

Email: l.welte@queensu.ca

Summary

The arch of the foot stretches and recoils in response to an applied load. In walking and running, it is unclear whether a reduction in applied force, or the windlass mechanism is responsible for arch recoil. We used high-speed x-ray and ground reaction forces to assess the timing of the load on the foot, the initiation of the windlass mechanism, as well as peak ankle and arch dorsiflexion. We found that the onset of arch recoil in walking is much later than the initiation of the windlass mechanism. Instead, load on the arch and/or arch-ankle coupling may play a larger role in initiating arch recoil than the windlass mechanism.

Introduction

The arch of the foot is mobile in both walking and running. In general, the arch moves in a spring-like manner [1], flattening in response to load and recoiling when the load is released. However, the windlass mechanism, whereby metatarsal-phalangeal joint (MTPJ) dorsiflexion raises the arch, is also credited with enabling arch recoil in walking and running [2]. While the windlass mechanism statically raises the arch [3], it is unknown whether it initiates arch recoil in propulsion, or if the arch recoils simply because forces on it are declining.

Recently, we showed that arch mobility enables ankle motion in running propulsion [4]. The propulsive phase is well modelled by a rebounding mass-spring system, which is theoretically in sync with the arch's recoil. However, arch recoil and ankle power are substantial in walking [5], despite more inverted-pendulum and less spring-like behavior. Using biplanar x-ray, we compare the timing of arch recoil and ankle dorsiflexion to peak loads in walking and running to understand how the arch-spring contributes to propulsion and to measure windlass mechanism timing relative to arch recoil.

Methods

Four participants walked and ran in minimal shoes over force plates while a high-speed biplanar x-ray system captured their foot and ankle motion. CT-generated models were used to semi-automatically measure the position and orientation of medial arch bones, toe and tibia [6]. Each bone had an inertial co-ordinate system. The dorsiflexion axes of the talus and tibia aligned with a cylinder fit to the tibial and talar domes.

“Propulsion” was the instant after the anterior-posterior force became anterior. Tait-Bryan YZX angles measured the rotation of the talus to the tibia (ankle), the first metatarsal to the calcaneus (arch) and the MTPJ (as an indication of an engaged windlass mechanism). The timing and magnitude of peak ankle, arch, and MTPJ dorsiflexion were measured in walking and running.

Results and Discussion

MTPJ dorsiflexion and propulsion occur simultaneously (Figure 1). In running, they coincide with the start of arch recoil; in walking, the arch flattens for the first half of propulsion before it recoils. Peak arch and ankle dorsiflexion are simultaneous: in running, these maxima are synchronized with propulsion; in walking, they are aligned later in stance with the second vertical ground reaction force peak.

Additionally, peak arch dorsiflexion was similar between walking and running (diff = $2 \pm 2^\circ$), while peak ankle dorsiflexion was higher in running (diff = $11 \pm 3^\circ$). When visualizing the bone motion at peak ankle dorsiflexion in running, the tibia appeared close to its end range of motion on the talus, substantially more anterior than in walking.

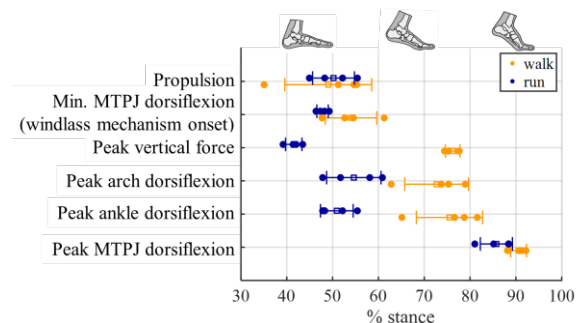


Figure 1: The timing in % stance of peak ankle, arch and toe dorsiflexion in walking and running for each participant, as well as the windlass mechanism onset, the transition to propulsion from the anterior-posterior force and the peak vertical force.

Conclusions

The synchronized onset of ankle plantarflexion, arch recoil and the windlass mechanism in running supports the arch's contribution to a spring-like propulsion. In walking, our results suggest that the windlass mechanism does not initiate arch recoil, as the onset of MTPJ dorsiflexion would have initiated arch plantarflexion. Instead, arch recoil seems to be initiated by the vertical load on the arch and may be related to peak ankle dorsiflexion. The arch and ankle dorsiflexion peaks occur simultaneously in walking and running, despite different peak ankle dorsiflexion, and position of the tibia on the articular surface of the talus. The arch and ankle appear to be intricately linked in propulsive function.

References

- [1] Ker RF et al. (1987). *Nature*, **325**: 147–149.
- [2] Hicks JH. (1953). *J. Anat.*, **87**: 345–357.
- [3] Welte L et al. (2018). *J. R. Soc. Interface*, **15**: 20180270.
- [4] Welte L (2020). *PhD Dissertation*. p. 64-81
- [5] Farris DJ et al. (2012). *J. R. Soc. Interface*, **9**: 110–118.
- [6] Akhbari B et al. (2019) *J. Biomech.*, **92**: 120–125.

A comparison of multisegment foot kinematics between younger and older adults during walking

Nayeli Marcial¹, Victoria Chester¹, Usha Kuruganti¹

¹Andrew and Marjorie McCain Human Performance Laboratory, University of New Brunswick, Fredericton, Canada

Email: nayeli.marcial@unb.ca

Summary

Older adults exhibit different gait patterns compared to younger adults [1]. The aim of the study was to examine age-related differences in multisegment foot (MSF) kinematics during walking. Results indicate that older adults, when compared to younger adults, show significant differences in MSF kinematics, such as decreased range of motion (ROM) of the midfoot relative to the calcaneus and reduced joint mobility of the midfoot when walking. Examining age-related MSF kinematic differences may lead to a greater understanding of typical and atypical foot mechanics and function in older adults.

Introduction

During gait, the foot and ankle have important roles such as attenuating shock at impact, providing stability and support of the lower limb, and aiding in forward propulsion of the body [2]. It is plausible that changes in foot function may result in impaired movement patterns which is known to increase with age. However, the interrelationship between age-related differences in foot mechanics and physical function are not clear [1]. The use of MSF models could provide insight about the functional significance of motion occurring within the foot as well as alterations due to age. Only a few studies have used an MSF model to determine the age-related differences in foot kinematics during walking [1-4] and further research is warranted. The purpose of this study was to compare MSF kinematics between younger and older adults during walking at a self-selected speed.

Methods

Sixteen young participants (8 males, 8 females, mean age 23.62±3.73 years, mean weight 69.1±16.4 kg, mean height 1.71±0.12 m) and fifteen older participants (8 males, 7 females, mean age 71.64±5.94 years, mean weight 82.9±16. kg, mean height 1.71±0.12 m) with no known lower-extremity disease/disorder/injuries were recruited. A12-camera Vicon T160 motion capture system (Oxford Metrics Group Ltd., UK), sampling at 100 Hz, was used to track thirty-six retro-reflective markers (9 mm diameter) were placed on the medial and lateral tibia and anatomical landmarks of the foot using a modified version of a 5-segment MSF model used [5]. Three-dimensional relative angles and planar angles of the foot segments were computed. Significant group differences ($p < 0.05$) in range of motion, mean max and min peak relative angles between foot segments, and time of occurrence of these peaks were analyzed using a one-way ANOVA or if indicated, Kruskal-Wallis test. Statistical analyses were completed using R Studio (RStudio 2018, RStudio, Inc., USA).

Results and Discussion

The results suggest that older adults demonstrate significantly different MSF kinematics compared to younger adults during gait (Figure 1). These age-related differences included decreased mean peak plantarflexion (PF) of the calcaneus-shank angle (older: $-13.3 \pm 6.52^\circ$,

younger: $-5.31 \pm 17.08^\circ$) with a delay to peak onset (older: $66.49 \pm 18.19\%$; younger: $56.49 \pm 18.19\%$ gait cycle). A decreased ROM was also evident for the older group ($-21.10^\circ \pm 1.97^\circ$) compared to younger ($-22.23^\circ \pm 1.42^\circ$). The older group had reduced mean max eversion of the midfoot-calcaneus angle (older: $12.47 \pm 5.02^\circ$; younger: $18.10 \pm 3.95^\circ$). The ROM was thereby slightly decreased (older: $5.85^\circ \pm 0.18^\circ$, younger: $7.19^\circ \pm 0.37^\circ$), whereas the time to max peak eversion was decreased (older: $28.68 \pm 27.98\%$, younger: $28.68 \pm 27.98\%$ gait cycle) of the midfoot-calcaneus. Moreover, the older group had reduced mean max adduction of the midfoot-calcaneus (older: $3.59 \pm 6.19^\circ$; younger: $9.93 \pm 6.37^\circ$), as well as decreased ROM ($5.20 \pm 0.45^\circ$, younger: $5.83 \pm 0.27^\circ$). Further, the older group had increased time to min peak adduction (older: $36.46 \pm 16.56\%$, younger: $33.26 \pm 16.26\%$ gait cycle) and time to max peak adduction (older: $59.96 \pm 8.29\%$ younger: $59.49 \pm 5.24\%$ gait cycle) of the mid-cal angle. Additionally, the older group had reduced mean peak abduction of the metatarsus-midfoot angle (older: $-2.46 \pm 7.84^\circ$, younger: $-13.23 \pm 6.06^\circ$), but there were no differences in the ROM. Further, the older group had increased time to min peak abduction (older: $36.92 \pm 27.63\%$, younger: $30.36 \pm 27.14\%$ gait cycle) and time to max peak abduction (older: 42.14 ± 16.86 , younger: $37.66 \pm 12.54\%$ gait cycle) of the met-mid angle. These findings suggest a less propulsive gait pattern and reduced mobility of the foot, especially the midfoot.

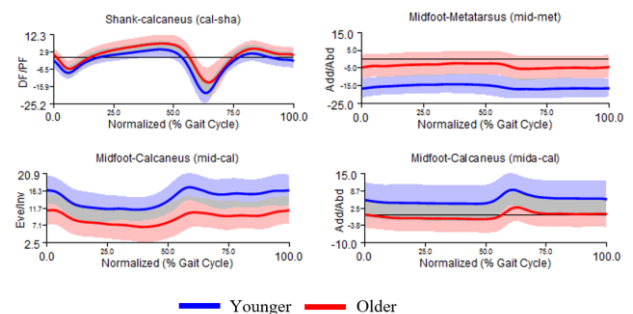


Figure 1. Mean cal-sha, mid-cal and met-mid angles of younger and older adults (solid line with standard deviation band).

Conclusion

MSF analyses will improve our understanding of foot mechanics and function in younger and older adults. Further, such data could aid in distinguishing between typical and atypical gait patterns in older adults. Future studies should include a larger sample size and range of walking speeds to corroborate these findings.

Acknowledgements

Funding from the Natural Sciences and Engineering Research Council (NSERC) of Canada.

References

- [1] Arnold et al. (2014), *Gait Posture*, 39:689-94.
- [2] Legault-Moore et al. (2012), *J Clin Med Res*, 4:259.
- [3] Lee et al. (2017), *J Foot Ankle Res*, 10:29.
- [4] Van Hove et al. (2017), *Medicine*, 96:1-7.
- [5] Leardini et al. (2007), *Gait Posture*, 25:453-462.

Lower Extremity Joint Moment Angular Impulse during Gait Transitions

Li Jin¹, Michael E. Hahn^{2,3}

¹Dept. of Kinesiology, San Jose State University, San Jose, CA, USA

²Neuromechanics Lab and ³Bowerman Sports Science Clinic, Dept. Human Physiology, University of Oregon, Eugene, OR, USA
Email: li.jin@sjsu.edu

Summary

This study investigated lower extremity joint extensor moment angular impulse (I_{joint}) during the walk to run transition (WRT) and run to walk transition (RWT) processes. We found I_{ankle} and I_{knee} contributed to more than 80% of the total lower extremity support moment impulse. Additionally, gait transitions significantly change I_{knee} after the transition step.

Introduction

Walking and running have different whole-body center of mass dynamic patterns [1]. The transition between the walking inverted pendulum and the running spring mass paradigm is primarily determined and modulated by lower extremity kinetic factors [2]. Both the WRT and RWT require lower extremity extensor muscles to support the body moving forward. Joint level moment angular impulse represents the joint moment effect over time and it is regarded as the end-effect of muscle functions in human locomotion [2,3].

This study aimed to investigate lower extremity joint extensor moment angular impulse (I_{joint}) during the WRT and RWT processes. Since joint kinetic parameters are known to increase with locomotion speed, we hypothesized that I_{joint} would increase during the WRT and decrease during the RWT.

Methods

Ten healthy subjects (50.7 ± 6.0 years, 173.4 ± 11.4 cm, 69.7 ± 14.9 kg) participated in this study. Subjects were asked to complete treadmill WRT (1.8 – 2.4 m/s) and RWT (2.4 – 1.8 m/s) protocols, with acceleration and deceleration set to 0.1 m/s^2 and -0.1 m/s^2 , respectively. We selected five steps for data analysis: transition step (S0); two steps before transition (S–2, S–1); two steps after transition (S1, S2).

Stance phase joint extensor moment angular impulse (I_{joint}) was calculated as the sum of all stance phase extensor joint moment integrated over time within each joint [3]. Total lower extremity joint support moment impulse (I_{total}) was calculated as the sum of I_{ankle} , I_{knee} and I_{hip} during stance phase. I_{joint} was examined for differences between joints and steps via the 2-way ANOVAs (joint \times step) for WRT and RWT in SPSS (V22.0, IBM, Armonk, NY). I_{total} was examined using a 1-way ANOVA to compare between the five steps tested during WRT and RWT, respectively.

Results and Discussion

I_{ankle} was higher than I_{hip} at all steps during both WRT and RWT. Within I_{knee} , we found significant differences between

steps before and after transition: S–2 was lower than S1 and S2, and S–1 was lower than S1 during WRT; during RWT, I_{knee} at S1 was lower than S–2 and S–1 (Figure 1).

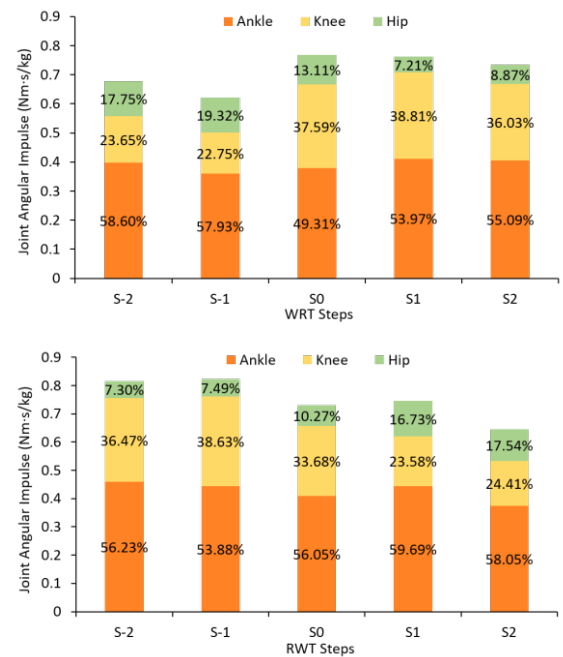


Figure 1: Joint extensor moment angular impulse in WRT (top) and RWT (bottom) steps.

I_{ankle} contributed to around 50% of I_{total} among all steps during both transitions. This indicates ankle plantar flexor moment would compensate for the changeable stance time length, and this would be helpful to maintain a relatively consistent I_{ankle} output during both transitions. Future assistive device design should consider the ankle plantar flexor moment compensatory mechanism in response to the change of locomotion tasks, speeds and stance time.

Conclusions

Both the I_{ankle} and I_{knee} played more dominant roles to support the body during both WRT and RWT processes. Gait transitions significantly change I_{knee} after the transition step.

Acknowledgments

This work was supported by the Betty Foster McCue Scholarship at the University of Oregon.

References

- [1] Segers V et al. (2007). *J Exp Biol.*, **210**: 578-85.
- [2] Pires NJ et al. (2014). *J Exp Biol.*, **217**: 3519-27.
- [3] DeVita P et al. (2000). *J Appl Physiol.*, **88**: 1804-11.

Posture (slouched versus erect sitting) affects upper limb maximal voluntary contraction levels: preliminary results

A. Tomezzoli¹, B. Fréchède¹, S. Duprey¹

¹LBMC UMR_T9406, Univ Lyon, Univ Claude Bernard Lyon 1, Univ Gustave Eiffel, IFSTTAR, F69622, Lyon, France
Email: aurelie.tomezzoli@univ-eiffel.fr

Summary

A slouched, versus erect sitting posture, is known to affect shoulder abduction isometric maximal voluntary contraction (MVC) levels. This study investigated the impact of 2 sitting postures on shoulder abduction, elbow flexion and wrist flexion MVCs. Fourteen participants (3 men, 11 women, 23.7±4.6 years) were randomly placed in a slouched or erect sitting posture, using oral instructions and light touch. Isometric MVCs were measured by a uniaxial load cell. The maximal of 3 MVCs was extracted for each joint (0-20° wrist flexion, 90° elbow flexion and 90° shoulder abduction in the scapula plane) in each posture, and then compared w.r.t posture using t-tests. In the erect posture, mean isometric MVC was 13.1% higher ($p<0.01$) for wrist flexion, 14.1% ($p<0.01$) for elbow flexion and 11.7% (NS) for shoulder abduction.

Introduction

Upper limb musculoskeletal disorders are a major public health issue. Biomechanical parameters and individual susceptibility are some of the risk factors for these diseases [1]. Besides, a slouched, versus erect sitting posture, decreases individual functional capacities for shoulder abduction isometric maximal voluntary contraction (MVC) [2]. Thus, posture modifications might be a key to limit musculoskeletal disorders' occurrence.

The goal of this study was to assess the impact of two sitting postures (erect vs slouched) on wrist, elbow and shoulder isometric MVCs. Preliminary results are reported here.

Methods

Fourteen participants (3 men, 11 women, 23.7±4.6 years) were recruited after ethical endorsement (CPP N°2020-A00573-36). Their spinal curvatures were increased or decreased using oral instructions and light touch, to reach erect or slouched stable, easily maintained postures, in a random order. Wrist flexion MVC was measured at 0-20° of wrist flexion, with 90° of elbow flexion and 10° of shoulder abduction, forearm supine. Elbow flexion MVC was measured at 90° of elbow flexion, with 10° of shoulder abduction. Shoulder abduction MVC was measured at 90° of abduction in the scapula plane, *i.e.* 45° of flexion. Upper limb and trunk stabilization were performed manually and using an armrest. The participants were asked to maintain their posture and keep their eyesight horizontal while they pulled a flat foam-padded device connected to a 500N TME F480TC uniaxial load cell by a wire rope (Figure 1). Recorded oral encouragements provided guidance for a two second progressive rise, then for a three second sustained maximal contraction. Three trials, separated by a minimal one-minute rest, were performed in each posture for each

joint. If between trials maximal difference exceeded 25%, a 4th trial was performed and the most divergent trial was considered unrepresentative of the posture and thus discarded.

Raw data were smoothed using a 4th order Butterworth filter with a cutoff frequency of 1 Hz. The maximal value of each set of three trials was extracted. Finally, the effect of posture was assessed using paired t-tests, after variable transformation to insure their normal distribution.



Figure 1: Elbow isometric MVC measurement device.

Results and Discussion

In the erect posture, mean isometric MVC was 13.1% ($p<0.01$) higher for wrist flexion, 14.1% ($p<0.01$) for elbow flexion and 11.7% (NS) for shoulder abduction.

Posture seems to be one of the most important explanatory factors for MVC intra-individual variability, after tiredness and pain [3]. Postural induced scapula position modifications [2] might explain its impact on MVCs. The effect size found by Kebaetse for shoulder abduction MVC was higher (16.2% instead of 11.7% here) [2], which could be explained by the degree of arm rotation or spinal posture characteristics.

Conclusions

Posture seems to modify individual upper limb functional capacities, which had already been reported for shoulder capacities. The present study expands this result to wrist and elbow joints. Thus, posture could impact the risk of musculoskeletal disorders as well as athletic performances for the whole upper limb.

References

- [1] Brière J et al. (2015). *Des indicateurs en santé travail: les troubles musculo-squelettiques du membre supérieur en France*; INVS.
- [2] Kebaetse M et al. (1999). *Arch Phys Med Rehabil*, **80(8)**: 945-50.
- [3] Nuzzo JL et al. (2019). *J Appl Physiol*, **126(3)**: 513-43.

Effect of operating setting on muscle activity of the upper body during tree harvester simulation

J. Toner¹, U. Kuruganti¹, J. Ketterling², V. Chester¹,

¹Andrew and Marjorie McCain Human Performance Laboratory, Faculty of Kinesiology, University of New Brunswick, Fredericton, Canada

²J.D. Irving Woodlands Division, Fredericton, New Brunswick, Canada

Email: jc526075@dal.ca

Summary

Forest machine operators are exposed to a variety of musculoskeletal stressors including repetitive strain injury, back and shoulder pain, and discomfort. This study examined the effects of operator skill level and operating settings on muscle activity of the upper body while operating a tree harvesting simulator. The results of this study showed that there were differences in upper limb muscle activity due to operating settings. In addition, novice participants demonstrated greater muscle activity than experienced operators suggesting differences due to experience. The results of this study may help to better understand the muscular demands of this type of work and develop improved work protocols.

Introduction

The integration of machinery has reduced the risk of manual material handling within the tree harvesting industry. While the operation of mechanized harvester machines does not require large force contractions, the continuous and repetitive nature of the work can result in muscular discomfort and fatigue. The workload in the upper extremities of the workers operating forestry machines for long hours has been associated with discomfort and pain. [1, 2].

Methods

Fifty-four (n=54) individuals participated in the study (49 males, 5 females) and were categorized as novice (Age: 29.4 ± 7.4; Weight (kg): 76.9 ± 12.5; Height (m): 1.8 ± 0.1), experienced (Age: 34.7 ± 10.2; Weight (kg): 93.8 ± 16.3; Height (m): 1.8 ± 0.7) or advanced (Age: 37.9 ± 11.2; Weight (kg): 101.8 ± 11.7; Height (m): 1.8 ± 0.1). Novice participants were recruited by word of mouth and experienced/advanced operators were recruited from a forestry company. Muscle activity was monitored using bipolar surface electromyography (EMG) placed over the flexor digitorum (FD), flexor carpi radialis (FCR), anterior deltoid (AD), upper trapezius (UT), and posterior deltoid (PT) muscle groups. EMG were acquired wirelessly (Due-Pro, OT Bioelettronica, Turin, Italy). Participants used a Ponssee tree harvesting simulator to simulate cutting trees. Participants started by completing an orientation using a standard crane speed. Then, participants were asked to cut 15 trees in 15 minutes using three randomized crane speeds; slow, standard and fast. Furthermore, the experienced and advanced operators completed an additional trial using a sensitive joystick setting. The sensitive joystick mimicked a challenging condition that more experienced operators would typically face when harvesting trees. The EMG amplitude of each signal was normalized to the individual's maximum isometric voluntary contraction. Muscle activity amplitude was estimated using the Root Mean Square (RMS) value. Median frequency (MF) was calculated at the beginning (after 1 minute) and end of the Simulator trial (~15 minutes) and compared to estimate fatigue. Statistical analysis of variance (ANOVA) and pairwise t-tests were conducted to test for significant differences in mean RMS and MF percent changes across the various operating and joystick settings. All of the statistical tests were compared for significance using a p-value less than the alpha value, set at 0.05

Results and Discussion

Figure 1 presents the mean RMS EMG data across muscles for the three crane speeds for novice participants. During the slow speed condition novice participants demonstrated significantly lower mean

RMS of the left PT using the fast speed (12.8 mV). Similarly, novice participants also showed significantly less mean RMS of their right forearms with the slow speed (16.4 mV (FCR); 15.3 mV (FD)) than the standard speed setting (17.7 mV; (FCR) 17.6 mV (FD)). In contrast, novice participants showed significantly greater mean RMS of their left forearms with the slow speed (14.9 mV (FCR); 19.4 mV (FD)) than the standard speed setting (13.7 mV; (FCR) 17.0 mV (FD)). While operating the sensitive joystick, experienced participants demonstrated significantly higher mean RMS in their right AD (14.4 mV) and lower mean RMS in both the left (12.8 mV), and right (21.6 mV) FCR, than using the standard speed (11.8 mV (AD); 23.6 mV (Right FCR); 12.5mV (Left FCR)). While there were differences detected in EMG amplitude, no significant differences were detected in the MF between the beginning and the end of the trial for any condition. Previous research [3] has shown decreases in the MF after 4 hours of Simulator use suggesting fatigue. The lack of significant differences in the MF in this study may be due to the shorter duration of the simulator operation (15 minutes) and the low force contractions used to operate the machine.

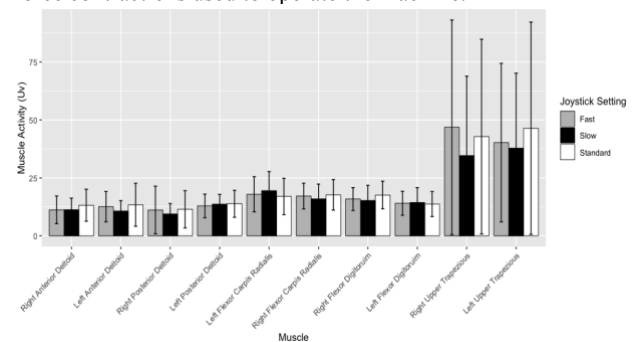


Figure 1: Mean RMS (uV) across all speed settings of novice participants

Conclusions

Ergonomic field studies of this industry are lacking as it is difficult to obtain comprehensive data while operators are cutting trees in the woods. Forest machine simulators provide an opportunity to further study this population. Overall, increases in muscle activity were found in all participants, however the regions affected varied according to skill level. The lack of significant differences in the frequency data suggests that future research should include longer testing to be more reflective of a typical work shift. The present findings suggest that there are differences in the muscles recruited during harvester operations depending on the skill level of the operator. The information will help employers to develop more focused training for operators using controls that minimize muscle requirements and develop skill.

Acknowledgments

We would like to acknowledge JDI Woodlands for provision of the simulator and Mr. Andre Cyr for his valuable insight

References

- [1] Østensvik, et al. (2008). *Int. J. Ind. Ergon.*38. 1017-1027.
- [2] Østensvik, et al. (2009). *Ergonomics*, 52:12, 1556-1567.
- [3] Kuruganti, et al. (2011). *Work*.39:4, 491-498.

Beyond Euler/Cardan analysis: true glenohumeral axial rotation during arm elevation and rotation

Klevis Aliaj^{1,2}, Heath B. Henninger^{1,2}

¹Department of Orthopaedics, University of Utah, Salt Lake City, Utah, United States of America

²Department of Biomedical Engineering, University of Utah, Salt Lake City, Utah, United States of America

Email: klevis.aliaj@utah.edu

Summary

Based on Euler/Cardan analysis, prior investigations have reported up to 80° of glenohumeral (GH) external rotation during arm elevation, varying by plane of elevation (PoE) [1, 2]. This (apparent) axial rotation incorrectly quantifies the rotation around the humerus' longitudinal axis because it assumes a sequence-specific path [3]. In this investigation, (true) axial rotation was computed by following the actual humeral path. True GH axial rotation was not different than 0° during arm elevation and does not vary by PoE. Clinicians want to understand the physically motivated true axial rotation [4], and thus it should be reported in kinematic analyses.

Introduction

Euler/Cardan analyses report up to 80° of GH external rotation during arm elevation, which is dependent on the PoE [1, 2]. However, this (apparent) axial rotation assumes a sequence-specific path for the humerus. Clinicians want to understand the physically motivated (true) axial rotation, and rely on laboratory analyses to inform their understanding of underlying shoulder biomechanics. This is critical for the GH joint since its motion cannot be visually ascertained in common clinical settings. True GH axial rotation has not been previously measured *in vivo*, and its difference from apparent axial rotation is unknown. We hypothesized that true GH axial rotation was 0° and did not vary by PoE during arm elevation.

Methods

This analysis was performed on kinematic data previously collected for healthy shoulder kinematics [5]. Humerus and scapula motions were imaged at 100 Hz using a custom biplane fluoroscopy system in 20 healthy subjects (10M/10F; 42±17 yrs; right-hand dominant) while performing coronal, scapular and forward elevations, and external rotation in adduction, and in 90° of abduction. Model-based markerless tracking was utilized to ascertain 3D bone kinematics.

Apparent axial rotation was computed using the $xz'y''$ and $yx'y''$ sequences. True GH axial rotation was computed by projecting GH angular velocity onto the humerus' longitudinal axis and integrating the resulting scalar value from the start of the motion to each timepoint [3]. One-dimensional statistical parametric mapping was utilized to: compare apparent vs. true GH axial rotation and GH axial rotation vs. 0°; and detect differences in axial rotation by PoE.

Results and Discussion

In contrast to apparent GH axial rotation, true axial rotation does not differ by PoE and is not different than 0° during arm elevation at higher elevation angles (Fig. 1A, one Euler sequence shown for clarity). The signed spherical area

between the sequence-specified and actual humeral trajectory – which does not represent an actual rotation around the humerus' longitudinal axis – accounts for the difference between apparent and true axial rotation (Fig. 1B). Euler/Cardan analysis misrepresents axial rotation leading prior studies to measure substantial GH axial rotation and differences between PoEs during arm elevation.

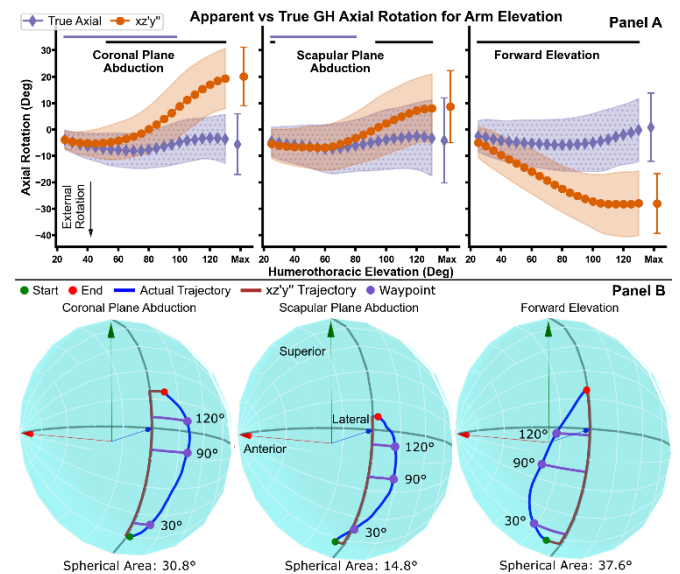


Figure 1: **A:** The solid purple line indicates true axial rotation $\neq 0^\circ$ and solid black line indicates true \neq apparent axial rotation. **B:** The spherical area between the actual (blue) and sequence-specified (brown) humeral trajectory quantifies differences between true and apparent axial rotation in **A**.

Conclusions

Clinically relevant quantification of axial rotation is important because biomechanics literature informs clinical understanding of shoulder biomechanics – especially for the GH joint since its motion cannot be visually ascertained. Clinicians can more reliably interpret the physically motivated true axial rotation (i.e. there is minimal humeral rotation during thump up arm elevation). True axial rotation should be reported in future studies of shoulder kinematics.

Acknowledgments

Funding from: NIH R01 AR067196.

References

- [1] Meskers C.G.M. et al. (1998). *Clin Biomech*, **13**: 280-92.
- [2] Ludewig P.M. et al. (2009). *J Bone Jnt Surg*, **91**: 378-89.
- [3] Miyazaki S. et al. (1991). *J Biomech Eng*, **113**: 270-5.
- [4] Zatsiorsky V. (1998). *Kine Humn Motn; Humn Kinetics*.
- [5] Kolz C.W. et al. (2021). *J Biomech*, **117**: 110266.

Biomechanics during controlled forward descents on outstretched arms in response to Fall Arrest Strategy Training (FAST) in older men and women

Pifko, J.¹, Arnold, C.², Farthing, J.P.¹, Lanovaz, J.¹

¹College of Kinesiology, University of Saskatchewan, Saskatchewan, SK, Canada

²School of Rehabilitation Science, University of Saskatchewan, Saskatchewan, SK, Canada

Email: justin.pifko@usask.ca

Summary

Upper body injuries commonly arise from forward falls in older adults. Research examining sex-related differences and the effect of training to improve capacity to reduce injury risk during simulated forward fall arrest biomechanics in older adults is lacking. We assessed 55 older adults (29 women) who completed three testing sessions evaluating biomechanics during a controlled forward descent on outstretched hands before and after Fall Arrest Strategy Training (FAST). Upper extremity loading and energy absorption requirements were reduced after the intervention. Older men had different descent mechanics compared to older women, but both groups responded similarly to FAST.

Introduction

More than 50 percent of injuries from falls in older adults occur in the upper body. Reaching hands forward is a common reaction to protect the body from injury during a forward fall [1]. One option to mitigate fall injury risk is to improve fall arrest capacity with an exercise intervention program. While women have been the focus of most fall prevention studies, injuries such as head trauma can occur equally between sexes [2]. Sex-related biomechanical changes after fall injury prevention programs in older adults is unknown. Our purpose was to quantify fall arrest capacity in older men and women in response to a unique intervention program.

Methods

Older adults completed three testing sessions: Baseline, Pre (after a 12-week control), and Post (after 12 weeks of FAST). FAST was led by two physical therapists for 45 minutes twice per week and focused on goals to improve upper extremity (UE) strength, reaction time, and movement time in combination with fall prevention goals – balance, strength, function, and mobility.

In the testing sessions, participants completed forward descents similar to the downward portion of a push-up at a body lean of 60° from horizontal using a custom apparatus [3]. Initially, participants had 90° shoulder flexion, elbows extended, and hands shoulder-width apart. A neutral spine with extended knees, feet together, and ankles in 90° dorsiflexion were used throughout the descent. Participants descended to a target of 90° elbow flexion in approximately 1.5 s following a metronome. Three trials were captured and averaged for each participant.

Bilateral force platforms (OR6-7, AMTI, Watertown, MA, fs=2000Hz) recorded hand reaction forces while a motion capture system (VICON, Centennial, CO, fs=200Hz) collected bilateral 3D UE kinematics. Outcome variables included elbow range of motion (eROM), maximum ground reaction forces (mxGRF), peak elbow moment (eMOM; normalized to height and body weight), elbow stiffness (eSTF), and overall energy absorption (OE; normalized to height and body weight) [4]. Independent *t*-tests compared sex demographics and separate 3 x 2 (time x sex) mixed-design ANOVAs with repeated measures examined outcome variables.

Results

Seventy-eight participants were enrolled in the study, and 55 older adults (29 women) completed all testing sessions. There was no significant age difference between sexes ($\bar{x}_M=73.5\pm 8.2$ years, $\bar{x}_W=69.7\pm 6.9$ years, range=60-93 years, $p=0.062$). Older men were significantly taller and heavier than older women, although body mass index was similar (M:28.7±3.6m²kg⁻¹, W:27.8±5.5m²kg⁻¹, $p=0.447$). FAST attendance between sexes was similar (M:82.5±13.6%, W:81.2±14.4%, $p=0.722$).

No sex or time effects were seen for eROM (Table 1). mxGRF showed a main effect of time ($p<0.001$, Base-Post, Pre-Post) and sex (M>W, $p=0.007$). Sex main effects were seen for eMOM (M>W, $p<0.001$) and eSTF (M>W, $p=0.009$). A time main effect was found for OE ($p=0.018$, Pre-Post).

Discussion and Conclusion

After the FAST program, participants shifted load distribution away from their UE during the descent movement and subsequently reduced UE OE demands. While older men applied higher forces and had higher eMOM and eSTF than older women, the intervention had similar effects on the controlled forward descent biomechanics.

Acknowledgments

Funding by the Saskatchewan Health Research Foundation.

References

- [1] DeGoede, KM, et al. (2003). *J Gerontol A Biol Sci Med Sci*, **56A**(9), 413-420
- [2] McIntyre, A, et al. (2018). *Evidence-based Review of Moderate to Severe Acquired Brain Injury*
- [3] Lattimer, L, et al. (2017). *JAPA*, **25**(3), 474-81
- [4] Sran, MM, et al. (2010). *J Gerontol A Biol Sci Med Sci*, **65A**(3), 312-7

Table 1: Outcome variable data from controlled forward descents separated by sex across each testing session (mean±SD).

	eROM M (°)	eROM W (°)	GRF M (%BW)	GRF W (%BW)	eMOM M (Nm/Nm)	eMOM W (Nm/Nm)	eSTF M (Nm/Nm/°)	eSTF W (Nm/Nm/°)	OE M (J/J)	OE W (J/J)
Base	70.2±14.4	74.5±12.8	20.1±2.8	18.1±2.2	0.018±0.004	0.016±0.003	0.008±0.002	0.007±0.002	2.24±0.53	2.10±0.42
Pre	70.9±14.1	76.7±10.8	19.4±3.1	18.7±2.7	0.018±0.004	0.016±0.003	0.008±0.003	0.007±0.002	2.19±0.48	2.35±0.52
Post	71.0±14.3	74.3±12.0	17.7±2.0	16.8±2.1	0.017±0.003	0.015±0.003	0.008±0.002	0.007±0.003	2.10±0.48	2.00±0.39

Effect of crutch fit on scapular motion and trapezius muscle activation

Gregor Kuntze¹, Yarmaghan Afzal², Janet L. Ronsky², Ranita H.K. Manocha³

¹Faculty of Kinesiology, University of Calgary, Calgary, Canada

²Schulich School of Engineering, University of Calgary, Calgary, Canada

³Division of Physical Medicine & Rehabilitation, University of Calgary, Calgary, Canada.

Email: gkuntze@ucalgary.ca

Summary

This study examined differences in upper and middle trapezius activation and scapular kinematics in response to changes in axillary crutch fit. Longer than standard fit crutches led to greater scapula upward rotation and greater activation intensity of the upper and middle trapezius. Shorter than standard fit crutches led to greater scapular downward rotation but no differences in EMG intensity.

Introduction

Crutches that are too long or too short may affect motion of the shoulder complex, contributing to injury of muscles, tendons, ligaments and nerves [1]. There is a knowledge gap regarding the effects of axillary crutch length on the kinematics of the shoulder complex and activity of associated muscles. This study examined the effects of longer and shorter than standard fit crutches on scapular kinematics and activation intensities of the upper and middle trapezius.

Methods

Nine men participated in axillary crutch-assisted gait ($1.40 \pm 0.07 \text{ ms}^{-1}$) using crutches that were 5cm longer and shorter than a standard fit (REB18-1045). Scapular kinematics (Motion Analysis, USA, 240 Hz) and upper and middle trapezius electromyography (EMG, Biovision, Germany, 2400 Hz) were recorded. Segment angles were computed in Visual3D (C-Motion, USA) and EMG data were processed in Matlab (MathWorks, USA) using a wavelet approach [2]. Long and short condition EMG intensities were normalized to the total intensity (TI) of the standard condition, where $TI = \text{sum of intensities across wavelets and time}$. EMG TIs of the first activation peak (Figure 1) were computed. Statistical analyses of maximum scapular rotation angles, and upper and middle trapezius TIs were performed in SPSS (IBM, USA) using Wilcoxon Signed Tanks Tests ($\alpha=0.05$).

Results and Discussion

Longer than standard crutches resulted in greater scapular upward rotation ($p=0.008$) and greater TI of upper ($p=0.028$) and middle trapezius ($p=0.008$) (Table 1). Shorter than

standard fit crutches resulted in greater downward rotation of the scapula ($p=0.008$). TIs did not differ between short and standard fit conditions ($p>0.05$).

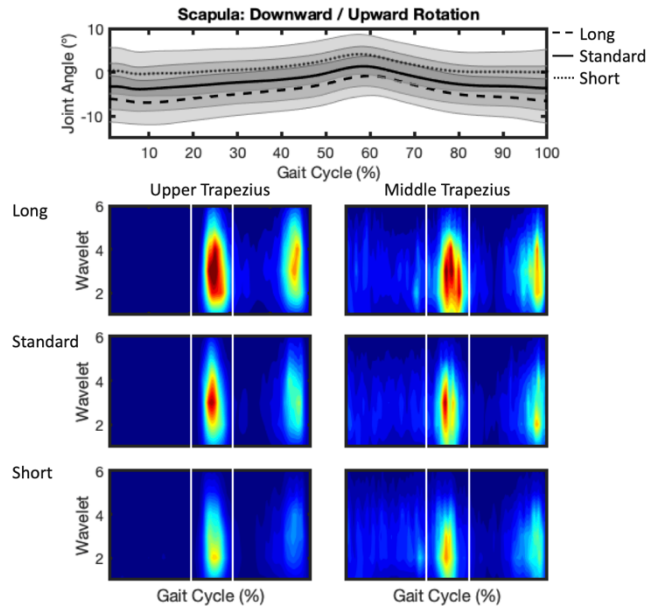


Figure 1: Effects of crutch fit on scapula rotation (°) and trapezius EMG intensities (red=high, blue=low). Vertical white lines indicate the period of interest for total EMG intensity analysis.

Conclusions

Longer crutches increased scapular upward rotation and caused greater trapezius muscle activation intensities. These findings may be relevant to individuals with conditions including rheumatoid arthritis, Ehlers-Danlos syndrome, hemophilia and paraplegia, who may have a limited capacity to compensate for the greater mechanical and neuromuscular demands of crutches that are too long [1].

References

- [1] Manocha et al (2020). *PM&R*, DOI: [10.1002/pmrj.12514](https://doi.org/10.1002/pmrj.12514).
- [2] von Tscharnar (2000). *J Electromyogr Kinesiol.* **10**(6): 433–45.

Table 1: Effects of crutch length on scapula rotation angle and trapezius muscle total intensity.

	Long Mean (SD)	Standard Mean (SD)	Short Mean (SD)	Long-Standard MD (95%CI)	p-value	Short-Standard MD (95%CI)	p-value
Max Downward/Upward Scapula Angle	-0.7 (5.0)	1.4 (4.5)	4.2 (4.1)	-2.2 (-3.1, -1.2)	0.008	2.7 (2.0, 3.5)	0.008
Total Intensity Upper Trapezius	0.67 (0.34)	0.48 (0.21)	0.36 (0.22)	0.20 (0.01, 0.38)	0.028	-0.12 (-0.28, 0.04)	0.110
Total Intensity Middle Trapezius	0.50 (0.25)	0.35 (0.15)	0.29 (0.13)	0.16 (0.07, 0.24)	0.008	-0.06 (-0.16, 0.04)	0.173

Age-Related Changes to Triceps Surae Muscle-Subtendon Interaction Dynamics During Walking

William H. Clark¹ and Jason R. Franz²

¹Department of Ecology and Evolutionary Biology, Brown University, Providence, RI, USA

²Joint Department of Biomedical Engineering, UNC Chapel Hill and NC State University, Chapel Hill, NC, USA

Email: jrfranz@email.unc.edu

Summary

Ankle moment and power generation is largely governed by the interaction between the triceps surae muscles (i.e., gastrocnemius and soleus) and the Achilles subtendons (i.e., distinct bundles of tendon fascicles arising from each muscle). Here, we investigated the interaction between triceps surae muscle and subtendon behaviour as a determinant for reduced ankle push-off in older adults. Our findings suggest that the capacity for sliding between subtendons facilitates independent muscle actuation in young adults but restricts that actuation in older adults. The resultant disruption in contractile behavior may contribute to hallmark reductions in push-off intensity during walking in older adults.

Introduction

The gastrocnemius (GAS) and soleus (SOL) muscles of the triceps surae undergo different fascicle kinematics and contribute differently to powering locomotion [1]. These differences may be facilitated by the Achilles tendon (AT), which is comprised of distinct bundles of tendon fascicles (“subtendons”) that originate from each muscle. Evidence of non-uniform displacement patterns within the AT suggests that sliding between subtendons may facilitate independent muscle actuation. Yet, in older adults, we have observed more uniform AT tissue displacements that correlate with reduced ankle moment generation during walking [2]. Here, we investigated differences in GAS vs. SOL muscle behavior as a determinant of reduced ankle moment generation. First, we hypothesized that, compared to young, older adults would have more uniform AT tissue displacements that would be accompanied by smaller differences between GAS and SOL muscle length-change. Second, we hypothesized that differences between GAS and SOL muscle length-change would correlate with peak ankle moment generation.

Methods

9 young (24±4 yrs, 4F) and 9 older (74±4 yrs, 3F) adults walked on a treadmill for 1 min each at 1.2 m/s with and without: (1) a 5% body weight horizontal aiding force (decrease ankle moment) and (2) a 5% body weight horizontal impeding force (increase ankle moment), as shown in Fig. 1A. A 60 mm ultrasound transducer recorded cine B-mode images through the right medial GAS and SOL at 76 fps. Simultaneously, a 38 mm ultrasound transducer recorded ultrasound radiofrequency data of the right leg free AT at 155 fps enabling synchronized assessment of two equally sized tendon depths – superficial (GAS) and deep (SOL). Post collection, we quantified time series of GAS and SOL fascicle lengths [3] and subtendon displacements [4], averaged across 2 strides per condition. We report stance-phase differences in

longitudinal muscle length change (i.e., GAS-SOL) and AT non-uniformity (i.e., superficial-deep). Mixed factorial ANOVAs tested for the effect of age and condition (1.2 m/s, aiding, and impeding) on peak ankle moment, GAS-SOL longitudinal muscle length change, and AT non-uniformity.

Results and Discussion

In support of our hypotheses, older adults walked with 49% more uniform AT tissue displacements ($P < 0.05$) that were accompanied by 17% smaller differences between GAS and SOL muscle length-change ($P < 0.05$). Only young adult muscle-level behavior correlated with AT non-uniformity and peak ankle moment generation (Fig. 1B-C).

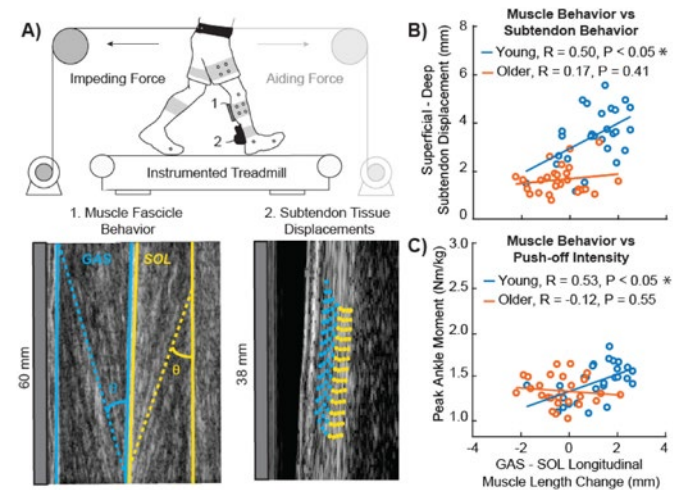


Figure 1: (A) Depiction of experimental protocol. Muscle behavior correlated with subtendon behavior (B) and peak ankle moment (C) in young, but not older adults. *significant ($P \leq 0.05$) correlation.

Conclusions

Our findings suggest that the capacity for sliding between subtendons facilitates independent triceps surae muscle actuation in young adults but restricts that actuation in older adults. The resultant disruption in muscle contractile behavior may contribute to hallmark reductions in push-off intensity (e.g., ankle moment) during walking in older adults.

Acknowledgments

Funded by NIH (R01AG051748, F31AG060675).

References

- [1] Fukashiro S, et al. (2006). *J Appl Biomech*, **22**: 131-47.
- [2] Franz JR, et al. (2015). *J Appl Physiol* (1985), **119**: 242-9.
- [3] Farris DJ, et al. (2016). *Comput Methods Programs Biomed*, **128**: 111-8.
- [4] Chernak Slane L, et al. (2014). *J Biomech*, **47**: 750-4.

Regional variability of shear wave velocity is different between passive and active muscle

Allison B. Wang^{*1,4}, Kristen L. Jakubowski^{*1,2,4}, Eric J. Perreault¹⁻⁴, Sabrina S.M. Lee²

¹Department of Biomedical Engineering, ²Department of Physical Therapy and Human Movement Sciences, ³Physical Medicine and Rehabilitation Northwestern University, Chicago, IL, USA ⁴Shirley Ryan AbilityLab, Chicago, IL, USA; ^{*}Co-first authors
Email: bwang15@u.northwestern.edu

Summary

Quantifying regional stress and material properties in passive and active muscle is useful for understanding force transmission and muscle contraction dynamics. However, directly measuring stress and material properties *in vivo* remains a challenge. Shear wave velocity (SWV) is sensitive to muscle material properties and stress and has been shown to be sensitive to regional heterogeneity in the biceps brachii under passive loading. However, it is unknown if similar regional variations exist in the highly compartmentalized tibialis anterior (TA) and if these variations change under active contractions. We investigated SWV across the proximal, belly, and deep regions of the TA under passive and active loading. We found regional variations in SWV under passive loading but none during active contractions. More studies are needed to determine if similar regional variability exists in other compartmentalized muscles. Studies using SWV should control for regional variability when investigating passive muscles.

Introduction

An individual muscle can have different compartments with distinct fiber architecture, fiber types, and innervation patterns. Strain within individual compartments is different under passive [1] and active loading [2]. These differences may be linked to regional variations in material properties and stress within the muscle. Heterogeneity in stress and material properties can influence muscle contraction dynamics and force transmission. However, current methods cannot make direct measurements of stress and material properties *in vivo*. Shear wave velocity (SWV) is a promising measurement as it is sensitive to differences in material properties and stress [3]. Previously, we have used SWV to detect heterogeneity within the bicep brachii muscle under passive conditions. However, it is unclear if these regional variations also occur in highly compartmentalized muscles, like the tibialis anterior (TA) where there is evidence of regional strain heterogeneity [4]. It is also unclear how the regional variations differ between active and passive loading where the stress inducing mechanism is vastly different. Therefore, we aim to investigate if SWV is different between compartments (proximal, belly, and deep) of the TA during passive and active loading. We hypothesize that, due to strain variability, SWV will vary across the proximal, belly, and deep regions of the TA.

Methods

Eight healthy young adults participated in the study. Shear wave ultrasound data (SuperSonic Imagine) was measured at the proximal, belly, and deep regions of the muscle (Fig. 1a) at several ankle angles (passive condition: maximum dorsiflexion and plantarflexion, and at the midrange of ankle range of motion; active condition: midrange ankle angle). Torque and electromyography (EMG) data were simultaneously collected with the EMG as visual feedback during the active trials. Participants performed isometric contractions of the TA by actively dorsiflexing at different levels of activation (5 – 40% maximum voluntary

contractions in 5% increments). SWV² is reported as it has been shown to be linearly related to changes in shear modulus and stress [3]. Linear mixed-effects models were used for statistical analyses.

Results and Discussion

Under passive conditions, SWV² increased with TA lengthening ($p < 0.001$), but the effect varied across different regions ($p < 0.001$; Fig. 1b). At the longest length, SWV² in the deep region was 5.5 m²/s² greater than in the proximal region ($p < 0.05$). Under active conditions, SWV² increased linearly with muscle activation ($p < 0.001$), but the relationship between SWV² and activation was not different across regions ($p = 0.14$; Fig. 1c). During active conditions, inter-subject variability was much higher than passive conditions. The different patterns of regional variations between passive and active muscle may be related to different regional variations in stress or material properties between passive lengthening and active contractions.

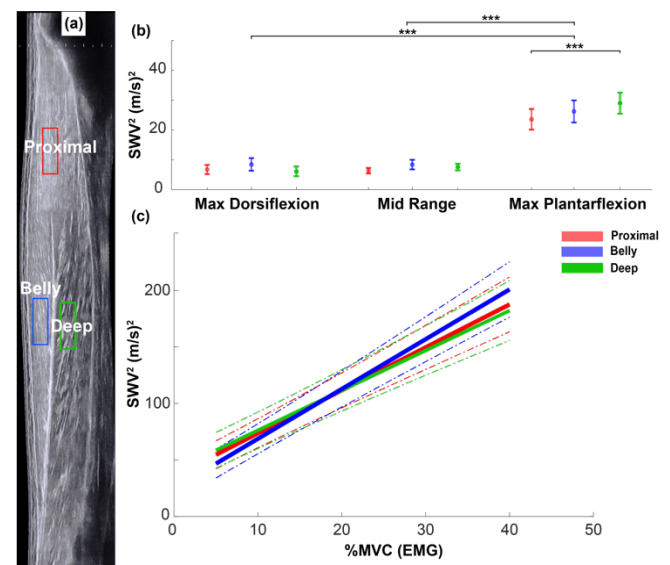


Figure 1: (a) Different regions within the tibialis anterior where SWV measurements were taken. Regional difference of shear wave velocity under passive lengthening (b) and active contraction (c).

Conclusions

We found regional variations of SWV² in the TA under passive loading, but not during active contractions. When using SWV² in the TA under passive loading, the imaging region needs to be considered. More studies are needed to determine if results are similar for other muscles that have a compartmental design.

References

- [1] Bol M et al. (2015). *J Mec Beh Biomed Mater*, 51:25-39.
- [2] Bennett HJ et al. (2014). *J Biomech*, 47(12):3050-3055.
- [3] Bernabei M et al. (2020). *J App Phy*, 128(1):8-16.
- [4] Jensen et al. (2016). *J Biomech*, 49(14):3430-3436.

Is there passive force-mediated enhancement of active force in skeletal muscles?

E.K. Moo^{1,2}, R. K. Korhonen², and W. Herzog¹

¹University of Calgary, Calgary, Canada, ²University of Eastern Finland, Kuopio, Finland,
Email: ekmo@ucalgary.ca

Summary

Aside from the regular Calcium (Ca^{2+})-dependent mechanism, active force production in skeletal muscle is also mediated by passive force, especially at high load. We wanted to quantify the amount of additional force that can be attributed to this force-mediated mechanism, by activating the muscle-tendon unit (MTU) of the mouse tibialis anterior that was held at a constant length but was activated at different levels of force. We found a result opposite to that expected; i.e., the active force generated at high passive force was lower than that produced at low passive force. Further research is needed to understand the influence of passive force on active force production.

Introduction

Skeletal muscle contraction has been thought to mainly involve Ca^{2+} -dependent series of events in which Ca^{2+} binds to troponin C to expose myosin-binding sites on actin, which in turn allows for the formation and cycling of cross bridges. Recent studies show that active force production is enhanced by passive force, especially at high loads [1-3]. This force-mediated mechanism acts through ‘awakening’ super-relaxed cross bridges by force, thus increasing the total number of cross-bridges for increased production of active force. However, the amount of additional force contributed by the ‘force-awakened’ cross bridges remains unclear. Therefore, the goal of this study was to quantify the active force produced by intact MTU that was stretched to the same length but activated at different levels of force. We posited that MTU activated at higher force generates higher active force in a manner consistent with the literature [1-3].

Methods

Intact MTU of tibialis anterior muscles of 8-10 week-old male C57/BL6 mice ($N = 7$) were stretched to long length (4 mm longer than resting length, 36 – 40% strain) corresponding to the descending limb of the active force-length curve using a custom-built miniature dynamometer. At the target length, the MTU was activated isometrically for 1.13s either instantaneously or following 10s of stress relaxation. The MTU was allowed to recover at the resting length for 3 min between trials. In separate trials, the MTU was stretched to the target length and held isometrically without activation to measure the stress relaxation of the passive force. Muscle force was recorded by a force transducer. For trials where activation was triggered instantaneously at the target length, the active force was derived either by subtracting the peak passive force from the total measured force (case 1, Fig. 1B, blue dotted curve) or by subtracting the stress-relaxation curve spanning the activation duration from the total force curve (case 2, Fig. 1B, blue solid curve). The active force resulting from activation following 10s relaxation was determined by subtracting the passive force prior to activation from the total measured force (case 3, Fig. 1B, green solid curve). The active force was divided into six time segments (Fig. 1B, vertical dotted lines), and force impulses for case 2 and case 3 were compared for each time segment.

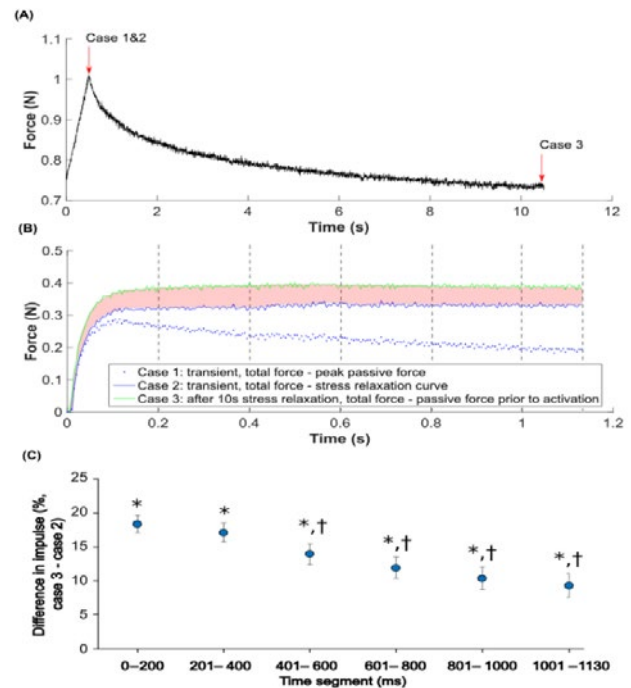


Figure 1: (A) Stress relaxation when the MTU was held passively at the target length for 10s, (B) active force produced when the MTU was activated either instantaneously (left arrow in (A), blue curve, case 1&2), or following 10s of stress relaxation (right arrow in (A), green curve, case 3). (C) Difference in impulse between active forces derived for case 2 and case 3 (red shaded area in (B)), for time segments indicated in (B). * denotes significant difference from zero, and † indicates significant difference compared to 0-200ms and 201-400ms time segments, as well as among each other. Error bars: ± 1 standard error of the mean.

Results and Discussion

The ratio of active to passive force was 0.16 ± 0.10 at the target MTU length. Following 10s stress relaxation, the passive force dropped by approximately 30% (Fig. 1A). The force impulses generated by the MTU activated following stress relaxation (case 3) were 9 – 18% higher than those when the MTU was activated at peak passive force (Fig. 1C, case 2) at all time points. This difference in force impulse decreased with activation time (Fig. 1C), which coincided with the decay of passive force with time (Fig. 1A).

Conclusions

We found that, at the same MTU length, the active force produced at high passive force was lower than that produced at low passive force, leading to the rejection of our hypothesis. Further research is needed for understanding the force-mediated production of active force.

References

- [1] Hooijman et al. (2011). *Biophys J* **100**, 1969–1976.
- [2] Naber et al. (2011). *J Mol Biol* **411**, 943–950.
- [3] Linari et al. (2015). *Nature* **528**, 276–279.

3D Soleus Model Predicts Regional Muscle Displacements that are Consistent with Dynamic MRI Measures

Katherine R. Knaus¹, Remziye Erdogan¹, Geoffrey G. Handsfield², Silvia S. Blemker¹

¹Department of Biomedical Engineering, University of Virginia, Charlottesville, VA, USA

² Auckland Bioengineering Institute, Auckland, NZ; Email: ker4e@virginia.edu

Summary

The soleus muscle's aponeurosis morphology is complex, and its effects on mechanical output are poorly understood. We developed a finite element model (FEM) of 3D soleus architecture that allows for examination of the effects of aponeurosis morphology and we validated the model by comparison with dynamic MRI. The model predicts regional variations in muscle displacements that are consistent with measurements from cine DENSE (Displacement Encoding with Stimulated Echoes) magnetic resonance imaging (MRI).

Introduction

The soleus muscle plays an important role in walking by generating plantarflexion (PF) power. Knowledge of soleus function is currently limited by understanding of the role of this muscle's complex structure. The soleus has an internal anterior aponeurosis (AA) attached to the tibia and fibula that splits the muscle into compartments [1]. Fascicles in the posterior compartment (PC) insert onto the posterior aponeurosis (PA) which is continuous with the Achilles at the muscle-tendon-junction (MTJ), while fascicles in the anterior compartment (AC) insert onto the median septum (MS) that protrudes from the PA and interdigitates with the AA [1]. While the aponeurosis morphology is well described, the effects of this morphology on the behavior of fascicles within the compartments is not well understood. Our goals were to (i) create an FEM representing these 3D structures to examine morphologic effects and (ii) verify model-predicted tissue displacement by comparing to *in vivo* soleus displacements.

Methods

A 3D model of the soleus muscle was created with AC, PC, AA, PA, and MS structures using MRI segmentation of the lower limb of one subject (22 years, 191 cm, 88.4 kg). Model geometry was meshed into tetrahedral elements and fiber directions were assigned to each element. Muscle fascicles originated on the AA surface and inserted onto the PA surface. Muscle and aponeurosis were transversely isotropic materials. To simulate active lengthening, the soleus was activated to 75% while the PA at the MTJ was displaced 20 mm distally and the attachments of the AA to bones were fixed (Fig 1A).

Static images were collected for eight subjects (24±3 years, 175±13 cm, 66±12 kg) in an axial plane (resolution 0.49 x 0.49 mm²) at approximately one third of the soleus muscle's length as they lay prone and plantarflexed. Cine DENSE images were acquired in the same plane as subjects repeated ankle motion using a non-ferrous exercise device so that rotation of inertial disks resulted in active lengthening of PF muscles [2]. Time-varying out-of-plane tissue displacement was determined in DENSE images (Fig 1C). Average muscle displacement near each aponeurosis was found in regions of interest (ROI) defined in static images and normalized by the

range in the peak frame (Fig 1B). Displacements in FEM axial plane (Fig 1D) were compared to DENSE results (Fig 1E).

Results and Discussion

The FEM predicted that the greatest average axial plane distal displacement was located near the PA and MS while the least displacement was located near the AA (Fig 1D,E). All 8 subjects showed behavior similar to the model; tissue in the PA ROI had the greatest normalized displacement, followed by the MS and AA (Fig 1C,E), so differential displacement was positive in both compartments. Nonuniform displacement indicates motion of both the PA and MS relative to the AA which will affect the fascicle kinematics in the PC and AC.

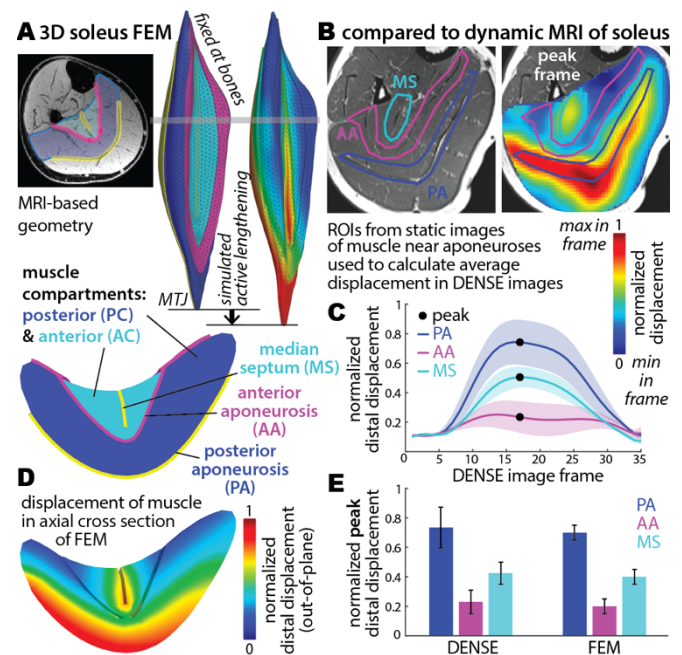


Fig 1: A) MRI-based soleus FEM predictions and B) DENSE MRI measurements from 8 subjects of E) differential tissue displacement during active lengthening in muscle regions near the aponeuroses.

Conclusions

FE simulations predict soleus muscle tissue displacements that depend on aponeurosis structure. Dynamic MRI reveals similar patterns of *in vivo* tissue displacement that correspond with static images of aponeurosis morphology. The FEM enables us to investigate effects of aponeurosis morphology and material properties on regional muscle displacement.

Acknowledgments

Thanks to Niccolo Fiorentino, Emily Kehne, & Darryl Thelen for MRI acquisition contributions and grant #R01AG051748.

References

- [1] Hodgson J et al. (2006). *J Morphology*, **267**: 584-601.
- [2] Fiorentino N et al. (2012). *J Biomechanics*, **45**: 647-652.

Does increasing passive force at the start of activation increase the total isometric force of muscles?

Siwoo Jeong¹, Kiisa C. Nishikawa¹

¹Department of Biological Sciences, Northern Arizona University, Flagstaff, AZ, USA

Email: Kiisa.Nishikawa@nau.edu

Summary

The total isometric force of a muscle has been regarded as the sum of the passive and active force. However, recent studies have suggested that the passive titin-based force might change upon activation if N2A titin binds to actin. If the titin-based force changes upon muscle activation, then the passive component of total force might not be constant. To test this hypothesis, a passive stretch and hold was performed to increase passive force, then maximal isometric contraction was established at three different times during the holding after stretch. We found that increasing passive force at the start of activation had no effect on total isometric force compared to normal passive tension at the same length but with no passive stretch. This finding suggests that titin-based passive force of muscles must change as a result of activation.

Introduction

Total isometric force is assumed to represent the sum of the titin-based passive force and the active cross-bridge force [1], since titin is in parallel with cross-bridges and titin is the main source of passive tension of striated muscles [2]. However, previous research suggests that titin structure changes upon muscle activation due to Ca²⁺-dependent titin-actin binding [3], which might affect the titin-based passive force as well. We hypothesized that total isometric force should increase with increasing passive force at the start of activation unless titin-based passive forces change when a muscle is activated. To test this hypothesis, we activated muscles isometrically at varying times after passive stretch when the passive tension was decreasing due to stress relaxation. Our working hypothesis is that if isometric contraction starts before the increased titin force due to passive stretch has dissipated, then total isometric force should be greater than the purely isometric force unless titin structure changes.

Methods

Six whole soleus muscles were isolated from wild-type mice. Muscles were passively stretched from 1.1L₀ to 1.15L₀ at 1L₀/s and held isometrically for 50, 300 or 1000ms before activation at 1.15L₀. For comparison, total isometric force was also measured at 1.15L₀ with no previous stretching. Instantaneous stiffness was measured in all trials

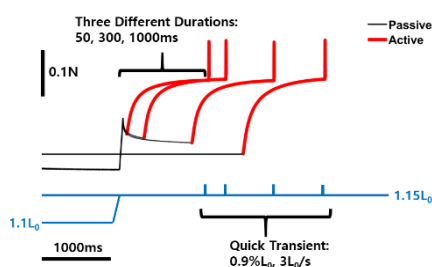


Figure 1: Muscle force (upper), length (lower) and measurement of instantaneous stiffness.

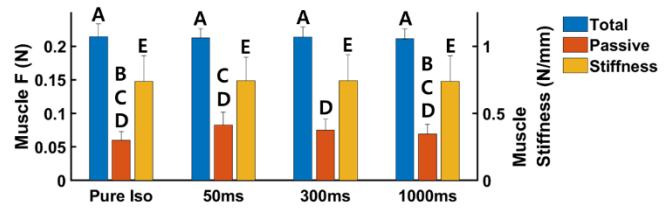


Figure 2: Mean (+1SD) total isometric force, passive force at the start of activation and instantaneous stiffness at maximal isometric force. Bars not connected by the same letter are significantly different (Bonferroni, $p < 0.05$).

using a quick strain transient (0.9%L₀, 3L₀/s, Fig. 1). One-way repeated measures ANOVA was used to compare total isometric force, passive force and instantaneous stiffness between different hold durations and the pure isometric contraction. Bonferroni corrections were used for post-hoc comparisons to identify differences between conditions.

Results and Discussion

Passive forces at 50 and 300ms were significantly greater than passive force with no stretching ($p = 0.014$, 50ms; $p = 0.032$, 300ms). Passive force at shorter hold duration was significantly greater than passive force at longer duration ($p = 0.011$, 50ms vs. 300ms; $p = 0.006$, 50ms vs. 1000ms; $p = 0.017$, 300ms vs. 1000ms), suggesting that passive force decreased as hold duration increased. Total isometric force and instantaneous stiffness did not differ significantly ($p > 0.05$) regardless of passive force at the start of activation (Fig. 2).

Given the in parallel connection between cross-bridges and titin and same isometric cross-bridge force at same muscle length, total isometric force should increase with the titin-based passive force unless the titin-based force changes during muscle activation.

Conclusions

Our results show that isometric force and stiffness were independent of the titin-based passive force at the start of activation. This finding suggests that the process of muscle activation involves more than simply adding cross-bridge force to passive force. Instead, it appears that titin force, cross-bridge force, or both are altered by muscle activation.

Acknowledgments

This research was funded by a grant from the National Science Foundation (IOS-2016049).

References

- [1] Hill AV (1950). *Nature*, **166**: 415-419
- [2] Linke WA et al. (1998). *Proc Natl Acad Sci*, **95**: 8052-8057
- [3] Dutta et al (2018). *Sci Rep*, **8**: 14575.

Comparison of Data Reduction Techniques and their Effect on Neural Network Performance

Fabian Hoitz^{1,2}, Vinzenz von Tscharnner¹, Jennifer Baltich³, Benno Nigg^{1,2}

¹Biomedical Engineering, Schulich School of Engineering, University of Calgary, Calgary, Alberta, Canada

²Human Performance Laboratory, Faculty of Kinesiology, University of Calgary, Calgary, Alberta, Canada

³Brooks Sports Inc., Seattle, Washington, United States

Email: Fabian.hoitz@ucalgary.ca

Summary

This work compared five techniques for data reduction and their effect on the performance of a neural network that was trained for gait recognition. Layer-wise relevance propagation was found to be the best technique for data reduction and ease of functional interpretation.

Introduction

Current trends in biomechanics include studies with large datasets [1]. While multivariate analyses (e.g., neural networks) benefit from such volumes and create astonishing results [2], functional interpretations of these extensive datasets remain challenging. It is often of interest to discern important aspects that contribute relevant information from less important aspects that are irrelevant and mostly contribute noise [3]. Data reduction techniques, such as principal component analysis (PCA), may help to isolate relevant aspects of a given dataset that would facilitate a functional interpretation without affecting the great performances of multivariate analyses.

The purpose of this work was, therefore, to compare multiple data reduction techniques in their effect on the performance of a neural network that was trained for gait recognition (i.e., identify individuals based on their gait pattern).

Methods

A neural network was trained to recognize fifty participants (12 males [mean ± std]: 33.5 ± 8.9 years, 95.6 ± 27.2 kg, 179 ± 6.4 cm; 38 females [mean ± std]: 35.2 ± 9.4 years, 69.8 ± 13.2 kg, 164.7 ± 6.3 cm) based on their gait patterns. A gait pattern consisted of 3D joint angle trajectories (Hip, Knee, and Ankle) and Ground Reaction Forces of a single step that were collected during overground running trials (3.5 m/s ± 15 %) along a 30 m indoor runway on two days that were eight weeks apart. All 1200 variables of a single gait pattern were ranked by either their relevance (derived via layer-wise relevance propagation [4]), their loading on the first principal axis (derived via PCA), their order (ascending vs. descending), or simply at random. The networks performance was then evaluated iteratively with an increasing number of variables (1-1200) according to the five ranking conditions.

Results and Discussion

Figure 1 shows the networks accuracy as a function of the number of variables used for the gait recognition task according to the five ranking conditions. To achieve acceptable accuracies (≥ 80 %), a minimum of 200 variables (selected via LRP or RND) was necessary.

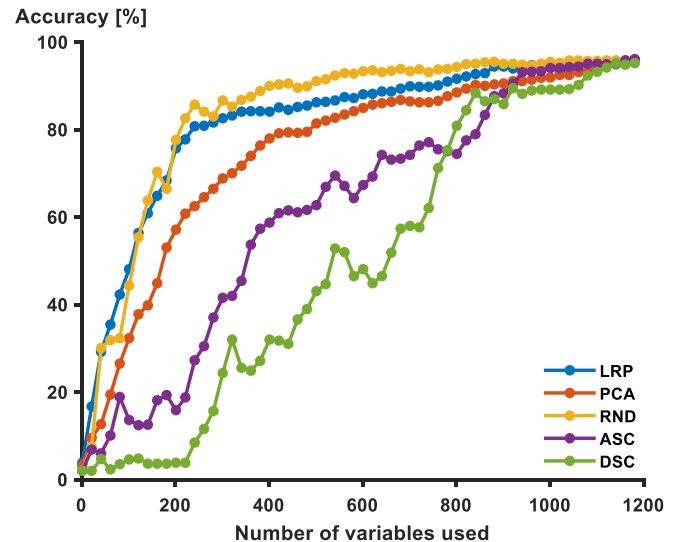


Figure 1: Neural network performance as a function of the number of variables used for gait recognition in five ranking conditions: layer-wise relevance propagation (LRP), principal component analysis (PCA), random (RND), ascending (ASC), and descending (DSC).

While a random selection of variables resulted in similar performances as variables selected via layer-wise relevance propagation, their functional interpretation remains unclear. For variables selected via layer-wise relevance propagation, one can conclude that they represent those variables that are most important for a recognition of individuals by gait.

Conclusions

Layer-wise relevance propagation may reduce large datasets to only those variables that are most vital for gait recognition.

Acknowledgments

We would like to thank Alberta Innovates and Alberta Advanced Education for their support of Mr. Hoitz's doctoral research by means of the Alberta Innovates Graduate Student Scholarship for Data-enabled Innovation.

References

- [1] Phinyomark A et al. (2018). *J Med Biol Eng.* **38(2)**:244-60.
- [2] Chau T. (2001). *Gait Posture.* **13(2)**:102-120.
- [3] Halilaj E et al. (2018). *J Biomech.* **81**:1-11.
- [4] Hoitz F et al. (2021), *PLoS One*. In review.

Prediction of Parkinsonian Gait in Older Adults with Dementia using Joint Trajectories and Gait Features from 2D Video

Andrea Sabo^{1,2}, Sina Mehdizadeh¹, Andrea Iaboni¹, Babak Taati^{1,2,3}

¹ KITE, Toronto Rehabilitation Institute, University Health Network, Toronto, Canada

² Institute of Biomedical Engineering, University of Toronto, Toronto, Canada

³ Department of Computer Science, University of Toronto, Toronto, Canada

Email: Babak.Taati@uhn.ca

Summary

Advances in machine learning have facilitated extraction of 2D joint trajectories from videos of natural gait collected outside of the clinic. This work evaluates regression models for predicting parkinsonism severity in gait on the UPDRS-gait scale in previously unseen participants. Traditional linear, random forest, and ordinal logistic regression models, as well as recently introduced spatial temporal graph convolutional networks are investigated for this task. Results on a dataset of natural gait in older adults with dementia suggest regression models that use both 2D joint trajectories and engineered gait features as input outperform models that use just joint trajectories or just gait features.

Introduction

Up to 60% of older adults with dementia develop parkinsonism when treated with antipsychotic medication. Consumer-grade cameras can unobtrusively monitor medication induced fluctuations of parkinsonism severity in gait in non-clinical settings. Recent advances in pose-tracking algorithms have facilitated extraction of trajectories of key joints in color video, presenting an opportunity to leverage deep learning models trained on 2D joint trajectories to predict clinical scores of parkinsonism severity in gait.

Methods

Joint trajectories from 2160 natural walking bouts of 38 older adults with dementia were extracted from standard video using Alphapose. A trained annotator labelled 324 bouts from 14 participants (age: 76.2 ± 8.7 years) with scores of parkinsonism on the gait criterion of the Unified Parkinson's Disease Rating Scale (UPDRS-gait). Eight gait features (cadence, number of steps, average step width, average margin of stability, the coefficient of variation of step width and time, the symmetry index of step times) were calculated from the joint trajectories [1, 2].

Linear, random forest, as well as immediate and absolute threshold variants of ordinal logistic regression were investigated for prediction of UPDRS-gait scores using these eight gait features as input. Leave-one-subject-out cross-validation (LOSOCV) was used to train models on walks from all but one participant and evaluate on the held-out participant. Model hyperparameters were tuned using 10-fold cross validation using validation sets selected from the training set.

Spatial temporal graph convolutional networks (ST-GCNs) are machine learning models that can leverage the innate spatial structure of skeleton trajectories [3]. ST-GCN models were trained to regress to UPDRS-gait scores using only joint trajectories, or both joint trajectories and gait features as input in a separate analysis. Hyperparameter tuning on three model

backbones, three temporal kernel sizes, and six dropout rates per model was performed using a LOSOCV scheme with five-fold cross-validation for each participant.

For all experiments, the macro-averaged F1-score per class on the validation set was used to select the model configuration used for evaluation on the held-out test participant.

Results and Discussion

Table 1 presents the test set accuracy, mean absolute error, and F1-score for the top performing models using gait features, joint trajectories, or both as input. The immediate threshold ordinal logistic regression model was the top performing model on only gait features, while 10 layer ST-GCN backbones introduced in [3] achieved the highest validation macro-averaged F1-scores using joint trajectory data, with and without gait features.

Table 1: Test Accuracy, MAE, and F1-score for Top Models

Input Data	Accuracy	Mean Absolute Error (MAE)	Macro F1-score
Gait Features	0.406	0.766	0.333
Joint Trajectories	0.352 ± 0.013	0.712 ± 0.036	0.321 ± 0.013
Joint Trajectories + Gait Features	0.411 ± 0.027	0.688 ± 0.008	0.372 ± 0.019

Conclusions

On a challenging dataset of natural walking bouts of older adults with dementia, regression models that combine both joint trajectories and gait features achieve better regression to parkinsonism severity in gait than models that only use gait features or joint trajectories as input.

Acknowledgments

This work was supported by the Walter and Maria Schroeder Institute for Brain Innovation and Recovery; KITE, Toronto Rehabilitation Institute; National Sciences and Engineering Research Council (NSERC, Canada) discovery grant (RGPIN 435653); Alzheimer's Association (USA) & Brain Canada (New Investigator Research Grant NIRG-15-364158); FedDev Ontario; the Vector Scholarship in Artificial Intelligence; and the Ontario Graduate Scholarship.

References

- [1] Ng KD et al. (2020). *IEEE J. Transl. Eng. Heal. Med.* **8**: 1.
- [2] Sabo A et al. (2020). *J Neuroeng Rehabil.* **17**: 97.
- [3] Yan S et al. (2018). *AAAI Conf. Artificial Intelligence.* **32**: 1.1.

Predicting ground reaction force waveforms from accelerometers during uphill and downhill running: A recurrent neural network solution

Ryan S. Alcantara¹, W. Brent Edwards², Guillaume Y. Millet³, & Alena M. Grabowski¹

¹Department of Integrative Physiology, University of Colorado Boulder, Boulder, CO, USA

²Faculty of Kinesiology, University of Calgary, Calgary, AB, Canada

³Laboratoire Interuniversitaire de Biologie de la Motricité, Univ Lyon, UJM-Saint-Etienne, Saint-Etienne, France

Email: ryan.alcantara@colorado.edu

Summary

Ground reaction forces (GRFs) are important for understanding the biomechanics of human movement. However, the measurement of GRFs is generally limited to laboratory environments. We present a recurrent neural network (RNN) capable of predicting normal (i.e., perpendicular to surface) GRF waveforms in near real-time across a range of speeds (2.5, 3.33, and 4.17 m/s) and slopes (0° , $\pm 5^\circ$, $\pm 10^\circ$) using accelerometers mounted to the sacrum and foot. The average \pm SD root mean squared error (RMSE) and relative RMSE (rRMSE) between experimentally-measured GRFs and RNN predictions across 19 subjects was 0.16 ± 0.04 BW and $6.4 \pm 1.5\%$, which is less than prior studies that predicted time-normalized vertical GRFs during level-ground running (RMSE = 0.20 BW; rRMSE = 13.9%). Our novel approach provides a technique to accurately estimate a runner's normal GRFs in a variety of outdoor environments, provide biomechanical feedback during a run, and longitudinally monitor biomechanical variables.

Introduction

Inertial measurement units (IMUs) have been used to measure kinetic and kinematic variables outside the laboratory setting [1,2], but IMUs cannot directly measure GRFs during running. Prior work has used neural networks to predict the entire GRF waveform during the stance phase of running from IMU data [3,4]. These networks required preliminary identification of the stance phase and normalization to the duration of a step or contact time, resulting in a loss of temporal information [3,4]. Additionally, prior work predicted GRF waveforms during level-ground running, but not uphill or downhill running. A method for predicting the normal GRF waveforms using IMUs across a range of running slopes, while maintaining the temporal component, could allow researchers and clinicians to predict kinetic and kinematic variables in outdoor environments. We sought to develop an RNN to predict normal GRF waveforms across a range of slopes and speeds using data from accelerometers.

Methods

19 subjects ran for 30-s on a force-measuring treadmill at five slopes (0° , $\pm 5^\circ$, $\pm 10^\circ$) and three speeds (2.5, 3.33, and 4.17 m/s) per slope. One biaxial accelerometer was adhered to the sacrum and two uniaxial accelerometers to the right shoe during all trials. Accelerometers on the shoe were used to classify foot strike patterns as rearfoot, midfoot, or forefoot [5], and sacral acceleration data were divided into overlapping 12-ms windows, allowing the RNN to iteratively predict the measured normal GRF waveform frame-by-frame. The average, SD, and range of values for each 12-ms window of

accelerometer data were included as RNN input features, along with the subject's body mass, height, slope, running speed, and percentage of a trial's steps classified as a rearfoot, midfoot, or forefoot strike. We assessed the accuracy and generalizability of the RNN using leave-one-subject-out cross validation, which provided an ensemble of RMSE and relative RMSE (rRMSE) values when comparing the normal GRF waveform predicted by the RNN to that measured by the force-measuring treadmill.

Results and Discussion

Predictions of each subject's normal GRF waveform had a average \pm SD RMSE of 0.16 ± 0.04 BW and rRMSE of $6.4 \pm 1.5\%$ across all conditions (Figure 1). The RNN predictions had a lower RMSE during slow uphill running (2.5 m/s, $+10^\circ$; RMSE = 0.13 ± 0.07 BW) compared to fast downhill running (4.17 m/s, -10° ; RMSE = 0.20 ± 0.05 BW). RNN prediction error was less than the error of neural networks used in prior studies (RMSE = 0.21 BW; rRMSE = 13.9%), which were limited to time-normalized vertical GRF waveforms only during level-ground running [3,4].

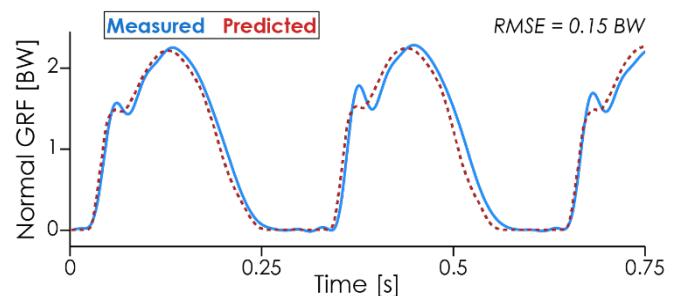


Figure 1: Representative subject's experimentally-measured normal GRF waveform (solid blue line) and RNN prediction (dashed red line) at 3.33 m/s and 0° slope.

Conclusions

We developed an RNN that uses accelerometer data to predict the continuous normal GRF waveform across a range of running slopes and speeds with greater accuracy than prior studies. Additionally, the RNN does not require preliminary identification of the stance phase, maintains the temporal component, can be applied to up- and downhill running, and allows for near real-time predictions of the normal GRF waveform due to the recurrent nature of the neural network.

References

- [1] Clermont et al. (2019). *J Appl Biomech*, **35**: 401-9.
- [2] Kiernan et al. (2018). *J. Biomech*, **73**: 201-209.
- [3] Dorschky et al. (2020). *Frontiers Bioeng Biotech*, **8**: 604.
- [4] Johnson et al (2020). *IEEE*, **68**: 289-297.
- [5] Giandolini et al. (2104) *J. Biomech*, **47**: 1588-1593.

Classifying Individuals With and Without Ankle Sprain History Using Machine Learning Techniques

Monica K. Russell^{1,2}, Oluwatoyosi BA Owoeye^{3,5}, Carolyn A. Emery^{2,3,4}, William B. Edwards^{1,2}

¹Biomedical Engineering Graduate Program, University of Calgary, Alberta, Canada

²Human Performance Laboratory, Faculty of Kinesiology, University of Calgary, Alberta, Canada

³Sport Injury Prevention Research Centre, Faculty of Kinesiology, University of Calgary, Alberta, Canada

⁴Pediatrics and Community Health Sciences, Cumming School of Medicine, University of Calgary, Alberta, Canada

⁵Department of Physical Therapy and Athletic Training, Doisy College of Health Sciences, Saint Louis University, St. Louis, MO, USA

Email: monica.russell@ucalgary.ca

Summary

Force platform data were collected for sixteen youth/young adults (ages: 15-30; 14 females, 2 males; 8 matched pairs) during a single leg balance (SLB) task. Eight participants had a history of significant ankle sprain (resulting in at least 3 days of time loss and requiring medical attention) 3-15 years prior, and eight participants had no history of lower extremity injury. Discrete measurements from the force plate data were fed into three machine learning (ML) algorithms [logistic regression, support vector machine (SVM), and a random forest] to classify participants into injured versus uninjured groups. All three ML classifiers yielded prediction accuracies greater than 0.5 (Logistic regression = 0.763 ± 0.134 , SVM = 0.731 ± 0.138 , Random forest = 0.644 ± 0.133). Future directions for this work will include a larger sample size and use of neural networks to examine weights used to classify participants.

Introduction

Ankle sprain injuries are the most common injury in youth sport [1]. Literature suggests ankle sprain injuries can lead to ligament proprioceptor damage, resulting in impaired balance [2]. Although ML in biomechanics is increasingly popular, few studies have used ML to classify individuals based on kinetic parameters [3].

The objective of this project was to compare the prediction accuracies of three ML algorithms to classify individuals with and without ankle sprain history based on force platform measurements during an SLB task.

Methods

Sixteen youth/young adults (ages: 15-30; 14 females, 2 males; 8 matched pairs) attended one testing session during which force platform data were collected during an SLB task. Eight participants had history of significant ankle sprain 3-15 years prior and eight participants had no history of lower extremity injury. For the SLB task, the participant balancing, eyes open, on each leg for 70 seconds for three trials per leg. The force platform data were used to calculate average centre of pressure (CoP) coordinates, 95% ellipse, and CoP path length. The injured leg of the previously injured group was compared to the nondominant leg of the control group.

Three machine learning algorithms were developed in Python using SciKit Learn software: logistic regression, SVM, and a random forest. CoP parameters were fed into the ML classifiers. Repeated stratified k-fold validation was used to validate the classifiers.

Results and Discussion

Logistic regression had the 'Cs' value set to the default value of 10. This resulted in a classification accuracy of 0.763 ± 0.134 . SVM was performed using a third-degree polynomial, gamma set to 0.01, and C set to 0.1 resulted in a classification accuracy of 0.731 ± 0.138 . The random forest algorithm had 100 decision trees, which used Gini impurity measures and had a maximum number of 2 branches. This resulted in a classification accuracy of 0.644 ± 0.133 .

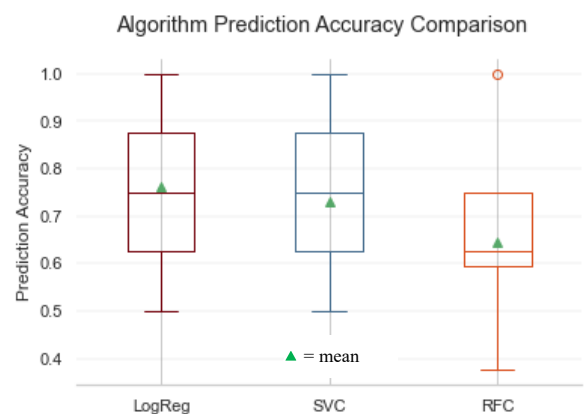


Figure 1: Median prediction accuracies and interquartile ranges of three machine learning techniques, calculated over 20 folds.

Conclusions

ML classifiers show potential for separating individuals with and without ankle sprain history based on kinetic differences in a single leg balance task. Logistic regression and SVM performed better than random forest. Further work is necessary in examining neural networks to determine what variables have the greatest impact on classification.

Acknowledgments

We would like to acknowledge sponsor support from Vi Riddell Paediatric Rehabilitation Research Program Chair in Paediatric Rehabilitation. This study was funded by the Canadian MSK Research Network (CIHR FRN: CFI-148081).

References

- [1] Valderrabano et al. (2006). *Am J Sports Med*, **34**(4), 612-620.
- [2] Akbari M. et al. (2006). *JRRD*, **34**(7), 819-824.
- [3] Halilaj E et al. (2018). *J.Biomech*, **81**, 1-11.

Two-Dimensional Video-Based Analysis of Human Gait using Pose Estimation

Jan Stenum^{1,2}, Cristina Rossi^{1,3}, Ryan T. Roemmich^{1,2}

¹Center for Movement Studies, Kennedy Krieger Institute, Baltimore, MD, USA

²Department of Physical Medicine and Rehabilitation, The Johns Hopkins University School of Medicine, Baltimore, MD, USA

³Department of Biomedical Engineering, Johns Hopkins University, Baltimore, MD, USA

Email: jstenum1@jhmi.edu

Summary

Recent advances in markerless pose estimation algorithms enable automated analysis of human movement from digital video recordings. Human gait analysis is commonly undertaken by reporting to a laboratory equipped with a 3D motion capture system. Here, we compare spatiotemporal gait parameters and kinematics acquired by motion capture and via pose estimation of healthy human gait. We found group mean errors between motion capture and pose estimation of 0.01 s for temporal gait parameters (step time, stance time, swing time and double support time), 0.018 m for step lengths and 0.03 m s⁻¹ for gait speed; mean errors were 4.0°, 5.6° and 7.4° for sagittal plane hip, knee and ankle angles. The accuracy with which gait parameters were estimated in the current study suggest that pose estimation is a promising technique to analyze human gait.

Introduction

Markerless pose estimation algorithms offer new possibilities for analysis of human movement outside of the laboratory. OpenPose [1] is one such algorithm that has received attention for its use in gait analysis [2]. It is of interest to clinicians and researchers to test how accurately a range of gait parameters can be estimated by applying OpenPose to digital videos of human gait. Here, we compared spatiotemporal gait parameters and kinematics obtained with sagittal plane videos of healthy human gait against simultaneously collected 3D motion capture data.

Methods

We used a freely available dataset of over-ground walking sequences of 31 healthy adults [3]. Gait sequences were simultaneously recorded with a 3D motion capture system (100 Hz) and digital videos (25 Hz). Digital videos were obtained from left and right sagittal plane views of the walkway. We used OpenPose to track 25 body keypoints (including left and right ‘hip’, ‘knee’, ‘ankle’, ‘small toe’ and ‘big toe’) in the videos. Spatiotemporal gait parameters (step time, stance time, swing time, double support time, step length and gait speed) and sagittal plane kinematics (hip, knee and ankle angles) were independently calculated from each measurement system (3D motion capture and OpenPose views). We developed a MATLAB workflow that used the x-y image coordinates of the body keypoints from the OpenPose output to calculate gait parameters (available at <https://github.com/janstenum/GaitAnalysis-PoseEstimation>). All parameters were calculated as individual participant mean values across the walking bout. We evaluated OpenPose by

calculating errors (absolute differences) between measurement systems.

Results and Discussion

Group mean errors (and maximal error) between motion capture and OpenPose were: 0.01 s (0.04 s) for temporal gait parameters (step time, stance time, swing time and double support time), 0.018 m (0.050 m) for step length and 0.03 m s⁻¹ (0.09 m s⁻¹) for gait speed. Mean errors of sagittal plane kinematics across the gait cycle were: 4.0° for hip, 5.6° for knee and 7.4° for ankle angles.

Errors between motion capture and OpenPose in the current study were less than previously reported values of minimal detectable change for spatiotemporal gait parameters and sagittal plane hip and knee angles in inter-session, test-retest studies of healthy human gait [4]. This suggests that spatiotemporal gait parameters and hip and knee angles can be estimated by OpenPose with the accuracy needed to detect changes in the gait pattern in healthy humans. We found that errors between left and right OpenPose views were less than errors between OpenPose and motion capture for all gait parameters suggesting that occlusion does not affect the calculation of gait parameters with OpenPose.

We found that errors for individual steps were occasionally high for step length (range of -0.202 to 0.204 m) and that the errors were systematically affected by the participants’ position relative to the camera; however, step length errors tended to cancel out when step lengths were averaged across the bout. Videos used in this study were obtained from stationary cameras placed ~3 m from the walkway at a height of ~1.3 m with a sagittal plane view; it is unknown how the results generalize to other data collection setups. Furthermore, the current study analyzed healthy human gait; it is possible that pose estimation may differ for pathological gait.

Conclusions

We have shown that a range of spatiotemporal gait parameters and kinematics can be estimated by OpenPose with the accuracy required to detect changes in healthy human gait [5].

References

- [1] Cao Z et al. (2021). *IEEE T Pattern Anal*, **43**: 172-86.
- [2] Kidziński et al. (2020). *Nat Commun*, **11**: 4054.
- [3] Kwolek B et al. (2019). *Multimed Tools Appl*, **78**: 32437-65.
- [4] Wilken JM et al. (2012). *Gait Posture*, **35**: 301-7.
- [5] Stenum J et al. (2020). *bioRxiv*, <https://doi.org/10.1101/2020.07.24.218776>.

Simulating the Effects of Body Weight Loading on the Arch of the Foot Using a Dynamic Model of the Foot and Ankle

Rostam S. Kojouri¹, Sorin Siegler¹, Alberto Leardini², Claudio Belvedere², Maria Ruiz¹

¹Department of Mechanical Engineering, Drexel University, Philadelphia, PA

²Movement Analysis Laboratory, IRCCS Istituto Ortopedico Rizzoli, Via di Barbiano 1/10, 40136 Bologna, Italy

Email: rsk86@drexel.edu

Summary

A subject specific, image-based 3D dynamic model of the foot and ankle was developed in this study based on an earlier validated model of the hindfoot. This model, able to simulate a variety of loading conditions, was used in this study to investigate the effect of body weight on arch kinematics and the plantar pressure distribution. The model was validated for this activity by comparing arch height and plantar pressure distribution against experimental data obtained from the subject from which the model was created. Excellent agreement between model and experimental results were obtained.

Introduction

Three-dimensional (3D), subject-specific, image-based models of the foot and ankle complex can be used as both tools to better understand the biomechanics of the structure, as well as predictive planning tools for medical diagnosis. This project involves the development of a subject specific dynamic model of the foot and ankle capable of accurately reproducing its passive mechanical behavior of the foot and ankle under diverse loading conditions. The current dynamic model expands on an existing model of the hindfoot [1] by including the midfoot and forefoot and a mobile fibula with all the corresponding ligamentous constraints. The current study focuses on the validation of this new model (Fig.1) by examining changes in the foot structure during axial loading to full body weight simulating quiet standing on one foot.

Methods

Imaging data of the geometry and orientation of the bones of the foot and ankle were obtained from Weight Bearing Computer Tomography (WBCT by CurveBeam™) scans of an individual, taken first while the subject was in the sitting position with no load applied to the scanned leg followed by a second scan with the subject in the standing position on one leg where the scanned leg was axially loaded to full body weight. A plantar pressure device (Pedar™ by NOVEL, Inc) measured the foot-to-ground pressure distribution (Fig. 2).

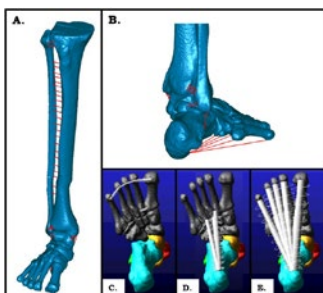


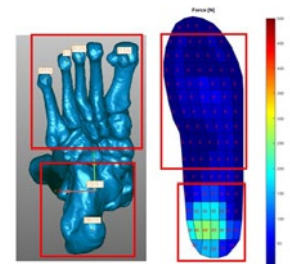
Figure 1: The dynamic model of the foot including elements representing: (A) the tibio-fibular ligaments, (B) the ligaments of the ankle joint complex, (C) the intermetatarsal ligaments, (D) the long-plantar ligament, (E) the plantar fascia.

The new features compared to the earlier hindfoot model [1] include the inclusion of a mobile, ligament constrained fibula, mid-foot and fore-foot bones and ligaments, and additional ligaments such as the plantar aponeurosis and long plantar ligament. The accessory sesamoids of the first metatarsal and navicular were modeled as bodies rigidly fixed to their associated bones to account for the increased areas of potential contact. The ligaments and fascia of the midfoot and forefoot spanning non-adjacent bones (e.g., the long plantar ligament) were implemented using tension-only spring elements. No a-priori kinematic constraints were applied in the model and its complex response to applied loads was exclusively the result of the ligament constraints and the bone-to-bone contact. Contact between the foot and the ground, modelled as a rigid flat surface, including static and dynamic friction allowing the foot the ability to slide on the floor. Simulations were performed starting with the foot flat on the ground in neutral position and then applying a vertical axial load to the tibia loading it slowly from zero to full body weight.

Results and Discussion

For the validation of the model, change in arch height and pressure distribution under the foot was compared between the experimental weight bearing CT data and the dynamic model. Arch height, defined as the perpendicular distance between the center of mass of the navicular and the floor, was 6.48 mm, experimentally and 5.31 mm for the model. The cumulative pressure under the midfoot and forefoot was 27.97 kPa experimentally and 39.27 kPa from the model, and the pressure under the hindfoot was 114.02 kPa experimentally and 104.07 kPa from the model.

Figure 2: Comparison of the plantar pressure distribution under body weight between the model and the experimental data obtain through the Pedar™ Novel, Inc. system.



Conclusions

A dynamic model of the foot and ankle was used to simulate the response of the foot to axial loads simulating standing. The height of the arch and the plantar pressure obtained through the model compared well to experimental data thus providing partial validation.

References

[1] Imhauser et al. (2008) *J Biomech.* **41(6)**: 1341-1349.

Measuring and modelling *in vivo* human gracilis passive force-length property

Lomas S. Persad¹, Benjamin I. Binder-Markey³, Alexander Y. Shin¹, Richard L. Lieber², and Kenton R. Kaufman¹

¹Department of Orthopedic Surgery, Mayo Clinic, Rochester, MN

²Shirley Ryan AbilityLab and Hines VA Medical Center, Chicago, IL

³Drexel University, Philadelphia, PA

Email: Kaufman.Kenton@mayo.edu

Summary

Understanding passive mechanical properties of healthy muscle is required to create models that mimic human muscle properties. In this study, the passive force-length relationship of the gracilis muscle was explicitly defined based on experimentally measured passive force and sarcomere length. Our results show that the gracilis is very compliant and current muscle models overestimate the passive force of this muscle.

Introduction

Human muscle is remarkable in its ability to produce both active and resistive forces that are necessary for mobility and stability of the human skeleton. One key aspect of muscle is its passive mechanical properties. Studies have shown that the passive mechanical properties of muscle changes due to disease, trauma and ageing. Therefore, it is important to understand the passive mechanics of healthy muscle. Passive properties of skeletal muscle vary from fibers to bundles in mouse, rabbit and human muscles. Thus, deducing passive mechanical properties of muscle from biopsy samples may be ill-advised [1]. No studies have reported on passive properties directly measured from whole human muscle.

Current predictions of whole muscle passive tension rely on models that are based on animal data obtained from a variety of species. There has been no direct experimental validation of current passive force-length models used in current musculoskeletal models that simulate human movement. Therefore, the aim of this study is to measure *in vivo* passive tension-length data for whole human muscle using a novel method. These experimental data were then compared to the standard passive force-length models from models [2, 3, 4].

Methods

Passive tension and sarcomere lengths were obtained from nine patients undergoing gracilis muscle transfer surgery. During surgery the leg was positioned in four joint configurations (JC) designed to gradually lengthen the gracilis muscle. *In vivo* passive tension at each JC was measured using a buckle force transducer (BFT) placed on the distal gracilis external tendon. Muscle tissue samples were clamped and excised at three of the four JC that corresponded to a knee flexion angle of 130°, 90° and 0°. The samples were formalin fixed within the clamp to determine the sarcomere length at each JC via laser diffraction. A natural exponential curve [5] was fitted to experimentally measured force-sarcomere length data to model the passive-elastic behavior of the gracilis muscle. Reported human sarcomere lengths are within a range of 70% to 130% of its optimal length [6]. For this reason,

experimental data and model predictions were compared at a normalized length of 1.3.

Results and Discussion

The experimental data clearly demonstrate that the gracilis muscle is more compliant when compared to the current models (Figure 1). Although models based on frog fibers performed better, all models overestimated passive force.

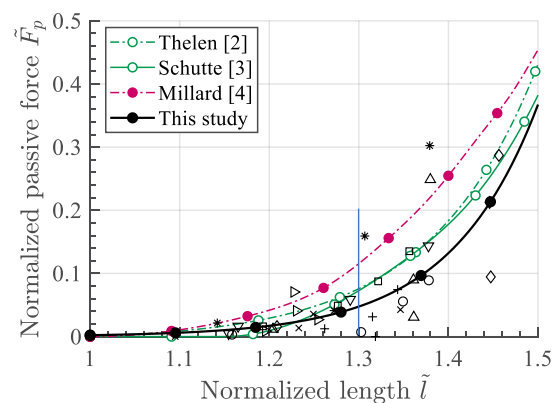


Figure 1: Comparison between measured gracilis passive force-length relationship and passive force-length models. Thelen [2] and Schutte [3] models were derived from passive properties of frog fibers while Millard [4] was derived from rabbit whole muscle data. The exponential curve was fitted ($r^2=0.95$) to experimental force-sarcomere length data for individuals shown by each symbol ($n=9$).

The Thelen, Schutte and Millard models overestimated normalized passive force by 60%, 53% and 143% respectively.

Conclusions

Current force-length models overestimate the passive tension of this human muscle. The gracilis appears to be very compliant compared to other human muscle however further research is needed to investigate this.

Acknowledgments

Supported by VA funding 1 I01 RX002462.

References

- [1] Ward SR et al. (2020). *Front. Physiol.*, **11**: 1-9.
- [2] Thelen DG (2003). *J. Biomech. Eng.*, **125**:70-77.
- [3] Schutte LM et al. (1993). *IEEE Trans. Rehabil. Eng.*, **1**:109-125.
- [4] Millard M et al. (2013). *J. Biomech. Eng.*, **135**: 1-11.
- [5] Magid A and Law DJ (1958). *Science.*, **230**: 1280-1282.
- [6] Burkholder TJ and Lieber RL (2001). *J. Exp. Biol.*, **204**: 1529-1536.

The Effects of Extracellular Matrix and Sarcomere Length Changes in Cerebral Palsy on Muscle Stiffness

Ryan N. Konno¹, Nilima Nigam¹, James M. Wakeling^{1,2}, Stephanie A. Ross²

¹Department of Mathematics, Simon Fraser University, Burnaby, Canada

²Department of Biomedical Physiology and Kinesiology, Simon Fraser University, Burnaby, Canada

Email: rkonno@sfu.ca

Summary

Cerebral palsy (CP) is an upper motor neuron lesion that results in alterations in skeletal muscle structure, which have a substantial impact on muscle mechanics. In this study we investigated the whole muscle response to changes in the microstructure as a result of CP using a three-dimensional computational model. We found that when the muscle was stretched, there is a larger effect from the extracellular matrix than sarcomere length on passive stiffness. These results provide us with a deeper understanding of the influence of each change in the individual microstructural components that may occur due to CP.

Introduction

Skeletal muscle is a complex material that has many organizational levels. It is composed of muscle fibres embedded in a background material which includes a matrix of collagen fibres, capillaries, and other cells.

The effects of structural changes resulting from CP, including the extracellular matrix (ECM) stiffness and volume fraction and sarcomere length, have been investigated through experimental studies; however, they have been found to vary between subjects and muscle groups [1]. Using a modelling approach we examined the individual contribution of different microstructural changes to muscle that may occur due to CP to passive whole muscle behaviour.

Methods

To investigate the effects of CP, we used a three-dimensional continuum model for skeletal muscle developed in [2,3]. The mathematical model consists of a fibre-reinforced nonlinearly elastic material. One-dimensional fibres are embedded within a base material, which describes contributions from the ECM and cellular components. We varied the volume fraction and stiffness of the ECM in the muscle, as well as the length of the sarcomeres. Changes in the sarcomere length led to changes in the passive force-length properties of the fibres.

To determine the effects of these different parameters on whole muscle stiffness, we conducted passive lengthening simulations. The optimal length for the sarcomeres was increased relative to healthy muscle tissue by up to 75% (c_{sarco}). The ECM volume fraction was varied between 2% and 60% of the muscle volume, and the ECM stiffness was increased and decreased by 33% of the stiffness for healthy muscle.

Results and Discussion

Our results showed that the nonlinear behaviour of the ECM resulted in larger contributions of the ECM to muscle stiffness at longer lengths. The sarcomere length, however, had less effect on the muscle stiffness at longer lengths (Figure 1),

which agrees with experimental findings that fibres contribute less than ECM to muscle stiffness [1]. Additionally, increases in the sarcomere passive stiffness strictly in the along-fibre direction decreased the stretch that occurred transverse to the muscle fibres. This demonstrates that the three-dimensional behaviour of muscle can be influenced by changes occurring in the muscle fibres only. Using this model we have been able to investigate the individual effects from microstructural components that can vary due to CP and develop a deeper understanding of how changes to these components may affect the muscle stiffness in patients with CP.

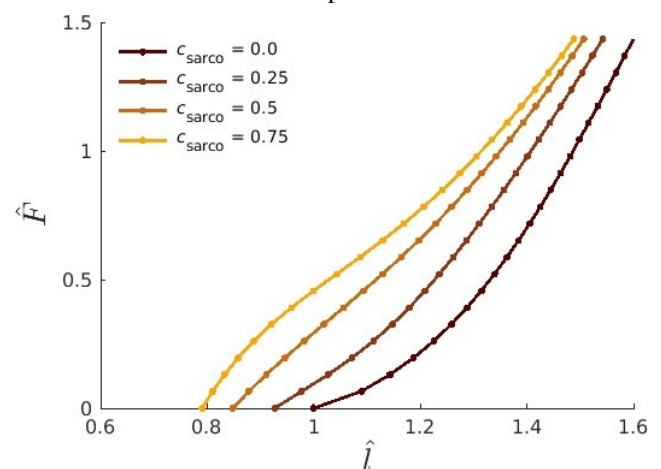


Figure 1: Plot of force normalized by maximum isometric force (\hat{F}) against length normalized by optimal length (\hat{l}), which demonstrates the effect of the shift (c_{sarco}) in the sarcomere force-length relationship on whole muscle mechanics.

Conclusions

Using our modelling approach, we were able to isolate the role of individual microstructural components in whole muscle mechanics in a way that is not possible experimentally. We found that changes in ECM properties have a greater impact on whole muscle stiffness than increases in sarcomere length. These results provide insight into the microstructural mechanisms that underlie increased whole muscle stiffness in CP.

Acknowledgments

We would like to acknowledge funding from NSERC Discovery Grants to NN and JMW.

References

- [1] Lieber RL et al. (2019). *J. Appl. Physiol.*, **126**:1492-1501.
- [2] Wakeling JM et al. (2020). *Front. Physiol.*, **11**: 813.
- [3] Konno et al. (2020). *PLoS ONE.*, (In Review).

Sharing the load: Strategies for modelling loads in OpenSim simulations of two-handed lifting

Mohammadhossein Akhavanfar¹, Thomas K. Uchida², Allison L. Clouthier¹, Ryan B. Graham¹

¹School of Human Kinetics, Faculty of Health Sciences, University of Ottawa, Ottawa, Ontario, Canada

²Department of Mechanical Engineering, Faculty of Engineering, University of Ottawa, Ottawa, Ontario, Canada

Email: ryan.graham@uottawa.ca

Summary

Appropriately modelling the interaction between the hands and external loads in OpenSim simulations of lifting is a difficult yet important problem. In this work, we introduce and compare five approaches of varying complexity. Approaches 1 and 2 have been employed in previously published research; Approaches 3–5 were developed as part of the current work. These modelling approaches were tested using a two-handed lifting scenario. We demonstrate that the modelling approach may result in considerably different spinal forces and, thus, must be chosen carefully in computational studies of lifting.

Introduction

Musculoskeletal models are commonly used to estimate spinal loads using Static Optimization (SO) [1]. The external load contact forces and moments (LCF&M) acting on the hands have a substantial effect on the results of SO during lifting tasks. LCF&M are often oversimplified in computational studies of lifting and the effect of various LCF&M modelling approaches on spinal loads has not been investigated. This study explores five approaches to model LCF&M in OpenSim [2] and evaluates the effect of these modelling approaches on the predicted spinal loads for one participant during two-handed lifting tasks.

Methods

Experiment: One male participant (20 yr, 185 cm, 73.9 kg) performed various symmetric stoop and squat lifting/lowering tasks with different speeds of movement and different loads in the hands. Marker data were collected for the participant and the load (Box) at 120 Hz using 10 Vicon Vantage V5 cameras. Motion cycles were cropped to begin and end when the load lifted off and returned to the floor, respectively.

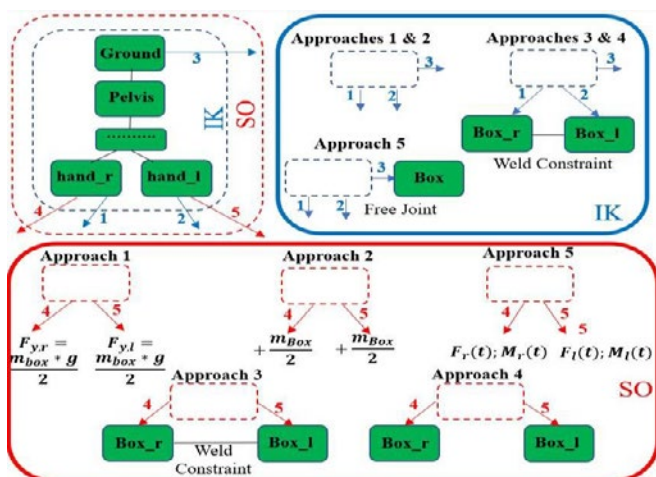


Figure 1. Topology of the model. Blue and red borders indicate the methods used for inverse kinematics (IK) and static optimization (SO) calculations, respectively. Green denotes OpenSim bodies.

LCF&M Modelling Approaches: Although the validated spine model from Bruno et al. [3] was used in this study, the presented LCF&M modelling approaches (Figure 1) are generalizable to other OpenSim lifting models. Approaches 1 and 2 do not consider the box kinematics. In Approach 1, a gravity-oriented half-load was applied to each hand; in Approach 2, the mass of each hand was increased by half of the box mass. In Approaches 3 and 4, a closed kinematic chain was formed for the IK analysis, but for Approach 4, an open-tree structure was used in SO to reduce the computational cost. In Approach 5, the kinematics of the body and box were calculated separately, and LCF&M were calculated as a function of time using an optimization procedure.

Results and Discussion

During stoop lifting with 20 kg, the maximum difference in the maximum L5/S1 resultant force was found between Approaches 1 and 5 (582 N). When lowering the load, the difference between Approaches 1 and 2 was greater than other approaches (539 N). Modelling Approaches 3–5 suggest that, during lifting, the maximum loads on the spine do not necessarily occur at maximum upper body flexion, which corroborates *in vivo* measurements [4]. However, Approach 1 cannot capture this phenomenon because it does not consider any acceleration of the load. Nevertheless, Approach 1 has been used in many lifting studies due to the ease of application, or because the simulated tasks were static.

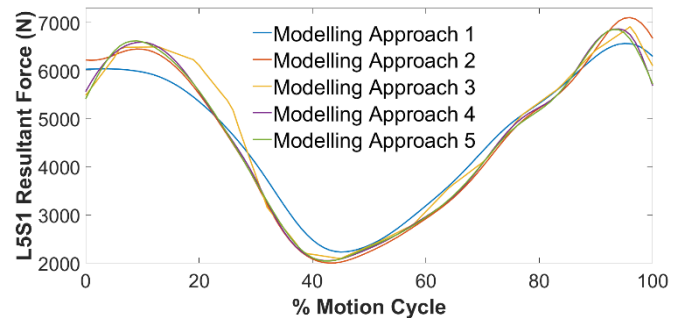


Figure 2. L5/S1 resultant forces during 20 kg stoop lifting.

Conclusions

LCF&M modelling approaches alone can substantially affect the estimated spinal loads during lifting tasks in OpenSim models. The comprehensive evaluation of our modelling approaches during stoop and squat, three speeds of movement, and two lifting loads will be presented at the conference.

References

- [1] Akhavanfar et al. (2019). *J. Biomech.*, **91**: 61–68.
- [2] Seth et al. (2018). *PLoS Comput. Biol.*, **14**: e1006223.
- [3] Bruno et al. (2015). *J. Biomech. Eng.*, **137**: 081003.
- [4] Damm et al. (2020). *J. Biomech.*, **102**: 109517.

Personalized gait modifications improve pain and slow cartilage degeneration in individuals with medial knee osteoarthritis: a one-year randomized controlled trial

Scott D. Uhlrich^{1,2}, Valentina Mazzoli^{1,2}, Amy Silder^{1,2}, Andrea Finlay², Feliks Kogan¹, Garry E. Gold¹, Scott L. Delp¹, Gary S. Beaupre^{1,2}, Julie A. Kolesar^{1,2}

¹Stanford University, Stanford, California, USA

²VA Palo Alto Healthcare System, Palo Alto, California, USA

Email: suhlrich@stanford.edu

Summary

Personalized foot progression angle (FPA) modifications effectively reduce the peak knee adduction moment (KAM), but the long-term efficacy of this intervention for medial knee osteoarthritis (OA) is not known. We conducted a randomized controlled trial comparing personalized FPA modifications to sham gait retraining. After one year, the FPA modification group had a reduced peak KAM, improved medial knee pain, and less cartilage degeneration compared to the sham group, demonstrating that FPA modifications are a promising treatment for medial knee OA.

Introduction

FPA modifications can reduce the peak KAM, which is related to medial knee OA progression [1]. Personalizing these modifications is important to maximally reduce the KAM [2] and may improve clinical outcomes compared to uniformly-prescribed modifications [3,4]; however, the long-term efficacy of this intervention is unknown. We hypothesized that, compared to sham gait retraining, adopting a personalized FPA modification would improve pain and function, reduce the peak KAM, and slow quantitative MRI metrics of OA progression over one year.

Methods

Sixty-eight individuals with medial knee OA enrolled in this clinical trial (NCT02767570), and 49 completed it. During an initial gait analysis (year 0), participants walked naturally, then were given vibrotactile feedback instructing them to toe-in and toe-out by 5° and 10° relative to their natural FPA. Participants were randomized into an *altered FPA* group that was trained to walk with the FPA modification that maximally reduced their peak KAM, and a *consistent FPA* (sham) group that was trained to walk more consistently with their natural FPA. During six once-per-week gait retraining visits, participants received biofeedback to learn their target FPA. They were also instructed to walk with this FPA outside of the lab. Refresher gait retraining visits occurred at four, six, nine, and 12 months (year 1) post-enrollment.

MRI scans (3T) were acquired at the year 0 and year 1 visits to measure $T_{1\rho}$ (TSL=1, 10, 30, 60 ms, FSL=500 Hz) and T_2 (3D qDESS, TE1/TE2=7.54/42.38 ms) relaxation times. The femoral cartilage was segmented and registered between visits, and the average voxelwise changes in $T_{1\rho}$ and T_2 in the medial weightbearing region were computed. Changes in numeric rating scale (NRS) medial knee pain, WOMAC pain and function, KAM, $T_{1\rho}$, and T_2 were compared between year 0 and 1 with a per-protocol analysis using t-tests ($\alpha=0.05$).

Results and Discussion

The *altered FPA* group's $5.1\pm 20.1\%$ reduction in peak KAM at year 1 was greater than ($p=0.003$) the $4.8\pm 11.4\%$ increase in the *consistent FPA* group. The *altered FPA* group also reduced their NRS medial pain by more than the *consistent FPA* group ($p=0.001$, Figure 1a); however, there were no significant between-group differences in WOMAC pain ($p=0.113$) or function ($p=0.274$). The reduction in $T_{1\rho}$ in the *altered* compared to the *consistent FPA* group ($p=0.013$, Figure 1b) suggests that offloading the medial compartment slowed or reversed the proteoglycan depletion characteristic of OA progression. There was not a significant between-group difference in T_2 ($p=0.944$).

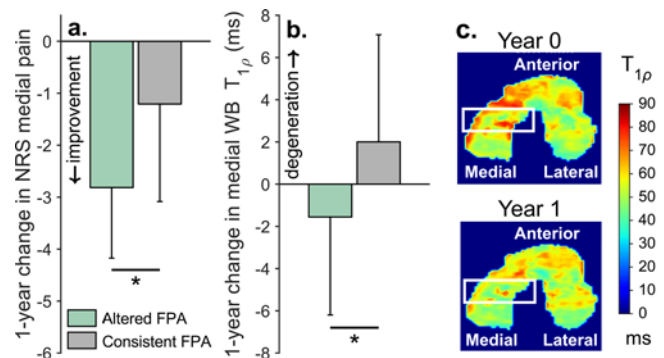


Figure 1: The *altered FPA* group had greater improvements in NRS pain (a) and reductions in $T_{1\rho}$ in the medial weightbearing (WB) region of the femoral cartilage (b) compared to the *consistent FPA* group ($*p<0.05$). $T_{1\rho}$ decreased over time in the medial WB region (outlined) of an *altered FPA* subject's femoral cartilage (c).

Conclusions

For individuals with medial knee OA, personalized FPA modifications reduced joint loading, improved NRS pain, and slowed cartilage degeneration compared to sham gait retraining, but did not significantly improve function. FPA modifications may become an effective tool in the multimodal treatment of medial knee OA.

Acknowledgments

This work was supported by award I01 RX001811 from the US Department of Veterans Affairs Rehab. R&D Service.

References

- [1] Miyazaki T, et al. (2002). *Ann. Rheum. Dis.*, **61**: 617-22.
- [2] Uhlrich S, et al. (2018). *J. Biomech.*, **66**: 103-10.
- [3] Hunt M, et al. (2018). *Osteoarthr. Cartil.*, **26**: 901-11.
- [4] Cheung R, et al. (2018). *Osteoarthr. Cartil.*, **26**: 1479-86.



Poster Abstracts

Analysis of Biomechanical Characteristics during the Drop-Landing Phase with Bionic Shoes: A Pilot Study

Huiyu Zhou^{1,2}, Ukadike C. Ugbole^{1,2}, Nicholas F. Sculthorpe², Julien S. Baker^{1,3}, Yaodong Gu¹

¹Faculty of Sports Science, Ningbo University, Ningbo, Zhejiang, China

²School of Health and Life Sciences, University of the West of Scotland, South Lanarkshire, Scotland, UK

³Department of Sport, Physical Education and Health, Hong Kong Baptist University, Kowloon Tong, Hong Kong

Email: B00385863@studentmail.uws.ac.uk

Summary

Traditionally, shoes have been used for protecting the foot and providing functional support. Normal footwear that provides stability and support functions for the foot could result in overprotection. Consequences of this may include that overprotection influences and reduces the function of lower limbs.

Introduction

This study is motivated by an original idea of “Barefoot shoes” which has led to the creation of unstable shoes [1]. After years of evolution, the cuticle of the human foot has gradually degraded, suggesting that the protection and advancement in footwear is still of importance. Based on these necessary factors, we have designed bionic shoes (BS) by combining the functions of barefoot and shoe protection. The objective of this study was to investigate possible differences in the lower limb kinetics and kinematics based on single-leg landing (SLL) when using normal shoes (NS) and BS. We hypothesized that BS will result in higher knee joint angles, compared with NS during a SLL phase.

Methods

15 male subjects volunteered for the study (Age 23.4 ± 1.14 years, height 177.6 ± 4.83 cm, body weight (BW) 73.6 ± 7.02 kg). There were two kinds of experimental shoes used in the landing experiments to detect the changes in the lower limbs whilst performing the landing task.

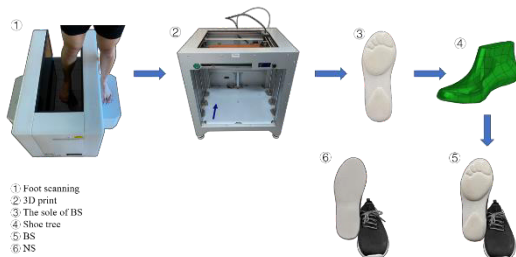


Figure 1: Illustration of shoe making procedure from initial idea to finished product.

Results and Discussion

The statistical parametric mapping (SPM) analysis using paired t-tests in figure 2 shows the significant differences between the NS and BS during the SLL phase.

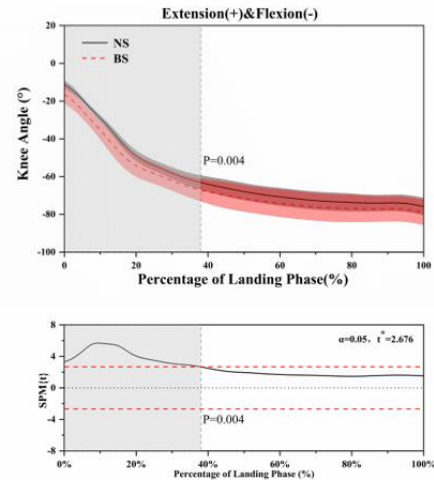


Figure 2: shows the kinematic differences using NS and BS in the knee angle. For the knee angle during extension and flexion, significant differences ($p=0.004$) between NS and BS were found during the SLL phase.

The soft landing could increase knee flexion angles and reduce impact forces. This may provide more landing velocities over a longer time period, which could result in decreased anterior cruciate ligament injuries [2]. We can conclude that BS may reduce lower limb injuries in the knee joint when performing a drop SLL from a 40cm height.

Conclusions

We found that when using BS to perform a SLL phase, the knee flexion angles have bigger flexion angles than those observed using NS.

Acknowledgments

This study was funded by the by Key Project of the National Social Science Foundation of China (19ZDA352), National Natural Science Foundation of China (No. 81772423), NSFC-RSE Joint Project (81911530253), and K. C. Wong Magna Fund in Ningbo University.

References

- [1] Zhou H et al. (2018). Unstable structure to adjust lower limb motion based on oxford foot model in order to control foot arthritis. *Osteoporosis Int.*, **29**:S151-S151 Someauthor PQ. (YEAR) *Some Book Title*; Publisher.
- [2] Li L et al. (2020). Falling as a strategy to decrease knee loading during landings: Implications for ACL injury prevention. *J Biomech.*, **109**: 1099

Can Intraoperative Intra-Articular Loads Predict Knee Joint Laxity? A Cadaveric Simulator Study

Darshan S. Shah¹, Orcun Taylan¹, Matthias Verstraete², Pieter Berger³, Hilde Vandenneucker³, Lennart Scheys^{1,3}

¹Institute for Orthopaedic Research and Training (IORT), KU Leuven, Leuven, Belgium; ²Orthosensor Inc., Dania Beach, USA;

³Division of Orthopaedics, University Hospitals Leuven, Leuven, Belgium

Email: dssiitb@gmail.com

Summary

Soft tissue balancing, vital for joint stability following total knee arthroplasty (TKA), is quantified intraoperatively during passive motions; however, postoperative patient satisfaction is based on active functional outcomes. Although our cadaveric study found no correlation between intraoperative joint loads and postoperative joint kinematics, a stark difference in joint load distributions was observed between passive and active tasks, necessitating further research in quantifying postoperative joint stability.

Introduction

Joint stability is crucial for successful functional outcomes following TKA [1]. While clinical assessment of knee joint laxity typically relies on passive manual tests, like the varus-valgus rotations at multiple flexion angles [2], the goal is to have the desired postoperative joint laxity for active motions, like walking. Soft tissue balancing, vital in TKA to achieve an optimal level of joint laxity, can be quantified intraoperatively by using instrumented tibial inserts [1]. This study aimed at correlating intraoperative joint loads and postoperative joint kinematics during laxity tests and functional tasks.

Methods

Four recipients of the European Knee Society Travelling Fellowship 2019 visiting our institution were assigned a fresh-frozen lower limb each to plan and perform posterior-stabilised TKA. An instrumented tibial insert (Verasense, Orthosensor, USA) was used to measure intraoperative joint loads at fixed flexion angles (0°-30°-60°-90°). Specimens were then subjected to varus-valgus laxity tests and mounted on a validated knee simulator [3] to perform squatting with actively loaded quadriceps. The instrumented insert captured intra-articular loads, while tibiofemoral kinematics were recorded with an optical motion capture system. The Pearson correlation test was used to assess the relationship between intraoperative intra-articular load and tibial abduction angle during laxity tests for each specimen ($p < 0.05$).

Results and Discussion

Laxity tests revealed greater stiffness in extension ($1.7 \pm 1.2^\circ$) than in flexion ($4.4 \pm 2.4^\circ$) for a joint moment of 10 Nm (Figure 1). A mean Pearson correlation factor (r) of -0.63 was observed between intraoperative intra-articular load and tibial abduction angle during laxity tests ($r_{\max} = -0.99$, $p < 0.001$; $r_{\min} = -0.07$, $p = 0.35$), with statistically significant correlation observed only for one of the four specimens.

Peak intra-articular loads for intraoperative measurements were observed in extension, with the medial load higher than the lateral load for three out of the four specimens; however,

peak loads for active squatting were observed in deep flexion, with lateral loads higher for all specimens (Figure 2).

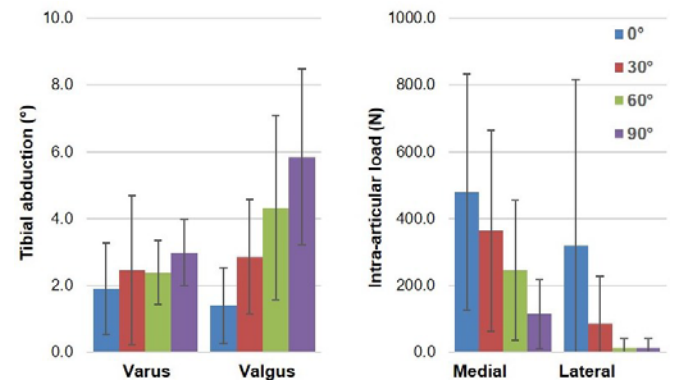


Figure 1: Tibial abduction during laxity tests and intraoperative joint loads at various flexion angles (Mean±SD for four specimens).

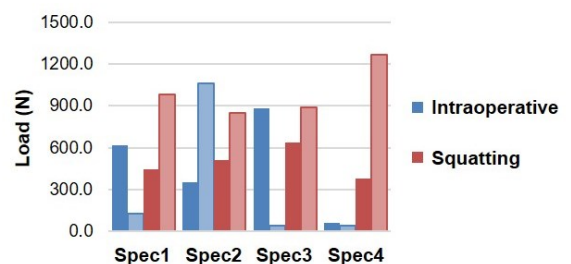


Figure 2: Peak loads in medial (dark) and lateral (light) compartments measured intraoperatively (blue) and during active squatting (red) for each specimen.

Despite an expected increase in varus-valgus laxity and a corresponding decrease in intra-articular loads with increasing knee flexion, no correlation was observed between the two parameters. However, intra-articular load distribution during active squatting was starkly different from the passive condition, which must be considered when assessing postoperative joint stability. A limitation of the study was that the instrumented tibial inserts were commercially calibrated only until 310N.

Conclusions

Intraoperative joint loads and postoperative laxity kinematics were not correlated, despite following expected trends. However, the discrepancy in joint loading during passive and active motions necessitates further research to associate joint stability to intra-articular loads during functional motions.

References

- [1] Roche et al. (2014). *Orthop Clin N Am*, **45**: 157-165.
- [2] Pederson et al. (2019). *J Biomech*, **82**: 62-69.
- [3] Victor et al. (2009). *JBJS Am*, **91(6)**: 150-163.

A proposal for the definition of anatomical reference systems for the bones of the foot and ankle complex

Michele Conconi¹, Alessandro Pompili¹, Nicola Sancisi¹, Alberto Leardini², Stefano Durante², Claudio Belvedere²

¹Department of Industrial Engineering - DIN, University of Bologna, Italy

²Movement Analysis Laboratory, IRCCS Istituto Ortopedico Rizzoli, Bologna, Italy

Email: michele.conconi@unibo.it

Summary

This study proposes a new method for the definition of anatomical reference system (ARS) for the bones of foot and ankle based on morphological and functional criteria, meant for the 3D description of the foot posture. The method shows high inter- and intra-operator precision ($<1^\circ$ and $<1\text{mm}$), providing a 3D characterization of the foot arches, which agrees with standard planar measures. Clinically sound ARS are needed to fully exploit the recent advances in the 3D description of the foot posture made possible by weight-bearing CT.

Introduction

Establishing ARS is fundamental to report and compare measurements in clinically relevant terms [1]. So far, foot posture has been assessed radiographically [2], where only planar measures are possible, while foot motion has been investigated through gait analysis, defining ARS by external palpation of anatomical landmarks and grouping bones in rigid segments [3]. Three-dimensional scanning techniques opened the way for a deeper investigation of the foot architecture: in recent fluoroscopic studies, ARS were proposed for the hindfoot based on bone morphology [4]. A thorough definition of ARS for each bone in the foot and ankle complex is however still missing, yet necessary to fully exploit the potentiality presented by 3D investigations. Principal inertial axes may be used [5], but their clinical interpretation is often difficult. Aiming at the description of both posture and kinematics of the foot and ankle, we propose a CT-based morphological approach for the definition of ARS for every bone in the complex. To show its effectiveness, the approach is used to compare the medial-longitudinal and the transverse arches in healthy and flat feet. Inter- and intra-operator sensitivity is also addressed.

Methods

We analyzed one healthy foot and one flatfoot. These were scanned in a Weight-Bearing CT. The 3D models of all the foot bones were reconstructed by a semi-automatic segmentation process (DICE $> 95\%$). To define ARS, overall bone and joint geometry was analyzed. For the talus: z axis coincides with the axis of a truncated cone, fitted on the surface articulating with the tibia, pointing laterally; origin O is the mid-point of the cone height; x axis is the projection on the plane normal to z of the vector from O to the center of a sphere fitting the talar head, pointing anteriorly; y axis is computed accordingly. For the intermediate cuneiform: origin O is the bone centroid; x axis is the mean of the normals of plains fitting surfaces articulating with scaphoid and first metatarsus, pointing anteriorly; z axis is the mean of the normals of plains

fitting surfaces articulating with medial and lateral cuneiform, pointing laterally; y axis is computed accordingly. For the sake of conciseness, the remaining ARS are only depicted graphically (fig 1). ARS were defined three times by the same operator and once by three different operators to assess the robustness of the procedure. To describe the arches, angles were extracted from the ARS orientation using a variation of the Grood & Suntay notation (cardan sequence: z-y-x). The medial longitudinal arch is defined by the flexion angle of calcaneus, talus, medial cuneiform and first metatarsus. The transverse arch is defined by the abduction angle of medial, intermedial, lateral cuneiform and cuboid.

Results and Discussion

The anatomical reference systems for each bone are shown in fig. 1. The inter- and intra-operator mean precision was $0.67^\circ \pm 0.72^\circ$ and $0.57^\circ \pm 0.82^\circ$ for rotations, and 0.59 ± 1.09 and 0.33 ± 0.77 mm for the translations, respectively. The proposed ARS make it possible to describe and distinguish among healthy and pathological arches (fig. 1). If the Djian-Annonier angle is computed from the proposed ARS, the amplitude of the medial longitudinal arch is 112.7° and 145.7° . Values are in line with the literature [6].

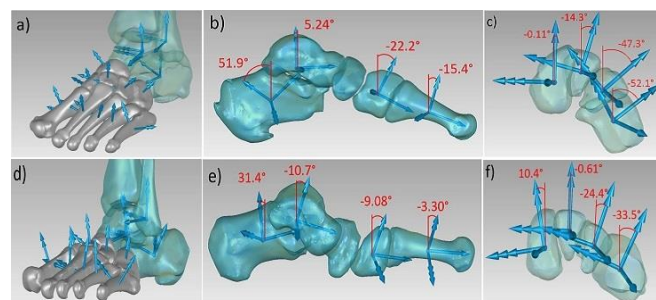


Figure 1: Healthy (a-c) and flat (d-e) foot. a) d) representation of the reference systems for each bone. b) e) bone angles across medial longitudinal arch. c) f) bone angles across transverse arch.

Conclusions

The proposed ARS provide a valuable clinical description and a basis for further 3D characterization of the foot and ankle complex behavior.

References

- [1] Wu et al. (2002). *J. of Biomech.*, **35**: 543-548.
- [2] Carrara et al. (2020). *Foot&Ank Surg.*, **26**: 509-517.
- [3] Della Croce et al. (2005). *Gait&Post.*, **21**: 226-237.
- [4] Parr et al. (2012). *J. of Biomech.*, **45**: 1103-1107.
- [5] Coburn et al. (2007). *J. of Biomech.*, **40**: 203-209.
- [6] Canavese et al. (2018). *Foot&Ank. Surg.*, **24**: 453-45.

Muscle activity and fatigue in the context of musculoskeletal health complaints in high string musicians

Dirk Möller¹, Nikolaus Ballenberger¹, Bronwen Ackermann², Christoff Zalpour¹

¹Department of Movement and Rehabilitation Science, University of Applied Sciences, Osnabrück, Germany

²The University of Sydney, Medical School, Discipline of Biomedical Science, Sydney, Australia

Email: d.moeller@hs-osnabrueck.de

Summary

Playing-related musculoskeletal disorders (PRMD) are very common among musicians with a higher prevalence in the group of high string players (violin and viola). A commonly suggested risk factor for these injuries includes asymmetrical playing as well as muscle fatigue.

Fifteen musicians (7 with and 8 without PRMD) went through a standardized protocol that examined the influence of muscle fatigue on muscle activity patterns between and within these groups by means of surface electromyography.

Changes in muscle activity patterns were observed between and within both groups, however these changes varied significantly depending on group affiliation. In addition, the overall muscles of the right arm and the left forearm muscles showed different fatigue behavior, with the PRMD group showing stronger signs of muscular fatigue.

Based on these results, it may be possible to identify compensatory or inefficient muscle activity patterns. This can support the development of targeted management strategies.

Introduction

Instrumentalists are exposed to numerous risk factors that can cause a PRMD [1]. Different loads during music playing can lead to an overload of the neuromusculoskeletal system. High string musicians (violin/viola) are particularly vulnerable to this due to their asymmetrical playing style. This leads to an unphysiological stress, particularly in the area of the upper extremities. The consequence can be a modification of muscle activity patterns during music performance.

The aim of this study was to investigate whether changes occur in muscle activity patterns and fatigue behavior during high string performance over a prolonged playing period, and whether this is influenced by a PRMD.

Methods

Fifteen professional or university high string musicians were recruited and then divided into a PRMD (n=7) and a non-PRMD (n=8) group. All musicians played a chromatic scale, then an individual “hard” or “heavy” piece of music for one hour, followed by a repeat of the chromatic scale. Surface electromyography (sEMG) data were recorded from 16 muscles of the arm, shoulder and trunk on both sides of the body. Primary outcome was the muscle activity measured by sEMG. Two parameters were collected, (1) the percentage of muscle activity in relation to the respective maximum strength during the time course of the chromatic scales and (2) the low frequency spectrum during the one-hour playing. Differences between and within groups as well as the low

frequency spectrum were analyzed using linear mixed models.

Results and Discussion

Changes in muscle activity patterns were observed between the beginning and the end of the trial, however these changes varied significantly depending on whether the musicians were suffering PRMDs or were without PRMDs (fig. 1). In addition, low frequency spectrum changes were observed in the overall muscles of the right arm (p=.04) and the left forearm flexors (p=.05) following the one hour of playing in musicians with a PRMD, compared to those without a PRMD, consistent with signs of muscle fatigue.

These results are consistent with other studies that describe a modification of muscle activity [2]. A possible explanation for this modification is a redistribution of muscle activity because of pain or movement inhibition to protect the neuromusculoskeletal system [3]. The sEMG analysis strategy used in this study proved to be a suitable tool for a detailed analysis of muscle activity and provides information on differences in muscle activity between musicians with and without PRMD.

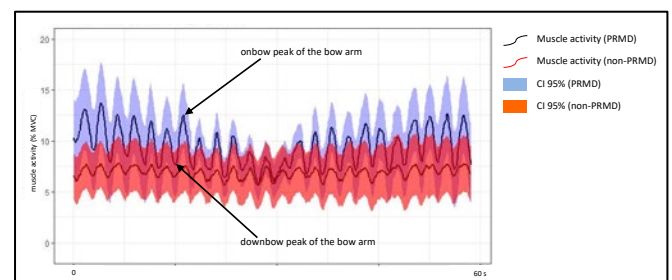


Figure 1: Example of changes in muscle activity pattern. Muscle activity of the right lower trapezius over time during the chromatic scale pretest. Mean muscle activity of each group including the corresponding 95% CI (shaded regions).

Conclusions

Differences of muscle activity appear between high string musicians with and without PRMD. Based on these results, it may be possible to identify compensatory or inefficient muscle activity patterns. This can support the development of targeted management strategies for high string musicians.

References

- [1] Ackermann B et al (2012). *Med Probl Perform Art*, **27**:181–187.
- [2] McCrary JM et al (2016). *Med Probl Perform Art*, **31**:125–131.
- [3] Hodges PW and Tucker K (2011). *Pain*, **152**:S90–S98.

ACL injury prevention in high knee flexion conditions: a new musculoskeletal model

D. Pavan¹, S. Van Rossom², H. Hoang², I. Jonkers², Z. Sawacha^{1,3}

¹University of Padua, Dept. of Information Engineering, Italy;

²KU Leuven, Dept. of Movement Sciences, Belgium; ³University of Padua, Dept. of Medicine, Italy

Email: all.pavandavide@federugby.it

Summary

Epidemiological studies underline high anterior cruciate ligament (ACL) injury and reinjury rates.

Although gait analysis has already identified biomechanical variables strongly related with ACL ruptures, a demanding task is likely to be needed to investigate knee biomechanics in trained athletes.

The present contribution addresses ACL injury prevention through musculoskeletal modelling (MSM), with a dedicated model developed for high knee flexion tasks, having enhanced degrees of freedom (DOFs) at the knee and ligaments.

Introduction

ACL injuries are instantly disabling and in the majority of cases will require surgery and long rehabilitations; moreover, reinjury has a higher occurrence rate than first ACL injury [1].

MSM implements experimental measurements with estimates of important variables, as muscle and joint forces, and could be applied focusing on ACL injury prevention [2]. Among the available musculoskeletal models, one with enhanced knee DOFs and ligaments [3], and one specifically developed for the squatting task [4] have been identified, along with the one developed by Delp [5]. The aim of the present work is to develop a knee model which overcomes the limitations of the currently available ones, in simulating the knee biomechanics during deep flexion tasks for ACL injury prevention purposes.

Methods

Ten healthy athletes were recruited (mean±SD; age=25,6±1,5 years; BMI=21,7±2,4 Kg/m²). Each participant performed three repeated monopodal squats: reflective markers were placed as in [6] and data were acquired by means of 3D stereophotogrammetry (BTS Smart-E, 6 cameras, 60 Hz) and 1 force plate (Bertec FP6040, 960 Hz); an electromyography system (BTS Free1000, 8 channels, 1000 Hz) recorded the activation of: Rectus Femoris, Biceps Femoris Caput Longus, Tibialis Anterior, Gastrocnemius Lateralis. MOTO-NMS [7] and OpenSim [8] were adopted, and scaling, inverse kinematics, inverse dynamics, and static optimization (SO) computed. Experimental EMG envelope peak occurrence within the task were compared with the related SO outcome (Wilcoxon signed-rank, $\alpha=0.05$) for validation purposes as in [6]. A new knee model was developed, with enhanced knee DOFs and ligaments repositioned based on published cadaveric geometries [9]. Data were further processed according to [3-5] and results of each simulation compared with the model proposed herein (rm-ANOVA, Tukey post-hoc, $\alpha=0.05$).

Results and Discussion

Results showed differences (Fig.1) mainly associated to the number of knee DOFs (i.e. [4,5] vs the one proposed and [3]).

Xu model showed task-related issues, while Delp, Catelli and the current model showed good compliance with the squat task, even though the models reported in [4,5] have limited DOFs at the knee and no ligaments.

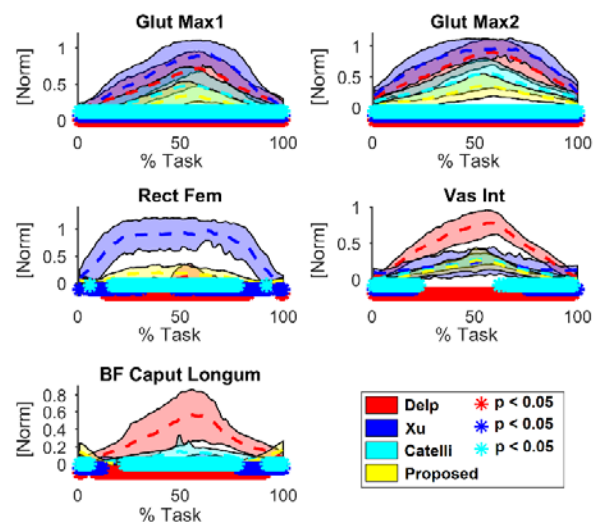


Figure 1: Gluteus maximus 1, Gluteus maximus 2, Rectus femoris, Vastus intermedius, and Biceps femoris caput longum normalized activations. Models: Delp, Xu, Catelli, proposed. Significant differences are flagged referring to the proposed model comparison with the model relative to the flag color in the legend.

Conclusions

The current study allowed comparing the performances of different knee models in critical conditions, providing further insights on the knee biomechanics during the squat task. The former could be adopted for ACL injury risk evaluation, to better inform the clinical decisions making and to aid in planning prevention and post-rehabilitation return on field programs.

References

- [1] Paterno MV et al, *Am J Sport Med*, **42**:1567-73, 2014.
- [2] Reinbolt JA et al, *Procedia IUTAM*, **2**:186-98, 2011.
- [3] Xu H et al, *Comp Method Biomec*, **18**:1217-24, 2015.
- [4] Catelli DS et al, *Comp Method Biomec*, **22**:21-4, 2019.
- [5] Delp SL et al, *IEEE T Biomed Eng*, **37**(8):757-67, 1990.
- [6] Scarton, A et al, *Gait & Posture*, **58**:194-200, 2017.
- [7] Mantoan A et al, *Source Code BiolMed*, **10**:1-14, 2015.
- [8] Delp et al, *IEEE T Biomed Eng*, **54**:1940-50, 2007.
- [9] Belvedere C et al, *J Biomech*, **45**:1886-92, 2012

Design principles, mechanical testing and functional evaluation of a novel custom dynamic Ankle-Foot Orthosis for drop-foot patients

Caravaggi P.¹, Rogati G.¹, Baleani M.², Fanciullo C.¹, Cinquepalmi A.¹, Cevolini F.⁴, Berti L.¹, Lullini G.¹, Zomparelli A.⁵, Ortolani M.¹, Boriani L.³, Leardini A.¹

¹IRCCS Istituto Ortopedico Rizzoli, Laboratorio di Analisi del Movimento, Bologna, Italy

²IRCCS Istituto Ortopedico Rizzoli, Laboratorio di Tecnologia Medica, Bologna, Italy

³IRCCS Istituto Ortopedico Rizzoli, Chirurgia delle Deformità del Rachide, Bologna, Italy

⁴CRP Technology, Modena, Italy

⁵University of Southern Denmark, Dept. of Technology and Innovation, Odense, Denmark

Email: paolo.caravaggi@ior.it

Summary

Ankle Foot Orthoses (AFO) improve foot clearance in the swing phase of walking in patients suffering from drop-foot. While standard-size off-the-shelf AFOs are normally suitable to support the foot and ankle, patients with concomitant morphological and postural alterations of the foot and lower limb need custom solutions. In this study, a dynamic custom AFO made of fiber-glass reinforced polyamide was designed according to the 3D shape of the leg and foot and manufactures via Selective Laser Sintering (SLS). An original setup replicating natural ankle plantar/dorsiflexion and Finite Element Analysis (FEA) were used to assess AFO mechanical properties and material stress levels during physiological deformations. Functional evaluation was performed via gait analysis on a small cohort of drop-foot patients. While confirmation on a larger population of drop-foot patients is required, the custom AFOs resulted in improved gait parameters and more comfortable than off-the-shelf orthoses.

Introduction

Dynamic AFOs can be prescribed to address a deficit of the main ankle dorsiflexor muscles in drop-foot patients, mostly due to neuromuscular pathologies. 3D scanning devices and additive manufacturing technology have been shown to allow designing and production of custom AFOs with improved fit and comfort [1, 2]. This study reports design principles, analysis of the mechanical properties, and functional evaluation in a small cohort of drop-foot patients, of a novel dynamic custom AFO manufactured via SLS of fiber-glass reinforced polyamide powder. The AFO aims at supporting the foot, correcting for foot postural alterations and providing better comfort with respect to standard off-the-shelf orthoses.

Methods

Two patients (67 years, 83 kg, 1.80 m; 80 years, 96 kg, 1.95 m) suffering from drop-foot due to lumbar disc herniation and spine surgery volunteered in the study. The patients' foot and lower limb were scanned in bipedal upright posture using a Kinect-based 3D scanner (fig. 1a) [3]. Custom AFOs were designed in Blender (fig. 1b) (Blender Foundation, Amsterdam), and manufactured via SLS of fiber-glass reinforced polyamide powder (Windform GT®, CRP Technology, Modena). AFOs were tested for mechanical properties using an ad-hoc setup replicating the AFO deformation during the stance phase of walking (fig. 1c, bottom). FEA was used to assess stresses in the regions subjected to the larger deformations under the same boundary conditions (fig. 1c, top). Functional evaluation was performed using the IOR-gait lower limb protocol

[4] in three conditions (fig. 1d): 1) without the AFO; 2) wearing the custom AFO, and 3) wearing a standard off-the-shelf AFO in polyethylene (Molla di Codivilla, Ottobock). The perceived comfort was scored via a 0-10 VAS scale.

Results and Discussion

The subjects walked at faster speed and with increased stride length wearing the custom AFO (0.91 ± 0.04 m/s; 1.22 ± 0.03 m) with respect to both the Codivilla (0.85 ± 0.03 m/s; 1.17 ± 0.03 m) and the no-AFO (0.67 ± 0.01 m/s; 1.09 ± 0.02 m) conditions. The ankle maximum dorsiflexion in the swing phase was larger while wearing the custom AFO (-16.9 ± 0.3 deg) with respect to the no-AFO condition (-33.4 ± 0.4 deg). The custom AFO resulted overall more comfortable than the Codivilla (9.7 vs. 7.3). Moreover, it scored higher in the shank support (9.6 vs. 7.5), in the plantar aspect (9.8 vs. 3.5) and in the perceived elastic return (9.7 vs. 6.9).

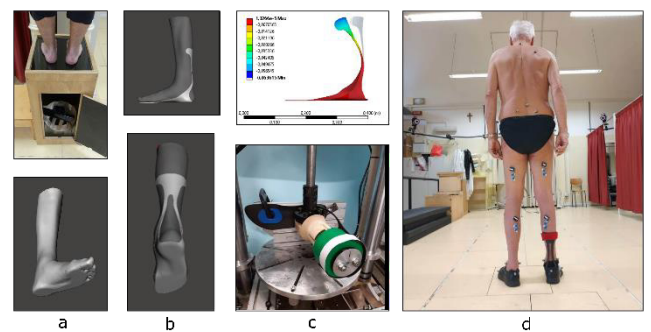


Figure 1: a) Leg and foot scan via Kinect-based sensor; b) design of the custom AFO via Blender; c) FEA of the AFO subjected to 15 deg ankle dorsiflexion (top), and corresponding bench-testing (bottom); d) functional evaluation via gait-analysis of one patient.

Conclusions

While confirmation on a larger population of drop-foot patients is required, this pilot study has shown that custom AFOs may be used to improve patients' gait and comfort with respect to standard off-the-shelf orthoses. Further customization of the mechanical properties with respect to subject-specific functional impairments and physical demand should be sought.

References

- [1] Telfer S et al. (2012). *BMC Musculoskeletal Disord*, **13**: 84
- [2] Wojciechowski E et al. (2019). *J Foot Ankle Res*, **12**(1): 11
- [3] Rogati G et al. (2019). *J Foot Ankle Res*, **12**(1): 1-8
- [4] Leardini A et al. (2007). *Gait&Posture*, **26**(4): 560-7

EFFECTS OF TAI CHI EXERCISE ON POSTURAL STABILITY AMONG THE ELDERLY DURING STAIR DESCENT UNDER DIFFERENT LEVELS OF ILLUMINATION

Yaya Pang¹, Li Li², Qipeng Song¹

¹College of Sports and Health, Shandong Sport University, Jinan, China

²Department of Health Sciences and Kinesiology, Georgia Southern University, Statesboro, 30460, USA

Corresponding author: Dr. Qipeng Song, songqipeng@sdpei.edu.cn

Summary

The elderly prone to stair descent falls under low illumination. Tai Chi, a traditional Chinese conditioning exercise, has been proved to improve postural stability by altering movement pattern, gait, and proprioception. This study investigates whether Tai Chi exercise could improve postural stability during stair descent under high and low illumination. Three groups of elderly women who practice Tai Chi, brisk walking, and no exercise were included. They descended from a simulated staircase. Decreased horizontal velocity, center of mass (COM) sway, and increased foot clearance were observed among the Tai Chi group, compared with other groups. Compared with under high illumination, Tai Chi participants decreased horizontal velocity, loading rate, braking impulse, and increased inclination angle COM sway, center of pressure displacement under low illumination. Tai Chi participants were more sensitive to the difference in illumination and took corresponding strategies to stabilize their bodies during stair descent.

Introduction

Recent reports have identified that stair gait falls account for 26% of all self-reported falls [1] and have become the leading cause of accidental death for the elderly [3]. Stair descent imposes significant challenges to movement control in people of all ages [2], but especially to the elderly due to the functional decline in many of their physiologic systems. Tai Chi is a traditional Chinese conditioning exercise. It has been proved that Tai Chi could improve postural stability in the elderly by altering their movement pattern, gait, and proprioception [4,5]. A kind of exercise that could improve postural stability in the elderly during high-risk activities, such as stair descent under low illumination, remains unclear.

Methods

Three groups of elderly women who practice Tai Chi (TC), brisk walking (BW), and no exercise (NE) were included. Each participant was asked to complete one testing session per day for a total of three testing sessions. In each session, the participants were asked to descend the staircase step over step under different illumination conditions. A simulated staircase with six steps was constructed for data collection in this study. Two force plates (KISTLER, 9287BA and 9281CA, Switzerland) were embedded in the third and fourth steps, to collect ground reaction force data at a sample rate of 1000 Hz. The stair descent test was recorded (100 Hz) by an eight-camera motion analysis system (Vicon, Oxford Metric, England). Descriptive analysis was conducted with the mean and

standard deviations for both kinematic and kinetic variables. Subgroup comparisons were assessed via respective 95% confidence intervals of mean difference. The confidence interval of mean difference values between groups was calculated by using the one-way ANOVA post hoc pairwise comparison with Bonferroni adjustment. The confidence interval of mean difference values between two illumination levels was calculated by using paired-sample t-test.

Results and Discussion

Horizontal velocity was lower in TC group compared with BW group (95% CI: -125.09 to 3.46) and decreased under low illumination in TC (95% CI: 15.23-105.07) and BW groups (95% CI:54.22-99.78). TC group had a greater foot clearance than BW (95%CI: 24.96-45.41) and NE (95% CI: 3.39-38.93). There were no significant group differences for head and trunk inclination angles. Under low illumination, the TC group had a higher head inclination angle (95% CI: -8.03 to -1.32), whereas BW and NE groups had higher trunk inclination angles (95% CI: -4.38 to -0.99; -4.06 to -1.47, respectively). TC group had a smaller COM_{ml} Sway than walking (95% CI: -19.32 to 0.31) and no exercise participants (95% CI: -23.97 to -3.59). All the three groups increased their COM_{ml} Sway (95% CI: -15.26 to -5.87, -18.15 to -4.32, -11.08 to -2.19, respectively) under low illumination. TC group had a lower loading rate than the BW group (95% CI: -5.75 to -0.02). Under low illumination, TC group decreased their loading rate (95% CI: 0.86-4.34), braking impulse (95% CI: 0.001-0.005), and increased their COP_{ap} (95% CI: -92.76 to -2.82) and COP_{ml}(95% CI: -26.50 to -3.47). Under low illumination, BW group increased their COP_{ml} (95% CI: -34.07 to -2.08).

Conclusions

TC group adjusted their movement pattern to increase postural stability during stair descent. Furthermore, the TC group were more sensitive to the difference in illumination and took corresponding strategies to stabilize their bodies during stair descent.

References

- [1] Antonio et al (2014). *Gait Posture*, **40**(3):429-434.
- [2] Novak et al (2012). *Applied Ergonomics*,**52**:275-284.
- [3] Buckley et al (2005). *Gait Posture*, **22**(2):146-153.
- [4] Chang et al (2016). *Research in Sports Medicine (Print)*, **24**(1):84-93.
- [5] Sun et al (2016). *Research in Sports Medicine (Print)*, **24**(2):145-156.

Quantification of arm swing during walking in healthy adults and patients with idiopathic Parkinson's disease

Elke Warmerdam^{1,2}, Robbin Romijnders^{1,2}, Clint Hansen¹, Gerhard Schmidt², Walter Maetzler¹

¹Department of Neurology, Kiel University, Kiel, Germany

²Faculty of Engineering, Kiel University, Kiel, Germany

Email: e.warmerdam@neurologie.uni-kiel.de

Summary

Arm swing has a high clinical relevance, especially in patients with idiopathic Parkinson's disease. This study developed an accurate inertial measurement unit-based algorithm to quantify arm swing during walking of healthy adults and patients with idiopathic Parkinson's disease. The algorithm was sensitive enough to detect differences between healthy older adults and patients with idiopathic Parkinson's disease, and can be applied to both clinical and daily-living data.

Introduction

A swinging motion of the arms characterizes gait. A reduction or asymmetry in the swinging motion is often seen in patients with idiopathic Parkinson disease (IPD) and could be a potential prodromal and progression marker of IPD, highlighting the need of an accurate assessment tool. The aim of this study was to develop and validate an algorithm that quantifies arm swing during walking that can be used in both clinical and daily-living environments.

Methods

Walking data were collected during treadmill walking from 15 healthy participants and 13 patients with IPD. An inertial measurement unit (IMU) and a marker cluster measured with an optical motion capture system were attached to the wrists of the participants. From the gyroscope data of the IMU, main amplitude, peak angular velocity, sideways amplitude, regularity, coordination and asymmetry of arm swing were calculated. A principal component analysis was performed to calculate the parameters in the main swing direction and make the algorithm robust to different wearing locations on the forearm. The peaks in the first principal component were detected to obtain the peak angular velocity. The data was then integrated and filtered with a moving average filter to obtain the angle which was used for the calculation of the amplitude. The regularity of the arm swing was calculated based on the autocorrelation of the angular velocity. The coordination between the left and right arm was based on a normalized cross-correlation. The asymmetry between both arms was extracted from the average arm swing amplitude of each arm. The angle and angular velocity were also calculated from the optical motion capture data to validate the arm swing parameters from the algorithm.

Results and Discussion

A Bland-Altman analysis was performed for the comparison between the IMU-derived and optical-derived data (Figure 1). The analysis resulted in small errors (Table 1). The comparison of the IMU-derived parameters between the two

groups even showed that differences between healthy adults and patients with IPD can be detected with the algorithm. This all makes the algorithm a valid and accurate tool to quantify arm swing during walking. In combination with a gait detection algorithm it could also be used to analyse daily-living data.

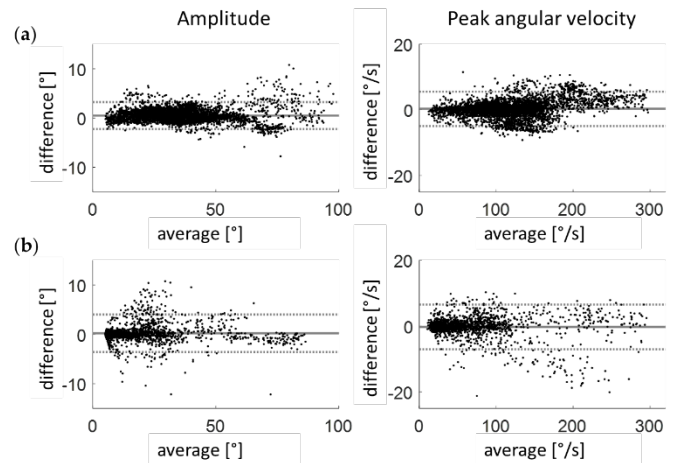


Figure 1: Bland-Altman plots with the arm swing amplitude and peak angular velocity for the healthy adults (a) and patients with IPD (b). On the x-axis the average of the IMU and optical results and on the y-axis the IMU minus the optical results.

Table 1: Error measures of IMU-derived arm swing data, compared to optical system-derived data.

		Healthy adults	Patients with IPD
Amplitude [°]	Systematic error	0.5	0.2
	Random error	2.7	3.8
	Absolute error	1.1	1.1
Peak angular velocity [°/s]	Systematic error	0.3	-0.3
	Random error	5.3	6.8
	Absolute error	1.9	2.0

Conclusions

An accurate arm swing algorithm was developed for both healthy adults and patients with IPD.

Acknowledgments

This research was funded by Keep Control from the EU's Horizon 2020 research and innovation program under the Marie Skłodowska-Curie grant agreement number 721577.

One-shot learning for personalized golf swing monitoring to overcome motion variability between users

Myeongsu Kim¹, Jung Kim¹, Suhyung Park¹

¹ Dept. Mechanical Engineering, Korea Advanced Institute of Science and Technology, Daejeon, Korea

Email: myeongsu@kaist.ac.kr

Summary

During motion monitoring with wearable devices, some users suffer from low estimation accuracy according to the motion variability between users. In the previous study about golf swing segmentation using an inertial measurement unit (IMU), one out of 20 skilled golfers revealed an exceptionally large estimation error. To overcome this, we personalized the segmentation algorithm with one-shot learning using the user's single swing sample. One-shot learned convolutional neural network (CNN) reduced the estimation error more than four times compared to the simple fine-tuning method. One-shot learning overcame the motion variability between users by adapting the golf swing segmentation model using a single motion sample from the new user and personalized the motion monitoring algorithm.

Introduction

Motion monitoring using wearable devices is widely applied and getting more attention in daily activities, sports, and clinical fields. Since the variability in the human body's movement appears due to individual characteristics, the accuracy of the estimated motion metrics to be monitored may decrease depending on the users. In the golf swing segmentation study using IMU, one out of 20 skilled golfers revealed an exceptionally large segmentation error for the address point [1]. However, building a vast motion dataset to learn and overcome a wide range of motion variability is time-consuming and expensive.

Meta-learning, or learning to learn, trains a model on various learning tasks to solve new learning tasks using only a few training samples [2]. If the individual users are considered as the learning tasks of the meta-learning, the motion variability might be overcome by adapting the model with a few motion samples of the new user. If only one training sample is used to adapt the model, it is called one-shot learning.

Therefore, in this study, we proposed a personalized golf swing monitoring using one-shot learning to overcome motion variability between users.

Methods

To verify that one-shot learning can personalize the model, we applied the method to the CNN, which segments golf swing phases from 6-axis IMUs attached to body parts [1]. The comparison was carried out between the following four models: a) CNN from Kim and Park [1], b) reproduced version of model a, c) fine-tuned from model b with one training sample of a new user, d) one-shot learning, or adapted to one training sample of a new user after meta-learning, applied to model b.

A total of 389 swing samples [1] from 20 skilled golfers with drivers and 7-irons were used. Subject 20, who revealed an exceptionally large segmentation error of the address point, was set as a new user (task). The one-shot learning algorithm was built based on ANIL [3], which simplified the inner loop of MAML [2] to offers computational improvements. Training and calculations were performed in Python 3.8.5 and PyTorch 1.7.1 environments.

Results

As a result of applying four models to subject 20, model d with one-shot learning demonstrated extremely smaller estimation errors of an average of 46 ms and 20 ms from the head and waist IMU, respectively, compared to all other models, including fine-tuned model c (Figure 1). As a result of applying four models to each of all 20 subjects, the standard deviation of the errors between subjects with model d significantly decreased compared to the reproduced model b from 60 ± 43 ms to 62 ± 21 ms using the head IMU, and from 54 ± 62 ms to 60 ± 19 ms using the waist IMU.

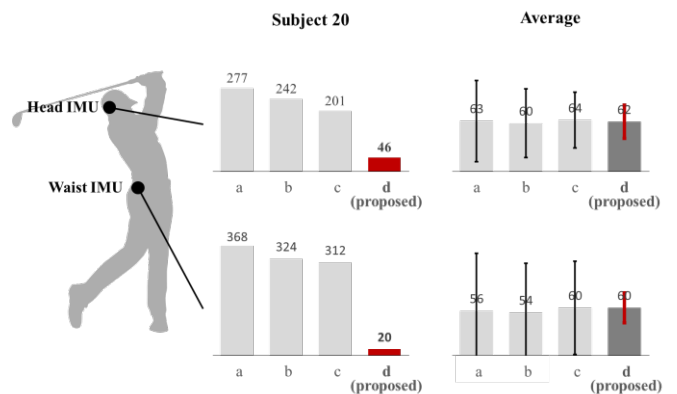


Figure 1: Comparing segmentation errors (ms) of the address point during golf swing between model a, b, c, and d (proposed).

Conclusions

One-shot learning can personalize motion monitoring algorithms to overcome the motion variability between users by adapting them to individual users with various motion characteristics.

Acknowledgments

The authors thank Hyunho Jeong and Seongwoong Hong for their technical advice.

References

- [1] Kim M and Park S (2020). *Sensors*, **20.16**: 4466.
- [2] Finn C et al. (2017). *ICML*, **3**.
- [3] Raghu A et al. (2020). *ICLR*, **2**.

Identifying the Objective of Human Behavior using Inverse Reinforcement Learning: A Case of Human Postural Control

SeongWoong Hong¹, Jung Kim¹ and Sukyung Park¹

¹Department of Mechanical Engineering, Korea Advanced Institute of Science and Technology, Daejeon, Korea
Email: sukyungp@kaist.ac.kr

Summary

Finding the objective of the human behavior can provide useful insight into the motion, but selecting the form of the objective function highly depends on the investigator's intuition. Inverse Reinforcement Learning can be a solution to learn the objective function directly from the behavior observation. Hence, we apply IRL to learn the objective of human behavior from its observation. The reference observations are created with a similar controller to the human postural control. This IRL architecture learns the reference objective function successfully. In the future, it could be extended to learn the objective of real human behaviors.

Introduction

When analyzing a specific behavior, an objective can provide valuable insight into that behavior. Some human behaviors could be represented by an optimized behavior of objective function by the CNS, and the behaviors could be successfully understood by that objective. However, the investigator should select the form of the objective function through their intuition to represent the objective of the behavior. Therefore, we suggest the architecture that could learn the objective from the observation of the behavior that does not depend on the investigators' intuition.

Inverse Reinforcement Learning (IRL) is used to find the objective of the behavior that was assumed as near-optimal of the objective [1]. Therefore, we try to find the objective assuming that human behavior is near-optimal according to the objective. In this study, we apply this architecture to known behavior before applying it to human behavior, and we successfully learned the objective through this architecture.

Methods

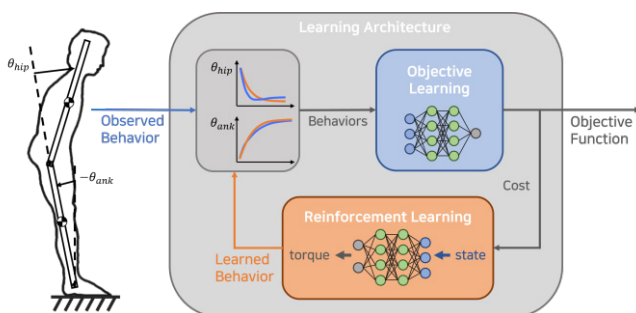


Figure 1: Overall architecture for learning the objective function

The target behaviors are produced to follow the Linear-Quadratic Regulator (LQR) objective which well describes the human postural control [2]. When the behavior follows the objective near-optimally, the observation can be assumed as a sample from the probability distribution according to the objective function value. The probability distribution is

modeled as (Eq. 1). The objective function and control policy are each updated iteratively to maximize the likelihood of the probability distribution over the observed behavior and to minimize the expected objective and the entropy of the policy [1]. Proximal Policy Optimization [3] is used to optimizing this control policy update rule.

$$p(\tau) = \frac{1}{Z} \exp(-c_{\theta}(\tau)) \quad (\text{Eq. 1})$$

The target behavior follows the noisy PD controller that optimizes randomly selected LQR objective function and have a gain noise that follow the gaussian $0.25 \times N(0, I)$. The simulator for learning control policy is modeled as 2-segment uniform inverted pendulum both have 5kg mass and 1m length.

Results and Discussion

We compared the control policy following the learned objective and the reference control policy for the randomly selected initial point (Fig. 2).

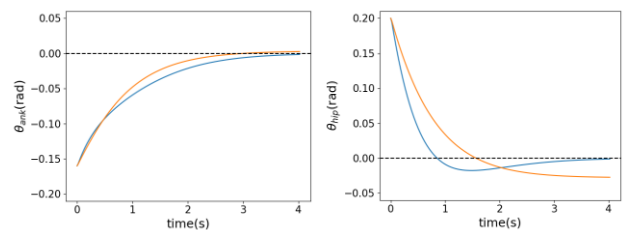


Figure 2: Each joint angles that follow the reference policy(blue) and learned policy(orange)

The learned control policy showed similar behavior to the reference motion for various initial states other than the selected one. Through this, we concluded that the objective was learned well.

Conclusions

The objective could be learned directly from the observation without the intuition about the form of the objective. This architecture reproduces the objective without information about the objective so it may learn more complex behavior's objective. In the future, it could be extended to learn the objective of human behaviors.

Acknowledgments

Thanks to Korea Advanced Institute of Science and Technology Biomechanics Lab members for thoughtful discussions.

References

- [1] Finn, Chelsea et al. (2016). *ICML*, **48**: 49-58.
- [2] Art. D. Kuo (1995). *IEEE Trans Bioed Eng*, **42(1)**: 87-101
- [3] Schulman, John et al. (2017). *arXiv*, **1707.063**

CLASSIFICATION OF CHILDREN WITH FRAGILE X SYNDROME BASED ON GAIT ANALYSIS: A SUPERVISED CLUSTERING APPROACH

W. PIATKOWSKA¹, M. ROMANATO¹, F. SPOLAOR¹, A. HUANG¹, F. CIBIN¹, A. CINIGLIO¹, R. POLLI², A. MURGIA² Z. SAWACHA^{1,3}

¹ Department of Information Engineering, University of Padova, Italy

² Department of Women and Children Health, University of Padova, Italy

³ Department of Medicine, DIMED, University of Padova, Italy

Email: weronikajoanna.piatkowska@studenti.unipd.it

Summary

Fragile X Syndrome (FXS) is a genetic condition, mainly characterized by intellectual disability, behavioral problems and musculoskeletal alterations. Somatic mosaicism for pre and full mutation, can be a strong phenotype modulator of the FXS clinical manifestations [1]. Therefore the aim of the present contribution was to develop a gait analysis driven classification of FXS children with classical full mutation of the FMR1 gene (FX-FM) and the ones who carried a full mutation with mosaicism (FX-M). Different supervised classification techniques were applied to a set of kinematic and sEMG data and the dataset who could better discriminate between the two populations of subjects was investigated. By including only sEMG parameters a better classification with 90,9 % of performance was provided.

Introduction

FXS is the leading form of inherited intellectual disability and autism spectrum disorder, caused by a tri-nucleotide CGG repeat expansion in the promoter region of the FMR1 gene [1]. Somatic mosaicism for pre and full mutation can be a strong phenotype modulator of the FXS clinical manifestations [1]. In FXS subjects musculoskeletal manifestations [1] justify a referral for gait analysis.

Supervised classification is used to determine the relation between a set of input parameters and a target variable[2]. In this contest it was driven by gait analysis parameters and adopted in order to distinguish between FX-FM and FX-M.

Methods

After appropriate informed consent by the parents, 12 FX-FM children (mean \pm SD age 10,69 \pm 3,67 years and BMI 18,82 \pm 4,09 Kg/m²) and 5 FX-M children (mean \pm SD age 9,00 \pm 3,35 years and 18,70 \pm 2,34 BMI Kg/m²), were evaluated at the BiomovLab and at the Women and Children Health Department (University of Padua). Kinematics and sEMG data were simultaneously acquired through 4 synchronized cameras (GoPro Hero3, 30fps) and an sEMG system (8 channels FreeEmg, BTS, 1000Hz) that collected the activity of Tibialis Anterior (TA), Gastrocnemius Lateralis (GL), Rectus Femoris (RF) and Biceps Femoris (BF). Each subject performed several gait trials and at least three trials per subject were processed. The following sEMG parameters were extracted: duration of muscle contraction, onset and offset activation timing [3], peak of the envelope and its occurrence [4] and number of co-contractions and their occurrence. The following kinematic parameters were estimated: minimum and maximum hip, knee and ankle joints angles, their range of motion (ROM) [5]. A supervised classification was performed

by means of 7 different classifiers: Decision Tree, Random Forest, CN2 Rule Induction, SVM, k-NN, Neural Network and Naïve Bayes and 2 different sets of vectors were used: S1. only sEMG parameters; S2. only kinematic parameters.

Results and Discussion

The best classification on a training set (66% of subjects) was obtained by applying the Neural Network algorithm for both S1 and S2; and this was further tested on the test set (33% of subjects) (Tab.1). Statistically significant differences ($p < 0.05$) between groups of subjects were detected on sEMG parameters but not on the kinematics (Fig. 1).

Table 1: Performance of the most performant classification algorithms on training and test data.

SET OF VECTORS	S1	S2
ALGORITHM	Neural Network	Neural network
TRAINING SET ACC (%)	98,5	83,1
TEST SET ACC (%)	90,9	84,8

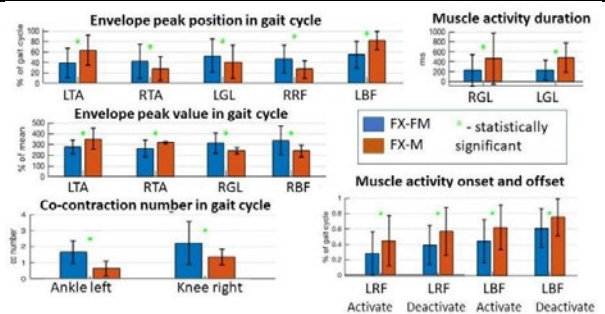


Figure 1: EMG parameters in subjects classified as FX-FM and FX-M by Neural Network classifier, *-statistically significant difference ($p < 0.05$)

Conclusions

Both kinematics and sEMG parameters showed their ability to discriminate between FX-FM and FX-M thus showing their potential to be used in support decision making applications.

References

- [1]Hagerman RJ et al. (2017). *Nat Rev Dis Primers*, 3, 17065
- [2]Alloghani M et al. (2020). *Springer Int. Publishing*, Cham, pp. 3–21.
- [3]Bonato P et al. (1998). *IEEE Trans Biomed Eng*, 45(3):287-99
- [4]Sawacha Z, and Spolaor F et al. (2012). *Gait Posture*, 35(1):101-5
- [5]Sartori M et al. (2015) *Neurophysiol* 114: 2509–2527

FFH Detection Using SVM with SMOTE, Normalization, and Univariate Feature Selection

Bummo Koo¹, Jongman Kim¹, Yejin Nam¹, and Youngho Kim^{1,*}

¹Department of Biomedical Engineering and Institute of Medical Engineering, Yonsei University, Republic of Korea
Email: *younghokim@yonsei.ac.kr

Summary

FFH (Fall-from-height) detection using various machine learning algorithms was performed in this study. Twenty healthy male volunteers performed 15 non-FFH, 5 low-hazard-FFH and 1 high-hazard-FFH. An IMU was placed on the 7th thoracic vertebrae (T7). FFHs were successfully detected with an high accuracy (98.3%) by SVM (Support Vector Machine) with SMOTE, normalization, and univariate feature selection.

Introduction

ILO [1] reported that the fatality rate observed for FFH is the highest among industrial accidents. As for the medical emergency, time is a critical factor for patients who are exposed to trauma [2]. This study aims to detect FFH using SVM with SMOTE, normalization, and univariate feature selection.

Methods

20 healthy volunteers performed 15 non-FFH, 5 low-hazard-FFH and 1 high-hazard-FFH (Table 1). An IMU sensor was positioned on the T7. Totally, 48 feature vectors were extracted from 3-axis acceleration and 3-axis angular velocity. Three pre-processing techniques were applied: SMOTE (Synthetic Minority Oversampling Technique), normalization, and univariate feature selection.

Table 1: Experimental Protocol

Non-FFH	sitting quickly and getting up, sitting on the floor and getting up, climbing up and down stairs, climbing up and down a ladder, working with a pickaxe, lifting(front), lifting(back), lifting(side), 0.7m jump, walking on a beam, walking on a beam with luggage in one hand, shoveling, stretching, climbing up and down a scaffold, moving up and down in an elevator
Low-hazard FFH	forward trip, lateral trip, backward slip, forward trip, fainting
High-hazard FFH	0.7m forward FFH

Table 2: Performance of classifiers for FFH detection

Pre-processing Technique	Accuracy (%)						
	Two-class			Three-class			
	FFH	Non-FFH	Total	Low-hazard FFH	High-hazard FFH	Non-FFH	Total
None	85.6	96.4	93.3	92.0	0	96.9	91.1
SMOTE	90.6	93.8	92.9	56.7	63.3	89.3	80.3
SMOTE +Normalization	98.9	100.0	99.7	92.9	90.0	100.0	97.9
SMOTE +Normalization + Feature selection	98.9	99.8	99.5	94.7	96.7	99.6	98.3

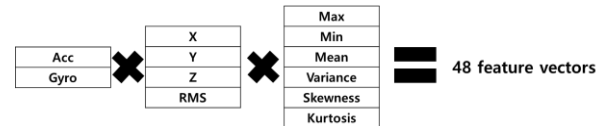


Figure 1: Feature vectors

The SVM classifier was applied with RBF kernel. Data from 10 subjects were used to train the classifier and those from the remaining 10 subjects were used to test the classifier.

Classification was conducted in two ways: two-class and three-class. Two-class represents non-FFH vs. FFH, and three-class represents non-FFH vs. low-hazard FFH vs. high-hazard FFH.

Results and Discussions

Since SMOTE is an oversampling approach that creates synthetic minority class samples [3], it did not improve the overall performance, but was able to create a balanced algorithm. Normalization improved the performance by reducing deviations between feature vectors. In addition, the feature vector selection contributed to improve the performance by solving the curse of dimensionality.

Conclusions

FFHs were successfully detected with an high accuracy (98.3%) by applying SVM with SMOTE, normalization and univariate feature selection. The present technique would be helpful to save the FFH victims by increasing the golden time.

Acknowledgments

Research supported by MSIT (#2018R1D1A1B07048575) and MOTIE (#20006386), Korea.

References

- [1] ILO. (2020). Top Causes of Global Construction Fatalities, and How to Avoid Site Risks
- [2] Harmsen A.M.K. et al. (2015). *Injury*, **46**: 602-609
- [3] Chawla N.V. et al. (2002). *J. Artif. Intell. Res.*, **16**:341-378

sEMG-based Finger Posture Recognition considering the Re-wearing of an Armband Sensor

Jongman Kim¹, Bummo Koo¹, Yejin Nam¹, Youngho Kim¹

¹Department of Biomedical Engineering and Institute of Medical Engineering, Yonsei University, Republic of Korea
Email: younghokim@yonsei.ac.kr

Summary

In this study, finger posture recognition algorithm was developed using armband-type-sEMG sensor and ANN classifier. In the re-wearing, the classification accuracy (CA) depended on the feature vector and the number of training data (TRN). Feature vectors with the high CA showed a strong linear relationship(LR) in inter-session. The present study can be useful to select the feature vector and the number of the training data to design the sEMG-based posture recognition.

Introduction

sEMG signal is useful to the pattern recognition (PR) algorithm for classification of the user's motion or intention. Most previous studies tried to avoid the misclassification, and the sEMG sensors on the specific muscle were usually used to minimize the effect of electrode shift in sEMG-based PR system [1]. However, these previous studies were difficult to use by non-experts and did not perform well when the sensors were worn again in daily life [2]. This study presents the sEMG-based finger posture recognition algorithm using the various feature vectors in the re-wearing of the sensor.

Methods

Ten healthy adults were recruited to perform twelve finger postures in MVC of 20% (rest, spread, cylindrical/spherical grasp, palmar/lateral/tip pinch, V-sign, O.K., scissor, finger-pointing, thumb-up). A pre-developed armband sensor [3] was aligned on flexor carpi radialis of the right lower arm. Each posture was repeated twice with ten times donning and doffing of the sensor. Twenty-one time-domain feature vectors were calculated using the filtered (10-250Hz) sEMG signal. The predefined threshold values [4-5] and additional threshold values as in eq (1) were applied to the feature vectors. Pearson's correlation coefficients (PCCs, r) were used to analyze the LR of inter-session ($0 < \text{weak} \leq 0.3 < \text{moderate} \leq 0.7 < \text{strong} \leq 1.0$). The 10-fold cross-validation was performed using an ANN classifier with a single feature vector by the different training data. The MATLAB and IBM SPSS Statistics 25 were used for the classification and the statistical analysis (Kruskal-Wallis test).

$$\text{Threshold Value} = T \times \text{RMS}_{\text{sEMG in REST}} \quad (T=0:0.5:10) \quad (1)$$

Results and Discussion

CA increased with the increased the number of training data for all feature vectors, but there was no significant difference in the range of TRN 1 to TRN4 and TRN5 to TRN9. In TRN9, the high CAs in ZC, WAMP, MYOP and SSC were 77.8 ± 5.0 % with a threshold of 15.0mV ([5] $r=0.840$), 79.3 ± 4.9 % with a threshold of 9.9mV ($T=3.0$, $r=0.855$), 79.7 ± 4.5 % with a threshold of 8.3mV ($T=2.5$, $r=0.857$) and 77.2 ± 5.5 % with a threshold of 15mV ([5], $r=0.843$), respectively. However, no

significant differences in CA were observed for ZC, WAMP, MYOP and SSC with the range of $2.5 \leq T \leq 9.5$, $1.5 \leq T \leq 8.5$, $1.0 \leq T \leq 6.0$ and $2.5 \leq T \leq 9.5$, respectively. VAR showed the highest CA (81.6 ± 13.1 % with $r=0.709$).

As for the re-wearing of the sensor, the additional training data was useful to improve the CA, and the feature vectors with a strong LR showed high CA ($\geq 60.0\%$). CA of higher than 70.0% was obtained for the feature vectors with $r \geq 0.8$.

Table 1: CA and PCCs of each feature vectors

Features	CA (%)			PCCs (r)
	TRN1	TRN5	TRN9	
IEMG	65.6±10.4	77.4±5.6	81.0±4.8	0.821
MAV	65.5±10.2	77.2±5.5	80.9±5.2	0.821
MAV1	65.5±10.6	77.0±5.4	80.1±5.5	0.819
MAV2	63.1±8.7	75.3±5.0	79.6±4.4	0.792
SSI	61.2±10.5	77.4±5.1	81.6±5.2	0.709
VAR	61.3±11.0	77.3±5.1	81.6±5.3	0.709
TM3	48.0±6.1	59.4±6.0	60.8±8.0	0.379
TM4	52.9±9.3	66.6±8.8	67.6±11.2	0.395
TM5	42.6±6.9	46.5±7.3	46.0±9.0	0.229
RMS	65.1±10.1	77.4±5.3	81.0±5.3	0.811
LOG	65.4±9.4	73.8±5.2	78.2±5.0	0.844
WL	64.7±9.9	76.8±5.2	80.7±4.8	0.816
AAC	64.9±10.1	76.6±5.7	81.0±4.5	0.816
DASDV	63.9±10.7	77.1±5.1	80.6±4.9	0.807
MAVSLP	25.4±2.5	30.3±2.3	30.9±2.8	0.006
ZC	63.8±8.6	72.8±5.5	77.08±5.0	0.840
WAMP	65.8±8.4	75.0±5.0	79.3±4.9	0.855
MYOP	66.4±9.2	75.2±5.0	79.7±4.5	0.857
SSC	64.3±8.4	72.7±5.4	77.2±5.5	0.843
AR	24.7±4.7	32.4±5.4	35.9±5.8	0.265
CC	24.7±4.7	32.3±5.5	36.5±5.9	0.291

Conclusions

The robustness on the re-wearing the sensor is important in sEMG-based PR system for non-expert and daily life. In this study, CA was improved by the additional training data, and inter-session PCCs correlated well with the CA depending on the feature vectors. The present study suggested that various finger postures could be recognized using an armband sensor, and the problem of the re-wearing the sensor could be solved using the feature vectors with a high inter-session PCCs.

Acknowledgments

This research was supported by The Bio & Medical Technology Development Program (NRF-2017M3A9E2063270) through the National Research Foundation of Korea (NRF) funded by the Ministry of Science and ICT.

References

- [1] Shi et al. (2018). Biocybern. Biomed. Eng., 38(1): 126-135.
- [2] Young, et al., IEEE T BIO-MED ENG, 59(3): 645-652, 2012.
- [3] Kim et al. (2019). Int. J. Precis. Eng. Manuf., 20(11): 1997-2006.
- [4] Phinyomark et al. (2009). J. Comput. 1(1): 71-80.
- [5] Tkach et al. (2010). J. Neuroeng. Rehabil., 7(1): 1-13.

Cerebral Palsy Gait Classification based on 3D Motion Capture Data using Deep Convolutional Neural Network

Joong-on Choi¹, Eun Sook Park¹, Dongho Park¹, Beomki Yoo¹, Dain Shim¹, Sehee Kim², Dong-wook Rha¹

¹Dept. and Research Institute of Rehabilitation Medicine, Yonsei University College of Medicine, Seoul, Korea

²Department of Biomedical Engineering, Yonsei University Wonju College, Gangwon, Korea

Email: medicus@yonsei.ac.kr

Introduction

Classifying gait patterns into several categories for gait analysis is helpful for clinical decision making; managing muscle spasticity, surgical lengthening of the shortened muscles, and applying orthosis to improve gait patterns. However, the gait pattern classification is still conducted with subjective judgement and the personal experience of healthcare providers.

In this study, we proposed a deep learning model to classify gait patterns in children with cerebral palsy (CP) through a combination of some of the extracted kinematic data based on 3D motion capture system.

The proposed deep learning model was trained using specific data made from custom datasets and evaluated for model performance. Then, the results were compared with clinical classification by experienced physician and trainee physician [1].

Methods

1. Custom Dataset

- The four gait patterns (True equinus, Jump knee, Apparent equinus, Crouch) were classified according to the widely used definition by Rodda et al. [2].

- 267 children with bilateral CP for model train & validation, 91 for model test.

- From 3D motion capture kinematic data, the custom datasets were reconstructed with joint kinematics (hip, knee and ankle) (6) and marker coordinates data (sacrum, anterior superior iliac spine, thigh, knee, tibia, ankle, and toe) (26) from the sagittal plane.

2. Deep Convolutional Neural Network (DCNN)

- The model was constructed to train time-series data using Conv1D. These convolutional layers were layered to form DCNN.

3. Comparison with experienced and trainee physician

- We compared the results of learned model to those of physicians' classification using the same patients' data to validate the model.

Results and Discussion

On test datasets, we obtained the accuracy(71.6), precision(69.0), recall(68.9), f1_score(68.1) and ROC-AUC(Fig.1) as classification performance metrics.

Table 1 showed that overall classification accuracy of the model was lower than experienced physician, but higher than trainee physician.

Especially in Jump knee, our model showed lower accuracy compared to physicians' classification and hard to discriminate it from True equinus.

However, our model showed higher accuracy in Apparent equinus and Crouch even compared to the classification accuracy of experienced physician. (Fig. 2)

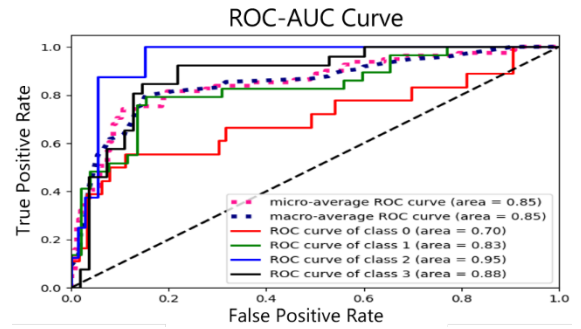


Figure 1. ROC-AUC for test dataset

(*class0-Jump knee, class1-Apparent equinus, class2-Crouch, class3-True equinus)

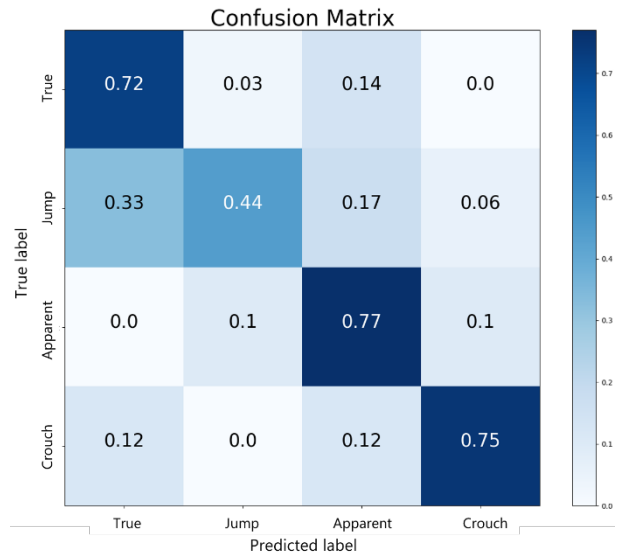


Figure 2. Confusion Matrix for test dataset

Conclusions

The higher classification accuracy of our model compared to the trainee physician was an encouraging result. Furthermore, deep learning analysis is expected to help physicians make more objective and fast clinical decisions.

However, further study is needed to optimize the model for better performance and apply a motion analysis model using 2D walking videos.

References

- [1] Dong Jin Kim, et al. (2011). *Ann Rehabil Med* 2011; 35: 354-360.
- [2] J. Rodda, et al. (2001) *European Journal of Neurology* 2001, 8 (Suppl. 5): 98-108

Table 1: The accuracy of the experienced, trainee rater's visual-based classification and classification accuracy of our model.

	True equinus	Jump knee	Apparent equinus	Crouch gait	Overall Accuracy
Experienced physician	88.5%	90.0%	61.8%	63.8%	75.8%
Trainee physician	61.5%	85.0%	29.4%	72.7%	56.0%
Our model	72.4%	44.4%	76.7%	75.0%	71.6%

Upper Body Posture Monitoring Using Inertial Measurement Units and Recurrent Neural Network

Hao-Yuan Tang¹, Ting-Yu Su^{1,2}, and Hsiang-Ho Chen^{1,2}

¹School of Biomedical Engineering, Taipei Medical University, Taipei, Taiwan
Email: hchen@tmu.edu.tw

Summary

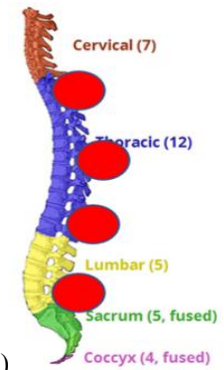
An athletic fit shirt imbedded with 4 IMU's sensors and machine learning algorithm was developed for sitting posture recognition tasks by seven static sitting postures classification (N=8). Time domain features served as input to a deep long short-term memory-based recurrent neural network (LSTM-RNN) architecture. The performance test explores the relevance between sensor information and postures. The overall results in performance indicated that IMU-based data and LSTM-RNN structural scheme was appropriate for sitting posture recognition.

Introduction

The main factor related to adult spinal deformity (ASD) is inappropriate postures e.g. poor sitting posture and following physiological stress on the vertebral which may cause spinal fractures. In clinical practices, the most common examinations for spinal deformity are traditional radiography and MRI with less invasiveness and higher precision, however, because of time and cost consumption, these tools cannot give rapid enough upper body postures information to patients. Upper body postures recognition (UPR) related to spinal pressure is investigated to understand people's behavior. Compared to diagnostic tools such as X-rays, wearable inertial measurement sensors (IMU), composed of a gyroscope, an accelerometer and a magnetometer, have received more and more attention in human activities recognition tasks. The purpose of this study is to evaluate the appropriateness of an IMU-based scheme and the LSTM-RNN for measurement of spine curvature provided an efficient option for posture recognition.

Methods

An athletic fit shirt imbedded with 4 IMU's sensors and machining learning algorithm was developed for UPR tasks in seven static sitting postures: upright/slump/flat back sitting, right/left bending, and right/left twisting. Four IMUs with 9 degrees of freedom were uniformly distributed in the range of thoracolumbar spine to acquire kinematics information in the spine (N=8) with controlled trial procedures. Time and frequency domain features, as input data in sequence-to-sequence classification tasks, a deep long short-term memory (LSTM) neural network architecture was used in the performance test to explore the relevance between sensor information and postures.



(a) prototype of system (b) relative positions to spine
Figure 1: Sensors distribution during human trials

Results and Discussion

The averaged accuracy of 7 classes is $99.0 \pm 0.3\%$ and F1-score ups to 0.966 ± 0.012 . The best performance is on humpback recognition and the worst is on right twisting. To evaluate the performance in the training model, we input a test sequence into this model and the accuracy is 81.2%, which indicated a slight overfitting. Also, we found the less sensors we used, the worse performance the model had, and the upper sequence of sensors combination can give better performance due to different distance to the rotational center of the upper body.

Conclusions

The overall results in performance evaluation indicated this IMU-based scheme was appropriate for measurement of spine curvature and that LSTM-RNN provided an efficient option for this application.

Acknowledgements

This work was supported by the ROC Ministry of Science and Technology (MOST 109-2221-E-038-007).

References

- [1] Petropoulos A et al. (2017) *IEEE 7th ICCE-Berlin*:5-9.
- [2] Mutegeki R and Han DS (2020) *International Conference on Artificial Intelligence in Information and Communication (ICAIIIC)*: 362-6.
- [3] Kang SW et al. (2017) *Sensors* 17: 2560.

Table 1: Interesting data from well-executed experiments. The data have been arranged in an interesting and clear manner.

States	Lean	Left bending	Left twisting	Right bending	Right twisting	Slump	Upright
Accuracy(%)	99.3	99.4	99.1	99.1	98.9	99.2	98.3
F1-score	0.975	0.976	0.966	0.967	0.960	0.974	0.942

A Biomechanical Testing Platform for the Stability and Mobility Assessment of Extracapsular Stabilization of Cranial Cruciate Ligament-Deficient Dogs

Wei-Ru Hsu¹, Cheng-Chung Lin², Ching-Ho Wu^{1*}

¹Institute of Veterinary Clinical Science, School of Veterinary Medicine, National Taiwan University, Taiwan

²Department of Electrical Engineering, Fu Jen Catholic University, Taiwan

Email: chinghowu@ntu.edu.tw

Summary

This study aimed to demonstrate a testing platform designed for the kinematics assessment of extracapsular stabilization (ECS) in cranial cruciate ligament deficient (CCLD) dogs. The testing platform was consisted of a custom-made jig and a motion capture system. The testing platform was used to evaluate *in vitro* the surgical outcome of ECS with bone anchors at two different pairs of isometric attachment sites. The jig was devised to drive the full range of flexion and extension, craniocaudal translation and internal rotation of the stifle joint in three-dimensional (3-D) space. The results showed that ECS tended to diminish the tibial cranial motion but increased excessive tibial external rotation in comparison to those of intact stifle. The testing platform was demonstrated to allow identify the changes of the post-surgical stability of the canine stifle joint.

Introduction

Cranial cruciate ligament disease is one of the most common causes of lameness in dogs. The biomechanical outcome after surgical correction for CCLD has been widely investigated. However, there were only a few studies that evaluated the reconstructed stifle in terms of 3-D kinematics. The study aimed to present a custom-made, high-mobility testing platform, which allowed quantify six-degrees-of-freedom kinematics of the stifle joint during various testing protocols and enabled to assess the performance of extracapsular stabilization.

Methods

The testing jig was designed to drive the full range of flexion and extension, craniocaudal translation and internal rotation of the stifle joint in 3-D space (Figure 1). The top plate of the jig was adjustable by the four vertical retractable columns. The proximal femur was affixed to a metal fixture via two 2.5-mm Steinmann pin, which was attached to the top plate with a bolt. A sliding base connecting with a torsionmeter on the bottom plate hold the distal end of the tibia, which provided stabilization during tests and allowed torque measurement during internal/external rotation of the stifle joint. A motion capture system (VICON, Oxford Metrics Group, Oxford, UK) was employed to record the motions of the stifle joint.

Three cadaveric pelvic limbs were harvested from three donors (Age: 5-14 y/o; BW: 7.0-16.8 kg). Each specimen was tested under different CCL condition: intact, CCLD, and repaired with ECS using bone anchors. Two 3.5-mm stainless steel anchors (Securos inc., Massachusetts, USA) were placed and connected with 80 lbs nylon leader line (NLL, Securos inc., Massachusetts, USA). Under the tension that cranial

drawer test became negative in stifle angle of 135°, the NLL was fixed with 80 lbs crimp clamp (Securos inc., Massachusetts, USA) The ECS group was divided into two subgroups, each with different chosen pair of isometric points (F2-T1 and F2-T3). The craniocaudal drawer tests and tibial internal rotation tests were conducted for each CCL conditions.

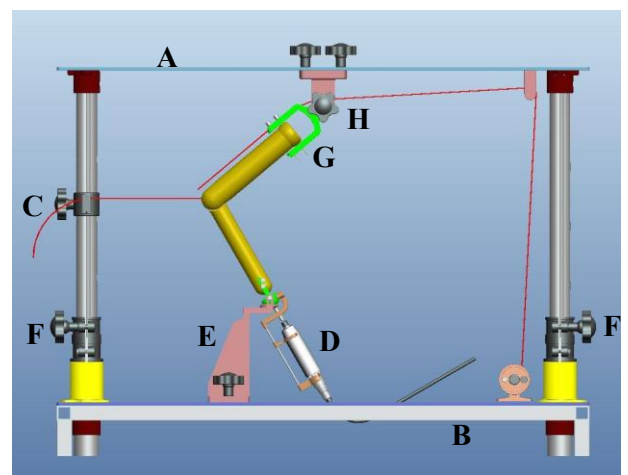


Figure 1: The schematic representation of the custom-made testing platform consisted of (A) a top plate, (B) a bottom plate, (C) a suture providing the cranial force, (D) a torsionmeter, (E) a sliding base, (F) fixation screws, (G) a metal fixture and (H) a bolt.

Results and Discussion

Tibial cranial translation of CCLD group was notably greater than that of intact group. The magnitude of internal rotation was greater in CCLD group in comparison to those of intact group, and both the ECS groups led to less tibial internal rotation comparing to both intact and CCLD group, which was in agreement with previous studies [1]. The new testing platform allowed 3D measurement of translation and rotation stability of the stifle joint at various positions of the hindlimb under precisely controlled loads.

Conclusions

A new biomechanical testing platform specifically devised for the kinematics assessment of canine limbs was constructed. The testing platform was demonstrated to enable identifying the changes of the post-surgical stability of the canine stifle joint.

References

- [1] Cinti F et al. (2015). *J Small Anim Pract*, **56**: 398-406.

Acute Effects of Transcranial Direct Current Stimulation on Dynamic Postural Stability in Healthy Young Adults

Baofeng Wang, Songlin Xiao, Liqin Deng, Changxiao Yu, Weijie Fu*
 School of Kinesiology, Shanghai University of Sport, Shanghai, China
 Email: fuweijie@sus.edu.cn

Summary

This study aims to investigate the acute effects of transcranial direct current stimulation (tDCS) on postural control in healthy young adults. Eight healthy male adults were recruited. All participants were asked to complete a dynamic postural stability task before and immediately after a 20-minute session of either anodal tDCS (a-tDCS) or sham tDCS (s-tDCS). Results showed that compared to the pre-intervention and s-tDCS group, the displacement of the center of pressure (COP) and the center of gravity (COG) was significantly decreased during a Y-balance task in the a-tDCS group. This suggests that a-tDCS can effectively improve the dynamic stability of healthy young adults.

Introduction

Postural control plays a major role in daily activities [1]. The maintenance of balance is controlled by the integration of sensory information and complex interaction between musculoskeletal and neurological systems [2]. Recently, the non-invasive brain stimulation technique emerged and has been widely used to improve postural control in the elderly. As one of the non-invasive brain stimulation technique, tDCS is a method stimulating specific brain regions by applying a constant weak current to the scalp. Therefore, this study aims to investigate the effects of tDCS on dynamic postural control in healthy young adults.

Methods

In this double-blinded sham-controlled study, eight healthy male adults (age: 25.9 ± 1.5 yrs, height: 1.75 ± 0.06 m, weight: 72 ± 17.8 kg) without exercise habits were asked to complete assessments of dynamic postural stability before and immediately after a 20-minute session of either a-tDCS or s-tDCS at two visits separated by one week. For the dynamic postural stability test, participants performed a Y-balance task (anterior, posteromedial, posterolateral directions) with a non-dominant leg on the force plate. The period and distance from the start position to the point of maximum reach in each direction was defined as analysis period and reach distance, respectively. Two-way repeated-measures analysis of variance was used to examine the effects of tDCS on the COG and COP excursion.

Results and Discussion

There were no significant main effects and interactions for the reached distance in both a-tDCS and s-tDCS groups (Table 1). The significant intervention by time interaction effects for the COG excursion at the posterolateral and posteromedial directions, COP excursion at the posterolateral direction were observed ($p < 0.05$). The results of the post-hoc analysis showed that compared to pre-intervention and s-tDCS, a-tDCS significantly decreased the COG excursion at the posterolateral and posteromedial directions, COP excursion at the posterolateral direction (Figure 1).

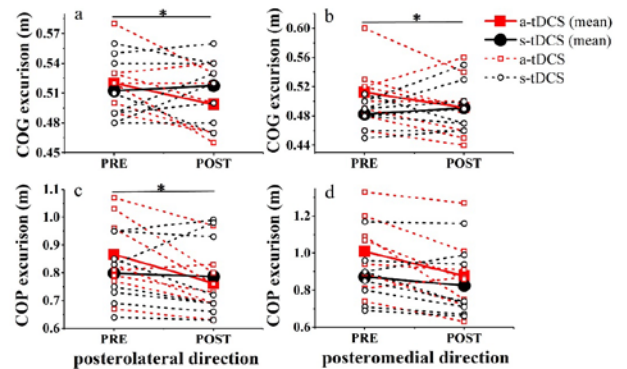


Figure 1: The changes of the center of gravity and center of pressure excursion before and immediately after a-tDCS and s-tDCS. COG: center of gravity, COP: center of pressure, *Significantly changes in the a-tDCS group, $p < 0.05$

Conclusions

A-tDCS could significantly decreased the displacement of the COG and COP compared to the pre-intervention and s-tDCS. This suggests that a-tDCS can effectively improve the dynamic stability of healthy young people.

Acknowledgments

This study was supported by NNSFC (11772201, 11932013), NKRDPC (2019YFF0302100), DPSCEC (19SG47).

References

- [1] Guo Z et al. (2020). *Frontiers in Aging Neuroscience*, **12**: 275.
- [2] Baharlouei H et al. (2020). *Comprehensive Review*, **50**: 119-131.

Table 1 The effects of a-tDCS and s-tDCS on reach distance

Direction	Time	a-tDCS	s-tDCS	Interaction (p value)	Time (p value)	Group (p value)
Anterior (%)	pre	76 ± 5	76 ± 5	0.53	0.75	0.92
	post	76 ± 3	77 ± 6			
Posterolateral (%)	pre	130 ± 8	132 ± 9	0.08	0.35	0.78
	post	134 ± 6	130 ± 8			
Posteromedial (%)	pre	115 ± 10	117 ± 11	0.24	0.42	0.86
	post	116 ± 14	113 ± 12			

Evaluation of Position and Variability of the Center of Pressure During Walking with Limited Knee Flexion

Seobin Choi, Jieon Lee, Gwanseob Shin

Department of Biomedical Engineering, Ulsan National Institute of Science and Technology, Ulsan, Republic of Korea
Email: gshin@unist.ac.kr

Summary

Stiff-Knee Gait, which is a common abnormal gait pattern, might cause loss of balance and falls. However, the isolated effect of limited knee flexion on the center of pressure (COP) movement has not been well studied. This study examined how walking with limited knee flexion would influence the position and variability of the COP.

Introduction

Stiff-Knee Gait (SKG) is a typical abnormal gait pattern following a stroke, spinal cord injury, and cerebral palsy, and it is known to reduce knee flexion range during the swing phase of the gait cycle [1]. Individuals with limited knee flexion may trip over obstacles and falls. Previous research has shown that the asymmetry and variability of COP movement are considered an indirect gait stability assessment [2]. However, the isolated effect of limited knee flexion on the movement of the COP has not been well studied. Therefore, this study aimed to examine how walking with limited knee flexion would influence the COP position and variability.

Methods

Sixteen healthy young male participants were recruited. The means (and standard deviations) of their age, height, body weight, and foot length were 23.1 (3.0) years, 173.4 (2.1) cm, 69.9 (8.1) kg, and 25.1 (0.7) cm, respectively. They walked on a 10-m walkway equipped with a 1.5m pressure platform (Zebris FDM 1.5; zebris Medical, Isny, Germany). They walked under four different conditions (Normal, L60, L40, and L20 conditions): normal and limited knee flexion of their left knee up to 60, 40, 20 degrees, respectively, at a self-selected comfortable speed. For the limited knee flexion walking, participants wore a hinged knee brace that permitted knee joint rotation from full extension to 120 degrees flexion. Their position and variability of the intersection point of the COP between both feet were captured by the pressure platform and compared between the four walking conditions. One-way repeated measure ANOVA and Tukey's post-hoc tests were conducted with a significance criterion of $p < 0.05$.

Results and Discussion

ANOVA found significant effects of the walking conditions on the anterior-posterior, lateral symmetry of the COP position and variability (Table 1). Tukey's post-hoc test showed that the position and variability of the COP were significantly different between the L20 and the normal walking conditions. The participants shifted their COP posteriorly and laterally on the left side while walking with limited knee flexion up to 20 degrees, compared to normal walking. The increase in the anterior-posterior and lateral symmetry variability was also observed during the L20 walking compared to normal walking. The limited knee flexion would change the position of COP and increase gait asymmetry and variability. The abnormal shifting of the COP could be a compensatory behavior to reduced foot-ground clearance associated due to the limited knee flexion. This finding may help assess gait stability and safety, and design guidelines for preventing falls for individuals with SKG.

Conclusions

Study findings show that limited knee flexion during walking might affect the dynamic balance, and it may be a risk factor for fall accidents who have stiff knee joints.

Acknowledgments

This research was supported by a grant of the Korea Health Technology R&D Project through the Korea Health Industry Development Institute (KHIDI), funded by the Ministry of Health & Welfare, Republic of Korea [HI19C1234].

References

- [1] Kerrigan, D. C., Gronley, J., & Perry, J. (1991). Stiff-legged gait in spastic paresis. A study of quadriceps and hamstrings muscle activity. *Am. J. Phys. Med. Rehabil.*, **70**(6), 294-300.
- [2] Hamacher, D., Singh, N. B., Van Dieën, J. H., Heller, M. O., & Taylor, W. R. (2011). Kinematic measures for assessing gait stability in elderly individuals: a systematic review. *J. R. Soc. Interface.*, **8**(65), 1682-1698.

Table 1: The position and variability of the COP, with p-values of ANOVA and Tukey results.

	Normal	L60	L40	L20	P-value
Anterior (+) /Posterior (-) position (mm)	0.7 ± 5.3 (A)	-0.6 ± 6.1 (AB)	-2.8 ± 4.8 (B)	-7.0 ± 7.1 (C)	<0.001
Lateral symmetry (Left (-), Right (+)) (mm)	-0.5 ± 4.3 (A)	0.5 ± 4.5 (A)	-2.3 ± 5.9 (AB)	-7.6 ± 12.3 (B)	0.002
Anterior/Posterior variability (mm)	2.5 ± 1.7 (A)	2.7 ± 1.1 (A)	2.5 ± 1.2 (A)	4.1 ± 2.2 (B)	0.005
Lateral symmetry variability (mm)	2.6 ± 1.5 (A)	3.6 ± 1.4 (AB)	3.7 ± 2.1 (AB)	4.6 ± 2.4 (B)	0.002

Note. Values given are group means ± standard deviation. Means with no letter in common are significantly different between walking conditions ($p < 0.05$) in Tukey's test.

Visualising Load Distribution of the Knee Throughout Kneeling Tasks

Simon Thwaites¹, Mark Rickman,^{1,2} Dominic Thewlis¹

¹Centre for Orthopaedic and Trauma Research, Adelaide Medical School, The University of Adelaide, Adelaide, Australia

²Department of Orthopaedics and Trauma, Royal Adelaide Hospital, Adelaide, Australia

Email: simon.thwaites@adelaide.edu.au

Summary

This work aimed to visualise the loading distribution of specific anatomical landmarks of the knee throughout various kneeling tasks. Force sensitive resistors (FSRs) were used to determine which structures were contacting the ground. Heatmaps of kneeling load distribution, and normalised vertical ground reaction forces (F_z) between left and right knees of 14 healthy participants were generated across two sessions. This study demonstrates an effective technique for visualising kneeling load distribution about the knee. This work is intended to inform future projects investigating the origins of anterior knee pain after fracture related surgery.

Introduction

Kneeling is an important activity of daily living. Trauma, degenerative conditions such as osteoarthritis, or the after-effects of local surgery may all lead to difficulty or the inability to kneel [1]. The anatomical structures contacting the ground changes with varying kneeling postures [2]. Previous work [3] has focused on the magnitude of applied loads but techniques for visualising which structures are contacting the ground requires further investigation. The aim of this study was to develop a technique for visualising loading distribution about the knee throughout kneeling.

Methods

Eight 12.7 mm circle diameter FSRs (Delsys, Boston, Massachusetts, USA, 2000 Hz) were placed about the right knee of 14 healthy participants (M/F: 7/7, age: 26.4 ± 2.5 years, height: 171.8 ± 4.9 cm, mass: 68.5 ± 12.8 kg). Four FSRs were placed in a line from the inferior pole of the patella (IPP) to the tibial tuberosity (TT); two FSRs were placed medially and laterally to this line, respectively. F_z data were captured using two in-ground force platforms (AMTI Optima, Watertown, Massachusetts, USA, 2000 Hz). Data were recorded using Vicon Nexus 2.9 (Vicon Motion Systems Ltd, Oxford, UK). Participants performed upright kneeling (60 secs) and reaching tasks: forward, back, left, and right (5 secs). Participants underwent a second session after a minimum three-day break. Matlab 2019b (MathWorks, Natick, Massachusetts, USA) and R 4.0.3 (R Core Team, Vienna, Austria) were used for data analysis. All participants provided informed consent.

Results and Discussion

The heatmaps (Figure 1) are a 4 x 3 array representing the average FSR activation of the right knee on the ground as if viewed from above. Columns 1, 2, and 3 are the medial 2 x FSRs, the 4 x FSRs located from the IPP to the TT, and the

2 x lateral FSRs. The TT and distal aspect of the patella tendon were active for all kneeling conditions.

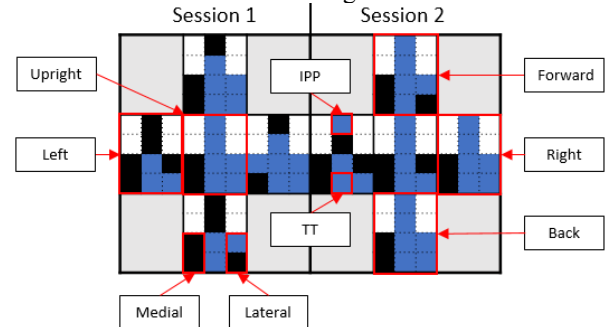


Figure 1: Average FSR activation of the right knee during kneeling tasks. Black = no activation, blue = activation, white = no FSR placed.

The intra-class correlation coefficient (ICC(2,1)) of the F_z showed good-to-excellent [4] intersession repeatability between left and right sides for all kneeling tasks except for upright kneeling on the left side (Table 1), which may be in-part more variable due to the increased recording time.

Table 1: Mean normalised F_z data (bodyweight (standard deviation)) and ICCs for left and right knees during kneeling tasks.

Task	Side	Session 1	Session 2	ICC
		Mean (SD)		
Upright	Left	0.46 (0.03)	0.47 (0.04)	0.35*
	Right	0.47 (0.04)	0.46 (0.06)	0.74 [†]
Forward	Left	0.28 (0.09)	0.30 (0.09)	0.81 [‡]
	Right	0.33 (0.10)	0.32 (0.08)	0.87 [‡]
Back	Left	0.28 (0.09)	0.28 (0.09)	0.85 [‡]
	Right	0.28 (0.09)	0.28 (0.08)	0.88 [‡]
Left	Left	0.51 (0.13)	0.51 (0.12)	0.67 [†]
	Right	0.24 (0.06)	0.24 (0.05)	0.89 [‡]
Right	Left	0.21 (0.05)	0.22 (0.06)	0.80 [‡]
	Right	0.54 (0.15)	0.51 (0.13)	0.82 [‡]

* poor, ** fair, [†] good, [‡] excellent [4]

Conclusions

The TT and distal patella tendon were most commonly loaded during kneeling. Most kneeling tasks were performed with good-to-excellent F_z intersession repeatability between left and right sides. FSR activation coupled with F_z data provides valuable insights into the magnitude and locations of applied load during kneeling. This study demonstrates an effective technique for visualising kneeling load distribution about the knee.

References

- [1] Weiss et al. (2002) *Clin Orthop Relat Res*, **404**:172–188.
- [2] Palmer et al. (2002) *J Bone Joint Surg Br*, **84**(2): 220-2.
- [3] Xu et al. (2017) *Appl. Ergon*, **58**: 308-13.
- [4] Cicchetti (1994) *Psychol. Assess*, **6**(4): 284–290.

Effects of dual-task training on gait in stroke patients: a meta-analysis

Zhang Xueyi¹, Wan Xianglin¹

¹Beijing Sport University, Beijing, China

Email: yicoia@qq.com

Summary

A systematic review and meta-analysis were performed to investigate effects of dual-task training on gait in stroke patients. The effect of dual-task training on the improvement of gait in stroke patients is better than that of conventional rehabilitation training, but the advantage of dual-task training in the improvement of gait speed in stroke patients may be affected by the time of intervention.

Introduction

Stroke is a common disease and the first cause of death in China. The average annual increase of the first incidence is 8.3%[1], and the recurrence rate 1 year after the first stroke is as high as 12.4%[2]. It is crucial to help patients recover functional disorders through various rehabilitation methods. The recovery of independent walking ability is the basis of improving the quality of life of stroke patients. Studies have found that dual-task training intervention can more effectively improve walking ability, and improve the independence of daily activities and quality of life of patients[3]. The purpose of this study is to systematically evaluate the effects of dual-task training on gait and balance of stroke patients, in order to provide reference for rehabilitation training programs of stroke patients.

Methods

The systematic review protocol described in the Preferred Reporting Items for Systemic Reviews and Meta-Analysis statement (PRISMA) were adopted to guide the review process. Keyword search was performed in Pubmed, Web of science, Cochrane Library, Embase, CNKI and Wanfang Database. All meta-analysis has been performed in Revman 5.4 software. A random-effect model was estimated given a P-value less than 0.05 for the Cochran's W test or I² statistics at or above 50%; otherwise, a fixed effect model was estimated.

Results and Discussion

A total of 15 RCTs involving 509 patients were included. The results of meta-analysis showed that the dual-task group was better than the control group in improving the gait speed, step length, stride length, cadence, and the difference was

statistically significant (Table 1). The results of subgroup analysis showed that when the intervention time was less than 4 weeks, dual-task was more effective in improving the gait speed of stroke patients (Figure 1). There was no statistical difference between the dual-task group and the control group when the intervention time was more than 4 weeks. Compared with previous studies, this meta-analysis covers a wider range of dual-task training types and provides a more comprehensive and reliable systematic evaluation result.

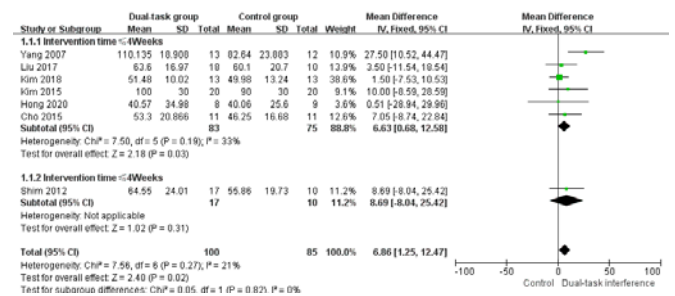


Figure 1: subgroup analysis of gait speed

The results of subgroup analysis indicated that dual-task training had certain advantages on gait speed of stroke patients in the short term, but might gradually lose the advantages in the long term. This conclusion suggests that in the middle and late stage of rehabilitation training for stroke patients, it may be necessary to change the training program for further intervention of patients.

Conclusions

(1) The effect of dual-task training on the improvement of gait in stroke patients is better than that of conventional rehabilitation training; (2) The advantage of dual-task training in the improvement of gait speed in stroke patients may be affected by the time of intervention. Due to the limitation of the quantity and quality of included studies, more high-quality studies are required to verify above conclusions.

References

- [1] Guan T, Ma J, Li M, et al. (2017). *Neurology*, **89**: 53-61.
- [2] Mi D, Jia Q, Zhang H, et al. (2012) *PLoS One*, **7**: e51406.
- [3] Chuang L L, Lin Y H, Lien Y S, et al. (2017) *Eur J Neurol*, **24**: 218.

Table 1: Meta-analysis results of gait outcome indicators.

Outcome	Heterogeneity test results		Meta-analysis Results	
	p-value	I ²	MD(95%)	p-value
Gait speed	0.27	21%	6.86(1.25,12.47)	0.02
Step length	0.21	32%	3.26(0.90,5.61)	0.007
Strike length	0.2	29%	7.23(4.16,10.29)	<0.00001
Cadence	0.98	0%	5.02(3.22,6.81)	<0.00001

Effects of Transcranial Direct Current Stimulation on Dynamic Postural Control: A Meta-Analysis

Changxiao Yu¹, Songlin Xiao¹, Baofeng Wang¹, Bin Shen¹, Weijie Fu^{1*}

¹ School of Kinesiology, Shanghai University of Sport, Shanghai, China

*corresponding author: E-mail: fuweijie@sus.edu.cn

SUMMARY

The purpose of this study was to investigate the effect of a-tDCS on dynamic postural control compared to sham stimulation, and confirm whether a-tDCS can be used as an effective ergogenic technology to improve postural control. Based on the PRISMA guidelines, this meta-analysis was performed until November 2020 in the Google Scholar, PubMed, and Web of Science. English full-text studies with sham-controlled, randomized, single/double-blinded experimental design whereby healthy adults were included. The results showed a-tDCS can significantly enhance the dynamic postural control in healthy adults.

INTRODUCTION

Dynamic postural control as the essential motor function plays an important role in our daily life, which often coincides with non-postural cognitive tasks [1]. Over recent years, increasing cortical excitability could enhance mental and physical performance has been widely accepted. As a promising technique, anodal transcranial direct current stimulation (a-tDCS) strengthens synaptic connections [2], promotes postural control [3], and improves motor sensation [4]. However, the results of a-tDCS are inconsistent or cannot be replicated. The purpose of current study is to investigate the effect of a-tDCS on dynamic postural control for healthy adults during different experimental tasks.

METHODS

We searched the following databases: Google Scholar, PubMed, and Web of Science before November 2020. The key search terms were the following: “tDCS” or “transcranial direct current stimulation” and “postural control” or “motor control” or “physical performance”. Studies that met the following criteria were included: (1) English full-text articles; (2) the design of the study was randomized, double/single-blinded, sham-controlled; (3) the application of a-tDCS for healthy adults; (4) the outcome measures include before and immediately after the trials; (5) perform dynamic postural control tasks.

The data used for meta-analysis are as follows: the speed of walking under single and dual tasks and the reaction time.

RESULTS AND DISCUSSION

Seventeen studies (424 participants) were included in the systematic review, and six of which for meta-analysis. The meta-analysis indicated that significant enhancement was found comparing a-tDCS vs. sham stimulation on dynamic postural control (Figure 1). There was no age-related process under dual-task conditions using a-tDCS over targeted brain areas in dynamic task performance. Additionally, a-tDCS has a significant reduction in reaction time for both the young and older populations (Figure 2).

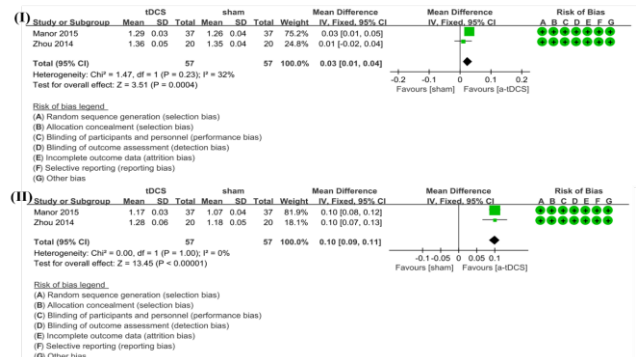


Figure 1: Forest plot showing mean different from the comparison of walking speed between a-tDCS and sham stimulation in single (I) and dual task (II) conditions during dynamic postural control.

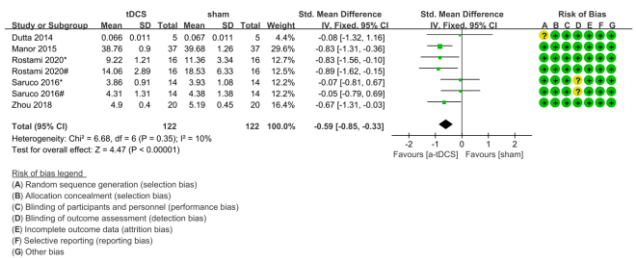


Figure 2: Forest plot showing standardized mean different from the comparison of reaction time between a-tDCS and sham stimulation in dynamic postural control tasks. Rostami 2020* - the time of TUG test; Rostami 2020# - the time of the Modified Figure of Eight Walk; Saruco 2016* - the time of a CONDITION × TEST interaction; Saruco 2016# - the time of a CONDITION × TEST × DIFFICULTY interaction.

CONCLUSION

Compared with sham stimulation, a-tDCS can significantly enhance the capabilities of dynamic postural control. Future studies should use larger sample sizes and imaging technology for in-depth study of brain mechanisms.

ACKNOWLEDGEMENTS

This study was supported by NNSFC (11772201, 11932013), NKRDP (2019YFF0302100), DPSCEC (19SG47).

REFERENCES

- [1] Yogev-Seligmann G et al. (2008). *Mov Disord*, Vol **23**, 329-342.
- [2] Kaski D et al. (2012). *J Neurophysiol*, Vol **107**, 2493-2505.
- [3] Manor B et al. (2015). *J Cognitive Neurosci*, Vol **28**, 1-7.
- [4] Peterka R.J. (2004). *J Neurophysiol*, Vol **91**, 410-423.

Evaluation of Trunk Muscles during Horseback Riding Therapy on Children with Cerebral Palsy

Kenichi Kaneko¹, Yoshiya Kawanori², Hitoshi Makabe³, Kiyoshi Yonemoto², Kazuyuki Mito⁴

¹Graduate School of Economics and Management System, Fuji University, Iwate, Japan

²Faculty of Social Welfare, Iwate Prefectural University, Iwate, Japan

³Department of Physical Therapy, Juntendo University, Tokyo, Japan

⁴Department of Informatics, The University of Electro-Communications, Tokyo, Japan

Email: kaneko@fuji-u.ac.jp

Summary

We examined the differences of the activity pattern of the trunk muscles during horseback riding therapy between healthy children and two low-birth weight children with cerebral palsy (CP) using electromyography (EMG). In the children with CP, the characteristics of the muscle activity pattern in the lumbar region showed low activity during horseback riding in comparison with that of healthy children. The proportion of EMG activity at the cervical region for the total muscle activities of trunk muscles was larger than that at the lumbar region in the children with CP. The children with CP had better control of trunk posture during horseback riding therapy mainly during the activities of the cervical muscles. It was suggested that the proportion of EMG activity of the cervical muscles and the lumbar muscles might also be a useful index for evaluating the horseback riding intervention for the children with CP.

Introduction

Horseback riding therapy is one of the rehabilitation methods for spinal injury or brain damage [1]. Over the past few years a considerable number of studies have been made on the effects of horseback riding therapy [e.g.: 2]. These results obtained in the present review show the potential benefit of horseback riding therapy in improving gross motor function in children with CP. What seems to be lacking, however, is an effective method of quantitative evaluation for horseback riding therapy from the viewpoint of biomechanics, and more experimental research is needed. The purpose of this study was to estimate the characteristics of muscle activity pattern in trunk muscles during horseback riding therapy. The proportion of surface EMG activity at the cervical region for the total muscle activities of trunk muscles was examined by root-mean-square (RMS) of the EMG. The values of proportion of RMS (%RMS) were compared between the children with CP and healthy children.

Methods

The subjects comprised two low-birthweight children with CP (a 10-year old and a 3-month old girl, a 10-year old and a 3-month old boy, respectively) and two healthy children (a 9-year old and a 3-month old girl, an 8-year old and a 10-month old boy, respectively) as a control. Two subjects with CP had been receiving horseback riding therapy for over 7 years. The horseback riding therapy was approximately 30 minutes in duration and was performed once weekly. The surface EMG values were recorded bilaterally from the four trunk muscles during the horseback riding therapy at the riding course. The muscle activity was quantified by the value of root-mean-square (RMS) for the surface EMG during the horseback riding. The mean values of RMS were compared between the children with CP and the normal children in each muscle. A proportion of RMS for the muscle activity amount at the trunk

was evaluated as a %RMS. The values of %RMS were compared between the cervical region and the lumbar region. For comparisons of %RMS, a chi-square test for independence was performed to investigate the independent difference with significance levels of 0.01.

Results and Discussion

The %RMSs values were compared between the children with CP and the healthy children and are shown in Figure 1. The proportion of EMG activity at the cervical region for the total muscle activities of trunk muscles was larger than that at the lumbar region in the children with CP. The chi-square test for independence showed statistical differences of 1%. The values of mean power frequency (MPF) of surface EMGs for the lumbar region were higher in the children with CP compared with that of the healthy children. The previous study showed the benefits of horseback riding therapy for improving gross motor function in the children with CP [2]. Our results suggested that there is a relationship between the characteristics of trunk muscle activity and the strategy of controlling the trunk posture during the horseback riding therapy in the children with CP.

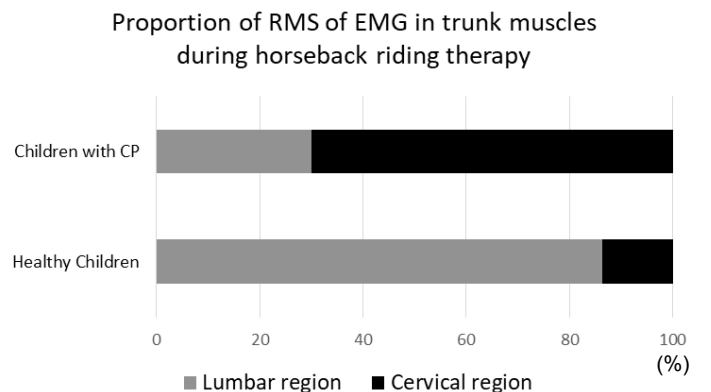


Figure 1: The value of mean %RMS from the lumbar muscles (Rectus abdominis and Erector spinae) and the cervical muscles (Splenius capitis and Trapezius) was compared between the children with CP and healthy children.

Conclusions

The proportion of the value of RMS for the cervical muscle and the lumbar muscle might be a useful index for estimation of the effectiveness of horseback riding intervention for the children with CP.

Acknowledgments

This work was supported by KAKENHI (20H01709).

References

- [1] Koca TT and Ataseven HT (2016). *North Clin Istanbul*, **2**: 247-252.
- [2] Gundos-Sanchez L et al. (2020). *Children (Basel)*, **7**: doi: 10.3390/children7090106.

Effects of Different Pressure Lower-Body Compression Garments on Proprioception

Siyao Wang¹, Hanjun Li²

^{1,2}Sports Science College, Beijing Sports University, Beijing, China

Email: 1178449559@qq.com

Summary

To study the effects of different pressure lower-body compression garments (CGs) on proprioception. Male students ($n=18$) from Beijing Sports University were selected as participants in tests. Participants were required to perform in three trial conditions: wearing conventional shorts, low-pressure CGs and high-pressure CGs. These conditions were randomized for each subject. Participants were required to perform an active joint repositioning task with conducting a secondary cognitive task. The result was assessed by measuring repositioning error from baseline measures. The repositioning error while wearing high-pressure CGs was significantly reduced ($P=0.04$). The effect of high-pressure CGs on proprioception was obvious. The high-pressure CGs significantly improved the ability of repositioning in the joint repositioning task with conducting a secondary cognitive task, which showed that CGs could improve the ability of proprioception. And it seems that the improvement of proprioception has relation with the pressure increase.

Introduction

Balance is mainly depended on the visual system, the vestibular system and proprioception [1]. In a randomized controlled trial for institutionalized older adults, Luis Espejo-Antúnez [2] found that a proprioceptive exercise program demonstrated significant improvements compared with the control group in areas such as functional mobility, musculoskeletal endurance, balance, gait, and risk of falls in institutionalized older adults. This shows the importance of proprioception to balance, and it is by affecting proprioception that compression garments (CGs) affects balance.

Methods

Participants: Eighteen healthy and active males (20.61 ± 2.29 yrs, 175.28 ± 3.36 cm, 70.22 ± 6.63 kg) from Beijing Sports University volunteered to participate in this study. An eight camera motion analysis system was used to sample the participants' repositioning angle. Subjects' 3D trajectories were captured by using a motion capture, measurement and analysis software using the plug-in gait full body model. Twenty-one spherical shaped retro-reflective markers were used to define rigid, linked segments of the participant (pelvis, thighs, shanks and feet) during each trial. The 3D trajectories of the reflective markers (14 mm diameter) were computed with a dynamic accuracy of 0.5 mm. Participants were required to use their dominant legs to carry out an active (knee-joint) repositioning task while conducting a concurrent secondary task. They performed in three trial conditions: wearing conventional shorts, low-pressure CGs (pressure on quadriceps femoris = 8.0 kPa) and high-pressure

CGs (pressure on quadriceps femoris = 17.5 kPa). These conditions were randomized for each subject. The secondary task (random word generation) was designed to make conscious attention away from the repositioning task. The target angle for the repositioning task was a random angle from 30 to 45, respectively, to reduce learning effects. Statistical analyses were performed by using Statistical Package for Social Science (V. 25.0, SPSS Inc.). The experimental data was expressed as mean \pm standard deviation (mean \pm std). The post-hoc test used the LSD test.

Results and Discussion

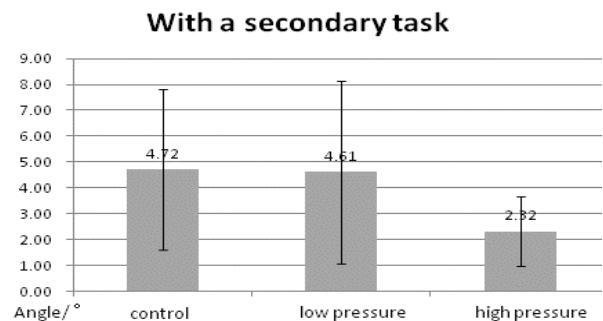


Figure 1: the error of reposition

The repositioning task is a general experiment to measure the proprioception. In this experiment, we use a knee-joint repositioning task. The cognitive task is added to interfere with the conscious attention, to maximize the effects of different pants on proprioception. Figure 3 shows the knee-joint repositioning task without conducting a concurrent secondary task. It can be seen that the difference between the reposition while wearing conventional shorts has the smallest error, and low-pressure CGs get the largest one.

Conclusions

High-pressure CGs is more conducive to reducing the error in reposition with a secondary task. Proprioception is very important when conscious control was gone. It shows that CGs could improve the ability of proprioception, and it seems that the improvement of proprioception has relation with the pressure increase.

References

- [1] Anne D. K. (2020) Exploring the Contribution of Proprioceptive Reflexes to Balance Control in Perturbed Standing. *Front. Bioeng. Biotechnol.*, 28 August 2020, **8**:866
- [2] Luis Espejo-Antúnez (2020) The Effect of Proprioceptive Exercises on Balance and Physical Function in Institutionalized Older Adults: A Randomized Controlled Trial. *Archives of Physical Medicine and Rehabilitation* 2020, **101**:1780-8

Comparison of foot kinematics of toe walking in the able-bodied to spastic equinus gait of cerebral palsy

Beomki Yoo¹, Wonhee Lee¹, Dongho Park¹, Dain Shim¹, Joong-on Choi¹, **Dong-wook Rha**¹

¹Department and Research Institute of Rehabilitation Medicine, Yonsei University College of Medicine, Seoul, Republic of Korea

Email: medicus@yonsei.ac.kr

Summary

Various neurological and musculoskeletal disorders can induce pathologic toe walking, also called equinus gait, and lead to changes in foot kinematics during walking[1]. Knowledge of foot kinematics during toe walking by non-disabled individuals is necessary to understand changes in foot kinematics during pathologic toe walking. Foot kinematics of spastic equinus gait of cerebral palsy were different from those of toe walking in young non-disabled persons.

Introduction

Toe walking is a gait without the heel-strike during the stance phase. Various neurological and musculoskeletal disorders can induce pathologic toe walking, also called equinus gait, and lead to changes in foot kinematics during walking[1]. Knowledge of foot kinematics during toe walking by able-bodied individuals is necessary to understand changes in foot kinematics during pathologic toe walking. In this study, we compared foot and ankle kinematics between toe walking in young non-disabled persons and spastic equinus gait of cerebral palsy.

Methods

The study group was consisted of fifteen young non-disabled adults (7 males and 8 females, age 23.1 ± 2.5 years old) and fifteen children(3-18 years of age) with spastic cerebral palsy who had true equinus gait pattern(maximum ankle dorsiflexion during stance phase was less than 5 degrees). The group of non-disabled persons walked in two conditions: Heel-toe walking(HW) and comfortable height toe walking(CTW) that kept lifting their heels to a height that was most comfortable for walking. All of participants walked at self-selected comfort speed through 10-meter pathway. Each trial was recorded using a 6-camera motion analysis system (MX-T10, Vicon, UK) and kinematic data were calculated. A modified Helen Hayes marker set for lower limbs and Oxford Foot Model for foot and ankle were used for analysis. Foot kinematics between each group were analyzed by paired t-test and student t-test using SPM.

Results and Discussion

Between HT and CTW in non-disabled group, there were no differences in foot kinematics on coronal plane. The hindfoot internal rotation and the forefoot abduction were higher for CTW than HW during stance phase ($p < 0.05$)(Fig. 1). Between CTW and spastic equinus gait, the hindfoot inversion was higher for spastic equinus gait during mid stance phase($p < 0.05$). The hindfoot internal rotation and the

forefoot abduction was higher for spastic equinus gait than CTW during swing phase($p < 0.05$)(Fig. 2).

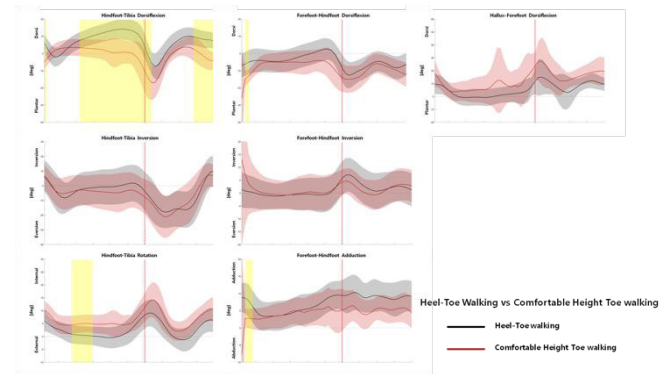


Figure 1. Between HW and CTW, mean kinematic angle of the hindfoot relative to the tibia, the forefoot relative to the hindfoot, and the hallux relative to the forefoot during the gait cycles of participants. Statistically significant differences are represented by yellow band. All of the kinematic angle curves were normalized over the gait cycle.

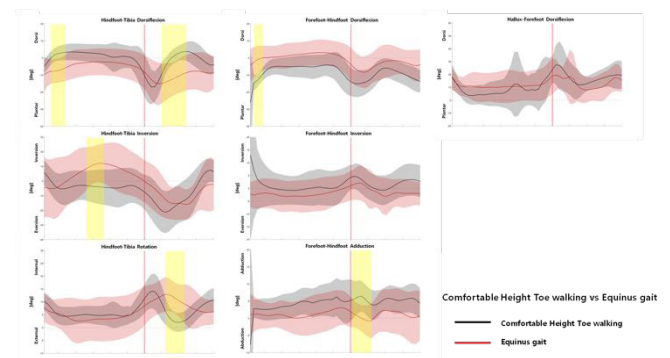


Figure 2. Between CTW and spastic equinus gait, mean kinematic angle of the hindfoot relative to the tibia, the forefoot relative to the hindfoot, and the hallux relative to the forefoot during the gait cycles of participants. Statistically significant differences are represented by yellow band. All of the kinematic angle curves were normalized over the gait cycle.

Conclusions

Foot kinematics of spastic equinus gait of cerebral palsy were different from those of toe walking in young non-disabled persons.

References

- [1] J.J. Ruzbarsky, D. Scher, E. Dodwell(2016). *Current opinion in pediatrics* 28(1) : 40-46

Systematic Review of In Vivo Foot and Ankle Kinematics during Gait Measured Using a Dual Fluoroscopic Imaging System

Dongqiang Ye¹, Xiaole Sun¹, Cui Zhang^{1,2}, Shen Zhang¹, Xini Zhang¹, Shaobai Wang¹, Weijie Fu¹

¹ School of Kinesiology, Shanghai University of Sport, Shanghai, China

² Shandong Institute of Sport Science, Jinan, China

Email: fuweijie@sus.edu.cn

Summary

The dual fluoroscopic imaging system (DFIS) is a potential valuable measuring tool that can detect small differences in the six degree-of-freedom (6DOF) in foot and ankle joints, especially when wearing shoes for both healthy and pathological populations. Thus, DFIS application is greatly important to understand the role of foot and ankle in human movement, identify abnormal joint movements and cure foot and ankle diseases.

Introduction

The foot and ankle joints play an important role in dynamic activities of the human body and are always the focus of biomechanics and medicine to prevent injury and speed up recovery [1]. While the technical deficiencies in traditional medical imaging methods limit the study of in vivo foot and ankle biomechanics. DFIS provides accurate and non-invasive measurements of dynamic and static activities in joints of the body (Figure 1). This paper evaluates existing literature that used DFIS to measure the in vivo kinematics of the foot and ankle during various activities in healthy and pathologic populations to provide effective theoretical support and constructive research direction for the future study of human foot and ankle.

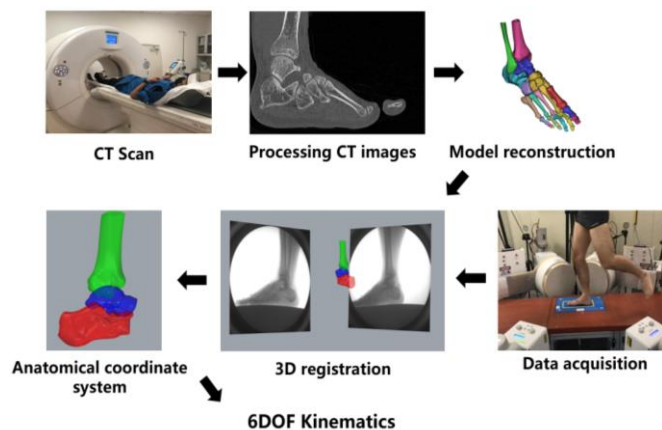


Figure 1: Process of DFIS in determining in-vivo foot and ankle kinematics

Methods

This systematic review was conducted following the Preferred Reporting Items for Systematic Reviews and Meta-Analyses guidelines [2]. PubMed, WoS, and EBSCO databases were searched from inception to April 2020 for related biomechanical studies that used DFIS. 20 experimental studies were identified after excluding the duplicated and irrelevant articles (Figure 2).

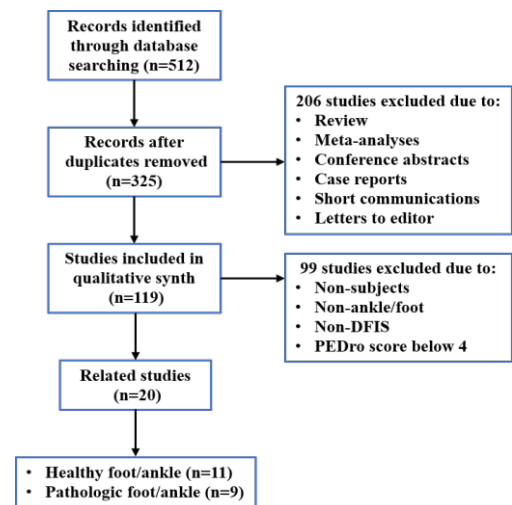


Figure 2: Literature search and study selection.

Results and Discussion

Included studies were categorised into healthy populations and injured conditions. Main findings: 1) the tibiotalar and subtalar joints are capable of 6DOF motion during activities for healthy people in barefoot conditions, 2) the minimalist shoes could not mimic barefoot running; meanwhile, the motion control shoes decreased the navicular drop compared with barefoot and minimal shoes, 3) patients with lateral ankle ligament sprains (LAS) and chronic ankle instability showed larger anterior/posterior translation and inversion of the tibiotalar joint than healthy control during walking and stair descent, and 4) the ankle brace thought to protect the foot neither limits anterior translation and plantarflexion of the subtalar joints nor improves abnormal foot movements.

Conclusions

DFIS has incomparable advantages compared with traditional biomechanical measurement methods. It detects small but substantial differences in foot and ankle 6DOF kinematics for healthy and pathological populations, especially those LAS patients. Therefore, future research should broaden the application of DFIS in foot and ankle biomechanics and even kinesiology.

Acknowledgments

This study was supported by NNSFC (11772201), NKRDPC (2019YFF0302100), DPSCEC (19SG47), TDFSM (2018107).

References

- [1] Tenforde A et al. (2016). *Phys Med Rehabil Clin N Am*, 27: 121-137.
- [2] Liberati A et al. (2009). *PLoS Med*, 6: e1000100.

Comfort Assessments in a Pneumatic Cuff System

Yejin Nam¹, Jongman Kim¹, Bummo Koo¹, SungHyuk Song², Youngho Kim¹

¹Department of Biomedical Engineering and Institute of Medical Engineering, Yonsei University, Korea

²Department of Robotics & Mechatronics, Korea Institute of Machinery & Materials, Korea

Email: younghokim@yonsei.ac.kr

Summary

The comfort in the binding parts of a wearable robot is essential for the human-robot interaction which can cause skin lesions and pressure ulcer. VAS (visual analogue scale) was used to quantify the comfort. The assessment was performed on four different levels of pressure using a pneumatic cuff on the thigh, the shank, and the knee. The comfort was analyzed using the temperature, PI index and SpO₂. The more pain was found in the thigh than in the shank or the knee. The present study would be helpful to determine an optimal binding parts for a standing wearable robot.

Introduction

With the development of robot technology, the wearable robot has been widely used [1]. Human-robot interfaces refers to the physical interaction between the user and the wearable robot. If an excessive load persists, it can lead to soft tissue damage such as pressure ulcers [2]. It is necessary to define a comfortable binding part in a standing wearable robot. The interface pressure depends on the cuff design and the human anatomy. With the pressure for a relatively long time, the temperature and the oxygen saturation in the blood also change.

Methods

Twenty healthy subjects (10 males and 10 females, age: 23.7±1.9years, height: 170.1±8.3cm, weight: 68.8±11.4kg) participated in the experiment. Measurements were made at 5 different locations (anterior/posterior of the thigh(TA/TP), anterior of the knee(K), and anterior/posterior of the shank(SA/SP)) using a pressure sensor (14x14cm, Pliance, Novel, Germany), a pneumatic cuff (DTS-2000s, DS Maref, Korea), a temperature sensor (RDXL6SD, Omega, Canada), a PPG sensor (Ubpulse 360, Laxtha, Korea) and a SpO₂ sensor (PM100N, Covidien, Ireland). The cuff pressure was set in 10, 20, 30 and 40 kPa. VAS ('0': no pain, '10': worst possible pain) was obtained based on VAS = 1 for 10kPa of the thigh after applying pressure for 2 min. The temperature was measured under the cuff. PPG and SpO₂ were attached to the distal ends of fingers and toes, respectively. Areas of interests were defined as three different masks (medial, center and lateral) to analyze the pressure distribution. Statistical analysis was performed using IBM SPSS Statistics 25 (IBM, New York, NY, USA) ($p < 0.05$).

Results and Discussion

The interface pressure and VAS increased with the increasing cuff pressure. Larger pressure was observed in the medial parts of TA and K. In SA and SP, the medial and lateral parts

showed higher pressure than the center part. Large pressure in the center part was shown in only TP. No significant differences in the mean pressure were found among the thigh, the knee and the shank. No significant gender difference in the mean pressure was also observed.

Table 1: VAS for cuff pressures in different locations

Pressure [kPa]	TA	TP	K	SA	SP
10	1.02 ± 0.45	0.68 ± 0.36	0.15 ± 0.20	0.24 ± 0.29	0.29 ± 0.35
20	2.30 ± 0.93	1.90 ± 0.70	1.12 ± 0.47	1.08 ± 0.45	1.07 ± 0.68
30	4.01 ± 1.20	3.64 ± 1.16	2.22 ± 1.01	2.04 ± 0.86	1.95 ± 1.33
40	5.48 ± 1.60	5.52 ± 1.69	3.21 ± 1.42	3.24 ± 1.45	3.14 ± 1.62

Table 1 shows VAS values for different cuff pressures at each location. The change in VAS as well as VAS itself were the largest in the thigh. Results showed no significant differences in temperature, SpO₂ and PI index for different cuff pressures. The increase in cuff pressure did not increase the temperature in that location even though the temperature increased due to the long period wearing. Localized pressures affected neither oxygen supply to the entire body nor PI index. SpO₂ would not be reliable to determine comfort because of the motion artifact.

Conclusions

VAS, interface pressures, temperature, PI index and SpO₂ were measured to determine the comfort in different cuff pressures for the lower extremity. Even though no significant differences in the interface pressure was found, the more pain was found in the thigh when the same pressure was applied. Temperature, PI index and SpO₂ would not be good indicators for the comfort assessment.

Acknowledgments

This work was supported by National Research Council of Science & Technology (NST, Korea Government).

References

- [1] MYLAEUS, A., et al. (2019) *Robotics and Well-Being*, 2019, 149-156.
- [2] KERMAVNAR, Tjaša, et al. (2020) *Human factors*, 2020, 0018720820908758.

The Differences between Bonded and Frictional Contact Settings in Foot-Sneaker Finite Element Analysis

Yang Yi^{1,2}, Zhu Xiaolan^{2,1}

¹Institute for Sports and Human Sciences, Beijing Sport University, Beijing, China

Email: 1114181977@qq.com

Summary

In finite element analysis, different contact settings will affect the accuracy of simulation results. In order to obtain a reliable foot-sneaker coupling model, this experiment compared the simulation results of binding contact and friction contact models to discuss the problem of contact surface setting in finite element simulation of foot and ankle, so as to provide an optimal contact setting for future research in this field.

Introduction

Finite element analysis had been widely used in researches of mechanical changes of foot skeletons, ligaments, plantar aponeurosis and other soft structures. However previous studies have not provided a uniform standard for the setting of bonded contact and frictional contact between foot-shoe connection [1].

By comparing the measured results with the simulated results to analyze which contact model is more accurate. And to determine a more realistic connection model through the simulated results of bonded contact and frictional contact.

Methods

CT scan was performed to obtain the foot-shoe imaging data of one subject(67kg) wearing experimental shoes and CT data saved as DICOM files. The Mimics19.0 and Ansys19.1 software were used to reverse model the foot-sneaker finite element model. By setting the connection of foot and shoe as bonded contact and frictional contact(frictional coefficient 0.5) to get two coupled finite element models. The contact between shoe and support plate was set as frictional contact with frictional coefficient 0.6 and those two coupled models should be used to simulate human static standing when force reaction was half weight(328N) [2]. Through Pedar-x pressure insole to measure plantar pressures of subject under static standing. In order to obtain more accurate comparison result, the plantar was divided into 10 regions [3], A-J, both pressure insole result and simulation. And the peak plantar pressure of these 10 regions was selected for comparison analysis and it would be compared with simulation data.

Results and Discussion

The bonded contact model has a poor simulation effect on the peak pressure of the forefoot, with a maximum error of 1576.7% but friction contact model has a peak pressure error of only 55.9% in the same region. It means that the friction contact is

closer to the actual working condition than the bonded contact..

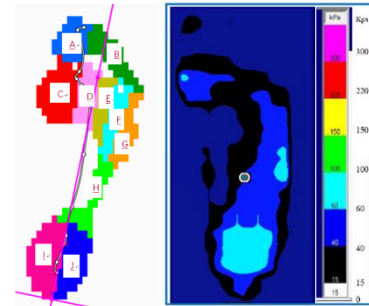


Figure 1: Plantar regions(left) and pressure insole result(right).

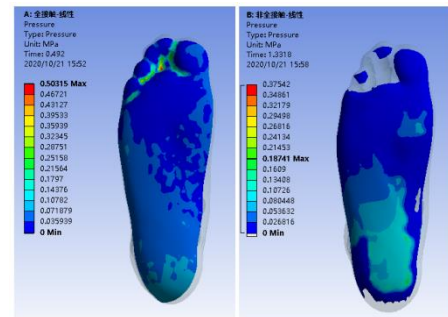


Figure 2: Bonded contact result (left) and frictional contact result(right).

Any model must be doing validation before mechanical simulations [4]. Although heel pressures of these two contact models were very close to measured results, the finite element model of foot-shoe without verification of other plantar regions shouldn't be used in simulation study.

Conclusions

The friction contact model can accurately reflect the mechanical changes of the foot inner structures and plantar pressures. It is suggested that the frictional contact setting of foot-sneaker connection should be carried out in the future finite analysis.

References

- [1] Cheung J T et al.(2009). *Footwear science*, **1(1)**:31-46
- [2] Wang Y et al.(2018). *J Orthop Translat*, **12**:55-65
- [3] Akrami Mohammad et al.(2018) *Biomechanics and Modeling in Mechanobiology*, **17(2)**:559-576
- [4] Hicks J L et al.(2015). *J Biomech Eng*,**137(2)**:20905.

Evaluation of Muscle Function by Mechanomyography during Dynamic Contraction using Microphone and Accelerometer

Yuki Haruta, Kazuyuki Mito, Aya Shirai, Tota Mizuno, Naoaki Itakura.

Department of Informatics, The University of Electro-Communications, Tokyo, Japan

Email: h2030093@edu.cc.uec.ac.jp

Summary

The purpose of the present investigation was to examine the mechanomyogram (MMG) with dynamic behavior. Six adult males (mean \pm SD age = 23 \pm 1) were performed concentric muscle action of the forearm flexion from 40deg to 140deg. To measure MMG, a microphone and an accelerometer were placed on the biceps branch muscle. The MMG signal was calculated microphone's MMG amplitude (MMGmic) and accelerometer's MMG amplitude (MMGacc) every 10deg of elbow flexion. We found that MMGmic was increased as the elbow flexion increased. However, there was not an increase in MMGacc. The result was considered that there were effects of mechanical artifacts such as body movement with the accelerometer. Therefore, it was considered that the microphone was suitable for measuring the MMG with dynamic behavior.

Introduction

The MMG is mechanical vibration by the lateral expansion of active muscle fibers [1]. MMG is important as a way to obtain biometric information. To measure MMG, an accelerometer was widely used. However, this transducer has a problem of susceptibility to mechanical artifacts. Research of this problem made progress and it was found that a microphone of the transducer was preferred for measuring MMG during static behavior because effects of mechanical artifacts with a microphone were less than an accelerometer in case of static behavior [2]. Although MMG with a microphone during static behavior was studied, MMG with a microphone during dynamic behavior was not studied. Therefore, the microphone will need to study the effectiveness of the microphone during dynamic behavior. In this study, we examine the MMG during dynamic behavior using a microphone and an accelerometer.

Methods

The subjects were six adult males (mean \pm SD age = 23 \pm 1). Microphone and accelerometer were placed on the biceps branch muscle with double-sided tape and a bipolar electrode was placed similarly to measure electromyogram (EMG). Elbow flexion was recorded while measuring MMG and EMG.

In the first, the maximum voluntary contraction (MVC) was measured. Then the subjects were asked to the flexed elbow from 40deg to 140deg and performed three trials at the velocity and under the weight. The velocities of the order were 10deg/s and 20deg/s. The weights corresponded to approximately 20% MVC and 40% MVC. The subjects took a rest for five minutes each the velocities and the weights

MMG and EMG amplitudes were estimated as the mean of the root mean square (RMS) of three trials. The values of RMS were calculated every 10deg of elbow flexion between 60deg and 120deg.

Results and Discussion

Fig.1 presents the relationship between RMS and elbow flexion at 40% MVC. There was an increase in EMG from 60deg to 120deg. There was an increase in MMGmic as well. However, there was not an increase in MMGacc. If we showed Fig.1, we find the difference in the velocities. There was a comparative increase in EMG and MMG. Similar propensities were shown at 20% MVC.

EMG RMS reflects the level of recruitment and firing rates of the motor units. The propensity of MMGmic was similar to the propensity of EMG. This result is considered that MMGmic reflected the level of recruitment and firing rates of the motor units without effects of mechanical artifacts. The difference between MMGmic and MMGacc was considered that there were effects of mechanical artifacts with the accelerometer as well as during static behavior.

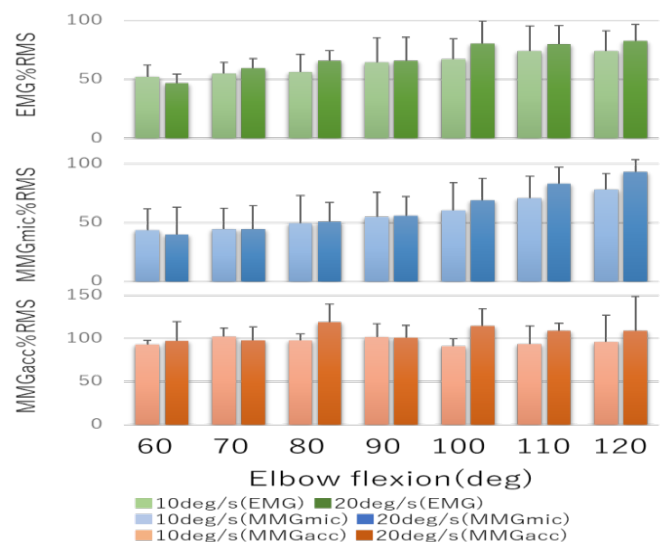


Figure 1: The relationship between elbow flexion and %RMS in EMG and MMG

Conclusions

This study investigated MMG with a microphone and an accelerometer during dynamic behavior and compared them. The result indicated MMGmic was increased and MMGacc was not increased as elbow flexion increased. These findings suggest that the microphone was suitable for measuring the MMG during dynamic behavior as well as during static behavior.

References

- [1] Orizio C et al. (1996), *Journal of Biomechanics*. **29**, 475-481
- [2] Watakabe M et al. (2001), *Medical and Biological Engineering and Computing* **39**, 195-201

The Functional Role of Collagen Content in the Human Cartilage Cell Microenvironment

Awuniji Linus¹, Ari Ronkainen², Rami Korhonen¹, Petri Tanska¹

¹University of Eastern Finland, ²Kuopio University Hospital

Email: awuniji.linus@uef.fi

Summary

Recently, we observed that collagen content in the cartilage pericellular matrix (PCM, a narrow region around cartilage cells) is reduced in human osteoarthritis. However, it is unknown how this content reduction affects cell volume, and thus, potentially cell synthesis. Here, we conducted a parametric multiscale modeling analysis using experimentally characterized human cartilage material properties to simulate how the changes in the PCM collagen content alter cell volumes following mechanical loading. The parametric analysis was conducted for the superficial and middle zone cartilage. We observed that the PCM collagen content modulates cell volume in a tissue depth specific manner. Reduced PCM collagen content reduced cell volume increase in the superficial zone (up to ~20%), but barely affected cells in the middle zone (changes less than 1%).

Introduction

Cartilage cells, chondrocytes, synthesize collagen, and proteoglycan (PG) molecules of the extracellular matrix (ECM). Their turnover is affected by the mechanical forces experienced by the cells and these mechanical signals are modulated and transferred to cells by the PCM [1]. Recent studies have suggested that PG content alterations that occur, especially during early phases of osteoarthritis, may alter the volumetric deformation of chondrocytes [2]. This may lead to altered cell synthesis. Recently, we observed that collagen content is reduced in the PCM of the middle zone cartilage during early osteoarthritis in human tissue [3]. However, it is unknown how these collagen content alterations contribute to the cell deformation. Thus, this study aimed to conduct a parametric investigation on how changes in the pericellular collagen content modulate cell volume using a computational multiscale modeling approach.

Methods

An axisymmetric ($h = 2.83$ mm, $r = 4$ mm) model of bulk cartilage was constructed in Abaqus/CAE (Providence, RI USA). A fibril-reinforced poroelastic swelling (FRPES) model with measured human cartilage properties, i.e. mechanical material parameters, depth-wise collagen architecture, collagen content and PG content, was used [4]. Two distinct zones were defined according to cartilage thickness, superficial zone: 0-10% and middle zone: 10-25%. Additional cell-level submodels representing the chondrocyte microenvironment (cell, PCM, and local ECM) were constructed at the center of each zone. The structure and composition of the PCM were based on the experiments and literature [1, 3]. After swelling equilibrium was established, a stress-relaxation test (10% compression at 10 μ m/s followed by a 20 min relaxation) in indentation geometry (indenter diameter = 1 mm) was imposed on the bulk cartilage model,

while the cell-level submodel was driven by the displacements and pore pressures of the bulk model. A parametric analysis was conducted by varying the PCM collagen content to assess its effect on cell volume change and aspect ratio after relaxation. This analysis also included an experimentally detected decrease in the human PCM collagen content; from healthy to -20% [3] in osteoarthritis. The average composition of healthy tissue served as a reference.

Results and Discussion

Changes in cell volume were zone specific. In the superficial cartilage, the mechanical loading resulted in an increased cell volume when compared to the initial swelling equilibrium state (Figure. 1A). Reduction in the PCM collagen content reduced this cell volume increase. In the middle zone, mechanical loading resulted in decreased cell volume when compared to the initial swelling equilibrium state (Figure. 1B). Reduction in the PCM collagen content barely affected the cell volume change (cell volume change was less than 1%).

Earlier both increased and decreased cell volumes have been observed experimentally and computationally in the superficial zone of cartilage [2]. Increased cell volume has been earlier linked mostly to cartilage softening in OA, allowing greater cell expansion in mechanically loaded cartilage. Here, analogously, the cell volume increase in the superficial zone is likely related to the relatively soft human cartilage, compared to other species.

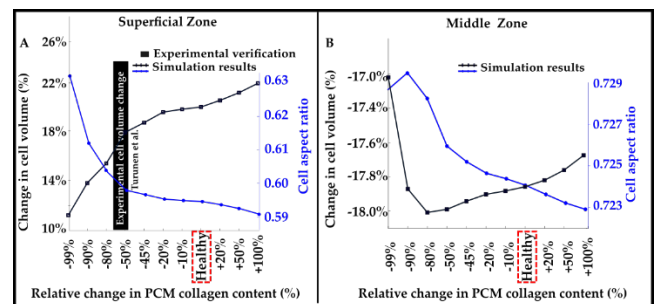


Figure 1: Simulated cell volume changes in the superficial and middle zone human cartilage.

Conclusions

Following mechanical loading of cartilage *in situ*, the PCM collagen content alters cell volume in a depth-specific manner, with superficial zone cells being more sensitive to the PCM collagen content changes than the middle zone cells.

References

- [1] Wilusz et al. (2012). *Matrix Biol.*, **6**: 320-327.
- [2] Turunen et al. (2013). *Osteoarthr. Cartil.*, **21**: 164146.
- [3] Linus et al. (2020). *Trans. Orthop. Res. Soc.*, 66:386.
- [4] Ebrahimi et al. (2020). *Ann. Biomed. Eng.*, **48**:2887-2900.

ROLE OF ACTIN FILAMENT IN DYNAMIC CHANGES OF INTRANUCLEAR STRAIN INDUCED BY CYCLIC STRETCHING

T. ASAKAWA¹, S. Tsukamoto¹, N. Takesue¹, N. Sakamoto¹

¹Mechanobiology Laboratory, Department of Mechanical Systems Engineering, Tokyo Metropolitan University, Tokyo, Japan
Email: asakawa-takumi@ed.tmu.ac.jp

Summary

Mechanical stimuli such as cell-substrate cyclic stretching are transmitted to the nucleus via actin filaments and thought to changes in cell function and morphology with changes in gene expression, but the mechanisms behind these relationships are still unclear. Here, we investigated changes in intranuclear strain induced by continuous cyclic stretching. The strain in the center of the nucleus induced by substrate stretching was higher than that in the periphery before the application of cyclic stretching. After exposure to continuous cyclic stretching for 15 min, strain at both the central and peripheral regions of the nucleus increased. Inhibition of actin filament polymerization abolished the changes in local strain caused by cyclic stretching. These results indicate that the local strain in the nucleus changes in response to cyclic stretching, and actin filaments play an important role in its change.

Introduction

Cells change their morphology and function in response to mechanical stimuli from the surrounding environment [1]. Mechanical stimuli transmitted from the cell-substrate through actin filaments cause nuclear deformation, which has been recently recognized as an important factor regulating chromatin structure and transcription factor binding to DNA [2]. Since the structure of actin filaments as well as mechanical properties of the nucleus changes in response to mechanical stimuli [3, 4], dynamic changes of nuclear deformation caused by mechanical stimuli need to be elucidated to understand the role of nuclear deformation in cell responses. We have developed a technique to evaluate cell-substrate stretching-induced nuclear strain with consideration of its heterogeneity [5]. In the present study, we investigated the changes of local intranuclear strain in a cell under a cyclic stretching condition.

Methods

To evaluate intranuclear strain induced by the substrate stretching, fluorescence images of the nucleus in a cell-seeded in a stretch chamber (Strex, Japan) were taken before and after applying a 10% step-stretching of the chamber using a custom-made uniaxial stretching device equipped on the stage of an inverted microscope (Olympus, Japan), and Von Mises equivalent strain then calculated with Ncorr according to the method previously reported [5]. Cells before and after exposure to continuous cyclic stretching for 15 min were evaluated. To assess the role of actin cytoskeletons, cells were treated with 1 μ M cytochalasin D, an inhibitor of actin filament polymerization, for 15 min prior to the continuous cyclic stretching.

Results and Discussion

The nuclear strain in the central region caused by the substrate stretching was higher than that in the periphery before the application of continuous cyclic stretching (Fig. 1), which is consistent with our previous work [5]. After exposure to continuous stretching for 15 min, nuclear strains at both the central and the peripheral regions increased. Treatment with cytochalasin D abolished the changes in the local strain caused by continuous cyclic stretching (data not shown), suggesting that force transmission through actin filaments is crucial for changes in intranuclear strain induced by exposure to continuous cyclic stretching. There are two possible mechanisms that cause the changes of intranuclear strains by continuous cyclic stretching; changes of actin filament structure which affects force transmission to the nucleus [4], and changes in the deformability of the nucleus. We will perform further studies to elucidate these mechanisms that causes the changes of local strain.

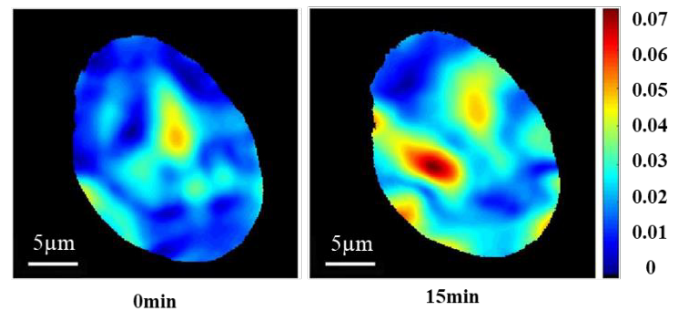


Figure 1: Von Mises equivalent strain distribution under a 10% step-stretching condition (before (0 min), and after exposure to continuous cyclic stretching for 15 min).

Conclusions

The present study shows that local nuclear strain increased after being subjected to cyclic stretching, and the actin filaments are thought to be responsible for the change of the nuclear strain.

Acknowledgments

This study was supported in part by Grants-in-Aid for Scientific Research from MEXT of Japan (Nos. 17H0277, 18H03521, and 18K19934).

References

- [1] Scaffidi et al. (2005). *Nat Med*, 11: 440-445.
- [2] Wang et al. (2009). *Nat Rev Mol Cell Biol*, 10: 75-82.
- [3] Hamed et al. (2012). *Plos One*, 10: e4584.
- [4] Le et al. (2016). *Nat. Cell Biol*, 18: 864-875.
- [5] Tsukamoto et al (2021). *J. Biomech*, 119: 110292.

Dynamic responses of cells govern the boundary instability at the closing wound

Hyuntae Jeong¹, Jinwook Yeo¹, Seunghwa Ryu^{*1}, and Jennifer H. Shin^{*1}

¹Dept. Mechanical Engineering, Korea Advanced Institute of Science and Technology, Daejeon, Republic of Korea

Email: jhst2914@kaist.ac.kr

Summary

Motions and forces in cells play critical roles in many pathophysiological events. Especially, wound healing requires dynamic responses of cells to achieve the boundary closure, which includes migration of active leader cells and tensional forces to tug the follower cells. Interplays between these two factors result in a complex interfacial landscape. Here, we investigated the correlations in dynamic responses of cells that give rise to interfacial instabilities. We found that the density-based cellular pressure governed the development of the instability in the boundary landscape, and the frequency of these instabilities was shown to correlate directly to the closure speeds of the wound.

Introduction

Cells' dynamic behaviors, marked by motions and forces, arise as consequences of complicated biochemical interactions amongst proteins and macromolecules within the cells. The dynamic behavior of individual cells also determines the collective functions of cell clusters through the physical responses amongst neighboring cells in various physiological events [1]. Especially, the wound closure is predominantly achieved by the collective cell migration of the epithelial cell layer resulting in boundary proceedings. Many studies have reported the boundary movement-induced interfacial instabilities that stemmed from the heterogeneously distributed collective motions near the boundary [2]. The interfacial instability presents varying curvatures whose values correlate with the cellular forces near the curve. Therefore, understanding this instability phenomenon would be fundamental to modeling the wound closures.

Methods

As an epithelial tissue model for wound healing, we used the normal kidney epithelial cell line, Madin-Darby Canine Kidney (MDCK). We patterned a silicon wafer with engravings of various geometries to use it as a mold to fabricate a polydimethylsiloxane (PDMS)-based stencil. We then put the stencil on the culture dish with cell suspension and waited until the cells were grown to ~90% confluency. Then, the PDMS stencil was carefully removed to make undamaged wound shapes. Migrations and forces of cells were visualized by DPIV(Digital Particle Image Velocimetry) and TFM(Traction Force Microscopy), respectively, to quantify the mechanical behaviors of the cells.

Results and Discussion

During the wound closures, interfacial instability was formed due to the differential accumulation of cellular motilities near the boundary. The constantly protruding cells at the wound boundary formed the finger-like extrusions, and retarded cells between two adjacent fingers exhibited concave

edges. The spreading area of the following cells simultaneously changed according to the proceeding speeds of the leading front. The overly compressed cells behind the concave edge gave the expansion pressure to the adjacent cells, then the novel streamlines were formed. By these sequential processes of physical features, the vacant area at the concave edge was closed. Consequently, we found that the interfacial instability was formed by the heterogeneously distributed migrating cells and was modified by cellular pressures amongst adjacent cells.

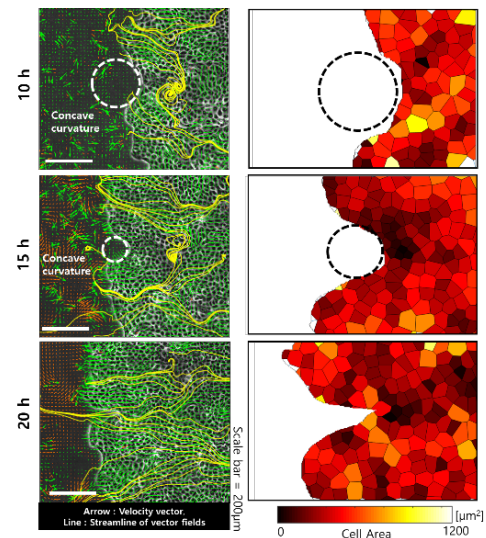


Figure 1: Interfacial instability correlated to the physical behaviors of cells near the boundary.

Conclusions

Here, we analyzed the formation of interfacial instabilities during the wound closure for advancing the knowledge about this complex phenomenon in terms of dynamic responses between cells. The visualized physical traits, especially the cellular migrations and shapes, demonstrated the interesting mechanisms for regulating the interfacial instability not in a stochastic manner. We expected these results would be a fundamental source for developing the mechanical model for wound closures.

Acknowledgments

This research was supported by Basic Science Research Program through the National Research Foundation of Korea (NRF) funded by the Ministry of Education, Science and Technology (NRF-2020M3A9E4039658).

References

- [1] Juliane Zimmermann et al. (2016). *PNAS*, **10**: 2660-2665.
- [2] Ricard Alert et al. (2019) *Phys. Rev. Lett*, 12:088104.

Hypoxic postconditioning on astrocyte activation in a 3D cortical stroke model

Mong Lung Steve Poon¹, Eunmin Ko¹, Eunyong Park¹, Jennifer H. Shin^{1,*}

¹The Shin Lab, Department of Mechanical Engineering, Korea Advanced Institute of Science and Technology, South Korea
Email: j_shin@kaist.ac.kr

Summary

Hypoxic postconditioning (HPC) has been shown to protect brain from secondary reperfusion injury after stroke. However, the optimal protocol for HPC has not been investigated. The current study aims to examine the effect of HPC on the functional recovery of the brain cells after stroke using a 3D spheroidal cortical stroke model. Based on astrocyte activation indicated by GFAP expression, we found that single hypoxia treatment most significantly enhanced the GFAP expression of astrocytes within the cortical stroke model.

Introduction

Hypoxic postconditioning (HPC) has emerged as a promising strategy to block secondary reperfusion injuries after stroke [1]. A variety of treatment protocols for HPC had been examined, including single hypoxia treatment for 1h or 2h or repeated intermittent hypoxia treatments for 1h or 2h with 24h intervals. Nonetheless, a few studies have reported the protective effect of HPC among different protocols. Therefore, we aim to investigate the optimal protocol for HPC using a 3D cortical stroke model based on astrocyte activation as indicated by GFAP expression.

Methods

Primary rat cortical cells were isolated from postnatal day 1-2 Sprague Dawley rat pups. Dissociated cortical cells were mixed with the culture medium (Neurobasal-A, B27 (1X), GlutaMAX (100X), and Penicillin–Streptomycin (1X)). The cell suspension was seeded onto the 96-well round-bottom Ultra-low attachment (ULA) plate and incubated at 37°C with 5% CO₂. Half of the culture medium was replaced with fresh medium every three days. Stroke induction was achieved by oxygen-glucose deprivation-reoxygenation (OGD-R). In brief, samples on day 7 were suspended in the culture medium without GlutaMAX and exposed to hypoxia (1% O₂) for 4h, followed by 24h of reoxygenation. For hypoxic postconditioning (HPC), single hypoxia treatment for 2h (1HPC) and three (3HPC) or five (5HPC) intermittent hypoxia treatments for 2h spaced at 24h intervals were applied to the samples after reoxygenation with 1% O₂ and normal culture medium. All samples were collected 144h after reoxygenation.

Results and Discussion

After a stroke, astrocytes become reactive, exhibiting increasing GFAP expression. These reactive astrocytes are essential to tissue remodeling and restoration of cellular integrity [2]. Therefore, to examine the effect of HPC in promoting functional recovery, GFAP within the cortical

spheroids was immunostained. Stroke induction by OGD-R significantly enhanced GFAP expression compared to the control. 1HPC further upregulated the GFAP expression. However, 3HPC significantly suppressed the GFAP expression compared to 1HPC. 3HPC and 5HPC shown no significant difference in GFAP expression. This result suggested that 1HPC best enhanced the astrocyte activation within the cortical stroke model.

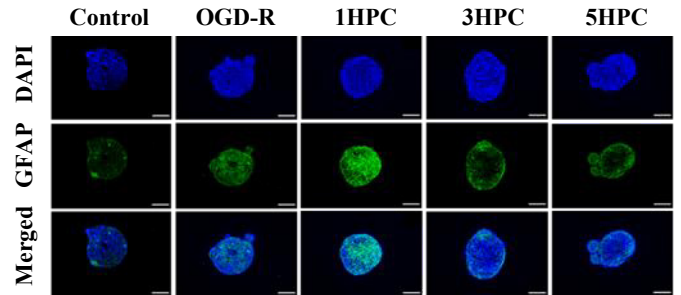


Figure 1: Immunofluorescent images of GFAP (green) and DAPI (blue) in cryosectioned cortical spheroids. Scale bars represent 200 μm.

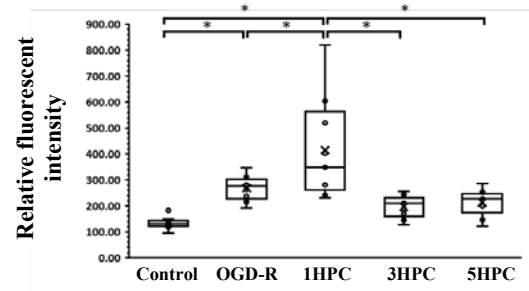


Figure 2: Box plots of relative fluorescent intensity of GFAP expression within the cortical spheroids. Data are expressed as means ± S.D. (* $p < 0.05$).

Conclusions

Single hypoxia has the greatest potential to promote astrocyte activation and hence promote functional recovery of the brain after stroke. Our study emphasizes the need to consider the differential effect of HPC on stroke under varying protocols.

Acknowledgments

This work is based on research that has been conducted as part of the KAIST-funded Global Singularity Research Program for 2020.

References

- [1] Hong.L. N. et al.(2018) *Exp. Neurol.*, **306**: 177-189
- [2] Li. et al. (2008) *Blood Flow Metab.*, **28**: 468-481

Biophysical response of human bronchial epithelial cells to biocides

Tae Yoon Kwon¹, Jaeseong Jeong², Eunyoung Park¹, Youngbin Cho¹, Dongyoung Lim², Ung Hyun Ko¹, Jennifer H. Shin¹, and Jinhee Choi²

¹Department of Mechanical Engineering, KAIST, 291 Daehakro, Daejeon, 34034, Republic of Korea

²School of Environmental Engineering, University of Seoul, 163 Seoulsiripdaero, Seoul, 02504, Republic of Korea
Email: j_shin@kaist.ac.kr, jinhchoi@uos.ac.kr

Summary

This study investigated the physical traits and mechano-stress response of human bronchial epithelial cells, BEAS-2B, to two different biocides, PHMG and CMIT/MIT, known as toxic components in humidifier disinfectants. When exposed to these biocides, the cells exhibited distinct average responses in their biophysical traits, and the heterogeneity in the responses was significantly higher in CMIT/MIT treated cells. Traction and intercellular stresses of the cellular monolayer were also measured over 24 hours based on live imaging data where two biocides showed remarkably distinct temporal responses. Based on the temporal stress evolution over 24 hours, protein and gene expressions were analyzed at specific time points for further confirmation of the changes in the physiological state of the cells. This study will contribute to the proper management of hazardous biocides related to humidifier disinfectants.

Introduction

Changes in the physical parameters of the cells can be important indicators of stress response because they are closely associated with changes in cellular functions. Physical traits allow continuous monitoring over a long culture time based on live-imaging data from which the morphological features and the stresses at the cell-matrix and cell-cell adhesions can be conveniently assessed.

From 2006 to 2011, fatal lung injury was observed, which later confirmed the chemical disinfectants (PHMG and CMIT/MIT) used in household humidifiers as the causal agents. In this study, we conducted the various real-time imaging-based cell-mechanical analysis using these two biocides on human lung cells.

Methods

BEAS-2B cells were obtained from American Type Culture Collection and cultured under a normal culture condition. Polyacrylamide (PA) gel (3kPa) and collagen type I were used to construct *in vitro* measurement platform. Traction and intercellular stress were measured based on the displacements of the fluorescent beads embedded in the PA gel. For the monolayer stress analysis, we cultured BEAS-2B cells on circular patterned collagen. This circular island was created by PDMS stencil to allow selective attachment of the cells only inside the circular pattern.

Results and Discussion

We characterized the cell and nuclear size, nuclear aspect ratio and cell traction based on single-cell measurements. While the

average responses of all 4 parameters were not significantly different, the degree of dispersion measured by standard deviation was remarkably higher in CMIT/MIT treated conditions.

Traction and intercellular stress of cells in the monolayer were also measured. The stress of PHMG and CMIT/MIT treated condition exhibited unique temporal responses compared to that of control during 24hours (Figure 1). We also investigate the expression of actin structures by immunofluorescence imaging and specific biomarkers (TGF- β and pSMAD-2) by western blot at two specific time points based on temporal stress evolution.

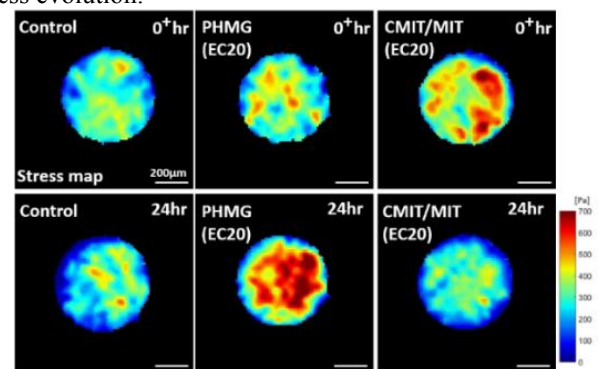


Figure 1: Temporal evolution of stress map.

Conclusions

This study highlights the strength of live imaging-based biophysical analysis that can provide a temporal portrait of the cellular response over a long time. The comparative analysis between CMIT/MIT and PHMG enabled better understanding of less studied substance, CMIT/MIT, in relation to a more studied substance, PHMG. Furthermore, this study is meaningful in that it can contribute to the proper management of hazardous biocides related to humidifier disinfectants.

Acknowledgments

This work was supported by the Korean Ministry of Environment under the 'Environmental Health R&D Program' (2017001370001) and National Research Foundation of Korea (NRF) grants funded by the Korean Government (NRF-2020M3A9E4039658).

References

- [1] Kim, S et al. (2016). *Environ. Health Toxicol*, **31**: e2016025.
- [2] Prasad, A et al. (2019) *Trends Biotechnol*, **37**: 347-35

Arm Profile Score represents ability of activity using upper limb in individual with stroke.

Dain Shim¹, Deog Young Kim¹, Joong-on Choi¹, Dongho Park¹, Beomki Yoo¹,
Dong-wook Rha¹

¹ Department and Research Institute of Rehabilitation Medicine, Yonsei University College of Medicine
Email: medicus@yonsei.ac.kr

Summary

Arm Profile Score (APS) is a simple index that evaluates severity of upper limb movement pathology based on kinematic data. The correlation between APS and the clinical upper limb function test in hemiplegic persons with stroke was measured. APS correlated moderately with the BBT and JHFT, which measure the ability of the activity using the upper limb.

Introduction

The 3D upper limb motion analysis is increasingly used to measure the impairment of the upper limb in persons with stroke, but it is difficult to interpret the enormous kinematic data. [1]

Arm Profile Score (APS) and Arm Variable Scores (AVS) are quantitative measurements that compare the characteristics of upper limb kinematics in individuals with motor impairments to those of non-disabled persons in a direct and simple way. [2]

The purpose of this study is to investigate whether the APS and AVS derived from 3D motion analysis reflect the upper limb function in hemiplegic persons with stroke.

Methods

A total of 74 individuals with stroke (44 males, 30 females; mean age 60±15.3 years) who could perform the Reach and Grasp Cycle [3] were recruited. Upper extremity subscale of the Fugl-Meyer assessment (FMA-UE), Box and Block Test (BBT), Jebsen-Taylor Hand Function Test (JHFT) were conducted. Computerized motion analysis was conducted during the Reach & Grasp Cycle include 4 tasks; reaching out to the cup and grabbing the cup, lifting the cup to the mouth, putting the cup back in its original position, and putting the hand back in place.

APS was calculated from root mean square error of the kinematic data of the subject with upper limb motor impairment compared to the mean kinematic value of non-disabled persons as a reference data. APS can be decomposed into 10 AVS representing each joint of upper extremity; thorax (3), shoulder (3), elbow (1), wrist (3) joints. [2] To evaluate correlations of APS and AVS with clinical upper limb function tests, the Spearman rank coefficient was used.

Results and Discussion

APS during Reach & Grasp Cycle showed moderate negative correlation with BBT score ($r^s = -0.581$; $p < 0.01$). (Table. 1)

Especially, AVS of wrist rotation showed moderate negative correlation with BBT score ($r^s = -0.513$; $p < 0.01$).

APS during Reach & Grasp Cycle showed moderate positive correlation with most items of JHFT ($r^s = 0.460-0.526$; $p < 0.01$). Especially, AVS of shoulder abduction/adduction showed moderate positive correlation with writing and lifting large object items of JHFT ($r^s = 0.433-0.520$; $p < 0.01$).

APS correlated moderately with BBT and JHFT, which measure the activity ability using the upper limb. But APS showed no significant correlation with FMA-UE, which measures physical function rather than ability of activity using upper limb.

Table 1: Spearman rank correlation between upper limb function measurements and the APS in hemiplegic persons with stroke.

	APS
Box and Block Test (n=67)	-0.581**
Jebsen Taylor hand function test (n=39)	
Writing	0.365*
Turning cards	0.363*
Lifting small objects	0.336*
Simulated feeding	0.460**
Stacking checkers	0.486**
Lifting Large, Light object	0.492**
Lifting Large, Heavy object	0.526**

* $P < 0.05$ by Spearman's rank correlation test

** $P < 0.01$ by Spearman's rank correlation test

Conclusions

BBT and JHFT, measuring limitation of upper limb activities, showed moderate correlation with APS. However, FMA-UE, measuring impairments of upper limb functions and structures, showed no significant correlation with APS. APS may be able to reflect activity limitation better than functional impairments of upper limb.

References

- [1] Joanne M Wagner et al. (2008). *Physical Therapy*, **88**; 652–663.
- [2] Ellen Jaspers et al. (2011). *Gait & Posture*, **34**: 227-233.
- [3] Erin E. Butler and Jessica Rose (2012). *J Biomech*, **45**; 945-951.
- [4] Federica Corona et al. (2018). *Clinical Biomechanics*, **51**: 45-51.

Lumbar and pelvis statistical shape model to characterize population shape variations

Nikita Ghosh¹, Justin Fernandez¹, Joe Baker³, Ju Zhang¹, Peter Robertson², Julie Choisine¹

¹Auckland Bioengineering Institute, University of Auckland, New Zealand

²Mercy Hospital, Auckland, New Zealand

³School of Medicine, University of Auckland, New Zealand

Email: ngho752@aucklanduni.ac.nz

Summary

Degenerative Disc Disease (DDD) is a major musculoskeletal disorder often surgically operated using fusion implants and associated with high failure rates. Statistical shape models (SSM) can predict patient-specific geometry to better predict clinical outcomes. By performing principle component analysis on vertebrae, sacrum and pelvis the main modes of shape variation within the population was captured. The predictive capability of SSM was compared between with and without integrating bone measurements. The results showed that with the measurements, SSM can better predict the bone shapes by 0.38mm (average across all of the bones) in case of RMS. For Dice score it improved by 3.5%, 2.3%, 3.5%, 2.4%, 3% and 1.35% respectively.

Introduction

DDD is a major musculoskeletal disorder often surgically operated using fusion implants. However, the surgery is associated with high failure rates (up to 40%), with only 25% of failures may be revised [1]. SSM can predict patient-specific geometry and compare intersubjective variability to better predict clinical outcomes. Therefore, the aim of this study was to compare the prediction accuracy of lumbar vertebrae, pelvis and sacrum bone shapes with different input measurements to the SSM.

Methods

De-identified CT scans (Siemens, Munich, Germany) from 79 healthy adult participants were collected (43 F, 45 ±6 y.o.). A total of 70 L1, L2 and L3, 67 L4, 68 L5, 64 sacrum and pelvic surfaces were segmented using Mimics (Materialise, Belgium) and remeshed using 3Matics. Template meshes were built for each vertebral level, sacrum, and pelvis. Bones coordinate system were built for each template according to the ISB standard [2]. Manually reconstructed bone surfaces were fitted and aligned to each template meshes for nodal correspondence. A PCA was performed on each vertebral level, sacrum and pelvis using an in-house python library, GLAS2 [3]. Based on the PCA outcome we extracted the

weights from 69 principal component and imported it in a Partial Least Square Regression (PLSR) along with the patient's age and sex. Additional bone measurements were included to the PLSR such as vertebral height length and width (for L1 to L5), sacrum's S1 upper plateau length and width and pelvic ASIS and PSIS distances. A leave one out analysis (LOO) was performed to understand the predictive power of each model; with and without bone measurements. Prediction accuracy was quantified by computing the Root Mean Square (RMS) error of the Euclidian distance and the Dice score quantified between the SSM-predicted shapes and CT-reconstructed shapes.

Results and Discussion

For L1-L5, the first three PCs accounted for 1) the vertebral body height, 2) posterior arch shape variation, and 3) superior, inferior articular process variations respectively. For the pelvis and sacrum, the first and second PCs described 1) bone height and 2) width variation and the third PC described iliac width (pelvis) and superior articular process (sacrum) shape variation. For the SSM models, the comparison between RMS and dice score for the 7 bones are shown in Table 1. In this work, we have developed a SSM of the lumbar vertebrae, sacrum, and pelvis on 72 healthy participants. We also aimed to compare the predictive capability of SSM considering with and without landmarks. Our results demonstrated that when we consider the anatomical landmarks in our SSM, the results improve significantly.

Conclusions

Bone shape prediction of the lumbar vertebra, sacrum and pelvis were more promising considering integrating bone measurement as input to the SSM.

References

- [1] Murray et al.(2013), *JAMA*:310:591-608.
- [2] Wu et al. (2002). *JOB* 35: 543-548.
- [3] Zhang et al. (2014), *CMBBE*: 2:3, 176-185.

Table 1: RMS error (average ±SD) of Euclidian distances (mm) and Dice score between CT reconstructed and SSM predicted bone for L1 to L5, sacrum and pelvis. SSM 1 represent the model without bone measurement (only age and sex) and SSM2 includes bone measurement in the SSM input.

	L1		L2		L3		L4		L5		Pelvis		Sacrum	
	RMS	Dice												
SSM1	2.1 ±0.5	0.86	2.1 ±0.5	0.87	2.4 ±0.6	0.85	2.3 ±0.6	0.85	3.1 ±0.7	0.83	6.5± 1.6	0.68	5.5 ±1.5	0.74
SSM2	1.6 ±0.2	0.89	1.7 ±0.3	0.89	2.1 ±0.5	0.88	2.1 ±0.4	0.87	2.5 ±0.5	0.85	6.4 ±1.4	0.70	4.9 ±1.4	0.75

Evidence Literature Summary: Patellofemoral pain in adolescents and objective test routines for the movement analysis laboratory

Josephine Meissner¹, Katharina Hermes¹, Annika Stampfler², Beat Göpfert³

¹Health Division, Bern University of Applied Sciences, Bern, Switzerland

²BZG, Bildungszentrum Gesundheit Basel-Stadt, Münchenstein, Switzerland

³Department Biomedical Engineering, University of Basel & University Children's Hospital Basel; Switzerland

Email: beat.goepfert@unibas.ch

Summary

Patellofemoral pain in adolescents is a common pathology but there are no standardized test routines for movement analysis laboratories. An evidence literature summary could not find any specific information for adolescents. An extended literature search found some functional tests for adults. The described tests suggest, that squatting and climbing stairs should be used as progress parameters.

Introduction

Patellofemoral pain (PFS) in adolescents and adults is one of the most common pathologies of the musculoskeletal system [1]. Up to 30% of adolescents are affected by this pain, especially girls and physically active people [2]. The cause of PFS is largely unclear [3]. Because of this, there are no clear guidelines for treatment. Physiotherapy is usually the first intervention in PFS. [4].

Methods

A literature search on PFS, test routines and adolescents was carried out. Due to a lack of studies, adults were included in a second search until May 17 2020.

- Used Databases: PubMed, Embase, Web of Science, Cochrane Library, Google Scholar.
- Articles published by May 17, 2020
- Evaluating the risk of bias (GATE-Frame, DELBI)
- Rating the Grade of Recommendation (A-E) based on the OCEBM Level of Evidence (Oxford Centre for Evidence Based Medicine)

Results

No literature could be found in relation to the question of objective PFS test routines and adolescents. Nonetheless, a study was included in the analysis because it provided meaningful insights. Eleven articles were included in the adult literature search (Tab 1).

Table 1: Summary table of the included articles. VGRF = Vertical Ground Reaction Force; EMG = electromyography; ↑ = climb up; ↓ = go down; DELBI = German Guideline Evaluation Instrument

Author	Tests	Level of Evidence	Risk of Bias
Adolescent			
[6]	neuromuscular control mechanisms	Level 2	low
Functional tests in adults			
[7]	VGRF during stair climbing↑↓	Level 2	moderat
[8]	Squatting; Stair ↑↓; Step-down	Level 1	low
[9]	Various gait parameter	Level 2	low
[10]	Squatting; Stairs ↑↓	Level 1	high
[11]	Stairs ↑↓; Forward/Lateral Step-down; etc.	Level 3	moderat
[12]	Squatting; Stairs ↑; Step-down	Level 1	moderat
[13]	Squatting; Stairs ↑; Step-down; Lunge; etc.	Level 1	low
[14]	Squatting; Stairs ↑↓; Lateral ↓; Step-down; etc. (DELBI)	–	–
EMG in adults			
[15]	frequency domain vs. time domain	Level 2	low
[16]	frequency domain vs. time domain	Level 2	moderat
[17]	frequency domain vs. time domain	Level 2	low

As part of this work, a study was found that examines and compares the reliability of various functional tests [5].

Discussion

- Functional tests like squatting and climbing and descending stairs are best suited.
- As reliable are described: Lateral and forward step-down as well as the single leg hop test.
- For EMG measurements, it is recommended to measure in the frequency domain instead of the time domain.
- Due to possible different causes of PFS in adolescents and adults, the suggested tests can only be used with caution.
- Inconsistent test execution makes it difficult to compare the functional tests.

Grades of recommendation for the various tests according to OCEBM [18].

- Squatting and climbing stairs
- EMG measurements using the frequency domain
- Frontal Plain Projection Angle during SLS; Lateral and Forward Step-down; Vertical Ground Reaction Force during the forward step-down

Conclusions

The articles reviewed did not provide consistent evidence of the accuracy of the tests. The results suggest that functional tasks such as squatting and climbing stairs should be used as progress parameters. In the future, standardized tests with homogeneous samples will have to be carried out.

References

- Glaviano et al. (2015). IJSPT.
- Witvrouw et al. (2014). BJSM.
- Smith et al. (2018). PLOS ONE.
- Witvrouw et al. (2014). BJSM.
- Lopes Ferreira et al. (2019). Gait and Posture.
- Galloway et al. (2018). AJSM.
- Briani et al. (2018). Knee.
- Cook. Et al. (2012). Physiotherapy.
- Leibbrandt; Louw (2018). J Bodyw Mov Ther.
- Leibbrandt, Louw (2017). SAJP
- Lopes et al. (2019). Gait and Posture.
- Nunes et al. (2013). Physical Therapy in Sport.
- Papadopoulos et al. (2015). Sports Med Open
- Willy, et al. (2019). JOSPT.
- Briani et al. (2015). Clinical Biomechanics.
- Motealleh et al. (2011). MJIRI.
- Pazzinatto et al. (2015). Motriz: Rev. Ed. Fís. [
- Phillips et al. (2009). OCEBM.

Kinematics Comparison of Two Posterior Stabilized Knee Implants During Daily Activities

Chang Shu¹, Fangjian Chen¹, Michael Bates², Ronald W. Singer² and Nigel Zheng¹
¹The University of North Carolina at Charlotte, NC, ²OrthoCarolina, NC, USA
 Email: nzheng@uncc.edu

Summary

Posterior stabilized (PS) TKA implant is the optimal choice for patient who needs knee replacement surgery but has relatively weak posterior cruciate ligament (PCL). It is important to assist surgeons to identify appropriate PS implants due to their different philosophy of design. This study compared two popular PS implants (Journey II, Persona) kinematically for level walking and stair ascending and found the significant differences between the implants.

Introduction

Total knee arthroplasty (TKA) is the most common surgical procedure aiming at reducing pain and improving physical function for patients with end-stage knee osteoarthritis. Posterior-stabilized (PS) knee implants were designed for patients with an incompetent or attenuated PCL [1]. The amount of bone resection may be related to the risk of popliteus tendon injury [2]. The aim of this study was to compare two PS knee implants (Journey II from Smith & Nephew, Persona from Zimmer) with healthy controls. 3-D knee joint kinematics of TKA patients and control group were compared during five daily activities such as level walking (LW) and stair ascending (SA). We hypothesized that there was no significant difference of two selected implants in 3D knee joint motion during daily activities.

Methods

20 patients with Journey II (J), 20 patients with Persona (P) implant and 11 healthy subjects (CG) were recruited. Both implant groups were tested pre-op and 6-month post-op using a motion capture system (FX 40, VICON). Due to the pandemic, only 10 patients with J and 8 patients with P completed the 6-month post-op tests. The knee joint kinematics were computed using a custom developed MATLAB program (MathWorks Inc.) One-way ANOVA was performed with 0.05 alpha level.

Results and Discussion

There were no significant differences in demography and pre-op knee joint kinematics between two groups. Group P had a knee flexion deficit during these activities (Fig.1). Group J had a closer range of motion (ROM) as CG than group P. AP

Table 1: Knee joint flexion/extension (deg), anterior/posterior translation (mm) and their range of motion (ROM) at 6-month post-op. *: significant difference between two implants.

	Level Walking			Stair Ascent		
	P	J	CG	P	J	CG
Flex.	66±9	72±9	74±6	100±9	106±9	108±10
Ext.	17±8	15±7	17±5	23±7	20±7	24±6
ROM	50±8*	57±5	57±7	79±6	86±6	83±8
Ant.	4±3	3±3	-2±3	1±5	-4±7	-3±3
Post.	-13±8*	-24±11	-26±11	-21±13*	-42±19	-41±15
ROM	17±6*	27±9	24±8	22±12*	39±15	31±13

translation in group J was closer to normal knee than patients in group P. Group P exhibited a significant deficit in posterior translation (Figure.1). The statistical significances were found between the two groups (Table.1). Although the joint rotation at the early stance phase was similar, the maximum knee flexion and ROM were different. Similar results for AP translation, the posterior translation and ROM were different between the two implants. Thus, the hypothesis was rejected. The difference may be linked to the different designs in cam-post shape of two implants. Further research is needed to explore the causes of these differences in knee joint movement and develop an optimal PS implant design.

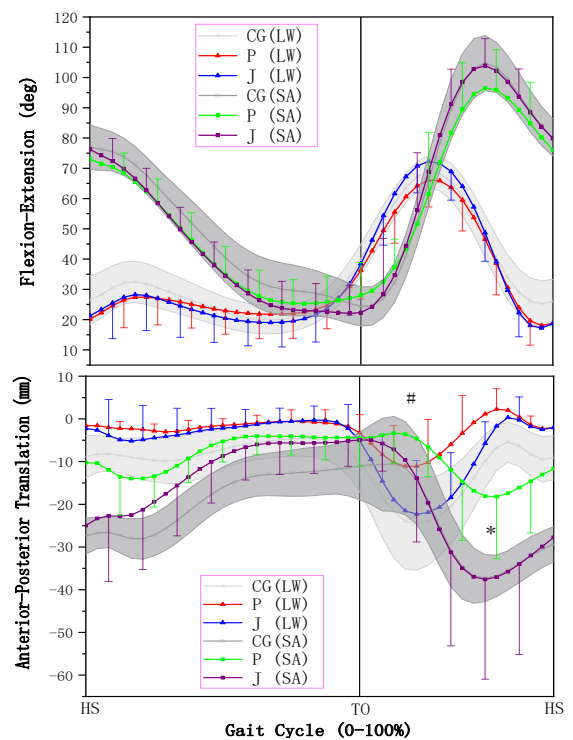


Figure 1: Knee flexion(+)/extension(-) and anterior(+)/posterior(-) translation. # and * represent the significant difference between group P and group J in terms of level walking (LW) and stair ascent (SA), respectively.

Conclusions

Findings from this study indicated implant design had influence on the functional improvement. Furthermore, it will provide useful information to PS knee implant design.

Acknowledgments

This study is funded by Smith and Nephew through an Investigator Initiated Study award.

References

- [1] Conditt, Michael A., et al. *J.Arthroplasty* 19.7: 107-112.
- [2] Takubo, Akihito., et al. *BMC MSD* 21: 1-7.

The effects of Joint Hypermobility Syndrome on the kinematics and kinetics of the vertical jump test.

Najla. Alsiri^{1,2}, Mary Cramp¹, Sue Barnett¹ Shea Palmer¹

¹Human Analysis Laboratory, University of the West of England, Bristol, United Kingdom

²Al-Razi Orthopedic and Rehabilitation Hospital, Capital Governance, Kuwait.

Email: dr.alsiri@outlook.com

Summary

This study presents a novel exploration of the biomechanics of the lower limb joints in adults with JHS during a high intensity physical task - the vertical jump test (Figure 1). This study showed that people with JHS are able to actively stiffen their joints during a high intensity task. Considering that multiple joint hypermobility is the primary feature in JHS. These changes can be considered dominant and should be maximized during rehabilitation to improve the activity of people with JHS.

Introduction

Biomechanical impairments are not apparent during walking in people with Joint Hypermobility Syndrome (JHS). This research explored biomechanical alterations during a higher intensity task, vertical jumping.

Methods

This cross-sectional study compared a JHS group (n=29) to a healthy control group (n=30). Joint kinematics and kinetics were recorded using a Qualisys motion capture system synchronized with a Kistler platform. Independent sample t-tests and standardized mean differences (SMD) were used for statistical analysis.

Results and Discussion

No significant statistical or clinical differences were found between groups in joint kinematics and jump height ($p \geq 0.01$). Sagittal hip and knee peak power generation were statistically lower in the JHS group during the compression phase ($p \leq 0.01$), but not clinically relevant ($SMD < 0.5$). Clinically relevant reductions were found in the JHS group knee and ankle peak moments during the compression phase, and hip and knee peak power generation during the push phase

($SMD \geq 0.5$), although these were not statistically significant ($p \geq 0.01$).

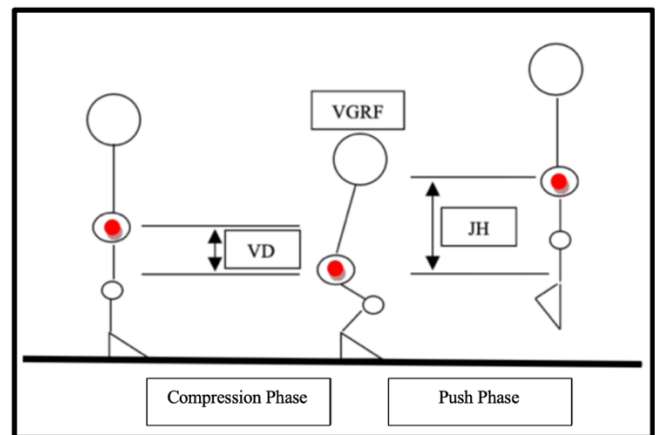


Figure 1: A drawing illustrating the jump test phases: compression and push phase. The compression phase is the phase between still standing to the lowest reached distance before the jump. The push phase is the phase between the first frame after the lowest reached distance to the maximum height reached. A pelvis marker; the red dot, was used to measure vertical displacement and jump height. VD = vertical displacement, VGRF = vertical ground reaction force, JH = jump height.

Conclusions

The JHS group achieved a similar jump height but with some biomechanical alterations. Further understanding of the joint biomechanical behavior could help to optimize management strategies for JHS, potentially focusing on neuromuscular control and strength/power training.

Are biomechanics during gait associated with the structural onset and progression of lower limb osteoarthritis? A systematic review and meta-analysis.

Nicole D'Souza¹, Jesse Charlton², Jane Grayson¹, Sarah Kobayashi¹, Laura Hutchison¹, Michael Hunt², Milena Simic¹

¹Faculty of Medicine and Health, University of Sydney, Australia

²Graduate Programs in Rehabilitation Sciences, Faculty of Medicine, University of British Columbia, Vancouver, Canada.

Email: ndso3565@uni.sydney.edu.au

Summary

The objective of this systematic review and meta-analysis is to evaluate if gait biomechanics are associated with increased risk of structurally diagnosed onset or progression of lower limb osteoarthritis (OA). Twenty out of the twenty-one included studies found an association between at least one biomechanical measure and structural onset/progression defined by image-based changes/ conduct of replacement surgeries. PROSPERO: CRD42019133920

Introduction

Osteoarthritis is one of the leading contributors to disability [1] in the world and is associated with a considerable economic burden to the individual, healthcare system, and the community [2]. In the attempt to reduce this burden, an understanding of the modifiable risk factors of disease onset and/or progression is needed. One of the key emerging risk factors for understanding OA onset and progression is theorised to be the loading of weight-bearing joints during gait [3].

Methods

A systematic review of Medline and Embase was conducted from inception to November 21st, 2020. Records were screened, data extracted, and methodological quality assessed by two independent reviewers. Included studies reported gait biomechanics at baseline, and either structural imaging or joint replacement outcomes in lower limb at follow-up. The primary outcome was the Odds Ratio (OR) (95% confidence interval (CI)) of the association between biomechanical measures and structural OA outcomes with data pooled, where possible, for meta-analysis.

Results and Discussion

Twenty-one studies reporting 28 different biomechanical measures and 10 OA imaging outcomes were included. Eighteen studies investigated knee OA progression; two of these also investigated knee OA onset. Three studies investigated hip OA progression. No longitudinal studies were found in relation to biomechanics and the risk of ankle OA or progression. Study quality score ranged from 14-20 out of 21

points. All but one study (95%) reported a significant association between at least one biomechanical outcome and OA onset or progression. There was an association between frontal plane kinematics and kinetics with medial tibiofemoral OA progression, and sagittal plane kinetics with patellofemoral and hip OA progression. Meta-analyses demonstrated increased odds of medial tibiofemoral OA progression with greater baseline early stance peak knee adduction moment (KAM) (Figure 1) (OR: 2.00 [95%CI: 1.04-3.84]), and varus thrust prevalence (Figure 2) (OR: 2.00 [95%CI: 1.32-2.98]).

Early stance peak KAM and medial tibiofemoral OA progression



Figure 1: The association between early stance peak KAM and medial tibiofemoral OA progression.

Varus thrust and medial tibiofemoral OA progression

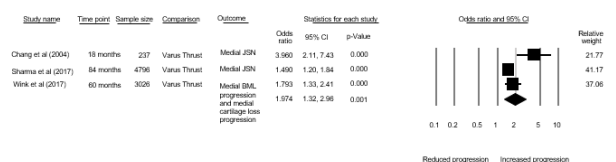


Figure 2: The association between varus thrust and medial tibiofemoral OA progression.

Conclusions

There is evidence that certain gait biomechanics are associated with an increased odds of OA onset and progression in the knee, and progression in the hip.

References

- [1] Vos et al. (2015). *The Lancet*, **386**: 743-800
- [2] Kingsbury et al. (2014) *Rheumatology*, **53**: 937-947
- [3] Andriacchi et al. (2004). *Annals of Biomedical Engineering*, **32**: 447-45

Influence of ankle joint angle on Achilles tendon stiffness

Evan D. Crotty¹, Laura-Anne M. Furlong², Andrew J. Harrison¹

Biomechanics Research Unit, Department of Physical Education and Sport Sciences, University of Limerick, Limerick, Ireland¹
School of Sport, Exercise and Health Sciences, Loughborough University, Loughborough, UK

Email: evan.crotty@ul.ie

Summary

Tendon stiffness (K_T) is a widely examined musculoskeletal measure due to its reported links with muscle-tendon unit performance and as a potential injury risk factor. This study examined the influence of ankle joint angle (θ_{ANK}) on K_T and the inter-day reliability of K_T across θ_{ANK} . K_T was measured during maximal voluntary plantarflexion contractions at three θ_{ANK} . A significant difference was not observed between K_T measured at the three θ_{ANK} however, K_T at the dorsiflexion θ_{ANK} demonstrated the best inter-day reliability. Measuring K_T at the dorsiflexion θ_{ANK} may improve the reliability of the measure when examining K_T across multiple time periods.

Introduction

K_T is commonly examined using B-mode ultrasound and dynamometry during isometric contractions [1] but can be methodologically challenging. Variability in K_T can be attributed to a number of reasons including measurement equipment, inherent individual variation, and methodological issues e.g. tendon moment arm measurement and ankle joint rotation [1]. Researchers commonly examine K_T at a neutral θ_{ANK} of 0° with the knee at 180° . Limited research has examined the influence of different θ_{ANK} on K_T , and the reliability of K_T acquired during dynamometry and ultrasound-based protocols. The study aims to investigate changes in K_T across θ_{ANK} . The objectives are: 1) to determine the inter-day reliability of K_T across θ_{ANK} , 2) to examine K_T changes across θ_{ANK} , and 3) to identify the main factors influencing K_T reliability.

Methods

Fourteen physically active individuals (7 ♂, 7 ♀) performed isometric maximal voluntary plantarflexion contractions at three θ_{ANK} (-10° plantarflexion (PF), 0° (NE), 10° dorsiflexion (DF)) on a calibrated dynamometer (Con-trex, Dubendorf, Switzerland) on two occasions separated by 7 days. The distal aponeuroses of the gastrocnemius medialis were visualized using a 128-element linear ultrasound probe (Telemed, Vilnius, Lithuania) during the contractions. Tendon force was estimated by dividing ankle moment by the tendon moment arm. Tendon elongation was digitized and corrected for elongation due to joint rotation. Resting tendon

length was calculated at rest with the knee at 180° and ankle joint plantarflexed at -20° . K_T was calculated as the slope of the force elongation (relative K_T), and force strain (absolute K_T) relationship between 10% and 90% of maximal tendon force. A one-way repeated measures ANOVA and Bonferroni post-hoc test examined K_T differences across θ_{ANK} . Inter-day reliability was examined using intra-class correlation coefficient (ICC), mean difference (Mdiff), coefficient of variation (CV), and effect size (ES).

Results and Discussion

Reliability: K_T at the DF θ_{ANK} demonstrated the best inter-day reliability for relative and absolute K_T (Table 1). Further investigation of the components that contribute to the calculation of K_T showed that time to maximum tendon force demonstrated improved inter-day reliability (ICC = 0.651) at the DF θ_{ANK} compared to other θ_{ANK} (PF ICC = 0.268, NE ICC = 0.255). Time to maximum tendon force is a factor in calculating tendon strain rate, and tendon strain rate is known to influence calculated K_T [2]. Thus, improved inter-day reliability of this component of tendon strain rate may contribute to the improved reliability of K_T at the DF θ_{ANK} .

Ankle angle: K_T tended to increase as θ_{ANK} moved from PF toward DF (Table 1). No significant difference was observed between the three θ_{ANK} for K_T measures.

Conclusions

K_T measured at the DF θ_{ANK} demonstrated improved inter-day reliability, potentially due to a participant's ability to produce a more uniform tendon strain rate at this θ_{ANK} . Examining K_T at this θ_{ANK} could improve the reliability of K_T for studies examining the influence of mechanical loading on tendon adaptation over multiple time periods.

Acknowledgements

The authors would like to acknowledge the Irish Research Council for supporting this research.

References

- [1] Pearson SJ and Onambele GL (2012). *J Mech Behav Biomed Mater.* **5**: 291-297.
- [2] Theis N et al. (2012). *J Electromyogr Kinesiol.* **22**: 947-53.

Table 1: Mean (\pm s) K_T values, and inter-day reliability measures

	Mean (\pm s)				ICC	Mdiff (%)	CV (%)	ES (d)
	Day 1		Day 2					
Relative K_T (N/mm)								
PF	88.9	40.1	85.3	37.6	0.598	3.96	24.82	0.095
NE	97.0	34.7	89.7	32.7	0.341	7.54	20.48	0.180
DF	103.7	27.2	98.8	26.7	0.756	4.66	9.57	0.254
Absolute K_T (N/Strain)								
PF	162.4	71.7	162.3	80.1	0.579	0.40	24.89	0.000
NE	172.1	62.0	169.1	72.6	0.410	1.80	20.30	0.144
DF	190.7	57.3	187.4	62.8	0.818	1.74	8.69	0.085

Assessment of role of iron in neural circuitry of motor intention on performance of Brain-Computer Interfaces

Jagriti Natraj^{1,2}, Vijayakumar Chinnadurai²

¹Modern School, Barakhamba Road, Delhi, India

²NMR Division, Institute of Nuclear Medicine and Allied Sciences, DRDO, Delhi, India

Email: jagritinatraj@gmail.com

Summary

Developing Brain-Computer Interfaces (BCI) with reproducible and stable Information Transfer Rate (ITR) is challenging as many cognitive and neural factors [1] influence an individual's ability to perform a specific cognitive task. One such factor is dysregulation of brain iron metabolism [2] which profoundly affects neurophysiological mechanisms, neural connectivity and brain structures. This study attempts to understand whether dysregulation of ferritin iron in motor and frontal lobes of individuals plays a significant role in fluctuation in ITR of the BCI system for early prediction of motor intention in hand gripping task. The study further presents novel microstate-based Motion Related Cortical Potential (MRCP) neural information as input information for deep learning models.

Introduction

The neural circuitry of motor intention is complex and varies inter-individually based on functional, structural and metabolic differences. This poses a challenge in developing a motor intention decoding BCI system with stable ITR. Recently, dysregulation of ferritin-iron deposited in brain regions was found to affect dementia and motor disorders. This study thus aims to understand the influence of iron deposited in the neural circuitry of motor intention on the ITR of the BCI system that classifies motor intention. The study also presents novel microstate-based MRCP neural information for training Long Short Time Memory–Stacked Autoencoder (LSTM-SAE) algorithms [3].

Methods

80 healthy, non-anemic, right-handed volunteers participated in simultaneous EEG-fMRI and Susceptibility Weighted Imaging (SWI) through 3T MRI and 32 Channel MR Compatible EEG systems. Each volunteer performed 90 randomized motor tasks of hand grip and release. The acquired data was subjected to the methodology illustrated in (Figure 1) consisting of two analyses: the development of a Deep neural BCI system based on microstate MRCP neural information, and the quantification of iron in the neural circuitry of motor intention. MRCP microstate analysis was carried out by collecting MRCP (0.2Hz to 2.5 Hz) [4] from pre-processed EEG prior to every motor action and the data was subjected to k-mean based microstate EEG analysis. The resultant microstates were back fitted to every

individual's EEG data and subsequently used to train the deep learning system LSTM-SAE. The performance of the trained BCI system was assessed by estimating its classification accuracy and ITR. Additionally, the neural circuitry of motor intention was estimated by subjecting MRCP information to EEG informed fMRI analysis. Then the SWI images were preprocessed and subjected to Quantitative Susceptibility Mapping (QSM) [5] for ferritin-iron quantification in the neural circuitry of motor intention. Finally, the estimated iron quantity was correlated with the ITR of the BCI system of the individual.

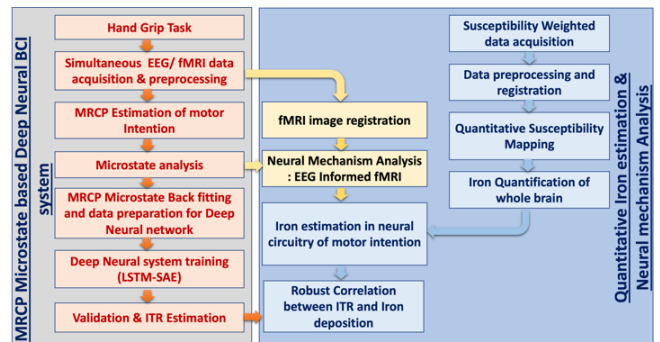


Figure 1: Overview of methodology employed

Results and Discussion

The performance of trained MRCP based LSTM-SAE BCI system is correlated with the iron quantification in the neural circuitry of motor intention as shown in (Table 1). It was found that Cerebellum, Lingual, Medial Frontal, Pre and Postcentral gyri have significant engagement during motor intention and corresponding iron quantification is observed to be correlating negatively with the ITR of the BCI system.

Conclusions

Iron dysregulation in the cerebellum, motor, frontal and cortical regions in healthy people is strongly associated with the neural engagement of motor intention and thus affects the ITR of the BCI system.

References

- [1] Myrden, Chau (2015). *Front. Hum. Neurosci.*, **9**: 308-319
- [2] Ravanfar et al. (2021). *Front. Neurosci.*, **15**: 41-72
- [3] Sangheer, Kotb (2019). *Sci Rep*, **9**: 19038
- [4] Shakeel et al. (2015). *CMMM*, **2015**: 34621
- [5] Vinayagamani et al. (2020). *JMRI*, **5**: 23-37

Table 1: Performance of microstate-based MRCP in LSTM-SAE BCI system and correlation with iron in neural circuitry of motor intention

Grip task intention	Classification Accuracy	Information Transfer Rate (ITR)	Significant robust correlation (p<0.001) observed between iron deposition and ITR values									
			Cerebellum		Lingual Gyrus		Middle Frontal Gyrus		Precentral Gyrus		Postcentral Gyrus	
			Right	Left	Right	Left	Right	Left	Right	Left	Right	Left
Left Hand	90.2 ± 9.1%	12.37±0.7	-0.39	-0.32	-0.46	-0.32	-	-0.36	-0.42	-0.32	-0.4	-
Right Hand	89.1 ± 9.9%	12.2 ± 0.9	-	-0.45	-0.41	-0.39	-	-0.45	-	-0.32	-	-0.35

Imaging and Image Processing Pipeline for Enhanced Connective Tissue MRI

M. Randika Perera¹, Leo Dang^{2,3}, Samantha Holdsworth^{2,3}, Geoffrey Handsfield¹

¹Auckland Bioengineering Institute, The University of Auckland, Auckland, New Zealand

²Mātai Medical Research Institute, Tāirawhiti-Gisborne, New Zealand

³Dept. Anatomy and Medical Imaging, The University of Auckland, Auckland, New Zealand

Email: mper162@aucklanduni.ac.nz

Summary: Recent interest in musculoskeletal connective tissues—e.g. tendon, aponeurosis, and fascia—has motivated *in vivo* medical imaging of these tissues, particularly using MRI. Due to the rapid T2* decay properties of collagenous tissues, advanced ultrashort echo time (UTE) MRI sequences are useful to produce images with high signal[1-2]. UTE MRI is now practical for connective tissue imaging, but limitations still exist, especially in signal and contrast. Image post processing can be implemented to improve feature extraction, particularly for thin tissues that may otherwise be obscured in images. Here we outline image processing methods suitable for enhancing MRI of the thin musculoskeletal connective tissues of aponeurosis and fascia.

Keywords: Connective Tissue, MRI, fascia, aponeurosis, imaging, image processing, feature extraction.

Introduction: MRI of fascia and aponeurosis is important for biomechanics and modeling applications of the musculoskeletal system, for anatomical assessment and probing clinical pathologies such as myofasciitis or compartment syndrome. The challenge of imaging these tissues with MRI has motivated the exploration of image processing methods that may enhance imaging and modeling of fascia and aponeurosis. We present four image processing techniques for fascia and aponeurosis imaging, and we identify and segment aponeurosis and fascia in processed images.

Methods: MRI was conducted on three participants on two different 3T MRI scanners which had different sequences available to trial. All images were collected using dual-echo ultrashort echo time (UTE) non-Cartesian MRI. Images collected on a 3T Siemens Skyra were acquired with a 2D stack of spirals sequence[3]. Images collected on a 3T GE Signa Premier were acquired with a 3D radial cones sequence[4]. In-plane spatial resolution was between 0.3x0.3 mm² and 0.5x0.5 mm² and the slice thickness was between 3mm and 5mm.

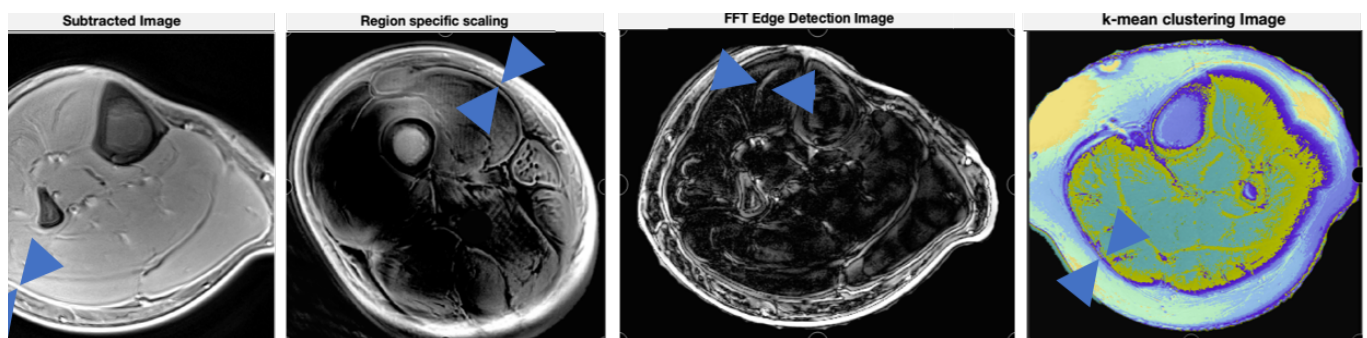
Tissue localization Methods: *Dual-echo image subtraction:* We use subtraction between the UTE image and the short TE image from our dual echo protocol to enhance connective tissue contrast. *Region specific scaling:* Region specific scaling was applied to reduce the signal intensity of unwanted tissues in one of the dual-echo images such that those signals cancel with less residual noise. This is useful for fat or muscle signal suppression to improve connective tissue contrast. *FFT edge detection:* Edge detection was implemented using a high-pass filter in the Fourier domain. This approach highlights the transition between muscle and internal connective tissue, resulting in high contrast in aponeurosis. *K-means Clustering:* Applied over dual-echo UTE images, this identifies regions by intensity and connectedness. In generic k-means clustering, each data point belongs to the cluster with the nearest mean. In our case, this approach identifies unique regions within the image that may not be easily identifiable via naked eye inspection.

Results and Discussion: Images of fascia and aponeurosis from our image processing methods are shown in Fig 1, regions of interest displaying fascia and/or aponeurosis are highlighted with arrows. Fascia was identified to run along the peripheral surface of muscle structures with widths between 1mm and 1.5mm. Aponeurosis width in the tibialis anterior was 1.8±0.2mm.

Conclusion: This work suggested several feature extraction image processing methods that could be used to enhance the MR signal quality of connective tissue in UTE MRI. Results demonstrate that fascia and aponeurosis are identifiable and measurable and suggest that these techniques improve imaging and modeling of thin connective tissues from MRI.

Acknowledgement: Authors thank Michael Carl from GE Healthcare, Anna Lydon from CAMRI & Paul Condon from Mātai Medical Research Institute for assistance with scanning.

References: [1] Robson et al.(2003).27:825–846. [2] Handsfield et al.(2020),Front. Sports Act. Living.2:70. [3] Qian et al.(2008), Magn Reson Med.60:135–145.[4] Ma et al.(2017), NMR in Biomed.30: 3709.



Demonstration of techniques. Blue markers on the images show fascia and aponeurosis locations (A) image subtraction reveals high signal, high contrast images of

Detailed Correlation Between Coronary Artery Disease and Tissue Speckle Tracking

Srisakul Chaichuum¹, Su-Chen Chang¹

Chih-Lin Chan², Yi-Ting Wu², Chu-Ying Hsu², Shou-Ju Chiang MD, PhD^{1,2}, Hsiang-Ho Chen PhD¹

¹Lab of Tissue Mechanics, Graduate Institute of Biomedical Materials and Tissue Engineering, Taipei Medical University, Taiwan

²Division of Cardiology, Dept. Internal Medicine, Taipei City Hospital Yangming Branch, Taipei, Taiwan

Email: d825108005@tmu.edu.tw

Summary

This study aims to investigate the correlations of cardiac mechanical parameters in tissue speckle tracking measurement and the coronary artery stenosis diagnosed by cardiac catheterization in patients with clinically diagnosed coronary artery disease (CAD). The actual stenosis rate in catheterization proved the evidence of this technique to assess coronary artery condition and implied the application of non-invasive method of tissue speckle tracking to evaluate the CAD.

Introduction

It is widely known that cardiovascular disease is a leading cause of mortality worldwide. CAD, a major adverse cardiac event is coronary stenosis, which is the underlying cause of ischemia, myocardial infarction, and sudden cardiac death. Although coronary angiography is the gold standard method to identify a blockage in cardiac vessels, catheterization is relatively invasive compared to other methods. Echocardiography is the most accessible and cost-effective technique routinely used for these patients. This non-invasive imaging model can detect the presence, extent and severity of the disease. Emerging ultrasound procedures such as tissue Doppler imaging, and the speckle tracking method are generally required as the first-line clinical utility [1]. Particularly, speckle tracking echocardiography can characterize cardiac mechanics [2].

Methods

The clinical practice in the cardiology department at Taipei City Hospital Yangming Branch has been studied since August 2020. All suspected CAD patients (n=53) were recruited as selection criteria by clinical diagnosis. Among the patients, 140 vessels were evaluated by coronary angiography and echocardiography. All patients underwent comprehensive transthoracic imaging as clinically indicated to rule out significant valvular heart disease. All biological parameters derived from tissue Doppler imaging were collected for further analysis. The echocardiographic views, in standard apical 4 chambers, 3 chambers, and 2 chambers from tissue speckle tracking were selected to quantify the left ventricle myocardial strain using EchoPAC software ; GE, Norway. The vessel strains of three main arteries ; right coronary artery (RCA), circumflex artery (LCX), and left anterior descending artery (LAD) were quantified (Figure 1) in longitudinal strain of each wall (Figure 2). The studied vessels were categorized and diagnosed by cardiac catheterization. The luminal stenosis of three main arteries were quantified

angiographically. A stenosis rate of over 70% was regarded as severe stenosis. The results of vessel-supplied tissue tracking and catheterization were compared with each other. The risk factors hypertension, diabetes mellitus, and serum lipid profile were also determined. The statistic analysis was done using SPSS software.

Results and Discussion

In total, 140 vessels in 53 patients were evaluated. The longitudinal strain of each vessel supplied area in severe stenosis vessels (n=39) (13.3 ± 6.4) was smaller than that of the insignificant stenosis vessel (n=101) (15.5 ± 5.2), $p = 0.04$. The results revealed that LAD, LCX and RCA vessel strain could be used to predict the stenosis condition in each coronary artery.

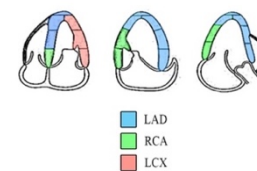


Figure 1: Myocardium is supplied by LAD, RCA and LCX.

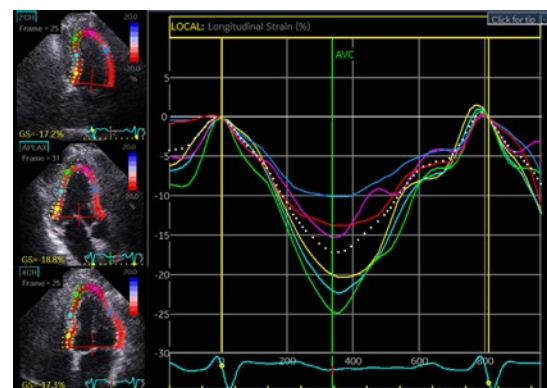


Figure 2: Myocardium was evaluated by tissue speckle tracking.

Conclusions

The tissue speckle tracking can be evaluated in each myocardial segment to determine each vessel strain. The vessel strain is correlated to the actual stenosis condition in CAD patients.

References

- [1] Xiaoyu Han et al. (2020). *BMC Cardiovasc Disord*, **20**: 362.
- [2] Shuo-Ju Chaing et al. (2014). *Circ J*, **78**: 419-42.

Differences in mechanical properties of hurdle bars

Ryo Iwasaki^{1,2}, Hiroyuki Nunome¹, Shariman Ismadi Ismail^{3,4}

¹ Faculty of Sports and Health Science, Fukuoka university, Fukuoka, Japan

² The United Graduate School of Education, Tokyo Gakugei University, Tokyo, Japan

³ Graduate school of Sports and Health Science, Fukuoka University, Fukuoka, Japan

⁴ Faculty of Sports Science and Recreation, Universiti Teknologi MARA, Shah Alam, Malaysia

Email: r-iwasaki@fukuoka-u.ac.jp

Summary

The present study aimed to investigate the differences in mechanical properties of hurdle bars. Bending test was performed on two hurdle bars made from different materials: ABS plastics and natural wood. From the bending test, load–deformation property was computed. The results of bending test were fitted with a regression line. There was a significant difference between the slopes of two regression lines. The wood bar was found to be more resistant to likely loads than the ABS bar. This finding suggests that materials used for the hurdle bar should consider when estimating the effect of hurdle hitting on race outcomes.

Introduction

In hurdle events, hitting hurdle has been known to have a negative impact on race performance, and its magnitude is dependent on the hitting part of the body [1] and may also be explained by the mechanical properties of hurdle bars. However, the mechanical properties of hurdle bars have never been investigated to date. Therefore, this study aimed to investigate the differences in mechanical properties of hurdle bars.

Methods

Two hurdle bars: made from ABS plastic and natural wood, were used for bending test. The test was performed five times to measure the deformation of the centre of bar against incremental loads (up to 10 kg from the World Athletics regulation [2]). A marker was attached to the centre of bar to detect its resultant deformation. A high-speed camera (FASTCAM Mini AX, Photron, Japan) was used to record the loaded deformations of the bars at 500Hz. Resultant deformation perpendicular to the bar was calculated using a motion analysis system (Frame-DIAS V, DKH, Japan). From this data, load–deformation property was computed as the relationship between the incremental loads (kg) and the resultant deformations (mm). In addition, the shore A hardness of each bar was measured at five points of each bar surface using shore A durometer (HTTK-37A, Tekcoplus Ltd., HKG). The results of bending test were fitted with a regression line. Analysis of covariance (ANCOVA) was used to compare the regression line slopes between the two conditions. A student's t-test was used to compare the shore A hardness between the two conditions. Significance level was set at $\alpha < 0.01$.

Results and Discussion

Figure 1 shows the load–deformation property of ABS and wood bars. The slope of the regression line of the wood bar was steeper than that of the ABS bar, and there was a significant difference between the slopes ($p < 0.01$). This finding indicated that the wood bar is more resistant to the given likely loads than the ABS bar. This could be affected by shore A hardness. In terms of shore A hardness, the wood bar was significantly harder than the ABS bar (Wood bar: 93.5 ± 0.8 HA, ABS bar: 87.1 ± 0.7 HA, $p < 0.01$). A previous study speculated that hitting hurdles might not affect overall performance in the 110-m hurdle race [3], thereby conflicting with another study [1]. These inconsistent findings may have been partially affected by the differences in mechanical properties of hurdle bars. Thus, this finding suggests that a detailed investigation on the material of the bar is necessary to estimate the exact impact of hitting hurdles on resultant race outcomes.

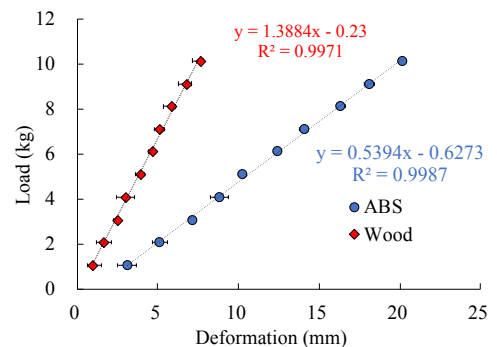


Figure 1: The load-deformation property between ABS and Wood

Conclusions

The present study demonstrated a clear difference in the mechanical property of hurdle bars made from ABS plastic and natural wood. This difference may affect the impact force of hitting hurdle and should be taken into account when examining its exact effect on race outcomes.

References

- [1] Iwasaki et al. (2020). *ISBS Proc.*, **38**:268–271.
- [2] World Athletics. (2020). <https://www.worldathletics.org/about-iaaf/documents/book-of-rules>, pp42–45, (accessed 4th. March. 2021).
- [3] Pollitt et al. (2018). <https://www.worldathletics.org/about-iaaf/documents/research-centre>, (accessed 4th. March. 2021).

Reliability of measuring ACL injury risk associated knee morphology in adolescent females

Bhushan Borotikar^{1,2}, Trent Guess³, Tinashe Mutsvangwa², Emily Leary³, Dana Duren³, Donna Pacicca⁴, Antonis Stylianou⁵

¹Symbiosis Centre for Medical Image Analysis, Symbiosis International University, Pune, India

²Division of Biomedical Engineering, University of Cape Town, Cape Town, South Africa

³University of Missouri, Columbia, USA

⁴Dept. of Orthopaedic Surgery, Children's Mercy Hospital, University of Missouri-Kansas City, Kansas City, USA

⁵School of Computing and Engineering, University of Missouri-Kansas City, Kansas City, USA

Email: bhushan.borotikar@scmia.edu.in

Summary

A comprehensive examination of early adolescent and adolescent knee morphologies associated with ACL injury provides critical knowledge of potential underlying risk, aiding efforts in injury prevention, ligament reconstruction and rehabilitation for this population. In this work, we characterize 11 morphological features of the tibia and femur that have a reported association with anterior cruciate ligament (ACL) injury risk using two raters and repeated measures. Measurements were conducted on retrospectively acquired MRI database of 36 healthy girls aged 13 to 18 years.

Introduction

The number of pediatric and adolescent ACL reconstructions has dramatically increased over the past decade [1]. Due to chondral and meniscus injury in an unstable knee, reconstructive ACL surgery is often the preferred treatment for skeletally immature patients. Adolescent individuals with ACL injury experience reduced knee related quality of life, increased risk for early-onset knee osteoarthritis, and high re-injury rates. Greater understanding of risk factors for ACL injury is key to injury prevention. Studies on the occurrence of ACL risk knee morphologies in pediatric populations, especially early adolescent and skeletally immature populations are limited. In this study we report on the reliability of MRI-based anatomical parameters associated with ACL injury risk around the knee joint in a healthy female adolescent population.

Methods

MRI datasets of adolescent girls between 13 to 18 years were retrospectively acquired (n = 36) from the Children's Mercy Hospital, Kansas City's radiology department. The data usage protocol was approved by the institutional review board. Each dataset was anonymized and examined by a radiologist for anatomical integrity and abnormality. Based on the literature,

11 morphological parameters were selected and manually measured (3D Slicer, ver. 4) in each acquired dataset. An instructive guideline was created based on the literature available for each of the parameters. Two independent and medically trained observers measured these parameters. Each observer performed the measurements twice. Inter-observer reliability was defined by intraclass correlation coefficient (ICC), using a two-way mixed effects ANOVA [3]. Intra-observer reproducibility was also defined by ICCs, using a two-way ANOVA and considering the choice of the observer as fixed effects [3]. All the ICCs were obtained using Matlab (Mathworks Inc., Natick, MA, USA).

Results and Discussion

ICC for Intra-observer repeatability ranged from 0.43 to 0.96 and ICC for inter-observer reliability ranged from 0.01 to 0.86 (Table 1). Bicondylar width, femoral notch angle and femoral trochlear depth measures were found to be highly reliable and repeatable within and between the observers). Low reliability found in lateral femoral condylar ratio and Beck angle could be attributed to ambiguous instructions and guidance from the literature, which are open to observer interpretation.

Conclusions

Achieving reliability in measuring the ACL risk factors is crucial for determining injury risk population and monitoring those. This study emphasizes the importance of clear and unambiguous guidelines in determining these measures.

Acknowledgments

This study was partially funded by the University of Missouri South Africa Education Program (UMSAEP).

References

- [1] Nogaro M et al. (2020). *Bone Joint J*, **102-B(2)**: 239-45.
- [2] Shrout P & Fleiss J (1979). *Psychol Bulletin*, **86**: 420-428.

Table 1: Mean anatomical measures associated with ACL injury risk from both the observers. ICC-intra1 and ICC-intra2 are the ICCs for intra-observer reproducibility for observer 1 and 2 respectively. ICC-inter is the ICC for inter-observer reliability. (SD: Standard Deviation)

	Inter-condylar width	Bi-condylar width	Notch width index	Notch angle	Femoral trochlear angle	Femoral trochlear depth	Posterior medial tibial slope	Posterior lateral tibial slope	Beck angle	Lateral tibial plateau length	Lateral femoral condylar ratio
	mm	mm	ratio	degree	degree	mm	degree	degree	degree	mm	ratio
Mean	18.05	64.64	0.27	59.35	132.28	6.13	7.10	6.91	49.86	34.89	67.54
SD	2.11	3.17	0.03	10.72	9.45	1.66	3.89	3.77	5.67	2.94	5.42
ICC-intra1	0.73	0.91	0.61	0.86	0.93	0.93	0.43	0.52	0.49	0.85	0.43
ICC-intra2	0.88	0.95	0.84	0.94	0.96	0.88	0.74	0.48	0.82	0.92	0.86
ICC-inter	0.34	0.83	0.23	0.86	0.58	0.72	0.4	0.36	0.36	0.16	0.01

The effect of low back pain on plantar pressure during gait

Clara Leyh^{1,2}, Véronique Feipel^{1,2}

¹Laboratory of Functional Anatomy, Université Libre de Bruxelles (ULB), Belgium

²Laboratory of Anatomy, Biomechanics and Organogenesis, Université Libre de Bruxelles (ULB), Belgium

Email: clara.leyh@ulb.be

Summary

To evaluate the effect of low back pain (LBP) on the plantar pressure distribution, 125 subjects suffering of LBP and 94 healthy controls walked at three different self-selected speeds on the GAITRite instrumented walkway. While patients with LBP walked slower at fast speed, the results showed an integrated pressure (P*t), a peak pressure and an active area impacted by LBP. Subjects with LBP increased P*t at preferred and fast speeds at the lateral forefoot. Furthermore, subjects with LBP displayed an increase of P*t and peak pressure in the heel region at slow speed, as well as decreased P*t and peak pressure in the medial forefoot. Even if gait velocity was not identical between groups at fast speed, the results emphasize different foot loading and gait patterns in patients suffering from LBP.

Introduction

The foot provides essential support during standing and gait. But in case of low back pain (LBP), especially with associated sciatica caused by nerve compression, a decrease of proprioceptive inputs and outputs on the foot sole and abnormal motion patterns could lead to changes in plantar pressure [1-2]. Because gait speed does not affect plantar pressure uniformly [3] and that patients with LBP are known to walk slower with shorter steps [4], a specific attention should be paid to the study of plantar pressure in subjects with LBP compared to healthy ones.

The aim of this study was therefore to evaluate the effect of low back pain on the evolution of plantar pressure parameters during gait at the lateral and medial heel, mid- and forefoot.

Methods

125 low back pain subjects (LBP) and 94 healthy controls (HC) walked barefoot three times at three different self-selected speeds (slow, preferred, fast) over the GAITRite electronic walkway, (length: 6,1 m, CIR Systems). The order of gait speeds was randomized. Average values over all three trials were computed.

Each footprint is divided in 12 trapezoids (six medial and six lateral) by the GAITRite Gold software (version 3.9) and for each section, four plantar pressure variables are computed: **P*t** (integrated pressure over time in one zone, expressed as a percentage of the overall integrated pressure over time), **peak time** (first time point at which one or more sensors in a zone were at their maximum level, expressed in seconds), **area** (sum of the active sensor areas within a zone; expressed in centimeters square) and **peak pressure** (maximum pressure per zone, expressed as a percentage of the overall maximum pressure per foot) [5]. To simplify the results, the data of the 12 trapezoids were assembled in 6 sections defined as medial and lateral fore-, mid- and hind-foot.

Normality of data distribution was explored. Repeated measures ANOVA were completed to analyze differences in pressure parameters between groups. Tukey HSD test were

computed to explore interactions between groups, pressure zones, and velocity. Level of significance was set at $p < 0.05$.

Results

No statistical differences were observed between CG and LBP groups for age and gender. Gait velocity was similar in both groups at slow and preferred speeds, but CG walked significantly faster (+9%) at fast speed compared to LBP ($p < 0.001$).

No group effect was found for peak time. LBP displayed a small but significant increase in active area compared to CG ($p = 0.03$). At fast speed, CG presented a 1% significantly lower P*t ($p = 0.005$) and area ($p = 0.0003$) than LBP. A velocity-zone-group interaction was observed for P*t ($p < 0.0001$) (Figure 1) and peak pressure ($p = 0.0004$). At preferred and fast gait speeds, LBP presented higher P*t values than CG at the lateral forefoot. At slow speed, P*t was greater in LBP in the lateral and medial rearfoot while it was lower than in CG at the medial forefoot. At slow speed, LBP presented lower peak pressure at the medial forefoot and higher peak pressure than CG at the heel.

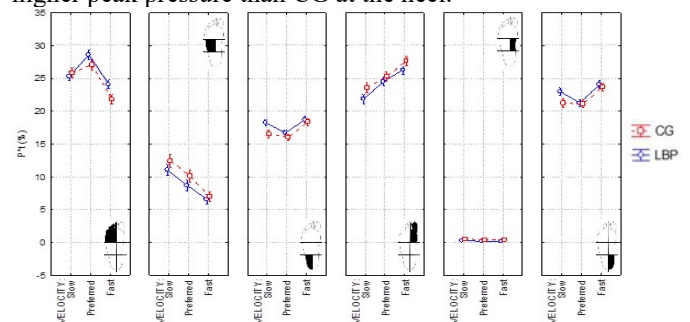


Figure 1: P*t average and standard errors for each foot zone at slow, preferred and fast speed in LBP and CG.

Conclusions

The results do not correspond to those of the literature where [1] no differences were found between chronic LBP and control groups and where [2] the emphasis was on the asymmetry in plantar pressure between the affected leg and the (healthy) lower limbs of control subjects.

Besides, a gait speed normalization should be effective to observe if, at fast speed, subjects with LBP presented indeed lesser peak pressure at the medial forefoot [3]. This is of interest because it impacts the push off phase of gait and suggests different roll-over pattern for subjects with LBP compared to controls. In addition, it may reflect a protection mechanism to avoid pain or reduced proprioception.

References

- [1] Anukoolkarn K et al. (2015) *J Med Assoc Thai*, **98**: 896-901
- [2] Lee JH et al. (2011) *J Phys Ther*, **23**: 923-926
- [3] Rosenbaum D et al. (1994) *Gait posture*, **2**: 191-197.
- [4] Keefe FJ (1985) *Pain*, **21**: 153-161.
- [5] Titianova EB (2004) *J Electromyogr Kinesiol*, **14**: 275-281.

Effects of different custom-made insoles on pressure-time integrals in cavus feet during running

Mujia Ma¹, Hui Liu², Qingquan Song¹

¹Beijing Sport University, Beijing, China

²China Institute of Sport and Health Science, Beijing Sport University, Beijing, China

Email: 573677921@qq.com

Summary

Custom-made insoles could dispersion the plantar pressure and relieve pain by high pressure for the cavus feet. The purpose of this study was to investigate the effect of different custom-made insoles on pressure-time integrals (PTI) in cavus feet during running. The results showed that two types of insoles reduced the PTI for medial/lateral forefoot and medial hell, and arch support insole also reduced the PTI for big toe. However, arch support structure of insole increased the PTI for medial and lateral arch.

Introduction

Compared to neutral feet, cavus feet is characterized of high PTI which are related to foot pain [1]. Custom-made insoles redistributed the plantar pressure concentrated by the cavus feet, and relieved the impact as well as pain by high pressure [2]. It was reported that cavus feet with forefoot valgus should raise forefoot lateral wedge in the insole [3].

The purpose of this study was to investigate the effect of different custom-made insoles on PTI in cavus feet during running. It was hypothesized that arch support insole reduced PTI for cavus feet.

Methods

Eight cavus feet and eight normal feet were screened using arch height index (AHI). The AHI for normal feet is 0.33 ± 0.01 , and the cavus feet is 0.40 ± 0.03 and average forefoot valgus angle is 11.0° . There were no significant differences in heights, weights and feet lengths between the two groups.

There were two different types of custom-made insoles for cavus feet, including the arch support insole (ASI), arch support with 6° lateral wedge increased of forefoot insole (AS+ FWI). All the custom insoles were designed using Easy CAD software. The EVA block were engraved using a CNC milling machine, and the insole were polished using a grinding machine.

Each footprint was divided into 11 recorded areas using the Pedar-X system as the subject running at 3.0m/s. PTI (kPa.s) were extracted for each area. PTI was calculated as the product of the pressure and the time over which it was applied.

T-test was used to investigate the PTI differences between the normal feet and each condition of cavus feet. One-way repeated measure ANOVA was used to investigate PTI differences between the two insoles of cavus feet. The alpha level for all statistical tests was set at 0.050.

Results and Discussion

The result showed that the PTI in the cavus feet none-insole (NI) was greater for the WF, MH, LH compare to neutral feet. The AS and AS+FWI were greater than that of neutral feet for MA. The ASI and AS+FWI demonstrated smaller PTI in the WF, MF, CF, MH compared to the NI. And the BT of PTI in the ASI was smaller than the NI. However, the MA and LA of PTI in ASI and AS+FWI was greater than the NI (Figure 1).

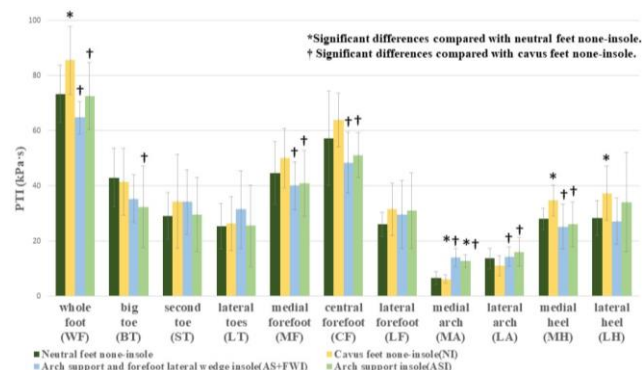


Figure 1: The PTI of neutral feet and different condition of cavus feet during running

Previous studies showed that cavus feet have a greater PTI and proportion of pain in the heel, forefoot, and toes than the neutral feet [1]. In this study, cavus feet have more PTI for the heel. Wearing ASI and AS+FWI could reduce the PTI for MH. Although there are no differences in PTI between cavus feet and neutral feet in forefoot, the PTI for MF and CF is decreased after wearing insoles. Furthermore, the ASI also reduced the PTI for BT, which can effectively alleviate the pain in MH, MF and CF with cavus feet, even in BT. However, wearing insoles increase the PTI for MA and LA, and thus increased the pressure and contact time, which would stretch the stiff arches and cause soft tissues injury in cavus feet.

Conclusions

Arch support insole and arch support with forefoot lateral wedge insole reduced the pressure-time integrals, in which arch support insole is more effective in reducing pressure-time integrals for big toe. The arch support structure of insole may increase the arches injury, which should be considered.

References

- [1] BURNS J et al. (2005). *CLIN BIOMECH. Journal*, 20(9): 877-82.
- [2] JUNG-KYU C et al. (2015). *BIO-MED MATER ENG. Journal*, 26 Suppl 1(s1): S705.
- [3] NAJJARINE A. (2008) *The orthotic revolution*; Publisher.

Predictive simulation of walking with weak ankle plantar-flexor using an AI gait controller

Young-Jun Koo¹, Mingi Jung¹, Seungbum Koo¹

¹Department of Mechanical Engineering, Korea Advanced Institute of Science and Technology, Daejeon, Republic of Korea
Email: skoo@kaist.ac.kr

Summary

Predictive gait simulations can help understand mechanical pathways of joint injuries. A musculoskeletal model and muscle controller are required to run predictive gait simulations. The objective of this study was to perform predictive gait simulations of a human musculoskeletal model with weak plantar flexor muscles using a reinforcement learning-based muscle controller. Gait data of a healthy subject was obtained. A musculoskeletal model with 92 muscles and 8 actuatable joints was constructed in the RaiSim dynamics simulation environment. A muscle controller was trained for the dynamics model to mimic the kinematics of a subject's gait via deep reinforcement learning. Maximum strengths of ankle plantar flexors of the musculoskeletal model were reduced to make an injured model. Normal and injured models were simulated using the trained muscle controller. Ankle plantar flexion and hip extension angles were reduced in the injured model, which conforms to previous clinical studies.

Introduction

Predictive simulations of human walking help to understand the pathomechanics of musculoskeletal disorders. However, the predictive simulation requires a muscle controller. Recently, controllers of a musculoskeletal model for various activities were predicted using deep reinforcement learning (RL) [1]. The objective of this study was to obtain a muscle controller for walking using deep RL and to perform predictive simulations of ankle plantar flexor weakness using the trained controller.

Methods

The study was approved by the institutional review board at Korea Advanced Institute of Science and Technology. A normal gait at self-selected walking speed was obtained for a healthy male subject. A three-dimensional full-body musculoskeletal model of 31 degree-of-freedom (DoF) was constructed in the RaiSim (Fig. 1). Ninety-two muscles were modeled according to the Hill-type muscle model. Musculoskeletal geometries and their parameters were obtained from a published model [2].

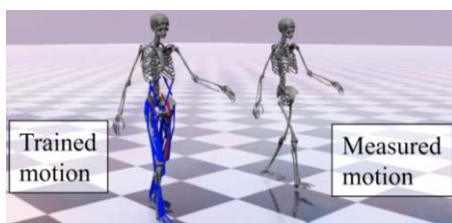


Figure 1: Reinforcement learning of a musculoskeletal model for normal walking

The musculoskeletal model was trained using a deep RL method, proximal policy optimization. A controller for the 92 muscle excitations and eight joint torques was trained to

mimic the measured gait motion of a subject. Maximum strengths of ankle plantar flexors (gastrocnemius and soleus) were reduced to 75%, 50%, and 25% of its original strength to make ankle plantar flexor weakness models. The normal and injured models were simulated using the muscle controller obtained from normal walking training.

Results and Discussion

The decrease in the maximum strengths of plantar flexors affected kinematics of the ankle and hip (Fig. 2). Ankle plantar flexion angles at push-off were 7.3°, 10.3°, 2.7°, -1.5° for 0%, 25%, 50%, and 75% decreases in the maximum strengths of plantar flexors, respectively. Hip extension angles at push-off were 25.8°, 25.5°, 21.3°, 15.2° for 0%, 25%, 50%, and 75% decreases in the maximum strengths of plantar flexors, respectively. The range of motions of the hip joint decreased as the maximum strengths of plantar flexors decreased. Previous studies reported that the hip flexion might compensate plantar flexor weakness [3], and the hip extension angle and range of motion of the hip were decreased in old adults with weak plantar flexor muscles [4]. Our predictive simulations conformed to previous clinical studies [3, 4].

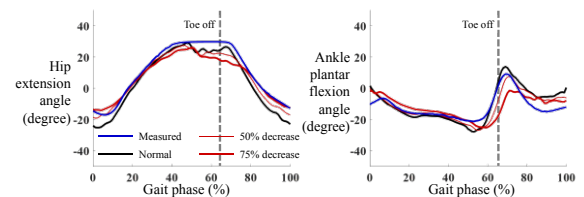


Figure 2: Kinematics of hip and ankle joints in the sagittal plane

Conclusions

A muscle controller of a high DoF musculoskeletal model was successfully created for gait simulation. The effect of weak ankle plantar flexor muscles on gait kinematics could be simulated using the muscle controller. This study would help understand the effect of muscle pathology and post-treatment on gait kinematics.

Acknowledgments

This work was supported by the Basic Science Research Program through the NRF (NRF-2020R1A2C2006057) of South Korea and the Samsung Research Funding Center of Samsung Electronics under Project Number SRFC-IT1902-01.

References

- [1] Lee S et al. (2019) *ACM T Graphic* **38(4)**:1-13
- [2] Rajagopal A et al. (2016) *IEEE T Bio-Med Eng* **63(10)**:2068-2079
- [3] Anderson DE & Madigan ML (2014) *J Biomech* **47(5)**:1104-1109
- [4] Monaco V et al. (2009) *Clin Biomech* **24**:493-498

ISB recommendations for skin-marker-based multi-segment foot kinematics

Alberto Leardini¹, Julie Stebbins², Howard Hillstrom³, Paolo Caravaggi¹, Kevin Deschamps⁴, Anton Arndt^{5,6}

¹Movement Analysis Laboratory, IRCCS Istituto Ortopedico Rizzoli, Bologna, Italy

²Oxford Gait Laboratory, Oxford University Hospitals NHS Foundation Trust, UK

³Leon Root, MD Motion Analysis Laboratory, Hospital for Special Surgery, New York, USA

⁴Faculty of Movement & Rehabilitation Sciences, KULeuven, Bruges, Belgium

⁵The Swedish School of Sport and Health Sciences, Stockholm, Sweden

⁶Karolinska Institute, Stockholm, Sweden

Email: leardini@ior.it

Summary

The present work [1] includes recommendations for multi-segment foot modelling, including the grouping of the foot bones, definition of landmarks and other anatomical references, experimental issues in motion data collection, analysing and reporting relevant results and finally designing clinical and biomechanical studies in large populations by selecting the most suitable protocol for the specific application. These recommendations may also be applied when writing manuscripts and abstracts.

Introduction

The foot is anatomically and functionally complex, and thus an accurate description of intrinsic kinematics requires multiple segments. This has led to the development of many multi-segment foot models [2,3]. These models differ in the number of segments, bony landmarks, marker set, anatomical axes and frames, joint convention, neutral positions etc. The terminology used is inconsistent and frequently confusing. Therefore the aim of this paper is to provide standardized recommendations covering both the use of established models, as well as designing new ones.

Methods

The International Society of Biomechanics has previously published proposals for standards regarding kinematic and kinetic measurements in biomechanical research; in the present work multi-segment foot modeling (MFM) is addressed. ISB is not prescribing here a particular set of standard definitions to be used in all applications, but rather aims to recommend a set of standards for collecting, calculating and reporting relevant joint kinematics data.

Results and Discussion

Recommendations when using an established MFM are here reported. Those for designing a novel MFM and the topics requiring further investigation are reported in the paper [1].

- Define a standard operating protocol for skin marker placement consistent with the MFM used.
- Assess your own intra-rater and inter-rater repeatability.
- Define a standard and repeatable procedure for raw data processing (gap filling, smoothing, filtering, etc.).
- Establish whether bony segment motion relative to a global reference system or joint motion between body segments is reported; distinguish also between 3D joint rotations and two-dimensional projection angles.

- Use the terminology recommended previously [4].
- Collect a static trial in bipedal up-right posture, i.e. hindfoot stance position, to serve as a metric for the calculation of deformity based deviations.
- Collect a second static trial, when the foot is in 'subtalar neutral position', to serve as a weight-bearing anatomical reference alignment; both of these positions to be used as off-sets for setting an origin for the MFM kinematic graphs.
- Determine the foot type of your cohort(s).
- Compare your final kinematic results, with corresponding results from the literature.
- Discuss comprehensively the issues mentioned above and specify how these may have affected your results.



Figure 1: Diagram representing possible technical and anatomical references in MFM. The longitudinal (i.e., mid-diaphyseal) axis of the bone (in red) can be represented as the line (black) joining two relevant anatomical landmarks (black circles); these landmarks are tracked by the external skin markers (grey spheres and axis).

Conclusions

It is becoming increasingly common to use MFM in biomechanical and clinical applications. Evidence suggests they provide adequate sensitivity for reporting joint motion and for distinguishing pathological from typically developing feet. But it is important that the selected MFM is well understood in order to generate accurate results and interpret the findings appropriately. Studies using these models should also use and report established references.

References

- Leardini A et al. (2021). *J Biomech*, in-press.
- Deschamps K et al. (2011). *Gait Posture*, **33**: 338–349.
- Leardini A et al. (2019). *Gait Posture* **69**: 50–59.
- Wu G et al. (2002) *J Biomech*, **35**(4):543-8

Investigation of the function of walking shoes equipped with spring on the heel during gait

H. Funakoshi¹, Y. Usami¹, K. Kubota¹, T. Kokubun^{1*}

¹ Saitama Prefectural University, Saitama, 343-8540, Japan,

*Email: kokubun-takanori@spu.ac.jp

Summary

This study aimed to investigate the effect of heel springs on gait, comparing walking shoes equipped with or without the spring model in gait on a treadmill. We evaluated kinetics, kinematics, and electromyography (EMG) data in five healthy elderly and six young adults. All subjects show a significant difference between shoes with and without springs in knee and ankle angle, ground reaction force (GRF), stride length, EMG data of gluteus medius. Additionally, EMG of Rectus femoris and Biceps femoris long head tend to decrease in spring shoes, but there is no significant difference. We suggest that spring shoes have the possibility of providing propulsive force association with changing kinetic control in gait.

Introduction

Shoes play an important role in predicting systemic disability during exercise. Recently, a variety of shoes for walking are sold. However, each effect of their feature has not yet to be investigated. The detailed impact on the gait of shoes with a unique mechanism that springs on the heel have not been clarified. The feature of these shoes is a high heel with spring and enough base of support. Several studies have reported that walking with high heel shoes changes dynamics [1]. Therefore, we compared high heel shoes with or without the spring to investigate the pure effect of spring.

Methods

Five healthy elderly (mean age \pm SD; 70.3 \pm 2.6, 3 males, 2 females) and six young (21.0 \pm 0.0, 6 males) walked on a treadmill at 0.6m/s, 0.8m/s, 1.0m/s with two conditions: 1) shoes equipped with 6.0cm height spring on the heel (spring shoes), 2) the same model of spring shoes but spring doesn't work (non-spring shoes). We analyzed gait data from a three-dimensional motion analysis system, a treadmill with a ground reaction force (GRF) sensor and a surface electromyogram. The lower limb angle, the center of mass (COM), stride, and EMG of gluteus medius (GMED), Rectus femoris (RF), and Biceps femoris long head (BF), medial gastrocnemius (MGAS) were used. Paired t-test using MATLAB2020 was used to compare the biomechanical variables between the different shoes. The level of significance was chosen as $p < 0.05$.

Results and Discussion

Of course, the spring affects in stance phase. In spring shoes, regardless of age, an anterior component of GRF in pre swing (PSw) (Arrow 1) was significantly increasing. A backward component in Mid Stance (MSt) (Arrow 2) and the vertical component of GRF in MSt (Arrow 3) and PSw (Arrow4) showed a significant increase only in young and all subjects (Figure 1).

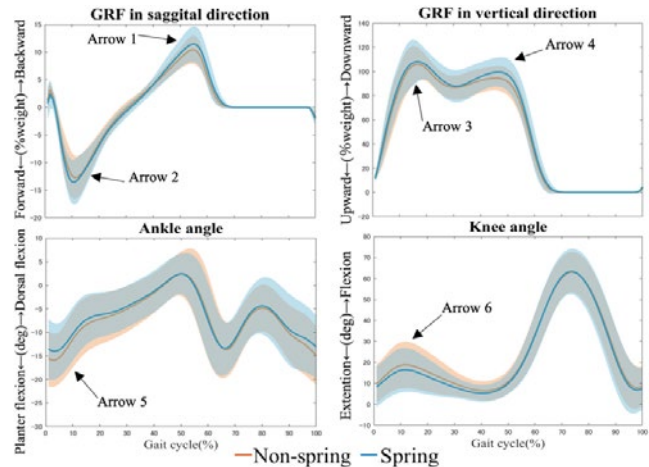


Figure 1: GRF of %weight and ankle and knee angle

Increasing GRF may mean Elastic force of the spring; increasing during Initial Contact to MSt indicate shortening of the spring and in releasing in PSw. Then, Increasing COM variation show elasticity of spring (Table 1).

Table 1: GRF of %weight and ankle and knee angle

±SD(%)	Elderly			Young			All Subject		
	Non spring	Spring	p-value	Non spring	Spring	p-value	Non spring	Spring	p-value
Stride	49.4±8.3	51.7±9.0	0.01*	55.0±7.9	59.4±8.4	<0.01*	52.5±8.4	55.9±9.4	<0.01*
COM variation(S)	1.3±0.4	1.7±0.5	<0.01*	1.5±0.3	1.7±0.4	<0.01*	1.4±0.4	1.7±0.4	<0.01*
GMED mean(LR)	55.3±34.8	60.5±35.2	0.20	61.4±28.4	67.8±30.8	<0.01*	58.6±31.1	64.5±32.6	<0.01*
BF mean(LR)	49.3±10.8	43.5±7.4	0.04*	42.4±35.0	39.8±31.4	<0.01*	45.5±23.3	41.5±23.9	0.20
RF mean(LR)	70.6±31.5	64.7±26.7	0.09	64.2±20.3	64.6±25.5	0.8729	67.8±26.8	64.7±25.7	0.18
MGAS mean(PSw)	66.0±16.4	69.1±18.3	0.09	44.6±13.1	45.2±10.0	0.7578	54.3±18.1	56.1±18.6	0.19

Additionally, expand the stride length without increasing the activity of lower limb muscle (Table 1) also strengthen the case for elasticity of the spring generates propulsive force. On the other hand, the activity of GMED is significantly increasing in young and all subjects. GMED may control the COM by braking the trunk in loading response (LR). Especially, young subjects showed a significant difference in GRF and a significant increase in GMED activity. Therefore, the young can handle spring shoes more effectively than the elderly by applying force to the spring.

Conclusions

Spring shoes can invest gait with propulsive force with increasing of GRF, although there are differences of effect size depending on age.

References

- [1] Stefanyshyn DJ et al. (2000). J. Appl. Biomech, 16: 309-319.

THE EFFECT OF FUNCTIONAL BIOMECHANICS GARMENT FOR WALKING.

Toshinori Miyashita^{1,2}, Shou Katayama³, Ayane Yamamoto³, Kodai Sakamoto¹, Masashi Kitano^{1,5}, Raita Takasaki⁴, Shintarou Kudo^{1,2,3}

1 Graduate school of health sciences, MORINOMIYA University of Medical Sciences, Osaka prefecture, Japan.

2 Inclusive medical science research institute, MORINOMIYA University of Medical Sciences, Osaka prefecture, Japan.

3 Department of Physical therapy, MORINOMIYA University of Medical Sciences, Osaka prefecture, Japan.

4 Department of Acupuncture, Morinomiya University of Medical Sciences, Osaka prefecture, Japan.

5 Yamamuro Orthopedics clinic, Toyama prefecture, Japan.

Email: miyashita.osaka@gmail.com

Summary

We developed that Functional biomechanics garments (FBG) with the function of the walking assistance based on the biomechanics of the gait. This study was to investigate the effect of FBG compared to other garments using a biomechanical method. The participants were divided into the FBG group, Compression garments (CG) groups, and Other brands garments (OBG) groups. The spatio-temporal data, the kinematics, kinetics, and Dynamic Joint Stiffness (DJS) during gait were calculated using three-dimensional gait analysis system. The walking speed was increased, and DJS of the hip decreased at Terminal Stance (TSt) by wearing the FBG.

Introduction

Wearing compression garments (CG) not only enhance performance in various sports [1, 2], but may also be applied to walking training on a daily basis. We have developed a functional biomechanics garment (FBG) designed to support the kinematics and kinetics of the lower extremity based on the walking mechanism during the stance phase. The FBG is a compression garment that adheres from the buttock to the heel. The characteristics of the FBG are a mix of different elastic parts to support accurately lower extremity movement (i.e., lower extremity joint moment) at the stance phase during walking. The purpose of this study was to investigate the effect of FBG compare other garments using a biomechanical method.

Methods

Forty-eight males (age 21.7±3.1 years, height 1.74±5.4 m, weight 64.1±7.3 kg) participated in this study. The participants were divided into of the FBG group, Compression garments (CG) groups and Other brands

garments (OBG) groups. All participants measured the baseline and each condition at the usual walking speed. The spatio-temporal data were measured, and the kinematics, kinetics and Dynamic Joint Stiffness (DJS) at the lower extremity during gait were calculated using a three-dimensional gait analysis system. A two-way ANOVA with repeated measurements was performed to compare groups among pre-walking with the post. ($p < 0.05$).

Results and Discussion

The walking speed was increased by wearing the FBG. The DJS of hip joint at Terminal Stance was FBG 0.033±0.014, CG 0.049±0.016, OBG 0.049±0.015 ($p < 0.05$). The passive elastic moment by the high elasticity part of the hip joint front in the FBG supported the internal hip flexion moment. Therefore, the FBG was able to increase the hip extension angle while decreasing the internal hip flexion moment. Accordingly, the FBG decreased hip DJS in the TSt and affected walking speed.

Conclusions

The FBG decreased hip DJS in the TSt and affected walking speed. The FBG has a biomechanical effect.

Acknowledgments

This work was supported by Toyota Tsusho Corporation and Fukusuke Corporation.

References

- [1] Marqués-Jiménez D, et al. (2018). J Sports Med Phys Fitness, 58: 1642-1651.
- [2] Angelakos I, et al. (2020) J Hum Kinet, 71: 59-68.

Table 1: Comparison of spatio-temporal data and Dynamic Joint Stiffness (DJS)

Measures	Groups	Wearing garment		Two-way ANOVA			Post-hoc	
		Pre	Post	Within Group differences	Between intervention differences	Effect of interactions		
		ave (SD)	ave (SD)					
Walking speed (m/s)	FBG	1.44 (0.12)	1.54 (0.12)	<0.01	<0.05	0.416	FBG>CG FBG>OBG ($p < 0.05$)	
	CG	1.40 (0.13)	1.42 (0.15)					
	OBG	1.35 (0.13)	1.42 (0.11)					
DJS (Nm/kg/degree)	Hip joint at TSt	FBG	0.051 (0.024)	0.033 (0.014)	<0.05	<0.05	0.140	FBG>CG ($p < 0.05$)
		CG	0.055 (0.015)	0.049 (0.016)				
		OBG	0.051 (0.013)	0.049 (0.015)				

average (ave), standard deviation (SD)

LONG-TERM TAI CHI PRACTITIONERS PERFORMED BETTER UNDER DUAL-TASK CONDITION DURING STAIR ASCENT

Zhufeng Shao¹, Li Li², Qipeng Song¹

¹College of Sports and Health, Shandong Sport University, Jinan, China

²Department of Health Sciences and Kinesiology, Georgia Southern University, Statesboro, 30460, USA

Corresponding author: Dr. Qipeng Song, songqipeng@sdpei.edu.cn

Summary

Stair walking contributed to 26% of self-reported falls and became the leading cause of accidental death for the elderly[1]. The risk of falls increases while performing a physical-cognitive dual-task (DT). We aimed to investigate performance under DT condition during stair ascent among people with more than 10-years Tai Chi (TC) practices. It would be helpful for the elderly if TC can be proved to improve their performance under cognitive-related conditions.

Introduction

Declining physical and cognitive functions increase the challenge of stair ascent among the elderly [2,3]. The ability to move while simultaneously performing a secondary cognitive task is essential to daily living activities. Still, there are more high fall risks under a stair ascent environment.

Tai Chi (TC) is a traditional Chinese conditioning exercise. It integrates training in balance, flexibility, and neuromuscular coordination with some cognitive components, resulting in benefits to body performance during stair ascent among the elderly. Therefore, this study was performed to investigate TC practitioners' performance under DT conditions during stair ascent.

Methods

Thirty healthy elderly individuals recruited for the study, including fifteen 10-year regular Tai Chi (TC) practitioners and fifteen no exercise (NE) history.

A simulating staircase with six steps, two force platforms (KISTLER, Switzerland) embedded in the 3rd and 4th steps, was constructed for data collection. Force data, sampling rate at 1000 Hz, were collected synchronously with kinematic data, an eight-camera motion analysis system (Vicon, England), sampling rate of 100 Hz. The participants were asked to walk from the starting position to ascend the stair setup in a step-over-step manner under condition DT. Meanwhile, the participants were asked to subtract seven from a given three-digit number ranging from 100 to 999 at the starting position. A successful stair ascent trial was defined as a trial in which

the participant continuously ascended from the end to the top of the staircase.

The kinematics and kinetics variables include horizontal velocity, foot clearance, step frequency, head/trunk inclination angle, hip/knee/ankle angle, loading rate, medial/lateral/propulsive/ braking impulse. The confidence interval of mean difference values between groups was calculated by using independent T-tests comparison. Significant differences were confirmed if the respective 95% confidence intervals(CI) of mean difference did not cross 0. Effect size(Cohen's d) and statistical power were also calculated for each dependent variable. Thresholds for effect sizes statistics were: 0.2, trivial; 0.6, small; 1.2, moderate; 2.0, large; and over 2.0, very large.

Results and Discussion

Selected descriptive statistics of the kinematic variables are presented in Table 1. Compared with the NE, TC practitioners had a lower trunk inclination angle (TC_{DT}=10.08°, NE_{DT}=19.12°; CI95%:-15.88/-2.19; moderate effect).

Compared with NE practitioners, TC practitioners had superior gait strategies to increase body stability and could perceive the potential risks brought from DT and changed their gait strategies to increase performance to prevent falls.

Conclusions

1 Under DT condition, body stability decreased among NE and remained unchanged among TC practitioners.

2 TC practitioners performed better during stair ascent compared with NE practitioners.

Acknowledgments

This work was funded by the Introduction and cultivation plan of young innovative talents of the Shandong Provincial Department of Education (2019-183)

References

- [1] J.G.Buckley et al. (2005). *Gait Posture*, **22**: 146-153.
- [2] F.Gaillardin et al. (2018) *Exp.Gerontol*, **106**: 74-79.
- [3] K.Watanabe et al. (2017). *Gait Posture*, **52**: 26-32

Table 1: Partly kinematic variables during dual-task stair ascent

Variables	Tai Chi (TC) practitioners	No exercise (NE) practitioners
Trunk inclination angle(mean±SD, °)	10.08±5.66	19.12±11.25
Subgroup comparisons(95%CI,°)	a) -15.88/-2.19	-1.63/6.82
Effect Size and Power	moderate; 0.86	small; 0.21

a) Between-group differences of TC and NE practitioners under DT condition; Significant differences in **bold** font

A Longitudinal Analysis of Change of Gait Stability in Older Adults with Dementia

Sina Mehdizadeh, Mohammadreza Faieghi, Andrea Sabo, Hoda Nabavi, Avril Mansfield, Alastair J. Flint, Babak Taati, Andrea Iaboni

KITE-Toronto Rehabilitation Institute, University Health Network, Toronto, ON, Canada

Email: sina.mehdizadeh@uhnresearch.ca

Summary

We measured changes in gait stability over a 10-week period in a group of hospitalized older adults with dementia to determine which factors were associated with its changes. Fifty-four individuals admitted to a specialized dementia inpatient unit participated in this study. A markerless motion capture system was used to record participants' natural gait. Multilevel growth models were developed with gait stability as the independent variable and clinical and demographic variables as predictors. Gait stability decreased over this period. Gait stability of men decreased more than that of women, associated with an increased sacrum lateral movement over time. The sacrum mediolateral range of motion decreased in those with mild neuropsychiatric symptoms, but increased in those with more severe neuropsychiatric symptoms. Our study provides evidence of worsening of gait stability, mainly due to difficulty in controlling the center of mass in older adults with dementia.

Introduction

Mobility in older adults with dementia can be affected by factors such as hospitalization, and use of antidepressants [1,2]. Monitoring of mobility status in older adults with dementia is important, because a decline in mobility not only has an impact on activities of daily living such as walking, but also increases the risk for falls. Current tools of monitoring mobility provide clinical observations about mobility status, but do not reveal the underlying biomechanical changes associated with mobility decline. These approaches are also subjective and infrequent and miss subtle changes occurring slowly over long periods of time [3]. Recent advances in markerless motion capture allow for longitudinal, unobtrusive, and frequent daily-life assessment of gait over time in older adults with dementia. The aims of this study were, therefore, to i) describe changes in gait stability (as the main cause of falls in walking) over 10 weeks in older adults with advanced dementia and to determine which demographic and clinical factors were associated with its change over 10 weeks.

Methods

Fifty-four individuals admitted to a specialized dementia inpatient unit participated in this study. A vision-based markerless motion capture system (incorporating a Microsoft Kinect v2 camera) was used to record participants' natural

gait. The estimated margin of stability (eMOS) was measured as the measure of gait stability in walking. In addition, participants' sacrum mediolateral range of motion (ML ROM) was measured as an estimation of their center of mass motion. Multilevel growth models were used with these two gait measures as the independent variables and clinical and demographic variables as predictors.

Results and Discussion

Over the course of 10 weeks, gait eMOS decreased (coefficient= -0.09 cm per week, $p=0.003$) indicating worsening of gait stability. In addition, the eMOS declined in men (Figure 1A) ~2 mm per week more than in women ($p= 0.002$). Over this period, men's sacrum ML ROM also increased (Figure 1B) on average 1.1 cm per week more than women ($p=0.02$). Moreover, while the sacrum ML ROM decreased for those with low neuropsychiatric symptoms, it was increased for those with higher neuropsychiatric symptoms (coefficient= 0.03 cm per week, $p=0.02$).

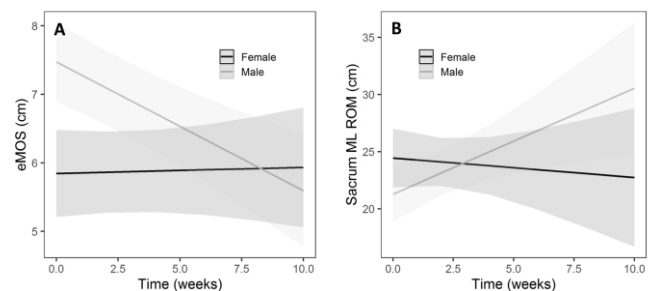


Figure 1: Plot of interaction effects A) sex on eMOS, B) sex on sacrum ML ROM.

Conclusions

Our findings demonstrate the worsening of gait stability was due to inability of participants to control their lateral center of mass movement which itself was associated with neuropsychiatric symptoms.

References

- [1] Dementia in hospitals. Canadian Institute for Health Information; 2015.
- [2] de Vos AJBM, et al. (2012) *BMC Geriatrics*. **12**:7.
- [3] Helvik AS, et al. (2014). *BMC Geriatrics*. **14**:45..

FUNCTIONAL INSOLES IMPROVE PLANTAR PRESSURE DISTRIBUTION DURING RACE WALKING

Xinrui Zhang¹, Wei Sun¹, Cui Zhang², Li Li³, Qipeng Song¹

¹College of Sports and Health, Shandong Sport University, Jinan, China

²Lab of Biomechanics, Shandong Institute of Sport Science, Jinan, 250102, China

³Department of Health Sciences and Kinesiology, Georgia Southern University, Statesboro, 30460, USA

Corresponding author: Dr. Qipeng Song, songqipeng@sdpei.edu.cn

Summary

This study investigated the effectiveness of functional insoles on plantar distribution during race walking to reduce the high plantar pressure and force on race walkers, who tend to suffer from overuse injury. A total of 20 male race walkers were recruited as participants. Each participant completed a race walking with functional or regular insoles. Plantar pressure data collected. A two-way analysis of variance with repeated measure was used to determine the difference between the two conditions among ten different plantar regions. Results showed that functional insoles reduce the peak pressure in the metatarsophalangeal joints and heels. Functional insoles have the potential to reduce the overuse injury risks at these parts. Functional insoles could also reduce the risks of foot and leg injuries.

Introduction

Fifty-kilometer race walking is the longest track and field event and involves distances that are approximately 7.8 km longer than those in marathons. A 67 kg individual walking 50 km must absorb about 2016 tons cumulative impact on each foot[1]. Thus, race walkers are prone to overuse injuries, such as blisters, metatarsalgia, stress fractures, and knee pains, in their lower extremities.

In this study, arch-supported functional insoles were used to reduce plantar pressure loading. We aimed to determine the effects of functional insoles on the plantar pressure distribution during race walking.

Methods

A total of 20 male race walkers were recruited from the provincial race walking team of Shandong, China. Each participant walked at an average race walking speed (3.5–3.8 m/s) for 400 m in his or her race walking shoes under two conditions in random order: (1) with a functional and (2) with a regular insole. Two sets of timing doors of the Smartspeed system were used to calculate the walking speed. Insole data were collected for ten consecutive steps during the last 100 m of each 400 m walk[2].

Plantar pressure insoles were used to collect plantar pressure data. During the test, peak pressures of eight anatomical sub-regions and GRF of the whole foot were calculated. Ten anatomical sub-regions were identified as the medial heels (Hm), lateral heels (HI), medial arch (Vm), lateral arch (VI), five metatarsal-phalange joints (MPJs): M1, M2, M3, M4, and M5, and the hallux (T1). Two-way analysis of variance (ANOVA) with repeated

measures was used to compare plantar pressure among ten different parts of the foot and between the two conditions. The significance level was set at 0.05.

Results and Discussion

This study demonstrated that the arch-support functional insoles reduce the peak pressure at all tested areas, except for the M5 and arch areas with increased pressure at the Vm area (Figure 1). The GRF exhibits a typical bimodal pattern (Figure 2). With functional insoles, the first peak decreased ($P=0.034$), where the second peak remained unchanged ($P=0.078$).

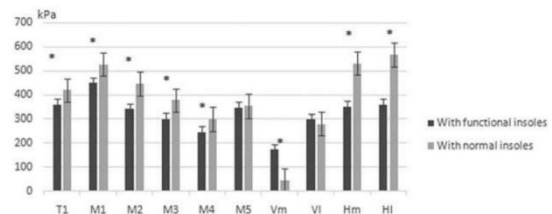


Figure 1: Peak pressures on plantar areas.

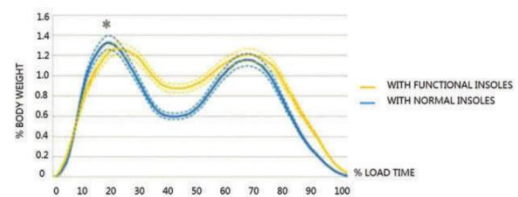


Figure 2: GRF in the vertical direction

Conclusions

During race walking, the peak pressure in the MPJs (except M5) and heels were reduced by arch-supported functional insoles. The reduction in the first GRF peak also suggests that the insoles absorb the vertical shock during the heels' strike phase and thus prevent the potential injury risks in the foot and leg.

Acknowledgments

This work was funded by the Introduction and cultivation plan of young innovative talents of Shandong Provincial Department of Education (2019-183)

References

- [1] Dowling et al. (2004). *International Obesity*, **28**:1514–1519.
- [2] De Cock et al. (2005). *Gait Posture*, **21**:432–439.
- [3] Song, Q.P et al. (2013) *Chinese Sports*, **5**:335–339.

Population Study of Kinematic Gait Parameters for Biometric Application

Gunwoo Park¹, Seungbum Koo^{1*}

¹Musculoskeletal Biodynamics Lab, Korea Advanced Institute of Science and Technology, Daejeon, Republic of Korea

Email: skoo@kaist.ac.kr

Summary

Studies on human walking as a behavior biometric have emerged with the advance of video processing methods. Among those, model-based procedures reconstruct motion from acquired images to compare it. Our work is about how motion data can be individualized. Kinematic parameters suggested by previous gait analysis were extracted from the captured motion of 488 subjects. Comparing total variance and intra-class variance of each parameter, we could explain how each feature remains invariant for different gait trials.

Introduction

Gait kinematics has been studied for various aspects of its application for biometric systems. Since gait data is usually captured as a sequence of images, existing studies comprise both model-free and model-based approaches [2]. Gait shape reconstruction precedes model-based works, while model-free works directly extract features from an image. Model-based studies have quantified three-dimensional shapes introducing a set of biomechanical parameters [1]. We aimed to explain how the parameters are distributed and whether they are consistent for each identity.

Methods

From a motion capture system with multiple optical cameras and markers, we captured the natural walking of sampled 500 subjects. Gait data from 12 subjects were excluded because of experimental errors such as missing markers. Gait data of 248 males (average age 36.8 (SD 17.2) years) and 240 females (average age 37.4 (SD 16.3) years) were used for the study. The time-series position of 17 landmarks was extracted. (Figure 1)

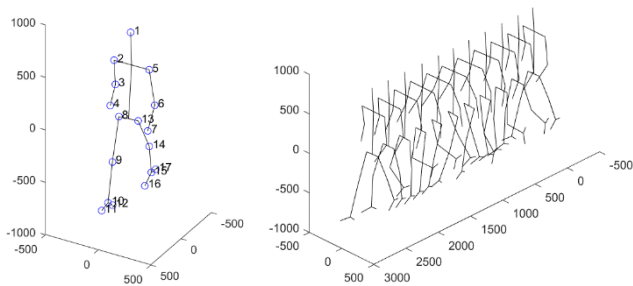


Figure 1: Gait data description

For each subject, we used four gait cycles. A gait cycle was set as a sequence of walking motion from a right heel strike to

the next right heel strike. The data contains information about the hip, knees, shoulders, and elbows. We extracted maximum flexion and extension for the joints as kinematic parameters, as well as overall shape such as stride length, width, and foot angles during the stance phase. The parameters were calculated from gait kinematics using scripts written at Matlab (2020a, MathWorks, Natick, MA, USA). Variation properties of each parameter were calculated. Total variance and intra-class variance are compared since how the feature is invariant depends on its intra-class and inter-class variation [3].

Results and Discussion

The intra-class variance was calculated as the variance of four gait trials of each subject. The parameter could be directly compared by scaling intra-class variance with total variance. If a scaled value is lower, it can be regarded that the feature is robust. (Table 1) The scaled intra-class variance was in the range of between 2% and 8%, except for step width, which was 26.3%.

Conclusions

The range shows that gait kinematics can be used for biometric individualization to some extent. Though stride and step width can be observed on the same scale, step width had much less total variance. Therefore, step width may not be discriminative in practice. Knee flexion showed the smallest scaled value of intra-class variance, which implies it may be a robust feature of gait. We showed that the gait model could be used for individualization by analyzing kinematic parameters. Many recent methods use machine learning algorithms to extract features from gait. This study will provide a useful baseline and information to analyze the resulting parameters.

Acknowledgments

This work was supported by the Basic Science Research Program through the NRF (NRF-2020R1A2C2006057) and Projects for Research and Development of Police Science and Technology through CRDPST and KNPA (PA-C000001) funded by the Ministry of Science and ICT of Republic of Korea.

References

- [1] Roberts et al. (2017). *Phys Ther Rehabil*, **4**, 6.
- [2] Connor et al. (2018). *CVIU*, **167**, 1-27.
- [3] Carreiras et al. (2014) *ICINCO*, vol. **2**, 765-772

Table 1: Total variation / Intra-class variation for gait kinematic parameters. Unit of stride and step length is mm, and angles are radian.

	Stride	Step width	Foot angle	Hip flexion	Hip extension	Knee flexion	Shoulder flexion	Shoulder extension
Total variance	13859	972	29.27	<0.01	<0.01	<0.01	<0.01	<0.01
Intra-class variance	926	256	1.22	<0.01	<0.01	<0.01	<0.01	<0.01
Scaled variance (%)	6.69	26.32	4.18	3.37	2.67	2.30	7.62	5.44

A Kinematic Comparison of Overground and Treadmill Walking Using AI-based Gait Controllers

Mingi Jung¹, Young-Jun Koo¹, Seungbum Koo¹

¹Department of Mechanical Engineering, Korea Advanced Institute of Science and Technology, Daejeon, Republic of Korea
Email: skoo@kaist.ac.kr

Summary

We used reinforcement learning to make gait controllers with two-layer neural networks for overground and treadmill walking in a dynamic simulation environment. Motion capture data of a subject was acquired during overground walking and used as a reference motion. Gait controllers were trained using an imitation learning technique to follow the reference motion during overground and treadmill walking simulations. First, we evaluated kinematic differences of the gaits with the trained gait controllers against the reference motions. Second, we compared the hip and knee angles between overground and treadmill cases.

Introduction

A number of studies reported differences in the body kinematics during overground and treadmill walking. The treadmill motor power and the change in treadmill speed during different phases of walking have been studied as potential causes in the differences [1]. Meanwhile, there is still a lack of understanding on the physics and physiology behind it. As a first step toward it, we aimed to create three-dimensional gait controllers of a humanoid model that can walk on overground and treadmill to compare the kinematics during the two conditions eliminating physiological differences.

Methods

Twelve motion capture cameras were used to obtain a subject's walking motion data, and it was processed into kinematic data by using OpenSim. The dynamic simulator RaiSim was used for reinforcement learning. The ground was made to learn overground walking, and a treadmill moving at a subject's average speed was made to learn treadmill walking. Each network was learned using the reward functions of DeepMimic [2]. Each controller network consists of 2 hidden layers of 256 units. This is shown in figure 1.

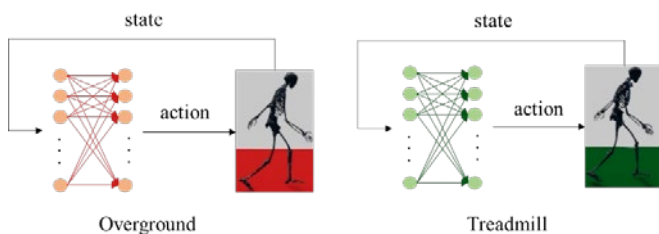


Figure 1: Training loops in both cases using neural networks

The human body model consists of joints with a total of 25 degrees of freedom (DoF). The hip joint has 3 DoF, and the knee joint has 1 DoF. The state has 86 dimensions (D): the pelvis's height, orientation, linear velocity, angular velocity (1D, 3D, 3D, 3D), the angle of each joint (25D), the angular velocity of each joint (25D), gait phase (1D), terrain

recognition (25D). The actions are the PD targets of each joint. The network parameters were updated using PPO.

When walking on the treadmill in the real world, the power of the treadmill is not infinite. Therefore, to make it similar to the actual walking, the noise between -0.1 m/s and 0.1 m/s was given every 0.01 seconds to treadmill velocity.

Results and Discussion

For the comparison between the reference motion and the simulated motions, the root mean square (RMS) difference of the knee flexion angle and hip flexion angle were 2.1 degrees and 5.2 degrees, respectively, for the overground walking simulation. In the case of treadmill walking, the RMS difference of the knee flexion angle and hip flexion angle were 2.5 degrees and 6.2 degrees, respectively. The gait controller for overground walking had a slightly lower difference.

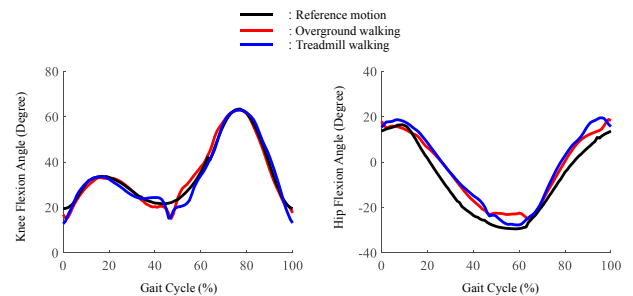


Figure 2: Knee and hip flexion angles

When the body kinematics during the two conditions were compared, the maximum knee flexion angles and the maximum hip flexion angles were both larger in the treadmill walking simulation by 0.1 degrees and 0.7 degrees, respectively. The knee ranges of motion and the hip ranges of motion were also larger in the treadmill walking by 2.3 degrees and 3.3 degrees, respectively.

Conclusions

Gait controllers of the three-dimensional humanoid model were successfully trained for overground and treadmill walking simulations. This approach would help understand the underlying physics and physiologies for different gait kinematics during overground and treadmill walking.

Acknowledgments

This work was supported by the Basic Science Research Program through the NRF (NRF-2020R1A2C2006057) of South Korea and the Samsung Research Funding Center of Samsung Electronics under Project Number SRFC-IT1902-01.

References

- [1] Tielke, A. et al. (2019). *Scientific reports*, 9(1):1-12.
- [2] Peng, X. B. et al. (2018). *ACM Transactions on Graphics (TOG)*, 37(4): 1-14

Developmental Plasticity of Locomotor Economy in an Avian Bipedal Model

Talayah Johnson, Kavya Katugam, Ian Dechene, Suzanne M. Cox, Stephen J. Piazza, Jonas Rubenson
Biomechanics Laboratory, Department of Kinesiology, The Pennsylvania State University, University Park, PA, USA
Email: taj5199@psu.edu

Summary

Whether adaptations in locomotor metabolic economy occur across an individual's life span remains unclear. Here, we used an avian bipedal model to assess the potential that locomotor economy responds plastically to altered loading history during growth. A remarkably low costs of carrying limb mass after chronic growth-period limb-loading demonstrate that locomotor economy may indeed be tuned to specific habitual conditions. Findings from this study have implications for understanding the impact of childhood activity level on locomotor energetics.

Introduction

Over an evolutionary time scale, natural selection has resulted in specializations for animal locomotor economy [1]. Whether adaptations in locomotor economy occur across an individual's life span, however, remains less clear. For example, it remains debated how and if running economy in humans is altered due to training [2]. A recent study that eliminated high-intensity activity during the growth period in an animal model showed no effect on locomotor economy [3]. The results of this study suggest that locomotor economy might not respond plastically to altered amounts of exercise during growth and may be robust to changes in life history.

To understand better the scope of developmental plasticity of locomotor economy, we adopted a bipedal model (guinea fowl) that permitted drastic alteration of musculoskeletal loads across the growth span. We achieved this by increasing distal limb mass experimentally by a factor of ~ 2.5x over the maturation period. We hypothesized locomotor economy responds plastically to altered load levels during growth and adapts in a manner that is tuned to the habitual loading environment.

Methods

Twelve 1-day old guinea fowl (*Numida meleagris*) were obtained (Privett Hatchery, Portales, NM) and raised in large circular floor pens. At one week of age, animals were randomly assigned to a control group (CON, n=6) and a limb-loaded experimental group (LL, n=6). A lead strip with mass equal to 3.3% of the individual's body mass was chronically added to the right leg of the LL group throughout growth (adjusted weekly). Starting at three weeks of age, each group was exercised three times per week by herding animals around a circular course in four 5-minute intervals for a total of 20 minutes.

Metabolic power was measured during standing and during treadmill walking ($0.5 \text{ m}\cdot\text{s}^{-1}$) using a flow-through metabolic chamber system [2]. Metabolic power was measured in the habitual condition (CON= unloaded, LL=loaded) as well as in their novel condition where an equivalent leg mass (3.3% body mass) was added to the CON group and the load was removed from the LL group. Lastly, we used an interlimb design to investigate load carrying economy on the habitually loaded leg versus the habitually unloaded leg in the LL group. Between 3-5 trials were recorded per condition and the order of conditions was randomized.

Results and Discussion

The LL group carried the added limb load more economically (26%) compared to the CON group (Fig. 1B). Surprisingly, the large addition in habitual limb mass in LL did not result in a difference in walking metabolic power compared to unloaded walking in the CON group (Fig. 1A). There was also a significant lower cost ($p = 0.05$) associated with carrying the additional mass on the habitually loaded leg (right) compared to the habitually unloaded leg (left). These findings support our hypothesis that locomotor economy adapts to altered loading history during growth, and in particular highlighted by the remarkably economical load carrying in LL. Nevertheless, contrary to our hypothesis, the CON group did not have a lower metabolic cost than the LL group in the unloaded conditions (Fig. 1C).

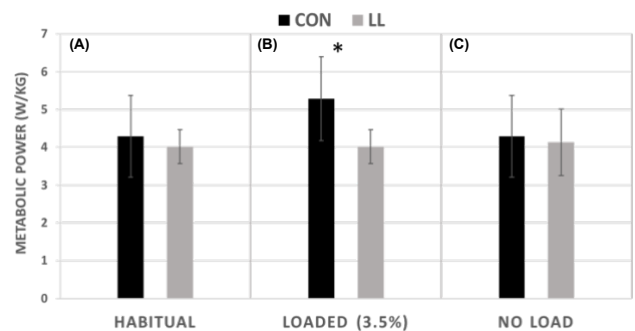


Figure 1: (a) : Comparison of net body-mass specific metabolic power in the habitual conditions (CON =Unloaded, LL= limb-loaded), the 3.3% BM loaded condition, and the unloaded condition. * $p < 0.05$.

Overall, our results support our hypothesis that locomotor economy responds plastically to altered amounts of load/functional demand during growth and is tuned to the habitual loading environment. The exception was the unloaded group comparison. The similar cost of unloaded walking between CON and LL may occur if the mechanical energy saving associated with removing the mass in the LL group is offset by muscles operating sub-optimally (e.g. unfavourable force-length-velocity effects). The musculoskeletal factors leading to altered economy are currently being explored.

Significance

Here we provide new evidence that locomotor economy can be altered based on the loading history during growth. These data have important implications for understanding the long-term effects of childhood activity and inactivity. Further analysis may determine the importance of the growth period on permanent adult locomotor energetics and biomechanics.

Acknowledgments

Supported through NIH Grant R21AR071588.

References

- [1] Alexander, R.M. (2003). *Principles of Animal Locomotion*, Princeton University Press, Princeton NJ.
- [2] Fletcher, J.R. et al. (2017). *Front Physiol*, 8: art 433, p 1-15.
- [3] Cox et al (2020). *J. Appl. Physiol.*, 128:1, p

Plantar fascia stiffness is related to the foot arch deformability and performance in single-leg drop jump

Hiroto Shiotani^{1,2}, Natsuki Sado³, Keisuke Kurumisawa¹, Junya Saeki^{1,2}, Yasuo Kawakami¹
¹Waseda University, Saitama, Japan. ²Japan Society for the Promotion of Science, Tokyo, Japan.
³University of Tsukuba, Ibaraki, Japan.
 Email: h.shiotani@asagi.waseda.jp

Summary

This study aimed to examine the relationships of the plantar fascia (PF) stiffness with the foot arch deformability and performance in single-leg drop jump. We found that PF shear wave velocity (an index of tissue stiffness: SWV) was related to the peak values of the foot arch deformation in the stance phase and jump performance. Our findings suggest that stiffer PF is associated with less foot arch deformability and superior performance in dynamic exercises.

Introduction

The foot arch is lowered and stretched out while bearing load in the stance phase, and then recoils as the load is removed. This spring-like property of the foot arch helps to attenuate impact forces and store/release elastic strain energy [1]. We previously found that the foot arch deformability during passive ankle and metatarsophalangeal joint angle changes depends on PF SWV [2]. Besides, a previous study reported that even when intrinsic muscles' contractions were inhibited by a tibial nerve block, the foot arch deformability during walking and running was not substantially changed [3]. These findings suggest that PF stiffness may regulate the foot arch deformability even in dynamic exercises, and thereby related to the exercise performance. To test this hypothesis, we examined the relationships of PF SWV with the foot arch deformability and performance in single-leg drop jump, which is a simplified bouncing-gait model.

Methods

Twelve healthy males (age 23.3 ± 2.7 years; mean \pm SD) participated in this study. PF SWV was measured at its proximal, middle, and distal sites in the longitudinal direction with supersonic shear imaging. Then, SWV values at the three sites were averaged to obtain the representative value of PF SWV over its length [2]. A three-dimensional motion capture system and a force plate were used to capture multi-segment foot kinematics and kinetics data during maximal single-leg drop jump. The peak values of the arch angle (the sagittal plane rotation of the metatarsal segment relative to the calcaneal segment) and arch length (Euclidean distance between the calcaneus and the second metatarsal head) in the stance phase were calculated as the measures of the foot arch deformability. The jump performance was assessed as jump height and the reactive strength index (jump height relative to contact time: RSI), which was calculated from the vertical component of ground reaction force. Pearson product-moment correlation coefficients were calculated to examine the relationship between measured variables ($\alpha = 0.05$).

Results and Discussion

PF SWV was significantly related to the peak values of the arch angle ($r = -0.593$, $p = 0.042$, Figure 1A) and arch length ($r = -0.652$, $p = 0.022$), jump height ($r = 0.623$, $p = 0.030$) and RSI ($r = 0.615$, $p = 0.033$, Figure 1B). There were no significant relationships between the measures of the foot arch deformability and jump performance ($p > 0.05$).

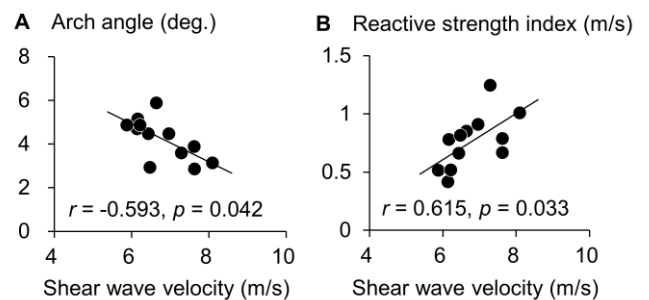


Figure 1: Relationships of PF SWV with the peak value of the arch angle (A) and RSI (B) with the regression lines.

A negative correlation between PF SWV and the peak arch angle demonstrates that the foot arch deformability during single-leg drop jump can be partly explained by PF stiffness. Additionally, as PF is extending from the calcaneus to the proximal phalanges, the peak arch length is conceivable as a measure of PF lengthening as well as the arch deformability. Thus, the relationship between PF SWV and the peak arch length can be interpreted that stiffer PF results in less lengthening, and thereby leading to smaller deformation of the foot arch upon loading. Furthermore, the measures of jump performance were correlated with PF SWV but not with the foot arch deformability. These results suggest that stiffer PF is associated with superior jump performance whereas the foot arch deformability does not affect the jump performance.

Conclusions

In this study, we found that PF SWV was related to the peak values of arch angle and arch length, jump height, and RSI in single-leg drop jump. Our findings suggest that stiffer PF is associated with less foot arch deformability and superior performance in dynamic exercises.

References

- [1] Ker RF et al. (1987). *Nature*, **325**: 147-149.
- [2] Shiotani H et al. (2020). *J. Appl. Physiol.*, In Press.
- [3] Farris DJ et al. (2019). *PNAS*, **116**: 1645-1650.

ADAPTATIONS OF FOOT FUNCTION WHEN HOPPING ON A DAMPED SURFACE

Jonathon V. Birch^{1,2}, Luke A. Kelly², Andrew G. Cresswell², Sharon J. Dixon¹ & Dominic J. Farris¹

¹Sport & Health Sciences, College of Life & Environmental Sciences, University of Exeter, Exeter, EX1 2LU, United Kingdom

²School of Human Movement & Nutrition Sciences, The University of Queensland, Brisbane, QLD 4072, Australia

Corresponding author email: jb1015@exeter.ac.uk

Summary

Humans account for dissipative work performed by a damped surface by altering their leg mechanics and increasing the active contribution from muscle [1]. However, prior work has not considered the contribution of our feet. Here we examined the adaptations of foot and ankle function and the contributions of the intrinsic foot muscles to this mechanism.

Introduction

Storing and returning energy is an important function of our feet; allowing us to redirect our centre of mass with great efficiency [2]. We have shown previously that humans modify this function to harness energy stored and returned from an elastic surface operating in series with the foot, reducing their active contribution to work [3]. This was at odds with prior work that showed contributions from the foot's intrinsic muscles to increase during shod gait in running shoes [4]. We propose that running shoes, in fact, act as a damper in series with the foot, rather than a spring as proposed previously. As such, here we tested the hypothesis that humans increase their active contribution to work at the foot and ankle to replace dissipated energy when hopping on a damped surface.

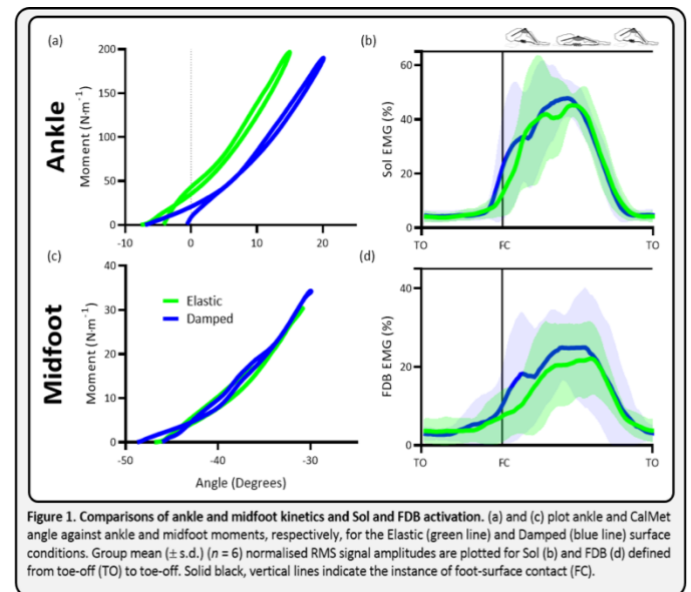
Methods

Eight participants hopped in place at 2.2 Hz on an adjustable platform in two damping configurations; Damped, and Elastic. Because we were interested in examining the effect of surface damping, the surface stiffness of each condition was matched. Three-dimensional kinematic and kinetic data were recorded in Qualisys Track Manager (Qualisys) alongside muscle activation from abductor hallucis (AH), flexor digitorum brevis (FDB), soleus (Sol) and tibialis anterior (TA). Kinematic and kinetic data were processed in Visual3D (C-Motion) to calculate sagittal plane joint angles, moments and work of the ankle and midfoot using a multi-segment foot model. EMG data were processed in Matlab (Mathworks). Raw signals were band-pass filtered before root mean square (RMS) envelopes were computed and normalised for each participant to the peak amplitude recorded on the Elastic surface condition.

Results and Discussion

In an effort to replace energy dissipated during the Damped platform configuration, positive work at both the ankle and midfoot increased

significantly with respect to hopping performed on the Elastic surface; $t(8)=3.314$, $p=0.001$ and $t(8)=4.289$, $p=0.004$, respectively (Table 1). This burst of work is evident at the end of the propulsive phase of the hop in the moment versus angle plots presented in Figure 1 (panels a and c). The generation of work at both ankle and midfoot appears to be linked to signal amplitudes and greater integrated EMG during contact recorded in the Damped condition in Sol ($t(7)=3.673$, $p=0.014$) and FDB ($t(7)=3.505$, $p=0.017$) (Figure 1, panels b and d).



Conclusions

Foot mechanics and muscle activations appear to be altered on a damped, compared to elastic surface to account for dissipated energy. This has applications for the design of wearable devices and footwear.

References

- [1] Moritz et al. (2004). *J. Appl. Physiol.*, **96**: 1996-2004.
- [2] Ker et al. (1987) *Nature*, **325**: 147-149.
- [3] Birch et al. (2019) [Conference presentation] ISB.
- [4] Kelly et al. (2016) *J. R. Soc. Interface*, **13**(119).

Table 1. Comparisons of ankle and midfoot kinetics. Group mean (\pm s.d.) ankle and midfoot kinetics for the Elastic and Damped surface conditions ($n=8$). N.b. negative and positive work performed during loading and unloading phase of hop, respectively.

	Surface condition		
	Elastic	Damped	
Ankle	Negative work (J/kg)	-0.42 \pm 0.09	-0.47 \pm 0.10
	Positive work (J/kg)	0.38 \pm 0.07	0.47 \pm 0.09*
	Quasi-stiffness (Nm/kg/deg)	0.15 \pm 0.03	0.14 \pm 0.03
Midfoot	Negative work (J/kg)	-0.05 \pm 0.03	-0.07 \pm 0.03
	Positive work (J/kg)	0.04 \pm 0.02	0.07 \pm 0.03**
	Quasi-stiffness (Nm/kg/deg)	0.03 \pm 0.01	0.03 \pm 0.01

*, ** denotes a statistically significant difference between the elastic and damped surface conditions, $p < 0.05$ and $p < 0.01$, respectively.

Knee and ankle joint stiffness during running with different runway surfaces

Zihan Yang^{1,2}, Feng Qu², Zhiyi Zheng³, Songhua Yan¹ and Kuang Zhang¹
¹School of Biomedical Engineering, Capital Medical University, Beijing, CHINA
²College of Sport science, Beijing Sport University, Beijing, CHINA
³Sports Science Laboratory, Anta (China) Co., Ltd., Fujian, CHINA
 Email: 226909999@qq.com

Summary

The present study examined knee and ankle joint stiffness on both the cement runway and plastic runway. While the knee joint play an important role for shock attenuation, the ankle joint become stiffer when running in the same speed range. This significant change on the knee and the ankle may be related to the greater risk of the knee soft-tissue and the Achilles tendon injuries [1].

Introduction

During running on a hard surface, the knee joint play an important role for shock attenuation, while the ankle joint is used much less in this capacity [2]. It is reasonable to expect that running on a cement runway requires less knee joint stiffness for shock attenuation than on a plastic runway. Therefore, the purpose of this study is to investigate the change in the knee and ankle joint stiffness during running on two surfaces.

Methods

Eight healthy male rearfoot runners (22.63 ± 3.74 yr, 65.65 ± 4.76 Kg, 172.75 ± 2.92 cm) completed three running trials at 3.33 ± 0.15 m/s were recruited. Kinetic data and kinematic data were captured with a force plate and an 8-camera motion capture system. Cement runway and plastic runway were laid at least 8m from start point to the force plate. Stiffness (K) for the ankle and knee joints was determined for the shock attenuating phase as the change in joint moment divided by the change in joint angle [3]. A paired t test at significance level $\alpha = 0.05$ was used to determine effect of surface type for the joint stiffness.

Results and Discussion

Results are presented in Figure 1 and Table 1. For knee joint, cement runway significantly demands less Δ moment and K_{knee} ($p < 0.001$) than plastic runway, no significant change observed in Δ angle ($p > 0.05$). For ankle joint, cement runway significantly demands more Δ moment and K_{ankle} ($p < 0.001$) than plastic runway, no significant changed observed in Δ angle ($p > 0.05$).

Conclusions

To accommodate a harder runway, the knee joint was less stiffness to absorb shock and ankle joint were more stiffness to resistance lower limb folding than plastic runway. Our results provide insight into the role of lower limb joint

stiffness for running on different runways and may shed light on higher risk of the Achilles tendon injury [1].

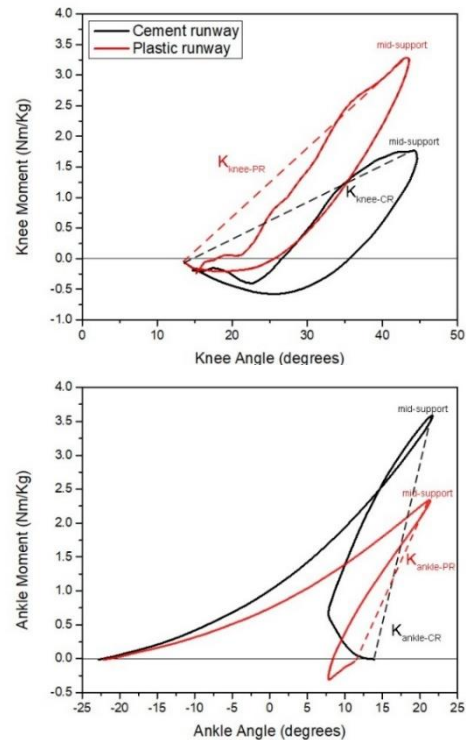


Figure 1: Mean joint stiffness at knee (top), and ankle (bottom). Solid lines indicate the joint moment and joint angle relation, dash lines indicate joint stiffness. Black indicates cement runway, red indicates plastic runway.

Table 1: The change in joint angular and moment of knee and ankle (K in $N^*m/kg/degree$) during running on cement and plastic runway.

	Cement runway		Plastic runway	
	Knee	Ankle	Knee	Ankle
Δ angle	29.97 ± 4.2	7.85 ± 4.08	28.44 ± 6.36	10.13 ± 2.79
Δ moment	1.85 ± 0.43	3.60 ± 0.39	3.52 ± 0.63	2.38 ± 0.26
Stiffness	0.06 ± 0.01	0.62 ± 0.41	0.13 ± 0.04	0.26 ± 0.11

Acknowledgments

This project was supported by ANTA Sports.

References

- [1] Lorimer et al. (2016). *Sports Med*, **46**:1921-1938.
- [2] Derrick et al. (1998). *MED SCI SPORT EXER*, **30**: 128-135.
- [3] Hamill et al. (2009). *RES SPORTS MED*, **17**: 260-273.

GaitSense: Estimation of knee joint angle for Sit-to-Stand (STS) movement activity in Osteoarthritis

Sitesh kumar^{1,2}, Gunjan P.^{2,1}

¹Biomechanics Research Lab, SynerSense Private Limited, Ahmedabad, India

²Dept. of Biodesign Medical Technology, SynerSense Private Limited, Ahmedabad, India

Email: gpatel.sns@gmail.com

Summary

Estimation of joint range of motion while performing dynamic activity day to day activity is important in diagnosing various musculoskeletal and neurological disorders. In this study we have used an inertial sensor based device developed by GaitSense to estimate and compare the knee joint angle of an Osteoarthritis (OA) patient with a healthy subject while performing dynamic STS movement activity. Results obtained for OA and normal subjects are compared to see variability in knee joint angle pattern in the sagittal plane while performing the same activity.

Introduction

In India, there are an estimated 104 million elder age group population. Physical therapy in geriatrics helps to strengthen the muscles and reduce the risk of imbalance and individuals return to their prior level of functioning, and encourage activities and lifestyle changes as specific to Sit-to-stand (STS) activity. Conventionally, Opto-electronic motion capture and video camera based systems are widely used to characterise sit-to-stand motion activity [1]. Thus, Motion capture systems have high capital cost and are limited to controlled settings. Present time, wearable inertial measurement unit (IMU) based device which can be easy to use in indoor or outdoor settings and monitors the physical therapy exercises improvement that provides reliable and accurate outcome measures [2,3].

This study presents the wearable IMU based motion capture (GaitSense) device, which is wireless, markerless and automated joint kinematic evaluation during STS which could be applied to monitor physical therapy rehabilitation in a wide variety of musculoskeletal disorders. The STS study was performed in indoor and outdoor settings. The STS data accuracy of the knee joint range of motion estimated for a single Sit-to-Stand cycle activity within suggested range and differentiate between normal and OA orthopedic disordered that the GaitSense can be considered as alternative method for motion capture.

Methods

The developed GaitSense device's each node comprises 3-axis accelerometer and 3-axis angular velocity sensor. For obtaining knee joint angle range of motion during the performed activity of STS in the sagittal plane, we require to place 4 nodes on both the lower limbs. A pair of nodes are placed laterally on the left and right side of the shank and thigh segments. Goniometer reading of knee joint angles at sitting and standing position was recorded to calibrate device at same time.

The subject is then instructed to perform 5 cycles of STS activity and the IMU data while performing the activity is recorded wirelessly.

The recorded data is processed using GaitSense proprietary sensor fusion algorithm to estimate knee joint range of motion in the sagittal plane. Post-processing of the data was done using the GaitSense proprietary software to obtain and represent the joint range of motion in standard format. The data was collected in both indoor and outdoor settings on the leveled ground surface.

Results and Discussion

The result obtained in the form of a joint angle graph replicates the goniometer readings of knee joint angle motion pattern in the sagittal plane during the dynamic activity of sit to stand. The output graph shows the difference of 13.6 degree in maximum knee joint angle between OA and normal subject.

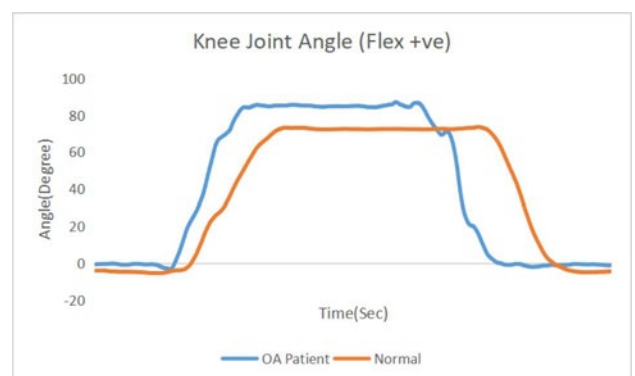


Figure 1: Knee flexion/extension joint range of motion in OA and normal subject while performing STS movement activity.

Conclusions

GaitSense device is capable of estimating joint range of motion of knee joint during dynamic activity like sit to stand, squat etc. This result could further be extended for joint angles about the other two axes i.e. in the frontal and transverse plane. Further clinical study is needed to validate the GaitSense system setup in healthy and pathological conditions.

References

- [1] Bolink et al. (2016). Med. engg & physics, 38(3), 225-231.
- [2] Daniel L. et al. (2018). Healthcare. Journal, 6(1), 21.
- [3] Kanai et al. (2016) BMC geriatrics, 16(1), 1-10.

Predictive tracking of the knee position for mobile x-ray imaging

Seungwoo Yoon¹, Seungbum Koo¹

¹Department of Mechanical Engineering, Korea Advanced Institute of Science and Technology, Daejeon, Republic of Korea
Email: skoo@kaist.ac.kr

Summary

The mobile biplane X-ray imaging system requires imaging of a target human joint while it moves. This study proposes a control algorithm that reduces the tracking error between the X-ray system and the target joint. Since the target joints that move at a high speed must be tracked, the time delay causes a large tracking error. A neural network was designed to predict future joint position to compensate for the time delay. The neural network was trained with a treadmill walking data for 60 seconds, and the position of the knee after 130 ms was estimated with a 1.4 mm error. The servo motor was driven with the predicted value. The target joint tracking RMS error between the servo motor and the target joint was 5.6 mm.

Introduction

Many biplane X-ray imaging systems have been studied to obtain accurate kinematics of human joints [1]. Among them, a mobile biplane X-ray imaging system was developed to capture a wider range of motion [2]. It was important for such equipment that the motor tracks the target joint position with little error. Since human joints moved at high speed around 1 m/s, there was a large error due to time delay. A neural network was designed to predict future joint position to compensate for the time delay.

Methods

Reflective motion capture markers were attached on the lower limbs of subjects with the Plug-in Gait marker set protocol and walked on a treadmill at 5 km/h. The position of the marker attached to the knee joint was measured at 100Hz cycle using the motion capture system of the VICON cameras. The linear actuator (5kW, Mitsubishi) was driven according to the measured target joint position. The linear actuator was driven by loading a vertical motor of about 100 kg (Figure 1). The walking data was transmitted to the linear actuator at 10ms cycles, and the position is feedback controlled by the motion controller (MR-MC240, Mitsubishi).

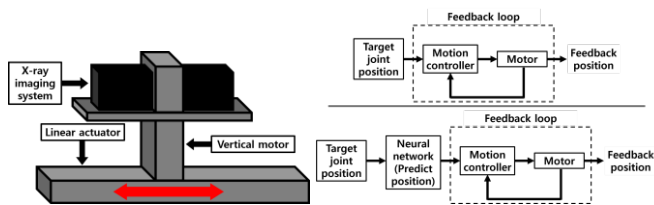


Figure 1: Mobile X-ray imaging system schematic design (left) and Feedback control loop (right, top) & Feedback control loop with neural network (right, bottom)

We designed a neural network to compensate for the error due to the time delay. The neural network had three hidden layers and 40 nodes. The neural network was trained using a

supervised learning algorithm to predict the future position after 130 ms by receiving 13 previous target joints position. The training data set consisted of 60 seconds of treadmill walking data captured at 100 Hz.

Results and Discussion

The target joint position after 130 ms was estimated with the RMS error of 1.4 mm. The graph of driving the motor with the predicted positions using the neural network is shown in Figure 2. When only the feedback control of the motion controller was used, the tracking RMS error was 79.9 mm. When the neural network and feedback control were utilized, the tracking RMS error was 5.6 mm.

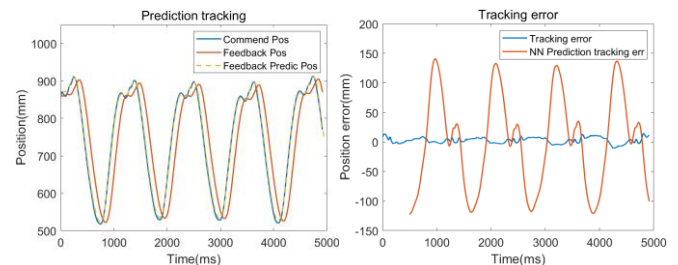


Figure 2: Compare trajectory between Motion controller & Motion controller + position Predictor (left) and tracking error (right)

In [2], when the Look-Ahead-Trajectory-Prediction and feed-forward control were applied for tracking the target joints, the tracking error was reported to be within 40 mm. Our equipment is not yet ready to take X-ray images, so a fair comparison is difficult, but we have confirmed that the tracking error can be reduced to 5.6 mm using a network-based predictive control.

Conclusions

We developed and operated a system that accurately tracks the joint by predicting the position of the knee joint while walking. This study would be helpful in developing a mobile biplane X-ray system that acquires X-ray images of lower limb joints during walking.

Acknowledgments

This work was supported by the Basic Science Research Program through the NRF (NRF-2020R1A2C2006057) of South Korea and the Samsung Research Funding Center of Samsung Electronics (SRFC-IT1902-01).

References

- [1] Hoshino Y & Tashman S (2012) *Knee Surg Sport Tr A* **20(7)**:1268-1275
- [2] Guan, S. et al. (2015). *IEEE T MED IMAGING* **35(1)**: 326-33

Identifying and comparing hip-knee coordination patterns in instep and punt kicking using functional data analysis

Liwen Zhang¹, Edward Gunning², Andrew J. Harrison³, Hui Liu⁴, Norma Bargary²
¹Biomechanics Lab, School of Sport Sciences, Beijing Sport University, Beijing, China
²Dept. Mathematics and Statistics, University of Limerick, Limerick, Ireland
³Dept. Physical Education and Sport Sciences, University of Limerick, Limerick, Ireland
⁴China Institute of Sport and Health Science, Beijing Sport University, Beijing, China
 Email: 328083341@qq.com

Summary

This study used functional data analysis (FDA) to understand hip-knee coordination patterns during instep and punt kicking. Three-dimensional kinematic data were obtained for 11 male soccer-majored college students performing the two kicking tasks. Bivariate functional principal components (BfPCs) for the hip and knee functions were extracted to determine key coordination patterns and the differences between kicking tasks and individual subjects. BfPC1 and BfPC2 suggested differences between individual subjects in the later portions of kicking movement, while BfPC3 and BfPC4 suggested differences between kicking tasks in the earlier portions. The relationships between these coordination patterns and hamstring length were explored to identify potential risk factors for hamstring injury.

Introduction

FDA is a family of statistical techniques and has excellent applicability to biomechanical data since it considers the entire sequence of measurements in a time-series as a single curve rather than as a series of discrete parameters [1]. Hip-knee coordination during instep and punt kicking and its relationship with hamstring lengthening are still unclear.

This study aimed to use BfPCA to (1) identify hip-knee coordination patterns during instep and punt kicking and determine how they differ between the two kicking tasks, and individual subjects, (2) qualitatively examine the potential relationships between the hip-knee coordination patterns and hamstring lengths during the two kicking tasks.

Methods

Eleven male soccer-majored college students with right foot dominance volunteered to participate. Reflective markers were attached. The participant then performed 3 successful trials for each of the instep kicking and punt kicking tasks. The sagittal hip and knee angles of each trial were calculated as the Cardan angles. The kicking movement was divided into the acceleration and follow-through phases. The muscle-tendon unit lengths of the biceps femoris, semimembranosus and semitendinosus were determined as the distance between the two attachment points of the muscle [2] and normalised to the respective muscle length in an upright posture.

BfPCs for the hip and knee angles of each trial were extracted. Angle-angle plots were used to visualise the BfPCs. A positive multiple of the BfPC was added to the mean hip-knee curve at equally spaced points and joined by an arrow. A positive score is indicated by '+ + +' and a negative score is indicated by '- - -'.

Results and Discussion

The first 4 BfPCs accounted for 93% of the total variation. BfPC1 captured variation in the knee angle at later stages of the kicking movement (Figure 1), while BfPC2 described the coordinated range of hip and knee angle throughout the kicking movement. Differences in scores on BfPC3 suggested that individuals displayed greater hip flexion when performing punt kicking compared with instep kicking, particularly before ball contact. Results from BfPC4 indicated that individuals displayed greater knee flexion before ball contact when performing punt kicking compared with instep kicking.

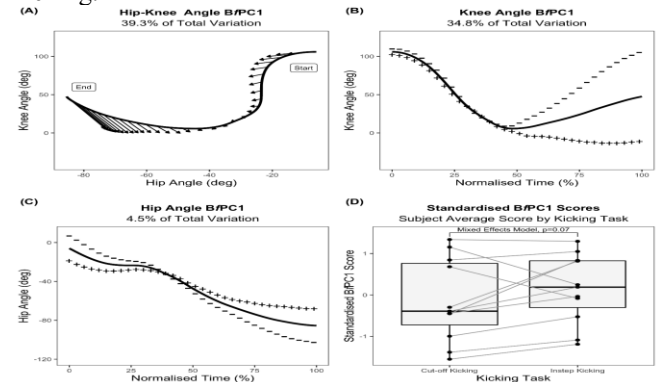


Figure 1: The first BfPC for hip-knee joint coordination.

Examining the impact of BfPC1 on hamstring muscle-tendon unit length, predictably a higher score meant that hamstrings underwent continued lengthening until the point of maximal hip flexion, reaching peak length later in the follow-through phase. A higher score on BfPC2 indicated that the hamstrings were at shorter lengths and thus at relatively lower potential risk for injury when kicking a ball.

Conclusions

Task and inter-individual hip-knee coordination differences were found in the acceleration and follow-through phase respectively. Kicking with a greater peak knee flexion angle throughout the kicking movement especially in the later portion of the follow-through phase is a good kicking strategy for preventing a hamstring injury. This study demonstrates the potential that FDA possesses to provide novel insights for complex movements in sports biomechanics with pairs of kinematic variables that are time series in nature.

References

- [1] Ryan, W et al. (2006). *Sports Biomech*, 5: 121-138.
- [2] Zhang, L. (2020) *J Biomech*, 99: 10

Electromyography recordings of the tensor fascia lata muscle during dynamic tasks: A comparison of surface and fine-wire electrodes

Manuela Besomi¹, Wolbert van den Hoorn¹, Bill Vicenzino¹, Paul W. Hodges¹

¹The University of Queensland, NHMRC Centre of Clinical Research Excellence in Spinal Pain, Injury and Health, School of Health and Rehabilitation Sciences, Brisbane, Qld 4072, Australia

Summary

The tensor fascia lata (TFL) is a small fusiform muscle that is active during flexion, abduction, and internal rotation of the hip. Surface electrodes are usually used to make electromyographic (EMG) recordings from the TFL, which are more susceptible to crosstalk from surrounding muscles. Differences in the pattern of TFL activity between surface and fine-wire recordings have not been investigated. EMG was simultaneously recorded from the TFL muscle with surface and fine-wire electrodes during step-up and step-down tasks. Although the pattern of TFL activity was variable between participants for both electrode types, it was clear-cut that surface recordings revealed activity that was absent in the fine-wire recordings, which strongly suggests contamination of surface recordings by activity from adjacent muscles. However, some participants showed opposite results (higher activity with fine-wire recordings than surface). Fine-wire recordings were more prone to artefacts.

Introduction

Although most existing studies have used surface electrodes to record EMG from the TFL muscle [Besomi et al., 2020], its small size and close proximity to other muscles make these recordings susceptible to crosstalk [Besomi et al., 2019]. Recent systematic review on muscle structure and activation of the TFL has identified that all EMG studies used surface electrodes for comparison of pattern of activity between participant groups [Besomi et al., 2020]. It is unclear whether the bursts of TFL EMG reported with surface recordings arise from TFL or represent crosstalk from underlying and surrounding muscles (e.g., gluteus medius and minimus, sartorius, rectus femoris, and iliacus).

Methods

Eight healthy and physically active volunteers (5 females, 3 males; mean \pm SD age 28 ± 6 years; height 1.70 ± 0.07 m; mass 65.6 ± 10.3 kg; BMI 22.8 ± 3.4 kg/m²) participated in this study. EMG signals of the TFL muscle were recorded with surface and fine-wire electrodes (inserted under guidance of ultrasound). Participants performed five trials of step-up and step-down tasks wearing their preferred footwear, followed by three maximum voluntary isometric contractions (MVICs). EMG data were band-pass filtered (50–500 Hz for both electrode types) with a zero-lag fourth-order Butterworth filter. EMG signals for all trials were visually inspected for artefacts. EMG data were rectified and subsequently smoothed with a 10-Hz, fourth-order zero-lag low-pass Butterworth filter, and were subsequently amplitude-normalised to the MVIC (expressed as %). Statistical parametric mapping (SPM) was used to statistically compare the patterns of activation between electrode types.

Results and Discussion

The pattern of TFL EMG from surface and fine-wire recordings varied between participants in both tasks. Some participants showed an additional major peak with surface recordings that was not apparent in the fine-wire recordings, and others showed the opposite. SPM revealed one supra-threshold cluster (between 10-15%) exceeding the critical threshold ($t^* = 3.516$, $p = 0.013$) during the step-up task. The MVIC normalised amplitude of surface recordings was significantly greater than fine-wire recordings during this period (Figure 1).

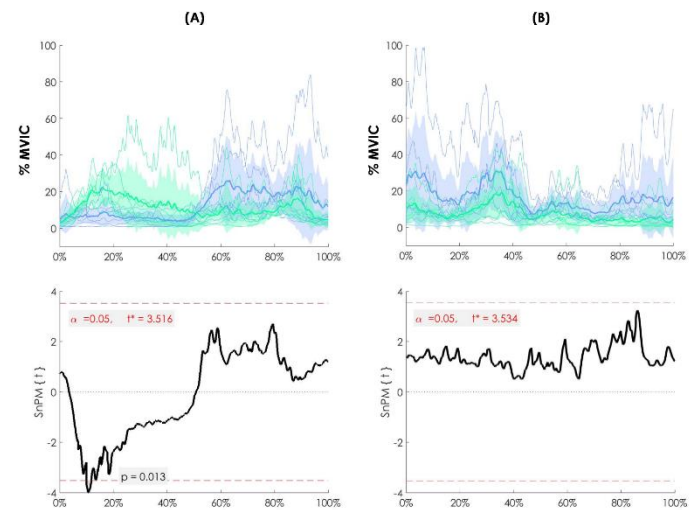


Figure 1: Comparison of EMG pattern of the TFL normalised to MVIC between surface (green) and fine-wire (blue) electrodes during step-up (A) and step-down (B). Bold line represents the group mean and shaded area the group standard deviation

During the step-up task, activation of other hip flexor muscles will be present and could have been recorded by the surface electrode. It is possible that fine-wire EMG recordings were greater during the late phase of the tasks because of the normalisation procedure. If MVIC for surface recordings included contribution of adjacent muscles, amplitude used for normalisation might exceed the muscle's true MVIC and thus lead to underestimating activation as a proportion of MVIC for that phase. Lower activation in surface EMG might also be explained by methodological issues from each electrode.

Conclusions

Surface EMG recordings of TFL are affected by crosstalk. For studies that aim to understand the specific activation of TFL, fine-wire recordings are recommended considering the limitations of this technique.

References

- [1] Besomi M et al. (2020). *Sports Med*, 50: 965–985
- [2] Besomi M et al. (2019). *JEK*, 48: 128-144

Removing artificial jumps from kinematic recordings with multiple cameras

Charlotte Le Mouel¹, Marc H. E. de Lussanet^{1,2}

¹Movement Science, University of Münster, Münster, Germany

²OCC Center for Cognitive and Behavioral Neuroscience, University of Münster, Münster, Germany

Email: lussanet@uni-muenster.de

Summary

In standard marker-based motion capture systems, the 3D position of each marker is reconstructed from the 2D views of a set of cameras. When the subset of cameras viewing a given marker changes, the reconstructed marker position jumps suddenly from one frame to the next. Although these jumps are often small (0.1 – 1 mm), they cause drastic errors in speed estimates (up to 0.5 m/s), especially for high frame rates (120 – 500 Hz). The problematic of these artificial jumps requires heavy filtering of kinematic data. We propose and compare methods for identifying and removing such jump artifacts. We validate these methods on kinematic data of both static balance and running recorded at two different frequencies using two different motion capture brands. Both methods reliably remove jump artifacts while keeping the original signal intact, and largely improve estimates of marker speed.

Introduction

The recording of kinematic data using modern high-speed cameras combines high spatial accuracy (typically 0.1 – 1 mm) with very high recording speeds (typical frame rates of 100-500 Hz). The 3D position of each marker is reconstructed from the 2D views of a set of cameras. The reconstructed marker position may be inaccurate if the initial calibration of the cameras' position is insufficient or the lens correction does not compensate fully for the nonlinearities of the cameras [1]. Although reconstruction errors are typically small (less than 1 mm), they depend on the subset of cameras viewing the marker. The subset of cameras changes the marker is obstructed from the view of one of the cameras or moves in or out of a camera's field of view. As a result, when the subset of cameras viewing a marker changes, a small jump in the reconstructed marker position (typically less than 1 mm) occurs from one sample to the next. Especially with rapid frame rates, this causes a drastic inaccuracies (spikes) in marker speed.

Typically, the problem is dealt with by severe smoothing of the data with a low pass filter that introduces real artifacts to the recorded kinematics. Thus, the kinematic jump problem represents a limiting factor to the effective accuracy of kinematic recordings.

We developed and tested numerical methods for removing artificial kinematic jumps without introducing artifacts into the kinematic signal. These artifacts involve transients, such as the heel-stroke during running, and drift due to the incomplete removal of jumps. Furthermore we test the stability of the filter with different measurement frequencies.

Methods

The methods involve the following steps. First, possible steps in the raw kinematic recording are identified. Second, the appropriate threshold to include as many steps as possible while ignoring transients in the recordings such as

heel strike and very fast movements. Third, removing possible drift from the thus cleaned signal.

We validated the methods on four datasets: 1. Treadmill running recorded at 500 Hz and down-sampled versions of the same recordings. Special attention was given to markers with frequent jumps due to partial masking, to ones with transient kinematics due to the heel strikes and to the fastest ones. 2. Walking along a track of several meters with special attention with special attention given to moving in and out of camera view. 3. Static balance recordings with a dense placement of foot markers. 4. Simulated sinusoidal motion with the negative phases replaced by zeros, with added noise and jumps. The stability of the method was further tested by applying it several times on the already processed signal.

Results and Discussion

The resulting method has an automatic threshold detection, providing objective criterions. Further, we got excellent velocity and acceleration signals by Savitzky-Golay differentiation.

The validation showed robust behavior of the new method, independent of the capture frequency, the movement velocity and kinematic transients such as heel strikes during running. At low frequencies, the new method became somewhat less selective for the heel strike. Steps due to calibration errors and nonlinearities of the cameras could be removed alike and irrespective of movement velocity, translation and partial occlusion.

The drift correction could keep the error with respect to the recorded signal below the size of the steps at all times.

Conclusions

The proposed novel method for removing kinematic jumps is highly selective and reliable in all tested conditions. It is the first one available and is advised for kinematic recordings with multiple cameras.

Matlab and Python scripts are made available on Github [1].

References

- Chiari L, Della Croce U, Leardini A, and Cappozzo A (2005). Human movement analysis using stereophotogrammetry. Part 2: instrumental errors. *Gait Posture*, **21**: 197–211.
- Le Mouel C and de Lussanet MHE (2019). Method for removing artificial steps from kinematic recordings. *GitHub*.

Micro-Biopsy Fiber Mechanics from the Medial Gastrocnemius of Dancers

Paige E. Rice¹, Sophia Nimphius¹, Kiisa Nishikawa²

¹School of Medical and Health Sciences, Edith Cowan University, Joondalup, WA, Australia

²Department of Biological Sciences, Northern Arizona University, Flagstaff, AZ, United States of America

Email: p.rice@ecu.edu.au

Summary

Human single muscle fiber and muscle fiber bundle mechanics have historically been performed on Bergström needle (5-6 mm) muscle biopsy samples (~60 mg). Here, we demonstrate that muscle fiber mechanics can be performed on muscle samples (~15 mg) from 14G micro-biopsy needles (2.1 mm), which are far less invasive, more feasible for laboratories that do not have access to a medical doctor, and pose less risk to the participant. To our knowledge, these are the first passive muscle fiber mechanics data from dancers.

Introduction

Muscle micro-biopsies are a practical technique for physiologists and biophysicists to further knowledge surrounding human muscle properties. Up until now, Bergström muscle biopsies have been the sole technique for researchers investigating human muscle fiber mechanics [1, 2]. The aims of this study were to 1) determine whether muscle fiber mechanics could be investigated using medial gastrocnemius (MG) micro-biopsy samples, and subsequently 2) report passive muscle fiber characteristics of dancers.

Methods

Healthy female dancers (n = 15; age = 24.2 ± 5.0 yrs.; height = 163.8 ± 4.6 cm; body mass = 61.1 ± 8.9 kg; dance training = 19.6 ± 4.9 yrs.) volunteered to participate in this study and gave informed consent. Topical lidocaine was used to numb the area of the biopsy. Three muscle samples (~45 mg of tissue) were taken using a micro-biopsy needle (SuperCore™ Semi-Automatic Biopsy Instrument, with co-axial needle, 14 G, 6 cm, Argon Medical, Frisco, TX) from the dancers' MG.

Muscle samples were immediately placed in 2 mL of skinning solution and stored at -30°C for one month prior to permanent storage in -80°C until the day of the experiment [1]. On the day of experiments, muscle fibers (2-3 mm in length) were teased from samples in relaxing glycerol (50:50). Muscle fibers were attached with acetone-based glue to length lever controller (Aurora Scientific Inc., Model 315C, Ontario, Canada) and force transducer pins (Model 400A). A high-speed camera (Aurora Scientific Inc., HVSL 901C, Ontario, Canada) was used to adjust fibers to a starting average sarcomere length (SL) of 2.4 μm. Muscle fiber cross-sectional area (CSA) was determined with an ocular micrometer (50X).

Muscle fibers (n = 50) were passively stretched from an average SL of 2.4 μm to 3.0 μm at 0.015 μm/s, 0.04 μm/s, and in five ramping increments at 0.12 μm/s (Figure 1). Trials were separated by three minutes of rest. Muscle fiber stress was calculated as force divided by muscle fiber CSA. Peak stress and average stress from the last second of each corresponding stretch-hold were reported.

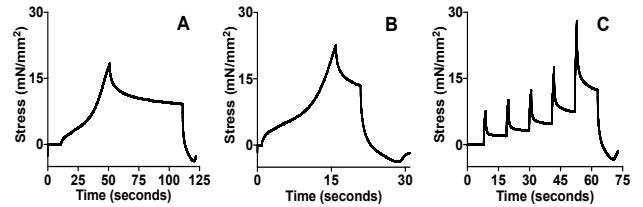


Figure 1: Example data from a passive muscle fiber during A) slow (0.015 μm/s), B) moderate (0.04 μm/s), and C) ramp stretch (0.12 μm/s) from an average SL of 2.4 to 3.0 μm.

Results and Discussion

Passive peak stress of muscle fibers increased with stretch velocity (Figure 2). The data are comparable to previous human MG fiber studies, and suggest that micro-biopsies can be used to investigate the intrinsic and adaptable properties of human muscle fibers [3].

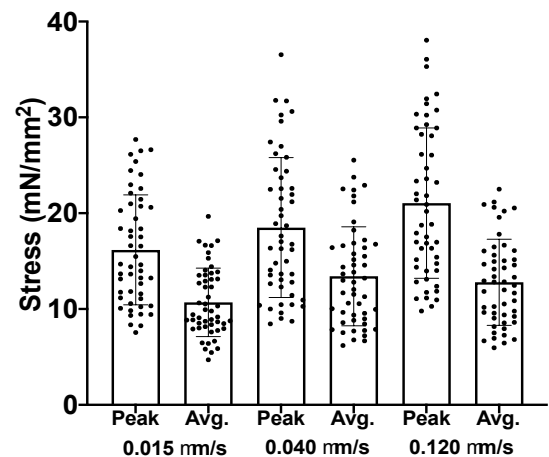


Figure 2: Passive peak stress at an average SL of 3.0 μm after slow, moderate, and the fifth ramp stretch (see Fig. 1).

Conclusions

Based on the comparable results of fiber mechanics between techniques, micro-biopsy samples are a viable alternative to Bergström biopsies to investigate fiber mechanics.

Acknowledgments

We thank Chris Rand, Aubrey Funke, and Anthony Hessel. This study was funded by a Doctoral Grant from the US National Strength and Conditioning Association.

References

- [1] Malisoux L et al. (2006). *J Appl Physiol*, **100**: 771-779.
- [2] Pinnell RAM et al. (2019). *J Biomech*, **91**:164-169.
- [3] Matthewson MA et al. (2014). *J Orthop Res* **32**(12):1667-1674.

Influence of Intermittent Blocking of Visual Information on Corticomuscular Coherence during Walking

Hitoshi Makabe¹, Ai Ogawa², Misuzu Awano³, Kenichi Kaneko⁴

¹Faculty of Health Science, Juntendo University, Tokyo, Japan. ²Sothern Tohoku Hospital, Fukushima, Japan.

³Shonai Amarume Hospital, Yamagata, Japan. ⁴Department of Economy, Fuji University, Iwate, Japan.

Email: h.makabe.lv@juntendo.ac.jp

Summary

The purpose of this study was to clarify the influence of intermittent blocking of visual information on walking parameters and corticomuscular coherence (CMC). Twelve healthy young persons participated in this study. Subjects walked at a comfortable speed for 10 minutes with and without intermittent blocking of visual information. The subjects' visual information was blocked intermittently by the liquid crystal shutter goggle with 10 Hz blinking frequency under the two conditions with the duty ratio of 30% and 70%. No blocking of visual information was the control condition. EEG was recorded from Cz, and EMG was recorded from the right tibialis anterior (TA). Walking parameters (speed, walking rate, step length) and the peak value of Cz-TA coherence in the beta band (13-30Hz) were evaluated. There was no significant difference in walking parameters at intermittent blocking of visual information with the duty ratio of 30% and 70%. The peak value of Cz-TA coherence in the beta band significantly decreased at intermittent blocking of visual information with the duty ratio of 70% compared to that of no blocking. These results suggested that intermittent blocking of visual information in young adults during walking mainly affected the modulation of CMC, but it did not even cause the change of walking parameters.

Introduction

There is still little consensus on the influence of intermittent blocking of visual information on walking parameters and corticomuscular coherence (CMC) during walking [1]. This study aimed to clarify the influence of intermittent blocking of visual information on walking parameters and CMC.

Methods

Twelve healthy young men (age: 21.2 ± 0.8 years, height: 169.8 ± 6.9 cm, weight: 65.5 ± 7.4 kg) participated in this study. The study was approved by the ethics committee for Yamagata Prefectural University of Health Sciences (approval number 1809-19) and was performed by the Declaration of Helsinki. Subjects walked a 20m 8-shaped walking path at a comfortable speed for 10 minutes. Measurement conditions were the following three conditions. The liquid crystal shutter goggle blocked the subjects' visual information with 10 Hz blinking frequency under two conditions with the duty ratio of 30% and 70%. No blocking of visual information (without the liquid crystal shutter goggle) was the control condition. Walking parameters of speed, walking rate, and step length were evaluated above the three conditions. Electroencephalogram (EEG) and electromyogram (EMG) were measured during walking using a 4-channel Ganglion Board (Open BCI) at the 200Hz sampling frequency. EEG activity was recorded through unipolar silver electrodes placed

at Cz by the international 10-20 system. Surface EMG electrodes of Ag/AgCl (Kendal H124SG, 30mm×24mm, interelectrode distance 2cm) were placed at the proximal 1/3 of the tibialis anterior (TA) muscle of the right leg. EEG and EMG electrode impedances were kept below 5k Ohm. The Welch algorithm calculated EEG-EMG coherence (Cz-TA coherence) for Cz-TA in theta (4-8Hz), alpha (8-13Hz), beta (13-30Hz), and gamma (30-40Hz) bands (window width: 256 points, overlapping 128 points, resolution 0.78 Hz). Walking parameters and peak values of Cz-TA coherence in the four bands were evaluated in the above three conditions. The evaluation parameters were compared between no blocking and intermittent blocking with the duty ratio of 30% and 70% using repeated-measures ANOVA. Statistical significance was given for P-values smaller than 0.05.

Results and Discussion

There was no significant difference in walking parameters during intermittent blocking of visual information with the duty ratio of 30% and 70%. The peak value of Cz-TA coherence in the beta band significantly decreased at intermittent blocking of visual information with the duty ratio of 70% compared to that of no blocking. These results suggested that intermittent blocking of visual information in young persons during walking mainly affected the modulation of CMC, but it did not even cause the change of walking parameters.

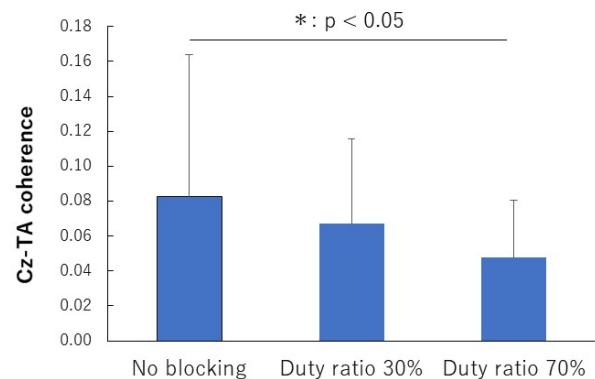


Fig. 1 Cz-TA coherence in beta band during walking

Conclusions

Intermittent blocking of visual information with the duty ratio of 70% in young persons during walking mainly affected the modulation of CMC, but it did not even cause the change of walking parameters.

References

[1] Spedden ME et al. (2019). *Neurobiol Aging*, **78**: 29-41.

Balance-Dexterity Task Performance In and Out of An Episode of Low Back Pain

Jiayi Tang¹, Hai-Jung Steffi Shih^{1,2}, Yue Ai¹, K. Michael Rowley¹, and Kornelia Kulig¹

¹Division of Biokinesiology and Physical Therapy, University of Southern California, Los Angeles, CA, USA

²Department of Biobehavioral Sciences, Teachers College, Columbia University, New York, NY, USA

Email: jiayit@usc.edu

Summary

This study explored trunk control during symptomatic and asymptomatic periods for individuals with recurrent low back pain (rLBP) and compared them with the back-healthy individuals using the Balance-Dexterity Task (BDT). Findings revealed that individuals with rLBP exhibited reduced center-of-pressure (COP) velocity when they were in remission compared to when they were in pain, and when compared to the back-healthy controls (CTRL).

Introduction

Based on a former study, we hypothesized trunk kinematics during a dynamic balance task would be altered compared to the back-healthy individuals [1]. This motor control dysfunction may contribute to the recurrence of pain [1]. So it is necessary to explore task performance for people with rLBP when they are in pain and in remission. The purpose of this study was to investigate trunk control, dexterity, and steadiness in and out of an episode of rLBP and compare them to CTRL. We hypothesized that persons with rLBP in remission would have similar steadiness (COP velocity) and dexterity (ability to maintain compression force) and less frontal plane trunk coupling compared to CTRL. We also hypothesized that in active pain, individuals with rLBP would exhibit increased frontal plane trunk coupling compared to when they were in remission due to a “tighter” trunk control triggered by pain [2].

Methods

19 individuals with rLBP (F=13, M=6; 25.3±5.2 years) and 19 matched CTRLs (F=13, M=6; 26.9±3.4 years) performed the BDT. rLBP group was first tested when they were in pain (rLBP-A, Visual Analog Scale (VAS) = 38.9±19.2 mm), then in remission (rLBP-R, VAS = 1.4±2.4 mm).

The BDT required participants to compress a stable block or an unstable spring with one limb (dexterous limb) to maintain an individualized force target while standing on the supporting limb [3]. With the recorded data from corresponding force plates under both feet (sampling frequency = 1500 Hz), COP velocity under the supporting limb and vertical force variability under the dexterous limb were analyzed. Frontal plane trunk coupling was calculated as the coefficient of determination (R^2) between thorax and pelvis angles, which were modeled from marker-based kinematic data recorded by a motion capture system. The statistical analysis was conducted using linear mixed-effects models. The analysis was first conducted between rLBP-A and rLBP-R. If no differences were found, then rLBP-A and rLBP-R were pooled and compared to CTRL.

Results and Discussion

Across rLBP-A and rLBP-R, participants had greater COP velocity ($p<.001$), greater vertical force variability ($p<.001$), and less trunk coupling ($p=.0135$) when compressing the spring than the block (condition main effect). Trunk coupling was not statistically different between rLBP-A and rLBP-R ($p=.695$) or between rLBP and CTRL ($p=.327$). There were no differences in dexterity between rLBP-A, rLBP-R ($p=.363$), and CTRL ($p=.421$). rLBP-R had reduced COP velocity compared to rLBP-A ($p=.029$) and CTRL ($p=.011$) (Fig 1).

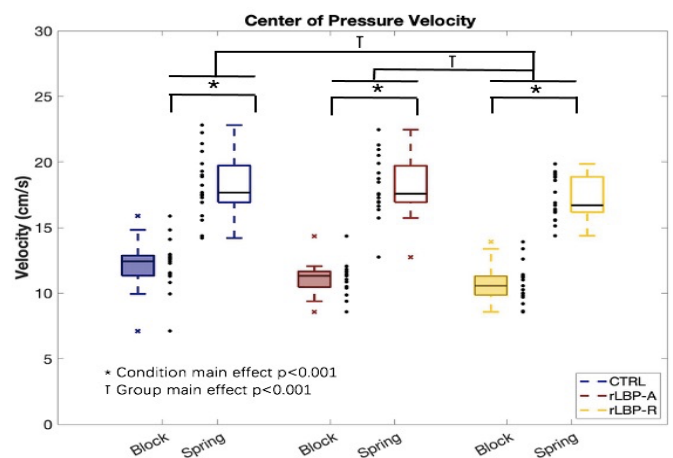


Figure 1: COP velocity during block and spring conditions in CTRL, rLBP-A, rLBP-R

Conclusions

Contrary to our hypothesis, individuals with rLBP did not alter frontal plane trunk coupling in and out of a painful episode, nor were they different from CTRL. Instead, individuals in remission showed a lower COP velocity compared to when they were in pain and the CTRL. This may indicate that frontal plane trunk coupling was altered independently of task performance. These results suggest that persons with rLBP have greater steadiness during symptom remission, which may be attributed to psychosocial influences such as fear of movement.

Acknowledgments

Funded by the ISB Matching Dissertation Grant to Shih.

References

- [1] Rowley et.al, (2019). *J Orthop Sports Phys Ther*, **49**:679-681.
- [2] Van Dieen et.al, (2019). *J Orthop Sports Phys Ther*, **49**: 370-379.
- [3] Rowley et.al, (2018). *J Biomech*, **80**:79-87.

The mechanical arrangement of the human semitendinosus muscle as assessed with shear wave elastography

Adam Kositsky^{1,2,3}, David J. Saxby^{1,2}, Kim Lesch⁴, Rod S. Barrett^{1,2}, Heikki Kröger⁵, Olli Lahtinen⁶, Laura E. Diamond^{1,2}, Rami K. Korhonen³, Lauri Stenroth³

¹School of Allied Health Sciences, ²Menzies Health Institute Queensland, Griffith University, Gold Coast, Queensland, Australia

³Department of Applied Physics, ⁴Faculty of Health Sciences, University of Eastern Finland, Kuopio, Finland

⁵Department of Orthopaedics, Traumatology and Hand Surgery, Kuopio University Hospital, Kuopio, Finland

⁶Diagnostic Imaging Center, Department of Clinical Radiology, Kuopio University Hospital, Kuopio, Finland

Email: adam.kositsky@griffithuni.edu.au

Summary

The mechanical arrangement of the human semitendinosus (ST), a hamstring muscle comprised of two anatomically in-series compartments, remains unknown. Using two-dimensional shear wave elastography (2D-SWE), we acquired the shear modulus of both ST compartments at ten knee joint angles. We found no differences in shear modulus-angle curve parameters between the two compartments. As shear modulus is linearly related to muscle force [1], our results suggest forces are equally distributed along the ST and thus the two ST compartments can be considered mechanically in-series.

Introduction

The ST is divided by a tendinous inscription into proximal (ST_{prox}) and distal (ST_{dist}) compartments, each with separate nerve branches [2]. As the two compartments are anatomically in-series, it is typically assumed they are also mechanically in-series in humans [3]. However, structures anatomically in-series do not necessarily bear identical loads and thus are not always mechanically in-series [4]. Further, potential imbalances in force between ST_{prox} and ST_{dist} may increase the risk of muscle injury [2]. As the shear modulus obtained with 2D-SWE can provide an indirect measure of muscle force [1], characterizing the passive shear modulus-angle relationship of ST_{prox} and ST_{dist} using 2D-SWE might suggest differences in force distribution between ST compartments. Thus, the aim of this study was to compare the passive shear modulus-angle curves of ST_{prox} and ST_{dist}.

Methods

The Young's modulus of ST_{prox} and ST_{dist} was obtained from 14 prone-positioned participants ($n=11$ bilateral, $n=3$ unilateral) with a 44 mm linear ultrasound transducer (9L; Logiq E9, GE Healthcare) (Figure 1A). Following preconditioning, three 2D-SWE images from each of ST_{prox} and ST_{dist} were acquired at 10° intervals from 90° to 0° (full extension) of knee flexion. Knee joint angle and semimembranosus myoelectric activity (to verify hamstring passive state) were monitored in real-time (ME6000, Mega Electronics). Young's modulus values were divided by three to obtain shear modulus [1]. A piecewise exponential model was fit to the data to obtain parameters from the shear modulus-angle curve: slack angle (the angle at which shear modulus starts to increase), slack shear modulus, and "alpha" (the slope of the increase in shear modulus) [5] (Figure 1B). The effects of leg and compartment on slack angle, slack shear modulus, and alpha were assessed with a linear mixed model.

Results and Discussion

There were no main effects of leg (slack angle: $p=0.054$; slack shear modulus: $p=0.319$; alpha: $p=0.471$) or compartment (slack angle: $p=0.480$; slack shear modulus: $p=0.141$; alpha: $p=0.220$) (Figure 1C-E). There were also no interactions between leg and compartment for slack angle ($p=0.419$), slack shear modulus ($p=0.564$), or alpha ($p=0.370$).

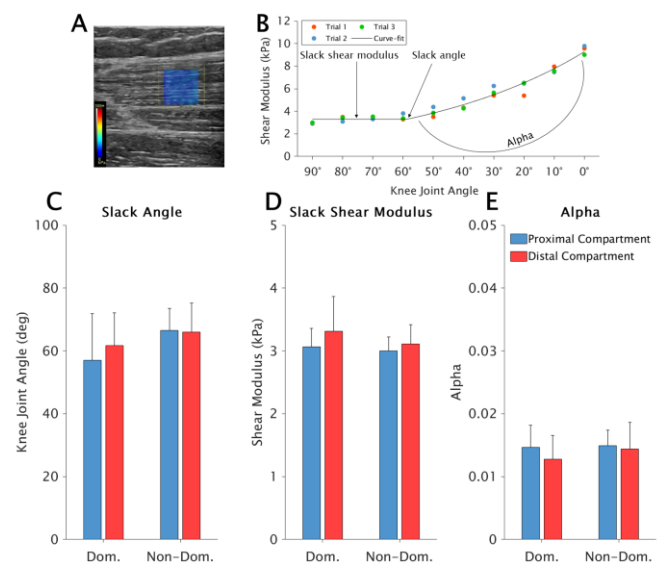


Figure 1: Example elastography image (A) and piecewise curve-fit (B). Shear modulus-angle curve parameters of the semitendinosus compartments of dominant and non-dominant legs (C-E).

Conclusions

The lack of differences in shear modulus-angle curve parameters between the proximal and distal ST compartments suggests an equilibrium of forces between the two human ST compartments and thus a mechanically in-series arrangement.

Acknowledgments

ISB Student International Travel Grant, the Erasmus+ programme of the European Union, the Academy of Finland.

References

- [1] Hug F et al. (2015). *Exerc. Sport Sci. Rev.*, **43**: 125-133.
- [2] Edgerton VR et al (1987). *Medicine Sport Sci.*, **26**: 12-23.
- [3] Ward SR et al. (2009). *Clin. Orthop. Relat. Res.*, **467**: 1074-1082.
- [4] Herzog W (2019). *BMC Biomed. Eng.*, **1**: 28.
- [5] Koo TK et al. (2014). *Clin. Biomech.*, **29**: 33-39.

Surgical Positioning of the Hip Joint Center During Total Hip Arthroplasty and its Effects on Muscle and Hip Joint Reaction Forces.

Jasvir S. Bahl¹, John B. Arnold², David J. Saxby³, Mark Taylor⁴, Lucian B. Solomon^{1,5}, Dominic Thewlis¹

¹Centre for Orthopaedics and Trauma Research, Adelaide Medical School, The University of Adelaide, Adelaide, Australia.

²Alliance for Research in Exercise, Nutrition, & Activity (ARENA), Allied Health and Human Performance, University of South Australia, Adelaide, Australia. ³Griffith Centre of Biomedical and Rehabilitation Engineering (GCORE), Menzies Health Institute Queensland and Advanced Design and Prototyping Technologies Institute (ADAPT), Griffith University, Gold Coast, Australia.

⁴The Medical Devices Research Institute, College of Science and Engineering, Flinders University, Adelaide, Australia.

⁵Department of Orthopaedics and Trauma, Royal Adelaide Hospital, Adelaide, Australia.

Email: Jasvir.bahl@adelaide.edu.au

Summary

Careful implant positioning during total hip arthroplasty (THA) is important to reduce muscle and joint forces during walking. However, current understanding of this relationship is based on simulation or mathematical models and often neglect true radiographical findings or fail to consider individual gait patterns. Here, we used pre-and post-operative computed tomography (CT) and 3D gait analysis to determine the effect of surgical placement of the hip joint center (HJC) during THA on hip abductor and hip joint reaction forces during walking.

Introduction

Considerable research effort has focussed on reconstructing the HJC during THA to provide a mechanical advantage to the hip abductors, which contribute to the most of any hip muscle group to the hip joint reaction force [1]. The aim of this study was to determine the effect of HJC reconstruction on the hip abductor and hip joint reaction forces.

Methods

Thirty-five patients undergoing primary THA for osteoarthritis (OA) were recruited from a single public hospital in Australia (mean age: 66 (SD 14) years, mean BMI: 24 (SD 5) kg.m⁻²). Subjects walked at a self-selected pace where a 10-camera motion analysis system (Vicon, Oxford, UK) system tracked marker trajectories and two force platforms recorded ground reaction forces. Pre-and post-operative CT of the pelvis and proximal femurs were obtained and reconstructed using the Scan-IP module (Simpleware,UK). The pre-operative hip HJC was determined using the center of a sphere fitted to the femoral head and its location was expressed relative to the center of a sphere fitted to the acetabulum. For the post-operative HJC location, the pre-and post-operative reconstructed models were aligned, where the post-operative femoral head location was expressed in the pre-operative acetabulum reference frame, allowing for the change in HJC location to be determined. To estimate muscle and joint reaction forces, a generic musculoskeletal model (Gait 2392) was scaled to the subject's anthropometry using the MAPClient [2], where the hip joint geometry was personalized from CT data. Muscle forces and hip joint reaction forces were computed using the available tools in OpenSim. To determine the effect of surgical change to HJC location alone paired samples *t*-test was used to test the

difference in the peak resultant hip reaction force when the pre-operative model was adjusted to represent the surgical change in HJC location, without any change in the pre-operative motion capture data.

Results and Discussion

Surgical change to the HJC reduced the magnitude of hip abductor muscle force (mean difference: -162 N, SD 187, *p* <.001) and the resultant peak hip reaction force (mean difference: -151 N, SD 324, *p* = .009) (Figure 1). Medial and proximal location of the HJC had the greatest influence on hip joint reaction forces, explaining 52% and 40% of the variance, respectively. For each millimeter of medialization, the peak resultant hip reaction force reduced by 35 N, (SD 7) and for each millimeter of proximal change, the peak resultant hip reaction force reduced by 28 N (SD 9).

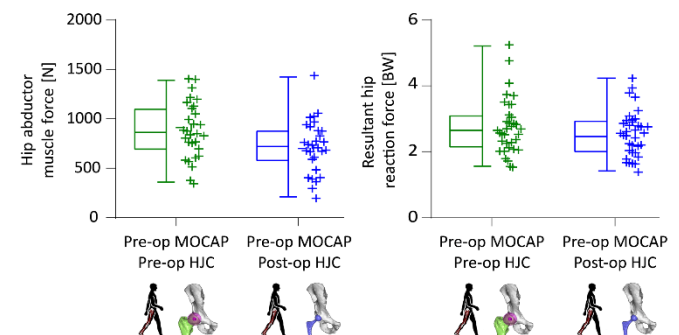


Figure 1: The effect of surgical change to the HJC on peak abductor muscle forces (left) and resultant hip joint reaction forces (right).

Conclusions

Medial and proximal location of the HJC resulted in the greatest reduction in hip abductor and hip reaction forces. Changes in the medial direction were most influential to reduce hip joint reaction forces, indicating an emphasis be placed on HJC medialization to increase the hip abductor moment-arm and reduce hip joint reaction forces, with consideration of proximal placement if the available bone stock is sufficient to achieve implant stability.

References

- [1] Correa TA et al. (2010). *J Biomech*, **43**: 1618-1622.
- [2] Zhang J et al. (2014). *ISBMS In: Biomed Sim*, **8789**

Optimal Design of Elastic Ankle Exoskeleton Using Optimal Control of Musculoskeletal Model

Karthick Ganesan, Abhishek Gupta

Department of Mechanical Engineering, Indian Institute of Technology Bombay, Mumbai, India

Email: karthick.ganesan@iitb.ac.in

Summary

Finding optimal stiffness is critical to the design of elastic ankle exoskeletons. Musculoskeletal simulations can be a promising alternative to laborious experiments in this regard. Here we use optimal control based musculoskeletal simulations to find the optimal stiffness of an elastic ankle exoskeleton. The stiffness found from simulations were similar to that found from experiments, proving the utility of this approach.

Introduction

Elastic ankle exoskeletons are of light weight, simple in construction, yet have the potential for reducing the metabolic cost of walking. However the stiffness of these exoskeletons has to be chosen optimally, otherwise it can even have negative effect on the metabolic cost due to the interplay between the plantarflexor muscles and tendon [1]. Researchers have used springs of different stiffness values in experiments to arrive at the optimal stiffness. Musculoskeletal simulations can complement experiments. Although simple lumped parameter models have been used [2], they did not consider the dynamics of all limb segments and assume fixed kinematics. Optimal control based predictive simulations can overcome these limitations. Here we use this approach to optimize the stiffness of an elastic ankle exoskeleton.

Methods

We used a 2D version of the Rajagopal's [3] musculoskeletal model, with 12 degrees of freedom and 28 muscles. Contact elements were defined on the plantar surface of each foot. The muscles were replaced by muscle model proposed by de Groote et al [4].

The goal was to determine the states and controls of the model, and the stiffness of the bilateral exoskeletons that minimized a cost functional subject to the skeleton and muscle dynamics, and task constraints with respect to the bounds on states, controls, stiffness (0 – 250 Nm/rad) and final time. The cost functional had a tracking term and a muscular effort term. The tracking term consisted of the squared difference between values of the model variables and the reference variables (generalized coordinates and speeds, and the ground reaction forces). For reference values we used the mean experimental values from the literature. The reference values for pelvic tilt and lumbar degrees of freedom were set as zero. The generalized speeds for the pelvis and lumbar degrees of freedom were not tracked. The weights for tracking and effort terms were tuned to produce realistic metabolic cost without exoskeleton.

We solved the optimal control problem numerically using direct collocation. The optimal control problem was

converted into a nonlinear programming problem through hermite-simpson transcription with 25 nodes. This was achieved using CasADi solver in OpenSim Moco [5]. IPOPT was used as the NLP solver. Stiffness of the exoskeleton was treated as a static parameter.

Results and Discussion

The optimal stiffness found was 34 Nm/rad which is close to that found through experiments. The metabolic cost reduction at this stiffness was 3.2%. We also tested the metabolic cost with different stiffness values and found that they were less, compared to that of optimal stiffness. One of the limitations of our study is that we used a two dimensional model to reduce the computational time. Another limitation is that we used experimental gait data for tracking. By increasing the weight on the effort term we can do a predictive simulation.

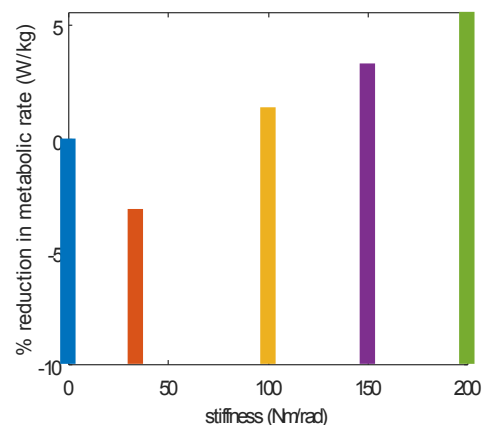


Figure 1: Percent reduction in metabolic rate for range of stiffness.

Conclusions

We demonstrated the use of optimal control based musculoskeletal simulations to optimize the stiffness of elastic ankle exoskeleton. This approach can be extended to other exoskeletons and parameters. This approach will be particularly useful for designing exoskeletons for pathological populations since conducting many experiments on them is difficult.

References

- [1] Collins SH et al. (2015). *Nature*, **522**: 212-215.
- [2] Sawicki GS and Khan NS (2016). *IEEE Trans Biomed Eng*, **63(5)**: 914-923.
- [3] Rajagopal A et al. (2016). *IEEE Trans Biomed Eng*, **63(10)**: 2068-79.
- [4] De Groote F et al. (2016). *Ann Biomed Eng*, **44(10)**:2922-36.
- [5] Dembia CL et al. (2020). *Plos One*, **pcbi.1008493**.

Estimations of Knee Joint Loading Using Generalized Methods and Muscle Recruitment Strategies

Kieran J. Bennett¹, Claudio Pizzolato², Saulo Martelli³, Jasvir S. Bahl¹, Arjun Sivakumar¹, Gerald J. Atkins¹, L. Bogdan Solomon^{1,4}, Dominic Thewlis¹

¹Centre for Orthopaedics and Trauma Research, School of Medicine, The University of Adelaide, Adelaide, SA, Australia.

²Griffith Centre of Biomedical and Rehabilitation Engineering, Griffith University, Gold Coast, QLD, Australia ³Science and Engineering Faculty, School of Mechanical Medical & Process Engineering, Queensland University of Technology, Brisbane, QLD, Australia. ⁴Department of Orthopaedics and Trauma, Royal Adelaide Hospital, Adelaide, SA, Australia

Kieran.Bennett@adelaide.edu.au

Summary

Estimations of joint loading are critical to evaluate joint disease and functional outcomes. However, the muscle recruitment strategy which best mimics joint loads measured *in vivo* remains unclear. This study compared the performance of three methods: (1) static optimization; (2) EMG-assisted, and; (3) an inverse EMG-informed stochastic method. Static optimization resulted in root mean square errors of 674 N and 196 N, while the EMG-assisted method errors were 413 N and 153 N. The stochastic method provided a spectrum of knee forces containing the *in vivo* target measurements and a spread consistent with the uncertainty on the inputs.

Introduction

Joint loadings have been associated with onset and progression of musculoskeletal diseases, such as knee osteoarthritis. Musculoskeletal models can estimate joint loading, overcoming the inability to perform direct *in vivo* measurements. However, contention still remains around the optimal method to simulate muscle recruitment strategies that accurately estimate joint loading. Using data from instrumented knee replacements as ground truth, we compared three methods for simulating muscle recruitment to estimate internal joint loading at the knee during walking.

Methods

Data were obtained from the Grand Challenge Competition to Predict *in-vivo* Knee Loads (challenges four, five, and six) [1]. Static and over ground gait trials were used. A generic full-body musculoskeletal model [2] was scaled using static marker data in MAPClient [3]. Musculotendon lengths [4] and muscle maximum isometric strengths [5] were tailored to subjects. Marker trajectories and ground reaction forces were used for inverse kinematics, inverse dynamics, and static optimization (SO) in OpenSim [2]. Electromyography (EMG) data were used for the Calibrated EMG Informed Neuromusculoskeletal Toolbox (CEINMS), and to inform constraints for the inverse EMG-informed stochastic method [7]. We used 8-11 EMG signals from large superficial muscles. In CEINMS, seven degrees of freedom were driven in EMG-assisted mode. In the stochastic method, one million solution samples were taken per frame, and muscles forces were constrained within one standard deviation of the CEINMS solution. Other muscles were constrained to half of their maximum possible force. The measured loading from the prostheses was used as the ground-truth for model validation.

Results and Discussion

For datasets where subjects walked abnormally (Challenge 5, Fig 1), SO significantly over predicted second peak loading

(1390 N error), while CEINMS was able to account for altered neuromusculoskeletal control during late stance (182 N second peak load error). The stochastic method produced a solution space encompassing the measured load, except for between 27-32%. Root mean square errors (RMSE) for SO and CEINMS were 674 N and 413 N respectively. In challenge 6, both SO and CEINMS accurately predicted knee JCF with RMSE of 196 N and 153 N respectively. The stochastic method produced a solution space which includes the *in-vivo* target measurement up to 90% of stance.

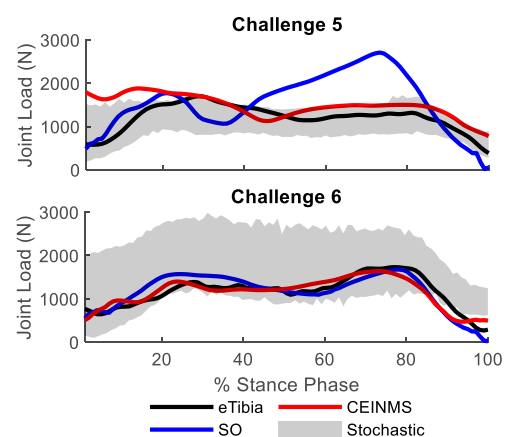


Figure 1: Measured (eTibia) and estimated knee joint loading using SO, CEINMS, and the stochastic method of muscle recruitment.

Conclusions

Estimations of joint loading were obtained using different methods of simulating muscle recruitment. Overall, CEINMS produced better estimates of joint loading compared to SO. The stochastic method provided a spectrum of knee forces containing the *in vivo* target measurements and can allow for further exploration into muscle recruitment and its effect on joint loading.

Acknowledgments

This project was funded by the NHMRC (ID: 1126229) and the ARC (DP180103146; FT180100338; IC190100020).

References

- [1] Fregly B.J. et al. (2012) *J Orthop Res.* **4**: 503-513
- [2] Delp S. et al. (2007) *IEEE TBME.* **54**: 1940-1950
- [3] Zhang J. et al. (2014) *ISMBS.* **2014**: 182-192
- [4] Modenese L. et al. (2016) *J. Biomech.* **49**: 141-148
- [5] Handsfield J. et al. (2014) *J. Biomech.* **47**: 631-638
- [6] Pizzolato C. et al. (2015) *J. Biomech.* **48**: 3929-3936
- [7] Martelli S. et al. (2015) *Interface Focus.* **5**: 20140094

Effect of sagittal alignment parameters on intervertebral compression forces in asymptomatic adolescent girls, during a pubertal growth spurt, using a thoracolumbar musculoskeletal model

Mohammad Amin Shayestehpour^{1,*}, Hamed Shayestehpour², Christian Wong³ and John Rasmussen²

¹Department of Mechanical Engineering, Sharif University of Technology, Tehran, Iran

²Department of Materials and Production, Aalborg University, Aalborg East, Denmark

³Department of Orthopedics, University Hospital of Hvidovre, Hvidovre, Denmark

Email: mohammadaminshayestehpour77@gmail.com

Summary

Sagittal alignment of the spine alters during the pubertal growth spurt. Using a musculoskeletal model, we simulated these alterations by choosing Thoracic Kyphosis and Sagittal Vertical Alignment as variable parameters. Results indicated that, by increasing these parameters as the posterior inclination of the spine decreases through the growth spurt, the intervertebral compression forces of the thoracolumbar spine increase.

Introduction

Adolescent Idiopathic Scoliosis (AIS) occurs most often in adolescent girls. This is a deformity in the frontal plane. However, this concurs with natural changes in sagittal plane alignment in their spinal pubertal growth. Previous studies indicate that the adolescent spine tends to be more posteriorly inclined earlier in the growth spurt, then Thoracic Kyphosis (TK) and Sagittal Vertical Alignment (SVA) increase in a way that posterior inclination decreases during further pubertal development [1, 2].

Methods

We utilized a recently developed thoracolumbar musculoskeletal model [3] to obtain the variation of normalized intervertebral joint compression (NJC) force caused by alteration of TK and SVA, and then investigate the NJC trend through the growth spurt.

TK is the sagittal Cobb angle between the T4 and T12 vertebrae, and SVA is the horizontal distance between the C7 vertebra and the posterior superior sacrum. Positive SVA means C7 is placed posteriorly to Sacrum. Parameter values during the growth spurt were obtained from previous studies. [1, 2]. In this study, TK and SVA were simulated in the range of 28 to 39 degrees and -20 to 43 mm respectively.

We represented the reclined segment (RS) of the spine by the number of vertebrae that are posteriorly inclined relative to the horizontal plane [1]. This parameter was employed to identify the proper growth direction line on the surface. Typical RS in growth is considered to be 8 to 10 posterior vertebrae, which were illustrated as dashed lines (Figure 1).

We acquired the growth direction line considering that TK and SVA increase and RS decreases, to describe typical TK, SVA and RS development in the growth spurt.

Results and Discussion

We considered the T8-T9 NJC as a function of TK and SVA (Figure 1) because T8 is the most common apical vertebra in AIS. However, the trend was the same for all the lower

thoracic and lumbar regions. NJC increased with increasing TK and SVA but NJC is more sensitive to SVA than TK.

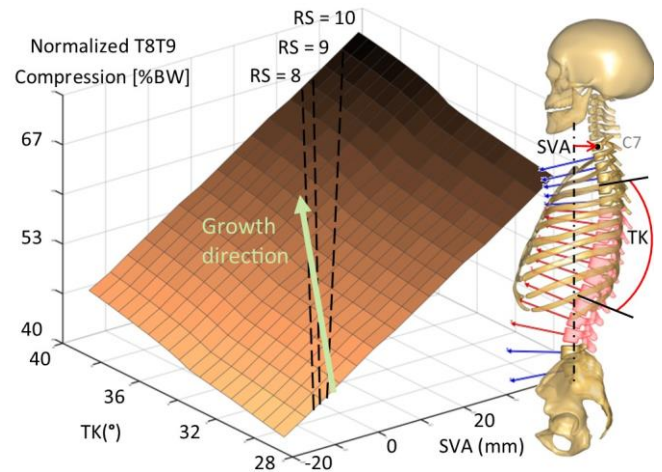


Figure 1: The T8-T9 NJC as a function of TK and SVA. The compression is normalized to body weight [BW]. TK and SVA are defined on the right and the reclined segment (RS) is shown in red. The spine arrows show the inclination of each vertebra. The dashed lines on the surface show constant RS of 8, 9, and 10 reclined vertebrae, which include L3 up to T8, T7, and T6, respectively.

Using the growth direction line, we infer that NJC is higher in the later stages of growth for adolescent girls. Moreover, we found a positive correlation between NJC and RS.

Conclusions

The intervertebral joint compression in T8-T9 increases with TK as well as SVA, and the combination of parameter development typical for the growth spurt causes a net increase of joint compression. It may be speculated that the balance between increasing spinal compression forces and evolving resistance to load in the adolescent spine can play a role in the pathomechanism of AIS. The perspectives of this thoracolumbar musculoskeletal model may contribute to investigating this question in the future.

Acknowledgments

The project has received funding from the European Union's Horizon 2020 research and innovation programme under the Marie Skłodowska-Curie grant agreement NO. [764644].

References

- [1] Schlösser et al. (2015). *Eur. Spine J.*, 24: 1158–1167.
- [2] Mac-Thiong et al. (2011). *Eur. Spine J.*, 20: 586–590.
- [3] H. Shayestehpour et al. (2021), *Multibody Syst Dyn*, Accepted.

Improving Muscle Geometry through Via-Point Optimization

C.V. Simon¹, F.C.T. van der Helm¹, T. Geijtenbeek¹

¹Biomechanics and Human-Machine Control, Delft University of Technology, Delft, The Netherlands

Email: t.geijtenbeek@tudelft.nl

Summary

Accurate representation of muscle lengths and muscle moment arms is crucial for musculoskeletal modeling. A common approach is to model muscle geometry using via-points fixed to specific bodies. A downside of this approach is that the way in which moment arms change with motion is often unintuitive and leads to inaccurate or suboptimal moment arms – especially for joints with multiple degrees of freedom (DOFs). We used optimization to determine via-point placement so that moment arms matches reference data over a range of motion as closely as possible. We found this approach to drastically improve existing via-point models, approaching accuracy of more advanced methods that use wrapping surfaces.

Introduction

The via-point method is a popular approach for modeling muscle geometry in musculoskeletal models [1]. It is easy to comprehend, visualize and implement, while being computationally far less expensive than more advanced methods based on wrapping surfaces [2]. The latter is specifically important for predictive simulations, where muscle lengths and moment arms are evaluated many times and often form a performance bottleneck.

Typically, the locations of via-points are tuned manually to match cadaver or imaging data. The downside of this approach is that selecting these points is unintuitive, since only segments that cross a joint are relevant. This leads to moment arms being inaccurate or suboptimal when considering the full range of motion of a joint. This problem is especially prevalent for multi-DOF joints that allow a large range of motion. The use of *conditional* via-points is an attempt to mitigate these issues [1], but this method instead leads to discontinuities with multi-DOF joints.

In our study we attempt to use optimization methods for determining via-point placement, in such a way that the resulting muscle moment arms match a ground truth over a specified range of motion, which is either based on real-world studies or models that use more advanced wrapping surfaces.

Methods

The goal of our optimization is to optimize via-points V in such a way that the squared difference between the moment arms M and ground truth M_{ref} is minimized over the relevant range of motion, determined by the set of joints J and corresponding degrees-of-freedom Q . The error $E(V)$ to be minimized corresponds to:

$$E(V, Q) = \frac{1}{|J||Q|} \sum_{j \in J} \sum_{q \in Q} \|M_j(V, q) - M_{ref,j}(q)\|^2$$

For our ground truth, we used data from experimental moment arm studies [3], supplemented by data from a musculoskeletal model that uses wrapping surfaces for muscle geometry [2]. We used the model from [1] as a starting point for our optimization, which was performed using Nelder-Mead [4], a non-differentiable optimizer based on the simplex method.

Results and Discussion

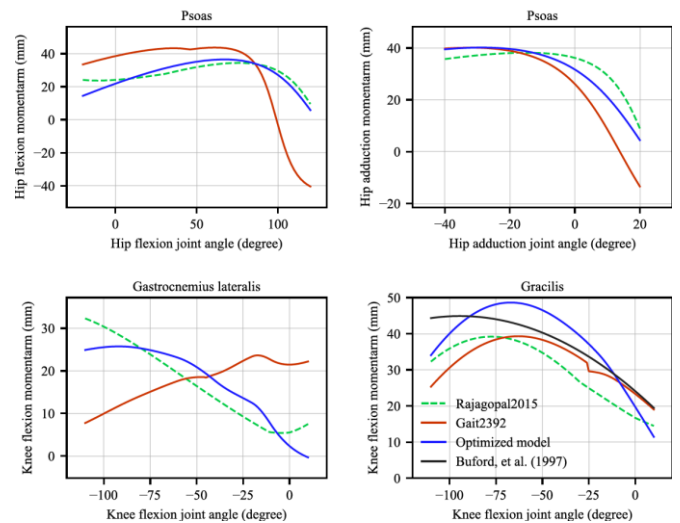


Figure 1: Optimized muscle moment arms compared to existing models [1,2] and experimental data [3]

After optimization, the moment arms of muscle paths described by via-points are able to match our ground truth remarkably well (see Figure 1, blue lines). Especially the psoas and gastrocnemius muscles show significant improvement compared to [1]. A full statistical analysis will be presented in a separate study.

Conclusions

The via-point method turns out to be remarkably capable for describing muscle moment arms over a range of motion. After using optimization methods to leverage their full capacity, via-point based models can approach the fidelity of more advanced and more computationally expensive methods based on wrapping surfaces.

References

- [1] Delp S et al. (1990), *IEEE Trans. Biom. Eng* **8**:757-767
- [2] Rajagopal A et al. (2016), *IEEE Trans. Biom. Eng.* **63**(10): 2068-2079
- [3] Buford WL et al. (1997), *IEEE Trans. Biom. Eng.* **5**(4): 367-379
- [4] Nelder JA and Mead R (1965), *The computer journal* **7**(4): 308-313

The difference of bilateral tibial load in patients with unilateral anterior cruciate ligament reconstruction during jogging

Ting Long¹, Hanjun Li¹

¹School of Sport Sciences, Beijing Sport University, Beijing, China

Email: longting0817@163.com

Summary

The risk of knee osteoarthritis is significantly increased after anterior cruciate ligament reconstruction (ACLR), and tibial contact force is associated with the development of knee osteoarthritis. Therefore, the bilateral tibial load of ACLR patients during jogging was calculated based on the neuromusculoskeletal model. The result showed the peak value of tibia compression force on the healthy side was significantly higher than that on the ACLR side, which may lead to insufficient recovery of articular cartilage or subchondral bone to withstand increased post-operative physical activity, leading to knee osteoarthritis.

Introduction

The risk of knee osteoarthritis is significantly increased after ACLR, and tibial contact force is associated with the development of knee osteoarthritis. Therefore, the calculation of tibial contact force in daily activities can deepen the understanding of the pathogenesis of knee osteoarthritis in ACLR patients and provide a theoretical basis for the development of rehabilitation strategies.

The aim to this study is to calculate the bilateral tibial load of ACLR patients during jogging and to analyze bilateral differences.

Methods

Seven ACLR patients were selected as subjects (3 males and 4 females, 1.5 to 3.5 years after surgery). The 14-camera Qualisys infrared motion capture system, Kistler 3D force measuring table and Delsys wireless EMG were used to synchronize the kinematics, dynamics and EMG data of the subjects when jogging.

A personalized neuromusculoskeletal model was established by combining scaling in OpenSim and calibration in CEINMS [1]. The Inverse Kinematics tool and Inverse Dynamics tool in OpenSim were used to calculate the joint angle and joint net moment. In CEINMS software, the EMG-assisted model was used to calculate the muscle force during jogging. On this basis, the contact force of the knee joint was analyzed by the JointReaction tool in OpenSim and the tibial contact force was obtained.

The paired sample t test was used to analyze the difference between the healthy side and the surgical side of the subjects.

Results and Discussion

The bilateral tibia compression force during jogging was shown in **Figure 1**. The peak value of tibia compression force on the healthy side was significantly higher than that on the

ACLR side ($P=0.039$). At the peak value of tibia compression force on the healthy side, the muscle force of quadriceps femoris on the healthy side was significantly higher than that on the ACLR side ($P=0.010$). The knee flexion angle on the healthy side was significantly higher than that on the ACLR side ($P=0.042$), and the dorsiflexion angle of the ankle joint on the healthy side was significantly higher than that on the ACLR side ($P=0.046$).

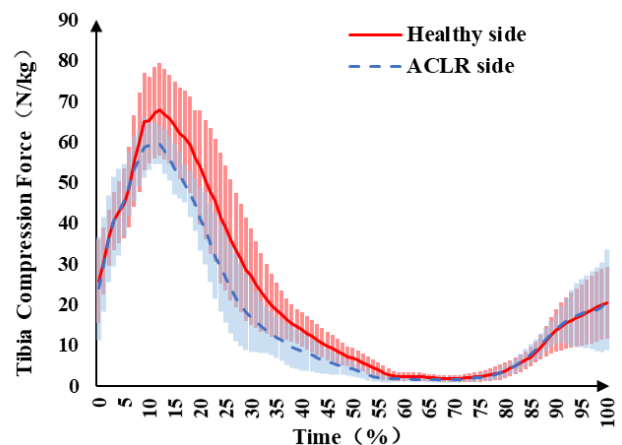


Figure 1: Bilateral tibia compression force during jogging.

The muscle force of quadriceps on the ACLR side was significantly less than that of the contralateral during the stance phase of jogging. This may be the reason why the tibial compression force on the ACLR side of the knee is less than that on the contralateral side.

In addition, the reduced compression force of the knee joint and tibia of ACLR may lead to insufficient recovery of articular cartilage or other joint tissues [2], so that the knee joint after ACLR surgery cannot withstand the gradually restored load intensity [3], leading to the occurrence of osteoarthritis.

Conclusions

Patients with unilateral ACLR show less tibial compression force on the ACLR side than on the healthy side during jogging, which may lead to insufficient recovery of articular cartilage or subchondral bone to withstand increased post-operative physical activity, leading to knee osteoarthritis.

References

- [1] Pizzolato, C. et al. (2015). *J Biomech*, **48**: 3929-3936.
- [2] Koo S. et al. (2007). *J Biomech*, **40**: 2962-2966.
- [3] Wellsandt, E. et al. (2016). *American Journal of Sports Medicine*, **44**: 143-151.

The effect of functional knee alignment on the knee contact forces during execution of closed kinetic chain rehabilitation exercises

Williane Bernardes¹, Amir Esrafilian¹, Paavo Vartiainen¹, Jari Arokoski², Rami Korhonen¹, Lauri Stenroth¹

¹Department of Applied Physics, University of Eastern Finland, Finland

²Department of Physical and Rehabilitation Medicine, Helsinki University Hospital and University of Helsinki, Helsinki, Finland

Email: williane.bernardes@uef.fi

Summary

Pain felt during exercises could be a reason for the reported low adherence of knee osteoarthritis (KOA) patients to the prescribed physical rehabilitation. Reducing the compressive loads on the knee regions affected by osteoarthritis may help to reduce the pain and improve adherence. In this study, the effect of functional knee alignment on the knee contact forces and external knee moments were evaluated during five exercises used in KOA rehabilitation. The alignment did not significantly affect the knee contact forces or external knee moments. Hence, alterations in the functional knee alignment may not be an effective strategy to unload specific regions of the knee in a rehabilitation setting.

Introduction

Physical rehabilitation is often prescribed for the treatment of KOA but patient adherence is low [1]. Pain felt during the exercises may be an explanation [2]. Unloading the knee regions affected by osteoarthritis may reduce the pain, and consequently, improve adherence and ultimately lead to better treatment outcomes. Alterations in the functional knee joint alignment have been used to redistribute joint loading in the knee during gait [3], which may potentially provide a feasible strategy also during the performance of closed kinetic chain rehabilitation exercises. This study aimed to assess if the distribution of the compressive knee joint contact forces (KCF) is altered when different alignments are used during closed kinetic chain rehabilitation exercises.

Methods

Eight healthy young adults (one female and seven males, 23.9 ± 5.2 yr. old) executed five exercises in three sets of seven repetitions using their right leg. Each set was performed with a different knee alignment in the frontal plane: neutral, medial, and lateral while marker trajectories, ground reaction forces and electromyography of 12 lower limb muscles from the right leg were recorded.

A musculoskeletal model designed for movements with high lower limb joint flexions [4] was modified to replicate a recently proposed quadriceps moment arm [5] and to include medial and lateral knee compartment [6]. Five repetitions per alignment were selected for the analyses and the simulated muscle activations were compared against the EMG signals. Knee alignment was quantified as the frontal plane projection angle (FPPA), defined as the angle between the vector from the ankle joint center to the knee joint center and the vector from the knee joint center to the hip joint center. The

data was time-normalized and averaged within the participant, exercise, and alignment. Ensemble average data was used for comparing the KCF between the alignments with non-parametric repeated measures ANOVA using statistical non-parametric mapping (SnPM).

Results and Discussion

The participants were able to perform the exercises with different knee alignments as evidenced by significant differences in the FPPA. However, the alignment had a minor to no effect on the magnitude and distribution of the KCF (Fig. 1), the external knee moments, and EMG activities.

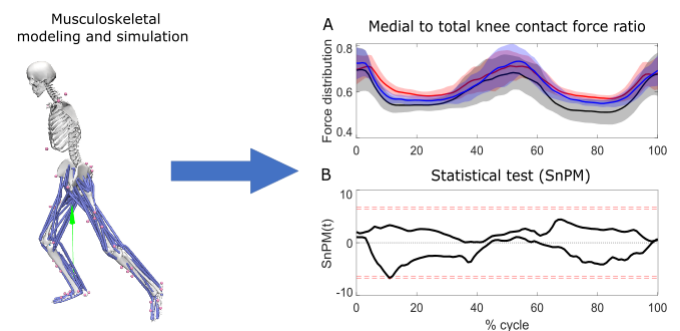


Figure 1: Mean (SD) of the medial to total compressive KCF ratio during forward-backward stepping exercise with lateral (red), medial (black), and neutral (blue) knee alignments (A) and the pair-wise comparison between neutral-lateral and neutral-medial using SnPM in which the upper and lower thresholds for significant differences between the knee alignments are represented by the red dotted lines (B).

Conclusions

Based on our results, different frontal plane knee alignments do not significantly alter the distribution of the compressive KCF, external knee moments, or lower limb muscle activities. Thus, altering the knee alignment may not be a successful strategy to unload the regions of interest of the knee while performing closed kinetic chain rehabilitation exercises.

References

- [1] Thomas, K. S. et al. (2002). *Br Med J*, **325(7367):752**.
- [2] Trevor B. Birmingham et al (2018). *Arthritis Care & Research*, **70(5):647-650**.
- [3] Walter, J. P. et al. (2010). *J Orthop Res*, **28(10):1348-54**.
- [4] Catelli, D. S. et al. (2019). *Comput Methods Biomech Biomed Engin*, **21-24**.
- [5] Bakenecker, P. et al. (2019). *J Biomech*, **86:225-231**.
- [6] Lerner, Z. F. et al. (2015). *J Biomech*, **48(4):644-50**.

Finite element solver based full-body musculoskeletal model for multiscale biomechanics

Shihao Li¹, Liming Shu^{1*}, Jiang Yao², and Sugita Naohiko¹

¹ Department of Mechanical Engineering, The University of Tokyo, Tokyo, Japan

² Dassault Systemes Simulia Corp., Johnston, RI, USA

*Email: l.shu@mfg.t.u-tokyo.ac.jp

Summary

Musculoskeletal modeling is a versatile computational method that gives a great insight into neuromuscular biomechanics of human movement. However, the calculation of subject-specific tissue-level mechanics with the musculoskeletal model is still an open issue. We proposed a finite-element-solver-based full-body subject-specific human musculoskeletal model which allows the synchronized calculation to provide the body and tissue level biomechanics with reasonable computation time and accuracy. Good consistency was found on knee joint rotations, muscle-tendon forces, and knee joint contact forces with experimental data.

Introduction

Musculoskeletal (MS) models that are available in software packages such as OpenSim and AnyBody are widely used in investigating body level biomechanics[1]. However, MS models are limited on the investigation of tissue-level biomechanics for lacking the ability to take material deformation into consideration. On the other hand, finite element (FE) methods are widely used in tissue biomechanics analysis, but the load conditions were often fixed, which means the inter-subject variances cannot be properly reflected. Recently, researchers have developed combined workflows of the MS model and FE method. Instead of directly incorporate the MS model into finite element workflow, the MS model was used to generate subject-specific input and boundary conditions for the FE model. This limited combination which only incorporated the one-way interaction enhanced the authenticity of the simulation. However, because of the difference in the ability to deal with deformation, the kinematics in the MS and FE workflows are supposed to be different. The variance in kinematics has a comprehensive influence on the muscle and joint reaction force calculation, which may reduce the accuracy. In this research, we proposed a subject-specific full-body FE-MS workflow. The model can concurrently predict the tissue and body level biomechanics, which means the kinematic and dynamic alterations between the MS and FE models are synchronized.

Methods

The generic FE-MS model developed in Abaqus CAE (Dassault Systems Simulia Corp., Providence, USA) is shown in Figure.1. The three-component Hill-type muscle model was modeled as 1D axial connector elements. The insertion coordinates and parameters were obtained from the ISB website[2]. The model was first scaled according to the motion capture data of each subject to obtain the subject-specific model. The inverse kinematics & dynamics were implemented using Abaqus Implicit Solver. Muscle optimization was performed to obtain the muscle force. With

all the initial state variables input into the model, the FE tissue is activated and the workflow starts iterating until the specified parameter converges. The data of the 6th grand challenge competition was used in the validation process. The patient data of DM who underwent total knee replacement with instrumented knee prosthesis were used to verify the proposed model from the aspects of muscle activation, joint kinematics, and joint contact force[3].

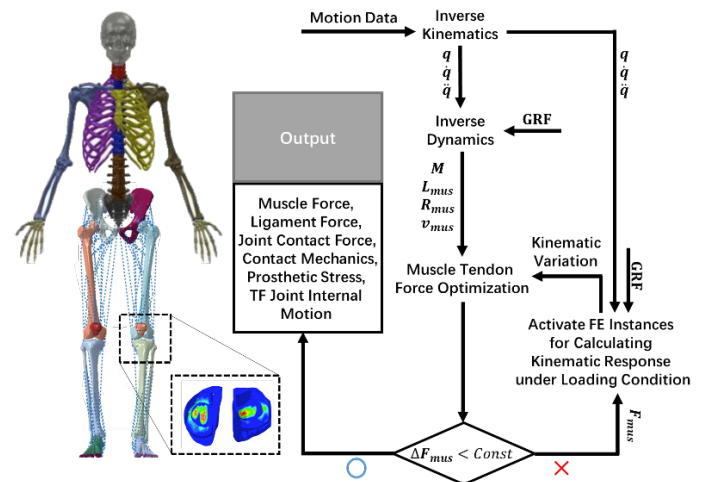


Figure 1: FE-MS model and workflow

Results and Discussion

The computation time for a single gait cycle on a desktop computer took approximately 30min. The muscle activation results of flexor-extensor muscles showed good consistency on trend with electromyography. Good agreement on magnitude and trend were found in both medial and lateral sides of the knee contact force. The prediction accuracy of the FE-MS model ($RMSE: 0.28$, $r^2: 0.90$) was high among the recent publications[4].

Conclusions

The proposed subject-specific FE-MS model presented a good prediction accuracy in terms of knee joint kinematics, dynamics, and muscle-tendon forces. It provides an approach for concurrent prediction of the body-level neuro-muscular biomechanics and the tissue-level biomechanics.

References

- [1] S. L. Delp. et al., 2007, *IEEE Trans. Biomed. Eng.* 54, 1940–1950.
- [2] S.L. Delp, et al., 1995, *Comput. Biol. Med.* 25, 21–34.
- [3] B.J. Fregly et al., 2012, *J. Orthop. Res.* 30, 503–513.
- [4] Chen Z et al., 2016, *Med Eng Phys*;38:708–16.

Pre-operative planning of high tibial osteotomy using musculoskeletal and finite element models

M. Kazemi¹, J. Zhang¹, T.F. Besier^{1,2}, A.P. Monk¹

¹Auckland Bioengineering Institute, University of Auckland, Auckland, New Zealand

²Department of Engineering Science, University of Auckland, Auckland, New Zealand

Email: mkaz010@aucklanduni.ac.nz

Summary

We developed a novel technique to perform the high tibial osteotomy (HTO) based on prediction of the load sharing along the tibiofemoral joint. This work is a bridge between musculoskeletal modelling and the finite element analysis which provides required information and tools for surgeons to plan and perform HTO intervention.

Introduction

HTO is a surgical procedure to delay the need for total knee replacement through correcting the frontal plane tibio-femoral alignment. A medial open wedge HTO is used for medial compartment osteoarthritis, whereby a surgeon makes a cut at the proximal tibia head and rotates the tibia in a valgus direction to offload the degenerated cartilage. Accurate pre-operative planning is essential to define the cut plane and valgus wedge angle in order to achieve the desired outcome. Frontal-plane x-ray is commonly used to define a correction angle, however, this does not account for the 3D articulating surface of the joint. We propose to provide a surgical plan by fitting a 3D model to the x-ray image and then simulating various cut orientations and predicting the changes in load distribution using a finite element model. Surgeons will be able to visualise the corrections and 3D print a wedge to accurately deliver the correct angle.

Methods

A 48-year-old male (mass 86 kg) with early-stage medial knee osteoarthritis consented to being a participant in this study, which was approved by the Auckland Hospitals Research and Ethics Committee. Partial tibia, fibula, and femur bones and knee cartilage layers were segmented from magnetic resonance images with additional scans covering the knee, hip and ankle joints. Statistical shape models of each corresponding bone were used to generate complete bones [1]. The articulating region of the bone and cartilage were then fit to the segmented data using radial basis functions to sub-millimetre accuracy. Anatomical landmarks were identified on triangulated meshes and used to define the coordinate system and HTO cut plane agreed by surgeon. Bone meshes were registered to the patient's Frontal-plane and oblique x-ray images to reproduce the joint at its full extension standing position. A finite element model of the knee was developed using FEBio [2]. Bone and cartilage were treated as rigid bodies, with the femur fixed at 6 degrees of freedom and tibia-fibula allowed to rotate in varus-valgus with flexion-extension prescribed based on the weight-bearing x-ray. A set of interval force vectors, with magnitude of half body weight and upward were exerted to the tibia base and the contact pressure (CP) along the medial and lateral knee were predicted after the model achieved static equilibrium. CPs were then obtained for a range of virtual valgus cut planes. Optimal cut plane and correct wedge

angles were determined by surgeon after viewing the medial and lateral CPs changes resulting from various valgus cut planes.

Results and Discussion

A range of valgus corrections and CPs were simulated and visualized on the tibial cartilage (Figure 1). By increasing the valgus angle, the peak CP along the medial articulation was gradually reduced. The surgeon received a spectrum of CP maps and selected the 8° valgus wedge (figure 1, left) to offload the medial compartment and equalise the forces through the medial and lateral tibial condyles [3]. A 3D template wedge was printed, sterilized, and used by the surgeon as a guide to deliver the correct valgus angle during the operation. Improvements to this workflow include the simulation of dynamic gait as boundary conditions to the FE model.

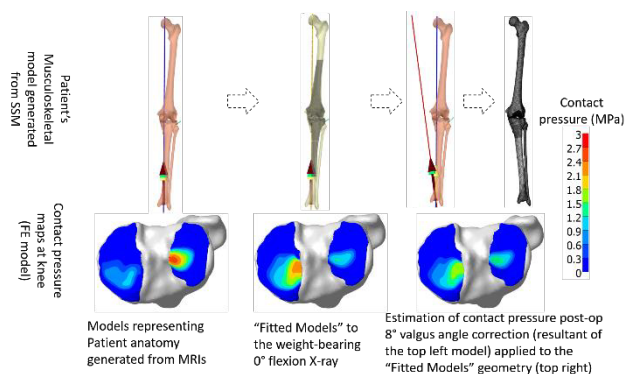


Figure 1: comparing the CP at the tibia cartilage. The pre-op mechanical axis (blue line), resultant post-op force vector (Red line) and its components (vectors).

Conclusions

To deliver a patient-specific HTO correction plan, we developed a finite element model of the knee from standard clinical MR and x-ray images. Using this workflow, surgeons can easily visualise various HTO correction angles and their influence on predicted CPs. A custom designed and printed wedge ensured the surgeon delivered the desired correction angle.

Acknowledgements

This research has been funded by the Auckland Bioengineering Institute, the Medical Technologies Centre of Research Excellence and Callaghan Innovation, NZ.

References

- [1] Zhang, J, et al. (2016). *J. of biomech.* 49(16): 3875-3881.
- [2] Maas SA. et al. (2012). *J. of biomech. eng.* 134(1).
- [3] Martay, J.L. et al. (2018). *The Knee*, 25(2), 286-295.

Is Hallux Valgus Responsible for Metatarsus Primus Varus?

Yuya OISHI¹, Hiroaki KUROKAWA², Shinichi KOSUGI³, Yasuhito TANAKA²,
Kohei AKIMOTO¹, Masataka YAMAMOTO^{1,4}, Hiroshi TAKEMURA¹

¹Tokyo University of Science, Chiba, Japan, ²Orthopedic surgery, Nara Medical University, Nara, Japan

³Kosugi Orthopaedic & Rheumatology Clinic, Osaka, Japan, ⁴Hiroshima University, Hiroshima, Japan

Email: 7520509@ed.tus.ac.jp

Summary

It is generally believed that the varus deformity of the first metatarsal occurs before hallux valgus (HV). To investigate the relationship between HV and metatarsus primus varus (MPV), the 3D bone position analysis by focusing on the alignment between the medial/intermediate cuneiforms and the first metatarsal was conducted. To evaluate the relationship between the MPV and HV, the correlation between the inclination angle of the first metatarsal and the HV angle was investigated. There was no significant correlation between them. The experimental results suggest that the MPV did not always occur before the HV.

Introduction

HV is a common structural disease of foot deformity. Yasuhito et al. reported that the HV is primarily caused by the MPV and the MPV is a major factor in the development of HV [1]. X-ray images are usually used for the evaluation of HV in clinical site, while 3D bone alignment between the medial/intermediate cuneiforms and the first metatarsal is difficult to analysis by the X-ray image. Little is known about the correlation between the HV angle and the inclination angle of the first metatarsal in consideration of the alignment between the medial and intermediate cuneiforms in 3D position. The aim of this study is to investigate the correlation between the first metatarsal direction based on cuneiforms and the HV angle by using 3D bone position analysis. We hypothesis that MPV is responsible for HV; the HV angle and the inclination of the first metatarsal could have a positive correlation.

Methods

The study included seven female participants (10 feet: 5 right, 5 left; 5 HV, 5 no HV, aged 70.9 ± 5.4 years) of whom five had ankle osteoarthritis. The 3D bone models were created from Computed Tomography (CT) image by using ITK-SNAP. A new coordinate system was proposed for the measurement of the MPV in consideration of the alignment between the medial/intermediate cuneiforms (Figure 1). The MPV was defined as the inclination of the first metatarsal from the Y-axis on the XY-plane.

Result and Discussion

Figure 2 shows the relation between the inclination of the first metatarsal on XY-plane and HV angle. The HV angle and the inclination of the first metatarsal did not have a positive correlation (correlation coefficient: -0.20). The hypothesis was rejected. There is a probability that the hallux valgus

(HV) occurs before varus deformity of the first metatarsal [2] or the MPV is not always responsible for HV.

Limitations of the study are the number of subjects was small and some of the subjects had ankle osteoarthritis. There is a possibility that ankle osteoarthritis affected the first metatarsal.

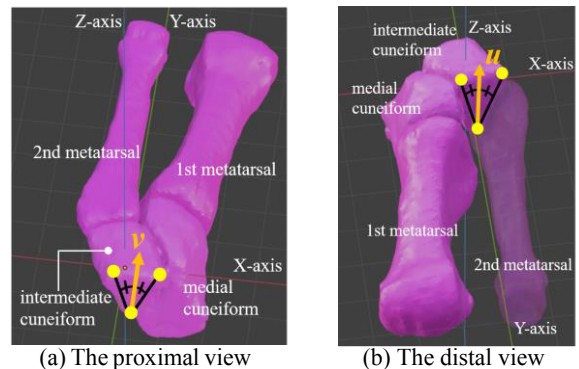


Figure 1: The proposed coordinate system definition. Origin: The average of six points (ex. yellow circles) used by a triangular approximation in two planes, proximal/distal planes of the intermediate cuneiform. X-axis: Cross-product Y- and Z-axes. Y-axis: The axis parallel to the 2nd metatarsal long axis. Z-axis: The average of bisectors in each proximal/distal plane of the intermediate cuneiform. The v and u -vector in the figure are a bisector in the proximal and distal plane of the intermediate cuneiform, respectively.

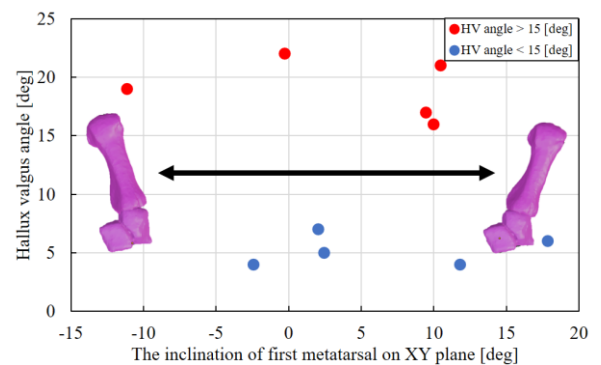


Figure 2: The relation MPV and HV.

Conclusions

The correlation between varus deformity of the first metatarsal based on cuneiforms and the HV angle was investigated. The experimental results suggest that the MPV did not always occur before the HV.

References

- [1] Yasuhito T et al. (2000). *Foot Ankle int*, **21**(8): 651-656.
- [2] Munuera PV et al. (2006). *Foot Ankle Int*, **27**(12): 1030-1035.

Cartilage thickness is coupled to bone shape in healthy knees and varies with sex

Marco T. Schneider¹, Nynke Rooks¹, Thor Besier^{1,2}

¹Auckland Bioengineering Institute, The University of Auckland, Auckland, New Zealand

²Department of Engineering Science, The University of Auckland, Auckland, New Zealand

Email: marco.schneider@auckland.ac.nz

Summary

The functional relationship between bone and cartilage is complex and is modulated by mechanical factors introduced by loading and motion. We investigated the coupled relationship between bone and cartilage morphology in a cohort of 51 knees as a function of sex, height, and body mass.

Introduction

Mature bone and cartilage have a location-dependent histomorphology that is developed in response to its specific loading history [1]. Bone size and shape can affect the contact area and the lines of action crossing the joint [2], while cartilage thickness influences the mechanical properties of cartilage [3] and the stresses and strains experienced in the tissue [2]. Scarce data exist on the relationship between bone shape and the spatial distribution of cartilage thickness, in terms of how this varies in a population, which has important implications for understanding the onset of osteoarthritis, development of surrogate and predictive models, and design of implants.

This study has two aims: first, to characterise the coupled variation in knee bone morphology and cartilage thickness distributions in knees with healthy cartilage. The second aim was to investigate this relationship as a function of sex, height, and body mass.

Methods

MR images of 51 healthy adult knees (28.4 ± 4.1 years) were obtained from a previous study [4]. The bones, including the femur, patella, tibia, and their corresponding cartilages were manually segmented and a published method [5] was adapted to train a statistical shape model of the femur, tibia, and patella and their cartilages.

A logistic regression classifier was trained to characterise sex related features, and multiple linear regression models were trained to characterise features related to height and body mass. 10-fold cross-validation was performed to evaluate the models' performance.

Results and Discussion

Cartilage thickness and its distribution was coupled to bone morphology, including both size (mode 1) and shape variations (mode 2 onwards). The first three modes described overall size, diaphysis size, femoral shaft angle, and corresponding spatial distribution of the cartilages (Figure 1). These modes were sex linked and could classify sex with an accuracy of 94.1% (95% CI [83.8%, 98.8%]) (Figure 2).

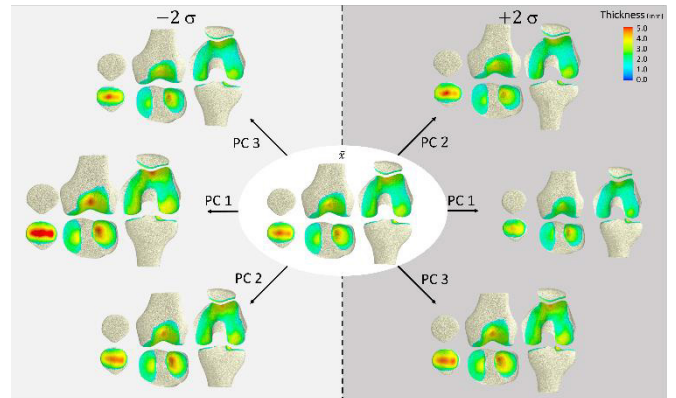


Figure 1. First three modes of coupled variation in the knee bones and cartilage.

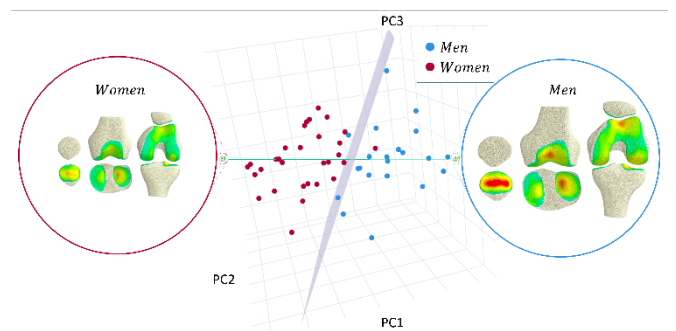


Figure 2. 3D scatter of the first three modes of the training set by sex, showing the decision boundary plane (grey) of the logistic regression model, and, a vector (green) that passes through the average male and female knee.

Two modes could predict height to an error of 4.8cm, while four modes could predict body mass to an error of 5.4kg.

Conclusions

Cartilage is thicker with increased bone size, diaphysis size, and decreased femoral shaft angle. Sexual dimorphism is present in these first three modes which can be used to classify sex. Shape features are also strongly correlated with height but weakly correlated with mass.

References

- [1] Carter DR et al. (2004). *Clin. Orthop. Relat. Res.*, **427**:69-77.
- [2] Anderson AE et al. (2010). *J. Biomech.*, **43**:1351-1357.
- [3] Thambyah A et al. (2006). *Osteoarthr. Cartil.*, **14**:580-588.
- [4] Draper C et al. (2006). *Osteoarthr. Cartil.*, **14**:931-937.
- [5] Schneider et al. (2018). *Osteoarthr. Cartil.*, **26**:1338-1344.

How do Bone Measurements Change with Growth in a Paediatric Population?

Laura Carman¹, Thor Besier¹, Julie Choisne¹

¹Auckland Bioengineering Institute, The University of Auckland, Auckland, New Zealand

Email: lcar475@aucklanduni.ac.nz

Summary

Understanding the change in bone shape and properties during growth is important for understanding how these factors deviate in children with movement disabilities, such as cerebral palsy. Statistical shape models (SSMs) of lower limb bones were built from a dataset of 333 children (aged 4-18 years). The aim of this study was to determine the changes in bone measurements with growth. No direct relationship was found between bone measurements and age, but relationships were found between bone measurements and the first principal component (PC) of the shape model.

Introduction

Clinical bone measurements are usually performed on a 2D X-ray or partial 3D CT/MRI scans of the patient. This has been shown to be inaccurate due to different methods of measurement being performed and the requirement for the landmarks to be in the same plane [1, 2]. A more consistent and accurate method for calculating bone measurements is by reconstructing bone shape in 3D. The aim of this study is to generate a population-based growth chart for clinical bone measurements for a typically developed paediatric population.

Methods

Post-mortem CT scans of 333 children (137 F, Age: 12 ± 5 Y, H: 148 ± 24 cm, M: 49 ± 22 kg) were obtained from the Victorian Institute of Forensic Medicine (VIFM, Melbourne, Australia). The lower limb bones were segmented and aligned according to the ISB coordinate system [3]. A SSM was generated for the femur, tibia/fibula, and pelvis using principal component analysis [4]. Bone measurements were taken from 3D bone geometry using an automated process. Measurements were taken for each bone in the dataset as well as from geometries projected along the first PC (percent variation Femur: 98%, Tibfib: 97%, Pelvis: 91%) of the SSM between ± 2 SD at intervals of 0.1. The bone measurements taken were for the femur: anteversion, neck shaft, bicondylar, and mechanical axis angle. For the tibia: tibial torsion and tibial mechanical angle. The relationship between these measurements and demographic data (age, height, mass, sex) was compared.

Results and Discussion

No definitive singular relationship between the measurements and anthropological factors were found. The relationship between femoral anteversion and age is shown in Figure 1 (top). When projecting along the first PC in terms of standard deviations (SDs), strong relationships were found between bone measurements and SDs for femoral anteversion, neck shaft angle, and tibial torsion.

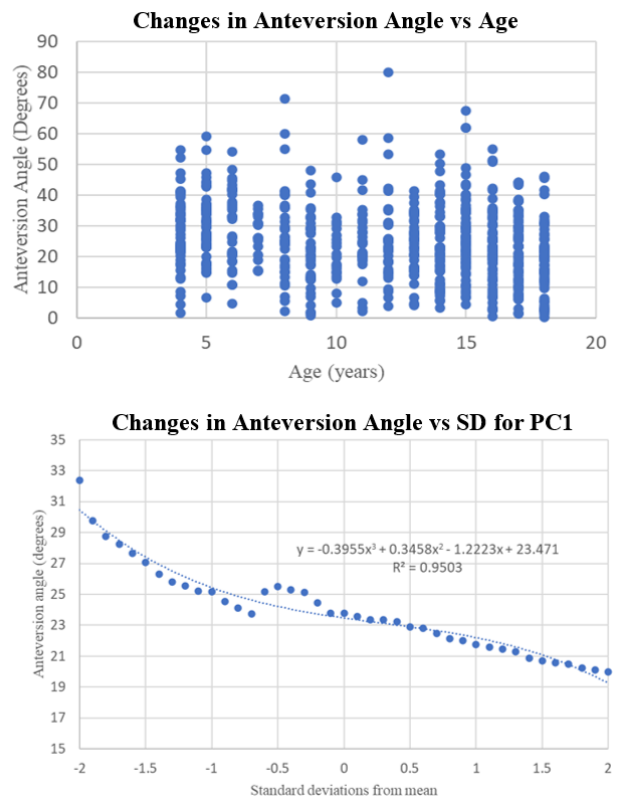


Figure 1: relationships of age and SDs with femoral anteversion

Conclusions

The shape model was shown to capture the variation within the dataset of femoral anteversion, neck shaft angle, and tibial torsion. It is likely that these measurements depend on multiple demographic measures in a multiplicative relationship. This relationship needs to be further analysed to determine the plausibility of the generation of a growth chart for these measurements which could be used clinically to determine the range of normal development.

Acknowledgments

Data from the VIFM made this research possible. This research is funded by the University of Auckland doctoral scholarship and the Health Research Council of NZ emerging researcher first Grant.

References

- [1] Lee et al. (2006). *Med. Biol. Eng. Comput.*, **44**: 895-906
- [2] Kaiser et al. (2016). *Arch. Orthop. Trauma Surg.* **146**: 1259-1264
- [3] Wu G et al. (2002). *J. Biomech.*, **35**: 543-548
- [4] Zhang J et al. (2016). *Med. Eng. Phys.*, **38**: 450-457

Increased Loading Rates During Gait Correlate with Morphology of Unaffected Hip in Juveniles with Treated Developmental Hip Dysplasia

Wei-Chun Lee^{1,2}, Tsan-Yang Chen¹, Chia-Hsieh Chang², and Tung-Wu Lu¹

¹ Department of Biomedical Engineering, National Taiwan University, Taiwan, R.O.C.

² Department of Orthopaedic Surgery, Chang Gung Memorial Hospital, Taiwan, R.O.C.

Email: agroup.lee@gmail.com

Summary

The current gait analysis study identified the loading and unloading rates of the ground reaction forces (GRF) during gait, and their correlations with the hip morphology in twenty juvenile patients with surgically treated unilateral DDH during toddlerhood. The loading rates on both the affected and unaffected sides were highly correlated to the acetabular index on the unaffected side, which was also significantly correlated with the peak unloading rates on the affected side. These results suggest that apart from regular follow-up of the affected hip, routine assessment of the morphological changes and/or increased loading rates of the unaffected hip is also important for early identification of any signs of insidious hip dysplasia and risk of premature degeneration of the cartilage.

Introduction

Abnormal loading rate was noted on affected side and unaffected side in the adolescent with unilateral DDH treated by Pemberton osteotomy [1]. So far as we know, no gait analysis study was about the correlation between the morphology and ground reaction forces during walking in the juvenile after DDH surgery. The purpose of the current study was to identify the loading and unloading rates of the GRF in the lower limbs during gait and their possible correlations with the bilateral hip morphology in juveniles who had been treated for DDH during toddlerhood.

Methods

Twenty patients who had been treated for unilateral dislocation of the hip by reduction surgery at an age of 2.2 ± 1.7 years participated in the current study. All subjects were able to walk without support. For each subject, the neck-shaft angle, acetabular index, and center-edge angle, femoral offset, acetabular depth ratio, articulo-trochanter distance (ATD), c/b ratio, and Alsberg angle were measured from anteroposterior X-ray images of the pelvis for both sides at the time of the gait study. Leg lengths of both sides were measured from a scenography. No leg length difference was found between left and right limbs (paired t-test, $p = 0.019$).

Each subject performed level walking at a self-selected pace on a 10-m walkway in a typical gait laboratory. The ground reaction forces (GRF) were gathered from three forceplates. At least three successful trials were obtained for each subject for subsequent analysis. The 1st and 2nd maximum peak vertical GRFs of either affected or unaffected limb were extracted. A correlation analysis between GRF variables and radiographic measurements were conducted using SPSS 20.0 (IBM, Armonk, New York, U.S.A.). All significance levels were set at $\alpha = 0.05$.

Results and Discussion

In the patient group, no significant differences were found in the morphological parameters between affected and unaffected sides. No significant between-side differences were found in the gait spatiotemporal parameters. No significant differences were found in the loading rates of vertical GRF between affected and unaffected sides (Fig. 1).

For the vertical GRF during initial contact, in general, the peak loading rates of both limbs were mainly correlated with the acetabular index of the unaffected side. The peak unloading rates of both limbs were also positively correlated with the acetabular index of the unaffected side. During loading response, peak loading rates of the affected limbs were positively correlated with the acetabular index and c/b ratio of the unaffected side, but those during both initial contact and loading response phases were negatively correlated with the center-edge angle of the unaffected side.

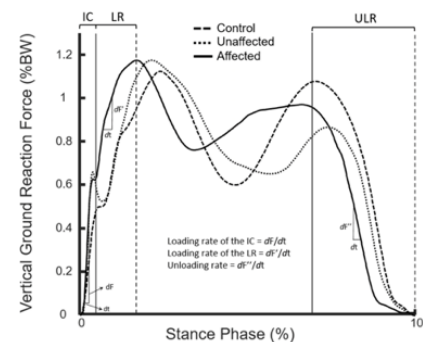


Figure 1: Curves of body-weight-normalized vertical ground reaction forces of the affected (solid line) and unaffected (dotted line) limbs of typical subjects in the DDH and Control group (dash line) during the stance phase of level walking.

Conclusions

In this study, high vertical GRF in the affected limb is correlated to the morphology of the unaffected hip, especially acetabular index. It is important to monitor the contralateral hip morphology to improve the clinical outcome of children after DDH surgery.

Acknowledgments

The authors are grateful for the financial support from the Chang Gung Memorial Hospital (CMRPG1F0131)

References

- [1] Chang, C.F., Wang, T.M., Wang, J.H., Huang, S.C., Lu, T.W., 2011. Adolescents after pemberton's osteotomy for developmental dysplasia of the hip displayed greater joint loading than healthy controls in affected and unaffected limbs during gait. *Journal of Orthopaedic Research* **29**, 1034-1041

Whole-body sagittal plane angular momentum during running in unilateral transfemoral amputees

Genki Hisano^{1,3}, Hiroto Murata^{2,3}, Daisuke Ichimura³, Motomu Nakashima¹, Hiroaki Hobara³

¹Tokyo Institute of Technology, Tokyo, Japan, ²Tokyo University of Science, Chiba, Japan

³National Institute of Advanced Industrial Science and Technology (AIST), Tokyo, Japan

Email: hisano.g.aa@gmail.com

Summary

Maintaining dynamic balance is essential to achieve continuous running without a fall. However, little is known about how the whole-body sagittal plane angular momentum (L) is regulated in unilateral transfemoral amputees (UTFAs) and the control of the affected (AL) and unaffected limbs (UL). We compared the positive and negative peaks of whole-body sagittal plane L between the AL–UL and UL–AL steps. No significant difference was observed in the positive peak, while the magnitude of negative peak during AL–UL step was significantly smaller than that of UL–AL step. These results suggest that UTFAs would require greater postural control demands to avoid the clockwise body rotation during UL–AL step than AL–UL step.

Introduction

Although the UTFAs are progressively taking part in running activities, a fear of falling is a major barrier for those who wish to run. To maintain dynamic balance for continuous running without falling, the whole-body L about the body center of mass should be regulated [1]. Generally, the whole-body sagittal plane L during running is balanced between two legs [1,2]. However, owing to the morphological asymmetry between AL and UL in UTFAs, the control of whole-body L during running would be a challenging task for this population. Thus, this study aimed to evaluate the sagittal plane dynamic balance during running in UTFAs using whole-body L .

Methods

Ten UTFAs participated in this study (age: 32.6 ± 10.6 years, height: 1.62 ± 0.09 m, mass: 57.0 ± 8.6 kg, mean \pm SD). Each participant performed maximal sprinting on a 40-m of runway, where seven force platforms and optical motion capture cameras were placed approximately 22 m from the starting line. Whole-body sagittal plane L was calculated using a 15-segment model (head, torso, pelvis, upper arms, forearms, hands, thighs, shanks and feet). In the present study, the inertial properties of prosthetic components are modeled using the method described in the previous study [3]. A positive L indicates a counterclockwise rotation as viewed from the right side. Furthermore, whole-body L was normalized by participant height, mass, and average running speed (5.84 ± 0.70 m/s). All variables were averaged across the four trials to serve as representative values for each participant. A paired t -test was performed to check the statistical differences in the positive and negative peaks of whole-body L between AL–UL and UL–AL steps. Statistical significance was set at $p < 0.05$.

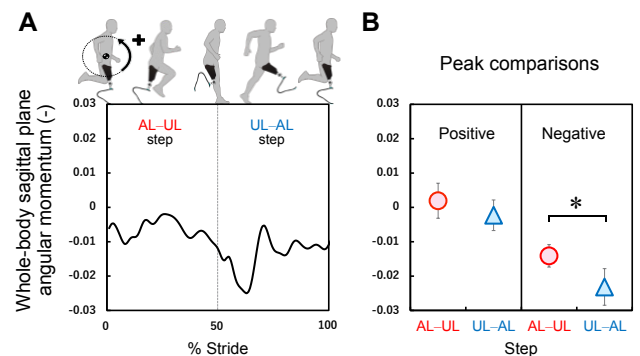


Figure 1: (A) A representative whole-body sagittal plane angular momentum during running over the AL stride cycle (recorded from one UTFA participant). (B) Shows the peak comparisons between AL–UL and UL–AL steps, where significant differences in the positive and negative peaks are indicated by the asterisk (*).

Results and Discussion

No significant difference was observed in the positive peak between AL–UL and UL–AL steps ($p = 0.07$). However, the magnitude of negative peak during AL–UL step was significantly smaller than UL–AL step ($p = 0.01$). A possible explanation for this phenomenon might be the mass difference between AL and UL. The larger magnitude of negative L with stance leg is counterbalanced by the smaller magnitude of positive L with swing leg throughout the running cycle in runners with and without transtibial amputation [1,2]. Because AL is the stance leg during AL–UL step, the reduced mass of AL might affect the smaller magnitude of negative L during AL–UL than UL–AL step.

A larger magnitude of negative whole-body L would lead to the clockwise body rotation. Therefore, current results suggest that UTFAs might require greater postural control demands for maintaining balance during UL–AL step than AL–UL step.

Conclusions

UTFAs displayed a similar positive peak, but a smaller magnitude for the negative peak in whole-body L during AL–UL step than UL–AL step. These results suggest that UTFAs would require greater postural control demands to avoid the clockwise body rotation during UL–AL step than AL–UL step.

Acknowledgments

This study was partly supported by JSPS KAKENHI (Grant Numbers 26702027 and 20J20572).

References

- [1] Sepp LA et al. (2019). *J. Biomech.*, **84**: 36-45.
- [2] Hinrichs RN (1987). *Int. J. Sport. Biomech.*, **3**: 242-263.
- [3] Namiki Y et al. (2019). *Biol. Open*, **8**(2): bio039206.

Proprioceptive Neuromuscular Facilitation Improves Symptoms in Older Adults with Knee Osteoarthritis

Peixin Shen¹, Qipeng Song², Dewei Mao^{1,2}

¹Biomechanics Lab, Beijing Sport University, Beijing, China

²Sport Biomechanics Lab, Shandong Sport University, Jinan, China

Email: deweimao@sdpei.edu.cn

Summary

Knee osteoarthritis (KOA) is a common disease associating with mechanical loading that causes limits functionality in older adults during daily activities. Proprioceptive neuromuscular facilitation (PNF) practices promote multiple-plane joint movements, which may improve medial loading distribution of the knee and increase joint range of motion (ROM). This study aims to examine the effects of a 6-week PNF intervention on joint ROM, and joint moments in the frontal plane in the elderly with KOA during walking. After the intervention, passive joint ROM increased in PNF participants. Peak external knee adduction moment decreased during walking. PNF could be recommended as one of the clinical treatments for KOA.

Introduction

Knee osteoarthritis (KOA) is the most common chronic degenerative disease associating with ageing and mechanical loading, resulting in dysfunction. Over 40% of adults 65 and older are KOA symptomatic, who experience smaller maximum knee and hip flexion angles during walking than their healthy counterparts [1]. Increased the medial load distribution of the knee is a contributor to increase joint stress and cartilage degradation, affecting gait pattern [2]. The peak external knee adduction moment (KAM) is a surrogate for medial loading which are often elevated in older adults with KOA compared to healthy counterparts [2].

Traditional treatments for KOA are hard to cause the change of joint moments in the frontal plane. Proprioceptive neuromuscular facilitation (PNF) may be beneficial for people with KOA. PNF's spiral-diagonal patterns allow joints to move in multiple planes, may increase joint movement and ROM [3]. Therefore, we aimed to examine the effects of a 6-week PNF intervention on range of motion, and frontal plane joint moments in older adults with KOA during stair descent.

Methods

Thirty-six people with KOA were randomly divided into the PNF and control (CTR) groups. The PNF group received PNF stretching, and the CTR group participated in a health lecture series, all for one-hour sessions, three times a week, for 6 weeks. Lower extremity passive flexion-extension joint ROMs from the affected leg were measured using standard goniometric procedures. Joint moments were measured using a motion analysis system with a force platform. Data were collected at weeks 0 and 6. Two-way (group by time) ANOVA with repeated measures was used to evaluate the intervention effects. Bonferroni-adjusted post-hoc pairwise comparison was used wherever appropriate. Cohen's d was used to represent the effect size of the post-hoc comparison.

Results and Discussion

Our results showed a significantly time*group interaction in the first peak KAM ($p=0.004$, $\eta^2p=0.291$), which decreased from week 0 to weeks 6 ($p<0.001$, Cohen's $d=0.83$) in the PNF group. A decreased KAM indicated decreased stress on the knee's medial compartment and a favorable treatment outcome for KOA. In the spiral and diagonal patterns, the therapist's proximal hand exerts resistance on the medial/lateral of the participant's knee joint, thereby enhancing the knee joint's movement on the frontal plane, that is, knee adduction/abduction movement. The frontal movement promoted abductors/adductors' activity, which played an important role in regulating the load distribution of the medial-lateral knee joint [4]. Our study confirmed that PNF practice is an effective intervention to balance loads in the medial and lateral compartments.

As shown in Figure1, compared to the control group, the PNF group increased passive hip, knee, and ankle ROM. Autogenic and reciprocal inhibition has traditionally been accepted as the neurophysiological explanation for the superior ROM gains that PNF stretching achieves [5]. They refer to a reduction in the excitability of a stretched muscle because of the inhibitory signals sent from the GTOs of the same muscle (autogenic inhibition) or GTOs of the antagonist muscle (reciprocal inhibition), respectively [5]. Both conditions occur when the GTOs in the tendons of the stretched muscle or in the antagonist muscle to the stretched muscle detect harmful stimuli (maximum stretching).

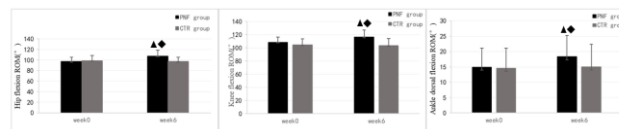


Figure 1. Passive joint range of motion of hip, knee and ankle.
▲ Denotes significant difference in the PNF group between weeks 0 and 6; ◆ Denotes significant difference compared with the control group at week 6.

Figure 1: Joint range of motions of hip, knee and ankle.

Conclusions

This study confirmed that a 6-week PNF intervention could decrease KAM and improve ROM in older adults with KOA during stair descent. PNF was an effective treatment for KOA to improve clinical symptoms.

References

- [1] Protopapadaki A et al. (2007). *Clin Biomech*, **22**: 203-10.
- [2] Chang AH et al. (2005). *Osteoarthritis Cartilage*, **23**: 10 99-106.
- [3] Weng MC et al. (2009). *Kaohsiung Journal of Medical ences*, **25**: 306-15.
- [4] Richards R et al. (2018). *The Knee*, **25**: 814-24.
- [5] Sharman et al. (2006). *Sports Med*, **36**: 929-39.

The effects of impaired foot plantar sensitivity on plantar pressure distribution during walking

Mengzi Sun^{1,2}, Kelsey Lewis², Fangtong Zhang¹, Feng Qu¹, Li Li^{2*}

¹Beijing Sport University, Beijing, 100084, China

²Georgia Southern University, Statesboro, 30460, USA

Email: lili@georgiasouthern.edu

Summary

We have studied the effects of foot cutaneous sensation deficit on gait by testing foot plantar sensitivity and plantar pressure distribution during walking. The results indicated the input of foot plantar cutaneous sensation affected the plantar pressure distribution during walking on the treadmill. The heel and fifth metatarsal suffered more pressure, where less pressure with the hallux location, with the loss of foot sole sensitivity.

Introduction

It was reported reducing plantar cutaneous causes no changes in plantar pressure distribution during walking in the healthy population [1]. And chronic sensory loss did not affect the plantar pressure distribution during walking in the peripheral neuropathy [2]. The effect of severity of foot sole sensitivity on plantar pressure is not clear. We aimed to explore the effects of impaired foot sole sensitivity on foot sole pressure distribution during walking.

Methods

Thirty-one participants were recruited and divided into three groups based on the foot sole sensitivity. Foot sole sensitivity was assessed in five locations of each foot (hallux, bases of first/fifth metatarsals, mid-sole, and heel) by 5.07-gauge Semmes-Weinstein monofilament. The Control group was scored at a full 10 on both feet. The less affected group (LA) ranged from 6 to 9 score. The participants with 0-5 scores named the more affected group (MA). Plantar pressure distribution of 10 walking steps was collected using the Novel system. The average pressure of the five areas corresponding to the monofilament testing over 10 steps was calculated. ANOVA with repeated measures was employed to exam the differences among the three groups.

Results and Discussion

Significant group differences detect at the hallux, fifth metatarsal, and heel (See **Figure 1** for more details). The average pressure underneath the hallux decreased from the Control (9.51±1.29%) to LA (7.77±2.73%, $p=0.021$, $d=0.762$),

and MA groups (7.08±1.59%, $p=0.002$, $d=1.643$). The average pressure below the fifth metatarsals of the MA group (1.46±0.41%) was greater than that of Control (1.06±0.27%, $p=0.005$, $d=1.136$) and LA groups (1.11±0.34%, $p=0.007$, $d=0.940$). The average pressure beneath the heel of the MA group (31.53±3.26%) was greater than that of both the Control (26.90±3.93%, $p=0.015$, $d=1.303$) and LA groups (26.94±6.17%, $p=0.008$, $d=0.918$). Significant differential effects of the foot sole sensitivity impairments were observed. Less (more) pressure was associated with more impairments at the hallux (heel) during walking.

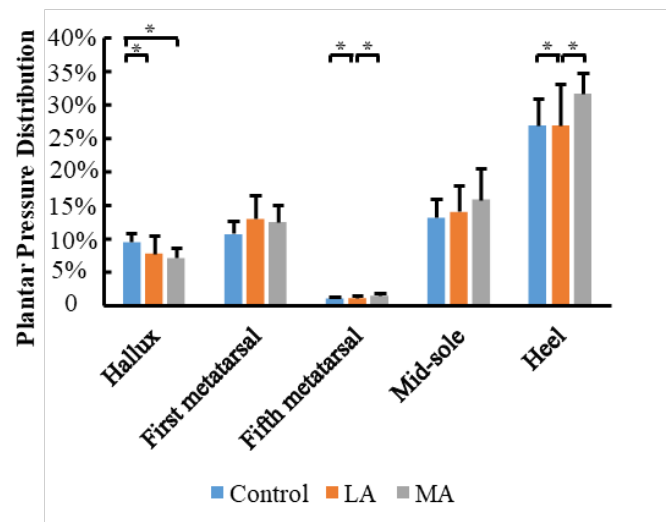


Figure 1. The plantar pressure distribution of five locations was showed. * indicate significant difference detected ($p < 0.05$) between groups.

Conclusions

Greater plantar pressure at the heel during walking was observed with severe loss of foot sole sensitivity. The opposite trend was detected at the hallux, where less pressure was detected with the most severely affected group.

References

- [1] Hohne A, Stark C. et al. (2009). *Clinical Biomechanics*. **24**: 308-313.
- [2] Zhang S, Li L. (2013). *Gait Posture*. **37**: 532-535.

Providing gravitational support using a direct-drive linear actuated assistive robot for shoulder rehabilitation

Soroosh Haji Hosseinnejad¹, Thor F Besier^{1,2}, Andrew J Taberner^{1,2} and Bryan P Ruddy^{1,2}

¹Auckland Bioengineering Institute, University of Auckland, Auckland, New Zealand

²Department of Engineering Science, University of Auckland, Auckland, New Zealand

Email: shos997@aucklanduni.ac.nz

Summary

We have developed an assistive robot intended for shoulder rehabilitation after stroke. Our robot consists of a single novel direct-drive linear actuator providing gravity compensation in all arm orientations. Our experimental results suggest that, when the robot fully supports the arm against gravity, the deltoid and trapezius muscles' effort reduce by ~60 %.

Introduction

Conventional rotary actuated assistive robots for stroke rehabilitation require complex mechanisms to be aligned with the instantaneous axes of rotation of the joint [1]. Although linear actuators offer a potential alternative, current off-the-shelf linear motors are unable to meet the main requirements for an assistive robot: back-drivability, high force density, compliance, and low mass. We have developed a novel linear motor [2] that is capable of meeting these requirements, producing a continuous force of 100 N from a 624 g device. Our assistive robot consists of one custom design direct-drive linear motor, attached to the arm and waist via two spherical joints (Fig 1) to lift the patient's arm in any directions. In this study, we present the results of using our assistive robot on healthy participants to investigate how robot assistance affects the shoulder muscles' effort during a series of abduction-adduction tasks.

Methods

Ten healthy right-handed volunteers (5 males, 5 females, aged 33.4 ± 6 years) with no history of shoulder injuries were selected for this study. The University of Auckland Human Ethics Committee approved this study, and all participants provided written informed consent before the experiment. All users wore the assistive robot supporting their right arms with only the supporting straps and waistband adjusted for each individual. We measured muscle activity from the anterior, medial, and posterior components of the deltoid (AntDel, MidDel, and PostDel, respectively), as well as the upper and middle components of the trapezius muscle (UPTrap, MidTrap respectively) using a Delsys Trigno electromyography (EMG) system (Natick, MA, USA) read with a National Instruments CompactRIO (Austin, TX, USA) at 1000 Hz. In the experiment, participants followed a predefined trajectory presented as a moving dot on a screen, by abducting and adducting their arm up to their shoulder height. The experiment was repeated under four conditions: a fixed assistive force of 0 %, 25 %, and 50 % of the participant's arm mass, and 100 % support using a position controller. The collected EMG data were high-pass filtered with a cut-off frequency of 30 Hz, fully rectified, and then

low-pass filtered with a cut-off frequency of 6 Hz; the average muscular activities are calculated for each trial.

Results and Discussion

The robot reduced the deltoid and trapezius muscle efforts by ~60 % on average when providing 100 % assistance compared to when it was off (Fig 1). Furthermore, providing 25 % assistance from the robot resulted a ~20 % decrease in middle trapezius and deltoid muscle activities. However, when the robot increased assistance to 50 % of the arm weight, the upper trapezius and anterior deltoid activities reduced by ~17 %, whereas other muscle activity only decreased ~7 %. Hence, the participant used their middle trapezius, posterior and medial components of the deltoid muscles more during the experiment, which is likely to control their arm's speed [3]. Finally, 50 % support from the robot showed similar muscular activation to when the participants performed the experiment without the robot and visually matched the arm's speed with the moving dot on the screen.

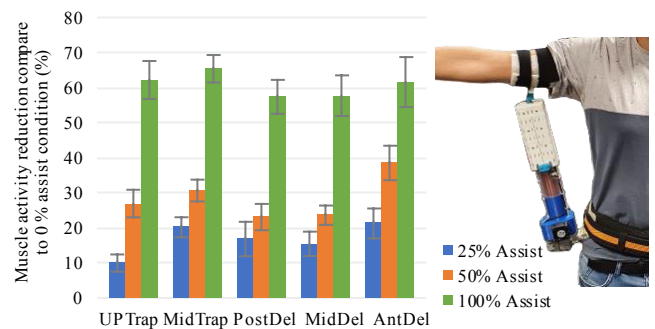


Figure 1: The robot illustration and its effect on the muscle effort.

Conclusions

This study demonstrates that our robot can assist the shoulder joint by providing gravitational support. When the arm was supported, the muscular effort of deltoid and trapezius muscle reduced by ~60 % during the abduction-adduction task.

Acknowledgments

The authors gratefully acknowledge the Medical Technologies Centre of Research Excellence (MedTech CoRE), funded by the Tertiary Education Commission of New Zealand, for supporting this research.

References

- [1] McBean J and Breazeal C (2004), *IROB*, 852-858
- [2] Haji Hosseinnejad S et al. (2020), *ECCE*, 1096-1101
- [3] Cools Ann et al. (2002), *J Orthop Sports Phys.* 221-229

Internal work could be used to estimate energy expenditure at various running intensities.

Bumjoon Kim¹, Jung Kim, Suhyung Park^{1*}

¹Department of Mechanical Engineering, Korea Advanced Institute of Science & Technologies, Daejeon, Korea

Email: suhyungp@kaist.ac.kr

Summary

To estimate energy expenditure during running, heart rates were widely used. However, mechanical work was also used to estimate energy expenditure at moderate-intensity running. In this study, we compared the correlations between heart rate, two mechanical work (external work, internal work), and energy expenditure at various running intensities. As a result, overall, internal work showed a similar correlation to heart rate with energy expenditure. However, correlations are different depends on running intensity. In conclusion, not only heart rate, internal work could be used to estimate energy expenditure at various intensities. However, if running intensity is fixed, we have to consider the characteristics of intensity.

Introduction

As running becomes a daily sport, many studies are being conducted to estimate energy consumption during running, which is one of the indicators of running performance. Of these, heart rate was the most used because it is related to oxygen supply [1]. However, some researchers had used mechanical work to estimate energy expenditure in certain intensity [2]. In this study, energy expenditure at various running intensities was measured and compared with heart rate and mechanical work (internal work and external work).

Methods

Eight subjects participated in this study. They ran for 10 minutes on the treadmill at high-intensity speed (>75%VO₂max), moderate-intensity speed (50~75%VO₂max), and light-intensity speed (<50%VO₂max). At the same time, metabolic energy, heart rate, ground reaction force, and lower limb motion were measured. Using these measured data, external work rate and internal work rate were calculated as follows; [3, 4].

$$\bar{P}_{ext} = \frac{\int_0^T \overline{GRF} \cdot \vec{v}_{com} dt}{T} \quad \text{Eq. (1)}$$

$$P_{int} = f \bar{s}^2 \left(1 + \left(\frac{d}{1-d} \right)^2 \right) q \quad \text{Eq. (2)}$$

\bar{P}_{ext} : average external work rate
 \overline{GRF} : ground reaction force
 \vec{v}_{com} : velocity of center of mass
 T : step duration
 P_{int} : internal work rate
 f : step frequency
 \bar{s} : progression speed
 d : duty factor
 q : compound dimensionless term

The average of the data 2 minutes before the end of each component was calculated to see a steady-state [2-4].

Results and Discussion

As a result, Pearson's correlation coefficient for HR, internal work rate, and external work rate was 0.56, 0.54, and 0.06, respectively (Figure1). Even though external work is

larger than internal work, the correlation of internal work is higher and similar to heart rate. When looking at each intensity, the correlation with external work was high in light intensity, and the correlation with internal work was high in high intensity. (Table 1). In light intensity, external work is the main because the speed is slow, but as the speed increases, the step width and step frequency increase. Therefore, the correlation is high because the internal work increases relatively significantly compared to the external work.

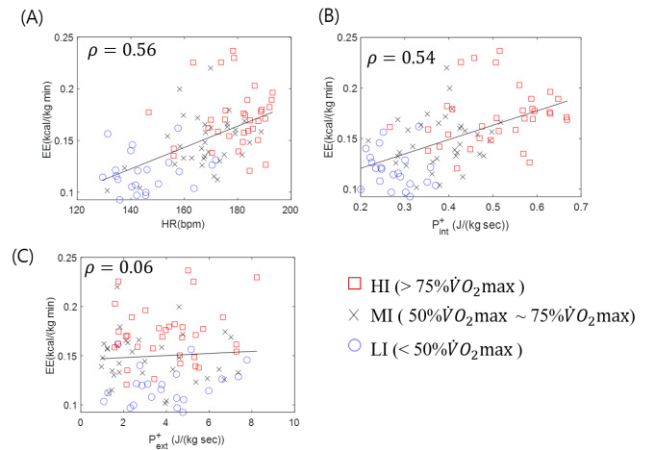


Figure 1: Pearson correlation between energy expenditure (EE) and (A) heart rate, (B) internal work rate, (C) external work rate, respectively.

Table 1: Pearson's correlation coefficient with energy expenditure

	LI (<50% VO ₂ max)	MI (50~75% VO ₂ max)	HI (>75% VO ₂ max)	Overall
Heart rate	0.12	0.38	0.05	0.56
Internal work rate	-0.21	0.16	0.19	0.54
External work rate	0.21	-0.08	0.05	0.06

Conclusions

In order to estimate energy expenditure, internal work rate could be used like heart rate. However, if running intensity is fixed, we have to consider the characteristics of intensity.

Acknowledgments

This paper is based on research that has been conducted as part of the KAIST-funded Global Singularity Research Program for 2021.

References

- [1] T. Beltrame et al. (2017). *Scientific reports*, **7**: 45738.
- [2] M. Zago et al. (2018) *J. of Biomech.*, **76**: 189-196.
- [3] Karl E. Zelik et al (2015). *The Company of Biologists*, **218**: 876-886.
- [4] Alberto E. Minetti (1998). *J. of Biomech.*, **31**: 463-468

Effects of Training Volume on Lower Limb Kinematics in Fast and Slow Running Speed Conditions in Elite Marathoners

Faning Zhang¹, Liqin Deng¹, Wing-Kai Lam², Fan Yang², Xini Zhang¹, Weijie Fu¹

¹School of Kinesiology, Shanghai University of Sport, Shanghai, China

²Li Ning Sports Science Research Center, Beijing, China

E-mail: fuweijie@sus.edu.cn

Summary

This study aimed to explore lower limb kinematics between elite marathoners with different training volumes at the speeds of 3m/s and 5m/s. The cadence, stride and sagittal plane lower-limb angles were collected during running. The results showed that hip and ankle angles at initial contact, and maximum hip flexion angle significantly increased in the HIGH group, but there were no significant differences on other kinematics variables. This study indicated that hip and ankle joints play a crucial role in controlling joint positioning at initial contact during running, and high-training volume may affect hip and ankle joints effectively.

Introduction

Running is one of the most popular and accessible sport activities, with more runners participating in marathons and half-marathons [1]. High-training volume is related to a better marathon performance and finished time [1]. The running performance is associated with proper lower limb kinematics [2], but the effect of weekly training volume on lower limb kinematics for different running speeds is currently unclear. Thus, the purpose of this study was to determine whether different runners with vary training volume would show distinct running mechanics at different running speeds.

Methods

Twelve healthy male elite marathoners (HIGH group: n=5, training volume: 180.0±40.0 km/week, age: 26.0±4.4 yrs, height: 172.8±4.7 cm, mass: 56.8±3.7 kg; LOW group: n=7, training volume: 88.6±32.2 km/week, age: 32.5±6.9 yrs, height: 174.9±5.7cm, mass: 64.9±7.3 kg). After warming up, all participants were asked to run over a treadmill at 3 m/s and 5 m/s for 3 minutes in a pair of running shoes (Li-Ning Boom, Beijing, China). The cadence, stride and sagittal plane lower-limb angles were collected by 8 VICON cameras during running. A 2×2 ANOVA was used to analyse lower limb sagittal kinematics (i.e., cadence, stride, joints angle at initial contact and maximum joint angle).

Table 1: Sagittal plane lower-limb angles between high-training and low-training volume groups.

Groups		Joint angle at initial contact (deg)			Maximum joint angle (deg)		
		Hip	Knee	Ankle	Hip flexion	Knee flexion	Ankle dorsiflexion
High-training	3 m/s	34.3±4.4*	-14.7±2.2	-3.2±4.4*	34.6±4.7*	33.7±4.2	14.9±2.5
	5 m/s	43.7±5.3*#	-18.0±1.9	-5.0±2.3*	44.6±6.8*#	38.9±4.7#	17.5±3.2
Low-training	3 m/s	29.4±4.4	-14.2±4	2.9±5	30.2±4.7	34.2±2.3	17.1±4.7
	5 m/s	36.5±5.1#	-13.7±4.1	0.74±7.8	37.2±3.9#	37.6±2.3#	17.4±6.1

Note: *: main effect of training volume, #: main effect of running speed, $P < 0.05$

Results and Discussion

The main effect of training volume indicated that compared to the LOW group, the HIGH group runners had larger hip and ankle angle at initial contact, and maximum hip flexion angle ($P < 0.05$, Table 1). The main effect of speed revealed that compared to running at 3m/s, hip flexion angle at initial contact, maximum hip and knee flexion angles, stride and cadence significantly increased at 5m/s ($P < 0.05$, Table 1, Figure 1).

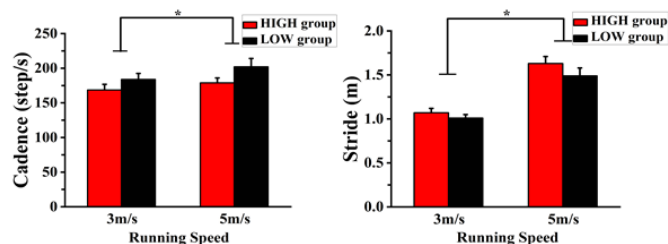


Figure 1: Cadence and stride between HIGH and LOW groups. *: main effect of speed, $P < 0.05$

Conclusions

The significant differences due to training volume found in hip and ankle angles at initial contact, and maximum hip flexion angle indicated that hip and ankle joint play a crucial role in joints motion control at initial contact during running, and high-training volume may affect hip and ankle joints effectively.

Acknowledgments

This study was supported by NNSFC (11772201), NKRDPC (2019YFF0302100), DPSCEC (19SG47), TDFSM (2018107).

References

- [1] Fokkema et al. (2020). *Sca J Med & Sci in Sports*, **30**: 1692-1704.
- [2] Thompson et al. (2017). *Integr Comp Biol*, **57**: 293-300

Shifts of tibiofemoral joint forces across the entire period of a half marathon

Tony Lin-Wei Chen^{1,3}, Wing-Kai Lam^{2,3}, Duo Wai-Chi Wong^{1,4}, Ming Zhang^{1,4}

¹Department of Biomedical Engineering, Faculty of Engineering, Hong Kong Polytechnic University, Hong Kong SAR, China

²Department of Kinesiology, Shenyang Sports Institute, Shenyang, China

³Li Ning Sports Science Research Center, Li Ning (China) Sports Goods Co. Ltd, Beijing, China

⁴Hong Kong Polytechnic University Shenzhen Research Institute, Shenzhen, China

Email: gilbertlam@li-ning.com.cn

Summary

Runners may adjust their gait patterns and joint loadings during a half marathon. This study investigated the changes of lower limb joint kinematics, muscle activities, and tibiofemoral joint forces in fourteen runners undergoing a half marathon. The kinematic and kinetic data were collected every 2 km (from 2 km to 20 km) and processed by a musculoskeletal model incorporating medial/lateral knee compartments. The simulations reported unchanged joint angulation, muscle co-contraction index, ground reaction force, and medial tibiofemoral contact force. Knee adduction moment was lower at 18 km than at 2 km and 6 km ($p = 0.001-0.002$). Lateral tibiofemoral contact force was reduced at 18 km, 16 km, 14 km, and 10 km compared to that at 2 km ($p \leq 0.045$). The medial-shifted tibiofemoral force might result from lower limb realignment to maintain running efficiency. The injury potentials of such joint loading redistribution remained to be clarified.

Introduction

Runners were thought to adjust their lower limb kinematics to cope with a prolonged run [1]. These body adjustments could influence loads on the tibiofemoral joint and thereby the injury risks. Joint contact force is the internal measure of the actual joint loading and is calculated as the primary variable in this study [2]. We also reported outcomes of joint kinematics and muscle activities at selected distance checkpoints.

We hypothesized that the runners would increase the hip joint excursion and reduce the knee flexion, muscle co-contraction, knee adduction moment, and tibiofemoral contact force as the half marathon progressed.

Methods

Fourteen experienced runners finished a half marathon on an instrumented treadmill. The kinematic and kinetic data were collected every 2 km (from 2 km to 20 km) and processed by a musculoskeletal model, which included an algorithm that calculated the distribution of the medial-lateral tibiofemoral contact forces. The computational simulations also reported lower limb joint kinematics, muscle activation, knee adduction moment. The co-contraction index of selected muscle pairs spanning the knee joint was calculated using a previously established method.

Results and Discussion

No significant changes were found in joint angulation, muscle co-contraction index, ground reaction force, and medial tibiofemoral contact force. Knee adduction moment (Figure 1) at 18 km were significantly lower than those at 2 km and 6 km ($p = 0.001-0.002$, $\gamma = 0.663-0.813$). Lateral tibiofemoral contact force reduced from 2 km to 10 km, 14 km, 16 km, and 18 km, respectively ($p \leq 0.045$, Hedges' $g = 0.216-0.859$). The results indicated that the external loads aligned closer to the lower limb's longitudinal axis as half-marathon progressed, whereby impacts during landing would be less absorbed by the works of soft tissue deformation but instead dispersed through segment collisions at the joint [3]. This may be an energy-saving strategy to increase race success while the injury risks behind it were unknown.

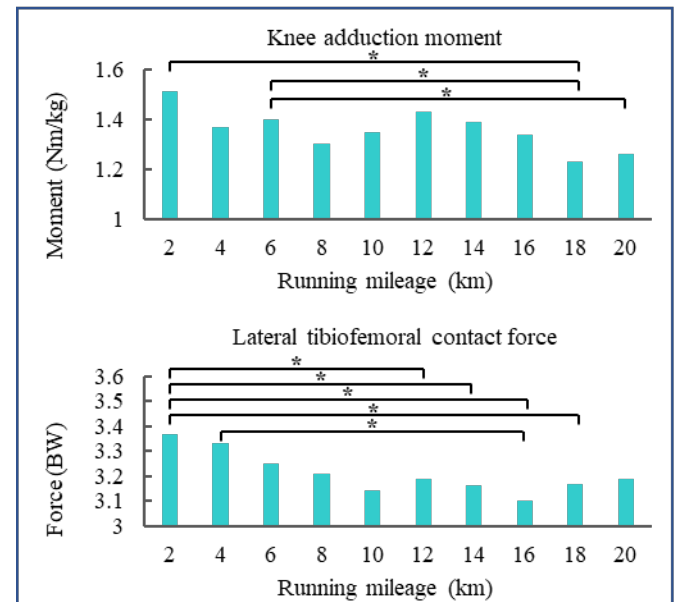


Figure 1: Knee adduction moment and lateral tibiofemoral contact force over the time course of a half marathon. * significant difference in pairwise comparisons.

Conclusions

Runners redistributed the knee joint loading during a half marathon to probably accommodate the effects of physical fatigue. Future studies were expected to explore its correlation with injury risks.

References

- [1] Giandolini M et al. (2016). *PLoS ONE*, **11**: e0151687.
- [2] Fong ICD et al. (2018). *Gait Posture*, **61**: 34-39.
- [3] Chan-Roper M et al. (2012). *J Sports Sci Med*, **11**:77-82.

Effects of Running Speeds and Footwear on Achilles Tendon Loading in Elite Marathoners with Different Training Volumes

Xini Zhang¹, Chenhao Yang¹, Wing-Kai Lam², Fan Yang², Liqin Deng¹, Songlin Xiao¹, Weijie Fu¹

¹School of Kinesiology, Shanghai University of Sport, Shanghai, China

²Li Ning Sports Science Research Center, Beijing, China

E-mail: fuweijie@sus.edu.cn

Summary

The purpose of this study was to investigate the Achilles tendon (AT) loading at different running speeds and footwear in elite marathon runners who trained with high- and low-training volumes (HIGH and LOW groups). All participants were instructed to run with two shoes at 3, 4, and 5m/s on an instrumented treadmill. The HIGH group had 1) greater ankle joint moment, AT force, average/peak loading rate, and less time to peak AT force than the LOW group; The HIGH group experienced greater AT force at 4 m/s and 5m/s, and ankle moment at 5m/s than those at 3m/s ($p < 0.05$). These results suggested that greater AT force could be advantageous in elite marathon runners who performed high-training volume, regardless of footwear and running speed.

Introduction

The Achilles tendon (AT) is the key anatomical structure to transmit the force from the triceps surae to the calcaneus. Elite marathon runners who performed high-training volume were demonstrated to have specific changes in morphologic and mechanical properties of AT (e.g. longer AT and greater AT force) [1]. However, it cannot be ignored the influence of footwear and running speeds on effective force transition by AT [2]. Thus, the purpose of this study was to investigate the effect of footwear and running speeds on AT loading in marathoners with different training volumes.

Methods

Twelve healthy male elite marathoners (HIGH group: n=5, training volume: 180.0±40.0 km/week, age: 26.0±4.4 yrs, height: 172.8±4.7 cm, mass: 56.8±3.7 kg; LOW group: n=7, training volume: 88.6±32.2 km/week, age: 32.6±6.9 yrs, height: 174.9±5.7 cm, mass: 64.9±7.3 kg) participated in this study. They were instructed to run with two pairs of shoes [Li-Ning Boom (L-N), E-Pebax midsole, 6-mm heel-to-toe drop, 152g; Nike Zoom Vaporfly 4% Flyknit (Nk), foam middle sole and carbon fiber outsole, 10-mm heel-to-toe drop, 195g] for 3 minutes at each of the running speeds (3, 4, and 5m/s) on an instrumented treadmill (Bertec Corp., Columbus, Ohio, USA). The ankle joint moment (M_A) and the mechanical properties [peak force (F_{AT}), time to peak force (T_{AT}), average (LR_{ave}), and peak loading rate (LR_{peak})] of the AT were calculated.

A mixed measures multivariate analysis of variance with an α set to .05 was used to examine the effects of training volumes, footwear, and running speeds on the AT loading (21.0, SPSS Inc., USA).

Results and Discussion

The ANOVA showed no interaction among three independent factors ($p > 0.05$). However, the main effects of training volumes and speeds were observed ($p < 0.05$). Specifically, the HIGH group had greater M_A , F_{AT} , LR_{ave} , and LR_{peak} , but smaller T_{AT} than the LOW group ($p < 0.05$, Figure 1). The HIGH group had greater F_{AT} at 4m/s and 5m/s, and M_A at 5m/s compared with the 3m/s, while F_{AT} only increased significantly at 5m/s in the LOW group ($p < 0.05$). These results suggested that the AT was more effective to transmit the force from the triceps surae to the calcaneus in the elite marathoners with larger training volume.

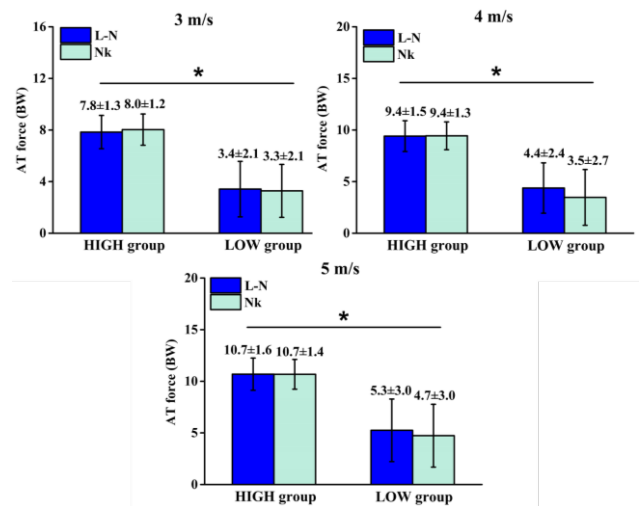


Figure 1: Comparison of AT force between two shoes in HIGH and LOW groups at running speeds of 3, 4, and 5m/s (*: $p < 0.05$).

Conclusions

The findings of this study suggested the similar acute effects between two tested shoes on the AT loading. The greater AT force and loading rate in marathon runners who trained with larger training volume training would benefit for effective force transition via AT.

Acknowledgments

This study was supported by NNSFC (11772201), NKRDPC (2019YFF0302100), DPSCEC (19SG47), TDFSM (2018107).

References

- [1] Kovács B et al. (2021). *Physiol Int*, **107**: 527-541.
- [2] Wearing SC et al. (2014). *Med Sci Sports Exerc*, **46**: 1604-1609.

Foot motion analysis using a stretch strain sensor during gait and running.

Kodai Sakamoto¹, Toshinori Miyashita², Masashi Kitano^{1,3}, Shintarou Kudo^{1,2,4}

¹ Graduate school of health science, Morinomiya University of Medical Sciences, Osaka, Japan

² Inclusive medical science research institute, Morinomiya University of Medical Sciences, Osaka, Japan

³ Yamamuro clinic, Toyama, Japan

⁴ AR-Ex medical research center, Tokyo, Japan

Email: kudo@morinomiya-u.ac.jp

Summary

The purpose of this study was to develop methods for the foot motion analysis using stretch strain sensor (STR). Foot kinematics during both walking and running on the treadmill were measured using both STR and optical motion capture system. STR was mounted over the skin between the navicular tuberosity and the sustentaculum tali. Difference from initial contact to maximum stretching value was defined as the S1, and difference from maximum and minimum value was defined as S2. Forefoot and hindfoot angular excursions with the same timing as S1 and S2 were calculated. Both S1 and S2 were assessed what angular excursion of the foot was reflected using multiple regression analysis. We found both S1 and S2 significantly related forefoot eversion/inversion excursion.

Introduction

Multi-segment foot analysis has acceptable reproducibility and accuracy. However, it is difficult to measure the foot kinematics with footwear and foot orthoses due to the need to mount the reflective markers on directly to the skin. We had proposed a measuring method using a stretch strain sensor (STR), thin enough to be inserted into the footwear, and it may provide an alternative solution for gait studies. The purpose of this study was to develop methods for the foot motion analysis using stretch strain sensor (STR).

Methods

The twenty-one normal volunteers were participated in this study. Foot kinematics during both walking(4km) and running (12km/h) on the treadmill were measured using the STR (C-stretch, Bando Chemical Industries, Japan) and a three-dimensional motion capture system(3DMocap) (Vicon MX system, Oxford Metrics Ltd., Oxford, England) sampling at 100 Hz, respectively. STR was mounted over the skin between

the navicular tuberosity and the sustentaculum tali. Difference from initial contact to maximum stretching value was defined as the S1, and difference between maximum and minimum value was defined as S2. Forefoot and hindfoot angular excursions with the same timing as S1 or S2 were calculated using the Oxford Foot Model using 3D Mocap. Both S1 and S2 were assessed what angular excursion of the foot was reflected in both walking and running using multiple regression analysis. Only items significantly correlated with S1 and S2 were used as independent variables. The significance level was $p < 0.05$.

Results and Discussion

The results of the multiple regression analysis were shown in table 1. Both S1 and S2 were significantly associated with forefoot eversion/inversion excursion, the STR most strongly reflected the forefoot frontal motion.

The previous study suggested that the talonavicular joint motion was largest in the foot, and it mainly occurs in the frontal planes with loading condition [1]. In this study, the STR was attached to straddle the talonavicular joint. The STR may be most strongly related to the forefoot frontal motion because the talonavicular joint motion stretched and shortened the STR.

Conclusions

The STR most strongly reflected the forefoot frontal motion. This method may be used in the future for measurement of foot kinematics while the subject is wearing the footwear and foot orthosis.

References

- [1] Kido M, et al. (2013). Clin Biomech (Bristol, Avon), **28**: 568-73.

Table 1: Multiple linear regression analysis for STR measurement using forefoot or hindfoot angular excursions.

	Dependent variable	Unstandardized coefficients	Standardized coefficients β	p	Adjusted R ²
S1 (walk)	Forefoot eversion	-0.573	-0.784	<0.01	-0.432
S2 (walk)	Forefoot eversion	-0.187	-0.366	<0.05	-0.728
S1 (run)	Forefoot eversion	-0.397	-0.545	<0.05	-0.592
S2 (run)	Forefoot inversion	-0.329	-0.527	<0.05	-0.443

Only items with the highest standardized coefficient β were listed in the table.

Effects of Training Volume and Running Shoes on the Patellofemoral Joint Loading in Elite Marathoners

Bin Shen¹, Wing-Kai Lam², Fan Yang², Xini Zhang¹, Songlin Xiao¹, Liqin Deng¹, Weijie Fu¹

¹School of Kinesiology, Shanghai University of Sport, Shanghai, China

²Li Ning Sports Science Research Center, Beijing, China

E-mail: fuweijie@sus.edu.cn

Summary

This study aims to explore the patellofemoral joint (PFJ) loading in elite marathoners with different training volumes when wearing different running shoes. The results found that running shoes had a similar effect on the PFJ loading. Marathoners with high-training volume experienced a lower peak knee extension moment (M_{EXT}) and peak patellofemoral joint stress (S_{PFJ}) compared to marathoners with low-training volume, which recommended a high-training volume for lowered risk of patellofemoral pain (PFP).

Introduction

PFP is one of the most frequently reported chronic injuries in runners [1]. Marathoners usually require a high volume of training. It is worth exploring whether the training volume can affect the load of PFJ in marathoners. Furthermore, high-end marathon racing shoes have been marketed and proven to have a better running economy and enable marathoners to achieve better athletic performance [2]. However, it remains unclear whether high-end shoes can prevent marathoners from a high loading of PFJ. Therefore, this study aimed to determine the PFJ load of marathoners with different training volumes when wearing different running shoes.

Methods

Twelve healthy male elite marathoners (HIGH group: n=5, training volume: 180.0±40.0 km/week, age: 26.0±4.4 yrs, height: 172.8±4.7cm, mass: 56.8±3.7kg; LOW group: n=7, training volume: 88.6±32.2 km/week, age: 32.5±6.9 yrs, height: 174.9±5.7cm, mass: 64.9±7.3kg) were recruited. Each participant randomly wore Nike Vaporfly 4% (Nk) and LI-NING Boom Marathon Racing Shoe ELITE (L-N) and ran at a speed of 5 m/s for 3 minutes on the Bertec instrumented treadmill (Bertec Corp., Columbus, Ohio, USA). Kinematic data was collected using Vicon T40 cameras (Oxford Metrics, UK).

Kinematics and ground reactional forces (GRF) of the right lower limb were processed using Visual 3D software (v5, C-Motion, Inc., USA). The peak M_{EXT} , peak knee flexion angle (θ_{FLX}), peak patellofemoral joint force (F_{PFJ}), and peak S_{PFJ} under different running shoes conditions were calculated. A

two-way ANOVA (Training volume × Shoe) was performed on all tested variables (21.0, SPSS Inc., USA).

Results and Discussion

There were no significant differences between the two groups in the peak θ_{FLX} and peak F_{PFJ} regardless of shoe types. However, there was a main effect of training volumes for peak M_{EXT} ($F=4.972$, $P=0.037$) and peak S_{PFJ} ($F=8.339$, $P=0.009$). Specifically, the HIGH group performed a lower peak M_{EXT} and peak S_{PFJ} compared to the LOW group (Figure 1).

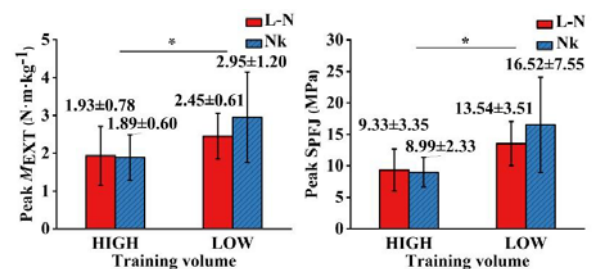


Figure 1: Comparison of the peak M_{EXT} and S_{PFJ} between high-training volume (HIGH) group and low-training volume (LOW) group with two types of shoes (L-N: LI-NING Boom Marathon Racing Shoe ELITE, Nk: Nike Vaporfly 4%) (* $P < 0.05$).

Conclusions

High-training volume marathoners experienced a lower peak M_{EXT} and peak S_{PFJ} compared to low-training volume marathoners, which indicated a lower risk of PFP via high-training volume regime [3]. Different high-end marathon racing shoes have minimal effect on PFJ loading (i.e., peak F_{PFJ} and S_{PFJ}) during running.

Acknowledgments

This study was supported by NNSFC (11772201), NKRDP (2019YFF0302100), DPSCEC (19SG47), TDFSM (2018107).

References

- [1] Taunton JE et al. (2002). *Br J Sports Med*, **36**: 95-101.
- [2] Hunter I et al. (2019). *J Sports Sci*, **37**: 2367-2373.
- [3] Thomas et al. (2010). *BMC Musculoskeletal Dis*, **11**: 201.

Table 1: PFJ characteristics of elite marathoners with different training volumes when wearing two running shoes.

Group	Peak M_{EXT} (N·m·kg ⁻¹) *		Peak θ_{FLX} (°)		Peak S_{PFJ} (MPa) *		Peak F_{PFJ} (BW)	
	L-N	Nk	L-N	Nk	L-N	Nk	L-N	Nk
HIGH	1.93±0.78	1.89±0.60	39.43±4.93	37.55±5.80	9.33±3.35	8.99±2.32	4.75±2.25	4.30±1.60
LOW	2.45±0.61	2.95±1.20	37.25±2.26	37.95±4.84	13.54±3.51	16.52±7.55	5.29±1.37	6.57±2.32

Notes: * indicates HIGH group vs. LOW group when regardless of the type of shoes, $P < 0.05$.

Effects of the arch span of a carbon-plated midsole on running shoe energy transformation— A finite element study

Tony Lin-Wei Chen^{1,3}, Wing-Kai Lam^{2,3}, Ben-Gang Yu³, Fan Yan³, Duo Wai-Chi Wong^{1,4}, Ming Zhang^{1,4}

¹Department of Biomedical Engineering, Faculty of Engineering, Hong Kong Polytechnic University, Hong Kong SAR, China

²Department of Kinesiology, Shenyang Sports Institute, Shenyang, China

³Li Ning Sports Science Research Center, Li Ning (China) Sports Goods Co. Ltd, Beijing, China

⁴Hong Kong Polytechnic University Shenzhen Research Institute, Shenzhen, China

Email: gilbertlam@li-ning.com.cn

Summary

An arched-shank design in a running shoe's midsole could facilitate energy return and improve running performance. The study investigated how different arch spans of the midfoot-shank would affect the shoes' energy flow during running through computational simulations. A runner performed running trials using a commercial running shoe, which featured an arched and carboned shank at the midfoot. Both of the runner's right foot and the shoe were finite-element modeled. The shoe model received virtual modifications on the shank's arch span and assembled with the foot model. Running simulations were conducted on the foot-shoe assemblies using the measured movement data. The results showed that increasing the arch span led to higher foot propulsive speed, shank energy return, and midsole energy return during gait propulsion. From the running efficiency perspective, we suggest that a running shoe including an arched midsole architecture considers a longer arch span to enhance its performance.

Introduction

A carbon shank in the midsole has been a mainstream design feature for high-performance running shoes recently. An elastic shank could reduce energy loss for the runners [1]. Despite the varied shank designs, most of the research attention has been paid to the stiffness of the shank material [2]. The effects of shank geometry were rarely examined, particularly for an arched shank. An arched shank recycles energy through a compress-decompress process, which could be influenced by changes in the arch spans. We hypothesized that a longer arch span would produce higher foot speed, increase shank deformation and midsole energy return during propulsion.

Methods

A finite element foot model was reconstructed from the MRIs of a healthy runner's right foot. A commercial running shoe (Jueying ARHQ245, Li Ning, China) with an arched shank was modeled and modified in virtual to produce four different arch spans (extra-short: 51 mm, short: 62 mm, long: 77 mm, extra-long: 92 mm). Thereby four foot-shoe model assemblies were created. The runner performed several running trials, which were processed with musculoskeletal modeling to generate a set of secondary movement variables. These variables served as the boundary conditions to set up the finite element analyses of running using each of the four model assemblies.

Results and Discussion

Since this study focused on the shoe's performance, we analyzed the energy transformation of 50% to 75% stance phase, during which the midsole bounced back for propelling the gaits. The extra-long arch span increased peak foot propulsive speed (by 22.6%–39.3%), shank energy return (by 41.4%–76.1%), and midsole material energy return (by 17.7%–35.0%) compared to the other three conditions. A longer arch span could reinforce the bending motion on the shank at midstance, which resulted in increased shank deformation and energy recycling. The reduced volume of cushioning material in the midsole for accommodating a longer shank design was offset by increased material strains and energy release during propulsion.

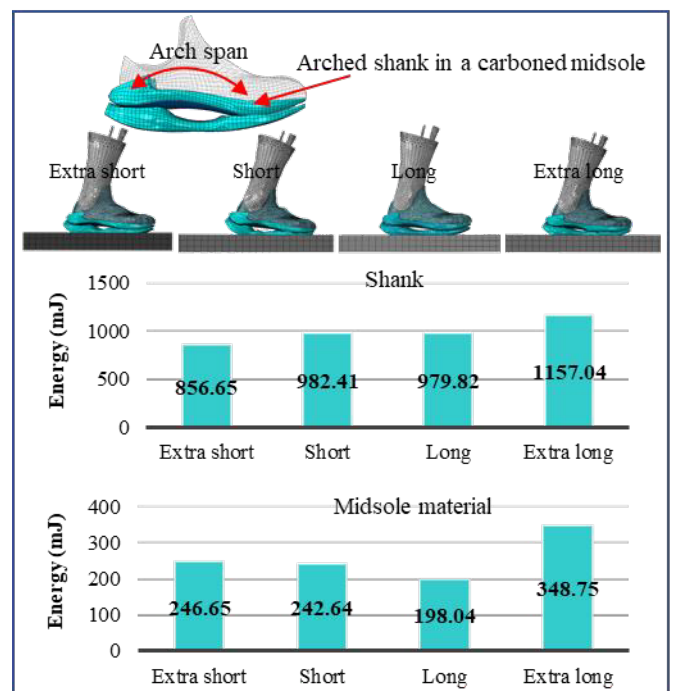


Figure 1: Energy return for propulsion (shank and midsole).

Conclusions

A running shoe using an arched-shank midsole system for energy saving/returning could consider a long arch span to enhance its performance during running.

References

- [1] Willwacher S et al. (2013). *J Appl Biomech*, **29**: 583-92.
- [2] Roy JP et al. (2006). *Med Sci Sports Exerc*, **38**: 562-9.

Influence of the Functional foot supporter on the foot motion during locomotion

Shintarou Kudo^{1,2}, Kodai Sakamoto¹

¹ Inclusive medical science research institute, Morinomiya University of Medical Sciences, Osaka, Japan

² Graduate school of health science, Morinomiya University of Medical Sciences, Osaka, Japan

³AR-Ex medical research center, Tokyo, Japan

Email: kudo@morinomiya-u.ac.jp

Summary

We have developed a functional foot supporter (FS) that the foot is thin and can be worn with various shoes. The purpose of this study is investigated influence of the FS on the foot motion during the locomotion. The strain of the foot which reflected on the eversion excursion of the foot during 3 trials which are walking(4km/h), running (12km/h) on the treadmill and over ground walking with comfortable speed were recorded using the Stretch strain sensor (STR). All trials were performed on barefoot without any supporter (BF) and with both FS and sham supporter (SS) at random. Strain of the foot with FS are significant difference with that of both BF and SS in all trials. The FS show to decrease eversion of the foot during loading phase of locomotion.

Introduction

Flatfoot deformity increase the risk of the overuse running injuries. The custom-made foot orthosis is known to be one of the effective footwears for running injuries, however, there is a need for something devices to prevention foot problems in every situation. We have developed a functional foot supporter (FS) that the footwear is thin and can be worn with various shoes. However, there are no evidence that FS can be influenced on the foot motion during the locomotion. The purpose of this study is investigated influence of the FS on the foot motion during the locomotion.



Figure 1: photograph of the functional supporter

Methods

The thirty feet of the thirty normal young volunteers with flatfoot deformity were participated in this study. Foot

motion during 3 trials which were walking(4km/h), running (12km/h) on the treadmill and over ground walking with comfortable speed were recorded using the STR (C-stretch, Bando Chemical Industries, Japan) with 100Hz. The STR was mounted over the skin between the navicular tuberosity and the sustentaculumtali. The difference strain from initial contact and maximum strain were calculated as loading strain reflected on eversion excursion of the foot with respected to the hind foot. All trials were performed on barefoot without footwear (BF) and with FS, sham supporter (SS) without supporting function at random. Difference strain each locomotion among the 3 supporters were assessed using repeated ANOVA with the Bonferroni test.

Results and Discussion

Strain value at each trail with 3 difference condition are shown in table1. Strain with FS are significant difference with that of both BF and SS in all trials. Thus, the FS can be decreased eversion of the forefoot during locomotion. The effects of the foot orthosis worn footwears can be assessed using footwear removing the window, because reflective markers can be captured by the infra-red cameras [1,2]. However, it decreases a rigidity of the shoes. Therefore, there is no evidence that foot orthosis can be influenced on the foot kinematics during locomotion with normal footwear. In this study, the FS we developed is designed to be reinforced the arch of the foot by thin and hard to stretch materials, and foot motion during locomotion is assessed using STR with thin and light. Therefore, FS showed to decrease eversion of the foot during loading phase of locomotion.

Conclusions

The FS can prevent to collapse the foot arch during the locomotion.

Acknowledgments

This work was supported by JSPS KAKENHI 19K19815.

References

- [1] Stearne SM et al. (2016). *Sci Rep*, **19**;6:19403.
- [2] Bishop C et al. (2015). *Gait Posture*, **41**: 295-599.

Table 1: difference Strain of the foot among the three condition

		Barefoot	Functional supporter	Sham supporter	p-value
treadmill	Gait (V)	2.15 ± 0.77	1.72 ± 0.80*	2.47 ± 0.79	0.01
	Running (V)	2.75 ± 0.96	1.97 ± 0.70*	2.81 ± 0.97	<0.01
over ground	Gait (V)	2.29 ± 0.84	1.87 ± 0.63*	2.61 ± 0.63	<0.01

*: significant difference with other conditions using *post hoc test*

FEM Driven plantar foot orthosis for diabetic foot prevention

A. Ciniglio¹, M. Palladino¹, A. Guiotto¹, F. Spolaor¹, A. Ianniello², E. Meggiato³, Z. Sawacha⁴

¹BiomovLab, Dept. Engineering Information, University of Padova, Padova, Italy

²Orthomedica S.r.l., Padova, Italy

³Podartis S.r.l., Crocetta del Montello, Italy

⁴Dept. Medicine, University of Padova, Padova, Italy

Email: zimi.sawacha@dei.unipd.it

Summary

Foot insoles are frequently prescribed in routine clinical practice to prevent or treat foot deformities or functional alterations. Currently adopted procedures for foot insoles manufacturing vary among clinical practitioners and manufacturers and decisions are mainly left to the experience of the ortho-prosthetic technician. Design frequently involves the use of cad-cam systems and, in the best case, static or, better, dynamic plantar pressure maps are considered. The aim of this contribution is to devise a simplified pipeline to provide ambulatory monitoring of dynamic foot function and to use this information to optimize plantar orthosis prescription for diabetic subjects. To this end both subject specific finite element models of the foot and of the plantar orthosis were developed.

Introduction

Diabetes mellitus is an epidemic disease: more than 422 million people worldwide presently suffer from T2DM and 10 years after disease onset, between 20 and 50% T2DM patients develop diabetes neuropathy, a major risk factor for diabetic foot problems. This represents the most common cause of non-traumatic amputation (Armstrong et al 2017). Although the use of optimized footwear combined with foot orthotics is inherently implemented in the clinical care path [1], foot orthosis prescription is currently based on clinical experience and static measures. With a re-ulceration risk of 65% in 5 years [1], there is an important potential to optimize foot orthosis prescription by accounting for dynamic foot biomechanical function [2]. As multi-scale modelling has proven to accurately predict both high plantar pressure and even more important internal tissue stresses [3] the aim of this contribution is to devise a simplified pipeline to apply this methodology in ambulatory conditions without the constraints of a gait laboratory.

Methods

The foot geometry of a cohort of 9 neuropathic diabetic subjects ((mean (SD) age 60.89(17.37) years and BMI 29.36(5.41) Kg/m²) was captured with a 3D scanner. Foot bones geometry was segmented from a database of neuropathic subjects foot MRI [4]. The foot bones were scaled based on every subject foot morphology (Abaqus). Each subject insoles geometries were scanned and meshed with tetrahedral elements (pipeline in Figure 1) and material properties were assigned according to the literature [3-4] and to the material characteristics declared by the insole

manufacturer. The vertical loads acquired during gait on a treadmill (2 km/h) through a PP insole system (PedarX, Novel gmbh) were applied in the FEM as boundary conditions. Loading response and midstance phases of the gait cycle were simulated [3] in 2 conditions: with and without the insole (see example in Figure 2). The comparison between the experimental PP and the simulated ones (peak and distribution) was used for validation purposes. Both simulated PP and internal Von Mises stresses in plantar soft tissues were compared across the different conditions (Root Mean Square Distance).

Results and Discussion

A good agreement was reached between the experimental and the simulated PP. Simulated insole did not completely succeed in assuring a better distribution of the PP but they reduced the Von Mises stresses.

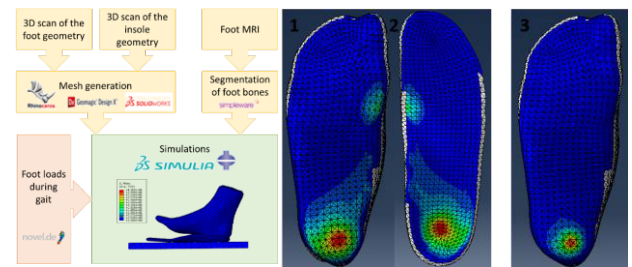


Figure 1: Left, the pipeline for the FEM creation; Right, the FEM simulation with (1,2) and without (3) the insole.

Conclusions

The behaviour of the insole was successfully simulated through the proposed pipeline by adopting a simple experimental protocol applicable in ambulatory condition. This approach can be used to predict the effects of the produced insole on the foot function thus resulting in an efficient tool for optimizing its design.

Acknowledgments

The study was conducted within the grant “S.F.I.D.A. Scarpa Funzionale Innovativa per Diabetici Attivi” – ID 10230017, financed by “POR FESR 2014 – 2020 Regione del Veneto, Azione 1.1.4 Bando Aggregazioni, DGR 711/2019”.

References

- [1] Armstrong et al. (2017). *SAGE*, **47**(2): 145-171.
- [2] Telfer et al. (2017). *J Biomech*, **60**: 157-161.
- [3] Scarton et al. (2018). *Gait & Posture*, **60**: 279-285.
- [4] Guiotto et al. (2014). *J Biomech*, **47**(12): 3064-3071.

Computational framework to perform parametric CFD studies from a patient-specific left atrium

Jorge Dueñas-Pamplona¹, Javier García¹, José Sierra-Pallares², César Méndez²,

Jorge Muñoz Paniagua¹, Javier Goicolea³, Francisco Castro²

¹Dept. de Ingeniería Energética. Escuela Técnica Superior de Ingenieros Industriales. Universidad Politécnica de Madrid (Spain)

²Dept. de Ingeniería Energética y Fluidomecánica. Escuela de Ingenierías Industriales. Universidad de Valladolid (Spain)

³Hospital Universitario Puerta de Hierro Majadahonda (Spain)

Email: jorge.duenas.pamplona@upm.es

Summary

Recently patient-specific Computational Fluid Dynamics (CFD) simulations have provided important insights to understand the flow behavior under diseases such as atrial fibrillation (AF), which tends to facilitate thrombus formation in the left atrium appendage (LAA). The mechanical relationship between the LAA geometry and the thrombosis risk is still unclear. Many LAA variables have been related with an increased risk, performing parametric CFD studies to evaluate the influence. However, less attention has been paid to the pulmonary veins (PV) orientation, which is known to have an important effect on left atrium (LA) flow patterns. The aim of this work is to present a computational framework to perform parametric studies for the evaluation of the influence of the PV orientations in LAA flow patterns during AF conditions.

Introduction

CFD techniques applied to patient-specific cardiac geometries in AF conditions aims to extend the existing knowledge about the thrombus formation process in the LAA, but the relationship between the thrombosis risk and the morphology of the LAA remains still unclear. Some of the previous CFD works have studied the influence of the dimensions of the LAA, the number of lobes, the ostium area, etc. However, the geometry and disposition of the PV, which present significant variations between patients and is known to affect to the left atrial flow patterns [1], has not been studied parametrically. The aim of this work is to find a convenient PV parametrization, providing a framework to perform parametric CFD studies from a patient-specific basis to evaluate the influence of the PV orientations in a physiological range.

Methods

In this study a CT imaging dataset and Doppler-echocardiogram of a cardiac patient has been provided by Hospital Puerta de Hierro of Madrid, acquired during sinus rhythm. The endocardial surface of the LA has been segmented, computing each slice through intensity thresholding, generating a 3D model compatible with CFD simulations. Doppler measurements granted patient-specific boundary conditions, making possible at the same time to validate the simulation.

The parametrization of the PV orientations is based in the angle projection of each PV in the projective planes, more specifically in the coronal and axial plane with respect to the sagittal plane (Figure 1). Since there are measurements of these angle projections available in previous clinical works

[2], the election of the angle projections as input variables for the parametric study allow us to generate a range of different physiological geometries. These eight variables were thus selected - the coronal and axial projection angle of each of the four PV - in order to launch a Design of Experiments (DOE). This way a range of different physiological PV orientations has been generated from a patient-specific basis. Then, CFD simulations have then been run by generating tetrahedral meshes from these geometries and the Doppler measurements as boundary conditions.

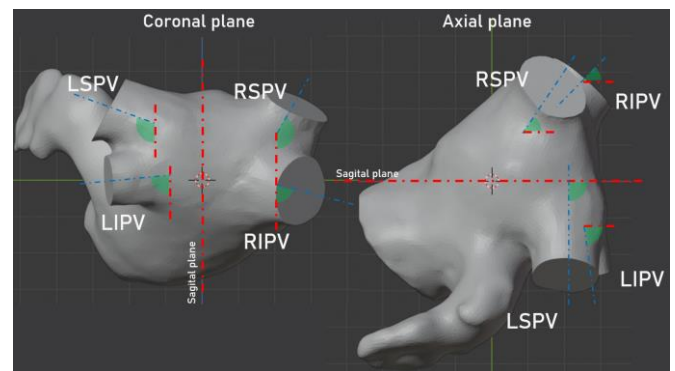


Figure 1: Sample of the projective angles employed to perform the parametrization. Coronal plane and axial plane are shown.

Results and Conclusions

This fully automated framework is able to generate a range of different physiological geometries from a patient-specific basis, opening the door to study the PV orientation influence on the LA flow patterns, and more specifically in the LAA thrombus formation process. Moreover, the workflow is valid to perform CFD simulations for both rigid and flexible atrium models.

Acknowledgments

This work was supported by Ministerio de Ciencia, Innovación y Universidades of Spain under contract **DPI2017-83911-R** and by the regional government of Castilla y León under contract **VA081G18**. We want to show our gratitude to the “Programa Propio - Universidad Politécnica de Madrid”.

References

- [1] Dahl, S.K. et al. (2012) *Cardiovascular Engineering and Technology*, **3**:269-281.
- [2] Mansour, M. et al. (2004). *Journal of cardiovascular electrophysiology*, **15**:387-393.
- [3] Buist, T.J. et al. (2016). *Journal of Cardiovascular Computed Tomography*, **10**: 251-257.

Assigning Trabecular Bone Material Properties to Total Hip Arthroplasty Finite Element Models of the Pelvis with Peri-prosthetic Osteolytic Lesions

Thomas M. Grace¹, Lucian B. Solomon^{1,3}, Gerald J. Atkins¹, Dominic Thewlis¹ and Mark Taylor²

¹Centre of Orthopaedic & Trauma Research, University of Adelaide, Adelaide, SA, Australia

²Medical Device Research Institute, College of Science and Engineering, Flinders University, Adelaide, SA, Australia

³Royal Adelaide Hospital, Adelaide, SA, Australia

Email: thomas.grace@adelaide.edu.au

Summary: A finite element analysis (FEA) based method for estimating strain distribution in the acetabulum with peri-prosthetic osteolytic (PPO) lesions was developed. The traditional total hip arthroplasty (THA) FEA approach of mapping material properties to trabecular bone geometry from patient CT scans is unfeasible for this method due to metal artefact. Therefore, five alternative approaches to assigning material properties to trabecular bone were tested and analysed. Analysis took into account; variability in acetabular strain values and distribution between approaches, simulation time and physiological validity of the values obtained. We consider applying constant generic material properties throughout trabecular bone geometry to be the most suitable of the five approaches tested.

Introduction: Published FEA THA models featuring acetabular PPO lesions use traditional methods of assigning material properties to trabecular bone [1] despite the effect of metal implants on CT clarity and Hounsfield Unit (HU) values [2]. The aim of this study was to perform a sensitivity analysis to determine which of five considered approaches of assigning trabecular material properties, whilst avoiding metal artefact, was most suitable within such models.

Methods: Two patients suffering from acetabular PPO (one with a unilateral THA implant *in situ* and one with bilateral THA implants *in situ*) were recruited and underwent both gait analysis and a CT scan. CT scans were segmented with a combination of thresholding, manual segmentation and Boolean operations. Volume meshes were generated from segmentations. FEA models were ran using these meshes and joint reaction forces were obtained from musculoskeletal modelling.

Five trabecular modelling approaches were outlined and tested. The first and second approaches involved assignment of one constant material property throughout the trabecular geometry aiming to represent generic healthy trabecular bone and 1+ years post-operative trabecular bone respectively. Approaches 3-5 were theoretically more physiologically realistic as trabecular bone material properties were assigned to three separate regions relative to the cup; superior, inferior and adjacent. Approach 3 assigned generic material properties to the superior and inferior regions and 1+ years material properties to the adjacent region. Approach 4 mapped material properties from the CT scans for the superior and inferior regions (as they were mostly unaffected by artefact) and assigned 1+ years material properties to the adjacent region. Approach 5

mapped material properties from the CT for all three regions however the material properties of the adjacent region were mapped from the contralateral side. Therefore, approach 5 was not possible for the bilateral THA patient.

Variability in acetabular strain values and distribution between approaches, physiological validity of the results and assembly and simulation time were all analysed.

Results and Discussion: There was little variance in strain values for approaches 2-4 implying no advantage to assigning different material properties to the superior, inferior and adjacent regions. For approaches 2 – 5 there were strain values that were considered physiologically unreasonable in the ilium with regards to theoretical yield (Fig. 1). There was consistency in the order of mean von Mises strain (lowest to highest) between the ilium, ischium and pubis for all approaches. This outcome was observed for both the unilateral and bilateral THA patient (with approach 5 excluded for the latter).

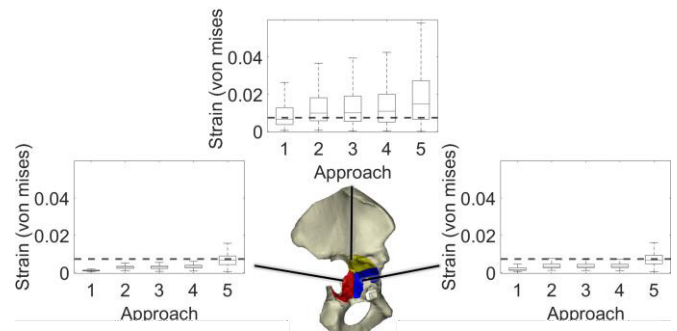


Figure 1: Box and whisker plots to demonstrate variability and in von Mises strain results between approaches for the unilateral THA patient. Dotted line indicates compressive yield value used to assess the physiological validity of the results.

Conclusions: Approach 1 (applying constant generic material properties throughout trabecular bone geometry) was considered the optimum approach of the five tested.

Acknowledgments: This study was supported by National Health and Medical Research Council (ID: 1126229)

References:

- [1] Munro JT et al. (2013). *J. Biomech*, **46**: 2529-2533
- [2] Gjestebj L et al. (2016). *IEEE Access*, **4**: 5826-5849

Construction of subject-specific foot finite element model based on foot surface scan

Yinghu Peng¹, Tony Lin-Wei Chen^{1,2}, Duo Wai-Chi Wong^{1,2}, Yan Wang^{1,2}, Ming Zhang^{1,2}

¹Department of Biomedical Engineering, Faculty of Engineering, The Hong Kong Polytechnic University, Hong Kong, China

²The Hong Kong Polytechnic University Shenzhen Research Institute, Shenzhen, China

Email: ming.zhang@polyu.edu.hk

Summary

Although a finite element (FE) foot model could assist the insole design, the modeling construction process is time-consuming and costly. This study aimed to assess and validate a simplified FE modeling method using merely the information of scanned foot surface. The foot surface and bone geometries from the Glasgow-Maastricht foot model were used as the template geometry. A set of anatomic landmarks was defined on the template foot surface and the target foot surface (the scanned foot). By matching the landmark position, a morphology-mapping algorithm was applied to scale the template foot surface and the encapsulated bone geometries to the target foot and create a subject-specific foot model. The scaled foot model was validated by comparing the predicted foot pressures with measurement. The proposed foot FE modeling approach could provide a fast and reliable foot pressure prediction, which would facilitate the orthotic design and optimization.

Introduction

A FE foot model could predict internal foot loading and verify the performance of an orthotic design. However, subject-specific foot modeling is challenging on a clinical basis because the modeling procedure can be time-consuming and costly. A simplified modeling method is needed to give quick but informative feedback on an orthotic treatment. This study proposed and validated a potential solution based on a foot surface scan and a model-scaling algorithm.

Methods

The right foot of a young male adult (height: 175cm, weight: 64 kg) was scanned under a minimal weight-bearing condition to construct the target foot model. Meanwhile, the Glasgow-Maastricht foot geometries in the Anybody software (AnyBody Technology, Aalborg, Denmark, version 6.0.5) was used as the template foot model [1]. To reduce the scaling complexity, we merged the bony segments in the template foot. The template foot model was scaled to the target foot geometries by matching predefined landmarks on the foot surface. The scaling process can be divided into two parts: affine transformations and built-in radial basis function (Fig. 1) [2].

The scaled foot model was meshed in Abaqus 6.14 (Dassault Systèmes, Vélizy-Villacoublay, France) with linear tetrahedral elements. The foot-ankle complex material properties were adopted from the literature [3]. The ground plate was loaded with 310N in against the plantar foot, and a 155N Achilles force was assigned to simulate a balanced standing condition.

Results and Discussion

The foot pressure distributions of balanced standing between model prediction and in-vivo measurement were compared (Fig.2). The predicted foot pressure showed a profile similar to the measurements. The peak foot contact pressures in model prediction and measurement were comparable (0.171 MPa and 0.163 MPa, respectively).

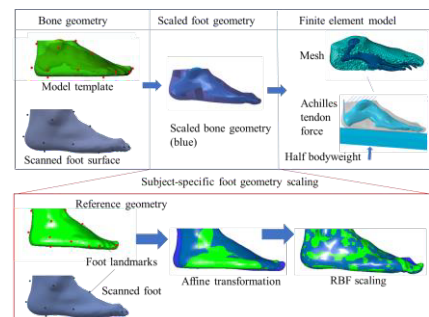


Fig. 1. Subject-specific foot geometry scaling for finite element model

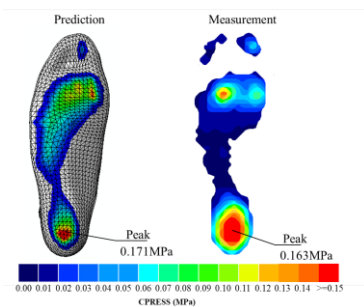


Fig. 2 Validation of the foot modeling with measurement during balancing standing

Conclusions

We proposed a quick and validated FE modeling method that could potentially be used for orthotic assessments in the clinic.

Acknowledgments

The work was supported by the National Natural Science Foundation of China [grant number 11732015, 11972315], General Research Fund granted by the Hong Kong Research Grant Council [grant number PolyU152065/17E].

References

- [1] Oosterwaal, M et al. (2016). *J Foot Ankle Res*, **9**: 1-10.
- [2] Marra MA et al. (2015). *J Biomech Eng*, 137:020904.
- [3] Peng Y et al. (2020). *Medicine Novel Tech Devices*. DOI: 10.1016/j.medntd.2020.100050.

Osteoporosis Vertebral Compression Fracture Finite Element Simulation and Expandable Bone Implant System Evaluation

Po-Yu Chen^{1,2}, Kit-Ieng Cheang^{1,2}, Bing-Shiang Yang^{1,2}

¹Department of Mechanical Engineering, National Chiao Tung University, Hsinchu City, Taiwan

²Department of Mechanical Engineering, National Yang Ming Chiao Tung University, Hsinchu City, Taiwan

Email: bsyang@nctu.edu.tw

Summary

We used finite element model (FEM) to simulate and evaluate the restored vertebral height result of using bone expandable implant in the state of osteoporosis vertebral compression fracture (OVCF) and verified our results with cadaveric experiment.

Introduction

With the aging society, osteoporosis has become the second most common endocrine disease in the world. It is characterized by low bone mass and microarchitectural degradation of bone tissue, which leads to a high chance of bone fragility and fracture susceptibility [1]. Patients with osteoporosis would be prone to have OVCF. The new minimally invasive surgery uses expandable implant to restore vertebral height. However, lack of biomechanical evidence on how the design of bone expandable implant affects the result of vertebral height restoration. It also takes considerable costs to refine the design and verify the functionalities through cadaveric experiments in the early stage of medical device development. This study established OVCF finite element model to verify the functionality of bone expandable implant and shorten the R&D process during initial design stage.

Methods

This study was divided into three parts. The first part was to establish a L1 OVCF finite element model. The second part was to verify our FEM model using a commercial device (T-type) with cadaveric experiment in device expansion. We primarily examine the implant height of T-type and the vertebral at the anterior, middle, and posterior height restorations (Figure 1). Lastly, we simulated the stress acting on the vertebral components in the state of OVCF.

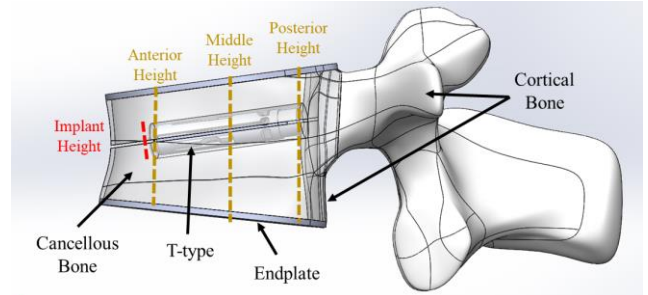


Figure 1: Vertebral components and height restoration. The black solid arrows are the vertebral components, yellow dotted lines are vertebral height restorations and red dotted line is implant height.

Results and Discussion

In the verification, the error of FEM simulation as compared to cadaveric experiment was 3.9%. The anterior, middle, and posterior height restorations in our FEM model were all overestimated with 1.283mm, 0.352mm, and 0.167mm respectively. The maximum stress in the cancellous bone caused by the bone expandable implant was 5.810 MPa; the maximum stress of the endplate stress at the front end was 3.258 MPa; the maximum stress of the cortical bone at the gap was 33.345 MPa (Figure 2).

Conclusions

We established an OVCF finite element model that can help the R&D team to evaluate the effectiveness of the bone expandable implant for intervening vertebral compression fracture.

References

- [1] Kanis JA (1994). "Assessment of fracture risk and its application to screening for postmenopausal osteoporosis: Synopsis of a WHO report." *Osteoporosis international*, 4: 368-381.

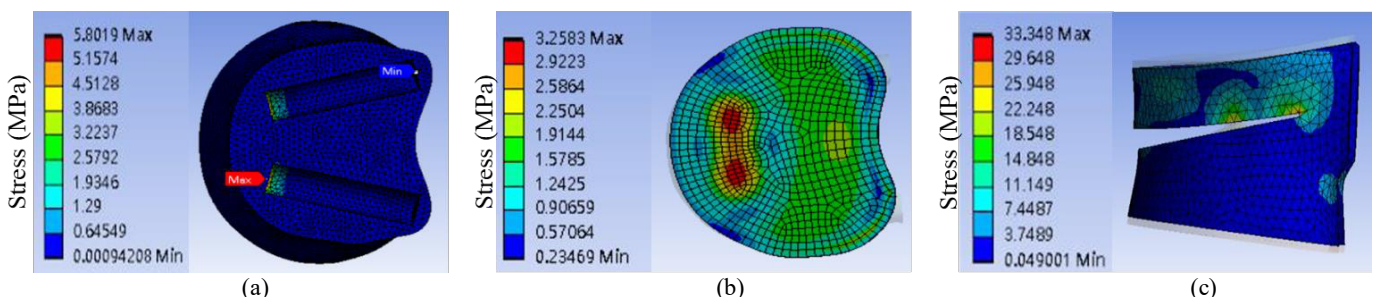


Figure 2: The stress acting on (a) Cancellous Bone (b) Endplate (c) Cortical Bone. The maximum stress (red area) of cancellous and endplate bone occurred at the front of T-type, and the maximum stress of cortical bone occurred at the gap.

Feasibility Analysis of Method for Obtaining Muscular Data of Forearm Using Musculoskeletal Simulation

T.L. Chen^{1,2}, B.S. Yang^{1,2}

¹Department of Mechanical Engineering, National Chiao Tung University, Hsinchu City, Taiwan

²Department of Mechanical Engineering, National Yang Ming Chiao Tung University, Hsinchu City, Taiwan

Email: bsyang@nctu.edu.tw

Summary

We used surface electromyography and musculoskeletal simulation software, OpenSim, to obtain the muscular data in wrist flexion and extension, and analyze the correlated level between two data.

Introduction

When tremor patients are having a botulinum toxin injection, it is important to define target muscle group and needle placement for the treatment [1]. However, there is a lack of ways to help doctors define which muscle causes tremor. Musculoskeletal simulation is a useful tool that can be used for biomechanical study. There are many studies used the muscle analysis tools in musculoskeletal simulation, OpenSim, such as computed muscle control (CMC), to simulate the muscle activation or muscle force, and surface electromyography (sEMG) signal was used for verification [2]. Nevertheless, sEMG signal is necessary when simulating the muscle activation or muscle force. According to the Hill-type muscle model, muscle generate force when muscle fiber contract, accompanied by the increase in muscle excitation. Huang and his colleagues [3] used optical motion capture system to capture the motions of upper arm, and evaluate shoulder disorder by simulating the muscle-tendon length in OpenSim without sEMG. However, simulation data in forearm muscles has not been verified. In this study, we aim to use OpenSim muscle-tendon length to develop a method for obtaining forearm muscle data without sEMG.

Methods

We recruited five healthy subjects (20-25 years old) for the experiment. In this study, concentric and eccentric contraction motions in extensor carpi radialis longus (ECRL) and flexor carpi ulnaris (FCU) would be measured with two sEMG sensors placed on the anatomy positions of these two muscles. Each subject outstretched his right arm, extended and flexed the wrist as much as they could. The movement

would be captured by optical motion capture system, and be imported into OpenSim for simulating muscle-tendon length. The electromechanical delay (EMD), which sEMG signal will happen about 30-100 (ms) earlier than the change in muscle-tendon [4]. To compare the profile of two data, the EMD would be considered by aligning the onset time of the sEMG data to the onset time of the muscle tendon length data of each subject. The Pearson correlation coefficient then be calculated using sEMG signal and muscle-tendon length varying with time.

Results and Discussion

According to the data, sEMG signal increase when muscle-tendon length decrease. The average Pearson correlation of the ECRL and FCU were both higher than 0.70 between OpenSim muscle-tendon length data and sEMG signal. These results represent that the OpenSim muscle-tendon length data is highly correlated ($r > 0.69$) with sEMG signal.

Conclusions

Our method successfully simulated the muscle-tendon length data of wrist flexion and extension using musculoskeletal simulation, and verified the simulation data with sEMG signal. Further research can be performed on tremor patients to explore the clinical applications.

References

- [1] Lee W-W and Jeon B. (2016). Practical Tips on Botulinum Toxin Injections *Botulinum Toxin Therapy Manual for Dystonia and Spasticity*; IntechOpen.
- [2] Seth A et al. (2019). *Frontiers in neurorobotics*, **13**: 90-90.
- [3] Huang P-H et al. (2016). *Development of a Diagnostic System for Shoulder Disorder Using Musculoskeletal Simulation*.
- [4] Cavanagh PR and Komi PV. (1979). *European Journal of Applied Physiology and Occupational Physiology*, **42**: 159-163.

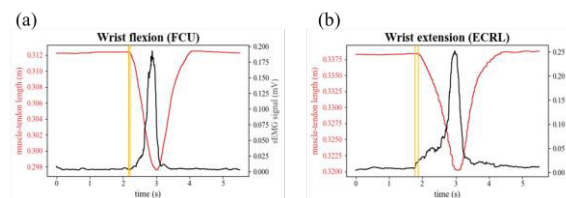


Figure 1: OpenSim muscle-tendon length data (red line) and sEMG signal (black line) versus time in wrist flexion and extension of (a) flexor carpi ulnaris (FCU) and (b) extensor carpi radialis longus (ECRL). The electromechanical delay (orange line) would be considered when calculating Pearson correlation.

An OpenSim-Based Musculoskeletal Model Controlled by Neural Oscillators That Generates Human Gait Patterns

Makoto Yoshida, Kazunori Hase

Dept. of Mechanical Systems Engineering, Graduate School of Systems Design, Tokyo Metropolitan University, Tokyo, Japan
Email: yoshida-makoto@tmu.ac.jp

Summary

In the investigations of human gait patterns, automatically generated patterns are useful because they are not affected by subjectivity by actual humans. Although a system that generates such patterns has been developed almost a couple of decades ago, it had not been used as widely as it deserves, probably due to the difficulty in data conversion. This system has been rewritten to be based on OpenSim, a widely used platform for biomechanical studies. A musculoskeletal model is controlled by a set of neural oscillators, a neuromimetic system capable of generating periodical signals suitable for gait control. A pair of neuron models acts as a neural oscillator, to which each rotational degree of freedom of the joints is assigned. The implementation of genetic algorithm to optimize the parameters of the set of neural oscillators with the criteria of maximizing the locomotive energy efficiency is underway.

Introduction

A significant difficulty in human gait analyses arises from the subjectivity of the participants of experiments. Automatic algorithms that generate gait patterns, free of subjectivity, play an important role to overcome this problem. Hase and Yamazaki developed a forward-dynamics simulation system employing a set of neural oscillators, and successfully generated three-dimensional human gait patterns [1].

In spite of the usefulness of the system, it had only been used by a limited number of researchers, probably because it did not offer the compatibility to any of the well-known data formats. We have ported the system to OpenSim 4.1 [2], a well-known platform for biomechanical studies, to make this system accessible to a wider population of researchers.

Methods

An OpenSim musculoskeletal model that reproduces the whole body of a human is constructed (Figure 1). Each joint was modeled as a single or a combination of rotational degrees of freedom.

This musculoskeletal model is controlled by a network of neuron models constructed according to that of Taga [3]. This neuromimetic controller that serves as a rhythmic pattern generator consists of paired neuron models. Each pair of neuron models acts as a neural oscillator, due to mutual inhibition of the neuron models in the pair. Each pair of neuron models is assigned to a rotational degree of freedom of a joint, where the state of a neuron model in a pair represents either the positive or the negative torque acting on the rotational degree of freedom, thus driving the

musculoskeletal model periodically. The states of the neuron models are modulated by a proportional-derivative feedback system employing some of the somatic senses, i.e. the joint angles, the ground reaction forces and the positions and the angles of the body segments with respect to the global coordinate system. The muscle force calculation is applied to the motion thus generated.

Results and Discussion

The implementation of genetic algorithm that optimizes the parameters of the set of neural oscillators with the criteria of maximizing the locomotive energy efficiency is underway. Although this system has not generated a single successful gait pattern so far, the authors are optimistic in completing the optimization by the date of the presentation, thanks to the experience on implementing a similar system [4].

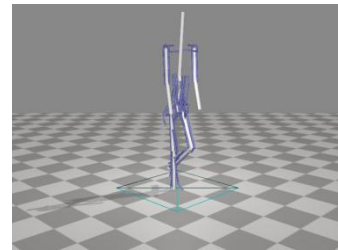


Figure 1: The musculoskeletal model. A neural oscillator is assigned to each rotational degree of freedom of the joints.

Since this system is not affected by subjectivity, this system may be used to find an optimal motion for walking in a variety of situations, e.g. that carrying some loads, that of a pregnant woman, that with prosthetic equipments, that with some pathology, the so-called Namba walking etc. This system may also be modified to simulate motions other than walking, e.g. skating, brachiation, cycling etc.

Conclusions

A system capable of generating three-dimensional human gait patterns has been rewritten as an OpenSim-based system. Implementation of the code to optimize the parameters of the neuromimetic controller is underway.

References

- [1] Hase K and Yamazaki N (2002). *JSME Int. J. Ser. C*, **45**: 1040-1050.
- [2] Seth A et al. (2018). *PLoS Comput. Biol.*, **14**: e1006223.
- [3] Taga G (1994). *Biol. Cybern.*, **73**: 97-111.
- [4] Yoshida M and Hase K (2019). *Proc. 17th ISCSB*, 19-20.

Estimation of Knee Ligament Forces During Non-resisted and Resisted Pedaling Using Finite Element Analysis

Yu-Ting Chen¹, Tzu-Yu Chou¹, Tung-Wu Lu^{1,2*}

¹Department of Biomedical Engineering, National Taiwan University, Taiwan

²Department of Orthopedic Surgery, School of Medicine, National Taiwan University, Taiwan

Email: twlu@ntu.edu.tw

Summary

Cycling is regarded as a gentle rehabilitation exercise for patients with knee ligament injury or surgery. However, improper pedaling conditions may cause damage on the knee musculoskeletal system damage. This study quantifies the forces transmitted in the anterior cruciate ligament (ACL), posterior cruciate ligament (PCL), medial collateral ligament (MCL), and lateral collateral ligament (LCL) during non-resisted and resisted pedaling using three-dimensional finite element analysis. According to the results, load on the PCL was much higher than the other ligaments for both resisted and non-resisted pedaling. It is recommended that patients with ACL injury or reconstruction but without PCL injury to perform pedaling as rehabilitation.

Introduction

Cycling is a common exercise in rehabilitation programs. It not only improves physical fitness, muscle strength, and function after treatments or surgeries but also avoids excessive ligament load [1]. Attempts were made to measure the strain in the knee cruciate ligament during cycling [2]. However, no method has been developed to measure the forces in the ligaments without employing invasive instruments. Due to the development of computer technology, finite element method has been widely used to achieve non-invasive estimation of *in vivo* joint soft tissue mechanics. This study aimed to compare the effects of resistance during cycling by analyzing loadings on the knee ligaments and to act as a reference for patients undergoing rehabilitation.

Methods

Twelve healthy subjects (age: 22.7±1.4 years; BMI: 22.6±3.6 kg/m²) were recruited and took CT and MRI images. They performed non-resisted and resisted pedaling under a speed rate of 30 rpm while the three-dimensional (3D) kinematics of the bones was measured using a 3D fluoroscopy method [3]. The resistance was set at 20 Nm to simulate the rehabilitation conditions. Laxity test was also performed on the subjects with KT-2000 arthrometer to obtain the displacement and force relationship.

In the finite element analysis process, models of the bones and ligaments were first constructed from CT and MRI images respectively. The attachments of ligaments were identified via a CT-to-MRI registration procedure. The bones were assumed to be rigid bodies and the material properties of the ligaments were assigned according to the data of laxity tests. Boundary conditions were obtained from the kinematics of 3D fluoroscopy. Resultant forces in the ligaments were then calculated by commercial finite element analysis software.

Results and Discussion

From the results (Figure 1 and 2), it was observed that the PCL bore forces 7-8 times greater relative to the other ligaments for both resisted and non-resisted cycling. Maximum loadings of the PCL occurred at crank angle of 0° while minimum loadings appeared at approximately 135°. The forces PCL transmitted in the process of 0° to 180° during non-resisted cycling were greater than that of resisted cycling. On the contrary, the results reversed from crank angle of 180° to 360°.

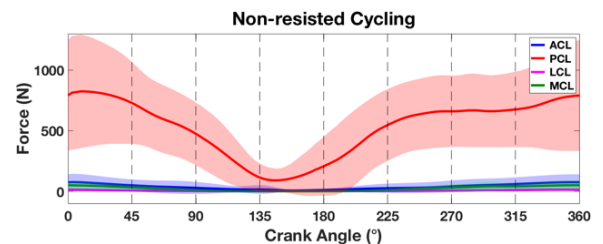


Figure 1: Ligament forces during pedaling without resistance

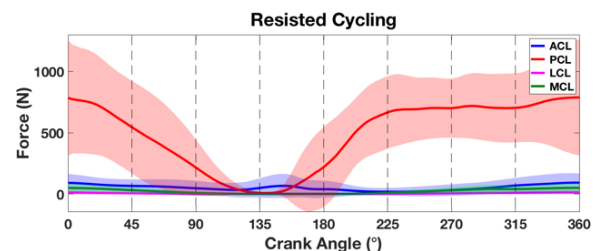


Figure 2: Ligament forces during pedaling with resistance

From the perspective of kinematics, since the position of the tibia was relatively posterior to the femur during the entire cycle of pedaling, the PCL would be stretched much more than the other ligaments to sustain joint stability. The lower forces in the PCL from 0° to 180° during resisted cycling compared to non-resisted cycling could be interpreted by the greater degree of internal rotation of the tibia obtained from the results of fluoroscopy, causing the PCL to become looser.

Conclusions

This study estimated and compared the forces in the knee ligaments during pedaling. The results indicated that non-resisted and resisted cycling could serve as appropriate rehabilitation exercises for patients with ACL injury, however, not suitable for patients with PCL injury or reconstruction due to the excessive loadings on the PCL.

References

- [1] Beynon, B. D., et al. (1995). *AJSM*, **23**(1), 24-34.
- [2] Fleming, B. C., et al. (1998). *AJSM*, **26**(1), 109-118.
- [3] Lin, C. C., et al. (2018). *Med Phys*, **45**(8), 3637-3649.

Simulating Subject-Specific Spine Mechanics: An Integrated Finite Element and Neuro-Musculoskeletal Modelling Framework

L. Meszaros^{1,2}, M. Hammer², J. Riede², P. Pivonka¹, J. Little¹, S. Schmitt²

¹Biomechanics and Spine Research Group, Queensland University of Technology, Brisbane, Australia

²Institute for Modelling and Simulation of Biomechanical Systems, Stuttgart, Germany

Corresponding author email: l2.meszaros@qut.edu.au

Summary

The aim of the current study is to integrate two different types of computational models (finite element and neuro-musculoskeletal) to simulate spinal motion in order to gain a greater understanding of the impact of spinal muscles on the mechanics in the thoracolumbar spine during forward flexion. All relevant structures were successfully included in both modelling workflows to directly simulate physiologically inspired motions. Analysis of the resulting finite element simulation shows a displaced spinal motion in the finite element model that was compatible with the simulated motion in the neuro-musculoskeletal spine model.

Introduction

Finite element (FE) analysis and multi-body (MB) modelling are computational methods commonly used as an effective tool in simulating human spine motion. The aim of the current study is to develop an integrated framework that allows to combine two different spine modelling methods. When combined, a more intrinsic understanding of spine biomechanics is provided, giving insight into the internal tissue mechanics for physiologically authentic motions. We adapted an established muscle-driven neuro-musculoskeletal (NMS) spine model developed in the in-house modelling framework *demoa* [1] to match the mechanical properties of a subject-specific osseoligamentous FE model of the spine [2] in order to provide temporal data for muscle forces.

Methods

The following sections detail the specific steps employed in order to generate models with compatible anatomy, soft tissue characteristics and initial conditions.

Anatomy: Both the NMS and FE models were personalised to include thoracolumbar spine, ribcage and pelvic anatomy for the Visible Man (VM) [3] using custom-developed image processing software, *Dicomtilt* [2]. The in-house preprocessor *calcman*, a tool for the calculation of 3D anthropometric data [1], was extended to allow the creation of subject-specific MB models based on CT-derived landmarks.

Muscles: A series of user-selected landmarks defined muscle attachment and deflection points in the thoracolumbar spine, sacrum and pelvis. Using custom-developed FE pre-processing software, *VirtuSpine* [2], these landmarks were used to create an osseoligamentous FE spine model with individual muscle threads modelled using axial connector elements (tension-only).

Ligaments: To match the nonlinear stiffness properties of the ligaments, an optimisation was performed using the

objective function of Least Squares on the literature-based stress-strain characteristics used in the FE model. The optimisation-derived characteristic points of the ligament stress-strain curve were implemented in the nonlinear modelling algorithm of the MB model.

Intervertebral (IV) discs: In order to equalise the models' IV coupling behaviour the 6D mechanical response of isolated IV discs from the FE model was encapsulated in different loading conditions and used to build individual surrogate models based on kernel methods for multiaxial non-linear approximation. These surrogate models mimic the forces and moments an IV disc exerts onto the endplates of adjacent vertebrae in the MB model.

Muscle forces were computed for a flexion movement using the developed subject-specific NMS model in a forward dynamics simulation. The NMS-derived temporal changes in muscle forces were applied via force amplitude data linearly ramped over the load step at the muscle connector elements in the FE model resulting in quasi-dynamic loading conditions.

Results and Discussion

The NMS modelling workflow was successfully adapted to simulate subject-specific anatomy and soft tissue properties. Similarly, the FE capability was advanced to define a subject-specific NMS loading regime using >200 individual muscle threads. Analysis of the FE model with NMS-derived muscles forces for a forward flexion motion, predicted a displaced spinal motion in the FE model that was compatible with the simulated NMS motion.

Conclusions

With the established framework, we have the capability to simulate NMS-derived, physiologically inspired motions in a FE model of the spine. This allows us to investigate the influence of spinal motion and muscle activation patterns on tissue level mechanics. All significant and relevant structures are now included in both modelling workflows to create identical models on FE and NMS level that together provide a finer resolution in discovering the influence of muscle synergies on joint mechanics. In future studies the developed approach will be applied on spinal pathologies.

References

- [1] Rupp TK et al. (2015) *Biomech Mod Mechanobiol.*, **14(5)**:1081-105.
- [2] Little JP and Adam CJ (2015) *CMBBE*, **18(6)**:676-688.
- [3] Ackerman MJ (1998) *Proc. IEEE*, **86(3)**:504-511.

Biomechanical analysis of the stick handling in field hockey: kinematics and kinetics assessment.

Alex Scadaferro¹, A. Ciniglio¹, G. Maistrello¹, F. Spolaor¹, A. Guiotto¹, F. Cìbin², Z. Sawacha^{1,3}

¹BiomovLab, Dept. Engineering Information, University of Padova, Padova, Italy

²BBSof S.r.l., Padova, Italy

³Dept. Medicine, University of Padova, Padova, Italy

Email: zimi.sawacha@dei.unipd.it

Summary

Injuries related to the practice of field hockey are very common, especially those regarding the lower limb joint biomechanics. The goal of this study is to understand whether females are more prone to lower limb injury risk than males while performing a hockey specific task, like a sprint done with an implement (the hockey stick). For this purpose, we have assessed two cohorts of subjects on field and compared the biomechanical variables related to the lower joint joints.

Introduction

Field hockey is a sport in which speed is the most important aspect in order to succeed. For this reason, hockey athletes are typically required to do several short sprints at high speed with the constraint of holding a hockey stick. Using the hockey stick while playing has been proved to affect players in terms of body posture and metabolic demand [1]. It should be further considered that injuries result not only in individual cost and can compromise the success of the team over the sporting season [1]. Furthermore, it has been shown that the joint kinematics was negatively affected by the use of the stick [2]. This study aims to compare female and male athletes in two different sprint conditions, and through the assessment of their lower limbs kinematics and kinetics, to evaluate their risk of injuries.

Methods

After signing informed consent, sixteen subjects (9 athletes of the female hockey team: mean (SD) age 21,56 (4,67) and BMI 22,01 (0,99) kg/m², 7 athletes of the male hockey team: mean (SD) age 22,00 (2,83) and BMI 23,71 (1,67) kg/m²) were acquired while performing two consecutive 10m sprints in two different conditions: one carrying the hockey stick with one hand and the other one carrying the hockey stick with two hands. Data were acquired by means of four GoPro Hero 3 cameras and plantar pressure insoles (Pedar X, Novel). An automatic tracking of feature software (TrackOnField, BBSof S.r.l.) and self-developed Matlab (R2017a) codes were used to estimate lower limbs (hip, knee and ankle) angles and moments [3]. The acquisition was performed directly on the field, while the athletes were performing the task. Seventeen retro-reflective markers were applied on each athlete according to a simplified version of the IORgait Marker Set

[4]. Only sagittal plane kinematics was considered. Normative bands were created (mean and standard deviation) of each variable for each tested condition and subject's cohort. Student T-test ($p < 0.05$) was applied (Lilliefors Test evaluation of normal distribution) in order to compare the biomechanical variables between the female and male cohort.

Results and Discussion

Statistically significant differences were observed between the two cohorts, especially in terms of lower limbs' hip joint rotations and knee moments. Higher hip flexion angles were observed in female athletes (Fig 1-left). An opposite trend was observed in the male athletes and higher knee moments were measured; female athletes recorded very high knee varus moments differently from male athletes that recorded low valgus moments (Fig 1-right).

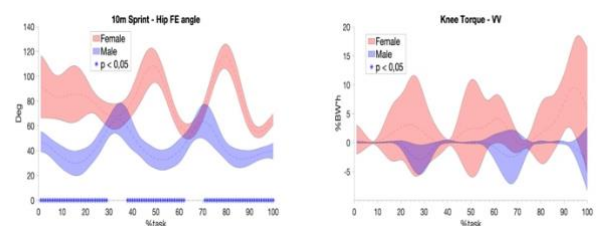


Figure 1: Left: Comparison between the hip angles of the two teams. Right: Comparison between the knee moments of the two teams.

Conclusions

Results of the present study highlighted differences between female and male hockey athletes while performing a sport specific task on field. A higher risk of lower limb injuries was assessed on the female athletes by considering the higher knee moment values on the coronal plane associated with higher flexion angles on all the lower limb joints.

References

- [1] Podgorski T. et al. (2011). *Hum Mov*, **12**: 108-123.
- [2] Wdowski MM. et al. (2013), *Sports Biomech*; **12**: 143-53
- [3] ACL Quick Check® patent: <https://www.bb-sof.com/>
- [4] Leardini A. et al. (2017). *Gait & Posture*; **26**: 560-571.

Intra-Subject Repeatability of Joint Angle Measurement During Skating on Synthetic Ice

Aminreza Khandan, Ramin Fathian, Jason Carey, Hossein Rouhani*

Mechanical Engineering, University of Alberta, Edmonton, Alberta

Email: hrouhani@ualberta.ca

Summary

High intra-subject repeatability in hockey players' kinematics is a requirement for athletic performance assessment based on joint angles; it, however, has not been studied yet for skating on synthetic ice. The objective of this study is to investigate the intra-subject repeatability of the joint angles during forward skating on synthetic ice. To this end, reflective markers were attached on four participants, and they were asked to skate forward on a synthetic ice area built on a motion capture lab. Using the marker trajectories, hip and knee joint angles were obtained. Then, the intrasubject repeatability of the joint angles was investigated. Good to excellent intra-subject repeatability was observed in the recorded joint angles during forward skating. Further studies with a higher number of participants on the real ice arena are required to reach a general conclusion.

Introduction

The key assumption in kinematic performance assessments for ice hockey is the high intra-subject repeatability of the measured joint angles. This assumption directly affects the reliability of the obtained angles to indicate the player's performance in a measurement session, and it has not been comprehensively investigated yet. This study aimed to investigate the intra-subject repeatability of the measured joint angles during forward skating on a synthetic ice area.

Methods

Four participants (age: 28 ± 1 years, body height: 176.5 ± 0.7 cm, body mass: 77.0 ± 7.7 kg, all male) were recruited to skate on a 14m-long synthetic ice area built on a motion capture lab. A 12 infrared camera motion capture system was used to measure the three-dimensional (3D) joint angles of the participants' lower limbs during skating. The 3D joint angles were obtained using the markers placed on anatomical landmarks following an experimental protocol suggested by Cappozzo et al. (1995) [1]. However, the markers on lateral and medial malleolus were attached to similar locations on the participant's skates to be visible by the cameras. Using the recorded marker trajectories, 3D hip and knee joint angles were calculated and expressed based on the joint coordinate system (JCS) in all captured strides in 20 skating trials, i.e.,

five strides for each participant. Following Kadaba et al. (1989) [2] and Growey et al. (1997) [3], the coefficient of multiple correlations (CMC) was utilized to investigate the intra-subject repeatability of the 3D joint angles during forward skating.

Results and Discussion

Intra-subject repeatability was excellent for the joint angles in the sagittal plane ($CMC = 0.93 \pm 0.03$) and good to excellent in other planes ($0.77 < CMC < 0.87$). The most repeatable joint angle was hip flexion-extension with $CMC = 0.96 \pm 0.01$. On the other hand, relatively lower repeatability in the hip internal-external rotation was observed ($CMC = 0.77 \pm 0.07$). Intra-subject repeatability of the 3D hip and knee angle measurements during skating on synthetic ice is presented in Table 1.

Conclusions

Although more data are needed before a general conclusion can be provided, the current observation confirmed good to excellent repeatability of the recorded joint angles during forward skating in a session. Also, the source of lower repeatability in some of the measured angles can be further studied; using other motion capture devices like inertial sensors will eliminate the errors due to marker reconstruction and marker misplacements. Finally, similar studies on real ice are required to investigate skaters' joint angle intra-subject variability during forward skating on ice.

References

- [1] A. Cappozzo, F. Catani, U. Della Croce, and A. Leardini (1995), Position and orientation in space of bones during movement: anatomical frame definition and determination, *Clinical biomechanics*, **10(4)**, 171-178.
- [2] M. P. Kadaba, H. K. Ramakrishnan, M. E. Wootten, J. Gainey, G. Gorton, and G. B. Cochran (1989), Repeatability of kinematic, kinetic, and electromyographic data in normal adult gait, *Journal of orthopaedic research*, **7(6)**, 849-860.
- [3] E. Growney, D. Meglan, M. Johnson, T. Cahalan, and K.-N. An (1997), "Repeated measures of adult normal walking using a video tracking system," *Gait & Posture*, vol. **6**, no. 2.

Table 1: Intra-subject repeatability of joint angle measurement during forward skating on synthetic ice expressed with coefficient of multiple correlations (CMC)

	Flexion/Extension		Adduction/Abduction		External/Internal rotation	
	Hip	Knee	Hip	Knee	Hip	Knee
CMC average	0.96	0.90	0.87	0.81	0.77	0.80
CMC standard deviation	0.01	0.06	0.05	0.11	0.07	0.08

Looking for the ideal sprint stride: how would sports results change if all strides were perfect

Andrey Pomerantsev

Institute of Physical Education and Sports, Lipetsk State Pedagogical P. Semenov-Tyan-Shansky University, Lipetsk, Russia

Email: a.pomerantsev.1981@gmail.com

Summary

World Athletics registers records in sprint running. Sprint race is a series of unique and non-repeating strides. Each step is a function of the previous steps and defines the next steps. The ideal step is the step that motor potential is realised to the greatest extent. Identifying the best step can serve as a running benchmark for a particular athlete, as well as an example for all athletes.

Introduction

If the best stride is considered as an ideal (reference) step, then it is possible to determine the time losses at each step due to the deviation from this one. The ideal strides of various sprinters can be compared to determine the best stride in the sport history.

Methods

The research is based on momentary velocity analysis in men's 100 m final at the 2009 IAAF World Championships in Berlin. The intracyclic velocity charts are taken from the IAAF official website [1]. Momentary velocity data is obtained by laser measurement system. We don't have the original numerical values of the momentary velocity, so we quantized the existing graphs. The quantization included mapping, scaling and interpolation points. It allows us to describe all features of the original curve in high degree of similarity. Based on this data momentary velocity graphs is reconstructed.

The graph shows that each oscillation corresponds to one running stride. The maximum peaks and the minimum troughs of the intracyclic contribute to a high average intracyclic speed [2]. We analysed the momentary speed of 3 outstanding sprinters in the history: Usain Bolt, Tyson Gay and Asafa Powell. These athletes won medals in the final race of the 2009 IAAF World Championship in Berlin and remain the best sprinters in history. One of them is the owner of the ideal sprint stride very likely. To determine the best stride we determined the average intracyclic speed for all running cycles.

Results and Discussion

Ideal stride is one that allows the highest average intracyclic speed in accordance with individual athlete's characteristics. Analysis reveals that the ideal step for all athletes is determined beyond of the starting acceleration and is not included in the final strides number (Figure1).

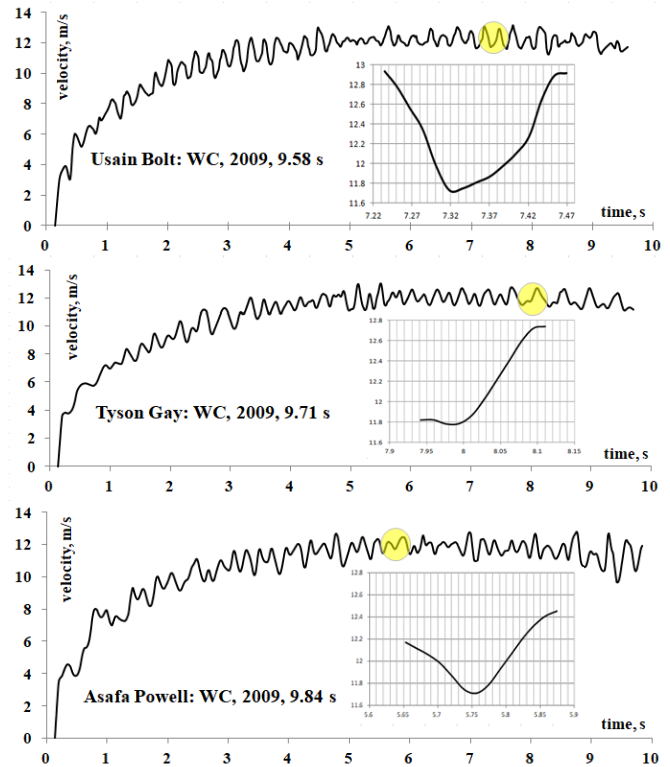


Figure 1: Momentary velocity vs time for medalists of 100m final at the 2009 IAAF World Championships in Athletics (quantized).

Computer calculation let to estimate the athletes' hypothetical results. In our cases we simulated that all strides would be identical and similar to the ideal stride after start acceleration (Table 1).

Table 1: Results of graphs analysis

Athletes	Velocity (average) of the ideal stride, m/s	Hypothetical results, s
Usain Bolt	12.30	9.42
Tyson Gay	12.19	9.50
Asafa Powell	12.08	9.54

Conclusions

The sports result in the sprint largely depends on athlete's motor potential realisation. Any deviation from the ideal stride will worsen sport performance.

References

- [1] Graubner R., & Nixdorf E. (2011). *New Studies in Athletics*, **26(1/2)**, 19-53.
- [2] Pomerantsev A.A. (2020). *Proceedings of 38th ISBS Conference*, **38 (1)**, 260-263.

Grip socks reduce in-shoe sliding but not actual change of direction performance

Charlotte. Apps, Jordan. Constable, Jonny. Dench, Brianna. Meyrick, Raekwame. Simpson, Jacob. Wright¹,

¹SHAPE Research Group, School of Science and Technology, Nottingham Trent University, Nottingham, United Kingdom

Email: charlotte.apps@ntu.ac.uk

Summary

It has become popular for team sport players to wear grip socks, which are marketed to reduce in-shoe slipping, and enhance speed and agility. We assessed these claims by quantifying in-shoe foot sliding using 3D motion capture, and measuring performance during change of direction manoeuvres. Foot sliding reduced in the tested grip socks, which was perceived by players to increase stability, comfort and speed. Yet, grip socks did not increase the coefficient of friction change or reduce time to complete a slalom course.

Introduction

Team sports necessitate frequent and rapid whole body changes of direction during matches [1], enabling players to evade opponents to perform a certain action that can influence the result of the game. Few studies have investigated the role of friction at the foot-shoe interface during changes of direction. Yet performance depends upon the foot position being maintained on the midsole platform to prevent time being lost from foot sliding whilst transitioning from deceleration to acceleration [2]. The aim of this study was to investigate if grip socks enhance actual and perceived change of direction performance by increasing the coefficient of friction and reducing in-shoe foot sliding.

Methods

Male recreational team sports players completed maximal effort change of direction manoeuvres (n = 10): a side cut (45°) and a complete turn (180°). Kinematic and kinetic data were collected with a 7-camera motion capture system (200 Hz) and a force plate (1000 Hz). In a separate visit participants (n =12) completed a slalom course to assess performance. Two sock conditions were tested: a regular athletic sports sock (RS) and a grip sock (GS) with rubber pads (7 x 9 mm) on the inside and outside sock material (LUX Sports). A standardised indoor football shoe was fitted to players that had holes in the shoe upper (30 mm Ø), and reflective markers attached to the midsole. The socks were cut in corresponding locations so markers were attached directly onto the dorsal foot skin overlaying the regions of the fifth metatarsal head (MH5) and base (MB5), and the lateral calcaneus (LC). During the change of direction manoeuvres, in-shoe foot sliding was determined from the maximum range of displacement between the foot and shoe markers between two frames after initial foot contact and two frames before toe-off, adapted from a previous study [3]. The mean coefficient of friction was calculated as the ratio of the horizontal to vertical ground reaction force during the loading and propulsive phase, defined as the first and second 50% period that in-shoe sliding was computed. The time taken to complete a 26 m slalom course was monitored [4] and subjective perception of

in-shoe grip, stability and comfort were measured with a 150 mm visual analogue scale [3]. Variables for each sock condition were averaged for each participant and compared statistically by paired t-tests (p<.05).

Results and Discussion

The GS tended to reduce in-shoe sliding across foot regions in both change of direction manoeuvres compared to the RS (Table 1). No differences were observed in the coefficient of friction during the loading or propulsive phases during the side cut or complete turn (Table 1).

Table 1: Maximum foot marker to shoe displacement (sliding) and coefficient of friction (COF) across participants.

Variable	Manoeuvre	RS	GS	p-value
MTH-shoe sliding (mm)	Side-cut	7.3 ± 2.0	5.8 ± 2.0	0.073
	Turn	13.7 ± 4.7	11.8 ± 1.9	0.096
MB5-shoe sliding (mm)	Side-cut	8.1 ± 2.7	6.7 ± 2.5	0.070
	Turn	11.6 ± 2.4	9.4 ± 1.2	0.002
LC-shoe sliding (mm)	Side-cut	7.0 ± 1.8	6.3 ± 1.8	0.465
	Turn	8.8 ± 2.6	6.2 ± 1.3	0.012
Loading phase COF	Side-cut	.40 ± .06	.39 ± .05	0.311
	Turn	.59 ± .06	.58 ± .06	0.350
Propulsive phase COF	Side-cut	.52 ± .03	.51 ± .06	0.654
	Turn	.61 ± .05	.60 ± .05	0.255

There was no difference in the time to complete the slalom course (p = .175), but participants' perceived in-shoe grip (p < 0.001), stability (p < 0.001) and comfort (p = 0.022) increased in GS compared to RS

Conclusions

Grips socks reduced in-shoe foot sliding during change of direction manoeuvres and were perceived to be more stable and comfortable. Future research needs to explore if this influences movement control and injury risk. The magnitude of foot sliding that grip socks reduced compared to regular socks is not sufficient to influence performance.

References

- [1] Bloomfield J et al. (2007). *Journal of Sports Science and Medicine*, **6**: 63-70.
- [2] Lafortune M (1997). *Journal of Applied Biomechanics*. **13**, 197-204.
- [3] Apps C et al. (2019). *Journal of Sports Sciences*, **38**, 206-213.
- [4] Sterzing T et al. (2009). *Footwear Science*. **1**, 5-17.

Reproducing the characteristics of muscle fatigue change through sEMG analysis based on joint mechanical work during upper limb repetitive rotation

Jinsung Jung¹, Jung Kim¹, Sukyung Park¹

¹Department of Mechanical Engineering, Korea Advanced Institute of Science and Technologies, Daejeon, Republic of Korea
Email: jinsungjung@kaist.ac.kr

Summary

In this study, a model capable of estimating the mean power frequency(MPF) of the sEMG from joint mechanical work data was proposed to reproduce the characteristics of muscle fatigue changes. sEMG signals and kinetic data of the upper limb were measured. The change characteristics of the estimation result through the proposed model were compared with the change characteristics of the sEMG MPF. Estimation using the proposed model showed lower NRMS error and a more similar ΔMPF value than linear regression. This result implies that the proposed model is more suitable than linear regression to estimate the sEMG MPF.

Introduction

Muscle fatigue, which can be measured through blood lactate concentration or sEMG[1], is widely used in human movement studies, including sports. However, it's challenging to obtain by a general user because of an invasive measurement method and the high price of measurement equipment. Therefore, unlike the previous methods, we tried to estimate the sEMG MPF, which means muscle fatigue, based on kinetic changes, and to reproduce the characteristics of the change due to muscle fatigue of the data.

Methods

The sEMG MPF of the upper arm muscles was modeled based on the upper limb joints' mechanical work, which can be obtained with inverse dynamics. From the fact that fatigued muscles' muscle fatigue decreases exponentially[2], a model for estimating the sEMG MPF was proposed.

$$\text{Estimated MPF}(\%) = 100 - \sum_{i=1}^{n_c} (c_s W_{s,i} + c_e W_{e,i}) e^{a(i-n_c)}$$

The model's parameters were determined through a nonlinear optimization that minimizes the objective function, which is defined as the square of the difference between the sEMG MPF and the estimated value. Nine subjects were recruited, and each subject performed six trials. In a single trial, subjects performed a crawl for 25 minutes with a 5 minutes break in the middle. The experiment was conducted on a swim bench (Figure 1). sEMG of the five upper arm muscles was measured, and the upper arm's kinetic data were collected from cameras and a force sensor.

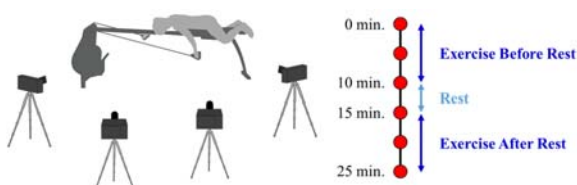


Figure 1: Experimental setup and protocol.

Results and Discussion

As a result of estimation through the proposed model, NRMS error of $20.48 \pm 8.45\%$ was shown for the measured sEMG MPF (Figure 2a, 2b). Two characteristics of change were observed: muscle fatigue progression speed (numerical differential) and the rise due to recovery (ΔMPF). Since the correlation between sEMG MPF and joint mechanical work was shown through linear regression in the previous study[3], the estimation was attempted through linear regression with the same number of parameters as the proposed model. The NRMS error of the numerical differential value was $23.82 \pm 109.73\%$ for linear regression estimation and $10.62 \pm 27.10\%$ for the estimate using the proposed model at the exercise after rest (Figure 2c). For each data, the difference between the data values at the start of exercise after rest and the end of exercise before rest was calculated (ΔMPF). ΔMPF of sEMG MPF was 13.26 ± 11.28 , the linear regression was 3.86 ± 11.85 , and the proposed model showed 8.60 ± 6.29 (Figure 2d). The proposed model reproduced ΔMPF value closer to the sEMG MPF.

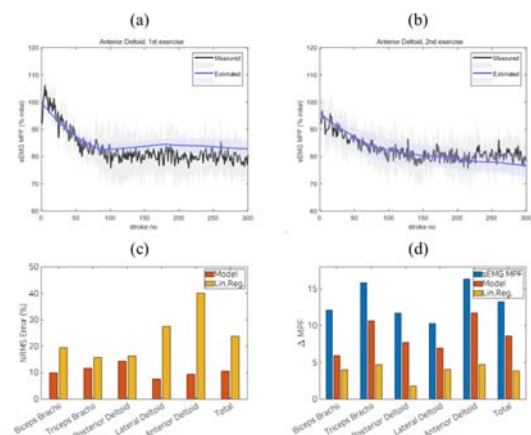


Figure 2 : (a) sEMG MPF and proposed model estimate result before rest and (b) after rest. (c) The numerical differential error of the proposed model and linear regression estimates. (d) ΔMPF of sEMG MPF, proposed model, and linear regression estimate.

Conclusions

As a result, the proposed model can estimate sEMG MPF with an error of about 20% and better reproduce sEMG MPF change characteristics than linear regression estimation.

References

- [1] Cifrek et al. (2009). *Clin Biomech*, **24**: 327-340.
- [2] Elfving et al. (2002). *Eur J Appl Physiol* **88**: 85-93.
- [3] Gonzalez-Izal et al. (2010). *J Electromyogr Kines*, **20**: 233-240.

Feedback-based running retraining for impact reduction: The relationship between peak tibial acceleration and step frequency

Pieter Van den Berghe^{1*}, Rud Derie^{1*}, Veerle Segers¹, Marc Leman², Dirk De Clercq¹

¹Dept. of Movement and Sports Sciences and ²IPEM, Ghent University, Ghent, Belgium

* Equal contribution, Email: pieter.vandenbergh@ugent.be, rud.derie@ugent.be

Summary

This study evaluated the feedback-induced effect of axial peak tibial acceleration (APTA) reduction on step frequency in two test centers. Ten runners with high APTA followed 3 weeks of gait retraining via auditory feedback on an athletic track at ~2.9 m/s. We developed a wearable system that stimulated a reduction in APTA of 30% via music-based biofeedback on the momentary APTA. Runners could freely explore biomechanical adaptations for lower impact running. Despite the substantial reduction in APTA observed in the athletic facility ($\Delta\bar{x}=-25.5\%$) and the laboratory ($\Delta\bar{x}=-26.9\%$), the relative changes in APTA and in step frequency were not linearly correlated. A retraining program based on auditory feedback can be completed outside the laboratory, with reproduction of lower impact running in the laboratory without the real-time feedback on APTA. Our data showed that altering step frequency was no generic motor strategy for APTA reduction in this sample of high impact runners.

Introduction

An increase in step frequency of 8.6% has decreased impact loading in high impact runners [1]. This impact loading was measured as the vertical loading rate of the ground reaction force, which correlates with the APTA during level over-ground running [2]. A strong negative linear relationship has been observed between the relative changes in step frequency and in APTA when varying the step frequency in running [3]. Hence, when stimulating a reduction in APTA with the use of biofeedback, we expected to observe a relationship between the relative changes in APTA and step frequency. The data were deliberately collected in two centers designed for over-ground running to improve confidence in the results.

Methods

Ten high impact runners (5M-5F, age: 32.1 ± 7.8 year, body height: 1.74 ± 0.11 m, mass: 71.5 ± 18.3 kg, running volume: 27 ± 10 km/week, APTA: 10.9 ± 2.8 g) completed a 3-week gait retraining program in an athletics facility. Six sessions of running at ~2.9 m/s were completed on an athletic track with real-time biofeedback aimed at reducing APTA by 30%. The wearable biofeedback system provided tempo-synchronized music that was superimposed with pink noise coupled to the momentary APTA. As main outcome of the gait retraining protocol, APTA was evaluated before the start and upon completion of the running program. An additional pre-post evaluation took place in a biomechanics laboratory. In this post-session, we asked the participants to replicate the running form in the absence of biofeedback. Step frequency was derived from the timing of consecutive APTAs. Changes were normalized to the absolute values obtained before the start of

the experiment [3]. Paired t-tests evaluated the changes in APTA. The Pearson correlation coefficient was calculated between the change in APTA and the change in step frequency for each of the test settings.

Results and Discussion

The APTA was substantially reduced in the athletic facility ($\Delta\bar{x} = -25.5\%$, $p = 0.008$, Cohen's $d = 1.08$). This decrease was not significantly different ($p = 0.798$, $d = -0.08$) from the relative decrease observed in the laboratory ($\Delta\bar{x} = -26.9\%$). Thus, following the retraining protocol, the group reproduced a form of lower impact running upon request in the absence of biofeedback in another setting. We observed substantial between-subjects variability in APTA reduction, but significant correlations between the changes in APTA and step frequency were absent both in the athletic facility (Figure 1) and in the laboratory ($p = 0.606$, $r = -0.186$). However, step frequency may still have influenced APTA on the individual level. A 3D gait analysis may improve insight into the mechanisms of APTA reduction during over-ground running.

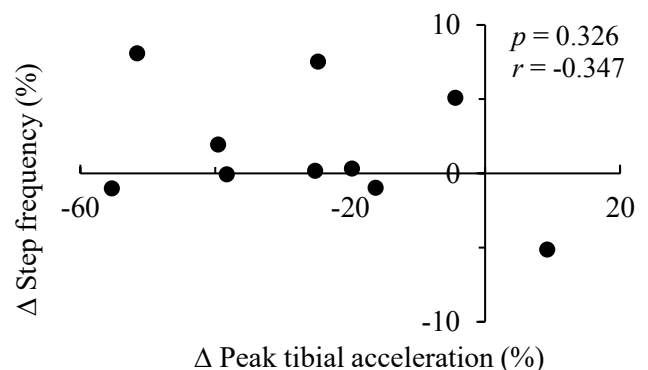


Figure 1: Relationship between individual mean changes (Δ) in APTA and step frequency during running on the athletic track.

Conclusions

The group of high impact runners successfully completed a biofeedback-driven retraining program outside the lab and could reproduce a form of lower impact running in another setting without the biofeedback. Altering step frequency was not the prominent strategy to reduce APTA in this cohort.

Acknowledgments

This study was supported by the FWO, the Industrial Research Fund (IOF) and the ISB's Matching Dissertation Grant 2019.

References

- [1] Willy R et al. (2016). *Scand J Med Sci Sports*, **26**:197–205
- [2] Clarke T et al. (1985). *J Sports Sci*, **3**:41–9.
- [3] Van den Berghe P et al. (2019). *J Biomech*, **86**: 238-242.

THE EFFECT OF CADENCES ON LOWER EXTREMITY BIOMECHANICS DURING STAIR ASCENT AND DESCENT

Qi Li, Ruixia Zhang, Shengnian Zhang

School of Kinesiology, Shanghai University of Sport, Shanghai, China

*corresponding author: E-mail: zhangsnx@163.com

INTRODUCTION

The U.S. Centers for Disease Control and Prevention (2007) states that more than half of all fall injuries are attributable to slope and stair walking [1]. The study found that the incidence of falls when stair ascent(77%) is more than three times that of stair descent(23%) [2]. However, the biomechanical mechanism of stair ascent(SA) and stair descent(SD) has not been clearly explained, and even joint moments at the lower extremity during SA and SD are still controversial.

METHODS

Thirteen healthy women were selected without lower limb injury (age:24±1.7 yrs, height:162.3±5.8m, body mass: 55.0±7.3kg), using an 8-camera VICON system (200 Hz) with 3 Kistler force plates (1000Hz) to synchronously collect the dynamics and kinematics data of the subjects ascending and descending stairs.

The staircase consists of five steps, each 17cm high. Three Kistler force plates are placed on the ground and the third and fourth steps. The subjects were asked to walk up and down stairs three times with low(70beats/min), optional(The normal cadence of each subject and is between high and low), and high(110beats/min) cadence, which is controlled by a metronome.

A Two-way ANOVA was used for statistical analysis of the experimental data, and the significance level α was set at 0.05 (21.0, SPSS Inc., USA).

RESULTS AND DISCUSSION

In both SA and SD, no significant differences were found in peak joint moments at the lower extremity during three cadences, the peak ankle moment is greater than that of the hip and knee at the low cadence, the peak knee moment is greater than that of the ankle and hip at the optional and high cadence. In SD, the ground reaction force at both high and optional cadence is greater than that at low cadence, and the difference is significant($p<0.05$).

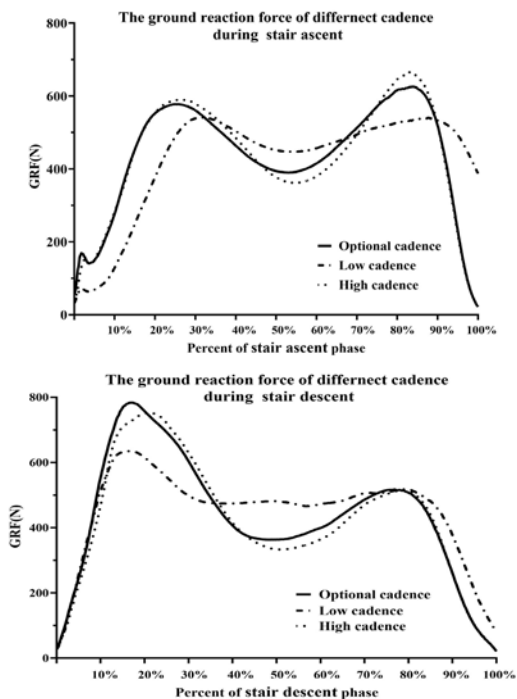


Figure 1: The ground reaction force of different cadence during stair ascent and descent phase

CONCLUSION

It is clear that SD is a process that more at risk of falling, the ground reaction force of SD under the three cadences is greater than that of SA. And a higher cadence may lead to a greater likelihood of falling. Future studies are needed to confirm the relationship between muscle co-activation and dynamics of SA and SD.

ACKNOWLEDGEMENTS

None.

REFERENCES

- [1] CDC. National Center For Injury, 2007.
- [2] STARTZELL J, OWENS D, LM, CAVANAGH P. Stair negotiation in older people: a review [J]. Journal of the American Geriatrics Society, 2000, 48(5): 567.

Table 1: The GRF and peak joint mement of lower limbs of different cadence during stair ascent and descent phase.

	SA-Low	SA-Optional	SA-High	SD-Low	SD-Optional	SD-High
peak GRF (N/kg)	10.76±2.61	12.01±2.68	12.51±2.55	12.73±3.00*	15.60±3.57*a	15.05±2.81*a
peak hip moment (Nm/kg)	0.75±0.20	0.86±0.23	0.85±0.22	0.72±0.24	0.96±0.35	0.87±0.28
peak knee moment (Nm/kg)	-1.37±0.40	-1.44±0.38	-1.45±0.38	1.37±0.40	1.44±0.38	1.45±0.38
peak ankle moment (Nm/kg)	1.5±0.23	1.31±0.24	1.4±0.28	1.21±0.36	1.28±0.25	1.34±0.35

Note: '*a' means there were significant differences between optional and high cadence and low cadence. In the index of peak joint moment, positive value represents extension moment and negative value represents flexion moment.

ANALYSIS OF FLAT SERVICE IN TENNIS

P.RAJINIKUMAR¹

¹Dept. of Exercise Physiology and Biomechanics, Tamil Nadu Physical Education and Sports University, Chennai, India. Email: rajinipkp88@gmail.com

Summary

The purpose of the study was to predict flat serve performance (speed and accuracy) based on the selected anthropometric, skill related fitness and biomechanical variables among elite tennis players. Thirty (N=30) male elite tennis players were selected at random and they were tested on their flat service performance (speed and accuracy) and the selected independent variables such as height, weight, arm length, leg length, grip strength, dynamic balance, co-ordination, arm power, leg power racket lowest point, and relative height of contact. Multiple regression statistical technique was used to predict the influence of selected independent variables on flat service performance Height, co-ordination, racket lowest point and relative height of contact were the predictors of flat serve performance in tennis.

Introduction

The serve has been the most important skill in professional players¹. The serve determines the success of a player, deciding the outcome of the match. The professional player's ability to produce high ball velocity to be the key elements of successful play, because it puts the opponent under stress and may hinder its return. In tennis, the serve is a sequence of motion referred to as a kinetic chain that begins with the lower limb action and followed by rotations of the trunk and the upper limb². In tennis, serve is one of the most important basic technique keys to success³. Tennis serve is the only closed skill a player has a full control on the trajectory path of the ball. But at the same time, it is difficult to master it involves the complex co-ordination of the lower and upper body segments. The purpose of the study was to predict flat serve performance (speed and accuracy) based on the selected anthropometric, skill related fitness and biomechanical variables among elite tennis players.

Methods

Thirty (N=30) male elite tennis players who had represented state and interuniversity competitions were selected from Chennai as the subjects of the study. They were selected at random from various tennis clubs, academies, colleges and universities from Chennai from a population of 70 male players. All the selected players were right hand players for the purpose of homogeneity. The age of the subjects ranged from 18 to 25 years. The independent variables such as

anthropometric variables namely height, weight, arm length and leg length and the skill related fitness variables namely, grip strength, dynamic balance, co-ordination, arm power and leg power were measured using standardized tests. The biomechanical variables such as ball release height, ball toss peak height, racket lowest point and relative height of contact were measured using max TRAQ 2D analysis software. Multiple regression statistical technique was used to predict the influence of selected independent variables on flat service performance. The Statistical Package for Social Sciences was used to analyze the data and alpha level of 0.05 was fixed to determine statistical significance.

Results and Discussion

Results showed that the multiple correlation co-efficient R=.983, which indicated that there was a high level of multiple correlation with flat service performance and nearly good predictor of dependent variable.

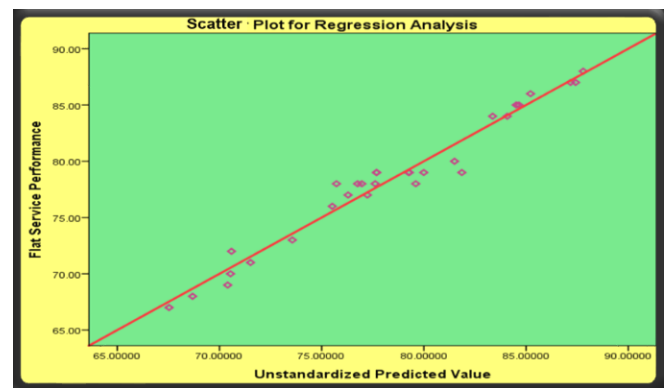


Figure 1: Scatterplot predicting flat service in tennis .

Conclusions

It was concluded that height (anthropometric variable), co-ordination (skill related fitness variables) and racket lowest point and relative height of contact (biomechanical variables) were the predictors of flat service performance (speed and accuracy) among elite men tennis players.

References

- [1] Johnson, C. D., McHugh, M. P., Wood, T., & Kibler, R. (2006). Performance demands of professional male tennis players. *British Journal of Sports Medicine*, **40**, 696-699.
- [2] Elliott, B., Fleisig, G., Nicholls, R. and Escamilla, R. (2003). Technique effects on upper limb loading in the tennis serve. *Journal of Science and Medicine in Sports*, **6**, 76-87.
- [3] Elliott, B. C. & Kilderry, R. (1983). *The Art of Science of Tennis*. Philadelphia, Saunders college Publishing.

Table 1: Results of Multiple regression analysis in prediction tennis flat service performance.

Model Summary				
Model	R	R Square	Adjusted R Square	Std. Error of the Estimate
1	.983 ^a	.966	.945	1.365

a. Predictors: (Constant), Racket Lowest Point, Dynamic balance, Co-ordination, Arm power, Relative height of Contact, Weight, Leg power, Grip strength, Leg length, Height, Arm length.

Kinematics Analysis of a Malaysian Female Elite Tenpin Bowler - A Case Study

Victoria Chin Quan Weoi², Yallini Selva¹, Viswanath Sundar¹

¹ Sports Biomechanics Centre, National Sports Institute of Malaysia, Kuala Lumpur, Malaysia

²Centre for Sport and Exercise Sciences, University Malaya, Kuala Lumpur, Malaysia

Email:viswabiomech@gmail.com

Summary

Tenpin bowling is a highly competitive sport that is popular in Malaysia. This study focuses on analysing the influence of lane oiling pattern on the kinematics of an individual bowler. Qualisys Track Manager and Visual 3D were used to identify and extract joint angles and angular velocities of the shoulder, elbow, wrist, hip, knee and ankle of three key variables (PH, FS & R). All investigated variables were analysed using the point biserial correlation. Several kinematic variables were identified to have a significant difference between bowling on short oil and long oil.

Introduction

Tenpin bowling is a popular sport with an estimation of more than 100 million players worldwide [1]. The technical skills of a tenpin bowling player are crucial in the delivery of a good throw. Previously, only two studies used 3D Motion Capture to analyse the kinematics of a bowler [2, 3]. However, none has investigated the influence of the oiling pattern on bowling lanes. The objective of this study is to investigate the influence of lane oiling pattern on the kinematics of a tenpin bowler.

Methods

One right-handed elite female Malaysian tenpin bowling athlete was recruited for this study (age 22, mass 55.15 kg, height 1.67m), the participant was briefed with the procedure and informed consent was obtained from all participants. A standard bowling ball (15lb) was used by the athlete. All data were collected in a sanctioned tenpin bowling alley. Eleven Oqus 7+ series infrared cameras (Qualisys AB 411 05, Goteborg, Sweden) at a frequency of 200Hz are used. Seventy-one, 12.5 mm reflective markers were attached to key body landmarks to create a 15-segment representation in Visual 3D v2020 (C-Motion Inc., Germantown, USA). Ten shots each from a total of 30 shots of short and long oil was chosen for further analysis. A 15-segment model in Visual

3D was used to calculate descriptive kinematic parameters. Key variables were calculated at three key instants; peak height (PH) (highest point of the backswing), foot slide (FS) (initial contact point of the foot to the lane during the last step), and release (R) (the point at which the bowling ball leaves the bowler's hand). Joint angles and angular velocities of the shoulder, elbow, wrist, hip, knee and ankle were identified. A point-Biserial correlation was conducted to analyse any relationship between oiling pattern and (kinematic) variables of the subject.

Results and Discussion

Point Biserial correlations results are displayed in (Table 1). Higher and lower shoulder abduction was found in short oil during peak height and release respectively. Higher right hip and knee angle during peak height was found in long oil patterns. During the foot slide, a higher left hip angle was found in short oil while a higher right wrist angle and velocity was found in a long oil pattern. Higher left dorsiflexion was also found in long oil during this phase.

Conclusions

This study has increased the understanding of kinematics between long and short oil patterns by highlighting the differences. Through this method, individualized technique identification could be provided to coaches for further improvisation.

Acknowledgments

This work was supported by the National Sports Institute of Malaysia.

References

- [1] Wiedman D. (2006). *Bowling: Steps to Success; Human Kinetics*
- [2] Klitgaard KK et al. (2017). *ISB, Abstract book: 271*
- [3] Rizal MR. (2013). *UM, Thesis*

Table 1: Point Biserial Correlation of investigated variables with oiling pattern.

Variables	Shoulder peak height angle Y	Right hip peak height angle	Right knee peak height angle	Wrist foot slide angle	Wrist foot slide angle velocity	Left hip foot slide angle	Left ankle foot slide angle	Shoulder release angle Y
Pearson correlation	-0.458*	-0.542*	0.634**	0.522*	0.802**	-0.454*	0.498*	0.668**
p-value	0.042	0.014	0.003	0.018	0.001	0.045	0.025	0.001

*Correlation is significant at the 0.05 level (2-tailed). **Correlation is significant at the 0.01 level (2-tailed).

Analysis of pacing strategy adopted by long-distance cross-country skiers

Xianshuang Yuan¹, Hui Liu²

¹Biomechanics Lab, School of Sport Science, Beijing Sport University, Beijing, China

²China Institute of Sport and Health Science, Beijing Sport University, Beijing, China

Email: y_x_s7508@163.com

Summary

This study analyzed the section speed and the velocity coefficients for 141 skiers in the 10-km (female, n=57) and 15-km (male, n=84) Chinese cross-country skiing races with the classic technique. Data were collected at 120Hz using six cameras. Every two cameras as a group placed at flat, uphill, and curve terrain were used for three-dimensional shooting. A two-way (distance and 3 levels of performance) repeated-measures ANOVA was conducted. Optimal pacing strategy during the race differs for males compared with females.

Introduction

Cross-country (XC) skiing is a complex endurance sport, in which an optimal pacing strategy is essential for desirable performance [1]. Studies on the pacing strategy of XC skiers are limited, especially for the Chinese skiers. The purpose of this study was to investigate the pacing strategy differences during long-distance XC skiing races in China related to the categories of performance level.

Methods

A total of 141 (57 females and 84 males) athletes finished the Chinese 10/15 km XC skiing races using the classic technique. The athletes were divided into 3 performance groups named L1, L2, and L3, in which L1 is the fastest, based on rankings. The time in each section of the race was measured using 6 synchronized 120Hz video cameras (FDR-AX700, Sony Inc., Tokyo, Japan). Every two cameras placed at flat, uphill, and curve terrain were used to capture the speeds for each athlete in each section. The main optical axis for the two cameras was about 90°. Velocity coefficient (%) was calculated as follows: velocity coefficient = 100% × (section velocity - mean velocity of the whole distance) / mean velocity of the whole distance. Two-way analysis of variance with repeated measures was used to examine the effects of performance level and distance (2*2) on the speed and velocity coefficient.

Results and Discussion

All the skiers adopted a positive pacing strategy, only the males in L1 used a reverse J-shaped pacing (Figure 1). This profile characteristics of males consisted with Bilodeau's report [2]. Significant effects of performance (p<0.001) and distance (p<0.001) on speed were observed for females. A moderate performance × distance interaction on speed was

observed, with speed difference between L1 and L3 ranging from 1.561 m/s (13850- 14458m) to 0.65 m/s (0 - 700m) and faster developing less decrease in speed during the whole course for males ($\eta^2 = 0.112, p = 0.023$). A large performance × distance interaction on the velocity variation of the whole course, with L1 presenting the smallest changes and the 0-700m section gained with the greatest variability, was shown for females ($\eta^2 = 0.383, p < 0.001$) and males ($\eta^2 = 0.154, p = 0.004$). This demonstrated that faster skiers had a more even pacing [3].

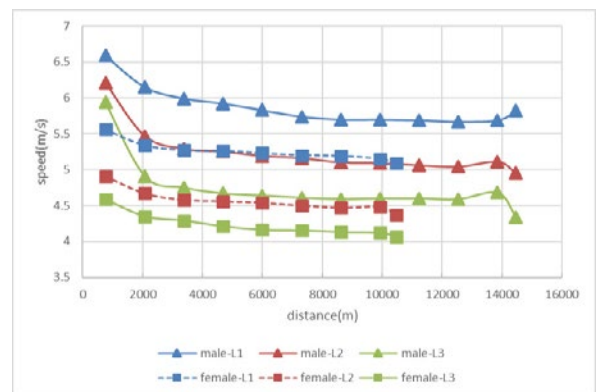


Figure 1: Speed profile of skiers across the race.

Conclusions

Faster skiers utilized a more even pacing. Furthermore, increasing speed in the final section was favorable for males. To optimize performance, it could be beneficial to increase their aerobic capacity through training.

Acknowledgments

This work was supported by the Performance-related Characteristics and Key Techniques of Scientific Talent Identification in Winner Sports under Grant No. 2018YFF0300404.

References

- [1] Stöggl T et al. (2018). *J Sport Health Sci*, 7: 381-393.
- [2] Bilodeau B et al. (1996). *Med Sci Sports Exerc*, 28: 128-138.
- [3] Nikolaidis PT et al. (2018). *J Sport Health Sci*, 7: 453-458.

Table 1: Mean velocity of each performance level skiers. Data are expressed as mean ± SD.

Sex	L1	L2	L3
Males	5.87 ± 0.07 m/s	5.23 ± 0.04 m/s	4.74 ± 0.05 m/s
Females	5.25 ± 0.12 m/s	4.56 ± 0.02 m/s	4.23 ± 0.04 m/s

Biomechanics of fast bowling in men's cricket using wearable sensors

Zia ul Rehman Tahir^{1,2}, Partha Mandal², Asad Kashif¹, Waqas Ahmad¹, Muhammad Tayyab Khan¹, Ammar Waheed¹, Abdul Samad¹, Amir Hussain¹, Muhammad Rizwan Yasin¹, Usama Murtaza¹, Usman Saleem¹, Muhammad Abdullah Arif¹

¹Department of Mechanical Engineering, University of Engineering and Technology Lahore, Pakistan

²School of Mechanical, Aerospace and Civil Engineering, The University of Manchester, United Kingdom

Email: ziartahir@uet.edu.pk

Summary

The recent developments in sports biomechanics have enabled the use of various motion capture systems to study the biomechanics of cricket. Fast bowling is known to be deceitful towards the batsman to reduce his delivery response time and effectiveness. Kinematics factors such as run-up speed, pre-delivery stride length, delivery stride length, lean back angle, and angular velocities of arm have been studied over the last two decades to correlate with ball release speed. The aim of this study is to correlate kinematic factors with ball release speed using an Inertial Measurement Unit (IMU) sensor-based motion capture system.

Introduction

Cricket has been the epicenter of sports for several decades now. The increasing global audience has attracted researchers to study and improve bowling techniques. One of the most crucial variables involved in fast bowling is the speed at which the ball is delivered [1]. Numerous human body kinematic factors have been studied to improve ball delivery. These include stride lengths, run-up speed, flexion angles, and angular velocity of each segment of body arm during delivery stride. Motion capture systems using marker-based optical systems have been implemented to study the significance of these factors, but no deterministic result has been concluded yet as to which kinematic factor contributes more to the ball delivery speed. These systems are commonly used in indoor environments but have limitations to use in outdoor environments. The sensor-based systems have the potential to be used in outdoor and even in-game situations.

Methods

Two male fast bowlers (semi-professional cricketers) volunteered for this study. Subject 1, aged 24 was a right-hand front-on fast bowler with an average ball speed of 65.3 ± 2.3 mph. Subject 2, aged 28 years old was a left-handed side-on fast bowler with an average ball speed of 64.47 ± 2.6 mph. The human body kinematic was measured by sensors-based motion capture systems using 17 IMUs developed by XSENS. This system is capable of measuring position, velocity, and acceleration (both translational and rotational) of 23 body segments. The ball release speed was measured using *K-Band*

Handheld Doppler Speed Radar with an accuracy of ± 1 mph. 30 delivery trials were recorded for each subject. Three kinematic parameters (run-up speed, pre-delivery stride length, delivery stride length) were calculated from the sensor data. These factors were calculated for both subjects and related with ball release speed to find correlation coefficient (*R*).

Results and Discussion

The mean values of kinematic parameters and the r-value of these parameters with ball release speed for both subjects are presented in Table 1. The correlation between run-up speed and ball release speed for both subjects is shown in Figure 1. Ball released speed showed significant dependency on the run-up speed, whereas, pre-delivery stride lengths showed negligible dependency for both subjects and delivery stride length yielded a slightly negative correlation coefficient.

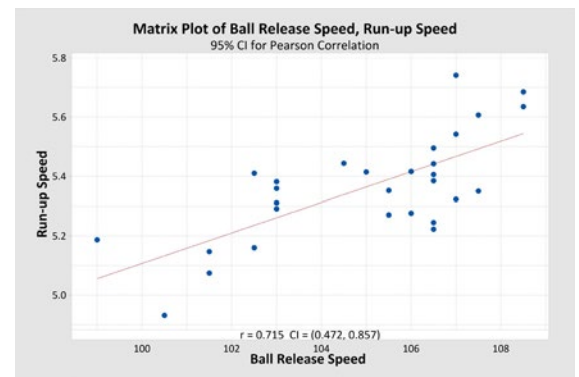


Figure 1: Correlation of run-up speed and ball delivery speed

Conclusions

This is a comprehensive biomechanics study of fast bowling using wearable sensors. The effects of kinematic parameters on ball release speed were investigated and it was found run-up speed is directly related to ball release speed, this is in accordance with previously published results using optical systems of motion capture. This study will help to investigate the biomechanics of bowling in outdoor environments.

References

[1] R.M. Bartlett et al. (1996). *Journal of Sports Sciences*.

Table 1: Statistical analysis including mean and correlation coefficients of both subjects.

Subjects	Mean Values			Correlation Coefficients (R)		
	Run-up Speed (km/h)	Pre-delivery stride length (m)	Delivery stride length (m)	Run-up Speed	Pre-delivery stride length	Delivery stride length
Subject 1	19.24	1.401	1.103	0.715	0.144	-0.181
Subject 2	20.96	1.591	1.788	0.356	0.105	-0.063

Combinations of release parameters for accurate baseball pitching

Ayane Kusafuka¹, Kazutoshi Kudo¹, Kimitaka Nkazawa¹

¹ Department of Life Science, Graduate School of Arts and Sciences, The University of Tokyo, Tokyo, Japan

Email: ayane422@g.ecc.u-tokyo.ac.jp

Summary

This study revealed that combinations of release parameters which determine the pitch location of baseball pitching. We focused on two strategies to improve the accuracy of the pitch locations, thereby increasing the reproducibility of individual parameters and coordinating covariation among parameters. To examine whether coordinated covariation is used by skilled pitchers, for hypothetical combinations of release parameters, in which the coordinated covariation was eliminated, the variability of the pitch location was simulated and compared to the measured pitch location. The results showed that there was little coordinated covariation for all release parameters and that the variability of the pitch locations was decreased by improving the reproducibility of the release angle.

Introduction

In various motor skills in sports, such as throwing, kicking, and hitting, accurately controlling a ball to a target position is one of the most important skills. The flight trajectory and final arrival position of the ball are physically determined by its state at the time of release or impact approximately. In baseball pitching, pitch location is determined by the combination of nine release parameters. If the state at the time of release is always the same, the ball will always arrive at the same position. However, it is known that there is always variability in each release parameter, even for skilled players. Therefore, the purpose of this study was to investigate the combinations of release parameters in pitching of skilled player to quantify the relationship between parameters which has an effect to improve accuracy of pitch location i.e., coordinated covariation.

Methods

The release parameters were obtained using TrackMan Baseball while eight skilled baseball pitchers to a target. Using a model to predict the pitch location from the release parameters [1] and the data randomization method [2,3], we simulated the variability of the vertical and horizontal pitch location when changing the relationship between the parameter i.e., one parameter varied individually. If the variability of the simulated pitch locations was larger than that of the measured ones, this was interpreted as an effect of a reduction in the variability of the pitch location the release parameters had (coordinated covariation). In the case where there was no or little coordinated covariation, increasing the reproducibility of individual release parameters was interpreted as effective. We defined the ratio of the variability of simulated pitch locations to the actual

ones as the index of covariation (IC) and a one-sample t-test was used to determine if the IC was greater than 1.

Results and Discussion

Significantly large ICs were not observed for all release parameters of all pitchers in either the vertical or horizontal pitch location ($M = 1.06$, 95% CI [0.97, 1.15], $t(7) = 1.50$, $p = 0.18$ in vertical; $M = 1.03$, 95% CI [0.91, 1.14], $t(7) = 0.66$, $p = 0.53$ in horizontal; Fig. 1 shows the result in vertical). This suggests that varying the relationships between release parameters does not significantly affect the variability in the pitch location (i.e., there is little coordinated covariation).

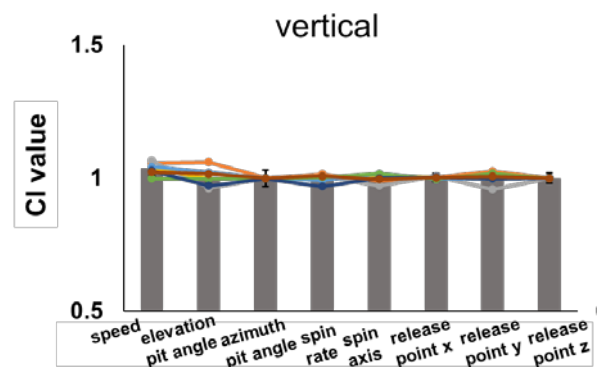


Figure 1: ICs for each release parameter in vertical pitch location.

The reason can be inferred by considering the effect of the variability of each release parameter on the pitch location. A previous study [3] found that the elevation pitching angle and the azimuth pitching angle have much larger effects on the vertical pitch location and horizontal pitch location, respectively, than other release parameters. In such a case, it is expected that compensating for the variability of the release angle by other parameters is difficult.

Conclusions

There was little coordinated covariation among all the release parameters of all pitchers in both the vertical and horizontal pitch locations. The variability of the pitch location can be decreased by improving the reproducibility of the release angle, rather than using a coordinated covariation relationship with other release parameters.

References

- [1] Ayane KUSAFUKA et al. (2020). *Frontiers in Sports and Active Living*, **2**: 36.
- [2] Kazutoshi KUDO et al. (2000) *Journal of Motor Behavior*, **32**: 337-345
- [3] Hermann MÜLLER and Dagmar STERNAD (2003). *Biological Cybernetics*, **89**: 22-23.

The applied analysis of kayaking ergometer with different drag resistance in kayak training: a plot study

Jiixiang Yan^{1,2}, Zhiqiang Liang³, Jianshe Li^{1,2}

¹ Faculty of Sports Science, Ningbo University, Ningbo, China

² Research Academy of Grand Health, Ningbo University, Ningbo, China

³ BMC Laboratory, School of Kinesiology, Shanghai University of Sport, China

Email: jiixiang0016@163.com

Summary

The purpose of this study was to evaluate the effect of two different kayaking ergometers (wind resistance, KWR; electronic resistance, KER) on training. Six elite male kayakers executed three trainings of 200m, 500m and 1000m on-water (TW) and two kayak ergometers. The significance testing was used to analyze the difference between KWR and KER on TW, the coefficient of variation (CV) was used to analyze the working stability of the two ergometers. The results showed that no significant difference was found between the TW and the two ergometers performance on 200m. In 500m and 1000m, the two kayak ergometers showed poorer sport performance than the TW. In addition, the results also show that both kayak ergometers have good stability. Therefore, KWR and KER can be used by athletes as a training device. But an athlete's TW performance could not be predicted by KWR and KER.

Introduction

Most kayakers rely on ergometers for training, especially in winter seasons [1,2]. The KWR calculate power via a mathematical relationship with the angular velocity of the flywheel. About KER, on the other hand, does not use the same approach [3]. Therefore, the purpose of this study was to analyze the kayaking ergometer with different drag resistance in kayak training.

Methods

Six elite male kayakers volunteered to participate in the study (age: 17±1 years; Height: 182±4.45cm; Weight: 75.5±5.47kg; Training years: 4.67±0.47 years).

The test was conducted on six separate days, it was performed on TW and two kayak ergometers respectively, in randomised order. Three different distances of 200m, 500m and 1000m were tested. Before the each test, the athletes had a 15-minute warm-up followed by a 2-minute rest. Participants were asked to perform at the highest level throughout the test on TW and on two ergometers.

The participants' performance on TW was collected by the testers, and the measured data on the display of the ergometers was downloaded. Shapiro-Wilk's Test was used to test the normal distribution of the data. Since the data were normally distributed, the independent samples T-test was used to test the significance of the TW and two ergometers performance. CV was used to analyze the stability of KWR and KER in test. Data were analyzed using SPSS 19.0 statistical software, and the significance level was set at $P < 0.05$.

Results and Discussion

In the 200m race, the difference between the two kayak ergometers and the TW performance was not found ($P > 0.05$) (Table 1). In 500m and 1000m sports, the two kayak ergometers showed slower athletic performance than TW ($P < 0.05$). Kayakers increase thoracolumbar extension and wider lateral bending range of motion during on water kayaking [4], over a long period of kayaking, these differences are magnified. The CV has good consistency when less than 10% [5]. Two kayak ergometers possess a stable CV (2.77 - 9.8 %) (Table 2).

Conclusions

These findings show that both kinds of kayak ergometers have good stability in operation. They can be used by athletes as a kind of land training device. But, an athlete's TW performance could not be predicted by KWR and KER.

References

- [1] Fleming N et al. (2012). *Journal of sports science & medicine*, 3: 430-437.
- [2] Fleming N et al. (2012). *Journal of sports science & medicine*, 1: 16-25.
- [3] Borges T O et al. (2017). *Int J Sports Physiol Perform*, 1-12.
- [4] Klitgaard K K, et al. (2020). *European Journal of Sport Science*, 21-25.
- [5] Jaqueline Alves Araújo et al. (2020). *International Journal of Sports Medicine*.

Table 1: Significance testing value of TW and two kayak ergometers performance.

ergometer	200m	500m	1000m
WKR	0.631	0.018	0
WER	0.888	0.007	0

Table 2: Typical Error of the Estimate as a Coefficient of Variation.

ergometer	200m	500m	1000m	Time	Pace	Speed	Watts	Consume
WKR	3.74%	6.58%	2.98%	2.77%	3%	2.77%	7.9%	5.73%
WER	3.26%	9.8%	4.6%	5%	3.87%	4.6%	7.57%	8.4%

GAIT VELOCITY INFLUENCE DYNAMIC GAIT STABILITY IN A DUAL-TASK PARADIGM

Jingwen Wang¹, Li Li², Wei Sun¹, Qipeng Song¹

¹College of Sports and Health, Shandong Sport University, Jinan, China

²Department of Health Sciences and Kinesiology, Georgia Southern University, Statesboro, 30460, USA

Corresponding author: Dr. Qipeng Song, songqipeng@sdpei.edu.cn

Summary

The effects of a concurrent cognitive or manual dual-task paradigm and gait velocity on dynamic gait stability (DGS) remain unclear. A total of 16 healthy young females descended a staircase under three different walking conditions: descend stairs only (single task), descend stairs while performing subtraction (cognitive dual-task), and descend stairs while carrying a glass of water (manual dual-task). An eight-camera Vicon motion analysis system and a Kistler force plate embedded into the third step of the staircase were used synchronously to collect kinematic and kinetic data. Gait velocity decreased and DGS increased with both cognitive and manual dual-task conditions. The center of mass–center of pressure inclination angle (IA) increased with gait velocity but decreased with the manual dual-task condition.

Introduction

Stair descent imposes significant challenges to dynamic gait stability (DGS) in people of all ages [1]. A dual-task involves performing a physical task while performing a concurrent cognitive (CT) or manual (MT) task. Previous studies revealed different dual-task effects on DGS. A possible explanation for the inconsistent results is the different variables used to measure DGS, including center of mass (COM) displacement, center of pressure (COP) displacement, COM–COP separation. IA formed by the vertical line and the projection of the vector onto the sagittal and frontal planes, was proposed to provide a more comprehensive assessment than the examination of COM or COP [2]. The greater the IA, the further the COM diverges from the COP, a fall can occur [3]. Changes in gait velocity caused by a dual-task paradigm may be another reason for DGS differences. The purpose of this study was to examine the relationship between velocity and a dual-task performance on DGS during stair descent. And address the importance of gait velocity in assessing the effects of a dual-task. We hypothesized that velocity would decrease under dual-task conditions. A concurrent dual-task condition would adversely affect DGS during stair descent, DGS would decrease with increasing gait velocity under a dual-task.

Methods

A total of 16 healthy young females participated in this study. All kinetic and kinematic data were obtained from a right foot single-support phase. The participants were instructed to descend the staircase step-over-step under three conditions: 1) single task; 2) cognitive dual-task; and 3) manual dual-task. Gait velocity and IA normality were tested using the Shapiro–Wilk test. One-way repeated-measures ANOVAs were employed to examine the first and second hypotheses. Multiple regression analysis was

used to predict the independent variables of IA (y) based on the dependent variable of velocity (x) during ST, CT, and MT conditions.

Results and Discussion

First, peak gait velocity decreased under CT or MT conditions and Peak velocity was also lower in MT than in CT. (CT velocity = 0.79 ± 0.09 ; MT velocity = 0.68 ± 0.08 ; ST velocity = 0.91 ± 0.11 m/s; Figure 1); Second, the peak IA_{AP} was less under the CT and MT dual-task conditions (CT_{AP} = $8.29 \pm 0.82^\circ$, $p = 0.019$; MT_{AP} = $7.16 \pm 0.89^\circ$, $p < 0.001$) than under the ST (ST_{AP} = $9.05 \pm 0.79^\circ$) and the peak IA_{ML} during MT (MT_{ML} = $5.95 \pm 1.02^\circ$, $p = 0.020$) was less than that during ST (ST_{ML} = $6.49 \pm 0.53^\circ$), our results failed to support our second hypothesis in both the anterior/posterior and medial/lateral directions, the decreased IA indicates improved DGS under CT or MT conditions during stair descent; Third, IA was positively related to gait velocity and negatively related to a concurrent MT (By regression equation $y = 4.976 + 4.365x - 0.768B$ and $y = 4.115 + 2.712x$ indicates the faster the peak velocity, the greater the IA_{AP} and IA_{ML}).

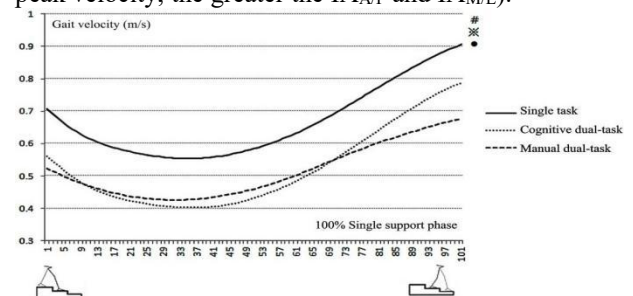


Figure 1: Descending velocity (y) of the single-support phase (x) during single-task and cognitive and manual dual-task conditions.

Conclusions

Gait velocity decreased under CT and MT. DGS decreased with increasing gait velocity during stair descent. Finally, the influence of gait velocity should be considered when assessing the effects of dual-tasks.

Acknowledgments

This work was funded by the Introduction and cultivation plan of young innovative talents of Shandong Provincial Department of Education (2019-183)

References

- [1] Hashish R et al. (2017). *Gait Posture*, **58**:409–414.
- [2] Hsue BJ et al. (2009). *Gait Posture*, **29**:465–470.
- [3] Reeves ND et al. (2008). *Gait Posture*, **28**:327–336.

THE EFFECT OF DIFFERENT ILLUMINATION LEVELS AND TAI CHI EXERCISE ON THE POSTURAL STABILITY OF THE ELDERLY DURING STAIR ASCENT

Qi Wang¹, Cui Zhang², Li Li³, Qipeng song¹

¹College of Sports and Health, Shandong Sport University, Jinan, China

²Lab of Biomechanics, Shandong Institute of Sport Science, Jinan, 250102, China

³Department of Health Sciences and Kinesiology, Georgia Southern University, Statesboro, 30460, USA

Corresponding author: Dr. Qipeng Song, songqipeng@sdpei.edu.cn

Summary

The effects of long-term Tai Chi exercise on postural stability of the elderly during stair ascent under high and low illumination were investigated. Forty-five healthy elderly women were divided into Tai Chi exercise (TC), brisk walking (BW) and no-exercise control (CON) groups. We use force platforms and a motion capture system to collect data. Under the high illumination, TC exhibited a greater loading rate and anteroposterior center of pressure (COP_{ap}) displacement and a lower braking impulse than CON. Under the low illumination, TC demonstrated greater COP_{ap} and mediolateral center of pressure (COP_{ml}) displacements and lower braking and lateral impulses compared with CON. The center of mass (COM_{ml}) sway in TC and CON were greater than BW. Therefore, low light increases the risk of falling, and Tai Chi practice can improve stability under this condition.

Introduction

The stability of the elderly is challenged during stair descent and ascent. Tai Chi is believed to improve the postural stability of the elderly. However, the veracity of whether low illumination could adversely affect the postural stability of the elderly remains unclear. If it does, then we should recommend what exercise to reduce the risk of it. Therefore, this study was performed to investigate the effects of Tai Chi exercise on postural stability of the elderly during stair ascent under high and low illumination. We hypothesize that Tai Chi practitioners can increase the postural stability of the elderly during stair ascent under low illumination.

Methods

Forty-five healthy elderly women were divided into Tai Chi exercise (TC), brisk walking (BW) and no-exercise control (CON) groups. We built a six-stage staircase and embedded force platforms in the third and fourth steps to collect ground reaction forces. The lux meter was placed 15-cm above the ground. In each session, the participant was asked to ascend the simulated staircase under high (300-lux) and low (3 lux) illumination levels [1]. The participants walk for 400-m at a self-selected pace as a level walking test before the stair ascent test, and took a one-minute rest between each test. In the experiment, we also used an eight-camera motion analysis system and 39 spherical markers. Descriptive analysis was conducted using the mean and standard deviations for both kinematic and kinetic variables.

Group and condition differences were examined using a mixed model two-factor ANOVA. Significance level set at 0.05.

Results and Discussion

Under the high illumination, the loading rate of BW and the COP_{ml} of TC were greater than those of CON (walking group, $W_{high}=4.92\text{BW/s}$, no-exercise group, $N_{high}=3.96\text{BW/s}$, 95%CI of the mean difference [CI_{95%}]:0.17/1.75; Tai Chi group, $T_{high}=0.032\text{m}$, $N_{high}=0.024\text{m}$, CI_{95%}:0.001/0.015). Under low illumination, TC demonstrated higher foot clearance, COP_{ap} and COP_{ml} displacements ($T_{low}=0.051\text{m}$, $N_{low}=0.040\text{m}$, CI_{95%}:0.003/0.018; $T_{low}=0.139\text{m}$, $N_{low}=0.117\text{m}$, CI_{95%}:0.002/0.044; $T_{low}=0.033\text{m}$, $N_{low}=0.024\text{m}$, CI_{95%}:0.001/0.016) and lower braking and lateral impulses than the CON ($T_{low}=10.88\text{BW/s}$, $N_{low}=14.56\text{BW/s}$, CI_{95%}:-6.63/-0.71; $T_{low}=2.32\text{BW/s}$, $N_{low}=3.76\text{BW/s}$, CI_{95%}:-2.87/-0.01). The lateral impulse in CON was greater under low illumination than under high illumination ($N_{high}=2.56\text{BW/s}$, $N_{low}=3.76\text{BW/s}$, CI_{95%}:-2.28/-0.22). Compared with the low illumination, the COP_{ap}, foot clearance, and head inclination angle of TC under the high illumination were lower ($T_{high}=0.121\text{m}$, $T_{low}=0.139\text{m}$, CI_{95%}:-0.029/-0.008; $T_{high}=0.043\text{m}$, $T_{low}=0.051\text{m}$, CI_{95%}:-0.014/0.002; $T_{high}=10.54^\circ$, $T_{low}=16.26^\circ$, CI_{95%}:-9.41/-2.04), and the trunk inclination angle and COM_{ml} of BW and CON under the high illumination were lower ($W_{high}=14.35^\circ$, $W_{low}=17.07^\circ$, CI_{95%}:-5.12/-0.30; $N_{high}=14.96^\circ$, $N_{low}=18.03^\circ$, CI_{95%}:-4.26/-0.33).

Conclusions

Low illumination increases the risk of falling. Tai Chi practitioners adopted appropriate strategies to maintain postural stability during stair ascent under low illumination.

Acknowledgments

This work was funded by the Introduction and cultivation plan of young innovative talents of Shandong Provincial Department of Education (2019-183)

References

- [1] Christina, K. A., & Cavanagh, P. R. (2002). *Gait & Posture*, **15**: 153–158.

Optimization of the whole-body motion to minimize the muscle-tendon length of biceps femoris long head during the late swing phase of high-speed running

Terumitsu Miyazaki¹, Norihisa Fujii²

¹Doctoral Program in Physical Education, Health and Sport Sciences, University of Tsukuba, Tsukuba, Japan

²Faculty of Health and Sport Sciences, University of Tsukuba, Tsukuba, Japan

Email: s1930497@s.tsukuba.ac.jp

Summary

Strain injuries in the biceps femoris long head (BFH) frequently occur during high-speed running. Stretching the muscle-tendon complex while generating muscle force is considered as one of the factors for strain injuries. To establish the optimal running motion that controls muscle-tendon dynamics, we aimed to optimize the whole-body motion by minimizing the muscle-tendon length of BFH using an angle-driven simulation during high-speed running. The results showed that the hip and knee flexion/extension angles were more sensitive joint angles than the other lower limb joint angles for minimizing the BFH length. The hip abduction/adduction and pelvic axial rotation angles also affected the BFH length. That optimization results were implicated an optimal running motion that reducing the risk of strain injuries in BFH.

Introduction

Strain injuries in BFH often occur during the late swing phase of high-speed running [1]. The late swing phase is defined from the timing of maximum knee flexion to the foot strike. BFH generates greater force while lengthening in this phase [2]. We aimed to optimize the whole-body motion using an angle-driven simulation that minimizes the BFH length during the late swing phase of high-speed running.

Methods

Fourteen male soccer players (mean age 20.2 years, body weight 67.4± kg, and height 173.6± cm) participated in this study. The participants completed the 50-m sprinting trials with their maximum effort in an outdoor track. The three-dimensional trajectories of markers that were attached to the whole-body were obtained using a motion-analysis system with three force platforms. An inverse kinematics algorithm was conducted after a filtering process to the trajectories [3].

To optimize the whole-body motion, an angle-driven simulation at each time step was conducted by minimizing the objective functions ($J(q)$) during the late swing phase. Residual forces and moments, which represent inconsistencies between the model's dynamics and experimental ground reaction forces, were not removed in this optimization. The objective function was the sum of two components: (1) the weighted (w) squared error between the experimental (q^{exp}) and simulated (q^{sim}) joint angles for each DoF (n_q) of the model. (2) the squared muscle-tendon length ratio of simulated (L^{sim}) to the experimental (L^{exp}) lengths.

$$J(q) = w \cdot \sum_{i=1}^{n_q} (q_i^{exp} - q_i^{sim})^2 + \{L_{bfh}^{sim}(q^{sim})/L_{bfh}^{exp}\}^2$$

The weighting factor (w) was perturbed from 1 to 10, to clarify the influences of the weighting factor on the results. The root means square errors (RMSE) for each joint and segment angle at each weighting factor were calculated before and after the optimizations.

Results and Discussion

As the weighting factor increased, the mean of RMSE values for the knee and hip joint angles tended to decrease, and the mean values of the ratio of simulated to experimental length (L^{sim}/L^{exp}) tended to increase (Fig. 1). When the weighting factor was 1, the mean and one standard deviation of RMSEs for the knee flexion/extension, hip flexion/extension, abduction/adduction, and external/internal rotation angles were 31.7 ± 2.8 [deg], 24.6 ± 4.6 [deg], 11.6 ± 5.5 [deg], and 3.3 ± 1.8 [deg], respectively (Fig. 1). The RMSEs for pelvic tilt, obliquity, and axial rotation angles were 0.3 ± 0.2 [deg], 1.2 ± 0.7 [deg], 23.6 ± 9.1 [deg], respectively. The results showed that the hip and knee flexion/extension angles were more sensitive factors for minimizing the BFH length than the other lower limb joint angles. The hip abduction/adduction and pelvic axial rotation angles also affected the BFH length. These results suggested that not only the hip and knee flexion/extension angles but also the hip abduction/adduction and pelvic axial rotation angles related to minimizing the BFH length.

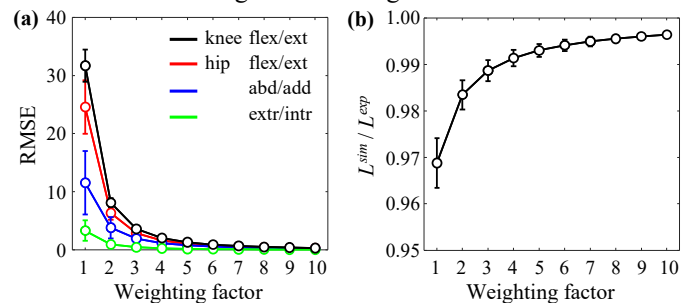


Figure 1: (a) The RMSEs for the hip and knee joint angles, and (b) the length ratio (L^{sim}/L^{exp}) at each weighting factor.

Conclusions

This study clarified the optimal running motions that minimize the BFH length during high-speed running. The results showed that the hip and knee flexion/extension, the hip abduction/adduction, and pelvic axial rotation angles affected minimizing the BFH length.

References

- [1] Woods C et al. (2004). Br J Sports Med, **38**: 36-41.
- [2] Chumanov ES et al. (2007). J Biomech, **40**: 3553-3562.
- [3] Lu TW et al. (1999). J Biomech, **32**: 129-134.

Does the canoe-kayak ergometer with the electromechanical drag force have a good performance during training?

Weilan He¹, Zhiqiang Liang², Guanliang Meng¹, Jianshe Li³, Yichen Lu⁴

¹ Administration Center of Zhejiang Water, Hangzhou, China

² School of kinesiology, Shanghai University of Sport, Shanghai China

³ Research Academy of Grand Health, Ningbo University, Ningbo, China

⁴ Zhejiang Pharmaceutical College, Ningbo, China

Email: irenehwl@163.com

Summary

CKE exhibited high stability coefficients in short, medium and long distances. The operation of the training equipment conformed to the actual application standards and can be used as a CK training equipment. With the increase of the test distance, CKE on-land specific physical training equipment runs better, and it can be used as a better choice for evaluating or testing the long-distance sports performance or aerobic capacity of kayak athletes.

Introduction

The real modern-style Canoe & kayak (CK) ergometer with wind resistance (CKR) appeared in 1988 after one-decade revolution [1]. Nowadays, ergometer has been an essential part of strength training facilities and specific stimulation equipment for CK training, aiming to improve the power output of athletes [2].

However, both of them are 'non-isokinetic' ergometers that is the biggest difference compared with water training. This design limitations of the CK ergometer at present likely limit the deep understanding on CK's characteristics. CK ergometer with electromechanical drag resistance (CKE) realizes isokinetic pattern based on the control from microcomputer. As so far no relevant study confirm effect of this ergometer; in order to test its effect on the training, we operated test on this device.

Methods

33 mixed-sexual canoe & kayak national team athletes participated this test (Figure 1). All participants had been fully informed about the whole test procedure. Before test, 5-10 mins were given athletes for warm-up and device preparation. After athletes had to finish 200m, 500m and 1000m training on the all ergometers. There was a 20-min break between the tests on two different ergometers in order to operate comparable experiment.

Data were collected by the electronic display station. Parameters including time (T), 500 split (500 S), stroke rate (SR), velocity (V), power (P) and calories (C) were used for analysis. Coefficient of variation (CV) and intraclass correlation coefficient (ICC), Pearson correlation test and T-test were used to analyze canoe-kayak equipment performance on the training.

Results and Discussion

Both CKE had a good running performance in longer distance (CV<0.15); CKE of kayak had a poorly correlated relationship with water performance. CKE of canoe had a poor performance at short distance training but had a good performance at long training distance (CV<0.15). CKE of canoe in 1000m had a highly correlated relationship with water performance ($r=0.73$). The significant differences of CKE were found in T and P.

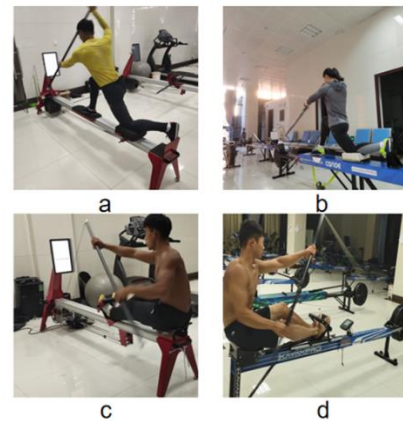


Figure 1: The test equipment in this experiment (a: CKE ergometer of canoe, b: CKR ergometer of canoe, c: CKE ergometer of kayak, d: CKR ergometer of kayak)

Conclusions

CKE had a good performance with the increase of training distance, which indicated that CKE would be used as a good equipment in longer distance training and test. However, short-distance event like 200m event was a difficult point of canoe-kayak technology research and development.

Acknowledgments

The authors would like to thank all rowers who took part in this study and for their efforts. And there is no conflict between authors.

References

- [1] LARSSON B et al (1988). A new kayak ergometer based on wind resistance. *Ergonomics*, **31**(11): 1701-1707..
- [2] TAMURA M et al (2016). Effects on the 50-meter full-power rowing of high school canoe kayak paddlers of exercises pulling with one hand with leg extension. *Research Journal of Sports Performance*, **8**.

THE BIOMECHANICAL CHARACTERISTICS AND RULES COULD IMPROVE INJURY RISKS DURING RACE WALKING

Xiaohui Duan¹, Li Li², Qipeng Song¹

¹Shandong Sport University, Jinan, 250102, China

²Department of Health Sciences and Kinesiology, Georgia Southern University, Statesboro, 30460, USA

Corresponding author: Dr. Qipeng Song, songqipeng@sdpei.edu.cn

Summary

The purpose of this study is to describe the biomechanical characteristics during race walking and identify whether the race walking rules could cause potential injury risks. Fourteen elite race walkers participated in this study. Rs-scan plantar pressure plate and three digital cameras were used to collect data during race walking and normal walking. Paired t-tests were used to detect differences. The results showed that during race walking, the peak pressure of lateral heel (HI) and medial heel (HM), The displacements of center of pressure (COP), ankle dorsiflexion, plantarflexion, knee extension, hip adduction, foot eversion, ankle angular velocity and average horizontal velocity were significantly larger than those during normal walking. The greater heel peak pressure and more ankle eversion may be the injury risks caused by the race walking rules.

Introduction

In recent years, race walking has grown in popularity, and the events of 5 and 10 km are becoming increasingly popular for casual athletes [1]. Few researches have examined peak pressure, COP and temporal parameters, such as total contact time and time to peak pressure, for race walkers, compared with the large numbers of researcher investigating the normal kinematics and kinetics of normal human walking and running [2]. As such, there is limited understanding of the kinematic and kinetic aspects of race walking.

Methods

Subjects: Fourteen elite race walkers (9 male, 5 female; age, 20.4±3.3 years [Mean (SD)]; height, 173.1±7.8 cm; body mass 59.8±9.6 kg) were recruited. Subjects had no history of lower limb pathology at the time of the study or in the preceding six months. All of them have given informed consent. Setting: The plantar pressure plate (Rs-scan International, 2m×0.4m×0.02m,) was used to collect plantar data. Two rubcor tracks (5m×0.4m×0.02m) were connected

the two sides of the plantar pressure plate to prevent the subjects from adjusting their walking style by aiming for the plate. Three 50 Hz digital cameras (Sony 9800, Japan) were placed approximately 5m away from the right, left front and right front of pressure plate edge, they were used to record the movement of the lower limb. Protocol: Race walkers walked on the plate with their training race walking speed and normal walking pattern respectively. In the current study, only the right foot plantar data was collected (Goble et al, 2003) and minimum of 5 valid trials were recorded and analyzed. Before testing, the subjects completed consent forms and were given sufficient time to warm up.

Results and Discussion

Our research regarded the high peak pressure of the heel areas as a potential risk factors of tibial foot injuries that is caused by the extended knee part of the race walking rule. and we believe eversion is another risk factor for injuries.

Table 1 shows the comparison of lower leg kinematic parameters between race walking and normal walking. The ankle dorsiflexion (P=0.003), ankle plantarflexion (P=0.002), ankle angular velocity (P=0.000), knee extension (P=0.000), hip adduction (P=0.038), foot eversion (P=0.013) and average horizontal velocity (P=0.000) during race walking were significantly greater than those in normal walking.

Conclusions

During race walking, The greater heel peak pressure and more ankle eversion may be the injury risks caused by the race walking rules.

References

- [1] Francis P.R; Richman N.M; Patterson P,(1998) Journal of Athletic Training; **33**:122-129.
 [2] Lafortune M, Cochrane A, Allison W (1989) Selected biomechanical parameters of race walking Excel **5**:15-1

Table 1: The comparison of low leg kinematic parameters between race walking and normal walking.

	Normal walking	Race walking	P
Ankle plantar flexion (°)	3.77±1.89	15.61±3.34	0.002**
Ankle angular velocity (°/s)	36.06±11.96	73.53±19.39	0.000**
Knee flexion (°)	39.95±10.40	25.47±7.93	0.182
Knee extension (°)	174.18±5.10	187.54±6.8	0.000**
Hip adduction (°)	6.51±2.61	9.63±2.69	0.038*
Foot eversion (°)	5.81±2.65	9.31±1.69	0.013*
Horizontal velocity (m/s)	1.77±0.17	3.15±0.31	0.000**

LONG-TERM TAI CHI PRACTITIONERS WERE LESS INFLUENCED BY THE DUAL-TASK PARADIGM DURING STAIR DESCENDING

Xiaoli Ma¹, LiLi², Wei Sun¹, Qipeng Song¹

¹Shandong Sport University, Jinan 250102, China;

²Department of Health Sciences and Kinesiology, Georgia Southern University, Statesboro, 30460, USA

Corresponding author: Dr. Qipeng Song, songqipeng@sdpei.edu.cn

Summary

Taking the stairs is common in daily life among the elderly under dual-task (DT) conditions; stair descending contributes to a high risk of falls among the elderly under dual-task (DT) conditions. The purpose of this study was to determine whether the practitioners of Tai Chi (TC) have lower fall risks under DT conditions during stair descending, compared with their no-exercise (NE) counterparts. Fifteen TC practitioners with at least 10 years of experience in TC and fifteen NE participants were recruited in this study. They were asked to descend a six-step staircase under single-task (ST) and DT conditions. An eight-camera motion analysis system and two force plates were used for data collection. Results showed the TC practitioners were less influenced by the DT paradigm than their NE counterparts. Our observations indicated that TC practitioners have lower fall risks under DT conditions during stair descending.

Introduction

The continuously increasing number of the stair-related injuries [1] has made stairs one of the most hazardous locations for fall accidents and the leading cause of accidental death for the elderly. Compared with level walking, stair descending demands a greater lower limb joint range of motion [2] and muscle strength [3], which imposes a significant challenge to postural control in the elderly. In a dual-task (DT) paradigm, the introduction of a concurrent task (mostly a cognitive task) during a primary task (mostly a physical task) leads to an increase in the risk of falls. Exercise has been proven effective in preventing falls and decreasing the risk of falls, and one of its most popular forms is TC. However, TC's potential as a mind-body exercise to reduce fall risks under DT conditions has not received considerable attention. Therefore, our study aims to investigate the effects of TC under the DT condition. We hypothesized that TC practitioners have lower fall risks under DT conditions during stair descending than their NE counterparts.

Methods

We recruited 25 participants, 13 in the TC group, with TC experience of 19.7±6.4 years, and 12 in the no-exercise (NE) group. A staircase with six steps was constructed for data collection. Two force platforms were embedded in the third and fourth steps of the staircase to collect ground reaction force data at a sample rate of 1,000 Hz. The participants were asked to ascend the staircase in a step-over-step manner under two conditions (ST and DT). All variables were collected by a Vicon system (kinematic sampling rate at 100 Hz) and then exported to Microsoft

Excel 2016 for further calculation. The group and condition effects were examined using a mixed model two-way ANOVA with a significance level set at 0.05.

Results and Discussion

Fig 1 presents the outcomes of the kinematic variables during stair descending. Our outcomes indicated that the lower fall risks under the TC group's DT condition might be related to some of their unique gait strategies, such as decreased walking velocity. Both groups took a more cautious gait strategy under the DT condition than under the ST condition, as represented by the increased foot clearance. Compared with the NE group, the TC group had higher foot clearance under both conditions during stair descending. TC group had lower head and trunk tilt angles than the NE group. TC exercise movements may be applied to stair descending when the TC group held their heads and kept their trunks erect under both conditions.

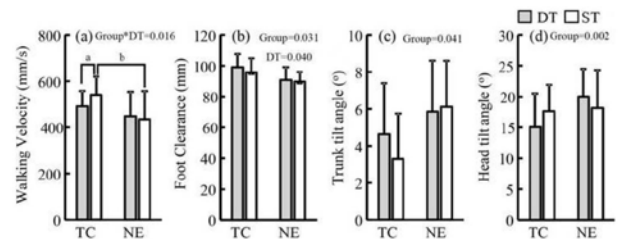


Figure 1: Kinematic variables during stair descent.

Conclusions

The TC group were less influenced by the DT paradigm than their NE counterparts. Our observations indicated that TC practitioners have lower fall risks under DT conditions during stair descending.

Acknowledgments

This work was funded by the Introduction and cultivation plan of young innovative talents of Shandong Provincial Department of Education (2019-183)

References

- [1] Blazewick DH, Chounthirath T, Hodges NL, Collins CL, Smith GA. (2018). *The American journal of emergency medicine*. 36:608-14.
- [2] Qu X. (2015). *J Biomech*. 48:4059-64.
- [3] Bosse I, Oberlander KD, Savelberg HH, Meijer K, Bruggemann GP, Karamanidis K. (2012). *Hum Mov Sci*. 31:1560-70.

BACKPACK WEIGHT INFLUENCE POSTURAL CONTROL AMONG CHILDREN WITH OBESITY DURING STAIR DESCENT

Xinheng Che¹, Cui Zhang², Li Li³, Qipeng Song¹

¹Shandong Sport University, Jinan, 250102, China

² Lab of Biomechanics, Shandong Institute of Sport Science, Jinan, 250102, China

³Department of Health Sciences and Kinesiology, Georgia Southern University, Statesboro, 30460, USA

Corresponding author: Dr. Qipeng Song, songqipeng@sdpei.edu.cn

Summary

This study investigates the effects of backpack weight on posture and gait patterns for children with obesity. A total of 16 obese (75.26 ± 15.99 kg) and 21 the control group (48.13 ± 9.52 kg) schoolboys were recruited. Two video cameras were used. Multivariate analysis of variance with repeated measures was employed. Obese children showed increased trunk and head forward inclination angle, gait cycle duration, stance phase, and decreased swing phase compared with the control group. The changes were observed even with an empty backpack in comparison with the control group and a 15% increase in backpack weight led to further instability and damage on their already strained bodies.

Introduction

Carrying a backpack is an activity in daily life for students. Many studies reported that excessive backpack weight results in back pain and muscle fatigue [1]. Our literature review did not show any study on the effects of backpack weight on posture, gait patterns of children with obesity. Obesity leads to a significant disadvantage in movement and discomfort in simple daily activities such as stair-climbing [2]. Large proportions of their body weight do not contribute to their movement performance. This study aimed to determine the effects of backpack weight on posture, gait pattern of male obese children in stair descent.

Methods

Each participant was asked to complete one testing session per day for a total of four testing sessions. The mean bodyweight was 75.26 ± 15.99 kg for children with obesity, and 48.13 ± 9.52 kg for control. The participant

was asked to carry a two strap backpack with both shoulders in a given backpack weight (0, 10, 15, or 20% of body weight) in each session. Two high-speed video cameras were placed 12 m from the walking track with an angle of 90° to record level walking and stair descent movements at a 100 Hz sampling rate. A two-way MANOVA with mixed design was performed to determine the effects of backpack weight and obesity condition. Significant level set at 0.05.

Results and Discussion

Compared to the control group, children with obesity showed increased trunk and head forward inclination angles ($p = 0.003$, $p = 0.001$), single and double support phase durations ($p = 0.030$, $p = 0.000$), and decreased swing phase duration ($p = 0.001$). See Table 1 for more details.

Conclusions

1. Children with obesity increased their trunk forward inclination angle, head forward inclination angle, and gait cycle durations in comparison to control when carrying a backpack weight between 0 to 20% of their body weight during stairs descent.
2. A backpack weight of more than 15% of body weight led to further instability and damage on the already strained bodies of children with obesity.

References

- [1] Johnson, Knapik, & Merullo (1995). *Perceptual and Motor Skills*, **81**:331–338.
- [2] Hills, & Parker, (1991). *Archives of Physical Medicine and Rehabilitation*, **72**: 403–407.

Table 1: Posture and temporal variables during stair descent (mean and standard deviation)

Load (% body weight)	Control				Obese			
	0%	10%	15%	20%	0%	10%	15%	20%
Trunk inclination angle (O)	5.54(2.6) ^a	6.78 (2.2) ^b	7.31 (2.4) ^b	7.57 (3.0) ^b	8.55(2.6) ^a	10.46 (3.8)	11.87(4.0) ^c	11.43(3.5) ^c
Head inclination angle (O)	18.3(11.2) ^a	16.29(10.6)	17.36 (8.9)	17.91(12.3)	22.68(10.1)	23.82 (8.1)	23.77 (10.0)	22.48(10.1)
Gait cycle duration (s)	0.96(0.1) ^a	0.96 (0.1)	0.93 (0.1)	0.99 (0.1) ^b	1.00(0.1) ^a	1.01 (0.2)	1.07 (0.2)	1.11 (0.2) ^c
Stance phase duration (%)	61.06(1.0) ^a	61.33 (1.7)	61.68(2.0) ^b	61.89(2.6) ^b	65.19(1.3) ^a	66.07 (2.1)	65.69 (2.6)	66.62(2.4) ^c
Swing phase duration (%)	38.94(1.1) ^a	38.67 (1.9)	38.32(1.6) ^b	38.11(2.1) ^b	34.81(1.3) ^a	33.93 (2.1)	34.65 (2.1)	33.38(2.4) ^c
Double support phase duration (%)	27.74(2.1) ^a	27.75 (3.2)	27.69 (3.1)	29.02(2.8) ^b	28.33(2.5) ^a	29.32 (3.0)	28.86 (2.6)	34.03(3.3) ^c

a: $p < 0.05$ between the average backpack loads of control and obese groups (shown in 0% backpack loads). b: $p < 0.05$ versus 0% in control group. c: $p < 0.05$ versus 0% in obese subjects.

Sex differences in foot kinematics and kinetics during drop-jump using a novel multi-segment foot model

Y. Sekiguchi¹, N. Ogihara², H. Hanawa³, T. Kokubun¹, N. Kanemura^{1*}

¹ Saitama Prefectural University, Saitama, 343-8540, Japan,

² University of Tokyo, Tokyo, 113-0033, Japan

³ University of Human Arts and Sciences, Saitama, 339-8555, Japan

*Email: kanemura-naohiko@spu.ac.jp

Summary

This study aimed to evaluate potential sex differences in foot mechanics during drop-jump by an inverse dynamic analysis using a newly-proposed multi-segment foot model. Thirty healthy adults (15 males, 15 females) performed drop-jumps. Inter-subject variabilities in joint angle and moment profiles during drop-jump were small. However, statistically significant sex differences were observed in metatarsophalangeal joint angle and moments during drop-jump. Biomechanical analysis based on the proposed multi-segment foot model may be useful to investigate pathogenetic mechanisms of foot injuries and disorders.

Introduction

It is generally accepted that the prevalence of foot injuries is greater in females than in males possibly because of higher joint laxity in females [1]. However, detailed kinematics and kinetics of the human foot during dynamic movements have not been sufficiently investigated mainly due to the lack of detailed foot model available to estimate internal forces and moments in the foot segment. The present study aimed to evaluate potential sex differences in foot kinematics and kinetics during drop-jump by an inverse dynamic analysis using our newly-proposed multi-segment foot model.

Methods

The proposed foot model had three segments: phalanx, forefoot, and hindfoot (Figure 1). Mass, center of mass, and moment of inertia of each segment were calculated based on the CT data of the foot from one healthy male subject (42 years old, 72 kg, 172 cm) using CAD software. The model was scaled by the cube root of the segment mass to create a subject-specific foot model.

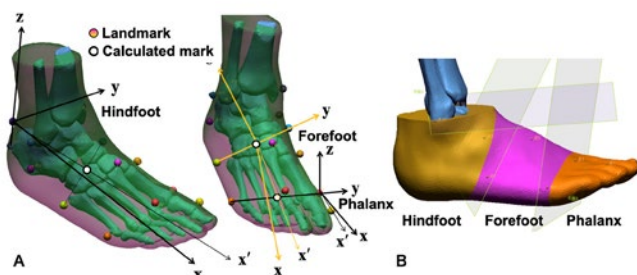


Figure 1: (A) The foot model definition; (B) The segmented foot based on the CT data

Thirty healthy adults (15 males, 15 females) performed drop-jumps. The participants were asked to land on the front and rear force-plates by their fore- and hindfoot, respectively. Trajectories of surface markers were collected using the Vicon Nexus 2.10.2, a three-dimensional motion analysis system (Vicon, Oxford, UK) with 20 infrared cameras at 100

Hz. The 3D rotation angles of the joints (ankle joint, midtarsal joint, and metatarsophalangeal joint: MTP joint) were described by y-x-z Euler angles. The joint moments were calculated by inverse dynamics analysis based on the Newton-Euler method. Sex differences were examined using the Wilcoxon rank-sum test, with a significance level of 5%.

Results and Discussion

The measured time-series of the joint angles were generally in good agreement with those reported in our previous study [2]. The joint angle and moment profiles (Figure 2) were found to be quite similar among the participants. Although there was no sex difference in the foot joint angles during quiet standing, dorsiflexion of the MTP joint was significantly larger in female than in male ($p < 0.01$). The timing of the peak plantarflexion moments was also significantly earlier in female than in male ($p < 0.01$).

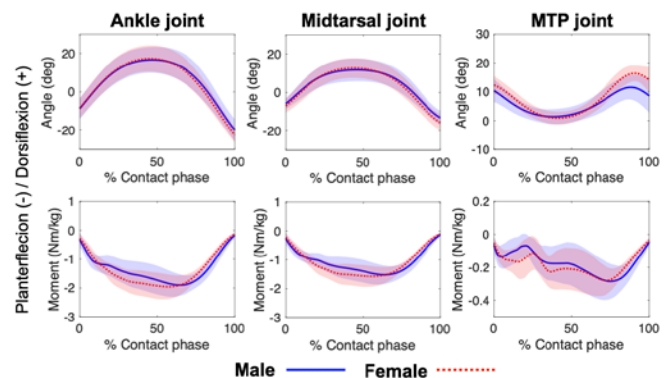


Figure 2: The joint angles and moments on the sagittal plane

Females may have taken a force-exertion strategy to compensate for higher joint laxity of the foot, since there were no sex differences in the kinematics of the ankle and midtarsal joints. The proposed model successfully extracted the differences in 3D motions and moments within the foot segment during drop-jumps between males and females.

Conclusions

The findings obtained from the proposed foot model possibly enhance our understanding of sex differences in dynamics of the foot during drop-jumps. The proposed multi-segment foot model may be useful to investigate pathogenetic mechanisms of foot injuries and disorders.

References

- [1] Shultz SJ et al. (2007). J. Orthop. Res, **25(8)**: 989-996.
- [2] Sekiguchi Y et al. (2020). J Med Biol Eng, **40(5)**: 757-765.

Acute effect of transcranial direct current stimulation on rowing endurance performance: a double-blind, randomized, crossover plot study

Zhiqiang Liang ¹, Xi Wang ¹, Fujia Jiao ¹, Jiaojiao Lü ¹, Yu Liu ²

¹School of Kinesiology, Shanghai University of Sport, China

²Institute of Sport Science, Shanghai University of Sport, China

Email: liang_sus@163.com

Summary

Aim of this study was to confirm effect of tDCS on rowing endurance performance by testing performance on the ergo of ten professional rowers. The result showed that rower after intervention of tDCS used minimum time to finish 5km compared with intervention of sham and baseline although no significant difference was found in performance parameters at statistics.

Introduction

As a new neuro-doping ergogenic technique transcranial direct current stimulation (tDCS) has been testified the positive influence on athlete performance [1]. A lots number of researches have suggested that tDCS not only improve the endurance performance of single joint exercise but also enhance the endurance performance of whole-body exercise [2]. And most of these studies have used cycling and running to test effect of tDCS on endurance performance as well as confirm that cycling is benefit from this way.

Both of cycling and rowing belong to the period sports event; however, there is only one research compared different stimulated intensity on rowing performance [3], and no research to confirm whether tDCS has the same effect on rowing endurance performance like cycling.

Taking research in this area may be provide some useful strategies on rowing performance, therefore, the aim of this study was to confirm this effect on rowing endurance performance. Based on previous studies, we hypothesed that tDCS would have a better performance compared with sham and none.

Methods

Ten professional female rowers voluntarily participated to this research and got the informed consent before test. Rowers had 5-15min to warm up and were asked to complete 5km on the ergometer at 20sr/min after 20min randomly stimulating by tDCS or sham and baseline respectively. When the 5km was finished, 10min-15min was give to cool down by ergo cycling. Each test was separated by for 48h at least.

Four halo sports (San Francisco, CA, United States) were used to complete 20min, 2mA tDCS and sham stimulation (ramp-down 30s). Three foam electrodes (4cmx6cm) were place over the Cz (anodal polarity), C5 and C6 (cathode polarity). 5km time (5kT), 500m/split (500-S),

power (P) and energy consumption (EC) was used to reflect endurance performance using one-way ANOVA by SPSS (version 26, SPSS, Chicago, IL, USA)

Results and Discussion

No significance was found in 5kT, 500-S, P and EC between intergroup during 5km endurance straining after three stimulated interventions (Table 1). However, compared with baseline(20:38.1±00:31.4), rower could fast complete 5km after intervention of tDCS (20:28.1±00:32.1) and sham (20:33.1±00:32.6) , and the tDCS was also better than sham (Figure 1).

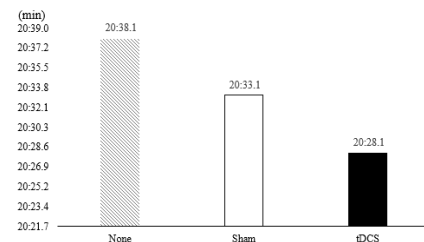


Figure 1: 5km endurance performance after different stimulated interventions

Conclusions

Although no significant difference in performance parameters was showed at statistics. Rower after stimulating by tDCS could use the less time to finish 5Km; tDCS might be as an effective way to improve rowing endurance performance

Acknowledgments

The authors would like to thank all rowers who took part in this study and for their efforts. This study was supported by grant from national natural science foundation of China (11932013) and MOE Foundation of Humanities and Social Sciences (19YJCZH115).

References

- [1] Edwards D J et al. (2017). Transcranial direct current stimulation and sports performance. *Frontiers in Human Neuroscience*, **11**:243-247.
- [2] Alix F et al. (2019). Short-term effects of anodal transcranial direct current stimulation on endurance and maximal force production. a systematic review and meta-analysis. *Journal of Clinical Medicine*, **8**(4):536-551.
- [3] Xiaoyun, L et al. (2018). Increased interhemispheric synchrony underlying the improved athletic performance of rowing athletes by transcranial direct current stimulation. *Brain Imaging & Behavior*, **13**(5):1324-1332.

Table 1: Parameter reflecting rowing endurance performance

Stimulation	5kT (Min)	500-S (Min)	P (W)	EC (J/h)
None	20:38.1±00:31.4	02:03.7±00:03.1	184.9±14.2	936.3±48.4
Sham	20:33.1±00:32.6	02:03.3±00:03.3	187.4±14.6	944.3±50.2
tDCS	20:28.1±00:32.1	02:02.7±00:03.2	189.7±14.5	952.2±49.8

PROPRIOCEPTIVE NEUROMUSCULAR FACILITATION IMPROVES DESCENDING MECHANICS AMONG KNEE OSTEOARTHRITIS PATIENTS

Bo Gao¹, Peixin Shen², Li Li³, Qipeng Song¹

¹College of Sports and Health, Shandong Sport University, Jinan, China

²Graduate School, Beijing Sport University, Beijing China

³Department of Health Sciences and Kinesiology, Georgia Southern University, Statesboro, 30460, USA

Corresponding author: Dr. Qipeng Song, songqipeng@sdpei.edu.cn

Summary

Knee osteoarthritis (KOA) is a common disease that causes pain and limits functionality in the elderly during daily activities, especially during stair descent. Proprioceptive neuromuscular facilitation (PNF) practices promote multiple-plane joint movements, which relieve pain and increase joint range of motion (ROM). We randomized 36 elderly with KOA who met the inclusive criteria into two groups: the twelve-week PNF intervention group and the control group. The aim of this study was to examine the effects of a 12-week PNF intervention on pain relief, ROM, and frontal plane knee moments in the elderly with KOA during stair descent. Compared to the control group, the PNF group showed a decreased pain score, increased passive hip, knee, ankle ROM, a decreased minimum knee flexion angle, and increased hip adduction moment (HAM) during stair descent.

Introduction

The prevalence of knee osteoarthritis (KOA) is associated with aging; over 40% of adults 65 and older are symptomatic [1]. Increased joint pain and decreased joint range of motion (ROM) are the most common complaints associated with KOA and confirmed by physical examinations. Stair walking requires greater functional ability than level walking for people with lower extremity disorders [2] and is influenced by knee pain [3]. In comparison with stair ascent, stair descent exhibits faster gait velocity [2] and knee angular velocity [4] in patients with KOA. Proprioceptive neuromuscular facilitation (PNF) practices promote movement at the joints in sagittal, frontal, and horizontal planes to achieve diagonal movements, which can relieve pain [5] and increase ROM [6].

Methods

PNF group included 36 participants who experienced 12-week PNF stretching. Participants (N=16) in the control group watched television or read magazines at the same time. The overall pain score (0-10) from the affected leg was self-assessed at the end of weeks 0, 6, and 12 by completing the Western Ontario and McMaster Universities Arthritis Index. Lower extremity passive flexion-extension joint ROMs from the affected leg were measured using standard goniometric procedures. One force platform (Kistler, 9287BAs), embedded in the 4th step from the bottom of the staircase, was used to collect ground reaction force data at a sampling rate of 1000 Hz.

The stair descent test was recorded by an eight-camera motion analysis system (Vicon, Oxford Metrics, Ltd.) at 100 Hz. Vicon Plug-In Gait model used to analyze data via a 13-segment whole-body model. Sagittal plane joint angle (representing the active ROM) and frontal plane joint moment were estimated using commercially available software (Visual 3d, C-motion). The normality of all

outcome variables was tested using the Shapiro-Wilk test. The mean and standard deviations for the kinematic and kinetic variables were subjected to descriptive analysis. A mixed model two-way analysis of variance was used to determine the PNF intervention effects and group differences on each of the outcome variables. A Bonferroni-adjusted post hoc analysis was conducted when time-group interaction was detected. Partial eta squared (η^2_p) was used to represent the effect size of main effect and interaction of two-way analysis of variance.

Results and Discussion

Significant time by group interactions were detected in pain scores, which significantly decreased from week 0 to weeks 6, then to week 12, in the PNF group, and were significantly lower in the PNF group compared with that in the control group at week 6. Significant time by group interactions was detected in ROM, which significantly increased from week 0 to weeks 6 and 12 in the PNF group. The ROMs were significantly greater in the PNF group than those in the control group at weeks 6 and 12.

This study confirmed that a 12-week PNF intervention could relieve pain without increasing KAM, enhance passive ROM, increase active knee flexion ROM, and increase HAM in the elderly with KOA during stair descent. These findings support that PNF practice is an effective intervention to relieve the symptoms and slow down the progression of KOA.

Conclusions

This study confirmed that a 12-week PNF intervention could relieve pain without increasing KAM, enhance passive ROM, increase active knee flexion ROM, and increase HAM in the elderly with KOA during stair descent.

Acknowledgments

This work was funded by the Introduction and cultivation plan of young innovative talents of Shandong Provincial Department of Education (2019-183)

References

- [1] Dawson J et al. (2004). *Rheumatology*, **43**: 497-504.
- [2] Hicks-Little CA et al. (2012). *Arthroplasty*, **27**: 1183-1189.
- [3] Whitcelo T et al. (2014). *Disabil Rehabil*, **36**: 1051-1060.
- [4] de Oliveira DC et al. (2014). *BMC Musculoskeletal Disord*, **15**:321.
- [5] Sharman MJ et al. (2006). *Sports Med*, **36**: 929-939.
- [6] Hindle KB et al. (2012). *Hum Kinet*, **31**: 105-113.

Development of Squat-Exercise Support System using Kinect Sensor for Persons with Intellectual Disabilities

Kazuyuki Mito¹, Yuta Nohara², Aya Shirai¹, Taeko Tajima³, Takeshi Kuwamoto³, Yoshiaki Takahashi³,

Tota Mizuno¹, Naoaki Itakura¹

¹Department of Informatics, The University of Electro-Communications, Tokyo, Japan

²Fixpoint Inc., Tokyo, Japan

³Nijinokai for Community Welfare, Tokyo, Japan

Email: k.mito@uec.ac.jp

Summary

Visual assistance is important for persons with intellectual disabilities to understand something. In this study, we have developed a squat-exercise support system for persons with intellectual disabilities. In the system, the human joint positions during the squat-exercise of the subject was detected by a Kinect sensor and the subject guided to correct movement by the animation. 16 persons with intellectual disabilities used this system and they were able to exercise more correctly than instruction by lecture movie.

Introduction

Persons with intellectual disabilities are lack exercise and they have a high risk of locomotor disorders. To prevent the deterioration of their mental and physical functions, physical measurements and exercise programs have been carried out at the welfare facility of the disabled. In the exercise program, the instructor shows the correct movement using the lecture movie and verbally conveys the part of the body that should be careful. They do not fully understand the meaning of the verbal explanation and cannot move correctly. The purpose of this study is to construct a training system that enables the person with intellectual disabilities to exercise correctly and effectively with visual support.

Methods

In this system, the joint positions of a whole-body during squats-exercise were detected by the Kinect for Windows v2 (Microsoft Japan Co., Ltd.), and the subject was instructed in the correct movement using the animation function. There were two types of squats: normal squats with both feet shoulder-width and wide squats with both feet wider than shoulder-width. The joint positions of the shoulders, hips, knees, and ankles were measured by the Kinect sensor and the knee joint angle was calculated from the joint positions of the ankle, knee, and hip. A correct squat-exercise was judged when the knee joint angle is maintained in the range of 70 to 120 degrees for 1.5 seconds. A figure of the user and the joint positions measured by the Kinect sensor was displayed on a large monitor in front of them. If the knee joint angle was less than 70 degrees, an animation of a downward arrow displayed and the user had to bend the knee further. If the knee joint angle was more than 120 degrees, an animation of an upward arrow displayed and the user had to extend the knee. When the knee joint angle was kept from 70 degrees to 120 degrees, a flame animation that means correct squat-exercise displayed on the thigh. A red circle gauge displayed above the user's head at the same time as the

flame animation, and after 1.5 seconds it turned light blue and counts as the correct squat. In wide squats, the system displayed a warning message if the width of both feet of the user was narrower than the width of the shoulders.

16 persons with intellectual disabilities (6 females and 10 males) aged 20 to 49 years (averaged: 31.6 ± 9.02 years) such as autism and Down's syndrome participated in the evaluation experiment of this system. The Kinect sensor and 50-inch monitor were installed at a height of 80 cm above the ground and the subjects lined up at 3.0 to 3.5 m from the Kinect sensor. Subjects performed normal-stance and wide-stance squat-exercise with both the lecture movie and the proposed system. In the lecture movie, subjects performed squat-exercise watching the correct behavior movie by the trainer. In the proposed system, the subjects performed squat-exercise while watching their body movement and the support animation on the monitor. In each condition, subjects performed the squat-exercise 10 times.

Results and Discussion

The percentage of correct squat-exercise was shown in Table 1. Data from two subjects who refused the experiment on the way were excluded from the results. In both normal and wide squat-exercises, the use of a proposed system significantly increased the correct percentage. In the cognitive ability test of an autistic person, it is reported that the visual information ability is higher than the auditory information processing ability [1]. Therefore, it is expected that the proposed system having a visual support function was effective.

Table 1: Correct percentage of squat-exercises (n=14)

Squat-exercise	Lecture method	Correct percentage (%)	t-test
Normal stance	Movie	62.1 ± 34.7	p<0.05
	Proposed system	88.6 ± 24.2	
Wide stance	Movie	44.4 ± 39.9	p<0.01
	Proposed system	87.1 ± 25.8	

Conclusions

In this study, the squat-exercise support system was developed using Kinect sensor and the animation function. The effectiveness of this system was recognized in the squat-exercise of persons with intellectual disabilities.

References

- [1] Prior MR. (1979) *J. Abnormal Child Psychology*, 7: 357-380.

Directional Dependence of Uniaxial Response Characteristics of the Porcine Thoracic Aorta

Manoj Myneni¹, Raghuvver L. Sridhar¹, K.R. Rajagopal¹, Chandler C. Benjamin¹

¹Department of Mechanical Engineering, Texas A&M University, College Station, TX, USA

Email: manojmyneni@tamu.edu

Summary

We studied the response of the porcine thoracic aorta under uniaxial extension using dumbbell shaped specimens oriented at 0°, 30°, 45°, 60°, 90° with the circumferential direction. The stress-strain curve shows a characteristic J-shape for all the specimens. Specimens oriented at 30° show an increasingly negative shear strain, while specimens at 45° and 60° depict a non-monotonic shear strain with increasing nominal stretch.

Introduction

Aorta is generally regarded to have an orthotropic material symmetry with respect to the circumferential-axial-radial planes[1]. Negligible twist undergone by animal aortas in their unloaded tubular forms during inflation-extension experiments led to this observation[2]. Most of the recent studies, however, are conducted on square or dumbbell shaped specimens obtained after cutting open the aorta along its length and flattening it[3]. All these studies restrict their testing to the specimens oriented along circumferential and axial directions. Material symmetry depends on the choice of the reference configuration, and it is possible that the material symmetry with respect to the tubular form of the aorta may be different from the material symmetry in the flattened form obtained after a longitudinal cut. The data presented here can be used to evaluate if the existing constitutive models of the thoracic aorta, which were proposed based on the assumption of orthotropic material symmetry, can be used to study the deformations from the flattened state. (Note: Arteries are not elastic solids. They are a mixture of solids and fluids. Refer to [4] for a review on problems with existing constitutive models almost all of which assume artery as an elastic solid, and the limitations of current experiments, many of which presume that the arterial wall is an elastic solid.)

Methods

Fresh porcine aortas (n=10) were harvested from a slaughterhouse on the Texas A&M University campus. Loose connective tissue was carefully removed, and the segment of the aorta between the end of the aortic arch and the third branching arteries was stored in 0.01M Phosphate Buffer Saline (PBS) solution at -20°C. After thawing overnight, the aorta was cut open along its length and dumbbell shaped specimens (Total length ~30mm, gauge length ~10mm, gauge width ~3mm, width of the wider portion of the specimen ~6mm) were punched out using an in-house machined punch. Images of the specimens were taken to measure the width and the thickness of the specimens. After clamping the specimen, Rust Oleum® spray paint and primer was used to create a speckle pattern on the intimal surface. A preload of <0.05N was applied to straighten the specimen. One of the clamps was displaced (by applying appropriate force) to produce a constant nominal stretch rate of 2%/s until a nominal stretch of 1.5. Seven preconditioning cycles were applied. The data was collected from the loading part of the next cycle. Images were captured for a Digital Image Correlation(DIC) analysis using Ncorr [4]. The Green strain (\mathbf{E}) obtained from Ncorr is

averaged over a 1.5 mm x 1.5mm region around the center of the specimen.

Results and Discussion

The mean curves for the specimens obtained from all the aortas are given in Figure 1. The nominal stress shows an inclined J-shaped dependence on the nominal stretch for the specimens oriented in all directions. The X-component (direction of the uniaxial displacement) of the Green strain increases with nominal stretch with a change of slope occurring at a nominal stretch between 1.3-1.4. This can be attributed to the straightening of the collagen fibers as they deform during loading. E_{yy} decreases with E_{xx} demonstrating a slope change occurring due to increased collagen fiber engagement. Circumferential (0°) and axial (90°) specimens show nearly zero shear strain (E_{xy}). The remaining specimens undergo shear during uniaxial extension with 45°, 60° specimens showing a non-monotonic E_{xy} with increasing E_{xx} .

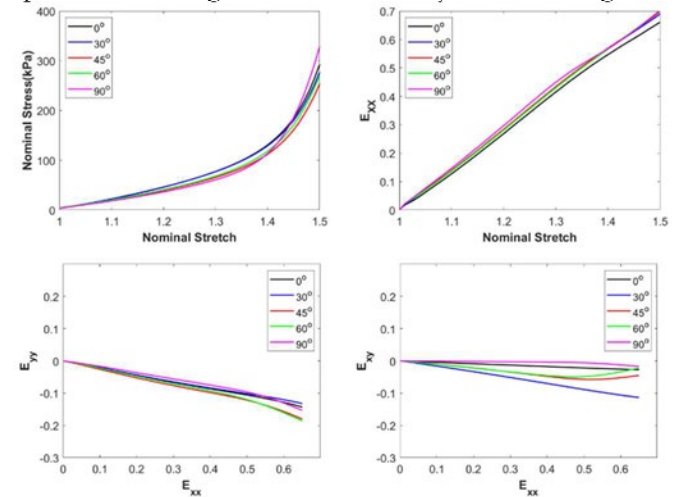


Figure 1: (a) Nominal Stress vs. nominal stretch (b) E_{xx} vs. nominal stretch (c) E_{yy} vs. E_{xx} (d) E_{xy} vs E_{xx}

Conclusions

Our study demonstrates the variation of the uniaxial stress-strain behavior with the direction in which the specimens are obtained after a longitudinal cut of the aorta. Specimens from all the directions depict a nearly overlapping stress-stretch relation, E_{xx} vs. stretch, and E_{yy} vs. E_{xx} . Strong anisotropy can, however, be observed in the E_{xy} - E_{xx} curve of 30°, 45° and 60° specimens, indicating the importance of testing specimens oriented along non- circumferential and non-axial directions.

Acknowledgments

We would like to thank Dr. Michael Moreno, Texas A&M University for providing the lab facilities to conduct the experiments.

References

- [1] Chuong et al. (1986). *J. Biomech. Eng.* **108(2)**: 189-192.
- [2] Patel et al. (1969). *Circ. Res.* **24**:1-8
- [3] Peña et al. (2015). *JMBBM.*, **50**: 55-69.
- [4] Rajagopal et al. (2020). *Aorta*, **8(4)**: 91–97
- [5] Blaber et al. (2015). *Exp. Mech.* **55**: 1105-1122.

Ventricle of terrestrial Anura is stiffer than that of aquatic Anura due to differences in collagen density

Megumi Ito¹, Shukei Sugita¹, Masanori Nakamura¹, and Yoshihiro Ujihara¹
¹Biomechanics Lab, Nagoya Institute of Technology, Nagoya, Japan
 Email: megumi1123ito@gmail.com

Summary

During the evolution of vertebrates, the hearts have undergone marked anatomical changes to adapt to different environments and lifestyles. The transition from aquatic to terrestrial life may have required the acquisition of the ability to circulate blood against the force of gravity. Here, we investigated the passive mechanical properties and histology of the ventricles of two species of Anura (frogs and toads) with different habitats, *X. laevis* (aquatic) and *B. j. formosus* (terrestrial). Pressure-loading tests demonstrated that the ventricle of *B. j. formosus* was significantly stiffer than that of *X. laevis*. Histological analysis revealed the collagen density of *B. j. formosus* was significantly higher than that of *X. laevis*. These results suggest that the ventricles become stiff in the process of terrestrialization by increasing ventricular collagen fibers.

Introduction

Vertebrate hearts have undergone marked morphological and structural changes to adapt to different environments and lifestyles in the course of evolution. However, it remained unclear how structural changes is related to evolutionary changes in mechanical properties. Amphibians are the first vertebrates that come to land. The transition from aquatic to terrestrial life requires the acquisition of the ability to support the body and to perform locomotion against gravity. It is therefore possible that mechanical properties of the ventricles that affect the pumping functions of the heart have changed in association with terrestrialization. Here, we evaluated the passive mechanical properties of the ventricles of two species of Anura (frogs and toads) with different habitats, *X. laevis* (aquatic) and *B. j. formosus* (terrestrial). Differences in the passive mechanical properties of the ventricles were discussed in light of the collagen density and the cardiomyocyte stiffness.

Methods

To analyze the passive mechanical properties of the ventricles, we obtained the relationship between the ventricular pressure and the ventricular volume by introducing cardioplegic solution into diastolic-arrested ventricle. To compare different-sized hearts, the ventricular volume was normalized with its weight. The second-harmonic generation (SHG) light from the collagen fibers of sliced ventricles was imaged under a multiphoton microscope (FV1200MPE, Olympus) [1]. The collagen density was quantitatively assessed by dividing the total intensity of SHG light by the area using ImageJ 1.53c. Sarcomere length of isolated ventricular cardiomyocytes [2] was determined by SarcOptiM [3], a plug-in for the ImageJ.

Results and Discussion

Typical examples of the pressure-normalized ventricular volume curves of *X. laevis* and *B. j. formosus* (Fig. 1). Larger pressures are required to expand the ventricles of *B. j.*

formosus than *X. laevis*, demonstrating that the ventricle of *B. j. formosus* was stiffer than that of *X. laevis*. The SHG light of the collagen fibers was observed in the myocardium, but it was more apparent in the outermost layer of ventricles in both animals. In both the outermost collagen layer of the ventricle and the myocardium, the collagen density of *B. j. formosus* was significantly higher than that of *X. laevis* (Fig. 2). Since collagen is a primary component to provide mechanical strength of tissues [4], *B. j. formosus* may have enriched collagen fibers and stiffened its ventricles to adapt to life on land. The sarcomere length of isolated cardiomyocytes of *X. laevis* and *B. j. formosus* was almost the same. Because sarcomere length determines the stiffness of cardiomyocytes [2], the stiffness of the cardiomyocytes of *X. laevis* and *B. j. formosus* was considered to be similar. These results suggest that the stiff ventricles of *B. j. formosus* compared to *X. laevis* is attributed to differences in collagen density, not in the stiffness of the cardiomyocytes.

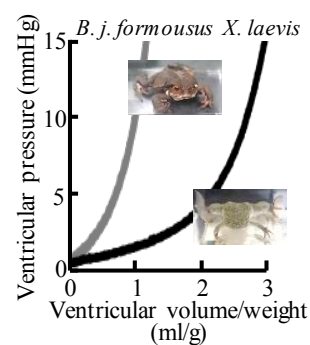


Fig. 1 Pressure-volume/weight curves

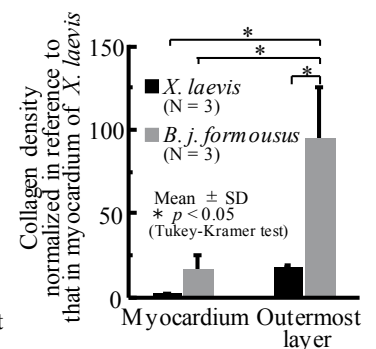


Fig. 2 Collagen density

Conclusions

In the present study, the passive mechanical properties and histology of the ventricles of aquatic *X. laevis* and terrestrial *B. j. formosus*. These results suggest that the ventricles of Anura become stiff in the process of terrestrialization by increasing collagen fibers of the ventricles.

Acknowledgments

This study was supported in part by KAKENHI (JP18K12055 and JP19K22962) from the Ministry of Education, Culture, Sports, Science and Technology (MEXT), Japan.

References

- [1] Sugita S et al. (2018). *Biomech. Model. Mechanobiol.* **17**: 577-587.
- [2] Honda T et al. (2018). *Kawasaki Med. J.* **44**: 1-17.
- [3] Pasqualin C et al. (2016). *Am. J. Physiol. Cell Physiol.* **311**: C277-283.
- [4] Spinale FG. (2007). *Physiol Rev.* **87**: 1285-1342

The importance of inertial measurement unit placement in assessing upper limb motion

Fredrik Öhberg, Gustav Höglund, Helena Grip

Dept. Biomedical Engineering, University Hospital of Umeå, Umeå, Sweden

Email: Fredrik.Ohberg@regionvasterbotten.se

Summary

Motion analysis using inertial measurement units (IMU) has emerged as an alternative to optical motion capture but still the validity and reliability of upper limb measurements varies between studies. The objective was to determine how sensor placement affects joint angle measurements during motion of the arm, shoulder, and scapula. Results show that sensor placement considerably affects the measured joint angle.

Introduction

Motion analysis provides an objective and detailed way to assess upper limb motion. Optical marker systems are the gold standard method, but they require remittance of patients to a clinical movement laboratory [1]. IMUs, consisting of gyroscopes, accelerometers, and magnetometers [2], are an alternative that can be used in ordinary clinics, since they require only wearable IMU-sensors, and a computer where data are registered and analysed. Still, clinical use of IMUs is limited, due to the lack of standardized and validated kinematic protocols [3] and because the validity and reliability for measuring upper limb motion has not been concluded [4]. One cause is that the sensors output is affected by skin and muscle movements. Such errors must be minimized by standardization of measurement protocols regarding biomechanical models, calibration procedures, and sensor placements.

To evaluate the treatment outcome, different measurement protocols are used, e.g., Modified Mallet scale [5]. Today, no study has investigated the impact of IMU sensor placement on joint angle measurements during upper limb motion measurements.

The objective was to evaluate the effect on joint angle measurements from distal and proximal sensor placements on arms, and from lateral and medial placements on the scapula, in a group of healthy individuals, while performing standardized arm movements included in the modified Mallet scale [5].

Methods

Five female and six male healthy participants with a mean age of 28 ± 6.5 years was recruited. Motion was assessed by a portable movement-analysis system, including seven IMU sensors (MoLab™, AnyMo AB, Umeå, Sweden). Two sensors were placed distally/laterally and proximally/medially on each body segment (forearm, upper arm, and scapula) except on thorax. The test procedure was standardized and consisted of nine arm-movement tasks based on the Modified Mallet Scale [5]. All tasks were repeated five times, where each task began with the right arm hanging vertically. The

joint angle (elevation/rotation for upper arm and scapula; Euler for elbow) where computed for both sensor positions. The linear relationship between angular data from the proximal/medial and distal/lateral sensor for each task and segment were analysed by a linear regression.

Results and Discussion

Scatter plots, together with the results of the linear regression and R^2 -values for the shoulder flexion/extension and forearm pronation/supination are illustrated in Fig 1 together with a description of the analysed planes. The results show that sensor placement has a considerable effect on motion measurement, which could explain the inconclusive validity and reliability reported in previous studies [4].

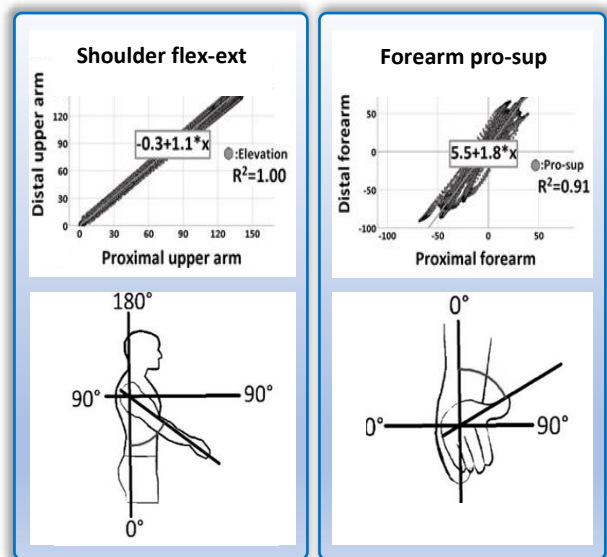


Figure 1: Top: Linear model. Bottom: Analyzed planes.

Conclusions

Sensor placement affects the obtained kinematic output differently, depending on the analyzed joint and plane of rotation.

References

- [1] Morrow MMB et al. (2017). *J Appl Biomech*, **33**:227-232.
- [2] Filippeschi A et al. (2017). *Sensors (Basel)*, **17**.
- [3] Petuskey K et al. (2007). *Gait Posture*, **25**: 573-9.
- [4] Poitras I et al. (2019). *Sensors (Basel)*, **19**.
- [5] Abzug JM et al. (2010). *J Pediatr Orthop*, **30**: 469-74.

Comparing Surface and Intramuscular Electromyography Patterns of the Brachialis Muscle during the Dynamic Elbow Movement.

Shota Date¹, Hiroshi Kurumadani¹, Yuko Nakashima², Akio Ueda¹, Toru Sunagawa¹

¹Biomedical & Health Sciences, Hiroshima University, Hiroshima, Japan

²Hiroshima University Hospital, Hiroshima, Japan

Email: sdate@hiroshima-u.ac.jp

Summary

This study aimed to compare the muscle activity of the brachialis (BR) between surface and intramuscular electromyography (EMG) in dynamic elbow movement. Six healthy subjects performed the active elbow flexion. The EMG signal was recorded from the BR. The coefficient of determination (R^2) of the muscle activity pattern between the surface and intramuscular EMG was assessed. The result showed that the mean R^2 was higher than 0.8, indicating the muscle activity patterns of surface and intramuscular EMG were statistically similar. Thus, it is suggested that the muscle activity of the BR can be assessed using surface EMG in dynamic elbow movement.

Introduction

The muscle activity of the BR has mainly been measured using intramuscular EMG [1], and there are a few studies using surface EMG [2]. Moreover, these studies using surface EMG have measured the muscle activity in a static condition (isometric contraction) [1, 2]. Therefore, it remains unclear whether the muscle activity of the BR can be assessed using surface EMG in a dynamic motion.

Methods

Six healthy right-handed volunteers participated in this study. They performed an active elbow flexion task with the non-dominant upper limb. The forearm positions during the task were supination, pronation, and neutral. Surface and intramuscular EMG were recorded from the BR using surface and fine-wire electrodes. Each electrode was set on the lateral sides of the distal upper arm where the muscle belly was superficial. The placement of the BR muscle belly was

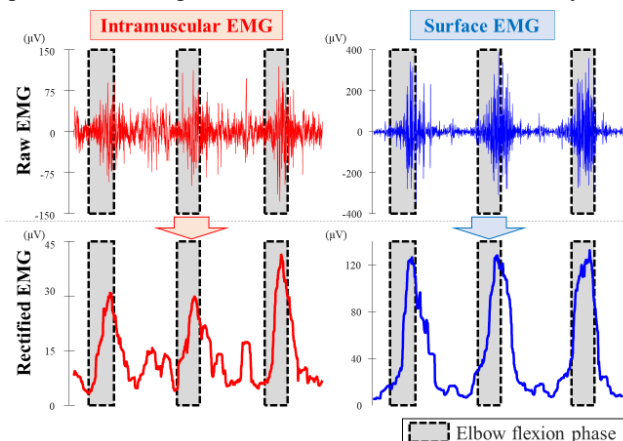


Figure 1. Intramuscular and surface EMG signals during the elbow flexion.

confirmed by ultrasonography. The EMG data were filtered, rectified, and then normalized by the peak values during the task (**Figure 1**). To compare the muscle activity patterns between the surface and intramuscular EMG, the coefficient of determination (R^2) of the patterns were assessed using regression analysis.

Results

As shown in **Figure 2**, the muscle activity of the BR tends to increase in the second half during elbow flexion. For comparing muscle activity patterns between the surface and intramuscular EMG, the R^2 of all subjects were higher than 0.8 in all forearm positions (Supination: $R^2 = 0.85 \pm 0.16$; Pronation: $R^2 = 0.92 \pm 0.08$; Neutral: $R^2 = 0.83 \pm 0.16$) (all $p < 0.05$). This result indicated that the muscle activity patterns of surface and intramuscular EMG were statistically similar.

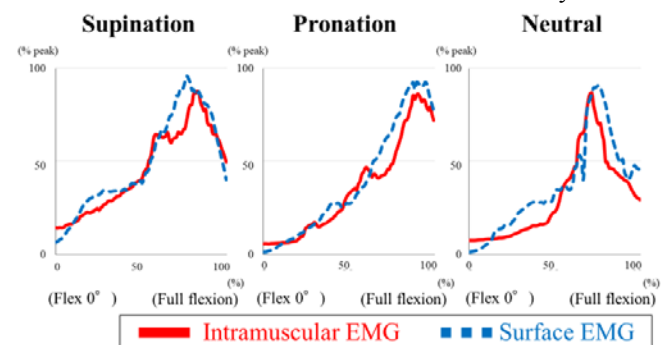


Figure 2. The muscle activity patterns of intramuscular and surface EMG.

Discussion

The BR has two heads: a superficial and a deep head. The superficial head is larger and places on anterolaterally [3]. Thus, in this study, it is considered that the surface and intramuscular EMG could be recorded from the surficial head of the BR.

Conclusions

It is suggested that the muscle activity of the BR can be assessed using surface EMG in the dynamic elbow flexion.

References

- [1] Basmajian JV et al. (1957), *J Bone Joint Surg Am*, **39-A**: 1106-1118.
- [2] Staudenmann D et al. (2015). *J Electromyogr Kinesiol*, **25**: 199-204.
- [3] Leonello DT et al. (2007). *J Bone Joint Surg Am*, **89**: 1293-1297

System identification to characterise shoulder stiffness in a functional posture at various levels of muscle contraction

Yahya Z. Yahya¹, Ian W. Hunter³, Thor F. Besier^{1,2}, Andrew J. Taberner^{1,2}, Bryan, P. Ruddy^{1,2}

¹Auckland Bioengineering Institute, The University of Auckland, Auckland, New Zealand

²Department of Engineering Science, The University of Auckland, Auckland, New Zealand

³Department of Mechanical Engineering, Massachusetts Institute of Technology, Cambridge, MA, US

Email: yyah724@aucklanduni.ac.nz

Summary

In this study, we present a method to quantify the function of the shoulder joint. This method is based on using system identification techniques to characterise shoulder joint stiffness in two degrees of freedom, internal/external rotation and horizontal abduction/adduction, at various levels of muscle voluntary contraction. Experiments have been conducted on six healthy participants. It has been verified that this method can successfully estimate shoulder stiffness and, therefore, it has potential to be used as a diagnostic tool for patients with shoulder disorders.

Introduction

The glenohumeral and scapulothoracic joints rely upon muscle for stability and normal function. Characterising muscles' influence on joint stiffness remains a challenge, but is important for understanding normal and pathological function. System identification can be used to characterise the mechanical stiffness, K , inertia, I , and viscous, B , parameters of human joints [1]. However, previous studies that have used system identification to investigate shoulder function did not evaluate the joint in functional postures [1,2].

The objective of this study was to use system identification to characterise the intrinsic mechanical properties of the shoulder joint during in/external rotation and horizontal ab/adduction at various levels of muscle activation. Shoulder stiffness, inertia and viscous properties were evaluated with the arm in an abducted, throwing posture.

Methods

Six male participants (age: 31 years \pm 5 years, body mass: 77 kg \pm 9 kg, and height: 1.77 m \pm 0.09 m), with no history of shoulder injury or neuromuscular disease, participated in this study.

A shoulder perturbation robot was developed to provide perturbations to the humerus in multiple degrees of freedom (DOF) [3]. Shoulder perturbations were performed in in/external rotation and horizontal ab/adduction, with the upper arm abducted to horizontal, elbow flexed to 90° and the palm of the hand facing forward. Maximum voluntary contractions (MVCs) in each DOF were performed. Then torque and angles were measured during stochastic binary sequence waveforms filtered by a low pass filter of 10 Hz cutoff frequency, while the participant was asked to maintain 0%, 10%, 20%, 30% and 40% of their MVC.

A parametric system identification approach was used to evaluate the stiffness, inertia and viscous properties from

angle and torque measurements [2] at each level of contraction.

Results and Discussion

As expected, across all participants, muscle activity resulted in changes to the stiffness and viscous parameters of the shoulder. The stiffness parameter, K , increased with the level of muscle contraction in internal rotation, external rotation, abduction and adduction. The viscous parameter, B , tended not to change with contraction.

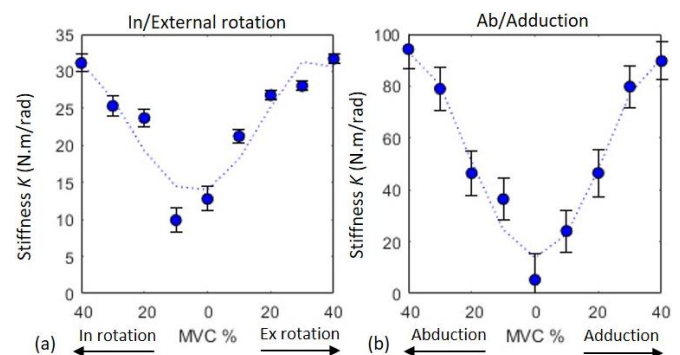


Figure 1. Stiffness parameters, K , and their 95% confidence intervals, for a typical participant, at various levels of contraction, (a) in/external rotation and (b) ab/adduction (right shoulder).

Previous studies [1,2] showed that the stiffness parameter, K , increased with contraction, and this is similar to what we found. Measuring shoulder stiffness in such a posture, where the shoulder is vulnerable to injury, is clinically important.

Conclusions

To conclude, shoulder joint stiffness was quantified in relevant posture and degrees of freedom. In the future, we will use this method to investigate shoulder pathology.

Acknowledgments

The authors would like to thank the Medical Centre of Research Excellence and the University of Auckland Faculty Research Development Fund for financial support.

References

- [1] Lipps D et al. (2015). *IFAC*, **48**:1369-1374.
- [2] Zhang L et al. (2000). *J Orthop Res*, **18**:94-100.
- [3] Yahya Y et al. (2020). *IEEE EMBC*, **42**: 4913-4916.

Assessing Upper Extremity Function by Applying a Sensor-Embedded Device

Charlie Chen Ma¹, Hsiao-Feng Chieh¹, Chien-Ju Lin^{1,2}, Fong-Chin Su^{1,2}

¹Department of Biomedical Engineering, ²Medical Device Innovation Center, National Cheng Kung University, Taiwan
Email: P88061041@gs.ncku.edu.tw

Summary

Upper extremity dysfunction could be occurred due to several disorders, diseases, or aging. It is crucial for clinicians to understand patients' upper extremity function (UEF) before offering treatments. However, current assessments of UEF are not digitized nor might be subjective by testers. This study offered a novel sensor-embedded holding device (SEHD) to digitized UEF evaluation, the results showed promising data to evaluate movement smoothness and grip strength which could offer objective clinical references for clinicians to understand each patient's UEF at site or remotely.

Introduction

Upper extremity dysfunctions could occur due to several diseases or systematic disorders, such as stroke, acute trauma, arthritis, aging, etc. Upper extremity dysfunctions are highly correlated to compromise quality of life. Therefore, to evaluate UEF is important to identify the problem and further customize rehabilitation programs for each individual.

There are many assessments for evaluating UEF which could be classified into groups: clinical tools, questionnaires, and functional test. However, most of the tests might not be able to be digitized or might be subjective that different testers might have different results from the same subject.

Therefore, this study focuses on designing a novel holding device to offer digitized upper extremity movement data and functional evaluation data for clinical references.

Methods

The SEHD includes one 6-axis IMU sensor, 14 force sensors and connects to MCU for further processing. The cylindrical outlook design of SEHD is due to the common shape for hand holding movements in the daily living.

13 young healthy individuals (male: female = 10:3, age = 25 ± 3) were recruited with signed consent form as subjects to perform tasks related to upper extremity movements.

Two movements were designed: (a) 2-step lifting, (b) maximum grip strength. The subjects were asked to practice once with each task and perform 3 trials for each task. The data were recorded and were processed by MATLAB.

Movement smoothness and force are the main parameters for this study. To calculate movement smoothness, based on Balasubramanian, S.'s study [1], log dimensionless jerk (LDLJ) would be most similar as what this study needs.

$$DLJ \triangleq \frac{-(t_2-t_1)^5}{v_{peak}^2} \int_{t_1}^{t_2} \left| \frac{d^2v(t)}{dt^2} \right|^2 dt$$

$$LDLJ \triangleq -\ln|DLJ|$$

The combined force of maximum grip of SEHD were recorded to understand the difference between SEHD and traditional grip test.

Results and Discussion

The movement of 2-step lifting could be divided into 4 phases, m0, m1 represents dynamic movement phases, s0, s1 represents static movement phases. The higher LDLJ number represent more jerk movements. The result (Figure 1.) showed during dynamic movement phases (m0 and m1) were not smooth as static movement phases (s0 and s1). The result could offer possible development of identify phases during movements, which could further apply in robotic designs.

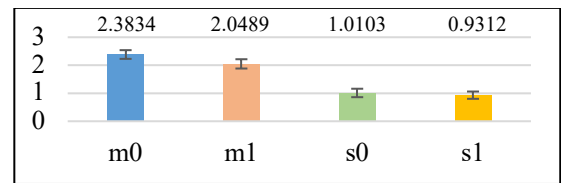


Figure 1: Movement smoothness (LDLJ) of 2-step lifting task, m0 represent first lifting dynamic movement, s0 represent holding phase after m0, m1 represent second lifting phase, and s1 represent holding after m1.

When comparing the SEHD maximum grip strength data with Jamar dynamometer, the result showed closely related (Table 1.) but not significant ($t = 0.091$, ns.). It could be due to the verbal instruction of the task that the researcher only ask subjects to grip SEHD as hard as they could, and the subjects did not place the fingers precisely on top of the sensors. However, the results were promising that the next version of the SEHD could offer force related data as clinical references.

Table 1: Grip strength comparison between Jamar dynamometer and SEHD

	Mean	N	Std. Deviation
Jamar	35.50000	13	9.067103
SEHD	39.47300	13	10.295808

Conclusions

This study focused on develop a novel sensor-embedded device for upper extremity functional evaluation. The main purpose of the device is to digitize evaluation data and offer proper clinical reference for clinicians to monitor the user's improvements and further to offer customized rehabilitation program for users.

Acknowledgments

Grant support from Taiwan Ministry of Science and Technology.

References

- [1] Balasubramanian, S et al. (2015). *J Neuroeng Rehabil*, 12, 112.

Quantify hand tremor of Parkinson's disease based on Channel State Information

Hui-Hsin Chen¹, Chi-Lun Lin²

^{1,2} Department of Mechanical Engineering, National Cheng Kung University, Tainan, Taiwan
Email: n16090023@gs.ncku.edu.tw

Summary

To provide physicians an objective way to consistently assess the severity of Parkinson's disease (PD), this study developed an approach to quantify the motor symptom via Wi-Fi channel state information (CSI). Our computer algorithm computed the frequency and duration of simulated hand tremors from the CSI data with an average accuracy of 90.94% and standard deviation of 3.53%.

Introduction

PD is a long-term neurodegenerative disease that mainly affects the motor functions of peripheral structures. Clinically, neurologists use Unified Parkinson's Disease Rating Scale to measure the progression of PD. However, different diagnoses may be made owing to the subjective judgment of professionals.

In this paper, we propose an innovative approach to quantify the hand rest tremor, which is a subtle motion and challenging to detect. This approach requires no intervention to the subject, captures no personally identifiable information, and allows long-term monitoring in the subject's natural state.

Methods

The proposed method captured the CSI of wireless communication links and recorded the multi-path fading effect in the environment. The contactless sensing was built by observing the corresponding relation between CSI variation and human activities.

We conducted experiments using the Linux 802.11n CSI Tool [1] with a TP-link Archer C60 commercial router (transmitter) and a Dell E6440 laptop (receiver). The network interface controller worked at a 5 GHz frequency band with a transmission rate of 1000 Hz. The experimental environment (Figure 1) is an enclosed classroom with existing desks and chairs.

A healthy participant, the only person in the room, imitated the hand tremor. The test was performed at 12 locations on the line perpendicular to line of sight (LOS) with equal distance of 50 cm and other 20 locations that uniformly spread in the room. The test at each location was repeated ten times with a frequency of shaking around 3-6 Hz [2] and a range of displacement fluctuation about 10-15 cm.

We applied the band-pass filter and principal component analysis to remove the noise from the CSI raw data and used energy-threshold segmentation to extract the target motion data. The frequency and duration of the motion were calculated. The participant also wore a MetaMotionR gyroscope (MBIENTLAB Inc., USA) on the wrist during the test with a sampling rate of 200 Hz to capture the reference data for evaluating the accuracy of our method.

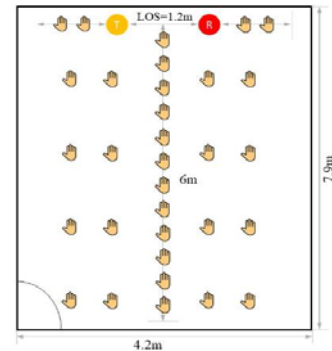


Figure 1: The experimental setup for the hand tremor detection. The 'T' denotes the transmitter, and the 'R' is the receiver.

Results and Discussion

Our algorithm was able to distinguish the active and rest states in the room. The influence of hand tremor induced wave crests in the received signals, as the center region framed by red dashed lines shown in Figure 2. We obtained the frequency and duration of hand tremor by computing the number of wave crests and their occurrence intervals. The results revealed that the accuracy of our approach was ranged from 85 to 95% (AVG. 90.94%, STD. 3.53%) by comparing with the gyroscope data. We also found that the measurement accuracy reduced as the motion location moved away from the LOS. Overall, the results showed that accurate motion detection could be achieved in the whole room.

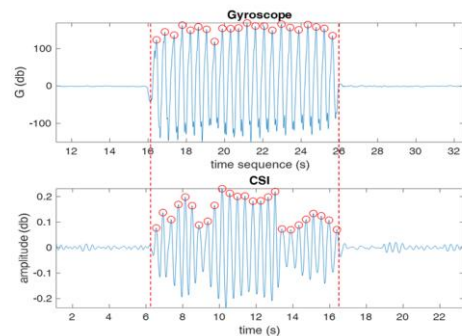


Figure 2: The results of the hand tremor detection using the gyroscope (top) and our approach (bottom).

Conclusions

We achieved non-contact PD symptom qualification with high accuracy by using the Wi-Fi CSI and robust signal processing methods. We overcame the restriction of the past research that subtle motion could only be sensed at designated positions and succeeded in detecting them in a whole room.

References

- [1] D. Halperin et al. (2011). *ACM SIGCOMM Computer Communication Review*, **41**: 53
- [2] A. Lemstra et al. (1999). *Neuroscience Letters*, **267**: 129-132

Positioning effects of GPS Sensors during running

Clint Hansen¹, Alina Schneider², Carl Schwenke², FalkPetzold², Stefan Kratzenstein²

¹Neurogeriatrics, University Hospital Kiel, Kiel, Germany

²CAU Motion Lab, Kiel University, Kiel, Germany

Email: c.hansen@neurologie.uni-kiel.de

Summary

GPS sensors are widely used in strength and conditioning (S&C) settings around the world. Preliminary results of eight sensors show little inter and intra sensor variability. In summary the sensors are suitable for S&C applications such as track and field or large pitch games.

Introduction

Measuring human movement during sports applications has a long standing tradition in biomechanics and especially in strength and conditioning (S&C). The systems vary and with the technological development training load estimations are more and more performed using GPS. The GPS sensors however often suffer from connectivity glitches introducing errors to the analysis. This becomes especially pertinent if training load parameters are assessed with multiple sensors e.g. to evaluate training load of a whole team. Previous work has reported that GPS sensors suffer from low acquisition frequencies or occlusion problems [1]. Applying signal processing techniques (e.g. filtering) could help to overcome some of those issues. In this work we test the intra and inter reliability of eight GPS sensors of the same brand to understand the overall bias introduced by the sensors positioning during a running task.

Methods

A distance of 200m was set at track and field stadium at the University Kiel. The test was performed by young healthy participants. In contrast to the manufacturer recommendation participants were equipped with eight GPS sensors attached to the back. 200m running trials were performed at 8 & 10km/h (2.22 & 2.78m/s). Data were collected and analyzed using the Titan Team Stats data processing tool.

Results and Discussion

A total of ten runs was performed. Here, we show the visualization from one sensor throughout the ten runs as a heatmap (Figure 1). The resulting distances are shown in Table 1.

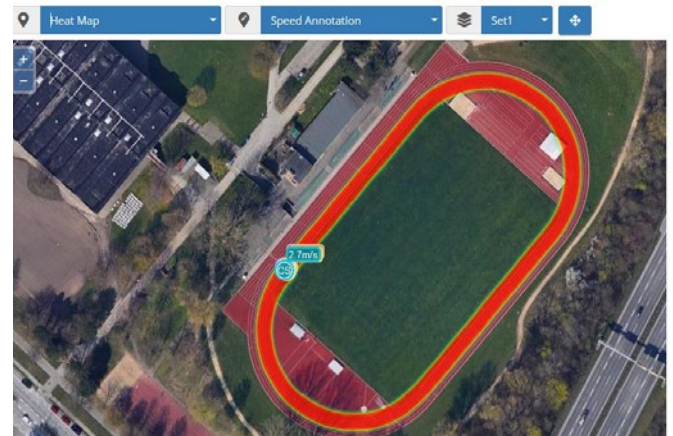


Figure 1: Heatmap showing the GPS units during the running trials on the track and field stadium .

Conclusions

The aim of this work was to present the potential errors introduced by positioning GPS sensors on various locations of the back of an athlete. The positioning introduced errors however on average the errors remain lower than eight percent. In addition to the positioning, the manual data analysis may have also introduced a bias resulting in those relative large absolute errors of 9.2m for the 10km/h and 8.7m for the 15km/h runs. Even though we need to account error in positioning the sensors on the back in a practice session, current GPS systems are a promising technology for tracking motions on the field.

References

- [1] Cummins et al. (2013). *Sports Med*, **43**,10, 1025-42.
- [2] Aughey (2011). *IJSSPP*, **6**, 3, 295-310.

Table 1: Results expressed as mean (standard deviation) [percentage error] of the executed running experiment.

	Sensor 1	Sensor 2	Sensor 3	Sensor 4	Sensor 5	Sensor 6	Sensor 7	Sensor 8
10km/h	188,14 (2,5) [5.9]	189,78 (3.1) [5.1]	191,7 (2.9) [4.2]	186,96 (1.5) [6.5]	188,3 (1.5) [5.8]	186,42 (5.4) [6.8]	198,16 (2.1) [0.9]	196,64 (1.1) [1.7]
15km/h	192,1(2.2) [4.0]	192,7(1.2) [3.7]	195,54(1.4) [2.2]	190,6(2.0) [4.7]	185,44(3.1) [7.3]	185,54(0.5) [7.2]	198,32(1.4) [0.8]	190,32(2.3) [4.8]

Evaluating The Validity Of An Inertial Measurement Unit For Determining Knee And Trunk Kinematics During Athletic Landing And Cutting Movements

Chia L.¹, Andersen J.¹, McKay M.¹, Sullivan J.¹, Megalaa T.¹, Pappas E.^{1,2}

¹Sydney School of Health Sciences, Faculty of Medicine and Health, The University of Sydney, Sydney, NSW, Australia

²University of Wollongong, Wollongong, NSW, Australia

Email: lclionelchia@gmail.com

Summary

Inertial Measurement Units (IMUs) are a promising alternative to laboratory-based motion-capture methods for the biomechanical assessment of athletic movements. The aim of this study was to investigate the validity of an IMU system for determining knee and trunk kinematics during landing and cutting tasks in sporting populations. Twenty-seven participants performed five cutting and landing tasks while their motion was simultaneously recorded using an optoelectronic motion capture system and an IMU system. Based on good-to-excellent correlation, reasonable accuracy (RMSE<5°), bias within 2°, and limits of agreements within 10°, we recommend the use of this IMU system for knee sagittal-plane range-of-motion (ROM) estimations during cutting, trunk sagittal-plane peak angle estimation during double-leg landing, trunk sagittal-plane ROM estimation for almost cutting and double- and single-leg landing tasks. Due to poor comparisons with the optoelectronic system, we currently do not recommend this IMU system for knee frontal-plane estimations.

Introduction

Knee injuries account for up to a third of severe injuries in sports involving high pivoting and landing demands such as basketball and soccer [1]. To reduce injury risk, a greater understanding of injury biomechanics is required. IMUs are convenient, cost- and time-effective devices that are promising alternatives to ‘gold-standard’ laboratory-based motion capture methods. However, current IMU algorithms are activity-specific, and their validity in sporting contexts remains limited. The aim of this study was to investigate the validity of an IMU system for determining knee and trunk kinematics during landing and cutting tasks for clinical and research applications in sporting populations.

Methods

Twenty-seven participants (14 males and 13 females, 28.7 ± 5.6 years, 1.7 ± 7.5m, 70.3 ± 15.2kg) performed five cutting

and landing tasks – anticipated 45° jump-stop cutting task to the right (CUTR) and left (CUTL) double-leg drop landing (DLL), and single-leg drop landing on the right (SLLR) and left leg (SLLL)– while their motion was recorded using a gold-standard optoelectronic motion capture system and an IMU system (Figure 1). Intra-class coefficients (ICC 2,1), Pearson’s *r*, root-mean-square error (RMSE), bias, and Bland-Altman limits of agreements between the motion capture and IMU systems were quantified for knee and trunk sagittal- and frontal-plane range-of-motion (ROM) and peak angles.

Results and Discussion

IMU validity was task-, joint-, and plane-dependent (QR Code links to full results). Based on good-to-excellent (ICC) correlation, reasonable accuracy (RMSE<5°), bias within 2°, and limits of agreements within 10°, our findings support the use of this IMU system for sagittal-plane estimations, especially for the knee and trunk during cutting, and the trunk during double-leg landing movements. Increasing trunk and knee flexion during landing and cutting movements is a common objective of knee injury prevention programs [2]. Due to poor comparisons with the optoelectronic system, we currently do not recommend this IMU system for knee frontal-plane kinematic estimations.



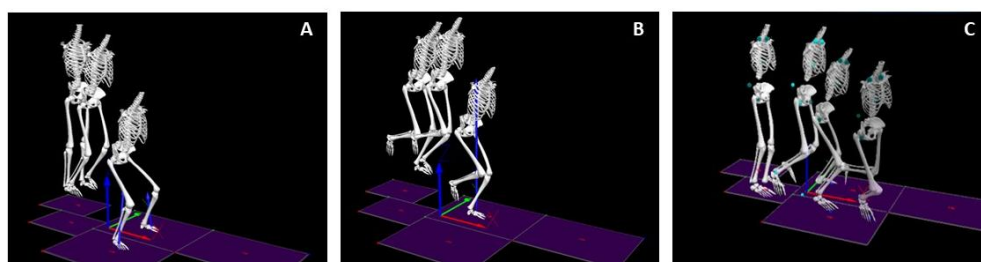
Conclusions

The IMU estimated sagittal-plane movements better than frontal-plane movements. IMU validity was task-, joint-, and plane-dependent. Fast athletic movements, such as those assessed in this study, present challenges for IMUs and further evaluation of algorithms, biomechanical models, sensor fixation and placement methods in sport-specific contexts should be performed before widespread usage.

References

- [1] Agel et al. (2007). *J Athl Train.* 42(2): 202
- [2] Fox (2018). *Sports Med.* 48(8): 1799-807

Figure 1: Illustrations of the (A) double-leg landing, (B) single-leg landing, and (C) anticipated jump-stop 45° cutting tasks



Is the Standing Long Jump Specific-Shoe really Necessary for Chinese Students?

Yang Song^{1,2,3}, Jialin Li⁴, István Bíró^{2,3} and Yaodong Gu¹

¹Faculty of Sports Science, Ningbo University, Ningbo, China

²Doctoral School on Safety and Security Sciences, Obuda University, Budapest, Hungary

³Faculty of Engineering, University of Szeged, Szeged, Hungary

⁴Ningbo University School of Medicine, Ningbo University, Ningbo, China

Email: guyaodong@hotmail.com

Summary

The purpose of this study was to investigate if the standing long jump specific-shoe (SS) can really help Chinese students achieve greater performance during the standing long jump test compared to normal sports shoe (NS). Eight participants (4 male and 4 female) performed six standing long jumps with jump distance and kinetic parameters collected utilizing long jump mat and Kistler force platform simultaneously. Both male and female participants tended to achieve greater jump distance in the SS condition, however, more research with larger sample size are warranted for further verification.

Introduction

The performance of standing long jump is often used as one of the best fitness tests to examine explosive power of the school students, especially in China [1]. Thus, many sports products companies introduced the standing long jump specific-shoe (SS), and claimed that SS can effectively enhance performance. The performance of standing long jump is highly associated with various factors based on previous studies [1,2]. Two questions arise, however. Firstly, few studies have attempted to explore the effect of different kinds of shoes on the quality of standing long jump. Moreover, the internal mechanisms contributed to this effect are consequently not so clear. Therefore, this study aimed to investigate if the SS can really help Chinese students achieve greater standing long jump performance.

Methods

A total of 8 university students (4 male and 4 female) were recruited. Participants reported no professional long jump experiences before. The study was approved by the Ethics Committee of Ningbo University and written informed consent forms were obtained. Conventional sports shoe and standing long jump specific-shoe with the same ethylene-vinyl acetate (EVA) midsole were used in this study (EU size 41-43, Figure 1). Participants were asked to perform 6 successful standing long jumps in each shoe. The jump distance was measured by a long jump mat and the kinetic data including vertical peak force (Fz), horizontal peak force (Fy) were collected by Kistler force platform (Kistler, Switzerland)

and then normalized to the participants' body weight (N). The traction coefficient (TC) was further calculated from the ratio of horizontal and vertical force [3]. A dependent-sample T-test was used to analysis the statistical differences of the jump distances and kinetic data. All data are presented as mean \pm SD and *P* was set at 0.05.



Figure 1: Experimental shoes (Left: SS; Right: NS)

Results and Discussion

The present study has found that both male and female participants tended to achieve greater jump distances when they jumped wearing SS (Table 1). The reason for the lack of significance may be the limited sample size. Further research with larger sample size must be done to verify the result.

The greater the TC is, the more one can lean forward [3]. It was found that the TC at take-off was significantly larger when jumped using SS (Table 1). Thus, it is deduced that the greater TC increases the horizontal length of the body's center of gravity, contributes to more horizontal force (which is also found in this study) and propulsive impulse, and further enhances performance [3].

Conclusions

It was found that SS may increase the jump distance partly due to the increased traction coefficient and horizontal force at take-off. However, more studies are warranted before it can be further verified.

References

- [1] Mackala K et al. (2013). J Strength Cond Res, **27**: 2674–2684.
- [2] Wakai M and Linthorne NP (2005). Hum Movement Sci, **24**: 81–96.
- [3] Kugler F and Janshen L (2010). J Biomech, **43**: 343–348.

Table 1: Comparison of long jump distance and kinetic parameters.

Variables	SS(Male)	NS(Male)	<i>P</i>	SS(Female)	NS(Female)	<i>P</i>
Jump Distance	222.70 \pm 18.28	208.90 \pm 10.91	0.05	178.60 \pm 17.72	171.20 \pm 21.35	0.41
Fy	5.93 \pm 1.33	5.15 \pm 1.17	0.01	6.94 \pm 2.23	5.59 \pm 1.92	0.002
Fz	12.00 \pm 3.58	12.77 \pm 3.87	0.09	14.45 \pm 3.32	14.18 \pm 3.80	1.00
TC	0.59 \pm 0.17	0.46 \pm 0.15	0.01	0.52 \pm 0.19	0.42 \pm 0.14	0.001

Development of snowboard force measurement system

Yun Chen¹, Ming Li¹, Wei Zhuang¹, YiWu Xiong¹, Yu Liu¹

¹School of Kinesiology, Shanghai University of Sport, Shanghai 200438

Email: 15617165575@163.com

Summary

With the approach of 2022 Beijing Winter Olympic Games, how to improve the performance of winter athletes quickly and efficiently has become the core issue of coaches and sports workers. In order to promote the scientific and effective training of skiers and promote the biomechanical research of skiing, based on the existing structure of snowboard, a three-dimensional force sensor and a high-precision data acquisition box are installed between the skis and the fixator components, and a snowboard force measurement system with high-precision XYZ triaxial force acquisition is designed, which provides technical support for improving the performance of skiers.

Introduction

Skiing in the Winter Olympic Games is an outdoor speed racing and skilful sport with the characteristics of wide range of motion. Due to its fast displacement speed and relatively complex movement technology, it is difficult for the existing laboratory to collect its dynamic data indoors [1]. The measurement of force is a necessary condition for the research and analysis of skiing biomechanics. Timely acquisition of the ground reaction force can help coaches and related researchers to analyze and diagnose the athletes' pedaling force. However, reviewing the existing findings, there is not enough accurate force measuring equipment to conduct a complete mechanical analysis of skiers' performance [2]. Therefore, in order to promote the scientific and effective training of skiers and promote the biomechanical research of skiing, it is necessary to develop relevant force measuring equipment to detect the stress state and performance of skiers in skiing. Based on this, the research team designed a snowboard force measurement system for skiers according to the characteristics of skiing and biomechanical technology.

Methods

The overall design : This product is a snowboard force measuring system, which is installed in the whole snowboard assembly, including two three-component force sensors, a set of high-precision data acquisition system, a SD

card, a power supply, etc. Based on the existing structure of the ski, a three-component force sensor and a high-precision data acquisition box are installed between the snowboard and the fixator component (Figure 1). Power supply interface, SD card slot interface and power switch are designed on the side, and the interface is covered by the corresponding cover plate to facilitate the training.

The three-component force sensor (including the transfer plate) is connected with the skis and the fixator components, and is divided into two front and back, which is used to measure the load changes in the training process of athletes. The high-precision data acquisition box is installed in the middle area of the two three-component force sensors, which can convert the analog signals of the two three-component force sensors into digital signals that are convenient for calculation and transmission. The three-component force sensor is made of aluminum alloy, while the high-precision data acquisition box is made of nylon and other plastic materials, which greatly reduces the quality of the whole system, while ensuring the strength and stiffness of the structure to meet the actual use requirements.

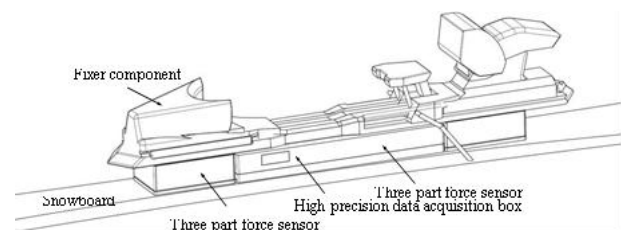


Figure 1: Schematic diagram of snowboard force measurement system

Key components : Three-component force sensor :

Three-component force sensor design, on the basis of the principle of strain electrical measuring temperature of output signal, high sensitivity, can effectively meet the training test requirements of skis force measurement and control system, and to prevent it in the process of skiing, snow because of the intense exercise into the force measurement and control system, both the closed and block processing (figure 2), to ensure that the skis force measurement and control system can meet the requirements of snow training.

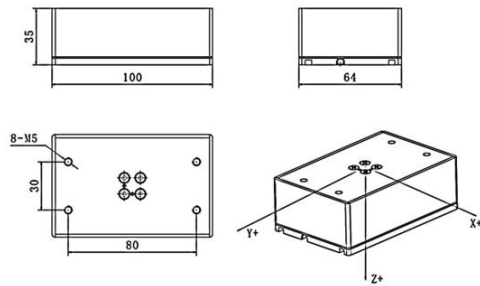


Figure 2: Three component force sensor contour diagram

High precision data acquisition system : The high-precision data acquisition system on the snowboard force measuring system includes signal conditioning circuit, A/D conversion circuit, data calculation, data transmission and storage modules. The analog signals of the two three-component force sensors can be converted into digital signals that are convenient for calculation and transmission, and the precision and speed of the output data can reach a higher level with the help of high-speed acquisition and machine learning algorithms and other technologies. The data of the high-precision data acquisition system is stored in the SD card in real time, and can be transmitted to the computer in real time, so that the customer can read and use it later.

- [1] Hu, C.H., et al., (2019) Skiing Simulation Based on Skill-Guided Motion Planning. *Computer Graphics Forum*. 38(6):66-78.
- [2] Klous, M., E. Muller, and H. Schwameder,(2014)Three-dimensional lower extremity joint loading in a carved ski and snowboard turn: a pilot study. *Comput Math Methods Med*. 14:340272.

Locomotor changes in knee osteoarthritis patients during a 6-minute walk test

Stuart C. Millar¹, Kieran Bennett¹, Mark Rickman² and Dominic Thewlis¹

¹Centre for Orthopaedic and Trauma Research, University of Adelaide, Adelaide, Australia

²Department of Orthopaedics and Trauma, Royal Adelaide Hospital, Adelaide, Australia

Email: stuart.millar@adelaide.edu.au

Summary

Several means have been proposed to assess the presence, severity and impairment associated with knee osteoarthritis (OA). Recent studies have suggested the use of physical performance tests to assess joint function for those with knee OA. This study investigated lower limb kinematics over the course of a 6-minute walk test (6MWT). Hip, knee and ankle joint angles were computed for the first and last minute of the 6MWT. Results indicated there to be no locomotor breakdown over the 6-minute period highlighting the 6MWT as a strong measure to quantify functional changes in people with knee OA.

Introduction

Knee osteoarthritis (OA) is a chronic condition affecting the entire joint and surrounding tissues, resulting in pain, stiffness and impaired movement [1]. While end-stage disease is most frequently treated with total knee replacement surgery, there is no definitive treatment option for people with mild-moderate knee OA – yet this is a significant target for pharmaceutical companies around the world. Recent regulatory approval processes now require, or at least strongly suggest, that joint function should form part of the assessment of efficacy of new treatments for knee OA. The 6-minute walk test (6MWT) has been consistently identified as a strong candidate tool for assessing function in people with knee OA [2]. The aim of this study was to investigate the stability of lower limb biomechanics during a 6MWT in people with moderate-severe knee OA.

Methods

Nineteen participants with knee OA were recruited for this study (Table 1). Gait data were collected in a single testing session during which participants were required to complete a 6MWT. Participants walked barefoot around a 20 m course with walking gait captured using a 10-camera Vicon Vantage system and two AMTI force platforms. Kinematic reconstruction of the data was undertaken in Visual 3D (V6, C-Motion Inc.). Gait speed and joint angles for the hip, knee and ankle were calculated during the first and last minute of the 6MWT. A paired samples t-test was performed to determine if there were changes in temporospatial or kinematic parameters between the first and last minute of the 6MWT. Additionally, a one-dimensional paired t-test was

performed in SPM1D [3] to determine if there was a difference in knee kinematics across a complete gait cycle.

Results and Discussion

Patient demographics and temporospatial measures from the 6MWT are presented in Table 1. There were no statistically significant differences in joint angles (Figure 1) or gait speed measured between data from the first and last minute of the test.

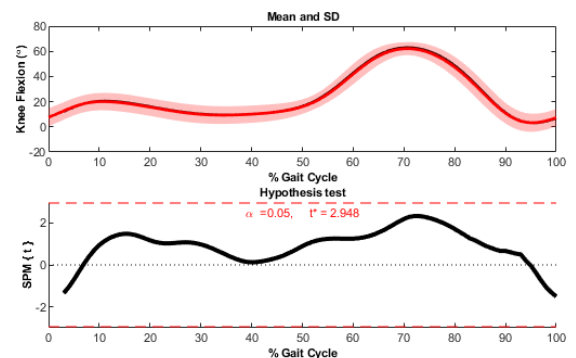


Figure 1: Mean and standard deviation for knee flexion during first (red) and last minute (black). The paired t-test shows no significant difference between the two groups across the entire gait cycle.

Conclusions

The data indicate there to be no breakdown of locomotor control across the course of the 6-minute period for knee OA sufferers. These data serve to support the notion that the 6MWT can be considered an appropriate performance test to quantify gait changes in people with knee OA when assessing the efficacy of treatments or interventions to reduce pain or improve function.

Acknowledgments

This study received funding from XALUD Therapeutics and the NHMRC (CDF ID: 1126229).

References

- [1] Haq I et al. (2003). *Postgrad Med J*, **79**:377-383.
- [2] Coleman G et al. (2020). *Arthritis Care Res.*, **72**:452-85.
- [3] Pataky TC. (2012). *Comput Methods Biomech Biomed Engin.*, **15**:295-301.

Table 1: Participant demographics and temporospatial parameters.

	Age (years)	Body Mass (kg)	BMI	KOOS Pain	KOOS Symptoms	6MWT Distance (m)	Gait Speed (m/s) First Min.	Gait Speed (m/s) Last Min.
Mean	62.8	96.1	32.0	39	38	366	1.24	1.23
SD	7.4	17.4	4.5	9	17	63	0.23	0.25

A Study on The Hip Joint Mechanism of The Exoskeletal Robot to Improve The Assistance Performance

Mingoo Jeong¹, Taeyeon Kim², Kyongchul Kong^{*}

^{1,2,*} Department of Mechanical Engineering, Korea Advanced Institutes of Science and Technology, Daejeon, South Korea
Email: mg.jeong@kaist.ac.kr

Summary

This paper proposes a new hip joint mechanism for an exoskeletal robot that can deliver the assisting torque without limiting the wearer's hip movement. The proposed mechanism allows all hip joint movements of the wearer and solves the rotation axis mismatch problem between the wearer and the robot.

Introduction

The human hip joint is one of the joints that play a significant role in daily human movements. As such, the hip joint impact on daily life is immense, so many researchers are developing exoskeletal robots to assist the hip joint [1, 2]. However, since the hip joint has the shape of a spherical joint, allowing all the hip joint movements with an exoskeletal robot is a challenging problem. Furthermore, if the rotation axis of the human and the exoskeletal robot are mismatched, the wearer must feel uncomfortable during motion. In this paper, a new mechanism of an exoskeletal robot for hip joint assistance is proposed to solve these difficulties.

Methods

Figure 1 shows the hip joint mechanism that was designed to solve the problem of rotation axis mismatch between the wearer and the robot and allow movement about all three rotation axes. In the proposed mechanism, a hinge joint and a prismatic joint are arranged in series on the back part, allowing the hip joint's internal and external rotation. There is also one hinge joint and a prismatic joint on the thigh side, so adduction and abduction motion can be allowed without any restrictions. In the case of flexion and extension, like other exoskeletal robots, one actuator is installed on each side to assist the movement. Furthermore, the robot is equipped with a backplate, so that the torque output from the actuator can be effectively transmitted to the trunk.

The experiment compares the difference in motion before and after wearing the robot to verify the proposed mechanism does not interfere with or limit the wearer's

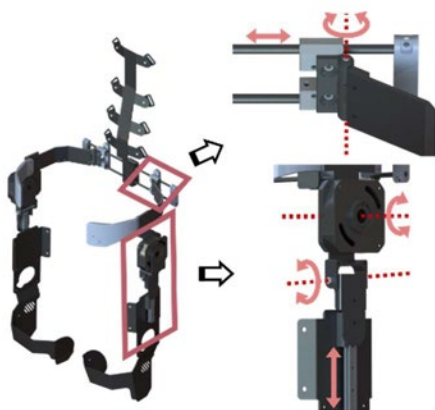


Figure 1 : The proposed hip joint mechanism

movement. Since the robot was customized for one person, the test subject consists of one person. The comparison motion was set as a walking motion, and a 3D motion capture system was used to measure the movement for each condition. The subject walked a 5m walking rail and performed a total of 10 walks for each situation. Besides, the subject performed the walking speed and the step length according to the subject's preference.

Results and Discussion

Figure 2 shows the motion of each joint in the sagittal plane. As can be seen through this, there is no significant difference in walking motion before and after wearing the robot. In addition, the walking speed with and without the robot was 1.393 m/s and 1.391 m/s, respectively, and the stride length was 1.386 m and 1.382 m, respectively. Therefore, through the above experimental results, it can be concluded that the proposed robot does not interfere with or limit the movement of the wearer.

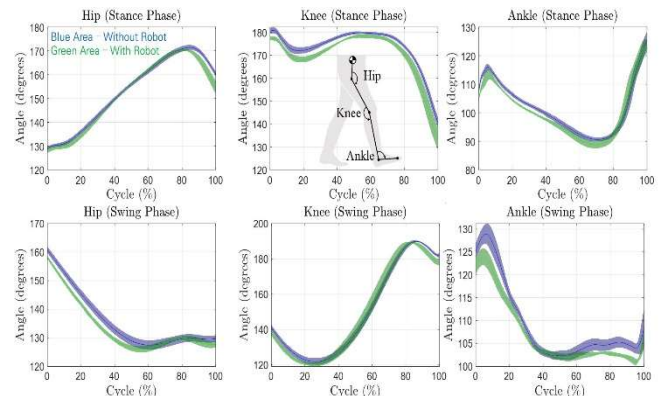


Figure 2 : Difference in motion in the sagittal plane

Conclusions

The mechanism proposed in this paper was devised to solve the mismatch of the rotation axis with the wearer while allowing all the wearer's hip joint motion. The effectiveness of this mechanism was verified by comparing the differences in gait motion. However, additional experiments are required to analyze the burden acting on the wearer more clearly.

Acknowledgments

This work was supported by the Technology Innovation Program (20007096, Super Human Robot Suit Project) funded By the Ministry of Trade, Industry & Energy (MOTIE, Korea)

References

- [1] Ting Zhang et al. (2018). *IEEE/ASME Transactions on Mechatronics*, **1**: 274-285.
- [2] Jongwoo Lee et al. (2020). *ICRA 2020*.

The 3D CoM kinematic estimation using a simple machine learning for portable gait monitoring

Myunghyun Lee¹, Kyoungchul Kong¹, Sukyung Park¹
¹Dept. Mechanical Engineering, KAIST, Daejeon, Republic of Korea
 Email: sukyungp@kaist.ac.kr

Summary

The center of mass (CoM) can be used as a major factor for gait monitoring. Therefore, many studies have tried to estimate the CoM kinematics using an inertial measurement unit (IMU) attached to the sacrum, but the estimation accuracy of velocity and acceleration was not high enough. In this study, we estimated the 3-axis CoM kinematics by first estimating CoM velocity using a machine learning. The change in velocity was estimated from the sacral IMU data using an artificial neural network (ANN), and the position and acceleration were derived by integrating and differentiating the velocity. We estimated the CoM kinematics with high accuracy, which reduced an error of up to 4 times compared to the sacral kinematics. With help of this accurate estimation method, it is expected that the CoM-based gait monitoring with a single IMU would be improved.

Introduction

The CoM is used as an indicator for gait monitoring. Since the CoM is not fixed to a specific part of the body, many gait analysis have used an IMU attached to the sacrum, which is most similar to the CoM[1]. However, the range and phase of motion of sacrum differ from that of the CoM[2]. In order to narrow the difference, many studies have tried to estimate the CoM kinematics using the sacral kinematics, but only focused on estimating the position[3]. However, a large error could occur by differentiating the estimated position to calculate the velocity and acceleration. To prevent a large error resulting from differentiating the position, highly accurate estimation method is required to estimate the CoM kinematic such as the velocity or the acceleration. In this study, the CoM velocity were estimated using machine learning, and the position and acceleration were estimated based on the estimated velocity.

Methods

To estimate the 3-axis CoM kinematics, the CoM velocity was estimated from the IMU data, and then the position and acceleration were calculated using the estimated velocity (Fig. 1). The sacral kinematics from an IMU were used to estimate the CoM velocity using an ANN. The walking speed was estimated from IMU data[1] and the velocity and position were derived by integrating the acceleration. The output was set as 3-axis CoM velocity with the average walking speed in the anteroposterior (AP) direction removed. The 3-axis acceleration and position were calculated using the estimated velocity added the estimated walking speed by IMU.

To verify the proposed method, 17 healthy subjects walked on the treadmill at four speeds (0.7, 1.0, 1.3 and 1.6 m/s) after signing the consent form approved by the KAIST IRB. The sacral kinematics were measured by a motion capture system and a sacral IMU. The CoM kinematics were calculated using the ground reaction forces measured by the force plates under

the treadmill. The estimation accuracy was verified by the normalized root-mean-square error (NRMSE) and RMSE between the measured and estimated CoM kinematics.

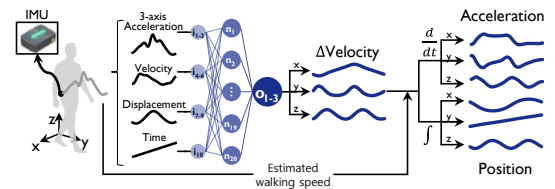


Figure 1: The CoM estimation method using machine learning

Results and Discussion

By estimating the change in velocity instead of absolute velocity, CoM velocity was estimated using machine learning from IMU data. The change in velocity could be estimated within 15% of the average NRMSE and within the average RMSE of 0.05m/s. With the estimated velocity change, the 3-axis position, velocity, and acceleration of CoM could be estimated (Fig. 2) within 17% of the average NRMSE except AP velocity. The average of RMSE were 5-57 mm for position, 0.029-0.102 m/s for velocity and 0.4-0.9m/s² for acceleration. Compared with the sacral kinematics from IMU, the estimation error was reduced by at least one-time (AP position) and up to four times (mediolateral (ML) acceleration).

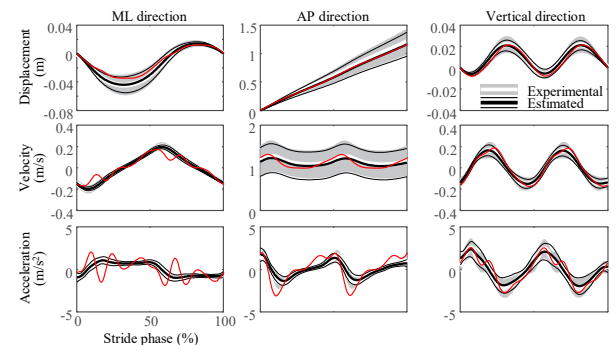


Figure 2: The CoM kinematics (red: sacral kinematics)

Conclusions

By first estimating the CoM velocity using machine learning, the CoM kinematic estimation from the sacral IMU could be improved. The CoM kinematic estimation method using a single IMU can be used for CoM-based gait monitoring.

Acknowledgments

This research was funded by the Ministry of Health & Welfare, Republic of Korea (# HJ20C0007).

References

- [1] Lee M and Park S (2020). *Sensors-Basel*, **20**(21): 6277.
- [2] Jeong B et al. (2018). *Gait Posture*, **62**: 333-341.
- [3] Floor-Westerdijk MJ et al. (2012). *Ieee T Bio-Med Eng*, **59**(7): 2080-2084.

Design and Verification of Bio-mimetic Knee Joint Mechanism for Exoskeletal robots

Taeyeon Kim¹, Mingoo Jeong² and Kyoungchul Kong*

^{1,2,*} Department of Mechanical Engineering, Korea Advanced Institute of Science and Technology, Daejeon, Republic of Korea
Email: ty.kim@kaist.ac.kr

Summary

A novel knee joint mechanism that mimics knee anatomy has been proposed to reduce misalignment. It consists of curved guide rails and bearings. The curve is designed based on human motion data. In this paper, the single pin joint and the proposed biomimetic joint are compared through experiments using pressure sensors. Pressure data between the human body and the frame was measured. The results showed that the bio-mimetic knee joint could improve the wearability by reducing misalignment.

Introduction

Knee is the most complex joint in the human body. While the knee bends, sliding and rolling occur in the sagittal plane. Thus, the instantaneous center of rotation of shank moves significantly with the flexion angle. However, many of well-developed exoskeleton robots have fixed pin knee joint structure[1]. If the robot frame and shank have different rotation axis, the exoskeleton will deviate from the human movement. This misalignment acts as the main factor of the unintentional repulsive force between the wearer and the robot system. Therefore, it is essential to decide the joints' structure so that it can smoothly follow the movements.

Methods

As shown in Figure 1(a), The curved guide rail acts like femur condyle. Three bearings that are fixed at the shank frame keep contact with this rail, maintain 1DOF movement. Two of them (yellow) support the weight like meniscus, and the top one (blue) prevents deviation like a ligament.

The shape of guide rail is designed using motion data of the shank with respect to the thigh. However, two bearings fixed at the shank will create two different trajectories as knee bent if the locations are arbitrary selected. For make continuous and simultaneous contact of two bearings, the trajectories need to be overlapped. Thus, it is necessary to optimize the bearings location. Figure 1(b) shows the optimized bearing trajectories and generated rail's shape. Using curve-fitting method, the result curve is derived which has minimum error. Bottom curve of the rail is generated by offset the result curve with bearing radius.

Evaluation and comparison the wearability by wearing the robot in real environment is necessary. The overall experimental process is shown in Figure 2(a). Air bladder made with silicon tube with pressure sensor [2] is chosen for measuring the repulsive pressure between human skin and robot's braces. Pressure sensor is attached to the both side of the shank. Assume that the human skin and the braces are elastic, then the measured pressure is proportional to the misalignment via Hook's law. For minimize the muscle activation effect, the wearer was seated in a chair and his shank were moved by a pulley.

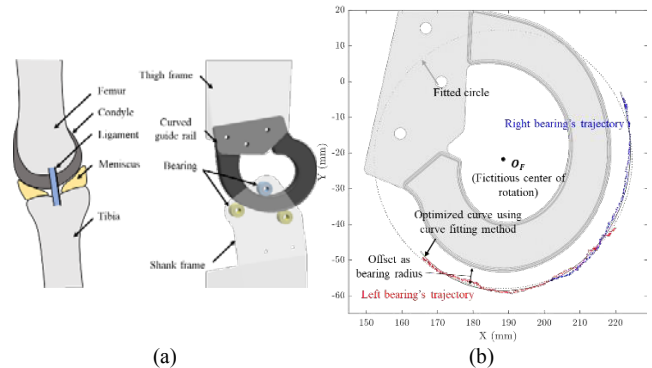


Figure 1: (a) Design method of the bio-mimetic joint. (b) Optimization result for curved guide rail

Results and Discussion

Pressure difference between front and rear side of the shank is plotted in Figure 2(b). As can be seen in the figure, the maximum pressure value and the sum of the absolute value of pressure are reduced about 70% when using bio-mimetic joint. Therefore, through this experiment, it was verified that the bio-mimetic joint greatly improved wearability.

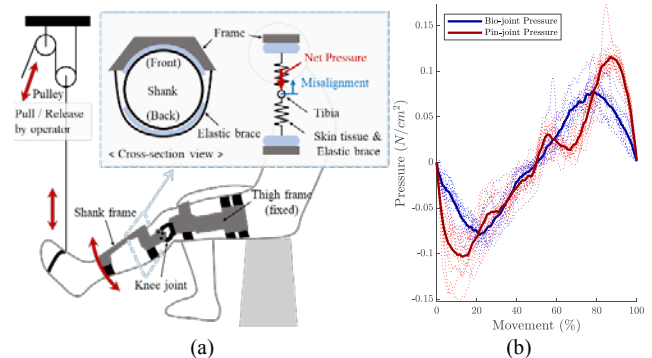


Figure 2: (a) Experimental procedure diagram. (b) Pressure data of bio-mimetic joint and pin joint.

Conclusions

Misalignment reduction using bio-mimetic knee joint is verified. A new direction for developing more comfortable exoskeletal device was established to compare the wearability according to the structural characteristics.

Acknowledgments

This work was supported by the Technology Innovation Program (20007096, Super Human Robot Suit Project) funded By the Ministry of Trade, Industry & Energy (MOTIE, Korea).

References

- [1] Cenciari et al. (2011). *IEEE International conference on rehabilitation robotics*, p. 1-6.
- [2] Kong, K., and Tomizuka, M. (2009). *IEEE/ASME Transactions on mechatronics*, 14(3), 358-370.

The repeated bout effect in the human medial gastrocnemius muscle: the influence of fascicle stretch elicited during different muscle contractions

Patricio A. Pincheira¹, Ben W. Hoffman^{1,2}, Andrew G. Cresswell¹, Timothy J. Carroll¹, Nicholas A. T. Brown³ and Glen A. Lichtwark¹

¹ School of Human Movement and Nutrition Sciences, The University of Queensland, QLD, Australia

² School of Health and Wellbeing, University of Southern Queensland, QLD, Australia

³ Research Institute for Sport and Exercise, University of Canberra, ACT, Australia

Email: uqpinch@uq.edu.au

Summary

The aim of this study was to determine the influence of muscle fascicle stretch elicited during eccentric (ECC) and isometric (ISO) contractions on the magnitude of exercise-induced muscle damage (EIMD) and the repeated bout effect (RBE). In 14 participants, we measured medial gastrocnemius' (MG) twitch torques and soreness scores before and after repeated bouts of ECC and ISO performed in contralateral legs. The results show that both contraction types elicited EIMD (i.e. reduction in torque) and a RBE (i.e. less soreness after the second exercise bout). However, the ISO condition caused less damage and less protection against muscle soreness two days after the repeated bout. Overall, our results suggest that the action of stretching an actively contracting muscle rather than sustained contractions at long lengths is more important for causing EIMD and a RBE in the MG.

Introduction

Controversy remains about whether EIMD and the RBE are caused by the process of stretching an actively contracting muscle (ECC), or whether damage arises due to the production of high force at long muscle lengths (ISO). This is particularly true for the MG, where fascicle stretch (and thus damage) is buffered by the Achilles tendon and the muscle's aponeurosis [1]. If high forces at long muscle lengths are important to elicit EIMD in the MG, at matched exercise volumes (i.e. time under tension), a bout of ISO should cause a larger, or similar, reduction in torque (i.e. contractile failure) and larger, or similar, increase in muscle soreness than a bout of ECC. If this is true, a bout of ISO may be more effective than a bout of ECC in protecting the muscle towards subsequent muscle damage from repeated bouts. As such, this study sought to compare the effect of ISO and ECC on MG markers of EIMD and the RBE.

Methods

Fourteen participants (11 male, age 26 ± 4 yrs, mass 74.6 ± 11 kg, height 178 ± 6 cm; 3 female, age 28 ± 8 yrs, mass 70.4 ± 6 kg, height 171 ± 7 cm) performed an initial bout of ISO with one leg at a long muscle length. Subsequently, the contralateral leg performed a bout of ECC as heel drop exercise. Seven days later, both legs performed the ECC condition. Time under tension (600 s) was matched between the ECC and ISO conditions. Twitch torque elicited by supramaximal peripheral nerve stimulation (i.e. the average peak torque of stimuli elicited at seven angles across the ankle

range of motion) and muscle soreness scores (participant's self-reported muscle soreness after a palpation test, reported using a 10-point analogue scale) were used to examine MG muscle damage before (PRE), two hours (2H) and two days (2D) after the bouts of exercise.

Results and Discussion

Both ECC and ISO conditions elicited EIMD and a RBE (Figure 1). However, ISO caused less damage 2H after the initial bout (14% less drop in twitch torque) and less protection 2H after the repeated bout (56% higher soreness) compared to ECC.

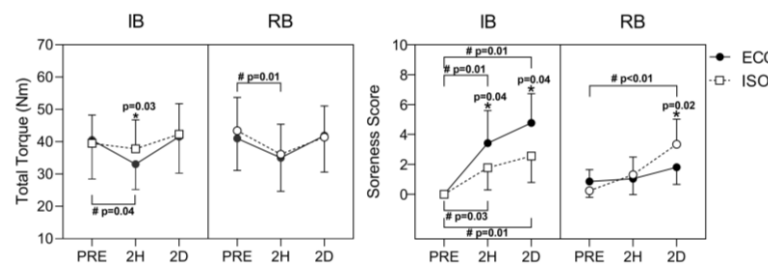


Figure 1: Markers of muscle damage. *Significant difference when comparing between the ECC and ISO contraction types. #Significant difference when comparing between timepoints (PRE, 2H, 2D) of the same contraction type. IB, initial bout; RB, repeated bout.

These results show that in the MG muscle, ECC elicits higher levels of muscle damage compared to ISO at a long muscle length, when time under tension is matched between the two conditions. Yet, the level of damage is considered to be low to moderate and is expressed mainly as an increase in soreness rather than changes in muscle force producing capacity. Both ECC and ISO are able to produce a RBE. Nevertheless, the protection conferred by the latter is less. This suggests that ISO do not produce enough muscle damage during the IB, and/or that significant muscle damage cannot be elicited in vivo in MG due to its capacity to buffer fascicle stretch via its elastic properties [1].

Conclusions

The process of stretching an actively contracting MG seems to provide a distinct stimulus for damage, more so than isometric contraction of MG at long lengths.

References

- [1] Hoffman BW et al. (2014). *J. Appl. Physiol*, **11**: 1455-1462

Relationship between A2 Pulley Venting and resultant Flexor Tendon Superficialis Slack

Tyler Shipley, William Adcock, Karl Bilderback, Tara Saxena, Jennifer Walt, Shane Barton, and Giovanni Solitro
Louisiana State University Health Shreveport, Shreveport, Louisiana
Email: gsolit@lsuhsc.edu

Summary

Discrepancies in documented outcomes of A2 pulley venting in flexor tendon repair indicate a need for further study of the biomechanical sequelae of venting. The purpose of this study is establishing whether difference exists in flexor slack that develops between fingers and if there is a threshold of venting at which point a significant increase in slack develops.

Introduction

It is understood that the A2 pulley along with the A4 pulley is crucial in prevention of flexor tendon bowstringing. However, occasionally during repair of flexor tendon lacerations the pulley must be released. Compared to partial excision of the A2 pulley, increased gliding resistance has been documented with intact A2 pulley in flexor tendon repair. Ruptures and inadequate flexion have also been documented as complications of flexor tendon repair with an intact A2 pulley. The purpose of this study is to assess the effect of incremental A2 pulley release on flexor tendon slack. Reduction of such surgical complications will lead to proper finger kinematics and more rapid return to activities of daily living. Our hypothesis is that full release of the A2 pulley leads to significant increase in tendon slack and there is difference among fingers on the exhibited slacks.

Methods

After receiving IRB exemption, 18 fingers (79±10yo) were isolated from fresh frozen cadavers. Transverse metacarpal pins were used to fix the hand to a custom apparatus (see Figure 1), which allowed control of tendon excursion while monitoring the loading. With a running lock stitch, the flexor digitorum superficialis (FDS) and extensor digitorum were tied to the apparatus which tested fingers by imposing an alternate displacement with loads ranging from 30±1 N to 2 N on the FDS in flexion. Each A2 pulley configuration was cycled 100 times into a force plate to 90 degrees of proximal interphalangeal joint flexion. The A2 pulley was sequentially incised in 20% increments until full release. Paired T-tests for means were performed between index and middle fingers and between ring and middle fingers to identify at which extent of pulley venting the fingers would show different slacks at a level of significance of 0.05.

Results and Discussion

The index fingers showed average of 0 mm slack at intact A2 pulley, 1.78 mm slack at 20 percent release, 3.03 mm slack at 40 percent release, 4.18 mm slack at 60 percent release, 5.01 at 80 percent release, and 7.05 mm at full release (see Figure 1). The middle fingers showed average of 0 mm slack with intact A2 pulley, 0.93 mm at 20% release, 1.7 at 40 % release,

2.35 mm at 60% release, 2.86 mm at 80% release, and 4.43 at full release. Ring fingers had average of no slack at intact A2 pulley, 2.06 mm at 20%, 3.2 at 40 %, 4.3 at 60%, 5.43 at 80%, and 6.36 at full release.

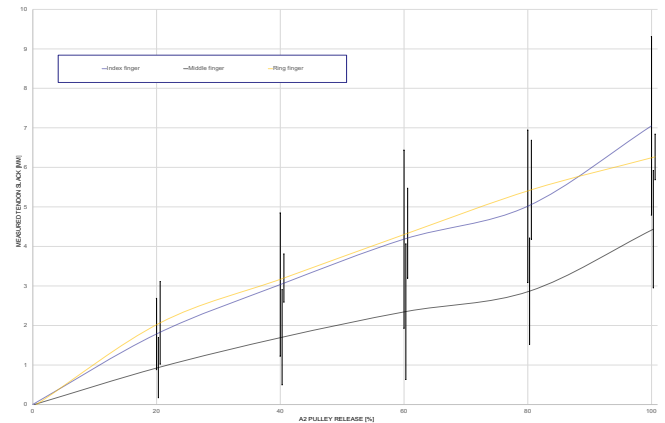


Figure 1: Pulley slack in relation to incremental A2 pulley release.

In a previous study, losses in joint flexion was documented with venting, however a direct relationship between venting and slack underlying this mechanism was not proposed (Tomaino et. al, 1998). The present study that indicate incongruence of slack development in the fingers, in which the index and ring fingers are more prone to slack than is the middle finger. Further research is needed to fully understand the sliding mechanism of the flexor tendon in presence of surgical repair and consequential adhesions. We did not associate the resultant slack to what could be potentially recovered through physical therapy and further research is needed for this specific purpose.

Conclusions

At the time of surgery it must be considered that there is direct proportionality between the A2 venting used in flexor repair and slack. The differences in slack between fingers demonstrates that each finger needs to be treated differently.

Acknowledgments

We would like to thank Mr. Alan Ogden for his assistance in performing the experiments.

References

- [1] Bunata RE et al.(2011). *Journal of Hand Surgery*. **36**:1316-1322.
- [2] Dy CJ and Daluiski A (2013). *Hand Clin*. **29**:235-242
- [3] Lilly SI and Messer TM (2006). *Journal of the AAOS*. **14**: 387-396.
- [4] Tomaino M et al. (1998). *JHS British and European*. **23**: 50-52.

Archery gesture segmentation with wearables in both able-bodied and Paralympic athletes

E Vendrame¹, L Rum², L Truppa¹, V Belluscio², G Vannozi², A Lazich³, E Bergamini², A Mannini^{1,4}

¹Istituto di Biorobotica, Scuola Superiore Sant'Anna, Pisa, Italy; ²Università degli Studi di Roma Foro Italico, Roma, Italy;

³Centro Veterani della Difesa, Roma, Italy; ⁴IRCCS Fondazione Don Carlo Gnocchi, Firenze, Italy

Email: eleonora.vendrame@santannapisa.it

Summary

This work assesses the feasibility of wearable magneto-inertial measurement units (MIMUs) for the segmentation of the archery shooting technique in athletes with and without disability. MIMU-based segmentation was validated against stereophotogrammetry, showing good reliability.

Introduction

Archery is a sport accessible to a wide range of people and can be practiced by both athletes with and without disability on a level playing field. Archery shooting technique consists in a sequence of movements which is consistently repeated. The main phases of the shot cycle – draw, aim, follow through – are defined by specific upper limb movements [1]. To date, the segmentation of the whole cycle has been mainly obtained through manual video analysis [1]. Wearable solutions, such as electromyography (EMG) or MIMUs, were devised only for the identification of the arrow release instant [2,3]. However, athletes with disability were never included in any of these investigations. For this reason, this preliminary work aims at proposing a wearable setup for the identification of the main events of the shot cycle, assessing its validity in both athletes with and without disability.

Methods

The experimental setup includes four MIMUs (Xsens, Netherlands, sampling rate 100 Hz) synchronized with an optoelectronic system (Vicon, UK, sampling rate 200 Hz). MIMUs were bilaterally positioned on forearm and upper arm, while markers were attached on both acromion processes, elbows and wrists. One non-disabled elite archer and one Paralympic athlete affected by spastic tetraparesis participated in the study. Participants shot 3 ends of 6 arrows at a target positioned at 10 meters from the shooting line. The time instants of four events within the shot cycle - bow lifting, arm stabilization, arrow release, bow lowering - were first identified from the optoelectronic data and then from MIMUs signals. Visual detection of the events was performed using bow-wrist marker trajectory in the vertical direction and it was considered as gold standard. The proposed event detection from MIMUs signals was performed using the angular velocity in the coronal plane of the bow-upper arm. The criteria considered for the identification of the events for the two measurement systems were the same for both the athletes,

and are provided in Figure 1. Non-parametric Bland-Altman analysis was performed to compare the agreement of the two techniques, with acceptable limits of ± 200 ms considering the sampling rate and the sport gesture characteristics ($\sim 6\%$ of total shooting time).

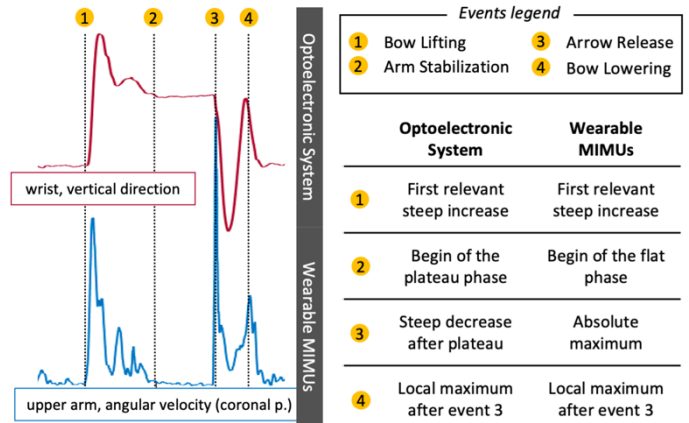


Figure 2: Events detected for the task segmentation. For the sake of readability, signals from the Paralympic athlete only were reported.

Results and Discussion

Bland-Altman analysis revealed an overall good agreement between the two measurement systems (Table 1). In particular, a strong agreement was found for the arrow release and bow lifting events in both athletes. The arm stabilization and bow lowering events showed wider limits of agreement between the two measurement systems, with a slightly lower accuracy found in the athlete with disability.

Conclusions

The proposed wearable setup based on MIMUs proved to be an overall reliable solution for the archery technical gesture segmentation in athletes with and without disability. Further studies will focus on validating this result on a larger cohort of athletes and on identifying phase-specific key performance indicators to support athletes and coaches during training.

References

- [1] Callaway AJ et al. (2017). *J. Sports Sci.*, **35**: 1142-1147.
- [2] Tinazci C (2011) *Procedia Eng.*, **13**: 290-296.
- [3] Taha Z et al. (2016). *Procedia Eng.*, **147**: 145-150.

Table 1: Limits of agreement from Bland-Altman analysis.

	<i>Limits of Agreement (mean, confidence limits 95%) [ms]</i>			
	<i>Bow Lifting</i>	<i>Arm Stabilization</i>	<i>Arrow Release</i>	<i>Bow Lowering</i>
Able-Bodied Athlete	-15, [43, -52]	10, [150, -50]	0, [33, -23]	0, [104, -107]
Impaired Athlete	30, [50, -51]	-45, [77, -205]	0, [27, -27]	70, [235, -169]

DIC-based stress-shielding analysis in compression of CoCrMo porous structures for orthopedic implants

Caravaggi P.¹, Rogati G.¹, Pagani S.³, Brogini S.³, Leardini A.¹, Fini M.³, Fortunato A.², Belvedere C.¹, Liverani E.²

¹Movement Analysis Lab, IRCCS Istituto Ortopedico Rizzoli, Bologna, Italy

²Department of Industrial Engineering, Università di Bologna, Bologna, Italy

³Complex Structure of Surgical Sciences and Technologies, IRCCS Istituto Ortopedico Rizzoli, Bologna, Italy

Email: paolo.caravaggi@ior.it

Summary

Joint replacement represents the gold-standard surgical treatment to preserve joint motion in end-stage osteoarthritis. One of the main biomechanical causes for aseptic late failure of orthopedic implants is the stress shielding. This is normally due to the larger stiffness of the implant with respect to that of the adjacent bone, causing periprosthetic bone resorption due to reduced loading at the peri-implant bone. The aim of the study is to present a method for the in-vitro evaluation of strain distribution between bovine bone specimens and Cobalt-Chromium-Molybdenum (CoCrMo) scaffolds with different porosity in compression. Full-density samples appeared to rigidly transfer the compression force to the bone which was subjected to large deformations ($2.2 \pm 0.3\%$ at 15 kN). The scaffolds made of 1000 μm pores cubic-cells allowed for a smoother load transfer to the bone and thus may decrease the stress-shielding of orthopedic implants.

Introduction

One of the main biomechanical causes for aseptic failure of orthopaedic implants is the stress shielding [1]. This is caused by uneven load distribution across the bone due to a stiff metal prosthesis component, leading to periprosthetic bone resorption and eventually to implant loosening and failure. To reduce the stress shielding and to improve osseointegration, biocompatible porous structures suitable for orthopaedic applications were developed [2, 3]. Aim of this study was to propose a novel in-vitro model of the interaction between metal lattice structures and bovine cortical bone in compression.

Methods

Full density and lattice structures with a nominal porosity of 43.5% (S750) and 63.2% (S1000) obtained by the repetition of 1.5 mm edge cubic elements were manufactured via Laser Powder Bed Fusion (SISMA MYSINT100, Vicenza, Italy) of CoCrMo powder, and characterized for mechanical properties using standard compressive testing. Local deformation and strains of metal samples coupled with fresh bovine cortical bone samples were evaluated using Digital Image Correlation (DIC) analysis via GOM Correlate (vers. 2.0.1) up to failure in compression. Visualization and quantification of the local strain gradient across the metal-bone interface was used to assess

differences in mechanical behaviour between structures which could be associated to stress-shielding in compression.

Results and Discussion

Stiffness and local mechanical properties of lattice and bone were consistent across samples (Table 1). Full-density metal samples appeared to rigidly transfer the compression force to the bone which was subjected to large deformations ($2.2 \pm 0.3\%$ at 15 kN). Larger porosity lattice was associated to lower stiffness and elastic modulus, and to a smoother load transfer to the bone (Fig 1).

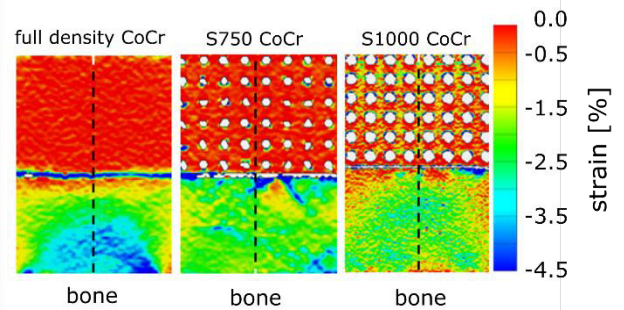


Figure 1: DIC-based analysis showing color map of local strains in three CoCrMo-bone sandwiches at 14-15 kN compressive load.

Conclusions

While tested on a limited sample size, the proposed in-vitro model appears robust and repeatable to assess the local mechanical interaction of metal samples suitable for orthopaedic applications with the bone tissue. According to the present results, CoCrMo scaffolds made of 1000 μm pores cubic cells may allow for a smoother load transfer to the bone when used as constitutive material of orthopaedic implants, which could result in lower stress-shielding with respect to a full-density metal implant.

References

- [1] Huiskes R et al. (1992). *Clin. Orthop. Relat. Res.*, **274**:124–134.
- [2] Hazlehurst K. et al. (2013). *Mater. Des.* **51**: 949–955.
- [3] Caravaggi P. et al. (2019). *J. Biomed. Mater. Res. Part B*, **107**: 2343–2353

Table 1: Mechanical properties of isolated porous structures and bone in compression.

	Young modulus [GPa]	Yield strength [MPa]	Ultimate strength [MPa]
S750	23.2 \pm 1.3	246.7 \pm 20.2	653.3 \pm 3.5
S1000	13.6 \pm 4.0	88.3 \pm 7.6	289.3 \pm 9.6
Bone	8.4 \pm 0.4	133.5 \pm 16.3	137.5 \pm 20.5

A gait pattern comparison between healthy adults and neurological patients at different walking speeds

Elke Warmerdam¹, Felix von der Recke¹, Clint Hansen¹, Walter Maetzler¹

¹Department of Neurology, Kiel University, Kiel, Germany

Email: e.warmerdam@neurologie.uni-kiel.de

Summary

Aging and neurological diseases are known to influence the gait pattern. This study compares the gait patterns of healthy young adults, healthy older adults, Parkinson patients and stroke patients with each other during different walking speeds. For all groups, the increase in speed showed a decrease in step time and an increase in step length, but no change in step width. There were significant differences in the gait parameters between the young adults and the other groups, no significant changes were found between older adults and neurological patients. These results suggest an increased risk of gait disorders in healthy older adults.

Introduction

Gait disorders are common in their occurrence and can be caused by pathological processes, but also by the physiological aging process. The consequences of these gait disorders are an increased rate of hospitalisation and death. [1] This study focusses on a better understanding of gait deficits in the aging population and neurological patients walking at different speeds.

Methods

Forty-nine participants consisting of four different groups took part in this study (Table 1). The participants completed five meters of steady state walking at slow, preferred and fast speed. Participants were measured with a 3D optical motion capture system. Gait velocity, step time, step length and step width were calculated. The changes in gait parameters with speed were analysed with a repeated measures ANOVA, the differences between the groups were analysed with a one-way ANOVA.

Table 1: Number and age of the participants

	Young adults	Older adults	Parkinson patients	Stroke patients
N (female)	17 (4)	10 (2)	14 (4)	8 (2)
Age, yrs ± SD	32 ± 9	73 ± 6	64 ± 10	64 ± 12

Results and Discussion

All participants modified their velocity, step time and step length between the different speed conditions. The step width did not significantly change between the three trials. Between preferred and fast speed, both the neurological patients and older adults (OA) groups showed no significant changes of their step length. The young adults (YA) showed a significantly higher velocity and longer step length than the other groups. No significant changes were found between the gait parameters of the older adults and the gait parameters of the neurological patients (Figure 1).

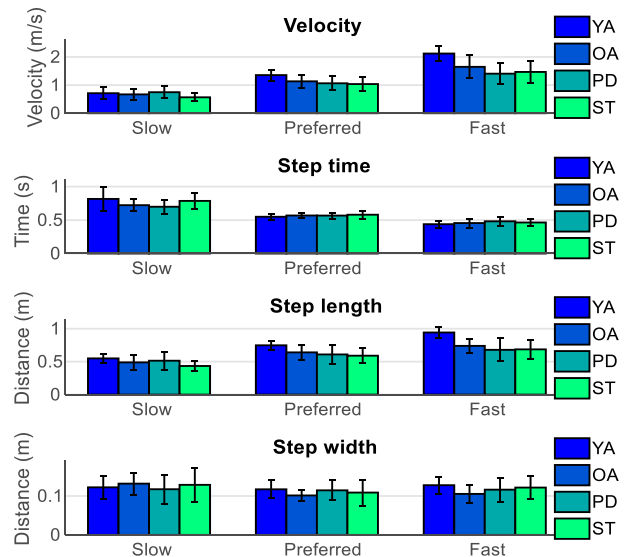


Figure 1: Alteration of gait parameters during different walking speeds

The similarities between the gait pattern of OA and neurological patients suggest that the neurological disorder is not the only cause of changes in the gait pattern and that supposedly healthy OA also have an increased risk of gait disorders and the associated consequences.

Conclusions

We demonstrate that OA and neurological patients have lower gait velocities and smaller step lengths than YA. No differences were found between the OA and neurological patients. This highlights the risk of age-related gait disorders and suggests that only a part of the gait disorders seen in neurological patients are caused by the disease.

Acknowledgments

This research was funded by Keep Control from the EU's Horizon 2020 research and innovation program under the Marie Skłodowska-Curie grant agreement number 721577.

References

[1] Verghese et al. (2006), *Journal of the American Geriatrics Society*, **54**: 255-261

Effect of Fatigue on Hip, Knee and Ankle Proprioception During a Golf Specific Fatigue Protocol.

Henry H. Hunter¹, Graeme G. Sorbie², Fergal M. Grace³, Antonio Dello Iocono¹, Julien S. Baker⁴, Ukadike C. Ugbohue¹

¹School of Health and Life Sciences, University of the West of Scotland, South Lanarkshire, Scotland, UK

²Division of Sport and Exercise Sciences, Abertay University, Dundee, DD1 1HG, UK

³Faculty of Health, Human Movement & Sport Sciences, Federation University Australia, Ballarat, Victoria, Australia

⁴Department of Sport, Physical Education and Health, Hong Kong Baptist University, Kowloon Tong, Hong Kong

Email: henry.hunter@uws.ac.uk

Summary

The purpose of this pilot study was to determine whether muscle fatigue generated by a golf specific fatiguing protocol would have an effect on proprioception and kinematic parameters of both left and right hip knee and ankle joints during the six phases of the golf swing. Five healthy, right handed male subjects participated in this pilot study respectively. The participants were asked to perform 125 golf swings using various clubs whilst being recorded with a 3D Motion capture System. A subset of swings were calculated as Pre-Fatigue and Post Fatigue for evaluation purposes. All data was then analysed and the results compared using both descriptive and inferential statistics.

Introduction

The golf swing is a complex movement of the whole body that encompasses the Sagittal, Frontal and Transverse planes. Several golf related studies have been carried out to improve performance in this field with regards to physical conditioning, mood, injury prevention and swing mechanics. According to studies [1] and [2] hip and knee mechanics can be substantially altered whilst fatigued. However, [3] points out that both “golf specific fatigue did not relate to the initial lower body sagittal plane angles at address nor was simulated golf specific fatigue related to peak transverse plane pelvis and trunk rotational velocities (or their timings) in a manner that indicates a relationship to resultant club head velocity and shot consistency”.

Methods

Five healthy, right handed male subjects participated in this pilot study (Height 176.8 + 27cm, Weight 71.48 + 33.8 kg) respectively. Participants were asked to perform 125 golf swings using various clubs (5 x 5 iron, 60 x 7 iron, 5 x 9 iron, 55 x Driver). Kinematic angle data of both left and right hip, knee and ankle joints in the Frontal (X), Sagittal (Y), and Transverse (Z) planes were recorded using a Vicon Nexus Bonita (Oxford Metrics Ltd) Motion Capture system operating at 250Hz. A Vicon plug in gait Lower Body Model was selected with 16 retro-reflective markers placed on the correct anatomical positions of the lower limbs and four on the shaft of the golf club. This allowed for correct identification of the six golf phases. The first five swings of the Driver and 7 Iron were extracted and used as “Pre-Fatigue” with the last 5 swings of the study stored as “Post-Fatigue” for evaluation and comparison purposes. All joint angle data was stored in Degrees (^o).

A paired t-test was used to compare the differences between the Pre-Fatigue and Post-Fatigue swings with respect to their corresponding joint angles. Significance was set to P = 0.05.

Table 1: t-test Pre-Fatigue v Post-Fatigue

Joint Angle (deg)	Coordinate	Address		Top of Backswing		Acceleration		Impact		Early Follow Through		Late Follow Through	
		Driver	7 Iron	Driver	7 Iron	Driver	7 Iron	Driver	7 Iron	Driver	7 Iron	Driver	7 Iron
LAnkleAngles	X	0.074	0.598	0.136	0.593	0.457	0.014	0.427	0.036	0.708	0.066	0.732	0.976
	Y	0.083	0.894	0.008	0.190	0.111	0.063	0.045	0.175	0.249	0.621	0.885	0.119
	Z	0.065	0.761	0.008	0.122	0.155	0.110	0.083	0.248	0.483	0.714	0.444	0.050
LHipAngles	X	0.079	0.925	0.007	0.250	0.411	0.008	0.119	0.008	0.102	0.069	0.212	0.267
	Y	0.587	0.808	0.012	0.253	0.417	0.340	0.084	0.827	0.033	0.904	0.169	0.155
	Z	0.834	0.895	0.067	0.552	0.011	0.785	0.320	0.393	0.472	0.893	0.166	0.174
LKneeAngles	X	0.107	0.912	0.005	0.368	0.361	0.027	0.598	0.029	0.512	0.010	0.064	0.150
	Y	0.645	0.689	0.036	0.100	0.682	0.349	0.385	0.965	0.898	0.522	0.030	0.875
	Z	0.536	0.682	0.606	0.420	0.328	0.580	0.639	0.198	0.885	0.081	0.425	0.928
LPelvisAngles	X	0.651	0.028	0.383	0.163	0.303	0.123	0.285	0.109	0.281	0.137	0.365	0.862
	Y	0.333	0.026	0.381	0.349	0.381	0.001	0.357	0.001	0.380	0.004	0.335	0.004
	Z	0.597	0.058	0.412	0.053	0.760	0.023	0.565	0.027	0.557	0.0496	0.321	0.382
RAnkleAngles	X	0.023	0.415	0.090	0.910	0.326	0.181	0.443	0.195	0.660	0.344	0.425	0.912
	Y	0.473	0.519	0.250	0.114	0.107	0.950	0.232	0.972	0.214	0.907	0.016	0.985
	Z	0.488	0.602	0.325	0.125	0.080	0.963	0.199	0.921	0.172	0.999	0.025	0.715
RHipAngles	X	0.166	0.909	0.245	0.457	0.611	0.005	0.416	0.021	0.339	0.213	0.227	0.895
	Y	0.718	0.760	0.151	0.731	0.451	0.799	0.344	0.334	0.009	0.318	0.405	0.053
	Z	0.323	0.356	0.463	0.187	0.400	0.957	0.375	0.835	0.354	0.407	0.163	0.107
RKneeAngles	X	0.937	0.866	0.521	0.787	0.570	0.085	0.913	0.022	0.875	0.008	0.954	0.139
	Y	0.211	0.398	0.537	0.585	0.599	0.228	0.979	0.321	0.342	0.243	0.298	0.239
	Z	0.209	0.198	0.597	0.642	0.548	0.146	0.470	0.089	0.355	0.130	0.419	0.055
RPelvisAngles	X	0.651	0.028	0.651	0.163	0.278	0.123	0.215	0.109	0.204	0.137	0.587	0.862
	Y	0.333	0.026	0.275	0.349	0.214	0.001	0.264	0.001	0.179	0.004	0.338	0.004
	Z	0.597	0.058	0.066	0.053	0.301	0.023	0.478	0.027	0.468	0.0496	0.881	0.382

Results and Discussion

There were significant differences (P>0.05) observed throughout the study with the exception of the Y and Z axes of the Right Knee Angle during all phases with both Driver and 7 Iron and also the 7 Iron at the Top of the Backswing for all joint angles. However, the scattering pattern of data displayed as significant differences does highlight similarities for both the Driver and shorter 7 Iron club particularly at the phases of the swing with higher Club Head Speed (CHS) (Acceleration, Impact and Early Follow Through).

Conclusions

The results of this study show that there were no significant differences displayed for the Y and Z axes of the Right Knee Angle during all phases with both clubs. The variability in the p values with respect to the joint angle and golf swing phases highlight the changes between the Pre-Fatigue and Post-Fatigue swings.

References

- [1] Lucci N et al. (2011). *J. Sci. Med. Sport*, **14** (5): 453–459
- [2] Miller PK et al. (1976). *Percept. Mot. Skills*, **42** (1): 135–138.
- [3] Higdon NR et al. (2012). *Sport. Biomech.*, **11** (2): 190–196.

A procedure for measuring the kinematics of the foot and ankle complex through Weight-Bearing CT

Alessandro Pompili¹, **Michele Conconi**¹, Nicola Sancisi¹, Alberto Leardini², Stefano Durante², Claudio Belvedere²

¹Department of Industrial Engineering - DIN, University of Bologna, Italy

²Movement Analysis Laboratory, IRCCS Istituto Ortopedico Rizzoli, Bologna, Italy

Email: michele.conconi@unibo.it

Summary

The aim of this work is to propose and validate a semi-automatic procedure, including bone segmentation and ICP-based bone registration, for the reconstruction of bone kinematics in the foot and ankle through Weight-Bearing CT. The semi-automatic segmentation is compared to manual one and the overall accuracy of the procedure is addressed.

Introduction

Several methods are available to measure the human bone absolute and relative motion from in-vitro and in-vivo experiments [1]. When the structures under investigation become complex and the number of bones to be tracked grows, motion is often reconstructed from a series of static 3D scans [2]. In this case, the challenge is to define a fast yet accurate procedure for the elaboration of the dataset. Typically, this involves segmentation and registration: assessing the accuracy and the computational time of these operations is crucial. The aim of this study is to propose a procedure consisting in a semi-automatic segmentation, evaluated in terms of processing time and DICE score with respect to a manual segmentation, and an automatic ICP-based registration process. Also, a method for the accuracy quantification of the reconstructed bone motion is proposed.

Methods

The full procedure for bone kinematics reconstruction is based on two steps: 1) segmentation of all scans, 2) registration of each bone of a reference scan to the corresponding bone model in each scan.

Semiautomatic segmentation is tested on three feet, scanned in a Cone Beam CT. Firstly, each foot is divided into two parts by cropping the CT scan in Slicer 4.10, to reduce the amount of data to be processed at once. The segmentation is carried out in MITK software: firstly, bones are identified by a single bound threshold (fig. 1.1), whose lower bound is manually varied between 280 and 400 Hounsfield Units to minimize the overlap among bones. If necessary, bones are further manually separated (fig. 1.2). Then, each bone segmentation is completed by morphological operation: closing (structuring element: ball; radius:18 mm) and filling (fig. 1.3). A smoothed stl model is then created. To assess the

quality of segmentations, DICE score [3] was used, comparing manually and semiautomatically segmented talus, intermediate cuneiform and first metatarsus, for all the feet.

Anatomical reference systems for each bone are defined at the neutral scan. Bone registration is performed by an ICP-based automatic algorithm defined in Matlab (fig 1.4) from the neutral to the specific scan, to define bone kinematics. To assess the accuracy of the overall procedure, bone motion is simulated with a set of 5 synthetic scans obtained by applying 5 rigid rototranslations to the DICOM files of the neutral position through Slicer and by resampling them. The transformations are chosen randomly within the foot range of motion. These scans are processed with the procedure and the computed kinematics is compared with the imposed motion. For the sake of simplicity, analysis is limited to 2 feet and to talus, intermediate cuneiform and first metatarsus.

Results and Discussion

DICE score has a minimum value of 94.5% for the intermediate cuneiform and a maximum value of 98% for the talus. The average value is $96.4\% \pm 1.0$, higher than what found in the literature for fully automated segmentation algorithms [3]. The process time is about 2 hours to segment a foot scan (14 bones excluding toes). The operator time is mainly devoted to the separation of the cuneiforms. In comparison, manual segmentation requires 12 hours. The overall registration accuracy is $0.37^\circ \pm 0.30^\circ$ and 0.09 ± 0.08 mm. The worst accuracy is in the reconstruction of the intermediate cuneiform ($0.53^\circ \pm 0.23^\circ$ and 0.09 ± 0.08 mm). The lowest values are found for talus $0.13^\circ \pm 0.06^\circ$ and 0.09 ± 0.09 mm.

Conclusions

A fast and accurate semiautomatic procedure for computing the bone kinematics of the foot-ankle complex is presented. The need of an operator to guide the segmentation is balanced by the high accuracy achievable. This procedure has been successfully employed for the investigation of 3 feet.

References

- [1] Kessler et al. (2019). *Bioeng. & Biotech.*, **7**: 199.
- [2] Neu et al. (2001). *J. of Biomech.*, **34**: 1429-1438.
- [3] Fu et al. (2017). *Phy in Med. & Bio.*, **62**: 2812.

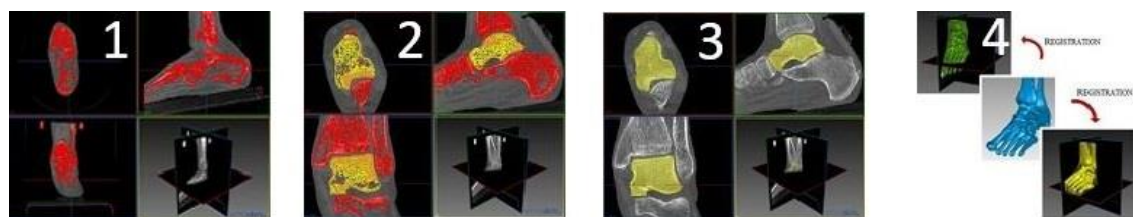


Figure 1: The procedure: 1) bone identification by thresholding. 2) manual separation of the bones. 3) bone mask closing and generation of the stl. 4) bone registration among CT scans.

The project RefLabPerform - Development of a reference laboratory for the evaluation of playing- and performance-related dysfunctions of performing artists to derive individual prevention and rehabilitation strategies

Dirk Möller, Florian Avermann, Christoff Zalpour

Department of Movement and Rehabilitation Science, University of Applied Sciences, Osnabrück, Germany
Email: d.moeller@hs-osnabrueck.de

Summary

Performing artists are a socially relevant group through numerous forms such as dance, music or singing. In contrast to competitive athletes, however, medical and therapeutic care tends to be inadequate, which is seen as a contributing factor to the high prevalence of musculoskeletal complaints in this group. The project RefLabPerform is developing a reference laboratory for the assessment of neuromusculoskeletal disorders with the support of physiotherapeutic diagnostic methods in combination with biomechanical motion analyses. This also includes the automatized merging of physiotherapeutic assessment results with biomechanical analysis results to an individual treatment recommendation with decentralized health care suggestions for a home-based therapy on evidence-based prevention and rehabilitation strategies.

Introduction

Performing artists are exposed to high levels of strain, e.g. from rehearsals or performances. This is comparable to the strains of athletes, but performing artists additionally strive for the perfect dance performance or the perfect sound in a concert. Competitive athletes receive optimal medical care in their sport clubs, olympic or state sports centers. In contrast to this, there is no nationwide supply of performing artists, only on their own initiative they get a better medical care. A consequence of this inadequate supply is the high prevalence of neuromusculoskeletal complaints.

The aim of RefLabPerform is to develop a reference laboratory for the assessment of neuromusculoskeletal disorders using manual physiotherapeutic assessment methods in combination with biomechanical motion analysis.

Methods

Several work packages are carried out systematically (fig. 1):

1. Identification of the specific requirement profiles for the different performing artist groups.
2. Development of the individual physiotherapeutic protocols, prevention and rehabilitation strategies as well as the biomechanical setup and the technical routines of the laboratory.
3. At the same time, various biomechanical analysis protocols will be developed and at the end of this work package these protocols will be merged with the physiotherapeutic protocols.
4. Overlapping with the previous work packages, the reference laboratory will be continuously tested for application and feasibility. Clinical and biomechanical

data will be merged and checked on the basis of individual case studies from various groups of performing artists.

As a part of an iterative agile software development process, the results flow back into the previous work packages in order to optimize them and then test them again.

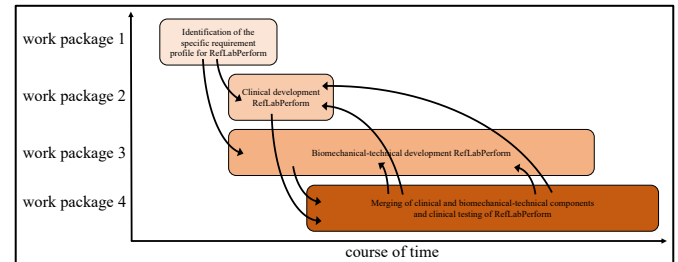


Figure 1: Overview of the work packages and their content-related iterative interaction for the development of RefLabPerform.

The biomechanical setups are individually adjusted to the respective performing artist groups, so that an optimal data collection can take place from a temporal and qualitative point of view. Therefore, a mixture of different biomechanical capture methods is also considered (fig. 2).

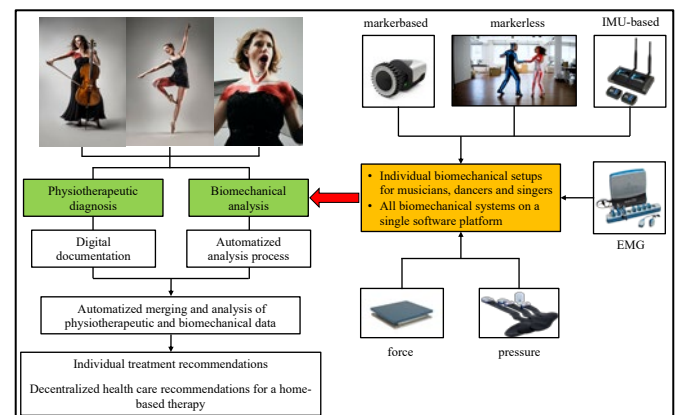


Figure 2: Structure of data collection and application possibilities of the biomechanical assessments according to individual requirements of the performing artists.

Results and Discussion

At the end of this project a functional and proven reference laboratory for the comprehensive clinical and biomechanical analysis of performing artists will be developed.

Conclusions

This reference laboratory will be specialized for the diagnosis and treatment of neuromusculoskeletal disorders of performing artists using manual physiotherapeutic assessment methods and the biomechanical motion analysis.

Step length asymmetry is associated with fear of falling activity avoidance in persons with unilateral transtibial amputation

Noah J. Rosenblatt¹,

¹Center for Lower Extremity Ambulatory Research, Rosalind Franklin University of Medicine and Science, North Chicago, USA

Email: noah.rosenblatt@rosalindfranklin.edu

Summary

The extent to which gait symmetry in persons with transtibial amputation (pTTA) should be a rehabilitation goal is questionable. Given that step length (SL) asymmetry in pTTA may impart stability, we explored the extent to which gait asymmetry in this population was associated with perceptions of gait that can impact activity. Symmetry indices (SI) for spatiotemporal gait parameters were correlated with measures of balance and gait self-efficacy, based on which we conclude that longer prosthesis side steps and single support time may promote self-efficacy and limit fear of falling (FoF)-related activity avoidance

Introduction

Low balance confidence and FoF are prevalent yet overlooked issue among prostheses users [1] that can significantly limit activity. Many studies have evaluated gait characteristics associated with FoF in intact older adults, but, to our knowledge none have done so in pTTA. Whereas older adults display fairly symmetric gait, asymmetry is common in persons with amputation. For example, pTTA often display greater SL with their prosthesis. However, as this may represent a functional adaptation to, rather than a negative consequence of, amputation that helps to maintain stability and prevent a backward [2], leveraging SL asymmetry to ensure stability may facilitate balance confidence and reduced FoF; SL asymmetry may serve as a marker of self-efficacy. We evaluated the association between i) step length asymmetry and ii) measures of balance and gait self-efficacy as well as FoF-related activity avoidance. We also evaluated the associations between symmetry indices for other gait characteristics associated with FoF in intact older adults and the latter outcomes.

Methods

This is a secondary analysis of data collected on 17 pTTA (5 F/12 M, 58.8±12.6 yrs) at the start of a larger intervention trial, prior to any intervention. Passive reflective markers were placed on body, after which participants walked across a 10m laboratory walkway 10-20 times at a self-selected pace. For each limb, the following were averaged across steps: SL; step width (SW); step time (ST); percent single support (%SS); single support time (SST); percent double support (%DS) and double support time (DST), consider only for the DS phase following heel strike of a given limb. Symmetry indices (SI) were calculated as the between-limb difference relative to the between-limb mean (SI>0 indicates

prosthetic side (P) values greater than non-prosthetic (NP) side). The following surveys were completed: i) Activity-specific Balance Confidence (ABC) scale to assess balance self-efficacy, a strong correlate of FoF; ii) Modified Gait Self Efficacy Scale (mGES) to assess gait self-efficacy; iii) Fear of Falling Avoidance Behavior Questionnaire (FFABQ), e.g. level of agreement with “due to my FoF I avoid walking”; iv) One item from the Prosthetic Evaluation Questionnaire (PEQ) that states “Over the past 4 weeks, rate how satisfied you have been with how you are walking”. Gait variables and survey measures were correlated.

Results and Discussion

PSL but not NPSL was significantly associated with all survey measures (Table 1). However, only FFABQ, was associated with SL SI. Neither limb-specific measures nor SI measures for SW, ST, % SS, %DS or DST were significantly associated with any survey measures. However, SST SI was significantly associated with ABC and PEQ walk (Figure 1); greater PSST relative to NPSST was associated with greater confidence and gait satisfaction.

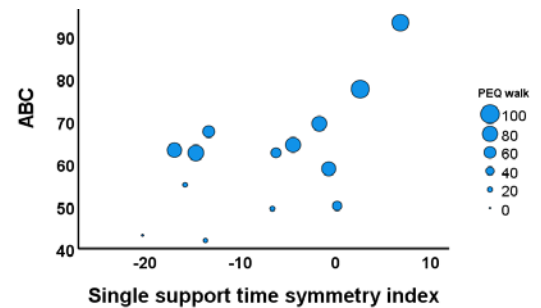


Figure 1: ABC vs. SST SI; bubble size relative to PEQ question.

Conclusions

Longer P side steps (reliant on NP push off) and longer relative PSST (reliant on P side balance) may promote self-efficacy and limit FoF-related activity avoidance. Fostering symmetry in rehabilitation may not be desirable.

Acknowledgments

This work was funded by DoD award W81XWH-17-1-06

References

- [1] Miller WC et al (2002) *Phys Ther*, **82**: 856-65
- [2] Hak L et al. (2014) *Phys Ther*, **94**: 1480-88

Table 1: Correlation coefficients (p-values) for associations between survey measures and SL measures

	PSL	NPSL	SL SI
ABC (higher = greater efficacy)	0.608 (0.010)	0.378 (0.135)	0.341 (0.180)
mGES (higher = greater efficacy)	0.570 (0.027)	0.290 (0.295)	0.422 (0.117)
FFABQ (higher = more avoidance)	-0.729 (0.002)	-0.371 (0.173)	-0.572 (0.026)
PEQ question (higher = more satisfaction)	0.539 (0.047)	0.421 (0.134)	0.212 (0.466)

Multi-digit Force Coordination in Patients with Trigger Digit using Machine Learning and Deep Learning

Kien Tran¹, Hsiao-Feng Chieh¹, Chien-Ju Lin^{1,2}, Po-Tsun Chen³, Fong-Chin Su^{1,2}

¹Department of Biomedical Engineering, ²Medical Device Innovation Center, National Cheng-Kung University, Tainan

³School of Physical Therapy, Chang Gung University

Email: tkien.billy@gmail.com

Summary

This research presents a machine learning approach to analyze multi-digit force coordination in subjects with and without trigger digit symptoms.

Introduction

Trigger digit (TD) is a common symptom in hand, that affects motor coordination, and results in hand functional impairment. Previous studies used cylindrical grasp to investigate finger force coordination during precision grasping of TD patients. Data characterizing five-digit force coordination is commonly high-dimensional, complex, and dynamic. There is a lack of studies to process this type of data in dynamic and multivariate ways. To compensate for this problem, it will be interesting to utilize machine learning method of predictive models for data mining.

The purpose of this study is to first develop a machine learning and deep learning model to classify healthy subjects and trigger digit patients. After that, we analyze the post-trained model to investigate applied force differences between two group of subjects

Methods

Forty-four healthy subjects (39.5 years \pm 7.6) and fifty-four TD patients (57.6 years \pm 8.0) with involved digit were included in this research. Patients with affected digit include 11 patients with thumb, 7 patients with index finger, 17 patients with middle finger, 12 patients with ring finger, 3 patients with index and ring fingers, and 4 patients with middle and ring fingers.

The participants performed a grasping task: grasped and lifted the simulator to the height of 20 cm then hold it stably for at least three seconds and lowered it to the original position.

A machine learning model (Random Forest) and a deep learning model (1D-CNN) are used to map force data to given subject status. Two models are trained and validated by 10-fold cross-validation in intra-subject (trial-mixed) and inter-subject (subject-mixed) datasets. A separated testing set was also used to test the performance of the two models. The Random Forest model is analyzed by feature importance calculation. The 1D-CNN model is analyzed by Grad-CAM.

Results and Discussion

Cross-validation and testing mean accuracy of RF are 79% and 85% for intra-subject while 81% and 86% for inter-subject. Cross-validation and testing accuracy of 1D-CNN are

84% and 85% for intra-subject while 71% and 77% for inter-subject.

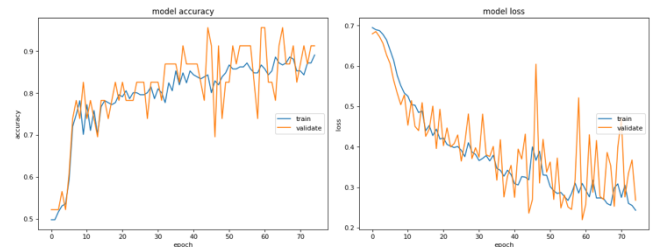


Figure 1: Accuracy and loss graph of model training.

Feature importance shows that the duration of trials is the most important. Grad-CAM model shows that the model pays most attention to the holding phase

Conclusions

By using machine learning methods, we can classify healthy subjects and trigger digit patients. The duration of trials is an important factor that should be controlled in the experiment setting. The stability holding phase reveals important features and should be investigated in future studies.

Acknowledgments

Grant support from Taiwan Ministry of Science and Technology.

References

- [1] P.-T. Chen, C.-J. Lin, I.-M. Jou, H.-F. Chieh, F.-C. Su, and L.-C. Kuo, "One digit interruption: the altered force patterns during functionally cylindrical grasping tasks in patients with trigger digits," *PloS one*, vol. 8, no. 12, p. e83632, 2013.
- [2] P.-T. Chen, I.-M. Jou, C.-J. Lin, H.-F. Chieh, L.-C. Kuo, and F.-C. Su, "Is the control of applied digital forces during natural five-digit grasping affected by carpal tunnel syndrome?," *Clinical Orthopaedics and Related Research*, vol. 473, no. 7, pp. 2371-2382, 2015.
- [3] H. Y. Chiu, H. Y. Hsu, L. C. Kuo, J. H. Chang, and F. C. Su, "Functional sensibility assessment. Part I: develop a reliable apparatus to assess momentary pinch force control," *Journal of orthopaedic research: official publication of the Orthopaedic Research Society*, vol. 27, no. 8, pp. 1116-21, Aug 2009.
- [4] V. M. Zatsiorsky and M. L. Latash, "Multifinger prehension: an overview," (in eng), *J Mot Behav*, vol. 40, no. 5, pp. 446-76, Sep 2008.

Inter-session repeatability of markerless motion capture gait kinematics

Robert Kanko¹, Elise Laende¹, W. Scott Selbie², Kevin J. Deluzio¹

¹Mechanical and Materials Engineering, Queen's University, Kingston, Canada

²Theia Markerless, Inc., Kingston, Canada

Email: r.kanko@queensu.ca

Summary

This study examined the repeatability of lower limb gait kinematics measured using *Theia3D* markerless motion capture software and compared the results to previously reported repeatability of marker-based systems [1-4]. Subjects' joint angle waveforms were found to be consistent across multiple sessions. The average inter-trial variability (2.5°) was slightly greater and the average inter-session variability (2.8°) was slightly lower than previously reported for marker-based systems, indicating that markerless motion capture is somewhat less affected by multi-session protocols than marker-based systems.

Introduction

Three-dimensional (3D) human movement analysis is a widely used tool to quantify individuals' movement patterns, particularly gait. These data have typically been collected using marker-based motion capture, which relies on skin-mounted markers that require expert operators for their placement, dedicated laboratory space for their use, non-negligible subject preparation time, and the sacrifice of subject comfort while collecting data.

Markerless motion capture is a quickly evolving technology that offers an alternative to measure human movement with fewer practical limitations. *Theia3D* (Theia Markerless Inc., Kingston, Canada) is one such system which uses deep neural networks trained on >500,000 labelled images of humans in the wild to estimate the position of subjects' anatomical landmarks in videos recorded by an array of synchronized cameras. The objective of this work was to determine the repeatability of lower-limb gait kinematics measured using *Theia3D* and compare the results to previously reported values for marker-based systems.

Methods

Eight healthy adults (2/6 female/male, mean: age 30.3 years, height 173.8 cm, mass 69.0 kg) each attended three separate collection sessions separated by an average of 8.5 days, wearing their own everyday clothing of choice. During each session, subjects performed five over-ground walking trials at self-selected speeds while synchronized video data were recorded using eight Sony RX0 II video cameras (Sony Corp., Minato, Japan). Videos were processed in *Theia3D* to obtain 3D pose estimates which were further analyzed in *Visual3D* (C-Motion Inc., USA). Measures of inter-trial and inter-session variability of lower limb joint angles were calculated based on an established method [1] and compared to previously reported values for marker-based systems [1-4].

Results and Discussion

The time required for each session was typically between five and ten minutes. Session average joint angle waveforms showed that subjects' gait patterns were measured consistently across all three sessions (Figure 1).

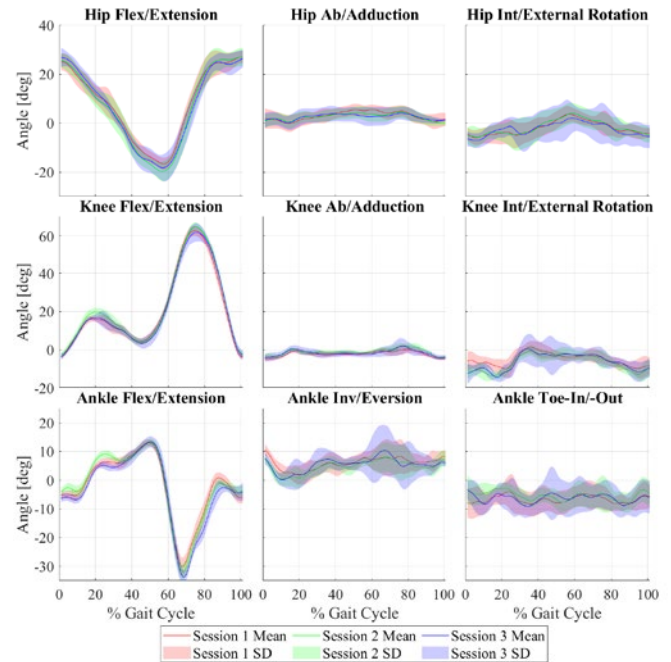


Figure 1: Mean +/- SD joint angle patterns for three sessions from one representative subject, measured using *Theia3D*.

The average inter-trial variability of the markerless gait kinematics was 2.5°, the largest among the included studies by a margin of 0.1°. The average inter-session variability of the markerless gait kinematics was 2.8°, the smallest among the included studies by a margin of 0.2°.

Conclusions

The results demonstrate that gait kinematics measured using *Theia3D* are somewhat less affected by the use of a multi-session protocol compared to marker-based systems. The slight increase in inter-trial variability in combination with the decreased inter-session variability and ease of data collection is an acceptable compromise because of the potential for substantially more accessible data collections.

References

- [1] Schwartz MH et al. (2004). *Gait Posture*, **20**: 196-203.
- [2] Manca M et al. (2010). *Gait Posture*, **32**: 282-284.
- [3] Caravaggi P et al. (2011). *Gait Posture*, **33**: 133-135.
- [4] Kaufman K et al. (2016). *Gait Posture*, **49**: 375-38.

NOVEL COMPUTER VISION AND DEEP LEARNING APPROACHES FOR TRACKING 3-D SPINE MOTION DURING DYNAMIC TRUNK FLEXION USING AN RGB-D CAMERA

Ryan B. Graham^{1,2}, Wantuir C.R. Junior¹, Kristen Beange², Alistair Boyle¹, Matthew P. Mavor¹

¹School of Human Kinetics, Faculty of Health Sciences, University of Ottawa, Ottawa, ON, Canada

²Ottawa-Carleton Institute for Biomedical Engineering (OCIBME), Ottawa, ON, Canada

Email: rgraham@uottawa.ca

Summary

The overall goal of this work was to develop an inexpensive and portable tool capable of quantifying lumbar spine motion in the field using a red-green-blue-depth (RGB-D) time-of-flight camera. Specifically, we created a novel framework that takes the RGB-D data and manipulates them to measure 3-D lumbar spine kinematics during dynamic trunk flexion. To achieve our goal, we carried out two independent research studies: 1) the development and validation of a custom computer vision method to track infrared (IR) reflective markers from raw depth data to calculate 3-D spine angles; and 2) development and validation of a custom four module convolutional neural network (CNN; SpineNet) to track and automatically segment regions of each participant's back to calculate 3-D kinematics without the use of any markers.

Introduction

In order to better understand motor control and biomechanical differences between low back pain patients and healthy controls, researchers and clinicians often observe movement patterns and quality during pre-defined tasks (e.g., trunk flexion-extension) [1]. Recently, a great amount of work has been undertaken to validate the use of portable inexpensive sensors such as inertial measurement units (IMUs) to measure 3-D spine motion during dynamic tasks in the field [2]; however, an alternative approach is to use RGB-D cameras [3]. While many research studies have been carried out in the biomechanical domain using RGB-D cameras [3], few have attempted to measure spine motion [4], and none have done so during dynamic trunk flexion tasks with or without markers. Through two studies we aimed to address this research gap.

Methods

Study 1: 12 healthy young adults (6M, 6F) were recruited to perform repetitive spine flexion-extension, with infrared reflective marker clusters placed over their T₁₀-T₁₂ spinous processes and sacrum, and motion capture data were recorded simultaneously by one RGB-D camera and a 10-camera optoelectronic motion capture system. Custom computer vision algorithms were developed to extract spine angles from depth data. Root mean square error (*RMSE*) was calculated for continuous Euler angles, and intraclass correlation coefficients (*ICC*_{2,1}) were calculated between min, max, and average range of motion angles in all movement planes for both systems.

Study 2: A single RGB-D camera captured infrared, depth, and colour image data of 15 male participants performing two batteries of 10 cycles of repetitive trunk flexion-extension under two conditions: marked (i.e., hand drawn markers on key anatomical locations on the back) and unmarked. The collected data were used to create a custom four module convolutional neural network (CNN; SpineNet) (Figure 1 – based on [5]) to segment the back into upper, lower, and spine regions and then to extract lumbar spine kinematics. SpineNet

was trained and tested on ten marked participants in a train:test ratio of 80:20. Images of five additional participants without markers were used to evaluate model generalizability.

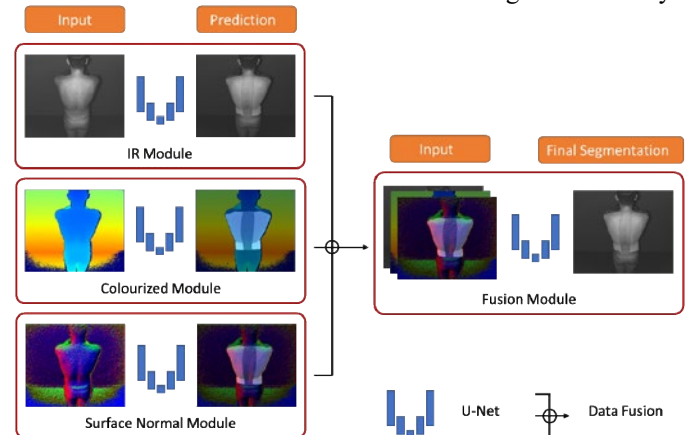


Figure 1. CNN architecture. Each RGB-D camera data stream was used as input for each of the three individualized U-Net modules. Individual modules' anatomical segmentation predictions were then fused and used as input for the final U-Net segmentation module.

Results and Discussion

Study 1: *RMSE* in angles between the two calculation methods were very low across all movement axes ($RMSE \leq 2.05^\circ \pm 0.97^\circ$), and *ICC*_{2,1} values were good to excellent across all axes ($0.849 \leq ICC_{2,1} \leq 0.979$). Bland-Altman plots revealed that, on average, the RGB-D camera slightly underestimated lumbar flexion-extension angles (-1.88°) and overestimated lumbar lateral bending and axial twisting angles ($\leq 0.58^\circ$).

Study 2: Quantitative image segmentation analysis on marked data had good similarity (frequency weighted intersection over union ≥ 0.8087) and accuracy (mean pixel accuracy ≥ 0.8855) between the prediction and ground truth across all modules. Qualitative image segmentation analysis on unmarked data showed that colourized and surface normal modules presented a more robust class morphology throughout frames than infrared and fusion modules. Kinematic analysis on unmarked participants showed that flexion-extension angles exhibited movement profiles (i.e., shape, timing, and peaks) that are comparable to similarly collected data from previous research.

Conclusion

This work provides proof for using a single RGB-D camera for assessing lumbar kinematics with or without markers.

Acknowledgments

Funding provided by NSERC and the Ontario ERA program.

References

- [1] van Dieën et al. (2019). *JOSPT* **49**: 370-9. [2] Beange et al. (2019). *J Biomech* **97** : 109356. [3] Clark et al. (2019). *Gait Posture* **68** : 193-200. [4] Macpherson et al. (2016). *J Biomech* **49** : 474-8. [5] Rahman et al. (2017). *IEEE ICME*, 991-6.

A SUPERVISED CLASSIFICATION OF CHILDREN WITH FRAGILE X SYNDROME AND CONTROLS BASED ON KINEMATIC AND SEMG PARAMETERS.

W. PIATKOWSKA¹, M. ROMANATO¹, F. SPOLAOR¹, F. CIBIN¹, A. CINIGLIO¹, A. HUANG¹, R. POLLI², A. MURGIA², Z. SAWACHA^{1,3}

¹ Department of Information Engineering, University of Padova, Italy

² Department of Women and Children Health, University of Padova, Italy

³ Department of Medicine, DIMED, University of Padova, Italy

Email: weronikajoanna.piatkowska@studenti.unipd.it

Summary

Fragile X Syndrome (FXS) is a genetic condition, mainly characterized by intellectual disability, behavioral problems and musculoskeletal alterations. In order to classify FXS subjects' motor deficits for assisting in clinical decision making, a supervised classification was performed by adopting kinematics and sEMG parameters combined together or isolated as input variables. The set of parameters that was more efficient in discriminating between FXS subjects and controls was determined.

Introduction

FXS is the leading form of inherited intellectual disability and autism spectrum disorder, caused by a tri-nucleotide CGG repeat expansion in the promoter region of the FMR1 gene [1]. In these subjects, the frequent musculoskeletal manifestations, such as ligamentous laxity and flat foot [1], justifies a referral for gait analysis evaluation.

Supervised classification is generally used to find the relation between the input parameters and the target variable [2] that in our contest is represented by the presence of musculoskeletal alterations associated with FXS. The aim of the present study was to find out which set of gait and sEMG analysis parameters were the most useful to discriminate between controls and FXS subjects, for assisting in clinical decision making.

Methods

After appropriate informed consent by the parents, 20 FXS children ((FX) mean (\pm SD) age and BMI respectively of 10,00 (\pm 3,74) years and 18,57 (\pm 3,46) Kg/m²) and 16 controls ((CS) mean (\pm SD) age of 10,22 (\pm 3,19) years and 22,84 (\pm 3,93) BMI of Kg/m²), were evaluated at the Bioengineering of Movement Laboratory of the Department of Information Engineering and at the Women and Children Health Department of the University of Padua. Kinematics and sEMG data were simultaneously acquired through four synchronized cameras (GoPro Hero3, 30fps) and an 8 channel sEMG system (FreeEmg, BTS, 1000Hz) that collected the activity of Tibialis Anterior (TA), Gastrocnemius Lateralis (GL), Rectus Femoris (RF) and Biceps Femoris (BF). Each subject performed several gait trials and at least three trials per subject were processed. The following sEMG parameters were extracted: duration of muscle contraction, onset and offset activation timing [3], peak of the envelope and its occurrence [4] and number of co-contractions and their occurrence. The following kinematic parameters were also estimated: minimum and maximum values of lower limb joints angles (hip, knee and ankle) and their range of motion

(ROM) [5]. Supervised classification by means of 7 different classifiers was performed: Decision Tree, Random Forest, CN2 Rule Induction, SVM, k-NN, Neural Network and Naïve Bayes on 3 different sets of vectors: S1 sEMG parameters only; S2 kinematic parameters only; S3 combined sEMG and kinematic parameters.

Results and Discussion

The best classification on a training set (66% of subjects) were obtained by applying k-NN algorithm for S2 and Random Forest for S1 and S3; hence it was further tested on a test set (33% of subjects) (Table 1 and Fig. 1).

Table 1: Performance of the most performant classification algorithms on training and test data.

Set of vectors	S1	S2	S3
Algorithm	Random Forest	k-NN	Random Forest
Training set acc (%)	98,3	100,0	99,2
Test set acc (%)	98,3	100,0	96,7

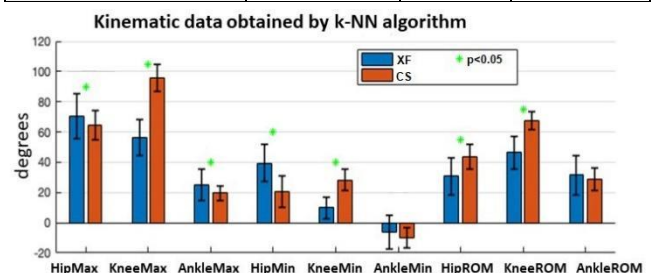


Figure 1: Kinematic parameters in subjects classified as FX and CS by k-NN classifier, *-statistically significant difference (p<0.05)

Conclusions

All the analyzed solutions allowed a good classification of FXS subjects, yet using only kinematic data allowed a better classification. This suggests that the most evident differences in motor control between CS and FX subjects can be detected by analysing kinematic parameters.

References

- [1] Hagerman RJ et al. (2017). *Nat Rev Dis Primers*, 3, 17065
- [2] Alloghani M et al. (2020). *Springer Int. Publishing*, Cham, pp. 3–21.
- [3] Bonato P et al. (1998). *IEEE Trans Biomed Eng*, 45(3):287-99
- [4] Sawacha Z, and Spolaor F et al. (2012). *Gait Posture*, 35(1):101-5
- [5] Sartori M et al. (2015) *Neurophysiol* 114: 2509–2527

Ankle Joint Quasi-Stiffness of Quiet Unperturbed Standing in Chiari Malformation: A Fast Fourier Transform Approach

Brittany N. Sommers¹, Brian L. Davis¹

¹Center for Human Machine Systems, Mechanical Engineering Department, Cleveland State University, Cleveland, Ohio, USA
Email: b.n.sommers@vikes.csuohio.edu

Summary

Ankle joint quasi-stiffness (AJ-QS) is a commonly reported parameter in gait but not upright standing. The AJ-QS calculation of upright standing is more ambiguous due to the instantaneous fluctuations of the center-of-pressure (COP). This abstract presents a novel technique for quantifying AJ-QS in upright standing via a Fast Fourier Transform (FFT). This method identifies the natural frequency of COP trajectories and uses the equations of motion of a second order inverted pendulum to calculate AJ-QS. This method is advantageous as it (1) is not influenced by instantaneous fluctuations of muscular noise, and (2) allows for consideration of the entire COP signal. This study involved 30-second, unperturbed standing trials on individuals with Chiari Malformation (CM), a neuromuscular condition arising from the cerebellum. Joint stiffness is a main qualitatively reported symptom of CM, however this is the first study to quantitatively report AJ-QS in CM.

Introduction

Chiari Malformation (CM) is a congenital neuromuscular condition occurring from a descent of the cerebellar tonsils into the foramen magnum. There is no cure for CM, however a decompression surgery can be implemented to reduce pain from specific symptoms. Suboccipital headaches, joint stiffness, and loss of motor control are a few of the commonly reported symptoms of CM. [1]

During quiet standing, the ankle joint complex is influenced by rotations about the ankle to maintain alignment of the center-of-mass (COM) over the heel [2]. Often, the ankle joint is modeled as a single inverted pendulum, where center-of-pressure (COP) fluctuations are used to realign the COM [2]. In gait, ankle-joint quasi stiffness (AJ-QS) is calculated as the relationship between the ankle torque and ankle angle. This method in upright standing is not practical due to the instantaneous fluctuations of muscle dynamics on the COP. Thus, using a FFT to calculate the natural frequency of the COP, we can estimate AJ-QS from the relationship of undamped natural frequency, stiffness, and inertia. To the authors knowledge, this is the first study to (1) Quantify AJ-QS using an FFT, and (2) to Quantitatively report AJ-QS in individuals with CM.

Methods

The study consisted of six CM participants with decompression surgery (CM-D) and six CM participants without (CM-ND). All participants were female. Participants were asked to stand on an AMTI force plate with their eyes open, feet together, and hands comfortably at their sides for 3, 30-second trials to obtain the anterior-posterior (AP) COP trajectories. Data were recorded at 1000 Hz, and down

sampled to 100 Hz for analysis. COP trajectories were zero-centered before applying the FFT to determine the natural frequency. Natural frequency (ω_n) and stiffness (k) are then related by the equation:

$$\omega_n = \sqrt{\frac{k}{(I_T)/2}}$$

Where I_T is the total moment of inertia of the body, divided in half to account for the distribution of two feet standing on one force plate. I_T anthropometric values were obtained [2] and rotations were considered about the distal axis for each segment.

Results and Discussion

The CM-D group presented higher average AJ-QS, natural frequencies (ω_n), and peak power spectral density (pPSD) values from the FFT than CM-ND. With the limited sample size, only pPSD was significant ($p = 0.032$).

Table 1: Group averages of quasi-stiffness and FFT variables

Group	AJ-QS [kgm ² s ⁻²]	ω_n [Hz]	pPSD [db/Hz]
CM-D	0.098 ± 0.089	0.098 ± 0.062	82.0 ± 47.9
CM-ND	0.068 ± 0.096	0.076 ± 0.046	23.5 ± 19.1

It is hypothesized that the CM-D group has more severe cerebellar damage than the CM-ND group, as decompression surgery is only performed for more severe malformations. Feedback to the cerebellum affects postural sway. Higher natural frequencies and greater power distributions are seen in the group with more neural pathway damage, and *vice versa*.

Conclusions

To the authors knowledge, this abstract presents the first instance of quantifying ankle joint quasi-stiffness in quiet, unperturbed standing via FFT. This method eliminated the need for motion capture data and is not sensitive to muscular noise. This method revealed the affect of cerebellar damage on natural frequency of the system and mechanical stiffness of the ankle joint. The authors expect to have control data for comparison by the time of the conference.

Acknowledgements

Acknowledgements are made to the Conquer Chiari Foundation for their generous funding to this study.

References

- [1] Milhorat TH et al. (1999). *Neurosurgery*, **44**: 1005 - 1017
- [2] Winter DA. (1990). *Biomech & MC of Hum. Mov.*; Wiley

Ground Reaction Forces during Anteriorly-loaded Overground Walking

Jiyun Ahn¹, Caroline Simpkins¹, Meng-Wei Lin¹, Feng Yang¹

¹Department of Kinesiology and Health, Georgia State University, Atlanta, GA 30303, USA

Email: jahn12@gsu.edu

Summary

This study examined the effects of anterior load carriage on ground reaction forces (GRFs) in the sagittal plane during overground level walking. The hypothesis was that anterior loading would change the GRFs during overground walking. Thirty healthy young adults were assigned into three groups (no load, 10%, and 20% body weight (bw)) and their GRFs were measured. The results did not show any significant group-related difference in the peak values of the vertical, forward (or propulsive), and backward (or braking) GRFs.

Introduction

Falls are a significant workplace accident leading to a diverse outcomes such as injuries and economic strain [1]. The literature highlights the frontal load as one of the major occupational fall hazards. The existing studies about front-weighted walking mainly focused on the kinematic gait parameters. Despite meaningful, these parameters may not provide comprehensive information explaining the potential impact of front load carriage on gait. It is necessary to study how the front load carriage affects the kinetic aspect of human gait, in particular the GRFs. A recent study used the GRF as an outcome measurement [2]. It reported that the peak GRF increased among the loaded groups by an amount of the carried weight than unloaded groups. However, there are limitations associated with this previous study. First, participants in this past study walked on a treadmill. The controlled gait speed could have altered the natural gait pattern when walking over the ground. Therefore, the finding from the previous study may not be applicable to overground walking. Second, the GRFs were reported in Newtons but not normalized in the previous study. Given that the loaded groups carried an extra weight, it is intuitive that their absolute GRFs would be greater than the unloaded groups. To address these two limitations, we conducted this present study to test how frontal load alters the normalized peak GRFs during overground level walking. It was hypothesized that the frontal load carriage alters the peak GRFs during overground walking.

Methods

Thirty healthy young adults (24.83 ± 4.96 y/o) were randomized into three groups: no load (Group 1), 10% (Group 2), and 20% bw (Group 3). Each participant had three walking trials on a 10-m walkway at their preferred speed without load. Then, Groups 2 and 3 walked three more trials with their assigned load assembled in a sandbag. During walking, the loaded groups were instructed to hold the sandbag against their abdomen using both hands in a symmetric way and try to maintain the height of the load. Group 1 completed another three normal walking trials without a load.

Two force plates (ATMI) embedded in the middle section of the walkway collected the GRFs during all walking trials. The vertical, forward, and backward GRFs were filtered and normalized by the weight of the body-load system (including the weight of the human body and the external load). The peak GRF in each direction was determined as the maximum value of the respective GRF over a gait cycle. One-way ANOVA compared the dependent variables (peak vertical,

forward, and backward GRFs) with the load level as the factor (0% vs. 10% vs. 20% bw). SPSS 25 (IBM) was used with a significance level of 0.05.

Results and Discussion

The results did not show a significant load level-related effect on GRFs in all three directions ($p = 0.89, 0.88,$ and 0.20 respectively for vertical, propulsive, and braking forces, Figure 1). Our hypothesis that the frontal load changes the GRFs while walking was not supported. A recent study reported significant differences in peak GRFs when participants carrying a front load walk on a treadmill [2]. However, the non-normalized GRFs in the previous study could introduce a confounding effect due to the variations in the body weight between groups. In the current study, the GRFs were normalized to the combined weight of the human body and the load. As stated, the normalized GRFs did not exhibit a load-related difference. Furthermore, participants in our study walked over the ground instead of on a treadmill. The GRF information should more closely reflect the natural human walking in our study than the previous one.

The finding of similar peak vertical GRF between groups in this present study did not agree with another previous study that reported an additional frontal load increases the normalized peak vertical GRF during walking [3]. The discrepancy could be due to the difference in selecting the peak vertical GRF between the two studies. In the previous study, the peak vertical GRF was determined as the maximum vertical GRF during the loading phase of the gait cycle, while the current study selected the global peak value over the entire gait cycle. Further studies should examine the change in the GRFs while carrying a front load heavier than 20% bw.

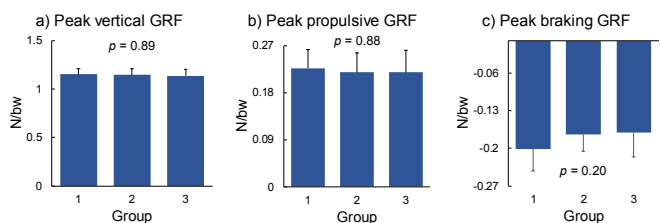


Figure 1. Between-group comparisons of the peak GRF in three directions: a) vertical, b) forward, and c) backward during overground walking.

Conclusion

Anteriorly carrying up to 20% bw may not change the normalized peak GRFs in sagittal plane during overground walking among young adults.

Acknowledgements

The authors thank all members in Biomechanics Lab at Georgia State University for assisting the data collection.

References

- [1] Webster, T. (2000) *Compensation and working conditions*; p. 28-38.
- [2] James, C. R. (2015), *Hum. Mov. Sci.* **44**:327-337
- [3] Cham, R. and Redfern, M. S. (2004). *Occup Ergon*, **4**: 11-26

Automatic Identification and Segmentation of Balance-Related Tasks Using Markerless Motion Capture

Kieran J. Eveleigh¹, Elysia Davis¹, Elise Laende¹, Scott Selbie², Stephen H. Scott³, Kevin Deluzio¹

¹Department of Mechanical & Materials Engineering, Queen's University, Kingston, Canada

²Theia Markerless Inc., Kingston, Canada, ³Department of Biomedical & Molecular Sciences, Queen's University, Canada
Email: kieran.eveleigh@queensu.ca

Summary

An algorithm was developed to identify the onsets and offsets of seven balance-related tasks performed consecutively in a circuit, using data from a markerless motion capture system. The algorithm identified events 116 times faster than two raters. Intraclass correlation coefficients for all task onsets and offsets were between 0.999-1.000.

Introduction

Many clinical assessments of balance include multiple tasks that are performed in succession [1]. Patient performance is often assessed qualitatively. An alternate approach is to use motion capture systems, but it can be laborious to identify key task features such as the beginning and end of a motor action.

The purpose of this study was to (1) develop an algorithm to identify the starts and ends of seven distinct balance-related tasks using data from a markerless motion capture system and (2) to compare the algorithm's performance to manually identified tasks.

Methods

This investigation was carried out in the Human Mobility Research Laboratory (Queen's University, Kingston, ON) and was approved by the institutional ethics review board. Fifteen adults (8 female, mean (SD) age: 34.5 (17.2) years, height: 172.0 (7.8) cm, weight: 75.0 (10.7) kg) participated in this study after providing informed consent.

Participants completed seven balance tasks as part of a larger circuit of clinical assessments. Balance tasks included: tandem stance (TS), functional reach (FR), single limb stance (SLS), shoulder abduction (SA) and rotation (SR), standing hip abduction (HA) and quiet standing on foam with eyes closed (QS). Each participant performed five trials of the circuit, while eight synchronized video cameras recorded video data at 60 Hz.

Kinematic measures were extracted from video data using Theia3D (Theia Markerless, Inc., Kingston, ON) and filtered in Visual3D (C-Motion Inc., Germantown, MD) using a generalized, cross-validatory spline smoothing and differentiation function with a cutoff frequency of 5 Hz. Matlab (MathWorks, Natick, MA) was used for data analysis.

Full body segment kinematic data were used to identify onsets and offsets of the tasks, regardless of the order in which they were performed. All tasks were identified according to the same approach: onsets and offsets of potential instances of a task were identified using primary kinematic features [2], and true occurrences of each task were identified using multiple secondary requirements. The algorithm was developed using pilot data, then tested using the data collected in this study.

Two raters independently used video data to identify the onset and offset of each balance-related task by frame number for one randomly selected trial from each participant. The time taken to label all tasks within a trial was recorded.

The algorithm's performance was compared to the two raters using a two-way, mixed-effects, absolute agreement, single measures intraclass correlation coefficient (ICC). All ICC estimates and their 95% confidence intervals (CI) were calculated using SPSS (SPSS Inc., Chicago, IL).

Results and Discussion

The algorithm identified all seven balance-related tasks in each of the 15 trials. The average processing time for a single trial for the algorithm was 6 s, compared to 697 s for the raters. ICC estimates for all tasks (Table 1) showed excellent reliability [1], indicating that the algorithm can be used to replace the manual segmentation of multiple tasks within a dataset of kinematic measures.

Conclusions

The algorithm introduced in this paper can identify the onsets and offsets of seven balance-related tasks commonly featured in clinical assessments. It shows potential to expedite the segmentation of tasks within large motion capture datasets from balance-related studies, without compromising the correct identification of task onsets and offsets.

Acknowledgments

This study was funded by an Ontario Research Fund-Research Excellence grant (RE09-112).

References

- [1] Horak FB et al. (2009). *Phys. Ther.*, **89**: 484-498.
- [2] Coderre AM et al. (2010). *NRR*, **24**: 528-541.

Table 1: Intraclass Correlation Coefficients and 95% CI's Comparing Task Onsets (+) and Offsets (-) Identified Algorithmically and Manually.

Tasks	TS +	TS -	FR +	FR -	SLS +	SLS -	SA +	SA -	SR+	SR -	HA +	HA -	QS +	QS -
ICC	1.000	1.000	0.999	1.000	0.999	1.000	0.999	1.000	1.000	1.000	1.000	1.000	1.000	1.000
95% CI	0.999, 1.000	0.963, 1.000	0.985, 1.000	0.997, 1.000	0.955, 1.000	0.997, 1.000	0.983, 1.000	1.000, 1.000	0.999, 1.000	1.000, 1.000	0.999, 1.000	0.999, 1.000	0.998, 1.000	0.999, 1.000

Improved Balance Control Following Distance Learning of Yoga in Novice Practitioners

Pranavi L. Depur¹, Belle P. Ponce de Leon¹, Andrew Y. Cho¹, Joshua A. Vicente¹, Jacob W. Hinkel-Lipsker, Ph. D.¹
¹Move-Learn Lab, California State University, Northridge, California, USA
 Email: movelearnlab@gmail.com

Summary

Due to the recent COVID-19 pandemic, there is interest among the lay public to implement effective virtual fitness paradigms. Yoga is a common form of at-home exercise that can be instructed in multiple ways—including live (synchronous) sessions or asynchronous video. In this study we examined how novice yoga practitioners learned using these different pedagogical methodologies in terms of balance control over an 8-week intervention. Early results indicate that the group that practiced using a mix of synchronous and asynchronous modalities showed the greatest improvement in balance control, followed by synchronous, while the fully asynchronous group was least effective. These results indicate that yoga practiced in an online format improves balance control, which can be highly useful to those who do not have access to traditional in-person classes, and that distance learning should incorporate both asynchronous and synchronous components.

Introduction

Yoga is known to have many health benefits such as improved flexibility, strength, and balance control [1,2]. However these benefits have been largely unexplored when yoga is practiced via distance learning. Due to the COVID-19 pandemic, most exercise forms have moved to an online platform. Methods of instruction are generally categorized into synchronous practice where the instructor and learner are practicing in real time, asynchronous practice, where learners practice on their own time utilizing content created by the instructor, or mixed practice, which integrates both methods [3]. Based on research in online (non-fitness) education, a blended approach is the most effective in learning outcomes [3]. Due to the growing proliferation of at-home exercise models it is necessary to determine which method of content delivery is the most effective for yoga practitioners. The purpose of this study was to assess the effects of synchronous, asynchronous and mixed online content delivery from an 8-week yoga program designed for novice yoga practitioners. We hypothesized that a blend of the two modalities would lead to the greatest improvement in balance control (e.g., center of mass sway and velocity).

Methods

Fifty-three novice participants between the ages of 18 and 65 were recruited for the study to participate in an online 8-week yoga program. Before and after the intervention, participants met over video conferencing with a member of the research team and engaged in a series of balance tests randomized in order, which included a single leg stance pose with the eyes closed, a tree pose, and an eagle pose. Markers were placed on the participants' approximate center of mass in the frontal and sagittal planes. Participants were recorded

during performance of these poses, and two-dimensional motion analysis software was used to track center of mass (COM) position. Marker coordinate data were used to quantify center of mass excursion (displacement), velocity, and total distance traveled during each pose. Following baseline testing, participants were randomly assigned to either an asynchronous, synchronous or mixed group, all of whom were instructed to complete a minimum of two classes per week where attendance was recorded. After program completion, participants again met with a member of the research team virtually to perform the balance tests using the same methodology as before.

Results and Discussion

Preliminary results ($n = 3$) demonstrate that all approaches yielded improvement to balance control; however, the mixed approach was the most effective form of instruction as their COM velocity was slowest when comparing pre-testing results with post testing results (Figure 1). Similar improvements were observed in terms of COM total excursion as well as the total distance traveled during the balance poses.

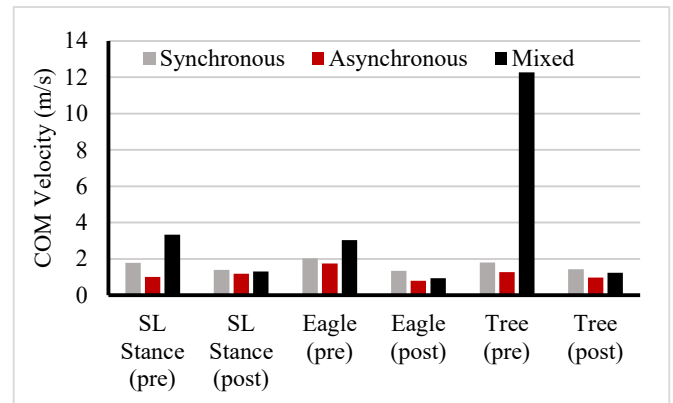


Figure 1: Pre and Post-test COM Velocity across all groups

Conclusions

This study yielded large improvements in balance control, especially for those who used a mixed methodology. Future yoga interventions should implement both synchronous and asynchronous methods, and ensuing research should study whether different populations (e.g., older adults) respond similarly to this intervention.

References

- [1] D. E. Laaksonen, et al. (2002). *Diabetes Care*, vol. 25:1612–1618,
- [2] M. D. Tran et al. (2001). *Preventive Cardiology*, vol. 4: 165–170
- [3] N.T. Butz, and R.H. Stupinsky (2016). *The Internet and Higher Education*, vol. 28: 85-95

Functional calibration to improve kinematic analysis in the clinics using inertial measurement units

Clint Hansen¹, Baraah Chebil¹, Elke Warmerdam^{1,2}, Robbin Romijnders^{1,2}, Kirstin Hansen¹, Walter Maetzler¹

¹Neurogeriatrics, University Hospital Kiel, Kiel, Germany

²Digital Signal Processing and System Theory, Kiel University, Kiel, Germany

Email: c.hansen@neurologie.uni-kiel.de

Summary

Preliminary results show that functional calibration methods are not only feasible in the clinical setting but also allow to improve the accuracy of the joint kinematics using inertial measurement units (IMU).

Introduction

Measuring human movement in clinical settings has a long standing tradition in biomechanics. The systems vary and with the technological development movement analyses are more and more performed using IMUs. The IMUs however suffer from drift, introducing errors to the analysis. This becomes especially pertinent if gait parameters are assessed based on multiple sensors e.g. to evaluate the kinematics of a patient. Previous work has already provided solutions to overcome those problems for single sensor or single joint configurations [1] or either using post processing techniques to the lower body kinematic chain [2]. In this work we use a functional calibration method, an accelerometer-based correction tool, which ultimately allows to collect kinematic data in a magnetically disturbed spot.

Methods

The Short Physical Performance battery (SPPB) was performed at the University hospital Kiel with healthy and neurogeriatric participants [3]. The SPPB assesses lower extremity physical function: 3 standing balance tests, a 4-meter walk at usual pace, and 5 unassisted chair stands. Participants were equipped with seven IMUs attached to the lower back, the thighs, the shanks and the feet. A functional walking trial was collected to overcome problems with magnetically disturbed clinical environment and applied to the SPPB trials. Data were collected using the MyoMotion data processing tool. The data collection is ongoing with a target sample size of 50.

Results and Discussion

Currently 15 participants have conducted the SPPB in the clinical setting including the functional walking

calibration. The calibration procedure can be performed by all participants. Here, we show the data from one healthy participant (female, 50 years). The resulting walking kinematics are shown in (Figure 1).



Figure 1: Sagittal joint angles (hip, knee, ankle) and the corresponding inter-joint coordination plots (hip vs. knee angle) of the left and right side.

Conclusions

The aim of this work was to present the feasibility of a calibration method to measure kinematics during the SPPB. The functional walking method proved to be feasible and produce stable results, is robust, and relatively simple to administer. Functional calibration methods are a promising direction for future wearable health monitoring systems when tracking motions in magnetically disturbed areas, such as the clinical ward [3].

References

- [1] Muller et al. (2017). *IEEE J BHI* **21**(2):312-319.
- [2] Kong et al (2016). *Sensors*, **16**(12)
- [3] Geritz et al. (2020) *BMC Geriatrics*, **20**, 45.

A Preliminary Study Comparing the Effects of Concurrent and Terminal Visual Feedback on Standing Balance in Older Adults

Jamie Ferris¹, Vincent J. Barone¹, Kerby Shedden¹, Noel C. Perkins¹, Kathleen H. Sienko¹

¹University of Michigan, Ann Arbor, MI, USA

Email: jcferris@umich.edu

Summary

Reductions in older adults' abilities to balance can lead to increased fall risk and other negative health effects. Balance training with a physical therapist improves balance performance and health outcomes, but access is limited by the cost and availability of physical therapy. Consequently, home-based training technologies may increase access to preventative and therapeutic balance training. This preliminary study compared the immediate and post-training effects of concurrent and terminal visual feedback to inform the design of a visual-feedback based home balance training technology.

Introduction

Concurrent visual feedback increases training efficacy under certain conditions and has been implemented in research settings [1]. However, concurrent visual feedback cannot be used to support all types of balance training exercises (e.g., exercises performed with eyes closed or head movements). In contrast, terminal feedback has the potential to support a broader range of exercises and could be provided with ubiquitous technology such as a smartphone. The guidance hypothesis predicts that concurrent feedback yields greater immediate improvement and terminal feedback yields greater retention of improvement. However, these effects vary by task and type of feedback, and the differences in the effects of concurrent and terminal visual feedback during balance training are not well understood [2]. Therefore, the objective of this study was to perform a preliminary comparison of the immediate and post-training effects of concurrent and terminal visual feedback on older adult balance performance to inform the design of home-based balance training technologies.

Methods

Nineteen healthy older adults participated in a single-day crossover study during which they performed multiple repetitions of standing with feet together on a foam surface while receiving either concurrent or terminal visual feedback. For each feedback type, participants completed 19 total trials consisting of four baseline trials (without feedback) followed by five repetitions of three trials (two with feedback and one without).

Postural sway data were collected using an inertial measurement unit (MTx, XSens) on the lower back and were used to calculate angular position and velocity performance features. The effects of both types of feedback were analyzed using linear mixed-effects models ($\alpha = 0.05$). The effects of training with feedback (i.e., the effects of an increase in trial number with feedback) were evaluated using the model

results, and the post-training effects of feedback (i.e., the differences between baseline trials and the final trial completed without feedback) were evaluated using subsequent contrasts.

Results and Discussion

Effects of training with feedback: Measures of sway angle (root mean square angle from vertical, RMS; 95th percentile confidence interval elliptical fit area, EA) decreased throughout the training session regardless of the type of feedback (RMS $p < 0.001$; EA $p = 0.001$). However, mean sway velocity increased with concurrent feedback ($p = 0.009$) and decreased with terminal feedback ($p < 0.001$), suggesting that participants used concurrent feedback to make many rapid postural corrections while they used terminal feedback to make fewer slow adjustments.

Post-training effects of feedback: Following the completion of the concurrent feedback training protocol, sway angles returned to baseline values (RMS $p = 0.935$; EA $p = 0.529$) and mean sway velocity decreased to below baseline values ($p < 0.001$). In contrast, following the completion of the terminal feedback training protocol, sway angles and sway velocity both decreased to below baseline values (RMS $p = 0.022$, EA $p = 0.007$, mean velocity $p < 0.001$).

Conclusions

Both types of feedback yielded sway reductions during training. However, in the context of this study, only training with terminal visual feedback yielded small, short-term, single-task sway reductions following the completion of the training protocol. While the implication of these findings is limited by the short training duration, these preliminary results suggest that terminal visual feedback may be a viable alternative to concurrent visual feedback. Terminal visual feedback should therefore be further investigated for use in at-home balance training technologies because it may support a broader range of exercises, be compatible with smartphone platforms, and offer the potential for improved training retention.

Acknowledgments

This project was supported by the University of Michigan Rackham Graduate Student Research Grant.

References

- [1] Halická Z et al. (2011). *Act Nerv Super Rediviva*, **53**: 67-71.
- [2] Goodwin JE and Goggin NL (2018). *Perceptual and Motor Skills*, **125**: 1160-1172.

Changes in postural dynamics can be captured by a Wii Balance Board during standing tasks

Takashi Sado¹, Kota Z. Takahashi¹ & Mukul Mukherjee¹

¹Department of Biomechanics, University of Nebraska at Omaha, Omaha, NE USA
email: tsado@unomaha.edu, web: <https://www.unomaha.edu/college-of-education/cobre/>

INTRODUCTION

Variability during postural sway has been shown to characterize healthy and pathological systems. Specifically, persistence from center of pressure displacement (i.e., how variability of postural control fluctuates over time) is a useful description of postural control in healthy populations [1] and in the investigation of pathologies such as Parkinson's disease and developmental disorders. However, obtaining such measurements outside of a laboratory setting is not simple. This is because portable laboratory-grade force platforms are expensive.

Our previous study showed that the Nintendo Wii Balance Board (WBB), a cost-effective portable device was able to accurately quantify persistence and anti-persistence behaviors of postural sway in the anterior-posterior direction compared to force platform (FP) in healthy populations [2]. However, typically studies use the center of pressure displacement. In a recent study, the point-to-point velocity of the center of pressure (COPv) was shown to be more sensitive in capturing the persistence and anti-persistence behavior in postural control [3]. Therefore, the purpose of this study is to determine the effects of task conditions on postural dynamics measured using a WBB.

METHODS

Seventeen healthy volunteers were recruited (3 females; mean age 24.5 ± 4.5 years). All participants performed three different conditions for 3 minutes: quiet standing on both legs with eyes open, quiet standing on both legs with eyes closed and standing on one leg with eyes open.

The WBB was placed centrally upon a flush mounted laboratory grade FP. The data was collected at 600 Hz for the FP, while it was collected at 30 Hz for the WBB. The data from FP was down-sampled to 30 Hz. From the COP displacement data, COPv was calculated for the WBB and FP. DFA was used to analyze the persistence and anti-persistence characteristics of the COPv in the anterior-posterior and mediolateral directions. First, inflection point was determined manually as the first time the persistence behavior shifted to anti-persistence behavior. Based on this, the alpha value of the short-term scale region (persistence) and long-term scale region (anti-persistence) was calculated. The level of statistical significance was set at $p < 0.05$.

RESULTS AND DISCUSSION

One-way repeated ANOVA revealed that there was a significant condition effect in alpha value of short scale region (alpha-short) in the AP ($p = 0.014$) and the ML ($p = 0.048$)

directions. Inflection point, where the persistence behavior switched to anti-persistence behavior for the first time, also showed significant condition effect in AP ($p = 0.001$) and ML ($p = 0.014$). Post-hoc pairwise comparisons indicated that alpha-short for eyes closed standing was larger than one leg standing in AP ($p = 0.015$). Although there was no statistical significance ($p = 0.051$), it is interesting to see that in comparison to quiet standing, eyes closed standing has higher persistence. The eyes closed standing also showed earlier inflection point compared to the quiet eyes open standing ($p = 0.027$). In ML, one leg standing showed smaller alpha-short value compared to the eyes open quiet standing ($p = 0.004$), and had much earlier inflection point compared to the eyes closed standing ($p = 0.044$). These results showed that WBB can capture the changes in persistence behavior of COPv between the standing conditions.

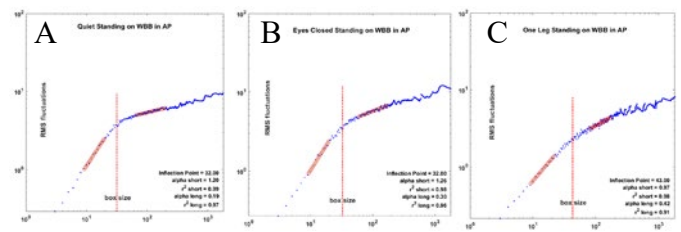


Figure 1A-C: Representative DFA data of COPv on WBB in AP of the same participant performing quiet normal standing with eyes open (1A), eyes closed standing (1B), and one leg standing (1C).

CONCLUSIONS

In this study, postural sway variability of COPv from WBB was analyzed using DFA. It was found that WBB can capture the changes of persistence in velocity of postural sway and is sensitive to task conditions. Future studies will compare how accurately WBB captures the persistence and anti-persistence of postural sway (COPv) compared to the gold standard, the FP.

REFERENCES

1. Rand, TJ, et al. *Ann Biomed Eng.* **43(11)**, 2017.
2. Meade, ZS, et al. *J. Biomech.* **100**, 2020
3. Rand, TJ, et al. *Exp. Brain Res.* **236**, 2018.

ACKNOWLEDGEMENTS

This study was supported by the COBRE grant (1P20GM109090-01) from NIGMS/NIH, a NASA EPSCoR Research grant (80NSSC18M0076) and an AHA AIREA award (18AIREA33960251). In addition, intramural GRACA and FUSE grants from the UNO also provided support.

Evaluation of Postural Sway for Remote Monitoring of Vestibular Rehabilitation

Timothy P. Zehnbaauer¹, Nathan T. Pickle¹, Paulien E. Roos¹,

¹CFD Research Corporation, 701 McMillian Way NW, Suite D. Huntsville, AL 35806

Email: paulien.roos@cfdr.com

Summary

Vestibular rehabilitation is an effective treatment for reducing dizziness and falls in older individuals. In this study, we investigated measurements from a low-cost commercial inertial sensor (IMU) as the basis for assessing postural sway during remote treatment. We found that an outcome measure based on jerk is dependent on sensor placement but effectively distinguished between some balance tasks and may be effective for tracking patient progress.

Introduction

Vestibular rehabilitation is effective in reducing dizziness and falls in older individuals and improving gait and overall quality of life [1]. Rehabilitation targets head and eye coordination (e.g., vestibular ocular reflex (VOR) exercises) as well as balance, such as standing on one foot. However, patient adherence remains a major problem due to frequency of visits required and accessibility to care [2]. With the recent increased acceptance of telehealth solutions, tools are needed to quantitatively assess patients' progress remotely. In this study, we explored the use of a parameter based on jerk (time rate of change of acceleration) as an indicator of the smoothness of postural sway to distinguish between different balance conditions [3]. In addition, we evaluated different sensor locations to determine whether a sensor placed on the head could be used to assess both VOR and balance exercises.

Methods

To determine the validity of using jerk to assess postural sway during balance exercises, we had one healthy subject (male, 26 years old) perform 12 trials of 3 balance exercises after providing written informed consent to a protocol approved by the IRB at CFD Research: neutral standing posture, standing on one leg only with eyes open, and standing on one leg only with eyes closed. Half of the trials were performed with a sensor fixed to the head, and the other half while the sensor was fixed to the lower back. The subject was instructed to perform the exercise for one minute while looking straight and remaining as still as possible. Accelerometer data were collected using a MetaMotionR (MbiEntLab Inc, San Francisco, CA) sensor secured at either the 5th lumbar vertebrae level (L5) using a Velcro strap or on the forehead using a headband.

Accelerometer data were filtered using a 4th order zero-phase shift low-pass Butterworth filter with a 3.5Hz cutoff. To assess postural sway the integral of the square of the magnitude of jerk in the anterior/posterior and medial/lateral directions was used [3]:

$$\frac{1}{2} \int_0^t \left(\left(\frac{dAccAP}{dt} \right)^2 + \left(\frac{dAccML}{dt} \right)^2 \right) dt \quad (1)$$

where *AccAP* and *AccML* are accelerations in the anterior/poster and medial/lateral directions respectively. Lower values tightly controlled postural sway.

Unpaired t-tests were performed to determine the difference between means of conditions. A Bonferroni pair-wise correction was applied to account for multiple comparisons ($\alpha=0.05/3=0.017$).

Results and Discussion

Results indicated a statistically significant difference between balancing on one foot with eyes closed compared to balancing on one foot with eyes open and neutral standing when using a sensor placed on L5 (Table 1). For all other conditions, the difference in means was not statistically significant after Bonferroni correction. While a head sensor would be especially advantageous for assessing vestibular rehabilitation exercises, as most other exercises involve repetitive head movements, we were unable to distinguish between the three conditions using a sensor placed on the head.

Table 1: Mean (S.E.) jerk parameter value in each condition with sensor on the head or 5th lumbar vertebrae (L5). Significant differences ($p<0.017$) relative to eyes closed indicated by '*'.

	<u>Postural Sway Smoothness (m²/s⁵)</u>		
	Standing	Eyes Open	Eyes Closed
L5	1.2·10 ⁻³ (2.6·10 ⁻⁴)*	5.9·10 ⁻² (1.9·10 ⁻²)*	1.1 (0.23)
Head	6.6·10 ⁻³ (1.4·10 ⁻³)	0.11 (3.1·10 ⁻²)	1.5 (0.46)

Conclusions

We demonstrated that postural sway can be accurately assessed using data from a low-cost IMU sensor placed on the lower back to compute a jerk-based parameter. The head-mounted sensor did not distinguish between conditions, so our results suggest that an L5-mounted sensor is necessary. These results provide justification for future studies to test the effectiveness of this method to assess severity of vestibular dysfunction and track patient progress over time.

Acknowledgments

Research reported in this publication was supported by the NIDCD (NIH Award R44DC017408). The content is solely the responsibility of the authors and does not necessarily represent the official views of the NIH.

References

- [1] Whitney SL et al. (2016). *Curr. Treat. Options Neurol.* **18(3)**: 13.
- [2] Soto-Varela A et al. (2017). *J. Laryngol. Otol.*, **131(3)**: 232-238.
- [3] Mancini M et al. (2011). *Parkinsonism Relat. Disord.* **17(7)**: 557-562.

Characterizing the feasibility of Progressive Gait Perturbation Protocol for Individuals Poststroke

Hala E. Osman¹, Antonie J. van den Bogert², Ann Reinthal³, and Debbie Espy³

¹ Cleveland State University, Department of Biomedical Engineering, Cleveland, OH, USA

² Cleveland State University, Department of Mechanical Engineering, Cleveland, OH, USA

³ Cleveland State University, College of Sciences and Health Professions, Cleveland, OH, USA

Email: h.osman@vikes.csuohio.edu

Summary

We identified minimal performance characteristics under which our treadmill gait perturbation protocol (FLP) was feasible for individuals post stroke. For those able to complete the protocol, it was able to demonstrate fall resistance improvements. Participants who did not meet the minimal conditions were included as a gait speed only group (GSP). Despite the unsuitableness of the protocol for people with extremely slow gait speeds or otherwise very impaired gait, our full protocol was in fact feasible for adults' post stroke with generally slower gait speeds and significant balance challenges, the group for whom this type of measure is useful.

Introduction

Treadmill-based gait perturbation protocols have been shown to hold potential as balance assessment tools using simulated slips to induce adaptive full body stability responses and falls reduction [1].

Research has found that high-intensity, treadmill-slip training improved older adults' gait speed and another study found that a progressively-increasing intensity protocol had advantages over the progressively-decreasing protocol as not all participants could tolerate such high intensity training [2].

However, these protocols were not individualized to meet each person's balance and motor ability. Thus, our goal was to scale the initial perturbation magnitude based on the individual's maximum gait speed and balance ability as measured by the Mini-BEST.

Methods

Participants were asked to identify when their comfortable, natural, but safe speed (NWS) on the treadmill had been reached. After resting as needed, they were asked to walk to find their maximum walking speed (MWS). The treadmill then ran at each participant's NWS throughout the perturbation testing sessions.

To scale and ensure appropriateness to each individual, the initial perturbation was based on the individual's maximum gait speed and balance ability as measured by the Mini-BEST. The initial perturbation magnitude (mPer) was calculated based on the participant's MWS and their Mini-BEST score: for scores from 19 – 23, mPer = 55% of MWS, 24 -25 mPer = 75% of MWS, and 26 - 28 mPer = 95% of MWS.

The same initial mPer was used for pre-and post- intervention testing. A stepwise progression based on trial outcome was followed to modulate the mPer for subsequent trials.

Results and Discussion

We identified conditions under which this full perturbation protocol (FLP) was feasible for individuals post stroke. Specifically, necessary conditions are: (1) gait speed greater than 0.2 m/s to generate a noticeable perturbation; (2) able to walk on the treadmill without holding the handrail for the 90 sec trials to elicit solely a stepping strategy for recovery; and (3) able to walk on both force plates (each foot landing consistently on its side of the treadmill) to trigger perturbations under the unaffected leg. Participants who did not meet these conditions were included as a gait speed only protocol group (GSP). Mini-BEST score was higher in the FLP than GSP group (Figure 1).

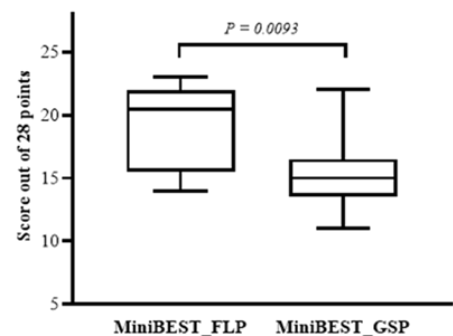


Figure 1: Mini-BEST score was higher in the FLP than GSP group.

Twenty-two participants completed pre- and post-testing: 12 were able to complete the FLP and 10 completed the GSP only. NWS was different from MWS at pre and post-test and NWS was faster at post-testing than pre as was MWS.

Conclusions

The present study has enhanced our understanding of the possible use of this methodology as a direct approach for assessing reactive responses and potentially could be used as an alternative to fall data collection.

References

- [1] F. Yang and Y.C. Pai (2013). *J. Biomech*, **46**: 63–69.
- [2] X. Liu et al. (2016). *J. Biomech.*, **49**: 135–140.

Multifractal Analysis of Quiet Standing in the Young and Old

John H. Challis

Biomechanics Laboratory, The Pennsylvania State University, Pennsylvania, United States

Email: jhc10@psu.edu

Summary

The center of pressure during quiet standing can reveal insights into the control of movement. This study analyzed quiet standing with eyes open and eyes closed for a young subject group and an older subject group. The multifractal spectra of the center of pressure data were computed, and indicated that all signals were multifractal in nature. This property is indicative of the processes controlling quiet standing operating at different time scales – the system has multiplicative cascade dynamics.

Introduction

When human stand still, they do not stand perfectly still they have body sway. This body sway is typically analyzed by extracting various metrics from the motion of the center of pressure. It has been suggested that the center of pressure motion reflects two processes operating over different time scales [1]. These results suggest that the control of standing has multiplicative cascade dynamics, that is that system behavior is dependent on the interactions from system components which operate over different time scales. For such a system the output should demonstrate multifractal fluctuations. Therefore, the purpose of this study was to examine the multifractal properties of center of pressure data to examine if quiet standing demonstrates multiplicative cascade dynamics, and to determine if there were different properties between young and old subjects.

Methods

The analysis was performed on a public data set of force plate data of human quiet standing [2]. The analyzed data came from 27 young subjects, (height: 1.71 ± 0.11 m; mass 70.3 ± 17.8 kg; age: 23.1 ± 4.3 years; 15 males and 12 females) and 22 older subjects (height: 1.61 ± 0.09 m; mass 68.7 ± 11.2 kg; age: 67.8 ± 6.1 years; 11 males and 11 females). The subjects stood still for three 60 s trials with their eyes open, and a further three trials with their eyes closed. Force plate data were collected at 100 Hz for all trials.

Center of pressure data were tested for data normality using the Jarque-Bera test [3]. The Detrended Fluctuation Analysis (DFA) determines for a signal its statistical self-affinity, thus revealing underlying signal properties [4]. A drawback of the DFA of a signal is that second moment-fluctuations only are assessed but by considering higher order moments a multifractal DFA (MDFA) can be determined [5]. Therefore, for these data the MDFA was used and from that analysis the multifractal spectrum determined. From this spectrum the multi-fractal spectrum width, range of the q^{th} -order singularity exponents, was computed as an indication of the range of different scale invariant structures in the time series. In addition, the average velocity of the center of pressure

was computed as was the area of the center of pressure motion [6].

Results and Discussion

All data demonstrated a lack of normality, as indicated by the Jarque-Bera test. Normality is a necessary condition for data demonstrating fractal like properties. It also indicates data which is not well described by basic statistical analyses (e.g., computation of signal mean and standard deviation).

The center of pressure velocity was greater with eyes closed than with eyes open, it was statistically different between these conditions for each subject group ($p < 0.05$). Comparison between groups indicated a greater center of pressure velocity for the older subjects compared with the younger subjects, these differences were statistically different for each condition ($p < 0.05$).

For the center of pressure area there was no statistically significant differences between conditions for each subject group, or between groups for the same condition. The method for determine center of pressure area assumes normality of the data [6], which is violated for these data.

The multifractal spectra of the center of pressure data indicated that the signals for both groups and all conditions were multifractal, indicative of processes operating at different time scales. For standing there are multiple systems contributing to the maintenance of upright standing, with both neurological and physiological processes operating at different speeds and therefore time scales. The multi-fractal spectrum widths were not statistically different between groups or conditions, except for the older group when eyes closed was compared with eyes open ($p < 0.05$). For the older group the spectrum width narrowed with eyes closed, possibly due to the removal of one source of feedback.

Conclusions

Center of pressure data from quiet standing contains multiple fractal processes, indicating that the center of pressure arises from multiplicative cascade dynamics.

References

- [1] Collins JJ, & De Luca CJ. (1994). *Physical Review Letters*, **73**(5), 764-767.
- [2] dos Santos DA, et al. (2017). *PeerJ*, **5**, e3626.
- [3] Jarque CM, & Bera AK. (1987). *International Statistical Review*, **55**(2), 163-172.
- [4] Peng, CK et al. (1994). *Physical Review E*, **49**(2), 1685-1689.
- [5] Kantelhardt JW et al. (2002). *Physica A*, **316**(1-4), 87-114.
- [6] Oliveira LF., Simpson DM, & Nadal, J. (1996). *Physiological Measures*, **17**, 305-312.

Simple model of arch support: relevance to Charcot Neuroarthropathy

Shaye M. Tiell¹, Brian L. Davis², G. R. McMillan³, L. P. Goss³, J. W. Crafton³

¹The University of Akron, Akron, OH, USA

²Cleveland State University, Cleveland, OH, USA

³Innovative Scientific Solutions Inc., Dayton, OH, USA

Email: smt125@uakron.edu

Summary

Charcot neuropathy is a common complication resulting from poorly controlled diabetes and peripheral neuropathy leading to the collapse, and ultimately breakdown, of the midfoot. Mechanically, a compromised arch support is likely associated with slippage at the distal and proximal interface regions of the foot's plantar surface and the adjacent support surface. Systems for monitoring interface shear stresses could potentially assess this slippage. However, correlation between arch collapse and interface shear stresses needs verified. Thus, a model was developed using a multi-body dynamics package. The model's predictions matched interfacial shear stresses during upright stance. Of clinical relevance, when the stiffness of the plantar spring (representing aponeurosis and intrinsic muscles) was reduced by 10%, the frictional force difference increased by about 6.5%. Clinical implications are that, while arch lengthening of less than 2mm might be difficult to measure in a gait lab, using shear sensors under the foot should allow repeatable assessment of arch support.

Introduction

Charcot neuropathy is a common complication resulting from poorly controlled diabetes and peripheral neuropathy leading to the collapse, and ultimately the breakdown, of the midfoot. Mechanically, it is likely that a compromised arch support would be associated with slippage at the distal and proximal interface regions of the plantar surface of the foot and the adjacent support surface [1-4]. This slippage, although difficult to quantify with standard motion capture systems used in a gait laboratory, could potentially be assessed with systems for monitoring interface shear stresses. However, before investing in such systems, a correlation between arch collapse and interface shear stresses needs to be verified.

Methods

A sagittal plane model of a foot was developed using a multi-body dynamics package (MSC Adams). This model mimicked a subject swaying back and forth, and was constructed to show the dependence of interface stresses on altered arch support (see Figure 1).

Results and Discussion

The model's predictions matched typical interfacial shear data: lengthening of the arch of 1-2mm, sway oscillations of 0.22-0.33 seconds and frictional force differences (calcaneus relative to forefoot) of 60N (see Figure 2). Of clinical relevance, when plantar spring stiffness (representing aponeurosis and intrinsic muscles) was reduced by 10%, the frictional force difference increased by about 6.5%.

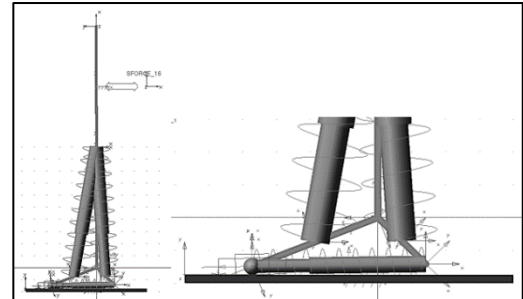


Figure 1: Initial foot model developed with MSC Adams software: (left) An upright subject is represented, (right) close-up view.

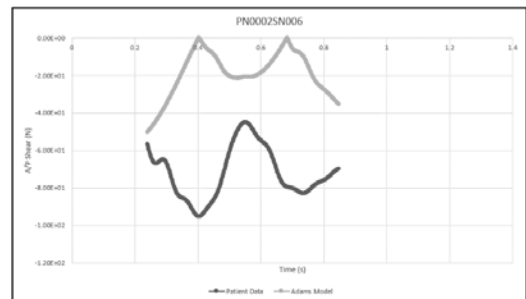


Figure 2: Computational model compared to patient trial data. Note that the sign convention for the experimental data is arbitrary – in this case, the negative peaks of the experimental data match the positive peaks in the model data.

Conclusions

The clinical implications of this study are that, while arch lengthening of less than 2mm might be difficult to measure reliably in a gait lab, using shear sensors under the forefoot and hindfoot should allow arch support to be assessed in a repeatable manner. For patients at risk for arch collapse, measuring shear differences between forefoot and hindfoot regions may provide opportunities for early intervention.

Acknowledgments

This work was supported by the National Institutes of Health 1R41DK125238-01.

References

- [1] Strotman et al. (2016). *Foot & ankle international*, 37(11), 1255-1263.
- [2] Chantelau et al. (2006). *Exp Clin Endocrinol Diabetes*. 114(3):118-23.
- [3] Davis et al. (2017). *J. Biomech.* 52, 176-178.
- [4] Jeffcoate et al. (2005). *Lancet*, 366(9502):2058-61.

Do relaxed sarcomeres return to their original length following repeated activations?

First I. Meng Li¹, Second II. Walter Herzog², Third III. EngKuan Moo³

¹Human Performance Lab, Kinesiology, University of Calgary, Canada

^{2,3} Human Performance Lab, Faculty of Kinesiology, University of Calgary, Canada

Email: meng.li2@ucalgary.com

Summary

Sarcomere length non-uniformities are thought to be the primary cause for many mechanical properties of skeletal muscle. However, despite its importance, it is not known if sarcomere length non-uniformities occur randomly or are determined by structural and contractile properties of muscles. In this study, we identified that passive sarcomere length non-uniformities are not random and are likely associated with the properties, isoform and concentration of titin molecules in sarcomeres.

Introduction

Sarcomeres in muscles, fibres, and myofibrils are known to be non-uniform in skeletal muscle of vertebrates [1-3]. These non-uniformities differ substantially between passive and active muscles. Sarcomere length non-uniformities have been associated with major functional and mechanical properties of skeletal muscles, such as muscle “creep” extension of the plateau of the force-length relationship, residual force depression, and residual force enhancement. Despite this apparent importance of sarcomere length non-uniformities in muscle function, the factors determining these non-uniformities are unknown. It is not even known if these non-uniformities arise randomly from the proposed instabilities of sarcomeres on the descending limb of the force-length relationship, or if they are determined uniquely by structural and/or contractile sarcomeric proteins in the passive and active muscle state. The purpose of this study was to determine if sarcomere non-uniformities in passive myofibrils arise randomly or are determined and similar for multiple activation/deactivation cycles.

Methods

18 myofibrils with 356 individual sarcomeres were used for this study. Myofibrils were obtained from psoas muscles of seven female rabbits age ≥ 6 months. Prior to each experiment, the average sarcomere lengths of the myofibrils were set at 2.7 μm , 3.2 μm , and 3.6 μm . The individual sarcomere lengths at these initial lengths were measured and are referred to as R₀. Myofibrils were then activated for 5s, and relaxed for 2 minutes, and this activation/relaxation process was repeated for three times, giving three additional individual sarcomere lengths in the relaxed state referred to as R₁, R₂, and R₃. For visualization (Figure 1), sarcomeres were divided depending on their initial, R₀, lengths into short, n = 76, SL = 2.5 \pm 0.27 μm (black); short-medium, n = 116, SL = 2.9 \pm 0.25 μm (red); medium-long, n = 111, SL = 3.4 \pm 0.24 μm (green), and long, n = 50, SL = 3.9 \pm 0.31 μm (yellow). Sarcomere lengths at R₀-R₃ were measured between the centroids of the A-bands using light microscopy (Zeiss Axiovert 200M, Zeiss, 40x, NA

0.75 \times 2.5 Opti-over), and a custom-designed program that identified the A- and I-bands based on light intensity patterns.

Results and Discussion

Sarcomere lengths tended to return to their initial values following three activation and deactivation cycles; that is, short sarcomeres tended to remain short and long sarcomeres tended to remain long. Approximating the first (R₀) and the last (R₃) sarcomere length values for all 356 sarcomeres, a regression line through a zero y-intercept has a slope of nearly 1.0 and a coefficient of variation r² of, indicating that sarcomeres tend to return to similar lengths, and definitely do not go to arbitrary lengths after each activation/deactivation cycle. This result then suggests that sarcomere length non-uniformities are governed by some structural component inherent to the sarcomere.

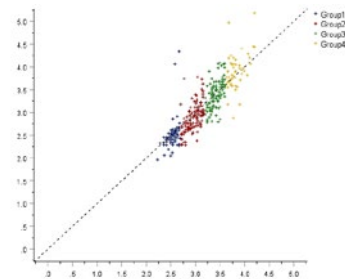


Figure 1: Linear Regression of R₀ and R₃ for the Four Groups.

Since the structural protein titin is the virtually exclusive provider of passive force, and since all sarcomeres in a myofibril are arranged in series, and thus must transmit the same force, it seems reasonable that the number of titin molecules in a sarcomere might determine its passive length.

Conclusions

We conclude from the results of this study that passive sarcomere length non-uniformities are not random but are caused by passive structural element non-uniformities at the level of sarcomeres, likely associated in some way with the number or inherent stiffness of titin molecules.

Acknowledgments

This study was supported by the Chinese Speed Skating Association, CIHR, NSERC, CRC and the Killam Foundation.

References

- [1] Moo, E.K. and Herzog, W. (2018). *Sci. Rep.* 8, 15235.
- [2] Edman, K.A. and Reggiani, C (1984). *J. Physiol.* 351, 169–198.
- [3] Bartoo, M.L et al. (1993). *J. Muscle Res. Cell Motil.* 14, 498–5.

Classification of Autism Gait Patterns in Children Using Multisegment and Single Segment Foot Kinematic Data

Ashirbad Pradhan¹, Victoria Chester¹

¹Andrew and Marjorie McCain Human Performance Laboratory, Faculty of Kinesiology, University of New Brunswick, Fredericton, Canada

Email: ashirbad.pradhan@uwaterloo.ca

Summary

This study examined the retrospective classification of gait patterns in children with autism using both traditional single segment foot (SSF) and multisegment foot (MSF) kinematic data. Results suggest that gait patterns in autism and controls can be classified with a high accuracy of 90.7% using features from a combination of MSF data. MSF data could provide a better understanding of atypical ankle motion in children with autism.

Introduction

Previous research has shown that children with autism walk with atypical ankle kinematics and kinetics^{1,2}. To date, no studies have examined multisegment foot kinematics in children with autism. The purpose of this study was to: 1) determine the optimal multisegment foot kinematic features for classifying autism/control gait patterns in children, and 2) determine whether SSF angle data, MSF angle data, or both combined are more accurate for classifying autism/control gait patterns in children.

Methods

Nineteen children (n=19) diagnosed with autism between the ages of 6-15 years (16 males, 3 females, age=10.4±2.9 yrs; height: 1.42±0.1 m; weight: 41.2±17.0 kg) and twenty-four controls (n=24) between the ages of 6-18 years (12 males, 12 females, age=12.1±3.34 yrs; height: 1.51±0.1 m; weight: 47.0±17.0 kg) participated in the study. A 12 camera T160 Vicon motion capture system (Oxford Metrics Group, Oxford, UK), sampling at 100 Hz, was used to track the 3D trajectories of 36 reflective markers (9mm diam.) placed on each participant's skin. The MSF model³ consisted of 4 rigid segments, including the shank (Sha), calcaneus (Cal), midfoot (Mid), and forefoot (Met). The SSF³ consisted of the shank and foot. For all relative angles in each model, a feature-set was generated that included the angular value at heel-strike (HS) and toe-off (TO), range-of-motion (ROM), maximum (MAX) and minimum (MIN) angle during stance (ST) and swing (SW), and the corresponding time of occurrence. The feature-sets from each angle served as input for linear discriminant analysis (LDA) models for classifying gait patterns between the two groups. For the performance evaluation, a leave-one-out cross-validation was employed, and the mean accuracy, sensitivity, and specificity were reported. Additionally, the entire feature set was ranked according to their F-score values to determine predictor importance. All data analysis was performed using Matlab (Mathworks, Inc. Natick, MA, USA).

Results and Discussion

Maximum accuracy of 90.7% and sensitivity of 89.5% were obtained for classifying autism and control groups using

features from Cal_Met+Cal_Mid+Mid_Met+Sha_Cal (Table 1). This was higher than the accuracy of individual feature sets which ranged from 70.9%-79.1% including the SSF model (75%.6). However, when all feature subsets were combined the accuracy reduced slightly (89.5%). The reduction was distinct in the sensitivity values which reduced to 86.8%. This suggests that the MSF angles have better classification performance than the SSF angle for classifying autism and control gait patterns. Also, a combination of MSF feature-sets is found to have better performance than individual models.

Table 1: Classification of Autism/Control gait patterns.

MSF Angles	Accuracy	Sensitivity	Specificity
Sha_Foot (SSF)	0.779	0.658	0.875
Cal_Met (MSF)	0.791	0.737	0.833
Cal_Mid (MSF)	0.791	0.684	0.875
Mid_Met (MSF)	0.709	0.447	0.792
Sha_Cal (MSF)	0.756	0.605	0.750
Cal_Met+Cal_Mid+Mid_Met+Sha_Cal	0.907	0.895	0.917
All features (MSF+SSF)	0.895	0.868	0.917

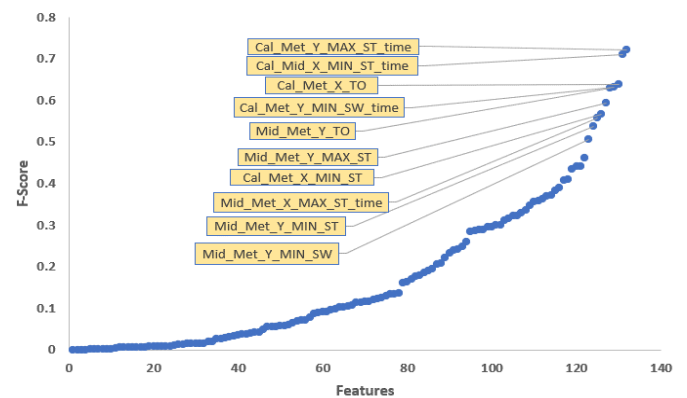


Figure 1: F-Score ranking of MSF angles-based features.

Conclusions

Examining MSF data may help identify atypical gait patterns in children with autism, thus leading to a greater understanding of foot mechanics and function. This would assist in more effective treatments and thus provide an improved quality of life.

References

- [1] Calhoun, M et al. (2011). *Cli. Biomech.*, 26(2), 200-206.
- [2] Ilias, S et al (2016). *IEEE IEACon* (pp. 275-279).
- [3] Leardini et al. (2017). *Gait & posture*, 25(3), 453-462.

Firefighter turnout gear limits the ability to lift while maintaining a neutral spine posture

Danielle R. Carnegie¹, David M. Frost¹, Alex Boersma², Tyson A.C. Beach¹

¹Musculoskeletal Biomechanics and Injury Prevention Lab, University of Toronto, Toronto, Canada

²Toronto Fire Services, Toronto, Canada

Email: danielle.carnegie@mail.utoronto.ca

Summary

This study assessed the effect that wearing motion-restricting firefighter turnout gear had on maximal reach distance when constrained to lift with a neutral lumbar spine posture. Firefighters performed a series of maximal reach tasks while wearing pieces of turnout gear required on-duty (i.e., fire protection gear and station wear). The results indicated that wearing fire pants and/or fire jacket reduces how far firefighters are able to reach for an object without rounding their spine. In contrast, fire boots and station wear did not significantly influence reach distance. This suggests that the motion-restricting effects of required protective equipment limit firefighters' ability to reach for low-lying objects without flexing the lumbar spine.

Introduction

Low back disorders (LBD) account for 68% of all injuries sustained by emergency responders (e.g., firefighters, paramedics) [1]. In firefighters, 43% of LBD have been linked to manual lifting tasks (e.g., patient transfer, equipment handling, victim rescue) [1]. To reduce lifting related low-back disorder risk, it is often recommended to limit lumbar spine flexion during lifting tasks. However, there is also evidence that when lower extremity joint motion is experimentally restrained, greater sagittal plane lumbar spine motion is observed in order for performers to accomplish the same lifting task [2]. Further, there is some evidence to suggest that the protective turnout gear worn by on-duty firefighters reduces available joint range-of-motion [3] which may influence available movement solutions while on the job. However, the influence this restrictive gear has specifically on lifting mechanics is unknown. The purpose of the study was to determine the influence of each component of firefighter turnout gear on maximal reach distance attainable while maintaining a neutral lumbar spine.

Methods

Thirty-eight firefighters completed a series of maximal reach tasks, which involved lowering a wooden dowel as far as possible while wearing a custom spine motion restraint [4]. Four different combinations of fire gear were worn with and without boots: 1) station wear (innermost layer of protective equipment worn at all times); 2) fire pants only (worn overtop station gear when called to emergency); 3) fire jacket only (with air tank); and 4) full gear. Three repetitions of each condition were performed, and foot position was controlled. A control condition was also performed wearing comfortable shorts and a t-shirt. Maximal reach distances (i.e., the distance from the knuckles to the ground when the firefighter was at their lowest reach position) were averaged

across three repetitions then compared via general linear model with one within-participant factor (condition).

Results and Discussion

Compared to the control condition, wearing fire pants or jacket alone (i.e., with and without boots) reduced maximal reach distance by 8 cm ($p < 0.001$), while full gear reduced maximal reach distance by 13 cm ($p < 0.001$). The influence of fire pants and fire jacket alone were not significant ($p = 1.000$). Station wear did not significantly influence maximal reach distance, as compared to control ($p = 0.294$). Within all tasks, wearing boots did not influence reach distance compared to not wearing boots ($p > 0.05$) (Figure 1).

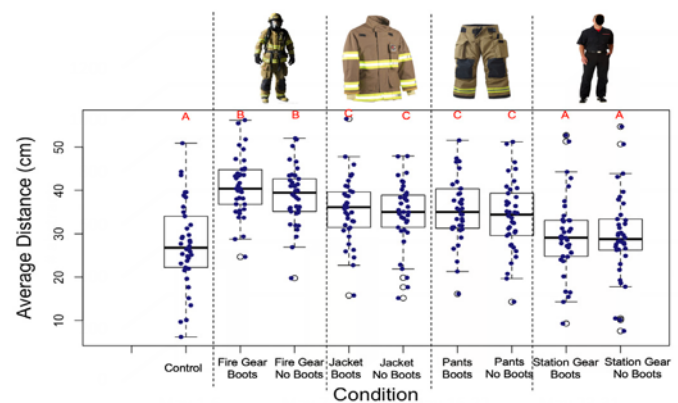


Figure 1: Maximal reach distance averaged across three repetitions for each condition. Control refers to comfortable clothing condition. Different letters indicate that conditions are significantly different ($p < 0.05$). Box plots display group data with median, upper and lower quartiles, and whiskers display max and min values excluding outliers. Outliers (greater or less than 1.5 times interquartile range) are shown as black circles. Solid blue dots represent individual data points (mean value of three reps).

Conclusions

Wearing fire gear reduces the depth firefighters can reach while maintaining a neutral lumbar spine. Thus, the general recommendation to limit spine motion when lifting may not be implementable by firefighters (or other first responders) who must wear motion-restricting protective equipment.

Acknowledgments

Study funded by the Centre of Research Expertise for the prevention of Musculoskeletal Disorders Seed Grant.

References

- [1] Frost D et al. (2015). *Work*, **52**: 835-42.
- [2] Beach TAC et al. (2014). *Work*, **47**: 221-34.
- [3] Ciesielska-Wrobel I et al. (2017). *Ergo*, **60**: 997-1007.
- [4] Zehr JD et al. (2018). *J Electromyogr Kin*, **39**: 104-13.

Does the time of day influence the clinical assessment of muscle strength in men and women?

Inaê de Oliveira Marcelo¹, Karine Josibel Velasques Staelben^{1,2}, Gabrielly Dalcanale Martins¹, Marcos Roberto Kunzler¹, Felipe P. Carpes^{1,2}

¹Applied Neuromechanics Research Group, Laboratory of Neuromechanics, Federal University of Pampa, Uruguai, RS, Brazil

²Programa de Pós-Graduação Multicêntrico em Ciências Fisiológicas, Federal University of Pampa, Uruguai, Brazil

Email: inaemarcelo.aluno@unipampa.edu.br

Summary

We set out to determine the influence of time of day on muscle strength assessment in men and women. Considering common parameters considered in the clinical evaluation of lower limbs strength, it seems that leg asymmetries and sex need to be considered in the clinical examination, but the time of the day has less influence on the results.

Introduction

The maximal isometric strength can be higher in the late afternoon [1]. In the clinical context, an influence of the time of the day on strength may have impact on the assessment of injury risk factors, identification of leg asymmetries, and sports performance [2]. Here we determine whether the time of the day influences muscle strength in men and women.

Methods

Twenty-two men (n=12) and women (n=10) with mean±standard deviation age 27±5 years, height 1.69±0.11m, body mass 71±12kg, physically active, were assessed concerning the maximal isometric strength for knee extension and flexion, and hip abduction, bilaterally, by handheld dynamometry (Microfet 2). Muscle strength was measured in Newton and torques were estimated by the product of strength by shank (knee torque), and leg length (hip torque), and normalized to the individual body mass. The peak and mean values from three trials were considered. Each participant was evaluated in the morning (8:00AM to 12:00AM) and in the evening (6:00PM to 10:00PM) with at least 36 h in between, in randomized order for morning and evening, under controlled temperature and light. Generalized estimated equations with three factors, time of day (morning and evening), limb preference (preferred and non-preferred), and sex (male and female), were used to identify the main effects and interactions. The significance level was set at 0.05.

Results and Discussion

Preferred leg showed higher peak (p=0.008, Figure 1A) and mean (p=0.002, Figure 1B) knee extension torques for both men and women. Men were stronger than women for peak (p=0.001, Figure 1C) and mean (p=0.001, Figure 1D) knee extension torques, and peak hip abduction torque (p=0.004, Figure 2A). The mean hip abduction torque showed an interaction between sex and time of day (p=0.048), with the men showing higher hip abduction torque in the morning (p=0.042, Figure 2B) and higher torques than women regardless of the time of the day (p≤0.024, Figure 2B). Knee flexors did not show main effects or interactions (p≥0.158). The higher torques found for men compared to women [3] and leg asymmetries between [4] agree with previous studies. It suggests caution when assuming one limb as representative of the contralateral. While an effect of the time of the day was not clear, the higher hip abduction torque in the morning deserves

investigation with a larger sample, which was not possible to be accomplished during the experiments reported.

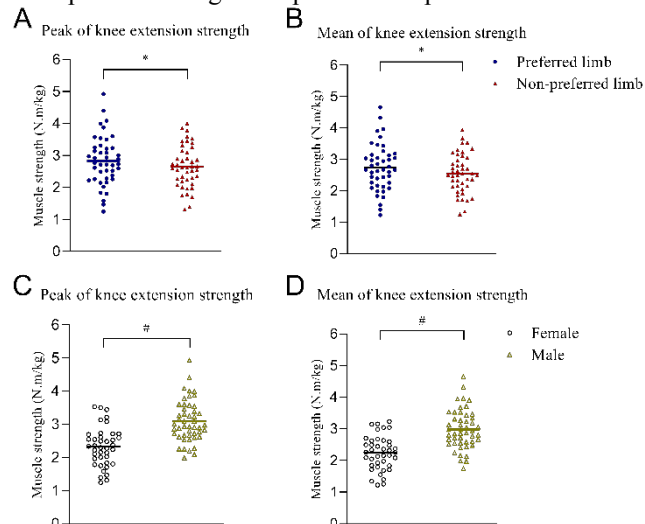


Figure 1. Effect of the limb (A-B) and sex (C-D) on peak and mean values of the knee muscle strength. (A-B) * Indicates a difference between limbs. # Indicates a difference between sexes.

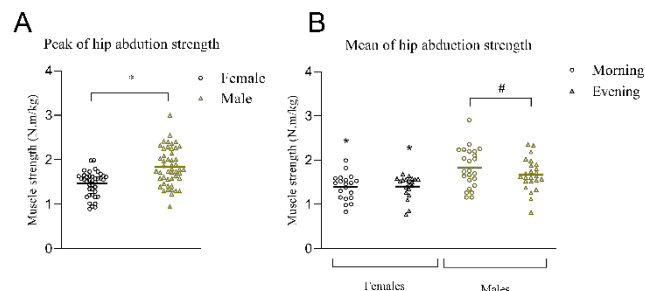


Figure 2. Effect of the sex (A-B) and shifts (B) on peak and mean values of the hip muscle strength. *Indicates a difference between sexes. # Indicates a difference between shifts.

Conclusions

Hip strength was influenced by the time of the day in men. Regardless of the time of the day, leg asymmetries require attention for both men and women.

Acknowledgments

FPC, IOM, and KJVS are supported by CNPq – Brazil.

References

- [1] Douglas CM, Hesketh SJ, Esser KA. (2021). *Physiology (Bethesda)*. 1: 44-51.
- [2] Suchomel TJ, Nimphius S and Stone MH (2016) *Sports Med.* 10: 1419-49
- [3] Thorborg K, Bandholm T, Hölmich P. (2013) *J Sci Med Sport.* 5: E1-3
- [4] Perry MC et al (2007). *Eur J Appl Physiol.* 5: 553-61
- [5] Wilson, BR et al (2017). *J. Sport Rehabil.* 5: 445-5

Gluteal Activation Cues Reduce Peak Acetabular Contact Pressure During Squatting in Persons with Femoroacetabular Impingement Syndrome: A Finite Element Analysis Study

Jordan Cannon, Christopher M. Powers
 Division of Biokinesiology and Physical Therapy
 University of Southern California, Los Angeles, CA
 Email: cannonjo@usc.edu

Summary

Diminished gluteal muscle activation in persons with femoroacetabular impingement syndrome (FAIS) has been proposed to contribute to symptomatic impingement. The purpose of this pilot project was to investigate if targeted gluteal muscle activation during squatting could reduce impingement kinematics and peak acetabular contact pressure. Our preliminary results suggest that cueing persons with FAIS to activate gluteal musculature reduces hip internal rotation and in doing so reduces peak acetabular contact pressure.

Introduction

Femoroacetabular impingement syndrome (FAIS) is a motion-related clinical disorder resulting from abnormal hip joint morphology [1]. Mechanical impingement, in which the aspherical femoral head (cam morphology) abuts with the acetabular rim, is created with simultaneous deep hip flexion, internal rotation, and adduction. The area of impingement on the anterior-superior acetabulum corresponds with the location of intra-articular joint damage in FAIS [2]. The gluteal musculature are of interest in FAIS [3] given their ability to avoid impingement during squatting by producing hip external rotation and abduction motion. The purpose of this pilot study was to investigate if targeted gluteal muscle activation during squatting could reduce impingement kinematics and acetabular contact pressure, while shifting the location of peak contact pressure away from the anterior-superior acetabular rim.

Methods

A 3D finite element (FE) model of the hip joint was developed from a male with a diagnosis of FAIS (32 years, 1.79 m, 70.9 kg). Kinematic, kinetic, and surface EMG of 6 hip muscles were collected while the participant performed two bodyweight squat tasks. First, an unconstrained squat to maximum depth with a self-selected stance width and foot position. Next, in the same stance position, the participant was provided coaching cues to increase gluteus maximus and medius activation. Nine squats were collected for each condition, with movement speed and arm position controlled. An EMG-driven musculoskeletal model estimated bone-on-bone contact forces at the hip joint during squatting [4]. Subject-specific input parameters to the FE model included 3D hip joint kinematics and bone-on-bone contact forces at peak hip flexion for each squat condition, as well as acetabulum and proximal femur geometry.

Table 1: Hip joint angles (°) at peak hip flexion input to the FE model.

	Flexion	Abduction	Internal Rotation
Squat	130	33	17
Squat + Gluteal Activation	128	31	10

Bony geometry was obtained from CT scans of the pelvis and proximal femur to create a 3D model of the symptomatic (left) hip. The acetabulum and femur were modelled using homogeneous, isotropic, triangular continuum shell elements with an elastic modulus of 17.0 MPa and a Poisson ratio of 0.30. Quasi-static loading simulations were performed using a nonlinear FE solver in Abaqus using a hard contact algorithm, with a surface-to-surface, finite sliding contact, and a surface coefficient of friction of 0.02. Peak contact pressure was analyzed at peak hip flexion during each of the squat conditions.

Results and Discussion

Hip flexion and abduction were similar between squat conditions, however internal rotation was reduced by 7° during the trials with the gluteal activation cues (Table 1). In the cued trials, peak acetabular contact pressure decreased from 8.49 to 3.84 MPa and the location of peak pressure shifted away from the anterior-superior acetabular rim. (Figure 1). The findings of this preliminary analysis highlight the influence of hip internal rotation in contributing to mechanical impingement during squatting. Specifically, modest reductions in internal rotation resulted in a 55% decrease in acetabular contact pressure.

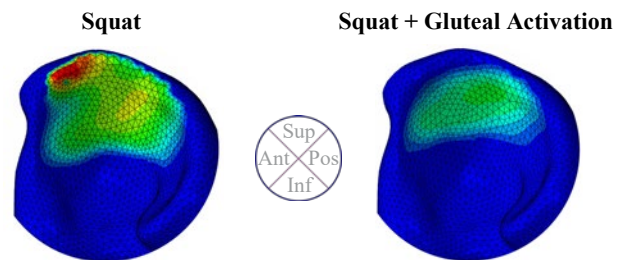


Figure 1: Acetabular contact pressure at peak hip flexion.

Conclusions

Our preliminary results suggest that gluteal activation cueing during squatting reduces hip internal rotation and in doing so reduces peak acetabular contact pressure. This finding highlights the importance of the gluteal musculature in minimizing impingement kinematics during deep squatting.

Acknowledgments

We acknowledge the financial support provided by the International Society of Biomechanics Matching Dissertation Grant and USC Division of Biokinesiology & Physical Therapy.

References

- [1] Griffin, DR et al (2016). *BJSM*, **50**(19): 1169-1176.
- [2] Tannast et al (2008). *Clin. Orth. Rel. Res.*, **466**(2): 273-280.
- [3] Cannon et al (2020). *Physical Therapy*, **100**(5): 788-797.
- [4] Cannon et al (2021). *J. Biomechanics*, **116**: 110240.

Lower Extremity Kinetics Following an Achilles Speedbridge: A Case Study

Kevin A. Valenzuela¹, Justin Demoss¹, Anaya Blade¹, Alfredo Cervantes¹, Hunter J. Bennett²

¹Movement Science Lab, Department of Kinesiology, California State University Long Beach, CA, USA

²Neuromechanics Lab, Department of Human Movement Science, Old Dominion University, Norfolk, VA, USA

Email: kevin.valenzuela@csulb.edu

Summary

Longitudinal effects of an Achilles repair due to bone spurs and Achilles tendinopathy remain unknown. Following a 16-week longitudinal analysis of lower extremity biomechanics, it was determined that pre-operative kinetic patterns return at approximately 12-weeks post-operative. Peak VGRF and plantarflexion moments during the push-off of stance phase during gait are reduced at 8 weeks post-op.

Introduction

Achilles tendinopathy represents approximately 5-18% of injuries in distance runners [1]. Runners who exhibit Achilles tendinopathy display reduced gait speed during walking [2]. The injury presents a reduced peak dorsiflexion angle [3] but no differences on peak impact forces [4].

While restricted dorsiflexion is commonly seen, less is known about the longitudinal kinetic effects of Achilles tendinopathy following an Achilles repair surgery. Therefore, the purpose of this study was to longitudinally assess lower extremity kinetics following an Achilles repair.

Methods

A 35-year old male (1.85m, 86.4kg) presented right Achilles insertional tendinitis and a large retrocalcaneal bone spur which had fractured and was partially embedded in the Achilles tendon. One week before the operation, the subject completed over ground walking trials at a gait velocity of 1.0m/s. Qualisys Oqus cameras and Bertec force plates were used to collect 3D marker data and ground reaction forces.

The subject then underwent an Achilles tendon repair and a bone spur excision. The excess calcaneal bone was removed and smoothed down. The fragments were removed from the tendon. An Arthrex Speedbridge was used to reattach the tendon under normal resting tension.

Following six weeks of no weight bearing, the subject was able to begin walking. The pre-operative testing was repeated at 8-, 12-, and 16- weeks post-operatively. Peak ankle, knee, and hip joint moments and vertical ground reaction forces (VGRF) were assessed during the stance phase of the operated limb.

Results and Discussion

There was an inability to achieve a gait speed of 1.0 m/s at 8-weeks post-operation (0.89 m/s was the fastest achievable speed). Peak loading VGRF did not change post-operatively (Figure 1), however, push-off VGRF did significantly decrease at 8 weeks post-operatively. By 16 weeks it was close to pre-operative levels.

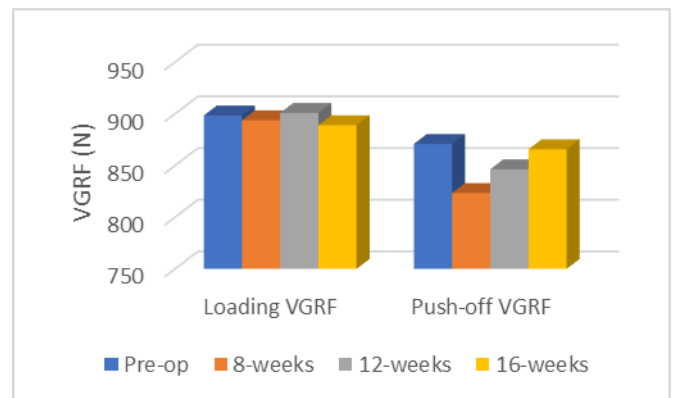


Figure 1: Peak loading and push-off VGRF (N).

There was a sharp decline in peak plantarflexion moments (push-off) at 8-weeks post-operative (Figure 2) but this returned closer to pre-operative levels by 16-weeks.

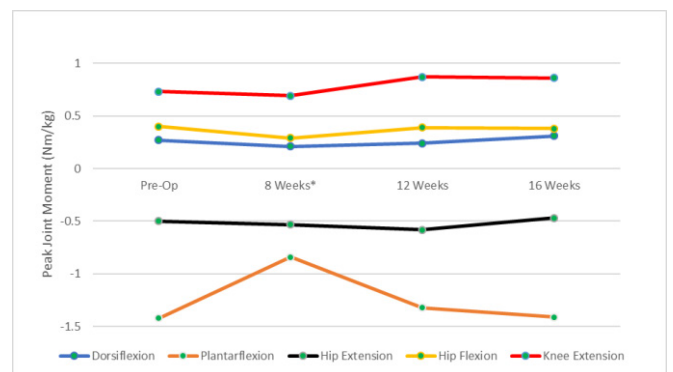


Figure 2: Peak joint moments (Nm/kg) during stance phase.

Six weeks of non-weightbearing caused reduced abilities in the performance of the ankle plantarflexors, which was evident in the reduced peak plantarflexion moment during push-off.

Conclusions

Normal gait patterns are evident at approximately 12 weeks post-operatively in slow gait speeds. Push-off forces and peak joint moments return closer to pre-operative levels by 12-weeks. However, running was not occurring at 16 weeks.

References

- [1] McCrory JL et al. (1999). *Med Sci Sports Exer*, **31**: 1374-1381.
- [2] Kim SJ et al. (2015). *J Sport Sci Med*, **14(2)**: 284-289.
- [3] Hein T et al. (2014). *Scand J Med Sci Spor*, **24(3)**: 201-212.
- [4] Azevedo LB et al. (2008). *BR J Sport Med*, **43**: 288-292.

Is the dissipative energetic behavior of the human heel associated with thermal changes?

Nikolaos Papachatzis¹, Dustin R. Slivka², Iraklis I. Pipinos³, & Kota Z. Takahashi¹

¹Department of Biomechanics, University of Nebraska at Omaha, Omaha, NE, USA

²School of Health and Kinesiology, University of Nebraska at Omaha, Omaha, NE, USA

³Department of Surgery, University of Nebraska Medical Center, Omaha, NE, USA

email: npapachatiz@unomaha.edu, web: cobre.unomaha.edu

Summary

During walking, the heel's function is analogous to a shock-absorber that dissipates energy (negative net-work), which may be essential to minimize tissue damage. The laws of thermodynamics state that the dissipated energy may increase the heels' temperature. Although, our experimental setup increased the heel's negative work. The results showed no strong association between the heel's negative work and the heel's temperature changes. It is possible that the heel's mechanical work was dissipated as sound and not heat – although a direct measure of sound is needed to verify this conclusion. Additionally, we are currently investigating alternative hypotheses to determine whether other factors could explain increases in foot temperature, such as shear force and increased blood flow.

Introduction

During human walking, the leading limb collides with the ground and performs negative work [1]. It is now well established that a large portion of this collision work is performed by the foot, particularly the heel [2,3]. Energy absorption (or dissipation) maybe be beneficial as a protective mechanism to minimize trauma or injuries [4]. However, it is currently unclear where the foot's energy goes or how the body absorbs or dissipates this energy. One possibility is that the heels' energy is dissipated as heat. The thermodynamics laws state that the dissipated energy may increase the heels' thermal energy (i.e., increase temperature), potentially explaining the increases in heel temperature during walking [5]. Currently, it is unclear whether the heel's mechanical energy can induce thermodynamic responses. Understanding the relationship between biomechanics and temperature regulation may be valuable for improving diagnoses for foot complications, such as the formation of diabetic foot ulcers that are thought to arise due to impaired ability to dissipate heat [6]. Here, we used walking with added mass to increase the heel's negative work [3] and investigated its effect on thermodynamic responses. We hypothesized that the heel's temperature would increase when walking with added mass. We also hypothesized that the increase in temperature is related to increased energy absorbed (i.e., negative work) and energy dissipated (i.e., net negative work) by the heel.

Methods

A total of 20 healthy young adults (5 females, 15 males; age: 24.4±2.8 yrs; height: 1.74.61±0.07 m; mass: 83.6±21.2 kg; means± s.d.) walked over-ground on force plates and for 10 minutes on a treadmill (both at 1.25 m/s). Participants carried (via weight vest) three different levels of symmetrical loads: 0%; no added body mass, 15%, and 30% of their body mass. The over-ground walking conditions were used to collect foot mechanics data (kinematic & kinetic), whereas the treadmill conditions were used to measure the foot temperature data. We quantified the mechanical power and work done by the

foot using a unified-deformable analysis [7]. To isolate the heel contribution, we computed the work when the center-of-pressure was underneath the heel segment during the early stance phase [3,8]. An estimate of the total work over the 10 minutes of treadmill walking was calculated by multiplying the average work per step measured in over-ground trials by the number of steps taken in 10 minutes of treadmill walking. Temperature measurements were taken immediately before and after each treadmill condition at the bottom of the right foot, including the heel pad. We computed the change in temperature of the heel before and after each walking condition. A one-factor repeated-measures ANOVA was used to determine the effect of the added mass on the dependent variables. When a significant main effect was found, a Bonferroni post hoc analysis was conducted for pair-wise comparisons. We used a linear mixed models test to examine the relationship between foot temperature changes (before and after walking) and foot energy dissipation. The significance level was set to $\alpha = 0.05$ for all the statistical tests.

Results and Discussion

Our hypotheses were not supported as there was no significant increase in heel temperature between added mass walking conditions ($p=0.138$, Figure 1), despite an increase in the magnitude of negative work ($p=0.003$, Figure 1). Neither the negative nor the heel's net work was associated with increased heel temperature ($p=0.535$ & $p=0.661$, respectively). Future studies are needed to test alternative hypotheses related to energy dissipation mechanisms such as sound, shear forces, and blood flow, which may lead to novel insights for understanding the causes of diabetic foot complications [6].

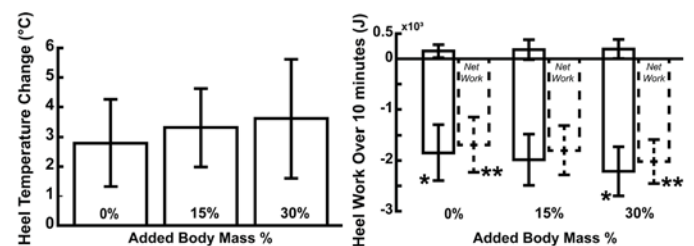


Figure 1: (Left side) The heel's temperature increased after 10min. of walking, but there was no significant effect of added mass on change in temperature ($p=0.138$). **(Right side)** The added mass significantly increased the magnitude of the heel's negative ($p=0.002$) and net ($p=0.003$) work over 10 minutes of treadmill walking, but not the positive work ($p=0.265$). The asterisks indicate significance (*: negative work; **: net work) (N=20).

References

- [1]. Kuo AD., et al. *Exercise and sport sciences reviews*, **33**(2), 88-97, 2005.
- [2]. Honert EC & Zelik KE. *Human movement science*, **64**, 191-202, 2019
- [3]. Papachatzis N, et al. *Journal of Experimental Biology*, **223**, 12, 2020.
- [4]. Wearing S., et al. *Medicine and science in sports and exercise*, (**46**),8, 1588-1594, 2014.
- [5]. Reddy PN., et al. *Gait & posture*, **52**, 272-279, 2017
- [6]. Armstrong DG., et al. *The American journal of medicine*, **120**(12), 1042-1046, 2007
- [7]. Takahashi KZ., et al. *Journal of biomechanics*, **45**(15), 2662-2667, 2012
- [8]. Bruening DA & Takahashi KZ., *Gait & posture*, **62**, 111-116, 201.

The effects of using a rehabilitation technology on foot muscles strength in people with diabetic neuropathy: A preliminary data analysis

Jane S. S. P. Ferreira¹, Ronaldo H. Cruvinel-Júnior¹, Jady L. Veríssimo¹, Érica Q. Silva¹, Renan L. Monteiro¹, Isabel C. N. Sacco¹

¹ Department of Physical Therapy, Speech, and Occupational Therapy, School of Medicine, University of São Paulo, São Paulo, Brazil
Email: janesuelen@usp.br

Summary

The reduction of strength of the foot muscles represents one of the main musculoskeletal alterations due to diabetic neuropathy. The implementation of an internet-based exercise protocol appears as a promising strategy to minimize these muscular alterations. This study provides insight into the effects of this internet-based foot-ankle exercises on foot strength in neuropathic patients.

Introduction

Diabetic Peripheral Neuropathy (DPN) affects the muscle and joint structures of the foot and ankle [1]. These include alterations in the joints surrounding tissues, reducing their range of motion, and reduction in functionality and strength due to deterioration of the intrinsic foot and lower leg muscles [2]. Therefore, self-care strategies are an interesting option for prevention and treatment of more serious dysfunctions and complications, such as ulcer formation and amputation. We believe that an internet-based exercise protocol, focusing on strengthening the foot muscles, in which the person can self-manage, can be an efficient preventive strategy for further musculoskeletal dysfunctions in this population.

Methods

At present, we are conducting a superiority randomised controlled trial on the efficacy of a 12-week internet-based foot-ankle therapeutic exercise program guided by the Diabetic Foot Guidance System – SOPeD (www.soped.com.br) to treat musculoskeletal disorders in people with DPN at age between 18 to 65. The present abstract reports the results of a preliminary analysis of a total of 14 subjects, 6 in the intervention group and 8 in the control group.



Figure 1: Hallux and toes strength test using an emed pressure platform (A-Baseline, B- after 12 weeks of intervention).

At the beginning of the intervention protocol, the user had a face-to-face supervision on how to perform the exercises, after the allocation by the physiotherapist in order to give the initial guidance on the use of SOPeD. The other sessions were followed remotely via software. All participants in the study received calls every two weeks. The strength of the participant's foot muscles was evaluated 2 times (T0 - baseline, T12 - after 12 weeks of treatment). The strength of

the flexor muscles of the hallux and toes were evaluated using an emed® -q100 pressure platform (Figure 1) [3].

Results and Discussion

So far, no changes have been observed for foot strength (Figure 2). Others studies had observed an improvement in the ankle-foot complex muscle strength after applying a supervised foot exercise protocol for 12 weeks. However, the measures of strength evaluation used by these studies were different: Francia et al. [4] used ankle dynamometry that focuses on evaluating the strength of the extrinsic muscles. The study of Sartor et al. [5], although focusing on intrinsic musculature, used a manual strength test. In our study, we used a pressure platform, which can be considered a reliable method for measuring indirectly the strength of the foot intrinsic muscles. Thus, different outcomes can be expected when compared with the current literature. In addition, the data presented are from a limited sample, so significant changes in strength may not have been detected.

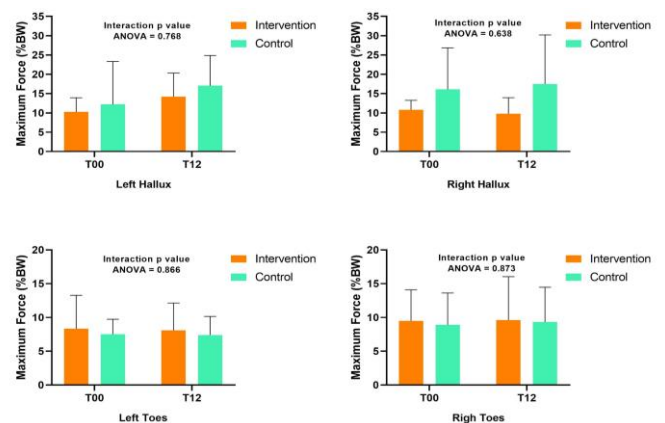


Figure 2: Comparison of the mean of the hallux and toes strength after 12 weeks of intervention.

Conclusions

The implementation of an internet-based foot-ankle therapeutic exercise program emerges as a promising rehabilitation strategy, although these preliminary data do not demonstrate statistically significant differences in foot muscle strength.

References

- [1] Sinacore DR et al. (2013). *J Foot Ankle Res*, **6**: 1-9.
- [2] Cheuy VA et al. (2013) *Clin Biomech.*, **28**:1055–1060.
- [3] Mickle KJ. (2008) *Clin Biomech.*, **23**: 662-720.
- [4] Francia P. (2015) . *Ital J Anat Embryol*, **120**: 21-32.
- [5] Sartor CD. (2014) *BMC Musculoskelet Disord*, **15**: 1-13

Effect of maturation and limb dominance on knee flexion and extension torque in adolescent athletes

Joanna C. Geck¹, Teresa E. Flaxman¹, Nicholas J. Romanchuk¹, Sasha Carsen³, Daniel L. Benoit^{1,2}

¹School of Human Kinetics, University of Ottawa, Ottawa, ON, Canada

²School of Rehabilitation Sciences, University of Ottawa, Ottawa, ON, Canada

³Department of Surgery, University of Ottawa, Ottawa, ON, Canada

Email: joanna.geck@uottawa.ca

Summary

Contralateral or uninjured limbs are commonly used to compare quadriceps and hamstring strength data for return-to-play readiness in adolescents after sustaining an ACL injury. While it is useful to know if there is a between-limb strength deficit, it is also critical to determine how the growing patient compares to their maturing peer. As such, we present the change in isometric knee flexion and extension torque in adolescent male and female athletes over a year span. Results indicated a greater increase in torque between visit one and two for the dominant (D) limb knee extension compared to the non-dominant (nD) limb. Smaller differences in torque were observed for knee flexion.

Introduction

Sustaining an ACL injury causes strength deficits that can be linked to arthrogenic muscle inhibition and muscle atrophy [1], leading to impairment in voluntary quadriceps and hamstring muscle activation [2]. This impairment affects both the injured and healthy contralateral limb as well [3]. Therefore, the practice of using the “healthy” contralateral limb as the “gold standard” when assessing readiness for return to sport is flawed, in particular in the maturing population where natural increases in strength are to be expected. The purpose of this study was, therefore, to describe the change in knee flexion/extension strength over a typical rehabilitation period (9-12 months) in healthy adolescent population. Strength may be affected by limb dominance and was also compared. We hypothesize that both flexion and extension would present significant between-limb differences across visits.

Methods

Seventy-one uninjured participants between the ages of 12 and 18 years were recruited via convenience sampling through sporting associations in the Ontario/Gatineau region. Thirty-six of these participants came for a second evaluation 7-15 months later. Participants had no previous ACL injury, and no lower extremity injury in the 6 months prior to testing and were experiencing no pain in the lower extremity prior to testing.

Limb dominance was defined as the leg they would choose to kick a soccer ball at a maximum distance. Maximum voluntary isometric contractions (MVICs) were recorded using an isokinetic dynamometer (Biodex System-4). Knee flexion and extension was tested in a seated position with the knee flexed to 60° and hip to 90°. Participants completed three trials per limb for each isometric contraction. Verbal encouragement and visual feedback encouraged participants to produce a maximum effort. The average of the three trials was normalized to body mass, and the peak torque value was used for data analysis. Limb symmetry was indicated by the

ratio between the nD and D torque values, with a ratio <.90 being deemed clinically significant.

Results and Discussion

Data from the first (n=71) and second (n=36) were consolidated to provide normative data and evaluate limb symmetry. A paired t test revealed significant differences between limbs during flexion (D=1.48 Nm/kg, SD=0.289; nD=1.40 Nm/kg, SD=0.258, p<0.002) and extension (D=2.94 Nm/kg, SD=0.527; nD =2.79 Nm/kg, SD=0.498, p<0.001) (Figure 1).

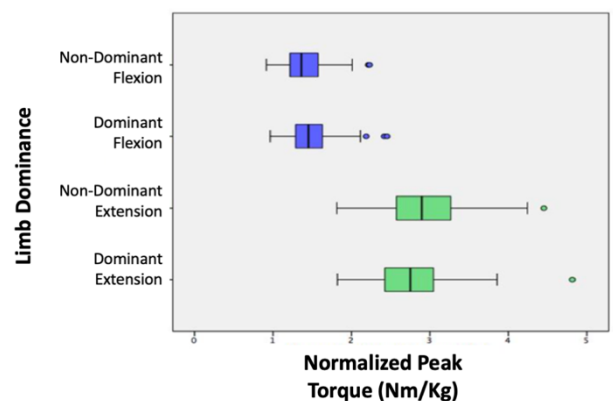


Figure 1: Normative knee flexion and extension isometric torque values for adolescent athletes (“minimum”, first quartile (25%), median, third quartile (75%), “maximum”). Open circles are a representation of moderate outliers. (blue: flexion, green: extension; visit 1 and 2, n= 36)

A subgroup analysis of the participants with two visits (n=36), using a two-way ANOVA, indicated an interaction between limb dominance and visit number during knee extension, highlighting a significantly greater change in torque values for the D limb (150.5Nm) compared to the nD limb (136.5Nm) across visits (p < 0.001). Limb symmetry ratios revealed that after the second visit the number of cases that presented ratios less than .90 were doubled (Visit 1=11, Visit 2=22) indicating the importance of considering limb dominance in the maturing population.

Conclusions

Our findings suggest that (1) strength increases over a 7-15 month period in youth maturation and (2) the effect of limb dominance on strength also increases. It is reasonable to conclude that youth with an ACL injury would normally experience similar changes. As such, using the contralateral limb strength to gauge readiness for return-to-sport after ACL injury is a flawed metric. These patients must also be considered with respect to the expected changes of maturation and limb dominance.

References

- [1] Palmieri-Smith et al. (2008). *CSM*, 3: 405-424.
- [2] Urbach et al. (1999). *MSSE*, 12:1691-1696.
- [3] Urbach et al. (2002). *IJSM*, 4: 231-236.

Upper and Lower Body Inter-Segmental Coordination During Unsupervised Gait of Older Adults with Dementia

Lina Musa^{2,1}, Sina Mehdizadeh¹, Alastair Flint^{3,6}, Avril Mansfield^{2,7}, Babak Taati^{1,4,5}, Andrea Iaboni^{1,3,6}

¹Kite Research Institute, University Health Network, Toronto, ON, Canada

²Rehabilitation Sciences Institute, University of Toronto, Toronto, ON, Canada

³Department of Psychiatry, University of Toronto, Toronto, ON, Canada

⁴Department of Computer Science, University of Toronto, ON, Canada

⁵Vector Institute for Artificial Intelligence, Toronto, ON, Canada

⁶Centre for Mental Health, University Health Network, Toronto, ON, Canada

⁷Sunnybrook Research Institute, Toronto, ON, Canada

Email: l.musa@mail.utoronto.ca

Summary

Impairment in mechanical stability while walking contributes to falls in people with dementia [2]. The aim of this study was to determine if inter-segmental coordination of the upper and lower body segments during natural gait is predictive of stability and falls. Episodes of walking were captured using a vision-based system and analysed over the first 2 weeks to obtain a measure of the cross-correlation between upper and lower body segments. The cross-correlation between upper and lower body segments revealed a maladaptive pattern of walking.

Introduction

People with dementia fall frequently and impaired mechanical stability while walking is an important predictor of falls in dementia [2,3]. Mechanical stability is the relationship between the center of mass (COM) and the boundaries of the base of support (BOS). In healthy individuals, shifts in the COM (upper body) outside of the BOS are stabilized through adaptations through foot placement (lower body) [1]. The coordination of the upper and lower body joints may thus be used to examine impairments in mechanical stability in people with dementia.

Methods

We analyzed data from an observational study using a vision-based gait monitoring system, that incorporated a Kinect camera. Joint coordinates from 2 weeks of unsupervised walks of 52 individuals were used to derive measures of coordination. We examined the cross correlation between a spine marker and knee markers (right and left) in the frontal plane as the measure of coordination.

Results and Discussion

Preliminary analysis of 30 participants (mean 7.83 walks per participant) revealed a median lag of -4.76% (range -16.21% to 6.52%), where negative lags indicate peak knee abduction occurs before peak spine abduction in a single gait cycle. Most participants (60%) had negative lags, representing a maladaptive gait pattern. To maintain the COM within the BOS, lateral foot placement should not precede COM movement. This may be indicative of impaired mechanical stability. Lag times were also highly variable within individuals (median lag time variability = 10.49%, range 7.64% to 16.38%).

Conclusions

Most of the participants with dementia demonstrated poor temporal coordination of their upper and lower body segments, with significant variability. Future analyses will examine the relationship between upper and lower body inter-segmental coordination and mechanical stability and fall risk.

Acknowledgments

Canadian Institutes of Health Research, Alzheimer Association and The Walter and Maria Schroeder Institute for Brain Health and Recovery.

References

- [1] Bruijn SM and Van Dieën, JH (2018) *J R Soc Interface*, **15(143)**: 20170816.
- [2] Mehdizadeh et al. (2019) *J Gerontol A Biol Sci Med Sci*, **75(6)**: 1148-1153.
- [3] Mehdizadeh et al. (2020) *JAMDA*

Biomechanical improvement and timing for total knee arthroplasty surgery

Chang Shu¹, Fangjian Chen¹, Michael Bates², Ronald W. Singer² and Nigel Zheng¹

¹The University of North Carolina at Charlotte, NC, ²OrthoCarolina, NC, USA

Email: nzheng@uncc.edu

Summary

Patients with osteoarthritis are always wondering when is the optimal time for surgery. This study focuses on the timing of TKA surgery by analysis of young cohort and elder cohort who had undergone TKA preoperatively and postoperatively. The kinematics data from the motion capture system was compared between two groups. It is concluded that the young patients had better improvement in gait speed, balance test and expectation & satisfaction score.

Introduction

Patient age, radiographic, and symptoms are typically considered as the three crucial timing factors in choosing the osteoarthritic patients for total knee arthroplasty (TKA) [1]. Due to the limited lifespan of the knee implant, younger patient always treated with nonsurgical options first. However, it is reported that the younger TKA patients would potentially benefit from the surgery than the elder TKA patients [2]. The purpose of this study was to evaluate the associations among the age cohorts, the biomechanical outcomes and patient satisfaction and expectation score in order to comprehend the age factor in timing of TKA.

Methods

39 posterior-stabilized TKA subjects were recruited and tested preoperatively (pre-op) and 21 of them postoperatively (post-op), with 7 subjects (age <60, 55±2.5) in young group and 10 subjects (age>65, 68±3) in elder group (Table 1). Motion data, clinical assessment (Time up-go, sit to stand, and balance test using BIODEX) and knee society score were collected during each visit. Motion data during walking was collected at 120 Hz (FX 40, VICON) and biomechanical variables were computed using a custom MATLAB program. The improvement was defined by the difference between preoperative and postoperative surgery. One-way ANOVA was performed and the significance level was set as 0.05.

Results and Discussion

There were no significant differences in pre-op biomechanical variables between the two groups. There were significant differences in the flexion-extension improvement in the stance phase. Greater heel strike angle could explain that gait speed was significantly increased in young group (Table 1). Both groups had similar improvement in varus-valgus and axial rotation following TKA (Fig. 1). The young group had greater improvement in expectation and satisfaction than elder group (Table 1). Single leg (with implant) balance test results showed young group had better performance than elder group. Young group had 52% improvement and was significantly better than the elder group (14%). This indicated that the young patient restored their muscle strength much better.

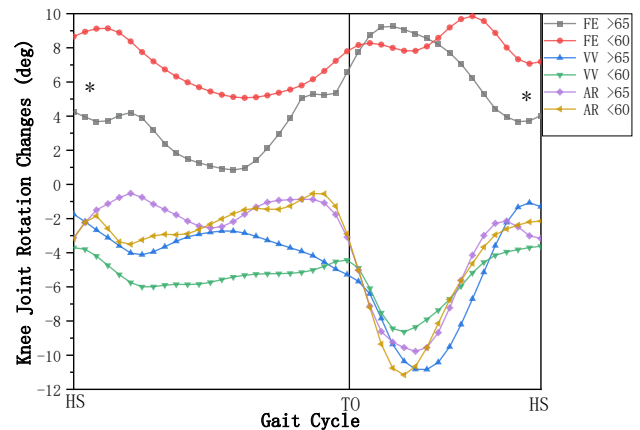


Figure 1: Knee joint rotation improvement during walking. FE: Flexion(+)/Extension(-), VV: Varus(-)/Valgus(+), AR: Internal(-)/External(+). HS: heel strike, TO: toe-off. Statistical analysis was performed between young and elder group. *: p<0.05.

Conclusions

Both groups had very similar improvement on knee joint rotation except greater flexion at stance phase. The better subjective assessment was found in young patients. Overall, the young group had slight better outcomes.

Table 1: Subject demography and variables. *: p<0.05 between the pre-op and post-op. #: p<0.05 between two groups post-op.

	Demography			Expectation & Satisfaction		Gait speed (m/s) #		Stance time (s)		Surgical single leg balance test score#	
	Gender	Ht (cm)	BW (kg)	Pre-op	Post-op	Pre-op	Post-op	Pre-op	Post-op	Pre-op	Post-op
Young	2F/5M	1.77	100	29±9	42±12*	0.93±0.14	1.03±0.11*	0.81±0.11	0.79±0.09	3.5±0.8	2.5±1.0*
Elder	4F/6M	1.69	104	30±7	39±11*	0.83±0.11	0.87±0.16	0.88±0.17	0.81±0.08*	3.9±1.2	3.8±1.1

References

- [1] Chang C B, et al. (2010). *J. Orthop Trauma*, **11(1)**: 21-27.
- [2] Ghomrawi H M K, et al. (2020). *JBJS*, **102(6)**: 468-476.

Acknowledgments

This study is funded by Smith and Nephew through an Investigator Initiated Study award.

Sex and anterior cruciate ligament injury effects on isometric and isokinetic force production in a paediatric population

Christine C. Smith¹, Nicholas J. Romanchuk², Michael J. Del Bel³, Sasha Carsen⁴, Daniel L. Benoit¹⁻³

¹School of Human Kinetics, University of Ottawa, Ottawa, ON, Canada

²Ottawa-Carleton Institute for Biomedical Engineering, University of Ottawa, Ottawa, ON, Canada

³School of Rehabilitation Sciences, University of Ottawa, Ottawa, ON, Canada

⁴Department of Surgery, Division of Orthopedic Surgery, University of Ottawa, Ottawa, ON, Canada

Email: dbenoit@uottawa.ca

Summary

The purpose of this study was to determine if sex and/or anterior cruciate ligament (ACL) injury affect peak torque values produced during isometric and isokinetic knee flexion and extension tasks in ACL-injured (ACL*i*) and uninjured (CON) paediatric males and females. Uninjured controls display a higher mean limb symmetry index (LSI) for isokinetic extension torque compared to ACL-injured patients, however, the opposite is true for isokinetic flexion torque. There were no interaction effects found, therefore, strength deficits following an ACL injury are not dependent on the individual's sex. However, it was determined that leg dominance should be considered when assessing knee joint function as it relates to paediatric rehabilitation guidelines.

Introduction

There is no consensus on appropriate ACL return-to-activity (RTA) guidelines for paediatric athletes [1]. Current practice may be inadequate given that 21.3% - 38.1% of paediatric patients sustain an ACL re-injury, and only 56-63% returning to preinjury level of sport participation [1, 2]. Through the use of isometric and isokinetic knee flexion and extension data, we can gain insight on muscular functional performance and thus rehabilitation status [3]. However, to date, no research has examined if interaction effects exist between sex and injury status regarding lower-limb strength in youth. Therefore, the purpose of this study was to determine if sex and injury status affect peak torque values produced during isometric and isokinetic knee flexion and extension tasks in paediatric male and females with and without an ACL*i*.

Methods

Sixty-five (46 females) ACL*i* patients with confirmed ruptures and 70 (39 females) control participants were recruited to participate in this study. All participants performed maximal voluntary isometric and isokinetic knee flexion and extension tasks on an isokinetic dynamometer (System 4 Pro, Biodex Medical Systems, Inc., New York, USA). Isometric contractions were performed in a seated position with the knee joint held at 60° of flexion. Isokinetic knee flexion and extension was performed at 60°/s for a total of 44 repetitions. Peak torques were identified during the

isometric and isokinetic tasks and normalized to each participant's body mass (Nm/kg). Limb symmetry indexes (LSI) were then calculated for each limb (non-dominant/dominant and injured/contralateral limb). Two-way ANOVAs ($\alpha=.05$) were used to evaluate the effect of sex (male vs. female) and injury status (ACL*i* vs. CON) in isometric and isokinetic torques and LSIs.

Results and Discussion

Uninjured controls had higher mean LSIs for isometric extension torque compared to ACL*i* patients ($p<.001$; Table 1). For the isokinetic task, control participants had higher mean LSIs for isokinetic extension torque compared to ACL*i* ($p=.002$); however, ACL*i* patients had a higher mean LSI for isokinetic flexion torque ($p=.013$). As well, males demonstrated a higher mean LSI compared to females for the isokinetic flexion torque ($p<.050$). No interaction effects were seen in either task.

The results indicate that strength deficits (LSIs) following an ACL injury are not dependent on the individual's sex. The higher isokinetic flexion LSI in the injured individuals is likely due to the confounding factor of leg dominance. Since the dominant limb is typically stronger (Table 1), and 60.4% of the ACL-injured patients injured their dominant limb, the resulting strength deficit would not appear in the LSI.

Conclusions

Leg dominance significantly affects isometric and isokinetic torque measurements at the knee in adolescent males and females. Since these measures are commonly used to assess rehabilitation in ACL*i* patients by comparing the injured to healthy limbs, those results may be biased by this limb dominance effect and must be considered. Further research is needed to evaluate the influence of limb dominance in ACL*i* strength deficit measures and how these may be used to inform the rehabilitation process and RTA evaluations.

References

- [1] Heath *et al.* (2019). *Am J Sports Med*, **47** (1): 41-51
- [2] Ardern *et al.* (2011). *Br J Sports Med*, **45** (7): 596-606
- [3] Davies *et al.* (2017). *Curr Rev Musculoskelet Med*, **10**: 307-314.

Table 1: Means and standard deviations of peak isometric/isokinetic torques: dominant (DOM), non-dominant (NDom), contralateral (CON), and injured (INJ) limbs.

		LSI: Isometric Extension	LSI: Isokinetic Flexion	LSI: Isokinetic Extension
<i>ACL Injured</i>	<i>Males</i>	0.830 ± 0.14	1.11 ± 0.27	0.837 ± 0.16
	<i>Females</i>	0.847 ± 0.25	0.991 ± 0.17	0.900 ± 0.25
<i>Controls</i>	<i>Males</i>	1.02 ± 0.16	0.973 ± 0.10	0.970 ± 0.16
	<i>Females</i>	0.958 ± 0.12	0.962 ± 0.14	1.03 ± 0.18

Knee joint kinetics during stationary cycling for unilateral total knee arthroplasty patients

Erik T. Hummer^{1,2}, Tanner T. Thorsen³, Joshua T. Weinhandl³, Harold Cates⁴, Songning Zhang³
¹Center for Mobility and Rehabilitation Engineering Research, Kessler Foundation, West Orange, NJ, USA
²Dept. of Physical Medicine & Rehabilitation, Rutgers New Jersey Medical School, Newark, NJ, USA
³Dept. of Kinesiology, Recreation, and Sport Studies, University of Tennessee, Knoxville, TN, USA
⁴Tennessee Orthopaedic Clinics, USA

Email: ehummer@kesslerfoundation.org

Summary

The purpose of this study was to compare the knee joint kinetics of unilateral total knee arthroplasty (TKA) patients during stationary cycling. The results display that replaced limbs have a decreased peak knee extension moment (KEM) compared to their non-replaced limbs, which is consistent with results during gait.

Introduction

TKA patients walk with decreased peak KEM in their replaced limbs [1]. This unloading is indicative of quadriceps weakness or pain during motion. Stationary cycling is a common exercise task used for TKA rehabilitation due to the lower tibiofemoral compressive forces [2]. However, there is limited information on whether the peak KEM inter-limb differences found during gait are present during stationary cycling. The purpose of this study was to examine the knee joint kinetics of TKA patients during stationary cycling.

Methods

Fifteen unilateral TKA patients (10 males, 5 females, 64.3 ± 8.2 yrs) were recruited from an orthopedic clinic and were operated by the same orthopedic surgeon (8.6 ± 2.4 months post-op, cruciate retaining = 14, bi-cruciate stabilizing = 1).

Participants cycled on stationary cycle ergometer (Excalibur Sport, Lode B.V., Groningen, Netherlands) in two randomized workrate conditions (80 and 100 Watt) at a cadence of 80 RPM. The ergometer was adjusted for each participant. Participants cycled for one-minute in each condition, with data collection occurring in the final 10 seconds. Three-dimensional motion capture (240 Hz, Vicon Motion Inc., Oxford, UK) and pedal reaction force (PRF) data (1200 Hz, Type 9027C, Kistler, Switzerland) were collected.

Five individual revolutions were truncated for data analysis and processed in Visual3D (C-Motion Inc., Germantown, MD, USA). A 2 x 2 (limb x workrate) repeated measures ANOVA was run with an alpha of 0.05.

Results and Discussion

There was a main effect of limb for peak KEM ($p = 0.034$) as well as for peak vertical PRF ($p = 0.038$). The replaced limbs had a 21.3% lower peak KEM and 5.3% lower peak vertical PRF (Table 1). Additionally, replaced limbs had a significantly lower peak posterior PRF ($p = 0.018$) compared to non-replaced limbs. Inter-limb differences found for peak KEM were similar to those during gait, with decreased KEM in replaced limbs. The KEM in replaced limbs could be due to decreases in both vertical and posterior PRFs. Interestingly, increases in workrate by 20 W did not alter knee joint moments, which has been previously reported [3]. There were no differences between limbs for peak knee abduction moment (KAbM) ($p = 0.376$). There was only a main effect of workrate for peak vertical PRF ($p < 0.001$) with a larger force at 100 Watt compared to 80 W (Table 1).

Conclusions

Unilateral TKA patients cycled with a reduced peak KEM in their replaced compared to non-replaced limbs. This indicates an unloading of the replaced limbs, similar to findings in gait. When increasing intensity via workrate in cycling, increments of 20 W may be ideal to not exacerbate inter-limb loading differences found in peak KEM.

Acknowledgments

Funding was provided by the Matching Dissertation Grant of International Society of Biomechanics with matching funds from the University of Tennessee, Knoxville.

References

- [1] Wen C et al. (2019). *J Biomech*, **89**: 40-47.
- [2] D'Lima DD et al. (2008). *Clin Orthop Relat Res*, **11**: 2605-11.
- [3] Fang Y et al. (2016). *Med Sci Sports Exerc*, **48**: 260-266.

Table 1: Pedal reaction forces (N) and knee joint moments (N*m) for replaced and non-replaced limbs at 80 and 100 W (mean ± STD)

	80 Watt		100 Watt		Interaction	P values	
	Replaced	Non-Replaced	Replaced	Non-Replaced		Limb	Workrate
Vertical PRF	210.2±42.2	227.3±43.7	233.9±39.3	241.7±43.2	0.144	0.038	<0.001
Posterior PRF	-54.4±15.9	-65.7±22.1	-55.5±15.7	-65.6±17.8	0.677	0.018	0.855
KEM	18.7±5.2	24.7±6.9	19.8±5.1	24.2±7.0	0.375	0.034	0.750
KAbM	-7.4±4.0	-13.1±7.5	-12.3±9.0	-12.8±6.2	0.204	0.376	0.146

Evaluating Muscle Recruitment during Lower Trapezius Early-Stage Exercises Performed below 90° Shoulder Elevation

Herrera. Maria C¹, Garcia. Jonathan,¹ Dickerson. Clark¹

¹Department of Kinesiology, University of Waterloo, Waterloo, ON, Canada

Email: m6herrer@uwaterloo.ca

Summary

sEMG activity from serratus anterior (SA), lower trapezius (LT), middle trapezius (MT), and upper trapezius (UT) was recorded from 32 healthy participants while performing four shoulder rehabilitation exercises targeting LT strengthening. No exercise performed below 90° of shoulder elevation had statistically similar LT activity as the gold standard overhead Y Prone exercise. However, side lying external rotation and wall angel exercises still achieved low UT/LT ratios. Wall angel and the side lying external rotation exercises may be useful early-stage shoulder rehabilitation protocol exercises to promote LT activation while achieving a low UT/LT ratio.

Introduction

LT assists scapular control and rotation and is often weak with scapular dysfunction [1]. LT strength development is crucial in scapular control dysfunction. Protocols often include high shoulder elevation exercises, which are often impossible in dysfunctional shoulders. “Y prone” is one of the most common exercises [Figure 1] [2]. A lack of research on more feasible LT exercises below 90° shoulder elevation exists. Exercises with high activation of LT and lower activation of UT are recommended to optimize scapular muscle balance [1]. This study compared EMG activity four periscapular muscles and the UT/LT ratio during low arm elevation exercises with the Y prone exercise.

Methods

Thirty-two (15M/17F) right hand dominant healthy persons participated. sEMG was recorded during five exercises (seated press up, side lying external rotation, side lying flexion, and wall angel, and Y prone) [Figure 1]. One-way repeated measures ANOVAs were used to compare muscular recruitment and UT/LT ratio across exercises ($p < 0.05$). A Post-hoc Tukey-Kramer test was used to find significantly different means from each other ($p < 0.05$).

Results and Discussion

No exercise performed below 90° of shoulder elevation had similar lower trapezius activity as Y Prone ($p < 0.0001$).

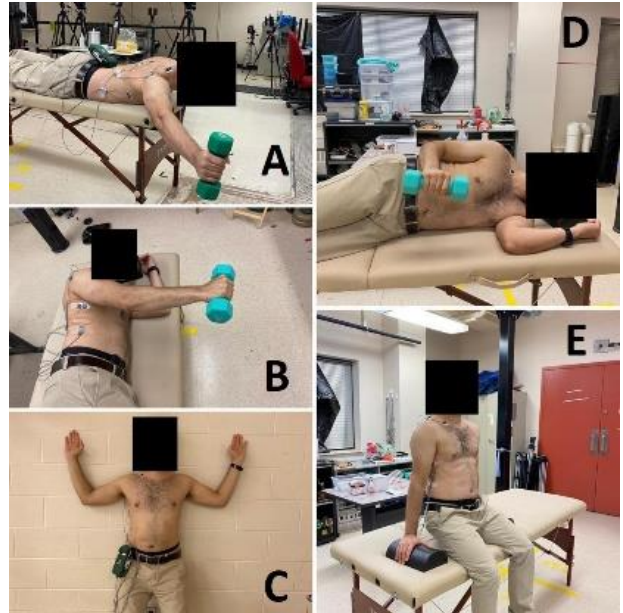


Figure 1: A: Y prone, B: Side lying flexion, C: Wall angel, D: Side lying external rotation, E: Seated Press Up

However, side lying external rotation and wall angel exercises demonstrated the highest LT activation peak and a low significant UT/LT ratio [Table 1].

Conclusions

Wall angel and the side lying external rotation exercises are considered safe and feasible to be implemented in an early-stage shoulder rehabilitation protocol to promote a combination of high LT muscle activation with a low UT/LT ratio.

Acknowledgments

This project was partially funded through an NSERC Discovery Grant held by Dr. Clark Dickerson, 311895-2011.

References

- [1] Cools AM et al (2007) *Am J Sports Med* **35**: 1744–1751.
- [2] Sgroi TA et al (2018) *Curr Rev Musculoskelet Med* **11**: 86-91

Table 1: sEMG activity in the evaluated muscles and UT/LT ratio across exercises. Points not sharing a letter are statistically different ($p < 0.05$).

	Y prone (%MVC)/ Level**	Wall Angel (%MVC)/ Level**	Seated Press Up (%MVC)/ Level**	Side lying external rotation (%MVC)/ Level**	Side lying flexion (%MVC)/ Level**
LT	74.9±26.6/ A	45.8±27.2/ B	23.1±14.9/ D	42.8±30.7/ B	32.5±20.3/ C
UT	46.6±22.3/ A	25.7±11.2/ B	13.2±7.9/ C	10.5±5.8/ C	25.0±12.9/ B
MT	62.1±23.0/ A	37.6±15.6/ B	7.9±14.6/ D	27.6±14.5/ C	35.5±17.3/ B
SA	32.1±22.2/ B	19.9±10.5/ C	42.3±30.5/ A	12.1±9.6/ D	21.8±12.7/ C
Ratio UT/LT	72.4±33.5/ C	75.6±41.9/ C	171.5±135.9/ A	47.2±39.0/ D	110.6±87.6/ B

**Post-hoc Tukey- Kramer HDS test

National Biomechanics Day: Past, Present, and Future

Lisa N. MacFadden^{1,4}, Felipe P. Carpes^{2,4}, Justin P. Waxman⁴, Paul DeVita^{3,4}

¹Sanford Sports Science Institute, Sanford Health, Sioux Falls, South Dakota, United States

²Department of Health Sciences, Universidade Federal do Pampa, Uruguaiana, Rio Grande do Sul, Brazil

³Department of Kinesiology, East Carolina University, Greenville, North Carolina, United States

⁴The Biomechanics Initiative, Parent Organization of National Biomechanics Day, Earth

Email: lisa.macfadden@sanfordhealth.org

Summary

National Biomechanics Day (NBD) has grown over the last five years into a worldwide celebration of all things biomechanics. Biomechanists have participated in 392 NBD events in [28 nations](#), reaching over 29,000 students and 950 teachers. Through its unprecedented growth as a unique, fun-filled Biomechanics STEM and STEAM event, NBD has become part of the Biomechanics firmament. Here we present a brief history of NBD, review current initiatives and successes, and present our vision of the future.

From small beginnings come great things – Proverb

National Biomechanics Day (NBD) began in 2016 with the distant goal of teaching biomechanics in high schools across the U.S. and it's raison d'etre was fully explained in the visionary, "[Why National Biomechanics Day](#)," [1]. The first NBD event was an unqualified success with over 2,000 high school students and teachers participating in 48 biomechanics experiences across the United States. Stemming from this success, the NBD outreach initiative grew to hundreds of synchronous events around the world. To date, over 29,000 students and teachers have participated in ~400 NBD events in 28 countries. Inspirational photos and videos from NBDs across the years and around the world can be seen [HERE](#).

The future depends on what you do today – Ghandi

Since 2016, NBD has connected biomechanics labs around the world through coordinated events broadcasted on social media channels, innovative and creative competitions, articles in lay and science journals, newspaper and television news stories, music playlists, fun and wild graphics advertisements, among other exposures. NBD has also supported and collaborated with 17 different biomechanics societies and 37 commercial biomechanics companies. Anecdotally, faculty and students have commented that the value of annual society meetings has increased because of the relationships fostered through NBD, creating more opportunities for networking and collaborating. We suspect that the less formal guidelines for promoting an NBD event may have positively impacted people involved with biomechanics, which felt comfortable to promote small events, of low budget, and leveraging new ideas and initiatives to popularize and share biomechanics content.

Today, many individual and student driven outreach events now exist due to the impact and leadership of NBD. These include the Biomechanics On Our Mind ([BOOM](#)) podcast, [The Biomechanist](#) network for biomechanics, and the [Sports Biomechanics Lecture Series](#). Newly formed, focused biomechanics societies have energetically affiliated with

NBD, including the Black Biomechanist Association (BBA) and International Womxn in Biomechanics (IWB). NBD has also introduced students from historically underrepresented groups to biomechanics at a rate we hope will enhance diversity in biomechanics. By 2017, over 50% of student participants were female and 50% of student participants were non-Caucasian. We assume that NBD being promoted globally, including in developing countries, contributes to successfully reaching and promoting underrepresented groups.

As more high school students are introduced to biomechanics, and more graduate students, faculty, and private companies are connected through NBD, the community is developing a foundation that inspires young people to make their own impact on the field.

The best way to predict the future is to create it – Lincoln

In 2019, The Biomechanics Initiative (TBI) was created as the parent organization for NBD. Through TBI, support for other initiatives has been possible thanks to donations from [sponsoring organizations](#). This year, TBI & NBD are offering funding opportunities in collaboration with biomechanics societies (ASB and ISB) and affiliates (BBA and IWB) to support NBD events that reached more diverse populations. Additional funding opportunities were provided in Australia and Brazil to support NBD events where financial limitations would have prevented schools from participating (Australia) and to promote biomechanics research opportunities for high school students (Brazil). Future grants and scholarships are planned to help young biomechanists impact biomechanics.

Go forth and set the world on fire – Ignatius of Loyola

National Biomechanics Day has led to grassroots growth in biomechanics and spurred many new exciting directions for our outreach efforts. As we look to the future, we are excited about the opportunities that TBI and NBD will create for the biomechanics community. We aim to inspire others to share their passions with students and each other so that our community and impact on society can grow. A dream that started with the goal of integrating biomechanics into the high school curriculum has grown into a global vision that will continue to build communities, initiatives, and programs that revolutionize how we train future generations of biomechanists and inspire and support one another. Together, we will make Biomechanics the Breakthrough Science of the 21st Century!

References

[1] DeVita, P. (2018). *J Biomech*, **71**:1-3.

Development of a Hands-on, Wearables Course as an Alternative for Physiology Labs

Patrick Mayerhofer, Jim Carter, Max Donelan

Department of Biomedical Physiology and Kinesiology, Simon Fraser University, Vancouver, Canada

Email: pmayerho@sfu.ca

Summary

Here we present a remote alternative to a traditional physiology lab course. We developed a customizable, inexpensive, microcontroller-based hardware kit with devices that can measure different physiological variables. We also developed open-access software to program the hardware for data collection and analyze the collected data, which we share in online repositories. With customizable lab manuals and supplementary video tutorials, all freely available online, students learn to conduct physiological experiments, by collecting and analyzing data (e.g.: EMG, ECG, kinematics).

Introduction

Delivering a remote, hands-on lab course in physiology can be challenging. During the COVID-19 pandemic, we developed an inexpensive, customizable hardware kit along with fully open-source teaching resources to help educators deliver their physiology lab courses remotely. These resources allow educators to teach students how to do hypothesis-driven physiological experiments, without the need for students to have previous coding or electronics experience. Additionally, all of our resources are fully customizable, allowing educators to fit the requirements of their respective physiology courses.

Course Principles

Before developing our course resources, we defined multiple key principles. First, the whole system must be wearable. All measurement systems should be able to run battery powered and store data. Second, students should not require technical experience for taking the course. Setting up the hardware should work without soldering, and the number of wires and devices for a measurement system should be small. Students also should not require prior coding knowledge to set up software for the measurement systems and the data analysis. Third, all resources should be financially accessible. The hardware kit should be relatively inexpensive (~cost of a textbook), all the software required should be open-source, and the instructional materials should be open-access. Lastly, the workload for educators to develop a similar course should be minimal. All hardware, software, and instructional materials should be customizable. Following these principles will allow students to conduct insightful experiments on different physiology systems.

Course Design

Our hardware kit consists of commercially-available electronic components, with a microcontroller as its base and a suite of physiological sensors. The microcontroller is a small computer that reads, alters, and outputs signals from and to other devices in the system. To make the hardware kit wearable, a 9V battery powers the system and a data logger stores

the data on a memory card, eliminating the need to be tethered to a computer. To make the system solderless and minimize the number of wires, all devices in the kit connect to the microcontroller with no more than three wires. Digital, analog, or communication via a specific one-wire protocol called “Qwiic”, are all possible. Our particular hardware kit (Fig 1) is ~\$120 US. It can be customized with different sensors depending upon instructional needs.

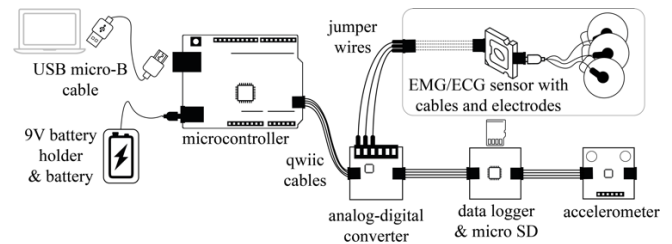


Figure 1: Components of our hardware kit.

To support students without prior coding experience, we share our codes in open-access GitHub repositories. To make all software open-source, we chose the Arduino Integrated Development Environment (IDE), a commonly used programming platform for microcontrollers, to program our hardware, and Python, the fastest growing programming language in the world, for data analysis [1]. Educators can download, customize, and share all code using GitHub. For lab manuals, we use open-access Google Docs to allow educators to copy and edit documents, as well as share them with collaborators and students. To help students set up measurement systems and analyze data, we created a YouTube channel with supplementary video tutorials. To customize this library, educators can create their own YouTube library with videos from our channel and their own additional content. These resources allow educators to rapidly implement labs for students to conduct EMG, ECG, and kinematics experiments. And they can be leveraged to develop new labs for different physiological systems.

Conclusions

Our course resources are available online [2]. We taught this course for the first time in Fall 2020. In their homes, students learnt how to build measurement systems, acquire and analyze real physiological data, trouble-shoot problems, and interpret results. Our resources can support universities to set up their own hands-on, customized wearables physiology lab courses.

Acknowledgments

Funded by NSERC Discovery Grant to JMD.

References

- [1] Srinath KR (2017). *IRJET*, 4: 354-357.
- [2] Mayerhofer P et al. (2020). *SFU BPK Wearables – Lab Overview*, http://bit.ly/3popKqg_SFU_BPK_Wearables

Pilot study: Performance benefit of young athletes using a video-based feedback and instrumented starting blocks in athletics sprint start

Beat Göpfert¹, Edith Bek¹, Alina J. Tittel¹

¹ Department Biomedical Engineering, University of Basel & University Children's Hospital Basel; Switzerland
Email: beat.goeppfert@unibas.ch

Summary

An Instrumented video-based movement analysis is rarely used in local teams with young athletes (U16), due to availability and knowledge. A pilot study, in which an athletic sprint start was done, showed, that young athletes today benefit in their practice because they are often used working with video-based teaching tool and thus were able to optimize their movement pattern.

Introduction

In athletics, the sprint start from the starting block initiates the beginning of sprint race and is seen as an important part of the race. Especially in young athletes "A good start gives a good feeling for the race", but the movement pattern of the start is very demanding and requires a lot of practice, muscular coordination and power. As a fast and complex movement, it is also demanding for coaches to identify the optimal movement pattern for different athletes with different performance and skill levels. Nowadays video analysis methods are often used in high-performance athletes, but rarely in young athletes (U16). The goal of this pilot study was to evaluate the benefit of video-based feedback a with instrumented starting blocks during the sprint start in athletics.

Methods

7 young athletes (14 y, 5 f, 2 m) of a local athletic team participated in this pilot study, while performing a sprint start over 10 m, using instrumented starting blocks with two 3D-forceplates (KI-Sprint-System, Kistler AG, Winterthur, CH). 3 starts were recorded with a high-speed camera (100 Hz) during 3 independent indoor practice sessions. There were 2 weeks of regular practice between each measurement session. After the first and second measurement session, each athlete got an individual written feedback incl. videos with proposed adjustments for the following measurement session. The changes in starting performance (force direction, step length, step time) were analyzed and compared between the 3 sessions.

Results and Discussion

The results showed that most of the athletes had a smaller push-off force angle, resulting in an 8% increase of the horizontal push-off force and a slight longer first step of the rear leg of 10% (4 cm). Furthermore, in the set position the center of mass moved 17% (4cm) in direction of the starting line, which allows to produce higher horizontal force [1]. The individual temporal parameters of the ground-contact and flight phases have not changed much in the 3 sessions, except for the ground contact time of the first step, which became in avg. 0.012sec. longer. This resulted to an mean in-

crease of the total starting time for the first two steps of 0.015sec in Session 3 compared to Session 1. Unfortunately, due to the COVID-19 pandemic, the regular practice had to be interrupted for 3 months, 4 weeks after the 3rd measurement session. Therefore, the results of the few competitions in late summer are not very meaningful.



Figure 1: Athlete using the KI-Sprint-System during the pilot-measurement

Conclusions

Conclusion for the start performance:

The results show that beside the maximum muscular power during push-off and ground contact: (a) Optimizing the push-off-angle more towards a more forward than upward movement [2] and (b) the maximal capable and controllable angular velocity and power in the hip-joint, are some of the critical factors for a good starting performance in young athletes in the athletics sprint start.

Conclusion for the coaching process:

The pilot measurement showed that young athletes today can improve their technique well with the help of video analyzes and biomechanical measurement. In addition, it is helpful for coaches to get objective parameters in order to set priorities in the training program. It should be kept in mind that in a possible future coaching career, athletes are more likely to use such technologies if they are already familiar with and could benefit from it.

Acknowledgments

We thank the athletes for participating and Kistler AG, Winterthur for providing the KI-System in the pilot study

References

- [1] Mann R.V.; Murphy A. 2018, The mechanics of Sprinting and Hurdling, Mann R.V, Las Vegas NV, USA
- [2] Colyer, S. L. *ISBS Proceedings Archive* 37.1 (2019): 495.

Active learning strategies using surface electromyography improve the undergraduate student's understanding of neuromuscular human movement control

Carlos De la Fuente,^{1,2,3} Álvaro S Machado,¹ Marcos R Kunzler,¹ Mauricio Delgado,² Felipe P Carpes¹

¹Applied Neuromechanics Research Group, Federal University of Pampa, Brazil; ²Physical Therapy career, Health Sciences Department, Pontificia Universidad Católica de Chile, Chile; ³Clinica MEDS, Chile.
Email: delafuente@gmail.com

Summary

Here we describe the potential of laboratory activities integrating theoretical and hands-on aspects using active methodologies and surface electromyography (sEMG) to improve comprehension about neuromuscular human movement control in undergraduate students without a previous background in biomechanics.

Introduction

In many health sciences careers the initial studies of the human body involve the acquisition of biology and anatomy knowledge. However, these biological topics are often presented disconnected from mechanical elements of movement including the effects of gravity, inertia, or torques [1]. We hypothesized that combining a strategy to stimulate critical thinking skills and an active methodology of learning into biomechanics lab using sEMG would result in a better understanding of the link between the neuromuscular system and mechanical elements of human movement in undergraduate students without a previous background in biomechanics.

Methods

Retrospectively, we analyzed the difficulties and advances of students to solve problems related to the links between the neuromuscular system and mechanical elements of human movement for 482 second-year physiotherapy students attending a human movement analysis course from 2013 to 2018. The problems included tasks such as bipedal standing, shoulder elevation, handgrip test, weightlifting, and walking. The sEMG signals were collected from the main superficial muscles that are active during the performance of these tasks under diverse conditions like altering workload, movement speed, amplitude, and fatigue level. sEMG signals were online processed during the classes and served to illustrate the concepts. We employed discussions in small groups, oral presentations of outcomes, and round tables with questions from the students. The difficulties and advances of students were qualitatively described. The students' grades in the lab activities, the overall course grades, and the students' self-reports were considered in the data analysis. All the students had no specific biomechanics background. To quantify how the grade in the laboratory activities explained the final grade of the overall course, we performed linear regression with an alpha set to 5%.

Results and Discussion

Figures 1 and 2 summarize the results. Students reported difficulties when activities addressed aspects involving basic anatomy knowledge, the understanding of concentric and eccentric muscle actions, and the effects of an external and

internal couple of forces across the joints. Common difficulties involved lack of reasoning and discussion about how the joints are actively stabilized and generate movement from the muscle activation. However, better integration between muscle activation and mechanical outputs to control movements occurred after each activity. The laboratory grades explained the overall course grades ($p < 0.001$, R-square = 0.427).

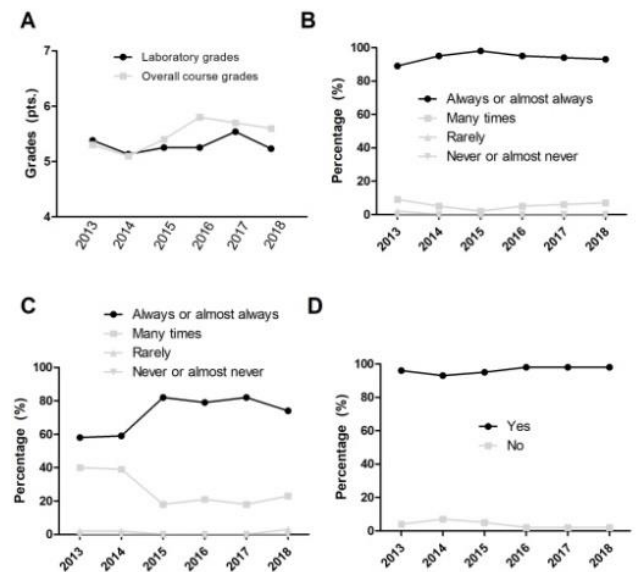


Figure 1: Self-reported time series. A. Grades. B. Real-life examples involved in the course. C. Critical thinking involved in the course. D. Satisfaction with the course.

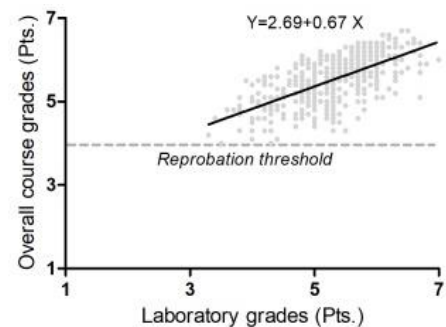


Figure 2: Regression analysis.

Conclusions

Active learning strategies using sEMG facilitate the understanding of neuromuscular human movement control in undergraduate students without a previous background in biomechanics.

References

[1] Webb AL, et al. (2019). *Clin Anat.* 32(8):974-1007.

Micromovements, low back pain, and computer task performance during prolonged sedentary postures

Liana M. Tennant¹, Jackie D. Zehr¹, Jessa Buchman-Pearle¹, Jack P. Callaghan¹

¹Department of Kinesiology, University of Waterloo, Waterloo, Canada

Email: liana.tennant@uwaterloo.ca

Summary

Lumbar spine fidgeting early in standing and often in sitting are thought to reduce transient low back pain (LBP) related to these postures. Posture and LBP may also affect productivity. During two, 2-hour exposures, there was no effect of standing-induced LBP on the frequency of lumbar fidgets in either sitting or standing. For a data entry computer task, productivity was the same between LBP groups in sitting but was reduced in standing in participants with standing-induced LBP. There was no effect of posture or LBP group on typing performance or score on a reading comprehension test (GRE). Thus, performance of demanding computer tasks while standing may decline in individuals with standing-induced LBP performing the same task seated.

Introduction

Micromovements of the lumbar spine, including fidgets, may have a complex relationship with transient low back pain (LBP) development in prolonged sedentary postures [1-4]. For sitting, lumbar fidgets may minimize sitting-induced LBP [1]; in standing, fewer fidgets in the first 15 minutes may predispose individuals to LBP [3]. Sitting or standing is thought to have little effect on productivity for typing tasks [5]. Our aim was to explore how fidget frequency may differ for individuals with standing-induced LBP in both sitting and standing, and the interaction of posture and LBP on computer task performance. We expected that standing-induced LBP developers would show similar fidget patterns regardless of posture, and that LBP may worsen task performance.

Methods

Twelve back-healthy adults (6 males, age: 24 ± 3 y, height: 1.70 ± 0.12 m, mass: 66.8 ± 12.7 kg) completed two hours of data entry, typing, and an online simulated Graduate Record Examination (GRE) in equal time allotments and in a randomized order while standing and sitting on separate days. Lumbar spine posture was measured at 250 Hz with triaxial accelerometers at S1 and L1 (ADXL335, Analog Devices, MA, USA). LBP was recorded on a 100 mm visual analog scale every 20 minutes. LBP was noted if pain exceeded 10 mm from baseline [3].

Accelerometer data were filtered at a 1 Hz cut-off using a dual-pass low-pass Butterworth filter. Lumbar flexion angle was calculated as the difference in accelerometer inclination. Lumbar fidgets were identified by comparing each frame of angle data to the moving average, such that: $|\bar{x}_w - x_i| > 3SD_w$, where \bar{x}_w and SD_w are the average and standard deviation of a moving window (size $w = 50$ s), centred on point x_i [2]. Maximum fidget duration was 4 s. Fidget frequency was normalized to time. Mixed general linear models were used to

investigate fidget frequency (fidgets/min), typing (words/min (WPM)), data entry (entries/min), and GRE score (%) between standing pain developers (PD) and standing non-pain developers (ND), in sitting and standing ($\alpha < 0.05$).

Results and Discussion

Six participants developed LBP in standing. There was no difference in lumbar fidget frequency between postures ($p = 0.84$). Contrary to our hypothesis, there was no difference in fidget frequency between LBP pain groups ($p = 0.81$), nor an interaction effect ($p = 0.25$) (Figure 1).

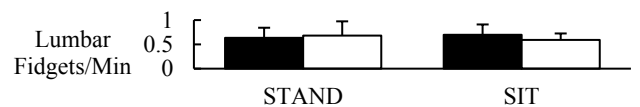


Figure 1: Fidgets in PDs (■) and NDs (□) in sitting and standing.

In partial support of our hypothesis, for data entry, productivity was similar for both pain groups in sitting but worsened in standing in the PDs ($p < 0.01$) (Figure 2a). Neither posture nor pain group affected typing ($p > 0.19$, $n = 11$ – one outlier removed) or GRE score ($p > 0.48$) (Figure 2).

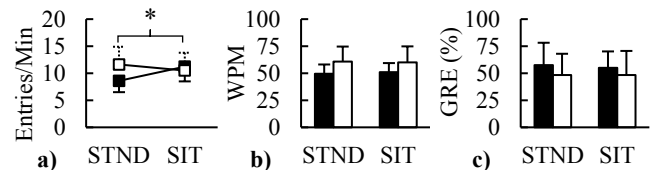


Figure 2: a) Data entry b) Typing, and c) the GRE scores in standing PDs (■) and NDs (□), in sitting and standing (STND). Significant interaction effect ($p < 0.05$) denoted with an (*).

Conclusions

Any relationship between lumbar fidgets and LBP may be too nuanced for gross fidget behaviour to be similar between standing and sitting [3]. Standing-induced LBP worsened performance in standing data entry, possibly due to the many demands of the task (attention, mousing, and typing) and pain distraction, as only one participant developed LBP in sitting.

Acknowledgments

Funding was provided by NSERC (RGPIN-2016-04136). JC is supported by a Canada Research Chair (950-228146).

References

- [1] Greene RD et al. (2019). *Ergonomics*, **62**: 1415-1425.
- [2] Dunk, NM and Callaghan JP (2010). *Work*, **35**: 3-14.
- [3] Gallagher KM and Callaghan JP (2015). *Hum Mov Sci*, **44**: 111-121.
- [4] Gallagher KM et al. (2011). *Gait Posture*, **34**: 490-495.
- [5] Karakolis T et al. (2016). *Ergonomics*, **59**: 1275-1287.

Sex-specific neuromuscular adaptations to fatigue in a repetitive pointing task while sitting on a sit-stand stool

Chen Yang¹, Yiyang Chen¹, Erika Renda¹, Julie N Côté¹

¹Biomechanics of Occupational and Sport Laboratory, Department of Kinesiology and Physical Education, McGill University, Montreal, Canada

Email: chen.yang4@mail.mcgill.ca

Summary

This study quantified the sex differences in muscle activation adaptation to fatigue when sitting on a sit-stand stool. Participants performed a repetitive pointing task until task terminal while we collected the electromyographic data of the upper body muscles. Results showed that females and males adopted different activation strategies. Females demonstrated greater activation and variability of the prime movers. This highlighted the importance of considering sex differences when recommending sit-stand stool as an alternative workstation.

Introduction

Muscle fatigue can be induced by repetitive occupational task and may lead to neuromuscular adaptations [1]. Previous studies have noted alterations of muscle activation amplitude, variability, and frequency with fatigue [2]. Recently more and more ergonomic workstations have been recommended to avoid impairments from prolonged work. Sit-stand stools intend to avoid the disadvantages of both standing and sitting. Previous studies focused on the kinematic, physiological changes when adopting sit-stand stool. However, how the muscle activity adjusts with fatigue when utilizing a sit-stand stool remains unknown.

Methods

Young healthy adults (n = 29, 15 males) were recruited to perform a repetitive pointing task (RPT) on a sit-stand stool (Muvman®, aeris-Impulsmobel GmbH & Co.KG, Germany) [3]. EMG data was recorded using a Delsys EMG system (Delsys Inc., Boston, MA, USA; Fs = 2000 Hz) using surface electrodes placed on: Upper Trapezius (UT), Anterior Deltoid (AD), Middle Deltoid (MD), Triceps Brachii (TRI), Biceps Brachii (BIC), and Left and Right Erector Spinae (LES and RES). EMG and perceived neck/shoulder exertion data was collected in the last 30 seconds of every minute during RPT. The task was terminated when perceived exertion score reached 8 out of 10. The first and last 30-second trials were recognized as the non-fatigued (NF) and fatigue-terminal (FT) trials.

EMG data were filtered (dual-pass 4th-order Butterworth bandpass filter, 20–500 Hz). Root mean squares (RMS) of EMG amplitude were averaged across forward movements to obtain one RMS value per muscle. The corresponding standard deviation (SD) of the RMS and Median Power Frequency (Mdpf) were also calculated. Generalized estimating equations (GEEs) were used to detect effects of sex and fatigue condition on EMG variables in each muscle.

Results and Discussion

The RMS of all measured muscles increased after fatigue, confirming that the task induced fatigue in all muscles. The RMS of AD and TRI was greater in females compared to males. At NF, the RMS of MD was greater in females. However, the sex difference disappeared at FT. Sex differences were found in the RMS of AD (p=0.008), MD (p=0.003), and TRI (p=0.013) (Figure 1), i.e. in the prime movers only, rather than the stabilizer muscles. Similarly, the SD of activation in all the muscles increased after fatigue as well. Besides, females exhibited higher activation variability in AD (p<0.0001) and TRI (p=0.028) compared to males independently from fatigue. In terms of Mdpf, sex differences were observed in UT (p<0.0001), AD (p<0.0001), MD (p<0.0001), and BIC (p=0.023). Females showed higher firing frequency in these muscles compared to males. Combined with the RMS results of AD and MD, the greater activation amplitude and higher activation frequency in females may imply that females experienced a higher exertion at deltoid during the task. Besides, greater activation and variability of prime mover muscles (AD and TRI) suggest that the task was more demanding of the prime movers of females than those of males.

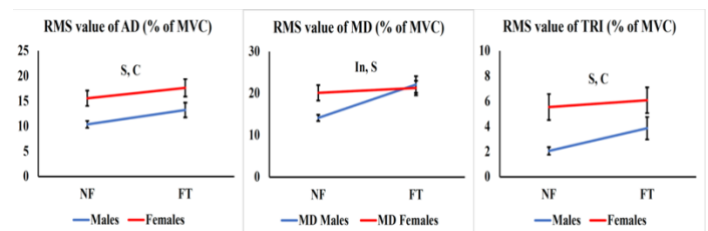


Figure 1: RMS results of AD, MD, and TRI. *IN, S, and C stands for interaction effect, sex effect, and condition effect, respectively.

Conclusions

Sex differences exist in EMG adaptations to muscle fatigue induce by a repetitive arm task while sitting on a sit-stand stool. Females may have experienced a higher exertion of prime movers during the task. Sex differences need to be considered when recommending sit-stand stools.

Acknowledgments

This study was supported by Fonds de recherche du Québec – Santé (FRQS) PhD training award (File number: 271870)

References

- [1] Bigland-Ritchie B et al. (1983). *J. Neurophysiol*, 50(1).
- [2] Antle D M et al. (2015). *Int. J. Ind. Ergon*, 45: 98-106.
- [3] Fuller J R et al. (2009). *J Electromyogr Kinesiol*, 19(6).

Sex-Specific Effects of Anti-Fatigue Lenses on Discomfort, Kinematics and Performance during a Seated Computer Task

Samuel Lamanuzzi¹, Geneviève Gill¹, & Julie N. Côté^{1,2}

¹Department of Kinesiology and Physical Education, McGill University, Montreal, Quebec, Canada

²Occupational Biomechanics and Ergonomics Laboratory, Michael Feil and Ted Oberfeld/CRIR Research Centre, Jewish Rehabilitation Hospital, Laval, Quebec, Canada

Email: Samuel.Lamanuzzi@mail.mcgill.ca

Summary

Anti-fatigue lenses (AFL) claim to offer health benefits. However, no studies have measured their impact on discomfort, biomechanical outcomes, or computer work performance, or how these effects differ between the sexes. Twenty-four University students and regular computer users (n = 12 males) were recruited. Participants underwent two 90-minute computer sessions with AFL or placebo lenses. Visual analogue scales (VAS) for eye strain, neck/shoulder and other body discomfort were recorded, with performance measures, electromyographic (EMG) upper trapezius (UT) amplitude and variability and head/neck kinematics. Discomfort increased over time, more in females (eye strain and neck/shoulder: $p < 0.001$; other body regions: $p = 0.013$). UT EMG amplitude for females was negatively correlated to eye strain in the placebo group. UT EMG variability for males wearing AFL was negatively correlated to eye strain. Neck flexion was positively correlated to eye strain for males wearing placebo lenses, suggesting sex-specific effects of AFL.

Introduction

AFL show multiple benefits, such as glare reduction and near vision magnification [1,2]. These benefits claim to reduce eye strain, neck pain, trapezius muscle activity and other symptoms associated with musculoskeletal discomfort [1,2,3,4]. However, no study has objectively examined the outcomes of AFL on performance, eye strain and musculoskeletal characteristics in university students and how they might differ between the sexes. The objective of this study was to determine the effectiveness of AFL on visual and musculoskeletal discomfort, EMG UT activity amplitude and variability, kinematics and performance outcomes in males and females. We hypothesized that AFL wear would reduce eye strain and musculoskeletal discomfort in both sexes. In addition, that AFL would improve the performance for both sexes while minimizing UT EMG activity, neck flexion and head protraction, while increasing UT muscle variability.

Methods

Twenty-four university students and regular computer users (n = 12 males; mean age = 23 ± 2.3 years) were recruited. Participants underwent two 90-minute seated computer sessions with either AFL or placebo lenses in random order. VAS for eye strain, neck/shoulder and other body discomfort were recorded, along with typing speed and errors. UT EMG activity was measured using surface electrodes (Delsys), and tridimensional head/neck kinematics was quantified using

motion capture (Vicon). Main and interaction effects of Condition (AFL vs. Placebo), Time and Sex were analyzed using ANOVA. Relationships between variables were analyzed using Pearson/Spearman's correlational analysis.

Results and Discussion

Eye strain and discomfort to the neck/shoulder ($p < 0.001$) and other body regions ($p = 0.013$) significantly increased with time, more so in females. It has been speculated that extended periods of sustained computer work can stimulate low levels of constant muscle activity which could explain the observed musculoskeletal discomfort found in our study [5]. In the placebo lens condition, there was a negative correlation between UT EMG amplitude and eye strain ($r(18) = -.49, p = .05$), with a greater impact in females ($r(7) = -.681, p = .05$). UT EMG variability for males wearing AFL was negatively correlated to eye strain ($r(9), -0.622, p = 0.041$). This is in line with past results suggesting a health-protective effect of high motor variability [6]. There was a significant positive correlation between eye strain and neck flexion in males wearing the placebo lenses ($r(7), 0.705, p = 0.034$). Excessive glare during computer work of 10 minutes has been shown to increase UT muscle blood flow and induce a more forward-bent posture, eliciting a specific visual stress response [7].

Conclusions

Sex-specific effects of AFL are suggested during a 90-minute seated computer task. There seems to be a clear, sex-specific link between the visual and musculoskeletal system while wearing AFL, since females experienced greater ratings of discomfort throughout the entire task. This could lead to sex-specific recommendations for AFL wear.

References

- [1] Aghilinejad, M. et al. (2016). *Medical Journal of the Islamic Republic of Iran*, **30**: 473 - 473.
- [2] Ide, T. et al. (2015). *Asia-Pacific Journal of Ophthalmology*, **4**(2): 80-5.
- [3] Cagnie, B. et al. (2017). *Environmental Health and Preventive Medicine*, **22**(1): 8-8.
- [4] Zetterberg, C. et al. (2013). *Journal of Electromyography and Kinesiology*, **23**(5): 1190-1198.
- [5] Wahlström, J. (2005). *Occupational Medicine (Oxford, England)*, **55**(3): 168-76.
- [6] Madeleine, P. and Farina, D. (2008). *European Journal of Applied Physiology*, **102**(3): 325-333.
- [7] Mork, R. et al. (2018). *International Archives of Occupational and Environmental Health*, **91**(7): 811-830

Relationship between the global movement of the hand and the forearm muscles during typing

T. Ito¹, H. Funakoshi¹, Y. Sekiguchi¹, N. Kanemura¹, T. Kokubun^{1*}

¹ Saitama Prefectural University, Saitama, 343-8540, Japan.

*Email: kokubun-takanori@spu.ac.jp

Summary

This study aimed to examine the relationship between the global movement of the hand (GMH) and the forearm muscles during typing. Seven healthy adults input Japanese sentences. The Unchanging Typists (UT) group consisted of subjects with lower than average right-hand GMH, and the Changing Typists (CT) group consisted of subjects with higher GMH. There was a significant difference in GMH between the groups ($p < 0.05$). There was no significant difference in muscle activities between the groups. These data indicated that although GMH can affect the spatiotemporal efficiency of typing movements, maintaining a static home position is not necessarily an explanatory factor that reduces the cost of forearm muscle activities during typing.

Introduction

The fingers and hands used for keystrokes depend on the individual's typing style [1]. The UI and o keys are located on the right side of the QWERTY keyboard, so they are repeatedly inputted by the fingers of the right hand in the case of Japanese sentences. While most typists move their entire hand toward the key to be typed, the others have a spatiotemporally efficient strategy of keeping their hand in a static home position during typing. However, the relationship between these strategies and the forearm muscle activities is not clear. This study aimed to show the relationship between changes in the GMH and forearm muscle activities during Japanese text input.

Methods

Seven healthy adults volunteered in the experiment. We used a 3D motion capture system, surface EMG and QWERTY keyboard. Infrared-reflecting markers were attached to landmarks and measured kinematics parameters (Figure 1). Surface EMG was attached to the right side of four forearm muscles (Table 1). Subjects entered the sentence of about 5,000 characters in Japanese. The UT group and the CT group data were compared using the unpaired t -test ($p < 0.05$).

Results and Discussion

The location mapping of the right wrist, hand, and index finger for UT and CT group (Figure 1).



Figure 1: Mapping of UT group (upper) and CT group (lower).

There was a significant difference in the GMH between the groups. ($p < 0.05$). Comparisons of physical and kinematics parameters and muscle activities between groups showed no significant differences.

Table 1: Physical and kinematics parameters and muscle activities.

	Unchanging (n=3)	Changing (n=4)	p
global movement of the hand: GMH (mm/sec)	15.6 ± 0.2	40.7 ± 10.2	*0.02
Wrist width (cm)	6.6 ± 0.1	6.7 ± 0.5	0.93
Index finger length (cm)	8.9 ± 0.4	9.7 ± 0.7	0.17
Typing time (sec)	533.3 ± 270.0	209.8 ± 25.6	0.22
Changes of Wrist radial/ulnar deviation (deg/sec)	5.2 ± 1.6	11.8 ± 4.9	0.14
Changes of MP abduction/adduction deviation (deg/sec)	15.2 ± 3.8	25.4 ± 4.5	0.07
%MVC : Flexor carpi radialis (%)	1.0 ± 0.3	1.6 ± 0.6	0.27
%MVC : Flexor carpi ulnaris (%)	0.6 ± 0.2	1.0 ± 0.7	0.45
%MVC : Extensor carpi radialis (%)	3.0 ± 1.5	1.3 ± 0.4	0.13
%MVC : Extensor carpi ulnaris (%)	4.0 ± 2.8	2.7 ± 0.8	0.51

In the CT group, the index finger entered the 'u' key and vowels such as 'i' and 'o' key, and the home position was changed at any time. This strategy may be controlled by changes in hand posture due to forearm muscle activities and changes in segment position due to proximal muscles. Therefore, we did not observe an increase in forearm muscle activities.

Conclusions

The GMH can affect the spatiotemporal efficiency of typing movements. Maintaining a static home position is not necessarily an explanatory factor that reduces the cost of forearm muscle activities during typing movements.

References

[1] Anna Maria Feit et al. (2016). CHI, ACM, 4262-4273.

Combining wearable sensors and machine learning to monitor low back loading and injury risks in material handling

Emily S. Matijevich^{1,*}, Peter Volgyesi² and Karl E. Zelik¹

¹Department of Mechanical Engineering, Vanderbilt University, Nashville, TN, USA

²Institute for Software Integrated Systems, Vanderbilt University, Nashville, TN, USA

Email: em.matijevich@gmail.com

Summary

We discovered a promising wearable solution for practical, automated, and accurate monitoring of low back loading during manual material handling. Using signals from a trunk inertial measurement unit and pressure insoles together with a Gradient Boosted Decision Tree algorithm has the potential to provide a practical (relatively few sensors), accurate (up to $r^2 = 0.89$), and automated way (using wearables) to monitor time series lumbar moments across a broad range of material handling tasks. This promising wearable solution has the potential to transform low back injury risk assessment, monitoring, and prevention in various industries. Full results and discussion are published in [2].

Introduction

Low back disorders are a leading occupational health problem and about one in four workers reports dealing with low back pain [1]. Overexertion injuries are consistent with a fatigue failure process due to repetitive loading on the low back. There are opportunities to use low back loading and fatigue failure insights to understand and reduce the risk of overexertion injuries (e.g., through ergonomic assessments, or continuous, personal monitoring of injury risk). While wearable sensors provide a promising tool for unconstrained, continuous monitoring of low back loading, there remains a need for a solution that requires a small number of wearable sensors (to be practical to implement in industry) and provides validated estimates of low back loading for a range of work-relevant tasks (to ensure accuracy).

Methods

Ten participants each performed about 400 manual material handling tasks (lifting, lowering and moving boxes of varying masses) in a motion analysis lab while we synchronously collected data from lab-based instrumentation and from wearable sensors. Wearable sensors included inertial measurement units (IMUs) and pressure insoles. Then, we developed wearable sensor algorithms using various combinations of wearable sensor signals (algorithm inputs), machine learning techniques, and our lab-based gold-standard estimates of low back loading, specifically lumbar extension moment (algorithm target). We quantified how the number of sensors used influenced algorithm estimation accuracy and identified the most important subset of sensors for low back load estimation.

Results and Discussion

As expected, maximum algorithm accuracy increased with the number of sensor locations (Fig. 1). While single sensor solutions (e.g., using a trunk IMU only) provided moderate

correlations of lumbar moment (up to $r^2 = 0.74$), these solutions failed to capture increases in lumbar loading when objects of varying mass were lifted. Alternatively, an algorithm using two sensors (e.g., a trunk IMU and pressure insoles) provided more accurate estimates of lumbar moment (up to $r^2 = 0.89$) and captured key trends in elevated back loads when objects of varying mass were lifted. Additionally, this two sensor solution sacrificed minimal accuracy compared to an algorithm using sensors distributed over six body locations ($r^2 = 0.89$ vs. $r^2 = 0.92$, respectively). For monitoring lumbar loading during manual material handling there appears to be a sweet spot for accuracy and practicality that uses pressure insoles and a single IMU.

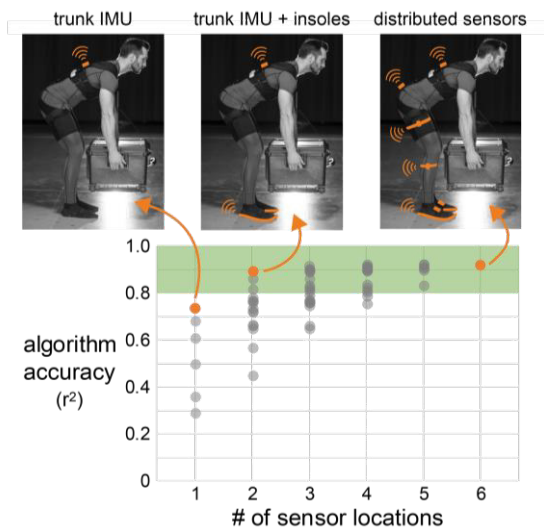


Figure 1: Maximum algorithm accuracy increased with number of sensor locations. Algorithm accuracy is average coefficient of determination across participants (r^2). Orange dots represent the distributed sensor algorithm (right) and the highest accuracy algorithms using one (left) and two (center) sensor locations.

Conclusions

Combining a trunk IMU and pressure insoles with a Gradient Boosted Decision Tree algorithm has the potential to provide practical, automated, and accurate monitoring of low back loading, opening new opportunities to manage and reduce low back injury risks in material handling.

Acknowledgments

Funding: National Institutes of Health (R01EB028105).

References

- [1] Yang, H et al. (2010) *J Manipulative Physiol Ther* **39**: 459-472
- [2] Matijevich et al. (2021). *Sensors*. 21(2), 340.

Correlation Between Wear Region of Shoes and Contact Region During Early Gait

Rosh Bharthi¹, Sarah L Hemler¹, Kurt E Beschorner¹

¹Department of Bioengineering, University of Pittsburgh, Pittsburgh, United States

Email: roshbhar@pitt.edu

Summary

As shoe treads wear over time, people are exposed to increased risk of slip and fall accidents. Identifying the time during a gait cycle when wear occurs is needed to better understand shoe wear progression to develop design changes that mitigate its effect. The purpose of the study was to determine the timepoint in a gait cycle where the contact region best aligns with the shoe wear region. The results show that these regions match well for some individuals at early in stance (~17 ms after heel contact). Other individuals have poorer matches between the worn region and the contact region occurring later in stance (33 ms - 83 ms after heel contact). Future directions include determining if the bimodal distribution is representative with a larger sample size and determining the wear mechanisms relate to shoe wear for both these wear conditions.

Introduction

Shoe treads exhibit wear over time, notably in the heel region. As a result, the drainage capacity and the friction performance of these shoes degrades, which can lead to slip and fall accidents [1]. Predicting shoe wear can provide insight on tread design changes that will improve tread durability. An impediment to developing these predictions is a lack of understanding of the gait cycle times that contributes to wear. The goal of the study was the determine the timepoint during the gait cycle that is most relevant to wear.

Methods

Four participants were provided with two shoe designs (SR Max, SafeTStep). Participants walked over a frustrated total internal reflection (FTIR) plate, while a camera beneath the plate recorded tread contact regions during stance. Participants then wore each pair of shoes in their workplace for up to 12 months. At the end of the wear period, pictures were taken of the worn heel tread to record the worn region. Custom image analysis code (MATLAB) was used to identify the contact region from the FTIR images and the worn region from the shoe tread pictures. For the FTIR images, the image was cropped to isolate the contact region, and brightness thresholds were used to identify the contact region. For the worn region, a user used a spline crop to identify the region with visible wear. The centroid of the contact and wear regions were recorded to the heel. Nine FTIR images (encompassing the first 83 ms of stance) were analyzed for each shoe and participant to capture the shoe contact region over time. To describe the timepoint most relevant to wear, the resultant distance between the contact centroid and the wear region was calculated for each frame. The frame where this distance was minimized was selected as the most relevant time. This time and the resultant distance were described.

Results and Discussion

The distribution for the stance time that best matched the wear region was bimodal: participants with centroid overlap occurring at 17 milliseconds (early stance wear) and participants with centroid overlap at timepoints greater than 30 milliseconds (ranging from 33 ms to 83 ms). For the early stance wear group, strong agreement exists between the worn region and contact region at 17 milliseconds (Figure 1). For the other group, the wear regions did not match as well despite the centroid coordinates matching closely. Commonly, the wear region would be located at the lateral edge of the heel, yet the contact region spans the entire width of the shoe, encompassing a larger portion.



Figure 1: Comparison of contact region 17ms after heel contact (left) and wear region after 10 months of use (right). The blue cross indicates the heel marker, and the red and green crosses indicate the centroids. Both regions are located at the lateral edge of the heel.

This analysis shows that the location of wear exists in the shoe region that is in contact early in the gait cycle (i.e., within the first 100 milliseconds after heel contact). Shoe wear models can be developed to incorporate biomechanical parameters (shoe angles, forces, etc.) at these earlier time points to predict wear location and pattern [2]. Additionally, the bimodal distribution of relevant times suggest that different gait styles may lead to different types of wear. Some wear may occur due to the shoe sliding at heel contact at foot contact (abrasion wear), while other wear may occur due to the normal and shear loading that occurs later in stance (fatigue failure) over a time range instead of a specific time [3,4]. This finding may suggest different wear mechanisms or patterns for each group.

Conclusions

The wear region is correlated with early instances in the gait cycle for some but not all participants. Further analysis, especially with a larger sample size, could help determine if this categorization is required for accurate shoe wear models.

References

- [1] Sundaram VH et al. (2020). *J biomechanics*, **105**: 109797.
- [2] Moghaddam SRM et al. (2019). *Wear*, **422**: 235-241.
- [3] Hemler SL. (2021). *Gait & Pos*. In Review.
- [4] Yamaguchi T. (2019). *Biotribology*, **19**: 100101.

A Scoping Review on the Applications of Machine Learning for Primary Work-Related Musculoskeletal Disorder Prevention

Victor C.H. Chan¹, Gwyneth B. Ross¹, Allison L. Clouthier¹, Steven L. Fischer², Ryan B. Graham¹

¹School of Human Kinetics, Faculty of Health Sciences, University of Ottawa, Ottawa, Canada

²Department of Kinesiology, Faculty of Health, University of Waterloo, Waterloo, Canada

Email: vchan017@uottawa.ca

Summary

To determine the applications of machine learning (ML) used for the primary prevention of work-related musculoskeletal disorders (WMSDs), a scoping review was conducted using seven literature databases. Of 3,201 unique results, 122 original articles were deemed relevant for inclusion. Articles were classified as a contribution to one of six steps within a primary WMSD prevention research framework [1]. The steps with the most contributions from ML techniques were the development of interventions (35.2%), followed by risk factor identification (23.0%); the fewest contributions were for intervention implementation (4.1%). Over a quarter (25.4%) of all articles were published in 2020. These findings provide a mapping for the use of ML techniques in primary WMSD prevention and should help identify future opportunities.

Introduction

Primary WMSD prevention is a leading focus for researchers, clinicians, and organizations alike, and the growing feasibility to collect and process large amounts of data welcomes ML techniques. Such techniques can model non-linear interactions between numerous variables and may be better suited for understanding the complex etiology of WMSDs and subsequently prevent their occurrence. As the use of ML techniques for these purposes are relatively novel, a scoping review was conducted. The purpose was to determine how ML techniques have been used for primary WMSD prevention in the steps outlined by van der Beek et al. [1].

Methods

A literature search strategy centred around machine learning, musculoskeletal disorders, and occupation was developed using the Medline database then translated to Embase, Cochrane Central Register of Controlled Trials, PsycInfo, IEEE Xplore, SPORTDiscus, and Scopus databases. The seven databases were searched on December 3, 2020 and articles were included if: 1) they were published on January 1, 1990 or later; 2) they were original research; 3) ML technique(s) were used to develop their system/framework and/or used to produce the final results; and 4) the work represents an effort to prevent WMSD occurrence, as defined using the WMSD prevention framework [1]. Title & abstract screening and full-text review were completed by two researchers using Covidence systematic review management software (Covidence, Victoria, Australia), and the results were reported according to the PRISMA guidelines. Included articles were classified as contributions to one of six steps of the WMSD prevention framework [1] as outlined in Figure 1.

Results and Discussion

The searches returned 4,627 results, with 1,426 identified as duplicates. The full-text of 246 articles were reviewed for eligibility, with a final of 122 articles included. The number

of articles classified to each step of the primary WMSD prevention research framework is presented in Figure 1.

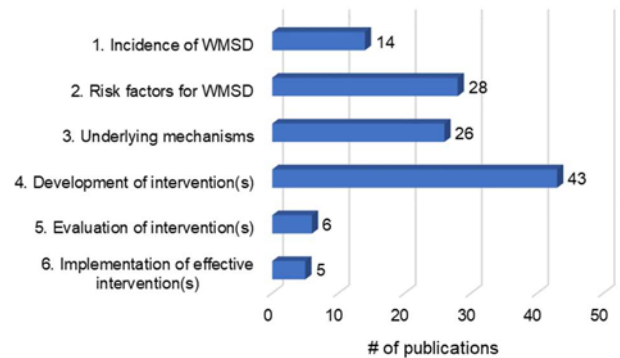


Figure 1: The number of research articles employing ML techniques found at each step of the primary WMSD prevention framework [1].

Articles in step 1 used text and data mining techniques with large databases to autocode and quantify WMSD incidences. Step 2 articles were characterized by unsupervised learning algorithms (e.g., *k*-means clustering) to identify potential risk factors amongst subgroups. Most articles classified for step 3 augmented existing biomechanical methods used for studying WMSD etiology, such as developing load prediction models that do not rely on musculoskeletal modelling. Articles in step 4 primarily presented systems for automated, real-time, ergonomic worker assessment using wearable sensors or computer vision-based methods. Articles in step 5 generally evaluated ML-based interventions, and step 6 consisted of articles that used ML to determine which jobs face the highest risk for WMSDs, warranting intervention implementation. Artificial neural networks, decision tree-based algorithms, and support vector machines were the most commonly-employed ML techniques, present in 42.6%, 18.0%, and 13.9% of articles, respectively. Publications from 27 countries were included, and the United States of America published the largest proportion of relevant articles (42.6%).

Conclusions

The use of ML techniques is rapidly growing in all industries, including for primary WMSD prevention. The most common usage has been to develop automated, real-time worker assessment systems. Many opportunities still exist at every step of WMSD prevention, especially for research regarding intervention evaluation and implementation.

Acknowledgements

NSERC and the Ontario Early Researcher Award Program.

References

- [1] van der Beek AJ et al. (2017). *Scand. J. Work Environ. Health*, **43**: 526-539

Drift-free algorithm for estimating muscle fascicle length from ultrasound images

Tim. J. van der Zee^{1,2}, Arthur D. Kuo^{2,1}

¹Faculty of Kinesiology, University of Calgary, Calgary, AB, Canada

²Biomedical Engineering Graduate Program, University of Calgary, Calgary, AB, Canada

Email: tim.vanderzee@ucalgary.ca

Summary

Ultrasound imaging is valuable for non-invasively estimating muscle lengths *in vivo*, especially when performed computationally to avoid subjective decision-making. An effective analysis technique is to use optic flow to track displacements from image sequences, but with sensitivity to integration drift for longer sequences. We here present an alternative algorithm that objectively estimates fascicle length from ultrasound images, without drift sensitivity. The algorithm estimates fascicle angles and derives their lengths between identified aponeuroses. Length estimates of human vastus lateralis in healthy subjects (N = 9) compared well (root-mean-square deviation, RMSD < 0.80 cm) to manual estimates from independent observers (n = 3). The algorithm had a higher coefficient of multiple correlation (CMC) with manual estimates than state-of-the-art optic flow algorithms (0.94 vs. 0.88-0.90 respectively), suggesting higher accuracy. The algorithm may extrapolate fascicle lengths that extend beyond the image frame, and requires minimal manual intervention.

Introduction

Muscle fascicle length may be estimated from ultrasound images using automated techniques. A challenge for automation is that images are typically noisy and offer few identifiable features that may be tracked across successive images. The optic flow approach avoids feature tracking by accumulating flow across sequences to yield fascicle displacements. But longer sequences of images are subject to drift, so that the displacement at the end of a periodic contraction cycle may not match the beginning. Another challenge is subjective decision-making, with manual estimation of the first image as initial condition for subsequent automation^[1,2]. We propose that fascicle lengths may be estimated without optic flow, and that automated identification of aponeuroses can reduce manual intervention. We demonstrate this approach with an open-source algorithm^[3,4].

Methods

The algorithm uses a three-step procedure: (1) filtering for line detection, (2) fascicle angle detection, and (3) trigonometric extrapolation. We applied it to estimate fascicle lengths from vastus lateralis ultrasound images in healthy subjects (N = 9).

The image filtering step is to highlight line-like structures, namely the aponeuroses and fascicles. As with any filter, contrast and other parameters may be set manually, but we found it efficient to identify aponeurosis lengths and angles with a minimally trained support vector machine (SVM). For the fascicles, a technique known as the Hough transform^[5] can identify lines and their angles without explicitly tracking

features. Finally, trigonometric extrapolation determines fascicle length L_{fas} from fascicle angle α , aponeurosis angle β and the distance between superficial and deep aponeuroses T_{muscle} (see Figure 1). We devised the algorithm in Matlab and trained aponeurosis detection with only nine sample images (one each from nine subjects). We compared the algorithm's length estimates against manual estimates by independent human observers (n = 3).

Results and Discussion

Algorithm fascicle length estimates increased with human observer estimates (slope: 0.99 ± 0.01 , estimate $\pm 95\%$ c.i., linear regression, see inset Figure 1), with algorithm-human differences comparable to human-human differences (RMSD: 0.77-0.79 cm vs. 0.66-0.82 cm respectively). The uncorrected CMC between algorithm and human estimates was 0.94, which is higher than reported for state-of-the-art optic flow algorithms (i.e. 0.88^[1]-0.90^[2]). In addition, algorithm estimates were produced considerably faster (107 images·min⁻¹, i5 processor) than human estimates (~1-2 images·min⁻¹). The algorithm may be used for objectively estimating muscle length changes.

Superficial aponeurosis

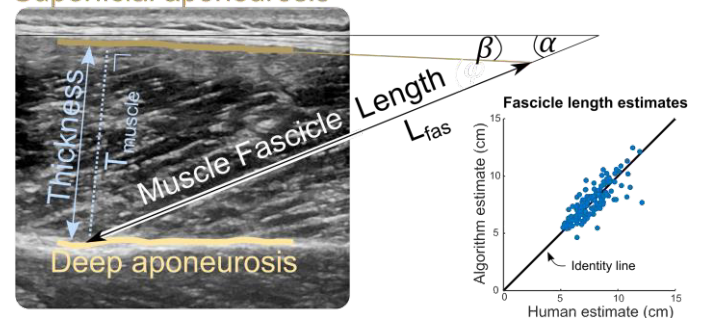


Figure 1. Ultrasound image from vastus lateralis with identified aponeuroses and estimated fascicle angle. Trigonometric extrapolation then estimates fascicle length. Inset at right: algorithm fascicle length estimate versus mean of human observer (n=3) estimate.

Conclusions

A freely available algorithm estimates muscle fascicle length from ultrasound images, with minimal manual intervention and no drift sensitivity, yielding accuracy comparable to state-of-the-art.

References

- [1] Farris DJ and Lichtwark GA (2016). *Comput. Methods Programs Biomed.*, **128**: 111-118.
- [2] Drazan JF et al. (2019). *PeerJ.*, **7**: e7120.
- [3] github.com/timvanderzee/ultrasound-automated-algorithm
- [4] [biorxiv.org/content/10.1101/2020.08.23.263574v1](https://doi.org/10.1101/2020.08.23.263574v1)
- [5] Duda RO and Hart PE (1971). *Comm. ACM*, **15**: 11-15.

Patient and implant performance between satisfied and dissatisfied total knee replacement patients

Jordan S. Broberg^{1,3}, D.D.R. Naudie^{1,2,4}, B.A. Lanting⁴, J.L. Howard⁴, E.M. Vasarhelyi⁴, and M.G. Teeter¹⁻⁴

¹Department of Medical Biophysics, Schulich School of Medicine & Dentistry, Western University, London, Canada

²Robarts Research Institute, London Canada; ³Lawson Health Research Institute, London, Canada

⁴Department of Surgery, Schulich School of Medicine & Dentistry, Western University, London, Canada

Email: jbroberg@uwo.ca

Summary

This study compares groups of satisfied and dissatisfied total knee replacement (TKR) patients to determine if there are any objective differences in implant migration, kinematics, and patient function between groups. No major objective differences existed between satisfied and dissatisfied TKR patients, however patients dissatisfied with their function reported higher levels of pain and more unmet expectations.

Introduction

TKR often successfully reduces pain and returns function to the affected joint, however one fifth of patients are still dissatisfied following their operation. It is unclear why many patients feel this way, but there are thought to be multiple contributing factors. Wearable sensors and radiostereometric analysis (RSA), a stereo x-ray technique used for obtaining implant migration and joint kinematics, are two modalities available that could uncover potential factors in patient dissatisfaction. The goal was to compare the implant migration, joint kinematics, and objective measurements of patient function between satisfied patients and dissatisfied patients to determine if any have a role in post-operative patient dissatisfaction following TKR.

Methods

Patients answered the Knee Society Score (KSS) and were split into "Satisfied" and "Dissatisfied" groups based on their response to three questions on functional satisfaction. RSA was used to measure implant migration at multiple time points up to 1-year post-operatively. At 1-year post-operatively, an additional series of RSA images were acquired at different knee flexion angles to investigate joint kinematics, including medial and lateral anteroposterior (AP) tibiofemoral contact and AP translation during early (0-40°), mid (40-80°), and deep (80-max) flexion, given as a percentage of the tibial baseplate (0% being most posterior, 100% being most anterior). A Timed-Up-and-Go (TUG) test was performed with wearable sensors pre-operatively and at 1-year post-operatively to obtain objective measures of function, including total test time and mean flexion range of their operative limb during the test. Patients also completed questionnaires including the Short Form 12 (SF-12), the Western and McMaster Universities Osteoarthritis Index (WOMAC), and the University of California, Los Angeles (UCLA) Activity Score, and the KSS.

Results and Discussion

There were 31 patients in the Satisfied group and 18 in the Dissatisfied group. The Satisfied group had more tibial

migration at 6-weeks (mean difference (MD)=0.13 mm, $p=0.002$), but not at 3-months ($p=0.07$), 6-months ($p=0.83$), and 1-year ($p=0.17$). AP contact position throughout flexion can be seen in Figure 1. No differences were found between groups in medial AP translations in early flexion ($p=0.29$), mid flexion ($p=0.22$), or deep flexion ($p=0.48$). Laterally, there were no differences in AP translation in early flexion ($p=0.24$) and deep flexion ($p=0.51$), but the dissatisfied group had more posterior translation in mid flexion (MD=2.7%, $p=0.04$). No differences were found between groups in total TUG test time pre- ($p=0.88$) and one-year post-operatively ($p=0.80$), or mean flexion range pre- ($p=0.79$) and one-year post-operatively ($p=0.76$). From the questionnaires, the Dissatisfied group reported worse WOMAC Pain (MD=11.8, $p=0.01$) and Function (MD=19.4, $p=0.0003$) Scores, UCLA Activity Scores (MD=1.12, $p=0.04$), and KSS Functional Expectations Scores (MD=2.62, $p<0.0001$).

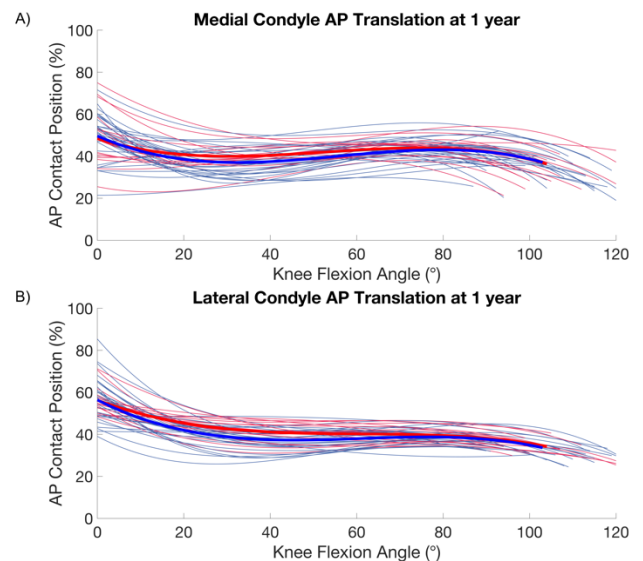


Figure 1: AP contact position on the A) medial and B) lateral condyles throughout flexion. Blue lines indicate satisfied patients and red lines indicate dissatisfied patients. Thicker coloured lines represent the means of the groups.

Conclusions

No major differences existed between satisfied and dissatisfied TKR patients when considering implant migration, joint kinematics, and objective measurements of patient function. However, patients dissatisfied with their function reported higher levels of pain and more unmet expectations, suggesting that to improve the functional satisfaction rate of TKA, focus should be on managing residual pain and setting realistic expectations.

Investigation of the Biofidelity of the MIL-Lx Foot

Julia de Lange¹, Cheryl E. Quenneville^{1,2}

¹School of Biomedical Engineering, McMaster University, Hamilton, Canada

²Department of Mechanical Engineering, McMaster University, Hamilton, Canada

Email: quennev@mcmaster.ca

Summary

Injury risk to the lower leg as a result of car crashes is evaluated in the tibia using Anthropomorphic Test Devices (ATDs). The axial impact response of three lower leg representations, cadaveric ‘intact’ specimens, the ‘MIL-Lx’ ATD and an ‘adapted’ legform (combining cadaveric feet with the MIL-Lx tibia) were assessed. They were fitted with an instrumented boot and impacted at sub-failure energies. Results suggest that the MIL-Lx foot is stiffer and dissipates less energy than cadaveric feet. This study provided regional loading data for the isolated cadaveric foot, for improved future ATD foot designs.

Introduction

Foot and ankle injuries from car crashes continue to increase in severity and incidence [1]. Injury risk to this region is grouped and evaluated using load cells in the tibia of Anthropomorphic Test Devices (ATDs). Although the impact response of the ATD tibia has been investigated to improve biofidelity (leading to the development of the MIL-Lx), the foot has historically been ignored. As load is transmitted through the foot/ankle to the tibia, injury assessments are directly affected by the biofidelity of the foot. Furthermore, while ATDs are valuable tools with load cells to collect forces and act in a repeatable manner, they do not undergo injuries. In contrast, cadaveric testing is advantageous as it allows for the identification of fracture limits, locations and mechanisms. The objective of this study was to develop a technique to mount cadaveric feet to an ATD tibia, to isolate the foot and investigate the potential differences in load transmission.

Methods

Six cadaveric lower legs (‘intact,’ 80 ± 12 years, 3 male) were supported in a pneumatic impacting apparatus and fitted with an instrumented boot. The boot insole has an array of eight piezoresistive sensors, divided into fore-, mid-, and hindfoot regions. They were axially impacted at 5 m/s (sub-failure energies), and force distribution and net force on the boot insole were recorded for each impact.

The Military Lower Extremity (‘MIL-Lx’, Humanetics Innovative Solutions) was similarly impacted, with boot measures as well as tibia load cell forces and moments recorded. The cadaveric specimens were then disarticulated at the ankle joint, preserving surrounding soft tissue. The distal tibia and fibula were optically scanned to 3D print a mating surface for the talus (minimizing unnatural stress concentrations). The 3D printed component was mounted to the MIL-Lx and included attachment points to suture tendon and ligament bundles. Each cadaveric foot was mounted to the

adapted structure (‘adapted’) and tested at similar impact conditions, with boot measures and tibia load cell measurements recorded.

Results and Discussion

No significant differences in net boot forces were found among lower leg representations, suggesting that overall reaction force at the plantar surface was comparable ($p=0.5$). No statistical differences were found among lower leg representations for the forefoot force ($p=0.7$) or hindfoot force ($p=0.2$) regions, however the intact specimen midfoot readings were significantly higher than the ‘adapted’ and the MIL-Lx midfoot readings ($p<0.05$, Figure 1). Furthermore, the proximal and distal tibia load cells recorded significantly higher forces in the MIL-Lx than the ‘adapted’ leg, ($p<0.05$), suggesting the MIL-Lx foot is stiffer and dissipates less energy than cadaveric feet.

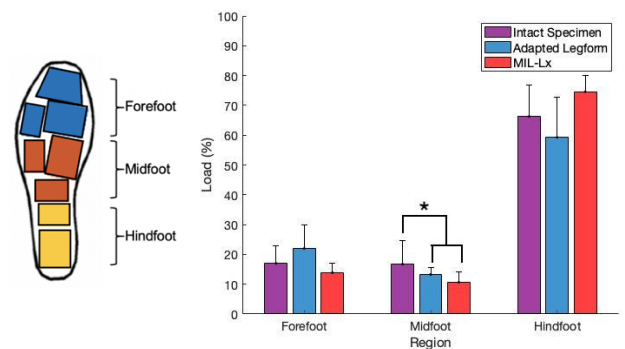


Figure 1: Regional loading comparisons of lower leg representations (* = $p<0.05$).

Forces measured on the plantar surface of the foot were over 35% higher than forces measured in the tibia, which is unsurprising when considering the direction of loading. By focusing on isolated cadaveric feet, while also collecting tibia load data, this study assessed the impact characteristics of feet specifically.

Conclusions

This study developed a technique that combines collecting the realistic loading response of cadaveric feet with industry relevant ATD metrics and used it to impact three lower leg forms. Results suggest the MIL-Lx foot may be an overly stiff representation of cadaveric feet, so these data may be used for an improved ATD foot design.

References

- [1] Richter, M. *et al.* (2001). *J. Orthop. Trauma*, **15**: 287-293.

Occupant Kinematic Prediction Model During Rear End Collisions

Kyle Van Housen¹, Sean D. Shimada, PhD¹

¹Biomechanical Consultants of California

Summary

The goal of this paper was to determine continuous equations representative of time-dependent acceleration and velocity profiles for an occupant's head during rear-end collisions. These curves were designed to be generated based on the change in velocity of the vehicle. These results can be used for injury prediction and calculations of HIC.

Introduction

Rear end collisions are the most common form of motor vehicle collision. The National Highway and Traffic Safety Administration (NHTSA) reported there were over 2 million rear-end collisions in the United States in 2019 [1]. Thirty-one percent of the occupants sustained injuries, while seven percent were fatal [1]. Creating a model to accurately recreate occupant head kinematics during a motor vehicle accident would assist in determining injury thresholds and improving upon injury analyses. Ultimately, the outcome of the model can be used to improve occupant safety during motor vehicle crashes.

Methods

Atarod et al. [2] mounted accelerometers to the heads of ATD's and performed rear-end impacts at vehicle speeds ranging from 22.2 to 31.9 kph. Head acceleration traces from these crashes were imported into MATLAB, and a rational equation (Eq. 1) was fit to the waveform (Figure 1). Of the possible fits available in MATLAB, the polynomial fit was significantly better than other tested models. Through manipulations for individual parameters, it was found that the q3 coefficient had the most significant effect on peak value of the curve without drastically affecting other aspects of the curve's shape. By holding all other coefficients constant, we solved for q3 in terms of peak value which was used to scale the model to the appropriate head acceleration. The peak head acceleration point for different ΔV values were plotted from multiple sources [2], [3] and a linear regression was fit (R² = 0.9). Combining the regression between ΔV and peak head acceleration, and adjusting q3 based on this peak value allows the polynomial equation to adjust and give a continuous model for head acceleration. Integration of this model generates a graph for head velocity.

$$\frac{p1x^3 + p2x^2 + p3x + p4}{(x^2 + q1x^2 + q2x + q3)}$$

Equation 1. Fitted rational equation for head acceleration.

HIC was subsequently calculated based on the generated head acceleration curves using a standard 36 millisecond time interval with the peak value at its center.

Results and Discussion

Figure 1 shows the modeled head acceleration curve for a vehicle crash speed at 31.9 kph (peak acceleration of 38.5 g; HIC 62.7). To extend the range of speeds that this model can predict, more accelerometer data as acquired from Pasquesi et

al. [3] who tested rear-end crashes from 5.6 – 19.5 kph. Comparing the peak head accelerations from both sources [2],[3] to the values calculated from the model shows a correlation of 0.92. When overlaying the accelerometer data and the mathematically calculated acceleration, they overlap continuously in the general area where peak forces occur. During the interval after the peak head acceleration (t = 0.2-0.45) all the accelerometers record a dip below the x-axis. The model was unable to re-create this phenomenon while maintaining accuracy for the rest of the curve.

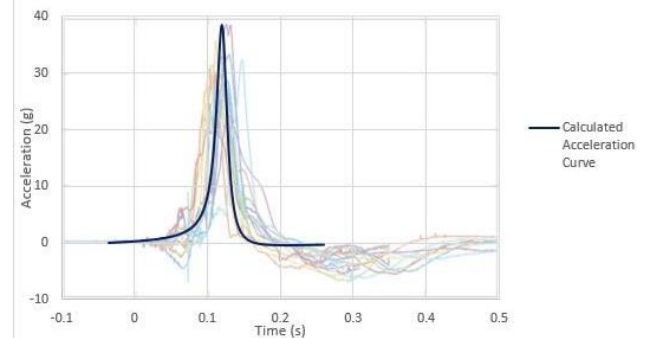


Figure 1. Modeled head acceleration for 45.5 kph crash overlaid on data from [1].

Conclusions

The resulting biomechanical model accurately recreated the peak value and general waveform of occupant head acceleration during a rear-end collision. However, this model was only validated for changes in velocities of 5.6 - 31.9 kph. The use of a continuous equation allows for subsequent mathematical operations to be performed. Although the generated curves do not recreate an early dip observed experimentally, forces acting during this time are unlikely to cause head injury. More work is needed to test this model in for a wider the range of velocities. The generated HIC values also need to be further validated.

References

- [1] "National Highway Traffic Safety Administration."
- [2] Atarod, M., "Occupant Dynamics during Moderate-to-High Speed Rear-End Collisions," SAE Technical Paper.2020-01-0516,2020, doi:10.4271/2020-01-0516. NHTSA, www.nhtsa.gov
- [2] Pasquesi, S.A., Bruno, A., Courtney, A., Imler, S.M. et al., "Risk of Concussion in Low- to Moderate-Speed Frontal and Rear-End Motor Vehicle Collisions Evaluated Using Head Acceleration-Based Metrics," SAE Technical Paper 2019-01-1218, 2019.

Most Severely Injured Body Regions in Near Side Motor Vehicle Collisions Involving Head Impact

Rachel L. Tanczos¹, Sean D. Shimada¹
¹Biomechanical Consultants, Davis, CA
 Email: rltanczos@ucdavis.edu

Summary

The National Automotive Sample System Crashworthiness Data System's (NASS-CDS), a publicly available database, was used to determine the most severely injured body regions of nearsided occupants during lateral motor vehicle collisions. The investigation was restricted to brain injured and non-brain injured occupants with evidence of a direct head impact. Brain injured occupants were more likely to have severe injuries to their torso, while non-brain injured occupants had higher frequency of severe spinal and extremity injuries.

Introduction

Motor vehicle accidents are one of the most prevalent causes of traumatic brain injury. Data from studies comparing frontal and lateral motor vehicle collisions supports an increased risk and severity of brain injuries in lateral collisions [1,2]. This investigation aimed to identify differences in the most severely injured body regions of brain and non-brain injured occupants who sustained head impacts in nearside collisions. The results may be used to identify potential differences in crash conditions and occupant kinematics in order to improve vehicle safety from lateral impacts.

Methods

MATLAB® was used to compile and filter datasets from NASS-CDS's publicly available database for the years 2001 to 2015. Concussive and internal organ injuries of the head were identified based on the Abbreviated Injury Scale (AIS) classification system. Injuries due to head impact were selected for using the database's direct contact variable (DIRINJ = 1). Occupants that were involved in a rollover, not between 16 and 60 years of age, or in a vehicle other than a passenger car were excluded. In addition to meeting all other filtering criteria, the group considered to be non-brain injured were required to have some other type of direct contact injury to their head.

The database variable "BODYREG" was used to identify the body region where occupants sustained their most severe injury. A normalized frequency of occurrence was then calculated. Multiple entries were recorded for occupants' injuries of the same AIS severity across multiple body regions. Database years that used AIS 1990/1998 Update (AIS98) vs. AIS 2005 Update 2008 (AIS08) were analyzed separately and displayed as side-by-side histograms representing brain and non-brain injured occupants.

Results and Discussion

229 brain injured and 228 non-brain injured occupants met the filtering criteria. The head/skull region was the most common and severely injured body region for all occupants (Figure 1). For both the AIS98 and AIS08 analyses, compared to their respective non-brain injured occupants, brain injured occupants had higher normalized frequencies for the abdomen, chest, and head/skull. The non-brain injured occupants had higher normalized frequencies for the cervical spine, lower extremity, shoulder, thoracic lumbar spine, and upper extremity. These results suggest brain injured occupants are more likely to be involved in more severe collisions that also cause their torso to contact the interior of the vehicle. Non-brain injured occupants may more frequently use their extremities to brace for impact. The face and hip regions had contrasting trends between AIS98 and AIS08 data.

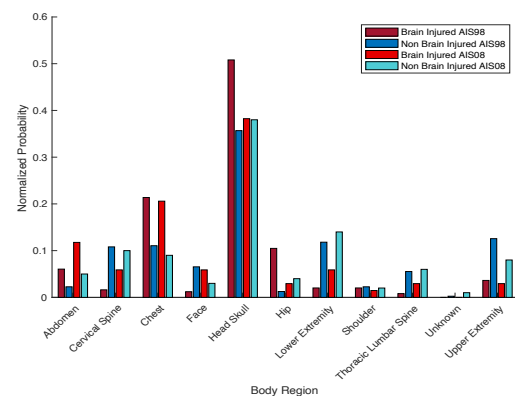


Figure 1: Distribution of most severely injured body regions in nearside collisions involving direct head contact.

Conclusions

When direct head contact occurs, nearsided occupants were most likely to sustain their most severe injury to their head or skull. Brain injured occupants were more likely to have severe injuries to their torso, while non-brain injured occupants had higher frequency of severe spinal and extremity injuries. To further update the analysis and resolve trend discrepancies for the face and hip, future work will convert AIS98 codes to AIS08 codes for a combined dataset. Comparing the severity scores of the most severe occupant injuries would add another layer of analysis.

References

- [1] Bazarian JJ et al. (2004). *Ann. Emerg. Med.*, **44**: 142-152.
- [2] Compagnone C et al. (2008) *IRCOBI Conference*: 115-121.

High Risk Glenohumeral Joint Forces During Three Pull-Up Techniques

Caryn A. Urbanczyk¹, Joseph A.I. Prinold¹, Peter Reilly², Anthony M.J. Bull¹

¹Musculoskeletal Mechanics Lab, Dept. Bioengineering, Imperial College London, London, UK

²Imperial NHS Trust, Imperial College London, London, UK

Email: c.urbanczyk17@imperial.ac.uk

Summary

Descriptive laboratory study of loading patterns during performance of three different pull-up variants using optical motion capture and computational modelling. Glenohumeral (GH) joint stress and stability patterns vary across techniques, but all achieve torso elevation as a primary objective and arm depression as a secondary event. Relative upper limb and torso positioning is clinically relevant in upper extremity injury rehabilitation. Alleviating dysfunction and increasing strength relies on managing stress.

Introduction

There are strong links between overhead activities and shoulder pathology. Common injuries among athletes regularly performing such activities include impingement, tendonitis, and rotator cuff tears [1]. Heavily loaded training tasks, such as pull-ups are an effective strength training and rehabilitation exercise that require high muscle force maintained over a large range of motion [2]. However, care should be taken in progressing pull-ups to the loading rates in functional demands. This study used computational modelling to examine loading patterns during pull-ups and highlight risks to vulnerable musculoskeletal structures.

Methods

Optical motion tracking (200Hz) and a force platform (1000Hz) under a free-standing pull-up apparatus, captured kinematics and kinetics of 11 male subjects without history of shoulder pathology, during 5 trials each of 3 different pull-up types: pronated front grip, pronated wide grip, and supinated reverse grip. Recorded data provided input to the UK National Shoulder model (UKNSM) [3]. GH joint forces and glenoid contact patterns were analyzed by repeated measures ANOVA with Tukey HSD ($\alpha < 0.05$). Further results from these study methods are described in [4].

Results and Discussion

GH joint reaction forces were similar in front and wide pull-ups ($p = 0.11$), but the reverse pull-up was significantly larger (Figure 1; $p < 0.025$). Peak GH joint force was 3.1 times body weight (xBW) in the front pull-up, 2.6 xBW in the wide pull-up, and 8.8 xBW in the reverse pull-up.

All glenoid contact patterns start in the posterior / inferior quadrant at the bottom of the pull-up motion and move diagonally into the anterior / superior quadrant at the top of the pull-up motion. Contact patterns near the glenoid rim indicate decreased relative shoulder stability. Wide pull-ups show highest percent of frames within 0.5mm of the glenoid rim ($16.1 \pm 11.4\%$) at the start of the pull-up (Figure 2c). Front pull-ups show fewer frames near the glenoid rim ($10.8 \pm 9.6\%$) but indicate instability at bottom and top of pull-up motion (Figure 2a). Reverse pull-ups display the most centralized

force locus, with substantially fewer frames near the glenoid rim ($4.4 \pm 8.1\%$; Figure 2b). Differences between mean glenoid contact patterns are reflected in the Fréchet distance, where distance from wide to front and reverse patterns was $27.01 \pm 7.5\text{mm}$ and $35.5 \pm 6.3\text{mm}$, respectively, while Fréchet distance between front and reverse was $22.8 \pm 11.1\text{mm}$.

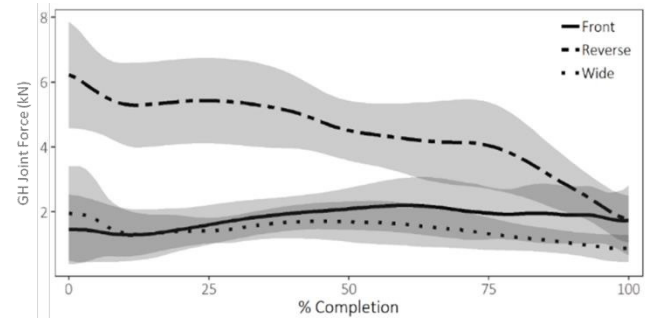


Figure 1: Resultant GH joint force in each pull up type (mean \pm sd)

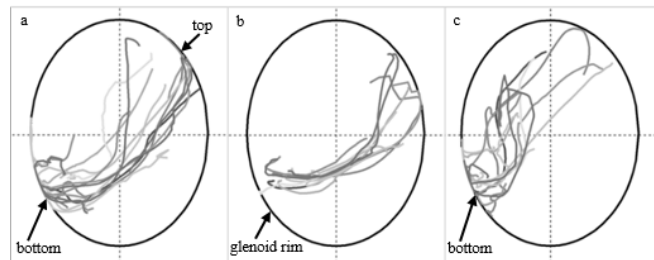


Figure 2: Glenoid contact patterns for each subject in the a) front, b) reverse, & c) wide pull-ups, arrows indicate pattern locations near the glenoid rim at start (bottom) and end (top) of pull-up motion.

Conclusions

Pull-ups promote shoulder strength by leveraging extreme scapulohumeral positioning. All variants prioritize teres major and latissimus dorsi to depress the arm, but each also uses other muscles. Wide pull-ups show humeral head translation near the glenoid rim indicating instability. The predominately posterior pattern implies activation of middle deltoid, while the centralized pattern in the reverse pull-up suggests rotator cuff activity to stabilize the GH joint; a necessity when supporting much higher joint forces. Shoulder rehabilitation and strength & conditioning programs should incorporate all three pull-up variants with systematic progression to provide global strengthening of torso and upper limb musculature.

References

- [1] Kibler W. (1998) Am J Sports Med. 26(2): 325-337.
- [2] Prinold J. & Bull AMJ. (2016) J Sci Med Sport. 19(8): 629-635.
- [3] Charlton I. & Johnson G. (2006) Proc Inst Mech Eng H 220(8): 801-812
- [4] Urbanczyk C. et al., (2020) Scand. J. Med. Sci. Sports. 30(11): 2205-2214

Classification of ACL Reconstructed Running Dynamics Using Common Gait Features

Yannis K. Halkiadakis¹, Helia Mahzoun Alzakerin¹, Kristin D. Morgan¹

¹Department of Biomedical Engineering, University of Connecticut, Storrs, CT 06269 USA

Email: yannis.halkiadakis@uconn.edu

Summary

The objective of this study was to employ machine learning to classify between healthy and pathological gait. Common gait features such as stride time, peak knee angle, and loading rate, extracted during running, were determined to successfully differentiate between healthy controls and post anterior cruciate ligament reconstruction individuals with an accuracy of 92%. The resulting model has the potential to be utilized in the clinic to evaluate successful rehabilitation.

Introduction

Post anterior cruciate ligament reconstruction (ACLR) patients continue to show altered running gait years after surgery [1-3]. This altered gait is associated with the development of knee osteoarthritis, thus restoring normal gait would be a step forward in limiting the onset of this disease [1]. Machine learning can be a valuable tool in this field because it aids in the identification of gait parameters that can be used as measures of successful rehabilitation. This type of machine learning model can be used to assess running performance to determine if the post-ACLR individuals' gait has normalized. Differences in spatiotemporal parameters, sagittal plane kinematics, and limb loading between healthy and post-ACLR individuals are all clinically meaningful measures to evaluate healthy biomechanics. Therefore, we hypothesized that these common gait parameters can be used to create a strong machine learning model that can classify between healthy controls and post-ACLR participants.

Methods

Fifteen post-ACLR participants (age: 18.7 ± 4.4 yrs; height: 1.7 ± 0.1 m; mass: 68.1 ± 10.5 kg; running speed: 2.7 ± 0.3 m/s) and 15 healthy controls (age: 18.5 ± 3.7 years; height: 1.7 ± 0.1 m; mass: 66.7 ± 11.3 kg; running speed: 2.7 ± 0.4 m/s) ran on an instrumented treadmill collecting at 1200 Hz (Bertec Corporation, Columbus, Ohio). Participants were fit with fifty-six markers and a 10-camera motion capture system (Motion analysis Corporation, Santa Rosa, CA) collected marker data at 200 Hz. Marker placement followed the protocol described by Noehren et al. (2013) [3].

After a five-minute warmup, participants ran at a self-selected speed for one minute. Stride times, swing times, and average loading rate were extracted from the vertical ground reaction force (vGRF) data. Loading rate was normalized by body weight (BW). The marker trajectory data was used to calculate the sagittal plane knee angle. The knee angle upon impact and peak angle during swing were recorded. T-tests were performed to compare the gait parameters between the two groups ($\alpha=0.05$). A 60%-40% training-testing split was used to develop, train, and test the model. Multiple algorithms including the support vector machine (SVM) model were tested using the training data. Model performance was based

on the assessment of the receiver operating curve (ROC) using test data.

Results and Discussion

The stride time, swing time, and sagittal plane peak knee angle during swing phase were significantly lower in the post-ACLR individuals than the controls, while the average loading rate and the knee angle at impact were significantly greater (Table 1).

Table 1. Comparison of the mean gait parameters of interest for the healthy controls and post-ACLR individuals.

Gait Parameters	ACLR Group	Control Group	P-value
Stride Time (s)	0.35 ± 0.02	0.39 ± 0.05	0.02*
Swing Time (s)	0.07 ± 0.02	0.09 ± 0.03	0.05
Peak Knee Angle Swing (°)	95.6 ± 8.2	103.3 ± 11.2	0.04*
Knee Angle at Contact	21.6 ± 4.8	16.0 ± 5.0	<0.01*
Loading Rate (BW/s)	12.1 ± 5.5	6.1 ± 3.4	<0.01*

*Indicates the means are significant different ($\alpha=0.05$)

The SVM model outperformed other models in every category, showing an accuracy of 92%, recall of 86%, precision of 100%, and area under the ROC curve of 0.93. The results supported the hypothesis as common gait parameters were able to classify between healthy controls and post-ACLR individuals. Looking at the parameters, loading rate was significantly higher in the post-ACLR participants with no significant difference in impact peak, indicating an altered limb loading strategy. The post-ACLR group also landed with greater knee angle at contact, possibly to help redistribute the load at the knee. Lastly, the post-ACLR group exhibited decreased stride and swing times, even though running speed was not significantly different between groups suggesting that a greater percentage of the running gait cycle was spent in stance, helping to maintain balance.

Conclusions

This study demonstrated that common gait parameters are strong enough metrics to effectively delineate between altered running strategies in healthy controls and post-ACLR individuals. The model can be integrated in a clinical setting to assess rehabilitation performance. Future models could introduce measures of asymmetry between the reconstructed and non-reconstructed limbs to improve model performance.

Acknowledgments

We would like to thank Dr. Brian Noehren for providing the data for this study.

References

- [1] Butler et al. (2009) *Br. J. Sports Med.*, **43**: 366-370.
- [2] Mahzoun Alzakerin et al. (2020) *IEEE EMBC Conf.*, **42**: 4811-4814.
- [3] Noehren et al. (2013). *Med Sci Sports Exerc*, **45**: 1340-1347.

Use of Pressure-Measuring Insoles to Characterize Center of Pressure Length and Width under Simulated Reduced Gravity Conditions

C. Ison¹, C. Neilsen², J. DeBerardinis², M. Trabia², J.S. Dufek¹

¹Department of Kinesiology and Nutrition Sciences, University of Nevada Las Vegas, Las Vegas, NV, USA

²Department of Mechanical Engineering, University of Nevada Las Vegas, Las Vegas, NV, USA

Email: christian.ison@unlv.edu

Summary

Exercise under reduced gravity conditions is used by clinicians for individual recovering from lower extremity injuries. The effect of reduced gravity exercise on kinetics and kinematics of lower extremities and plantar pressure have been observed. However, the relationship between variations in the center of pressure (COP) under reduced gravity conditions is not well understood. We used pressure-measuring insoles to better understand this problem.

Introduction

Rehabilitation of persons experiencing a lower extremity injury requires careful assessment and monitoring. Full body weight bearing activities may potentially exacerbate pain and disrupt recovery due to the magnitude of forces applied to the injured tissues and joints [1]. Therefore, limited weight bearing activities are often implemented, which requires full understanding of gait and how loads are transmitted. Researchers have suggested that COP path length and width may determine preventative fall risk strategies, especially among the geriatric population [2]. We explored the changes of COP under different gravity conditions to understand this supposition and consider its potential clinical application.

Methods

Plantar pressure was measured using pressure measuring insoles (Medilogic GmbH, Schonefeld, GE). Gravity conditions were simulated on a treadmill (AlterG, Inc., USA). Twenty-nine healthy, (27 males, 2 females; age 24.7 ± 4.04 ; mass = 72.36 ± 13.52 kg; height = 1.67 ± 0.04 m) volunteers participated in this cross-sectional experiment. After providing informed consent (IRB#1510671-2), participants completed two 3.5-minute walking trials on the treadmill at 100% (normal gravity) bodyweight (BW), 40% and 20% (reduced gravity) BW. The plantar pressure insole data were recorded under each of these gravity conditions and sensors' location and coordinates were identified following the specifications of the insole manufacturer. The sensor data were processed as previously described [3]. Processed data were used to generate the COP coordinates. More details can be found in [4]. Each COP length and width were normalized with respect to the length and width of the insole the participant wore during the experiment. Two one-way repeated measures ANOVAs ($\alpha=0.05$) were used to test COP length and width differences across gravity conditions.

Results and Discussion

Table 1 shows the mean normalized COP length and width over the three gravitational conditions. A repeated measures

ANOVA with a Greenhouse-Geisser correction determined that average COP path length differed significantly ($p<0.05$) among gravity conditions (Table 1). Post hoc tests using the Bonferroni correction revealed that the 100% BW condition was significantly greater than the 40% and 20% BW conditions. However, there were no significant differences observed between 40% and 20% BW conditions ($p=0.259$). A repeated measures ANOVA with a Greenhouse-Geisser correction determined that average COP path width differed significantly among gravity conditions ($p<0.05$; Table 1). Post hoc tests using the Bonferroni correction revealed that the 100% BW condition was significantly different than the 40% and 20% BW conditions. There were no significant differences observed between 40% BW condition and the 20% BW condition ($p=0.134$). While COP length decreased with unweighting, COP width increased. This latter observation may be useful to increase stability and decrease fall susceptibility for those recovering from injury.

Table 1. Normalized center of pressure length and width in mm (mean \pm standard deviation) for each gravity condition.

	100% BW	40% BW	20% BW
COP Length	0.63 \pm 0.06	0.45 \pm 0.19	0.39 \pm 0.17
COP Width	0.11 \pm 0.02	0.15 \pm 0.03	0.17 \pm 0.22

Conclusions

We found that a walking task at three gravitational conditions in healthy individuals is mainly characterized by a decrease in COP path length and increase in COP width as gravity is reduced (Table 1). Reduced gravity minimizes heel contact and requires more effort for lateral stabilization. The findings from this study may prove beneficial for clinicians as they develop rehabilitation strategies to effectively unload the individual's body weight to perform safe exercises. Future studies are needed to further corroborate the findings from this study.

References

- [1] T. Kawae, et al. (2017). *J. Phys. Ther. Sci.*, vol. 29, no. 8, pp. 1444–1448, doi: 10.1589/jpts.29.1444.
- [2] H. Qiu and S. Xiong (2015). *Int. J. Ind. Ergon.*, vol. 47, pp. 37–44, 2015, doi: 10.1016/j.ergon.2015.02.004.
- [3] D. E. Lidstone, J. DeBerardinis, J. S. Dufek, and M. B. Trabia (2019). *Foot*, vol. 39, pp. 1–10, doi: 10.1016/j.foot.2019.01.009.
- [4] J. DeBerardinis, C. Neilsen, DE Lidstone, J.S. Dufek and M.B.Trabia (2020). *J. Rehabil Assistive Technol Engineer*, vol 7, pp. 1-12, doi: 10.117

In vitro mechanical effects of a specific neurodynamic mobilization of the superficial fibular nerve: a preliminary study

Lavoie F-A^{1,2}, St-Pierre M-O^{1,2}, Paquin J-P³, Gilbert K.K.⁴, Ellis Richard⁵, Sobczak Stéphane^{1,2}

¹Research Chair in Functional Anatomy, Université du Québec à Trois-Rivières (UQTR), Trois-Rivières, Canada. ²Dept. Human Anatomy, UQTR, Trois-Rivières, Canada. ³Dept. of health sciences, Université du Québec à Chicoutimi. ⁴Texas Tech University Health Sciences Center, Lubbock, TX, USA. ⁵Dept. of physical therapy, Auckland Institute of Technology, Auckland, New Zealand.

Email: felix-antoine.lavoie@uqtr.ca

Summary

Neurodynamic mobilizations (NM) in rehabilitation are commonly used in the treatment of peripheral nerve neuropathies. NM can be used to exploit biomechanical principles to induce displacement and strain on nerve tissue to influence neuropathic pain. To date, there is no evidence about the effectiveness of NM technique sequence for the treatment of neuropathies of the superficial fibular nerve (SFN). We used displacement transducers to measure linear displacement to calculate strain of the SFN while applying a specific NM of the SFN, applied in different hip positions, in unembalmed cadavers in order to evaluate its biomechanical influence. Results showed that adjacent joint (ankle) motions are the most important in order to produce linear strain in the SFN.

Introduction

The incidence of SFN entrapment neuropathy is about 3,5% in people presenting with chronic lower limb pain [1]. Although surgery has a success rate of about 80% [2], surgery presents risks and may not be readily available. Conservative management can include physical rehabilitation and manual therapy. Among manual therapy modalities, NM can have a prevalent role in the assessment of entrapment neuropathies. These techniques are based on biomechanical principles in order to assess mechanosensitivity in patients by inducing linear strain to a specific nerve [3, 4]. For the moment, no data supports the ability of the technique proposed in the literature for inducing SFN strains.

Objective 1: To evaluate strain on the SFN using a sequence described in reference literature. **Objective 2:** To determine if a difference in strain exists at different Straight Leg Raise (SLR) position during a complete sequence.

Methods

The SFN from three lower limbs of two unembalmed cadavers were exposed at the exit from the crural fascia on the lower 1/3 of the antero-lateral leg. A displacement sensor was inserted into the SFN 2cm distally from the emergence point to measure linear displacement during the application of the specific NM. Strain (ϵ) was measured using displacement data using standard linear strain equation: $\epsilon = \Delta L/L_0$. The specific sequence of movement applied at four different SLR positions (0°/30°/60°/90°) was: Maximal ankle plantar flexion (PF) followed by maximal ankle inversion (INV), SLR and 35° of hip ADD. Each position was maintained two seconds to obtain stable data. Normalization of strain was performed after INV at 100% in order to eliminate inter-subject variability and obtain SLR data. Optitrack motion capture system was used to control range of motion during the experiment.

Results and Discussion

The preliminary results demonstrated that the specific NM sequence tends to produce strain at all hip positions described previously (Figure 1). Hip SLR and ADD seem to have a lesser influence on total strain when compared to ankle PF and

INV who are the main contributors of strain. PF is constantly the most contributing movement to the overall strain during NM followed by INV. Although producing a positive amount of strain, ADD seems to be the least contributing motion of all the NM sequence (Table1). SLR position has an influence on total strain (Fig. 1) with 90° producing the most at 14,3% when normalizing data after max FP+INV.

Table 1. Relative contribution % of motions on total strain (SD) at different SLR positions.

Motion	SLR position			
	0°	30°	60°	90°
PF	78.3 (10,5)	88.9 (7.10)	76.9 (14.8)	77.7 (16.6)
INV	18.6 (11.0)	8.1 (7.0)	10.8 (6.5)	9.1 (5.6)
SLR	0.0	0.9 (0.5)	8.6 (5.2)	11.3 (11.2)
ADD	3.1 (0,5)	2.1 (2.1)	3.7 (4.6)	1.9 (2.3)

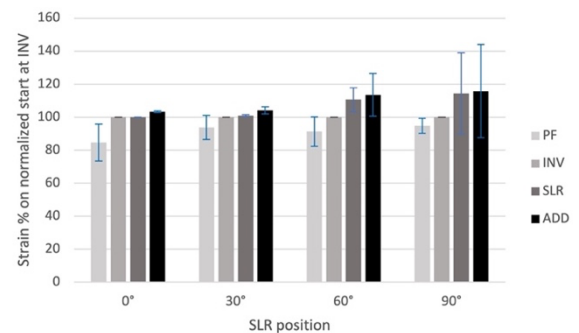


Figure 1. Evolution of normalized strain during mobilization. 100% is considered the normalized start following INV

Conclusions

Ankle motions may be considered the most important in order to evaluate mechanosensitivity. Although the lumbar plexus is known to pass medially to the axis of ABD/ADD, hip ADD is a contributor (weak) to SFN strains during NM and evaluation. This could be explained by an “anchor” at the ischial tuberosity/hamstring tendon acting as a pulley modifying the proximal set point of the sciatic nerve. There seems to be an effect of different SLR position on total linear strain as higher angles of hip flexion seem to produce more strain.

Acknowledgments

The research team would like to recognize the people who donated their bodies to UQTR’s anatomy laboratory to enable biomechanical research and anatomical studies

References

- [1] Styf, J., & Morberg, P. (1997). *TJBS. British volume*, 79-B(5), 801-803.
- [2] Matsumoto, J. et al. *Neurologia medico-chirurgica*, 58(7), 320-325.
- [3] Shacklock, M. (1995). *Neurodynamics. Physiotherapy*, 81(1), 9-16.
- [4] Butler, DS (1991) *Mobilisation of the Nervous System*, Churchill Livingstone.

Drop height and sex differences in anterior cruciate ligament force during unilateral drop landings

Jake A. Melaro¹ & Joshua T. Weinhandl¹

¹Dept. of Kinesiology, Recreation and Sport Studies, University of Tennessee, Knoxville, TN, USA

Email: jmelaro@vols.utk.edu

Summary

Anterior cruciate ligament (ACL) injury rates are thought to be influenced by sex factors and movement intensity (i.e. drop height), though their combinatory effects are unknown. Male and female unilateral drop landing data were collected to model ACL loading. Analysis showed that ACL forces were actually greater in men than women and statistically similar at different drop heights.

Introduction

120,000+ ACL injuries are diagnosed annually, of which 40% are non-contact injuries and 75% of all ACL injuries require surgery [1,2]. These injuries result in substantial losses in terms of playing time, and present a major economic burden. Further, sex differences and drop height have been implicated as non-contact ACL risk factors. Previous works have examined the isolated effects of sex and drop height on ACL loading and lower extremity joint biomechanics [3], yet interaction effects between these factors have yet to be investigated during unilateral drop landing tasks. Therefore, this study sought to elucidate any effects on ACL loading and lower extremity biomechanics due to sex, drop height, or their interaction during unilateral drop landings.

Methods

Forty college-aged, recreationally-active men (n=20, 80.35±11.26 kg, 1.80±0.05 m) and women (n=20, 61.32±8.08 kg, 1.63±0.05 m) completed unilateral landings off of 30- and 50-cm tall boxes while GRF (2000 Hz, Bertec) and 3-D positional (200 Hz, Vicon) data were collected.

These data were exported to Visual3D for lower extremity joint kinematic and kinetic calculations. Peak joint moments and angles, as well as joint angles at initial contact were identified. Joint angle and moment data were then imported into OpenSim (v3.3, <http://simtk.org>) where the static optimization tool was used in conjunction with a modified 3 degrees-of-freedom knee model. The static optimization analysis produced estimated muscle forces needed for knee-spanning muscles subsequently input into a previously established knee model [4] to estimate 3-D ACL forces and stress. Individual 2×2 repeated measures ANOVAs were used to assess drop height (within-subject) and gender (between-subject) differences for ACL loading and lower extremity joint kinematic and kinetic variables. *A priori* significance was set at $p < 0.05$ and Cohen's *d* effect sizes were reported for effect size interpretations.

Results and Discussion

No interaction effects were observed, though unilateral drop landings exposed men to significantly greater peak sagittal ($p=0.001$; $d =0.51$) and resultant ($p=0.005$; $d =0.45$) ACL forces than women.

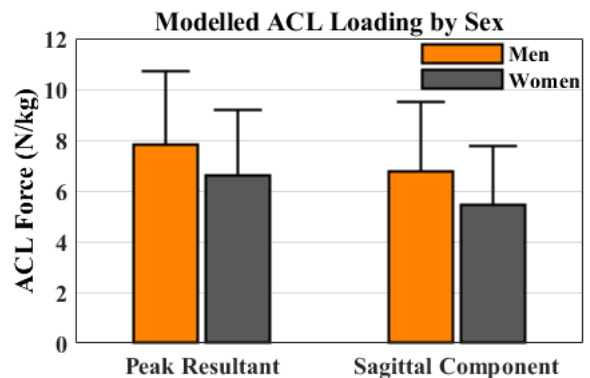


Figure 1: Modeled ACL resultant and sagittal forces.

Men also exhibited greater peak knee internal rotation ($p=0.016$; $d =0.38$) but smaller hip abduction ($p<0.001$; $d =0.67$) moments than women. Interestingly, women landed with greater peak hip internal rotation ($p<0.001$; $d =0.59$), peak knee flexion ($p<0.001$; $d =0.63$) and abduction ($p<0.001$; $d =0.76$), and plantarflexion at initial contact ($p<0.001$; $d =0.59$) compared to men.

The 50-cm drop height conditions produced greater peak hip ($p=0.001$; $d =0.55$), knee ($p<0.001$; $d =1.09$), and ankle ($p<0.001$; $d =0.70$) extension moments than the 30-cm drop height. Peak hip adduction ($p<0.001$; $d =0.80$) and knee flexion ($p=0.002$; $d =0.50$) and external rotation ($p=0.001$; $d =0.50$) angles were observed at the greater drop height. Finally, initial contact hip ($p=0.036$; $d =0.33$) and ankle ($p=0.043$; $d =0.31$) flexion, hip adduction ($p<0.001$; $d =1.25$), and hip ($p=0.025$; $d =0.35$) and knee ($p=0.002$; $d =0.50$) external rotation at increased with drop height.

Conclusions

Lower extremity joint kinematics and kinetics are altered during unilateral landings from different heights between men and women. Surprisingly, the modeled ACL loading was greater in the male, not female, participants when performing unilateral drop landings from different heights. These results are surprising when considering women incur ACL injuries at greater rates than men and the observed joint angles and moments present in the current investigation. Future research should seek to elucidate the mechanism(s) behind altered ACL loading between sexes during unilateral landings.

References

- [1] Gornitzky AL et al. (2016). *Am J Sports Med*, **44**: 2716-23.
- [2] Joseph AM et al. (2013). *J Athl Train*, **48**: 810-17.
- [3] Moktarzadeh H et al. (2017). *J Biomech*, **60**:181-187.
- [4] Weinhandl JT et al. (2016). *Comput Methods Biomech Biomed Engin*, **19**: 1550-56.

Effects of ACL Reconstruction on *In Vivo* Quadriceps Contractile Behavior and Association with Knee Joint Biomechanics

Amanda E. Munsch¹, Alyssa Evans-Pickett², Hope Davis-Wilson^{2,3}, Brian Pietrosimone², Jason R. Franz¹
¹Applied Biomechanics Lab, Joint Dept. of Biomedical Engineering, UNC-CH and NCSU, Chapel Hill, NC, USA
²MOTION Science Institute, Dept. of Exercise and Sport Science, UNC-CH, Chapel Hill, NC, USA
³Physical Medicine and Rehabilitation, University of Colorado Anschutz Medical Campus, Aurora, CO, USA

Email: aemunsch@live.unc.edu

Summary

Our purpose was to quantify the effects of anterior cruciate ligament reconstruction (ACLR) on vastus lateralis (VL) fascicle length change behavior and the association thereof with gait biomechanics. Because active quadriceps muscles resist muscle-tendon unit (MTU) lengthening during weight acceptance, we hypothesized that ACLR limbs with known deficits in quadriceps force generation would exhibit more fascicle lengthening despite less MTU lengthening than contralateral and uninjured control limbs. We also hypothesized that fascicle length change in the ACLR limb would correlate with knee biomechanics during weight acceptance. As hypothesized, only the involved limb in individuals with ACLR exhibited VL lengthening during weight acceptance, which we interpret in the context of strength deficits and changes in series elastic tendon mechanical properties. Conversely, only the contralateral limb demonstrated associations between VL contractile behavior and knee biomechanics, perhaps to compensate after ACLR.

Introduction

Insufficient quadriceps force production and altered knee joint biomechanics after ACLR may contribute to a heightened risk of osteoarthritis. Changes in walking biomechanics frequently manifest in early stance via smaller peak knee extensor moments (pKEM), and reduced knee flexion excursion for the ACLR limb compared to the contralateral and uninjured control limbs [1,2]. Despite widespread recognition that muscle force is governed not only by muscle activation and size but also by contractile state, no study to our knowledge has quantified *in vivo* quadriceps contractile behavior during walking in individuals with ACLR or examined correlations between *in vivo* quadriceps contractile behavior and joint biomechanics. We suspect that the altered gait biomechanics often associated with OA development after ACLR arise in part from an incomplete understanding of quadriceps muscle function in walking and changes thereof following ACLR.

Methods

We quantified bilateral VL contractile behavior (i.e., fascicle length and pennation) via cine B-mode ultrasound imaging [3] and gait biomechanics (i.e., vGRF, pKEM, and KFE) via standard gait analysis in 16 individuals with ACLR (age: 20.1±4.1 years, since ACLR: 7.4±1.2 months) who walked on an instrumented treadmill. We compared outcomes between limbs with paired samples t-tests and to outcomes collected from 11 uninjured control participants (age: 23.8±2.5 years)

with independent samples t-tests. Finally, we identified associations between measures of fascicle length and gait biomechanics using linear regressions.

Results and Discussion

Despite 19% less VL MTU lengthening in the ACLR limb compared to the contralateral limb ($p < 0.01$), the VL fascicle on the ACLR limb lengthened (0.23 ± 2.13 cm) whereas the contralateral limb fascicle shortened (-2.66 ± 3.74 cm, $p < 0.01$) in manner similar to uninjured controls (-1.30 ± 2.32 cm, $p = 0.05$). We may see more lengthening in ACLR limb fascicles due to a combination of insufficient strength, inhibition, and altered patellar tendon mechanics from graft removal. Ultimately, the eccentric action of the VL fascicles, unique to ACLR limbs, suggests that these muscles may succumb to the task demands of MTU lengthening during weight acceptance. VL length and length change behavior correlated with change in MTU length, change in KEM, and pKEM, but only in the contralateral limb ($p \leq 0.04$). These contralateral limb correlations may allude to a greater influence of quadriceps muscle action in governing knee joint biomechanics, which may serve to compensate for ACLR limb deficiencies.

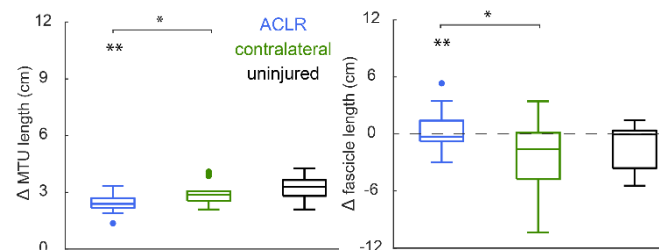


Figure 1. Change in VL MTU length (left) and VL fascicle length (right) between heel-strike and instant of pKEM.

Conclusions

In vivo quadriceps muscle behavior may serve as a marker of recovery or a target for therapeutic intervention relevant to the risk of post-traumatic osteoarthritis in individuals with ACLR.

Acknowledgments

Supported by a grant from NIH (R21AR074094).

References

- [1] Davis-Wilson HC et al. (2020). *MSSE*, **52**: 785-794.
- [2] Roewer BD et al. (2011) *J Biomech*, **44**: 1948-53.
- [3] Munsch AE et al. (2020). *PeerJ*, **8**: e9509.

Optimization vs Unscented Filtering for Measuring Walking Motion using IMUs

Anirudh S. Bhateja¹, Ted Yeung², Thor F. Besier², Benjamin J. Fregly¹

¹Rice Computational Neuromechanics Lab, Department of Mechanical Engineering, Rice University, Houston, TX, USA

²Auckland Bioengineering Institute and Department of Engineering Science, University of Auckland, Auckland, New Zealand

Email: asb13@rice.edu

Summary

This study applied optimization and unscented Kalman filter methods to an 18-DOF lower body model to convert synthetic inertial measurement unit (IMU) data into corresponding joint angles. Tracking errors produced by both methods were compared using overground and treadmill walking data. The optimization method was more accurate and robust, although it required more computation time.

Introduction

IMUs could provide an attractive alternative to video motion capture systems for measuring walking in a non-laboratory setting. The two most common methods for converting IMU data into corresponding joint angle data are optimization and unscented Kalman filtering. While optimization methods are more flexible, unscented filtering methods are generally faster computationally. This study compares these two methods using noisy synthetic IMU data generated from actual video motion capture walking data.

Methods

Experimental video motion capture and IMU data were collected from a single subject who performed overground and treadmill walking trials. For an initial static trial, three reflective markers were placed on each IMU consistent with IMU local coordinate systems. OpenSim model scaling [1,2] was performed to scale a generic 3D OpenSim model [3] and attach dynamic markers and IMUs to the pelvis (6 DOFs) and lower body segments (6 DOFs per leg). Next, OpenSim inverse kinematics was performed to calculate pelvis and lower body joint angles as well as corresponding synthetic IMU measurements. Finally, synthetic noise was added to the synthetic IMU data to emulate actual IMU data.

For one overground and one treadmill walking trial, pelvis and lower body joint angles were recovered from the noisy synthetic IMU data using a nonlinear least squares optimization method and a standard unscented filter method, both implemented in Matlab. For each time frame, the optimization method adjusted the kinematic model's joint positions, velocities, and accelerations to minimize errors between model and synthetic IMU data (including integrated IMU orientations, velocities, and positions) and between model and integrated joint positions and velocities. All numerical integration was performed using an implicit method.

Results and Discussion

Overall, the optimization method was more accurate and robust than was the unscented filter method. While the unscented filter was only slightly less accurate for 4 seconds

of overground walking (Fig. 1), it completely diverged for 30 seconds of treadmill walking. In contrast, the optimization method tracked the correct joint positions well for the duration of the treadmill walking trial (average RMS errors of < 2 mm for translations and < 1 deg for rotations for last 3 seconds). Thus, the optimization method could entrain the kinematic model to the natural system dynamics, while the unscented filter method could not. The main drawback of the optimization method was increased computational cost, though no effort was made to improve it.

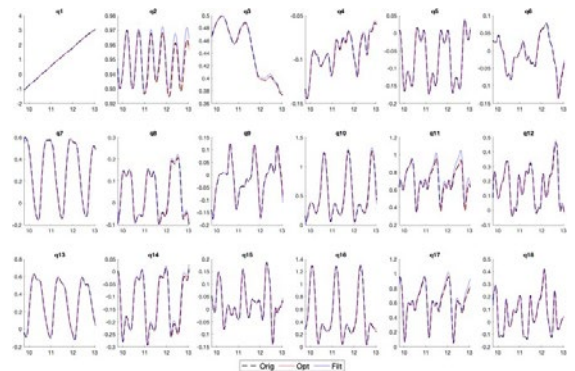


Figure 1: Optimization vs. filtering for overground walking.

Both methods required parameter tuning to achieve the best tracking of the original joint angles. The optimization method required identifying different cost function weights for position, velocity, and acceleration errors and was relatively insensitive to the selected values. In contrast, the unscented filter method required state and measurement covariance along with α , β , and κ algorithm parameter values and was more sensitive to the selected values.

Conclusions

The optimization method produced more accurate and robust joint angle tracking than did the unscented filter method but at the cost of increased computation time. The next step will be to repeat the evaluation using actual IMU data that can be properly synchronized with the motion capture data.

Acknowledgments

This work was by the National Science Foundation under award number 1805896.

References

- [1] Delp SL et al. (2007). *IEEE*, **55**: 1940-50.
- [2] Seth A et al. (2018). *PLoS*, **14**(7): e1006223.
- [3] Rajagopal A et al. (2016). *IEEE*, **63**,10: 2068-79.
- [4] Van der Merwe R and Wan EA (2001). *IEEE*, **6**: 3461-4.

Eight-Week Individualized Gait Modification Intervention to Reduce Knee Adduction Moment: Preliminary Analysis of a Randomized Controlled Trial

Bryndan Lindsey¹, Yakun Wang², Scott Bruce², Nelson Cortes¹

¹ Sports Medicine Assessment, Research & Testing (SMART) Laboratory, George Mason University, Manassas VA

² Department of Statistics, George Mason University, Fairfax VA

Email: ncortes@gmu.edu

Summary

Our preliminary analysis of a randomized controlled trial (RCT) investigating the effects of an individualized 8-week gait retraining intervention on KAM demonstrates that prior findings in quasi-experimental studies (often using healthy participants) are replicable using more rigorous study designs on the target population.

Introduction

Increased first peak internal knee abduction moment (KAM) due to altered gait mechanics has been associated with increased knee osteoarthritis (KOA) severity [1]. Gait modifications using real-time biofeedback have shown to be effective in reducing KAM. Prior studies, however, have largely relied on single-session designs with healthy participants, limiting generalizability. Additionally, the majority of studies have not screened KOA patients in regards to which modification is most beneficial to reduce KAM, despite evidence of large variability in individual responses to different modifications [2]. Our purpose was to evaluate preliminary data from a RCT investigating the effect on KAM of an individualized 8-week gait modification intervention.

Methods

Eight patients with medial compartment KOA completed the intervention. Patients first performed a baseline screening session consisting of 10 normal, trunk lean, and toe-in walking trials. Patients were randomized into either the intervention group (where the modification used was that which most reduced KAM compared to normal walking) or control group. Those in the intervention group completed 20 minutes of training once-per-week for 8 weeks using a previously described wearable inertial measurement unit (IMU) system [3] (Figure 1). The protocol for the control group matched the intervention, however, with normal walking. KAM was collected at week 5, 1-week, and 1-month post-intervention where participants were asked to walk with their learned modification. A mixed effects linear regression model was developed to assess changes in KAM across sessions and groups while accounting for correlation due to repeated measurements from patients.

Table 1: Estimated change in KAM from baseline to posttests for intervention group using mixed effects linear regression.

Posttest	Estimate (SE)	P-value	95% CI
1	0.111 (0.070)	0.164	(-0.061,0.284)
2	0.057 (0.031)	0.114	(-0.019,0.133)
3	0.086 (0.022)	0.008	(0.033, 0.139)

Results and Discussion

Of the patients randomly assigned to the intervention group, all three most reduced KAM using trunk lean gait. The remaining five were assigned to the control group. Estimated change in KAM from baseline for the intervention group (Table 1) showed a significant reduction in KAM during the final posttest ($p < 0.01$). The control group (not shown) did not show any significant changes in KAM across sessions.

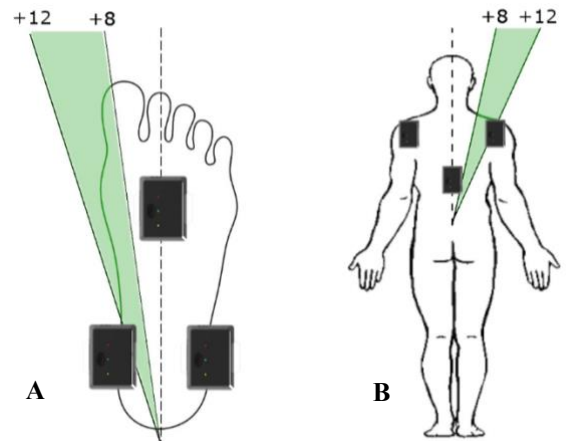


Figure 1: Gait modification schematic for (A) toe-in gait, and (B) trunk lean gait. Black nodes represent the placement of IMU nodes on the body. The nodes on the dashed lines computed joint kinematics in real-time while the others provided haptic feedback. If during training, a patient was not within their prescribed modification range (8° - 12° toe-in or trunk lean compared to baseline) they would be provided haptic feedback. If they were under the prescribed range during toe-in, the medial node would vibrate and vice versa. If they were under the prescribed range during trunk lean, the node on the side of the studied limb would vibrate and vice versa. Patients were instructed to attempt to walk so that they were provided no feedback.

Conclusions

Our preliminary results provide strong support for prior quasi-experimental studies showing that gait modification strategies are effective to reduce KAM in both healthy and KOA samples. In addition, it is clear from the results of the baseline screening process that different patients will find certain modifications much superior to others. Future research should attempt to highlight if there are certain variables that indicate which modification a patient may respond best to.

References

- [1] Sharma L et al. (1998). *Osteoarth. Cartil.* **26**: 1425-37.
- [2] Eddo O. (2017). *IJKSS.* **5**: 35-55.
- [3] Lindsey B (2020). *Knee.* **27**: 102-110.

HOME-BASED FOOT-ANKLE EXERCISES PROGRAM ORIENTED BY A BOOKLET CHANGED POSITIVELY FOOT MOTION DURING GAIT IN PEOPLE WITH DIABETIC NEUROPATHY

Érica Q. Silva¹, Jady L. Veríssimo¹, Renan L. Monteiro^{1,2}, Jane S.S.P. Ferreira¹, Ronaldo H. Cruvivel-Júnior¹, Marcos Duarte³, Isabel C.N. Sacco¹

¹Universidade de São Paulo, Faculdade de Medicina, São Paulo, SP, Brazil

²Department of Biologic and Health Science, Federal University of Amapá, Macapá, AP, Brazil

³Biomedical Engineering Program, Federal University of ABC, Rua Arcturus, 3, São Bernardo do Campo, SP, Brazil.

Email: icsacco@usp.br / ericaqueiroz10@usp.br

Summary

We aimed at identifying the effect of a home-based foot-ankle exercises program oriented by a booklet in foot-ankle kinematics during gait in people with diabetes and neuropathy (DPN). Twenty participants were randomly allocated to usual care (control group [CG]) or usual care plus home-based foot-ankle exercises (intervention group [IG]) for 8 weeks. Preliminary results showed that IG increased hallux relative to forefoot (first metatarsal) range of motion (ROM) and decreased maximum forefoot relative to hindfoot (midfoot motion) dorsiflexion during gait. The home-based exercise programme showed preliminary positive changes in foot motion during gait of people with DPN.

Introduction

DPN leads to progressive losses in muscle strength, distal joints motion, sensibility, which can result in important changes in gait biomechanics[1,2]. Therapeutic foot-ankle exercises may be beneficial for people with DPN and were recommended for the first time in the most recent guidelines of the International Working Group on the Diabetic Foot[3]. However, it is not yet a worldwide strategy when prevention of ulcer formation is considered. A home-based program guided by a booklet can be an efficient preventive strategy for stimulating self-management, especially when physiotherapy is not regularly recommended for this population. Therefore, we sought to evaluate the effect of a foot-ankle exercises program oriented by a booklet in gait biomechanics in people with DPN through an randomized controlled trial.

Methods

Twenty participants of both sexes with clinical diagnosis of type 1 or 2 diabetes and DPN were randomly allocated to usual care CG (55.3±8.9yrs) or usual care plus home-based foot-ankle exercises IG (58.1±3.6yrs) and assessed at baseline (T00) and Week 8 (T08) by 3D displacements of passive reflective markers tracked by 8 cameras at 100 Hz (VERO, Vicon). Plug-In Gait and Oxford Foot Model [4] setup protocols were used. Participants walked barefoot at a comfortable, self-selected speed on a walkway and 10 valid steps of each side were acquired. Digitisation and 3D reconstruction were performed in NEXUS software. Kinematic data were filtered using a zero-lag 2nd-order low-pass filter (6 Hz). Kinematics were computed with the open-source Python package pyCGM2 replicating the Vicon Plug-In Gait protocol and Plug-In of Oxford Foot Model. The variables calculated were ROM of first metatarsal, midfoot, rearfoot and tibia joints relative to the proximal segment. Comparisons between T00 and T08 within each group were performed by paired t-test to all variables (p<0.05).

Results and Discussion

After 8 weeks, IG increased hallux relative to the forefoot ROM (first metatarsal joint) (p <0.001). A difference of 3.2 (-6.4 to 0.07) degrees was observed, suggesting an improvement in foot motion at a crucial gait phase when the first metatarsophalangeal joint is required for propulsion. IG showed a decrease in the maximum forefoot relative to hindfoot dorsiflexion (midfoot motion) (p=0.029). A difference of 5.0 (6.7 to 9.3) degrees was observed, suggesting an increase in the midfoot stiffness during push-off, favouring the midtarsal joint locking mechanism, resulting in a changeover from a flexible foot during weight acceptance to a rigid foot structure during propulsion. IG also presented a decrease in the maximum forefoot relative to tibia dorsiflexion (p<0.001) with a difference of 3.1 (1.95 to 4.15) degrees. The CG presented an increase in the hindfoot relative to tibia dorsiflexion ROM (p=0.027) of 3.7 (-6.9 to -0.5) degrees that can be explained by either a placebo effect or the supervision of usual care.

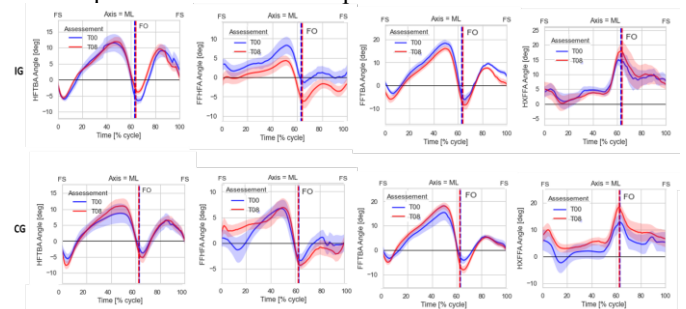


Figure 1: Ensemble averaged kinematics of the hindfoot (HFTBA), midfoot (FFHFA), tibia (FFTBA) and hallux (HXFFA) joints in degrees (deg) relative to the proximal segment. Blue colour indicates baseline assessment (T00), red colour indicates Week 8 assessment (T08). Error bars represent standard error. FS indicates foot strike, vertical lines (FO) indicate foot off event in the gait cycle.

Conclusions

This is the first study to evaluate biomechanical outcomes specifically related to DPN losses using a specialised foot-exercises program guided by a booklet and it showed positive preliminary changes in hallux, forefoot and midfoot motion during gait.

Acknowledgments

CAPES (financial code 001) for providing funding to ES and JV; CNPQ for IS; FAPESP for ES (2017/15449-4), RM (2017/17848-3), JF (2019/02522-0) and RCJ (2019/06405-9).

References

- [1] Shun, C. et al. (2004). *Brain* **127**.
- [2] Riandini, T. et al. (2018). *Acta Diabetol.* **55**, 155–164.
- [3] Schaper, N. C. et al. (2020). *DMRR.* **36**, 1–10.
- [4] Stebbins, J., et al (2006). *Gait Posture* **23**, 401–410.

Evaluation of a clinical walking test among unilateral lower-limb amputees

Hananeh Younesian^{1,2}, Raphaël Ouellet^{1,2}, Thomas Legrand^{1,2}, Katia Turcot^{1,2}

¹Center for Interdisciplinary Research in Rehabilitation and Social Integration (CIRRIS), Quebec, Canada

²Department of kinesiology, Laval University, Quebec, Canada

Email: Hananeh.younesian.1@ulaval.ca

Summary

Clinicians are commonly using six-minute walk test (6MWT) to evaluate rehabilitation progress and needs in individual with lower-limb amputation (iLLA). In this study, we evaluated the intensity and spatiotemporal parameters of 6MWT using inertial sensors and heart rate sensor. Our findings showed that both workload and pain level increased over 6MWT. However, cadence and stance duration decreased and increased, respectively. Deterioration of spatiotemporal parameters could be due to physiological and pain-related fatigue.

Introduction

The main goal of rehabilitation in iLLA is to improve mobility and lifestyle in iLLA [1]. Recently, wireless and light-weight inertial measurement units (IMUs) combined with heart rate (HR) sensor bring new inputs during the evaluation of 6MWT in iLLA [2]. Hence, clinicians were able to assess spatiotemporal parameters over 6MWT as well as workload among iLLA. In continuity of previous work, the objective of this study was to evaluate the intensity and spatiotemporal parameters over 6MWT in iLLA.

Methods

Eleven unilateral iLLA (4 trans-femoral, 7 trans-tibial) participated in this study. The HR sensor (Polar® RS800CX™, Kempele, Finland, 1000 Hz) was placed below the chest muscles. Two synchronized IMUs (Physilog®4, Lausanne, Switzerland, 200 Hz) were attached on top of each shoe. Cadence and stance ratio were selected as spatiotemporal parameters. Pain level was estimated using a VAS score (0-10) before and after the 6MWT. The HR, cadence and stance ratio were classified in six intervals of one minute (I1-I6). Mean and variability (SD) of each interval were computed. The HR were normalized using the age-predicted maximal heart rates ($HR_{max} = 220 - \text{age}$) to represent intensity of workload. Non-parametric repeated measures ANOVA (nparLD) test, with Bonferroni corrections were used to analyze mean and variability of HR performance and spatiotemporal parameters over 6MWT using R statistical software. A significant difference was set at a p level $< .05$.

Results

Mean of age and body mass index were 57.91 ± 6.22 yrs and 24.57 ± 6.22 kg/m^2 , respectively. Mean distance travelled during the 6MWT was 321.93 ± 128.04 m. VAS score after 6MWT was significantly higher than before 6MWT ($p = .016$). Our results showed that the mean of normalized HR gradually increased over 6MWT (I1: 61.59 ± 10.73 $HR_{max}\%$, I6: 70.15 ± 12.26 $HR_{max}\%$) ($p < .05$). Variability of HR during the

first interval of the 6MWT was significantly higher than others ($p < .01$) (Figure 1).

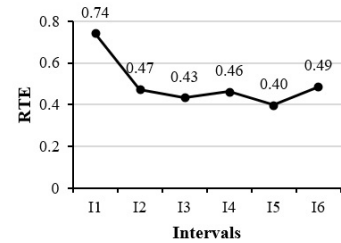


Figure 1: Relative treatment effect (RTE) variability of HR.

Cadence in I1 (AL: 100.16 ± 20.18 ; nAL: 103.07 ± 18.7 steps/min) and I2 were higher than I3, I4, I5 and I6 (AL: 96.76 ± 21.93 ; nAL: 98.63 ± 21.32 steps/min) during 6MWT ($p < .05$). Mean of stance ratio in I6 (63.39 ± 3.27 gait cycle%) and I5 were significantly longer than I4, I3, I2 and I1 (61.99 ± 3.35) in AL. Likewise, stance ratio in I5 (64.40 ± 4.08 gait cycle%) was longer than I1 (63.33 ± 2.63 gait cycle%) in nAL ($p = .042$) (Figure 2).

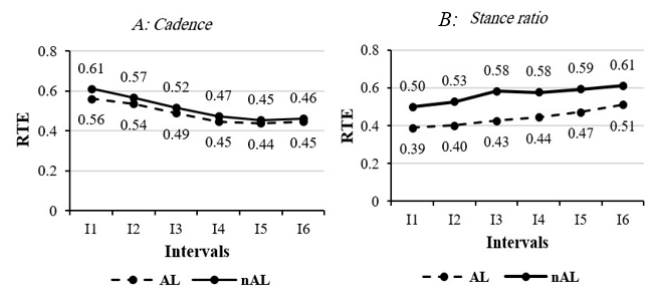


Figure 1: Relative treatment effect (RTE), cadence and stance ratio. AL: amputated leg, nAL: non-amputated leg.

Discussion and Conclusion

Variability of HR over the first interval of 6MWT was higher than over the others which can reflect high level of stress due to the test (white coat effect) [3]. Diminished HR variability after the first interval of 6MWT might reflect reduction of mental stress of clinic visit. Workload and the normalized mean of HR increased over 6MWT in iLLA. However, cadence decreased and stance ratio increased over 6MWT which can be due to physiological and pain-related fatigue [3].

Acknowledgments

We would like to thank all the participants for their time.

References

- [1] Treweek S et al. (1998). *Prosthet Orthot Int*, **3**:178-185.
- [2] Beausoleil S et al (2019). *Gait Posture*, **72**:40-45.
- [3] Aaronson (1999). *Image J Nurs Sch*, **1**: 45-50.

Foot Progression Angle Modifications that Maximally Reduce the Knee Adduction Moment do not Decrease Medial Knee Contact Force

Kirsten A. Seagers¹, Scott D. Uhlich^{1,2}, Janelle Kaneda¹, Julie Kolesar^{1,2}, Gary S. Beaupre^{1,2}, Scott L. Delp¹

¹Stanford University, Stanford, CA, USA

²Department of Veterans Affairs Healthcare System, Palo Alto, CA, USA

Email: kseagers@stanford.edu

Summary

The knee adduction moment (KAM) is a surrogate metric for medial compartment knee loading, which is correlated with medial knee osteoarthritis (OA) progression. Gait modifications, like changing the foot progression angle (FPA), are often prescribed to maximally reduce the KAM. Selecting modifications in this manner does not reduce medial knee contact force (MCF), but MCF can be reduced by 6.4% ($p < 0.001$) if it is used as the selection metric for an FPA modification.

Introduction

Compressive joint loading is related to OA progression [1], but joint loads cannot be directly measured *in vivo* in a native knee, only estimated with musculoskeletal modeling. The KAM is used as a surrogate measure of joint loading [2]. Gait modifications, like changing the FPA, aim to decrease the KAM to slow the progression of medial knee OA [3]. It is understood that the KAM does not fully explain changes in MCF, yet it is the most common target for load-reducing knee OA interventions [4]. While KAM is easier to estimate, mechanobiology suggests that compressive force transmitted through the medial compartment may be a better metric of tissue-level strains that damage the cartilage microstructure [1]. The purpose of this study was to investigate how FPA modifications selected to reduce the KAM affect MCF. This work investigates three hypotheses: (1) FPA modifications selected to maximally reduce peak KAM (i.e., KAM-reducing modification) decrease peak MCF during initial training; (2) the KAM-reducing modification results in a persistent reduction in peak MCF after one year and (3) FPA modifications selected to maximally reduce peak MCF (i.e., MCF-reducing modification) will result in larger peak MCF reductions than the KAM-reducing modification.

Methods

Forty-nine individuals with radiographic and symptomatic medial knee OA participated in a 1-year gait retraining study. The intervention group ($n=24$) was taught to walk with the KAM-reducing modification, an FPA modification (5° or 10° toe-in or toe-out change) that maximally reduced their peak KAM, using biofeedback. The control group ($n=25$) also received biofeedback to reinforce their natural FPA. Twenty steps were analyzed for the following trials: natural gait and KAM-reducing modifications at week 1, and the retrained KAM-reducing modification at week 52. MCF was estimated using OpenSim 4.0 with muscle forces estimated using a static optimization algorithm that minimizes the sum of squared muscle activations. Wilcoxon

signed rank and Mann Whitney U tests compare MCF ($\alpha=0.05$) within and between subject groups, respectively.

Results

Intervention subjects reduced their peak KAM by 12% with the KAM-reducing modification during week 1 but did not significantly reduce peak MCF (1.2%, $p=0.33$). At week 52, there was no statistical difference in peak MCF between the KAM intervention group and control group ($p=0.63$). Yet, an average 0.13 BW reduction in peak MCF could be achieved with an MCF-reducing modification, which was greater than ($p=2.93 \times 10^{-4}$) the KAM-reducing modification (Figure 1).

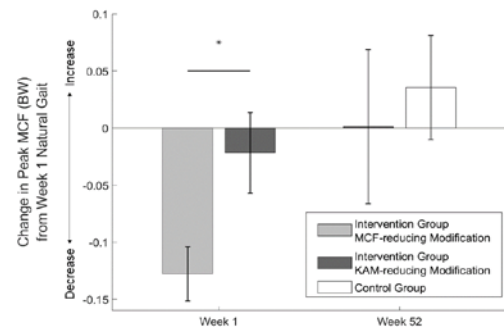


Figure 1: Peak MCF changes from week 1 natural gait for the intervention (grey) and control group (white). At week 1, MCF-reducing modifications (light grey) reduce peak MCF more than the KAM-reducing modification (dark grey).

Conclusions

FPA modifications that are selected to maximally reduce KAM do not decrease average peak MCF; however, average peak MCF was reduced by 6.4% ($p=2.98 \times 10^{-4}$) when it was used as the gait modification selection metric. Future work is needed to identify the most effective targets for load-reducing interventions.

Acknowledgments

This work was supported by the NSF Graduate Research Fellowship Program and the US Dept. of Veterans Affairs Rehabilitation R&D Service (I01 RX001811).

References

- [1] Andriacchi et al. (2004). *Ann Biomed Eng*, **32**: 447-57.
- [2] Miyazaki et al. (2002). *Ann Rheum Dis*, **61**: 617-22.
- [3] Shull et al. (2013). *J Orthop Res*, **31**: 1020-25.
- [4] Walter et al. (2010). *J Orthop Res*, **28**: 1348-54.
- [5] Rajagopal et al. (2016). *IEEE Trans Biomed Eng*, **63**: 20168-79.
- [6] Lerner et al. (2015). *J. Biomech*, **48**: 644-50.

Are medial and lateral tibiofemoral compressive forces different in uphill compared to level walking for patients following total knee arthroplasty?

Tanner Thorsen, Chen Wen, Songning Zhang

Biomechanics and Sports Medicine Lab, The University of Tennessee, Knoxville, Tennessee

Email: tthorsen@vols.utk.edu

Summary

The purpose of this research was to determine how knee joint compressive forces change during uphill walking as compared to level walking in both the replaced and non-replaced limbs of patients with total knee arthroplasty (TKA). TKA patients experience greater knee compressive force in their non-replaced limb during uphill walking.

Introduction

Uphill walking is a necessary part of daily living that has also become popular in exercise and TKA rehabilitation. TKA patients exhibited lower knee extension moments than did healthy controls in both the replaced and non-replaced limbs and the replaced limb of TKA patients exhibited lower peak knee extension moment at 10° and 15° incline compared to the non-replaced limb [1].

Variables such as knee extension moment have been correlated to tibiofemoral compressive force in level walking, however, these variables do not directly indicate the magnitude or behavior of compressive forces [2]. Recent developments of musculoskeletal modeling have provided the ability to estimate total (TCF), medial (MCF), and lateral (LCF) knee joint compressive force [3]. The purpose of this research was to determine how tibiofemoral joint compressive forces change during 10° uphill walking compared to level walking of TKA patients.

Methods

Twenty-five TKA patients (11 male 14 female, 68.6 ± 4.9 years, 22.1 ± 11.7 months since surgery) walked at self-selected pace at 0° (level walking) and 10° incline five times on a customized adjustable ramp system which was instrumented with two force platforms (1200 Hz, AMTI, Watertown, MA, USA). Three-dimensional (3D) kinematics (240 Hz, Vicon, Oxford, UK) and ground reaction force (GRF) were collected simultaneously.

An open-source musculoskeletal capable of resolving knee TCF, MCF, and LCF was used to perform the musculoskeletal simulations [3]. Static optimization and joint reaction analysis

were used in OpenSim to determine muscle activations and TCF, MCF, and LCF during level and uphill walking.

A 2x2 (slope: level and 10° × limb: replaced and non-replaced) repeated measures analysis of variance (ANOVA) was used to detect differences between slope and limb conditions and their interaction (SPSS). An α level of 0.05 was set a priori and adjusted for post hoc comparisons such that the interaction $\alpha < 0.0125$.

Results and Discussion

Peak loading-response TCF, MCF, and LCF were greater during uphill walking than level walking for the non-replaced limb (Table 1). During uphill walking peak loading-response TCF, MCF, and LCF were smaller in the replaced limb compared to the non-replaced limb. During level walking, the replaced and non-replaced limb experienced rather comparable joint loading, however the replaced limb experienced reduced joint loading in relationship to the non-replaced limb during uphill walking. Differences in joint loading between replaced and non-replaced limbs were not present during level walking, suggesting compensation from the replaced limb during the more difficult task. Furthermore, the distribution TCF (MCF vs. LCF) highly favors MCF at 86% and 87% of TCF for the replaced limb and non-replaced limbs, respectively. During uphill walking, the distribution of TCF shifts laterally such that MCF accounts for 75% and 74% of TCF for the replaced and non-replaced limbs, respectively.

Conclusions

It is difficult to make direct conclusions about the benefit of uphill walking following TKA, as it promotes a more balanced loading (MCF vs. LCF) of the knee joint during stance, however these benefits come at the expense of increased loading at the non-replaced limb.

References

- [1] Wen C et al. (2019) *J Biomech*, **89**: 40-47.
- [2] Walter JP. (2010) *J Orthop Res*, **28**: 1348-1354.
- [3] Lerner ZF et al. (2015) *J Biomech*, **48**: 644-650.

Table 1: Peak knee compressive forces (BW) during level and uphill waking: mean ± standard deviation.

Variables	Level	Level	10° Ramp	10° Ramp	p value		
	Replaced Limb	Non-Replaced Limb	Replaced Limb	Non-Replaced Limb	Limb	Slope	Int
TCF	-3.03 ± 1.10	-2.86 ± 1.09 ^a	-3.47 ± 1.31 [#]	-4.04 ± 1.27	0.004	0.343	0.004
MCF	-2.62 ± 0.78	-2.50 ± 0.84 ^a	-2.60 ± 0.88	-3.00 ± 0.79	0.126	0.383	0.008
LCF	-0.59 ± 0.50 ^a	-0.45 ± 0.42 ^a	-1.03 ± 0.56	-1.21 ± 0.65	< 0.001	0.782	0.012

Note: ^a: significantly different of the same limb from ramp walking, [#]: significantly different from the Non-Replaced limb at the same slope.

Dynamic Gait Stability During Anteriorly Loaded Treadmill Walking

Caroline Simpkins¹, Jiyun Ahn¹, Meredith Wells¹, Feng Yang¹

¹Department of Kinesiology and Health, Georgia State University, Atlanta, GA, USA

Email: claubacher1@student.gsu.edu

Summary

This study examined the effects of anteriorly-loaded treadmill walking on dynamic stability in young adults. Participants were randomized into three groups: 0% or no load, 10% body weight (*bw*), 20% *bw*. Center of mass (COM) dynamic gait stability was found to be comparable across all groups at touchdown (TD) and liftoff (LO) during gait. To maintain stability during loaded walking, subjects leaned their trunk backward while keeping a similar step length.

Introduction

Anterior load carriage during walking is common in activities of daily living and many occupations. Carrying a load in front of the body can affect gait patterns and increase the risk of falls [1]. Due to the advantages of using a treadmill, it has been broadly employed in previous work to investigate the effect of front load carriage on gait parameters while participants walk on a treadmill [2]. The variability of gait parameters has been used as an index of fall risk. Dynamic gait stability is another measurement of the human body's dynamic balance and the risk of falling during walking [3]. An examination of how front load carriage influences dynamic gait stability could provide novel insight into the impact of front load carriage on the risk of falls. However, it remains completely unknown how front load carriage impacts dynamic gait stability during treadmill walking. The purpose of this study was to inspect the effects of anteriorly-loaded treadmill walking on dynamic gait stability in healthy young adults. We hypothesized that front load carriage would affect dynamic gait stability during treadmill walking.

Methods

Thirty healthy young adults (24.83 ± 4.96 years) were randomly allocated to three groups: 0% or no load (Group 1), 10% body weight (*bw*) (Group 2), 20% *bw* (Group 3). The load was assembled by filling sand bags with various weights into a fitness sandbag. Before loaded treadmill walking, participants walked on the treadmill unloaded for 10 minutes to warm up. Self-selected walking speed (in m/s) was also determined during the warm-up. After finishing three 30-sec treadmill trials at self-selected speed with either no load (Group 1) or the assigned load (Groups 2 and 3), participants completed three walking trials at a set treadmill belt speed of 1.2 m/s. This pre-set gait speed could remove confounding effects due to the uncontrolled speed. Groups 2 and 3 carried the sandbag against their abdomen using both hands in a symmetric posture maintaining load height with both elbows flexed about 90°.

Full-body kinematics were collected from 26 reflective markers on the body landmarks through a motion capture

system (Vicon, UK). Two more markers were attached at both sides of the sandbag. Marker paths were filtered. Two characteristic gait events (TD and LO) were identified based on foot kinematics. The body-load system's COM position was calculated from the filtered marker paths. The two components of the COM motion state (position and velocity) were calculated relative to the rear part of the base of support (or the lead heel) and normalized by foot length and the square root of the product of body height and gravitational acceleration, respectively. Dynamic gait stability at both events was calculated as the shortest distance from the COM motion state to the limit against backward balance loss [3]. Trunk angle (°, +: lean backward) at TD and LO in the sagittal plane and step length (/body height) were calculated from the marker paths. Dependent variables (dynamic stability at TD and LO, trunk angle at TD and LO, and step length) were compared between groups using one-way ANOVA. SPSS 25 (IBM) was used and α level of 0.05 was applied.

Results and Discussion

No significant differences were found between groups for dynamic stability at TD ($p = 0.205$) and LO ($p = 0.122$, Table 1). Trunk angle showed significant group-related differences at TD and LO (both $p < 0.001$). All groups took a similar step length ($p = 0.344$).

	Group 1	Group 2	Group 3
Stability-TD	0.05±0.03	0.04±0.02	0.04±0.02
Stability-LO	0.22±0.04	0.16±0.10	0.19±0.02
Trunk angle-TD	-1.27±4.66	3.86±2.07	9.08±2.51
Trunk angle-LO	1.16±4.59	5.09±3.42	10.48±2.87
Step length	0.35±0.03	0.34±0.03	0.36±0.02

Table 1: Comparisons of outcome measures (mean ± SD).

The results reject our hypothesis. To maintain stability during loaded walking, subjects leaned their trunk backward in the loaded groups to maintain the body-load system COM's position relative to the base of support. As the gait speed is the same across groups, dynamic stability was not different between groups.

Conclusions

Anterior load carriage of up to 20% *bw* may not alter dynamic gait stability in young adults during treadmill walking at a set-speed.

References

- [1] Owings et al. (2004). *J. Biomech.*, **37**: 935-938.
- [2] Padulo et al. (2014). *MLTJ*, **4**: 159-162.
- [3] Yang, F. (2016). *Handbook of Human Motion*; 1-22.

Danger Ahead: Fatigued Obstacle Negotiation in an Unpredictable Environment

Joshua A. Vicente¹, Nicole M. Stoehr¹, Maria Ayala¹, Michael Weise¹,
Sean M. Rogers, DAT¹, Jacob W. Hinkel-Lipsker, PhD¹

¹Move-Learn Lab, Department of Kinesiology, California State University, Northridge, California, USA
Email: movelearnlab@gmail.com

Summary

This study investigated the impact of physical fatigue on an individual's ability to navigate randomized and unexpected obstacles during locomotion. Participants completed a series of obstacle negotiation trials in the dark, then underwent a fatiguing protocol, before completing another series of negotiation trials. Results revealed that participants had a significant decrease in leading toe and trailing toe clearance and a significant increase in leading heel clearance when fatigued. Additionally, participant fitness level significantly predicted where participant foot placement while approaching the obstacle. These results indicate that physical fatigue impacted participant's crossing mechanics. Implications from this study may be of interest to occupational work and safety associations to reduce workplace injuries for employees in physically demanding positions/fields.

Introduction

A prominent cause of non-fatal work-related injuries is attributed to slips, trips, and falls [1]. While it is known that fatigue has a direct impact in navigating obstacle navigation, most of the literature surrounds the geriatric population and is not based around the working population [2]. Thus, the goal of this study is to explore the impact of physical fatigue on young, physically-fit individuals' ability to negotiate unpredictable obstacles. We hypothesized that participants would exhibit a riskier crossing behavior (e.g., lower foot clearance) when fatigued.

Methods

Twenty-one participants were recruited and chosen for this study based on their respective cardiovascular (CV) fitness levels so that our results would reflect the potential outcomes of individuals with active, physically-demanding occupations. All participants were between 18 and 35 years of age, and were classified to have an above average level of cardiovascular fitness.

Participants were instructed to walk through a darkened pathway over a randomly placed hurdle that upon approach would be illuminated by a motion detection light. This setup was modelled to simulate an unpredictable workplace environment with limited to no visibility (Figure 1.).

To analyse participants' crossing mechanics, three-dimensional motion capture collected coordinate data and associated spatiotemporal measurements. Additionally, multiple linear regressions were performed to determine if any anthropometric or demographic variables predicted spatiotemporal negotiation mechanics.

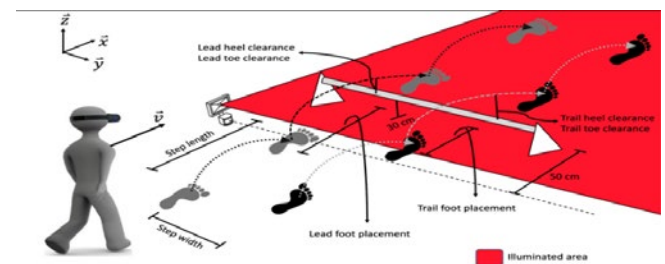


Figure 1: Layout of Obstacle Trial Attempt after Fatigue Protocol.

Results and Discussion

Participants exhibited a significantly lower leading toe and trailing heel clearance. Participants also stepped closer to the obstacle prior to clearing it when fatigued, placing them at greater risk for foot contact and a subsequent likelihood of tripping. They also walked at a significantly faster gait velocity, which may have reduced the time available to them to coordinate motion over the obstacle, which may also be disadvantageous for obstacle negotiation. Finally, participant CV levels were a significant predictor of leading and trailing foot placement the step before negotiation, where those with lesser fitness stepped closer to the obstacle—a potentially riskier behavior as it provides them with less time to control the trajectory of their foot [3].

Conclusions

Reductions to the participants' clearance margins suggest a diminished ability to coordinate the lower extremities, reflecting a riskier obstacle negotiation behavior when in a physically-fatigued state. With increased fatigue, an increase in work-related injuries like slips trips and falls could potentially occur in physically demanding occupations.

References

- [1] Change et al. (2016). *Ergonomics*, 7: 861-883.
- [2] Helbostad et al. (2018). *Gait and Posture*, 66: 235-236.
- [3] Patla et al. (1999). *Exp Brain Res*, 128: 441-450

Modeling Spatial Asymmetry in Visuomotor Coordination

Kolby Brink, Aaron Likens, and Nicholas Stergiou

¹Department of Biomechanics, University of Nebraska at Omaha, Omaha, NE USA

email: kolbybrink@unomaha.edu

Presentation Preference: Podium

INTRODUCTION

Coordination is foundational to human movement¹. One prominent model of coordination is the Haken-Kelso-Bunz (HKB) which predicts change in relative phase between two oscillators according to the following equation:

$$\dot{\phi} = \Delta\omega - a \sin(\phi) - 2b \sin(2\phi) - \sqrt{Q}\zeta_t,$$

where $\Delta\omega$ quantifies differences in natural periods between the oscillators. The ratio, b/a , models the collective frequency of coordinated oscillation. $\sqrt{Q}\zeta_t$ is a noise term with strength Q . $\Delta\omega$ is an ‘imperfection parameter’ that predicts deviations in relative phase, ϕ , due to timing differences in oscillators. Another possibility is that deviations of ϕ might result from asymmetries in spatial alignment of oscillators, such as in visual motor coordination. We propose two possible mechanisms for modeling asymmetry based on a modified HKB model:

$$\dot{\phi} = \Delta\omega + \Delta s - a \sin(\phi - \eta) - 2b \sin(2\phi) - \sqrt{Q}\zeta_t$$

Two potential terms, Δs and η , can model the effects of spatial asymmetries of oscillators. Both predict shifts in mean relative phase, $\bar{\phi}$, away from stable fixed points. Only the Δs parameter predicts a shift in $SD_{\bar{\phi}}$, a decrease in the stability of coordination. This study was designed to distinguish which, if either, of those parameters best models spatial asymmetry.

METHODS

10 healthy adults (26.4 ± 6.87 years, 7 males, 3 females) participated in this study. A 6-camera system (Optotrak, NDI) measured upper body movement at 100 Hz. The aim was to investigate the effects of reference frame alignment on the form and stability of visuomotor coordination. Participants coordinated their arm movements with a visually displayed sinusoidally oscillating stimulus (S_{Sine}). Forearm movements

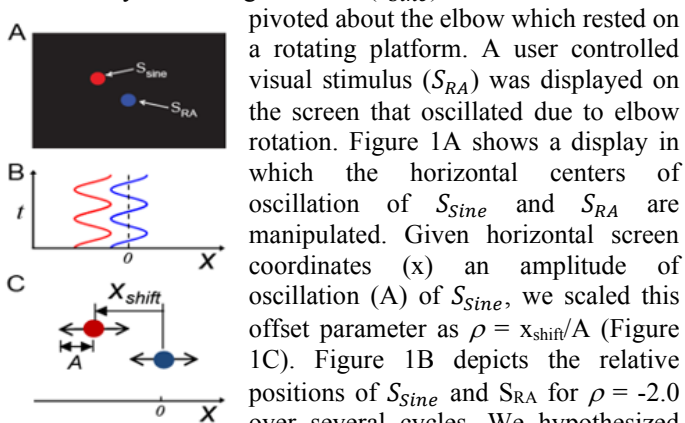


Figure 1. See Text

pivoted about the elbow which rested on a rotating platform. A user controlled visual stimulus (S_{RA}) was displayed on the screen that oscillated due to elbow rotation. Figure 1A shows a display in which the horizontal centers of oscillation of S_{Sine} and S_{RA} are manipulated. Given horizontal screen coordinates (x) an amplitude of oscillation (A) of S_{Sine} , we scaled this offset parameter as $\rho = x_{shift}/A$ (Figure 1C). Figure 1B depicts the relative positions of S_{Sine} and S_{RA} for $\rho = -2.0$ over several cycles. We hypothesized that particular spatial offsets will be preferred. To test this hypothesis, we

studied preferences for particular spatial arrangements of S_{Sine} and S_{RA} that arise from initial arrangements of $\rho = -3, -2, -1, 0, 1, 2$ or 3 . Participants were free to move the location of S_{RA} as

long as they could comfortably perform anti-phase and in-phase coordination. Subjects performed 3 trials for each phase (in-phase, anti-phase) $\times \rho$ pair, each lasting 60 seconds. 3 practice trials were given at $\rho = 0$ to familiarize subjects with the task.

Analysis Strategy. We computed instantaneous relative phase between S_{Sine} and S_{RA} for all trials, along with circular means and standard deviations.² We then modeled $\bar{\phi}$ and $SD_{\bar{\phi}}$ as a function of ρ and phase (inphase/antiphase) in separate Bayesian multilevel models developed specifically for circular/directional dependent variables.³

RESULTS AND DISCUSSION

Estimates in Table 1 replicate well known differences between required phases because the 95% credible intervals defined by LB and UB do not overlap. Modeling results in Table 2 show

Table 1. Estimated circular descriptive statistics for $\bar{\phi}$ as a function of required phase. Estimates are in radians.

	Mean	Mode	SD	LB	UB
Anti-phase	-2.82	-2.87	0.13	-2.98	-2.59
In-phase	0.14	0.12	0.03	0.08	0.21

that most slope estimates indicate that a one unit change in ρ predicts a negative change in $\bar{\phi}$ because credible intervals do not contain 0. Models relating ρ and $SD_{\bar{\phi}}$ (not reported to due to space) found no evidence of such a relationship, implying that Δs may not be useful in modeling asymmetry effects.

Table 2. Slope estimates for ρ predicting $\bar{\phi}$

Slopes	Mean	SD	Mode	LB	UB
β_c	-0.18	-0.22	0.23	-0.31	0.14
AS	-0.08	-0.08	0.15	-0.22	-0.02
SAM	-0.08	-0.09	0.06	-0.20	-0.02

Note: β_c = Slope at inflection point, AS = Average Slope, SAM = Slope at Grand Mean, LB/UB = Upper and lower bounds of 95 % credible interval from Bayesian estimates.

CONCLUSIONS

Results suggest that, in the current context, spatial asymmetries may best be modeled via the η parameter in the modified HKB model. Future work will investigate the extent to which this modification transfers to other conditions of asymmetry.

REFERENCES

1. Kelso, J., MIT PRESS, (1995).
2. Lamb, P.F., et al. *Clinical Biomech.*, (2014) **29(5)**, 484-493.
3. Cremers, J. et al, *Frontiers in psychology* (1994). **9**, 2040.

ACKNOWLEDGEMENTS

This work was supported by NIH P20GM10909 and a Pilot Project Award to A. Likens from the Center for Research in Human Movement Variability and the NIH.

Effectiveness of a speed control based on auditive feedback during metabolic cost trials

L. Lagos Hausheer^{1,2}, R.L. Bona¹, C.M. Biancardi¹

¹LIBiAM, Dept. of Biological Sciences, CENUR L.N., Universidad de la República, Paysandú, Uruguay

²Departamento de Kinesiología, Facultad de Medicina, Universidad de Concepción, Chile

Email: lagoskinesiologo@gmail.com

Summary

The metabolic cost of transport (C) at variable speed, including gait transitions, has been determined through a series of experiments on a treadmill (Lab) and in the field (F). The Lab trials were replicated in the F by using an auditive feedback. The C in F was affected by a positive speed bias: the average speed was around 50% higher than in the Lab. Therefore the C adjusted for the real speed was lower in the F than in the Lab.

Introduction

The metabolic cost of locomotion (C) at variable speed in real conditions has been poorly investigated [1]. Our experiments were designed to study the C during acceleration cycles around the walk-run (W-R) transition speeds, both on a treadmill (Lab) and in the field (F). One of our hypotheses was that the C in the F would be higher than in the Lab.

Methods

24 trained males signed an informed consent and participated in the investigation. The study was approved by the local Ethical Committee.

First, each subject was asked to perform three trials on a treadmill (T2100, GE Healthcare, USA), at variable speeds organized in two ascending and descending ramps, in order to determine the W-R transition speed (Ts). Then, a personalized ascending and descending speed ramp was designed, centered on the transition speed and ranged from Ts-20% to Ts+20%, each step lasting 5 s. Each ramp cycle lasted 50 s, and was repeated 5 times, for a total trial time of 250 s. Gas exchanges and heart rate(HR) were measured by a portable metabograph (K5, Cosmed, Italy). Only the last 50 s cycle was used to take the steady state oxygen uptake and carbon dioxide production. The step frequency (Sf) during the Lab trials was recorded, and used as audio guide for the F trials, which were performed on a regular course track in the Paysandú Sport Center. Speed progressions in F were controlled afterwards by analysing the GPS data of the K5 equipment.

Results and Discussion

The C in the F at the same theoretical speed was higher than in the Lab (Table and Fig. 1). However the actual speed

detected by GPS was around 150% of the Lab speed. Therefore, the C in the F was lower, thus in a range of speed not comparable to the Lab. For this reason our hypothesis could not be proven.

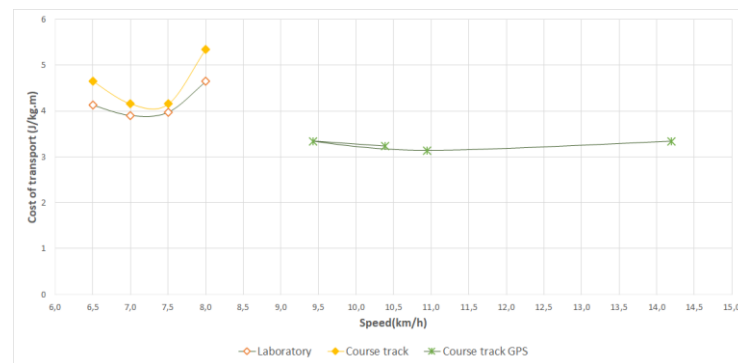


Figure 1: Metabolic Cost of transport laboratory, course track and course track GPS.

The auditive feedback, based on the assumption that the same Sf would lead to the same speed, is, compared to other systems, simple and inexpensive [1, 3]. However it has proved unreliable in these complex trials. The subjects were able to maintain the Sf but at a larger, on average, stride length (SI) [2], suggesting different mechanical behaviours in Lab vs F. This difference explains the different C for unit distance.

Conclusions

The speed control is a critical point in order to determine the C, because wrong assumptions could lead to misinterpretation of the results. Spatio-temporal and mechanical parameters should also be taken into account: it's one of our goals in the continuation of this project.

References

- [1] Minetti AE et al. (2013). *J.Appl.Physiol.*, **114**: 498-503.
- [2] García-Pinillos F et al. (2019). *Gait&Posture*. **68**: 72-77
- [3] Hoelzl G (2009). *Int. Conf. Mob. Comp. Ap. S.* Springer

Table 1: C at different speeds and conditions. **ANOVA p<0,005 and DUNN' POST HOC p<0,005 GPS and C, GPS and L.

	6.5 km/h Ts		7.0 km/h Ts		7.5 km/h Ts		8.0 km/h Ts	
	C	GPS	C	GPS	Cost	GPS	Cost	GPS
Laboratoy	4,133 ± 0,567	—	3,936 ± 0,360	—	4,010 ± 0,318	—	4,645 ± 0,291	—
Course track	5,090 ± 2,078	—	4,638 ± 1,329	—	4,406 ± 1,576	—	6,008 ± 1,380	—
Course track GPS	3,234 ± 0,836	9,960 ± 0,835 (153 %)	3,340 ± 0,537**	9,510 ± 0,538 (146%)	3,139 ± 1,003**	10,860 ± 1,003 (167%)	3,340 ± 0,909**	9,960 ± 0,910 (153%)

Ts: transition speed; C: Metabolic Cost of transport (J/kg.m) Mean ± Stand.dev ; GPS: GPS Speed (km/h) mean ± Stand.dev - % respect to Ts

Differences in ground reaction forces between children, adults, and elder people during walking

Rafael R. Baptista¹, **Mauricio Delgado-Bravo**², Marcus F. Viera³, Alvaro Reyes⁴, Gustavo S. Heidner⁵

¹School of Health and Life Science, Pontifícia Universidade Católica do Rio Grande do Sul, Porto Alegre, Brazil

²Departamento de Ciencias de la Salud, Facultad de Medicina, Pontificia Universidad Católica de Chile, Santiago, Chile

³Escuela de Kinesiología, Universidad Andrés Bello, Viña del Mar, Chile

⁴Bioengineering and Biomechanics Laboratory, Universidade Federal de Goiás, Goiania, Brazil.

⁵East Carolina University, Greenville, USA.

Email: rafael.baptista@pucrs.br

Summary

Studying the parameters of the ground reaction force (GRF) during gait allows classifying them weight acceptance and impulse strategies during the vita cycle. In this study, we focused on comparing these variables between gait in children, adults, and older adults. We found differences between these parameters in different axes when comparing these strategies in children versus older people.

Introduction

The clinical and biomechanical analysis of gait during the lifespan should be implemented to control alterations in daily life activities and the appearance of pathological processes in the elderly [1]. The study of the ground reaction forces is very important to provide an accurate description of the gait among age groups. This approach enables the collection of several parameters regarding gait biomechanics such as force-time characteristics, peaks of vertical and anterior-posterior ground reaction force components, spatiotemporal parameters, and impulses. These data can be used by researchers, physiotherapists, clinicians, or others interested in human movement as a tool to assess interventions, investigate the patient's walking pattern, diagnose gait disorders, compare different populations, among other applications. Larish et al. [2] described healthy gait patterns in older adults like walk velocity and its relationship with the economy of movement, as well as kinetic data, like the vertical and anterior-posterior ground reaction forces peak.

The purpose of this study was to compare gait ground reaction forces and derived parameters between children, young and older adults. We hypothesized that ground reaction forces and impulses would increase from children to young adults and decrease from young adults to older adults. Also, we hypothesized that the walking velocity would increase from children to young adults, and decrease from young adults to older adults, with the time parameters adapting to accommodate such alterations during the lifespan.

Methods

Twenty-five children, thirty adults, and thirty-three older adults participated in this study. This investigation used a non-probability sampling process of intentional type, in which subjects were selected through a direct approach. Exclusion criteria were comprised of (i) a history of neuromusculoskeletal injuries, and (ii) have been submitted to an orthopedic/neurological surgery in the past two years that

could interfere with the participants ability to walk. Each participant performed five trials, walking at a self-selected pace, while wearing sports footwear, on a 6.0 m long by a 1.4 m wide walkway with 8 embedded force platforms (BTS Bioengineering, Milan, Italy). A Python 3 (Python Software Foundation; v3.8.1) script was developed to visually inspect and calculate the mean of the peaks of vertical forces and anteroposterior forces and their respective times across all steps. It also calculated the impulses using Simpson's rule to numerically integrate the area under the time-force curve. Normality assumptions were evaluated using the Shapiro-Wilk test. The intraclass correlation coefficient (ICC) was calculated to estimate the reliability of GRF parameters. A one-way analysis of co-variance (ANCOVA) was used to determine differences between groups in GRF parameters adjusted by gait velocity. Pairwise comparisons after ANCOVA were adjusted using Scheffé method. The magnitude of between group differences were also analyzed using Eta squared (η^2) effect size. Results were considered significant at $p \leq 0.05$. All analyses were performed using STATA 15.0.

Results and Discussion

A one-way analysis of variance revealed that gait velocity was significantly higher in children in comparison to older adults ($p=0.031$). The one-way analysis of co-variance revealed that overall, gait velocity had a significant inverse effect in GRF parameters in all groups. The children group had a significantly higher first peak force (F1) and lower second peak force (F2) in comparison with adults and older adults. Time to peak forces (T1, T2, T3) were significantly lower in children in comparison with adults and older adults. Similarly, impulse of loading response and midstance and total impulse of the vertical GRF were significantly lower in children in comparison with adults and older adults.

Conclusions

There are differences between the parameters of gait force, time and impulse, for the anteroposterior and vertical axes when comparing children and the elderly people.

References

- [1] Hausdorff, J.M. (2005). *J Neuro Engineering Rehabil*, **2**, 19.
- [2] Larish, P. E, et al. (1988). *Ann. N. Y. Acad. Sci.*, vol. **515**, no. 1 Central Deter, pp. 18–32.

Impact of foot progression angle and/or lateral trunk lean gait modifications on lower limb joints external moments

T. Legrand^{1,3}, H. Younesian^{1,3}, N. Equey¹, A. Campeau-Lecours^{2,3}, K. Turcot^{1,3}

¹Kinesiology Department, Université Laval, Québec, Canada

²Mechanical Engineering Department, Université Laval, Québec, Canada

³Center for Interdisciplinary Research in Rehabilitation and Social Integration, Québec, Canada

Email: thomas.legrand.1@ulaval.ca

Summary This study highlights the importance to consider the biomechanical consequences of gait modifications on the ankle and hip before considering a clinical application of gait retraining approaches.

Introduction Gait retraining as a non-invasive prospective approach to restore mechanical loading at the knee joint and slowing down knee osteoarthritis (OA) progression shows great promise [1]. However, the impact of gait modifications such as an increase in foot progression angle (FPA) or lateral trunk lean (LTL) on the ankle and hip is not yet well understood [1]. Thus, the goal of this study is to provide insight on the impact of FPA and LTL on the sagittal and frontal external moments at the ankle and hip in a cohort of healthy participants. We hypothesize that there is an optimum, for which an increase in FPA and/or LTL minimize the knee adduction moment (KAM) without increasing significantly the frontal and sagittal external moments at other surrounding joints during gait.

Methods A total of 23 healthy participants (age: 35.6±5.10y.o.; height: 1.73±0.09m; weight: 74.4±12.60kg, 10 women) were equipped with a 6 degrees of freedom marker set on both lower limbs and the pelvis following the International Society of Biomechanics standards [2, 3]. Marker trajectories were recorded at 100Hz using a motion capture system (9 cameras, Vicon motion system, Oxford, UK) and filtered using the predicted mean-squared error adaptive filter (Nexus software, version 2.6). Ground reaction forces were collected at 1000Hz for each lower limb using an instrumented treadmill with two embedded force plates (Bertec, Columbus, OH, USA).

Participants performed 12 walking trials in each condition (i.e., normal gait and with gait modifications [LTL at 5 or 10° and/or FPA at 10, 15 and 20°]). Self-selected comfortable gait speed kept constant throughout the experiment on the treadmill. Gait modifications were delivered through a visual feedback placed on a screen in front of the participant.

The kinematic and kinetic data were time-normalized to 101 samples from 0% (heel strike) to 100% (subsequent toe-off) to represent the stance phase of gait. The flexion and adduction external moments for the dominant lower limb joints were extracted, normalized to body weight and height (%BW·Ht) and averaged over eight gait cycles.

Statistical Parametric Mapping (SPM) was used to statistically compare the whole kinetic stance phase between walking conditions.

Results and Discussion A FPA of 10°, 15° and 20° significantly increased the hip sagittal moment in late stance ($p < 0.001$) and the hip frontal moment in early, mid and late stance ($p < 0.001$). An LTL of 5° and 10° significantly decreased the ankle sagittal moment in early stance ($p <$

0.001) and increased it in mid-stance ($p < 0.001$). It also significantly increased the hip sagittal moment in early and late stance ($p < 0.001$). A combination of FPA and LTL significantly increased the ankle and hip sagittal moment mid-stance ($p < 0.001$) and the hip frontal moment in early and late stance ($p < 0.001$).

The hypothesis that an optimum where the KAM is minimized while the external moments at the ankle and hip are kept constant or decreased was not confirmed. While not all the gait modifications performed by the participants in this study reduced the KAM, they significantly increased the sagittal moment at the ankle and the frontal moment at the hip (Figure 1). Therefore, highlighting the importance of better understanding the impact of a gait modification on the neighboring joints.

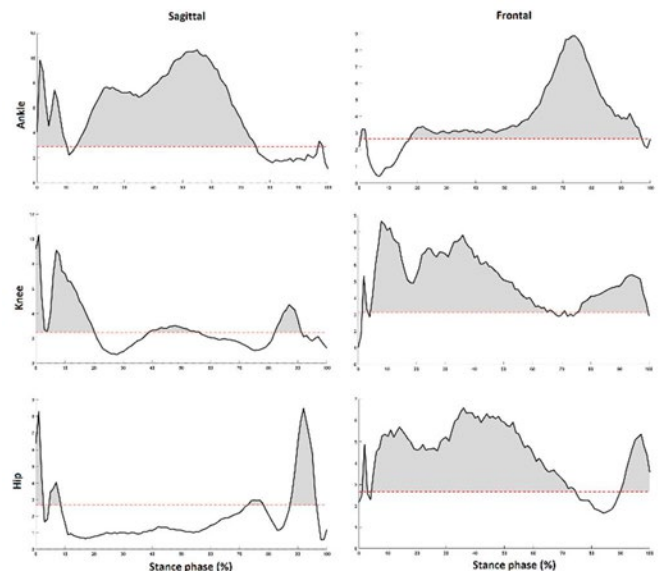


Figure 1: Statistical non-parametric mapping one-way repeated measures ANOVA conducted on the sagittal and frontal external moments at the ankle, knee and hip comparing the 12 walking conditions.

Conclusions This study highlights the importance to consider the biomechanical consequences of gait modifications on the ankle and hip before considering a clinical application of gait retraining approaches.

Acknowledgments This work was supported by the Natural Sciences and Engineering Research Council of Canada (CRSNG-2016-06001).

References

- [1] Bowd J. et al. (2019). *ARRCT*, 1;3: 100022.
- [2] Wu and Cavanagh. (1995). *J. Biomech*, 28;10: 1257-1261.
- [3] Wu et al. (2002). *J. Biomech*, 35;4: 374-386.

Spinal Reflexes can Produce a Variety of Bipedal Gaits

T. Geijtenbeek¹, F.C.T. van der Helm¹

¹Biomechatronics and Human-Machine Control, Delft University of Technology, Delft, The Netherlands

Email: t.geijtenbeek@tudelft.nl

Summary

Spinal reflexes are known to be important for legged locomotion, but their exact contribution and relation to other spinal circuits are poorly understood. We use predictive simulation from first principles to gain insight in the capabilities of spinal reflexes, using a biologically plausible neuromuscular controller that mimics proprioceptive reflex pathways as described in neuroscientific literature. After optimization, this relative simple control strategy was able to produce stable bipedal walking and running gaits that resemble real-world data, both for planar and 3D models. Our model is expected to have several clinical applications.

Introduction

The way in which spinal circuitries contribute to human locomotion is a long-standing open research question. Neuromusculoskeletal simulations can be useful for unraveling these underlying mechanisms, as they allow systems-level studies with fine-grained control. However, existing simulation studies typically use a *finite state machine* to select feedback pathways and gains based on the active phase of the gait cycle (swing, stance, etc.) [1]. This is problematic, since there is no direct neurological evidence for such systems, while the hand-crafted states and transitions are domain-specific and do not generalize to other behaviors.

We developed a neuromuscular controller that solely mimics established spinal reflex pathways [2], and optimized its parameters for high-level gait objectives. Surprisingly, our simple network was able to produce a variety of walking and running gaits, and generalized to 3D models.

Methods

Neural network. The input to our spinal control network consists of group Ia afferents from spindle sensors (modeled as a weighted combination of muscle length and velocity), group Ib afferents from Golgi tendon organs (muscle tendon force), and vestibular afferents that represent relative head position and velocity. Ia afferents connect directly to homonymous motoneurons (MN) and Ia inhibitory interneurons (IaIN), which reciprocally inhibit antagonist MNs. Ib afferents connect to Ib interneurons (IbIN), which connect either inhibitory or facilitatory to MN and other IbINs. Renshaw cells (RC) recurrently inhibit MNs and IaINs (see Figure 1, left). Neural excitation is modeled as a rectified weighted (k_{ij}) sum of base b_i and its inputs $\{X_I, \dots, X_n\}$:

$$I_i(t) = \max(0, b_i + \sum[k_{ij}X_j(t - \Delta t_{ij})])$$

Neural delays Δt_{ij} are proportional to the length of the pathway, based on experimental data. Two-way connection delays for hip, knee and ankle muscles are 10ms, 20ms and 35ms respectively. One-way vestibular delay is 100ms.

Optimization. The crux is in finding the right weights k_{ij} and biases b_i . After finding suitable initial values, we optimized the parameters using single shooting in SCONE [3], based on target velocity, energy expenditure and joint load.

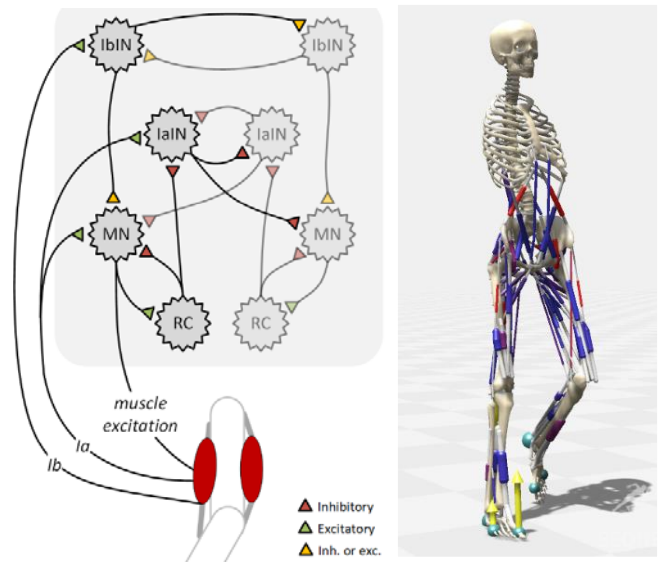


Figure 1: left: spinal control circuits, right: 3D simulation model

Results and Discussion

After optimization, our neuromuscular controller could produce walking and running gaits that match real-world data. Results were on-par or better than control schemes with much more elaborate control, yet our control strategy generalizes better to running gaits, as well as 3D models. This enables a range of clinical applications and could help in the development of assistive devices. Our controller can potentially be augmented with additional interneurons and afferents to further increase its capabilities.

Conclusions

Our results demonstrate proprioceptive reflexes to be a remarkably powerful musculoskeletal control primitive. Even though we know other circuits, such as central pattern generators, play an important role in gait, we might need to re-evaluate their relation and dependencies

Acknowledgments

This research was funded by the NWO VENI program 15153.

References

- [1] Geyer, H., & Herr, H. (2010). *IEEE Trans. Neural Systems and Rehabilitation Engineering*, **18**(3), 263–273.
- [2] Côté, M. P., et al. (2018). *Frontiers in Physiology*, **9**:784
- [3] Geijtenbeek, T. (2019). *Journal of Open Source Soft*, **4**(38)

Walking aid selection for non-weight bearing ambulation: effects on stance limb plantar force, walking speed, perceived exertion, and device preference in adults 50 years of age and older

David C. Kingston¹, Kassondra Collins², Samuel K Essien², Audrey R. Zucker-Levin²

¹Department of Biomechanics, University of Nebraska Omaha, Omaha, USA

²School of Rehabilitation Science, University of Saskatchewan, Saskatoon, Canada

Email: dkingston@unomaha.edu

Summary

Young adults accommodate the increased energy expenditure, coordination, stance limb and hand discomfort associated with walking aids for non-weightbearing (NWB) ambulation, but it is unknown if adults over 50 years of age have such tolerance. The objective of this study was to determine how walking aid selection affects stance limb plantar force, walking speed, perceived exertion, and device preference in mature adults. Twenty-one participants walked 200 m unaided and NWB with three walking aids: crutches, walker, and wheeled knee walker (WKW). An in-shoe sensor measured plantar force, each walk was timed, perceived exertion (RPE) was reported using the BORG CR-10 scale, and device preference was self-identified. Using a WKW for NWB ambulation reduced stance foot plantar force, maintained unaided walking speed and perceived exertion, and was preferred to crutches or a walker.

Introduction

Walking aids are prescribed to offload injured lower extremities. Little consideration has been given to the effect of device selection on stance foot loading and exertion in mature adults. Standard walking aids, such as crutches and walkers, cause axillary/hand pain and/or stance limb pain in 68% of users when used for NWB ambulation [1,2]. Understanding how diverse walking aids effect stance limb plantar force, walking speed, step frequency, and RPE will help guide clinical recommendations for patient use.

Methods

This study was a prospective, randomized cross-over design. Participants were 50 years of age or older and in good overall health with no self-reported conditions that would affect walking. Walking aids were fitted to each participant. Participants choose their stance foot while the other was completely unloaded.

An insole force sensor (LoadSol®, Novel Inc., St. Paul MN) was fitted in the shoe of the stance foot to wirelessly record

plantar force at 100 Hz [3]. Participants then completed four NWB walking trials of 200 m, on a straight 50 m indoor path free of any obstructions with a randomized presentation of walking aid. Time to complete each walking trial was used to calculate self-selected walking speed. Participants stated their RPE and were given two minutes rest after each trial. Participants ranked walking aid preference. Individual steps were identified using a 50 N threshold from plantar force timeseries data. Steps occurring within 30-60 sec of each trial was reported as step frequency. One-way repeated measures ANOVAs were performed for each outcome variable with an a priori $\alpha = 0.05$ and Bonferroni correction for multiple comparisons.

Results and Discussion

Average plantar force was at least 75% lower when participants used a WKW when compared to other walking aids (Table 1). Self-selected walking speed did not differ between unaided walking or when using the WKW (Table 1). Step frequency was at least 27% higher in unaided walking but not different amongst walking aids (Table 1). RPE was 72% lower for unaided walking and 50% lower for WKW use when compared to crutches or a walker (Table 1). Participants overwhelmingly preferred the WKW over other walking aids as 20 of 21 participants stated they would use it as opposed to crutches or a walker.

Conclusions

Reduced plantar forces, maintenance of self-selected walking speed, and a minimal increase to RPE may justify the prescription of the WKW over other walking aids for ambulation.

References

- [1] Bertrand et al. (2017). *AmJPhysMedRehab*, **96**: 894-903.
- [2] Patel et al. (2016). *Foot*, **28**:7-11.
- [3] Burns et al (2019). *JSportSci*, **37**: 1129-1138.

Table 1: Summary walking parameters and rating of perceived exertion (RPE). Values that share superscripted letters (a-d) are not different at the $p < 0.05$ level. Bold values emphasize significantly different values. WKW represents wheeled knee walker.

Condition	Average plantar force (N)		Self-selected walking speed (m/s)		Step frequency (steps/min)		RPE (0-10)	
	Mean	95% CI	Mean	Range	Mean	Range	Mean	Range
Unaided	345.3 ^a	307.6-382.9	1.41 ^a	1.18-1.68	57.9^a	28-70	1.6 ^a	1-4
Crutches	433.9^b	380.4-487.4	0.76^b	0.29-1.24	39.1 ^b	24-50	5.7^b	3-8
Walker	480.0^b	420.9-539.2	0.42^c	0.23-0.74	37.1 ^b	26-54	6.1^b	4-8
WKW	84.6^{b,c}	57.5-278.4	1.31 ^a	0.8-2.0	42.3 ^b	28-54	2.7 ^a	1-6

Data Collection Settings Influence Total Body Angular Momentum: Effects of Walking Speed and Participant Sex

Jackson Lordall¹, Alison Oates¹, Joel Lanovaz¹
¹University of Saskatchewan, Saskatoon, SK, CA
 E-mail: Jackson.Lordall@usask.ca

Summary

The study explored the influence of setting on total body angular momentum during walking at different speeds in male and female young adults. Settings impacted ranges of total body angular momentum while walking at slow and self-selected speeds, with the greatest ranges in a laboratory setting and the smallest ranges in an outdoor setting. There were larger ranges of total body angular momentum at slow speeds and smaller ranges at self-selected and fast speeds. Total body angular momentum in the frontal plane was greater for males, independent of setting and speed condition.

Introduction

Recent developments in wearable sensor technology allow complex measures of behaviour to be explored outside of a laboratory setting. Total body angular momentum (H) during walking is highly regulated to maintain stability [1-3]. An increase in the range of H suggests reduced control of angular motion about the total body centre of mass [1]. The objective of the current study was to explore how H is affected by setting when walking at different speeds in male and female young adults.

Methods

Healthy young adults walked in four different settings: laboratory (10m); standard hallway (20m); large indoor open space (20m); and outdoors along an open pathway (20m). Participants walked at three different speeds (slow, self-selected, and fast) following standardized verbal instructions. The order of settings and walking speed conditions were block-randomized. Participants wore an inertial-based full body kinematic data collection system (Xsens Awinda, Culver City, CA, fs=60Hz). The range for anterior-posterior (AP) and medial-lateral (ML) H over a stride (H_{AP} and H_{ML}) were computed with a 16-segment model [4] using data from the middle strides of each trial (~440 strides/participant). H data were normalized to participant height, walking speed, and mass [2,3]. A 4 x 3 x 2 (setting x walking speed x participant sex) RM ANOVA was conducted for each dependent variable. Significant interaction effects were investigated using multiple RM ANOVAs with adjusted pairwise comparisons. Violations of sphericity were corrected using the Greenhouse-Geiser correction and significance was set at $\alpha = 0.05$.

Results and Discussion

A total of 14 males (age = 23 ± 4 yrs; height = 181 ± 7 cm; mass = 79 ± 1 kg) and 15 females (age = 22 ± 4 yrs; height = 170 ± 7 cm; mass = 70 ± 2 kg) participated. Outlier analysis excluded data for one female. Significant setting x speed interactions for H_{AP} ($F(3.358, 87.296) = 13.496, p < .001$) and H_{ML} ($F(2.523, 65.603) = 11.033, p < .001$) were found (Figure 1). Values for H_{AP} and H_{ML} were significantly larger in the slow condition, regardless of setting. For the self-

selected condition, H_{AP} was greater in the lab compared to the large indoor area and outdoor setting, and in the hallway compared to outdoors. For the slow condition, H_{AP} was greater in the lab compared to the hallway, large indoor area, and outdoors; and greater in the hallway and large indoor area compared to outdoors. For the slow condition, H_{ML} was greater in the lab compared to the large indoor area and outdoors, and in the hallway compared to outdoors. No setting effects were found for the fast condition. There was a significant main effect of sex for H_{ML} (male = $.034 \pm .008$, female = $.028 \pm .007, F(1, 26) = 5.937, p = .022$).

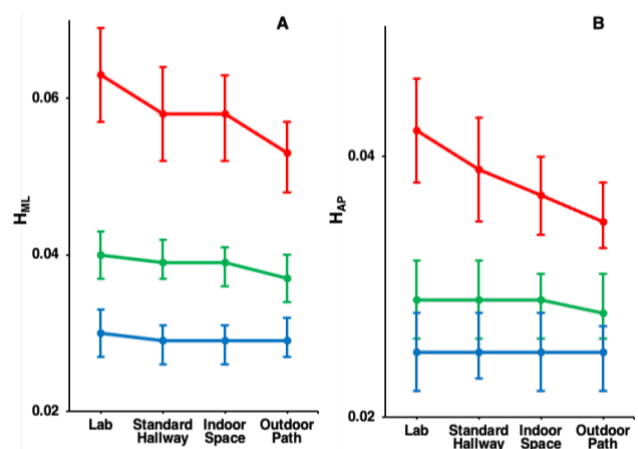


Figure 1: Mean H data (+/- 95%CI, A: H_{ML} , B: H_{AP}) in different settings at different walking speeds (slow, self-selected, fast).

Data suggest that ranges of H increase as walking speed decreases, aligning with previous research [3]. Settings had a greater influence on H in the slow condition, suggesting that having individuals walk at different speeds can provide insight on mechanisms of locomotor control. Setting influenced AP and ML angular momentum at slow walking speeds and in the AP direction at self-selected speeds, suggesting that H during walking in laboratory settings may not be reflective of H during walking in indoor and outdoor non-laboratory settings. H_{ML} was greater for males, independent of settings and speed condition, which could be partly due to greater ML trunk ranges of motion in young adult males [5]; however, further exploration is required to explain these sex-based differences.

Conclusions

H was influenced by settings during walking at slow and self-selected speeds, with larger ranges of H in a laboratory setting. H_{ML} was greater for males which could be related to sex-based differences in locomotor control [5].

References

- [1] Begue J et al. (2019). *Exp. Gerontol.*, **127**: 110714.
- [2] Herr H et al. (2008). *J. Exp. Biol.*, **211**: 467-481.
- [3] Bennett BC et al. (2010). *Hum. Mov. Sci.*, **29**: 114-124.
- [4] De Leva P. (1996). *J. Biomech.*, **29**: 1223-1230.
- [5] Bruening DA et al. (2015). *Gait Posture*, **41**: 540-545.

Adaptations in mechanical limb power and metabolic energy cost after chronic growth-period limb loading

Katugam, K¹, Johnson, T¹, Dechene, I¹, Cox, SM^{1,2}, Piazza, SJ¹, Rubenson, J¹.

¹Department of Kinesiology, Pennsylvania State University

²Department of Ecology and Evolutionary Biology, University of California, Irvine

Email: kavya@psu.edu

Summary

How locomotor mechanics and energetics are affected by long-term alterations to external loading during growth remains largely unknown. Here we test whether a reduction in mechanical limb work contributes to a lower cost of carrying externally-applied limb mass after chronic loading. We find that animals subjected to increased limb loading across their growth period do not adapt their mass-specific mechanical power during limb swing to achieve a lower walking metabolic power.

Introduction

Humans and other animals adapt to expend the least amount of energy to complete a movement task, both over acute [1,2] and evolutionary timeframes [3]. Whether adaptations in locomotor economy occur in response to altered life history (e.g. environmental fluctuations, or training in humans) remains less clear. Furthermore, the mechanical underpinning to developmental adaptations in locomotor economy have not been well explored.

Here we test the hypothesis that a reduction in mechanical limb work contributes to the lower cost of carrying externally-applied limb mass after chronic loading. Specifically, we hypothesize that (1) limb-loaded animals (LL) locomote with added mass using less mechanical power (Watts/kg) than control (CON) animals, (2) the increase in mechanical power between unweighted and weighted conditions will be smaller for LL animals than CON animals, and finally (3) if mechanical power is a strong determinant of the metabolic plasticity.

Methods

To study the effect of load stimulus on locomotor mechanics and energetics, we applied a mass equal to 3.5% body mass unilaterally to the lower limb of a group of guinea fowl continuously from 1-16 weeks of age (limb-loaded group, LL; n = 6). We raised a second group of birds in the same conditions but with no external limb loading (CON group; n = 6). At 16 weeks of age, we measured the metabolic power of walking on a treadmill at 0.5 m/s in both unilaterally-loaded and non-loaded conditions. The mass-specific power of walking of unilateral limb loading was 26% greater in the CON group compared to the LL group (p = 0.03). The power of walking in the habitual condition (limb loaded in LL; unloaded in CON) was the same for both groups, despite the LL group moving substantially more limb mass.

Birds limb joints and body segments were marked and video recorded (Point Grey, Grasshopper 3, Richmond, BC) walking for 20-second bouts at 0.5 m/s, both loaded and

unloaded. An inverse dynamic formulation was used to compute instantaneous joint power during the swing-phase. Work (joules/kg) was computed per animal per load condition by integrating each instantaneous joint power curve and summing across all joints. Positive mechanical power (watts/kg) was computed by dividing the positive work of the swing phase by the stride time. Five strides were used to generate averages per animal per load condition.

Results and Discussion

Average total swing-phase positive power for LL animals when compared to CON animals was 55% greater for the unweighted condition (p = 0.15), and 22% greater for the weighted condition (p = 0.067). Average total swing-phase positive power of the habitual conditions for each group (unweighted for CON, 3.5% weighted for LL) were significantly different, with LL habitual power being 109% greater than CON habitual (p = 0.01).

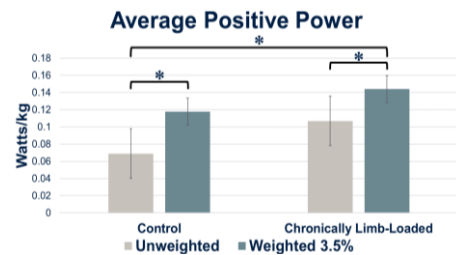


Figure 1: Average positive power (watts/kg) computed across 5 swing phases per group per condition.

Conclusions

Contrary to our hypothesis, animals subjected to increased limb loading across their growth period do not adapt their mass-specific mechanical power during limb swing to achieve a lower metabolic power. Surprisingly, LL animals exhibit comparatively greater mechanical power, despite their lower metabolic power. The lower mechanical power in CON may represent an offloading strategy, but one that incurs a higher metabolic cost. Future directions for this work include analyses of limb mechanics of the contralateral limb, as well as adaptations to muscle architecture/physiology.

Acknowledgments

Supported by NIH Grant R21AR071588.

References

- [1] Alexander RM. (2003). *Prin Animal Loc*, Princeton Univ. Press.
- [2] Hoyt & Taylor (1981) *Scienc*
- [3] Snell-Rood EC (2012). *Integr Comp Biol*, **52**: 31-42

Stepping kinematics indicate minimal disruptions to balance control when linking the arms and legs during walking

Daisey Vega¹, Helen J. Huang², Christopher J. Arellano¹

¹Center for Neuromotor and Biomechanics Research, Dept. of Health and Human Performance, Houston, Texas, USA

²Dept. of Mechanical and Aerospace Engineering, Orlando, Florida, USA

Email: dvega2@cougarnet.uh.edu

Summary

Using the arms to assist the legs during treadmill walking provides both mechanical and metabolic benefits. Our stepping kinematic analyses reveal little to no changes in walking balance, suggesting that linking the arms and legs may be useful for gait rehabilitation.

Introduction

Coordinating the active use of the arms with the motion of the legs shows promise for gait rehabilitation [1]. In recent work, we developed a rope-pulley system that links the arms and legs during treadmill walking [2; Fig. 1]. We discovered that the arms harnessed energy from the treadmill via the rope connection which provided an assistive force to the body. This significantly reduced the need for propulsion and the net metabolic power required to walk. However, we observed greater arm swing ranges with rapid transitions and greater collision forces, which may have disrupted the control of balance from step-to-step. Disrupting a patient's ability to maintain balance could increase fear of falling, hinder walking recovery and/or lead to a direct fall. Therefore, understanding if and to what extent balance control was compromised would help determine if this type of assistive approach could feasibly translate to clinical users. As indicators of balance, we quantified step width, step length, step time, and variability. We hypothesized that these indicators of balance control would remain the same when walking normally and when walking with the arm-leg assistive device.

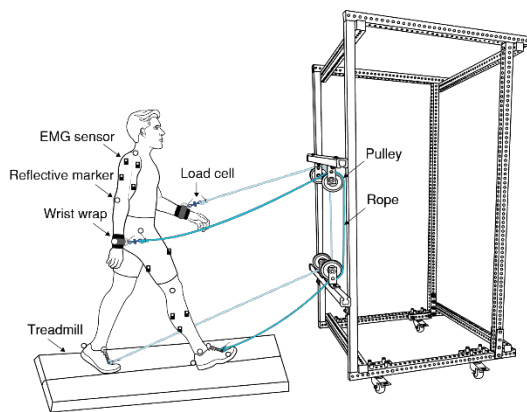


Figure 1: Arm-leg rope pulley system.

Methods

Eight young, healthy subjects (3 women, 5 men) participated in the study. Subjects performed two randomized walking trials: (1) Normal and (2) Assisted (walking with the arm-leg pulley system) on a treadmill at 1.25 m/s. A twelve-camera motion capture system recorded the 3-D positions of reflective

body markers (100 Hz) during the last 3 min of each 7 min trial. We calculated foot placement from the left and right heel marker positions and used 288 steps as the minimum number of steps for all subjects. We calculated average and standard deviation values for all step parameters. We then normalized step width and length by leg length (% LL), and step time by $\sqrt{LL/g}$. Paired sample *t*-test, or the non-parametric Related Samples Wilcoxon Signed Rank test, were performed.

Results and Discussion

When compared to normal walking, we found that linking the arms and legs during assisted walking revealed no significant differences in step length and step time ($p > 0.05$). However, subjects increased their step width by 31% ($p = 0.012$, Fig. 2). Despite adjustments in step width, the variability of step width and step length did not differ between conditions ($p > 0.05$). Step time variability, however, increased by 39% compared to normal walking ($p = 0.008$, Fig. 2).

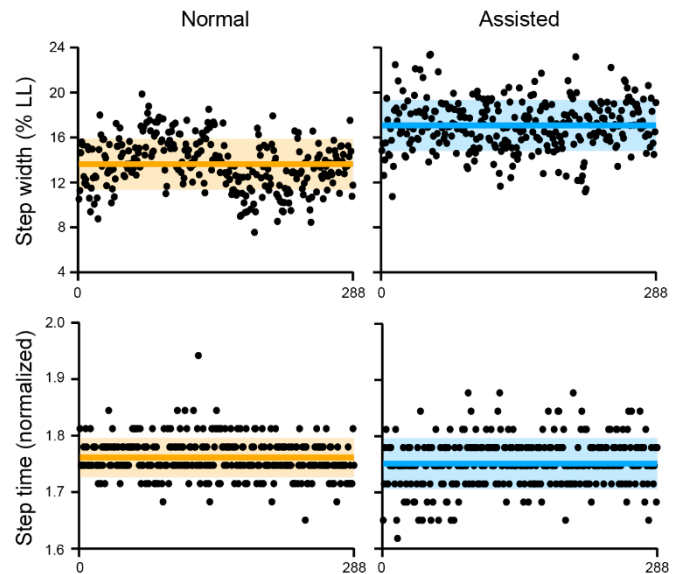


Figure 2: Representative data for both conditions ($n = 1$). Average and SD values shown as solid lines and shaded regions, respectively.

Conclusions

Our step-to-step kinematic analyses reveal minimal disruptions to balance control when linking the arms and legs during walking. Our future work aims to test this assistive device in patients recovering from a spinal cord injury.

References

- [1] Ferris DP et al. (2006). *Exerc Sport Sci Rev.*, **34**: 113-120.
- [2] Vega D and Arellano CJ. (2021). *J Neuroeng Rehabil.*, In review.

Lower-limb impact loading and bone stimulus in children during a week-long protocol

Danilo S. Catelli¹, Sasha Carsen² and Mario Lamontagne¹

¹ Human Movement Biomechanics Laboratory, School of Human Kinetics, University of Ottawa, Canada

² Children's Hospital of Eastern Ontario, Ottawa, Canada

Email: danilo.catelli@uottawa.ca

Summary

Step counting and chart logs are insufficient for quantifying activity types/levels/intensity in the pediatric population. Wireless inertial sensor units were able to differentiate activity intensity based on step impact levels between very and less active children. This study demonstrates the potential of a week-long protocol to self-monitor step intensity activity and to compare lower-limb impact loads, impact symmetry and bone stimulus in active and less-active children.

Introduction

Excessive physical activity and loading of the proximal femoral growth plate are considered determinants to the development of cam-type hip morphology [1,2]. Physical activity monitoring based on step counting, only, gives limited information about activity intensity or limb loading. Impact loading and load symmetry of the lower-limbs provide supplementary metrics about limb overload, that can be used to monitor bone load stimulus [3], and to the development of cam-type hip morphology. Specific physical activities and intensity may be linked to several forms of pediatric injury and development. Step counting and patient/family logs are insufficient for accurately quantifying and comparing activity types/levels/intensity in the pediatric population. The purpose of this study is to (1) demonstrate the potential of a week-long protocol data outcome to self-monitor step intensity activity in children; and to (2) compare lower-limb impact loads, impact symmetry and bone stimulus in active and less-active children.

Methods

Nine healthy children, five considered very active (VA, over 1,000 steps/h, 1F/4M, 10±3 years old, BMI 14±2 kg/m²), and four less-active (LA, less than 1,000 steps/h, 1F/3M, 10±3 years old, BMI 16±4 kg/m²) were monitored for 6 to 12h/day for five consecutive days. Two wireless inertial sensor units (IMU) sensors (Blue Trident, IMeasureU, NZ) recorded and computed the participant's physical activity intensity. The sensors were strapped just above the malleolus on both legs. The data were collected and pre-processed using STEP software (IMeasureU, NZ) to obtain the step count and acceleration normalized by gravity (g) of each step, and exported in Matlab (MathWorks, USA) to further analysis. All variables were time-normalized per hour. Step Impact (SI) was classified by low (below 5g), medium (6 to 20g) and high (over 21g) accelerations. Impact load (IL) was calculated based on the sum of each intensity created from every SI. Symmetry indexes were computed for the low, medium and high impact steps. Bone stimulus was computed per day [3].

Results and Discussion

VA averaged 44% greater number of steps/hour (1235±286) than LA (853±159). Within the total number of steps, the proportional SI for the VA group was 68±11% (823±156 steps/h) in the low, 25±9% (320±168 steps/h) in the medium, and 7±4% (92±53 steps/h) in the high levels; compared to 63±7% (540±115 steps/h), 29±7% (249±86 steps/h) and 7±0% (64±14 steps/h) of the LA, respectively. Symmetry indexes were very similar between the groups for low (VA:1±0%, LA: 2±1%), medium (VA:3±1%, LA: 4±4%) and high impacts (VA:5±4%, LA: 5±1%). VA averaged 58% greater IL per minute (76±30 n_{step}*g/min) than LA (51±13 n_{step}*g/min), but similar bone stimulus per day (VA:260±29, LA:253±11).

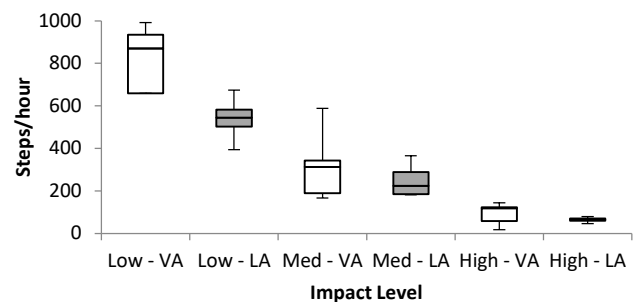


Figure 1: Average and standard deviation of steps per hour performed by the very active (VA, white) and less active (LA, gray) participants, separated by step impact levels (low, medium and high).

Conclusions

Wireless inertial sensor technology was able to differentiate activity intensity based on step impact levels between VA and LA children. The VA children performed more steps/hour in all SI levels, and as well as the LA, with very similar proportion among the three impact levels. The higher standard deviation found in medium and high impact levels for the VA group, can be an evidence that not all children within that group reached the step count during sports activities, but perhaps prolonged low-impact daily activities (e.g. walking to the school). The VA children showed 58% higher IL/hour when compared to LA, but the similar bone stimulus outcomes (due to its saturation over time) [3], can be indicative that this type of metric creates a limitation for prolonged data collections. This type of protocol illustrates a more precise indicator of activity level and intensity than step count alone. Likewise, this type of protocol allows minimal or no physical interaction between researchers and volunteers, and can offer an opportunity to collect motion data during periods when people are carrying out physical distancing measures.

References

- [1] Jamieson P et al. (2017). *Hip Symp COA/CORS*, 125.
- [2] Carsen S et al. (2014) *Clin Orthop Relat Res*, **472**:430-6.
- [3] Beaupre GS and Orr TE (1990). *J Orthop Res*, **8**: 651-661.

Novel Clamp Protocol Examines Cause-Effect Relations Between Propulsive Force, Walking Speed, and Cost of Transport

Richard E. Pimentel¹, Jordan N. Feldman¹, Michael D. Lewek², Jason R. Franz¹

¹Joint Dept. of BME, UNC Chapel Hill and NC State University, USA ²Division of Physical Therapy, UNC Chapel Hill, USA
Email: rickypim@live.unc.edu

Summary

This study sought to examine cause-effect relations between peak propulsive force (F_P), walking speed, and metabolic cost of transport in young adults. In different experimental trials, we clamped walking speed or peak F_P using targeted biofeedback and a self-pace treadmill controller. We show in part that walking with larger/smaller F_P yields faster/slower walking speeds. These cause-effect relations may inform the time course of gait changes due to age and disease and build confidence that interventions designed to increase peak F_P may translate to improved walking speed.

Introduction

Walking speed serves as a simple surrogate for human health status and ambulatory function. The selection of walking speed in healthy young adults is often attributed to minimizing the metabolic cost of transport (CoT). However, declines in walking speed due to age or disease are frequently accompanied by smaller propulsive forces (F_P) during push-off. Thus, F_P is considered a biomechanical determinant of walking speed. However, no study to our knowledge has established empirical cause-and-effect relations between F_P , walking speed, and CoT, even in healthy young adults. Our purpose was to: (1) investigate if F_P governs the selection of walking speed using real-time targeted biofeedback and self-pacing treadmill control, and (2) quantify how metabolic energy cost shapes the relation between F_P and walking speed. We ultimately aim to better understand the time course of gait changes due to age or disease and to inform targeted interventions.

Methods

Ten young unimpaired adults have thus far participated (5F/5M; age: 25.2 ± 5.8 years, typical overground walking speed: 1.40 ± 0.10 m/s, typical F_P : 21.5 ± 2.4 %BW). We first determined participants' typical overground walking speed (4 passes of 30 m). Next, participants completed five 5-minute trials on a dual-belt instrumented treadmill at a fixed speed.

We recorded participants' average peak F_P at their typical speed as well as at $\pm 10\%$ and $\pm 20\%$ of that speed in randomized order (speed clamp). Participants then walked for 5 minutes each on the same treadmill in a self-paced mode while responding to a visual biofeedback paradigm to target their average peak F_P from each of the fixed-speed trials (F_P clamp). The self-paced mode adjusted speed in real-time based on subjects' anterior-posterior position on the treadmill. We measured rates of oxygen consumption and carbon dioxide production, which were averaged over the final 2 minutes of each trial to calculate net metabolic CoT using standard procedures. We averaged speed and F_P over the same time period. A two-way repeated measures ANOVA analyzed differences in walking speed, F_P , and CoT between clamp types (fixed-speed vs. F_P targeting) and condition intensity.

Results and Discussion

Subjects increased and decreased F_P and CoT in response to faster and slower walking speed and increased and decreased walking speed and CoT in response to larger and smaller F_P , respectively (p -values < 0.05 , Figure 1). Significant condition \times clamp interaction effects revealed that walking speed and CoT were less sensitive to the F_P clamp versus the speed clamp when decreasing condition intensity. In other words, participants selected faster speeds at a higher CoT for those conditions despite identical F_P . Additionally, F_P was less sensitive to the F_P clamp when increasing condition intensity; we were surprised to find that participants walked at the same speed and with the same CoT despite lower F_P .

Conclusions

We provide evidence that walking with larger/smaller F_P yields faster/slower walking speeds paralleled by changes in CoT in young adults. However, these cause-effect relations are more complex than previously appreciated and are not always governed by minimizing metabolic cost of transport.

Acknowledgments

Funded by NIH (R01AG058615)

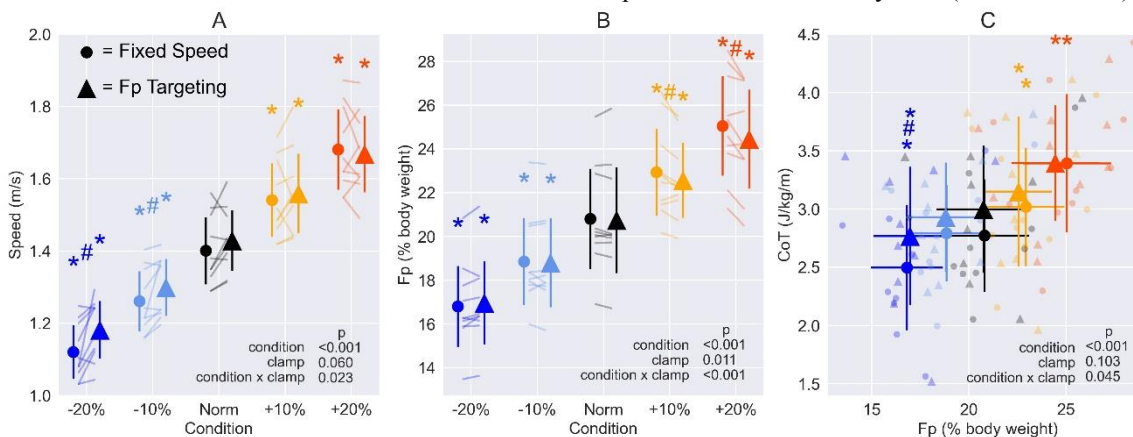


Figure 1. (A) Speed and (B) F_P across condition intensities for each clamp type (prescribed speed vs prescribed F_P) and (C) resultant changes in metabolic cost of transport. Asterisks (*) indicate a significant ($p < 0.05$) pairwise difference versus preferred condition (Norm). Hashtags (#) indicate a significant ($p < 0.05$) pairwise difference between clamp types.

Contribution of the transverse arch to *in vivo* foot stiffness in humans

Ali Yawar¹, Lucia Korpas¹, Shreyas Mandre², and Madhusudhan Venkadesan¹

¹Department of Mechanical Engineering and Materials Science, Yale University, New Haven, CT, USA

²Mathematics Institute, University of Warwick, Coventry, UK

Email: ali.yawar@yale.edu

Summary

The human foot is stiff enough to withstand ground forces and not bend severely when walking and running. The foot's medial longitudinal arch and transverse tarsal arch are key contributors to this bending stiffness. The transverse arch is hypothesized to stiffen the foot by coupling sagittal plane midfoot bending with the stretching of intermetatarsal tissues. This cross-axis coupling hypothesis has so far only been tested in cadaveric feet. However, active muscle contraction is known to influence the stiffness contribution of the longitudinal arch, and may similarly affect transverse arch function. We tested this hypothesis *in vivo* by increasing intermetatarsal stiffness at the forefoot and measured the resulting change in the foot's bending stiffness in standing human volunteers. We find that the cross-coupling hypothesis carries over *in vivo*, and suggest strategies for foot stiffness augmentation in clinical and athletic settings.

Introduction

The cross-axis coupling hypothesis arising from the foot's transverse tarsal arch was recently tested in static loading experiments on cadaveric feet [1]. Surgically incising the intermetatarsal tissues led to a significant loss of foot bending stiffness [1], suggesting a coupling between midfoot bending stiffness in the sagittal plane and transverse intermetatarsal stiffness. While cadaveric studies identify the contribution of passive tissues to the baseline stiffness of the foot, muscle activity is known to modulate around it [2]. Such modulation is well understood in the context of the longitudinal arch, but muscles with insertions in the transverse arch could similarly influence its stiffness contribution. This motivates an *in vivo* test of the cross-axis coupling hypothesis. We wrapped elastic tape around the forefoot to increase intermetatarsal stiffness and measured the resulting change in foot stiffness to assess the extent of the cross-axis coupling. If the hypothesis holds *in vivo*, we expect foot stiffness to increase upon taping.

Methods

We used two methods to measure the change in foot stiffness. First, the height of the midfoot above ground h when supporting half bodyweight on the forefoot provided an indirect midfoot stiffness measure. Second, we used the windlass mechanism of the foot to deliver a perturbative midfoot torque by externally dorsiflexing the toes by $\Delta\theta$ and measured the change in midfoot height Δh . The ratio $\Delta h/\Delta\theta$ is inversely proportional to the midfoot stiffness K . All measurements were made in standing human subjects under three conditions (Figure 1a): (i) *free* - with no tape, (ii) *tape* - with the forefoot tightly wrapped, and (iii) *control* - with loosely wrapped tape. Subjects received live feedback to maintain consistent half bodyweight load under the ball of the foot. Free and taped stiffness measures were normalized by the control condition, and compared using a one-way ANOVA and pairwise comparisons between conditions.

Results and Discussion

Forefoot taping led to an increase in both measures of foot stiffness. Midfoot height with the forefoot tape was significantly greater than the control condition (mean \pm std. error = $2.0\% \pm 0.4\%$, $p < 0.0001$), but not in the free condition ($-0.5\% \pm 0.3$, $p = 0.12$) (Figure 1b). The stiffness K found using the perturbative torque was significantly greater in the taped condition than the control ($76\% \pm 19\%$, $p = 0.0002$), but not in the free condition ($4\% \pm 19\%$, $p = 0.82$) (Figure 1c). These results show that cross-axis coupling between midfoot stiffness and transverse intermetatarsal stiffness is present *in vivo*. Therefore, the muscle activity involved in forefoot bodyweight support does not disrupt this coupling. The finding and the methodology to experimentally alter midfoot stiffness paves the way for future studies to investigate how the transverse tarsal arch and the cross-axis coupling it introduces could influence dynamical foot stiffness modulation during locomotion. Our non-invasive foot taping protocol may find application in the management of disorders that cause a loss of foot stiffness, and in the augmentation of foot stiffness in athletic settings.

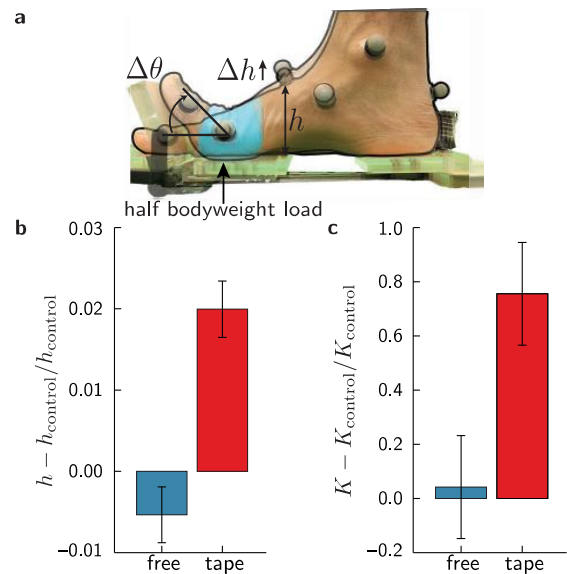


Figure 1: Foot stiffness change because of forefoot taping. a. A foot in the taped condition, showing the measured midfoot height h , and the change in height Δh upon dorsiflexion of the toes by $\Delta\theta$. Bar plots of b, the midfoot height and c, the stiffness estimated using the perturbative midfoot load in the free and taped conditions relative to control. Whiskers show standard error of the mean (n=7).

Conclusions

Cross-axis coupling due to the transverse arch significantly contributes to *in vivo* foot stiffness.

References

- [1] Venkadesan M et al. (2020) *Nature* **579** 97-100
- [2] Kelly LA et al. (2014) *J. R. Soc. Interface* **11** (93), 20131188

Movement decreases muscle and tendon stiffness compared to torque and angle matched isometric conditions

Kristen L. Jakubowski^{1,2,4}, Daniel Ludvig^{1,4}, Sabrina S.M. Lee², Eric J. Perreault¹⁻⁴

¹Department of Biomedical Engineering, ²Department of Physical Therapy and Human Movement Sciences, ³Physical Medicine and Rehabilitation, Northwestern University, Chicago, IL, USA; ⁴Shirley Ryan AbilityLab, Chicago, IL, USA
Email: kristen.jakubowski@northwestern.edu

Summary

While muscle and tendon govern ankle impedance, it remains unknown how the muscle and tendon contribute to the decrease in ankle impedance during movement compared to postural conditions. This is largely due to a lack of *in vivo* measurement techniques for quantifying muscle and tendon impedance during movement. We recently developed a novel measurement technique that simultaneously quantifies muscle, tendon, and ankle impedance. This study uses our technique to determine how muscle and tendon govern ankle impedance between posture and movement. We observed that the decrease in ankle impedance during movement is mainly driven by decreased muscle impedance with a small, unexpected decrease in tendon impedance. Unlike postural conditions where ankle impedance is primarily governed by the tendon, during movement, muscle and tendon impedance were similar. These data provide the first *in vivo* measurements on how muscle and tendon govern ankle impedance between posture and movement.

Introduction

Ankle impedance during movement is decreased compared to postural conditions [1]. However, it is unknown how changes in the muscle or tendon, the structures that govern ankle impedance, drive this decrease. This gap is largely due to a lack of *in vivo* measurement techniques to quantify muscle and tendon impedance during movement. We recently developed a novel *in vivo* measurement technique using ultrasound to address this overall gap [2]. Using this technique, this ongoing study aims to determine how the contribution from the muscle and tendon to ankle impedance differs between posture and movement. Previous *in situ* muscle impedance measurements suggest that muscle impedance varies not only between posture and movement but also within a movement between concentric and eccentric contractions [3]. In contrast, tendon impedance scales with force and, to our knowledge, does not vary between force-matched postural and movement conditions. Thus, we hypothesize that the decrease in ankle impedance during movement is due to decreased muscle impedance.

Methods

Three young adults were seated with their right foot rigidly secured to a rotary motor and 6-degree-of-freedom load cell. The motor controlled the position of the ankle while subjects produced voluntary plantarflexion torque at 15% of their maximum. The motor moved the subject's ankle through a 20-degree sinusoidal motion resulting in periods of eccentric and concentric contractions. Four isometric conditions were also tested (Figure 1a) within the same range as the imposed movements. Small stochastic perturbations were superimposed on the large sinusoidal movement and isometric conditions to quantify ankle impedance [2]. Muscle and tendon displacement was measured using B-mode ultrasound to track the medial gastrocnemius muscle-tendon junction. We estimated ankle, muscle, and tendon impedance from the collected data [2]. Here we present the stiffness component of these impedances.

Results and Discussion

Ankle and muscle stiffness decreased by an average of 42% and 62%, respectively, during movement relative to isometric conditions ($p < 0.001$ for both; Figure 1b & c). More surprisingly, we also found that tendon stiffness decreased by an average of 27% during movement ($p < 0.001$; Figure 1d). No difference was observed between concentric and eccentric contractions for ankle, muscle, or tendon stiffness. The muscle was 2.6x stiffer than the tendon during postural conditions but only 1.4x stiffer during movement. Since the muscle and tendon are connected in series, the stiffness of the ankle is dominated by the most compliant component. These results indicate that the tendon dominated ankle mechanics in the tested isometric conditions, but muscle and tendon contributed more evenly during movement.

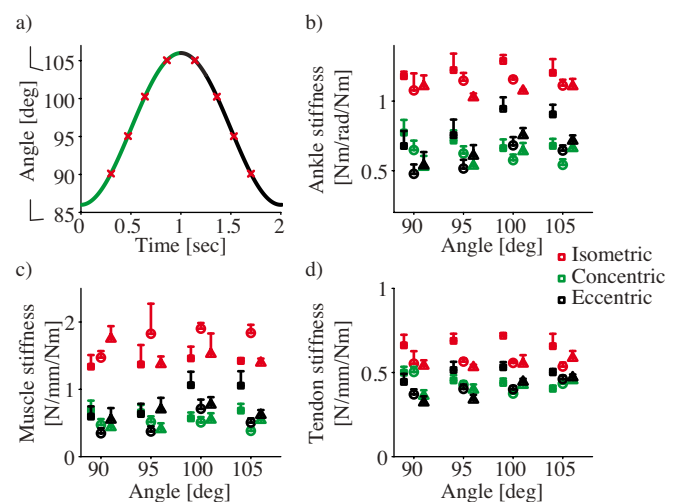


Figure 1: (a) During the movement condition, ankle angle was varied to produce concentric (green) and eccentric (black) contractions. Isometric contractions at matched angles were performed (red x's). Comparisons between ankle (b), muscle (c), and tendon (d) stiffness during the concentric, eccentric, and isometric contractions. Different symbols represent different subjects, and subjects are offset for ease of viewing.

Conclusions

Applying our novel technique, we demonstrate that the contribution from the muscle and tendon to ankle impedance differs between posture and movement. Prior to this work, muscle and tendon impedance could only be estimated. These data provide the first *in vivo* reference on how muscle and tendon govern ankle impedance during movement.

References

- [1] Rouse et al (2014). *IEEE Trans. Biomed. Eng.* **22(4)**: 870-878
- [2] Jakubowski et al (2020). *Eng. Med. Biol. Soc. Ann.* 4819-4822
- [3] Ettema and Huijing (1995). *J. Biomech.* **27**: 1316-1368

Knee extensor moment increases with reduced moment arm in running and walking

Mitchell G.A. Wheatley¹, Darryl G. Thelen², Daniel P. Borschneck³, Kevin J. Deluzio¹, Michael J. Rainbow¹

¹Department of Mechanical and Materials Engineering, Queen's University, Kingston, Canada

²Department of Mechanical Engineering, University of Wisconsin-Madison, Madison, USA

³Department of Surgery, Kingston General Hospital, Kingston, Canada

Email: mitchell.wheatley@queensu.ca

Summary

The patella extends the moment arm of the knee extensor mechanism, but it is less clear how its motion contributes to variation in the moment arm during stance. In this study, we used a lower-limb musculoskeletal model with a twelve degrees-of-freedom knee to simulate patella kinematics in walking and running. We compared variation in the moment arm to the variation in the moment caused by the knee extensors. We hypothesized that the knee extensor moment would increase with moment arm length. However, we found that the knee extensor moment increased with a decrease in moment arm in both walking and running. Future research will investigate muscle force contributions to knee velocity with variation in moment arm.

Introduction

The patella contributes to knee extension by increasing the knee extension moment arm and altering its mechanical contribution throughout the gait cycle [1]. The moment caused by the knee extensors can be calculated by multiplying the force from knee extensor muscles acting on the tibia with the knee extensor moment arm. Reducing the mechanical advantage by decreasing the extension moment arm may reduce the muscle shortening requirement during concentric contraction and may benefit joint velocity [2]. Moment arm advantages have been studied at the ankle [2], but there remains a lack of understanding of moment arm contributions at the knee in walking and running, due to the difficulty of measuring *in vivo* motion of the patella paired with muscle and ligament forces.

Musculoskeletal modelling is an approach that can be used to investigate *in vivo* tibiofemoral and patellofemoral mechanics [3]. Optimization algorithms are used to solve for secondary kinematics of the tibiofemoral joint and six degrees-of-freedom patellofemoral joint kinematics, as well as muscle and ligament forces. The objective of this study was to determine relationship of knee extensor moment production to moment arm length in walking and running. We hypothesized that the knee extensor moment would increase with an increase in moment arm.

Methods

Mean bone and cartilage geometry was calculated from a previously collected dataset of fourteen healthy knee MRIs [4]. Optical motion capture and GRF data were recorded for walking and running trials from ten participants. We incorporated kinematics and mean geometries into a validated, lower-limb musculoskeletal model with muscles, ligaments, and a twelve degrees-of-freedom knee joint. We sectioned gait depending on if the knee was flexing or extending and calculated the rotation axis of the knee as the change in pose of the tibia from the first frame of each section to the last frame of the same section. Knee extension

moment arms were calculated using a geometric method during stance [5].

We represented the knee extensor moment by the product of patellar ligament force normalised to body weight and moment arm. F-tests determined if the correlation between moment and moment arm length were non-zero with an alpha of 0.05 for each trial and section of stance. We performed linear regressions of each trial and section to determine the trend of the relationships. T-tests determined if the means of the slopes were non-zero.

Results and Discussion

Correlations between moment and moment arm length were all non-zero ($p < 0.004$) (Figure 1). The slopes of the sections and trials were non-zero ($p < 0.001$). There average slope for walking (-103.3 N/kg) and running (-298.8 N/kg) trials were both negative. These trends represent a decrease in moment arm with an increase in knee extensor moment in both walking and running. Higher forces in running allowed the peak running moment to be 112% larger than the peak walking moment walking and running had similar ranges of moment arm.

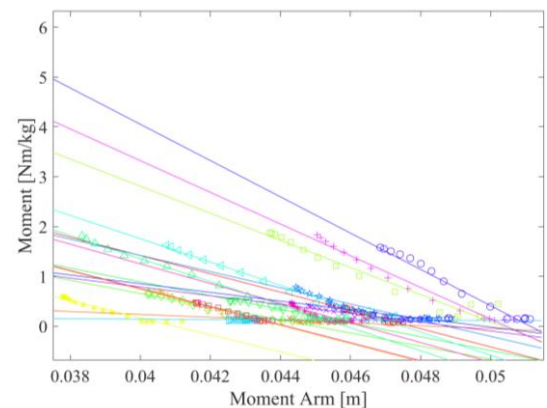


Figure 1: Linear regressions of correlations between moment and moment arm for the first section of stance in walking and running.

Conclusions

Contrary to our hypothesis, the knee extensor moment increased with a decrease in moment arm in both walking and running. Further research is required to determine how the increased force in running relates to muscle force-velocity properties and its contribution to knee extension velocity, though moment arms were similar in walking and running during stance.

References

- [1] Ellis, MI et al. (1980). *Eng Med*, **9**(4): 189-94.
- [2] Lee, SSM et al. (2009). *J Exp Biol*, **212**(22): 3700-7.
- [3] Lenhart, RL et al. (2015). *Ann. Biomed. Eng.*
- [4] Clouthier, AL et al. (2019). *Med Eng Phys*, **66**: 47-55.
- [5] Krevolin JL et al. (2004). *J Biomech*, **37**(5): 785-8.

Simulation-Based Exploration of the Anterior Drawer Test in Juvenile Patient Populations

Alexandria Mallinos¹, Brian Davis, Ph.D¹, Kerwyn Jones, MD²

¹Cleveland State University, Cleveland, OH, USA, ²Akron Children's Hospital, Akron, OH, USA

Email: a.mallinos@vikes.csuohio.edu

Summary

Every year, there will be more than 200,000 ACL tears in the US alone. In this study, the goal was to develop baseline knee models that accurately predict anterior tibial displacement when undergoing an anterior drawer test and provide a starting point for further knee model investigations. The models were able to predict tibial displacement measurements that are statistically similar to those obtained in clinical settings.

Introduction

Knee arthrometers have been used to evaluate the structural integrity of the anterior cruciate ligament (ACL). The purpose of this study was to establish baseline specimen-specific computational juvenile knee models that accurately predict the anterior drawer test (ADT). This study utilized data on normal ACL laxity measurements obtained using knee arthrometers [1-3]. These data were used to compare the anterior translation of the finite element representations (FER) of the knee joints under anterior loads of 67, 89, and 133 N.

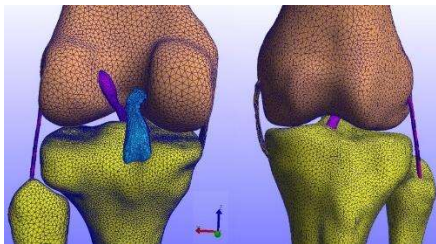


Figure 1: Sagittal plane view of the finite element model.

Methods

A total of 22 CT images of juvenile knees were utilized. The patients selected had no ACL pathologies and no bony deformations (ages: 9-18, males: n=16, females: n=6). 3D Slicer was used to convert the CT images into a three-dimensional representation of the bony anatomy. The bony anatomy was uploaded into FEBio to construct each tibiofemoral joint (Fig.1). The bones were defined as rigid bodies while the ligaments were modeled as incompressible transversely isotropic Mooney-Rivlin. The material properties of each bone and ligament were obtained from the Open Knee User's Guide and the ligament stl files were utilized for each model [4]. To replicate the ADT, the femur was fixed in all degrees of freedom while the tibia-fibula was only allowed anterior-posterior translation (y-axis). An anteriorly directed force was applied to the tibia-fibula at 67, 89, and 133 N.

Results and Discussion

The FER of the juvenile knees provides a realistic depiction of the ADT data obtained using knee arthrometers. The model predicted tibial displacement fell within the range of the experimental data (Fig. 2). The computer simulated models exhibited similar behavior to the experimental data by

increasing in anterior tibial displacement with each loading force level: 4.4 mm, 5.4 mm, and 7.3 mm. A two-sample t-test ($\alpha=0.05$) was used to analyze the differences between the experimental and predicted data for each force level. The calculated p-values (0.27, 0.49, 0.15) were all greater than α which concludes that there are no significant differences between the experimental and simulated ADT.

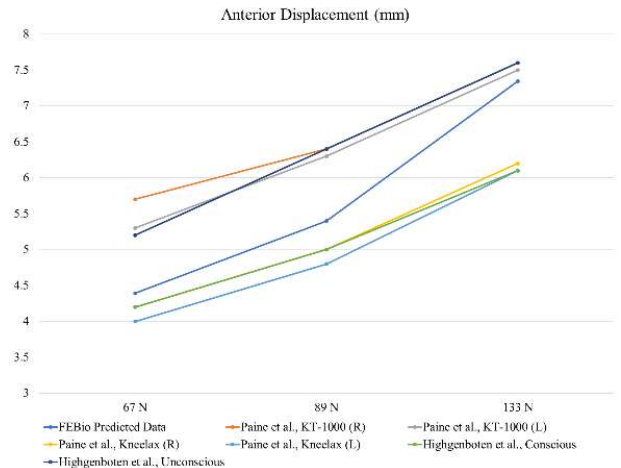


Figure 2: Graphical representation of the FEBio predicted anterior displacement versus the experimental data published in the literature using a knee arthrometer.

Simulations run at 67 and 89 N fell within the midrange of the clinical studies. This is a novel and important advancement because it provides a solid foundation at which to assess the in vivo biomechanics of the knee and its ligaments. At 133 N, the mean ADT is skewed towards the higher end of the experimental range. A possible factor as to why this occurs at higher forces can be due to natural physiological barriers such as the muscles and skin that prevent excessive anterior tibial translation and are not represented in the models.

Conclusions

Despite the limitations of this study, the FER were able to accurately simulate the ADT, predicting tibial displacement that is representative of the clinical data available in the literature.

References

- [1] Highgenboten, C. L., et al., (1992). KT-1000 arthrometer: conscious and unconscious test results using 15, 20, and 30 pounds of force. *Am J Sports Med*, 20(4), 450-454.
- [2] Paine, R., et al. (2012). Comparison of Kneelax and KT-1000 knee ligament arthrometers. *J. Knee Surg*, 25(2), 151.
- [3] Rangger C, et al. Diagnosis of an ACL disruption with KT-1000 arthrometer measurements. *Knee Surg Sports Traumatol Arthrosc*. 1993;1(1):60-66.
- [4] Erdemir, A., & Sibole, S. (2010). Open knee: a three-dimensional finite element representation of the knee joint. User's guide, 1(0).

Lower Extremity Biomechanical Demands of a Bend and Pick-Up Task in Healthy, Older Adults

Moore, J¹; Kanwar, K¹; Lee, H¹; Cai, G¹; Hawkes, R²; and Salem, G¹

¹University of Southern California, Los Angeles, CA

²University College London, London, UK

Email: jaredmoo@usc.edu

Summary

In order to improve/maintain health-related quality of life in older adults, it is important develop adherent exercise programs and examine the physical demands they engender. Golf is a multimodal activity that provides multiple fitness benefits for older adults [1]. An activity commonly overlooked is the bending task to tee or mark a ball (MTB). The purpose of this pilot work was to investigate the lower extremity (LE) demands of this task and compare the results to common exercises for older adults, such as bodyweight squatting. Our results demonstrated similar or greater LE demands during the MTB task compared to bodyweight squatting.

Introduction

Aging is associated with decreased muscle mass and a corresponding drop in muscular strength, which decreases functional capacity and increases fall risk [2]. Golf is a multimodal exercise activity that encompasses multiple aspects of fitness including: aerobic training through walking, high-velocity swings, squatting, balance and cognitive challenges, and social interaction. One aspect of golf that is commonly overlooked is the repeated squatting maneuver to tee and pick up a ball. The purpose of this pilot study was to quantify the sagittal plane lower extremity mechanical demands of this task and to compare these demands to those associated with squatting activities in older adults.

Methods

Fifteen healthy, right-handed, older adults whom did not currently golf were enrolled in a 10-wk, 2x/wk, golf program with fitness testing before and after the intervention. During follow-up testing, participants were asked to perform a ‘mark the ball’ (MTB) task, during which they placed a marker behind a ball before picking the ball up to return to an upright position. Lower extremity sagittal-plane internal net joint moments were calculated from kinematic and kinetic data using a lower extremity marker-based 11-camera Qualisys motion capture system (Qualisys, Sweden) and Visual3D software (C-motion Inc, USA). The participants stood with each foot on a forceplate (AMTI, USA) while they completed 3 trials of the MTB task. Peak moments were averaged across trials for the right and left limbs at the ankle, knee, and hip. Support moments were also calculated [3]. Differences between moments in the left and right limbs were evaluated using Hedge’s g effect sizes [4].

Results and Discussion

Participants completed 283/300 (94%) sessions and there were no adverse events (AE’s) during the program. Table 1 displays average peak net extensor/plantarflexor moments presented as mean±SD with Hedge’s g effect sizes for differences between limbs. There was a smaller net joint moment about the left knee with a moderate effect size that coincided with greater left hip

loading with a large effect size during the MTB task. There was no difference in the support-moment between limbs. All participants were right-handed which may have led to higher demands on the left hip while marking the ball with their right hand.

Moment (Nm/kg)	Left	Right	Hedge’s g
Ankle	0.61±0.10	0.60±0.09	0.10
Knee	0.47±0.26	0.67±0.43	0.55
Hip	1.28±0.17	0.96±0.29	1.30
Support	2.27±0.38	2.13±0.52	0.30

Table 1: Average peak net extensor/plantarflexor moments during MTB task and Hedges g effects sizes for differences between limbs.

The MTB task mimics a squatting task and is done repeatedly over the course of play. Our participants performed this task an average of 24 times during 9 holes of golf. Comparing the lower extremity joint demands of this task to squatting in similar age healthy older adults, the MTB task creates similar or greater joint moments compared to bodyweight squatting and chair squatting [5]. Thus, MTB appears to provide a sufficient demand that could improve lower extremity strength. These types of demands should be investigated alongside more common analyses of the golf swing and traditional exercises. The differences shown in knee and hip loading between limbs should be acknowledged and considered when determining exercises appropriate for individuals with knee or hip osteoarthritis, which is an increasing risk in older adults. The results from this study show that the goal of the task being performed should be considered as the demand may shift between joints depending on that goal.

Conclusions

This work is important in helping to determine safe and adherent exercise programs that also supply the necessary demands to influence strength improvements in older adults. Older adults also have other needs in an exercise program, such as social interaction, that can help to promote adherence. Golf is a multimodal exercise activity that encompasses multiple aspects of fitness that includes an MTB activity that mimics the loading of bodyweight squats in older adults shown here. This activity is performed multiple times throughout golf play and is interspersed within other physically demanding activities such as swings, balance control, and walking over uneven terrain.

Acknowledgments

This research was funded by R&A Grant GHA0012017.

References

- [1] DuBois A et al. (In Press). *Int J Golf Sci*.
- [2] Moreira NB et al. (2018). *Arch Gerontology & Geriatrics*, **77**: 57-63.
- [3] Winter DA. (1980). *J Biomechanics*, **13.11**: 923-927.
- [4] Lakens D. (2013). *Front in Psych*, **4**: 863.
- [5] Flanagan S et al. (2003). *Med Sci Sports Exerc*, **35.4**: 635-643

Validation of a non-invasive intra-abdominal pressure measurement tool in living and cadaveric specimen

N. Jacobson¹, M. Driscoll¹

¹McGill University, Montreal, Canada

Email: mark.driscoll@mcgill.ca

Summary

Prolonged increase in intra-abdominal pressure (IAP) is a life-threatening condition occurring in between 20 and 50% of intensive care unit patients. IAP is typically measured using urinary bladder pressure (UBP): an invasive, disputed method of measurement. Given the dangers associated with increased IAP, and the invasive nature of popularized measurement methods, it is the effort of this research to validate a novel, non-invasive tool for IAP measurement. In a cohort of 14 participants, IAP was measured with the novel device and compared to published ideal values at four body positions: supine, inclined, sitting and standing. Pearson correlation (r) between tested and literature based ideal IAPs revealed high correlation between results with r of 0.982 ($p < 0.0001$). Further, direct IAP measurements via UBP were compared in 4 cadavers to the novel device. These tests presented r values of 0.129 ($n = 21$). Positive results indicate the need for further research on the novel device, particularly in larger and wide-spread samples.

Introduction

Intra-abdominal pressure (IAP) is the pressure contained in the abdominal compartment [1]. High IAP is a life-threatening condition, typically diagnosed in intensive care units by urinary bladder pressure (UBP) measurement [2, 3]. Previous research has indicated the feasibility of a novel, non-invasive suction technique for measuring IAP [4]. Therefore, it is the objective of this study to validate said novel system for IAP measurement against existing popularized methods, namely, UBP.

Methods

The IAP of four fresh cadavers (1 male, 3 female) was measured using the popularized method of UBP, as suggested by the World Society on Abdominal Compartment Syndrome (WSACS), alongside the novel device [2]. Measurements were taken with cadavers in supine and inclined positions, 5 cm subxiphoid. The correlation between the two measurement tools was evaluated with Pearson's correlation (r), where r greater than 0.7 is deemed "high" correlation [5].

In addition, 14 living participants (7 male, 7 female) were tested with the novel device, 5 cm subxiphoid, in supine, inclined, sitting, and standing positions. Participants were tested without abdominal activation and at end-exhalation. Measured IAPs were compared to "ideal" IAP values, as suggested in literature.

Results and Discussion

Pearson correlation between ideal IAP values from literature and living participants was 0.982 ($p < 0.0001$).

Results are illustrated by the given Bland-Altman plot given in Figure 1.

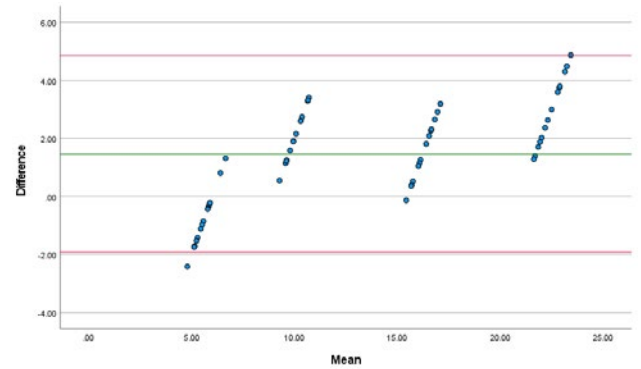


Figure 1: Bland-Altman plot comparing "ideal" data versus the novel device. Clusters indicate (from left to right) supine, inclined, sitting and standing positions.

Pearson correlation between UBP and the novel device on cadaveric specimen was 0.129 ($p < 0.6$) ($n = 21$), indicating negligible correlation, though with insufficient data. The average (standard deviation) absolute error between measured and actual results was 3.1 (2.8) mmHg.

Conclusions

A novel, non-invasive IAP measurement system was evaluated against "ideal" literature values, as well as benchmark cadaveric UBP measurements. Results demonstrated high correlation between measurement sets in living participants, and negligible correlation in cadaveric specimen. Negligible results may be attributed to uncertainty in the experimental setup of control measurements. Therefore, though promising in its results, it is recommended to consider a wider sample of varying BMI and baseline IAP in future research.

Acknowledgments

The authors wish to express gratitude to Mr. Trevor Cotter and Mr. Lorne Beckman for their assistance in preparing and performing clinical studies.

References

- [1] Malbrain M et al. (2014). *Anesthesiol. Int. Ther.*, **46**: 433–450.
- [2] Roberts D et al. (2016). *Surg. Int. Care Med.*, **39**: 621–644.
- [3] Papavramidis T et al. (2011). *J. Emerg. Trauma, Shock*, **4**: 279–291.
- [4] Jacobson N and Driscoll M (2020). *J. Med. Device*, **MED-20-111**.
- [5] Mukaka M (2012). *Malawi Med. J.*, **24**: 69-71.

Development of a Novel Tibiofemoral Dynamic Unloading Knee Brace with Air Bladder Insert and Wearable Control Box

Run Ze Gao¹, Kendal Marriott², Paula Hao-Fan He², Clark R. Dickerson², Monica R. Maly², Carolyn L. Ren¹

¹Dept. of Mechanical and Mechatronics Engineering, Waterloo, Canada

²Dept. of Kinesiology, Waterloo, Canada

Email: rzgao@uwaterloo.ca

Summary

A proof of concept dynamic unloading brace for managing medial tibiofemoral osteoarthritis was tested against force-sensitive resistors to verify its unloading pressure applied to the lateral knee. The dynamic knee brace was created by combining an off-the-shelf varus/valgus brace (Medi Soft OA light) with a soft air bladder insert powered by a wearable control box. Preliminary testing proved that two 60-gram pumps fluidically connected in parallel achieved clinically relevant unloading pressures within 250 ms of inflation, allowing for dynamic unloading during every step.

Introduction

Commercially available unloading braces for managing medial tibiofemoral osteoarthritis (OA) are all passive. The biggest issue with unloader knee braces is poor adherence due to discomfort and bulkiness [1,2]. However, discomfort due to constant unloading force remains problematic. Thus, we added dynamic unloading capabilities to a brace. The novelty of this technology involves applying an unloading pressure during only the stance phase of gait and removing this pressure during the swing phase. A soft air bladder powered by a wearable control box replaces the knee brace's original cushion at the hinge. The soft air bladder's inflation and deflation are triggered by a feedback control using a pair of inertial measurement units. This proof of concept study focused on observing the unloading pressures experienced on the medial knee during activation of the soft air bladder.

Methods

A prototype of the unloader brace was fitted on the right knee of a healthy male (age 25 years, Body Mass Index 23.7). The control box's internal components were placed on a table (Figure 1(a)). A Tekscan force-sensitive resistor array sensor was placed between the skin-contact fabric and soft air bladder on the lateral knee. Pressure maps indicating the location and magnitude were captured during standing at the following time points: the brace donned passively, 250 ms after inflation and 15 ms after deflation of the soft air bladder.

Results and Discussion

In the passive condition (i.e. when wearing the inactivated brace), the pressure observed on the medial knee was 374 mbar. In the inflated condition, the pressure observed was 436 mbar. In the deflated condition, the pressure observed was 218 mbar (Figure 1(b)).

15 ms of deflation was chosen for dynamic unloading during every step to not over-deflate and still achieve clinically relevant unloading pressure during the stance phase. Lastly, the minimum unloading pressure level should be tolerable by the user during the swing phase.

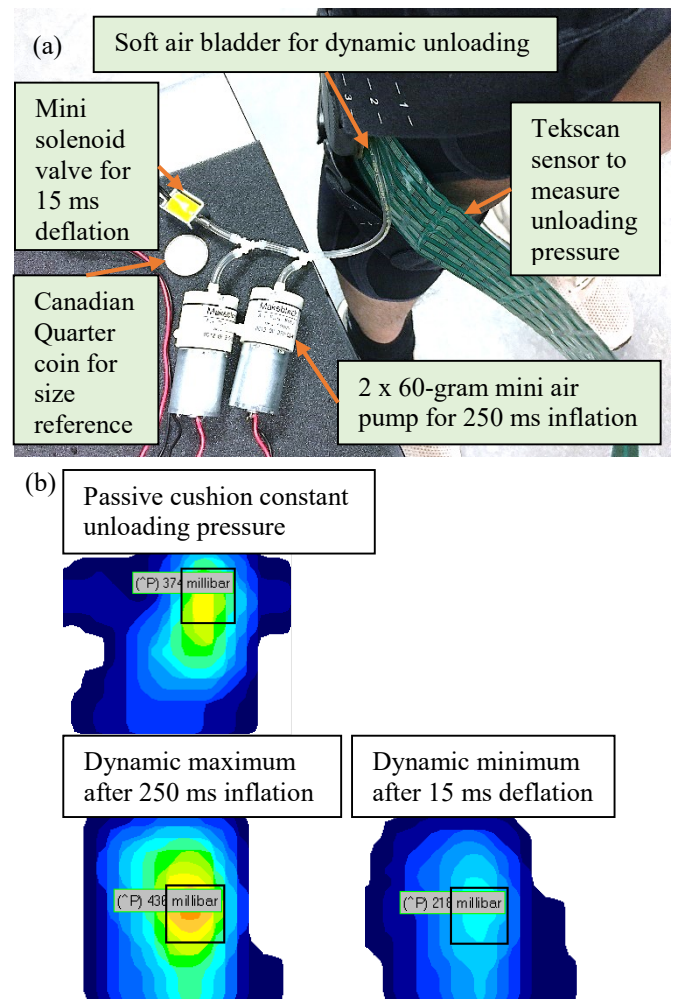


Figure 1: (a) Testing setup. (b) Testing results.

Conclusions

This proof of concept showed that a dynamic knee brace with clinically relevant unloading pressure and timing during each step with a truly wearable control box is possible. Future work will involve incorporating IMUs for feedback control of the timing for actuating the unloading pressures.

Acknowledgments

The authors would like to acknowledge the University of Waterloo Interdisciplinary Trailblazer Fund, NSERC, and Ontario Government for funding work presented herein.

References

- [1] Della Croce et al. (2013). *PM&R*, **5**: 816–824.
- [2] Squyer et al. (2013). *Clin. Orthop. Relat. Res.*, **471**: 1982–1991.

A NOVEL, PHYSIOLOGIC BIOMECHANICAL TESTING SYSTEM OF PROXIMAL HUMERUS FIXATION

Jeffrey Olson MD¹, Patrick Williamson MS², Kaveh Momenzadeh MD², Nadim Kheir MD, Edward Rodriguez MD, PhD³, Ara Nazarian, PhD²

¹Harvard Orthopedic Surgery Residency Program, Boston, MA

²Musculoskeletal Translational Innovative Initiative, Beth Israel Deaconess Medical Center, Boston, MA

³Department of Orthopaedic Surgery, Beth Israel Deaconess Medical Center, Boston, MA

Email: pmwill@bu.edu

Summary

We describe a novel method of biomechanical testing of proximal humerus locking plate fixation using a previously validated shoulder testing system mimicking passive shoulder abduction. We report normative glenohumeral joint reactive forces and compare interfragmentary gap displacement between bicortical and unicortical locking screw fixation during cyclic abduction loading.

Introduction

Proximal humerus fractures present a challenge to treating orthopedic surgeons due to osteopenia, fracture comminution, and inadequate fixation. Fractures commonly fail in varus malalignment with head screw cut out. [1] Previous biomechanical cadaveric studies have evaluated locking plate fixation through axial and torsional loading of the proximal humerus. [2] The goal of this study was to use a novel biomechanical shoulder testing system mimicking physiologic passive glenohumeral abduction to test strength of proximal humerus fixation.

Methods

Specimen Preparation and Fixation

Four fresh-frozen cadaveric shoulders were used. A dectopectoral approach exposed the proximal humerus. Proximal humerus locking plates were used with five 3.5 mm locking screws in the humeral head and three 3.5mm non-locking cortical shaft screws. For condition one, screws 2 mm short of the subchondral bone were placed, achieving unicortical purchase only. For condition two, screws were placed minimally penetrating through the subchondral bone, achieving bicortical fixation. Fluoroscopy confirmed screw placement. A surgical neck osteotomy with a 5 mm gap was made. The scapula and humerus were potted in 2-part epoxy (Smooth-Cast 300q and PMG Smooth-on Inc., Macungie, PA) and loaded onto the biomechanical testing device.

Biomechanical Device and Testing

Specimens were tested using a previously validated 7 degree of freedom cadaveric shoulder testing system. [3] Two hundred abduction cycles, from 45 to 90° of glenohumeral abduction per condition were passively applied per specimen. Interfragmentary gap motion was measured using the position of two electromagnetic sensors (240Hz, Liberty, Polhemus, Rochester, VT) rigidly affixed to the proximal humerus and humeral shaft. The maximum gap displacement during testing was taken as the maximum change in position between sensors. A 6DoF load cell (Mini58 IP65/IP68, ATI, Apex, NC) beneath the scapula was used to measure joint reactive force during motion. Statistical analysis was performed in MATLAB.

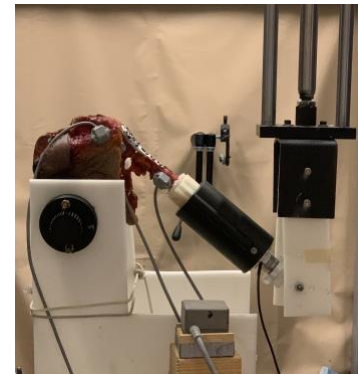


Figure 1: Biomechanical Shoulder Testing System

Results and Discussion

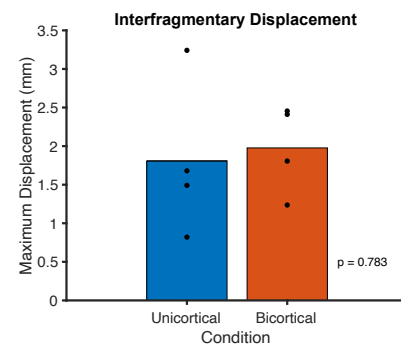


Figure 2: Maximum Interfragmentary displacement over 200 passive scapular plane abduction cycles.

There was no statistically significant difference in maximum interfragmentary gap displacement between the two conditions (Figure 1). The mean (SD) joint reactive force measured across specimens under the two conditions was 37.84 (3.0) N.

Conclusions

We describe a novel method of testing proximal humerus fixation in fresh frozen cadavers, using a previously validated testing system, simulating physiologic loading of the proximal humerus. We provide normative joint reactive force data for reference in future testing of proximal humerus fixation.

Acknowledgments

The authors would like to thank the Orthopedic Research Education Foundation (OREF) for funding this study.

References

- [1] Clavert et al. (2010). *J Shoulder Elbow Surg.* **19**; 489-494
- [2] Jabron et al. (2018). *BioMed Eng Online.* **17**;47
- [3] Entezari et al. (2012). *Bone Joint Res.* **1(5)**;78-8

To filter, or not to filter force plate data for jump height determination?

Brendan L. Pinto, Jack P. Callaghan

Department of Kinesiology, University of Waterloo, Waterloo, ON, Canada

Email: blpinto@uwaterloo.ca

Summary

Previous evidence has recommended against low pass filtering force plate data when calculating jump height. However, this evidence used unfiltered force plate data as the criterion. The purpose of this investigation was to examine the effect of low pass filtering on jump height calculated from force plate data, using a kinematic criterion. Contrary to previous evidence, low pass filtering with a low cut-off frequency appears to improve the estimation of jump height.

Introduction

Previous evidence has advised against low pass filtering force plate data when calculating jump height [1, 2]. Filtering can alter the frequency content of the signal and is suspected to be the highest source of error when compared to other analysis procedures in determining jump height. However, these investigations used unfiltered force plate data as the criterion. The effects of low pass filtering on jump height calculated from force plate data, were evaluated using a kinematic criterion that directly measures the whole-body vertical displacement that the force plate calculation aimed to estimate.

Methods

Thirty-four counter-movement jumps from 12 participants (6 female; mean \pm SD age 24 ± 4 years; mass 73.4 ± 17.6 kg; height 1.74 ± 0.08 m) were each single pass (SP) and dual pass (DP) filtered, with cut-off frequencies of 100, 50 and 5 Hz. Unfiltered and filtered data from each jump were used to calculate jump height using the take-off velocity summed with take-off displacement method [3].

A single marker on the third lumbar vertebrae was used to record vertical displacement. This captured the displacement of the torso while limiting the influence of limb, ribcage and pelvis posture. This criterion matched the assumption of point mass made by the force plate calculation and was thus more appropriate than estimating centre of mass (COM) using a rigid link model (the force plate calculation does not account for changes in COM due to body posture redistribution during flight).

Paired differences between the criterion and jump heights calculated from the unfiltered and six filtered force plate signals, were analyzed using a linear mixed effects model. If the ANOVA from this model indicated a significant main effect of filter condition ($\alpha=0.05$), pairwise comparisons of the estimated marginal means (EMM) were conducted with a Tukey adjustment ($\alpha=0.05$).

Results and Discussion

The 5 Hz SP data had the lowest paired difference with the criterion, followed by the 5 Hz DP filtered data. Both conditions were significantly different from each other (pairwise comparison $p<0.001$) and all other conditions (pairwise comparison $p<0.001$), whereas the other filter conditions did not differ from each other (pairwise comparison $p>0.997$). It is possible that filtering with a low cut-off frequency, models the second order nature of the biomechanical system to improve the biofidelity lost when calculating jump height from the force plate assuming point mass.

Table 1: EMM and 95% confidence limits (CL) of the paired jump height difference for each condition relative to the criterion.

Filter Condition	EMM (cm)	Lower 95% CL	Upper 95% CL
Unfiltered	-1.86	-2.38	-1.34
100 Hz SP	-1.85	-2.37	-1.34
50 Hz SP	-1.84	-2.36	-1.32
5 Hz SP	-0.82	-1.34	-0.30
100 Hz DP	-1.86	-2.38	-1.34
50 Hz DP	-1.86	-2.38	-1.34
5 Hz DP	-1.30	-1.82	-0.78

Conclusions

Contrary to previous evidence, low pass filtering with a low cut-off frequency improves the calculation of jump height from force plate data. Future investigation should elucidate this effect and if there is a biomechanical purpose to filtering the force time signal, as this may also inform the analysis of other force plate outcome measures.

Acknowledgments

The authors acknowledge funding from the Natural Sciences and Engineering Research Council of Canada.

References

- [1] Street et al. (2000). *J Appl Biomech*, **17**(1):43-54.
- [2] Harry et al. (2020). *J Strength Cond Res*, doi: 10.1519/jsc.0000000000003611.
- [3] Moir (2008). *Meas Phys Educ Exerc Sci*, **12**(4):207-218.

Timing of gait events affect time-continuous analysis outcomes

Eric C. Honert¹, Todd C. Pataky²

¹Human Performance Lab, Faculty of Kinesiology, University of Calgary, Calgary, Alberta, Canada

²Department of Human Health Sciences, Kyoto University Graduate School of Medicine, Kyoto, Japan

Email: eric.honert@ucalgary.ca

Summary

Time continuous analyses, such as statistical parametric mapping (SPM), have been increasingly used in biomechanics research. Currently, it is not known how sensitive time-continuous analyses are to timing variability that occur in gait data. We evaluated this sensitivity by examining the frequency of significant SPM outcomes for lower limb joint powers between two walking speeds for 40 different stride definitions, based on repeatable lower limb gait events. Our findings demonstrate that gait interventions (e.g. changes in walking speed) can induce temporal shifts in gait events, which can in turn affect time-continuous outcomes. Understanding that time-continuous analyses are sensitive to the timing of gait events may enable researchers to better understand the outcomes and limitations of these methodologies that inform injury prevention, device development and basic understanding of biomechanics.

Introduction

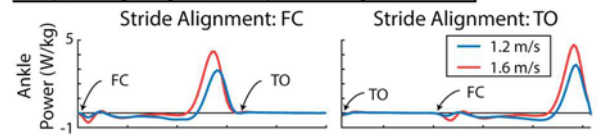
It has become increasingly common to utilize time-continuous analyses (e.g. SPM, principal component analysis) to examine biomechanical data. One methodological consideration for time continuous algorithms is curve registration [1]. It is common practice in gait analysis to linearly register curves based on a single event such as foot contact. This linear alignment allows for inherent timing variability of gait events [2]. However, it is not known how timing variability of gait events affects time-continuous analysis outcomes.

Methods

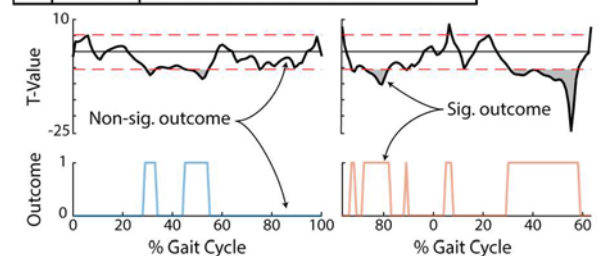
Ten subjects from [3] were reprocessed to understand how gait event timing variability affects SPM outcomes. For conciseness, data from only 1.2 and 1.6 m/s during level ground walking are reported. Lower limb joint powers were segmented and aligned based on 40 different gait events (Fig. 1: Step 1). We use the term ‘stride definition’ to refer to a gait event-based definition of stride. Repeatable gait events were determined from lower limb joint and segment kinematics, joint kinetics as well as ground reaction forces. For each subject and stride definition, 10 strides were analyzed. SPM paired t-tests compared the subject-averaged curves for each stride definition between the two walking speeds using `spm1d` ($\alpha=0.05$, www.spm1d.org). For each SPM test, we recorded whether there was or was not statistical significance with a binary outcome of “1” or “0”, respectively, at each time point (Fig. 1: Step 2). This binary outcome for each stride definition was time-shifted to temporally align the outcomes (Fig. 1: Step 3). These shifted outcomes were finally averaged together across all 40 stride definitions to provide the frequency of statistical outcomes (Fig. 1: Step 4).

Results and Discussion

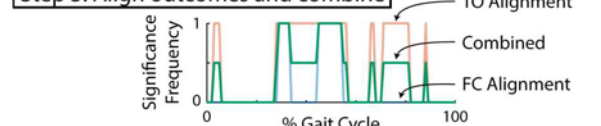
Step 1: Align signal on repeatable gait feature



Step 2: Compute SPM t-test and outcomes



Step 3: Align outcomes and combine



Step 4: Examine across 40 stride definitions

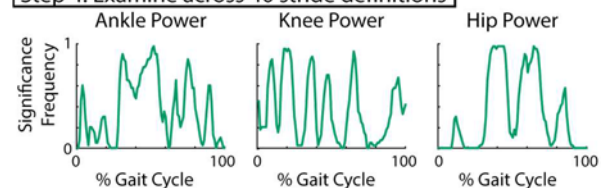


Figure 1: Determining frequency of statistical outcomes for joint powers with data aligned by foot contact (FC) and toe-off (TO) and with data aligned by 40 different gait events.

Statistical outcomes from joint powers were sensitive to stride definitions defined throughout the gait cycle (Fig. 1, Step 4). This sensitivity arose due to variable timing of gait events in the data. In the future, researchers should consider performing multiple SPM tests with alternative event-based stride definitions to quantify this timing variability and sensitivity.

Conclusions

Investigators are encouraged to test alternative event-based stride definitions to ensure robust conclusions from time-continuous analyses.

References

- [1] Helwig NE et al. (2011). *J. Biomech.*, 44: 561-566.
- [2] Giakas G and Baltzopoulos V. (1997) *Gait Posture.*, 5: 189-197.
- [3] Honert EC and Zelik KE. (2019) *Hum. Mov. Sci.*, 64: 191-202.

Analysing the impact of sensor placement on the quality of sEMG signals on the human forearm

Schimmer J.¹, Ganguly A.¹, Mombaur K.²

¹Optimization, Robotics and Biomechanics, Institute of Computer Engineering, Heidelberg University, Heidelberg

²Chair in Human-Centred Robotics & Machine Intelligence, University of Waterloo, Waterloo

Email: schimmer@stud.uni-heidelberg.de

Summary

Surface electromyography (sEMG) is increasingly used in next-generation wearable assistive devices to facilitate user in-loop controls and replace state machine controllers such as exoskeletons and prosthetics. Conventionally, muscle bellies are chosen as sEMG affixation sites to ensure high quality recordings. However, the muscle bellies are not always accessible, often due to the design of wearable assistive devices and hence, alternative sites are sought to record reliable sEMG signals. In this study, 5 muscles in the forearm region of 10 subjects were chosen which are responsible for wrist flexion and extension as well as ulnar and radial deviation. sEMG signals were recorded from the muscle belly, 1cm proximal and distal to the muscle belly of each muscle, respectively. The study demonstrates that some alternative sites indeed offer reliable sEMG signals, but it does not intend to replace the conventional sEMG practice.

Introduction

The majority of upper limb replacements are so-called passive prosthesis [1]. In order to develop these wearable assistive technologies, primary data from myoelectric as well as kinetic measurements have to be recorded. sEMG signals are conventionally measured from the muscle belly but this study indicates that reliable sEMG recordings can be derived on sites away from the muscle belly.

Methods

The arm of each subject was palpated for 5 muscles, FCR, FCU, ED, and AN in order to locate appropriate sites to place the sEMG electrodes. Electrodes were placed on those muscle bellies, 1 cm distal and 1 cm proximal to it. The subjects carried out 10 different tasks, including resting and Maximal voluntary isometric contraction used to normalise the obtained data. The mean amplitude of each period was used for further evaluation.

For every muscle placement one ANOVA per period was carried out, including all 10 subjects and all 3 different electrode placements resulting in 10 F-values per muscle. To investigate correlation between measurements the Pearson correlation coefficient (PCC) was calculated for the conventional and distal placement as well for conventional and proximal placement of each muscle. Finally to further compare the placements Bland-Altman Plots (BAP) were computed.

Results and Discussion

No ANOVAs show a significant difference between the placements. This has been a prerequisite for further investigation of correlation and similarity which makes it possible to interpret similarity of the placements. However the different affixation sites showed a high correlation with PCCs > 0.90. Whereas, the BAPs indicated that some placements yield equal results while others failed to pass this test. An exemplary set of results is given for the FCU in Figure 1.

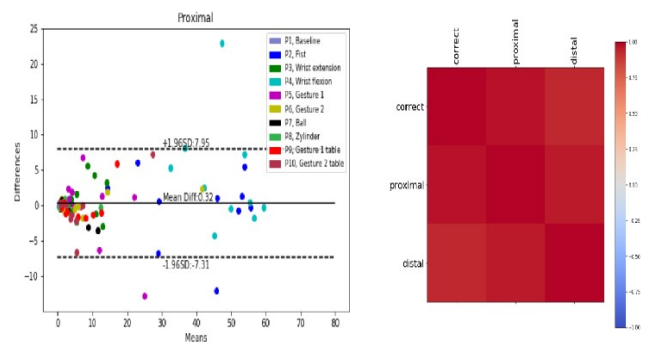


Figure 1: Bland-Altman Plot and PCC for Flexor carpi ulnaris .

Conclusions

Most of the tested muscles showed reliable similarity in at least one of the alternative placement sites. Even placements which failed to fulfil the conditions of the BAP acquired high correlation and might be useful for prosthesis development. This study shows that alternative sEMG sites can be used when muscle belly of the target muscle in question may not be easy to access. This is often found in wearable devices being driven by EMG.

Acknowledgments

We thank all participants who volunteered for this study. The project is partly funded by the EIT Health 19340.

References

1. Maat, B. et al. (2018). *Prosthet Orthot Int*, **42**: 66-74.
2. Carkeet, A. et al. (2015). *Optom Vis Sci*. **92**: e71-80

Stochastic Resonance and Heaviness Perception of an Ocluded Object

Alli Grunkemeyer¹, Aaron D. Likens¹

¹Department of Biomechanics, University of Nebraska at Omaha, Omaha, NE USA

Email: agrunkemeyer@unomaha.edu

Summary

We are investigating a novel means to enhance haptic perception of wielded objects. Specifically, we are interested in the effect of low amplitude vibratory noise, when applied to a limb, when perceiving the weight of an occluded wielded object. This research project, if successful, would contribute new theoretical knowledge about the role and structure of neuromuscular noise in the perception of wielded objects. Stochastic resonance is a newly introduced phenomenon and when applied to perception it can advance the theoretical literature in this topic and apply it to human movement variability.

Introduction

Heaviness perception is the ability to use haptic feedback from effortful touch to determine the weight of a wielded object [1]. The perception of an object being wielded does not rely solely on the object's mass, but muscular effort as well. When an object is wielded, torques and moments of inertia are produced. The inertia tensor contains those moments and provides information about how mass is distributed in a rigid body. The corresponding eigenvalues and eigenvectors of the inertia tensor have been related to an object's perceived magnitudes (e.g., weight) and directions (e.g., orientation with respect to hand), respectively (**Figure 1a**) [2]. The inertia tensor can be visualized as an ellipsoid, as seen in **Figure 1b**, which is produced in effect from the constraints related to the position of the limb. In this study, we will manipulate the eigenvectors associated with an object in relation to the limb.

Recent studies have also provided evidence that adding noise to a weak stimulus can enhance a person's ability to detect it [2]. Introducing a subthreshold (vibrational) stimulus embedded with noise may, in some cases, improve sensations gained from limb movements [1]. We hypothesize that adding vibrotactile noise of various forms will improve accuracy in perceiving heaviness of a wielded object (**Figure 2**).

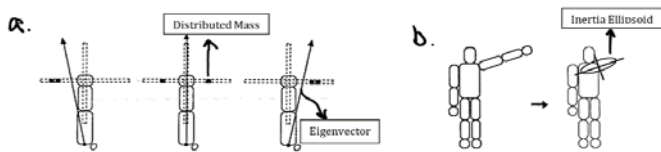


Figure 1. (a) Effect of varying mass loads on eigenvectors. **(b)** Inertia ellipsoid of upper limb.

Methods

Ten adults (18-45 years of age) will be seated for the duration of the trial with a BM3C tactor fastened to the humerus of the subject as seen in **Figure 2**.

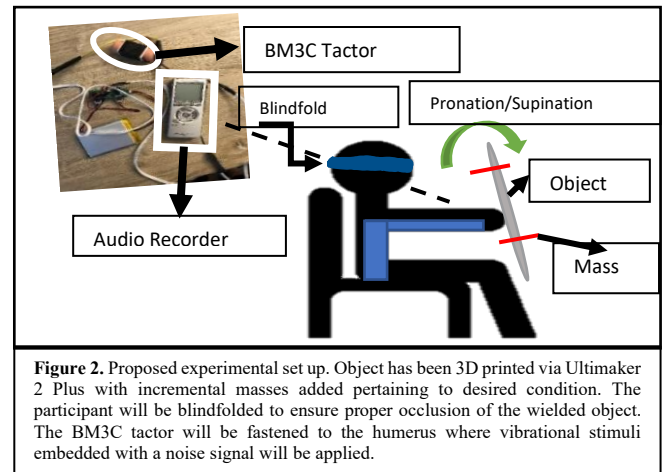


Figure 2. Proposed experimental set up. Object has been 3D printed via Ultimaker 2 Plus with incremental masses added pertaining to desired condition. The participant will be blindfolded to ensure proper occlusion of the wielded object. The BM3C tactor will be fastened to the humerus where vibrational stimuli embedded with a noise signal will be applied.

Vibrational stimuli will be introduced via the tactor with different signals of colored noise, or signals produced by stochastic processes varying in power spectral slope. Noise (3) \times mass (6) combinations will be presented. Each condition of noise and mass will be introduced randomly. Subjects will rate the heaviness of the object by stating their perceived proportion of mass added on a scale of 1-10.

Expected Results and Discussion

The study will be introduced as a 3x6 repeated measures design with the first factor being noise, along with the second factor, mass. Mass will be added in increments of 20% all the way up to a max 100% mass increase. Based on previous literature as well as what we know about the various impacts of coloured noise on biological systems, it is expected that with the addition of pink noise to the system, the accuracy of heaviness perception will be the greatest compared to white noise and the control group as the mass increases.

Conclusions

Introducing a noise as a subthreshold vibration is hypothesized to improve the heaviness accuracy of a given wielded object. Pink noise is expected to display the highest level of accuracy considering the exploratory patterns conveying fractal properties the subjects will exert. These fractal properties are common in most biological systems, therefore producing a more accurate identification of weight.

References

- [1] Pagano et al. (1998) *Journal of Applied Biomechanics*, **14**: 331-359.
- [2] Nozaki et al. (1999) *Physical Review Letters*, **82**: 2402-2405.

SEX DIFFERENCES AND FATIGUING MOVEMENT EFFECTS ON TASK-SPECIFIC STABILITY

Hasanbarani F.¹, Yang C.¹, Bailey C.A.¹, Slopecki M.¹, Côté J.N.¹

¹ Department of Kinesiology and Physical Education, McGill University, Montreal, QC H2W 1S4, Canada

Email: fariba.hasanbarani@mcgill.ca

Summary

There are several internal factors that affect task-specific stability. However, the sex-specific effects of fatigue on the stability of arm kinematics during a repetitive pointing task (RPT) remain unidentified. We quantified the stability (variability) of an RPT using the Un-Controlled Manifold (UCM) approach. Participants performed the RPT while arm and trunk kinematics was captured by a 3D system in both fatigue and non-fatigue conditions. Results showed good and bad variability more in women compared to men after fatigue, which may reflect an underlying mechanism of sex differences in musculoskeletal disorders.

Introduction

According to the principle of abundance, a living system uses all elemental variables (EVs) to produce movement, which leads to variability in EVs to keep performance-related variables stable and accomplish a task. Synergy and Motor Equivalence concepts in the UCM framework have been developed to explain the motor control processes that may underlie task-specific stability. The motor equivalence analysis quantifies the amount of deviation in the space of elemental variables that occurs in two directions; one that preserves the performance variable (good variance, ME), and the other one that affects it (bad variance, nME). Synergy index ($\Delta V > 0$) and inequality of $ME > nME$ represent stability (more good variability) in performing a task. Although previous studies showed an increase of synergy after fatigue [1], this approach has never been used to study the sex-specific multi-joint adaptations in tasks with multiple upper limb joints. We aimed to study the effects of fatigue and sex differences on an RPT's stability using the Motor equivalence model in UCM's framework.

Methods

Healthy adults ($n = 26$, 13F; age: 35.3 ± 10.6 yrs.) performed an RPT by moving their dominant arm between a proximal target and a distal target in a standing position (Fig 1) until near fatigue (Borg CR10 rating 8/10). Tridimensional kinematics of pelvis, trunk, upper arm, forearm, and hand

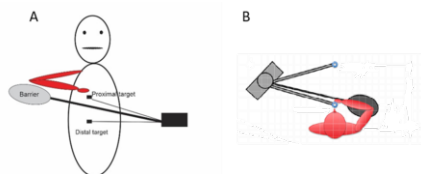


Figure 1: Experimental setup

segments were captured by high-resolution cameras (Vicon) every minute. ΔV and ME and nME (Equation 1) were computed in MATLAB using the specific equations [2, 3].

$$\text{Eq1: } nME = \frac{\sum_{j=0}^n |nME_j|}{\sqrt{n \times DoF_{PV}}} \quad ME = \frac{\sum_{j=0}^n |ME_j|}{\sqrt{n \times DoF_{EV-PV}}}$$

In SPSS, a mixed-effect analysis of variance with the factors of Sex (woman vs. man) * Phase (early vs. middle vs. late) * Condition (NF vs. FT) on Component (ME vs. nME) and synergy index (ΔV_z) were used with $P \leq 0.05$.

Results and Discussion

Results showed $\Delta V > 0$ and $ME > nME$ for women and men, reflecting the EV synergies stabilizing the end-point coordinate in Non-Fatigue and Fatigue conditions. Moreover, the movement phase during which the sex differences occurred changed with fatigue, suggesting different time-dependent compensatory mechanisms (Fig 2).

The effect of Condition * Sex ($p = .01$) and Bonferroni comparisons showed higher ME (by 0.19 ± 0.1 rad) and nME (by 0.15 ± 0.09 rad) in women related to men after fatigue, which reflect more good variability and bad variability in women compared to men.

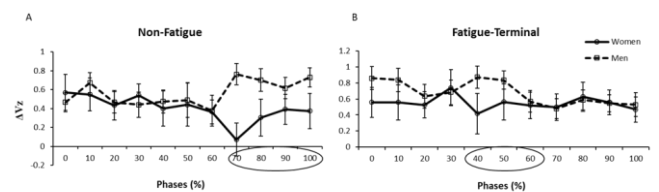


Figure 2: ΔV in NF and FT conditions for both women and men. The significant differences are shown with Circles.

Conclusions

Despite showing comparable endurance, women fulfilled the task similar to men; nevertheless, they showed an increase in the bad variability, which could explain the mechanisms underlying sex differences in musculoskeletal disorders.

Acknowledgments

We thank Dr. Mark Latash for data analysis suggestions and Kim Emery for her assistance with data collection.

References

- [1] Sing T et al. (2010). *Journal of neurophysiology*, **103**:2990-3000.
- [2] Hasanbarani F & Latash ML (2020). *Motor Control*, **24**:1-15
- [3] Mattos D et al. (2015). *Experimental brain research*, **233**: 487-50.

Movement Preferences of the Wrist and Forearm Combined During Activities of Daily Living

Scott Tew¹, Will Anderton¹, Spencer Ferguson¹, Joshua Hernandez¹, Steven K. Charles^{1,2}

¹Mechanical Engineering and ²Neuroscience, Brigham Young University, Provo, UT, USA
Email: skcharles@byu.edu

Summary

We characterized the combined behavior of the wrist and forearm during activities of daily living. Subjects spent 50% of their time in the central 20% of their functional range of motion, and movement speed dropped off exponentially. Interestingly, subjects often merged the dart-thrower's motion (DTM) with a twist from pronation to supination (similar to a hand-to-mouth movement). Given its importance in many activities (e.g. eating and grooming), the prevalence of this action is not surprising. However, it suggests that the importance of the DTM may not lie in itself, but rather in combining with pronation-supination to bring objects toward the head.

Introduction

Although the wrist and forearm function together during activities of daily living (ADL), few studies have investigated the *combined* kinematics of wrist flexion-extension (FE), wrist radial-ulnar deviation (RUD), and forearm pronation-supination (PS). In addition, most past studies investigating the kinematics of these three degrees of freedom (DOF) have focused on the functional range of motion (fROM) needed to perform activities of daily living, or else on the impact of fractures, neurological disorders, surgical procedures, or orthotic devices on the maximum range of motion (mROM) in these DOF. However, the behavior of the wrist and forearm *within* the fROM has received relatively little attention. Here we characterized natural wrist and forearm behavior throughout the entire space spanned by PS, FE, and RUD.

Methods

Ten young, healthy participants (5 male, 5 female) were instrumented bilaterally with electromagnetic motion capture sensors (trakSTAR by Ascension Technologies, Burlington, VT) on the acromion, distal upper arm, distal forearm, and back of the hand. Each participant performed 24 ADL, with 5 repetitions per ADL, for a total of 120 actions. Most ADL were selected from past studies to allow comparison. Sensor data were converted into joint angles, resulting in joint configuration (FE, RUD, PS) over time for each of the 120 actions of each subject. From joint configurations we extracted the following movement preferences: mean configuration, distribution of configurations, path direction, distribution of speed (combined across all three DOF), and common configurations at different speeds.

Results and Discussion

Combining the kinematic data resulted in three-dimensional data clouds (Figure 1), from which we extracted movement preferences in each of the three projection planes (FE-RUD, FE-PS, PS-RUD). *Mean configuration (centroid) and mROM:* The mean configuration, averaged across all ADL and subjects, was $12^\circ \pm 20^\circ$ of extension, $3^\circ \pm 12^\circ$ of ulnar deviation,

and $16^\circ \pm 27^\circ$ of pronation (mean \pm STD). Centroids of motion were not aligned ($p < 0.001$) with the anatomical origin in any of the three DOF. *Distribution of configurations:* The distribution of joint configurations was not uniform for any projection ($p < 0.0001$) but roughly mimicked the shapes of mROM in each projection plane. *Path direction:* The directions of movement were not uniformly distributed ($p < 0.001$) among any of the DOF. For example, in the FE-RUD plane, movements in the direction of the dart-thrower's motion (DTM) were about three times more common than movements perpendicular to that direction. *Speed:* The distribution of movement speed was well-fit by an exponential with a decay constant of 62.9 deg/s, indicating that 25%, 50%, and 75% of the velocities were under 18, 44, and 87 deg/s, respectively. *Common configurations at different speeds:* At low speeds, the configuration was roughly uniformly distributed in direction. However, at higher speeds, certain movement directions became more common. Specifically, the most common movement directions at high speeds were the DTM with a twist from pronation to supination.

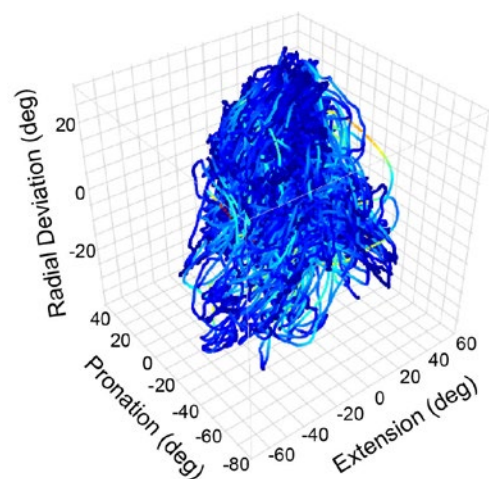


Figure 1: Wrist and forearm joint configuration over time during ADL. Hotter colors indicate higher movement speeds.

Conclusions

From the measures analyzed, it is evident that wrist and forearm behavior during ADL favors certain movement configurations, directions, and speeds. One preference was of particular interest: at high speeds, the most common movement combined the DTM with PS. This pattern is what is required to pick up an object in front of one's body (pronation and extension, with some radial deviation) and place it close to the head (supination and flexion, with some ulnar deviation). We hypothesize that the importance of the DTM may not lie in itself, but rather in its role with PS of bringing objects toward the head.

Information in EMG within and between pedal cycles

Jaylene S. Pratt¹, Stephanie A. Ross¹, Emma F. Hodson-Tole², James M. Wakeling¹

¹Department of Biomedical Physiology and Kinesiology, Simon Fraser University, Burnaby, BC, Canada

²Musculoskeletal Science and Sports Medicine Research Centre, Manchester Metropolitan University, Manchester, UK

Email: jaylene_pratt@sfu.ca

Summary

EMG signals contain small fluctuations between data points across time. Although small fluctuations were historically attributed to motor system noise, recent work found the order of these fluctuations contains information relevant to motor control. In a cyclic task, EMG can fluctuate within a burst of excitation, between the excitation and quiescent periods of a cycle, and across multiple cycles. It is unknown how these sources of variation affect the measurement of structure in EMG. We used pedaling to explore the order of fluctuations or 'structure' in EMG that occurs both within and between cycles. We constructed square wave signals that lack fluctuations within an excitation burst and fluctuations across multiple pedal cycles and compared the structure of these signals to that of experimental EMG intensities using Entropic Half Life (EnHL) analysis. We found that the EnHL is primarily affected by variation between the excitation and quiescent periods of a cycle.

Introduction

Small fluctuations within EMG collected during gait are thought to reveal information about underlying motor control [1, 2]. This has been assessed using Entropic Half-Life (EnHL) analysis during cycling, which quantifies the timescale at which regularity in a signal decays [3]. At present, we do not know how variation within and between cycles in the EMG signal affects the EnHL. In this study we use measured and constructed EMG signals to explore structure within and between pedal cycles.

Methods

In order to determine the sources of variation that are responsible for the rate of decay of structure in an EMG signal, we compared measured with constructed EMG signals where we altered the sources of variation in the signals. We collected EMG from nine participants and six muscles of the lower limb during cycling at a constant cadence and resistance. EMG signals were resolved into intensities, where the intensity is a close approximation to the power in the EMG. We determined the duration of each excitation burst and rest period, as well as the average intensity of each burst. Using these burst and rest durations and average intensities, we constructed five square waves that lacked variation within a burst of excitation (Figure 1). Square waves 2-4 possessed variation in time, intensity, or both between multiple cycles. Square wave 1 lacked variation between multiple cycles. To construct square wave 5, we randomized the order of each cycle in square wave 4 to remove information related to the order of multiple cycles but maintain a random variation between cycles. We analyzed the EnHL of all square waves and compared these to the EnHL of the EMG intensities.

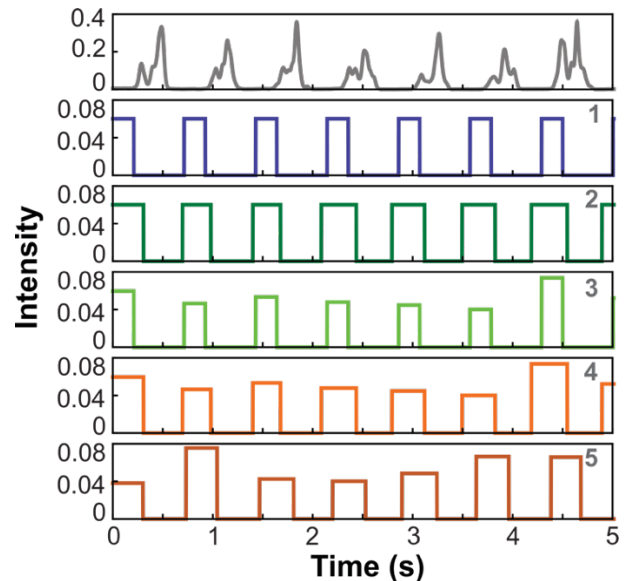


Figure 1: Measured and constructed EMG signals from the vastus medialis of a representative participant. From top to bottom: EMG intensity, and square waves 1-5.

Results

The EnHL of square wave 1 (with constant burst and rest parameters) was longer than all other analyzed signals. All square waves with variable burst and rest durations or variable intensity had similar EnHL values to the EMG intensities. The EnHL of the square wave with randomized cycle order was similar to the EnHL of the square wave with preserved cycle order (square waves 5 and 4, respectively).

Discussion and Conclusions

Although the EMG intensities contained variation within a burst of excitation, these variations did not contribute to the EnHL. This is shown through the similar EnHL between the square waves and the EMG intensities. Variation across multiple cycles contributed to the EnHL, as the EnHL of square wave 1 was longer than all other signals. However, the order of this variation did not contribute to the EnHL as the EnHL was unaffected when cycle order was randomized. The EnHL was thus primarily influenced by variation in the burst and rest durations and the average EMG intensities.

References

- [1] Hodson-Tole EF and Wakeling JM (2017). *Front. Physiol.*, **8**: 679.
- [2] Wakeling JM and Hodson-Tole EF (2018). *Med. Sci. Sports Exerc.*, **50**: 2518-2525.
- [3] Zandiyeh P and Von Tscherner V (2013). *Physica A*, **392**: 6265-6272.

Ultrasound estimates of muscle quality: correcting for the confounding effect of subcutaneous fat.

Heiliane de Brito Fontana^{1,2}, Jonathan N. Muller¹, Juliana Y. Passos Karam¹, Fabio J. Lanferdini¹

¹Biomechanics Laboratory, Federal University of Santa Catarina, Florianopolis, Brazil

² School of Biological Sciences, Federal University of Santa Catarina, Florianopolis, Brazil

Email: heiliane.fontana@ufsc.br

Summary

Subcutaneous fat is a major confounding factor when comparing echo intensity (EI) of skeletal muscle sonograms. We used exogenous fat to analyze the confounding effect of fat thickness on muscle echo intensity. Equations for improved accuracy in estimates of muscle quality in obese/overweight are provided.

Introduction

EI of skeletal muscle sonograms has been used as an estimate of muscle quality in individuals with various phenotypes. Until now, most studies that correct ultrasound-based estimates of muscle quality for the confounding effect of subcutaneous fat have counted on the equations developed by Young et al. [1].

However, their experiment consisted in changing fat thickness by applying different levels of pressure with the ultrasound (US) probe on the skin, which is expected to lead to changes in tissue parameters that may influence the speed of US wave propagation, producing changes in EI that do not represent the effect of subcutaneous fat thickness [2].

In this study, we aim to provide an unbiased estimate of the effect of subcutaneous fat thickness on EI scores. Fat thickness was modified by adding exogenous fat layers over the skin, and the resulting change in EI was analyzed. This experimental approach allowed us to mimic the effects of increasing fat thickness (attenuation and changes in ROI relative position) on EI estimates of muscle quality.

Methods

Ten healthy subjects (age 28.0±5.6 years, height 1.70±0.11 m and body mass 67.8±11.9 kg) participated in this study.

Sonograms were taken from the tibialis anterior mid-belly with the ultrasound probe longitudinally aligned with the muscle and perpendicular to the skin. (Figure 1).

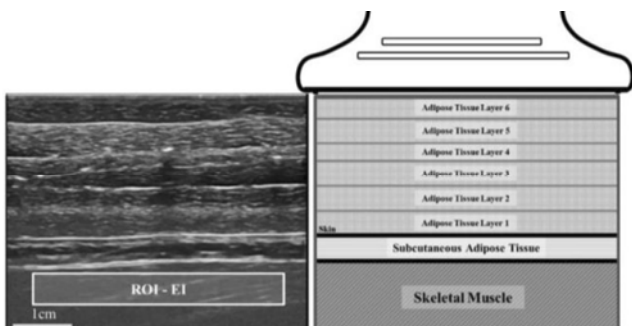


Figure 1: The average of three independent B-mode sonograms (40-mm depth and 60-dB gain) for each condition (no fat and for 6 additional exogenous layers) was used in the analysis.

Results and Discussion

A significant effect of adipose thickness (AT) was observed on EI ($p < 0.001$, Figure 2).

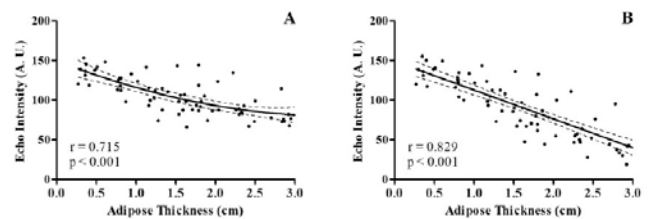


Figure 2: EI scores decrease as fat thickness increases. This confounding effect on EI differs between sonograms with focus fixed at 1 cm (A) and with focus adjusted to the ROI (B).

Correcting equations (with standard errors) for sonograms without (i) and with (ii) focus adjustment are presented:

$$(i) EI_{corrected} = EI_{measured} - 5.0054 \cdot AT^2 + 38.30836 \cdot AT$$

$$(ii) EI_{corrected} = EI_{measured} + 39.2297 \cdot AT$$

The confounding effect of subcutaneous fat thickness on EI estimates of muscle quality leads to an underestimation of the negative impact of obesity/overweight on muscle health [3,4] and may lead to erroneous conclusions regarding chronic exercise induced changes in muscle quality and differences in muscle quality between men and women or between muscles and muscle regions [5,6]. The slope of the relationship between subcutaneous fat thickness and EI observed by [1] with tissue compression differs substantially from the one observed in our study (Figure 2A). Differences may be explained by the nature of the experiment conducted by [1], which does not allow for the quantification of the independent effect of fat thickness, and also by the limited range of fat thickness tested in their experiment.

Conclusions

US estimates of muscle quality should be corrected for the confounding effect of subcutaneous fat and the correction should take into account whether focus is adjusted to the muscle region of interest or not. To our knowledge, this is the first study to systematically analyze the confounding effect of fat thickness as an independent factor and the provided equations can be used for improved accuracy in estimates of muscle quality in obese/overweight subjects/patients.

References

- [1] Young et al. *Muscle Nerve*. 52(6):2015
- [2] Ishida et al. *Middle East J Rehabil Health Stud*. 3(2):2016
- [3] Oranchuk et al. *Appl Physiol Nutr Metab*. 45(7):2020
- [4] Ryan et al. *Appl Physiol Nutr Metab*. 41(10):2016
- [5] Wong et al. *J Ultrasound*. 23(4):2020
- [6] Stock et al. *Appl Physiol Nutr Metab*. 45(11):2020

Probabilistic DTI tractography demonstrates better consistency with ultrasound estimates of muscle fascicle lengths in comparison to deterministic methods

Divya Joshi^{1,2}, Amy Adkins^{1,2}, Wendy Murray^{1,2,3}, Julius P.A. Dewald^{1,2,3}, Carson Ingo^{2,4}

¹Department of Biomedical Engineering, ²Department of Physical Therapy & Human Movement Sciences, ³Department of Physical Medicine & Rehabilitation, ⁴Department of Neurology, Northwestern University Feinberg School of Med., Chicago, IL
 Email: divyajoshi@u.northwestern.edu

Summary

We establish, for the first time, feasibility of probabilistic DTI tractography in skeletal muscles, as compared to the deterministic methods prevalent in literature. Probabilistic methods estimated fascicle lengths more consistent with ultrasound measurements and produced more variability, which suggests heterogeneity previously only identified in cadaveric measurements.

Introduction

Musculoskeletal structure has traditionally been investigated using cadaveric specimens, while *in vivo* measurements are made with ultrasound (US). More recently, magnetic resonance (MR) based diffusion tensor imaging (DTI) has emerged as a promising approach that can non-invasively capture skeletal muscle architecture while overcoming limitations posed by ultrasonic and cadaveric methods.

In order to estimate muscle fascicle length properties, DTI can be implemented by using either deterministic tractography, which computes a binary fiber direction at each voxel, or probabilistic tractography, which produces a probability distribution of fiber direction at each voxel [1]. While it has been shown that probabilistic tracking more reliably reconstructs crossing fibers within a voxel, the two methods have yet to be compared for musculoskeletal tractography. Due to the computational burden of probabilistic methods, previous literature in skeletal muscle DTI has predominantly used deterministic algorithms [2]. Here, we explore the differences seen when using both methods and compare the results to previously obtained ultrasound measurements.

Methods

Diffusion-weighted images of both upper arms were acquired in two male, age-matched individuals using a spin-echo echo planar imaging sequence (voxel resolution=1.25x1.25x5 mm³, diffusion gradient b=450 s/mm², 12 directions with 3 averages). High resolution T1 anatomical images were also obtained to guide the identification and segmentation of the biceps brachii muscle and its inner tendon.

Deterministic and probabilistic tractography was initiated from the same segmented seedmask of the biceps brachii muscles. Deterministic tractography was run using DSI Studio with the following parameters: angular threshold=10°, step size=0.5 mm, and minimum length=20 mm. Probabilistic tractography was run using FSL with the following parameters: maximum fibers per voxel=2, burnin period=1000, and step size=0.5 mm. Probabilistic tractography had a 400-fold greater expenditure of time than deterministic tractography. Resulting tracts from both

algorithms were constrained using anatomical boundaries and fit to polynomial curves, from which fascicle lengths were measured and compared to previously reported US results [3].

Results and Discussion

Both tractography methods were able to capture fascicles across the entire muscle region, resulting in an order of magnitude more fascicles than were captured using ultrasound, which can only estimate superficially located fibers (Figure 1) due to limited field of view inherent to US. Both DTI methods produced shorter fascicles than ultrasound. Probabilistic methods yielded an average of 57.6% longer median fascicles, which were more consistent with ultrasound measurements, than deterministic methods.

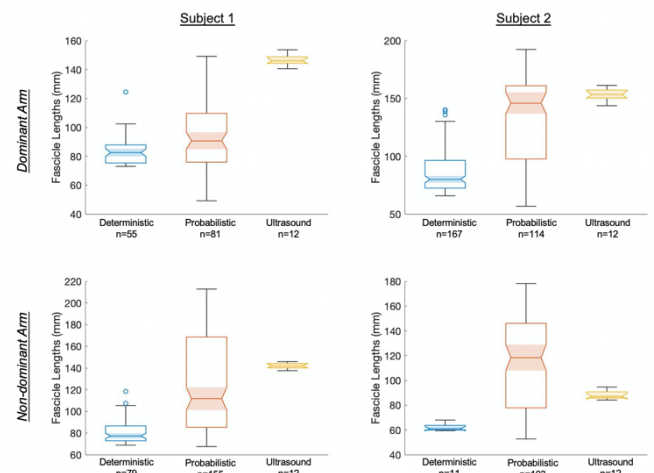


Figure 1: Fascicle length measured by deterministic and probabilistic tractography, and 2D ultrasound [3].

Conclusions

Probabilistic tractography can estimate an increased number of fascicle length measurements, which are closer to previously reported results. Additionally, it has potential to capture a more heterogeneous sample of fascicles, which has previously only been explored via cadaveric methods [2].

Acknowledgments

This work was done with the support of National Institutes of Health awards R01HD084009, R03HD094615, and predoctoral fellowship T32EB025766 awarded to DJ.

References

- [1] Sarwar, T. et al. (2019). *Magn. Reson. Med.*, **81**: 1368-1384.
- [2] Damon BM. et al. (2017). *NMR Biomed.*, **30**.
- [3] Adkins AN. et al. (2020). *bioRxiv*.

Open vs closed articular architecture of the forearm for an analysis of muscle recruitment during throwing motions

Claire Livet¹, Théo Rouvier², Charles Pontonnier¹, Georges Dumont¹

¹Univ Rennes, Inria, CNRS, IRISA – UMR 6074, F-35000 Rennes, France

²Institut de Biomécanique Humaine Georges Charpak, Arts et Métiers ParisTech

Email: claire.livet@ens-rennes.fr

Summary

The osteoarticular architecture of the forearm can be modeled by an open or a closed-loop. This study aims to compare the impact of the chosen architecture on the muscle activity for overhead throwing motions. Preliminary results show similar muscle behaviors with both models.

Introduction

Musculoskeletal modeling can analyze human motion from kinematics to muscle activity. The impact of modeling on the kinematic reconstruction of the motion has been studied [1]. This pilot study aims at comparing activations estimated with a full-body musculoskeletal model presenting an open-loop (OLM) [2] or a closed-loop (CLM) [3] model at the forearm during overhead throwing motions.

Methods

The OLM is based on [4] for the lower limb and [2] for the upper limb. Muscle activations are estimated by the following static optimization under the respect of dynamic equations [5]:

$$\min_a \sum_{i=1}^m a_i^2$$

$$\text{s. t. } \begin{cases} 0 \leq a_i \leq 1, \forall i \in \llbracket 1, m \rrbracket \\ H(q)\dot{q} + C(q, \dot{q}) = R(q)F_{max} \odot a \end{cases}$$

The muscle force model is $F_m = F_{max}a$, with a the muscle activations. q are the degrees of freedom, $H(q)$ is the mass matrix, $C(q, \dot{q})$ is the Coriolis matrix and the effect of external forces, $R(q)$ is the moment arm matrix from [6].

The CLM is based on [4] for the lower limb and [3] for the upper limb. The forearm contains a closed loop modeled by constraints $h(q) = 0$, contributing to dynamic equations via its Jacobian K and Lagrange multipliers λ [7]. The muscle recruitment problem is now:

$$\min_{a, \lambda} \sum_{i=1}^m a_i^2$$

$$\text{s. t. } \begin{cases} 0 \leq a_i \leq 1, \forall i \in \llbracket 1, m \rrbracket \\ H(q)\dot{q} + C(q, \dot{q}) = R(q)F_{max}(q) \odot a + K^T \lambda \end{cases}$$

The study was implemented in CusToM [9], an open-source Matlab toolbox for musculoskeletal modeling. Geometrical and inertial parameters were extracted from [10] and scaled to the subject (1m74, 64kg) using the CusToM scaling routine. The raw data for 18 throwing trials were taken from [11].

Measured EMGs and activations computed from OLM and CLM were compared with phase error metrics [8].

Results and Discussion

OLM and CLM had similar results while compared to EMG measurements (Figure 1). This was confirmed by the OLM and CLM comparison, with phase errors under 25%.

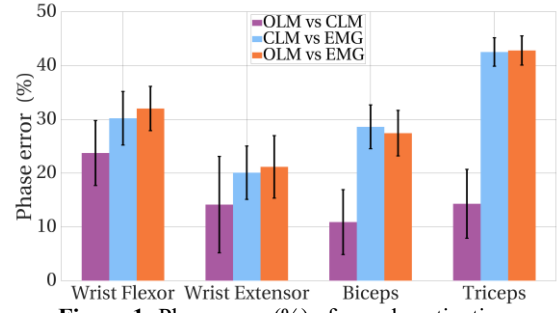


Figure 1: Phase error (%) of muscle activations

OLM and CLM were expected to have similar behaviors. However, adding constraints in the dynamic equations may impact the muscle recruitment to give a better match with measurements. We can see that constraints did not have a strong impact on these specific motions and that none of OLM or CLM fairly match EMG data. This could be explained by the small number of solids in the CLM and the relatively low level of solicitation related to this motion.

Conclusion

Finally, it seems that CLM did not bring any improvement compared to OLM for studying throwing motion. A similar study should be done for a larger cohort to validate these preliminary results. The same comparison could be done for shoulder models, using more complex constraints.

References

- [1] Duprey, S. et al. (2017). *J Biomech*, **62**, 87–94.
- [2] Holzbaur, K. R. S. et al. (2005). *Ann Biomedical Eng*, **33**(6), 829–840.
- [3] Pennestrì, E et al. (2007). *J Biomech*, **40**(6), 1350–1361.
- [4] Klein Horsman M. D. et al. (2007) *Clin Biomech*, **22**(2):239–247.
- [5] Pedotti A et al. (1978). *Math Biosci*, **38**(1-2):57–76.
- [6] Rankin, J. W., & Neptune, R. R. (2012). *J Biomech*, **45**(9), 1739–1744.
- [7] Featherstone, R. (2008). *Rigid Body Dynamics Algorithms*.
- [8] Schwer, L. E. (2007). *Eng Comput*, **23**(4), 295–309.
- [9] Muller, A. et al. (2019). *JOSS*, **4**(33), 927.
- [10] Dumas, R., Chèze, L., & Verriest, J. P. (2007). *J Biomech*, **40**(3), 543–553.
- [11] Cruz Ruiz, A. L. et al. (2017). *Appl Bionics Biomech*, **40**(3), 543–553.

A quantitative test of soft tissue work analysis in human walking

Koen K. Lemaire¹, Arthur D. Kuo^{1,2}

¹Faculty of Kinesiology, ²Biomedical Engineering Program, University of Calgary, Calgary, AB, Canada

Email: koen.lemaire@ucalgary.ca

Summary

Inverse dynamics is widely used to quantify the joint torque and work during walking, assuming rigid segments. But many body tissues are not rigid, and soft tissue deformations are expected to passively dissipate some energy. New analysis techniques quantify that dissipation, but with few direct tests of their validity during walking. We therefore evaluated soft tissue work analysis, by artificially adding non-rigid dissipatory elements to the body—flexible air pumps—for which the amount of dissipation was quantified independently. We performed soft tissue work analysis for normal walking and walking with artificial dissipation, and evaluated the accuracy of the dissipation estimate. We found that the soft tissue work calculated from the artificial soft tissue conditions was much larger than that calculated from normal walking, and was close to the values obtained from independent mechanical characterization. We also found the observed dissipation to be well quantified by distal foot power. We conclude that soft tissue work can be accurately quantified during walking, particularly if associated with the foot.

Introduction

Inverse dynamics analysis uses dynamic equilibrium between rigid bodies to quantify joint torques, based on measured kinematic variables and ground reaction forces. The body is not entirely rigid, as indicated by observations of net positive joint work [1], even though there is negligible net work done over a stride of periodic walking. A previously proposed analysis quantifies the work of soft tissue deformations [1], using the discrepancy between summed joint work and change in total mechanical energy (including body center of mass and peripheral motions). Here, we quantitatively test this analysis by introducing an experimental manipulation of artificial soft tissues mounted under the feet that dissipates a known amount of energy. We tested whether the soft tissue analysis could quantify the artificial energy dissipation, to determine its validity for human walking.

Methods

We performed inverse dynamics and soft tissue work analysis for walking with and without artificial soft tissues. The manipulation was a flexible air pump attached to the bottom of each shoe. One human subject walked in both conditions on an instrumented treadmill at three speeds (0.7 – 1.1 m/s), while kinematic data of the feet, shanks, thighs and trunk were recorded [2], along with ground reaction forces. (The test focused on a mechanical perturbation and analysis, and not on variation between human subjects.) Inverse dynamics analysis was performed on about 50 seconds of data for each trial [1]. From these results, total mechanical power, sum of joint power, distal foot power, and soft tissue power were calculated [1,2]. Total mechanical power was quantified as the sum of center of mass power (using ground reaction forces and including soft

tissue motion) and peripheral power (from motion relative to the center of mass), from which subtracting summed joint power yielded soft tissue power. Distal foot power was quantified as the 6-DOF joint power between ground and foot [2]. For each of these variables, net work was calculated by integration with respect to time.

Results and Discussion

We found that walking with artificial soft tissue resulted in substantially more soft tissue dissipation (94, 102, 111 J/stride for both feet) than normal walking (8, 9, 13 J/stride), for all three speeds (Figure 1). The amount of additional energy dissipated during one step with the artificial soft tissue (about 40 J) was close to that observed during a single compression of the air pump (39 J), quantified in a separate experiment. This dissipation largely agreed with net distal foot work, which was 10, 12 and 16 J/stride for normal walking and 101, 112 and 119 J/stride for walking with artificial soft tissue.

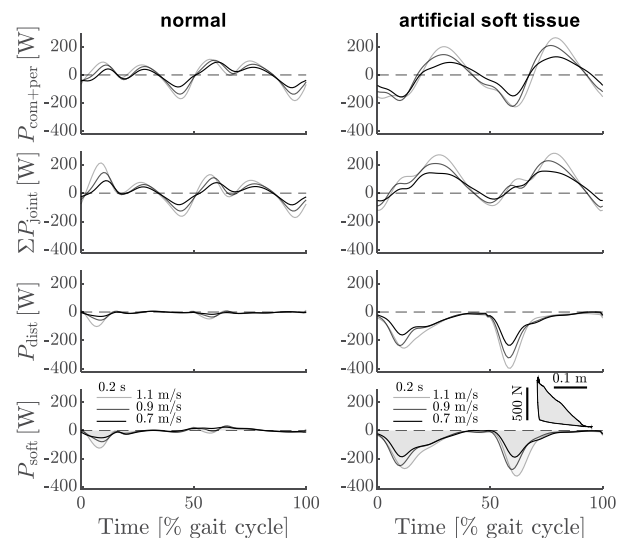


Figure 1: Total mechanical power, sum of joint power, distal foot power and soft tissue power as a function of normalized stride time. Data is average over strides (starting left heel strike). Each line corresponds to a trial at a different speed, as indicated by the legend, which also serves as scale bar for the time axis. The inset (bottom right) shows one work loop for a separate decompression cycle of the air pump, in the vertical dimension. Shaded areas indicate net work done.

Conclusions

The additional energy dissipation of an artificial soft tissue is well quantified by both soft tissue work analysis and distal foot power. Whereas distal foot power should be applicable to deformation of the foot, soft tissue analysis should quantify the energy dissipated in deformations throughout the body.

References

- [1] Zelik KE et al. (2015) *J. Exp. Biol.*, **218**: 876-886.
- [2] Honert EC & Zelik KE (2019) *H. Mov. Sci.*, **64**: 191-202.

Can Electrically Induced Contractions Replicate Walking in Microgravity?

Thomas J. Abitante^{1,2,3}, Mary L. Bouxsein², Kevin R. Duda³, Dava J. Newman¹

¹Human Systems Lab, Massachusetts Institute of Technology, Cambridge Massachusetts

²Harvard Medical School, Boston Massachusetts,

³Draper Laboratories, Cambridge Massachusetts

Email: abitante@mit.edu

Summary

Neuromuscular Electrical Stimulation (NMES) is an electrical pulse that elicits muscular contractions, which can potentially reduce bone loss in astronauts. External Force output of the Vastus Medialis, Vastus Lateralis, and Hamstring muscle group from NMES-induced isometric contractions of the knee were measured (n=1), and applied to biomechanical knee and hip models to estimate the internal forces. The muscle and joint reaction forces were then applied to a finite element analysis (FEA) of the femur to produce a strain model. The peak trabecular tensile and compressive strains were 1391 and -2095 microstrain ($\mu\epsilon$) respectively. Peak cortical tensile and compressive strains were 715 and -890 $\mu\epsilon$ respectively, which is comparable to estimated peak $\mu\epsilon$ during walking. Therefore, it is possible that a daily application of NMES can replicate the daily strain stimulus one would experience with recommended daily walking doses (\approx 5,000 steps).

Introduction

Astronauts in microgravity experience muscle and bone loss and are required to exercise daily. For future long duration missions, alternative methods are being investigated to reduce mass and logistical requirements. Neuromuscular Electrical Stimulation (NMES) is a technique that sends electrical pulses via skin electrodes to elicit an involuntary muscular contraction. NMES has previously been applied to reduce bone loss in spinal cord injury patients [1], and therefore is a potential method to reduce bone loss in astronauts [2]. Bone is thought to respond to its daily strain stimulus, which is determined by the peak strain experienced and total loading cycles [3]. Strain experienced on the femur from walking has previously been estimated by both finite element analysis (FEA) [4] and *in-vivo* studies [5]. In addition, studies have estimated the total number of daily steps required to maintain bone density at healthy levels (\approx 5000) [6]. In order to determine potential effective of a NMES regimen for use with astronauts, a FEA strain model of the femur during isometric NMES contractions against a fixed resistance was created.

Methods

Isometric contraction force of the Vastus Medialis (VM), Vastus Lateralis (VL), and Bicep Femoris/Semitendiosus muscles of one subject were measured while seated with the knee at 90°. For each muscle, the amplitude of the NMES pulse was increased to a subjective, maximum tolerable level. The internal muscle and reaction forces were estimated using simple knee and hip biomechanical models, and the forces were applied to a Finite Element Analysis (FEA) of the femur. A 4th generation Standard Femur Model [7], which is composed of a cortical shell and a distal and proximal cancellous components, was used with the Abaqus CAE software. A linear tetrahedron element mesh of approximately

uniform size (1.2mm) was implemented with literature derived bone mechanical properties and muscle origin points.

Results and Discussion

Figure 1 displays the peak principal strains ($\mu\epsilon$) along the z axis of the proximal trabecular femur. The overall peak tensile and compressive strains were 1391 and -2095 ($\mu\epsilon$).

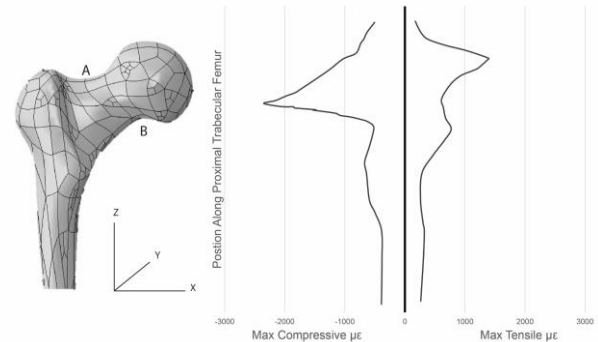


Figure 1: The trabecular peak principal strains ($\mu\epsilon$) along nodal paths within x-z plane that bisected the model y axis. The peak tensile and compressive strains were at points A and B.

Peak principal tensile and compressive strains measured on the cortical surface of the femoral neck were 715 and -890 $\mu\epsilon$ and occurred superficial to the trabecular peaks. These results are comparable to those observed *in vivo* (1198, -393 $\mu\epsilon$) and FEA (752, -859 $\mu\epsilon$) walking studies [4,5].

Conclusions

This study demonstrated that isometric contractions from NMES can produce peak bone strains akin to walking. If 5,000 daily steps (2,500 per leg) is able to maintain bone health on Earth [6], a NMES regimen of similar repetitions could possibly be used to reduce bone loss in astronauts in microgravity. The addition of another cross hip joint muscle, the rectus femorus, in leui of the VM and VL could further increase the strain, potentially reducing the required number of repetitions, increasing practicality. Future research aims include 1) repeating the analysis for subjects of varying leg size, strength, and gender, as individuals can have a wide range of responsiveness and tolerance to NMES, and 2) performing co-contractions of the knee extensors and flexors to create isometric contractions without a fixed resistance to replicate microgravity conditions.

References

- [1] Dudley-Javorski S et al (2012) *Osteo Int.* 23: 2335-46
- [2] Abitante TJ et al (2020) *ASCEND Conf Proc.*
- [3] Carter DR et al (1989) *J Biomech.* 22: 231-44
- [4] Edwards W et al (2016) *J Biomech.* 49: 1206-13
- [5] Aamodt A et al (1997) *J Ortho Res.* 15: 927-31
- [6] Boyer KA et al (2011) *Osteoporosis Int.* 22: 2981-88
- [7] Polgar K et al (2003) *Proc Inst of Mech Eng.*

Foot Joint Stiffness Effects on Maximum Vertical Jumps

Daniel J. Davis, John H. Challis

Biomechanics Laboratory, The Pennsylvania State University, Pennsylvania, United States

Email: djd426@psu.edu

Summary

Shoe and foot stiffness may play a role in athletic performance. The present investigation used a musculoskeletal model of maximum vertical jumping to clarify mechanisms of potential performance enhancement. Overall, increased passive midtarsal joint stiffness and increased toe flexor strength had little effect, whereas increased shoe longitudinal bending stiffness increased jump height by over 1.5%.

Introduction

The longitudinal bending stiffness (LBS) of athletic footwear has received considerable attention with regards to running and jumping performance. Stefanyshyn & Nigg (2000) reported increased jump heights with stiffer shoes, proposing that less negative work at the metatarsophalangeal (MTP) joint was at least in part responsible. Recently, investigators have reported that the muscles of the foot can alter the stiffness of the foot's joints [2], which could perhaps also be beneficial for vertical jump performance. The purpose of the present analysis was then to determine the mechanisms by which model shoe and foot joint stiffness changes influence maximum vertical jump performance.

Methods

A two-dimensional direct dynamics model with 11 muscles/muscle groups (gluteus maximus, vasti, rectus femoris, hamstrings, gastrocnemius, soleus, tibialis posterior, peroneus brevis/longus, flexor digitorum/hallucis longus) was created in OpenSim (v4.0). Muscle excitation time-histories were optimized to maximize jump height and were the same across model variations. The effects of shoe LBS were determined by altering passive MTP joint dorsiflexion stiffness values to approximate flexible (baseline) and stiff shoe conditions. Passive joint moments were used to enforce biologically relevant ranges of motion and stiffnesses [3], with systematic variations from baseline midtarsal joint stiffness used to examine its influence on jump performance. Lastly, the extrinsic toe flexor's maximum isometric forces were increased from baseline to model the effects of strengthening these muscles.

Results and Discussion

Modelling an increase in shoe LBS had the largest effect on jump performance, increasing jump height by nearly a centimeter between the baseline and most stiff shoe conditions. This was accompanied by 5.4 Nm (21.7%) greater peak MTP joint moment and about 16% less negative work between conditions. Increasing shoe LBS also increased the proportion of vertical ground reaction force on the model's toe segment, effectively increasing the plantarflexion moment arm (Table 1).

The least stiff midtarsal joint condition reduced vertical jump height compared to the baseline condition by 2 mm but jump height did not differ between baseline and the most stiff midtarsal joint conditions. Peak joint moments were about 5 Nm different between the least stiff and baseline conditions, and the midtarsal joint extended 2.5 degrees more in the least stiff condition compared to the baseline condition (Table 1).

Increasing the maximum isometric force capacity of the model's toe flexor muscles by 20% increased vertical jump height by 2 mm. The proportion of the vertical ground reaction force on the toe segment was increased, albeit to a lesser extent than in the increased shoe LBS condition (Table 1). MTP joint negative work was reduced by 4% compared to the baseline condition.

Conclusions

Foot joint stiffness and muscle strength changes influenced maximum vertical jump performance much less than externally supplementing MTP joint stiffness. Passive foot joint properties and foot muscle strength therefore likely contribute less to maximum jump performance than footwear choices.

References

- [1] Stefanyshyn DJ & Nigg BM. (2000). *Med & Sci in Sports & Exercise*, **32**(2): 471-476.
- [2] Farris DJ, Birch J, & Kelly L. (2020). *J R Soc Interface*, **17**(168): 20200208.
- [3] Erdemir A & Piazza SJ. (2004). *J Biomech Eng*, **125**(2): 237-243.

Table 1: Maximum vertical jump performance and foot joint kinematics and kinetics from models of varying joint stiffness and muscle strength. LBS: longitudinal bending stiffness; vGRF: vertical ground reaction force.

Model Condition	Jump Height (m)	Max MTP Joint Angle (deg.)	Max MTP Joint Moment (Nm)	Max Midtarsal Joint Angle (deg.)	Max Midtarsal Joint Moment (Nm)	Proportion of vGRF on Toe Segment
Baseline	0.384	27.2	24.9	14.4	92.6	56.1%
Stiffest LBS	0.391	22.0	30.3	14.8	97.8	63.9%
Least Stiff Midtarsal Joint	0.382	25.3	24.0	16.9	87.3	57.6%
Stronger Toe Flexors	0.386	26.9	24.4	14.4	92.9	57.2%

Effects of Maturation on Estimated ACL Loading in Adolescent Female Soccer Players

Lauren E. Schroeder¹, Kevin R. Ford², Audrey E. Westbrook², Jeffrey B. Taylor², Anh-Dung Nguyen^{2,3}, Joshua T. Weinhandl¹

¹Department of Kinesiology, Recreation, and Sport Studies, The University of Tennessee, Knoxville, TN, USA

²Department of Physical Therapy, High Point University, High Point, NC, USA

³Division of Athletic Training, West Virginia University, Morgantown, WV, USA

Email: lschroel@vols.utk.edu

Summary

ACL injuries are the most common medically disqualifying injury in female youth soccer. Alterations in biomechanical and neuromuscular control have been identified throughout the maturation process, potentially affecting ACL loading (F_{ACL}). However, it is unknown how ACL loads change throughout maturation. Fifty-nine adolescent female soccer players, classified into prepubescent, pubescent, and post-pubescent, completed unanticipated cutting trials. Musculoskeletal modeling was used to estimate F_{ACL} , and peak F_{ACL} was compared between groups. No significant differences in peak F_{ACL} between groups were present.

Introduction

Age significantly affects anterior cruciate ligament (ACL) injury rates in female soccer, with players 15 years or older exhibiting an almost twofold increased injury rate compared to younger players. Sex disparities in ACL injury rates increase after the onset of adolescence, suggesting the rapid musculoskeletal changes that occur significantly contribute to ACL injury rates. Musculoskeletal modeling allows researchers to estimate ACL loading (F_{ACL}), providing insight into how kinematic and neuromuscular changes affect ACL loading through the maturation process. Understanding these changes throughout maturation could aid in improving ACL injury prevention programs. Therefore, the purpose of this study was to compare estimated ACL loading between maturation groups in young female soccer players. It was hypothesized that the more mature females would exhibit greater F_{ACL} compared to less mature females.

Methods

Motion capture data from 59 adolescent female soccer players completing unanticipated cutting trials (CUT) off the dominant leg were used. Participants were classified into three maturation groups based on their predicted adult stature percentage [1]: prepubertal (PRE: $n = 17$, age: 10.3 ± 0.6 yrs, ht: 1.38 ± 0.07 m, mass: 34.23 ± 4.49 kg), pubertal (PUB: $n = 20$, age: 11.8 ± 0.9 yrs, ht: 1.52 ± 0.07 m, mass: 43.64 ± 6.50 kg), and post-pubertal (POST: $n = 22$, age: 15.1 ± 1.6 yrs, ht: 1.62 ± 0.06 m, mass: 54.54 ± 10.40 kg).

Musculoskeletal simulations of the CUT trials were conducted in OpenSim (v3.3, <http://simtk.org>). Inverse

kinematics and inverse dynamics were used to calculate joint angles and moments from a subject-specific scaled musculoskeletal model [2]. Joint torques were decomposed into net muscle forces using static optimization. A Joint Reaction Analysis was used to obtain anteroposterior knee joint reaction forces, using muscle forces from static optimization as inputs. Finally, a previously established data-driven model was utilized to estimate F_{ACL} , using the anteroposterior knee reaction force and knee flexion angle [3].

Peak F_{ACL} during stance phase was identified. To see how mass affects F_{ACL} , two separate one-way ANOVAs were performed on peak F_{ACL} between the three maturation groups, one using the raw F_{ACL} and the other using F_{ACL} normalized to body weight (SPSS, $\alpha = 0.05$).

Results and Discussion

Both raw and normalized peak F_{ACL} and standard deviations for the three maturation groups are presented in Table 1. Our hypothesis was not supported. There were no significant differences in both raw F_{ACL} : $F(2,56) = 2.684$, $p = 0.077$, $\eta^2_p = 0.087$, and normalized F_{ACL} : $F(2,56) = 2.511$, $p = 0.090$, $\eta^2_p = 0.082$. However, a medium η^2_p effect size was detected in both analyses. Raw F_{ACL} increased from PRE to PUB in a way that reflected body mass increases, but changes in raw F_{ACL} from PUB to POST were small and did not reflect the increase in body mass between groups, possibly implying a movement strategy to reduce ACL loading in the POST group.

Conclusions

Our results revealed no significant differences in estimated raw and normalized F_{ACL} between maturation groups during unanticipated cutting in young female soccer players. Future analyses should consider examining movement strategies between groups, as well as adjusting the model to better reflect age and sex of the participant by altering body segment mass and inertial parameters, as well as muscular parameters.

References

- [1] Westbrook AE et al. (2020) *PLoS One*, **15**: e0233701.
- [2] Lai AM, et al. (2017). *Ann Biomed Eng.* **45**: 2762-74.
- [3] Weinhandl JT et al. (2016). *Comput Methods Biomech Biomed*, **19**: 1550-6.

Table 1: Mean \pm SD raw (N) and normalized (BW) peak F_{ACL} between maturation groups.

	Raw Peak F_{ACL} (N)	Normalized Peak F_{ACL} (BW)
PRE ($n = 17$)	664.80 \pm 181.02	1.99 \pm 0.48
PUB ($n = 20$)	828.56 \pm 307.45	1.96 \pm 0.69
POST ($n = 22$)	865.20 \pm 313.70	1.63 \pm 0.52

Dynamic foot model to study the syndesmotic variation during the rotation of the ankle

Maria Ruiz¹, Rostam S. Kojouri¹, Sorin Siegler¹

¹Biomechanics Lab, Department of Mechanical Engineering, Drexel University, Philadelphia, PA

Email: mr3393@drexel.edu

Summary

A dynamic computational model of the foot, which includes the full tibia and fibula bones, the ankle joint and the midfoot bones up to the metatarsals, is used to study the effect of ankle rotation in the proximal and distal tibiofibular syndesmotic joints. Dorsiflexion/plantarflexion and external/internal rotations are simulated, and the predictions of the model are checked with previous published data as a validation method.

Introduction

The syndesmotic joint ensures the stability of the ankle. An excessive widening of the distal fibula from the tibia, might lead to joint sprains or injured ligaments. Yet, syndesmotic flexibility is crucial to allow for proper rotation of the foot. Due to the importance of this joint, several studies have been carried out to understand its properties.

In this project, a 3D subject specific model of the foot and ankle is used to study the syndesmotic width variation as the ankle rotates. The relationship between the proximal fibula and tibia is also analyzed, since it is closely related to the syndesmosis of the ankle. Measuring the syndesmotic opening on CT scans is limited to 2D images; using markers on skin during gait is not very reliable either, since the slightest of displacements from these markers may lead to incorrect monitoring of the joint motion. As opposed to these, the computational model provides high precision in 3D for all sorts of situations. This analysis also serves as a validation for the model by matching its predictions to previously published data.

Methods

While the original computational model kept the fibula and tibia completely fixed [1], the fibula is released for all 6 degrees of freedom in this project, which allows for the analysis of the syndesmotic joint. Apart from the ankle ligaments the model had, the proximal and distal tibiofibular ligaments, as well as the interosseus membrane, had to be included to connect the fibula to the tibia. The midfoot bones were another addition to the computational model since they can have an effect in the behavior of the ankle during certain activities. All the ligaments were assumed to act as tension-only springs, with individual non-linear strain properties. Contact between the bones is assumed to be frictionless and no penetration is allowed. The articulating bone surfaces have also been offset to compensate for cartilage.

The computational model is set to rotate passively in dorsiflexion/plantarflexion and external/internal rotation. These two rotations have been proven to have the largest effect on the syndesmosis. For that, the simulation will be set

up with the tibia completely fixed, while the other bones are free to move in any directions as controlled by the ligaments and the contact mechanics. An axial load of half body weight is applied upwards to serve as ground force reaction. At the same time, a rotational moment is applied to the foot for each of the two directions. Thus, matching the experimental set-up of cadaveric studies that were published in the past, where variations in syndesmosis in the proximal and distal sides were recorded [2,3].

Results and Discussion

As the foot is made to go through a moment of 10Nm for dorsiflexion/plantarflexion, its rotation ranges 40°. It can be seen during the simulation, that when the foot goes into dorsiflexion, a coupling of slight external rotation is produced, which pushes the fibula 1.3mm away from the tibia. When a moment is applied in external/internal rotation, the foot rotates 34°, and the syndesmosis widens up to 2mm. The foot internally rotated barely affects the position of the fibula, while in external position, the talus pushes the fibula from the tibia, thus increasing the syndesmotic width (Figure 1). This particular test is very commonly carried out during clinical procedures to test typical syndesmotic injuries.

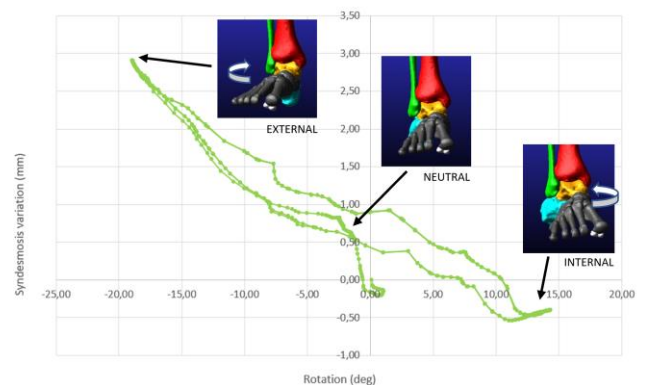


Figure 1: Syndesmotic width variation during external/internal rotation of the foot.

Conclusions

This computational model of the foot and ankle proved to be very powerful to further understand the biomechanics of the foot under different conditions. Besides, the data from the simulations match the same patterns to previous published results, which increases the reliability of the model.

References

- [1] Imhauser et al. (2008) *J Biomech.* **41(6)**: 1341-1349.
- [2] Bragonzoni et al. (2006). *Arch Orthop Trauma Surg.* **126**: 304-308
- [3] Soavi et al. (2000) *FAL.* **21(4)**: 336-34

Verification of a Method to Examine the Effects of a Knee Brace on Joint Loading and Muscle Activity

Ryan C.J. Baxter¹, Scott C.E. Brandon², Janet L. Ronsky¹

¹Schulich School of Engineering, University of Calgary, Calgary, AB, Canada

²School of Engineering, University of Guelph, Guelph, ON, Canada

Email: ryan.baxter2@ucalgary.ca

Summary

Knee braces are commonly prescribed for knee osteoarthritis (OA) to reduce pain and improve user function. The Levitation brace from Spring Loaded Technology (SLT) was designed to reduce forces in all compartments of the knee by lowering quadriceps muscle activity, a predictor of knee joint contact force. Here we verify a 3-D musculoskeletal (MSK) modelling method to evaluate the effect of the Levitation brace on knee joint loading and quadriceps muscle activity during gait for the first time. We verify that knee extension moment and quadriceps activity are reduced when the brace is applied versus when the brace is not, as expected. Further model development is required in order to assess potential differences in compartmentalized knee joint contact forces.

Introduction

Musculoskeletal (MSK) computer modelling approaches are commonly used to estimate knee joint contact forces from measured biomechanical data [1]. A wide variety of methods and models can be applied for solving joint contact forces under different conditions, making verification an important step in determining the effectiveness of these models [2].

Knee braces are prescribed for knee OA, a debilitating MSK disease, as assistive devices to reduce pain and improve function for the user. The SLT Levitation knee brace was designed to reduce forces in all three compartments of the knee, by lowering the tensile quadriceps muscle forces that compress the knee joint [3]. This is achieved using a silicon liquid spring to store energy during knee flexion and return energy to assist in knee extension. A previous 2-D modelling study shows reduced quadriceps and knee contact forces with the Levitation brace [4], but 3D knee contact forces have yet to be assessed. The objective of this study is to verify a 3-D MSK modelling method to examine the effects of the Levitation brace on knee joint loading and quadriceps muscle activity. By applying an external moment to the knee, the brace is expected to reduce knee contact forces, knee extension moment and quadriceps activity, which are the measures used to verify the model performance. The results will provide valuable insight to inform design modifications.

Methods

In-vivo walking data collected for a single participant for the second “Grand Challenge” MSK modelling competition was used as the raw input data [3]. Kinematic data from marker trajectories and ground reaction force (GRF) data was collected and used to inform a generic MSK model, using OpenSim [1]. The model, comprised of 18 segments and 92 muscle-tendon actuators, was scaled using static trial data. The model was augmented to include an expression-based coordinate force at the knee joint to represent the Levitation knee brace (data provided by SLT). Two conditions were

analyzed: brace ‘on’ and brace ‘off’, to verify that the model predicts decreases in knee measures with the brace external moment applied. Inverse kinematics (IK) were determined with the gait data. IK results and GRF data were filtered (dual-pass, 2nd-order Butterworth filter, 6 Hz and 12 Hz cutoff frequencies, respectively) to calculate inverse dynamics. Residual reduction was applied and internal knee extension moments were determined and compared between bracing conditions. Muscle forces during walking were solved using static optimization techniques. Quadriceps muscle forces were compared between braced and unbraced conditions in order to verify that the brace decreased muscle force output. Knee joint contact forces calculated using joint reaction analysis were compared to evaluate differences with bracing.

Results and Discussion

Applying the simulated brace resulted in reduced knee extension moment up to 33% (Fig.1) and quadriceps muscle activity between 4-17% compared to the unbraced condition, verifying the successful implementation of the brace modelling method. Knee contact forces showed no substantial differences between conditions, which was not surprising given the low flexion angles associated with walking and brace angular force profile. Future work will focus on analyzing movements involving greater knee flexion ranges and developing a more sophisticated model.

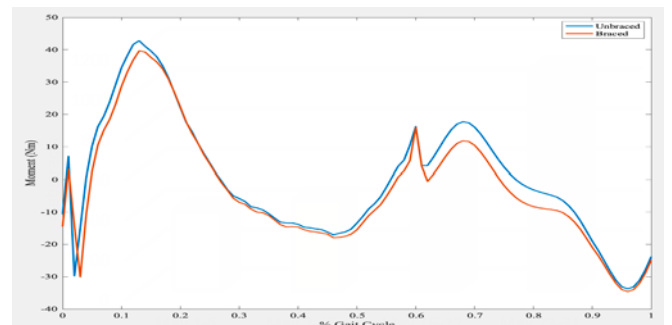


Figure 1: Knee extension moment across gait cycle.

Conclusions

The modelling method incorporating the Levitation brace was successfully verified producing results to evaluate differences between simulated braced and unbraced conditions for knee joint loading and muscle activity. Further research is required to assess potential knee joint contact force reductions with this brace in greater ranges of knee flexion/extension.

References

- [1] Lerner et al. (2015). *J.Biomech*, **48(4)**:644-650. [2] Kinney et al. (2013). *J.Biomech. Eng*, **135(2)**:0210121-0210124.
- [3] Shelburne et al. (2006). *J.Orthop*, **24(10)**:1983-90. [4] McGibbon et al. (2021). *Front. Bioeng. Biotechnol*, **8:604860**.

Effect of Muscular Fatigue on ACL Loading in Healthy and ACL-Reconstructed Females

Shelby Peel^{1,2}, Jake Melaro¹, Jeff Reinbolt¹, Songning Zhang¹, Liesel Schneider¹, John Sorochan¹, Joshua Weinhandl¹

¹University of Tennessee, Knoxville, TN, USA, ²High Point University, High Point, NC, USA

Email: speel@genevaUSA.org

Summary

Females are 16 times more likely to sustain a second anterior cruciate ligament (ACL) injury compared to their healthy female counterparts. Many of these females return to sport after ACL-reconstruction (ACL-R). Muscular fatigue is a hypothesized risk factor for female athletes. Previous studies suggest both fatigue and previous ACL-R can independently influence ACL loading (F_{ACL}). Seven healthy and four ACL-R females completed five anticipated cutting trials pre- and post- a fatigue protocol. Musculoskeletal modeling was used to estimate F_{ACL} pre- and post-fatigue. No significant differences were found in F_{ACL} between groups or fatigue.

Introduction

Up to 83% of ACL-R athletes return to their pre-injury sport, however 10 to 30% may sustain a secondary ACL injury. Re-injury of the ACL-R leg is multifactorial, such as altered lower extremity mechanics and altered muscle activity. However, lesser understood factors, such as muscular fatigue, could play a role in ACL reinjury. Previous research has shown that fatigue can influence lower extremity ACL-injury risk mechanics in both healthy and ACL-R females. However, it is unknown if fatigue can influence F_{ACL} . Therefore, the purpose of this study was to investigate the effects of fatigue on F_{ACL} pre- and post- during a laboratory-based fatigue protocol in healthy and ACL-R females.

Methods

Seven healthy (23.0 ± 2.6 yrs, 69.2 ± 6.9 kg; 1.66 ± 0.6 m) and four ACL-R (21.8 ± 2.1 yrs, 67.3 ± 4.8 kg; 1.68 ± 0.6 m) recreationally active females volunteered to participate in this study. Participants first completed a 5-minute self-selected warm-up, followed by five box land-and-cut trials from a 30 cm box placed $\frac{1}{2}$ their height from the force plates. They completed a laboratory-based fatigue protocol, then performed five additional box land-and-cut trials.

A 12-camera motion capture system (200Hz, Vicon) and a force platform (2000Hz, AMTI) were used to collect marker coordinate and GRF data, respectively. Musculoskeletal simulations of the pre- and post-fatigue trials were conducted in OpenSim (v3.2, <https://simtk.org/>). Inverse kinematics and inverse dynamics were used to calculate joint angles and moments from a participant-specific scaled musculoskeletal model [1]. Static optimization was used to decompose joint torques into net muscle forces. Anteroposterior knee joint reaction forces using the muscle forces obtained from static optimization were computed using the JointReaction Analysis in OpenSim. Finally, anteroposterior knee joint reaction force was used to estimate F_{ACL} relative to the tibial coordinate system using a previously established mathematical ACL model [2,3].

Differences in F_{ACL} across the entire stance phase between healthy and ACL-R females pre- and post-fatigue was examined via one-dimensional statistical non-parametric mapping (SnPM{F}) 2x2 ANOVAs (group x fatigue). Significance was set at $p < 0.05$.

Results and Discussion

There was no statistically significant group main effect, fatigue main effect, or group \times fatigue interaction found for F_{ACL} between healthy and ACL-R females pre- and post- a fatigue protocol ($p > 0.05$). The lack of significance could be attributed to small, uneven sample sizes in the two groups. Descriptively, F_{ACL} magnitude was lower in both the healthy and ACL-R groups post-fatigue, with the lowest magnitude observed in the ACL-R group at 0.91 BW. Kinematic and kinetic changes at the hip post fatigue in this group could indicate a compensatory mechanism to help stabilize the knee and reduce loading on the ACL post-fatigue.

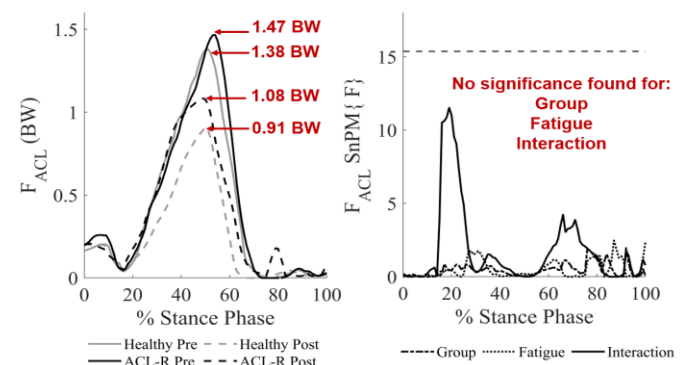


Figure 1: Mean ensemble curves for F_{ACL} pre- and post-fatigue between healthy and ACL-R females (A) and its respective SnPM{F} output (B) from 0 to 100% of stance phase.

Conclusions

The study reported no significant differences in F_{ACL} pre- and post-fatigue in healthy and ACL-R females. Differences in methodology and fatigue protocols, as well as small sample size most likely led to the lack of significant differences in the current study. However, given the limitations to the study, future research should focus on increasing sample size and to grasp a better understanding of how F_{ACL} is influenced by fatigue and prior ACL surgical intervention.

References

- [1] Lai AM, et al. (2017). *Ann Biomed Eng.* **45**:2762-2774.
- [2] Kernozek TW and Ragan RJ (2008). *Clin Biomech.* **23**:1279-1286.
- [3] Weinhandl JT, et al. (2016). *Comput Methods Biomech Biomed Engin.* **19**:1550-1556.

Evaluating Anthropometrically Scaled Models of Lateral Pinch to Characterize the Pediatric Hand

Tamara Ordonez Diaz¹, Jennifer A. Nichols¹

¹J. Crayton Pruitt Family Department of Biomedical Engineering, Gainesville, FL, USA

Email: tordonezdiaz@ufl.edu jnichols@bme.ufl.edu

Summary

Musculoskeletal models provide a powerful approach for examining the human hand. We examined lateral pinch simulations using a generic model of the wrist and thumb anthropometrically scaled to represent heights reported across childhood, puberty, older adolescence, and adulthood. Results demonstrated the potential of anthropometrically-scaled generic models to study hand strength across the lifespan, while also highlighting that muscle control strategies may adapt as we age. We concluded that anthropometric scaling can accurately represent age characteristics of the population.

Introduction

Generic musculoskeletal models are often developed using average data from healthy adult males. Thus, subject-specific or scaled-generic models are needed to represent pediatric populations. To what extent scaled-generic models can accurately represent the spectrum of strength profiles across the pediatric population is unknown. The objective of this study was to evaluate the accuracy of these models by measuring maximum pinch strength, comparing muscle control strategies, and evaluating isometric force scaling.

Methods

Twenty models were scaled from a generic model of the adult wrist and thumb [1] to represent the full range of height (1st, 15th, 50th, 80th, and 97th percentile) for four ages: 7, 12, 16, and 30 years [2]. For each model, five lateral pinch simulations were performed in OpenSim v. 3.3. Given the contribution of the *flexor pollicis longus* (FPL) is more than 50% for lateral pinch [3], the first set of simulations maximally activated the FPL to simulate maximum pinch strength. Simulations employing different muscle control strategies (50th percentile male, age-matched, and literature-based) were then designed to generate the maximum force required for typical activities of daily living. The final set of simulations increased the maximum isometric force of all muscles by a factor of 2. The maximum pinch strength simulations were compared to published experimental data to identify if these models could represent the strength produced at distinct ages [4-9]. To examine how representative the generic muscle control strategy was, the effect of using various control strategies was evaluated. Doubling the maximum isometric force explored the force-length relationship between the muscle's isometric force and lateral pinch force achieved. Paired t-tests were performed to compare the maximum lateral pinch force across age groups for all simulations.

Results and Discussion

Anthropometric scaling successfully captured age-dependent differences in pinch strength during simulations that maximally activated the FPL (Fig. 1). However, the model's

ability to represent the pediatric population is limited. The 7 y/o models failed to reach the target force of 40 N with all muscle control strategy simulations. Notably, the age-matched muscle control strategy simulations resulted in models activating the extrinsic thumb muscles similarly to published data, but the simulations also heavily relied on the wrist muscles to achieve the target force. Literature-based control strategy simulations failed to run to completion for models scaled below 0.75 corresponding to 132 cm (4 ft. 4 in.) height and showed no improvement for all other models. Linearly scaling the muscle force-generating capacity of all muscles resulted in a nonlinear relationship of maximum lateral pinch force achieved and maximum isometric force.

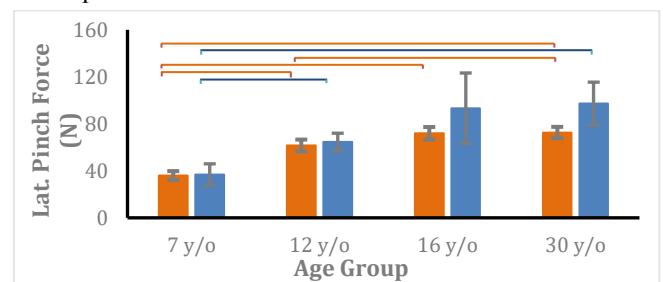


Figure 1. Lateral pinch force versus age for the maximum pinch simulations (orange) compared to experimental data (blue). Error bars represent standard deviation across height.

Given our simulations suggest that muscle recruitment may shift as we age, these models could be used to study how children adapt as their muscles develop and grow stronger. Our simulations were also able to highlight the complexity of the force-length relationship, and how it changes with age and task. The current simulation set-up prevented models younger than 7 y/o to reach completion. However, developing scaled-generic models to represent toddlers will further exemplify whether these results apply to the entire pediatric population.

Conclusion

Anthropometrically scaled hand models have the potential to represent the scope of strength profiles across the pediatric population. Modeling height difference with age is a critical step toward representing the full diversity of the population. This work motivates future research to elucidate how various musculoskeletal disorders and age-related changes in muscle strength and activation patterns influence hand strength.

References

- [1] Nichols et al. 2017. *J Biomech.* **58**:97-104.
- [2] CDC. 2012. *Vital & Health Statistics.* 11.
- [3] Goetz et al. 2012. *J Hand Surg Am.* **37**:2304-09.
- [4] Ager et al. 1984. *Am J Occup Ther.* 107-113.
- [5] Mathiowetz et al. 1986. *Am J Occup Ther.* **40**:705-711.
- [6] Fain et al. 2016. *J Hand Ther.* **29**:483-488.
- [7] Mathiowetz et al. 1985. *Arch Phys Med Rehabil.* **66**:69-72.
- [8] Mohammadian et al. 2014. *Iran J Public Health.* **43**:1113-22.
- [9] Smet et al. 2006. *J Pediatr Orthop.* **15**:426-427

Alignment of the Normal Ankle Joint in Neutral Bilateral Standing in Six Degrees of Freedom

Jordan Stolle¹, Maria Ruiz Rincón¹, Dhwanit Vispute¹, Rena Mathew¹, Francois Lintz², Cesar Netto³, Alessio Bernasconi⁴, Sorin Siegler¹

¹Department of Mechanical Engineering, Drexel University, Philadelphia, PA, 19103, USA

²Clinique de l'Union, Toulouse, France

³University of Iowa, Iowa City, IA, 52242, USA

⁴University of Naples Federico II Via Pansini n 5, 80131, Naples, Italy

Email: jts376@drexel.edu

Summary

Various pathologies affect bone alignment in the ankle joint, changing not only the alignment of the joint itself, but also the interaction between its articulating surfaces. Previous definitions have been developed to describe the misalignment of the ankle joint, two of these being the Saltzman angle [1] and the Foot Ankle Offset [2]. These measures, however, do not examine misalignment in all six degrees of freedom. This study examines the parameters of alignment, coverage, and congruity to quantify the alignment of normal ankle joints in six degrees of freedom.

Introduction

Alignment in this study is examined via a three-dimensional model comparing the translation and rotation of the tibia, talus, and calcaneus. Anatomical frames are defined for the talocrural joint, subtalar joint, and ankle joint complex to quantify the rotation and translation of the joints. Additionally, coverage, defined as the proportion of the articular cartilage region on the bone covered by the contralateral bone, and congruity, defined as the ratio between the standard deviation of the distance map and the average distance within the covered region are calculated, and a database of these measures are compiled and analyzed.

Methods

Over 100 non-symptomatic subjects were chosen for this study, with the ankle joint CT scanned via Weight-Bearing CT with a resolution of .3mm. 3D bone models were extracted from the CT scan images for the tibia, fibula, talus, and calcaneus. In order to establish the relative orientation of the bones, reference frames were first fully defined for the tibia, talus, and calcaneus. The rotations and translations of the joints were then defined using 313 (z-x-z) Euler angles to define the anatomical frames for the talocrural (Figure 1), subtalar, and ankle joint complex. The anatomical frames were then analyzed using MATLAB to determine the translation in and rotation around the anterior-posterior, medial-lateral, and proximal-distal axes.

For the analysis of coverage and congruity, the ankle joint articular surfaces were identified on the superior aspect (Figure 2a) and the inferior aspect (Figure 2b) of the talus.

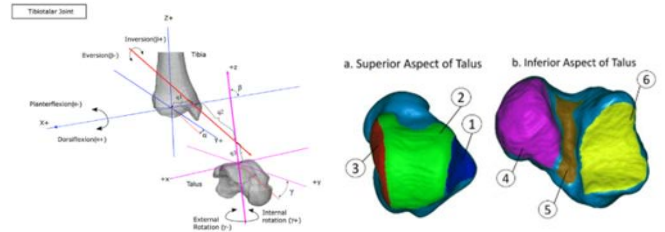


Figure 1: Anatomical Frame of Talocrural Joint

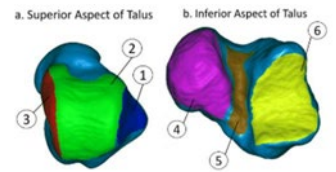


Figure 2: Articulating Surfaces of the a) Ankle Joint and b) Subtalar Joint

Distance maps describing the surface-to-surface distance distribution were produced for each of the regions of interest (Figure 2). The coverage and congruity were calculated from these distance maps for each specimen.

Results and Discussion

Average coverage and congruity results are displayed in Table 1. Average alignment values in each of the three anatomical frames are displayed in Table 2.

	Coverage	Congruity
Talar Dome	82.49	50.79
Medial Surface	65.45	55.01
Lateral Surface	63.49	58.17
Posterior Surface	82.46	55.23
Central Surface	79.04	66.28
Anterior Surface	33.45	44.52

Table 1: Coverage and Congruity of the Joint Surfaces of the Talus

Conclusions

The alignment, coverage, and congruity parameters determined for normal subjects within this study form a basis for comparison against pathological specimens to identify differences in the pathological cases.

References

- [1] Saltzman CL, El-Khoury GY. The hindfoot alignment view. *Foot Ankle Int*, 1995; 16: 572-576
- [2] Lintz F, Welck M, Bernasconi A, Thornton J, Cullen NP, Singh D, et al. 3D biometrics for hindfoot alignment using weightbearing CT. *Foot Ankle Int.*, 2017;38:684-9

Talocrural Rotation (degrees)			Subtalar Rotation (degrees)			AJC Rotation (degrees)			Talocrural Translation (mm)			Subtalar Translation (mm)			AJC Translation (mm)		
ML	AP	PD	ML	AP	PD	AP	ML	PD	ML	AP	PD	ML	AP	PD	AP	ML	PD
2.93	87.74	0.97	2.96	93.46	0.75	6.71	88.85	4.83	1.40	1.57	-1.64	-0.71	6.29	-30.84	-4.87	1.61	-28.91

Table 2: Average Alignment Values for the Talocrural, Subtalar, and Ankle Joint Complex

How do Dry Needling and High-Intensity Focused Ultrasound Affect the Mechanical Properties of Supraspinatus Tendons?

Sujata Khandare¹, Ali A. Butt¹, Molly Smallcomb², Jacob Elliott², Julianna C. Simon^{1,2}, Meghan E. Vidt^{1,3}

¹Biomedical Engineering, Pennsylvania State University, University Park, PA, USA

²Graduate Program in Acoustics, Pennsylvania State University, University Park, PA, USA

³Physical Medicine & Rehabilitation, Penn State College of Medicine, Hershey, PA, USA

Email: uuk72@psu.edu

Summary

Tendon injury treatments have reported mixed success rates and their mechanical implications are unknown. Our goal was to compare the mechanical effects of dry needling (DN), and high-intensity focused ultrasound (HIFU). Fifty *ex vivo* rat supraspinatus tendons were divided into: sham, DN, and 3 HIFU parameter sets: HIFU-1, HIFU-2, and HIFU-3 (n=10/group). Tendons were mechanically tested after treatment exposure to determine elastic modulus, stiffness, and percent relaxation. Outcomes suggest that DN diminishes tendon elastic properties. HIFU preserves elastic properties, with HIFU-1 performing better than HIFU-2 and HIFU-3.

Introduction

Tendon or ligament injuries at the shoulder represent 81% of all musculoskeletal injuries reported annually [1]. Injured tendons are mechanically inferior, compromising function. Conservative therapies, like dry needling (DN), are widely used; however, DN is invasive and has mixed success rates [2]. As tendons are required to withstand high physiological loads, there is a need for treatments that do not diminish tendon mechanical properties while promoting healing. High-intensity focused ultrasound (HIFU) is an emerging non-invasive therapy that directs ultrasound energy into a well-defined focal volume [3]. Different parameters of HIFU, like pulse length and treatment duration, can be varied to emphasize either tissue heating or acoustic cavitation. In this study, 3 different HIFU parameter sets chosen to emphasize acoustic cavitation were evaluated mechanically and compared to DN and sham.

Methods

Fifty *ex vivo* rat supraspinatus tendons were divided into: sham, DN, HIFU-1, HIFU-2, and HIFU-3 (n=10/group). For DN, a 30G needle (Tai-Chi, Suzhou, Jiangsu, China) was inserted and quickly removed from the central portion of the tendon 5 times over 12s. HIFU was performed at 1.5MHz with peak +ve and -ve pressure of 89MPa and 26MPa, respectively. The central portion of the tendon was exposed to 1ms pulses @10Hz for 60s for HIFU-1, 10ms pulses @1Hz for 15s for HIFU-2, and 5ms pulses @1Hz for 60s for HIFU-3. Following treatment exposure, tendons were mechanically tested using an MTS 858 Mini Bionix (MTS Systems Corp., Eden Prairie, MN) mechanical testing system, using an established testing protocol [4]. Tendon elastic and viscoelastic properties, including elastic modulus and stiffness, and percent relaxation, respectively, were determined. Statistical analysis was performed using ANCOVA, with sex as covariate, and coefficient of variation in SAS (SAS Institute, Inc., Cary, NC, v9.4), with significance at p<0.05.

Results and Discussion

Fifty samples were successfully tested; 4 measures were removed as outliers (>2SD outside mean). Elastic modulus of sham was higher than DN (p=0.0280), HIFU-2 (p=0.0476), and HIFU-3 (p=0.0450); modulus of HIFU-1 was higher than DN (p=0.0459) (Fig.1a). Stiffness of sham was higher than DN (p=0.0334); stiffness of HIFU-1 was higher than DN (p=0.0045) and HIFU-2 (p=0.0136) (Fig.1b). Percent relaxation of sham (60.85±15.4%) was higher than DN (50.17±7.6%; p=0.0247) and HIFU-2 (48.90±6.1%; p=0.0069; 1 outlier removed). Results suggest that DN causes a decline in tendon elastic properties. HIFU preserves elastic properties better than DN, with HIFU-1 performing better than HIFU-2 and HIFU-3. Although the percent relaxation of sham was higher than DN and HIFU-2, the coefficient of variation of sham (25.3%) was higher than DN (15.2%) and HIFU-2 (12.4%), possibly due to a higher number of male rats used in sham.

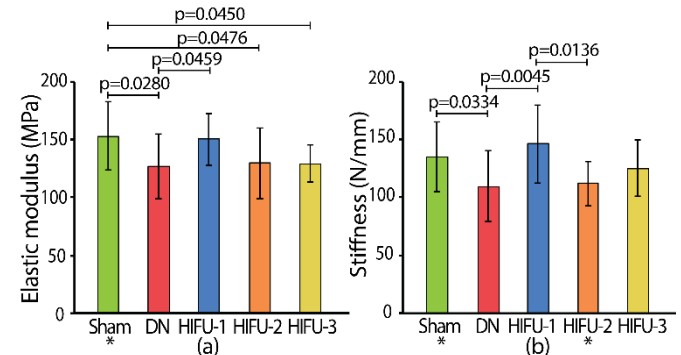


Figure 1: (a) Elastic modulus and (b) stiffness of *ex vivo* rat supraspinatus tendons exposed to sham, dry needling (DN), or 3 parameter sets of high-intensity focused ultrasound (HIFU-1; HIFU-2; HIFU-3) settings. *(n-1) samples due to outlier being removed.

Conclusions

Tendon mechanical properties in the HIFU-1 group were similar to sham, suggesting that HIFU-1 does not diminish tendon mechanical properties and should be investigated as an alternative, non-invasive treatment for tendon injuries. Further studies are needed to better understand the *in vivo* mechanical and healing effects of DN and HIFU.

Acknowledgments

NIH R21EB027886; NSF GRFP DGE1255832 (Smallcomb).

References

- [1] Yelin E et al. (2016) *The burden of musculoskeletal diseases in the United States*; Semin. Arthritis Rheum.
- [2] Krey D et al. (2015). *Phys. Sportsmed.* **43**; 80–6.
- [3] Dubinsky TJ et al. (2008). *AJR* **190**; 191-9.
- [4] Huang TF et al. (2004). *Ann. Biomed. Eng.* **32**; 336–4.

Spatial Distribution of Material Properties Influences Gross and Regional ACL Load Bearing Function

Jillian E. Beveridge, Snehal K. Chokhandre, Ellen M. Klonowski, Kayla Malby, Elise I. Baron, Ahmet Erdemir
Musculoskeletal Research Center & Department of Biomedical Engineering, Cleveland Clinic, Cleveland, USA
Email: beverij2@ccf.org

Summary

We show that locally assigned ACL material properties based on the distribution of MR T_2^* relaxation times alters the estimate of tissue reaction force and stress-strain distributions during an anterior drawer test.

Introduction

The native in vivo function of the anterior cruciate ligament (ACL) and its bearing on long-term joint health following repair or reconstruction remains ill-defined. To this end, we are developing a computational pipeline to estimate the role of localized ACL tissue properties and their influence on tibiofemoral contact mechanics using a computational model that incorporates quantitative magnetic resonance (MR) imaging properties. Here, we describe our approach and preliminary results.

Methods

Subject & data acquisition. A computational model of the porcine anterior cruciate ligament was developed from an 18-month old male Yucatan minipig. All animal procedures were reviewed and approved by our institutional animal care and use committee. MR images were acquired in vivo on a 3T scanner to ascertain tibiofemoral and ACL geometry (double echo steady state sequence; 0.36x0.36x0.7mm resolution) [1] and ACL T_2^* relaxation time (gradient multi-echo sequence; 0.42x0.42x0.8mm resolution) [2]. **Model parameters:** After manual segmentation, bone surfaces were represented using triangular meshes and the ACL was meshed using linear tetrahedral elements with a mesh density comparable to MR image resolution. Bones were modeled as rigid bodies, and the ACL as a deformable transversely isotropic Mooney-Rivlin material. The ligament was attached to the bones by tie constraints between the surface nodes of the ligament at insertion sites and the bony rigid bodies. Any wrapping of the ligament around bone surfaces was modeled as frictionless contact. A posterior femoral translation of 3 mm was prescribed to simulate an anterior drawer test. **ACL load simulations:** Three conditions were simulated: (1) homogeneous healthy ligament; (2) homogeneous weak ligament; and (3) heterogeneous ligament based on the spatial distribution of MR T_2^* relaxation times by scaling the local element material coefficients (C1, K, C3, C5) to range between zero and healthy values (Table 1). C2=0; C4=116.22; and lam_max=1.046 MPa parameters were constant across all simulation conditions.

Table 1: Model material properties (units in MPa).

	(1) Healthy	(2) Weak	(3) Heterogeneous
C1	1.95	0.0195	0 - 1.95
K	146.41	1.4641	0 - 146.41
C3	0.0139	0.00139	0 - 0.0139
C5	535.039	5.35039	0 - 535.039

Finite element analysis was conducted using FEBio (v2.9). For each simulation, fiber stretch and effective stress distributions were inspected and the reaction forces at 3 mm anterior drawer were extracted.

Results and Discussion

Under the simulated anterior drawer test, total reaction forces for healthy, weak, and heterogeneous ACL conditions were 398N, 3.98N and 321N, respectively. Effective stress varied across conditions, with the MR T_2^* -based heterogeneous model demonstrating the greatest variation which was particularly evident between adjacent ligament regions at the proximal third of the ACL (red vs. blue arrows, Figure 1).

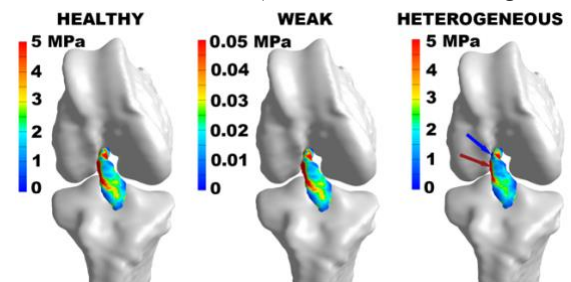


Figure 1: Effective stress distribution across the 3 ACL conditions. Fiber stretch distribution was similar to effective stress results with the heterogeneous ACL demonstrating the greatest magnitude of localized regional variation.

Our results suggest that greater ACL computational model sensitivity might be achieved by scaling the material properties according to the spatial distribution of MR T_2^* relaxation times. The 20% reduction in estimated reaction force between healthy homogeneous and heterogeneous models is substantial. Given injured or repaired ligament will likely have a much larger variation in material properties with a tendency towards a higher proportion of weaker ligament [3], taking into account the spatial distribution of weaker regions is likely to be critical for accurately estimating the in vivo mechanical behaviour and (re)injury risk of healing or remodeling ACL.

Conclusions

Preliminary model outputs show sensitivity to our approach and supports further model development.

Acknowledgments

We thank Ariel Schwartz for her technical assistance and our funding agencies: NIH NIAMS R00-AR069004 and the Cleveland Clinic MSRC Pilot Program.

References

- [1] Kim J et al. (2020). *OAC*, **28**: 1539-1550. [2] Beveridge JE et al. (2017) *J Biomech*, **56**: 117-121. [3] Beveridge JE et al. (2017) *JOR*, **36**: 1701-1709.

Analyze the effect of the anterior oblique ligament injury and first dorsal interosseous function upon thumb CMC joint subluxation: a cadaver study

¹Yueh-Ning Chu, ^{3,4,5}Hsiu-Yun Hsu, ^{4,5}Li-Chieh Kuo, ^{1,2,5*}Tai-Hua Yang

¹Department of Biomedical Engineering, ²Department of Orthopaedic Surgery, National Cheng Kung University Hospital, College of Medicine, ³Department of Physical Medicine and Rehabilitation, National Cheng Kung University Hospital, College of Medicine, ⁴Department of Occupational Therapy, College of Medicine, ⁵Medical Device Innovation Center, National Cheng Kung University, Tainan, Taiwan
Email: dd2006tw@gmail.com

Summary

Although there is still a difference between using the cadavers and the real situation, our study might provide information not only to understand the importance of AOL for the stability of the CMC joint but also to refer the standard in the force and movement mode in clinical examination or traditional rehabilitation programs. In muscle training, for the thumb CMC joint instability, according to results, the training programs included the FDI muscle strengthening could provide stability for subjects with joint problems in some situations. But from another point of view, the joint distance was decreased after FDI training. If applied to some cases that already had OA or bone spurs around the joint, it would cause these groups to have more severe pain or accelerate the production of OA.

Introduction

Since instability of the thumb carpometacarpal (CMC) joint is such a common issue, but nowadays, there are still many kinds of opinions and methods in the clinical examinations and treatments [1,2]. In this study, we set cadaver models to simulation the modified thumb abduction stress test and frequent functional movement to analyze the CMC joint distance in different muscle loadings. Besides that, we also investigate how the joint change after the AOL ligament injury and whether the hand intrinsic muscle training can provide good joint stability after ligament damage.

Methods

A total six left hands was performed in this study. A custom mechanism [3] was used to imitate the subject of performing a thumb abduction stress test and key pinch movement at various muscle maximal loading in different conditions, such as removing the anterior oblique ligament (AOL) and strengthening the FDI muscle. Then, we created 3D images by computer tomography (CT) and calculated the geometric center distance of the thumb CMC joint using software from all experimental data. The paired t-test and one-way ANOVA were used to analyze and set a p-value defined less than 0.05 as statistical significance.

Results and Discussion

Without removing the soft tissue around the CMC joint, the joint distance increased between 0% and 50% maximal loading in the abduction movement but decreased when the force reaches 75%. However, in key pinch movement, the joint distance was significantly increased as loading increases (P=0.015). After removed the AOL ligament compared with

those who have not been removed, the joint distance increased and reaches a statistically significant under 0% tension (P=0.005) in the abduction and significantly increased at 0% (P=0.005) and 50% (P=0.016) maximal loading in a key pinch. When added to the FDI muscle training, the joint distance reduced compared to before and had statistically significant at 50% and 100% loading in both movements (P<0.01). (Figure 1.) Those data can find out that while the applied force increases, the joint distance also increases gradually. Additionally, after removed the AOL, the joint distance had increased. It means that AOL plays an essential role in stabilizing the thumb CMC joint for movement. It demonstrated that the joint distance decreased after the imitation of the FDI training program in both movements.

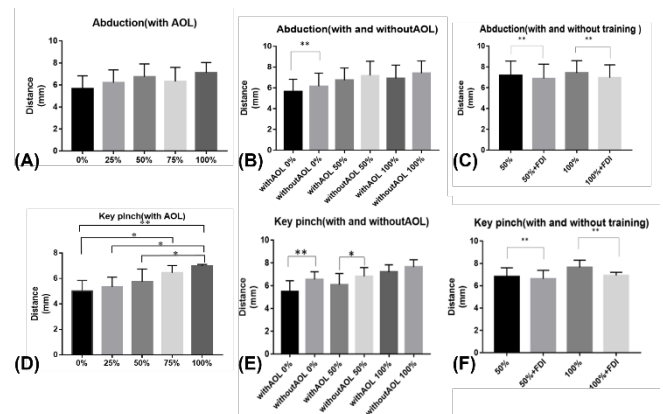


Figure 1: Distance values of abduction and key pinch movement (A) with the AOL of abduction (B) without the AOL of abduction (C) FDI muscle training of abduction (D) with the AOL of key pinch (E) without the AOL of key pinch (F) FDI muscle training of key pinch

Conclusions

Our result provides a useful reference for clinical stuff as making rehabilitation programs and common suggestions for subjects suffering from joint instability.

Acknowledgments

Special thanks to all Department of Radiology members, National Cheng Kung University Hospital, College of Medicine in NCKU.

References

- [1] Wolf, J.M., et al. (2009). *The Journal of hand surgery*, **34(8)**: 1402-1406.
- [2] Adams, J.E., et al. (2018). *HAND*, **13(1)**: 40-44.
- [3] Kuo, L.-C., et al. (2018). *Journal of Medical and Biological Engineering*, **38(5)**:724-734

Transfemoral prosthesis user stumble recovery responses for both limbs across swing phase

Maura E. Eveld, Shane T. King, Karl E. Zelik, and Michael Goldfarb
 Department of Mechanical Engineering, Vanderbilt University, Nashville, TN USA
 Email: maura.e.eveld@vanderbilt.edu

Summary

In order to inform fall prevention interventions, four transfemoral prosthesis users who use the Ottobock C-Leg were tripped 3-4 times per limb during treadmill walking using our custom stumble perturbation system. Stumble recovery responses were analyzed along with participant age, prosthesis type, and swing percentage of perturbation.

Introduction

Transfemoral prosthesis users fall 200x more often than age-matched controls [1]. In order to develop interventions (e.g., prostheses, training) to decrease this population's fall incidence, it is important to understand the deficiencies in the recovery strategies attempted by the individuals as well as the shortcomings in the function of their prescribed prostheses.

For able-bodied adults, responses to perturbations depend on the timing of the perturbation during swing phase and the age of the individual. Typically prescribed prosthetic knees have various joint designs (e.g., single-axis, polycentric) and control schemes (e.g., fixed vs. variable damping), aspects that affect their behavior following perturbations. Thus, understanding how these factors (i.e., age, swing phase, and prosthesis type) affect recovery responses, and how they interact, is crucial to ultimately providing beneficial interventions. While a few studies (e.g., [2,3]) have contributed to this knowledge gap, the cumulative number of data points remains too small to draw strong inferences regarding the nature of such recovery responses, and how prosthesis functionality might mitigate or aggravate the likelihood of a fall.

The overarching goal of our study is to analyze a case series of obstacle stumble events accounting for a range of participant ages, prosthesis types, and points in swing phase. For this abstract we investigate a subset of this case series in order to hold one variable constant (prosthesis type). Specifically, we aim to characterize the strategies attempted and fall outcomes of Ottobock C-Leg users for each limb across swing phase.

Methods

Four Ottobock C-Leg users were recruited for a stumble perturbation experiment. Each participant experienced 3-4 unexpected obstacle perturbations to each limb, targeted to occur in early, mid, and late swing phase, while walking on a treadmill at 0.8 m/s. The custom obstacle perturbation system and protocol used are detailed in [4]. For each stumble, the recovery strategy attempted (as defined in [2, 4]) and fall outcome (fall identified as >50% bodyweight measured by a load cell in-line with overhead harness) were reported, as well as the swing percentage of the perturbation. Ground-reaction forces and kinematic data were collected, and joint-level kinematics/kinetics were computed.

Results and Discussion

Swing percentage of perturbation, recovery strategy attempted, and fall outcome are reported for each stumble (Figure 1). Full results/analyses will be presented at the conference; here we highlight a few key results. *Stumbles to sound-side swing phase:* The older participants (P1, P2) never recovered, regardless of swing phase percentage, while the younger participants (P3, P4) recovered from all but one perturbation. The participants who fell were unable to initiate swing in early/mid-stance with their prosthetic limb. These results align with studies of older able-bodied adults, who fall more often due to slower reaction time and less muscle strength. *Stumbles to prosthetic-side swing phase:* Three participants recovered from all mid/late-swing perturbations with a lowering/delayed lowering strategy; the C-Leg's resistance to flexion increases during the extension portion of swing phase (when these perturbations occurred), which prevented buckling and facilitated a lowering step. However, these recoveries involved substantial thigh abduction (avg 31+/-7 deg) to clear the obstacle in the following step due to the C-Leg's insufficient knee flexion; P2's lack of thigh abduction (13 deg) inhibited his ability to clear the obstacle, resulting in a fall.

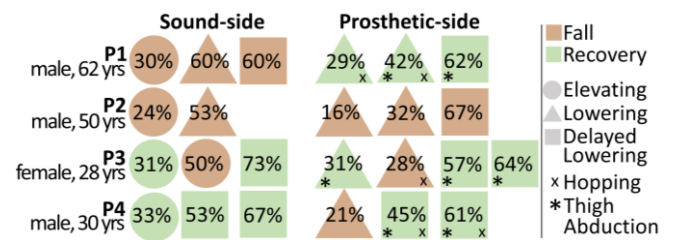


Figure 1: Swing percentage of perturbation (number), recovery strategy attempted (shape, symbol), and fall outcome (color) for each stumble for four C-Leg users.

Conclusions

For sound-side stumbles, the two older C-Leg users had more difficulty recovering than the two younger participants; they may benefit from assistance initiating prosthetic swing in early/mid-stance. For prosthetic-side stumbles, while flexion resistance prevented prosthetic knee buckling at perturbation, substantial thigh abduction was still essential to recover from mid/late-swing perturbations; additional prosthetic knee flexion in the following step may improve responses.

Acknowledgments

Funding from NIH R01HD088959 and the NSF GRFP.

References

- [1] Hafner BJ et al. (2007). *Arch Phys Med Rehab*, **88**:207-217.
- [2] Shirota C et al. (2015). *JNER*, **12**: 79.
- [3] Campbell JH et al. (2020). *RATE*, **7**:1-10.
- [4] Eveld ME & King ST et al. (2019). *JNER*, **16**: 69.

Motor Unit Action Potential Features For Robust Motion Classification

Michael D. Twardowski¹, Michael D. Chan¹, John P. Chiodini¹, Serge H. Roy¹, Paola Contessa¹, Gianluca De Luca¹, and Joshua C. Kline¹

¹Delsys, Inc and Altec Inc, Natick, MA

Email: mtwardowski@delsys.com

Summary

We investigated the feasibility of using our Motor Unit Drive (MU Drive) neural interface for prosthetic control to provide robust motion classification performance at varying muscle contraction intensities. MU Drive employs algorithms for extracting motor unit action potential (MUAP) features from surface electromyographic (sEMG) signals. We trained and tested a motion classifier using the MUAP-features extracted with MU Drive to discriminate 6 different motions of the wrist and hand from sEMG signals detected from 4 muscles of the upper arm across a range of contraction intensities. Our results demonstrated robust motion classification with a median of 93.3% accuracy and an average delay of 137 ms.

Introduction

Efforts to improve prosthetic control have led to the development of neural interfaces that employ pattern recognition algorithms trained on myoelectric features from sEMG signals collected from several sites on the residual limb to map the various intended motions of the user. This approach however is confounded by variations in muscle contraction intensity that occur during normal operation of prostheses and that diminish the discriminability of myoelectric features and result in low classification accuracies [1, 2]. To overcome the limitations of traditional myoelectric features, our group has developed MU Drive, a neural interface that employs decomposition methods to access MUAP-based features from the individual MUAP firings within the sEMG signal [3], which are the individual components for controlling force and motion. Our prior work has demonstrated that MU Drive can provide responsive real-time proportional control signals across a range of muscle activation levels [3]. We now investigate the potential of employing MU Drive to extract MUAP-features for enabling robust identification of motion classification and intent.

Methods

Ten healthy subjects with intact limbs volunteered for this research study (5 males, 5 females; age=33.6±16.2). We placed Trigno™ Galileo 4-pin mini-grids over four muscles of the upper-limb that control motions of the hand and wrist—the extensor digitorum communis, the flexor digitorum profundus, the pronator teres, and the biceps brachii—and recorded sEMG signals during repeated trials of 6 different motions of the hand and wrist—finger flexion & extension, wrist flexion & extension, forearm pronation & supination—performed at targeted muscle activation levels of 30%, 60%, and 100% maximum voluntary sustained activation (MVSA). We filtered the sEMG signals from 20–450 Hz and digitized them at 2.222 kHz using a Trigno™ EMG acquisition system (Delsys Inc.). Features indicative of MUAP shape and

amplitude were then extracted using MU Drive in 100 ms non-overlapping windows and used to train a linear discriminant analysis (LDA) classifier, commonly used in prosthetic applications. For each subject, we trained their LDA classifier using 22% of their motion data, and tested its performance on the remaining 78% of motion data. We timed the algorithm to gauge its real-time efficacy.

Results and Discussion

MU Drive successfully extracted MUAP-features from each non-overlapping 100 ms window with an average 37.0±1.8 ms computational delay. The LDA classifier demonstrated an average accuracy of ranging from 89.8 to 94.4% across all motions and muscle intensities tested – values substantially higher than those reported in previous studies of traditional myoelectric features [1]. (**Table 1**).

Table 1: Classifier accuracies at 30%, 60%, and 100% MVSA levels.

Classifier	MVSA	MVSA60	MVSA30
LDA	94.4±4.8%	91.6±13.9%	89.8±12.6%

Overall, the LDA classifier achieved a median accuracy of 93.3%, indicating that MUAP-features extracted using MU Drive enable motion classification that is robust to changes in muscle contraction intensity.

Conclusions

These results support the feasibility of our MU Drive neural interface system to robustly detect movement intent at varying intensities of muscle contraction. Future research will refine and integrate motion classifiers based on MUAP-features with proportional control demonstrated in our previous work [3] to provide a comprehensive MU Drive system for improved control of prostheses, and robotics systems.

Acknowledgments

This research was supported by the De Luca Foundation, Delsys Inc., and the NICHD (award number R44HD094626).

References

- [1] Campbell E et al (2020). *Sensors*, **20**:1613.
- [2] Scheme, E et al (2013). *J Prosthet Orthot*, **25**:2.
- [3] Twardowski MD et al. (2019). *J Neural Eng*, **16**:016012.

Exploring Effects of Prosthetic Ankle and Toe Joint Range of Motion on Activities of Daily Living

Rachel H. Teater¹, Kirsty A. McDonald², Karl E. Zelik¹

¹Department of Mechanical Engineering, Vanderbilt University, Nashville, TN, USA

²Department of Exercise Physiology, University of New South Wales, Sydney, NSW, Australia

Email: rachel.h.teater@vanderbilt.edu

Summary

We are exploring if the addition of ankle or toe joint range of motion could improve the ability of lower limb prosthesis users (LLPUs) to perform activities of daily living: sit-to-stand, squatting, lifting, and lunging. We are collecting data with participants performing these tasks wearing their prescribed passive prosthesis and also the Vanderbilt Powered Ankle (used to emulate design changes in prosthetic ankle and/or toe articulation). Preliminary results from a transtibial LLPU on their prescribed prosthesis show highly asymmetric lower limb loading across tasks, with the intact limb experiencing significantly greater loads than the prosthetic limb.

Introduction

Most LLPUs wear a passive ankle-foot prosthesis where the ankle joint and foot keel are locked at a fixed angle. A significant percentage of these LLPUs live with mobility challenges that affect their ability to carry out daily activities and live independently [1]. Surveys of transtibial LLPUs have found that 11% cannot stand-up from a chair, 25% cannot pick up an item off the floor, 41% cannot get up from the floor, and 40% do not have independent household mobility [1,2]. Many daily tasks such as standing up from a chair, lunging forward, or squatting down involve ankle and toe flexion in healthy individuals – degrees of freedom that are limited or not included in most passive prosthetic feet. Limitations in ankle and toe joint mobility may contribute to task performance deficits or lead to unsafe compensation strategies. For instance, prosthetic device limitations may lead unilateral LLPUs to perform tasks in a highly asymmetric manner, overloading their intact lower limb and thus contributing to overuse injury or degenerative joint disorder risks. Prosthetic design modifications could potentially improve their comfort, safety, or ability to complete certain daily tasks, or do so with less overloading of their intact lower limb. To investigate this, we aim to characterize how LLPUs perform common everyday movements while wearing their prescribed passive ankle-foot device, and assess if adding prosthetic ankle and toe joint range of motion aids LLPUs by improving functional ability, symmetry, and/or perceived stability.

Methods

Through reviewing the scientific literature and interviewing local LLPUs, physicians, and prosthetists, we identified several tasks that LLPUs often avoid or find challenging and have the potential to be improved by modifying prosthetic ankle-foot design. We are now conducting a human movement study evaluating transtibial LLPUs during these identified tasks: sit-to-stand, lifting, squatting and lunging. To address the first objective, we are collecting data with users performing variations of all tasks in their prescribed passive prosthesis. We then use the Vanderbilt Powered

Ankle to emulate various device design modifications that may improve the ability of LLPUs to complete these tasks, i.e., adding ankle and/or toe joint flexion/extension. We are collecting participant feedback on perceived effort, stability, and comfort as well as motion capture and ground reaction force (GRF) data.

Results and Discussion

Preliminary data from one transtibial LLPU (K4 mobility level) wearing his prescribed prosthesis (Fillauer AllPro) are presented here. The participant was able to complete all tasks, but expressed that standing up from a low chair and lunging with his prosthesis forward were extremely difficult. Vertical GRFs during tasks that are expected to be symmetric (sit-to-stand, squatting, lifting) showed the intact limb often experienced more than twice the load of the prosthetic limb (Fig. 1A-C). When lunging with the intact limb forward, the participant's intact limb experienced approximately nine times more force than the prosthetic limb (Fig. 2D). Initial healthy control data indicates that the leading limb usually experiences only about twice the force of the prosthetic limb during lunging. This study is ongoing and additional findings will be shared at the conference.

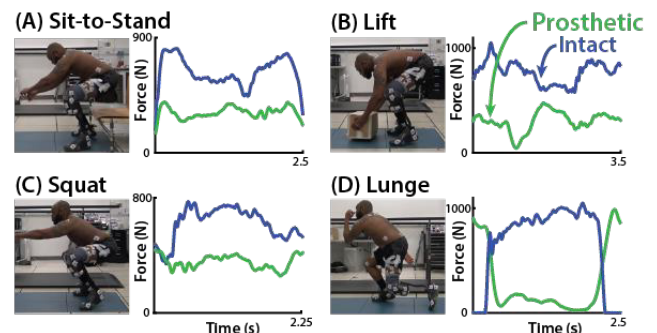


Figure 1: Vertical GRF of a transtibial LLPU performing (A) sit-to-stand, (B) lifting (10 kg), (C) squatting, and (D) lunging with his prescribed prosthesis.

Conclusions

Preliminary results indicate that LLPUs adopt a high degree of asymmetry to complete common tasks, and there may be opportunities to improve symmetry, stability, or functional ability through prosthetic design modifications to the ankle or toes.

Acknowledgments

This research is supported by NIDILRR (90IFRE0001) and NIH (T32EB021937). Dr. Bastas is thanked for his insights.

References

- [1] Gauthier-Gagnon C et al. (1999). *Arch Phys Med Rehabil.*, **80**: 706-713.
- [2] Davies B and Datta D (2003). *Prosthet Orthot Int.*, **27**: 186-190.

Bone contact differences of conical and cylindrical endoprostheses for transtibial percutaneous osseointegrated prostheses

Carolyn E. Taylor^{2,3}, Heath B. Henninger^{2,3}, Kent N. Bachus^{1,2,3}

¹Department of Veterans Affairs, Salt Lake City, Utah, United States of America

²Department of Orthopaedics, University of Utah, Salt Lake City, Utah, United States of America

³Department of Biomedical Engineering, University of Utah, Salt Lake City, Utah, United States of America

Email: carolyn.taylor@utah.edu

Summary

This research developed, validated, and utilized virtual implantation of transtibial percutaneous osseointegrated (OI) endoprostheses for prosthetic limb attachment. The area of virtual bone in contact with two virtual endoprosthesis designs (cylindrical and conical) were analyzed. The results indicate that for transtibial residual limbs greater than 20% residual length, a conical endoprosthesis has a greater ratio of contact area to bone removed when compared to a cylindrical endoprosthesis. Neither design appears optimal for very short amputations of less than 20% residual length due to a high rate of cortical penetration through a thin non-circular medullary canal. Though transfemoral OI attachment systems have demonstrated clinical success in transtibial amputees, this research suggests that not all transfemoral designs are suited for transtibial use, and further research is necessary before utilizing existing percutaneous OI systems for these patients.

Introduction

Percutaneous OI systems are used to attach prosthetic limbs to the residual bone of an amputee. Most clinical systems rely on conically shaped press-fit or cylindrically threaded fixation to create intimate contact of the endoprosthesis surface to the host bone to encourage skeletal fixation. All devices used clinically were initially developed for the femur, then applied in the tibia [1, 2] without translational research to support either similar, or better clinical results. While there has been some success, continued reports of aseptic loosening [3] indicate that endoprosthesis design may need to be customized for the transtibial population. This research used virtual implantation to estimate contact between the bone and simplified conical and cylindrical endoprosthesis designs.

Methods

Virtual implantation procedures were validated on 27 cadaver tibias using a conically shaped design [4] as a template for systems with circular cross-section. Part comparison between virtual and surgical preparations confirmed accuracy within CT resolution of 1 mm.

Then, CT scans were obtained and reconstructed for 20 specimen pairs (40 bones). Virtual implantation was conducted using commercially available software (3-Matic

v13.0, Materialise, Plymouth, MI). A 3 cm long, conical (2° taper angle) and a 3 cm long cylindrical endoprosthesis shape were virtually implanted into the medullary canal of these bones at 20, 30, 40, 50, 60, 70, and 80% residual length. The percent of bone-endoprosthesis contact and the percent of bone volume removed during implantation were calculated. The ratio of these two values indicates the amount of bone-endoprosthesis contact per volume removed, and normalized the data.

Results and Discussion

For the short residual limbs of less than 20% residual length, 72% resulted in cortical penetration at the proximal tip, independent of the design of the endoprosthesis. This also occurred in 50% of cylindrical implantations and 20% of the conical implantations at 80% residual length (Table 1). All instances where the bone penetrated completely through the cortex were removed from compiled results.

Comparing cylindrical to conical designs showed that the cylindrical implants achieved 12.0±6.5% more bone-endoprosthesis contact, but with 4.8±2.5% more bone removed (Table 1). Except for the 20% residual length, all the independent residual lengths showed that when the contact area data was normalized with the bone removal data, that the cylindrical endoprosthesis achieved the greater contact at the expense of greater amounts of bone removed. Therefore, while the cylindrical design may result in greater bone contact, it also removes bone that could compromise the structural integrity of the construct. In contrast, the conical design is more efficient by achieving approximately 30% more contact per unit bone removed.

Acknowledgments

Research funding from the US Department of Veterans Affairs Rehabilitation Research and Development Service (#I01RX001246), the US Army Medical Research and Materiel Command (#W81XWH-15-C-0058).

References

- [1] Hoyt, BW, et al.(2020)*Expert Rev Med Devices*;17:17-25.
- [2] Thesleff, A, et al.(2018)*Ann Biomed Eng*;46:377-391.
- [3] Haque, R, et al.(2020)*BMJ Open*;10:e038346.
- [4] Drew, AJ, et al.(2020)*Clin Biomech*; 72:108-114.

Table 1: Endoprosthesis fit summary (Mean±SD) *Significant difference between cylindrical and conical endoprosthesis (p≤0.05).

Amputation Level (%)	Average Implant Size	Failure (N, N=40 total)		Contact (%)		Bone Removed (%)		% Contact / % Removed	
		Cylindrical	Conical	Cylindrical	Conical	Cylindrical	Conical	Cylindrical	Conical
20	26±3	30	29	37.6±5.9*	30.6±4.2*	7.4±1.0*	5.4±.7*	5.1±0.7*	5.7±0.6*
30	19±2	8	8	52.5±8.2*	42.5±6.8*	9.6±3.0*	6.8±2.2*	5.9±1.6*	6.7±1.8*
40	15±2	0	0	66.8±9.0*	49.4±6.7*	8.6±2.7*	5.3±1.9*	8.4±2.2*	10.3±2.8*
50	12±1	0	0	80.4±7.8*	63.9±9.9*	10.0±3.1*	6.0±2.2*	8.8±2.9*	11.9±4.1*
60	11±1	0	0	87.0±6.6*	73.9±7.3*	12.2±3.7*	7.6±2.7*	7.7±1.9*	10.5±2.8*
70	12±2	1	0	95.4±4.3*	86.7±6.8*	19.7±5.6*	13.1±4.1*	5.2±1.4*	7.2±2.1*
80	16±2	20	8	98.6±3.5*	96.7±3.5*	35.2±8.4*	28.4±8.2*	3.0±0.9*	3.7±1.3*

Variable Stiffness Foot provides Users with Adjustment of Knee and Ankle Mechanics

Kieran M. Nichols¹, Peter G Adamczyk¹

¹Mechanical Engineering, University of Wisconsin-Madison, Madison, WI, USA

Email: knichols4@wisc.edu

Summary

The Variable Stiffness Foot prosthesis can modulate its forefoot stiffness through the deflection of a compliant cantilever-beam keel and adjustable support fulcrum. Participants tested the effects of this modulation on leg mechanics in walking using three different VSF stiffnesses. As the VSF stiffness increased, participants exhibited less dorsiflexion and more plantarflexor moment, more knee extension, more knee flexor moment, and less power flow through the ankle. These modulations could be controlled to aid users in walking across various terrain or different speeds.

Introduction

The Variable Stiffness Foot (VSF) is an energy storage and return (ESR) prosthesis that can passively store and return energy through the deflection of a compliant cantilever-beam forefoot keel [1]. It is a semi-active prosthesis [1] that allows real-time control of stiffness that can be dependent on the type of activity (standing, flat ground walking, ramp and stairs walking). The VSF prototype's effective stiffness is modulated by a support fulcrum moved by a motor and belt.

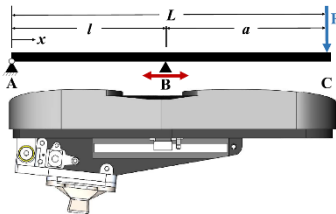


Figure 1: side drawing of the VSF highlighting the cantilever mechanics [1].

Previous studies in prosthetics found that increased range of motion for stairs and ramps is associated with improved gait [2]; a stiffer ankle (increased moment for small change of angle) is helpful for standing stability [3]; and a compliant forefoot returns more energy to the rest of the body [4]. We hypothesized that increasing forefoot stiffness would lead to decreasing ankle dorsiflexion angle, increasing peak ankle moment, and decreasing uniform deformable body power (related to decreasing energy returns in push-off), along with increasing knee extension angle and knee flexor moment.

Methods

Seven persons with trans-tibial amputation walked across two force plates (one foot on each plate) in a motion capture lab. The participants walked with three different VSF stiffness settings (compliant-1, medium-2, and stiff-3; each scaled to each person's body mass) for 3 trials at 1.1 ± 0.1 m/s.

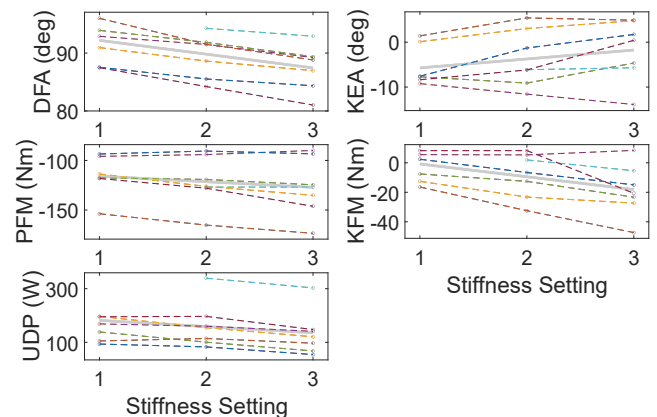
Motion and force data were processed to estimate joint angles and moments using standard inverse dynamics, and power flow through the ankle from the prosthesis using a deformable body model (Unified Deformable power, UDP) [5]. Peak values of ankle dorsiflexion angle (DFA), plantarflexor moment (PFM), midstance knee extension angle (KEA) and

knee flexor moment (KFM), and UDP were computed for each stride on the prosthetic side and averaged across the three trials for each stiffness setting. Mixed linear effects models were used to estimate the sensitivity of these metrics to stiffness settings, their significance (p-value), and the coefficients of determination (r^2) of their regressions.

Results and Discussion

Stiffer VSF settings led to reduced DFA ($r^2=0.97$, $p<0.0001$), increased KEA ($r^2=0.88$, $p=0.0001$), more negative PFM ($r^2=0.95$, $p<0.0001$), more negative KFM ($r^2=0.88$, $p=0.0001$), and reduced UDP ($r^2=0.97$, $p<0.0001$) during toe off, which correlates with reduced push off energy. Interestingly, more extended knee angle was associated with more negative knee flexor and ankle plantarflexor moments.

Figure 2: mixed linear effect trends for ankle and knee angles, moments, and UD power. The grey bar represents the mixed linear effects fit of all subjects for the given metric. Plantarflexion/flexor (ankle) and flexion/flexor (knee) are in the negative direction.



Conclusions

The VSF enables modulation of mechanical outcomes through controlled stiffness. Automated, real-time stiffness control could enable adaptation to terrain conditions such as sandy, muddy, wet or icy ground as well as stairs and ramps, or to alter biomechanical loads such as undesirable knee moments.

Acknowledgments

This work was supported by NIH HD074424 and institutional funds from the University of Wisconsin-Madison.

References

- [1] Glanzer et al. (2018). *IEEE TNSRE*, **26.12**: 2351- 2359.
- [2] Torburn et al. (1994). *Clin. Orthopaedics*, **303**: 185-192.
- [3] Adamczyk et al. (2015). *IEEE TNSRE*, **23**: 776-785.
- [4] Hansen et al. (2010). *Gait & posture*, **32.2**: 181-18
- [5] Takahashi et al. (2012). *Biomechanics*, **45.15**: 2662

EFFECTS OF A PHYSIOTHERAPY EXERCISE PROGRAM FOR FOOT-ANKLE IN PEOPLE WITH DIABETES ON FOOT KINEMATICS DURING GAIT

Renan L. Monteiro^{1,2}, Érica Q. Silva¹, Jane S. Ferreira¹, Ronaldo H. Cruvinel-Júnior¹, Jady L. Verissimo¹, Marcos Duarte³,

Isabel C.N. Sacco¹

¹Universidade de Sao Paulo, Faculdade de Medicina, São Paulo, SP, Brazil

²Department of Biologic and Health Science, Federal University of Amapá, Macapá, AP, Brazil

³Biomedical Engineering Program, Federal University of ABC, Rua Arcturus, 3, São Bernardo do Campo, SP, Brazil.

Email: icsacco@usp.br / renanlm@usp.br

Summary

Recently, foot-ankle exercises have been recommended for people with diabetic neuropathy (DPN) risk 1 and 2; however the effects of this type of intervention on foot motion during gait is yet to be determined. We designed a randomized controlled clinical trial RCT (NCT02790931) aiming to evaluate the effects of a 12-week physiotherapeutic foot-ankle exercises supervised program on foot-ankle kinematics in people with DPN. Fifty-six subjects were enrolled in this study and were allocated into the control (CG) and intervention groups (IG). Plug-In Gait and Oxford Foot Model setup protocols were used for gait kinematic acquisition at baseline and 12 weeks after the intervention. After the intervention, IG compared to CG increased forefoot relative to hindfoot dorsiflexion range of motion (ROM) ($p < 0.0131$) during gait stance phase.

Introduction

DPN evolves progressively with sensitivity and motor deficits including vibratory, thermal, tactile, proprioception sensitivities, atrophy of foot-ankle extrinsic and intrinsic muscles, foot deformities, and all these alterations usually ended up affecting gait mechanics and balance [1,2]. Physiotherapeutic supervised exercises targeting foot-ankle function may be beneficial for people with DPN and they are now part of international guideline recommendations for people at risk of diabetic foot disease. Few RCTs evaluated the effects of foot-related strengthening and mobility exercises in different outcomes - especially biomechanical outcomes - the majority are of low quality, present small effect sizes, and do not involve exercises that specifically target the main musculoskeletal dysfunction in people with DPN. This study aimed to assess the effect of a 12-week physiotherapeutic foot-ankle exercises supervised program on foot-ankle kinematics in DPN people.

Methods

Fifty-six participants of both sexes with clinical diagnosis of type 1 or 2 diabetes and DPN were randomly allocated to CG ($n=26$, 61.3 ± 8.48 yrs) or IG ($n=30$, 63.0 ± 10.7) and foot-ankle kinematics were evaluated at baseline (T0) and week 12 (T12) after face-to-face physiotherapeutic foot-ankle exercises by 8 cameras at 100 Hz (VERO, Vicon). Plug-In Gait and Oxford Foot Model setup protocols were used. Participants walked barefoot at a self-selected speed on a walkway and 3 valid steps (stance phase) on left side were acquired. Digitisation, 3D reconstruction of the markers' positions and filtering of kinematic data were performed in NEXUS software (v. 2.10.3). Kinematic data were processed using a zero-lag 2nd-order low-pass filter (6Hz). Kinematics were computed with the open-source Python package pyCGM2 (www.pycgm2.github.io) replicating the Vicon Plug-In Gait protocol and Plug-In of Oxford Foot Model. The variables calculated were: ROM of

first metatarsal, midfoot and rearfoot joints relative to the proximal segment. Comparisons between groups and assessments (T00 and T12) were performed by 2-way ANOVAs (groups and repeated measures) to each variable followed by Bonferroni post hoc ($p < 0.05$).

Results and Discussion

After 12 weeks, the IG improved ROM of forefoot relative to hindfoot dorsiflexion, and the difference to the CG was 2.6 degrees ($p < 0.0131$), suggesting a better foot adaptability during stance phase [3], because the increase in the forefoot relative to hindfoot dorsiflexion may assist the arch raising mechanism at the end of stance phase. There were no other differences in any other biomechanical variable.

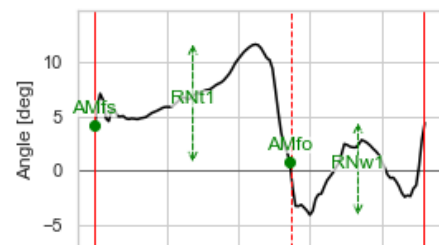


Figure 1: Example of a kinematic temporal series with forefoot relative to hindfoot dorsiflexion (degrees). RNt1 = dorsiflexion degree

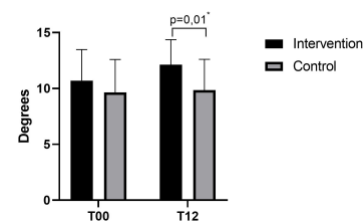


Figure 2: Forefoot relative to hindfoot dorsiflexion (degrees) mean and standard deviation for Intervention and control groups at baseline (T00) and week 12 (T12).

Conclusions

This study evaluated foot-related biomechanical outcomes after 12 weeks of foot-ankle exercise protocol focused on improving intrinsic foot muscle functionality and showed positive changes in the IG on forefoot relative to hindfoot dorsiflexion, suggesting a better foot adaptability during gait stance phase.

Acknowledgments

CAPES (financial code 001) for providing funding to ES and JV; CNPQ for IS; FAPESP for RM (2017/17848-3), JF (2019/02522-0) and RCJ (2019/06405-9).

References

- [1] Shun, C. et al. (2004). *Brain* **127**.
- [2] Riandini, T. et al. (2018). *Acta Diabetol.* **55**, 155–164
- [3] Ghanem, I. et al. (2019). *J Child Orthop.* **13**(2), 134-146

Effects of Short-Term Cycling Intervention on Knee Biomechanics in Cycling with Augmented Visual Biofeedback for Patients with Total Knee Arthroplasty

Songning Zhang¹, Erik T. Hummer², Jared Porter¹, Harold Cates³

¹Department of Kinesiology, Recreation, and Sport Studies, University of Tennessee, Knoxville, TN, USA

²Center for Mobility and Rehabilitation Engineering Research, Kessler Foundation, West Orange, NJ, USA

³Tennessee Orthopaedic Clinics, Knoxville, TN, USA

Email: szhang@utk.edu

Summary

The purpose of this study was to examine effects of short-term cycling intervention with augmented feedback of vertical pedal reaction force (PRF) on asymmetry and inter-limb biomechanical differences in patients with total knee arthroplasty (TKA). The results showed that asymmetry indices (AI) for knee extension moment (KEM) showed clinical improvements after the intervention.

Introduction

Patients with TKA experience inter-limb differences of vertical ground reaction force and KEM in walking [1] and cycling [2]. These inter-limb differences persist following rehabilitation and may lead to contralateral knee osteoarthritis and TKA. Intervention may improve the observed asymmetry. There is a lack of information on effects of cycling interventions for this patient group. The purpose of this study was to examine the effects of short-term cycling intervention with augmented feedback of vertical PRF on asymmetries of vertical PRF and KEM and biomechanical inter-limb differences in patients with TKA.

Methods

Ten unilateral TKA patients attended a 6-session cycling intervention over two weeks and were tested on their cycling biomechanics before and after the intervention. During the intervention, participants were provided with visual biofeedback on their vertical PRFs of both lower limbs and asked to reduce AI below 10% during training bouts. Each session included multiple 5-minute cycling training bouts.

During the two test sessions, participants cycled on cycle ergometer (Excalibur Sport, Lode) in two randomized workrate conditions [80 and 100 Watts (W)] at a cadence of 80 RPM. Participants cycled for one-minute in each condition, with data collection occurring in the final 10 seconds. Three-dimensional motion capture (240 Hz, Vicon) and PRF data (1200 Hz, Kistler) were collected. A one-way repeated ANOVA was used to evaluate AIs and a 2 x 2 (limb x time) repeated measure ANOVAs were run on the mean

data for the discrete secondary variables for 80 and 100 W conditions separately. Effect size (ES) was assessed using partial eta squared (η^2_p).

Results and Discussion

After intervention, vertical PRF AI decreased from 5.4% to -3.0% at 80 W ($p = 0.256$, $\eta^2_p = 0.141$) and 1.4% to -3.9% at 100 W ($p = 0.479$, $\eta^2_p = 0.064$). KEM AI decreased from 25.7% to 15.7% at 80 W ($p = 0.499$, $\eta^2_p = 0.052$) and 23.6% to 13.7% at 100 W ($p = 0.395$, $\eta^2_p = 0.092$). The ANOVA results for secondary variables showed peak posterior PRF at 100 W increased following the intervention compared to pre-training (Table 1). Additionally, there was significantly greater posterior PRF in the non-replaced limb for 80 and 100 W compared to replaced limb. Peak KEMs for both work rates were lower for the replaced limb (Table 1). Additionally, the replaced limbs showed decreased knee extension ROM compared to the non-replaced limbs.

These results suggest that the short-term cycling intervention with augmented biofeedback did reduce KEM asymmetry by 10% with medium ES, indicating a clinically relevant reduction [3].

Conclusions

While not statistically significant, reductions in KEM asymmetry of 10% or greater could indicate clinically relevant changes. The cycling intervention paired with augmented feedback may be beneficial in reducing the asymmetry during stationary cycling.

Acknowledgments

Supported by the Matching Dissertation Grant of International Society of Biomechanics and the University of Tennessee, Knoxville.

References

- [1] Wen C et al. (2019) *J Biomech*, **89**: 40-47.
- [2] Hummer et al. (in press) *J Biomech*.
- [3] Buddhadev et al. (2018) *J Appl Biomech*, **34**: 306-311.

Table 1: Secondary variables of PRF (N) and KEM (N•m) for replaced and non-replaced limbs (mean ± STD).

	Pre-Training		Post-Training		interactio	P (η^2_p)	
	Non-	Replaced	Non-	Replaced		Limb	Time
80 W							
Vertical PRF	233.2±43.9	209.8±43.8	221.0±39.2	223.6±40.9	0.210(0.1)	0.534(0.050)	0.622(0.032)
Posterior PRF	-66.1±21.7	-52.3±16.9	-67.6±19.1	-56.9±18.0	0.627(0.0)	<0.001 (0.765)	0.066(0.328)
KEM	25.5±6.6	17.9±5.2	24.5±6.9	20.1±7.3	0.405(0.0)	0.001 (0.734)	0.681(0.020)
100 W							
Vertical PRF	249.3±47.9	209.8±43.8	212.9±83.7	218.0±81.4	0.473(0.0)	0.922(0.001)	0.300(0.133)
Posterior PRF	-71.0±18.7	-55.4±18.4	-75.2±19.7	-64.0±16.6	0.410(0.0)	0.003 (0.691)	0.012 (0.570)
KEM	27.0±6.0	19.9±5.3	28.1±7.2	23.5±6.8	0.383(0.0)	0.002 (0.724)	0.053(0.391)

Assessment of DcEF stimulation on the neuronal function using *in vitro* stroke model

E. M. Ko¹, E. Y. Park¹, U. H. Ko¹ and Jennifer H. Shin^{1†}

¹Dept. of Mechanical Engineering, KAIST, Republic of Korea

[†] Corresponding author, j_shin@kaist.ac.kr

Summary

Stroke is one of the leading causes of death and the primary cause of disability. Rehabilitation treatments using exogenous electrical stimulation (ES) have been utilized successfully in a clinical setting, but the precise mechanism of how ES works remain elusive. In this study, we first established a 3D stroke model by forming multicellular spheroids and applying oxygen-glucose deprivation and reperfusion (OGD-R). We then tested the effectiveness of ES on the cells of the stroke model based on the changes in the phenotypes and gene/protein expressions. We found the compromised neuroplasticity after OGD-R stimulation and the partial recovery of neuroplasticity by electrical stimulation.

Introduction

According to a recent report, a stroke occurs in one out of five persons during a lifetime and has become one of the leading causes of death and primary cause of disability worldwide. Recent studies have shown that the ES can increase brain plasticity and improve rehabilitation efficiency. However, the poor understanding of the mechanism poses many obstacles to the clinical application of the ES. Therefore, we employed 3D multicellular spheroids that can simulate the brain's three-dimensional microenvironment to examine their morphological and biological changes following the ES treatment.

Methods

Cells were extracted from the cortex of postnatal one-day rats and maintained in Neurobasal™ Medium with 2% B-27™ Supplement (50X), 1% GlutaMAX™ Supplement and 1% Penicillin/Streptomycin. To form 3D cellular spheroids, the cell suspension was plated on 96-well Corning® Ultra-Low Attachment Products. Also, the oxygen-glucose deprivation and reperfusion (OGD-R: 5% CO₂, 94% N₂, 1% O₂, 4 hours) process was utilized to construct a stroke model on the Day 7 of the *in vitro* culture. For ES, dcEF was applied at 2.0V/cm for 1 hour. 2D spreading assay was performed to examine cellular morphology on a poly-d-lysine (PDL) coated cover glass after the ES, and immunofluorescence staining was performed after three days to check any ES-induced morphological changes. Total RNA was extracted 30 minutes after the ES, followed by qPCR to assess the genetic changes.

Results and Discussion

Based on immunostained images, we found number and density of neurites decreased after OGD-R compared to those of the control, which recovered slightly following the ES. Considering that many scientists have used the number and density of neurites as indicators of structural neuroplasticity, we found that both OGD-R and electrical stimulation had

immediate effects on the plasticity change in an opposite manner.

When the expression of neuroplasticity-related genes (Arc, C-fos, Zif268) were assessed, significant increases were shown in Arc (6.5 folds) and C-fos (3.4 folds) in the normal brain model and C-fos (7.1 folds) and Zif268 (1.9 folds) in the stroke model compared to non stimulated group. Furthermore, when comparing the conditions without the ES, the stroke model exhibited a significant increase in Arc (4.6 folds) and a significant decrease in Zif268 (2.6 folds) compared to the control. The ES seemed to increase neuroplasticity because at least two of the neuroplasticity indicators were significantly increased by the ES in all conditions. Also, we found the response to electrical stimulation varies before and after OGD-R. Based on that results, we could infer that OGD-R stimulation affects signals related to neuroplasticity.

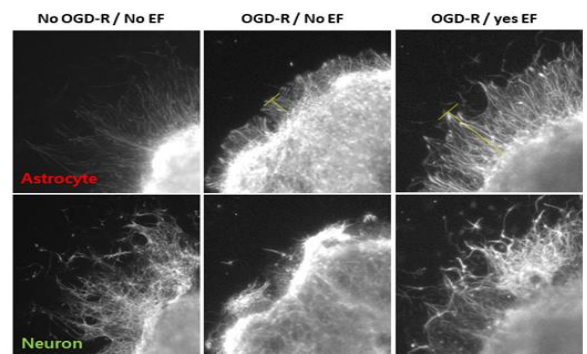


Figure 1: Immunofluorescence staining results in normal brain model, stroke model with and without electrical stimulation conditions (Astrocyte: GFAP, Neuron: Tuj1).

Conclusions

We found a significant decrease in neurite length and density after OGD-R and a partial increase after electrical stimulation. Also, we found increasing neuroplasticity markers by electrical stimulation in both the normal brain and stroke brain and change in the reaction by OGD-R. It is necessary to experiment on the common markers of neurite change and neuroplasticity to identify the relationship between OGD-R and electrical stimulation.

Acknowledgments

This work was supported by the global singularity project grant funded by the Korea Advanced Institute of Science and Technology (KAIST)(N11210052).

References

- [1] LAPCHAK, Paul A et al (2011). *Journal of neurochemistry*, 116.1: 122-131.
- [2] GESUETE et al (2011). *STROKEAHA*, 110.603266

Predicting Gait Events from Handle Forces in an Instrumented Posterior Walker

Evan A. Dooley^{1,2}, Allison M. Lehmann¹, Marshall W. Tumperi², Shawn D. Russell^{1,2}

¹Motion Analysis & Motor Performance Laboratory, UVA Dept. of Orthopaedic Surgery, Charlottesville, VA, USA

²Dept. of Mechanical & Aerospace Engineering, University of Virginia, Charlottesville, VA, USA

Email: dooley@virginia.edu

Summary

The human-device interface of patients using a posterior walker is not well understood. In this study, how users load a posterior walker is analyzed through utilization of a posterior walker with instrumented handles. Through collection of CP and typically developed users walking with this instrumented walker, we found a consistent local maximum of downward and forward force occurs prior to foot strike and foot off.

Introduction

Human gait has been studied extensively. How assistive devices, such as posterior walkers, affect gait is much less well defined. The interaction between the human and the device must be understood, given many individuals with walking disorders, due to neuromuscular disabilities, such as cerebral palsy (CP), use assistive devices to aid their mobility [1].

In the case of the posterior walker, introducing powered wheels could be highly beneficial to the user. Specifically, children with CP typically are weaker and fatigue faster than their typically developed (TD) peers, and have been shown to do 59% more work per unit mass, on average, than TD children [2]. Posterior walkers are used by people with CP to decrease load on their lower limbs and increase their stability. These benefits come at the metabolic cost of pulling the walker along with them. Powering the walker would negate this effort. Additionally, adding a control to this power could allow energy to be injected into the gait cycle to further increase the gait efficiency of the user. In order to apply this control appropriately, the location of the user in their gait cycle must be known. The aim of this work is to show that gait events can be detected from forces applied by the user to the handles of the posterior walker.

Methods

A typical posterior walker (Nurmi Neo, Ottobock) was instrumented at both handles with a 6 DoF load cell (LC, ATI) to capture all forces (1000Hz) applied through the handles of the walker. 9 TD users (15.6 ± 5.7 y.o.; 3F) and 14 CP users (12.2 ± 3.5 y.o.; 5F) walked, with this instrumented walker, at their self-selected walking speed along a level, straight path. Walking kinematics were collected using an 8 camera motion capture system (Vicon) at 100 Hz. Gait events were determined from collected motion capture data, and one stride was defined as foot strike to ipsilateral foot strike. A minimum of 65 strides of each subject were used in this analysis. LC force data was filtered at 3 Hz [3], segmented to the stride, and then normalized by excursion of force over the stride to investigate the pattern of loading on the walker handles.

Results and Discussion

In the TD population (blue in Fig. 1), a consistent pattern of a local minimum in the vertical direction is applied by the user before ipsilateral foot strike and contralateral foot off (relative to load cell, listed in Table 1). The CP group shows a much larger variance in this pattern across the group. When looking at each CP subject, it is seen that a consistent strategy for loading the walker is adopted. The group variation arises from different strategies adopted by users.

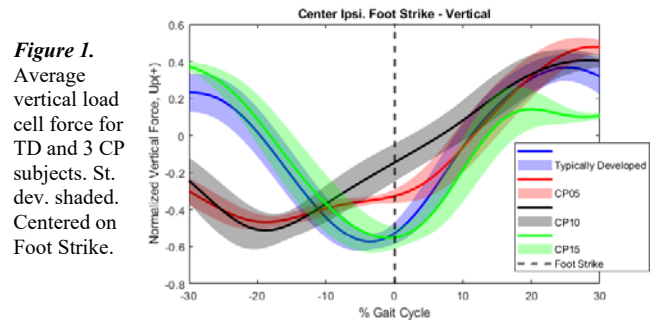


Figure 1. Average vertical load cell force for TD and 3 CP subjects. St. dev. shaded. Centered on Foot Strike.

Given the small within-subject standard deviation in LC minimum to gait event (mean ± 4.17 %GC), a method of event detection could be developed for the TD population, then this control method could be tuned to each specific walker user to account for the inter-subject variation seen in the population with CP. A similar pattern occurs in the loading of the axial direction, and relative to foot off.

Table 1. Location of load cell pattern characteristic relative to gait event. Reported as % Gait Cycle (±SD).

Axis	LC Min. Leading Ipsilateral Foot Strike		LC Min. Leading Contralateral Foot Off	
	TD	CP Group	TD	CP Group
Downward	3.5 (±2.5)	3.94 (±7.25)	15.27 (±2.5)	17.44 (±5.67)
Forward	3.1 (±3.0)	5.0 (±10.3)	14.89 (±3.2)	13.94 (±7.82)

This shows that we can predict gait events based on the characteristics of the load applied to the handles of the walker in a non-pathologic population. This ability will allow us to investigate ways to increase the gait efficiency of the user walking with a posterior walker. However, more investigation is necessary of the pathologic population, to find which users may benefit most from the additional aid offered by a powered posterior walker.

Conclusions

Gait events can be predicted from handle usage. This will enable us to develop more efficient walker designs to help increase the mobility of users.

References

- [1] Park ES et al. (2001). *Yonsei Med. J.*, 42: 180-184. [2] Russell SD et al. (2011). *J. Biomech.*, 27: 99-107. [3] Alwan M et al. (2004). *IEEE Conf. Med & Bio Soc.*

Protocol for Improving Familiarity with a Lower-Limb Robotic Exoskeleton in Able-Bodied, First-Time Users

Jan Lau¹, Katja Mombaur¹

¹Canada Excellence Research Chair Human Centered Robotics and Machine Intelligence Lab, Dept. Systems Design Engineering, University of Waterloo, Waterloo, Canada

Emails: jan.lau@uwaterloo.ca, katja.mombaur@uwaterloo.ca

Summary

Various lower-limb robotic exoskeletons have been created to target different healthcare needs, but no research has been done on developing a proper procedure for users to get accustomed to wearing and moving with one, and the instruction manuals provided are insufficient. A pre-test was conducted to observe the challenges of wearing an exoskeleton for the first time. Pre-test results showed safety concerns and a steep learning curve. This paper outlines a protocol that can potentially improve first-time users' comfort to interact with an exoskeleton. Since the execution of the full procedure was disrupted by a lab closure due to COVID-19 restrictions, the full experimental results will be presented at the conference.

Introduction

Lower-limb robotic exoskeletons have been developed for applications such as spinal cord injury (SCI) and stroke rehabilitation. So far, no procedures are available to help familiarize users how to move with one. Although instruction manuals are provided, the information is either insufficient or lacking in this regard.

A pre-test with two subjects was performed to identify the actions of a first-time user wearing an exoskeleton. The tasks were sit-to-stand, stand-to-sit, and walking. They experienced difficulty balancing when performing sit-to-stand, had lower back pain, and were startled from the exoskeleton's predefined gait pattern due to the lack of familiarity in motor interaction. Both are young, healthy, and able-bodied graduate students, which leads to the assumption that the initial exoskeleton experience would be worse with patients. Therefore, a need exists for a protocol that can better prepare able-bodied, first-time users to move with an exoskeleton.



Figure 1: A startled pre-test subject lost balance when walking.

Methods

The device used is the Twin developed by Istituto Italiano di Tecnologia (IIT). Made for people with SCI, its four actuators enable flexion/extension at the hips and knees [1]. The experiment includes ten subjects who are evenly divided into control and experimental groups.

The significance of each exercise is explained to the subject to better retain the information [2]. Protocol is shown below.

Preparation (Control + Experimental groups)

1. Adjust the forearm crutches appropriate to the subject.
2. Create a new profile of the subject on the Twin tablet.

Tutorial (Experimental group only)

1. Perform crutches exercises without exoskeleton.
 - a. Bring crutches backwards while sitting.
 - b. Perform sit-to-stand and stand-to-sit with crutches.
 - c. Walk around with crutches
 - d. Practice turning by pivoting.
 - e. Repeat 1c but shift weight to stationary leg for each step.
2. Demonstrate Twin's sit-to-stand, stand-to-sit, and walking motions without subject wearing it.
3. Don Twin and safety harness on subject.
4. Lift subject 30 cm off the ground with a patient lift.
5. Activate walking motion to familiarize subject with Twin's gait pattern without the risk of falling.

Exo Session (Control + Experimental groups)

1. Perform sit-to-stand and stand-to-sit wearing Twin.
2. Walk in Twin while being supported by a person.
3. Walk in Twin while being supported by a lift.

System Usability Scale (SUS), NASA Task Load Index (TLX), and a customized survey are used for measuring Twin's usability, subjects' mental workload, and subject's comfort level respectively. The customized survey is completed twice – before Tutorial/Exo Session and after Exo Session – to record how the comfort levels have changed. SUS and TLX are completed after the Exo Session. The selection of these questionnaires was inspired by the ones used for evaluating the don/doff procedure of a wrist exoskeleton [3].

Results and Discussion

Due to COVID-19, the full procedure that would have been executed in mid-January 2021 was disrupted by a lab closure. Full experimental results will be presented in the conference.

Conclusions

The protocol introduced could potentially improve user-exoskeleton interaction and the support provided by the device. In the future, it will be adjusted to geriatric users.

Acknowledgments

This research was undertaken thanks to funding from the Canada Excellence Research Chairs Program.

References

- [1] C. Vassallo et al. (2020) *ICRA*, 1778-1784.
- [2] C. Wickens et al. (2003) *An Introduction to Human Factors Engineering*; Pearson.
- [3] C. Lambelet et al. (2020). *J Neuroeng Rehabil*, **17**: 132.

Youth Running Biomechanics: The Influence of Footwear on Kinetics and Kinematics.

Andrew G. Traut, MS^{1,3}, JJ Hannigan, PhD^{2,3}, Justin A. Ter Har, MS^{1,3}, Christine D. Pollard, PhD, PT^{2,3}

¹Program in Kinesiology, Oregon State University-Cascades, Bend, Oregon, USA.

²Program in Physical Therapy, Oregon State University-Cascades, Bend, Oregon, USA.

³School of Biological and Population Health Sciences, Oregon State University, Corvallis, Oregon, USA.

Email: trautan@oregonstate.edu

Summary

This study investigated the effects of different footwear on running biomechanics in youth. Fourteen male participants (8-12 years old) ran in 3 different footwear conditions (barefoot, traditional, and minimal shoes) and had lower extremity kinematics and vertical ground reaction force characteristics collected and analyzed. Results showed that running barefoot and in minimal shoes significantly increased the average vertical loading rate (AVLR), when compared to traditional shoes. Increased AVLR has been associated with increased risk of running injury. There were also significant changes in sagittal plane knee and ankle kinematics. This is a unique analysis of the effects of footwear on the running biomechanics in youth, and the first study to specifically evaluate the effects of footwear on AVLR in youth. The dramatic effect on AVLR provides insight into the relative risk of overuse injury with minimal shoe or barefoot running in youth.

Introduction

The biomechanics of running injuries have been extensively studied in adults [1-3], but very little research has been conducted with youth, particularly related to footwear. The purpose of this study was to compare running biomechanics (loading rate and sagittal plane knee and ankle kinematics) in male youth between 3 different footwear conditions.

Methods

Fourteen active male youth (8-12 years old) participants had running biomechanics (ankle and knee sagittal plane kinematics and vertical ground reaction force characteristics) collected and analyzed using an 8-camera 3-D motion capture system (Vicon) and in-ground force plates (AMTI) in three different footwear conditions (barefoot, traditional, and minimal shoe). (Figure 1) A post-hoc visual analysis of foot strike was also performed.



Figure 1: The two types of shoes used in this study. Left, minimal shoe (Xero Prio Youth). Right, traditional shoe (New Balance 880)

Results and Discussion

The AVLR was significantly greater running barefoot (173.86 bodyweights/second (BW/s)) and in the minimal shoe (138.71 BW/s) compared to the traditional shoe (78.06 BW/s),

($p < 0.001$). (Figure 2) There were significant differences between shoes for knee flexion at initial contact (KFIC) ($p = 0.002$), knee sagittal plane excursion (KSE) ($p < 0.001$), peak dorsiflexion (PDF) ($p < 0.001$) and dorsiflexion at initial contact (DFIC) ($p = 0.028$). Barefoot KFIC ($14.02 \pm 4.15^\circ$) was significantly greater than in the minimal ($10.51 \pm 5.73^\circ$) and traditional shoe ($9.44 \pm 5.60^\circ$). KSE in the traditional shoe ($27.42 \pm 4.70^\circ$) was significantly greater than barefoot ($20.97 \pm 4.01^\circ$) and in the minimal shoe ($23.94 \pm 5.91^\circ$). PDF barefoot ($14.03 \pm 3.10^\circ$) was significantly less than the minimal ($18.38 \pm 4.82^\circ$) and traditional shoe ($20.06 \pm 2.74^\circ$). DFIC in the traditional shoe ($3.43 \pm 3.93^\circ$) was significantly greater than barefoot ($0.24 \pm 2.65^\circ$). No participants displayed a transition to, or any instances of, forefoot strike during this study.

Dramatically increased AVLR is noteworthy because of the association with injury, specifically tibial and metatarsal stress fractures [2] and plantar fasciitis [3]. The lack of any instances of forefoot strike is counter to a recent literature review which concluded that minimal shoes may encourage the development of a forefoot strike running pattern in youth [4].

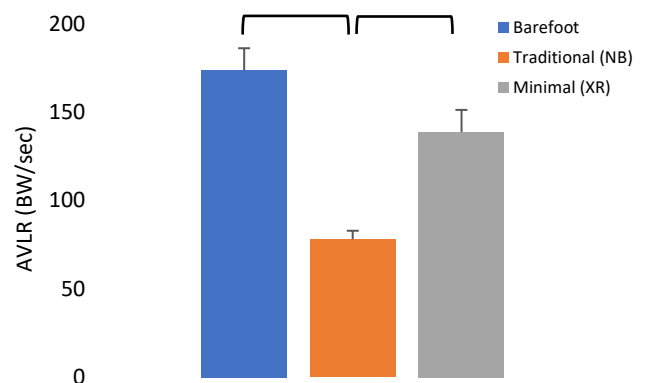


Figure 2: Average Vertical Loading Rate in bodyweights per second. Significant differences are bracketed.

Conclusions

Footwear significantly affected the running biomechanics of youth and caused immediate alterations in sagittal plane ankle and knee kinematics as well as AVLR. Acutely, running barefoot or in a minimal shoe dramatically increased the AVLR, which has been associated with injury, compared to a traditional shoe.

References

- [1] van Gent et al. (2007). *Br J Sports Med.* **41**: 469-480
- [2] Zadpoor et al. (2011). *Clin Biomech.* **26**: 23-28.
- [3] Pohl et al. (2009). *Clin J Sport Med.* **19**: 372-376.
- [4] Krabak et al. (2019). *Curr Sport Med Rep.* **18**: 53-59

The effect of fixation location and footwear type on peak impact accelerations from a consumer-grade IMU during running

Christopher Napier^{1,2}, Richard W Willy³, Brett C Hannigan², Ryan McCann³, Carlo Menon^{2,4}

¹Department of Physical Therapy, University of British Columbia, Vancouver, Canada

²School of Mechatronic Systems Engineering, Simon Fraser University, Metro Vancouver, Canada

³School of Physical Therapy and Rehabilitation Science, University of Montana, Missoula, USA

⁴ETH, Zurich, Switzerland

Email: chris.napier@ubc.ca

Summary

Biomechanical loads (e.g. vertical peak positive acceleration; PPA) from research-grade inertial measurement units (IMUs) have been correlated with lab-based metrics (e.g. ground reaction force loading rate) and running-related injuries (e.g. tibial stress fracture). Most commercially available IMUs are mounted either on the shoelaces or embedded in the insole and their validity has not been investigated. The purpose of this study was to assess the validity of two commercially available IMUs during running when compared to a research-grade tibia-mounted IMU. A secondary aim was to determine the effect of footwear on validity. We found poor to moderate validity between a tibia-mounted IMU and two commercially available IMUs located on the shoelaces and insole. Footwear (level of cushioning) also influenced the degree of validity, suggesting that both location of fixation and type of footwear should be taken into account in future research and in clinical applications.

Introduction

Wearable technology has made it possible for runners to quantify biomechanical loads (e.g. peak positive acceleration; PPA) using commercially available inertial measurement units (IMUs). Vertical PPA of the tibia has been associated with running-related injuries (e.g. tibial stress fracture) [1] and has been correlated with the vertical ground reaction force loading rate [2]. However, while PPA is often measured in a lab setting at the tibia, consumer-grade IMUs are often fixated on the shoelaces or embedded in the insole. The effect of these fixation locations on the magnitude of the PPA is unknown. Therefore, we aimed to assess the validity of two commercially available IMUs during running when compared to a tibia-mounted IMU. A secondary aim was to determine the effect of footwear on validity.

Methods

Healthy runners ran on a treadmill at their preferred speed in three footwear conditions (neutral, minimalist, maximalist). Three IMUs were affixed at the distal tibia (IMeasureU, Vicon, Oxford, UK), shoelaces (RunScribe, San Francisco, USA), and insole (Plantiga, Vancouver, Canada). Intraclass correlation coefficients (ICC_{2,1}) were calculated for PPA between the tibia-mounted IMU (IMU-Tibia) and the commercially available IMUs for each footwear condition.

Table 1: Validity of peak positive acceleration (PPA) from a lace-mounted and insole-embedded inertial measurement unit (IMU) in three different footwear conditions. Values represent ICC_{2,1} with 95% confidence interval. † $p < .05$

Criterion Reference	Footwear Condition	Plantiga Insole (PPA)	RunScribe (Impact)
Tibia-mounted IMU	Neutral	0.62 (-0.08, 0.87) [†]	0.60 (-0.06, 0.85) [†]
	Minimalist	0.31 (-0.90, 0.75)	-0.72 (-3.46, 0.34)
	Maximalist	0.74 (0.24, 0.91) [†]	0.72 (0.24, 0.90) [†]

Significance was set at $p < 0.05$.

Results and Discussion

Using the IMU-tibia as the criterion reference for PPA, ICC_{2,1} values for the RunScribe and Plantiga IMUs were significant in neutral and minimalist footwear conditions only, ranging from 0.60 to 0.74 (Table 1), representing poor to moderate validity [3]. ICC values of >0.90 are considered desirable for clinical measurements [3]. As such, both devices may have some clinical limitations for use as a proxy for vertical PPA at the tibia. Further, footwear had a clear effect on the validity of the signal from both devices, with the minimalist footwear resulting in insignificant correlations and the maximalist condition resulting in the highest correlations.



Figure 1: Tibia-mounted (IMeasureU), lace-mounted (RunScribe), and insole-embedded (Plantiga) inertial measurement units.

Conclusions

Our findings indicate that two commercially available IMUs located on the shoelaces and insole represent poor to moderate validity when acting as a surrogate for a tibia-mounted IMU for vertical PPA. Footwear (level of cushioning) also influences the degree of validity. Location of fixation and type of footwear, therefore, should be taken into account in future research and in clinical applications.

Acknowledgments

Funding support from an NSERC Post-doctoral Fellowship (CN) and the Canada Research Chair Program (CM).

References

- [1] Milner CE et al (2006). *Med Sci Sports Exerc*, **38**:323-28.
- [2] Hennig EM & Lafortune MA. (1991) *IJSB*, **7**:303-09.
- [3] Portney LG and Watkins MP (2009). *Foundations of Clinical Research*; FA Davis Company.

TRICEPS SURAE MUSCLE-TENDON PROPERTIES AS DETERMINANTS OF THE METABOLIC COST IN TRAINED LONG-DISTANCE RUNNERS

Esthevan Machado¹, Fábio J. Lanferdini², Edson S. da Silva¹, Jared R. Fletcher³, Jeam M. Geremia¹, Marco A. Vaz¹, Leonardo A. Peyré-Tartaruga¹

¹Laboratório de Pesquisa do Exercício, Universidade Federal do Rio Grande do Sul, Porto Alegre, RS, Brazil

²Laboratório de Biomecânica, Universidade Federal de Santa Catarina, Florianópolis, SC, Brazil

³Department of Health and Physical Education, Mount Royal University, Calgary, AB, Canada

Email: esthevanmachados@gmail.com

Summary

This study verified which muscle architecture and tendon property variables of the triceps surae are determinants of running metabolic cost (Cr) in trained long-distance runners. Ultrasound and isokinetic dynamometry were used to determine the muscle-tendon unit structural and mechanical variables. The Cr was evaluated by the running economy test. Cr at submaximal velocities (12 and 16 km.h⁻¹) was mainly determined by greater gastrocnemius medialis pennation angle, larger Achilles tendon cross-sectional area, and lower maximal tendon stress.

Introduction

The muscle-tendon unit is one of the most important structures for human running due to its role in generating tension and storing (and releasing) elastic energy [1]. During each running stride, the muscles produce force and perform mechanical work, while the lower-limb tendons store and release elastic energy, reducing Cr [1]. However, as the triceps surae muscle generates tension actively, it seems to be the dominant structure determining the Cr. Thus, this study aimed to determine which triceps surae muscle architecture and tendon property variables are related to Cr.

Methods

Seventeen trained male long-distance runners (34.2 ± 7.4 years) participated in this study (Ethics Committee approval number: 2.437.616). Ultrasound was used to determine the muscle architecture [fascicle length (FL), pennation angle (PA) and muscle thickness (MT)] of the gastrocnemius medialis (GM), gastrocnemius lateralis (GL) and soleus (SO), and the Achilles tendon cross-sectional area (CSA), resting length and elongation as a function of plantar flexion torque during maximal voluntary plantar flexion. From these data, Achilles tendon force-elongation and *stress-strain* relationships were determined. Then, Cr was measured during submaximal steady-state running (5 min) at 12 and 16 km.h⁻¹ on a treadmill. Stepwise multiple linear regression was used to determine the relationship between independent variables (tendon resting length, CSA, force, elongation, stiffness, stress, strain, Young's modulus, FL, PA and MT) with Cr (J.kg⁻¹.m⁻¹) at 12 and 16 km.h⁻¹.

Results and Discussion

Greater GM's PA and larger Achilles tendon CSA were Cr determinants at 12 km.h⁻¹, whereas greater GM's PA and

lower Achilles tendon stress were Cr determinants at 16 km.h⁻¹ (Table 1).

GM's PA is higher in long-distance runners than sprinters and non-active subjects [2]. Greater PA is determined by a higher number of myofibrils per fiber (i.e., higher in-parallel sarcomere numbers), thereby increasing muscle force [3]. Thus, the entire muscle needs to recruit fewer motor units to perform the same task, probably decreasing Cr. However, we were unable to find studies relating PA with Cr. Moreover, a large Achilles tendon CSA and lower tendon stress may be associated with an improvement in the tendon's ability to store and release elastic energy [5] and with a better force distribution by tendon area [6], improving muscle-tendon force transmission and running economy by decreasing Cr.

Table 1. Determinants of the Cr at 12 and 16 km.h⁻¹.

Depend. Variable	R ²	P-value	Indicator	Standardized Coefficients (β)	P-value
Cr-12 (J.kg ⁻¹ .m ⁻¹)	0.48	0.010	CSA (mm)	-0.514	0.019
			PA-GM (°)	-0.429	0.043
Cr-16 (J.kg ⁻¹ .m ⁻¹)	0.57	0.003	PA-GM (°)	-0.528	0.010
			Stress (MPa)	0.494	0.014

CSA (Achilles tendon cross-sectional area); PA-GM (Gastrocnemius medialis PA); Cr-12 and Cr-16 are running metabolic costs at 12 and 16 km.h⁻¹, respectively.

Conclusions

Cr in trained long-distance runners is determined by greater GM's PA, due to a higher in parallel sarcomere number that increase muscle force. Larger Achilles tendon CSA and lower tendon stress increase the tendon's ability to store and release elastic energy, with better force distribution per tendon area at submaximal velocities (12 and 16 km.h⁻¹).

Acknowledgments

The authors would like to thank the Pró-Reitoria de Pesquisa (PROPESQ), UFRGS for financial support.

References

- [1] Kram et al. (2000). *Exerc Sport Sci Rev*, **28**:138-143.
- [2] Abe et al. (2000). *Med Sci Sports Exerc*, **32**:1125-1129.
- [3] Blazevich (2006). *Sports Med*, **36**:1003-1017.
- [4] Monte et al. (2020). *J Sports Med Phys Fitness*, **60**:198-205.
- [5] Rosager et al. (2002). *Scand J Med Sci Sports*, **12**:90-98.

Mechanical Symmetry in Elite Middle Distance Runners

Geoffrey T. Burns¹, Kenneth M. Kozloff¹, Jessica M. Zandler¹, Ronald F. Zernicke¹

¹University of Michigan, Ann Arbor, Michigan, USA

Email: gtburns@umich.edu

Summary

Gait asymmetries are linked to running experience and ability, yet observations in elite-level runners and across large ranges of speeds are limited. This investigation explored symmetries of mechanical characteristics in elite and sub-elite middle distance runners across 10 speeds. Both groups exhibited low levels of asymmetry, and the elite runners had further reduced asymmetry in their intra-stride vertical oscillations and step characteristics. These data provide evidence and context for using mechanical symmetry metrics in athlete monitoring.

Introduction

Gait asymmetries are a common focus of coaches and clinicians for assessing running biomechanics. Greater movement symmetry has been associated with greater performance capacities [1,2], and inducing step asymmetries decreases one's running economy [3]. As a potential barometer for athlete development, training adaptation, and injury rehabilitation [4], a more comprehensive understanding of asymmetry patterns in highly developed runners would validate its efficacy as an assessment tool.

Observations in elite runners have, generally, been restricted to single speeds [1], yet asymmetries are modulated by speed in recreational runners [2]. Middle distance runners are a revealing population in which to explore speed-dependent mechanical patterns, as their training encompasses a large breadth of speeds [5].

The goal of the current study was to examine system-level mechanical symmetry and its variability via spring-mass behavior [6] in world-class middle distance runners within and across a wide range of training and racing speeds.

Methods

Ten elite level (E) male middle distance (MD) runners (1500 m: 3:37.3±3.6s) and 10 highly trained male sub-elite (SE) MD runners (1500 m: 4:07.6±3.7s) were recruited. They ran on a treadmill instrumented with a pressure platform at 4 low-intensity speeds for 4 min (E: 12-18 km/hr; SE 10-16 km/hr) and 6 high-intensity speeds for 30 s (E: 20-25 km/hr; SE 18-23 km/hr). Temporal measures were continuously recorded.

Spatiotemporal (i.e., contact time (t_c), flight time (t_f), duty factor (DF), step length (SL), and step frequency (SF)) and spring-mass (i.e., leg stiffness (k_{leg}), vertical stiffness (k_{vert}), and vertical oscillation (VO)) characteristics were calculated [7]. An asymmetry index (AI) [4] for each stride cycle and a rolling AI were calculated within each speed for each subject. Coefficients of variation were calculated within each speed. The effects of ability (E vs. SE) and speed were assessed with linear mixed-effects models. Model coefficients were assessed for significance at a type I error control of $p < 0.05$.

Results and Discussion

For each runner (mean±SD), 1770±79 stride cycles were captured across the 10 speeds. Both groups exhibited low intra-stride AIs across all measures, including (grand mean ± standard error): t_c (1.6±0.1%), t_f (2.9±0.1%), DF (1.6±0.1%), SL (1.4±0.1%), SF (1.4±0.1%), k_{leg} (4.1±0.2%), k_{vert} (2.9±0.1%), and VO (2.8±0.1%). Rolling AIs yielded similar results across all measures. These results are consistent with their high experience and performance levels [1,2]. Both groups increased their AIs across speeds for SL, SF, k_{leg} , and k_{vert} . AIs decreased across speeds for t_f , and there was a significant group interaction (Figure 1).

E runners had lower AIs across speeds for VO (-0.4%) (Figure 1), SL (-0.2%), and SF (-0.2%), consistent with elite long distance runners at a single speed [1] and suggestive of greater movement efficiency [3].

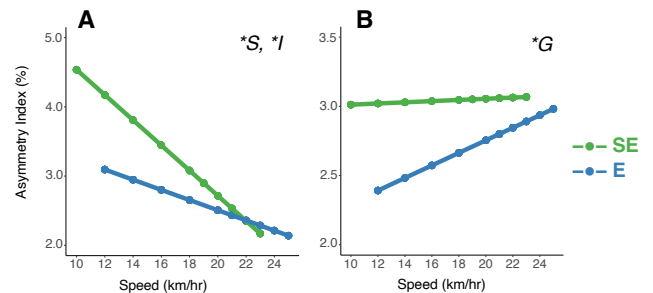


Figure 1: Asymmetry indices within strides across speeds for (A) flight time and (B) vertical oscillation. Significant effects are indicated as *G (group), *S (speed), and *I (interaction).

There were no group differences in AI variability within speeds. However, in both groups, variability in the AI increased as speed increased for t_c , t_f , DF, k_{leg} , and k_{vert} .

Conclusions

Highly trained MD runners with high performance capacities exhibited low levels of gait asymmetries. Elite-level runners exhibited greater symmetry in their vertical oscillations and step characteristics. Asymmetries were also speed-dependent in both groups. Monitoring and analysis of system-level gait asymmetries in runners may have useful application in informing individual-specific development trajectories, performance opportunities, and rehabilitation strategies.

References

- [1] Cavanagh P et al. (1977). *Ann N Y Acad Sci*, **301**:321-345
- [2] Mo S et al. (2020). *Hum Mov Sci*, **71**: 1-10
- [3] Beck ON et al. (2018) *Eur J Appl Physiol*, **118**:2147-2154
- [4] Zifchock RA et al. (2006). *J Biomech*, **39**: 2792-2797
- [5] Sandford GA and Stellingwerf T. *Front Sports Act Living* **1**:1-8
- [6] Blickhan R (1989). *J Biomech*, **22**: 1217-1227
- [7] Morin JB et al. (2005). *J Appl Biomech*, **21**:167-180

In silico modeling of tibial fatigue life in physically active males and females during different exercise protocols

Elliot Paul¹, Anup Pant¹, Stephanie George¹, John Willson², Stacey Meardon², Ali Vahdati¹

¹Department of Engineering, College of Engineering and Technology, East Carolina University, Greenville, NC, USA

²Department of Physical Therapy, College of Allied Health Sciences, East Carolina University, Greenville, NC, USA
Email: vahdatia18@ecu.edu

Summary

This study combined gait analysis, musculoskeletal modeling, finite element analysis, and a fatigue life prediction algorithm to investigate the effect of different exercise protocols on the tibial fatigue life in physically active males and females. Our results showed that both higher running speed and sex could be determinants of tibia stress injuries.

Introduction

The prevailing understanding of the bone stress injuries (BSI) etiology points to multi-factorial injury mechanisms, in part caused by repetitive, cyclical loading [1]. *In silico* studies of training habits, including changes in running speed, landing patterns, and other factors on tibial stress injury formation, can provide important insights into BSI prevention. This study aimed to computationally examine the effect of different exercise protocols on tibial fatigue life in a sample of male and female runners during walking and three speeds of running.

Methods

Three male and three female participants running >16 km/week were extracted from an existing data set (Meardon et al., accepted) and analyzed for this study. All subjects were between 19-24 years. Four gait conditions were tested and analyzed in this study: walking (1.3 m/s), preferred running and $\pm 10\%$ preferred running speed. Next, all participants underwent magnetic resonance imaging (MRI) of their right tibia with a 1.5-T scanner (Philips Achieva). A previously established musculoskeletal model was used to estimate muscle forces across the stance phase [2]. Finite element analysis was conducted in FEBio [3] through an automated MATLAB (MathWorks Inc) script. The models were fixed at the proximal end of the tibial shaft and loads were applied at the distal end of the shaft. The probability of failure accounting for repair and adaptation was calculated based on the approach developed previously [4,5] over 100 days. Subject-specific loading frequency was normalized by assuming the same running/walking distance of 4.8 km/day for all subjects.

Results and Discussion

Our results showed that the probability of BSI formation was generally lower for slower gait conditions (Figure 1). Furthermore, female subjects, on average, had a higher mean peak probability of failure (the probability of failure on day 100) in all four gait conditions. Furthermore, we observed

differences in spatial distribution and magnitudes of strain and stress predicted in the tibia by finite element analysis under different gait conditions.

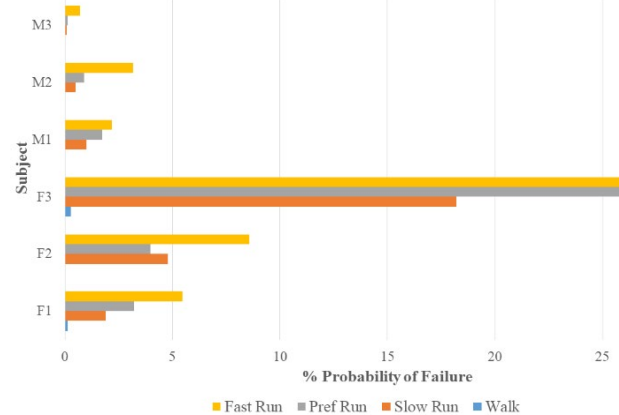


Figure 1: Peak probability of tibial fatigue failure for each subject and gait condition (M =male, F = female).

Conclusions

Our *in silico* results using subject-specific images suggests markedly reduced fatigue life in both sexes when progressing from a walk to run and with increasing running speed, supporting previous research. Tibial fatigue life in females was disproportionately reduced with increasing speed compared to males. We posit that sex-based differences in tibia shape and gait mechanics underpin the reduced fatigue life observed in this study and the increased incidence of BSI in females.

Acknowledgments

In part supported by the National Science Foundation under Grant No. EEC-1659796 and EEC-1359183. The authors would like to thank Dr. David Taylor and Dr. Brent Edwards for insightful email correspondence on their past work.

References

- [1] D.B. Burr, R.B. Martin, M.B. Schaffler, E.L. Radin, *J. Biomech.* 18 (1985) 189–200.
- [2] T.R. Derrick, W.B. Edwards, R.E. Fellin, J.F. Seay, *J. Biomech.* 49 (2016) 429–435.
- [3] S.A. Maas, B.J. Ellis, G.A. Ateshian, J.A. Weiss, *J. Biomech. Eng.* 134 (2012).
- [4] D. Taylor, E. Casolari, C. Bignardi, *J. Orthop. Res.* 22 (2004) 487–494.
- [5] B.W. Edwards, D. Taylor, T.J. Rudolph, J.C. Gillette, T.R. Derrick, *Clin. Biomech.* 25 (2010) 372–377.

Female Runners Demonstrate a Greater Decrease in Knee Flexion with Age than Males

Heather M. Hamilton¹, Max R. Paquette², Rumit Singh Kakar¹

¹Old Dominion University, Norfolk, VA, USA; ²University of Memphis, Memphis, TN, USA
Email: hmcco006@odu.edu

Summary

Increased age is associated with decreased peak dorsiflexion and knee flexion in male and female runners. Females demonstrate a greater decline in peak knee flexion compared to males with age, which may contribute to decreased shock absorption. It is important to understand sex differences in biomechanics of aging runners to maximize performance and minimize risk of running-related injury (RRI).

Introduction

Aging runners demonstrate changes in running biomechanics, specifically decreased ankle and knee joint excursion [1-3]. Limited evidence suggests males and females demonstrate different changes in running biomechanics with age [4], which may be related to unique physiological changes that females experience during the aging process that affect the musculoskeletal system [5]. It is therefore important to consider separate-sex analyses when studying the effects of age on running biomechanics. The purpose of this study was to determine the relationship between age and lower extremity running kinematics separately for male and female runners at two different speeds.

Methods

Male (n = 33) and female (n = 46) runners (ages 18-65 years) ran at self-selected long distance (JOG) and maximal running (MAX) pace on a treadmill. Lower extremity joint kinematics were collected using 3D motion capture (Vicon®). Linear regression was used to determine the relationship between age and sagittal plane peak joint angles of the dominant limb during stance phase for male and female participants. Speed was controlled for in the first block of the regression model.

Results and Discussion

In males for JOG (2.83 ± .51 m/s), there was a significant negative relationship between age and peak knee flexion, and the relationship between age and peak ankle dorsiflexion neared significance (Table 1). For MAX (4.41 ± .71 m/s), there was a negative relationship between age and peak knee flexion only. In females for JOG (2.66 ± .30 m/s) and MAX (3.80 ± .61 m/s), there were significant negative relationships between age and peak dorsiflexion and peak knee flexion

(Table 1). For JOG, there was a significant age by sex interaction effect for peak knee flexion ($p = .022$) (Figure 1). No other significant interaction effects were observed ($p > .082$). Results show that age influences peak knee flexion and perhaps more so in females compared to males. Females demonstrate a greater decline in peak knee flexion with age compared to males, which may reflect increased knee joint stiffness [1]. Findings are consistent with studies reporting decreased ankle and knee excursion in aging runners [1-3].

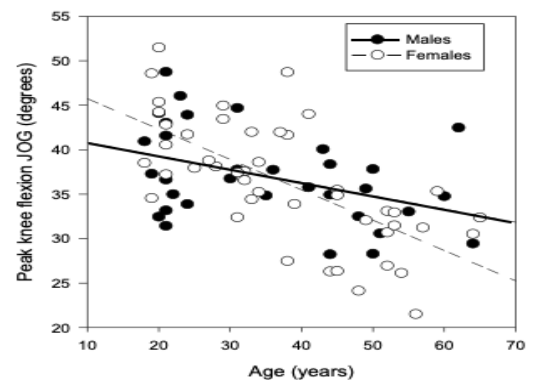


Figure 1: Relationships between age and peak knee flexion (JOG).

Conclusions

Decreased knee flexion as observed here may suggest increased knee stiffness, which has been reported as a predictor of RRI [6]. Female runners over the age of 50 years are more likely to experience RRI [7]. It is therefore important to understand the sex differences in aging-related changes in running biomechanics to develop training and rehabilitation programs in this population.

References

- [1] Fukuchi RK and Duarte M (2008). *J Sports Sci*, **26**: 1447-1454.
- [2] Fukuchi RK et al. (2014). *Clin Biomech*, **29**: 304-310.
- [3] Devita et al. (2016). *Med Sci Sports Exerc*, **48**: 98-106.
- [4] Boyer et al. (2017). *J Sports Sci*, **35**: 2225-2231.
- [5] Bondarev et al. (2018). *Menopause*, **25**: 1432-1441.
- [6] Messier et al. (2018). *Am J Sports Med*, **46**: 2211-2221.
- [7] Taunton et al. (2003). *Br J Sports Med*, **37**: 239-244.

Table 1: Linear regression results for relationship between age and kinematic variables for JOG and MAX speeds. IC = initial contact, TO = toe-off. * denotes $p < .05$.

	Males (n = 33)				Females (n = 46)			
	JOG		MAX		JOG		MAX	
	Mean (SD)	$R^2(p\text{-value})$	Mean (SD)	$R^2(p\text{-value})$	Mean (SD)	$R^2(p\text{-value})$	Mean (SD)	$R^2(p\text{-value})$
Peak dorsiflexion (°)	11.2 (6.2)	.18 (.056)	11.5 (6.2)	.13 (.167)	10.1 (5.6)	.50 (< .001)*	10.0 (5.6)	.40 (< .001)*
Peak knee flexion (°)	37.0 (5.2)	.20 (.035)*	38.0 (5.7)	.24 (.035)*	36.4 (6.9)	.45 (< .001)*	37.0 (7.3)	.43 (< .001)*
Hip flexion IC (°)	9.0 (11.4)	.01 (.844)	10.0 (12.1)	.10 (.287)	8.2 (6.7)	.04 (.442)	8.8 (7.7)	.02 (.732)
Hip extension TO (°)	26.1 (10.8)	.09 (.230)	28.2 (12.6)	.05 (.527)	30.4 (10.1)	.02 (.688)	31.9 (11.6)	.01 (.772)

The Effect of Increasing Step Rate on Foot Progression Angle During Running

Kathryn A. Farina¹, Michael E. Hahn¹

¹Bowerman Sports Science Clinic, University of Oregon, Eugene, Oregon, USA

Email: kfarina@uoregon.edu

Summary

Foot progression angle (FPA), a measure of transverse foot orientation, may influence rearfoot motion and injury risk. The effects of increasing step rate (SR), a popular gait retraining technique, on FPA are unknown. Twenty runners ran at their preferred, +5%, and +10% of preferred SR, and FPA was calculated. A significant difference in FPA between the preferred and +10% condition was observed, indicating increasing SR may be a tool for altering FPA during running.

Introduction

Increasing SR during running has become a popular method in gait retraining for injury prevention and recovery. FPA is a measure of the degree of toe-out or toe-in orientation of the foot [1]. Excessive toe-out may lead to increased pressure on the medial side of the foot, and could influence rearfoot eversion, a potential mechanism related to common running related injuries [1,2,3]. The purpose of this study was to assess the effects of increasing step rate on FPA during running.

Methods

Twenty runners (11 male; 24.9 ± 8.7 years old; 173.7 ± 9.8 cm; 64.7 ± 11.3 kg; 34.5 ± 17.1 miles per week) gave informed consent to participate in this IRB-approved study. Participants had to run at least 15 miles per week, and be pain free at the time of testing. Participants ran on a force-instrumented treadmill (Bertec, Columbus, OH) while marker position data (Motion Analysis Corp., Rohnert Park, CA) were collected ($f_s = 1000$ and 200 Hz, respectively) under three conditions while wearing standardized, neutral shoes (Brooks Launch). Participants ran at their preferred running pace (3.33 ± 0.4 m/s) at preferred SR, +5%, and +10% of preferred SR for three minutes each. Participants were cued by metronome set to goal SR for each of the increased conditions. Twenty strides were recorded during the final minute of each condition.

Data were analyzed using Visual3D v5 (C-Motion Inc., Germantown, MD). Marker coordinate and force plate data were filtered with a 4th order lowpass Butterworth filter at 10 and 30 Hz, respectively. FPA was calculated as the relative difference between the rearfoot segment and the lab coordinate system in the transverse plane. The FPA at initial contact was tested using a repeated measures ANOVA for comparison between SR conditions. Statistical parametric mapping (SPM) was used to test for differences throughout stance.

Results and Discussion

Significant differences were observed between SR conditions, with the preferred SR (175 ± 7) being significantly lower than

the +5% (185 ± 9) and +10% (192 ± 9) conditions ($p < 0.001$), confirming that the SR protocol was effective. Repeated measures ANOVA revealed a significantly greater toe-out orientation (more negative) at initial contact in the preferred SR condition (-7.72 ± 5.5) compared to the +10% condition (-7.03 ± 5.5) ($p = 0.041$), but not the +5% condition (-7.29 ± 5.6) (Figure 1). No clusters during stance reached critical threshold in SPM analysis.

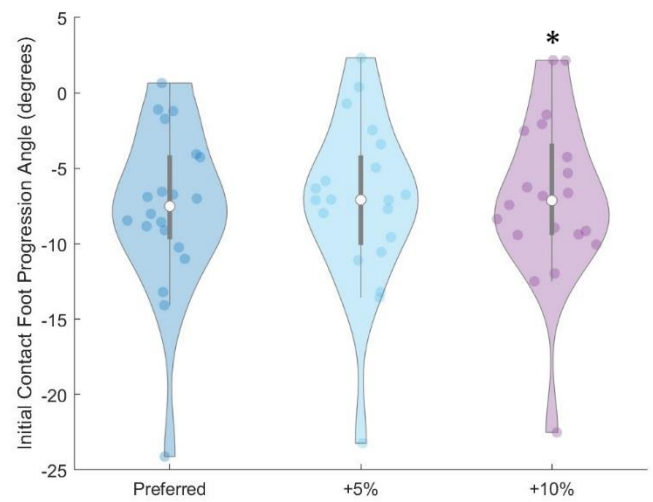


Figure 1: Violin plot showing distribution of FPA at initial contact between the preferred, +5%, and +10% SR conditions. Negative values indicate a toe-out orientation. * = significant difference from preferred condition.

The majority of participants displayed FPA at initial contact between 5 and 10 degrees of toe-out. There was a wide distribution in angles, likely due to varying foot strike patterns among participants. However, the majority of participants displayed a less toed-out initial angle with increased SR. Although significant, these changes were small, with the difference in mean values between the preferred and +10% condition only being 0.7 degrees (range: 0.01-3.27 degrees), raising the question of practically meaningful effect.

Conclusions

These findings indicate that increasing SR may be a feasible gait retraining method to alter FPA during running, and potentially reduce rearfoot eversion. More research is needed to understand the influence of SR on rearfoot motion, FPA, and these effects on running related injury development and rehabilitation.

References

- [1] Cibulka MT et al. (2016). *IJSPT*, **11**: 400-408.
- [2] Lai Y et al. (2014). *Clin Biomech*, **29**: 196-200.
- [3] Mousavi S et al. (2021). *Gait Posture*, **83**: 201-209.

Transverse thorax-pelvis movement patterns in runners with and without mild non-specific low back pain

Maria Jesús Celedón,² Carlos De la Fuente,^{1,2,3} Liege B Porto,¹ Karine JV Stolben,¹ Eliane C Guadagnin,¹ Felipe P Carpes.¹
¹Applied Neuromechanics Research Group, Federal University of Pampa, Brazil; ²Physical Therapy career, Health Sciences Department, Pontificia Universidad Católica de Chile, Chile; ³Clinica MEDS, Chile.

Email: msceledon@uc.cl

Summary

It remains unclear how a pain condition leads to changes in mobility of runners with low-back pain (LBP). We evaluated runners with and without mild LBP and found an out-phase pattern (segments rotating in opposite directions) for thorax-pelvis coordination. This pattern tends to overload the lumbar region by inducing larger rotations, which can be a determinant factor for mild LBP in runners.

Introduction

Two intersegmental patterns for thorax-pelvis coordination have been studied in runners with and without LBP [1]. The in-phase pattern occurs when the pelvis and thorax rotate in the same direction, whereas in the out-phase pattern pelvis and thorax rotate in opposite directions [1]. It is unclear whether mild LBP may influence these kinematics characteristics of the running or whether runners without pain also show an in-phase or out-phase pattern. Here we investigate the presence of the in-phase or out-phase thorax-pelvis patterns in runners with and without mild LBP.

Methods

This experiment was approved by the local institutional ethics committee (IRB #78835317.8.0000.5323) and included 20 trained runners. Among them, 10 (4 women) had mild LBP, with age 40(8.7) years old and an Oswestry score of 10.5(4.8) point, and 10 (4 women) had no LBP, with age 37.2(6.1) years old and an Oswestry score of 0.0(0.0) points. They should have run at least 15 km per week in the past 12 months. The 3D kinematics analysis was performed during treadmill running at a speed corresponding to 75% of their personal best 5 km time [10.7 (1.3) km/h for runners without LBP and 10.3 (1.2) km/h for runners with LBP]. The movement was captured after they ran 5 kilometers. Fifteen infrared cameras (Vicon Motion Systems) tracked the full-body plug-in-gait set markers at 120 Hz. Data were low-pass filtered with a 4th order Butterworth filter and cut-off frequency of 6 Hz. The runners were grouped by an in-phase or out-phase pattern by comparing their rotation directions in the whole time series. From the entire 10 running cycles at kilometer 5th, the absolute mean angle in the transverse plane between the thorax and pelvis was estimated. After confirming the normal data distribution, the patterns groups were compared with a two-tailed independent t-test and 5% alpha. The proportion of runners showing each coordination pattern was also described.

Results and Discussion

At the transverse plane, the angle between thorax-pelvis for the in-phase pattern was 24.6(9.0) degrees, and for the out-phase was 52.7(6.6) degrees ($P < 0.001$, Figure 1). It suggests that a larger rotation of the lumbar region is found in runners with and without LBP. This may lead to increased motor

control demands in the lumbar region. When comparing the groups, an out-phase pattern was more prevalent among runners with mild LBP. Although not evaluated here, this coordination pattern may alter lower limb kinematics, like the stride length, and further influence the running technique. On the other hand, debilitating pain may cause stiff joints. The heterogeneity findings (the proportion between with and without pain) may indicate different running adaptations across the participants. In consequence, it raises some questions: is the nervous system adjusting the thorax-pelvis pattern to reduce pain/speed resulting in an in-phase pattern? Has a percentage of out-phase pattern been an insufficient adjusted pattern, a sign of uncontrolled or recovered runners? How does the pattern change to face the pain in runners? What are the physiological thresholds of in-phase or out-phase patterns that the nervous system can have?

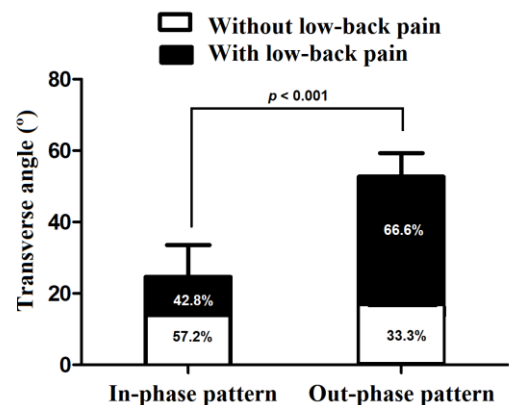


Figure 1: Transverse angle of thorax-pelvis for the in-phase and out-phase pattern and proportion of the patients with and without low-back pain.

Conclusions

The out-phase pattern was more commonly observed among runners with mild LBP. However, a causative model, where the pain modulates the thorax-pelvis pattern, is needed to understand better how and why the lumbar region kinematics' adjustments occur during running.

Acknowledgments

We acknowledge I. Nordetti and V. Carbone for technical support.

References

- [1] Seay JF et al. (2014). *European Journal of Sport Science*, 14(6): 563–568.

Quantifying Change Of Direction Movements In Youth Soccer Players Using Wearable Technology

Mathieu Chin, BSc¹, Lauren Benson, PhD¹, Aki-Matti Alanen, PT, MSc¹, Carla van den Berg, MSc¹, Kati Pasanen, PT, PhD^{1,2,3,4}

¹Sport Injury Prevention Research Centre, Faculty of Kinesiology, University of Calgary, Calgary, Canada

²Alberta Children's Hospital Research Institute, University of Calgary, Calgary, Canada

³McCaig Institute for Bone and Joint Health, University of Calgary, Calgary, Canada

⁴Tampere Research Center of Sports Medicine, UKK Institute, Tampere, Finland

Email: mathieu.chin@ucalgary.ca

Summary

Using inertial measuring unit (IMU), this study looked to determine the differences in mean peak acceleration between the dominant and non-dominant leg amongst male and female youth soccer players during preplanned 135°, 90° and 180° change of direction (COD) movements.

Introduction

Soccer is one of the most popular sports worldwide with over 265 million players. Being a sport with high rates of change of direction movements (COD), there is also a high incidence of traumatic non-contact knee and ankle injuries, with the majority of ankle and knee injuries occurring in non-contact movements, such as those seen in COD movements [1, 2].

The use of wearable devices has allowed researchers to better understand sport movement patterns beyond a typical laboratory setting [3]. There is a paucity of research which quantifies the movements of youth soccer players during a COD movement using wearable technology. This study will contribute objective IMU data to the youth soccer literature on leg-to-leg differences during COD movements.

Methods

Cross-sectional study. Sixty-one male (n=29) and female (n=32) youth soccer players between the age of 15-17 were recruited using a convenience sample. Athletes were fitted with an IMU (Shimmer3) with corresponding 4K video being recorded as they performed consecutive 135° cut turn, 90° cut turn, and 180° pivot turn using both legs. Video analysis was completed using Dartfish 10 to identify the timing of the movements with accelerometer data being processed using MATLAB. T-tests were conducted to determine leg-to-leg differences with p<0.05. Statistical analysis was completed using Stata software.

Main Outcome Measures

Primary outcomes from this study were obtained using IMU devices containing triaxial accelerometers, which recorded the mean peak accelerations of final foot contacts (acceleration, m/s²) comparing the players' dominant leg to their non-dominant leg.

Results

Mean peak acceleration was greater in the dominant leg turn when compared to the non-dominant leg turn for the 180°

COD movements for both males (Dominant: 55.6 (SD: 8.3) m/s², Non-dominant: 51.3 (SD: 7.7) m/s²; p=0.0336) and females (Dominant: 45.4 (SD: 8.8) m/s², Non-dominant: 40.8 (SD: 6.4) m/s²; p=0.0326). There was no statistical significance for the 135° and 90° COD movements.

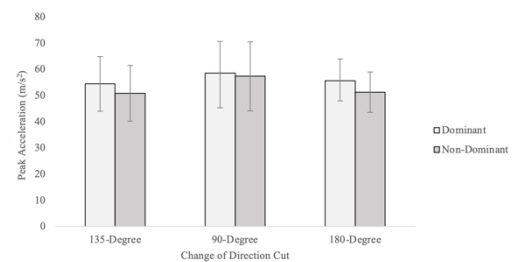


Figure 1. Comparison of the mean peak acceleration in the dominant and non-dominant leg in male youth soccer players.

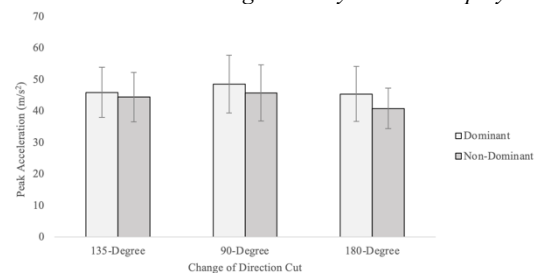


Figure 2. Comparison of the mean peak acceleration in the dominant and non-dominant leg in female youth soccer players.

Conclusion

Youth soccer players may exhibit greater mean peak acceleration and loading in their dominant leg when performing a 180° COD movement. Future analysis can monitor mean peak accelerations over time to better understand its relationship to injury and training.

Acknowledgements

The Sport Injury Prevention Research Centre is one of the International Research Centres for Prevention of Injury and Protection of Athlete Health supported by the International Olympic Committee.

References

- [1] Emery et al. (2006). Clin J Sport Med; 16: 20-26.
- [2] Pasanen et al. (2017). Scand J Med Sci Sports; 27(6), 643-649.
- [3] Li et al. (2016). Sports Health, 8(1), 74-78.

A systematic review: Long range correlations in running gait

Taylor J Wilson¹ & Aaron D. Likens¹

¹Department of Biomechanics, University of Nebraska at Omaha, Omaha, NE USA

Email: twilson50@unomaha.edu

Summary

Long range correlations (LRCs) are apparent in human walking and running gait and are indicative of a healthy system. A systematic review (SR) was completed to determine the typical LRC patterns in running. 20 articles were included in the SR. LRCs in running gait tend to be similar to the LRCs in walking gait, with fatigue contributing to a negative effect on the LRCs.

This SR could have implications on training guidelines for coaches and physical therapy methods to increase the LRCs in running gait for healthier functioning. More research is needed to determine how LRCs depend on running surface and what effect disease has on LRCs of running gait.

Introduction

Much research has been dedicated to measuring the health benefits of running, but only a few studies have examined how running patterns change over time. Long range correlations (LRCs) characterize the degree to which movements are correlated from one moment to the next. LRCs are found in many human activities, including walking and running. Assessing LRCs is important because the presence of LRCs has been associated with health, while the absence of LRCs has been noted as a marker of disease [2]. Hence, more research is needed to understand the meaning of LRCs in running gait.

A systematic review (SR) was completed to look at the effects of running gait on LRCs and the implications this could have on human health, performance, and rehabilitation. The aims of this review were to: identify the typical LRC patterns in human running gait, the effect that running/walking has on LRCs, the effect of injury/disease on running gait, and the effect that surface has on the LRCs of running gait.

Methods

PRISMA guidelines were followed for this SR. PubMed, IEEEExplore, Scopus and Web of Science were searched until November 2020 using the SR tool Rayyan. Exclusion criteria were: Non-experimental studies, non-humans, walking only, non-running, non-LRC analysis, and non-experiments. Two independent raters (TW, AL) screened articles for exclusion.

Results and Discussion

200 studies fell within our criteria. After review and deliberation, 20 articles were included in our SR. Our review revealed that, in general, gait characteristics of running seem indicative of LRCs and are similar to those found in walking gait. LRCs are apparent in both treadmill (TR) and overground running (OR). Results comparing OR and TR, however, are mixed, with some papers showing TR produces greater LRCs [5], while others show the opposite trend [3].

Surprisingly, we did not find any studies comparing LRCs as a function of health; however, two articles directly measured the effect of injury on the LRCs in running gait. One of those articles found only small differences in LRCs between injured and non-injured runners [6], compared to a significant difference in LRCs between the two groups [7]. The fatigue state of the runner may determine the magnitude of LRCs: One article showed a U-shaped trend in LRCs with highest levels of LRCs at the beginning and end of a run [8]. Other articles showed a linear decrease in LRCs with fatigue [1]. Speed may produce a similar U-shaped LRC trend in running gait [5], but this effect was not consistent in this review [6].

Conclusions

We conducted this review to uncover the typical LRCs of running gait in several contexts. With mixed results, our review suggests that, like walking, running gait exhibits patterns of LRCs that seem to vary according where running takes place and the state of the runner. If, as our review implies, fatigue produces measurable changes in LRCs, then tracking LRCs in a workout program could enhance injury prevention measures and speed up recovery. Our results also suggest new training possibilities that could enhance adaptability of the system. Training outside the preferred speed may increase LRCs, which could, in turn, improve recovery times and prevent injury. Furthermore, measuring the LRCs of locomotion is highly recommended due to its good reliability [4], and non-invasive nature compared to other methods of recording fatigue, like taking lactate levels and measuring intramuscular EMG signals during a run.

More research is needed to determine how LRCs depend on running surface. By determining the surface that produces the highest LRCs, this will benefit coaches/physical therapists to prescribe appropriate surfaces for their athletes/patients to improve healthier functioning. Lastly, our review suggests a strong need for further research into the timing of gait when running; due to mixed results concerning running surface, no research related to disease and running, and the relatively low number of papers that have investigated LRCs in this context.

References

- [1] Brahm CM, et al. (2020). *Gait Posture*.
- [2] Cavanaugh JT, et al. (2017). *J Neurol Phys Ther*, **41**(4): 245-51
- [3] Fairley JA, et al. (2010). *Hum Mov Sci*, **29**: 987-98
- [4] Fuller JM, et al. (2018). *Sports Biomech*. **36**: 702-05
- [5] Lindsay TR, et al. (2014). *Percept Mot Skills*. **118**(2):331-46
- [6] Mann R, et al. (2015). *Scand J Med Sci Sports*. **25**: 638-45
- [7] Meardon SA, et al. (2011). *Gait Posture*. **33**: 36-40
- [8] Mo S, et al. (2018). *Gait Posture*. **64**: 7-11

The Between-day Repeatability for Peak Tibial Acceleration During Track Running

Zoe Y.S. Chan^{1,2}, Hannah Dimmick¹, Angela Senevirathna¹, Reed Ferber¹

¹Faculty of Kinesiology, University of Calgary, Calgary, Canada

²Department of Rehabilitation Sciences, The Hong Kong Polytechnic University, Hong Kong

Email: zoe.chan1@ucalgary.ca

Summary

Tibial acceleration measurements must be reliable to ensure validity for longitudinal studies. This study determined the reliability of measuring peak tibial acceleration during overground track running, on three separate days, each averaged over a range of five to 200 strides. Overall, peak tibial acceleration measurements showed moderate to good between-session reliability. Averaging the peaks from 50 or more strides is required to achieve good reliability.

Introduction

Peak tibial accelerations (PTA) can be measured by an inertial measurement unit (IMU) and is considered practical for assessing and monitoring runners outside of the lab [1,2]. One previous study reported excellent within-session reliability but poor-to-moderate between-day reliability [2]. However, the study only analyzed four strides taken from separate short running bouts within the lab. These results may not be fully applicable to real-world running assessments, where PTA is measured for consecutive strides over longer runs and outside of lab conditions. Moreover, analysis of additional running strides has been suggested to improve IMU reliability [2,3]. Currently, there is a lack of evidence to fully assess the between-day reliability of PTA averaged over multiple consecutive strides. The number of strides needed to obtain adequate reliability is also yet to be determined. Hence, the aims of this study were to determine between-day reliability of axial PTA measured continuously during an overground run and determine if averaging more strides would improve between-day reliability.

Methods

Eleven recreational runners (6F, 5M; age = 23.9 ± 3.8) participated in this study. All participants completed three identical testing sessions at an indoor running track (200 m). Session 2 and 3 were conducted within one week (range: 1-7; median: 3 days) and three weeks (range: 16-30; median: 22 days) from the first session (Baseline).

During each session, an IMU containing a tri-axial accelerometer (Shimmer3®; Shimmer Inc., Ireland) was securely attached to the anteromedial aspect of the right tibia, with the y-axis aligned with the long axis. After a 5-minute warm-up, participants ran along the running track at a self-selected speed (3.15 ± 0.37 m/s) for 2 km. Acceleration data were sampled at 500 Hz.

Acceleration data were low pass filtered at 70 Hz. Data collected during the first and last minute were discarded to account for the acceleration and deceleration phases. Peaks identified within each stride cycle from the y-component of

the acceleration data were considered axial PTA and these values were averaged across the first 5, 10, 15, 20, 50, 100, 150 and 200 strides for subsequent analyses.

Test-retest reliability was evaluated by intraclass correlation coefficients (ICC_{2,k}) calculated using a two-way mixed effects model, mean of k measurements with absolute agreement. Values of <0.5, 0.5-0.75, 0.75-0.9 and >0.9 were interpreted as poor, moderate, good and excellent, respectively [4].

Results and Discussion

Paired *t*-tests showed no significant difference in mean PTA between Baseline and Session 2 ($p=0.10-0.39$) or Session 3 ($p=0.06-0.15$). When Baseline was compared to Session 2, ICC ranged from 0.73 to 0.86 (see Figure 1) and reliability was considered good when a minimum of 10 strides were used for analysis and peaked when using more than 50 strides. For Baseline compared to Session 3, ICC ranged from 0.64 to 0.73 and reliability was considered good when using more than 50 strides for analysis.

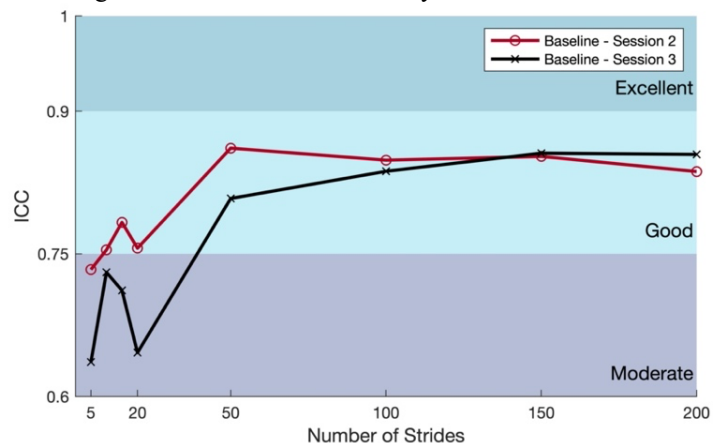


Figure 1: Between-session reliability of PTA averaged across different number of strides.

Conclusions

Axial PTA showed moderate to good between-session reliability for overground running. Future studies should average axial PTA over at least 50 strides for good reliability.

References

- [1] Sheerin et al. (2018) *Sports Biomech*, **17**(4): 531-540.
- [2] Van den Berghe P et al. (2019). *J Biomech*, **86**: 238-242.
- [3] Aubol KG et al. (2020). *J Appl Biomech*, **36**: 457-459.
- [4] Koo TK BC and Li MY (2016). *J Chiropr Med*, **15**(2): 155-163.

Potential influence of stiffening elements on metatarsal-phalangeal joint flexion and running economy

Scott L. Tucker¹, Natalie Harold², Sarah R. Chang², David Boone²

¹FastEquation Inc. Portland OR, USA

²Orthocare Innovations LLC Edmonds WA, USA

Email: Scott.Tucker@vimazi.com

Summary

Composite plates inserted into the midsoles of running shoes have gained popularity while their mechanics and interaction with human biomechanics remain unclear. Horizontal and vertical ground reaction force data from distinct plantar regions combined with 3D motion capture reveal that a composite plate may not alter the time, magnitude, or distribution of force on the plantar surface, and therefore, would not contribute to increased running economy.

Introduction

The proliferation of running shoes constructed with composite plates and stiffening elements has been motivated by an attempt to improve running economy and facilitate faster times in competition. The technology has gained wide adoption within the manufacturing industry and the running community despite the absence of a plausible mechanism¹. This study analyzes the ground reaction forces (GRF) from spatially distinct plantar regions together with 3D motion capture. Our results provide possible indications on how footwear stiffening elements may impact running economy. The analysis reveals how the propulsion forces of each foot region change with time for a 2nd class lever (foot-ankle)² and how the forces may not be altered in the presence of a stiffening plate.

Methods

Vertical GRF (vGRF), horizontal GRF (hGRF), and motion capture measurements were made simultaneously for 10 healthy human participants and 120 trials of barefoot walking and running on a 10 m gait lab runway. All individuals provided written informed consent for the IRB approved study. The runway was equipped with an embedded force plate, Matscan system (Tekscan Inc.), and 3D motion detection (Vicon).

The Matscan dense grid of force sensors allowed precise delineation of the plantar regions, their respective vGRF profiles, and temporal alignment with hGRF measurements from the force plate (Fig. 1). The foot, ankle, and leg markers' trajectories were overlain on the GRF profiles to correlate lever function with plantar regional force and time.

Results and Discussion

vGRF direction is determined by the position of the center of mass (CoM) relative to the center of force on the plantar surface. During the first portion of the ground contact phase, the CoM lies posterior to the center of force and the hGRF is directed rearward, creating a braking force that decelerates the CoM³. vGRF amplitude is at maximum when the CoM is directly above the center of force, the calcaneus is at its lowest elevation, and the metatarsal-phalangeal joints (MPJ) have no flexion. hGRF becomes forward directed as the CoM moves anterior to the center of force and the metatarsal and phalangeal regions account for the entire GRF.

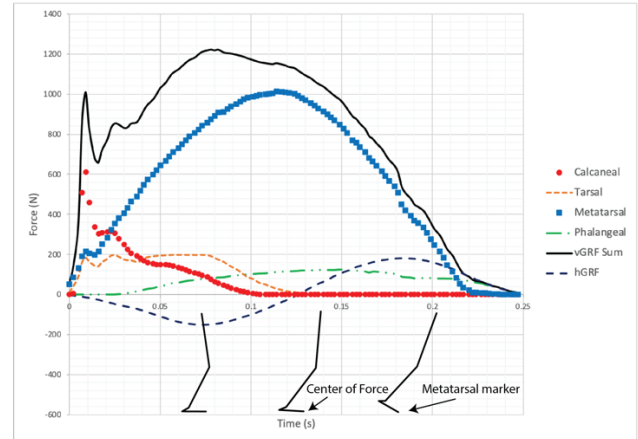


Fig. 1. Plantar regional vGRF and total hGRF with leg trajectory snapshots aligned with force profile time, in a running trial.

In the foot-ankle 2nd class lever, the MPJs make up the fulcrum and also function as load bearing hinges. The vGRF data reveal how the distribution of force between the metatarsal and phalangeal regions remains constant during MPJ flexion, indicating that force is not transferred from metatarsals to phalanges and is consistent with the 2nd class lever configuration. This function allows the metatarsals to smoothly transmit leg force both vertically and horizontally throughout the stride and flexion at the MPJ.

Conclusion

A composite plate extending under the MPJ requires additional force in order to dorsiflex and may also reduce the range of motion at the MPJ². However, since the MPJ functions to maintain the distribution of force between the metatarsal and phalangeal regions during flexion, not to transfer force, the composite plate may not alter the external power consumed in accelerating the CoM. It follows that if a composite plate may not alter the external power output, but that it may increase the internal power required during MPJ flexion, then a composite plate may decrease, but may not increase running economy. Further study is warranted to establish the precise impact of stiffening plates crossing the MPJ.

References

- [1] Hoogkamer, et al. (2018). *Sports Medicine*, **48**(4), 1009-1019.
- [2] Roy, J. P. R., and Stefanyshyn, D. J. (2006). *Medicine & Science in Sports & Exercise*, **38**(3), 562-569.
- [3] Jenny, D. F. and Jenny, P. (2020). *Journal of Biomechanics*, **110**, 109948.

A Multiscale EMG-assisted Muscle-Force Driven Finite Element Analysis Pipeline to Investigate Knee Joint Mechanics in Functional Movements: Towards a Rapid Multiscale Modeling Toolbox

Amir Esrafilian¹, Lauri Stenroth¹, Mika E. Mononen¹, Paavo Vartiainen¹, Petri Tanska¹, Pasi A. Karjalainen¹, Juha-Sampo Suomalainen², Jari Arokoski³, David G. Lloyd⁴, Rami K. Korhonen¹

¹Department of Applied Physics, University of Eastern Finland, Kuopio, Finland

²Department of Clinical Radiology, Kuopio University Hospital, Kuopio, Finland

³Department of Physical and Rehabilitation Medicine, Helsinki University Hospital and University of Helsinki, Helsinki, Finland

⁴Griffith Centre of Biomedical and Rehabilitation Engineering (GCORE) | Menzies Health Institute Queensland | School of Allied Health Sciences, Griffith University, Queensland, Australia

Email: amir.esrafilian@uef.fi

Summary

Here, a novel multiscale musculoskeletal (MS) finite element (FE) modeling pipeline is established with a focus on a rapid clinically feasible assessment toolbox. To do this, an electromyography (EMG) assisted muscle-force driven FE model with fibril-reinforced poroviscoelastic (FRPVE) cartilages and menisci was coupled with an atlas-based FE modeling toolbox. The pipeline was then used to investigate the mechanical responses of knee cartilage and menisci during different activities and exercise of knee osteoarthritis (KOA) individuals. The pipeline showcases fast subject-specific MS-FE analysis of knee mechanics during functional activities.

Introduction

Knee mechanics (i.e., tissue stress and strain) are known as crucial quantities in the genesis of MS disorders. However, current multiscale simulations that estimate these quantities are time consuming and require in-depth modeling expertise, and therefore, cannot be used to assist clinical decision making. Hence, our primary aim was to introduce a novel multiscale MS-FE analysis pipeline focusing on its feasibility for a rapid clinical toolbox to investigate multilevel mechanics of the knee load-bearing tissue. Second, we used the pipeline to explore cartilage mechanics during different daily activities and rehabilitation exercises of individuals with KOA.

Methods

Fifteen KOA participants performed six different daily tasks and seven rehabilitation exercises while marker trajectories, ground reaction forces, and EMGs (from 8 muscles of the leg of interest) were recorded. Magnetic resonance images (MRI) were acquired to create FE models. The pipeline (Figure 1) exploited an EMG-assisted MS-FE model with FRPVE cartilages and menisci [1]. The EMG-assisted MS analyses were conducted within CEINMS toolbox [2]. To provide our workflow with rapid FE modeling, an atlas-based FE modeling toolbox [3] was adapted to create subject-specific FE model geometries consisted of femoral, tibial, and patellar cartilages, menisci, and knee ligaments.

Results and Discussion

The estimated joint contact force, contact area [4], and muscle activations were comparable with experiments. Creating models took less than one hour per subject and running the simulations took ~16-40 hours, depending on the task. This

makes the pipeline feasible for clinical assessments, compared to manual workflow that typically takes more than a week.

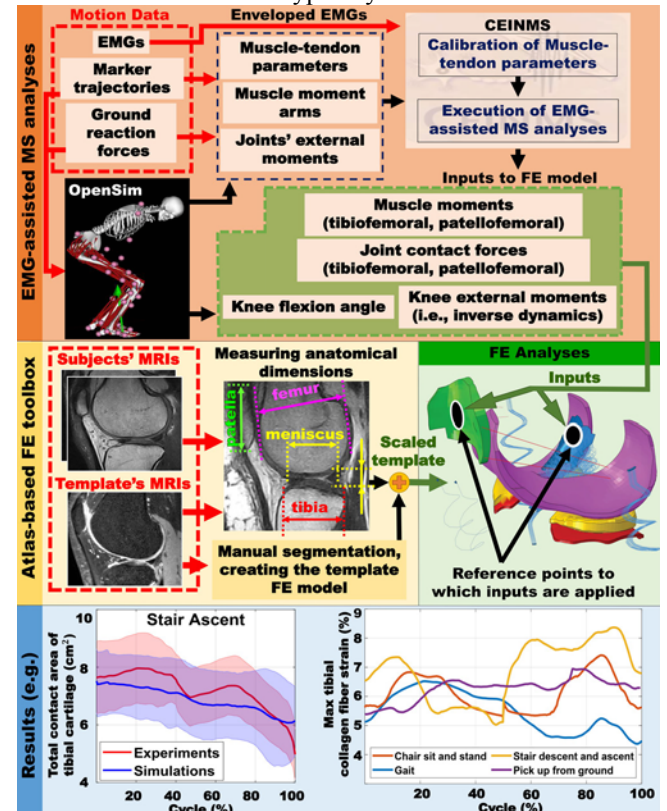


Figure 1. Illustration of the pipeline. Red arrows show raw inputs.

Conclusions

This study showcases the usability of the pipeline as a rapid MS-FE modeling toolbox to investigate in-depth tissue mechanics of various tasks and individuals with MS disorders (e.g., KOA) promisingly beneficial in clinical assessments.

Acknowledgments

Marie Skłodowska-Curie 713645; Academy of Finland 324529, 324994, 328920; ERDF A73200 and A73241

References

- [1] Esrafilian A et al. (2020), *IEEE Trans. Reh. Eng., In press*
- [2] Pizzolato C et al. (2015), *J Biomech*, **48**:3929-3936
- [3] Mononen M et al. (2018), *Ann. Biomed. Eng.*, **47**:1-13
- [4] Gilbert S et al. (2014), *J Biomech*, **47**:2006-20012

Development of a finite element model of the rat knee joint to estimate the articular cartilage biomechanics during gait

G. Orozco^{1,2}, K. Karjalainen¹, E. K. Moo³, L. Stenroth¹, P. Tanska¹, J. L. Rios³, T. Tuomainen¹, M. Nissi¹, H. Isaksson², W. Herzog³, and R. K. Korhonen¹

¹University of Eastern Finland, Kuopio, Finland, ²Lund University, Lund, Sweden, ³University of Calgary, Calgary, Canada
Email: gustavo.orozco@uef.fi

Summary

Abnormal loading of the knee after injuries or obesity is thought to contribute to the development of osteoarthritis (OA). Small animal models have been used for studying OA progression mechanisms. However, numerical models to study cartilage responses under dynamic loading in small animals have not been developed. Hence, a finite element (FE) model of a rat knee was created to evaluate cartilage biomechanical responses during gait. Model estimations showed that the greatest contact pressure, strain, and stress values occur in both medial and lateral compartments of the tibial plateau at ~85% of the stance phase. This approach can be used to investigate the biomechanical effects of gait abnormalities on cartilage tissue in rat knee joints.

Introduction

Abnormal loading of the knee joint after overuse, severe injuries, or obesity might lead to cartilage degeneration which contributes to the development of osteoarthritis (OA). Experimental animal models have been used in orthopaedic research for studying the progression of OA. In preclinical research, small animal models (e.g. rodents) are commonly used as they are cheaper and less time consuming for changes in primary outcomes to occur compared to large animal models. For example, rodent gait compensations have been evaluated in conjunction with biological markers of OA after ACL transection [1]. The effect of these compensations on cartilage loading and mechanics can be assessed using numerical models. However, computational models for joints of small animals have not been reported in the literature. Hence, our primary aim was to develop a FE model of the rat knee joint to evaluate the cartilage biomechanics during gait.

Methods

MRI protocol: An intact right lower limb of a cadaveric rat without known musculoskeletal disorders (Sprague Dawley, 56-week-old male) was imaged using an 11.74 T μ MRI scanner (MGE sequence, FOV (mm)=14.25x9.5x9.5, isotropic resolution: 37 μ m). The MRI data were used for segmenting the knee geometries in 3DSlicer (<http://www.slicer.org>). The geometries were imported into Abaqus where the FE mesh was constructed using 8-node hexahedral linear poroelastic (C3D8P) elements. **Musculoskeletal modeling:** A previously developed OpenSim musculoskeletal model of the rat lower limb was used to determine the joint loading during simulated gait [2]. The flexion-extension angle, moments, and translational knee forces were extracted and implemented into the FE model. **Biomechanical cartilage characterization:** Fibril-reinforced poroelastic (FRPE) material properties of rat cartilage were acquired using previous experimental indentation measurements [3]. The FRPE cartilage parameters were obtained by fitting the simulated stress-relaxation curve to the mean stress-relaxation curve of control group animals ($n=6$) [3]. **FE knee joint model:** Cartilages and

menisci were modeled using an FRPE material. The fitted FRPE material parameters, depth-dependent collagen fibril architecture, and fluid fraction distribution were implemented [4]. The tibial cartilage-bone interface was fixed in all directions and bones were assumed rigid. Following an initial contact step, the stance phase of the rat's gait was simulated (Figure 1).

Results and Discussion

Numerical results showed that the greatest contact pressure (0.25 MPa), reaction force (7.2 N), fibril strain (0.6%), maximum principal strain (3.5%), fluid pressure (9.2 MPa), and maximum principal stress (7.5 MPa) averaged over the contact area in the tibial cartilage surfaces were obtained at ~85% of the stance phase. This approach allows for future investigation of the biomechanical effects of pathological conditions in small animal preclinical OA models.

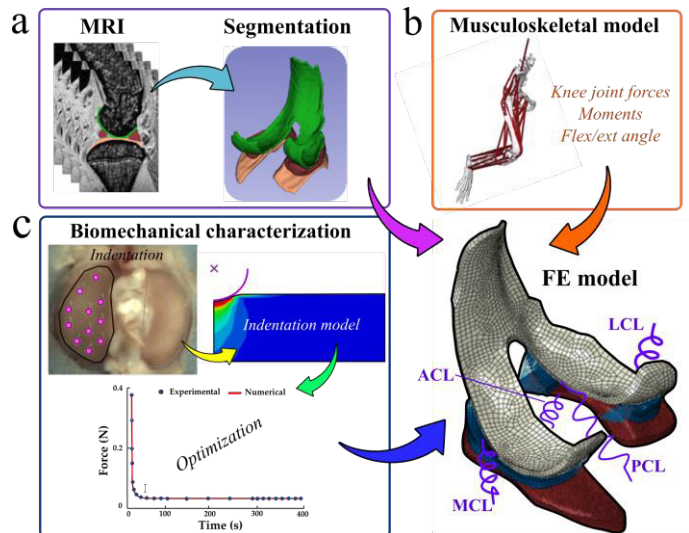


Figure 1: Workflow of the study. (a) Rat knee geometry, (b) motion and loading during gait from a musculoskeletal model, and (c) FRPE material properties from indentation tests were implemented into the FE model.

Conclusions

Our novel simulation approach can be utilized to evaluate the effect of knee joint disorders and gait impairments on cartilage biomechanical responses in small animal models.

Acknowledgments

ERA PerMed JTC2019, Academy of Finland, Päivikki ja Sakari Sohlberg and Maud Kuistila Memorial Foundations.

References

- [1] Jacobs et al. (2014). *Curr Pain Headache Rep.* **10**, 456
- [2] Johnson et al. (2008) *J. Biomech.* **41**, 610–619.
- [3] Rios et al. (2018). *Sports Medicine Open.* **4**, 15–25.
- [4] Ebrahimi et al. (2019). *Ann Biomed Eng.* **47**, 953–966.

Approximation method to calculate the elasticity tensor for hyperelastic finite element models

Manuel Lucas Sampaio de Oliveira¹, Thomas K. Uchida¹

¹Department of Mechanical Engineering, University of Ottawa, Ottawa, Ontario, Canada
Email: mdeol080@uottawa.ca

Summary

Rubber-like or hyperelastic materials are used in a broad range of applications, including vehicle tires, seals, base isolation of buildings, and biomedicine. Predicting the behaviour of these materials is crucial for design and analysis. In this work, we develop a user material in Ansys using an approximation formulation to improve computational performance during finite element analyses. The stress and strain produced by three constitutive models are compared to those of analytical models as well as built-in Ansys models. The approximation improves simulation time while introducing relatively small errors that may be acceptable in many applications.

Introduction

Hyperelastic models have been used to study the behaviour of many biological tissues including breasts, ligaments, arteries, and skin [1]. Many commercial software packages include built-in hyperelastic materials such as the Mooney–Rivlin and Yeoh models. These models assume that the material has isotropic properties; however, we often wish to include the effects of anisotropy by considering a strain energy that includes invariants associated with a preferred direction of stretch. Anisotropy can be useful for simulating polymers and fibered soft tissues such as ligaments [2] and muscles [3].

Ansys is a popular finite element analysis software and supports user material (“USERMAT”) subroutines to implement user-defined models. These subroutines provide as outputs the Cauchy stress and the tangent modulus, also referred to as the elasticity tensor or material Jacobian. The Cauchy stress is relatively straightforward to calculate; however, the tangent modulus is more complicated due to the presence of a fourth-order tensor, making the calculations more cumbersome to program and more time-consuming to evaluate. To reduce the computational expense of computing the elasticity tensor, we explore the use of an approximation of the tangent modulus proposed by Miehe [4]. This approximation relies on the perturbed deformation gradient and does not substantially compromise the convergence rate.

Methods

A USERMAT routine is implemented in Ansys in a systematic way, allowing one to easily implement different hyperelastic models. We test the Mooney–Rivlin and Yeoh models as well as the exponential form of the strain energy for an anisotropic material. The built-in Ansys model is used as the gold standard. A single-element cube is simulated under uniaxial, equitriaxial, shear, and torsion loads. We compare the stress and strain of our approximation and analytical model implementations against the built-in Ansys model. Finally, an analysis with different mesh refinement is performed to determine how the error is affected by mesh size.

The approximation method is based on perturbations of the deformation gradient. The performance of each model is assessed by calculating the normalized root-mean-square error (NRMSE) of stress and strain for N nodes:

$$\text{NRMSE} = \sqrt{\sum_{i=1}^N [(Predicted_i - Actual_i)/Actual_i]^2 / N}$$

Results

The average stress and strain errors were on the order of 10^{-2} to 10^{-4} for all models and loading conditions; normalized strain errors are shown in Figure 1. Specifically, the results are shown for four loading conditions: a uniaxial test with a displacement of 0.5 applied to one face with the opposite face constrained; an equitriaxial test with a displacement of 0.5 applied to three faces with the opposite faces constrained; a shear test with a lateral displacement of 0.5 applied to the top face with the bottom face constrained; and a torsion test where opposing 50 N forces are applied to the top and bottom faces.

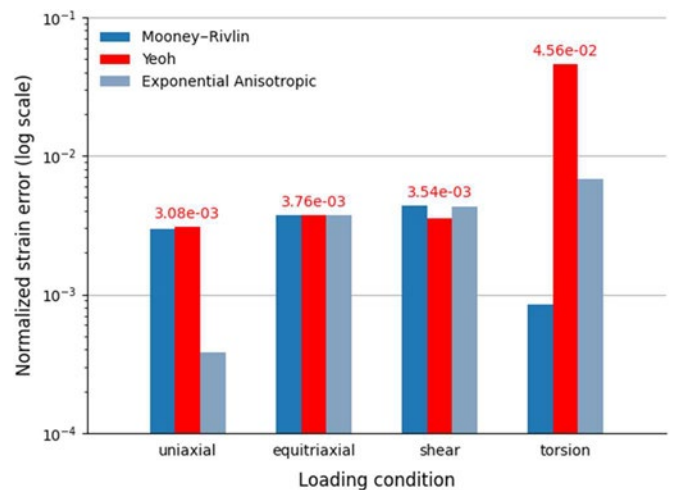


Figure 1: Normalized root-mean-square error in strain for three material models with approximation, in four loading conditions.

Conclusions

Analytical and approximate models all have relatively small errors when compared to the results from the built-in Ansys models. Complex models can be implemented easily and without substantial loss of precision using an approximation of the tangent modulus.

References

- [1] Chagnon G et al. (2015). *J. Elast.*, **120**: 129–160.
- [2] Peña E et al. (2007). *Int. J. Solids Struct.*, **44**: 760–778.
- [3] Blemker SS and Delp SL (2005). *Ann. Biomed. Eng.*, **33**: 661–673.
- [4] Miehe C (1996). *Comput. Methods Appl. Mech. Eng.*, **134**: 223–240.

A statistical shape model of the tibia-fibula complex: effects of age on reconstruction accuracy from anatomical landmarks

Olivia L. Bruce^{1,2}, Michael Baggaley¹, Lauren K. M. Welte³, Michael J. Rainbow³, W. Brent Edwards^{1,2}

¹Human Performance Laboratory, Faculty of Kinesiology, University of Calgary, Calgary, AB, Canada

²Biomedical Engineering Graduate Program, University of Calgary, Calgary, AB, Canada

³Department of Mechanical & Materials Engineering, Queen's University, Kingston, ON, Canada

Email: olivia.bruce@ucalgary.ca

Summary

A statistical shape model (SSM) was created for an active young adult population and used to predict tibia and fibula geometries for young and older adults from anatomical bony landmarks. Reconstruction errors with respect to computed tomography (CT) data were quantified and compared to errors from isometric scaling. The SSM estimated tibia and fibula geometries from landmarks with lower error (RMSE young = 1.62 mm, old = 2.12 mm), when compared to isometric scaling (RMSE young = 1.78 mm, old = 2.86 mm). The smaller errors for the young adults suggest a model specific to the population of interest provides excellent reconstruction accuracy; however, the SSM was still able to predict tibia and fibula geometries in older adults with 26% lower error than isometric scaling when shape variation is taken into account.

Introduction

Bone geometries in musculoskeletal models are commonly defined by isometrically scaling 'generic' models [1], which does not necessarily capture potentially important morphological differences among individuals. SSMs provide an alternative method to incorporate participant-specific bone geometry into musculoskeletal models as they can reconstruct geometry from anatomical landmarks. However, previous SSMs of the tibia and fibula were trained and tested on a wide range of ages [2,3]; a SSM more specific to the population of interest may provide better results. The aims of this study were to: (1) create a SSM of the tibia and fibula for a healthy young adult population and evaluate the accuracy of reconstructions from landmarks compared to isometric scaling, and (2) to evaluate reconstruction accuracy in older adults.

Methods

A SSM of the tibia-fibula complex was created using CT data from 41 young adults (22 F, 18-24 years). Nine landmarks were digitised on the bone surfaces. A leave-one-out analysis was performed, where a participant was removed from the SSM and reconstructed from the landmarks in two ways: (1) SSM-based reconstruction, where the average shape was morphed along eight principal components to match target landmarks, and (2) isometric scaling. Errors in surface geometry compared to CT segmentations were quantified. Landmarks were also digitised on bone surfaces of ten older adults (4F, 71-98 years). The SSM developed for the young adult group was used to reconstruct tibia and fibula geometries in the older group; reconstruction errors were again quantified and compared to isometric scaling. Wilcoxon signed-rank tests were performed to compare error measures between SSM and isometric scaling methods.

Results and Discussion

In the young group isometric scaling errors (median (IQR), RMSE = 1.78 (0.62) mm, maximum error = 5.84 (2.62) mm) were 51-54% lower compared to previous studies [2,3]. SSM reconstruction further reduced errors (RMSE = 1.62 (0.35) mm, maximum error = 5.12 (1.63) mm, $p < 0.001$, Fig. 1).

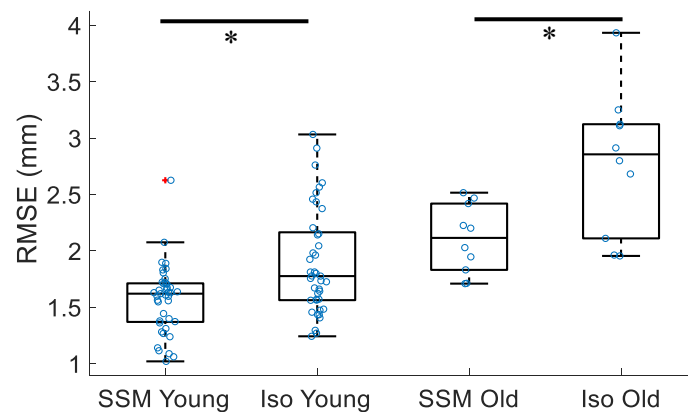


Figure 1: Root mean square errors for surface geometry reconstructions (SSM-landmark and uniform scaling methods) for young and older participants (circles). + represents an outlier. * indicates a significant difference between SSM and isometric scaling.

In the older group, errors were smaller in SSM (RMSE = 2.12 (0.63) mm, maximum error = 7.01 (1.28) mm) compared to isometric scaling (RMSE = 2.86 (1.08) mm, maximum error = 9.14 (4.19) mm, $p \leq 0.009$). Errors for both SSM and isometric scaling in the older group were generally larger than errors in the younger group but were still 22-34% lower compared to previous studies [2,3]. This may be explained in part by the use of more landmarks and principal components in SSM reconstructions as well as bone-surface landmarks in isometric scaling.

Conclusions

The SSM predicted tibia and fibula geometries from bony landmarks with high accuracy, improving upon isometric scaling. Errors were larger for the older adults, suggesting that some geometric variation due to age was not captured in the model; still, errors for older adults were low compared to previous studies. In summary, the SSM provided excellent reconstructions of the tibia-fibula complex in young adults and appears robust enough for older adults as well.

References

- [1] Delp S et al. (1990). *IEEE Trans Biomed Eng.* **37**:757-767
- [2] Nolte D et al. (2020). *Gait Posture.* **77**:269-275
- [3] Zhang J et al. (2016). *J Biomech.* **49**:3875-3881

Design and Evaluation of a Mixed Reality Spine Surgical Simulator Benchtop Configuration Based on the Workspace of Haptic Device and Simulator Users

Sneha Patel¹ and Mark Driscoll¹

¹Musculoskeletal Biomechanics Research Lab, Department of Mechanical Engineering, Faculty of Engineering, McGill University, Montreal, Canada

Email: mark.driscoll@mcgill.ca

Summary

Current surgical simulators have either virtual or physical components. In the present study, the surgical area is modelled virtually and physically therefore requiring matching reference models for natural manipulation of the surgical tools while interacting with the simulator. This study collected path trajectories of experienced spine surgeons in a novel spinal fusion surgical simulator and the workspace of the haptic device to determine the appropriate configuration of the mixed reality surgical simulator. The results suggest differences between users and the selected configuration encompassing the required workspace for the surgery.

Introduction

Minimally invasive spine surgeries are complicated and require complex motor skills due to the proximity of the spine to neural and vascular components and limited access to the surgical area. Without proper training serious complications can occur in these procedures [1].

Teaching hospitals strive to address the need for intensive training in this field while mitigating the risks associated with conventional training. Therefore, several use virtual reality simulators to provide residents a platform to improve their motor skills without risk to patients. In minimally invasive simulators, haptic feedback is essential due to the limited visual cues available from the surgical area. Therefore, most commonly, a haptic device or a physical model is used in the simulator [2, 3]. The purpose was thus to conceive a workspace, encompassing haptic and physical models, while enabling fluent surgical maneuvers.

Methods

First, the workspace adopted by experienced surgeons relative to that of the haptic device was evaluated, during surgical port insertion and discectomy, to optimize the design of the benchtop. This consisted of a model of the surgical area, sensors, and the haptic device. Kinematic analyses for the haptic device, were completed to develop the workspace of the haptic device. The haptic device modelled the tools and collected the path trajectory until the surgeons considered the task completed. Surgeons completed the same surgery on a cadaver before using the simulator to encourage fluid maneuvers. User trajectory was then superimposed on the haptic device workspace in order to determine the ideal configuration of the benchtop. Statistical analyses were then conducted to test the effects of surgical experience on the trajectory and workspace of the user in the simulator.

Results and Discussion

Figure 1 shows that the workspace of the user is always encompassed by the workspace of the haptic device. In figure 1(a) they have the freedom to move throughout the benchtop model. In figure 1(b) the user's movement is limited to the cylindrical port through which the procedure is completed.

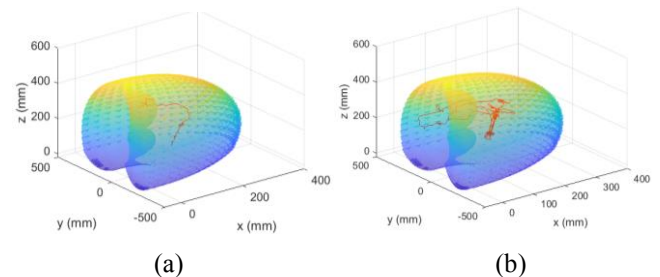


Figure 1: (a) Illustrates the trajectory of a surgeon, red, encompassed in the workspace of the haptic device for which heights were adjusted whereas (b) shows their trajectory through a cylindrical port during discectomy.

A Kruskal-Wallis Test assessed the trajectories of the subjects. Results of the analysis suggest user trajectories to be very different despite their surgical experience and that the selected configuration meets the needs of surgeons performing fusion surgery while enabling fluid maneuvers. The Spearman correlation compared the trajectory volume during each task versus the surgeons' experience. The results suggest a correlation between the two variables and the importance of this metric to assess the user in the simulator.

Conclusions

This study presents a method to determine and evaluate the configuration of a mixed reality surgical simulator using the workspace of the haptic device, the surgery workspace, and user trajectories in the simulator.

Acknowledgments

This work was supported in part by Natural Sciences and Engineering Research Council of Canada (NSERC) and MEDTEQ. The authors would also like to thank Entact Robotics Inc. for their support during this study.

References

- [1] A. J. Schoenfeld, et. al., (2011) *J. Bone Jt. Surg.*, **93**: 1577-82.
- [2] K. Atesok, et.al., (2012) *JAAOS*, **20**: 410-422.
- [3] T. R. Coles, et. al., (2011) *IEEE Trans Haptics*, **4**: 51-66.

Effect of Transverse Plane Alignment on Knee Contact Mechanics During Running

Peñaranda, D¹, Chen, R¹, Morgan, O³, Fragomen, A², Rozbruch, SR², Hillstrom, HJ^{2,3,4}, Hillstrom R^{2,4}

¹New York University, New York, NY, ²Hospital for Special Surgery, New York, NY,

³Anglia Ruskin University, Chelmsford, UK, ⁴Biomed Consulting, Inc., New York, NY

Email: HillstromH@HSS.edu

Summary

Running, a common recreational activity for maintaining health, has received little research in terms of knee joint contact mechanics. Further, there is a gap in knowledge for predicting knee contact mechanics before and after transverse plane deformity. A finite element model of the knee was employed to simulate corrective osteotomies and investigate changes in knee compartment contact mechanics. Our findings show that medial and lateral compartment stress can be modeled and simulated as a function of osteotomy angle.

Introduction

Lower limb malalignment in the sagittal, frontal, or transverse planes, is a common problem affecting individuals with osteoarthritis (OA). It is not clear how the initial posture or corrective osteotomies affects knee joint stress. Derotation osteotomy of the femur has been shown to treat either femoral retroversion or excessive anteversion [1]. Computational methods have been used to study lower limb malalignment and surgical repair. Still, there is paucity of in-vivo, in-vitro, and in-silico data from which the effect of transverse plane osteotomies upon knee contact mechanics may be predicted. The central hypothesis is that transverse plane osteotomies will modify medial and lateral compartment stress.

Methods

Our computational model was constructed from a 50-year-old, 65 kg male cadaveric specimen. MRI data of the left lower limb was segmented in Mimics (Materialise, Leuven) and exported to CATIA (Simulia, Vélizy-Villacoublay) to create 3D models of each tissue (bones, cartilage, meniscus, capsule and primary ligaments). The 3D tissue models were meshed and assembled in ABAQUS (Simulia, Vélizy-Villacoublay). The finite element model was augmented by including the patella and associated cartilage, ligaments, and the quadriceps-patellar tendon [2]. The native knee was in 35° of femoral anteversion (0° model), compared to 14±7.8° for the general population [3]. We simulated mid-femur transverse plane osteotomies of -20°, -10°, 0°, 20°, 30°, 40°, 50°, 55°, and 60° (retroversion (-) / anteversion (+)). All osteotomy corrections were made with respect to the native knee alignment of 35° degrees anteversion. Inverse dynamic forces and moments were acquired from the Leon Root, MD Motion analysis laboratory (height, weight, age, and sex matched). Specifically, the loading from 45% of the gait cycle, where peak internal/external moments occur, was applied. Input forces and moments were transformed to account for osteotomy correction angle. Von Mises and Tresca stress were computed for all tissues in the joint.

Results and Discussion

Different osteotomy angles provided varying medial and lateral compartment stress magnitudes at the cartilage-

cartilage and cartilage-meniscus interfaces (Fig. 1, Fig. 2). Fig. 1 illustrates the cartilage-meniscus stress in the medial and lateral compartments as a function of osteotomy angle, where 0° is the native alignment. In Fig. 2 the cartilage-cartilage interface is depicted for the medial and lateral compartments across all osteotomy angles.

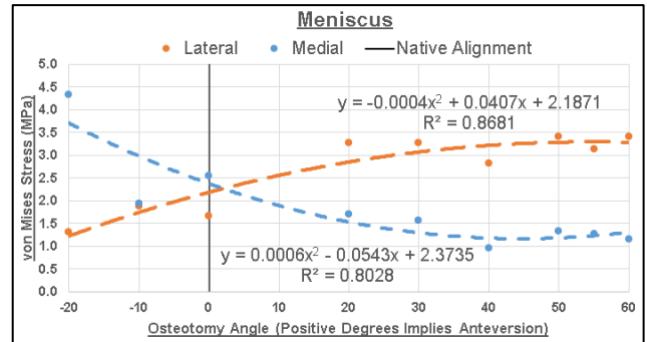


Fig. 1: Peak Meniscus von Mises Stress

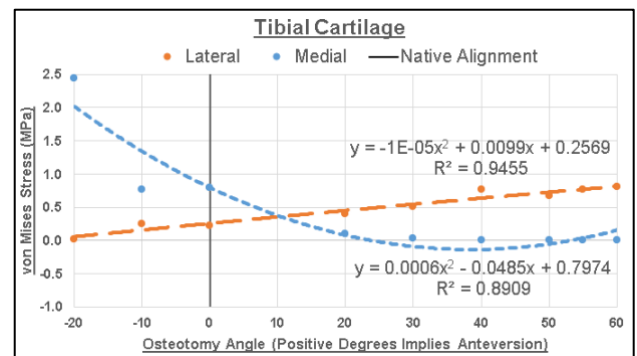


Fig. 2: Peak Tibial Cartilage von Mises Stress

Forces and moments were larger in the lateral compartment, as expected for running, for the anteverted osteotomies. As shown in Fig. 1 and Fig. 2, there is a trade-off between medial and lateral compartment stress as a function of osteotomy angle. The results depicted in this study correspond to the specific knee modeled and cannot be generalized. It is possible that other knees could have different peak stresses in different locations due to their different geometries.

Conclusions

In support of the hypothesis, simulation of medial and lateral compartment stress in running varied across transverse plane osteotomy angles. The anteverted osteotomies resulted in higher lateral compartment stress. This work represents a first step towards the development of surgical treatment planning tools to aid surgeons in making informed decisions when planning osteotomies.

References

- [1] Buly, R.L. et al. (2018) *J Am Acad Orthop Surg*.
- [2] Mootanah, R. et al. (2014) *CMBBE*
- [3] Bråten, M. et al. (1992) *Acta Orthop Scand*.

Learning from the Measurable: Predicting Changes in Hill-Type Muscle Parameters from Lateral Pinch

Kalyn M. Kearney¹, Joel B. Harley², Jennifer A. Nichols¹

¹J. Crayton Pruitt Family Department of Biomedical Engineering, University of Florida, Gainesville, United States

²Department of Electrical and Computer Engineering, University of Florida, Gainesville, United States

Email: kalynekearney@ufl.edu, joel.harley@ufl.edu, jnichols@bme.ufl.edu

Summary

Musculoskeletal models enable subject-specific analyses through controlled variation of biomechanical parameters. However, modeling even simple tasks requires assumptions about unmeasurable Hill-type muscle parameters. We tested an approach to estimate these parameters from simulated lateral pinch force using artificial neural networks. Our results suggest classifying muscle parameters from pinch force is feasible, but complex models may require more input features.

Introduction

Musculoskeletal models of the thumb are defined by over 109 independent biomechanical parameters [1]. Many of these parameters are difficult or impossible to measure *in vivo*, hindering development of subject-specific models. In this study, we present a data-driven approach to estimate the maximum isometric muscle force (unmeasurable parameter) from pinch force (measurable clinical outcome). Leveraging forward dynamic simulations and artificial neural networks (ANNs), we elucidate the role maximum isometric force of extrinsic muscles plays in lateral pinch force generation.

Methods

Four datasets of lateral pinch force were produced via forward dynamics in OpenSim v 3.3 [2]. A thumb model [1] was varied by adjusting maximum isometric force of the extrinsic thumb muscles [*abductor* (APL), *flexor* (FPL), and *extensor* (EPL) *pollicis longus* and *extensor pollicis brevis* (EPB)]. Datasets 1 through 4 contained 120, 1024, 3197, and 4096 simulations as 1-4 muscles were adjusted, respectively. The output of each simulation was a three-component pinch force vector versus time. The time-series force data was separately input into 2 ANNs: *feedforward* and *long short-term memory* (LSTM). Feedforward ANNs lack feedback within the structure [3], but are less computationally costly. LSTMs have feedback and thereby “memory” [4], which can aid study of time-dependent activities. Each ANN included 4 input nodes (time and three-component force vectors), 4 hidden nodes, and 1 hidden layer. Labeled data were grouped by whether the varied muscles were above (“High”) or below (“Low”) mean maximum isometric force. Modifying more muscles resulted in more labeled groups, requiring 2, 4, 8, or 16 output nodes for Datasets 1-4, respectively. Mean and standard deviation (SD) of thumb-tip force for each group were calculated. To reduce overfitting, 5-fold cross validation was used. Accuracies and losses were analyzed, and a two-sample t-test compared peak accuracies of each ANN and dataset.

Results and Discussion

The mean and distribution of final thumb-tip forces within Dataset 4 revealed the relative contributions of extrinsic

muscles (Figure 1). No overlap within 1 SD occurred between groups with a high FPL maximum isometric force and that with a low one. Little overlap occurred between groups of high and low APL maximum isometric force. Both ANNs saw a decrement in performance for datasets which altered more muscles. In the feedforward ANNs, the peak accuracy for Dataset 1 was 93.2%, but 37.4% for Dataset 4. For the LSTM ANNs, the peak accuracy for Dataset 1 was 93.8%, but 34.8% for Dataset 4. Losses became substantially less stable for more complex datasets for both ANNs. Two-sample t-tests revealed that only analysis of Dataset 2 produced significantly different peak accuracies ($p < 0.05$), which were higher for the LSTM than the feedforward ANN. Peak accuracies for all datasets were well above random guess.

The decrement in model performance for more complex datasets may be attributable to redundancies in muscle function. Notably, the EPL and EPB are extensors of the thumb, with the APL assisting in extension as well [5]. As Datasets 3 and 4 included changes to combinations of these muscles, the classification task of the ANN became more challenging. Optimization of ANN width and depth may benefit classification [6, 7], as well as the inclusion of more measurable inputs (e.g. kinematics, EMG)

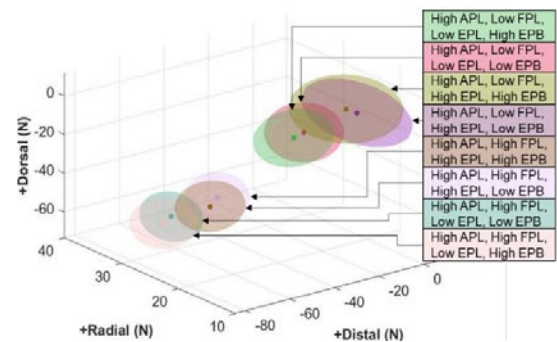


Figure 1: Thumb-tip forces for part of Dataset 4. Ellipsoid centers represent mean force and radii represent 1 SD

Conclusions

Our investigations tested the feasibility of using ANNs to predict muscle parameters from lateral pinch force. This framework is a first step toward estimating subject-specific muscle parameters from minimal, measurable data.

References

- [1] Nichols et al. (2017). *J Biomech*, **58**: 97-104.
- [2] Delp et al. (2007). *IEEE Trans Biomed Eng*, **54**: 1940-50.
- [3] Svozil et al. (1997). *Chemometr Intell Lab*, **9**: 43-62.
- [4] Hochreiter et al. (1997). *Neural Comput*, **9**: 1735-80.
- [5] Von Schroeder et al. (2001). *CORR*, **383**: 74-83.
- [6] Bengio et al. (2011). *Lecture Notes in Comput Sci*.
- [7] Hahn et al. (2005). *J Biomech*, **38**: 717-24.

Objectively Defining Design Parameters Associated with Self-Selected Lumbar Support Prominence

Jessa M. Buchman-Pearle, Kayla M. Fewster, Brendan L. Pinto, Jack P. Callaghan

Department of Kinesiology, University of Waterloo, Waterloo, Ontario, Canada

Email: jessa.bpearle@uwaterloo.ca

Summary

Participants self-selected lumbar support prominence (LSP) and vertical location in an automotive seat through a series of systematic adjustment trials. The average LSP setting was set for a one-hour driving simulation, followed by one final LSP adjustment trial. Multiple linear regressions revealed low to strong model fit between anthropometric characteristics and seated lumbar flexion, seatback average pressure, and contact area. Following the driving protocol, participants preferred changes to seat settings that decreased lumbar flexion and increased seatback pressure. These findings suggest that integrating subject-specific design parameters and methods for determining seat preference may reduce maladaptive tissue adaptations and discomfort associated with prolonged sitting.

Introduction

Automotive seat design parameters, such as the addition of a lumbar support prominence (LSP), has the potential to impact postural changes that may lead to low back pain during prolonged driving [1,2]. LSP preferences tend to vary across individuals, specifically between males and females [3]. Therefore, this study investigated subject-specific parameters which may alter LSP preference and associated variables, before and after a prolonged driving simulation.

Methods

Forty participants (21M/19F, mean height = 1.70 ± 0.10 m, mass = 72.1 ± 16.5 kg, BMI = 24.7 ± 3.8 kg/m², waist and hip circumference = 79.5 ± 13.6 and 97.6 ± 12.1 cm) completed six automotive seat-adjustment trials, a one-hour driving simulation, and one final seat-adjustment trial after driving. For the initial adjustment trials, three trials began with the LSP fully disengaged and down, and three with the LSP fully engaged and up, allowing the participant to freely position the LSP. The average chosen LSP setting (prominence and vertical location) was used for the prolonged driving simulation. Sagittal lumbar angles were calculated from triaxial accelerometers over the pelvis and L1. Seatback pressure distribution and motion of the trunk and pressure mat were also recorded.

Backward stepwise linear regressions were performed between participant anthropometry, standing lumbar angle, and lumbar sagittal range of motion on: 1) selected LSP, 2) seated lumbar flexion, 3) average seatback pressure, 4) seatback contact area, and 5) height of the centre of pressure (CoP) above the midpoint of the iliac crests. LSP was also input into the regressions for the remaining four dependent variables. Five two-way mixed ANOVAs ($\alpha = 0.05$) were performed to determine the effects of time and sex.

Results and Discussion

Significant regression models ($p \leq 0.005$) were produced for seated lumbar flexion, average seatback pressure, and

seatback contact area (Table 1). There was a significant main effect of time ($p \leq 0.017$) for all variables except LSP (Figure 1). There was a main effect of sex for contact area as area was 140.3 cm^2 greater for males than females.

Table 1: Summary of regression models which reached statistical significance ($p < 0.01$).

Dependent Variable	R	R ²	Independent Variable
Seated Lumbar Flexion	0.56	0.32	Standing lumbar angle
Average Pressure	0.44	0.19	LSP
Contact Area	0.73	0.53	Height and mass

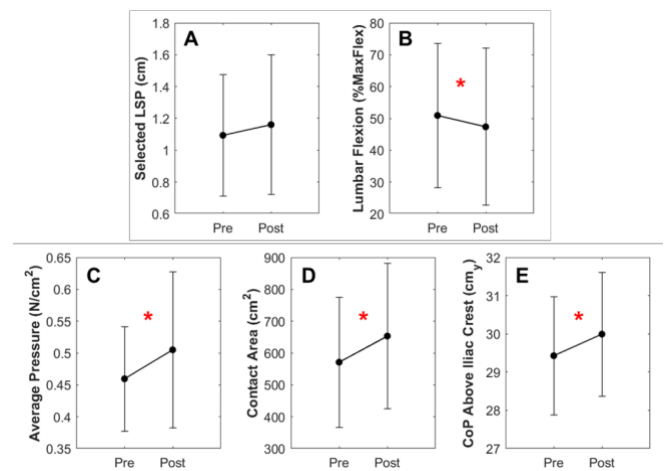


Figure 1: Pre- and post-driving simulation comparisons where red asterisks indicate a significant difference ($p < 0.05$).

Conclusions

The correlations between standing lumbar angle, height, mass, and dependent variables describing automotive seat preference suggests that these subject parameters should be considered in future automotive seat design. Additionally, the decrease in lumbar flexion and increase in seatback pressure without a significant change in LSP suggests that the method for seat-adjustment facilitates effective LSP selection across subjects. Further, utilizing this method may reduce the need for seat adjustments, wherein cueing short-term postural adjustments may be preferred.

Acknowledgments

The authors acknowledge funding from the Natural Sciences and Engineering Research Council of Canada. FCA Canada Inc. provided study materials and in-kind support for NSERC-ENGAGE funding.

References

- [1] Chen et al. (2005). *Scand J Work Environ Health*, **31**: 258-65.
- [2] De Carvalho & Callaghan. (2012). *Appl. Ergon*, **43**: 876-82.
- [3] De Carvalho & Callaghan. (2015). *Hum Factors*, **57**: 976-87.

Trunk Muscle Co-Activation In and Out of an Episode of Low Back Pain During the Balance-Dexterity Task

Yue Ai¹, Hai-Jung Steffi Shih^{1,2}, Jiayi Tang¹, K. Michael Rowley¹, and Kornelia Kulig¹

¹Division of Biokinesiology and Physical Therapy, University of Southern California, Los Angeles, CA, USA

²Department of Biobehavioral Sciences, Teachers College, Columbia University, New York, NY, USA

Email: yueai@usc.edu

Summary

We compared trunk muscle activation and co-activation during symptomatic and asymptomatic periods of persons with recurrent low back pain (rLBP) as well as back-healthy controls (CTRL) using the Balance-Dexterity Task (BDT). Persons who were actively in pain (rLBP-A) exhibited transverse plane trunk muscle co-activation patterns similar to CTRL, whereas persons in symptom remission (rLBP-R) demonstrated decreased co-activation of these muscles.

Introduction

Trunk control strategies in persons with rLBP are task-dependent, where submaximal tasks such as the BDT tend to elicit decreased activation compared to maximal tasks [1]. Previous research using the BDT suggests that rLBP individuals who were asymptomatic when tested showed reduced trunk kinematic coupling along with lower deep-to-superficial trunk muscle activation ratios compared to CTRL [2]. The influence of pain status in persons with rLBP on trunk muscle co-activation is unknown. Therefore, the purpose of this study was to investigate trunk muscle co-activation in and out of pain in persons with rLBP compared to CTRL. We hypothesized that persons with rLBP, regardless of pain status, will exhibit reduced trunk musculature co-activation compared to CTRL, and these individuals will have higher co-activation during their symptomatic periods compared to asymptomatic periods.

Methods

19 persons with rLBP (F=13, M=6; 25.3±5.2 years) and 19 matched CTRL (F=13, M=6; 26.9±3.4 years) were tested. rLBP were tested first in pain (Visual Analog Scale (VAS, 0-100): 38.9±19.2 mm), then out of pain (VAS: 1.4±2.4 mm).

The BDT required participants to stand on the supporting limb and exert a downward compression force onto either a stable block or an unstable spring with their non-stance limb to sustain an individualized force target. Surface EMG was used to collect activation levels for 8 muscles at 1500Hz (bilateral Longissimus, Rectus Abdominis (RA), External Oblique (EO), Gluteus Medius (GM)), and signals were processed using a 4th order Butterworth filter with a 50ms moving window. Activation amplitudes were normalized to the stable block condition. Muscle co-activation indices for 12 between-muscle pairings were derived using the Falconer and Winter method [3], where the co-activation levels for each muscle pairing were normalized to the sum of their individual activation levels. Statistical analysis was conducted using linear mixed-effects models.

Results and Discussion

All muscles showed significantly greater activation levels in the spring condition than the block condition ($p < 0.05$). Except for bilateral RA, all muscle pairings exhibited greater co-activation in the block condition than the spring condition ($p < 0.001$). rLBP-R showed less bilateral EO (R-L EO) co-activation than rLBP-A and CTRL, while no difference was found between rLBP-A and CTRL (Fig 1). No difference was found between rLBP-A and rLBP-R in other muscle pairings, so data was pooled between pain statuses and compared to CTRL. Pooled rLBP data showed greater decreases in right RA and right GM co-activation from block to spring in the rLBP group than the CTRL ($p = 0.035$).

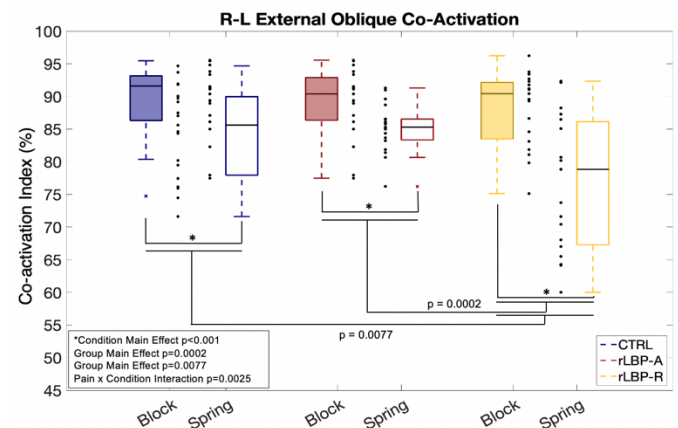


Figure 1: R-L EO Co-activation per condition and group.

Conclusions

Persons with rLBP exhibited more R-L EO co-activation in active pain than in remission, but the co-activation levels in active pain were not greater than those in CTRL. The lower co-activation of R-L EO during asymptomatic periods may cause excessive intersegmental motion as has been observed in this task previously [2] that may predispose persons to experience repeated bouts of pain.

Acknowledgments

Funded by the ISB Matching Dissertation Grant to Shih.

References

- [1] Van Dieen JH, et al. (2019). *J Orthop Sports Phys Ther*, 49: 370-379.
- [2] Rowley KM, et al. (2019). *J Orthop Sports Phys Ther*, 49: 887-898.
- [3] Falconer K and Winter DA. (1985). *Electromyogr Clin Neurophysiol*, 25: 135-149.

Exploring the Correlation Between Rotational and Translational Joint Passive Stiffness – A Porcine *in-vitro* Investigation

Kayla M. Fewster, Jeff M. Barrett, Jack P. Callaghan
 Department of Kinesiology, University of Waterloo, Waterloo, ON
 Email: kfewster@uwaterloo.ca

Summary

Different clinical test paradigms evaluating spine stiffness rarely agree, we hypothesized this may be because they assess different modes of loading. Translational anterior and posterior shear, and rotational flexion and extension stiffnesses were measured on 48 porcine functional spinal units. Linear regressions were performed between these measures. Only a weak positive correlation between posterior and extension stiffness was found.

Introduction

Spinal range of motion is an important clinical measure and can provide insight into the state of degeneration or injury of an intervertebral joint. This clinical significance has been emphasized through numerous *in-vitro* studies observing significant correlations between state of degeneration and structural properties of the functional spinal unit (FSU) [1–3]. However, *in-vivo* clinical assessments of spinal stiffness have weak correlations between one-another [4]. We hypothesized that these findings may be partially explained by anisotropy of the FSU and different loading paradigms across clinical testing. If the stiffness of isolated FSUs differs across loading paradigms, then it may explain the variability in findings from clinical assessments. Therefore, the purpose of this investigation was to quantify the relationships between rotational and translational stiffness *in-vitro*.

Methods

48 porcine cervical FSUs (20 C34, 28 C56) underwent rotation range of motion testing (ROM) ($\pm 8\text{Nm}$ moment applied at $0.5^\circ/\text{s}$) followed by translation ROM testing ($\pm 400\text{N}$ shear load applied to the caudal vertebra at $0.2\text{mm}/\text{s}$) while simultaneously exposed to 300N of compression. Porcine cervical FSUs were used as surrogates for the human lumbar spine due to the anatomical and functional similarities. Following testing, moment-angle curves from flexion-extension ROM testing and force-displacement curves from shear ROM testing, were created to quantify flexion and extension rotational stiffness and anterior and posterior shear translational stiffness. Correlations between all four measures were completed (RStudio, version 1.2.5033) and significant relationships were assessed at an *a-priori* level of significance (α) of 0.05.

Results and Discussion

Descriptive statistics for each outcome measure are presented in Table 1. No strong correlations ($R^2 > 0.80$) were observed between any of the outcome variables explored in this investigation (Figure 1). Of the six correlations completed,

only one was statistically significant. Specifically, posterior translational stiffness was weakly correlated with extension rotational stiffness ($p = 0.0146$; $R^2 = 0.123$).

Table 1: Summary of the stiffness values measured in the specimens along with standard deviations.

Anterior Stiffness (N/mm)	Posterior Stiffness (N/mm)	Flexion Stiffness (Nm/deg)	Extension Stiffness (Nm/deg)
61.0 ± 6.8	59.8 ± 4.4	0.903 ± 0.198	1.33 ± 0.40

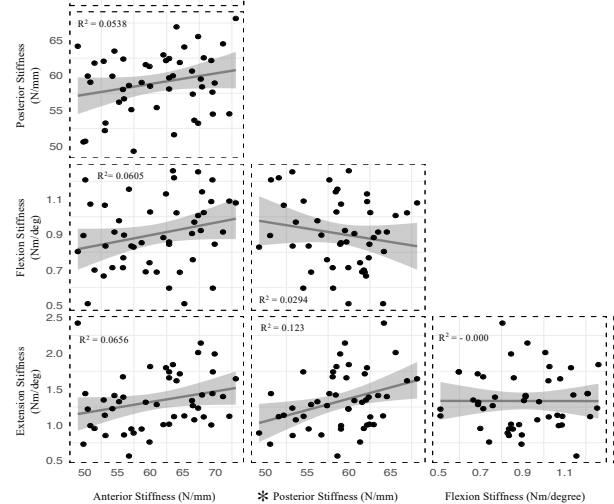


Figure 1: Correlations and their r^2 values for each of the six correlations completed. Overall, none of the variables explored in the study were highly correlated, and only extension and posterior stiffness values were significantly correlated.

Conclusions

This investigation demonstrated poor correlations between rotational and translational stiffness metrics. Such results support conflicting findings of tissue stiffness *in-vivo*. Results from this investigation suggest that clinicians should be cognizant of which degrees-of-freedom they are assessing in the spine, as their stiffness values may vary independently.

References

- [1] Fujiwara, A. (2000). *J. Spinal Disord.*, 13(5): 444-450.
- [2] Nachemson, AL. (1979). *Spine*. 4(1): 1-8
- [3] Sato, K. (1999). *Spine*. 24(23): 2468-2474.
- [4] Tennant, LM. (2020). *J. Appl. Biomech*. 36(6): 397-507

Reliability and accuracy of an on field methodology for ACL risk of injury screening

A. Ciniglio¹, M. Donadello¹, F. Spolaor¹, A. Guiotto¹, D. Pavan¹, F. Cibirin², Z. Sawacha^{1,3}

¹BiomovLab, Dept. Engineering Information, University of Padova, Padova, Italy

²BBSof S.r.l., Padova, Italy

³Dept. Medicine, University of Padova, Padova, Italy

Email: zimi.sawacha@dei.unipd.it

Summary

By considering the incidence of anterior cruciate ligament (ACL) injuries and the high reinjury rates, there is no agreement on which is the best criteria to plan the athletes return on field after ACL reconstruction [1]. The aim of this study is to identify a suitable protocol for assessing ACL injury biomechanics directly on the field, thus taking into account the role of the sport specific environment.

Introduction

Anterior cruciate ligament (ACL) injury is multifactorial and involves biomechanical, anatomical and neuromuscular factors, such as excessive knee valgus moments or large anterior tibial translation [2]. Hence, screening methods should be linked to the mechanical etiology of ACL injuries in order to effectively identify ‘at-risk’ athletes [3]. This study aims at validating the adoption of a biomechanical assessment that can be performed on the field by means of video cameras and plantar pressure for ACL injury risk assessment [4].

Methods

After signing informed consent, 7 subjects were acquired: 6 controls (age 27.3 ± 4.4 years, BMI 27.8 ± 1.9 kg/m²), 1 ACL-injured subject (ACL-S) 3 months after the surgery (age 27 years, BMI 22 kg/m²). Data were simultaneously acquired by means of a stereophotogrammetric system (6 TVC, BTS) synchronized with two force platforms (Bertec), a video-based system (8 TVC, GoPro Hero 7) and plantar pressure insoles (PedarX, Novel). Controls performed three mopedalic and bipodalic squats, while the ACL-S performed only bipodalic squats. Reflective markers were applied as in [5] and trajectories reconstructed through stereophotogrammetry and automatic tracking [4] (a self-developed software Track on Field (TOF), BBSof S.r.l., validated in [6] was used). Joint kinematics [5,6] and kinetics [4,5] provided through the following set-up were compared: Stereophotogrammetry and force plates (set-up_1) [5]; Stereophotogrammetry and plantar pressure (set-up_2) [4]; video cameras and force plates (set-up_3); video cameras and plantar pressure (set-up_4) [4]. Wilcoxon signed rank test ($\alpha=0.05$) was used to compare the data across the different set up and the asymmetry index (AI) was calculated [7]. The comparison between controls and ACL-S was performed through Wilcoxon rank sum test ($\alpha=0.05$). To assess the inter-operator variability of the video tracking the Standard Error (“SE”) [8] was calculated (2 operators).

Results and Discussion

Reliability and repeatability results showed good agreement between angles calculated with both systems, (Fig.1, Up) and a low inter-operator variability. In the comparison of the joint

moments across the different set-up, larger differences were observed in the monopodalic squats, especially in the central phase, at the hip joint, between set-up_1 and 4. Statistically significant differences were observed on joint angles, moments and the AI (Fig. 1, Down) between controls and ACL-S in every tested condition.

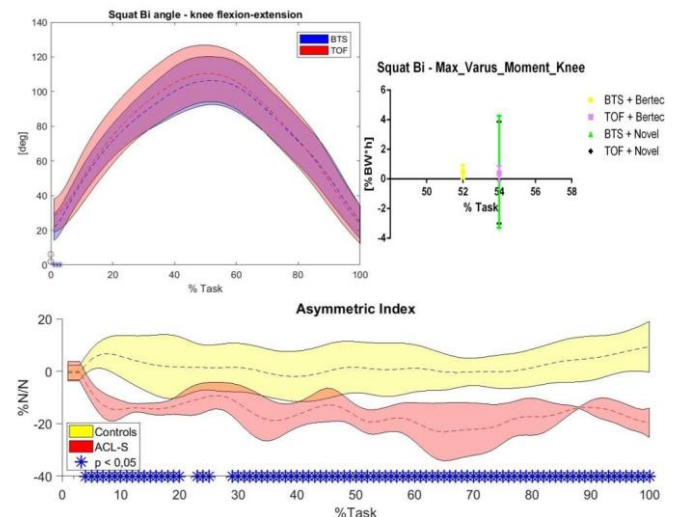


Figure 1: Up Left, the knee flexion-extension angle, BTS, in blue and TOF, in red. Up Right, the knee varus torque peak calculated for each set-up, value and occurrence within the task. Down, the AI, controls in yellow and ACL-S in red.

Conclusions

Reliability tests results’ are encouraging toward the adoption of set-up 4 which can be easily applied on field. Comparison in terms of joint kinetics, showed good agreement among the different evaluations. The significant differences observed between set-up_1 and 4 were mainly due to differences between force plate and plantar pressure measures.

References

- [1] Davies GJ et al. (2017). *Curr Rev Musculoskelet Med*, **10**(3): 307–314.
- [2] Shin et al. (2009). *J of Biomech*, **42**(3): 280-5.
- [3] Fox et al. (2016). *Sports Med*, **46**(5): 715-35.
- [4] ACL Quick Check® patent: <https://www.bb-sof.com/>
- [5] Del Din et al. (2011). *Med Biol Eng Comput*, **49**(7): 801-9.
- [6] Magalhães et al. (2013). *J Sports Sc & Med*, **58**: 194-200.
- [7] Jordan et al. (2018). *JSHS*, **7**: 416-424.
- [8] Schwartz et al. (2004). *Gait & Posture*, **20**: 196-20.

Multi-segment components of induced power generation during pitching in collegiate baseball players

Arnel Aguinaldo,¹ Kristen Nicholson,² Gordon Alderink³

¹Department of Kinesiology, Point Loma Nazarene University, San Diego, CA, USA

²School of Medicine, Wake Forest University, Winston-Salem, NC, USA

³Department of Physical Therapy, Grand Valley State University, Grand Rapids, MI, USA

Email: arnelaguinaldo@pointloma.edu

Summary

Using a full-body induced power analysis (IPA) of baseball pitching, we found that direct contributions to power of the throwing arm and ball velocity were primarily made by torques at the shoulder and by velocity-dependent effects.

Introduction

In an open kinetic chain such as baseball pitching, the velocity of the throwing arm is affected by the mechanical power through the chain via coordination of proximal-to-distal segmental motion, where muscular torques can induce accelerations of anatomically remote segments through dynamic coupling [1,2]. However, traditional inverse dynamics approaches are insufficient in decomposing the components of segmental motion that contribute to the energy and velocity of throwing arm [3]. Previous researchers have implemented induced acceleration analysis (IAA) models to perform this decomposition in baseball pitching but did not include lower body contributions [1,4]. Hence, the purpose of this study was to use a full-body IAA to examine how muscular and non-muscular torques contribute to the induced power of the throwing arm and to the forward velocity of a pitched ball in collegiate baseball players.

Methods

This retrospective study was approved by the institutional review board at Wake Forest University. Data from 17 collegiate pitchers (age = 20.4 ± 1.2 years, height = 1.87 ± 0.05 m, mass = 94 ± 7 kg) were examined from in-season pitching analyses. Each participant threw 12 various types of pitches to a catcher at a regulation distance (18.4 m) away from a mound instrumented with three force platforms (AMTI, Watertown, MA) while 3D motion data were captured at a sampling rate of 400 Hz using a marker-based motion analysis system (Qualisys, Göteborg, Sweden) [1]. Ground reaction force (GRF) data were collected at a sampling rate of 1000 Hz.

A 14-segment model was configured and implemented in Visual 3D (C-Motion, Germantown, MD). The joint accelerations were estimated using the following IAA equation:

$$\ddot{\theta} = I^{-1}(\theta)[\tau + V(\theta, \dot{\theta}) + g(\theta)]$$

where $\ddot{\theta}$ = generalized accelerations vector, I^{-1} = inverse of the system inertia matrix, τ = vector of the net muscular torques, $V(\theta, \dot{\theta})$ = vector due to velocity-dependent (Coriolis, centripetal) forces, and $g(\theta)$ = gravitational force. By taking the product of each force or torque component and the corresponding velocity vector, an induced power analysis (IPA) of the throwing arm was performed [1]. All IAA

equations were derived in SD/Fast (PTC, Cambridge, MA) and implemented in Visual 3D. The mechanical work of the throwing arm was computed via time integration of the induced power between the instants of maximum knee height in the stride phase and ball release. Likewise, the induced ball velocity was calculated by time-integrating the induced acceleration of each source.

Results and Discussion

The IPA showed that the velocity-dependent torque represented the largest proportion (65%) of the energy transferred to the arm at 0.93 ± 0.62 J/kg followed by the shoulder torque (29%). Only 6% of the power was directly induced by the motion of the other segments in the kinetic chain. This finding aligns with previous IPA studies which showed how pelvis and trunk motion indirectly contribute to the power of the throwing arm via the velocity-dependent torque [1,3]. Similarly, the results of this IAA indicated that the largest contributions to ball velocity came from the shoulder and velocity-dependent torques (Figure 1).

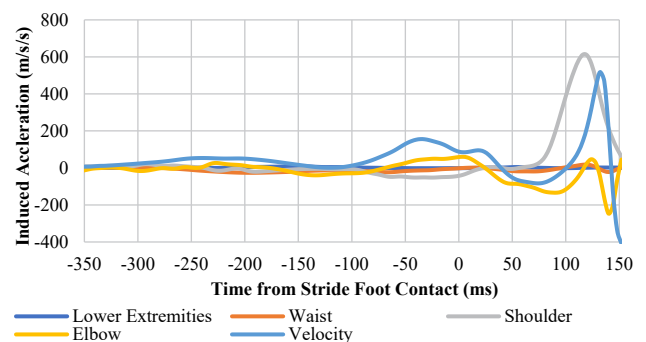


Figure 1: IAA components of a representative fastball pitch

Conclusions

These findings provide evidence to support the notion that the dynamic coupling effects of segmental motion are the primary contributors to the energy and velocity of the throwing arm.

Acknowledgments

The authors thank Tom Kepple of C-Motion for the development of the IAA plug-in and technical contributions.

References

- [1] Aguinaldo, A.L., et al., (2020). *Sports Biomechanics*, 1-7.
- [2] Alderink, G., et al., (2008). *Proceedings of the American Society of Biomechanics Meeting*, 5-6.
- [3] Naito, K., et al., (2011). *Sports Technology*, 4(1-2), 37.
- [4] Hirashima, M., et al., (2008). *Journal of Biomechanics*, 41(13), 2874-2883.

Center of Mass Vertical Velocity in Short Misses in the Basketball Shot

Casey Wiens¹, Jill L. McNitt-Gray^{1,2}

Departments of ¹Biological Sciences and ²Biomedical Engineering, University of Southern California, Los Angeles, CA, USA
Email: cwiens@usc.edu

Summary

When shooting a basketball, the body's center of mass velocity and the velocity generated by the arms determine the ball's velocity at release and, subsequently, the ball's flight trajectory. Misses short of the hoop are thought to be due to low body center of mass vertical velocity, which is regulated in part by the net vertical impulse generated during the ground contact. We hypothesized that short misses occur when the body's center of mass vertical velocity at release is lower than normal due to less net vertical impulse generated during ground contact. The results indicate less net vertical impulse generated during ground contact and longer time in the air before release contributed to low body center of mass vertical velocity in short misses. Identifying the cause of missed shot attempts for individual players is expected to provide meaningful insights when providing feedback and designing individualized training programs to improve accuracy.

Introduction

During a basketball shot, the ball velocity, angle, and distance to the rim at release determine the ball's trajectory. Ball velocity at release is influenced by the body's center of mass velocity – generated during the ground contact duration before release and altered by any time in the air before release – and the velocity generated by the arms [1]. A recent study indicated that the contribution of the body's center of mass vertical velocity (CM Vv) to the ball vertical velocity at release depends on the time of ball release relative to the body CM trajectory's apex during the shot [2]. When a player misses a shot short of the rim (short miss), coaches have suggested a lack of force generated during ground contact as a potential cause [3]. In this study, we hypothesized that lower CM Vv at release occurs in short misses compared to the successful shots made by the same player and that lower CM Vv at release was a result of less net vertical impulse generated during ground contact in the short misses compared to the successful shots made by the same player.

Methods

Seven recreational basketball players (4 female, university club and recreational leagues players) provided informed consent in accordance with the institutional review board for human subjects. Each participant attempted a minimum of 10 shots from 4.57 m (free throw line) and 6.02 m (American high school three-point line) distances.

Two portable force plates measured ground reaction forces (Kistler, 1200Hz) generated by each leg. The duration between ground departure and ball release defined time in the air before release. The CM Vv at ball release was calculated using net vertical impulse generated from shot initiation to ground departure and the time in the air before release.

Successful shots entered without touching the rim or touched the inside of the rim. Short misses were shots aligned with the rim but fell short of the rim.

Lower than normal CM Vv at ball release and net vertical impulse generated were magnitudes below the lower quartile (less than 75%) of all successful shots performed by the same player. Longer than normal time in the air before release were magnitudes above the upper quartile (more than 75%) of all successful shots performed by the same player.

Results and Discussion

Overall, 12 of the 118 shots analyzed were considered short misses. CM Vv at release was in the lower quartile in five of the 12 short misses: two from lower net vertical impulse generation and four from longer time in the air before release (Figure 1). Differences in CM Vv at release between successful and short shots at the same distance resulted from differences in net vertical impulse generated by the player during ground contact and time in the air before release (Figure 1). The greater the net vertical impulse generated, the greater the CM Vv available at ground departure. The longer the time in the air before release, the greater the reduction in the available CM Vv before release.

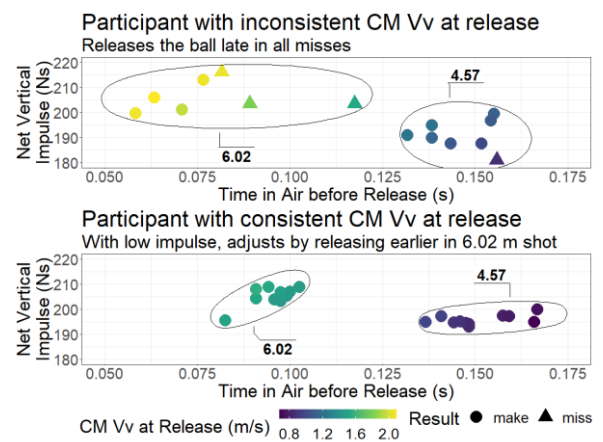


Figure 1. CM Vv at release, net vertical impulse, and time in air before release for two participants in shots from two distances.

Conclusions

A lower CM Vv – resulting from lower net vertical impulse generated during contact and longer time in the air before release – occurred in less than half of the shots that missed short of the rim. Short miss tendencies varied between players.

References

- [1] Hay JG. (1985). *Biomechanics Sport Tech*; Prentice-Hall.
- [2] Wiens C., McNitt-Gray JL. (2020) *ISBS*.
- [3] Filippi, A. (2011) *Shoot Like the Pros*; Triumph.

Correlation Between the Kinematic Analysis and the Field testing on the Efficiency of the Forehand Throwing on Ultimate Frisbee.

Salcedo E¹, Aedo E², Argothy R.¹⁻³

¹ Master of Physiotherapy in Sports and Physical Activity - Medicine School Facultad de Medicina National University of Colombia

² Biomechanics Laboratory - Applied Sports Science Unit (UCAD) - Ministry of Sports - Chile

³ Physical Culture Research Center (CICFI) - Military School of Cadetes - Bogotá Colombia

Email: reargothyb@gmail.com

Summary: the objective of this study is to evaluate the association between the systematic analyses of the forehand vs the field test of the throwing of the Frisbee. 15 athletes are evaluated (9 men's and 6 woman's) (age: 23 +- 4 years, weight 65.7 +- 12.3 kg) of a team of ultimate of high level that competes at national level. We realize a 3D analysis (qualisys System) and we place skin markers on the scapular waist, arms and core. The field test is performed with 20 throws of the Frisbee at 30 and 40 meters. It was found significant correlations between the throwing of the 30 mts, the angular speed of the acromion ($p = 0.028$) and the core inclination ($p = 0.028$). It was identified the importance of the bending angle of the elbow (average of $117^\circ \pm 15.2$, ($p = 0.044$)) on the distance of throwing. It is identified the systematic parameters that determine the effective sport gesture for the throwing at 30 and 40 meters

Introduction: On the ultimate Frisbee, perform throwing's with big distances is a competitive advantage to accumulate points in an efficient way, it's considered the speed of the throwing as a determinate variable to achieve greater distances of the disc. However the position that the athletes take is determinant to perform the sport gesture in a harmonic way and with a good energy transfer between the muscular segments that helps to prevent sport lesions and mechanic alteration that modify the sport performance. For this fields test are performed that allows to measure the efficiency of the throwing's. However, since it is a mix game, where men's and women's participate, several of the gestures performed are adopted to the texture and physical capacity and the accommodations that are learned on the course of the sport life. The objective of the present study is to determine the associations that exist between the field test (throwing of ultimate Frisbee) vs the Systematic analysis of the upper body and the core.

Methods: 15 athletes were participating, 9 man's, 6 woman's (Age: 23+- 4 old, weight: 65.7+- 12.3 kg) that are members of a team of ultimate that competes at national level. All the athletes has the right side as dominant hemibody. Two test were performed. 1) Tridimensional systematic analysis

through a 3D capture system (qualisys system), passive markers were placed on the right and left acromion, spinous apophysis of C7 and T10. Right epicondyles of the hummers and bilateral radial styloid process. The systematic variables were: angular speed of the acromion (left acromion – right acromion) bending angle of the upper body on the in coronal plane (C7 – T10) bending and extension angle of the elbow (acromion-lateral hummers epicondyle- radial styloid process) 2) technique test of the throwing and catching of the Frisbee at 30 and 40 meters. 20 throwing's are performed at each distance and is being qualified the amount of hits that has to get to the established point. A statistical analysis is performed through SPSS (v25) through the test of Pearson.

Results and discussion: Significant correlations are being observed about the throwing at 30 meters vs the angular speed of the acromion ($p = 0.028$) and core inclination on the coronal field ($p = 0.028$) and the elbow bending (average bending $117^\circ \pm 15.2$, ($p = 0.044$)). However, on the 40 meters only on the elbow bending significant correlations were observed. Like the angular speed on the shoulders that increases the speed of spin on the ultimate players (Sasakawa and cols (2017)),

Conclusion: And the sport gesture of the ultimate is related with a mayor angular speed of the acromion and the bending of the core, helps to the 30 meters throwing; perform a elbow bending close to 117° ensures accurate sport gesture on the throwings at 30 and 40 meters

References

- Zhang Z, et al. The Influence of X-Factor and Experience on the Quality of the Badminton Forehand Smash. *J Hum Kinet.* 2016
- Sasakawa K et al (2017): Biomechanics of increased spin velocity of flying discs during forehand throws by skilled and unskilled throwers, *Journal of Sports Sciences.*
- Sasakawa, K et al (2008). Biomechanical analysis of the sidearm throwing motion for distance of a flying disc: A comparison of skilled and unskilled Ultimate players. *Sports Biomechanics.*

Biomechanics of the landing for double salto backward stretched in the horizontal bar

Franklin de Camargo-Junior^{1,2}, Marko Ackermann³, Arturo Forner-Cordero², Luciano L. Menegaldo⁴, Luis Mochizuki¹, Júlio C. Serrão¹, Alberto C. Amadio¹

¹Biomechanics Laboratory, School of Physical Education and Sport, University of São Paulo, São Paulo, Brazil

²Biomechatronics Laboratory, Polytechnic School, University of São Paulo, São Paulo, Brazil

³University Center FEI, São Bernardo do Campo, Brazil

⁴COPPE, Biomedical Engineering, Federal University of Rio de Janeiro, Rio de Janeiro, Brazil

Email: fcamargo-junior@alumni.usp.br

Summary

The landing on the dismount of an apparatus in artistic gymnastics is one of the most challenging skills in this sport. This work investigates the determinant factors to spiked landing.

Introduction

In artistic gymnastics, a failure in the landing can take chances of podium in championships [1]. In order to reduce the chance of errors, dismounts are performed repeatedly during training sessions. The side effect of this practice is the increased exposure to the risk of musculoskeletal injury by mechanical overload or trauma [2,3]. The aim of this study was to clarify the determining biomechanical factors for optimal landing in artistic gymnastics (i.e., no step needed to achieve a rest state after contact with the ground).

Methods

An analytical interpretation model was proposed for the biomechanical factors governing the landing, based on an inverted pendulum system in which the gymnast was represented by the segment connecting the ankle joint center to the body center of mass (ank-CM) at the instant of collision. Selected by sampling (7 national elite gymnasts with international ranking) and methodological convenience (modeling and experimental), the dynamics of the horizontal bar dismount in double salto backward stretched (DSBS) was characterized. The Principal Component Analysis (PCA) was adopted to measure the predictive potential of the state variables defined by the biomechanical model for discriminating the success and failure conditions. Finally, a set of successful configurations was interpreted.

Results and Discussion

An almost absolute ability to discriminate between conditions (91% of cases) in the cumulative three axes of variability was revealed by the PCA. The combinations of angular momentum, angular position, angular velocity of the body and horizontal and vertical velocities of the CM were

considered sufficient to establish the ideal conditions for the DSBS in the pre-collision ().

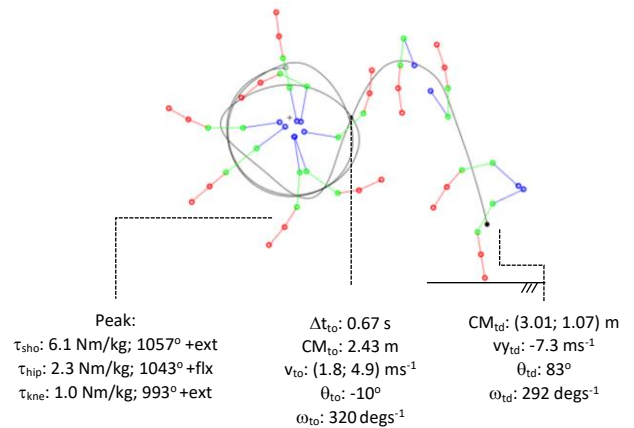


Figure 1: Biomechanical profile of the DSBS dismount.

Conclusions

The analytical model demonstrated a high sensibility for landing body angle, in which variations greater than 7 degrees make the landing in resting conditions unlikely, and a significant influence of angular momentum, angular velocity and linear velocity for the DSBD landing in the horizontal bar routine.

Acknowledgments

Acknowledgments to the Brazilian Olympic Committee, Brazilian Gymnastics Confederation and Artistic Gymnastics Center of São Caetano do Sul / Brazil.

References

- [1] Fédération Internationale de Gymnastique (2017). *Code of Points / MAG*.
- [2] Bruggemann, G-P. (2005). *International Society of Biomechanics in Sports Conference*, 16-24.
- [3] Gittoes, MJR; Irwin, G. (2012). *Sports Medicine, Arthroscopy, Rehabilitation, Therapy and Technology*, 4(1): 1-9.

Table 1: Summary of success determining factors for landing of DSBS.

	v_x	v_y	θ	ω	H_o
inferior limit	1.50	-7.42	81.63	261.89	-59.67 [#]
superior limit	1.80	-7.06	83.53	310.31	-46.91 [#]

Subtitle: (v_x and v_y) horizontal and vertical velocities, (θ) body angle, (ω) angular velocity and (H_o) angular momentum; (#) offset $H_o \rightarrow 0^+$.

Characterizing Tibial Accelerations and Exposure in Collegiate Basketball Players During Games and Practices

Jereme Outerleys^{1,2}, Mary Boussein^{2,3}, Miriam Bredella^{2,3}, Adam Tenforde^{1,2}, Thor Besier⁴, Irene Davis^{2,1}

¹Spaulding National Running Center, Spaulding Rehabilitation Hospital, Cambridge, USA ²Harvard Medical School, Boston, USA, ³Massachusetts General Hospital, Boston, USA ⁴University Of Auckland, Auckland, NZ

Email: jouterleys@bwh.harvard.edu

Summary

Musculoskeletal injury in sport result from acute high magnitude loads or cumulative exposure without adequate recovery. Monitoring loading during high impact sports such as basketball may help to identify risk for injury. Wearable sensors allow for the measurement of impacts in real-world game play and training. Practices result in the greatest exposure to impact events but at lower magnitudes compared to games. Cumulative exposure is increased for higher minute per game players which may result in increased risk for injury.

Introduction

Basketball is characterized by maneuvers such as jumping, cutting, and running that result in varying intensities of impact loads to the lower limbs. High magnitude loads and cumulative exposure throughout the season may increase risk of bone stress injury. Few studies have captured impact loads during live game play or longitudinally. The purpose of this study was to characterize the intensity and cumulative exposure of tibial accelerations in basketball players during games and practices.

Methods

One division III men's college basketball team, consisting of 17 players (mean (SD): height= 1.84 (0.07) m, weight = 82.1 (8.5) kg, age = 20 (2) years), were recruited for this study. All participants provided informed consent prior to the 2019-2020 season. Triaxial accelerations were collected throughout the regular season during games and practices using inertial measurement units (Blue Trident, IMeasureU, Auckland, NZ; 1600 Hz, +/- 200 g). IMUs were taped bilaterally to the distal antero-medial tibia by athletic training staff. Session footnotes were created to identify the beginning and end of games and practices. Data were uploaded to a web-based dashboard for step identification using a proprietary algorithm. The peak resultant tibial acceleration was identified for each step. Data were subsequently downloaded for further processing.

Total steps and the proportion of steps categorized as Low (<8g), Medium (8-25g), and High (>25g) accelerations were calculated for all sessions for each leg. Cumulative load (CL) was calculated as the cumulative sum of each step multiplied by its acceleration magnitude. Cumulative bone stimulus was

also calculated to incorporate the relative importance of the impact load magnitude to the number of load cycles [1].

All metrics were averaged between sides and then across players for practices and games, separately. Game and practice data were separated based on average minutes played per game. A high minutes (HM) group played > 10 mins. per game and a low minutes (LM) group played < 10 mins. Comparisons were made qualitatively between the HM and LM groups using median and interquartile ranges.

Results and Discussion

A total of 29 sessions were collected consisting of 9 games and 20 practices. A median of 6 games and 17 practices were collected per player. Practices had more steps and higher cumulative load than games in both HM and LM groups (Table 1). During games, the HM players had a 15% lower proportion of Low impacts compared to LM group. This reduction was accompanied by a 6-7% increase in High and Medium impacts. High variation in exposure and accumulation of impacts was evident between players due to minutes per game. Practices account for the majority of steps and cumulative exposure to impact accelerations throughout a basketball season. For players that play high minutes per game, however, cumulative bone stimulus was similar between games and practices. While more minutes per game results in more steps, the increased bone stimulus was due to an increased proportion of higher magnitude impacts during higher intensity game play.

Conclusions

Impact magnitudes and exposure during basketball are highly dependent on session type (practice vs game) and minutes per game. Higher impacts during increased game play may result in increased risk for injury.

Acknowledgments

Funding for this work was provided by the National Basketball Association and General Electric.

References

- [1] Beaupré et al. (1990). *J Orthop Res.*, 5: 662-70.

Table 1: Summary of Minutes played, Total steps, Proportion of total steps binned as Low, Medium and High Acceleration, Cumulative Load and Bone Stimulus during games and practices. Data presented as median (IQR). *Minutes played for games or session duration for practices.

Group (N)	Mins. Played*	Total Steps	Low Prop.	Med. Prop.	High Prop.	Cumulative Load	Bone Stimulus
HM Game (6)	22 (10)	4284 (1522)	0.49 (0.03)	0.33 (0.03)	0.15 (0.06)	28284.7 (6005.2)	261.9 (34.1)
LM Game (11)	4 (3)	1053 (522)	0.65 (0.11)	0.23 (0.08)	0.08 (0.01)	7145.7 (2877.1)	166.0 (41.1)
HM Practice (6)	122 (4)	8295 (1448)	0.64 (0.03)	0.27 (0.04)	0.08 (0.03)	40113.8 (8580.0)	257.8 (40.2)
LM Practice (11)	129 (6)	8544 (1405)	0.69 (0.05)	0.25 (0.04)	0.06 (0.02)	35795.3 (6515.5)	242.4 (76.6)

Role of Each Leg in Generating Linear and Angular Impulse in Baseball Pitching

Jun M Liu¹, Christopher Knowlton², Matthew Gauthier^{2,3}, Zach Tropp³, Antonia Zaferiou¹

¹ Musculoskeletal Control and Dynamics Lab, Dept. Biomedical Engineering, Stevens Institute of Technology, Hoboken, NJ, USA

² Rush University Medical Center, Chicago, IL, USA

³ Athletico Physical Therapy, Chicago, IL, USA

Email: jliu130@stevens.edu

Summary

We examined the roles of each leg in generating linear and angular impulse in pitching fastballs performed by professional pitchers. As previously reported, before ball release, the back leg generated forward linear impulse, while the front leg generated backwards linear impulse. Surprisingly, the back leg generated more forward angular impulse than did the front leg. This newly uncovered role of the back leg towards forward angular momentum can assist future training approaches.

Introduction

Ground reaction force (GRF) impulse can provide more information about the profile of the force-time curve and how the pitching action is performed than peak GRF alone [1]. Using energy flow analysis in young pitchers, it was reported that the back leg transfers linear power and the front leg generates rotational power [2]. This study compared the roles of each leg by studying the linear and angular impulse generated by the control of the GRF and moment about total body center of mass (TBCM).

Methods

Professional pitchers (n=4) volunteered for the study in accordance with the IRB. They pitched six to eleven fastballs from the stretch position on an instrumented mound while kinematic and kinetic data were collected (Bertec 1000/1080 Hz, Optitrack 250/360 fps). We excluded pitching trials that were rated unrepresentative/poor by the pitchers. The data were processed in MATLAB (Mathworks). The variables of interest were “X GRF”, the forward directed GRF, and “My”, the moment applied about the Y-axis passing through the TBCM (forward rotating moment) (Figure 1). These two variables were integrated to find the X Linear Impulse and Y Angular Impulse, respectively, for each leg and both legs (net) from the beginning of the push phase until ball release. The push phase began the last time Z GRF decreased before increasing to its peak. Within subject, paired T-tests were used to compare the impulse generated by each leg ($\alpha=0.05$).

Results and Discussion

The back leg generated positive X Linear Impulse, and the front leg generated negative X Linear Impulse, resulting in a net positive X Linear Impulse before ball release (Figure 2A). This led to forward momentum of the body. Both legs generated positive Y Angular Impulse, which led to forward rotation of the body towards accelerating the ball (Figure 2B). Surprisingly, the back leg generated more positive Y Angular Impulse than the front leg did.

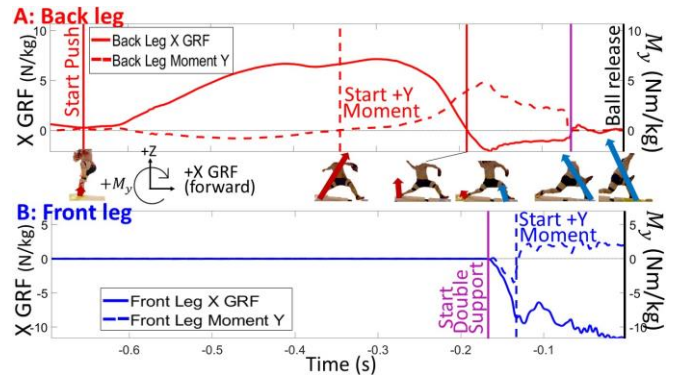


Figure 1: Exemplar X GRF and Moment about the Y-axis (My) vs. time applied by the (A) back and (B) front legs (Subject 2).

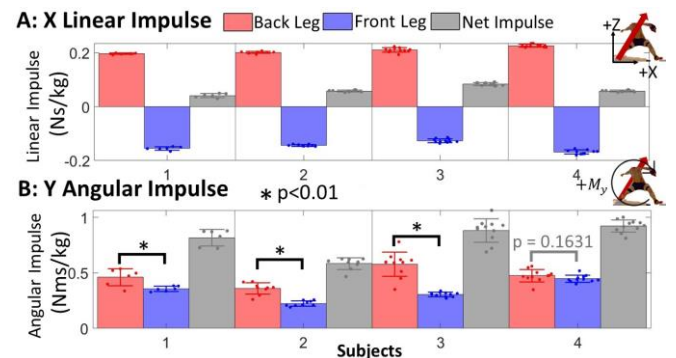


Figure 2: (A) X Linear Impulse and (B) Y Angular Impulse (B) for the back (red), front (blue), and net impulse (gray) during fastballs.

We found that the role of the back leg transitioned from linear propulsion to forward angular rotation before double support. We also found that the front leg initially generated negative Y Angular Impulse, slowing the forward rotation. To maximize forward rotation, it may be helpful to increase the back leg’s contribution to rotation and reduce the front leg’s negative Y Angular Impulse. Our future research will enroll more pitchers to better understand the role of each leg towards linear and angular momentum control.

Conclusions

This study uncovered the role of the back leg not only in linear propulsion, but also in generating more forward angular impulse than the front leg. Maximizing forward angular impulse may contribute to increased pitching performance.

Acknowledgements

This study is funded by Major League Baseball.

References

- [1] McNally MP et al (2015). *J. Strength Cond.Res.*, **29**(10)
- [2] Howenstein J et al (2020). *J. Biomechanics*, **108**

Clinical tests can predict trunk control during unilateral landings

Karine J.V. Stoelben^{1,2}, Evangelos Pappas³, Felipe P. Carpes^{1,2}

¹Applied Neuromechanics Research Group, Federal University of Pampa, Uruguaiiana, Brazil

²Programa de Pós-Graduação Multicêntrico em Ciências Fisiológicas, Federal University of Pampa, Uruguaiiana, Brazil

³The University of Sydney, Faculty of Medicine and Health, Sydney, NSW, Australia

Email: karinestaelben@gmail.com

Summary

Landing from a jump is associated with lower extremity injuries such as ACL ruptures. Clinical tests are commonly employed to detect altered movements that may be related to the risk for this injury. Here, we investigate the potential of clinical tests to predict trunk control during landing tasks. Knee and hip strength are the most important clinical outcomes related to trunk control during unilateral landings.

Introduction

Poor trunk control is a risk factor for ACL injury [1] and a frequent component of the mechanism of injury [2]. Evaluation and monitoring of this risk factor typically require expensive, time-consuming and complex laboratory tests. Sometimes biomechaical risk factors can be estimated by clinical tests more accessible to monitor athletes in the field [3]. However, the relationship between clinical tests and trunk control during drop landing has not been adequately investigated. Here we determine whether clinical tests can predict trunk biomechanics during the performance of unilateral landing tasks.

Methods

The local institutional ethics committee approved this study. Forty-seven recreational athletes (24±3 years old, 80±13 kg of body mass, 177±6 cm of height) completed a battery of clinical tests, and 3D kinematics assessment of unilateral drop jump tasks. Clinical tests were the Lunge, lateral step down, single, triple, and crossover hop tests, star excursion balance test (SEBT), knee flexor and extensor strength, and hip abductor and adductor strength (hand-held dynamometer). 3D kinetics and kinematics were sampled at 2000Hz and 200 Hz, respectively, during the landings. Trunk angles were determined at initial contact (threshold of 20N) and maximal knee flexion of the landing phase. Stepwise multiple regression analyses were performed for each dependent variable when $p \leq 0.20$ (Pearson's or Spearman's tests). Global effect size (f^2) was computed with interpretation: small to ≥ 0.02 , medium to ≥ 0.15 , and large to ≥ 0.35 .

Results and Discussion

The clinical tests predicted trunk sagittal angles for landing on the preferred and non-preferred legs (Figure 1, low to high effect sizes) and trunk frontal angles for the preferred leg (Figure 2, moderate to large effect sizes). Knee strength was the most important predictor of sagittal angles for both legs. For the frontal plane angles, hip abductor's strength had an important role.

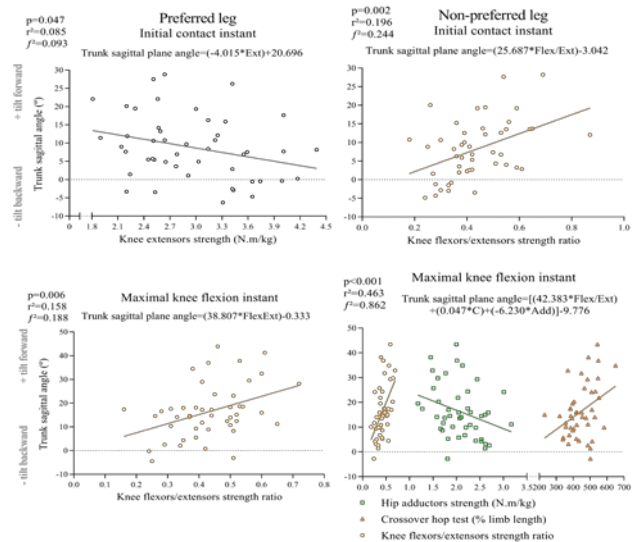


Figure 1: Trunk sagittal plane angles predicted by clinical outcomes.

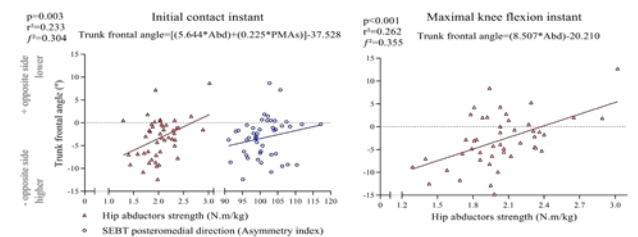


Figure 2: Trunk frontal plane angles predicted by clinical outcomes.

Trunk control during unilateral landings is associated with strength measures. This finding may have important clinical implications.

Conclusions

Trunk control during landing can be predicted by clinical tests. Knee and hip strength are the strongest clinical predictors of trunk control.

Acknowledgments

Conselho Nacional de Desenvolvimento Científico e Tecnológico for funding this research.

References

- [1] Hewett TE et al. (2010). *North Am J Sports Phys Ther*, **5**: 234-251.
- [2] Della Villa F et al. (2020). *Br J Sports Med*, **0**: 1-10.
- [3] Webster KE and Hewett TE (2019). *Sports Med*, **49**: 917-929.

Hip Range of Motion and Pitching Biomechanics in Adolescent Baseball Pitchers

Maxwell L Albiero, Wesley Kokott, DPT, Cody Dziuk, Janelle A Cross, PhD
 Department of Orthopaedic Surgery, Medical College of Wisconsin, Milwaukee, WI, USA
 Email: malbiero@mcw.edu

Summary

This study examined the relationship between an athlete's hip active range of motion (AROM) and pitching biomechanics. Clinical measurements of hip flexibility and pitching mechanics were recorded. Several significant correlations were discovered between AROM and biomechanical variables. These findings support the influence hip AROM has on pitching biomechanics and suggest greater movement at the hips allows for the kinematic chain to work at its maximal efficiency, increasing pitch velocity potential and decreasing risk for injury.

Introduction

Baseball pitching is a dynamic task that requires the use of the entire body as a kinematic chain to create upper extremity forces in the throwing arm which are used to release a high velocity pitch. These forces can lead to injury. Previous research has demonstrated the chain begins in the lower extremities and transitions to the upper extremity [1]. Insufficient hip range of motion (ROM) can arrest the throwing mechanics, thereby reducing energy transfer between the lower and upper extremities [2]. A pitcher who is able to more efficiently transfer energy up the chain will create greater forces in the upper extremity resulting in potential for greater ball velocity. However, a lack of proper throwing mechanics can result in these increased forces surpassing a physiologic threshold of the shoulder and elbow joints, creating injury [3]. The purpose of our study was to identify correlations between clinical hip active range of motion (AROM) measurements and pitching biomechanics.

Methods

Twenty-one adolescent male baseball pitchers (16.1 ± 0.8 years, 77.9 ± 8.3 kg, 183.9 ± 5.2 cm) from a competitive youth baseball program lacking a history of arm pain or throwing injury participated in this study. A certified physical therapist collected hip AROM measurements via a standardized protocol. A system of 8 Raptor-E cameras (Motion Analysis Corporation, Santa Rosa, CA) were positioned around an artificial mound to capture subjects pitching at 300 Hz. Forty-seven reflective markers were attached to subjects on anatomical landmarks and ten fastball pitches were recorded being thrown into a strike zone net positioned at a regulation distance of 18.4 m from the pitching rubber. The three fastest strikes were analyzed. Marker data was identified then filtered using a 13.4 Hz fourth-order Butterworth low-pass filter in Cortex software (Motion Analysis Corporation, Santa Rosa, CA). Biomechanics were calculated using Visual 3D software (C-Motion, Germantown, MD). SPSS statistical analysis

software (version 26, IBM Corporation, Armonk, NY) was used for data analysis with a significance level of $p < 0.05$.

Results and Discussion

Significant negative correlations were found at foot contact between torso rotation angle and back hip external rotation (ER) AROM, back hip abduction angle and back hip ER AROM, and lead hip abduction angle and back hip abduction AROM (Table 1). Stride length was positively correlated back hip extension AROM. Normalized elbow varus torque (EVT) was positively correlated with lead hip abduction AROM. Stride length and EVT are two commonly investigated variables in pitching biomechanics research. The results from this study demonstrate the impact hip AROM has on both of these, providing a greater understanding of the mechanics effecting these variables. The results also suggest back hip extension may be more vital than back hip abduction in generating a greater stride length due to the transition of the plane of motion seen in the back hip during the pitching motion.

Table 1: Significant correlations between pitching biomechanics and hip active range of motion

Kinematics at Foot Contact	r	p-value
Stride length and back hip extension AROM	.446	0.043*
Torso rotation angle and back hip ER AROM	-.468	0.032*
Back hip abduction angle and back hip ER AROM	-.474	0.030*
Lead hip abduction angle and back hip abduction AROM	-.458	0.037*
Kinetics		
Normalized elbow varus torque and lead hip abduction AROM	.435	0.049*

* Correlation significant at 0.05 level

Conclusions

Hip AROM has an important influence on pitching biomechanics, and flexibility should be evaluated when training to gain insight on a pitcher's mechanics and injury risk potential.

Acknowledgments

This study was funded by the Medical College of Wisconsin Department of Orthopaedic Surgery.

References

- [1] Aguinaldo A, et al. (2019). *Orthop J Sports Med*, 7: no. 2.
- [2] Laudner K, et al. (2010). *Am J Sports Med*, 38: 383-387.
- [3] Bushnell B, et al. (2010). *Am J Sports Med*, 38: 728-832.

Sagittal Plane Kinematics of Partnered and Individual Triple Steps in Swing Dancing

Meredith D. Wells¹, Feng Yang¹

¹Department of Kinesiology and Health, Georgia State University, Atlanta, GA, USA

Email: mwells19@student.gsu.edu

Summary

Despite its increasing popularity, swing dancing has not been thoroughly studied biomechanically, imposing challenges in understanding the movement patterns associated with swing dancing. The purpose of this study was to analyze the kinematics of the triple step to better understand the movement patterns related to swing dance.

Introduction

Swing dancing today refers to a cluster of dances developed between the 1920s and 1940s to the swing style of music [1]. Swing dancing remains popular today and continues to draw individuals to it with its lively music and social atmosphere [2]. Yet, there is limited research on the kinematics of the swing movements which restricts our ability to understand the demands placed on the body. Although swing dancing is generally performed with a partner, dancing individually also occurs. Therefore, it is of interest to check if the biomechanics differ between individual and partnered conditions.

The purpose of this initial study was to quantify the kinematics of the triple step (one of the most common swing dance elements) in the sagittal plane among recreational swing dancers while dancing individually and with a partner. It was hypothesized that few significant differences in the lower extremity joint positions would be seen between partnered and individual dance conditions.

Methods

Eight recreational swing dancers who completed at least 50 sessions of swing dancing in the prior year (age: 30.9 ± 4.7 years; height: 1.73 ± 0.07 m; mass: 73.6 ± 13.1 kg; swing dancing experience: 4.1 ± 3.1 years) participated in this study.

Participants completed a 5-minute dance warm-up, and then performed a triple step to the right individually (TSR) and with a partner (TSRP) in a random order. Three trials were collected for each. The triple step involves taking a small step to the side with one foot, bringing the second foot to meet the first, and then taking a larger step to the side with the first foot. Participants performed the dance element on vinyl flooring, to mimic a dance floor, wearing standardized socks.

Three-dimensional lower extremity kinematics were collected via 16 reflective markers using an 8-camera motion capture

system (Vicon, UK). Marker paths were low-pass filtered, and joint centers were calculated from the filtered marker paths and measured anthropometric parameters [3]. Joint angles at the ankle and knee during stance of each of the three steps within the triple step were calculated based on joint center data using inverse kinematics and were compared between dance conditions using paired *t*-tests. The significance level was set as 0.05.

Results and Discussion

Results from the *t*-test supported our hypothesis, indicating minimal significant differences between dance conditions in the triple step. Differences that were seen at the ankle include: greater peak dorsiflexion (DF) during the stance phase of the first ($p = 0.025$) and third ($p = 0.031$) steps of the TSR individually compared to partnered. Differences observed at the knee include: greater peak flexion during stance of the first ($p = 0.009$) and third ($p = 0.013$) steps of the TSR individually compared to partnered, and greater peak flexion at initial contact during the first ($p = 0.007$) and third ($p = 0.013$) steps of the TSR individually compared to partnered (Table 1).

These findings indicate that recreational swing dancers may move through a greater range of motion when practicing individually. The change in movement pattern when dancing with a partner may be due to the requirement to continuously match the partner's movements, requiring the dancers to be more careful when dancing with a partner to avoid hitting or stepping on them while dancing.

Conclusions

Results from this study illustrate that there are a few kinematic differences between dancing with and without a partner that need to be considered when planning training and performances. This also needs to be considered when analyzing the dance motion of individuals involved in partnered dances. However, further research with larger sample sizes is required in order to better understand the biomechanics of swing dancing.

References

- [1] Spring H. (1997). *American Music*, **15**: 183-207.
- [2] Fuller J. (2019) *Swing History*; CentralHome.com.
- [3] Pai YC, et al. (2006). *J of Biomech*, **39**: 2194-2204.

Table 1: Peak ankle and knee flexion angles of each step during the triple step to the right individually (TSR) and partnered (TSRP).

Step # & Limb	Max Ankle DF Angle		Max Knee Flexion Angle		Knee Flexion Angle @ IC	
	TSR	TSRP	TSR	TSRP	TSR	TSRP
1 (R)	16.85 ± 5.75	14.68 ± 3.18	40.38 ± 11.77	30.01 ± 11.14	39.56 ± 12.67	28.77 ± 11.86
2 (L)	22.64 ± 6.78	19.59 ± 7.21	35.00 ± 11.35	34.93 ± 10.16	24.97 ± 9.39	24.12 ± 10.65
3 (R)	14.03 ± 4.17	11.01 ± 3.78	32.53 ± 8.56	28.55 ± 10.34	32.29 ± 8.69	28.42 ± 10.45

Effects of dissociation on muscle activation and torque during stationary cycling

Milena A. dos Santos¹, Felipe P. Carpes²

Applied Neuromechanics Research Group, Laboratory of Neuromechanics, Federal University of Pampa, Uruguaiana, RS, Brazil
Email: milena.aguiar2008@hotmail.com

Summary

To listen to music while exercising indoors can have a dissociation effect on rate of perceived effort (RPE), but its effects on neuromuscular responses are not clear. Here we compared muscle activation and torque output between sessions of indoor cycling while listening or not to music as a dissociation stimulus. We found that exercise and music combined increased RPE, submaximal heart rate, and pedaling cadence, without effects on muscle activation and torque.

Introduction

Physical exercise can improve cognitive and physical capacities [1,2]. It has been found that dissociation between internal and external focus can influence exercise intensity, heart rate, effort perception, motivation, and pleasure [3]. Additionally, the attentional focus oscillation while listening to music can be a source of distraction [4]. Here we determine whether the music combined to the physical exercise affects neuromuscular activation and torques during cycling.

Methods

Thirteen health adults, healthy and physically active (6 women and 7 man) visited the laboratory for three times. The first was to determine the maximal power output using a LODE cycle ergometer. The second and third were to complete submaximal cycling trials at 50% of the maximal output. In the submaximal trials the participants listened or not to their preferred music songs in a range of 120-150 beats per minute, using earphones. RPE was quantified every 5 min (6-20 Borg Scale), while heart rate (Polar heart monitor), neuromuscular activation (sampled at 1.5 kHz using DTS Noraxon Inc.), and pedaling torque and cadence (measured every 2° with Lode Excalibur) were continuously recorded. Main effects and interactions considering the music condition (music vs no music) and the exercise time (start, middle, end) were verified using a general linear model ANOVA for repeated measures. Paired comparisons were performed by a dependent t-test or Wilcoxon test.

Results and Discussion

The music session elicited higher RPE ($p=0.003$, figure 1), heart rate ($p=0.04$) and pedaling cadence ($p=0.04$, figure 1). Main effects were not found for torque. No music effects were found for RMS and median frequency of the electromyographical signals, despite of a behavior indicating muscle fatigue (RMS increasing, median frequency decreasing along the exercise) for both the submaximal conditions. The higher pedaling cadence may suggest that an involuntary attempt to synchronize the music and the movement frequencies [5]. It may have affected the internal

load resultant of exercise (due to the higher RPE), without increasing exercise duration or external load.

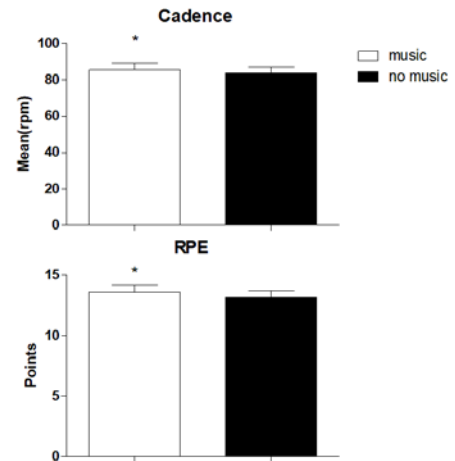


Figure 1. Cadence and RPE in the music and no music sessions. * $p<0.005$

Conclusions

Listening to preferred music during indoor cycling can be a strategy to increase internal load, especially cardiovascular demands, without increasing external load as quantified by muscle activation and torque output.

Acknowledgments

MAS is supported by Fundação de Amparo à Pesquisa do Estado do Rio Grande do Sul (FAPERGS, Brazil). FPC is funded by the Conselho Nacional de Desenvolvimento Científico e Tecnológico (CNPq-Brazil). Authors are grateful to Carlos De la Fuente for his technical support and the UFRGS for the loan of the LODE cycle ergometer.

References

- [1] Rueggsegger GN, Booth FW. (2018) *Cold Spring Harb Perspect Med.*;8(7).
- [2] Gaertner B, Buttery AK, Finger JD, Wolfsgruber S, Wagner M, Busch MA. (2018) *J Sci Med Sport.* 21(5):489–94.
- [3] Hutchinson JC, Karageorghis CI, Jones L. (2015) *Ann Behav Med.*;49(2):199–211.
- [4] Ekkekakis P, Parfitt G, Petruzzello SJ. (2011). *Sport Med.*;41(8):641–71.
- [5] di Fronso S, Tamburro G, Robazza C, Bortoli L, Comani S, Bertollo M. (2018) *Front Psychol.*;9(JUL).



CLINICAL ESTIMATION OF MOVEMENT BEHAVIOR PREDICTIVE OF GROUND REACTION FORCES DURING ATHLETIC TASKS



RACHEL K. STRAUB,¹ ALEX HORGAN,² ADAM J. BARRACK,¹ FRANKLIN ZHUANG,¹ RUBEN CUELLAR,¹ CHRISTOPHER M. POWERS¹

¹JACQUELIN PERRY MUSCULOSKELETAL BIOMECHANICS RESEARCH LABORATORY

DIVISION OF BIOMEDICAL & PHYSICAL THERAPY, UNIVERSITY OF SOUTHERN CALIFORNIA, LOS ANGELES, CA, USA

²TRINITY COLLEGE, DISCIPLINE OF PHYSIOTHERAPY, SCHOOL OF MEDICINE, DUBLIN, IRELAND

BACKGROUND

Given that elevated vertical ground reaction forces (vGRF) have been reported to contribute to various lower-extremity injuries,^[1,2] there is a need for a practical method to characterize movement behavior that is representative of elevated impact forces.

PURPOSE

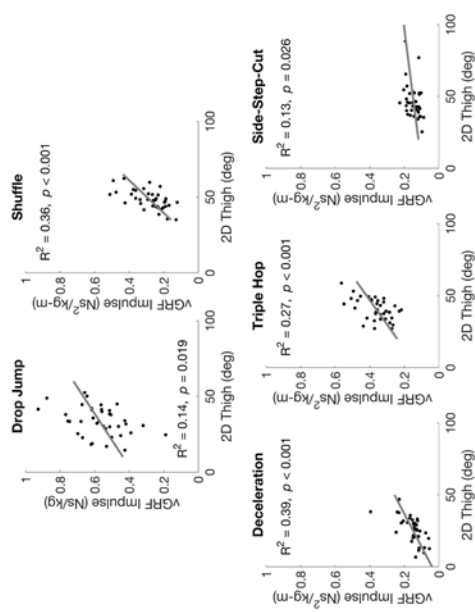
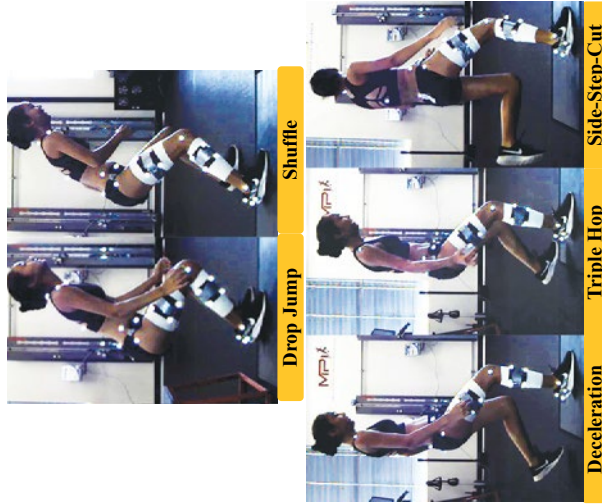
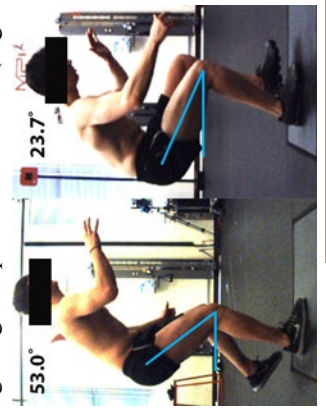
To determine if the thigh angle from 2D video could be used to predict the vGRF during athletic movements.

METHODS

Subjects: 39 healthy athletes (15 males, 24 females)
Biomechanical Assessment: Using a video-based system (Simi Motion), lower-extremity kinematics & kinetics (3D) with video (2D) were collected simultaneously during 5 tasks (Figure).

Outcomes Variables:

- (1) 1st Peak vGRF & vGRF impulses to 1st peak
- (2) 2D thigh angle at peak knee flexion (Figure)



CONCLUSIONS

The findings of the current study indicate that the 2D thigh angle can be used to approximate measures of vGRFs during various athletic tasks. Our findings suggest that the 2D thigh angle may have utility in the screening of athletes thought to be at risk for lower-extremity injury.

RESULTS

An increased 2D thigh angle predicted higher peak vGRFs for all tasks except cutting (R² = 0.17 to 0.47, all p < 0.01). However, an increased 2D thigh angle predicted a greater vGRF impulse for all 5 tasks (R² = 0.13 to 0.39, all p < 0.025) (Figure).

REFERENCES

- [1] Leppanen (2017). Am J Sports Med, 45: 386-393.
- [2] Abbott (2020). Phys Sportsmed, 48: 17-24.

Neuromuscular profile of the lower limb in Colombian female soccer players in the training process

Daza, M.¹, Ayala, D.¹, Aedo E.², Cubides J.³, Argothy, R.¹⁻³

¹ Sports Medicine – School of Medicine, National University of Colombia.

² Biomechanics Laboratory - Applied Sports Science Unit (UCAD) - Ministry of Sports - Chile

³ Physical Culture Research Center (CICFI) - Military School of Cadetes - Bogotá Colombia

E- mail: reargothyb@gmail.com

Summary (150 palabras máximo)

This study evaluates the neuromuscular profile of the lower limb in Colombian female soccer players, that are in the training school. Fifty-two soccer players participated (age 15.3 years \pm 1.01, weight 54.7 kg \pm 7.6, height 158.7 cm \pm 5.6). The countermovement jump (CMJ) and the isometric hamstring strength test (IHST) were performed using force platforms. The neuromuscular performance data of the CMJ vs Net Force hamstring were correlated with the asymmetry between the lower limbs. No associations were found between asymmetry and neuromuscular performance. A statistically significant association was found between JH, RSI, PP and PPV, which are markers of strength and explosive power of the lower body. According to the literature [1],[2] asymmetry between limbs has not augmented risk of injury, so it is necessary to perform the CMJ and IHST tests and the status of the extensor and flexor muscle chains of the lower body.

Introduction

Lower body asymmetries in female soccer players and their association with strength and power performance variables have been a subject of study in recent years. Risk factors related to knee and ankle injuries are now relevant, because there is a high rate of overuse injury and high training loads from high impact movements (landings), changes of direction (acceleration and deceleration) and muscle fatigue (hamstrings).

Constant monitoring of physical capacities and sports performance has been established to prevent lesions and identify the variables related to compensations in the body due to training and competition loads. It is currently not clear if risk of lesions is gender dependent or due to load adaptations.

The purpose of this study is to determine the neuromuscular profile of the lower limb of Colombian soccer players in the training process and its association with neuromuscular performance.

Methods

52 female soccer players in the training process (age: 15.3 \pm 1.01 years; weight: 54.7 \pm 7.6 Kg; height: 158.8 \pm 6.6 cm) were measured in the pre-season stage in this cross-sectional study. Two tests were performed: a) Countermovement jump test (CMJ) using force platforms (one platform for each leg). They performed 5 jumps and the best three were taken. b) Isometric hamstring strength test (IHST) was made in a supine position with 90° knee flexion and 90° hip flexion of the leg. In this position, the athlete applies heel pressure to the force platform for 3 seconds, three times on each leg with

a 30-second rest between each attempt. Correlational analysis was performed between the variables of the IHST and CMJ test using Pearson's correlation (SPSS-V25® software).

Results and Discussion

We found no correlation between the variables of the IHST vs the CMJ jump test. Likewise, no correlations were found between the asymmetries found in the IHST test, the eccentric and concentric impulse and eccentric asymmetries of the landing in the CMJ. However, there is a correlation between the variables of the CMJ test, such as jump height (JH) with respect to peak power (PP) ($p = 0.001$; $r=0.001$), relative strength index (RSI) ($p=0.001$; $r=0.001$), and the speed at peak power (PPV) ($p=0.001$; $r=0.001$). The PP with respect to JH ($p=0.001$; $r=0.001$), RSI ($p=0.001$; $r=0.001$) and PPV ($p=0.001$; $r=0.001$) and the RSI and PPV with respect to JH ($p=0.001$; $r=0.001$) and PP ($p=0.001$; $r=0.001$).

In our target population the CMJ test reported the neuromuscular profile of the variables JH, PP, RSI, PPV. The asymmetries found in CMJ and IHST were less than 10%, between the lower limbs. Loturco [1] and Bishop [2] found similar rates of asymmetry, on different populations. According to the literature [1],[2] asymmetry between limbs has not augmented risk of injury. Results correlate with previous studies where asymmetries do not correlate with neuromuscular performance.

Conclusions

Our target population is symmetrical. Asymmetry is not correlated with neuromuscular performance variables. The CMJ and IHST tests did not show associations, indicating that both tests should be performed to determine if there is compromise of extensor and flexor chain in the lower body. CMJ and IHST can be used as an indicator for evaluating overload, muscle fatigue, and hamstring-quadiceps ratio.

This is the first study, as far as we know, that has a target population with women that are in the training process. In this study the variables of JH, PP, RSI and PPV of Colombian female soccer players in the training process, can be the baseline for future investigations that help to demonstrate the associations of lower body injuries and the factors that affect neuromuscular performance under different loads.

References

- [1] Loturco, I. et al. (2019). *Biology of Sport*, **36(3)**:209-216
- [2] Bishop, C. et al. (2019) *JOURNAL OF SPORTS SCIENCES*. **38**:11-12, 1296-13

Functional Forearm Fatigue Response to Changing Stride Length in Baseball Pitchers

Ryan L. Crotin^{1,2}, Dan K. Ramsey³

¹Sports Performance Research Institute New Zealand, Auckland University of Technology, Auckland, NZ

³Department of Health Professions Education, School of Health Professions, D'Youville College, Buffalo, NY

Email: RLCrotin@gmail.com

Summary

Ulnar collateral ligament injuries are rampant in the sport of baseball where kinetic chain impacts stemming from misappropriation of stride length, or changes that occur in competition due to fatigue have not been evaluated for dynamic elbow stability effects.

Introduction

Stride length optimization has not been adequately researched in the sport baseball where previous work showed physiologic differences between relatively short and long strides, yet minimal differences in ball velocity [1,2] Maintenance of high velocity pitching demonstrated compensatory adaptation where pitchers have the ability to lengthen or shorten stride length to mitigate fatigue while radar velocity is unaffected and refutes its ability to identify adaptations in mechanics. What is unknown are the functional fatigue impacts on the flexor pronator mass, where stride length compensation may have deleterious effects on medial elbow stability. It was hypothesized that shortening stride length will increase functional forearm fatigue indicated by lowered grip strength after simulated play.

Methods

A cohort of 19 healthy and skilled competitive pitchers were recruited from collegiate and high school seasonal travel programs from across Western New York. Fifteen threw right-handed and 4 with their left hand (age 18.63 ± 1.67 years, height 1.84 ± 0.054 m, mass 82.14 ± 0.054 kg). Athletes were randomly assigned to throw in two simulated, 80-pitch games delivering the baseball at $\pm 25\%$ their desired stride. Optical 3D motion capture sampling at 240Hz (Vicon, Denver, CO) integrated with two embedded force plates sampling at 980Hz (Kistler, Amherst, NY) complete with a radar gun and LED display (Jugs Sports, Tualatin, OR) recorded biomechanics and competitive ball velocities.

Bilateral grip strength (Jamar Hydraulic Handgrip Dynamometer, Lafayette Instrument, Lafayette, IN) was tested prior to games and immediately after simulated play. Pitchers had 72 hours of recovery before their second simulated game in the crossover design. Grip data was collected seated with hips, knees and involved elbow bent at

90 degrees with a neutral wrist. Verbal encouragement was provided over a 3 second contraction, followed by 30 seconds rest between 3 repetitions for each arm. Statistical significance, determined *a priori*, was set at $p \leq 0.05$. Pairwise t-tests evaluated mean grip strength differences between stride length conditions.

Results and Discussion

Non-dominant grip strength was unchanged following simulated play indicating the need to evaluate functional forearm fatigue in the dominant arm. Functional forearm fatigue was not detected when strides were lengthened, however, our hypothesis was confirmed in the under-stride condition where strength decreased by approximately 2kg (Table1).

Previous modeling showed that within-subject variability in elbow valgus load can have more injurious impacts under fatigue, where decreased dynamic stabilization of the medial elbow decreased theoretical load capacity of the UCL [3]. Reduced stride length may be adopted to mitigate physiologic fatigue, however baseball pitchers may become less biomechanically efficient and demand more muscular effort from the medial elbow dynamic stabilizers [1].

Conclusions

Stride length optimization and compensatory stride length evaluation should involve measures of functional forearm fatigue to hallmark the degree of mechanical efficiency in the pitching delivery and thereby better understand stride length adjustment.

Acknowledgments

This work was supported by the Mark Diamond Research Fund at the University at Buffalo.

References

- [1] Crotin RL et al. (2014). *Med. Sci Sports Exerc*, **46**: 565-571.
- [2] Crotin RL and Ramsey DK. (2015) *Int. J. Perform. Anal*, **15**: 254-267.
- [3] Trigt B van et al. (2020). *Multidisciplinary Digital Publishing Institute Proceedings*, **49**: 107-113.

Table 1: Dominant Hand Absolute Grip Strength for Baseball Pitchers Throwing $\pm 25\%$ their Desired Stride

Stride Length Condition	Pre-Game (kg)	Post-Game (kg)	P-Value
Under-stride	45.1	42.2	0.02
Over-stride	44.6	43.4	0.21

The Effects of Drive-Leg Knee Valgus Angle on Ground Reaction Forces During Baseball Pitching

Anthony W. Fava^{1,1}, Jessica L. Downs^{1,2}, Hillary A. Plummer^{1,3}, Gretchen D. Oliver¹

¹Sports Medicine & Movement Lab, School of Kinesiology, Auburn University, Auburn, Alabama, USA

¹Email: awf0016@auburn.edu, jzd0075@auburn.edu, hplummer47@gmail.com, goliver@auburn.edu

Summary

This study analysed drive-leg kinematics and ground reaction forces (GRF) from the onset of the windup to follow-through of the pitching motion. Drive-leg knee valgus angle during windup was associated with GRF during the pitch; one GRF correlated with ball speed. At the start of the pitch, drive-leg knee valgus could be a strategy pitchers' use to get into a desired position to generate force and momentum. Following stride foot contact (SFC), drive-knee valgus may enable the foot of the drive leg to remain in position to create a GRF opposite the pitch direction. This can be accomplished by dragging the toe of the drive-leg foot helping to balance the pitcher and assisting the stride leg in decelerating the body's forward momentum.

Introduction

Sequential movements in baseball pitching allows power and energy to be produced and transferred from the lower extremities, through the trunk, to the distal segments of the arm and ultimately to the ball [1]. Stride-leg kinematic and temporal factors have been linked to improved performance [2]. Following SFC, pitchers with decreased stride-leg knee flexion and increased knee extension angular velocities were associated with higher pitch speeds [2]. Furthermore, pitchers with increased braking GRF following SFC had increased ball velocity [3].

Variations in drive-leg kinematics can influence force production and transfer thus affecting performance [1]. However, previous pitching research has not reported drive-leg kinematics that includes the wind-up motion. This study aimed to analyze drive-leg kinematics and GRF including the wind-up action to determine its effects at latter stages on the pitching motion.

Methods

Kinematic and GRF data were captured on 21 high school baseball pitchers (16.6 ± 3.1 yr; 180.1 ± 6.1 cm; 75.9 ± 10.5 kg) throwing fastballs from a mound at regulation distance (18.4 m). The three phases (P1-P3) of the pitching motion that were analyzed were: P1) stride foot lift to peak knee height, P2) peak knee height to SFC, P3) SFC to maximal shoulder external rotation. GRF (vertical, anterior-posterior, medial-lateral) and magnitude of the drive leg were measured using force plates and ball speed was assessed using a radar gun. Multiple regression was used to assess the relationship between drive-leg valgus angle and GRF. Correlation was used to determine the relationship between drive-leg GRF and ball speed.

Results

During P1, pitchers with increased drive-leg knee valgus angle had an increased anterior and medial drive-leg GRF during P3 ($r = .686, p = .025$) (Figure 1, Table 1). A significant correlation was found between maximum anterior drive-leg GRF during P3 and ball speed ($r = .434, p = 0.25$) (Table 1).

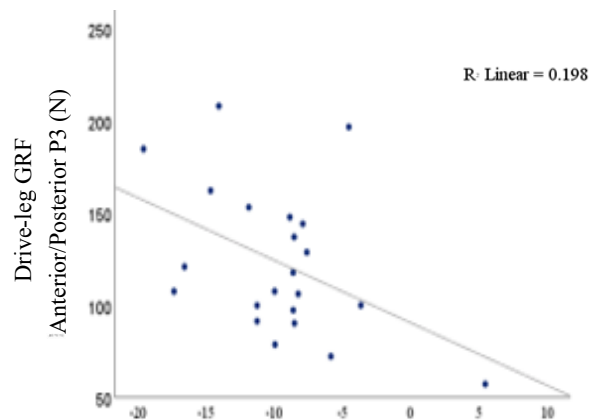


Figure 1: Drive-leg Knee Varus/Valgus Angle P1 (°).

Table 1: Means & St. Deviations; Knee Valgus, GRF, & Ball Speed.

Variable	Mean	SD
Drive Knee Varus/Valgus Angle P1 (°)	-9.62	5.38
Baseline Knee Varus/Valgus Angle (°)	-6.47	5.00
Drive-leg GRF Anterior/Posterior P3 (N)	125.28	39.73
Drive-leg GRF Medial/Lateral P3 (N)	56.23	53.54
Ball Speed (m/s)	31.91	2.75

Conclusions

The findings of drive-leg knee valgus during P1 (wind-up), resulted in pitchers producing medially directed drive-leg GRF in P3. Medial forces can be useful for stabilizing the lower body when transferring weight to the stride leg in preparing for trunk rotation in P3 (arm cocking). Additionally, an anterior force exerted by the drive-leg foot in P3 opposite to pitch direction may help decelerate the loading of the stride leg. This in turn, could affect temporal factors such as the timing of maximal shoulder external rotation, trunk rotation, and stride-leg knee extension. Pitchers may leverage drive-leg knee valgus to alter kinematics and GRF with the aims of augmenting their throwing technique. Future drive-leg studies should investigate the temporal effects of drive-leg knee valgus on the pitching motion.

References

- [1] Kibler, WB. et al. (2013). *Clin Sports Med.* **32**: 637-651.
- [2] Matsuo T. et al. (2001). *JAB.* **17**: 1-13.
- [3] Guido, JA. et al. (2012). *JSCR.* **26**: 1782-1785.

Ground Reaction Force Differences between Two Forms of Squats

Jason Wicke¹, Joseph Robbins, Sarah Myers

¹Human Motion Research Lab, William Paterson University, USA

Email: wickej@wpunj.edu

Summary

Ground reaction forces between the front and back squat were examined. Twenty weightlifters performed three squats at 85% of their specific 1-repetition maximum (1RM), 1) front, 2) back, and 3) bar on back with 1RM of front squat weight. The maximum anteroposterior (F_Y) and normalized vertical (F_Z) ground reaction forces were measured. Results showed an increased shearing force for the back squat, specifically during the completion of the squat, and a vertical force that decreased during the unweighing phase by approximately 50% of the total weight. These results suggest that weightlifters should initiate unweighing to stop the upward movement of the bar sooner, to reduce the larger shearing and ‘bouncing’ that appears to occur at the end of the lift.

Introduction

Squats are one of the most typical weight training exercises to build lower extremity strength. Front squats, where the bar is placed on the anterior of the body, result in a posterior lean, requiring greater muscles forces on the anterior portion of the legs. Conversely, back squats (bar on back) result in an anterior lean that places greater forces on the muscles of the posterior leg [1]. Significantly lower compressive forces and extensor moments were found at the knee during the front squat compared as compared to the back squat [2]. This study examined the maximum anteroposterior (shear) and vertical ground reaction forces while performing a front and back squat.

Methods

Twenty healthy college-aged males who were experienced weightlifters participated in the study. Prior to participation, an informed consent approved by the institutional review board was signed. Three trials in randomized order were performed: a front squat with a load of 85% of the participant’s one repetition maximum (1RM), a back squat with a load of 85% 1RM, and finally a back squat with the load of 85% of the participant’s front squat 1RM (FonB). Ground reaction forces in the anteroposterior direction (F_Y) and vertical direction (F_Z) were recorded on two BertecTM force plates. The F_Z data were normalized to the combined weight being lifted and the body weight of the participant. The dependent variables for this study were the maximum ground reaction force measures (F_Y and F_Z) and the independent variables were three phases of the squat (initiation, middle, completion) and the squat methods.

Results and Discussion

The max shearing forces (F_Y) were significantly greater during the completion phase of the back squat (Figure 1), though peak shear forces at the knees occur at 85-105° of

flexion [2]. Furthermore, max F_Y within each phase was significantly greater during the back squat and can be attributed to the larger weight, indicating that shearing forces at the feet are more dependent on the weight rather than the location of the bar.

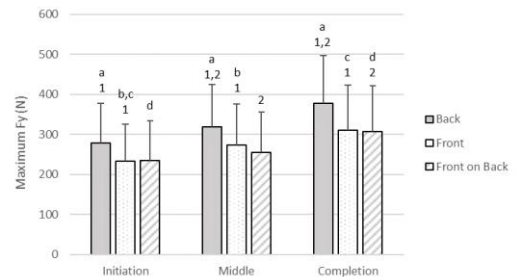


Figure 1: Max F_Y forces. letters = $p < 0.05$ within a squat across the phases / numbers = $p < 0.05$ between squats within each phase.

The normalized maximum F_Z were similar between squat methods (Figure 2), indicating that F_Z is primarily related to the total weight lifted. What was most surprising was the significantly lower F_Z (unweighing) that was produced right at the completion of the squat. For all three squats this unweighing reached approximately 50% of the total weight. It would be expected that with experienced lifters, deceleration of the bar to slow the ascent would be more gradual to avoid such large unweighing values at the completion of the lift.

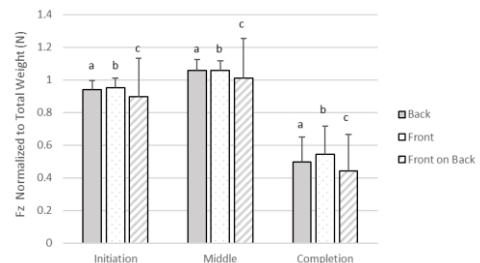


Figure 2: Max F_Y normalized to total weight. letters = $p < 0.05$ within a squat across the phases.

Conclusions

Shearing and vertical forces produced during a squat were examined. Absolute values indicated only slight differences between squats. A more gradual ascent may minimize bouncing at the completion of a lift, improving performance, and thus reducing the chance of injury.

References

- [1] Myer GD et al. (2014). *J. Strength Cond Research*, 36: 4-27.
- [2] Gullett JC et al. (2009). *J. Strength Cond Research*, 23: 284-292.

The Influence of Sports-Related Concussion on Cognition and Landing Biomechanics in Collegiate Athletes

Jason M. Avedesian¹, Tracey Covassin², Shelby Baez², Jennifer Nash³, Ed Nagelhout⁴, Janet S. Dufek¹
¹Department of Kinesiology and Nutrition Sciences, University of Nevada, Las Vegas, Las Vegas, NV, USA
²Department of Kinesiology, Michigan State University, East Lansing, MI, USA
²Department of Physical Therapy, University of Nevada, Las Vegas, Las Vegas, NV, USA
²Department of English, University of Nevada, Las Vegas, Las Vegas, NV, USA
 Email: jason.avedesian@unlv.edu

Summary

Collegiate athletes with and without a history of sports-related concussion (SRC) performed an unanticipated jump-landing task and neuropsychological testing. Group-based statistics and predictive models were performed to compare group differences on biomechanical and neuropsychological measures. Collegiate athletes with a history of SRC demonstrated significantly less knee flexion during the landing task compared to the control cohort. Knee flexion and neuropsychological variables related to attention and working memory were identified as the strongest predictors of SRC injury history.

Introduction

Athletes who sustain an SRC are at an approximately two times greater risk for lower extremity (LE) injury, often several months beyond full unrestricted return-to-sports [1,2]. However, the biomechanical and neuropsychological mechanisms associated with LE injury risk post-SRC have yet to be firmly elucidated.

This investigation sought to determine differences in landing biomechanics and neuropsychological performance in collegiate athletes with a history of SRC compared to matched controls. Additionally, various predictive models were performed to determine history of SRC based upon biomechanical and neuropsychological performance.

Methods

A total of 40 National Collegiate Athletic Association Division 1 athletes (20 SRC, 20 controls) performed biomechanical and neuropsychological testing. Each athlete in the SRC group was matched to one control athlete, controlling for sport, position, sex, and age (± 1 year).

Sport participation for the 20 athletes in the SRC group (age: 20.5 ± 1.3 years; time mean time since last SRC: 461 ± 263 days) and the 20 athletes in the control group (age: 19.8 ± 1.3 years; were as follows: football (n = 6), volleyball (n = 4), men's soccer (n = 3), women's soccer (n = 3), rowing (n = 2), field hockey (n = 1), and women's diving (n = 1)

Athletes completed unanticipated land-and-cut tasks on the dominant (DOM) and non-dominant (NDOM) limbs. Select kinetic and kinematic variables associated with LE injury risk were measured during biomechanical testing. Athletes performed two neuropsychological assessments: Immediate Post-Concussion Assessment and Cognitive Testing and Senaptec Sensory Station.

Results and Discussion

Group-based statistics revealed that the SRC group performed the landing task with significantly decreased knee flexion on both the DOM (SRC: 54.1 deg, control: 60.2 deg) and NDOM (SRC: 54.0 deg, control: 60.3 deg) limbs compared to controls. No other group differences were observed for biomechanical and neuropsychological variables.

Binary logistic regression (Multiple Object Tracking and NDOM knee flexion) and C5.0 decision tree algorithm (Verbal Memory, NDOM knee flexion, and Go / No Go total score) identified multiple biomechanical and neuropsychological predictors of SRC group membership (Figure 1).

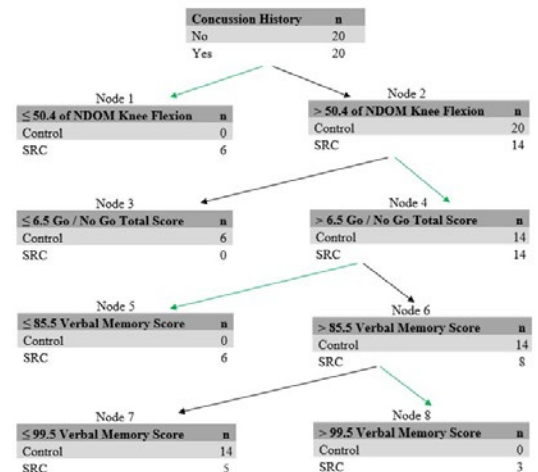


Figure 1: C5.0 decision tree identified NDOM knee flexion ≤ 50.4 deg, Go / No Go ≤ 6.5 , and Verbal Memory ≤ 85.5 and ≥ 99.5 as significant indicators of prior SRC injury history.

Conclusions

Collegiate athletes with a history of SRC display biomechanical movement patterns at the knee that may suggest a greater risk for LE injury. Biomechanical and cognitive performance may uniquely identify prior SRC history.

Acknowledgments

This project was supported by the International Society of Biomechanics Matching Dissertation Grant Program.

References

- [1] McPherson AL et al. (2018). *Am J Sports Med*, **47**: 1754-1762.
- [2] Reneker JC et al. (2019) *Musculoskeletal Sci Pract*, **42**: 173-185.

Inertial measurement unit for determining elbow torque during baseball pitching

Janelle A. Cross, PhD¹, Cody Dziuk, BS¹, Jessica M. Fritz, PhD¹

¹Department of Orthopaedic Surgery, Medical College of Wisconsin, Milwaukee, WI, USA

Email: jacross@mcw.edu

Summary

This study examined the use of an inertial measurement unit (IMU) sensor for determining elbow torque during baseball pitching. An optical motion capture system was used as the gold standard. An IMU sensor was placed near the subject's medial epicondyle on the throwing arm. The three fastest pitches thrown for a strike were analyzed. The resultant accelerations and calculated torques were compared between the motion capture and IMU systems. Significant positive correlations were found between the systems: medial elbow marker acceleration and resultant IMU acceleration, and elbow varus torque and IMU calculated torque. The IMU sensor could be an alternative to performing a full biomechanical analysis when concerned with elbow injury risk in pitchers.

Introduction

Overuse and improper pitching mechanics lead to increased elbow torque, and consequently increased risk of ulnar collateral ligament (UCL) injury and reconstruction [1,2]. The ability to quantify elbow torque daily throughout a throwing session, and cumulatively throughout an entire season would allow for more accurate tracking of UCL injury risk correlated with increased elbow torque. The purpose of this study was to examine an IMU sensor for determining elbow torque during baseball pitching.

Methods

Nineteen adolescent male baseball pitchers participated (16.0 ± 0.8 years, 77.4 ± 9.0 kg, 182.2 ± 5.3 cm). Each pitcher had at least 4 years of pitching experience with no current complaint of arm pain or history of throwing arm surgery. All subjects signed assent forms, and informed consent was obtained from their guardians prior to data collection. Eight Raptor-E cameras (Motion Analysis Corporation, Santa Rosa, CA) were positioned around an artificial mound to capture motion at 300 Hz. Forty-seven reflective markers were attached at specific landmarks. A Blue Trident IMU sensor (Vicon Motion Systems, Ltd.; Oxford, UK) was attached to the subject's throwing arm forearm, 4 cm below the medial epicondyle. IMU data was recorded using Vicon CaptureU software (Vicon Motion Systems, Ltd., Oxford, UK). Ten fastball pitches were recorded being thrown into a strike zone net positioned at a regulation distance of 18.4 m from the pitching rubber. The three fastest strikes were analyzed.

Marker data was identified then filtered using a 13.4 Hz fourth-order Butterworth low-pass filter in Cortex software (Motion Analysis Corporation, Santa Rosa, CA). Kinetics were calculated using Visual 3D software (C-Motion, Germantown, MD) [23]. Custom Python code was used to

extract and process the IMU data. The magnitude of the acceleration signal was calculated using the X, Y, and Z component signals. Forearm and hand lengths and masses were used to calculate a moment of inertia for each subject. The moment of inertia was used to calculate the torque using the resultant acceleration of the IMU. SPSS Statistics software (version 26, IBM Corporation, Armonk, NY) was used to analyze the data. Due to the difference in the scale of the acceleration magnitudes between the two systems, statistical analyses were focused on correlation tests. Associations examined were linear; thus, two-tailed Pearson correlation coefficients were used to determine correlations between the motion system and IMU metrics. A significance level of $p < .05$ was chosen.

Results and Discussion

The mean and standard deviations of the four key metrics compared are presented in Table 1. Significant positive correlations were found for both the medial elbow marker acceleration and resultant IMU acceleration ($r = 0.356$, $p = .007$), and the elbow varus torque and IMU calculated torque ($r = 0.559$, $p < .001$). The results from this study demonstrate that the Blue Trident IMU sensor could be an alternative to performing a full biomechanical analysis when concerned with elbow injury risk in pitchers. The acceleration metrics had a low to moderate positive correlation and the torque metrics had a moderate to strong positive correlation.

Table 1: Motion capture system and IMU mean and standard deviations

Elbow Marker Acceleration (deg/s ²)	367.6	±	39.4
IMU Acceleration (deg/s ²)	1333.7	±	487.1
Elbow Varus Torque (Nm)	60.8	±	16.2
IMU Calculated Torque (Nm)	60.0	±	22.3

Conclusions

The positive correlations between the motion capture system and IMU suggest the IMU sensor is reliable for coaches and athletes who do not have access to a motion capture system and has the advantage of daily use throughout a throwing season to cumulatively assess elbow torque while pitching.

Acknowledgments

Study was funded by the Medical College of Wisconsin Department of Orthopaedic Surgery.

References

- [1] Fleisig GS, et al. (2012). *Sports health*, 4:419-424.
- [2] Davis JT, et al. (2009). *Am J Sport Med*, 37:1484-1491.
- [3] Adhithia D, et al. (2015). *Proc of GCMAS*, 84-85.

Body Composition and Segmental Sequencing in Trained Softball Athletes

Kenzie B. Friesen¹, Gretchen D. Oliver²

¹College of Kinesiology, University of Saskatchewan, Saskatoon, Canada

²Sports Medicine and Movement Laboratory, School of Kinesiology, Auburn University, Auburn, USA

Email: kenzie.friesen@usask.ca

Summary

Segmental angular velocities of the trunk, shoulder, elbow, and wrist significantly differed between pitchers with a healthy body fat percentage (BF%) and a high BF%. While increased mass is often considered beneficial in pitching, differences in movement patterns exist according to body fat presence and should be further studied to understand how body composition can influence both performance and injury.

Introduction

Softball pitchers regularly present above-average body sizes despite reports that larger athletes are more susceptible to injury [1]. The windmill pitching motion is a sequential movement that requires proper coordination of segments to affect performance [2] and distal segment stress [3].

The purpose of this study was to examine the difference in segmental angular velocities of the trunk, shoulder, elbow, and wrist, between two groups of pitchers: 1) those with a healthy BF% (<32%) and 2) those with a high BF% (≥ 32%).

Methods

Forty high-school and college softball pitchers completed body composition testing via dual-energy x-ray absorptiometry and were placed into pitcher BF% groups. Kinematic data were captured at 240 Hz using an electromagnetic motion capture system synced with motion analysis software. Trunk rotation, shoulder flexion, elbow flexion, and wrist flexion angular velocities were defined according to ISB recommendations [4] and extracted over the final 101 frames prior to follow-through (defined as 100 ms following ball release). Statistical parametric mapping (SPM) was employed using MATLAB to complete a multivariate analysis of variance (MANOVA) over the 101 frames of data. Pitch velocity was also collected using a calibrated radar gun. An independent samples t-test was used to compare pitch velocity between the two groups of pitchers.

Results and Discussion

The SPM MANOVA {X₂} was statistically significant and showed that the two groups of pitchers differed at 74-75% and 92-99% of this portion of the movement (SPM{X₂}_{1,4} = 16.821, *p* = .041 and .006). The t-test revealed pitch velocity did not differ between pitcher groups, *t* = 1.484, *p* = .145.

Research notes larger athletes can possess increased segmental mass moments of inertia which can influence joint moments and angular accelerations [5]. Therefore, increased BF% may explain altered movement patterns during the windmill softball pitch. This has implications for performance, as research notes elite pitchers have better proximodistal sequencing [2]. Similarly, segmental sequencing differences between BF% groups may offer insight to pain and injury as research reports larger athletes have higher rates of injury [1].

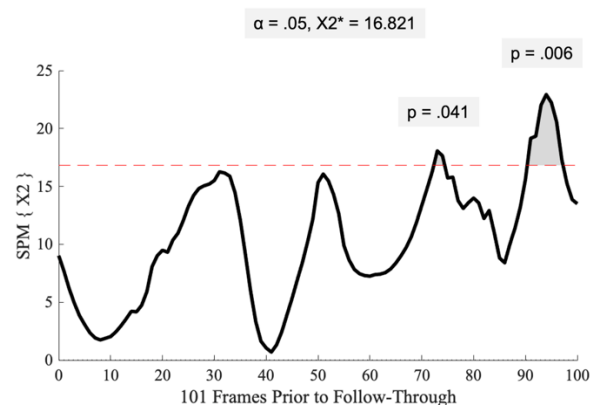


Figure 1: SPM analysis of the combined multivariate dependent variable (segmental angular velocities) during 101 frames of data prior to follow-through of the pitch. X₂* = SPM critical threshold.

Conclusions

Segmental sequencing differed between pitcher groups while pitch velocity did not. Therefore, the authors suggest that pitchers adopt different movement strategies to accommodate their physical characteristics and still reach comparable pitch outcomes. More research is needed to examine whether these sequencing differences are beneficial (increased pitch velocity) or detrimental (increased injury risk) to pitchers.

References

- [1] Oliver G et al. (2019). *Orthop. J. Sports Med.*, **7**: 2325967119865171.
- [2] Oliver G et al. (2010). *J. Strength Cond. Res.*, **24**: 0-2407.
- [3] Kibler W et al. (1995). *Baseball and Tennis*; Mosby.
- [4] Wu G et al. (2005). *J. Biomech.*, **38**: 981-99.
- [5] Fleisig et al. (1999). *J. Biomech.*, **32**: 1371-1375.

Table 1: Demographic data of the two separate groups of pitchers.

Pitcher Groups	Age (years)	Height (cm)	Mass (kg)	BF%	Pitch Velocity (mph)
Healthy BF%	16 ± 2	169.8 ± 6.9	64.8 ± 9.3	27.6 ± 2.5	56 ± 5
High BF%	15 ± 2	171.3 ± 5.9	83.5 ± 15.6	39.8 ± 5.1	54 ± 5

Should Major League Baseball Adjust the Mound Distance?

Megan S. Stewart^{1,2}, Alek Diffendaffer¹, Jon Slowik¹, Glenn Fleisig¹

¹The American Sports Medicine Institute, Birmingham AL, USA

²Concordia University of Chicago, River Forest, Illinois, USA

Email: megan.s.stewart19@gmail.com

Summary

With a decrease in runs scored, Major League Baseball (MLB) commissioned the American Sports Medicine Institute to conduct a biomechanical study looking at a potential change to distance of the pitching mound.

Introduction

Moving the mound backwards, farther from homeplate has also been suggested for increasing offense¹. The theory is that increased pitch velocity in today's game has reduced the time for the ball to reach homeplate, thus, lowering the ability for the hitter to react to the baseball. Therefore, increasing the distance between the pitching mound and homeplate may provide the hitter with an increase in time to see the baseball, swing, and make good contact. While an increase in the pitching distance may increase the offense, the effect on joint kinetics, pitching biomechanics, and injury risk must be determined. Therefore, the primary purpose of this research study was to determine the effect of pitching distance on adult baseball pitching biomechanics.

Methods

The research study was approved by the Institutional Review Board at St. Vincent's Health System (Birmingham, AL, USA). There was a total of 26 healthy, active collegiate pitchers (10 Division 1, 2 Division 2, 11 Division 3, 3 Junior College) were recruited to participate in this study. All of the testing was completed in an indoor biomechanics laboratory.

Anthropometric measures were collected and 38 retro-reflective markers were attached the participant at previously described^{10,16,17}.

Three-dimensional motion data of each pitcher were tracked with a 12-camera motion capture system sampling at 240 Hz with a three-dimensional residual threshold set at 0.45 ± 0.20 mm (Raptor System, Motion Analysis Corporation, USA). Ball kinematics were measured for the final 21 participants using a PITCHf/x system (SportsMEDIA Technology, Fremont, CA, USA). The first three pitches of each condition were excluded from the analysis to allow the pitcher to fully adapt to the pitching distance. The participant was unaware that these pitches would be excluded. Pitcher biomechanics and ball kinematics were calculated for the final five pitches for each mound condition.

Thirty-seven pitcher kinematic and kinetic variables were calculated as previously described^{13,15,17}. The initial ball velocity was measured at a location of 10ft in front of the pitching rubber. The final ball velocity was measured as the baseball crossed the front of homeplate. The length of ball

flight was defined as the total time it took the baseball to travel between these two abovementioned locations. Horizontal break of the baseball was defined as the maximum horizontal deviation from an imaginary straight-line path between the release point and the point where the pitch crossed the back tip of home plate. Vertical break of the baseball was defined as the maximum vertical deviation from an imaginary straight-line path between the release point and the point where the pitch crossed the back tip of home plate. For each pitching distance, strike percentage was calculated as the number of pitches within the PITCHf/x strike zone divided by the total number of pitches. For all of the pitching distances, the magnitudes of all parameters were averaged for each participant. A repeated measures analysis of variance (ANOVA) was utilized to detect significant differences among the pitching distances. When a significant difference ($p < 0.05$) was found, pairwise differences were analysed with a Tukey post-hoc test ($p < 0.05$).

Results and Discussion

The pitchers were (mean \pm SD) 19.7 \pm 1.2 years old, 73 \pm 2 in tall, and had a weight of 205 \pm 19 lbs. There were no significant differences seen for ball velocity, movement, or spin when pitching from the four mound heights for both the curveball and fastball. The mean ball velocity for the fastball and curveball was 88.4 \pm 6.06 mph and 70.2 \pm 5.95 mph respectively. There were twelve biomechanical variables (seven kinematic variables and five kinetic variables) that were found to be significantly different when comparing the mound height for the fastball pitches. When comparing mound height and curveballs, there were eight kinematic variables shown to be significantly different.

Conclusions

A moderate (up to 3.2 ft) increase in pitching distance will have no statistically significant effect on pitching kinematics or kinetics. The duration of ball flight increased with pitching distance, supporting the concept that moving the mound back would benefit hitters with more time to decide and execute their swing. However, the magnitudes of horizontal and vertical break also increased with pitching distance, potentially benefitting pitchers.

Acknowledgments

We would like to acknowledge Major League Baseball.

References

- [1] Stark J. Stark: Move back the mound? MLB and players' union are open to that - and more. *Athl.* Published online February 2019. <https://theathletic.com/804630/2019/02/06/stark-move-back-the-mound-mlb-and-players-are-open-to-that-more/>

Correlation of Glenohumeral Internal Rotation Deficit, Total Range of Motion, and Retroversion to Shoulder Kinetics in Collegiate Baseball Pitchers

Hannah L. Stokes¹, Marc Duemmler¹, Nigel Zheng¹, Koco Eaton²

¹Department of Mechanical Engineering and Engineering Science, University of North Carolina at Charlotte, NC, USA

²Tampa Bay Rays and University of South Florida, FL, USA

Email: nzheng@unc.edu

Summary

The study included 109 collegiate baseball pitchers and investigated correlations between shoulder rotational properties and shoulder kinetics during pitching. Pearson correlation tests were performed using SPSS. Retroversion had the most significant correlations to shoulder kinetics.

Introduction

Glenohumeral internal rotation deficit (GIRD), total range of motion (tROM), and retroversion (bony external range of motion) are related to shoulder injuries [1]. Higher joint loading has been shown to lead to more injury incidences [2]. GIRD and tROM are commonly assessed by team clinicians. The purpose of this study is to quantitatively investigate shoulder rotational properties related to GIRD, tROM, and retroversion and shoulder kinetics during baseball pitching. If correlations are found, this could improve the way shoulder rotational properties are monitored in order to reduce potential injuries from excessive forces and torques. We hypothesized that GIRD, tROM, and retroversion would have no significant correlation to shoulder kinetics.

Methods

The study included 109 collegiate baseball pitchers (height: 186±8 cm and weight: 85±9 kg). The study was approved by an institutional review board and all pitchers gave informed consent. All pitchers were healthy during biomechanical testing. The shoulder rotational test measured the end-point angle (EPA) and resistant onset angle (ROA) using a custom-made wireless device [3]. The test measured internal and external angles on both the throwing and non-throwing arm. tROM is defined as internal plus external EPA. Bilateral difference internal EPA is related to GIRD and bilateral difference external ROA is related to retroversion.

Pitching motion data was collected at 240 Hz with sixteen reflective markers using a motion capture system [4]. The ball speed was measured during pitching. A custom MATLAB program was created to use an inverse dynamics model to calculate anterior/posterior, superior/inferior forces, and internal/external rotation, horizontal adduction/abduction torques. Pearson correlation tests were performed using SPSS with an alpha set to 0.05.

Results and Discussion

Shoulder rotational properties had significant correlations with shoulder forces and torques (Table 1). Bilateral external ROA difference had significant correlations with superior/inferior forces, and internal rotation and horizontal adduction

torques. tROM had significant correlations with anterior force, external rotation and horizontal abduction torques. Bilateral internal EPA difference did not have any significant correlations. The shoulder rotational properties were not significantly correlated with ball speed.

Table 1: Pearson correlation values for shoulder rotational properties (ext: external, int: internal, bilat diff: bilateral difference) and shoulder kinetics, where * indicates $p < 0.05$.

	Forces			
	Anterior	Posterior	Superior	Inferior
Bilat Diff Int EPA	0.126	-0.087	0.089	-0.051
tROM	0.222*	-0.013	0.019	-0.113
Bilat Diff Ext ROA	-0.110	0.133	-0.291*	0.257*
	Torques			
	Internal	External	Horizontal Adduction	Horizontal Abduction
Bilat Diff Int EPA	0.028	0.099	0.036	-0.107
tROM	0.131	0.254*	-0.029	-0.166*
Bilat Diff Ext ROA	-0.259*	-0.016	-0.201*	-0.034

Findings emphasize that shoulder rotational properties should be monitored quantitatively in order to ultimately, improve performance and reduce injury. Correlations between GIRD and tROM with shoulder kinetics align with previously reported findings [5]. Further investigation is needed to determine if these correlations to kinetics are related to injury and surgery incidences.

Conclusions

GIRD, tROM, and retroversion are correlated with shoulder kinetics in college baseball pitchers. The bilateral difference in external ROA (retroversion) had the most significant correlations and should be closely monitored.

Acknowledgments

This study is funded by a Clinical Research Grant from Major League Baseball.

References

- [1] Wilk K et al. (2011). *Am J Sports Med*, **39**: 329-335.
- [2] Oyama S. (2012). *J Sport Health Sci*, **1**: 80-91.
- [3] Zheng N. (2011). *Int J Sports Med*, **33**: 463-468.
- [4] Zheng N et al. (2004) *Biomedical Engineering Principles in Sports*; Kluwer Academic/Plenum Publishers.
- [5] Lin H et al. (2020). *Int. J. Environ. Res. Public Health*, **17**:8211.

Are Distal Throwing Arm Kinematics Predictive of Maximum Elbow Valgus Torque in Youth Baseball Pitchers?

Tessa C. Hulburt¹, Garrett S. Bullock¹, Arnel L. Aguinaldo², Kristen F. Nicholson¹

1. Department of Orthopaedic Surgery, Wake Forest School of Medicine, Winston Salem, NC, USA

2. Department of Kinesiology, Point Loma Nazarene University, San Diego, CA, USA

Email: thulburt@wakehealth.edu

Summary

The purpose of this study was to determine if distal throwing arm kinematics calculated from fastball (FB), breaking ball (BB) and off-speed (OS) pitches are predictive of elbow valgus torque (EVT) in younger (13-15 years) and older youth athletes (16-18 years). Motion capture data and a generalized linear model with Lasso regularization found that kinematics from OS pitches thrown by younger youth pitchers were most association with EVT.

Introduction

Motion capture biomechanics has emerged as a vital tool to understand injury risk patterns and efficient mechanics in baseball pitching [1]. Biomechanics studies have investigated the lower extremity, trunk, and upper throwing arm, but little attention has been given to the distal throwing arm, particularly in youth pitchers [2]. The purpose of this study was to determine if distal throwing arm kinematics calculated from three pitch types are predictive of EVT in youth athletes aged 13-15 and 16-18 years.

Methods

Motion capture analyses were conducted on 52 pitchers aged 13-15 years (age: 14.8 ± 0.65 years, height: 1.78 ± 0.07 m, weight: 71.5 ± 11.6 kg) and 52 pitchers aged 16-18 years (age: 16.7 ± 0.5 years, height: 1.85 ± 0.07 m, weight: 83.1 ± 11.5 kg). A 41 reflective markerset and twelve-camera motion analysis system (Qualisys AB, Göteborg, Sweden) were used to collect pitching mechanics data. Ball velocity (BV) was recorded with a Trackman device (Trackman, Scottsdale, Arizona). Distal throwing arm kinematics were calculated with Visual3D (C-Motion, Inc. Germantown, Maryland). Pitching models were defined using the PitchTrak model [3], and segment coordinate systems were defined according to ISB recommendations [4]. EVT was normalized by body weight (N) and height (m). A generalized linear model with a Lasso regularization method was chosen due to multicollinearity within the kinematics dataset and the non-normal distribution of EVT data. This model calculated if 12 kinematic predictor variables were prognostic of EVT response variable by weighting each variable coefficient. Larger coefficients indicated a stronger association with EVT.

Results and Discussion

Kinematics from OS pitches thrown by youth players aged 13 to 15 years were most associated with EVT. Wrist flexion angle at maximum shoulder external rotation (MER) and ball release (BR) from this age group and pitch-type had a negative

and positive relationship with EVT, respectively. Forearm pronation at MER from younger youth OS pitches had a positive relationship with EVT. Both 10ms and 100ms after BR, ulnar deviation angle from younger youth OS pitches had predictive value for the response variable EVT. The only variable related to EVT in the older youth age group was wrist flexion at 10ms after BR in FB pitches. Younger youth player kinematics data from OS pitches may be associated with EVT because the OS pitch is often the last pitch-type learned after FB and BB pitches. Lack of skill and coordination with this pitch type may lead to potentially injurious elbow mechanics. Further, the average OS pitch ball speed for younger and older youth players was 73.6mph and 79.9mph, respectively. Despite the higher ball velocity, older youth player OS pitch kinematics were not associated with EVT, potentially indicating that older youth players develop the skill and coordination to throw OS pitches more safely.

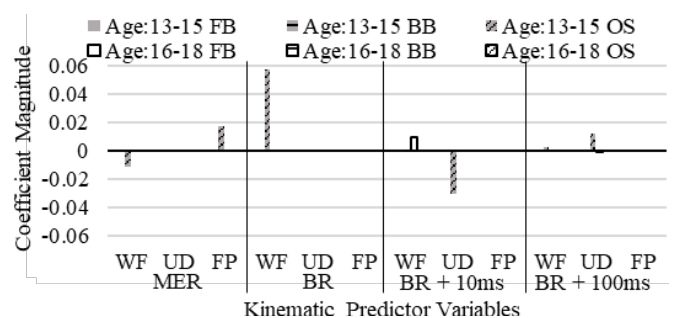


Figure 1. Kinematic coefficients associated with EVT for younger and older youth pitchers. Kinematic variables are wrist flexion angle (WF), ulnar deviation angle (UD), and forearm pronation angle at timepoints maximum external rotation (MER), ball release (BR), 10ms after ball release (BR + 10ms), and 100ms after ball release (BR + 100ms).

Conclusions

Distal throwing arm kinematics from OS pitches thrown by younger youth pitchers were most related to EVT. Proper mechanics should be emphasized to younger youth pitchers when throwing OS pitches to avoid increased stress to the medial elbow. Future work should include an analysis of distal throwing arm angular velocities and torques and comparison to skilled adult pitchers.

References

- [1] Davis JT et al. (2009). *Am. J. Sports Med.* **37**: 1484-1491.
- [2] Solomito MJ et al. (2004). *Sport. Biomech.* **13**: 320-331.
- [3] Aguinaldo AL et al. (2007). *J. Appl Biomech.* **23**: 42-51.
- [4] Wu G et al. (2005). *J. Biomech.* **38**: 981-99

Limb Symmetry During a Cutting Task in Athletes With and Without a History of Sports-Related Concussion

Warren O. Forbes¹, Jason M. Avedesian¹, Janet S. Dufek¹

¹Department of Kinesiology and Nutrition Sciences, University of Nevada Las Vegas, Las Vegas, NV

Email: warren.forbes@unlv.edu

Summary

Twenty athletes with a history of sports-related concussion (SRC) and twenty matched control athletes performed a land-and-cut task with their dominant and non-dominant limbs. An independent t-test was used to compare kinematic and kinetic variables prospectively linked to lower extremity (LE) injury risk between the dominant limb and the non-dominant limb during the task. Although there were no significant differences in limb asymmetry, there were differences in frontal plane kinetics at the knee joint that may predispose athletes in each cohort to increased LE injury risk.

Introduction

Athletes who sustain SRCs may have alterations to neuromuscular control that increase their risk of future non-contact LE injury [1]. The exact mechanisms of the relationship between SRC, altered neuromuscular control, and LE injuries are currently unknown.

A link between SRC history and limb asymmetry has been observed in elite athletes that may increase the risk of non-contact LE injury [2]. The Limb Symmetry Index Dominant/Non-Dominant (LSI-D/ND) has been used as a measure to quantify asymmetry between limbs (LSI-D/ND = dominant limb/non-dominant limb x 100) [3]. LSI-D/ND values should be greater than 90% to minimize the risk for sustaining an LE injury. The purpose of this study was to analyze the differences in LSI-D/ND between SRC athletes and a matched control group.

Methods

College athletes with a history of SRC (n = 20) and a control group of healthy athletes matched by sport, position, sex, and age (n = 20) were recruited for this study.

Athletes performed an unanticipated land-and-cut task. The task consisted of each athlete standing on a 60 cm box with a visual stimulus (FITLIGHT Corp., Aurora, Ontario, CA) positioned three meters away from the athlete. Various colors (eg, green, pink, blue, and red) were presented as the visual stimulus. Athletes were instructed to only respond to a green or red light. When a red or green light was presented, athletes were instructed to step off the box, land on both limbs and perform a 45-degree cutting movement to the left or right, respectively. A trial was considered successful if the athlete obtained full foot contact on the force platform and performed the correct land-and-cut maneuver in the direction corresponding to the color stimulus.

The kinetic and kinematic dependent variables of interest for the dominant (defined as the preferred limb for their respective sport) and non-dominant limbs were vertical ground reaction force (vGRF), peak knee extensor moment

(pKEM), peak knee abduction moment (pKAM), peak ankle dorsiflexion angle (pDF), peak knee flexion angle (pKF), and peak knee abduction angle (pKA). Separate independent t-tests were performed to compare LSI-D/ND for each dependent variable between the SRC and control groups.

Results and Discussion

There were no significant differences in LSI-D/ND between the SRC and control groups for vGRF, pKEM, pKAM, pDF, pKF, and pKA (p > .05).

Results indicated no significant differences in limb asymmetry between the SRC group and the control group. Every dependent variable, apart from pKAM, were within the acceptable LSI-D/ND range indicating minimized risk of LE injury. The LSI-D/ND for pKAM was 219% and 213% respectively for SRC and the control group. This indicates that the dominant limb, on average, had a peak knee abduction moment two times greater than that of the non-dominant limb. Further testing would be needed to assess the potential for frontal plane mechanics that could lead to LE injury.

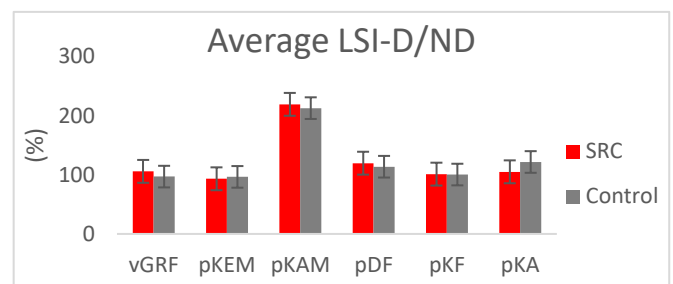


Figure 1. Limb Symmetry Dominant/Non-Dominant

Conclusions

Although LSI-D/ND was not significantly different between the SRC and control group, further research regarding limb asymmetry in athletes with an SRC history is necessary. While this study failed to identify any limb asymmetries between groups, analyzing each dependent variable individually may provide further insight regarding potential LE injury risk.

Acknowledgements

Partially supported by the International Society of Biomechanics Matching Dissertation Grant.

References

- [1] Howell DR, et. al. (2018). *Sports Med.* **48**: 1097-1115
- [2] Wilkerson GB, Nabhan DC, and Crane RT (2020). *J Athl Train.* **55**. 594-600.
- [3] van Melick N, et al. (2019). *Knee Surg Sports Traumatol. Arthrosc.* **27**. 549-55

Sprinting with prosthetic versus biological legs: an unfair advantage?

Owen N. Beck¹, Paolo Taboga², & Alena M. Grabowski^{3,4}

¹PoWeR Lab, School of Mechanical Engineering, Georgia Institute of Technology, Atlanta, GA, USA

²Biomechanics Lab, Dept. of Kinesiology, California State University, Sacramento, CA, USA

³Applied Biomechanics Lab, Dept. of Integrative Physiology, University of Colorado, Boulder, CO, USA

⁴Dept. of Veterans Affairs, Eastern Colorado Healthcare System, Denver, CO, USA

Email: obeck3@gatech.edu

Summary

Due to the world-class 400m running performances of athletes with prosthetic legs, many people assume that running-prostheses provide users an overall advantage over non-amputees during sprint races. These assumptions have caused athletics governing bodies to effectively prohibit the use of running-prostheses from sanctioned competition. Here, we show that no athlete with prosthetic legs, including the fastest such athletes, exhibit a single 400m performance metric that is superior to those achieved by elite non-amputees. Hence, the use of prosthetic legs during 400m running races cannot be considered unequivocally advantageous compared to the use of biological legs.

Introduction

Exceptional athletes with bilateral prosthetic legs have run 400m faster than the Olympic track and field qualifying standard. Yet, the potential for these athletes to race alongside non-amputee Olympians has been stifled by policymakers who assume that running-prostheses provide users an overall advantage versus non-amputee competitors. This assumption has been ill informed by the scientific literature, because there is no consensus regarding the *net effect* of running with prosthetic versus biological legs. Thus, we sought to determine whether athletes with bilateral prosthetic legs have inherent advantages versus non-amputees during 400m races by comparing athlete 400m performance metrics: initial race acceleration, maximum straight and curve running velocity, velocity at aerobic capacity, and sprint endurance. We reasoned that if an athlete with prosthetic legs exhibits a 400m performance metric that is superior to that achieved by elite non-amputees, prosthetic legs likely confer specific advantages to their users versus athletes with biological legs.

Methods

We quantified each 400m performance metric from the fastest male athlete with bilateral prosthetic legs (400m personal record (PR): 44.38 s) and compared his metrics to those of other elite male athletes with and without prosthetic legs. Statistically, we deemed athletes with prosthetic legs to exhibit a different 400m performance metric than non-amputees if they achieved a value outside the non-amputee range, and/or when our statistical tests revealed $\geq 95\%$ confidence that their best 400m performance metric was different from the mean of the comparison non-amputee cohort ($p < 0.05$).

Results

The fastest initial acceleration out of the starting blocks through 20 m from an athlete with prosthetic legs was 40% slower (>59 SDs) than the average of elite non-amputees (Fig. 1A) [1]. The fastest treadmill-running velocity achieved by athletes with prosthetic legs (11.4 m/s) was similar to, but not faster than that achieved by non-amputees (11.7 m/s). Athletes with prosthetic legs are estimated to slow $\geq 1.3\%$ more than non-amputees on an outdoor track curve versus on a straightaway. Notably, at a mutual running velocity (10 m/s), the fastest athlete with prosthetic legs exhibited similar ground reaction forces and stride kinematics as non-amputees ($<8\%$ & <2 SDs) [2]. The fastest $\dot{V}O_{2peak}$ from athletes with prosthetic legs (5.0 m/s) is nearly identical to that of non-amputee 400m athletes (PR: ≤ 48.03 s; Avg \pm SD: 4.9 ± 0.04 m/s) [2] and 19% (>3 SDs) slower than that of 10 km non-amputee distance-runners (PR: <32 min). The sprint endurance profile of the two fastest athletes with prosthetic legs was nearly identical to that of non-amputees ($<3\%$ & <1 SD; Fig. 1B) [2].

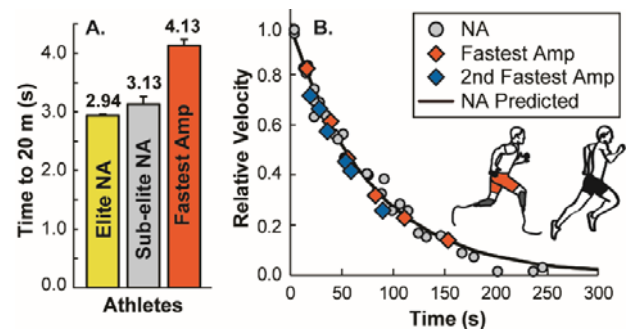


Figure 1. A. Avg \pm SD time to sprint from the starting blocks to 20 m for elite non-amputees (NA) [1], sub-elite NA [1], and the fastest athlete with prosthetic legs (AMP). B. The time that NA [2], as well as the two fastest AMP could sustain a treadmill running velocity relative to their maximum velocity [2].

Conclusions

Currently, no athlete with bilateral leg amputations using running-prostheses, including the fastest such athletes, has ever been reported to have a lab-tested 400m performance metric that is superior to that achieved by non-amputees. Therefore, the use of prosthetic legs during 400m running races cannot be considered unequivocally advantageous compared to the use of biological legs.

References

- [1] Rabita et al. (2015). *Scand J Med Sci Sports*. **25**: 583-594.
- [2] Weyand et al. (2009). *J Appl Physiol*. **107**: 903-911

CONCURRENT CHANGES IN MEDIAN NERVE DEFORMATION AND DISPLACEMENT DURING GRIPPING

Aaron M. Kociolek¹, Gabrielle Racine¹, Michael W. R. Holmes²

¹Biomechanics and Ergonomics Lab, School of Physical and Health Education, Nipissing University, North Bay ON, Canada

²Neuromechanics and Ergonomics Lab, Department of Kinesiology, Brock University, St. Catharines ON, Canada

Email: aaronk@nipissingu.ca

Summary

We investigated median nerve (MN) deformation and displacement in concert to elucidate carpal tunnel dynamics during forceful gripping. Twelve participants performed 3 different grip types (power, chuck, pulp) while ramping force up from 0% to 50% of maximal voluntary effort (MVE) and ramping force down from 50% to 0% MVE. Ultrasound of the transverse carpal tunnel demonstrated time-dependent changes in loading (ramping force up) versus unloading (ramping force down) for both MN deformation and displacement metrics. These results indicate that MN deformation is linked to its displacement during forceful gripping and may further suggest a viscoelastic effect due to strain of surrounding tissues, including the subsynovial connective tissue within the carpal tunnel.

Introduction

Finger exertions cause the flexor tendons in the carpal tunnel to displace palmarly, thus decreasing the distances between the flexor tendons and transverse carpal ligament [1]. Tendon displacement may, in turn, influence passive carpal tunnel structures, including the MN. Cowley et al. [2] showed the MN deformed during forceful gripping tasks, with the MN becoming more circular due to shortening in the radioulnar axis and lengthening in the palmar-dorsal axis. However, it remains unclear to what extent MN deformation is related to tendon dynamics. We evaluated MN deformation and displacement relative to the flexor tendons throughout loading and unloading of forceful gripping tasks to better elucidate tissue interactions within the carpal tunnel.

Methods

Twelve right-handed participants ramped isometric force up from 0% to 50% of MVE before ramping force down from 50% to 0% MVE for 3 different grip types (power, chuck, pulp). Grip forces were measured with a digital dynamometer (MIE Medical) at 1000 Hz in a custom LabVIEW program (National Instruments), which also provided participants with the force ramp matching profiles via visual display. The transverse carpal tunnel was imaged at the distal wrist crease using ultrasound (Vivid Q, 12L, General Electric) with an acquisition frequency of 13 MHz and a sample rate of 30 Hz. MN images were extracted from 0–50% in 10% increments of MVE during both the loading (ramping force up) and unloading (ramping force down) phases. Images were analyzed in Image J (National Institutes of Health) to determine MN cross-sectional area, circularity [$4\pi(\text{Area}/\text{Perimeter}^2)$], width (radioulnar axis), and height (palmar-dorsal axis) as well as the relative displacement between the MN and flexor digitorum superficialis tendon of

the middle finger (FDS-M). Three-way repeated measures ANOVAs tested the effects of grip type (power, chuck, pulp), grip force level (0%-50% in 10% increments of MVE) and ramp direction (loading versus unloading) on all deformation and displacement outcome variables ($\alpha = 0.05$).

Results and Discussion

We found a force level by ramp direction interaction on MN circularity ($F_{5,55}=3.18$, $p=0.014$). During loading, the MN became more circular from 0%-20% MVE, with no further change from 20%-50% MVE. These results fit a quadratic relationship. During unloading, there was a gradual decrease from 50%-0% MVE, which fit a linear relationship (Fig 1). Interestingly, MN displacement profiles during loading and unloading mirrored the deformation results. For example, the MN displaced ulnarly and dorsally relative to the FDS-M during the loading phase, but only up to 20% MVE with very little change thereafter. Conversely, the MN displaced radially and palmarly during unloading; however, displacement occurred gradually throughout the entire unloading phase from 50-0% MVE.

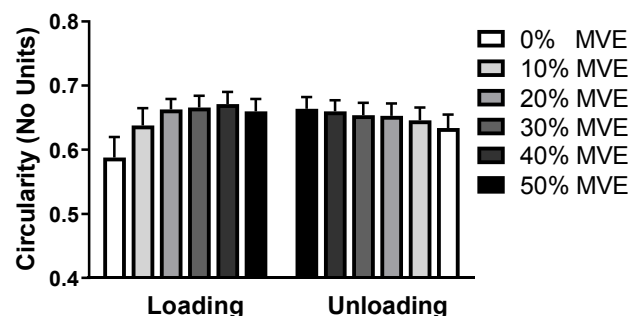


Figure 1: Mean (\pm standard error) median nerve circularity while ramping up (loading) and ramping down (unloading) grip force.

Conclusions

MN deformation and displacement both changed in a time-dependent manner, including differences in loading versus unloading. Therefore, the results indicated that deformation of the MN was linked to its displacement relative to the flexor tendons. Time-dependent changes may also suggest a viscoelastic effect due to strain of the surrounding subsynovial connective tissue within the carpal tunnel.

Acknowledgments

Natural Science and Engineering Research Council of Canada Discovery Grant # 2017-0409.

References

- [1] Gabra JN et al. (2016). *Med Eng Phys*, **38**: 1055-1062.
- [2] Cowley JC et al. (2017). *Clin Anat*, **30**: 470-478.

In-Vivo Measurement of Wrist Angles During the Dart-Throwing Motion Using Inertial Measurement Units

Gabriella Fischer^{1,2} and Michael A. Wirth¹, Simone Balocco³, Maurizio Calcagni¹

¹Division of Plastic Surgery and Hand Surgery, University Hospital Zurich, University of Zurich, Zurich, Switzerland

²Institute for Biomechanics, ETH Zurich, Zurich, Switzerland

³Dept. Mathematics and Informatics, University of Barcelona, Barcelona, Spain

Email: Gabriella.Fischer@usz.ch

Summary

This study investigates the clinically relevant dart-throwing motion (DTM) by comparing an inertial measurement unit based system (IMU) previously validated for basic motion tasks (BMT) with an optoelectronic motion capture system (OMC). Ten healthy volunteers performed the DTM equipped with both systems. Results of both systems were comparable, but bigger differences between the systems were found than in BMT and different possible reasons were identified in this study. Its easy applicability makes the IMU interesting for clinically measuring DTM range of motion (ROM).

Introduction

Movements in the wrist during activities of daily living often occur in an oblique plane from flexion-radial deviation to extension-ulnar deviation, this movement is referred to as DTM. The DTM is clinically relevant but its ROM is not usually clinically measured with goniometers due to the complexity of the movement [1] and systems like OMC capable of capturing this movement are very complex to use and require a laboratory setting. We investigated an easy to use IMU previously validated for motion analysis of BMT in the flexion/ extension and radial/ ulnar deviation planes [2] for this more complex movement by comparing it to the motion analysis gold standard, an OMC [3].

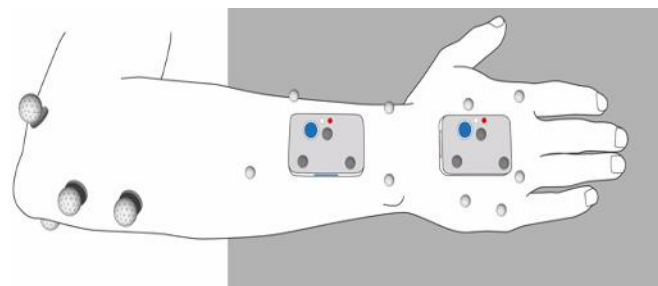


Figure 1: Sensor (IMU), skin marker (light grey, OMC1) and sensor marker (dark grey, OMC2) placement

Methods

Ten healthy volunteers were equipped with both OMC skin markers and IMU on their right hands as depicted in Figure 1 and performed the DTM a total of 10 times on two different days.

The kinematic evaluation of the OMC was based on marker clusters [4] and a functional determination of the wrist joint centre and flexion axis. Joint rotations were calculated according to an established protocol [5]. The kinematic evaluation of the IMU was carried out by the software included in the DyCare® system. The resulting mean \pm

standard deviation angle curves over all trials and subjects were aligned and compared. Absolute ROM in both movement axes were calculated for both systems as well as mean absolute differences (MAD) between the two systems.

Results and Discussion

We found ROM values of 99° for both systems in the flexion/ extension plane with a MAD of 7°. A ROM of 47° for the OMC1 and 62° for the IMU with a MAD of 17° in the radial- ulnar deviation plane was calculated. The calculated angle and velocity curves are depicted in Figure 2. The results show lower agreement between the systems than we found for BMT in an earlier study [1], possible explanations being a differently calculated orientation of the DTM plane for both systems and skin movement artefacts due to the weight of the sensors and skin markers at high velocity movements.

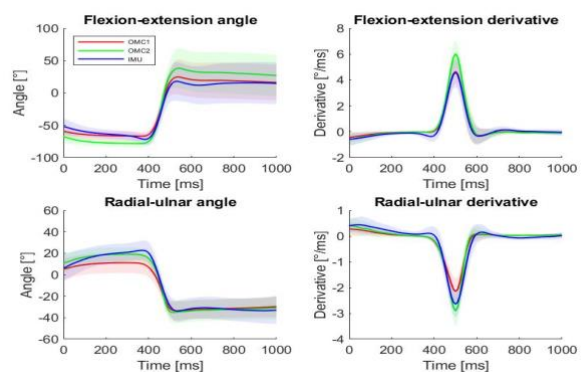


Figure 2: Wrist movement angles and movement speeds in the flexion/ extension and radial/ ulnar deviation plane during DTM

Conclusions

This study shows the challenge of comparing results of different kinematic motion capture systems for complex movements. Further investigations regarding calculation of the orientation of the DTM plane, probably using an imaging technique, would be helpful. Nevertheless, IMU are promising for future clinical application as they allow for measurement of dynamic and coupled wrist movements.

References

- [1] Reissner L et al. (2020). *J. Hand Surg. Eur. Vol.*, **45**: 501-507.
- [2] Wirth MA et al. (2019). *Sensors*, **19**: 5297.
- [3] Cuesta-Vargas AI et al. (2010). *Phys. Ther. Rev.*, **15**:462-473.
- [4] List R et al. (2013). *J. Strength Cond. Res.*, **27**:1529-38.
- [5] Grood ES et al. (1983). *J. Biomech. Eng.*, **105**:136-44.

There is no repeated bout effect on the torque-frequency relationship of the elbow flexors

Avery Hinks¹, Adam Hess¹, Mathew I. B. Debenham¹, Jackey Chen¹, Nicole Mazara¹, Keaton A. Inkol¹, Daniel T. Cervone¹, Lawrence L. Spriet¹, Brian H. Dalton², Geoffrey A. Power¹

¹Human Health and Nutritional Sciences, College of Biological Sciences, University of Guelph, Guelph, Ontario, Canada

²School of Health and Exercise Sciences, University of British Columbia, Kelowna, British Columbia, Canada

Email: ahinks@uoguelph.ca

Summary

High-intensity eccentric exercise can damage and weaken a muscle, and ‘the repeated bout effect’ (RBE) attenuates these impairments following a subsequent bout. It is unclear how the RBE influences torque production across a range of stimulation frequencies (i.e., the torque-frequency relationship). Nine males completed two bouts of high-intensity eccentric elbow flexions, separated by 4 weeks. A torque-frequency relationship was constructed 30 min to 7 days after both bouts. Indirect measures inferred the attenuation of damage in the second bout. Low and high frequencies recovered earlier than middle frequencies and there were no between-bout differences in torque at any frequencies. Therefore, there is not a RBE on the torque-frequency relationship of the elbow flexors.

Introduction

Unaccustomed high-intensity eccentric exercise damages and weakens a muscle, marked by decreased isometric strength and increased serum creatine kinase (CK) and self-reported soreness. Following the exercise, adaptations occur, then when an identical bout is performed several weeks later, damage and weakness are attenuated. This phenomenon is termed the repeated bout effect (RBE) [1,2]. Muscle damage can differentially affect low (~10 Hz) and high-frequency (~50 Hz) torque production, contributing to prolonged low-frequency force depression [1]. However, results in this area have been equivocal [3,4], and the RBE’s influence on torque across a range of stimulation frequencies is unclear.

Methods

Nine recreationally active males (24 ± 2 years, 74.7 ± 13.8 kg, 177.4 ± 6.6 cm) were recruited. Visits were split between Bout 1 and 2, 4 weeks apart. On a dynamometer at a 110° elbow angle, the current that elicited optimal twitch torque by percutaneous stimulation of the elbow flexors was first determined. An isometric maximal voluntary contraction (MVC) of the elbow flexors was then performed. A torque-frequency relationship was then constructed through tetanic stimulations (1000- μ s pulse width, 1-s duration) at 1, 6, 10, 20, 30, 40, 50, and 100 Hz. Participants then performed the eccentric exercise, which was 5 sets of 30 maximal isokinetic eccentric elbow flexions from 50° to 140° at $180^\circ/s$.

All baseline (BL) mechanical measures were repeated 30 min, 24, 48, 72, and 96 hr, and 7 days after the eccentric exercise. Serum CK (from the antecubital vein of the forearm) and self-reported soreness (visual analog scale) were also measured at baseline and throughout recovery. Data in figures are mean \pm standard error ($n=9$).

Results and Discussion

Serum CK, soreness, and MVC torque inferred the RBE’s attenuation of damage in Bout 2, with 820%, 19%, and 18% peak between-bout differences, respectively. A three-way ANOVA (bout[1-2] \times time[BL-7 days] \times frequency[1-100 Hz]) revealed a time \times frequency interaction ($P<0.01$) for tetanic torque, but no bout \times time \times frequency interaction ($P=0.12$). Hence, recovery was similar in both bouts, with Sidak-corrected t-tests showing lower (1-10 Hz) and higher frequencies (40-100 Hz) recovered by 24 hr, and middle-range frequencies (20-30 Hz) recovered by 48 hr (Figure 1).

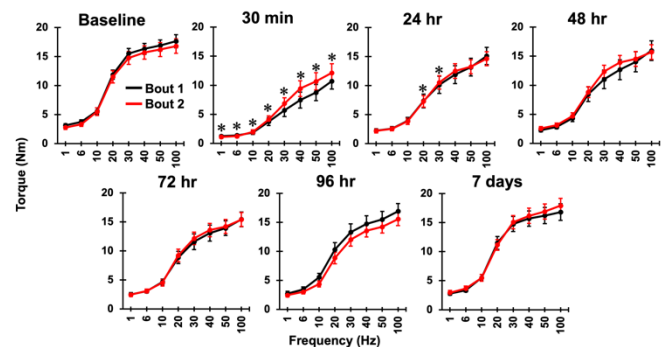


Figure 1: Recovery of the torque-frequency relationship following Bout 1 and 2. *Difference from baseline ($P<0.05$)

Contrary to our results, previous studies observed protection of 10, 15 and 100-Hz torque by the RBE 1-2 days post-exercise, albeit in lower-limb muscles [3,4]. Therefore, the RBE may affect the torque-frequency relationship of upper and lower-limb muscles differently. Future studies should explore peripheral mechanisms that may contribute to the longer lasting impairment of middle-range frequency torque production.

Conclusions

Elbow flexor torque production at middle-range frequencies experienced longer lasting impairment by eccentric exercise-induced weakness than at low and high frequencies. The RBE does not seem to mitigate these impairments.

References

- [1] Clarkson PM and Hubal MJ (2002). *Am. J. Phys. Med. Rehabil.*, **81**: 52-69.
- [2] Hinks A et al. (2020). *Appl. Physiol. Nutr. Metab.*, Epub ahead of print.
- [3] Kamandulis S et al. (2010). *Acta. Physiol.*, **198**: 91-98.
- [4] Bruce CD et al. (2020). *Appl. Physiol. Nutr. Metab.*, Epub ahead of print.

Effects of localized muscle fatigue on muscle activation during a multi-joint repetitive task

E. Renda^{1,2}, C. Yang^{1,2}, J.N. Côté^{1,2}

¹Department of Kinesiology and Physical Education, McGill University, Montreal, Canada

²Occupational Biomechanics and Ergonomics Laboratory, Michael Feil and Ted Obelfed/CRIR Research Centre, Jewish Rehabilitation Hospital, Laval, Canada

Email: erika.renda@mail.mcgill.ca

Summary

The objective of this study was to evaluate the effects of localized fatigue at different arm and trunk joints on electromyographical characteristics recorded during a multijoint, standing repetitive pointing task (RPT) performed with the dominant arm. We recruited 17 young adults. The activation amplitude (RMS), variability (SD) and mean power frequency (MnPF) were calculated for each of the pre-fatigue and post-fatigue RPT trials. Results show that activation of shoulder muscles was greater in all fatigue conditions. Results suggest that agonist (i.e. for the RPT: shoulder) muscles compensate by increasing their involvement during the arm task when either they, or other muscles, are locally fatigued.

Introduction

Previous research on musculoskeletal disorders identified muscle fatigue as one of the risk factors for its development [1]. Muscle fatigue can be defined as a decrease in the maximal force or power one produces for submaximal and/or dynamic contractions [2]. Only a few studies investigated the impact of localized muscle fatigue (i.e. induced by localized efforts of individual muscles involved in a multi-muscle task) on patterns of whole-body tasks [3]. Of those, studies which used electromyography (EMG) measures only evaluated the coordination and co-contraction of the fatigued trunk muscles during a task where the trunk was an agonist [3]. It is not clear how the activity patterns of various muscles involved in a multi-joint task would adapt when fatigue is induced locally at any muscle more or less involved in producing the task.

Methods

Seventeen young adults (8 males) without history of upper body injuries were recruited. Surface EMG electrodes were placed on: upper trapezius, pectoralis major, anterior and middle deltoid, biceps and triceps brachii, and left and right erector spinae. Subjects held a 0.7 kg weight and performed a Repetitive Pointing Task (RPT) in a standing position, moving the dominant index forward and backward at 1 Hz for 30 seconds (non-fatigued RPT (NFRPT)). Afterwards, they completed one shoulder, one elbow and one lower back fatiguing protocol in randomized order, separated by at least 30 minutes, where they held fixed weights and/or postures until exhaustion. Then, they performed the RPT again (after shoulder fatigue: SFRPT, after elbow fatigue: EFRPT, after trunk fatigue: TFRPT). RMS, SD and MnPF were calculated for each muscle during each RPT trial. The Least Significance Difference tests were applied between condition for each EMG variable for each muscle. To correct for type one errors, the Benjamini-Hochberg procedure was implemented.

Results and Discussion

SFRPT: Muscle activation was greater in middle deltoid (MD) compared to the other conditions (NFRPT: $p < 0.001$, EFRPT: $p = 0.024$, TFRPT: $p = 0.0032$), and in anterior deltoid (AD) compared to NFRPT condition ($p = 0.0032$). This demonstrates that when the shoulder muscles are fatigued, the prime movers mainly increased their muscle activation, likely by recruiting more and bigger motor units to keep up with the required pace and maintain the elevated arm posture and the movement performance. SD was greater in anterior deltoid (NFRPT: $p < 0.001$, EFRPT: $p = 0.0021$, TFRPT: $p < 0.001$) and middle deltoid (NFRPT: $p = 0.0015$, EFRPT: $p < 0.001$, TFRPT: $p < 0.001$) in SFRPT in comparison to the other three conditions. The increase in variability suggests that these muscles may be searching for new movement patterns to preserve performance in the presence of fatigue at that joint.

EFRPT: Upper trapezius variability in this condition was greater than in NFRPT ($p = 0.0024$), suggesting that this task's shoulder stabilizer was also searching for more motor unit rotation strategies to adapt to the elbow fatigue condition.

TFRPT: Middle deltoid activation amplitude was significantly greater compared to NFRPT ($p < 0.001$). A reason for this may be that since the trunk muscles are fatigued, the trunk is likely reducing its motion. With less trunk motion, a compensatory strategy would be to further engage the shoulder movers to move the arm from one target to the other.

Conclusions

Muscle activation adaptations to fatigue differ depending on which joint is locally fatigued during the multi-joint task. However, in all fatigued condition, the shoulder muscles compensate by increasing their involvement in the task. Results highlight compensatory strategies in muscles not fatigued, suggesting higher-level processes when adapting to fatigue to coordinate a multi-muscle task.

Acknowledgments

Support provided by Centre for Interdisciplinary Research in Rehabilitation of Greater Montreal (CRIR) and Fonds de Recherche Quebec-Santé (FRQS) doctoral support programs.

References

- [1] Iridiastadi H and Nussbaum MA. (2006). *Hum. Factors*, **48**:710-20.
- [2] Wang L et al. (2018). *Biomed. Res. Int.*, **2018**.
- [3] Gorelick M et al. (2003). *Appl. Ergon.*, **34**:317-25.

Effect of Thumb IP Joint Posture on CMC Joint Movement during Thumb Opposition

Hiroshi Kurumadani¹, Kazuya Kurauchi¹, Shota Date¹, Toru Sunagawa¹

¹Analysis & Control of Upper Extremity Function, Graduate School of Biomedical & Health Sciences, Hiroshima University, Hiroshima, Japan
Email: hkuruma@hiroshima-u.ac.jp

Summary

We examined whether the thumb interphalangeal (IP) joint posture affected the carpometacarpal (CMC) joint movement during thumb opposition. Twenty healthy adults conducted a thumb opposition task with two postural conditions: thumb IP joint extension and flexion. We recorded the three-dimensional thumb movement during tasks and then analyzed the thumb's joint angles and postural synergy in the conditions. The CMC joint angle and posture had become larger and more opposition in the thumb IP joint extension than the thumb IP joint flexion, respectively. We found that the thumb IP joint posture affected the CMC joint movement.

Introduction

The CMC joint of the thumb has a crucial role in thumb opposition; the evaluation of the CMC joint movement in thumb opposition is clinically important [1,2]. For the CMC joint evaluation, it has been discussed that the thumb IP joint posture affects the CMC joint movement in thumb opposition [3]. This study aimed to quantitatively examine the effect of the thumb IP joint posture on the CMC joint movement during thumb opposition.

Methods

Twenty healthy adults conducted a thumb opposition task with two conditions: thumb IP joint extension and flexion. We used the Kapandji test, which opposed the thumb at 11 positions (from 0 to 10 positions) [1,2], as the thumb opposition task.

We recorded the thumb movements during the task using a three-dimensional motion capture system. We computed the

flexion/extension, abduction/adduction, and pronation/supination angles of the CMC joint. Furthermore, we obtained the postural synergy of the thumb using principal component analysis. We compared the CMC joint angles and the postural synergy between the two conditions.

Results and Discussion

The CMC flexion angle had no differences between the thumb IP conditions at most Kapandji positions. The CMC abduction and pronation angles had significant differences between the thumb IP joint conditions; the CMC joint angles in the thumb IP joint extension were more abducted and more pronated than those in the thumb IP joint flexion (Figure 1). Postural synergy showed that thumb posture in the thumb IP joint extension had become more opposition than that in the thumb IP joint flexion. The adduction moment in the flexor pollicis longus muscle would be associated with these differences in the CMC joint movement. [4].

Conclusions

The thumb IP joint posture affects the CMC joint movement; thus, thumb opposition should be evaluated with thumb IP joint extension.

References

- [1] Kapandji IA. (1992). *J Hand Ther*, **5**: 102-106.
- [2] Kuroiwa T, et al. (2019). *J Hand Surg Eur*, **44**: 728-733.
- [3] Tonkin M. (2020). *J Hand Surg Eur*, **45**: 315-317.
- [4] Brand PW. (1999). *Clinical Mechanics of the Hand*, Mosby

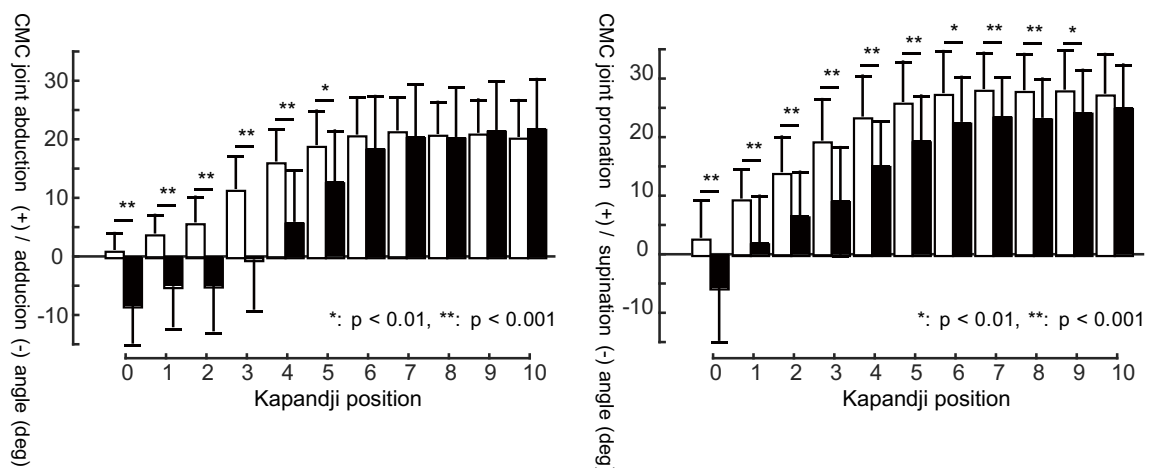


Figure 1. Joint angle of the thumb CMC joint abduction (left) and pronation (right). * and ** shows significant differences between the thumb IP joint extension (white) and flexion (black).

Carpal bone arch changes in response to carpal bone rotation

Andrew S Michalski, Jocelyn Hawk, Zong-Ming Li

Hand Research Laboratory, Departments of Orthopaedic Surgery and Biomedical Engineering

University of Arizona, Tucson, USA

Email: lizongming@arizona.edu

Summary

The hamate and trapezium were independently rotated to assess the influence of carpal bone motion on the carpal bone arch morphology. Carpal bone internal rotation decreased the carpal arch width. Hamate internal rotation reduced the cross-sectional area of the bone arch, but changes were small (<1.5%) at 10 degrees of rotation. The area remained invariant (-0.8% to 1.5%) in the 30 degree trapezium rotation range. These data suggest the space at the bone portion was relatively insensitive to carpal bone rotation within 10 degrees from the initial position.

Introduction

Carpal tunnel syndrome (CTS) is a peripheral nerve entrapment syndrome affecting hand function. CTS symptoms are minimized by reducing the compressive pressure on the median nerve accomplished through carpal tunnel release surgery or compressing the distal wrist to narrow the carpal arch [1]. Carpal arch narrowing has demonstrated improvements to median nerve compression attributable to the increased area of the ligament arch [2]. However, it is unknown how carpal bone rotation associated arch narrowing affects the bone arch space. The purpose of this study was to investigate how internal rotation of the hamate and trapezium would influence the dorsal bone arch of the carpal tunnel. We hypothesized internal rotation of the distal carpal bones would decrease the carpal arch width and decrease the cross-sectional area of the bone arch.

Methods

The carpal tunnel contents were evacuated from one cadaveric hand, and a medial balloon was inserted and pressurized to 10 mmHg using a solution of water and CT contrast agent. The complete hand was scanned using a clinical CT scanner. An axial slice at the distal tunnel, including the hook of hamate and ridge of trapezium (Figure 1), was identified for analysis.

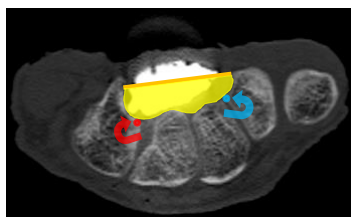


Figure 1: Carpal tunnel CT cross-section. Orange line is the carpal arch width. The yellow region is the carpal bone arch area. Hamate (red dot) and trapezium (blue dot) rotation occurs at 2-degree intervals about the point (arrows).

The carpal bones (hamate, capitate, trapezoid and trapezium) were manually segmented. Landmarks were manually identified on the hamate and trapezium surfaces, corresponding to the dorsal transverse carpal ligament insertion points, identified by the intersection of the carpal tunnel balloon and carpal bones. The line between these

landmarks corresponds to the carpal arch width (Figure 1, orange line). The other set of landmarks corresponds to the rotation points on the hamate (Figure 1, red point) and trapezium (Figure 1, blue point), identified by the innermost point on the carpal arch surface of each bone. The hamate or trapezium was independently and iteratively rotated 30 degrees about the rotation point at 2-degree intervals. Carpal bone arch area was defined as the area contained by the carpal bones' inner surfaces and the arch width line. The carpal arch width and area were measured at each rotation.

Results and Discussion

As the hamate or trapezium was internally rotated by 2-degree intervals, the carpal arch width progressively decreased. The arch width decreased by 4.5 and 3.1 mm at the 30-degree rotation of the hamate and trapezium. As the rotation angle of the hamate bone increased, the carpal bone arch area decreased, but the decrease was small (<1.5% at 10 degrees). As the trapezium was internally rotated, the carpal bone arch area varied within 1.5% (Figure 2).

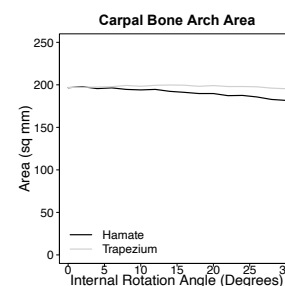


Figure 2: Measured carpal bone arch area with increasing internal rotation of the hamate (black) or trapezium (gray).

Narrowing of the carpal arch width has been shown to increase the ligament arch area [2-4], and this study showed that narrowing the arch by rotating the carpal bones within 10 degrees had a relatively small influence on the bone arch area. Our data suggests that internally rotating the distal carpal bones decreases the carpal arch width and does not affect the bone arch area. Further investigation is needed to understand the implications to the total carpal tunnel area.

Conclusions

Little change in the carpal bone arch area was observed with rotational perturbation to the carpal bones. These findings suggest that the carpal tunnel space is relatively insensitive to carpal bone motion, and the carpal ligament arch may play a more significant role in increasing the carpal tunnel cross-sectional area and decompressing the median nerve.

References

- [1] Yao Y et al. (2019). *J Orthop Transl*, **18**: 13-19.
- [2] Marquardt TL et al. (2015). *Clin Biomech*, **30**: 248-253.
- [3] Li ZM et al. (2013). *Clin Biomech*, **28**: 402-407.
- [4] Shen ZL & Li ZM. (2013). *J Appl Physio*, **114**: 225-229

INTER- AND INTRA-PARTICIPANT UNIFORMITY OF MUSCLE ACTIVATION DURING WRIST MOTION

Oluwalogbon O. Akinnola¹, Vasiliki Vardakastani¹, Angela E. Kedgley¹
¹Department of Bioengineering, Imperial College London, London, UK
 Email: o.akinnola16@imperial.ac.uk

Summary

The activity of seven forearm muscles were recorded during wrist flexion-extension, radial-ulnar deviation, and dart thrower's motion. Inter- and intra-participant comparisons showed people perform tasks with a consistent muscle activity pattern unique to them. The presence of co-contraction indicates that stability, not energy efficiency, may be a priority at the wrist.

Introduction

Electromyography (EMG) has been used to diagnose pathology and validate musculoskeletal models [1, 2]. Muscle activation patterns have been found to be similar for people performing the same task in the lower limb [3]. Standard activation patterns have not been reported for the upper limb, but it has been found that finger contact forces and moments are similar between people performing prehensile tasks [4]. This study seeks to establish if muscle activation patterns for fundamental and functional motions of the wrist are consistent both within and between people.

Methods

23 participants (1.71 ± 0.08 m, 68.26 ± 12.66 kg, 28.6 ± 4.60 years) took part in this study. Each participant performed three sets of five cycles of wrist flexion-extension (FE) radial-ulnar deviation (RUD), pronation-supination (PS), and dart throwing motion (DTM) with their dominant hand. The muscle activity of extensor digitorum communis (EDC), extensor carpi radialis (ECR), extensor carpi ulnaris (ECU), flexor digitorum superficialis (FDS), flexor carpi radialis (FCR), flexor carpi ulnaris (FCU), and pronator teres (PT) were recorded using surface EMG sensors (Delsys, Natick, MA). Statistical Parametric Mapping (SPM) non-parametric Multivariate ANOVA (MANOVA) was used to test for differences between the muscle activation patterns. The mean Pearson Correlation Coefficient (PCC) between the participants also calculated.

Results and Discussion

No difference was found within participants between the muscle activation patterns for each set of cycles. Activation

patterns for different motions performed by the same participant differed ($p < 0.01$). Post-hoc analysis found that activation patterns for all participants differed from all other participants in every motion ($p < 0.0002$). Qualitative comparison showed different levels of co-contraction (Figure 1). Mean PCCs varied between 0.40 – 0.66.

People showed a consistent muscle activation pattern when performing a specific motion repeatedly, but this pattern differed from one individual to another. Moderate correlation across participants for all the muscles was seen. Muscles have specific anatomical functions, so some correlation is expected but it was not strong. This could be different neuromuscular strategies or a consistent strategy applied to different physiology. Co-contraction was consistent in a participant across motions but varied across them. This ranged from co-activation of multiple synergistic agonists to activation of only a select few muscles. Literature showed extended activation increases metabolic cost [5] and proposed that co-activation of the antagonist muscles in the upper limb is adopted to manage unstable interactions with the environment [6]. Thus, wrist stability during motion may be more important than conserving energy to allow for precise manipulation. This has implications for the level of subject-specificity required for the development of musculoskeletal models of the wrist.

Conclusions

Our data indicate that physiological differences may lead to varying levels of co-contraction to achieve stability. The presence of co-contraction indicates that minimising energy expenditure is not a priority at the wrist.

References

- [1] Hogrel (2005) *Neurophys. Clin. Neurophys.*, **35**, 59–71.
- [2] Beaucage-Gauvreau et al. (2019) *Comput. Methods Biomech. Biomed. Engin.*, **22**, 451–464.
- [3] Hof et al. (2002) *Gait Posture*, **16**, 78–86.
- [4] Zatsiorsky et al. (2004) *Robotica*, **22**, pp. 231–234.
- [5] Moore et al. (2013) *J. Sci. Med. Sport. Aust.*, **17**.
- [6] Borzelli, et al. (2018) *PLOS ONE*, **13**

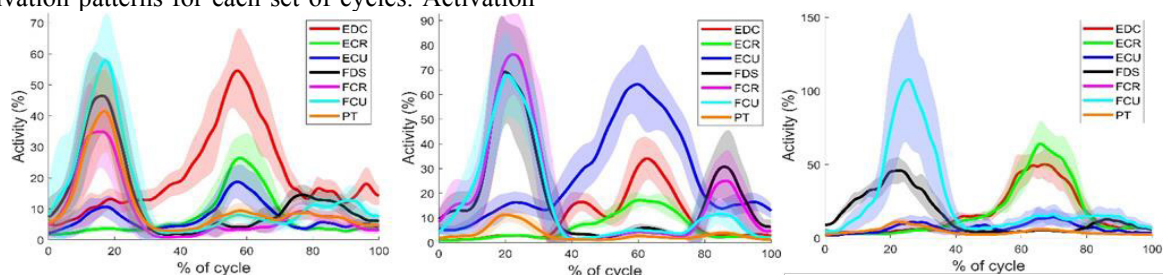


Figure 1: Mean (\pm 1STD) muscle activation patterns for three participants with different levels of co-contraction for 15 cycles of flexion-extension.

Capturing In-season Change of Direction Movement Pattern Variability in Youth Soccer Players with IMUs

Aki-Matti Alanen PT, MSc¹, Olivia Bruce MSc², Lauren Benson¹, Mathieu Chin BSc¹, Carla van den Berg MSc¹, Matthew J. Jordan PhD^{4,5}, Reed Ferber^{5,6,7}, Kati Pasanen PT, PhD^{1,3,8,9}

¹Sport Injury Prevention Research Center, Faculty of Kinesiology, University of Calgary, Calgary, Canada

²Human Performance Laboratory, Faculty of Kinesiology, University of Calgary, Calgary, Canada

³Alberta Children's Hospital Research Institute, University of Calgary, Calgary, Canada

⁴Canadian Sports Institute, Calgary, Canada

⁵Faculty of Kinesiology, University of Calgary, Calgary, Canada

⁶Running Injury Clinic, Calgary, Canada

⁷Faculty of Nursing, Cumming School of Medicine, University of Calgary, Calgary, Canada

⁸McCaig Institute for Bone and Joint Health, University of Calgary, Calgary, Canada

⁹Tampere Research Center of Sports Medicine, UKK Institute, Tampere, Finland

Email: akimatti.alanen@ucalgary.ca

Summary

Change of direction (COD) ability predicts sport performance and COD movement strategy is associated with sport injury.[1] Nevertheless, current laboratory-based testing methods lack ecological validity. Inertial measurement units (IMU) may assist practitioners to assess individual on-field COD movement patterns.

Introduction

A more acute COD cut angle increases tissue stress and strain that are thought to increase injury risk and these movements occur readily in soccer. IMUs provide the possibility of on-field COD analysis. However, there is no consensus on the relevant IMU signal features. Peak resultant acceleration is a commonly used feature in IMU based movement detection in sports.[3] The aim of this study was to analyze the individual within-season variability of accelerometer features in a COD test.

Methods

U15-U17 soccer players (n=7 females, n=12 males) performed two soccer-specific COD tests separated by two months.

Two bi-directional maximal effort COD maneuvers were performed at 3 cut angles (180°, 135° and 90°) and value from last trial was used. IMU sensors (Shimmer 3 IMU) were placed on both lower limbs and lower back. Trials were video recorded, tagged in Dartfish (Dartfish Live S) and synced with IMU data.

The penultimate foot ground contact (PFC) and final foot ground contact (FFC) were tagged for each limb. Peak resultant acceleration for PFC and FFC, time to peak acceleration, time between PFC and FFC and shock attenuation were extracted and used for analysis.

Results and Discussion

As a representative example of the variability observed in the outcome measures, intra-subject variability was found to be substantial for FFC peak acceleration (Figure 1). This was supported by poor to moderate intraclass correlation (ICC 3,1) coefficients between tests (ICC = 0.66, range for all

measures = -0.3 to 0.66) regardless of sensor placement. There were no systematic group changes observed that could be explained by the timing of the two tests.

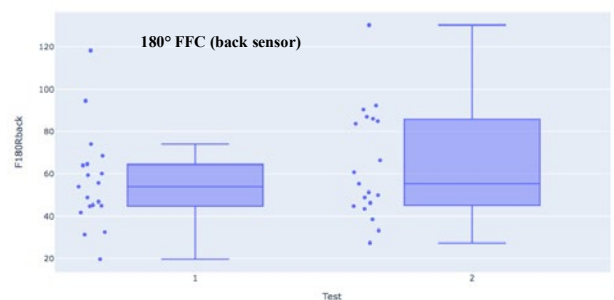


Figure 1: Individual Change in Peak Resultant Acceleration

Conclusions

As COD movement strategies are associated with sport injury, our data highlights the use of IMU technology to detect individual in-season change in COD patterns so that targeted training interventions can be applied to increase performance or decrease injury risk. A more thorough assessment of the reliability of the IMU signal features over a shorter time frame is needed. This would help practitioners to determine the stability of the measures, the number of tests that should be performed to establish the COD movement pattern, and relevant measures for sport performance and injury risk detection.

Acknowledgments

We thank all study participants and research assistants for their participation. The Sport Injury Prevention Research Center is one of the International Research Centers for Prevention of Injury and Protection of Athlete Health supported by the International Olympic Committee.

References

- [1] Sankey et al. (2020). *Whole-body dynamic stability*. *Am J Sports Med*, 104:109711.
- [2] Bloomfield et al. (2007). *Physical Demands of Different positions*. *J of Sport Sc and Med*; **6**: 63-70.
- [3] Chambers et al. (2015). *The Use of wearable microsensors*. *Sports Med*. **45**:1065-81

Classification of High Knee Flexion Postures Using Feature and Time-Series Based Distance Approaches

Annemarie F. Laudanski¹, Arne Küderle², Felix Kluge², Bjoern M. Eskofier², and Stacey M. Acker¹

¹Department of Kinesiology, University of Waterloo, Waterloo, ON, Canada

²Department of Computer Science, Friedrich-Alexander Universität, Erlangen, Germany

Email: annemarie.laudanski@uwaterloo.ca

Summary

Childcare workers spend a significant portion of their working hours adopting high knee flexion postures, despite their association with increased risk for musculoskeletal injury development. This study compared means of identifying these postures based on the classification of inertial data using both feature and time-series based distances, in order to identify a classifier capable of providing objective data on the demands of this occupation. Results suggest that comparing inertial based ankle, knee, and hip flexion angle estimates using Dynamic Time Warping distances as inputs to a k -Nearest Neighbor classification algorithm offers a promising means of identifying high flexion postures in childcare settings.

Introduction

Occupational exposures to high knee flexion postures, such as kneeling or squatting, result in increased risk of joint tissue degradation and osteoarthritis development [1]. Despite this association, frequent pain reporting, and a limited understanding of work-related exposures in childcare, few guidelines and little quantitative data exist to manage the adoption of these postures in workplace settings [2]. The objective of this study was therefore to compare classification approaches for inertial measurement unit (IMU) data in order to determine the most suitable means of identifying high knee flexion postures in occupational childcare settings.

Methods

Twenty participants completed 3 repetitions of 8 high flexion and 2 upright postures, frequently adopted in childcare, which were grouped into 6 movement categories (Table 1). Each participant was instrumented with 4 IMUs, attached to the base of the sacrum, the lateral aspect of the right upper and lower leg, and the superior aspect of the right mid-foot.

IMU signals were calibrated based on a 10-m walk and two isolated joint motion trials, consisting of rotations about the hip and the knee respectively, and flexion angles for the ankle, knee, and hip were subsequently estimated [3,4]. Two variations of a k -Nearest Neighbor (kNN) cross-validated classifier were developed and compared in order to determine the most robust approach for the identification of childcare related postures. In the first, time-domain features (maximum, minimum, mean, and standard deviation) for each flexion angle were extracted from consecutive windows of 500 ms, with a 50% overlap. These 12 features were combined with movement labels to create an ($n \times 13$) training dataset containing n trial windows, which were compared and classified based on Euclidean distances. The second classifier relied on a time-series based approach, where the training dataset was composed of movement labels and the

corresponding flexion angles, scale normalized between -1 and 1, combined tip to tail. Dynamic Time Warping (DTW) based distance metrics for classification were calculated between each of the ($n \times 344$) consecutive 2 s windows. For both training sets, a 5-fold cross validated nearest neighbor classifier ($k = 1$) was developed using 80% of the training data while the remaining 20% was withheld for testing.

Results and Discussion

Overall accuracies of 41.1% and 79.8% were reached when classifying postures through feature and time-series based kNN approaches respectively. Movement sensitivity and specificity can be found in Table 1. The highest rates of misclassification in the DTW-based approach were observed between unsupported and supported kneeling, suggesting that these postures could potentially be grouped into a single kneeling category if their separate study was not of interest.

Table 1: Sensitivity and specificity (%) for childcare postures classified using feature and time-series based kNN approaches.

Classifiers	Sensitivity		Specificity	
	Feature based kNN	DTW based kNN	Feature based kNN	DTW based kNN
Movement Categories				
Unsupported Kneeling (dorsiflexed, plantarflexed)	44.8	78.2	84.31	93.0
Supported Kneeling (single and double hand supported)	38.4	72.7	83.3	91.6
Squatting (flatfoot, heels-up)	42.5	84.9	86.4	96.0
Sitting on a child-sized and adult-sized chair	39.9	81.1	88.7	96.2
Standing still	45.3	83.3	97.6	99.4
Walking	33.8	95.5	95.4	99.3

Conclusions

While classification results must be validated in continuous data, as would be collected in childcare settings, the DTW-based nearest neighbor classification of time-series data offers promise for the identification of high flexion postures.

Acknowledgments

Funding provided by the Canadian Foundation for Innovation, NSERC Canada, and the ISB International Travel Grant.

References

- [1] Coggon, D et al. (2000) *Arthritis Rheum* **43**(7);p.1443-1449
- [2] Holtermann A et al. (2020) *Ann. Work Expo. Health* **64**(6); p.586-595
- [3] Seel, T et al. (2014) *Sensors* **14**; p.6891-6909
- [4] Küderle, A. et al. (2018) *Curr. Dir. Biomed. Eng* **4**(1);p.439-444

Validation of a wearable sensor OpenSense model for evaluating motor variability in gait

Christopher A. Bailey¹, Julie Nantel¹, Ryan B. Graham¹

¹School of Human Kinetics, University of Ottawa

Email: cbailey2@uottawa.ca

Summary

Stride-to-stride variability in gait is a factor associated with falls in older adults. Currently, there is no known inexpensive and opensource method available for evaluating variability of the underlying joint motions outside of the lab and clinic. We propose an inertial measurement unit (IMU) OpenSense model of joint angle variability. Trunk-down joint angles were estimated from optoelectronic and IMU motion capture, and variability was quantified by conventional and dynamical systems metrics. In a preliminary evaluation, IMU modelled variability patterns approximated optoelectronic patterns, with similar mean standard deviation (meanSD), statistical persistence (α), and maximum Lyapunov exponents (λ_{\max}). Preliminary findings suggest that the IMU-OpenSense model measured both the magnitude and dynamics of joint angle variability accurately during treadmill gait.

Introduction

Motor variability, the existing variability in sensorimotor actions like joint motions, is a control principle of gait linked to fall risk. Measurements include the inter-stride standard deviation to quantify the magnitude of variability [1] and dynamical systems metrics to quantify quality of stride-to-stride control [2]. Current kinematic evaluation methods select a non-portable evaluation of joint motion [1] or a portable but limiting evaluation of variability in segment motion [3]. An approach is still needed for a robust and portable evaluation of stride-to-stride joint control in gait. One potential approach is simulating inverse kinematics from segment-worn IMUs, which can estimate joint angles to $\sim 3^\circ$ of error [4]. Since many variability measurements are not limited by initial posture estimations by IMUs, there is high potential for accuracy. Thus, the objectives of this study were to test the validity of an IMU-driven model of joint angle variability in gait and the sensitivity of the model to varied gait conditions.

Methods

Young adults (N = 16, 8 females) will be recruited; data are available for one young male (aged 29 years). Motion data were acquired optoelectronically (Vicon Vantage) and by IMUs (Xsens Dot). Markers were placed according to the Rajagopal full body model [5] and IMU sensors were placed on the trunk, pelvis, thighs, shanks, and feet. The participant completed five 7-minute trials of treadmill gait under varied conditions: preferred speed (1.16 m/s), 70% preferred speed, 130% preferred speed, active arm swing at preferred speed, and arms-held at preferred speed. Optoelectronic and IMU motion data were input into the full body OpenSim model to simulate lower limb joint angles [5], using the OpenSense tool kit for IMU-to-segment calibration and inverse kinematics. Joint angles were partitioned into individual strides and synchronized between methods by the foot velocity profile.

Variability outcomes were the meanSD, scaling exponent α of range of motion, obtained via detrended fluctuation analysis,

and λ_{\max} of the continuous timeseries for each joint angle degree of freedom. IMU outcome validity (relative to optoelectronic) will be tested by established metrics and methods (e.g. root mean square error, intraclass correlation coefficients, Bland-Altman plots), and sensitivity will be analyzed by Condition*Method ANOVAs.

Preliminary Results

IMU variability patterns appeared to approximate optoelectronic patterns across lower limb joints in normal speed gait (e.g. left ankle dorsiflexion/plantarflexion in Figure 1).

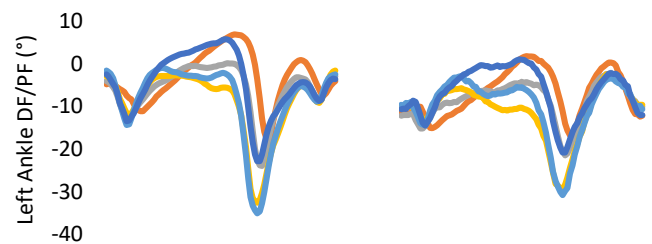


Figure 1. IMU (left) and optoelectronic-modeled (right) dorsiflexion/plantarflexion (DF/PF) in five consecutive, matched strides.

MeanSD, α , and λ_{\max} of left ankle dorsiflexion/plantarflexion were similar between the IMU and optoelectronic models, which was a consistent observation across joints and degrees of freedom (Table 1). This suggests that the IMU model accurately measured joint variability magnitude, persistence, and local dynamic stability in the young male. Further data acquisition is needed to verify this initial observation and to evaluate whether measurements are sensitive to changes across conditions and to interindividual differences.

Table 1. Left ankle dorsiflexion/plantarflexion variability outcomes.

	meanSD (°)	α	λ_{\max}
IMU	2.17	0.54	1.837
Optoelectronic	2.00	0.87	1.843

Acknowledgments

This project is supported by a uOttawa-CHEO Research Fellowship, NSERC, and the Ontario Early Researcher Award Program.

COVID-19 Note

Regretfully, COVID-19 delayed data acquisition. However, at the time of submitting this abstract, data can now be acquired and so completed results will be available in time for ISB 2021.

References

- [1] Bailey CA et al (2020). *J Biomech*, **99**:109574.
- [2] Cusumano JP et al (2013). *Hum Mov Sci*, **32**:899-923.
- [3] Helbostad et al (2007). *J Am Geriatr Soc*, **62A**:1010-15.
- [4] Seel T et al (2014). *Sensors*, **14** :6891-6909.
- [5] Rajagopal et al (2016). *IEEE Trans Biomed Eng*, **63**:2068-79.

Between-day and Between-condition Reliability for Accelerometer Measurements of Ground Contact Time

Hannah L. Dimmick¹, Zoe Y.S. Chan^{1,2}, Angela Senevirathna¹, Andrew J. Pohl¹, Reed Ferber¹

¹Faculty of Kinesiology, University of Calgary, Calgary, Canada

²Department of Rehabilitation Sciences, The Hong Kong Polytechnic University, Hong Kong

Email: hannah.dimmick@ucalgary.ca

Summary

Increase in the use of accelerometers to analyze gait variables, such as ground contact time, provides the potential for greater insight into real-world environments. However, care must be taken to avoid generalizing laboratory-based results to real-world conditions. This study sought to determine the reliability of ground contact time between an indoor track and outdoor run over the course of 3 days. Results showed that inter-day reliability for each condition was excellent, but intra-day reliability between conditions demonstrated only moderate agreement.

Introduction

Most studies using accelerometry to analyze “overground” running are performed on controlled surfaces (i.e. indoor tracks), whereas most runners exercise outdoors. Thus, research is warranted on whether data derived from controlled conditions can be reliably translated to less controlled, outdoor environments. Ground contact time (GCT) is a metric frequently used in biomechanical research and has been shown to be a valid predictor of running performance [1]. The aim of this study was to determine whether GCT measured by a back-mounted tri-axial accelerometer is reliable when measured across several days in either a controlled indoor run or an outdoor overground run.

Methods

Nine recreational runners (4F, 5M; age = 24.22 ± 4.12 yrs) completed 3 testing sessions on 3 separate days within a 21-day period. Each session involved two experimental protocols following a 5-minute warm-up: one 2km indoor run (200m track) and one 2km outdoor run, each at a self-selected speed (indoor = 3.15 ± 0.28 , outdoor = 3.06 ± 0.37 m/s). The order of conditions was randomized each day.

During each session, an inertial measurement unit (IMU) containing a tri-axial accelerometer (Shimmer3®; Shimmer Inc., Ireland: 200 Hz) was securely attached to the low back between L3-L5 vertebrae with orthogonal axis -x, y and z aligned in the mediolateral, vertical and anteroposterior directions.

Acceleration data were low pass filtered at 10 Hz and data were analyzed from the first 5-minute epoch of each condition, excluding the initial 30 seconds to account for the acceleration phase. GCT was calculated as the time difference between the initial contact and toe off for each stride and averaged across the 5-min epoch according to methods described by Benson et al. [2].

Between-session reliability for each condition was evaluated by intraclass correlation coefficients (ICC 2,k) calculated. Values of <0.5, 0.5-0.75, 0.75-0.9 and >0.9 were interpreted as poor, moderate, good, and excellent, respectively [3]. Between-condition reliability was evaluated using Bland-Altman limits of agreement (LoA)

for each day, and a two-way repeated measures ANOVA ($\alpha=0.05$) condition [indoor vs outdoor] \times day [1 vs 2 vs 3].

Results and Discussion

When GCT was compared across all three sessions, ICCs were 0.908 and 0.951 for the indoor and outdoor conditions, respectively, demonstrating excellent between-day reliability. This result suggests that GCT estimated from tri-axial accelerometers mounted on the low back is reliable over time when conditions are similar. For intra-day, between-condition analysis, there was no significant condition \times day interaction ($P=0.528$) or significant main effects for condition ($P=0.526$) or day ($P=0.951$). LoA for each day are shown in Figure 1. Although no significant differences were detected between days or conditions via ANOVA, only moderate agreement between conditions (mean bias=5.52 ms; LoA range 44.81-50.87 ms) can be observed. Thus, caution is warranted in presuming agreement for GCT across conditions.

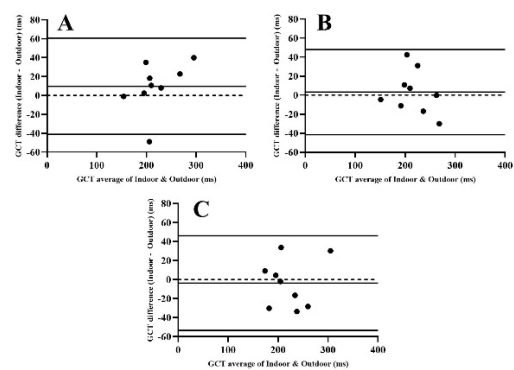


Figure 1: Bland-Altman LoA plots of GCT for (A) day 1, (B) day 2, and (C) day 3. Mean bias and 95% limits of agreement are represented by the solid lines.

Conclusions

GCT derived from a single, back-mounted tri-axial accelerometer demonstrated excellent between-day reliability within surface condition, but only moderate between-condition reliability. These results should be considered in future studies when extrapolating indoor accelerometry data to outdoor overground conditions, as well as by manufacturers of wearable devices that report this metric.

Acknowledgments

This study was funded by the NSERC CREATE We-TRAC Training Program and an NSERC Discovery Grant.

References

- [1] Hayes P and Caplan N (2012) *J. Sports Sci.*, **30**(12): 1275-1283.
- [2] Benson LC et al. (2019) *Sensors*, **19**(7): 1483.
- [3] Koo TK and Li MY (2016). *J Chiropr Med*, **15**(2): 155-163.

Using Wearable Technology to Quantify Adherence to a Neuromuscular Training Warm-Up in Youth Basketball and Soccer Players

Lauren C. Benson^{1,2}, Anu M. Räisänen³, Sartaj S. Sidhu⁴, Carolyn A. Emery^{4,8}

¹Department of Sports Medicine, United States Olympic and Paralympic Committee, Colorado Springs, USA

²Faculty of Kinesiology, University of Calgary, Calgary, Canada

³Department of Physical Therapy Education, College of Health Sciences, Western University of Health Sciences, Lebanon, USA

⁴Sport Injury Prevention Research Centre, Faculty of Kinesiology, University of Calgary, Calgary, Canada

⁵McCaig Bone and Joint Institute, Cumming School of Medicine, University of Calgary, Calgary, Canada

⁶Alberta Children's Hospital Research Institute, University of Calgary, Calgary, Canada

⁷Department of Community Health Sciences, Cumming School of Medicine, University of Calgary, Calgary, Canada

⁸Department of Pediatrics, Cumming School of Medicine, University of Calgary, Calgary, Canada

Email: lauren.benson@ucalgary.ca

Summary

Youth athletes wore an IMU on their lower back while completing a neuromuscular training warm-up program with concurrent video recording. The videos were evaluated to determine if athletes completed the prescribed exercise volume. Algorithms were developed to quantify exercise volume from the IMU signal. Excellent algorithm accuracy suggests that IMUs may be used to quantify exercise volume during a neuromuscular training warm-up program.

Introduction

Sport injuries among youth can have long-term consequences, such as the increased risk of osteoarthritis [1]. Neuromuscular training (NMT) warm-up programs are effective in preventing injuries in youth sports [2]. Ensuring that the athletes are performing the NMT warm-ups as prescribed is critical to achieve the benefits of NMT warm-up programs [3].

Monitoring exercise volume through direct observation or video recording is time consuming and difficult to conduct in a team setting. Inertial measurement units (IMUs) may be effective at measuring the volume of some exercises by leveraging their ability to record impacts and changes in orientation. The purpose of this study was to evaluate the accuracy of using IMUs to measure exercise volume during a NMT warm-up in basketball and soccer.

Methods

Participants were female and male youth basketball and soccer players performing single leg jumps (front to back), double leg jumps (in place), Nordic hamstring curls, and/or single leg balance exercises as part of a NMT warm-up prior to their typical practice. Video of the exercises was recorded, and participants wore an IMU on their lower backs. A physiotherapist evaluated the videos and determined if each

participant performed the prescribed exercise volume for each exercise. Algorithms were developed for each exercise to count the number of repetitions based on the IMU signal. The repetitions counted using the algorithms were compared to the gold standard from the physiotherapist evaluation in terms of accuracy, precision, and recall.

Results and Discussion

A total of 91 (39 female, 52 male) youth athletes performed at least one of the four warm-up exercises. There was greater than 0.94 accuracy, precision and recall for all exercises except single leg balance which had accuracy of 0.889, precision of 0.897 and recall of 0.956. The single leg jump algorithm classified all sets correctly (Table 1). The high classification accuracy is consistent with other algorithms that use IMUs to count repetitions during gym exercises [4].

Conclusions

IMUs may be used to quantify exercise volume for exercises that involve both impact during landing and changes in orientation during rotations. Using IMUs to monitor exercise volume could be used to explore the association between exercise volume during a NMT warm-up and injuries.

Acknowledgments

The University of Calgary Sport Injury Prevention Research Centre is one of the International Research Centres for Prevention of Injury and Protection of Athlete Health supported by the International Olympic Committee.

References

- [1] Thomas AC et al. (2017). *J Athl Train*, **52**: 491-496.
- [2] Brunner R et al. (2019) *Br J Sports Med*, **53**: 282-288.
- [3] Steffen K et al. (2013). *Br J Sports Med*, **47**: 794-802.
- [4] Soro A et al (2019). *Sensors*, **19**: 714.

Table 1: Algorithm Performance.

Exercise	Total Sets	Accuracy	Precision	Recall
Single Leg Jumps	95	1.000	1.000	1.000
Double Leg Jumps	91	0.945	0.974	0.962
Nordic Hamstring Curls	49	0.959	0.957	1.000
Single Leg Balance	126	0.889	0.897	0.956

Validation of In-Shoe Force Sensors for Measuring Ground Reaction Forces During Walking

Kaleb Burch¹, Sagar Doshi¹, Erik Thostenson¹, Jill Higginson¹

¹University of Delaware, Newark, Delaware, USA

Email: kburch@udel.edu

Summary

Fabric-based nanocomposite pressure sensors [1] placed in shoes were validated for measurement of ground reaction forces (GRF). A detailed calibration and validation approach is presented. The sensors exhibit good agreement with force plate (FP) measurements for six subjects walking at 3 speeds.

Introduction

Quantification of GRF, particularly maximum vertical GRF, offers clinical value for applications such as detecting overloading during a partial weight-bearing regimen [2]. Consequently, wearable sensors such as pressure-sensitive shoe sensor (SS) systems [3] have been designed with the goal to continuously record GRF during daily life. This study seeks to introduce a simple SS system and validate it against FP measurements for quantification of peak and absolute maximum GRF during walking.

Methods

Ten subjects (age: 23.3 ± 2.5 years, mean \pm std; mass: 75.2 ± 18.2 ; 5 male and 5 female) performed calibration trials and then walking trials on an instrumented treadmill (Bertec Corp, Worthington, OH, USA). FPs recorded GRF (2000 Hz) and an Arduino Uno Rev3 (mean frequency of 28Hz) recorded resistance from sensors on the hindfoot and forefoot. Calibration trials involved 3 repetitions of shifting one's body weight (BW) onto and off of individual sensors. Six total 30-second walking trials were conducted with 2 repetitions each of 3 speeds (0.5 m/s; 1.0 m/s; 1.5 m/s); order was randomized.

The loading phase of the calibration trials was used to calibrate sensor resistance to force. Walking trials were evaluated using cross validation, where all 8 subsets of data that include 1 trial each at all 3 speeds were considered. Within each subset, the following process was carried out. The two FP peak forces from 12 gait cycles (GCs) per trial were extracted, as well as both SS forces at those times. SS forces were scaled to approximate FP force using the least-squares method. Then, 12 steps from each of the 3 trials not used for calibration were used to compare SS with FP using the Bland-Altman method. This analysis was performed on 2 sets of data: (1) both GRF peaks (2PK) in each GC and (2) the maximum GRF (MAX) in each GC. Results were evaluated

in terms of mean of difference (MoD) and reproducibility coefficient (RPC).

Results and Discussion

GRF of the SS system closely matched the FP in shape and magnitude (Figure 1). The Bland-Altman results showed varying levels of agreement across subjects (Table 1). Results varied depending on whether 2PK or MAX was considered. Under the 2PK assessment, the MoD was less than 2% for all but one subject. Likewise, RPC was less than 24% for all but one subject. Under the MAX assessment, the MoD was less than 4% for all subjects. RPCs ranged from 8.5 – 33.8%; most subjects were around 10%. This is comparable to another SS study [3] that obtained an estimated RPC of 10.4%.

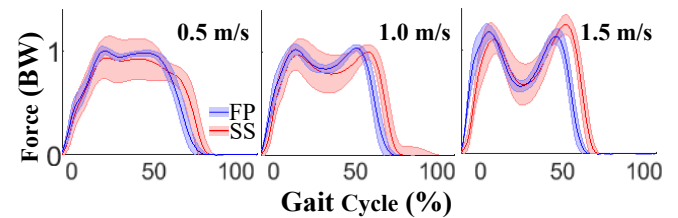


Figure 1. GRF curves (mean \pm std) for SS and FP from all 6 subjects over all GC at each speed. Results from a representative subset of data, identified by proximity to mean RPC, are used.

We expect that these sensors could be useful for providing feedback on overloading for patients prescribed with a partial weight-bearing regimen [2].

Conclusions

This sensor system offers reasonable maximum force measurements for walking at 3 different speeds.

Acknowledgments

UNIDEL Foundation, Inc

References

- [1] Doshi et al. (2018) *ACS Sens.* **3**: 1276-1282.
- [2] Hurkmans et al. (2012) *Arch Phys Med & Rehab*, **93**: 565-570.
- [3] Howell et al. (2013). *IEEE Trans Bio Eng*, **60**: 3284-3290.

Table 1. MoD and RPC for each subject, reported as mean \pm standard deviation, which are obtained from the 8 outcomes from the cross-validation. Both MoD and RPC are expressed as percentages of the measured peak values.

Subject	1	2	3	4	5	6	Mean	
Condition	Variable							
Two Peaks	MoD (%)	-1.8 ± 1.2	-1.8 ± 1.7	-7.7 ± 2	-0.6 ± 0.7	-0.8 ± 5.6	-0.5 ± 1.8	-2.2 ± 2.76
	RPC (%)	23.9 ± 0.9	22.6 ± 1	42.9 ± 3.6	16.8 ± 1.4	23.3 ± 2.3	14.9 ± 2.1	24.07 ± 9.94
Maximum	MoD (%)	0.8 ± 1.1	0.7 ± 2	-4 ± 1.4	1.6 ± 1.7	4.1 ± 5.3	1.4 ± 1.3	0.4 ± 2.69
	RPC (%)	8.5 ± 0.4	19.5 ± 0.8	33.8 ± 1.2	9.3 ± 1.7	11.3 ± 3.6	10.2 ± 1.6	15.43 ± 9.84

A Weighed K-Nearest Neighbors classifier as a tool for identification of activities of daily living in subjects with Parkinson's Disease

Alberto I. Perez-Sanpablo¹, Claudia Hernandez-Arenas², Jimena Quinzaños-Fresnedo², Alicia Meneses Peñaloza³, Arturo Gonzalez-Mendoza¹, Ivett Quiñones-Uriostegui¹

¹Human Motion Analysis and Rehabilitation Engineering Lab, National Institute of Rehabilitation Luis Guillermo Ibarra Ibarra, Mexico City, Mexico

²Neurologic Rehabilitation Department, National Institute of Rehabilitation Luis Guillermo Ibarra Ibarra, Mexico City, Mexico

³Pediatric Rehabilitation Department, National Institute of Rehabilitation Luis Guillermo Ibarra Ibarra, Mexico City, Mexico

Email: albperez@inr.gob.mx

Summary

Inertial measurement units (IMUs) are promising to evaluate quality of movement during activities of daily living (ADL) of subjects with Parkinson's Disease (PD). Here we introduced a classifier to identify ADL. In total 179555 observations were analyzed. Classifier reached an accuracy higher than 99%. Therefore, the classifier has potential to support monitoring of PD subjects using IMUs.

Introduction

Inertial measurement units (IMUs) are promising to evaluate quality of movement during activities of daily living (ADL) performed by people with movement disorders, particularly people with Parkinson's Disease (PD), due to their accuracy, ubiquitousness, unobtrusiveness, and low cost [1][2][3]. IMUs applications comprise detection and monitoring of motor fluctuations. However, most studies reported in literature have limitations related monitoring during free living conditions where ADL are performed. Therefore, we introduced a classifier to identify ADL performed by subjects with PD which could be helpful to support monitoring using IMUs.

Methods

To build the classifier and to test its ability to detect ADL, it was necessary to register movement data of six common ADL performed on one session during on medication state of PD subjects. Four IMUs shimmer3 (Shimmer Research Ltd, Dublin, Ireland) were used to collect data at a sampling frequency of 50Hz. IMUs were located on foot, thigh, pelvis, and wrist. Free-living environment conditions were simulated at the Hospital. Five PD subjects participated in the study (mean age: 63.5±2.6 years, mean Hoehn-Yahr score: 2). Movement data of six common ADL tasks were recorded in random order. IMU data were filtered using a lowpass 2nd order Butterworth filter with a cutoff frequency of 5 Hz. IMU data was smoothed using a moving average filter with a window size of 6.4 s. Institutional research and ethics committees approved the measuring protocol. All subjects and parents gave their informed consent. WKNN classifier was calculated using 13 predictors based on accelerometer, magnetometer, and gyroscope data on each single axis (X, Y,

Z) and 3D resultant. WKNN classifier training and evaluation was done in MATLAB R2019a (Natick, MA, USA) leaving out 50% of data.

Results and Discussion

In total 179555 observations were analyzed. WKNN classifier was validated using leaving out 50% of data. WKNN classifier reached an accuracy, precision, sensitivity, and specificity higher than 99%, a false negative rate and a false discovery rate <1%, and an area under the curve higher than 0.99, see Table 1.

Table 1: Confusion Matrix

		Predicted Class					
		1	2	3	4	5	6
True Class	1	14021	8	10	3	12	0
	2	13	11761	7	4	1	2
	3	9	2	7279	12	4	1
	4	4	4	4	12767	12	6
	5	2	0	8	4	33922	6
	6	1	0	2	4	4	9978

Conclusions

The introduced a classifier has potential to identify ADL performed by subjects with PD which could be helpful to support monitoring using IMUs.

Acknowledgments

Research supported by the Mexican National Council of Science and technology grant number: CONACYT PEI PROINNOVA 251032

References

- [1] Lonini L, et al (2018). *Npj Digit. Med.* **1**
- [2] Nguyen H, et al (2018). *IEEE Trans. Neural Syst. Rehabil. Eng.* **26** 197–204
- [3] Rovini E, et al (2017). *Front. Neurosci.* **11**

Use of an inertial sensor for anaerobic resistance tests

Andrés Cervantes V.^{1,2}, Julieta del C. Díaz de la G.², Domingo Rangel M.¹

¹Centro de Física Aplicada y Tecnología Avanzada, Universidad Nacional Autónoma de México, Querétaro, México

²Licenciatura en Fisioterapia, Facultad de Medicina, Universidad Nacional Autónoma de México, Ciudad de México, México

Summary

This study shows the development of an anaerobic power test, using its own inertial device for its implementation. The test consisted of carrying out one minute of continuous countermovement type jumps (CMJ), following the vertical jumps specifications of Bosco's protocol. The results obtained in the evaluation were able to correspond with the variables sought by the continuous jump resistance tests [1], taking into account that the presented system has a considerably lower cost when compared to laboratory instruments commonly used for this type of tests. The acceleration data of the developed system were previously validated, using as a reference the MetaMotion R sensor, from the company MbiEntLab, obtaining a significant correlation ($r = 0.9389$; $p < 0.0001$). This study presents us with an alternative for the application of this test, where it is possible to obtain the fatigue indices sought by the original protocol, using a lower cost equipment.

Introduction

The importance of biomechanics in sports analysis lies in the comparison of quantitative movement data [2]. In the search to achieve quantitative measurement of body mechanics in its most natural way without significantly interfering with movement, biomechanics has worked to describe certain sports gestures based on information from inertial sensors, this implies not having the spatial trajectory in coordinates, but only with the linear acceleration and/or the angular velocity of a body segment, and thus have the facilities that an inertial system provides in the measurement process [3].

The continuous jump test for one minute is an anaerobic endurance test, which uses Bosco's protocol of vertical jumps and measures mainly anaerobic power levels through increased contact times, and resistance to fatigue to through the decrease in flight times over the minute [1].

Methods

The presented system was placed on the subject's lower back, at the level of the sacrum. Starting in an upright position on both feet with hands on hips, the subject received the start and end signal of the test, performing countermovement jumps (CMJ) at maximum effort from start to finish, carrying out the full movement indicated by Bosco's protocol of the CMJ jump, with hands on hips at all times, and knees straight in the air. The system worked with the preset parameters, which are 50Hz sample rate and +/- 16g range on all three accelerometer axes.

Results and Discussion

Using the data series obtained in the test, a data handling was carried out using the magnitude of the acceleration, oriented with the signs measured by the vertical axis of the system. Finally, the jump takeoff and landing points were identified (Figure 1), using the corresponding acceleration peaks. In this way, by measuring the time intervals between the peaks, it was possible to obtain the flight time, contact and total times of the test, from which the fatigue resistance parameters are determined.

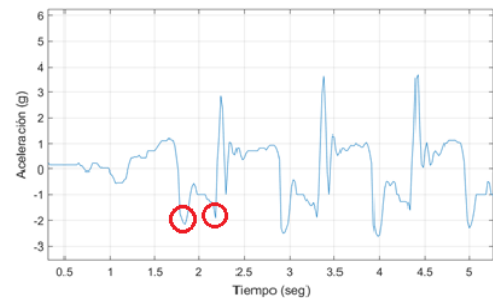


Figure 1: Acceleration vs. time data graph of the continuous jump test, with the identification of peaks signaled, corresponding to takeoff and landing of the jump.

Using the flight time values, the percentages of decrease of this were obtained, in intervals of 10 seconds (Table 1), with respect to the maximum value.

Time intervals	10 (s)	20 (s)	30 (s)	40 (s)	50 (s)	60 (s)
ToF decrease parameter	0.94	0.9	0.87	0.79	0.63	0.42

Table 1: Table of parameters for the reduction of flight time during the test, corresponding to the fatigue resistance indices.

In the same way, it was possible to obtain the contact times, total jump time and acceleration peaks for take-off and landing for each of the jumps.

Conclusions

This application method allows us to obtain functional results, comparable with those of the original protocol [1], using tools that allow the test to be applied in any condition and which are inexpensive.

References

- [1] Jandova S., Musilek M., Martin A.J., Cochrane D., Rozkovec J. (2017) Take-off efficiency: transformation of mechanical work into kinetic energy during the bosco test. *Human Movement*, 18(3): 34–39.
- [2] A. Leardini, F. Biagi, A. Merlo, C. Belvedere, M. Grazia-Benedetti. (2011) Multi-segment trunk kinematics during locomotion and elementary exercises. *Clinical Biomechanics*, 26: 562-571.
- [3] Hugo G. Espinosa, Jim Lee, Daniel A. James, (2015) The Inertial Sensor: A Base Platform for Wider Adoption in Sports Science Applications. *Fitness Research*, 4: 13-20.

Comparisons Between Researcher-Placed and Subject-Placed Wearable Sensors

Matthew C. Ruder¹, Michael Hunt², Dylan Kobsar¹

¹Department of Kinesiology, McMaster University, ON, Canada; ²Department of Physical Therapy, University of British Columbia, BC, Canada

Email: matthew.ruder@gmail.com

Summary

Wearable sensors allow research to move out of the lab and collect data in the real world. One potential application for these sensors could be to monitor disease progression of knee osteoarthritis. The subject-placement of sensors may become useful in such applications, but this may influence the reliability of these data. Therefore, this study assessed the reliability of outcome measures from researcher-placed sensors and subject-placed sensors within and between sessions. The results suggest that the subject-placed sensors have comparable reliability to researcher-placed sensors for most metrics. Future research should evaluate if reliability could be further improved with new post-processing methods.

Introduction

Knee osteoarthritis affects more than 5 million Canadians and over 32 million Americans, making it one of the most common musculoskeletal diseases. Knee joint loading has been used to assess disease state and progression, along with the presence of a varus thrust (i.e., abrupt lateral knee motion or peak frontal plane angular velocity during stance) [1,2]. Wearable sensors offer the ability to collect similar data in more ecologically valid, real-world settings and over longer periods of time. While this may further support the monitoring of disease states and progression, it may often require the self-placement of sensors. Additionally, given the ongoing shift to remote data collections with COVID-19, there is a need to better understand the effect of subject sensor placement on the reliability of wearable sensor metrics.

Therefore, the purpose of this study was to assess the reliability of wearable sensor metrics between a researcher-placed sensor and a subject-placed sensor within and between two in-lab data collections. It was hypothesized that vertical (V) and resultant (R) acceleration impact peaks would display excellent reliability with researcher-placed and subject-placed sensors for both within- and between-session reliability. However, we expected to observe reduced between-session reliability for other axis-specific metrics such as anteroposterior (AP) and mediolateral (ML) accelerations impact peaks, as well as frontal plane angular velocity peaks, especially in subject-placed sensor conditions.

Methods

Nine healthy, pain-free young adults were recruited for this study. Each participant attended two data collection sessions with 5-7 days between collections. During each session, the participant was instructed to place a 9-axis IMU (Shimmer 3, 100Hz, Shimmer Sensing, Dublin, IE) on their left shank at the medial inferior tibial tuberosity. Following participant placement of the sensor, an experienced researcher carefully placed another sensor at the same location on the right shank. Participants were then instructed to complete ten 8m over-ground walking trials. Participants walked at their preferred gait speed and all trials were within $\pm 10\%$ of this speed.

The variables of interest were V, ML, AP, and R acceleration impact peaks and frontal plane angular velocity peaks during stance. Within-session reliability was assessed by comparing the average from all steps in the first 5 trials to those in the last 5 trials within session 1. Between-session reliability was assessed by comparing the average from all steps in the first 5 trials in session 1 to the first 5 trials in session 2. An ICC (2,k) was used to assess reliability, with <0.5 , $0.50-0.75$, $0.75-0.90$, and $0.90+$ defined as poor, fair, good, and excellent reliability.

Results and Discussion

V and R acceleration impact peaks displayed good to excellent reliability (ICC: 0.87-0.96) in all cases. Similarly, all other researcher-placed sensor metrics displayed excellent reliability (ICC: 0.91-0.94). For subject-placed sensors, only ML impact peaks displayed excellent between-session reliability (ICC=0.96), while AP impact peaks and frontal plane angular velocity peaks were fair (ICC: 0.68-0.74), possibly due to a misalignment between axes. See Table 1.

Conclusions

The between-session reliability for subject-placed sensors appears to be comparable to that of an experienced researcher for measuring V and R impact peaks, as well as ML impact peaks. However, lower levels of reliability may be present in other metrics, such as angular velocity used as an estimate of varus thrust. Future research is needed to evaluate if the reliability of subject-placed wearable sensors can be improved through an automated post-processing alignment correction.

References

- [1] Chang et al., (2004). *Arthritis Rheum*, **50**:3897–3903.
- [2] Costello et al., (2020). *Clin Biomech*, **80**:1052

Table 1: ICC values for acceleration and angular velocity peaks, with lower and upper bounds.

		Mediolateral Acceleration	Vertical Acceleration	Anteroposterior Acceleration	Resultant Acceleration	Frontal Plane Angular Velocity
Within Session	Researcher-placed	0.98 (0.94-0.99)	0.98 (0.91-0.99)	0.96 (0.70-0.99)	0.97 (0.87-0.99)	0.98 (0.93-1.00)
	Subject-placed	0.97 (0.84-0.99)	0.97 (0.86-0.99)	0.79 (0.14-0.95)	0.97 (0.87-0.99)	0.99 (0.94-1.00)
Between Session	Researcher-placed	0.94 (0.75-0.99)	0.90 (0.54-0.98)	0.92 (0.66-0.98)	0.87 (0.46-0.97)	0.91 (0.60-0.98)
	Subject-placed	0.96 (0.84-0.99)	0.96 (0.83-0.99)	0.74 (0.00-0.94)	0.94 (0.60-0.99)	0.68 (0.00-0.92)

Examining the association of backward walking velocity with forward balance control in healthy adults

Kirat Shukla¹, Joel Lanovaz¹, Jonathan Farthing¹, Gary Linassi², Alison Oates¹

¹College of Kinesiology, University of Saskatchewan, Saskatoon, Canada

²College of Medicine, Department of Physical Medicine and Rehabilitation, University of Saskatchewan, Saskatoon, Canada

Email: kirat.shukla@usask.ca

Summary

The association between backward walking velocity and balance control measures in forward walking was examined in healthy adults. The results demonstrated that specific measures of balance control in forward walking were significantly correlated with backward walking velocity.

Introduction

Gait velocity during forward walking is one of the most frequently reported outcomes and has been used to assess balance control and predict the risk of falls, recurrence of falls, and cognitive decline with increasing age [1,2]. Backward walking velocity, while not a common measure, has been shown equal to or better in identifying individuals with a history of falls compared to commonly used measures such as the timed up and go test [3]. In addition to using backward walking as a rehabilitation exercise [4], studies report it as a clinically useful test of balance to discriminate fallers from non-fallers [3,5], individuals with Parkinson's disease from healthy controls [6], and to highlight gait dysfunction in children with cerebral palsy [7]. The purpose of this study was to explore the relationship between backward walking velocity and balance control during normal forward walking and a challenging task of forward tandem walking. The primary hypothesis was that backward walking velocity would positively correlate with the magnitude of forward balance control measures and negatively correlate with variability of those same measures.

Methods

Thirty-five healthy adults (28.4±8.8 years) performed five trials each for forward, backward, and tandem walking along a 10-m walkway in a lab environment. Trials were completed in random order at the participants' preferred speed. Kinematic data were collected using a motion capture system (fs = 100 Hz, Vicon Motion Systems, Denver, CO) and low pass filtered at 8 Hz using a 4th order Butterworth filter. Processing and calculation of outcome variables were completed offline using custom-written scripts (MATLAB R2019b; MathWorks, Natick, MA). Balance control during forward and tandem walking was characterized using margins of stability (MOS) in the anteroposterior (AP) and mediolateral (ML) directions (average and variability) over a stride and variability of step length and step width during normal forward walking. Variability of MOS and stepping measures were calculated as the standard deviation (SD) of the mean. An increase in the MOS magnitude and a reduction in the variability of the MOS and stepping measures were interpreted as increased balance control. Data were examined

for normality using the Shapiro-Wilk test. Balance control measures were correlated with backward walking velocity using Pearson's r for normally distributed data and Spearman's ρ for non-normal data ($\alpha=0.05$).

Results and Discussion

Backward walking velocity was positively correlated with the magnitude of the MOS in the AP direction during normal walking ($r = .710, p < .001$) and negatively correlated with the variability of the MOS in the AP direction during tandem walking ($\rho = -.451, p < .05$). The results suggest individuals with a higher backward walking velocity are more stable in the sagittal plane during forward and tandem walking. This relationship warrants further investigation into individuals with a higher risk of falls. The significant correlations from this study are in line with previously published results in which backward velocity was significantly correlated with performance on clinical tests of balance [8]. The lack of relationships between backward walking velocity and forward balance control in the ML direction ($p > .05$) and the variability of stepping measures ($p > .05$) may be due to the nature of the population (healthy) and should be examined further since balance control in the ML direction has shown to be a predictor of falls [9].

Conclusions

The primary purpose of this study was to examine the relationship between backward walking velocity and balance control in healthy adults. Participants with faster backward walking velocity had better AP dynamic balance control in forward and tandem walking. These results provide further evidence for the utility of backward walking as a clinical test of balance. Backward walking could be useful as a dynamic balance control measure for researchers and clinicians.

Acknowledgments

Funding was provided by the College of Graduate and Postdoctoral Studies and College of Kinesiology (University of Saskatchewan).

We would like to thank all the participants who volunteered for the study.

References

- [1] Menant JC. et al. (2014) *Ageing Res. Rev.*, **16**: 83-104
- [2] Peel NM et al. (2019) *J. Gerontol. A Biol. Sci. Med. Sci.*, **74**: 943-948
- [3] Carter V. et al. (2019) *J. Geriatr. Phys. Ther.*, **42**: 249-255
- [4] Yang et al. (2005) *Clin. Rehabil.*, **19**: 264-273
- [5] Fritz et al. (2013) *Gait Posture*, **37**: 593-597
- [6] Hackney ME and Earhart GM (2009) *Mov. Disord.*, **24**: 218-223
- [7] Cappellini G et al. (2018) *J. Neurophysiol.*, **119**: 1153-1165
- [8] Maritz et al. (2017) *Phys Ther Rehabil.*, **4**: 14
- [9] Lord SR. et al. (1999) *J. Am. Geriatr. Soc.*, **47**: 1077-1081

Sex and height effects on unilateral landing on hip joint loading, ground reaction forces, and lower extremity kinematics

Joshua M. Lardie¹, Bobbie S. Irmischer², Joshua T. Weinhandl¹

¹Biomechanics/Sports Medicine Lab, University of Tennessee, Knoxville, Tennessee

²Old Dominion University, Norfolk, Virginia

Email: jlardie@vols.utk.edu

Summary

Femoroacetabular impingement (FAI) is increasing in diagnosis amongst athletic populations and is a highly estimated cause of hip pain of the general population. Increased GRFs as well as altered ROM have been associated with impingement morphologies. These are seen through alteration of landing mechanics and heights. Healthy subjects completed unilateral drop tests from 30 and 50-cm heights. Female participants demonstrated increased peak GRF (pGRF), peak hip joint force (pHJF), hip ROM in the frontal and sagittal plane compared to males, suggesting gender-based risk factors. Height also increased pGRF, pHJF, and ROM, similarly to gender-based differences.

Introduction

FAI diagnoses have been rapidly increasing amongst adolescents and adults. With an estimated 22-55% of all hip pain caused by these impingement pathomorphologies, incidence rates are as high as 10-15% of the general population. Traditionally associated with aging populations, strong links have emerged with athletic participation [1,2]. Increased risks of injury potential have been associated with modified landing mechanics such as single leg and cutting tasks, as well as increased landing height [3]. As height increases, BW normalized GRF increases, with more energy absorption necessary from the lower body [4]. With unilateral and cutting task landings, the largest kinematic differences are related to frontal plane motion at the hip and knee [5].

Methods

Eighty-three recreationally active subjects ages 18-35 participated in the study. Inclusion criteria included at least 30 minutes of exercise and one jumping related exercise performed per week, with no history of lower extremity surgery, no injury in the past 6 months, and no condition that impaired the ability to jump or land. 3D marker coordinate data (200 Hz, Vicon, Centennial, CO, USA) and kinetic data (2000 Hz, Bertec, Columbus, OH, USA) were collected using single retro-reflective markers placed on the skin over anatomical landmarks as well as rigid four-marker cluster plates, serving as tracking markers.

A successful trial consisted of the participant dropping off a 30-cm and 50-cm box without the contralateral limb contacting the ground, landing with their entire intended foot on the force plate without hopping or jumping, and maintaining arms crossed high across the chest.

Visual3D as well as OpenSim were used for creating subject specific models and calculating discrete and continuous kinematic and kinetic variables. A 2x2 analysis of variance was performed in SPSS for each discrete variable while

continuous variables were compared using ensemble curve analyses.

Results and Discussion

	Males	Females	30-cm	50-cm
Peak Force (BW)				
pGRF #*	3.47 ± 0.49	3.66 ± 0.52	3.28 ± 0.43	3.85 ± 0.43
pHJF #*	9.26 ± 2.34	10.18 ± 1.98	8.79 ± 1.91	10.65 ± 2.11
Loading Rate (BW/s)				
pGRF #*	58.97 ± 12.76	62.59 ± 13.23	53.87 ± 10.45	67.69 ± 11.76
ROM_i				
Hip Flexion #*	6.94 ± 3.18	8.48 ± 3.89	7.08 ± 3.35	8.34 ± 3.80
Hip Adduction #*	4.70 ± 2.44	6.45 ± 2.96	4.08 ± 2.00	7.08 ± 2.78
Hip Rotation *	6.41 ± 3.35	5.72 ± 2.84	5.40 ± 2.88	6.73 ± 3.21
Ankle Dorsiflexion #*	32.39 ± 9.26	32.93 ± 8.49	31.91 ± 9.05	33.41 ± 8.66
ROM_L				
Hip Flexion *	17.31 ± 8.76	19.23 ± 10.24	15.53 ± 8.12	21.01 ± 10.11
Hip Adduction #*	13.04 ± 5.65	18.86 ± 8.15	11.46 ± 5.00	20.80 ± 6.65
Hip Rotation #*	10.87 ± 5.47	8.86 ± 3.54	8.75 ± 3.79	10.97 ± 5.26
Ankle Dorsiflexion *	44.32 ± 1.60	45.20 ± 7.94	43.23 ± 9.18	46.30 ± 9.32
# Significant main effect for sex (p<0.05)				
* Significant main effect for landing height (p<0.05)				

Table 1: Group means and STD for discrete variables.

Significant differences between continuous forces and landing heights were identified for GRF between 1-29%, and HJF between 14-25% and 77-100% of the landing phase. Significant main effects for sex and height were identified for pGRF, pHJF, GRF loading rate, ROM initial contact (ROM_i), hip flexion and adduction, ROM_i ankle dorsiflexion, and ROM landing (ROM_L) hip adduction and rotation. Females landed with +0.19 BW pGRF, +0.92 BW pHJF, and +3.62 BW pGRF loading rate compared to males. Landings from 50-cm incurred +0.57 BW pGRF and +1.86 BW pHJF, with loading rates +13.82 BW/s pGRF and +28.46 BW/s pHJF compared to 30-cm landings. All ROM_i angles except ankle dorsiflexion were greater for 50-cm than 30-cm landings as well as all ROM_L angles. These results might suggest that modified landing mechanics can place added stress associated with FAI development in athletic populations.

Conclusions

In conclusion, females demonstrated increased pGRF and pHJF, increased hip ROM flexion and adduction compared to their male counterparts. Increases in landing heights yielded similar increases in pGRF and pHJF.

References

- [1] Colvin AC et al. (2012). *Trends in Hip Arthro.*, **94**: 23.
- [2] Groh MM & Herrera J (2009). *Curr. Rev. in Msk.Med.*, **2**: 15-117.
- [3] Weinhandl JT et al. (2015). *The Knee*, **22**: 298-303.
- [4] Ali N et al. (2014). *The Knee*, **21**: 38-46.
- [5] Kernozek TW et al. (2005). *Med. & Sci. in Sp. & Ex.*, **37**: 1003-1012.

Tasks used when determining return-to-activity in paediatric patients following an anterior cruciate ligament reconstruction: a systematic review

Nicholas J. Romanchuk¹, Holly Livock², Kenneth J. Lukas³, Michael J. Del Bel⁴, Daniel L. Benoit⁴, Sasha Carsen²

¹Ottawa Carleton Institute for Biomedical Engineering, University of Ottawa, Ottawa, Canada

²Division of Orthopaedic Surgery, Children's Hospital of Eastern Ontario Research Institute, Ottawa, Canada

³University of Dublin, Trinity College, College Green, Dublin 2, Dublin, Ireland

⁴School of Rehabilitation Sciences, University of Ottawa, Ottawa, Canada

Email: dbenoit@uottawa.ca

Summary

The purpose of this systematic review was to identify the most commonly used tasks when determining unrestricted return – to-activity (RTA) following an anterior cruciate ligament reconstruction (ACLR) in paediatric patients. The literature was reviewed according to the Preferred Reporting Items for Systematic Reviews and Meta-Analyses guidelines (PRISMA). A total of 25 articles met all criteria for review; of which, strength (14/25 studies) and hopping (9/25 studies) tests were the most commonly used RTA tasks. Current RTA criteria have focused on easily collected metrics such strength and hopping distance, despite limited evidence supporting their use in a paediatric population.

Introduction

Anterior cruciate ligament (ACL) rupture is a debilitating knee injury associated with sequela such as joint degeneration [1]. Unfortunately, following an ACL reconstruction (ACLR), rates of either ACL graft failure or contralateral ACL rupture ranges from 17-30% in paediatric patients [2]. A contributing factor to the high re-injury rate in this population may be the lack of consensus regarding the appropriate criteria for allowing RTA post-operatively. By reviewing the literature, future interventions can build more effective RTA assessments through the validation of current RTA criteria and the implementation of new criteria according to identified literature gaps. Thus, the purpose of this systematic review was to determine the most commonly used criteria when assessing RTA readiness post-ACLR in paediatric patients.

Methods

Following PRISMA guidelines, a systematic search was performed of Medline/PubMed, Cochrane, Embase, CINAHL, and SPORTDiscus electronic databases. Studies were included if they specified the criteria used to determine RTA following an ACL reconstruction and included paediatric patients (≤ 18 years old). The quality of each study was assessed using the validated Methodological Index for Non-Randomized Studies. The primary outcome of interest was the RTA task(s) used by each study when determining clearance to full activities.

Results and Discussion

A total of 25 articles met all criteria for review. Strength (14/25 studies) and hopping (9/25 studies) tests were the most commonly used tasks when deriving RTA criteria (Table 1). A limb symmetry index of $>90\%$ was the most common

threshold for determining RTA. In addition, only 2/25 studies used an objective assessment of movement quality before RTA.

Table 1: Frequency of tasks reported in the literature when accessing RTA in adolescents

Task	No. of Studies
Isokinetic Strength	9
Anterior Hop	7
Triple Hop	6
Cross Hop	4
Timed-Hop	2
Isometric Strength	2
Single Heel Raise	2
Single Leg Dip	2
Tuck Jump	2
Shuffle T-Test	2
Sprint/Cutting T-Test	2
Vertical Jump	1
T-Balance Test	1
Shuttle Run	1
Sprint and Back Paddle	1
Sprint Stop and Go	1
Cutting 90°	1
Side Shuffle 90°	1

Conclusions

Despite the high rate of ACL re-injuries in paediatric and adolescent patients, there is substantial variability in the use and reporting of paediatric RTA criteria following an ACLR. With limited available evidence to support paediatric RTA decision making, it is not surprising there is no consensus on the appropriate criteria for determining RTA. Current criteria have focused on easily collected metrics such strength and hopping tests, despite evidence suggesting they are ineffective at reducing the risk for re-injury [3]. Although infrequently used in the current literature, clinicians may benefit from the inclusion of patient reported outcome measures and lower-limb kinematics in their RTA assessments.

Acknowledgments

The authors would like to thank the Ontario Graduate Scholarship, Natural Sciences and Engineering Research Council of Canada, the Arthroscopy Association of North America, and the University of Ottawa.

References

- [1] Oiestad BE et al. (2011). *Br. J. Sports Med.*, **45**: 583-8
- [2] Wiggins AJ et al. (2016). *Am. J. Sports Med.*, **44**: 1861-76
- [3] Webster KE et al. (2019). *Sports Med.*, **49**: 917-29.

Design of a Swelling Suture Anchor for Improved Fixation to Osteoporotic Bone

Nicholas Anastasi¹, Rena Mathew¹, Victoria McDonald¹, Giuseppe Palmese², Moein Taghvaei², Jianwei Tu², Sorin Siegler¹

¹Department of Mechanical Engineering, Drexel University, Philadelphia, PA, 19103, USA

²Department of Chemical Engineering, Drexel University, Philadelphia, PA, 19103, USA

Email: naa94@drexel.edu

Summary

Rotator cuff repairs (RCRs) are common orthopedic procedures which require the application of suture anchors [1]. The humeral head, where the suture anchors are inserted, is of low density particularly when osteoporosis is present, resulting in failure of the suture anchor due to low pullout strength [2]. This study aims to improve fixation of suture anchor in RCR by utilizing a swelling co-polymeric material [3] integrated into a unique suture anchor design. By controlling the swelling characteristics of the material, the swelling suture anchor (SSA) provides better fixation and promotes osteointegration for improved long-term anchor fixation.

Introduction

With a swelling anchor, swelling strain can be utilized for effective anchor fixation as opposed to the tradition shear strain of screws which is low in low density bone. By allowing the material to swell after implantation the SSA can affix itself within low density bone without damaging it. Additionally, the SSA has a refixation capability as compared to a traditional suture anchor [3].

The purpose of this study is to develop and evaluate a SSA optimized for osteointegration and fixation into low density bone. The swelling and mechanical properties of the material, such as strength and porosity, were characterized.

Methods

Cylindrical samples of the swelling material with varying diameters of 4, 5, and 8 mm were created. The swelling characteristics were evaluated by placing the samples in saline solution and allowing them to swell for 33 days. During this time the weight and volume increase was periodically measured. Then the samples were removed from the saline solution and mechanically tested. Mechanical testing consists of compression under cyclic load followed by testing to failure.

Results and Discussion

Within the initial 24 hours the material nearly reached its peak swelling capability as seen in Fig. 1. After the 33-day swelling period the average percent change in diameter of the samples was 6.24% and the average percent change in weight was 9.99%. The swelling material has a dry compressive strength of 120 MPa and a wet compressive strength of 47 MPa. The dry modulus of the material is 1.7 GPA and the wet modulus is 0.9 GPA. As a reference, the average compressive strength of cancellous bone is 10-20 MPa and the modulus is 0.2-0.5 GPA. As can be seen from these results (Fig. 2), the swelling co-polymer losses a significant amount of its mechanical

properties while become more ductile. In the swelling state the mechanical properties match well those of cancellous bone thus minimizes stress shielding as oppose to a metal anchor.

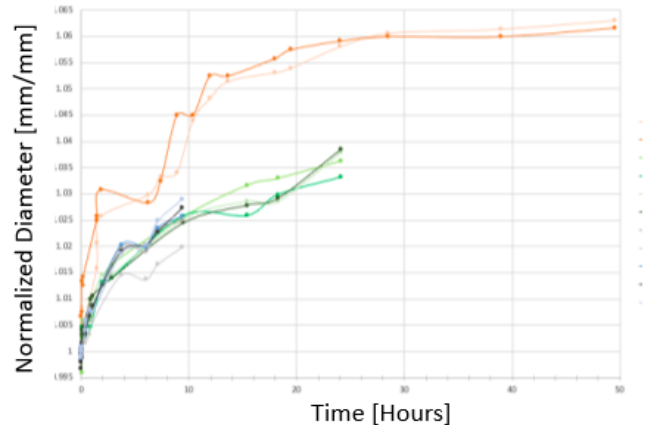


Figure 1: Swelling characterization of the material

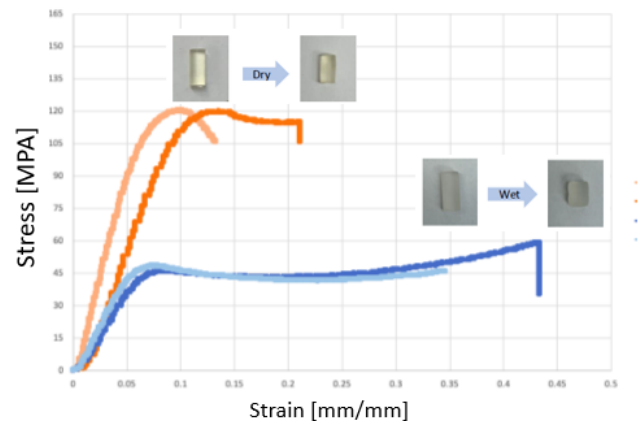


Figure 2: Mechanical characterization of swelling material

Conclusions

The unique properties of the swelling co-polymer makes it a good candidate for implementation in suture anchors that improve fixation to cancellous bone and promote osteointegration.

References

- [1] Colvin, A. C. et al. (2012). *JBJS*, 94: 227-233.
- [2] Benson, E. C. et al. (2010). *Arthroscopy*, 26: 310-315
- [3] Abusafieh, A. et al. (1997). *J Bio Mat Res*, 38: 314-3

Increased postural threat alters control of dynamic stability in response to external perturbations that induce a step

Noah J. Rosenblatt¹, Shirali Shah¹, Marco Avolos¹

¹Center for Lower Extremity Ambulatory Research, Rosalind Franklin University of Medicine and Science, North Chicago, USA

Email: noah.rosenblatt@rosalindfranklin.edu

Summary

The mechanisms by which fear of falling increases fall risk are poorly understood. While increased anxiety in response to postural threat affects postural control during standing and following non-stepping perturbations, the effect on stepping responses remains unknown. We compared dynamic stability when healthy young adults utilized a step to regain stability in response to an external perturbation applied while standing overground (OG) versus a raised platform. Regardless of stepping direction, participants initiated a step significantly earlier and under significantly less instability while on the platform. Participants also took significantly shorter recovery steps on the platform. Under conditions of increased postural threat, healthy young subjects adopt a cautious strategy in which they are less willing to allow instability, triggering steps prior to conditions that would otherwise do so.

Introduction

FoF affects ~35% of adults >60 years of age and increases fall risk. FoF can lead to avoidance of activities and in turn deconditioning, which can precipitate falls. Older adults with FoF may also perceive everyday environmental challenges, e.g., small obstacles, as more threatening than would a non-fearful older adult, which may incite excessive anxiety and impact postural posture and balance [1]. One way to isolate the extent to which psychological versus physiological changes may negatively impact posture and balance, and in turn fall risk, in older adults with FoF is to have young adults perform tasks under conditions of increased postural threat. i.e., standing on a raised surface. When standing at a height, young adults impart greater volitional control over posture [2]. In general, increased threat alters neuromuscular control of standing postural [3]. While altered postural control may increase the likelihood of balance loss, falls ultimately occur due to an inappropriate recovery response, most often in the form of a step to extend the base of support. The purpose of this study was to evaluate the effects of postural threat on the compensatory stepping response in healthy young adults.

Methods

Ten healthy young adults participated. Passive reflective markers were placed on bony landmarks and postural perturbations were applied in the anterior and posterior directions using a waist mounted spring scale while participants stood OG and on 1m raised platform (PF). The spring was pulled to a set load while the participant resisted. At random intervals the load was released, and the participant was instructed to avoid stepping. If successful, the load was increased; otherwise, the load was repeated. Loading ceased after steps were taken on two consecutive trials at a given load, which defined the stepping threshold. For the two trials at the stepping threshold, we extracted the following from motion capture data and averaged across trials: i) time to recovery

foot off (FO); ii) margin of stability (MOS) at recovery foot off relative to the mean MOS for the 100ms prior to load release (MOS_{FO}); iii) MOS at recovery foot contact (MOS_{FC}) taken relative to the stepping limb; iv) recovery step length and time. Two-way repeated ANOVAs (factors of stepping direction and surface - OG vs PF) and correlations were used to assess effects and relationships among variables.

Results and Discussion

Posterior, but not anterior stepping thresholds were significantly lower PF vs OG. However, the between surface loading differences were unassociated with any other between-surface changes. Regardless of stepping direction, participants reacted more quickly during PF; time to FO was significantly reduced and MOS_{FO} was significantly greater (Figure 1), with a strong association between the two ($r=-0.825$; $p<0.001$). Posterior steps during PF were taken before instability ensued ($MOS_{FO}=4.1\pm 3.8$ cm). Participants took significantly shorter recovery steps during PF, but step time was unaffected. Increased stability during the recovery step for PF resulted from an extrapolated center of mass that remained closer to the border of the stance foot, contributing to a significantly greater MOS_{FC} despite the shorter step.

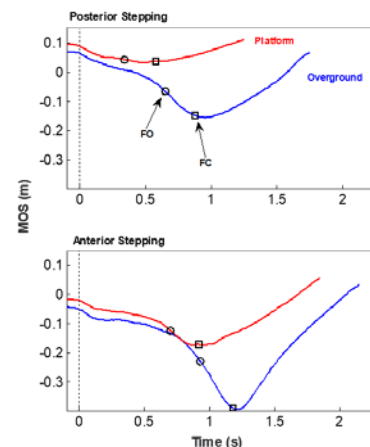


Fig 1: Weighted group average MOS curves for non-stepping limb

Under increased postural threat, healthy young adults adopt a cautious strategy. While this could be protective against falls in older adults with FoF, it may also have unintended negative consequences, e.g., reduced processing time, altered attentional demands. Additional work is needed.

Conclusions

The control of dynamic stability following a postural perturbation eliciting a step is affected perceived postural threat.

References

- [1] Young W et al. (2015). *Gait & Posture*, 41(1): 7-12.
- [2] Carpenter MG et al. (2001). *Exp Brain Res*, 138(2):210-18
- [3] Carpenter MG et al. (2004). *J Neurophysiol*, 92(6):3255-65

The relationship between 2D and 3D sacropelvic measurements

Nikita Ghosh¹, Justin Fernandez¹, Joe Baker², Peter Robertson³, Julie Choisne¹

¹Auckland Bioengineering Institute, University of Auckland, New Zealand

²School of Medicine, University of Auckland, New Zealand

³Mercy Hospital, Auckland, New Zealand

Email: ngho752@aucklanduni.ac.nz

Summary

Degenerative Disc Disease is a musculoskeletal disorder often surgically operated using fusion implants and associated with high failure rates. The aim of this study was 1) to compare the sacropelvic parameters, usually measured preoperatively in 2D, and their 3D measurement from pelvis and sacrum bone reconstruction; 2) understand the correlation between the bone shape and the sacropelvic parameters. Calculated 3D angles were not statistically different to the 2D measured angles. The distances calculated from a 3D perspective were statistically different to the ones measured in 2D. Sacrum shape has a moderate correlation with pelvic incidence.

Introduction

Degenerative Disc Disease is a major musculoskeletal disorder often surgically operated using fusion implant devices. The International Spine Study Group has reported that the success of the surgery relies on the optimal values of sacropelvic parameters [1]. Quantitative measurements of the sacropelvic parameters are usually performed on 2D sagittal/frontal X-rays pre surgery. The information obtained from the projection of 2D angles are supposedly limited compared to the parameters calculated in 3D. Therefore, the aim of this study were to 1) compare sacropelvic parameters measured in 2D and 3D and 2) understand the correlation between sacropelvic parameters and bone shape.

Methods

De-identified CT scans (Siemens, Munich, Germany) from 79 healthy adult participants were collected (43 F, 45 ±6 y.o.) with sacrum and pelvis segmented using Mimics (Materialise, Belgium). An orthopaedic surgeon measured 2D sacropelvic parameters: anterior pelvic angle (AP), pelvic incidence (PI), sacral table angle (STA), projection angle (PA), femorosacropelvic angle (FSPA), pelvisacral angle (PSA), crest pubic distance (CPD), crest sacrum distance (CSD), inlet (ID) and outlet distances (OD) on the sagittal and frontal slices of the CT scan images. Each bone surface were fitted to template meshes and assigned the ISB coordinate system [2]. A Python code was used to find each pelvic and sacrum landmarks needed to calculate the 3D aforementioned sacropelvic parameters automatically from the fitted meshes. The comparison between 2D and 3D measurements was done using a dependent t-test on each of the angles.

A Principal Component Analysis (PCA) was performed on each bone using a python library [3] to understand the shape variation of the pelvis and sacrum. Pearson correlation coefficient (R) were determined from the PCA projected weights and the calculated 2D sacropelvic parameters.

Results and Discussion

Sacropelvic parameters of the calculated 3D measurements and measured 2D angles and distances are shown in Table 1. No statistically significant difference were found between 2D and 3D angles measurements while the crest-pubic, crest-sacral and inlet distances showed significant differences. This difference is likely due to two reasons. First, the SSM calculated distances are taken in 3D space which will always be larger than when projected onto a 2D plane. Second, the 2D calculated distances highly depends on the CT scan slice chosen for measurements. These results look promising to be able to use the SSM with a regression algorithm to predict clinical angles without the need for extensive scans. The first and second principal components (PC) for the sacrum and pelvis described 1) bone height and 2) bone width variation. The third PC described the iliac width in the pelvis and superior articular process shape variation in the sacrum. The R-value between sacrum's width (PC2) and PI shows a moderate correlation (0.537). However, no significant correlation were observed between the other sacropelvic angles and pelvic/sacrum bone shape.

Conclusions

We found statistical differences in the 2D versus 3D measurements of crest-pubic, crest-sacral and inlet distances but no significant differences in angle measurements. We also found that sacrum width is moderately correlated with the pelvic incidence angle.

Acknowledgement

We would like to thanks the Wishbone Orthopaedic Research Foundation of New Zealand, Callaghan Innovation and the Auckland Bioengineering Institute for funding this research.

References

- [1] Glassman et al. (1976). *Spine*; 30: 682-8
- [2] Wu et al. (2002). *JOB* 35: 543-548.
- [3] Zhang et al. (2014), *CMBBE*: 2:3, 176-185.

Table 1: Average ±SD of sacropelvic angles (°) and distances (mm) calculated in 3 dimension (3D) and measured in 2D slices. *** p<0.001

	AP	PI	STA	PA	FSPA	PSA	CPD ***	CSD ***	ID ***	OD
2D	20 ±3	51 ±9	61 ±21	18 ±11	69 ±10	42 ±15	89 ±10	100 ±8	121 ± 8	118± 10
3D	21 ± 4	50 ±10	61 ±21	18 ± 12	68 ±9	42 ±14	92 ± 12	99 ± 16	125 ± 10	123 ± 12

Musculoskeletal simulations of high knee flexion tasks – knee ligaments geometry definition

D. Pavandavide¹, S. Van Rossom², H. Hoang², I. Jonkers², C. Sawacha^{1,3}

¹University of Padua, Dept. of Information Engineering, Italy

²KU Leuven, Dept. of Movement Sciences, Belgium ³University of Padua, Dept. of Medicine, Italy

Email: all.pavandavide@federugby.it

Summary

Anterior cruciate ligament (ACL) injuries are immediately disabling, and require long rehabilitation periods, in order to return to the previous level of competition. Addressing the prevention through musculoskeletal modelling (MSM) allows for the estimation of variables not otherwise measurable.

The present work aims to define knee ligaments geometry in a musculoskeletal model, focusing on ACL injury prevention.

Introduction

The majority of knee and ACL injuries are often identified as non-contact injuries [1]: they occur when forces applied to the ligament are greater than the loads it can withstand [2] – in order to be effective, screening methods should be linked to ACL mechanical etiology [2]. MSM has already been successfully applied in clinic to assess musculoskeletal disorders [3]. A musculoskeletal model with enhanced degrees of freedom (DOF) at the knee and knee ligaments has been identified in literature [4], although not specifically developed for deep flexion tasks. Some works [5,6] have been identified reporting rotations on the frontal and transverse plane [5], and ligaments elongation and spatial orientation [6] in relation to passive knee flexion up to 130 degrees.

The present contribution aims to define the 3D ligaments geometry in a musculoskeletal model having enhanced DOF at the knee, focusing on high knee flexion tasks simulation.

Methods

Once digitalized the data published in [5,6], the insertions of 11 ligament bundles have been redefined through an iterative algorithm: 1. once simulated the knee flexion as in [5], the models' ligaments 3D geometry and elongation are compared with [6] by means of RMSD and Pearson's correlation; 2. comparison are performed only when ligament elongation is higher than its resting length. 3. a tentative insertions cloud is then computed and a simulation run for each combination of tentative insertions. 4. breaking condition are set as the best insertions combination result, equal to the insertions combination given as input. 5. the optimization procedure is performed several times for each bundle, restarting the process with slightly different initial conditions, to avoid for suboptimal solutions, and the best overall solution is stored with the corresponding parameter values.

Results and Discussion

Ligaments geometry optimization results (Fig. 1) showed good compliance with [6] geometries and elongation rates,

both in terms of correlation and RMSD, when the ligament elongation was higher than its resting length.

The repositioned ligaments geometry and the elongation pattern showed good compliance with [6] throughout the knee flexion. Both ligaments lever arms end force exertion are affected by these parameters during MSM simulations, hence by adopting the proposed methodology outcomes would be in line with knee physiology in simulating high knee flexion tasks.

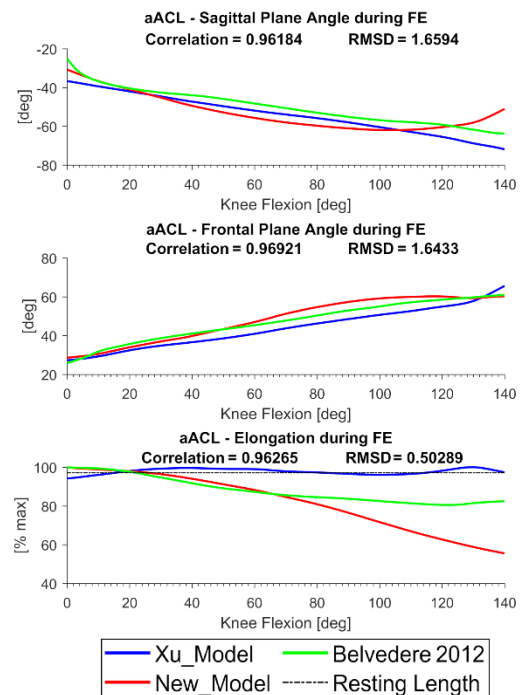


Figure 1: ACL anteromedial bundle - frontal and transverse plane projection of the angle formed against the vertical tibial axis, and ligament elongation trough knee flexion.

Conclusions

The proposed knee model could be adopted for knee injury prevention screening in high knee flexion tasks and support the clinical decision making in readmitting an injured athlete to trainings and competitions.

References

- [1] Boden BP et al, *J Am Ac Orthop Sur* **18**: 520–27, 2010.
- [2] Shin CS et al, *J Biomech*; 42:280-85, 2009.
- [3] Scarton, A et al, *Gait & Posture*, 58:194-200, 2017.
- [4] Xu H et al, *Comp Method Biomec*, **18**:1217-24, 2015.
- [5] Belvedere C et al, *J Orthop Res*, **27**: 1426–31, 2009.
- [6] Belvedere C et al, *J Biomech*, **45**:1886-92, 2012.

Musculoskeletal Modelling – relevance of model anatomical consistency

Michele Conconi¹, Erica Montefiori², Nicola Sancisi¹, Claudia Mazz²

¹ Department of Industrial Engineering - DIN, University of Bologna, Italy ²INSIGNEO Institute for In Silico Medicine – Department of Mechanical Engineering, The University of Sheffield, Sheffield, UK
Email: michele.conconi@unibo.it

Summary

No consensus exists on how to model human articulations within musculoskeletal models (MSKM). We propose to evaluate a joint model based on their anatomical consistency (AC), i.e. by quantifying ligament and cartilage deformation associated to its motion: to be consistent with articular physiology this deformation should be minimum. We compared AC of three ankle joint models with increasing personalisation and showed that a higher personalisation better complies with the expected physiological behaviour.

Introduction

MSKM are widely adopted to estimate muscle and joint forces during motion tasks. Many different joint models and kinematic chains (KCs) have been proposed, from simple spherical or revolute joints to complex parallel mechanisms or coupling equations between the joint degrees of freedom. Guidelines for the definition of MSKM were proposed [1], but no consensus exists on the best KCs, mainly due to validation complexity. Rather than validation, we propose to use the concept of AC to compare different KCs. In agreement with articular physiology, a common assumption in MSKM is that joints are workless [1]. For this to hold true, no significant tissue deformation should occur within the joint during motion. AC can thus be determined by quantifying the ligament and cartilage deformation associated with joint motion. This concept was tested by computing the internal forces associated with tissue deformation for three different ankle models, characterised by an increasing level of personalisation. Through dynamic simulations of gait, the effect of these internal forces on the output of the three analysed models was also quantified.

Methods

Gait analysis and medical resonance imaging (MRI) were collected from 10 juveniles (1:9 m:f, 11.6 ± 3.1 y.o., 45.2 ± 17.9 kg, 1.44 ± 0.15 m) as part of the MD-Paedegree project. For each subject, three lower-limb MSKM were built, differing from each other for the definition of the ankle model. The first model (scaled generic, SGJ) was obtained from marker-based scaling of the generic OpenSim model gait2392 [2]. The second one (morphological fitting-based, MFJ) was identified via morphological fitting of a cylinder to the MRI-segmented talar surface [3]. The third one was a 1-degree of freedom joint with a spatial floating-axis, defined by optimising the transmission of contact forces, i.e. maximising joint congruence (MCJ) [4]. Attachment regions of the tibio-calcaneal (TiCa) and fibulo-calcaneal (FiCa) ligaments were identified on MRI and were represented by their single most isometric fibre [5] with a bilinear elastic characteristic. Cartilages were modelled with the elastic foundation approach. Ligament elongation and cartilage co-

penetration associated with the ankle motion were computed for each model over the ankle range of motion. A standard inverse OpenSim pipeline, including Static Optimisation and Joint Reaction Analysis, was run to estimate ankle moment, muscle forces and joint forces. The pipeline was run first ignoring (scenario 1, S1) and then considering (scenario 2, S2) the ankle joint internal forces resulting from tissue deformation. Differences in maximum ankle moment (normalised by body mass and height), and amplitude of ankle contact forces (normalised by body weight, BW) between S1 and S2 were investigated for the three models.

Results and Discussion

SGJ exceeded 30% of ligament elongation for both FiCa and TiCa (Table 1), above the physiological isometric threshold of 5% [5]. MFJ and SGJ showed non-physiological cartilage co-penetration. Internal forces due to tissue deformation (S2) caused a dramatic alteration of ankle moment and contact forces in SGJ (Table 2). MFJ and MCJ ankle moments were in line with average values reported in a previous work for the same cohort [3], but MFJ failed to provide reasonable values for contact forces under S2. Differences between S1 and S2 should be minimum to comply with ankle physiology. These differences provide a good indication of the AC of a joint model.

Table 1: Maximum tissue deformation across the cohort

	MCJ	MFJ	SGJ
FiCa elongation [%]	3.5	8.2	50.7
TiCa elongation [%]	5.9	17.9	32.6
Cartilage co-penetration [mm]	-0.5	-2.4	-5.4

Table 2: Maximum difference between S1 and S2 across the cohort

	MCJ	MFJ	SGJ
Plantarflexion moment [N/kg]	0.0	0.2	13.3
Ankle contact force [BW]	0.8	6.8	120.8

Conclusions

Quantification of AC provides a solid criterion for the comparison of different joint models and personalisation strategies. A low AC raises concern about MSKM outputs credibility. When investigating specific subjects, a level of AC similar to the one of MCJ is recommended.

Acknowledgments

Supported by the UK EPSRC (EP/K03877X/1 and EP/S032940/1) and by the EU MD-Paedegree (CN:600932).

References

- [1] Hicks JL et al. (2015). *J Biomech Eng*, **13**: 020905
- [2] Delp S et al. (1990). *IEEE Trans Biomed Eng* **3**: 757-67
- [3] Montefiori E et al. (2019). *J Biomech*, **85**: 27-36.
- [4] Conconi M. et al. (2015). *J Biomech*, **48**: 2960-7
- [5] Leardini A et al. (1999). *J. Biomech.* **3**: 111-8.

Cadaveric Knee Simulator in Orthopaedic Training: Quantifying Joint Kinematics for Active Functional Motions

Darshan S. Shah¹, Orcun Taylan¹, Pieter Berger², Luc Labey³, Hilde Vandenneucker², Lennart Scheys^{1,2}

¹Institute for Orthopaedic Research and Training (IORT), KU Leuven, Leuven, Belgium; ²Division of Orthopaedics, University Hospitals Leuven, Leuven, Belgium; ³Dept of Mechanical Engineering, KU Leuven, Leuven, Belgium
Email: dssiitb@gmail.com

Summary

Orthopaedic training is typically based on passive joint assessment; however, postoperative patient satisfaction depends on successful outcomes during active functional tasks. This study aimed at introducing cadaveric simulators to surgical fellows to provide quantitative and dynamic assessment of the joint following total knee arthroplasty (TKA). Significant differences observed in postoperative joint kinematics between passive and active tasks indicated the benefits of integrating joint simulators in orthopaedic training.

Introduction

Orthopaedic training sessions, although vital for surgeons to understand postoperative joint function, are primarily based on passive and subjective joint assessment. However, cadaveric knee simulators, commonly used in orthopaedic research [1], could potentially benefit surgical training by providing quantitative kinematic assessment of the joint for active functional motions. The integration of cadaveric simulators in orthopaedic training was explored with recipients of the European Knee Society Travelling Fellowship visiting our institution in 2018 and 2019. The aim of the study was to introduce the fellows to a knee joint simulator in order to observe the surgical impact of TKA on the dynamic joint behaviour.

Methods

Eight fellows were assigned a fresh-frozen lower limb each to plan and perform posterior-stabilised TKA using patient-specific instrumentation. Specimens were tested in the native and postoperative conditions on a validated knee simulator [2]. All fellows participated in the *in vitro* testing protocol, which included passive flexion (0°-120°), active squatting (35°-100°) and varus-valgus laxity tests (at 0° and 90°). Tibiofemoral kinematics were recorded with an optical motion capture system and compared between native and postoperative conditions using a linear mixed model (α : $p < 0.05$). The detailed kinematic analysis was also discussed with the fellows.

Results and Discussion

Postoperative tibial abduction was closer to neutral than the native condition during squatting, although differences were not statistically significant ($p > 0.28$). Passive flexion resulted in higher tibial internal rotation post-TKA ($p < 0.05$), while squatting resulted in lower internal rotation post-TKA ($p < 0.033$) (Figure 1). Postoperative joint stiffness was greater in extension ($1.4 \pm 1.2^\circ$) than in flexion ($4.4 \pm 2.0^\circ$) for a joint moment of 10 Nm.

In vitro experimental testing on the knee simulator provided the fellows with new quantitative parameters for postoperative joint assessment. Although trained at different institutions, all fellows followed certain standard intraoperative guidelines while performing TKA, such as achieving neutral tibial abduction and avoiding internal tibial rotation [3], albeit at a static knee flexion angle. However, postoperative tibiofemoral kinematics exhibited differences for passively and actively loaded motions (Figure 1). Thus, traditional orthopaedic training could be further enhanced by the inclusion of cadaveric simulators replicating functional joint motions, as was also the unanimous opinion of all participating fellows in their positive feedback.

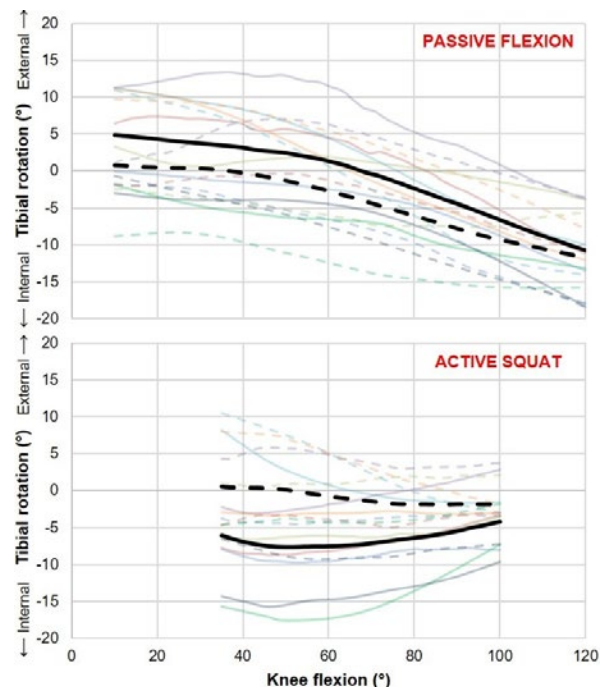


Figure 1: Tibial rotation during passive flexion and active squatting in native (solid) and postoperative (dotted) states. Data shown for each specimen (light colours) and mean across specimens (black).

Conclusions

Postoperative joint kinematics differed significantly for active squatting as compared to passive flexion, thereby indicating the potential contribution of cadaveric joint simulators in objectifying and improving surgical training.

References

- [1] Heyse et al. (2018). *Knee Surg Traum*, **26**: 1767-1775.
- [2] Victor et al. (2009). *JBJS Am*, **91**(6): 150-163.
- [3] Gromov et al. (2014). *Acta Orthop* **85**(5): 480-487.

Assessing the mechanical properties and stress distribution in dynamic Ankle-Foot Orthoses bench testing and FEA

Cara **Caravaggi P**, Rogati G.¹, Cinquepalmi A.¹, Compagnoli A.³, Fognani R.², Leardini A.¹, Calci Novati M.²

¹ IRCCS Istituto Ortopedico Rizzoli, Laboratorio di Analisi del Movimento, Bologna, Italy

² IRCCS Istituto Ortopedico Rizzoli, Laboratorio di Tecnologia Medica, Bologna, Italy

³ Dept. of Technology and Innovation, University of Southern Denmark, Odense, Denmark

Email: paolo.caravaggi@ior.it

Summary

This study is part of a larger investigation aimed at developing a novel dynamic custom Ankle-Foot Orthosis (AFO) to improve function and comfort in patients not satisfied with standard solutions. Within this aim, a setup capable to replicate the biomechanical conditions characterizing the AFO in gait was developed. The setup allows to simulate the dorsi/plantar flexion an AFO is subjected to in the stance phase of walking. The setup was tested in a sample of standard and custom AFOs made of fiber-glass reinforced polyamide. Finite Element Analysis (FEA) was used to assess the stress distribution in the custom AFOs using the same boundary conditions. The setup showed high repeatability in assessing AFO stiffness and appeared flexible to adapt to different sizes and dimensions. The stiffness of the custom AFOs was consistent with that of similar-size off-the-shelf AFOs and the maximum Von Mises stress was lower than the material's yield strength.

Introduction

AFOs are prescribed to address a deficit of the main ankle dorsiflexor muscles in drop-foot patients. While standard-size off-the-shelf AFOs are suitable to support the foot and ankle, these do not account for subject-specific morphology for ankle deficit and functional demand, and do not address concomitant morphological and postural alterations of the foot. Measuring the mechanical properties of AFOs is a key element to provide each patient with the right AFO [1]. However no standard setup for testing AFOs is currently available [2, 3]. In this study, a setup capable to replicate the AFO flexion during the stance phase of gait was developed. The setup has been tested for intra-sample repeatability and sensitivity to inter-sample difference in measuring AFO stiffness of custom and off-the-shelf orthoses.

Methods

A setup based on a servo-hydraulic testing machine (Biaxial Mini Bionix 858, MTS) capable to replicate the biomechanical conditions characterizing the AFO during the stance phase of walking was developed (Fig.1). Within the apparatus, the plantar aspect of AFO is fixed, while the calf shell is free to rotate about the load frame axis, which is aligned with the ideal ankle joint axis according to anatomical proportions. In order to allow physiological dorsi/plantarflexion, the calf strap constrains the upper border of the calf shell on a plastic cylinder free to slide along and to rotate around the "leg" axis. The rotational actuator applies 15 deg under angular displacement control while the torque cell (axial-torsional load cell 662.20D, MTS) measures the AFO resisting torque to flexion. Stiffness of the AFO [Nm/deg] is determined as the average slope of the torque/angle curve (fig 1, right) across five test repetitions. In the present study, two AFOs

were designed and manufactured via Selective Laser Sintering of fiber-glass reinforced polyamide powder (Windform GT, CRP Technology, Modena) customised for two drop-foot patients, and 6 standard polyethylene AFOs (*Molla di Codivilla*, Ottobock) – two samples for each small, medium, and large sizes – were tested for mechanical properties with the proposed setup. FEA was used to assess Von Mises stress in the regions subjected to the larger deformations and the overall stiffness of each design under the same boundary conditions of the bench testing.

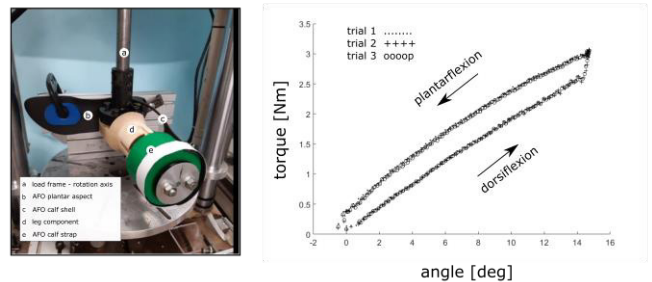


Figure 1: Left, one of the custom AFOs in the testing rig. Right, torque/angle scatter plots in three 0-15-0 deg deformation-controlled dorsi/plantarflexion cycles.

Results and Discussion

For all AFOs, torque/angle plots were highly repeatable across the five test repetitions. For each size, the measured stiffness of the *Molla di Codivilla* AFOs was consistent between left and right samples. Small and medium sizes presented a similar stiffness of about 0.17 Nm/deg, whereas the large size showed the largest average stiffness (0.28 Nm/deg). The two custom AFOs showed an average stiffness of 0.18 Nm/deg and 0.26 Nm/deg. FEA confirmed that Von Mises stress was lower than the yield strength of the material (56.2 MPa) at 15 deg flexion.

Conclusions

While confirmation on a larger sample of AFOs is required, the present setup appears capable to characterize AFOs mechanical properties in realistic biomechanical conditions. The mechanical characterization will allow to accurately measure the stiffness of current off-the-shelf orthoses and to verify if the stiffness of the laser sintered custom AFOs is consistent with the nominal design values.

References

- [1] Masilkauskaitė E et al. (2019). *Disabil Rehabil Assist Technol.* 14(1):1-13.
- [2] Kobayashi T et al. (2011). *J Rehabil Res Dev.* 48(5): 565-76.
- [3] Gregman D et al. (2009). *Gait&Posture*, 30(2): 144-149.

Kinematic Analysis of the Human Body using Machine Learning Technique

Zia ul Rehman Tahir^{1,2}, Partha Mandal², Usman Saleem¹, Muhammad Abdullah Arif¹, Ammar Waheed¹, Muhammad Taimoor Adil¹, Muhammad Rizwan Yasin¹, Muhammad Tayyab Khan¹, Usama Murtaza¹

¹Department of Mechanical Engineering, University of Engineering and Technology Lahore, Pakistan

²School of Mechanical, Aerospace and Civil Engineering, The University of Manchester, United Kingdom

Email: ziartahir@uet.edu.pk

Summary

The biomechanical data of human body was measured using inertial measurement unit (IMU) sensors for *The Timed Up and Go* (TUG) test. The test was recorded using a simple RGB camera and the video was analyzed using a machine learning (ML) approach. This study aims to evaluate the accuracy of biomechanical data estimated from 2D video source using machine learning method against data measured using 3D IMU's sensors.

Introduction

Commonly used system for motion tracking is marker based optical systems using stereoscopic cameras, these systems are commonly used in indoor environment. Wearable sensors based on IMUs using a biomechanical model are comparatively fast systems and are capable of working in outdoor environment. These systems are expensive and skilled persons are required for their operation. ML techniques for estimation of kinematics of human body using computer vision algorithms and neural networks developed over past few years have proven to be revolutionary for data collection. Machine learning techniques using single RGB 2D camera source are gaining attraction due to their accessibility and minimal cost. *OpenPose* is a pose estimation technique consisting of neural networks, which is utilized, and output is processed to obtain kinematic data [1]. A large set of biomechanical data can be obtained for motion capture in clinical and sports kinematic analysis. The accuracy of kinematic data estimated using these techniques is questionable due to less reported comparison with physically measured data using either an optical system or sensor-based system.

Methods

The TUG test is commonly used to assess mobility of a person and require both static and dynamic balance. The TUG test was selected to compare results of inertial measurement system and machine learning approach. Human body kinematic data was measured using inertial measurement system containing 17 IMUs (XSENS MVN Awinda), the system measures kinematics of 23 body segments. A single RGB camera synchronized with IMU's was used to record videos.

The test was performed on 15 healthy subjects and ten trials of each subject were recorded. The displacement (horizontal and vertical) of three body segments (head, sternum and pelvis) measured by inertial system was used as reference to compare with ML technique. The video data was parsed into

frames, which were processed through a multistage Convolutional Neural Network (CNN), converting the feature maps of the input frame into the part confidence maps and part affinity fields which were further processed to obtain the required location of the segments for each frame. The location was assimilated into position of segments from the frame after scaling to physical dimensions of the setup.

CNN was trained using the *Body25* Caffe model with high accuracy flags. The neural networks were deployed on an ubuntu-based Linux server utilizing Tesla T4 GPUs, however, potentially can be scaled for locally and commercially available server execution. The estimated kinematic data was compared with reference data and accuracy evaluation was conducted on the basis of the Mean Absolute Error (MAE).

Results and Discussion

The horizontal and vertical position was represented as x -axis and z -axis respectively. The MAE for three segments for a single subject is presented in Table 1. The maximum MAE of three segments in horizontal and vertical position was 0.1370 m and 0.0878 m respectively. The errors in horizontal direction are comparatively high due to perspective and fisheye effect. The horizontal and vertical position of head using both systems is shown in Figure 1. The distinguishing characteristics of the kinematic displacement graphs were considerably conserved for kinematic analysis in both z -axis and x -axes.

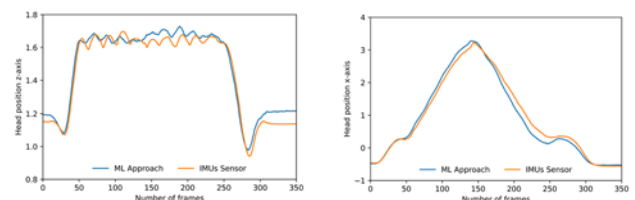


Figure 1: Head position z -axis (left) and x -axis (right)

Conclusions

The results of ML technique are in good agreement with inertial measurement system with a maximum MAE of 0.1370 m. The use of this technique is very cheap compared to using IMUs systems. The results of this study can be used for accurate assessment of clinical biomechanics especially TUG test.

References

- [1] Z. Cao and G. Hidalgo Martinez and T. Simon and S. Wei and Y. A. Sheikh (2019). *IEEE Transactions on Pattern Analysis and Machine Intelligence*, **8765346**.

Table 1: Average of Mean Absolute Error from three segments

Position	Sternum		Pelvis		Head	
	z -axis	x -axis	z -axis	x -axis	z -axis	x -axis
Mean Absolute Error (m)	0.0697	0.1075	0.0878	0.1044	0.0437	0.1370

BrokenPose by we need custom models for markerless motion analysis

Neil Cronin^{1,2}

¹Neuromuscular Research Centre, Faculty of Sport and Health Sciences, University of Jyväskylä, Finland

²School of Sport and Exercise, University of Gloucestershire, UK

Email: neil.j.cronin@jyu.fi

Summary

The emergence of deep neural networks has enabled kinematic analysis outside of a lab and without expensive equipment. A method from computer science, pose estimation, can be used to detect body landmarks via a process called supervised learning, which requires “training” images to be manually labelled. Several open-source algorithms exist for this purpose but they are not tailored to the needs of biomechanists: the training data were labelled via crowdsourcing, so the body parts that they detect are not always relevant or accurate. This in turn results in poor kinematic estimates. One solution is to use custom models, which allow the “marker set” to be chosen. In this work I compare 2D joint angles computed using pre-trained and custom models, demonstrating the superiority of the latter.

Introduction

The emergence of deep neural networks has enabled joint angles to be computed without expensive cameras or reflective markers. Markerless detection of human body landmarks is achieved using an approach from computer science called “pose estimation”. With additional post-processing, joint angles can then be computed. Several open-source algorithms allow body landmarks to be detected in real-time [1,2], but the landmarks that they detect often do not coincide with those typically used in biomechanical motion analysis. As an alternative, it is possible to train a custom model (e.g. using DeepLabCut [3]) where the specific marker set can be chosen. In this work I compare joint angles obtained using pre-trained and custom models, as well as manual analysis, for a range of human movements.

Methods

Various common movements were examined from 8 participants (mean age: 26±3 females) including running on a treadmill and clinical tests that allow for a stationary camera position (e.g. sit-to-stand, lower limb ab/adduction, lumbar side flexion). Videos were processed in 3 ways: manual analysis, with an OpenPose pre-trained model [1] and with a custom model developed in DeepLabCut and a marker set that more closely resembled those used in biomechanics studies. Primarily single plane movements were chosen for simplicity, and because the use of pose estimation for markerless 3D joint angle prediction is still in its infancy (see [4]).

Results and Discussion

Compared to manual analysis, a custom DeepLabCut model yielded more similar joint angle estimates than the OpenPose

pre-trained model (Figure 1). For all movements, across a whole repetition or stride, mean differences in hip angle were 10.1° (control vs. OpenPose) and 6.2° (manual vs. DeepLabCut). Corresponding values for knee angle were 15.8° and 5.1° respectively.

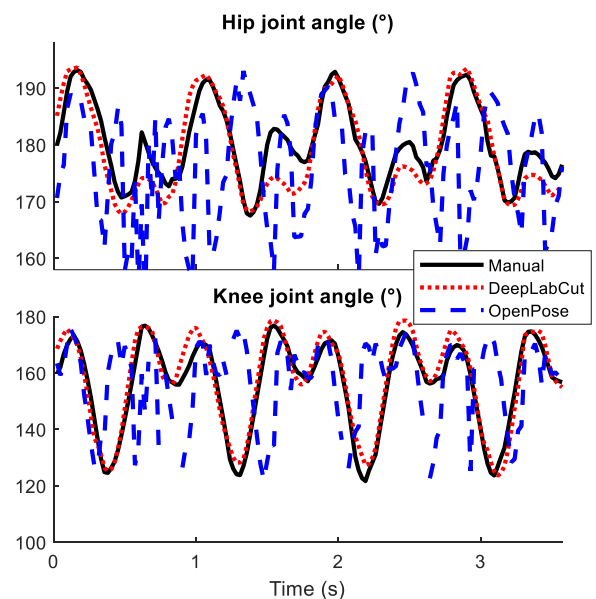


Figure 1: Hip and knee joint angles during running computed using 3 methods: manual analysis (Manual), a pre-trained model (OpenPose) and a custom model (DeepLabCut).

Conclusions

Accurate markerless motion analysis requires neural network models trained in accordance with the needs of biomechanists. For 2D analysis, this can be achieved using custom models combined with transfer learning to minimise the required volume of training data.

Acknowledgments

Academy of Finland (decision number: 323473) Roope Uitto and Leonora Vlaanderen the groups of Irene Davis (Harvard Medical School) and Benedicte Vanwanseele (KU Leuven).

References

- [1] Cao et al. (2018). *arXiv:1812.08008*.
- [2] Kane G et al. (2020) *Comp Sys Bio Neuro*, DOI: 10.7554/eLife.61909.
- [3] Mathis A et al. (2018). *Nat Neurosci*, 21: 1281-9.
- [4] Nakano N et al. (2020). *Front Sports Act Living*, DOI: 10.3389/fspor.2020.00050

Improved Balance Analysis Accuracy using a Functional Base of Support Model

Matthew Millard¹, Lizeth Sloot¹, Katja Mombaur²

¹Optimization, Robotics and Biomechanics Group, Heidelberg University, Germany

²Systems Design Engineering, University of Waterloo, Canada

Email: matthew.millard@uni-heidelberg.de

Summary

Mathematical balance models have the potential to identify people at risk of falling before an injury occurs. Many models of balance depend on an accurate geometric model of the base of support (BOS). The functional BOS (FBOS) of the human foot is smaller than its full outline because not all parts of the foot can support large loads. In this work, we measure the FBOS using center-of-pressure (COP) movements in barefoot and shod conditions.

Introduction

Several of the most general mathematical models of balance map [1] the state of the body to a balance point (BP) on the floor: if the BP can be enclosed by the BOS, the person will be able to transition to a statically stable standing pose. The dynamic balance margin (DBM) is the distance between a BP and the person's BOS. The DBM is useful for assessing balance performance, but its accuracy is affected by the BOS model's accuracy. Recently, we found that having a FBOS model, based on COP movements, allowed us to see systematic differences in balance control between older and younger adults previously obscured when using the full outline of the foot [2]. Here we define the FBOS as the convex region on the foot that can support at least half of the body's weight, a requirement of stable two-footed standing. Here we extend our pilot FBOS model [2] by evaluating the average FBOS of 11 adults when barefoot and shod.

Methods

We recorded the foot movements and ground forces of 11 typical adults while they stood on a force plate and slowly moved their COP through the largest loop possible while keeping the foot on the ground (Fig. 1). The resulting COP trajectories were resolved in a foot-fixed frame, the convex hull of the COP extracted, and normalized by bare foot

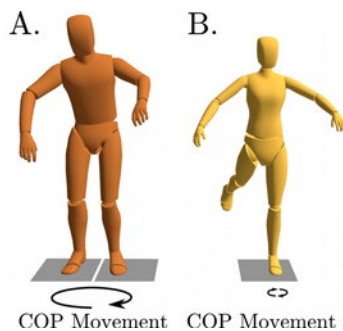


Figure 1: Double (A) and single-stance (B) FBOS tasks

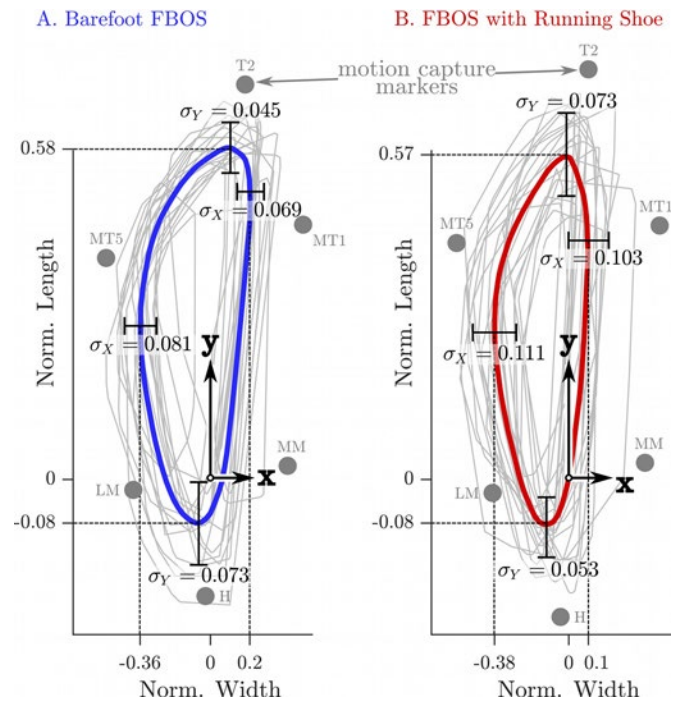


Figure 2: Barefoot (A) and shod (B) FBOS of the 11 participants length and width. The mean FBOS is evaluated by averaging across the convex-hulls of the two tasks (Fig. 1), and across the data from the left and right feet.

Results and Discussion

The average FBOS is smaller than the foot's outline and similar in size across both conditions (Fig. 2). The FBOS model would improve the accuracy of the DBM by 17% of foot length at the heel and toe, and 24% of foot width at the sides. In physical terms, the FBOS model would improve DBM accuracy by 5.1 cm at heel and toe, and 2.4 cm at the sides, for a 30cm by 10cm foot. Though this may seem small, centimeter differences in DBM can mean the difference between standing stably and having to take a step.

Acknowledgments

We gratefully acknowledge the Carl Zeiss-Foundation (Germany) for funding this work through project HeiAge.

References

- [1] Pratt et al. (2006). *In Fast Motions in Biomechanics and Robotics*. Springer, Berlin, Heidelberg.
- [2] Sloot et al. (2020). *FRONT SPOR ACT L*. 2

Differences in single leg postural control when assessed over time in professional rugby union players

Molly McCarthy-Ryan^{1,2}, Stephen Mellalieu^{1,2}, Chris Towers², Adam Bruton³, Isabel Moore¹

¹Cardiff School of Sport & Health Sciences, Cardiff Metropolitan University, Cardiff, UK

²Ospreys Rugby, Swansea, UK

³Department of Life Sciences, University of Roehampton, London, UK

Email: momccarthy-ryan@cardiffmet.ac.uk

Summary

Postural control has been defined as ‘the act of maintaining, achieving or restoring a state of balance during any posture or activity’ [1]. Traditionally, postural control is assessed through single leg stance, with the trial being analysed as a whole. Jonsson [2] proposed the need to analyse postural control in 5 second phases due to larger force variability within the first 5 seconds of the trial. The main finding of this study is that healthy elite rugby union players demonstrate differences in postural control between-phases for both eyes open (EO) and eyes closed (EC) trials. Although for EO trials the initial seconds (dynamic phase) showed larger variability across postural control variables, in line with Jonsson [2], whereas the dynamic phase in the EC task had the smallest variability.

Introduction

Jonsson [2] suggested postural control can be divided into two phases, dynamic and static, due to vertical force changing over time. No study has identified if this is the case for all postural control variables when assessing healthy elite male athletes. The aim of this study was to assess the changes in postural control over time in healthy elite rugby union players in single leg stance trials

Methods

Twenty-one injury free elite male rugby union players (weight 94.86±10.40kg; height 182.35±6.52cm; age 25±4 years), completed a single leg stance in two conditions: EO and EC. A total of 3 x 20 seconds trials were collected for each. Using the filtered data, the following variables were calculated: center of pressure (COP) Sway path (m), COP velocity (m.s⁻¹), and 95% ellipse area (m²). All variables were analysed in 5 second intervals; the first interval was 0 to < 5 seconds. The second interval was 5 to < 10 seconds; third interval 10 to <15 seconds and fourth interval 15 seconds to end of the trial.

Results and Discussion

When looking at the effect of EO and EC on change in postural control over time the pattern observed by Jonsson [2] as only witnessed in the EO trials, whereas the opposite was observed for EC trials, although changes over time were evident in both conditions. For EO trials sway path and mean COP velocity identified differences between interval one and two, one and three and one and four, whereas 95% ellipse area had differences between intervals one and two, one and three, two and four and three and four. However, for EC trials sway path identified differences between interval one and two, one and three, compared to COP velocity who identified differences between interval one and two, one and three and one and four and finally 95% ellipse area only had differences in intervals two and four. The results indicate acute postural control changes that occur for all variables over time in both EO and EC assessments of postural control.

Conclusions

In both EO and EC trials, changes in postural control occurred over time for all variables. Furthermore, the changes in postural control occur in different directions for EO and EC trials indicating that the different visual conditions interact with the sensorimotor system in unique ways. Postural control should be assessed in phases, with both EO and EC, where postural disturbances occur within the trial.

Acknowledgments

The lead author, Molly McCarthy-Ryan is funded by a Knowledge Economy Skills Scholarship (KESS 2). The authors would like to thank Ospreys Rugby for their collaborative partnership in this research.

References

- [1] Pollock A et al. (2000). *Clinical Rehabilitation*, **14**: 402-406.
- [2] Jonsson E et al. (2004). *Clinical Biomechanics*. **19**: 688-694.

Table 1: Mean ± standard deviations of postural control variables in relation to the four time intervals.

	Condition	Interval 1	Interval 2	Interval 3	Interval 4
Sway Path (m)	Eyes Open	0.25±0.08	0.23±0.09 ^a	0.23±0.07 ^b	0.23±0.08 ^c
	Eyes Closed	0.45±0.10	0.52±0.13 ^a	0.51±0.14 ^b	0.48±0.11
Mean COP velocity (m.s ⁻¹)	Eyes Open	0.051±0.016	0.046±0.0178 ^a	0.046±0.015 ^b	0.046±0.016 ^c
	Eyes Closed	0.090±0.021	0.104±0.027 ^a	0.101±0.029 ^b	0.098±0.020 ^c
95% ellipse area (m ²)	Eyes Open	0.001±0.0010	0.001±0.0003 ^a	0.001±0.0004 ^b	0.001±0.0010 ^{d e}
	Eyes Closed	0.002±0.0010	0.002±0.0010	0.003±0.0010	0.003±0.0001 ^d

^a Significant difference between Interval 1 and 2, ^b Significant difference between Interval 1 and 3, ^c Significant difference between Interval 1 and 4, ^d Significant difference between Interval 2 and 4, ^e Significant difference between Interval 3 and 4.

Foot and ankle joint coupling in balance and gait

Rosemary Dubbeldam¹, Lena I.G. Fennen¹, Heiko Wagner¹

¹Department of Movement Science, Institute of Sport and Exercise Sciences, University of Münster, Germany
Email: r.dubbeldam@uni-muenster.de

Summary

Foot and ankle joint coupling has been related to task and pathology. However, little is known about their coupling in balance. This study aims to assess coupling of foot and ankle joint movements in balance and gait. Therefore, gait and 1-limb stance of 17 healthy participants was recorded and the motion of the hallux, medial forefoot, midfoot, hindfoot and leg was calculated. The relationship between (non-)adjacent segments was assessed by fitting a linear regression model. Group average coefficients of determination and regression angles were derived. In balance, a strong relationship was found between hindfoot and medial forefoot eversion. In gait and balance, hindfoot exorotation and eversion were consistently related to medial forefoot dorsiflexion, and hindfoot eversion to hallux dorsiflexion. However, in balance, hindfoot inversion was related to hallux plantarflexion as compared to dorsiflexion in gait. Furthermore, more variance was demonstrated in balance, suggesting more variation in control compared to gait.

Introduction

Passive and active structures influence the movements of our body segments. Multiple studies have related pathology to changes in segment movement coupling, yielding insight in diagnosis and treatment options [1,2]. However, little is known about foot and ankle joint coordination during balance. The aim of this study is to analyse 3-dimensional coupling motion of (non-)adjacent foot and ankle joints in balance and compare them to those in gait.

Methods

A 3-dimensional movement analysis system was used to record gait and 2 trials of 1-limb stance with eyes closed of 17 participants (average 24 years, range 20-34 years). The motion of the hallux, medial forefoot, midfoot, hindfoot and leg was assessed [3]. Six coupled motions between segments were analysed by fitting a robust linear regression model [4]. The coefficient of determination (R^2) and regression angle (α) were derived for each stance phase in gait (at least 10 steps) and the 60 second balance trials. Average group values and corresponding standard deviations were assessed for gait and balance. In segment coupling plots, consistency was assumed, when both segments move together along the regression line and demonstrate synchronous turning points (Figure 1) [4].

Results and Discussion

In gait, hindfoot exorotation and eversion were consistently related to medial forefoot dorsiflexion (R^2 0.3 ± 0.3 , $\alpha = 6^\circ \pm 7^\circ$ and R^2 0.5 ± 0.3 , $\alpha = 11^\circ \pm 12^\circ$, respectively), and hindfoot eversion to hallux dorsiflexion (R^2 0.6 ± 0.2 , $\alpha = -7^\circ \pm 4^\circ$). In balance, the same consistent relationships were found for

hindfoot exorotation and eversion to medial forefoot dorsiflexion (both R^2 0.3 ± 0.3), and hindfoot eversion to hallux dorsiflexion (R^2 0.5 ± 0.3). However, the regression angles increased up to $10^\circ \pm 26^\circ$, $33^\circ \pm 25^\circ$, and $27^\circ \pm 22^\circ$, respectively (Figure 1). Consequently, in balance, hind foot inversion was related to hallux plantarflexion, compared to hallux dorsiflexion in gait, where the Windlass mechanism plays a role. Additionally, a consistent relationship between hindfoot and medial forefoot eversion was observed in balance (R^2 0.5 ± 0.3 , $\alpha = 33^\circ \pm 25^\circ$).

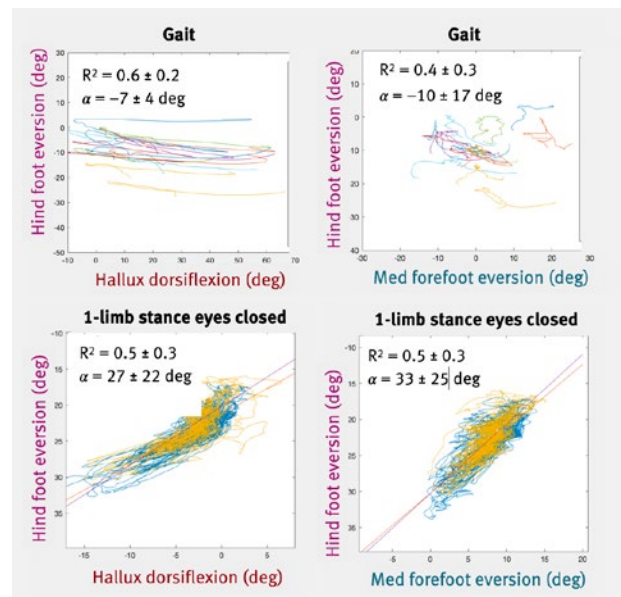


Figure 1: Foot segment coupling plots for gait (stance-phase of all participants) and 1-limb balance (2 trials of 1 participant). With average group R^2 and α .

Conclusions

The results suggest, that different active and passive structures influence balance compared to gait. Furthermore, between-subject variation was larger in balance than in gait. Individual balance control mechanisms and performance, may play a role. In future, assessment of relations between task performance, muscle activation and foot and ankle segment coupling may provide additional insight.

Acknowledgments

We would like to thank M. de Lussanet, M. Gerlach and J. Dietzsch for their contribution in the lab and data processing.

References

- [1] Doherty C et al. (2015). *Clin Biom*, **30**: 129-135.
- [2] Pohl MB et al. (2007). *Gait Post*, **25**: 295-302.
- [3] De Mits S et al. (2012). *J Orth Res*, **30**: 655-661.
- [4] Dubbeldam R et al. (2013). *Gait Post*, **37**: 159-164.

Intra and Intersession Reliability of Centre of Pressure Measures in Older Adults during Bipedal Static Postural Tests

Diana Soares, Iain Fletcher, Andrew Mitchell and Laura Charalambous
 Institute of Sport and Physical Activity Research, University of Bedfordshire, Bedford, UK
 Email: diana.soares@study.beds.ac.uk

Summary

Research investigating test-retest reliability of centre of pressure (CoP) measures during bipedal static postural tests in older adults is sparse. The aim of this study was to assess the intra (same day) and intersession (between days) reliability of nine CoP measures in older adults aged 65 to 79 years, to identify how many trials are needed to obtain a low coefficient of variance (CoV%) during bipedal static postural tests. Using a force plate, CoP sway path and mean speed were found to be the most reliable measures, but only in the eyes open (EO) condition. ML mean velocity was reliable in both EO and eyes closed (EC) conditions. Two trials of 30 seconds were sufficient to obtain an acceptable intra and intersession reliability in these CoP measures.

Introduction

The intrinsic variability of CoP measures, sampling duration and number of trials may affect the reliability and validity of postural stability outcomes [4,6]. Previous studies [1,3,4,5] have indicated how many trials and trial time are needed to obtain good reliability in several CoP measures in older adults. Sampling durations ranged from 30 to 120 seconds and number of trials from three to nine [1,3,5], or were not indicated [4]. Comparisons are hence difficult due to major variations across protocols. It is important that any differences observed in CoP measures are due to changes in the participants' postural control as opposed to random or systematic errors in the measurement procedure [2]. The aim of this study was to investigate the intra and intersession reliability of nine CoP measures to identify how many trials are needed to obtain acceptable reliability during a bipedal static postural test in older adults.

Methods

Eleven healthy older adults (70.2±2.7 yrs, 165±7.6 cm, 71.5±12.9 kg) volunteered to perform a bipedal static postural test with eyes open (EO) and eyes closed (EC) (blindfolded). Participants stood barefoot on a force plate (100Hz, Kistler) as still as possible, with feet hip width apart and arms hanging by their sides in both conditions. While looking at a 10x10 cm diameter black mark on a white board placed 2 m away from the participant, ten 30 seconds trials were randomly (EO or EC) conducted with seated rest periods of 1 min between each trial. Consistent foot placement was ensured between trials and sessions by placing an outline of the feet on top of the force plate. After 1 hour of seated rest, the test session was repeated to evaluate intrasession reliability and one week later to test intersession reliability. Using Microsoft Excel, CoP measures in both anterior-posterior (AP) and medial-lateral

(ML) directions were calculated for sway path (mm), mean speed (mm), maximum speed (mm·s⁻¹), peak velocity (mm·s⁻¹), mean velocity (mm·s⁻¹) and peak displacement (mm). Intra and intersession reliability for all CoP measures in each condition was estimated using the CoV% (SD/mean x 100) [2] and reliability scores were obtained (test-retest).

Results and Discussion

Results indicated that, in both EO and EC conditions, it was found an acceptable intersession reliability (CoV% < 20%) but not intrasession (CoV% < 20%) in all CoP measures. This might be due to the participants not being familiar to stand barefoot for 30 seconds without moving. Only CoP ML mean velocity presented an acceptable intra and intersession CoV% reliability scores in both EO (0.4% < 3.7%) and EC (3.1% < 1%) conditions, when two trials of 30 seconds were averaged. This is similar to previous studies [3,5], however they used two trials of 120 seconds with EO [3] and three trials of 75 seconds with EC [5], to obtain good reliability in this CoP measure. In the present study, intra and intersession variability did not reduced as more trials were averaged in either condition. CoV% plateaued for all variables by trial 3. When two trials were averaged, sway path and mean speed presented an acceptable intra (0.4%) and intersession reliability (2.7%) but only in the EO. This suggests that visual input may have an effect when estimating reliability in CoP measures in older adults during postural analysis in quiet stance.

Conclusions

CoP sway path and mean speed were the most reliable measures of static postural stability, but only in the EO condition when assessing older adults aged 65 to 79 years. In the EC condition, ML mean velocity is recommended. Two trials of 30 seconds were sufficient to obtain good intra and intersession reliability when using these CoP measures. Number of trials and visual conditions must be taken into account when investigating postural stability in this population as it may impact the efficacy of the results. Further investigation is needed to explain the superiority of some CoP measures in terms of reliability.

References

- [1] Corriveau et al. (2000). *Arch. Phys. M.*, **81**: 45-48.
- [2] Hopkins et al. (2000). *Sports Med.*, **30**: 1-15.
- [3] Lafond et al. (2004). *Arch. Phys. M.*, **85**: 896-901.
- [4] Li et al. (2016). *J. Phys. Ther.*, **8**: 1364-1367.
- [5] Lin et al. (2008). *Gait Posture*, **28**: 337-342.
- [6] Paillard & Noé (2015). *Biomed Res. Int.*, **15**: 1-15.

The effect of feet position on standing balance in pediatric patients with flat feet

A.M. Khodorovskaya¹, M.V. Savvina¹

Physiology and Biomechanics Research Laboratory. H. Turner National Medical Research Center for Children's Orthopedics and Trauma Surgery, Saint Petersburg, Russia;
Email: shulamif@mail.ru

Summary

This study aims to examine the effect of feet positions on standing balance in children with flat feet and its clinical applications.

Introduction

Pediatric flat feet are a very common concern for parents and one of the most frequent presenting complaints to a pediatric practice. The flat foot diagnosis can't be limited to a morphological examination [1]. It should be based on an accurate clinical and radiographic examination, as well as on functional and instrumental analysis such as stabilometry. An influence variation in foot position on standing balance in pediatric patients with flat feet has not been fully investigated..

Methods

Forty nine children with fixed flat feet aged between 9 and 12 years participated in this study. (23 girls and 26 boys). Weight: $46 \pm 6,3$ Kg; Height: $149,5 \pm 5,7$ cm; foot length: $24 \pm 2,7$ cm;) All subjects did not have any musculoskeletal or neurological disorders, as well as no history of surgeries and trauma of musculoskeletal structures on the lower limbs. The study conforms to the Declaration of Helsinki. Written informed consent was obtained from parents of all participants prior to the biomechanical examinations.

For the bipodal test, children were instructed to stand on the platform with arms hanging beside their body in two positions: 1) feet forming an angle of 30° degrees and heels apart-3 cm (group A); 2) feet parallel to each other and distance between the 2 ankle joint centers equal to the distance between the right and left anterior superior iliac spines (group B). For the monopodal test, patients stood on each of their lower limbs at the center of the platform.

The test was performed using Stabilan-02-stabilometric platform (ZAO OKB Ritm - Russia).Acquisition time was set at 20 seconds. The Closed Eyes test was performed before the Open Eyes one to the purpose of limiting the oculomotor control memory on balance keeping in Closed Eyes condition. The displacement of the Center of Foot Pressure (COP) was analyzed by assessing the standard indicators for the bipodal test as well as for the left leg and right-leg monopodal tests.

Statistical analysis. For comparison stabilometric variables between groups (group A and group B), the Student's t-test for independent samples was used. Normality of data was assessed through a Kolmogorov-Smirnov test. A significance level of $p \leq 0.05$ was set for all statistical procedures, and the SPSS v. 19 software was used.

Results and Discussion

Bipodal stabilometry showed that in group B scored significantly higher with respect to COP X mean ($p=0.0427$) during the eyes-closed condition than in group A in same condition. Monopodal stabilometry tests showed that leg corresponding to the side of the larger COP X mean displacement had scored significantly higher in COP Length($p=0.008$) and COP Speed ($p=0.003$) during the eyes-closed and the eyes-open condition.

Feet positions have an important role in controlling posture in a standing position. We hypothesized that patients in group B would have poorer standing postural control than patients in group A, because greatly reduces stability within the foot joints. The decreased stability may be due to reduced joint congruity and consequently an increased reliance on soft tissue structures This may explain why the patient in group B position had a significantly displacement position of the COP in the medio-lateral plane than the patients in group A and not in the antero-posterior plane. Assessment of the clinical parameters of the feet does not provide complete information about the degree of flat feet [2]. Stabilometry could can be used as an additional tool for assessing the severity of flat feet and also employed for monitoring for nonsurgical patients with flat feet.

Conclusion

The position of the feet affects the standing balance in patients with flat feet. Taking these results into account we recommend using a bipodal standing, with feet parallel to each and the distance between the 2 ankle joint centers equal to the distance between the right and left anterior superior iliac spines when performing stabilometry in pediatric patient with flat feet.

References

1. Ford S. E., Scannell B. P. (2017). *Foot and ankle clinics*, 22:643-656.
2. Sapogovskiy AV, Boyko AE.(2020). *Pediatric Traumatology, Orthopaedics and Reconstructive Surgery*, 8:407-416.

Limits of stability in cognitively healthy individuals and mild cognitive impairment (MCI)

Andresa M. C. Germano¹, Daniel Schmidt¹, Niclas Masuch¹, Thomas L. Milani¹

¹Department of Human Locomotion, Chemnitz University of Technology, Chemnitz, Germany

Email: andresa.germano@hsw.tu-chemnitz.de

Summary

We investigated balance control in mild cognitive impairment (MCI) compared to cognitively healthy controls. Although only differences between the young and old groups were found, correlations between cognitive and balance parameters were evident. Hence, further studies are needed.

Introduction

MCI causes structural and functional changes in the brain, being considered as a process between cognitive changes of normal aging and dementia diseases [1]. The increased rate of atrophy of affected brain regions negatively affects the ability to balance and leads to a higher risk of falls [2]. Still, studies regarding motor deficits in MCI show controversies. Therefore, we investigated balance control (limits of stability, LoS) in MCI patients compared to healthy controls. We hypothesized decreases in balance control in MCI and correlations between balance and cognitive parameters.

Methods

193 participants (MCI (82.7±2.4 yrs): 55♂, 35♀; older cognitively healthy individuals (OCH) (82.3±2.7 yrs): 35♂, 40♀; and young cognitively healthy individuals (YCH) (22.8±3.1 yrs): 15♂, 13♀) took part in the LoS balance tests. The groups were determined using the Montreal Cognitive Assessment (MoCA: value < 26 corresponds to MCI). Three trials of LoS were collected using a force plate (GK-1000 Koordinator, IMM Holding GmbH, 1kHz). The protocol consists of three phases: 1) 20s of quiet stance (COP_static); 2) the distance until the maximal forward leaning without losing balance (AP_displacement; normalized by foot length); and 3) maintenance of maximal forward leaning position for 10s (COP_limit). Mean±SD of the COP parameters were calculated for statistical analyses.

Results and Discussion

Gender differences were found (Table 1). Rejecting our hypothesis, differences between the groups were found in all parameters, but only between both older groups and YCH. This reflects age-related deteriorations. Interestingly, the same behavior can be observed in foot sensitivity [3], which could explain our balance results, since skin sensitivity contributes to the control of balance. Correlations between

balance and cognitive parameters support our hypothesis, showing that motor control is affected as consequence of brain damage in cognitively impaired (Figure 1). This is in line with a previous study [4], which also reported a low cognitive performance and increased postural instability.

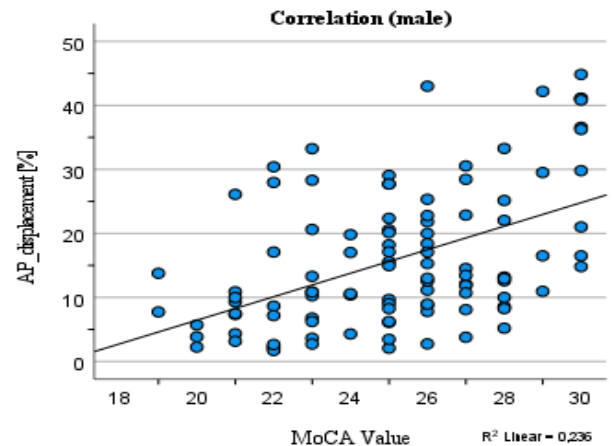


Figure 1: Exemplary: correlation between AP_displacement and MoCA value ($\rho = 0.470$, $p < 0.001$).

Conclusions

Aging effects were evident, but no additional decreased balance in MCI was present. However, correlations between balance and cognitive parameters were shown. Hence, further measurements are needed to provide insights into the brevity of motor control decline and information-processing structures in MCI.

Acknowledgments

This study (SENDA) was funded by the ESF and the SAB.

References

- [1] Chen W et al. (2013). *Shanghai Arch Psychiatry*, **25**: 119-120.
- [2] Makizako H et al. (2013) *BMC Neurol*, **13**: 102.
- [3] Gescheider GA et al. (1994). *Somatosens. Mot. Res.*, **11**: 345-357.
- [4] Leandri M et al. (2015). *J Alzheimers Dis*, **3**: 705-707.

Table 1: Mean±SD of balance data.

	COP_static [mm]		COP_limit [mm]		AP displacement [%]	
	male	female	male	female	male	female
YCH	92.5 ± 49.7	66.3 ± 43.3	88.4 ± 27.8	67.0 ± 18.9	34.6 ± 7.8 ^F	28.5 ± 6.2 ^F
OCH	223.5 ± 96.4 ^A	127.2 ± 60.3 ^A	115.8 ± 47.9 ^C	55.4 ± 25.2 ^C	13.6 ± 6.0	10.9 ± 7.8
MCI	254.8 ± 148.9 ^B	147.0 ± 81.4 ^B	100.7 ± 39.4 ^D	67.5 ± 36.6 ^D	12.4 ± 8.8	9.7 ± 5.2

^{A, B, C, D, E, and F} $p < 0.05$ of Mann-Whitney-U-Test (inter-gender). Differences between groups (for both genders): COP_static: YOH vs. OCH; YOH vs. MCI/ COP_limit: YOH vs. OCH/ AP displacement: YOH vs. OCH; YOH vs. MCI, all $p < 0.05$ (Mann-Whitney-U-Test).

The vertical balance control system in children with cerebral palsy is more synchronized compared to healthy children

Igor E. Nikityuk, Galina A. Ikoeva

H. Turner National Medical Research Center for Children's Orthopedics and Trauma Surgery, Saint Petersburg, Russia

E-mail: femtotech@mail.ru

Summary

The analysis of stabilometric examination of patients with mild and severe cerebral palsy (CP) at the age from 6 to 12 years was carried out. For comparison, healthy children of the same age were examined, each group of children consisted of 10 people. The results of the study showed a significant decrease in the stability of the vertical balance in both groups of patients with cerebral palsy in comparison with healthy children. However, a strong correlation was found between the parameters of the statokinesiogram: area S , length L , and amplitude A of the center of pressure (COP), which significantly exceeds that in healthy children and is most pronounced in severe CP. The pathologically increased ordering of the COP trajectory of statokinesiograms in CP patients is regarded as an indicator of a deficit in postural control.

Introduction

All forms of cerebral palsy impair the balance management system of the body. There are proposals to present postural control as a stochastic process. Such a principle of postural balance analysis may be more informative in comparison with the descriptive statistics methodology [1].

Methods

A stabilometric examination with open eyes (OE) and closed eyes (CE) of 3 groups of children, 10 people each, aged from 6 to 12 years, was carried out using the MBN Biomehanika complex. The first group - children with mild cerebral palsy, the second - children with severe cerebral palsy, the third - healthy children. The length of the trajectory passed by COP (L , mm), the area S (mm^2) of the stabilogram, and the average amplitude of COP oscillations - A (mm) were calculated. To study the relationship of signs, correlation analysis with Spearman coefficient r_s was used. Differences were considered statistically significant at $p < 0.05$.

Results and Discussion

In both groups of patients with cerebral palsy, pronounced disorders of postural balance with a significant increase of L , S and A parameters compared with healthy children ($p < 0,05$) were revealed. At the same time, the statistical differences between the stabilometric parameters of children with mild and severe cerebral palsy were not significant.

Correlation analysis showed an average inverse multiplicative relationship between parameters L , S (LFS) and A in the group of healthy children (OE: $r_s = -0.54$, CE: $r_s = -0.59$).

Higher modulus r_s values were found in the group of patients with mild cerebral palsy (OE: $r_s = -0.65$, CE: $r_s = -0.81$) (Fig. 1, a). The strongest correlation in modulus between the parameters was found in the group of patients with severe cerebral palsy (OE: $r_s = -0.92$, CE: $r_s = -0.93$) (Fig. 1, b).

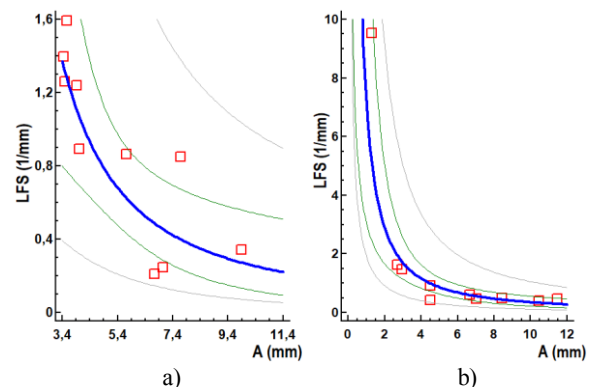


Figure 1: Regression line (blue) for the dependence of the LFS parameter of statokinesiograms on the range of variability A in children with CP in the test with opened eyes: a) mild degree; b) severe degree.

The increased ordering of the trajectory of the center of pressure in children with cerebral palsy was described earlier [2] and can be regarded as pathological [3]. The use of the stochastic approach is highly sensitive and can provide a deeper understanding of the mechanisms used by the postural control system in patients with cerebral palsy.

Conclusions

In patients with cerebral palsy, the vertical balance control system, despite severe disorders, is more synchronized in comparison with healthy children. Moreover, the relationship between the parameters of stabilometry in severe cerebral palsy is significantly higher than in mild.

References

- Riley MA et al. (1999). *Gait Posture*, 9: 65–78.
- Donker SF et al. (2008). *Exp Brain Res*, 184: 363–370.
- Goldberger AL. (1997). *Perspect Biol Med*, 40: 543–561.

Energy dissipation while landing from a jump

T. Toussaint¹, B. Schepens¹

¹Laboratory of Physiology and Biomechanics of Locomotion, Institute of Neuroscience (IoNS), Université catholique de Louvain (UCLouvain), Louvain-la-Neuve, Belgium
Email: thibaut.toussaint@uclouvain.be

Summary

This study highlights the mechanical behavior adjustments of the lower limbs when landing on the ground from a jump at different heights (i.e., when the amount of energy to be dissipated increases). We observe that the strategy is mainly tuned to get a safety margin in order to avoid bouncing on the ground or losing balance, and less to limit the mechanical constraints.

Introduction

When landing from a jump, we must be able to slow down our body and dissipate the energy gained during the fall in order to reach back a stable standing position without rebounding or losing balance. The motor control must therefore be adjusted to the amount of energy to be dissipated.

The landing can be divided into two phases (Figure 1) [1,2]. During the first phase, the center of mass of the body (*CoM*) goes down and the vertical component of the ground reaction force (vGRF) increases; this behavior assimilates the lower limbs to a linear spring. During the second phase, the *CoM* goes down and up while the vGRF mainly decreases; this behavior can be described by a spring associated with a damper allowing energy dissipation. To our knowledge, the way this model is modified as function of the amount of energy is unknown. Therefore, our aim is to analyze if and how the amount of energy shapes the biomechanical properties of the lower limbs (i.e., stiffness and damping).

Methods

Fifteen subjects (age: 22-31 yo) were instructed to perform a jump from a box of different heights (10, 30, 60cm) and land on both feet in a natural way. The vertical acceleration and the displacement of the *CoM* (a_v and S_v) were computed from the vGRF, which was recorded using force-platforms.

The biomechanical behavior of the lower limbs was assessed from $a_v - S_v$ by computing the stiffness (k_1) from touchdown (*TD*) until the maximum value of a_v (a_{v-peak}), and then the stiffness & damping coefficients (k_2 , c_2) until the standing position as described by Gambelli et al. (2015). In addition to a_{v-peak} , the lowest position of the *CoM* (S_{v-min}) and the minimum value of a_v (a_{v-min}) were measured (Figure 1). Note that if a_{v-min} reaches the value of -9.81 m.s^{-2} , the subject will rebound on the ground.

Results and Discussion

The model previously described (i.e., spring–spring&damper) yields good fit with our experimental data (mean $r^2 = 0.93$). When the amount of energy to be dissipated increases, the stiffness k_1 remains constant while the stiffness k_2 and the damping coefficient c_2 decrease. Accordingly, the impact of the ground increases ($a_{v-peak} \uparrow$), and the *CoM* reaches a lowest position ($S_{v-min} \uparrow$) while the minimum of a_v (a_{v-min}) remains constant. One interpretation of such behavior is that the biomechanical properties of lower limbs seem to be tuned to get a safety margin in order to avoid imbalance and rebound, rather than reducing the mechanical constraints.

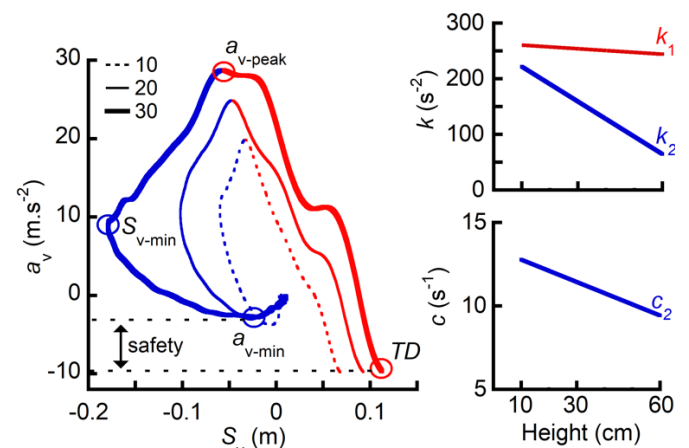


Figure 1: Grand mean of a_v as function of S_v from *TD* until the standing position. The spring-like phase is presented in red and the spring&damping-like phase is presented in blue. Each trace represents an experimental condition (jumps from 10 to 60 cm). The stiffness & damping coefficients (line of best fit) are presented as function of height.

Conclusions

When landing from a jump, the biomechanical properties of lower limbs are tuned according to the amount of energy to be dissipated. To deal with the increased amount energy to dissipate, the lower limbs behavior must be modified throughout landing (two distinct behaviors) and these modifications take part mainly during the second of landing.

Acknowledgments

This study was supported by “Fonds Spéciaux de Recherche” de l’UCLouvain (Belgium).

References

- [1] Gambelli et al. (2015). *Plos One*, e0141574.
- [2] Dyhre-Poulsen et al. (1991). *J Physiol*, **437** :287-304.

Anticipatory Postural Adjustments During Gait Initiation in People with Mild Chronic Low Back Pain

Rum Lorenzo¹, Russo Guri¹, Mannozzi Giuseppe¹, Laudani Luca², Macaluso Andrea¹

¹Laboratory of Bioengineering and Neuromechanics of Human Movement, University of Rome "Foro Italico", Rome, Italy

²Cardiff School of Sport and Health Sciences, Cardiff Metropolitan University, Cardiff, UK

Email: lorenzo.rum@uniroma4.it

Summary

Anticipatory Postural Adjustments and trunk flexion are fundamental mechanisms utilized prior to walking to produce optimal biomechanical conditions. Gait initiation kinematics in people with mild Chronic Low Back Pain (mCLBP) and healthy controls was collected with force plates and motion capture. Participants with mCLBP showed altered postural preparation with respect to healthy controls, which was also associated with thorax motion during gait initiation, but tends to disappear during the first step execution.

Introduction

Gait initiation is a transitory motor task requiring Anticipatory Postural Adjustments (APAs), which produce an initial motion of the feet Centre of Pressure (CoP) aiming at providing optimal balance and motor performance [1]. During this phase, a key functional role to generate the necessary forward momentum and initiate gait is also played by the forward leaning of the trunk [2]. However, it has been recently shown that neuro-mechanical control of the trunk is impaired in individuals with mild Chronic Low Back Pain (mCLBP) during walking and gait termination [3]. The present study aimed to investigate the effects of mCLBP on APAs and trunk kinematics during gait initiation.

Methods

Eleven healthy adults and 11 adults with mCLBP performed 10 gait initiation trials at their comfortable self-selected speed. Two force platforms (Fertec Corp, OH) were used to record the CoP trajectory during the preparation and execution of the first step. APAs' amplitude and duration, the initial posterior peak force and the step initiation latency with respect to the onset of ML CoP motion during step preparation were obtained. A motion capture system (Vicon, UK) was used to assess the absolute angular displacement of the thorax in the sagittal plane during step preparation and the first step length and width according to the Plug-in Gait model. Group comparison was performed by means of independent sample t-test or Mann-Whitney Test. A partial correlation analysis for repeated observation within subjects was performed to evaluate the relationship between sagittal thorax angular displacement and gait initiation parameters within each group.

Results and Discussion

Participants with mCLBP showed longer APAs duration and step initiation latency compared to healthy participants ($p = .012$ and $p = .001$, respectively) (Figure 1). No differences were observed for either APAs amplitude, first step spatio-temporal parameters or thorax kinematics ($p > .05$). Greater thorax forward flexion was positively correlated with step initiation

latency in mCLBP group and the posterior peak force in healthy participants (Table 1).

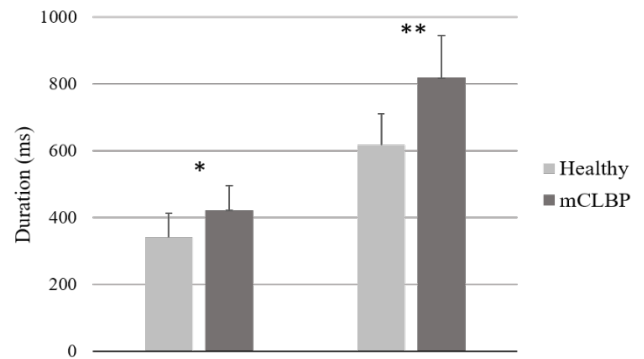


Figure 1: APAs duration (left) and step initiation latency (right). * $p < 0.05$, ** $p < 0.001$.

Table 1: Results of partial correlation analysis between sagittal thorax angular displacement ($^{\circ}$) and each parameter during gait initiation.

	Healthy		CLBP	
	r	p	r	p
APA amplitude (mm)	-.12	NS	-.21	NS
APA duration (ms)	-.17	NS	.19	NS
Step latency (ms)	.15	NS	.45	<.001
Posterior peak force (N)	.45	<.001	.18	NS

Conclusions

People with mCLBP initiate gait more cautiously than healthy controls by producing lower forces during postural preparation, as shown by the comparable APAs amplitude but the longer APAs duration. Interestingly, the longer step latency was positively associated with thorax forward flexion in participants with mCLBP, which suggests a link between APAs impairment and trunk motion, confirming the functional role played by the upper body in gait initiation. Taken together, these adaptations in postural preparation shown by people with mCLBP seem to be effective in preserving balance using a more cautious strategy, as shown by the lack of differences in the first step characteristics between this group and the healthy controls.

References

- [1] Iou E et al. (2017). *World J Orthop*, **8**: 815-828.
- [2] Laudani L et al. (2006). *J Electr Kin*, **1**: 603-610
- [3] Rum L et al. (2021). *Gait Posture*, **84**: 238-244

Video game based kinematic assessment using a Leap Motion Controller

Dominik Buchmann¹, Amartya Ganguly¹, Katja Mombaur²

¹Optimization, Robotics and Biomechanics, Institute of Computer Engineering, Heidelberg University

²Chair in Human-Centred Robotics & Machine Intelligence, University of Waterloo

Email: d.buchmann@stud.uni-heidelberg.de

Summary

Development of feasible assessment methods for hand kinematic analysis is of great importance in many clinical applications like physiotherapy and rehabilitation engineering. Motion analysis for kinematic assessments usually requires high end setups involving costly laboratory grade camera systems or similar detectors. Game based setups, using low cost consumer grade peripheral devices like the Xbox Kinect or the Nintendo Wii, promise repeatable and reproducible experiments for assessment. For this study a game for hand kinematic assessment was created which uses a Leap Motion Controller as the only tracking device needed. The game was then used to assess hand kinematics of the participants.

Introduction

A game-based approach to capture and assess hand kinematics, using a Leap Motion Controller (LMC) as the main peripheral, was developed in [1]. The analysis focused on the performance of able-bodied subjects performing pick and place operations in the virtual environment using a pinch grip. Data was compared inter trial and inter participant as well as against data from available database [2]. The game was a virtual take on the standard peg-test (NHPT) [3].

Methods

Ten participants, age: 22,3 (\pm 2), volunteered to take part in the experiment using only their stated dominant hand. Each participant was considered able-bodied in terms of being able to perform a pinch grip. Motion tracking was done using a well calibrated LMC in a portable setup with an estimated total latency of less than 100ms. Participants were shown a play through of the game but not given any rehearsal trials. Each participant then played the game three times whilst data was recorded for each trial and each participant separately. Data was timestamped, giving an overall time score, which also served as a secondary assessment of the participants motor skills.

Results and Discussion

All participants were able to successfully complete the experiment showing the stability of this game-based setup. The pinch strength parameter, given by the LMC was found to have an inverse correlation with the distance between the index finger and thumb tips. Normalising the tracked Pinch Strength then allows it to be compared against an actual force measurement, (Figure 1). Both data indicates a rapid increasing in the beginning of the grip phase with an

overshoot. The adaption phase using the LMC is less quickly or sometimes missing most likely due to absent physical feedback. Participants in general were able to better their time scores from an average of 74.1 seconds (\pm 39.69) to 38.6 seconds (\pm 11.68). Which suggests an adaptation phase occurred regarding the task.

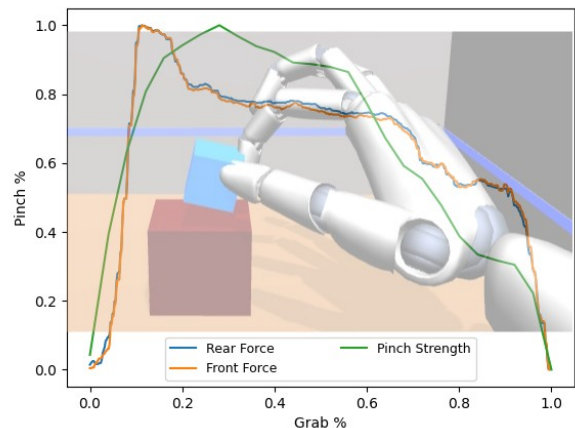


Figure 1: Course of the Pinch Strength compared against Force measurement on the iBox faces (Normalised) blended with a screenshot of the pick and place task in the virtual environment.

Conclusion

Similar to assessments using the NHPT, participants on average, decreased their overall used time needed to solve the operations along the trials. Compared against data resulting from actual force sensors shows that the pinch strength is not to be taken as an actual measurement of force but rather as an indicator of the current pinch pose. Furthermore, the data suggest that visual feedback given by the game might replace the missing physical feedback to some extent.

Acknowledgments

We thank all participants who volunteered for this experiment. We also thank our funders EIT Health 19340.

References

- [1] Dominik Buchmann (2020). *Interactive Visualisation to assess hand Kinematics*, Bachelor Thesis, University of Heidelberg
- [2] Martin-Brevet, S. et al. (2017). *PloS one*, **12**: e0178185.
- [3] Grice et al. (2003). *American Occupational Therapy Association*, **57**: 570-3.

A novel method to assess soft tissue overloading within the sole of the foot

Panagiotis Chatzistergos¹, Nachiappan Chockalingam¹

¹Centre for Biomechanics and Rehabilitation Technologies, Staffordshire University, Stoke-on-Trent, UK

Email: panagiotis.chatzistergos@staffs.ac.uk

Summary

This study explores the potential use of measurements of altered tissue biomechanics for the detection of overloading within the plantar soft tissue with potential application in the management of the diabetic foot. Overloading was simulated by repeatedly loading the centre of the heel to the threshold of pain. Overloading caused measurable stiffening in the areas where pressure was most intense.

Introduction

People with diabetes can gradually lose the protective sensation of pain in their feet leading to repeated overloading, diabetic foot ulceration (DFU) and even to amputation. In the absence of pain, soft tissue overloading is usually detected only after visible signs of DFU have developed and it is too late for effective prevention. This study aims to explore the possibility of detecting overloading based on the changes that overloading might cause in tissue stiffness.

Methods

Shear wave (SW) speed was measured (SL15-4, SuperSonic Imagine Ltd) in the axial plane at the centre the heel for 15 non-diabetic volunteers with normal sensitivity in their feet before and after overloading (age: 41y±10y, BMI: 26.8kg/m² ±5.7kg/m²). To minimise the effect of loading history the participants were asked to walk barefoot the length of the lab twice (≈80 steps) before baseline imaging (Figure 1a). Overloading was imposed by pressing a small cylinder (diameter=1cm) at the centre of the heel with a hand-held dynamometer (500N Cytec) until the participant indicated pain, at which point the heel was unloaded. This loading process was repeated ten times before imaging the heel again (Figure 1b). Pressure pain threshold (PPT) was recorded for each cycle by dividing the applied force over the loaded area. To see whether any possible changes in SW speed could be eliminated by preconditioning, SW imaging was repeated after walking barefoot the same distance as before (Figure 1c). At the end, SW speed was exported for five circular areas (diameter=5mm): three in the loaded area and two outside the loaded area (±1.25cm from the centre) (Figure 1).

Results and Discussion

Repeated measures ANOVA with Bonferroni correction for multiple comparisons revealed a statistically significant increase in SW speed in the left edge (position -0.5cm) of the loaded area which was not eliminated by walking (Table 1). Our previous work on the validation of SW elastography for the plantar soft tissue has indicated that changes in SW speed offer a reliable assessment of changes in initial stiffness[1]. Even though no other change in SW speed was statistically significant, a similar trend was also observed for the right edge

of the loaded area (position +0.5cm). Assuming a uniform distribution of loading the average (±STDEV) PPT for all participants was 0.55MPa(±0.36MPa). However, the pressure is likely to have been higher at the edges[2] which can explain the bigger changes in SW speed observed at the edges relative to the centre of the loaded area.

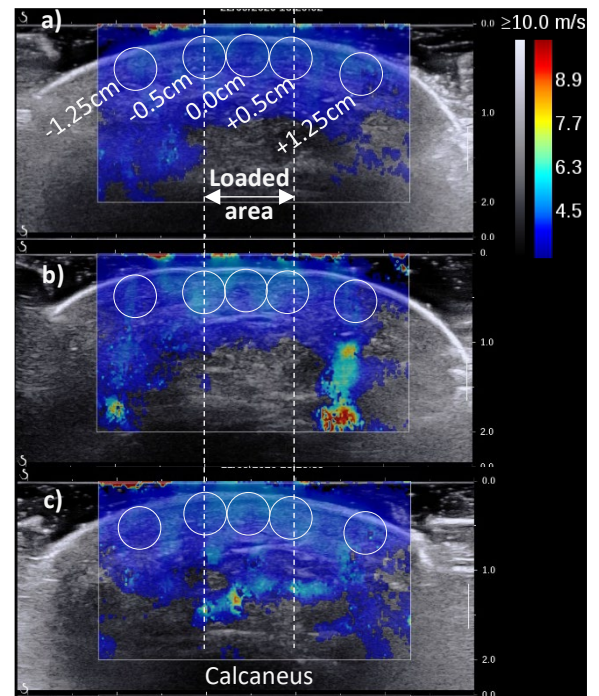


Figure 1: SW elastograms at baseline (a), after overloading (b) or after walking (c). The loaded area and circular areas for measuring SW speed at different distances from the centre are also shown.

Table 1: SW speed at different distances from the centre. Statistically significant changes relative to baseline are indicated with (*).

Distance from centre (cm)	Baseline	Overloading	Overloading & walking
-1.25	5.96(±1.57)	6.19(±1.63)	5.84(±1.61)
-0.50	6.01(±1.15)	6.47(±1.24)*	6.33(±1.20)*
0.00	5.88(±1.13)	6.11(±0.98)	5.89(±1.03)
+0.50	6.18(±1.46)	6.53(±1.36)	6.28(±1.55)
+1.25	5.93(±1.72)	5.58(±1.58)	5.34(±2.15)

Conclusions

Repetitive loading to the threshold of pain causes localised changes in tissue biomechanics which are detectable using SW elastography. Measurements of regional changes in SW speed could be used to study the effect of overloading on plantar soft tissue biomechanics.

References

- [1] Chatzistergos P et al. (2018). *J Biomech*, **28**:114–50.
- [2] Melia M et al. (2019). *Eur J Pain*, **23**:167–82.

Friction coefficients of cancellous bone densified with autologous bone-particles in uncemented fixation

Sebastian M. Zobel, Miriam Ruhr, Michael M. Morlock

Institute of Biomechanics, Hamburg University of Technology (TUHH), Hamburg, Germany

Email: sebastian.zobel@tuhh.de

Summary

A high bone volume to total volume ratio (BTV) is required in the close surrounding of uncemented implants as prerequisite for sufficient primary stability. This study investigated whether the friction against cancellous bone can be increased by densification with autologous bone-particles. Shear tests of native and densified samples against an implant-like surface were carried out. Densified samples showed a tendency of a higher static friction coefficient as well as a significant increase in sliding friction coefficient.

Introduction

The successful osseointegration of uncemented implants depends on the resistance of the bone-implant-interface to micromotion [1]. Shear forces between implant and bone are of major interest and are associated with the bone quantity and quality at the interface [2]. This study investigated whether the friction coefficients of cancellous bone against an implant-like surface can be increased by densifying the intertrabecular pores with autologous bone-particles.

Methods

Cancellous bone samples ($n = 24$) were taken from 6 pairs of human femoral heads (age 65 - 77) using a hollow-core drill ($\varnothing 25$ mm). One of each pair was densified while the other one was left native. For densification, 2 ml of trabecular bone particles - collected from the femoral heads - were quasistatically pressed into the testing surface ($\sigma = 0.5$ MPa, Zwick/Roell, Germany). The testing surface was created by cutting the bone samples in half, creating two cylindrical, corresponding samples. Both corresponding samples were then densified or left native. The microstructure of the samples was analyzed using a μ CT (Scanco Medical, Switzerland) to evaluate the amount and depth of the permeated particles. In the test setup, the corresponding samples were pressed symmetrically against an implant-like surface ($\sigma = 0.5$ MPa; Figure 1).

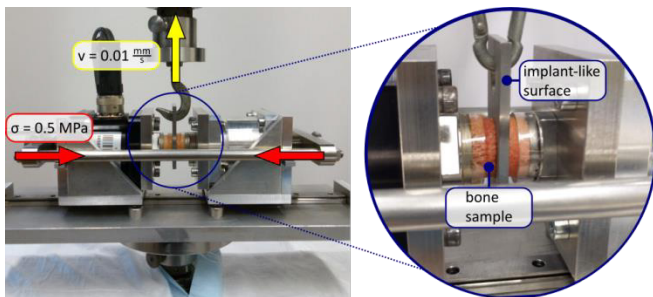


Figure 1: Experimental setup for shear testing of cancellous bone.

Results and Discussion

The densification with bone-particles increased the BTV significantly ($p = 0.002$). Increased BTV was associated with an increase in static ($p = 0.002$, $R = 0.814$) and sliding friction coefficient ($p = 0.033$, $R = 0.642$). The densified bone samples showed a tendency of higher static friction coefficient ($p = 0.080$), but a significant increase in sliding friction coefficient ($p = 0.043$; Figure 2) in comparison to the native samples.

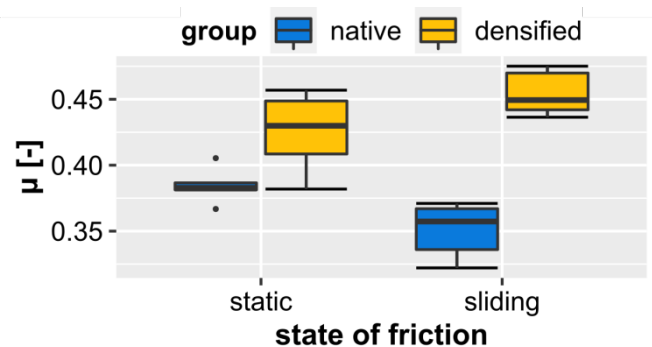


Figure 2: Boxplot of the static and sliding friction coefficients (μ) for the native and densified samples.

The densification depth was independent of the native BTV ($p = 0.618$). The amount of densification decreased with increasing BTV ($p = 0.041$). This resulted in higher densification for low dense bones. Though not significant, a negative correlation between the amount of densification and the increase in friction coefficients was found.

This might be due to the greater intertrabecular pores, in which bone particles clamp less under shear stress than in smaller pores. Hence, the increase in static friction might be a trend and the method of increasing friction coefficients with particle-based densification might be limited to medium dense bones. This needs to be further investigated.

Conclusions

Densifying medium dense, cancellous bone with autografted bone-particles might be beneficial in increasing the primary stability of uncemented implants. The results are specific to the implant-like surface studied and friction parameters are highly dependent on the investigated system. Therefore, further experiments are required to specify these.

References

- [1] Rancourt D et al. (1990) JBMR, **24**: 1503-1519.
- [2] Huwais S and Meyer EG, IJOMI, **32**: 27-36.

A Finite Element Investigation of the Tunability of Non-Pneumatic Tyres for Wheelchair Use

Otis Wyatt¹, Panagiotis Chatzistergos², Nachiappan Chockalingam², Evangelia Ganniari-Papageorgiou¹

¹School of Digital, Technologies and Arts, Staffordshire University, Stoke-on-Trent, UK

²Centre for Biomechanics and Rehabilitation Technologies, Staffordshire University, Stoke-on-Trent, UK

Email: evi.ganniari@staffs.ac.uk

Summary

The ability to tune, to the specific needs of an individual, the vertical and shear stiffness of a wheelchair tyre can improve comfort and reduce user energy expenditure. This level of tuning is not possible with existing pneumatic tyres but could be achieved using novel Non-Pneumatic Tyres (NPT). This Finite Element (FE) analysis offers the first verification of the tunability of NPTs for use in wheelchairs.

Introduction

A 1930s wheelchair had pneumatic tyres similar to the tyres used on wheelchairs today despite the disadvantages that have stayed the same for over almost a century [1]. These disadvantages include punctures, pressure maintenance and tuning [1]. Novel NPTs eliminate the first two disadvantages [2] and are also hypothesised to enable tuning vertical and shear stiffnesses separately (unlike pneumatic tyres) to create bespoke tyres that suit individual wheelchair user's needs.

Methods

A parametric FE analysis was conducted using ANSYS software to test the tunability of NPTs. A wheelchair NPT was designed with similar dimensions to pneumatic tyres and a honeycomb spoke design [3](Figure 1).

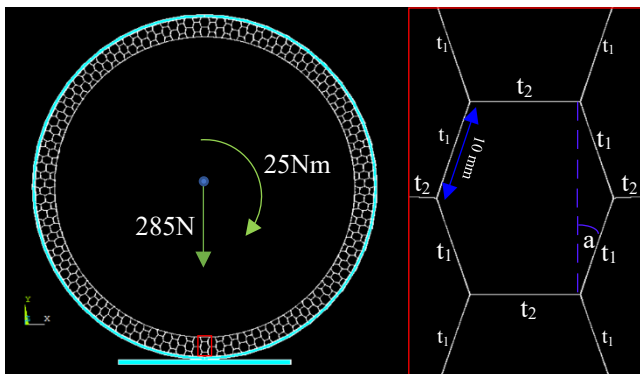


Figure 1: The design of the wheelchair NPT model (left). The spoke design parameters used in the parametric analysis are also shown (right).

The parameters studied were internal angle ($a^{\text{ref}}=19^\circ$); the thickness of parallel ($t_1^{\text{ref}}=1\text{mm}$) and perpendicular ($t_2^{\text{ref}}=1\text{mm}$) honeycomb plates to the radius. Parameters were adjusted to +/-10% of the reference values. A vertical force corresponding to 25% of an average person's body and wheelchair weight combined was applied to the tyre's central axis followed by a 25Nm rotational moment [4]. The vertical displacement (U) and rotation (R) of the central axis were used to assess changes in vertical and rotational stiffness respectively.

Results and Discussion

Changes to the interior angle and uniform thickness of the honeycomb spokes altered both vertical and shear stiffnesses to almost equal measures. Changes in the different orientations of the honeycomb plates had a more noticeable impact on only one of the two stiffnesses. Changes in the thickness of the honeycomb plates almost parallel to the radius of the tyre had a large effect on vertical stiffness and an almost negligible change in shear stiffness when the thickness was altered. On the contrary changes in the thickness of the perpendicular plates had a stronger effect on shear stiffness (Table 1).

Table 1: Honeycomb plate thickness adjustments indicating a decoupling of the tunability of vertical and shear stiffness.

Plate Orientation	Plate Thickness (mm)	U (mm)	% Change	R (°)	% Change
Parallel (t_1)	0.9	-7.01	13%	-0.297	0%
	1.0	-6.21	-	-0.297	-
	1.1	-5.33	-14%	-0.300	1%
Perpendicular (t_2)	0.9	-6.26	1%	-0.313	5%
	1.0	-6.21	-	-0.297	-
	1.1	-6.03	-3%	-0.282	-5%

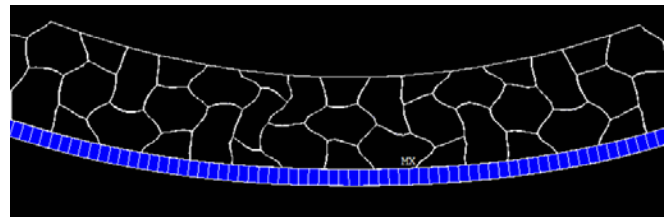


Figure 2: Buckling of the honeycomb spokes.

The loads applied to the tyre caused buckling of the honeycomb spokes (Figure 2). The non-linear mechanical response of the NPT means that optimal design will depend on the applied load magnitude. Further research is needed to develop a tuning method for wheelchair NPTs.

Conclusions

The initial results have determined that vertical and shear stiffnesses of an NPT can be tuned separately through alteration of different oriented honeycomb plates, but further research should be conducted to determine if other parameters affect these stiffnesses and if they could reduce manufacturing complexity.

References

- [1] Jaehyung Ju et al (2012). *Comp. Structures*, **94**: 2285
- [2] Libin Rajan et al (2019). *IJITEE*, **8**: 301
- [3] Wang et al (2020). *Int. J. Appl. Mech*, **12**: 2050024
- [4] Koontz et al (2006). *Asst Technol*, **18**: 75-96

Development of a Sensor Assembly to measure Vertical, Horizontal and Tilt Motion of the Glenoid Edge during the ASTM F08 Test

Leanne Laworth¹, Tim Peach², Vishvanath Gorotikar^{1,3}, Stephen Roche⁴, Sudesh Sivarasu¹

¹Division of Biomedical Engineering, Faculty of Health Sciences, University of Cape Town, Cape Town, South Africa

²Department of Biomedical Engineering, Ecole Polytechnique, France

³ Symbiosis Centre for Medical Image Analysis (SCMIA), Symbiosis International University, Lavale, Pune, India

⁴Department of Surgery, Groote Schuur Hospital, Cape Town, South Africa

Email: sudesh.sivarasu@uct.ac.za

Summary

The most common cause of failure of a shoulder joint prosthesis is loosening of the glenoid (scapular) component. The standardized test for evaluating glenoid loosening uses vertical displacement of the edges as a measure of loosening. However, laboratory experiments and finite element modeling studies have shown that the glenoid edge does not only move vertically, but also horizontally and with a rotational (tilt) motion. In this research an augmented ASTM test apparatus has been developed and tested that can measure all 3 types of motion of the glenoid edge, to better understand the behavior of the glenoid during loosening and hence inform future prosthesis designs.

Introduction

Current shoulder joint prostheses most often fail due to loosening of the glenoid (scapular) component. This loosening is attributed to eccentric loading of the edges of the glenoid component [1]. The American Society for Testing and Materials (ASTM) set out a standardized test to evaluate glenoid loosening, in which the glenoid is cyclically loaded and the vertical displacement of the edges is measured.

However, laboratory experiments [2] and computational finite element modeling (FEM) studies [3] of the glenoid under load have reported that the edges not only deflect vertically, but also horizontally and with a tilting motion as the material of the component is deformed. Therefore, the ASTM standardized test does not fully quantify the glenoid reaction to loading. This could be the cause of high percentage of recurrence surgeries due to glenoid component failures. This study proposes an augmented ASTM test rig to investigate the effect of eccentric loading patterns on the glenoid component's loosening process.

Methods

The augmented ASTM type test rig was developed with a specialized sensor assembly which can measure vertical, horizontal and tilt motions of the glenoid. The sensor assembly used two sets of 3 L-DT sensors which track the motion of rigid blocks, connected to the glenoid edges by lever arms.

An analytical algorithm used the sensor readings to calculate the motion of the center of each block, which was then converted to glenoid edge motion. This algorithm was coded into MATLAB and was validated *in-silico* by means of a Solidworks motion simulation. Pilot tests were performed on a glenoid component installed in bone substitute foam. In the

pilot test horizontal motion of the humeral head component was controlled, and the associated horizontal, vertical and tilt motions of the glenoid edges were measured.

Results and Discussion

The results show the sensor assembly system acquiring the three types of motion at the glenoid edge (Figure 1). In the figure the outputs from the three sensors on the left-hand block, connected to the left glenoid edge, are shown in relation to the position of the humeral head as it moved from the left to the right edges. These measurements were then converted to glenoid edge motion. The glenoid edge under load was compressed 0.8mm downwards (positive direction), 0.4mm horizontally to the left, and tilted outward by 5°. As the humeral head moved to the right edge, the left edge experienced tension, showing an upward motion of 0.4mm, a horizontal motion 0.4mm to the right and a tilt of 1° inward.

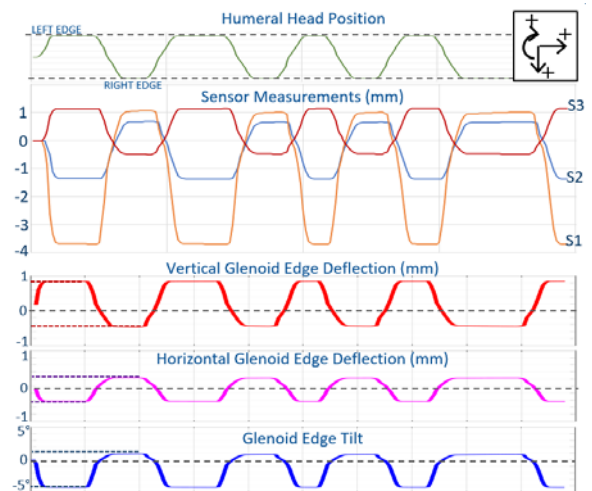


Figure 1: Sample results for four cycles of the humeral head from the left to right edge of the glenoid showing sensor measurements and corresponding glenoid edge deflection

Conclusions

This pilot study serves as a validation of the functionality of the measurement system, which can now be used to investigate the loosening behavior of a novel glenoid design, developed at the UCT Orthopedic Biomechanics Laboratory.

References

- [1] Favard, L., 2013, *OTSR 99s* S12-S21
- [2] Juniad, S. et al. , 2009 ‘ *J. Biomech* **43**, pp714-719
- [3] Dey, R., 2018 ‘ *Unpublished Doctoral Thesis, University of Cape Town*

Robot-based method for analysis of knee prostheses in human cadaveric knees

Adrián Gómez, M. Nusser¹, L. Kiener¹, G. Tschupp²

¹Biomechanical Engineering, Zurich University of Applied Sciences, Winterthur, Switzerland

Email: adrian.gomezdiaz@zhaw.ch

²Mathys AG, Bettlach, Switzerland

Summary

A new robot-based method was developed and evaluated to investigate the functionality of different knee prostheses in *in vitro* tests. A common method is the determination of the passive path, which describes a force- and torque-free knee flexion. This path provides the starting points for the stability tests. Using the robot as a reliable test device, the following requirements should be fulfilled: Automated determination of the force-free and torque-free state at 0° flexion and a high level of reproducibility and sensitivity. This study shows a new method to reliably find the starting point. To assess the measurement accuracy, 18 repetitions of a passive path were performed. To test the sensitivity, the passive path of a specimen was compared in the native state and with a medial side prostheses replacement. The new method meets all requirements for a reliable measurement and provides reproducible results.

Introduction

Despite research efforts to improve the functionality of knee prostheses, epidemiological studies show that postoperative pain, instability or loosening of the prosthesis are common [1]. Therefore, it is imperative to test prostheses not only mechanically but also functionally. Based on another study [2] a new robot-based method was developed and evaluated to investigate the functionality of different knee prostheses in human cadaveric knees. By using the robot as a reliable test device, the following points should be fulfilled: Automated determination of the force- and torque-free point at 0° flexion, high reproducibility, and sensitivity.

Methods

Preparation for *in vitro* testing in CAD 3D models are built based on CT scans of test specimen. Coordinate systems of tibia and femur according to Eckhoff et al. [3] and that of the robot clamp are defined and positioning adapters for the leg in the suspension cylinders are constructed.

Preparation for *in vitro* experiments in the laboratory:

At a distance of 28cm and 12cm above and below the joint line the bone is cut, and soft tissue is removed, respectively. The 3D-printed adapter is fixed to the bone stumps for exact

positioning in the aluminum cylinder, which is filled with bone cement. The densities of the tibial tissue and the tibia are then determined experimentally.

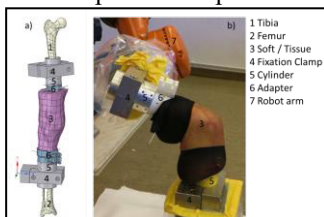


Figure 2: a) CAD-model, b) Robot set-up

Finding the force-free state at 0° flexion: The leg is clamped at 0° flexion. The load hanging on the robot arm can be calculated and is defined as a tare value in the robot program. The remaining forces at 0° degrees are the forces caused by the ligaments which the robot tries to cancel in order to obtain a force- and torque-free condition.

Reproducibility test: 18 passive paths of a medially and laterally supplied cadaveric knee were run through from 0° to 90° flexion while applying an axial load of 100N. The tolerances of the forces were 2.5N and of the moments 0.5Nm. **Sensitivity test:** A comparison of the passive path from 0° to 90° flexion of a specimen in the native state and with a medial knee prosthesis was performed.

Results and Discussion

Finding the force-free state at 0° flexion: Due to the exact determination of the mass and density distribution, the starting point can be found reproducibly and leads to a higher quality of the results. **Reproducibility test:** The largest standard deviation of the 18 trials with respect to anterior and posterior tibial translation occurred at 28° and is 0.5mm. The standard deviation calculated for internal and external rotation amounts to 0.3° at 38°. To date, no other robot-based studies have published their reproducibility, so a comparison was not possible. **Sensitivity test:** The difference between the passive path of the two conditions was greater than the standard deviation of the repeatability measurement. This indicates that the robot measures sensitively enough to reliably test prostheses.

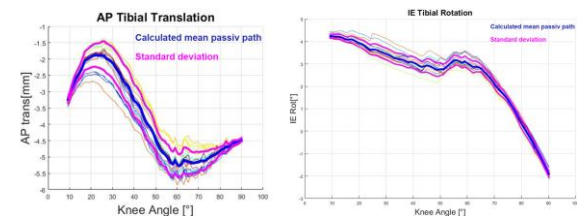


Figure 1: Left: Reproducibility of the anterior/posterior translation. Right: internal/external rotation during the passive path measurements displayed in knee coordinate system.

Conclusions

The results show that the described new test method, is very accurate. The robot can be used to perform functionality tests and helps to increase the physiological quality of prostheses.

Reference

- [1] Khan M et al. (2016). The Bone Joint Journal, **98**: 105–112
- [2] Most E et al. (2003). Clinical Orthopaedics and Related Research, **410**: 101–113
- [3] Eckhoff, DG (2005). J Bone Joint Surg Am, **87**: 71-80

Increased muscle activity in acoustic startle response among children with recurrent pain in the head/neck and abdomen due to chronic stress

Andersson ^{1,2}, Alfvén G³

¹Laboratory of Biomechanics and Motor Control, Swedish School of Sport and Health Sciences, Stockholm, Sweden

²Department of Neuroscience, Karolinska Institutet, Stockholm, Sweden

³Clintec, Karolinska Institutet, Stockholm, Sweden

Email: eva.andersson@gih.se

Summary

With recorded EMG amplitude and time parameters, increased resting activity and potentiated acoustic startle responses were observed in the muscles involved in stress tender patterns among children with recurrent psychosomatic pain.

Introduction

Children with recurrent pain of negative chronic stress origin from different locations have a characteristic pattern of tender points in the temporal, trapezoid, great pectoral and abdominal muscles. The aim was to study if acoustic startle reactions are higher, measured with increased EMG-responses, in muscles sites related to tender point pattern and the recurrent pain among those children as compared to healthy controls.

Methods

Forty-two children of both sexes (10-17 years) participated, whereof 19 in a pain (PAIN) group and 23 in a control (CON) group (mean age 12,7 and 13,0 years, respectively). Acoustic Startle Responses (ASR) were elicited with a 50-ms-duration stimulus of unexpected short white noise (USWN) at 105 dB with an instantaneous rise time in both ears via headphones. The subject was laying supine on a bench in a calm milieu. The stimulus was controlled with a digital audio-stimulator. Eight ASR were given with varying time intervals, usually between 1.5 and 2.0 min, similarly for all subjects¹. Surface EMG was recorded and analyzed (via Mega Electronic Ltd-system, Finland) for the six muscles OR-orbicularis oculi, TE-temporalis, TR-trapezius, PE-pectoralis major, RA-rectus abdominis and ES-erector spinae (L3-L4 level, 2-3 cm lateral to the spinal processes). The recording sites were similar to general tender point positions. The PAIN group had pain of "non-organic origin" recurring at least once a week for more than 3 months and affecting activity of daily life. Eighteen had abdominal pain in a mean of 37,2 (8-140) months all fulfilling diagnosis criteria of functional abdominal pain. All reported frequent headache, five backache and three shoulder pain. All described stress and anxiety problems and fulfilled six of

seven criteria for the diagnosis of psychosomatic pain². Eighteen children had nine of nine stress tender points and one had seven³. One child had school-stress-induced depression. All the children met the same paediatrician specialist at several sessions until diagnosis. The matched controls were without recurrent pain problems and in general good health. Fifteen were enrolled from four school classes, and eight from personal contacts. Socio-economic status was comparable in the two groups.

Results

The PAIN group showed significantly higher resting activity and higher acoustic startle response values ($p < 0,05$), than the CON group, for all six muscles together regarding the mean amplitude in the initial 100 ms (Tab. 1), the initial 200 ms, and during the burst of activity (start $\geq 10 \mu V$, end $\leq 10 \mu V$), as well as longer burst duration and shorter burst latency (ms). These results are based on average for all eight startle sound events (ASR) together. For PAIN compared to CON, all separate muscles showed generally higher values of EMG amplitudes and burst durations as well as shorter latencies for the burst onset in all measures with statistically significant differences or strong trends for several parameters and muscles.

Conclusions

The results show in children and adolescents how recurrent pain of negative stress, origin from the head, abdomen, back and chest, is associated with increased acoustic startle reaction and increased muscle tension in these regions, shown with EMG amplitude and EMG timing parameters for six muscles in the body. This study, showing increased muscle excitability in children with stress-induced pain in the head, neck and abdomen, may contribute to the understanding of the mechanisms underlying the broad problem of recurrent psychosomatic pain.

References

- [1] Lumenthal, T.D. (2005) *Psychophysiology* 4:1-15.
- [2] Alfvén, G. (2003). *Acta Paediatr.* 9:43-9.
- [3] Alfvén, G. (1993) *Acta Paediatr.* 8:400-403.

Table 1 Mean EMG-amplitude (± 1 SD) in μV for the initial 100 ms period after the startle sound for all six muscles together and separately for each muscle in the two groups of children (PAIN and CON). Each value represents an average for all eight startle sound responses (ASR) together.

Time interval from the startle sound	All muscles	OR	TE	TR	PE	RA	ES
100 ms PAIN	16 \pm 28	37 \pm 20	11 \pm 5	26 \pm 57	10 \pm 12	5 \pm 7	2,9 \pm 1,4
100 ms CON	9 \pm 12	28 \pm 19	7 \pm 5	7 \pm 8	5 \pm 6	4 \pm 6	1,4 \pm 1,4

Instrumenting human-robot interaction using a robot rollator simulator device

Frieder Krafft¹, Peter Wittlinger¹, Michael Herzog², Thorsten Stein², Lizeth H. Sloot¹

¹Institute of Computer Engineering, Heidelberg University, Heidelberg, Germany

²ioMotion Center, Institute for Sports and Sports Science, Karlsruhe Institute of Technology, Karlsruhe, Germany

Email: frieder.krafft@ziti.uni-heidelberg.de

Summary

Wheeled walkers, or simply called rollators, are used to support and stabilize movements in less mobile older persons. However, it is still unclear, how the interaction between older adults and the rollator influences movement control and stability. Especially as recent findings show that rollators can also increase the risk of falling. Therefore, comprehensive biomechanical analyses in healthy young and older participants are required for a better understanding of human-rollator-interaction. Therefore, the purpose of this study protocol is to close this gap due to its novel design.

Introduction

Falls are the primary cause of injury during daily life ambulation in older adults, with over 50% of people older than 80 years falling at least once a year [1]. Moreover, falls reduce the ability of independent living [1]. To enhance daily ambulation, rollators are prescribed to support and stabilize older persons [2]. Rollators are presumed to improve movement stability by increasing the base of support and to provide weight support by allowing the upper body to carry part of the body weight to compensate for lower limb weakness [2,3]. While these assumptions have yet to be experimentally validated [4], recent findings also show that rollators can actually increase fall risk [3]. The lack of biomechanical evaluation, including body movement and load transfer, is limiting our ability to understand this. As fall risk and human-rollator-interaction are task-dependent, it has been emphasized that analyses of various other movements (e.g., sit-to-stand) under normal and challenging floor conditions are required [3,4]. Therefore, height-adjustable force-sensing rollator handles, and a complicated set-up that allows for controlled measurement during different movement tasks and manipulations of the provided support, are necessitated for thorough biomechanical evaluation of rollator support.

Thus, the purpose of this study protocol is the comprehensive biomechanical analysis of human-rollator interaction with a novel instrumented robot rollator simulator device (Figure 1) in a young ($n = 35$ years) and older group ($n = 65$ years). The rollator simulator device allows for instrumented measurements of human-rollator interaction during different tasks, surface conditions, and different levels of support.

Study Protocol

To evaluate the role of rollator support during various activities of daily living, the following tasks are included: stance, sit-to-stand, stand-to-sit, gait initiation, and straight walking. To disentangle the supportive role of touch (proprioception) versus weight assistance, the tasks are performed unassisted, with light touch of the handles, and

with full leaning on the robot-rollator-handles. To understand the stabilizing effects of rollators under greater perturbations, the young participants will also perform the tasks under more challenging surface conditions, using a balance-board during stance and a dual-task (counting backwards) during the other tasks.

Human-rollator interaction analysis will be based on:

- center of mass (CoM) displacements and reaction forces at the handles to analyze control mechanisms
- stability measures (e.g., stability margin) to evaluate influences of the rollator on user's stability;
- joint kinetics to analyze potential load reductions to the legs and load increase to the trunk and arms.

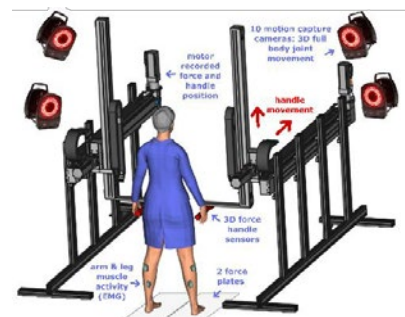


Figure 1: Robot rollator simulator device.

Results and Discussion

Data collection of the younger ($n = 15$) and older ($n = 10$) study group will be conducted up to May 2021. The generated data set will allow us to understand the stabilizing effect of full rollator support versus light touch support during various movement tasks under normal and challenging floor conditions. These findings will help to increase the user guidance for conventional rollators currently used by older adults. Furthermore, the results will also contribute to the development of assistive devices for a broader scope of movements in our continuously ageing population.

Acknowledgments

Research project is funded by the HEiKA – Heidelberg-Karlsruhe strategic partnership.

References

- [1] Ambrose et al. (2013). *Maturitas*, **5**: 51-56.
- [2] Schölein et al. (2017). *J Neuroeng Rehabil*, **14**: 18.
- [3] Costamagna et al. (2019). *PLoS One*, e0210960.
- [4] Lindemann et al. (2017). *J Gerontol A Biol Sci Med Sci*, **72**: 636-640.
- [5] Mundt et al. (2019). *Eur Rev Aging Phys*, **1**: 1.

Verónica Gracia-Ibáñez¹, Estor Barba-Lucena¹, Maria-Jesus Agost¹, Pablo Granell², Vicente Bayarri-Porcar¹, Alba Roda-Sales¹, Margarita Bergara¹, Joaquín L. Sancho-Cru¹

¹Department of Mechanical Engineering and Construction, Universitat Jaume I, Castellón de la Plana, Spain

²Consorci Hospitalari Provincial de Castelló, Castellón de la Plana, Spain

Email: vgracia@uji.es

Summary

Flexion active range of motion (AROM) of thumb joints and the functional one (FROM) of 35 osteoarthritis (HOA) patients were compared with those of healthy subjects, to determine the impact of range of motion changes on hand function. AROM and FROM were measured with a Cyberglove, and FROM were computed for the angles used while performing the Sollerman Hand Function Test (SHFT). 37% of HOA patients presented an AROM reduction of CMC flexion larger than 30%. For them, an impact larger than 30% was estimated in 6 ADL, with longer execution times but only slightly lower SHFT scores. The sum of flexion AROM values of the thumb joints was also analyzed to consider inter-joint compensation. Although partial compensation was detected, it was not enough to overcome functional problems.

Introduction

It has been proposed [1] inferring the functional impact of mobility reduction in joints caused by hand diseases through the analysis of the joint angles of healthy subjects while developing activities of daily living (ADL). However, due to the complexity of hand kinematics, motion of other joints might compensate the loss of mobility. In this work, we compare the flexion ranges of motion of thumb joints of hand HOA patients to those of healthy subjects and analyze the impact of range of motion changes on hand function.

Methods

AROM and FROM of the right-hand thumb were measured to 35 HOA patients using a Cyberglove (carpometacarpal - CMC-, metacarpophalangeal -MCP- and interphalangeal -IP-joints). FROM was computed as percentiles 5% and 95% of the angles used while performing the SHFT tasks. ROM, FROM and sum of flexion AROM of the three joints (sROM) were compared to those of healthy subjects [1, 2]. The functional impact in ADL was estimated according to [1] and compared to real functionality measured through the SHFT scores and times to develop each task.

Results and Discussion

37% of HOA patients (subsample A) presented an AROM reduction in CMC flexion larger than 30%. Table 1 shows AROM and FROM of healthy subjects (37.83 ± 8.07 years) and subsample A (69.9 ± 11.2 years). These patients with reduced AROM in CMC flexion present a reduction in IP flexion, as well as in FROM values in these joints (CMC and IP), but larger FROM in MCP flexion, to compensate for the constraints in the adjacent joints. This compensation may be

the origin of structural changes at MCP joint, which becomes into larger flexion AROM. However, this larger flexion does not compensate for the total sROM (Table 2) and is not enough to overcome functional problems, as patients needed longer times (Table 2) to execute those tasks where a functional impact was expected according to [1]: zipping and unzipping (T1), turning the handle (T2), fastening and unfastening buttons (T3), cutting with knife (T4), writing (T5), and pouring water (T6). Patients' age may have also contributed to these longer times [3]. However, SHFT scores are similar (Table 2).

Table 1: Statistics across subjects of AROM&FROM of patients of subsample A and healthy subjects, in degrees. Extension (E), Flexion (F), and abduction (A).

			CMC			MCP		IP	
			E	F	A	E	F	E	F
A R O M	Patients Subsample A	Mean	30	8	23	28	30	31	47
		Sd	8	6	3	8	14	19	14
	Healthy subjects [1]	Mean	26	42	20	21	26	37	75
		Sd	17	10	4	12	9	15	20
F R O M	Patients Subsample A	Mean	32	31	23	16	23	44	31
		Sd	2	8	0.5	4	3	4	2
	Healthy subjects [2]	Mean	21	38	23	20	16	37	42
		Sd	8	2	1	3	4	4	2

Table 2: Statistics across subjects of patients of subsample A and healthy subjects: execution time of tasks, sROM and SHFT scores.

		Execution time (s)						sROM (deg)	SHFT score
		T1	T2	T3	T4	T5	T6		
Patients Subsample A	mean	13	4	26	21	17	25	86	69.15
	sd	4	1	10	11	13	5	19	10.17
Healthy subjects	mean	8	3	22	11	6	21	170	72.15
	sd	2	1	6	3	1	3	23	2.20

Conclusions

Estimating the impact of AROM reduction from data of healthy subjects successfully identified which ADL were affected, as clearly longer execution times were found in all those tasks. Conversely, the SHFT scores hardly identified the functional problems, as they were only slightly diminished.

Acknowledgments

Projects PGC2018-095606-B-C21 (MCIU/AEI/FEDER,UE), G2020/067 (Regional Government) and UJI-2017-51.

References

- [1] Gracia-Ibáñez V. et al.(2017) *J. Hand Ther.* **30**(3)337-347.
- [2] Roda-Sales A. (2020) *J. Biomech.* **98**09512.
- [3] Singh H.P. et al.(2015) *Hand Surg.* **40**(3)298-309.

Hiking with total knee arthroplasty: In field kinematics in sloped walking in relationship to muscle strength

Judith Bleuel¹, Iris Mittendorfer¹, Igor Komnik², Steffen Willwacher³, Björn Michel¹

¹Institute of Motion Analysis and Sports Medicine, Garmisch-Partenkirchen Medical Center, Garmisch-Partenkirchen, Germany

²Institute of Biomechanics and Orthopaedics, German Sport University Cologne, Köln, Germany

³Department of Mechanical and Process Engineering, Offenburg University of Applied Sciences, Offenburg, Germany

Email: Judith.bleuel@klinikum-gap.de

Summary

Patients with total knee arthroplasty (TKA) and therapists fear overloading of the operated limb due to higher loads in sports. We showed that 5-14 month after surgery in field knee kinematics during downhill hiking and knee surrounding muscle strength in TKA patients were different from healthy controls (CON). Further muscle strengthening is recommended prior to return to hiking.

Introduction

Persons with TKA show kinematic differences during level walking and muscular impairments of the quadriceps and hamstrings muscles after surgery, as reported in laboratory studies [1,2]. Although an active lifestyle is recommended after TKA [3], potential kinematic deficits have not yet been investigated in field. Hiking is one of the most popular activities in the elderly. However, especially downhill walking is a challenging task for the knee joint and the surrounding musculature. We investigated the in field downhill walking kinematics during a hike in persons with TKA 5-14 months post-op and an age-matched CON in relationship to the muscle strength of the knee flexors and extensors.

Methods

Participants walked on a predetermined walking trail at self-selected pace wearing an inertial sensor system (XSens, Awinda, Enschede, Netherlands) for recording the 3d kinematics of the whole body. We evaluated sagittal plane hip, knee and ankle joint angles over the gait cycle at level walking and two different slopes. In addition, we measured the concentric and eccentric lower extremity isokinetic muscle strength of the knee flexors and extensors (Isomed2000, D. & R. Ferstl GmbH, Hemau, Germany) at two angular velocities (50°/sec, 120°/sec).

Results and Discussion

TKA patients (n = 19) had more extended knees during stance in the operated limb than CON (n = 19) under all walking conditions (p < 0,02). Differences rose with steeper slopes (Figure 1). Hip and ankle joint angles did not differ between the groups. Muscle strength was lower in TKA for both muscle groups and all measured conditions (Figure 2). The hamstrings to quadriceps ratio (H/Q) was higher in TKA than in CON for the operated resp. weak limb (50°/sec: TKA 86,82 ± 21,84; CON 66,98 ± 18,45; p = 0,01; 120°/sec: TKA 93,57 ± 22,94, CON 77,96 ± 24,00; p = 0,05). H/Q at 120°/sec correlated with maximum knee flexion angle during stance while walking downhill at moderate slope in the TKA

group (p < 0,02), showing lower maximal flexion with higher ratio.

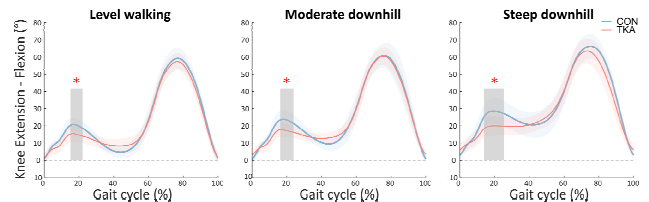


Figure 1: Sagittal knee joint angles over gait cycle during level, moderate, and steep sloped walking in TKA (red) and CON (blue). Gray areas display phases of significant differences (*p < 0,02).

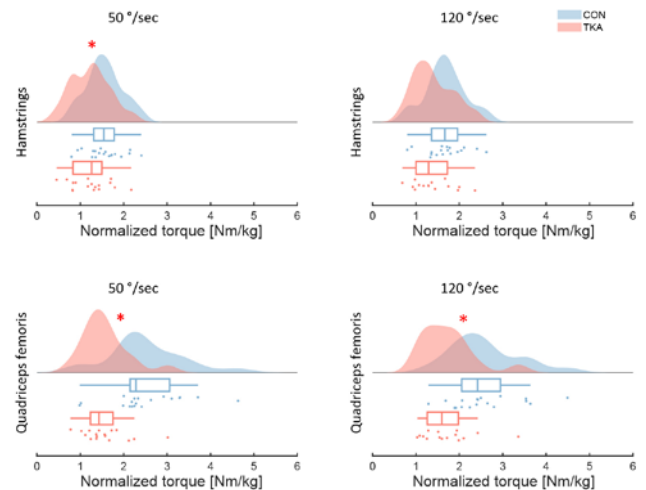


Figure 2: Raindrop plots, boxplots and distribution of single datapoints of normalized eccentric maximum torque (Nm/kg) of Hamstrings and Quadriceps at 50°/sec and 120°/sec in the operated limb of TKA (red) and weak limb of CON (blue) (*p < 0,05).

Conclusions

Even if rehabilitation was completed successfully, 5-14 month after TKA surgery muscle strength was still not sufficient to display normal gait pattern during downhill hiking. Further muscle strengthening after rehabilitation is recommended prior to return to hiking to prevent overloading.

Acknowledgments

The study was funded by the Dr. Auguste-Schaedel-Dantscher Stiftung für medizinische Forschung.

References

- [1] McClelland JA et al. (2007). *Knee*, **14(4)**: 253-263.
- [2] Schache MB et al. (2014). *Knee*, **21(1)**: 12-20.
- [3] Witjes S et al. (2016). *Sports Med*, **46**: 269-292.

Can knee valgus kinematics be predicted by clinical assessments during a unilateral landing task?

Karine J.V. Stoelben^{1,2}, Andressa L. Lemos^{1,2}, Evangelos Pappas³, Felipe P. Carpes^{1,2}

¹Applied Neuromechanics Research Group, Federal University of Pampa, Uruguaiiana, Brazil

²Programa de Pós-Graduação Multicêntrico em Ciências Fisiológicas, Federal University of Pampa, Uruguaiiana, Brazil

³The University of Wollongong, Wollongong, NSW, Australia

Email: karinestaelben@gmail.com

Summary

Here we investigate the potential of clinical tests to predict knee valgus kinematics during unilateral landing tasks in recreational male athletes. Lateral step down test, star excursion balance test, single and crossover hop test explain up to 26% of knee valgus in the preferred leg. Triple hop test explains up to 15% of knee valgus in the non-preferred leg. Clinical tests have the potential to be used as a screening tool for knee valgus kinematics.

Introduction

The risk of athletic knee injury is typically assessed in biomechanical laboratories, which can be time-consuming and expensive. Clinical tests can assess performance, quality of movement, and dynamic balance to guide clinical decisions [1]. However, the relationship between performance in clinical tests and knee valgus during unilateral drop landing, often a source of knee injury, is currently unclear. In this study, we determine whether performance in clinical tests can predict knee valgus during a unilateral landing task.

Methods

Forty-seven recreational athletes (24±3 years old, 80±13 kg of body mass, 177±6 cm of height) completed a battery of clinical tests and had 3D kinematics and kinetics measured during a drop jump task. Clinical tests were the Lunge, lateral step down (LSD), single, triple, and crossover hop tests, star excursion balance test (SEBT), knee flexor and extensor strength, and hip abductor and adductor strength (hand-held dynamometer). During unilateral drop jumps (preferred and non-preferred legs) 3D kinetics and kinematics were sampled at 2000 Hz and 200 Hz, respectively. Knee valgus angle was determined at initial contact (threshold of 20 N), at peak knee flexion, as well as for peak and range of motion values. The local institutional ethics committee approved this study (protocol number: 96793518.3.0000.5323). Pearson's or Spearman's tests were performed to examine the correlation between the dependent and independent variables. When $p \leq 0.20$ was present, stepwise multiple regression analyses were performed for each dependent variable. The global effect sizes (f^2) were also computed and interpreted as small ≥ 0.02 , medium ≥ 0.15 , and large ≥ 0.35 .

Results and Discussion

The clinical tests explained up to 26% of knee valgus angle variance (Figure 1). A larger prediction was found for the preferred leg mainly at initial contact (Figure 1A) and for peak values (Figure 1E).

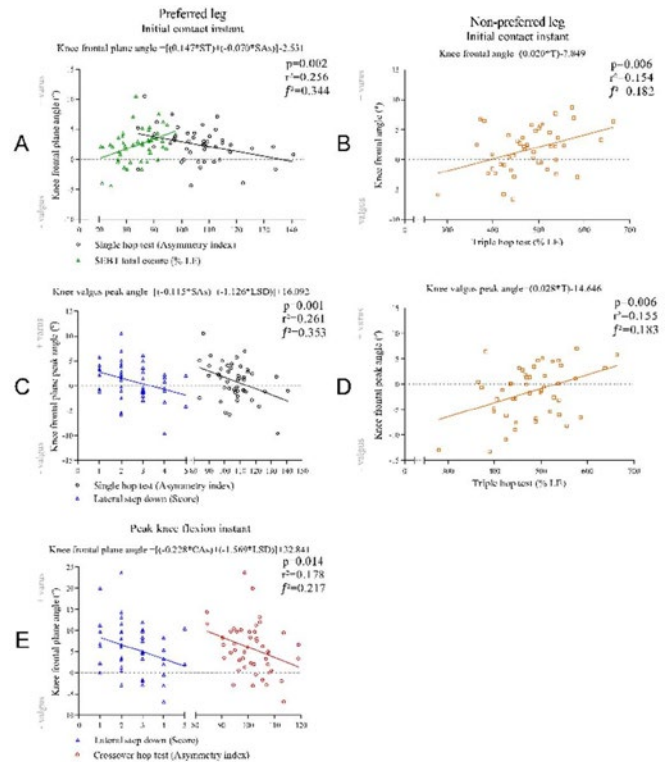


Figure 1: Knee valgus predicted by clinical outcomes.

The clinical test might be chosen according to leg preference. Preferred leg predictions combined one test of performance with one of quality of movement or dynamic balance, while non-preferred was predicted only by the performance test. The preferred leg may generally be recruited for actions requiring force and mobility, while the non-preferred leg may be more recruited for stabilization tasks [2].

Conclusions

Different combinations of clinical tests can predict up to 26% of knee valgus angle variability for preferred and non-preferred legs during unilateral landing tasks.

Acknowledgments

The authors acknowledge the funding from Conselho Nacional de Desenvolvimento Científico e Tecnológico.

References

- [1] Webster KE and Hewett TE (2019). *Sports Med*, **49**: 917-929.
- [2] Carpes FP, Mota CB & Faria IE (2010). *Phys Ther Sport*, **11**:136-142.

INFLUENCE OF MANDIBULAR RECONSTRUCTION EMPLOYING ILIAC CREST FLAP AND FIBULA FLAP ON THE LONG-TERM GAIT OF PATIENTS

Susanne Skiba¹, Sybele E. Williams¹, Florian Peters², Frank Hölzle², Catherine Disselhorst-Klug¹, Ali Modabber²

¹Department of Rehabilitation and Prevention Engineering, Institute of Applied Medical Engineering, RWTH Aachen University, Aachen Germany

²Department of Oral, Maxillofacial and Facial Plastic Surgery, University Hospital RWTH Aachen, Aachen, Germany
Email: skiba@ame.rwth-aachen.de

Summary

In maxillofacial surgery, facial bone defects are often reconstructed using autologous implants from the lower extremity. 43 patients, who underwent mandibular resection (22 iliac crest flap, 21 fibula flap) were assessed using clinical gait analysis on three different dates (preoperative, 3 - 14 months postoperative and 6 - 33 months postoperative). The results showed that changes in range of motion (ROM) of the patients in the iliac crest flap cohort persisted after an average of 16 months in all the joints considered, while patients in the fibula flap cohort primarily retained an increased ROM in the pelvis over a comparable period.

Introduction

Reconstruction of bony and soft tissue defects in the facial region after tumor disease or accidents is vital for patient functionality and welfare. In mandibular resection, facial bone defects are often reconstructed using autologous implants from donor sites in the lower extremity.

Previous studies have analyzed the influence of the donor site on gait in terms of pain, clinical scores, and parameters e.g. gait speed, cadence, step length, and range of motion (ROM) [1, 2]. However, a comparison with healthy gait patterns was missing. By assessing patients and their age-matched cohort this study aims to determine the influence of the selected donor site during mandibular resection on patients' postoperative kinematics and the long-term changes in the gait pattern.

Methods

Forty-three patients were divided into 2 cohorts based on the donor sites selected during mandibular resection. The iliac crest flap cohort consisted of 22 patients (16 male, 6 female, avg. age 56 ± 14 years), and the fibula flap cohort consisted of 21 patients (12 male, 9 female, avg. age 51 ± 16 years). The clinical gait of both cohorts was analyzed at one preoperative and two postoperative (median 3 - 7 months, median 13 - 14 months) appointments in a motion analysis laboratory. Using the Plug-in-Gait model (Vicon Nexus) the ROM for the pelvis, hip, knee and foot was calculated and normalized to a baseline composed of 203 steps from an age-matched healthy collective (121 male, 82 female) under identical conditions. Initial changes in gait were determined based on the difference between the first post- and preoperative appointments. Long-term effects were determined from the difference between the second post- and preoperative appointments.

Results and Discussion

The results of the ROM for each joint in the sagittal plane are summarized in Figure 1.

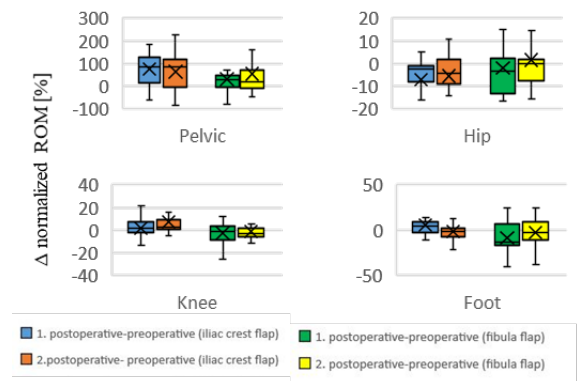


Figure 1: Differences in normalized range of motion (ROM) for 4 lower extremity joints (sagittal plane).

In the case of resection using iliac crest flap, patients showed a significant reduction in ROM postoperatively in the hip joint. Due to movement deficit, the ROM in the pelvis and knee joint significantly increased. In the long-term comparison, the ROM in the hip joint continued to reduce and the ROM of the pelvis and knee joint continued to increase. Patients in the fibula flap cohort showed a reduced ROM in dorsal plantar flexion due to the removal of muscular tissue. Movement compensation in the fibula flap cohort occurred primarily through increased pelvic tilt. With increasing time, the reduced ROM for dorsal plantar flexion regressed, but an increased pelvic tilt remained.

Conclusions

Mandibular resection with iliac crest flap led to a long-term change in the gait pattern for the pelvis, hip and knee joints. Resection with a fibula flap resulted in a sustained pelvic tilt in the sagittal plane.

References

- [1] Feuvrier D, Sagawa Jr Y, Béliard S, Pauchot J, Decavel P (2016). Long-term donor site morbidity after vascularized free fibula flap harvesting: Clinical and gait analysis. *Journal of Plastic, Reconstructive & Aesthetic Surgery*, 69:262-269.
- [2] Syczewska M, Krajewski R, Kirwil M, Szczerbik E, Kalinowska M (2018). Gait changes in patients after reconstruction of facial bones with fibula and iliac crest free vascularized flaps. *Acta of Bioengineering and Biomechanics*, Vol. 20, No.1, 20

Evaluation strategies for assessing finger motion in rheumatoid arthritis to estimate impaired hand function

Uday Phutane^{1,†}, Anna-Maria Liphardt^{2,†}, Johanna Bräunig^{3,†}, Johann Penner^{1,†}, Michael Klebl¹, Koray Tascilar², Martin Vossiek³, Arnd Kleyer², Georg Schett², Sigrid Leyendecker¹

¹Institute of Applied Dynamics, Friedrich-Alexander-Universität Erlangen-Nürnberg (FAU), Erlangen, Germany

²Department of Internal Medicine 3 - Rheumatology and Immunology, University Hospital Erlangen, FAU, Erlangen, Germany

³Institute of Microwaves and Photonics, FAU, Erlangen, Germany, [†]Equally contributed

Email: uday.phutane@fau.de

Summary

Hand function is impaired in patients with rheumatoid arthritis (RA) [1]. In addition to traditional methods for assessing hand function, optical measurements [2] can be used to observe changes occurring at the musculoskeletal level. We leverage marker-based measurement techniques to measure hand function [3] in healthy control participants and RA patients in a pilot study to determine relevant hand movements, which allow to differentiate between RA patients and healthy controls based on hand motion characteristics.

Introduction

Conventional assessment of lower musculoskeletal function in patients suffering from RA is performed by either questionnaires or basic functional test such as isometric grip strength or the Moberg-Picking-Up Test (MPUT) [3]. These can be aided with state-of-the-art technologies such as optoelectronic measurement systems (OMS) to quantify hand motion by tracking optical passive markers while performing the functional tests and activities of daily living. The aim of this study was to design an experimental setup that allows identifying differences in hand motion between healthy individuals and RA patients.

Methods

Patients diagnosed with rheumatoid arthritis and healthy control subject without known musculoskeletal disease participated in this study. Hand segments movement was recorded using a 29-marker set up, inspired by [2], with changes to tracking of thumb metacarpal. The subjects were instructed to perform a set of motions. Here, we focus on the performance of grip strength and MPUT, performed in the clinical setup (without markers) and with the OMS setup. Additionally, two simple motions of index and little finger tapping by metacarpal joint hyper-extension with a high frequency are performed and tracked by the use of a single marker on either fingertip. Differences in hand function between the two groups were modelled using a mixed-effects regression model with the person as a random effect. P-values < 0.05 indicate a significant difference in the respective outcomes between RA and Control participants.

Results and Discussion

Results are presented from measurements of 64 hands (35 healthy control hands and 29 RA patient hands) of 47 individuals. RA patients needed longer (mean \pm standard deviations) to complete the MPUT compared to controls in both the clinical (RA: 17.5 ± 4.7 s, Control: 14.1 ± 4.1 s, $p = 0.004$) and the OMS setup (RA: 20.3 ± 7.1 s, Control: $16.0 \pm$

4.5 s, $p = 0.007$). This increase in MPUT times when hand are equipped with markers is similar for control subjects and RA patients. Additionally, we show the normalized grip distance (distance between index and thumb tips, divided by the respective finger lengths) for a healthy control and an RA patient, as shown in Figure 1. The values for the distance between index and thumb fingers are 0.45 ± 0.11 and 0.52 ± 0.07 for the control individual and an RA patient, respectively. This suggests that the control individual was able to maintain the two fingers closer (lower mean), and was able to perform prehension with a higher degree of mobility (higher standard deviation), when compared with the RA patient.

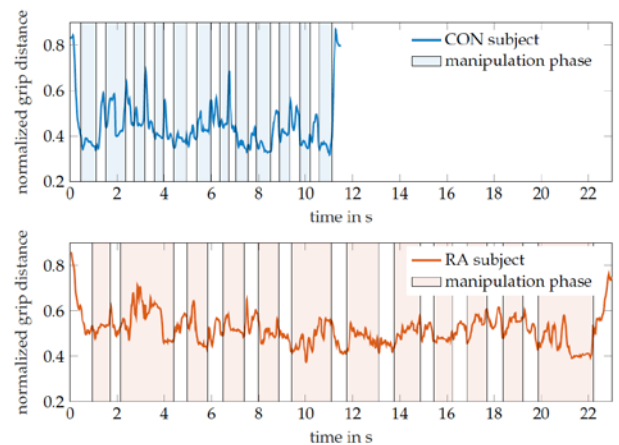


Figure 1: Normalized grip distance for a healthy control and an RA patient.

Conclusions

The use of OMS to assist in the characterization of hand movement opens new avenues in the characterization of hand motion in RA. The differences observed in the time to completion for the functional tests when using optical markers suggests the need of marker-less technologies.

Acknowledgments

The authors would like to thank the German Research Foundation (DFG) for funding the major instruments at the Institute of Applied Dynamics, FAU Erlangen-Nürnberg used in this study - reference number INST 90 / 985-1 FUGG.

References

- [1] Liphardt AM; et al. (2020). *ACR Open Rheuma.*, **2**: 734-750.
- [2] Sancho-Bru J.; et al. (2014). *Proc. Inst. Mech. Engineers.*, **228**(2): 182-189.
- [3] Ng, CL; et al. (1999). *Jour. Hand Therapy.*, **12**: 309-31

SAAC^{1,3}, F. SPOLAOR¹, W. PIATKOWSKA¹, F. CIIN¹, A. CINIGLIO¹, A. GUIOTTO¹, R. POLLI², A. MURGIA²

¹ Department of Information Engineering, University of Padova, Italy

² Department of Women and Children Health, University of Padova, Italy

³ Department of Medicine, DIMED, University of Padova, Italy

Email: sawacha@dei.unipd.it

Summary

Fragile Syndrome (FXS) is a genetic condition, mainly characterized by intellectual disability, behavioral problems and musculoskeletal alterations. Somatic mosaicism for pre and full mutation, can be a strong phenotype modulator of the FXS clinical manifestations [1]. This project aims to investigate association between abnormal motor control in FXS subjects with classical full mutation of the FMR1 gene (FX-FM) and the ones who carried a full mutation with mosaicism (FX-M). For this purpose kinematics and surface electromyography (sEMG) were acquired within standard clinical ambulatory conditions. Results showed reduced range of all lower limb joints in both groups and multiple activations of GL during gait in FX-FM subjects.

Introduction

FXS is the leading form of inherited intellectual disability and autism spectrum disorder, caused by a tri-nucleotide CGG repeat expansion in the promoter region of the FMR1 gene [1]. In FXS children characteristic musculoskeletal manifestations, which include hypotonia, joint laxity and flexible flat feet [6], may lead to non-physiological gait patterns [2], that justifies a referral for gait analysis. The aim of the present study was to identify the relationship between observed musculoskeletal manifestations and altered motor control in FXS children. Furthermore the presence of differences in motor control between FX-FM and FX-M was investigated. For this purpose kinematics and sEMG were acquired within standard clinical ambulatory conditions and sagittal plane kinematics and both duration, onset and offset of muscle activity during gait cycle were estimated.

Methods

After appropriate informed consent by the parents, 12 FXS children, of whom 7 FX-FM (mean±SD age and BMI respectively of 9,57±2,51 years and 18,97±5,54 Kg/m²) and 5 FX-M (mean±SD age of 9,00±3,74 years and 18,70 ±2,61 BMI of Kg/m²) and 19 controls ((CS) mean±SD age of 9,68±2,90 years and 21,52±4,61 BMI of Kg/m²), were evaluated at the at the BiomovLab and at the Women and Children Health Department (University of Padua). Kinematics and sEMG data were simultaneously acquired through 4 synchronized cameras (GoPro Hero3, 30fps) and an sEMG system (8 channels FreeEmg, BTS, 1000Hz) that collected the activity of Tibialis Anterior (TA), Gastrocnemius Lateralis (GL), Rectus Femoris (RF) and Biceps Femoris (BF). Each subject performed several gait trials and at least three trials per subject were processed.

Sagittal plane kinematics was obtained as in [3] and hip, knee and ankle flexion/extension joints rotations were computed together with spatio-temporal parameters; in terms of sEMG analysis duration of contraction and onset and offset activation timing was obtained [4].

Results and Discussion

Results consistently showed the presence of an altered muscle activity (Fig. 1): joint kinematics highlighted a reduced range of motion of all the lower limb joints in both FX-FM and FX-M, while onset and offset activation timing revealed that FX-FM subjects continuously activated and deactivates GL throughout the gait cycle, FX-M subjects displayed a muscle activity closer to controls.

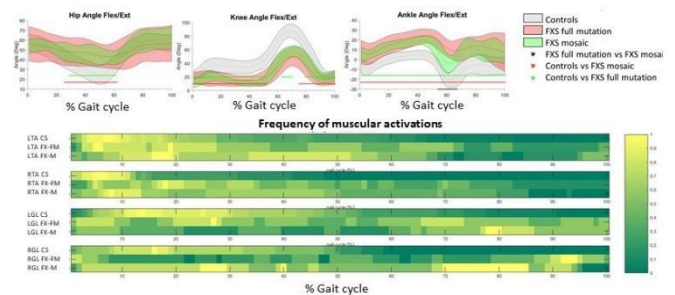


Figure 1: Top: Ankle, knee, hip sagittal plane angles in CS, FX-FM and FX-M groups. Bottom: Frequency of TA and GL activation in CS, FX-FM and FX-M subjects horizontal bars are color coded as in [5], according to the number of subjects in which muscle activity at each % of gait cycle is observed yellow: muscle activity is detected in all subjects, dark green: muscle is not active.

Conclusions

Results suggest that FX-FM subjects adopt a muscle compensatory mechanism to cope with the reduced range of motion in the lower limbs. The muscle alterations found in FX-M are milder than in FX-FM. Application of gait analysis in FXS subjects can be a useful tool to plan rehabilitation therapies.

References

[1] Hagerman RJ, et al. (2017) *Nat Rev Dis Primers*, **3**, 17065.
 [2] Davids JR, et al. (1990) *J Bone Joint Surg Am* **72**(6):889-96.
 [3] Colpe D, et al. (2017) *Gait & Posture* **55**:87-94.
 [4] Conato P, et al. (1998) *IEEE Trans Biomed Eng*, **45**(3):287-99.
 [5] Agostini V, et al. (2010) *Gait & Posture*; **32**, 285-289

Knee Joint Biomechanics Following Total Knee Arthroplasty with Posterior Stabilized Implants

Chang Shu¹, Fangjian Chen¹, Michael Bates², Ronald W. Singer² and Nigel Zheng¹

¹The University of North Carolina at Charlotte, NC, ²OrthoCarolina, NC, USA

Email: nzheng@uncc.edu

Summary

Posterior Stabilized TKA Implants are designed to be more kinematics consistent in the sagittal plane, but may also have impacts on biomechanics in the frontal plane. This study is to investigate the knee joint biomechanics of two popular PS implants (Journey II, Persona) in frontal plane for level walking and stair ascending. No significant differences were found between two implants and it is concluded that different PS implants have similar effect on frontal biomechanics.

Introduction

Abnormal valgus or varus positioning of the tibial component of a total knee arthroplasty (TKA) implant may cause increased possibility for loosening or implant wear and eventually lead to a revision surgery [1]. Adducting moments applied to the knee caused lift-off of the lateral femoral condyle from the bearing and increased the tendency toward dislocation [2]. The aim of this study was to compare the varus/valgus angle and loading of operated knee in level walking (LW) and stair ascending (SA) between two posteriors stabilized (PS) TKA implants - Persona (P) and Journey II (J), with the healthy control (CG). We hypothesized that there were no significant differences in varus/valgus angle and adduction/abduction moment of the knees with these implant at 6-month post-op during daily activities.

Methods

20 patients with Journey II implant and 20 patients with Persona implant were recruited and tested pre-op and some of them also tested at 6 months post-op. Due to the pandemic, only 10 patients with implant J and 8 patients with implant P and 11 healthy subjects (CG) were included in this study. All the knees in group P were done by the one surgeon and the group J was performed by the other surgeon. A 10-camera motion capture system (FX 40, VICON) was used to record motion data at 120 Hz. Two force plates (AMTI) were used to record ground reaction force at 1200 Hz. Subjects were instructed to perform each activity five times at a self-selected pace. A custom-developed and validated MATLAB program was used to perform the kinematic analysis. One-way ANOVA was performed (SPSS 21).

Table 1: Maximum knee valgus angle (deg) and adduction torque (BWxHt%) at 6-month post-op during level walking and stair ascending. *: significant difference between two implants.

	Level Walking			Stair Ascending		
	P	J	CG	P	J	CG
Valgus	16±4	13±3	15±2	13±4	11±5	14±4
Torque	1.5±0.7	1.9±0.7	2.0±0.8	1.7±0.8	2.3±0.8	1.7±0.3

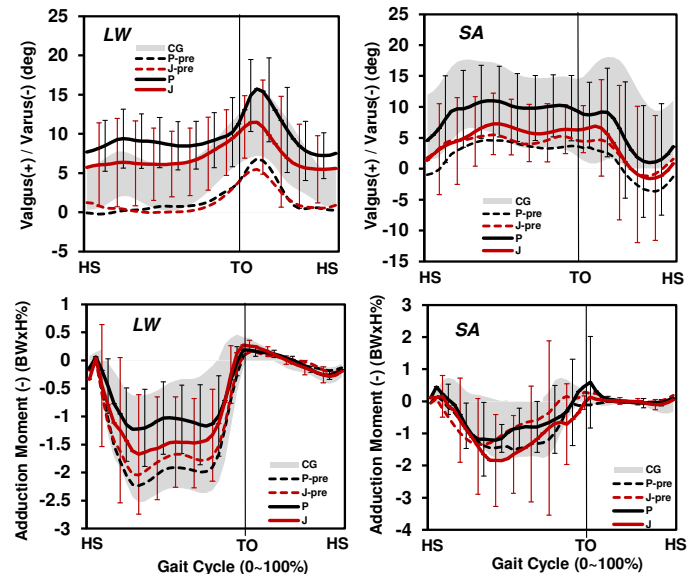


Figure 1: Knee varus/valgus (deg) and adduction/abduction moment (BWxHt%) during LW and SA.

Results and Discussion

No significant differences were found between two implant groups. Both groups exhibited similar valgus trend at 6-month post-op in LW, the maximum valgus angle of group P had greater changes than group J when the pre-post differences (P: 12±4, J:9±4, p=.11) were compared (Fig.1). The adducting moment of group P and group J were within the CG's range in LW. Neither group P or group J had the significant improvement during stair ascending. Considering stair ascending is the more demanding activity, muscles strength may not robust enough to perform it well at 6 months post-op. Further investigation on longer follow-ups of TKA patients may explain better in frontal plane knee biomechanics during daily activities. The findings suggested our hypothesis was approved, as there was no significant difference between the implant groups.

Conclusions

The PS TKA designs had similar influence on knee biomechanics in the frontal plane. The functional improvement at post-op would depend on demanding levels of daily activities.

Acknowledgments

This study is funded by Smith and Nephew through an Investigator Initiated Study award.

References

- [1] Werner W.F., et al. *J. of Biomech.* 38(2):349-355,2005.
- [2] Weale A.E., et al. *J. of Arthroplasty* 17(4) 475-483, 2002.

The effect of diabetic peripheral neuropathy on lower limb biomechanics: a systematic review and meta-analysis

Erica Bartolo MSc¹, Claudia Giacomozzi PhD², David Coppini MD³, Alfred Gatt PhD¹

¹Faculty of Health Sciences, University of Malta, Msida, MSD 2080, Malta

²Department of Cardiovascular Diseases, Dysmetabolic Diseases & Ageing, Italian National Institute of Health, Rome, Italy

³Diabetes & Endocrinology, Mater Dei Hospital, Msida, MSD 2080, Malta

E-mail: erica.bartolo.08@um.edu.mt

Summary

A systematic review and meta-analysis was performed to evaluate the effect of diabetic neuropathy on lower limb joint kinematics, kinetics, muscle activity and spatiotemporal parameters and their relationship to plantar pressure distribution. Sixteen studies fit the inclusion/exclusion criteria for qualitative synthesis and twelve studies were eligible for meta-analysis. Results show that, as a result of neuropathy, there may be decreased range of motion in the knee and ankle joints, resulting in limited dorsiflexion of the foot during heel strike and a resultant increase in peak plantar pressures during gait. However, overall, the current level of evidence is not sufficiently robust to determine whether altered gait patterns in individuals living with DPN are altering plantar pressures during gait and increasing the risk of ulceration. Further investigations are required to decrease heterogeneity in research.

Introduction

In the presence of diabetic peripheral neuropathy, plantar ulceration occurs on high plantar pressure areas due to the repetitive, excessive mechanical loadings which causes tissue breakdown. Through this systematic review and meta-analysis, it is hoped that the underlying mechanism of what causes tissue breakdown is understood by looking into the effect of neuropathy on lower limb joint kinetics and kinematics, muscle activity and plantar pressures.

Methods

A systematic literature search was done for studies published between January 2000 and June 2019, evaluating the effect of diabetic peripheral neuropathy on hip, knee, ankle and foot joint kinematics and kinetics, spatiotemporal parameters, electromyography and plantar pressures during gait.

Following a quality assessment of the sixteen studies included in this review, qualitative analysis and meta-analysis was performed on these outcome measures.

Results and Discussion

The qualitative and meta-analysis results in this review suggested that participants living with diabetic peripheral neuropathy exhibited reduced knee, ankle and rearfoot (Sha-Cal) kinematics, higher midfoot and rearfoot peak plantar pressures and higher PTI in the medial forefoot, lateral forefoot and midfoot regions. However, conflicting results were present between studies with regards to the spatiotemporal parameters and lower limb muscle activity. Further research is required, including larger sample sizes, to decrease heterogeneity of the meta-analysis results since there is paucity of information on the effect of diabetic peripheral neuropathy on the outcome measures assessed. Literature states that diabetic peripheral neuropathy may cause a decreased range of motion in the knee and ankle joints. This may produce inadequate dorsiflexion of the foot during initial stance phase of gait, thus redistributing plantar pressures to the midfoot and forefoot regions for longer periods during gait, resulting in tissue breakdown. Further research, examining the outcome measures assessed in this review in the presence of active ulceration, might offer a better understanding as to the underlying pathomechanics of tissue breakdown.

Conclusions

A clear understanding of the underlying biomechanical mechanism of the altered mechanical loadings might provide more accurate, patient-specific treatment options of ulceration and reduce the risk of reulceration and amputation rates in individuals living with diabetic peripheral neuropathy.

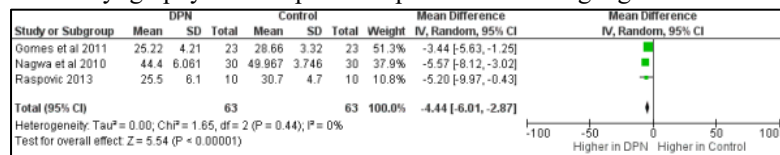


Figure 1: Meta-analysis performed on sagittal knee joint kinematics in DPN vs healthy controls

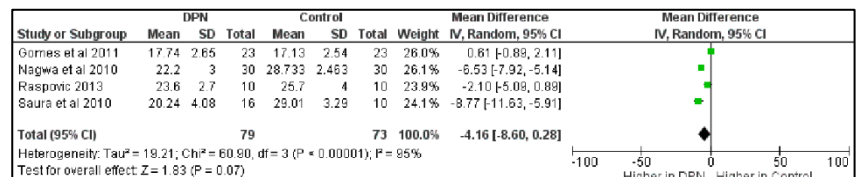


Figure 2: Meta-analysis performed on sagittal ankle joint kinematics in DPN vs healthy controls

Reliability of a portable system for motion analysis in children and young adults with treated obstetrical brachial plexus palsy

Helena Grip¹, Annika Wasberg¹, Lisa Jakobsson¹, Anna Källströmer², Fredrik Öhberg¹

¹Dept. Biomedical Engineering, University Hospital of Umeå, Umeå, Sweden

²Dep. of Surgical and Perioperative Sciences, Umeå University, Umeå, Sweden

Email: Helena.Grip@regionvasterbotten.se

Summary

There is a need for clinical systems that objectively assess the mobility of the upper extremities. Therefore, the aim of this study was to study the test-retest reliability of a portable motion analysis system in a small group of people with obstetrical brachial plexus palsy (OBPP).

Introduction

To decide if an intervention has improved the arm function for a person with OBPP, it is important that there the instrument is sensitive enough to measure changes in upper limb mobility.

In clinical practice, assessment of upper limb mobility is usually based on visual estimation and use of goniometers. The visual estimations result in scores on different scales, such as the modified Mallet scale (MMS) [1] and the Active Movement Scale [2], but these visual methods to measure elbow and shoulder angles do not correlate well to objective methods such as 2D movement analysis [3].

A technique to measure mobility of the shoulder that has been developed in the last decade is motion analysis with inertial measurement units (IMUs) containing accelerometers, gyroscopes and magnetometers [4]. This is a portable system that is non-invasive and requires no equipment other than the sensors and a computer. The aim of this study was to study the test-retest reliability of a portable motion analysis system based on IMUs in a small group of people with OBPP.

Methods

Six persons with OBPP, aged between 7-22 years and nine matched healthy controls (HC), aged 8-25 years took part in this study. A portable motion analysis system (MoLab™, AnyMo AB, Umeå, Sweden) with 7 IMU sensors were used for collecting joint angles from the upper extremities (i.e., scapula, upper arm, and forearm). All participants were examined on two different occasions to determine the test-retest reliability. Time between examinations was on average 5.8 days for the participants with OBPP and 4.1 days for the HCs. All participants were instructed to avoid any heavy physical activity of the upper extremities for two days before each examination. On both occasions the examination was carried out by the same test leader. The performed tasks in the examination were partially based on the MMS [1]. The joint angles examined were the humerothoracic joint (HT) and the scapulothoracic joint (ST). Like Cutti et al, [5] HT was described by three

independent angles: flexion-extension (HT-FE), abduction-adduction (HT-AB) and internal-external rotation (HT-ROT). ST kinematics was described by three independent angles: anterior-posterior tilt (ST-ANT), lateral-medial rotation (ST-LM) and protraction-retraction (ST-PR). For each task, range of motion (RoM) was calculated. Intraclass Correlation Coefficient (ICC) and Cronbach's alpha (α) were then calculated as a measure of test-retest reliability for the two test occasions for each group. Values >0.75 represent good reliability.

Results and Discussion

The test-retest reliability varied between tasks and joints as illustrated in Figure 1.

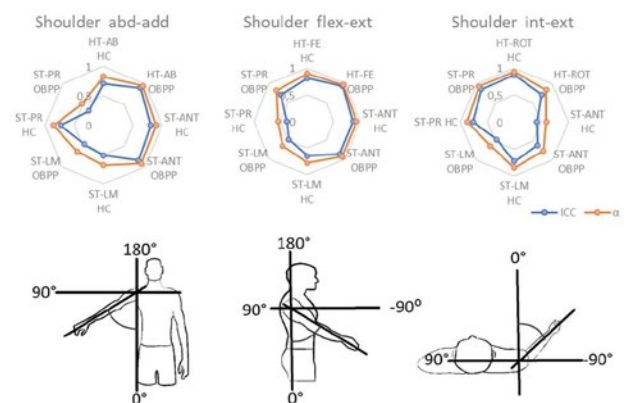


Figure 1: Top: illustrates ICC and α for range of motion in scapulothoracic (ST) and humerothoracic (HT) joints, for three shoulder tasks, in healthy controls (HC) and plexus patients (OBPP). Bottom: Analyzed movement planes (Shoulder abd-add, flex-ext and int-ext).

Conclusions

Measuring ROM of joint angles in different anatomical planes can give a good test-retest reliability for certain anatomical planes and anatomical joint. Before this technology can be implemented in clinical practice, larger studies are needed to determine the system's validity.

References

- [3] Bialocerkowski AE and Galea M. (2006). *J Brachial Plex Peripher Nerve Inj*, 1:5.
- [1] Abzug JM et al. (2010). *J Pediatr Orthop*, 30:469-74.
- [2] Curtis C et al. (2002). *J Hand Surg Am*, 27:470-8.
- [4] De Baets LR et al. (2017). *Gait & posture*, 57:278-294.
- [5] Cutti AG et al. (2008). *Medical&biological engineering& computing*, 46:169-178

Quadriceps Muscle and Pain During Daily Activities for Total Knee Arthroplasty Patients

Fangjian Chen¹, Chang Shu¹, Ronald Singer², Michael Bates², Nigel Zheng¹

¹University of North Carolina at Charlotte, NC, USA

²OrthoCarolina at Charlotte, NC, USA

Email: nzheng@uncc.edu

Summary

The objective of this study was to find the relationship between muscle activity of quadriceps and pain level. 25 total knee arthroplasty (TKA) patients were enrolled before and 6-months after surgery in this study. The electromyography (EMG) data from vastus lateralis and vastus medialis was processed to find the peak muscle activity and the duration of muscle activity. Pain levels were collected using Knee Society Score (KSS). Based on the correlation analysis performed for five daily activities, the relationships were found between pain and muscle activity.

Introduction

The total knee arthroplasty (TKA) was the most common to treat the end stage of knee osteoarthritis. Although many investigations have reported that TKA improved functional performance [1], many patients still have pain and dissatisfaction to performing household duties and leisure recreational activities. It is reported that the muscle activities of vastus lateralis (VL) and vastus medialis (VM) highly affected the performance of knee during daily activities [2]. The purpose of this study was to determine the relationship between muscle activity of both VL and VM with pain for TKA patients. We hypothesized that EMG of knee extensors were not affected by the pain level.

Methods

25 subjects with posterior stabilized TKA (M/F: 18/7, age: 61±6 years, BMI: 30±5 kg/m²) were recruited and tested preoperatively and 6-month postoperatively. The study protocol was approved by an institutional research board, and all participants gave written informed consent. Muscle activity of involved (VL) and (VM) were recorded using surface EMG (Noraxon) during level walking (LW), stair ascending (SA), stair descending (SD), ramp up (RU) and ramp down (RD). A custom MATLAB code was developed to perform EMG processing (remove bias, low pass filter (10Hz), rectification, and window averaging) [3]. Peak muscle activity (PMA) was found based on the muscle activated pattern. the duration of muscle activity (DMA) was determined as previously described [4]. The pain levels were collected using the KSS for LW and SA respectively. The correlation analysis was performed using SPSS with alpha set to 0.05.

Results and Discussion

No correlations had been found in PMA and MDA with pain during LW, RU, and RD for both muscles (Table 1, Fig. 1). Significant correlations were found between PMA and pain

level during SA and SD for both muscles. There was a significant correlation between DMA and pain level during SA for both muscles. The results showed that there were significant correlations between EMG and pain level for more demanding activities (stair ascending and descending).

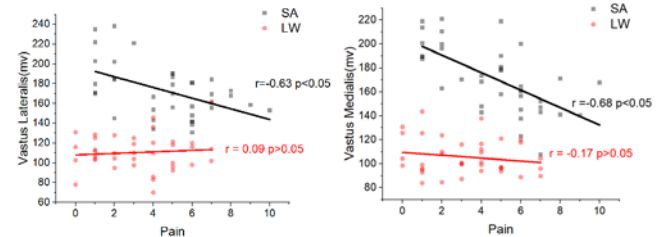


Figure 1: Correlations between PMA of both muscles and pain levels during level walking (LW) and stairs ascending (SA).

Table 1: The correlation analysis of PMA and DMA with pain level during daily activities for both muscles. (* p<0.05)

Activity	Parameters	VL	r	VM	r
Level	PMA (mv)	109±18	0.09	113±15	-0.17
Walking	DMA(%gait)	45±7	-0.15	42±9	-0.08
Stair	PMA (mv)	182±21	-0.63*	188±25	-0.68*
Ascending	DMA(%gait)	54±11	-0.45*	57±9	-0.42*
Stair	PMA (mv)	170±23	-0.56*	201±14	-0.58*
Descending	DMA(%gait)	53±20	0.08	60±24	-0.12
Ramp	PMA (mv)	96±18	-0.23	103±18	-0.18
Up	DMA(%gait)	48±10	0.12	45±6	0.13
Ramp	PMA (mv)	113±20	0.06	131±18	0.09
Down	DMA(%gait)	45±7	0.08	49±6	0.06

Conclusions

The pain level of the knee had an impact on the activities of knee extensors only during stair ascending and stair descending.

Acknowledgments

This study is funded by Smith and Nephew through an Investigator Initiated Study award.

References

- [1] Benedetti MG et al. (2003) *Clin Biomech*, **18**:871-876.
- [2] Ryan L. et al. (2005) *Orthopedic*, **23**:1083-1090.
- [3] Burden AM et al. (2003) *Electromyography*, **13**:519-532.
- [4] Van Boxtel et al. (1993) *Psychophysiology*, **30**:405-412.

Comparison between two mobile applications measuring shoulder elevation angle – A Validity Study

Fredrik Ohberg, Martin Gunn, Karolina Jonzén, Urban Edström and Nina Sundström
 Dept. Biomedical Engineering, University Hospital of Umeå Umeå, Sweden
 Email: Fredrik.Ohberg@regionvasterbotten.se

Summary

This study shows a comparison between two mobile applications (ErgoExposure and ErgoArmMeter) that can be used by ergonomists for measuring work-related shoulder exposure to poor working postures. ErgoExposure had better accuracy, but both applications seem viable to be used by ergonomists.

Introduction

Pain in shoulder and neck affects between 7-25% of the working population and one risk-factor is continuous manual work with elevated arms [1]. To quantify and compare these factors, ergonomists use tools that broadly divide into; 1) self-reported data, e.g. worker diaries; 2) observational methods that include both simpler techniques for systematic evaluation of risk factors and advanced software analysis that computes the specific variables from video recordings; and 3) direct measurements using equipment attached to the body for measuring e.g. movement [2]. To facilitate the evaluation of interventions, better objective tools are needed for measuring exposure to poor working postures. A mobile application for iPhone (ErgoExposure) has been developed that uses the internal accelerometers and gyroscope to measure the shoulder's elevation angle when attached to the upper arm.

The aim of this study was to test the validity of ErgoExposure by comparing it to an existing mobile application (ErgoArmMeter) developed by Wang et.al. [3]

Methods

Mobile phones were fastened to the upper arm of 11 test persons (6M/5F) who in turn performed 3 different tests: 1) static shoulder elevation (flexion and abduction) 2) dynamic arm swing at three different speeds and 3) two simulated work tasks (postal sorting and teaching, see Fig 1.). During the tests, the two mobile applications and the optical tracking system collected the change in shoulder elevation angle at each point in time. The results from both mobile applications were then compared to the results of the optical tracking system that was used as a gold standard.



Figure 1: Simulated work task. A) Postal sorting and B) Teacher.

Results and Discussion

For ErgoExposure the static test had an overall bias (flexion and abduction) of -0.97° with limits of agreement (LOA) -6.1° to 4.2° (see Fig. 2.) as compared with ErgoArmMeter that had an overall bias of -1.3° and LOA -7.6° to 5.2° . ErgoExposure resulted in an average root mean square difference (RMDS) of 3.06° with an increasing error at higher speeds, from 2.62° at slow-paced to 3.97° at fast-paced arm swings. ErgoArmMeter had a higher average RMDS of 7.44° and showed an increasing error at higher speed. The simulated work tasks showed similar results, ErgoExposure had an average RMDS of 1.79° with no clear difference between the tasks. ErgoArmMeter had a higher average RMDS of 3.21° , but showed differences between the tasks, average for postal sorting was 4.41° and for teacher 2.01° .

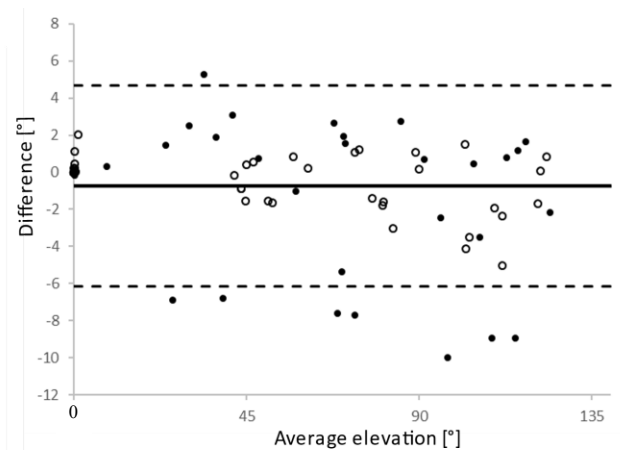


Figure 2: Bland Altman Plot of the static test.

Conclusions

Both apps showed results within reasonable margin from the optical tracking system, where the main error came from a time lag in the dynamic tests and the simulated work tasks. Compared to other methods, both apps give accurate results for measuring shoulder elevation. ErgoExposure seems to be appropriately viable to be used by ergonomists in practice.

References

- [1] Luime JJ et al. (2004). *Scand J Rheumatol*, **33**: 73-81.
- [2] David GC. (2005). *Occup Med (Lond)*, **55**: 190-199.
- [3] Yang L et al. (2017). *Appl Ergon*, **65**: 492-500.

INTEGRATED CONTACT ANALYSIS SUPPORT MODELING OF BIOMECHANICAL CONTACT OF SHOE SURFACES

Lasse Jakobsen¹, Filip G. Lysdal², Rasmus K. Jensen², Uwe G. Kersting^{2,3} and Ion M. Sivebæk¹

¹Department of Mechanical Engineering, Technical University of Denmark, Denmark

²Department of Health Science and Technology, Aalborg University, Denmark

³Department of Biomechanics and Orthopaedics, German Sport University Cologne, Germany

lasjak@mek.dtu.dk

INTRODUCTION

The contact mechanism between shoe and surface is crucial in order to avoid slipping and falling [1], enhance sporting performance or minimize the risk of sport injuries [2]. However, studying this contact mechanism, between footwear and surface, is challenging and violates the traditional Amontons–Coulomb’s law of friction, due to the viscoelastic outsole materials [3]. Hence, replicating the biomechanical test conditions are of great importance, when determining the friction properties of footwear [1]. The aim of this study is to present a test-setup able to replicate biomechanical relevant test conditions.

METHODS

The test-setup consisted of a steel frame designed to maintain the position of a shoe, mounted above a force plate (AMTI-OPT464508HF-1000, Advanced Mechanical Technology, Inc. Watertown MA, USA). The force plate is attached on top of a hydraulic platform (Serman-Tipsmark, Randerslev, Denmark), which makes it possible to move vertical and horizontal.

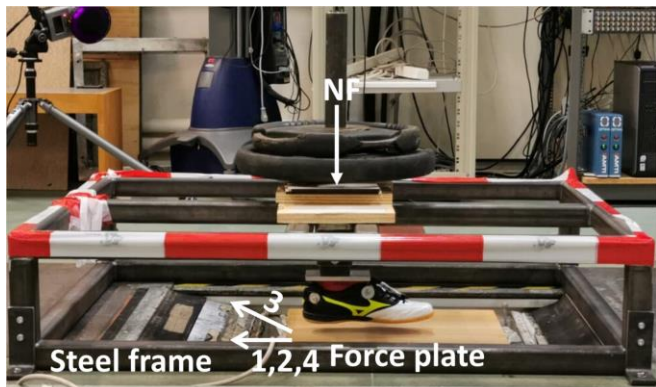


Fig 1 Illustration of the test-setup. Drag-test (1,2,4) impacting (3) illustrates platform movement directions.

An indoor Puma One size 43 (EU), (Puma, Herzogenaurach, Germany) and a square sample of a vinyl indoor sports floor (7.5 mm Taraflex - Evolution, Gerflor, Lyon, France) was used in the test-setup. Four different test conditions were performed: 1) Drag-test according to ISO 13287 (normal load (NL) 500 N, sliding velocity (S) 0.3 m/s) 2) Drag-test (NL 750 N, S 0.3 m/s) 3) Impacting, with the platform moving both horizontal and vertical (NL 750 N, S 1.0 m/s), and 4) Drag-test (NL 750 N, S 1.0 m/s). We recorded five trials of each condition.

Force data were filtered using a 2nd order Butterworth filter with a cut-off frequency of 30 Hz and 10 Hz, respectively. Zero-phase filtering was performed using MATLAB function Filtfilt, filtering both forward and reverse. All measurements

were synchronized using the kinematics of a retro-reflective marker by calculating cross-covariance and aligning data by circular shift. Ten empty force plate movements were recorded for each condition and used to subtract the inertial contribution from the hydraulics accelerating the force plate.

Coefficient of friction (μ) was calculated by $\mu = \frac{F_f}{F_n}$ from the computed normal force (F_n) and horizontal forces (friction force, F_f) [2].

RESULTS AND DISCUSSION

The μ was influenced by the test conditions, where higher normal loads and sliding velocities resulted in lower μ , which is in agreement with rubber friction theory [3]. The initial part of condition 3 mimics somewhat the initial contact, as in real-world walking or running, and shows a highly fluctuating μ , most likely caused by the minimal damping in the present setup. However, we still consider condition 3 to be more biomechanically relevant, compared to traditional one-direction sliding tests as per ISO 13287.

Adding impacts, and potentially also damping characteristics, in the mechanical tests of footwear could possibly contribute to a deeper understanding of the shoe-surface sliding and/or sticking phenomena.

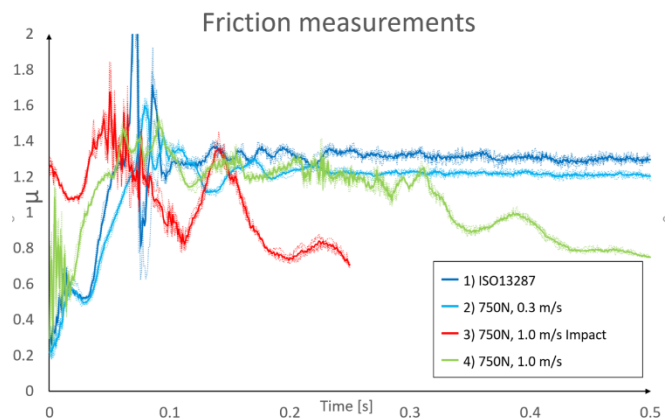


Fig 2 μ as function of time for the four different test conditions.

CONCLUSIONS

This study presents a new test setup that can characterize the tribological behavior of shoe and surface in a traditional way, by following the traditional ISO 13287 standards, but more importantly also being able to add a novel impacting approach to the test of footwear, which is arguably more biomechanically relevant.

REFERENCES

- [1] Chang WR, et al. (2001), *Ergonomics*, **44**: 1233-1261
- [2] Frederick EC. (1993), *ISBS-Conference*, **11**: 15-22
- [3] Persson N. (2001), *J Chem Phys*, **115**: 3840-3861, 2001

Functional Assessment for Passive and Active Back Supporting Exoskeletons

Jasper Johns, Ulrich Glitsch, Kai Heinrich

¹Institute for occupational safety and health (IFA), Sankt Augustin, Germany

Email: jasper.johns@dguv.de

Summary

In this study the supportive functions of one active and two passive industrial exoskeletons were quantified and compared to the acting hip moments of 12 subjects during a symmetrical lifting task. Determining the functional support of exoskeletons is a crucial step in analyzing their ability to effectively aid the user during strenuous working tasks. The demonstrated approach aimed to establish a protocol to assess the supportive function and the potential assistance provided by the used exoskeletons. The results demonstrate that for the active system, the achieved support level depends on the selected system settings, and that different support strategies could be adopted for the passive systems.

Introduction

Exoskeletons are a novel approach to reduce lumbar loadings in industrial workers by supporting the trunk based on a torque exerted at about hip joint level. They aim to support the erector spinae muscles and thus lower resulting compression forces acting along the spine. While previous studies have shown that exoskeletons can effectively reduce muscular activity [1], the analysis of the mechanically provided support has only been subject to few studies [2, 3]. By including the provided supportive torque into biomechanical models, it is possible to assess the direct effects of exoskeletons on internal loading of affected structures.

The goal of this paper was to quantify the provided support of three industrial exoskeletons and propose a protocol for their functional assessment.

Methods

One active (A) and two passive (P1, P2) exoskeletons were tested in this study. With the passive exoskeletons, direct force measurements were conducted to determine the contact forces transmitted by the exoskeleton chest pad to the user's sternum and movements were tracked with 40 markers (with 7 to 15 additional markers to track the exoskeleton motion) and a 12 camera vision system. For the active exoskeleton, internal sensors recorded motor torques and segment positions, and data could be accessed through an online interface.

Additionally, kinematic data of 12 subjects were collected during a repeated lifting task (20 kg) and a top-down inverse dynamic model was applied to calculate the acting hip joint moments. The respective supportive torque – flexion angle relationships of the exoskeletons were created and compared to the hip joint moments during unassisted lifting.

Results and Discussion

The tested exoskeletons provided different levels of support during certain phases of the lifting motion. While the absolute support provided by exoskeleton P1 reached an early peak of

26 Nm at around 40°, the support of P2 steadily increased until 54 Nm at 90° trunk flexion. The system settings of exoskeleton A were configured in a way that the flexion phase during lifting was completely unsupported and the electric motors delivered maximal output when the trunk extension was initiated. With the actuation only starting at the beginning of the trunk extension, the peak of 70 Nm was reached at 35° trunk flexion. Compared to the normalized hip moments during unsupported lifting, only exoskeleton A could provide substantial support during the last phase of unloaded extension. Systems P1 and P2 exhibited different support strategies, but both could only provide a fraction of the net joint moments around the hip as support during loaded trunk extension (Fig. 1).

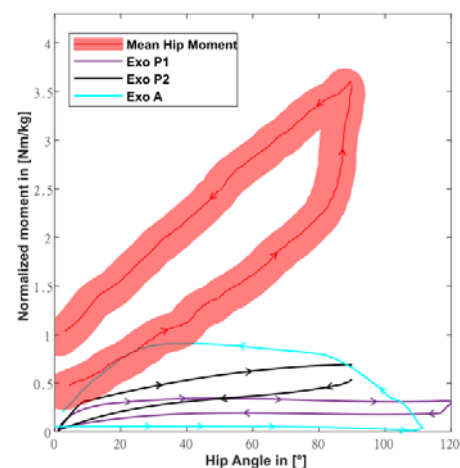


Figure 1: Comparison of the hip joint moments with the exoskeletons' supportive torques. Hip joint moments were normalized for corresponding subject weight and exoskeleton support for average subject weight.

The comparison of the hip joint moments and the provided supportive torque over a lifting cycle reveals the maximal estimated assistance provided by the tested exoskeletons.

Conclusions

For an appropriate analysis of the effect of exoskeletons on the loading of affected structures during industrial work tasks, it is important to consider the support provided by exoskeletons. Only by focusing on the multifaceted human-exoskeleton-interaction is it possible to judge their capability to effectively reduce musculoskeletal loading.

References

- [1] De Looze et al. (2016). *Ergonomics*, **59**, 671-681.
- [2] Koopman et al. (2020). *J Biomech*, **103**, 109486
- [3] De Quaries et al. (2019). *IIEE Transactions on Occupational Ergonomics and Human Factors*, **33**, 311-321.

Fracture behavior of a composite of bone and calcium sulfate/hydroxyapatite

Joeri Kok¹, Elin Törnquist¹, Deepak B. Raina², Sophie Le Cann³, Vladimir Novak⁴, Aurimas Sirka⁵, Lars Lidgren², Lorenzo Grassi¹, Hanna Isaksson^{1,2}

¹Biomedical Engineering, Lund University, Sweden; ²Orthopedics, Lund University, Sweden; ³CNRS, Paris, France

⁴Paul Scherrer Institute, Switzerland; ⁵Orthopedics and Traumatology, Lithuanian Univ. of Health Sciences, Lithuania
Email: Joeri.kok@bme.lth.se

Summary

The mechanical and structural properties of bone augmented with a calcium sulfate/hydroxyapatite (CaS/HA) biomaterial were evaluated. Plugs of human trabecular bone with and without addition of CaS/HA were imaged using synchrotron X-ray tomography. Loading was applied *in situ* during tomography. Mechanical and structural parameters were compared, and the crack propagation was followed. Adding CaS/HA increased the peak force and absorbed energy due to formation of microcracks in CaS/HA.

Introduction

New tools for reinforcing bone or fixation of orthopaedic implants are being investigated [1]. Calcium sulfate/hydroxyapatite (CaS/HA) based biomaterials are an attractive alternative owing to their injectability, osteoconductivity and mechanical properties. Despite the wide variety of applications the biomaterial is used in, the mechanical behavior of the composite of CaS/HA and bone on a microscale is still largely unknown. Current developments in imaging techniques allow for better investigation of the mechanics of bone-biomaterial interactions at the microscale. The aim of this study was to determine if and how bone augmentation with CaS/HA alters the fracture behavior of bone.

Methods

Eleven cylindrical plugs (Ø 6 mm, H 7.5 mm) were drilled from two human femoral heads (one male, one female). Bone marrow was removed from all plugs and CaS/HA was introduced into the 5 plugs by manual tapping. 1 plug of only CaS/HA was prepared. The plugs were imaged with synchrotron X-ray tomography (TOMCAT, PSI, Switzerland) (energy: 30 keV; scanning speed: ~2 min/scan; isotropic voxel size: 2.75 µm). Loading was performed *in situ* (displacement rate: 0.9 mm/min) and tomographs were taken at increments of 0.15 mm. Images of unloaded samples were used to obtain bone volume/total volume (BV/TV), CaS/HA volume/total volume (CV/TV), and trabecular thickness (Tb.Th). From the load curves, peak force (Fmax), stiffness (k) and work (W) were determined. One sample from each group was used for further image analysis, by selecting a region of interest where damage occurred. At each loadstep, cracks in this region were segmented. For the composite sample, a distinction was made between cracking in CaS/HA, cracking in bone and separation of the bone-CaS/HA interface.

Results and Discussion

The CaS/HA-only sample had the highest peak force, stiffness and work (Table 1). The resulting fracture for this sample was

brittle (Figure 1). The composite sample showed the most plastic behavior (Figure 1). During early loading, the CaS/HA matrix developed small cracks and started to separate from the bone at the interface. However, the force kept increasing and at the last loadstep the bone was still mostly intact. The bone-only sample showed large deformations before failing at a relatively low peak force.

Reinforcing bone with CaS/HA results in an increased peak force, stiffness, and work. Most interesting is the fracture behavior leading to the increase in absorbed energy, which is caused by the large amounts of micro-cracks that are formed in the CaS/HA before global failure.

Table 1: Median mechanical and structural properties.

	Bone	Composite	CaS/HA
Fmax [N]	56	265	479
k [N/mm]	122	497	792
W [Nmm]	34	91	131
BV/TV	0.21	0.21	-
CV/TV	-	0.44	0.99
Tb.Th [µm]	165	175	-

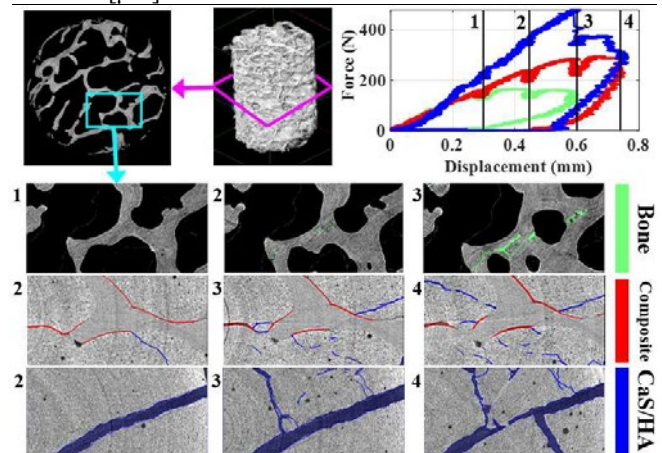


Figure 1: Force-displacement curves of the three samples and the crack evolution over the last three load steps (numbered). Cracks' localizations are colored blue (CaS/HA), green (bone), and red (bone-CaS/HA separation).

Acknowledgments

J. Engqvist and S. Hall for the load cell, BoneSupport AB for the CaS/HA material and Paul Scherrer Institut, Villigen, Switzerland for synchrotron beamtime at TOMCAT. We thank VINNOVA, the Swedish Agency for Innovation systems, and Marie Skłodowska-Curie grant No. 713645.

References

[1] Kok J. et al. (2019). *Clin. Biomech.*, **63**:172-178

Microscale compressive behavior of hydrated lamellar bone at high strain rates

Cinzia Peruzzi¹, Rajaprakash Ramachandramoorthy¹, Alexander Groetsch¹, Daniele Casari¹, Philippe Grönquist², Markus Rüggeberg², Johann Michler¹, Jakob Schwiedrzik¹

¹Empa, Swiss Federal Laboratories for Materials Science and Technology, Laboratory for Mechanics of Materials and Nanostructures, Thun, Switzerland

²Institute for Building Materials, ETH Zürich, Switzerland
Email: cinzia.peruzzi@empa.ch

Summary

Micropillar compression experiments were performed in ovine bone at two orientations, over seven orders of magnitude in strain rate and at a relative humidity of over 90%. These conditions were chosen to mimic the natural conditions of bone in a human body. The determined strain rate sensitivity is similar to the reported strain rate sensitivities of bone of other species and higher length scales. This suggests that it is an intrinsic property of the bone extracellular matrix. Furthermore, an increase in post-yield energy absorption and a thickening of the shear deformation bands were observed at high strain rates (10^2 s^{-1}). This study highlights the importance to examine bone at several length and time scales and under clinically relevant conditions.

Introduction

Bone is a hierarchically structured composite material. Its main components are collagen molecules, calcium phosphate minerals and water. Mineralized collagen fibrils are embedded into an extrafibrillar matrix and form lamellae, 3 to 7 μm thick layers that are wrapped around blood vessels forming osteons in cortical bone. In daily life, bones are subjected to mechanical loading at different strain rates, such as during walking ($5\text{--}80 \times 10^{-3} \text{ s}^{-1}$), sprinting ($5 \times 10^{-2} \text{ s}^{-1}$) and accidental falls (25 s^{-1}) [1]. Microscale tests have typically been conducted at quasi-static strain rates (up to 10^{-3} s^{-1}). In this study, we investigate the rate-dependent mechanical behavior of ovine bone micropillars at the lamellar length scale across seven orders of magnitude (up to $8 \times 10^2 \text{ s}^{-1}$), under physiologically relevant humidity conditions.

Methods

Micropillars were produced in cortical bone with a focused-ion beam (FIB) [2] using two samples from one ovine tibia. The samples are oriented in (axial) and perpendicular (transverse) to the main osteon direction. 93 micropillars (46 axial and 47 transverse) were fabricated with a diameter of $5.52 \pm 0.14 \mu\text{m}$ and a height of $10.35 \pm 0.68 \mu\text{m}$. Compression experiments were performed under ambient pressure and with a relative humidity greater than 90% using a custom-built nanoindenter. Quasi-static up to impact strain rates were used ($10^{-4} - 8 \times 10^2 \text{ s}^{-1}$). High resolution scanning electron microscope (HRSEM) imaging was conducted on all micropillars. To get a better insight into the deformation mechanisms six micropillars were selected for FIB cross sectioning and a further three micropillars that were compressed at high strain rates ($10^2 - 8 \times 10^2 \text{ s}^{-1}$) for scanning transmission electron microscopy (STEM) imaging.

Results and Discussion

Microscale lamellar bone exhibits a clear strain rate sensitivity being slightly more pronounced in axial ($m = 0.057$) than in transverse ($m = 0.041$) micropillars (Figure 1). The strain rate sensitivity is similar to reported values for bovine and human bone ($m = 0.06$) [1] suggesting it is an intrinsic property of the bone extracellular matrix.

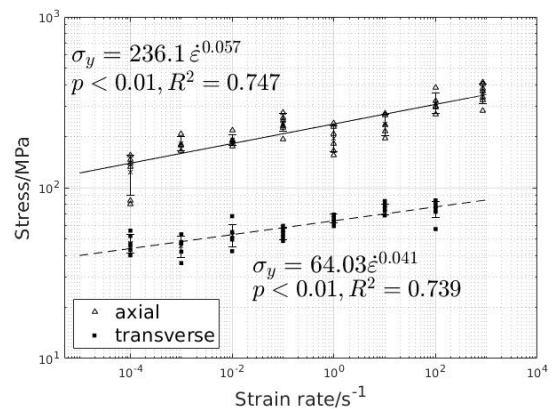


Figure 1: Expected yield stress extracted from axial and transverse micropillar compression tests at different strain rates.

In addition, an increase in the post-yield energy absorption and the thickening of shear bands as well as nucleation of multiple shear bands was observed for high strain rates (10^2 s^{-1}). This suggests that at high strain rates thin kink bands do not have sufficient time to propagate causing a change in deformation mechanism towards shear band nucleation and thickening.

Conclusions

The findings of this study illustrate the importance to investigate bone at several length and time scales and clinically relevant conditions.

Acknowledgments

This work was supported by Ambizione grant 174192 of the Swiss National Science Foundation.

References

- [1] D.R. Carter et al., (1976), *Science*, **194**, 1174-1176.
- [2] J. Schwiedrzik et. al., (2014), *Nature Materials*, **13**, 740-747.

Harry Duckworth¹, Adriana Azor^{1,2}, David J Sharp^{2,3}, Mazdak Ghajari²

¹Dyson School of Design Engineering, Imperial College London, UK

²The Computational, Cognitive and Clinical Neuroimaging Laboratory, Imperial College London, UK

³Care Research and Technology Centre, Dementia Research Institute, UK

Email: h.duckworth17@ic.ac.uk

Introduction

Finite element modelling of the brain has been used with increasing frequency to investigate brain biomechanics and pathology of injury [1]. Some models have considered the mechanical effects of vasculature on the response of the brain matter however there are only a small number of studies which investigate vasculature injury, and of these, the focus is bridging vein rupture, meaning diseases such as microbleeding and are unable to be investigated. Here we present a method for inclusion of the complete venous system in the brain from a T1 image and high resolution QSM image for finite element analysis.

Method

A high resolution QSM modality image of the vasculature was segmented using a combination of manual and semi-automatic tools in Mimics (Materialise Mimics Research 20.0). Thresholding was used to identify macroscale veins, a dynamic growth algorithm was used to manually segment remaining veins, and finally, a smart expansion algorithm was applied to add missing edges and discontinuities. The vasculature image was registered to the head segmentation and the centerlines/radii data was transformed to the head coordinate system.

Three steps were taken to build the Finite element (FE) model of the brain from the subjects T1 image. The subcortical structures were segmented using freesurfer, the cerebrospinal fluid (CSF) was segmented using fsl and the skull was created by thresholding the T1 image then removing the brain and CSF segmentation mask. Smoothing was applied at material interfaces.

Four head impact reconstructions were simulated in LS-DYNA for verification purposes [2]. CORA scores, a method for comparison of biomechanical reconstructions, were calculated for each receiver to verify the fidelity of the brain model. Simulations of injury events in sport, road traffic collision, and fall were ran on the model to investigate vasculature strains.

Results

A detailed FE model of the brain was created which included 46 parts, made up of the skull, meninges, CSF, cortical, and subcortical structures (figure 1 left). The biomechanics of the model was verified using head impact data with average CORA scores giving a good/fair biofidelity rating as specified in ISO/TR-9770 (figure 1 right).

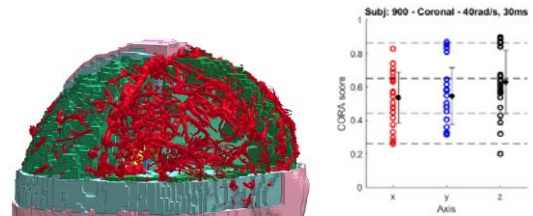


Figure 1 (L) FE brain model with complete venous system, (R) CORA scores for each receiver per axis for reconstruction of UVA900COR4 [2]

The venous system was successfully segmented and imported onto the brain model. Good alignment of anatomical features was seen and veins < 0.4mm diameter were successfully identified. Strains were seen to peak in patterns in the brain which could indicate pathology.

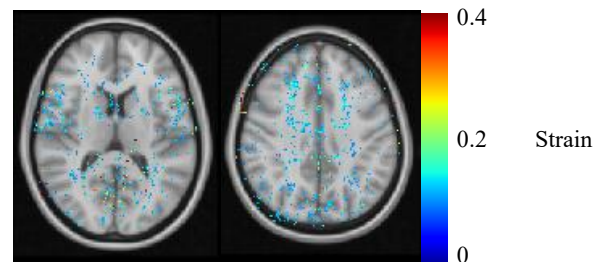


Figure 2 Axial slices of fall reconstruction showing distribution of strains < 0.15

Conclusions

Here we present the first FE brain model to use high resolution imaging for identification and inclusion of vasculature in the brain. The brain biomechanics were verified from head impact tests showing fair/good fidelity. Injury recreations show patterns of strain in perivascular region where vasculature injury is seen.

Acknowledgments

We thank Dr. H Mattern for providing the imaging data. This work was supported by EPSRC, grant number [EP/N509486/1](https://doi.org/10.1039/B509486G) and reference [2024686](https://doi.org/10.1039/B5024686G).

References

- [1] Dixit, P. et al. (2017). A Review on Recent Development of Finite Element Models for Head Injury Simulations. Archives of Computational Methods in Engineering 24(4): 979-1031.
- [2] Alshareef, et al., (2020). Biomechanics of the Human Brain during Dynamic Rotation of the Head. J. Neurotrauma 37(13): 1546-1555.

The Axial Impact Response and Plantar Load Distribution of the Hybrid III and MIL-Lx under Altered Ankle Postures

Julia de Lange¹, Cheryl E. Quenneville^{1,2}

¹School of Biomedical Engineering, McMaster University, Hamilton, Canada

²Department of Mechanical Engineering, McMaster University, Hamilton, Canada

Email: quennev@mcmaster.ca

Summary

Lower extremities injuries are frequent and debilitating in frontal automotive collisions. Two commonly used ATDs (the Hybrid III and MIL-Lx) were axially impacted at conditions representative of automotive collisions, at seven different ankle postures. Results suggest that initial ankle posture must be considered when conducting safety evaluations as the distribution of load and peak recorded tibia forces changed with differing ankle postures. Furthermore, the two surrogates and their respective injury criteria are not equivalent, and thus caution with their application must be used.

Introduction

In frontal automotive collisions, lower extremities are the most frequent site for “non-minor” injuries [1]. Anthropomorphic Test Devices (ATDs) are commonly used to assess injury risk in automotive applications, where the lower leg is typically instrumented with upper and lower tibia load cells. Injury risk is typically evaluated using these load cells based on peak axial force (F_z) or the Tibia Index (TI , a calculated metric of forces and moments), and sometimes foot acceleration. There are many limitations to the current methods of assessing injury risk to the lower extremities; injury tolerance testing conducted on cadavers position the lower leg in a 90° tibia/foot (neutral) posture, while vehicular occupants assume a range of postures while driving [2]. The purpose of this study was to assess the impact response of two common ATD lower legs: the Hybrid III (H3) and Military Lower Extremity (MIL-Lx) under altered ankle postures, to investigate whether this influences safety evaluations.

Methods

The ATDs were suspended at the knee clevis in a pneumatic impacting apparatus. The positioning of the ATDs was controlled *via* an ankle positioner and a force-sensing boot was fitted to each ATD, with sensors grouped by anatomical region and divided into the fore-, mid-, and hindfoot.

Axial impacts were delivered at a target velocity of 6 m/s and duration of 20 ms, intended to be in the range of realistic frontal collision conditions. Each ATD was impacted in seven ankle postures: neutral, 10°- and 20°-plantarflexion, 10°- and 20°-dorsiflexion, 15°-eversion with 10°-external rotation, and 15°-inversion with 10°-external rotation. Five repeated impacts were conducted at each posture. All data, including the two 5-axis tibia load cells and eight boot insole sensors, were recorded at 50 kHz.

Results and Discussion

The average impact velocity of the 70 impacts was 5.89 ± 0.16 m/s. For the impacts in which the ankle was positioned in

varying degrees of flexion, the footplate acceleration was 125 ± 10 G for the H3 and 127 ± 8 G for the MIL-Lx, showing no significant difference between ATD models ($p=0.43$). The impact duration was significantly higher ($p<0.05$) in the MIL-Lx (23.0 ± 2.0 ms) than the H3 (17.2 ± 1.0 ms). The H3 recorded significantly higher forces than the MIL-Lx in each posture (Figure 1).

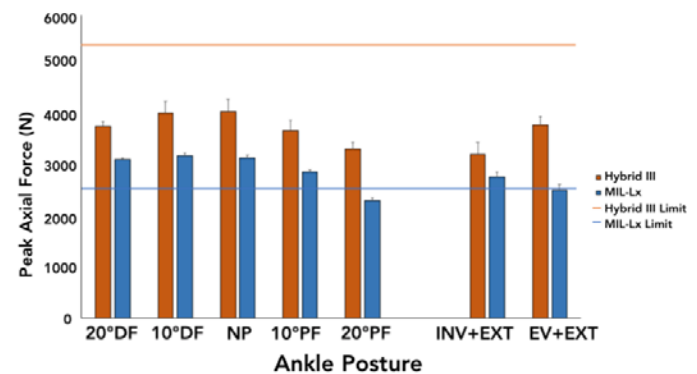


Figure 1: Peak axial force measurements in the tibia. The limits of each ATD are associated with a 10% risk of injury, indicating a passing or failing test.

The peak axial force showed a decreasing trend as the ankle was moved from dorsiflexion through neutral and into plantarflexion. Interestingly, the H3 would have ‘passed’ all tests, while the MIL-Lx would have ‘failed’ all tests, suggesting the two surrogates and their respective injury criteria are not equivalent. The MIL-Lx generally had a decreasing TI as the foot moved from a dorsiflexed ankle posture through to plantarflexion.

When examining the distribution of the load across the plantar surface of the foot, the hindfoot carried most of the load (average 72%). As the ankle rotated from neutral into plantarflexion, a portion of the hindfoot load was transferred to the other regions, primarily the forefoot.

Conclusions

This study emphasized the importance of selecting an appropriate surrogate as well as considering initial ankle posture when conducting safety testing for the lower extremity. This study also highlighted the importance of developing regional injury criteria for the foot and moving beyond the gross measures indicating global mechanics.

References

- [1] Yoganandan N et al. (2015) *Accidental Injury: Biomechanics and Prevention*; Springer Science + Business Media.
- [2] Behr M et al. (2009). *Accid. Anal. Prev.* **42**: 797-801

Knee biomechanics of single leg hop landings after primary anterior cruciate ligament repair and InternalBrace™ augmentation

Birte Coppers^{1,2}, Linda Bühl^{1,3}, Sebastian Müller¹, Corina Nüesch^{1,3,4,5}, Geert Pagenster⁶, Annegret Mündermann^{1,3,4,5}, Christian Egloff¹

¹Department of Orthopaedics and Traumatology, University Hospital Basel, Switzerland; ²Institute of Sport and Sports Science, Karlsruhe Institute of Technology, Germany; ³Department of Biomedical Engineering, University of Basel, Switzerland;

⁴Department of Clinical Research, University of Basel, Switzerland; ⁵Department of Spine Surgery, University Hospital Basel, Switzerland; ⁶Praxis Clarahof, Basel, Switzerland

Email: birte.coppers@googlemail.com

Summary

In this study patients 2 years after primary anterior cruciate ligament (ACL) repair with ligament augmentation showed no relevant deficits in knee biomechanics of their affected leg during landing from a single leg hop (SLH) compared to their contralateral leg and healthy controls.

Introduction

Good clinical outcomes and patient reported data after ACL repair with ligament augmentation have been reported [1,2]. However, the functional outcome of primary ACL repair with ligament augmentation is unknown. The aim of this study was to compare kinematics and kinetics during landing from a SLH between the affected and contralateral knee in patients after primary ACL repair with InternalBrace™ (Arthrex GmbH, USA) and with the non-dominant knee in healthy controls.

Methods

Ten patients 2 years after surgery (5f/5m; age: 32.2±8.7 years; BMI: 22.8±2.9 kg/m²; Tegner-Activity-Score: 4.6±1.1; IKDC: 89±9) and 10 age and sex matched controls (5f/5m; age: 31.8±9.0 years; BMI: 24.4±5.0 kg/m²; Tegner-Activity-Score: 4.4±2.0; IKDC: 98±3) performed SLHs for distance. Participants were instructed to jump for maximal distance and maintain balance for 2 seconds after landing. Knee kinematics and kinetics (sagittal plane) were recorded for five trials with a motion capture system (VICON, UK) using the plug-in-gait model and two force plates (Kistler AG, Switzerland). Data of the trial with the greatest distance was used for further analysis. Joint angles, power and ground reaction force parameters were compared within patients and between the affected leg of patients and the non-dominant leg of healthy controls using t tests (P<0.05).

Results and Discussion

We found no significant differences in the knee parameters between the affected and contralateral leg in patients (P>0.183) (Figure 1 a). Kinematic and kinetic parameters of the affected knee in patients did not differ significantly from those of the non-dominant knee in healthy controls (patients vs. controls; jump distance: 1.21±0.32 m vs. 1.21±0.34 m, P=0.778; flexion angle at initial contact: 12.8±6.4° vs. 13.4±6.0°, P=0.830; peak flexion angle: 54.9±15.6° vs.

56.4±6.6°, P=0.788; range of motion: 42.2±10.3° vs. 43.0±7.8°, P=0.836 (Figure 1 b); peak knee power: 6.6±4.9 W vs. 8.6±5.3 W, P=0.391; peak vertical ground reaction force: 377±96% body weight vs. 380±110% body weight, P=0.948). The variability especially in peak knee flexion angle was much greater among the affected legs of patients than among their contralateral leg and among controls.

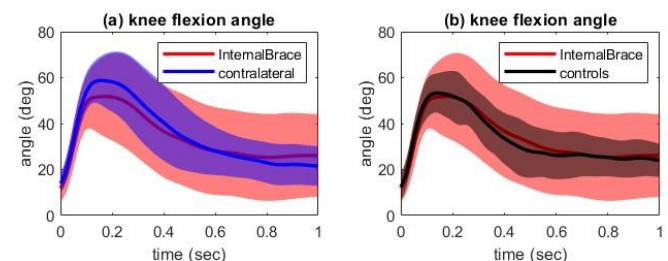


Figure 1: Knee flexion angle during first second after initial contact (0 sec) for the affected leg compared to patients' contralateral leg (a) and to non-dominant leg of controls (b).

Overall, the movement strategy and functional condition of the knee during landing appeared to be comparable to healthy knees, which is in contrast to previous results for patients after ACL reconstruction [3,4]. The biomechanical analysis further reflects comparable result of the jump distance between patients and controls.

Conclusions

This result is promising and supports the choice of surgical treatment of proximal ACL rupture with primary repair and InternalBrace™. Further studies are required to strengthen these results, to further explore the variability within the groups and to understand the role of proprioception, muscle strength and muscle coordination in the landing biomechanics from jumps in patients after ACL repair.

Acknowledgments

Funding: Department of Orthopaedics and Traumatology, University Hospital Basel; Deutsche Arthrose-Hilfe e.V.

References

- [1] Bodendorfer et al. (2017). *J Orth Rhe Sp Med*, **3**: 111
- [2] van Eck et al. (2018). *Am J Sports Med*, **9**: 2291-2298
- [3] Kotsifak et al. (2019). *Br J Sports Med*, **3**: 139-153
- [4] Lepley et al. (2018). *J Athl Train*, **2**: 144-159

New home exercise program for the Swiss Box Lacrosse National Team

Janis Brogle¹, Stephanie Ledermann¹ Philippe Merz² Beat Göpfert³

¹Health Division, Bern University of Applied Sciences, Bern, Switzerland

²BZG, Bildungszentrum Gesundheit Basel-Stadt, Münchenstein; Switzerland

³Department Biomedical Engineering, University of Basel, Basel

Email: janis.brogle@hotmail.com, stephanie.ledermann@bluewin.ch

Summary

Injury prevention is important in sport, unfortunately it is often forgotten in the daily routine. This quality control study of the new home exercise program of the Swiss national box lacrosse team was done as a physiotherapy bachelor thesis.

For this, the dynamic balance and strength of the shoulder external rotators of the throwing arm was measured at three points in time. Additionally, the influence of co-variables on the measurement results was analyzed.

Introduction

The Swiss Box Lacrosse National Team introduced a new home exercise program for injury prevention in view of the upcoming World Championship 2019 and due to many "non-contact" injuries during the last season. The prevention program addresses the most common injuries to the foot, knee and shoulder [1,2].

Methods

At three points in time, dynamic balance was measured with the Y-Balance Test. Additionally isometric strength of the shoulder external rotators of the throwing arm was measured with a handheld dynamometer.

The first phase served as a control phase and included the usual training. From the measured differences of the second phase, which served as the intervention phase, the differences of the first phase were subtracted to eliminate natural changes. This resulted in the final differences, which were tested for significance.

Various co-variables from the training diary, a health questionnaire and the implementation frequency of the new home exercise program were recorded and tested for a relationship with the changes in the measurement results.

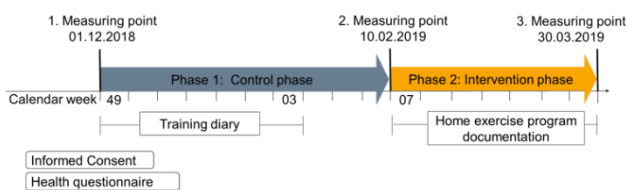


Figure 1: Quality control timeline

Table 1: final difference [Δ Phase 2 (3. measuring point – 2. measuring point) – Δ Phase 1 (2. measuring point – 3. Me measuring point)]

Total of participants (n=18)	Final difference Y-Balance left (%)	Final difference Y-Balance right (%)	Final difference Force measurement (Newton)
Mean (SD)	1.79 (6.08)	0.654 (5.86)	3.83 (62.9)
Median [Min, Max]	0.165 [-6.07, 16.0]	1.25 [-9.19, 12.4]	14.0 [-146, 107]
p-value	0.34	0.28	0.71

Results and Discussion

In 18 included subjects, the one-sample Wilcoxon test did not detect a significant change for either the Y-balance test or the isometric strength measurement of the external shoulder rotators at a significance level of 0.05. The p-values are 0.34 for the Y-balance test on the left, 0.28 for the Y-balance test on the right and 0.71 for the force measurement.

Only by means of Stepwise Model Selection a correlation of single co-variables with the final differences could be shown.

Conclusions

After the seven-week implementation of the home exercise program, no significant change in dynamic balance and isometric strength measurement of the external shoulder rotators was achieved. Lack of compliance, a small sample size and the quality criteria of the strength measurement doubt concerning the validity of the results [3,4]. The influence the co-variables have on the results cannot be determined in this study. Finally, we recommend paying more attention to the topic of injury prevention including the reliable implementation.

Acknowledgments

Swiss national box lacrosse team and team manager Mario von Jackowski

References

- [1] Staff of the Swiss Box Lacrosse National Team (2018). *modified prevention program*. 
- [2] Webb et al. (2014). *Orthopaedic Journal of Sports Medicine*.
- [3] Cools et al. (2014). *Journal of Shoulder and Elbow Surgery*, **23**: 1454-1461.
- [4] Riemann et al. (2010). *Journal of Shoulder and Elbow Surgery*, **19**: 1175-1183

Experimental Investigation of Human Head Interaction with Deformable Elastoplastic Unsecured Object placed in the Vehicle during Vehicular Frontal Crash

Jaroslav Hruby^{1,2}, Brad Parker Wham^{2,1}, Denek Krobot^{3,1}, Aldrich Galerian^{4,1}, Marek Semela^{5,1}

^{1,5}Institute of Forensic Engineering, Brno University of Technology, Brno, Czech Republic

^{2,4}Center for Infrastructure, Energy, and Space Testing, CU Boulder, Boulder, Colorado, United States of America

³Department of special and Combat Vehicles, Brno University of Defense, Brno, Czech Republic

Email: info@isb2021.com

Summary

The presented study described in this abstract deals with human head interaction during a vehicular frontal crash with the unsecured deformable object (impactor) placed in the vehicle. The primary study focuses on head injury determination through Head Injury Criterion (HIC) calculation and comparison of the HIC calculation with the well-known value of HIC equal to 1000. The value of HIC equal to 1000 represents a potential injury risk with a dangerous effect on the human health condition [1], [2].

Introduction

The study presented in this abstract deals with a familiar situation, when people are going on a trip via vehicle and place their luggage or objects of daily use in the car. When a vehicle accident happens, these objects are acting as projectiles with high kinetic energy. If these objects interact with vehicle occupant bodies, they may cause a severe injury.

The frontal vehicular crash situation is described with a focus on unsecured object vs. human head direct interaction. [1] The unsecured object assumed for the study is a plastic bottle, which is fully filled out with water without internal pressure. The bottle has a deformable body – elastoplastic effect. The model of the vehicle occupant is the Hybrid III 50th percentile male dummy for the frontal crash.

Methods

An experimental approach was used [1]. The experimental setup had these parts: Airgun (with pressure vessel and optical measuring barriers) Nylon body projectiles with different mass (0.5 [kg], 1 [kg], 1.5 [kg]) and plastic bottle deformable impact part Hybrid III 50th percentile male dummy with instrumentation vehicle seat with restraint system DA system DEWE A4.

HIC values (15 [ms]) were calculated through software NI DIADEM, including Crash Analysis Toolkit (specific math modules). HIC is calculated through formulas (1) and (2) [2].

$$HIC = \max_{t_1, t_2} \left\{ \left(\frac{1}{t_2 - t_1} \int_{t_1}^{t_2} a \, dt \right)^{2.5} (t_2 - t_1) \right\} \quad (1)$$

$$a = \sqrt{a_x^2 + a_y^2 + a_z^2} \quad (2)$$

The symbol a in Eq. (1) represents resultant head acceleration, and it is calculated from Eq. (2), where a_x , a_y , and a_z are components of "resultant" acceleration. Symbols t_1 and t_2 are a time interval for the HIC calculation process (15 [ms]).

Results and Discussion

Obtained experimental results show that the critical value of HIC is in impactor velocity interval from 40 [km/h]/1.5 [kg] to 50 [km/h]/ 1.0 [kg]. For an impactor with a weight of 0.5 [kg], the critical HIC value of 1000 was not obtained due to the airgun capabilities relying on the airgun pressure system construction. Figure 1 shows obtained experimental results in a graphical form with approximation curves from which higher HIC values and relating impactor velocities can be calculated – for impactors with a mass around 0.5 [kg].

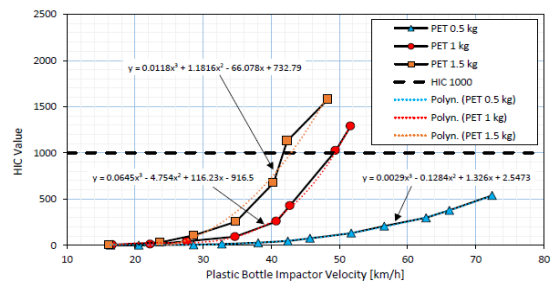


Figure 1: HIC (15 ms) values Obtained from Experimental Analysis and their Comparison with Critical HIC value 1000

The presented experimental study focuses only on the human head interaction with loosen object/impactor and is not taking into account interactions with airbags and other parts of the vehicle body. Also, the water behavior in the bottle is neglected when the bottle is filled out with water randomly – a verification study will be performed.

Conclusions

The study describes the head injury potential of a special type of impactor acting on a human head. Obtained results show the importance of the solved problem, but other experiments should be performed to understand and cover it.

References

- [1] Hruby J. et al. (2020). *vASB2020*, 5, 785.
- [2] G. Mc Henry, *ATB Users Group*, 18, 20

Table 1: Experimental Data Describing Critical Impactor Velocity Interval (and Mass) in which HIC (15 ms) Value 1000 is Expected

Velocity Interval/Mass [km/h]/[kg]	-/0.5	Velocity Interval/Mass [km/h]/[kg]	42.8 to 49.5/1.0	Velocity Interval/Mass [km/h]/[kg]	40.3 to 42.3/1.5
HIC Value Interval [-]	-	HIC Value Interval [-]	429 to 1023.2	HIC Value Interval [-]	675.6 to 1129.5

Influence of a Mixed Reality training on gait in people with mental disabilities

Laly Alexis^{1,2}, Biard Jean-Clément², Tixier Pierre-Alexandre², Ferrari Alexandra², Rosnet Elisabeth¹, Houel Nicolas¹

¹Université de Reims Champagne Ardenne, PSMS EA7507, Reims, France

²Laboratoire de Recherche et d'Etude sur le Mouvement, Nevers, France

Email: alexis.laly@univ-reims.fr

Summary

The aim of this study was to assess the impact of a three-month non-invasive weekly Mixed Reality (MR) activity on the gait of people with mental disabilities. Gait and cognition were analyzed before (T0) and after (T3) training. At T3, the subjects' walking speed, Walk Ratio, Functional Ambulation Performance Score and stride length had significantly increased, showing an improvement in gait mobility and stability. Cognition score has been maintained.

Introduction

Although not included in the diagnosis, people with mental or cognitive disabilities are subject to motor impairments. Cognitive and motor systems are interlinked. For instance, training working memory can increase the walking speed of ageing people [1]. From these cognitive-motor interactions, combined with recent technological developments, new therapeutic approaches are emerging. This includes Mixed Reality, whereby a headset can be used to superimpose virtual holographic elements with which it is possible to interact, on the real environment.

A MR activity can improve balance in healthy subjects [2], but its influence on the motor skills of mental disabled people has not been proved yet. The hypothesis is that cognitive-motor training using Mixed Reality will improve the subjects' motor skills objectified by gait parameters.

Methods

Eight residents from a home for disabled adults (mean±SD: age = 51.5±15.7 years old, height = 1.6±0.1 m, mass = 55.8±8.0 kg) participated to the study. Gait spatiotemporal parameters (STP) were assessed with a Zeno™ walkway gait analysis system and cognition was evaluated using MoCA (Montreal Cognitive Assessment) before (T0) and after (T3) training. The three-month weekly intervention consisted in using the application PopBallons™ (Actimage, France) on a Microsoft HoloLens 2® MR device for 15 to 25 minutes. Its purpose is to find, walk to and pierce virtual balloons with the finger. Both cognitive and motor functions are thus stimulated.

T3-T0 differences distribution normality was tested with a Shapiro-Wilk test. The significance of the changes in gait STP was therefore tested with a Student's t-test and a Wilcoxon test was used for the MoCA score difference.

Results and Discussion

Gait speed, Walk Ratio, Functional Ambulation Performance Score (FAPS) and stride length have significantly increased

after the three-month Mixed Reality intervention (Table 1). Mobility, balance, and gait stability seem to be enhanced, which is in line with previous studies results [1,2].

Table 1: Gait STP and MoCA before and after MR training

	T0		T3		p-value (*p < 0.05)
	Mean	SD	Mean	SD	
Speed (m/s)	0.63	0.21	0.75*	0.29	0.049
Stride Length (cm)	74.18	18.67	85.33*	22.27	0.018
Walk Ratio (cm/(step/min))	0.38	0.10	0.42*	0.07	0.012
FAPS	73.63	18.75	78.75*	18.66	0.029
MoCA	6.25	4.46	6.50	5.66	0.957

The current study's gait speed mean change (+19%) is similar to Azadian et al. (+22%) in which the activity carried out was only cognitive, but the training load was much higher (3*45min/week). Thus, a cognitive-motor Mixed Reality training appears more efficient than an only cognitive one to improve motor skills. Although riskier than computerized cognitive exercises, this MR task shows less risk and physical demands than traditional physical activity for frail people.

This greater effect might be due to the dual task character of the MR activity. Indeed, it has been shown that dual task training can improve both cognitive and motor functions [3]. Contrary to de Andrade et al. results, the current study does not reveal any MoCA improvement. Their intervention lasted nevertheless longer. The MoCA score might thus increase later in the case of a longer MR intervention. In any case, cognition did not significantly decrease.

Conclusions

To conclude, a three-month weekly Mixed Reality cognitive-motor training improves gait parameters in people with mental disabilities in spite of a low training load. Further research should focus on how MR could also improve cognition, with higher training loads or different MR activities.

Acknowledgments

We would like to thank Corinne Charbonnier and Thierry Le Goaziou, respectively president and director of Adapei 58, Lucile Ribet director of the "foyer de vie pour adultes handicapés Le Clos, Adapei 58, Saint-Andelain, France" and the whole caring staff.

References

- [1] Azadian et al. (2018). *J Bodyw Mov Ther*, **22**: 881-887.
- [2] Glueck and Han (2020). *Virtual Real*, **24**: 223-229.
- [3] de Andrade et al. (2013). *JAGS*, **61**: 1919-1926.

Gait asymmetry results in symmetric relative efforts between affected and unaffected side musculature in children with hemiplegic cerebral palsy

Kulmala JP¹, Haakana P¹, Nurminen J¹, Elina Ylitalo¹, Niemelä T¹, Marttinen-Rossi E¹, Mäenpää H¹ & Piitulainen H^{1,2}

¹Motion Laboratory, New Children's Hospital, University of Helsinki and Helsinki University Hospital, Helsinki, Finland.

²Faculty of Sport and Health Sciences, University of Jyväskylä, Finland.

Email: juhapekka.kulmala@gmail.com

Summary

Tendency to minimize the energy cost of walking is thought to be a central factor in determining the way individuals walk. However, the recent study on post stroke individuals suggest that factors other than energy cost minimization may gain importance in determining gait pattern among clinical populations [1]. The present study in children with hemiplegic cerebral palsy suggest that the preference of asymmetric gait pattern may arise from tendency to equalize relative efforts between affected and unaffected side musculature.

Introduction

Self-optimization hypothesis predicts that the central nervous system innately coordinates limb movements so that the resulting gait patterns coincide with the minimal energy expenditure. Evidence for this comes primarily from studies on unimpaired locomotion, which have shown that humans (and animals) self-select many gait parameters to minimize their energy expenditure, and even a small perturbation to preferred gait pattern, such as asymmetry, altered step length or width, increase the energy cost of walking. [2]

However, the recent findings of Nguyen et al. (2020) on post stroke individuals suggest that factors other than energy cost minimization may gain importance in determining preferred asymmetric gait pattern among clinical populations. The authors noted that persons with chronic stroke self-select an asymmetric gait despite being capable of walking more symmetrically; however, the energy cost of walking does not seem to be a central driver in gait asymmetry, because it did not differ between the self-selected asymmetric versus more symmetric gait, which was achieved using biofeedback. [1]

We hypothesized that a tendency to equalize relative efforts between affected and unaffected side musculature may be an important factor to explain the preference of asymmetric gait. We used children with hemiplegic cerebral palsy (CP) as a model to study this idea, because they walk asymmetrically due to compromised neuromuscular function of the affected side lower limb [3].

Methods

We examined gait pattern asymmetries and relative muscle efforts of the ankle and knee extensors between unaffected versus affected lower limbs in children with hemiplegic CP. Ten children with hemiplegic CP (13 yrs.) and 10 healthy peers (13 yrs.) performed gait and maximal two-leg hopping in motion analysis laboratory. To quantify relative efforts, muscle moments generated by knee and ankle extensors were quantified during gait and then related to maximum moments generated by the same muscle groups during the hopping test.

Results and Discussion

During walking at self-selected speed (1.22 ± 0.08 m/s) hemiplegic CP children demonstrated 0.04 s shorter contact time ($p=0.004$) and tendency towards smaller step length (2.1 cm, $p=0.1$) on the affected side compared to unaffected side. In the affected side, the walking-related ankle and knee extensor moments were 14% ($p=0.002$) and 41% ($p=0.007$) lower, respectively, compared to unaffected side (Fig. 1A). During all-out hopping test, the maximal moments developed in the affected side were 17% ($p=0.033$) and 27% ($p=0.021$) lower, respectively, in the ankle and knee extensors (Fig. 1B). However, no differences were found in the relative ankle ($p=0.103$) and knee ($p=0.292$) extensor muscle efforts in the affected versus unaffected lower limbs (Fig. 1C). This suggest that by shifting muscular contributions from the affected side to the unaffected side, children with hemiplegic CP can equalize the relative muscular efforts between limbs in walking.

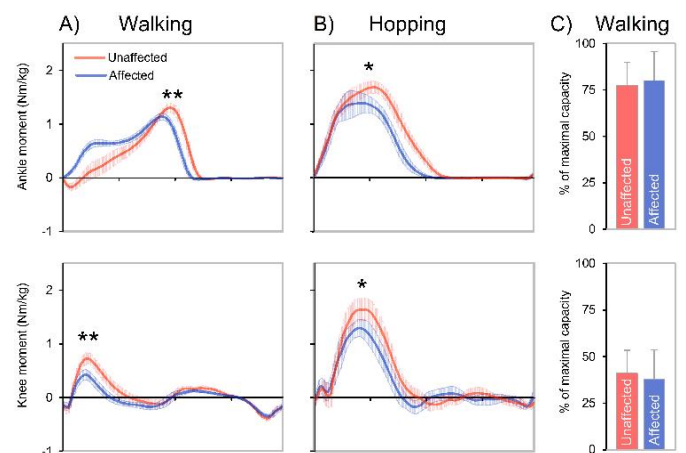


Figure 1. Muscle moments and relative efforts of the ankle and knee extensors.

Conclusions

Asymmetric gait in children with hemiplegic CP results in symmetric relative muscle effort in affected versus unaffected side ankle and knee extensors, which is likely an important strategy to prevent locomotor-induced muscle fatigue. These observations may also explain why gait asymmetry tend to be a very persistent in children with hemiplegic CP and why they often fail to adopt better, more symmetric gait patterns.

References

- [1] Nguyen et al. Journal of Neuro Engineering and Rehabilitation 2020
- [2] Saibine & Minetti. EJAP 2003
- [3] Riad et al. Clin Orthop Relat Res 2012

The effect of lower limb loss on the stability and variability of kinematics and muscle activations during walking

Natalie L. Egginton¹, Laura-Anne M. Furlong¹, Paul W Sanderson¹, Baihua Li², Matthew T.G. Pain¹

¹School of Sport, Exercise and Health Sciences, Loughborough University, UK

²School of Computer Science, Loughborough University, UK

Email: n.l.egginton@lboro.ac.uk

Summary

Maximum short and long term finite time Lyapunov exponents were estimated to determine stability of lower limb kinematics and muscle activations in lower limb amputees (AMP) and compared to able-bodied (AB) participants. Shank loss increases bilateral muscle activation variability and prosthetic limb ankle and bilateral hip angle instability.

Introduction

Typically, pathological gait is identified by comparing averaged gait cycles to a norm with variability defined as the standard deviation (SD) between cycles. These analyses assume cycle independence and that variation is random, contradicting the inherent dynamic nature of gait. Local stability quantifies the systems corrective response to perturbations. Knowledge of lower limb AMP gait dynamics may help prevention of falls. This study aimed to compare the stability and variability of AMP kinematics and muscle activations during walking to AB individuals.

Methods

Marker motion (250 Hz) and electromyography (EMG; 2000 Hz) data for twelve AB (male) and three unilateral transtibial AMP (2 male) participants, who had provided informed consent, were recorded during at least 15 mins of treadmill walking (AB: four, 4 minute, AMP: three, 5 minute trials) at overground preferred walking speed (AB: $1.46 \pm 0.2 \text{ m}\cdot\text{s}^{-1}$, AMP: $1.46 \pm 0.1 \text{ m}\cdot\text{s}^{-1}$). EMG was recorded from bilateral ankle (tibialis anterior, soleus, gastrocnemius lateralis and medialis), knee (rectus femoris, vastus lateralis, biceps femoris long head, semitendinosus) and hip (rectus femoris, biceps femoris long head, semitendinosus, gluteus maximus) musculature, locations determined with ultrasound.

Marker trajectories were lowpass filtered (12.2 Hz) and lower limb joint angles were calculated. Gait events were determined by kinematic algorithms [1,2]. EMG with impact spikes were replaced with a common signal matched for duration that preserved temporal features. EMG were: band pass filtered (20 – 450 Hz), demeaned, amplitude normalized, rectified, low pass filtered (6Hz), down sampled (250 Hz).

Trials were divided into two, 2 minute segments. Signals were time normalised to 101 data points. SD was calculated across the gait cycle and mean SD obtained. Maximum short (λ^*_s , 0 to 1 strides) and long (λ^*_L , 4 to 10 strides) term finite time Lyapunov exponents [3] were estimated to determine stability. Phase space was reconstructed using a time delay method. Optimal time lag and embedding dimension were determined by averaged mutual information [4] and false nearest neighbour [5]. EMG phase space was reconstructed in 8 dimensions, four joint muscle signals and time delay copies.

Results and Discussion

AB kinematic stability and variability were bilaterally similar and agree with previous literature [6]. AMP kinematic λ^*_s

differed from AB for the prosthetic limb ankle and bilateral hip (Table 1). Elevated prosthetic limb ankle angle λ^*_s implies increased instability and a slowed response to perturbations, due to the absence of a control system. Prostheses had repetitive joint movement, indicated by reduced variability (intact: $1.4 \pm 0.3^\circ$, prosthetic: $0.8 \pm 0.2^\circ$). Increased AMP hip angle λ^*_s may be due to a compensatory mechanism for the instability from the prosthesis, this instability was not reflected in the variability.

AMP EMG stability variables were comparable to AB (Table 1). All intact and prosthetic limb muscles displayed increased variability compare to the mean AB limbs (mean increase 25% and 41%, respectively).

Table 1: Mean (top) and standard deviation (bottom) of mean amputee (AMP, I: intact, P: prosthetic limb) and able-bodied (AB, L: left, R: right limb) bilateral short (λ^*_s) and long (λ^*_L) term Lyapunov exponents for joint kinematics and muscle activations.

		Ankle		Knee		Hip			
		λ^*_s	λ^*_L	λ^*_s	λ^*_L	λ^*_s	λ^*_L		
Kinematics	AB	L	0.52	0.06	0.96	0.08	0.66	0.07	
		R	0.09	0.01	0.07	0.01	0.08	0.01	
	AMP	I	0.49	0.06	0.99	0.08	0.66	0.07	
		P	0.12	0.01	0.07	0.01	0.11	0.01	
	EMG	AB	L	0.57	0.05	0.97	0.07	0.79	0.06
			R	0.08	0.01	0.06	0.01	0.14	0.01
AMP		I	0.83	0.06	0.96	0.06	0.73	0.06	
		P	0.11	0.01	0.04	0.01	0.14	0.01	
EMG	AB	L	0.23	0.04	0.22	0.03	0.22	0.03	
		R	0.03	0.01	0.03	0.01	0.03	0.01	
	AMP	I	0.23	0.03	0.23	0.03	0.23	0.03	
		P	0.03	0.01	0.05	0.01	0.06	0.01	
	AMP	I	0.24	0.03	0.25	0.03	0.25	0.03	
		P	0.01	0.01	0.00	0.00	0.01	0.00	
				0.21	0.02	0.21	0.02		
				0.03	0.01	0.03	0.01		

Conclusions

Lower limb loss increased prosthetic limb ankle and bilateral hip kinematic instability. No effect on muscle activation stability was observed but intact and prosthetic limb variability increased.

Acknowledgments

Funding Engineering & Physical Sciences Research Council.

References

- [1] Zeni JA. *et al.* (2008). *Gait Posture*, **27**: 710-714.
- [2] De Asha AR. *et al.* (2012). *Gait Posture*, **36**: 650-652.
- [3] Rosenstein MT. *et al.* (1993). *Physica D*, **65**: 117-134.
- [4] Fraser AM. (1986). *Dimensions and Entropies in Chaotic Systems*; Springer.
- [5] Kennel MB. *et al.* (1992). *Phys. Rev. A*, **45**: 3403-3411.
- [6] Dingwell JB. *et al.* (2001). *J Biomech Eng.*, **123**: 27-32.

□ Hip contact forces in paediatric patients with increased femoral antetorsion

□athalie Ale□ander^{1,2}, Elke □iehweger^{3,4,5}, Johannes Cip², Reinald G. H. □runner^{3,4,5}, Enrico De Pieri^{3,5}

¹ Laboratory for Motion Analysis, ² Department of Paediatric Orthopaedics, Children's Hospital of Eastern Switzerland, St. Gallen, Switzerland ³ Laboratory for Movement Analysis, ⁴ Department of Neuro-Orthopaedics, University of Basel Children's Hospital, Basel, Switzerland ⁵ Department of Biomedical Engineering, University of Basel, Basel, Switzerland
Email: enrico.depieri@unibas.ch

Summary

This study analyzed hip contact forces in paediatric patients with increased femoral antetorsion and healthy controls during gait by means of personalized musculoskeletal models based on individual morphological data. Hip contact forces were found to be less medially and less posteriorly oriented during early stance in patients with increased femoral antetorsion.

Introduction

Kinematic and kinetic gait deviations due to increased femoral antetorsion have been described in the literature [1,2]. Passmore et al. compared joint loadings using a generic and subject-specific musculoskeletal model in patients with increased femoral antetorsion and increased tibial torsion [2]. However, no study to date compared joint loadings between patients and controls. Furthermore, the orientation of the intra-articular forces might be of interest with regards to acetabular cartilage damage that could arise during adulthood in concomitance with other morphological alterations, such as femoroacetabular impingement syndrome [3]. Therefore, the aim of the current study was to analyze hip contact forces (HCFs) in patients with increased femoral antetorsion and controls using personalized musculoskeletal models based on individual morphological data.

Methods

Forty-two pediatric patients with isolated, CT-confirmed increased femoral antetorsion (26 females, mean age □ 12.8 years, mean antetorsion □ 39.4°) [1] and 9 healthy controls with MRI-confirmed normal torsion (5 females, mean age □ 12 years, mean antetorsion □ 21°) were included in this retrospective study. Patients were referred to gait analysis because of gait abnormalities going along with an increased femoral antetorsion $\geq 30^\circ$. Kinematic and kinetic data were recorded during 3D gait analysis using the Plug-In Gait model. The collected motion capture data was used as input for an inverse dynamics analysis (Any□ody Technology, Denmark) to evaluate HCFs, reported in a pelvis-based reference frame. Subject-specific models were created from a generic lower-limb model [4], which was scaled according to marker data from a static trial. The modelled femurs were morphed (Figure 1a) to match each subject's femoral antetorsion measurements. Differences in HCF 3-dimensional components between patients and control group were evaluated over the whole gait cycle through statistical parametric mapping (SPM) with two-tailed, two-sample t-tests ($\alpha = 0.05/3$).

Results and Discussion

Statistically significant differences in HCF components were observed between the two groups in various phases of the gait cycle (Figure 1b,c,d). The resulting HCFs were less medially and less posteriorly oriented during early stance in patients with increased femoral antetorsion, even though they also presented an overall lower HCF magnitude.

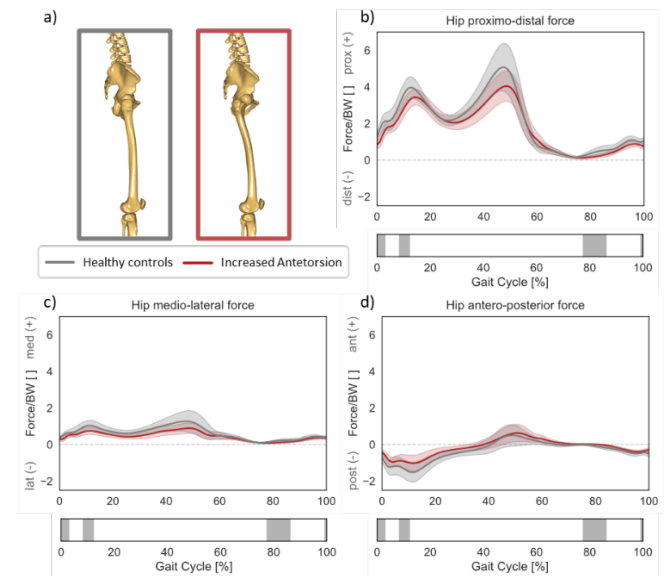


Figure 1: Predicted HCF 3D components in patients with increased femoral antetorsion (red) and controls (grey). Significantly different phases of the gait cycle are indicated below each force component.

Conclusions

A better understanding of the forces that are produced within the acetabulum is necessary to improve individual diagnoses and to optimally plan targeted realignment of the lower extremities. Future work should also focus on investigating how such morphological deformities can affect the mechanics of the adjacent joints and/or potentially impair muscle functionality.

References

- [1] Alexander N et al. (2019). *J Biomech*, **8** □ 167-174.
- [2] Passmore E et al. (2018) *Gait Posture*, **3**: 228-235.
- [3] Pascual-Garrido et al. (2019). *Clin Orthop Relat Res*, **4** □ □ 1021-1033.
- [4] De Pieri et al. (2018) *PLoS ONE*, **13** □ □

Comparison of the post-operative knee abduction-adduction angle measured during surgical navigation and treadmill gait: A preliminary study

X. Gasparutto¹, A. Bonnefoy-Mazure¹, R. Dumas², S. Armand¹, H. Miozzari³

¹Kinesiology Laboratory, Geneva University Hospitals, University of Geneva, Geneva, Switzerland

² Univ Lyon, Université Claude Bernard Lyon 1, Univ Gustave Eiffel, IFSTTAR, LBMC UMR_T9406, F69622 Lyon, France

³Dept. of orthopaedic surgery and trauma care, Geneva University Hospitals, Geneva, Switzerland

Email: xavier.gasparutto@hcuge.ch

Summary

Computer-assisted surgery (CAS) can provide real-time feedback of the knee kinematics during surgery. Understanding the link between this passive kinematics and the knee kinematics during gait could help surgeons evaluate the quality of the surgery. This study compared the adduction-abduction (AA) angle assessed by the surgeon during surgical navigation to AA during gait after total knee arthroplasty (TKA) for 8 patients. This preliminary study showed fair to moderate correlations between those angles but needs further investigations to increase the number of patients and clarify the results.

Introduction

Computer-assisted surgery (CAS) is intended to improve the accuracy and precision of component position and leg alignment during TKA [1], especially the correction of the knee AA angle [1]. During surgery, the surgeon has a real-time feedback of multiple parameters such as the passive knee range of motion, AA angle in function of the flexion, or ligament balance. The intra-operative passive movements applied by the surgeon to assess the knee function was showed to have no significant differences with an active movement without loading in a recent study [2]. However, there is currently no evidence that knee kinematics evaluated during this passive movement is similar to the knee kinematics during weight-bearing activities such as gait. Thus, the objective of this study is to compare AA angles assessed by the surgeon during surgical navigation to AA measured during gait after TKA.

Methods

Eight patients (median [IQR], 72 [10] years old, 159.0 [16.4] cm, 76.0 [49.7] kg, 6 females) undergoing primary TKA participated in this preliminary study. During surgery, after definitive TKA implantation, passive flexion-extension movements were measured with the Knee 3 CAS system (Brainlab, Germany) to assess passive knee kinematics. Three months after surgery, patients performed a standardized treadmill gait analysis [3] (KneeKG, Emovi, Canada) to assess active knee kinematics during walking at a comfortable self-selected speed.

The homogenization of conventions for knee kinematics computation was done based on the ISB recommendations [4]

and used the hip joint centre, medial and lateral femoral epicondyles and malleoli. Knee AA measured with navigation was expressed in function of knee flexion and fitted with a 3rd order polynomial [5]. The knee flexion measured during treadmill gait was used as input in the polynomial to estimate the AA value of navigation for a gait pattern of flexion. Finally, a Spearman correlation was performed between the AA angle curves measured during surgical navigation and treadmill gait for each patient. Correlations were classified in poor ($r < 0.2$), fair ($r: 0.21-0.40$), moderate ($r: 0.41-0.60$), good ($r: 0.61-0.80$) and very good ($r > 0.81$) [6].

Results and Discussion

Three patients had fair correlations and 5 had moderate correlations which indicates a link between passive and active weight-bearing knee kinematics (Table 1). Surprisingly, three correlations were positive and 5 were negative. This could be linked to the multiple differences between the measurements such as: passive and active conditions, intraoperative (with arthrotomy) and normal, closed condition, intra-cortical pins and external harness to fixate motion capture markers, or the pointing of the epicondyles: on the bone for navigation and on the skin for treadmill gait.

Conclusions

The results indicate a link between passive knee kinematics and active weight-bearing knee kinematics during gait. However, this preliminary study needs further investigations to increase substantially the number of patients and understand the differences in correlations sign between patients.

Acknowledgments

This study was funded by the 'Fondation Privée' of the Geneva University Hospitals .

References

- [1] Jones CW et al. (2018). *J. Arthro.*, **33**: 1989-93.
- [2] Grassi et al. (2020) *J Exp. Ortho.*, **7**:12.
- [3] Hagemeister et al. (2005), *J. Biomech.* **38**:1926-31.
- [4] Wu et al. (1995), *J. Biomech.* **28**:10:1257-61.
- [5] Walker et al. (1988), *J. Biomech.* **21**:11:965-74
- [6] Altman et al. (1999), *Practical statistics for medical research*, Chapman Ed.

Table 1: Correlation between passive knee AA and active weight-bearing knee AA post-surgery

Patients	1	2	3	4	5	6	7	8
r	-0.42	0.3	-0.3	-0.48	-0.58	0.44	-0.46	0.36
p	0.000	0.002	0.002	0.000	0.000	0.000	0.000	0.000

The change of foot clearance and cognitive performance between single and dual task conditions of healthy older adults and people with Parkinson's syndrome

Ulke Warmerdam¹, T. Eiken¹, Clint Hansen¹, Walter Maetzler¹

¹Department of Neurology, Kiel University, Kiel, Germany

Email: e.warmerdam@neurologie.uni-kiel.de

Summary

People with idiopathic Parkinson disease (IPD) and healthy older adults experience a change in gait and cognitive performance with aging and while performing actions simultaneously, which is common in everyday actions. This study explored the interaction between foot clearance and cognitive performance during dual tasking. IPD patients had higher dual-tasking costs in more complex cognitive tasks than healthy older adults. Healthy older adults prioritized the cognitive task, IPD patients did not prioritize any task.

Introduction

Aging affects gait and cognitive performance. People with idiopathic Parkinson disease (IPD) might even be more affected. Gait and cognitive performance are important factors for quality of life of the affected. One important gait parameter is foot clearance (maximum vertical height of the foot during the swing phase). A smaller foot clearance, as well as a lower cognitive performance can result in an increased risk of falling [1,2]. In everyday life, actions are often performed simultaneously which can potentially lead to an even smaller foot clearance. The aim of this study is to explore the interaction between foot clearance and cognitive performance during dual tasking.

Methods

Ten IPD patients (65 ± 11) and 12 healthy older adults (70 ± 9) were recruited. Gait analysis was performed with a 3D optical motion capture system (Qualisys A, Göteborg, Sweden). Cognitive performance was assessed with two tests on a smartphone: a simple reaction time test and a more complex Stroop-test, where subjects choose the number with the highest value. In the neutral part the numbers are in the same font size, in the congruent part the higher is bigger and in the incongruent part the higher is smaller. Gait was analysed on a 5 m walkway on which subjects repeatedly walked up and down. First these tasks were performed separately (single task) and afterwards the cognitive tests were performed while walking (dual task).

After the measurements, the difference between single-tasking and dual tasking performance was evaluated by calculating the dual tasking costs (DTC)

$$DTC(\%) = \frac{dual\ task - single\ task}{single\ task} * 100$$

Mann-Whitney-U-tests were performed for the comparison of the foot clearance, cognitive performance and the DTC.

Results and Discussion

No significant differences were found between healthy older adults and IPD patients regarding the foot clearance and the cognitive performance. Only for the most difficult testing situation (incongruent part of the Stroop test), the DTC were higher for the IPD group compared to the healthy older adults (Figure 1). Comparing DTC of cognitive performance with DTC of foot clearance showed that IPD patients did neither prioritize foot clearance nor cognition. However, healthy older adults prioritized cognition over foot clearance.

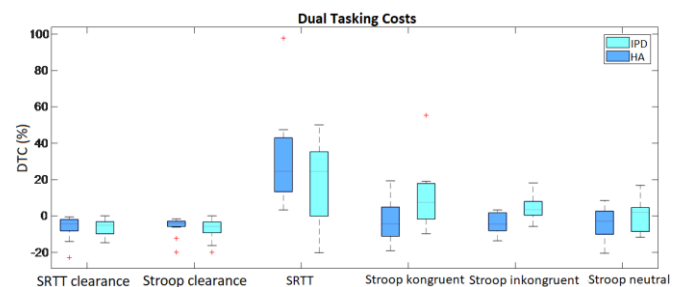


Figure 1: Dual Tasking Costs. IPD = idiopathic Parkinson disease, HA = healthy older adults, clearance = foot clearance during cognitive test, SRTT = simple reaction time test.

The groups did not significantly differ in the Montreal Cognitive Assessment (IPD 26 ± 2; older adults 25 ± 4), which might explain the lack of significant differences between the two groups looking at the cognitive performance. Healthy older adults might prioritize the cognition because of the absence of gait problems, which allows them to concentrate more on the cognitive performance. Vice versa, IPD patients may need to focus more on their gait, and might therefore divide their attention evenly over the cognitive and the walking task.

Conclusions

While there was no significant difference between IPD patients and healthy older adults regarding the foot clearance and the cognitive performance, the DTC of IPD patients were higher in more difficult cognitive tasks. IPD patients prioritize neither foot clearance nor the cognitive performance, while healthy older adults prioritize the cognitive task.

Acknowledgments

This research was funded by Keep Control from the EU's Horizon 2020 research and innovation program under the Marie Skłodowska-Curie grant agreement number 721577.

References

- [1] Alcock et al. (2016). *Journal of Biomechanics*, **49**: 2763-2769.
- [2] J Cohen et al.. (2016) *Maturitas* **93**: 73-77

The Role of Cutaneous Afferents on Mechanically Induced Stretch Reflex Excitability

Kelly A. Robb¹, Jordan D. Hyde¹, Lara A. Green¹, Stephen D. Perry¹

¹Department of Kinesiology & Physical Education, Wilfrid Laurier University, Waterloo, ON, CANADA

Email: robb8660@mylaurier.ca

Summary

Evidence from electrically evoked cutaneous reflexes support the role of foot sole cutaneous afferents in modulating the excitability of spinal motoneurons innervating muscles of the lower extremity. The purpose of this study was to employ a non-electrical method of facilitating cutaneous afferent feedback (adding texture to the walking surface) to investigate its effects on stretch reflex (SR) latency, peak magnitude and integrated EMG of the muscle burst. There was a significant positive relationship in texture response between SR burst and SR peak in both the anterior platform tilt direction ($r=0.495$, $p=0.01$) and the posterior platform tilt direction ($r=0.714$, $p<0.01$). Results of this study highlight the individual responses of cutaneous afferent facilitation on SR excitability.

Introduction

Evidence from electrically evoked cutaneous reflexes supports the role of foot sole cutaneous afferents in modulating the excitability of spinal motoneurons innervating muscles of the lower extremity [1]. This cutaneous reflex facilitation has been limited to electrical stimuli [2]; however, the effect of alternative cutaneous afferent facilitation methods, such as adding textured materials under the foot sole [3], on mechanically induced stretch reflex excitability remains unclear. The purpose of this study was to determine if the addition of texture, as a method of enhancing plantar-surface cutaneous mechanoreceptor feedback, will modify stretch reflex characteristics.

Methods

Thirty healthy young adults (23.2 ± 9 years) participated in 48 block-randomized walking trials of planned gait termination. Cutaneous afferent feedback was either 'non-facilitated' or 'facilitated' (texture added to the walking surface). The walking surface during the second last step of termination was unexpectedly manipulated to tilt in two directions: anterior or posterior. In the anteriorly tilted platform perturbations, the ankle moved into plantarflexion generating a stretch reflex (SR) response in the tibialis anterior (TA) muscle. In the posterior tilted platform directions, the ankle moved into dorsiflexion generating a stretch reflex response in the medial gastrocnemius (MG) muscle. All participants were instrumented with a standardized 12-IREM marker setup and kinematics were recorded with two Optotrak Certus cameras (SF=100Hz). Kinetic and EMG data were measured with three AMTI force plates (embedded flush to the walking platform) and a Noraxon Ultium EMG system (SF=1000Hz). The stretch reflex characteristics were comprised of 3 dependent variables: SR latency, as well as peak amplitude (SR Peak) and total amplitude of the agonist burst (SR burst) (Figure 1).

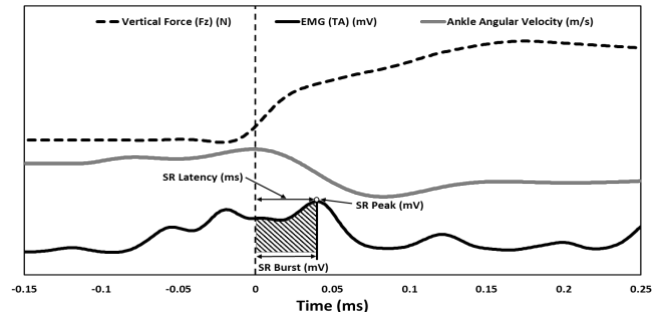


Figure 1: The vertical ground reaction force (F_z), ankle angular velocity, and EMG (TA) were used to calculate the SR latency (time, ms), SR peak (maximum amplitude of muscle burst, mV) and SR burst (integrated EMG, mV).

Results and Discussion

A significant interaction between the direction of platform tilt and cutaneous afferent facilitation on the SR peak ($F_{1,25}=4.25$, $p=0.042$) and SR burst magnitude ($F_{1,25}=8.52$, $p=.004$) was found. There was a significant positive response between SR burst and SR peak texture response in both the anterior platform tilt direction ($r=0.495$, $p=0.01$) and the posterior platform tilt direction ($r=0.714$, $p<0.01$) (Figure 2).

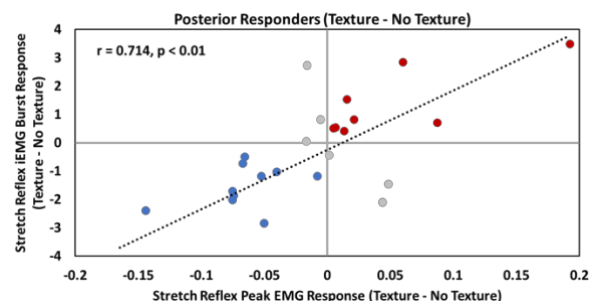


Figure 2: The relationship between responders (positive (red), negative (blue)) and non-responders (grey) in the posterior platform tilt directions between SR Peak and Burst.

Conclusions

As expected, there was no effect of texture on SR latency. Results of this study highlight the individual dependent responses of cutaneous afferent facilitation on SR excitability. This inter-subject variability is important in future studies exploring cutaneous afferent facilitation on SR excitability.

References

- [1] Fallon JB et al. (2005). *J. Neurophysiol*, **94**: 3795-3804.
- [2] Sayenko, DG et al. (2007). *Neurosci. Lett*, **415**: 294-298.
- [3] Viseux, FJ. (2020). *Neurophysiol. Clin*, **50**: 55-68

Application of deep learning based pose estimation methods for clinical gait outcome measures

Logan Wade¹, Laurie Needham¹, Murray Evans¹, Steffi Colyer¹, Darren Cosker¹, James Wilson¹, Polly McGuigan¹
¹Centre for Analysis of Motion, Entertainment Research and Applications, University of Bath, Bath, United Kingdom
 Email: lw2175@bath.ac.uk

Summary

Clinical gait analysis measures were compared between deep learning-based pose estimation methods (OpenPose, AlphaPose and DeepLabCut) and standard marker-based motion capture.

Introduction

Markerless motion capture employs deep learning-based pose estimation methods and has the potential to streamline data collection and processing. Such methods could improve the viability of gait analysis in a clinical environment. Numerous open-source pose estimation algorithms have been developed, but to date no comparison has been made between algorithms to examine their accuracy compared to marker-based motion capture. This study aims to compare clinical gait analysis measures (specifically those related to knee osteoarthritis), to examine if gait analysis performed by open-source markerless methods could be used for clinical applications.

Methods

Fourteen healthy participants performed over-ground constant speed walking while motion capture was obtained from 15 Qualisys cameras and 9 machine-vision cameras at 200 Hz. Image data from each machine-vision camera were processed using OpenPose[1], AlphaPose[2] and DeepLabCut[3]. 2D image plane coordinates from each pose estimation method were back-projected into the 3D space, where the intersect of the back-projected rays were taken to represent the 3D joint centre locations. Right ankle, knee and hip joint-centre locations were used to calculate step length, step width, velocity and planar joint angles over one stride. Outcome measures were compared using Bland-Altman and correlation analysis between marker-based and markerless methods.

Results and Discussion

AlphaPose presented the best agreement with marker derived methods across most variables, followed by OpenPose and DeepLabCut (Table 1). AlphaPose and OpenPose sagittal measures had a lower bias compared to frontal measures (Table 1) and this was especially evident in the frontal plane at the hip, which was systematically offset across the whole

stride for all methods (Figure 1). This systematic offset was likely due to erroneous manual identification of hip joint centre location within the training data of the markerless algorithms. Variability (SD of bias) was at best, 3.5 ° in the sagittal plane and 2.2 ° in the frontal plane, which may be too large to detect small meaningful changes during gait in some clinical conditions (Table 1). Therefore, these open-source methods are likely still too imprecise for many clinical applications.

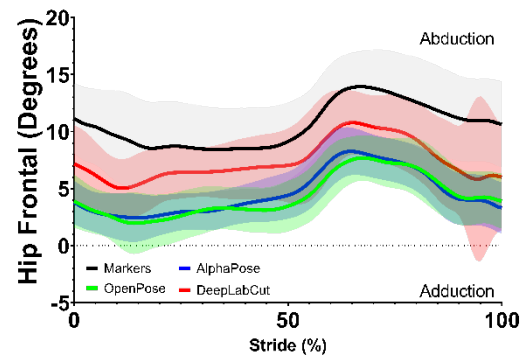


Figure 1: Mean (\pm SD) frontal plane hip joint angle.

Conclusions

The spatial measures produced by AlphaPose and OpenPose may be sufficiently accurate to detect changes in gait, however sagittal variability, frontal accuracy and frontal variability are currently too large for most clinical applications. Researchers and clinicians need to carefully consider the desired outcome measure and accuracy required for their specific application, before implementing these markerless motion capture methods in their current form.

Acknowledgments

This investigation was funded by CAMERA, the RCUK Centre for the Analysis of Motion, Entertainment Research and Applications, EP/M023281/1

References

- [1] Cao, et al. (2019). *IEEE Trans.* 43(1), 172-186.
- [2] Fang, et al. (2017). *In ICCV* (pp. 2334-2343).
- [3] Mathis, et al. (2018). *Nat neurosci*, 21(9), 1281-1289.

Table 1: Bias, standard deviation of bias and R^2 compared to marker-based method. Highlighted cells indicate the best score between methods.

Variable	Bias			SD of Bias			R^2		
	OpenPose	AlphaPose	DeepLabCut	OpenPose	AlphaPose	DeepLabCut	OpenPose	AlphaPose	DeepLabCut
Step Length (mm)	-3	-1	-18	9	8	65	0.989	0.990	0.691
Step Width (mm)	-5	-2	3	6	4	15	0.900	0.943	0.602
Velocity (mm/s)	3	10	-1	19	17	34	0.996	0.997	0.987
Knee Frontal (°)	2.6	2.1	2.2	2.5	2.2	4.3	0.722	0.779	0.410
Knee Sagittal (°)	0.1	-0.4	-0.6	3.5	4.2	8.3	0.973	0.962	0.861
Hip Frontal (°)	-6.2	-9.4	-3.2	2.9	2.8	3.6	0.496	0.508	0.349
Hip Sagittal (°)	3.5	2.8	3.8	3.6	4.2	4.7	0.950	0.934	0.910

Kinematic and gait parameters classification of obesity by means of principal component analysis: a preliminary study

N. Houel^{1,2}, C. Barelle³, C. Grubsztejn², M. Soudain-Pineau¹, S. Hanneton⁴

¹Université de Reims Champagne Ardenne, PSMS EA 7507, Reims, France

²ESO – Recherche, Ecole Supérieure d'Ostéopathie – Paris, Champs sur Marne, France

³Motion Analysis Accuracy and Performance (MAAP), Villeneuve le Comte, France

⁴Institut des sciences du sport Santé (URP 3625 – I3SP), Université de Paris, Paris, France

Email: Nicolas.houel@univ-reims.fr

Summary

Various spatiotemporal parameters alterations are observed in obese subjects. Principal component analysis (PCA) could improve subject's classification reducing optimal set of variables. Kinematics of fourteen subjects (with and without obesity) during walking was recorded. PCA showed that the two main principal components included the same variables: body mass index (BMI) and active range of motion (AROM) of ankle flexion. These variables could explain the different strategies in gait pattern of obese subjects.

Introduction

Obesity prevalence has increased continuously over the past decade. Obese subject's walking is mainly associated with a decrease of speed and various spatiotemporal parameters alterations according to their weight and age [1].

PCA can be used to minimize the optimal variables to be explored. The aim of the study is to propose a functional set of variables classification associated with obesity based on PCA.

Methods

Seven obese subjects (mean \pm standard deviation; age = 34.57 \pm 16.11 years, height = 1.73 \pm 8.19, BMI = 36.11 \pm 4.57) and seven paired normal weight subjects (BMI = 23.7 \pm 2.49) were selected according to their age and height. All subjects voluntarily performed six walking gaits at their preferred velocity. Subjects low body kinematics have been recorded according to an optoelectronic system (Vicon ® Nexus, 8 cameras, 100 Hz) synchronized to two force plates (AMTI ® Accugait, 1000 Hz). AROM were assessed for clinical estimation of: hip flexion and abduction, knee flexion and ankle plantar flexion. Subject speed, stride length, cadence, step length and stride time were also computed.

A normalized and centered PCA has been used to study the relations between the kinematics, spatiotemporal variables and BMI.

Results and Discussion

PCA showed that the two first principal components explained respectively, 74.8% and 23.4% of the result variance. These two principal components included the same variables: BMI and AROM of ankle. For the first principal component, contributions of BMI and AROM of ankle flexion were respectively -67.1% and 73.6%. For the second principal component, contributions of BMI and AROM of ankle were respectively 73.8% and 66.7% (figure 1). Decreasing AROM

of ankle associated with the increase of BMI seem to be the main variables to classify gait pattern of obese subjects.

Alterations in spatiotemporal gait parameters at preferred walking speed in obese adults have been currently reported [1]. Few studies have defined the influence of ankle muscular activity during gait in obese adults [2]. The preliminary results of the present study are in agreement with the hypothesis that ankle plantar flexion could mainly affect gait pattern and velocity of obese subjects at preferred speed [3].

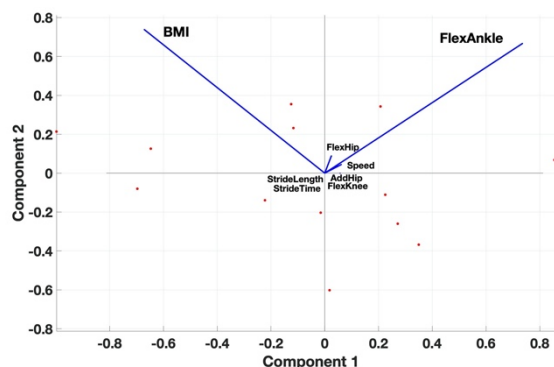


Figure 1: Variables contributions in the two principal components.

The first principal component could present one ankle plantar flexion self-optimization strategy in obese subjects in order to limit knee load associated with overweight [1]. The second component could present the muscular increased and prolonged ankle activities during the support phase in obese subjects [2]. In both cases, ankle play a determinant support to obese subjects in order to compensate AROM restrictions of hip and knee. The increase of subject's recruitment is needed to improve the validity of the PCA results.

Conclusions

PCA showed that BMI and AROM of ankle plantar flexion could be the main variables explaining the different strategies in gait pattern of obese subjects.

Acknowledgments

The authors wish to thank the management of Ecole Supérieur d'Ostéopathie - Paris for their support.

References

- [1] Ko S et al. (2010). *J.Biomech*, **43**: 1104-1110.
- [2] Maktouf W et al. (2020) *Exp.Gerontol*, **140**: 111054.
- [3] Kuo AD and Donelan JM. (2010). *Phys.Ther* **90**: 157-174.

Perturbed Treadmill Walking Effect on Cognitive Vigilance

Alex P. Moorhead¹, Giuseppe Lorenzini¹, Stefano Marelli¹, Enrico Marchetti¹, Marco Tarabini¹
¹Department of Mechanical Engineering, Politecnico di Milano, Milan, Italy
 Email: alexpatten.moorhead@polimi.it

Summary

Whole-body vibration (WBV) as experienced during work, recreation, and transportation, have potentially detrimental consequences on health [1]. The cognitive strain of WBV on subjects during dual tasks is less well known. In order to measure the effect of lateral WBV while walking on cognitive vigilance, a device was designed and manufactured by our lab for subjects to perform a Psychomotor Vigilance Test (PVT) while walking atop a laterally vibrating treadmill. Preliminary results show that PVT reactions times increase (worsen) during vibration, walking, and dual motor tasks, however, return to baseline after testing.

Introduction

Whole-body vibration (WBV) has been established as being potentially dangerous or beneficial depending on the exposure dosage [2]. The human response to vibration has also been shown to be dependent upon both posture and activity [3]. Employees who are exposed to WBV commonly must perform tasks which involve both physical and mental (dual task) vigilance. However, little research has studied the effects of WBV on cognitive performance during dual task scenarios. Understanding this is essential to creating safety and performance guidelines for WBV-exposed employees. To do so, subjects must be safely exposed to WBV while also having their cognitive vigilance evaluated.

Methods

Healthy male subjects 20-40 years old have been recruited to test the effect of lateral WBV on cognitive vigilance. Subjects performed five sessions of Psychomotor Vigilance Tests (PVT) in one day. One baseline PVT session is performed while standing without vibration or walking followed by three PVT sessions in randomized order to avoid a learning effect: walking without vibration, vibration without walking, and walking with vibration (dual task). Subjects then perform a final standing PVT session without walking or vibration. After each session, subjects are given a two minute rest.

To perform the PVT sessions, a custom device was developed using a Wemos Lolin D1 mini board, based on the ESP8266-EX microcontroller, connected to a speaker and two LED panels to create audiovisual stimuli, as well as a custom handheld push button to respond. A custom firmware was developed to manage the PVT device which communicates via Wi-Fi with a custom MATLAB (version R2018b, MathWorks; Natick, Mass., USA) script.

When the test is initiated, a panel of blue LEDs are illuminated while a speaker simultaneously emits a low frequency (LF) tone. After a random period of time (2-9 s) has elapsed, a second panel of green LEDs are illuminated and the LF tone switches to a high frequency (HF) tone. At the moment the

audiovisual stimuli change, the subject must react as quickly as possible by pressing the handheld button. The reaction time is measured by the microcontroller and sent to MATLAB. The system then provides a 1.5 s reset time when the lights and speaker are turned off. The sequence is repeated ten times per minute for five minutes resulting in fifty reaction times per trial session.

Results and Discussion

Preliminary results, as seen in Figure 1, show that both the mean and standard deviations of reaction times during a PVT test are greater when the subject is performing the test during exposure to vibration and is highest when walking.

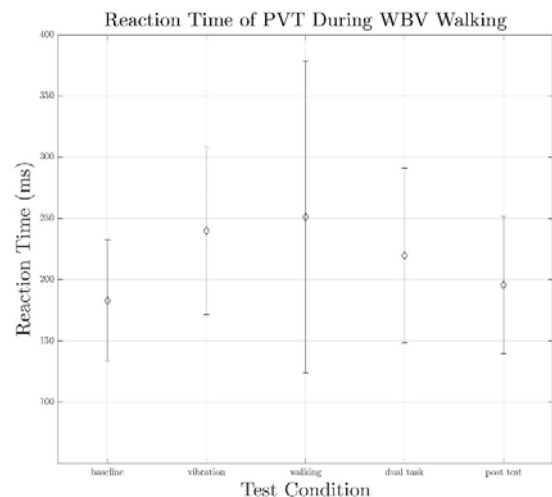


Figure 1: The mean (diamond) and SD (bars) reaction time of PVT tests across the five testing conditions.

Conclusions

While it was expected that dual task walking would result in the greatest increase in PVT reaction times, it appears that walking on its own creates the greatest strain on cognitive vigilance. It can be observed, however, that vibration has a similar (yet lesser) effect as well. Since results are currently preliminary, it will require greater subjects to statistically prove which treatment has the greatest effect on PVT times. Further investigation can help understand the limits of vibration safety as well as the cognitive performance of employees while performing dual occupational requirements.

References

- [1] Krajnak, K., (2018). *J. Toxicol. Environ Health B Crit Review*, **21** (5): 320-334.
- [2] International Standard (1997). *Mech Vib and Shock Eval of Hum Exp to WBV*; ISO 2631-1, **1**, 1:30.
- [3] Chadeaux et al. (2021). *Appl Erg*, **90**: in print

The effect of gait speed on plantar pressure data measured with the GAITRite instrumented walkway

Clara Leyh^{1,2}, Véronique Feipel^{1,2}

¹Laboratory of Functional Anatomy, Université Libre de Bruxelles (ULB), Belgium

²Laboratory of Anatomy, Biomechanics and Organogenesis, Université Libre de Bruxelles (ULB), Belgium

Email: clara.leyh@ulb.be

Summary

94 healthy controls and 125 subjects suffering of low back pain walked at three different self-selected speeds on the GAITRite instrumented walkway to evaluate the effect of gait velocity on plantar pressure distribution. Except for peak time, that decreased, with increasing gait speed, no medial midfoot pressure parameter changed with velocity. Peak pressure and integrated pressure (P*t) behaved almost likewise: they increased at the heel and decreased at the lateral forefoot when changing gait velocity from self-selected preferred gait speed. Contact area increased proportionately with gait speed at the lateral and medial heel and at the medial forefoot. We conclude that the GAITRite can highlight the effect of gait speed on plantar pressure distribution, despite its independence to anatomical landmarks.

Introduction

The GAITRite® walkway is a portable pressure-sensor mat that detects footfalls. Each footprint is represented by the GAITRite software as a quadrangle divided in 12 trapezoids (six medial and six lateral) for which it computes resistive plantar pressure parameters [1]. Since this pressure mat is easily (no patient preparation) and broadly used in clinics [2], it appears interesting to study if plantar pressure parameters, provided for each trapezoid, agree with previously reported data in the literature; with a special focus on the impact of gait speed on plantar pressure [3-4].

The aim of this study was therefore to evaluate, using the GAITRite, a 6,1 m long electronic walkway, the effect of slow, preferred and fast self-selected gait speeds on the evolution of plantar pressure parameters at the lateral and medial heel, mid- and forefoot in healthy subjects and subjects with low back pain.

Methods

94 healthy controls and 125 subjects with low back pain (LBP) walked barefoot three times at three different self-selected speeds (slow, preferred, fast) over the GAITRite walkway (CIR Systems). The order of gait speeds was randomized. Average values over all three trials were computed.

The GAITRite Gold software (version 3.9) computed, for each of the 12 footprint trapezoids, four dependent variables: **P*t** (integrated pressure over time in one zone, expressed as a percentage of the overall integrated pressure over time), **peak time** (first time point at which one or more sensors in a zone were at their maximum level, expressed in seconds), **area** (sum of the active sensor areas within a zone; expressed in square centimeters) and **peak pressure** (maximum pressure per zone, expressed as a percentage of the overall maximum pressure per foot). To simplify the results, the data of the 12 trapezoids were assembled in 6 sections defined as medial and lateral fore-, mid- and hind-foot.

Normality of all data distributions was explored. Repeated measures ANOVA were completed to investigate differences in pressure parameters between gait velocities. Tukey HSD test were computed to explore interactions between velocity and pressure zones. The level of significance was set at $p < 0.05$.

Results

All parameters were significantly different in terms of velocity ($p < 0,003$). A velocity-zone interaction was also found for all four parameters ($p < 0,0001$). Figure 1 shows the average peak pressure in the different zones and for all gait speeds.

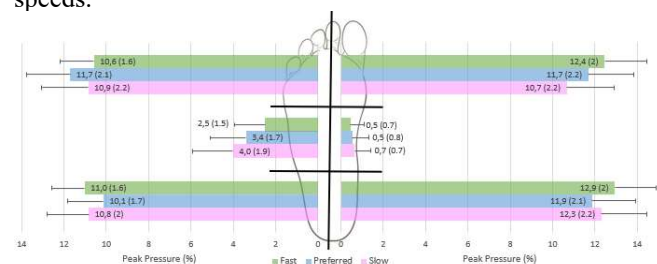


Figure 1: Peak pressure average and standard deviation for each foot zone and gait velocity (slow, preferred and fast).

Except for medial midfoot at preferred and fast speeds, **peak time** decreased for all pressure zones with velocity increase. No changes in **P*t**, **area** and **peak pressure** were found in the medial midfoot. In contrast, these parameters decreased significantly at the lateral midfoot with increasing gait velocity ($p < 0,0001$). **Area** increased proportionately with gait speed at the lateral and medial heel. In addition, at the medial heel, area was similar at preferred and fast speed. At the lateral hindfoot, **P*t** increased from preferred speed to slow and from slow to fast while **peak pressure** increased from preferred speed to slow or fast walking velocity. At the medial heel, **P*t** was equal at slow and preferred speed but increased at fast gait velocity; **peak pressure** increased from preferred speed to slow and from slow to fast. Lateral forefoot **area** was not influenced by gait velocity. **P*t** and **peak pressure** decreased in that zone from preferred to slow and/or fast speed, respectively. Medial forefoot **area**, **P*t** and **peak pressure** increased with increasing gait speed.

Conclusions

The results agree with those of the literature [3-4] and are of interest given the independency to anatomical landmarks or clinical regions of interest in the processing of the footprint mask by the GAITRite software. To evaluate the impact of LBP on plantar pressure, future studies are needed with a special care in controlling for gait speed differences.

References

- [1] Titianova EB (2004) *J Electromyogr Kinesiol*, **14**:275-281.
- [2] Bilney B et al. (2003) *Gait posture*, **17**: 68-74.
- [3] Rosenbaum D et al. (1994) *Gait posture*, **2**: 191-197.
- [4] Segal A et al. (2004) *Foot Ankle Int*, **25**: 926-933.

How does modulating load impact the limits of stability during walking? Inferences from simulated body-weight support and load carriage conditions

Yong Kuk Kim, Michelle Gwerder, Deepak K Ravi, William R Taylor, Navrag B Singh
Laboratory for Movement Biomechanics, Institute for Biomechanics, ETH Zurich, Switzerland

Summary

This study investigated the movement of the center of mass of the whole body (CoM) and the swing foot with respect to the boundaries formed by the base of support (BoS). The vision to get a better understanding of temporal co-ordination between CoM and feet placement. With different weight conditions, load-carriage resulted in adaptability in swing foot placement. Whereas, body-weight support resulted in instability, might allow better flexibility for upcoming stride.

Introduction

In order to walk continuously, CoM needs to be regulated over the BoS (Physical Boundary: B_p). While the spatial constraints imposed to achieve this task successfully are established [1], the temporal limits have not been fully understood. Time to contact (TtC) provides an estimate of the duration of contact with BoS in a continuous manner, and thus promises to fill the gap on temporal constraints. In addition, quantifying TtC on CoM vs. a particular extremity – swing foot – allows us to assess the temporal co-ordination (K, Figure 1B) needed to achieve walking stability [2].

Simulating weight bearing vs load carriage provide ideal conditions as not only are they encountered in daily life, they also perturb the swing foot dynamics. Therefore, the aim of this study was to investigate the TtC under body weight loading (via body-weight support vs. load carriage).

Methods

Twenty healthy participants (9 females; Mean(SD): 24(2) yr; 174.4(7.5) cm; 69.3(8.2) kg) performed in a randomized order: normal walking (Normg), 20% additional (20+), and 40% additional bodyweight (40+) with a weight vest as well as 20% less (20-) and 40% less bodyweight (40-) in a clinical harness system. Participants walked on a treadmill for 6 minutes each condition. 3D kinematics were obtained via an optical motion capture system (Vicon Motion Systems, UK) by placing 38 reflective markers over both lower limbs (Fig 1A) at 500 Hz. The centroid of 7 pelvis markers was used to estimate CoM. B_p (Fig 1A) was defined as the position (anteroposterior direction, AP) of the first metatarsal of the stance foot.

Results and Discussion

The CoM in Normg approached B_p at 72% (TtC_{CoM} approaching 0, Fig 1B), while the swing foot crossed B_p at 49% of swing phase(sp). Supporting body weight expedited (66% sp), while load carriage delayed the approach of CoM to B_p . The swing foot approached CoM (in AP) at ~12% sp (K=1, Fig 1B), and thereafter continued to lead CoM in the movement towards B_p . Supporting body weight delayed (~14% sp), while adding weight hastened (~10% sp) the approach of

the swing foot to CoM. When swing foot leads the CoM towards B_p it allows adaptability in foot placement [2] as seen in the load carriage condition. However, it might come at a cost of inflexibility, due to the delayed CoM approach to B_p might result in insufficient time to plan for the upcoming stride. With body-weight support, CoM lags the swing foot for a longer period of time inducing a considerably larger single limb stance phase (than Normg) resulting in unstable walking. Here, as the swing foot crosses the CoM late anticipatory, during the swing, adjustments might be difficult.

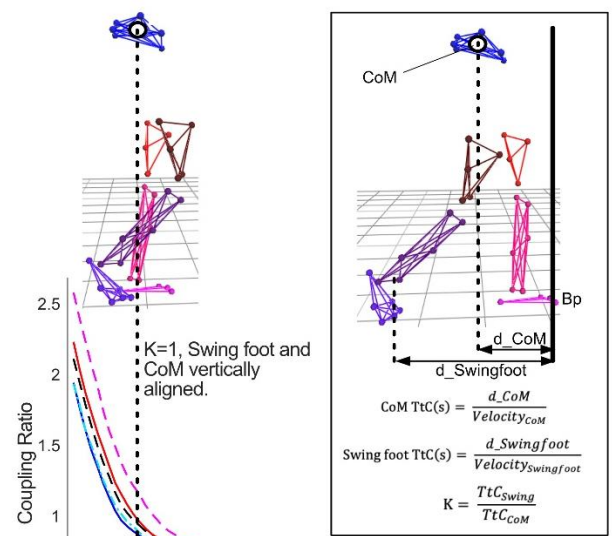


Figure 1A. Equations Ttc and K.

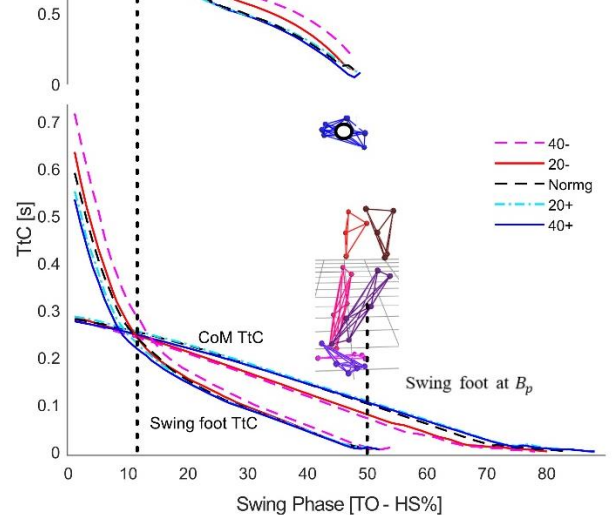


Figure 1B. Coupling Ratio (K) (above) and TtC (below) vs Swing Phase.

References

1. Hof, A.L., Hum Mov Sci, 2008. **27**(1): p. 112-25.
2. Remelius et al., Hum Mov Sci, 2014. **36**: p. 227-45.

Detecting Gait from a Shank-Worn Inertial Measurement Unit Using Harmonic Frequencies

Robbin Romijnders^{1,2}, Elke Warmerdam^{2,1}, Clint Hansen², Gerhard Schmidt¹, Walter Maetzler²

¹Digital Signal Processing and System Theory, Kiel University, Kiel, Germany

²Neurogeriatrics, University Hospital Kiel, Kiel, Germany

Email: robr@tf.uni-kiel.de

Summary

Preliminary results shows that harmonic frequency analysis of accelerations and angular velocities obtained with a shank-worn inertial measurement unit can be used to distinguish between walking and other cyclic activities.

Introduction

In [1], the authors have shown that gait can be distinguished from other cyclic activities by using harmonic frequencies. A foot-worn inertial measurement unit (IMU) was used to record accelerations and angular velocities during in-lab gait assessments and unsupervised semi-standardized gait tests in the home environment from 121 controls and 7 participants with Parkinson's Disease (PwP), respectively. Here, we extend their work by testing if the methods also apply to a shank-worn IMU.

Methods

A home-like assessment was performed at the University of Tübingen (details in [2]) where participants performed daily-life-relevant, non-instructed activities, including walking around in the hospital corridors, making coffee, and ironing clothing. Before each home-like assessment, the rigidity of the lower legs were checked (Item 3.3, UPDRS Part III [3]).

Participants were equipped with shank-worn IMUs attached at the frontal sides of each shank. Data were processed for the left and right shank independently. Data from the rigidity assessment and data from a manually extracted walking bout

were analyzed in the frequency domain to determine whether harmonic frequencies were present.

Results and Discussion

Here, we have analyzed the data from one participant diagnosed with Parkinson's Disease (male, 38 years). During walking the medio-lateral angular velocity signal shows a typical harmonic pattern, where minimally two harmonics can be observed in the frequency range up to 6 Hz, as indicated by the peaks (green square) at multiples of the fundamental frequency (red triangle) (Figure 1). For the rigidity assessment, the fundamental frequency is generally higher, and less harmonics (< 2) are observed.

Conclusions

The methods of [1] can be extended to shank-worn IMUs, although this needs to be validated with more participants and various non-walking cyclic activities.

Acknowledgments

This research was funded by Keep Control from the EU's Horizon 2020 research and innovation programme under the Marie Skłodowska-Curie grant agreement number 721577.

References

- [1] Ullricht et al. (2020). *IEEE J Biomed Health*, **24**(7): 1869-1878.
- [2] Pham et al. (2017) *Front Neurol*; **8**:457.
- [3] Goetz et al (2008). *Mov Disord*, **23**(15):2129-2170.

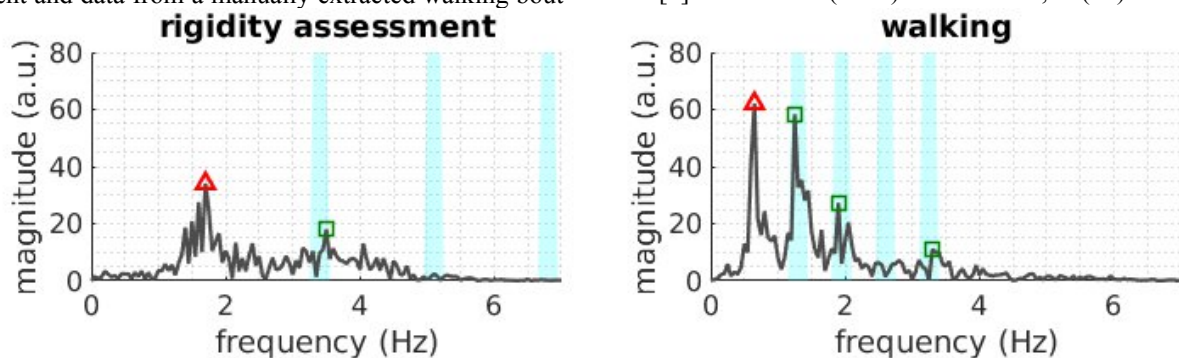


Figure 1: Frequency spectra of the rigidity assessment (left) and a walking bout (right). The red triangle indicates the dominant frequency, the green squares depict peaks indicating harmonics of the dominant frequency (the cyan background depicts the tolerance region in which we look for harmonics).

Moving from straight-line to curvilinear walking: effects on accuracy of marker-based gait event detections

Bonci Tecla¹, Scott Kirsty¹, Buckley Ellen¹, Salis Francesca², Bertuletti Stefano², Caruso Marco³, Cereatti Andrea³, Mazzà Claudia¹
¹ Department of Mechanical Engineering & INSIGNEO Institute for *in silico* Medicine, The University of Sheffield, Sheffield, UK
² Department of Biomedical Sciences, University of Sassari, Sassari, Italy and IuC BoHNeS
³ Department of Electronics and Telecommunications, Politecnico di Torino, Torino, Italy and IuC BoHNeS
 Email: t.bonci@sheffield.ac.uk

Summary

Stereophotogrammetry could be considered as an optimal solution for quantifying spatio-temporal gait outcomes from complete turning maneuver. Nevertheless, relevant algorithms estimating foot-to-ground events have been extensively validated for straight-line walking. This study showed that these approaches can indeed be translated to curvilinear walking with a minimal loss of accuracy.

Introduction

Spatio-temporal metrics are used to quantify functional gait limitations. These are traditionally extracted from straight-line walking (*s-walk*), even if their quantification while turning (*t-walk*) might be more sensitive in detecting impairments [1]. Quantification of spatio-temporal metrics relies on accurate identification of foot-to-ground gait events (GEs), for which stereophotogrammetry (SP) is a convenient solution if interested in multiple consecutive steps acquired during complex tasks. SP-GE algorithms, however, have been mostly validated on *s-walk* [2] and only on limited portions of *t-walk* [3]. This study will therefore aim to assess the GE reliability for *t-walk* of the method proposed by Zeni *et al.* [4].

Methods

Twenty healthy subjects (13 males, age: 29.7±9.0, BMI: 23.2±2.8 kg/m²) were included in this study, after providing written informed consent. They were asked to perform two motor tasks including 90- and 180-degree turns (Figure 1). Subjects were equipped with a wearable multi-sensor system (INDIP) including sixteen force-sensing resistors embedded in each pressure insole (PI) [5], thus providing reference GEs (r-GE). Twelve marker trajectories (10-camera Vicon T160; four markers on each foot and four on a rigid case on the lower back) were used to detect marker-based GE (m-GEs) [4] and the pelvic axes. The latter were used to detect: (i) initial (IC) and final contacts (FC) as maximal and minimal displacement of heel and toe markers with respect to a marker on the rigid case along the pelvic anterior/posterior axis, respectively; (ii) turns defined from thresholds on angular velocity and rotations around the vertical pelvic axis [1]. SP and INDIP signals ($f_s = 100\text{Hz}$) were synchronized as described in [5].

For each r-GE, the relevant time error (Δt) was calculated matching the closest m-GE event. Based on the identified

turns, Δt were classified as either curvilinear (Δt_c) or straight (Δt_s) walking error; sampling at 100 Hz imposes a minimal Δt of 10 ms. Descriptive statistics of Δt distributions were calculated in terms of accuracy (mean) and precision (standard deviation); statistical differences were evaluated with independent Mann-Whitney U tests (IBM SPSS 26).

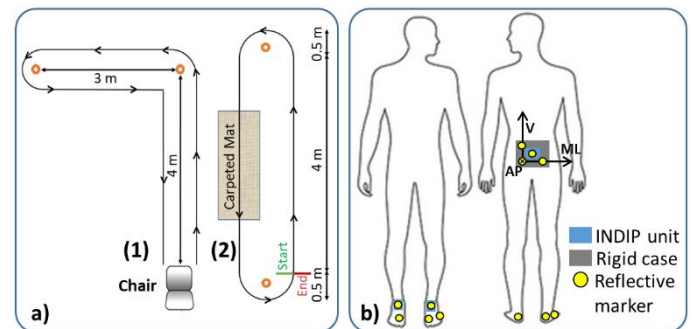


Figure 1: a) Motor tasks: L-Test (1) and surface test (2). b) Markerset, pelvic axes and INDIP units.

Results and Discussion

Table 1 shows results for 1298 GEs (669 ICs) and relevant Δt from 19 participants (data from one participant was discarded due to poor PI signal quality). Negligible differences in Δt were observed between the two walking conditions and only FC- Δt_c values were significantly larger than FC- Δt_s .

Conclusions

In conclusion, this study showed that kinematic data can be used to estimate GEs with a minimal loss of FC accuracy in curvilinear walking. The impact of such inaccuracies on other spatio-temporal metrics still needs to be assessed but is expected to be negligible.

Acknowledgments

This work is part of Mobilise-D (IMI2 Joint Undertaking, grant agreement No 820820).

References

- [1] El-Gohary M *et al.* (2014). *Sensors*, **14**(1): 356–69.
- [2] Bruening and Ridge (2014). *Gait Posture*, **39**(1): 472–77.
- [3] Ulrich B *et al.* (2019). *J. Biomech*, **91**: 69–78.
- [4] Zeni JA *et al.* (2008). *Gait Posture*, **27**(4): 710–14.
- [5] Salis F *et al.* (2020). *Proceedings of GNB 2020*.

Table 1: Gait event (GE) error values [s] observed for straight-line Δt_s and curvilinear Δt_c walking conditions.

GEs	Walking Condition	N (%)	Accuracy [s]	Precision [s]	25-perc [s]	Median [s]	25-perc [s]	Test Statistics
IC	Δt_s	51.4	-0.03	0.02	-0.04	-0.03	-0.02	$z = 1.963$
	Δt_c	48.6	-0.03	0.02	-0.04	-0.03	-0.01	$p = 0.050$
FC	Δt_s	47.9	-0.02	0.03	-0.03	-0.02	0.00	$z = -4.502$
	Δt_c	52.1	-0.03	0.03	-0.05	-0.02	-0.01	$p < 0.000$

Validity and reliability of a mobile insole to measure vertical ground reaction force during walking

Bernhard Dumphart¹, Markus Schimanko¹, Stefan Nöstlinger¹, Michael Iber², Brian Horsak¹, Mario Heller¹

¹St. Pölten University of Applied Sciences, Institute of Health Sciences, Austria

²St. Pölten University of Applied Sciences, Institute of Creative Media/Technologies, Austria

Email: bernhard.dumphart@fhstp.ac.at

Summary

Reliability and validity of a low-cost insole device to measure plantar pressure and force were evaluated. Reliability in terms of the intraclass correlation between a test and retest showed excellent agreement (≥ 0.9). In terms of validity, results indicated an overall high correlation ($R^2: 0.84$) between the insole and force plate data. Despite, some technical limitations, this insole device seems to be a promising alternative to measure plantar pressure and force in the field.

Introduction

Gait analysis (GA) has become an important tool for clinical decision-making in various patient groups [1]. The gold standard, 3DGA, allows describing kinematic and kinetic aspects of human locomotion. However, 3DGA is limited to specialized facilities, is expensive, and time-consuming. Being bound to a stationary laboratory is another limitation. For this reason, different types of wearables have recently been introduced and are gaining popularity. These allow the investigation of real-world scenarios, not in a confined research environment, but where patients perform their day-to-day activities. Nevertheless, new sensors and technologies need to meet certain quality criteria before they can be used. Therefore, this study investigates the validity and reliability of temporal and kinetic variables of a low-cost (~250€) mobile pressure insole device (stappone, stAPPtronics GmbH).

Methods

Ground reaction forces (GRF) sampled at 1000 Hz and insole-pressure data sampled at 100 Hz of the dominant leg from 48 healthy participants were recorded simultaneously during a test and retest, approx. 15 minutes apart. Five to eight valid trials per participant and session were recorded on a 10-meter walkway at a self-selected speed. Reliability was assessed by calculating the intraclass correlation coefficient (ICC, model 2,k) of discrete variables from averaged test and retest data of the insole. Variables comprised the first (F1) and second (F2) force peaks, the mid stance valley (MSV) and their timestamps in milliseconds. Validity was assessed by calculating the linear fit method (LFM) [2] between the signals of the GRF and the insole for each trial. All signals were filtered using a 4th-order Butterworth filter with a cutoff frequency of 10 Hz. For the LFM calculations, data was normalized to a range of 0 and 1 because the insole only measures relative loads expressed as bits between 0 and 1023 (dimensionless).

Results and Discussion

The ICC showed excellent agreements (≥ 0.9 , range of 95% confidence interval (CI): 0.71 – 0.99) for all temporal and

kinetic parameters. Results are in agreement to earlier studies reporting ICCs of 0.81 to 0.97 [3, 4]. Differences in sampling rate, testing protocols, sample heterogeneity and investigated parameters must be considered when comparing various studies. In terms of validity, the LFM results indicate an average R^2 value over all trials of 0.84 (± 0.08) with the 95% CI ranging between 0.84 and 0.85. This shows that on average 84% of the variance in the insole data can be matched by the variance in the GRF data, implying an overall good representation. The similarity of both systems is represented in Figure 1, where the mean and standard deviation of the GRF (black) and insole (blue) trials are compared. Nonetheless, local differences in some areas like the F1, F2 and the MSV can be recognized. These differences in peak height and timing might be attributed to a varying number and size of sensors in the heel and forefoot area of the insole. The rather wide standard deviation might be explained by a pre-load of the sensors due to constant contact of the foot with the insole in the shoe, even during swing.

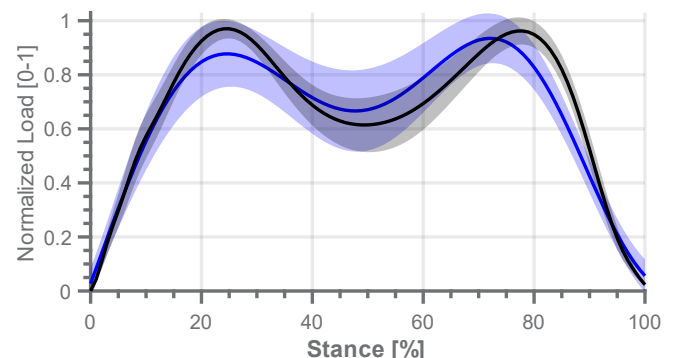


Figure 1: Mean and standard deviation of the normalized vertical GRF measured by the force plate (black) and the insole (blue).

Conclusions

The insole shows good results for both the reliability and validity criteria in a healthy sample. Further research on pathological gait is needed, but otherwise, the insole indicates a promising alternative in rehabilitation and field scenarios.

Acknowledgments

This work was funded by the Austrian Research Promotion Agency, FFG (Nr. 868220). We would also like to thank Anna-Maria Raberger for her great assistance.

References

- [1] T. A. L. Wren et al. (2020). *Gait Posture*, **80**: 274–279.
- [2] M. Iosa et al. (2014). *BioMed Res. Int.*, **2014**.
- [3] M. S. Oerbekke et al. (2016). *Gait Posture*, **51**: 116–124.
- [4] B. J. Braun et al. (2015). *J. Foot Ankle Res.*, **8**: 54.

Effect of aging and physical activity level on recovery within the stride during walking

Leopoldine Kury¹, Aitor Fernandez Menendez¹, Davide Malatesta¹

¹Institute of Sport Sciences of the University of Lausanne, University of Lausanne, Lausanne, Switzerland
Email: leopoldine.kury@unil.ch

Summary

This study aimed to investigate the effect of aging and physical activity level on pendular energy-saving mechanism in active and sedentary older (≥ 65 yr) and young individuals. Twelve sedentary older, 11 active older and 21 young individuals walked at $1.11 \text{ m}\cdot\text{s}^{-1}$ on an instrumented treadmill. Mechanics of walking were assessed. Compared to young individuals and independently of their physical level, older adults walked with a significant higher pendular recovery (+14; $P < 0.001$) and significant lower external mechanical work (-18%; $P < 0.001$). Recovery within the stride was significantly higher during the first half of the double contact phase and the second half of the single contact phase in older than in Y participants ($P \leq 0.01$). Our findings showed that older participants, seem to adapt their walking pattern to improve their pendular energy recovery in order to limit the external mechanical work, especially during the step-to-step transition phase.

Introduction

Physical activity seems to limit the physiological changes in walking performance due to aging. The aim of this study was to investigate the effect of aging and physical activity level on pendular energy-saving mechanism in active and sedentary older (≥ 65 yr) and young individuals.

Methods

Twelve sedentary older (SO 71.6 ± 4.3 yr), 11 active older (AO 71.5 ± 3.7 yr) and 21 young (24.3 ± 2.0 yr) individuals walked at $1.11 \text{ m}\cdot\text{s}^{-1}$ on an instrumented treadmill and mechanics of walking [positive external mechanical work (W_{ext}) and average and instantaneous pendular recovery within the stride [R(t)]] were assessed [1].

Results and Discussion

Compared to young individuals and independently of their physical level, older adults walked with a significant higher pendular recovery ($+14\% \pm 0.001$) and significant lower W_{ext} (-18% ± 0.001). R(t) was significantly higher during the first half of the double contact phase and the second half of the single contact phase in OA and SO than in Y ($P \leq 0.01$ Figure 1). The older individuals performed less W_{ext} during the push II phase, making kinetic (E_k) and potential (E_p) mechanical energies more out of phase, reducing the phase shift between the two curves in this phase. These findings corroborate previous one, showing that, compared with young individuals, older individuals performed an average of 10% less individual limb work during double contact phase [2]. As reported in obese individuals [3], older individuals seem to improve the pendulum mechanism to reduce the amount of W_{ext} .

During the single contact, the within-step analysis of pendular energy recovery showed that there were two zones in which older individuals had a skillful R(t) compared with young subjects. These zones were just before and slightly after the maximum E_p in the ascent and descent of the COM, respectively, in the middle of the single contact phase (Figure 1). In the former zone, older individuals improved the R(t) to minimize the W_{ext} necessary to increase the height of the COM. In the second zone, a smaller amount of E_p has to be absorbed by the muscles, favoring the transduction of E_p to E_k , as previously shown in African women carrying loads on their heads [1]. The only zone in which the young individuals had a higher R(t) than older subjects was in the transition between the mid- and terminal stance which may represent critical events in terms of gait dynamic stability and motor control [4] that penalize pendular energy transduction in older individuals.

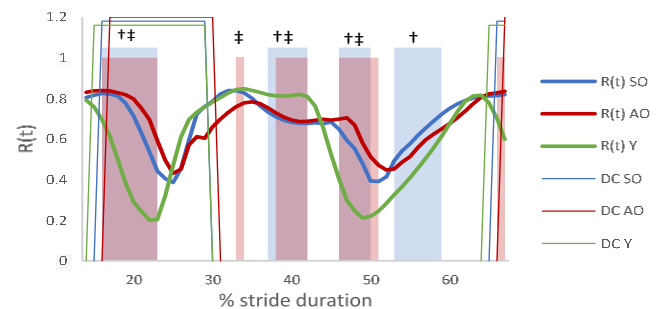


Figure 1: Recovery within the step [R(t)] as a function of the percent of stride duration (% stride duration) for the 3 groups (SO: sedentary older; AO: active older; Y: young). DC: double contact phase. † Significant difference between the sedentary older and young individuals (SO vs Y; $P \leq 0.05$); ‡ Significant difference between the active older and young individuals (AO vs Y; $P \leq 0.05$).

Conclusions

Compared with their young counterparts, older individuals, regardless of the level of activity, walk at $1.11 \text{ m}\cdot\text{s}^{-1}$ with lower W_{ext} and higher recovery. R(t) shows that older individuals improve pendular energy recovery in the phases of the step where they have to perform W_{ext} , especially at the beginning of the double contact phase during the step-to-step transition. Ageing specifically and not physical activity level seems to modify pendular recovery during walking.

References

- [1] Cavagna GA et al. (2002). *J Exp Biol*, **05**: 10.
- [2] Ortega JD and Farley CT (2007). *J Appl Physiol (1985)*, **10**: 2266-2273.
- [3] Fernandez Menendez et al. (2019). *J Appl Physiol (1985)*, **1**: 1250-1258.
- [4] Paret RS et al. (2010). *Gait Posture*, **3**: 429-435.

Residual force depression is increased following greater *in vivo* muscle shortening work

Brent J. Raiteri¹, Daniel Hahn^{1,2}

¹Human Movement Science, Faculty of Sport Science, Ruhr University Bochum, Bochum, Germany

²School of Human Movement and Nutrition Sciences, University of Queensland, Brisbane, Australia

Email: brent.raiteri@rub.de

Summary

This study aimed to reveal whether reducing muscle shortening work in the human tibialis anterior (TA) relative to that performed in a fixed-end contraction would reduce residual force depression (rFD). TA muscle fascicle shortening during active force production was reduced by lengthening TA's muscle-tendon unit (MTU) to effectively stiffen its MTU and steady-state torques following lengthening (Len) were compared with those attained during fixed-end reference contractions (Ref) at the same muscle activity level and MTU length. Preliminary results show that *in vivo* rFD increases with greater muscle shortening work and highlight that following Len muscle performance can be enhanced because of less preceding positive muscle work.

Introduction

A long-lasting tension deficit exists following active muscle shortening compared with fixed-end contractions at the same muscle length and activation level, which is termed rFD [1]. Although rFD is often assumed to be absent during human voluntary fixed-end contractions, rFD can exist because of initial muscle shortening during active force development, which occurs due to MTU compliance [2]. As rFD increases with increasing muscle shortening work in electrically-stimulated muscle [3], we tested whether a reduction in TA muscle fascicle shortening amplitude before reaching a given voluntary muscle activity level and MTU length would enhance steady-state dorsiflexion torque due to reduced rFD.

Methods

Pilot data was recorded from one healthy male participant who laid prone on a bench with their right foot secured to the footplate attachment of a dynamometer (IsoMed2000, D&R Ferstl GmbH, Germany). Voluntary fixed-end ramp-and-hold Ref contractions were performed over 12-s up to a constant muscle activity level of 30% of maximum voluntary contraction (MVC) at an ankle joint angle of 20° plantar flexion (PF). TA muscle activity was displayed as a 250-ms root-mean-square amplitude calculation and this signal was maintained within two horizontal lines spaced 6% MVC apart throughout each contraction. MTU-lengthening-hold contractions (Len) at a matched muscle activity level were also performed over the same duration, whereby TA's MTU was lengthened with a 20° PF rotation as muscle activity increased during the ramp phase of the ramp-and-hold contractions and then held constant for 10-s. The stretch velocity was 10°·s⁻¹ and therefore the ramp duration was 2-s to ensure that steady-state dorsiflexion torques and muscle fascicle lengths could be compared between Len and Ref at the same muscle activity level and MTU length.

TA muscle activity was recorded using surface EMG at 2000 Hz and bandpass analogue filtered between 10-500 Hz, prior to being sampled at 2000 Hz. TA muscle fascicles within its superficial compartment were imaged with B-mode ultrasound using a 60 mm veterinary transducer operating at ~154 Hz with an image depth of 40 mm (LV8-A2; Teled, Vilnius, Lithuania). Fascicle lengths (FLs) were determined offline in Matlab (R2019b, MathWorks, USA) by implementing a semi-automated tracking algorithm [4]. Net ankle joint torque and crank arm angle were recorded at 2000 Hz and synchronized with ultrasound and EMG recordings using a 16-bit A/D card within a Power1401 data acquisition interface (Spike2, CED, Cambridge, UK). rFD was estimated as the time-matched steady-state mean torque difference over 6-s between Len relative to Ref and expressed in % MVC.

Results and Discussion

Preliminary results show that steady-state TA muscle activity levels and TA FLs during Len (27.9% MVC and 58 mm) were similar to Ref (27.8% MVC and 58 mm). As expected, TA fascicles were found to shorten 4.5 mm less during the ramp phase of Len compared with Ref, where TA fascicles shortened 2.4 vs. 6.9 mm, respectively. This led to reduced rFD during Len as evidenced by an increased steady-state torque of 2.7% MVC compared with Ref, where torques were 45.3 and 42.6% MVC, respectively. This level of enhanced torque might be increased further when muscle shortening work is completely abolished [3] and this will be attempted in future experiments.

Conclusions

Preliminary results suggest that *in vivo* rFD can increase with greater TA muscle shortening work during submaximal voluntary dorsiflexion contractions. These findings highlight that reduced rFD can enhance muscle performance following MTU lengthening. Future research will investigate the relationship between *in vivo* muscle shortening work and rFD.

Acknowledgments

This work was supported by the German Research Foundation (DFG, grant #447345165).

References

- [1] Abbott BC and Aubert XM (1952). *J. Physiol.*, **117**: 77-86.
- [2] Raiteri BJ and Hahn D (2019). *Acta Physiol.*, **225**: 1-18.
- [3] Herzog W et al. (2000) *J. Biomech.*, **33**: 659-668.
- [4] Farris DJ and Lichtwark GA (2016). *Comput. Meth. Prog. Bio.*, **128**: 111-118.

Relationship between metatarsophalangeal joint flexors and lower limb strength—a preliminary investigation

Enrico Roma¹, Romain Tourillon^{1,2}, Antoine Michel¹, Pascal Edouard¹, François Fourchet², Guillaume Y Millet¹, Jean-Benoit Morin¹

¹University Saint-Etienne, France ²La Tour Hospital, Switzerland
Email: enrico.roma@univ-st-etienne.fr

Summary

This study evaluated the reliability of a method to measure the metatarsophalangeal joint (MPJ) flexion strength, offering insight for foot training. The relationship between lower limb and MPJ strength was also investigated, showing that the MPJ strength is an independent construct. Finally, quadriceps strength was shown to be the major predictor of dominant leg concentric jump impulse (DLCJI) while plantar flexion and MPJ strength did not contribute significantly.

Introduction

The foot is a complex joint system with multiple degrees of freedom and plays a role in athletic tasks. Its structure allows to transmit lower limb muscles force output to the ground and to generate forward propulsion. Consistent literature showed the relevance of foot strength in relation to performance or lower leg injury prevention [1], yet no study has investigated its relation to lower limb muscles strength. Besides, the literature lacks homogeneity in the assessment since the main action evaluated ranges from functional movement to toe flexion (TF) around the MPJ or interphalangeal joint (IJ) [2]. The present study evaluated the reliability of a MPJ flexion strength measure and its relation to lower limb muscles strength and DLCJI.

Methods

22 healthy volunteers, 25.8(5.7) years, 1.76(0.07) m, 71.1(11.2) kg were evaluated across two testing sessions, 3 to 5 days apart. Participants performed four MPJ flexion maximal voluntary isometric contractions (MVICs) with a custom-made ergometer placing the toes on a force platform (Kistler) with ankle joint in full plantar flexion and MPJ in dorsiflexion. Maximal force was determined as the highest peak force recorded from four MVICs. Three isometric MVICs of ankle plantar flexion at 0° and knee extension at 90° on an isokinetic dynamometer (Con-Trex) were performed. Maximal DLCJI during three countermovement jumps on two Kistler force plates were kept for the analysis. The four trials of the first session were used to test intra-session reliability. Intraclass correlation coefficients (ICC) were calculated using a 2-way mixed effect model, single measurement for absolute agreement. Coefficient of variation (CV) was computed as the mean of the intra-individual CV's. Standard error of prediction (SEP) and minimal detectable differences (MDD) were always reported [3], while Limits of Agreement (LoA) only for inter-session reliability. Results were reported as mean (SD) [min-max]. To predict the DLCJI, a hierarchical multiple regression was used.

Results and Discussion

In session one, the maximal force was 231 N (84) [67-413], versus 241 N (84) [106-416] in session two. According to the 95% CI, the ICC ranges between 'moderate' and 'good' for both intra-session and test-retest reliability. The mean force is higher to previously reported data [4], however, these studies used a TF gripping task. To our knowledge, this is the first study to evaluate maximal voluntary MPJ isometric flexion in maximal ankle plantar flexion. MPJ flexion strength did not correlate with knee extension ($r=0.17$, $t(22)=0.827$, $p=0.417$) and plantarflexion ($r=0.13$, $t(22)=0.622$, $p=0.5404$) peak force, neither in absolute nor in relative (lean body mass) terms. The MPJ strength appears as an untied construct compared to the overall lower limb strength, suggesting that it should be evaluated and possibly trained in a specific way. DLCJI can be explained only by knee extension of the variable considered (DLCJI, $\beta=0.32$, $t(22)=3.662$, $p=0.001$), $R^2=0.379$, $F(1, 22)=13.41$, $p=0.001$. Our results partially contrast previous findings [5], that reported a significant but low ($r=0.382$) correlation between CJI and TF strength, but without accounting for knee extension strength.

Table 1: Reliability statistics

	ICC	95% CI	CV (%)	SEP (N)	MDD 95% (N)	LoA-lower	LoA-upper
Intra-session	0.812	0.690-0.903	14.0	32.5	121		
Test-retest	0.880	0.738-0.947	7.8	28.7	109	-82.3	75.2

Conclusions

This study presents a moderate to highly reliable method to evaluate MPJ flexion strength. It may be useful to assess the effect of a training protocol targeting intrinsic and extrinsic toe flexors, as our data showed the specificity of this construct. Finally, it is suggested that when research aims to investigate the link between "functional task" and MPJ strength, considering the overall strength is important.

References

- [1] Van Der Merwe C et al. (2020). *Res Q Exerc Sport*. 7;1-8; [2] Soysa A et al. (2012). *J Foot Ankle Res*. 26;5:29. [3] Weir J. P. (2005) *J Strength Cond Res*, 19(1), 231-240. [4] Bruening DA et al. (2019). *BMC Musculoskelet. Disord.*, 20(1), 1-9. [5] Yamauchi J et al. (2020). *J Biomech*, 104, 109719.

Comparison of leg muscle activity levels during different fitness tests in elderly individuals using surface electromyography

Jonina Oddsson ¹, Weinback A², Godhe M^{1,3}, Andersson E^{1,3,4}.

¹Laboratory of Biomechanics and Motor Control, Swedish School of Sport and Health Sciences, ²Scandinavian College of Naprapathic Manual Medicine, ³Department of Molecular Medicine and Surgery, Karolinska Institutet, and ⁴Department of Neuroscience, Karolinska Institutet, Stockholm, Sweden

Email: jonina.oddsson@gih.se

Summary

Ten older adults participated in a study measuring activity levels in eight leg muscles during various submaximal and maximal fitness tests for field contexts¹⁻⁴. Several statistically significant differences emerged in comparisons of different fitness tests and maximal exercises, respectively. For example, fast walking gave significantly higher values for all hip and leg muscles compared to normal walking speed.

Introduction

Physical activity, including strength training, is a common form of training for seniors. A desire in certain training and test exercises for older adults is to be able to give specific advice to individuals based on how much different muscles are involved. Knowledge about activity levels for muscles in different test and training tasks can be obtained with electromyographic recordings (EMG). The aim of the study was to investigate in seniors muscle activity levels in eight different leg and hip muscles during some fitness tests and maximum voluntary contractions (MVC).

Methods

Ten seniors (women and men, 66-89 years, who regularly participate in supervised exercise at least once a week) performed six physical field context tests (primarily for the hip and leg muscles)¹⁻⁴. We also recorded 16 static maximum voluntary contractions (MVC), designed to maximally activate the gluteus maximus (GM), lateral hamstrings (BF-biceps femoris-caput longum, medial hamstrings (SEMI-semi-tendinosus/semimembranosus), rectus femoris (RF), vastus lateralis (VL), vastus medialis (VM), gastrocnemius (GASTR) and soleus (SOL) muscles. Surface EMG activity levels were analyzed regarding mean amplitude (mV) in each exercise. The EMG levels for each exercise, muscle and individual were expressed as a percentage of the highest measured value found in any of the assessed MVC exercises. Mean values (± 1 Standard Deviation, SD) were calculated for all participants' normalized EMG values. Statistically significant differences between the recorded exercises for each muscles' activity level (expressed as a percentage of MVC level) were calculated via one-way ANOVA followed by post-hoc Fisher LSD-test ($p < 0.05$).

Table 1 Mean EMG-amplitude values (\pm SD) in percentage of MVC in two of the assessed field-context fitness tests designed for seniors.

Fitness tests	GM	M	F	SEMI	RF	VL	VM	ASR	SOL
Five-repetition sit-to-stand ¹	17 \pm 17	18 \pm 11	19 \pm 14	38 \pm 13	39 \pm 14	39 \pm 16	15 \pm 7	10 \pm 10	
Timed up & go ³ from a chair & back ^{2,3}	10 \pm 14	5 \pm 9	9 \pm 11	3 \pm 8	30 \pm 12	3 \pm 12	40 \pm 20	59 \pm 20	

Results

High activity levels (% of MVC), were noted in a number of exercises. An example was a dominance in the muscles of the front thigh during the exercise "wall sit" i.e. a static sitting position without a chair, with 90° in the hip and knee joint. Here, the mean amplitude was for RF 42%, VL 50% and VM 49%, whereas the levels of the hip extensors were significantly lower, GM 9%, BF 7% and SEMI 6%, and the activity for the lower leg muscles SOL was then 24% and for GASTR 12%. In the 10-meter-walking-test⁴, which was performed both at a self-selected calm normal walking pace and walking as fast as possible, a significantly increased activity (\approx 15-35% higher values) was seen in all registered muscles, in the faster execution ($p < 0,05$). The mean EMG-levels in the fastest versus the normal walking speed were for GM: 25% vs 11%, BF: 36% vs 21%, SEMI: 41% vs 21%, RF: 57% vs 22%, VL: 34% vs 17%, VM: 50% vs 23%, GASTR: 53% vs 31%, SOL: 66% vs 48%. All three quadriceps muscles had obvious activity in the two tests "Five-repetition sit-to-stand" and "Timed-up-and-go" (TUG), while within the calf muscles the latter test, TUG, revealed higher activity (Tab. 1). The muscles within a synergy could show their highest EMG levels in separate MVC tasks, in which factors of importance could be i.e. how and where the external resistance was given in the MVC task, and if nearby joints were flexed or extended.

Conclusions

Several statistically significant EMG activity differences emerged for the muscles in the tests. It may be of interest to see which fitness tests result in higher respectively lower muscle activation for evaluations of leg strength and function in different health test contexts. Thus, results might be useful in various gym and clinical settings to give specific advice to older adults regarding how much different muscles are involved in certain training and test exercises.

References

- [1] Bohannon, R. W. (2006). *Percept Mot Skills*, **103**:215-22.
- [2] Bohannon, R. W. (2006). *J Geriatr Phys Ther*, **9**:64-8.
- [3] Rikli, R.E., et al. (2013). *Gerontologist*, **53**:255-67.
- [4] Morris, D.R., (2013). *J Am Heart Assoc*, **13**:e001105.

The utility and validity of high intensity intermittent exercise protocols for biomechanical injury preventive screening in male jump-landing athletes

Dermeulen Stefan^{1,3}, De Leecker Camilla^{1,3}, De Laiser Cedric¹, Boone Jan², Willems Tine¹, Vanrenterghem Jos³, Roosen Philip¹, and De Ridder Roel¹

¹Department of Rehabilitation Sciences, Ghent University, Ghent, Belgium

²Department of Movement and Sports Sciences, Ghent University, Ghent, Belgium

³Department of Rehabilitation Sciences, KU Leuven, Leuven, Belgium

Email: Stefan.Dermeulen@UGent.be

Summary

Over the last decade, the importance of fatigue as (modulating) risk factor for developing sports injuries has been emerging. This study investigated the utility and validity of two versions of a high-intensity intermittent exercise protocol to include in biomechanical injury preventive screening. Long-lasting fatigue-related alterations in cardiovascular and muscular characteristics were demonstrated after similar fatigue protocol versions, which either terminated after a fixed number of circuits, or terminated at a fixed subjective measure of exhaustion. Therefore, both fatigue protocols are deemed valid and can be utilized in biomechanical injury preventive screening in male jump-landing athletes.

Introduction

Fatigue reduces the capability to react properly to biomechanical demands of a rapidly changing physical environment [1] and can be considered as a modulator for risk factors for developing lower extremity injuries. Since previous biomechanical studies used fatigue protocols without having information about the extent to which fatigue effects persist in the protocol, validated fatigue protocols with sports specific characteristics are required. This study investigated the utility and validity of the high-intensity intermittent exercise protocol (HIIP) [2] and a modified version of 5 circuits (HIIP-5) to include in biomechanical injury preventive screenings. Whilst the former has the advantage of standardized level of exhaustion, the latter has the advantage of a fixed protocol duration. The purpose of this study was to determine the cardiovascular and muscular effects and the duration of these acute fatigue effects following the cessation of both versions of the fatigue protocol.

Methods

Twenty healthy male volleyball (n=10) and basketball (n=10) players, participated in this study. Physical performance, objective and subjective cardiovascular and muscular parameters were extracted continuously before and up to 30 minutes (0, 15, 30 minutes) after cessation of the HIIP and HIIP-5. Subjective scores of fatigue were extracted by means of the rate of perceived exertion for breathlessness (RPE-B) and legs (RPE-L). Objectively, mean counter-movement jump (CMJ) height and heart rate (HR) were continuously monitored and peak blood lactate levels were compared to resting values. The impact of each fatigue protocol on maximal concentric (CONC) muscle force of the quadriceps

was determined by means of isokinetic dynamometry (Biodex System 3 Pro[®]). Raw isokinetic muscle force data were filtered and imported in Matlab (Matlab, version 2020b) for individual curve analysis using IKD1D (www.ikd1d.org). Repeated measures ANOVA with Bonferroni-correction was applied to determine fatigue-related cardiovascular and/or muscular alterations using SPSS (IBM SPSS statistics 26) for discrete outcome variables and Statistical Parametric Mapping for torque-angle profiles (www.spm1d.org).

Results and Discussion

Scores for the RPE-B and RPE-L increased significantly, respectively up to 20 and 30 minutes following termination of both the HIIP and HIIP-5 ($p < 0,001$). Mean CMJ height decreased and HR increased significantly up to 30 minutes following cessation of the HIIP and HIIP-5 ($p < 0,001$). Peak blood lactate levels increased significantly after HIIP and HIIP-5 ($p < 0,001$). A significant main effect of HIIP and HIIP-5 was found for the isokinetic CONC muscle force of the quadriceps with a significant reduction at 0, 15 and 30 minutes post-fatigue compared to pre-fatigue ($p < 0,001$) (Figure 1).

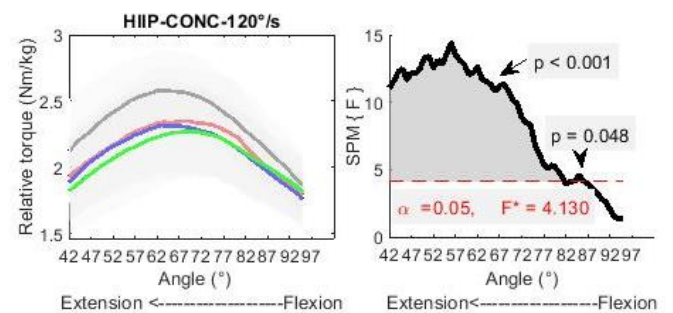


Figure 1: CONC torque-angle profiles for the quadriceps before and after HIIP. Black line pre-fatigue, red line post-fatigue 0 minutes, blue line post-fatigue 15 minutes, green line post-fatigue 30 minutes.

Conclusions

The HIIP and HIIP-5 seem valid tools to induce long-lasting cardiovascular and muscular fatigue effects and can be utilized in biomechanical injury preventive screening in male jump-landing athletes.

References

- [1] Benjaminse A et al. (2019). *Sports Med.* **49**: 565-586.
- [2] Whyte E et al. (2015). *J Athl Train.* **50**: 392-39.

Investigating osteoarthritis in the human hip using three-dimensional finite element models

James Osborne¹, Reza Samani¹, Jim Craig², Mohammad Akrami²

¹Medical School, College of Medicine and Health, Exeter E1 2LU, U.K.

²Department of Engineering, College of Engineering, Mathematics, and Physical Sciences, University of Exeter, Exeter E4 4UF, U.K.

Email: jo363@exeter.ac.uk

Summary

This project uses complex three-dimensional finite element models to investigate the impacts of osteoarthritic damage regarding loading patterns and stress points in the human hip. This study could show the isolation of the structure and exclusion of other factors that may influence biomechanics of the hip. This will ascertain the extent of the influence the osteoarthritic damage itself has upon locomotion and loading of the hip.

Introduction

Osteoarthritis (OA) is a term for the degeneration of cartilage present in joints in the body, causing stiffness and pain from bone contacting bone and the myriad of issues stemming from this contact [1]. Specifically, hip osteoarthritis refers to the damage of the articular cartilage found on the head of the femur and surface of the acetabulum, and the discomfort and impaired movement associated with these two bone surfaces rubbing together. Current literature suggests that this can cause a shift in loading of the hip, theorised to be the patient altering gait mechanics, therefore loading patterns, to alleviate the symptoms of osteoarthritis [2,3]. It could be the anatomy of the damaged cartilage influences loading patterns, even when isolated from patient attempts to alter the load. Through the creation of a complex three-dimensional finite element healthy hip model, it is possible to simulate differing loads placed upon the joint and the articular cartilage, and evaluate where specifically points of stress on the structure are located in a healthy human hip. An OA version of the complex three-dimensional human hip model was also created to undergo the same experimental process, yielding comparable data on stress points in the structure. Using this model, behavioral elements have been removed from the study, allowing an evaluation of the extent the articular cartilage itself plays a role.

Methods

MRI scans of a healthy human hip were taken from a 20-year-old female. The subject had no medical issues relating to the hip or spine [4]. This MRI data-set was then put into Mimics Research 21.0 software where the pelvis (including: partial ilium, complete ischium, partial pubis, and complete acetabulum with articular surface, acetabular fossa and acetabular labrum), femur (including: complete proximal end with femoral head articular cartilage), and ligaments (iliofemoral, the pubofemoral and ischiofemoral) were segmented and converted into a three-dimensional model (Figure 1). Subsequently, the model was copied the articular cartilage and femur head re-segmented to represent an OA hip. This involved the flattening of the superior side of the femur head and thinning of the cartilage [5]. Changes were made in line with clinical presentations of hip OA across multiple MRI scans found in the literature. These models were imported to finite element analysis software, ABAQUS. They were tested with varying loading and boundary conditions to analyse sensitivities. Material properties and loading values of differing tissue was taken from the literature.

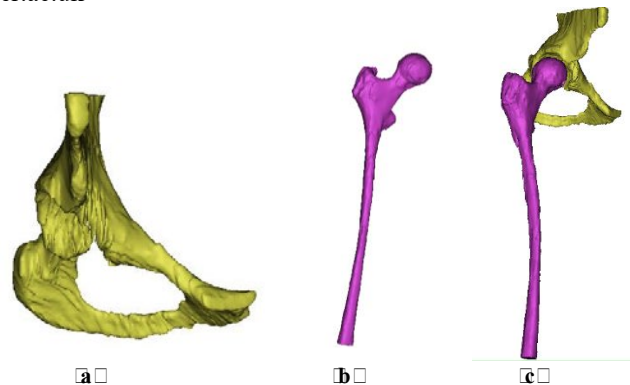


Figure 1: Rough draft models for cancellous femur (a), cancellous pelvis (b) and both combined (c). Set to model cortical bone, cartilage and ligaments.

Results and Discussion

The finite elements analysis showed a shift in loading patterns, even when separated from a human subject and their gait mechanics, due to the abnormal shape of the hip joint created by OA, in turn causing the OA model to possess differing stress points to the healthy model. The data provides evidence of the significant role the articular cartilage alone plays in loading patterns, helping to further our understanding of OA and its relationship with biomechanics.

The developed finite element model could be used as an asset for further research of the human hip including: investigating biomechanics of different clinical presentations of osteoarthritis, long term effect of altered gait mechanics on the hip, investigating new methods of total hip arthroplasty.

Conclusions

Articular cartilage and femur head structure resulting from OA changes the loading patterns of the human hip during gait, independent of loading patterns caused by patients altering gait mechanics themselves.

References

- [1] Arden N, Nevitt M. Osteoarthritis: Epidemiology. *Best Practice & Research Clinical Rheumatology*. 2006;10(1):3-25.
- [2] Constantinou M, Loureiro A, Carty C, Mills P, Barrett R. Hip joint mechanics during walking in individuals with mild-to-moderate hip osteoarthritis. *Gait & Posture*. 2017;53:162-167.
- [3] Meyer C, Wesseling M, Corten K, Nieuwenhuys A, Monari D, Simon J et al. Hip movement pathomechanics of patients with hip osteoarthritis aim at reducing hip joint loading on the osteoarthritic side. *Gait & Posture*. 2018;59:11-17.
- [4] Akrami M, Craig K, Dibaj M, Javadi A, Benattayallah A. A three-dimensional finite element analysis of the human hip. *Journal of Medical Engineering & Technology*. 2018;4(7):546-552.
- [5] Outry N, Paul C, Leroy J, Fredoux D, Migaud H, and Cotton A. Rapidly Destructive Osteoarthritis of the Hip: MR Imaging Findings. *American Journal of Roentgenology*. 2002;179:657-66

Relationship of contact time during cutting manoeuvres and lower extremity joint variability

Johanna Robbin^{1,2}, Patrick Mai², Leon Robertz², Mario Fleiter³, Uwe G. Kersting²

¹Faculty of Mechanical and Process Engineering, Offenburg University, Offenburg, Germany

²Institute of Biomechanics and Orthopaedics, German Sport University Cologne, Cologne, Germany

³Adidas AG, Herzogenaurach, Germany

Email: jrobbin@stud.hs-offenburg.de

Summary

Fast completion and short ground contact times (CT) during cutting and turning are essential performance parameters during sports games. Coordination is assumed to be important with high joint variability (JV) potentially compromising speed. In the present study, it was aimed to investigate the relationship between JV in the lower extremity and CT during a 135° cutting manoeuvre (CM). Overall, the correlation between CT and the adjusted coefficient of multiple determination (ACMD) showed an increase for joint angles and a decrease for moments from proximal to distal. The approach may be helpful to understand the relationship between performance and injury risk in complex tasks.

Introduction

Fast completion and short CT during CM are essential performance parameters during team sports [1]. JV, calculated by the ACMD [2], was linked to performance as joint coordination is assumed to be important for CM. However, the relationship between CT and JV has not been studied yet. Therefore, the purpose of this study was to investigate the relationship between 3D-JV of the lower extremity joints and CT during a 135° CM.

Methods

Twenty-three participants performed a minimum of fifteen 135° CM with maximum effort on artificial turf. Kinematic and kinetic data were acquired with a motion analysis system and a force plate. We calculated 3D lower extremity joint kinematics and kinetics of the right leg. ACMD of joint angles, joint moments, and ground reaction forces were computed. All parameters were correlated with CT by using Kendall's tau ($\alpha=0.05$).

Results and Discussion

We can see a trend to decreased angular JV from distal to proximal, while correlations are elevated in the sagittal plane. An opposite trend is seen for joint moments, while all ground reaction force components show very high ACMD values (Fig.1). JV and CT for the hip moment in the sagittal and frontal planes were strongly related, as was the knee moment in the frontal and transverse planes (Tbl.1). Likewise, the

sagittal hip angle and the transverse knee rotation plane were significantly related.

JV of ankle kinetics also relates to CT, while knee and hip kinetics and non-sagittal plane kinematics show weaker predictive value. It remains to be investigated how muscle contractions are controlled to maintain a stable force output while kinematics, in particular, vary substantially.

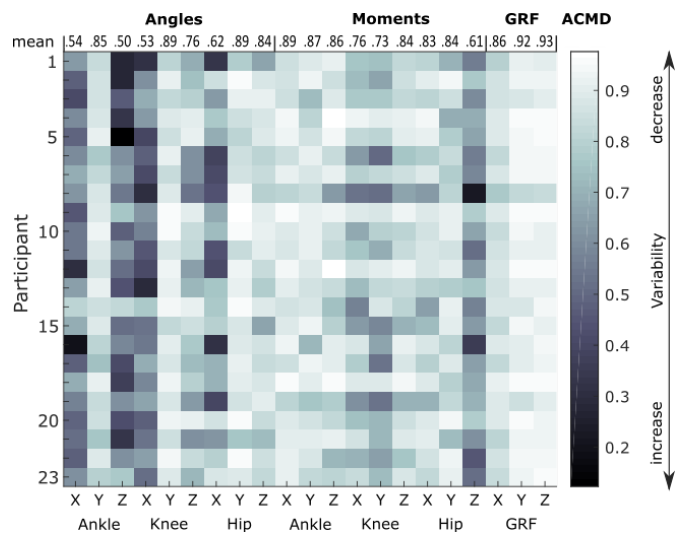


Figure 1: ACMD values of the lower extremity joint parameters and overall participants. X, Y, Z are frontal, sagittal and transverse plane.

Conclusions

CT as an indirect performance parameter is related to the variability of joint kinematics and kinetics during cutting manoeuvres. This connection could be important for performance improvements, prevention, or even the characteristics of injuries. Therefore, further studies should quantify the relationship between variability in cutting trials and injury risk.

Acknowledgments

Adidas AG., Herzogenaurach, Germany.

References

- [1] Schrödter et al. (2016). *Footw. Science*, **8**, 23-31.
- [2] Marshall et al. (2014) *J. Strength Cond. Res.*, **10**, 2845-2851.

Table 1: Results of significant correlations and effect sizes (Kendall's tau).

Parameters	Ankle moment transverse plane	Knee moment frontal plane	Knee moment transverse plane	Hip moment frontal plane	Hip moment sagittal plane
p	0,01	0,04	0,05	0,02	0,02
tau	-0,38	-0,30	-0,30	-0,34	0,35

Sex influence on the neuromuscular fatigue examined by a force-velocity concentric test

Rob Macchi¹, A. Santuz^{2,3}, A. Hays¹, F. Mercruyssen⁴, A. Arampatzis^{2,3}, C. Nicol¹

¹ ISM, CNRS Aix Marseille Univ, Marseille, France

² Department of Training and Movement Sciences, Humboldt-Universität zu Berlin, 10115 Berlin, Germany

³ Berlin School of Movement Science, Humboldt-Universität zu Berlin, 10115 Berlin, Germany

⁴ IAPS, University of Toulon, Toulon, France

Email: robin.macchi@gmail.com

SUMMARY

Recent studies suggest that women may be less fatigable than men, but this has been mostly studied in isometric test condition and in the acute recovery phase. This study assessed the sex influence on the delayed neuromuscular fatigue two and four days after a 20 km graded running race by using a pluri-articular horizontal force-velocity (HF- \square) test. Only men presented delayed performance decrease in power. Sex, but not recovery time, influenced the timing of the synergistic muscle activations patterns.

INTRODUCTION

Women are usually reported as less fatigable than men after a fatiguing running exercise [1]. However, this has mainly been assessed by monoarticular isometric tests which tend to overestimate the fatigue observed in pluriarticular tests [2]. On the other hand, previous studies have rarely detected any delayed fatigue in pure-concentric tests. Yet, no studies have assessed the fatigue-induced changes of the force-velocity relationship and in the associated muscle activation patterns. Our purpose was to analyze the influence of sex on the delayed neuromuscular fatigue after a 20 km graded running race by using a concentric pluriarticular test.

METHODS

Seventeen recreational runners (nine women) completed the race. They underwent three recording sessions: a week before the race (PRE), two and four days (2D and 4D) after the race. Delayed onset muscle soreness (DOMS) was quantified using a visual analogue scale (0-10). For each session, the HF- \square test was performed under four resistive conditions. Surface EMG activity of eight ipsilateral muscles was recorded synchronously with the bilateral force production. For each session, force-velocity (F- \square) and power-velocity (P- \square) relationships were quantified by the theoretical values of maximal force at null velocity ($\bar{F}0$), maximal velocity at null force ($\bar{V}0$) and the resulting $\bar{P}max$ [3]. Muscle synergies were extracted from the EMG signals through non-negative matrix factorization [4] and divided into motor modules (i.e., relative muscle contribution) and motor primitives (i.e., temporal coefficients) for the heaviest load.

RESULTS

Mixed ANOVAs showed DOMS in most muscles at 2D, but only for women in the hamstrings ($p < 0.001$). A sex \times time interaction was found for $\bar{V}0$ ($p < 0.025$) and $\bar{P}max$ ($p < 0.024$), but not for $\bar{F}0$ (Figure 1). Planned contrasts showed significant decreases at 2D only for men in $\bar{V}0$ ($p < 0.009$) and

in $\bar{P}max$ ($p < 0.004$). Regardless of the session and sex, three muscle synergies were extracted from EMG data. The first synergy referred to the movement initiation with a major influence of the knee extensors, especially in women ($p < 0.001$). There was a session effect on the relative contribution of knee extensors, flexors and ankle flexors to this synergy ($p < 0.033$) and in women the main activity of motor primitives was shifted later in time compared to men ($p < 0.001$). The second synergy (mid push-off) showed a similar involvement of all muscles. In women, the motor primitives of this synergy were narrower (i.e., shorter in duration) and shifted later in time compared to men ($p < 0.001$). The third synergy corresponding to the late push-off phase showed a main contribution of the ankle joint flexors and extensors, with no sex- or session-related differences in the timing of motor primitives.

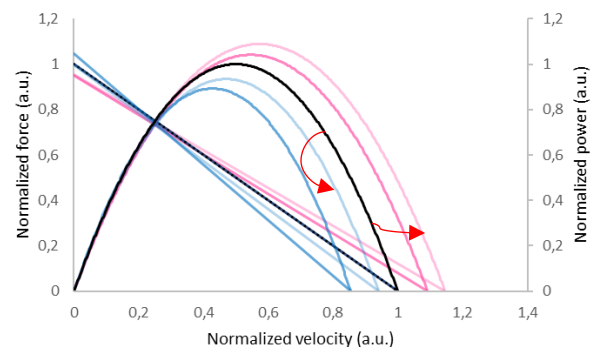


Figure 1 Normalized F- \square and P- \square relationships as compared to PRE (black curves) for men (blue curves) and for women (pink curves) at 2D and 4D (in bold and light, respectively)

DISCUSSION AND CONCLUSIONS

This study reveals a sex influence on the F- \square profile in a pluriarticular concentric test. Only men presented a 2D drop in performance. The relative muscle contributions to the movement initiation synergy were affected by both sex and session, suggesting that women modulate this synergy differently than men along the recovery. Sex also influenced the main activation timing of the initiation and mid push-off synergies. Taken together, our results suggest that the sex-specific organization of muscle synergies might explain the different timeline of recovery after a fatiguing run.

REFERENCES

- [1] Hunter SK et al. (2016). *MSSE*, **48**: 2247–2256
- [2] Chen TC et al. (2007). *J. Sports Sci.*, **5**: 55–63
- [3] Samozino P et al. (2012). *MSSE*, **44**: 313–322
- [4] Santuz A et al. (2018). *Sci. Rep.* **8**: 2740

Age-Related Lower Limb Muscle Co-Activation in Sit-to-Stand/Stand-to-Sit Performances

Anna Brinkmann¹, Sandra Lau², Conrad Fifelski-von Böhlen¹, Ole Meyer¹, Rebecca Diekmann¹, Andreas Hein¹

¹Assistive Systems and Medical Device Technology, Carl von Ossietzky University of Oldenburg, 26121 Oldenburg, Germany

²Geriatric Medicine, Carl von Ossietzky University of Oldenburg, 26121 Oldenburg, Germany

Email: anna.brinkmann1@uni-oldenburg.de

Summary

Dynamic muscle stability in functional tasks like Sit-to-Stand/Stand-to-Sit performances requires muscle co-activation of knee extensors and flexors. For a comparison of a geriatric patient and a healthy young subject, biomechanical and neurophysiological STS parameters were analyzed to determine muscle co-activation. Modified STS movement strategies induced higher co-activation in the geriatric patient due to sustained distribution of knee extensor and flexor muscle activity.

Introduction

Transitional movements in every-day life require active motor control units for horizontal and vertical displacement of the whole body's center of mass (CoM). During Sit-to-Stand/Stand-to-Sit (STS), balance control and coordination of the trunk and lower limbs are maintained through muscle co-activation (CA). Age-related physiological changes may lead to muscle weakness (1) and an increasing muscle CA during postural control (2) inducing altered movement patterns in functional tasks. Little is known about performance strategies of older, physically impaired persons during concentric and eccentric STS. Thus, the aim of the present pilot study was to focus on changes in biomechanical and neurophysiological STS parameters of a geriatric patient.

Methods

A geriatric patient (m, 68y, 1.70m, BMI: 35.90 kg/m²) and a young participant (m, 27y, 1.93m, BMI: 24.97 kg/m²) performed independently three series of a five timed STS (3). A standardized armless chair (0.45m seat height) was placed on a force plate in a laboratory setting (4). STS vertical CoMz velocity and acceleration were analyzed and phases defined according to (5). Unilateral EMG of Vastus Medialis (VM),

Rectus Femoris (RF) and Biceps Femoris (BF) were recorded (SENIAM guidelines), sampled (1 kHz) and amplified (2.5 kHz). EMG data was full-wave rectified, RMS filtered and normalized to STS peak value. Thus, relative muscle activation for concentric and eccentric STS was obtained and then used for the calculation of knee extensor (KE) and knee flexor (KF) CA ratios.

Results and Discussion

Existing differences in mechanical and muscle-specific STS parameters for the geriatric patient and the young participant are presented in Figure 1 and Table 1. Calculated CA ratios quantify the distribution of KE and KF activity for each STS phase (Figure 1). Lower CA ratios of the young participant indicate phasic muscle activation in which KE activity was followed by KF activity in concentric STS and reversed activity in eccentric STS. Predominantly higher CA ratios of the geriatric patient represent a more persistent KE and KF activity in concentric and eccentric STS indicating an altered movement strategy during postural control (6). The geriatric patient needed more time to rise from a chair and to adjust balance (7) (Figure 1, Table 1). In contrast, faster descending with high CA ratios led to a rigid posture reducing the degree of freedom and forced the patient to plump down onto the chair (8). The geriatric patient showed slower peak CoMz velocity and acceleration for both STS phases (Table 1).

Conclusions

This pilot trial was a proof-of-concept characterizing the distribution of muscle-specific parameters between concentric and eccentric STS performances for further application in studies. Results indicated changes in STS movement strategies inducing higher CA in the geriatric patient compared to a young study participant.

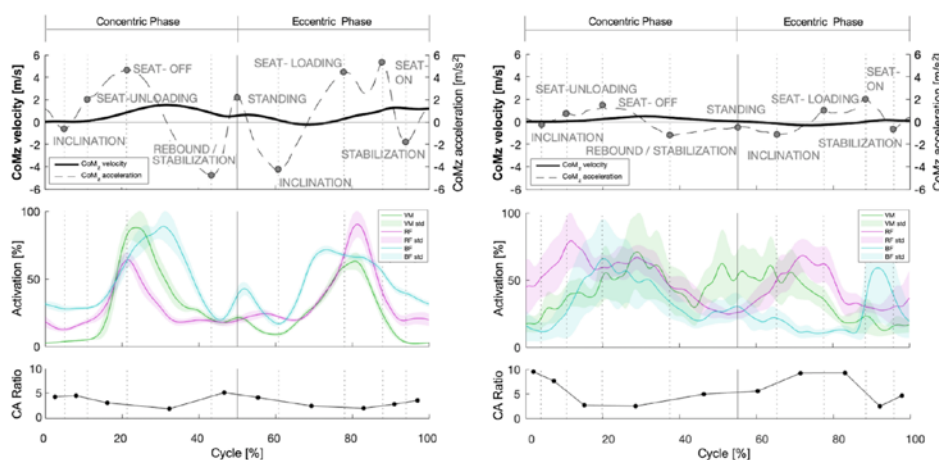


Figure 1: Mean CoMz velocity and acceleration, normalized mean EMG muscle activation plus standard deviation for three series of a five timed STS with respective KE/KF CA ratio for a young (left) and a geriatric (right) participant.

Table 1: Comparison of STS parameters of a young (total STS time: 2.1 s) and a geriatric participant (total STS time: 2.4 s).

Parameter	Concentric STS		Eccentric STS	
	Young	Geriatric	Young	Geriatric
Cycle	50.00 %	55.30 %	50.00 %	44.70 %
Rising/Descending	28.71 %	35.39 %	37.92 %	33.30 %
Stabilization	5.71 %	17.81 %	12.08 %	11.44 %
Peak CoMz Velocity	1.52 m/s	0.48 m/s	1.29 m/s	0.32 m/s
Peak CoMz Acceleration	4.78 m/s ²	1.20 m/s ²	5.34 m/s ²	2.04 m/s ²

References

- [1] Cruz-Jentoft A (2019). *Age Ageing*, **48**(1):16-31
- [2] Nagai K (2012). *J Gerontol A Biol Sci Med Sci*, **67**:882-9
- [3] Guralnik J (1995). *N Engl J Med*, **332**(9):556-61
- [4] Brinkmann A (2020). *Nanomaterials & Energy*, **9**:27-38
- [5] Krajl A (1990). *J Biomech*, **23**(11): 123-1138
- [6] Bernardi M (2004). *J Electromyogr Kinesiol*, **14**:401-10
- [7] Chorin F (2015). *Aging Clin Exp Res*, **28**(5):871-9
- [8] Tucker MG (2008). *Hum Mov Sci*, **27**:728-37

A new shoe sole technology that transfers the ground composition to the sole of the foot: a user experience evaluation

Bettina Sommer¹, Daniel Baumgartner², Roman P. Kuster^{2,3}, Michaela Wenger², **Christoph M. Bauer¹**

¹ Institute of Physiotherapy, School of Health Professions, Zurich University of Applied Sciences, Winterthur, Switzerland

² Institute of Mechanical Systems, School of Engineering, Zurich University of Applied Sciences, Winterthur, Switzerland

³ Division of Physiotherapy, Department of Neurobiology, Care Sciences and Society, Karolinska Institutet, Stockholm, Sweden

Email: christoph.bauer@zhaw.ch

Summary

A new, stimuli transmitting shoe sole technology transfers the ground composition mechanically to the sole of the foot when walking on uneven surfaces. Healthy participants evaluated the user experience of this sole technology.

All participants felt the stimuli transmission. The strongest sensation was in the forefoot region, where also most complaints occurred. Of the tested grounds like pavement and soft grounds, slight preferences were shown for nature trails, although preferences differed widely.

Introduction

With comfortable, shock-absorbing shoes, the mechanoreceptors of the sole of the foot are no longer stimulated. Consequently, a trend goes back to minimal shoes. However, also these have been shown to be insufficient to provide enough stimulation. This lack of stimulation leads to worse proprioception, which can lead to poor posture and to a risk of injuries. [1] Therefore, a new shoe sole technology is needed, which transfers the ground composition to the sole of the foot and may provide enough stability through an integrated foot bed.

Methods

The stimuli transmitting shoe sole technology is performed mechanically. The shoe sole consists of hard plastic balls, which are pushed towards the sole of the foot due to uneven surfaces (Figure 1).

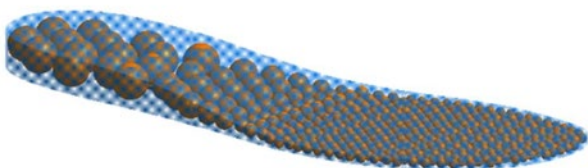


Figure 1: shoe sole technology with balls in orange

This shoe sole technology was evaluated by the user experience. Questionnaires covered walking sensation, comfort, complaints and intensity of sensory transmission. Answering options were on a Likert scale as well as open questions. The tests consisted of a two-week user study with the aim to evaluate the shoe sole in daily life as well as a one-hour monitored parcours evaluating the shoe sole on specific grounds (like stones, forest etc.). All participants were healthy with shoe size EU 38-43. The user study included 20 participants (Ø 64 years). Additionally, 10 persons (Ø 41 years) participated in the parcours.

Results and Discussion

Intensity: Most of the participants rated the stimulus transmission as very or rather strong. Nobody rated it as very weak. In the parcours, the strongest sensation was on coarse stones and pavement transitions, followed by the forest floor (Figure 2).

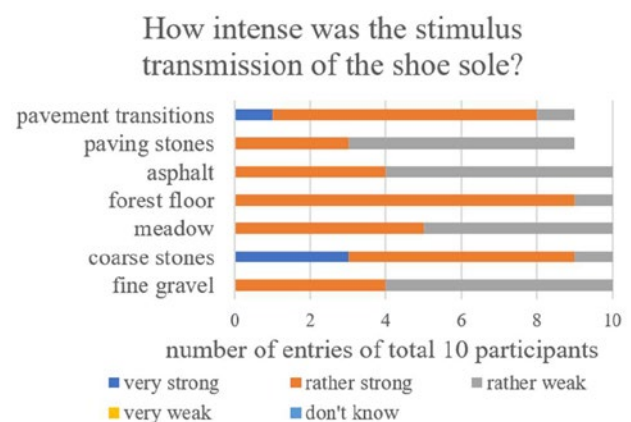


Figure 2: intensity of stimulus transmission depending on ground

Comfort & complaints: The majority perceived the shoe sole as very or rather comfortable. Participants perceived the stimuli strongest in the forefoot, where also most of the complaints occurred. The complaints were reported as tired feet, pain, pressure and burning feet, and occurred roughly every third day.

Ground composition: Nature trails seemed more comfortable than hard grounds, even though the opinions about hard grounds diverged. The most uncomfortable walking was on unpaved, downwards grounds.

Conclusions

All participants perceived the stimuli transmission of the shoe sole. However, the product polarizes. While some considered the stimuli as comfortable, others found them too strong. The forefoot was the part with the strongest stimuli sensation, but also with the most complaints.

Acknowledgments

The authors would like to thank Innosuisse for funding this study (LS-28381.1).

References

- [1] Altman and Davis (2012). *Current Sports Medicine Reports*, 11: 244-250

An Integrated Cloud Platform to Perform *In Silico* Standard Testing for Orthopedic Implants

Vincenzo Carbone, Alberto Palazzin, Marc-Antonio Bisotti, Roberta Bursi
 Research and Development, InSilicoTrials Technologies S.p.A., Trieste, Italy
 Email: vincenzo.carbone@insilicotrials.com

Introduction

Regulatory bodies impose stringent pre-market controls to certify the safety and compatibility of medical devices. However, internationally recognized standard tests may be expensive, time consuming and challenging for orthopedic implants because of many possible sizes and configurations. In addition, cost and time of experimental standard testing designed, developed, and used for generic devices may nullify the advantages of 3D-printed custom implants.

Modeling and simulation (M&S) can be used to virtually test medical devices before prototyping, helping manufactures and points-of-care to improve design reliability, speed up development process, and accelerate regulatory approval. We engineered an integrated cloud platform to perform *in silico* testing for orthopedic implants, assessing mechanical safety and electromagnetic compatibility in a completely virtual environment, in line with recognized standards and regulatory guidelines.

Methods

The InSilicoTrials.com platform contains two M&S tools for orthopedic implants: CONSELF and NuMRis.

CONSELF (conself.com) uses Salome-Meca 2017 to compute static implant stresses and strains on metallic orthopedic devices, following the requirements and considerations of ASTM F2996-20 Standard Practice for non-modular hip femoral stems [1] and ASTM F3161-16 Standard Test Method for total knee femoral components [2]. Simulation results were consistent with those reported in the two standards.

NuMRis (numris.insilicomri.com) uses ANSYS HFSS and ANSYS Mechanical 2019R3 to compute radio-frequency energy absorption and induced heating during magnetic resonance imaging in 1.5T and 3T MRI coils, replicating the ASTM F2182-19e2 Standard Test Method [3]. Simulation results were validated against *in vitro* measurements.

The integrated M&S workflow on the cloud platform allows the user to upload the 3D geometry and the material properties of the orthopedic implant to be tested, automatically set up the standard testing scenarios, run simulations and process outcome, with the option to summarize the results in accordance with current FDA guidance on M&S reporting [4].

Results and Discussion

The easy-to-use interfaces of InSilicoTrials tools run through commercial web browsers, requiring no specific expertise in computational methods or additional on-premises software and hardware resources, since all simulations are run remotely on cloud infrastructure.

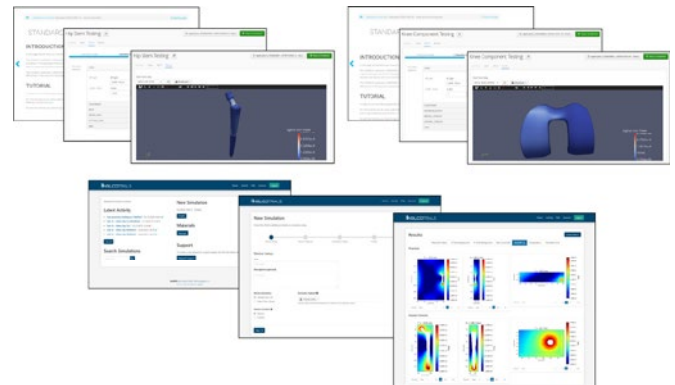


Figure 1: Web interface of the CONSELF and NuMRis tools.

The integrated cloud platform can be used to evaluate design alternatives, test multi-configuration devices, perform multi-objective design optimization, and identify worst-case scenarios within a family of implant sizes, thus reducing the amount of physical testing to be conducted.

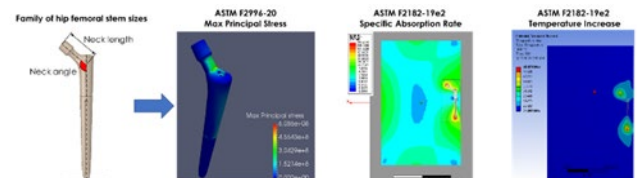


Figure 2: CASE EXAMPLE: Evaluate design alternatives and identify worst-case scenarios within a family of implant sizes.

Conclusions

InSilicoTrials.com is the first cloud platform offering a collection of M&S tools to perform *in silico* standard testing for orthopedic implants. The proposed tools allow to easily assess mechanical safety and electromagnetic compatibility of generic and custom devices before prototyping, preventing risks and criticalities for the patient, and helping manufacturers and points-of-care to accelerate time and reduce costs of device development.

The proposed platform promotes the broader adoption of digital evidence in preclinical trials, supporting the device submission process and pre-market regulatory evaluation, and helping accelerate regulatory approval.

References

- [1] ASTM F2996-20, *ASTM International*.
- [2] ASTM F3161-16, *ASTM International*.
- [3] ASTM F2182-19e2, *ASTM International*.
- [4] Reporting of Computational Modeling Studies in Medical Device Submissions, *FDA guidance*, September 2016.

Can tibio-talo-calcaneal arthrodesis help to assess the effect of the soft tissue artefacts in hindfoot kinematics

A. Naaim¹, P.A. Deleu^{1,2}, Devos Evernage², T. Leemrijse², L. Chize¹, R. Dumas¹

¹Univ Lyon, Univ Gustave Eiffel, LMC UMR T9406, F69622, Lyon, France

²Foot Ankle Institute, 5 Avenue Ariane, 1200 Brussels, Belgium

Email: alexandre.naaim@univ-lyon1.fr

Summary

Soft tissue artefacts (STA) is one of the main limitations for using motion capture. Foot joint arthrodeses are frequently performed in end-stage osteoarthritis. Tibio-talo-calcaneal (TTC) arthrodesis consists to fuse the joints between the calcaneus, the talus and the tibia together. One may expect that motion recorded during gait between the segments of the calcaneus and the shank would result only from STA. Four subjects who underwent a TTC arthrodesis performed a gait analysis with a modified version of the Rizzoli foot model. Effects of STA found for the shank-calcaneus dorsi-plantar flexion were larger than that reported in previous studies. This might be due to major skin sliding over the calcaneus for these subjects. Studies assessing subjects with TTC arthrodesis should interpret kinematic data with caution.

Introduction

Soft tissue artefacts (STA), the underlying movement between skin markers and their anatomical counterpart, remain one of the main limitations in using marker base motion analysis both in research and in clinical context [1]. Usually, STA can be evaluated using invasive protocols such as intracortical pins [2] or using imaging technology [3]. As a result, it might be difficult for a laboratory to evaluate how STA affect their measurements. A solution might arise for the ankle and foot joints. Foot joint arthrodeses are frequently performed in end-stage osteoarthritis. Tibio-talo-calcaneal (TTC) arthrodesis consists to fuse the joints between the calcaneus, the talus and the tibia. One may expect that motion recorded between the segments of the calcaneus and the shank would result from STA as the joints are fused. In this first feasibility study, the 3D kinematics of shank-calcaneus (Sha-Cal) joint of subjects with TTC arthrodesis was evaluated.

Methods

Three male and one female subjects (age: 46.5 ± 6.5 years, BMI: $31 \pm 8 \text{ kg.m}^{-2}$) with a TTC arthrodesis participated in this study. One subject had the surgical procedure at both feet. At least 12 months post-operatively, they performed a gait analysis. The participants were asked to walk at self-selected speed barefoot over a 10 m walkway.

Inter-segment foot kinematics were obtained using a motion-capture system of 10 Miquis cameras (Qualysis, Goteborg Sweden) at a 200Hz frequency. An adaptation of the Rizzoli foot model proposed by Deschamps et al. [4] was used. This model allowed to consider the Sha-Cal joint as the movement between the tibia and the calcaneus.

The effect of the STA was quantified as the mean range of motion (RoM) about the three joint axes during the five most

homogeneous trials (based on walking speed) and compared to the fluoroscopic results of Kessler et al. [2].

Results and Discussion

Table 1: Mean Range of Motion (RoM) in degree of the Sha-Cal joint during a gait cycle for all subjects

Subject	Mean RoM Dorsi-plantar flexion	Mean RoM Inversion-Eversion	Mean RoM Abduction-Adduction
S1 Left	7.1°	3.4°	1.7°
S2 Left	6.1°	1.4°	1.0°
S3 Right	7.2°	1.5°	0.2°
S4 Left	9.5°	3.6°	1.8°
S4 Right	9.3°	3.8°	2.1°
Mean (n = 5)	7.8°	2.8°	1.3°
StD (n = 5)	1.5°	1.2°	0.8°
STA in Kessler et al. [2] (n = 9)	2.5°	3.6°	4.3°

Surprisingly, our results differ from the findings of Kessler et al. [3] who used bi-plane fluoroscopy on asymptomatic subjects. In contrast to their results, this study found the largest effect of STA for dorsi-plantar flexion (STA effect appears 2 to 3 time larger). For the two other joint axes, the effect tends to be lower in our study.

During gait, STA is mainly due to skin sliding as opposed to muscle contraction or inertial effects. A possible explanation for this amplified effect found on dorsi-plantar flexion might be a major skin sliding over the calcaneus, with the TTC arthrodesis acting as a large “wrapping object” for the skin. As the movement of the other mobile joints occurs mainly in dorsi-plantar flexion, the STA effect tends to be larger about this joint axis.

Conclusions

A larger than expected effect of the STA on hindfoot joint kinematics was found in our study. It seems that Sha-Cal joint arthrodesis does not represent an efficient method to assess the effect of STA on the joint kinematics. In addition, studies assessing foot joint kinematics after TTC arthrodesis should interpret their results with caution as large STA were found for the hindfoot.

In future work, it could be interesting to evaluate this method on a larger sample and other fused foot joints.

References

- [1] Camomilla, et al. (2017). *J Biomech*, 1-4.
- [2] Nester, et al. (2007). *J Biomech*, **40**: 3412-3413.
- [3] Kessler et al. (2019) *Front Bioeng Biotechnol*
- [4] Deschamps et al. (2017) *Gait Posture*, **5**: 40-44

Reliability and Repeatability of a Methodology for Real World Gait and Posture Assessment in Children

Alfredo Ciniglio¹, Francesca Michieletto¹, Federica Cibirin³, Fabiola Spolaor¹, Annamaria Guiotto¹, Zimi Sawacha^{1,2}

¹Dept of Information Engineering, University of Padova, Italy

²Dept of Medicine, University of Padova, Italy

³BBSof S.r.l., Padova, Italy

Email: zimi.sawacha@dei.unipd.it

Summary

Assessing interventions for mobility disorders in children using real-life movement is still an unsolved problem and the possibility to transfer gait analysis to the real world conditions to prevent children postural alterations is attracting attention in the literature [1]. The aim of the study was to evaluate the reliability and repeatability of a methodology for forming movement analysis for mobility disorders assessment in children in real world conditions. To this extent commercial video-cameras and automatic tracking of features techniques were used. Results are encouraging as good reliability and repeatability were observed.

Introduction

Gait analysis is a process of instrumented measurement and evaluation of walking ability in patients, recognized as a useful assessment tool and a support in medical decision-making [2]. Standard gait analysis is performed within a gait laboratory by means of stereophotogrammetric systems. Recently great attention has been given to the possibility of assessing children's motion for gait and posture evaluation purposes, in real world conditions [1]. The aim of this study was to evaluate the reliability and repeatability of a methodology for gait and posture assessment in real world conditions by means of commercial video-cameras and automatic tracking of features techniques in children. This approach could be exploited in ambulatory conditions, in school or sport facilities, for the prevention of postural alterations in children with foot deformities [3], scoliosis [4] and temporomandibular disorders [5].

Methods

Eleven subjects (mean±SD age 9.7 ± 2.6 years, BMI 20.6 ± 3.5 kg/m²) were acquired simultaneously with a stereophotogrammetric system (6 TVC, 60-120 Hz, BTS) and 4 GoPro Hero 7 cameras. Each subject performed several gait cycles and 4 different set-up were adopted: reflective markers on anatomical landmarks ("BTS"), markers made with double colored tape ("Tape") [6], without applying any marker ("NoTape"). Reflective markers were applied as in [7] and trajectories were reconstructed through stereophotogrammetry ("BTS") or video tracking ("Marker"), using Track on Field (BBSof, S.r.l), based on a self-developed tracking of feature algorithm [6]; in the other 2 conditions (Tape and NoTape), a simplified version of [7] was applied and only video tracking was used to reconstruct anatomical landmarks trajectories. Joints angles were determined as in [6] for "BTS" and "Marker" set up, while

only sagittal plane kinematics was retrieved for "Tape" and "NoTape". Comparison among the four set-up was performed through the estimation of the mean root mean square distance (RMSD) and Wilcoxon signed-rank test ($p < 0.05$). For the inter-trial variability, the Coefficient of Multiple Correlation ("CMC") [8] was calculated for each biomechanical variable. Normative bands were created, for each condition, including only trials with a CMC > 0.7 [9]. To verify the inter-operator variability the Standard Error ("SE") [9] was calculated (2 operators).

Results and Discussion

Although statistically significant differences were observed, results showed that the 4 set up were comparable in terms of occurrence of the joint angles peak within the gait cycle (Fig. 1, right) and range of motion (Fig.1, left). Good inter-operator repeatability was found.

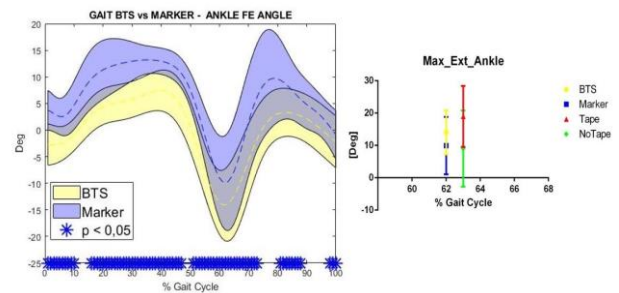


Figure 1: Left side: Ankle Flexion-Extension Angle, "BTS" & "Marker" asterisks indicate statistically significant differences; right side: Ankle Extension Angle Peaks

Conclusions

Results are encouraging toward the adoption of a wider use of motion analysis in real world conditions as in sport or rehabilitation facilities, and schools.

References

- [1] Wang et al. (2019). *Sensors*, **19**(8): 1925.
- [2] Benedetti et al. (2017). *Gait & Posture*, **58**: 252-260
- [3] Root et al. (1999). *JAPMA*, **89**: 268-269
- [4] Negrini et al. (2012). *SOSORT*, **7**:3
- [5] Mason et al. (2014). *Otolaryngologists*, **4**(4): e110.
- [6] Magalhães et al. (2013). *J Sports Sc & Med*, **58**:194-200
- [7] Leardini et al. (2007) *Gait & Posture*, **26**(4): 560-71.
- [8] Ferrari et al. (2010). *Gait & Posture*, **31**(4): 540-542
- [9] Schwartz et al. (2004). *Gait & Posture*, **20**: 196-203.

Summary

In recent years, high-density surface electromyography (HD-sEMG) is gaining more popularity. In this study, reliability of electrical activities of ankle dorsi-/plantar-flexors measured by HD-sEMG are evaluated during isometric contraction. Furthermore, multiple features are extracted from the collected signals to characterize the major muscles around the ankle. Measurements were conducted with different angle and percentages of the maximum voluntary contraction (MVC). Results show reliability of less than 10% variance. Features such as mean average value (MAV) and zero crossing (ZC) could be potentially useful to indicate muscle characteristics in clinical applications.

Introduction

HD-sEMG has been more and more applied to quantify spatial and temporal muscle activity [1-2], which can provide insights into new muscle characteristics. The aim of this study is to evaluate the reliability of HD-sEMG recordings of major ankle muscles during isometric contraction and extract features from the collected signals that can be used to characterize the muscles.

Methods

An experimental protocol was designed to collect HD-sEMG data (Quattrocento, OT Bioelettronica) from five muscles (medial and lateral gastrocnemius, soleus, peroneus longus and tibialis anterior) of the right lower leg of five healthy subjects (3F/2M, age: 28.6 ± 5.4 yrs, height: 169.0 ± 8.9 cm) at 30%, 50% and 70% MVC in plantarflexors and dorsiflexors, respectively. The grid was placed on each muscle according to a standardized protocol. The participants were asked to follow a trapezoidal force profile with 5 repetitions on the display with $\pm 10\%$ error allowed and 5s rest between each repetition. The torque was measured simultaneously using an ankle dynamometer. Each test constituted of 4 ankle angles in a randomized order (a neutral position at 0° , 7.5° and 15° plantarflexion and 10° dorsiflexion). To determine the reliability of the experimental setup, relative variance between measurements in two different days were evaluated. To investigate the characteristics of the muscles during the sub-MVCs, heatmaps of muscle activation were created and two common EMG features, namely MAV and ZC, were extracted.

Results and Discussion

The preliminary results of reliability show intra-subject variance as low as 1% for tibia anterior (TA). The highest variance of 9% was found for gastrocnemius medialis (GM). Heatmaps of the measured average differential EMG signal

in each electrode of the grid provide visual information on the spatial distribution and magnitude of activation in the muscles over the measured area (Fig 1a-c). Different subject recruit different part of the muscle to produce the same level of the MVC. The extracted MAV of tibia anterior was found to correlate with ankle angle, increasing from the dorsiflexion to plantarflexion positions. Moreover, analyzing the signal in frequency domain with ZC feature, we observed that the peaks of ZC slightly increased from the first to the last sub-MVC attempt (Fig 1d). The increased ZC could indicate a correlation between the frequency of the signal and MU temporal recruitment as well as possible fatigue.

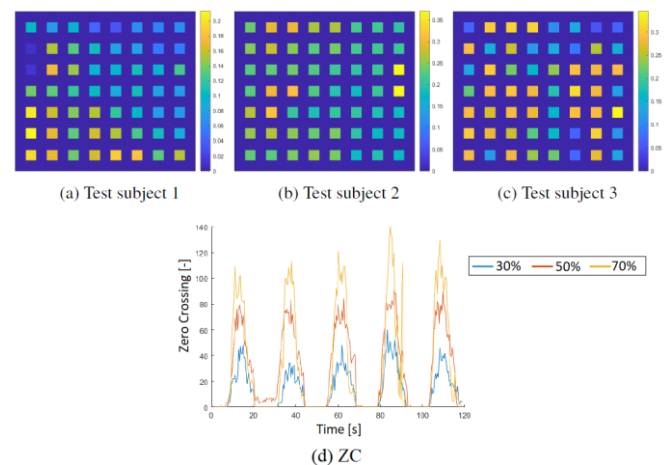


Figure 1: (a-c) Visualization of the spatial muscle activation of TA during isometric dorsiflexion (70% MVC and 0°). (d) ZC change of GM during isometric plantarflexion at 15° with sub-MVCs

Conclusions

Our preliminary study shows promising results in terms of intra-subject reliability. Multiple features were extracted from the collected signals and identified as a possible indicator for muscle characteristics such as muscle fatigue, activation, and spatial distribution of activation. This can be a helpful tool to assess the muscle contraction in different population and identify compromised areas of the muscles amongst others.

Acknowledgments

We would like to acknowledge financial support from Promobilia Foundation and (20039) Swedish Research Council (2018-04902).

References

- [1] Gea Drost et al. (2006) *J Electromyogr Kinesiol* 16:586-602
- [2] Di Girolamo M. et al. (2017) *Inform. Med. Unlocked* 9:255-263

A modified vertex-wise Bhattacharya metric to compare statistical shape models of pediatric ankle bones

A. Boutillon^{1,2}, A. Salhi^{1,2}, R. Bailly^{2,3}, M. Naffrechoux², S. Brochard^{2,3}, B. Borotikar^{2,3,4}

¹IMT Atlantique, Brest, France ²LaTIM, INSERM UMR 1101, Brest, France ³CHRU de Brest, Brest, France

⁴Symbiosis Centre for Medical Image Analysis, Symbiosis International University, Pune, India

Email: bhushan.borotikar@scmia.edu.in

Summary

We propose a method to compare healthy and pathological statistical shape models (SSM) of the pediatric talus. The proposed approach, based on a vertex-wise Bhattacharya metric, provides clinically relevant local similarity assessment and allows an evaluation of the musculoskeletal disorder impact on different bone regions. Experiments conducted on pediatric cohorts of healthy and equinus ankles illustrate the clinical potential of the methodology.

Introduction

The Bhattacharya coefficient, which measures the similarity between probability distributions, has already been used to compare SSM built from the same dataset but with different point-set registration algorithms [1]. A global overlap was computed on point-based probability distributions, and the returned value ranged from 0 (dissimilar) to 1 (similar).

However, in clinical practice, it is needed to compare two separate populations (healthy and pathological) and to assess the local modifications in shape conveyed by the disorder. Hence, rather than comparing the global shape distributions arising from the healthy and pathological populations, we propose to employ a vertex-wise Bhattacharya metric on selected bone regions.

Methods

MR images of 20 pediatric ankles (10 healthy and 10 equinus) were acquired using a 3T scanner after acquiring parental consent. An expert manually segmented the images to obtain the 3D meshes of the talus bone. A non-rigid alignment algorithm was used to obtain point-to-point correspondence between the 20 shapes [2]. We then created two SSMs, one each from the healthy and equinus populations, using the established correspondences [2]. The two SSMs were thus in point-to-point correspondence, and each point, in each SSM, was defined by a 3D distribution.

We selected 5 regions on the mean healthy talus bone (Fig. 1): posterior facet (PF), anterior facet (AF), articular surface for tibia (AST), articular surface for lateral malleolus (ASLM) and head (H). For each vertex in these regions, we computed the Bhattacharya overlap between the healthy and pathological 3D Gaussian distributions, based on their respective means and covariance matrices. Then for each region, we determined the mean, standard deviation (STD), minimum and maximum of the vertex-wise coefficients.

Results and Discussion

The obtained mean Bhattacharya overlap ranged from 0.36 to 0.41, indicating medium similarity between healthy and pathological SSM (Tab. 1). The minimum similarities were observed in region AF (0.19) and H (0.12), while the maximum appeared in region PF (0.63) and H (0.62). The visualization (Fig. 1) further illustrated that regions AF and H were the most impacted by the pathology.

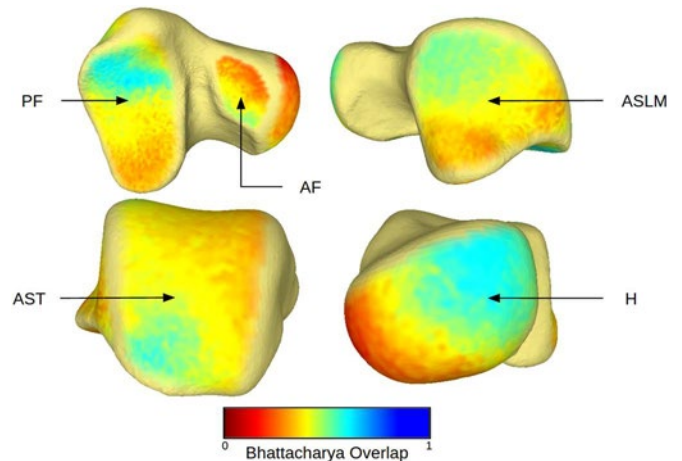


Figure 1: Visualization of the vertex-wise Bhattacharya overlap between healthy and pathological SSM on the 5 talus regions.

However, while the results appear promising, the proposed methodology is limited by the low sample size, which is due to the scarcity of pediatric datasets.

Conclusions

We presented a method, based on SSM and vertex-wise Bhattacharya metric, to assess the impact of the equinus pathology on the shape of the pediatric talus.

Acknowledgments

This work was funded by IMT, Fondation Mines-Télécom, Institut Carnot TSN (Futur & Ruptures). Data was acquired with the support of Fondation motrice (2015/7), Fondation de l'Avenir (AP-RM-16-041) and Innoveo (CHRU Brest).

References

- [1] Babalola K.O. et al. (2006). *MICCAI*, **4190**: 142-150.
- [2] Salhi A. et al. (2020). *Annals of BME*, **48**: 367-379.

Table 1: Mean, standard deviation, minimum and maximum of the vertex-wise Bhattacharya overlaps on the 5 talus regions.

	Talus region	PF	AF	AST	ASLM	H
Vertex-wise Bhattacharya overlap	Mean ± STD	0.41 ± 0.09	0.36 ± 0.08	0.41 ± 0.06	0.40 ± 0.06	0.40 ± 0.13
	Min / Max	0.25 / 0.63	0.19 / 0.53	0.28 / 0.59	0.27 / 0.54	0.12 / 0.62

Validation of kinematic models of the human whole body centre of mass

Charlotte Le Mouel¹,

¹Movement Science, University of Münster, Münster, Germany

Email: charlotte.lemouel@normale.fr

Summary

Characterising human movement and balance requires estimating the position of the whole body centre of mass (CoM). This is typically done using kinematic models, whose validity during dynamic movement is not known. During running, when the body is in the air, the acceleration of the CoM is equal to gravity. This study compares this ground truth to the CoM acceleration obtained from three different kinematic models. The state-of-the-art model has a mean error of 2.4 m/s². The simplified models have a larger error, up to 4.8 m/s². This error may be improved by combining kinematic and force plate recordings.

Introduction

To characterise human movement and balance, the external forces and torques acting upon the human body need to be estimated. The force and torque exerted by the ground reaction can be directly measured using force plates. To determine the torque exerted by weight however, the position of the whole body CoM must be estimated. This is typically done with kinematic recordings. The body is divided into segments and a model is used to determine the weight and CoM of each segment, which are then combined to obtain the whole body CoM.

The state-of-the-art kinematic model requires measuring the position of 38 markers [1], which is cumbersome and time consuming. Therefore, simplified versions of this model have been proposed. This study compares the accuracy of three kinematic models during dynamic movement.

Methods

Three kinematic models of the CoM were compared: 1. the state-of-the-art model, requiring 38 markers [1], 2. a simplified version requiring 13 markers [2], 3. the hip midpoint, requiring 4 markers.

The CoM position was reconstructed during running, smoothed using a Savitzky-Golay filter of order 3, and differentiated twice to obtain acceleration. Only the flight phases of running were analysed.

Results and Discussion

During the flight phase of running, the acceleration of the CoM is equal to gravity, i.e. null in the horizontal plane and downwards of amplitude 9.81 m/s². However, the mean acceleration calculated from all three kinematic models had a bias both in the vertical direction and in the horizontal plane. Downwards acceleration was overestimated by 0.7 m/s² for the full model, and by 1.2 m/s² for both the simplified and hip models. The bias in the forwards direction was largest for the hip model (-3.0 m/s²), followed by the simplified model (0.8 m/s²) then the full model (0.3 m/s²). The mean net error was also largest for the hip model (4.8 m/s²), followed by the simplified model (3.7 m/s²) then the full model (2.4 m/s²).

The state-of-the-art kinematic model of the CoM does not provide an accurate estimate of the CoM acceleration during

running. Simultaneous recordings of kinematics and ground reaction forces could provide improved estimates of CoM position.

Conclusions

The estimation of CoM position from kinematics has a mean error in acceleration of at least 2.4 m/s² during running. This error may be improved by combining kinematic and force plate recordings.

References

- [1] R. Dumas, L. Chèze, and J.-P. Verriest, "Adjustments to McConville et al. and Young et al. body segment inertial parameters," *J. Biomech.*, vol. 40, no. 3, pp. 543–553, 2007, doi: 10.1016/j.jbiomech.2006.02.013.
- [2] R. Tisserand, T. Robert, R. Dumas, and L. Chèze, "A simplified marker set to define the center of mass for stability analysis in dynamic situations," *Gait Posture*, vol. 48, pp. 64–67, Jul. 2016, doi: 10.1016/j.gait-post.2016.04.032.

Summary

Principal Component Analysis (PCA) has been extensively used to reduce hand kinematics because hand joints have coordinated movements (kinematic synergies). However, synergies are task-dependent and the variety of tasks the hands can perform during daily life is vast. The aim of this work is to identify a small set of tasks representative of the hand kinematic synergies during activities of daily living (ADL) by using an iterative PCA method. Kinematic synergies were extracted from 16 hand joint angles recorded to 24 healthy adults while performing 24 varied ADL. As a result, 6 ADL could be enough to obtain kinematic synergies with high level of similarity to those considering a wide set of varied ADL, and with little loss of range of movement.

Introduction

PCA has been extensively used to reduce hand kinematics in many fields, such as in prosthesis design, based on the fact that hand joints have coordinated movements (kinematic synergies) [1]. These synergies are obtained from the analysis of hand kinematics during the performance of some tasks. However, the variety of tasks the hands can perform during daily life is vast. The aim of this work is identifying a small set of tasks representative of the hand kinematic synergies during ADL.

Methods

Hand kinematics data from [2] were used (16 joint angles of 24 right-handed healthy adults while performing 24 varied ADL). A first PCA (eigenvalues, varimax rotation, standardized data) was applied to all the data to identify the kinematic synergies (²⁴PCi). Then, an iterative method was followed: in each step, the kinematic data was reduced by removing each ADL data one-by-one, and the resulting N datasets were used as input in N PCA (one PCA per each ADL, N=24-k, in the k-th step). In this case, a non-standard scaling was applied, using the mean and SD of the original

matrix. In each step, the dataset explaining highest variance was selected as input for the next step. This iteration was repeated until one ADL remained (k=23). Finally, the similarity between the synergies in each step (^{24-k}PCi) and the original ones (²⁴PCi) was checked by means of the angles between the vectors that represent both set of synergies, and the comparison of the scores of ^{24-k}PCi respect to ²⁴PCi.

Results

Five synergies (⁶PCi) representative of all the ADL were obtained from the first PCA (with 73.1% of the variability of the original data). Figure 1 (Left) shows the % of variance of the original data explained in each step of the iterative ADL removal, where a slight decrease is observed until arriving to a set with only 6 ADL. The 5 synergies (⁶PCi) from this set of 6 ADL explained 71.9% of the original data variance, and were quite similar to the original ones and with similar ranges in the coordinated movements (Figure 1, Right).

Discussion

The results suggest that a set with only 6 ADL (cleaning with a cloth, pouring water, putting a shirt on and doing buttons up, opening a door, talking by phone and putting shoes on and tying laces) could be enough to obtain the kinematic synergies underlying ADL, with high level of similarity to those considering a wide set of varied ADL and with little loss of range of movement. Some ADL provided high inter-subject variability. Therefore, it might be interesting to investigate the sample size required to obtain representative results of global population.

Acknowledgments

UJI-2017-51, PGC2018-095606-C21 (MCIU/AEI/FEDER, UE)

References

- [1] C. Della Santina, et al. (2017). *Front. Neurobot*, **11**:41.
- [2] Gracia-Ibáñez et al. (2017). *J. Hand Ther*, **30**: 337-347.

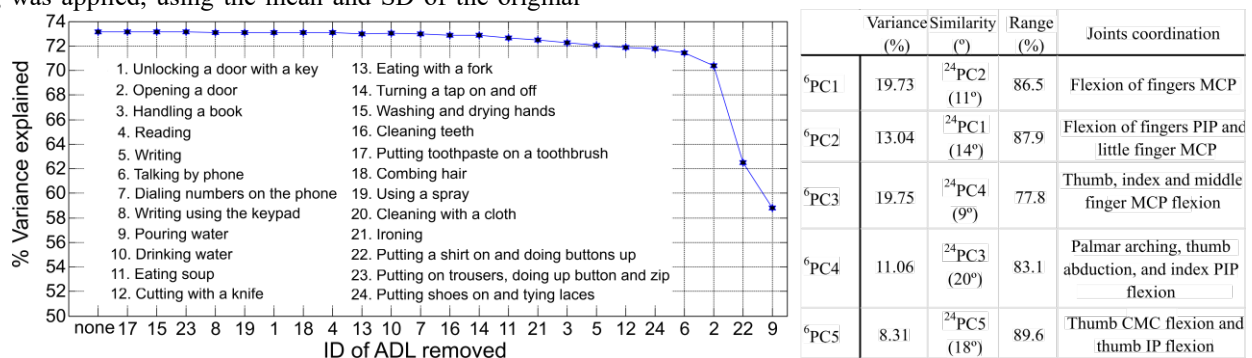


Figure 1: (Left) List of ADLs and plot of variance explained in each step of the iterative ADL removal. (Right) Description of ⁶PCi: Percentage of the original data variance explained by the ⁶PCi, similarity to which ²⁴PCi and corresponding angle, range of scores with respect to that of similar ²⁴PCi. Abbreviations: Carpometacarpal (CMC) Metacarpophalangeal (MCP) Proximal Interphalangeal (PIP)

Falling heads biomechanical and neuromuscular responses to head-neck perturbations

Isabell Wochner¹, Lennart Nölle¹, Oleksandr Martynenko¹, Syn Schmitt¹

¹Institute for Modelling and Simulation of Biomechanical Systems, Stuttgart Center for Simulation Science, University of Stuttgart, Germany

Email: isabell.wochner@simtech.uni-stuttgart.de

Summary

In this study, we conducted perturbations experiments (called ‘falling heads experiments’) to the head-neck complex to understand the involved reflexive responses. The volunteers were placed on a table with an additional trapdoor supporting the head. This trapdoor was suddenly released, leading to a free-fall movement of the head until the muscles’ reflexive responses stopped the downwards movement. We report the experimental results and enhance them by performing simulations with a reflex controller. The experimental dataset [1] can be used as a benchmark test to compare different muscle control strategies and validate existing human body models.

Introduction

Head and neck perturbations can lead to injuries in many different situations ranging from sports-related impacts to car accident scenarios. Such injuries are widely recognized as a significant public health concern [2,3]. They are induced by biomechanical forces such as contact or inertial forces that are transmitted to the brain, head or upper body. To better understand the underlying phenomena, we set up experiments perturbing the head-neck complex for two force directions (flexion and extension) with healthy participants of different ages and genders.

Methods

In the experiments, 17 volunteers were placed on a table in a supine and prone position. The subject’s head was supported by a trap door, which was unexpectedly released leading to the heads’ free-fall movement (see Fig. 1). We recorded the heads’ kinematic trajectory and the electromyographic signal of the *sternocleidomastoideus* and the *trapezius* muscle. Furthermore, we performed simulations matching this ‘Falling Head’ experiment using a simple stretch-based reflex controller.

Results and Discussion

First, we show a large difference in the individual reflexive responses between participants: The maximal falling height between participants varies between 3.2-14.9 cm, and latency times range between 17.67-86.67 ms (in the supine case). Second, the reflexive behavior depends on the directions of the perturbation force: in the prone case the participants tend to fall less (range between 0.5 – 8.3 cm vs 3.2-14.9 cm), and they display smaller linear and rotational peak accelerations (average rotational peak of 44.4 rad/s² vs 62.4 rad/s²). Third, we show that our neuro-musculoskeletal simulations using a reflex controller can predict similar responses compared to the experiments. Furthermore, this response can be modulated by simple control parameter adjustments (e.g. reflex thresholds). Based on this controller variation, we show that a higher sensitivity in the neuronal state (e.g. a higher threshold) reduces acceleration peaks, which might reduce injury risks.

Conclusions

The findings based on the experimental results of our study will help to improve existing and to develop potentially better Human Body Models and muscle control strategies.

Acknowledgments

This work was supported by the EU Horizon 2020 research and innovation program under grant agreement No. 768947 ‘OSCCAR’ and by the Deutsche Forschungsgemeinschaft (DFG, German Research Foundation) under Germany’s Excellence Strategy - E-C 2075 - 390740016 (SimTech).

References

- [1] Wochner, I. et al. (submitted 2020).
- [2] Genner A, et al. (2009) *Int. Emerg. Nurs.*, 1(1):52–59.
- [3] Rubiano, AM et al. (2015). *Nature*, 5(7578), S193-S197.

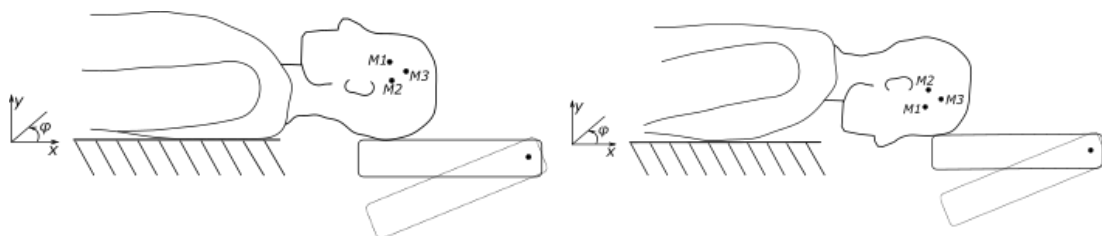


Figure 1: Sketch of volunteer placement in supine and prone position.

New approach on constitutive modeling of the pure titanium thermoplastic deformation

Jakub Bańcerowski¹, Marek Pawlikowski¹

¹ Warsaw University of Technology, Institute of Mechanics and Printing, Poland

Summary

Commercially pure titanium was compressed in high temperatures and under various strain rates in order to increase its strength by grain fragmentation. However, to fully control this complex thermomechanical process, proper constitutive equation had to be implemented. The experimental data was fitted to Arrhenius, Johnson-Cook, Khan-Huang-Liang and Anand equations to determine which model would be most useful in further work.

Introduction

Commercially Pure (CP) titanium as a biomaterial requires controlled plastic deformation processing to increase its strength [1]. This process is complex and dependent on many factors such as strain rate, temperature, coefficients of strain hardening and softening and others [2]. To ensure stability and repeatability of this process, constitutive equation must be applied [3]. In order to find the most accurate model for our process, several equations were selected and fitted to the data.

Methods

CP titanium (Ti) samples were compressed at elevated temperatures (775 K ÷ 875 K) at different strain rates ($\dot{\epsilon} = 10^{-2} \div 10^1$) to the constant strain $\epsilon = 0.6$ in a Gleeble thermomechanical simulator. The data from the experiment were used in the constitutive model constants identification.

According to literature the most commonly used constitutive equations were Arrhenius model (1), Johnson-Cook eq. (JC) (2) and Khan-Huang-Liang eq. (KHL) (3). Due to viscoplastic character of the deformation the Anand model (4) (usually employed for the solder processing modeling) was also chosen.

- Arrhenius model:

$$\dot{\epsilon} = A[\sinh(\alpha\sigma)] \exp\left(-\frac{Q}{RT}\right), \quad (1)$$

where $\dot{\epsilon}$ [s⁻¹] - strain rate, A , β , n_1 , n , $\alpha = \beta/n_1$ - material constants, Q [kJmol⁻¹] - activation energy of plastic strain, R - universal gas constant, T [K] - temperature, σ [MPa] - flow stress;

- Johnson-Cook eq.:

$$\sigma = (A + B\epsilon^n)(1 + C \ln \dot{\epsilon}^*) (1 - T^{*m}), \quad (2)$$

where A , B , n , m are material constants.

- Khan-Huang-Liang eq.:

$$\sigma = \left[A + B \left(1 - \frac{\ln \dot{\epsilon}}{\ln D_0^p} \right)^{n_1} (\epsilon^p)^{n_0} \right] \left(\frac{\dot{\epsilon}}{\dot{\epsilon}^*} \right)^C \left(\frac{T_m - T}{T_m - T_r} \right)^m \quad (3)$$

where A , B , C , m , n_1 are material constants, D_0^p is upper bound strain rate (arbitrarily chosen), T_m is melting temp., T_r is reference temp. (arbitrarily chosen).

- Anand eq.:

$$\dot{\epsilon}_p = A \exp\left(-\frac{Q}{RT}\right) \left[\sinh\left(\xi \frac{\sigma}{s}\right) \right]^{\frac{1}{m}} \quad (4)$$

where s , ξ , m are material constants. The common symbols in equations (1), (2), (3) and (4) denote the same quantities.

Results and Discussion

Models were fitted to data with the varying degrees of success. The Anand, JC and KHL models provide a good fit. The Arrhenius one is less adequate (Fig. 1). It is worth noticing that only Anand model is able to represent the whole range of deformation.

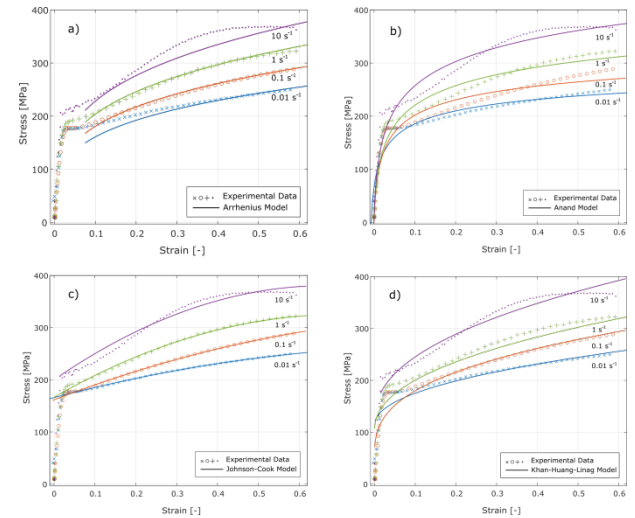


Figure 1: Stress-strain graphs and Arrhenius (a), Anand (b), JC (c), KHL (d) models for the 775 K deformation process.

Conclusions

The applied models provide precise fit in plastic deformation zone. JC is the most accurate for the higher strain rates. KHL model is the most precise one in plastic zone. Arrhenius model is the least precise. The most promising is however Anand model, due to its ability to predict material behavior during both, elastic and plastic deformation. The further work will include the finite element modelling of the titanium processing in order to find the best input parameters leading to desired material properties.

References

- [1] Sakai T et al. (2014). *Prog. Mater. Sci.* **60**:130-207.
- [2] Zhang S et al. (2015) *Mat Sci Eng A*, **641**: 29-36
- [3] Lin YC et al. (2011). *Mater Des.*, **32**: 1733-1759

Does Multibody Kinematic Optimization Increase Reliability of Knee Joint Angles and Moments Between Thigh Marker Clusters in High Knee Flexion?

Jessa M. Buchman-Pearle, Stacey M. Acker

Department of Kinesiology, University of Waterloo, Waterloo, Ontario, Canada

Email: jessa.bpearle@uwaterloo.ca

Summary

This study explored the sensitivity of peak knee joint angles and moments in high knee flexion to thigh marker cluster location and multibody kinematic optimization (i.e., constraining joint degrees-of-freedom). Peak knee flexion, abduction, and adduction angles and moments were calculated using six different thigh marker clusters, with and without multibody optimization for fifty participants in squatting and kneeling. The effect of marker cluster location (quantified by the effect size, η^2) decreased, however within-subject repeatability (quantified by the intraclass correlation coefficient, ICC(2,1)) increased. These findings suggest that, in high knee flexion, multibody optimization may not effectively compensate for thigh marker cluster-specific soft tissue artifact on an individual basis.

Introduction

Select marker placements [1] and data processing techniques, such as multibody kinematic optimization [2], have been shown to impact soft tissue artifact. The objective of this study was to explore if multibody optimization reduced differences in peak knee joint angles and moments from marker clusters localized to six different areas of the thigh in high knee flexion. An increase in within-subject reliability would suggest that multibody optimization may partially compensate for cluster-specific soft tissue artifact.

Methods

Motion of the lower limb and ground reaction force data during squatting and kneeling (Figure 1) were recorded from fifty participants. Six marker clusters were used on the thighs (Figure 1) and one on the shank. The peak knee flexion, abduction, and adduction angles and moments were calculated using each thigh marker cluster with and without multibody optimization. Multibody optimization was implemented in Visual 3D by applying translational constraints to the ankles, knees, and hips, as well as frontal and axial rotational constraints on the ankles. Effect sizes, to determine the effect of marker cluster location for each task and multibody optimization condition, were evaluated with the partial eta squared (η^2). Intraclass correlation coefficients [ICC(2,1)] were also calculated using a two-way mixed effects model to assess agreement across the marker clusters.



Figure 1: Heels-up squat (HS), dorsiflexed knee (DK), and plantarflexed knee (PK) and thigh marker cluster placement.

Results and Discussion

Of the 18 effect sizes calculated without multibody optimization, 3 were classified as medium (0.07-0.09) for the flexion moments and all others were classified as large (0.16-0.50). With multibody optimization, effect size classification decreased to small for the flexion moments (0.02-0.03), and medium for angles in HS (0.12-0.13) the abduction moment in HS (0.11), and the adduction moment in PK (0.06). All other effect sizes remained classified as large (>0.14).

Of the thirty-six ICCs, 21 were classified as poor, 13 as moderate, 1 as good, and 1 as excellent (Table 1). Multibody optimization improved ICC classification for the flexion angle in HS and PK (Table 1).

Table 1: ICC for peak knee joint angles and moments with (MO) and without (no MO) multibody optimization. Bolded ICCs were classified as moderate to excellent (>0.50).

Task	Flexion		Adduction		Adduction	
	No MO	MO	No MO	MO	No MO	MO
<i>Peak Angles</i>						
HS	0.75	0.92	0.60	0.38	0.57	0.20
DK	0.52	0.67	0.72	0.42	0.52	0.33
PK	0.45	0.66	0.70	0.37	0.59	0.34
<i>Peak Moments</i>						
HS	0.63	0.60	0.38	0.45	0.64	0.49
DK	0.40	0.38	0.46	0.32	0.61	0.33
PK	0.45	0.42	0.43	0.48	0.46	0.06

Conclusions

Large effect sizes and poor reliability with different marker cluster placements highlights the importance of consistent marker placement within and between subjects. Multibody optimization improved effect size classifications (decreased η^2) for 8 variables and improved reliability classification (increased ICC) for 2 variables. Collectively, these findings suggest that while multibody optimization may decrease differences in knee joint angles and moments between marker clusters across a sample, multibody optimization does not compensate for cluster-specific soft tissue artifact for a given participant. This is particularly apparent when evaluating tasks which elicit greater range of motion at multiple joints (i.e., DK and PK) [3] and outcomes in the frontal plane.

Acknowledgments

The authors acknowledge funding from the Natural Sciences and Engineering Research Council of Canada.

References

- [1] Stagni et al. (2005). *Clin Biomech*, **20**: 320-29.
- [2] Lu & O'Connor. (1999). *J. Biomech*, **32**: 129-34.
- [3] Hemmerich et al. (2006). *J. Orthop. Res.*, **24**: 770-81.

Periodic median filter for power line interference in force plate and bioelectric recordings

Marc [□□□de Lussanet](#)^{1,2}, Charlotte le Mouel¹

¹Movement Science, University of Münster, Münster, Germany

²OCC Center for Cognitive and Behavioral Neuroscience, University of Münster, Münster, Germany

Email: lussanet@uni-muenster.de

Summary

Power line interference (“hum noise”) is a common source of noise in recorded biological data. It has a frequency of 50 or 60 Hz with harmonics and temporal fluctuations in frequency, amplitude and wave shape. Various filters have been proposed, but these fluctuations often present severe problems, such as deformations. Also, steps in the data, e.g., in force plate recordings tend to produce “ringing” artifacts. We propose a periodic median (PM) filter to reliably remove hum of any harmonic composition. We compare the performance of this filter to that of two state-of-the-art filters on a combination of recorded and simulated force plate and EMG data. Our filter is robust to fluctuations in line frequency and unstable harmonics. It does not introduce border artifacts or ringing. The filter is validated on recorded and artificial data. The PM filter thus outperforms the best hum filters currently in use.

Introduction

Power line interference (“hum noise”) presents an old and well-known problem in diverse biological recordings, including bioelectric (EEG, ECG, EMG), biomagnetic (MEG) and kinetic (force plates) signals. In addition to the classical “Notch” filter, a large number of numerical filters for hum have been proposed. Modern filters exist, that do cope quite well with the typical instabilities of the hum noise, which are fluctuations in frequency, amplitude and harmonic composition. However, they introduce distortions of the signal during transient steps in the data, at the start and end of the recording and during sudden changes in the noise amplitude. For example, landing on a force plate will cause a sudden rapid change in the measured signal, and hum filters typically introduce Gibbs rippling or “ringing artifact” in the vicinity of the transient.

Methods

To remove the hum from a signal, the waveform of the hum over each period of the hum noise is estimated. First, a high-pass filter is applied to the signal (20 Hz cut-off, 4th order two-way Butterworth). The waveform of the filtered signal is then averaged on a sliding window of 50 successive periods of the hum frequency. For averaging, we take the median rather than the mean to improve robustness. This Periodic Median is then subtracted from the signal.

The Periodic Median filter (PM) is compared to two modern ones (gold standard), i.e., the Spectrum Interpolation (SI) filter [1] of FieldTrip [2] and the Fourier Decomposition Method (FDM) [3].

We compared the performance of the 3 filters on 1. artificial signals with a realistic frequency spectrum and hum, 2. hum-free EMG recordings (ground truth) with superimposed power line hum (recorded from non-loaded force plates), 3. force plate recordings of jumping (with hum).

Results and Discussion

All three filters had similar steady-state performance for removing a hum with constant amplitude from artificial signals. The performance of SI and FDM deteriorated at the beginning and end of the signal, and at sudden changes in the amplitude of the hum, whereas that of our novel PM filter did not. On the EMG recordings with added hum noise, the FDM filter showed considerable errors, particularly during strong muscle contraction. Both the SI and the PM filters performed well, with the PM showing slightly better performance than the SI during low muscle contraction, and slightly worse during large muscle contraction. During large muscle contraction, the error of the PM filter nevertheless remained below the amplitude of the hum and was negligible with respect to the amplitude of the signal.

When applied to force recordings of jumps, both SI and FDM showed substantial ringing in the vicinity of the jumps (for the FDM, the ringing amplitude was as much as four times the hum amplitude). The novel PM filter showed no ringing at all, and no increase of the error.

Conclusions

The here proposed novel PM filter is highly stable and highly reliable in all tested conditions, and performed equally well or outperformed both reference filters in almost all tests. We recommend its use for biological recordings with power line hum.

Matlab and Python scripts are made available on Github [4].

References

1. Leske S and Dalal SS (2019). *NeuroImage*, **189**: 763-776.
2. Oostenveld R et al. (2011). *Comput Intelligence Neurosci*, **011**: 9.
3. Singh P et al. (2019). In: Tanveer M □ Pachori R□, Eds, *Machine Intellig Signal Analysis*, 25–36. Springer, Singapore.
4. de Lussanet MHE and le Mouel (2019). Periodic median subtraction for hum noise. *GitHub*.

Studying the impact of internal and external forces minimization in a motion-based external forces and moments prediction method application to fencing lunges

Pauline Morin¹, Antoine Muller², Charles Pontonnier¹, Georges Dumont¹

¹Univ Rennes, CNRS, Inria, IRISA - UMR 6074, F-35000 Rennes, France

²Univ Lyon, Univ Gustave Eiffel, Université Claude Bernard Lyon 1, LBMC UMR_T 9406, F-69675 Lyon, France

Email: pauline.morin@ens-rennes.fr

Summary

External forces and joint torques have been jointly minimized in a motion-based external force prediction method. The prediction of external forces during a fencing lunge demonstrates the interest to consider joint torques during static phases of movements.

Introduction

In motion analysis studies, classical inverse dynamic methods require ground reaction forces and moment (GRF/M) to compute internal forces. Predicting GRF/M from motion capture makes it possible not to measure them. In such a prediction method, contact is handled through multiple points, making the inverse dynamics problem undetermined. Physiological assumptions (like minimizing external forces) in an optimization approach enable to determine the most plausible solution from the mathematical variety of force distribution solutions [1]. This abstract presents a pilot study questioning the implication of the internal forces (considering joint torques) in external forces prediction during a fencing lunge.

Methods

The present study is a pilot study considering 10 lunges executed by one fencer (1.86m, 78.6 kg) issued from [2]. Lunge motion consists in an explosive extension of the front leg accompanying an extension of the sword arm. It admits a static (preparing the attack) and a dynamic phase (the lunge itself). Motion capture markers (46 on standardized anatomical landmarks) were recorded with an optoelectronic motion capture system Qualisys (200Hz). The external forces were recorded with two AMTI force platforms (2000Hz). The GRF/M were predicted from an optimization approach considering a set of discrete contact points. The cost function was a combination of a quadratic sum of external forces $\|F\|^2$ and a quadratic sum of joint torques $\|\tau\|^2$ as follow:

$$\min_F \left(w_{ext} \frac{\|F\|^2}{F^{norm2}} + w_{int} \frac{\|\tau(F)\|^2}{\tau^{norm2}} \right)$$

At each frame, the quadratic sum of external forces was normalized by the square of the norm of the global external force F^{norm2} (computed from the inverse dynamic equilibrium). The quadratic sum of joint torques was normalized by the quadratic sum of joint torques considering equal to zero the external forces. The two terms were balanced by:

$$(w_{ext}, w_{int}) \in [0,1] \text{ s. t. } w_{ext} + w_{int} = 1$$

This method has been implemented in the CusToM Matlab toolbox [3].

The external forces were predicted for different values of (w_{ext}, w_{int}) : (1, 0), (0.75, 0.25), (0.5, 0.5), (0.25, 0.75) and (0,1). The efficiency of those predictions was evaluated comparing predicted GRF/M and force platforms data varying, in terms of RMSE. The results are presented for the static and the dynamic phases, detected visually on each trial.

Results and Discussion

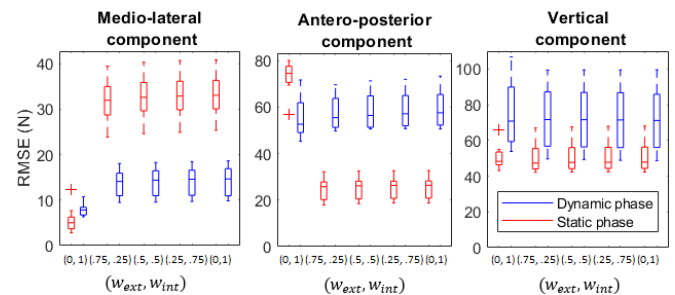


Figure 1: RMSE of the external force prediction for different (w_{ext}, w_{int}) values with a dynamic and static phase distinction.

The RMSE statistical repartition is presented in the Figure 1 for each resultant component. All non-zero values of w_{int} led to similar predictions in shape and amplitude. Considering joint torques in the prediction improved the antero-posterior component prediction and deteriorated the medio-lateral component prediction during the static phases. Considering joint torques in the cost function did not impact prediction during the dynamic phases. The studied motion admitted two easily identifiable phases (static and dynamic), and we may assume that joint torques were minimized during the static phase to let the fencer being relaxed before the assault. Any other motion may present specificities to be considered to find the best combination between internal and external forces to be minimized in the prediction.

In conclusion, minimizing joint torques and external forces in a motion-based external forces prediction method seems relevant for static phases of motions. A larger cohort should be considered to validate these preliminary results. Other motions presenting specific dynamical characteristics should also be considered.

References

- [1] R. Fluit, et al. (2014) J. Biomech 47(10):2321–2329.
- [2] Sorel A, et al. (2019). PLoS ONE
- [3] A. Muller, et al. (2019). J. Open Source Softwa. 4(33):92

CNN-based markerless motion capture approach: a pilot study

Silvia Zampato^{1,2}, Azza Bouleimen¹, Francesco Piemontese¹, Silvia Fantozzi²
Giorgio Gatta³, Matteo Cortesi³, Michele Rossi¹, Zimi Sawacha^{1,4}

¹Dept of Information Engineering, University of Padova, Padova, Italy

²Dept of Electrical, Electronic and Information Engineering, University of Bologna, Bologna, Italy

³Dept for Life Quality Studies, University of Bologna, Rimini, Italy

⁴Dept of Medicine, University of Padova, Padova, Italy

Email: zampatosil@dei.unipd.it

Summary

This pilot study introduces an innovative signal processing pipeline for a markerless motion capture system. In the proposed approach, the three-dimensional space pose and the joints angles are the results of a cascade of classifiers based on convolutional neural networks (CNN), which are applied to a set of time-synchronized video streams. This method is also applied to underwater (UW) data acquisitions, a challenging environment due to internal reflections and high levels of noise. In this analysis, lower limb joints flexion-extension angles are presented and compared with a state-of-the-art marker-based technique.

Introduction

Nowadays, clinically accepted optical systems are mostly marker-based. Despite the high accuracy they can achieve, there are some open issues: expensive instrumentation is required, markers can prevent the subjects from preserving a natural motion, occlusions and an overall long processing time can affect trajectories reconstruction. To overcome these problems, markerless techniques are gaining more and more relevance. In this study, we propose a deep learning-based motion capture pipeline as deep neural networks have been widely applied to images and video processing domains with success.

Methods

The proposed pipeline is highly modular, and flexible for future innovations. A set of synchronized cameras is placed around the scene and the data stream can be managed both online and offline. The former case tends towards a real-time application: the synchronized new frames are processed as soon as they are available. Whereas, in the latter case, the trials are assumed to be completed and the processing can exploit the information from the whole videos in order to improve accuracy. After the preprocessing step that extracts and undistorts the video frames, a cascade of a person detector [1] and a pose estimator [2] are applied to a set of synchronized frames. The result is a heatmap per each joint expressing the probability map of finding that particular joint on the 2D image. Then the 3D subject pose is triangulated and refined matching the anatomical constraints imposed by a subject-specific model acquired by laser scan. The final step calculates planar angles between the anatomical segments. The system was tested on 42 gait trials performed by 3 subjects (mean age 27.3 ± 5.5 years, mean BMI $21.3 \pm$

2.6 kg/m^2) acquired both in a laboratory environment (out-of-water, OW) and underwater (UW) in a swimming pool. Six synchronized UW color analog wide-angle cameras (720×576 resolution TS-6021PSC), were used and synchronized automatically with a custom-made application [3]. Calibration of the intrinsic parameters was performed OW, filming a black and white checkerboard and then corrected for UW condition [3]. A 12-control points calibration grid (2 m×1.1 m×1.1 m) was used for extrinsic calibration [3]. In order to assess reliability of the proposed approach, the same gait trials were processed by automatically tracking anatomical landmarks (Track on Filed, BBSOF S.r.l.) marked on the subjects skin with a black marker, according to [4]. Mean and Standard deviation, across trials, of each planar angle were computed for each technique and compared (Paired T Test $p < 0.05$).

Results and Discussion

No significant differences were observed between the two methods both OW and UW (Fig.1).

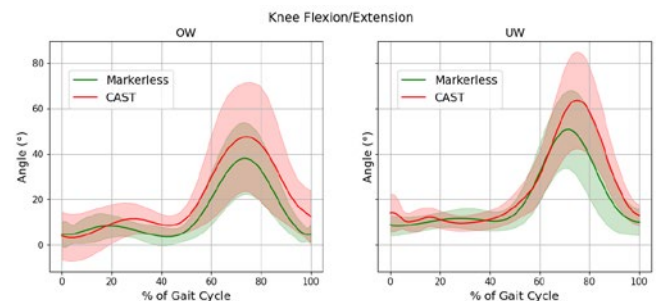


Figure 1: Knee flexion-extension angles during gait, same subject in different environments. Total number of gait cycles: markerless 12 (OW) and 31 (UW), CAST 4 (OW) and 9 (UW)

Conclusions

Despite the pose estimator was trained for non-clinical purposes, the joints' kinematics was reconstructed with remarkable accuracy.

References

1. Ren S. et al, *IEEE Transactions on Pattern Analysis and Machine Intelligence*, 39:1137-1149, 2017
2. Sun K. et al, *IEEE/CVF CVPR*, 5686-5696, 2019
3. Ceseracciu E. et al, *Journal of Biomechanics*, 44(12):2236-2242
4. Cappozzo A. et al, *Clinical biomechanics*, 10:171-178, 1995

Evaluating methods of calculating jump height from force plate data

Rendán L. Pinto, Jack P. Callaghan

Department of Kinesiology, University of Waterloo, Waterloo, ON, Canada

Email: blpinto@uwaterloo.ca

Summary

Jump heights calculated from force plate data using take-off velocity (TOV) and TOV summed with take-off displacement (TOV+s) were compared to whole body displacement measured by a single kinematic marker. This provided a criterion that matched the assumption of point mass made by the force plate calculation methods while directly recording representative whole body displacement. Conversely, estimating centre of mass (COM) from a rigid link model (RLM) would not match these assumptions. Results indicate that the TOV+s method provides greater accuracy and precision.

Introduction

Jump height can be calculated from force plate data using projectile motion equations. The TOV and TOV+s methods are preferred over the time in air method, which is influenced by landing posture [1,2]. Results from TOV and TOV+s methods have been compared to COM displacement derived from a kinematic RLM. However, COM from the RLM is sensitive to changes in body posture during flight, whereas the projectile motion calculation using force plate data assumes the body as a point mass. The purpose of this investigation was to compare the calculate jump height from the TOV and TOV+s methods to a kinematic criterion that matches the assumption of point mass made by the projectile motion calculation, while directly measuring actual whole body vertical displacement.

Methods

A single marker on the third lumbar vertebrae was used to record vertical displacement. This captured the displacement of the torso while limiting the influence of limb, ribcage and pelvis posture. This approach entailed fewer assumptions than the RLM while directly recording the vertical point mass displacement that the TOV and TOV+s methods attempt to estimate from the force plate data.

Thirty-four counter-movement jumps from 12 participants (6 female; mean \pm SD age 24 ± 4 years; mass 73.4 ± 17.6 kg; height 1.74 ± 0.08 m) were used to calculate the limits of agreement (LOA) between each force plate calculation method and the kinematic criterion. A linear mixed effects model was used calculate the variance components while accounting for the multilevel data structure [3].

Results and Discussion

The TOV+s method provided the best agreement with the kinematic criterion as the mean bias (dashed line Figure 1) was closer to the criterion (solid line at 0 cm Figure 1), with narrower limits of agreement (dotted lines Figure 1). However, this method still underestimated the criterion by up

to 4 cm and appears to be influenced by the magnitude of the jump as indicated by the slight negative trend with increasing jump magnitude (Pearson's $r = -0.59$, Figure 1).

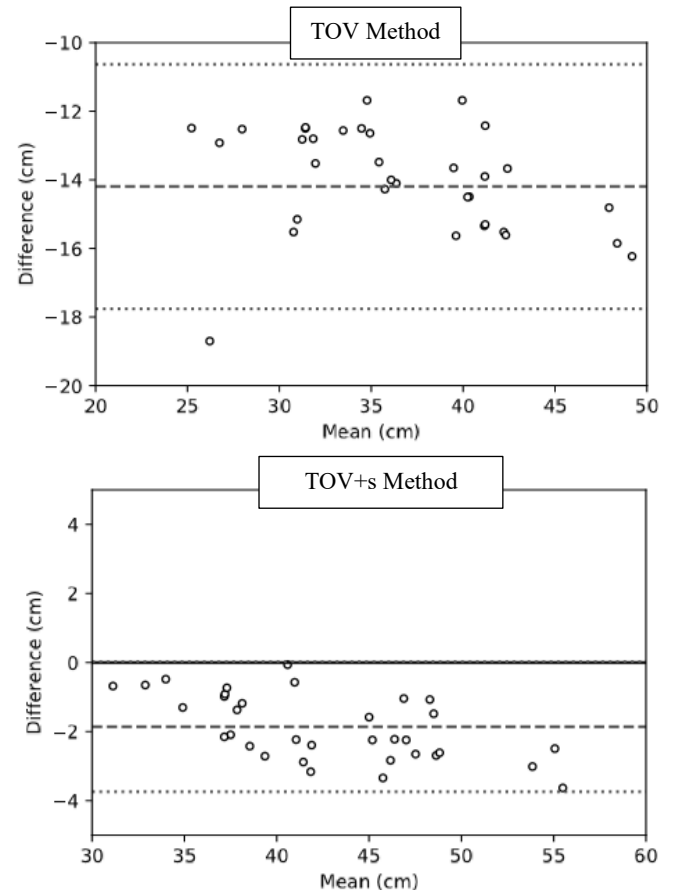


Figure 1: Bland and Altman plots for each method's agreement with the kinematic criterion.

Conclusions

Accounting for displacement at take-off using the TOV+s method provides higher accuracy and precision compared to the TOV method. Further investigation is required to assess the persisting error, towards developing improved estimates of jump height from force plate data.

Acknowledgments

The authors acknowledge funding from the Natural Sciences and Engineering Research Council of Canada.

References

- [1] Aragón (2000). *Meas Phys Educ Exerc Sci*, **4**(4):215-228.
- [2] Chiu & Dohlin (2020). *Meas Phys Educ Exerc Sci*, **4**(1):25-32.
- [3] Parker et al. (2016). *PLoS One*, **11**(12), e0168321.

A spot check to ensure comparability of stereophotogrammetric data in multicentric studies

Scott Kirsty¹, Conci Tecla¹, Alcock Lisa², Hansen Clint³, Schwickert Lars⁴, Gazit Eran⁵, Cereatti Andrea⁶, Mazzoni Claudia¹

¹ Department of Mechanical Engineering - INSIGNEO Institute for *in silico* Medicine, The University of Sheffield, Sheffield, UK

² Translational and Clinical Research Institute, Faculty of Medical Sciences, Newcastle University, Newcastle upon Tyne, UK

³ Kiel University and Department of Neurology, University Hospital Schleswig-Holstein, Campus Kiel, Kiel, Germany

⁴ Department for Geriatric Rehabilitation, Robert-Koch-Hospital, Stuttgart, Germany

⁵ Centre for the Study of Movement, Cognition and Mobility, Tel Aviv Sourasky Medical Centre, Tel Aviv, Israel

⁶ Department of Electronics and Telecommunications, Politecnico di Torino, Torino, Italy

Email: kscott3@sheffield.ac.uk

Summary

While many methods have been proposed to quantify the systematic error of stereophotogrammetric (SP) systems, they are underutilised and not commonly reported due to their complexity and need for additional equipment. In response, a simple spot-check has been designed adopting previously proposed methodology. This study demonstrates the use of this method and presents preliminary results of the systematic error quantified for three different SP systems.

Introduction

SP systems are widely used for the quantification of gait features and for estimating joint kinematics and kinetics. The laboratory set-up, capture volume, as well as the outcome of calibration procedures are critical aspects in the accuracy of a SP system [1]. Consequently, monitoring the accuracy and reliability of these systems is crucial to deploy laboratory quality assessment. Current practice on reporting systematic errors varies between manufacturers and usually does not entail the provision of easily readable feedback to compare errors on different days of use and between different systems. Although previous studies have assessed the error of different systems [2], a quick and cost-effective approach that could be easily performed before each use and can provide information about both linear and angular errors, is not yet available. To this end, this study aims to demonstrate the use of a simple spot-check to estimate the systematic error of different SP systems across multiple testing.

Methods

After calibration, following the manufacturers guidelines, the proposed spot-check was performed on three SP systems: SP1: 14 Canon cameras, capture volume 5x4m; SP2: 10 Canon T160 cameras, capture volume 7x4m; SP3: 12 Qualisys Miquis cameras, capture volume 6x4.5m.

Two trials were recorded using a wand comprising markers: 1) Static: a 5 s recording of the wand placed in the centre of the capture volume and 2) Dynamic: a recording of the operator moving the wand exploiting the full capture volume. Both trials were reconstructed and labelled following

manufacturers guidelines. The uncertainties ($Uncertainty = SD_E \times k$, where SD_E is the standard deviation of the error and k is the coverage factor, $k=3$) for the distances (D_1 and D_2 , Figure 1) and angles (θ_1 and θ_2) were calculated for the static trials. The root mean square errors of each distance and angle were calculated for the dynamic trials [3].

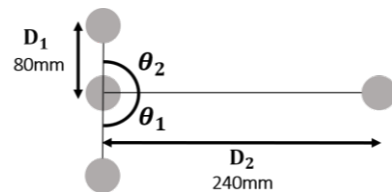


Figure 1: Distances and angles calculated from the active markers.

Results and Discussion

Table 1 summarises the results of the spot-checks performed on each system on 10 different days of data collection. Errors observed both within and between systems were low overall, with the error for the distances always under 2mm and 1.8° for the angles.

Conclusion

This study demonstrates the adoption of a simple method to monitor the level of systematic error in SP systems, regardless of manufacturer, number of cameras, capture volume and operators. This preliminary study is part of an ongoing data collection with a more comprehensive analysis of this method to be shared with the research community once completed, together with the computational tools that will ensure it may be embedded routinely within standardised protocols.

Acknowledgments

This work is part of the Mobilise-D project (IMI2 Joint Undertaking, grant agreement No 820820). This study was cofunded by Grönenthal.

References

- [1] Windolf et al. (2008). *J. Biomech.*, **41**: 2776-2780.
- [2] Conconi et al. (2021). *J. Biomech.*, **114**: 110-162
- [3] DiMarco et al. (2017). *Meas. J.*, **101**: 265-271.

Table 1: The mean and standard deviation of the error (E) for the distances and angles calculated during the spot check.

SP System	Static trial – Uncertainty				Dynamic trial – Root Mean Square Error			
	D1 _E [mm]	D2 _E [mm]	θ1 _E [deg]	θ2 _E [deg]	D1 _E [mm]	D2 _E [mm]	θ1 _E [deg]	θ2 _E [deg]
SP1	0.07±0.03	0.06±0.02	0.03±0.02	0.05±0.02	0.45±0.07	0.43±0.06	0.24±0.03	0.31±0.11
SP2	0.09±0.09	0.09±0.08	0.04±0.03	0.08±0.06	0.44±0.07	0.78±0.06	0.18±0.13	0.19±0.08
SP3	0.14±0.06	0.12±0.03	0.06±0.02	0.09±0.01	0.76±0.24	1.13±0.50	0.51±0.46	0.74±0.24

Influence of the Balance of Excitatory and Inhibitory Neurons on Reservoir Computing Performance

Myriam L. De Graaf^{1,3}, Luis Mochizuki², Frederik Thies¹, Heiko Wagner^{1,3}

¹Movement Science, University of Münster, Horstmarer Landweg 62b, 48149 Münster, Germany

²School of Arts, Sciences and Humanities, University of São Paulo, Brazil

³Otto Creutzfeldt Center for Cognitive and Behavioral Neuroscience, University of Münster, Germany

Email: mdegraaf@uni-muenster.de

Summary

While biological neural networks (NN) function under states of excitatory to inhibitory (EI-)balance, the number of neurons and their connections are not the same for these two groups. We investigated whether reservoir computing artificial neural networks (RC-NNs) also perform better with inequalities between the excitatory and inhibitory populations. Results show that networks generally perform better when inhibitory neurons have the upper hand.

Introduction

NNs function under states of EI-balance, meaning there is a relatively constant ratio between excitatory and inhibitory inputs to neural cells. This phenomenon has been theorized to be a mechanism to keep networks both stable as well as temporally irregular and chaotic. In firing rate RC-NNs [1,2], pools of neurons are randomly created without distinction between excitatory and inhibitory populations, with their connections in an even distribution around zero. The aim of this study was to assess the effect of fluctuating the E:I ratio of (1) neuron number, (2) connection percentage, and (3) connection strength, on the performance of RC-NNs. Based on the findings in nature, we expect that such maps should not be symmetrical in relation to the main diagonal.

Methods

All networks were trained and tested using locomotion data: slow walking, fast walking, and running. Kinematics and ground reaction forces were measured and, using the inverse dynamics option of the 3D muscle model called *Myonardo* (Predimo GmbH, Münster, Germany), transformed into spinal cord afferent and efferent signals, that functioned as the target signals (see Figure 1A). The network input was a context signal specifying the type of activity (binary signal) and the step frequency (via a sinusoid). The network was trained using FORCE [2]. For both populations, neuron number varied from 100-2000, connection percentage from 5-50% and connection strength from a factor of 0.25 to 4. Connection percentage and strength were tested for a combination of E:I ratios (4:1, 3:1, 2:1, 1:1 and vice versa).

Results and Discussion

Networks performed better if they had a higher number of inhibitory than excitatory neurons. A clear cut-off line between successful and non-successful networks was found ranging from a E:I of 2:1 for smaller networks and a slightly smaller ratio for larger networks (Figure 1B). For the connection percentage, a similar phenomenon was found

(Figure 1C). Here, the slope of the cut-off line gets steeper, increasing the number of successful networks, as the fraction of inhibitory neurons increases. For the connection strength, a relatively small island of success was found (Figure 1D). Networks performed better when excitatory strength was no higher than a factor 1, while inhibitory strength could be scaled up. General trends show that networks perform better when the inhibitory neurons have more influence. At first glance, this seems to go against what we see in nature, since the cortex might have four times as many excitatory than inhibitory neurons [3]. However, networks with a biologically relevant 4:1 ratio have been found to be successful in this study given that either the inhibitory connection percentage or connection strength is high enough.

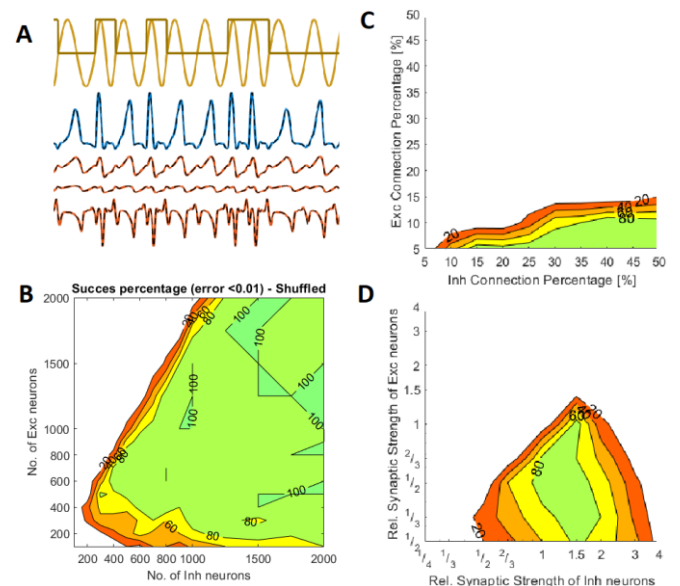


Figure 1: Example output of a successful network (A) and success percentages for varied number of neurons (B), connection percentage (C) and connection strength (D). Results in C and D are from a network with 1200 excitatory and 300 inhibitory neurons.

Conclusions

RC-NNs function better when the excitatory and inhibitory network number, connection percentage and connection strength are not equal, reflecting what we see in the human nervous system.

References

- [1] Verstraeten D et al. (2007). *Neural Netw*, 10: 391-403.
- [2] Sussillo D and Abbott LF (2009). *Neuron*, 63: 544-57.
- [3] Lombardi F et al. (2017). *Chaos*, 27: 047402

Relationship between neck flexion in neurodynamic tests and lower limb muscle activity

Dirk Möller¹, Harry von Piekartz¹, Kevin Maliszewski¹, David Snowdon¹

¹Department of Movement and Rehabilitation Science, University of Applied Sciences, Osnabrück, Germany
Email: d.moeller@hs-osnabrueck.de

Summary

Neck flexion has a proven effect on the mechanosensitivity of neurodynamic tests of the lower limb, but it is not clear whether this can be explained by an increased (intra-neural) tension of the neural tissue and/or by a protective reflex mechanism of the motor system. The aim of this study was to evaluate the relationship between range of neck flexion and muscle activity changes in the lower limb during neurodynamic tests.

All included subjects performed the neurodynamic straight leg raise test and slump test. Muscle activity of the hamstring, quadriceps and calf muscles and range of motion of the neck flexion were measured during these tests and correlations were calculated.

The study results substantiated an overall-segmental influence of passive neck flexion on muscle activity in the lower limb. The patterns potentially indicate a protective muscular mechanism in end of range neurodynamic positions.

Introduction

Neck flexion is a sensitizing maneuver for neurodynamic tests of the lower limb. It has a proven effect on the mechanosensitivity of these tests, but it is not clear whether this can be explained by an increased intra-neural tension and/or by a protective mechanism of the motor system. Previous research showed a relationship, but the muscular response of the lower limb on neck flexion is still not clear.

The aim of this study was to evaluate the relationship between range of neck flexion and muscle activity changes in the lower limb during neurodynamic tests.

Methods

Muscle activity (measured with electromyography) of the hamstring, quadriceps and calf muscles was measured in 30 healthy participants during neck flexion (measured with an inertial sensor system) in two neurodynamic tests (straight leg raise and slump). Correlations were calculated between increasing neck flexion and muscle activity during these tests.

Results and Discussion

Increasing neck flexion was significantly correlated to muscle activity during straight leg raise test ($r_s = -.61 - .76$; hamstrings > quadriceps > calf) as well as during slump test ($r_s = -.34 - .94$; hamstrings > calf > quadriceps) (tab. 1). Negative values represent muscle activity declined with increasing neck flexion. Figure 1 illustrates the time course of neck flexion and muscle activity during the slump test.

These results support the hypothesis of a complex protective mechanism based on reciprocal inhibition to protect the neural structures [1,2,3].

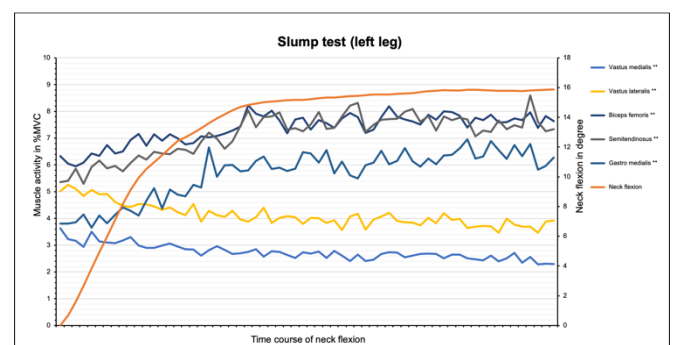


Figure 1: Activity of different muscles in the time course of the passive neck flexion during the slump test (left muscles, $**p < .01$)

Conclusions

Neck flexion in neurodynamic tests seems to have an influence on muscle activity of the lower limb. These muscle activity patterns during neck flexion supports clinical findings of an increase of symptoms and passive resistance in the lower limb during neurodynamic tests.

References

- [1] Bayoumi A and Ashby P (1989). *Exp Brain Res*, **76**:223-228.
- [2] Hall T et al (1998). *Man Ther*, **3**:140-146.
- [3] Szikszay T et al (2017). *J Back Musculoskeletal Rehabil*, **30**:1171-1186.

Table 1: Correlations of muscle activity and passive neck flexion for the neurodynamic tests straight leg raise test and slump test (SLR = Straight Leg Raise; r_s = Correlation coefficient according to Spearman; p = level of significance; $*p < .05$; $**p < .01$);

		SLR right		SLR left		Slump right		Slump left	
		r_s	p	r_s	p	r_s	p	r_s	p
right	Vastus medialis	-0,619	0,001**	-0,550	0,001**	-0,562	0,001**	0,804	0,001**
	Vastus lateralis	-0,185	0,198	-0,632	0,001**	-0,338	0,047*	0,904	0,001**
	Biceps femoris	-0,605	0,001**	-0,929	0,001**	0,918	0,001**	0,874	0,001**
	Semitendinosus	-0,614	0,001**	-0,863	0,001**	0,941	0,001**	0,914	0,001**
	Gastrocnemius medialis	0,701	0,001**	-0,471	0,001**	0,904	0,001**	0,570	0,001**
left	Vastus medialis	-0,343	0,015*	0,634	0,001**	0,830	0,001**	-0,856	0,001**
	Vastus lateralis	0,768	0,001**	-0,764	0,001**	0,649	0,001**	-0,803	0,001**
	Biceps femoris	-0,818	0,001**	-0,810	0,001**	0,443	0,008**	0,739	0,001**
	Semitendinosus	-0,694	0,001**	-0,814	0,001**	0,863	0,001**	0,677	0,001**
	Gastrocnemius medialis	0,661	0,001**	0,346	0,014*	0,736	0,001**	0,797	0,001**

Painful sinusoidal electrical stimulation decreases the firing rate of vastus medialis and lateralis motor units

Alessio Gallina¹, Girivasan Rajarathinam¹, Jacques Abboud², Jean-Sébastien Louin³, Deborah Falla¹

¹Centre for Precision Rehabilitation of Spinal Pain, School of Sport, Science and Exercise Science, University of Birmingham, UK

²Département des Sciences de l'Activité Physique, Université du Québec à Trois-Rivières, Trois-Rivières, Canada

³School of Kinesiology, University of British Columbia, Vancouver, Canada

Email: a.gallina@bham.ac.uk

Summary

We aimed to investigate whether painful electrical stimulation alters vastus medialis (VM) and lateralis (VL) motor unit recruitment strategies during isometric knee extension contractions. Twelve asymptomatic participants performed three 30s-long isometric knee extensions at 20% of their maximal voluntary contraction. In the middle 10s of each contraction, sinusoidal electrical stimulation at 4 Hz was delivered over the infrapatellar fat pad to induce a pain intensity of 4/10 (verbal analog scale). The firing rate of 51 single motor units was identified from surface high-density electromyographic recordings and averaged before, during, and after the painful stimulation. Friedman tests identified no difference in torque ($p=0.368$), but motor unit firing rate decreased during the painful part of the contraction compared to before ($p=0.001$) and after pain ($p=0.011$). Similar to injections of hypertonic saline solution in the infrapatellar fat pad, painful electrical stimulation alters VM and VL motor unit recruitment.

Introduction

A decrease in VM and VL motor unit firing rate is commonly observed when experimental knee pain is induced by injecting hypertonic saline solution in the infrapatellar fat pad [1]. Recent evidence shows that low-frequency sinusoidal electrical stimulation applied with surface electrodes over the infrapatellar fat pad elicits stable perception of pain over at least 60s, while allowing the recording of surface EMG with minimal artefacts [2]. We aimed to investigate if pain induced by low-frequency sinusoidal electrical stimulation replicates the alteration in motor unit recruitment strategies observed after injection of hypertonic saline solution as this could provide an alternative, non-invasive experimental pain model.

Methods

Twelve asymptomatic participants (2 women 27 ± 5 years old 176 ± 6 cm 76 ± 8 kg) participated in the study which was approved by the local ethics committee. Stimulation electrodes were placed over the medial and lateral sides of the infrapatellar fat pad. Electrical stimulation was delivered as a 4 Hz sine wave [2] at an intensity that induced a pain intensity of 4/10 on a verbal analog scale. Knee extension torque was measured using a Biodex dynamometer. High-density surface EMG signals were recorded from the VM and VL using a Sessantaquattro (OT Bioelettronica, Italy) and grids of 8x4 electrodes with 10 mm inter-electrode distance. Participants performed three 30s-long isometric knee extensions at 20% of their maximal voluntary

contraction. Painful electrical stimulation was delivered during the middle 10s of each contraction.

Single motor unit firings were identified using the Convolution Kernel Compensation algorithm [3]. Torque and firing rate of the identified motor units were averaged in epochs before (pre), during (pain), and after (post) the painful stimulation, and averaged across contractions. Friedman tests and Bonferroni-corrected Wilcoxon tests were used to identify differences between pre, pain and post.

Results and Discussion

Knee extension torque did not change during pain ($p=0.368$). Of the 51 single motor units identified across all participants, 40 fired continuously throughout the contraction. The firing rate of motor units was, on average, lower during pain compared to pre (0.43 [0.02, 0.74] Hz $p=0.001$) and post (0.26 [0.02, 0.74] Hz $p=0.011$), with no difference between pre and post ($p=1.00$). Additionally, 6 new motor units were recruited during pain, 4 were de-recruited, and 1 was recruited only after the end of the painful stimulation.

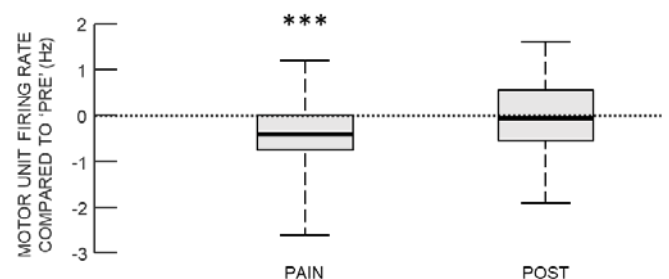


Figure 1: Change in motor unit firing rate between pre and pain, and between pre and post $p < 0.001$.

Similar to what has been observed after injection of hypertonic saline solution, we observed recruitment and de-recruitment of motor units. The smaller reduction in firing rate (0.4 Hz vs 1.2 Hz) compared to other studies [1] may be due to lower pain intensity or differences in the type and location of targeted receptors.

Conclusions

Pain induced with low-frequency sinusoidal electrical stimulation of the infrapatellar fat pad alters motor unit recruitment strategies of the vastus medialis and lateralis.

References

- Tucker K & Hodges P. (2009). *J Neurosci* **29**: 10820-6.
- Gallina A et al. (2021) *J Physiol* in press.
- Holobar A & Fazula D. (2007). *IEEE Sig Pr*; **55**: 487-96.

The Efficacy of Surface EMG Decomposition to Detect Motor Unit Firing Rates of the Lower-Limb Muscles During High Cadence Cycling

Brett Still^{1,2}, Franky Mulloy¹, Steven Lindley², Sandy Willmott¹, David Mullineaux¹

¹School of Sport and Exercise Science, University of Lincoln, UK ²Delsys Europe, Greater Manchester, UK
Email: bstill@lincoln.ac.uk

Summary

Advances in surface EMG decomposition have allowed a better understanding of motor unit firing rates during dynamic movement. However, the application has been limited to movements at relatively slow contraction speeds. The preliminary results presented here demonstrate the efficacy of surface EMG decomposition to detect motor unit firing rates of the lower limb muscles during whole limb dynamic movement at fast contraction speeds during cycling.

Introduction

Surface EMG decomposition provides useful insight into neuromuscular control. The application of surface EMG decomposition to the study of dynamic movement has been limited to relatively slow contraction speeds [1]. During dynamic motion, with relatively fast contraction speeds, there is a greater displacement of the surface EMG sensor relative to the underlying muscle fibers [2]. This additional motion may limit motor unit firing rate detection accuracy, subsequently reducing motor unit yield. For example, motor unit firing rates for the vastus lateralis during slow walking at 40 and 60 steps per minute were 13 ± 9 and 10 ± 7 respectively [1]. Whereas for isometric contractions of the vastus lateralis at 50%MVC, motor unit yields of up to 31 motor units per contraction have been reported [3]. To the authors knowledge limited research has attempted to detect motor unit firing rates during highly dynamic movements with faster contraction speeds beyond tasks such as bicep curls and level walking.

The aim of this preliminary investigation was to explore the efficacy of surface EMG decomposition for motor unit firing rate detection of multiple lower-limb muscles during high-cadence cycling activity.

Methods

Following informed consent and institutional ethical approval two recreationally active men (participant 1: age 37, height 175 cm, mass 67kg; participant 2: age 33, height 170 cm, mass 60 kg) completed 60 seconds of submaximal cycling at cadences of 60, 75, 90 and 105 RPM on an SRM ergometer. Surface EMG data was recorded for three bi-articular muscles (rectus femoris, biceps femoris and gastrocnemius medialis) and three mono-articulate muscles (vastus lateralis, semimembranosus and tibialis anterior) using Galileo surface EMG sensors (Delsys, Boston, USA).

Maximal power was determined with a 10 second sprint test at each cadence. During submaximal cycling participants were asked to match the target power of 40% max placed on a screen in front of them. Processing of the surface EMG data was conducted using proprietary decomposition algorithms (Delsys, Boston, USA). Accuracy of the algorithm was determined using the DSDC method [4].

Results and Discussion

Motor unit yields were successfully obtained for a number of muscles at higher cadences (Table 1). Data for the biceps femoris and semimembranosus was not successfully collected for participant 2 due to the sensors being dislodge during the trial. Motor unit yields for the lower-limb muscle are comparable at 60, 75, 90 and 105 RPM with a motor unit firing rate detection accuracy of > 90%.

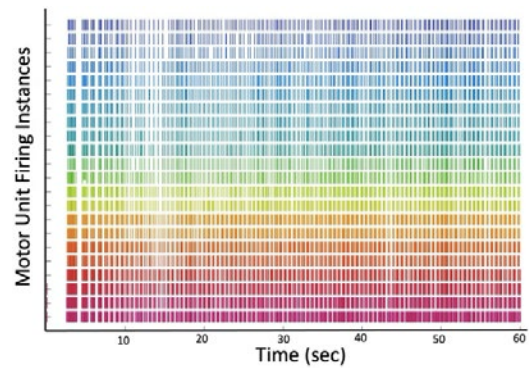


Figure 1: Motor unit firing instances for the rectus femoris during isokinetic cycling at 105 RPM and 40% max power for 60 seconds.

Conclusions

The preliminary results demonstrate the efficacy of surface EMG decomposition to accurately detect motor unit firing rates of the lower limb muscles during high cadence cycling. Motor unit yields presented here demonstrate that surface EMG decomposition can indeed be applied to highly dynamic activities for the assessment of neuromuscular control strategies.

References

- [1] DeLuca CJ et al. (2015). *J. Neurophysiol*, **113**: 1941-1951
- [2] Mesin L et al (2009). *J. Electromyogr. Kinesiol*, **19**: 719-726
- [3] Nawab SH et al (2010). *Clin. Neurophysiol*, **121**: 1602-1615
- [4] Kline JC et al. (2014). *J. Neurophysiol*, **112**: 2718-2728

Table 1: Motor unit yields (with DSDC detection accuracy > 90%) for six lower limb muscles during isokinetic cycling at four controlled cadences at 40% of maximal power for each cadence. Results are presented separately for participant 1 (column 1) and 2 (column 2).

	Rectus Femoris		Vastus Lateralis		Biceps Femoris		Semimembranosus		Gastrocnemius		Tibialis Anterior	
60 RPM	16	14	19	21	1	5	3	6	1	6	13	1
75 RPM	22	16	12	19	8	12	5	15	6	9	12	5
90 RPM	9	7	15	12	4	8	5	15	5	13	11	5
105RPM	22	14	12	23	1	-	8	-	5	8	7	10

The effect of load, speed and contraction phase on motor unit behaviour during a knee extension exercise

J. Heredia-Jimenez^{1,2}, E. Orantes-Gonzalez¹, J. Richards³, G. Chapman³, S. Lindley⁴

¹Human Behavior and Motion Analysis Lab (Hubema Lab). University of Granada. Ceuta, Spain.

²Dpt. Physical Education and Sport. Faculty of Education, Economy and Technology. University of Granada. Ceuta, Spain.

³Allied Health Research unit, University of Central Lancashire, UK

⁴Delsys Europe, Manchester, UK

Email: herediaj@ugr.es

Summary

Knee extension training has been typically used to gain strength in the quadriceps muscles and is frequently used in muscle building routines. The analysis of vastus medialis (VM) and vastus lateralis (VL) activity during knee extension exercises has been widely reported due to their role in the rehabilitation of conditions such as patellofemoral pain and ACL injury. Therefore, the aim of this study was to explore the effect of speed, load and contraction phase on motor unit behaviour in VL and VM using surface EMG decomposition (dEMG) during knee extension tasks in healthy subjects. The results obtained indicated that the motor unit firing rates increased with both load and speed, and were also greater during the concentric phase.

Introduction

Knee extension training has been typically used to increase strength in the quadriceps muscles [1] and is frequently reported due to its implications to musculoskeletal conditions at the knee [2]. With respect to the influence of the speed of movement on EMG activity, the amplitude of signals has been shown to increase in VM and VL at faster speeds during the eccentric phase of knee extension [3]. Although differences were seen between concentric and eccentric phases at lower speeds, no such differences have been observed at faster speeds (60°/s) [3]. The use of surface EMG decomposition (dEMG) to describe motor unit behaviour within muscles has previously been restricted to isometric tasks [5], however this has been recently reported during cyclic dynamic contractions [6]. The aim of this study was to explore the effects of speed, load and contraction phase on the motor unit firing rates in VM and VL during knee extension training tasks.

Methods

Twenty-three healthy adults (10 females and 13 males) volunteered and participated in this study. The average (standard deviation) age was 31 (9.0) years, height 1.79 (0.1) m and weight 78.5 (14.6) kg. Surface EMG signals were recorded at a frequency of 2222 Hz using two four-channel dEMG Trigno Galileo wireless sensors (Delsys Inc., Boston, USA). The dEMG sensors were attached to the skin using hypoallergenic double-sided tape over the VM and VL of the dominant leg of each participant. An additional two IMUs sensors (Trigno Avanti, Delsys Inc., Boston, USA) were attached to the skin on the thigh to record angular velocity at a frequency of 148Hz.

A knee extension machine (Technogym UK Ltd., WP, United Kingdom) was used to complete knee extension

training tasks with loads of 10% and 20% of body weight (BW), at 15 and 25 repetitions per minute (RPM). NeuroMap software v.1.1.0 (Delsys Inc., Boston, USA) was used to decompose the EMG signals from VM and VL into their constituent motor units. Motor units over an 80% accuracy threshold were then combined with the segment angular velocity data and imported into Visual 3D. The mean, maximum, and tertiles (upper, middle and lower) of the firing rates were then calculated for the different loads and speeds for both the eccentric and concentric phases of the knee extension training tasks. A three factor repeated measures ANOVA was used to explore the effects of load, speed and contraction phase, and any significant interactions were explored using post hoc paired t-tests. The statistical significance level was set to $p < 0.05$.

Results and Discussion

The repeated measures ANOVA showed that both muscles had significantly higher firing rates as both load and speed increased, approximately 13% and 8% respectively ($p < 0.001$ and $p < 0.05$), with the VM showing the greatest firing rates and changes (Figure 1). In addition, the concentric phase showed approximately 5% and 10% higher firing rates than the eccentric phase across all measures in the VL and VM respectively ($p < 0.001$). However, significant interactions were seen between load and contraction phase, and speed and contraction phase for the firing rates. Post hoc tests revealed significant differences between speeds across both loads in VM, whereas VL only showed significant differences between speeds at 20% BW. The higher firing rates indicate an increase in neuromuscular demand as load and speed are increased, which is also higher during the concentric phase, with VM showing the greatest changes to the different conditions.

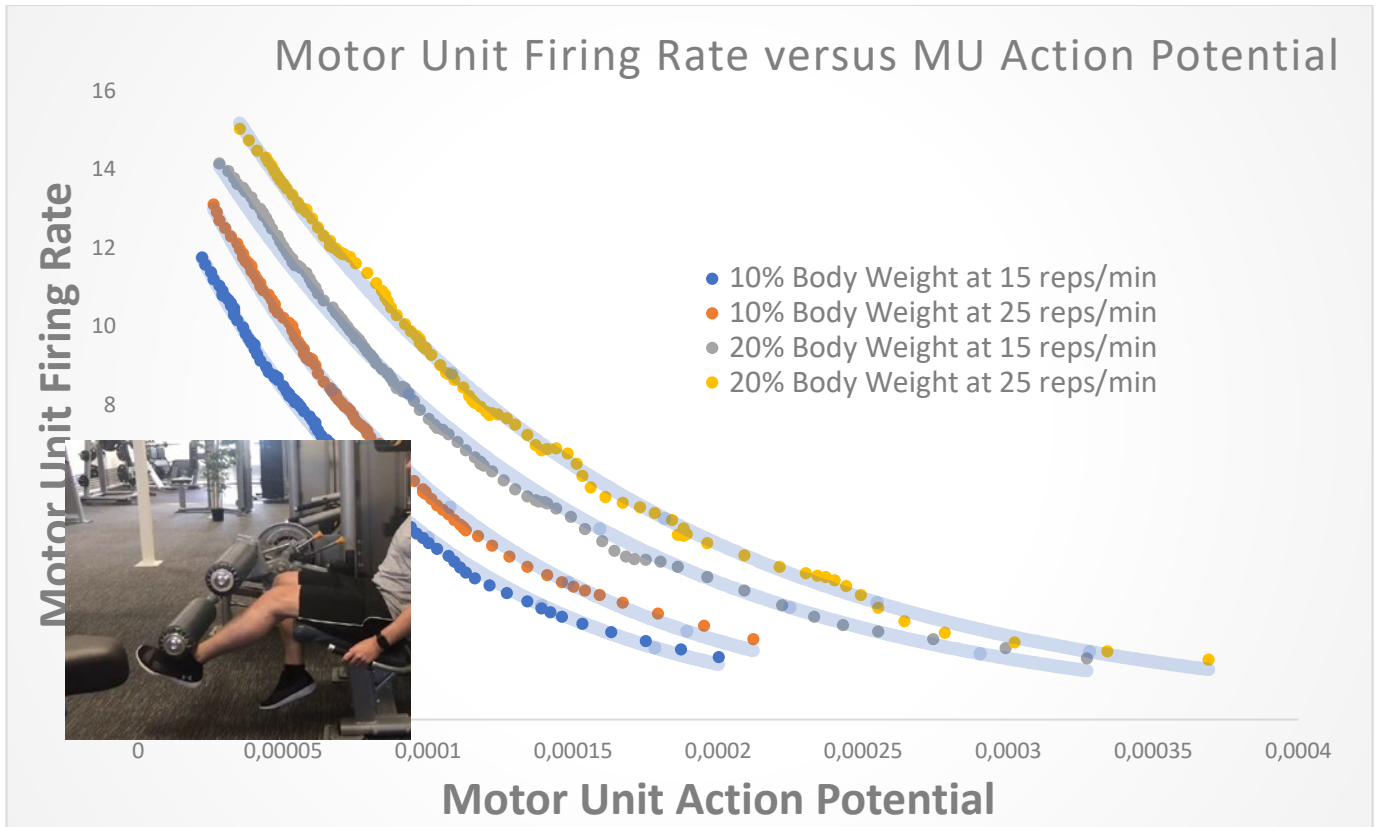
Conclusions

These findings highlight previously unreported effects of load, speed and contraction phase during knee extension exercises. These may yield important information on changes in motor unit behaviour and how such movements are controlled during different rehabilitation exercises.

References

- [1] Krisnan et al. (2014). *25th Pan Asian Conference of Sports*.
- [2] Irish et al. (2010). *J Strength Conditioning Research*. **5**:85-91
- [3] Haztel et al. (2012). *Open Sports Med J*, **6**: 42-7
- [4] Houghlum & Bertoti (2012). *Clinical Kinesiology*.
- [5] Del Vecchio et al. (2020). *J Electrom Kinesiol*. **53**:102426.
- [6] De Luca et al. (2015). *J Neurophysiol*. **113**:1941-51.

Figure 1. Vastus Medialis average firing rate versus peak motor unit amplitude in the different condition.



The effects of passive hyperthermia on muscle-tendon unit mechanical properties

A. Mornas^{1,2}, S. Racinais^{1,3}, F. Brocherie¹, M. Alhammoud³, R. Hager¹, Y. Desmedt¹, G. Guilhem¹

¹French Institute of Sport (INSEP), Laboratory Sport, Expertise and Performance (EA 7370), Paris, France

² Université de Paris

³ Aspetar Orthopaedic and Sports Medicine Hospital, Doha, Qatar

Email: adele.mornas@insep.fr

Summary

This study aimed to measure mechanical properties of *gastrocnemius medialis* (GM) muscle-tendon unit following heat exposure (HOT, 46-50°C), increasing core and muscle temperature, compared to control environment (CON, 26°C). Rate of force development (RFD) in the early phase (*i.e.*, <100 ms) was faster in HOT than CON while late RFD was unchanged. Peak fascicle shortening velocity was unaffected, joint force-velocity relationship shifted to the right while fascicle force-velocity properties remained similar between both conditions. Passive muscle stiffness and active Achilles tendon stiffness decreased with hyperthermia. These results could explain the change in early RFD in hot environment.

Introduction

Explosive force is commonly evaluated through the RFD, which is dependent of neural drive transmission, propagation of the action potential, excitation-contraction coupling processes and muscle force transmission [1]. RFD has been shown to increase with increasing core temperature [2]. This study aimed to evaluate the effect of hyperthermia on GM fascicle force-velocity relationship, passive muscle stiffness and active tendon stiffness to understand the localized mechanisms potentially involved in improved skeletal muscle contractility.

Methods

Sixteen young recreationally active participants performed two testing sessions in CON and then in HOT condition, core and muscle temperature reaching 38.4±0.3°C and 37.0±0.6°C in HOT. Participants laid prone with their knee fully extended and their ankle flexed at 90°. Mechanical and ultrasound data were collected across four procedures: electrically-evoked and maximal voluntary contractions (MVC), ballistic contractions, at 0, 1.5 and 3kg, and isometric ramp contractions from 0 to 90% of MVC peak force. Resting shear modulus was measured in GM in neutral ankle position.

Results and Discussion

Core and muscle temperature values were higher in HOT than CON (+1.42±0.5 and +3.0±1.0, respectively; $P < 0.001$). MVC

force showed a trend to be lower in HOT and voluntary activation was lower in HOT (Table 1). RFD increased in the early phase (RFD₀₋₁₀₀) while late RFD (RFD₁₀₀₋₂₀₀) was unchanged (Table 1). Peak fascicle shortening velocity (V_F) during electrically-evoked and voluntary contractions was not different between conditions (Table 1). Joint velocity at a given force was higher in HOT (Figure 1). Fascicle force-velocity properties relationship was unchanged (Figure 1). Muscle stiffness and active tendon stiffness decreased in HOT (Table 1).

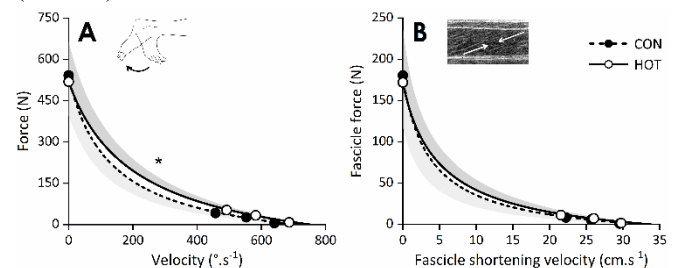


Figure 1: Mean joint force-velocity relationship (A) and mean fascicle force-velocity relationship (B) in CON and HOT. *, main effect of condition ($P < 0.05$).

Hyperthermia does not modify muscle contractility (*i.e.*, fascicle shortening velocity), but decreases the stiffness in soft tissues. The increase in RFD is potentially linked to upstream mechanisms such as the speed of nerve conduction [3].

Conclusions

The hyperthermia-induced increase in early RFD, is not related to changes in muscle contractility as reflected by similar force-velocity properties and reduced stiffness of soft tissues. The present study provides information on the determinants of human muscle performance in the heat.

References

- [1] Maffiuletti et al. (2016). *Eur J Appl Physiol*, **116**: 1091–1116.
- [2] Racinais et al. (2017). *Am J Physiol Regul Integr Comp Physiol*, **312**: 101–107.
- [3] Del Vecchio et al. (2019). *J Physiol*, **597**: 2445–2456.

Table 1: Mechanical parameters and muscle tendon properties in CON and HOT. *, significant differences between conditions ($P < 0.05$).

Mechanical parameters	CON	HOT	Muscle-tendon properties	CON	HOT
MVC force (N)	558 ± 128	531 ± 138	Peak V_F electrically-evoked ($cm.s^{-1}$)	13.6 ± 2.0	14.0 ± 2.1
VA (%)	97 ± 5	93 ± 11*	Peak V_F voluntary ($cm.s^{-1}$)	14.4 ± 5.3	15.8 ± 4.9
RFD ₀₋₁₀₀ ($N.s^{-1}$)	1097 ± 554	1397 ± 439*	V_0 fascicle ($cm.s^{-1}$)	32.7 ± 6.2	33.8 ± 8.5
RFD ₁₀₀₋₂₀₀ ($N.s^{-1}$)	1949 ± 620	1750 ± 607	F_0 fascicle (N)	180.3 ± 62.5	172.1 ± 67.0
V_0 joint ($°.s^{-1}$)	707 ± 109	752 ± 130	Muscle shear modulus (kPa)	15.6 ± 4.7	13.6 ± 4.9*
			Active tendon stiffness ($N.mm^{-1}$)	33.2 ± 8.5	28.5 ± 7.7*

3D Muscle Morphology and Intramuscular Fat of Lower Legs in Children with Cerebral Palsy

Antea Destro¹, Alexandra Palmerantz², Cecilia Lidbeck³, Sven Petersson⁴, Ferdinand von Walden³, Eva Pontén^{3,5}, Ruoli Wang¹

¹KTH MoveAbility Lab, Department of Engineering Mechanics, Royal Institute of Technology, Stockholm, Sweden

²Department of Physiotherapy, Karolinska University Hospital, Stockholm, Sweden

³Department of Women's and Children's Health, Karolinska Institute, Stockholm, Sweden

⁴Department of Medical Radiation Physics and Nuclear Medicine, Karolinska University Hospital, Stockholm, Sweden

⁵Department of Pediatric Orthopedic Surgery, Astrid Lindgren's Children Hospital, Stockholm, Sweden

Email: ruoli@kth.se

Summary

Children with cerebral palsy (CP) may undergo significant morphological and compositional alterations during growth that make their muscles smaller and weaker [1]. In the current study, we quantified 3D muscle morphological parameters and intramuscular fat fraction (IFF) in typically developing (TD) children and children with CP. The observed alterations in fascicle length (FL) and IFF can provide valuable information to evaluate musculoskeletal function in children with CP.

Introduction

Physical activity is limited among children with CP, thus IFF may rise compared to TD children, which has important impact for physical performance [2]. The aim of this study was to compare 3D morphological parameters, i.e., FL, and IFF of lower leg muscles in CP and TD groups.

Methods

Five children with CP (2M/3F, age 10.3 ± 3.1 yrs, height 138.1 ± 10.7 cm, weight 31.8 ± 6.9 kg) and eight TD children (3M/5F, age 9.3 ± 2.4 yrs, height 134.2 ± 13.4 cm, weight 30.4 ± 6.4 kg) voluntarily participated in the study approved by the local ethics committee. All the participants were scanned using a 3T MRI scanner (Siemens Trio) in a supine position, with 20° knee flexion and 10° ankle plantar flexion. T1-weighted, diffusion tensor (DT) and mDixon images were acquired for the lower legs. Muscle fascicle reconstruction was performed based on a previously reported pipeline [3] consisting of manual T1-weighted image segmentation, DTI registration, fiber tracking and parameter identification. IFF of all voxels in a muscle were calculated using the ratio of water and fat signal intensities [4]. For children with CP, quantification was made on the more affected side. For TD children, one side was randomly selected. Due to the low image quality and movement artifacts, mDixon images of three TD children and one child with CP were not included in the analysis.

Results and Discussion

The FL and IFF of medial gastrocnemius (MG) and tibialis anterior (TA) are summarized in Figure 1, where FL was normalized with respect to the body height. Compared to the TD group, the FL of MG was found 17.8 % longer in children with CP but 11.3 % shorter in TA. As expected, compared to the TD group, children with CP have higher IFF in both muscles, which was in line with a previous study [2].

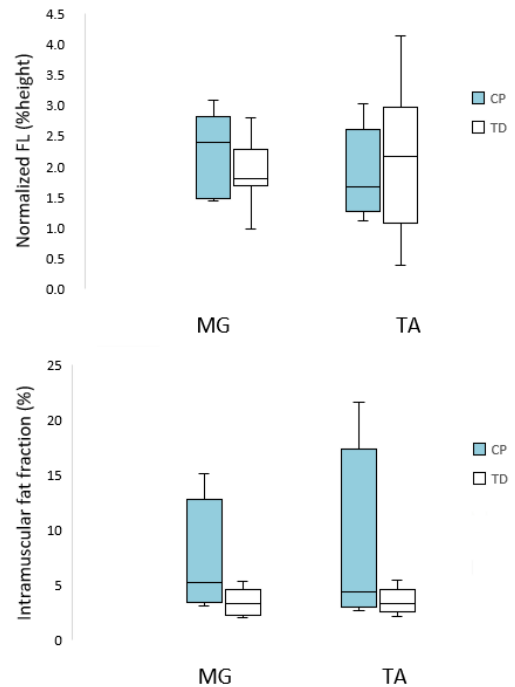


Figure 1: Normalized FL (top) and IFF (bottom) in MG and TA in children with CP (affected side) and TD group.

Conclusions

DTI and mDixon images were used to investigate FL and IFF in the lower leg muscles of children with CP. The preliminary results showed that children with CP had a longer FL in MG but shorter in TA. Higher IFF was found in both MG and TA in the CP group. Further analysis is needed to determine whether the morphological and compositional changes are related to muscle strength and overall joint function.

Acknowledgments

We would like to acknowledge financial support from Promobilia Foundation, Norrbacka-Eugenia Stiftelsen and Stockholm City Council.

References

- [1] Elder G et al. (2003). *Dev. Med. Child Neurol*, **45**: 542-550.
- [2] Noble JJ et al. (2014). *BMC Musculoskelet Disord*, **15**:236.
- [3] Körting C et al. (2019). *Sci. Rep*, **9**: 1-11.
- [4] D'Souza A et al. (2020). *Clin Biomech*, **80**: 1-7.

Reliability of regional measurements of gastrocnemius muscle fibre lengths obtained from diffusion tensor imaging

□ Aeles¹, F. Hug^{1,2}, T. Dick², □. □olsterlee³

¹Nantes University, Laboratory “Movement, Interaction, Performance” (EA 4334), Nantes, France

²The University of Queensland, School of Biomedical Sciences, Brisbane, QLD, Australia

³Neuroscience Research Australia □ University of New South Wales, Sydney, NSW, Australia

Email: jeroen.aeles@univ-nantes.fr

Summary

We tested the between-day reliability of diffusion tensor imaging (DTI) measurements of muscle fibre lengths in regions of varying size in the medial (MG) and lateral (LG) gastrocnemius muscles. The reliability increased with increasing size of muscle regions in which median lengths were measured, and varied considerably between individuals. These results should be taken into account when using DTI to measure local variations in muscle architecture.

Introduction

The architecture of a muscle, particularly the fibre length, contains important information regarding the muscle’s force generating capacity. DTI is a promising technique to non-invasively quantify *in vivo* muscle fibre lengths in 3 dimensions at high spatial resolution. While the technique has been shown to provide reliable measures of the average muscle fibre length and other architectural parameters in whole muscles [1], the reliability has not yet been tested for smaller muscle regions.

Methods

Previously published data from the MG and LG [1], collected in four women and four men was used in this study. Each participant was scanned on two separate days to obtain both T1-weighted and DTI MRI scans of the left lower leg on each day. Segmentations of MG and LG from the T1 MRI scans were used to define the muscle boundaries. On average, 4436 ± 1185 (MG) and 2755 ± 902 (LG) fibre tracts were fitted on the DTI with third-order polynomials and then linearly extrapolated to the muscle boundaries.

A grid of rectangles was overlaid on the muscle’s (local) frontal plane (Fig. 1). Three rectangle sizes were used: small, medium, and large, with heights of 20%, 25%, 25% of muscle length and widths of 10%, 20%, 33.3% of muscle width, respectively. Median fibre lengths of all fibres with midpoints inside a given rectangle were calculated and compared between days. The mean intra-class correlation (ICC) and standard error of measurement (SEM) between days were computed for each rectangle size and muscle.

Results and Discussion

An increasing rectangle size resulted in an increasing ICC for the median fibre lengths between days, in both muscles (Table 1). The mean ICC values ranged from moderate to good. However, we found a relatively large range of individual ICC values, with poor reliability in some participants. SEM values for both muscles followed a similar trend of decreasing values with increasing rectangle size. This suggests that with the largest rectangle sizes (□ 55 x 24 mm for the participant shown in Fig. 1), local median fibre lengths can be measured, on average, with good reliability.

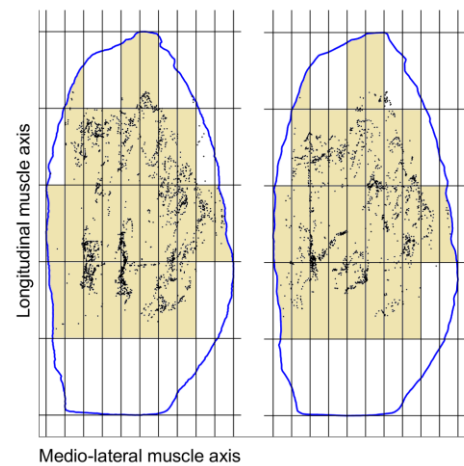


Figure 1: Frontal view of the same MG muscle on day 1 (left) and day 2 (right), with the small rectangle size overlaid. Muscle boundaries are outlined in blue □ black dots show fibre midpoints □ shaded rectangles contain midpoints in both scans and were used to determine the ICC and SEM of median fibre length measurements.

Conclusions

The reliability of DTI-based measurements of regional muscle architecture depends on the size of the region, with larger regions giving higher reliability. These results should be taken into account when using DTI to measure highly local variations in muscle architecture.

References

[1] □olsterlee □ et al. (2019). *J. Biomech.*, **8** □ 71-78.

Table 1: Mean [range] intra-class correlations (ICC) and standard error of measurement (SEM) results of the eight participants.

	ICC			Whole muscle [1]	SEM (mm)		
	Small	Medium	Large		Small	Medium	Large
MG	0.72 [0.41 - 0.91]	0.79 [0.36 - 0.91]	0.83 [0.40 - 0.95]	0.92	7.98 [1.52 22.84]	6.29 [1.02 26.58]	5.30 [0.68 25.56]
LG	0.64 [0.21 - 0.75]	0.68 [0.19 - 0.94]	0.81 [0.54 - 0.98]	0.84	11.22 [4.52 30.87]	9.68 [1.00 18.99]	5.67 [0.41 11.31]

Effect of muscle length on performance enhancement in a stretch-shortening cycle of the quadriceps femoris

Martin Groeber¹, Arnold Baca¹

¹Department of Biomechanics, Kinesiology and Computer Science in Sport, Centre for Sport Science and University Sport, University of Vienna, Vienna, Austria
Email: martin.groeber@univie.ac.at

Summary

The present work disputes the influence of the muscle length on the stretch-shortening cycle (SSC) performance enhancement. The focus of this work is on the history-dependent properties of this muscle action. 25 healthy adults have been tested at an isokinetic dynamometer, parameters of interest were the mechanical work during shortening and the steady-state isometric force after the dynamic phase.

Introduction

The isometric force or torque following eccentric or concentric muscle action is smaller (residual force depression, rFD) or greater (residual force enhancement, rFE) compared to an isometric reference contraction at the same muscle length and activation level [1]. rFE occurs at all muscle lengths but seems to be greater at long muscle lengths [2]. The contribution of rFE to a more relevant muscle action like the stretch-shortening cycle (SSC) should therefore also be greater at long muscle lengths. Thus, the focal point of this study was to examine the influence of different muscle lengths (meaning different angular positions) on the SSC performance enhancement.

Methods

Torque of 25 healthy young adults was measured during SSC conditions, shortening conditions (CON) and isometric reference conditions (ISO) using an isokinetic dynamometer. The tests were conducted at the quadriceps femoris of the right leg. Electrical stimulation was used for all contractions. Current was increased until 35% of maximal voluntary contraction was reached, this current was used for the whole experiment. The angular velocity and range of motion were always fixed to 60°/s and 30° respectively, but angular positions varied (CON: 50 - 20°, 80 - 50° or 110 - 80°; SSC: 20 - 50 - 20°; 50 - 80 - 50°, 80 - 110 - 80°). Full extension of the knee joint was defined as 0°.

Two-way ANOVA was used, the interaction (condition × angular position) and main effect was examined for the mechanical work during the shortening phase and the steady-state torque after the dynamic phase. The effect size was assessed with partial eta squared (η^2).

Results and Discussion

For mechanical work, no significant interaction (condition × angular position) was found ($p = 0.544$, $\eta^2 = 0.25$). Main effect for condition ($p < 0.001$, $\eta^2 = 0.435$) and angle ($p < 0.001$, $\eta^2 = 0.408$) revealed significant higher mechanical work with greater knee flexion angle and for the SSC condition. The percentage increase of mechanical work was nearly identical

at all different angle ranges (50 - 20°: 8.1%, 80 - 50°: 8.5% and 110 - 80°: 8.6%).

Two-way ANOVA revealed a significant interaction (condition × angle) ($p = 0.033$, $\eta^2 = 0.127$) for the steady-state torque. Main effect of angle was significant ($p < 0.001$, $\eta^2 = 0.636$), as well as the main effect for condition ($p < 0.001$, $\eta^2 = 0.296$). Further comparison with Bonferroni post hoc correction showed significant higher torque for the SSC condition compared with the CON condition at the greatest dynamometer angle ($p = 0.043$) (Figure 1). No statistical difference was found between CON: 50-20° and SSC: 20 - 50 - 20° ($p > 0.05$) and between CON: 80-50° and SSC: 50 - 80 - 50° ($p > 0.05$).

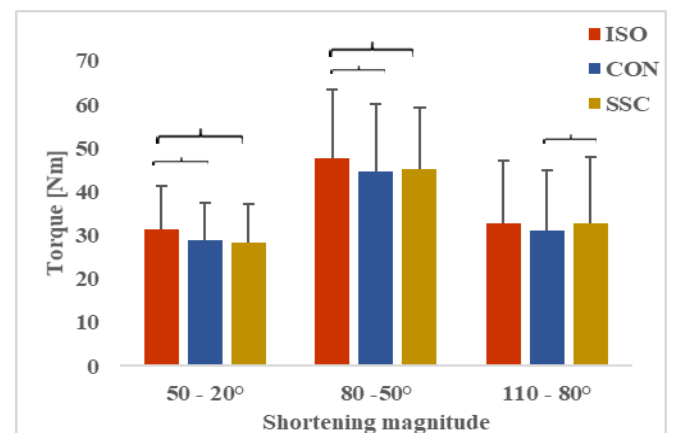


Figure 1: Steady-state torque of all tested contractions. Brackets indicate significant differences ($p < 0.05$).

The results imply, that mechanisms related to rFE are responsible for the less depressed steady-state torque after the SSC with the greatest angular position.

Conclusions

In conclusion, reduced rFD after the SSC contraction was only found at the condition with the greatest knee flexion angle (meaning longer muscle length). However, the percentage increase of mechanical work was independent of the angular position.

References

- [1] Herzog W. (2001) The nature of force depression and force enhancement in skeletal muscle contraction. *European Journal of Sport Science* 1,1-14.
- [2] Lakenecker, P., Raiteri, J., and Hahn, D. (2020). Force enhancement in the human vastus lateralis is muscle-length-dependent following stretch but not during stretch. *European journal of applied physiology* 120, 2597–2610.

Quantifying mechanical loading and elastic strain energy of the human Achilles tendon during walking and running

Mohamadreza Kharazi^{1,2}, Sebastian Bohm^{1,2}, Christos Theodorakis^{1,2}, Adamantios Arampatzis^{1,2}
¹Berlin School of Movement Science, Berlin, Germany

² Department of Training and Movement Sciences, Humboldt-Universität zu Berlin, Berlin, Germany

Email: mohamadreza.kharazi@hu-berlin.de

Summary

We assessed the in vivo Achilles tendon (AT) strain, loading and strain energy during walking and running using a novel experimental approach. The AT length behavior was measured by integrating ultrasound and kinematics. The curved-shape of the AT was assessed by small reflective skin-markers placed on the path of the AT from origin (notch in calcaneus bone) to insertion (junction to medial gastrocnemius). The misalignment of the myotendinous junction to the skin surface and potential displacement of the skin insertion marker relative to the bone were considered. The tendon loading and strain energy during gaits was assessed by fitting a quadratic function to the experimentally measured AT force-elongation curve obtained from maximum voluntary ramp contractions. We found the AT strain during running lower than reported thresholds for an effective stimulus for tendon adaptation, which may explain the lack of adaptation following running training reported earlier. Moreover, we found a recoil of AT strain energy in the early stance phase of running, which we suggest to be functionally relevant.

Introduction

The AT can adapt to external mechanical loading by increasing its stiffness. AT strain levels between 4.5 to 6.5 % were found to be effective to stimulate AT adaptation [1]. Previously, reported AT strains during running were in the suggested range of strain for tendon adaptation (i.e. 4.6 to 9 %). However, most studies that compared runners and untrained controls could not detect significant differences in AT stiffness [2]. The discrepancies between these findings might be the result of methodological limitations using simple planimetric model. Tendons feature elastic properties, enabling the storage and release of strain energy during gaits in favor of energy conservation and locomotor economy. Komi et al. (1990) [3] reported a reduction of the AT force in the early stance phase of running, suggesting an energy recoil of the AT after touchdown. This energy recoil might be functionally relevant for human running but has not been directly investigated yet.

Methods

Eleven participants (height = 177 ± 6 cm, body mass = 74 ± 9 kg, age = 29 ± 3 years) walked and ran at 1.4, 2.5 and 3.5 m/s on a treadmill. AT length was defined as a curve-path from the insertion at the calcaneus (notch) that follows a line of reflective markers placed on the skin above the AT to its origin at the gastrocnemius myotendinous junction (MTJ).

The MTJ was captured during gaits using ultrasound and tracked by a self-developed semi-automatic algorithm. The tracked positions were firstly projected to skin surface and then projected to the global coordinate system. The potential skin-to-bone displacement of the calcaneus skin marker (insertion) was assessed separately during a passive rotation of the ankle joint and ultrasound. AT force and strain energy during gaits were calculated by fitting a quadratic function to the separately experimentally measured AT force-elongation curve obtained from maximum voluntary ramp contractions.

Results and Discussion

The contribution of skin-to-bone displacement and projection of MTJ to the skin surface significantly affected AT length ($p < 0.05$). The maximum AT strain ranged from 4.0 to 4.9%, indicating an insufficient strain magnitude to induce adaptation, which can explain the lack of adaptive changes in AT stiffness of runners. We found an elastic energy recoil between 7.8 J (walking) and 11.3 J (running) during the propulsion phase. We further found a recoil of elastic strain energy by AT in the early stance phase of slow and fast running in order of 1.7 ± 0.6 J and 1.9 ± 1.1 J, respectively, which might be functionally relevant for running efficiency.

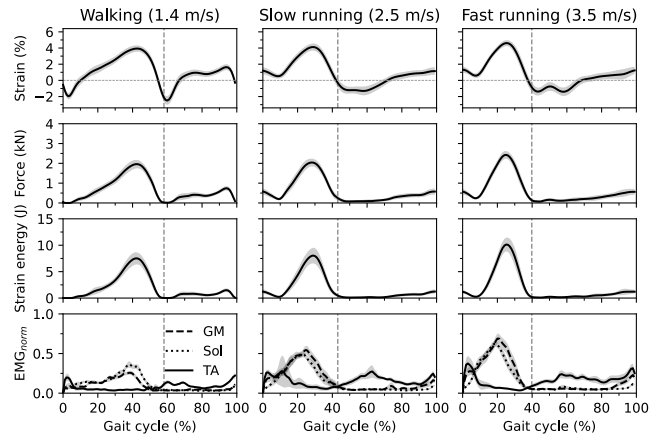


Figure 1: Achilles tendon strain, force and strain energy, as well as EMG-activity of the gastrocnemius medialis (GM), soleus (Sol) and tibialis anterior muscle (TA).

Conclusions

We found the AT strain during running is lower than previously reported and inadequate to initiate an adaption and provided the first evidence of elastic strain energy recoil in the early stance phase of running.

Reference

- [1] Lai et al. (2015). *J. appl*, **118** 1266-1275
- [2] Arampatzis et al. (2007). *J. Biomech*, **40**: 1946-1952
- [3] Komi et al. (1990). *J. Biomech*, **23**: 23-34

Ultrasound investigation of muscle size and muscle properties in transfemoral amputees

Susann Wolfram¹, Begum Seybek¹, Alvaro Dueñas Ruiz², Victor M. Encinas-Tobajas³

¹School of Health and Life Sciences, Teesside University, Middlesbrough, UK

²Institute of Biomedicine of Seville, Virgen del Rocío University Hospital, Sevilla, Spain

³Radiology Department, Virgen del Rocío University Hospital, Sevilla, Spain

Email: s.wolfram@tees.ac.uk

Summary

This study investigated muscular adaptations of the residual and sound limb of transfemoral amputees compared to able-bodied controls. We found a decrease in muscle thickness in the residual limb compared to the sound limb and controls but no change in muscle stiffness.

Introduction

Transfemoral (TF) amputation involves disinsertion of distal ends of thigh muscles and reinsertion to non-physiological sites. As a result, amputees must adapt to a new muscular state. Loss of muscle mass has been reported for some thigh muscles of the residual limb [1] but nothing is known about changes in muscle material properties.

The purpose of this study was to conduct a thorough investigation into thickness of the major thigh muscles and subcutaneous fat of TF amputees and to obtain a measure of muscle stiffness using shearwave (SW) elastography.

Methods

Thigh muscles of the residual limb (RES) and sound limb (SND) of six established TF amputees (3 males, 39.00 ± 6.22 years) and the left thigh of four able-bodied, age-matched controls (CON; 3 males, 38.75 ± 6.87 years) were studied. Participants provided informed consent and the study was approved by the ethics committee of Hospital Universitario Virgen del Rocío. Muscle thickness, subcutaneous fat thickness and SW velocity were measured from the mid-belly region of rectus femoris (RF), vastus medialis (VM), vastus lateralis (VL), adductor magnus (AM), biceps femoris (BF), semitendinosus (ST) and semimembranosus (SM). Muscle thickness, subcutaneous fat thickness and SW velocity were compared between RES, SND and CON with a One-Way ANOVA and Tukey's post-hoc test, where appropriate.

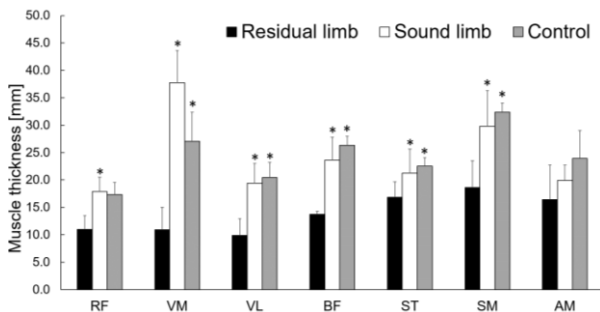


Figure 1 Muscle thicknesses of residual limb, sound limb and control. Error bars represent standard deviations. *Significant difference to residual limb ($p < 0.05$).

Results and Discussion

In agreement with previous studies [1,2], muscle thickness was significantly smaller for all RES muscles compared to SND and CON except AM (Figure 1), which may be due to muscle atrophy but could also be a result of surgical technique. The thickness of subcutaneous tissue did not differ for any of the areas between RES, SND and CON.

Interestingly, we did not find differences in SW velocity between the RES, SND and CON for most muscles. Only SW speed of BF was found to be significantly greater in CON compared to RES (Table 1). These findings indicate that muscle material stiffness is not related to muscle atrophy as was shown for the elderly [3]. Rather, changes in SW speed may reflect adaptations of muscle connective tissue.

Table 1: Shearwave velocities (with standard deviations) for all muscles. *Significant difference to residual limb ($p < 0.05$)

Muscle	Shearwave velocity [m/s]		
	Residual limb	Sound limb	Control
Rectus femoris	2.34 (0.41)	2.18 (0.26)	2.38 (0.68)
Vastus lateralis	3.27 (0.89)	2.42 (0.88)	2.32 (0.46)
Vastus medialis	2.78 (0.72)	2.23 (0.54)	2.49 (1.11)
Biceps femoris	2.54 (0.74)	3.47 (1.23)	3.47 (0.42)*
Semitendinosus	2.04 (0.34)	2.43 (0.45)	2.96 (0.78)
Semimembranosus	2.39 (0.58)	3.00 (0.9)	4.12 (1.04)
Adductor magnus	4.03 (0.88)	3.66 (0.84)	4.71 (0.25)

Conclusions

Muscular adaptations in TF amputees occur for the residual limb through a reduction in muscle size rather than a change in muscle material properties. These adaptations seem to affect the residual limb only but not the sound limb.

Acknowledgments

This project has received funding from the European Union's Horizon 2020 research and innovation program under grant agreement No. 825429.

References

- [1] Sherk, D et al. (2010). *Arch. Phys. Med.*, **91**: 1077-1081.
- [2] Schmalz, T et al. (2001) *Arch. Orthop. Trauma. Surg.*, **111**: 307-312.
- [3] Alfuraih, AM et al. (2019). *Aging Clin. Exp. Res.*, **31**: 1755-1763.

In vivo submaximal force-angle relationship of the quadriceps based on net joint torque and shear wave tensiometry

Tobias Weingarten¹, Patrick Bakenecker¹, Brent J. Raiteri¹, Daniel Hahn^{1,2}

¹Human Movement Science, Faculty of Sport Science, Ruhr University Bochum, Bochum, Germany

²School of Human Movement and Nutrition Sciences, University of Queensland, Brisbane, Australia

Email: tobias.weingarten@rub.de

Summary

Human muscle function is often evaluated using indirect measures such as net joint torque. We therefore used a new non-invasive technique known as shear-wave tensiometry to estimate the *in vivo* human quadriceps muscles' force-angle relationship at various muscle activity levels using patellar tendon wave speed measurements and net joint torque measurements. Preliminary data shows that tensiometry is more sensitive to changes in both passive and active muscle tension across knee joint angles.

Introduction

A muscle's force capacity depends on its length as described by its force-length relationship (F-l-r). When estimating the F-l-r of human muscles *in vivo*, muscle force cannot be measured directly. Often, external net joint torque is used as a substitute and force is estimated using lever-arm functions [1]. However, these approaches are problematic as subject-specific lever arms are often unknown and because net joint torque is influenced by gravitational forces and forces generated by agonist and antagonist muscles.

Recently, it has been shown that non-invasive tensiometry [2] might be able to overcome these problems. Tensiometry allows tendon load to be estimated by calculating the speed of a shear wave that is induced by a tap on the tendon. By assuming that tendon load is proportional to muscle force, the F-l-r can then be estimated based on more direct estimates of muscle force from tendon wave speed measurements. The aim of this study was to compare the submaximal F-l-r of the quadriceps obtained from both net joint torque and tendon wave speed measurements.

Methods

Preliminary data was recorded from one healthy participant who performed nine fixed-end ramp contractions at knee angles ranging from 30 to 110° of knee flexion (0° refers to extension) at 10° increments. Their right shank was fixed to the lever arm of a dynamometer (IsoMed2000, DOR Ferstl GmbH, GER) while they sat with 90° hip flexion. Contractions were based on the summed muscle activities of vastus lateralis (VL), vastus medialis (VM) and rectus femoris (RF), which was provided as a real-time visual biofeedback signal. During the contractions, the participant had to linearly increase their quadriceps activity such that after 3-s they matched 50% of their maximum activity observed during maximum voluntary contraction (MVC) at 70° knee flexion.

Torque and crank arm angle were recorded at 2 kHz. Muscle activity was recorded at 2 kHz by surface EMG (NeuroLog System NL905, Digitimer Ltd, UK). Patellar tendon wave

speed was calculated from the time delay of the shear wave induced by a piezoelectric stack actuator (PK4J-P2, Thorlabs, USA), as measured by two accelerometers (Model 352A26, PC Piezotronics, USA) attached over the skin nine millimeters apart. Accelerometer data was sampled at 100 kHz and synchronized with all other signals using a 16-bit A/D converter (Power1401, CED, UK).

Submaximal torque-angle and wave speed-angle relationships ($T-\theta$ -r and $Ws-\theta$ -r) for 5–50 % MVC EMG levels were constructed from the nine fixed-end contractions. The summed quadriceps activity was normalized to its maximum recorded at each angle during the ramp contractions up to 50% MVC and submaximal torque and wave speed were taken at the corresponding time points from 10–100% of the normalized signal (resulting in 5–50% activity). Torque and wave speed were measured at rest from the first 250ms of each fixed-end contraction and subtracted at each angle. The $T-\theta$ -r and $Ws-\theta$ -r data were fitted with a second order polynomial.

Results and Discussion

First results indicate a steep rise in wave speed at rest from 90° knee flexion, which was not observed using torque measurements. While passive torque is dominated by gravity acting on the leg attached to the dynamometer, wave speed at rest should reflect the tension in the quadriceps muscle-tendon units (MTUs). When considering the muscle and tendon as perfectly in series, this could indicate that beyond 90° knee flexion the passive tension of the muscle increases substantially.

The amplitude of the $Ws-\theta$ -r largely exceeded the amplitude of the $T-\theta$ -r. At 50% EMG activity, the lowest wave speed at 30° knee flexion equaled only 13% of the maximum wave speed at 70° knee flexion, whereas the minimum torque at 30° knee flexion equaled 60 % of the maximal torque at 70° knee flexion. One possible explanation could be related to joint geometry and the muscle's lever arm function that transforms tendon force into joint torque.

Conclusions

Our preliminary data suggest that standard measurements of net joint torque potentially do not reflect patellar tendon load and therefore the tension generated by the quadriceps' muscles.

References

- [1] Bakenecker P et al. (2019). *J. Biomech.*, **8**: 225-231
- [2] Martin JA et al. (2018). *Nat. Commun.*, **9**: 1-9

Investigating the influence of personalized musculoskeletal models on the calculated muscles and joints forces

Ahmed Soliman^{1,*}, Slawomir Kedziora¹, Jens Kelm², Torsten Gerich³, Stefan Maas¹

¹ Dept. of Engineering, Université du Luxembourg, 1359 Luxembourg, Luxembourg

²Chirurgisch-Orthopädisches Zentrum, 66557 Illingen/Saar, Germany

³Centre Hospitalier de Luxembourg, 1210 Luxembourg, Luxembourg

*Corresponding author: ahmed.soliman@uni.lu

Summary

It was the objective to analyze the influence of personalization of musculoskeletal models (MS) on muscle and contact joint forces for frequent daily movements. For normal gait cycle, we detect approximately 20% for some muscles attached to the pelvis, as well as for maximum hip-joint contact force.

Introduction

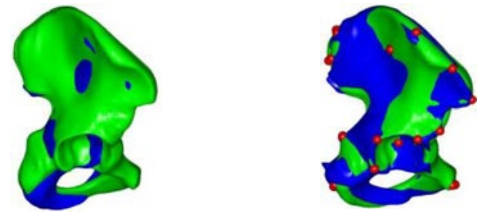
Over the past decades, numerous biomechanical studies were performed in order to investigate pelvis charging under physiological loading. Musculoskeletal Models (MS) proved already to provide precise muscle and contact forces. The latter were validated by measurements of instrumented implants [1], for this reason the muscles' forces can be assumed to be correct. However, an interesting question is the influence of personalization. The calculated muscles and joints contact forces may be utilized to predict stress states in pelvis bones and implants by using finite element (FE) software. In our study, the generic MS model of AnyBody software [2] is customized by matching the pelvis to the individual geometry ("morphing") of the SawBone pelvis [3]. As a result, muscle attachment points and joints centers shifted and results are compared.

Methods

In order to digitize the 4th gen. SawBones artificial pelvis, computed tomography (CT) was conducted and 593 Digital Imaging and Communications in Medicine (DICOM) images of 0.5 mm thickness were imported into ITK-SNAP [4] and a 3D model of the pelvis was segmented. The total number of 28 corresponding anatomical landmarks (red dots in Figure 1) on both pelvises are selected using Meshlab [5]. The landmark coordinates are used in anybody to scale the morphing. For the gait movement, the inverse dynamics analysis was done twice, once for the generic MS and then for the personalized model.

Results and Discussion

Figure 1(a), (b) show the two pelvises prior to and after morphing, respectively. As an example, the force of Gluteus Medius muscle for both models during normal gait is shown in Figure 2, which is considered as one of the most significant muscles of the lower limb. Though the pattern for both models is similar, there are deviations up to 24% for Left Heel Strike (LHS). The resulting Hip Joint Contact (HJC) force for both models show similar deviations up to \approx 20% for Right Heel Strike (RHS), well in line with experimental studies of Bergman et al. [1].



(a) Before Morphing

(b) After Morphing

Figure 1: Illustration of the differences between the generic and the morphed Anybody pelvis in MS models. AnyBody pelvis in blue, Sawbones pelvis (Target) in green, Controlling landmarks in red

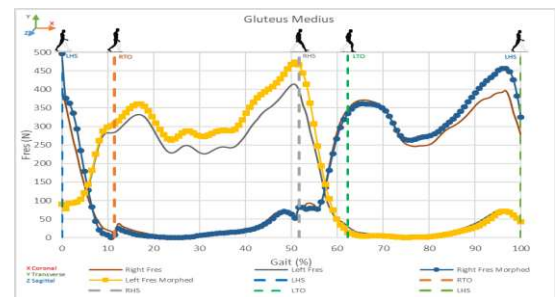


Figure 2: Force (Fres) of Gluteus Medius muscle of left and right leg for both generic and morphed AnyBody MS model

Conclusions

MS models allow full insight on muscle and joint contact forces. The personalized MS model shows similar shape of the calculated forces with clearly detectable deviations at distinct moments of the gait cycle. Hence, personalizing MS models can provide better results for individual biomechanical studies and for personalized implants.

References

- [1] Bergmann G, Deuretzbacher G, Heller M, Graichen F, Rohlmann A (2001), Strauss J, Duda GN. Hip contact forces and gait patterns from routine activities. *J Biomech* **34**(7): 859-871.
- [2] AnyBody. The AnyBody Modeling System. Aalborg (2017), Denmark: AnyBody Technology A/S.
- [3] Sawbones. Product Catalogue (2019). Available at: <http://www.sawbones.com/products>. Accessed July 1.
- [4] Paul A. Yushkevich, Joseph Piven, Heather Cody Hazlett, Rachel Gimpel Smith, Sean Ho, James C. Gee, and Guido Gerig (2006). User-guided 3D active contour segmentation of anatomical structures: Significantly improved efficiency and reliability. *Neuroimage* Jul 1; **31**(3):1116-28.
- [5] P. Cignoni et al. (2008) MeshLab: an Open-Source Mesh Processing Tool Sixth Eurographics Italian Chapter Conference, page 129-136.

Towards more effective training: A biomechanical comparison of three hamstring exercises

Bas van Hooren¹, Panayiotis Teratsias¹, Paul Willems¹, Sam van Rossum², Benedicte vanwanseele², Kenneth Meijer¹, Maarten Drost¹
¹NUTRIM School of Nutrition and Translational Research in Metabolism, Maastricht University Medical Centre, Department of Nutrition and Movement Sciences, Maastricht, The Netherlands

²Human Movement Biomechanics Research Group, Department of Movement Sciences, KU Leuven, Leuven, Belgium
 Email: basvanhooren@hotmail.com

Summary

This study aimed to characterize and compare lower-limb muscle forces, muscle activation, and biceps femoris muscle fascicle behavior between three hamstring exercises: the Nordic hamstring exercise (NHE), the single-leg Roman chair (RCH), and the single-leg deadlift (DL). Increases in fascicle length were largest in the NHE, followed by the DL and RCH. Peak knee joint moments were highest for the NHE, followed by the RCH and DL while peak hip joint moments did not differ.

Introduction

Risk factors for hamstring injuries include low hamstrings strength, short biceps femoris fascicles, and altered intermuscular coordination between the medial and lateral hamstrings [1]. A variety of exercises is being used to modify these risk factors in an attempt to prevent hamstrings injuries and improve performance. Knowledge about the muscle forces, relative load and activation of each muscle, and fascicle behavior during exercises is essential as this allows practitioners and researchers to target specific adaptations to maximize the effectiveness of the exercises. However, there is currently little evidence available on these aspects across different exercises. The aim of this study is therefore to characterize and compare lower-limb muscle forces, muscle activation, and biceps femoris muscle fascicle behavior between three hamstring exercises: the Nordic hamstring exercise (NHE), the single-leg Roman chair (RCH), and the single-leg deadlift (DL).

Methods

Ten male participants performed the NHE, RCH and DL in a randomized order with a 1RM load, while full-body kinematics, ground reaction forces, lower-limb surface muscle activation (EMG) and biceps femoris muscle fascicle behavior were measured. Joint moments and muscle forces were determined using OpenSim [2]. Linear-mixed models were used to compare outcomes between exercises.

Results and Discussion

Biceps femoris fascicles remained quasi-isometric before actively lengthening during the NHE and RCH, while they lengthened and subsequently shortened in the DL (Figure 1A). The increase in fascicle length was sig. larger in the NHE (30.8 ± 11.7 mm), compared to the DL or RCH (18.5 ± 5.2 and 17.8 ± 7.9 mm, respectively). Mean fascicle length was largest in the DL, followed by the RCH and NHE (130.1 ± 39.6, 92.8 ± 26.1 and 72.4 ± 14.6 mm, respectively), with all pairwise comparisons being significant. Peak knee joint

moments were highest for the NHE, followed by the RCH and DL (6.6 ± 1.2, 3.8 ± 1.3, 1.0 ± 0.4 N·m/kg, respectively (Figure 1B)). Peak hip joint moments and peak surface muscle activation did not significantly differ. Preliminary results indicate that the peak muscle forces for all hamstring muscles are highest in the NHE, followed by the RCH and DL.

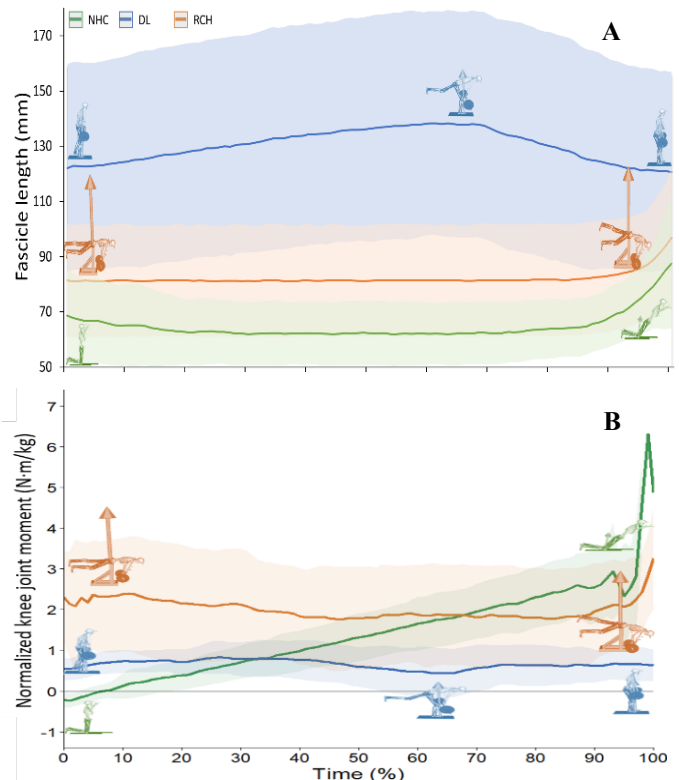


Figure 1 (A) Biceps femoris long head fascicle length, and (B) normalized knee joint moment during the NHE, RCH, and DL. Solid lines depict individual data, shaded areas between-subject SD.

Conclusions

The larger increase in fascicle length during the NHE suggests this exercise may be most effective to trigger fascicle length adaptation. The higher peak hamstring muscle forces in the NHE suggest this exercise may be most effective to increase strength in these muscles.

Acknowledgments

Bas van Hooren was funded by a Kootstra Talent Fellowship.

References

- [1] Bourne M. et al. (2020) *Prevention and rehabilitation of hamstring injuries* Springer.
- [2] Catelli. D. et al. (2018) *CMBBE*, 21-24.

A forward-dynamics tracking simulation using a combined rigid body - FEM model to predict knee meniscus loading

Benedikt Sagl¹, Colin R. Smith², John E. Lloyd³, Ian Stavness⁴

¹Competence Center Clinical Research, University Clinic of Dentistry, Medical University of Vienna, Vienna, Austria

²Laboratory for Movement Biomechanics, Institute for Biomechanics, ETH Zürich, Zürich, Switzerland

³Department of Electrical and Computer Engineering, University of British Columbia, Vancouver, Canada

⁴Department of Computer Science, University of Saskatchewan, Saskatoon, Canada

Email: benedikt.sagl@meduniwien.ac.at

Summary

This project uses a forward-dynamics tracking approach to compute muscle as well as knee joint forces from measured gait data using a musculoskeletal model combining rigid body bones, line actuators, and finite element meniscus bodies. This model will allow us to investigate meniscal loading during highly dynamic movements as well as the effect of meniscal injuries on knee loading.

Introduction

Dynamic musculoskeletal simulations using motion analysis data are a common tool in lower extremity biomechanics and have been used to investigate knee loading for a variety of tasks and disorders. Typically, these models use idealized rigid body joints to represent the knee, which does not allow for easy inclusion of deformable meniscus bodies. On the other hand, FE studies on meniscal loading are often computationally expensive and are mostly used for static or quasi-static investigations. In this project, we strive to use a rigid body model with included FE menisci to run forward-dynamics tracking simulations of various lower extremity tasks. This will allow us to investigate meniscal and articular cartilage loading during dynamic tasks from realistic, *in vivo* loading conditions.

Methods

We built a combined rigid body-FE body model of the knee that included femur, tibia, patella, and menisci bodies connected by six-degree-of-freedom joints, ligaments, and articular contact. Bone, cartilage, muscle, and ligament geometries as well as tissue parameters were taken from an existing OpenSim model [1] and imported into ArtiSynth [2] (www.artisynth.org). The lateral and medial menisci were modeled as FE bodies using a linear material model. Articular cartilage was modeled as elastic contact foundation layers. The Artisynth tracking controller [3] was first employed to run a muscle-driven forward-dynamics tracking simulation of a simple knee flexion task. The controller is currently being improved to track measured motion capture trajectories and ground reaction forces during a full gait cycle to investigate meniscal loading. To examine the effect of a meniscus tear we virtually resected the FE mesh and repeated simulations. Ultimately, we aim to visualize the effect of tears on the von Mises and maximum principal stresses of the menisci and the contact pressures of the cartilage.

Results and Discussion

Preliminary results computed for a dynamic knee flexion indicate increased loading of the anterior cruciate ligament and articular cartilage layers in knees with a torn meniscus and greater deformations in the meniscal bodies.

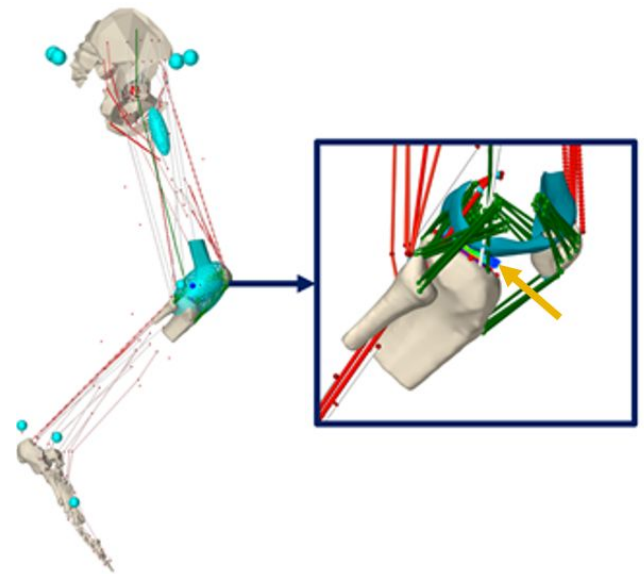


Figure 1: Dynamic leg model and detailed view of knee model; inset shows detailed knee set-up including FE meniscus (location indicated by a gold arrow)

Conclusions

We use a forward-dynamics tracking approach to perform muscle driven gait simulations that include FE representations of the meniscus. Simulations of meniscal tears can provide insight into surgical repair techniques and the role of meniscal damage in osteoarthritis.

References

- [1] Lenhart R et al. (2015). *Ann Biomed Eng*, **43**: 2675-2685.
- [2] Lloyd J et al. (2012) *Soft Tissue Biomechanical Modeling for Computer Assisted Surgery*; Springer.
- [3] Sagl B et al. (2019). *IEEE Trans Biomed Eng*, **66**: 335-342.

Estimated Hamstring Muscle Function During Sprinting is Sensitive to Modeling Methods

Carlie J. Ede, Glen M. Blenkinsop, Sam J. Allen

School of Sport, Exercise and Health Sciences, Loughborough University, UK

Email: c.ede@lboro.ac.uk

Summary

Musculoskeletal modelling of hamstring (HS) muscle function during the swing phase of sprinting was matched via three optimisation methods. Fibre length and velocity were similar in all methods, but increased muscle force during the early swing phase was found during dynamic optimisations.

Introduction

Musculoskeletal models are a valuable tool to investigate HS muscle function and injury risk during sprinting. Multiple methods are available to estimate muscle function, each with differing complexity. Static Optimisation (SO) solves the muscle indeterminacy problem by matching joint torques from inverse dynamics at discrete time steps, assuming a rigid tendon. Dynamic optimisations such as, Computed Muscle Control (CMC) and the newly released OpenSim Moco (0.4.0) employ forward dynamics approaches. CMC combines feedforward and feedback controllers to track experimental kinematics, while Moco utilises direct collocation. Previously, similar results have been reported between static and dynamic optimisations during walking and slow running [1], though the effects of these methods on estimated muscle function during dynamic activities is yet to be compared.

Methods

One male participant ran at $8 \text{ m}\cdot\text{s}^{-1}$ on an instrumented treadmill following informed consent and university ethical approval. Synchronised force (1000 Hz) and motion capture (250 Hz) data were recorded for 10 strides.

A generic OpenSim model [2] was scaled to the participant and modified to form a 2D planar model, reducing the size of the optimisation and focusing on primary muscle groups. The model had 14 degrees of freedom and comprised: 20 segments, 30 muscle-tendon actuators and 5 ideal torque actuators to control the torso and upper limbs. The optimal fibre length was adjusted to match the angle at maximum isometric force identified by Anderson [3]. Maximum isometric force was adjusted based on muscle volumes from

Miller [4], and the maximum contraction velocity was set at $20 \text{ fibre lengths}\cdot\text{s}^{-1}$.

Inverse kinematics was performed in OpenSim before force and kinematics were low pass filtered (20 Hz), cropped to a single representative swing phase, and inputted into SO, CMC and Moco. For all problems, residual actuators at the pelvis were added to account for dynamic inconsistencies and coordinate actuators were used to support the function of the lower limbs.

Results and Discussion

CMC required the highest coordinate reserves (combined RMS: 55.1 Nm), followed by SO (19.5 Nm) and Moco (2.0 Nm). Normalised fibre length was similar across methods, with a slightly lower peak in CMC (1.37) compared to Moco (1.40) and SO (1.42). In line with Thelen [5], peak fibre length, velocity and power were reported in late swing for all methods (figure 1). SO showed a peak force of 1189 N at 82% of swing, but almost zero force for the first 50%. Both CMC and Moco produced similar peak values in late swing, but peak force occurred within the initial 10% (CMC: 1689 N, Moco: 1515 N). This difference is likely due to increased co-contraction at the hip and knee after toe-off, which has been demonstrated with EMG data [6].

Conclusions

Force output from the three methods showed varied results. Algorithms that support muscle dynamics and co-contraction may provide better estimates of HS function during dynamic tasks such as sprinting.

References

- [1] Lin et al. (2011) *J Eng Med*, **226**: 103-112.
- [2] Lai et al. (2017) *Ann Biomed Eng*, **45**: 2762-74.
- [3] Anderson et al. (2007) *J Biomech*, **40**: 3105-13.
- [4] Miller et al. (2020) *Med Sci Sports Exerc*, Online
- [5] Thelen et al. (2005) *Med Sci Sports Exerc*, **37**: 1931-8.
- [6] Jonhagen et al. (1996) *Scand J Med Sci Sports*, **6**: 15-21

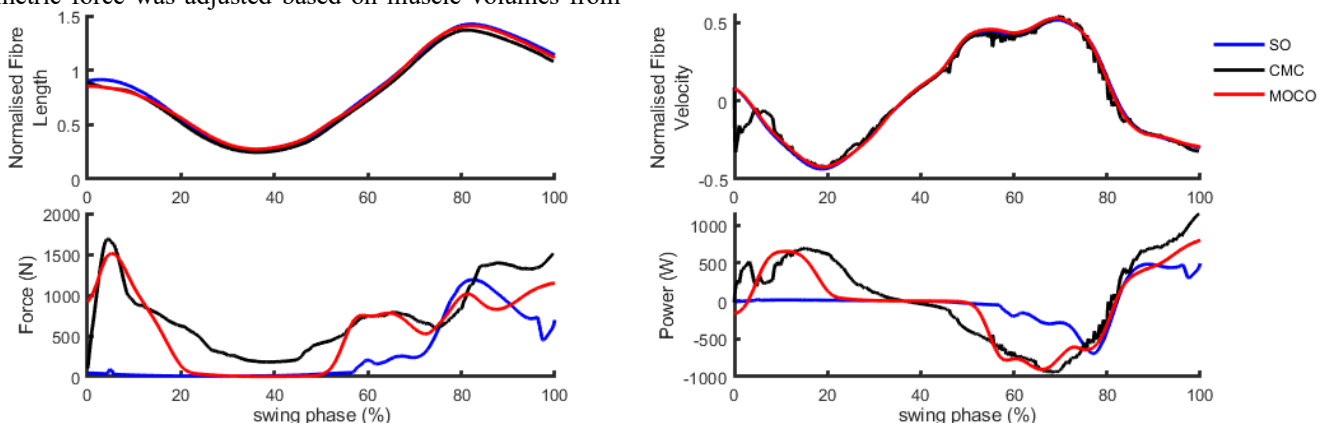


Figure 1: Normalised fibre length and velocity, muscle force and power of the biceps femoris long head (right leg) during the swing phase of an $8 \text{ m}\cdot\text{s}^{-1}$ running trial using static optimisation (SO, black), computed muscle control (CMC, blue) and OpenSim Moco (Red). Negative power represents eccentric contraction.

Musculoskeletal Models for Assessing Surgical Indications and Outcomes in Cerebral Palsy

Claude Foyford¹, Emma Pratt², Claudia Mazzoli¹

¹Department of Mechanical Engineering & Insigneo Institute for in silico Medicine, University of Sheffield, United Kingdom

²Sheffield Children's Hospital NHS Foundation Trust Gait Laboratory, Ryegate Children's Centre, United Kingdom

Email: cfhayford1@sheffield.ac.uk

Summary

Some surgical indications and outcomes in CP are based on joint kinematics derived from the conventional gait model and direct kinematics. Global optimization has however been proven to be more accurate. Using clinical gait analysis data of CP patients who underwent femoral derotation osteotomies, this study investigates three transverse plane kinematic measures (pelvic rotation, hip rotation, and foot progression angle) in addition to the Gait Profile Score and suggests that global optimisation with constrained models can equally quantify and predict relevant clinical changes and outcomes for use in clinical decision-making.

Introduction

Femoral Derotation Osteotomies (FDO) are used to correct torsional deformities such as excessive anteversions in children with cerebral palsy (CP). Outcomes are judged based on changes in transverse plane kinematics over stance such as pelvic rotation (PRot), hip rotation (HRot), and foot progression angle (FPA) [1]. Similarly, the Gait Profile Score (GPS) is used to quantify overall lower limb gait quality. These metrics are predominantly obtained from clinical gait analysis (CGA) using the conventional gait model (as implemented in the Plug-in-Gait model (PiG)). Global optimisation has been shown to be more accurate due to reducing skin tissue artefacts [2]. This is typically associated with musculoskeletal (MSK) models having additional joint constraints with respect to the PiG. This study hypothesized that using such a model and the global optimisation approach, clinical information equally relevant to that provided by the traditional gait analysis model can be obtained when looking at outcome quantification and prediction. This would support the case for adopting these MSK models, allowing to also estimate internal muscle and joint contact forces, in clinical protocols to improve decision-making.

Methods

Retrospectively collected CGA data for controls (n = 34) and CP patients with excessive femoral anteversion (FA, n = 26) were investigated. Each subject had at least 3 dynamic gait trials and FA had pre- and one or more post-surgery visits. PiG model (DoF: 3 at hip and knee, 2 at ankle) joint kinematics for all subjects were processed per the clinical protocol in Vicon Nexus. Scaled gait2392 models (Gen, DoF: 3 at hip, 1 at knee and ankle) were created for each subject and simulated in OpenSim 3.3 to estimate joint angles. Mean of PRot, HRot and FPA were calculated over stance. GPS was calculated per Baker et al, 2009. These metrics were summarised as mean and standard deviation. Additionally, correlation analysis between PiG and Gen estimates were

performed. Changes (Δ) in these metrics between visits were also compared.

Results

PRot, FPA and GPS scores of all limbs and observations were highly correlated ($R^2 > 0.7$) between PiG and Gen. Similarly, there was a greater than 89% (n = 81, all limbs) agreement between PiG and Gen estimates of positive or negative changes in GPS between observations.

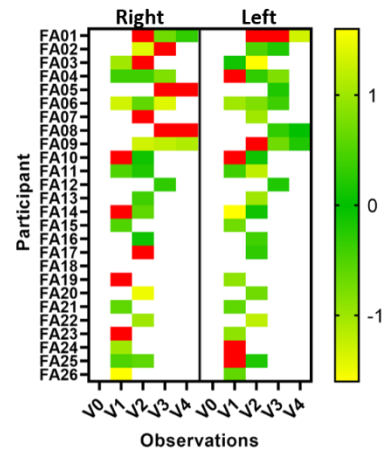


Figure 1: Differences between Δ (GPS) estimated by Gen and PiG. Red squares values exceeding 1.6° (minimal clinically important difference in GPS) as the limit of agreement between models.

Results showed great correlation and similarity between joint kinematics estimated by PiG and Gen as previously reported [3]. The exception to this was HRot where the Gen tended to estimate more externally rotated hip angles compared to the PiG observable as an offset between model estimates. This affected Gen GPS estimates and when HRot was omitted from the calculation, the percentage of agreement in estimates of change (Δ (GPS), Figure 1) increased. The decreased correspondence at the hip may be due to the Gen's inability to capture the different degrees of anteversion and further analysis is ongoing to understand this important aspect for this population. Overall, the Gen was able to detect the direction of change in metrics although magnitudes could be different.

Conclusion

These results suggest MSK models can be used to approximate changes in indications and outcomes after FDO in CP, similar to estimates from using the PiG model.

References

- [1] Schwartz M et al. (2014) *Gait Posture*, **39**: 778-783.
- [2] Lu T and O'Connor J. (1999) *J. Biomech.*, **32**: 129-134
- [3] Kainz H et al. (2017) *Gait Posture*, **54**: 325-33

A ligament-based enhancement via MRI in dynamic ankle modelling validated against corresponding experimental data

Belvedere C.¹, Siegler S.³, Campagnoli E.¹, Ferraro D.¹, Ruiz M.³, Durante S.², Leardini A.¹

¹Movement Analysis Laboratory & ²NTRAS, IRCCS Istituto Ortopedico Rizzoli, Bologna, Italy

³Department of Mechanical Engineering and Mechanics, Drexel University, Philadelphia, PAUSA.

Email: belvedere@ior.it

Summary

Reliable computational ligament-skeletal models are essential for the comprehension of the human ankle biomechanics. Although, a good level of approximation with respect to experimental data is reported, current models still need further improvements. This study reports a development of a validated in-silico model by including MRI-based mapping of a number of critical ligaments poorly investigated in the relevant literature. Comparisons in terms of load-displacement curves between standard and updated anatomical mapping revealed considerable improvements in simulation-to-measurement comparisons.

Introduction

A thorough comprehension of the stabilizing role of the ligaments at the Ankle Joint Complex (AJC) is important in biomechanics [1] and in clinics, for reliable diagnosis and personalized surgical treatments. Several subject-specific computational models have been developed, but only a few with a strong validation against experimental data [2]. Unfortunately, model inputs in terms of bone-ligament attachment mapping still employ improper information, especially in the case of structures of difficult identification. More subject-specific models should derive from more precise overall mappings data from state-of-the-art Magnetic Resonance Imaging (MRI). The aim of this study was to further enhance a validated ankle computational model by using subject-specific morphological data, including bones derived by Computer-Tomography (CT) and critical ligament attachments areas as by MRI. For the same model, resulting joint load-displacement curves will be compared with the corresponding from standard procedures. The effects deriving from the removal of one of these ligaments at a time are also analyzed.

Methods

Morphological data of ankle bones were obtained from CT (DE Rev HD 1700 GSI, GE; 0.6 mm slicing space and thickness) of one normal cadaver leg. Corresponding bone-ligament attachment areas were reconstructed from 3.0 T MRI (750W GEM ENAB, GE; Sag 3D cube). The following ligaments were mapped by an experienced radiologist: Anterior Talo-Fibular (ATFL), Posterior Talo-Fibular (PTFL), Calcaneo-Fibular (CFL), Anterior ATTL and Posterior (PTTL) Tibio-Talar, Tibio-Calcaneal (TCL), Tibio Spring (TSL), Interosseus Talo-Calcaneal (ITCL), and Cervical Ligament (CL), the latter two being of difficult access and here properly identified. AJC motion and load data, derived from imposed Internal-External (Int-Ext) and Inversion-Eversion (Inv-Eve) rotation torques were measured experimentally [3].

A validated computational ankle model [1,2] was utilized both in its standard ligament configuration, and after update via the above reported subject-specific ligament data. After proper cartilage compensations, 3D bone models were imported in ADAMS (MSC Software Corporation, USA-CA); all ligaments were modelled as tension-only force elements, whose number depends on the ligament size, with non-linear strain [1]. Int-Ext and Inv-Eve loads necessary to run dynamic simulations were extracted from the corresponding experimental torque signals. Model predictions, in terms of AJC load and angular displacement, were derived from standard and updated ligament configuration. The latter was used also to analyze the effect of removal of one ligament at a time, this meant to mimic realistic ankle injuries.

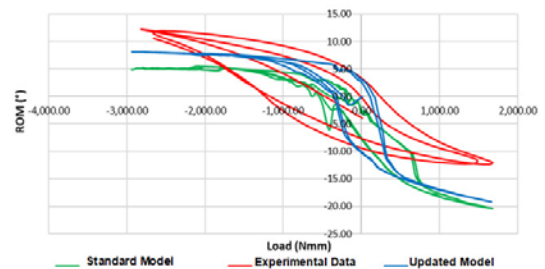


Figure 1: Int-Ext load-displacement: curves from experimental measurements, and those from the two different model predictions, i.e. with standard and updated ligament configurations.

Results and Discussion

When moving from standard to updated MRI-based ligament configuration, the difference in Int-Ext rotation range between model-based and experimental data dropped down by about ~50% (~40% in Int direction); marginal differences were observed in Inv-Eve range (~5%). Most of the observed changes are due to the mapping of ITCL and CL. Similarly between configurations, when ITCL is removed, Ext rotation increases of ~250%; when CL is removed Inv-Eve range increases of ~30% in both directions.

Conclusions

The reported differences confirm how computational models may benefit further from more subject-specific ligament mapping, especially for the most critical ones. Since a closer replication of experimental AJC laxity may derive from such mapping, this must be carried out with appropriate care.

References

- [1] Imhauser CW et al. (2008). *J.Biomech.*, **41**: 1341–1349.
- [2] Palazzi E et al. (2019) *J.Biomech.*, **98**: 109421.
- [3] Belvedere C et al. (2017) *J.Biomech.*, **53**: 97–10

Influence of optimization criteria on the prediction of knee-joint forces during walking and squatting

Heiko Wagner^{1,2}, Myriam L. de Graaf^{1,2}, Kim J. Boström¹, Marc H.E. de Lussanet^{1,2}, Christian Puta³, Luis Mochizuki⁴

¹Department of Movement Science, Institute of Sports and Exercise Sciences, University of Münster, Germany, ²Otto Creutzfeldt Center for Cognitive and Behavioral Neuroscience, University of Münster, Germany, ³Department of Sports Medicine and Health Promotion, University of Jena, Germany, ⁴School of Arts, Sciences and Humanities, University of Sao Paulo, Brazil
Email: heiko.wagner@uni-muenster.de

Summary

Several circumstances in daily living require minimization of forces acting on a joint. To investigate the relation between muscle forces and joint forces, a direct measurement of these variables is desirable. Rather than using invasive methods to directly measure joint forces, they can also be approximated using musculoskeletal models. Here, we investigate the accuracy of predicted forces in a knee joint during walking and squatting based on a computational musculoskeletal model, by comparing the predicted data with the corresponding real-life data gained from knee prostheses capable of measuring internal joint forces.

Introduction

Movement and non-movement related pain mostly influences the motor control and movement pattern of people with joint pain. Strategies to reduce pain involve, e.g., shifting the load to the non-painful leg, changing the gait pattern, or using gait assistant tools. To estimate the individual outcome of such strategies, it is desirable to know the joint and muscle forces as precisely as possible. However, for ethical reasons, a direct joint force measurement is problematic because of its invasiveness.

Here, we investigated the accuracy of predicted forces in a knee joint during walking and squatting based on a computational musculoskeletal model, by comparing the predicted data with the corresponding real-life data gained from knee prostheses capable of measuring internal joint forces [1]. Furthermore, we analyzed how different optimization strategies for neuromuscular activation patterns of bi- and uniarticular knee muscles can reduce knee joint forces.

Methods

The experimental basis for the analyses of the present study was the CAMS-knee dataset [1], which encompasses kinematic data, ground reaction forces and measured joint forces in the knee prostheses of six patients. For the computational modeling, a full body musculoskeletal model called *Myonardo* (Predimo GmbH, Münster, Germany) was used. With *Myonardo* we calculated the net joint torques to predict the muscle forces acting on each joint. To calculate the net joint torques, the kinematics of the body segments and the external GRF acting on each foot were applied to the skeletal model.

Subsequently, we compared the influence of two different optimization criteria on the predicted joint forces, namely (1)

minimizing muscle forces, and (2) minimizing resulting joint force.

Results and Discussion

The accuracy of the predicted knee joint forces depended on the optimization criterion, i.e. the optimization parameter s (Fig. 1, left). Minimum Root Mean Squared Error (RMSE) for parameter s was about 0.9. The standard deviations of the predicted and measured trajectories of the six patients were overlapping (Fig. 1, right).

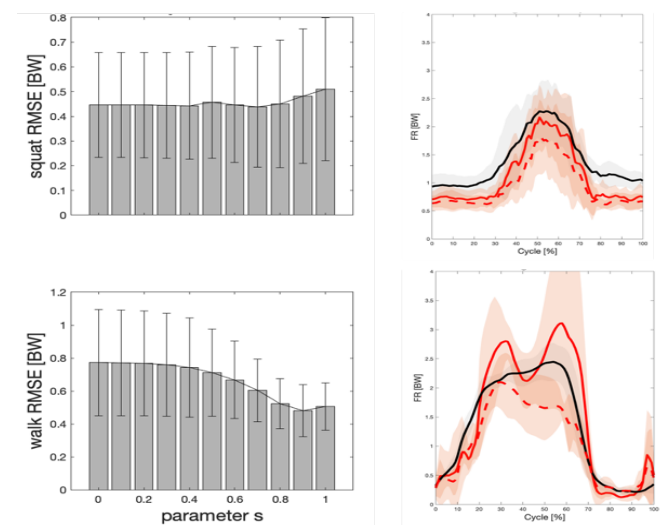


Figure 1: Left: RMSE between measured and predicted joint forces during squatting (1st row) and level walking (2nd row), and different parameters s ($s=0$ minimizes muscle forces, $s=1$ minimizes joint forces). Right: Predicted knee joint forces ($s=0$ red solid line, $s=1$ red dashed line), and measured knee joint forces (black).

Conclusions

We found that the accuracy of the predicted knee joint forces depends on the optimization criterion ($0 < s < 1$). Patients may adapt their neuromuscular activation pattern to reduce joint forces during locomotion or everyday movements.

Acknowledgments

We acknowledge the sources of the CAMS-Knee database (Laboratory for Movement Biomechanics, ETH Zurich, Julius Wolff Institute, Charité), and Predimo GmbH for providing the *Myonardo* software.

References

- [1] Taylor WR et al. (2017). *J. Biomech.*, **65**: 32-39

A note on the influence of tendon speed in musculoskeletal inverse dynamics

L. Joakim Holmberg, Alexandra Roser, Jonas Stålhand

Solid Mechanics, Dept. Management and Engineering, Institute of Technology, Linköping University, Linköping, Sweden
Email: Joakim.holmberg@liu.se

Summary

In the Hill model for muscle contraction, the split between the muscle and tendon is arbitrary and the problem lacks a unique solution. Commonly, a constant tendon length is assumed in simulation tools, but this assumption has not been thoroughly tested and may introduce unknown errors to the simulations.

We propose a new model that behaves like a friction clutch, includes an evolution law for the muscle length and non-zero tendon speed. Using a biceps curl simulation our model is compared to a state-of-the-art commercial muscle model (using zero tendon speed). Overall, the results are similar, but there is a difference in tendon speed of up to 3.3%.

Introduction

In 1938 Hill [1] proposed a mechanical muscle model: a contractile element, representing the muscle, in series with a spring, representing the tendon. This Hill model comprise features like length and contraction speed dependence on the generated force. Hill-type muscle models are used in musculoskeletal simulation tools, e.g., AnyBody [2].

The speed-dependent properties of muscles together with the serial arrangement require a split of the total length and total speed of the muscle-tendon into separate parts for the contractile muscle and the tendon. The measurable quantities are usually the total muscle-tendon length and speed along with the tendon force. Thus, the split between muscle and tendon becomes arbitrary. Because a muscle's force-length-speed characteristics refer to muscle contraction, not total muscle-tendon length, the problem lacks a unique solution and is ill-posed. One solution is to reformulate the problem into a differential-algebraic equation and solve for a set of initial conditions. However, it is generally assumed that the speed of the tendon is negligible and that the contractile speed of the muscle is the total muscle-tendon speed, e.g. in AnyBody. The effect of this substitution has not been thoroughly tested for musculoskeletal inverse dynamics.

Methods

We have previously proposed a modified muscle model where the contractile element behaves like a friction clutch [3,4,5] because of the similarity to the muscle contraction cycle; myosin heads attach to thin actin filaments, pull them inwards to the center of the sarcomere while the actin filaments also have a short and rapid outward slip. We have 3 elements in parallel: the contractile element; a passive element, modeled as a spring, that represents any stiffness in the muscle; and a viscous damper that represents any fluid in the muscle that would resist contraction. In series with these 3 elements is a spring representing the tendon. From the model's internal

mechanical power and the dissipation inequality we derived an evolution law for muscle contraction that facilitates the inclusion of tendon speed in the muscle model.

To assess the inclusion of tendon speed we compare results from our model with the Hill-type model in AnyBody using the brachialis muscle during an inverse dynamics simulation of a biceps curl. The external loading on the muscle, muscle properties and simulation times are the same or as close as possible. See Roser [5] for numerical and other details.

Results and Discussion

For all tested cases, the tendon speed is small but non-zero throughout the motion using our model (Figure 1). Thus, there is a difference between our model and AnyBody, which expressed as a tendon speed error percentage ranges from almost zero to 3.3%. The tendon speed error generally increases with increased muscle contraction speed. The resulting differences for max muscle force and muscle work were up to 16.9% and 6.5% respectively.

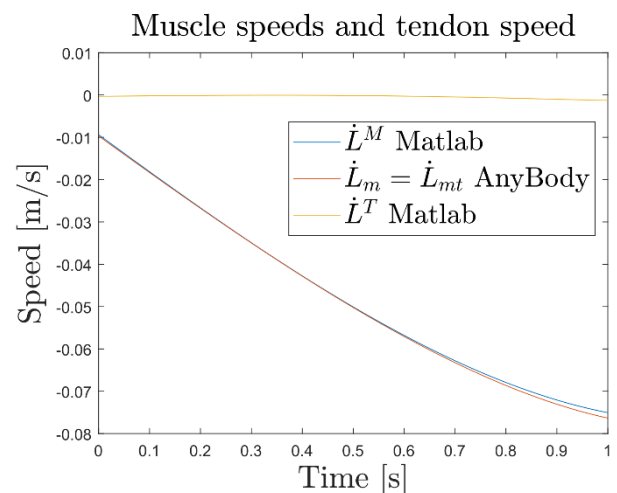


Figure 1: Speeds for our model (Matlab) and Anybody.

Conclusions

The effect of including tendon speed seems to be small, but not necessarily always negligible as is generally assumed.

References

- [1] Hill AV (1938). *Proc R Soc London B Biol Sci*, **126**: 136-195.
- [2] Damsgaard M et al. (2006). *Simul Model Pract Theory*, **14**: 1100-1111.
- [3] Sharifimajd B and Stålhand J (2013). *Biomech Model Mechanobiol*, **12**: 965-973.
- [4] Holmberg LJ et al. (2019). *Svenska Mekanikdagarna*, Stockholm, Sweden
- [5] Roser A (2019). *Master thesis*, Linköping University, Sweden

A Musculoskeletal Parameter Study of Scapula Characteristics Affecting Rotator Cuff Muscle Forces

Johanna F. Menze¹, Hanspeter Hess¹, Stephen J. Ferguson², Matthias Humstein³, Nicolas Gerber¹, Jürgen Burger¹, Kate Gerber¹
¹ sitem Center, University of Bern, Bern, Switzerland
² Institute for Biomechanics, ETH Zurich, Zurich, Switzerland
³ University Hospital Bern, Inselspital, Bern, Switzerland
 Email: johanna.menze@sitem.unibe.ch

Summary

A musculoskeletal shoulder model was applied to compare maximum rotator cuff forces (RC) during abduction and flexion to 120° with various scapula morphologies. Subscapularis (SB) and infraspinatus (IS) forces strongly increase with an upward glenoid inclination (GI) and acromion lateralization (AL) during abduction. Supraspinatus (SS) forces increase with an upward GI, but decrease with a higher AL.

Introduction

Clinical observations and experimental studies have shown that morphological characteristics of the scapula affect the incidence of RC tearing [1]. Understanding the biomechanics could allow the identification of high risk patients for symptomatic RC injuries. Continuous overstraining of the rotator cuff might cause the high incidence of RC tearing for scapula geometries with an upward tilted glenoid and a laterally extended acromion, corresponding to a high Critical Shoulder Angle (CSA) [2]. However, a systematic parameter study comparing the influence of GI and AL on RC muscle forces calculated by inverse dynamics is lacking to date.

This musculoskeletal study aims at comparing the influence of the GI and AL on the maximum RC muscle forces during abduction and flexion.

Methods

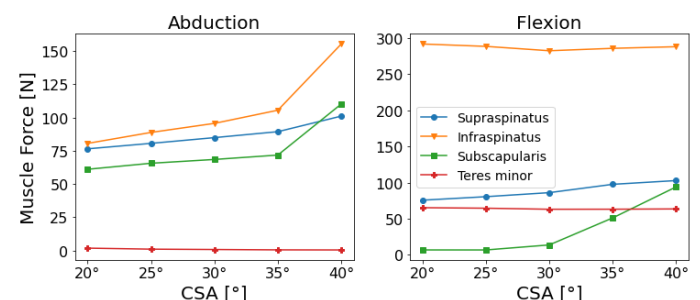
The musculoskeletal modeling was performed in Anybody 7.3 using the generic model (male, 75kg, 1.80m) of the repository AMMR v.2.3.1. Muscle forces were calculated based on inverse dynamics for shoulder abduction and flexion to 120° against a resistance of 25N and the maximum forces were subsequently compared. A parameter study was defined where the GI was altered while the AL remained unchanged, and vice versa. Both influence the CSA which was set to range from 20° to 40° to cover the population variations [3]. The chosen CSA range corresponds to a GI measure, the β -angle according to Maurer et al.(2012), from 64° to 91° for the first part and to an acromion index (AI) between 0.4 and 1.0 for the second part [4,5].

Results and Discussion

GI and AL variations have a stronger effect on RC forces during abduction than flexion (Figure 1 A, B). An increase of the CSA from 20° to 40° by GI changes, leads to a force increase of 93%, 67% and 31% in the IS, S \square and SS, respectively (Figure 1A). While an acromion medialization does not influence the RC forces, an AL also increases the IS

and S \square forces which suggests they might be crucial to provide shoulder stability [7]. The SS force during abduction decreases by 17% for a 40° CSA by AL (Figure 1 B) which accords with experimental studies showing that GI has a stronger effect on SS forces than AL [2].

A: Variation of glenoid inclination



B: Variation of acromion lateralization

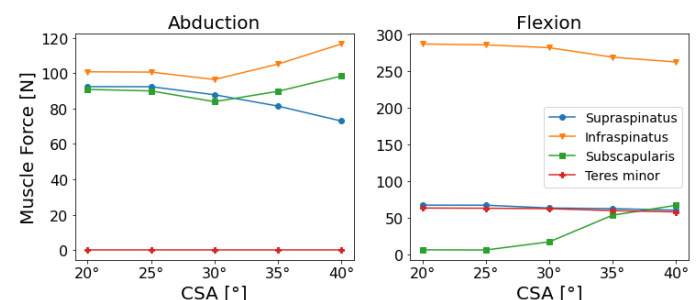


Figure 1: Maximum RC muscle forces during abduction and flexion from 0° to 120° for a range of Critical Shoulder Angles (CSA) varied by changing the GI (A) and the AL (B)

Conclusions

Using Anybody simulations it could be shown that S \square and IS are most sensitive to changes in AL and GI. This could imply they are the key muscles for shoulder joint stability. An upward GI appeared to be more important for SS loading than AL. Glenohumeral translations will be included in further investigations.

References

- [1] Moor et al. (2013). *Bone Joint J*, **95**: 935-941
- [2] Moor et al. (2016). *Clin Biomech*, **3**: 268-273
- [3] Stamiris et al. (2020). *Orthop Rev*, **1**: 8457
- [4] Maurer et al. (2012). *J Shoulder Elbow Surg*, **1**: 1096-1103
- [5] Nyffeler et al. (2006). *JBJS*, **88**: 800-805
- [6] Geeler et al. (2019). *J Orthop Res*, **3**: 205-210
- [7] Melis et al. (2010). *J Shoulder Elbow Surg*, **19**: 757-763

Assistance Level versus Metabolic Cost in a Biarticular Exoskeleton: A Simulation Study

Karthick Ganesan, Abhishek Gupta

Department of Mechanical Engineering, Indian Institute of Technology Bombay, Mumbai, India

Email: karthick.ganesan@iitb.ac.in

Summary

Finding how different assistance levels affect metabolic cost in exoskeleton assisted gait is an important goal in exoskeleton development. We used musculoskeletal simulation to explore the effect of different assistance levels in a biarticular knee-ankle exoskeleton for loaded walking. The results of this study can be used to choose appropriate assistance level in knee-ankle exoskeletons.

Introduction

Exoskeletons can augment the capacity of humans and enhance mobility in the disabled. Often it is required to understand how varied levels of assistance affect the metabolic cost. Experimental studies investigated the effect of varied assistance on metabolic cost for different exoskeletons [1]. Simulations can complement experiments. Simulations have shown how actuator joint locations affect the metabolic cost and have provided optimal device torque profiles [2]. Here we investigate how different levels of assistance affect metabolic cost in loaded walking with a biarticular knee-ankle exoskeleton.

Methods

We used OpenSim [3] for modeling and simulations. We used the scaled, mass adjusted musculoskeletal model and experimental gait data with load, without exosuit of one subject supplemented with the literature [2] for the simulations. The three dimensional musculoskeletal model has 39 degrees of freedom. Eight of the degrees of freedom were locked. For the simulations of loaded walking, the model has a 38 kg of load attached to the torso. We considered two cases: one with a monoarticular ankle exoskeleton and other with a biarticular knee-ankle exoskeleton. In case I, exoskeleton actuator was modeled as ideal torque actuator providing ankle plantar flexion torque and was implemented as CoordinateActuator in OpenSim. In case II, it was modeled as ideal force actuator producing force along a prescribed path, implemented using PathActuator. We used computed muscle control algorithm to estimate the muscle and actuator controls to track the experimental data. We used Umberger2010MuscleMetabolicsProbe to compute the metabolic cost.

The force produced by actuator is given by

$$F = x F_{opt} \quad (1)$$

Where x is the control signal to the actuator, varying from 0 to 1 and F_{opt} is the optimal force, the maximum force/moment that the actuator can produce. Varied levels of assistance were achieved by varying the optimal force parameter of the actuator.

Results and Discussion

With increased assistance, metabolic cost of walking reduces (Figure 1). Beyond a certain optimal force value, there is no significant decrease in metabolic cost. Minimizing the metabolic cost to the fullest extent may affect some other parameters such as joint loads or may alter the kinematics more. Designer can choose to provide a certain amount of assistance required to achieve a desired metabolic cost reduction based on constraints like device power, mass and cost. For different levels of assistance, optimal moment profile at ankle is shown (Figure 1). Here gait cycle begins with opposite toe off. Biarticular actuator produces more moment at the ankle compared to monoarticular actuator since it reduces the activity of gastrocnemius muscle in addition to soleus muscle. Biarticular actuator also increased activity of tibialis anterior muscle. Simulations with peak force values beyond the optimal value obtained from CMC simulations resulted in ankle reserve actuator producing more moment, giving unrealistic metabolic cost estimation.

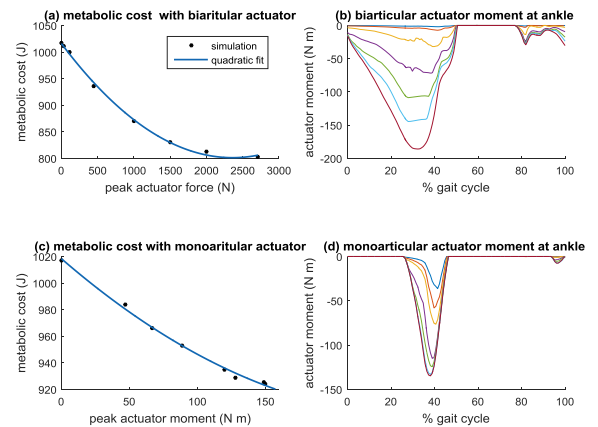


Figure 1: Metabolic cost versus peak actuator force/moment and actuator torque profile for different levels of assistance.

Conclusions

This abstract presents a framework for finding pareto optimal assistance profiles for exoskeletons. The results provide a reference for deciding the amount of assistance required and optimal torque profile for ankle and knee-ankle exoskeletons. This can be extended to other joints as well.

References

- [1] Quinlivan BT et al. (2017). *Sci. Robot*, **2**:eaah4416.
- [2] Dembia CL et al. (2017). *PLoS One*, **12**:e0180320.
- [3] Delp SL et al. (2007). *IEEE Trans. Biomed. Eng.*, **54**:1940-1950.

Motion based ground reaction forces and moments prediction method in a moving frame – a pilot study

L. Demestre¹, F. May¹, P. Morin¹, G. Nicolas², N. Lemaire², G. Dumont¹, C. Pontonnier¹

¹Univ Rennes, CNRS, Inria, IRISA – UMR 6074, F-35000 Rennes, France

²Univ Rennes, Inria, Laboratoire M2S, F-35000 Rennes, France

Email: louse.demestre@ens-rennes.fr

Summary

A motion-based method to predict ground reaction forces and moments (GRF/M) in a moving and/or non-horizontal frame has been developed. The motion of a subject located on a moving hand pallet truck has been recorded. The moving structure has been equipped with a force platform to compare predicted and measured GRF/M.

Introduction

Inverse dynamics methods are widely used in motion analysis studies to compute joint torques. The ground reaction forces and moments are required to solve the dynamic equilibrium of the subject studied. Measuring the GRF/M reduce the ecological aspect and constraint the movement area. Motion-based prediction methods are used to circumvent this limitation. All the existing methods regard the ground as a static and horizontal surface. In this abstract, an existing prediction method [1] is improved to expand its application to external forces coming from mobile and/or non-horizontal structures.

Methods

The force platform is composed of a 6-dofs force sensor (MCS10 5kN, 5000Hz, HBM) located between two steel plates. The motion capture data were recorded using an optoelectronic system (200 Hz, Qualisys). 43 reflective markers were placed on standardized anatomical landmarks of the human subject and 3 markers on the upper surface of the force platform. The force platform was laid down on a hand pallet truck. During a trial, the subject stood on the force platform, squatted once then successively lifted up each foot. During the subject's movement, an investigator pulled the hand pallet truck.

The GRF/M were predicted at each frame following two steps: contact detection and forces distribution. Firstly, a moving frame linked to the force platform was created using the 3D displacement of the 3 markers placed on it. Relative position and velocity thresholds between the moving contact surface and a set of discrete contact points under the subject's feet were tested. Secondly, the external forces applied on each prediction point were minimized with respect to the dynamic

equilibrium of the subject [1]. This method has been implemented in the CusToM Matlab toolbox [2].

Results and Discussion

A comparison between predicted and measured force on vertical direction (Fz) and moment on antero-posterior direction (My) for a sample trial is presented below (Figure 1):

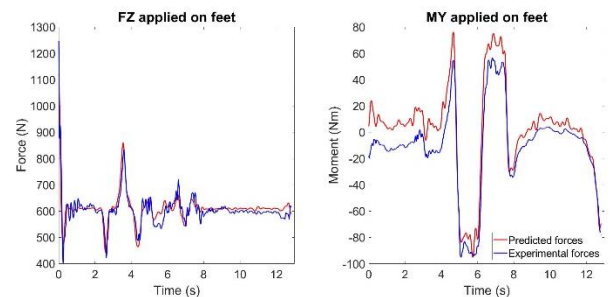


Figure 1: Predicted (red) and measured (blue) Fz (left) and My (right) applied on feet.

The RMSE errors between predicted and measured GRF/M curves for this trial are presented in the table below (Table 1). They are of the same order of magnitude as those obtained from the initial CusToM method [1]. The prediction method in moving frame presented here seems to open new applications to the initial one keeping the same accuracy. Nevertheless, more subjects and structure movements must be studied to draw suitable conclusion about this new method.

Conclusions

A motion-based GRF/M prediction method in a moving and/or non-horizontal frame has been proposed. Preliminary results shows that this new method is promising and needs to be evaluated with more subjects and more challenging structure motions. Such a method may be useful for many applicative studies in sports or ergonomics.

References

- [1] A. Muller, et al. (2020). *IEEE T Bio-Med Eng*, 67(2): 344-352.
- [2] A. Muller, et al. (2019). *J. Open Source Softwa*. 4(33):92

Table 1: RMSE errors between predicted and measured forces (FX, FY, FZ) and moments (MX, MY, MZ) curves as a function of time

Component	FX	FY	FZ	MX	MY	MZ
RMSE	14.7 N	30.9 N	27.5 N	9.5 N.m	14.7 N.m	1.0 N.m

Automatic generation of personalized skeletal models of the lower limb using the STAPLE toolbox

Luca Modenese¹, Jean-Baptiste Renault²

¹Dept Civil Engineering, Imperial College London, UK

²Aix-Marseille University, Marseille, France

Email: l.modenese@imperial.ac.uk

Summary

STAPLE (Shared Tools for Automatic Personalized Lower Extremity modelling) is an open source MATLAB toolbox that automates the creation of subject-specific models from three-dimensional bone geometries, normally obtained by segmentation of medical images. We compared automatic and manual models based on four anatomical datasets by quantifying the differences in their joint coordinate systems (JCS) and in joint angles and net moments calculated in gait analysis. Our findings suggest that the JCS of the automatic models were comparable to manual ones (within reported inter-operator variability) and differences observed in joint angles and moments for gait were due to JCS offsets and tibial mass estimation. The STAPLE toolbox is available at <https://simtk.org/projects/msk-staple>.

Introduction

Predicting the effect of physical treatments has been made feasible by recent improvements in simulation techniques [1]. However, clinical applications, e.g. in orthopedics, very often require highly personalized anatomical models of the musculoskeletal system to virtually modify the patient anatomy according to planned interventions. Currently there are no fully automatic methodologies for generating these models, which are built by trained operators in several hours, so strongly limiting the adoption of modelling outside research environments. In this work we introduce a MATLAB toolbox called STAPLE that enables the generation of subject-specific skeletal models using fully automatic workflows and compare joint parameters and results of a gait analysis from automatic and manual models.

Methods

Four anatomical datasets (age range: 14-85 yo, height: 1.71-1.8 m, mass: 45-87 kg, quality of segmented bone geometries: from excellent to low) were used as input to an automatic workflow consisting of a bone morphological analysis [2] streamlined with custom model-building scripts implemented in OpenSim 4.1 [3]. The models included five segments (pelvis, femur, tibia, talus and foot) and five joints (pelvis-ground: free joint, hip: spherical joint, tibiofemoral, talocrural and subtalar: hinge joints—12 degrees of freedom in total) defined as in [4]. Corresponding models were manually created by expert operators from the same anatomical datasets. Differences in JCS were quantified in terms of origin distance and axes orientation. For one of the datasets, joint angles and net joint moments were computed using OpenSim for six gait trials [5]. The resulting curves were compared using a two-tailed t-test (significance level $\alpha=0.05$) implemented in the *spm1d* (<https://spm1d.org>)

package, plus correlation coefficients and root mean squared errors (RMSE) for each couple of corresponding curves.

Results and Discussion

The automatic models were generated in less than 25s on a standard laptop. Differences of JCS origins ranged from 0.5 mm (hip joint) to 5.9 mm (subtalar joint), while the joint axes differed between 1° (knee joint) to 11° (subtalar joint). These values are comparable with inter-operator variability reported for manual models [6].

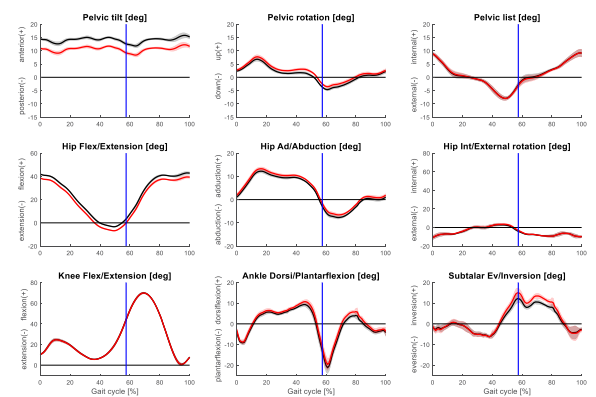


Figure 1: Comparison of gait kinematics estimated using an automatic (red lines) and a manual (black lines) lower limb model.

Correlation coefficients ≈ 0.99 ($p < 0.0001$) and RMSE $\approx 1^\circ$ were found for all joint coordinates except pelvis tilt and hip flex/extension, presenting 3.4° offset leading to significant differences in the t-test. The net joint moments differed prevalently in the swing phase of gait because of 25% difference in tibial mass estimation.

Conclusions

The STAPLE toolbox automatically generates subject-specific lower limb skeletal models comparable to manual procedures in negligible processing time and offers a platform for further developments in personalized modelling.

Acknowledgments

Imperial College Research Fellowship and Academy of Medical Sciences Springboard Grant [S/F004/1056] to LM.

References

- [1] Falisse et al. (2019). *Interface Journal*, **1**: 20190402.
- [2] Renault et al. (2018). *J Biomech*, **80**: 171–178.
- [3] Seth et al. (2018). *PLoS Comput Biol*, **14**: e1006223.
- [4] Modenese et al. (2018). *J Biomech*, **3**: 108–118.
- [5] Montefiori et al. (2019). *Ann Biom Eng*, **4**: 2155–2167.
- [6] Martelli et al. (2015). *J Biomech*, **18**: 1555–1563.

Evaluation of the impact of different scaling approaches in the model based muscle forces estimation during locomotion in Parkinson's disease subjects

Marco Romanato¹, Francesca Colpin¹, Daniele Colpe², Cimi Sawacha^{1,3}
¹Department of Information Engineering, University of Padova, Padova, Italy
²Fresco Parkinson Center, Villa Margherita, S. Stefano, Vicenza, Italy
³Department of Medicine, University of Padua, Padua, Italy
 Email: romanato@dei.unipd.it

Summary

The aim of our work was to apply the most appropriate musculoskeletal scaling approach in order to characterize differences between healthy and Parkinson's disease (PD) subjects.

Introduction

PD is a progressive pathological condition characterized by a dopamine deficiency. Gait alterations are a well-known hallmark of PD patients [1]. Recently, the authors detected further signs of motor impairments in PD's neural strategies, as the timing of the muscle activation peak during the gait cycle and a difference in its amplitude [2] when compared with healthy subjects. Electromyography (EMG) is not representative of the subject's strength and currently, no studies investigated the possibility to assess strength in terms of muscle forces as a biomarker of disease progression in PD subjects. A possible way forward is the use of musculoskeletal modeling which allows the non-invasive estimation of muscle forces.

Methods

Five control subjects ((CS), age=57.8±5.6 years, BMI=27.3±3.9 kg/m²) and five PD subjects (age=62.8±11.4 years, BMI=27.1±2.9 kg/m²) were acquired with a 6-camera motion capture system (60Hz, BTS), synchronized with 2 force plates (960Hz, Bertec) and an 8-channels EMG system (1000Hz, BTS) that recorded bilaterally the activities of 4 muscles: Rectus Femoris, Biceps Femoris, Gastrocnemius Lateralis (GL) and Tibialis Anterior (TA). Data were processed in OpenSim and two different scaling approaches were considered: the standard linear scaling (LS) and the muscle optimizer (MO) scaling [3]. For the latter, two different sets of muscles were used during the process, one including all the muscles of the model (MO_FULL), and one including muscles only spanning knee and ankle joints (MO_MIN). Three different scaled models were obtained for each subject, then inverse kinematics, and static optimization were performed. RMSE between CS predicted and experimental EMGs was computed to assess the physiological

validity of the models. Muscle forces were compared via Wilcoxon Signed Rank test, as no evidence of normality assumption was verified.

Results and Discussion

RMSE (Table 1) reported a comparable physiological behavior of the investigated models, suggesting no significant loss of information between the approaches. Muscle forces obtained for LS and MO_MIN models denoted statistically significant differences in GL and TA (Figure 1).

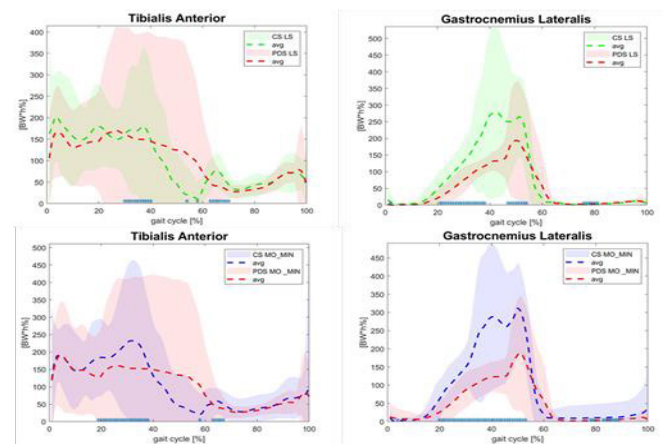


Figure 1: TA and GL muscle forces for CS and PD generated both for LS and MO_MIN scaling approaches.

Conclusions

The MO scaling approach resulted in an enhanced method to detect subject-specific modifications in the lower limb strength production in PD when compared to CS, thus no loss of physiological information was noticed. Further studies are needed to generalize these outcomes.

References

- [1] D. Colpe et al, Gait & Posture, 52:87-94, 2017.
- [2] F. Spolaor et al, Gait & Posture, 57:53-54, 2017.
- [3] L. Modenese et al, Journal of Biomech, 49:141-8, 2016.

Table 1: Mean RMSE ± standard deviation of experimental activations for the three different models.

	Rectus Femoris	Tibialis Anterior	Gastrocnemius Lateralis	Biceps Femoris
LS	0.25±0.07	0.25±0.10	0.17±0.09	0.20±0.08
MO_FULL	0.26±0.09	0.28±0.10	0.23±0.10	0.18±0.08
MO_MIN	0.26±0.10	0.28±0.10	0.22±0.09	0.18±0.08

Individual muscle contributions to knee bone-on-bone forces occurring during a maximal forward braking and backward acceleration in elite athletes

Rodrigo M. Mateus¹, Ventura Ferrer-Roca², Filipa Joia¹, António P. P. Veloso¹

¹Faculty of Human Kinetics, University of Lisbon, Cruz Quebrada, Portugal

²High Performance Center (CAR), Sant Cugat del Valles, Spain

Email: apveloso@fmh.ulisboa.pt

Summary

Most of the high-level sports movements are related to accelerations, or decelerations of the body, to produce direction changes. The aim of this work is to estimate muscle contributions to the knee bone-on-bone forces during a maximal forward braking and backward acceleration in elite athletes. Scaled generic musculoskeletal models, consisting of 12 segments, 23 degrees of freedom, and 92 musculotendon actuators were used in OpenSim. Anterior, compressive, and medial knee bone-on-bone forces occur during this task. The *vasti* are the main contributors to these forces along all three directions. The results of this work present a preventive approach to understand the injury mechanisms of knee injuries during deceleration tasks.

Introduction

Improving joint stabilization during high-impact tasks plays a key factor to be accounted for in training programs that increase muscle coordination and strength. In addition to this, knowledge about how joint kinematics and muscle forces affect knee joint loading, whilst performing ballistic tasks remains scarce. The use of computational modeling allied with non-invasive experimental techniques to study injury mechanisms is an advantageous approach. To this end, the main purpose of this study is the identification of the main muscle contributors to the bone-on-bone forces exerted at the knee joint whilst performing a maximal forward braking and backward acceleration in elite athletes.

Methods

Fourteen elite male team-sports injury-free athletes participated in this study (age: 22 ± 4 years, height: 185 ± 4 cm, weight: 77 ± 11 kg). Kinematic and kinetic data were collected using 8 infrared cameras (Qualisys) working at a frequency of 300Hz and 2 force plates (Kistler). Muscle and joint contact forces were attained through OpenSim [1]. The musculoskeletal model was manually scaled to match each subject's anthropometry. A residual reduction algorithm (RRA) step was used to minimize errors related to kinematic inconsistencies and modelling assumptions. Muscle forces were estimated using a Static Optimization (SO) optimization technique. The forces obtained from SO and the adjusted kinematics from RRA were used for this analysis. Muscle contributions to the bone-on-bone forces were estimated based on [2].

Results and Discussion

As expected from this task, the joint reaction forces at the knee are the highest along the A/P direction, being applied anteriorly on the tibia. These forces along the fore – aft direction recorded at the knee, are related to the fact that the muscles that exerted the most force in this task, *vasti*, are inserted in this joint. In addition to this, the hamstrings act as a minor contributor to the anterior bone-on-bone forces. Compressive forces along the vertical directions are applied at the knee joint. Once again, compressive force contributions by the *vasti* are also predominant. Slight contributions by the *soleus* are also of note. Along the mediolateral direction, at the knee joint, the medial bone – on – bone forces are key to the realization of the task, as they help maintaining the knee in a neutral position. Along this direction, the *vasti* are the main contributors.

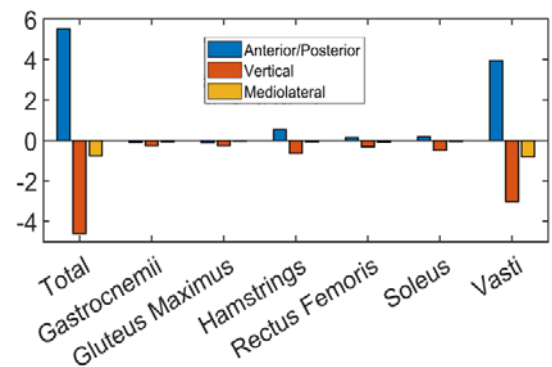


Figure 1: Main muscle contributions to bone-on-bone forces at the knee joint, given in terms of body weight.

Conclusions

The results from this work show that the main knee extensors are the primary producers of the knee bone-on-bone forces. Since the loadings at the knee joint and their contributions are interesting unknowns, their estimation is an important step to better understand the mechanisms behind an abrupt A/P deceleration task.

Acknowledgments

This work was supported by CIPER-FCT (I³D unit 447, project reference UIDB/00447/2020).

References

- [1] S. L. Delp et al.(2007), IEEE Trans. Biomed. Eng.,**54**: 1940–1950.
- [2] Sasaki, K. and Neptune, R.R.(2010), *Journal of biomechanics*, **43**:2780–278

Dynamic estimation of soft tissues stiffness of lower limb segments during squatting

Y. I. Sacha¹, G. Lafon¹, Vincent Bonnet^{2,3}, Rachid Aissaoui⁴, Raphaël Dumas¹

¹ Univ Lyon, Univ Gustave Eiffel, LMC UMR IT 9406, F-69622 Lyon, France

²LISSI, Univ. Paris-Est-Créteil, 94000 Créteil,

³LAAS/CNRS, Univ. Toulouse, F-31400, Toulouse, France

⁴Dépt Génie des systèmes, École de technologie supérieure, Montréal, Canada

Email: raphael.dumas@univ-eiffel.fr

Summary

This study presents a new numerical approach based on skin markers and fluoroscopy-based knee joint kinematics to estimate soft tissues stiffness of the thigh and of the shank segments during a squat movement.

Introduction

Modelling the interface between the lower limb segments and a socket, orthosis or exoskeleton is of crucial importance for the design, modelling, control and the assessment of such devices. For that purpose, soft tissues stiffness is a key parameter. It has been estimated in static condition [3] and for given anatomical loading direction [2]. In dynamic conditions, the soft tissue stiffness is more generally studied to model the so-called *wobbling mass effect* [1]. In this context, this study aims to estimate translational and rotational soft tissues stiffness at the thigh and shank levels during a squat movement, a daily living dynamic activity, by extending the vibrational analysis method called smooth orthogonal decomposition (SOD), a method already developed for soft tissue artifact (STA) analysis in [1].

Methods

Fluoroscopy-based implants and skin markers positions for 6 patients (5 males and 1 female, 68 ± 5 years, 88 ± 12 kg, 1.73 ± 0.04 m) with knee prostheses have been recording at 25Hz and 100Hz, respectively. One trial per subject of a squat movement was analyzed [4]. Data was down sampled to 25Hz. The SOD method [1], was extended here in order to compute the rotational stiffnesses in the 3 Dofs of the anatomical coordinate system of the thigh or the shank.

Results and Discussion

In average, and for all subjects in the 3 anatomical directions, the translational and rotational stiffness coefficients were respectively equal to 2.2 ± 0.3 kN/m (median and IQR) and 17 ± 6.5 Nm/deg for the shank. The results for the thigh segment are much lower i.e. 0.5 ± 0.1 kN/m and 5.2 ± 2.3 Nm/deg. Figure 1 represents the stiffness coefficients along the longitudinal directions of the segments. The translational stiffness estimated by the SOD method are lower than the one computed experimentally with instrumented exoskeleton cuff [3] (see Figure 1). These differences could be due to the type of tissue involved by the STA that represents mainly the behavior of the skin while other methods may involve deeper tissues. Rotational stiffness coefficients computed in this study revealed to be

higher than from literature [3]. This may be due to different muscular contraction levels and external loadings (static condition vs. squat movement).

The main limit of the proposed methodology relies on the experimental setup (number and location of the skin markers) and on the retained imaging method (mono-plane fluoroscopy).

Nevertheless, the SOD method used in this study is a new numerical approach in soft tissues characterization during dynamic activities. The main benefit over traditional approach is to obtain task dependent stiffness coefficients. Investigating such approach paves new ways to deal efficiently with the increasing amount of fluoroscopic data for various activities and various devices (STA and socket or orthosis studies). Moreover, the results derived from the proposed stiffness estimation method could improve external devices conception, modelling and evaluation.

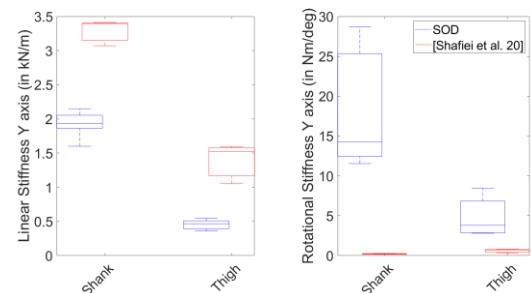


Figure 1: Translational and rotational stiffness coefficients along the longitudinal direction, with SOD method during squatting compared with literature report [3]

Conclusions

This study extends the approach of Dumas et al. [1] by adding the computation of rotational soft tissues stiffness of both thigh and shank segments during squatting. When compared to the literature [3], the estimated stiffness coefficients were lower for the translational stiffness and higher for the rotational ones. This may be due to different tissue and/or different loadings involved during squatting. Nevertheless, this dynamic estimation of soft tissues stiffness seems to be promising in the context of human interface modelling with external devices.

References

- [1] Dumas et al. (2017). *J BIOMECH*, 47-52.
- [2] Liu et al. (1995). *J REHABIL RES DEV*, 3(1): 135-40.
- [3] Shafiei et al. (2020). *J MECH ROBOT*, 1(1): 011007.
- [4] Taylor et al. (2017). *J BIOMECH*, 5: 3

Impact of the Quadratus Lumborum Muscle on the Lumbar Spine Joint Efforts via a Parametrized Model

Simon Hinnekens¹, Philippe Mahaudens², Christine Detrembleur², Paul Fiset¹

¹IMMC/MEED, Université catholique de Louvain, Louvain-la-Neuve, Belgium

²IREC/NMSK, Université catholique de Louvain, Brussels, Belgium

Email: simon.hinneken@uclouvain.be

Summary

The quadratus lumborum (QL) is a deep muscle whose activity is difficult to record. A parametrized musculoskeletal model allowed to study its influence on the lumbar spine efforts for a prone back extension exercise. Activating more QL fascicles increased the normal and shear forces at each intervertebral lumbar level and modified the orientation of the disc internal fibers.

Introduction

Musculoskeletal models allow to improve the knowledge of the human body. Using models gives the possibility to study the influence of one or several parameters for which there is few or no data. In this study, the parameter is the activation fraction of the quadratus lumborum (QL) muscle whose activity is difficult to assess via non-invasive measurements.

Methods

On the basis of a fully articulated thoracolumbar spine and rib cage model published previously [1], a model of a 25-year-old man (height 175cm and mass 78 kg) was developed for a prone back extension exercise carried out in the Sorensen test posture [2]. The model included lumbar (LP), dorsal paravertebral (DP) muscles and the QL muscle [3]. A deterministic muscle distribution based on maximal isometric forces was used. The activated QL fraction can be modulated from 0 to 40%, reducing *de facto* the activation of both LP and DP muscles. The model can consequently be parametrized via the activated QL fraction.

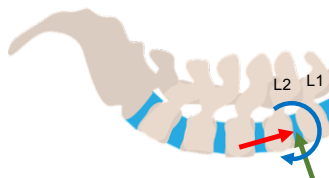


Figure 1: Intervertebral resultant efforts – normal force in red, shear in green and bending moment in blue – from L2 to L1 vertebral segment. Drawn arrows define positive values.

Efforts – forces and torques – (Figure 1) produced at each lumbar (Lx) intervertebral disc (IVD) levels were computed.

Results and Discussion

For a given activated QL fraction, the normal force (Figure 2 top) at each IVD increases when coming closer to the pelvis. It is due to the greater number of muscles in the lower area of the lumbar spine, which induces a larger force resultant from those muscles. Shear (Figure 2 middle) does not show any logical sequence. It is found mainly at L5/L4 level. The bending moment reflects how internal fibers in each IVD are

oriented. For a QL fraction below 20% (Figure 2 bottom), the positive bending moment at L5/L4 level indicates that the posterior fibers of the IVD are in compression while the anterior fibers are in traction. For all the other levels, the negative bending moment induces the opposite trend. A possible explanation is that most of muscles involved in the model act at L5/L4 level which results in pulling L4 upwards. Above L5/L4 level, each segment might be seen as a cantilevered beam.

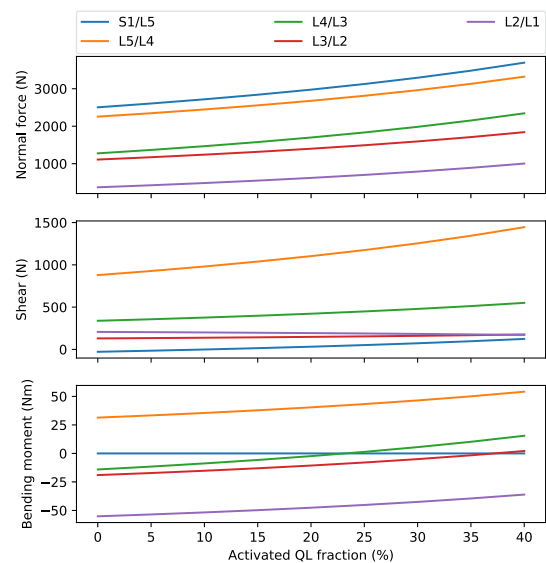


Figure 2: Efforts at each IVD in the lumbar spine.

When the activated QL fraction increases, normal and shear forces increase in most of the IVD levels reflecting the larger force resultant from the QL muscle, itself due to shorter lever arms of its fascicles. The bending moment decreases in cantilevered segments which results in less forces in IVD internal fibers. The positive bending moment at L5/L4 level is reinforced, involving greater forces in IVD fibers.

Conclusions

This study showed the influence of the QL muscle on the lumbar spine efforts during a prone back extension exercise. Further work will focus on the possible experimental validation.

References

- [1] Bruno AG et al. (2015). *J Biomech Eng*, **137**: 081003.
- [2] Demoulin C et al. (2006). *Joint Bone Spine*, **73**: 43-50.
- [3] Hinnekens S et al. (2020). *Comput Methods Biomech Biomed Eng*, **23**: S142-144

Impact of femur length scaling errors on estimate muscle and joint contact forces at all joints

Willi Koller¹, Arnold Baca¹, Hans Kainz¹

¹Department of Biomechanics, Kinesiology and Computer Science in Sport, Centre for Sport Science and University Sports, University of Vienna
Email: willi.koller@univie.ac.at

Summary

Musculoskeletal simulations are widely used in the research community. Marker-based scaling approaches include errors due to inaccuracies in marker placements. The aim of this study was to evaluate the influence of scaling errors due to a misplaced lateral epicondyle marker on simulation results in a systematic and comprehensive way. Magnetic resonance images from a child with cerebral palsy and a typically developing child were used to create a subject-specific reference model for each child. These reference models were modified to mimic scaling errors. Subsequently, musculoskeletal simulations with OpenSim were performed with all models. Joint kinematics, joint kinetics, muscle forces and joint contact forces were compared between the reference and altered models. Observed scaling errors influence simulation results at all joints due to the global optimization approach used in musculoskeletal simulations. Our findings can be used to estimate potential errors due to marker-based scaling approaches in previous and future studies.

Introduction

Musculoskeletal simulations are widely used in the research community [1,2]. The locations of surface markers are mostly used to scale a generic model to the participant's anthropometry. Marker-based scaling approaches include errors due to inaccuracies in marker placements [3,4]. The aim of this study was to evaluate the influence of scaling errors due to a misplaced lateral epicondyle marker on simulation results in a systematic and comprehensive way.

Methods

Motion capture data and magnetic resonance images from a child with cerebral palsy (CP) and a typically developing (TD) child were used to create a subject-specific reference model for each child. These reference models were modified to mimic scaling errors due to inaccurately placed lateral epicondyle markers, which are frequently used to scale the thigh and shank segments. The thigh length was altered in 1% steps from the original length and the shank length was accordingly adjusted to keep the total leg length constant. Thirty additional models were created, which included models with an altered thigh length of $\pm 15\%$. Subsequently, musculoskeletal simulations with OpenSim were performed with all models (Figure 1). Joint kinematics, joint kinetics, muscle forces and joint contact forces (JCF) were compared between the reference and altered models by analyzing the waveforms and computing the root-mean-square-error.

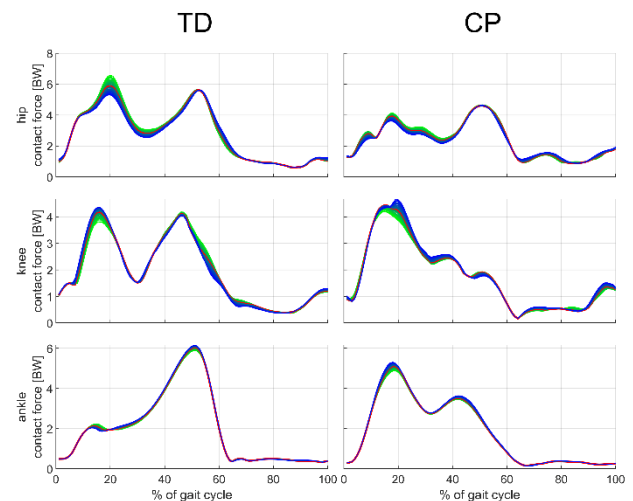


Figure 1: Comparison of joint contact forces of the TD (left column) and the CP child (right column) including all modified models. The red line shows the mean waveforms of the reference model. Green lines represent the models with shorter femur length while blue lines show the models with increased femur length.

Results and Discussion

The investigated scaling error influenced joint kinematics and joint kinetics by up to 9.4° (hip flexion angle) and 0.15 Nm/kg (knee flexion moment), respectively. Maximum muscle and JCF differences of 46% (medial gastrocnemius) and 72% (hip JCF) bodyweight, respectively, were observed between the reference and altered models. Scaling errors mainly changed the magnitude but not the shape of most analyzed parameters. The influence of scaling errors on simulation results were similar in both participants.

Conclusions

Scaling errors due to misplaced lateral epicondyle markers influence simulation results at all joints due to the global optimization approach used in musculoskeletal simulations. Our findings can be used to estimate potential errors due to marker-based scaling approaches in previous and future studies.

References

- [1] G.K. Lenton et al. (2018). PLoS ONE **13** 11
- [2] A. Seth et al. (2018). PLoS Comput Biol **14**
- [3] H. Kainz et al. (2017). J. Appl. Biomech **33** 354-360
- [4] U. Della Croce et al. (2005). Gait Posture. **21** 226-237

Predictive simulations of step initiation to study origins of age-related changes in weight shifting

Wouter Muijres¹, Maarten Afschrift^{1,2}, Friedl De Groot¹

¹Human Movement Biomechanics Research Group, KU Leuven, Leuven, Belgium

²Robotics, Automation and Mechatronics, KU Leuven, Leuven, Belgium

Email: wouter.muijres@kuleuven.be

Summary

Incorrect body weight shifts are a common cause of falls in elderly. Here, we used predictive simulations of stepping to study the effect of muscle weakness on weight shifting strategies. The backward center of pressure (COP) excursion when preparing to step decreases with age. In contrast, the simulated backward COP excursion increased when weakening the model. Hence, our simulations suggest that weakness is not the main cause of age-related changes in weight shifting.

Introduction

One out of three older adults fall each year. A common cause for falling in older individuals is incorrect body weight shifts. Step initiation is a suitable task to study weight shifting since successful initiation of a step prerequisites a series of well described weight shifts, such as the backward movement of the COP when preparing to step. With age, weight shifting strategies change. Older adults initiate steps with smaller ankle torques and decrease backward COP excursion [1]. The relative contribution of different age-related changes in the neuro-musculoskeletal system, such as muscle weakness and decreased sensory acuity, to altered weight shifting remains unclear. It is hard to study these relative contributions experimentally since aging affects different factors simultaneously. However, in computer simulations, model parameters can be altered to mimic age-related changes and their isolated influence on movement can be evaluated. Here we apply a previously developed gait simulation framework [2] to step initiation. We demonstrate that (1) simulated stepping captures main features of experimentally observed stepping and (2) how the framework can be used to study the effect of muscle weakness, which is common in aging.

Methods

To simulate step initiation, we used a 2D OpenSim model with 10 degrees of freedom. Ankles, knees, and hips were actuated by 18 Hill-type muscles. The metatarsal and back joints were torque-actuated. Foot-ground contact was modeled by 3 Hunt-Crossley contact spheres per foot. Stepping was simulated by solving for muscle and torque controls that optimized performance [see 2] while imposing the initial and final states and step duration. At the initial and final times, the model was in a static upright position and the final state was translated 0.4 m forward with respect to the initial state. We evaluated the effect of (1) speed by varying step duration and (2) muscle weakness by reducing the maximal isometric force of all muscles by 30%.

Results and Discussion

We compared simulated kinematics for different step durations (Figure 1) with experimental data on gait initiation at different speeds as experimental data on stepping at different speeds was not available [3]. Simulated and experimental hip, knee, and ankle angle trajectories were qualitatively similar. Both in experiments and simulations, hip and knee angle amplitude increased with increasing speed. In agreement with observations, weakening the model resulted in reduced peak ankle torques. In contrast with observations, simulated backward COP excursion increased. Hence, our simulations suggest that age-related changes in weight shifting strategy are not due to weakness. We will extend our model to test whether increases in sensory noise or changes in task-level goals, e.g. prioritizing stability over effort, explains age-related changes in weight shifting.

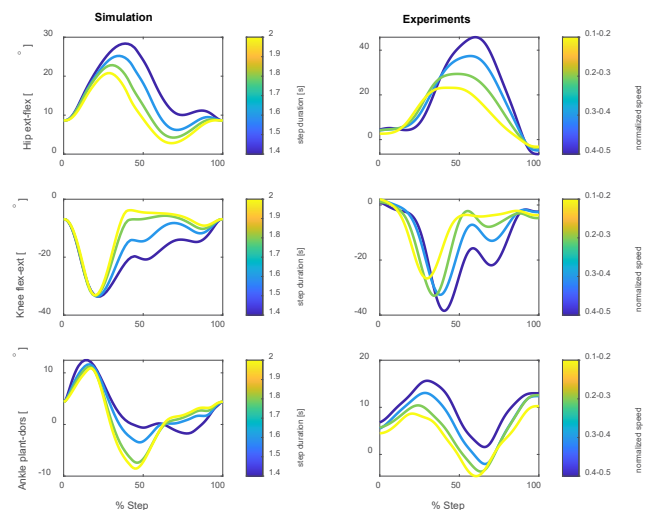


Figure 1: Simulated and experimental (reproduced from [3]) swing leg joint angles of the hip, knee, and ankle. In experiments, speed was normalized by $\sqrt{\text{body height } x \text{ g}}$.

Conclusions

Our previously developed framework to simulate gait also captures important features of other tasks such as gait initiation, and is a potentially powerful tool to explore causal relationships between age-related changes in the neuro-musculoskeletal system and weight shifting strategies.

Acknowledgements

FDG was funded by FWO (FWO research project G088420).

References

- [1] Khanmohammadi R *et al.* (2015) *Brain Res.* **1629**: 240–249
- [2] Falisse A *et al.* (2019) *J. R. Soc. Interface* **16**:
- [3] Stansfield B *et al.* (2018) *Gait Posture* **61**: 331–338

□ **high musculoskeletal model best predicts muscle excitations at different walking speeds** □

Israel Luis¹, Lara Wehrmeyer¹, Maarten Afschrift², Friedl De Groot², Elena M. Gutierrez-Farewik¹

¹KTH MoveAbility Lab, Dept. Engineering Mechanics, KTH Royal Institute of Technology, Stockholm, Sweden

²Department of Movement Sciences, KU Leuven, Leuven, Belgium

Email: ailp@kth.se

Summary

We estimated muscle excitations based on motion capture data of walking at seven speeds using three musculoskeletal models that differed mainly in parameters that define isometric muscle strength and passive muscle forces. We compared estimated muscle excitations to recorded EMG signals for eleven muscles. The *Lai-Arnold* model that combined high muscle strength with low passive muscle forces best captured changes in muscle activity with speed. None of the models estimated EMG patterns in hamstrings, rectus femoris or gluteus muscles accurately.

Introduction

Several musculoskeletal models have been refined to study human locomotion in recent years [1]-[4]. Hamner et al. modified the default OpenSim model [1] to simulate running [2]. Rajagopal et al. modified muscle parameters based on MRI data from healthy individuals and elderly cadavers [3] and Lai et al. further improved this model to compensate for excessive passive forces at knee and hip joints as observed in cycling [4]. These modifications might yield different muscle excitation predictions using the same experimental motion data and muscle redundancy solver [5], yet this hypothesis has not been tested at various walking speeds. This study aims to evaluate which model most accurately predicts muscle excitations at different walking speeds.

Methods

Marker trajectories (icon 16), ground reaction forces (AMTI Optima), and electromyography (EMG) were collected from 10 able-bodied subjects walking at 55%, 70%, 85%, 100%, 115%, 130% □ 145% of their preferred walking speed. EMG signals were collected from 11 lower limb muscles using bipolar surface electrodes (Myon aktos). These muscles were: biceps femoris (BF), semitendinosus (ST), vastus lateralis (VL) □ medialis (VM), rectus femoris (RF), gluteus maximus (GMA) □ medialis (GMED), tibialis anterior (TA), gastrocnemius lateralis (GL) □ medialis (GM) and soleus (SO). EMG signals were normalized to each subject's maximum activations during a high vertical jump.

Recorded data were processed (inverse kinematics and inverse dynamics) using OpenSim 4.1 based on three different musculoskeletal models: *Hamner* [2], *Rajagopal* [3], and *Lai-Arnold* [4], and scaled to each subject's dimensions. Muscle redundancy was solved by minimizing squared muscle activations using direct collocation [5]. Predicted and recorded muscle excitations were compared qualitatively.

Results and Discussion

All models captured main trends of muscle excitation time series in VA, VL, GM, GL, SO, and TA as observed in EMGs in that their magnitudes increased with walking speed. They, however, predicted delayed SO excitation (Figure 1) and did not reliably predict RF excitation at midstance. *Rajagopal* and *Lai-Arnold* tended to underestimate BF and ST excitation in late swing. *Hamner* tends to overestimate SO, GMA □ and GMED in stance □ its plantarflexor muscle parameters, specifically maximum isometric force, seem less suitable for simulations of high walking speeds than the other models. Limitations in surface EMG recording and data processing may have contributed to the observable discrepancies in measured and predicted muscle excitation.

Conclusions

Estimated changes in predicted muscle excitations with increasing walking speed in VA, VL, GM, GL, SO, and TA are similar between models. Predicted BF, ST, RF, GMA □, and GMED vary among the different models and do not agree with measured EMG as closely, even with the modifications of *Rajagopal* and *Lai-Arnold*. Among the models, *Lai-Arnold* better predicts muscle excitations for walking than *Rajagopal* and seems more suitable for higher speeds than *Hamner*.

References

- [1] Delp et al. (1990). *IEEE Trans Biomed Eng*, **37**: 757-76736
- [2] Hamner et al. (2010). *J Biomech*, **14**: 2709-2716
- [3] Rajagopal et al. (2016). *IEEE Biomed Eng*, **3**: 2068-2079
- [4] Lai et al. (2017). *Ann Biomed Eng*, **45**: 2762-2774
- [5] De Groot et al. (2016). *Ann Biomed Eng*, **44**: 2922-2936

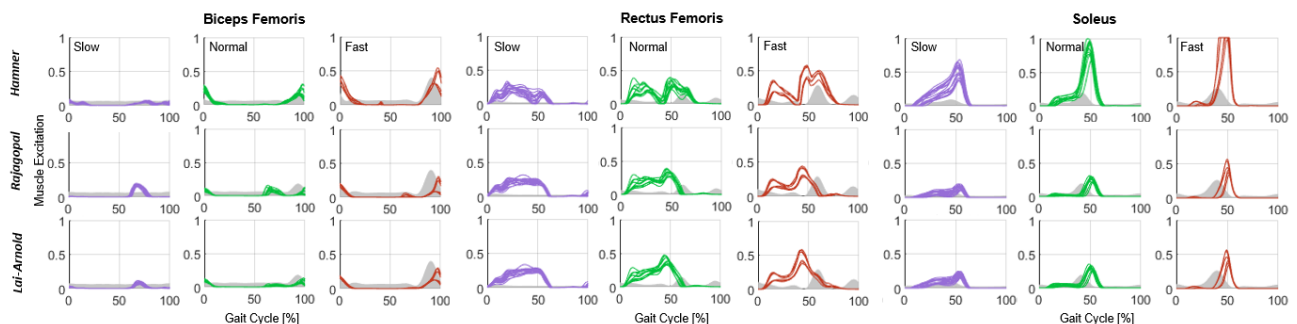


Figure 1: Predicted (colored) and recorded (gray) muscle excitation (0-1 scale) of BF, RF and SO at 55% (“slow”: purple), 100% (“normal”: green) and 145% (“fast”: red) preferred walking speed in 1 representative subject, computed with *Hamner* (top), *Rajagopal* (middle) and *Lai-Arnold* (bottom) models.

Validation assessment of a novel technique for restoring native collateral ligament strains in total knee arthroplasty

Orcun Taylan¹, Ignace Ghijssels², Josh Slane¹, Hans J. den Wyngaert², Alex Demurie², Hendrik P. Delpont¹, Lennart Schey¹
¹Institute for Orthopaedic Research and Training, Department of Development and Regeneration, KU Leuven/University Hospitals Leuven, Belgium ²Alma, Eeklo, Belgium
 Email: orcun.taylan@kuleuven.be

Summary

Soft tissue balancing is one of the most important factors for a successful knee arthroplasty however, there is no consensus for the most appropriate surgical technique. This *in-vitro* study aimed to assess to what extent a novel Patella-in-Place tensioner balancing (PIP) technique restores the biomechanical behavior of the native knee. Our findings showed that the PIP technique seemed to restore knee joint kinematics and collateral ligament strains better in passive than in dynamic conditions, i.e. squatting. Care must be taken when translating intraoperative assessments of knee balance during passive flexion to loaded conditions.

Introduction

Although soft tissue balancing is vital for successful total knee arthroplasty (TKA), there is no consensus for the most appropriate technique towards an optimally balanced TKA and the associated restoration of native joint function [1]. We aimed to use a cadaveric knee simulator to assess the biomechanical impact of a novel Patella-in-Place tensioner balancing (PIP) technique, which aims to restore native collateral ligament behavior without any ligament release.

Methods

Eight fresh-frozen legs were dissected and the soft tissue around the knee was removed, while preserving the joint capsule, ligaments and tendons. The native specimens were mounted on a validated physiological knee simulator [2] and subjected to passive flexion (10°-120°) and squatting motions (35°-100°) the latter with actively controlled quadriceps tendons. Specimens then underwent a single-radius cruciate-retaining TKA (Stryker Triathlon, MI, USA) using the PIP surgical technique, followed by the same tests. Extensometers (MTS, Minnesota, USA) were affixed to the superficial collateral ligaments to measure strain, while a motion capture system (Icon, Oxford, UK) was used to obtain tibiofemoral kinematics. Tibiofemoral kinematics and collateral ligament strains were compared between pre- and post-operative conditions using a linear mixed model (p<0.05).

Results and Discussion

As compared to the native condition, post-operative tibiofemoral kinematics revealed similar medial and lateral translations during passive flexion (Fig.1). Moreover, strain behaviors for medial and lateral collateral ligaments were statistically different only in deep flexion and mid-flexion, respectively (Fig.2). For squatting, the post-operative condition exhibited a more pronounced medial pivot configuration. Conversely, the post-operative medial

collateral ligament strain significantly differed from the native condition from mid-flexion onwards, while the lateral collateral ligament strain differed in mid-flexion.

Increased post-operative MCL strain (Fig.2) could be attributed to greater tibial internal rotation resulting in increased lateral translations following TKA during squatting.

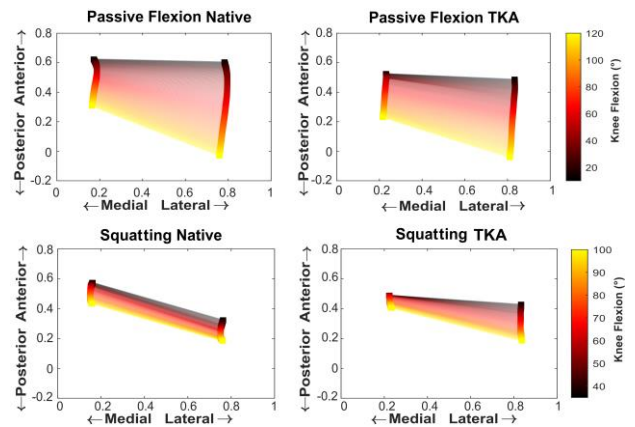


Figure 1: Mean femoral rollback patterns (normalized to tibial plateau geometry) across eight specimens in the native condition (left) and following TKA (right) throughout the range of flexion during passive flexion (top) and squatting (bottom).

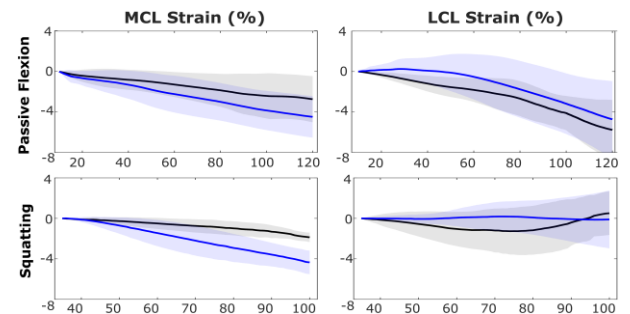


Figure 2: Collateral ligament strains (mean±SD across eight specimens) in the native (black) and post-operative (blue) conditions during passive flexion (top) and squatting (bottom).

Conclusions

The PIP technique seemed to restore joint kinematics and strains better in passive condition as compared to squatting. Care must be taken when translating intraoperative assessments of knee balance during passive flexion to loaded conditions.

References

[1] Walker et al. (2018). EFFORT, 3:614-619
 [2] Victor et al. (2009). J Bone Joint Surg, 91:150-163

A numerical model to simulate crack propagation in articular cartilage under cyclic loading

Gustavo A Orozco^{1,2}, Petri Tanska¹, Anna Gustafsson², Hanna Isaksson², and Rami K. Korhonen¹

¹Department of Applied Physics, University of Eastern Finland, Kuopio, Finland

²Department of Biomedical Engineering, Lund University, Lund, Sweden

Email: gustavo.orozco@uef.fi

Summary

Severe joint injuries frequently involve cartilage defects which propagate after mechanical loading. The propagation of these tears may contribute to the development of post-traumatic osteoarthritis (PTOA). Predictive tools would provide insights into crack growth in injured tissue. Here, we developed a numerical model to estimate crack propagation under dynamic loading. Computational predictions were compared to experiments reported in the literature. Our numerical estimations corresponded well with the experimental results suggesting that our approach may help in developing better tools for predicting crack propagation in soft tissue after injury.

Introduction

Traumatic joint injuries often involve cartilage tears which contribute to the development of PTOA. This degenerative disease includes a decrease in the mechanical properties, volume, and thickness of the tissue. After the injury, the size of the cartilage defects increases due to the limited tissue healing capacity. Previous experimental investigations have studied crack growth and fracture toughness to understand their role during cartilage degeneration [1]. However, there are no numerical predictive models on crack growth in cartilage under dynamic loading. Thus, we aimed to develop a model capable of simulating crack propagation under tensile cyclic loading. Numerical estimations were calibrated using previously reported experimental crack propagation results [1].

Methods

Numerical model: A 2-D FE model was constructed in Abaqus (v2018) to predict crack growth. The specimen dimensions and loading protocol (Figure 1) were replicated from literature [1]. The cartilage specimen with dimensions of 10 x 10 mm, including a notch of 2.26 mm in the middle, was meshed with 7506 elements (CPE4P). **Cohesive damage model:** A cohesive element set (COH2D4) was used along a line ahead of the notch to represent the experimentally observed crack propagation direction. A traction-separation constitutive response was assumed to the cohesive element set. Damage initiation was modeled using a maximum nominal stress criterion (σ_f). Moreover, a damage evolution law based on the fracture energy (G_f) with a linear softening was adopted. **Boundary and loading conditions:** The loading protocol was simulated based on the experiments [1]. The bottom of the specimen was fixed, and a uniform tensile displacement was applied to the top nodes. Initially, 15% strain was applied to the model in tension and held for 5s. This was followed by a 5% sinusoidal loading amplitude (1

Hz) imposed for 2,000 cycles. **Model calibration:** Articular cartilage was modeled as a poro-hyper-viscoelastic material. Poro-hyperelastic properties were adopted from the literature [2,3], but the damage initiation stress σ_f , fracture energy G_f , and viscoelastic Prony-parameters were calibrated by fitting the simulated progression (crack length) to the experimental data [1] using an iterative optimization approach (Matlab).

Results and Discussion

Our numerical predictions corresponded well with the reported experimental crack growth under tensile dynamic loading showing greater crack length with an increasing number of loading cycles (MSE=0.0029). The fitted values for the σ_f (4.72 MPa) and G_f (1.1 N/mm) were within the range reported in previous studies [4,5]. However, more experiments and different loading frequencies are required to fully validate our computational approach.

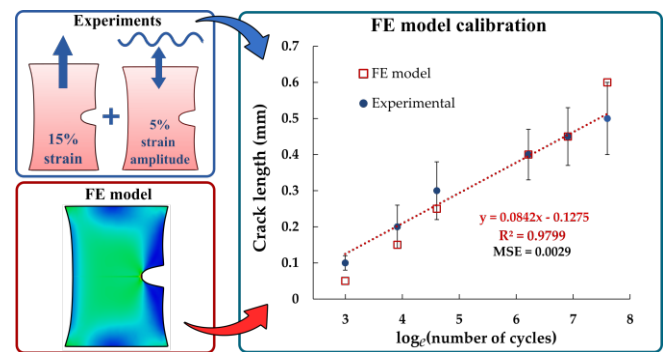


Figure 1: A FE model was developed to estimate crack propagation under dynamic loading. The sample dimensions and loading conditions were adopted from a previous study [1]. Our model was able to reproduce the crack growth observed in the experiments.

Conclusions

Our numerical predictions corresponded well with the experimental results. This cohesive crack model provides a novel platform for predicting tear propagation in injured tissue.

Acknowledgments

ERA PerMed JTC2019, and Pivikki ja Sakari Sohlberg and Maud Kuistila Memorial Foundations.

References

- [1] Sadegui H. et al. (2018). *JBMMB*. 40-46.
- [2] Pawaskar et al. (2011) *J Biomech*. **44** 1536–1542.
- [3] Keenan et al. (2013) *J Appl Biomech*. **9** 292–302.
- [4] Chin-Purcell & Lewis (1996). *J Biomech Eng*. **118** 545-556
- [5] Stok & Oloyede (2007). *Clin Biomech*. 725-735

Repeatability of cartilage oligomeric matrix protein kinetics in response to a walking stress test

Simon Herger^{1,3}, Michael Hächler^{1,5}, Anna-Maria Liphardt⁶, Christian Egloff^{1,3,4}, Corina Nüesch^{1,2,3,4}, Annegret Mündermann^{1,2,3,4}
¹Department of Orthopaedics and Traumatology and ²Department of Spine Surgery, University Hospital Basel; ³Department of Biomedical Engineering, ⁴Department of Clinical Research and ⁵Department of Sport, Exercise and Health, University of Basel, all Basel, Switzerland; ⁶Department of Internal Med. 3 – Rheumatology and Immunology, Friedrich-Alexander-University Erlangen-Nuremberg (FAU), Universitätsklinikum Erlangen, Erlangen, Germany
 Email: simon.herger@unibas.ch

Summary

In two experiments separated by 2-7 days, we compared sCOMP concentrations before and after the same 30-min walking stress test. sCOMP concentrations showed good to excellent repeatability between the two measurements.

Introduction

Articular cartilage blood marker concentrations and load-induced marker kinetics were proposed to serve as surrogate parameter for articular cartilage metabolism and its response to load [1]. One of these markers is serum cartilage oligomeric matrix protein (sCOMP), a cartilage constituent that is involved in collagen fibril organization [2] and serum concentrations may represent cartilage turnover or degeneration [3]. The purpose of this study was to determine the repeatability of load-induced changes of sCOMP concentration after 30-minutes treadmill walking.

Methods

Ten healthy subjects (5 male, 5 female; median [interquartile range], age 27 [26–29] years; body mass: 62.5 [58.5–79.7] kg; height: 1.70 [1.63–1.76] m; body mass index: 22.2 [21.8–23.5] kg/m²) completed the same walking stress test in two measurements within 6 [4-7] days. On each day, venous blood samples were collected after 60-min of rest before (t₀), immediately after (t₁) and 30-min after (t₂) a 30-min treadmill walking stress. Samples were aliquoted and frozen to -80°C until analysis. sCOMP concentrations were assessed using a commercial enzyme-linked immunosorbent assay (BioVendor, Modrice, CZ). Steps were counted with a hip-worn accelerometer (GTX3+ ActiGraph, Pensacola, USA). Because of the small sample size, non-parametric tests (sign tests) were used to detect significant differences in the number of steps during the test and absolute sCOMP concentrations between test days and between time points of the stress test. We computed intraclass correlation coefficients (ICCs) to determine the repeatability of sCOMP concentrations between test days across all and for each time point.

Results and Discussion

A priori self-selected walking speed was 1.38 [1.31-1.39] m/s. The number of steps taken during the 30-min walk did not differ between day 1 and day 2 (day 1: 3336 [3261-3465] steps; day 2: 3328 [3298-3516] steps; P=0.754).

sCOMP concentrations at t₀, t₁ and t₂ were 528.4 [463.3-643.5], 632.2 [565.6-757.1] and 533.4 [487.8-617.7] ng/ml on day 1 and 516.2 [440.5-623.7], 608.3 [582.8-757.0] and 475.4

[460.3-598.2] ng/ml on day 2. Concentrations did not differ between measurements (t₀: P=0.344; t₁: P=0.754; t₂: P=0.344). The ICC for sCOMP across all time points was 0.869. The ICCs for each time point were 0.706, 0.864, and 0.910 for t₀, t₁ and t₂, respectively. sCOMP increased from t₀ to t₁ (day 1: P=0.022; day 2: P=0.002) and decreased from t₁ to t₂ (day 1: P=0.022; day 2: P=0.002) (Figure 1).

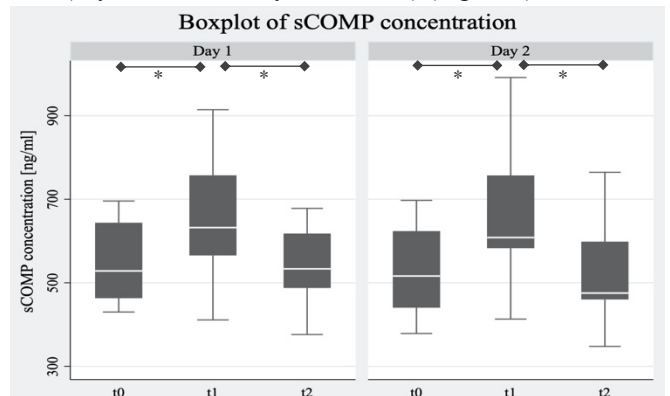


Figure 1: Boxplot of sCOMP concentration at timepoints t₀, t₁, and t₂ for the measurements on day 1 and day 2 (n=10). Significant differences are indicated as * p<0.05.

Conclusions

Serum concentrations of sCOMP appear to be consistent between days. Moreover, the overall load-induced increase of sCOMP after a walking stress test followed by a decrease is repeatable between days. While in most subjects the concentration kinetics in the sCOMP mechanoreponse appears to be remarkably consistent, some variability between measurements was observed in a few subjects. Because the two measurements were separated by only 7 days or less, physiological or metabolic variations are unlikely to cause such differences. The good to excellent day to day repeatability in load-induced blood marker kinetics in healthy subjects further support the feasibility of a well-controlled walking stress test to study the effects of biological variations and interventions on articular cartilage marker kinetics in response to ambulatory load.

Acknowledgments

Funding: Swiss National Science Foundation (SNSF #320030_184912).

References

- [1] Roberts et al. (2019). *EJAP*, **119**: 2401-2420
- [2] Acharya et al. (2014). *Matrix Biol.*, **37**: 102-111.
- [3] Erhart-Hledik et al. (2012). *OA Cartil.*, **20**: 1309-1315.

The Effect of Abduction Angle and Infraspinatus Load on Supraspinatus Articular Surface Strain

Patrick M Williamson^{1,2}, Thomas J. Noonan², Kaveh Momenzadeh, MD,² Mohammad Reza Abbasian, MD², Arun J. Ramappa, MD², Joseph P. DeAngelis, MD², Ara Nazarian, Ph.D.²

¹Boston University, Mechanical Engineering Department, Boston, Massachusetts, USA

²Musculoskeletal Translational Innovation Initiative, Carl J. Shapiro Department of Orthopaedic Surgery, Beth Israel Deaconess Medical Center and Harvard Medical School, Boston, MA, USA

Email: pmwill@bu.edu

Summary

We have quantified the articular surface strain of human cadaveric supraspinatus tendon for varying simulated abduction angles and infraspinatus load using a custom positioning system mounted on an Instron load frame and opensource digital image correlation analysis (NCCorr).

Introduction

Articular-sided partial rotator cuff tears are common and may be symptomatic or asymptomatic. [1] Classically, Nakajima et al. reported that the tendon's articular side is more vulnerable to tensile load than the bursal side, [2] which may be related to the random orientation of collagen fibers in this region. However, there is little evidence to determine which articular-sided tears are stable and which may progress. It has been shown in cadaveric studies that surface tendon strain is associated with tear progression and that the supraspinatus and infraspinatus tendons interact mechanically. [3] In this study, a single infraspinatus load was applied and the glenohumeral abduction angle was kept constant. Therefore, we aimed to assess 1) the effect of infraspinatus load and 2) glenohumeral abduction angle on the articular surface strain of the supraspinatus using a custom positioning system mounted on a material testing system and digital image correlation analysis.

Methods

Specimen Preparation and Fixation

Two fresh-frozen healthy left cadaveric shoulders (one male, one female – mean age 57.5) were dissected of all tissue, leaving the supraspinatus and infraspinatus tendon and muscle units intact. No attempt was made to separate the interface between the tendons. The humeral head was resected to allow perpendicular line-of-sight to the tendon's articular surface at low abduction angles.

The specimens were potted in two-part epoxy (Smooth-Cast 300q and PMG Smooth-on Inc., Macungie, PA) and fixed in a custom positioning system mounted on an Instron load frame (8511, Norwood, MA). This system allows for changing the angle of the humerus relative to the loading axis of the Instron to simulate altered abduction angle. The articular surface of the supraspinatus was sprayed with hematoxylin stain to speckle the surface for image analysis. The supraspinatus was rigidly clamped to the Instron loading axis, and the infraspinatus was loaded along its physiological line of action via Krackow stitch and pulley system.

Data Acquisition

The supraspinatus was preloaded according to a previous study, namely 10 cycles from 10-50 N at 0.125mm/s. [3] It were then loaded to 200N for three cycles at 0.333m/s. The infraspinatus was statically loaded to 5, 10, 15, 20, and 25lbs,

while the humerus was oriented to simulate 90° of glenohumeral abduction. Then, the infraspinatus was loaded to 20lbs while the humerus was rotated to simulate 90°, 80°, 70°, and 60°. During loading, a CMOS microscope camera (PL-A662, Pixelink) was positioned to capture images of the tendon's articular surface at 2Hz.

Data Analysis

The articular surface strain on the supraspinatus tendon at 200N was estimated using an opensource digital image correlation package (NCCorr). [4] This analysis tracks the speckled surface between images to estimate the surface deformation, then calculates the strain associated with that deformation. The average supraspinatus surface strain at 200N for three cycles was calculated for each condition – abduction angle and infraspinatus load. One-way repeated measures ANOVA tests were conducted to compare the effect of abduction angle or infraspinatus load on articular supraspinatus surface strain.

Results and Discussion

With this sample size, altering infraspinatus load or increasing glenohumeral abduction angle between 60° and 90° had no significant effect on the articular surface strain ($P > 0.45$ and 0.35 , respectively).

Articular Supraspinatus Tendon Surface Strain

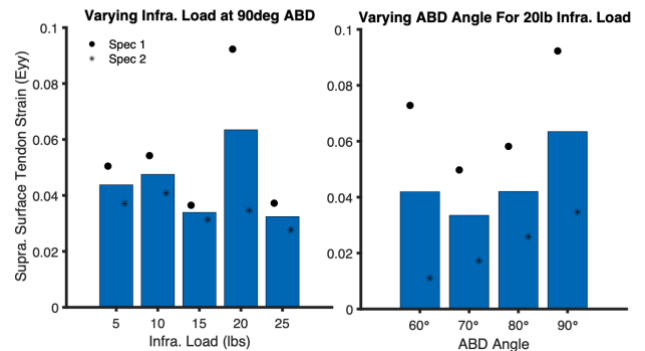


Figure 1: Articular Supraspinatus Tendon Surface Strain.

Conclusions

The articular surface strain may not be affected by abduction angle or infraspinatus load, but additional specimens will help to elucidate this relationship.

References

- [1] Milgrom J *One Joint Surg*. 1995;77(2):296-8
- [2] Nakajima T *J Shoulder Elbow Surg*. 1994 Mar;3(2):79-87
- [3] Andarawis-Puri NJ *Orthop Res*. 2010 Jul;28(7):846-51
- [4] *Laber Exp Mech* 55, 1105–1122 (2015)

A Predictive Simulation Study into the Effect of Below-Knee Prosthesis Alignment on Metabolic Cost

Anne D. Koelewijn^{1,2}, Marlies Nitschke¹, Antonie van den Bogert²

¹Machine Learning and Data Analytics Lab, Faculty of Engineering, Friedrich-Alexander Universität Erlangen-Nürnberg, Erlangen, Germany

²Parker Hannifin Laboratory for Human Motion and Control, Department of Mechanical Engineering, Cleveland State University, Cleveland, Ohio, USA

Email: anne.koelewijn@fau.de

Summary

We investigated the effect of below-knee prosthesis alignment on metabolic cost in simulation. Metabolic cost was reduced when the prosthesis was abducted or externally rotated, though not significantly. Further research should investigate how joint reaction forces are affected by prosthesis alignment.

Introduction

Metabolic energy expenditure and joint reaction forces are important gait variables when evaluating a prosthesis. Many studies have evaluated their relation to prosthesis stiffness (e.g. [1]), but little research has investigated how these variables are affected by prosthesis alignment. Prostheses fit depends on the experience of the prosthetist [2]. When a prosthesis is misaligned, the loading of the legs changes [2], which likely affects metabolic cost and joint loading.

Previous work has shown that a sagittal plane alignment change of a below-knee prosthesis increases metabolic cost [3], but no such study investigated transverse and frontal plane alignments changes. A predictive simulation study could provide insight into metabolic cost and joint loading without requiring a costly and time-consuming experiment. Therefore, we compared predictive gait simulations with different below-knee prosthesis alignments to investigate how an alignment change affects joint loading and metabolic cost.

Methods

Predictive simulations were generated using the approach described in [4]. The below-knee prosthesis was modeled as a rotational ankle spring with a stiffness of 600 Nm/rad and a damping ratio of 15 Nms/rad [5]. The reference alignment was the original model alignment. The prosthesis alignment was then changed by introducing 5 and 10 degree offsets between the femur and the prosthesis in flexion, extension, abduction, adduction, and internal and external rotation.

Trajectory optimization problems were solved to simulate gait with all prosthesis alignments. Muscle stimulations were found to create a periodic gait trajectory while minimizing muscular effort and tracking normal gait data [6]. 50 virtual participants were drawn with a random mass, body mass index, isometric muscle force, optimal contractile element

length, and maximum shortening velocity. Tendon slack length was adjusted to not change the total muscle length.

Results and Discussion

5 virtual participants were discarded since an unrealistic local optimum was found for at least one alignment. An ANOVA test found statistically significant differences ($p < 0.0001$) in metabolic cost, calculated using Umberger's model [7], between alignments (table 1). A multiple comparisons test showed that only the 10-degree flexion alignment was significantly different from the reference. Similar to [3], metabolic cost increased with a sagittal alignment change. Metabolic cost was reduced 1% with a 10-degree abduction or external rotation alignment. Even such a small difference might be beneficial to persons with a transtibial amputation.

We also found that alignment changed joint moments and muscle activations. Therefore, joint reaction forces are likely altered as well. These changes were small for the external rotation, indicating that the energy expenditure reduction requires only small loading changes. Further analysis should identify any favorable changes in joint loading.

Conclusions

We conclude that metabolic cost is not significantly altered by prosthesis alignment, though small reductions might be achieved. Kinetic results suggest that joint reaction forces are altered. Further analysis of joint reaction forces is required to completely understand the effect of prosthesis alignment.

Acknowledgments

This research was supported by adidas AG, the National Science Foundation, Grant No. 1344954, and by a Graduate Scholarship from the Parker-Hannifin Corporation.

References

- [1] Major MJ et al. (2014). *Clin Biomech*, **29.1**: 98-104.
- [2] Fang L et al. (2007). *Clin Biomech*, **22.10**: 1125-1131.
- [3] Schmalz et al. (2002). *Gait & Posture*, **16.3**: 255-263.
- [4] Nitschke M et al. (2020). *Sci Rep*, **10.1**: 1-12.
- [5] Zmitrewicz RJ et al. (2007). *J Biomech*, **40.8**: 1824-1831
- [6] Horst, F et al. (2019). Mendeley Data, V2.
- [7] Umberger BR (2010). *J R Soc Interface*, **7.50**: 1329-1340.

Table 1: Average metabolic cost of predictive simulations over 45 virtual participants with different prosthesis alignments.

Alignment	Reference	Flexion		Extension		Abduction		Adduction		Internal Rotation		External Rotation	
		5	10	5	10	5	10	5	10	5	10	5	10
Offset in degrees													
Metabolic Cost (J/kg/m)	3.03	3.06	3.11	3.04	3.04	3.02	2.99	3.05	3.06	3.04	3.04	3.02	3.00

Cleveland Barnett¹, Liam D. Hughes¹, Amy E. Sullivan², Gerda Strutzenberger^{3,4}, Jodie L. Levick¹, Maria Cisele¹ and Alan R. De Asha^{1,5}

¹School of Science and Technology, Nottingham Trent University, UK.

²University Hospitals of Derby and Burton NHS Trust, UK.

³Universitätsklinik Balgrist, Switzerland.

⁴Department of Sport and Exercise Science, University of Salzburg, Austria.

⁵C-Motion, Inc., USA.

Email: cleveland.barnett@ntu.ac.uk

Summary

The selection of prosthetic componentry and their inherent mechanical function is critical for mobility in those with limb loss. Individuals with transfemoral amputation use both knee and ankle-foot components for mobility. The current study suggests that using a microprocessor-controlled knee with a hydraulically-articulating ankle-foot improves mobility, when compared to less functionally advanced components.

Introduction

Individuals with unilateral transfemoral (UTF) amputation make use of both knee and ankle components for locomotion. Hydraulically-articulating ankle-foot components (HAD) have been shown to reduce trip risk [1] and increase mobility [2], whereas microprocessor-controlled knee (MPK) components reduce fall incidence [3]. Overcoming mobility and safety issues through prosthetic prescription can result in economic benefits to healthcare systems [4]. However, the benefits of combining HAD and MPK are not clear. Therefore, the aim was to investigate the effects of ankle-foot and knee component combinations on minimum toe clearance, gait stability and inverted pendulum model adherence in UTFs during level walking.

Methods

Nine people with unilateral transfemoral amputation (52.8 ± 9.7 years, 1.8 ± 0.06 m, 83.3 ± 13.0 kg.) walked at a self-selected speed along a 13m walkway in four prosthetic combinations using an MPK or non-MPK (NMPK) knee component, with either a HAD or rigid (RIG) ankle-foot component (all components manufactured by Bionica, Basinstoke, UK). The order of prosthetic combinations was randomised across participants. Reflective markers were attached to the whole body and kinematics were recorded using a 13-camera motion capture system (Qualisys A1, Gothenburg, SE). Gait stability, and safety were represented by the margins of stability and minimum toe clearance, respectively.

Results and Discussion

Walking speed was highest in the MPKHAD combination, followed by the MPKRIG, NMPKHAD and the NMPKRIG combinations ($F(3,24) = 4.50$, $p < 0.01$, $\eta_p^2 = 0.36$). Gait stability was higher in the intact vs. prosthetic limb,

particularly in MPK trials. Minimum toe clearance was higher in the prosthetic limb, particularly when using an NMPK.

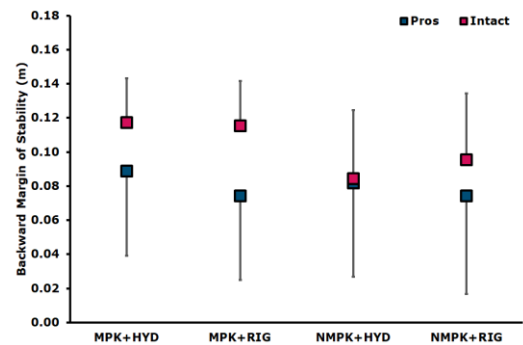


Figure 1. Backward Margin of Stability for all four prosthetic combinations and both the prosthetic and intact limbs.

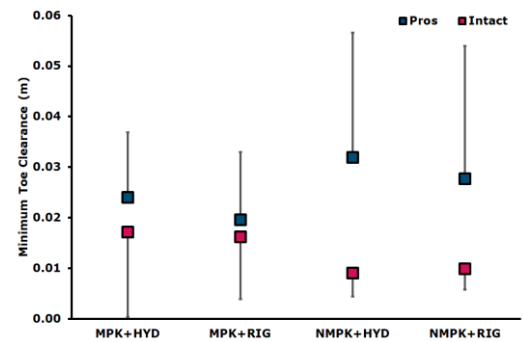


Figure 2. Minimum toe clearance for all four prosthetic combinations and both the prosthetic and intact limbs.

Conclusions

Using a microprocessor-controlled knee combined with a hydraulically-articulating ankle-foot results in mobility benefits, when compared to non-microprocessor-controlled knee and rigid ankle-foot components.

References

- [1] Johnson L et al. (2014). *J Rehabil Res Dev*, **51**: 429-37.
- [2] Barnett CT et al. (2018). *J Prosthet Orthot*, **30**: 158-64.
- [3] Kaufman, KR et al. (2018). *Clin Biomech*, **58**: 116-22.
- [4] Chen C et al. (2018). *J Neuroeng Rehabil*, **15**: 49-59.

Impact of the acetabular component thickness on the implantation process and primary stability

Miriam Ruhr¹, Johanna Baetz¹, Klaus Pueschel², Michael M. Morlock¹

¹Institute of Biomechanics, Hamburg University of Technology, Hamburg, Germany

²Department of Legal Medicine, University Medical Center Hamburg-Eppendorf, Hamburg, Germany

Email: miriam.ruhr@tuhh.de

Summary

A major complication in total hip arthroplasty is cup loosening that may occur due to insufficient primary stability. The role of the cup design and the impaction process was analyzed within this study. Acetabular cups of different thickness were impacted in human acetabula. Cup deformation, cup seating and the lever out moment were evaluated. Thin-walled cups expressed higher primary stability. Excessive number of strikes may enhance the risk of cup loosening due to a release of cup deformation.

Introduction

Insufficient primary stability of acetabular components is a complication resulting in early cup loosening. Available cup designs vary in thickness, which plays a role for the implantation process and primary stability. This study investigated the effect of cup design on the implantation process and the resulting primary stability.

Methods

Two different cup designs (ca. 3 mm and 4 mm thickness, n=10 each, DePuy Synthes) were implanted in ten excised human pelvises (69 ± 3 years). Impaction was performed with constant energy (3.5 J, Kincise, DePuy Synthes) until no further cup seating was observed by a 3D digital image correlation system (Aramis 3D, GOM). Cup deformation was determined using strain gauges at the inner surface. Contact between bone and implant was analyzed with conducted laser scans. The lever out moment was used as a measure for primary stability.

Results and Discussion

Thin-walled cups displayed higher strains ($p = 0.006$) and a higher lever out resistance compared to thick-walled cups ($p < 0.001$; Figure 1).

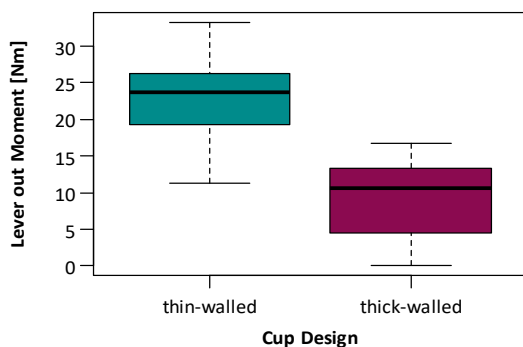


Figure 1: Higher lever-out moments for thin-walled cups.

Higher cup deformation, as well as low number of strikes, were associated with an increase in primary stability ($p = 0.039$, $R^2 = 0.24$). An increasing number of strikes resulted in strain release during the impaction progress ($p = 0.016$, $R^2 = 0.39$; Figure 2). The seating curves revealed a correlation between a high number of strikes and small seating steps at the end of the impaction ($p = 0.002$, $R^2 = 0.72$).

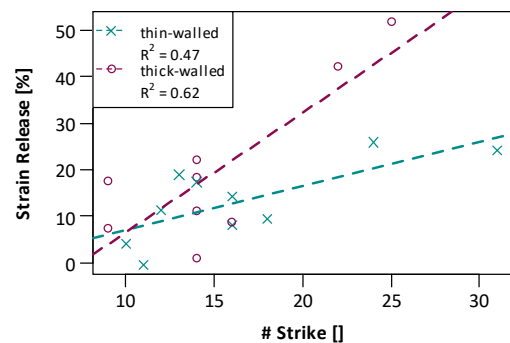


Figure 2: The strain release during cup impaction increased for high number of strikes.

Sufficient cup seating without over-impaction showed to be critical for initial cup fixation. Over-impaction is associated with bone damage and a negative influence on primary stability. Sufficient seating promotes cup deformation, as well as it restricts over-impaction due to further cup seating. For thin-walled cups, sufficient seating can be achieved with lower energy input, reducing the risk of bone damage.

Conclusions

Thin-walled cups facilitate the prevention of impaction errors, which might promote early cup migration. Sufficient cup seating with low impaction energies reduces the risk of over-impaction and bone damage. Additional strikes should be avoided as soon as no further seating is observed. Excessive cup deformations have to be prevented since they can cause incomplete liner seating or excessive liner deformation, which might disturb the bearing tribology.

Acknowledgments

The financial and material support of DePuy Synthes, Leeds, UK is gratefully acknowledged.

Variability between Surgeons in Total Hip Arthroplasty

Tobias Konow¹, Johanna Aetz¹, David Everland², Tim Board³, Frank Lampe⁴, Klaus Püeschel⁵, Michael M. Morlock¹

¹Institute of Biomechanics, TUHH - Hamburg University of Technology, Hamburg, Germany

² Belfast Arthroplasty Research Trust, Belfast, Northern Ireland

³ Wrightington Hospital, Lancashire, Great Britain

⁴ Schön Klinik Hamburg Eilbek, Hamburg, Germany

⁵ Department of Legal Medicine, UKE - University Medical Center Hamburg-Eppendorf, Hamburg, Germany

Email: tobias.konow@tuhh.de

Summary

Complications such as implant loosening and periprosthetic fractures (PPF) are often related to the surgical process in total hip arthroplasty (THA). This study investigates the variability within the surgical process between highly experienced surgeons. Variations were observed regarding stem positioning, sizing, press-fit and contact area. These even exist between experienced surgeons and may affect the PPF risk influenced by positioning and sizing.

Introduction

Implant loosening and PPF are major complications in uncemented THA. Complications decrease with increasing experience and surgical volume [1]. Specific surgical parameters, indicative for these complications, have yet to be identified. The goal was to determine the extent of variability between highly experienced surgeons. Selected parameters were chosen (implant size, position, densification, press-fit and contact area) which bear the potential to determine differences in PPF risk.

Methods

Primary hip stems (Corail, Depuy Synthes) were implanted in sixteen cadaveric femora (67 ± 8 years) by three experienced surgeons (surgeon A: n=6; surgeon B: n=6; surgeon C: n=4). All femora were qCT scanned and the BMD determined at three different time instances: native, with the reamed cavity, and after stem insertion. Stem tilt and canal-fill-ratio (CFR) were analyzed using the initial and implantation scans. Proximal densification at the bone-implant-interface was determined by computing the change in BMD between initial and cavity scans [2]. Press-fit and contact area were analyzed using a surface-to-surface comparison with the superimposed cavity and implantation scans.

Results and Discussion

High variability between surgeons was observed regarding press-fit ($p < 0.014$, Figure 1a) and contact area ($p < 0.011$). No differences between surgeons were observed for bone densification ($p < 0.751$, Figure 1b). Large variations were found in terms of implant sizing (CFR, $p < 0.021$, Figure 1d). A trend was observed regarding the stem tilt ($p < 0.073$, Figure 1c) and

A stem tilt towards varus might increase PPF risk as it increases bone stresses [3]. Larger implants increase the PPF risk, while smaller implants may reduce primary stability [4].

Bone densification appears to be influenced by the instruments rather than the surgeon [2]. The observed differences in contact area and press-fit may be linked to different stem impaction forces, which were not documented, as well as variations in BMD and technique. Including less experienced surgeons in the analysis may further increase the observed variability, partly explaining the relation between the number of THA surgeries and the risk for complications [1].

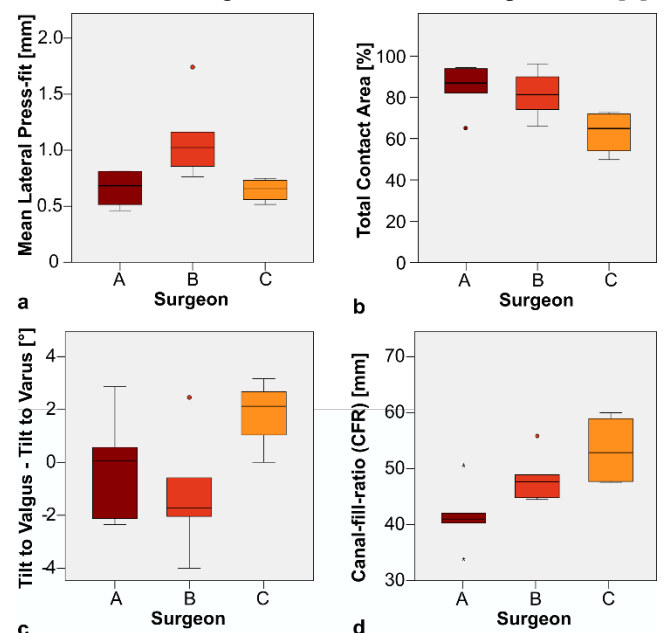


Figure 1 a) Variability in the lateral press-fit. b) Variability in the bone implant contact area. c) Valgus-varus tilt of the stem in the femur. d) CFR as a measure for the chosen implant size.

Conclusions

Variations exist even between experienced surgeons. Reported variations in implant position and size may have an impact on the PPF risk, as already shown in literature. Whether and to what extent other parameters affect PPFs is yet to be determined.

Acknowledgments

DePuy Synthes financially supported the study.

References

- [1] Konow T, et al. (2021). *Bone Jt. J.*, **Accepted manuscript**.
- [2] Aetz J, et al. (2019). *J Orthop Res*, **37**: 1580-1589
- [3] Tadross T, et al. (2000). *J Arthroplasty* **15**, 47-51
- [4] Spina M, Scalvi A (2020). *Acta Biomater* **91**, 1-9

Are different foot models able to detect the same changes in kinematics due to foot orthoses □

Tomas Klein¹, □raham □Chapman,² Ondrej Lastovicka¹, Miroslav Janura¹, Jim Richards²

¹Faculty of Physical Culture, Palacký University Olomouc, Olomouc, Czech Republic

²Allied Health Research unit, University of Central Lancashire, UK

Email: tomas.klein@upol.cz

Summary

There has been significant progress in the field of multi-segment foot modelling over the past few decades. However, the ability of the different foot models to detect the same changes in kinematics due to foot orthoses has not been fully explored. This study used SnPM to determine if the same kinematic differences exist in the time series with and without foot orthoses using two previously reported foot models. Foot kinematics of thirty-two participants was recorded using the Oxford foot model and a 6DOF model. The rearfoot to tibial results show both models being in agreement in 86.4% of cases with both models being able to detect changes in 61% of the variables explored. However, the forefoot relative to the rearfoot showed agreement between the models in only about half of the cases, with an opposite effect seen 23% of the time.

Introduction

There has been significant progress in the field of multi-segment foot modelling over the past few decades and enough evidence now exists to support the use of multi segment foot models in clinical populations, however to date there is little evidence on the use of such models to explore changes in kinematics when using foot orthoses within shoes [1]. Although the particular foot models have been used to explore the effect of foot orthoses on foot kinematics [2], the comparison of various foot models' ability to detect this effect remains unknown. Therefore, the aim of this study was to compare the ability of two commonly used foot models, the six-degrees-of-freedom CAST foot model (6DOF) and the Oxford Foot model (OFM), to detect changes in the rearfoot to tibial and forefoot to rearfoot kinematics during the stance phase of gait when using a foot orthosis.

Methods

An eight camera □icon vantage □5 (Oxford Metrics, UK) motion capture system was used to collect three-dimensional kinematic gait data. Participants were fitted with uniform correctly sized rubber-soled shoes and walked at a self-selected speed under two different orthotic conditions □no foot orthosis and foot orthoses with a medial heel bar positioned under the sustentaculum tali. Retroreflective markers for lower limb model and both foot models were placed on the anatomical landmarks and shoes accordingly. A standard 14 mm marker was used instead of posterior calcaneus wand marker for the OFM. Seventeen walking trials were captured for each condition, order of which was randomized with both models applied simultaneously. Kinematic data were processed in □icon Nexus 2.10 and exported to C3D format. Gait events were identified manually based on linear

acceleration, velocity and visual inspection of the heel and toe marker trajectories. □oth the OFM and 6DOF were applied in □usual 3D (C-Motion, USA). Data were normalized to 100% of the stance phase. As the D'Agostino-Pearson K2 test failed to confirm time series data normality, a non-parametric version of vector field statistical analysis technique, statistical non-parametric mapping (SnPM) was used. The observed effects of the medial heel bar were compared between the two models, and the possible outcomes of □ the same effect, no effect for both models, a separate effect of either the 6DOF or OFM, or an opposite effect of the models.

Results and Discussion

Thirty-two healthy participants (16 males) who were all right side dominant with a mean age, body weight and height of 22.9 ± 3.5 years, 67.9 ± 10.4 kg and 173.7 ± 10.3 cm, respectively. The overall results across all planes and phases for rearfoot to tibia show both models being in agreement in 86.4% of the cases and both models being able to detect change over the other in approximately 7% of cases. Despite the different tracking markers and anatomical definition of the segments, which can explain differences in the values obtained from the two models, the ability to detect the same effect of medial heel bar remains high. In the forefoot to rearfoot kinematics agreement between the models was seen in about half of the cases, with the 6DOF being able to detect change over the OFM in 17% of cases, and the OFM being able to detect change over the 6DOF in 9% of cases. However, in almost a quarter of the cases the opposite effect was observed. The greater disagreement between the models in the forefoot to rearfoot kinematics can be explained by the different anatomical definitions of the tarsal-metatarsal segment and the different tracking markers used.

Conclusions

According to our study results, when used to explore the effect of foot orthoses on rearfoot, both models perform in strong agreement. In forefoot the agreement drops to about 50% with 6DOF detecting around twice as much changes over the OFM. However, the study cannot answer the question, which model is correct.

Acknowledgments

This work was supported by the Palacký University Olomouc Internal grant [IGA□FTK□2018□014].

References

- [1] Leardini A et al. (2019). *Gait & Posture*, □9: 50-59.
- [2] Klein T et al. (2021). *Gait & Posture*, 84: 93-101.

Vasja Plešec¹, Gregor Harih¹

¹Laboratory for Intelligent CAD systems, Faculty of Mechanical Engineering, University of Maribor, Slovenia

Email: vasja.plesec@um.si

Summary

Inadequate fit, volume change of the limb and overheating of the limb are still the main problems limiting the use of prostheses. In this study, we compared different types of prosthetic liners using a newly developed generic 2D numerical prosthesis-liner-limb model, thus providing a tool to assess the suitability of each liner objectively. The better insight into the biomechanical behavior of the prosthesis-liner-limb system helps us to develop new materials and shapes suitable for prosthetic liners. The obtained results in terms of contact pressure serve as a comfort criterion - we want the lowest contact pressure over the largest area. On the other hand, we also want maximum stability with minimum relative displacement between components. By analyzing the contact pressure and relative displacement of different liners with the developed model, we compared the liners directly, thus finding the best solution for the given boundary condition.

Introduction

In recent years, total surface bearing (TSB) prostheses in combination with silicone liners have prevailed. The idea of such an implementation is to distribute the contact pressure over as large an area as possible and thus minimize it. The main problems with the use of TSB prostheses are: providing a good fit, the change in volume of the limb, and the increased temperature of the limb due to the low thermal conductivity of silicone liners. All of this can lead to discomfort that can develop into chronic pain and deep tissue injury [1]. With an improved liner-socket system, the duration of using the prosthesis can be extended, and the patient's mobility increased.

There are only a limited number of liners with generic properties that cover all subjects (commercial liners are not custom made for specific patient) [2]. Obtained results of contact pressure, displacements and strains can show us which liners are better in terms of comfort and stability and hence optimize the liner numerically.

Methods

We utilized a previously developed generic axisymmetric 2D numerical model, which significantly reduces computation time, simplifies control over boundary conditions and still provides accurate results.

We used homogenous hyper-elastic material model for soft tissue, and liners [2,3], while a linear-elastic model was used for bone and prosthesis [2,4]. Material models were obtained from previous studies where the models were also validated. We defined three load cases that included all the critical moments during the use of the prosthesis (Figure 1).

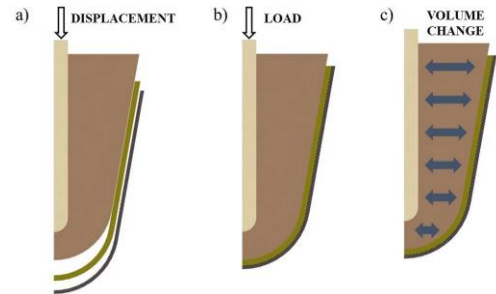


Figure 1: Schematic representation of load cases: a) liner and socket donning; b) applying load; c) change in the soft tissue volume.

Results and Discussion

The results obtained give us an insight into the behaviour inside the socket. The contact pressure at the tissue-liner and the liner-socket interface helps us to assess comfort, as minimizing and distributing it over a larger area protects the residual limb from damage and provides greater comfort.

The incompressibility of the silicone liner provides good overall pressure distribution. On the other hand, such a liner can be uncomfortable when the residual limb changes volume. In terms of adapting to the volume change, a liner with controlled compressibility could be the better option, but we must be careful not to compromise stability.

Conclusions

The developed numerical model allows a relative comparison of different types of prosthetic liners, which serves us as an objective tool in the development of new liners and sockets. The results show that different liner properties are desirable for different load cases. To improve comfort while maintaining the patient's stability, the compressible liners with nonlinear behaviour should be investigated in the future.

Acknowledgments

The authors acknowledge the financial support from the Slovenian Research Agency (research core funding No. P2-0063).

References

- [1] Sankaran et al. (2019). *IEEE 2019*, Proceedings: 77-81
- [2] Cagle et al. (2016). *A dissertation*, University of Washington.
- [3] Kallin et al. (2019). *arXiv preprint arXiv*, 1907.13340.
- [4] Ramalho et al. (2020). *Materials Today*, Proceedings.

Ground reaction forces during walking of people with traumatic bilateral major lower limb amputations.

Brieuc Panhelleux¹, Biranavan Sivapuratharasu¹, Alison H. McGregor¹, Anne K. Silverman²

¹Department of Surgery and Cancer, Imperial College London, London, United Kingdom

²Department of Mechanical Engineering, Colorado School of Mines, Golden, CO, United States

Email: b.panhelleux19@imperial.ac.uk

Summary

People with bilateral transfemoral amputation (TFA) have higher vertical and lower propulsive ground reaction forces (GRFs) during walking than people with bilateral through the knee (TKA) or transtibial amputation (TTA). People with bilateral TKA and TTA have similar GRFs, but people with bilateral TFA and TKA have different GRF peak forces during gait and should be separately considered in future work.

Introduction

Bilateral lower limb amputation (LLA) results in altered gait kinematics and kinetics [1]. While GRFs in people with unilateral amputations are well documented, there are limited data for bilateral amputation at all LLA levels. While less common than unilateral amputation, bilateral amputation is prevalent in blast injury survivors. In addition, TKA and TFA are often grouped together in biomechanical studies of people with amputations, and potential differences between these groups remain unclear. Thus, we evaluated peak GRFs of bilateral TTA, TKA, and TFA and an able-bodied group.

Methods

Ten people with bilateral, traumatic lower-limb amputations and nine able-bodied controls (34yo, 84kg, 182cm, all males) walked at self-selected speed on a level walkway containing two embedded force plates (Kistler Instrumente AG, 1000 Hz). Participants with amputations included five bilateral TFA (34yo, 76kg, 165cm, all males), three bilateral TKA (32yo, 94kg, 178cm, all males) and two bilateral TTA (46yo, 100kg, 187cm, all males). All participants walked across the walkway at least five times with both feet hitting consecutive force plates. Vertical and A/P peak GRFs were normalized by body weight and compared across the different levels of amputation and to the control group. Peak forces and average walking speed were evaluated across groups with an ANOVA ($\alpha=0.05$). When significant main effects were found, pairwise comparisons using a Tukey's HSD test ($\alpha=0.05$) were done.

Results and Discussion

People with bilateral TFA had higher peak vertical and braking but lower propulsive GRFs compared to those with

bilateral TKA and TTA while having a slower walking speed than TTA (Table 1). These results suggest that sagittal plane GRFs of TFA were more vertically directed than A/P directed, supporting body weight. Greater peak vertical GRFs in TFA compared to controls, even when they were walking at a much slower speed, may have implications for long term joint health in this group. Bilateral LLA at all amputation levels lack the function of the ankle plantarflexors, which explains the lower propulsive peak compared to able-bodied controls for people with TFA and TTA. The higher vertical peak GRFs and lower propulsive forces during gait in TFA compared to TKA suggest that TKA should not be grouped with TFA and requires further study of biomechanical outcomes. Further, TKA had similar GRF peak values to TTA, but further study is needed with a greater sample size. GRFs for all levels were consistent with prior studies. Specifically, GRF peak values for bilateral TTA were similar to prior work [1]. Vertical and braking GRF peak values for bilateral TFA are larger than prior results in people with unilateral TFA, but propulsive peak values were similar [2]. Further, while there are limited data about TKA, GRF peak values were similar to the values reported for a single unilateral TKA [3].

Conclusions

These results suggest that bilateral TKA and TFA should not be grouped together for biomechanical studies and that bilateral TKA may be considered an alternative to TFA when TTA is not feasible. TFA had higher vertical peak forces and lower propulsive peak forces than other LLA levels.

Acknowledgments

This work was conducted under the auspices of the Royal British Legion Centre for Blast Injury Studies at Imperial College London. We thank the Royal British Legion for financial support.

References

- Gard SA. (2007) *J Rehabil Res Dev.*, **44**: 491–501.
- Zhang T, et al. (2019) *Gait Posture.*, **71**: 219–226.
- Tang J, et al. (2017) *Med Eng Phys.*, **49**: 131–139.

Table 1: Mean (standard deviation) walking speed, and vertical and A/P GRF peak values in percent body weight and associated statistical results. ^a and ^b Indicate statistically significant pairwise differences from TFA and Control respectively ($p<0.05$).

	TFA (n=5)	TKA (n=3)	TTA (n=2)	Control (n=9)	Main effect
Walking speed (m/s)	0.95 (0.07) ^b	0.96 (0.09)	1.07 (0.12)	1.22 (0.05) ^a	p=0.032
Vertical Peak 1 (%BW)	113.85 (13.39) ^b	95.66 (14.43) ^a	99.67 (6.34) ^a	103.46 (16.62) ^a	p<0.001
Vertical Peak 2 (%BW)	101.45 (8.44)	90.97 (8.37) ^{a,b}	92.49 (10.39) ^{a,b}	102.16 (9.78)	p<0.001
Braking Peak (%BW)	-13.50 (4.32) ^b	-12.04 (3.57) ^{a,b}	-9.23 (4.96) ^a	-14.05 (6.75) ^a	p<0.001
Propulsive Peak (%BW)	9.44 (1.62) ^b	11.25 (2.66) ^a	10.94 (4.88) ^{a,b}	16.50 (7.13) ^a	p<0.001

A Method to Autonomously Monitor the Performance of Rehabilitation Exercises

Asaad Sellmann¹, Désirée Wagner¹, Catherine Disselhorst-Klug¹

¹Department of Rehabilitation and Prevention Engineering, Institute of Applied Medical Engineering, RWTH Aachen University, Aachen, Germany

Summary

Low Back Pain (LBP) patients are facing a higher risk of injury through missing guidance and control in an out-patient environment. IMU sensors were used to detect movements and record accelerations along the back during exercise performance. 30 healthy subjects performed three different exercises: Prone-Rocking, Bird-Dog and Rowing according to two conditions: clinically prescribed exercise (CPE) and mimicking a typical compensatory movement (TCM). The order of these conditions and exercises was randomised.

From the processed IMU signals a set of N parameters was utilized to train a classifier to distinguish CPE from TCM. The method developed was shown to be effective for the exercises investigated. The results showed that the classification achieves an accuracy of up to 98%.

Introduction

Low Back Pain (LBP) is prevalent in western society and a common reason for a medical consultation [1, 2]. The exercises typically prescribed in the rehabilitation of LBP are designed to optimize muscle activation and coordination, reduce pain, and improve patients' quality of life. Unfortunately, 70% of patients do not rigorously perform the prescribed exercises [3]. This reduces the effectiveness of rehabilitation and increases the risk of secondary injury. Thus, methods to monitor the execution of rehabilitation exercises outside of clinical or rehabilitation environments are needed to minimize secondary injury.

Methods

Thirty healthy subjects (15 males/15 females) without a history of back pain participated in this study. The subjects' ages ranged from 18 to 35 years with an average age of 27.4 ± 2.5 years. Three IMU sensors were used to detect movements of the back and to record accelerations. Volunteers were asked to perform three exercises according to two conditions: clinically prescribed exercise (CPE) and mimicking a typical compensatory movement (TCM). The three exercises were Prone-Rocking, Rowing and Bird-Dog, where the latter needed to be performed on each side of the body. In each case a subject executed 3 sets of 6 repetitions

for every exercise. The order of the conditions i.e. CPE and TCM and exercises was randomised.

To minimize any errors introduced through outliers, the data points of six repetitions (set) were averaged per sample point. In this manner pre-processed accelerometer readings from the 3 sensors were used to calculate a series of features based on nine signals (x-, y- and z-axis per sensor). Through feature selection processes a set of N features was selected for each exercise based on their ability to discriminate between CPE and TCM. The best set of features per exercise was used to train a simple binary decision tree to classify exercise performance.

Results and Discussion

The method of feature selection and decision tree training introduced provides a classification accuracy of up to 98.9% for Prone-Rocking using only one feature (**Table 1**). However, it has to be mentioned that the results for Rowing indicate that there might be limitations to the system which may require an adjustment of the sensor set.

Conclusions

By analyzing the main axes of movement in the three selected exercises, it can be concluded, that the method developed can be applied to all exercises that include movements of spine and head with slight adjustments of the sensor positions.

Acknowledgments

We gratefully acknowledge the funding for this work by the *Bundesministerium für Bildung und Forschung*, Germany.

References

- [1] J.K. Freburger et al. (2009). The rising prevalence of chronic low back pain, *Arch Intern Med*, **169**: 251-258.
- [2] G.B. Andersson (1999). Epidemiological features of chronic low-back pain, *Lancet*, **354** 581-585.
- [3] N.A. Beinart et al. (2013). Individual and intervention-related factors associated with adherence to home exercise in chronic low back pain: a systematic review, *Spine J*, **13** 1940-1950.

Table 1: Best performing features per exercise and the resulting prediction accuracy when used for training a binary classification tree. X, Y and Z indicate the direction of linear acceleration in the IMU sensor which is denoted by numbers 1, 2 and 3.

Exercise	Bird-Dog both sides	Prone-Rocking	Rowing
Features	RMS Euler Angles ref. Gravity 1, Variance Z3	Variance Y2	RMSZ3, max α 1,2, KurtosisY2, Variance X3
Accuracy	98.3%	98.9%	82.8%

Biophysical effects of steering on asynchronous and synchronous submaximal handcycle ergometry in able-bodied men

Cassandra Kraaijenbrink^{1,2}, Riemer J.K. Vegter^{2,3}, Nils Ostertag¹, Luc Janssens^{4,5}, Yves Vanlandewijck⁵, Lucas H.V. van der Woude^{2,3,6}, Heiko Wagner¹

¹Department of Movement Science, Institute for Sport and Exercise Sciences, University of Münster, Münster, Germany; ²Centre for Human Movement Sciences, University Medical Centre Groningen, University of Groningen, Groningen, the Netherlands; ³Peter Harrison Centre for Disability Sport, School of Sport, Exercise and Health, Loughborough University, Loughborough, United Kingdom; ⁴Electrical Engineering (ESAT) TC, Campus Group T Leuven, KULeuven, Leuven, Belgium; ⁵Department of Rehabilitation Sciences, Faculty of Movement and Rehabilitation Sciences, KULeuven, Leuven, Belgium; ⁶Centre for Rehabilitation, University Medical Centre Groningen, University of Groningen, Groningen, the Netherlands
Email: kraaijen@uni-muenster.de

Summary

Outdoor, real-life handcycling requires both propulsion and steering. On the other hand, during indoor testing or training, a fixed ergometer is used, which has no steering requirements. The effects of steering on the metabolic strain were investigated for both asynchronous and synchronous straightforward handcycling. Handcycling technique was studied by means of the propulsion and steering torque as a cause for a change in metabolic strain. For synchronous handcycling, metabolic strain or handcycling technique did not change, regardless of the steering requirements. For asynchronous handcycling, however, an increased metabolic strain is found when steering is required. In order to cancel out unwanted steering movements, participants need to change their handcycling technique, as could be shown by the propulsion and steering torque. For testing or training handcyclists, who have a synchronous set-up in real-life, a synchronous ergometer set-up is advised.

Introduction

During outdoor handcycling the front wheel axis is to rotate freely around the steer axis. This results in a combined requirement of propulsion and steering. The handcycle cranks are mostly mounted synchronously (parallel). Arm cycle ergometers, on the other hand, are often fixed to the wall or floor and cranks are mostly mounted asynchronously (anti-phase). The aim of the study is to evaluate the biophysical effects of combining propulsion and steering requirements in both asynchronous and synchronous submaximal handcycle ergometry.

Methods

Sixteen able-bodied male novices volunteered in this experiment. The set-up consisted of an instrumented handcycle ergometer that allows 'natural' steering, which could be fixed at the steering axis [1]. Four submaximal steady-state exercise conditions were evaluated: asynchronous versus synchronous and fixed versus steering. All participants practiced 3x4 minutes in each of the four conditions in a counterbalanced order, with 2 minutes rest in between. Finally, they handcycled (4 minutes) in each of the four conditions, with 10 minutes rest in between, while metabolic outcomes, ergometer kinematics and kinetics were recorded using bilateral instrumented handlebars with 3D

force sensors and optical encoders. Before statistical analyses, the data of one participant was removed, as this data was found to be recorded wrongly.

Results and Discussion

Steering requirements have an effect on several metabolic outcomes, including mechanical efficiency ($P = .003$, $r = -.55$), due to an increase in strain during asynchronous handcycling. In the Asyn Fixed condition, the force produced at the handlebars causes a peak propulsion torque simultaneously with a peak steering torque (Figure 1). As the steer axis is fixed, no steering movements are created. To avoid the high peaks in steering torque, the propulsion torque pattern is different in the Asyn Steer condition. Hence, participants have another handcycling technique whenever steering is required. In the synchronous handcycling conditions, almost no steering torque is produced, so that the same technique can be used in the fixed and steer condition.

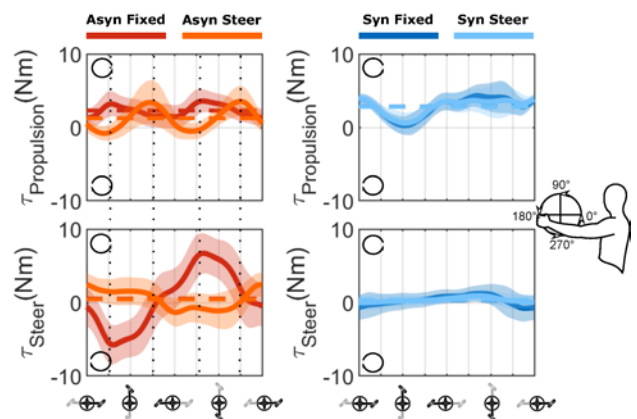


Figure 1: Bilateral propulsion and steering torque profile (mean cycle, $n=570$ (15 participants*38 cycles per participant)).

Conclusions

To test or train handcyclists, who have a synchronous crank mode in their daily handcycle, a synchronous crank set-up of the ergometer is advised, as exercise performance in terms of metabolic strain and torque production is independent of steering requirements in that mode.

References

- [1] Verellen J et al. (2012). *Sport Technol.*, 5: 65-73

Implications of a familiarization phase with a robot-assisted rehabilitation system on motor performance during simulated daily activities

Sybele E. Williams¹, Catherine Disselhorst-Klug¹

¹Department of Rehabilitation and Prevention Engineering, Institute of Applied Medical Engineering – Helmholtz Institute, RWTH Aachen University, Aachen, Germany.
Email: williams@ame.rwth-aachen.de

Summary

The aim of this initial study was to test whether a familiarization phase with an end-effector robot-assisted rehabilitation system could ensure that patients performed more physiological movements during rehabilitation. 2 simulated daily activities, involving the upper limb were investigated under 2 conditions: (i) unconstrained arm movement and (ii) with a passive robot-arm coupled to the test subject's forearm. 23 healthy subjects were assessed during 2 test sessions, at least a week apart. The familiarization phase was included only in the first test session. Analysis of kinematic data recorded, showed differences in movement performance under both conditions. The familiarization phase did not reduce differences within a test session. However, a training effect seemed to reduce performance differences at the second test session.

Introduction

End-effector robotic rehabilitation systems support early intervention using high intensity, task-oriented exercises. It was reported that healthy subjects showed increased muscular activation while performing robot-assisted movement tests [1]. This has implications for the use of robot-assisted rehabilitation systems since poor motor learning may negatively affect rehabilitation goals. This study investigated the introduction of a familiarization phase to an end-effector robot-assisted rehabilitation system during selected movement tests in order to assess the effect of such familiarization and changes in movement performance..

Methods

23 healthy subjects (10 males, 13 females, avg. age: 25 ± 2.70 yrs.) were measured during two test sessions, at least 1 week apart. The measurement protocol had 3 phases: (i) simulated daily activities with unconstrained arm, (ii) a familiarization phase with robot, and (iii) simulated daily activities with robot. The 'robot' condition infers that the subject's forearm is coupled to the passive robotic arm. Two versions of the test protocol were used, a complete protocol with all 3 phases and a second, which omitted phase (ii). During testing, each subject sat in a standardized position before the robotic arm LBR Med (KUKA), which was mounted on a special table. Data was recorded using a 3D motion analysis system (Vicon). Two movement tasks were investigated Cup to Box and Cup to Mouth (CBCM) and Sorting Elements (SE). The familiarization phase involved a 'reach-to-touch' test. Joint angles in the elbow and shoulder were determined using a suitable biomechanical model [2]. Three performance indices (PI) were used to compare

movements: PI1: duration, PI2: velocity profile symmetry, and PI3: range of motion (ROM).

Results and Discussion

Results are presented for the sequence Cup to Mouth of the movement task CBCM. This comprised 2 main movement sequences: S1 - lift cup up to mouth from table, S2 – return cup to table.

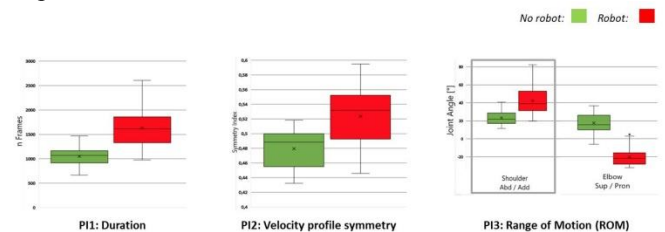


Figure 1: Comparison of performance indices for 2 conditions (robot/no robot).

The duration of the movement (PI1) was significantly longer in the robot condition ($F(1)=84,942$, $p<0.01$). This could be caused by the mass inertia and braking effect of the robotic arm. Acceleration time during S1 was slightly longer than the deceleration during S2 in the robot condition. The difference in elbow supination/ pronation was significant ($F(1)=188,79$, $p<0.01$). Greater abduction in the shoulder joint was also significant in the condition 'robot' ($F(1)=62,438$, $p<0.01$). In the 'robot' condition the ROM was negative, which suggests that subjects performed a pronation while lifting the cup.

Conclusions

While the introduction of a familiarization phase did not reduce differences in movement performance within a test session, differences were smaller at the second test session. This may be due to a training effect of the initial test session.

Acknowledgments

Funding was provided by i2-CoRT (Innovation and Implementation acceleration for Complex Rehabilitation Technology), Interreg Euregio Meuse-Rhine program.

References

- [1] Becker, S. et al. (2019) Comparison of muscular activity and movement performance in robot-assisted and freely performed exercises. *IEEE Trans Neural Syst Rehabil Eng.* **27**: 43-50.
- [2] Williams, S. et al. (2006) An upper body model for the kinematical analysis of the joint chain of the human arm. *J Biomech.* **39**: 2419-29.

F-A-I-T-H-kids method: A pilot evaluation of the clinical efficiency

Noemi Bochsler¹, Adina Meyer¹, Lukas Stammeler², Beat Göpfert³

¹Health Division, Bern University of Applied Sciences, Bern, Switzerland

²BZG, Bildungszentrum Gesundheit Basel-Stadt, Münchenstein; Switzerland

³Department Biomedical Engineering, University of Basel & University Children's Hospital Basel; Switzerland

Email: noemi.bochsler@bluewin.ch, adinameyer@livenet.ch

Summary and Introduction

From 2012, the program called “functional analysis and individual training for children with muscular hypotonia” (F-A-I-T-H-kids) has been delivered by the Swiss physiotherapist Jens Hentschel in an interdisciplinary cooperation with speech and myofunctional therapists [1]. Children affected by muscular hypotonia have often been sent from speech or myofunctional therapists to physiotherapy. Muscular hypotonia is usually described as a symptom of underlying neurological diseases, but not yet as an independent and classified pathology. In cases where no cause of a hypotonia can be detected and the etiology remain unclear; the authors of this paper coined the term «Constitutional Muscular Hypotonia». The aim of this study is to examine the clinical efficacy of the F-A-I-T-H-kids method with children diagnosed of constitutional muscular hypotonia. Furthermore, the authors intend to call attention for this issue as well as the interdisciplinary correlation.

Methods

- P:** Children with constitutional muscular hypotonia and myofunctional deficits
- I:** 18 physiotherapy units of 30 minutes within the F-A-I-T-H-kids method supplied by weekly home training
- C:** Every child represents its own control object, no comparison between the participants
- O:** Parameters for symmetry and trunk force such as y-balance test, plank test and trunk-symmetry test according to Hentschel, myofunctional tests such as palatogram and spring scale test, health questionnaire, adherence of home training

Study design: Prospective quality control trial with surveys before and after the interventional time, three probands have been tested

Data evaluation: Due to the small number of participants the results have not been statistical evaluated

Ethics: This study has been registered by Business Administration System for Ethics Committees (BASEC), it has not been defined as ethically obligated

Results and Discussion

All the participants showed a statistical improvement in the myofunctional tests. A few of them were detected as clinically relevant. In the Y-balance test, only one participant achieved improvement, though not clinically relevant. In the trunk-symmetry test according to Hentschel, all participants improved considerably. The result of the plank test showed a

clinically unimportant improvement of two participants and a slight worsening of the third.

Due to the Covid-19 pandemic, the authors were only able to recruit five participants for the clinical trial. Out of this group, two participants did not complete the entire intervention period. The small number of participants as well as the partially inconsistent results measured by the authors hinder an accurate answer to the scientific question. In general, a positive trend for the efficacy of the F-A-I-T-H-kids method can be shown. Resulting from these, only a few minimal clinical important differences (MCID) were achieved. The interpretation of the results was difficult due to the lack of evidence for quality criteria in myofunctional tests. The chosen metrical assessments have only been examined fragmented in the sighted literature. Therefore, the authors created the described trunk-symmetry test according to Hentschel. This test shows potential in its further development of objectivity and accuracy.

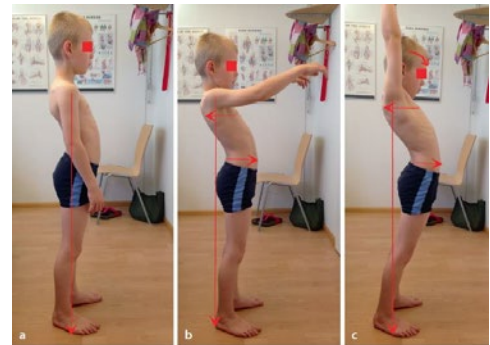


Figure 1: A boy with constitutional muscular hypotonia showing its typical pattern during movement of the arms straight in front of him. a) Hanging arms, the perpendicular goes through the middle of the feet; b) Arms in 100 degree of shoulder flexion, the perpendicular through the shoulder raises behind the heels c) Arms in maximal shoulder flexion, a maximal ventral translation of the pelvis as well as a cervical spine flexion can be observed [1].

Conclusions

There is a wide variance according the results of this study, which are partially contradictory and can be traced back to the small sample size. Although the results show a positive tendency, the authors cannot make a definitive conclusion about the efficacy of the F-A-I-T-H-kids method. Therefore, the authors recommend the verification of the effectiveness of the F-A-I-T-H-kids method in further studies as well as the evaluation of the applied quality criteria.

References

- [1] Codoni, S., Spirgi-Gantert, I., & Jackowski, J.A. von (Hrsg.). (2019). *Funktionsorientierte Logopädie: Der Einfluss von Haltung und Bewegung auf Schlucken, Sprechen und Sprache*. Springer

Impact of foot strike pattern on ankle plantar flexor muscle function during running at different speeds

K. Balint¹, Sebestyén K¹, Csala D¹, Pólinkó G.², Petridis L.², Tihanyi J.¹

¹University of Physical Education, Department of Kinesiology, Budapest, Hungary

² University of Physical Education, Research Center for Sport Physiology, Budapest, Hungary

Email: k.balint828@gmail.com

Summary

In recent years forefoot strike running style has been idolized as a superior running technique since most of the elite east African distance runners with world class performance use it. However, most of the elite marathon runners use rearfoot strike [1]. Therefore, we investigated if there is any difference in muscle function between fore and rearfoot strike running. In this study we demonstrate that muscle activation level is unaffected by the foot strike style in competitive Caucasian runners.

Introduction

Forefoot strike and rear foot strike pattern has a distinctive kinematic difference regarding the degree of ankle and knee joint rotation [2] which can affect the muscle-tendon interaction [3]. We think that the higher knee rotation during rearfoot strike compared to forefoot running can decrease the efficiency of the gastrocnemii muscles [3], but soleus muscle can compensate it with higher activation level. Therefore, the aim of this study was to investigate the difference within the ankle plantar flexor muscle function/activation between forefoot and rearfoot strike running during different running speeds.

Methods

Fourteen male and female competitive distance runners volunteered for this study. The participants ran on a motorized treadmill at three running speeds: 12, 14 and 16 km⁻¹ with rearfoot strike and with forefoot strike pattern. During running we measured lower leg kinematics and the electromyographical activity (EMG) of ankle plantar flexor muscles simultaneously. In the case of medial gastrocnemius, we mounted electrodes on the proximal, middle and distal region of the muscle. To test statistically the difference between joint angular displacement and EMG amplitudes we used SPM analysis in Matlab.

Results and Discussion

As expected, we found that there is a statistical difference between foot strikes in ankle joint rotation during early stance phase. In opposed to previous findings we did not detect relevant difference in knee joint rotation between rear and forefoot strike running at any speed. We expected to detect significant difference in EMG activity of the proximal region of the medial gastrocnemius due to the assumed difference in

knee joint rotation. However, there was no difference in knee joint rotation and as a consequence we did not find statistical difference in EMG activity (Figure 1.) of the investigated muscles between different foot strike patterns irrespectively of running speeds. The difference in initial foot strike ankle angle between rear and forefoot strike also suggests an increased muscle-tendon unit lengthening during forefoot strike running, and also a different Achilles tendon moment arm length, since the moment arm length is angle dependent [4].

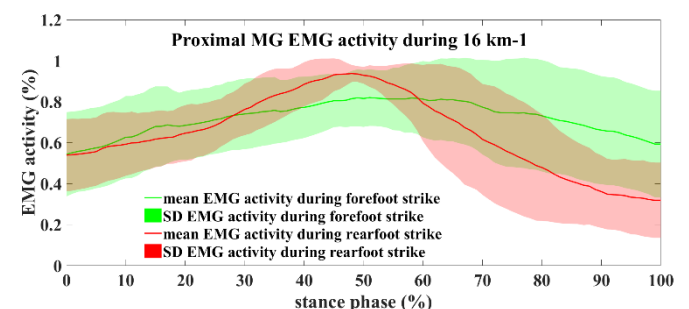


Figure 1: Difference in EMG activity of the medial gastrocnemius proximal region during forefoot and rearfoot strike running at 16 km⁻¹ speed.

Therefore, it can be assumed that a longer Achilles tendon moment arm at initial foot strike during forefoot strike running can result in similar EMG activity to that of rearfoot strike running. We did not measure the resting or dynamic length of Achilles tendon moment arm length therefore this assumption needs to be investigated in future studies.

Conclusions

In summary we did not find any difference in EMG activity of the plantar flexor muscles between forefoot strike and rearfoot strike running in opposed to previous reports and despite of the difference in ankle joint rotation between the two conditions. We can assume that for competitive distance runners changing the foot strike pattern has not associated with short term beneficial effects on the neuromuscular activation level.

References

- [1] Novacheck T. (1998). *Gait and posture*, 11: 77-95.
- [2] Hanley et al. (2019). *J. Biomech*, 91: 54-60
- [3] Wong et al. (2020). *Sci Rep*, 10: 5872
- [4] Deforth et al. (2019). *Foot*, 38: 91:94

Ben Sauer¹, Andrew Greenhalgh¹, Bettina Karsten², Mark Burnley³, Daniel Muniz-Pumares¹

¹ School of Life and Medical Sciences, University of Hertfordshire, Hatfield, United Kingdom

² European University of Applied Science (EUFH), Berlin, Germany

³ Endurance Research Group, School of Sport and Exercise Sciences, University of Kent, Chatham Maritime, United Kingdom
Email: b.hunter3@herts.ac.uk

Summary

We investigated whether local dynamic stability (LDS) is affected by the intensity domain in which running is performed. Ten trained male runners completed four running trials to task failure at speeds below (95%), equal to (100%), and above (105 and 115%) critical velocity (CV). The local dynamic stability (LDS) of the sacral marker was calculated using the Lyapunov exponent (LyE). Our results showed LDS during running reduced throughout running trials performed in the severe intensity domain. Alterations to sacral dynamics suggest that peripheral fatigue mechanisms may be predominantly responsible for changes in LDS.

Introduction

Gait stability can be quantified by measures of LDS quantified using LyE [1]. The LyE computes the ability of the motor system to attenuate small perturbations and can be affected by mechanical and sensory inputs [2]. Further to mechanical and sensory mechanisms, metabolites such as H⁺ and lactate are thought to affect gait stability, exerting inhibitory effects on α -motoneurons by activating fatigue-sensitive muscle afferents [3].

The critical velocity (CV) demarks the heavy and severe intensity exercise domains. Above the CV, the severe intensity domain is characterised by an inexorable rise of metabolites including lactate and H⁺ [4]. Below CV, in the heavy intensity domain, a metabolic steady state can be maintained. The influence of exercise intensity domains on LDS is poorly understood. Therefore, the purpose of this study was to examine changes to LDS in the heavy and severe intensity exercise domains.

Methods

Ten trained males (age: 29.3 ± 10.1 years; mass: 72.1 ± 9.6 kg) provided written informed consent and completed the study. Four constant velocity runs to task failure were performed at velocities corresponding to 95%, 100%, 105%, and 115% of the estimated CV (CV₉₅, CV₁₀₀, CV₁₀₅, and CV₁₁₅) in a randomised order. Pulmonary gas exchange was measured breath-by-breath using a gas analyser (MetaLyzer 3, Cortex Biophysik, Leipzig, Germany). Kinematics of markers placed on the sacrum and right second metatarsal head were captured using a 14-camera high speed motion capture system sampling at 200 Hz (Motion Analysis Corp., Santa Rosa, CA). The sacral marker was used to approximate COM dynamics. Heel strikes of 80 consecutive strides were identified immediately after the initial 15 strides and prior to the final 5 strides in each trial. The sacrum marker velocity in the frontal, sagittal, and transverse planes of 80 strides was time-normalised to 8000 data points, corresponding to 100

data points within each stride. A time-delay of 10 was used based on the Average Mutual Information algorithm and a dimensionality of four was estimated using False Nearest Neighbour algorithm. Local dynamic stability of the sacral marker was assessed using the LyE estimation using the method defined by Rosenstein et al. [5]. Low values of LyE indicate greater stability and vice versa.

A one-way ANOVA was performed to test the effects of velocity on time to task failure (T_{lim}), end pulmonary $\dot{V}O_2$, blood [La] responses and rate of change in LyE ($\Delta LyE/\Delta time$) in the mediolateral (LyE_{ML}), anteroposterior (LyE_{AP}), and vertical (LyE_V) directions.

Results and Discussion

There was a significant effect of velocity on T_{lim}, blood [La], and end pulmonary $\dot{V}O_2$ ($p < 0.001$, Table 1). One-way ANOVA revealed the rate of increase of LyE_{ML} in trials performed at CV₁₁₅ was greater than in trials performed at CV₁₀₀ ($p < 0.001$) and CV₉₅ ($p < 0.001$, Figure 1).

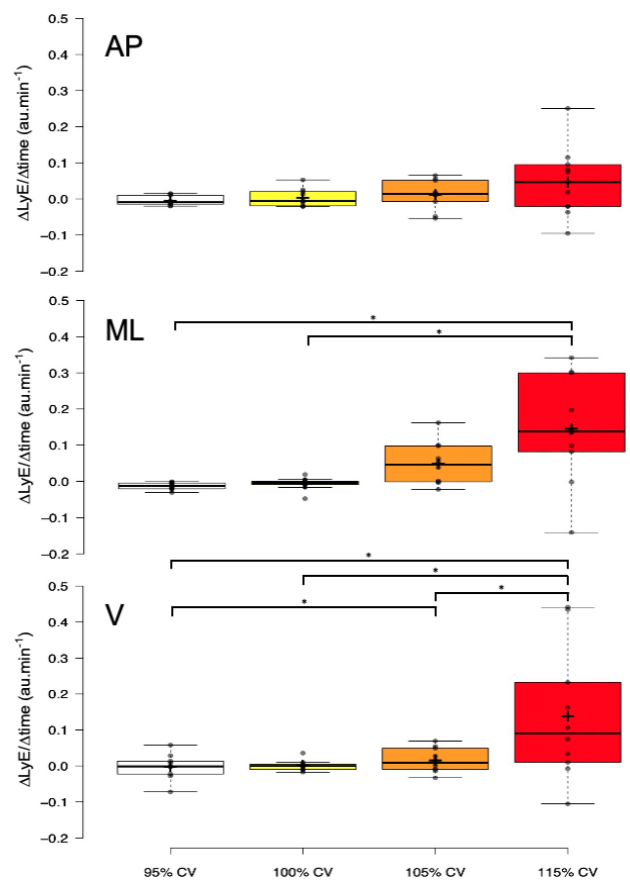


Figure 1: Changes to LyE during trials performed below (95% CV), at (100% CV), and above (105% CV and 115% CV) critical velocity. Asterisks denote sig. dif. ($p < 0.05$)

Similarly, greater rate of increases in LyE_{\square} were evident at $C_{\square 115}$ compared to all other conditions ($p \square 0.05$). Significantly greater rate of change in LyE_{\square} was found during trials performed at $C_{\square 105}$ when compared to $C_{\square 95}$ ($p = 0.039$).

Increased rates of LyE change were only demonstrated above CV, suggesting that stability is affected by metabolic rate. Exercise above the CV is associated greater levels of peripheral fatigue with a precipitous flux of metabolites and depletion of high-energy phosphates, and typically terminated when these reach a critical value [3]. It has been postulated that compromised stability after exercise is due to metabolites associated with exercise above CV, such as H^+ ions and lactate [2]. However, inconsistent rates of change in LDS_{ML} at the end of trials in $C_{\square 105}$ when compared to $C_{\square 115}$ suggest that the metabolic environment is one variable of potentially many that affect LDS during running.

It is possible that during the current study, diminished LDS was evident due to limited degrees of freedom permitted by treadmill running. This may have limited the adaptability of running velocity and movement patterns when compared to overground running. Moreover, we cannot be entirely sure of

the levels of peripheral and central fatigue at task failure. However, given the low SEE of C_{\square} estimates and pulmonary responses in the current study, and the noted physiological responses in the severe intensity domain, it is reasonable to assume task failure coincided with considerable peripheral fatigue.

Conclusions

Local dynamic stability of the sacral marker in ML and \square directions during running reduced at a greater rate in the severe intensity domain when compared to running at or below C_{\square} . These findings suggest that peripheral fatigue mechanisms may be predominantly responsible for changes in LDS of the centre of mass during treadmill running.

References

- [1] Mehdizadeh (2018). *Gait Posture*, **0**: 241-250.
- [2] Peterka (2002). *J. Neurophysiol*, **88**: 1097-1118.
- [3] Paillard (2012). *Neurosci Biobehav Rev*, **3**: 162-176.
- [4] Poole et al. (2016). *Sports Med Exerc Sci*, **48**: 2320-2334.
- [5] Rosenstein et al. (2018). *Phys. D.*, **5**: 117-134.

Table 1: Trial parameters, pulmonary $\dot{V}O_2$, and blood [La] responses during trials performed below (95% CV), at (100% CV), and above (105% CV and 115% CV) critical velocity

	95% CV	100% CV	105% CV	115% CV
Velocity ($m \cdot s^{-1}$)	3.71 ± 0.38	3.94 ± 0.42	4.21 ± 0.42	4.64 ± 0.49
T_{lim} (min)	$20.00 \pm 0.00^{a,d,f}$	$16.68 \pm 4.41^{b,e,f}$	$8.03 \pm 2.36^{c,d,e}$	$3.27 \pm 0.67^{a,b,c}$
$\dot{V}O_2$ at T_{lim} ($L \cdot min^{-1}$)	$3.27 \pm 0.30^{a,b}$	3.40 ± 0.35^b	3.53 ± 0.39^a	3.37 ± 0.40
B[La] ($mmol \cdot L^{-1}$)	$4.45 \pm 1.38^{a,c,e}$	$7.25 \pm 1.84^{b,d,e}$	$9.03 \pm 1.98^{c,d}$	$9.48 \pm 1.52^{a,b}$

Values are expressed as Mean \pm SD. T_{lim} , time to task failure; HR, heart rate. Mean values in the same row sharing the same superscript letters are significantly different from each other $P < 0.05$.

The relationship between running speed and footfall sounds during overground running

Peter Dam¹, Cristina Pircoveanu², Anderson Souza Oliveira²

¹ Department of Health Science and Technology, Aalborg University, Aalborg, Denmark

² Department of Materials and Production, Aalborg University, Aalborg, Denmark

Email: oliveira@mp.aau.dk

Summary

The sound of footfalls has been suggested to be an effective measure of running impact properties. Therefore, present study aimed to investigate the relationship between running speed (RS) and footfall sound during overground running. Thirty-one recreational runners performed 3 x 3-minutes of overground running. Ground reaction force, RS, and sound of footfalls were assessed. The impact peak force, vertical loading rate, impact peak sound and late peak sound all increased as a function of RS. A correlation analysis showed that the sound properties are superior in describing RS than force parameters. The use of footfall sound showed to be an effective method of investigating running impact properties.

Introduction

Running induces remarkable lower limbs loading, which has been quantified using peak vertical impact force (IPF) and vertical loading rate (LR) [1]. There is a close relationship between RS and vertical force parameters [2], and new evidence has proposed the use of footfall sounds to investigate running impact properties using single [3] and multi-directional recordings [4]. Since sounds of footfalls during running may be an alternative to investigate running impact properties, the aim of present study was to investigate the relationship between RS, vertical ground reaction force and sound properties of running footfalls recorded using multiple microphones and ground reaction forces.

Method

Thirty-one recreational runners performed 3 x 3-minutes overground running on a 20m obround running track containing a ground reaction force platform embedded at the middle of one of the straights. Participants were asked to run at different RS, varying from 2 m/s to 6 m/s. Vertical ground reaction force, head kinematics and surround sound waves from four microphones located equidistantly around the force platform [4] were recorded throughout the protocol. The IPF, LR, and peak impact sound (averaged across the four microphones) within the first 30% stance (SP) were calculated for each step on the force platform. Subsequently, RS was computed from head kinematics and steps were divided into four speed categories: ≤ 2.5, 2.5-3, 3-3.5 and >3.5 m/s. A total of 1005 steps were analyzed (≤ 2.5 m/s: 229 steps, 2.5-3 m/s: 296 steps, 3-3.5 m/s: 204, >3 m/s: 286 steps). Non-parametric Kruskal-Wallis tests with Bonferroni correction were used to investigate the effect of RS on the dependent variables. Moreover, Pearson correlations were computed between RS vs IPF, LR and SP. For all tests, the significance level was set to $p \leq 0.05$.

Results and Discussion

The IPF, LR and SP values, all increased as a function of RS, statistically different from each other ($p < 0.01$). Although this was expected for the force parameters [2],

our study revealed that sounds of footfalls are also sensitive in revealing speed-related changes in running impact properties. Moreover, weak, and moderate correlations were present between RS vs IPF ($r = 0.36, p < 0.01$) and RS vs LR ($r = 0.47, p < 0.01$). Interestingly, SP demonstrated the greatest (moderate) correlation with RS ($r = 0.55, p < 0.01$, Figure 1). These results suggest that early peak sounds captured from multiple directions were more related to RS than traditional force parameters (IPF and LR). A previous study using similar sound recording technique has demonstrated the relationship between the sound and force parameters are highly affected by the number and location of the microphones [4]. Therefore, multi-directional sound properties may be an alternative to investigate running impact properties.

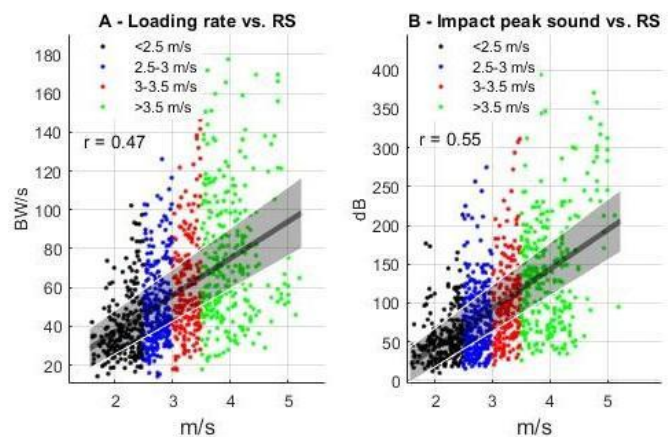


Figure 1: Depicts the correlations between Loading rate (A) and the impact peak sound (B) with each speed category represented by a color and the Pearson correlation coefficient (r).

Conclusion

The use of multi-directional sound recordings demonstrated sensitivity to capture speed-related changes in running footfall sounds. Moreover, the early peak sounds of running stance presented greater relation to RS, reiterating the relevance of sound recordings to investigate running impact properties. Future research should aim to use multi-directional sound capturing from microphones attached to the shoe. This could potentially provide a robust and relevant method to investigate running impact properties in realistic conditions.

Acknowledgements

The work was supported by Kulturministeriet [FPK.2018-0048].

References

- [1] Milner et al. (2006). *Med. Sci Sports Exerc.* **38**:323–328.
- [2] Reine et al. (2014). *MSSE*, **4**:1595–1603.
- [3] Phan et al. (2017). *J Sports Sci*, **35**:1636-1642.
- [4] Pircoveanu et al. (2020). *J Sports Sci*, **39**:267-274.

Music-based biofeedback induced running gait adaptations for lower impact running

Rud Derie¹, Pieter van den Berghe¹, Joeri Gerlo¹, Marc Leman², Dirk De Clercq¹, Geerle Segers¹

¹Department of Movement and Sports Sciences, Ghent University, Ghent, Belgium

²IPEM, Department of Arts, Music and Theatre Sciences, Ghent University, Ghent, Belgium

Equal contribution, Email: rud.derie@ugent.be - pieter.vandenbergh@ugent.be

Summary

The present study provides novel insights in the running style adaptations employed by high impact runners who completed a retraining outside the laboratory. Real-time music-based feedback on tibial shock was provided in a randomized controlled trial design. Gait analysis was conducted pre and post retraining. Runners allocated to the biofeedback condition succeeded in lowering their impact characteristics by 27-29% using two distinct strategies. (1) A more pronounced rearfoot strike or (2) switching to a non-rearfoot strike. This indicates that, at least two strategies are apparent to reduce tibial shock during over-ground running.

Introduction

Real-time biofeedback on impact during gait-retraining proved to play a role in reducing running injuries, and altering biomechanical variables associated with it [1-3]. A full understanding of how runners achieve their goal directed over-ground gait-retraining is limited. Therefore we aimed to describe kinematic changes of high impact runners following a lower impact running retraining program.

Methods

Twenty high impact runners completed in a gait-retraining study consisting of six twenty-minute over-ground running sessions. Participants were assigned to a biofeedback (n=10) or a music-only (n=10) placebo condition. The biofeedback consisted of an amount of pink noise, distorting the tempo-synchronized music, based on the momentary tibial shock (the max positive acceleration (g) of the tibia during the first 50ms of stance) [3]. We asked subjects to run with music as pure as possible. Gait analysis took place over-ground in a lab pre and post intervention. Subjects ran at $2.9 \pm 0.2 \text{ m}\cdot\text{s}^{-1}$ across a 30-m instrumented runway. The refined strike index of five footfalls was determined [4]. We also used vertical instantaneous loading rate of the vertical ground reaction force ($\text{N}\cdot\text{s}^{-1}$) as a lab-based measure of impact. Statistics were done using a linear mixed-model in SPSS.

Results and Discussion

The experimental group successfully reduced both the tibial shock ($\Delta\bar{x}=-27\%$) and vertical instantaneous loading rate ($\Delta\bar{x}=-29\%$) (Table 1), similar to a previous proof of concept study [3]. There were inter-individual strategies to achieve lower impact running. Two subjects opted for a non-rearfoot

strike pattern, while the remaining eight subjects were able to lower their impact while using a more pronounced rearfoot strike (Figure 1). Both strategies were earlier cross-sectionally characterized by a lower impact loading [4].

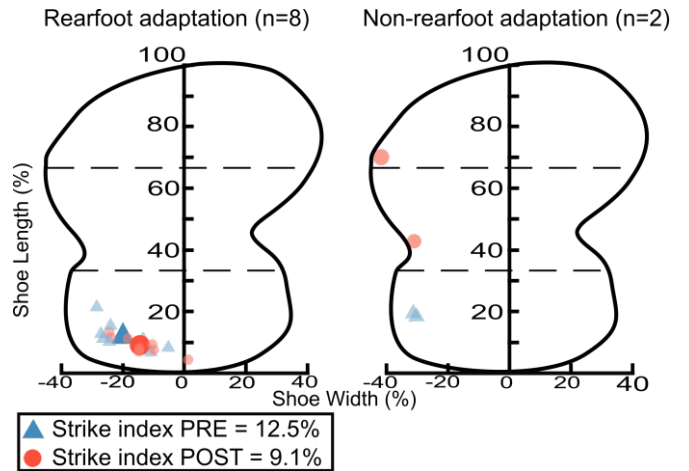


Figure 1: Initial points of contact on the shoe sole changed from pre (blue squares) to post (red dots) retraining. Individual and mean data are represented by respectively tiny and big markers. Mean data is shown for the rearfoot adaptation (left). The strike index of the music-only group remained unchanged (12%).

Conclusions

An overground gait-retraining program with musical biofeedback on tibial shock successfully reduced impact loading. distinct adaptations were present as impact reduction was achieved by adopting either a non-rearfoot strike or a more pronounced rearfoot strike. Further research should seek if other running gait adaptations also contribute to the realized impact reduction.

Acknowledgments

FWO (FWO.3F0.2015.0048.01) | EU - Interreg (Nano4Sports) | Ugent Industrial Research Fund (IOF)

References

- [1] Chan et al. (2018). *Am J. Sports Med.*, 388-395.
- [2] Clansey et al. (2014). *MSSE.*, 5: 973-981.
- [3] van den Berghe et al. (2021). *Sci Rep*, accepted.
- [4] reine et al. (2016). *JOSS.*, 15: 1556-1564.

Table 1: Tibial shock (TS) and vertical instantaneous loading rate (VILR) from pre to post gait retraining - Mean (SD)

	Group	PRE	POST	p-val		PRE	POST	p-val
TS (g)	Biofeedback	8.10 (2.34)	5.92 (1.81)	0.011	VILR ($\text{N}\cdot\text{s}^{-1}$)	101.08 (29.9)	72.57 (24.5)	0.006
	Music-only	7.23 (2.17)	7.59 (2.66)			81.73 (22.01)	84.18 (24.48)	

Running power estimation using body-worn inertial sensors: in-lab validation and sensor location comparison

Salil Apte¹, Mathieu Falbriard¹, Frederic Meyer², Benoit Mariani³, Gregoire P. Millet², Kamiar Aminian¹

¹Laboratory of Movement Analysis and Measurement, EPFL, Lausanne, Switzerland

²Institute of Sport Science, University of Lausanne, Lausanne, Switzerland

³Gait Up SA, EPFL Innovation Park, Bâtiment C, 1015 Lausanne, Switzerland

Email: salil.apte@epfl.ch

Summary (max. 150 words)

This study aimed to estimate mechanical power (MP) during level and inclined running. We equipped 34 participants with inertial measurement units (IMUs) on the feet, shank, sacrum, wrist, and head, to compare the accuracy of MP power estimated from each location. Participants ran on an instrumented treadmill, at speeds ranging from 8–14 km/h, and slopes from -20 – +20%. To estimate stepwise MP, we created two machine-learning models using 15 features based on gait temporal parameters, running speed, body mass, and statistical measures of IMU signals. Mechanical power, determined from the antero-posterior ground reaction forces, was used as reference for the leave-one-out cross-validation method. The lowest RMSE was $11.1 \pm 4.8\%$ (shank) and $20.9 \pm 14.2\%$ (head) for flat and inclined running respectively. These results show the promise of IMUs to estimate MP, even with the use of a single sensor.

Introduction

Feedback of running mechanical power (MP) can be a promising tool for training and pacing strategies, but commercially available running power meters are not accurate enough [1]. Current analytical models focus either on the characterization of overall race performance [2] or on the power requirement while running on flat terrain [3]. An approach based on wearable inertial measurement units (IMUs) has shown promise, but requires data from 15 body segments [4]. Neither of these approaches are suitable for accurate real-time feedback of MP. To address this, we developed and validated two machine-learning (ML) models, for flat and inclined running, to estimate stepwise MP using one IMU on either feet, shank, sacrum, wrist, or head.

Methods

We equipped 34 healthy participants with IMUs on the above-mentioned locations. The participants ran on an instrumented treadmill, at combinations of speeds ranging from 8–14 km/h, and slopes from -20 – +20%. Figure 1 presents the overall setup. For the ML model, we used data from 10 participants for feature selection and from 24 participants for training and testing using leave-one-subject-out cross-validation. We selected 15 features based on gait temporal parameters [5], running speed, body mass, and statistical measures of the filtered IMU signals to develop the model. The data was balanced using random oversampling [6] and the input features were scaled using robust z-score normalization [7]. Training was done using the LASSO method [8], with mechanical power estimated from the antero-posterior ground reaction forces (GRF) [9] as reference. To estimate stepwise MP using every sensor location, separate ML models were developed for flat and inclined running.

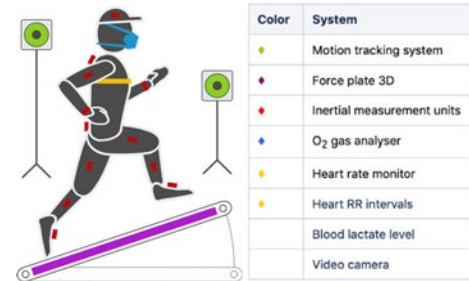


Figure 1: In-lab sensor setup for data collection of 34 healthy subjects

Results and Discussion

Across individual sensor locations, the lowest RMSE (Table 1) was $11.1 \pm 4.8\%$ and $20.9 \pm 14.2\%$ for flat and inclined running respectively. Shank and head sensors provided the best results for flat and inclined running respectively, while the wrist sensors performed second best for both running modalities. The estimation accuracy showed similar order of magnitude across all locations. Unlike the ML model for flat running, the one for inclined running used vertical speed as feature and had a lower accuracy. These results were used as a starting point for the design of a sensor setup for conveniently providing real-time feedback based on MP. We demonstrated the utility of this work in a field study with 13 runners, with an IMU on the wrist used for estimating MP and providing real-time feedback.

Table 1: % RMS error (median \pm IQR) for different sensor locations

Location	Level running	Inclined running
Foot	12.6 ± 5.7	23.0 ± 13.4
Wrist	12.2 ± 6.2	21.7 ± 12.7
Sacrum	14.2 ± 6.2	25.3 ± 15.2
Head	12.8 ± 7.7	20.9 ± 14.2
Shank	11.1 ± 4.8	27.1 ± 20.6

Conclusions

Our results show the promise of IMUs to estimate MP, even with when a single sensor is used. Estimation accuracy of the ML model can be improved further by combining features from sensors on different body segments.

References

- [1] Jaén-Carrillo D. et al. (2020). *Sensors*, **22**: 6482
- [2] Mulligan M. et al. (2018) *PloS one*; **13(11)**: e0206645
- [3] Jenny D.F. & Jenny P. (2020). *J. Biomech*, **110**: 109948
- [4] Fohrmann D. et al. (2019). *ISBS proceedings*, **37(1)**: 145
- [5] Falbriard M. et al. (2018). *Fr. in Physiol.*, **9**: 610
- [6] Pes B. (2020). *IEEE access*, **8**: 13527:13540
- [7] Jain A. et al. (2005). *Pattern Recognition*, **38(12)**: 2270-2285
- [8] Tibshirani R. (1996) *J R Stat Soc Series B*; **58(1)**: 267-288
- [9] Rabita G. et al. (2015). *Scand J Med Sci Sports*, **25(5)**: 583-594

Runners don't bounce - power economy in springless legged locomotion

Scott L. Tucker¹, Natalie Harold², Sarah R. Chang², David Boone²

¹FastEquation Inc. Portland OR, USA

²Orthocare Innovations LLC Edmonds WA, USA

Email: Scott.Tucker@vimazi.com

Summary

The discovery of impact impulses from discrete plantar structures led to a plantigrade running theory that models vertical and horizontal ground reaction forces (GRF) from 2D center of mass (CoM) motions. The accuracy of the theory's predictions results from treating tendon elasticity and compliant tissues not as springs, but as mechanical resistors. When applied to legged locomotion with a flight phase (i.e. running), mass-spring-damper (MSD) predictions conflict with observations and the laws of motion. Specifically, the frequency of impact force and the direction of CoM motion are incompatible with bounce. By applying the theoretical framework of plantigrade running to the computation of power and running economy, we demonstrate that the most economical locomotion system results from the elimination of springs.

Introduction

MSD models of GRF profiles for horizontal human running assume tendons function with spring-like properties [1]. Fundamental to this concept is the conversion of kinetic energy into spring potential energy and the return of some portion of the spring energy in the form of work done on the mass. Assuming some frictional losses, the solution to this equation is damped harmonic motion with a predictable frequency and amplitude. Given the boundary conditions for legged locomotion (striding) at human velocities (<10 m/s) in a gravitational field where the point of impact (foot) is anterior to the CoM, there are no real solutions that incorporate damped harmonic motion.

The theoretical framework for Plantigrade Running (PR), based entirely on measurable parameters and $F=ma$, describes running dynamics as the superposition of a high frequency gravitational impact force at landing and a low frequency muscular propulsion force to create liftoff. The framework predicts the force amplitudes, periods, and sequential timing for each plantar region (calcaneal, tarsal, metatarsal, phalangeal) according to velocity, stride length, and strike pattern, which sum to equal the overall GRF profile.

Methods

The hypothesis that plantar force amplitudes and frequencies are a function of CoM energetics was tested in a controlled barefoot experiment including 270 trials using a Matscan system (Tekscan Inc.) operating at 476 Hz. All individuals provided written informed consent for the IRB approved study. The healthy participants ran according to taped stride length markers, a metronome, and prescribed strike pattern on a level 60 m indoor runway. The dense grid of force sensors allowed precise delineation of the plantar regions, their respective vGRF profiles, and timing of touchdown for each region (Fig. 1).

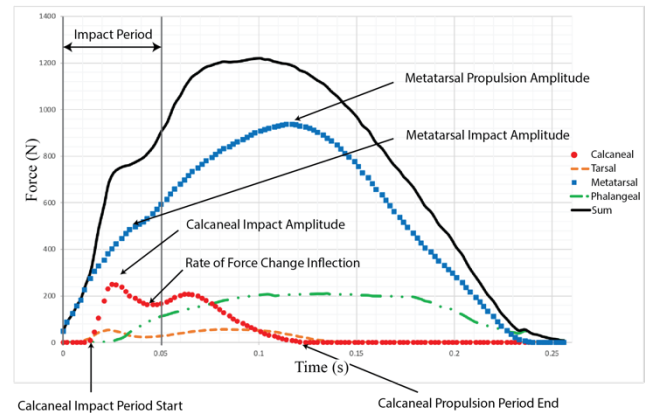


Fig. 1. Plantar regional vGRF trials example with forefoot strike

Results and discussion

Impulse amplitudes and periods were clearly discernable for each plantar region (impact: $p=0.006$ $r^2=0.999$ and propulsion $p=0.005$ $r^2=0.999$) in 100% of the trials and support rejecting the null hypothesis. Foot strike pattern was quantified by defining the parameter FT as the time differential between calcaneal contact and metatarsal contact. Changes in FT correlate with the relative distribution of impact force between calcaneal and metatarsal regions, but do not change total impact force [2]. FT does not correlate with propulsion forces. Together these data support the theory and physical model that the gravitational kinetic energy dissipates during the period of impact. The result is consistent with the observation that horizontal and vertical CoM momentum are not reversed during impact, thereby excluding the possibility of damped harmonic motion.

Conclusion

External power, the work to move the CoM vertically and achieve liftoff velocity over time, decreases with increasing cadence, due to the shorter stride lengths and lower trajectory heights during the flight phase [3]. Spring activity during the propulsion phase would increase energy loss, and therefore, increase external power consumption due to frictional losses. Total running economy at any given speed will be determined by the cadence-driven external power and the cadence-driven muscular (internal) power consumption.

References

- [1] Alexander, R. (1990) *International Journal of Robotics Research*, **9**(2), 53-61.
- [2] Perl, et al. (2012). *Med Sci Sports Exerc*, **44**(7), pp.1335-43.
- [3] Jenny, D. F. and Jenny, P. (2020). *Journal of Biomechanics*, **110**, 109948.

The physiological and biomechanical adaptations to acute fatigue on running economy and pelvic-thorax coordination in sub-elite runners

Craig Hicks, Robert A. Needham, Nachiappan Chockalingam

Centre for Biomechanics and Rehabilitation Staffordshire University, Stoke-on-Trent, UK.

Email: Ch56@staff.staffs.ac.uk

Summary

This study investigated the effect of fatigue on running economy and pelvic-thorax coordination. Ten sub-elite runners performed two 10-minute runs at their ventilatory threshold. Between each 10-minute run participants performed a localised eccentric fatigue protocol. A significant difference in $\dot{V}O_2$ uptake was found between pre-post fatigue runs. Similar pelvic-thorax coordination patterns were noted in all three planes between the pre-post fatigue runs. However, an increase in thorax forward lean in the sagittal plane was noted across the entire gait cycle in the post-fatigue run that could have impacted on running economy.

Introduction

Quantifying the coordination between the thorax and pelvis during running may have implications with performance and injury risk. For example, pelvic-thorax coordination during running may detail desired movement strategies that inform on the position and control of the centre of mass (COM) [1]. In addition, trunk and pelvis posture is thought to be one of the several factors that may influence running economy (RE) [2]. However, there is limited research on the relationship between RE and trunk kinematics, although research has shown that running when fatigued can increase trunk flexion [3]. This study investigated the effect of fatigue on running economy and pelvic-thorax coordination.

Methodology

Ten sub-elite male distance runners (age, 33.8 ± 13.9 years, height, 178.5 ± 11.4 cm and mass, 76 ± 12.3 kg) took part in two laboratory visits. A maximal $\dot{V}O_2$ max test was conducted using breath by breath analysis (Metalyzer 3B cortex Leipzig Germany). to gain participants ventilatory threshold. Seven days later, participants performed two 10-minute runs on a treadmill (model t9700HRT, vision fitness) at their individual ventilatory threshold. Between each 10-minute run participants performed a localised eccentric muscle fatigue protocol consisting of 100 box jumps off a 40cm box with 20 seconds recovery between each jump. Marker coordinate data was captured at 200 Hz using a 17-camera motion capture system (VICON, Oxford, UK). Thorax and pelvis segment angles were processed in Visual3D (C-motion Inc, MD, USA) Vector coding was used

to quantify pelvic-thorax coordination [4]. $\dot{V}O_2$ uptake was analysed during the final minute of each 10-minute run.

Results & discussion

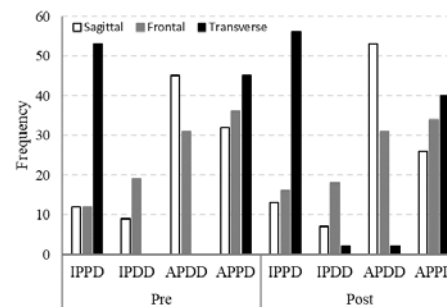


Figure 1: Average frequency count on pelvic-thorax coordination during running across the gait cycle in the sagittal, frontal and transverse plane. (IPDD – inphase proximal dominance / (IPDD – inphase distal dominance / (APDD – antiphase distal dominance / (APPD – antiphase proximal dominance).

In the current study, 3D pelvic-thorax coordination patterns during the pre-fatigue run confirmed the results of a previous study [1]. Coordination patterns during the post-fatigue run did not differ to the pre-fatigue run. However, there was a significant increase ($p < 0.07$) in $\dot{V}O_2$ uptake during the final minute of the post-fatigue run (39.9 ± 6.2 ml/min/kg) compared to the final minute of the pre-fatigue run (38.4 ± 4.3 ml/min/kg). While not highlighted from vector coding analysis, sagittal plane kinematic waveforms highlighted an increase in thorax flexion across the entire gait cycle during the final minute of post-fatigue run. This postural adaptation following induced fatigue is in line with a previous study [3].

Conclusion

This study highlighted that an increase in thorax forward lean as a result of being in a fatigued state may impact on running economy due to an increased $\dot{V}O_2$ uptake.

References

- [1] Preece SJ et al. (2016). *Hum mov sci*, **45**, 110-118.
- [2] Folland JP et al. (2017). *Med sci sports and exerc*, **49** 1412-1423.
- [3] Koblbauer IF et al. (2014). *J sci med sport*, **1** 419-424.
- [4] Needham RA et al. (2020). *The Foot*, **44**:01678.

Effect of the wear of city shoes on the variables characterizing the foot / ground interaction

Éliot Polomé^{1,2}, Nicolas Théveniau¹, Cédric Vigier¹, Raphaël Dumas², Thomas Robert²

¹CTC, Comité Professionnel de Développement Économique Cuir Chaussure Maroquinerie, Lyon, France

²Université Lyon, Université Gustave Eiffel, LEMC UMR 519406, F69622, Lyon, France

Email: epolome@ctcgroupe.com

Summary

This study examined the effect of the wear of city shoes on different variables characterizing the foot / ground interaction during gait analysis and during physical tests. Gait analysis variables did not change while physical tests revealed significant decreased with wear of the shoe.

Introduction

During locomotion, the shoes deteriorate over the multiple steps a person has taken. Wear occurs both on the sole and on the upper (loss and fatigue of material, formation of holes, etc.). However, there is little information on the rate of deterioration as the number of steps increases, nor on its impact on the gait characteristics. Information only exists regarding the rate of deterioration over increasing mileage for running shoes [1, 2, 3]. Therefore, this study examined the effect of the wear of city shoes on gait.

Methods

Six healthy men (age 36.8 ± 7.8 years, height 1.78 ± 0.03 m, body mass 74.9 ± 6.1 kg) received a new pair of city shoes (Stan Smith, Adidas, DE) which they were required to wear during their working day for a period of 60 days. Step counts were determined using an ONWALK 900 pedometer (Newfeel, Decathlon, FR).

The participants carried out three series (initial test, 30-day test and 60-day test) of gait analysis on a dual-belt instrumented treadmill (Ortec, Columbus, OH, USA) with two imposed speeds (3 and 5 km/h). Acquisition frequency was set at 2000 Hz. Before each acquisition, two physical tests were carried out on the shoe in order to evaluate the effect of the wear on the sole and the upper: generating homogeneous shock at the base of the sole to assess the transfer coefficient of the sole and flexing the shoe in the forefoot with an angle of 45 degrees to assess the longitudinal flexibility in flexion.

Data processing was carried out using MATLAB software. Data from the treadmill was filtered (Butterworth low-pass 4th order, cut-off frequency of 50 Hz). The heel-strike and toe-off events were detected using the vertical ground reaction forces (vGRF), with a threshold set at 5% of the body weight. The following variables were observed: number of steps from the pedometer, initial peak vertical ground reaction force (IPF), loading rate of the vertical force from touchdown to the first peak vertical force (FLR), breaking peak anteroposterior ground reaction force (bPPF), propulsive peak anteroposterior ground reaction force (pPPF) from the treadmill and transfer coefficient of the sole (TCS) and longitudinal flexibility in flexion (LFF) from the

physical tests. ANOVA with repeated measures was employed to assess wear effect, α was set at 0.05.

Results and Discussion

After 60 days, participants have performed $379\,161 \pm 110\,000$ steps, corresponding to $6\,319 \pm 1\,835$ steps per day of use. Table 1 shows that gait analysis variables did not change between initial and 60-day tests. Conversely the physical tests revealed significant decreased in TCS and LFF between initial and 30-day tests. No further change was observed between 30-day and 60-day tests. As expected, gait kinetic variables were dependent on velocity.

Table 1: Gait analysis and physical variables during walking for initial, 30-day and 60-day tests. Mean (SD) data of each variables. *Significant difference between 3 and 5 km/h. ** Significant difference between initial and 30-day / 60-day tests.

Variable	Initial test		30-day test		60-day test	
	3 km/h	5 km/h	3 km/h	5 km/h	3 km/h	5 km/h
IPF (BW)*	1.01 (0.046)	1.19 (0.056)	1.01 (0.045)	1.20 (0.064)	1.02 (0.042)	1.19 (0.050)
FLR (BW/S)*	4.52 (0.978)	7.98 (0.509)	4.64 (0.808)	8.07 (0.772)	4.63 (0.470)	8.04 (0.413)
BPF (BW)*	-0.127 (0.011)	-0.219 (0.02)	-0.133 (0.021)	0.223 (0.019)	-0.124 (0.013)	-0.219 (0.014)
PPF (BW)*	0.135 (0.013)	0.231 (0.015)	0.137 (0.02)	0.238 (0.019)	0.145 (0.014)	0.244 (0.022)
TCS (%)	24.4 (7.91)		10.1 (10.6) **		8.2 (7.8) **	
LFF (daN)	0.636 (0.074)		0.298 (0.062) **		0.320 (0.078) **	

Thirty days and about 200 000 steps were sufficient to demonstrate wear of the shoes (degradation of their mechanical properties). Although the physical measures did not evolve during the second month, tests will be performed to assess further changes. The changes in the shoe revealed by the physical tests did not affect the foot / ground interactions, possibly due to participant adaptations [4] - that we plan to further investigate - or lack of sensitivity of these kinetic variables due to the fact that walking is a less dynamic activity than running.

Conclusions

While ground reaction forces during gait remains unaltered, physical tests allow to characterize some alteration of the materials of a shoe after one month of wearing.

References

- [1] Wang et al. (2010). *Footwear Science* **3**: 141-47.
- [2] Chambon et al. (2014). *J Sports Sci* **11**:1013-22.
- [3] Herbaut et al. (2017). *Gait Posture* **54**: 123-28.
- [4] Kong et al. (2009). *Br J Sports Med* **10**: 745-49.

The effect of footwear on lower extremity joint functional indices in distance running

Patrick Mai¹, Gillian Weir², Markus Kurz³, Matthieu B. Trudeau⁴, Joseph Hamill², and Steffen Willwacher^{1,5}

¹Institute of Biomechanics and Orthopaedics, German Sport University Cologne, Cologne, Germany

²Biomechanics Laboratory, University of Massachusetts Amherst, Amherst, MA, USA

³Sports Tech Research Centre, Mid Sweden University, Östersund, Sweden

⁴Brooks Running Inc., Seattle, WA, USA

⁵Department of Mechanical and Process Engineering, Offenburg University, Offenburg, Germany

Email: p.mai@dshs-koeln.de

Summary

Understanding lower extremity leg joint functions (JFs) is essential for the design of technical devices to assist locomotion. In running, footwear is the interface between the foot and the ground, modulating the distribution of mechanical work across joints [1]. However, little is known about how footwear can redistribute joint work and thus change the JFs. Here we analyzed the JFs for running in different footwear conditions by using the joint functional indices (JFIs). We found that the JFs were significantly affected by the type of footwear. The strut index of the ankle and knee increased in more minimal footwear. We found an inverse relationship between footwear minimalism and the spring index. We suggest that the type of footwear used should be considered when designing passive or active e.g. biomechatronic systems.

Introduction

The JFIs describe the lower extremity JFs based on mechanical joint work as spring, damper, motor, and strut elements [2]. It has been shown that the JFs of the lower extremities adapts to various task demands. However, the influence of footwear on the JFs in running has not been studied yet. Therefore, the purpose of the study was to quantify if the JFIs are affected by the type of footwear used.

Methods

We determined lower extremity sagittal plane joint biomechanics (n=103) with a motion capture system and a force plate during overground running (3.5 m/s). Participants ran with three types of shoes (minimal, Sock; neutral, Brooks Glycerine; support, Brooks Adrenaline). We calculated the JFIs for the stance phase of running [2]. Friedman's test and effect sizes (Kendall's W) for each JFIs were determined to quantify the influence of footwear on the JFs.

Results and Discussion

We found the strongest footwear effects at the ankle and the knee joint (Tab.1). The strut index of the ankle and knee joint was higher in the minimal compared to the cushioned footwear conditions (Fig.1). In contrast, the spring index of the ankle and knee joint was higher in more cushioned footwear. We observed a significantly higher damping index for the minimal compared to the cushioned shoe condition. We further observed a high footwear effect for the damping index of the knee joint induced by the minimal shoe. Differences in JFs might be caused by changes in the footfall pattern and the associated load and work redistribution while running in a more minimal shoe.

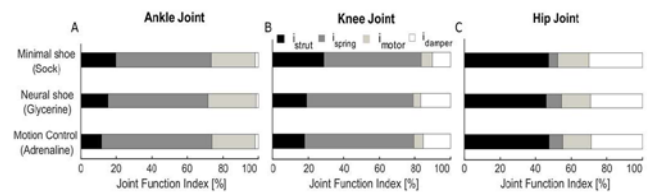


Figure 1: Lower extremity JFIs for the three footwear conditions.

Conclusions

Footwear can affect the JFs in running. Therefore, footwear should be considered when evaluating training interventions and designing, e.g. biomechatronic systems for the assistance of human locomotion. In this context, further studies might also explore the relationship between JFIs and injury risk.

Acknowledgments

Brooks Sports Inc., Seattle, WA, USA.

References

- [1] Fuller et al. (2016). *J Athl Train*, **10**: 806-812.
- [2] Farris et al. (2017) *R.Soc. open sci.*, **4**: 160901.
- [3] Qiao et al. (2016) *J. Biomech.*, **1**: 66-72.

Table 1: Effect sizes (Kendall's W) for each JFI. Bold effect sizes indicate a significant footwear effect (Friedman test, $p < 0.05$).

	Ankle Joint	Knee Joint	Hip Joint
Strut Index	0.52	0.52	0.03
Spring Index	0.31	0.24	0.14
Motor Index	0.09	0.06	0.03
Damper Index	0.01	0.46	0.02

The effect of running shoes' milage on lower limb muscle actiCity

□□ abenicht¹ □ S. Kratzenstein^{1,2}

¹ Institute of Sport Science, Kiel University, Germany □ ² CAU Motion Lab, Kiel University, Germany,
Email: stefan.kratzenstein@email.uni-kiel.de

Summary

Previous studies showed that the mechanical properties of running shoes change with increasing milage, which requires an adaptation of muscle responses to continuously changing load to protect the musculoskeletal system from injuries. Furthermore, the runner must decide when the original shoe properties are worn out. An autonomous quantification of biomechanical key parameters could provide an individual assessment of increasing pathological impacts. This study quantifies the muscle activity as a direct motor response to ground impacts and aims to investigate changes in the integrated EMG (iEMG) within 500km of running. The activity of four lower limb muscles was quantified every 100km and compared to iEMG while running un-worn reference shoes. The results revealed no systematic, intra-individual changes in the muscle response. It remains unclear whether the iEMG was not suitable to identify changes in activity patterns or the range of usage did not lead to effective changes of the mechanical properties.

Introduction

The mechanical properties of running shoes change with increased usage [1]. Here, most studies analysed ground reaction forces to quantify the physiological response to these changes. Only very few studies quantified changes in muscle activity [2]. Recommendations for a shoe substitution range from 300-1000km, depending on i.e. runners' weight and shoe type. An autonomous analysis, which identifies physiological thresholds could enable runners to individually identify the time when the original mechanical properties are worn-out. In this study, we quantify the iEMG during ground contact of four lower limb muscles and evaluate changes considering the runner's feedback on shoe comfort.

Method

Eight recreational runners participated in this study. Each runner was considered as single case study, since the heterogeneity of the cohort included age, gender, performance level, and shoe type. All runners were equipped with two identical new pairs of running shoes, whereas one pair was kept un-worn as the reference shoe (REF), while the other pair (TRA) was worn for at least 500km within the regular training. The muscle activity of the left biceps femoris (□F), gastrocnemius med. (GM), peroneus longus (PL), and the tibialis ant. (TA) was measured every 100km during 3 x 8min (warm-up, TRA shoe, REF shoe) treadmill runs at a sub-maximal velocity. The order of REF and TRA was randomized with 4min rest between the sessions.

EMG electrodes placement and signal processing were conducted according to SENIAM recommendations [3]. The EMG (myon320, prophysics, 1000Hz) data collection

included at least 25 ground contacts. iEMG was calculated for each cycle. Student t-test was applied to test for intra-individual differences between the shoes.

Results and Discussion

The average differences ($n \geq 25$ ground contacts) in iEMG over all athletes, here focussing on the final difference from REF after 500km, range from 0.02 ± 0.004 (□F), -0.01 ± 0.002 (TA), 0.02 ± 0.003 (PL), and -0.01 ± 0.003 (GM). All differences are significant ($p \leq 0.05$). Figure 1 shows exemplary results for a male runner ($m \approx 78\text{kg}$) after 500km.

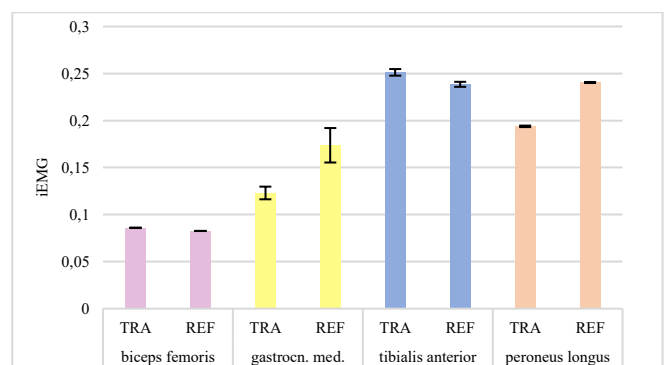


Figure 1 □ Averaged iEMG ($n \geq 25$ ground contacts) of one runner after running 500km

The results show individual characteristics and changes of the iEMG. It remains unclear whether the iEMG is not suitable to identify smaller changes due to its already high variation within each trial or the milage of 500km did not lead to effective changes in the shoe's mechanical properties, although this would contradict the runner's feedback about decreasing comfort. Furthermore, it should be considered that the large number of involved muscles leads to a high number of degrees of freedom to response to the load change, which cannot be recorded in a single measurement.

Conclusion

This study showed the sensibility and the individuality of muscle activity. Although there are differences in the muscle activity while running in the TRA or the REF, these differences are not consistent. An EMG analysis alone seems not to provide a reliable indicator of the need to change the running shoes.

References

- [1] Heidenfelder, Sterzing □ Milani (2009). *Footwear Science*, 1:16-17.
- [2] Escamilla et al. (2020). *Int J Environ Res Public Health*, 5: 5-17.
- [3] Hermens et al. (2000). *Journal of Electromyography and Kinesiology*, 10: 361.

Predictive neuromuscular simulation of the sit-to-walk movement

van der Kruk, Eline¹ & Geijtenbeek, Thomas.¹

¹Biomechanical Engineering, Delft University of Technology, Delft, the Netherlands

Email: e.vanderkruk@tudelft.nl

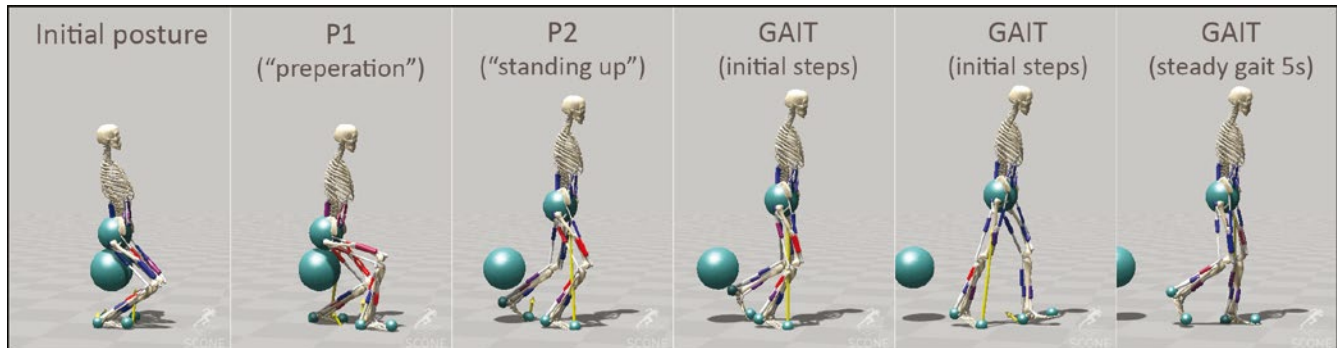


Figure 1: Images from the predictive sit-to-walk simulation using CMA-ES optimization of three controllers (GAIT, P1, P2) in SCONE.

Summary

Progression of neuromuscular decline often leads to incorrect or insufficient compensation strategies, both through altered muscle recruitment and changes in movement trajectories. Predictive neuromuscular simulations are an effective tool for discovering those strategies, enabling clinicians to design treatments that are both more effective and efficient for prolonging the mobility of the patient. In this study we have developed a predictive neuromuscular model that can simulate the sit-to-walk movement using SCONE.

Introduction

The treatment of age-related mobility impairments is increasingly relevant in our ageing societies. These impairments typically do not arise at the onset of age-related physical decline, due to the redundancy of the human movement system. Functional redundancy is the redundancy in the muscle architecture of the human body; the result of functional redundancy is compensation. Most state-of-the-art musculoskeletal studies (inverse/forward) however do not account for compensation: they use prescribed movements (kinematics) to study decline of variables. Predictive models that generate kinematics *de novo* have the potential to simulate the capacity versus compensation relationship, since they can generate new movement trajectories. The aim of this study is to develop a predictive neuromuscular model that can simulate the sit-to-walk movement, an important daily life activity.

Methods

The musculoskeletal model is based on an OpenSim [1] model representing a male adult with height of 1.80m and a mass of 75kg. The model has 10 DOF (2D model) and is actuated by 22 Hill-type muscle-tendon units. Contact force between the feet and the ground and between the buttocks and the chair were modelled with Hunt-Crossley force spheres (two at the foot, one at the pelvis, one at the chair). Our sit-to-walk controller consists of a gait controller (GAIT) based on [2] and a two-phase stand-up controller (P1, P2) based on proprioceptive feedback from muscle

length feedback (L), tendon force feedback (F), and constant excitation (C). The delayed feedback pathways were both monosynaptic and antagonistic. The controller was developed and optimized in SCONE [3] using a shooting-based optimization method. The 152 free parameters were optimized to minimize the gross cost of transport, at a prescribed minimum gait velocity, while avoiding falling, ligament injury, and excessive head motion. We ran multiple parallel optimizations with the same initial guess and used the best set as start for the next set of optimizations. Final results were compared to recorded kinematics (Vicon), ground reaction forces, and EMG from young (18-35 year) and older (>65 year) adults (N=50) [4], in which participants were asked to stand up and walk to a table, at self-selected (5x) and fast speed (5x).

Results and Discussion

The predictive 2D lower limb model was able to simulate a sit-to-walk movement that matches real-world kinematic recordings. The experimental study showed that >80% of the older adults used their arms to push off while standing up in a daily life setting. To allow for realistic compensation, we are working on a 3D upper- and lower limb model.

Conclusions

With its current limitations the developed model was not able to simulate all daily life compensation strategies in sit-to-walk, but the model does simulate the sit-to-walk movement well for some strategies.

Acknowledgments

NWO-ENW Rubicon Grant 019.173EN.023, 2018

References

- [1] Lower Limb Extremity Model 2010, OpenSim
- [2] Geyer & Herr (2010). A muscle-reflex model that encodes principles of legged mechanics produces human walking dynamics and muscle activities.
- [3] Geijtenbeek, T (2019). SCONE: Open Source Software for Predictive Simulation of Biological Motion.
- [4] Van der Kruk & Bull (ISB 2021), Unrestricted age-related compensation in a daily life sit-to-walk task.

Estimating safe rehabilitation movements for rotator-cuff injuries from musculoskeletal modeling

Micah Prendergast¹, Tom Driessen², Luka Peternel³, Ajay Seth¹

¹Department of Biomechanical Engineering, Delft University of Technology, Delft, Netherlands

²Clinical Technology, Faculty of 3mE, Delft University of Technology, Delft, Netherlands

³Department of Cognitive Robotics, Delft University of Technology, Delft, Netherlands

□Authors contributed equally

Email: a.seth@tudelft.nl

Summary

We developed a simulation workflow to estimate rotator-cuff muscle strains and to explore 3D shoulder movements that minimize strain in rotator-cuff muscle tendons. Our findings reveal that the shoulder can be mobilized within a large workspace of low strain, which could be adopted during physical therapy to safely increase the range-of-motion of the shoulders of patients with rotator-cuff injuries.

Introduction

Shoulder injuries are common with rotator-cuff tears alone occurring at a rate of 50% among individuals over 60 [1]. With rehabilitation, it often takes a year for patients to recover normal range-of-motion (RoM) and strength. Immobilization after surgery and limited RoM during rehabilitation, particularly in the early stages, limit the risks of reinjury, but also delay recovery. Reinjury is associated with strains in torn or sutured tendons of rotator-cuff muscles. Our aim is to find rehabilitation movements with increased RoM while limiting reinjury risk during the recovery from a rotator-cuff injury.

Methods

We employed a musculoskeletal model of the shoulder [2] (Fig. 1(a)) to explore the passive movements of the glenohumeral joint while estimating the tendon strains in the affected rotator-cuff muscle(s). Muscle strains were computed by solving for muscle forces necessary to hold the shoulder in a given position using static optimization to resolve individual muscle activations and forces in OpenSim [3]. An entire workspace of tendon strains was computed for each rotator-cuff muscle for glenohumeral joint positions that span its RoM. From this workspace, low strain trajectories and subspaces were visualized and identified. The musculoskeletal model was then used to visualize shoulder motions along low strain paths. A strain of 1% was used to highlight regions of low reinjury risk. These regions were compared to the passive RoM of physical therapy movements prescribed post-surgery [4].

Results and Discussion

Large regions of low rotator-cuff strain were found in the movement space of the shoulder as were regions of high strain (Fig. 1). Strains were particularly sensitive to internal and external rotation of the glenohumeral joint. Identified regions of low rotator-cuff strain were typically larger than those prescribed during physical therapy.

The strain spaces from our musculoskeletal model indicate that shoulder movements can be planned in such a way that they minimize strain and limit the risk of reinjury. □y estimating strains that cannot be perceived by the therapist, the model could provide therapists with visual and/or vibrotactile feedback of strains to keep motions safe during physical therapy when applying shoulder movements in real-time.

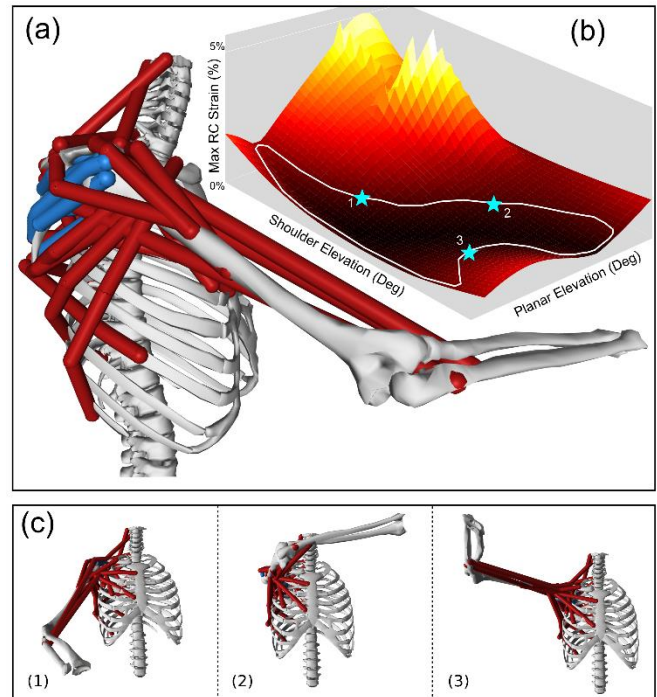


Figure 1: (a) OpenSim shoulder model used to estimate strains in specific rotator-cuff muscle tendons. (b) 3D surface plot showing the max strain experienced by any tendon of the rotator-cuff muscles at every pose (specified by glenohumeral joint angles) in the reachable workspace. The weight of the arm is assumed to be supported in such a way that the shoulder is moved passively (with minimal muscle activation related to gravity compensation). In white is an example trajectory (movement) that traverses a large range-of-motion at low rotator-cuff tendon strain. (c) Sample of the shoulder model in selected poses (1), (2) and (3) along the low-strain trajectory. Note, two degrees of freedom are shown for visualization, however our strain maps include axial rotation for full motion of the glenohumeral joint.

Conclusions

Our musculoskeletal simulations reveal a large range of shoulder movements that pose minimal risk of rotator-cuff reinjury. We hope this work will enlighten and encourage physical therapists to explore these movements during the rehabilitation of rotator-cuff injuries and limit losses in RoM and thereby speedup the recovery of their patients.

References

- [1] Thigpen et al. (2016). *J Shoulder Elbow Surg.*, □5:521-35.
- [2] Seth et al. (2019). *Front. Neurobot.*, **13**:90
- [3] Seth et al. (2018). *Plos Comp. Bio.*, **14**□e100622.
- [4] Meijden et al. (2012). *Int. J. Sports Phys. Ther.*, □(2) 197-218.

Kinematics and muscle activation patterns during a 30min walking test in patients with symptomatic lumbar spinal stenosis and healthy controls

Corina Nüesch^{1,2,3,4}, Filippo Mandelli^{1,3,4,5}, Stefan Schären¹, Cordula Netzer¹, Annegret Mündermann^{1,2,3,4}

¹Department of Orthopaedics and Traumatology and ²Department of Spine Surgery, University Hospital Basel; ³Department of Biomedical Engineering and ⁴Department of Clinical Research, University of Basel; ⁵Department of Orthopaedics, University Children's Hospital Basel, all Basel, Switzerland; Email: corina.nueesch@usb.ch

Summary

Patients with symptomatic lumbar spinal stenosis have higher paravertebral and hip abductor muscle activation at the beginning of a 30min walking test compared to healthy controls that further increases at the end of the test in the longissimus thoracis muscle.

Introduction

Patients with symptomatic lumbar spinal stenosis (sLSS) suffer from pain and functional limitations such as a limited walking distance [1] or altered pelvic acceleration compared to healthy people [2]. After onset of claudication symptoms, increased postural sway [3] and increased forward flexion of the trunk [4] have been reported. Paravertebral muscle activation and forward trunk flexion during walking decreased after decompression surgery, [4]. The aim of this study was to compare muscle activation patterns of hip abductor and paravertebral muscles and joint kinematics during walking between patients with sLSS and healthy persons and to investigate whether these patterns change during a 30min walking test.

Methods

Twenty patients (12 female, 8 male; age, 70.4±8.5 years; body mass index (BMI), 26.8±4.0 kg/m², Oswestry Disability Score (ODI), 28.9±13.1) with sLSS scheduled for decompression surgery and 19 healthy subjects (11 female, 8 male; age, 63.0±10.1 years; BMI, 24.1±3.4 kg/m²; ODI, 1.2±2.2) performed a 30min walking test along a 200m corridor with continuous measurement of surface electromyography and 3D accelerations (myon, Switzerland) of the gluteus medius, multifidus and longissimus thoracis muscles. Every 3 min, sagittal kinematics of the ankle, knee and hip joint were recorded with seven inertial sensors (RehaGait, Hasomed, Germany). In case of onset of symptoms that caused patients to pause, the test was ended prematurely. Accelerometer signals of the longissimus sensor were used to determine the heel strikes of 20 consecutive steps at the beginning and end of the walking test [5]. EMG envelopes were calculated using

a moving average filter (window size, 100 ms) and normalized to the peak activity at the beginning of the walking test. Differences in muscle activation patterns and joint kinematics between patients and controls (independent sample t test) and between beginning and end of the walking test (paired t tests) were determined using statistical parametric mapping (www.spm1d.org; P<0.05).

Results and Discussion

The patients walked slower (1.00±0.19 vs. 1.26±0.10 m/s, P<0.001) and for a shorter time (22.8±10.7 vs 30min; P=0.006) compared to healthy controls. Patients had less ankle plantarflexion (54-67% gait cycle (gc), P=0.002) and less hip extension (39-47%gc, P=0.029), as well as higher muscle activation of the multifidus (25-38%gc, P<0.001), longissimus (24-47%gc, P<0.001 and 70-94%gc, P<0.001) and gluteus medius (21-37%gc, P<0.001) than controls (Figure 1). In patients, right longissimus muscle activity was higher at the end of the test compared to the beginning (+16%, 0-5%gc and 97-100%gc, P=0.016 and P=0.035).

Conclusions

The more continuous and for longissimus even increasing muscle activity during the walking test may be related to the reported greater lumbar flexion in patients with LSS [4]. The slower walking speed and slightly altered kinematics might be caused by nerve dysfunction due to increasing epidural pressure [6] and indicate other adaptations in the gait patterns to relieve pain during walking. Whether these altered muscle activation patterns and kinematics during walking can be influenced by surgery and following rehabilitation still needs to be investigated.

References

- [1] Loske S et al. (2018). *Spine J*, **18**: 2195-2204.
- [2] Bumann H et al. (2020). *Spine J*, **20**: 112-120.
- [3] Nagai K et al. (2014) *J Spinal Disord Tech*, **27**: 136-142.
- [4] Goto T et al. (2017). *Gait Posture*, **51**: 149-152.
- [5] Zijlstra W and Hof AL (2003). *Gait Posture*, **18**: 1-10.
- [6] Takahashi K et al. (1995). *Spine*, **20**: 2476-2749

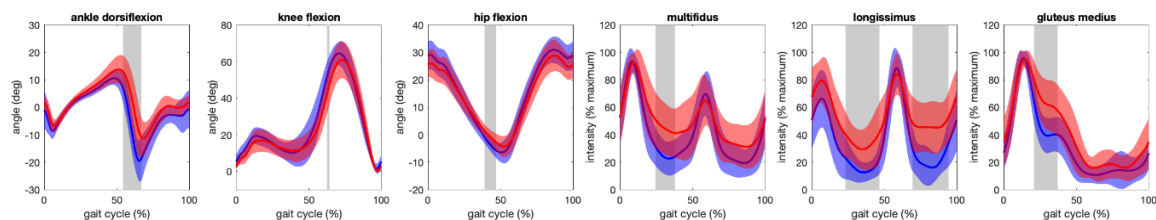


Figure 1: Mean ± 1 standard deviation of right joint angles and muscle activation pattern of sLSS patients (red) and healthy controls (blue). Grey areas indicate time periods with significant differences between patients and controls (P<0.05).

Altered timing in trunk rotation with the ToneFit Reha compared to Nordic Walking in people with low back pain

Eveline S. Graf, Carole A. Pauli, Bettina Sommer

Institute of Physiotherapy, School of Health Professions, Zurich University of Applied Sciences, Winterthur, Switzerland

Email: eveline.graf@zhaw.ch

Summary

This study compared the trunk rotation during walking with the ToneFit Reha (TFR), a product with push-pull resistance handles, and Nordic Walking. The TFR resulted in a delayed reversal of trunk rotation towards the end of the second double support phase. This change in timing allowed to manage the challenged balance when walking with the TFR.

Introduction

Physical activity is widely used for the treatment of low back pain (LBP) [1]. Nordic Walking (NW) has been used as an exercise to increase the benefits of walking in such population resulting in increased core stability [2].

The ToneFit Reha (TFR) is a newly developed product, worn around the waist (Figure 1). It mimics normal walking but with added push-pull handles with adjustable resistance. The TFR is intended for rehabilitation, allowing individual settings for each person and each side of the body. The aim of this study was to determine the effect of walking with the TFR on trunk rotation compared to NW.

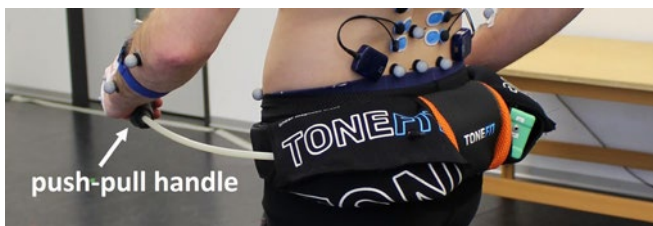


Figure 1: ToneFit Reha.

Methods

Ten participants with LBP (age 42.1 ± 5.4 years, mass 71.4 ± 8.0 kg, height 172.1 ± 5.2 cm) were recruited. After signing informed consent, retro-reflective markers were added to the spine [3] and arm and a familiarization period for each condition was allowed. Each participant performed ten trials with NW followed by the TFR at the same speed.

Marker trajectories were recorded using 12 Vicon cameras (240 Hz, Vicon Vantage, Vicon Motion Systems Ltd, UK). Trunk rotation angles, shoulder flexion angles as well as durations of double and single support phases were averaged over the left and right side and of all trials per participant for statistical analysis. A paired t-test with Bonferroni adjustment resulting in a significance level of 0.01 was used to determine statistically significant differences between conditions.

Results and Discussion

While the peak contralateral trunk rotation angle did not differ between TFR and NW, the peak occurred later during

TFR. Further, the first double support phase was significantly longer while the second single support phase was significantly shorter for TFR (Figure 2). The timing of the peak shoulder flexion (indicating the reversal of the arm movement) did not differ between TFR (43% of gait cycle) and NW (45% of gait cycle).

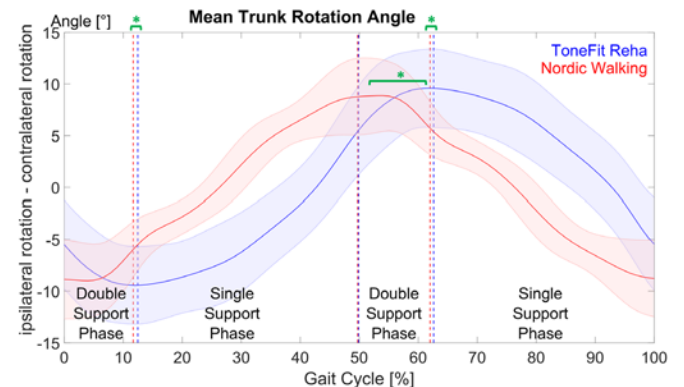


Figure 2: Mean trunk rotation angle [in degrees] during gait cycle [in percent], blue = ToneFit Reha, red = Nordic Walking, green: sign. difference ($p < 0.01$).

During TFR, the push-pull movement with the handles needed to be counterbalanced by the trunk. Changing the direction of the trunk rotation while simultaneously generating enough force to stabilize against the applied force at the handles, is a challenging task. It is concluded that this challenge was met by delaying the directional change of the trunk rotation towards the end of the second double support phase. The increased base of support during this phase provides more stability to the body. Also, due to this delay, the leading arm was closer to the body when the change of trunk rotation occurred. Therefore, the lever arm was smaller resulting in less force needed in the trunk to keep the upper body stable.

Conclusions

The TFR caused significant changes in the timing of the trunk rotation to manage the increased challenges due to instability. If this added challenge in stability and the chosen strategy is beneficial for rehabilitation, will need to be determined in future research.

Acknowledgments

The authors acknowledge the entire project consortium and the funding agency Innosuisse (Nr. 26022.1 PFLS.LF)

References

- [1] Bloxham S et al. (2016). *Healthcare (Basel)*, **4**: 1-12.
- [2] Zoffoli L et al. (2016). *Gait Posture*, **46**: 57-62.

3D Characterisation of Isolated Disc Specimens Subject to Cyclic Loading

Shahid Ayward, A.W. Miles, P.S. Keogh, S. Gheduzzi

Department of Mechanical Engineering, University of Bath, Bath, United Kingdom

Email: sh2616@bath.ac.uk

Summary

Defining the viscoelastic behaviour of spinal specimens is critical to understanding the biomechanics of the healthy, damaged and surgically modified spine. A method using MATLAB SimScape to tune a non-linear Kelvin element to spinal load-displacement curves is proposed to fully characterise behaviour. The model matches experimental dissipated energy with a mean difference of 4% and allows full characterisation of the intervertebral disc behaviour.

Introduction

Back pain affects around 80% of the population and research in the field has been prominent since the mid 1900s [1]. The most widespread technique for analysing spinal test data uses linear least squares regression to calculate gradients of load-displacement curves from specimens subject to cyclic loading [1, 2]. It is favoured for simplicity but relies on assumptions which neglect viscoelastic characteristics.

Loaded cyclically, spinal specimens exhibit a time-dependent response in an S-shaped hysteresis loop [3]. This response can be approximated using a polynomial or double sigmoid function but these approaches give non-unique solutions defined by parameters without useful physical representation. A computational method for tuning non-linear viscoelastic models to spinal load-displacement data has been developed to fully characterize behaviour using spring and damper elements. This method expands on that introduced by Panjabi (1991) [4]. The model comprising a non-linear Kelvin element (Figure 1 left) is implemented.

Methods

Three thoracic porcine functional spinal units were obtained and dissected into isolated disc (ISD) specimens. During testing, specimens were wrapped in moist tissue and plastic wrap to prevent dehydration. A 500N preload was applied for a 30-minute equilibration period prior to 6-axis stiffness testing at a constant rate of 0.1 Hz (amplitudes in Figure 1).

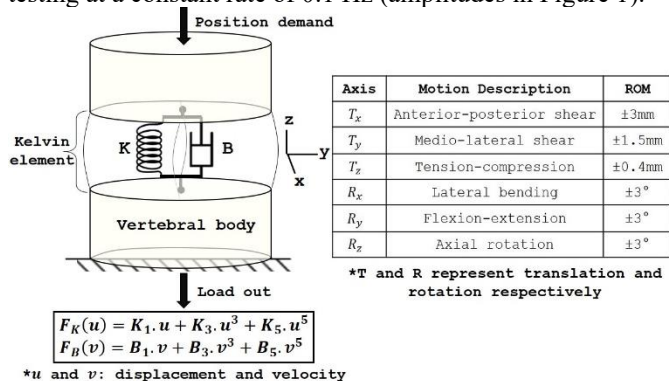


Figure 1: Viscoelastic model of disc and axis motion descriptions

The non-linear Kelvin model was implemented in MATLAB Simulink R2020b using the SimScape library. Solution coefficients were determined with an optimization cost function using sum of squared errors with a non-linear least squares optimization method and a Trust-Region-Reflective algorithm [5].

Results and Discussion

Figure 2 shows an example of the fit obtained by the model for a single cycle in axial rotation.

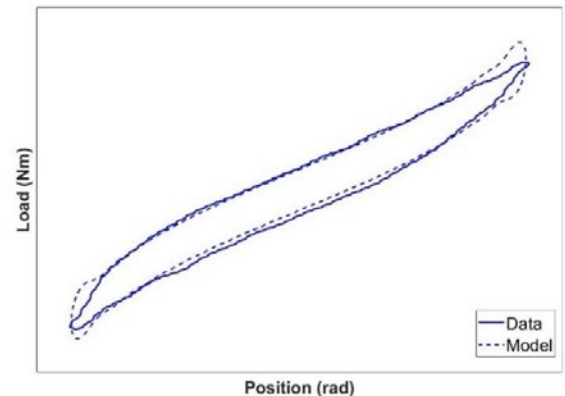


Figure 2: Viscoelastic model and fit obtained for axial rotation

The mean % difference between area enclosed by the model and experimental curves is below 4%, indicating the model's ability to represent dissipated energy.

At solution, the primary coefficients K_1 and B_1 showed average percentage deviations from mean less than 24%. However, for higher order coefficients, this repetition decays.

Conclusions

The agreement between dissipated energy in the experiment and model data and repetition in primary coefficients shows good potential for use of this method. The method illustrates that non-linear viscoelastic models can be used to fully describe spinal ISD load-displacement curves. Further work

Acknowledgments

The authors wish to express their gratitude to the Enid Linder Foundation for their continued support of this PhD project.

References

- [1] Panjabi M.M. et al. (1976). *J.Biomech*, **9**: 185-192
- [2] Gardner-Morse M.G. et al. (2004). *J.Biomech*, **37**: 205-212
- [3] Ozkaya N. et al. (2016). *Fundamentals of biomechanics: Equilibrium and deformation*, 4th edition, Springer
- [4] Panjabi M.M. (1991). *BioMed Mater and Eng.*, **1**: 203-214
- [5] MathWorks, (2020). Simulink® Design Optimization™: User's Guide (R2020b). Retrieved January 2021

Comparison of three approaches for calculating the CoM acceleration based on video analysis and plantar pressure data

Ale Scaldaferro¹, Alfredo Ciniglio¹, Giacomo Maistrello¹, Fabiola Spolaor¹, Annamaria Guiotto¹, Federica Cibin², Zimi Sawacha^{1,3}

¹iomov Lab, Dept. Engineering Information, University of Padova, Padova, Italy

²SoF S.r.l., Padova, Italy

³Dept. Medicine, University of Padova, Padova, Italy

Email: zimi.sawacha@dei.unipd.it

Summary

The objective of this study is to find a strategy to estimate the acceleration of the center of mass (CoM) of the hockey player while doing a sprint task. The data are acquired directly on the field so the methodology used to calculate the acceleration must be usable without the instrumentation of a motion analysis laboratory. For that reason, we compared three different methods for calculating the acceleration of the centre of mass: the first considered the instantaneous acceleration of the anatomical point L5, the second considered the anthropometric formula of De Leva and the third considered the Winter's formula.

Introduction

Field hockey is a competitive, high intensity sport game and one of the most popular team sports now played around the world. In this study we acquire data relative to a 10m sprint task, made by athletes of a female elite-hockey team, holding the hockey stick with one hand. The main purpose of this contribution is to analyze the Center of Mass (CoM) acceleration of the players while they are performing the hockey-specific task previously described. To this extent three approaches were adopted: 1. Track the anatomical point L5 2. Apply the anthropometric formula of De Leva [1] 3. Apply the Winter's formula [2] using plantar pressure data.

Methods

Nine female athletes signed the informed consent and took part in the study (mean ± SD age: 21.56 ± 4.67 years, BMI: 22.01 ± 0.99 kg/m²). The players were acquired, directly on field, while performing a 10m sprint holding the hockey stick with one hand, by means of four synchronized GoPro Hero 3 cameras and a Novel Pedar plantar pressure system. For performing the video tracking, the application TrackOnField (SoF S.r.l.) was used, while to implement the three different approaches for calculating the CoM acceleration Matlab codes were developed. The following pipeline was used: 1. The 3D trajectory of the anatomical point L5 was extracted from the video sequences and its instantaneous acceleration was calculated. 2. To apply the anthropometric formula of De Leva [1], the anthropometric measure of the athletes was retrieved from the anatomical landmarks and the CoM trajectory calculated. 3. The center of pressure data (CoP) was extracted from the plantar pressure system and the Winter's [2] (1) formula was applied to calculate the CoM acceleration (CöM) as follows:

$$\text{CoP} - \text{CoM} = k \cdot \text{CöM} \quad (1)$$

where k is the ratio between the inertial moment of the human body and the product of the body force of the subject and the height of the CoM:

$$k = \frac{I}{W * h}$$

Results and Discussion

The results showed a good agreement between the first two methods: the anthropometric approach and the trajectory of the anatomical point L5 (Fig.1). Meanwhile, CoM acceleration calculated using the Winter's formula was lower compared to the other two methods.

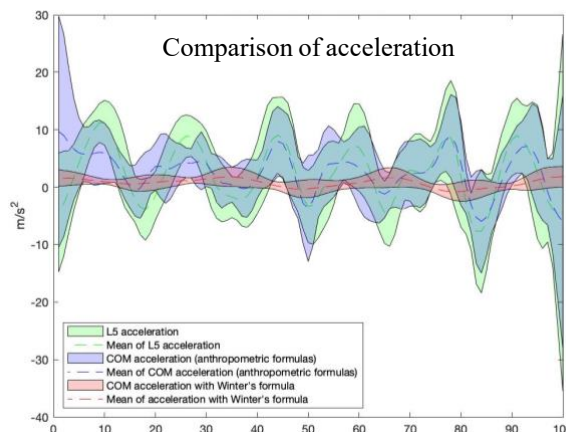


Figure 1: In the figure is reported the comparison across the acceleration extracted from L5, the anthropometric approach and the Winter's formula.

Conclusions

This study showed that in dynamic conditions, CoM acceleration could be estimated using different approaches but, only in two of the considered cases this led to comparable results. For validation purposes this approach should be further applied in static condition with the aid of a force plate that could represent a gold standard.

References

- [1] De Leva P et al. (1996). *J Biomech*, 9: 1223-1230.
- [2] Winter DA. (2009) *Biomechanics and Motor Control of Human Movement* John Wiley & Sons Inc.

Trunk center of mass position during a 90° cut in soccer players who go on to ACL injury and those who do not

C. Dix¹, Amelia Arundale², Holly Silvers-Granelli³, Ryan Zarzycki⁴, Adam Marmon⁵, Elisa Arch⁶, Lynn Snyder-Mackler¹

¹Biomechanics and Movement Science Program; Department of Physical Therapy, University of Delaware, Newark, DE, USA

²Ichan School of Medicine Mount Sinai Health System, New York, NY, USA; Red Bull Athlete Performance Center, Thalguva, Austria

³Velocity Physical Therapy, Los Angeles, CA, USA

⁴Department of Physical Therapy, Arcadia University, Glenside, PA, USA

⁵Lite Cure LLC, Newcastle, DE, USA

⁶Kinesiology and Applied Physiology, University of Delaware, Newark, US

Email: cdix@udel.edu

Summary

Trunk center of mass (COM) position at initial contact of a 90° cut was compared between soccer players who went on to ACL injury and those who did not. Measures of COM position were assessed at initial contact (IC) and peak knee abduction moment (PKAM) with no significant differences between injured and uninjured players. These findings suggest that trunk COM at IC and PKAM are not influencing risk of ACL injury when cutting.

Introduction

Anterior cruciate ligament (ACL) injuries are a prevalent injury among women's soccer players, and many occur during cutting maneuvers without contact from another player [1,2]. High knee abduction moments have been identified as a lower extremity biomechanical risk factor for non-contact ACL injury [3]. Shifting the trunk laterally toward the stance foot has been shown to increase knee abduction moments by increasing the moment arm between the ground reaction force and knee joint [4]. Additionally, trunk lateral displacement after a sudden force has previously been used to identify athletes who go on to knee injury [5]. However, trunk displacement during a sport-specific task has not been studied prospectively before. Thus, the purpose of this study was to determine whether two methods of trunk COM position during a 90° cut differentiate between soccer players who went on to ACL injury and those who did not.

Methods

Forty-one NCAA D1 and D2 women's soccer players completed preseason motion analysis of a 90° cut. Kinematic and kinetic data were recorded simultaneously using an 8 camera system and an embedded force plate. The trunk model used iliac crest and acromion markers to define the proximal and distal segments respectively, and a rigid cluster of tracking markers was placed on the trunk. The trunk was modelled as a cylinder and a universal segment depth of 0.12m was applied. Position of the trunk COM was also calculated at initial contact (IC) and peak knee abduction moment (PKAM) relative to proximal tibia (COM_k) and relative to the foot (COM_f). Position was normalized to leg length, and (-) position indicated the COM was medial to the knee. Throughout the season, each team's respective athletic trainer recorded injuries and four non-contact ACL injuries were reported at the conclusion. The right and left limb of the uninjured participants were averaged so that each uninjured participant contributed a single healthy limb and each injured participant contributed a single ACL injured limb to our statistical model [6]. Independent t-tests were used to determine whether COM position differed between players who

went onto ACL injury and those who did not. Alpha was set a priori at p<0.05.

Results and Discussion

There were no significant differences between injured and uninjured participants at IC for COM_i or COM_f (Table 1). There were also no significant differences between injured and uninjured participants at PKAM for COM_i or COM_f (Table 1). Although uninjured players demonstrated a slightly more medial trunk COM position when measured relative to the foot, these results suggest trunk COM position does not differ between soccer players who go on to ACL injury and those who do not during a sport-specific task.

Variable, event	Mean±SD (m)		p-value	Effect Size
	Uninjured (N=37)	Injured (N=4)		
COM _i , IC	-0.30±0.06	-0.30±0.1	0.95	D=0.03
COM _f , IC	-0.26±0.06	-0.24±0.05	0.50	D=0.37
COM _i , PKAM	-0.89±0.15	-0.84±0.05	0.51*	η ² =0.01
COM _f , PKAM	-0.80±0.08	-0.67±0.17	0.13*	η ² =0.06

Table 1. Descriptive statistics for COM measures and results of independent t-tests at initial contact (IC) and peak knee abduction moment (PKAM) for soccer players completing a cutting task. *Unequal variances between groups so Mann-Whitney U test utilized.

Conclusions

These results suggest that trunk COM position at initial contact and at peak knee abduction moment may not be primary factors in lower extremity risk for ACL injury during cutting maneuvers. While larger frontal plane moments have been indicated to influence risk of non-contact ACL tears in the past, the present findings do not highlight any differences. The small number of injuries that occurred in our sample suggest further study may be warranted.

Acknowledgments

Funding sources: NIH: NIH T32 HD007490.

References

- [1] Brophy et al. (2015). *Sports Health.*, 7: 244-249.
- [2] Agel J et al. (2005). *Am J Sports Med.*, 33: 524-530.
- [3] Hewett T et al (2005) *Am J Sports Med.* 33 492-501.
- [4] Hewett T et al (2009). *Br J Sports Med.*, 43: 417-422.
- [5] Zazulak B et al (2007). *Am J Sports Med.*, 35: 1123-1130.
- [6] Dix C et al (2020). *Int J Sports Phys Ther.*, 15: 928-930.

SMARTPHONE-BASED DEMOCRATIZATION OF VERTICAL JUMP HEIGHT ESTIMATE

Guido Mascia¹, Alessandro Valenti¹, Valentina Camomilla¹

¹Interuniversity Centre of Bioengineering of the Human Neuromusculoskeletal System, University of Rome “Foro Italico”, Italy

Email: g.mascia@studenti.uniroma4.it

Summary

A method for estimating vertical jump height directly from smartphone measures is presented, aiming to democratize this computation. Two multiple linear regressions, combining time-frequency and anthropometric quantities, were devised to correct for soft tissue wobbling. The height computed from force platforms measures was used as gold standard.

Introduction

Vertical jump height (h) is commonly used to analyze lower limb power generation both in clinical and sport context. Height is often computed through force platforms (FPs), although Inertial Measurement Units (IMUs) are becoming more and more popular, given their reduced cost and size. However, critical issues in h estimation with IMUs exist, mostly related to the inertial effects of wobbling masses, as part of a wider phenomenon known as soft tissue artefact (STA), also dependent on IMU location. Smartphones are devices within everyone’s reach whose internal IMUs can be exploited as a handy-but-bulky source of information. Hence, the aim of this study is to estimate accurate jump height from time-series measured with a smartphone. Reduction of STA-related errors is achieved by devising reliable multiple linear regression models (MLR) that embeds time-frequency and anthropometric quantities.

Methods

Seventeen participants (11M, 6F; age: 26.8 ± 4.7 years; height: 1.7 ± 0.1 m; mass: 72.0 ± 13.6 kg) were recruited. To each of them, biceps, triceps, subscapular, and superior-anterior iliac crest (B, T, S, and I, respectively) skinfold lengths were measured. They performed 3 countermovement (CMJ) and 3 squat (SJ) jumps on a FP, bringing the smartphone at the chest and maintaining the elbows at the waist height to limit the effects of arm swing. Smartphone measures were performed using the app Phyphox [1]. Smartphone IMU data were aligned to the world reference frame according to [2]. Variational Mode Decomposition (VMD) was applied to IMU acceleration signal to obtain three components, each centered around a central frequency [3]: the low-frequency (f_3) component was associated with the jump; the mid- and high-frequency (f_1, f_2) with the inertial effects due to wobbling masses. Moreover, the negative acceleration peak after the take-off instant (NP), the positive acceleration peak (PP) and their

ratio (R_{PN}) were taken into account as associated with upward/downward arm swing and inertial effects. Take-off velocity method was used to compute h (FP), \hat{h} (IMU) and \hat{h} (MLR). Two MLRs were devised, one for CMJ (MLR_{CMJ}), one for SJ (MLR_{SJ}). Best-subset regression method with k-fold cross validation was used to select the best subset of variables to be included in each MLR. A scheme of the procedure is presented in Figure 1.

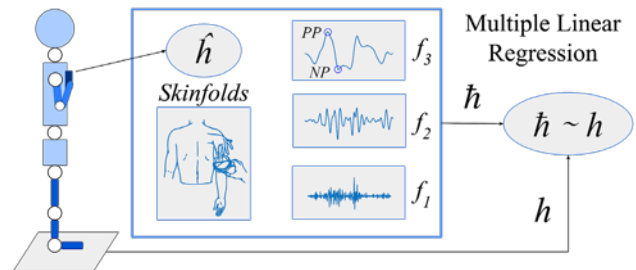


Figure 1: Schematic depiction of the procedure for \hat{h} estimation.

Results and Discussion

Mean average errors with respect to h showed that \hat{h} was erroneous by 6 ± 5 cm and 5 ± 4 cm for CMJ and SJ, respectively. The \hat{h} estimated with MLR_{CMJ} showed an average error of 2 ± 1 cm, while the one computed through MLR_{SJ} showed 2 ± 2 cm average error. MLR_{CMJ} predictors explained the 83.8% ($R^2 = .855$, $F(5, 43) = 50.66$, $p < 10^{-16}$) of h variation, while MLR_{SJ} explained the 75.9% ($R^2 = .779$, $F(4, 45) = 39.6$, $p < 10^{-14}$). The coefficients and significance levels of these MLRs are shown in Table 1. MLRs obtained without considering skinfolds had no significant predictors and poorer performance (an average error: of 3 ± 2 and 2 ± 2 cm; R^2 : .664 - .701, respectively for CMJ and SJ), and were not reported.

Conclusions

A democratization attempt for h estimation was made. The use of an unaided smartphone for h estimation led to large errors either for CMJs or SJs. The two proposed MLRs largely reduced the error in h estimation for both tasks.

References

- [1] Staacks S et al. (2018). *Phys. Educ.*, **53**: 045009.
- [2] Rantalainen T et al. (2020). *Med. Sci. Sports*, **30**: 38-45.
- [3] Dragomiretskiy K and Zosso D (2013). *IEEE Trans. Signal Process.*, **62**: 531-544.

Table 1: MLRs coefficients and their respective R^2 . Significance level legend: *** $p < 0.001$; ** $p < 0.01$; * $p < 0.05$; § $p < 0.1$.

	constant	\hat{h}	B	T	S	I	f_3	R_{PN}	R^2
MLR_{CMJ}	.385***	.101§	-.004**	-.005***	-.004**	-	-.08***	-	.855
MLR_{SJ}	.161***	.31***	-	-	-.009***	.005***	-	.034***	.779

Relationships between strength, jump and kinematic variables during resisted sled sprinting

Katja Magdalena Osterwald^{1,2}, David Kelly^{1,2}, Ciaran O Cathain^{1,2}

¹Department of Sport and Health Sciences, Athlone Institute of Technology, Athlone, Ireland

²SHE Research Group, Athlone Institute of Technology, Athlone, Ireland

Email: katja.magdalena.osterwald@gmail.com

Summary

Resisted sprinting involves adding a load to the movement of sprinting, to improve specificity and is believed to increase strength specific to sprinting [1]. However the addition of load may negatively impact running mechanics. It is to assume that maximum strength influence this change in kinematics, however this is currently unknown. The main purpose of this research was to examine the relationships between change in kinematics and 1RM back squat (BS) and hip thrust (HT) strength measures. Further, the relationships were examined between several mechanical measures assessed (1RM), vertical jumps (CMJ, DJ), and the performances obtained by athletes in different sprint distances with different loading conditions.

Introduction

Resisted sprint training increases the athlete's ability to produce horizontal and vertical forces during sprinting [2-4]. Multiple systematic reviews have demonstrated positive effects of resisted sprint training on sprint performance across multiple loading conditions. Petrakos et al. (2016) found that resisted sled sprinting is an effective method to improve sprint performance, specifically in the early acceleration phase [5]. Despite this not all findings are consistent, and this may be due to varying levels of strength [6]. It is unknown whether heavy loading is violating kinematic specificity for stronger athletes in the same manner as for weaker. This is interesting to know for coaches, as stronger athletes might be able to handle a higher overload without displaying changes in sprint kinematics.

Methods

This study analyzed the relationship between levels strength and kinematic variables of field sport athletes and sprinters while towing a sled of varying resistances (10%, 20% and 30% decreases in maximum velocity) using a between-within repeated measures design. Thirty-three athletes completed 3 testing days. This included a familiarization day and two experimental days, which were separated by a minimum of 48 hours. Participants completed numerous 40 m sprints on an indoor running track at each of the above listed loading conditions as well as 1RM and vertical jumps. Sprints were recorded for examination on two different High-Speed Cameras. Kinematic analysis was undertaken with Dartfish Software (Fribourg, Switzerland). The tools incorporated into Dartfish high speed video analysis software facilitate the slowing down and magnification of video images to calculate joint angles. Joint (trunk, hip, knee and ankle angles) and segment angle (thigh, shank, foot) variables were calculated for the two first contacts of the right foot during the acceleration and one within maximum velocity phases of each

trial [7]. All angles were measured at toe-off (TO) and touch down (TD) [8].

Results and Discussion

Significant negative correlations were found between strength measures and change in joint angles (hip, knee and trunk) for each loading condition. Further, significant negative correlations were found between maximum strength and unloaded sprint times ($r=0.44-0.47$ for BS; $r=0.71-0.72$ for HT). Significant negative correlations were found between jump height and sprint time. Controversy, no significant correlations were found between peak power and sprint time. Moreover, maximum strength measures and jump performance measures showed no correlations, except for BS and peak power of the CMJ ($r=0.77$).

Conclusions

The study indicates that stronger athletes might be able to handle a higher overload without displaying changes in sprint kinematics. This may have important implications in terms of training adaptations. Maximum strength measures may explain some of the responses of athletes during RSS and coaches should ensure athletes develop squat and HT strength.

References

- [1] Martnez-Valencia, M.A. et al. (2015). Effects of Sled Towing on Peak Force, the Rate of Force Development and Sprint Performance during the Acceleration Phase. *Journal of Human Kinetics*, **46**: 139–187.
- [2] Kawamori, N. et al. (2014b). Effects of weighted sled towing on ground reaction force during the acceleration phase of sprint running. *Journal of Sports Sciences*, **32**: 1139–1184.
- [3] Morin, J. et al. (2017). Very-heavy sled training for improving horizontal-force output in soccer players. *International journal of sports physiology and performance*, **12**: 840–844.
- [4] Morin, J.B. et al. (2012). Mechanical determinants of 100-m sprint running performance. *European Journal of Applied Physiology*, **112**: 3921–3951.
- [5] Petrakos, G. et al. (2016). Resisted Sled Sprint Training to Improve Sprint Performance: A Systematic Review. *Sports Medicine* **46**: 381–400.
- [6] Murray, A. et al. (2005). The effect of towing a range of relative resistances on sprint performance. *Journal of Sports Sciences*, **23**: 927–962.
- [7] Bergamini, E. (2011). *Biomechanics of sprint running: a methodological contribution*.
- [8] Lockie, R.G. et al. (2003). Effects of resisted sled towing on sprint kinematics in field-sport athletes. *Journal of strength and conditioning research*, **17**: 760–767.

Training to be an Olympic ski jumper in less than four years – a joint level perspective on the early development of simulated ski jump take-off performance in young athletes participating in a talent transfer program

Paavo Partainen¹, Pasi A Karjalainen¹, Lauri Stenroth¹

¹Department of Applied Physics, University of Eastern Finland, Finland

Email: lauri.stenroth@uef.fi

Summary

We investigated the development of lower limb mechanics in simulated ski jump take-off in a group of novice ski jumpers aiming for the 2022 Winter Olympics with less than four years of ski jump training and compared the novice jumpers to a group of experienced jumpers. Surprisingly, only modest differences between the novice and experienced jumpers were found after the initial few months of ski jump training and the differences were further diminished during a 6-month follow-up.

Introduction

China's talent transfer program aims for success in the 2022 Winter Olympics by recruiting young talented athletes from summer sports to winter sports. The program provides a unique opportunity to examine early sport discipline-specific development in talented athletes exposed to a new sport. The purpose of this study was to investigate how technical aspects and performance of simulated ski jump take-off (imitation jump) evolves during the initial stages of training and how they compare against experienced ski jumpers.

Methods

Thirteen young Chinese males (age 15-18 y.) aiming for the ski jump competition at the 2022 Winter Olympics with less than four years of sport-specific training participated in the study. The athletes performed five maximal effort imitation jumps while ground reaction forces and lower body kinematics were recorded with two force plates (1000 Hz) and eight cameras (250 Hz). The athletes were first tested 2-3 months after entering the program (baseline) and a second time 6 months later. Nine experienced male ski jumpers from the Finnish national team (age 19-24 y.) served as a comparison group. Lower limb kinematics and joint moments were calculated in OpenSim [1]. Joint powers were calculated as the cross-product of the joint angular velocity and joint moment. Work done at each joint was calculated as the integral of the joint power with respect to time. Joint kinematics and kinetics were compared between the groups and test sessions using statistical parametric mapping and pelvis vertical velocity at take-off and contribution of each joint to the total joint work using t-tests.

Results and Discussion

Pelvis vertical velocity at take-off increased by 6% ($p=0.010$) during the 6 months in novices but did not differ from the experienced athletes at baseline ($p=0.2103$) or at 6-month ($p=0.8109$) time points. Knee extensor moment (Figure 1) and power were higher at the early push-off and

the hip joint was more flexed throughout the movement in the experienced jumpers. In the late push-off, novices generated higher ankle power. The differences between the groups were lowered during the 6 months but remained statistically significant. At baseline, the contribution of the knee joint work to the total joint work was larger ($p=0.049$) and the ankle joint contribution was smaller ($p=0.002$) in the experienced compared to the novices. After 6 months, ankle joint contribution was still lower in the experienced compared to the novice ($p=0.010$). Greater between-jump variability was found in the novice jumpers in the knee joint angle, angle, moment, power, and work.

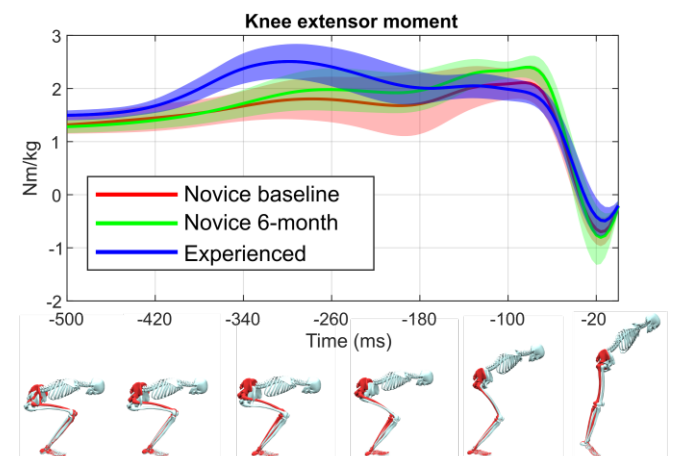


Figure 1: Knee extensor moment (mean and SD) during the push-off phase of the imitation jump from novice and experienced ski jumpers. Group average lower limb and torso kinematics is presented with the skeleton (red, novice-white, experienced). The torso is drawn only for the experienced group for clarity.

Conclusions

Ski jump take-off performance, as measured by pelvis vertical velocity at take-off, did not differ between novice and experienced ski jumpers. However, the relative contribution of joint work across the lower limb joints differed and between-jump variability was greater in the novice compared to experienced ski jumpers. The results indicate that technical rather than physical performance aspects differentiate novices from experienced ski jumpers.

Acknowledgments

The research was conducted in HUMEA laboratory of University of Eastern Finland (www.uef.fi/humea) and supported by ERDF-projects A73200 and A73241.

References

- [1] Seth A et al. (2011). *Procedia IUTAM*, 1, 212-232.

Validation of a monocular camera based method to obtain 3D kinematics in strength training

L. Noteboom^{1,2}, M.J.M. Hoozemans¹, H.E.J. Geeger^{1,2}, F.C.T. van der Helm²

¹Faculty of Behavioral and Movement Sciences, Vrije Universiteit Amsterdam, the Netherlands

²Department of Biomechanical Engineering, Delft University of Technology, the Netherlands

Email: l.noteboom@vu.nl

Summary

Camera-based motion capture has the potential to take kinematic analysis out of the lab and into the field in sports science. In the present study, the kinematic accuracy of a new deep-learning based method, requiring only one simple camera, is evaluated during strength training tasks.

Introduction

Both the state-of-the-art optoelectronic measurement system (OMS), as well as the marker-less motion capture alternative, the Microsoft Kinect, are dealing with restrictions in set-up time, capture volume and light sensitivity, which limits their applicability outside a controlled environment [1]. Recent developments in the field of deep-learning present marker-less motion capture methods, requiring only one simple camera, and therewith yielding the potential of bringing movement analysis into the field [2]. The aim of the present study is to validate the 3D kinematics obtained from this method during strength training exercises.

Methods

Five male subjects each performed fifteen repetitions of two upper-body strength exercises: the lateral fly (LF) and the biceps curl (BC). Motions were simultaneously recorded by three systems: OMS (gold standard), Microsoft Kinect and a normal camera. Two different upper-body biomechanical models were created: one for the OMS in accordance with ISB recommendations [3], and one for the marker-less systems, adjusted for the different input coordinate set. Euler angles were calculated for the shoulder [3] during the LF, and the elbow flexion angle was calculated during the BC. Statistical analysis included RMSD and Pearson's correlation (r) of joint angle time series, and an ICC agreement for peak joint angles between Camera and OMS and between Kinect and OMS.

Results and Discussion

Results are summarized in table 1. For the Kinect, compared to OMS, mean correlations ranged from weak to excellent (0.21-0.989), with mean RMSD's ranging from 5 to 13 degrees. For the camera, compared to OMS, mean correlations

ranged from moderate to excellent (0.47-0.996), with mean RMSD's ranging from 4 to 8 degrees. Thus, the camera seemed to capture these movement cycles with reasonable accuracy, and seemed to outperform the Kinect, especially in tracking the shoulder endo-/exorotation rotation angle, as shown in Fig.1, and the shoulder elevation plane angle. However, when absolute peak values were considered, the low ICC's of the camera for all angles indicated an unacceptable agreement (ICC), which appeared to be due to both systematic errors and inconsistencies between trials and individuals. Considering the agreement on peak values, the Kinect appeared to be advantageous, although still unacceptable in most cases.

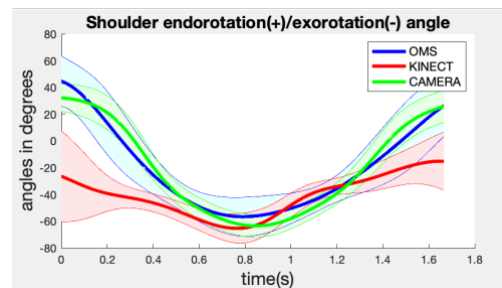


Figure 1: Shoulder endo-/exorotation angle during LF, captured by OMS (blue), Kinect (red) and camera (green), presented as mean \pm 1SD (shaded) over all trials and all subjects.

Conclusions

The deep-learning based camera method seems a promising tool to capture 3D kinematics within a sports environment, indicated by reasonable correlations and RMSD's when compared to the gold standard and Kinect. However, for capturing single (peak) values the camera method needs to be improved in future research before this method can be applied in the sports practice.

References

- [1] van der Kruk E and Reijne MM (2018). *Eur J Sport Sci*, **18**: 806-819.
- [2] Pavllo D et al. (2019). *IEEE/CVF Conference*: 7753-7762
- [3] Wu G et al. (2005). *J biomech*, **38**: 981-992.

Table 1: Between-systems RMSD and Pearson's r of joint angle time series, with Mean \pm SD over subjects, and ICC agreement on peak values.

Variable	Kinect - OMS			Camera-OMS		
	RMSD (Mean \pm SD)	r (Mean \pm SD)	ICC	RMSD (Mean \pm SD)	r (Mean \pm SD)	ICC
Shoulder elevation angle (deg)	4.79 \pm 3.88	0.98840 \pm 0.0039	0.86	3.92 \pm 4.12	0.9964 \pm 0.0019	0.30
Shoulder elevation plane angle (deg)	9.86 \pm 9.22	0.21 \pm 0.69	0.48	6.00 \pm 0.99	0.47 \pm 0.46	0.14
Shoulder endo-/exorotation angle (deg)	13.40 \pm 9.03	0.57 \pm 0.32	0.68	7.81 \pm 5.69	0.95 \pm 0.02	-0.16
Elbow flexion/extension angle (deg)	7.68 \pm 9.67	0.989 \pm 0.004	0.22	7.24 \pm 9.34	0.990 \pm 0.003	0.05

A deterministic model of the Bottom turn Technique

Micael De Sousa¹, Miguel Moreira¹, António P. Veloso¹, Vera Moniz-Pereira¹

¹ Universidade de Lisboa, Faculdade de Motricidade Humana, CIPER, LBMF, Lisboa, Portugal

Email: micaelf.sousa@gmail.com

Summary

The aim of this study was to determine the critical features of the surf Bottom-Turn (BT) manoeuvre. To accomplish this goal, a deterministic model was built. A panel constituted by biomechanists and surf coaches critically analysed the model and the derived critical features. The consensus version is now being analysed by the top National coaches so that a qualitative tool, aiming at assessing the BT technique, can be developed.

Introduction

Surf is a sport where the main manoeuvres are performed on the top of the waves. The most common trajectory, after standing up, is going down in the wave and turn to the side of the wave that will break to go up again. This manoeuvre, named Bottom-Turn (BT), is, therefore, fundamental to the ride of the surfer and one of the first to be taught.

In order to assess the BT technique, surf coaches use a qualitative approach, supported on direct or video observation., as collecting quantitative data in the sea is very difficult [4].

One important step of the qualitative approach is the development of the deterministic model. This process starts with the establishment of the main objective(s) of the task, and then progresses by identifying and judging the relationship between the result and each factor that produces the result [2], allowing a more systematic approach, and less subjected to past experience bias, determination of the critical features [6].

The purpose of this study was to establish a deterministic model and to determine the critical features of the BT technique.

Methods

MS and VMP developed the first version of the model and table of critical features based on the work done by Hay and Reid (1982) and other studies using the same approach. All doubts and disagreements were noted. Then two experts, one in biomechanics (APV) and other in surf (MM), were invited to analyse and discuss the model and the critical components. Based on all comments a consensus version was created.

Results and Discussion

The main goal of a surfer is to obtain the highest score possible. Although the BT alone is not punctuated, the fact that it will affect the score of the following manoeuvre led us to establish the judges' score as the main goal, as it is the case of other sports like gymnastics and diving [2]. The next box is the trajectory shape, which is the global criterion commonly used by the judges to distinguish a good from a

bad BT. Further, because the main goal of the BT is to place the surfer at the pocket of the wave [5] (trajectory precision) with postural control (the surfer should be able to maintain balance throughout the manoeuvre) and velocity (the surfer should arrive at the pocket of the wave with the highest possible velocity), the flowing boxes of the model include trajectory precision, postural control and velocity

Following the example of other theoretical model obtained for the Change of Direction of 90° and 180° [3] one of the factors responsible from a good precision, is the head orientation that allows the surfer to see the wave breaking and should lead the movement. The precision is further determined by the trunk rotation and body leaning into the curve that follows.

The postural control be accomplished by using a large base of support, lowering the COM [1] and leaning into the curve.

The velocity of a surfer Centre Gravity at the top of the wave, will be influenced by the velocity at the take-off and the change in velocity generated by the surfer. The first is influenced by height of the wave, the inclination of the wave and wave speed. The second, is influenced by the impulse that the surfer produces.

Both the postural control and the change in velocity are dependent on trunk and lower limb flexion-extension patterns throughout the movement.

Conclusions

A theoretical model of the BT technique was built based on Hays' framework [2]. The critical features derived from the model include: the head orientation, knee flexion/extension angle, the use of the rail (body leaning), hand positioning during body leaning, trunk rotation, and BT duration and trajectory shape. The motion was then divided in temporal phases and a table of critical components was created accordingly. We are now interviewing the top National Coaches to integrate their views and learn about their acceptance regarding the model and critical features established.

Acknowledgments

This work was supported by CIPER-FCT (project reference UID/DTP/00447/2020)

References

- [1] Forsyth JR et al (2018). *Aerial*, **28(5)**: 1615-1624.
- [2] James G. Hay. *Human Motion*, Prentice-Hall, Inc. 1982.
- [3] Hewit JK (2012). Change of direction, *7(3)*: 82-88
- [4] Mendez-Villanueva (2010). *Assessment*: 24(1): 135-139
- [5] Moreira M (2014). *Qualitative Task*, 42(42): 245- 257
- [6] Powers PNR (1999). *Biomechanical*, 19(12) 799-806

Lateral Heel Release Reduces ACL strain in Simulated Backward Twisting Falls

Ryo Ueno^{1,2}, Dieter Heinrich¹, Kurt Schindelwig¹, Nathaniel A. Gates², Nathan D. Schilaty², Werner Nachbauer¹

¹ Department of Sport Science, University of Innsbruck, Innsbruck, Austria

² Department of Orthopedic Surgery, Mayo Clinic, Rochester, Minnesota, USA

Email: ryo.ueno@uibk.ac.at

Summary

Anterior cruciate ligament (ACL) strain was estimated via a finite element (FE) knee model during various conditions of simulated backward twisting fall with and without a lateral heel release. Lateral heel release reduced ACL strain by 6-91% relative to simulations conducted with lateral toe release.

Introduction

Bindings with lateral heel release mechanism have been developed to reduce ACL injury risk in backward twisting falls, which is one of the most frequent ACL injury mechanisms in skiing [1]. However, their efficacy in the reduction of ACL loading remains unclear. The purpose of this study was to simulate the effect of lateral heel release on ACL strain during backward twisting fall simulated with a FE model.

Methods

An experimental binding release test was performed with a lateral toe release binding and a lateral heel release binding. Lateral forces were applied on the ski tail and increased until the binding released under various pre-applied normal forces (0, 0.5 and 1 body weight (BW) of 70 kg person) and load application location (25, 35 and 45 cm behind from the center of binding). Recorded release forces were applied quickly within 60 ms on a previously developed and validated specimen-specific FE knee model [2]. Inertial properties of boot-ski-binding system were added to the model. The knee angle was set at 25° and the femur was fixed. A minimal quadriceps-hamstring force of 120 N was constantly applied. The kinetic and kinematic parameters, including knee flexion angle, hip internal rotation, load application time and quadriceps-hamstrings force were changed from the highest and lowest ACL strain condition to cover more variations of backward twisting falls. The estimated ACL strain and knee kinematics up to binding release were compared between lateral toe and lateral heel release.

Results and Discussion

The lateral heel release decreased ACL strain by 6-32 % relative to lateral toe release (Fig. 1-a). The highest ACL strain of 8.1 % from a lateral toe release binding decreased to 5.7 % with a lateral heel release binding. For lateral heel release, the peak ACL strain of 6.1 % was derived from 45cm-1BW trial. The largest change in kinematics due to the lateral heel release was always found in the knee abduction angle that ranged between 11-40 % decrease relative to lateral toe release.

By changing the parameters for the base conditions (45cm-0BW as lowest and 25cm-1BW as highest ACL strain trials),

the lateral heel release decreased ACL strain by 31-91% relative to lateral toe release except for the condition with hip internal rotation (Fig. 1-b). Longer loading time of 120 ms increased ACL strain 123-168% relative to base conditions. This derived peak ACL strain of 21.7% within all simulations with lateral toe release and was decreased to 13.6% with lateral heel release.

The binding with lateral heel release includes two pivot points. It can release whenever medio-lateral force was applied on ski tip or tail [3]. The pivot is on toe for heel release whereas it is on heel for toe release. Thus, lateral heel release will be triggered with smaller lateral force due to a longer moment arm when lateral force is applied on ski tail, relative to lateral toe release. This resulted in lower knee abduction angle and ACL strain, and would decrease ACL injury risk during variations of backward twisting fall.

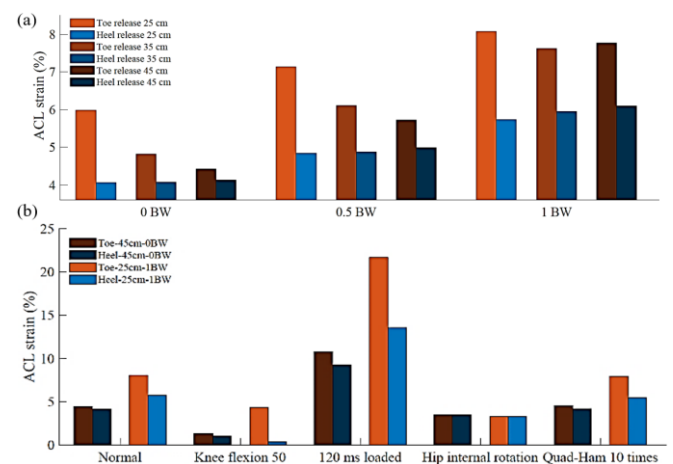


Figure 1: Comparisons of peak ACL strain between lateral toe release binding (red) and lateral heel release binding (blue).

Conclusions

Lateral heel release might reduce ACL injury risk as it decreased ACL strain during various conditions of simulated backward twisting fall compared to lateral toe release.

Acknowledgments

The authors acknowledge funding from NIH grants R01AR056259.

References

- [1] Johnson R et al. (2003). *Skiing Trauma and Safety*. ASTM International.
- [2] Navacchia A et al. (2019). *J Orthop Res.* **3**: 1730-1742.
- [3] St-Onge N et al., (2004). *Med Sci Sports Exerc.* **3**: 1218-1225.

Inertial Measurement Units to estimate drag forces and power output during standardised wheelchair tennis coast-down and sprint tests

Thomas Rietveld¹, Barry S. Mason², Vicky L. Goosey-Tolfrey², Lucas H.V. van der Woude^{1,2,3}, Sonja de Groot^{1,4,5}, Riemer J.K. Vegter^{1,2}

¹University of Groningen, University Medical Center Groningen, Center for Human Movement Sciences, Groningen, The Netherlands, ²Peter Harrison Centre for Disability Sport, School of Sport Exercise & Health Sciences, Loughborough university, Loughborough, United Kingdom, ³University of Groningen, University Medical Center, Center for Rehabilitation, Groningen, The Netherlands, ⁴Amsterdam Rehabilitation Research Center Reade, Amsterdam, the Netherlands, ⁵Department of Human Movement Sciences, Faculty of Behavioural and Movement Sciences, VU University, Amsterdam, the Netherlands
Email: t.rietveld@umcg.nl

Summary

The purpose of this study was to describe and explore an inertial measurement unit-based method to analyse drag forces and external power loss in wheelchair tennis, using standardised coast down and 10m sprint tests. Drag forces and power output were explored among different wheelchair-athlete combinations and playing conditions (tyre pressure, court surface). Eight wheelchair tennis players participated in this study. Three inertial measurement units (IMUs) were placed on the frame and axes of the wheels of their wheelchair. All players completed coast-down trials and 10m sprints with different tyre pressures on hardcourt surface. One athlete completed additional tests on a clay and grass tennis-court. A higher tyre pressure led to lower drag forces during coast-down tests on hardcourt surface. The current prediction of power output was successfully implemented during coast-down testing, unfortunately the power prediction during 10m sprints were difficult to accomplish.

Introduction

Wheelchair tennis is part of all grand slam tournaments like Wimbledon & Roland Garros. Unfortunately, there is a lack of wheelchair tennis specific knowledge. One of the key areas identified by wheelchair tennis players is the interaction between tyre pressure and surface competed on. The purpose of this study was to describe and explore an inertial measurement unit-based method to analyse drag forces and external power loss in wheelchair tennis, using standardised coast down and 10m sprint tests. Drag forces and power output were explored among different wheelchair-athlete combinations and playing conditions (tyre pressure, court surface).

Methods

Eight highly trained wheelchair tennis players participated in this study. Three inertial measurement units (IMUs) were placed on the frame and axes of the wheels of their wheelchair. All players completed a set of three standardised coast-down trials and two 10m sprints with different tyre pressures on hardcourt surface. One athlete completed additional tests on a clay and grass tennis-court.

Results and Discussion

Coast-down based drag forces of 4.8-7.2N and an external power loss of 9.6-14.4W at a theoretical speed of 2 m/s were measured on hardcourt surface. A higher tyre pressure led to lower drag forces during coast-down tests on hardcourt surface ($F_r(4) = 10.7$, $p = 0.03$) (Fig 1). For the single athlete an external power loss of 10.4, 15.6 and 49.4W respectively for the hardcourt, clay and grass. The current prediction of power output was successfully implemented during coast-down testing, unfortunately the power prediction during 10m sprints were difficult to accomplish.

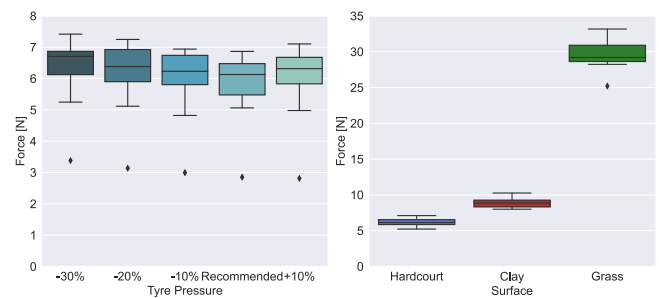


Figure 1: Differences in tyre pressures (left) and surfaces (right)

Conclusions

This research showed the added value of coast-down testing in wheelchair tennis, by the prediction of drag forces and power loss. The usefulness and sensitivity of these measures was illustrated by the negative effect of reduced tyre pressure on the necessary power output for the group of athletes. Albeit measured in only one person, court type is a more important factor to consider, with clay showing almost 1.5 times higher drag forces compared to hardcourt, while grass showed even five times higher drag forces compared to hardcourt.

Acknowledgments

The authors would like to thank the UK Lawn Tennis Association for the provided courts, players and financial resources, in particular special thanks to Alex Cockram. Also big thanks to all players for their participation.

Biomechanical alterations as potential risk factors for ACL re-injury in soccer: a systematic review

Sanchez-Alvarado A

Clinical Exercise Science, University of Potsdam, Potsdam, Germany

Email: sanchezalvarado@uni-potsdam.de

Summary

ACL injuries in soccer threaten the athlete's career as high reinjury rates remain. To ensure a safe return to sport, a comprehensive understanding of potential biomechanical risk factors being present after reconstruction is required. Therefore, this systematic review aimed to identify biomechanical alterations as potential risk factors for ACL re-injuries in soccer players. A literature search was conducted in PubMed and Web of Science databases. Article rating was based on NIH quality assessment tools, according to study type. Out of 185 unique articles, 9 met the inclusion criteria, which was restricted to case-control or prospective study designs (rated between 6-9 for the 8 case-control articles, and 8 for the prospective study). Although the occurrence of several biomechanical alterations was identified, their predictive value for ACL re-injury is limited as only one prospective study was included, and therefore, their clinical relevance remains unclear.

Introduction

A high rate of Anterior Cruciate Ligament re-injury in athletes has been reported in the literature [1,2]. Biomechanical alterations have been identified in soccer player following the initial ACL injury, however, their clinical relevance and predictive value for future ACL injuries remains in discussion [3,4]. Therefore, this systematic review aimed to identify potential biomechanical alterations associated with an ACL re-injury as risk factors in soccer players.

Methods

This systematic review followed the PRISMA guidelines, and the literature search was conducted in PubMed and Web of Science databases until December 2020. The inclusion criteria were defined as: (1) investigations of ACL re-injuries in soccer with functional, kinematic, and kinetic outcomes, (2) case-control (CC) or prospective study (PS) designs, and (3) English language only. Study quality was rated by the NIH quality assessment tools (NIQA), based on study type (both out of 12 total points). The alterations were divided into differences between ACLR and controls (CAC), and intra-individual ACLR differences (IAD).

Results and Discussion

Nine out of 185 unique articles met the inclusion criteria. There were 8 CC studies (NIQA: 6-9), and 1 PS (NIQA: 8). Table 1 displays the summarized significant mean differences found between groups (CAC) and intra-individuals (IAD).

The highest significant differences in soccer players with ACLR compared to controls, respectively, (3 CC, NIQA: 7-9)

revealed increased asymmetries in jump height ($24.1 \pm 13.7\%$ vs $10.5 \pm 7.8\%$), and Reactive Strength Index asymmetries ($27.9 \pm 14.5\%$ vs $13.1 \pm 9.9\%$) during 10 seconds vertical hops (10SVH) tests and higher variability couplings angles (mean difference 23.3° vs 16.2°) in a side-cutting maneuver (SCM). Five CC showed increased landing errors, lower jump distances, lower hip abduction, and external rotation, lower ankle inversion, and higher knee extension angles during jump-based assessments.

Other reported assessments were countermovement jump (CMJ), single-leg drop vertical jump (SLDVJ), isokinetic testing at $60^\circ/s$ and $300^\circ/s$ (IK60, IK300), and leg-press tests.

Table 1: Summary of highest significant differences

Category	Study type	Significant differences (mean difference)
BAC	CC	<ul style="list-style-type: none"> ↑ jump height asymm. (13.6%) @10SVH ↑ RSI asymm. (14.8%) @10SVH ↑ joints variability (7.05°) @SCM ↑ LESS in a fatigued state (3 err.) @CMJ ↓ gastrocnemius EMG ($\approx 10\%$) unplan.
IAD	CC	<ul style="list-style-type: none"> ↓ jump height (3.2 cm) inv. leg @10SVH ↓ RSI (0.11 m/s) inv. leg @10SVH ↓ RSI (0.16 m/s) inv. leg @SLDVJ ↓ peak torque (48%) inv. leg @IK60 ↓ peak torque (27%) inv. leg @IK300 ↓ hip flex. angle (21.28°) unplan. ↓ knee flex. angle (22.67°) unplan. ↓ hip ext. moment (0.57 Nm/kg) unplan. ↓ peak pressure (115.17 KPa) unplan.
	PS	<ul style="list-style-type: none"> ↓ RFD ($>20\%$) @6 mo. vs preinjury

Intra-individual comparisons in ACLR athletes displayed main differences between involved (inv.) and uninvolved legs, and unplanned (unplan.) and planned landing, during jump-based and isokinetic testing. Finally, one prospective investigation found an increased risk of re-injuries by reduced rates of force development (mean difference $\approx 20\%$) during isometric leg-press tests after 6 months of ACLR.

Conclusions

Despite the occurrence of several biomechanical alterations, their predictive value is limited as only one prospective study was included. Without further longitudinal investigations the clinical relevance of found alterations remains unclear.

References

- [1] Wiggings A. et al. (2016). Am J Sports Med, **44**: 1861-1876.
- [2] Paterno M. (2014) Am J Sports Med, **42**: 1567-1573.
- [3] Colpi P. et al. (2016). Muscles, Ligaments Tendons J., **4**: 480-485.
- [4] Paterno M. et al. (2017), OJSM, **4**: 1-7

The Simulation of Kayak Paddle Blade Based on Individual Stroke Technique Characteristics

Andrey Pomerantsev

Institute of Physical Education and Sports, Lipetsk State Pedagogical P. Semenov-Tyan-Shansky University,
Lipetsk, Russia

Email: a.pomerantsev.1981@gmail.com

Summary

Spatial reconstruction of the real stroke underwater trajectory allowed identifying the individual characteristics of the kayaking technique. Simulation of hydrodynamics forces based on genuine blade geometry and real stroke trajectory let to see the shortcomings of existing paddles. Besides that the proposed approach allowed to simulate the most appropriate paddle for a particular athlete considering his technique features.

Introduction

Sports technique of each athlete is unique [1]. The aim of the study was to model the paddle that takes into consideration the individual biomechanics characteristics of the technique.

Methods

Two high-speed video cameras Fastec InLine (1000 fps) were used to fix the coordinates of markers placed on surface part of the paddle. Using this data 3D underwater stroke trajectory was reconstructed (Figure 1).

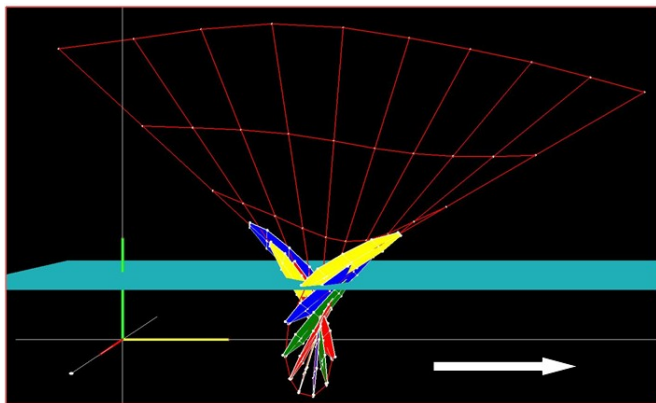


Figure 1: Spatial reconstruction of the stroke trajectory

The next step was virtual reconstruction of the genuine blade geometry and its integration with real stroke trajectory. Pressure at each point of the blade was calculated using computer simulations. Pressure depended on hydrodynamic characteristics incoming water flow and the orientation of the blade in space [2]. We determined the combinations hydrodynamics forces (drag and lift) for all parts of the blade as well as the spatial superposition of forces and its projection on the course of the kayak [3]. After that we started to change paddle blade form. During numerous iterations with various blade parameters (spatial petals orientation, petals area) optimal geometry of the paddle was found. The

hypothetical paddle will maximally appropriate for specific athlete with unique technique.

Results and Discussion

The study revealed that different blade areas have different efficiency in performing the stroke. The maximum efficiency is registered on the distal section of the blade. This paddle part provides the greatest propulsive effect on the boat during entire stroke. The proximal blade section produces a braking effect colliding with incoming flow of water by outer side of the paddle.

The calculated blade is still theoretical (Figure 2). When creating a physical model it may be difficult to provide strength for a multiblade paddle. Another scientific dilemma is that the new paddle will change the hydrodynamic forces. It means that the kayaking technique will change and the athlete will not be able to repeat the same trajectory.

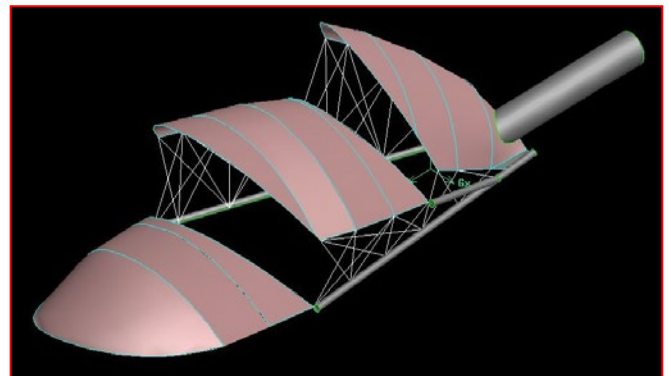


Figure 2: Multiblade paddle

Conclusions

A new approach to design of paddle blade based on the spatial reconstruction of the stroke. It contains a huge potential for improving sports paddles taking into consideration the individual features of the sport technique.

Acknowledgments

The author is grateful to a member of the Russian national canoe team Kirill Luchkin for his participation in the study.

References

- [1] Warmenhoven J. et al. (2018) *Sports Med.*, **48**: 2703–2714.
- [2] Caplan N. et al. (2007) *J. Sports Sci.* **25(9)**: 1025–34.
- [3] Morgoch D. et al. (2016) *11th conf. of the ISEA*, Delft.

Toe flexor strength in elite female gymnasts compared to toe flexor strength trained men

Philipp Goldmann^{1,2}, M. Sedler^{1,2}

¹Institute of Biomechanics and Orthopaedics, German Sport University Cologne, Germany

²German Research Centre of Elite Sport, German Sport University Cologne, Germany

Email: goldmann@dshs-koeln.de

Summary

The strength of toe flexor muscles (TF) seems to create a good prerequisite for jump performance. Since gymnastics is a typical jumping and landing sport, we expected increased TF strength in elite gymnasts. The analysis showed that elite female gymnasts' TF revealed 80% to 86% higher strength compared to male sport students, and the same strength level compared to TF strength-trained men. TF in elite gymnastics seem to be highly loaded and have to be of particular interest for training and performance enhancement.

Introduction

There is some evidence that intrinsic foot muscles propel the body forward during locomotion [1]. Nearly 80% of intrinsic foot muscles consists of toe flexor muscles (TF) [2] proceeding from the heel to the distal phalanges of the toes. TF strength capacity has the potential to enhance jump performance [3]. Since the ability to jump is a performance-limiting factor in gymnastics, we hypothesized that elite female gymnasts' TF strength is higher than in male sport students, but similar to TF strength-trained men.

Methods

28 female gymnasts (15 ± 2 y, 47 ± 9 kg, 1.56 ± 0.09 m) of the German national team and a basic control group of sport students ($n = 28$, 25 ± 3 y, 77 ± 8 kg, 1.83 ± 0.06 m) performed three maximum voluntary isometric contractions (MVC) of TF for each foot. TF strength was determined by measuring the moment about the transverse axis of a custom-made dynamometer in 25 degrees toe dorsiflexion. The external moments of force about the axis represented the moments of force produced by the TF [3]. The best of three trials was used for further analysis. Peak moments were determined as the mean value of a 2 s time window of the plateau region. Data were compared to a previous study with the same dynamometer, where a TF strength training group (15 men, 24 ± 4 y, 77 ± 9 kg, 1.85 ± 0.07 m) performed a heavy resistance TF strength training with 90% of MVC for 7 weeks [3]. Statistics: Kolmogorov-Smirnov, unpaired t-test.

Results and Discussion

TF strength significantly differed ($p < 0.001$) between elite female gymnasts (left: 0.41 ± 0.08 Nm kg⁻¹, right: 0.45 ± 0.09 Nm kg⁻¹) and male sport students (left: 0.22 ± 0.05 Nm kg⁻¹, right: 0.25 ± 0.06 Nm kg⁻¹). There were no significant differences ($p > 0.05$) between the TF strength of elite female gymnasts and the male strength training group after 7 weeks of TF strength training (left: 0.38 ± 0.07 Nm kg⁻¹, $p = 0.07$, right: 0.40 ± 0.08 Nm kg⁻¹, $p = 0.07$).

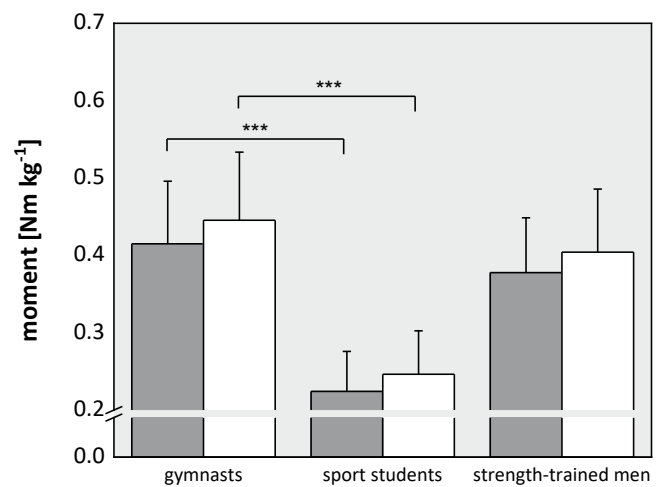


Figure 1: Moments about the dynamometer's axis normalized to body mass caused by TF contraction for the left (grey) and right (white) foot ($p < 0.001$)

Adolescent female gymnasts showed 80% to 86% higher TF strength than male sport students, but nearly the same strength level as adult men after 7 weeks heavy resistance TF strength training [3].

Conclusions

TF in elite gymnastics seem to be highly loaded and have to be of particular interest for training and performance enhancement.

References

- [1] Farris et al. (2019). *PNAS*, **116**: 1645-1650.
- [2] Kura et al. (1997). *Anat Rec*, **49**: 143-151.
- [3] Goldmann et al. (2013). *J Sport Sci*, **31**: 424-433.

The applied analysis of kayaking ergometer with different drag resistance in kayak training: a plot study

Jiaxiang Yan^{1,3}, Zhiqiang Liang², Jianshe Li^{1,3}

¹ Faculty of Sports Science, Ningbo University, Ningbo, China

² School of Kinesiology, Shanghai University of Sport, China

³ Research Academy of Grand Health, Ningbo University, Ningbo China

Email: jiaxiang0016@163.com

Summary

The purpose of this study was to evaluate the effect of two different kayaking ergometers (wind resistance, KWR; electronic resistance, KER) on training. Six elite male kayakers executed three trainings of 200m, 500m and 1000m on-water (TW) and two kayak ergometers. The significance testing was used to analyze the difference between KWR and KER on TW, the coefficient of variation (CV) was used to analyze the working stability of the two ergometers. The results showed that no significant difference was found between the TW and the two ergometers performance on 200m. In 500m and 1000m, the two kayak ergometers showed poorer sport performance than the TW. In addition, the results also show that both kayak ergometers have good stability. Therefore, KWR and KER can be used by athletes as a training device. But an athlete's TW performance could not be predicted by KWR and KER.

Introduction

Most kayakers rely on ergometers for training, especially in winter seasons [1,2]. The KWR calculate power via a mathematical relationship with the angular velocity of the flywheel. About KER, on the other hand, does not use the same approach [3]. Therefore, the purpose of this study was to analyze of kayaking ergometer with different drag resistance in kayak training.

Methods

Six elite male kayakers volunteered to participate in the study (age: 17±1 years; Height: 182±4.45cm; Weight: 75.5±5.47kg; Training years: 4.67±0.47 years).

The test was conducted on six separate days, it was performed on TW and two kayak ergometers respectively, in randomised order. Three different distances of 200m, 500m and 1000m were tested. Before the each test, the athletes had a 15-minute warm-up followed by a 2-minute rest. Participants were asked to perform at the highest level throughout the test on TW and on two ergometers.

The participants' performance on TW was collected by the testers, and the measured data on the display of the ergometers was downloaded. Shapiro-Wilk's Test was used to test the normal distribution of the data. Since the data were normally distributed, the independent samples T-test was used to test the significance of the TW and two ergometers performance. CV was used to analyze the stability of KWR and KER in test. Data were analyzed using SPSS 19.0 statistical software, and the significance level was set at $P < 0.05$.

Results and Discussion

In the 200m race, the difference between the two kayak ergometers and the TW performance was not found ($P > 0.05$) (Table 1). In 500m and 1000m sports, the two kayak ergometers showed slower athletic performance than TW ($P < 0.05$). Kayakers increase thoracolumbar extension and wider lateral bending range of motion during on water kayaking [4], over a long period of kayaking, these differences are magnified. The CV has good consistency when less than 10% [5]. Two kayak ergometers possess a stable CV (2.77 - 9.8 %) (Table 2).

Conclusions

These findings show that both kinds of kayak ergometers have good stability in operation. They can be used by athletes as a kind of land training device. But, an athlete's TW performance could not be predicted by KWR and KER.

References

- [1] Fleming N et al. (2012). *Journal of sports science & medicine*, 3: 430-437.
- [2] Fleming N et al. (2012). *Journal of sports science & medicine*, 1: 16-25.
- [3] Borges T O et al. (2017). *Int J Sports Physiol Perform*, 1-12.
- [4] Klitgaard K K, et al. (2020). *European Journal of Sport Science*, 21-25.
- [5] Jaqueline Alves Araújo et al. (2020). *International Journal of Sports Medicine*.

Table 1: Significance testing value of TW and two kayak ergometers performance.

Ergometer	200m	500m	1000m
WKR	0.631	0.018	0
WER	0.888	0.007	0

Table 2: Typical Error of the Estimate as a Coefficient of Variation.

Ergometer	200m	500m	1000m	Time	Pace	Speed	Watts	Consume
WKR	3.74%	6.58%	2.98%	2.77%	3%	2.77%	7.9%	5.73%
WER	3.26%	9.8%	4.6%	5%	3.87%	4.6%	7.57%	8.4%

Joint moments have greater impact on vertical jump height than joint angular velocities

Marin Zedler^{1,2}, Jan-Peter Goldmann^{1,2}

¹Institute of Biomechanics, German Sport University Cologne, Cologne, Germany

²German Research Centre of Elite Sport Cologne, German Sport University Cologne, Cologne, Germany

Email: m.zedler@dshs-koeln.de

Summary

The differences in joint moments and joint angular velocities between good and poor performers of the countermovement jump (CMJ) were investigated ex-post-facto. Good performers showed sig. higher joint moments and joint angular velocities at the hip, knee, and ankle joint than poor performers (except for hip angular velocity). Since the effect sizes were greater in favor of joint moments, the authors suggest that it is more crucial to provoke high joint moments in athletic training rather than high angular velocities to improve the performance of ballistic movements such as the vertical jump.

Introduction

The ability to maximally accelerate one's body from rest or after a preceding countermovement is a critical limitation in athletic performance (e.g. vertical jumping). To accelerate the body's COM during a vertical jump, the hip, knee, and ankle joint must generate a high mechanical power. Since joint mechanical power is the product of joint moment and joint angular velocity, a given power output can be achieved by different relative contributions of those two components. Good performers of the vertical jump show higher mechanical power at the hip, knee, and ankle joint than poor performers [1]. Moreover, it is valuable knowledge for athletic coaches if there are differences in the joint moments and joint angular velocities between good and poor performers.

Methods

An ex-post-facto-experiment has been applied to the database of the German Research Centre of Elite Sport Cologne, which encompasses vertical jump performance diagnostics of young athletes in North-Rhine-Westphalia (10 infrared cameras, 120 Hz, VICON Motion Systems, Oxford, UK; 2 force plates, 1080 Hz, Kistler Winterthur, Suisse; inverse two-dimensional model Alaska Dynamicus, Alaska, Chemnitz, Germany). For the analysis, the database was sorted by countermovement jump height resulting in a group of *good* (0.35 - 0.40 m jump height, n = 52, male, 17.4 ± 3.5 yrs., 70.2 ± 12 kg) and a group of *poor* (0.20 - 0.25 m jump height, n = 52, male, 14.4 ± 1.4 yrs., 60.0 ± 11.7 kg) performers. The group differences in the time series of hip, knee, and ankle joint moments and angular velocities were investigated by using statistical parametric mapping.

Results and Discussion

During the negative phase of the CMJ there is no difference in the angular velocities between *poor* and *good*, whereas during the positive phase, the *good* group shows sig. greater peak angular velocities at the knee (105.1 ± 12.3°/s, p = 0.001) and ankle joint (99.4 ± 14.9°/s, p = 0.01) than the *poor* group (93.3 ± 13.6°/s, 87.3 ± 17.6°/s). Regarding the external joint flexion moments, a sig. difference between the two groups was found for all joints. The joint moments of the *good* group were sig. higher at the hip (1.9 ± 0.4 Nm/kg vs. 1.4 ± 0.3 Nm/kg, p = 0.001), knee (1.1 ± 0.2 Nm/kg vs. 0.9 ± 0.2 Nm/kg, p = 0.001) and ankle joint (1.5 ± 0.2 Nm/kg vs. 1.2 ± 0.1 Nm/kg, p = 0.001) than those of the *poor* group. Additionally, the effect sizes of the differences in joint moments were larger than the effect sizes of the differences in angular velocities (hip: d = 1.7 (0.3), knee: d = 1.0 (0.8), ankle: d = 2.1 (0.7)), which indicates that the ability to generate higher joint moments might be more crucial in the performance of vertically directed ballistic movements than joint angular velocities.

Table 1: Peak joint moments and angular velocities at the hip, knee and ankle joint during maximal CMJ (* sig. difference to low).

	Joint Moment [Nm/kg]		Angular Velocity [°/s]	
	<i>poor</i>	<i>good</i>	<i>poor</i>	<i>good</i>
Hip	1.4 ± 0.3	1.9 ± 0.4***	44.7 ± 8.8	47.3 ± 7.5
Knee	0.9 ± 0.2	1.1 ± 0.2***	93.3 ± 13.6	105.1 ± 12.3***
Ankle	1.2 ± 0.1	1.5 ± 0.2***	87.3 ± 17.6	99.4 ± 14.9**

The difference in hip moments was present for the longest time during the jump phase (58-94 %), which confirms the importance of this joint also found by [2]. Interestingly, the higher hip moments did not lead to a significant increase in hip angular velocity, which implies a proximal to distal energy transfer through biarticular muscles [3].

Conclusions

These findings suggest that athletic training should focus on provoking high joint moments rather than high angular velocities to improve vertical jump height.

References

- [1] Lees M, Kanelis (2007). *SLE Conference*, 19-21.
- [2] Lees et al. (2004). *J Strength Cond Res*, 18(4), 787-791.
- [3] Jacobs et al. (1996). *J Biomech*, 29(4), 513-523.

Kinematics of elite board paddling in rescue sports

Stefan Kratzenstein^{1,2}, E. Prella³, T. Franz³ & J. Wohlers²

¹CAU Motion Lab, Kiel University, Germany, ²Institute of Sport Science, Kiel University, Germany

³DLRG Rescue Sports, Team Germany

Email: stefan.kratzenstein@email.uni-kiel.de

Summary

The systematic optimization of movement strategies in board paddling requires the identification of relevant kinematical parameters. In rescue sports, these parameters only exist as trainer's experiences and individual case observations, which need to be validated considering the competition-specific profile. In this pilot study, the movements of 16 athletes of Team Germany are recorded during a 5-minute all-out ergometer test to (1) validate existing movement guidelines, (2) evaluate the use of a new paddle ergometer, and (3) derive specific questions for further analysis. The analysis of the shoulder, hip, and knee joint movements resulted in significant correlating movement patterns. Only two athletes differed from the group by a significantly more upright upper body posture. The results emphasized the need to include performance parameters to conclude the effectiveness of the movement pattern. Specific questions about the role of movement specialization and the transferability of lab results to open water conditions were derived.

Introduction

Board paddling is a discipline of beach competitions in rescue sports. The lack of a description of the basic paddling movement restrains the evaluation of techniques that deal with external environmental conditions (e.g. waves) and for coping with tactical manoeuvres on water. The athlete's motor competence is considered to be an intentional variation of a basic movement pattern to solve the situational task. Thus, this study aimed to analyse the kinematics of board paddling under standardized conditions to systematically derive further questions regarding the more complex situation on the water during races.

Methods

16 elite athletes from Team Germany (8 males, age 22±3 years) were analysed. It was assumed that the movement patterns of this cohort are highly automated. Nevertheless, the athletes had no experience of paddling on the ergometer, which was developed exclusively for this study. The ergometer (WEKA Sport, Powerbox, AUT, Fig.1) had independent parallel ropes with flat hand paddles. The maximum braking power was 60kg per rope.

The 3D motion analysis included the analysis of the right shoulder, hip, and knee joints in the sagittal plane and was conducted with an inertial measurement unit system (Noraxon, myo-motion, US). The warm-up was followed by a calibration of the sensors and a 5-minute all-out test, which corresponded to a competition-specific load protocol. 30s time segments were recorded in the 1st, 3rd, and final minute.

An ANOVA was conducted to prove the data for differences between athletes and between time points.

Results and Discussion

Significantly correlating movement patterns and no differences between kinematic parameters were found for all joint angles within the entire cohort. The only exceptions were found for two athletes who paddled with an elevated centre of mass position. Further studies are required to investigate if this posture is intended to allow dynamic reactivity and is therefore a result of the athletes' specialization in a heavy swell.

In addition, all athletes reported that ergometer paddling differs significantly from paddling on the water in terms of intensity, volume, and body posture. The following investigations need to compare the ergometer directly with paddling on water to evaluate the transferability of the analysis output of standardized ergometer analyses to training practice.

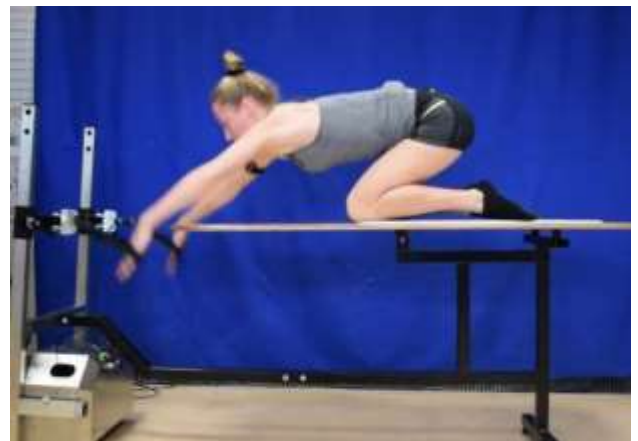


Figure 1: Athlete in catch position on the board paddle ergometer.

Conclusions

In this study, we quantified the basic movement of elite athletes. Further questions were systematically derived from the results, which are fundamental for subsequent projects, which aim to identify the individuality of the athletes and to develop standardized movement and performance analysis.

Acknowledgments

We acknowledge the support of Jana Emken during the data collection and the reliable cooperation with Team Germany and the DLRG.

EFFECTS OF TAI CHI EXERCISE ON POSTURAL STABILITY AMONG THE ELDERLY DURING STAIR DESCENT UNDER DIFFERENT LEVELS OF ILLUMINATION

Yaya Pang¹, Li Li², Qipeng Song¹

¹College of Sports and Health, Shandong Sport University, Jinan, China

²Department of Health Sciences and Kinesiology, Georgia Southern University, Statesboro, 30460, USA

Corresponding author: Dr. Qipeng Song, songqipeng@sdpei.edu.cn

Summary

The elderly prone to stair descent falls under low illumination. Tai Chi, a traditional Chinese conditioning exercise, has been proved to improve postural stability by altering movement pattern, gait, and proprioception. This study investigates whether Tai Chi exercise could improve postural stability during stair descent under high and low illumination. Three groups of elderly women who practice Tai Chi, brisk walking, and no exercise were included. They descended from a simulated staircase. Decreased horizontal velocity, center of mass (COM) sway, and increased foot clearance were observed among the Tai Chi group, compared with other groups. Compared with under high illumination, Tai Chi participants decreased horizontal velocity, loading rate, braking impulse, and increased inclination angle COM sway, center of pressure displacement under low illumination. Tai Chi participants were more sensitive to the difference in illumination and took corresponding strategies to stabilize their bodies during stair descent.

Introduction

Recent reports have identified that stair gait falls account for 26% of all self-reported falls [1] and have become the leading cause of accidental death for the elderly [3]. Stair descent imposes significant challenges to movement control in people of all ages [2], but especially to the elderly due to the functional decline in many of their physiologic systems. Tai Chi is a traditional Chinese conditioning exercise. It has been proved that Tai Chi could improve postural stability in the elderly by altering their movement pattern, gait, and proprioception [4,5]. A kind of exercise that could improve postural stability in the elderly during high-risk activities, such as stair descent under low illumination, remains unclear.

Methods

Three groups of elderly women who practice Tai Chi (TC), brisk walking (BW), and no exercise (NE) were included. Each participant was asked to complete one testing session per day for a total of three testing sessions. In each session, the participants were asked to descend the staircase step over step under different illumination conditions. A simulated staircase with six steps was constructed for data collection in this study. Two force plates (KISTLER, 9287BA and 9281CA, Switzerland) were embedded in the third and fourth steps, to collect ground reaction force data at a sample rate of 1000 Hz. The stair descent test was recorded (100 Hz) by an eight-camera motion analysis system (Vicon, Oxford Metric, England). Descriptive analysis was conducted with the mean and

standard deviations for both kinematic and kinetic variables. Subgroup comparisons were assessed via respective 95% confidence intervals of mean difference. The confidence interval of mean difference values between groups was calculated by using the one-way ANOVA post hoc pairwise comparison with Bonferroni adjustment. The confidence interval of mean difference values between two illumination levels was calculated by using paired-sample t-test.

Results and Discussion

Horizontal velocity was lower in TC group compared with BW group (95% CI: -125.09 to 3.46) and decreased under low illumination in TC (95% CI: 15.23-105.07) and BW groups (95% CI:54.22-99.78). TC group had a greater foot clearance than BW (95%CI: 24.96-45.41) and NE (95% CI: 3.39-38.93). There were no significant group differences for head and trunk inclination angles. Under low illumination, the TC group had a higher head inclination angle (95% CI: -8.03 to -1.32), whereas BW and NE groups had higher trunk inclination angles (95% CI: -4.38 to -0.99; -4.06 to -1.47, respectively). TC group had a smaller COM_{ml} Sway than walking (95% CI: -19.32 to 0.31) and no exercise participants (95% CI: -23.97 to -3.59). All the three groups increased their COM_{ml} Sway (95% CI: -15.26 to -5.87, -18.15 to -4.32, -11.08 to -2.19, respectively) under low illumination. TC group had a lower loading rate than the BW group (95% CI: -5.75 to -0.02). Under low illumination, TC group decreased their loading rate (95% CI: 0.86-4.34), braking impulse (95% CI: 0.001-0.005), and increased their COP_{ap} (95% CI: -92.76 to -2.82) and COP_{ml}(95% CI: -26.50 to -3.47). Under low illumination, BW group increased their COP_{ml} (95% CI: -34.07 to -2.08).

Conclusions

TC group adjusted their movement pattern to increase postural stability during stair descent. Furthermore, the TC group were more sensitive to the difference in illumination and took corresponding strategies to stabilize their bodies during stair descent.

References

- [1] Antonio et al (2014). *Gait Posture*, **40**(3):429-434.
- [2] Novak et al (2012). *Applied Ergonomics*,**52**:275-284.
- [3] Buckley et al (2005). *Gait Posture*, **22**(2):146-153.
- [4] Chang et al (2016). *Research in Sports Medicine (Print)*, **24**(1):84-93.
- [5] Sun et al (2016). *Research in Sports Medicine (Print)*, **24**(2):145-156.

Effect of exercise on muscle oxygen saturation during the posterior 11 hours

A. Gandia-Soriano¹, I. Catalá-Vilaplana², M.T. Pellicer-Chenoll³, J.L. Bermejo-Ruiz³, A. Encarnación-Martínez², J.I. Priego-Quesada^{1,2}

¹Biophysics and Medical Physics Group (GIFIME), Dept of Physiology, University of Valencia, Valencia, Spain

²Research Group in Sport Biomechanics (GIBD), Dept of Physical Education and Sports, University of Valencia, Valencia, Spain

³Dept of Physical Education and Sports, University of Valencia, Valencia, Spain

Email: j.ignacio.priego@uv.es

Summary

The objective of this preliminary study was to assess the effect of exercise on muscle oxygen saturation (SmO₂) in the posterior hours. Higher values of SmO₂ were obtained after exercise, with the peak value 5h after exercise.

Introduction

The interest in measuring SmO₂ during exercise using near-infrared spectroscopy (NIRS) methods is increasing due to its non-invasive nature and price affordability [1]. SmO₂ measurement has been observed as a useful physiological indicator of athlete's exertion [1] or muscle oxygenation availability during exercise in different hypoxia scenarios [2].

However, there is a lack of knowledge about if SmO₂ values could be related with the fatigue level after exercise. Therefore, the objective of this preliminary study was to assess the effect of exercise on SmO₂ in the posterior hours.

Methods

13 physically active participants volunteered to participate in the study (mean ± standard deviation: age 38 ±7 years, height 174.5 ±8.0 cm, body mass 74.5 ±9.6 kg and body fat percentage 16.7 ±6.2%). Participants signed the written consent form, and the study was approved by the University of Valencia ethics committee. From the 13 participants, 6 participated as control and 7 as experimental. SmO₂ of experimental participants were measured between 7:30 and 8:30 am (pre), then they performed exercise and were measured immediately after exercise (Post), 2 h, 5 h and 11 h after exercise (Post2, Post5, Post11). Exercise consisted in running 10 km at competition pace and performing 2 sets of 5 repetitions of 10m sprints. Controls did not perform exercise and were not measured in the Post moment (condition).

SmO₂ was measured using the NIRS instrument Humon. Humon was attached to the middle of the participant's quadriceps using a strap with a hook-and-loop fastener. Measurement was performed during 3 min and mean, minimum and maximum values of SmO₂ were obtained using a Garmin watch (model Fenix 5) and the Wko 5 application. Due to the low sample size, differences between control and experimental groups were assessed using Cohen's d Effect Size (ES).

Results and Discussion

Similar results were obtained for mean, minimum and maximum values. Experimental and controls did not differ in the Pre measurement (ES=0.1), but after exercise, experimental groups presented always higher values (ES=0.6 in Post2, and ES=0.5 in Post11), with the higher differences in the Post5 (ES=2.5) (Figure 1).

Conclusions

The preliminary results of this study suggests that SmO₂ data could be used as an indicator of the posterior physiological effect of exercise. Future studies should increase sample size and test the effect of different fatigues.

Acknowledgments

This study was funded by "Conselleria de Innovación, Universidades, Ciencia y Sociedad Digital de la Generalitat Valenciana" (Proyectos Emergentes GV/2020/050).

References

- [1] Farzam P. et al. (2018). *Physiol. Rep.*, **6-7**: e13664.
- [2] Girard O. et al. (2021). *Eur J Appl Physiol*, **121**: 95-107
- [3] Crum E.M. et al. (2017). *Eur J Sport Sci*, **17-8**: 1037-1043

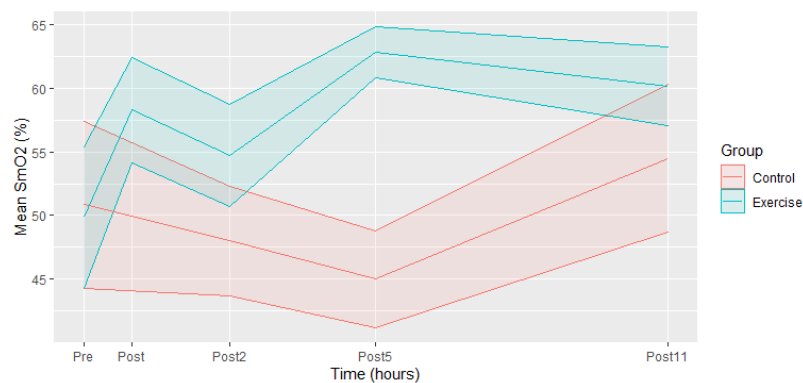


Figure 1: Mean ±SD of mean muscle oxygen saturation (SmO₂) of control and experimental groups.

Mechanical work as a (key) determinant of metabolic cost in human locomotion: handcycling and handcycling-driven watercraft

Luca P. Ardigo¹, Gabriela Fischer²

¹Department of Neurosciences, Biomedicine and Movement Sciences, University of Verona, Italy

²Department of Physical Education, Federal University of Santa Catarina, Florianópolis, Brazil

Email: luca.ardigo@univr.it

Summary

It were reviewed recent findings on the mechanical determinants of metabolic cost during human locomotion, obtained by using a mechanical approach based on the König theorem (the “Fenn-Cavagna-Minetti” approach, FCM). Recent developments in analytical methods and of their applications allowed to better understand the mechanical-bioenergetic interaction in handcycling and handcycling-driven navigation. In spite of some investigations on biomechanics and bioenergetics variables other than total mechanical work, FCM was applied to the study of handcycling by Fisher [1] who, beyond the power against air resistance (W'_a) and rolling resistance, (W'_r) computed also the power needed to sustain the movements of the whole-body center of mass of the handbike-subject complex (W'_{bcom}). Over the investigated speed range, W'_a and W'_r in addition to W'_{bcom} (substantial fraction of total external power) were observed to increase with effect on a *pendulum*-like energy recovery, too. FCM could be applied to studies on handcycling-driven navigation, as well.

Introduction

Handcycling is a relatively new mode of paracycling available to athletes with disabilities. Over the years, investigated physical activity variables (besides performance time and distance travelled) have been related to handbike configuration, body segments and crank kinematics and submaximal or peak/*maximum* (crank) power output [1]. Researches have also investigated metabolic variables such as aerobic/anaerobic threshold, peak/*maximum* heart rate, oxygen consumption [1], lactate concentration, respiratory exchange *ratio*, rates of perceived exertion, locomotion (apparent) efficiency (total mechanical work/metabolic cost of transport [CoT] [1]) and muscular activation. It were reviewed recent findings on the mechanical determinants of CoT during handcycling and handcycling-driven navigation, obtained by using FCM [2,3].

“Fenn-Cavagna-Minetti” approach in handcycling

The “Fenn-Cavagna-Minetti” approach was applied to the study of handcycling by Fisher [1] who, beyond W'_a and W'_r , computed also W'_{bcom} . Over the investigated speed range (2.8-8.5 m s⁻¹), W'_a was observed to increases from 6 to 145 W, W'_r from 27 to 54 W (with lower values on macadam compared with tartan) and W'_{bcom} from 10 to 57 W (Figure 1). The latter is thus a substantial fraction total external power (~20%). In addition, in the study of Fisher [1], energy recovery was observed to range from 40 to 50% (and to decrease linearly with speed) suggesting some *pendulum*-

like energy-saving mechanism (Figure 2), and the mechanical internal power was observed to be almost negligible (5-7 W).

Handwaterbike

A spin-off topic is represented by biomechanical and energetic assessment of synchronous arm cranking with human powered watercrafts (i.e. the handwaterbike) for people with disabilities [4]. The FCM could be used in this contest, as well as in future studies on handcycling, to provide researchers and disability field professionals with original and applicable findings.

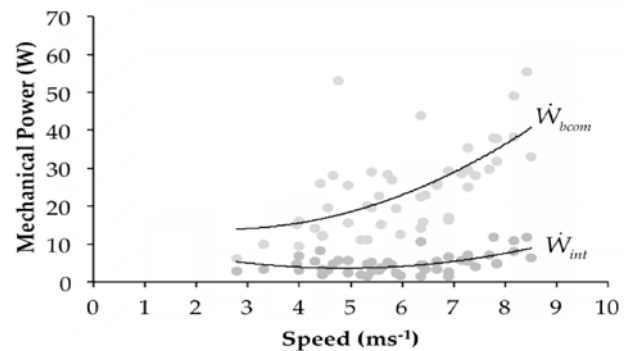


Figure 1: W'_{bcom} and W'_{int} over handcycling speed.

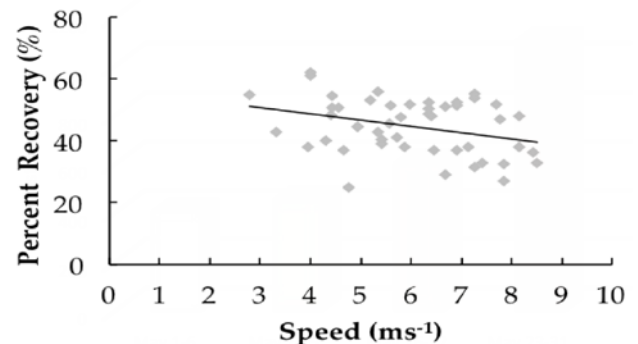


Figure 2: Energy recovery (Percent Recovery) over handcycling speed.

References

- [1] Fischer G (2013). *Bioenergetics and biomechanics of handbiking: focus on spinal cord injured athletes*; Ph.D. Thesis, University of Verona.
- [2] Cavagna GA et al (1963). *J. Appl. Physiol.*, **18**: 1-9.
- [3] Cavagna GA and Kaneko M (1977). *J. Physiol.*, **268**: 467-481.
- [4] Fuglsang T et al (2017). *Front. Physiol.*, **8**: 635.

Using In-Fibre Bragg Grating Sensors within the Periodontal Ligament Space of an Intact Swine Premolar: A Cross-Verification with a Representative Finite Element Model

Kathryn P Houg¹, Alejandro Matos Camarillo¹, Michael R Doschak², Tracy Popowics³, Christopher Dennison¹, Dan Romanyk^{1*}

¹Department of Mechanical Engineering, University of Alberta, Edmonton, AB, Canada

²Faculty of Pharmacy & Pharmaceutical Sciences, University of Alberta, Edmonton, AB, Canada

³University of Washington School of Dentistry, Seattle, Washington, USA

*Email: dromanyk@ualberta.ca

Summary

The Periodontal Ligament (PDL) provides physical attachment between the tooth and surrounding alveolar bone. In-Fibre Bragg Grating sensors (FBG) have been used to measure repeatable strains from within the PDL space during displacement-controlled tests. Cross-verification was used to compare the FBG strains to physical strains within the PDL estimated from a linear elastic finite element (FE) model. Results suggest that the FBG can be used as a proxy for change in strain, as a change in FBG strain was linearly related to the corresponding change in FE strain.

Introduction

The PDL is a connective tissue that provides attachment between the tooth root and surrounding alveolar bone. The PDL mechanical properties are vital to understanding how the tooth-PDL-bone complex (TPBC) will respond to external loads, such as chewing or orthodontics [1]. The PDL is known to have a narrow and irregular width (0.06-0.25 mm in humans [2]) making the implementation of traditional strain sensors within an intact TPBC challenging [2,3]. FBGs are small (0.125 mm diameter), flexible, optical sensors that can be placed within the PDL space of an intact TPBC [2]. FBG strain measurements have been shown to be repeatable; however, the accuracy has not been studied. The objective of this work was to compare the FBG measured strains to those estimated through FE analysis to determine the suitability of FBG measurements in predicting PDL mechanics.

Methods

Swine second premolars (n=14) were subjected to displacement-controlled tests with an FBG placed in the PDL space. Each premolar was subjected to two different quasi-static displacements. After preconditioning, 10 trials from each displacement were used and the mean peak strain measurements were calculated for each displacement. An experimental ratio was calculated for each mandible, dividing the mean strain from the first displacement by the second.

A representative FE geometry was created from Microcomputed Tomography (μ CT) scans (SkyScan 1076; Bruker-MicroCT, Kontich, Belgium, at: 100 kV, 110 μ A, 17.2 micron resolution). A linear elastic FE model was created using ANSYS (ANSYS Academic Research Mechanical, Release 2020 R1, Canonsburg, PA, USA, total elements (SOLID187): 829,822). The tooth, bone, and PDL had a Young's Modulus of 20 GPa [5], 13 GPa [5], and 0.46 MPa, respectively. All materials had a Poisson's ratio of 0.30. FE strains were taken from the approximate location of the FBG (Figure 1), determined from μ CT scans. An FE ratio was

calculated in the same manner as for the experimental ratio. A linear regression between the experimental and FE ratios was completed to determine the suitability of using FBG measures to predict change in strain.

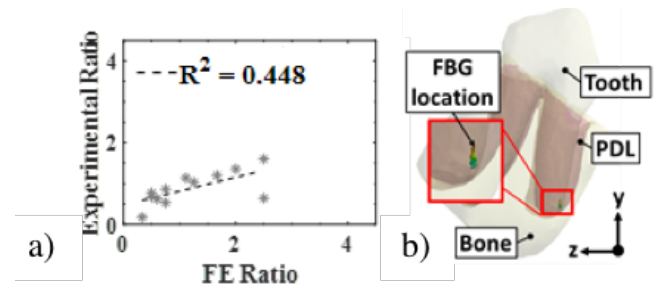


Figure 1: a) Linear regression between experimental and FE ratios
b) Representative FE model indicating FBG location

Results and Discussion

The linear regression between experimental and FE strain ratios was statistically significant (p-value=0.017) and it was found that the FE ratio was capable of predicting 44.8% of the variation in the experimental ratio ($R^2=0.448$) (Figure 1). The linear relationship implies that a change in FBG output measurements can be used to predict the change in physical strains within the PDL. This is significant as this sensing method would allow for measuring the change in strain within the PDL at various time points during temporal studies without having to sacrifice and dissect the PDL.

Conclusions

FBG sensors can be used as a proxy for change in physical PDL strain over time. This preliminary relationship shows promise; however, more work must go into the effects of other external mechanical stimuli (e.g., effect of loading rate).

Acknowledgments

This work was supported by the American Association of Orthodontics Foundation, and the Natural Science and Engineering Research Council of Canada.

References

- [1] Proffit WR et al. (2013). *Contemporary Orthodontics*; Elsevier.
- [2] Romanyk DL et al. (2017). *J Biomech*, **54**: 117-122.
- [3] Fill TS et al. (2011). *J Dent Biomech*, **2011**:312980.
- [4] Qian et al. (2009). *Dental Materials*. **25**:1285-1292.
- [5] Nikolaus A et al. (2017). *J Mech Behav Biomed Mater*, **67**: 61-73

Multi-scale constitutive model of human trabecular bone

Krzysztof Jankowski¹, Marek Pawlikowski¹

¹Institute of Mechanics and Printing, Warsaw University of Technology, Warsaw, Poland

Email: krzysztof.jankowski.wip@pw.edu.pl

Summary

The aim of this study was to formulate new multi-scale constitutive model of human trabecular bone. The model takes into account visco-elastic properties of human bone trabeculae, i.e. hysteresis loop, load rate dependency and stress relaxation. Calibration of visco-elastic constants was based on nanoindentation tests performed on trabeculae and relaxation test performed on whole sample. The constitutive model was formulated to implement it in finite element analyses. The validation presented in the study was based on the results from compression test and simulation of this test.

Introduction

The constitutive model can be used to numerically model bone behavior and to predict all or some of the bone-related disorders, as well as to understand the relationship between bone and implants.

Methods

The cuboid bone sample 9.8 x 9.6 x 9.6 mm was cut out from bone specimen resected from a femoral head of a 63-year-old patient during a hip replacement surgery. The 3D model of this sample was created from μ CT images (Figure 1).

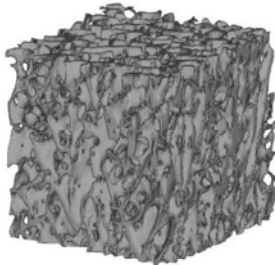


Figure 1: Model of a bone sample.

The micro-indentation tests were carried out on different trabeculae from the sample. A spherical diamond indenter tip was used. The tests were conducted until the maximal force values 300 mN, 500 mN and 700 mN were reached at the load and unload rates 500 mN/min and 1000 mN/min. A total of 18 tests were conducted. During relaxation test bone sample was compressed until strain value 0.01 was reached and then the change of the force was registered for 500 sec. Compression test was conducted on the cuboid bone sample with the same strain value. To model human bone behavior in micro- and macro-scale we proposed a non-linear visco-elastic constitutive model of general form:

$$\mathbf{S} = \int_0^t g(t-s) \frac{\partial \mathbf{S}^e}{\partial s} ds, \quad (1)$$

where: \mathbf{S} – second Piola-Kirchhoff stress tensor, \mathbf{S}^e – elastic second Piola-Kirchhoff stress tensor, $g(t) = g_\infty + \sum_{i=1}^n g_i \cdot \exp(-t/\tau_i)$, g_i are characteristic amplitudes and τ_i –

relaxation times. In this equation s represents the historical time, whereas t is the current time [1, 2]. The form of \mathbf{S}^e was derived from the Mooney-Rivlin strain energy density Ψ :

$$\Psi = c_{10}(I_1 - 3) + c_{01}(I_2 - 3), \quad (2)$$

where: c_{10} , c_{01} are hyperelastic material constants, I_1 and I_2 – first and second strain invariants, respectively. The relaxation times τ_i and the value of n were determined by fitting the curve described by (1) to the relaxation test in compression performed on bone sample. The elastic constants c_{10} , c_{01} and the visco-elastic constants g_i were determined on the basis of micro-indentation tests using an indirect method based on finite element analyses [3] implementing the proposed constitutive model (1) into Abaqus[®] software by means of User-Supplied subroutine. Both the indentation and compression tests were simulated. To validate our constitutive model the results from simulation were compared to results from experiment.

Results and Discussion

In Figure 2 the results of the constitutive model validation is graphically presented. The curve obtained from compression test is shown by means of squares and the FE analysis curve with a solid line. Reasonable accordance between the model and experiment is clearly visible.

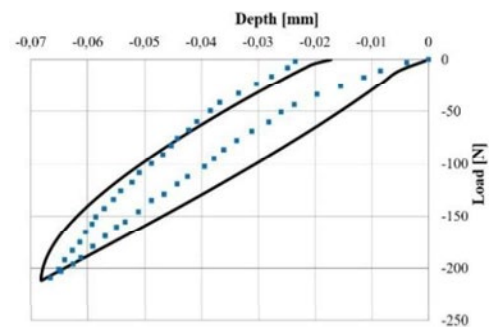


Figure 2: Validation of the constitutive model: experiment (squares) and FE simulation (solid line).

Conclusions

The formulated multi-scale constitutive model for human trabecular bone proved to be capable to model visco-elastic properties of bone both in micro and macro scale. It can be utilized to simulate more accurately bone behavior and also to predict its reaction to various types of load conditions.

References

- [1] Pawlikowski et al. (2016). *Biocybern Biomed Eng.*, **36**: 491-498.
- [2] Pawlikowski et al. (2018). *J Mech Behav Biomed Mater.*, **85**: 162-169.
- [3] Goh et al. (2004). *Mech Time-Depend Mater*, **8**: 255-2.

Reliability and validity of a robotic manipulator to reproduce quasi-static physiological humerus motions

F. Moissenet¹, C. Rastoll², D. Gonzalez², N. Foukia², M. Lauria², S. Armand¹ and N. Holzer³

¹ Kinesiology Laboratory, University of Geneva and Geneva University Hospitals, Geneva, Switzerland

² Geneva School of Engineering, Architecture and Landscape - HEPIA, Geneva, Switzerland

³ Department of Surgery, Geneva University Hospitals, Geneva, Switzerland

Email: florent.moissenet@unige.ch

Summary

This study aimed to assess the reliability and validity of a robotic manipulator to reproduce quasi-static humerus motions based on operator-induced humerus motions on cadaveric specimens. Reliability, quantified by the root mean square difference (RMSD) between a motion cycle and the related average across specimens, motions and cycles was 0.28 ± 0.13 mm and $0.15 \pm 0.08^\circ$ for humerus position and orientation, respectively. Validity, quantified by the RMSD between a cycle and the related operator-induced motion, was 0.58 ± 0.56 mm and $0.22 \pm 0.12^\circ$ for humerus position and orientation, respectively.

Introduction

Biomechanical testing of human joints is commonly performed using universal testing machines [1]. While providing precise position and force measurements, the related protocols are often limited to only one or two degrees of freedom (DoF) [2]. To overcome this issue, several studies have been oriented toward the use of robotic manipulator with multiple DoFs [1,3,4]. However, to the best of our knowledge, these protocols remain performed in extra-corporal conditions by fixing a bony segment and mobilizing another one. In the context of the shoulder complex, such an approach may produce results quite far from physiological bone movements of this kinematic chain with various DoFs. The aim of this study was to assess the reliability and validity of a robotic manipulator to reproduce quasi-static humerus motions based on operator-induced movements on cadaveric specimens.

Methods

Five female cadaveric specimens (77.4 ± 9.99 years) were obtained for the study. None of the 10 shoulders had degenerative joint disease or previous ligamentous injury. Specimens were placed on and attached to a vertical support to ensure that the thorax was held rigidly to the table. Each humerus was cut approximately 15.5 cm distal to the humeral head centre, potted in a custom 3d-printed cylinder by use of the bone cement (Palacos LV, Heraeus, Germany), and rigidly fixed to the end-effector of a robotic manipulator (KUKA LBR iiwa 14 R820, KUKA, Germany). The 3D trajectories of a set of cutaneous reflective markers placed on thorax and upper limb [5] were previously recorded using a 11-camera optoelectronic system sampled at 100 Hz (Oqus5, Qualisys, Sweden) during operator-induced humerus motions (flexion-extension, abduction-adduction, internal-external rotation at 0° of flexion, horizontal flexion-extension, vertical traction

and horizontal compression). These trajectories were gap-filled, filtered (2nd order Butterworth filter, 6 Hz cut-off) and used to compute the position and orientation of a segment coordinate system defined on the humeral 3d-printed cylinder. The resulting trajectory and quaternion were sent to ROS (Robot Operating System, version 16.04.6 “Kinetic”) and the manipulator motion planning was computed by inverse kinematics. Finally, the manipulator reproduced the humeral motions (27 cycles per motion) and the reliability and validity of the humerus position and orientation were assessed. As the motion velocity was not constrained, a dynamic time warping approach was used to map the compared time-series and the RMSD was then computed between the resulting mapped data for each humerus motion cycle. The reliability of the robotic manipulator was then quantified by the RMSD between a motion cycle and the related average across all cycles. Similarly, the validity of the robotic manipulator was quantified by the RMSD between a motion cycle and the related operator-induced motion. This protocol was approved by the Cantonal Commission for Research Ethics (2020-00598).

Results and Discussion

Concerning the humerus position, the average RMSD related to reliability and validity were respectively 0.28 ± 0.13 mm and 0.58 ± 0.56 mm across specimens, motions and cycles. Concerning the humerus orientation, the average RMSD related to reliability and validity were respectively $0.15 \pm 0.08^\circ$ and $0.22 \pm 0.12^\circ$ across specimens, motions and cycles. The reliability of the humerus (i.e. the manipulator end-effector) position and orientation agrees with the manufacturer values ($\pm 0.1^\circ$).

Conclusions

Regarding the present reliability and validity of the robotic manipulator to reproduce quasi-static physiological humerus motions, the proposed methodology will now allow to develop various experimental cadaveric protocols to robustly assess joint kinematics in quasi-static conditions.

References

- [1] Aliaj K et al. (2020). *Plos ONE*, **15(11)**:e0242005.
- [2] Beitzel K et al. (2014). *Am J Sports Med*, **42(9)**:2141:2148
- [3] Lee J et al. (2020). *J Shoulder Elbow Surg*, **In press**.
- [4] Pastor MF et al. (2016). *Arch Orthop Trauma Surg*, **136**:1513-15419
- [5] Wu G et al. (2005). *J Biomech*, **38**:981-992

Foot health technology for the diabetic high risk foot – A systematic Review

Claire Saliba Thorne MSc¹, Alfred Gatt PhD¹, Clifford DeRaffaele PhD¹, Abdurahman Azena², Cynthia Formosa PhD¹

¹ Faculty of Health Sciences, University of Malta

² Middlesex University, Malta

Email: claire.saliba-thorne.08@um.edu.mt

Summary

This systematic review analyzed the existing literature on technologies used to read and measure both in-shoe pressures and skin temperatures. All studies have shown excellent index test validity and only a few tested for the reliability of the device. None of the studies tested for responsiveness of the device. Quality assessment results scored high-risk in ‘applicability’, and low risk in view of ‘use if index test’. The data outlined in this review confirms that further improvement, reliability testing and clinical validation of the developed systems is required despite the results of excellent performance in detecting changes of in-shoe skin temperature and pressure.

Introduction

When the skin is subjected to continuous plantar stresses in the diabetic high-risk foot, the skin temperature at the area of stress rises, weakening the ability of the surrounding tissues to resist biomechanical abnormalities. To date, monitoring of skin temperature and plantar pressure mapping measurement, can only be obtained separately using a thermographic camera and an in-shoe pressure device, a technique which can result as both expensive and time consuming. In view of this, researchers have been attempting to develop and validate innovative in-shoe devices that can serve as an alternative to the current impractical technologies that are currently available. The aim of this systematic review is to provide a more rigorous analysis of existing literature related to the technologies used to read and measure both in-shoe plantar pressures and skin temperature.

Methods

A systematic review of the literature related to the topic was searched in database sources such as Medline OVID, Cochrane Library, PubMed, CONAHL, PROSPERO, and Elsevier. Outcome measures of interest included validity, reliability and responsiveness of in-shoe temperature and/or pressure mapping device used, and characteristics and quantity of sensors used, anatomical landmarks and statistical analysis used to interpret the data. Quality of evidence and risk of bias was evaluated using the QUADAS-2.

Results and Discussion

This study was first to provide a comprehensive understanding of the currently available technologies developed to measure in-shoe plantar pressures and temperature. Nineteen studies were included in this review. The majority of studies used a small sample and recruited healthy participants. All studies have shown index test validity and only a few tested for the reliability of the device. None of the studies tested for responsiveness of the device. Quality assessment results scored high-risk in view of ‘patient selection’, ‘use of reference standard’ and ‘applicability’, and low-risk in view of ‘use if index test’ and ‘flow and timing’. In-shoe technologies are generally developed to monitor only one of these parameters. Current evidence is not robust enough to confirm the reliability and validity of a such an innovative device vis-à-vis the early identification of ulcer development. By confirming valid and reliable measurement of peak plantar pressures and skin temperature, the clinician can have an objective risk assessment on which to base his/her clinical reasoning [1] which is highly commended by health care guidelines [2] and is proven to reduce ulcer development by 70% [3].

Conclusions

The data outlined in this review confirms that further improvement, reliability testing and clinical validation of the developed systems is required. The type of information gathered from this review, can be useful in identifying functioning characteristics of mentioned devices to develop an innovative, low cost, reliable and valid, in-shoe pressure and temperature measuring device that can be used as an alternative to current technology to predict the risk of ulceration prior to tissue breakdown.

References

- [1] Bus, S.A. et al. (2016). IWGDF guidance on the prevention of foot ulcers in at-risk patients with diabetes. *Diabetes Metabolism Research Review* **32**, 16–24. 12.
- [2] Lavery, L.A. et al. (2016). WHS guidelines update: diabetic foot ulcer treatment guidelines. *Wound Repair and Regeneration* **24**, 112–26.
- [3] Armstrong, D.G. et al. (2007). Skin temperature monitoring reduces the risk for diabetic foot ulceration in high-risk patients. *American Journal of Podiatric Medicine* **120**(12):1042–6.

Movement quality in subjects with osteoarthritis and after total joint arthroplasty assessed by a single accelerometer

Jill Sijmmerzaal¹, Kristoff Corten³, Rob van der Straaten², Annick Timmermans², Ilse Jonkers¹, Benedicte Vanwanseele¹

¹Human Movement Biomechanics Research Group, Department of movement sciences, KU Leuven, Belgium

²REAL Rehabilitation Research Centre, Faculty of Rehabilitation Sciences, Hasselt University, Belgium

³Department of Orthopaedics, Ziekenhuis Oost Limburg, Belgium

Email: jill.emmerzaal@kuleuven.be

Summary

We investigated movement quality in terms of symmetry, complexity, smoothness, and stability in hip or knee osteoarthritic and non-arthritic people and following total knee arthroplasty (TKA), using linear and non-linear measures assessed by a single lower trunk accelerometer. We detected differences in gait pattern between arthritic and non-arthritic subjects that surpassed the minimal detectable change. We observed normalisation of most symmetry measures after TKA. Further, the initial deterioration in movement complexity did not recover over time. Moreover, a less stable gait pattern was detected at one-year post-TKA compared to asymptomatic controls. These results show that a single trunk worn accelerometer can characterise movement quality before and after a total joint arthroplasty.

Introduction

Hip and knee osteoarthritis (OA) are common, disabling musculoskeletal disorders. They are a leading cause of lower extremity disabilities [1]. Symptomatic OA is characterised by pain, stiffness, physical disabilities, and difficulties in performing daily life activities [1]. Patient-reported outcome measures are frequently used to assess daily functionality in arthritic subjects; however, they lack biomechanical insight [2]. Inertial measurement units have shown the ability to measure functionality in terms of gait symmetry, complexity, smoothness, and stability in a natural environment. However, the discriminant ability of these parameters in arthritic versus non-arthritic subjects is still mostly unexplored. The purpose was to evaluate which movement quality variables derived from a single trunk worn IMU can distinguish the gait pattern of arthritic compared to non-arthritic subjects. Second, we evaluated these variables' sensitivity to capture changes in gait properties during one year following total knee arthroplasty.

Methods

Twenty patients with hip OA, 18 patients with knee OA and 20 asymptomatic controls participated in this study. Seventeen of the 18 subjects with knee OA were followed for one year postoperatively. The participants were equipped with a single trunk worn IMU (MVN BIOMECH Awinda, Xsens Technologies, 60 Hz) and were instructed to walk back and forth along a 10m walkway at a self-selected speed. During pre-processing, sensor tilt was corrected, and the left-right steps were recognised using the anteriorposterior and mediolateral acceleration signal. The separate walking trials were concatenated to one long time trial. The movement

quality parameters: gait symmetry (step-stride regularity and Harmonic Ratio), complexity (sample entropy), smoothness (Spectral Arc Length), and stability (Maximum Lyapunov Exponent) were calculated from the raw acceleration signal in three directions. We established the parameters' minimal detectable change using test-retest data from the asymptomatic controls to determine if measured differences surpassed naturally occurring measurement variability. We used the Mann-Whitney U test for group differences between asymptomatic controls and hip or knee OA subjects. To assess how the parameters evolve after a TKA, Friedman's chi-square ANOVA was conducted. When a significant difference was found ($\alpha < 0.05$), a Wilcoxon signed-rank test with a Bonferroni correction ($\alpha < 0.005$) was calculated to test for differences between time-point.

Results and Discussion

We found that both arthritic groups had a more asymmetrical gait pattern than non-arthritic subjects. Furthermore, hip OA subjects had a more intermittent movement pattern than asymptomatic controls. At one year post-TKA, we see an initial deteriorating followed by improvement in gait symmetry—and an initial deterioration in movement complexity that does not recover over time. Moreover, at one-year post-TKA, patients display a more unstable gait pattern in long-term stability measure compared to asymptomatic individuals.

Conclusions

A single lower back accelerometer can be used to characterise movement quality before and after a total joint arthroplasty. We see a recovery of most symmetry measures, but a more unstable and less complex gait pattern at follow-up. These results show the ability to monitor these variables in a free-living environment to inform personalised rehabilitation of gait symmetry, stability, complexity, and smoothness.

Acknowledgments

This research was funded by FWO-TM (ref T004716N).

References

- [1] Woolf, AD., et al. (2003). *Bull World Health Organ* **81**(9), 646-645
- [2] Hodt-Clifton C., et al. (2011). *J Rehabil Med.*, **43** 787-793.

Lyapunov estimation from smartphone acceleration signals – Comparison between elderly and young adults

Abime Al Abiad^{1,2}, Thomas Robert¹, Alerie Renaudin², Enguerran Houdry³, Carlos El Khoury³

¹ Univ Lyon, Univ Gustave Eiffel, LMC UMR T9406, F69622, Lyon, Fr

² AME-GEOLOC, Univ Gustave Eiffel, F44344 Dougenais, Fr

³ Medipole, Equipe de Recherche, Villeurbanne, Fr

Email: thomas.robert@univ-eiffel.fr

Summary

Short-term maximum Lyapunov exponent (LyE) has been proven useful in identifying gait instability in fall-prone aged adults. This study aims at demonstrating the feasibility of estimating LyE using very simple set-up (smartphone – simple walking protocol) which could be used to monitor the LyE evolution for elderly adults.

Introduction

It is essential to identify falling risks and instability measures to reduce falls within the elderly population. The LyE has gained increasing interest in the present literature. In the context of gait stability, the LyE quantifies the motor system's ability to recover from small perturbation and maintain dynamic stability in the presence of kinematic variability which increases with age. LyE has been successfully measured by [1] using a non-aligned inertial measurement unit (IMU). To date, LyE has not been measured using smartphone IMU. Smartphone IMUs have been proved to be practical in terms of gait analysis. There is no restriction in terms of smartphone IMU signal's quality for LyE calculation. Measuring gait instability during a simple walking protocol, 6-minute walk test (6MWT), using smartphone accelerometer data can greatly benefit clinicians and individuals in terms of affordability and accessibility. Therefore, in this study, we aim at demonstrating the feasibility of estimating LyE using very simple set-up (smartphone – 6MWT) which could be used to monitor the LyE evolution for elderly adults.

Methods

Six elderly (72 ± 6 y, 6 men, 89 ± 23 kg, 170 ± 6 cm) and six young adults (26 ± 6 y, 4 women and 2 men, 66 ± 7 kg, 168 ± 9 cm) volunteered for this study. The participants had no history of falls. Each participant signed an informed consent. Participants walked in a corridor back and forth for 6 minutes with a smartphone, One plus 7, placed in a sport's belt at the waist. The acceleration signal was recorded at 100 Hz using a customized application. Because of the phone power-dependent sampling frequency, the recorded acceleration signal is resampled to 100 Hz. The LyE is calculated on the mediolateral (ML), anterior-posterior (AP), and vertical (V) acceleration components and on the acceleration norm (N). Pre-processing methods before LyE calculation of the four signals are similar to those found in [2]. No filtration was done because of the unwanted effects of filtering nonlinear signals. 150 consecutive strides are analyzed for each case. Signals are time-normalized to contain 15,000 samples. The chosen time delay is 10 samples and, the embedding dimension selected is

5. The LyE is estimated on 0 to 50 samples using the Python package nolds [3] and the Rosenstein et al. algorithm.

Results and Discussion

Average LyE calculated on the V, ML, AP, and N signals for old and young adults are shown in figure 1. The LyE showed no difference between elderly and young adults and no difference between signal types.

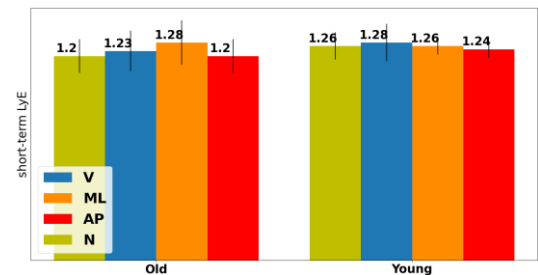


Figure 1: Short-term Lyapunov (Lye) exponent calculated on vertical (V), mediolateral (ML), anterior-posterior (AP) components of acceleration, and acceleration norm (N) for old and young adults.

Due to the lack of standardized methodology, disparate LyE values for young and elderly adults are present in the literature [4]. Still values of LyE obtained in this study are within the range found in the literature [4]. Moreover, the findings that young and elderly with no history of falls present similar LyE is in line with the previous study [5] where negligible differences between healthy old and young adults were found.

The feasibility study is the first to show that it is possible to assess the LyE using a smartphone and a simple over-ground walking protocol. This evaluation, that can be either performed by a clinician or by the person himself at home, represents an interesting possibility to monitor the risk of fall. Further investigations are on-going on a larger database including elderly with a history of falls. A follow-up of elderly fall occurrences is also considered. Future results will provide additional information regarding the validity of this measure to detect an early increase risk of fall.

References

- [1] Bruijn SM et al. (2010). *Ann Biomed Eng*, **38**: 2588–2593.
- [2] Bruijn SM et al. (2009). *J Biomech*, **42**:1506–1512.
- [3] Schölzel C. (2019). doi: 10.5281/zenodo.3814723
- [4] Mehdizadeh S. (2018). *Gait Posture*, **60**: 241–250
- [5] Lockhart T. E. and Liu J. (2008). *Ergonomics*, **51**:1860–1872

The Performance of a Flexible Implantable Strain Sensor Under Replicated *In Vivo* Conditions

Maomi Adam¹, Liang Chang¹, Byron Llerena Cambrano², Roland König³, William R. Taylor¹, Colin R. Smith¹

¹Laboratory for Movement Biomechanics, Institute for Biomechanics, ETH Zurich, Zurich, Switzerland

²Laboratory of Biosensors and Bioelectronics, ETH Zurich, Zurich, Switzerland

³Center for Communications Systems, Zurich University of Applied Sciences, Winterthur, Switzerland

Email: bt@ethz.ch

Summary

A passive strain sensor was developed using novel flexible electronic technologies with the aim to wirelessly measure *in vivo* human Achilles Tendon (AT) strain. Mechanical testing performed on the sensor in air and submerged in a saline bath at different temperatures demonstrated high performance and wireless data transmission under replicated *in vivo* conditions. The calibration curve remained linear and distinct signal changes were observed for strain steps of 0.1% in all conditions.

Introduction

Early loading rehabilitation following AT rupture appears key to restoring the healthy tendon length and stiffness necessary for a full functional recovery. We developed a highly compliant implantable strain to monitor AT healing and inform data driven rehabilitation. For the sensor to reach this goal, it must achieve the necessary strain resolution and range to accurately capture AT elongation under dynamic *in vivo* conditions.

Methods

A stretchable capacitive sensor was fabricated by embedding two conductive AuTiO₂ nanowire layers in series with a coil antenna in PDMS, allowing the whole unit to work as an inductor-capacitor-resistor circuit. A readout system was developed to wirelessly measure the sensor resonance frequency (RF) at 1024 Hz. Stretching the sensor reduces the distance between the two nanowire layers, and thus the capacitance and RF, allowing an indirect strain measurement. One sensor was stretched in a tensile machine (Zwick Roell ZDO-F0.5TS) while the RF was wirelessly measured (Figure 1A). Tests were performed under four conditions: the sensor in air or submerged in Phosphate-buffered saline (PBS) water, and the wireless data transfer across air or PBS water. Calibration and resolution tests were performed under displacement control in the four conditions after 50 cycles of pre-conditioning (0-25%):

Calibration: To characterize the relationship between the applied strain and the measured RF (Fig 1C), each sensor was stretched from 0% to 25% strain in 1% steps maintained for 30s. The RF value was averaged on 3 seconds.

Resolution: The smallest measurable strain variation was established by performing 10 cycles of 3 steps of ± 0.1%, 0.2% and 0.5% strain around the 5%, 10% and 15% strain levels (Fig 1C).

Temperature: One sensor was then set at a fixed length and the RF was measured while the PBS was heated from 22 to 45°C.

Results and Discussion

Calibration: The slope of the sensor remained almost perfectly linear between 0% and 25% in all conditions (R²0.99), a range that exceeds expected *in vivo* AT strains. However, submerging the sensor in PBS caused a shift in the baseline RF, likely due to swelling.

Resolution: The strain steps of 0.1% were observable in all conditions and at all strain levels. This resolution exceeds the necessary threshold to capture clinically relevant *in vivo* strain variations in the human AT during dynamic activities.

Temperature: The sensor RF increased linearly with temperature (R²0.99): a 2°C increase leads to a sensor signal change equivalent to 0.1% strain.

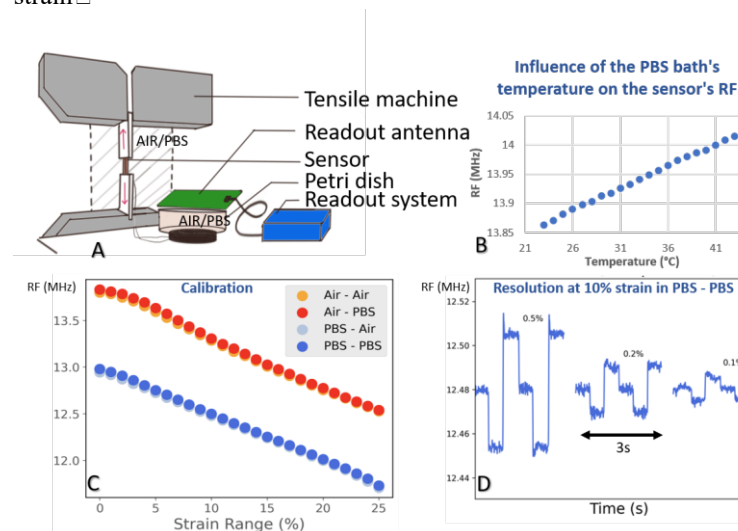


Figure 1: A. Experimental setup. B. Influence of the temperature on the sensor RF. C. Calibration curves of the sensor in 4 conditions. D. Resolution for 3 different strain steps.

Conclusions

Our novel sensor demonstrated in a saline environment with representative *in vivo* conductivity properties that it has the strain range and resolution needed to perform *in vivo* AT measurements. Upcoming implantations in sheep will demonstrate *in vivo* sensor function and biocompatibility over a two-month period.

Acknowledgments

This research was funded by the Swiss Excellence Scholarship (FCS) and the Swiss National Funding (SNF).

A NOVEL METHOD FOR EQUINE GAIT EVENT DETECTION

Eloise V. Briggs¹, Claudia Mazza¹

¹Department of Mechanical Engineering and INSIGNEO Institute for in silico Medicine, University of Sheffield, Sheffield, United Kingdom
Email: evbriggs1@sheffield.ac.uk

Summary

Accurate detection of hoof on and off events is essential to equine gait assessment. This study aimed to propose and validate inertial sensor-based methods of gait event detection, exploring different sensor placement and signal processing methods. A mixed cohort of eleven horses wore sensors on the left hooves, pasterns and canons. Walk and trot strides were recorded on asphalt. Gait events detected from pastern and cannon sensors were compared to reference, hoof-detected events. Pastern-based methods were the most accurate and precise, incurring mean errors of 1ms to 6ms, depending on the limb, gait and event. No horse-dependent effects were seen. Thus, developed methods were validated to enable reliable gait event detection from a mixed cohort of horses.

Introduction

As interest in analysing equine gait in real world conditions increases, so too does demand for validated quantification methods which use portable measuring systems [1]. Consequently, several methods based on inertial measurement units (IMUs) have now been proposed for detecting gait as an alternative to traditional force plate-based methods [2,3,4,5]. However, these have been restricted to validation under lab conditions, often with a limited cohort of horses. This research aimed to propose and validate methods of gait event detection using IMUs attached to the pasterns and canons.

Methods

Eleven horses (eight geldings, three mares; 154(21)cm; 12(8)years) were recruited to wear IMUs attached to the left hooves, pasterns and canons (Fig 1). Shimmer3 IMUs (Dublin, Ireland) collected data (200Hz) using triaxial gyroscopes (± 2000 deg/s), magnetometers (± 49 Ga) and accelerometers ($\pm 16g$ m/s² canons; $\pm 200g$ m/s² hooves, pasterns). Horses were led in a 25m straight line at walk and trot, three passes per gait on asphalt.

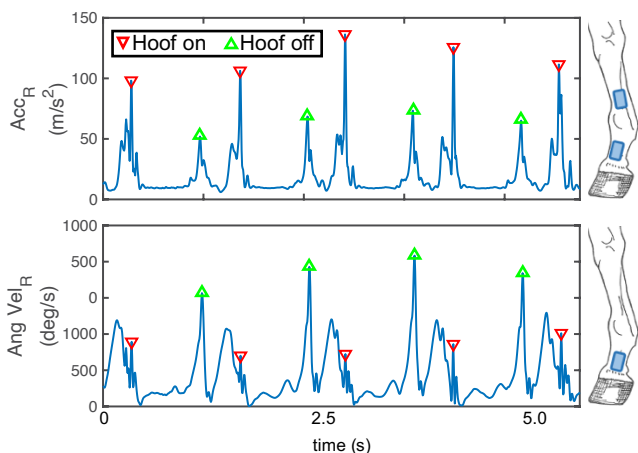


Figure 1: illustration of the two novel data processing methods to detect hoof on and off

Timing of gait events were detected from cannon IMUs using two state of the art methods [3,4] and from canons and pasterns using two novel methods, based on identification of peaks in the resultant angular velocity (pasterns; Fig 1, bottom) or resultant acceleration (pasterns or canons; Fig 1, top). The hoof on and off timings obtained using these methods were compared to event timings detected by a hoof-based, reference method [5]. The performance of each method for detecting events was assessed in terms of the mean error (*accuracy*) and distribution of these errors (*precision*). Results were investigated for significance using repeated measures ANOVA techniques.

Results and Discussion

Novel cannon methods consistently outperformed application of literature methods, incurring mean errors (standard deviations) ranging from magnitudes of 1(19)ms to 15(33)ms, compared to 4(27)ms to 161(412)ms. Novel methods may be more robust than the alternatives for use in the field as they use only resultant data streams so exact IMU orientation is less important, reducing inter-user variability and effects of IMU movement during data collection. Pastern methods (Table 1) proved superior to novel cannon methods, with errors of 2(9)ms to 5(11)ms compared to 1(19)ms to 15(33)ms for forelimbs; and 1(12) to 6(14)ms compared to 1(15) to 7(14) hindlimbs. Differences were significant ($p < 0.001$) for all events except forelimb events at walk. Furthermore, no horse-dependent effects were revealed by statistical analysis, suggesting the developed methods were consistent across the highly varied range of horses.

Table 1: Errors (ms) incurred by the most accurate and precise pastern methods to detect gait events

Gait	Forelimb		Hindlimb	
	Hoof on	Hoof off	Hoof on	Hoof off
Walk	-5(11)	3(16)	2(10)	6(14)
Trot	-2(9)	4(34)	1(12)	2(9)

Conclusions

Methods have been developed which are able to accurately and precisely detect gait events from a varied cohort of horses using pastern mounted IMUs. This will facilitate future studies under field conditions.

Acknowledgments

This study was supported by the UK EPSRC (EP/K03877X/1, EP/S032940/1) and Worldbase Ltd.

References

- [1] Egan et al. (2019). *Equ. Vet. J.*, 51, 813-24
- [2] Olsen et al. (2012). *Sensors*, 12(6), 8145-56
- [3] Sapone et al. (2020). *Sensors*, 25(3), 469-74
- [4] Bragança et al. (2017). *Equ. Vet. J.*, 49, 545-51
- [5] Tijssen et al. (2020). *PLoS ONE*, 15(6): e02332

Improved accelerometer assessed physical activity patterns after an eight-week exercise intervention.

Godhe M^{1,2}, Ekblom Ö¹, Ekblom M¹, Pontén M¹, Andersson E^{1,2}.

¹Laboratory of Biomechanics and Motor Control, Swedish School of Sport and Health Sciences, Stockholm, Sweden

²Department of Molecular Medicine and Surgery, Karolinska Institutet, Stockholm, Sweden

Email: manne.godhe@gih.se

Summary

Older adults participating in an eight-week intervention with guided physical activity two times per week improved physical activity (PA) and reduced sedentary behaviour (SB) measured with accelerometers. The result of this study may contribute valuable knowledge in designing of proper public health strategies targeting healthier physical activity patterns in older adults.

Introduction

Many beneficial health outcomes are associated with SB and PA in older adults.¹ However, research is scarce or lacking regarding supervised exercise-interventions with accelerometer measured SB and PA including reliability assessments in older adults. The aim of this study was to determine if eight-weeks of regular supervised exercise would have any effect on physical activity patterns in older adults. For comparison, a control group, not receiving supervised exercise, performed similar pre- and end-tests intervals. Reliability of the accelerometer with two separate pre-tests measures was also investigated.

Methods

Seventy-eight older adults exercised (65-91yrs, 61,5% women) and 43 participated in a control group (65-88yrs, 69,8% women). The exercise group performed combined aerobic and strength-training, twice/w à 1 h. Accelerometer assessments (GT3X+, Actigraph) for the exercise group were performed three times, two times before the intervention (Pre-1 and Pre-2) and one test in the last week of the 8-week-exercise-period (End).² The control group performed one pre-test and one end-test at corresponding intervals, without receiving any supervised physical activity. Accelerometer data was analyzed using the vector magnitude (VM) of all three-axis in 60s epochs, with previously validated cut-points for physical activity intensities related to METs.^{3,4}

Results

There was a significant difference in the exercise-group from Pre-1 to End-test in both absolute minutes (min/w) and relative to daily wear time (%); in moderate-to-vigorous-PA (MVPA +41 min/w and 8% of-total-daily-wear-time), light-intensity (LPA+228 min/w and 3.9% of-total-daily-wear-time), Sedentary (SED) -time (-254 min/w and -4.7% of-total-daily-wear-time) and SED-bouts-à-10 min (-320 min/w and -5.7% of-total-daily-wear-time), (see Figure 1). The control group showed only significant differences from pre-1-to-End-test in % of-total-daily-wear-time for LPA (+2.3%) and SED-time (-2.7%). Total-daily-counts in the End-test increased for controls (+6,7%) but significantly more for the exercise group (+17,3%). Between the exercise groups' two pre-tests, no significant difference was observed, except for percent of wear time in total-PA (+4.6%) and SED-total (-2.4%).

Conclusions

Older adults participating in supervised exercise increased light and moderate- to vigorous PA and decreased time in SB, which is of importance because elderly being less sedentary and more physically active reduce risks of disease and morbidity. Furthermore, a good repeatability was shown from the two pre-tests.

References

- [1] Lee, I.M. et al. (2012). Physical Activity Series Working Group. *Lancet*. **380**:219-29.
- [2] Jarrett, H. et al. (2015). *Journal of Physical Activity and Health*, **12**: 382-387.
- [3] Diniz, T.A. et al. (2017) *Journal of aging and physical activity*, **25**:20-26.
- [4] Heesch, K.C., et al. (2018) *International journal of behavioral nutrition and physical activity* **15**: 119.

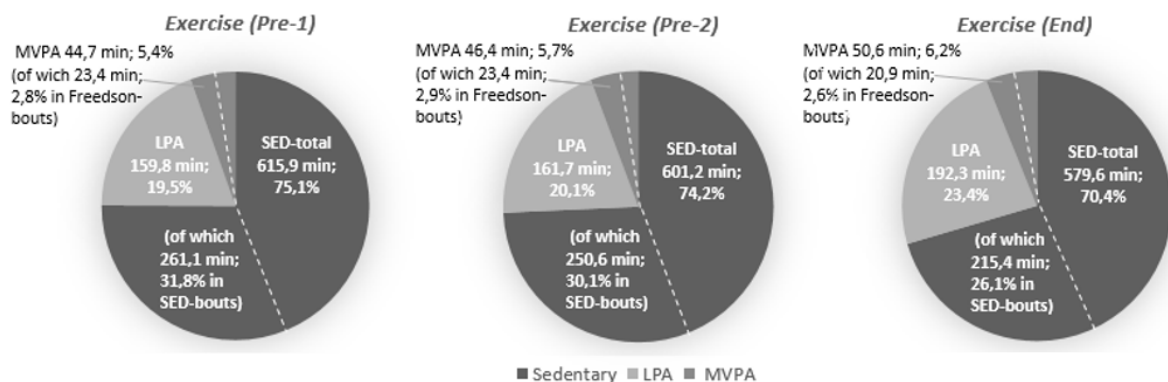


Figure 1. Physical activity patterns in the exercise group from three measures: Pre-1, Pre-2 and End, illustrated with the average absolute time per day (min); and as percentage of daily wear time (%) in SED, LPA and MVPA.

Validation of a LiDAR-based player tracking system during football-specific tasks

Theodoros M Bampouras¹, Neil M. Thomas²

¹Lancaster University, Lancaster Medical School, Faculty of Health and Medicine, Lancaster, United Kingdom

²Liverpool John Moores University, School of Sport and Exercise Sciences, Faculty of Science, Liverpool, United Kingdom

Email: t.bampouras@lancaster.ac.uk

Summary

Tracking players' movements is important for monitoring and optimization of training load. A novel LiDAR-based system purports to accurately measure velocity and acceleration of player movements. The study examined the validity of this system against a 3D motion analysis system. Two competitive football players completed nine sport-specific movements trials, recorded concurrently by the LiDAR and 3D systems. Instantaneous velocity and acceleration, and time spent within key performance indicator (KPIs) bands were compared between systems. RMSE and R^2 assessed agreement and goodness of fit, respectively. T-tests compared time within each KPI band. Velocity and acceleration RMSE values were low, while R^2 showed high agreement across all movements. Differences in time spent within each KPI band were mostly trivial. These results show that the LiDAR-based system can provide valid measures of velocity and acceleration in football-specific tasks, thus providing accurate tracking of players and calculation of relevant KPIs.

Introduction

Recent advances in electronic performance and tracking systems (EPTS) have allowed tracking football players' movements in training and competition [1], avoiding injuries and overload by monitoring and optimising training load and progression [2]. Additionally, live tactical changes are facilitated by in-game physical and tactical performance assessment. A new LiDAR-based system (Sportlight[®] LiDAR) purports to provide accurate velocity and acceleration metrics derived from player movements, with little set up time, no markers and high portability.

The aim of the study was to examine the validity of LiDAR against a 'gold standard' 3D motion analysis system (Icon).

Methods

Two competitive football players (age: 18 years, height: 1.74 ± 0.01m, mass: 66.5 ± 7.8kg, playing experience at this level: 3 years) completed nine trials each of six sport-specific movements, consisting of straight-line sprints, cuts, and curved runs. Trials were recorded concurrently by four LiDAR units and a 64-camera Icon system. Instantaneous velocity and acceleration, and time spent within key performance indicator (KPI) bands (defined by velocity and acceleration thresholds) were compared between systems. Agreement and goodness of fit were evaluated by root mean

square error (RMSE) and coefficient of determination (R^2), respectively. Time spent within each KPI band, as an indicator of work volume, was assessed with t-tests for statistical significance and Cohen's d for effect size.

Results and Discussion

Velocity RMSE ranged from 0.04m s⁻¹ to 0.14m s⁻¹ across all movements and acceleration RMSE ranged from 0.16m s⁻² to 0.7m s⁻², showing small deviation of the LiDAR system values from the Icon ones. R^2 values for velocity and acceleration ranged from 0.88 to 1.00 across all movements, indicating high agreement between the two systems. Finally, differences between systems in time spent within each KPI were trivial, except for Sprint and High deceleration where small differences were found (Table 1).

Table 1. Key performance indicators (KPIs) for velocity and acceleration. Velocity thresholds: slow (≥ 0.3 m·s⁻¹ and < 1.6 m·s⁻¹); moderate (≥ 1.6 m·s⁻¹ and < 4.2 m·s⁻¹); fast (≥ 4.2 m·s⁻¹ and < 5.5 m·s⁻¹); very fast (≥ 5.5 m·s⁻¹ and < 6.9 m·s⁻¹); and sprint (≥ 6.9 m·s⁻¹). High acceleration threshold: ≥ 3 m·s⁻². High deceleration threshold: < 3 m·s⁻². 3D and LiDAR data presented as mean ± SD. p: significance value ($\alpha = 0.05$). Cohen's d: effect size. RMSE: root mean square error.

	3D	LiDAR	p	Cohen's d	RMSE
<i>Velocity KPI</i>					
Slow	9.70 ± 2.94	9.42 ± 2.78	0.024	0.098 (trivial)	0.545
Moderate	24.97 ± 5.08	24.77 ± 5.13	0.005	0.04 (trivial)	0.33
Fast	6.19 ± 1.37	6.20 ± 1.33	0.908	0.005 (trivial)	0.25
Very fast	3.01 ± 0.92	2.97 ± 0.90	0.315	0.044 (trivial)	0.164
Sprint	0.21 ± 0.21	0.16 ± 0.23	0.119	0.264 (small)	0.158
<i>Acceleration KPI</i>					
High acceleration	19.79 ± 4.87	19.52 ± 4.82	0.002	0.057 (trivial)	0.413
High deceleration	4.95 ± 1.27	4.54 ± 1.25	< 0.001	0.325 (small)	0.488

Conclusions

The present results suggest that practitioners and coaches can use the LiDAR-based system to monitor workload through KPIs derived from velocity and acceleration, with no trade-off between portability and accuracy.

References

- [1] Buchheit M and Simpson M. (2017). *Int J Sports Physiol Perform*, **11**: S235-S241.
- [2] Akenhead R and Nassis GP. (2016). *Int J Sports Physiol Perform*, **11**: 587-593

Step count is related to habitual weight bearing asymmetry in the workplace: An occupational study in hotel employees

Alison N. Agres, Sónia A. Alves, Georg N. Duda
 Julius Wolff Institute, Charité –Universitätsmedizin Berlin, Berlin, Germany
 Email: alison.agres@charite.de

Summary

Although standing is often suggested to promote health in the sedentary workplace, extensive standing results in accumulated joint load from prolonged weight bearing and can consequentially lead to musculoskeletal pain. Weight bearing asymmetries apply asymmetric loads, which can exacerbate this problem, but could also serve as an indicator for imbalanced musculoskeletal loading. Here, we analyzed weight bearing asymmetry in an occupational setting and found that hotel workers that took more steps during a work shift exhibited improved overall weight bearing symmetry. These results imply that periods of dynamic movement can improve weight bearing asymmetry, which can break up extended static periods in active and sedentary workplaces.

Introduction

In the workplace, standing is typically recommended in order to avoid long sedentary periods. These static postures offer increased muscle activity versus sitting [1], yet prolonged standing still leads to detrimental musculoskeletal symptoms [2]. Longer periods of weight bearing (WB) lead to the accumulation of excessive joint loads that can precede occupational injury [3], which can accelerate when WB is asymmetric. It remains unclear how an individual's relative activity level, as determined by steps, affects overall WB asymmetries. Thus, the aim of this study was to determine the relationship between step count and side-to-side differences in weight bearing during a typical workday. In order to achieve this, instrumented insoles measured WB during shift work in active hotel employees.

Methods

Twenty participants (14 females, 31.9±7.9 years, 24.8±4.2 kg.m²) employed at five local hotels in reception, service, and housekeeping departments were recruited. The local ethics committee approved protocols and participants gave written informed consent. Each participant received an iPod and a pair of instrumented insoles (loadsol, novel GmbH), then instructed on data collection. Participants wore insoles for a minimum of one work shift within two weeks. Insoles recorded the overall plantar force from each foot, transmitted via Bluetooth to the iPod for local storage. Upon equipment recovery, raw data was downloaded. A custom-step recognition script (RStudio Inc.) identified periods of static and dynamic loading. The weighted Universal Symmetry Index (wUSI) [4] determined overall side-to-side load asymmetry over the entire measurement for each participant, where 0% indicates perfect symmetry and 100% indicates total asymmetry. After normality tests, one-way analyses of variance examined the effect of group on step count and wUSI values (p=0.05). A Pearson correlation examined the

relationship between the mean number of steps per shift and overall wUSI across all participants.

Results and Discussion

In an average shift, reception workers took fewer steps (3210±2424, p<0.01) compared to service and housekeeping (14729±4597 and 14874±3783, respectively). The overall proportion of dynamic loading was 14% in the reception group, compared to 40% in service, and 39% in housekeeping. A negative correlation was found between overall wUSI and mean number of steps taken per shift (Figure 1; $r = -0.540$; $p = 0.014$).

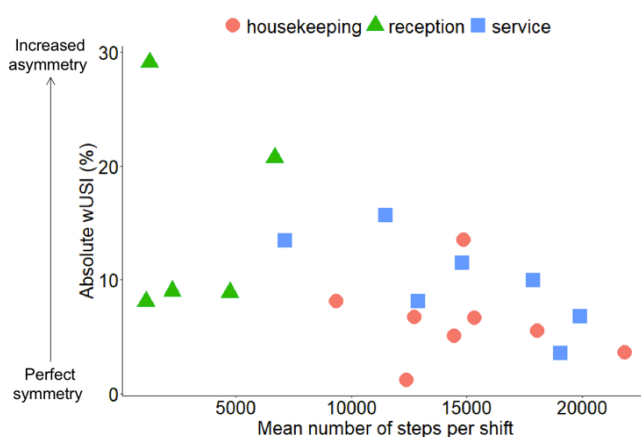


Figure 1: Absolute weighted universal symmetry index (wUSI) versus mean steps per shift for participant from the housekeeping (pink circles) reception (green triangles) and service (blue squares).

Of note, many participants exceeded a wUSI of 10%, which corresponds to levels of asymmetry measured during crutch-assisted gait in healthy participants in a gait laboratory [4]. These results further underline the disparity between laboratory measurements and real-life workplace settings. Further work in expanded cohorts should aim to understand weight bearing symmetry and its relationship to physical activity and musculoskeletal health.

Conclusions

Increased dynamic activity, measured by steps taken, corresponds to improved WB symmetry during a shift in active hotel workers. Prolonged static WB activity, such as standing, correlates to decreased WB symmetry or increased WB asymmetry.

References

- [1] Gao Y et al. (2017) *Med Sci Sport Exer*, **49**:1927–34.
- [2] Coenen P et al (2017) *Gait Posture*. **58**:310-8.
- [3] Kumar S. (2001). *Ergonomics*. **44**:17-47.
- [4] Alves et al. (2020) *Front. Bioeng. Biotechnol*, **8**: 57951.

An Automatic Inertial Measurement Unit Alignment Pipeline in Human Motion Measurement

Summary

This study presents an automatic pipeline to detect and correct misalignment in the Inertial Measurement Unit (IMU) - based human motion measurement. Novel algorithms were proposed and tested to successfully reduce IMU misalignment errors with great potential to an easy and reliable calibration.

Introduction

Movement injury is increasingly recognized as a global public health concern as ageing occurs worldwide in recent years, which calls for accurate and timely medical diagnosis and well-designed rehabilitation scheme for patients. (IMU)-based human motion tracking system, characterized by considerable accuracy, friendly costing, and low dependency on utilizing occasion, plays a more and more significant role in the clinical treatment process. However, misalignment could be caused by magnetic distortion during measurement, resulting in inaccurate joint angle estimation and failure in motion reconstruction. This study aims to develop a pipeline integrated with novel algorithms to automatically detect motion phase and correct IMU misalignment.

Methods

The experiment was conducted using a wireless IMU system (Trigno Avanti, Delsys, USA) and an electronic compass. Six IMUs were attached to a plane with corresponding axes pointing to the same direction (Y-axis to the global south). After keeping IMUs still for 5 to 10 seconds, the plane was rotated around the global up axis with a pitch motion in a range of -60° to 60° .

An algorithm based on the Riemannian distance on $SO(3)$ space was developed for the motion phase detection. The Riemannian distance is considered to be an intrinsic representation of rotation [1] to quantify relative motions between two adjacent frames and is calculated as

$$d = \frac{1}{\sqrt{2}} \log(\|R_1^T R_2\|_F)$$

where $\|\cdot\|_F$ denotes the Frobenius norm of the matrix. In addition, a high-order median average filter was utilized to smooth the processed signal to improve the threshold-based motion phase detection.

An algorithm to correct the IMU misalignment was also proposed: first, the projection of Y-axis was calculated with a reference to the global coordinate frame; next, an average projection was calculated which was a considerable rotation standard; finally, a rotation around the global Up axis was

performed on the direction cosine matrix of each frame to ensure the Y-axis pointing to the same direction.

Results and Discussion

Fig. 1 gives a visualization of different motion phase during a representative experiment. By calculating the Riemannian distance between adjacent frames, the motion phases were detected. The algorithm could be applied to detect the still-to-move transition and simplify a calibration procedure in human motion tracking which often requires a manual segmentation of a static anatomical position.

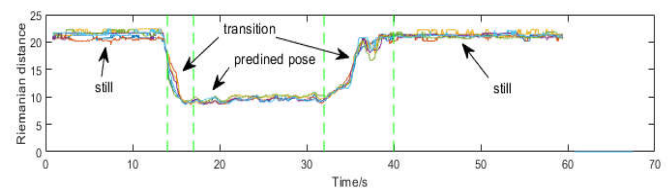


Figure 1: A representative result of motion phase detection. Green dash lines represent the boundary of motion phases.

As shown in the Fig. 2 (a), the IMU misalignment error decreased from 13° to 5.0° after the application of predefined pose and correction algorithm. The reduction was lower than 32.9% reduction as reported in the other study [2]. The repeatability test of ten experiments showed that the error was decreased from $13^\circ \pm 18^\circ$ to $5^\circ \pm 5^\circ$ (Fig. 2b); the correction algorithm further improved the precision with a variation of 0° (c), which was best when compared to the other algorithms [3].

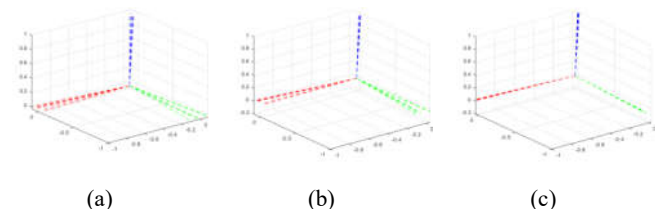


Figure 2: IMU coordinate frame with reference to global frame (a) before correction (b) after predefined pose (c) after correction algorithm.

Conclusions

The pipeline has shown to successfully improve the accuracy and precision in the IMU-based misalignment correction.

References

- [1] Yutao L et al. (2019) *Measurement*, **142**: 1-9,
- [2] Jehong L et al. (2018) *IEEE T IND ELECTRON*, **65**:1408-1419
- [3] Zhiqiang Z et al.(2015) *IEEE T BIO-MED ENG*, **62**:553-560

COVID-19 Impact on Physical Activity: A COVISTRESS Questionnaire Evaluation

Ugbole U.C.^{1,2}, Maïlys Clinchamps³, Julien S. Baker⁴, Baodong Gu¹, Frédéric Dutheil³

¹Faculty of Sports Science, Ningbo University, Ningbo, Zhejiang, China

²School of Health and Life Sciences, University of the West of Scotland, South Lanarkshire, Scotland, UK

³Physiological and Psychosocial Stress, LaPSCo, CNRS, Preventive and Occupational Medicine, WittyFit, University Hospital of Clermont-Ferrand, CHU Clermont-Ferrand, Université Clermont Auvergne, Clermont-Ferrand, France

⁴Department of Sport, Physical Education and Health, Hong Kong Baptist University, Kowloon Tong, Hong Kong

Email: u.ugbolue@uws.ac.uk

Summary

A global health emergency based on the COVID-19 outbreak was declared on the 30th of January 2020. Countries more susceptible to the COVID-19 situation included those with compromised, weak or vulnerable healthcare systems. During the COVID-19 global pandemic it became apparent that the lives of the citizens of the world would be affected from a public health, lifestyle and economy perspective. As a consequence, the spread of the COVID-19 pandemic continued to grow which gave rise to observing quarantine measures, social distancing measures, hospitalisation / bed rest measures and risks of physical inactivity brought about by immobilisation. This study aims to evaluate the effect of COVID-19 on leisure physical activity among 10,121 participants using a validated COVISTRESS questionnaire.

Introduction

The COVISTRESS network recently published a COVID-19 study associated with physical activity, sedentary action and psychological emotion [1]. Research in this area remains ongoing and continues to broaden. New COVISTRESS (<http://www.covistress.org/index-en.html>) questionnaires are developed ever so often to meet the demands of society in response to the changes brought about by the COVID-19 pandemic. On a global scale the impact of the COVID-19 pandemic continues to affect the lives of white-collared and blue-collared workers in our communities. Majority of these workers become emotionally distressed. In view of the first and second waves of the coronavirus, stringent lockdowns have been stipulated and as a consequence has led to reductions in physical activity levels and a rise in depression. This abstract highlights the impact COVID-19 has had on number of hours performed by the COVISTRESS questionnaire participants in terms of physical activity per week.

Methods

Participants were recruited via the application of the convenience and snowball sampling technique. All participants that satisfied the recruitment criteria were granted online access to the COVISTRESS questionnaire. 10,121 participants (Male: 2850, Female: 6292) completed the questionnaire. Of the 10,121 participants 979 did not indicate their sex. Two observational study scenarios were evaluated namely “Prior” to COVID-19 pandemic and “Currently”, i.e., during the COVID-19 period. Specific

information requested included number of hours of leisure physical activity per week “Prior” to the Coronavirus Pandemic and “Currently”. All these components were evaluated using a Spearman correlation (r) and the MAS with an intensity scale ranging from 0–100.

Table 1 Descriptive statistics showing the “Prior” and “Currently” dataset summary of the MAS intensity scale

Physical Activity Measurement	Assessment "Before" COVID-19 (Mean ± SD)	Assessment "Now" during COVID-19 (Mean ± SD)
Female: Number of hours of leisure physical activity per week	8.32 ± 7.29	5.99 ± 6.08
Male: Number of hours of leisure physical activity per week	10.39 ± 8.61	7.75 ± 7.61

Results and Discussion

Both males and females displayed similar output measures (Table 1). A stronger correlation between “Prior” COVID-19 and “Currently” was also observed among the Males ($r = 0.720$) in comparison to the Females ($r = 0.639$). The results presented in this abstract provide insightful information pertaining to physical activity using the COVISTRESS MAS intensity scale. On completion of the current dataset analyses, a 90% compliance was achieved with respect to completed COVISTRESS questionnaires.

Conclusions

A detailed assessment and report on the impact of physical activity has been presented. The aim of this study was achieved through the effective use and interpretation of the COVISTRESS questionnaire. These findings from the COVISTRESS questionnaire are encouraging and provide a platform from which future studies and collaborations across different countries can be fostered.

Acknowledgments

The authors would like to thank the COVISTRESS Network and all the participants involved in the study.

References

[1] Ugbole UC et al. (2020). *J. Clin. Med.*, **9** (10) 3352.

Effect of total contact cast on lower limb kinematics and kinetics during walking gait

Aoife Healy¹, Ilias Theodorakos², Panagiotis Chatzistergos¹ and Nachiappan Chockalingam¹

¹Centre for Biomechanics and Rehabilitation Technologies, Staffordshire University, Stoke on Trent, UK

²Univ Lyon, Univ Gustave Eiffel, LBMC UMR_T9406, F69622, Lyon, France

Email: a.healy@staffs.ac.uk

Summary

This study examined the effect of the use of total contact cast (TCC) on the range of motion and loading of the ankle, knee and hip joints during walking. While wearing the TCC, ankle kinematics and loading were significantly reduced and altered knee and hip kinematics were observed. The effect of a TCC on internal joint loading was quantified.

Introduction

TCC is widely used in the management of diabetic foot ulceration by offloading the foot and ankle. Wearing a TCC is known to significantly change the biomechanics of gait but its effect on internal joint loading is not fully understood. A possible increase in knee or hip joint loading could have a detrimental effect on comfort and increase the risk for injury. In this context, the aim of this study is to quantify the changes in lower limb joints caused by the use of a TCC.

Methods

Twelve participants were selected based on sex (6 males, 6 females), height (short, average, tall) and BMI (healthy, obese) with no known medical conditions, participated in the study. Participants performed walking trials with TCC (Figure 1a) and without TCC. Casting was done using a novel wood and biodegradable plastic casting material (Woodcast®, Onbone Oy, Espoo, Finland) [1,2].

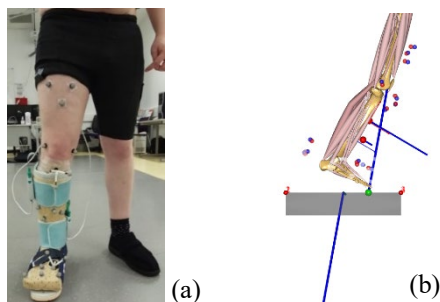


Figure 1: (a) Lower limb casted with TCC; (b) AnyBody musculoskeletal model.

Two force plates (AMTI, USA), a Vicon motion capture system (Vicon, OMG, Oxford, UK), and F-Scan pressure measurement system (Tekscan Inc., Boston, USA) provided measurements that served as inputs to subject specific musculoskeletal models that were developed in the AnyBody Modelling System (AMS) v 6.1.0, based on the "MoCap_LowerBody" model (Figure 1b). Simulations were performed to obtain joint kinematics and joint reaction forces.

Results and Discussion

One way (cast condition) repeated measures ANOVA with two between subject factors (sex, BMI) revealed a significant reduction for the TCC trials for talocrural plantarflexion, subtalar eversion and hip flexion, while knee flexion was significantly increased (Table 1). For the kinetic variables, the TCC resulted in significantly reduced talocrural proximodistal and mediolateral, and subtalar anteroposterior and mediolateral reaction forces, and a reduction in the peak vertical ground reaction force. Hip loading was not significantly affected by the TCC. A significant interaction was observed between the TCC and BMI for the knee proximal force; knee proximal force decreased for the obese participants when they wore the TCC (No TCC 4.7 BW vs. With TCC 4.1 BW), while it increased for the healthy participants (No TCC 4 BW vs. With TCC 5.4 BW). The healthy participants used a more upright posture with a less flexed knee and hip, which resulted in significantly increased knee proximal force.

Table 1: Significantly different variables ($p < 0.05$) between conditions (Mean (SD)).

Variable	p	No TCC	With TCC
Vertical ground reaction force (BW)	0.002	1.13 (0.06)	1.08 (0.07)
Talocrural plantarflexion angle (°)	0.002	23.8 (6.6)	17.2 (5.0)
Subtalar eversion angle (°)	0.037	-6.1 (8.5)	-12.4 (8.2)
Knee flexion angle (°)	0.011	11.6 (8.3)	28.4 (17.6)
Hip flexion angle (°)	0.047	18.8 (14.3)	9.3 (19.4)
Talocrural proximodistal force (BW)	0.017	-7.7 (2.1)	-5.9 (1.5)
Talocrural mediolateral force (BW)	0.040	1.7 (0.6)	1.3 (0.4)
Subtalar anteroposterior force (BW)	0.004	6.1 (1.8)	4.0 (1.4)
Subtalar mediolateral force (BW)	0.048	-0.6 (0.7)	-0.0 (0.7)

Conclusions

Participants used different movement strategies based on their BMI to overcome the restricted ankle movement imposed by the TCC. While results support the use of TCCs where a reduced foot and ankle loading is required, longitudinal studies are needed to understand the effect of altered knee and hip kinematics and knee loading on individuals using a TCC.

Acknowledgments

This research was funded by Woodcast®. The funders had no role in study design, data collection and analysis, or preparation of this abstract.

References

- [1] Chatzistergos P. et al. (2020). *Clin Biomech*, **77**: 105064.
- [2] Martynov I. et al. (2020). *Bone Joint J*, **102**:1405-1411.

Determining the optimal limb symmetry index threshold for classifying anterior cruciate ligament injury status in pediatric patients

Nicholas J. Romanchuk¹, Michael J. Del Bel², Celine I. Girard¹, Teresa Flaxman³, Sasha Carsen⁴, Daniel L. Benoit²

¹Ottawa Carleton Institute for Biomedical Engineering, University of Ottawa, Ottawa, Canada

²School of Rehabilitation Sciences, University of Ottawa, Ottawa, Canada

³Children's Hospital of Eastern Ontario Research Institute, Ottawa, Canada

⁴Division of Orthopaedic Surgery, Children's Hospital of Eastern Ontario Research Institute, Ottawa, Canada

Email: dbenoit@uottawa.ca

Summary

The objective of this study was to determine the optimal limb symmetry index (LSI) cut-off threshold for classifying anterior cruciate ligament (ACL) deficient and uninjured paediatric patients. Forty-two ACL injured patients (ACLi) and 69 matched uninjured controls (CON) performed isometric strength and hopping tasks. Classification trees (CT) were then trained according to different LSI cut-off thresholds. A LSI threshold of 89% had the highest Mathew's Correlation Coefficient (MCC) with 0.662, a specificity of 93%, and a sensitivity of 70%. Thus, based on our analysis, it appears the 89-90% LSI cut-off is an appropriate threshold for separating the hopping and strength performance of ACL injured paediatric participants.

Introduction

Following a paediatric ACL reconstruction the risk for a subsequent ACL injury is extremely high, with approximately 17-30% of paediatric patients sustaining a second ACL injury within two years [1]. Despite the high rate of re-injury, no consensus exists for what performance thresholds should be reached prior to return-to-activity (RTA). In adult populations, most contemporary RTA guidelines recommend a >90% LSI for single-leg hopping and strength tests; however, there is limited evidence supporting the >90% threshold in paediatric patients. In fact, research suggests that LSIs used by paediatric orthopaedic surgeons can range from 75-95% [2]. Therefore, the purpose of this study was to determine which LSI cut-off threshold should be used when classifying ACL deficient and uninjured paediatric patients.

Methods

Forty-two ACLi patients (30 females; 10-18 years old) and 69 CON (36 females; 10-18 years old) were recruited for this study. Participants performed isometric knee extension and flexion tasks on an isokinetic dynamometer. Jump distance and time were also recorded during series of single-leg hopping tasks. LSIs were calculated as injured/uninjured limb for ACLi and non-dominant/dominant limb for CON. LSIs with significant between group (ACLi vs CON) differences (independent *t*-tests), were used in a machine learning algorithm. LSIs were then converted from percentage to categorical 'pass/fail' grades according to cut-off thresholds ranging from 70-100%. CTs were then fit to the converted categorical data at each cut-off threshold. Ten-fold cross-validation was used to determine the optimal tree complexity. Model performance was evaluated according to Mathew's Correlation Coefficients (MCC), sensitivity and specificity.

Results and Discussion

Statistically significant differences ($p < 0.05$) were identified in the maximum anterior, lateral and triple hop distances, timed 6m hop, and knee extension strength LSIs. These variables were then included in a machine learning algorithm. When the data was converted from percentage to categorical 'pass/fail' grades using LSI cut-off thresholds, a plateau in the MCCs occurred between LSIs thresholds of ~85-90%. A LSI threshold of 89% had the highest MCC with 0.662, as well as a specificity of 93% and a sensitivity of 70%.

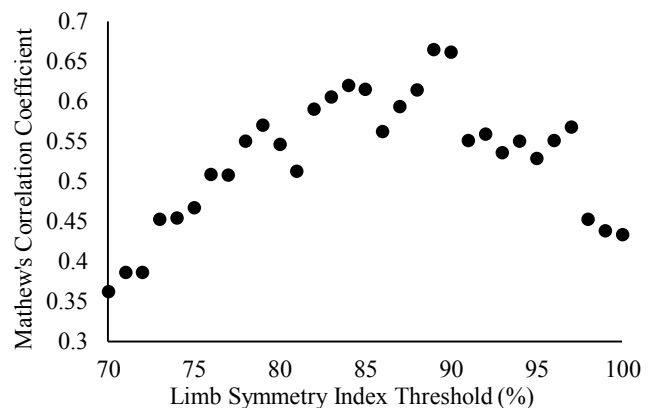


Figure 1: The classification tree MCCs according to different limb symmetry index cut-off thresholds.

Conclusions

By applying a machine learning model at different LSI cut-off thresholds we were able to determine that LSI thresholds in the 85-90% range provided the most accurate classification of paediatric ACL injury status (Figure 1). Thus, based on our analysis, it appears the 90% LSI cut-off is an appropriate threshold for separating the hopping and strength performance of ACLi and CON paediatric participants. Finally, considering that assigning LSI cut-off thresholds improves the interpretability of the functional tests while also offering an accurate classification for injury status, our findings suggest that LSI thresholds are viable in a clinical environment.

Acknowledgments

The authors would like to thank the Ontario Graduate Scholarship, Natural Sciences and Engineering Research Council of Canada and the University of Ottawa.

References

- [1] Wiggins AJ et al. (2016). *Am. J. Sports Med.*, **44**: 1861-76
- [2] Greenberg EM et al. (2019). *Orthop. J. Sport Med.*, **7**: 1-14

A dynamic model of the ankle joint with artificial articular surfaces and its validation against corresponding experiments

Daisy Ferraro^{1,2}, Claudio Felvedere¹, Alberto Leardini¹, Maria Ruiz³, Sorin Siegler³

¹Movement Analysis Laboratory, IRCCS Istituto Ortopedico Rizzoli, Bologna, Italy

²James Watt School of Engineering, University of Glasgow, Scotland, UK

³Department of Mechanical Engineering and Mechanics, Drexel University, Philadelphia, PA, USA

Email: daisyferraro@tiscali.it

Summary

In-silico models are essential for understanding the biomechanics of the human ankle joint. However, prior to their use, validation against experimental data is required. The goal of this study was to further develop one of these models to include artificial articular surfaces designed to mimic the natural geometries of one anatomical specimen and to validate it against corresponding experimental data via a dynamic simulation approach. The loading conditions for the dynamic simulations were obtained from the in-vitro experiment on the corresponding anatomical specimen. Model predictions, in terms of angular displacements of the ankle joint complex (AJC), compared well with the experimental results, thus demonstrating that such model is a good reproduction of the anatomical specimen. When provided with the same physiological loading conditions, all artificial surfaces were able to reflect the mechanics of the joint with natural surfaces.

Introduction

The difficulty in accessing the internal parts of the AJC during in-vitro experiments is being overcome by the introduction of in-silico models with the potential to improve the surgical techniques and clinical outcomes of Total Ankle Replacement. In particular, an image-based model including three-dimensional bone geometries, cartilage compensation, and ligament fibre recruitment was developed [1,2] and validated against experimental data [3,4] using standard sinusoidal curves.

In the present study, the model was extended to include artificial articular surfaces and its predictions were compared to experimental data using the corresponding loading curves from the experiments.

Methods

Morphological details of the ankle bones were obtained from medical imaging of an anatomical specimen and cartilage compensations were added at the articulations. The 3D bone geometries were imported in ADAMS (MSC Software Corporation, California, USA), where the ligaments were modelled as tension-only force elements with non-linear strain [1,2]. Artificial articular surfaces (a cylindrical surface, a standard cone with medial apex, and a skewed cone with lateral apex) designed to replace the natural shapes were virtually implanted on the model.

The loading conditions used to run the dynamic simulations were extracted from the corresponding experimental internal-external rotation and inversion-eversion torques [3,4]. Model predictions, in terms of angular displacement of the AJC, were compared to the experimental kinematics.

Results and Discussion

The application of the corresponding loading conditions in the model produced load-displacement curves that were very similar to the experimental ones (Figure 1). Moreover, the model predictions reflected the pattern depicted by the experimental results, according to which the joint with standard conical surfaces allows the greatest internal-external rotation and inversion-eversion range of motion (29° and 30°), closely followed by the joint with cylindrical surfaces (27° and 29°) and skewed conical surfaces (26° and 29°). On the other hand, the joint with natural surfaces is characterised by the smallest range of motion, suggesting that such surfaces, together with the ligaments, provide a more constraining effect.

The application of the physiological loading conditions from the natural joint to the joint with three different artificial surfaces showed that all surfaces are good at replicating the motion of the natural joint, which was found to be smaller by just 0-3° depending on the type of surface and torque applied.

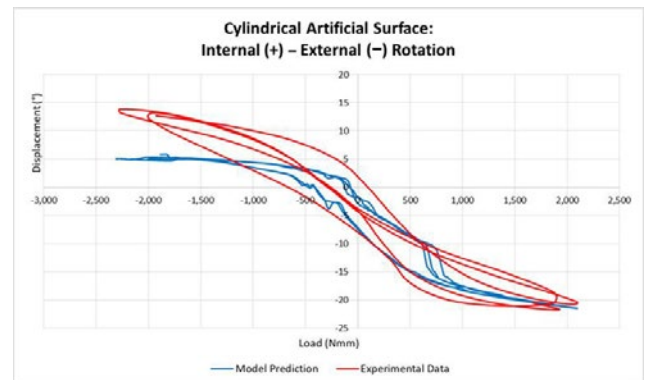


Figure 1: A typical load-displacement graph comparing experimental data (red) and model prediction (blue).

Conclusions

This study has shown that experimental data can be used to further validate the model, whose predictions with artificial surfaces were found to be better than those with natural surfaces. The results presented suggest that this model can be used for future works on prosthetic devices for total ankle replacement with various articular surface geometries.

References

- [1] Imhauser CW et al. (2008). *J.Biomech.*, **41**: 1341–1349.
- [2] Palazzi E et al. (2019) *J.Biomech.*, **98**: 109421.
- [3] Felvedere C et al. (2017) *J.Biomech.*, **53**: 97–104.
- [4] Felvedere C et al. (2018) *J.Biomech.*, **5**: 159–163.

JOIN THE
LARGEST
COMMUNITY
USING
**GOLD
STANDARD**
MOTION
MEASUREMENT
TOOLS

VICON

www.vicon.com/lifesciences

Tues 27th July – 15.30-16.00
Vicon panel discussion
hosted by Dr Kim Duffy

Weds 28th July – 12.15-12.45
Vicon live demo:
'comparing two shoe types
while hopping'

PROUD TO
SPONSOR



xsens

Attend our workshops
at ISB2021

1 **Generating automated reports with Xsens, bridging the gap between data and analysis**

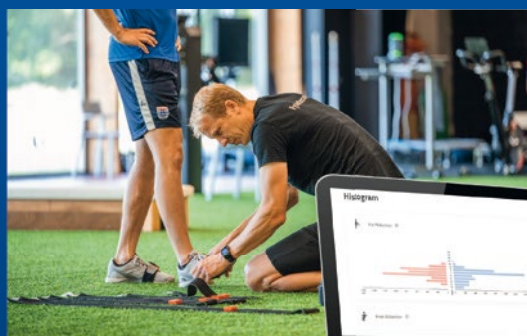
JULY 27TH
3:30PM-4:00PM

With MVN Reports you can easily generate automated reports for Health, Ergonomics and Sports. Powered by the new Xsens MotionCloud platform, MVN Reports instantly present complex movement data in an accessible, easy-to-read report. In this workshop we will show you how you can easily generate an automated Gait Analysis report with MVN Reports.

This report is automatically generated on the Xsens MotionCloud platform. The data is processed in the unique 'Xsens Sensor Fusion Engine, providing accurate and validated data. All that's required is an Xsens MVN motion capture setup and access to Xsens MotionCloud.

During this workshop, we would like to give you an insight in the functionalities of MVN Reports and the reports roadmap. Also, we would like to give you an in-depth introduction to the Gait Analysis report specifically.

In as little as a few minutes, a full standardized report with relevant data for that specific application is created. Also, the motion data is visualized as a 3D avatar.



2 **Sneak peek: ACL patient tracking platform generates immediate objective results**

JULY 28TH
12:15PM-12:45PM

Objective measurements can now be visualized in automated reports as part of a new platform aimed at improving the rehabilitation phase of an ACL patient. Xsens MotionCloud generates a Knee Assessment Report which contains objective results of nine knee stability tests like 'single hop for distance' or a 'drop vertical jump'. Joint angles, distances, symmetries and automated LESS are visualized in the report.

The MotionCloud report is integrated into a patient tracking platform, where it is combined with the results of patient surveys (IKDC, Tegner, etc.) training specific programs and other measurement. This platform aids a physiotherapist to monitor a patient through the rehab phases, keeping the patient motivated. A dashboard displays the criteria that need to be met to elevate a patient to the next phase.

www.xsens.com



Thank You!

Congress sponsor

QUALISYS
Motion Capture Systems

Major sponsors

VICON

XSENS

Basic Sponsor

novel.de

Qualisys Partners

DELSYS
WEARABLE SENSORS
FOR MOVEMENT SCIENCES

AMTI
FORCE AND MOTION

h/p/cosmos

NORAXON

Minor Sponsors

cometa

sagemotion

simi
reality motion systems

*The
Motion Monitor*

Sponsor

